Technetium Complexes with Labile Ligands

and

Coordination Chemistry of Organoselenium and -tellurium Compounds

Inaugural-Dissertation
to obtain the academic degree
Doctor rerum naturalium (Dr. rer. nat.)

submitted to the Department of Biology, Chemistry, Pharmacy
of Freie Universität Berlin

by

Maximilian Roca Jungfer

2022

The work for the present dissertation has been conducted between Oct 2018 and Dez 2021 under the guidance of Prof. Dr. Ulrich Abram at the Institute of Chemistry and Biochemistry (Department of Biology, Chemistry, Pharmacy) of the Freie Universität Berlin and Prof. Dr. Ernesto Schulz Lang at the Departamento de Química of the Universidade Federal de Santa Maria in Santa Maria, Rio Grande do Sul, Brazil.

I hereby declare that the dissertation submitted is my own work. All direct or indirect sources used are acknowledged as references.

1st reviewer: Prof. Dr. Ulrich Abram

2nd reviewer: Prof. Dr. Roger Alberto

Date of defense: 25.04.2022

Acknowledgement

Firstly, I want to express my gratitude to my supervisor Prof. Dr. Ulrich Abram for the opportunity to work on the special fields of technetium and chalcogen chemistry in his research group. Furthermore, I want to thank him for his kind support, advice and guidance. I am especially grateful for the encouragement and the freedom to follow and develop my own ideas and interests within these projects. I will not forget the lessons about Tom Bombadil and work on further improving my sometimes-lengthy wording. I am very grateful for all that I learned from you and I am glad that I accepted the offer to work in your group.

Secondly, I humbly express my gratitude to Prof. Dr. Roger Alberto for being the second reviewer of this thesis but also for the discussions about technetium carbonyl chemistry, which enabled me to learn a lot and often challenged my beliefs in a critical, productive way.

I want to thank Prof. Dr. Ernesto Schulz Lang for the opportunity to come to Brazil, work in his laboratory and for showing me the endorsing Brazilian serenity. Thank you for the wonderful stay with your neighbors, the lovely food, the great trip to the canyon, the fishing, the Ubajara jungle and cave tours and of course the great trip to Fortaleza. You and Elida are some of the kindest people I have met over the last years and for that I am truly grateful.

I want to thank Dr. Adelheid Hagenbach for her continuous friendship, the measurements of the crystal structures and her understanding ears in many situations

My special thanks are directed to Cassia Delgado and Dr. Sarah Hildebrandt who delivered an initial amount of bis(2-aminophenyl)diselenide as well as Jacqueline Grewe for the preparation of $(NBu_4)[ReOCl_4]$ and $[ReOCl_3(PPh_3)_2]$. I want to thank Falk Wenzlaff for the repeated syntheses of several technetium starting materials. Furthermore, I want to thank Jacqueline Grewe for her continuous support from organizational matters to the supportive company in the hospital during my Master-Thesis days. Thank you for everything!

I am grateful for the many students that either directly participated in some part of my research or worked on their independent projects with me: Johann Plaschke, Arseniy Galashov, Laura Elsholz, Moritz Johannes Ernst and Johanna Krüger. Thank you for your efforts and support!

I want to thank Detlef Wille and Rita Friese for the elemental analyses.

I want to thank Fabian Klautzsch for the introduction to the ESI-MS measurement and the whole BioSupraMol facility for the measurement of several spectra.

I want to thank the whole present and former Abram and Schulz Lang groups for the friendly welcome, the barbecues, the show lectures and everything else. You guys know who you are, and you know you rock. Nevertheless, I want to express special gratitude to Dr. Anna Grunwald, Domenik Nowak, Dr. Federico Salsi, Jonas Genz, Dr. Clemens Scholtysik, Dr. Carlos Rojas and Dr. Bruna Possato for the fun days in the lab and beyond. Distinctly, I want to thank Dr. Abdullah Abdulkader, Guilhem Claude and Moritz Johannes Ernst for our numerous discussions about analytics, chemistry, and slice of life. In this regard I also want to acknowledge the same for our kind Brazilian visitors Dr. Camila Nunez Cechin, Jéssica Fonseca Rodrigues, Dr. Felipe Dornelles da Silva, Dr. Sailer dos Santos as well as the wonderful souls of Prof. Dr. Roberta Cargnelutti, Prof. Dr. Barbara Tirloni and Prof. Dr. Vânia Schwade who made the last but amazing day in Brazil unforgettable for me.

I am thankful for the introduction into theoretical calculations from Prof. Dr. Paulo Cesar Piquini, the physicist who broke down the fundamentals for a mere chemist to grasp some of the possibilities offered by DFT also for synthetic chemistry.

I want to thank the DAAD for the financial support to go to Brazil and the Dahlem Research School for the financial support during the first year of my doctoral studies.

I would also like to thank my family and friends for the understanding and support throughout the whole doctorate, especially to my loving partner Laura John and to my mother Michaela Roca Padilla. Thank you to everyone for keeping me sane, your support was crucial to the success of this thesis.

Table of Contents

1 Introduction

1.1 Technetium Complexes

The first artificially produced element, technetium, was originally isolated from neutron-bombarded molybdenum sheets.[1] Consequently, the element was named after the Greek word *technetos*, meaning artificial or man-made.[1] After its initial discovery, technetium was also proven to exist on earth in natural uranium ores with a miniscule natural abundance given that it is mainly formed by spontaneous nuclear fission - a highly improbable event.[1] In a similar way, the majority of the currently produced technetium results from the nuclear fission of uranium in standard ^{235}U-fueled nuclear reactors.[2,3] One of the most probable fission products of the ^{235}U nucleus is the nuclide ^{99}Mo.[2,3] ^{99}Mo, however, is unstable and decays with a relatively short half-life of 66 h to give mainly the excited nuclear isomer ^{99m}Tc.[2,3] ^{99}Tc results from the relaxation of the ^{99m}Tc nucleus to the ground-state under γ-emission and ultimately decays with a half-life of ca. 200 000 years to stable ^{99}Ru.[2,3] The two nuclear reactions leading to the two common nuclides of technetium, ^{99m}Tc and ^{99}Tc, and the radioactive decay properties involved are shown in Figure 1.

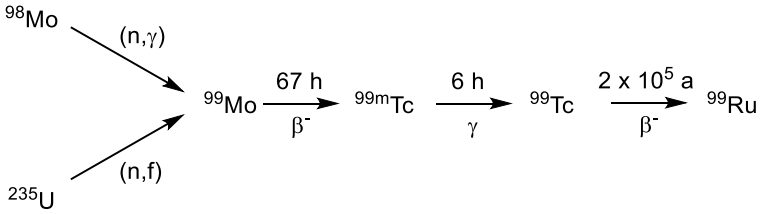

Figure 1. Nuclear reactions involved in the production of ^{99}Mo and its radioactive decay.[3]

The most important application of technetium concerns the metastable nuclear isomer ^{99m}Tc, which is used in nuclear medicine for single photon emission computed tomography (SPECT) due to its beneficial γ-decay properties such as a low energy and a reasonable half-life of 6 h.[2,4] The mother nuclide of ^{99m}Tc, ^{99}Mo, for such applications is mainly produced from controlled nuclear fission reactions through the exposure of suitable targets containing ca. 20% of the fissile uranium isotope ^{235}U to the high neutron flux of a nuclear reactor.[2,3] Nuclear medical applications of ^{99m}Tc were sparked by the introduction of the ^{99}Mo/^{99m}Tc generator system in the early 1960s, where a steady formation of ^{99m}Tc-pertechnetate by the β^- decay of immobilized ^{99}Mo-molybdate enabled the in-house production of ^{99m}Tc as well as the formation of the corresponding imaging agents.[2,5,6] Ever since that time a major interest in the chemistry of technetium revolved around the development of novel chelators and imaging agents with an improved and specific biodistribution.[2,4,6] The structures of

three important ^{99m}Tc-based imaging agents are shown in Figure 2.[4,6] The hexakisisocyanide complex ^{99m}Tc-sestamibi is a myocardial imaging agent and the most frequently used radiopharmaceutical diagnostic agent, while the also commonly used technetium(V) oxido complexes ^{99m}Tc-HMPAO and ^{99m}Tc-MAG3 are used as imaging agents for cerebral and renal imaging respectively.[4,6,7]

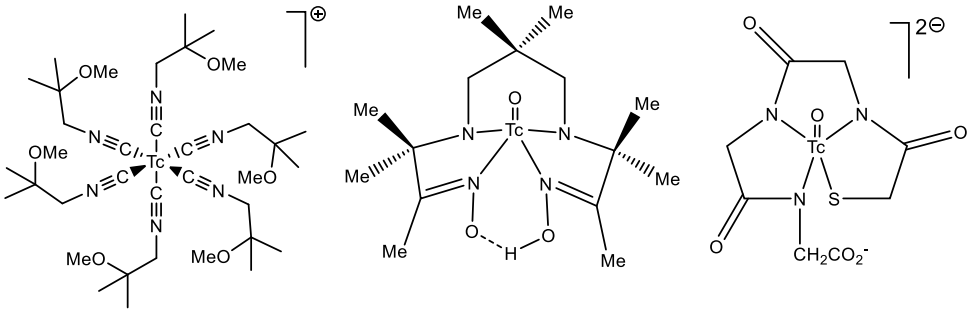

Figure 2. The structures of three important ^{99m}Tc-based radiopharmaceutical imaging agents.[4,6,7]

Interestingly, nuclear medicine is not the only important aspect of technetium chemistry. ^{99}Tc forms and accumulates alongside numerous other long-lived fission products in the ^{235}U-enriched fuel that powers most nuclear reactors.[2,8,9] The fission yield of ^{99}Tc is high with ca. 6% and contributes ca. 10% to the total mass of fission products.[2,3] In such reactors, the ^{235}U nuclei are cleaved in a nuclear reaction by the impact of a neutron of sufficient energy under the emission of heat and excess neutrons or convert to even heavier elements by neutron capture.[2,8,10] An initial enrichment of fissile ^{235}U to ca. 3% is required in a potential fuel to sustain a nuclear fission cascade. [2,8,10] The prevalent isotope in natural uranium is ^{238}U resulting in a consequently low abundance of ^{235}U of ca. 0.71%.[8,9] Until the fuel is too depleted in the fissile nuclide ^{235}U to provide a sufficiently high neutron flux to support the self-sustaining nuclear fission chain-reaction, the released thermal energy can be harvested and converted into electrical power.[8,9] Nuclear fuel that no longer fulfils the requirements of an efficient self-sustaining nuclear fission reaction is considered spent nuclear fuel.[8,9] Spent nuclear fuel represents the largest portion of high-level radioactive waste produced by human-kind.[9] It mainly consists of UO_2 (ca. 96%) that still contains significant amounts of fissile ^{235}U alongside fission and decay products as well as transuranium elements formed by neutron capture.[8,9] Therefore, the recovery of the nuclear fuel ^{235}U (and fissile plutonium) from spent nuclear fuel has been extensively studied to reduce the requirement for fresh uranium ore, which finally culminated in the development of nuclear fuel recycling processes.[11] The flow-chart for one commercial process, the classical plutonium uranium reduction extraction (PUREX) process, is given in Figure 3.

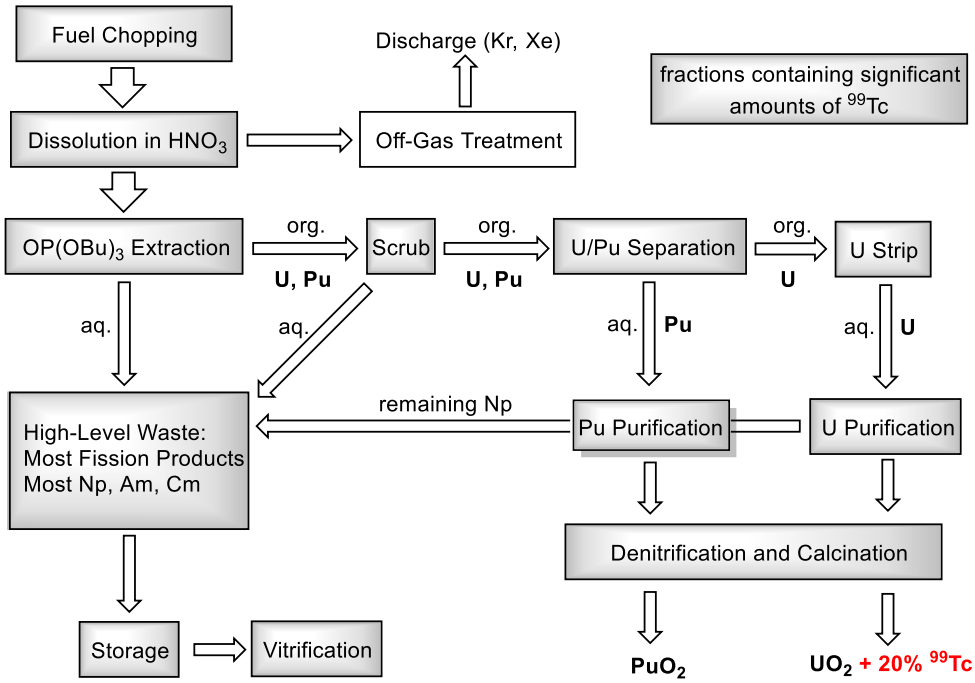

Figure 3. Flow-chart for one of the classical plutonium uranium reduction extraction (PUREX) processes where ^{99}Tc is contained in every product and waste fraction.[11]

Besides the recovery of uranium, a main aim of the PUREX processes is the volumetric reduction of high-level waste, which is accompanied by a significantly increased volume of low-level waste. Since ^{99}Tc is present throughout all fractions of the nuclear fuel recycling process, the nuclide majorly contributes to the high-level and low-level waste generated by the process.[2,10,11] The enrichment of ^{235}U in the uranium that is recovered through the PUREX process is too low for the direct regeneration of the nuclear fuel and, thus, ^{235}U is further enriched from the mixture in the same way natural uranium is processed.[8,10] ^{235}U and ^{238}U are separated through gaseous diffusion or through gas-phase centrifugation of the volatile uranium hexafluoride, UF_6.[8,10,11] In contrast to natural uranium, however, the uranium stream obtained through the standard PUREX procedure shown in Figure 3 contains ca. 20% of the technetium generated during nuclear fission.[2,12] If technetium is not removed from the uranium stream before the re-enrichment procedure, highly volatile technetium species form under the oxidizing conditions applied.[2] Most notably, the hexafluoride TcF_6 or related fluorides and oxyfluorides cause major environmental hazards as they are easily released into the environment through the discharge of polluted airstreams.[2,12] Nowadays, strict regulations limit the allowed discharge of ^{99}Tc at the enrichment sites.[13-16] Consequently, over 99% of the initially contained technetium has to be separated from uranium during the PUREX procedure before the re-enrichment to limit the unavoidable release of the artificial element.[2,12,17] In the early days of the nuclear fuel recycling, the Sellafield reprocessing plant alone discharged a total activity of ca. 300 TBq (≈ 0.5 t;

specific activity of ^{99}Tc: 6.2·10^{8} Bq/g) of ^{99}Tc between 1978 and 1980.[12-16] An adjusted PUREX process that accounts for technetium is shown in Figure 4.

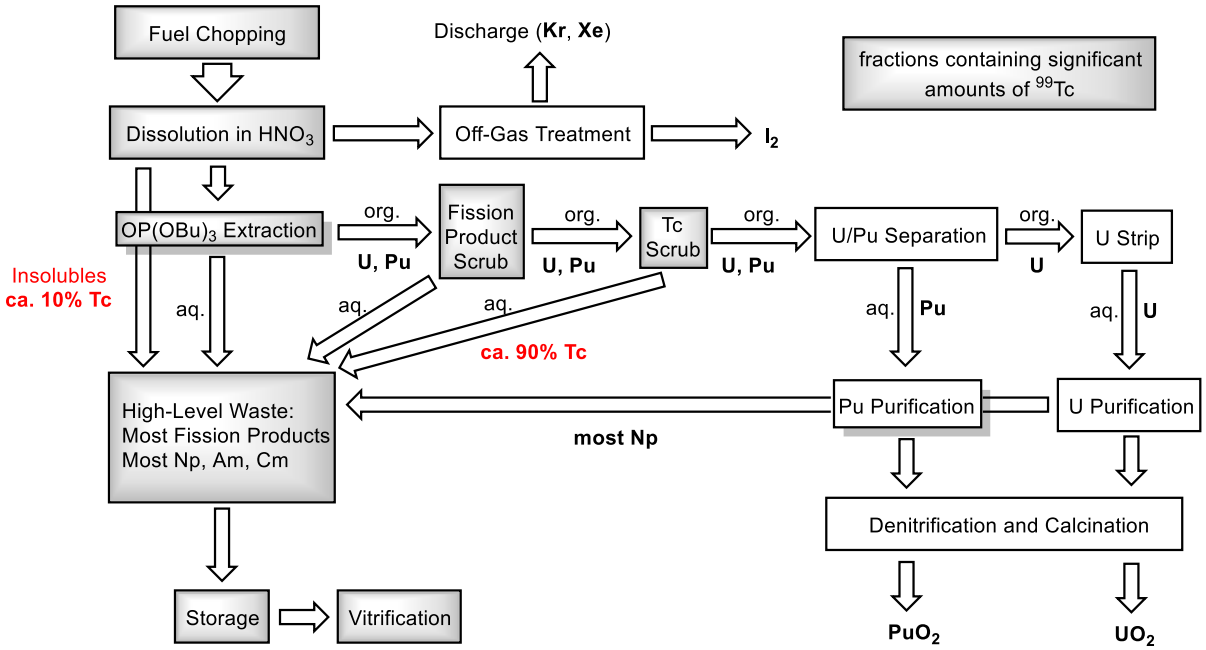

Figure 4. Flow-chart for a technetium-accounted plutonium uranium reduction extraction (PUREX) process where ^{99}Tc is contained in the waste fractions, but not in the products.[11]

Even with the implementation of strict regulations and the accounting for technetium in the nuclear fuel reprocessing, the resultant high-level radioactive waste containing technetium presents an environmental concern with regard to the final deposition in a nuclear waste containment repository, while the discharge of low-level radioactive waste may still carry significant amounts of technetium into the environment.[2,9,17-20] Parallelly, the accidental release of technetium into the environment poses a risk that cannot be prevented entirely as has been seen through the leakage of dissolved technetium into the ground water at problematic nuclear waste sites such as the Hanford wastewater tanks.[12,17,21-25] Overall, the Hanford waste site alone contains ca. 0.9 PBq (≋ 1.5 t) of ^{99}Tc in ca. 200 m³ of high-level radioactive waste as remnants of the plutonium production for nuclear weapon development during the Manhattan project.[17,21-25] Due to its omnipresence in nuclear waste, high environmental mobility and the long half-life of ca. 200 000 years, ^{99}Tc is one of the major concerning factors in the nuclear waste produced by the use of nuclear power.[2,9,12,17,18,20]

Technetium, once an element of low natural abundance, has made its way into the biosphere and the lithosphere not only through the continuous release by nuclear fuel recycling plants but also through the uncontrolled release by nuclear disasters such as the Chernobyl catastrophe.[12,20,26] Other contributing factors include the testing (and use) of nuclear arsenal and weaponry that also released large amounts of radioactive fission products into the environment.[12,20] In comparison, the long-term

accumulation of technetium in the environment through the continuous release of ^{99m}Tc (and thus ^{99}Tc) through medical applications of the element cannot be denied but plays a minor role.[2,12,20] The ultimate biological and geochemical fate of technetium, however, is largely unknown although an increasing amount of the element has undisputedly entered the human habitat.[12,20]

Thus, four main pillars govern the interest in the chemistry of technetium:

1. Radiopharmacy
2. Behavior in the nuclear fuel cycle
3. Behavior in the environment
4. Behavior towards biologically relevant ligands

In the light of these four main challenges in technetium chemistry, it is imperative to assess the basic inorganic, organometallic and coordination chemistry of technetium through the synthesis and characterization of defined molecular species and the study of their properties. Given the numerous and complex redox processes present in all these areas especially highly reduced and highly oxidized complexes play a major role. Exemplarily, complexes containing the $\{^{99}Tc(CO)_3\}^+$-motif were found in problematic nuclear waste sites such as the Hanford waste-water tanks.[21-25] In this context the study of the basic chemistry of technetium hydrides and especially the chemistry of technetium carbonyl hydrides became relevant and has been considered in this thesis (Publication 1: *Organometallics*, **2021**, *40*, 3095-3112).

The fundamental chemistry of technetium hydrido complexes revolving around $[TcH_3(PPh_3)_4]$ and the derived technetium(I) carbonyl hydride $[TcH(CO)_3(PPh_3)_2]$ have been studied. The potential of the seven-coordinate trihydride complex as a starting material for other hydrido complexes of technetium was evaluated and especially the reactions of $[TcH(CO)_3(PPh_3)_2]$ with inorganic and organic Brønsted acids and their reversible carbonylation/decarbonylation behavior were investigated. The immediate displacement of H_2 in such protonation reactions provides a viable and flexible method for the systematic preparation of the scarcely studied chemistry of *mer*-tricarbonyl complexes of technetium. ^{99}Tc NMR spectroscopy was revealed as a convenient and powerful tool to distinguish di- and tricarbonyl complexes as well as the *mer*- and *fac*-isomers of the formed products.

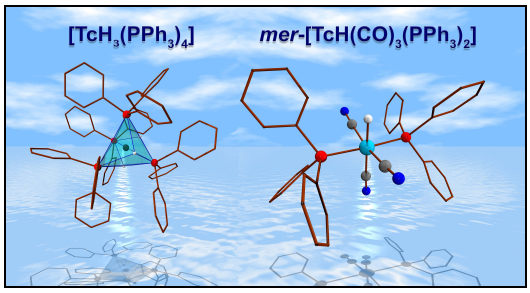

Organometallics, **2021**, *40*, 3095-3112.

Commonly, hydrido complexes are good starting materials for further reactions with other ligands due to their reactivity. Since the protonation of $[TcH(CO)_3(PPh_3)_2]$ inevitably proceeds through an intermediate H_2-complex, it became interesting to investigate the protonation of $[TcH(CO)_3(PPh_3)_2]$ with Brønsted acids of less-coordinating counter-ions to isolate a defined functional analog of the 16 e^- metallo Lewis-acidic $[Tc(CO)_3(PPh_3)_2]^+$. The protonation of $[TcH(CO)_3(PPh_3)_2]$ with protic acids of weakly coordinating anions results in the formation of the $[Tc(OH_2)(CO)_3(PPh_3)_2]^+$ cation even in the absence of water and when using the oxonium acid $[H(OEt)_2][BArF_{24}]$. In situ NMR spectroscopy suggests the formation of water by the protolysis of diethylether from the oxonium cation at the highly Lewis-acidic $\{Tc(CO)_3(PPh_3)_2\}^+$ fragment. A near-quantitative and scalable synthesis of the $[Tc(OH_2)(CO)_3(PPh_3)_2]^+$ cation enabled the study of its reactivity, which has been done in publication 2 (*Inorg. Chem.* **2021**, *60*, 16734-16753).

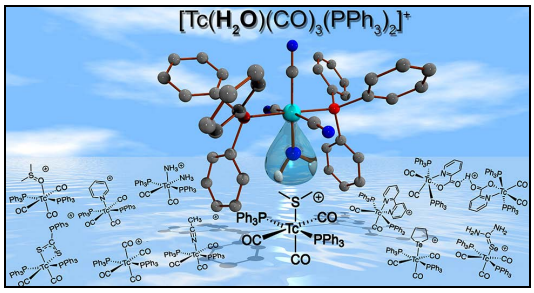

Inorg. Chem. **2021**, *60*, 16734-16753.

The $[Tc(OH_2)(CO)_3(PPh_3)_2]^+$ cation was shown to be a valuable synthon for the preparation of stable and inert or unstable and labile technetium(I) complexes with neutral ligands having C, O, N, S, Se and Te donor atoms formally derived from the unsaturated 16 e^- metallo Lewis-acidic $[Tc(CO)_3(PPh_3)_2]^+$. One of the highlights of this work was the isolation of the stable mixed carbonyl ammine complex *cis-cis-trans*-$[Tc(NH_3)_2(CO)_2(PPh_3)_2]^+$ which was ultimately supported by a ^{15}N-labeled isotopic study and X-ray diffraction. Among others, the first unidentate selenoether complexes have been structurally characterized and the first telluroether complexes of technetium were prepared. Thioether complexes of the type $[Tc(SR_2)(CO)_3(PPh_3)_2]^+$ have a potential as highly reactive, non-protic substitutes for $[Tc(OH_2)(CO)_3(PPh_3)_2]^+$ as synthons for the 16 electron compound $[Tc(CO)_3(PPh_3)_2]^+$. ^{99}Tc NMR proved an invaluable tool for the characterization and structural assessment of the resulting complexes even in complex mixtures.

The high reactivity of the $[Tc(OH_2)(CO)_3(PPh_3)_2]^+$ cation with neutral ligands immediately suggested a similar reactivity towards anionic ligands due to charge compensation. Surprisingly, the coordination chemistry of technetium with many fundamental anionic inorganic ligands with relevance to nuclear waste sites such as nitrite, nitrate, azide, chalcogenocyanates, tetraoxidometallates and more have only been studied scarcely. The reactions of $[Tc(OH_2)(CO)_3(PPh_3)_2]^+$ with seemingly simple anionic ligands, however, proved surprisingly complex. An overview of the reactions of $[Tc(OH_2)(CO)_3(PPh_3)_2]^+$ with various fundamental anionic ligands has been published in publication 3 (*Inorg. Chem.* **2022**, *61*, 2980-2997).

The course of reactions of $[Tc(OH_2)(CO)_3(PPh_3)_2]^+$ with azide sources depends on the nucleophilicity of the reagent. For sodium azide, a surprising preference for the nucleophilic attack at one of the carbonyl ligands has been observed. Reactions with chalcogenocyanates initially form complexes that are coordinated through the ligands chalcogen atom but quickly isomerize to give the nitrogen coordinated products. The isomerization was slow when the potassium salt of selenocyanate was employed and a mixture of *Se*- and *N*-bound products was isolated. In contrast reactions with potassium cyanate and thiocyanate only yield the *N*-bound isomers. The sole formation of the N-bound selenocyanato product was achieved using the weakly coordinating cation bis(triphenylphosphonio)iminium, revealing a non-innocence of the cations in reactions of technetium complexes with anionic ligands. The N-bound NCSe-complex is not stable and slowly eliminates elemental selenium to give the stable cyanido complex. Mixed carbonyl nitrito and nitrato complexes of technetium were shown to engage in reversible carbonylation/decarbonylation processes. Both ligands coordinate to technetium in η^1 and η^2 modes. The first complex of technetium with an unsubstituted borohydrido ligand was structurally characterized revealing further insight into the possible intermediates and products formed in redox processes involving technetium. The mixed-valence complex $[Tc^{I}(OTc^{VII}O_3)(CO)_3(PPh_3)_2]$ containing both technetium(I) and technetium(VII) is obtained from the reaction of $[Tc(OH_2)(CO)_3(PPh_3)_2]^+$ with pertechnetate salts. Heating solutions of the mixed-valence compound in non-coordinating media results in the formation of a η^2-TcO_4^- complex due to the decarbonylation of $[Tc^{I}(OTc^{VII}O_3)(CO)_3(PPh_3)_2]$. If such reactions are performed in coordinating solvents, dicarbonyl solvent complexes are obtained instead. Both, the solvent and the η^2-$Tc^{VII}O_4^-$ complexes easily comproportionate to give the stable technetium(IV) oxide. The value of ^{99}Tc NMR was shown to characterize complex mixtures and identify subtle changes in the coordination sphere of technetium.

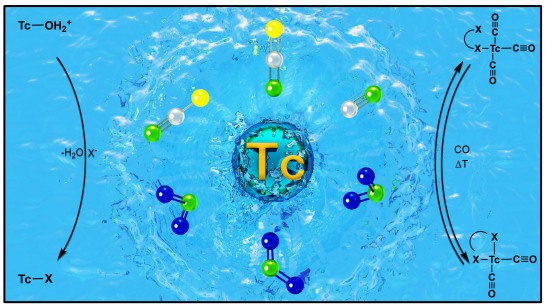

Inorg. Chem. **2022**, *61*, 2980-2997.

Given that not only small inorganic but also organometallic ligands may form under the conditions technetium is exposed to in nuclear waste repositories, in biological systems or in the environment also knowledge about the little developed fundamental organometallic chemistry of technetium becomes crucial. As the previously used synthon $[Tc(OH_2)(CO)_3(PPh_3)_2]^+$ is protic, a different starting material was desired for the work with organometallic reagents. Consequently, the labile and highly reactive dimethylsulfide complex $[Tc(SMe_2)(CO)_3(PPh_3)_2]^+$ was introduced as a functional analog of $[Tc(CO)_3(PPh_3)_2]^+$, where non-protic conditions were required. This approach towards a better understanding of the organometallic chemistry of technetium is presented in publication 4 (*Inorg. Chem.* submitted).

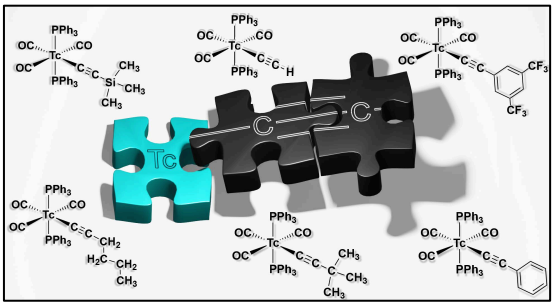

Inorg. Chem. submitted.

The organometallic chemistry based on the $\{Tc(CO)_3(PPh_3)_2\}^+$ fragment was studied systematically and led to the formation of air- and water-stable organometallic technetium complexes such as $[TcMe(CO)_3(PPh_3)_2]$, $[TcPh(CO)_3(PPh_3)_2]$ and $[Tc(Cp)(CO)_2(PPh_3)]$. The use of organolithium reagents for a transmetallation procedure proved crucial due to the high affinity of the starting materials for halides, which prohibited the use of Grignard reagents. Reactions with alkynols gave the first technetium cyclooxycarbene complexes and reactions with acetylenes in the presence of a base as well as reactions with lithium acetylides resulted in the first complexes of technetium containing ligands coordinating through a $\{C\equiv C\text{-}R\}^-$ moiety. The neutral alkynyl technetium species $[Tc(C\equiv C\text{-}R)(CO)_3(PPh_3)_2]$ contain the organometallic ligand in an end-on binding mode. ^{99}Tc NMR spectroscopy proved its value as a tool for the structural determination of ^{99}Tc complexes and to distinguish carbon-based donor ligands.

A relatively well-studied group of organotechnetium compounds are cyclopentadienyl complexes. Recently, the $\{Tc(NO)(Cp)(PPh_3)\}^+$ fragment became available[27] and a further insight into its chemistry becomes interesting taking into account that the analogous rhenium fragment $\{Re(NO)(Cp)(PPh_3)\}^+$ acts as a versatile and highly reactive Lewis-acid towards many ligands. The related work is contained in publication 5 (*Organometallics*, **2019**, *38*, 4471-1178).

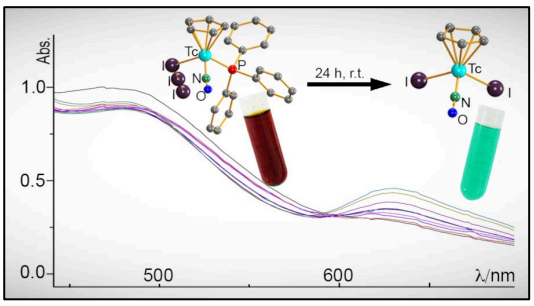

Organometallics, **2019**, *38*, 4471-1178.

The chemistry of complexes with the general structure $[Tc(X)(NO)(Cp)(PPh_3)]$ was investigated for several different anionic donor ligands. Sometimes an unexpected reactivity was observed. $[Tc(NO)(Cp)(PPh_3)(Cl)]$ reacted with HI to give $[Tc(NO)(Cp)(PPh_3)(I_3)]$ instead of $[Tc(NO)(Cp)(PPh_3)(I)]$. The triiodido complex decomposed by an internal redox reaction to give $[Tc^{II}(I)_2(NO)(Cp)]$. According to the experimental EPR spectrum, the unpaired electron of the paramagnetic complex is not fully localized at the technetium atom but delocalized towards the Cp^- ligand. DFT calculations explained this interaction as the spin-density of the singly occupied molecular orbital (SOMO) in $[Tc^{II}(NO)(Cp)(I)_2]$, which partially expands into the cyclopentadienyl moiety. Another surprising result is the formation of the *S*-bound thiocyanato complex $[Tc(NO)(Cp)(PPh_3)(SCN)]$, while the majority of technetium complexes with the pseudohalogenido ligand contain *N*-bound isocyanato ligands. On the basis of DFT calculations, $[Tc(NO)(Cp)(PPh_3)(SCN)]$ was revealed to be the kinetic product of this reaction, while the thermodynamically more stable product is $[Tc(NO)(Cp)(PPh_3)(NCS)]$. The theoretically predicted thermal isomerization was then proven experimentally by *in situ* ^{99}Tc NMR spectroscopy.

The organometallic chemistry based on the $\{Tc(NO)(Cp)(PPh_3)\}^+$-fragment is limited by the formation of the dimeric cation $[\{Tc(NO)(Cp)(PPh_3)\}_2\text{-}\mu\text{-}Cl]^+$,[28] which was sought to be overcome by the use of the sterically somewhat more demanding phosphite-based Kläui ligand. As the Kläui ligand is commonly discussed as an alternative to both Cp^- and trispyrazolylborate, a similar reactivity was expected. The surprising outcome of these reactions is described in publication 6 (*Z. Allg. Anorg. Chem.* **2022**, e202100316).

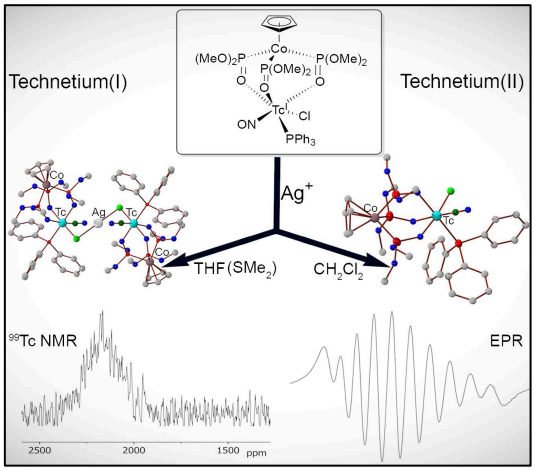

Z. Allg. Anorg. Chem. **2022**, e202100316.

Reactions of the technetium(I) starting material $[Tc^{I}(NO)(PPh_3)(L^{OMe})Cl]$ with $AgPF_6$ in dichloromethane lead to the oxidation of technetium and the formation of the cationic technetium(II) species $[Tc^{II}(NO)(PPh_3)(L^{OMe})Cl]^+$. The isostructural but paramagnetic cation is easily distinguished from the diamagnetic starting material through the absence of an NMR resonance but the observation of an EPR signal. A similar reaction in a mixture of THF and dimethylsulfide resulted in the formation of the unexpected silver-bridged technetium(I) dimer $[\{Tc^{I}(NO)(PPh_3)(L^{OMe})Cl\}_2Ag](PF_6)$. The silver-bridged dimer exists in a dynamic equilibrium with the technetium(I) starting material $[Tc^{I}(NO)(PPh_3)(L^{OMe})Cl]$ and $Ag(PF_6)$ as indicated by the line-broadening observed in the ^{99}Tc NMR spectrum of $[\{Tc^{I}(NO)(PPh_3)(L^{OMe})Cl\}_2Ag](PF_6)$. Ultimately, the silver-bridged dimer is not stable in solution and undergoes decomposition under formation of $[Tc^{I}(NO)(PPh_3)(L^{OMe})Cl]$, elemental silver and the technetium(II) salt $[Tc^{II}(NO)(PPh_3)(L^{OMe})Cl](PF_6)$, that was obtained from reactions performed in dichloromethane. The different technetium-containing products can be separated by extraction and well-distinguished by IR, NMR and EPR spectroscopy.

A surprising redox behavior may not only be observed for technetium complexes with the metal in low oxidation states but also for those containing the metal in high oxidation states. An illustrative example for the interplay of the redox behavior of technetium complexes in high and low oxidation states is the previously mentioned comproportionation reaction of the mixed-valcence complex $[Tc^{I}(OTc^{VII}O_3)(CO)_3(PPh_3)_2]$. The high oxidation-state redox chemistry of technetium is governed by the properties of technetyl $\{TcO_3\}^+$ species and have major implications for the speciation of technetium in nuclear waste solutions. Therefore, the basic reduction chemistry of pertechnetate in highly acidic media is not only relevant to the general chemistry of technetium, but also to nuclear waste treatment. Work about the chemistry of pertechnetate salts in super acidic media is contained in publication 7 (*Angew. Chem. Int. Ed.* **2021**, *61,* e202113777).

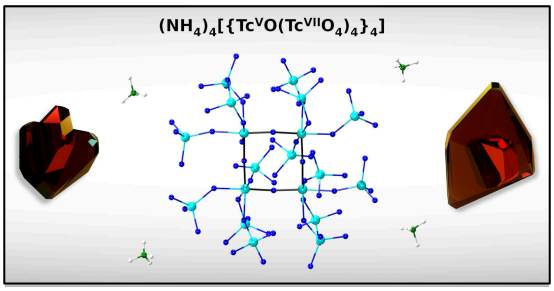

Angew. Chem. Int. Ed. **2021**, *61*, e202113777.

Ammonium pertechnetate reacts with triflic acid under initial formation of pertechnetyl triflate, which undergoes spontaneous redox processes to give technetium(VI) and ultimately technetium(V) complexes. ^{99}Tc NMR spectroscopy was confirmed as a powerful tool also for the structural elucidation of ^{99}Tc complexes with technetium in the oxidation states +7 and +5. Besides the highly reactive triflate complex $[Tc^{V}O(OTf)_5]^{2-}$, the study revealed the surprising formation of the previously unknown, mixed-valence ammonium polyoxometallate salt $(NH_4)_4[\{Tc^{V}O(Tc^{VII}O_4)_4\}_4]$. The latter is related to tech-red, a mysterious and volatile technetium oxide of relevance to the nuclear waste processing and storage.

1.2 Chalcogen compounds

In the previous section, chalcogen-based ligands were already introduced in the form of chalcogenoethers. Another form of chalcogen-based ligands are anionic chalcogenolates. Arylchalcogenolate donor units of the lighter chalcogens oxygen and sulfur are valuable and common building blocks in flexible ligand classes such as Schiff' bases. Metal complexes containing such flexible ligands often take part in catalytic reactions.[29-44] The use of the heavier chalcogens selenium and tellurium in such ligands allows a modulation of the properties of the metal complexes. Our knowledge about selenolato and tellurolato complexes in contrast to thiolato and alcoholato complexes is mainly restricted by their limited stability and limitations on synthetic routes for their preparation.[45-56] Nevertheless, such compounds often have unique optical or electrical properties.[57,58] Organoselenolates and tellurolates are usually prepared directly before use by the reduction of the more stable dichalcogenides.[45,46] Unfortunately, a precise control of the reaction conditions is commonly required and especially reactions with metal ions in their high oxidation states are problematic due to a parallel reduction of the metal ions.[45,46] A reasonable way to avoid the parallel reduction of the high-valent metal ions might be the use of starting materials, which contain phosphine ligands.[59] When phosphine ligands are released during the reactions of such precursors, they may then act as *in situ* reducing agents. A method for the preparation of defined chalcogenolato complexes containing rhenium in the oxidation state "+5" based on this hypothesis is presented in publication 8 (*Eur. J. Inorg. Chem.* **2019**, *47*, 4974-4984).

Triphenylphosphine ligands, which are released during reactions of $[ReOCl_3(PPh_3)_2]$ or $[Re(NAr)Cl_3(PPh_3)_2]$ were found to represent ideal reducing agents for the reduction of dichalcogenides, since they have a defined stoichiometry by design. Although such reactions require oxygen-free conditions, the presence of water was found to be crucial to obtain the products in reasonable yields. A suggested mechanism attributes the need for water in these reactions to the cleavage of an intermediate phosphonium species, which can be cleaved by water to release the chalcogenol(ate) and $OPPh_3$. The formation of the stable phosphorus-oxygen double bond is concluded as a reasonable driving force of the reaction. Additionally, the precise control of the reaction conditions (solvent, water-content, etc.) is crucial for the success of such reactions and a number of different protocols was derived depending on the observed reactivity, solubility and stability of the corresponding rhenium starting materials and products.

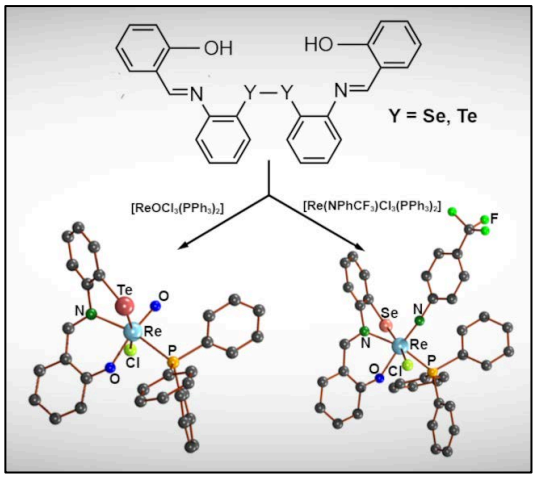

Eur. J. Inorg. Chem. **2019**, *47*, 4974-4984.

The proposed mechanism for the rhenium-induced reduction of dichalcogenides by released phosphine ligands shows the potential for an extension of this synthetic approach to other transition metals. Chalcogenolato complexes of nickel, palladium or platinum, which contain Schiff' base fragments, are generally interesting regarding their applications as single-molecule precursors, for catalysis and their optoelectronic properties.[31-44] Therefore, reactions of suitable nickel, palladium and platinum phosphine complexes with dichalcogenides were studied experimentally and by DFT calculations in publication 9 (*Eur. J. Inorg. Chem.* **2020**, *45*, 4303-4312).

Indeed, phosphine-containing Ni^{II}, Pd^{II} and Pt^{II} complexes react analogously to the previously discussed rhenium(V) complexes. No reduction of the metal ions was observed and the chalcogenolato complexes were easily prepared in high yield. This led to the question, why triphenylphosphine – normally a reducing agent of insufficient strength for the reduction of the heavier dichalcogenides – was able to reduce them effectively under the applied conditions. A computational study supports the hypothesis that a coordination of the intact dichalcogenide moiety results in an increased electrophilic nature in the sense of a positive polarization of the uncoordinated chalcogen atom of the dichalcogenide. Finally, the calculations reveal that

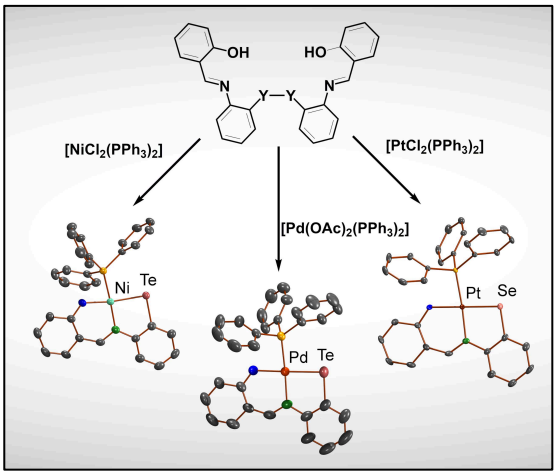

Eur. J. Inorg. Chem. **2020**, *45*, 4303-4312.

the enlargement and intensity increase of the σ-hole on the back-side of the dichalcogenide upon coordination to the metal are the prevalent reasons for the feasible reduction of dichalcogenides with triphenylphosphine. Consequently, the calculations show that the feasibility of a reduction by triphenylphosphine is increased by the introduction of electron-withdrawing substituents on the dichalcogenide moiety, which has a similar effect. Finally, an oxidation of the complexes with elemental iodine did not lead to defined high-valent nickel, palladium and platinum complexes but resulted in the formation of a zwitterionic organotellurium(II) diiodide species: {[(HO)C_6H_4-(CHN$^+$H)-C_6H_4-TeI_2] · $OPPh_3$}. The same compound is obtained in somewhat better yields by the oxidation of the corresponding ditelluride with elemental iodine in the presence of triphenylphosphine oxide.

For palladium, also a different mechanism for the reduction of the dichalcogenides is possible: via the formation of transient palladium(IV) species or intermediate palladium(0) species.[51-55] Complex mixtures of several polynuclear complexes are commonly formed during such reactions.[51-55] Contrarily, such a redox behavior is not known for nickel and the analogous disulfide Schiff' base $\{L^S\}_2^{2-}$ forms monomeric or dimeric nickel(II) complexes containing the intact disulfide moiety, where one of the disulfide sulfur atoms coordinates to the metal ion.[42,43] For both metals, the formation of supramolecular products is poorly understood in terms of the aggregation into defined chalcogen-metal clusters. Thus, it became interesting to study reactions of the dichalcogenides with phosphine-free palladium(II) and nickel(II) starting materials. Indeed, reactions with palladium(II) acetate lead to chalcogenolato-based clusters, while the reaction with nickel(II) acetate lead to clusters containing coordinated dichalcogenides. A survey of the observed reactivity and structural diversity has been assessed in publication 10 (*Inorg. Chem*. **2022**, *61*, 3785–3800).

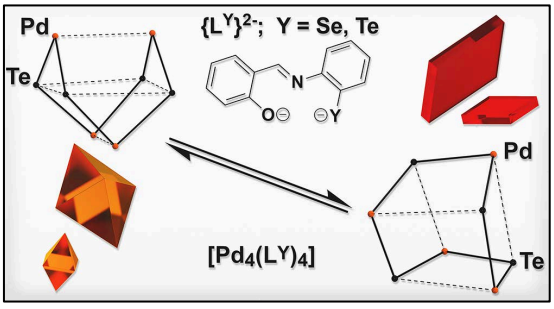

Inorg. Chem. **2022**, *61*, 3785–3800.

Reactions of the salicylidene Schiff' base-functionalized dichalcogenides $\{HL^Y\}_2$ (Y = Se, Te) with palladium(II) acetate led to the isolation of the tetrameric palladium clusters $[Pd_4(L^Y)_4]$. Two isomers with a different arrangement of the central Pd_4Y_4 unit, but with an identical chemical composition could be isolated and structurally characterized for the first time. To give a rationale for the formation of one isomer over the other, a reduced density gradient analysis based on DFT calculations was performed. In agreement with the solid-state structures, the analysis revealed the short Pd...Pd and Pd...Te contacts in both isomers as weak van der Waals contacts. In reactions of $\{HL^Y\}_2$ (Y = Se, Te) with nickel(II) acetate, the dichalcogenides were not cleaved. Instead, the intact, deprotonated dichalcogenides act as pentadentate ligands with an {*O*,*N*,*Y*,*N*,*O*} donor set and give the trimeric complexes [Ni-μ^2-κ^2-(Ni{κ^5-L^Y}$_2$)$_2$-μ^2-$(OAc)_2$]. The nickel clusters as well as the palladium clusters appear to be fluxional in solution as is indicated by ESI mass spectrometry. After prolonged storage in air, the tellurium complex [Ni-μ^2-κ^2-(Ni{κ^5-L^{Te}}$_2$)$_2$-

μ^2-$(OAc)_2$] decomposes by hydrolysis of the central nickel(II) acetate unit and oxidation of all tellurium atoms to tellurium(IV). The formed hexanuclear cluster [Ni_2-κ_5-(Ni_4-κ_6-μ_6-{($L^{Te}{}_2O_3$)($L^{Te}O_2$)$_2$}$_2$)-μ_2-$(H_2O)_2$] is a rare example of a defined compound containing tellurinic anhydride and tellurinate units. Remarkably, the combination of tellurinic anhydride and tellurinate units acts as a ligand framework for the nickel ions in an unprecedented fashion.

As described in publication 10, metal complexes with dichalcogenide ligands can be sensitive to oxidation and can form telluroxane-based ligands derived from tellurinic anhydride and tellurinate. Similarly, organotellurium halides are often sensitive to hydrolysis, which leads to the formation of chaotic and ill-defined telluroxane networks. Under certain conditions, however, the hydrolysis of *in situ* generated $[PhTeI]_x$ leads to the formation of the defined, giant and bowl-shaped organotelluroxane clusters. The syntheses and properties of such supramolecular clusters were investigated experimentally and theoretically in publication 11 (*Angew. Chem. Int. Ed.* **2021**, 60, *28*, 15517–15523).

Giant clusters of general composition [{$(PhTe)_{19}O_{24}$}$_2I_{18}$] are dimeric and consist of two {$(PhTe)_{19}O_{24}$} telluroxane half-shells connected by an inner layer of halide ions. They are robust enough to be transferred into the gas-phase as is indicated by mass-spectrometric analyses. The whole cluster can act as a supramolecular host towards guest molecules, which are accommodated in the central cavity. Additionally, the central telluroxane unit of each half-shell can act as a crown-ether like ligand to coordinate metal ions. The addition of metal ions such as Ca^{2+} or lanthanide^{3+} ions to the central telluroxane unit results in a change of the telluroxane network and interestingly, the deep red-brown color of the non-coordinating parent compound is lost upon coordination of a Ca^{2+} ion in each half-shell. Density function theory calculations reveal a shift of the maximum UV/VIS absorption lines to lower wave lengths due to an extension of the delocalization of electron density within the telluroxane network and, thus, rationalize the discoloration.

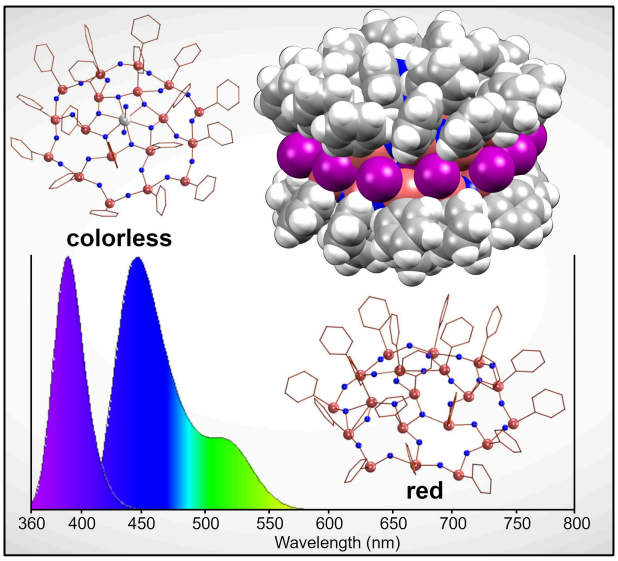

Angew. Chem. Int. Ed. **2021**, 60, *28*, 15517–15523.

2 Summary

In the first part of this thesis, the general coordination and organometallic chemistry of technetium was explored. The preparation and reactivity of technetium hydrido complexes based on an improved synthetic protocol for the scalable synthesis of the technetium(III) hydride $[TcH_3(PPh_3)_4]$ was investigated. As a result, the technetium(I) hydride *mer-trans*-$[TcH(CO)_3(PPh_3)_2]$ became available in scalable amounts, which led to the isolation of a variety of structurally similar technetium(I) complexes containing two or three carbonyl ligands through its reactions with Brønsted acids. Reactions with Brønsted acids of weakly coordinating counter-ions resulted in the formation of the labile aqua complex *mer-trans*-$[Tc(OH_2)(CO)_3(PPh_3)_2]^+$ that has been used as a labile starting material for ligand exchange reactions with various ligands of general interest to the coordination chemistry of technetium. The non-protic dimethylsulfide surrogate *mer-trans*-$[Tc(SMe_2)(CO)_3(PPh_3)_2]^+$ was developed and successfully used for the preparation of novel organometallic technetium complexes, for example the isolation of the first acetylido complexes of technetium was accomplished. Throughout these studies, a series of structurally related compounds containing the *mer*-$\{Tc(CO)_3\}^+$ or *cis*-$\{Tc(CO)_2\}^+$ cores was prepared, that enabled a detailed evaluation of structural relationships among technetium complexes having the same core structure but different ligands. Most importantly, ^{99}Tc NMR spectroscopy was proven as an invaluable and highly specific tool for the analysis of the low-valent technetium carbonyl species. Besides carbonyl complexes, also the chemistry of the low-valent technetium(I) complexes $[Tc(NO)(Cp)(PPh_3)Cl]$ and $[Tc^{I}(NO)(PPh_3)(L^{OMe})Cl]$ has been investigated. Finally, the reduction chemistry of pertechnetate in highly acidic media was studied resulting in the characterization of the previously unknown, mixed-valence ammonium polyoxometallate salt $(NH_4)_4[\{Tc^{V}O(Tc^{VII}O_4)_4\}_4]$.

In the second part of this thesis, the coordination chemistry of organoselenium- and tellurium compounds was studied. A method for the easy and reliable preparation of organochalcogenolato complexes from dichalcogenides and metal phosphine complexes was developed using reduction-sensitive Schiff' base substituted dichalcogenides as model compounds. The coordination of one chalcogen atom of the dichalcogenide increases the reactivity of the second chalcogen atom through an increase in its electropositive σ-hole and, thus, enables the nucleophilic attack of the *in situ* released reducing agent. The method was expanded from the originally studied rhenium(V) oxido and arylimido complexes to nickel, palladium and platinum complexes in the oxidation state +2. With phosphine-free starting materials, the Schiff' base substituted dichalcogenides form clusters of varying structure. For the first time, the interconversion of the gyrobifastigial and cuboid-like structures of tetrameric

Pd_4Chal_4 central units for compounds with the same chemical composition has been observed. Lastly, large bowl-shaped telluroxane clusters have been investigated. The coordination of the central unit of each half-shell in the large telluroxane-clusters to calcium in a crown-ether-like fashion led to a loss in color. The shift of the UV-VIS absorption could be explained by DFT calculations due to an increased delocalization of electron density in the telluroxane framework.

3 Zusammenfassung

Im ersten Teil der vorliegenden Arbeit wurde die allgemeine Koordinations- und Organometallchemie des Technetiums untersucht. Die Darstellung und Reaktivität von Technetiumhydridokomplexen wurde dabei auf Basis einer optimierten und skalierbaren Synthese des Technetium(III)-Hydrids $[TcH_3(PPh_3)_4]$ untersucht. Das Technetium(I)-Hydrid *mer-trans*-$[TcH(CO)_3(PPh_3)_2]$ wurde infolge dieser Arbeiten in skalierbarer Menge verfügbar. Reaktionen von *mer-trans*-$[TcH(CO)_3(PPh_3)_2]$ mit Brønsted-Säuren erlaubten die Isolation und Charakterisierung einer Vielzahl strukturell ähnlicher Technetium(I)-Komplexe mit zwei oder drei Carbonylliganden. Dagegen führten Reaktionen mit Brønsted-Säuren schwachkoordinierender Anionen zur Bildung des Komplexes *mer-trans*-$[Tc(OH_2)(CO)_3(PPh_3)_2]^+$. Dieser Komplex erwies sich aufgrund seines labilen Wasserliganden als geeignete Startverbindung für Ligandenaustauschreaktionen mit vielen für die Koordinationschemie des Technetiums interessanten Liganden. Das nicht-protische Analogon *mer-trans*-$[Tc(SMe_2)(CO)_3(PPh_3)_2]^+$ besitzt einen labilen Dimethylsulfidliganden und wurde für die Synthese metallorganischer Technetiumkomplexe entwickelt. Die Verwendung von *mer-trans*-$[Tc(SMe_2)(CO)_3(PPh_3)_2]^+$ führte beispielsweise zu einer zuverlässigen Route für die Darstellung der ersten Technetiumacetylido- und -cyclooxycarbenkomplexe. Insgesamt wurde im Rahmen dieser Studien eine Reihe strukturell verwandter Verbindungen mit den Strukturmotiven *mer*-$\{Tc(CO)_3\}^+$ und *cis*-$\{Tc(CO)_2\}^+$ dargestellt. Der Zugang zu dieser Reihe und die einfache Erweiterung durch die entwickelten, verallgemeinerbaren Synthesewege ermöglichte eine systematische Auswertung der strukturellen Variationen in Technetiumkomplexen mit gleicher Grundstruktur aber unterschiedlichen Liganden. Hierbei erwies sich insbesondere die ^{99}Tc-NMR-Spektroskopie als unersetzliches und hochspezifisches Werkzeug für die Charakterisierung, Analyse und Differenzierung der niedervalenten Technetium(I)-Carbonylspezies. Neben Carbonylkomplexen wurde auch die Chemie der niedervalenten Technetium(I)-Nitrosylverbindungen $[Tc(NO)(Cp)(PPh_3)Cl]$ und $[Tc^{I}(NO)(PPh_3)(L^{OMe})Cl]$ untersucht. Abschließend wurde die Reduktionschemie des hochvalenten Pertechnetatanions in stark sauren Lösungen beleuchtet, wobei unteranderem das zuvor unbekannte, gemischtvalente Ammoniumpolyoxometallat-Salz $(NH_4)_4[\{Tc^{V}O(Tc^{VII}O_4)_4\}_4]$ charakterisiert und isoliert wurde.

Im zweiten Teil dieser Arbeit wurde die Koordinationschemie von Organoselen- und -tellurverbindungen untersucht. Eine einfache und zuverlässige Methode für die Synthese von Organochalcogenolatokomplexen aus Diorganodichalcogeniden und Metallphosphankomplexen wurde am Beispiel von reduktionsempfindlichen Schiff'schen Basen modifizierten Dichalcogeniden entwickelt. Die Koordination eines Chalcogenatoms der Dichalcogenideinheit erhöhte dabei die

Reaktivität des zweiten Chalcogenatoms durch die Vergrößerung und Intensivierung des σ-Lochs an der Rückseite der Chalcogen-Chalcogen Bindung. Diese Erhöhung der Polarität erlaubt den nukleophilen Angriff des *in situ* freigesetzten Reduktionsmittels PPh_3. Diese Methode konnte von den ursprünglich untersuchten Rhenium(V)-Oxido- und -Arylimidospezies auch auf Nickel-, Palladium- und Platinkomplexe der Oxidationsstufe +2 ausgeweitet werden. Mit phosphanfreien Startverbindungen der Metalle Nickel und Palladium reagierten die Schiff' Basen substituierten Dichalcogenide unter Bildung von Clustern variabler Struktur. Insbesondere konnte die Umwandlung der gyrobifastigialen und würfelähnlichen Strukturen der zentralen Pd_4Chal_4-Einheit ineinander erstmals für Cluster der gleichen Zusammensetzung beobachtet werden. Abschließend wurden große, schüsselförmige Telluroxancluster untersucht. Die kronenetherähnliche Koordination von Calciumionen durch die zentrale Telluroxaneinheit in jeder Halbschale führte zu einer Entfärbung. Die Verschiebung der UV-VIS-Absorption konnte mithilfe von DFT-Rechnungen hauptsächlich einer erhöhten Delokalisierung der Elektronendichte im Telluroxannetzwerk zugeordnet werden.

4 Publications

1. Roca Jungfer, M.; Elsholz, L.; Abram, U. "**Technetium Hydrides Revisited: Syntheses, Structures, and Reactions of [$TcH_3(PPh_3)_4$] and [$TcH(CO)_3(PPh_3)_2$]**", *Organometallics*, **2021**, *40*, 3095–3112. Featured on the cover of volume 40 issue 18 (published 09/2021).

2. Roca Jungfer, M.; Abram, U. **"[$Tc(OH_2)(CO)_3(PPh_3)_2]^+$: A Synthon for Tc(I) Complexes and its Reactions with Neutral Ligands"**, *Inorg. Chem.* **2021**, *60*, 16734-16753.

3. Roca Jungfer, M.; Elsholz, L.; Abram, U. **"Technetium(I) Carbonyl Chemistry with Small Inorganic Ligands"**, *Inorg. Chem.* **2022**, *61*, 2980-2997.

4. Roca Jungfer, M.; Abram, U. **"Technetium and the C≡C triple bond: Unlocking air- and waterstable technetium acetylides and other organometallic complexes"**, *Inorg. Chem.* submitted.

5. Ackermann, J.; Abdulkader, A.; Scholtysik, C.; Roca Jungfer, M.; Hagenbach, A.; Abram, U. "**[$Tc^{I}(NO)X(cp)(PPh_3)$] Complexes (X^- = I^-, I_3^-, SCN^-, $CF_3SO_3^-$ or CF_3COO^-) and Their Reactions**", *Organometallics*, **2019**, *38*, 4471-1178.

6. Roca Jungfer, M.; Ernst, M. J.; Hagenbach, A.; Abram, U. **"[{$Tc^{I}(NO)(L^{OMe})(PPh_3)Cl$}$_2$Ag]($PF_6$) and [$Tc^{II}(NO)(L^{OMe})(PPh_3)Cl$]($PF_6$): Two Unusual Technetium Complexes with a "Kläui-type" Ligand"**, *Z. Anorg. Allg. Chem.* **2022***,* e202100316.

7. Zegke, M.; Grödler, D.; Roca Jungfer, M.; Haseloer, A.; Kreuter, M.; Neudörfl, J. M.; Sittel, T.; James, C. M.; Rothe, J.; Altmaier, M.; Klein, A.; Breugst, M.; Abram, U.; Strub, E.; Wickleder, M. S. **"Ammonium pertechnetate in mixtures of trifluoromethanesulfonic acid and trifluoromethanesulfonic anhydride"**, *Angew. Chem. Int. Ed.* **2021***, 61,* e202113777*.*

8. Roca Jungfer, M.; Hagenbach, A.; Schulz Lang, E.; Abram, U. "**Rhenium(V) Complexes with Selenolato- and Tellurolato-substituted Schiff' Bases – Released PPh_3 as a Facile Reductant**", *Eur. J. Inorg. Chem.* **2019**, *47*, 4974–4984.

9. Roca Jungfer, M.; Schulz Lang, E.; Abram, U. "**Reactions of Schiff Base-Substituted Diselenides and -tellurides with Ni(II), Pd(II) and Pt(II) Phosphine Complexes",** *Eur. J. Inorg. Chem.* **2020**, *45*, 4303–4312.

10. Roca Jungfer, M.; Schulz Lang, E.; Abram, U. "**Solvents and Ligands Matter: Structurally Variable Palladium and Nickel Clusters Assembled by Tridentate Selenium- and Tellurium-Containing Schiff Bases",** *Inorg. Chem.* **2022**, *61*, 3785–3800.

11. Kirsten, L.; Fonseca Rodrigues, J.; Hagenbach, A.; Springer, A.; Pineda, N. R.; Piquini, P. C.; Roca Jungfer, M.; Schulz Lang, E.; Abram, U. "**Large Telluroxane Bowls Connected by a Layer of Iodine Ions**", *Angew. Chem. Int. Ed.* **2021**, *60*, 15517–15523.

4.1 Technetium Hydrides Revisited: Syntheses, Structures, and Reactions of $[TcH_3(PPh_3)_4]$ and $[TcH(CO)_3(PPh_3)_2]$

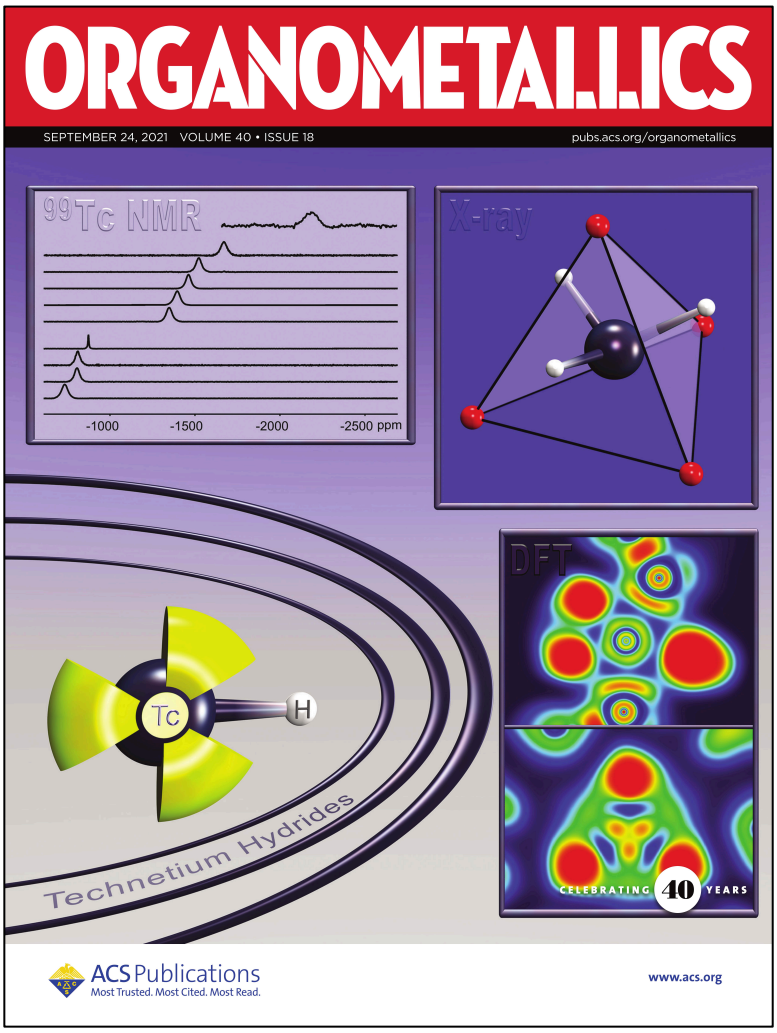

Reproduced with permission from Roca Jungfer, M.; Elsholz, L.; Abram, U. *Organometallics*, **2021**, *40*, 3095–3112.

DOI: 10.1021/acs.organomet.1c00274

For Supplementary Material see A.1.

Author Contributions:

Maximilian Roca Jungfer and Ulrich Abram designed the project. Maximilian Roca Jungfer performed the synthesis and characterization of the compounds, performed DFT calculations, calculated the X-ray structures and wrote a draft of the manuscript. Laura Elsholz performed some of the experiments and DFT calculations during a research internship under the supervision of Maximilian Roca Jungfer. Ulrich Abram supervised the project, provided scientific guidance and suggestions, and corrected the manuscript. Maximilian Roca Jungfer and Ulrich Abram designed the cover picture of the issue.

ORGANOMETALLICS

pubs.acs.org/Organometallics Article

Technetium Hydrides Revisited: Syntheses, Structures, and Reactions of $[TcH_3(PPh_3)_4]$ and $[TcH(CO)_3(PPh_3)_2]$

Maximilian Roca Jungfer, Laura Elsholz, and Ulrich Abram*

Cite This: *Organometallics* 2021, 40, 3095−3112 Read Online

ACCESS | Metrics & More | Article Recommendations | Supporting Information

ABSTRACT: Optimized synthetic approaches to $[TcH_3(PPh_3)_4]$ (**1**) and *mer-trans*-$[TcH(CO)_3(PPh_3)_2]$ (**5**) as key compounds of the technetium hydrido chemistry are reported. They give access to pure and stable samples of the complexes. The solid-state structures of the two title compounds have been determined. Reactions of $[TcH_3(PPh_3)_4]$ with monodentate basic phosphines such as PMe_2Ph or PMe_3 lead to mixtures of mixed-phosphine complexes of the compositions $[TcH_3(PR_3)_n(PPh_3)_{4-n}]$ (n = 1−3), from which the mixed-phosphine trihydride complex $[TcH_3(PPh_3)_2(PMe_3)_2]$ (**2**) could be isolated. Spectroscopic data and DFT calculations suggest a fluxional structure between a capped trigonal prism and a pentagonal bipyramid. Reactions of the monohydride *mer-trans*-$[TcH(CO)_3(PPh_3)_2]$ (**5**) with HX (X = Cl, Br, I) give $[TcX(CO)_3(PPh_3)_2]$ (**6**) complexes in good yields, while *mer-trans*-$[Tc\{\eta^1\text{-}O(CR)O\}(CO)_3(PPh_3)_2]$ (**7**) or *cis*−*trans*-$[Tc\{\eta^2\text{-}OO(CR)\}(CO)_2(PPh_3)_2]$ (**8**) complexes are formed with carboxylic acids depending on the substituent R and the conditions applied. Chelate formation of the formato ligand can also be obtained by thermal decarbonylation of the isolated *mer-trans*-$[Tc(\eta^1\text{-}O(CH)O)(CO)_3(PPh_3)_2]$ (**7a**) complex. The latter reaction is reversible, and the tricarbonyl compound is reformed when $[Tc\{\eta^2\text{-}OO(CH)\}(CO)_2(PPh_3)_2]$ (**8a**) is exposed to CO gas. Reactions of $[TcH(CO)_3(PPh_3)_2]$ (**5**) with phenyl seleninic acid (PhSeOOH) in methanol give the tetranuclear cluster $[\{Tc(CO)_3\}_3(\mu^3\text{-}OH)(\mu^2\text{-}O(SePh)O)_3\{Tc(CO)_3\}]$ (**10**) and a small amount of the bridged dinuclear oxalato complex $[Tc_2(CO)_6(ox)(OPPh_3)_2]$ (**11**). The latter compound is the result of a complex reaction, which involves a metal-induced oxidation of methanol to formate and a subsequent C−C coupling of two formato ligands. The plausibility of the proposed mechanism is supported by the fact that the dimeric oxalato complex is much more efficiently formed when the formato complex $[Tc\{\eta^1\text{-}O(CH)O\}(CO)_3(PPh_3)_2]$ (**7a**) is directly reacted with PhSeOOH. Exclusively the monomeric oxalato complex $[Tc(\eta^2\text{-}oxH)(CO)_2(PPh_3)_2]$ (**12**) is formed during a reaction of *mer-trans*-$[TcH(CO)_3(PPh_3)_2]$ (**5**) with oxalic acid. The remaining proton of the Hox^- ligand of $[Tc(\eta^2\text{-}oxH)(CO)_2(PPh_3)_2]$ (**12**) can be removed by NEt_3, and the ion pair $(HNEt_3)[Tc(\eta^2\text{-}ox)(CO)_2(PPh_3)_2]$ (**13**) is formed.

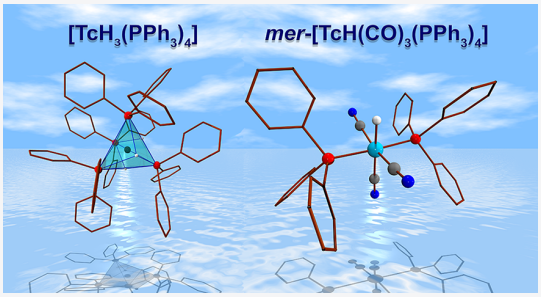

INTRODUCTION

In contrast to the coordination chemistry of its higher congener rhenium, where many hydrido complexes are known and play an important role in a number of catalytic processes,[1−7] reports about compounds with technetium−hydrogen bonds are scarce.[8−23] Only some of them have been characterized unambiguously, e.g., by single crystal X-ray crystallography. This includes mononuclear compounds such as $[TcH(N_2)(dppe)_2]$,[13] $[TcH\{\eta^2\text{-}N,S\text{-}HNC(NH_2)S\}(PMe_3)_4](PF_6)$,[15] or $[Tc(H_2)Cl(dppe)_2]$,[16] the binuclear compound $[Tc_2\text{-}\mu\text{-}H(\mu\text{-}C,N\text{-}C_5H_4N)(py)_2(CO)_6]$,[19] but also the trinuclear clusters $[Tc_3\text{-}\mu\text{-}H_3(CO)_{12}]$[18,21] and $[Tc_3H(CO)_{14}]$[20] or some borohydride compounds.[22,23] The structure of the iconic $K_2[TcH_9]$ was determined by comparison of its powder data with those of the rhenium analogue.[10] Some of the compounds are shown in Chart 1. Most of the well-explored Tc hydrides have limited potential as precursors. $[TcH_9]^{2-}$ is not suitable as a starting material for the preparation of other technetium hydrides due to its

Chart 1. Selected Hydrido/Dihydrogen Complexes of Technetium[10,13,16,18,23]

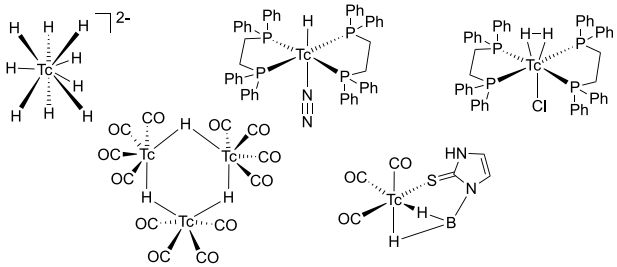

Received: May 4, 2021
Published: June 22, 2021

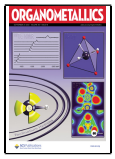

intrinsic instability: it cannot be obtained in sufficient amounts and/or purity. It is nearly insoluble and only short-term-stable in KOH solutions at low temperatures.[10] Although several hydrido and dihydrogen complexes can be derived from the 16-electron dppe complex $[TcCl(dppe)_2]$, their formation is exclusively limited to this bisphosphine ligand system.[11,13,16]

Compounds such as $[Tc_2\text{-}\mu\text{-}H(\mu\text{-}C,N\text{-}C_5H_4N)(py)_2(CO)_6]$[19] or the trinuclear carbonyl hydrides $[Tc_3\text{-}\mu\text{-}H_3(CO)_{12}]$[18] and $[Tc_3H(CO)_{14}]$[20] are formed in only moderate yields during not fully understood hydrolytic processes. Another potential technetium hydrido starting material, $[TcH(CO)_5]$, can only be prepared in trace amounts, is unstable, and produces a major radiation protection concern due to its volatility.[9]

Finally, another hydrido compound with an interesting reactivity was introduced in 1995: $[TcH(CO)_3(PPh_3)_2]$ (**5**).[17] It can be prepared from $[TcH_3(PPh_3)_4]$ (**1**). Unfortunately, the synthesis of $[TcH_3(PPh_3)_4]$ has never been published in a journal but can be found in the doctoral thesis of Jessica Cook.[24] $[TcH_3(PPh_3)_4]$ was described as an unstable compound, which rapidly decomposes to unattractive, less defined dark products. Nevertheless, this report motivated us to reinvestigate syntheses, structures, and reactivities of the trihydride and its reaction product with carbon monoxide: $[TcH(CO)_3(PPh_3)_2]$ (**5**).

RESULTS AND DISCUSSION

Synthesis and Properties of $[TcH_3(PPh_3)_4]$ (1). The trihydride can be prepared from $[TcCl_4(PPh_3)_2]$, PPh_3, and $Na(BH_4)$. In the original procedure,[24] ethanol has been used as solvent, in which $[TcCl_4(PPh_3)_2]$ is almost insoluble. This results in a heterogeneous reaction, from which the product was isolated as a finely powdered solid. The product has been described as a rather unstable compound, which decomposes even under Ar, N_2, or H_2 atmospheres and an "unusual" ^1H NMR spectrum with an unexpected additional hydride signal in addition to the expected quintet has been reported.[24] This may indicate the presence of at least one additional compound, which might also be responsible for the intrinsic instability of the product. We performed the synthesis of **1** following this protocol, and the described behavior is well reproducible including the described instability of the obtained finely powdered solid, the color of which gradually darkens even under argon or dihydrogen, and after a few days only a dark brown, insoluble solid is left (see Figure 1). Solutions of this material in dry, argon-saturated solvents quickly start to deposit a black insoluble solid and the decomposition was complete within 6 h.

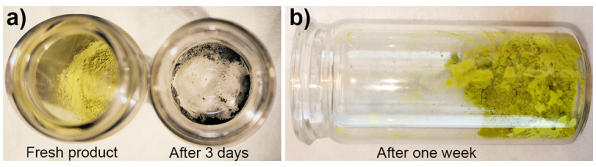

Figure 1. Samples of $[TcH_3(PPh_3)_4]$ (**1**) obtained by different procedures: (a) Product prepared following the previous protocol with ethanol as solvent,[24] directly after isolation and after storage for 3 days in a refrigerator under an Ar atmosphere, and (b) product of the optimized synthesis after storage for 7 days at room temperature on air.

Supposing that the detected impurity contained in the material might be the reason for its instability, we tried to find an improved procedure. Fortunately, only a few modifications of the originally reported conditions were required. When the reaction between $[TcCl_4(PPh_3)_2]$, PPh_3 and $Na(BH_4)$ is performed in a mixture of toluene, ethanol, and hexane (for details see Experimental Section), the coprecipitation of undesired side-products is minimized. In the course of the reaction, the almost insoluble technetium(IV) complex dissolves completely before the bright yellow, crystalline product precipitates with a high purity. The product of this procedure can be stored for at least six months in a refrigerator without additional precautions such as inert gas atmosphere. Figure 1 shows pictures of the products obtained from both procedures immediately after their isolation and after storing them for several days. It becomes clear that the improved synthetic procedure increases the stability of the product as a solid. An obvious disadvantage is the lower solubility of the crystalline product compared to the finely powdered trihydride obtained from the older protocol. Together with the inherent instability of the reactive compound in solution, this hinders the measurement of ^{13}C, ^{31}P, or ^{99}Tc NMR spectra of sufficient quality, but does not restrict its suitability as a precursor for ligand exchange reactions.

The spectroscopic data derived for the crystalline material are consistent with those of the finely powdered material synthesized by the protocol reported by Cook.[24] The ^1H NMR spectrum of the crystalline material shows a quintet signal in the hydride region at −7.21 ppm ($^2J_{P-H}$ = 37 Hz) (but not the "additional signal" reported in ref 24), and its IR spectrum shows a broad, diagnostic ν(Tc−H) stretch at 1890 cm^{-1}. The presence of a single band suggests a symmetric arrangement of the three hydrido ligands as is observed in some other phosphine trihydride complexes.[16] Therefore, the structure of **1** should resemble a C_{3v} symmetric capped octahedron with a capping PPh_3 ligand over the H−H−H face of a P_3H_3-octahedron, in which each hydrido ligand is equivalently positioned *trans* to a phosphine ligand. Given the low-lying d_{xz} and d_{yz} orbitals in all three possible CN7 geometries, diamagnetism is expected for such Tc(III) complexes having a d^4 configuration. This is in accord with the observation of resolved NMR spectra.

The novel procedure for the synthesis of compound **1** allows the growth of single crystals of the product suitable for an X-ray structure determination. Large, yellow-green crystals were obtained directly from a severely dilute reaction mixture, where no product precipitated at room temperature. They are formed after storing such a solution overnight in a refrigerator, while the remaining solution contained decomposition products as is indicated by its dark brown color. The identity of this material with the microcrystalline solid described above was checked by comparison of their IR spectra.

The crystal structure of **1** reveals the expected capped octahedral coordination environment around the technetium atom. A representation of the coordination sphere of technetium and the coordination polyhedron are shown in Figure 2. Table 1 contains some selected bond lengths and angles. First, the four phosphine ligands form a trigonal pyramid with three basal and one apical phosphorus atoms. The Tc−P bond to the apical atom P4 (2.249(1) Å) is shorter than those to the phosphorus atoms of the basal plane (2.473(1)−2.4937(9) Å). While the latter Tc−P bond lengths are in the normal range for Tc−P single bonds, the Tc−P4

https://doi.org/10.1021/acs.organomet.1c00274
Organometallics 2021, 40, 3095−3112

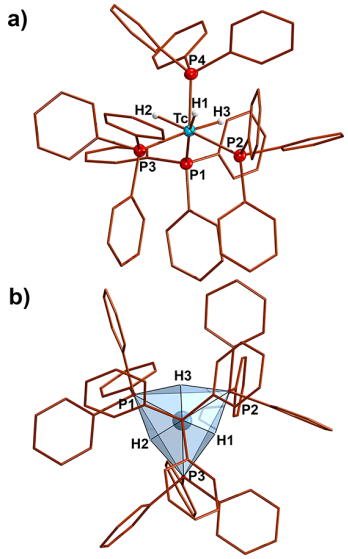

Figure 2. (a) Solid-state molecular structure of **1** with the located hydrido ligands and (b) the coordination polyhedron around technetium.

Table 1. Selected Bond Lengths (Å) and Angles (deg) in the Solid-State Structure of $[TcH_3(PPh_3)_4]$ (1)

P1−Tc	2.4824(9)	Tc−H1	1.54(2)
P2−Tc	2.4937(9)	Tc−H2	1.64(5)
P3−Tc	2.473(1)	Tc−H3	1.55(4)
P4−Tc	2.249(1)		
P4−Tc−P3	113.11(3)	P3−Tc−H2	74(2)
P4−Tc−P1	115.20(3)	P1−Tc−H2	75(2)
P3−Tc−P1	104.15(3)	P2−Tc−H2	178(2)
P4−Tc−P2	114.73(4)	H1−Tc−H2	112(2)
P3−Tc−P2	105.36(3)	P4−Tc−H3	71(2)
P1−Tc−P2	103.06(3)	P3−Tc−H3	175(1)
P4−Tc−H1	69.4(9)	P1−Tc−H3	72(1)
P3−Tc−H1	78(1)	P2−Tc−H3	74(1)
P1−Tc−H1	172.8(9)	H1−Tc−H3	105(2)
P2−Tc−H1	69.7(9)	H2−Tc−H3	107(2)
P4−Tc−H2	67(2)		

bond is among the shortest experimentally determined Tc−P distances.[25] Only for the 16e⁻ compound $[Tc^{I}(dppe)_2Cl]$ and for a few Tc(III) complexes Tc−P bond lengths shorter than 2.3 Å have hitherto been reported.[16,26−28] The positions of the hydrido ligands have been determined from the final Fourier maps of the refinement of the crystal data and Tc−H bond lengths of 1.54(2), 1.55(4), and 1.64(5) Å have been derived. It is known that M−H bond lengths derived from X-ray diffraction experiments are commonly too short due to the elusive physical nature of the hydrido ligand electrons in such complexes,[29] but no neutron diffraction data on technetium hydrido complexes have hitherto been reported. Thus, we can compare the data obtained for the hydride **1** exclusively with the limited number of X-ray structure determinations on technetium hydrides. Only for two of them, the position of terminal hydrido ligands could be resolved experimentally, namely for $[TcH(N_2)(dppe)_2]$ with a Tc−H bond length of 1.7(1) Å and for $[TcH_4(PPh_2Me)_4](BF_4)$ with Tc−H distances of 1.87 Å.[13,24] The H−H distances in $[TcH_3(PPh_3)_4]$ are between 2.44 and 2.64 Å and indicate the presence of classical hydrido ligands.

The spectroscopically derived coordination polyhedron, a capped octahedron, has been checked with the SHAPE software.[30−34] Although there is by far no perfect fit with one of the common polyhedra of coordination number 7, a capped octahedron (7-COC) is the closest one.[35] The determined SHAPE measure of 9.28906 reflects a significant deviation from the ideal polyhedron, but can readily be explained by the obviously large bond length differences of the Tc−H and Tc−P bonds.

Reactions of $[TcH_3(PPh_3)_4]$ (1) with Monodentate Phosphines. The first reactions performed with **1** as synthon were somewhat restrained by the inherent instability of the compound. Nevertheless, J. Cook succeeded with the isolation of $[TcH(H_2)(dppe)_2]$ (dppe = 1,2-bis(diphenylphosphino ethane) and $[TcH_3(PPh_2Me)_4]$. The dihydrogen ligand of the former compound is labile and can be replaced by a reversible reaction with N_2. The product of this reaction, $[TcH(N_2)(dppe)_2]$, can also be prepared in a feasible procedure directly from $[TcCl_4(PPh_3)_2]$[36] and has been used for a number of ligand exchange reactions affecting exclusively the axial dinitrogen and/or hydrido ligands.[37−40] $[TcH_3(PPh_2Me)_4]$ is a relatively unreactive compound and does not exchange its phosphine ligands. But, unlike $[TcH_3(PPh_3)_4]$, which decomposes on treatment with HBF_4, this compound can be protonated, and $[TcH_4(PPh_2Me)_4](BF_4)$ has been isolated and characterized spectroscopically and by X-ray diffraction.[24]

Since reactions of $NaBH_4$ with $[TcCl_4(PR_3)_2]$ complexes containing tertiary phosphines such as $P(C_6H_{12})_3$, $P(C_6F_5)_3$, $P(C_6H_4F)_3$, PMe_2Ph or PBu_3 only gave unattractive, black-brown mixtures, we attempted exchange reactions with the same phosphines starting from **1** These attempts also ended less encouraging, since only highly soluble, instable products were obtained. The results are in a line with similar experiments undertaken before with trihydrides of technetium and rhenium.[24,41]

Only during the reaction of $[TcH_3(PPh_3)_4]$ (**1**) with PMe_3, highly sensitive and very soluble yellow crystals of $[TcH_3(PPh_3)_2(PMe_3)_2]$ (**2**) could be isolated by the addition of $MeOH/H_2O$ to the reaction mixture after the complete dissolution of the starting material. The crystals decompose quickly in a vacuum and are only moderately stable in solution. Nevertheless, some instructive NMR data of the product could be collected. The ^1H NMR spectrum of the complex shows a quintet located at −5.88 ppm with a $^2J_{P-H}$ coupling constant of 22.05 Hz, suggesting coupling to four either equivalent or very similar ^{31}P nuclei. Since the methyl and phenyl resonances correspond to each two PMe_3 and PPh_3 ligands, the differences in the coupling constants to the different phosphines are probably not resolved or equal by chance. The hydrido ligands can, thus, either quickly exchange with each other $(H,(H)_2/H,(H_2)$ binding motifs) or they are in general chemically equivalent in solution as in the parent trihydride **1** having a symmetric H,H,H arrangement. Also in some dppe/PPh_3 and $P(OPh)_3/PPh_3$ mixed ligand trihydrido complexes of the higher congener rhenium the coupling constants between the hydrido ligands and the phosphorus nuclei were equivalent and quintets were observed.[42,43] Unfortunately, no ^{31}P NMR resonance could be resolved for **2**. This is not unexpected for phosphine complexes of technetium, where scalar couplings with the large quadrupole moment of ^{99}Tc (Q = −0.19 Å ×

https://doi.org/10.1021/acs.organomet.1c00274
Organometallics 2021, 40, 3095−3112

10^{-28} m^2)[43,44] commonly result in extreme line-broadenings, which make the resolution of ^{31}P NMR spectra frequently impossible.[44,45] The large quadrupole moment is also the reason for a drastic line-widening of the related ^{99}Tc NMR signals of compounds with a low local symmetry.[46] For the hydride **2** we recorded a ^{99}Tc NMR resonance at −2009 ppm (line width: ∼6350 Hz).

The obvious diamagnetism of the compound can be explained in two ways: either **2** shows (H,H,H) coordination of the three hydrides and is, thus, a rare example of a seven-coordinate d^4 Tc(III) complex with a detectable ^{99}Tc NMR resonance or the isolated product is better described as a d^6 technetium(I) mixed hydrido-dihydrogen complex. The IR spectrum of the complex shows an intricate pattern of three bands in the ν(Tc−H) region. A complication of the IR patterns of hydrido complexes has been reported previously and is either due to changes in the complex geometry or an inequivalence in the binding mode of the hydrido ligands (e.g., H,H,H; (H_3); $H(H_2)$; or $H(H)_2$ patterns).[42,47] After a simple phosphine substitution under retention of the geometry and general trihydride structure, a two-band spectrum should be expected, while a d^6 configuration with $H,(H)_2$ or $H,(H_2)$ binding patterns should produce more bands. Thus, we carried out a series of DFT calculations on the B3LYP/(Stuttgart1997, lanl2dz, 6-311G**) level to get more information about the hydride coordination and support for one of the interpretations of the observed spectral features. A pentagonal bipyramid and a capped trigonal prism (as distortions of the capped octahedron) were regarded. It turned out, that the ν(Tc−H) vibration is in either case weakened upon coordination of more basic PMe_3 compared to PPh_3. A full substitution of all PPh_3 ligands by PMe_3 results in a slight preference of ca. 3 kJ/mol for the pentagonal bipyramid with a H−P−H−P−H plane, while calculations on the higher B3LYP/x2c-TZVPPall-s level suggest a 8 kJ/mol preference for the capped trigonal antiprismatic arrangement (see Supporting Information). The resulting structure should therefore exhibit some fluxionality around these two ideal orientations. For neither of the regarded structures a real $H,(H_2)$ or $H,(H)_2$ binding motive of the hydrido ligands upon partial substitution of PPh_3 with PMe_3 can be securely deduced. The shortest H−H contact in the bicapped trigonal prismatic structure is 1.66 Å, while that in the pentagonal bipyramidal structure is 1.64 Å. The frequency analyses of both optimized structures show three vibrational M−H modes with a similar intensity distribution as observed in the experimental spectrum.

Figure 3 shows a visualization of the Electron Localization Functions (ELF) for the calculated structures of $[TcH_3(PR_3)_4]$ complexes at the B3LYP/(Stuttgart 1997, lanl2dz, 6-311G**) level. On the basis of the experiments and the comparison with the DFT calculations, we assign the isolated compound as $[TcH(H)_2(PPh_3)_2(PMe_3)_2]$ with two PMe_3 ligands oriented *trans* to two (almost) nonclassical hydrido ligands, an apical PPh_3 ligand and the second one in a trigonal plane together with the two PMe_3 ligands (see structural sketch in Scheme 1). Additional details are given in the Supporting Information.

Unlike $[TcH_3(PMePh_2)_4]$,[24] the mixed PPh_3/PMe_3 hydride complexes from the reaction described above, could not be protonated to the corresponding $[TcH_4(PPh_3)_n(PMe_3)_{4-n}](BF_4)$ (n = 1−3) species. Attempted reactions with $Et_2O{\cdot}HBF_4$ gave only intractable solutions, from which no products could be isolated. A corresponding reaction with $Et_2O{\cdot}HCl$ in dry benzene, however, gave immediately a bright yellow solution,

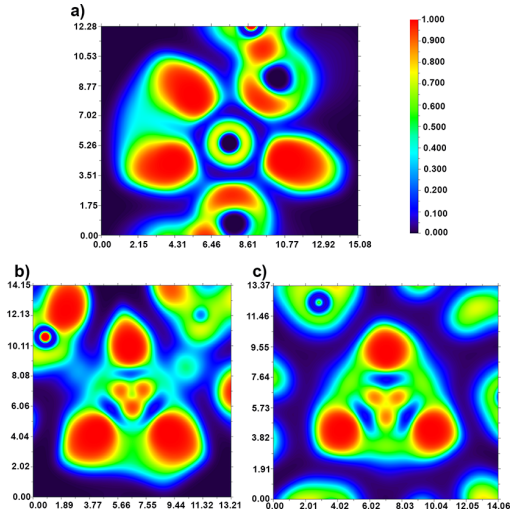

Figure 3. ELF mapping for the calculated structures of (a) PBP-$[TcH_3(PMe_3)_4]$, (b) COC-$[TcH_3(PMe_3)_4]$, and (c) COC-$[TcH_3(PPh_3)_4]$ at B3LYP level (sections through the central H,H,H planes). Note that the calculation base on the ECP approximation and, thus, the ELFs might be distorted (lengths in Bohr).

from which yellow blocks of $[TcCl_3(PMe_3)_3]$ (**4**)·$OPPh_3$ could be isolated. The abstraction of the hydrides during such reactions comes not completely unexpected and the reformation of $[TcCl_4(PPh_3)_2]$ from the hydrido complex **1** in chlorinated hydrocarbon solvents has been observed before.[24] The structure of $[TcCl_3(PMe_3)_3]$ with cocrystallized $OPPh_3$ is similar to that reported for $[TcCl_3(PMe_3)_3]{\cdot}(PhNCO)_3$.[15] Details are discussed in the Supporting Information.

When solutions of **1** are exposed to CO, the formation of the monohydride $[TcH(CO)_3(PPh_3)_2]$ (**5**) can be achieved. This has first been reported in the PhD thesis of J. Cook,[24] and some insertion reactions into the Tc−H bond of the compound were performed.[17] Some modifications in the reported protocol (particularly the use of toluene as solvent and an extension of the reaction time) allow the isolation of **5** in high purity and with an almost quantitative yield. IR and NMR data are identical with the reported ones.[24] In addition, we recorded a broad ^{99}Tc NMR signal at −2210 ppm ($\nu_{1/2}$ ∼ 9200 Hz).

Monoclinic single crystals of **5** suitable for X-ray diffraction were obtained by recrystallization from THF/pentane solutions. Figure 4 depicts an ellipsoid plot of the molecular structure. Selected bond lengths and angles are contained in Table 2. The coordination sphere of technetium is a distorted octahedron with the two triphenylphosphine ligands in *trans* position to each other. Thus, the three carbonyls are in a meridional arrangement. This is rare in the coordination chemistry of technetium, where only three more compounds with this coordination mode have been studied by crystal structure determination,[17,48,49] while the majority of 87 of the structurally studied compounds possess a facial coordination.[25] The C1−Tc−C3 angle of 163.1(2)° clearly indicates that the steric stress in **5** can be minimized by bending the related carbonyl ligands toward the hydrido ligand. The Tc−H bond length of 1.72(3) Å is slightly longer than those in **1** but in the range found for the other few technetium hydrides.[13,24]

After crystallization of **5** from toluene/ethanol, a triclinic polymorph of the compound was isolated (a = 9.8450(4) Å,

https://doi.org/10.1021/acs.organomet.1c00274
Organometallics 2021, 40, 3095−3112

Scheme 1. Synthesis of $[TcH_3(PPh_3)_4]$ and $[TcH(CO)_3(PPh_3)_2]$ and Their Reactions with PMe_3, Hydrogen Halides, and Carboxylic Acids

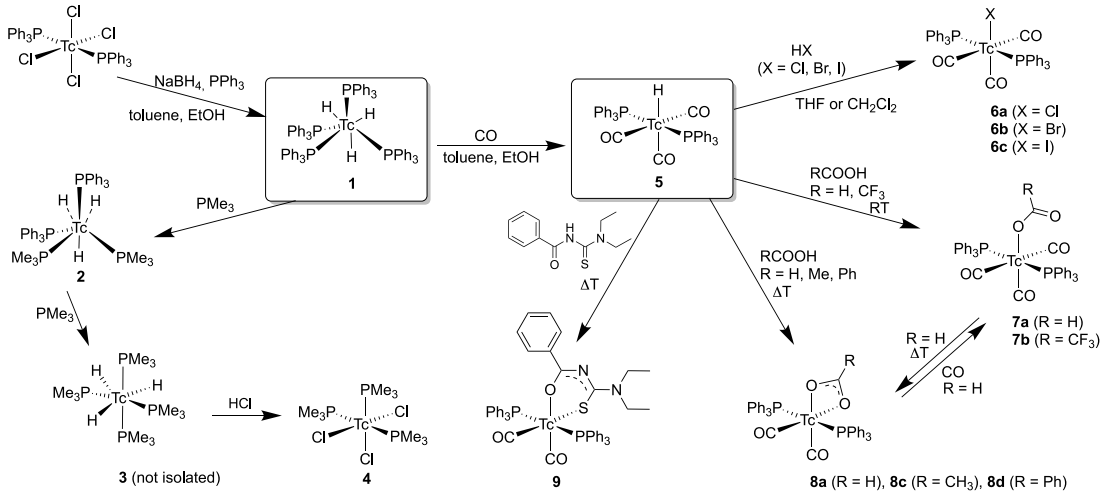

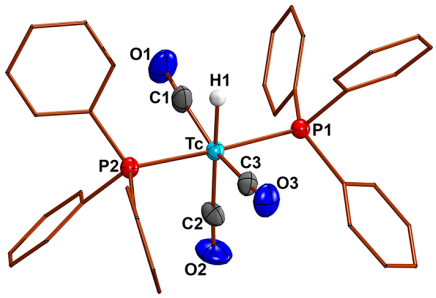

Figure 4. Molecular structure of **5**. Ellipsoids are depicted at 50% probability. Hydrogen atoms bound to carbon atoms and further labels are omitted for clarity.

b = 10.5678(5) Å, c = 17.9662(6) Å, α = 75.816(2)°, β = 77.711(2)°, γ = 65.441(2)°). A second monoclinic polymorph crystallized from dry THF/acetonitrile mixtures (a = 13.670(1) Å, b = 13.923(1) Å, c = 17.951(2) Å, β = 104.899(7)°). Details are reported in the Supporting Information.

The ready synthesis of **5** offers a chance to study the coordination behavior of compounds containing the *mer*-$[Tc(CO)_3(PPh_3)_2]^+$ and $[Tc(CO)_2(PPh_3)_2]^+$ cores in more detail. The hydride **5** reacts with HX solutions (X = Cl, Br, I) at room temperature under formation of $[TcX(CO)_3(PPh_3)_2]$ complexes and H_2 gas. It should be mentioned that the corresponding fluorido complex could not be prepared in this way or by a procedure using HF·py (see Supporting Information).

The interest in such compounds dates back to 1965,[50,51] when the first syntheses of such compounds have been attempted, but it took until 1992 before $[TcCl(CO)_3(PPh_3)_2]$ could first be characterized unambiguously by X-ray diffraction.[48] With the synthesis of the complete series of $[TcX(CO)_3(PPh_3)_2]$ complexes (X = H, Cl, Br, I) and their complete structural characterization, we can now also shade some light in the hitherto inconclusive reports of spectroscopic data for these complexes. Particularly, there exist different

Table 2. Selected Bond Lengths (Å) and Angles (deg) in the Solid-State Structures of $[Tc(X)(CO)_3(PPh_3)_2]$ Complexes 5 (X = H), 6a (X = Cl),[48] 6b (X = Br), 6c (X = I), and $[Tc(HNNPh\text{-}4\text{-}Bu^t)(CO)_3(PPh_3)_2](PF_6)$[17,a]

	$[TcH(CO)_3(PPh_3)_2]$	$[TcCl(CO)_3(PPh_3)_2]$[48]	$[TcBr(CO)_3(PPh_3)_2]$[b]	$[TcI(CO)_3(PPh_3)_2]$	$[Tc(HNNPh\text{-}4\text{-}Bu^t)(CO)_3(PPh_3)_2](PF_6)$[17]
Tc–C1	1.972(4)	1.979	1.959(5)	1.998(3)	1.999
Tc–C2	1.939(4)	1.887	1.900(5)	1.889(3)	1.910
Tc–C3	1.943(4)	1.983	1.986(6)	2.009(4)	1.985
Tc–P1	2.4025(8)	2.4404	2.4370(7)	2.4593(7)	2.453
Tc–P2	2.4097(8)	2.4454	2.4463(7)	2.4624(8)	2.461
Tc–X	1.72(3)	2.5055	2.6217(6)	2.8352(3)	2.157
X–Tc–C1	84(1)	92.60	88.32(2)	87.0(1)	92.6
X–Tc–C2	175(1)	178.84	176.6(2)	174.98(9)	178.0
X–Tc–C3	79(1)	96.4	95.4(2)	97.64(9)	89.7
X–Tc–P1	91(1)	88.51	86.58(2)	86.82(2)	86.9
X–Tc–P2	86(1)	87.34	91.70(2)	88.81(2)	86.8
C1–Tc–C2	100.6(2)	86.3	88.3(2)	88.0(1)	86.1
C1–Tc–C3	163.1(2)	171.0	175.6(4)	175.4(1)	177.5
C2–Tc–C3	96.3(2)	84.7	87.9(3)	87.4(1)	91.6

[a]The molecular labeling schemes of complexes taken from the literature are adopted to those of Figures 4 and 5. [b]Values refer to the main component of the 85:15 disorder between Br^- and one of the *cis* CO ligands.

https://doi.org/10.1021/acs.organomet.1c00274
Organometallics 2021, 40, 3095–3112

values for the ^{99}Tc NMR chemical shifts (most probably due to the presence of different isomers in the studied solutions, keeping in mind that most of the syntheses started from pentacarbonyl or *fac*-tricarbonyl technetium complexes).[24,48,50−54] With the de novo syntheses of the complexes from an already pre-established *mer-trans*-arrangement of the carbonyl and phosphine ligands, we unequivocally confirm the chemical shifts of *mer-trans*-$[TcCl(CO)_3(PPh_3)_2]$ (**6a**) and *mer-trans*-$[TcBr(CO)_3(PPh_3)_2]$ (**6b**) to be −1461 ppm ($\nu_{1/2}$ ∼ 3110 Hz) and −1534 ppm ($\nu_{1/2}$ ∼ 4300 Hz). This linearly fits with the chemical shift we observed for *mer-trans*-$[TcI(CO)_3(PPh_3)_2]$ (**6c**) at −1670 ppm ($\nu_{1/2}$ ∼ 3920 Hz) and nicely corresponds to the different donor properties of the corresponding halogen atoms.

Since the number of structurally characterized series of technetium complexes with different halogen donors in low oxidation states is limited, we determined the crystal structures of the bromido and the iodido complexes. Ellipsoid representations of the molecular structures are shown in Figure 5. Selected bond lengths and angles are compared with those of other $[TcX(CO)_3(PPh_3)_2]$ complexes (X = H, Cl, (HNNPh-4-Bu^t)) in Table 2.

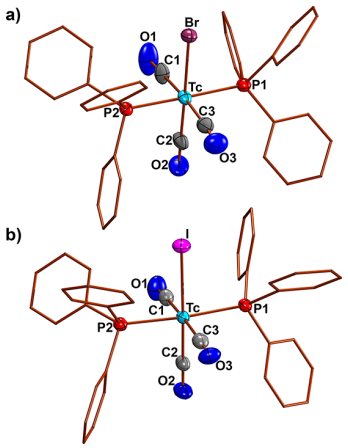

Figure 5. Molecular structures of (a) $[TcBr(CO)_3(PPh_3)_2]$ (**6b**) and (b) $[TcI(CO)_3(PPh_3)_2]$ (**6c**). Thermal ellipsoids are depicted at 50% probability. Hydrogen atoms and further labels are omitted for clarity.

The technetium atoms in **6b** and **6c** are coordinated in distorted octahedral fashions with the PPh_3 ligands in *trans* positions to each other and three meridionally coordinated CO ligands. In contrast to the situation in **5**, where the two carbonyl ligands in *cis* position to H^- are bent toward the hydride, they are bent away from the halido ligand. This is also observed for $[TcCl(CO)_3(PPh_3)_2]$ (**6a**) and can be attributed to the differences in size of H^- and the halido ligands.

Reactions of $[TcH(CO)_3(PPh_3)]$ (5) with Carboxylic Acids and Other Proton Sources. Reactions of **5** with carboxylic acids are strongly dependent on the π-basicity of the acid and the conditions applied. Monodentate coordination of the carboxylate and the formation of $[Tc\{\eta^1\text{-}O(CR)O\}(CO)_3(PPh_3)_2]$ (**7**) complexes is observed under mild conditions and/or when using less π-basic carboxylic acids such as CF_3COOH. When, however, the reactions are carried out at higher temperatures or when relatively π-basic carboxylic acids are used, decarbonylation and the formation of chelate complexes is observed. On closer inspection of these reactions, we found that two factors are important: the Brønsted acidity of the carboxylic acid and the π-basicity of the corresponding carboxylate anion. This can be reasoned with an increased *cis*-effect or *cis*-labilization due to coligands with high π-basicity when they are in *cis*-position to π-acidic ligands such as CO. A similar tendency toward increased coordination strength of the second oxygen donor of the carboxylate group with increased π-basicity was previously described in ^{99}Tc NMR studies on the substitution series from *fac*-$[Tc(CO)_3(OH_2)_3]^+$ to *fac*-$[Tc(CO)_3(OC(R)O)_3]^{2-}$ compounds.[55] A similar *cis*-labilization resulting in a decarbonylation has also been observed for terphenylisocyanide complexes of manganese of the type *mer-trans*-$[Mn\{\eta^1\text{-}O(CR)O\}(CO)_3(CNAr^{Dipp2})_2]$ (Ar^{Dipp2} = 2,6-(2,6-(i-Pr)$_2C_6H_3$)$_2$-C_6H_3.). The products, $[Mn\{\eta^2\text{-}OO(CR)\}(CO)_2(CNAr^{Dipp2})_2]$, represent ultimately useful synthons for the generation of the highly unsaturated, divacant metallo Lewis-acid $[Mn(CO)_2(CNAr^{Dipp2})_2]^+$ and its solvent adducts.[56] As in the manganese example, the decarbonylation reaction of the technetium carboxylato complexes is reversible in the presence of an excess of CO gas. However, for a convenient isolation of the η^1-derivatives, the acidity of the carboxylic acid must be sufficient to protonate **5** effectively at room temperature and its π-basicity must be low enough not to induce decarbonylation even at room temperature. Two illustrative examples are the reactions with acetic acid and trifluoromethyl acetic acid. All our attempts to isolate $[Tc\{\eta^1\text{-}O(CCH_3)O\}(CO)_3(PPh_3)_2]$ failed. We observed the instantaneous formation of $[Tc\{\eta^2\text{-}OO(CCH_3)\}(CO)_2(PPh_3)_2]$ (**8c**) due to the relatively high π-basicity of acetate. For the stabilization of the complex with monodentate acetato coordination, such solutions must be kept under an CO atmosphere or the products must rapidly be precipitated. In the latter case, however, the obtained solids contain significant amounts of the chelate complex and any attempts of purification result in further decarbonylation. Contrarily, the reaction of **5** with CF_3COOH generally gives almost exclusively (**7b**). The high acidity of CF_3COOH and the low π-basicity of its anion prohibits the formation of significant quantities of the dicarbonyl compound even after prolonged heating in toluene.

The $[Tc\{\eta^1\text{-}O(CR)O\}(CO)_3(PPh_3)_2]$ (**7**) and $[Tc\{\eta^2\text{-}OO(CR)\}(CO)_2(PPh_3)_2]$ (**8**) derivatives can easily be distinguished by their IR and ^{99}Tc NMR spectra. The complexes of type **7** show four carbonyl stretches in their IR spectra. Three bands around 2050 cm^{-1}, 1960 and 1900 cm^{-1} correspond to the *mer*-tricarbonyl unit, while a broad band between 1400 and 1700 cm^{-1} can be assigned to the carboxylate pseudoallyl system. In comparison, the technetium dicarbonyl complexes $[Tc\{\eta^2\text{-}OO(CR)\}(CO)_2(PPh_3)_2]$ (**8**) show a total of three carbonyl bands: two corresponding to the metal carbonyls at ca. 1940 and 1860 cm^{-1} and the third relatively broad band between 1400 and 1700 cm^{-1} is that of the carboxylate pseudoallyl system. These findings are consistent with the previously reported IR bands found in the carboxylato complexes $[Tc\{\eta^2\text{-}OO(CR)\}(CO)_2(PPh_3)_2]$ (R = Ph_2CH, $PhCH_2$, CCl_3), which were prepared by reactions of RCOOLi with **6a**.[57]

Both types of technetium carboxylato complexes show relatively broad ^{99}Tc NMR resonances with half-line widths between 3000 and 4000 Hz, but can readily be distinguished by their chemical shifts. While the tricarbonyl species resonate at chemical shifts between −1350 ppm and −1400 ppm, the

https://doi.org/10.1021/acs.organomet.1c00274
Organometallics 2021, 40, 3095−3112

signals of the dicarbonyl complexes appear between −700 and −800 ppm. Surprisingly, the chemical shift range of the η^2-carboxylato complexes differs significantly from the ^{99}Tc NMR chemical shift range observed for the dithiocarboxylato complexes $[Tc\{S(CR)S\}(CO)_2(PPh_3)_2]$ (R = NEt_2, P-$(OMe)_2$, OMe), which show characteristic and narrow triplets between −1270 ppm and −1500 ppm with $^1J_{Tc-P}$ coupling constants of ca. 550−600 Hz and half-line widths between 100 and 300 Hz.[58]

There is surprisingly little structural information about technetium complexes with simple carboxylic acids or carboxylates, and only a few compounds have been studied by X-ray crystallography.[25] In most of the compounds, the carboxylates act as bridging ligands between two metal atoms. Mononuclear complexes have preferably been studied with trifluoroacetic acid.[45,59,60] Thus, the three $[Tc\{\eta^2\text{-}OO(CR)\}(CO)_2(PPh_3)_2]$ complexes **8a**, **8c**, and **8d** of the present study represent the first crystallographic proof of the existence of chelate bonded technetium complexes with simple carboxylato ligands. However, it should be mentioned that the formation of corresponding formato and acetato complexes has been concluded before from spectroscopic data.[24] The reported IR and NMR data are in accord with our findings, but we cannot confirm the reported inertness of the compounds. Compound **8a** readily reacts with CO when solutions of these complexes are heated under a CO atmosphere. No such reactivity could be confirmed for the corresponding chelates with acetate and benzoate.

For comparison, we undertook X-ray crystal structure determinations on a series of $[Tc\{\eta^1\text{-}O(CR)O\}(CO)_3(PPh_3)_2]$ (**7**) and $[Tc\{\eta^2\text{-}OO(CR)\}(CO)_2(PPh_3)_2]$ (**8**) complexes. Ellipsoid representations of the corresponding formato complexes are shown in Figure 6 as representatives for the two classes of compounds. Plots of the other compounds are shown in the Supporting Information. A summary of selected bond lengths and angles is given in Table 3.

In the compounds **7a** and **7b**, the octahedral coordination environment around technetium is similar to that in the halido complexes retaining the *mer-trans* orientation of the carbonyl and phosphine ligands. The two carbonyl ligands positioned *cis* to the carboxylato ligands are less tightly bound compared to the *trans* oriented carbonyl ligand. The O4−C4−O5 bond angles of ca. 129° as well as the similar C4−O4 (ca. 1.26 Å) and C4−O5 (ca. 1.23 Å) bond lengths indicate delocalization of the electron density in the pseudoallyl system. The Tc−O4 bond lengths of 2.184(4) Å in the η^1-formato and 2.162(3) Å in the η^1-trifluoroacetato complex are in the range of the technetium−oxygen single bond in the previously studied trifluoroacetato complexes.[45,59,60]

Since the complexes of type **8** represent the first technetium complexes with chelate-bound, simple carboxlates, the related structural motifs shall be discussed a little more in detail. The Tc−C bond lengths in the dicarbonyl complexes with chelate-bonded carboxylates show values between 1.84 and 1.87 Å and are, thus, somewhat shorter than the corresponding bonds in the complexes **7**. This is in accord with the values found for related dicarbonyl compounds of technetium such as $[Tc(\eta^2\text{-}ArN\cdots X\cdots NAr)(CO)_2(PPhMe_2)_2]$ (X = C, N), $[Tc(\eta^2\text{-}O,N\text{-}diazepine)(CO)_2(PPh_3)_2]$, $[Tc\{\eta^2\text{-}S(COMe)NPh\}(CO)_2(PPh_3)_2]$, $[Tc\{\eta^2\text{-}S(CNHPh)S\}(CO)_2(PPh_3)_2]$ or $[Tc(\eta^2\text{-}O,N\text{-}\{(C_3H_2NS)N{=}CHC_6H_4O\})(CO)_2((PPh_3)_2]$.[58,61−64] They show a similar bonding situation with technetium−carbonyl distances between 1.87 and 1.90 Å.

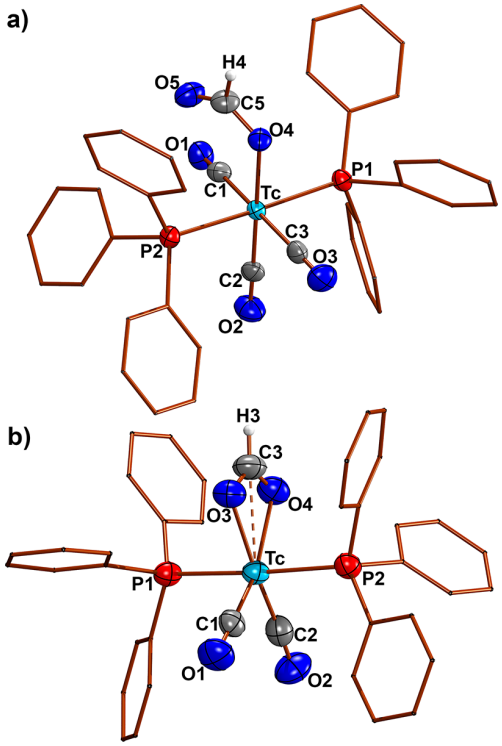

Figure 6. Molecular structures of (a) $[Tc\{\eta^1\text{-}O(CH)O\}(CO)_3(PPh_3)_2]$ (**7a**) and (b) $[Tc\{\eta^2\text{-}OO(CH)\}(CO)_2(PPh_3)_2]$ (**8a**). Ellipsoids are depicted at 50% probability. Hydrogen atoms that are not bound to the formato ligands and further labels are omitted for clarity.

The technetium−oxygen bonds in the η^2-carboxylato complexes are also in the range of normal single bonds but slightly longer than in the $[Tc(\eta^1\text{-}O(CR)O)(CO)_3(PPh_3)_2]$ compounds. The almost equal C−O bond lengths in the carboxylate ligands and the O3−C3−O4 angles of ca. 120° reflect an almost ideal trigonal symmetry around the carboxylato carbon atoms. Interestingly, the η^2-benzoato ligand in **8d** is not entirely flat. The phenyl ring is tilted from the TcCOO plane by a torsion angle of ca. 20° indicating a lower degree of delocalization of the carboxylic group with the ligand backbone.

The *cis*-angles between the carbonyl carbon atoms and the carboxylic oxygen atoms are between 101° and 112° and, thus, deviate strongly from the ideal 90°. This is also seen in the *trans*-angles between the same atoms, which are between 159° and 169°. Both findings are readily explained with the small bite-angles of the carboxylic groups, which are between 58 and 59°.

The distances between the Tc atoms and the carbon atoms of the chelate-bonded carboxylates are ca. 2.58 Å. A comparison with the distances between technetium and the central atoms in the previously reported dicarbonyl pseudoallyl complexes $[Tc(\eta^2\text{-}ArN\cdots X\cdots NAr)(CO)_2(PPhMe_2)_2]$ with X = C or N (2.68−2.71 Å), $[Tc(\eta^2\text{-}O,N\text{-diazepine})(CO)_2(PPh_3)_2]$ (2.61 Å), $[Tc\{\eta^2\text{-}S(COEt)N\}(CO)_2(PPh_3)_2]$ (2.78 Å), and $[Tc\{\eta^2\text{-}S(CNHPh)S\}(CO)_2(PPh_3)_2]$ (2.94 Å) shows that these distances are mainly influenced by the donor atoms of the pseudoallyl ligands.[58,60−64] On the basis of these compounds, a dependence of the Tc···C distance in complexes with pseudoallyl ligands on the nature of the neighboring

https://doi.org/10.1021/acs.organomet.1c00274
Organometallics 2021, 40, 3095−3112

Table 3. Selected Bond Lengths (Å) and Angles (deg) in the Solid-State Structures of $[Tc\{\eta^1\text{-}O(CH)O\}(CO)_3(PPh_3)_2]$ (7a), $[Tc\{\eta^1\text{-}O(CF_3)O\}(CO)_3(PPh_3)_2]$ (7b), $[Tc\{\eta^2\text{-}OO(CH)\}(CO)_2(PPh_3)_2]$ (8a), $[Tc\{\eta^2\text{-}OO(CCH_3)\}(CO)_2(PPh_3)_2]$ (8c), and $[Tc\{\eta^2\text{-}OO(CPh)\}(CO)_2(PPh_3)_2]$ (8d)[a]

	7a	7b		8a	8c	8d
Tc−C1	1.982(9)	2.034(3)	Tc−C1	1.841(5)	1.870(2)	1.858(4)
Tc−C2	1.883(7)	1.874(3)	Tc−C2	1.866(6)	1.870(2)	1.849(4)
Tc−C3	1.973(9)	1.960(3)	Tc−O3	2.233(3)	2.213(1)	2.221(2)
Tc−O4	2.183(4)	2.162(2)	Tc−O4	2.246(3)	2.231(1)	2.220(3)
Tc−P1	2.435(2)	2.4377(8)	Tc−P1	2.419(1)	2.4211(4)	2.430(1)
Tc−P2	2.457(2)	2.4489(8)	Tc−P2	2.428(1)	2.4360(4)	2.430(1)
C1−O1	1.141(8)	1.109(4)	Tc···C3	2.568(6)	2.581(2)	2.570(4)
C2−O2	1.151(7)	1.169(4)	C1−O1	1.172(6)	1.156(2)	1.162(5)
C3−O3	1.140(8)	1.132(4)	C2−O2	1.172(6)	1.159(2)	1.174(4)
C4−O4	1.262(8)	1.259(4)	C3−O3	1.239(7)	1.262(2)	1.263(4)
C4−O5	1.232(9)	1.222(5)	C3−O4	1.252(7)	1.267(2)	1.274(4)
O4−Tc−C1	96.0(2)	93.1(1)	O3−Tc−C1	101.4(2)	167.42(6)	105.3(1)
O4−Tc−C2	179.3(3)	176.5(1)	O3−Tc−C2	169.9(2)	105.90(6)	166.2(1)
O4−Tc−C3	88.5(2)	91.3(1)	O3−Tc−P1	87.5(1)	93.88(3)	86.11(7)
O4−Tc−P1	88.8(1)	85.91(6)	O3−Tc−P2	92.5(1)	84.20(3)	92.03(7)
O4−Tc−P2	89.0(1)	86.71(6)	O4−Tc−C1	159.4(2)	109.01(6)	164.4(1)
P1−Tc−C1	86.9(2)	90.9(1)	O4−Tc−C2	112.2(2)	164.11(6)	107.0(1)
P1−Tc−C2	91.8(2)	91.5(1)	O4−Tc−P1	89.4(1)	85.16(3)	91.84(7)
P1−Tc−C3	89.92(2)	91.21(9)	O4−Tc−P2	85.6(1)	91.81(3)	85.69(7)
P2−Tc−C1	93.2(2)	90.6(1)	O4−Tc−O3	58.0(1)	58.63(4)	59.14(9)
P2−Tc−C2	90.4(2)	95.9(1)	C1−Tc−C2	88.5(2)	86.58(7)	88.6(2)
P2−Tc−C3	90.2(2)	87.81(9)	P1−Tc−C1	91.3(2)	86.93(5)	87.7(1)
P1−Tc−P2	177.75(9)	172.54(3)	P1−Tc−C2	89.9(2)	92.87(4)	94.5(1)
C1−Tc−C2	84.3(3)	84.6(2)	P2−Tc−C1	94.4(2)	86.58(7)	94.5(1)
C1−Tc−C3	174.4(3)	175.2(1)	P2−Tc−C2	89.1(2)	94.42(5)	86.9(1)
C2−Tc−C3	91.2(3)	91.1(2)	P1−Tc−P2	174.10(5)	176.95(1)	177.44(4)
O4−C4−O5	128.2(7)	129.4(3)	O3−C3−O4	121.4(5)	118.8(1)	119.5(3)

[a]The atomic labeling scheme has been adopted from Figure 6.

atoms can be derived. They increase in the order *O,O* < *O,N* < *N,N* < *S,N* < *S,S*.

The protonation of complex **5** and the decarbonylation of the compounds **7** have been studied by DFT calculations on the B3LYP level of theory in dichloromethane solution. The obtained free-energy differences correlate well with the experimental observations. Expectedly, the protonation of **5** by RCOOH and the formation of $[Tc\{\eta^1\text{-}O(CR)O\}(CO)_3(PPh_3)_2]$ complexes and H_2 is thermodynamically more favored, when the acidity of RCOOH is high. The energies for the protonation involving PhCOOH and CH_3COOH favor the starting materials by insignificant energy values (0.1 and 0.4 kJ/mol), which are within the margin of error of the method. Therefore, it can be safely assumed that the protonation by them is energetically least favored across the group and only a small energy gain is involved. The CO labilization is well-represented by the free-energy differences in the $[Tc\{\eta^1\text{-}O(CR)O\}(CO)_3(PPh_3)_2]$ vs $[Tc\{\eta^2\text{-}OO(CR)\}(CO)_2(PPh_3)_2]$ + CO couples. The loss of CO is most feasible for benzoate and acetate with a difference in free energy of ca. 12 kJ/mol, respectively, while there is only a slight tendency of 3 kJ/mol in the case of formate. In the case of the trifluoroacetate, the release of CO is impeded by an energy barrier of ca. 16 kJ/mol. Details are given in the Supporting Information.

The hydride abstraction from **5** is not restricted to carboxylic acids, but also occurs with other proton sources. We have probed this by the reaction with *N,N*-diethyl-*N*′-benzoylthiourea (HEt_2btu). The coordination chemistry of technetium and rhenium with such potentially chelating ligands has been studied extensively, which allows comparisons with a variety of related Tc complexes.[65−67] The reaction resulted in the formation of the bright yellow dicarbonyl complex $[Tc(S,O\text{-}Et_2btu)(CO)_2(PPh_3)_2]$ (**9**).

Deprotonation and the formation of an *S,O* chelate is strongly suggested by the spectroscopic data of the product. The IR spectrum of the product does not show any NH band and the $\nu_{C=O}$ stretch of the benzoylthiourea is bathochromically shifted (1409 cm^{-1} in **9** vs 1660 cm^{-1} in the uncoordinated ligand). The large degree of delocalized electron density inside the chelate ring and beyond is supported by the detection of a hindered rotation around the exocyclic C-NEt_2 bond in the ^1H NMR spectrum of the complex. The ^{31}P NMR signal of **9** is broad as observed for all other compounds of this study. The ^{99}Tc NMR resonance of the chelate is found at −1119 ppm, which is expectedly in the middle of the chemical shift range observed for the η^2-carboxylato complexes containing an *O,O* donor set and the previously reported $[Tc\{SS(CR)\}(CO)_2(PPh_3)_2]$ (R = NEt_2, $P(OMe)_2$, OMe) complexes containing an *S,S* donor set.[58]

Single crystals of compound **9** suitable for X-ray diffraction were obtained by slow evaporation of a toluene/methanol solution. An ellipsoid plot of the molecular structure is shown in Figure 7 and selected bond lengths and angles are summarized in Table 4. The spectroscopically detected strong delocalization of electron density in the chelate ring is confirmed by the determined bond lengths. This also includes the relatively short exocyclic C4−N1 bond and explains the

https://doi.org/10.1021/acs.organomet.1c00274
Organometallics 2021, 40, 3095−3112

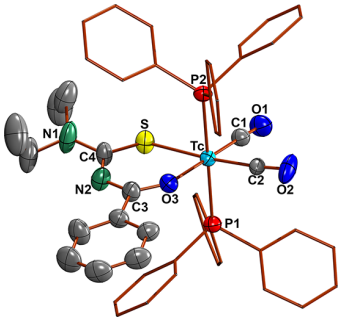

Figure 7. Molecular structure of **9**. Ellipsoids are depicted at 50% probability. Hydrogen atoms and further labels are omitted for clarity.

Table 4. Selected Bond Lengths (Å) and Angles (deg) in 9

Tc−C1	1.872(7)	C2−O2	1.144(6)
Tc−C2	1.892(6)	O3−C3	1.274(6)
Tc−O3	2.140(4)	C3−N2	1.330(7)
Tc−S	2.475(2)	N2−C4	1.353(8)
Tc−P1	2.450(2)	C4−S	1.687(7)
Tc−P2	2.455(2)	C4−N1	1.371(8)
C1−O1	1.164(7)		
O3−Tc−C1	177.7(2)	S−Tc−O3	85.4(1)
O3−Tc−C2	97.3(2)	C1−Tc−C2	84.4(3)
O3−Tc−P1	90.3(1)	P1−Tc−C1	88.2(2)
O3−Tc−P2	87.8(1)	P1−Tc−C2	91.9(2)
S−Tc−C1	92.9(2)	P2−Tc−C1	93.8(2)
S−Tc−C2	175.7(2)	P2−Tc−C2	87.1(2)
S−Tc−P1	91.44(6)	P1−Tc−P2	177.66(7)

hindered rotation around this bond, which has been detected by NMR.

Interestingly, the chelating ligand is not entirely planar, but twisted along the C3(O1)−N2−C4(S1)−N1Et$_2$ axis around C4. While the benzoyl amide moiety C3(O1)−N2 in the ligand is planar, a torsion of the thiourea moiety C4(S1)−N1Et$_2$ by ca. 20° out of the plane is observed. The torsion of thiourea and the benzoyl amide moieties has been observed before in some other technetium complexes containing benzoylthioureato or the derived thiocarbonylbenzamidinato ligands with torsion angles between 2° and 32°.[65−67] The resulting *O,S* bite angle of the Et$_2$btu$^-$ ligand is 85.4(1)°.

Reactions of [TcH(CO)$_3$(PPh$_3$)$_2$] (5) with PhSeOOH. Unexpected results were obtained from reactions of **5** with phenyl seleninic acid (PhSeOOH). A summary of the isolated products and their reactions is given in Scheme 2.

We performed the experiment in order to synthesize a compound, which is suitable for a comparison with the obtained benzoato complex. However, a complex of the composition [Tc{η^2-OO(SePh)}(CO)$_2$(PPh$_3$)$_2$] could not be isolated from such reactions and ^{99}Tc NMR spectra of the crude reaction mixtures indicate the formation of a variety of Tc(I) compounds depending on the solvents and the reaction time. The signal of the starting material **5** at −2208 ppm quickly disappears independent of the reaction medium. However, sharp ^{99}Tc resonances are observed in two groups of signals (−400 to −600 ppm with a main signal at −582 ppm and −750 to −900 ppm with a main signal at −765 ppm) when the products of the reaction in toluene/MeOH/H$_2$O were studied (Figure 8a).

Scheme 2. Reactions of 5 with Phenyl Selenic Acid and Oxalic Acid

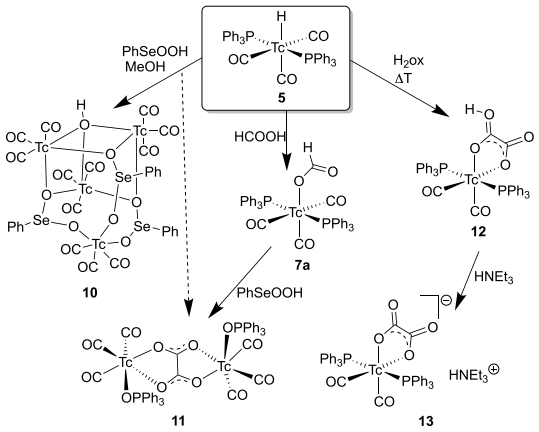

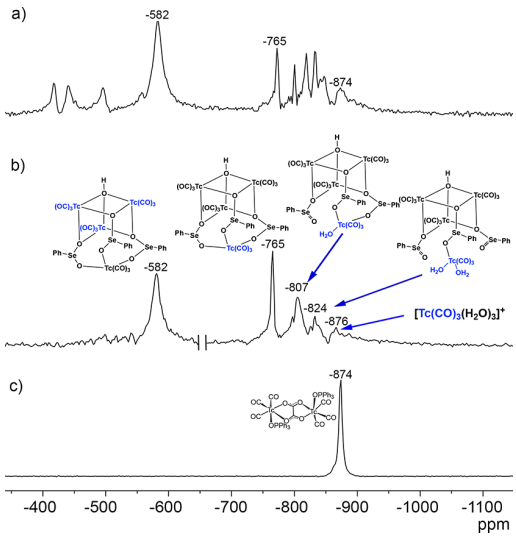

Figure 8. ^{99}Tc NMR spectra of (a) a CH$_2$Cl$_2$ extract of the crude residue obtained from a reaction between **5** and PhSeOOH in toluene/MeOH/H$_2$O, (b) a solution of **10** in (moist) CH$_2$Cl$_2$, and (c) a solution of **11** in CH$_2$Cl$_2$.

We tentatively assigned the resonances between −770 and −900 ppm to mixed-ligand *fac*-{Tc(CO)$_3$}$^+$ complexes with aqua ligands. This is in accordance with previous studies.[55] The resonances between −400 and −600 ppm presumably belong to complexes containing phenylseleninato and aqua or hydroxido ligands. A ^{31}P NMR resonance at 28 ppm indicates the coformation of OPPh$_3$.

Crystallization of the crude residue gave single crystals of a colorless main product and a few pale yellow crystals depending on the recrystallization conditions. The main product was obtained by recrystallization from CH$_2$Cl$_2$/pentane and identified as [{Tc(CO)$_3$}$_3$(μ^3-OH)(μ^2-O(SePh)-O)$_3$Tc(CO)$_3$}] (**10**)·(OPPh$_3$)·0.25 pentane by X-ray diffraction. An ellipsoid representation of the cluster structure is shown in Figure 9. Selected bond lengths and angles can be found in Table 5.

All technetium atoms in the cluster are coordinated octahedrally with three facial carbonyl ligands. The *mer*/*fac* isomerization of the carbonyl units in the starting material can

https://doi.org/10.1021/acs.organomet.1c00274
Organometallics 2021, 40, 3095−3112

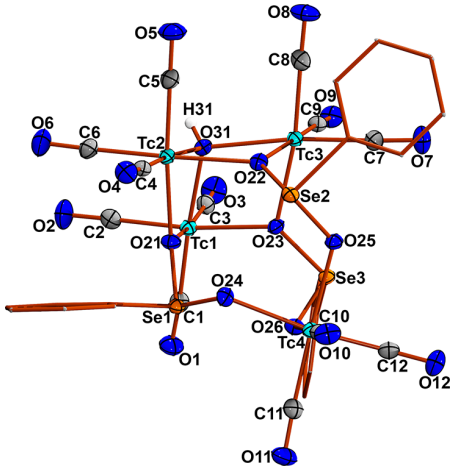

Figure 9. Molecular structure of $[\{Tc(CO)_3\}_3(\mu^3\text{-}OH)(\mu^2\text{-}O(SePh)\text{-}O)_3\{Tc(CO)_3\}]$ (**10**). Ellipsoids are depicted at 50% probability. Phenyl hydrogen atoms and further labels are omitted for clarity.

Table 5. Selected Bond Lengths (Å) and Angles (deg) in 10

Tc1–O31	2.116(2)	Tc2–O31	2.177(2)
Tc3–O31	2.207(2)	Tc1–O21	2.198(2)
Tc1–O23	2.197(2)	Tc2–O21	2.144(2)
Tc2–O22	2.204(2)	Tc3–O22	2.235 (2)
Tc3–O23	2.166(2)	Tc4–O24	2.194(2)
Tc4–O25	2.211(2)	Tc4–O26	2.139(2)
Se1–O21	1.766(2)	Se1–O24	1.669(2)
Se2–O22	1.732(2)	Se2–O25	1.657(2)
Se3–O23	1.723(2)	Se3–O26	1.751(2)
Tc1–O21–Se1	125.80(9)	O21–Se1–O24	105.9(1)
Se1–O24–Tc4	124.8(1)	Tc1–O23–Se3	134.8(1)
O23–Se3–O26	105.06(9)	Se3–O26–Tc4	121.4(1)
Tc2–O21–Se1	132.9(1)	Tc3–O23–Se3	119.9(1)

be understood by the oxidative removal of the PPh_3 ligands from the coordination sphere of technetium. The reduced steric stress allows the formation of the more stable *fac*-arrangement of the carbonyl ligands. Three of the $\{Tc(CO)_3\}^+$ units are chemically equivalent and connected by a μ^3-hydroxido bridge. They are additionally bridged by three μ^2-phenyl seleninato ligands. The second oxygen atoms of the three phenyl seleninato ligands coordinate a fourth $\{Tc(CO)_3\}^+$ unit in a tripodal fashion. Thus, the forth technetium atom has another coordination environment than the others and is not embedded in the pseudocubane structure of the $[\{Tc(CO)_3\}_3(OH)(PhSeOO)_3]^-$ unit. The bonding parameters within the tricarbonyl units are not remarkable and also the technetium oxygen bond lengths fit the expected region of technetium oxygen single bonds well. Surprisingly, two different bonding situations are found for the phenyl seleninato ligands and indicate a stronger delocalization of the electron density in the ligand comprising Se3 compared with the two others. The solid-state structure is stabilized by a hydrogen bond between the hydroxido ligand to the oxygen atom of the adjacent, cocrystallized triphenylphosphine oxide.

The structural features derived from the solid-state structure with two different $\{Tc(CO)_3\}^+$ units are well reflected by the ^{99}Tc NMR spectrum of the cluster giving two signals at −582 and −765 ppm (Figure 8b). The $\{Tc(CO)_3\}^+$ unit comprising Tc4 seems to establish only weak bonds to the $PhSeOO^-$ ligands of the $[\{Tc(CO)_3\}_3(\mu^3\text{-}OH)(O(SePh)O)_3]^-$ entity, which can readily be cleaved in solution by the interaction with solvent molecules. This reactivity is illustrated by the ^{99}Tc NMR spectrum of Figure 8b, which has been measured in (moist) CD_2Cl_2. Clearly three signals of products resulting from a stepwise hydrolysis are resolved at −807, −824, and −876 ppm. The chemical shift of the latter one is identical with that of the $[Tc(CO)_3(H_2O)_3]^+$ cation.[46] A similar behavior has also been observed upon dissolution of **10** in other coordinating solvents such as acetonitrile.

The tricarbonyltechnetium(I) groups of the trimeric $[\{Tc(CO)_3\}_3(\mu^3\text{-}OH)(\mu^2\text{-}O(SePh)O)_3]^-$ pseudocubane unit are not involved in a similar solvolytic degradation. The proton of the bridging hydroxido ligand is observed as a single broad resonance at 8.30 ppm in the ^{1}H NMR spectra of such solutions, while the resonances of the water protons are very broad and shifted to ca. 0.5 ppm due to the fluxional coordination of the $\{Tc(CO)_3\}^+$ fragment.

As already mentioned above, we could isolate a small amount (about 3% yield) of faint yellow crystals as a minor side product of the reaction of **5** with PhSeOOH. They grew by fractional crystallization of the reaction mixture from a mixture of toluene, methanol, water, and diethyl ether. Surprisingly, the IR spectrum of the crystals shows a carbonyl band at 1626 cm^{-1} in addition to two sharp bands at 2036 and 1925 cm^{-1}. The additional band appears in the same region as the ν_{CO} bands in the previously discussed carboxylato complexes. A relatively narrow ^{99}Tc-NMR signal ($\nu_{1/2}$ = 576 Hz) was observed at −874 ppm and the ^{31}P NMR spectrum showed a $OPPh_3$ resonance at 44 ppm.

A single-crystal X-ray diffraction study of the compound finally revealed the formation of the dimeric oxalato complex *fac-fac*-$[Tc_2(ox)(CO)_6(OPPh_3)_2]$ (**11**). An ellipsoid representation of the compound is shown in Figure 10 and selected bond lengths and angles are summarized in Table 6.

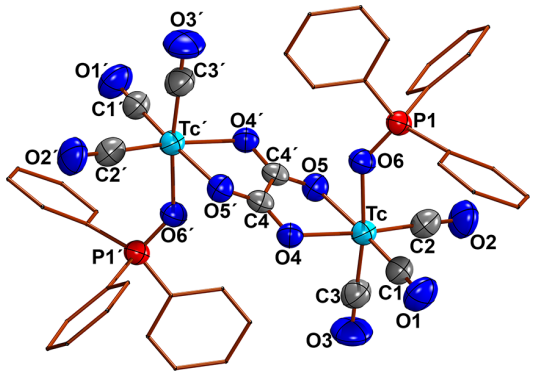

Figure 10. Molecular structure of **11**. Ellipsoids are depicted at 50% probability. Hydrogen atoms and further labels are omitted for clarity. Symmetry code: (′) 1 − *x*, 1 − *y*, −*z*.

Compound **11** is a centrosymmetric molecule with a center of inversion in the middle of the C–C bond of the bridging oxalato ligand. The coordination spheres of the technetium atoms are completed by three facial carbonyl and one $OPPh_3$ ligands each. The central $\{(CO)_2Tc(ox)Tc'(C'O')_2\}$ unit is almost planar with a maximum deviation of 0.2830 Å for O5′ (r.m.s. 0.1536 Å). The Tc–O (oxalate) bonds are somewhat shorter than those in the complexes **8** and fall in the range found for complexes of type **7** (Table 3). This can easily be

https://doi.org/10.1021/acs.organomet.1c00274
Organometallics 2021, 40, 3095–3112

Table 6. Selected Bond Lengths (Å) and Angles (deg) in 11

Tc−C1	1.885(4)	Tc−C2	1.885(4)
Tc−C3	1.884(4)	Tc−O4	2.166(2)
Tc−O5	2.178(2)	Tc−O6	2.163(2)
C4−O4	1.250(4)	C4−C4′	1.539(6)
C4−O5′	1.246(4)	O6−P1	1.491(2)
O4−Tc−O5	76.39(8)	Tc−O6−P1	138.5(1)
Tc−O4−C4	112.8(2)	Tc−O5−C4′	111.9(2)
O4−C4−5′	116.8(3)	O5−C4′−C4	118.0(3)

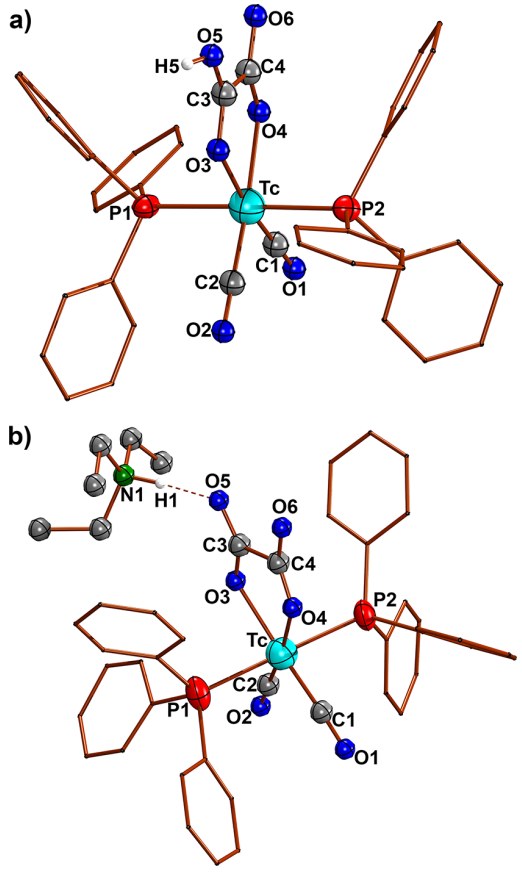

Figure 11. Molecular structures of (a) $[Tc(\eta^2\text{-oxH})(CO)_2(PPh_3)_2]$ (**12**) and (b) $(HNEt_3)[Tc(\eta^2\text{-ox})(CO)_2(PPh_3)_2]$ (**13**). Ellipsoids are depicted at 50% probability. Hydrogen atoms and further labels are omitted for clarity.

Table 7. Selected Bond Lengths (Å) in 12 and 13

	12	13
Tc−C1	1.863(9)	1.84(2)
Tc−C2	1.853(8)	1.84(2)
Tc−O3	2.207(5)	2.19(1)
Tc−O4	2.209(5)	2.16(1)
Tc−P1	2.441(2)	2.442(5)
Tc−P2	2.422(2)	2.434(4)
O3−C3	1.261(8)	1.31(2)
O4−C4	1.231(8)	1.19(2)
C3−O5	1.244(8)	1.24(2)
C4−O6	1.252(9)	1.27(2)
C3−C4	1.535(9)	1.59(3)

understood by the 1,2-coordination of the oxalato bridge. The Tc−C bonds are the normal range for Tc carbonyls.

The formation of an oxalato ligand as a result of a reaction between the Tc hydride **5** and phenyl seleninic acid is surprising. Nevertheless, several mechanisms for the formation of oxalic acid or oxalate from simple starting materials such as CO, methanol, or formic acid have been discussed before.[68−70] In the present case, two of these mechanisms seem to be reasonable. One is a methanol mediated CO/CO-coupling type reaction, while the second mechanism involves the oxidation of methanol to formic acid or formate followed by the subsequent dehydro-dimerization to give oxalic acid or oxalate. Keeping in mind that PhSeOOH is a mild oxidant and the retention of the three respective carbonyl ligands, particularly the oxidation pathway should have some probability.

To show that the reaction indeed proceeds via formic acid or formate (resulting from the oxidation of the solvent methanol), we studied the course of the same reaction, but with the addition of formic acid. The dehydro-dimerization should be much more feasible under such conditions. And indeed, in situ ^{99}Tc NMR spectra of the reaction mixture showed the rapid formation of two major resonances at −758 and −805 ppm, which could potentially be assigned to the bridged dimeric complexes $[Tc_2\{\mu^2\text{-}\eta^1\text{-}O(CH)O\}_2(CO)_6(PPh_3)_2]$ and $[Tc_2\{\mu^2\text{-}\eta^1\text{-}O(CH)O\}_2(CO)_6(OPPh_3)_2]$ on the basis of their chemical shifts (see also a proposed mechanism in the Supporting Information). After an analogous workup as described above (evaporation of both the aqueous and organic phases), the solution of the residue in CH_2Cl_2 showed similar ^{99}Tc resonances as in the previous experiment with two distinctions. First, the intensity and number of resonances in the mixed carboxylato/aqua region between −750 to −900 ppm increased, while the resonances in the mixed aqua or hydroxido/phenylseleninato region between −400 and −600 ppm disappeared (with the exception of the $[\{Tc(CO_3)\}_3(\mu^3\text{-}OH)(O(SePh)O)_3]^-$ cluster signal at −582 ppm). Second, the resonance of $[Tc_2(ox)(CO)_6(OPPh_3)_2]$ at −875 ppm is now the second main product of the mixture. Thus, the addition of formic acid favors the formation of the dimeric oxalato complex by bypassing the oxidation of MeOH and avoids the formation of the species giving resonances between −400 and −600 ppm. Recrystallization of the crude residue from CH_2Cl_2/pentane gave pure $[Tc_2(ox)(CO)_6(OPPh_3)_2]$ in ca. 50% yield.

Although an exact mechanism for the observed dehydro-dimerization of formate cannot be formulated unambiguously on the basis of the available data, it is highly probably that the formation of the C−C bond is metal supported. The proposal of a mechanism is deposited in the Supporting Information. As a strong hint for the proposed reaction pathway we regard the fact that the tricarbonyl units are retained at both technetium atoms and the novel oxalato ligand appears as bridge between the two units.

All our attempts to synthesize the dimeric complex directly from **5** and oxalic acid failed. Reactions between the hydrido complex and oxalic acid result in gas evolution and the formation of $[Tc(\eta^2\text{-oxH})(CO)_2(PPh_3)_2]$ (**12**) as the sole product. The compound is only sparingly soluble and precipitates as a yellow solid in good yields. A broad band at 3547 cm^{-1} in the IR spectrum of the compound gives a hint that at least one of carboxylic groups remained protonated. The ^{99}Tc chemical shift of −875 ppm is in the range of

https://doi.org/10.1021/acs.organomet.1c00274
Organometallics 2021, 40, 3095−3112

complexes with chelate-bonded carboxylates. Thus, the formation of a neutral dicarbonyl complex is strongly indicated.

In contrast to the other carboxylic acids regarded in this study, the hydrogenoxalato ligand can adopt two different η^2-modes: as 1,1- or 1,2-chelate (as observed for **11**). We evaluated both binding modes by DFT calculations on the B3LYP level in CH_2Cl_2 solution. The η^2-OO(CCOOH) binding mode is energetically disfavored by ca. 17 kJ/mol over the η^2-O(C(O)C(OH))O binding mode. Additionally, the decarbonylation of $[Tc\{\eta^1\text{-}O(CCOOH)O\}(CO)_3(PPh_3)_2]$ under formation of $[Tc\{\eta^2\text{-}O(C(O)C(OH))O\}(CO)_2(PPh_3)_2]$ is favored by ca. 10 kJ/mol.

Finally, the formation of a compound with the predicted structure of **12** was proven by X-ray diffraction. Figure 11a shows an ellipsoid plot of its molecular structure. Selected bond lengths are summarized in Table 7. The oxalato ligand is indeed bonded as a 1,2-chelate with Tc−O bond lengths of 2.207(5) and 2.209(5) Å. There is a widespread equalization of the four C−O bond lengths in this ligand, which also indicates that the hydrogen atom (H5) is disordered over two positions (at the oxygen atoms O5 and O6).

The remaining carboxylic group of compound **12** can easily be deprotonated, e.g., by a reaction with NEt_3. The sparingly soluble starting material rapidly dissolves in CH_2Cl_2 upon addition of the amine. The progress of the reaction can be monitored by ^{99}Tc NMR spectroscopy, where a shift of the signal from −875 ppm to −967 ppm is observed. A colorless solid of $(HNEt_3)[Tc(\eta^2\text{-ox})(CO)_2(PPh_3)_2]$ (**13**) can be precipitated by the addition of pentane to such solutions.

An ellipsoid representation of the molecular structure of **13** is shown in Figure 11b. It can clearly be seen that a hydrogen bond between the ammonium cation and the complex anion is established. The bond lengths (see Table 7) inside the complex are not significantly influenced by the deprotonation of the peripheral carboxylic group.

CONCLUSIONS

Improved procedures allow the synthesis of the hydrido complexes $[TcH_3(PPh_3)_4]$ and $[TcH(CO)_3(PPh_3)_2]$ in good yields and high purity. The syntheses can readily be scaled up to a millimolar level.

Through reactions of $[TcH(CO)_3(PPh_3)_2]$ with hydrogen halides, dihydrogen is evolved and the related *mer,trans*-$[TcX(CO)_3(PPh_3)_2]$ (X = Cl, Br, I) complexes are formed in good yields. Similar reactions with carboxylic acids of sufficient Brønsted acidity and anions with low π-acidity (such as formic acid of trifluoroacetic acid) give similar products: $[Tc(\eta^1\text{-}O(CH)O)(CO)_3(PPh_3)_2]$ and $[Tc\{\eta^1\text{-}O(CH)O\}(CO)_3(PPh_3)_2]$. Decarbonylation and the formation of $[Tc\{\eta^2\text{-}OO(CR)\}(CO)_2(PPh_3)_2]$ complexes is observed when the carboxylates possess a sufficient π-basicity. Formic acid represents a borderline case, where a reversible carbonylation/decarbonylation was observed.

An interesting result was obtained from a reaction of $[TcH(CO)_3(PPh_3)_2]$ with phenyselenic acid in the presence methanol: the unexpected formation of oxalate by a C−C coupling reaction. There are strong hints that this coupling is metal-driven and formato ligands, which are formed by the oxidation of MeOH, play a crucial role. More detailed mechanistic studies on this unusual type of reaction will be required to understand this fascinating reaction. In light of potential applications, such experiments should be done, e.g., with nonradioactive elements of group 7, in the future.

^{99}Tc NMR spectroscopy has been proven to be a valuable tool for the evaluation of the content of reaction mixtures of the diamagnetic technetium complexes under study. A collection of the chemical shifts and line widths of representative complexes can be found in Table 8. The tricarbonyl species *mer*-$[TcX(CO)_3(PPh_3)_2]$ (X = H, Cl, Br, I, O(CH)O and $O(CF_3)O$) show resonances between −1350 ppm and −2208 ppm with a decreasing shielding of the ^{99}Tc nucleus in the order $H^- > I^- > Br^- > Cl^- > CHOO^- > CF_3COO^-$. Thus, they can clearly be distinguished from the related dicarbonyltechnetium(I) complexes with signals between −736 ppm and −1119 ppm. It shall be mentioned that the dicarbonyl region overlaps with the region where *fac*-tricarbonyl complexes commonly resonate.

Table 8. ^{99}Tc NMR Data of the *trans-mer*-Tricarbonyl and *cis-trans*-Dicarbonyl Complexes of This Study and Their Reaction Products (Solvent for All Data: CD_2Cl_2)

	chem. shift [ppm]	$\nu_{1/2}$ [Hz]
$[TcH(CO)_3(PPh_3)_2]$	−2208	9180
$[TcI(CO)_3(PPh_3)_2]$	−1670	3920
$[TcBr(CO)_3(PPh_3)_2]$	−1534	4296
$[TcCl(CO)_3(PPh_3)_2]$	−1461	3114
$[Tc(\eta^1\text{-}O(CH)O)(CO)_3(PPh_3)_2]$	−1396	4086
$[Tc(\eta^1\text{-}O(CF_3)O)(CO)_3(PPh_3)_2]$	−1350	3667
$(HNEt_3)[Tc(\eta^2\text{-ox})(CO)_2(PPh_3)_2]$.	−967	1614
$[Tc(\eta^2\text{-oxH})(CO)_2(PPh_3)_2]$	−875	3265
$[Tc(\eta^2\text{-}OO(CCH_3))(CO)_2(PPh_3)_2]$	−811	2862
$[Tc(\eta^2\text{-}OO(CPh))(CO)_2(PPh_3)_2]$	−806	3061
$[Tc(\eta^2\text{-}OO(CH))(CO)_2(PPh_3)_2]$	−736	4028

Surprisingly, the technetium nucleus in $[TcH(H)_2(PPh_3)_2(PMe_3)_2]$ is less shielded than the one in $[TcH(CO)_3(PPh_3)_2]$. Furthermore, the presence of hydrido ligands appears to increase the line widths of the ^{99}Tc resonances.

EXPERIMENTAL SECTION

General Considerations. Unless otherwise stated, reagent-grade starting materials were purchased from commercial sources and either used as received or purified by standard procedures. Solvents were dried and deoxygenated according to standard procedures. HEt_2btu and $[TcCl_4(PPh_3)_4]$ were prepared as previously described.[71,72]

Physical Measurements. NMR spectra were recorded at 20 °C with JEOL 400 MHz multinuclear spectrometers with a relaxation delay of 10 μs. The values given for the ^{99}Tc chemical shifts are referenced to pertechnetate. IR spectra were recorded with a Shimadzu FTIR 8300 spectrometer as KBr pellets. The following abbreviations were used for the intensities and characteristics of IR absorption bands: vs = very strong, s = strong, m = medium, w = weak, sh = shoulder.

Radiation Precautions. ^{99}Tc is a long-lived weak β^- emitter (E_{max} = 0.292 MeV). Normal glassware provides adequate protection against the weak beta radiation when milligram amounts are used. Secondary X-rays (bremsstrahlung) play a significant role only when larger amounts of ^{99}Tc are handled. All manipulations were done in a laboratory approved for the handling of radioactive materials.

X-ray Crystallography. The intensities for the X−ray determinations were collected on STOE IPDS II or on Bruker D8 Venture instruments with Mo Kα or Cu Kα radiation. The space groups were determined by the detection of systematical absences. Absorption corrections were carried out by multiscan or integration methods.[73,74] Structure solution and refinement were performed with the SHELX program package.[75,76] Hydrogen atoms were derived from the final Fourier maps and refined or placed at calculated positions and treated

https://doi.org/10.1021/acs.organomet.1c00274
Organometallics 2021, 40, 3095−3112

with the "riding model" option of SHELXL. The representation of molecular structures was done using the program DIAMOND 4.2.2.[77]

Additional information on the structure determinations is contained in the Supporting Information and has been deposited with the Cambridge Crystallographic Data Centre.

Computational Details. DFT calculations were performed on the high-performance computing systems of the Freie Universität Berlin ZEDAT (Curta)[78] using the program package GAUSSIAN 16.[79] The gas phase and solution geometry optimizations were performed using coordinates derived from the X-ray crystal structures using GAUSSVIEW and Avogadro.[80,81] The polarizable continuum model (PCM) with the integral equation formalism variant (IEFPCM) was used to implicitly simulate the solvent dichloromethane. The calculations were performed with the hybrid density functional B3LYP.[82−84] The double-ζ pseudopotential LANL2DZ basis set with the respective effective core potential (ECP) was applied to P.[85] The Stuttgart relativistic small core basis set with the corresponding ECP was applied to Tc.[86,87] The 6-311+G** basis set was used to model all other atoms in the calculations regarding the carbonyl complexes.[88,89] The 6-311G** basis set was applied for C and H in the calculation of the trihydrido complexes.[88] Only for the assessment of the energetic differences in $[TcH_3(PMe_3)_4]$ isomers, the all-electron basis set x2c-TZVPPall-s was employed for all atoms.[90] The system size of the other complexes quickly became prohibitive for the use of all-electron basis sets. All basis sets as well as the ECPs were obtained from the EMSL database.[91] Frequency calculations after the optimizations confirmed the convergence. No negative frequencies were obtained for the given optimized geometries of all compounds. The entropic contribution to the free energy was corrected for low-energy modes using the quasi-harmonic approximation of Grimme[92] as implemented in the freely accessible python code *GoodVibes* of Funes-Ardoiz and Paton with a cutoff at 300 cm^{-1}.[93] Further analysis of orbitals, charges, electron localization function (ELF), etc., was performed with the free multifunctional wave function analyzer *Multiwfn*.[94] Visualization of the electrostatic potential maps was done with GAUSSVIEW.[80]

Syntheses of the Complexes. *$[TcH_3(PPh_3)_4]$ (1)·2 Toluene.* $[TcCl_4(PPh_3)_2]$ (1.2 g, 1.6 mmol) and PPh_3 (10.7 g, 40.8 mmol, 26 equiv) were suspended in toluene (30 mL) in a 500 mL flask. A suspension of freshly ground $NaBH_4$ (653 mg, 17.3 mmol, 11 equiv) in ethanol (6 mL) was quickly added under vigorous stirring. Additional ethanol (9 mL) was added, while immediately a violent evolution of dihydrogen started and a color change from deep green to orange-brown occurred. The mixture was stirred for 20 min, after which time the bubbling rate decreased and no residual green starting material was visible in the slurry. Hexane (12 mL) was added to the suspension under stirring. The stirring was stopped and more hexane (18 mL) was slowly added. This mixture was kept unagitated at room temperature for 30 min to finish the precipitation. The formed yellow crystalline solid was filtered of and copiously washed with acetone and water. Finally, it was washed with pentane and quickly dried in air before storage in the refrigerator. Yield: 1.92 g (1.4 mmol, 88%). IR (KBr, $\tilde{\nu}$, cm^{-1}) 1890 (m, ν_{Tc-H}). ^1H NMR (C_6D_6, ppm) −7.21 (quint., $^2J_{H,P}$ = 36.5 Hz, Tc−H), as given in ref 24. No ^{31}P and ^{99}Tc spectra could be recorded due to the low solubility of the crystalline material.

Some large yellow green single crystals of $[TcH_3(PPh_3)_4]$·2 toluene for X-ray diffraction were obtained from a highly dilute reaction mixture of $[TcCl_4(PPh_3)_2]$ (71 mg, 0.1 mmol) and PPh_3 (681 mg, 2.6 mmol, 26 equiv) and freshly ground $NaBH_4$ (42 mg, 1.1 mmol, 11 equiv) in a toluene/ethanol mixture (18 mL/4 mL). The reaction was performed as stated above and the resulting clear brown-yellow solution was stored in a refrigerator overnight resulting in the formation of single crystals alongside reddish-black decomposition products.

$[TcH_3(PPh_3)_2(PMe_3)_2]$ (2). The synthesis and all manipulations were carried out using standard Schlenk technique. A solution of PMe_3 (1 mmol, 1.0 mL of a 1 M solution in THF) was added to a suspension of **1** (138 mg, 0.1 mmol) in benzene (1 mL). After stirring for 1 h, additional benzene (4 mL) was added to the light green suspension. After stirring for an additional 1.5 h at room temperature, the green suspension became a clear, deep green solution. Methanol (20 mL) was added to the mixture resulting in the formation of bright yellow microcrystals. Water (0.5 mL) was added to complete the precipitation. After storage in the refrigerator for 3 h, the microcrystals were filtered off and washed with MeOH and pentane. After drying in air, they were stored in the refrigerator under argon. Yield: 38 mg (0.04 mmol, 40%). IR (KBr, $\tilde{\nu}$, cm^{-1}) 1957 (w, ν_{Tc-H}), 1896 (m, ν_{Tc-H}), 1871 (m, ν_{Tc-H}). ^1H NMR (C_6D_6, ppm) 8.16−7.99 (m, 12H, PPh_3), 7.14−7.08 (m, 12H, corrected for benzene overlap, PPh_3), 7.08−7.00 (m, 6H, PPh_3), 0.91 (d, 18H, $^2J_{H,P}$ = 20.04 Hz, PMe_3), −5.82 (3H, p, $^2J_{H,P}$ = 22.05 Hz, Tc−H). ^1H NMR (CD_2Cl_2, ppm) −6.47 (3H, s, Tc−H). ^{99}Tc NMR (C_6D_6, ppm) −2008 (s, $\nu_{1/2}$ = 7095 Hz). ^{99}Tc NMR (CD_2Cl_2, ppm) −1981 (s, $\nu_{1/2}$ = 2976 Hz). The ^{31}P NMR spectrum has not been observed due to quadrupolar coupling with the ^{99}Tc nucleus.

$[TcH(CO)_3(PPh_3)_2]$ (5). The synthesis of this compound was performed adopting the procedure given in ref 17. with some modifications, which resulted in higher yields. Toluene (20 mL) was saturated with CO gas over 1.5 h. Solid **1** (828 mg, 0.6 mmol) was added in a strong stream of CO. Within 1.5 h, the insoluble starting material dissolved resulting in a clear yellow solution. The mixture was stirred in a continuous CO stream for a total of 4 h. Then, ethanol (40 mL) was added, which resulted in the formation of a colorless precipitate. The mixture was stored in the refrigerator overnight to complete the crystallization. The colorless microcrystals of **5** were filtered off, washed with ethanol (6 mL) and pentane (6 mL) before drying in air. Yield: 411 mg (0.58 mmol, 97%. Reducing the CO exposure to 2 h, lowers the yield significantly. IR (KBr, $\tilde{\nu}$, cm^{-1}) 2023 (w, $\nu_{C\equiv O}$), 1929 (vs, $\nu_{C\equiv O}$). ^1H NMR (CD_2Cl_2, ppm) 7.63−7.47 (m, 12H, PPh_3), 7.47−7.26 (m, 18H, PPh_3), −4.86 (1H, t, $^2J_{H,P}$ = 19.66 Hz, Tc−H). ^1H NMR (THF-d_8, ppm) 7.65−7.54 (m, 12H, PPh_3), 7.43−7.30 (m, 18H, PPh_3), −4.75 (1H, t, $^2J_{H,P}$ = 20.04 Hz, Tc−H). ^1H NMR (benzene-d_6, ppm) 7.93−7.76 (m, 12H, PPh_3), 7.08−6.89 (m, 18H, PPh_3), −4.12 (1H, t, $^2J_{H,P}$ = 20.08 Hz, Tc−H). ^{99}Tc NMR (CD_2Cl_2, ppm) −2208 (s, $\nu_{1/2}$ = 9180 Hz). The ^{31}P NMR spectrum has not been observed due to quadrupolar coupling with the ^{99}Tc nucleus. Single crystals suitable for X-ray diffraction have been obtained by layered diffusion of pentane into a thf solution, CH_3CN into a THF solution and ethanol into a toluene solution of the complex.

$[TcCl(CO)_3(PPh_3)_2]$ (6a). A concentrated Et_2O·HCl solution (1 mL, prepared from 3 mL conc. HCl in 20 mL Et_2O followed by drying with $MgSO_4$) was added to a suspension of **5** (25 mg, 0.04 mmol) in dichloromethane (1 mL). After stirring for 30 min, MeOH (10 mL) was layered on the top of the reaction mixture and it was stored in the refrigerator overnight. **6a** deposited as a colorless solid, which was filtered off, washed with methanol and then pentane. Yield: 27 mg (0.04 mmol, quantitative). IR (KBr, $\tilde{\nu}$, cm^{-1}) 2054 (w, $\nu_{C\equiv O}$), 1958 (vs, $\nu_{C\equiv O}$), 1904 (vs, $\nu_{C\equiv O}$). ^1H NMR (CD_2Cl_2, ppm) 7.73 (s, 12H, PPh_3), 7.43 (s, 18H, PPh_3). $^{31}P\{^1H\}$ NMR (CD_2Cl_2, ppm) 36 (s, broad, $\nu_{1/2}$ = 3025 Hz). ^{99}Tc NMR (CD_2Cl_2, ppm) −1461 (s, $\nu_{1/2}$ = 3114 Hz).

$[TcBr(CO)_3(PPh_3)_2]$ (6b). Concentrated $HBr_{(aq)}$ (3 drops) was added to a suspension of **5** (35 mg, 0.05 mmol) in THF (1 mL). An immediate evolution of H_2 was observed. After stirring for 5 min, MeOH (9 mL) was added to complete the precipitation of **6b**. The colorless powder was filtered off, washed with methanol and pentane, and dried in air. Yield: 39 mg (0.05 mmol, 99%) IR (KBr, $\tilde{\nu}$, cm^{-1}) 2058 (w, $\nu_{C\equiv O}$), 1960 (vs, $\nu_{C\equiv O}$), 1917 (vs, $\nu_{C\equiv O}$), 1906 (sh, $\nu_{C\equiv O}$). ^1H NMR (CD_2Cl_2, ppm) 7.61 (s, 12H, PPh_3), 7.42 (s, 18H, PPh_3). $^{31}P\{^1H\}$ NMR (CD_2Cl_2, ppm) 51 (s, broad, $\nu_{1/2}$ = 858 Hz). ^{99}Tc NMR (CD_2Cl_2, ppm) −1534 (s, $\nu_{1/2}$ = 4296 Hz). Single crystals suitable for X-ray diffraction have been obtained by diffusion of pentane into a CH_2Cl_2 solution of the complex.

$[TcI(CO)_3(PPh_3)_2]$ (6c). A concentrated solution of Et_2O·HI (4 mL, prepared from conc. HI (0.25 mL) in Et_2O (6 mL) followed by drying with $MgSO_4$) was dropwise added to a suspension of **5** (36 mg, 0.05 mmol) in dichloromethane (1 mL). After stirring for 5 min,

https://doi.org/10.1021/acs.organomet.1c00274
Organometallics 2021, 40, 3095−3112

pentane (10 mL) was layered on the top of the mixture, which was then stored in the refrigerator overnight. Colorless microcrystals of **6c** deposited, which were filtered off, washed with diethyl ether (which removes traces of a brown color) and pentane. After drying, greyish microcrystals were obtained. Yield: 38 mg (0.05 mmol, 91%). IR (KBr, $\tilde{\nu}$, cm^{-1}) 2048 (m, $\nu_{C\equiv O}$), 2002 (w, $\nu_{C\equiv O}$), 1960 (vs, $\nu_{C\equiv O}$), 1904 (vs, $\nu_{C\equiv O}$). ^1H NMR (CD_2Cl_2, ppm) 7.74 (s, 12H, PPh_3), 7.42 (s, 18H, PPh_3). $^{31}P\{^1H\}$ NMR (CD_2Cl_2, ppm) 28 (s, broad, $\nu_{1/2}$ = 2264 Hz). ^{99}Tc NMR (CD_2Cl_2, ppm) −1670 (s, $\nu_{1/2}$ = 3920 Hz). Single crystals suitable for X-ray diffraction have been obtained by diffusion of acetone into a CH_2Cl_2 solution of the complex.

*[Tc{η^1-O(CH)O}(CO)$_3$(PPh$_3$)$_2$] (**7a**).* Formic acid (1 mL) was added to a suspension of **5** (72 mg, 0.1 mmol) in dichloromethane (1 mL) and heated on reflux for 10 min. After stirring for additional 20 min, MeOH (9 mL) was layered on the top of the mixture, which was then stored in the refrigerator overnight. Gray microcrystals of **7a** deposited during this time. They were filtered off, washed with methanol and then pentane, and dried on air. Yield: 59 mg (0.08 mmol, 78%). IR (KBr, $\tilde{\nu}$, cm^{-1}) 2050 (w, $\nu_{C\equiv O}$), 1958 (vs, $\nu_{C\equiv O}$), 1909 (vs, $\nu_{C\equiv O}$), 1609 (m, ν_{COO}). ^1H NMR (CD_2Cl_2, ppm) 7.56−7.27 (m, 30H, PPh_3). $^{31}P\{^1H\}$ NMR (CD_2Cl_2, ppm) 41 (s, broad, $\nu_{1/2}$ = 2996 Hz). ^{99}Tc NMR (CD_2Cl_2, ppm) −1396 (s, broad, $\nu_{1/2}$ = 4086 Hz). Single crystals suitable for X-ray diffraction have been obtained by diffusion of MeOH into a CH_2Cl_2 solution of the complex.

*[Tc{η^1-O(CCF$_3$)O}(CO)$_3$(PPh$_3$)$_2$] (**7b**)·0.5 Toluene.* CF_3COOH (3 drops) was added to a suspension of **5** (68 mg, 0.1 mmol) in toluene (2 mL). The resulting clear, reddish-pink solution was heated under reflux for 30 min after which the color of the solution had turned yellow. Upon cooling, MeOH (10 mL) and H_2O (20 mL) were added. The mixture was left for slow evaporation of the organic solvents for 2 days. The formed colorless crystals were filtered off and dried in the air. They were suitable for X-ray diffraction. Yield: 60 mg (0.07 mmol, 68%). IR (KBr, $\tilde{\nu}$, cm^{-1}) 2068 (s, $\nu_{C\equiv O}$), 1963 (vs, $\nu_{C\equiv O}$), 1854 (vs, $\nu_{C\equiv O}$), 1672 (m, ν_{COO}). ^1H NMR (CD_2Cl_2, ppm) 7.62−7.38 (2m, 30H, PPh_3), 7.30−7.11 (2m, 2/3 of 5H, toluene-ArH), 2.35 (s, 2/3 of 3H, toluene-CH_3). ^{19}F NMR (CD_2Cl_2, ppm) −76.6 (s). $^{31}P\{^1H\}$ NMR (CD_2Cl_2, ppm) 37 (s, broad, $\nu_{1/2}$ = 3045 Hz). ^{99}Tc NMR (CD_2Cl_2, ppm −1350 (s, $\nu_{1/2}$ = 3667 Hz).

*[Tc{η^2-OO(CH)}(CO)$_2$(PPh$_3$)$_2$] (**8a**).* (a) Formic acid (1 mL) was added to a suspension of **5** (35 mg, 0.05 mmol) in toluene (1.5 mL). An evolution of H_2 and the formation of a clear, colorless, biphasic solution was observed. The biphasic mixture was heated under reflux for 30 min resulting in a color change to faint yellow-green in the upper phase. MeOH (9 mL) was carefully added and the mixture was then stirred vigorously resulting in the precipitation of colorless microcrystals. The mixture was stored in the refrigerator for 2 h to complete the crystallization. The formed **8a** was filtered off, washed with MeOH and finally with a small amount of pentane. After drying in air, analytically pure colorless microcrystals were obtained. Yield: 35 mg (0.05 mmol), 97%).

(b) **8a** is also formed by heating a solution of **7a** in toluene for 30 min. The conversion is quantitative based on the ^{99}Tc NMR spectra. IR (KBr, $\tilde{\nu}$, cm^{-1}) 1940 (vs, $\nu_{C\equiv O}$), 1859 (vs, $\nu_{C\equiv O}$), 1546 (m, ν_{COO}). ^1H NMR (CD_2Cl_2, ppm) 7.44 (s, 30H, PPh_3), 6.97 (1H, s, CH). $^{31}P\{^1H\}$ NMR (CD_2Cl_2, ppm) 44 (s, broad, $\nu_{1/2}$ = ca. 3226 Hz). ^{99}Tc NMR (CD_2Cl_2, ppm) −736 (s, $\nu_{1/2}$ = 4028 Hz). Single crystals suitable for X-ray diffraction have been obtained by diffusion of methanol into a CH_2Cl_2 solution of the complex.

*[Tc{η^2-OO(CCH$_3$)}(CO)$_2$(PPh$_3$)$_2$] (**8c**).* Acetic acid (1 mL) was added to a suspension of **5** (100 mg, 0.14 mmol) in toluene (1.5 mL). The resulting slurry was heated under reflux for 30 min. Upon cooling, microcrystals of **8c** deposited. To complete the precipitation, MeOH (9 mL) was added and the mixture was stored in the refrigerator overnight. The formed crystals were filtered off, washed with MeOH and pentane, and dried in air. Yield: 96 mg (0.13 mmol, 92%). IR (KBr, $\tilde{\nu}$, cm^{-1}) 1937 (vs, $\nu_{C\equiv O}$), 1859 (vs, $\nu_{C\equiv O}$), 1520 (m, ν_{COO}). ^1H NMR (CD_2Cl_2, ppm) 7.56−7.27 (m, 30H, PPh_3), 0.48 (3H, s, CH_3). $^{31}P\{^1H\}$ NMR (CD_2Cl_2, ppm) 48 (s, broad, flat, $\nu_{1/2}$ = ca. 4000 Hz, $^1J_{Tc-P}$ ca. 400 Hz). ^{99}Tc NMR (CD_2Cl_2, ppm) −811 (s, $\nu_{1/2}$ = 2862 Hz).

*[Tc{η^2-OO(CPh)}(CO)$_2$(PPh$_3$)$_2$] (**8d**).* Benzoic acid (31 mg, 0.25 mmol) and **5** (35 mg, 0.05 mmol) were suspended in toluene (1 mL). The resulting slurry was heated under reflux for 1 h to give a clear colorless solution. After cooling, MeOH (9 mL) was added and microcrystals of **8d** deposited. To complete the precipitation, the mixture was stored in the refrigerator for 3 h. The crystals were filtered off, washed with MeOH and pentane, and dried in air. Yield: 39 mg (0.05 mmol, 97%). IR (KBr, $\tilde{\nu}$, cm^{-1}) 1936 (vs, $\nu_{C\equiv O}$), 1859 (vs, $\nu_{C\equiv O}$), 1508 (m, ν_{COO}). ^1H NMR (CD_2Cl_2, ppm) 7.46 (s, 12H, PPh_3), 7.37 (s, 20H, PPh_3+OOCPh), 7.08−6.88 (m, 3H, OOCPh). $^{31}P\{^1H\}$ NMR (CD_2Cl_2, ppm) 48 (s, broad, $\nu_{1/2}$ = ca. 4225 Hz). ^{99}Tc NMR (CD_2Cl_2, ppm) −806 (s, $\nu_{1/2}$ = 3061 Hz). Single crystals suitable for X-ray diffraction have been obtained by diffusion of methanol into a saturated CH_2Cl_2 solution of the compound.

*[Tc(η^2-O,S-Et$_2$btu)(CO)$_2$(PPh$_3$)$_2$] (**9**).* HEt_2btu (27 mg, 0.11 mmol) was added to a suspension of **5** (80 mg, 0.11 mmol) in toluene (1 mL). The resulting slurry was heated under reflux for 30 min. MeOH (25 mL) was added and the mixture was stored in the refrigerator overnight. The formed off-white precipitate consisted of a mixture of **9** and **5**. It was filtered off and the remaining deep yellow filtrate was kept for slow evaporation at room temperature. The resulting pure yellow crystals of **9** were collected by filtration and washed with MeOH and pentane. After drying, yellow microcrystals were obtained. A second crop of crystals was harvested from the deep yellow filtrate after complete evaporation of the solvent. They were suitable for X-ray diffraction. Yield: 51 mg (0.06 mmol, 51%). IR (KBr, $\tilde{\nu}$, cm^{-1}) 2031 (w, $\nu_{C\equiv O}$), 1933 (vs, $\nu_{C\equiv O}$), 1853 (vs, $\nu_{C\equiv O}$), 1409 (m, $\nu_{C=O}$). ^1H NMR (CD_2Cl_2, ppm) 7.60−7.53 (m, 12H, PPh_3), 7.53−7.48 (m, 2H, btu-Ph), 7.45−7.38 (m, 3H, btu-Ph), 7.30−7.15 (m, 20H, PPh_3), 3.47 (2H, q, $^3J_{H-H}$ = 7.1 Hz, η^2-btu-NCH_2CH_3), 3.28 (2H, q, $^3J_{H-H}$ = 7.0 Hz, η^2-btu-NCH_2CH_3), 0.92 + 0.91 (6H, 2t, $^3J(0.92\ ppm)_{H-H}$ = 7.1 Hz, $^3J(0.91\ ppm)_{H-H}$ = 7.0 Hz, η^2-btu-NCH_2CH_3). $^{31}P\{^1H\}$ NMR (CD_2Cl_2, ppm) 40 (s, broad, flat, $\nu_{1/2}$ = ca. 4625 Hz, $^1J_{Tc-P}$ ca. 460 Hz). ^{99}Tc NMR (CD_2Cl_2, ppm) −1119 (s, $\nu_{1/2}$ = 2496 Hz).

*[{Tc(CO)$_3$}$_3$(μ^3-OH)(μ^2-O(SePh)O)$_3${Tc(CO)$_3$}] (**10**)·(OPPh$_3$).* Solid PhSeOOH (47 mg, 0.25 mmol) was added to a suspension of **5** (35 mg, 0.05 mmol) in toluene (1 mL). The evolution of H_2 was observed and the color changed to bright yellow. The mixture was heated under reflux for 30 min to give a clear yellow solution. MeOH (12 mL) was added. The solution was then added to a mixture of H_2O (ca. 40 mL) and Et_2O (10 mL). The solution was left for evaporation resulting in the formation of colorless crystals and a yellow oil. The residue was extracted with CH_2Cl_2 (0.5 mL) and filtered. Pentane (9 mL) was layered on the top and the mixture was stored in the refrigerator overnight. The formed colorless crystals were filtered off, washed with pentane, and dried in air. Yield: 18 mg (0.01 mmol, 91%). IR (KBr, $\tilde{\nu}$, cm^{-1}) 2029 (s, $\nu_{C\equiv O}$), 1904 (vs, $\nu_{C\equiv O}$). ^1H NMR (CD_2Cl_2, ppm) 8.30 (s, broad, 1H, μ^3-OH), 7.98−7.16 (3m, 30H, ArH). $^{31}P\{^1H\}$ NMR (CD_2Cl_2, ppm) 30 (s). ^{99}Tc NMR (CD_2Cl_2, ppm) −582 (s, $\nu_{1/2}$ = 1646 Hz), [{**Tc** $(CO)_3$}$_3$(μ^3-OH)(μ^2-O(SePh)O)$_3$]$^-$), −765 (s, $\nu_{1/2}$ = 292 Hz, [η^3-({Tc-$(CO)_3$}$_3$(μ^3-OH)(μ^2-O(SePh)O)$_3$){**Tc** $(CO)_3$}]).

*[Tc$_2$(CO)$_6$(ox)(OPPh$_3$)$_2$ (**11**).* Formic acid (2 drops) was added to a suspension of **5** (35 mg, 0.05 mmol) in toluene (1 mL). After 2 min, solid PhSeOOH (47 mg, 0.25 mmol) was added to the stirred solution. The formation of H_2 was observed and the color changed to bright yellow. The mixture was heated under reflux for 30 min to give a clear yellow solution. MeOH (12 mL), water (ca. 40 mL) and diethyl ether (10 mL) were added to the clear yellow solution. The mixture was left for evaporation, which gave colorless crystals and a yellow oil. The residue was extracted with CH_2Cl_2 (0.5 mL). The extract was filtered, pentane (9 mL) was layered on the top and the mixture was stored in the refrigerator overnight. The formed crystals were filtered off, washed with pentane, and dried in air. Yield: 13 mg (0.01 mmol, 51%). IR (KBr, $\tilde{\nu}$, cm^{-1}) 2036 (s, $\nu_{C\equiv O}$), 1925 (vs, $\nu_{C\equiv O}$), 1626 (m, ν_{COO}). ^1H NMR (CD_2Cl_2, ppm) 7.65−7.58 (m, 12H, $OPPh_3$), 7.31−7.24 (m, 12H, $OPPh_3$). $^{31}P\{^1H\}$ NMR (CD_2Cl_2,

https://doi.org/10.1021/acs.organomet.1c00274
Organometallics 2021, 40, 3095−3112

ppm) 42 (s, $\nu_{1/2}$ = 65 Hz). ^{99}Tc NMR (CD_2Cl_2, ppm) −874 (s, $\nu_{1/2}$ = 576 Hz).

*[Tc(η^2-Hox)(CO)$_2$(PPh$_3$)$_2$] (**12**).* Oxalic acid (11 mg, 0.11 mmol) was added to a suspension of **5** (35 mg, 0.05 mmol) in toluene (1 mL). The resulting colorless suspension was heated under reflux, upon which the mixture became a clear, orange-red solution. After ca. 5 min of heating, the formation of a light yellow precipitate was observed. Heating under reflux was continued for a total of 30 min. Then, MeOH (9 mL) were added and the mixture was stored in the refrigerator for 1 h to complete the precipitation. The yellow precipitate was filtered off and washed with methanol and pentane, and dried in air. The product is poorly soluble in common solvents. Yield: 36 mg (0.05 mmol, 94%). IR (KBr, $\tilde{\nu}$, cm^{-1}) 3547 (m, broad, $\nu_{O-H(COOH)}$) 2046 (w, $\nu_{C\equiv O}$), 1957 (vs, $\nu_{C\equiv O}$), 1879 (vs, $\nu_{C\equiv O}$), 1718−1628 (m, complicated band pattern, ν_{COO}). ^{1}H NMR (CD_2Cl_2, ppm) 7.59−7.29 (m, 30H, PPh$_3$). ^{99}Tc NMR (CD_2Cl_2, ppm) −875 (s, $\nu_{1/2}$ = 3265 Hz). Single crystals suitable for X-ray diffraction have been obtained by evaporation of a saturated CH_2Cl_2 solution.

*(HNEt$_3$)[Tc(η^2-ox)(CO)$_2$(PPh$_3$)$_2$] (**13**).* **12** (25 mg, 0.03 mmol) was suspended in CD_2Cl_2 (0.5 mL). NEt_3 (3 drops) was added, causing the complete dissolution of the sparingly soluble starting material and the formation of a colorless solution. The product was precipitated with hexane (9 mL) resulting in the formation of colorless microcrystals. They were filtered off, washed with pentane, and dried. Yield: 27 mg (0.03 mmol, 96%) IR (KBr, $\tilde{\nu}$, cm^{-1}) 2900 (complex band pattern, ν_{N-H}), 2500 (w, broad, ν_{N-H}), 2033 (w, $\nu_{C\equiv O}$), 1942 (vs, $\nu_{C\equiv O}$), 1852 (vs, $\nu_{C\equiv O}$), 1649 (m, broad, ν_{COO}). ^{1}H NMR (CD_2Cl_2, ppm) 7.46 (s, 12H, PPh$_3$), 7.35 (s, 18H, PPh$_3$). ^{31}P{^{1}H} NMR (CD_2Cl_2, ppm) 40 (s, very broad, flat, $\nu_{1/2}$ = ca. 4500 Hz). ^{99}Tc NMR (CD_2Cl_2, ppm) −967 (s, $\nu_{1/2}$ = 1614 Hz). Single crystals suitable for X-ray diffraction have been obtained by evaporation of a saturated CH_2Cl_2/hexane solution.

■ ASSOCIATED CONTENT

Supporting Information

The Supporting Information is available free of charge at https://pubs.acs.org/doi/10.1021/acs.organomet.1c00274.

Crystallographic tables, bond lengths, angles and ellipsoid plots; Spectroscopic data (PDF)

Accession Codes

CCDC 2081313−2081329 contain the supplementary crystallographic data for this paper. These data can be obtained free of charge via www.ccdc.cam.ac.uk/data_request/cif, or by emailing data_request@ccdc.cam.ac.uk, or by contacting The Cambridge Crystallographic Data Centre, 12 Union Road, Cambridge CB2 1EZ, UK; fax: +44 1223 336033.

■ AUTHOR INFORMATION

Corresponding Author

Ulrich Abram − *Institute of Chemistry and Biochemistry, Freie Universität Berlin, 14195 Berlin, Germany;* orcid.org/0000-0002-1747-7927; Email: ulrich.abram@fu-berlin.de

Authors

Maximilian Roca Jungfer − *Institute of Chemistry and Biochemistry, Freie Universität Berlin, 14195 Berlin, Germany*

Laura Elsholz − *Institute of Chemistry and Biochemistry, Freie Universität Berlin, 14195 Berlin, Germany*

Complete contact information is available at: https://pubs.acs.org/10.1021/acs.organomet.1c00274

Notes

The authors declare no competing financial interest.

■ ACKNOWLEDGMENTS

We acknowledge the assistance of the Core Facility BioSupraMol supported by the DFG and High-Performance-Computing (HPC) Centre of the Zentraleinrichtung für Datenverarbeitung (ZEDAT) of the Freie Universität Berlin for computational time and support.

■ REFERENCES

(1) Chatt, J.; Coffey, R. S. Hydrido-complexes of Rhenium which contain Tertiary Phosphines. *J. Chem. Soc. A* **1969**, 1963−1972.

(2) Cotton, F. A.; Luck, R. L. Reduction of $ReCl_5$ in the Presence of $PMePh_2$ To Give mer-$ReCl_3(PMePh_2)_3$, $ReCl(\eta^2\text{-}H_2)(PMePh_2)_4$, $ReH_3(PMePh_2)_4$, or $ReCl(CO)_3(PMePh_2)_2$, Depending on Conditions. *Inorg. Chem.* **1989**, *28*, 2181−2186.

(3) Lunder, D. M.; Green, M. A.; Streib, W. E.; Caulton, K. G. Structure and Reactivity of $ReH_4(PMe_2Ph)_4^+$. *Inorg. Chem.* **1989**, *28*, 4527−4531.

(4) Cotton, F. A.; Luck, L. L. X-ray Crystal Structure of $ReH_5(PPh_3)_3$ and Variable-Temperature T_1 Studies on $ReH_5(PPh_3)_3$ and $ReH_5(PMe_2Ph)_3$ in Various Solvents: Are T_1 Measurements Reliable in Predicting Whether Polyhydride Complexes Contain Molecular Hydrogen Ligands? *J. Am. Chem. Soc.* **1989**, *111*, 5757−5761.

(5) Lee, J. C. Jr.; Yao, W.; Crabtree, R. H.; Rüegger, H. Fluxionality in $[ReH_5(PPh_3)_2(pyridine)]$. *Inorg. Chem.* **1996**, *35*, 695−699.

(6) Jiang, Y.; Blaquet, O.; Fox, T.; Berke, H. Catalytic CO_2 activation Assisted by Rhenium Hydride/$B(C_6F_5)_3$. Frustrated Lewis Pairs-Metal Hydrides Functioning as FLP Bases. *J. Am. Chem. Soc.* **2013**, *135*, 7751−7760.

(7) Jin, H.; Zhu, Z.; Jin, N.; Xie, J.; Cheng, Y.; Zhu, C. CO-enabled rhenium hydride catalyst for directed C(sp^2)-H bond alkylation with olefins. *Org. Chem. Front.* **2015**, *2*, 378−382.

(8) Floss, J. G.; Grosse, A. V. Technetium Analogues of Rhenohydrides. *J. Inorg. Nucl. Chem.* **1960**, *16*, 44−47.

(9) Hileman, J. C.; Huggins, D. K.; Kaesz, H. D. Derivatives of Technetium Carbonyl. Synthesis and Properties of the Carbonyl Halides and the Pentacarbonyl Hydride. *Inorg. Chem.* **1962**, *1*, 933−938.

(10) Ginsberg, A. P. Transition Metal-Hydrogen Compounds. III. Dipotassium Enneahydridotechnate(VII). *Inorg. Chem.* **1964**, *3*, 567−569.

(11) Kaden, L.; Lorenz, B.; Schmidt, K.; Sprinz, H.; Wahren, M. Darstellung und Charakterisierung von Dihydridochloro-bis[1,2-bis(diphenylhosphino)-ethan]-technetium(III). *Z. Chem.* **1981**, *21*, 232.

(12) Kaden, L.; Lorenz, B.; Wahren, M. Kurze Originalmitteilungen: Komplexkatalyse mit Technetiumverbindungen. Hydrierung von Alkenen und Hydridokomplexe des Technetiums. *Isotopenpraxis* **1982**, *18*, 400−403.

(13) Struchkov, Y. T.; Bazanov, A. S.; Kaden, L.; Lorenz, B.; Wahren, M.; Meyer, H. Kristall- und Molekülstruktur von Hydridobis-[1,2-bisdiphenylphosphanoethan]distickstofftechnetium(I). *Z. Anorg. Allg. Chem.* **1982**, *494*, 91−97.

(14) Roseberry, A. M.; Davison, A.; Jones, A. G. Synthesis of $Tc(NO)(PPh_3)_3(H)_2$: a novel hydrido complex of technetium. *Inorg. Chim. Acta* **1990**, *176*, 179−181.

(15) Watson, P. L.; Albanese, J. A.; Calabrese, J. C.; Ovenall, D. W.; Smith, R. G. Synthesis and Structural Characterization of Trimethylphosphine Complexes of Technetium(III). *Inorg. Chem.* **1991**, *30*, 4638−4643.

(16) Burrell, A. K.; Bryan, J. C.; Kubas, G. J. Synthesis of the 16-Electron Complex $TcCl(dppe)_2$ and Its Reaction with Hydrogen To Give *trans*-$Tc(H_2)Cl(dppe)_2$: The First η^2-Dihydrogen Complex of Technetium. *J. Am. Chem. Soc.* **1994**, *116*, 1575−1576.

(17) Cook, J.; Davison, A.; Davis, W. M.; Jones, A. G. Insertion Chemistry of $HTc(CO)_3(PPh_3)_2$. *Organometallics* **1995**, *14*, 650−655.

(18) Alberto, R.; Schibli, R.; Schubiger, P. A.; Abram, U.; Hübener, R.; Berke, H.; Kaden, T. A. A simple single-step synthesis of

[$^{99}Tc_3H_3(CO)_{12}$] from [$^{99}TcO_4$]$^-$ and its X-ray crystal structure. Application to the production of no-carrier added [$^{188}Re_3H_3(CO)_{12}$]. *Chem. Commun.* **1996**, 1291−1292.
(19) Zuhayra, M.; Lützen, U.; Lützen, A.; Papp, L.; Henze, E.; Friedrichs, G.; Oberdorfer, F. C-H Bond Activation of Coordinated Pyridine: Ortho-Pyridyl-Ditechnetiumhydridocarbonyl Metal Cyclus. Crystal Structure and Dynamic Behavior in Solution. *Inorg. Chem.* **2008**, *47*, 10177−10182.
(20) Sidorenko, G. V.; Miroslavov, A. E.; Grigorev, M. S.; Gurzhiy, V. V.; Lumpov, A. A.; Mikhalev, V. A.; Suglobov, D. N. Hydrolysis of $Tc(CO)_6^+$ cation in aqueous solutions. Crystal and molecular structures of the identified products: $Tc_2(CO)_{10}$ and $Tc_3H_3(CO)_{12}$. *Radiochemistry* **2011**, *53*, 44−50.
(21) Miroslavov, A. E.; Shishkina, A. P.; Sidorenko, G. V.; Gurzhiy, V. V.; Maltsev, D. A.; Kurysheva, E. V. Hydrolysis of Hexacarbonyltechnetium(I) Cation: Formation and Structure of Technetium Carbonyl Hydride $^{99}Tc_3H(CO)_{14}$. *Inorg. Chem.* **2020**, *59*, 9239−9243.
(22) Maria, L.; Paulo, A.; Santos, I. C.; Santos, I.; Kurz, P.; Spingler, B.; Alberto, R. Very Small and Soft Scorpionates: Water Stable Technetium Tricarbonyl Complexes Combining a Bis-agostic (u^3-H, H, S) Binding Motif with Pendant and Integrated Bioactive Molecules. *J. Am. Chem. Soc.* **2006**, *128*, 14590−14598.
(23) Garcia, R.; Paulo, A.; Domingos, Â.; Santos, I.; Ortner, K.; Alberto, R. Re and Tc Complexes Containing B-H···M Agostic Interactions as Building Blocks for the Design of Radiopharmaceuticals. *J. Am. Chem. Soc.* **2000**, *122*, 11240−11241.
(24) Cook, J. A. *Synthesis and Reactivity of Technetium Hydrides*. Doctoral thesis, Massachusetts Institute of Technology, 1995.
(25) *Cambridge Structural Database*, Release 5.40, April 2020.
(26) Pietzsch, H.-J.; Tisato, F.; Refosco, F.; Leibnitz, P.; Drews, A.; Seifert, S.; Spies, H. Synthesis and Characterization of Novel Trigonal Bipyramidal Technetium(III) Mixed-Ligand Complexes with SES/S/P Coordination (E = O, $N(CH_3)$, S). *Inorg. Chem.* **2001**, *40*, 59−64.
(27) de Vries, N.; Cook, J.; Jones, A. G.; Davison, A. Technetium-(III) Complexes with the Tetradentate "Umbrella" Ligand Tris(*o*-mercaptophenyl)phosphinate: X-ray Structural Characterization of $Tc(P(o\text{-}C_6H_4S)_3)(CNC_3H_7)$ and $Tc(P(o\text{-}C_6H_4S)_3)(CNC_3H_7)_2$. *Inorg. Chem.* **1991**, *30*, 2662−2665.
(28) Marvelli, L.; Bergamini, P.; Marchi, A.; Bersani, G.; Ferretti, V.; Bertolasi, V. Direct formation of new water soluble Re and Tc complexes containing PTA (1,3,5-triaza-7-phosphaadamantane) from their permetallated salts. Reactivity and X-ray crystal structures. *Inorg. Chim. Acta* **2018**, *470*, 352−359.
(29) Teller, R. G.; Bau, R. Crystallographic studies of transition metal hydride complexes. *Struct. Bonding (Berlin)* **1981**, *44*, 1−82 and references cited therein.
(30) Llunell, M.; Casanova, D.; Cirera, J.; Alemany, P.; Alvarez, S. *SHAPE Program for the Stereochemical Analysis of Molecular Fragments by Means of Continuous Shape Measures and Associated Tools*, version 2.1; 2013. http://www.ee.ub.edu/index.php?option=com_jdownloads&Itemid=529&view=viewcategory&catid=4.
(31) Pinsky, M.; Avnir, D. Continuous Symmetry Measures. 5. The Classical Polyhedra. *Inorg. Chem.* **1998**, *37*, 5575−5582.
(32) Casanova, D.; Cirera, J.; Llunell, M.; Alemany, P.; Avnir, D.; Alvarez, S. Minimal Distortion Pathways in Polyhedral Rearrangements. *J. Am. Chem. Soc.* **2004**, *126*, 1755−1763.
(33) Cirera, J.; Ruiz, E.; Alvarez, S. Shape and Spin State in Four-Coordinate Transition-Metal Complexes: The Case of the d^6 Configuration. *Chem. - Eur. J.* **2006**, *12*, 3162−3167.
(34) Casanova, D.; Alemany, P.; Bofill, J. M.; Alvarez, S. Shape and Symmetry of Heptacoordinate Transition-Metal Complexes: Structural Trends. *Chem. - Eur. J.* **2003**, *9*, 1281−1295.
(35) Cirera, J.; Ruiz, E.; Alvarez, S. Continuous Shape Measures as a Stereochemical Tool in Organometallic Chemistry. *Organometallics* **2005**, *24*, 1556−1562.
(36) Kaden, L.; Lorenz, B.; Schmidt, K.; Sprinz, H.; Wahren, M. Darstellung des Technetium-Distickstoff-Komplexes Bis[1,2-bisdiphenylphosphinoethan]distickstofftechnetium. *Z. Chem.* **1979**, *19*, 305−306.
(37) Abram, U.; Abram, S.; Beyer, R.; Münze, R.; Kaden, L.; Lorenz, B.; Findeisen, M. Mixed-ligand complexes of technetium. II. $[Tc(dppe)_2(R\text{-}NC)_2]^+$ complex (dppe = bis(diphenylphosphino)-ethane; R = tert. butyl, cyclohexyl). *Inorg. Chim. Acta* **1988**, *148*, 141−142.
(38) Abram, U.; Beyer, R.; Münze, R.; Stach, J.; Kaden, L.; Lorenz, B.; Findeisen, M. Mixed-ligand complexes of technetium. III. Synthesis and characterization of [bis(diphenylphosphino)ethane]-tetrakis(trimethylphosphite)technetium(I) hexafluorophosphate, [Tc-(DPPE)(TMP)$_4$]PF_6. *Polyhedron* **1989**, *8*, 1201−1204.
(39) Kaden, L.; Findeisen, M.; Lorenz, B.; Schmidt, K.; Wahren, M. $HTc(N_2)(DPPE)_2$ as starting material for mixed-ligand complexes of technetium(I). *Inorg. Chim. Acta* **1992**, *193*, 213−215.
(40) Kaden, L.; Pombeiro, A. J. L.; Wang, Y.; Abram, U. Mixed-ligand complexes of technetium. XIII. A new and facile synthesis, structure and electrochemical behaviour of *trans*-$[Tc(dppe)_2(but.NC)_2](PF_6)$ · ethanol (dppe = bis(diphenylphosphino)-ethane, but.NC = tert.butylisocyanide). *Inorg. Chim. Acta* **1995**, *230*, 189−192.
(41) Freni, M.; Romiti, P. New phosphite complexes of rhenium. *Inorg. Nucl. Chem. Lett.* **1970**, *6*, 167−170.
(42) Freni, M.; Demichelis, R.; Giusto, D. Hydrido and halogenohydrido complexes of rhenium(III). *J. Inorg. Nucl. Chem.* **1967**, *29*, 1433−1439.
(43) Wendlandt, D.; Bauche, J.; Luc, P. Hyperfine structure in Tc I: experiment and theory. *J. Phys. B: At. Mol. Phys.* **1977**, *10*, 1989−2002.
(44) Abram, U.; Lorenz, L.; Kaden, L.; Scheller, D. Nitrido Complexes of Technetium with Tertiary Phosphines and Arsines. *Polyhedron* **1988**, *7*, 285−289.
(45) Ackermann, J.; Abdulkader, A.; Scholtysik, C.; Roca Jungfer, M.; Hagenbach, A.; Abram, U. $[Tc^I(NO)X(Cp)(PPh_3)]$ Complexes (X- = I^-, I_3^-, SCN^-, $CF_3SO_3^-$, or CF_3COO^-) and Their Reactions. *Organometallics* **2019**, *38*, 4471−4478.
(46) Mikhalev, V. A. ^{99m}Tc NMR Spectroscopy. *Radiochemistry* **2005**, *47*, 319−333 and references cited therein.
(47) Moehring, G. A.; Walton, R. A. Reactivity of the Polyhydride Complexes $[ReH_5(PPh_3)_3]$, $[ReH_3(dppe)_2]$ (dppe = $Ph_2PCH_2CH_2PPh_2$), $[ReH_3(PPh_3)_3L]$, and $[ReH_4(PPh_3)_3L]PF_6$, (L = MeCN or Bu^{t}NC) towards Electrophiles and Nucleophiles. *J. Chem. Soc., Dalton Trans.* **1987**, 715−720.
(48) Alberto, R.; Herrmann, W. A.; Kiprof, P.; Baumgärtner, F. Multiple Bonds between Main Group Elements and Transition Metals. 95. Synthesis and Reactivity of $[TcCl(CO)_3[P(C_6H_5)_3]_2$: Novel Technetium Complexes of 1,4,7-Triazacyclononane and Hydridotris(pyrazolyl)borate. *Inorg. Chem.* **1992**, *31*, 895−899.
(49) Claude, G.; Salsi, F.; Hagenbach, A.; Gembicky, M.; Neville, M.; Chan, C.; Figueroa, J. S.; Abram, U. Structural and Redox Variations in Technetium Complexes Supported by *m*-Terphenyl Isocyanides. *Organometallics* **2020**, *39*, 2287−2294.
(50) Hieber, W.; Lux, F.; Herget, C. Über Kohlenoxidverbindungen des Technetiums. *Z. Naturforsch., B: J. Chem. Sci.* **1965**, *20*, 1159−1165.
(51) Mazzi, U.; Bismondo, A.; Kotsev, N.; Clemente, D. A. Phosphine carbonyl-technetium(I) and -technetium(III) complexes. *J. Organomet. Chem.* **1977**, *135*, 177−182.
(52) Davison, A.; Kronauge, J. F.; Jones, A. G.; Pearlstein, R. M.; Thornback, J. R. Tc NMR Spectroscopy of Technetium(I) Phosphine and Phosphite Complexes. *Inorg. Chem.* **1988**, *27*, 3245−3246.
(53) Findeisen, M.; Kaden, L.; Lorenz, B.; Wahren, M. ^{99}Tc NMR Spectroscopy on Neutral and Cationic Tc(I) Carbonyl Complexes. *Inorg. Chim. Acta* **1988**, *142*, 3−4.
(54) O'Connell, L. A.; Pearlstein, R. M.; Davison, A.; Thornback, J. R.; Kronauge, J. F.; Jones, A. G. Technetium-99 NMR Spectroscopy: Chemical Shift Trends and Long Range Coupling Effects. *Inorg. Chim. Acta* **1989**, *161*, 39−43.

https://doi.org/10.1021/acs.organomet.1c00274
Organometallics 2021, 40, 3095−3112

(55) Suglobov, D. N.; Miroslavov, A. E.; Sidorenko, G. V.; Gorshkov, N. I.; Lumpov, A. A. Complexation of $Tc(CO)_3^{+}$aq with Anions of Monobasic Carboxylic Acids in Aqueous Solutions: A ^{99}Tc NMR Study. *Radiochemistry* **2005**, *47*, 50−53.
(56) Agnew, D. W.; Moore, C. E.; Rheingold, A. L.; Figueroa, J. S. Controlled cis Labilization of CO from Manganese(I) Mixed Carbonyl/Isocyanide Complexes: An Entry Point to Coordinatively Unsaturated Metallo-Lewis Acids. *Organometallics* **2017**, *36*, 363−371.
(57) Marchi, A.; Rossi, R.; Duatti, A.; Zucchini, G. L.; Magon, L. Preparation and characterization of mixed amido, carboxylato or thiazolato carbonyl(phosphine)technetium(I) complexes. *Transition Met. Chem.* **1986**, *11*, 164−166.
(58) Lorenz, B.; Findeisen, M.; Schmidt, K. Synthese, Charakterisierung und Tc-99-NMR-Spektren von Technetium-Carbonyl-Komplexen mit Dithioliganden. *Isotopenpraxis* **1991**, *27*, 266−267.
(59) Balasekaran, S. M.; Spandl, J.; Hagenbach, A.; Köhler, K.; Drees, M.; Abram, U. Fluoridonitrosyl Complexes of Technetium(I) and Technetium(II). Synthesis, Characterization, Reactions, and DFT Calculations. *Inorg. Chem.* **2014**, *53*, 5117−5128.
(60) Balasekaran, S. M.; Hagenbach, A.; Drees, M.; Abram, U. $[Tc^{II}(NO)(trifluoroacetate)_4F]^{2-}$ - synthesis and reactions. *Dalton Trans.* **2017**, *46*, 13544−13553.
(61) Marchi, A.; Marvelli, L.; Rossi, R.; Bertolasi, V.; Ferretti, V. Technetium and rhenium carbonyl complexes with 1,4-benzodiazepine derivatives: X-ray crystal structure. *Inorg. Chim. Acta* **1998**, *272* (1−2), 267−273.
(62) Rossi, R.; Marchi, A.; Aggio, S.; Magon, L.; Duatti, A.; Casellato, U.; Graziani, R. The chemistry of heteroallyl derivatives of technetium. Reactivity of $[TcNCl_2(PPh_3)_2]$ and $[Tc(CO)_3Cl(PPh_3)]$ with thiazetidine ligands, crystal structures of $[Tc(CO)_2(PPh_3)_2\{PhN = C(OEt)S\}]$ and $[TcN(Cl)(PPh_3)\text{-}\{PhN = C(OEt)S\}]$. *J. Chem. Soc., Dalton Trans.* **1990**, 477−481.
(63) Marchi, A.; Rossi, R.; Duatti, A.; Magon, L.; Bertolasi, V.; Ferretti, V.; Gilli, G. Reactions of the technetium(I)carbonyl complexes $[Tc(PMe_2Ph)_3(CO)_2Cl]$ and $[Tc(PPh_3)_2(CO)_3Cl]$ toward pseudo-allyl ligands such as triazenido, formamidinato, and acetamidinato. Crystal structures of $[Tc(PMe_2Ph)_2(CO)_2(p\text{-}CH_3C_6H_4N = N{=}NC_6H_4CH_3\text{-}p)]$ and $[Tc(PMe_2Ph)_2(CO)_2(C_6H_5N = C(CH_3){=}NC_6H_5)]$. *Inorg. Chem.* **1985**, *24*, 4744−4748.
(64) Rossi, R.; Marchi, A.; Magon, L.; Duatti, A.; Casellato, U.; Graziani, R. Synthesis and characterization of new technetium(I) and rhenium(I) Schiff base complexes. Crystal structure of $[M(PPh_3)_2(CO)_2\{(C_3H_2NS)N = CHC_6H_4O\}]$ (M = Tc, Re; C_3H_2NS = Thiazol-2-yl). *Inorg. Chim. Acta* **1989**, *160*, 23−28.
(65) Huy, N. H.; Abram, U. Rhenium and Technetium Complexes with N,N-Dialkyl-N'-benzoylthioureas. *Inorg. Chem.* **2007**, *46*, 5310−5319.
(66) Huy Nguyen, H.; Deflon, V. M.; Abram, U. Mixed-Ligand Complexes of Technetium and Rhenium with Tridentate Benzamidines and Bidentate Benzoylthioureas. *Eur. J. Inorg. Chem.* **2009**, *21*, 3179−3187.
(67) Salsi, F.; Portapilla, G. B.; Simon, S.; Roca Jungfer, M.; Hagenbach, A.; de Albuquerque, S.; Abram, U. Effect of Fluorination on the Structure and Anti-Trypanosoma cruzy Activity of Oxorhenium(V) Complexes with S,N,S-Tridentate Thiosemicarbazones and Benzoylthioureas. Synthesis and Structures of Technetium(V) Analogues. *Inorg. Chem.* **2019**, *58*, 10129−10138.
(68) Schuler, E.; Ermolich, P. A.; Shiju, N. R.; Gruter, G.-J. M. Monomers from CO_2: Superbases as Catalysts for Formato-Oxalate Coupling. *ChemSusChem* **2021**, *14*, 1517−1523.
(69) Lakkaraju, P. S.; Askerka, M.; Beyer, H.; Ryan, C. T.; Dobbins, T.; Bennett, C.; Kaczur, J. J.; Batista, V. S. Formate to Oxalate: A Crucial Step for the Conversion of Carbon Dioxide into Multi-carbon Compounds. *ChemCatChem* **2016**, *8*, 3453−3457.
(70) Riemenschneider, W.; Tanifuji, M. Oxalic acid. In *Ullmann's Encyclopedia of Industrial Chemistry*; Wiley-VCH: Weinheim, 2002. DOI: 10.1002/14356007.a18_247.
(71) Beyer, L.; Hoyer, E.; Hennig, H.; Kirmse, R.; Hartmann, H.; Liebscher, J. Synthese und Charakterisierung neuartiger Übergangsmetallchelate von 1,1-Dialkyl-3-benzoyl-thioharnstoffen. *J. Prakt. Chem.* **1975**, *317*, 829−839.
(72) Mazzi, U.; de Paoli, G.; Di Bernardo, P.; Magon, L. Complexes of technetium(IV) and (III) with phosphines. *J. Inorg. Nucl. Chem.* **1976**, *38*, 721−725.
(73) Sheldrick, G. M. *SADABS*; University of Göttingen: Germany, 1996.
(74) Coppens, P. *The Evaluation of Absorption and Extinction in Single-Crystal Structure Analysis*; Crystallographic Computing: Copenhagen, Muksgaard, 1979.
(75) Sheldrick, G. M. A short history of SHELX. *Acta Crystallogr., Sect. A: Found. Crystallogr.* **2008**, *A64*, 112−122.
(76) Sheldrick, G. M. Crystal structure refinement with SHELXL. *Acta Crystallogr., Sect. C: Struct. Chem.* **2015**, *C71*, 3−8.
(77) *Diamond−Crystal and Molecular Structure Visualization Crystal Impact, vers. 4.6.5, 2021*; Putz, H., Brandenburg, K., Eds.; GbR: Bonn, Germany, 2021.
(78) *High Performance Computing (HPC) System Curta at Freie Universität Berlin*; Freie Universität Berlin, 2020. DOI: 10.17169/refubium-26754.
(79) Frisch, M. J.; Trucks, G. W.; Schlegel, H. B.; Scuseria, G. E.; Robb, M. A.; Cheeseman, J. R.; Scalmani, G.; Barone, V.; Petersson, G. A.; Nakatsuji, H.; Li, X.; Caricato, M.; Marenich, A. V.; Bloino, J.; Janesko, B. G.; Gomperts, R.; Mennucci, B.; Hratchian, H. P.; Ortiz, J. V.; Izmaylov, A. F.; Sonnenberg, J. L.; Williams-Young, D.; Ding, F.; Lipparini, F.; Egidi, F.; Goings, J.; Peng, B.; Petrone, A.; Henderson, T.; Ranasinghe, D.; Zakrzewski, V. G.; Gao, J.; Rega, N.; Zheng, G.; Liang, W.; Hada, M.; Ehara, M.; Toyota, K.; Fukuda, R.; Hasegawa, J.; Ishida, M.; Nakajima, T.; Honda, Y.; Kitao, O.; Nakai, H.; Vreven, T.; Throssell, K.; Montgomery, J. A. Jr.; Peralta, J. E.; Ogliaro, F.; Bearpark, M. J.; Heyd, J. J.; Brothers, E. N.; Kudin, K. N.; Staroverov, V. N.; Keith, T. A.; Kobayashi, R.; Normand, J.; Raghavachari, K.; Rendell, A. P.; Burant, J. C.; Iyengar, S. S.; Tomasi, J.; Cossi, M.; Millam, J. M.; Klene, M.; Adamo, C.; Cammi, R.; Ochterski, J. W.; Martin, R. L.; Morokuma, K.; Farkas, O.; Foresman, J. B.; Fox, D. J. *Gaussian 16*, Revision B.01; Gaussian, Inc.: Wallingford, CT, 2016.
(80) Dennington, R.; Keith, T. A.; Millam, J. M. *GaussView*, Version 6; Semichem Inc.: Shawnee Mission, KS, 2016.
(81) Hanwell, M. D.; Curtis, D. E.; Lonie, D. C.; Vandermeersch, C.; Zurek, E.; Hutchison, G. R. Avogadro: An advanced semantic chemical editor, visualization, and analysis platform. *J. Cheminf.* **2012**, *4*, 17.
(82) Vosko, S. H.; Wilk, L.; Nusair, M. Accurate spin-dependent electron liquid correlation energies for local spin density calculations: a critical analysis. *Can. J. Phys.* **1980**, *58*, 1200−1211.
(83) Becke, A. D. Density-functional thermochemistry. III. The role of exact exchange. *J. Chem. Phys.* **1993**, *98*, 5648−5652.
(84) Lee, C.; Yang, W.; Parr, R. G. Development of the Colle-Salvetti correlation-energy formula into a functional of the electron density. *Phys. Rev. B: Condens. Matter Mater. Phys.* **1988**, *B37*, 785−789.
(85) Wadt, W. R.; Hay, P. J. Ab initio effective core potentials for molecular calculations. Potentials for main group elements Na to Bi. *J. Chem. Phys.* **1985**, *82*, 284−298.
(86) Andrae, D.; Häußermann, U.; Dolg, M.; Stoll, H.; Preuß, H. Energy-adjusted ab initio pseudopotentials for the second and third row transition elements. *Theor. Chim. Acta* **1990**, *77*, 123−141.
(87) Martin, J. M. L.; Sundermann, A. Correlation consistent valence basis sets for use with the Stuttgart-Dresden-Bonn relativistic effective core potentials: The atoms Ga-Kr and In-Xe. *J. Chem. Phys.* **2001**, *114*, 3408−3420.
(88) Krishnan, R.; Binkley, J. S.; Seeger, R.; Pople, J. A. Self-consistent molecular orbital methods. XX. A basis set for correlated wave functions. *J. Chem. Phys.* **1980**, *72*, 650−654.
(89) Clark, T.; Chandrasekhar, J.; Spitznagel, G. W.; Schleyer, P. V. R. Efficient diffuse function-augmented basis sets for anion

calculations. III. The 3-21+G basis set for first-row elements, Li-F. *J. Comput. Chem.* **1983**, *4*, 294−301.
(90) Franzke, Y. J.; Treß, R.; Pazdera, T. M.; Weigend, F. Error-consistent segmented contracted all-electron relativistic basis sets of double- and triple-zeta quality for NMR shielding constants. *Phys. Chem. Chem. Phys.* **2019**, *21*, 16658−16664.
(91) Schuchardt, K. L.; Didier, B. T.; Elsethagen, T.; Sun, L.; Gurumoorthi, V.; Chase, J.; Li, J.; Windus, T. L. Basis Set Exchange: A Community Database for Computational Sciences. *J. Chem. Inf. Model.* **2007**, *47*, 1045−1052.
(92) Grimme, S. Supramolecular Binding Thermodynamics by Dispersion-Corrected Density Functional Theory. *Chem. - Eur. J.* **2012**, *18*, 9955−9964.
(93) Paton, R.; Funes-Ardoiz, I. *bobbypaton/GoodVibes: GoodVibes*, ver. 3.0.0. DOI: 10.5281/zenodo.3346166.
(94) Lu, T.; Chen, F. Multiwfn: A multifunctional wavefunction analyzer. *J. Comput. Chem.* **2012**, *33*, 580−592.

https://doi.org/10.1021/acs.organomet.1c00274
Organometallics 2021, 40, 3095−3112

4.2 $[Tc(OH_2)(CO)_3(PPh_3)_2]^+$: A Synthon for Tc(I) Complexes and its Reactions with Neutral Ligands

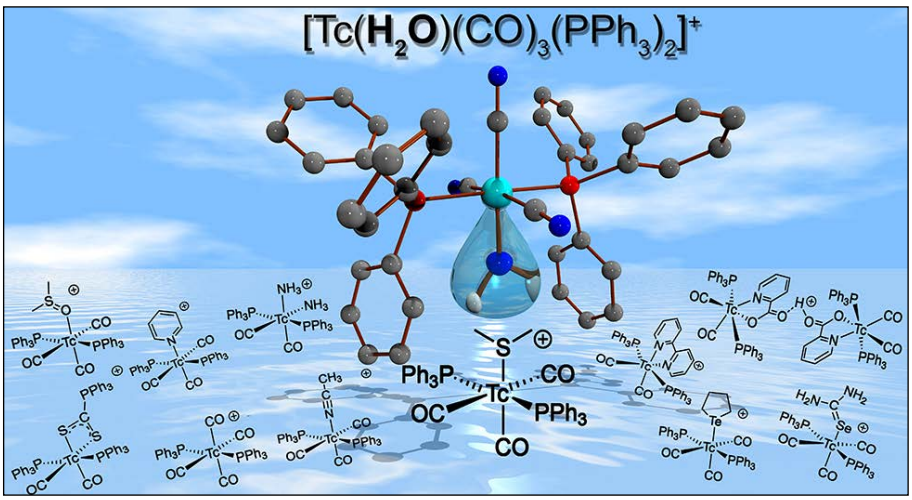

Reproduced with permission from Roca Jungfer, M.; Abram, U. *Inorg. Chem.* **2021**, *60*, 16734–16753.

DOI: 10.1021/acs.inorgchem.1c02599

For Supplementary Material see A.2.

Author Contributions:

Maximilian Roca Jungfer and Ulrich Abram designed the project. Maximilian Roca Jungfer performed the synthesis and characterization of the compounds, calculated the X-ray structures, and wrote a draft of the manuscript. Ulrich Abram supervised the project, provided scientific guidance and suggestions, and corrected the manuscript.

Inorganic Chemistry

pubs.acs.org/IC Article

$[Tc(OH_2)(CO)_3(PPh_3)_2]^+$: A Synthon for Tc(I) Complexes and Its Reactions with Neutral Ligands

Maximilian Roca Jungfer and Ulrich Abram*

Cite This: *Inorg. Chem.* 2021, 60, 16734−16753 Read Online

ACCESS | Metrics & More | Article Recommendations | Supporting Information

ABSTRACT: A scalable synthesis of the novel and highly reactive $[Tc(OH_2)(CO)_3(PPh_3)_2]^+$ cation is described. The ligand-exchange chemistry of this compound with neutral ligands coordinating through C, N, O, S, Se, and Te has been explored systematically. The complexes either retain the original *mer-trans* tricarbonyl core under exclusive exchange of the aqua ligand or form dicarbonyl complexes by thermal decarbonylation. Ligand exchange reactions starting from $[Tc(OH_2)(CO)_3(PPh_3)_2]^+$ proceed under mild conditions and are generally almost quantitative. Some of the formed complexes are remarkably stable and inert, while others provide products with one labile ligand for further reactions. The derived complexes of the type $[Tc(L)(CO)_3(PPh_3)_2]^+$ and $[Tc(L)_2(CO)_2(PPh_3)_2]^+$ represent an interesting opportunity for the development of ^{99m}Tc complexes with potential use in radiopharmacy. The ready displacement of the aqua ligand highlights the synthetic value of $[Tc(OH_2)(CO)_3(PPh_3)_2]^+$ as a reactive entry point for further studies in the little explored field of the organometallic chemistry of technetium.

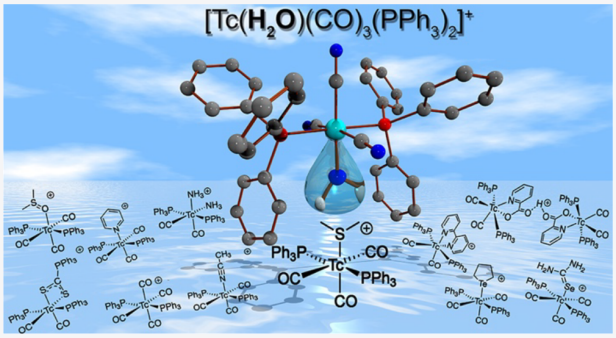

INTRODUCTION

The high intrinsic stability of organometallic technetium(I) complexes makes them exceptional candidates for potential radiopharmaceutical applications with the medicinally relevant nuclear isomer ^{99m}Tc. This is impressively demonstrated by ^{99m}Tc sestamibi—a highly inert d^6 hexakisisonitrile complex, which has been used extensively for myocardial imaging since the 1990s.[1−6] Modern approaches toward novel technetium radiopharmaceuticals also address bis(arene) compounds[7−9] and cyclopentadienyl complexes.[10−13] Particularly the latter group of compounds is frequently stabilized by the $\{Tc^I(CO)_3\}^+$ core, which can be provided in aqueous solution as the $[Tc(CO)_3(OH_2)_3]^+$ complex for ^{99}Tc as well for the clinically relevant gamma emitter ^{99m}Tc.[14−19] The aqua ligands of this compound can be readily exchanged by biologically relevant ligands and give, thus, access to potential pharmaceuticals.[14−20]

Despite the importance of the technetium chemistry in aqueous media, there are surprisingly few structural reports about Tc complexes with aqua ligands. Of course, there are a number of oxido and nitrido complexes, where water sometimes appears as a strongly labilized ligand *trans* to O^{2-} and N^{3-};[21−32] but this is the most labile coordination position in such molecules, and the replacement of such aqua ligands does not represent a synthetic approach to stable ligand exchange products. In addition to some instable chlorido complexes of technetium(V) and -(IV),[32−34] there exist to the best of our knowledge hitherto only three compounds, in which aqua ligands have been proven by X-ray structural analysis (Chart 1). This involves the Tc(III) cation $[TcCl_2(OH_2)(tacn)]^+$ (tacn = 1,3,6-triazacyclononane),[35] a cationic Tc(I) complex with DPPE (DPPE = 1,2-bis(diphenylphosphino)ethane),[36] and a neutral tricarbonyltechnetium(I) complex.[37] Particularly the latter compound seems to be interesting for nuclear medical considerations, since it belongs to the family of

Chart 1. Technetium Complexes with Aqua Ligands

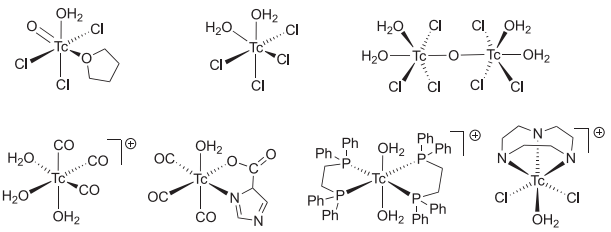

Received: August 23, 2021
Published: October 18, 2021

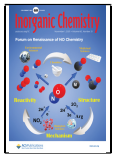

Scheme 1. Synthesis of $[Tc(OH_2)(CO)_3(PPh_3)_2](X)$ Salts (X = $BArF_{24}^-$, BF_4^-, OTf^-) and Their Reactions with DMF and DMSO

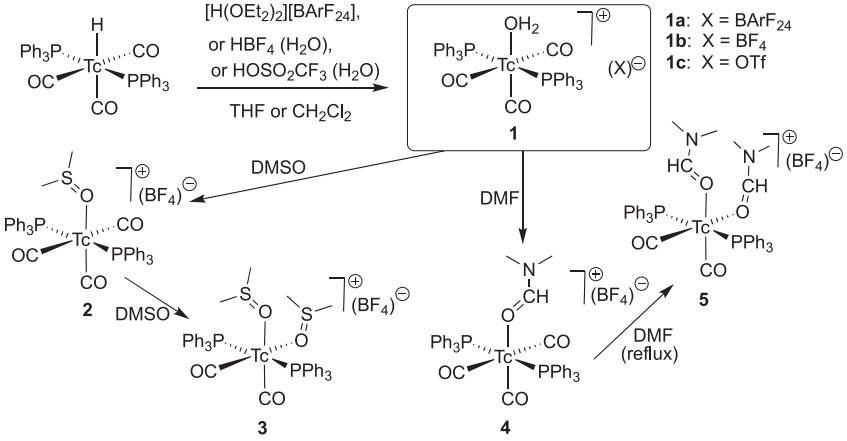

tricarbonyltechnetium(I) complexes, that originates from the (structurally not yet fully characterized) $[Tc(CO)_3(OH_2)_3]^+$ cation.[38] In contrast to the analogous rhenium cation[39,40] and despite several attempts, $[Tc(CO)_3(OH_2)_3]^+$ has not yet been characterized crystallographically. Several pH-dependent protonation/condensation and ligand exchange reactions are expected for aqua complexes of technetium, as has been found for the corresponding $[Re(CO)_3(OH_2)_3]^+$ cation.[39,41−46]

In a recent paper, we studied the reactivity of hydrido complexes of technetium and anticipated the formation of a well-defined synthon for the metallo Lewis acid $[Tc(CO)_3(PPh_3)_2]^+$ by protonation of *mer-trans*-$[TcH(CO)_3(PPh_3)_2]$.[47] Since the target has only one highly Lewis acidic vacant side, it offers the unique possibility for a systematic study of the general coordination chemistry of *mer-trans*-$[Tc(L)(CO)_3(PPh_3)_2]^{+/0}$ and related complexes. This may allow access to bench-stable but nevertheless highly reactive products, which are of potential value for the further development of the organometallic chemistry of technetium. In the present work, we describe the synthesis of the cationic technetium(I) complex $[Tc(OH_2)(CO)_3(PPh_3)_2]^+$ and its reactions with small ligands having C, N, O, S, Se, or Te donor atoms.

RESULTS AND DISCUSSION

$[Tc(OH_2)(CO)_3(PPh_3)_2]^+$ and Similar Solvent Complexes. In continuation of our recent work on hydrido complexes of technetium,[47] we attempted the preparation of the dihydrogen complex $[Tc(H_2)(CO)_3(PPh_3)_2]^+$ by protonation of the monohydride $[TcH(CO)_3(PPh_3)_2]$ with acids of weakly coordinating anions. The dihydrogen complex could act as a functional equivalent to the metallo Lewis acid $[Tc(CO)_3(PPh_3)_2]^+$ due to the expected lability of the dihydrogen ligand. Similar intentions date back to 1995, when such a protonation had been attempted with triflic acid. However, an immediate H_2 evolution was observed, and the isolated product was assigned to a composition of "$[Tc(OTf)(CO)_3(PPh_3)_2]$" on the basis of its spectroscopic data.[48] Therefore, we used Brookhart's acid, $[H(OEt_2)_2](BArF_{24})$, for a similar reaction. It contains the even less coordinating $(BArF_{24})^-$ anion, from which we expected the stabilization of the dihydrogen complex. However, all attempts to isolate $[Tc(H_2)(CO)_3(PPh_3)_2]^+$, even under strictly dry and inert conditions, failed. We isolated the aqua complex $[Tc(OH_2)(CO)_3(PPh_3)_2](BArF_{24})$, instead in reasonable yields (Scheme 1). Single crystals of $[Tc(OH_2)(CO)_3(PPh_3)_2](BArF_{24})$ (**1a**)·$0.5CH_2Cl_2$ were obtained directly from such a reaction mixture. The formation of an aqua complex is consistent with observations made with the analogous rhenium cation $[Re(H_2)(CO)_3(PPh_3)_2]^+$. This dihydrogen complex was prepared *in situ* from $[ReH(CO)_3(PPh_3)_2]$ and Brookhart's acid, and its existence is highly probable on the basis of spectroscopic data.[49] However, also the rhenium complex could not be isolated and rapidly decomposed under formation of $[Re(OH_2)(CO)_3(PPh_3)_2]^+$. Traces of water from the glass surface of the reaction vessels were used to explain the formation of this product.[49]

We repeated the reaction between $[TcH(CO)_3(PPh_3)_2]$ and $[H(OEt_2)_2](BArF_{24})$ in carefully dried and degassed CD_2Cl_2 or thf-d_8. *In situ* NMR data of the reaction mixtures show that even under such conditions and when the reactions are performed in PTFE NMR tubes, the formation of the aqua complex could not be avoided. We attribute the decomposition of coordinated diethyl ether at the highly Lewis acidic $[Tc(CO)_3(PPh_3)_2]^+$ center in the highly Brønsted acidic reaction medium as the source for the coordinated water. A similar reaction pattern has been observed before on a phenylmercury compound.[50] Interestingly, the observed decomposition is slower in thf-d_8, probably due to the stabilization of the unsaturated intermediate by the donor solvent. Further information about the *in situ* NMR experiments including a proposed mechanism is given in the Supporting Information.

Since even the use of the $(BArF_{24})^-$ anion could not stabilize the intermediate dihydrogen complex and exclusively the aqua complex is formed, it became interesting to isolate the $[Tc(OH_2)(CO)_3(PPh_3)_2]^+$ cation with less exotic counterions in reasonable yields. Since water is a better ligand than BF_4^- or OTf^-,[51] these anions are suitable candidates; and indeed, reactions of $[TcH(CO)_3(PPh_3)_2]$ with HBF_4 or triflic acid and water give $[Tc(OH_2)(CO)_3(PPh_3)_2](BF_4)$ (**1b**) and $[Tc(OH_2)(CO)_3(PPh_3)_2](OTf)$ (**1c**) in good to excellent yields.

The formation of the aqua complex is easily verified by the appearance of a ^{99}Tc NMR resonance at −1232 ppm ($\nu_{1/2}$ = approximately 5000 Hz), while the signal of $[TcH(CO)_3(PPh_3)_2]$ at −2208 ppm disappears. The ^{99}Tc resonance of $[Tc(OH_2)(CO)_3(PPh_3)_2]^+$ is downfield-shifted by 100 ppm

https://doi.org/10.1021/acs.inorgchem.1c02599
Inorg. Chem. 2021, 60, 16734−16753

with respect to neutral complexes with the same donor set and geometry around technetium, e.g., the $[Tc\{\eta^1\text{-}O(CR)O\}(CO)_3(PPh_3)_2]$ complexes (R = H, CF_3).[47]

Interestingly, the three isolated salts exhibit different splitting patterns in the ν_{O-H} regions of the IR spectra (Figure 1). Only that of $[Tc(OH_2)(CO)_3(PPh_3)_2](BArF_{24})$ (**1a**)

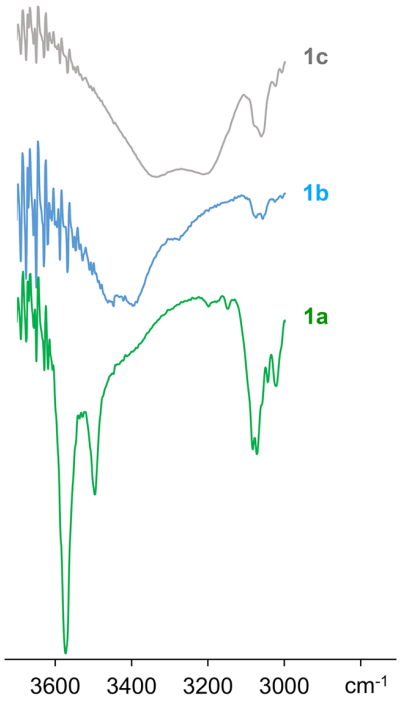

Figure 1. ν_{O-H} Region of the IR spectra of **1a**, **1b**, and **1c** recorded in KBr.

shows two sharp bands at 3572 and 3495 cm^{-1}, while those of **1b** and **1c** contain very broad double maxima between 3300 and 3500 cm^{-1} (**1b**) and between 3200 and 3300 cm^{-1} (**1c**). This indicates the formation hydrogen bonds between the aqua ligands and the counterions in the latter two cases. The positions of the experimentally observed bands correspond with the expectation that such interactions should be stronger for the OTf^- ion compared to BF_4^-.

The spectroscopic results are confirmed by X-ray diffraction data of the three salts. Indeed, the solid-state structure of **1a** contains isolated $[Tc(OH_2)(CO)_3(PPh_3)_2]^+$ cations, while dimeric structures were observed for **1b** and **1c** (Figure 2). The formation of strong hydrogen bonds between each two complex cations seems to be characteristic for the BF_4^- and OTf^- salts of the $[Tc(OH_2)(CO)_3(PPh_3)_2]^+$ cation. It has also been found in a monoclinic polymorph of **1b** and the etherate $[Tc(OH_2)(CO)_3(PPh_3)_2](BF_4)\cdot Et_2O$, which was obtained after crystallization from CH_2Cl_2/Et_2O. Further details about these compounds are given in the Supporting Information.

It is interesting to note that some hydrogen bonding interactions between the aqua ligands and the counterions resist the dissolution of the complexes in CD_2Cl_2. The ^1H chemical shifts and line widths of the OH_2 proton resonances are surprisingly dependent on the anion: $(BArF_{24})^-$ δ = 1.51 ppm, $\nu_{1/2}$ = 37 Hz; $(BF_4)^-$ δ = 2.97 ppm, $\nu_{1/2}$ = 4 Hz; $(OTf)^-$ δ = 1.25 ppm, $\nu_{1/2}$ = 17 Hz.

The technetium atoms in all solid-state structures containing $[Tc(OH_2)(CO)_3(PPh_3)_2]^+$ have an equivalent octahedral coordination environment with two axial triphenyl phosphine ligands and three meridional carbonyl ligands. The equatorial plane is completed by the weakly bound aqua ligand. As in the other few complexes containing the *mer*-$\{Tc(CO)_3\}^+$ motif,[47,52−54] the bonds between Tc and the two carbonyl ligands in the *trans*-position to each other are weakened compared to the third CO ligand, which has another ligand (here water) in the *trans*-position. The Tc−O(water) bond lengths are similar to those in other Tc complexes containing aqua ligands.[21−37] One of the few structural differences between the three solid-state structures are the C1−Tc−O10 and C3−Tc−O10 angles. They are significantly smaller (83.9(1)°, 86.9(1)) in the $BArF_{24}^-$ salt than in the two hydrogen-bridged dimers (90.34(7)° to 93.20(8)°), in which the two carbonyl ligands are slightly bent away from the H-bonded anions.

The aqua complexes are stable as solids but gradually decompose in solution under formation of the $[Tc(CO)_4(PPh_3)_2]^+$ cation, which can finally be isolated in yields up to 50%. The complementary decomposition product is most probably $[Tc(OH_2)_2(CO)_2(PPh_3)_2]^+$ as is concluded from a

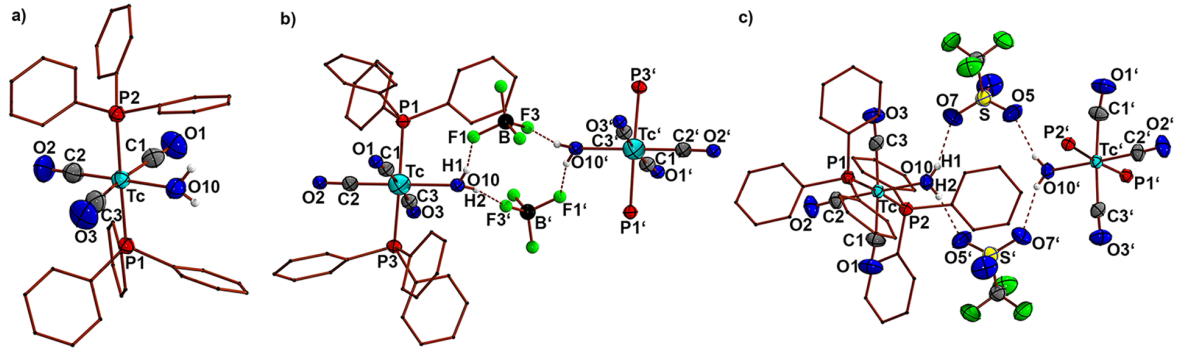

Figure 2. Structure of the $[Tc(OH_2)(CO)_3(PPh_3)_2]^+$ cation in a) **1a** (Tc−C1 1.984(3) Å, Tc−C2 1.884(3) Å, Tc−C3 2.012(3) Å, Tc−O10 2.235(2) Å; C1−Tc−O10 86.9(1)°, C3−Tc−O10 83.9(1)°) and sections of the dimeric structures of b) **1b** (Tc−C1 1.991(3) Å, Tc−C2 1.877(3) Å, Tc−C3 1.983(3) Å, Tc−O10 2.227(2) Å, H1−F1 1.85(4) Å, H2−F3′ 1.83(3) Å (′1−*x*, 1−*y*, −*z*); C1−Tc−O10 92.5(1)°, C3−Tc−O10 91.1(1)°) and c) **1c** (Tc−C1 1.995(2) Å, Tc−C2 1.883(2) Å, Tc−C3 1.992(2) Å, Tc−O10 2.218(1) Å, H1−O7 2.06(3) Å, H2−O5′ 1.94(3) Å (′1−*x*, 1−*y*, 1−*z*); C1−Tc−O10 93.20(8)°, C3−Tc−O10 90.34(7)°).

https://doi.org/10.1021/acs.inorgchem.1c02599
Inorg. Chem. 2021, 60, 16734−16753

^{99}Tc NMR signal at −801 ppm ($\nu_{1/2}$ = 3300 Hz), that means in the typical region for dicarbonyltechnetium(I) complexes.[47] Unfortunately, the diaqua species could not be isolated as a final proof for the assumed CO/OH_2 exchange. It subsequently decomposes under formation of intractable, oily deposits. The formation of these deposits is slower in THF-d_8 than in CD_2Cl_2 suggesting some stabilization by the donor solvent as mentioned above.

Even when the intermediate formation of $[Tc(OH_2)_2(CO)_2(PPh_3)_2]^+$ could not be proven unambiguously in the decomposition of $[Tc(OH_2)(CO)_3(PPh_3)_2](BF_4)$ described above, the decarbonylation and the formation of defined dicarbonyl species are confirmed for reactions of **1b** with dimethyl sulfoxide (DMSO) or dimethyl formamide (DMF). A compound of the composition $[Tc(DMSO)_2(CO)_2(PPh_3)_2](BF_4)$ (**3**) is the final product with DMSO, while a similar reaction with DMF gives first the monosubstitution product $[Tc(DMF)(CO)_3(PPh_3)_2](BF_4)$ (**4**), which can be isolated in crystalline form. It is converted into the dicarbonyl complex $[Tc(DMF)_2(CO)_2(PPh_3)_2](BF_4)$ (**5**) when the reaction is performed at elevated temperatures (Scheme 1). The complete consumption of **1b** in such reactions and the formation of the solvent complexes can easily be checked by the absence of the characteristic splitting of the water band in the IR spectra of the products. The decarbonylation can be followed by the ^{99}Tc NMR resonances. For the two DMF complexes, they appear at −1245 ppm (**4**) and −736 ppm (**5**).

The formation of $[Tc(DMSO)_2(CO)_2(PPh_3)_2]^+$ is nearly quantitative over prolonged reaction times at room temperature, and the complex can be isolated as the BF_4^- salt in good yields. All our attempts to isolate pure $[Tc(DMSO)(CO)_3(PPh_3)_2]^+$ (**2**) were without success. An *in situ* NMR monitoring of the reaction between **1b** and DMSO in CD_2Cl_2 showed that only in the first step of the reaction a considerable amount of $[Tc(DMSO)(CO)_3(PPh_3)_2]^+$ (**2**) (δ = −1176 ppm, $\nu_{1/2}$ = 4532 Hz) is formed. The decarbonylation and the formation of $[Tc(DMSO)_2(CO)_2(PPh_3)_2]^+$ (δ = −739 ppm, $\nu_{1/2}$ = 480 Hz), however, could not be avoided, and already immediately after dissolution of the starting material in DMSO, the formation of the dicarbonyl compound starts. Interestingly, the reaction in DMSO initially does not produce considerable amounts of $[Tc(CO)_4(PPh_3)_2]^+$. Further information about the *in situ* reaction of **1b** with DMSO is given in the Supporting Information.

Given the limited number of available solid-state structural data of technetium complexes with coordinated DMSO or DMF ligands,[55,56] we undertook X-ray diffraction studies on single crystals of compounds **3**, **4**, and **5**. The structures of the complex cations of **3** and **4** are depicted in Figure 3. Details regarding compound **5** are contained in the Supporting Information. The only other two structurally characterized technetium complexes with DMSO ligands are the Tc(IV) compounds $[TcCl_3(DMSO)_3]^+$ and $[\{TcCl_3(DMSO)_2\}_2(\mu\text{-}O)]$.[55] The observed Tc−O bond lengths of 2.035−2.121 Å in these complexes are clearly shorter than those in $[Tc(DMSO)_2(CO)_2(PPh_3)_2]^+$. The solid-state structure of the $[Tc(DMF)(CO)_3(PPh_3)_2]^+$ cation (Figure 3b) in compound **4** shows the same general features as discussed for the aqua complex. The technetium atom is in a distorted octahedral coordination environment. The only other crystallographically studied technetium complex with a coordinated DMF ligand is $[TcCl_3(DMF)(PPh_3)_2]$ with a Tc−O bond length of 2.12 Å.[56] The Tc−O4 bond in $[Tc(DMF)(CO)_3(PPh_3)_2](BF_4)$ is

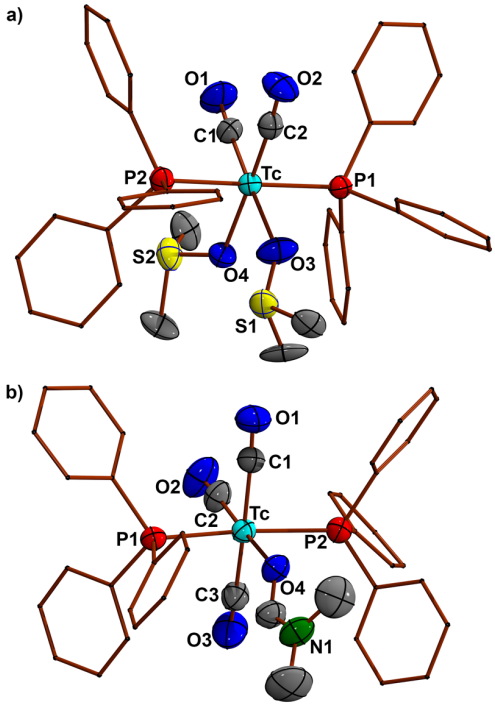

Figure 3. Structures of the complex cations of a) $[Tc(DMSO)_2(CO)_2(PPh_3)_2](BF_4)$ (**3**) (Tc−C1 1.856(4) Å, Tc−C2 1.853(5) Å, Tc−O3 2.189(3) Å, Tc−O4 2.219(3) Å) and b) $[Tc(DMF)(CO)_3(PPh_3)_2](BF_4)$ (**4**) (Tc−C1 2.003(5) Å, Tc−C2 1.882(5) Å, Tc−C3 1.976(5) Å, Tc−O4 2.168(4) Å; C1−Tc−O4 88.9(2)°, C3−Tc−O4 97.7(2)°).

longer by 0.05 Å due to the *trans*-influence of the carbonyl ligand. It should, however, be mentioned that it is still 0.05 Å shorter than the Tc−O4 bond in the aqua complex **1b** indicating that DMF is bound more tightly to technetium than the aqua ligand.

The bond lengths and angles given for compound **4** refer to a triclinic polymorph, which crystallized as a pentane solvate from a CH_2Cl_2/pentane mixture. A monoclinic polymorph of $[Tc(DMF)(CO)_3(PPh_3)_2](BF_4)$ was obtained by slow evaporation of the dichloromethane reaction mixture at room temperature. Further information is given in the Supporting Information.

The high reactivity of compound **1** even toward solvent molecules and the easy scalability of the whole preparation sequence for its synthesis encouraged us to test its potential as a starting material for exchange reactions with ligands having other donor atoms.

Reactions with Carbon-Donor Ligands. With the increasing interest in organotechnetium compounds, also reactions with simple monodentate carbon-donor ligands are relevant. Thus, we studied some reactions of $[Tc(OH_2)(CO)_3(PPh_3)_2]^+$ (**1**) with CO, CS_2, and isocyanides.

In the previous section, we already mentioned the formation of the tetracarbonyl complex $[Tc(CO)_4(PPh_3)_2]^+$ (**6**) as a decomposition product of $[Tc(OH_2)(CO)_3(PPh_3)_2]^+$. Since in this reaction the tetracarbonyl cation is formed by a "ligand scrambling" process between two molecules of **1**, only an unsatisfactory maximum yield of 50% can be obtained. Additionally, purification operations are required to obtain a

https://doi.org/10.1021/acs.inorgchem.1c02599
Inorg. Chem. 2021, 60, 16734−16753

Scheme 2. Reactions of $[Tc(OH_2)(CO)_3(PPh_3)_2](X)$ Salts (X = $BArF_{24}^-$, BF_4^-, OTf^-) with Carbon-Donor Ligands

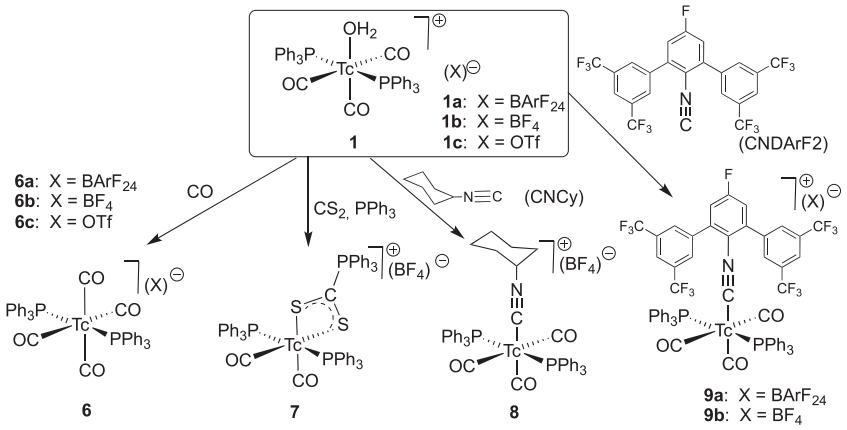

highly pure product. Similar restrictions hold true for previous routes to salts of complex **6**.[48,57]

When solutions of **1a**, **1b**, or **1c** in CH_2Cl_2 are exposed to a stream of CO gas, an immediate, clean, and quantitative formation of the corresponding $[Tc(CO)_4(PPh_3)_2]^+$ salts is observed within a few minutes even at room temperature (Scheme 2). The ^{99}Tc NMR spectrum of $[Tc(CO)_4(PPh_3)_2]^+$ shows a single resonance at −1888 ppm. The $(BArF_{24})^-$ and $(BF_4)^-$ salts were obtained in crystalline form by diffusion of pentane or hexane directly into the dried reaction mixtures. The structure of the $[Tc(CO)_4(PPh_3)_2]^+$ cation of compound **6b** is shown in Figure 4. Further information about the structural data of compounds **6a** and **6c** can be found in the Supporting Information.

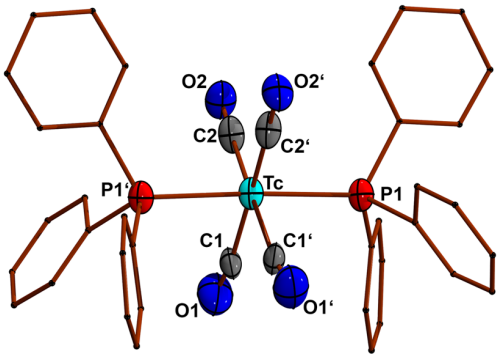

Figure 4. Structure of the complex cation of $[Tc(CO)_4(PPh_3)_2](BF_4)$ (**6b**) (Tc−C1 1.939(10) Å, Tc−C2 2.035(1) Å). Symmetry operation: ′1−*x*, 1−*y*, *z*.

With respect to the extraordinarily clean reaction between **1b** with CO, we attempted the synthesis of the corresponding thiocarbonyl derivative via a reaction of **1b** with CS_2 and PPh_3 as a sulfur scavenger. The reaction mixture turned purple upon prolonged heating, and a dark oil separated after the addition of pentane. Dissolution in CH_2Cl_2 and diffusion of pentane into this solution gave stable, purple crystals of $[Tc(S_2CPPh_3))(CO)_2(PPh_3)_2](BF_4)$ (**7**)·CH_2Cl_2 (Scheme 2). The formation of triphenylphosphoniodithioformate has occasionally been observed as a result of the attack of PPh_3 to coordinated carbon disulfide or by the insertion of CS_2 into phosphorus−metal bonds.[58] The zwitterionic compound is unstable in isolated form but is stabilized upon coordination to transition metal ions. There are only a few structural reports about one iridium complex and a small number ruthenium compounds.[59−62] Consequently, technetium complexes or such with other "group 7" metals with S_2CPPh_3 are not yet known.

Figure 5 shows the structure of the complex cation of complex **7**. The P-CS_2 unit has the same arrangement around

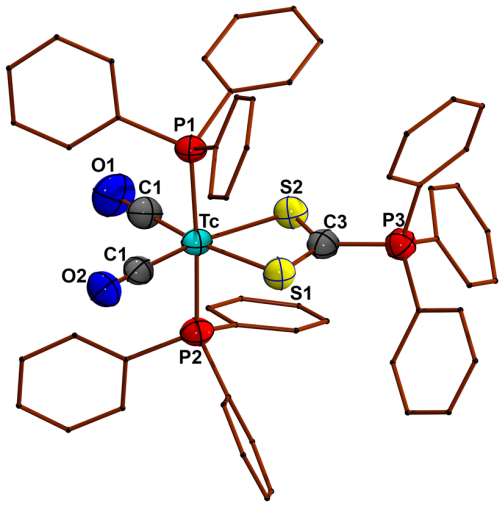

Figure 5. Structure of the complex cation of $[Tc(S_2CPPh_3)(CO)_2(PPh_3)_2](BF_4)$ (**7**) (Tc−C1 1.904(4) Å, Tc−C2 1.872(5) Å), Tc−S2 2.476(1) Å, Tc−S2 2.509(1) Å, S1−C3 1.668(5) Å, S2−C3 1.682(4) Å, C3−P3 1.811(5) Å, Tc···C3 2.931(4) Å).

the central carbon atom as in the previously structurally characterized complexes of this rare ligand.[59−62] The bond lengths indicate a large degree of delocalization in the electronic structure of the CS_2 moiety within the zwitterionic adduct. The C−S bond lengths are virtually identical and short enough to represent CS double bonds, while the C3−P3 bond length is in the range of a normal single bond. The Tc−S bond lengths are somewhat elongated as commonly found in complexes with carbonyl ligands in the *trans*-position.

The ^{31}P NMR spectrum of $[Tc(S_2CPPh_3)(CO)_2(PPh_3)_2](BF_4)$ (**7**) shows a broad resonance at 18 ppm for the two axial PPh_3 ligands and a narrow resonance at 25 ppm for the

https://doi.org/10.1021/acs.inorgchem.1c02599
Inorg. Chem. 2021, 60, 16734−16753

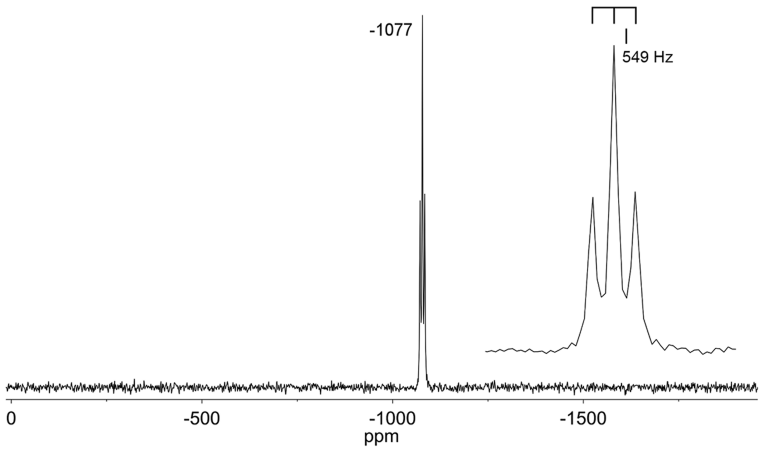

Figure 6. ^{99}Tc NMR spectrum of compound **7** in CD_2Cl_2 with a well-resolved ^{31}P coupling.

S_2CPPh_3 adduct. A drastic line broadening of ^{31}P signals for P atoms, which are directly bonded to the quadrupolar nucleus ^{99}Tc, is frequently found for complexes with low local symmetry. This is commonly explained by scalar couplings between the two nuclei, which in many cases make the ^{31}P signals practically invisible.[63,64] The large quadrupole moment of ^{99}Tc ($Q = -0.19 \cdot 10^{-28}$ m^2)[65] is also the reason for the commonly observed line-broadening of related ^{99}Tc signals.[66] In some rare cases, however, the lines remain small as is the case with compound **7** and some structurally related dithiocarbamato, dithiophosphato, and xanthogenato complexes of technetium(I).[67] Figure 6 illustrates the ^{99}Tc NMR spectrum of **7** with a Tc–P coupling to the axial PPh_3 ligands of 549 Hz. Such couplings are in accord with those observed in the other few $[Tc(L)(CO)_2(PPh_3)_2]$ complexes, where L represents chelating dithioligands.[67−70]

Despite the fact that with the development of ^{99m}Tc sestamibi an isonitrile complex of technetium(I) became one of the most used radiopharmaceuticals worldwide,[1,2] the fundamental coordination chemistry of technetium with this class of ligands is relatively little explored. Most of the Tc isocyanide complexes contain the metal in low oxidation states.[68−70] In a recent report, also the access to corresponding nitrido and phenylimido complexes of technetium(V) is described.[71] The stabilization of high oxidation states became possible by the use of sterically encumbered terphenylisocyanides, which allowed the tuning of bonding properties in a wide range. One of these ligands (CNDArF2, Scheme 2) has also been used for a reaction with compound **1b**.

The addition of CNDArF2 or CNCy to a suspension of $[Tc(OH_2)(CO)_3(PPh_3)_2](BF_4)$ in CH_2Cl_2 leads to the immediate dissolution of the starting materials and the formation of inert $[Tc(CNR)(CO)_3(PPh_3)_2](BF_4)$ salts (R = Cy, $C_6H_2F(C_6H_3(CF_3)_2)_2$). Even prolonged heating with a large excess of isocyanide did not lead to dicarbonyl complexes. The ^{99}Tc chemical shifts of the products are very similar to those of the tetracarbonyl complex. However, the line widths of the resonances are as broad as that of the aqua complex. We undertook a single-crystal X-ray analysis of the cyclohexylisocyanide complex **8**. The structure of the complex cation is depicted in Figure 7. The bond between technetium and the isocyanide is slightly longer than the Tc-CO bonds. This is not unexpected and is in accord with other carbonyl/isocyanide mixed-ligand complexes of technetium. The

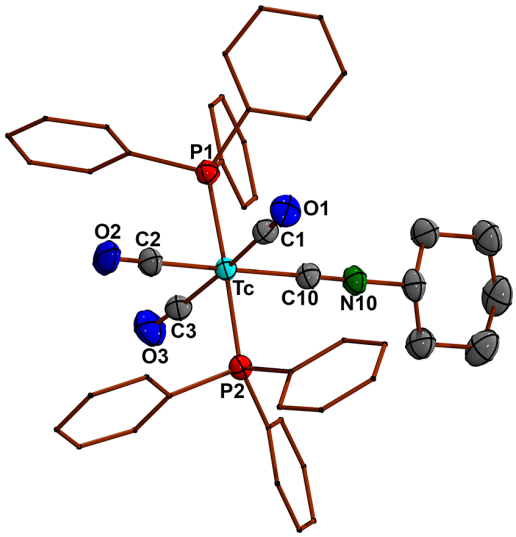

Figure 7. Structure of the complex cation of $[Tc(CNCy)(CO)_3(PPh_3)_2](BF_4)$ (**8**) (Tc–C1 1.988(5) Å, Tc–C2 1.956(5) Å, Tc–C3 2.025(5) Å, Tc–C10 2.098(5) Å, C10–N10 1.148(6) Å; C1–Tc–C10 89.4(2)°, C3–Tc–C10 95.9(2)°).

structure of CNDArF2 complex **9** resembles that of **8**. However, the X-ray data are of low quality, and thus, the corresponding bond lengths and angles shall not be discussed here. Nevertheless, the topology of the coordination sphere can be derived unambiguously.

For both isocyanides, no back-donation from technetium into the C≡N bond can be derived from the X-ray data and from the corresponding IR stretches. The $\nu_{C\equiv N}$ frequencies are found at 2203 cm^{-1} for **8** and 2153 cm^{-1} for **9**. This is at higher wave numbers compared with the values for the uncoordinated ligands (2136 cm^{-1} for CNCy and 2118 cm^{-1} for CNDArF2).

In contrast to $[Tc(CO)_4(PPh_3)_2]^+$,[48,57] the mixed carbonyl isocyanide complexes $[Tc(CNR)(CO)_3(PPh_3)_2]^+$ do not react with oxy bases under formation of oxycarbenes. Instead, the starting materials can be recovered unchanged during the first 2 h, while a longer exposure to hot $NaOH/CH_3CN$ leads to the formation of intractable black-brown decomposition products.

https://doi.org/10.1021/acs.inorgchem.1c02599
Inorg. Chem. 2021, 60, 16734−16753

Scheme 3. Reactions of $[Tc(OH_2)(CO)_3(PPh_3)_2](BF_4)$ with Some Nitrogen-Donor Ligands

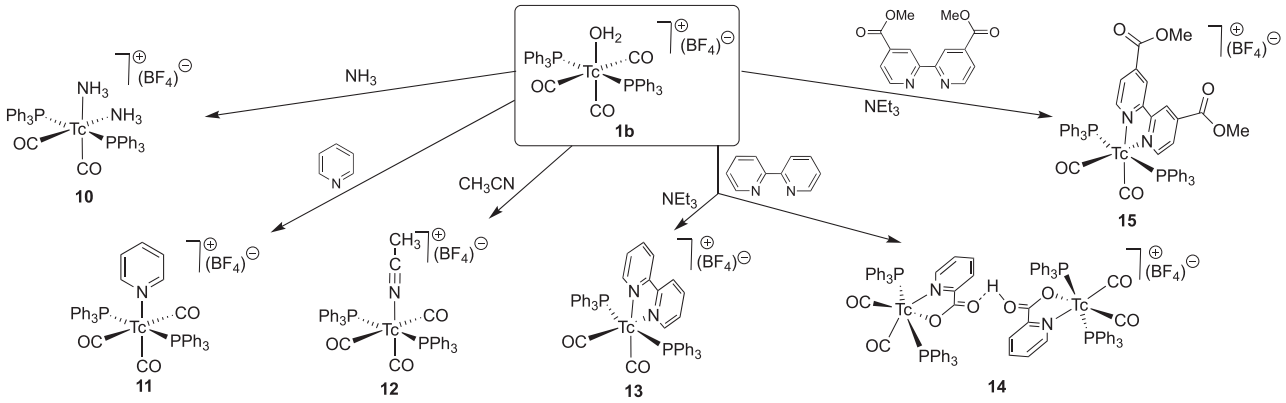

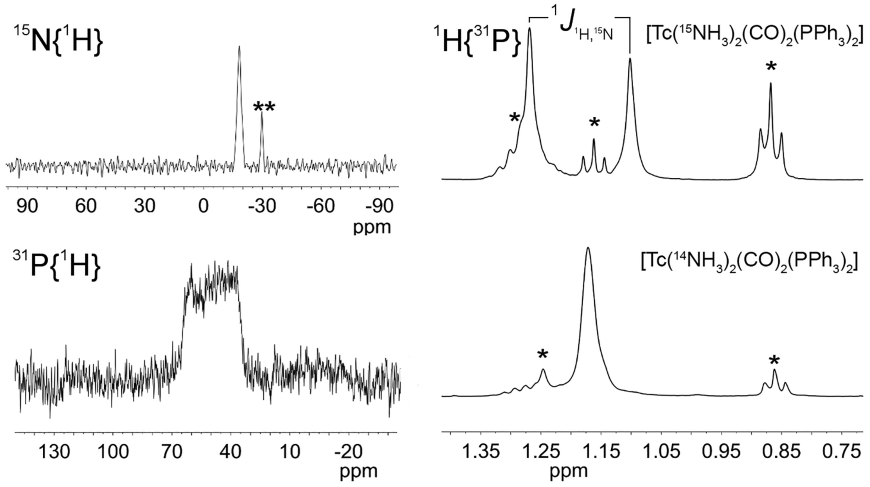

Figure 8. Fractions of the ^{15}N, ^{31}P, and ^{1}H NMR spectra of $[Tc(NH_3)_2(CO)_2(PPh_3)_2](BF_4)$ (**10**) in CD_2Cl_2 (** NH_4^+ ions, * solvent).

Reactions with Nitrogen-Donor Ligands. The importance of nitrogen-donor ligands for the coordination chemistry of technetium as for that of any other transition metal is obvious. Thus, they also played and play an important role in the designing of ligand systems for nuclear medicine, and many well-optimized chelators with N-donor atoms serve in routine imaging procedures.[3−5] Here, however, the focus of our interest shall be set to some fundamental reaction patterns of $[Tc(OH_2)(CO)_3(PPh_3)_2](BF_4)$ (**1b**) with simple ligands such as NH_3, acetonitrile, and imines. A summary of the performed reactions and their products is given in Scheme 3.

Complexes containing carbonyl and ammine ligands simultaneously are scarce in the entire coordination chemistry. Only 28 of such compounds could be isolated in crystalline form and studied by X-ray diffraction.[71] No such technetium compounds are known up to now, and also the overall number of known ammine complexes of technetium is strongly limited.[72−76] Nevertheless, there should be a good chance to access them, having in mind that a number of related rhenium complexes have been isolated.[77−84]

Thus, we performed a reaction of $[Tc(OH_2)(CO)_3(PPh_3)_2](BF_4)$ with ammonia giving colorless crystals of the diammine complex $[Tc(NH_3)_2(CO)_2(PPh_3)_2](BF_4)$ (**10**). The product shows a ^{99}Tc NMR resonance with a chemical shift of −1232 ppm and a half-line width similar to that of the starting material. However, no splitting of the residual water band in the IR spectrum of the product was evident, and the integral ratio of PPh_3 protons to the ammine ligand protons was approximately 30:6. An isotope labeling experiment with $^{15}NH_3$ unequivocally confirmed the presence of ammonia in the product by the appearance of a broad ^{15}N NMR resonance at −18.2 ppm and the splitting of the ammine ^{1}H NMR resonance into a doublet (Figure 8). The $^{1}J_{H-15N}$ coupling constant of 67 Hz is in accord with related coupling constants measured for $^{15}NH_3$ complexes of platinum.[85−87] The $^{31}P\{^{1}H\}$ resonance of complex **10** follows the broadening pattern described above. The observed almost rectangular peak shape, however, is indicative of a partially resolved coupling between the phosphorus nuclei and the nuclear spin of ^{99}Tc of 9/2. The expected ten-line pattern is poorly resolved, and the resulting $^{1}J_{P-Tc}$ coupling constant of ca. 500 Hz can only be approximated by line-width considerations as has been done for similar cases, e.g., the ^{1}H NMR resonance of $[TcH_9]^{2-}$.[88]

Finally, a single-crystal X-ray diffraction study confirmed that not only the aqua ligand is exchanged but additionally one of the carbonyl ligands (Figure 9a). The Tc−N bond lengths in this complex are longer by about 0.1 Å than those in the three previously structurally characterized ammine complexes of technetium (ca. 2.17 Å).[75,76] This is due to the strong *trans*-influence of the carbonyl ligands. The structural features of the

https://doi.org/10.1021/acs.inorgchem.1c02599
Inorg. Chem. 2021, 60, 16734−16753

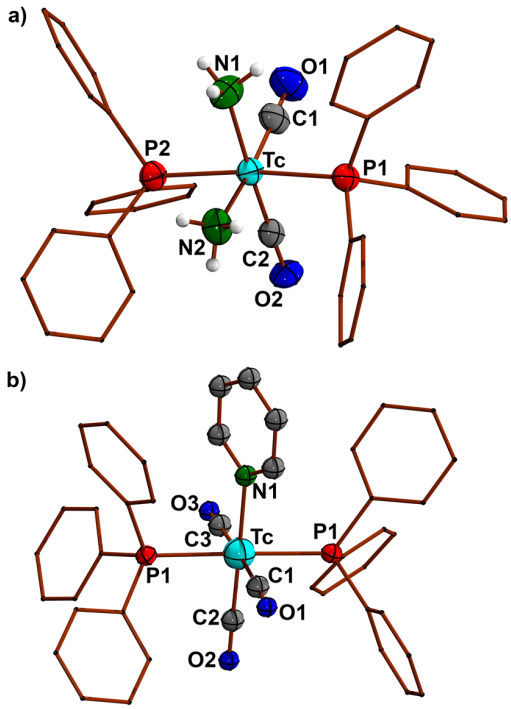

Figure 9. Structures of the complex cations of a) $[Tc(NH_3)_2(CO)_2(PPh_3)_2](BF_4)$ (**10**) (Tc–C1 1.876(5) Å, Tc–C2 1.839(5) Å, Tc–N1 2.261(2) Å, Tc–N2 2.239(2) Å) and b) $[Tc(py)(CO)_3(PPh_3)_2](BF_4)$ (**11**) (Tc–C1 1.993(6) Å, Tc–C2 1.889(8) Å, Tc–C3 1.985(6) Å, Tc–N1 2.226(6) Å, 1; C1–Tc–N1 90.7(3)(2)°, C3–Tc–N1 93.2(3)°).

carbonyl ligands are similar to those previously discussed. The solid-state structure of **10** is supported by hydrogen bonds between the ammine ligands and the BF_4^- counterion.

In contrast, reactions of **1b** with acetonitrile or pyridine lead to the replacement of only the aqua ligands. The ^{99}Tc resonances of the products are observed at chemical shifts of −1328 ppm and −1504 ppm, which perfectly fit the region of tricarbonyl complexes. The two complexes were additionally characterized by single-crystal X-ray diffraction. Unfortunately, the quality of the data set of the acetonitrile complex $[Tc(CH_3CN)(CO)_3(PPh_3)_2](BF_4)$ (**12**) was poor. Nevertheless, the composition and connectivity of the complex are verified unambiguously. Some more details are contained in the Supporting Information. The structure of the complex cation of $[Tc(py)(CO)_3(PPh_3)_2](BF_4)$ (**11**) is shown in Figure 9b. The structure of the pyridine complex reveals a nonlinear, twisted binding mode (twist angle ca. 21°). The Tc–N bond length of the pyridine complex (2.226(6) Å) is shorter than those we observed in the ammine complex, which might be attributed to the weak π-acidity of the pyridine ligand.

Our attempts to introduce a second pyridine ligand by prolonged heating of complex **11** with additional pyridine failed. We only obtained another polymorph of the complex with cocrystallized pyridine, $[Tc(py)(CO)_3(PPh_3)_2](BF_4)\cdot py$ (see Supporting Information). A similar result was observed when boiling complex **12** in acetonitrile.

An unexpected product was obtained during the reaction of **1b** with bipyridine (bpy). When the reaction was performed without special precautions in CH_2Cl_2, the immediate formation of a purple solution was observed. After heating, two ^{99}Tc resonances were observed in such mixtures: a main resonance at −952 ppm and a minor component at −1039 ppm. The two signals appear in the typical region for dicarbonyltechnetium(I) species. The latter one could be assigned to the expected complex $[Tc(bpy)(CO)(PPh_3)_2](BF_4)$ (**13**), while that at −952 ppm belongs to a completely unexpected reaction product: $[\{Tc(N,O\text{-}C_5H_4N\text{-}COO)(CO)_2(PPh_3)_2\}_2H](BF_4)$ (**14**). It was isolated from an acetone/diethyl ether mixture as yellow crystals in a yield of approximately 30%.

The nature of compound **14** as a picolinic acid complex was confirmed unambiguously by X-ray diffraction. Figure 10

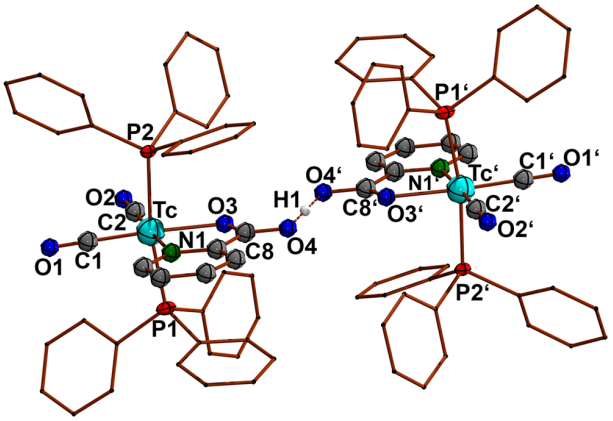

Figure 10. Structure of the complex cation of $[\{Tc(N,O\text{-}C_5H_4N\text{-}COO)(CO)_2(PPh_3)_2\}_2H](BF_4)$ (**14**) (Tc–C1 1.871(10) Å, Tc–C2 1.898(8) Å, Tc–N1 2.194(8) Å, Tc–O3 2.168(5) Å, O3–C8 1.261(8) Å, C8–O4 1.258(9) Å, O4···H10 1.20(6) Å).

depicts the structure of the dimeric complex cation $[\{Tc(N,O\text{-}C_5H_4N\text{-}COO)(CO)_2(PPh_3)_2\}_2H]^+$, in which two complex species are connected by a hydrogen bond. The formation of such dimers is not unknown in the solid-state chemistry of picolinic acid. It is frequently accompanied by zwitterionic organic derivatives but has also been found as a structural motif of metal complexes.[89,90] The Tc–N bond length in **14** of 2.194(8) Å is slightly shorter than in the pyridine complex **11**, and the Tc–O bond is in the same range as those in the recently studied technetium complexes with monodentate carboxylato ligands.[47]

The unanticipated formation of picolinic acid during reactions with bipy has been observed before;[91,92] but in the reported examples, also (partially strong) oxidants were involved, while this is not the case in the reaction under study. Thus, it is highly probable that a metal-mediated oxidation with air is responsible for the formation of the picolinato ligand. Such an assumption is in a line with a recent observation, where the parent complex of compound **1**, $[TcH(CO)_3(PPh_3)_2]$, promoted the oxidation of methanol to formate and a subsequent C–C coupling reaction, which finally gives oxalic acid.[47] It is probable that in both cases the unsaturated Lewis acid $[Tc(CO)_3(PPh_3)_2]^+$ plays a crucial role. This presumption is supported by the fact that the formation of complex **14** is completely suppressed when a base such as NEt_3 is added to the reaction mixture of **1b** and bpy in CH_2Cl_2. That way, yellow crystals of $[Tc(bpy)(CO)_2(PPh_3)_2](BF_4)$ (**13**) are formed in an almost quantitative yield, and no

https://doi.org/10.1021/acs.inorgchem.1c02599
Inorg. Chem. 2021, 60, 16734−16753

signs for the formation of the picolinic acid complex were observed, even after prolonged treatment with moist solvents and under aerobic conditions.

The stability of the chelate **13** and the ease of its formation indicate that it might be a suitable platform for bioconjugation with the medicinally relevant isotope ^{99m}Tc.

Although the present paper does not focus the search for radiopharmaceutical solutions, we tested the reactivity of an ester-substituted bipyridine under the experimental conditions applied for bpy and the stability of the formed product. The reaction of **1b** with 4,4′-dimethoxylcarbonyl-2,2′-bipyridine (bpy^{COOMe2}) was straightforward and gave the corresponding product $[Tc(bpy^{COOMe2})(CO)_2(PPh_3)_2](BF_4)$ (**15**) in quantitative yield.

Single crystals of $[Tc(bpy^{COOMe2})(CO)_2(PPh_3)_2](BF_4)\cdot 2CH_2Cl_2$·acetone were obtained by slow evaporation of a solution of the complex in an acetone/CH_2Cl_2/diethyl ether mixture. A representation of the structure is given in Figure 11.

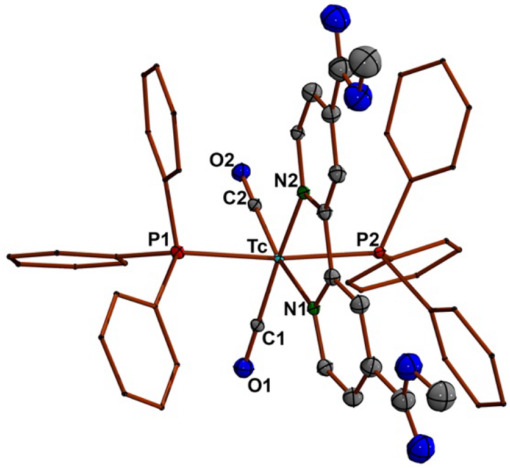

Figure 11. Structure of the complex cation of $[Tc(bpy^{COOMe2})(CO)_2(PPh_3)_2](BF_4)$ (**15**) (Tc–C1 1.896(10) Å, Tc–C2 1.904(8) Å, Tc–N1 2.169(9) Å, Tc–N2 2.159(9) Å).

Although all complexes of this study having nitrogen-donor ligands seem to be rather inert and stable, the bpy complexes have the shortest Tc–N bond lengths and, thus, may be regarded as particularly robust. The bipyridine ligand in compound **15** is bonded as tight as in the other two structurally characterized mixed carbonyl/bpy complexes of technetium(I) $[TcCl(CO)_3$(4,5-diazafluorene-9-one aroylhydrazone)] (Tc–N = 2.22–2.23 Å)[93] and $[Tc(CO)_3(bpy)Cl]$ (Tc–N = 2.17–2.19 Å)[94] or in the robust isocyanide/bpy cation $[Tc(bpy)(CN^tBu)_4]^+$ (Tc–N = 2.15–2.17 Å).[95]

Reactions with Sulfur, Selenium, and Tellurium Donors. Some reactions of $[Tc(OH_2)(CO)_3(PPh_3)_2](BF_4)$ with oxygen-donor ligands such as DMSO or DMF have already been discussed in a previous chapter of this communication, and it became clear that stable products with ethers such as THF, diethyl ether, or dioxane could not be isolated. Having in mind the "soft" character of Tc(I), attempts with not too bulky diorganosulfides, -selenides, or -tellurides should be more promising.

Indeed, $[Tc(OH_2)(CO)_3(PPh_3)_2](BF_4)$ readily reacts with small neutral dialkylchalgogenides such as dimethylsulfide (SMe_2), diethylsulfide (SEt_2), dimethylselenide ($SeMe_2$), dimethyltelluride ($TeMe_2$), tetrahydrothiophene (tht), tetrahydroselenophene (thse), and tetrahydrotellurophene (thte). No reaction, however, was observed with the more bulky diphenylsulfide. A summary of the performed reations and their products is given in Scheme 4.

The products can be obtained in good to excellent yields directly from the reaction mixtures by the addition of pentane. No residual aqua complex was contained in the precipitated solids. This has been proven by the inspection of their IR spectra, where no splitting of the water band is indicated. The dialkylchalcogenide complexes **16**–**22** are stable as solids. Most of them could be isolated in crystalline formed and studied by X-ray diffraction. During the measurement of their IR spectra in KBr pellets (this technique was required for radiation protection reasons), however, we found some evidence for the formation of $[TcBr(CO)_3(PPh_3)_2]$; this means a partial exchange of the dichalcogenides in favor of Br^-. A similar observation has been made for $[Tc(OH_2)(CO)_3(PPh_3)_2]^+$. We attribute this behavior to a certain reactivity of the complexes even in solid solutions. Since the chemistry of technetium with small and labile (and/or sensitive) diorganochalcogenide ligands is scarce, we have studied the reactivity and characteristics of the obtained complexes in more detail.

Scheme 4. Reactions of $[Tc(OH_2)(CO)_3(PPh_3)_2](BF_4)$ with Some Sulfur, Selenium, and Tellurium Donor Ligands

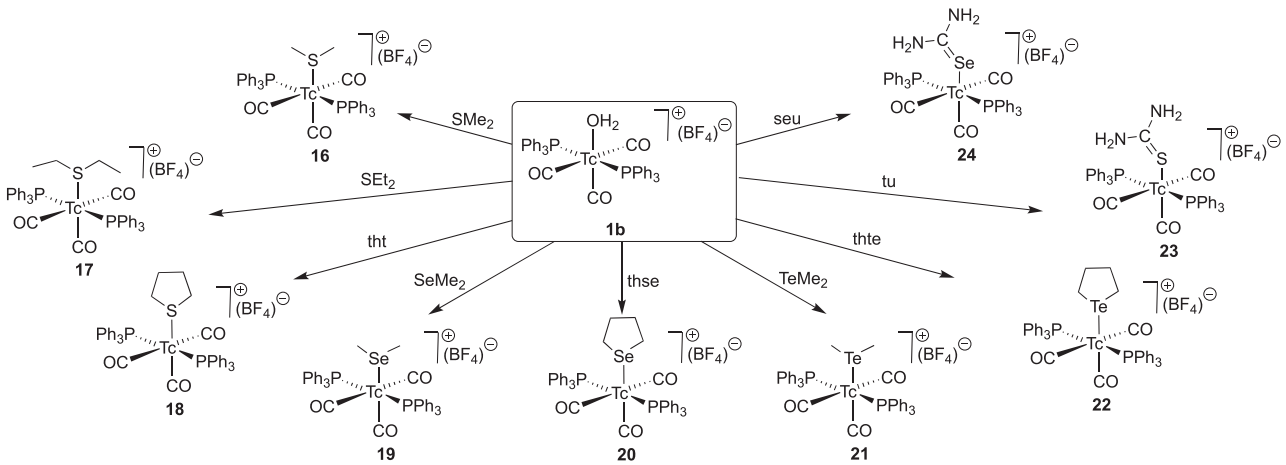

https://doi.org/10.1021/acs.inorgchem.1c02599
Inorg. Chem. 2021, 60, 16734–16753

Particularly the selective and controlled exchange of the (volatile) SMe_2 or tht ligands in compounds **16** and **18** may make these complexes excellent precursors for ongoing studies with the highly reactive Lewis acid $[Tc(CO)_3(PPh_3)_2]^+$, particularly for organometallic approaches, where $[Tc(OH_2)(CO)_3(PPh_3)_2]^+$ with the aqua ligand as a leaving group is sometimes unfavorable.

The lability of the thioether complexes becomes evident in their NMR spectra. Upon dissolution of the pure, water-free complexes, the thioether ligands exchange with residual water of the deuterated solvent. This process is reversible, and after the addition of an excess of the corresponding thioether, the thioether complexes are reformed quantitatively (Scheme 5).

Scheme 5. Equilibrium between $[Tc(OH_2)(CO)_3(PPh_3)_2]^+$ and $[Tc(SR_2)(CO)_3(PPh_3)_2]^+$ Complexes

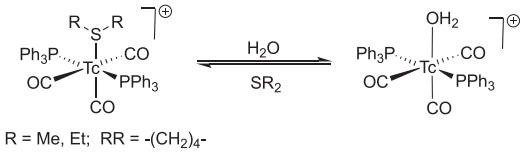

Two different sets of ^1H resonances are observed for coordinated and uncoordinated tht, SEt_2, and SMe_2 in the ^1H NMR spectra of the complexes. This means that the related exchange between the coordinated and uncoordinated ligands is slow on the NMR time scale. Furthermore, the SMe_2 and SEt_2 complexes show a higher exchange percentage with the residual water than the tht complex **18**. The progress of the ligand exchange can readily be monitored by ^1H or ^{99}Tc NMR spectroscopy. This is exemplarily demonstrated for the reactions of compounds **17** and **18** with the water from moist CD_2Cl_2 and the subsequent addition of an excess of SEt_2 or tht (Figure 12).

Although the structural chemistry of technetium complexes with sulfur donors is well-studied and hundreds of crystal structures are available,[71] a basic understanding of the binding properties of monodentate neutral sulfur donors cannot be concluded. To the best of our knowledge, there are only three structural reports on nonchelated thioether complexes of technetium: $[TcCl_4(SR_2)_2]$ (SR_2 = tht, 1,4-thioxane) and $[TcBr_5(tht)]^-$.[55,96] Thus, we undertook X-ray structure analyses on all three new derivatives. The solid-state structures of their cations are shown in Figure 13. The technetium atoms are coordinated in a distorted octahedral fashion. Generally, the Tc−S bond lengths in the cations of the present study are

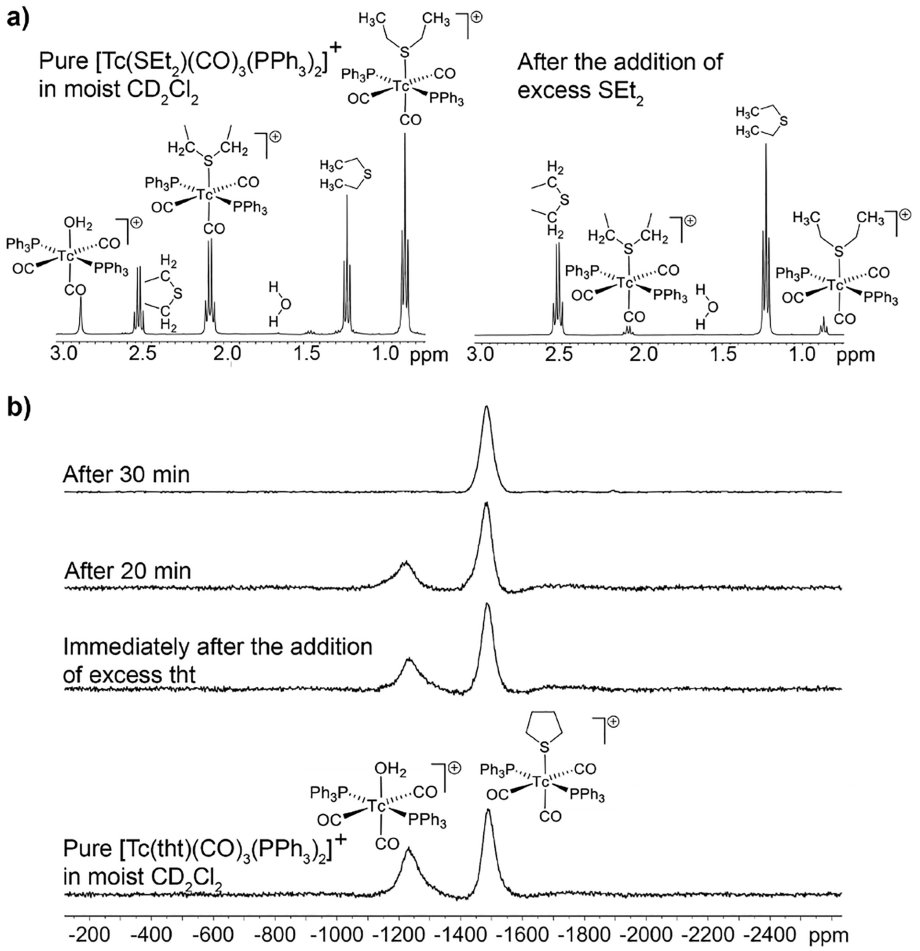

Figure 12. a) Fraction of the ^1H NMR spectrum of $[Tc(SEt_2)(CO)_3(PPh_3)_2](BF_4)$ in moist CD_2Cl_2 before and after the addition of excess SEt_2 and b) ^{99}Tc NMR spectra of $[Tc(tht)(CO)_3(PPh_3)_2](BF_4)$ in moist CD_2Cl_2 before and after the addition of excess tht.

https://doi.org/10.1021/acs.inorgchem.1c02599
Inorg. Chem. 2021, 60, 16734−16753

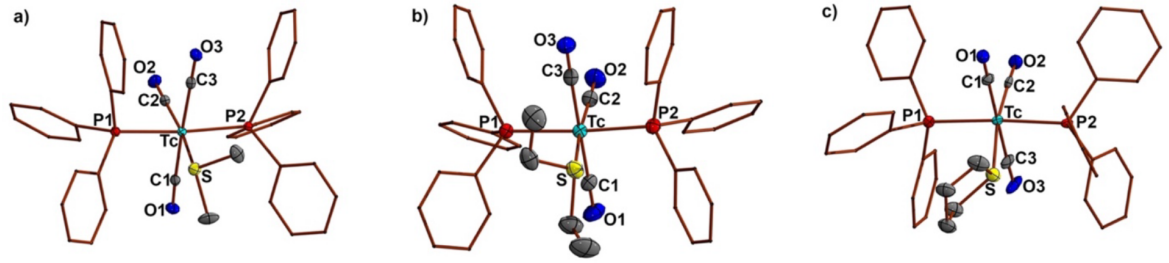

Figure 13. Structures of the complex cations in a) **16** (Tc−C1 1.979(2) Å, Tc−C2 1.926(2) Å, Tc−C3 2.013(2) Å, Tc−S 2.5347(8) Å; C1−Tc−S 90.99(5)°, C3−Tc−S 88.7(6)°), b) **17** (Tc−C1 1.970(3) Å, Tc−C2 1.913(3) Å, Tc−C3 2.008(3) Å, Tc−S 2.5412(8) Å; C1−Tc−S 91.6(1)°, C3−Tc−S 91.4(8)°), and c) **18** (Tc−C1 1.979(7) Å, Tc−C2 1.928(7) Å, Tc−C3 1.994(8) Å, Tc−S 2.519(2) Å; C1−Tc−S 93.3(2)°, C3−Tc−S 86.6(2)°).

the longest so far experimentally determined Tc−S bond lengths with the only exception of $[TcNCl_2(P,P,S\text{-}\{PPh_2(CH_2CH_2)\}_2S)]$, where the Tc−S distance is ca. 2.8 Å and hardly represents a real Tc−S bond.[97] Thus, the weak bonding of the thioethers, which is strongly suggested by their observed lability in solution, is confirmed by their solid-state structures. Interestingly, even the spectroscopically observed differences in the ligand exchange rates between the three thioethers discussed above are reflected by the Tc−S bond lengths detected in the solid state (2.541 Å (SEt_2) > 2.534 Å (SMe_2) > 2.519 Å (tht)).

Surprisingly, the analogous selenium and tellurium compounds are clearly more inert than the thioether complexes. Only for compound **19** some $SeMe_2/H_2O$ exchange is detected in moist solvents. The ^{1}H NMR spectrum of $[Tc(SeMe_2)(CO)_3(PPh_3)_2](BF_4)$ (**19**) in moist CD_2Cl_2 also shows in addition to the resonance of the coordinated selenoether that of the uncoordinated compound. The sum of their integrals perfectly fits with the expected 30:6 ratio beween the aromatic and aliphatic protons for this compound. The $^2J_{H,Se}$ coupling constant in the ^{77}Se satellites is reduced from 10.08 to 9.10 Hz upon coordination.

Within the series of the tetrahydrochalcogenophene complexes, the observed ring inversion barrier increases along the group. The barrier for the ring inversion in the tetrahydrotellurophene complex $[Tc(thte)(CO)_3(PPh_3)_2](BF_4)$ (**22**) is high enough that two distinct signals are observed for the α_{axial}-/$\alpha_{equatorial}$-protons. Contrarily, the metal-bound five membered rings in the tetrahydrothiophene and tetrahydroselenophene complexes **18** and **20** can freely invert their configuration at room temperature, which gives a single resonance for each set of chemically equivalent protons. The signals in the tetrahydrotellurophene complex **22** were unambiguously assigned by a NOESY experiment. The relative strength of the NOESY cross-peaks of the α-thte protons with the *o*-protons of the axial PPh_3 ligands allows for the assignment of the α_{axial} protons due to the larger 1,7-diaxial interaction observed for the multiplet at ca. 2.4 ppm. The difference in shielding between the two geminal protons is likely due to the ring current of the adjacent PPh_3 moieties, which shields the equatorial protons more than the axial ones. The NOESY spectrum is shown in Figure 14. The shielding of the ^{99}Tc nuclei in the complexes decreases from sulfur to tellurium, reflecting the more metallic and electropositive character of the Se and Te donor atoms. Expectedly, the chemical shifts of the sulfur and selenium complexes are closer to each other than to those of the corresponding tellurium complexes.

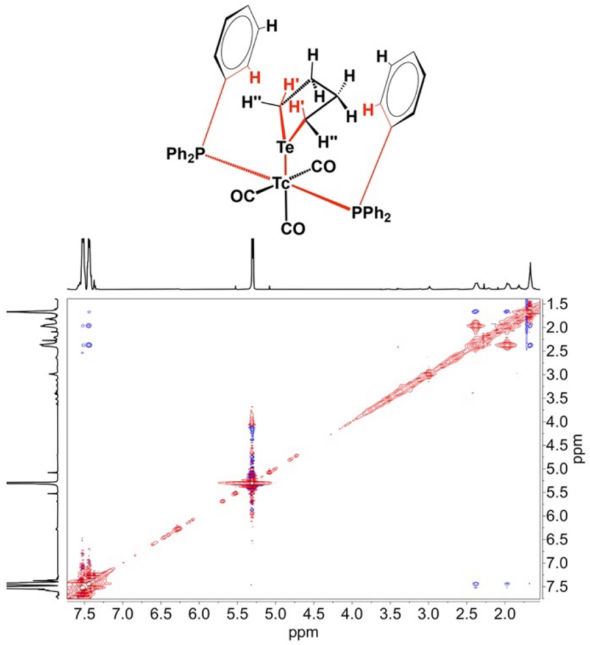

Figure 14. Phase-sensitive ^{1}H−^{1}H-NOESY spectrum of $[Tc(thte)(CO)_3(PPh_3)_2](BF_4)$ (**22**). Blue refers to negative phases, while red corresponds to positive phases.

Complexes of technetium with selenium and tellurium donor ligands are rare. There are only four structural reports on complexes containing Tc−Se−C bonds: $[Tc^{III}(SeAr)_3(PPh_3)(CH_3CN)]$,[98] $[Tc^{V}O(SeAr)_4]^-$,[98] $[Tc^{V}O(i\text{-}mns)_2]^-$, and $[Tc^{V}N(i\text{-}mns)_2]^{2-}$ (i-mns^{2-} = 1,1-dicyanoethene-2,2-diselenolate).[99,100] Additionally, there are two complexes with organotellurium ligands: $[Tc^{III}(TeAr)_3(PPh_3)(CH_3CN)]$ and $[Tc^{V}O(TeAr)_4]^-$.[98] So far, no structural data for low-valent technetium complexes or such for seleno- or telluroethers of technetium are available.

Figure 15 shows the structures of the complex cations of $[Tc(SeMe_2)(CO)_3(PPh_3)_2](BF_4)$ (**19**) and $[Tc(thse)(CO)_3(PPh_3)_2](BF_4)$ (**20**). The technetium atoms in both compounds are coordinated octahedrally. The Tc−Se bond lengths are 2.6370(5) Å and 2.6416(5) Å. This means that they are much longer than those found for the other technetium complexes with organoselenium ligands (Tc^{III}: 2.37−2.39 Å, Tc^{V}: 2.48−2.53 Å).[98−100] This is most probably due to the steric strain and the *trans*-influence of the carbonyl ligands.

https://doi.org/10.1021/acs.inorgchem.1c02599
Inorg. Chem. 2021, 60, 16734−16753

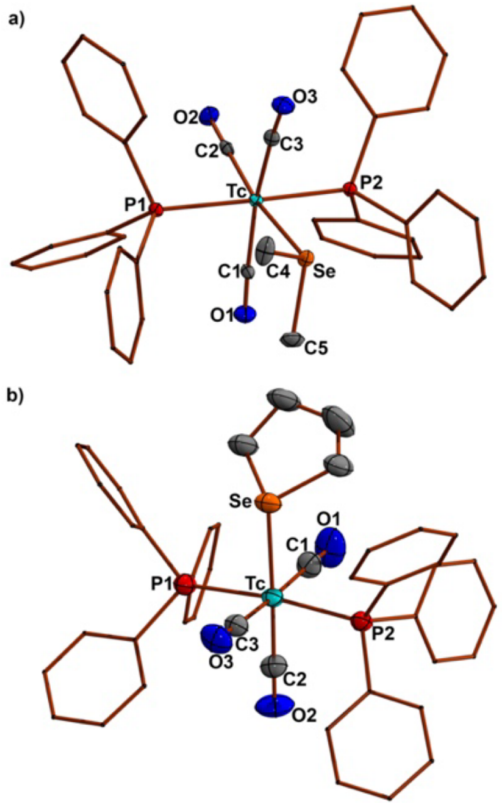

Figure 15. Structures of the complex cations of a) $[Tc(SeMe_2)(CO)_3(PPh_3)_2](BF_4)$ (**19**) (Tc–C1 1.987(6) Å, Tc–C2 1.914(4) Å, Tc–C3 1.995(6) Å, Tc–Se 2.6370(5) Å; C1–Tc–Se 89.0(2)°, C3–Tc–Se 80.0(2)°) and b) $[Tc(thse)(CO)_3(PPh_3)_2](BF_4)$ (**20**) (Tc–C1 1.976(4) Å, Tc–C2 1.918(3) Å, Tc–C3 1.992(3) Å, Tc–Se 2.6416(5) Å; C1–Tc–Se 91.6(1)°, C3–Tc–Se 84.31(9)°).

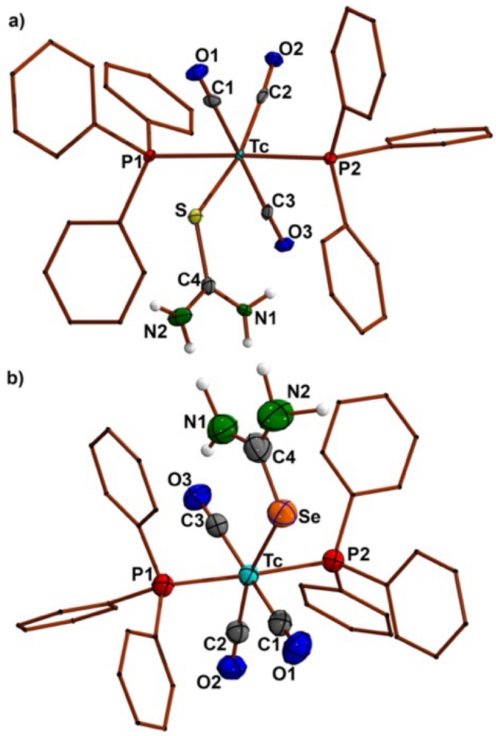

Figure 16. Structures of the complex cations of a) $[Tc(tu)(CO)_3(PPh_3)_2](BF_4)$ (**23**) (Tc–C1 2.005(5) Å, Tc–C2 1.915(5) Å, Tc–C3 1.981(5) Å, Tc–S 2.529(1) Å; C1–Tc–S 77.3(2)°, C3–Tc–Se 99.9(2)°) and b) $[Tc(seu)(CO)_3(PPh_3)_2](BF_4)$ (**24**) (Tc–C1 1.992(8) Å, Tc–C2 1.903(9) Å, Tc–C3 1.975(8) Å, Tc–Se 2.654(1) Å; C1–Tc–Se 75.7(3)°, C3–Tc–Se 102.0(3)°).

In addition to the chalcogenoethers described above, we attempted reactions of **1b** with thiourea and selenourea. Both ligands readily react with the aqua complex and give the expected products $[Tc(tu)(CO)_3(PPh_3)_2](BF_4)$ (**23**) and $[Tc(seu)(CO)_3(PPh_3)_2](BF_4)$ (**24**) in good to quantitative yields. Unfortunately the corresponding unsubstituted tellurium compound is not accessible to complete the series.

As found for the chalcogenoether complexes, the ^{99}Tc NMR resonance of the sulfur compound **23** is less downfield-shifted than that of the selenium analog **24**. Overall the ^{99}Tc nuclei in the chalcogenourea complexes are somewhat more shielded than in the corresponding chalcogenoether complexes. This may be attributed to the mesomeric chalcogenolate structure of these ligands.

Since there are only two structural reports on thiourea complexes of technetium and none on selenourea complexes,[101,102] we determined the solid-state structures of the two novel chalcogenourea complexes. They are shown in Figure 16. Both complexes have a strongly distorted octahedral coordination environment around technetium. The main distortions result from the relatively small C2–Tc–S/Se angles of 166.8(2)° for the thiourea and 164.6(2)° for the selenourea complex. These values are clearly smaller than those found in the diorganochalcogenide complexes. In contrast to the diorganochalcogenides, the chalcogenourea moieties are less bent away from the PPh_3 ligands.

There is a considerable degree of delocalized electron density inside the ligands. This is indicated by the short C4–N bond lengths of around 1.3 Å. These partial double bonds as well as the relatively long C4–S/Se distances of 1.707(6) Å and 1.814(12) Å are consistent with a partial chalcogenolate character of the two chalcogenourea ligands. The amine groups of the chalcogenourea moieties stabilize the solid-state structures by the formation of hydrogen bonds with the $(BF_4)^-$ anions. Further information is given as Supporting Information.

The selenourea complex is hydrolytically unstable in acidic solutions and readily loses elemental selenium.

CONCLUSIONS

mer-trans-$[Tc(OH_2)(CO)_3(PPh_3)_2](BF_4)$ is a bench-stable functional analogue of the unsaturated Lewis acid $[Tc(CO)_3(PPh_3)_2]^+$. It can be prepared in excellent yields and with high purity by a scalable synthesis. The compound can be used as a highly reactive synthon for the synthesis of novel complexes having the *mer-trans*-$\{Tc(CO)_3(PPh_3)_2\}^+$ and *cis–trans*-$\{Tc(CO)_2(PPh_3)_2\}^+$ cores. This has been tested by reactions with a variety of neutral ligands having different donor atoms and coordination properties.

Thermal decarbonylation, which gives the *cis–trans*-$\{Tc(CO)_2(PPh_3)_2\}^+$ core, was observed with oxygen-donor solvents such as DMSO or DMF, NH_3, and bpy ligands.

Some of the resulting complexes with carbon and nitrogen donors are robust enough to be considered for potential

https://doi.org/10.1021/acs.inorgchem.1c02599
Inorg. Chem. 2021, 60, 16734–16753

applications using the medicinally relevant nuclear isomer ^{99m}Tc.

Monodentate thioethers readily replace the aqua ligand of $[Tc(OH_2)(CO)_3(PPh_3)_2](BF_4)$. The formed products are air-stable as solids, but the thioether ligands are labile in solution and can be exchanged by better donors. This means, compounds such as $[Tc(SMe_2)(CO)_3(PPh_3)_2](BF_4)$ or $[Tc(tht)(CO)_3(PPh_3)_2](BF_4)$ may serve as synthetic alternatives for the title compound, when the protons of the aqua ligand are troublesome for the intended reactions.

EXPERIMENTAL SECTION

General Considerations. Unless otherwise stated, reagent-grade starting materials were purchased from commercial sources and either used as-received or purified by standard procedures. Solvents were dried and deoxygenated according to standard procedures. $[TcH(CO)_3(PPh_3)_2]$ was prepared as previously described.[47] Dimethylselenide,[103] dimethyltelluride,[103] tetrahydroselenophene,[104] tetrahydrotellurophene,[104] CNDArF2,[105] and $[H(OEt_2)_2](BArF_{24})$[106] were prepared according to the literature procedures.

Physical Measurements. NMR spectra were recorded at 20 °C with JEOL 400 MHz multinuclear spectrometers. The values given for the ^{99}Tc chemical shifts are referenced to pertechnetate. IR spectra were recorded with a Shimadzu FTIR 8300 spectrometer as KBr pellets. The following abbreviations were used for the intensities and characteristics of IR absorption bands: vs = very strong, s = strong, m = medium, w = weak, sh = shoulder.

Radiation Precautions. ^{99}Tc is a long-lived weak β^- emitter (E_{max} = 0.292 MeV). Normal glassware provides adequate protection against the weak beta radiation when milligram amounts are used. Secondary X-rays (bremsstrahlung) play a significant role only when larger amounts of ^{99}Tc are handled. All manipulations were done in a laboratory approved for the handling of radioactive materials.

The radioactivity of the technetium-containing samples also precluded the use of analytical techniques, which work with "open samples" such as combustion analysis or mass spectrometry.

X-ray Crystallography. The intensities for the X-ray determinations were collected on STOE IPDS II or on Bruker D8 Venture instruments with Mo Kα radiation. The space groups were determined by the detection of systematical absences. Absorption corrections were carried out by multiscan or integration methods.[107,108] Structure solution and refinement were performed with the SHELX program package.[109,110] Hydrogen atoms were derived from the final Fourier maps and refined or placed at calculated positions and treated with the "riding model" option of SHELXL. The representation of molecular structures was done using the program DIAMOND 4.2.2.[111] Some remaining crystallographic problems are commented on in the respective cif files and/or in the Supporting Information.

Additional information on the structure determinations is contained in the Supporting Information and has been deposited with the Cambridge Crystallographic Data Centre.

Syntheses. *$[Tc(OH_2)(CO)_3(PPh_3)_2](BArF_{24})$ (**1a**)·0.5CH_2Cl_2.* A flask containing $[TcH(CO)_3(PPh_3)_2]$ (71 mg, 0.1 mmol) was evacuated and subsequently flushed with Ar. The procedure of evacuation and filling with the inert gas was repeated three times. $(HOEt_2)(BArF_{24})$ (94 mg, 0.1 mmol) was added under a strong flow of argon. After three additional cycles of evacuation and Ar flushing, the solid mixture was cooled to −78 °C (dry ice/acetone). Dry, degassed CH_2Cl_2 (3 mL) was added. H_2 evolution occurred immediately, and the light yellow mixture was warmed to room temperature. After stirring at room temperature for 5 min, the mixture was layered with pentane (10 mL). The solution was stored in a refrigerator overnight, which resulted in the precipitation of colorless blocks of $[Tc(OH_2)(CO)_3(PPh_3)_2](BArF_{24})$·0.5$CH_2Cl_2$. They were filtered off, washed copiously with pentane, and dried in air. A minor second crop in the form of an analytically identical gray powder (10 mg) was obtained from the filtrate upon evaporation and addition of pentane to the residue. The obtained crystals were suitable for X-ray diffraction. Yield: 123 mg (0.077 mmol, 77%). IR (cm^{-1}): 3570 (m, ν_{O-H}), 3495 (w, ν_{O-H}), 2072 (w, $\nu_{C\equiv O}$), 1983 (vs, $\nu_{C\equiv O}$), 1933 (vs, $\nu_{C\equiv O}$). ^{1}H NMR (CD_2Cl_2, ppm): 7.70 (9H, s, *p*-Ar**H**), 7.52 (32H, s, *o*,*m*-Ar**H**), 1.51 (2H, s, $\nu_{1/2}$ = 37 Hz, Tc−O**H**$_2$). ^{19}F NMR (CD_2Cl_2, ppm): −62.8 (s, $ArCF_3$). ^{11}B NMR (CD_2Cl_2, ppm): 7.6 (s). ^{31}P NMR (CD_2Cl_2, ppm): 42 (s, $\nu_{1/2}$ = 1780 Hz). ^{99}Tc NMR (CD_2Cl_2, ppm): −1225 (s, $\nu_{1/2}$ = 5659 Hz).

*$[Tc(OH_2)(CO)_3(PPh_3)_2](BF_4)$ (**1b**).* $[TcH(CO)_3(PPh_3)_2]$ (448 mg, 0.63 mmol) was suspended in THF (2 mL). Water (8 drops) was added. A solution of HBF_4·Et_2O (1.2 g, ca. 6.8 mmol, 50−55% w/w) in diethyl ether was added dropwise. H_2 evolution was observed, and the color of the mixture changed to yellow-brown. After 5 min, diethyl ether (24 mL) was added to the yellow solution resulting in the formation of flocculent colorless microcrystals. The mixture was stored in a refrigerator for about 5 h, after which time solid, gray $[Tc(OH_2)(CO)_3(PPh_3)_2](BF_4)$ had deposited. The solid was filtered off and washed copiously with diethyl ether to remove residual HBF_4. After a final washing with pentane, the light gray microcrystals were dried in air. From the combined filtrate and washing solutions, a neglectable amount (ca. 10 mg) of additional colorless microcrystals can be isolated. Crystals suitable for X-ray diffraction were obtained by recrystallization from CH_2Cl_2/pentane, CH_2Cl_2/Et_2O, THF/pentane, and THF/Et_2O. Yield: 508 mg (0.62 mmol, 99%). IR (cm^{-1}): 3451 + 3367 (br, ν_{O-H}), 2072 (w, $\nu_{C\equiv O}$), 1983 (vs, $\nu_{C\equiv O}$), 1933 (vs, $\nu_{C\equiv O}$). ^{1}H NMR (CD_2Cl_2, ppm): 7.63−7.42 (30H, 2m, Ar**H**), 2.97 (2H, s, $\nu_{1/2}$ = 4 Hz, Tc−O**H**$_2$). ^{19}F NMR (CD_2Cl_2, ppm): −145.0 (s, $^{10}BF_4$), −145.1 (s, $^{11}BF_4$). ^{11}B NMR (CD_2Cl_2, ppm): 5.7 (s). ^{31}P NMR (CD_2Cl_2, ppm): 36 (s, $\nu_{1/2}$ = 2834 Hz). ^{99}Tc NMR (CD_2Cl_2, ppm): −1229 (s, $\nu_{1/2}$ = 5122 Hz).

*$[Tc(OH_2)(CO)_3(PPh_3)_2](OTf)$ (**1c**).* $[TcH(CO)_3(PPh_3)_2]$ (35 mg, 0.05 mmol) was suspended in THF (1 mL). Neat triflic acid (3 drops) was added, which resulted in the immediate evolution of H_2. After 5 min, water (6 mL) was added to the faint yellow solution resulting in the formation of a flocculent precipitate. The precipitate was filtered off and washed copiously with water and finally with methanol. A second crop of colorless powder (ca. 12 mg) was obtained from the combined filtrate and washing solutions. The colorless powder was dried in air. Crystals suitable for X-ray diffraction were obtained by slow evaporation of a CH_2Cl_2 mixture. A slow decomposition of the product was observed during this procedure. Yield: 40 mg (0.05 mmol, 93%). IR (cm^{-1}): 3333 + 3210 (br, ν_{O-H}), 2072 (w, $\nu_{C\equiv O}$), 1989 (vs, $\nu_{C\equiv O}$), 1924 (vs, $\nu_{C\equiv O}$), 1875 (w, $\nu_{C\equiv O}$). ^{1}H NMR (CD_2Cl_2, ppm): 7.71−7.27 (30H, 2m, Ar**H**), 1.25 (2H, s, $\nu_{1/2}$ = 17 Hz, Tc−O**H**$_2$). ^{19}F NMR (CD_2Cl_2, ppm): −77.8 (s, Tc−O_3SCF_3), −78.9 (s, O_3SCF_3). The ^{31}P NMR resonance was too broad to be observed due to a combination of fluxionality and couplings with the quadrupole moment of ^{99}Tc. ^{99}Tc NMR (CD_2Cl_2, ppm): −1245 (s, $\nu_{1/2}$ = 5043 Hz).

*$[Tc(DMSO)(CO)_3(PPh_3)_2](BF_4)$ (**2**).* DMSO (3 drops) was added to a suspension of $[Tc(OH_2)(CO)_3(PPh_3)_2](BF_4)$ (41 mg, 0.05 mmol) in CH_2Cl_2 (1.5 mL). The clear, light yellow solution was stirred for 5 min and then filtered over a small bed of $MgSO_4$ to remove the released water. The $MgSO_4$ was washed with CH_2Cl_2 (2 × 0.5 mL), and the combined filtrate and washing solutions were layered with pentane (8 mL). After storage in a refrigerator overnight, a mixture between $[Tc(DMSO)(CO)_3(PPh_3)_2](BF_4)$ and $[Tc(DMSO)_2(CO)_2(PPh_3)_2](BF_4)$ precipitated. The solid was filtered off, washed with pentane (4 × 3 mL), and dried in air. Yield: 28 mg (0.03 mmol, 64%). IR (cm^{-1}): 2060 (w, $\nu_{C\equiv O}$), 1964 (vs, $\nu_{C\equiv O}$), 1931 (vs, $\nu_{C\equiv O}$), 1844 (vs, $\nu_{C\equiv O}$). ^{1}H NMR (CD_2Cl_2, ppm): 7.63−7.37 (30H, 2m, Ar**H**), 1.83 (6H, s, S**CH**$_3$), ^{99}Tc NMR (CD_2Cl_2, ppm): −1179 (s, $\nu_{1/2}$ = 4609 Hz).

*$[Tc(DMSO)_2(CO)_2(PPh_3)_2](BF_4)$ (**3**)·toluene.* Dimethyl sulfoxide (1 drop) was added to a suspension of $[Tc(OH_2)(CO)_3(PPh_3)_2](BF_4)$ (15 mg, 0.02 mmol) in CH_2Cl_2 (0.5 mL). The clear solution was stirred for 2 min and then layered with pentane (6 mL). After storage in the refrigerator overnight, colorless needles of $[Tc(DMSO)(CO)_3(PPh_3)_2](BF_4)$ formed in an oily layer of DMSO at the bottom. The supernatant was decanted, and the crystals and the DMSO were

https://doi.org/10.1021/acs.inorgchem.1c02599
Inorg. Chem. 2021, 60, 16734−16753

dissolved in toluene and kept in air for evaporation of residual CH_2Cl_2. After 2 days, large colorless plates of $[Tc(DMSO)_2(CO)_2(PPh_3)_2](BF_4)$·toluene formed, which were filtered off, washed with toluene (2 × 0.5 mL) and pentane (3 × 3 mL), and dried in air. They were suitable for X-ray diffraction. Yield: 16 mg (0.02 mmol, 96%). IR (cm^{-1}): 2029 (w, $\nu_{C\equiv O}$), 1931 (vs, $\nu_{C\equiv O}$), 1844 (vs, $\nu_{C\equiv O}$). ^1H NMR (CD_2Cl_2, ppm): 7.66−7.40 (30H, 2m, Ar**H**), 7.31−7.04 (4H, 2m, MePh**H**), 2.34 (3H, s, PhC**H**$_3$), 1.90 (10H, s, SC**H**$_3$). ^{19}F NMR (CD_2Cl_2, ppm): −152.2 (s, shoulder, $^{10}BF_4$), −152.2 (s, $^{11}BF_4$). ^{11}B NMR (CD_2Cl_2, ppm): −1.2 (s). ^{99}Tc NMR (CD_2Cl_2, ppm): −736 (unresolved t, $\nu_{1/2}$ = 772 Hz, $^1J_{Tc-P}$ = ca. 658 Hz). The ^{31}P NMR resonance was too broad to be observed due to couplings with the quadrupole moment of ^{99}Tc.

*[Tc(DMF)(CO)$_3$(PPh$_3$)$_2$](BF$_4$) (**4**).* Dimethylformamide (1 drop) was added to a suspension of $[Tc(OH_2)(CO)_3(PPh_3)_2](BF_4)$ (15 mg, 0.02 mmol) in CH_2Cl_2 (0.5 mL). The clear solution was stirred for 2 min and then layered with pentane (6 mL). After storage in the refrigerator overnight, colorless needles of $[Tc(DMF)(CO)_3(PPh_3)_2](BF_4)$·pentane formed. They were filtered off, washed with pentane (3 × 3 mL), and dried in air. They were suitable for X-ray diffraction but quickly lost lattice solvent. Yield: 16 mg (0.02 mmol, 96%). IR (cm^{-1}): 2072 (w, $\nu_{C\equiv O}$), 1973 (vs, $\nu_{C\equiv O}$), 1908 (vs, $\nu_{C\equiv O}$), 1850 (m, $\nu_{C\equiv O}$), 1651 (vs, $\nu_{C=O}$). ^1H NMR (CD_2Cl_2, ppm): 7.57−7.38 (30H, m, Ar**H**), 6.06 (1H, s, **H**C(O)NMe$_2$), 2.37 (3H, s, NC**H**$_3$), 2.34 (3H, s, NC**H**$_3$). ^{19}F NMR (CD_2Cl_2, ppm): −152.8 (s, $^{10}BF_4$), −152.8 (s, $^{11}BF_4$). ^{11}B NMR (CD_2Cl_2, ppm): −1.1 (s). ^{31}P NMR (CD_2Cl_2, ppm): 36 (broad). ^{99}Tc NMR (CD_2Cl_2, ppm): −1245 (s, $\nu_{1/2}$ = 5002 Hz).

*[Tc(DMF)$_2$(CO)$_2$(PPh$_3$)$_2$](BF$_4$) (**5**).* $[Tc(OH_2)(CO)_3(PPh_3)_2](BF_4)$ (15 mg, 0.02 mmol) was dissolved in dimethylformamide (0.75 mL). The clear solution was heated under reflux for 10 min after which time the color had changed to yellow. The solution was filtered over a small bed of Na_2SO_4 to remove the released water. Na_2SO_4 was washed with dimethylformamide (2 × 0.25 mL). The combined filtrate and washing solutions were layered with diethyl ether (9 mL). After storage in a refrigerator overnight, colorless needles formed. The crystals were filtered off, washed with diethyl ether (3 × 3 mL) and pentane (3 × 3 mL), and dried in air. Single crystals for X-ray diffraction were obtained from CH_2Cl_2/toluene. Yield: 16 mg (0.02 mmol, 95%). IR (cm^{-1}): 1937 (vs, $\nu_{C\equiv O}$), 1844 (vs, $\nu_{C\equiv O}$), 1645 (vs, $\nu_{C=O}$). ^1H NMR (CD_2Cl_2, ppm): 7.72−7.16 (30H, m, Ar**H**), 6.53 (2H, s, **H**C(O)NMe$_2$), 2.42 (6H, s, NC**H**$_3$), 2.31 (6H, s, NC**H**$_3$). ^{19}F NMR (CD_2Cl_2, ppm): −152.9 (s, $^{10}BF_4$), −152.9 (s, $^{11}BF_4$). ^{11}B NMR (CD_2Cl_2, ppm): −1.1 (s). ^{99}Tc NMR (CD_2Cl_2, ppm): −852 (t, $\nu_{1/2}$ = 797 Hz, $^1J_{Tc-P}$ = 658 Hz). The ^{31}P NMR resonance was too broad to be observed due to couplings with the quadrupole moment of ^{99}Tc.

*[Tc(CO)$_4$(PPh$_3$)$_2$](BArF$_{24}$) (**6a**)·0.25CH$_2$Cl$_2$.* CO gas was bubbled through a solution of $[Tc(OH_2)(CO)_3(PPh_3)_2](BArF_{24})$ (41 mg, 0.026 mmol) in CH_2Cl_2 (1 mL) for 20 min. The solution was then filtered over a small bed of $MgSO_4$ to remove the released water. The $MgSO_4$ was washed with CH_2Cl_2 (0.5 mL), and the combined filtrate and washing solutions were layered with hexane (10 mL). After storage in a refrigerator for 3 h, colorless needles formed, which were filtered off. The crystals of $[Tc(CO)_4(PPh_3)_2](BArF_{24})$·0.25 CH_2Cl_2 were washed with pentane (3 × 3 mL) and dried in air. The crystals were suitable for X-ray diffraction. Yield: 40 mg (0.025 mmol, 98%). IR (cm^{-1}): 2010 (vs, $\nu_{C\equiv O}$). ^1H NMR (CD_2Cl_2, ppm): 7.74 (9H, s, *p*-Ar**H**), 7.61−7.46 (35H, 6m, *o*,*m*-Ar**H**). ^{19}F NMR (CD_2Cl_2, ppm): −62.8 (s, $ArCF_3$). ^{11}B NMR (CD_2Cl_2, ppm): 7.6 (s). ^{31}P NMR (CD_2Cl_2, ppm): 33 (s, $\nu_{1/2}$ = 4340 Hz). ^{99}Tc NMR (CD_2Cl_2, ppm): −1895 (s, $\nu_{1/2}$ = 2643 Hz).

*[Tc(CO)$_4$(PPh$_3$)$_2$](BF$_4$) (**6b**).* CO gas was bubbled through a solution of $[Tc(OH_2)(CO)_3(PPh_3)_2](BF_4)$ (81 mg, 0.1 mmol) in CH_2Cl_2 (1 mL) for 10 min. The solution was then filtered over a small bed of $MgSO_4$ to remove the released water. The $MgSO_4$ was washed with CH_2Cl_2 (0.5 mL), and the combined filtrate and washing solutions were layered with hexane (10 mL). After storage in a refrigerator overnight, colorless crystals formed. The crystals of $[Tc(CO)_4(PPh_3)_2](BF_4)$ were filtered off, washed with pentane (3 × 3 mL), and dried in air. Single crystals were obtained by layered liquid/liquid diffusion of pentane into a CH_2Cl_2 solution of the compound. Yield: 78 mg (0.1 mmol, 99%). ^{99}Tc NMR (CD_2Cl_2, ppm): −1886 (s, $\nu_{1/2}$ = 2420 Hz). The other analytical data are consistent with the previously published analyses.[48,57]

*[Tc(η^2-SSCPPh$_3$)(CO)$_3$(PPh$_3$)$_2$](BF$_4$) (**7**).* A suspension of $[Tc(OH_2)(CO)_3(PPh_3)_2](BF_4)$ (41 mg, 0.05 mmol) in THF (1 mL) was added to a solution of PPh_3 (262 mg) and CS_2 (0.5 mL) in THF (1 mL). A clear yellow solution formed immediately upon heating the mixture to reflux. The mixture quickly turned reddish purple upon heating. After 5 min, pentane (12 mL) was added, which resulted in the separation of a purple oil. After storage in the refrigerator for 3 h, the yellow solution was decanted, and the deep red oil was washed with pentane. The oily residue was extracted with acetone to give a deep purple-red solution. After evaporation of the acetone, the residue was recrystallized by liquid/liquid diffusion of Et_2O into a CH_2Cl_2 solution. The resulting purple crystals were filtered off, washed with pentane (3 × 3 mL), and dried in air. They were suitable for X-ray diffraction. Yield: 7 mg (0.04 mmol, 13%). IR (cm^{-1}): 2008 (w, $\nu_{C\equiv O}$), 1960 (vs, $\nu_{C\equiv O}$), 1890 (sh, $\nu_{C\equiv O}$), 1875 (vs, $\nu_{C\equiv O}$). ^1H NMR (CD_2Cl_2, ppm): 7.95−6.95 (45H, 6m, Ar**H**). ^{19}F NMR (CD_2Cl_2, ppm): −150.2 (s, $^{10}BF_4$), −150.2 (s, $^{11}BF_4$). ^{11}B NMR (CD_2Cl_2, ppm): −0.8 (s). ^{31}P NMR (CD_2Cl_2, ppm): 25.1 (s, $\nu_{1/2}$ = 24 Hz), 17.5 (s, $\nu_{1/2}$ = 290 Hz). ^{99}Tc NMR (CD_2Cl_2, ppm): −1077 (t, $\nu_{1/2}$ = 248 Hz, $^1J_{Tc-P}$ = 549 Hz).

*[Tc(CNCy)(CO)$_3$(PPh$_3$)$_2$](BF$_4$) (**8**).* CNCy (2 drops) was added to a suspension of $[Tc(OH_2)(CO)_3(PPh_3)_2](BF_4)$ (41 mg, 0.1 mmol) in CH_2Cl_2 (1 mL) and stirred for 5 min. The resulting clear solution was filtered over a small bed of Na_2SO_4 to remove the released water. Na_2SO_4 was washed with CH_2Cl_2 (3 × 0.5 mL), and the combined filtrate and washing solutions were layered with pentane (12 mL). After storage in a refrigerator overnight, colorless microcrystals formed. The crystals were filtered off, washed with pentane (3 × 3 mL), and dried in air. Single crystals suitable for X-ray diffraction were obtained by layered liquid/liquid diffusion of diethyl ether into a CH_2Cl_2 solution of the compound. Yield: 39 mg (0.04 mmol, 86%). IR (cm^{-1}): 2203 (m, $\nu_{C\equiv N}$), 2079 (m, $\nu_{C\equiv O}$), 1989 (vs, $\nu_{C\equiv O}$), 1977 (vs, $\nu_{C\equiv O}$). ^1H NMR (CD_2Cl_2, ppm): 7.54 (30H, s, Ar**H**), 1.60−0.88 (11H, 4s, CNC$_6$**H**$_{11}$). ^{19}F NMR (CD_2Cl_2, ppm): −154.1 (s, $^{10}BF_4$), −154.2 (s, $^{11}BF_4$). ^{11}B NMR (CD_2Cl_2, ppm): 3.2 (s). ^{31}P NMR (CD_2Cl_2, ppm): 36 (s, $\nu_{1/2}$ = 2362 Hz). ^{99}Tc NMR (CD_2Cl_2, ppm): −1884 (s, $\nu_{1/2}$ = 4600 Hz).

*[Tc(CNDArF2)(CO)$_3$(PPh$_3$)$_2$](BArF$_{24}$) (**9a**).* A suspension of CNDArF2 (13.6 mg, 0.025 mmol) in CH_2Cl_2 (0.5 mL) was added to a solution of $[Tc(OH_2)(CO)_3(PPh_3)_2](BArF_{24})$ (40 mg, 0.025 mmol) in CH_2Cl_2 (0.5 mL) and stirred for 15 min. The resulting clear solution was filtered over a small bed of $MgSO_4$ to remove the released water. The $MgSO_4$ was washed with CH_2Cl_2 (0.5 mL), and the combined filtrate and washing solutions were layered with pentane (10 mL). After storage in a refrigerator overnight, clear, colorless needles formed. The crystals were filtered off, washed with pentane (3 × 3 mL), and dried in air. $[Tc(CNDArF2)(CO)_3(PPh_3)_2](BArF_{24})$ was obtained quantitatively and solvent-free, as the clear crystals dampened quickly throughout the drying procedure as a consequence of solvent loss. Yield: Quantitative. IR (cm^{-1}): 2153 (m, $\nu_{C\equiv N}$), 2073 (m, $\nu_{C\equiv O}$), 2002 (vs, $\nu_{C\equiv O}$). ^1H NMR (CD_2Cl_2, ppm): 7.91 (2H, s, Ar**H**), 7.75 (8H, s, B-*o*-Ar**H**), 7.62−7.31 (27H, 2s+2m, 6 *o*-P-Ar**H**, 3 *p*-P-Ar**H**, ^{CNDArF}Ar**H**), 7.26−7.15 (13H, m, 6 *o*-P-Ar**H**, 3 *p*-P-Ar**H**, ^{CNDArF}Ar**H**), 6.71−6.58 (2H, m, H_2O). ^{19}F NMR (CD_2Cl_2, ppm): −62.8 (24F, s, B-*m*-$ArCF_3$), −62.9 (12F, s, CN-*m*-$ArCF_3$), −103.5 (1F, t, $^4J_{F,H}$ = 7.65 Hz, CN-*p*-F). ^{11}B NMR (CD_2Cl_2, ppm): 7.6 (s). ^{31}P NMR (CD_2Cl_2, ppm): 36 (s, $\nu_{1/2}$ = 1827 Hz). ^{99}Tc NMR (CD_2Cl_2, ppm): −1879 (s, $\nu_{1/2}$ = 6159 Hz).

*[Tc(CNDArF2)(CO)$_3$(PPh$_3$)$_2$](BF$_4$) (**9b**).* CNDArF2 (55 mg, 0.1 mmol) was added to a suspension of $[Tc(OH_2)(CO)_3(PPh_3)_2](BF_4)$ (81 mg, 0.1 mmol) in CH_2Cl_2 (2 mL) and stirred for 15 min. The resulting clear solution was filtered over a small bed of $MgSO_4$ to remove the released water. The $MgSO_4$ was washed with CH_2Cl_2 (0.5 mL), and the combined filtrate and washing solutions were layered with pentane (12 mL). After storage in a refrigerator overnight,

https://doi.org/10.1021/acs.inorgchem.1c02599
Inorg. Chem. 2021, 60, 16734−16753

colorless microcrystals formed. The crystals were filtered off, washed with pentane (3 × 3 mL), and dried in air. Yield: 118 mg (0.09 mmol, 88%). IR (cm^{-1}): 2153 (m, $\nu_{C\equiv N}$), 2079 (m, $\nu_{C\equiv O}$), 2004 (vs, $\nu_{C\equiv O}$), 1973 (vs, $\nu_{C\equiv O}$). ^1H NMR (CD_2Cl_2, ppm): 8.11−6.91 (38H, 4m, Ar**H**). ^{19}F NMR (CD_2Cl_2, ppm): −62.8 (12F, s, CN-*m*-$ArCF_3$), −103.5 (1F, t, $^4J_{F,H}$ = 7.67 Hz, CN-*p*-F), −153.1 (s, $^{10}BF_4$), −153.1 (s, $^{11}BF_4$). ^{11}B NMR (CD_2Cl_2, ppm): −1.2 (s). ^{31}P NMR (CD_2Cl_2, ppm): 37 (s, $\nu_{1/2}$ = 3115 Hz). ^{99}Tc NMR (CD_2Cl_2, ppm): −1903 (s, $\nu_{1/2}$ = 5515 Hz).

*[Tc(NH$_3$)$_2$(CO)$_2$(PPh$_3$)$_2$](BF$_4$) (**10**).* $NH_{3(aq)}$ (2 drops) was added to a suspension of $[Tc(OH_2)(CO)_3(PPh_3)_2](BF_4)$ (41 mg, 0.05 mmol) in CH_2Cl_2 (1 mL). The initial bubbling quickly ceased, and the resulting clear solution was stirred for 10 min. The excess water was removed by filtration over a small bed of Na_2SO_4. Na_2SO_4 was washed with CH_2Cl_2 (2 × 0.5 mL), and the combined filtrate and washing solutions were layered with pentane (12 mL). After evaporation of the solvents at room temperature overnight, colorless cubes formed. The crystals were suspended in pentane, filtered, washed with pentane (3 × 3 mL), and dried in air. The isolated cubes were suitable for X-ray diffraction. Yield: 40 mg (0.05 mmol, 98%). IR (cm^{-1}): 3354 (s, ν_{N-H}), 3275 (m, ν_{N-H}), 2081 (m, $\nu_{C\equiv O}$), 1983 (vs, $\nu_{C\equiv O}$), 1940 (vs, $\nu_{C\equiv O}$), 1863 (vs, $\nu_{C\equiv O}$). ^1H NMR (CD_2Cl_2, ppm): 7.77−7.33 (30H, 3m, Ar**H**), 1.36−1.19 (6H, 6s, $\nu_{1/2}$ = 9 Hz, Tc−N**H**$_3$). ^{19}F NMR (CD_2Cl_2, ppm): −149.4 (s, $^{10}BF_4$), −149.5 (s, $^{11}BF_4$). ^{11}B NMR (CD_2Cl_2, ppm): −2.3 (s). ^{31}P NMR (CD_2Cl_2, ppm): 50 (unresolved dec., $\nu_{1/2}$ = 4962 Hz, $^1J_{P-Tc}$ = ca. 500 Hz). ^{99}Tc NMR (CD_2Cl_2, ppm): −1237 (unresolved t, $\nu_{1/2}$ = 1720 Hz, $^1J_{Tc-P}$ = ca. 550 Hz).

[Tc(^{15}*NH$_3$)$_2$(CO)$_2$(PPh$_3$)$_2$](BF$_4$).* $^{15}NH_3$ was generated by a reaction of solid $^{15}NH_4Cl$ (178 mg, 3.15 mmol) with an excess of solid KOH (529 mg, 9.45 mmol) upon gentle heating and condensed into a trap cooled with liquid nitrogen. A solution of $^{15}NH_{3(aq)}$ was prepared by dissolution of the thawing $^{15}NH_3$ in water (4 drops) and used immediately. Two drops of this solution were added to a suspension of $[Tc(OH_2)(CO)_3(PPh_3)_2](BF_4)$ (83 mg, 0.1 mmol) in CH_2Cl_2 (1 mL). The initial bubbling quickly ceased, and the resulting clear solution was stirred for 30 min. The excess water was removed by filtration over a small bed of Na_2SO_4. Na_2SO_4 was washed with CH_2Cl_2 (2 × 0.5 mL). Pentane (12 mL) was added to the combined filtrate and washing solutions to precipitate the product as colorless microcrystals. The microcrystals were filtered off, washed with pentane (3 × 3 mL), and dried in air. Yield: 79 mg (0.1 mmol, 97%). IR (cm^{-1}): 3343 (s, ν_{N-H}), 3275 (m, ν_{N-H}), 3213 (m, ν_{N-H}), 2081 (m, $\nu_{C\equiv O}$), 1981 (vs, $\nu_{C\equiv O}$), 1969 (vs, $\nu_{C\equiv O}$), 1938 (vs, $\nu_{C\equiv O}$), 1921 (vs, $\nu_{C\equiv O}$), 1853 (vs, $\nu_{C\equiv O}$), 1850 (vs, $\nu_{C\equiv O}$). ^1H NMR (CD_2Cl_2, ppm): 7.77−7.33 (30H, 3m, Ar**H**), 1.20 (6H, d, $\nu_{1/2}$ = 7 Hz, $^1J_{H-15N}$ = 67 Hz, Tc−^{15}N**H**$_3$). ^{19}F NMR (CD_2Cl_2, ppm): −149.6 (s, $^{10}BF_4$), −149.7 (s, $^{11}BF_4$). ^{11}B NMR (CD_2Cl_2, ppm): −2.3 (s). ^{31}P NMR (CD_2Cl_2, ppm): 50 (unresolved dec., $\nu_{1/2}$ = 5120 Hz, $^1J_{P-Tc}$ = ca. 510 Hz). ^{99}Tc NMR (CD_2Cl_2, ppm): −1236 (unresolved t, $\nu_{1/2}$ = 1487 Hz, $^1J_{Tc-P}$ = ca. 550 Hz). ^{15}N NMR (CD_2Cl_2, ppm): −18.3 (82%, s, $\nu_{1/2}$ = 152 Hz), −29.8 (18%, s, $\nu_{1/2}$ = 51 Hz).

*[Tc(py)(CO)$_3$(PPh$_3$)$_2$](BF$_4$) (**11**).* Pyridine (2 drops) was added to a suspension of $[Tc(OH_2)(CO)_3(PPh_3)_2](BF_4)$ (45 mg, 0.05 mmol) in CH_2Cl_2 (1 mL) and stirred for 5 min. The resulting clear yellow solution was filtered over a small bed of Na_2SO_4 to remove the released water. Na_2SO_4 was washed with CH_2Cl_2 (3 × 0.5 mL), and the combined filtrate and washing solutions were layered with pentane (12 mL). After storage in a refrigerator overnight, colorless crystals formed. The crystals were filtered off, washed with pentane (3 × 3 mL), and dried in air. The obtained crystals were suitable for X-ray diffraction. Yield: 45 mg (0.05 mmol, 95%). IR (cm^{-1}): 2068 (w, $\nu_{C\equiv O}$), 1981 (vs, $\nu_{C\equiv O}$), 1921 (vs, $\nu_{C\equiv O}$), 1865 (m, $\nu_{C\equiv O}$). ^1H NMR (CD_2Cl_2, ppm): 7.75 (2H, s, py**H**), 7.68−7.12 (31H, m, Ar**H**), 6.81 (2H, s, py**H**). ^{19}F NMR (CD_2Cl_2, ppm): −153.9 (s, $^{10}BF_4$), −153.9 (s, $^{11}BF_4$). ^{11}B NMR (CD_2Cl_2, ppm): −3.1 (s). ^{31}P NMR (CD_2Cl_2, ppm): 38 (s, $\nu_{1/2}$ = 3477 Hz). ^{99}Tc NMR (CD_2Cl_2, ppm): −1328 (s, $\nu_{1/2}$ = 3219 Hz).

*[Tc(NCCH$_3$)(CO)$_3$(PPh$_3$)$_2$](BF$_4$) (**12**).* Acetonitrile (2 drops) was added to a suspension of $[Tc(OH_2)(CO)_3(PPh_3)_2](BF_4)$ (29 mg, 0.04 mmol) in CH_2Cl_2 (1 mL) and stirred for 5 min. The resulting clear yellow solution was filtered over a small bed of Na_2SO_4 to remove the released water. Na_2SO_4 was washed with CH_2Cl_2 (3 × 0.5 mL), and the combined filtrate and washing solutions were layered with pentane (12 mL). After storage in a refrigerator overnight, colorless needles formed. The crystals were filtered off, washed with pentane (3 × 3 mL), and dried in air. Yield: 25 mg (0.03 mmol, 83%). IR (cm^{-1}): 2290 (vw, $\nu_{C\equiv N}$), 2073 (w, $\nu_{C\equiv O}$), 1967 (vs, $\nu_{C\equiv O}$), 1956 (s, $\nu_{C\equiv O}$). ^1H NMR (CD_2Cl_2, ppm): 7.54 (30H, s, Ar**H**), 1.57 (3H, s, NCC**H**$_3$). ^{19}F NMR (CD_2Cl_2, ppm): −153.7 (s, $^{10}BF_4$), −153.7 (s, $^{11}BF_4$). ^{11}B NMR (CD_2Cl_2, ppm): −3.1 (s). ^{31}P NMR (CD_2Cl_2, ppm): 41 (s, $\nu_{1/2}$ = 5302 Hz). ^{99}Tc NMR (CD_2Cl_2, ppm): −1503 (s, $\nu_{1/2}$ = 2728 Hz).

*[Tc(bpy)(CO)$_2$(PPh$_3$)$_2$](BF$_4$) (**13**).* 2,2′-Bipyridine (5 mg, 0.03 mmol) was added to a suspension of $[Tc(OH_2)(CO)_3(PPh_3)_2](BF_4)$ (24 mg, 0.03 mmol) in CH_2Cl_2 (2 mL). NEt_3 (2 drops) was added, and the resulting yellow solution was heated under reflux for 10 min. Et_2O (6 mL) was added, and the heating was continued for another 10 min. After cooling to room temperature, the mixture was layered with pentane (12 mL). After storage in a refrigerator overnight, yellow needles precipitated. The microcrystalline precipitate was filtered off, washed with pentane (3 × 3 mL), and dried in air. Yield: 26 mg (0.03 mmol, 97%). IR (cm^{-1}): 2005 (vw, $\nu_{C\equiv O}$), 1948 (vs, $\nu_{C\equiv O}$), 1863 (vs, $\nu_{C\equiv O}$). ^1H NMR (CD_2Cl_2, ppm): 8.12 (2H, d, $J_{H,H}$ = 8.4 Hz, bpy**H**), 7.86−7.70 (4H, m, bpy**H**), 7.31 (6H, t, $J_{H,H}$ = 6.9 Hz, Ar**H**), 7.27−7.14 (24H, m, Ar**H**), 6.68 (2H, t, $J_{H,H}$ = 6.5 Hz, bpy**H**). ^{19}F NMR (CD_2Cl_2, ppm): −152.3 (s, $^{10}BF_4$), −152.3 (s, $^{11}BF_4$). ^{11}B NMR (CD_2Cl_2, ppm): −2.0 (s). ^{31}P NMR (CD_2Cl_2, ppm): 47 (s, $\nu_{1/2}$ = 2132 Hz). ^{99}Tc NMR (CD_2Cl_2, ppm): −1105 (s, $\nu_{1/2}$ = 2466 Hz).

*[{Tc(N,O-C$_5$H$_4$N-COO)(CO)$_2$(PPh$_3$)$_2$}$_2$H](BF$_4$) (**14**).* 2,2′-Bipyridine (21 mg, 0.1 mmol) was added to a suspension of $[Tc(OH_2)(CO)_3(PPh_3)_2](BF_4)$ (41 mg, 0.05 mmol) in CH_2Cl_2 (1 mL) and stirred for 5 min. The resulting deep purple solution was heated under reflux for 5 min. After cooling to room temperature, it was filtered over a small bed of Na_2SO_4 to remove the released water. Na_2SO_4 was washed with CH_2Cl_2 (3 × 0.5 mL), and the combined filtrate and washing solutions were layered with pentane (9 mL). After storage in a refrigerator overnight, a small amount of a colorless precipitate formed. The precipitate was filtered off. The filtrate was evaporated, and the purple residue crystallized by layered diffusion of Et_2O into an acetone solution. The formed yellow crystals were filtered off, washed with pentane (3 × 3 mL), and dried in air. The formed crystals contained quickly evaporating solvent. Crystals suitable for X-ray diffraction were obtained by slow evaporation of an acetone/Et_2O solution of the complex. Yield: 12 mg (0.01 mmol, 30%). IR (cm^{-1}): 1944 (vs, $\nu_{C\equiv O}$), 1861 (vs, $\nu_{C\equiv O}$), 1655 (w, $\nu_{C=O}$). ^1H NMR (CD_2Cl_2, ppm): 8.28 (1H, d, $J_{H,H}$ = 5.3 Hz, py**H**), 7.63 (1H, t, $J_{H,H}$ = 7.8 Hz, py**H**), 7.41−7.30 (18H, m, Ar**H**), 7.26−7.19 (12H, m, Ar**H**), 7.18−7.11 (2H, m, py**H**). ^{19}F NMR (CD_2Cl_2, ppm): −152.4 (s, $^{10}BF_4$), −152.5 (s, $^{11}BF_4$). ^{11}B NMR (CD_2Cl_2, ppm): −2.0 (s). ^{99}Tc NMR (CD_2Cl_2, ppm): −987 (s, $\nu_{1/2}$ = 4994 Hz). The ^{31}P NMR resonance was too broad to be observed due to couplings with the quadrupole moment of ^{99}Tc.

*[Tc(bpy^{COOMe2})(CO)$_2$(PPh$_3$)$_2$](BF$_4$) (**15**).* 4,4′-Dimethoxycarbonyl-2,2′-bipyridine (10 mg, 0.04 mmol) was added to a suspension of $[Tc(OH_2)(CO)_3(PPh_3)_2](BF_4)$ (31 mg, 0.04 mmol) in CH_2Cl_2 (1.5 mL). NEt_3 (1 drop) was added, and the resulting yellow solution was heated under reflux for 10 min to give a clear yellow-orange solution. After cooling to room temperature, the mixture was layered with diethyl ether (6 mL) and pentane (6 mL). After storage in a refrigerator overnight, yellow needles precipitated. The microcrystalline precipitate was filtered off, washed with pentane (3 × 3 mL), and dried in air. Crystals suitable for X-ray diffraction were obtained by slow evaporation of a CH_2Cl_2/acetone/diethyl ether solution of the compound. Yield: 38 mg (0.04 mmol, 96%). IR (cm^{-1}): 2014 (vw, $\nu_{C\equiv O}$), 1944 (vs, $\nu_{C\equiv O}$), 1873 (vs, $\nu_{C\equiv O}$), 1856 (vs, $\nu_{C\equiv O}$), 1734 (vs, $\nu_{C=O}$). ^1H NMR (CD_2Cl_2, ppm): 8.54 (2H, s, bpy**H**), 8.04 (2H, d, $J_{H,H}$ = 5.7 Hz, bpy**H**), 7.32 (6H, d, $J_{H,H}$ = 5.9 Hz, Ar**H**), 7.28−7.08 (26H, m, Ar**H**, bpy**H**), 4.04 (6H, s, bpyC(O)OC**H**$_3$). ^{19}F NMR (CD_2Cl_2, ppm): −152.6 (s, $^{10}BF_4$), −152.6 (s, $^{11}BF_4$). ^{11}B NMR

https://doi.org/10.1021/acs.inorgchem.1c02599
Inorg. Chem. 2021, 60, 16734−16753

(CD_2Cl_2, ppm): −2.1 (s). ^{31}P NMR (CD_2Cl_2, ppm): 36 (s, $\nu_{1/2}$ = 5650 Hz). ^{99}Tc NMR (CD_2Cl_2, ppm): −1082 (s, $\nu_{1/2}$ = 2694 Hz).

*[Tc(SMe$_2$)(CO)$_3$(PPh$_3$)$_2$](BF$_4$) (**16**).* SMe_2 (2 drops) was added to a suspension of $[Tc(OH_2)(CO)_3(PPh_3)_2](BF_4)$ (41 mg, 0.05 mmol) in CH_2Cl_2 (1 mL) and stirred for 5 min. The resulting clear solution was then filtered over a small bed of Na_2SO_4 to remove the released water. Na_2SO_4 was washed with CH_2Cl_2 (3 × 0.5 mL), and the combined filtrate and washing solutions were layered with pentane (12 mL). After storage in a refrigerator overnight, colorless crystals formed. The crystals were filtered off, washed with pentane (3 × 3 mL), and dried in air. The obtained, greasy shimmering crystals were suitable for X-ray diffraction. Yield: 33 mg (0.04 mmol, 77%). IR (cm^{-1}): 2070 (w, $\nu_{C\equiv O}$), 1983 (vs, $\nu_{C\equiv O}$), 1964 (s, $\nu_{C\equiv O}$). ^{1}H NMR (CD_2Cl_2, ppm): 7.53 (30H, s, Ar**H**), 1.67 (6H, s, Tc−S(C**H**$_3$)$_2$). ^{19}F NMR (CD_2Cl_2, ppm): −153.0 (s, $^{10}BF_4$), −153.1 (s, $^{11}BF_4$). ^{11}B NMR (CD_2Cl_2, ppm): −3.3 (s). ^{31}P NMR (CD_2Cl_2, ppm): 35 (s, $\nu_{1/2}$ = 2991 Hz). ^{99}Tc NMR (CD_2Cl_2, ppm): −1488 (s, $\nu_{1/2}$ = 3534 Hz). The given NMR data correspond to the pure compound after addition of excess SMe_2 (see Results and Discussion).

*[Tc(SEt$_2$)(CO)$_3$(PPh$_3$)$_2$](BF$_4$) (**17**).* SEt_2 (0.5 mL) was added to a suspension of $[Tc(OH_2)(CO)_3(PPh_3)_2](BF_4)$ (41 mg, 0.05 mmol) in CH_2Cl_2 (1 mL) and stirred for 5 min. The resulting clear solution was then filtered over a small bed of Na_2SO_4 to remove the released water. Na_2SO_4 was washed with CH_2Cl_2 (3 × 0.5 mL), and the combined filtrate and washing solutions were layered with pentane (12 mL). After storage in a refrigerator overnight, colorless crystals formed. The crystals were filtered off, washed with pentane (3 × 3 mL), and dried in air. The obtained crystals were suitable for X-ray diffraction. Yield: 40 mg (0.05 mmol, 90%). IR (cm^{-1}): 2070 (w, $\nu_{C\equiv O}$), 1981 (vs, $\nu_{C\equiv O}$), 1962 (s, $\nu_{C\equiv O}$). ^{1}H NMR (CD_2Cl_2, ppm): 7.54 (30H, s, Ar**H**), 2.09 (4H, q, $J_{H,H}$ = 7.4 Hz, Tc−S(C**H**$_2$CH$_3$)$_2$), 0.87 (6H, t, $J_{H,H}$ = 7.4 Hz, Tc−S(CH$_2$C**H**$_3$)$_2$). ^{19}F NMR (CD_2Cl_2, ppm): −152.3 (s, $^{10}BF_4$), −152.3 (s, $^{11}BF_4$). ^{11}B NMR (CD_2Cl_2, ppm): −2.2 (s). ^{31}P NMR (CD_2Cl_2, ppm): 44 (s, $\nu_{1/2}$ = 2207 Hz). ^{99}Tc NMR (CD_2Cl_2, ppm): −1466 (s, $\nu_{1/2}$ = 4148 Hz). The given NMR data correspond to the pure compound after addition of excess SEt_2 (see Results and Discussion).

*[Tc(tht)(CO)$_3$(PPh$_3$)$_2$](BF$_4$) (**18**).* Tetrahydrothiophene (2 drops) was added to a suspension of $[Tc(OH_2)(CO)_3(PPh_3)_2](BF_4)$ (41 mg, 0.05 mmol) in CH_2Cl_2 (1 mL) and stirred for 5 min. The resulting clear solution was then filtered over a small bed of Na_2SO_4 to remove the released water. Na_2SO_4 was washed with CH_2Cl_2 (3 × 0.5 mL), and the combined filtrate and washing solutions were layered with pentane (12 mL). After storage in a refrigerator for 2 days, colorless crystals formed. The crystals were filtered off, washed with pentane (3 × 3 mL), and dried in air. The obtained, greasy shimmering crystals were suitable for X-ray diffraction. Yield: 31 mg (0.04 mmol, 70%). IR (cm^{-1}): 2072 (w, $\nu_{C\equiv O}$), 1981 (vs, $\nu_{C\equiv O}$), 1964 (s, $\nu_{C\equiv O}$). ^{1}H NMR (CD_2Cl_2, ppm): 7.54 (30H, s, Ar**H**), 2.25 (4H, s, Tc−S(C**H**$_2$CH$_2$)$_2$), 1.55 (4H, s, Tc−S(CH$_2$C**H**$_2$)$_2$). ^{19}F NMR (CD_2Cl_2, ppm): −153.8 (s, $^{10}BF_4$), −153.8 (s, $^{11}BF_4$). ^{11}B NMR (CD_2Cl_2, ppm): −3.6 (s). ^{31}P NMR (CD_2Cl_2, ppm): 37 (s, $\nu_{1/2}$ = 2426 Hz). ^{99}Tc NMR (CD_2Cl_2, ppm): −1485 (s, $\nu_{1/2}$ = 4147 Hz). The given NMR data correspond to the pure compound after addition of excess tht (see Results and Discussion).

*[Tc(SeMe$_2$)(CO)$_3$(PPh$_3$)$_2$](BF$_4$) (**19**).* $SeMe_2$ (0.1 mL) was added to a suspension of $[Tc(OH_2)(CO)_3(PPh_3)_2](BF_4)$ (41 mg, 0.05 mmol) in CH_2Cl_2 (1 mL) under an Ar atmosphere and stirred for 5 min. The resulting clear solution was filtered over a small bed of Na_2SO_4 to remove the released water. Na_2SO_4 was washed with CH_2Cl_2 (3 × 0.5 mL), and the combined filtrate and washing solutions were layered with pentane (12 mL). After storage in a refrigerator overnight, colorless crystals formed. The crystals were filtered off, washed with pentane (3 × 3 mL), and dried in air. The obtained cuboid crystals were suitable for X-ray diffraction. Yield: 42 mg (0.05 mmol, 95%). IR (cm^{-1}): 2066 (w, $\nu_{C\equiv O}$), 1979 (vs, $\nu_{C\equiv O}$), 1962 (s, $\nu_{C\equiv O}$). ^{1}H NMR (CD_2Cl_2, ppm): 7.63−7.47 (30H, s, Ar**H**), 1.57 (6H, s, ^{77}Se satellites: $^2J_{H,Se}$ = 9.10 Hz, Tc−Se(C**H**$_3$)$_2$). ^{19}F NMR (CD_2Cl_2, ppm): −152.7 (s, $^{10}BF_4$), −152.7 (s, $^{11}BF_4$). ^{11}B NMR (CD_2Cl_2, ppm): −2.2 (s). ^{31}P NMR (CD_2Cl_2, ppm): 43 (s, $\nu_{1/2}$ = 2081 Hz). ^{99}Tc NMR (CD_2Cl_2, ppm): −1551 (s, $\nu_{1/2}$ = 4378 Hz).

*[Tc(thse)(CO)$_3$(PPh$_3$)$_2$](BF$_4$) (**20**).* A solution of freshly distilled tetrahydroselenophene (0.25 mL) in CH_2Cl_2 (0.5 mL) was added to a suspension of $[Tc(OH_2)(CO)_3(PPh_3)_2](BF_4)$ (41 mg, 0.05 mmol) in CH_2Cl_2 (1 mL) under an argon atmosphere and stirred for 5 min. The resulting clear solution was filtered over a small bed of Na_2SO_4 to remove the released water. Na_2SO_4 was washed with CH_2Cl_2 (3 × 0.5 mL), and the combined filtrate and washing solutions were layered with pentane (12 mL). After storage in a refrigerator overnight, colorless crystals formed. The crystals were filtered off, washed with pentane (3 × 3 mL), and dried in air. The obtained, greasy shimmering crystals were suitable for X-ray diffraction. Yield: 40 mg (0.04 mmol, 86%). IR (cm^{-1}): 2068 (w, $\nu_{C\equiv O}$), 1981 (m, $\nu_{C\equiv O}$), 1960 (s, $\nu_{C\equiv O}$), 1906 (s, $\nu_{C\equiv O}$). ^{1}H NMR (CD_2Cl_2, ppm): 7.61−7.41 (30H, s, Ar**H**), 2.18 (4H, s, Tc−Se(C**H**$_2$CH$_2$)$_2$), 1.61 (4H, s, Tc−Se(CH$_2$C**H**$_2$)$_2$). ^{19}F NMR (CD_2Cl_2, ppm): −152.7 (s, $^{10}BF_4$), −152.8 (s, $^{11}BF_4$). ^{11}B NMR (CD_2Cl_2, ppm): −2.2 (s). ^{31}P NMR (CD_2Cl_2, ppm): 39 (s, $\nu_{1/2}$ = 2142 Hz). ^{99}Tc NMR (CD_2Cl_2, ppm): −1556 (s, $\nu_{1/2}$ = 4574 Hz).

*[Tc(TeMe$_2$)(CO)$_3$(PPh$_3$)$_2$](BF$_4$) (**21**).* A solution of freshly distilled $TeMe_2$ (0.1 mL) in hexane (1 mL) was added to a suspension of $[Tc(OH_2)(CO)_3(PPh_3)_2](BF_4)$ (44 mg, 0.05 mmol) in CH_2Cl_2 (2 mL) under an argon atmosphere and stirred for 5 min. The resulting clear solution was then filtered over a small bed of Na_2SO_4 to remove the released water. Na_2SO_4 was washed with CH_2Cl_2 (3 × 0.5 mL), and the combined filtrate and washing solutions were layered with pentane (12 mL). After storage in a refrigerator overnight, colorless microcrystals formed. The flocculent needles were filtered off, washed with pentane (3 × 3 mL), and dried in air. Yield: 51 mg, quantitative. IR (cm^{-1}): 2062 (m, $\nu_{C\equiv O}$), 1970 (vs, $\nu_{C\equiv O}$), 1950 (s, $\nu_{C\equiv O}$), 1931 (s, $\nu_{C\equiv O}$). ^{1}H NMR (CD_2Cl_2, ppm): 7.61−7.43 (30H, s, Ar**H**), 1.28 (6H, s, ^{125}Te satellites: $^2J_{H,Te}$ = 18.07 Hz, Tc−Te(C**H**$_3$)$_2$). ^{19}F NMR (CD_2Cl_2, ppm): −152.4 (s, $^{10}BF_4$), −152.5 (s, $^{11}BF_4$). ^{11}B NMR (CD_2Cl_2, ppm): −2.2 (s). ^{31}P NMR (CD_2Cl_2, ppm): 46 (s, $\nu_{1/2}$ = 2075 Hz). ^{99}Tc NMR (CD_2Cl_2, ppm): −1739 (s, $\nu_{1/2}$ = 4677 Hz).

*[Tc(thte)(CO)$_3$(PPh$_3$)$_2$](BF$_4$) (**22**).* A solution of freshly distilled tetrahydrotellurophene (0.25 mL) in CH_2Cl_2 (0.5 mL) was added to a solution of $[Tc(OH_2)(CO)_3(PPh_3)_2](BF_4)$ (41 mg, 0.05 mmol) in CH_2Cl_2 (1 mL) under an argon atmosphere and stirred for 5 min. The resulting clear solution was filtered over a small bed of Na_2SO_4 to remove the released water. Na_2SO_4 was washed with CH_2Cl_2 (3 × 0.5 mL), and the combined filtrate and washing solutions were layered with diethyl ether (12 mL). After storage in a refrigerator, the formed colorless precipitate was filtered off, washed with pentane (3 × 3 mL), and dried in air. Yield: 35 mg (0.04 mmol, 72%). IR (cm^{-1}): 2064 (w, $\nu_{C\equiv O}$), 1971 (vs, $\nu_{C\equiv O}$), 1946 (s, $\nu_{C\equiv O}$). ^{1}H NMR (CD_2Cl_2, ppm): 7.65−7.24 (30H, s, Ar**H**), 2.46−2.32 (2H, s, Tc−Te(C(H)**H**$_{axial}$CH$_2$)$_2$), 2.04−1.89 (2H, s, Tc−Te(C(H)**H**$_{equatorial}$CH$_2$)$_2$), 1.74−1.62 (4H, s, Tc−Te(CH$_2$C**H**$_2$)$_2$). ^{19}F NMR (CD_2Cl_2, ppm): −153.0 (s, $^{10}BF_4$), −153.0 (s, $^{10}BF_4$). ^{11}B NMR (CD_2Cl_2, ppm): −3.4 (s). ^{31}P NMR (CD_2Cl_2, ppm): 37 (s, $\nu_{1/2}$ = 2203 Hz). ^{99}Tc NMR (CD_2Cl_2, ppm): −1750 (s, $\nu_{1/2}$ = 4531 Hz).

*[Tc(tu)(CO)$_3$(PPh$_3$)$_2$](BF$_4$) (**23**).* Thiourea (11 mg, 0.15 mmol) was added to a suspension of $[Tc(OH_2)(CO)_3(PPh_3)_2](BF_4)$ (43 mg, 0.05 mmol) in CH_2Cl_2 (1 mL) and stirred for 5 min. The resulting clear solution was filtered over a small bed of Na_2SO_4 to remove the released water. Na_2SO_4 was washed with CH_2Cl_2 (3 × 0.5 mL), and the combined filtrate and washing solutions were layered with pentane (9 mL). After storage in a refrigerator overnight, colorless crystals formed. The crystals were filtered off, washed with pentane (3 × 3 mL), and dried in air. The obtained crystals were suitable for X-ray diffraction. Yield: 46 mg, quantitative. IR (cm^{-1}): 3468 (s, ν_{N-H}), 3321 (s, ν_{N-H}), 3219 (s, ν_{N-H}), 2070 (m, $\nu_{C\equiv O}$), 1973 (vs, $\nu_{C\equiv O}$), 1944 (vs, $\nu_{C\equiv O}$), 1630 (vs, $\nu_{C=S}$). ^{1}H NMR (CD_2Cl_2, ppm): 7.89−7.17 (30H, m, Ar**H**), several broad ^{1}H NMR resonances were observed between 6.99 and 0.98 ppm. ^{19}F NMR (CD_2Cl_2, ppm): −150.0 (s, $^{10}BF_4$), −150.0 (s, $^{11}BF_4$). ^{11}B NMR (CD_2Cl_2, ppm): −2.2 (s). The ^{31}P NMR resonance was too broad to be observed due to a combination of fluxionality and couplings with the quadrupole

https://doi.org/10.1021/acs.inorgchem.1c02599
Inorg. Chem. 2021, 60, 16734−16753

moment of ^{99}Tc. ^{99}Tc NMR (CD_2Cl_2, ppm): −1544 (s, $\nu_{1/2}$ = 4237 Hz).

*[Tc(seu)(CO)$_3$(PPh$_3$)$_2$](BF$_4$) (**24**).* Selenourea (12 mg, 0.1 mmol) was added to a suspension of $[Tc(OH_2)(CO)_3(PPh_3)_2](BF_4)$ (41 mg, 0.05 mmol) in CH_2Cl_2 (1 mL) and stirred for 5 min. The resulting clear solution was filtered over a small bed of Na_2SO_4 to remove the released water. Na_2SO_4 was subsequently washed with CH_2Cl_2 (3 × 0.5 mL), and the combined filtrate and washing solutions were layered with pentane (9 mL). After storage in a refrigerator overnight, colorless crystals formed. The crystals were filtered off, washed with pentane (3 × 3 mL), and dried in air. The obtained crystals were suitable for X-ray diffraction. Yield: 35 mg (0.04 mmol, 76%). IR (cm^{-1}): 3452 (m, ν_{N-H}), 3310 (m, ν_{N-H}), 3215 (m, ν_{N-H}), 2062 (m, $\nu_{C\equiv O}$), 1967 (vs, $\nu_{C\equiv O}$), 1942 (vs, $\nu_{C\equiv O}$), 1632 (vs, $\nu_{C=Se}$). ^{1}H NMR (CD_2Cl_2, ppm): 7.71−7.29 (30H, m, Ar**H**), several broad ^{1}H NMR resonances were observed between 6.99 and 0.98 ppm. ^{19}F NMR (CD_2Cl_2, ppm): −149.8 (s, $^{10}BF_4$), −149.9 (s, $^{11}BF_4$). ^{11}B NMR (CD_2Cl_2, ppm): −2.2 (s). The ^{31}P NMR resonance was too broad to be observed due to a combination of fluxionality and couplings with the quadrupole moment of ^{99}Tc. ^{99}Tc NMR (CD_2Cl_2, ppm): −1590 (s, $\nu_{1/2}$ = 5741 Hz).

■ ASSOCIATED CONTENT

Supporting Information

The Supporting Information is available free of charge at https://pubs.acs.org/doi/10.1021/acs.inorgchem.1c02599.

Crystallographic tables, bond lengths angles, and ellipsoid plots and spectroscopic data (PDF)

Accession Codes

CCDC 2103082, 2103086−2103109, 2104393, and 2106108 contain the supplementary crystallographic data for this paper. These data can be obtained free of charge via www.ccdc.cam.ac.uk/data_request/cif, or by emailing data_request@ccdc.cam.ac.uk, or by contacting The Cambridge Crystallographic Data Centre, 12 Union Road, Cambridge CB2 1EZ, UK; fax: +44 1223 336033.

■ AUTHOR INFORMATION

Corresponding Author

Ulrich Abram − *Institute of Chemistry and Biochemistry, Freie Universität Berlin, D-14195 Berlin, Germany;* orcid.org/0000-0002-1747-7927; Email: ulrich.abram@fu-berlin.de

Author

Maximilian Roca Jungfer − *Institute of Chemistry and Biochemistry, Freie Universität Berlin, D-14195 Berlin, Germany*

Complete contact information is available at: https://pubs.acs.org/10.1021/acs.inorgchem.1c02599

Notes

The authors declare no competing financial interest.

■ ACKNOWLEDGMENTS

The experimental assistance of Laura Elsholz (FU Berlin) is gratefully acknowledged. Additionally, we are thankful for the support from the Core Facility 1249 BioSupraMol.

■ REFERENCES

(1) Jones, A. G.; Abrams, M. J.; Davison, A.; Brodack, J. W.; Toothaker, A. K.; Adelstein, S. J.; Kassis, A. I. Biological studies of a new class of technetium complexes: the hexakis(alkylisonitrile)-technetium(I) cations. *Int. J. Nucl. Med. Biol.* **1984**, *11*, 225−234.

(2) Kronauge, J. F.; Mindiola, D. J. The Value of Stable Metal-Carbon Bonds in Nuclear Medicine and the Cardiolite Story. *Organometallics* **2016**, *35*, 3432−3435.

(3) Bartholomä, M. D.; Louie, A. S.; Valliant, J. F.; Zubieta, J. Technetium and gallium derived radiopharmaceuticals: comparing and contrasting the chemistry of two important radiometals for the molecular imaging era. *Chem. Rev.* **2010**, *110*, 2903−2920.

(4) Papagiannopoulou, D. Technetium-99m radiochemistry for pharmaceutical applications. *J. Labelled Compd. Radiopharm.* **2017**, *60*, 502−520.

(5) Abram, U.; Alberto, R. Technetium and rhenium − coordination chemistry and nuclear medical applications. *J. Braz. Chem. Soc.* **2006**, *17*, 1486−1500.

(6) Kuntic, V.; Brboric, J.; Vujic, Z.; Uskokovic-Markovic, S. Radioisotopes Used as Radiotracers in vitro and in vivo Diagnostics: A Review. *Asian J. Chem.* **2016**, *28*, 235−411.

(7) Benz, M.; Braband, H.; Schmutz, P.; Halter, J.; Alberto, R. From Tc^{VII} to Tc^{I}; facile syntheses of bis-arene complexes $[^{99(m)}Tc(arene)_2]^+$ from pertechnetate. *Chem. Sci.* **2015**, *6*, 165−169.

(8) Meola, G.; Braband, H.; Jordi, S.; Fox, T.; Blacque, O.; Spingler, B.; Alberto, R. Structure and reactivities of rhenium and technetium bis-arene sandwich complexes $[M(\eta^6\text{-arene})_2]^+$. *Dalton Trans.* **2017**, *46*, 14631−14637.

(9) Meola, G.; Braband, H.; Hernández-Valdés, D.; Gotzmann, C.; Fox, T.; Spingler, B.; Alberto, R. A Mixed-Ring Sandwich Complex from Unexpected Ring Contraction in $[Re(\eta^6\text{-}C_6H_5Br)(\eta^6\text{-}C_6R_6)](PF_6)$. *Inorg. Chem.* **2017**, *56*, 6297−6301.

(10) Wald, J.; Alberto, R.; Ortner, K.; Candreia, L. Aqueous one-pot synthesis of derivatized cyclopentadienyl-tricarbonyl complexes of ^{99m}Tc with an *in situ* CO source: Application to a serotoneric receptor ligand. *Angew. Chem., Int. Ed.* **2001**, *40*, 3062−3066.

(11) Peindy N'Dongo, H. W.; Liu, Y.; Can, D.; Schmutz, P.; Spingler, B.; Alberto, R. Aqueous synthesis of $[(Cp\text{-}R)M(CO)_3]$ type complexes (Cp = cyclopentadienyl, M = Mn, ^{99m}Tc, Re) with bioactive functionalities. *J. Organomet. Chem.* **2009**, *694*, 981−987.

(12) Frei, A.; Spingler, B.; Alberto, R. Multifunctional Cyclopentadienes as a Scaffold for Combinatorial Bioorganometallics in $[(\eta^5\text{-}C_5H_2R^1R^2R^3)M(CO)_3]$ (M = Re, ^{99m}Tc) Piano-Stool Complexes. *Chem. - Eur. J.* **2018**, *24*, 10156−10164.

(13) Masi, S.; Top, S.; Boubekeur, L.; Jaouen, G.; Mundwiler, S.; Spingler, B.; Alberto, R. Direct Synthesis of Tricarbonyl-(cyclopentadienyl)rhenium and Tricarbonyl(cyclopentadienyl)technetium Units from Ferrocenyl Moieties - Preparation of 17α-Ethynylestradiol Derivatives Bearing a Tricarbonyl-(cyclopentadienyl)technetium Group. *Eur. J. Inorg. Chem.* **2004**, *2004*, 2013−2017.

(14) Alberto, R.; Schibli, R.; Abram, U.; Egli, A.; Knapp, F. F. R.; Schubiger, P. A. Potential of the "$[M(CO)_3]^{+}$" (M = Re, Tc) Moiety for the Labeling of Biomolecules. *Radiochim. Acta* **1997**, *79*, 99−150.

(15) Alberto, R.; Schibli, R.; Egli, A.; Schubiger, A. P. A Novel Organometallic Aqua Complex of Technetium for the Labeling of Biomolecules: Synthesis of $[^{99m}Tc(OH_2)_3(CO)_3]^+$ from $[^{99m}TcO_4]^-$ in Aqueous Solution and Its Reaction with a Bifunctional Ligand. *J. Am. Chem. Soc.* **1998**, *120*, 7987−7988.

(16) Alberto, R.; Schibli, R.; Waibel, R.; Abram, U.; Schubiger, A. P. Basic aqueous chemistry of $[M(OH_2)_3(CO)_3]^+$ (M = Re, Tc) directed towards radiopharmaceutical application. *Coord. Chem. Rev.* **1999**, *190−192*, 901−919.

(17) Alberto, R. The Chemistry of Technetium−Water Complexes within the Manganese Triad: Challenges and Perspectives. *Eur. J. Inorg. Chem.* **2009**, *2009*, 21−31.

(18) Grundler, P. V.; Helm, L.; Alberto, R.; Merbach, A. E. Relevance of the Ligand Exchange Rate and Mechanism of *fac*-$[(CO)_3M(H_2O)_3]^+$ (M = Mn, Tc, Re) Complexes for New Radiopharmaceuticals. *Inorg. Chem.* **2006**, *45*, 10378−10390.

(19) Duatti, A. Review on ^{99m}Tc radiopharmaceuticals with emphasis on new advancements. *Nucl. Med. Biol.* **2021**, *92*, 202−216.

(20) Li, Bo; Hildebrandt, S.; Hagenbach, A.; Abram, U. Tricarbonylrhenium(I) and -technetium(I) Complexes with Tris-

(1,2,3-triazolyl)phosphine Oxides. *Z. Anorg. Allg. Chem.* **2021**, *647*, 1070−1076.
(21) Jurisson, S.; Lindoy, L. F.; Dancey, K. P.; McPartlin, M.; Tasker, P. A.; Uppal, D. K.; Deutsch, E. New oxotechnetium(V) complexes of N,N′-ethylenebis(acetylacetone imine), N,N′-ethylenebis(salicylideneamine), and o-phenylenebis-(salicylideneamine). X-ray structures of the complexes of N,N′-ethylenebis(acetylacetone imine) and N,N′-ethylenebis-(salicylideneamine). *Inorg. Chem.* **1984**, *23*, 227−231.
(22) Baldas, J.; Boas, J. F.; Colmanet, S. F.; Mackay, M. F. Preparation and structure of bis(tetraphenylarsonium) *trans*-aquatetracyanonitridotechnetate(V) pentahydrate. ESR studies of the $[TcN(CN)_4(OH_2)]^{2-}/[TcNCl_4]^-$ System. *Inorg. Chim. Acta* **1990**, *170*, 233−239.
(23) Marchi, A.; Rossi, R.; Magon, L.; Duatti, A.; Casellato, U.; Graziani, R.; Vidal, M.; Riche, F. Technetium(V) nitrido complexes with tetra-azamacrocycles: monocationic and neutral octahedral complexes containing the $[TcN]^{2+}$ core. Crystal structure of $[TcN(L^1)H_2O]\cdot 2H_2O$ (H_2L^1= 1,4,8,11-tetra-azacyclotetradecane-5,7-dione). *J. Chem. Soc., Dalton Trans.* **1990**, 1935−1940.
(24) Baldas, J.; Colmanet, S. F.; Williams, G. A. Preparation of the technetium(VI) aquanitrido complexes $(NEt_4)[TcNX_4(OH_2)]$ (X= Cl or Br). Crystal structures of $(NEt_4)[TcNBr_4(OH_2)]$ and $Cs_2[TcNCl_5]$. *Inorg. Chim. Acta* **1991**, *179*, 189−194.
(25) Stassinopoulou, C. I.; Mastrostamatis, S.; Papadopoulos, M.; Vavouraki, H.; Terzis, A.; Hountas, A.; Chiotellis, E. Synthesis and structure of oxotechnetium(V) complexes of N,N′-ethylenebis-(acetylacetone thioimine) and N,N′-ethylenebis(benzylacetone thioimine). *Inorg. Chim. Acta* **1991**, *189*, 219−224.
(26) Bertolasi, V.; Ferretti, V.; Gilli, P.; Marchi, A.; Marvelli, L. Structure of *trans*-aquanitrido(1,4,8,11-tetraazacyclotetradecan-5-onato-N,N′,N″,N‴)technetium(V) chloride dihydrate. *Acta Crystallogr., Sect. C: Cryst. Struct. Commun.* **1991**, *C47*, 2535−2539.
(27) Baldas, J.; Boas, J. F.; Colmanet, S. F.; Rae, A. D.; Williams, G. A. Preparation and ESR studies of salts of crown ether complex cations and nitridotechnetium(VI) anions: structures of the twinned 'infinite sandwich' [Cs(18-crown-6)][$TcNCl_4$] complex and of [Rb(15-crown-5)$_2$] [$TcNCl_4(OH_2)$]. *Proc. R. Soc. London, Ser. A* **1993**, *442*, 437−461.
(28) Kani, Y.; Takayama, T.; Inomatam, S.; Sekine, T.; Kudo, H. Synthesis and Structure of Nitridotechnetium(V) Complex of Tetradentate Amine Oxime $[TcN(pnao)(H_2O)]^+$. *Chem. Lett.* **1995**, *24*, 1059−1060.
(29) Kani, Y.; Takayama, T.; Sekine, T.; Kudo, H. Crystal structures of nitridotechnetium(V) complexes of amine oximes differing in carbon chain lengths. *J. Chem. Soc., Dalton Trans.* **1999**, 209−214.
(30) Marchi, A.; Marvelli, L.; Cattabriga, M.; Rossi, R.; Neves, M.; Bertolasi, V.; Ferretti, V. Technetium(V) and rhenium(V) complexes of biguanide derivatives. Crystal structures. *J. Chem. Soc., Dalton Trans.* **1999**, 1937−1944.
(31) Kurti, L.; Papagiannopoulou, D.; Papadopoulos, M.; Pirmettis, I.; Raptopoulou, C. P.; Terzis, A.; Chiotellis, E.; Harmata, E.; Kuntz, R. R.; Pandurangi, R. S. Synthesis and Characterization of Novel ^{99g}Tc(V) and Re(V) Complexes with Water-Soluble Tetraaza Diamido Dipyridino Ligands: Single-Crystal X-ray Structural Investigations of Mono- and Dinuclear Complexes. *Inorg. Chem.* **2003**, *42*, 2960−2967.
(32) Brugnati, M.; Marchesi, E.; Marchi, A.; Marvelli, L.; Bertolasi, V.; Ferretti, V. Reactivity of $[MO]^{3+}$ (M = Tc, Re) core towards 2-mercapto-1,3-azole ligands. Formation of a new organometallic complex of Re(IV) and X-ray crystal structures. *Inorg. Chim. Acta* **2005**, *358*, 363−375.
(33) Yegen, E.; Hagenbach, A.; Abram, U. $[TcCl_4(H_2O)_2]$ and $[Cl_3(H_2O)_2TcOTc(H_2O)_2Cl_3]$ − two molecular intermediates of the hydrolysis of technetium(iv). *Chem. Commun.* **2005**, 5575−5577.
(34) Oehlke, E.; Alberto, R.; Abram, U. Synthesis, Characterization, and Structures of R_3EOTcO_3 Complexes (E = C, Si, Ge, Sn, Pb) and Related Compounds. *Inorg. Chem.* **2010**, *49*, 3525−3530.
(35) Braband, H.; Abram, U. Technetium Complexes with Triazacyclononane. *Inorg. Chem.* **2006**, *45*, 6589−6591.
(36) Hübener, R.; Abram, U.; Hiller, W. trans-Bisaquabis[1,2-bis(diphenylphosphino)ethane]technetium(I) tetraphenylborate. *Acta Crystallogr., Sect. C: Cryst. Struct. Commun.* **1994**, *C50*, 188−190.
(37) Mundwiler, S.; Kundig, M.; Ortner, K.; Alberto, R. A new [2 + 1] mixed ligand concept based on $[^{99(m)}Tc(OH_2)_3(CO)_3]^+$: a basic study. *Dalton Trans.* **2004**, 1320−1328.
(38) Alberto, R. The "Carbonyl Story" and Beyond; Experiences, Lessons and Implications. *ChemBioChem* **2020**, *21*, 2743−2749.
(39) Herrick, R. S.; Ziegler, C. J.; Cetin, A.; Franklin, B. R. Structure of the triaquatricarbonylrhenium(I) Cation and its Conjugate base. *Eur. J. Inorg. Chem.* **2007**, *2007*, 1632−1634.
(40) Sokolov, M. N.; Abramov, P. A.; Peresypkina, E. V.; Virovets, A. V.; Fedin, V. P. In situ generation of H_2Se and hydrothermal synthesis of new polynuclear rhenium carbonyl polyselenides. *Polyhedron* **2008**, *27*, 3259−3262.
(41) Alberto, R.; Egli, A.; Abram, U.; Hegetschweiler, K.; Gramlich, V.; Schubiger, P. A. Synthesis and reactivity of $[NEt_4]_2[ReBr_3(CO)_3]$. Formation and structural characterization of the clusters $[NEt_4]$-$[Re_3(\mu^3\text{-}OH)(\mu\text{-}OH)_3(CO)_9]$ and $[NEt_4][Re_2(\mu\text{-}OH)_3(CO)_6]$ by alkaline titration. *J. Chem. Soc., Dalton Trans.* **1994**, 2815−2820.
(42) Alberto, R.; Schibli, R.; Egli, A.; Schubiger, P. A.; Herrmann, W. A.; Artus, G.; Abram, U.; Kaden, T. A. Metal carbonyl syntheses XXII. Low pressure carbonylation of $[MOCl_4]^-$ and $[MO_4]^-$: the technetium(I) and rhenium(I) complexes $[NEt_4]_2[MCl_3(CO)_3]$. *J. Organomet. Chem.* **1995**, *493*, 119−127.
(43) Herrick, R. S.; Brunker, T. J.; Maus, C.; Crandall, K.; Cetin, A.; Ziegler, C. J. Aqueous preparation and physiological stability studies of $Re(CO)_3$(tripodal) compounds. *Chem. Commun.* **2006**, 4330−4331.
(44) Grundler, P. V.; Salignac, B.; Cayemittes, S.; Alberto, R.; Merbach, A. E. Mechanistic Changeover for the Water Substitution on fac-$[(CO)_3Re(H_2O)_3]^+$ Revealed by High-Pressure NMR. *Inorg. Chem.* **2004**, *43*, 865−873.
(45) Salignac, B.; Grundler, P. V.; Cayemittes, S.; Frey, U.; Scopelliti, R.; Merbach; Hedinger, R.; Hegetschweiler, K.; Alberto, R.; Prinz, U.; Raabe, G.; Koelle, U.; Hall, S. Reactivity of the Organometallic *fac*-$[(CO)_3Re(H_2O)_3]^+$ Aquaion. Kinetic and Thermodynamic Properties of H_2O Substitution. *Inorg. Chem.* **2003**, *42*, 3516−3526.
(46) Alberto, R.; Schibli, R.; Waibel, R.; Abram, U.; Schubiger, A. P. Basic aqueous chemistry of $[M(OH_2)_3(CO)_3]^+$ (M=Re, Tc) directed towards radiopharmaceutical application. *Coord. Chem. Rev.* **1999**, *190−192*, 901−919.
(47) Roca Jungfer, M.; Elsholz, L.; Abram, U. Technetium Hydrides Revisited: Syntheses, Structures and Reactions of $[TcH_3(PPh_3)_4]$ and $[TcH(CO)_3(PPh_3)_2]$. *Organometallics* **2021**, *40*, 3095.
(48) Cook, J. Synthesis and Reactivity of Technetium Hydrides. Doctoral thesis, Massachusetts Institute of Technology, 1995.
(49) Heinekey, D. M.; Radzewich, C. E.; Voges, M. H.; Schomber, B. M. Cationic Hydrogen Complexes of Rhenium. 2. Synthesis, Reactivity, and Competition Studies. *J. Am. Chem. Soc.* **1997**, *119*, 4172−4181.
(50) Sarazin, Y.; Wright, J. A.; Bochmann, M. Synthesis and crystal structure of $[C_6H_5Hg(H_2NSiMe_3)][H_2N\{B(C_6F_5)_3\}_2]$, a phenyl−mercury(II) cation stabilised by a non-coordinating counter-anion. *J. Organomet. Chem.* **2006**, *691*, 5680−5687.
(51) Beck, W.; Sünkel, K. Metal Complexes of Weakly Coordinating Anions. Precursors of Strong Cationic Organometallic Lewis Acids. *Chem. Rev.* **1988**, *88*, 1405−1421.
(52) Cook, J.; Davison, A.; Davis, W. M.; Jones, A. G. Insertion Chemistry of $HTc(CO)_3(PPh_3)_2$. *Organometallics* **1995**, *14*, 650−655.
(53) Alberto, R.; Herrmann, W. A.; Kiprof, P.; Baumgärtner, F. Multiple Bonds between Main Group Elements and Transition Metals. 95. Synthesis and Reactivity of $[TcCl(CO)_3[P(C_6H_5)_3]_2$: Novel Technetium Complexes of 1,4,7-Triazacyclononane and Hydridotris(pyrazolyl)borate. *Inorg. Chem.* **1992**, *31*, 895−899.

https://doi.org/10.1021/acs.inorgchem.1c02599
Inorg. Chem. 2021, 60, 16734−16753

(54) Hieber, W.; Lux, F.; Herget, C. Über Kohlenoxidverbindungen des Technetiums. *Z. Naturforsch., B: J. Chem. Sci.* **1965**, *20*, 1159−1165.
(55) Hagenbach, A.; Yegen, E.; Abram, U. Technetium Tetrachloride as A Precursor for Small Technetium(IV) Complexes. *Inorg. Chem.* **2006**, *45*, 7331−7338.
(56) Rochon, F. D.; Melanson, R.; Kong, P.-C. Reaction products of ammonium pertechnetate(VII) with triphenylphosphine and crystal structures of mer-$Tc(PPh_3)_2Cl_3(DMF)\bullet 2PPh_3$ and $NH_2(CH_3)_2^+$DMAH$^+$ $[TcCl_6]^{2-}\bullet PPh_3O$. *Can. J. Chem.* **1991**, *69*, 397−403.
(57) Cook, J.; Davison, A. Nucleophilic attack on coordinated CO in $[Tc(CO)_4(PPh_3)_2]BF_4$. *J. Organomet. Chem.* **1996**, *507*, 47−51.
(58) Galindo, A.; Miguel, D.; Perez, J. Phosphine-carbon disulfide adducts, S_2CPR_3: versatile ligands in coordination chemistry. *Coord. Chem. Rev.* **1999**, *193*−*195*, 643−690.
(59) Ghiassi, K. B.; Walters, D. T.; Aristov, M. M.; Loewen, N. D.; Berben, L. A.; Rivera, M.; Olmstead, M. M.; Balch, A. L. Formation of a Stable Complex, $RuCl_2(S_2CPPh_3)(PPh_3)_2$, Containing an Unstable Zwitterion from the Reaction of $RuCl_2(PPh_3)_3$ with Carbon Disulfide. *Inorg. Chem.* **2015**, *54*, 4565−4573.
(60) Boniface, S. M.; Clark, G. R. The Crystal and molecular structure of triphenylphosphoniodithiocarboxylato-SS′-carbonylbis-(triphenylphosphine)iridium(I) tetrafluoroborate. $[Ir(S_2CPPh_3)(CO)(PPh_3)_2]BF_4$. *J. Organomet. Chem.* **1980**, *188*, 263−275.
(61) Lo, Y.-H.; Fong, Y.-H.; Tong, H.-C.; Liang, Y.-R.; Kuo, T.-S.; Huang, C.-C. Synthesis and characterization of O-methyldithiocarbonate and triphenylphosphoniodithiocarboxylate complexes containing a tris(pyrazolyl)borato (Tp) ligand. *Inorg. Chem. Commun.* **2010**, *13*, 331−333.
(62) Leung, W.-H.; Chan, E. Y. Y.; Lam, T. C. H.; Williams, I. D. Ruthenium thiocarbonyl and phosphoniodithiocarboxylate complexes with an oxygen tripod ligand. *J. Organomet. Chem.* **2000**, *608*, 139−145.
(63) Abram, U.; Lorenz, B.; Kaden, L.; Scheller, D. Nitrido Complexes of Technetium with Phosphines and Arsines. *Polyhedron* **1988**, *7*, 285−289.
(64) Grunwald, A. C.; Scholtysik, C.; Hagenbach, A.; Abram, U. One Ligand, One Metal, Seven Oxidation States − Stable Technetium Complexes with the "Kläui Ligand. *Inorg. Chem.* **2020**, *59*, 9396−9405.
(65) Wendlandt, D.; Bauche, J.; Luc, P. Hyperfine Structure in Tc I: experiment and theory. *J. Phys. B: At. Mol. Phys.* **1977**, *10*, 1989−2002.
(66) Mikhalev, V. A. ^{99}Tc NMR Spectroscopy. *Radiochemistry* **2005**, *47*, 319−333.
(67) Lorenz, B.; Findeisen, M.; Schmidt, K. Synthese, Charakterisierung und Tc-99-NMR-Spektren von Technetium-Carbonyl-Komplexen mit Dithioliganden. *Isotopenpraxis* **1991**, *27*, 266−267.
(68) Sattelberger, A. P; Scott, B. L.; Poineau, F. Technetium Organometallics. In *Comprehensive Organometallic Chemistry III*; Mingos, D. M. P., Crabtree, R. H., Eds.; Elsevier: 2007; pp 833−854 and references cited therein, DOI: 10.1016/B0-08-045047-4/00077-7.
(69) Miroslavov, A. E.; Lumpov, A. A.; Sidorenko, G. V.; Levitskaya, E. M.; Gorshkov, N. I.; Suglobov, D. N.; Alberto, R.; Braband, H.; Gurzhiy, V. V.; Krivovichev, S. V.; Tananaev, I. G. Complexes of technetium(I) (^{99}Tc, ^{99m}Tc) pentacarbonyl core with π-acceptor ligands (tert-butyl isocyanide and triphenylphosphine): Crystal structures of $[Tc(CO)_5(PPh_3)]$OTf and $[Tc(CO)_5(CNC(CH_3)_3)]ClO_4$. *J. Organomet. Chem.* **2008**, *693*, 4−10.
(70) Miroslavov, A. E.; Polotskii, Y. S.; Gurzhiy, V. V.; Ivanov, A. Y.; Lumpov, A. A.; Tyupina, M. Y.; Sidorenko, G. V.; Tolstoy, P. M.; Maltsev, D. A.; Suglobov, D. N. Technetium and Rhenium Pentacarbonyl Complexes with C2 and C11 ω-Isocyanocarboxylic Acid Esters. *Inorg. Chem.* **2014**, *53*, 7861−7869.
(71) *Cambridge Structural Database*, Release 5.42; Update May 2021.
(72) Eakins, J. D.; Humphreys, D. G.; Mellish, C. E. New Compounds in which Technetium has a Low Valency. *J. Chem. Soc.* **1963**, 6012−6016.
(73) Armstrong, R.; Taube, H. Chemistry of trans-Aquonitrosyltetraamminetechnetium(I) and Related Studies. *Inorg. Chem.* **1976**, *15*, 1904−1909.
(74) Heitzmann, M. W.; Yang, G. C.; Ford, L. A.; Benson, W. R. Electron spin resonance spectroscopy studies of 99Tc in aqueous solutions. *J. Labelled Compd. Radiopharm.* **1981**, *18*, 535−543.
(75) Lu, J.; Clarke, M. J. Modulation of Tc-NX (X = O or S) bonds by π-Acceptor Ligands. *J. Chem. Soc., Dalton Trans.* **1992**, 1243−1248.
(76) Balasekaran, S. M.; Spandl, J.; Hagenbach, A.; Köhler, K.; Drees, M.; Abram, U. Fluoridonitrosyl Complexes of Technetium(I) and Technetium(II). Synthesis, Characterization, Reactions, and DFT Calculations. *Inorg. Chem.* **2014**, *53*, 5117−5128.
(77) Lindner, E.; Bouachir, F.; Weishaupt, M.; Hoehne, S.; Schilling, B. Das Verhalten von Mono- und Diorganylphosphansulfiden gegenüber Metallcarbonylsystemen. XX. Darstellung, Eigenschaften und Kristallstruktur von Ammin(tetracarbonyl) (dimethylthiophosphinito) rhenium. *Z. Anorg. Allg. Chem.* **1979**, *456*, 163−168.
(78) Li, J.; Miguel, D.; Morales, M. D.; Riera, V. Carbon−Sulfur Bond Cleavage of S_2CPR_3 Ligands in Dinuclear Complexes Promoted by Reduction and Protonation. *Organometallics* **1998**, *17*, 3448−3453.
(79) Pomp, C.; Wieghardt, K.; Nuber, B.; Weiss, J. Synthesis and reactivity of $[LRe(NO)(CO)(NCO)]^+$ (L = 1,4,7-triazacyclononane). Kinetics and mechanisms of its formation and transformation of $[LRe(NO)(CO)X]^{n+}$ (X = NH_3, Cl^-, HCO_2^-, $CF_3SO_3^-$) and other species. Crystal structure of $[LRe(NO)(CO)(NH_3)]Br_2$. *Inorg. Chem.* **1988**, *27*, 3789−3796.
(80) Herrick, R. S.; Ziegler, C. J.; Sripothongnak, S.; Barone, N.; Cupelo, R.; Gambella, A. Preparation and characterization of rhenium (I) tricarbonyl dithiocarbamate compounds; $Re(CO)_3(S_2CNMe_2)(L)$. *J. Organomet. Chem.* **2009**, *694*, 3929−3934.
(81) Alvarez, M. A.; Garcia, M. E.; Garcia-Vivo, D.; Iglesias, E. H.; Ruiz, M. Synthesis of the Unsaturated $[MMoCp(\mu\text{-}PR_2)(CO)_5]^-$ Anions (M = Mn, R = Ph; M = Re, R = Cy): Versatile Precursors of Heterometallic Complexes. *Eur. J. Inorg. Chem.* **2017**, *2017*, 1280−1283.
(82) Franklin, B. R.; Herrick, R. S.; Ziegler, C. J.; Cetin, A.; Barone, N.; Condon, L. R Reactions of the $Re(CO)_3(H_2O)_3^+$ Synthon with Monodentate Ligands under Aqueous Conditions. *Inorg. Chem.* **2008**, *47*, 5902−5909.
(83) Meiere, S. H.; Brooks, B. C.; Gunnoe, T. B.; Carrig, E. H.; Sabat, M.; Harman, W. D. Dihapto Coordination of Aromatic Molecules by the Asymmetric π-Bases {TpRe(CO)(L)} (Tp = hydridotris(pyrazolyl)borate; L = ^{t}BuNC, PMe_3, pyridine, 1-methylimidazole, or NH_3). *Organometallics* **2001**, *20*, 3661−3671.
(84) Zobi, F.; Spingler, B.; Alberto, R. Guanine and Plasmid DNA binding of Mono- and Trinuclear fac-[Re(CO)3]+ Complexes with Amino Acid Ligands. *ChemBioChem* **2005**, *6*, 1397−1405.
(85) Marek, R.; Lyčka, A. ^{15}N NMR Spectroscopy in Structural Analysis. *Curr. Org. Chem.* **2002**, *6*, 35−66.
(86) Martin, G. J.; Martin, M. L.; Gouesnard, J. P. $^nJ^{15}N \sim X$ Coupling Constants. In *^{15}N-NMR Spectroscopy. NMR Basic Principles and Progress*; Springer: Berlin, Heidelberg, 1981; Vol. *18*, DOI: 10.1007/978-3-642-50172-2_7.
(87) Burrows, A. D.; Mingos, D. M. P.; Lawrence, S. E.; White, A. J. P.; Williams, D. J. Platinum(II) phosphine complexes of dicarboxylates and ammonia: crystal structures of $[\{Pt(PPh_3)_2\}_2\{\mu\text{-}1,3\text{-}(O_2C)_2C_6H_4\}_2]$, $[\{Pt(PPh_3)_2(NH_3)\}_2\{\mu\text{-}1,4\text{-}(O_2C)_2C_6H_4\}][PF_6]_2$ and *cis*-$[Pt(PPh_3)_2(NH_3)_2][NO_3]_2$. *J. Chem. Soc., Dalton Trans.* **1997**, 1295−1300.
(88) Ginsberg, A. P. Transition Metal-Hydrogen Compounds. III. Dipotassium Enneahydridotechnate(VII). *Inorg. Chem.* **1964**, *3*, 567−569.
(89) Shaikh, N.; Panja, A.; Banerjee, P.; Kubiak, M.; Ciunik, Z.; Puchalska, M.; Legendziewicz; Vojtisek, P. Pyridine-2,6-dicarboxylate and perchlorate bridged hydrogen bonded 1D chains involving

https://doi.org/10.1021/acs.inorgchem.1c02599
Inorg. Chem. 2021, 60, 16734−16753

manganese(III)-cyclam moiety: synthesis, X-ray crystal structures and magnetic study. *Inorg. Chim. Acta* **2004**, *357*, 25−32.
(90) Impert, O.; Katafias, A.; Wrzeszcz, G.; Muziol, T.; Hryniewicz, K.; Olejnik; Chrzanowska, M.; van Eldik, R. Synthesis and detailed characterization of cis-dichloridobispicolinatoruthenate(III) as solid and in solution. *J. Coord. Chem.* **2016**, *69*, 2107−2120.
(91) Zhu, X.; Liu, Y.; Liu, C.; Yang, H.; Fu, H. Light and oxygen-enabled sodium trifluoromethanesulfinate-mediated selective oxidation of C−H bonds. *Green Chem.* **2020**, *22*, 4357−4363.
(92) Constable, E. C.; Housecroft, C. E.; Kariuki, B. M.; Mahmood, A. Where Did All the bpy Go? − Synthesis, Crystal and Molecular Structure of 4-Nitropicolinic Acid Monohydrate. *Supramol. Chem.* **2006**, *18*, 299−303.
(93) Barbazán, P.; Hagenbach, A.; Oehlke, E.; Abram, U.; Carballo, R.; Rodríguez-Hermida, S.; Vázquez-López, E. Tricarbonyl Rhenium-(I) and Technetium(I) Complexes with Hydrazones Derived from 4,5-Diazafluoren-9-one and 1,10-Phenanthroline-5,6-dione. *Eur. J. Inorg. Chem.* **2010**, *2010*, 4622−4630.
(94) Kurz, P.; Probst, B.; Spingler, B.; Alberto, R. Ligand Variations in [ReX(diimine)$(CO)_3$] Complexes: Effects on Photocatalytic CO_2 Reduction. *Eur. J. Inorg. Chem.* **2006**, *2006*, 2966−2974.
(95) O'Connell, L. A.; Dewan, J.; Jones, A. G.; Davison, A. Technetium(I) Isocyanide Complexes with Bidentate Aromatic Amine Ligands: Structural Characterization of [Tc$(CNtBu)_4$(bpy)]-PF_6, a Complex with "Tc(III) Character. *Inorg. Chem.* **1990**, *29*, 3539−3547.
(96) Hagenbach, A.; Abram, U. Tetrahydrothiophene complexes of technetium(IV). *Inorg. Chem. Commun.* **2004**, *7*, 1142−1144.
(97) Tisato, F.; Refosco, F.; Porchia, M.; Bolzati, C.; Bandoli, G.; Dolmella, A.; Duatti, A.; Boschi, A.; Jung, C. M.; Pietzsch, H.-J.; Kraus, W. The Crucial Role of the Diphosphine Heteroatom X in the Stereochemistry and Stabilization of the Substitution-Inert [M(N)-(PXP)]$^{2+}$ Metal Fragments (M = Tc, Re; PXP = Diphosphine Ligand). *Inorg. Chem.* **2004**, *43*, 8617−8625.
(98) Noschang Cabral, B.; Kirsten, L.; Hagenbach, A.; Piquini, P. C.; Patzschke, M.; Schulz Lang, E.; Abram, U. Technetium complexes with arylselenolato and aryltellurolato ligands. *Dalton Trans.* **2017**, *46*, 9280−9286.
(99) Bandoli, G.; Mazzi, U.; Abram, U.; Spies, H.; Münze, R. Synthesis and X-ray crystal structure of tetraethylammonium bis(1,1-dicyanoethene-2,2-diselenolato)oxotechnetate(V), [Et_4N][TcO-(Se_2C=C$(CN)_2)_2$]. *Polyhedron* **1987**, *6*, 1547−1550.
(100) Abram, U.; Abram, S.; Stach, J.; Dietzsch, W.; Hiller, W. Technetium Complexes with 1,1-Dicyanoethene-2,2-diselenolate,i-mns^{2-}. The Crystal Structure of $(Bu_4N)_2$[TcN(i-mns$)_2$]. *Z. Naturforsch., B: J. Chem. Sci.* **1991**, *B46*, 1183−1187.
(101) Baldas, J.; Colmanet, S. F.; Ivanov, Z.; William, G. A. Preparation and Structure of [{Tc^VN(thiourea)$\}_4$(edta)$_2$]•6H_2O: the First Example of a Cyclic Nitrido-bridged Tetrameric Technetium Complex. *J. Chem. Soc., Chem. Commun.* **1994**, *18*, 2153−2154.
(102) Abrams, M. J.; Davison, A.; Faggiani, R.; Jones, A. G.; Lock, C. J. L. Chemistry and Structure of Hexakis(thiourea-*S*)technetium(III) Trichloride Tetrahydrate, [Tc$(SC(NH_2)_2)_6]Cl_3$•4H_2O. *Inorg. Chem.* **1984**, *23*, 3284−3288.
(103) Kuhn, N.; Faupel, P.; Zauder, E. Ein einfaches Verfahren zur Synthese von [EMe_3]I und EMe_2 (E = Se, Te). *J. Organomet. Chem.* **1986**, *302*, C4−C6.
(104) Levanova, E. P.; Grabel'nykh, V. A.; Elaev, A. V.; Russavskaya, N. V.; Klyba, L. V.; Albanov, A. I.; Korchevin, N. A. Novel Route to the Synthesis of Chalcogenolanes, and 1,2-Dichalcogenaepanes. *Chem. Heterocycl. Compd. (N. Y., NY, U. S.)* **2012**, *47*, 1345−1352.
(105) Ditri, T. B.; Carpenter, A. E.; Ripatti, D. S.; Moore, C. E.; Rheingold, A. L.; Figueroa, J. S. Chloro- and Trifluoromethyl-Substituted Flanking-Ring m-Terphenyl Isocyanides: H6-Arene Binding to Zero-Valent Molybdenum Centers and Comparison to Alkyl-Substituted Derivatives. *Inorg. Chem.* **2013**, *52*, 13216−13229.
(106) Brookhart, M.; Grant, B.; Volpe, A. F., Jr. [(3,5-$(CF_3)_2C_6H_3)_4$B]$^-$[$H(OEt_2)_2]^+$: A Convenient Reagent for Generation and Stabilization of Cationic, Highly Electrophilic Organometallic Complexes. *Organometallics* **1992**, *11*, 3920−3922.
(107) Sheldrick, G. M. *SADABS*; University of Göttingen: Germany, 1996.
(108) Coppens, P. *The Evaluation of Absorption and Extinction in Single-Crystal Structure Analysis*; Crystallographic Computing: Copenhagen, Muksgaard, 1979.
(109) Sheldrick, G. M. A short history of SHELX. *Acta Crystallogr., Sect. A: Found. Crystallogr.* **2008**, *A64*, 112−122.
(110) Sheldrick, G. M. Crystal structure refinement with SHELXL. *Acta Crystallogr., Sect. C: Struct. Chem.* **2015**, *C71*, 3−8.
(111) *Diamond - Crystal and Molecular Structure Visualization*; Crystal Impact - Dr. H. Putz & Dr. K. Brandenburg GbR: Bonn, Germany.

https://doi.org/10.1021/acs.inorgchem.1c02599
Inorg. Chem. 2021, 60, 16734−16753

4.3 Technetium(I) Carbonyl Chemistry With Small Inorganic Ligands

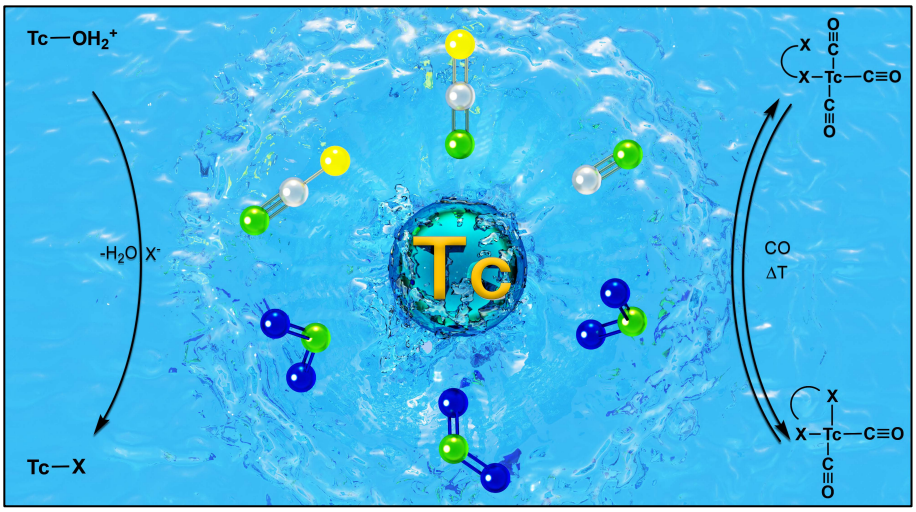

Reproduced with permission from Roca Jungfer, M.; Elsholz, L.; Abram, U. *Inorg. Chem.* **2022**, *61*, 2980-2997.

DOI: 10.1021/acs.inorgchem.1c03919

For Supplementary Material see A.3.

Author Contributions:

Maximilian Roca Jungfer and Ulrich Abram designed the project. Maximilian Roca Jungfer performed the synthesis and characterization of the compounds, performed DFT calculations, calculated the X-ray structures and wrote a draft of the manuscript. Laura Elsholz performed some of the experiments and DFT calculations during a research internship under the supervision of Maximilian Roca Jungfer. Ulrich Abram supervised the project, provided scientific guidance and suggestions, and corrected the manuscript.

Inorganic Chemistry

pubs.acs.org/IC Article

Technetium(I) Carbonyl Chemistry with Small Inorganic Ligands

Maximilian Roca Jungfer, Laura Elsholz, and Ulrich Abram*

Cite This: *Inorg. Chem.* 2022, 61, 2980–2997 Read Online

ACCESS | Metrics & More | Article Recommendations | Supporting Information

ABSTRACT: $[Tc(OH_2)(CO)_3(PPh_3)_2](BF_4)$ has been used as a synthon for reactions with small inorganic ligands with relevance for the treatment of nuclear waste solutions such as nitrate, nitrite, pseudohalides, permetalates (M = Mn, Tc, Re), and BH_4^-. The formation of bond isomers and/or a distinct reactivity has been observed for most of the products. $[Tc(NCO)(CO)_3(PPh_3)_2]$, $[Tc(NCS)(CO)_3(PPh_3)_2]$, $[Tc(CN)(CO)_3(PPh_3)_2]$, $[Tc(N_3)(CO)_3(PPh_3)_2]$, $[Tc(NCO)(OH_2)(CO)_2(PPh_3)_2]$, $[Tc(\eta^2\text{-}OON)(CO)_2(PPh_3)_2]$, $[Tc(\eta^1\text{-}NO_2)(CO)_3(PPh_3)_2]$, $[Tc(\eta^2\text{-}OONO)(CO)_2(PPh_3)_2]$, $[Tc(\eta^1\text{-}ONO_2)(CO)_3(PPh_3)_2]$, $[Tc(\eta^2\text{-}OO(CCH_3))(CO)_2(PPh_3)_2]$, $[Tc(\eta^2\text{-}SSC(SCH_3))(CO)_2(PPh_3)_2]$, $[Tc(\eta^2\text{-}SSC(OCH_3))(CO)_2(PPh_3)_2]$, $[Tc(\eta^2\text{-}SSC(CH_3))(CO)_2(PPh_3)_2]$, $[Tc(\eta^2\text{-}SS(CH))(CO)_2(PPh_3)_2]$, $[Tc(OTcO_3)(acetone)(CO)_2(PPh_3)_2]$, $[Tc(OTcO_3)(CO)_3(PPh_3)_2]$, and $[Tc(\eta^2\text{-}HHBH_2)(CO)_2(PPh_3)_2]$ have been isolated in crystalline form and studied by X-ray crystallography. Additionally, the typical reactivity patterns (isomerization, thermal decomposition, hydrolysis, or decarbonylation) of the products have been studied by spectroscopic methods. ^{99}Tc NMR spectroscopy has proved to be a particularly useful tool for the evaluation of such reactions of the diamagnetic technetium(I) compounds in solution.

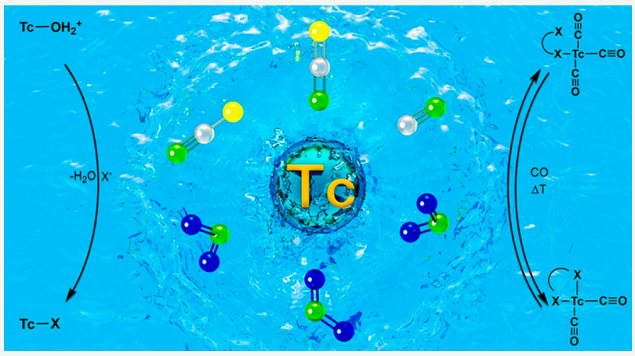

INTRODUCTION

Detailed knowledge about the coordination chemistry of technetium with small inorganic ligands is imperative to assess the possible speciation of technetium in the environment and at problematic nuclear waste sites such as the Hanford wastewater tanks. Particularly, interactions with small nitrogen-containing ligands such as nitrite, nitrate, or azide may contribute to the omnipresent potential explosion hazard formed by transition-metal complexes in conjunction with the high level of radioactivity present in these containers.[1−5] The existence of low-valent organotechnetium compounds such as carbonyls in nuclear waste solutions has been proven, and thus, an assessment of hitherto unknown complexes of technetium carbonyl complexes with small inorganic ligands also becomes important.

Although an isocyanide compound of technetium(I), the highly inert d^6 hexakis(isonitrile) complex ^{99m}Tc-Sestamibi (Chart 1), has been the workhorse for nuclear medical myocardial imaging for decades,[6−12] the organometallic chemistry of this element can still be regarded as relatively little explored.[13] The development of a normal-pressure synthesis for *fac*-$[Tc(CO)_3(OH_2)_3]^+$ and related compounds opened the door for a detailed exploration of the chemistry of such complexes.[14−20] Thus, reasonable numbers of *fac*-tricarbonyltechnetium(I) complexes have been prepared with the long-lived β^- emitter ^{99}Tc as well as for the medicinally invaluable γ emitter ^{99m}Tc by the exchange of the three aqua ligands. The choice of donor atoms and the charge of such ligands have a major effect on the stability of the resulting metal complexes, as has been found for several donor atom constellations.[16−21]

Chart 1. Fundamental Organotechnetium Complexes

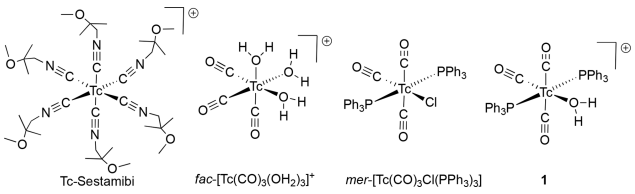

In contrast, much less is known about the structural chemistry of compounds with a *mer*-$[Tc(CO)_3]^+$ core. The first synthesis of such a compound, *mer,trans*-$[Tc(CO)_3Cl(PPh_3)_2]$, succeeded via a reaction of $[TcOCl_4]^-$ with PPh_3 under a CO atmosphere.[22] A second example of a *mer*-$\{Tc(CO)_3\}$ compound was formed by the isomerization of a *fac*-$\{Tc(CO)_3\}$ complex under the influence of a sterically

Received: December 16, 2021
Published: February 2, 2022

https://doi.org/10.1021/acs.inorgchem.1c03919
Inorg. Chem. 2022, 61, 2980−2997

encumbering isocyanide.[23] A more systematic study of the structural chemistry and reactivity of such complexes is contained in two very recent papers, which are based on the reactivity of the hydrido complex $[TcH_3(PPh_3)_4]$.[24,25] A key compound of this series is the bench-stable cationic aqua complex *mer,trans*-$[Tc(OH_2)(CO)_3(PPh_3)_2]^+$ (**1**; Chart 1), which can be regarded as a functional analogue of the unsaturated Lewis acid $[Tc(CO)_3(PPh_3)_2]^+$. This highly reactive synthon can be prepared in a scalable synthesis and has been tested in a variety of reactions with neutral ligands having different donor atoms and coordination properties.[25] Depending on the ligands applied, novel *mer*-$[Tc(L)(CO)_3(PPh_3)_2]^+$ complexes or thermal decarbonylation products could be isolated.

The observed high reactivity and the structural variety of the obtained products stimulated us to perform reactions of **1** with small inorganic ligands with particular relevance in the coordination chemistry of transition metals, which have found hitherto little or no attention in the related chemistry of technetium. This includes ligands of general interest for the aforementioned treatment of nuclear waste solutions such as nitrate, nitrite, pseudohalides, or BH_4^- but also potentially ambidentate ligands such as chalcogenocyanates. A collection of the ligands used is summarized in Chart 2.

Chart 2. Ligands Used Throughout this Study

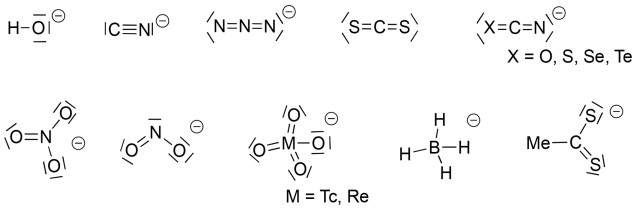

RESULTS AND DISCUSSION

Halides and Hydroxide. The hydrido complex *mer*-$[TcH(CO)_3(PPh_3)_2]$ readily reacts with HCl, HBr, or HI in organic solvents with practically quantitative formation of *mer*-$[TcX(CO)_3(PPh_3)_2]$ (X = Cl (**2a**), Br (**2b**), I (**2c**)) complexes (Scheme 1).[24] A similar preference for heavier halido ligands has been observed during reactions of *mer*-$[Tc(OH_2)(CO)_3(PPh_3)_2]^+$ (**1**). Exemplarily, the formation of the bromido complex **2b** is occasionally even observed in KBr pellets of pure complex **1**.[25] Thus, it is not surprising that the complexes **2a**–**c** can be prepared by simple H_2O/X^- exchange reactions starting from compound **1**. Alkaline or organic ammonium chlorides, bromides, and iodides are suitable X^- sources and give high yields of the *mer*-$[TcX(CO)_3(PPh_3)_2]$ (X = Cl, Br, I) complexes. However, it should be noted that we also observed the formation of considerable amounts of these compounds during other frequently unexpected or even undesired reactions. Thus, the bromido complex **2b** is the main product of the reaction of **1** with the Grignard reagent PhMgBr instead of the desired phenyl compound and the iodo complex **2c** is the sole technetium-containing product of reactions of **1** with $(SeMe_3)I$ or NaI_3. In the latter reaction, the triiodide ion is quantitatively cleaved and I_2 could be identified as a side product. No signs for the formation of an intermediate triiodido complex, e.g. by ^{99}Tc NMR spectroscopy, have been observed. Such a course of the reaction is surprising, since we recently observed a clear preference for triiodide coordination on another technetium(I) core: a reaction of $[Tc(NO)Cl(Cp)(PPh_3)]$ with HI gave preferably $[Tc(NO)I_3(Cp)(PPh_3)]$ and the corresponding iodo complex could only be isolated when trimethylsilyl iodide was used instead of HI.[26]

Scheme 1. Reactions of $[Tc(OH_2)(CO)_3(PPh_3)_2]^+$ with Halide Ions and KOMe

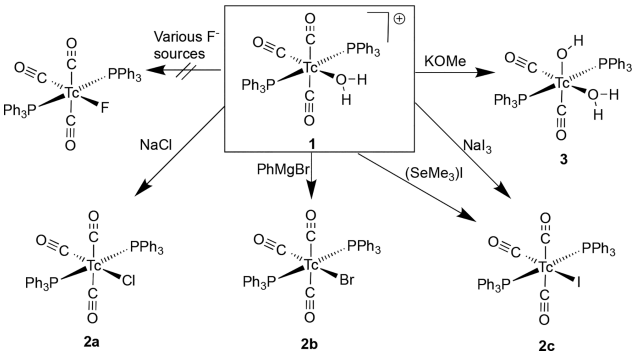

Another interesting aspect of the reactivity of **1** is the fact that, despite the obvious high tendency of the formation of *mer*-$[TcX(CO)_3(PPh_3)_2]$ complexes with X = Cl, Br, I, the corresponding fluorido species could not be isolated. All our attempts to synthesize it with various fluoride sources such as NBu_4F, KF, CsF, [K(18-crown-6)]F, and (PPN)F (PPN^+ = bis(triphenylphosphonio)iminium cation) did not allow the isolation of a defined low-valent fluorido complex but resulted in a complex mixture formed by a quick decarbonylation of intermediate fluorido compounds. Such a behavior is not completely unexpected, bearing in mind that only a few Tc(I) or Tc(II) complexes with fluorido ligands have been isolated up to now. All the previous work has been performed on different nitrosyl- or carbonyl-based systems,[27−30] while the present study has been done with a single starting material: **1**. The results thus allow a direct comparison of the reactivities of the different halides and may directly contribute to a better understanding of the behavior of technetium species in (acidic) nuclear waste solutions, where all of the halide ions used are present.

Given the similarity between the fluorido ligand and the hydroxido ligand, we attempted the deprotonation of the aqua ligand of complex **1** to give the hydroxido complex $[Tc(OH)(CO)_3(PPh_3)_2]$. The reaction of $[Tc(OH_2)(CO)_3(PPh_3)_2](BF_4)$ with KOMe in MeOH, however, gave a yellow solid of the composition $[Tc(OH)(OH_2)(CO)_2(PPh_3)_2]$ (**3**). The decarbonylation of the starting material can be proven by ^{99}Tc NMR spectroscopy. The signal of **1** at −1229 ppm disappears and a new signal appears at −859 ppm, which is in the typical range of dicarbonyltechnetium(I) complexes.[25] The ^{1}H NMR spectrum of the product of this reaction confirms the presence of OH^- and OH_2. No ^{11}B or ^{19}F resonances were observed, in accord with the proposal of a neutral species. The nature of compound **3** as a mononuclear species cannot be proven entirely on the basis of the obtained spectroscopic data, particularly with regard to the absence of a sharp IR band for the terminal OH^- ligand, which can be explained by the potential formation of hydrogen bonds. In general, the reaction of **1** with the strong π-donor OH^- is very similar to that with F^-, with the difference being that the neutral hydroxo species

https://doi.org/10.1021/acs.inorgchem.1c03919
Inorg. Chem. 2022, 61, 2980−2997

quickly deposits as a yellow solid and thus the ongoing decomposition of the product, which has been observed for fluoride, is prevented. The formation of hydroxide-bridged cluster compounds,[25,28,31] as is occasionally observed for *fac*-$\{Tc(CO)_3\}^+$ units, should be precluded in the present case by the presence of two PPh_3 ligands.

^{99}Tc NMR spectroscopy is a valuable tool for an evaluation of the behavior of such compounds in solution. Although the signals are frequently broad, they can be reliably observed and the detected chemical shifts clearly depend on the technetium core (dicarbonyl compounds, −730 to −970 ppm; *mer*-tricarbonyl compounds, −1350 to −2200 ppm) and the donor atoms.[24] Figure 1 depicts the spectra of the starting material **1**,

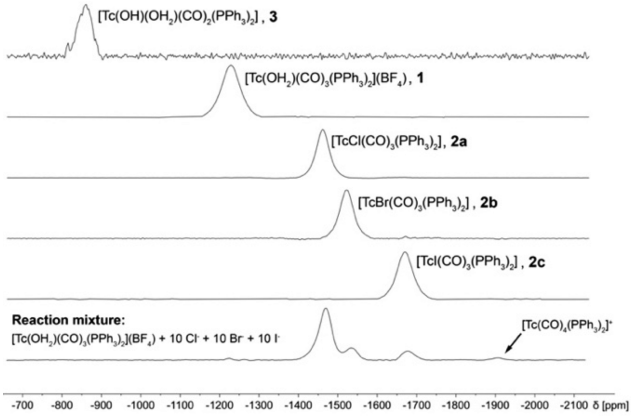

Figure 1. ^{99}Tc NMR spectra of $[Tc(OH_2)(CO)_3(PPh_3)_2](BF_4)$ and its reaction products with halides and KOMe. Note that the spectra of complexes **1**−**3** have been measured in different windows optimized for the signals of the detected compounds. The spectrum of the reaction mixture has been optimized for the intensity of the signal at −1700 ppm.

the halido complexes **2a**−**c**, and the decarbonylation product **3**. Additionally, we provide the spectrum resulting from a solution of **1** in CH_2Cl_2, which was treated with 10 equiv each of $(NBu_4)Cl$, $(NBu_4)Br$ and $(NBu_4)I$. It is evident that the exchange of the aqua ligand is fast and practically quantitative, but it can also be derived that the formation of the chlorido complex is clearly preferred over its analogues with the heavier halogenides.

A similar reaction with a corresponding $(NBu_4)Cl/(NBu_4)Br/(NBu_4)I/(NBu_4)F$ mixture gave a variety of additional technetium(I) compounds, which involve more dicarbonyl complexes, but also an isomerization of the *mer*-$[Tc(CO)_3]^+$ core to a *fac*-$[Tc(CO)_3]^+$ unit becomes evident. This is most probably a result of the prior removal of one or both PPh_3 ligands. The spectrum of this reaction mixture is given in the Supporting Information.

Pseudohalides. Reactions of pseudohalides with $[Tc(OH_2)(CO)_3(PPh_3)_2](BF_4)$ are more complex, since they can act as ambidentate ligands (OCN^-, SCN^-, $SeCN^-$), readily decompose under the influence of acidic reaction centers ($SeCN^-$, $TeCN^-$), or attack carbonyl ligands as nucleophiles (N_3^-) (see Scheme 2). The latter reaction has been observed in an early survey of the coordination chemistry of $[Tc(CO)_4(PPh_3)_2](BF_4)$, where the formation of reasonable amounts of the isocyanato complex $[Tc(CO)_3(NCO)(PPh_3)_2]$ has been observed during a reaction with sodium azide.[32] No evidence, however, was found for the formation of the corresponding azido complex.

A similar reactivity pattern is observed during the reaction of $[Tc(OH_2)(CO)_3(PPh_3)_2](BF_4)$ with NaN_3, where also the formation of cyanate was detected. The isocyanato complex $[Tc(NCO)(OH_2)(CO)_2(PPh_3)_2]$ (**4**) is the main product, and single crystals of this compound were separated in the form of large yellow blocks. It should be noted that in this case the nucleophilic attack on a carbonyl ligand is surprisingly preferred over the simple replacement of the aqua ligand by N_3^-. The ^{99}Tc NMR signal of **4** is relatively narrow and shows a triplet with a chemical shift of −975 ppm and $^1J_{Tc-P}$ value of 582 Hz. This is the typical behavior for such dicarbonyl complexes and has been observed before for a number of related solvent complexes.[24,25] Additionally, two minor side products were detected: (i) an amorphous colorless solid with a ^{99}Tc NMR resonance at −1113 ppm and (ii) a small amount of colorless, needlelike crystals of $[Tc(N_3)(CO)_3(PPh_3)_2]$ (**5**) (^{99}Tc chemical shift −1459 ppm). The attack of N_3^- on the carbonyl ligands can be suppressed when the less nucleophilic trimethylsilyl azide (TMS-N_3) is used as an azide source. Compound **5** is formed in such a reaction as the sole product in almost quantitative yield. The azido complex is stable in air but is light-sensitive and during the X-ray diffraction study of this compound a considerable decomposition was observed under the influence of the X-ray beam.

Scheme 2. Reactions of $[Tc(OH_2)(CO)_3(PPh_3)_2]^+$ with Pseudohalides

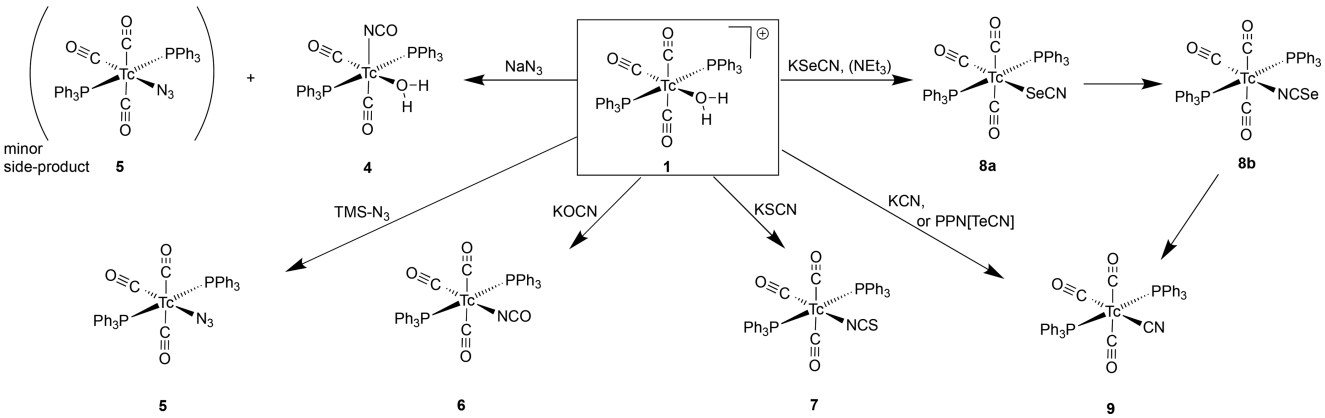

https://doi.org/10.1021/acs.inorgchem.1c03919
Inorg. Chem. 2022, 61, 2980−2997

Figure 2 depicts ellipsoid plots of the solid-state structures of complexes **4** and **5**, which are the first crystallographically

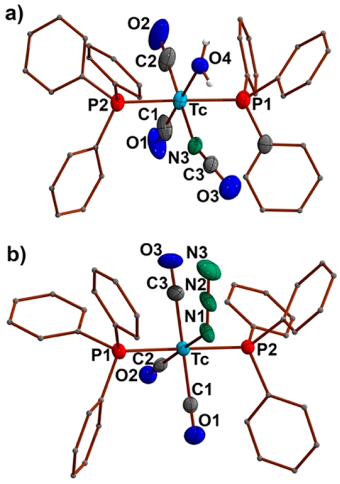

Figure 2. Solid-state structures of (a) $[Tc(NCO)(OH_2)(CO)_2(PPh_3)_2]$ (**4**) (Tc−C1 1.818(4) Å, Tc−C2 1.841(8) Å, Tc−N3 2.141(5) Å, Tc−O4 2.288(4) Å, C3−N3 1.062(7) Å, C3−O3 1.279(7) Å; Tc−N3−C3 162.0(5)°, N3−C3−O3 178.3(7)°) and(b) $[Tc(N_3)(CO)_3(PPh_3)_2]$ (**5**) (Tc−C1 2.019(8) Å, Tc−C2 1.89(1) Å, Tc−C3 1.962(9) Å, Tc−N1 2.14(1) Å, N1−N2 1.15(2) Å, N2−N3 1.18(1) Å; Tc−N1−N2 124(1)°, N1−N2−N3 178(1)°).

studied isocyanato and azido complexes of technetium. The general assembly of compound **4** is similar to that of other dicarbonyl bis(triphenylphosphine) complexes of technetium: two axial triphenylphosphine ligands and two *cis*-oriented carbonyl ligands are present in the octahedral coordination sphere, which is completed by two additional ligands in positions *trans* to the two carbonyl ligands. In **4**, these are an aqua ligand and an isocyanato ligand. The almost linear Tc−N−C bond (162.0(5)°) supports the N-coordination of the ambidentate ligands, and a Tc−N bond length of 2.141(5) Å has been found. This is similar to the values in the azido complex **5** or the isocyanato and isothiocyanato complexes $[Tc(NCO)(CO)_3(PPh_3)_2]$ (**6**) and $[Tc(NCS)(CO)_3(PPh_3)_2]$ (**7**) (*vide infra*). The aqua ligand in **4** has a Tc−O bond length of 2.288(4) Å and is clearly longer than that in the cationic starting material **1**. The Tc−O bond lengths in **1** are ca. 2.23 Å depending on the anion. The solid-state structure of **4** represents a hydrogen-bonded dimer, where the hydrogen atoms of the aqua ligand interact with the oxygen atom of the isocyanato ligand of an adjacent molecule (see the Supporting Information).

The general structure of the azido complex **5** is similar to those of the previously described *mer*-$[Tc(L)(CO)_3(PPh_3)_2]^+$ complexes, with the azido ligand adopting a bent coordination mode (Tc−N−N angle 124(1)°). This coordination angle allows an easy differentiation of the azido ligand from the related triatomic isocyanato ligand, which coordinates linearly to technetium. The Tc−N bond length in **5** is in the common range for Tc−N single bonds, and the short N−N bond lengths inside the azido moiety indicate a large degree of delocalization within the ligand. This is also reflected by the almost linear N1−N2−N3 bond angle of 178(1)°.

As mentioned above (Scheme 2 and ref 32), the treatment of carbonyl complexes with sodium azide delivers isocyanato complexes in reasonable yields. A better and more convenient access, however, is the reaction of **1** with KOCN, which gives $[Tc(NCO)(CO)_3(PPh_3)_2]$ (**6**) in good yield and in high purity. The product deposits as a colorless solid. It shows a ^{99}Tc resonance at −1553 ppm, which is clearly shifted from that of the starting material at −1229 ppm. In previous studies,[24,25] we observed that $[Tc(L)(CO)_3(PPh_3)_2]^+$ complexes with oxygen donor ligands show ^{99}Tc NMR resonances between −1180 and −1400 ppm, while the nitrogen donor complex $[Tc(NCCH_3)(CO)_3(PPh_3)_2]^+$ shows a ^{99}Tc NMR chemical shift of −1503 ppm.[25] Thus, the new resonance is preferably assigned to an N-bound isocyanato complex. The final proof of the assignment is given by a single-crystal X-ray diffraction analysis of crystals grown from a CH_2Cl_2/hexane mixture (Figure 3a). The technetium atom shows a distorted-

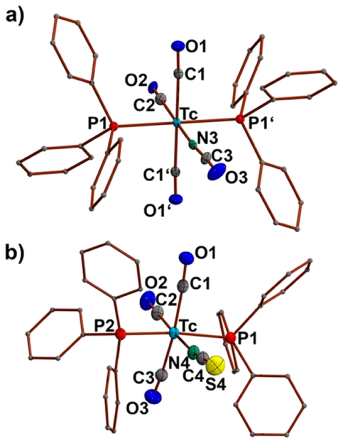

Figure 3. Solid-state structures of (a) $[Tc(NCO)(CO)_3(PPh_3)_2]$ (**6**) (Tc−N3 1.99(1) Å, C3−O3 1.24(2) Å, C3−N3 1.18(2) Å; C1−Tc−N3 90.4(7)°, C2−Tc−N3 179(2)°, C1′−Tc-N3 89.6(7)°, P1−Tc−N3 90.8(7)°, P1′−Tc-N3 89.2(7)°, N3−C3−O3 174(3)°, Tc−N3−C3 173(3)°) and (b) $[Tc(NCS)(CO)_3(PPh_3)_2]$ (**7**) (Tc−C1 1.983(2) Å, Tc−C2 1.899(2) Å, Tc−C3 1.977(2) Å, Tc−N4 2.140(1) Å, C4−S4 1.625(2) Å, C4−N4 1.160(2) Å; C1−Tc−N4 92.41(6)°, C2−Tc−N4 176.84(6)°, C3−Tc−N4 99.82(6)°, P1−Tc−N4 86.51(4)°, P2−Tc−N4 84.04(4)°, N4−C4−S4 179.2(2)°, Tc−N4−C4 169.1(1)°). Symmetry code: (′) $-x, -y + 1, -z + 1$.

octahedral coordination geometry with three meridional carbonyl ligands, two triphenylphosphine ligands in positions *trans* to each other, and an isocyanato ligand *trans* to one of the carbonyl ligands.

The procedure applied for the synthesis of the isocyanato complex **6** can also be used for the corresponding isothiocyanato compound. A reaction between the aqua complex **1** and KSCN results in the selective formation of a single species with a ^{99}Tc NMR resonance at −1518 ppm. This value falls in the range of N-bound ligands, which is not unexpected with regard to the fact that with only one exception all structurally studied technetium complexes with SCN^- establish N-coordination to this ligand.[33−39] The only exception from this general trend was observed during a reaction of the organometallic technetium(I) compound $[Tc(NO)Cl(Cp)(PPh_3)]$ with KSCN.[26] A single-crystal X-ray study on the product $[Tc(NO)(SCN)(Cp)(PPh_3)]$ doubtlessly confirmed an S-coordination of the ambidentate ligand. In solution, however, a slow isomerization to the thermodynamically more stable isothiocyanato complex was observed by ^{99}Tc NMR.[26] In the present case, $[Tc(NCS)(CO)_3(PPh_3)_2]$ (**7**) is the sole product formed. Even at low

https://doi.org/10.1021/acs.inorgchem.1c03919
Inorg. Chem. 2022, 61, 2980−2997

temperature there was no evidence for the formation of the "kinetic" S-bonded product.

Finally, an X-ray structure analysis of the light pink single crystals confirmed the isothiocyanato coordination in **7** (Figure 3b). Two polymorphs of the compound were crystallized. The values for the monoclinic structure (space group $P2_1/c$) are used in the following discussion, while those of a triclinic polymorph (space group $P\bar{1}$) are given in the Supporting Information.

As in the isocyanato complex, the technetium atom shows a distorted-octahedral coordination geometry with three meridional carbonyl ligands, two triphenylphosphine ligands in positions *trans* to each other, and an isothiocyanato ligand *trans* to one of the carbonyl ligands. The Tc−N4 bond is 2.140(1) Å and thus significantly shorter than those of the related pyridine complex $[Tc(py)(CO)_3(PPh_3)_2]^+$ (2.226(6) Å) and the ammine complex $[Tc(NH_3)_2(CO)_2(PPh_3)_2]^+$ (2.24−2.26 Å) as well as those observed in the chelate complexes $[Tc(bpy^{COOMe2})(CO)_2(PPh_3)_2]^+$ (2.16−2.17 Å) and $[\{Tc(N,O\text{-}C_5H_4N\text{-}COO)(CO)_2(PPh_3)_2\}_2H]^+$ (2.194(8) Å).[25] The bond lengths in the isothiocyanato ligand indicate a strong delocalization of electrons among the three atoms. As in the previously characterized isothiocyanato complexes of technetium, the ligand is bound rather linearly to technetium with a Tc−N4−C4 angle of 169.1(1)°.

The heavier chalcogenocyanates $SeCN^-$ and $TeCN^-$ are unstable and readily decompose with formation of elemental selenium or tellurium and CN^-. Such reactions proceed rapidly in acidic media, and thus, it is not surprising that they are also observed with the highly Lewis acidic technetium complex **1**. After the addition of KSeCN to solutions of **1**, an immediate formation of an insoluble red solid of elemental selenium is observed. The decomposition can be avoided by the addition of the base NEt_3 to the aqua complex prior to the addition of selenocyanate. A mixture of the selenocyanato and isoselenocyanato complexes is formed. They can be unambiguously assigned by ^{99}Tc NMR spectroscopy. One signal appears at −1518 ppm (practically the same chemical shift as observed for the isothiocyanato complex **7**), while the second (major) signal is shifted downfield and is observed at −1654 ppm. Such downfield shifts are typical for series of chemically related compounds, in which single donor atoms are systematically replaced (e.g., Cl/Br/I in the complexes shown in Figure 1 or S/Se/Te in related chalcogenoether complexes).[25] Thus, an assignment of the signal at −1654 ppm to *mer*-$[Tc(SeCN)(CO)_3(PPh_3)_2]$ (**8a**) and that at −1518 ppm to *mer*-$[Tc(NCSe)(CO)_3(PPh_3)_2]$ (**8b**) seems to be justified. This assumption is supported by the observation that the Se-bound complex isomerizes into the N-bound complex. When the mixture was heated for only 5 min, the major amount of the Se-bound isomer **8a** converted into **8b** (Figure 4). An attempt to complete the isomerization by leaving the sample overnight at room temperature resulted in the complete consumption of **8a**. In parallel, an ongoing decomposition of **8b** proceeded, which could be easily detected by the sedimentation of elemental red selenium and the appearance of an additional ^{99}Tc NMR signal at −1901 ppm, which can be assigned to *mer*-$[Tc(CN)(CO)_3(PPh_3)_2]$ (**9**). The selenium abstraction proceeds slowly at room temperature over a time span of about 2 weeks but is complete within a few hours when the samples are heated.

Interestingly, we found that the use (PPN)SeCN (PPN^+ = bis(triphenylphosphonio)iminium) instead of KSeCN as the selenocyanate source leads to the exclusive formation of **8b**. We attribute the different reactivities to coordinating interactions between K^+ ions and the N-donor site of the ambidentate $SeCN^-$ ion and, thus, a partial inhibition of this position for the reaction with technetium. In solutions with the less coordinating PPN^+ cation, such interactions are excluded and the N-donor atom is fully available for complex formation with the transition metal.

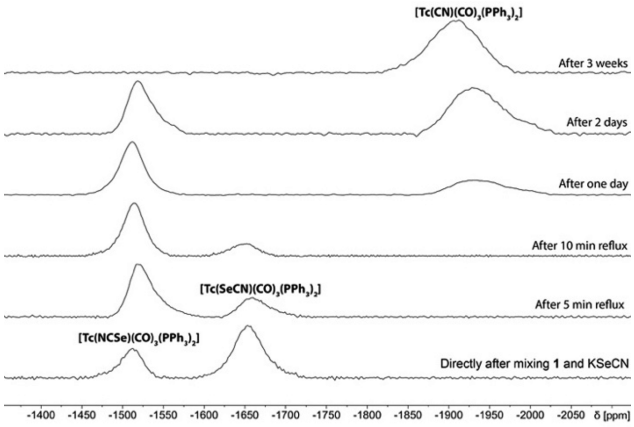

Figure 4. ^{99}Tc NMR spectra of a solution of **1** after the addition of KSeCN, showing the isomerization of the selenocyanato complex **8a** into the isoselenocyanato complex **8b** followed by selenium abstraction with formation of the cyanido complex **9**.

From reactions of (PPN)TeCN with **1** or with the nonprotic precursor $[Tc(SMe_2)(CO)_3(PPh_3)_2][BF_4]$ we could not isolate products with coordinated $TeCN^-$ ligands. This is not unexpected with regard to the instability of tellurocyanate in solution. However, there was also no spectroscopic evidence for any such compounds, even when the reactions were performed at −78 °C. Instead, the immediate formation of the cyanido complex **9** and the parallel sedimentation of elemental tellurium was evident. Attempts to follow either the selenium or the tellurium elimination reaction spectroscopically using ^{15}N-enriched seleno- or tellurocyanates were not successful.

Given the different reactivities of the chalcogenocyanates, we performed DFT calculations on the B3LYP level in an implicit solvent model for the solvent dichloromethane. We successfully located a transition state for the unimolecular isomerization reaction for each chalcogenocyanate using a simple PMe_3 model instead of the much more expensive PPh_3 ligands for calculations. The chalcogenocyanate moiety coordinates to technetium in a side-on way in the isomerization reaction. Obviously, the energy barrier for the isomerization increases along the group, while the chalcogen-bound isomer is energetically increasingly more favored along the group (Figure 5). This is in accord with the isolation of the isocyanato and isothiocyanato complexes **6** and **7**. The observed formation of the selenocyanato complex **8a** in comparison to the isoselenocyanato complex **8b** and the thermal isomerization of **8a** to **8b** can be understood in terms of a kinetic control leading to the selenium-coordinated isomer, while the nitrogen-bound isomer can be considered the thermodynamic product of the reaction.

Pure $[Tc(CN)(CO)_3(PPh_3)_2]$ (**9**) can of course also be prepared in high yields by the reaction of **1** with KCN. It shows a ^{99}Tc resonance at −1930 ppm, which is in the same range as those of analogous isocyanide complexes [Tc(CNR)-

https://doi.org/10.1021/acs.inorgchem.1c03919
Inorg. Chem. 2022, 61, 2980−2997

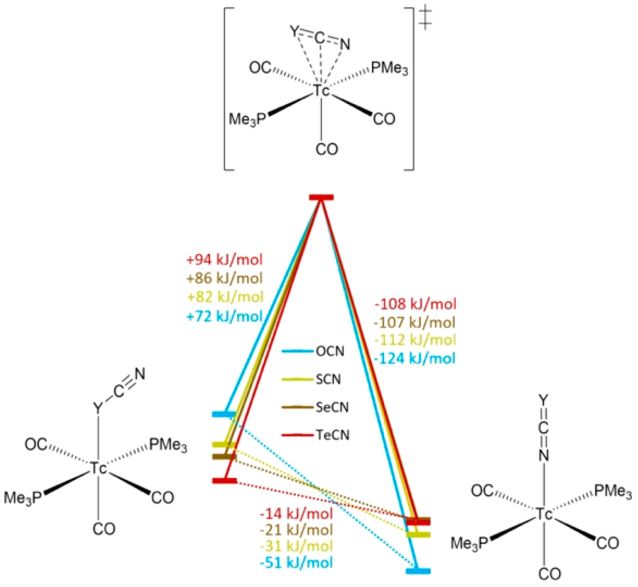

Figure 5. Calculated free energies for the unimolecular isomerization of the model complexes $[Tc(NCY)(CO)_3(PMe_3)_2]$ (Y = O, S, Se, Te). The values refer to the energy differences.

$(CO)_3(PPh_3)_2]^+$ (R = Cy, −1884; R = CN^{DArF2}, −1879 to −1903 ppm) and the tetracarbonyl cation $[Tc(CO)_4(PPh_3)_2]^+$ (−1886 ppm).[25] To date there have only been 10 structural reports on technetium cyanido complexes,[40] and only one of them has technetium in a low oxidation state, the $[Tc(CN)_3(CO)_3)]^{2-}$ anion.[41] Thus, we studied the structure of complex **9** by X-ray diffraction. A triclinic polymorph was obtained from CH_2Cl_2. Unfortunately, the cyanido ligand was crystallographically indistinguishable from the carbonyl ligands, as emphasized by the symmetry-related generation of CN from CO. Further information is given in the Supporting Information. Finally, the methanol solvate **9**·MeOH crystallized from a CH_2Cl_2/MeOH mixture, where the cyanido ligand was easily identified due to its nearly linear hydrogen bonding with the cocrystallized MeOH (Figure 6).

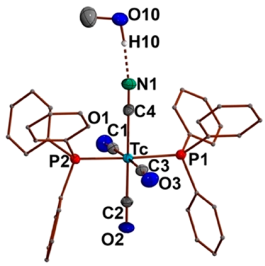

Figure 6. Solid-state structure of $[Tc(CN)(CO)_3(PPh_3)_2]$ (**9**) in **9**·MeOH (Tc−C1 2.003(2) Å, Tc−C2 1.945(2) Å, Tc−C3 1.972(2) Å, Tc−C4 2.135(2) Å, C4−N1 1.136(3) Å, N1···H10 1.80(4) Å, O10−H10 1.07 Å; O10−H10−N1 171(3)°).

The general geometry around technetium in **9**·MeOH resembles that of the other meridional tricarbonyl complexes. The Tc−C4 bond length of 2.135(2) Å is significantly longer than the Tc−C bonds of the carbonyl ligands. It is in the normal range of Tc−C bonds for cyanido ligands in the 10 previously characterized cyanido complexes of technetium.[40] The Tc−C2 bond in a position *trans* to the cyanido ligand is 1.945(2) Å and hence somewhat longer than those in other structurally related meridional tricarbonyl complexes of technetium such as the isocyanide complex $[Tc(CNCy)(CO)_3(PPh_3)_2]^+$.[25]

Nitrite and Nitrate. Nitrogen oxides or nitroxide anions are common components in nuclear waste solutions, and such ions can also serve as models for interactions of the radiometal technetium with environmental compartments. Additionally, there have hitherto been no reports about isolated nitrato or nitrito complexes of technetium, to the best of our knowledge. Since particularly the NO_2^- ion belongs to the classic "Werner-type" ligands,[42] more knowledge about its coordination chemistry with technetium would be most welcome. Scheme 3 summarizes the reactions performed, and it becomes clear that the ambidentate behavior of nitrite also plays a role in its complexes with technetium.

Scheme 3. Synthesis and Chemical Behavior of Nitrito and Nitrato Complexes of Technetium

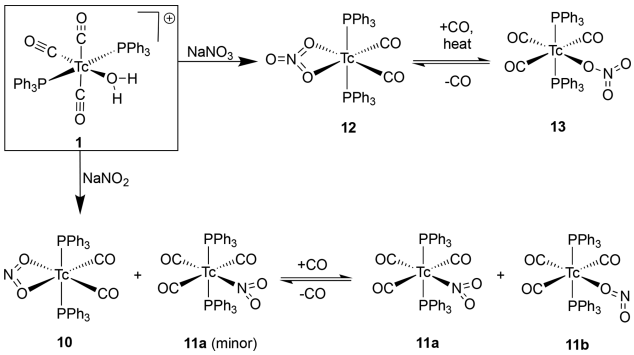

$[Tc(OH_2)(CO)_3(PPh_3)_2](BF_4)$ reacts with $NaNO_2$ or $NaNO_3$ with formation of $[Tc(\eta^2\text{-OON})(CO)_2(PPh_3)_2]$ (**10**) and $[Tc(\eta^2\text{-OONO})(CO)_2(PPh_3)_2]$ (**12**). The formation of dicarbonyl fragments is strongly supported by the presence of two $\nu_{C\equiv O}$ bands in the IR spectra of **10** (1871 and 1946 cm^{-1}) and **12** (1879 and 1952 cm^{-1}) and ^{99}Tc signals at −629 (**10**) and −820 ppm (**12**), which is in the expected range for dicarbonyls (*vide supra*).[24,25] Interestingly, compound **12** is obtained as the sole product during such reactions, while some traces of a η^1-tricarbonyl complex remained even in the isolated solid of compound **10**.

X-ray structural analyses on **10** and **12** (Figure 7) confirm the dicarbonyl structures derived from the spectroscopic data. They are the first structurally studied nitrate and nitrite compounds of technetium. The technetium atoms are coordinated octahedrally with the general dicarbonyl bonding motif. The coordination sphere is completed by NO_3^- or NO_2^- ligands, which coordinate to technetium in a bidentate fashion with Tc−O bond lengths between 2.181(5) and 2.227(3) Å. The bite angle of both ligands is small at 57.3(2) and 57.3(3)°, respectively, which is in line with the angle observed in η^2-carboxylato complexes.[25] For the carboxylato complexes, they can also be understood as being coordinated through a pseudoallylic system. The distances between technetium and the central nitrogen atoms are ca. 2.64 Å and therefore slightly longer than the Tc−C distances observed for the carboxylate complexes (ca. 2.58 Å).[25] The distances between technetium and the central atoms of the previously reported dicarbonyl pseudoallyl complexes $[Tc(\eta^2\text{-ArN}\cdots X\cdots NAr)(CO)_2(PPhMe_2)_2]$ with X = C, N (2.68−2.71 Å),

https://doi.org/10.1021/acs.inorgchem.1c03919
Inorg. Chem. 2022, 61, 2980−2997

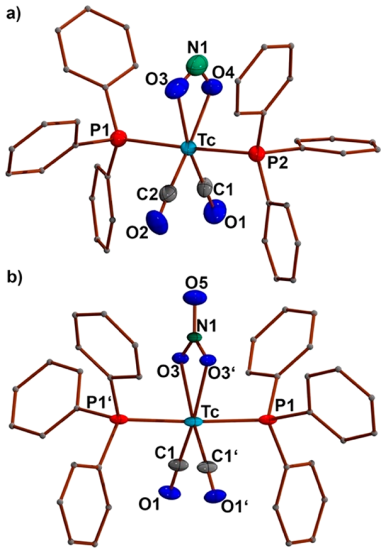

Figure 7. Solid-state structures of (a) [Tc(η^2-OON)$(CO)_2(PPh_3)_2$] (**10**) (Tc−C1 1.868(7) Å, Tc−C2 1.881(8) Å, Tc−O3 2.211(5) Å, Tc−O4 2.181(5) Å, O3−N1 1.30(1) Å, N1−O3 1.25(1) Å, Tc···N1 2.64(1) Å; O3−Tc−O4 57.3(3)°, O3−N1−O4 111.5(7)), and (b) [Tc(η^2-OONO)$(CO)_2(PPh_3)_2$] (**12**) (Tc−C1 1.875(5) Å, Tc−O3 2.227(3) Å, O3−N1 1.271(4) Å, N1−O4 1.240(8) Å, Tc···N1 2.644(6) Å; O3−Tc−O3′ 57.3(2)°, O3−N1−O3′ 114.2(5). Symmetry code: (′) $-x + 1, y, -z + 3/2$.

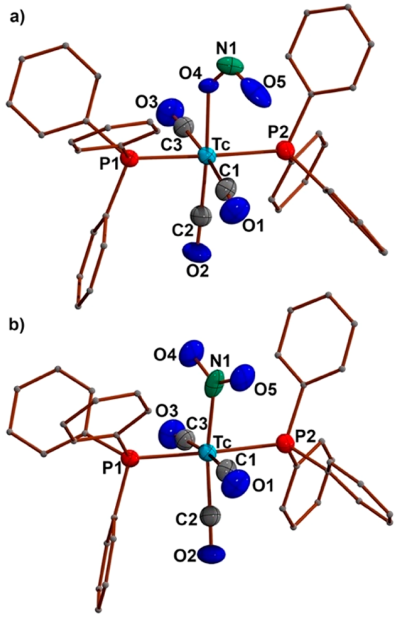

Figure 8. Solid-state structures of the two bond isomers (a) [Tc(η^1-ONO)$(CO)_3(PPh_3)_2$] (**11a**) (Tc−C1 1.967(5) Å, Tc−C2 1.910(4) Å, Tc−C3 1.986(5) Å, Tc−O4 2.159(6) Å, O4−N1 1.19(1) Å, N1−O5 1.22(2) Å; C1−Tc−O4 102.2(2)°, C2−Tc−O4 174.2(3)°, C3−Tc−O4 82.1(2)°, P1−Tc−O4 86.4(2)°, P2−Tc−O4 91.3(2)°, Tc−O4−N1 133.6(9)°, O4−N1−O5 109(1)°) and (b) [Tc(η^1-NO_2)$(CO)_3(PPh_3)_2$] (**11b**) (Tc−C1 1.967(5) Å, Tc−C2 1.910(4) Å, Tc−C3 1.986(5) Å, Tc−N1 2.20(2) Å, O4−N1 1.22(2) Å, N1−O5 1.27(2) Å; C1−Tc−N1 84.5(3)°, C2−Tc−N1 166.8(3)°, C3−Tc−N1 100.2(3)°, P1−Tc−N1 92.1(4)°, P2−Tc−N1 85.4(4)°, Tc−N1−O4 120(2)°, Tc−N1−O5 117(1)°, O4−N1−O5 124(2)°).

[Tc(η^2-*O,N*-diazepine)$(CO)_2(PPh_3)_2$] (2.61 Å), [Tc{η^2-SN(COEt)}$(CO)_2(PPh_3)_2$] (2.78 Å), and [Tc{η^2-SS(CNHPh)}$(CO)_2(PPh_3)_2$] (2.94 Å) indicate that not only does the type of *donor atom* have an influence on this parameter as concluded previously[43−47] but also the identity of the *central atoms* of the pseudoallyl ligands is essential.

The structurally related formato complex [Tc(η^2-OO(CH))$(CO)_2(PPh_3)_2$] reversibly binds CO and forms the complex [Tc(η^1-O(CH)O)$(CO)_3(PPh_3)_2$] with a monodentate carboxylato ligand. It binds or releases carbonyl ligands depending on the conditions.[25] A similar reactivity has been observed for the nitrito complex **10**. Faint yellow-green solutions of **10** react at room temperature with an excess of CO gas with immediate discoloration. The resulting solution shows two ^{99}Tc resonances at −1305 ppm ($\nu_{1/2}$ = 3594 Hz) and −1431 ppm ($\nu_{1/2}$ = 3544 Hz), which suggest the presence of tricarbonyl isomers with O- and N-bonded η^1-nitrito ligands. Similar equilibria have been suggested for the analogous rhenium complexes, but in this case nitrogen−metal interactions had only been suspected on the basis of IR spectral data and mechanistic considerations but not observed directly.[48] For the technetium complexes of the present study they have been confirmed unambiguously by an X-ray structural analysis. In the single crystals obtained from the colorless mixture, both bond isomers [Tc(η^1-ONO)$(CO)_3(PPh_3)_2$] (**11a**) and [Tc(η^1-NO_2)$(CO)_3(PPh_3)_2$] (**11b**) are cocrystallized in a 60:40 ratio. Figure 8 contains structure plots of both isomers.

The general octahedral ligand arrangement around technetium in both **11a** and **11b** is that of the classic meridional tricarbonyl core. In **11a**, the coordination sphere is completed by an O-coordinating η^1-nitrito ligand, while in **11b** the coordination sphere is completed by an N-coordinating η^1-nitro ligand. Both ligands show a torsion of ca. 27° from the equatorial plane. The technetium−oxygen bond in **11a** is 2.159(6) Å, while the technetium−nitrogen bond in **11b** is somewhat longer at 2.20(2) Å. The average N−O bond lengths are smaller in **11a** in comparison to **11b**, which can be understood as a lowered degree of double-bond character in the nitro in comparison to the nitrato moiety.

Interestingly, the ratio between **11a** and **11b** is not influenced by changes in the reaction parameters (e.g., reaction time and reaction temperature). In contrast to the nitrito complex **10**, the nitrato complex **12** does not react with CO gas at room temperature. Nevertheless, the η^1- complex [Tc(η^1-ONO_2)$(CO)_3(PPh_3)_2$] (**13**) is formed when **12** is heated in the presence of CO gas. This can be concluded from the appearance of a ^{99}Tc resonance at −1275 ppm ($\nu_{1/2}$ = 3594 Hz), which rapidly disappears with re-formation of the signal at −820 ppm (compound **12**) when the sample is opened and stored at room temperature.

With the assignment of the ^{99}Tc NMR signal at −1275 ppm to compound **13**, it is highly probable that the N-bonded nitrite species **11b** is the compound that was detected as a minor side product during the synthesis of the chelate **10**.

We investigated the de- and recarbonylation reactions of the nitrito and the nitrato complexes using DFT calculations at the B3LYP level with an implicit solvent model for CH_2Cl_2. For a PMe_3 model, we located transition states for all reactions involved, including the isomerization between **11a** and **11b** (Figure 9).

Borane and Boranate. Alkali-metal and tetrabutylammonium boranates as well as solvent adducts of BH_3 are common reductants for the synthesis of low-valent technetium compounds.[16,17,48−50] Especially, boronates are also under

https://doi.org/10.1021/acs.inorgchem.1c03919
Inorg. Chem. 2022, 61, 2980−2997

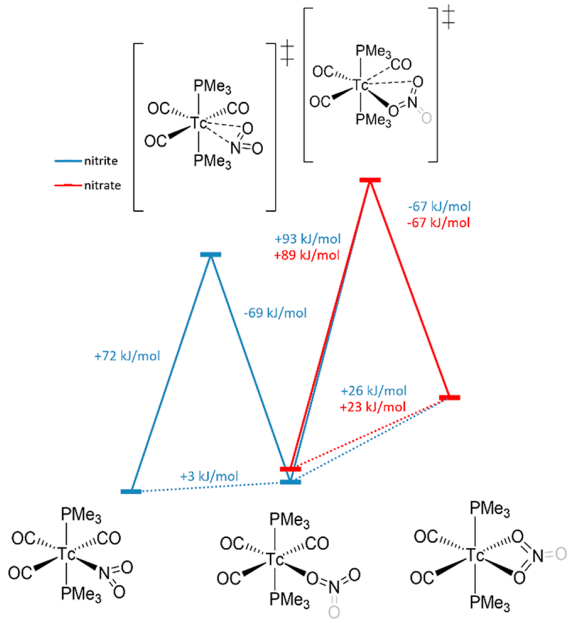

Figure 9. Calculated free energies for the isomerization and decarbonylation reactions of the model complexes $[Tc(NO_x)(CO)_3(PMe_3)_2]$ and $[Tc(NO_x)(CO)_2(PMe_3)_2]$ (x = 2, 3).

permanent consideration as components for hydrogen storage materials and play a role in the nuclear fuel cycle.[51−53] In this context BH_4^- complexes with several transition-metal ions have also been isolated including a few rhenium compounds.[54,55]

Reactions of **1** with $LiBH_4$ or $(NBu_4)BH_4$ did not result in a simple exchange of the aqua ligand and the formation of $[Tc(\eta^1\text{-}HBH_3)(CO)_3(PPh_3)_2]$ or $[Tc(\eta^2\text{-}HHBH_2)(CO)_2(PPh_3)_2]$. An immediate evolution of borane was observed and $[TcH(CO)_3(PPh_3)_2]$ (**14**) was formed almost quantitatively according to the ^{99}Tc NMR spectrum of the reaction mixture. However, when solutions of **14** were additionally treated with BH_3·THF and heated to reflux, an additional ^{99}Tc resonance was observed at −964 ppm. This is the region of dicarbonyl compounds and a strong hint for the formation of $[Tc(\eta^2\text{-}HHBH_2)(CO)_2(PPh_3)_2]$ (**15**) (Scheme 4).

Scheme 4. Addition of BH_3·THF to the Hydrido Complex $[TcH(CO)_3(PPh_3)_2]$

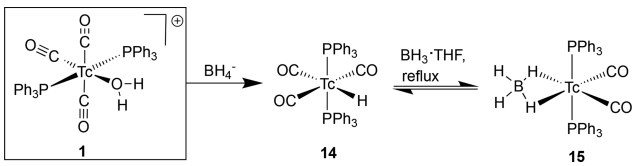

The observed reaction is not quantitative. A maximum conversion of 20% was observed after ca. 5 min, independent of the borane concentration and the temperature. However, the addition of pentane to such solutions allows the isolation of both complexes in crystalline form. Colorless blocks of $[TcH(CO)_3(PPh_3)_2]$ (**14**) and yellow plates of $[Tc(\eta^2\text{-}HHBH_2)(CO)_2(PPh_3)_2]$ (**15**) could be clearly distinguished in the resulting solid and were hand-picked for the X-ray diffraction study. The IR spectrum confirmed the dicarbonyl core by the presence of two ν_{CO} bands at 1886 and 1956 cm^{-1}.

^{1}H and ^{99}Tc NMR spectra of the product mixture are shown in Figure 10. The borohydride ligand gives a broad ^{1}H NMR

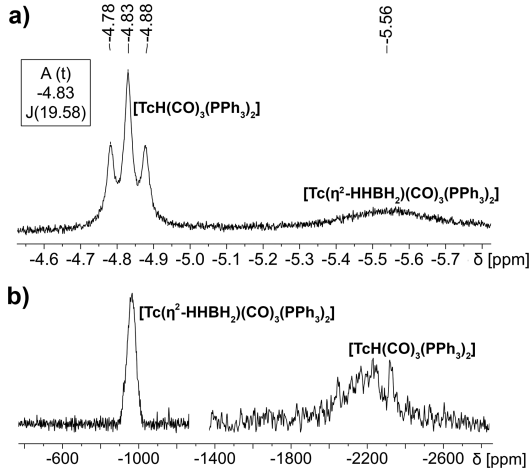

Figure 10. (a) ^{1}H and b) ^{99}Tc NMR spectra of a mixture of compounds **14** and **15**. Note that the ^{99}Tc spectrum had to be measured in two windows.

resonance at −5.56 ppm, indicating the full fluxionality of the four hydrides, and a ^{99}Tc NMR resonance in the established dicarbonyl region at −963 ppm.

The solid-state structure of $[Tc(\eta^2\text{-}HHBH_2)(CO)_2(PPh_3)_2]$ (**15**) is shown in Figure 11. The technetium atom is

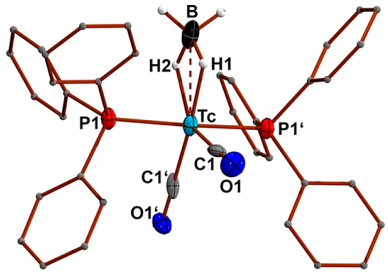

Figure 11. Solid-state structure of $[Tc(\eta^2\text{-}HHBH_2)(CO)_2(PPh_3)_2]$ (**15**) (Tc−C1 1.847(6) Å, Tc−C2 1.885(4) Å, Tc1−H1 1.79(7) Å, Tc1−H2 1.95(5) Å, Tc···B 2.50(1) Å).

coordinated octahedrally with two *cis*-oriented carbonyl ligands and two *trans*-oriented PPh_3 ligands. The short Tc−C bond lengths are consistent with a dicarbonyl species and support the η^2-BH_4^- interpretation. For an appropriate refinement, the B−H distances in **15** were restrained to an average distance of 1.14 Å. The resulting Tc−H distances are asymmetric at 1.95(5) and 1.79(7) Å. The resulting H1−Tc−H2 bite angle is 50(2)°. The distance between technetium and the central boron atom is 2.50(1) Å. As **15** is the first technetium complex with an unsubstituted borohydride (BH_4^-) ligand, we can only compare it with two other structurally characterized imidazole-substituted borohydride complexes of technetium: $[Tc\{\kappa^3\text{-}S,H,S\text{-}H(\mu\text{-}H)B(tim^{Me})_2\}(CO)_3]$ and $[Tc\{\kappa^3\text{-}S,H,H\text{-}H(\mu\text{-}H)_2B(tim^{Me})\}(CO)_3]$ (timMe = 2-mercapto-1-methylimidazolyl).[56,57] The borohydride in $[Tc\{\kappa^3\text{-}S,H,S\text{-}H(\mu\text{-}H)B(tim^{Me})_2\}(CO)_3]$ is stabilized by two additional mercaptoimidazole substituents, and its coordination is stabilized by the

https://doi.org/10.1021/acs.inorgchem.1c03919
Inorg. Chem. 2022, 61, 2980−2997

formation of an *S,H,S*-chelate. The Tc−H distance in this "η^1-complex" is 1.65(6) Å, and the Tc−B distance is 2.834(5) Å.[56] In the "η^2-complex" $[Tc\{\kappa^3\text{-}S,H,H\text{-}H(\mu\text{-}H)_2B(tim^{Me})\}(CO)_3]$, where the borohydride is stabilized by one additional imidazole substituent and additionally an *S,H,H*-chelation stabilizes the coordination of the two hydrido bridges, the Tc−H distances are 1.89(3) and 1.94(3) Å with a Tc−B distance of 2.329(3) Å and a H−Tc−H bite angle of 62(1)°.[57] Thus, the Tc−B distance in **15** is intermediate between those observed for the single-agostic complex $[Tc\{\kappa^3\text{-}S,H,S\text{-}H(\mu\text{-}H)B(tim^{Me})_2\}(CO)_3]$ and the double-agostic complex $[Tc\{\kappa^3\text{-}S,H,H\text{-}H(\mu\text{-}H)_2B(tim^{Me})\}(CO)_3]$. Expectedly, the bite angle in **15** is somewhat smaller in comparison to that in $[Tc\{\kappa^3\text{-}S,H,H\text{-}H(\mu\text{-}H)_2B(tim^{Me})\}(CO)_3]$. The Tc−H bond lengths are in line with the interpretation of one Tc-hydridic H donor atom (as in the parent hydrido complex) and a second agostic coordination side of the BH_3 moiety.

Acetate, Thioacetate, and Dithioacetate. Previously,[24] we found that $[TcH(CO)_3(PPh_3)_2]$ reacts with acetic acid with immediate loss of a carbonyl ligand, resulting in the formation of $[Tc\{\eta^2\text{-}OO(CMe)\}(CO)_2(PPh_3)_2]$ (**16**). This contrasts with the reaction of formic acid, where the formation of the corresponding dicarbonyl $[Tc\{\eta^2\text{-}OO(CH)\}(CO)_2(PPh_3)_2]$ or tricarbonyl $[Tc\{\eta^1\text{-}O(CH)O\}(CO)_3(PPh_3)_2]$ species is dependent on the conditions applied. A missing link in these previous studies was the elusive complex $[Tc(\eta^1\text{-}O(CMe)O)(CO)_3(PPh_3)_2]$. Thus, we anticipated that the tricarbonyl complex might be stabilized under favorably mild and quick reaction conditions, which became possible with complex **1** as the starting material. However a reaction with **1** (Scheme 5) also resulted in the immediate and exclusive formation of the decarbonylated product **16**. A similar result was obtained during the reaction of **1** with potassium thioacetate, where the released water immediately hydrolyzed the thioacetate with subsequent decarbonylation and formation of the acetato chelate **16** in high yields.

Scheme 5. Reactions of $[Tc(OH_2)(CO)_3(PPh_3)_2]^+$ with Acetate, Thioacetate, and Dithioacetate

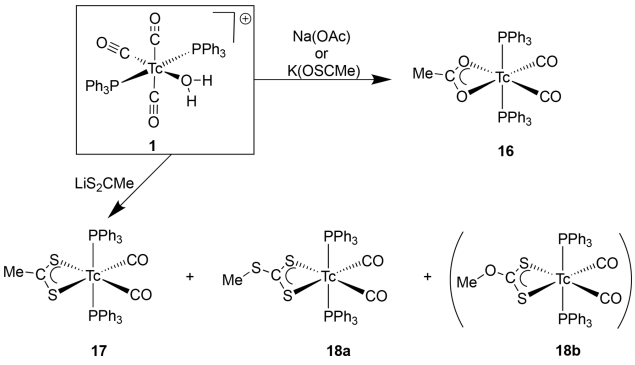

With respect to the previously discussed experiences with the different chalcogenocyanates, the obtained results lead to the question of what reactivity can be expected with dithiocarboxylates or related ligands. Such ligands are usually prepared *in situ* by the reaction of carbon nucleophiles on CS_2 due to the instability of the dithiocarboxylate moieties.[58] To keep the results comparable, we have chosen dithioacetate as a suitable target, although there are only 27 structurally characterized transition-metal complexes with this ligand coordinating in a η^2 mode.[40]

Lithium dithioacetate was prepared by the reaction of MeLi with CS_2 and added to a solution of **1**, which resulted in the formation of a mixture of two main yellow products (Scheme 5): the dithioacetato complex $[Tc\{\eta^2\text{-}SS(CMe)\}(CO)_2(PPh_3)_2]$ (**17**) and the methyltrithiocarbonato compound $[Tc\{\eta^2\text{-}SS(CSMe)\}(CO)_2(PPh_3)_2]$ (**18a**). A minor side product could be identified as the corresponding xanthate complex $[Tc\{\eta^2\text{-}SS(COMe)\}(CO)_2(PPh_3)_2]$ (**18b**), which is most probably formed during the workup procedure, where the products were precipitated by the addition of methanol. No evidence was found for the formation of the acetato complex **15** as a hydrolysis product.

The ^{99}Tc NMR spectra of the three products appear as relatively narrow triplets ($\nu_{1/2} \approx 350$ Hz, $^1J_{Tc-P} \approx 550$ Hz) between −1330 and −1410 ppm (see the Supporting Information). Such narrow ^{99}Tc NMR signals with ^{31}P couplings are typical for Tc(I) dicarbonyl complexes with chelating dithio ligands.[25,58−62]

An X-ray structural analysis revealed the cocrystallization of the two products **17** and **18a**. Figure 12 depicts their structures, which both contain technetium atoms in a distorted-octahedral environment. The main distortions result from the small S−Tc−S bite angles of ca. 70°. The Tc−S bond lengths in **17** are somewhat longer than those in **18a**. The Tc−C3 distance is shorter for the more tightly bound methyl thioxanthate ligand at ca. 2.88 Å in comparison to that in the dithioacetato complex, where a distance of ca. 3.09 Å is found. Both values are in the expected range for two sulfur donor atoms. The C−S bond lengths within the methyltrithiocarbonato ligand are unsymmetrical: the two technetium-coordinat-

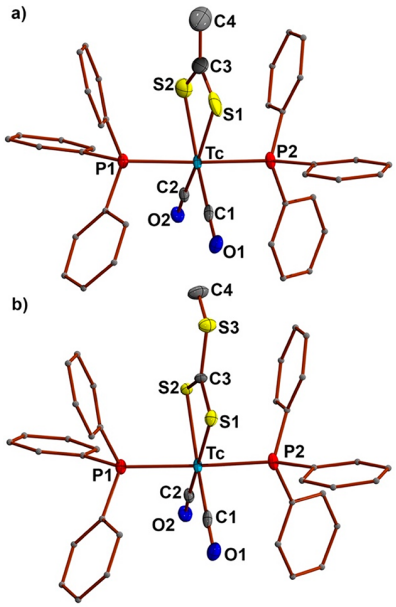

Figure 12. Solid-state structures of the two disordered, cocrystallized complexes (a) $[Tc(\eta^2\text{-}SS(CMe))(CO)_2(PPh_3)_2]$ (**17**) (Tc−C1 1.901(4) Å, Tc−C2 1.891(4) Å, Tc−S1 2.53(1) Å, Tc−S2 2.56(1) Å, C3−S1 1.75(3) Å, C3−S2 1.68(4) Å) and (b) $[Tc(\eta^2\text{-}SS(CSMe))(CO)_2(PPh_3)_2]$ (**18a**) (Tc−C1 1.901(4) Å, Tc−C2 1.891(4) Å, Tc−S1 2.51(1) Å, Tc−S2 2.501(8) Å, C3−S1 1.67(2) Å, C3−S2 1.69(3) Å, C3−S3 1.796(9) Å).

https://doi.org/10.1021/acs.inorgchem.1c03919
Inorg. Chem. 2022, 61, 2980−2997

ing sulfur atoms show partial double-bond character with C−S bond lengths of 1.67(2) and 1.69(3) Å in comparison to the clear single bond between C3 and S3 of 1.796(9) Å. In comparison, the C−S bond lengths in the dithioacetato ligand of **16** are slightly asymmetrical. S1 is bound with a single bond of 1.75(3) Å, while S2 is bound with a double bond of 1.68(4) Å.

The formation of the methyltrithiocarbonato ligand can be attributed to the thermal instability of the dithioacetate.[58] Neither **17** nor **18a** binds CO with re-formation of tricarbonyl complexes even on exposure to CO for longer periods. Thus, they reflect the reactivity of compound **16**, which contains the relatively π-basic acetato ligand.

The experimental findings that the acetato and dithioacetato complexes show a similar resistance against CO addition and re-formation of tricarbonyl complexes lead to the question of whether this is generally the case for the corresponding carboxylates and dithiocarboxylates (also bearing in mind that electronic parameters in the backbone of carboxylates frequently influence the reactivity of such complexes).

The dithioformato ligand is structurally closely related to both the nitrito and formato ligands, which both show reversible CO binding. The dithioformato complex $[Tc(\eta^2\text{-}SS(CH))(CO)_2(PPh_3)_2]$ (**20**) is easily formed by an insertion of CS_2 into the hydride bond of $[TcH(CO)_3(PPh_3)_2]$.[63] In contrast to the formation of the dithioacetato complex discussed above (Scheme 5), we found clear evidence for the intermediate formation of the tricarbonyl complex $[Tc(\eta^1\text{-}S(CH)S)(CO)_3(PPh_3)_2]$ (**19**), as is indicated in Scheme 6.

Scheme 6. Insertion of CS_2 Into the Tc−H Bond of $[TcH(CO)_3(PPh_3)_2]$

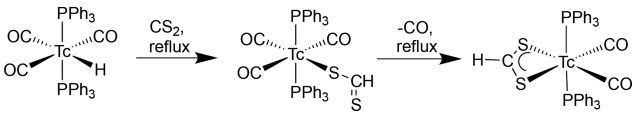

The reaction of compound **14** with CS_2 (Scheme 6) does proceed at room temperature with a reasonable rate. When the mixture was heated in toluene, however, it turned yellow and the formation of two technetium(I) species was detected at −1498 ppm (**19**) and −1250 ppm (**20**) by ^{99}Tc NMR (see Supporting Information), while the signal of the starting material disappeared. Both new resonances are narrow and show well-resolved triplets with $^1J_{Tc-P}$ values of ca. 580 Hz. The signal of compound **19** disappears after a reaction time of approximately 5 min, and the chelate complex **20** can be isolated in crystalline form in good yields. It should be mentioned that compound **19** with the η^1-bonded dithioformate could not be re-formed by the reaction of **20** with CO. This result is a clear contrast to the behavior to the corresponding formato complex.[24]

Single crystals of **20** grew by slow evaporation of a toluene/MeOH mixture. Figure 13 shows the solid-state structure of the complex. The dithioformato ligand is disordered over two positions with an occupation of ca. 50:50 with one of the carbonyl ligands. The general ligand arrangement is the same as in the previously discussed dithio complexes. Similarly to the dithioacetato ligand in **17**, the C−S bond lengths are somewhat asymmetrical in the dithioformato ligand.

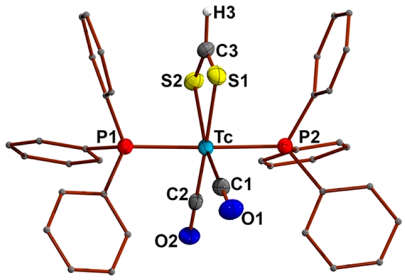

Figure 13. Solid-state structure of $[Tc(\eta^2\text{-}SS(CH))(CO)_2(PPh_3)_2]$ (**20**) (Tc−S1 2.505(1) Å, Tc−S2 2.461(3) Å, C3−S1 1.61(1) Å, C3−S2 1.71(1)/1.65(2) Å; S1−Tc−S2 70.55(9)°; S1−C3−S2 119.7(6)°).

Pertechnetate, Perrhenate, Permanganate. Since pertechnetate or, depending on the pH or composition of the solution, other pertechnetic compounds are doubtlessly the main technetium species in nuclear waste solutions, it is essential to understand the reaction behavior of related species in such solutions (also toward other technetium compounds). Therefore, we undertook some experiments with compound **1** and MO_4^- salts (M = Tc, Re, Mn).

The addition of NH_4TcO_4 or NH_4ReO_4 to compound **1** in a THF/water mixture results in a color change, and light yellow crystals of $[Tc(OTcO_3)(CO)_3(PPh_3)_2]$ (**21**) or $[Tc(OReO_3)(CO)_3(PPh_3)_2]$ (**22**) are obtained in good yields by slow evaporation of the THF. Expectedly, an analogous reaction with $KMnO_4$ results in an immediate oxidation of technetium and the formation of $KTcO_4$. In parallel, MnO_2 deposits from the reaction mixture (Scheme 7).

Scheme 7. Reactions of $[Tc(OH_2)(CO)_3(PPh_3)_2]^+$ with Pertechnetate and Perrhenate and Subsequent Decarbonylation and Decomposition Reactions

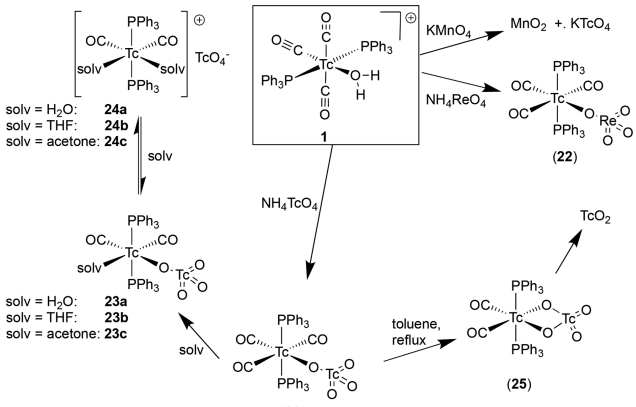

The crystal structure of the mixed-valence technetium complex **21** was determined for the unsolvated and benzene-solvated complex. Details about the solid-state structure of the benzene solvate are given in the Supporting Information. The structure of **21** derived from the solvent-free crystals is shown in Figure 14.

The coordination sphere of the technetium atom Tc1 in **21** shows the usual *mer-trans* orientation of CO and PPh_3. The oxygen bridge between the two technetium atoms is expectedly asymmetrical with a Tc1−O4 bond length of 2.153(3) Å and a Tc2−O4 bond length of 1.739(3) Å. The Tc2−O4 bond is

https://doi.org/10.1021/acs.inorgchem.1c03919
Inorg. Chem. 2022, 61, 2980−2997

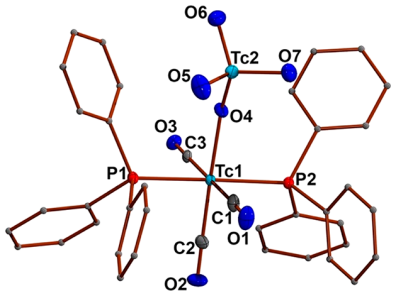

Figure 14. Solid-state structure of $[Tc(OTcO_3)(CO)_3(PPh_3)_2]$ (**21**) (Tc1–C1 2.018(4) Å, Tc1–C2 1.894(4) Å, Tc1–C3 1.971(4) Å, Tc1–O4 2.153(3) Å, Tc2–O4 1.739(3) Å, Tc2–O5 1.700(4) Å, Tc2–O6 1.698(3) Å, Tc2–O7 1.708(3) Å).

somewhat longer than those of Tc2 to the other multiply bonded oxygen atoms, indicating some $\{TcO_3\}^+$ character of this group. The bridging Tc1–O4–Tc2 angle is bent (148.7(2)°). The same structure is observed for the analogous rhenium compound $[Re(OReO_3)(CO)_3(PPh_3)_2]$.[64]

There are only two other structurally characterized technetium complexes with pertechnetato ligands: the dinuclear compound $[Tc_2(acetate)_4(OTcO_3)_2]$ and the mixed-valence polyoxometalate $[(TcO)_4(OTcO_3)_{16}]^{4-}$, which contains four technetium(V) oxido units, each coordinated by four pertechnetato ligands.[65−67] The Tc–$OTcO_3$ bond lengths in $[(TcO)_4(OTcO_3)_{16}]^{4-}$ have an average value of 2.003 Å, while the average TcO–TcO_3 bond length is 1.777 Å. The terminal Tc=O bond lengths are unexceptional. It should be mentioned that there are also a few more pertechnetato complexes that are relevant for the speciation of technetium in nuclear waste solutions, the actinide complexes $[UO_2(TcO_4)_2(OPPh_3)_3]$, $[Th(TcO_4)_4(OPPh_3)_4]$, and $[(NpO_2)_2(TcO_4)_4(H_2O)_3]$, which also contain monodentate or bridging pertechnetato ligands.[68,69]

The tricarbonyl pertechnetato complex **21** gives ^{99}Tc resonances at 41 and −1137 ppm (Figure 15a), while the spectrum of the perrhenato complex **22** (Figure 15b) expectedly shows only one ^{99}Tc signal in the region of the tricarbonyl complexes (−1166 ppm).

Many of the previously regarded *mer*-$[Tc(L)(CO)_3(PPh_3)_2]$ complexes underwent a thermal decarbonylation when they were heated in coordinating solvents or when chelate formation of the ligand L was possible. Such reactions did not proceed for the perrhenato complex **22**. For compound **21**, however, we observed both reaction pathways depending on the conditions applied. When a solution of $[Tc(OTcO_3)(CO)_3(PPh_3)_2]$ (**21**) in wet THF was heated, the signal of the starting material at −1137 ppm disappeared and three resonances in the typical "dicarbonyl" region appeared: two overlapping signals at −762 ppm and one at −854 ppm. The latter signal belongs to the already known diaqua cation $[Tc(OH_2)_2(CO)_2(PPh_3)_2]^+$.[25] The two overlapping resonances likely can be assigned to the rapidly exchanging complexes $[Tc(OTcO_3)(THF)(CO)_2(PPh_3)_2]$ and $[Tc(OTcO_3)(H_2O)(CO)_2(PPh_3)_2]$. This is supported by the ^{99}Tc NMR resonances observed in the pertechnetate region: a resonance at 31 ppm corresponds to $[Tc(OTcO_3)(H_2O)(CO)_2(PPh_3)_2]$, while a resonance at 37 ppm can be assigned to $[Tc(OTcO_3)(THF)(CO)_2(PPh_3)_2]$. Finally, the resonance of uncoordinated TcO_4^- anions is detected at 17 ppm.

Similar solvent adducts were observed when **21** was heated in acetone, where the formation of several new dicarbonyl and pertechnetate species were observed *in situ*. The related spectra are shown in the Supporting Information.

Finally, from this reaction a crystalline compound, $[Tc(OTcO_3)(acetone)(CO)_2(PPh_3)_2]$ (**23c**)·acetone, could be isolated. A solution of this compound shows a broad signal in the dicarbonyl region with a flat-topped peak shape at −803 ppm. The peak shape is attributed to an overlap between the resonances of compound **23c** and the solvent adduct $[Tc(OTcO_3)(H_2O)(CO)_2(PPh_3)_2]$ (**23a**), which is formed by the dissolution of **23c** in wet CH_2Cl_2. This interpretation is supported by the detection of two signals in the pertechnetate region at 37 and 31 ppm.

The X-ray structure analysis of the isolated yellow single crystals of the acetone complex **23c** unambiguously prove the existence of such solvent complexes (Figure 16). The

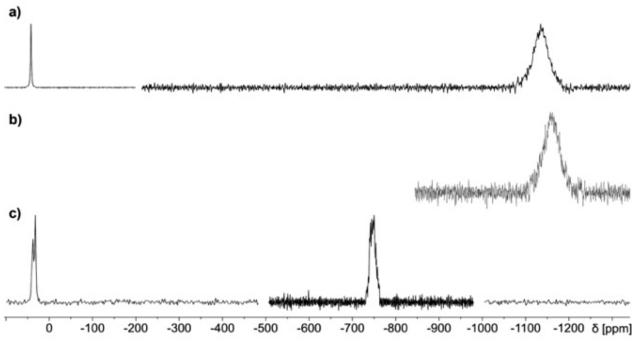

Figure 15. ^{99}Tc NMR spectra of (a) $[Tc(OTcO_3)(CO)_3(PPh_3)_2]$ (**21**), (b) $[Tc(OReO_3)(CO)_3(PPh_3)_2]$ (**22**) and (c) $[Tc(OTcO_3)(acetone)(CO)_2(PPh_3)_2]$ (**23c**). Note that the ^{99}Tc NMR spectra had to be measured in different windows.

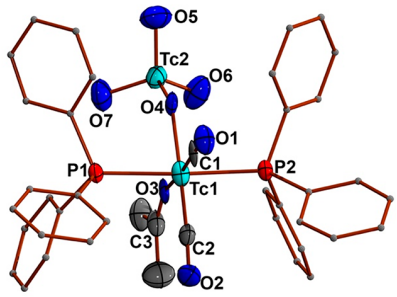

Figure 16. Solid-state structure of $[Tc(OTcO_3)(acetone)(CO)_2(PPh_3)_2]$ (**23c**) (Tc1–C1 1.74(1), Tc1–C2 1.82(2), Tc1–O3 2.142(9), Tc1–O4 2.182(9), Tc2–O4 1.750(8) Å).

compound is the first technetium complex in which a coordination of acetone to technetium has been proven (bearing in mind that acetone is frequently used as a solvent for reactions with pertechnetate and methyl ethyl ketone is a common extractant for TcO_4^-). The coordination environment of the central technetium atom in **23c** is as expected, with the two carbonyl ligands having $OTcO_3^-$ and acetone in *trans* positions. Since the crystal quality for the structure determination was limited, a detailed discussion of bond lengths and angles shall not be given here. Details are provided in the Supporting Information.

A subsequent reaction of compounds **23** in coordinating solvents results in an ongoing ligand exchange, which applies

https://doi.org/10.1021/acs.inorgchem.1c03919
Inorg. Chem. 2022, 61, 2980−2997

not only to the solvent molecules but also to the pertechnetato ligands. Finally, they are replaced and the cationic bis(solvent) complexes **24** are formed as additional products. In CH_2Cl_2/THF/acetone/water solutions, a stepwise increase in complexity arises from the formed mixture, with the products containing each of these solvents, which are readily detected by ^{99}Tc NMR (see the Supporting Information). Their ratio depends on the concentration of the respective solvents.

Similar experiments with **21** in absolutely dry, degassed toluene result in the final formation of a black sediment of the stable decomposition product $Tc^{IV}O_2$. This can be understood by a synproportionation between the Tc(I) and Tc(VII) atoms in **21** and would preferably proceed via a chelate-bonded pertechnetato ligand. The intermediate formation of $[Tc(\eta^2\text{-}OOTcO_2)(CO)_2(PPh_3)_2]$ (**25**) is supported by the fact that in the reaction mixture the ^{99}Tc NMR signal of **21** gradually disappears and in the supernatant solution over the black solid a highly symmetrical dicarbonyl species with a chemical shift of −798 ppm ($\nu_{1/2}$ = 98 Hz) can be detected, while the pertechnetate resonance at 41 ppm persisted (Figure 17). A

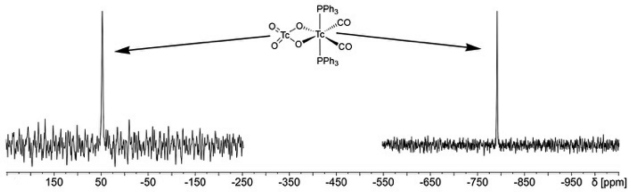

Figure 17. ^{99}Tc NMR spectrum of $[Tc(\eta^2\text{-}OOTcO_2)(CO)_2(PPh_3)_2]$ (**25**).

high and rigid symmetry around the technetium atom in the dicarbonyl part of the molecule is concluded from the narrow line width of the signal, since the line broadening of ^{99}Tc NMR signals is frequently related to symmetry parameters or dynamic effects.[70] Remarkably, the pertechnetato signal at 41 ppm is relatively broad ($\nu_{1/2}$ = 174 Hz) in comparison to those of the monodentate pertechnetato ligands (*vide supra*) or uncoordinated TcO_4^-.[70] It is not yet clear if this is the result of a fluxional behavior or if a second pertechnetate component is present.

The decomposition of the pertechnetato complex **21** with formation of TcO_2 requires elevated temperatures. Thus, we found no evidence for the formation of the chelate complex **25** and a subsequent synproportionation in boiling acetone or THF. The formation of dicarbonyl complexes with solvent ligands (compounds **23** and **24**) might support the stabilization of the mixed-valent technetium complexes, but it should be mentioned also that an attempted reaction of compound **21** in boiling benzene did not result in the formation of compound **25** and/or TcO_2. Only the benzene solvate of complex **21** could be recovered from such solutions in quantitative yields (*vide supra*). This information might also be of relevance for the elevation of the speciation of technetium compounds in nuclear waste solutions.

CONCLUSIONS

The organometallic, bench-stable aqua complex *mer,trans*-$[Tc(OH_2)(CO)_3(PPh_3)_2](BF_4)$ reacts with a large variety of small inorganic ligands with exchange of the aqua ligand. The reaction pathway and the nature of the products strongly depend on the donor atoms of the ligands and the reaction conditions. Donor solvents frequently participate in the reactions and establish equilibria between different complexes.

Many products could be isolated in crystalline form. Thus, the present study introduces the first technetium complexes with nitrato, nitrito, azido, isoselenocyanato, and BH_4^- ligands. An ambidentate bonding behavior could be unambiguously confirmed for nitrite and $SeCN^-$ ligands.

The obtained results may have some implications in the evaluation of technetium-containing nuclear waste solutions on consideration of the following facts.

(i) Carbonyl species contained in such solutions are reactive, and their speciation is not restricted to the $[Tc(OH_2)_3(CO)_3]^+$ cation.
(ii) Carbonyl species can form complexes with nitrate and nitrite ions, which are common in such solutions.
(iii) The related nitrito and nitrato complexes can establish bond isomerism and induce decarbonylation reactions.
(iv) Technetium carbonyls form complexes with potentially hazardous azide species, but also a nucleophilic attack of N_3^- on CO with subsequent cyanate formation has been observed.
(v) Common reducing agents such as BH_4^- can form complex species with technetium(I) carbonyls.
(vi) Even the behavior of pertechnetate is not innocent in its role as a ligand for the coordination of low-valent technetium species.

^{99}Tc nuclear magnetic resonance proved to be an invaluable tool for the study of these systems. The differentiation between different binding modes of ambidentate ligands as well as the decarbonylation/recarbonylation was easily achieved through the use of ^{99}Tc resonances. In general, dicarbonyls are formed when highly π-basic or strong σ-donors attack.

EXPERIMENTAL SECTION

General Considerations. Unless otherwise stated, reagent-grade starting materials were purchased from commercial sources and either used as received or purified by standard procedures. Solvents were dried and deoxygenated according to standard procedures. $[TcH(CO)_3(PPh_3)_2]$, $[Tc(OH_2)(CO)_3(PPh_3)_2][BF_4]$, and $[Tc(OH_2)(CO)_3(PPh_3)_2][BF_4]$ were prepared as previously described.[24,25] Trimethylselenonium iodide and PPN^+ salts were prepared according to literature procedures.[71,72]

Physical Measurements. NMR spectra were recorded at 20 °C with JEOL 400 MHz multinuclear spectrometers. The values given for the ^{99}Tc chemical shifts are referenced to potassium pertechnetate in water. IR spectra were recorded with a Shimadzu FTIR 8300 spectrometer as KBr pellets. The following abbreviations were used for the intensities and characteristics of IR absorption bands: vs = very strong, s = strong, m = medium, w = weak, sh = shoulder.

Radiation Precautions. ^{99}Tc is a long-lived, weak β^- emitter (E_{max} = 0.292 MeV). Normal glassware provides adequate protection against the weak β radiation when milligram amounts are used. Secondary X-rays (bremsstrahlung) play a significant role only when larger amounts of ^{99}Tc are handled. All manipulations were done in a laboratory approved for the handling of radioactive materials.

X-ray Crystallography. The intensities for the X-ray determinations were collected on STOE IPDS II or Bruker D8 Venture instruments with Mo Kα radiation. The space groups were determined by the detection of systematic absences. Absorption corrections were carried out by multiscan or integration methods.[73,74] Structure solution and refinement were performed with the SHELX program package.[75,76] Hydrogen atoms were derived from the final Fourier maps, refined or placed at calculated positions, and treated with the "riding model" option of SHELXL. The representation of molecular structures was done using the program DIAMOND 4.2.2.[77]

https://doi.org/10.1021/acs.inorgchem.1c03919
Inorg. Chem. 2022, 61, 2980−2997

Additional information on the structure determinations is contained in the Supporting Information and has been deposited with the Cambridge Crystallographic Data Centre.

Computational Details. DFT calculations were performed on the high-performance computing systems of the Freie Universität Berlin ZEDAT (Curta)[78] using the program package GAUSSIAN 16.[79] The gas-phase and solution geometry optimizations were performed using coordinates derived from the X-ray crystal structures using GAUSSVIEW and Avogadro.[80,81] The polarizable continuum model (PCM) with the integral equation formalism variant (IEFPCM) was used to implicitly simulate the solvent dichloromethane. The calculations were performed with the hybrid density functional B3LYP.[82−84] The double-ζ pseudopotential LANL2DZ basis set with the respective effective core potential (ECP) was applied to P, S, Se, and Te.[85] The Stuttgart relativistic small-core basis set with the corresponding ECP was applied to Tc.[86,87] The 6-311+G** basis set was used to model C, H, O, and N atoms.[88,89] All basis sets as well as the ECPs were obtained from the EMSL database.[90] Frequency calculations after the optimizations confirmed the convergence. No negative frequencies were obtained for the given optimized geometries of all compounds. The entropic contribution to the free energy was corrected for low-energy modes using the quasi-harmonic approximation of Grimme[91] as implemented in the freely accessible python code GoodVibes of Funes-Ardoiz and Paton with a cutoff at 300 cm^{-1}.[92] Further details are contained in the Supporting Information.

Syntheses. *mer-[TcX(CO)$_3$(PPh$_3$)$_2$] (X = Cl (**2a**), Br (**2b**), I (**2c**)).* A solution of NaX (Cl, 6 mg; Br, 12 mg; I, 18 mg, 0.12 mmol) in water (1 mL) was added to a suspension of [Tc(OH$_2$)(CO)$_3$(PPh$_3$)$_2$][BF$_4$] (18 mg, 0.02 mmol) in CH_2Cl_2 (1 mL). After the resulting biphasic mixture was stirred for 10 min, water (3 mL) was added and the organic phase was separated. The separated organic phase was dried by filtering over a small bed of Na_2SO_4. The aqueous phase was extracted twice with CH_2Cl_2 (1 mL), which was then also dried over Na_2SO_4. The combined extracts were left for evaporation overnight. Colorless microcrystals of **2a**−**c** were isolated. Yield: **2a**, 13 mg (0.02 mmol, 96%); **2b**, 14 mg (0.02 mmol, 93%); **2c**, 13 mg (0.02 mmol, 85%). The analytical data are as reported earlier.[25]

*[TcBr(CO)$_3$(PPh$_3$)$_2$] (**2b**) from a Grignard Reagent.* A solution of PhMgBr (0.5 mL, 1 M, in THF) was added dropwise to a suspension of [Tc(OH$_2$)(CO)$_3$(PPh$_3$)$_2$][BF$_4$] (85 mg, 0.1 mmol) in dry, degassed THF (2 mL) under Ar. After the resulting clear yellow-orange solution was stirred for 1 h, the solvent was evaporated under vacuum. The residue was extracted with toluene (5 × 2 mL). The volume was reduced to ca. 0.5 mL under vacuum, and 6 mL of pentane were added to precipitate a crude mixture of Mg salts and the product (88 mg). Extraction of the technetium compounds with CH_2Cl_2 followed by crystallization from CH_2Cl_2/pentane resulted in the formation of crystals of **2b**, which were filtered off, washed with pentane, and dried in air. The crystals were suitable for X-ray diffraction. Yield: 50 mg (0.06 mmol, 60%). The product is spectroscopically identical with **2b** prepared by literature methods.[25]

*[TcI(CO)$_3$(PPh$_3$)$_2$] (**2c**) from SeMe$_3$I.* $SeMe_2$ (0.5 mL, freshly distilled from 5.5 g of $SeMe_3I$) was added to a suspension of [Tc(OH$_2$)(CO)$_3$(PPh$_3$)$_2$][BF$_4$] (41 mg, 0.05 mmol) in CH_2Cl_2 (1 mL). The resulting clear solution was stirred for 1 min and then filtered over a small bed of Na_2SO_4 to remove the released water. The Na_2SO_4 was washed with CH_2Cl_2 (2 × 0.5 mL). The combined filtrate and washing solutions were layered with pentane (15 mL). After storage in a refrigerator overnight, colorless crystals formed. The crystals were filtered off, washed with pentane (3 × 3 mL), and dried in air. The crystals were suitable for X-ray diffraction. Yield: 27 mg (0.03 mmol, 65%). The product obtained is spectroscopically identical with **2c** prepared by literature methods.[25]

*[TcI(CO)$_3$(PPh$_3$)$_2$] (**2c**) from NaI$_3$.* A freshly prepared red solution of NaI_3 (NaI, 2.8 mg, 0.02 mmol; I_2, 4.7 mg, 0.02 mmol) in THF (0.5 mL) was added to a suspension of [Tc(OH$_2$)(CO)$_3$(PPh$_3$)$_2$][BF$_4$] (15 mg, 0.02 mmol) in THF (0.5 mL). The resulting clear, orange-red solution was stirred for 15 min. The addition of MeOH (9 mL) resulted in the precipitation of golden yellow microcrystals. The crystals were filtered off, washed with MeOH (3 mL) and hexane (3 × 3 mL), and dried in air to give 5 mg of **2c**. Slow evaporation of the filtrate resulted in the formation of a second crop (8 mg) of the product as large yellow crystals. The crystals were suitable for X-ray diffraction. Yield: 13 mg (0.02 mmol, 84%). The product obtained is spectroscopically identical with **2c** prepared by literature methods.[25]

*[Tc(OH)(H$_2$O)(CO)$_2$(PPh$_3$)$_2$] (**3**).* Solid KOMe (5 mg, 0.07 mmol) was added to a suspension of [Tc(OH$_2$)(CO)$_3$(PPh$_3$)$_2$][BF$_4$] (15 mg, 0.02 mmol) in MeOH (0.5 mL), resulting in the formation of a yellow suspension. After the resulting suspension was stirred for 30 min, the light yellow precipitate was filtered off. It was washed with MeOH (2 × 2 mL) and pentane (3 mL). After drying in air, a yellow powder was obtained. Yield: 14 mg (0.02 mmol, 98%). IR (cm^{-1}): 2013 (vw, $\nu_{C\equiv O}$), 1967 (w, $\nu_{C\equiv O}$), 1940 (s, $\nu_{C\equiv O}$), 1906(sh, $\nu_{C\equiv O}$), 1861 (vs, $\nu_{C\equiv O}$). ^{1}H NMR (CD_2Cl_2, ppm): 7.72−6.97 (30H, m, Ar*H*), 2.58 (1H, s, O*H*), 1.55 (2H, s, OH_2). ^{31}P NMR (CD_2Cl_2, ppm): 54 (s, $\nu_{1/2}$ = 5852 Hz). ^{99}Tc NMR (CD_2Cl_2, ppm): −859 (s, $\nu_{1/2}$ = 3920 Hz).

*[Tc(NCO)(OH$_2$)(CO)$_2$(PPh$_3$)$_2$] (**4**).* A solution of NaN_3 (10 mg, 0.15 mmol) in MeOH (0.5 mL) was added to a suspension of [Tc(OH$_2$)(CO)$_3$(PPh$_3$)$_2$][BF$_4$] (23 mg, 0.03 mmol) in CH_2Cl_2/MeOH (1 mL/0.5 mL). After the resulting clear solution was stirred for 5 min, water (2 mL) and CH_2Cl_2 (1 mL) were added. The separated organic phase was dried by filtering over a small bed of $MgSO_4$. $MgSO_4$ was washed with CH_2Cl_2 (2 × 0.5 mL), and the combined filtrate and washing solutions were left for evaporation overnight. The beige residue was crystallized from CH_2Cl_2/hexane, filtered, and washed with pentane. After drying in air, a mixture of colorless and yellow crystals was obtained, which mainly consisted of **4**, while traces of **5** and an unidentified impurity were present. Yield: 18 mg (0.02 mmol, 86%). IR (cm^{-1}): 2106 (s, $\nu_{N=C}$), 2033 (s, $\nu_{C\equiv O}$), 1948 (vs, $\nu_{C\equiv O}$), 1917 (vs, $\nu_{C\equiv O}$), 1871 (s, $\nu_{C\equiv O}$). ^{1}H NMR (CD_2Cl_2, ppm): 7.62 (12H, s, Ar*H*), 7.45 (18H, s, Ar*H*). ^{99}Tc NMR (CD_2Cl_2, ppm): −975 (t, $\nu_{1/2}$ = 502 Hz, $^1J_{Tc-P}$ = 582 Hz). The ^{31}P NMR resonance was too broad to be observed due to couplings with the quadrupole moment of ^{99}Tc.

*[Tc(N$_3$)(CO)$_3$(PPh$_3$)$_2$] (**5**).* Trimethylsilyl azide (66 μL, 0.5 mmol) was added to a suspension of [Tc(OH$_2$)(CO)$_3$(PPh$_3$)$_2$][BF$_4$] (41 mg, 0.05 mmol) and CsF (0.05 mmol, 8 mg) in THF (2 mL). The orange-red suspension was stirred for 2.5 h, while slow gas evolution was observed. The volume of the resulting solution was reduced to ca. 0.5 mL. Hexane (10 mL) was added to complete the precipitation. The formed precipitate was filtered off and washed with hexane (3 × 3 mL), water (2 × 2 mL), ethanol (2 × 2 mL), and hexane (2 × 3 mL). After drying in air, a colorless powder was isolated. Recrystallization was done from CH_2Cl_2/pentane. Yield: 37 mg (0.05 mmol, 99%). IR (cm^{-1}): 2058 (sh, $\nu_{C\equiv O}$), 2034 (s, $\nu_{N=N}$), 1954 (vs, $\nu_{C\equiv O}$), 1913 (vs, $\nu_{C\equiv O}$), 1846 (m, $\nu_{C\equiv O}$). ^{1}H NMR (CD_2Cl_2, ppm): 7.62 + 7.46 (30H, s, Ar*H*). ^{31}P NMR (CD_2Cl_2, ppm): 34 (s, $\nu_{1/2}$ = 3683 Hz). ^{99}Tc NMR (CD_2Cl_2, ppm): −1452 (s, $\nu_{1/2}$ = 3222 Hz).

*[Tc(NCO)(CO)$_3$(PPh$_3$)$_2$] (**6**).* Solid KOCN (8 mg, 0.1 mmol) was added to a suspension of [Tc(OH$_2$)(CO)$_3$(PPh$_3$)$_2$][BF$_4$] (15 mg, 0.02 mmol) in CH_2Cl_2/MeOH (1 mL/1 mL). After the resulting clear solution was stirred for 1 h, MeOH (6 mL) was layered on top. The cloudy solution was left for diffusion overnight. The formed colorless microcrystals were filtered from the remaining MeOH, washed with MeOH (6 mL) and pentane (3 mL), and dried in air. Yield: 12 mg (0.02 mmol, 87%). IR (cm^{-1}): 2237 (vs, $\nu_{C=N}$), 2056 (w, $\nu_{C\equiv O}$), 2007 (w, $\nu_{C\equiv O}$), 1964 (vs, $\nu_{C\equiv O}$), 1937 (vs, $\nu_{C\equiv O}$), 1915 (s, $\nu_{C\equiv O}$), 1850 (vs, $\nu_{C=O}$). ^{1}H NMR (CD_2Cl_2, ppm): 7.85−7.14 (30H, m, Ar*H*). ^{31}P NMR (CD_2Cl_2, ppm): 38 (s, $\nu_{1/2}$ = 3254 Hz). ^{99}Tc NMR (CD_2Cl_2, ppm): −1553 (s, $\nu_{1/2}$ = 3104 Hz).

*[Tc(NCS)(CO)$_3$(PPh$_3$)$_2$] (**7**).* A solution of KSCN (10 mg, 0.1 mmol) in MeOH (1 mL) was added to a suspension of [Tc(OH$_2$)(CO)$_3$(PPh$_3$)$_2$][BF$_4$] (41 mg, 0.05 mmol) in CH_2Cl_2/MeOH (0.5 mL/0.5 mL). After the resulting reddish brown solution was stirred for 5 min, water (2 mL) and CH_2Cl_2 (1 mL) were added. The separated organic phase was dried by filtering over a small bed of Na_2SO_4. The Na_2SO_4 was washed with CH_2Cl_2 (2 × 0.5 mL), and the combined filtrate and washing solutions were left for evaporation

https://doi.org/10.1021/acs.inorgchem.1c03919
Inorg. Chem. 2022, 61, 2980−2997

overnight. The formed reddish crystals were suspended in pentane, filtered, and washed with pentane (3 × 3 mL). The crystals were suitable for X-ray diffraction. Yield: 24 mg (0.03 mmol, 62%). IR (cm^{-1}): 2085 (vs, $\nu_{C\equiv N}$), 2046 (vs, $\nu_{C\equiv O}$), 1950 (vs, $\nu_{C\equiv O}$), 1929 (vs, $\nu_{C\equiv O}$). ^1H NMR (CD_2Cl_2, ppm): 7.62 (12H, s, Ar*H*), 7.48 (18H, s, Ar*H*). ^{31}P NMR (CD_2Cl_2, ppm): 39 (s, $\nu_{1/2}$ = 3597 Hz). ^{99}Tc NMR (CD_2Cl_2, ppm): −1518 (s, $\nu_{1/2}$ = 2523 Hz).

*[Tc(NCSe)(CO)$_3$(PPh$_3$)$_2$] (**8a**)/[Tc(SeCN)(CO)$_3$(PPh$_3$)$_2$] (**8b**).* A solution of KSeCN (15 mg, 0.1 mmol) in THF (1 mL) was added to a suspension of $[Tc(OH_2)(CO)_3(PPh_3)_2][BF_4]$ (41 mg, 0.05 mmol) and NEt_3 (1 drop) in THF (1 mL) at ca. −40 °C. After the resulting yellow solution was stirred for 10 min, the mixture was warmed to room temperature. A mixture of water and methanol (1 mL/3 mL) was added, resulting in the formation of a light yellow precipitate. The mixture was cooled in a refrigerator for 1 h to complete the precipitation. It was filtered, washed with H_2O (3 × 2 mL) and pentane (3 × 3 mL), and dried in air to give a colorless powder. The product is much more soluble in methanol in comparison to all other complexes of the $[TcX(CO)_3(PPh_3)_2]$ series. Yield: 23 mg (0.03 mmol, 53%). IR (cm^{-1}): 2083 (m, $\nu_{C\equiv N}$), 2048 (w, $\nu_{C\equiv O}$) 1954 (s, $\nu_{C\equiv O}$), 1933 (s, $\nu_{C\equiv O}$), 1861 (m, $\nu_{C\equiv O}$). ^1H NMR (CD_2Cl_2, ppm): 7.62 (12H, s, Ar*H*), 7.45 (18H, s, Ar*H*). ^{31}P NMR (CD_2Cl_2, ppm): 34 (s, $\nu_{1/2}$ = 2341 Hz). ^{99}Tc NMR (CD_2Cl_2, ppm): −1509 (s, $\nu_{1/2}$ = 3061 Hz, Tc-NCSe), −1649 (s, $\nu_{1/2}$ = 3544 Hz, Tc-SeCN).

*[Tc(CN)(CO)$_3$(PPh$_3$)$_2$] (**9**) from KCN.* A solution of KCN (18 mg, 0.28 mmol) in MeOH (0.5 mL) was added to a suspension of $[Tc(OH_2)(CO)_3(PPh_3)_2][BF_4]$ (31 mg, 0.04 mmol) in CH_2Cl_2/MeOH (1 mL/0.5 mL). After the resulting clear solution was stirred for 5 min, water (2 mL) and CH_2Cl_2 (1 mL) were added. The separated organic phase was dried by filtering over a small bed of $MgSO_4$. The $MgSO_4$ was washed with CH_2Cl_2 (2 × 0.5 mL), and the combined filtrate and washing solutions were left for evaporation overnight. The formed colorless crystals were suspended in hexane, filtered, and washed with pentane (3 × 3 mL). After drying in air, colorless microcrystals were obtained. In contrast to other complexes of the type $[TcX(CO)_3(PPh_3)_2]$, the product is quite soluble in acetone. The product is sparingly soluble in CH_2Cl_2. The crystals were suitable for X-ray diffraction. Yield: 19 mg (0.03 mmol, 68%).

*[Tc(CN)(CO)$_3$(PPh$_3$)$_2$] (**9**) from KSeCN.* A solution of KSeCN (16 mg, 0.1 mmol) in MeOH (1 mL) was added to a suspension of $[Tc(OH_2)(CO)_3(PPh_3)_2][BF_4]$ (37 mg, 0.04 mmol) in CH_2Cl_2/MeOH (0.5 mL/0.5 mL). Red selenium precipitated immediately, and MeOH (10 mL) was added shortly after. The precipitated mixture of **8a**,**b**, **9**, and elemental selenium was filtered off, washed with MeOH (3 × 2 mL), and dried in air (40 mg). Slow evaporation of the filtrate gave colorless crystals of **9**·MeOH, which were suitable for X-ray diffraction. The crystals were filtered off and washed with MeOH. Yield: 11 mg (0.02 mmol, 30%).

*[Tc(CN)(CO)$_3$(PPh$_3$)$_2$] (**9**) from (PPN)TeCN.* A solution of (PPN)-TeCN (100 mg, 0.1 mmol) in dry, degassed THF (1 mL) was added to a suspension of $[Tc(OH_2)(CO)_3(PPh_3)_2][BF_4]$ (41 mg, 0.05 mmol) and NEt_3 (0.2 mL) in dry, degassed THF (1 mL) at ca. −40 °C. Black tellurium powder precipitated immediately, and a mixture of water and methanol (3 mL/6 mL) was added. The mixture was extracted with CH_2Cl_2 (3 mL). The separated organic phase was dried by filtering over a small bed of Na_2SO_4. The Na_2SO_4 was washed with CH_2Cl_2 (2 × 0.5 mL), and the combined filtrate and washing solutions were left for evaporation. The gray-brown residue was suspended in pentane and filtered off. It was washed with pentane to give an off-white powder. Yield: 15 mg (0.03 mmol, 41%). IR (cm^{-1}): 2116 (w, $\nu_{C\equiv N}$), 2054 (w, $\nu_{C\equiv O}$), 1960 (vs, $\nu_{C\equiv O}$), 1935 (vs, $\nu_{C\equiv O}$). ^1H NMR (CD_2Cl_2, ppm): 7.72 (12H, s, Ar*H*), 7.45 (18H, s, Ar*H*). ^{31}P NMR (CD_2Cl_2, ppm): 36 (s, $\nu_{1/2}$ = 1542 Hz). ^{99}Tc NMR (CD_2Cl_2, ppm): −1901 (s, $\nu_{1/2}$ = 5907 Hz).

*[Tc(η^2-OON)(CO)$_2$(PPh$_3$)$_2$] (**10**).* A solution of $NaNO_2$ (8 mg, 0.12 mmol) in water (1 mL) was added to a suspension of $[Tc(OH_2)(CO)_3(PPh_3)_2][BF_4]$ (18 mg, 0.02 mmol) in CH_2Cl_2 (1 mL). After the resulting biphasic mixture was stirred for 1 h, water (3 mL) was added and the organic phase was separated. The separated organic phase was dried by filtering over a small bed of Na_2SO_4. The water was extracted twice with CH_2Cl_2 (1 mL), and the extracts were then dried over Na_2SO_4. The combined extracts were left for evaporation overnight. Light yellow-green crystals of $[Tc(\eta^2\text{-}OON)(CO)_2(PPh_3)_2]$ (**10**) formed. They were suspended in pentane, filtered, washed with pentane (3 × 3 mL), and dried in air. They were suitable for X-ray diffraction. Traces of $[Tc(\eta^1\text{-}NO_2)(CO)_2(PPh_3)_2]$ (**11a**) could not be removed. Yield: 16 mg (0.02 mmol, 100%). IR (cm^{-1}): 1946 (vs, $\nu_{C\equiv O}$), 1871 (vs, $\nu_{C\equiv O}$). ^1H NMR (CD_2Cl_2, ppm): 7.43 (30H, s, Ar*H*). ^{31}P NMR (CD_2Cl_2, ppm): 46 (s, $\nu_{1/2}$ = 2341 Hz). ^{99}Tc NMR (CD_2Cl_2, ppm): −629 (s, $\nu_{1/2}$ = 4530 Hz).

*[Tc(η^1-NO$_2$)(CO)$_3$(PPh$_3$)$_2$] (**11a**)/[Tc(η^1-ONO)(CO)$_3$(PPh$_3$)$_2$] (**11b**).* CO(g) was bubbled through a light yellow solution of $[Tc(\eta^2\text{-}OON)(CO)_2(PPh_3)_2]$ (**10**) in CH_2Cl_2 (1 mL). A colorless solution formed after 1 min. The products were crystallized by the addition of hexane and slow evaporation, yielding plates of $[Tc(\eta^1\text{-}NO_2)(CO)_3(PPh_3)_2]$ (**11a**)/$[Tc(\eta^1\text{-}ONO)(CO)_3(PPh_3)_2]$ (**11b**). The crystals were filtered, washed with pentane (3 × 3 mL), and dried in air. Crystals suitable for X-ray diffraction were obtained by slow evaporation of a saturated CH_2Cl_2/MeOH solution. Yield: quantitative. IR (cm^{-1}): 2052 (w, $\nu_{C\equiv O}$), 1964 (vs, $\nu_{C\equiv O}$, **11a**), 1946 (m, $\nu_{C\equiv O}$, **11b**), 1913 (m, $\nu_{C\equiv O}$, **11b**), 1871 (vs, $\nu_{C=O}$, **11a**). ^1H NMR (CD_2Cl_2, ppm): 7.62 (12H, s, Ar*H*), 7.45 (18H, s, Ar*H*). ^{99}Tc NMR (CD_2Cl_2, ppm): −1305 (s, $\nu_{1/2}$ = 3594 Hz, η^1-ONO), −1431 (s, $\nu_{1/2}$ = 3544 Hz, η^1-NO_2). The ^{31}P NMR resonances were too broad to be observed due to couplings with the quadrupole moment of ^{99}Tc.

*[Tc(η^2-OONO)(CO)$_2$(PPh$_3$)$_2$] (**12**).* A solution of $NaNO_3$ (3 mg, 0.04 mmol) in water (1 mL) was added to a suspension of $[Tc(OH_2)(CO)_3(PPh_3)_2][BF_4]$ (17 mg, 0.02 mmol) in CH_2Cl_2 (1 mL). After the resulting biphasic mixture was stirred for 15 min, the organic phase was separated and dried by filtering over a small bed of Na_2SO_4. The light yellow-green solution was left for evaporation overnight. The resulting colorless residue was partially dissolved in CH_2Cl_2 (0.5 mL) and reprecipitated with pentane (12 mL). The light yellow-green powder of $[Tc(\eta^2\text{-}OONO)(CO)_2(PPh_3)_2]$ (**12**) was filtered, washed with pentane (3 × 3 mL), and dried in air. Crystals suitable for X-ray diffraction were obtained by slow evaporation of a CH_2Cl_2/MeOH mixture. Yield: 15 mg (0.02 mmol, 97%). IR (cm^{-1}): 1952 (vs, $\nu_{C\equiv O}$), 1879 (vs, $\nu_{C\equiv O}$), 1524 (vs, $\nu_{N=O}$). ^1H NMR (CD_2Cl_2, ppm): 7.73−7.23 (30H, m, Ar*H*). ^{99}Tc NMR (CD_2Cl_2, ppm): −820 (s, $\nu_{1/2}$ = 4165 Hz). The ^{31}P NMR resonance was too broad to be observed due to couplings with the quadrupole moment of ^{99}Tc.

*[Tc(η^1-ONO$_2$)(CO)$_3$(PPh$_3$)$_2$] (**13**).* CO(g) was bubbled through a light yellow solution of $[Tc(\eta^2\text{-}OONO)(CO)_2(PPh_3)_2]$ (**12**) in CH_2Cl_2 (1 mL). After the mixture was heated to reflux, a colorless solution formed. It was heated for 5 min. After this time, the ^{99}Tc NMR spectrum of the mixture indicated the complete conversion of **12** into $[Tc(\eta^1\text{-}ONO_2)(CO)_3(PPh_3)_2]$ (**13**). All attempts to isolate **13** in crystalline form resulted in the regeneration of dicarbonyl **12**. ^{31}P NMR (CD_2Cl_2, ppm): 39 (s, $\nu_{1/2}$ = 3511 Hz). ^{99}Tc NMR (CD_2Cl_2, ppm): −1275 (s, $\nu_{1/2}$ = 3594 Hz).

*[Tc(η^2-HHBH$_2$)(CO)$_2$(PPh$_3$)$_2$] (**15**).* A solution of BH_3·THF (0.5 mL, 0.5 mmol, 1 M) was added to $[TcH(CO)_3(PPh_3)_2]$ (35 mg, 0.05 mmol) in 0.5 mL of THF under Ar. The mixture was heated to reflux for 5 min. It turned yellow, and an off-white solid started to precipitate. Pentane (9 mL) was added, and the mixture was stored in a refrigerator overnight. The resulting light yellow precipitate was filtered off, washed with pentane, and dried in air to give a yellowish mixture of $[TcH(CO)_3(PPh_3)_2]$ with ca. 20% $[Tc(\eta^2\text{-}HHBH_2)(CO)_2(PPh_3)_2]$ (**15**). Crystals suitable for X-ray diffraction were obtained from the filtrate. Yield/recovery: 17 mg. Analytical data are only given for **15**, although the sample also contained a significant amount of $[TcH(CO)_3(PPh_3)_2]$. IR (cm^{-1}): 2479 (w, $\nu_{B-H,terminal}$), 2440 (w, $\nu_{B-H\cdots Tc}$), 2021 (w, $\nu_{B-H/Tc-H}$), 1956 (m, $\nu_{C\equiv O}$), 1886 (m, $\nu_{C\equiv O}$). ^1H NMR (CD_2Cl_2, ppm): −5.56 (s, $\nu_{1/2}$ = 116 Hz, Tc−B*H*$_4$). ^{99}Tc NMR (CD_2Cl_2, ppm): −964 (s, $\nu_{1/2}$ = 5075 Hz).

*[Tc(η^2-OO(CCH$_3$))(CO)$_2$(PPh$_3$)$_2$] (**16**) from NaOAc.* A solution of NaOAc·3H_2O (14 mg, 0.1 mmol) in MeOH (1 mL) was added to a suspension of $[Tc(OH_2)(CO)_3(PPh_3)_2][BF_4]$ (23 mg, 0.03 mmol) in CH_2Cl_2/MeOH (0.5 mL/0.5 mL). After the resulting clear yellow

https://doi.org/10.1021/acs.inorgchem.1c03919
Inorg. Chem. 2022, 61, 2980−2997

solution was stirred for 5 min, water (2 mL) and CH_2Cl_2 (1 mL) were added. The separated organic phase was dried by filtering over a small bed of Na_2SO_4. The Na_2SO_4 was washed with CH_2Cl_2 (2 × 0.5 mL), and the combined filtrate and washing solutions were left for evaporation overnight. The formed colorless crystals were suspended in pentane, filtered off, and washed with pentane (1 × 3 mL). They were suitable for X-ray diffraction. Yield: 25 mg (0.03 mmol, 60%).

*[Tc(η^2-OO(CCH$_3$))(CO)$_2$(PPh$_3$)$_2$] (**16**) from Potassium Monothioacetate.* A suspension of potassium monothioacetate (4 mg, 0.04 mmol) in H_2O (1 mL) was added to a suspension of [Tc(OH_2)-$(CO)_3(PPh_3)_2$][BF_4] (15 mg, 0.02 mmol) in CH_2Cl_2 (1 mL). The biphasic mixture was stirred for 15 min, during which time the organic phase turned yellow. The separated organic phase was dried by filtering over a small bed of Na_2SO_4. The Na_2SO_4 was washed with CH_2Cl_2 (2 × 0.5 mL), and the combined filtrate and washing solutions were left for evaporation overnight. The orange-yellow residue was partially dissolved in CH_2Cl_2 (0.5 mL) and reprecipitated with pentane, filtered off, and washed with pentane (1 × 3 mL). A beige powder of **16** was obtained. Yield: 12 mg (0.02 mmol, 88%). The analytical data are as reported previously.[25]

*[Tc{η^2-SSC(CH$_3$)}(CO)$_2$(PPh$_3$)$_2$] (**17**) and [Tc{η^2-SSC(SCH$_3$)}-(CO)$_2$(PPh$_3$)$_2$] (**18a**).* A red-orange solution of Li(SSCCH$_3$) (ca. 0.8 M) was prepared by the addition of a MeLi solution (1 mL, 1.6 M) to a solution of CS_2 (122 mg, 1.6 mmol) in dry, degassed THF (1 mL). An aliquot (0.08 mmol, 0.1 mL) of the thus-prepared solution was added dropwise to a suspension of [Tc(OH_2)$(CO)_3(PPh_3)_2$][BF_4] (15 mg, 0.02 mmol) in THF (0.5 mL). Large colorless crystals precipitated immediately, which were dissolved by the addition of MeOH (9 mL). The mixture was left for evaporation for 2 days. The formed yellow plates were filtered off and washed with a small amount of MeOH (2 × 0.5 mL) and pentane (3 × 3 mL). After drying, the yellow plates were suitable for X-ray diffraction. The crystals consist of cocrystallized [Tc{η^2-SS(CCH_3)}$(CO)_2(PPh_3)_2$] (**17**) and [Tc{η^2-SS($CSCH_3$)}$(CO)_2(PPh_3)_2$] (**18a**). Yield: 12 mg (0.02 mmol, 80%). IR (cm^{-1}): 1938 (vs, $\nu_{C\equiv O}$), 1865 (vs, $\nu_{C\equiv O}$), 1481 (broad, $\nu_{C=S}$, **16**), 1433 (broad, $\nu_{C=S}$, **15a/b**). ^{1}H NMR (CD_2Cl_2, ppm): 7.60 (12H, 2s, Ar*H*), 7.38 (18H, 2s, Ar*H*), 1.86 (2H, s, η^2-SSCSCH_3) 1.47 (1H, s, η^2-SSCCH_3). ^{99}Tc NMR (CD_2Cl_2, ppm): −1339 (t, $\nu_{1/2}$ = 345 Hz, $^1J_{Tc-P}$ = 559 Hz, η^2-SSCCH_3), −1374 (t, $\nu_{1/2}$ = 317 Hz, $^1J_{Tc-P}$ = 611 Hz, η^2-SSCOCH_3), −1409 (t, $\nu_{1/2}$ = 349 Hz, $^1J_{Tc-P}$ = 593 Hz, η^2-SSCSCH_3). The ^{31}P NMR resonances were too broad to be observed due to couplings with the quadrupole moment of ^{99}Tc.

*[Tc(η^2-SS(CH))(CO)$_2$(PPh$_3$)$_2$] (**20**).* CS_2 (1 mL) was added to a suspension of [TcH$(CO)_3(PPh_3)_2$] (16 mg, 0.02 mmol) in toluene (0.5 mL) and heated to reflux for 5 min. MeOH (9 mL) was added, and the solution was left for evaporation for 2 days. The formed yellow crystals were filtered off and washed with MeOH (2 × 1 mL) and pentane (2 × 3 mL). After drying in air, yellow plates that were suitable for X-ray diffraction were obtained. If necessary, traces of **19** could be removed by heating in toluene for an additional 5 min. Yield: 15 mg (0.02 mmol, 88%). IR (cm^{-1}): 2045 (w, $\nu_{C\equiv O}$), 1946 (vs, $\nu_{C\equiv O}$), 1869 (vs, $\nu_{C\equiv O}$). ^{1}H NMR (CD_2Cl_2, ppm): 10.12 (1H, s, η^2-SSC*H*), 7.61 (12H, s, Ar*H*), 7.39 (18H, s, Ar*H*). ^{99}Tc NMR (CD_2Cl_2, ppm): −1250 (t, $\nu_{1/2}$ = 404 Hz, $^1J_{Tc-P}$ = 583 Hz). The ^{31}P NMR resonance was too broad to be observed due to couplings with the quadrupole moment of ^{99}Tc.

*[Tc(OTcO$_3$)(CO)$_3$(PPh$_3$)$_2$] (**21**).* Water (0.2 mL) was added to a suspension of NH_4TcO_4 (4 mg, 0.02 mmol) and [Tc(OH_2)-$(CO)_3(PPh_3)_2$][BF_4] (15 mg, 0.02 mmol) in THF (1 mL) to give a yellow solution. The mixture was stirred for 30 min. After evaporation of the THF overnight, yellow crystals formed. The crystals were suspended in MeOH (2 mL) and filtered. After washing with MeOH (3 × 3 mL), they were dried in air. Yield: 13 mg (0.02 mmol, 83%). IR (cm^{-1}): 2073 (m, $\nu_{C\equiv O}$), 1964 (vs, $\nu_{C\equiv O}$), 1923 (vs, $\nu_{C\equiv O}$), 1865 (w, $\nu_{C\equiv O}$), 912 (vs, $\nu_{Tc=O}$). ^{1}H NMR (CD_2Cl_2, ppm): 7.63−7.52 (12H, m, Ar*H*), 7.52−7.43 (18H, m, Ar*H*). ^{31}P NMR (CD_2Cl_2, ppm): 36 (s, $\nu_{1/2}$ = 2969 Hz). ^{99}Tc NMR (CD_2Cl_2, ppm): 41 (s, $\nu_{1/2}$ = 208 Hz, OT*c*O$_3$), −1137 (s, $\nu_{1/2}$ = 3996 Hz).

*[Tc(OReO$_3$)(CO)$_3$(PPh$_3$)$_2$] (**22**).* NH_4ReO_4 (7 mg, 0.02 mmol) and [Tc(OH_2)$(CO)_3(PPh_3)_2$][BF_4] (15 mg, 0.02 mmol) were dissolved in THF/water (1 mL/5 drops). The mixture was stirred for 30 min and turned yellow-green. After evaporation of the THF overnight, a yellow precipitate formed under a greenish aqueous phase. The precipitate was suspended in 0.5 mL of water and filtered. After washing with additional water, the greenish impurities were removed by washing with MeOH (2 × 1 mL). Drying in air gave a yellow powder of **22**. Yield: 6 mg (0.01 mmol, 38%). IR (cm^{-1}): 2073 (m, $\nu_{C\equiv O}$), 1964 (vs, $\nu_{C\equiv O}$), 1923 (vs, $\nu_{C\equiv O}$), 1863 (m, $\nu_{C\equiv O}$), 927 (vs, $\nu_{Re=O}$). ^{1}H NMR (CD_2Cl_2, ppm): 7.62−7.52 (12H, m, Ar*H*), 7.52−7.44 (18H, m, Ar*H*). ^{31}P NMR (CD_2Cl_2, ppm): 38 (s, $\nu_{1/2}$ = 4463 Hz). ^{99}Tc NMR (CD_2Cl_2, ppm): −1166 (s, $\nu_{1/2}$ = 4063 Hz).

*[Tc(OTcO$_3$)(acetone)(CO)$_2$(PPh$_3$)$_2$]·acetone (**23c**).* A suspension of [Tc$(OTcO_3)(CO)_3(PPh_3)_2$] (10 mg, 0.01 mmol) in acetone (0.5 mL) was heated to reflux for 5 min. Pentane (6 mL) was added to the resulting yellow solution, and the mixture was left to evaporate. Overnight, yellow microcrystals formed. They were suspended in pentane (1 mL), filtered off, washed with pentane (2 mL), and dried in air. Crystals suitable for X-ray diffraction were obtained from the diffusion of acetone vapor into a powder of [Tc($OTcO_3$)-$(CO)_3(PPh_3)_2$]. Yield: 7 mg (0.01 mmol, 70% based on Tc). IR (cm^{-1}): 2079 (vw, $\nu_{C\equiv O}$), 1942 (vs, $\nu_{C\equiv O}$), 1852 (vs, $\nu_{C\equiv O}$), 1705 (m, $\nu_{C=O}$, acetone in lattice), 1672 (m, $\nu_{C=O}$, Tc−O=CMe_2), 905 (m, $\nu_{Tc=O}$), 870 (m, $\nu_{Tc=O}$), ^{1}H NMR (CD_2Cl_2, ppm): 7.62 (12H, s, Ar*H*), 7.47 (18H, s, Ar*H*), 2.12 (8H, s, acetone). ^{99}Tc NMR (CD_2Cl_2, ppm): 37 (s, $\nu_{1/2}$ = 588 Hz, [Tc(OT*c*O$_3$)(acetone)$(CO)_2(PPh_3)_2$]), 32 (s, $\nu_{1/2}$ = 240 Hz, [Tc(OT*c*O$_3$)$(H_2O)(CO)_2(PPh_3)_2$]), −803 (s, $\nu_{1/2}$ = 1643 Hz, [T*c*$(OTcO_3)$(solv)$(CO)_2(PPh_3)_2$]).

■ ASSOCIATED CONTENT

Supporting Information

The Supporting Information is available free of charge at https://pubs.acs.org/doi/10.1021/acs.inorgchem.1c03919.

Crystallographic tables, bond lengths angles, ellipsoid plots, and spectroscopic data (PDF)

Accession Codes

CCDC 2127177−2127192 contain the supplementary crystallographic data for this paper. These data can be obtained free of charge via www.ccdc.cam.ac.uk/data_request/cif, or by emailing data_request@ccdc.cam.ac.uk, or by contacting The Cambridge Crystallographic Data Centre, 12 Union Road, Cambridge CB2 1EZ, UK; fax: +44 1223 336033.

■ AUTHOR INFORMATION

Corresponding Author

Ulrich Abram − *Institute of Chemistry and Biochemistry, Freie Universität Berlin, D-14195 Berlin, Germany;* orcid.org/0000-0002-1747-7927; Email: ulrich.abram@fu-berlin.de

Authors

Maximilian Roca Jungfer − *Institute of Chemistry and Biochemistry, Freie Universität Berlin, D-14195 Berlin, Germany*

Laura Elsholz − *Institute of Chemistry and Biochemistry, Freie Universität Berlin, D-14195 Berlin, Germany*

Complete contact information is available at: https://pubs.acs.org/10.1021/acs.inorgchem.1c03919

Notes

The authors declare no competing financial interest.

■ ACKNOWLEDGMENTS

We gratefully acknowledge support from the Core Facility 1249 BioSupraMol.

REFERENCES

(1) Levitskaia, T. G.; Anderson, A.; Chatterjee, S. D.; Cho, H. M.; Rapko, B. M.; Peterson, J. M.; Walter, E. D.; Washton, N. M. *Speciation and Oxidative Stability of 23654; EMSP-RPT-024*, Rev. 0; U.S. Department of Energy: 2014.

(2) Lukens, W. W.; Shuh, D. K.; Schroeder, N. C.; Ashley, K. R. *Behavior of Technetium in Alkaline Solution: Identification of Non-Pertechnetate Species in High-Level Nuclear Waste Tanks at the Hanford Reservation. 11 Sep 2003*; 20 p; American Chemical Society Meeting, Fall 2003; New York, NY (United States), 7−11 Sep 2003; AC03-76SF00098; Also available from OSTI as DE00817638. PURL: https://www.osti.gov/servlets/purl/817638-gLf1u2/native/.

(3) McGregor, D.; Burton-Pye, B. P.; Howell, R. C.; Mbomekalle, I. M.; Lukens, W. W., Jr; Bian, F.; Mausolf, E.; Poineau, F.; Czerwinski, K. R.; Francesconi, L. C. Synthesis, Structure Elucidation, and Redox Properties of ^{99}Tc Complexes of Lacunary Wells-Dawson Polyoxometalates: Insights into Molecular ^{99}Tc-Metal Oxide Interactions. *Inorg. Chem.* **2011**, *50*, 1670−1681.

(4) Lukens, W. W.; Shuh, D. K.; Schroeder, N. C.; Ashley, K. R. Correction to "Identification of the Non-Pertechnetate Species in Hanford Waste Tanks, Tc(I)-Carbonyl Complexes. *Environ. Sci. Technol.* **2004**, *38* (1), 229−233.

(5) Chatterjee, S.; Holfeltz, V. E.; Hall, G. B.; Johnson, I. E.; Walter, E. D.; Lee, S.; Reinhart, B.; Lukens, W. W.; Machara, N. P.; Levitskaia, T. G. Identification and Quantification of Technetium Species in Hanford Waste Tank AN-102. *Anal. Chem.* **2020**, *92*, 13961−13970.

(6) Jones, A. G.; Abrams, M. J.; Davison, A.; Brodack, J. W.; Toothaker, A. K.; Adelstein, S. J.; Kassis, A. I. Biological studies of a new class of technetium complexes: the hexakis(alkylisonitrile)-technetium(I) cations. *Int. J. Nucl. Med. Biol.* **1984**, *11*, 225−234.

(7) Kronauge, J. F.; Mindiola, D. J. The Value of Stable Metal-Carbon Bonds in Nuclear Medicine and the Cardiolite Story. *Organometallics* **2016**, *35*, 3432−3435.

(8) Bartholomä, M. D.; Louie, A. S.; Valliant, J. F.; Zubieta, J. Technetium and gallium derived radiopharmaceuticals: comparing and contrasting the chemistry of two important radiometals for the molecular imaging era. *Chem. Rev.* **2010**, *110*, 2903−2920.

(9) Papagiannopoulou, D. Technetium-99m radiochemistry for pharmaceutical applications. *J. Labelled Compd. Radiopharm.* **2017**, *60*, 502−520.

(10) Abram, U.; Alberto, R. Technetium and rhenium - coordination chemistry and nuclear medical applications. *J. Braz. Chem. Soc.* **2006**, *17*, 1486−1500.

(11) Kuntic, V.; Brboric, J.; Vujic, Z.; Uskokovic-Markovic, S. Radioisotopes Used as Radiotracers in vitro and in vivo Diagnostics: A Review. *Asian J. Chem.* **2016**, *28*, 235−411.

(12) Abrams, M. J.; Davison, A.; Jones, A. G.; Costello, C.; Pang, H. Synthesis and Characterization of Hexakis(alkyl isocyanide) and Hexakis(aryl isocyanide) Complexes of Technetium(I). *Inorg. Chem.* **1983**, *22*, 2798−2800.

(13) Sattelberger, A. P.; Scott, B. L.; Poineau, F. Technetium Organometallics. In *Comprehensive Organometallic Chemistry III*; Mingos, D. M. P.; Crabtree, R. H., Eds.; Elsevier: 2007; pp 833−854 and references cited therein.

(14) Alberto, R. The "Carbonyl Story" and Beyond; Experiences, Lessons and Implications. *ChemMedChem.* **2020**, *21*, 2743−2749 and references cited therein.

(15) Duatti, A. Review on ^{99m}Tc radiopharmaceuticals with emphasis on new advancements. *Nucl. Med. Biol.* **2021**, *92*, 202−216.

(16) Alberto, R.; Schibli, R.; Abram, U.; Egli, A.; Knapp, F. F.; Schubiger, P. A. Potential of the "$[M(CO)_3]^{+}$" (M = Re, Tc) Moiety for the Labeling of Biomolecules. *Radiochim. Acta* **1997**, *79*, 99−150.

(17) Alberto, R.; Schibli, R.; Egli, A.; Schubiger, A. P.; Abram, U.; Kaden, T. A. A Novel Organometallic Aqua Complex of Technetium for the Labeling of Biomolecules: Synthesis of $[^{99m}Tc(OH_2)_3(CO)_3]^{+}$ from $[^{99m}TcO_4]^{-}$ in Aqueous Solution and Its Reaction with a Bifunctional Ligand. *J. Am. Chem. Soc.* **1998**, *120*, 7987−7988.

(18) Alberto, R.; Schibli, R.; Waibel, R.; Abram, U.; Schubiger, A. P. Basic aqueous chemistry of $[M(OH_2)_3(CO)_3]^{+}$ (M = Re, Tc) directed towards radiopharmaceutical application. *Coord. Chem. Rev.* **1999**, *190−192*, 901−919.

(19) Alberto, R. The Chemistry of Technetium-Water Complexes within the Manganese Triad: Challenges and Perspectives. *Eur. J. Inorg. Chem.* **2009**, *2009*, 21−31.

(20) Grundler, P. V.; Helm, L.; Alberto, R.; Merbach, A. E. Relevance of the Ligand Exchange Rate and Mechanism of *fac*-$[(CO)_3M(H_2O)_3]^{+}$ (M = Mn, Tc, Re) Complexes for New Radiopharmaceuticals. *Inorg. Chem.* **2006**, *45*, 10378−10390.

(21) Duatti, A. Review on ^{99m}Tc radiopharmaceuticals with emphasis on new advancements. *Nucl. Med. Biol.* **2021**, *92*, 202−216.

(22) Mundwiler, S.; Kundig, M.; Ortner, K.; Alberto, R. A new [2 + 1] mixed ligand concept based on $[^{99(m)}Tc(OH_2)_3(CO)_3]^{+}$: a basic study. *Dalton Trans.* **2004**, 1320−1328.

(23) Alberto, R.; Herrmann, W. A.; Kiprof, P.; Baumgartner, F. Multiple Bonds between Main Group Elements and Transition Metals. Synthesis and Reactivity of $TcCl(CO)_3[P(C_6H_5)_2]_2$: Novel Technetium Complexes of 1,4,7-Triazacyclononane and Hydrotris-(pyrazolyl)borate. *Inorg. Chem.* **1992**, *31*, 895−899.

(24) Claude, G.; Salsi, F.; Hagenbach, A.; Gembicky, M.; Drance, M. J.; Neville, M.; Chan, C.; Figueroa, J. S.; Abram, U. Structural and Redox Variations in Technetium Complexes Supported by *m*-Terphenyl Isocyanides. *Organometallics* **2020**, *39*, 2287−2294.

(25) Jungfer, M. R.; Elsholz, L.; Abram, U. Technetium Hydrides Revisited: Syntheses, Structures and Reactions of $[TcH_3(PPh_3)_4]$ and $[TcH(CO)_3(PPh_3)_2]$. *Organometallics* **2021**, *40*, 3095−3112.

(26) Roca Jungfer, M.; Abram, U. $[Tc(OH_2)(CO)_3(PPh_3)_2]^{+}$: A Synthon for Tc(I) Complexes and Its Reactions with Neutral Ligands. *Inorg. Chem.* **2021**, *60*, 16734−16753.

(27) Ackermann, J.; Abdulkader, A.; Scholtysik, C.; Jungfer, M. R.; Hagenbach, A.; Abram, U. $[Tc^{I}(NO)X(Cp)(PPh_3)]$ Complexes (X^{-} = I^{-}, I_3^{-}, SCN^{-}, $CF_3SO_3^{-}$, or CF_3COO^{-}) and Their Reactions. *Organometallics* **2019**, *38*, 4471−4478.

(28) Balasekaran, S. M.; Spandl, J.; Hagenbach, A.; Köhler, K.; Drees, M.; Abram, U. Fluoridonitrosyl Complexes of Technetium(I) and Technetium(II). Synthesis, Characterization, Reactions, and DFT Calculations. *Inorg. Chem.* **2014**, *53*, 5117−5128.

(29) Stepanova, E. S.; Gurzhiy, V. V.; Tyupina, M. Y.; Miroslavov, A. E.; Sidorenko, G. V.; Lumpov, A. A. Does $[TcF(CO)_5]$ exist? The crystal and molecular structure of $[Tc(CO)_3(OH)_{0.49}F_{0.51}]_4\cdot[Tc(CO)_5(BF_4)]$. *Dalton Trans.* **2016**, *45*, 8428−8432.

(30) Balasekaran, S. M.; Hagenbach, A.; Spandl, J.; Abram, U. The Reaction of $Cs_2[Tc(NO)F_5]$ with BF_3 in Acetonitrile: Formation and Structure of $[\{Tc(NO)(CH_3CN)_4\}_2(\mu\text{-}F)](BF_4)_3$. *Z. Anorg. Allg. Chem.* **2017**, *643*, 1146−1149.

(31) Balasekaran, S. M.; Hagenbach, A.; Drees, M.; Abram, U. $[Tc^{II}(NO)(trifluoroacetate)_4F]^{2-}$ - synthesis and reactions. *Dalton Trans.* **2017**, *46*, 13544−13552.

(32) Alberto, R.; Schibli, R.; Egli, A.; Abram, U.; Abram, S.; Kaden, T. A.; Schubiger, P. A. Steps towards $[(C_5Me_5)TcO_3]$: Novel synthesis of $[(C_5Me_5)Tc(CO)_3]$ from $[\{Tc(\mu^3\text{-}OH)(CO)_3\}_4]$ and oxidation of $[(C_5Me_5)M(CO)_3]$ (M = Tc, Re) with Br_2. *Polyhedron* **1998**, *17*, 1133−1140.

(33) Cook, J.; Davison, A. Nucleophilic attack on coordinated CO in $[Tc(CO)_4(PPh_3)_2]BF_4$. *J. Organomet. Chem.* **1996**, *507*, 47−51.

(34) Trop, H. S.; Davison, A.; Jones, A. G.; Davis, M. A.; Szalda, D. J.; Lippard, S. J. Synthesis and Physical Properties of Hexakis-(isothiocyanato)technetate(III) and -(IV) Complexes. Structure of the $[Tc(NCS)_6]^{3-}$ Ion. *Inorg. Chem.* **1980**, *19*, 1105−1110.

(35) Williams, G. A.; Bonnyman, J.; Baldas, J. Structural Studies of Technetium Complexes. X* The Crystal Structure of Tetraphenylarsonium Hexakis(isothiocyanato)technetate(IV)- Dichloromethane (1/1). *Aust. J. Chem.* **1987**, *40*, 27−33.

(36) Hauck, J.; Schwochau, K. Zur Kristallstruktur komplexer Technetium-Verbindungen. II. $[(CH_3)_4N][Tc^{V}(NCS)_6]$. *Inorg. Nucl. Chem. Letters* **1973**, *9*, 927−929.

(37) Hauck, J.; Schwochau, K. Zur Kristallstruktur komplexer Technetium-Verbindungen. I. $[(CH_3)_4N]_2[Tc^{IV}(NCS)_6]$. *Inorg. Nucl. Chem. Letters* **1973**, *9*, 303−304.

https://doi.org/10.1021/acs.inorgchem.1c03919
Inorg. Chem. 2022, 61, 2980−2997

(38) Baldas, J.; Bonnyman, J.; Williams, G. A. Structural Studies of Technetium Complexes. Part 4. The Crystal Structure of *trans, trans*-Acetonitriledi-isothiocyanato(nitrido) bis-(triphenylphosphine) technetium (V)-acetonitrile (1/0.5). *J. Chem. Soc., Dalton Trans.* **1984**, *5*, 833−837.
(39) Bandoli, G.; Mazzi, U.; Ichimura, A.; Libson, K.; Heineman, W. R.; Deutsch, E. An Isothiocyanato Complex of Technetium(II). Spectroelectrochemical and Single-Crystal X-ray Structural Studies on *trans*-$[Tc(DPPE)_2(NCS)_2]$, where DPPE = 1,2-Bis-(diphenylphosphino)ethane. *Inorg. Chem.* **1984**, *23*, 2898−2901.
(40) Rochon, F. D.; Melanson, R.; Kong, P.-C. Synthesis of new mixed-ligands Tc complexes containing monodentate phosphine and isothiocyanato ligands: Crystal structures of complexes $Tc(P(C_3H_7)_3)_2(NCS)_4$, $Tc(P(CH_3)_2Ph)_4(NCS)_2$ and $Tc(P(OCH_3)Ph_2)_4(NCS)_2 \cdot 1{:}2CH_2Cl_2$. *Inorg. Chim. Acta* **2000**, *300*, 43−48.
(41) *Cambridge Structural Database, Release 5.42*, Update May 2021.
(42) Kurz, P.; Spingler, B.; Fox, T.; Alberto, R. $[Tc^I(CN)_3(CO)_3]^{2-}$ and $[Re^I(CN)_3(CO)_3]^{2-}$: Case Studies for the Binding Properties of CN^- and CO. *Inorg. Chem.* **2004**, *43*, 3789−3791.
(43) Werner, A. Beitrag zur Konstitution anorganischer Verbindungen. *Z. Anorg. Chem.* **1893**, *3*, 267−330.
(44) Marchi, A.; Rossi, R.; Duatti, A.; Zucchini, G. L.; Luciano, M. Preparation and characterization of mixed amido, carboxylato or thiazolato carbonyl(phosphine)technetium(I) complexes. *Transition Met. Chem.* **1986**, *11*, 164−166.
(45) Marchi, A.; Marvelli, L.; Rossi, R.; Bertolasi, V.; Ferretti, V. Technetium and rhenium carbonyl complexes with 1,4-benzodiazepine derivatives: X-ray crystal structure. *Inorg. Chim. Acta* **1998**, *272*, 267−273.
(46) Rossi, R.; Marchi, A.; Aggio, S.; Magon, L.; Duatti, A.; Casellato, U.; Graziani, R. The chemistry of heteroallyl derivatives of technetium. Reactivity of $[TcNCl_2(PPh_3)_2]$ and $[Tc(CO)_3Cl(PPh_3)_2]$ with thiazetidine ligands, crystal structures of $[Tc(CO)_2(PPh_3)_2\{PhN = C(OEt)S\}]$ and $[TcN(Cl)(PPh_3)\{PhN = C(OEt)S\}]$. *J. Chem. Soc., Dalton Trans.* **1990**, 477−481.
(47) Marchi, A.; Rossi, R.; Duatti, A.; Magon, L.; Bertolasi, V.; Ferretti, V.; Gilli, G. Reactions of the Technetium(I) Carbonyl Complexes $[Tc(PMe_2Ph)_3(CO)_2Cl]$ and $[Tc(PPh_3)_2(CO)_3Cl]$ toward Pseudoallyl Ligands Such as Triazenido, Formamidinato, and Acetamidinato. Crystal Structures of $[Tc(PMe_2Ph)_2(CO)_2(p\text{-}CH_3C_6H_4N = N{=}NC_6H_4CH_3\text{-}p)]$ and $[Tc(PMe_2Ph)_2(CO)_2(C_6H_5N = C(CH_3){=}NC_6H_5)]$. *Inorg. Chem.* **1985**, *24*, 4744−4748.
(48) Rossi, R.; Marchi, A.; Magon, L.; Duatti, A.; Casellato, U.; Graziani, R. Synthesis and characterization of new technetium(I) and rhenium(I) Schiff base complexes. Crystal structure of $[M(PPh_3)_2(CO)_2\{(C_3H_2NS)N = CHC_6H_4O\}]$ (M = Tc, Re; C_3H_2NS = Thiazol-2-yl). *Inorg. Chim. Acta* **1989**, *160*, 23−28.
(49) Alberto, R.; Schibli, R.; Egli, A.; Schubiger, P. A.; Herrmann, W. A.; Artus, G.; Abram, U.; Kaden, T. A. Metal carbonyl syntheses XXII. Low pressure carbonylation of $[MOCl_4]^-$ and $[MO_4]^-$: the technetium(I) and rhenium(I) complexes $[NEt_4]_2[MCl_3(CO)_3]$. *J. Organomet. Chem.* **1995**, *493*, 119−127.
(50) Hildebrand, S. $(NBu_4)[Tc_2(\mu\text{-}Cl)_3(CO)_6]$ als Startverbindung für Technetiumtricarbonylkomplexe. Ph.D. Thesis, Freie Universität Berlin, 2018.
(51) Mundwiler, S.; Braband, H.; Alberto, R.; Mcgregor, D.; Howell, R. C.; Francesconi, L. C. Bis(tetraethylammonium)*fac*-Tribromotricarbonylrhenate(I) and Technetate(I). *Inorg. Synth.* **2014**, *36*, 149−155.
(52) Tarhan, C.; Cil, M. A. A study on hydrogen, the clean energy of the future: hydrogen storage methods. *J. Energy Storage* **2021**, *40*, 102676.
(53) George, L.; Saxena, S. K. Structural stability of metal hydrides, alanates, borohydrides of alkali and alkali-earth elements: A review. *Int. J. Hydrogen Energy* **2010**, *35*, 5454−5470.
(54) Kim, D. S.; Soderquist, C. Z.; Icenhower, J. P.; McGrail, B. P.; Scheele, R. D.; McNamara, B. K.; Bagaasen, L. M.; Schweiger, M. J.; Crum, J. V.; Yeager, D. J.; Matyas, J.; Darnell, L. P.; Schaef, H. T.; Owen, A. T.; Kozelisky, A. E.; Snow, L. A.; Steele, M. J. Tc Reductant Chemistry and Crucible Melting Studies, with Simulated Hanford Low-Activity Waste. *Pacific Northwest National Laboratory Report, PNNL-15131*, 2005.
(55) Gusev, D.; Llamazares, A.; Artus, G.; Jacobsen, H.; Berke, H. Classical and Nonclassical Nitrosyl Hydride Complexes of Rhenium in Various Oxidation States. *Organometallics* **1999**, *18*, 75−89.
(56) Liu, X.-Y.; Bouherour, S.; Jacobsen, H.; Schmalle, H. W.; Berke, H. The interaction of Lewis acidic boron derivatives with $Re(CO)_{5-n}(H(PMe_3)_n$ complexes. *Inorg. Chim. Acta* **2002**, *330*, 250−267.
(57) Maria, L.; et al. Very Small and Soft Scorpionates: Water Stable Technetium Tricarbonyl Complexes Combining a Bis-agostic (t^3-H, H, S) Binding Motif with Pendant and Integrated Bioactive Molecules. *J. Am. Chem. Soc.* **2006**, *128*, 14590−14598.
(58) Garcia, R.; Paulo, A.; Domingos, Ł.; Santos, I.; Ortner, K.; Alberto, R. Re and Tc Complexes Containing B-H···M Agostic Interactions as Building Blocks for the Design of Radiopharmaceuticals. *J. Am. Chem. Soc.* **2000**, *122*, 11240−11241.
(59) Grote, J.; Friedrich, F.; Berthold, K.; Hericks, L.; Neumann, B.; Stammler, H.-G.; Mitzel, N. W. Dithiocarboxylic Acids: An Old Theme Revisited and Augmented by New Preparative, Spectroscopic and Structural Facts. *Chem. - Eur. J.* **2018**, *24*, 2626−2633.
(60) Lorenz, B.; Findeisen, M.; Schmidt, K. Synthese, Charakterisierung und Tc-99-NMR-Spektren von Technetium-Carbonyl-Komplexen mit Dithioliganden. *Isotopenpraxis* **1991**, *27*, 266−267.
(61) Miroslavov, A. E.; Lumpov, A. A.; Sidorenko, G. V.; Levitskaya, E. M.; Gorshkov, N. I.; Suglobov, D. N.; Alberto, R.; Braband, H.; Gurzhiy, V. V.; Krivovichev, S. V.; Tananaev, I. G. Complexes of technetium(I) (^{99}Tc, ^{99m}Tc) pentacarbonyl core with c-acceptor ligands (tert-butyl isocyanide and triphenylphosphine): Crystal structures of $[Tc(CO)_5(PPh_3)]OTf$ and $[Tc(CO)_5(CNC(CH_3)_3)]ClO_4$. *J. Organomet. Chem.* **2008**, *693*, 4−10.
(62) Miroslavov, A. E.; Polotskii, Y. S.; Gurzhiy, V. V.; Ivanov, A. Y.; Lumpov, A. A.; Tyupina, M. Y.; Sidorenko, G. V.; Tolstoy, P. M.; Maltsev, D. A.; Suglobov, D. N. Technetium and Rhenium Pentacarbonyl Complexes with C2 and C11 ω-Isocyanocarboxylic Acid Esters. *Inorg. Chem.* **2014**, *53*, 7861−7869.
(63) Cook, J.; Davison, A.; Davis, W. M.; Jones, A. G. Insertion Chemistry of HTc(CO)3(PPh3)2. *Organometallics* **1995**, *14*, 650−655.
(64) Ardizzoia, C. A.; Cenini, S.; D'Alfonso, G.; la Monica, G.; Masciocchi, N.; Moret, M. A Re(I)-Re(VII) Complex by the Oxygenation Reactions of Re(I) Species - Reactivity and X-Ray Structural Characterization of $Re(CO)_3(PPh_3)_2(OReO_3)$. *Gazz. Chim. Ital.* **1992**, *122*, 515−520.
(65) Baturin, N. A.; German, K. E.; Grigoriev, M. S. Kryutchkov, Electronic, crystal and molecular structure of tetra(μ-acetato)-ditechnetium(III) dipertechnetate(VII). *Koord. Khim.* **1991**, *17*, 1375−1383.
(66) German, K. E.; Fedoseev, A. M.; Grigoriev, M. S.; Kirakosyan, G. A.; Dumas, T.; Den Auwer, C.; Moisy, P.; Lawler, K. V.; Forster, P. M.; Poineau, F. A 70-Year-Old Mystery in Technetium Chemistry Explained by the New Technetium Polyoxometalate $[H_7O_3]_4[Tc_{20}O_{68}] \cdot 4H_2O$. *Chem.-Eur. J.* **2021**, *27*, 13624−13631.
(67) Zegke, M.; Grödler, D.; Roca Jungfer, M.; Haseloer, A.; Kreuter, M.; Neudörfl, J. M.; Sittel, T.; James, C. M.; Rothe, J.; Altmaier, M.; Klein, A.; Breugst, M.; Abram, U.; Strub, E.; Wickleder, M. S. Ammonium Pertechnetate in Mixtures of Trifluorosulfonic Acid and Trifluoromethanesulfonic Anhydride. *Angew. Chem., Int. Ed.* **2022**, *61*, No. e202113777.
(68) Sarsfield, M. J.; Sutton, A. D.; May, I.; John, G. H.; Sharrad, C.; Helliwell, M. Coordination of pertechnetate $[TcO_4]^-$ to actinides. *Chem. Commun.* **2004**, 2320−2321.
(69) Fedosseev, A. M.; Budantseva, N. A.; Grigoriev, M. S.; Guermann, K. E.; Krupa, J.-C. Synthesis and properties of neptunium(VI, V) and plutonium(VI) pertechnetates. *Radiochim. Acta* **2003**, *91*, 147−152.
(70) Mikhalev, V. A. ^{99}Tc NMR Spectroscopy. *Radiochemistry* **2005**, *47*, 319−333.

https://doi.org/10.1021/acs.inorgchem.1c03919
Inorg. Chem. 2022, 61, 2980−2997

(71) Kuhn, N.; Faupel, P.; Zauder, E. Ein einfaches Verfahren zur Synthese von $[EMe_3]I$ und EMe_2 (E = Se, Te). *J. Organomet. Chem.* **1986**, *302*, C4−C6.
(72) Martinsen, A.; Songstad, J.; et al. Preparation and Properties of Some Bis(triphenylphosphine)iminium Salts, $[(Ph_3P)_2NJX$. *Acta Chem. Scand.* **1977**, *31a*, 645−650.
(73) Sheldrick, G. M. *SADABS*; University of Göttingen: 1996.
(74) Coppens, P. The Evaluation of Absorption and Extinction in Single-Crystal Structure Analysis. *Crystallographic Computing*; Munksgaard: 1979.
(75) Sheldrick, G. M. A short history of SHELX. *Acta Crystallogr.* **2008**, *A64*, 112−122.
(76) Sheldrick, G. M. Crystal structure refinement with SHELXL. *Acta Crystallogr.* **2015**, *C71*, 3−8.
(77) *Diamond - Crystal and Molecular Structure Visualization*; Crystal Impact.
(78) High performance computing (HPC) system Curta at Freie Universität Berlin.
(79) Frisch, M. J.; Trucks, G. W.; Schlegel, H. B.; Scuseria, G. E.; Robb, M. A.; Cheeseman, J. R.; Scalmani, G.; Barone, V.; Petersson, G. A.; Nakatsuji, H.; Li, X.; Caricato, M.; Marenich, A. V.; Bloino, J.; Janesko, B. G.; Gomperts, R.; Mennucci, B.; Hratchian, H. P.; Ortiz, J. V.; Izmaylov, A. F.; Sonnenberg, J. L.; Williams-Young, D.; Ding, F.; Lipparini, F.; Egidi, F.; Goings, J.; Peng, B.; Petrone, A.; Henderson, T.; Ranasinghe, D.; Zakrzewski, V. G.; Gao, J.; Rega, N.; Zheng, G.; Liang, W.; Hada, M.; Ehara, M.; Toyota, K.; Fukuda, R.; Hasegawa, J.; Ishida, M.; Nakajima, T.; Honda, Y.; Kitao, O.; Nakai, H.; Vreven, T.; Throssell, K.; Montgomery, J. A., Jr.; Peralta, J. E.; Ogliaro, F.; Bearpark, M. J.; Heyd, J. J.; Brothers, E. N.; Kudin, K. N.; Staroverov, V. N.; Keith, T. A.; Kobayashi, R.; Normand, J.; Raghavachari, K.; Rendell, A. P.; Burant, J. C.; Iyengar, S. S.; Tomasi, J.; Cossi, M.; Millam, J. M.; Klene, M.; Adamo, C.; Cammi, R.; Ochterski, J. W.; Martin, R. L.; Morokuma, K.; Farkas, O.; Foresman, J. B.; Fox, D. J. *Gaussian 16, Rev. B.01*; Gaussian, Inc.: 2016.
(80) Dennington, R.; Keith, T. A.; Millam, J. M. *GaussView, Ver. 6*; Semichem Inc.: 2016.
(81) Hanwell, M. D.; Curtis, D. E.; Lonie, D. C.; Vandermeersch, C.; Zurek, E.; Hutchison, G. R. Avogadro: An advanced semantic chemical editor, visualization, and analysis platform. *J. Cheminform.* **2012**, *4*, 17.
(82) Vosko, S. H.; Wilk, L.; Nusair, M. Accurate spin-dependent electron liquid correlation energies for local spin density calculations: a critical analysis. *Can. J. Phys.* **1980**, *58*, 1200−1211.
(83) Becke, A. D. Density-functional thermochemistry. III. The role of exact exchange. *J. Chem. Phys.* **1993**, *98*, 5648−5652.
(84) Lee, C.; Yang, W.; Parr, R. G. Development of the Colle-Salvetti correlation-energy formula into a functional of the electron density. *Phys. Rev.* **1988**, *B37*, 785−789.
(85) Wadt, W. R.; Hay, P. J. Ab initio effective core potentials for molecular calculations. Potentials for main group elements Na to Bi. *J. Chem. Phys.* **1985**, *82*, 284−298.
(86) Andrae, D.; Häußermann, U.; Dolg, M.; Stoll, H.; Preuß, H. Energy-adjusted ab initio pseudopotentials for the second and third row transition elements. *Theor. Chim. Acta* **1990**, *77*, 123−141.
(87) Martin, J. M. L.; Sundermann, A. Correlation consistent valence basis sets for use with the Stuttgart-Dresden-Bonn relativistic effective core potentials: The atoms Ga-Kr and In-Xe. *J. Chem. Phys.* **2001**, *114*, 3408−3420.
(88) Krishnan, R.; Binkley, J. S.; Seeger, R.; Pople, J. A. Self-consistent molecular orbital methods. XX. A basis set for correlated wave functions. *J. Chem. Phys.* **1980**, *72*, 650−654.
(89) Clark, T.; Chandrasekhar, J.; Spitznagel, G. W.; Schleyer, P. V. R. Efficient diffuse function-augmented basis sets for anion calculations. III. The 3-21+G basis set for first-row elements, Li-F. *J. Comput. Chem.* **1983**, *4*, 294−301.
(90) Schuchardt, K. L.; Didier, B. T.; Elsethagen, T.; Sun, L.; Gurumoorthi, V.; Chase, J.; Li, J.; Windus, T. L. Basis Set Exchange: A Community Database for Computational Sciences. *J. Chem. Inf. Model.* **2007**, *47*, 1045−1052.
(91) Grimme, S. Supramolecular Binding Thermodynamics by Dispersion-Corrected Density Functional Theory. *Chem.-Eur. J.* **2012**, *18*, 9955−9964.
(92) Paton, R.; Funes-Ardoiz, I.: https://zenodo.org/badge/latestdoi/16266/bobbypaton/GoodVibes. DOI: 10.5281/zenodo.3346166.

4.4 Technetium and the C≡C triple bond: Unlocking air- and water-stable technetium acetylides and other organometallic complexes

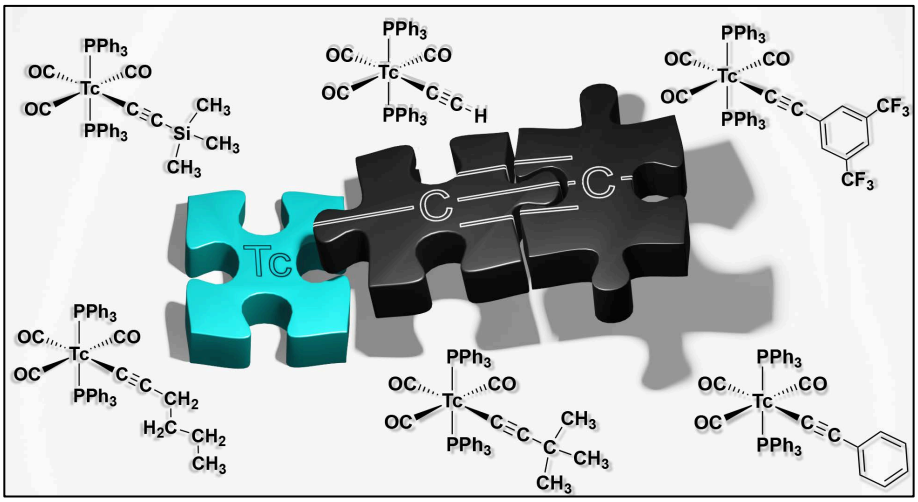

Reproduced with permission from Roca Jungfer, M. Abram, U.; submitted to *Inorg. Chem.* Jan./8th **2022**.

For Supplementary Material see A.4.

Author Contributions:

Maximilian Roca Jungfer and Ulrich Abram designed the project. Maximilian Roca Jungfer performed the synthesis and characterization of the compounds, performed DFT calculations, calculated the X-ray structures and wrote a draft of the manuscript. Ulrich Abram supervised the project, provided scientific guidance and suggestions, and corrected the manuscript.

Technetium and the C≡C triple bond: Unlocking air- and water-stable technetium acetylides and other organometallic complexes

Maximilian Roca Jungfer, Ulrich Abram*

Institute of Chemistry and Biochemistry, Freie Universität Berlin, Fabeckstr. 34/36, D-14195 Berlin, Germany

The first technetium complexes containing anionic alkynido ligands in an end-on coordination mode have been prepared by use of the non-protic, cationic precursor *mer-trans*-$[Tc(SMe_2)(CO)_3(PPh_3)_2]^+$. This cation acts as a functional analogue of the highly reactive 16-electron metallo Lewis acid $\{Tc(CO)_3(PPh_3)_2\}^+$ in reactions with alkynes, acetylides and other organometallic reagents. Such reactions give a variety of organometallic technetium complexes in excellent yields and enable the preparation of $[Tc(CH_3)(CO)_3(PPh_3)_2]$, $[Tc(Ph)(CO)_3(PPh_3)_2]$, $[Tc(Cp)(CO)_2(PPh_3)]$, $[Tc(=CCH_2CH_2CH_2O)(CO)_3(PPh_3)_2]^+$, $[Tc(=CCH_2CH_2CH_2CH_2O)(CO)_3(PPh_3)_2]^+$, $[Tc(C\equiv C\text{-}H)(CO)_3(PPh_3)_2]$, $[Tc(C\equiv C\text{-}Ph)(CO)_3(PPh_3)_2]$, $[Tc(C\equiv C\text{-}^tBu)(CO)_3(PPh_3)_2]$, $[Tc(C\equiv C\text{-}^nBu)(CO)_3(PPh_3)_2]$, $[Tc(C\equiv C\text{-}SiMe_3)(CO)_3(PPh_3)_2]$ and$[Tc\{C\equiv C\text{-}C_6H_3(CF_3)_2\}(CO)_3(PPh_3)_2]$. The bonding situation in the alkynyl complexes are compared to corresponding alkyl- and arylnitrile and -isonitrile complexes. $[Tc(N\equiv C\text{-}Ph)(CO)_3(PPh_3)_2](BF_4)$, $[Tc(C\equiv N\text{-}Ph)(CO)_3(PPh_3)_2](BF_4)$, $[Tc(N\equiv C\text{-}^tBu)(CO)_3(PPh_3)_2](BF_4)$ and $[Tc(C\equiv N\text{-}^tBu)(CO)_3(PPh_3)_2](BF_4)$ were prepared in high yields by ligand exchange reactions starting from *mer*,*trans*-$[Tc(OH_2)(CO)_3(PPh_3)_2](BF_4)$. The novel complexes were characterized by single crystal X-ray diffraction and spectroscopic methods. Especially ^{99}Tc NMR spectroscopy proved to be an invaluable and sensitive tool for the characterization of the complexes. DFT calculations strongly suggest similar bonding situations for the related alkynyl, nitrile and isonitrile complexes of technetium.

Introduction

The importance of the basic organometallic chemistry of the elements as the fundament for a rational chemical design is indisputable in many disciplines such as surface chemistry, material science, catalysis, bioorganometallic chemistry or medicinal chemistry. While the organometallic chemistry of most elements steeply develops to reveal an astonishing complexity of structure, binding and reactivity,[1-10] that of technetium has mostly been developed around carbonyl,[11-18] isonitrile,[18-26] arene[27-29] and cyclopentadienyl ligands.[30-44] Recently, also some *N*-heterocyclic carbene (NHC) complexes of technetium have been studied.[45-49] The related research is mainly attributed to the surprising stability of the resulting complexes containing Tc-C bonds and their potential for applications in radiopharmaceutical solutions.

Besides such application-driven endeavors, some fundamental work has been done starting in the early days of preparative technetium chemistry by pioneers of the organometallic chemistry such as W. Hieber or E. O. Fischer on the reactivity of coordinated carbonyl ligands with strong nucleophiles.[50-53] Another systematic study has been reported for complexes derived from the coordinatively unsaturated 16-electron complex $[TcCl(dppe)_2]$.[54] Relatively little is known about alkyl complexes containing technetium in high oxidation states,[55-57] or related aryl complexes.[44,48,58]

Detailed knowledge about this possibly vast but scarcely explored field of technetium chemistry is, however, of fundamental interest when thinking about the fact that the long-lived isotope ^{99}Tc (half-life ca. 200,000 years) is one of the most critical nuclear fission products, which is formed with a high fission yield of approximately 6 percent. Under the extreme conditions to which technetium compounds are exposed to at nuclear waste sites, several unexpected reactions may proceed. Thus, not only high-valent technetium compounds are present in such solutions, but also the reduction of technetium to low-valent compounds such as Tc(I) or Tc(II) carbonyls or nitrosyls has been observed under the influence of the radiation level present.[59-64]

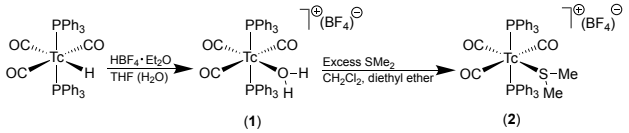

Scheme 1. Syntheses of *mer-trans*-$[Tc(OH_2)(CO)_3(PPh_3)_2](BF_4)$ (**1**) and *mer-trans*-$[Tc(SMe_2)(CO)_3(PPh_3)_2](BF_4)$ (**2**).

In recent communications, we described the syntheses of a number of complexes with the *mer-trans*-$\{Tc(CO)_3(PPh_3)_2\}^+$ or *cis-trans*-$\{Tc(CO)_2(PPh_3)_2\}^+$ motifs, which were either derived from reactions between the hydrido complex $[TcH(CO)_3(PPh_3)_2]$ and Brønsted acids,[65] or the cationic

technetium(I) complex *mer-trans*-$[Tc(OH_2)(CO)_3(PPh_3)_2]$-$(BF_4)$ (**1**) with a variety of neutral and anionic ligands.[66,67] The water ligand of the *mer-trans*-$[Tc(OH_2)(CO)_3(PPh_3)_2]^+$ cation is labile and, thus, the complex acts as a functional analogue of the highly reactive 16 e^- metallo-Lewis-acid $\{Tc(CO)_3(PPh_3)_2\}^+$ enabling the isolation of complexes with C, N, O, S, Se, Te, Cl, Br and I donor atoms.[66,67] A 'non-protic' alternative to the aqua complex **1** can be prepared by a reaction of compound **1** with dimethylsulfide. The resulting cationic complex $[Tc(SMe_2)(CO)_3(PPh_3)_2](BF_4)$ (**2**) can be obtained in a scalable reaction in high yields (Scheme 1). Reactions of both synthons with organometallic reagents are subject of the present work.

Results and Discussion

Methyl, Phenyl and Cyclopentadienyl Compounds

mer-trans-$[Tc(OH_2)(CO)_3(PPh_3)_2](BF_4)$, but also the non-protic synthon *mer-trans*-$[Tc(SMe_2)(CO)_3(PPh_3)_2](BF_4)$, show a high tendency to react with halides and form the corresponding technetium(I) halido complexes $[Tc(X)(CO)_3(PPh_3)_2]$ (X = Cl, Br, I). Such a reaction pathway was also observed during reactions with corresponding Grignard reagents, where no alkyl or aryl products could be obtained.[66] Such undesired side-reactions could be avoided by the use of methyllithium and phenyllithium, respectively. They lead in straight reactions to the formation of the corresponding methyl- and phenyltechnetium(I) compounds $[Tc(CH_3)(CO)_3(PPh_3)_2]$ (**3**) and $[Tc(Ph)(CO)_3(PPh_3)_2]$ (**4**), Scheme 2.

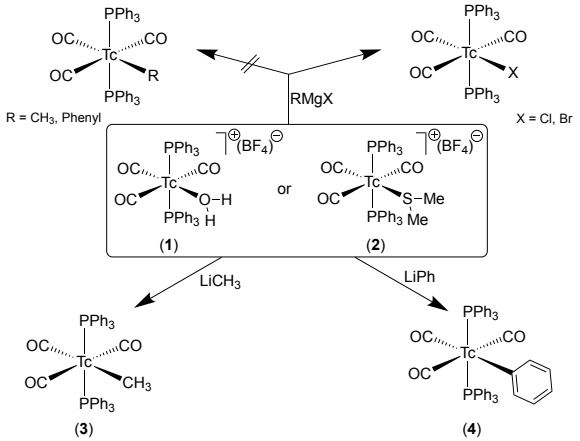

Scheme 2. Synthesis of $[Tc(CH_3)(CO)_3(PPh_3)_2]$ (**3**) and $[Tc(Ph)(CO)_3(PPh_3)_2]$ (**4**).

Expectedly, the reactions require the addition of precise amounts of organolithium reagents due to the electrophilic nature of the three carbonyl ligands. Obviously, also the BF_4^- anion is not innocent in both cases and preferentially reacts with the organolithium reagents, which consumes four equivalents of the added lithium compounds. In the case of the aqua complex, another equivalent of organolithium reagent is required due to the hydrolysis with the released H_2O. Consequently, reactions of $[Tc(OH_2)(CO)_3(PPh_3)_2](BF_4)$ require a precise addition of 6 equivalents of organolithium reagent for optimal yields, while 5 equivalents are required for reactions with $[Tc(SMe_2)(CO)_3(PPh_3)_2](BF_4)$.

The products are easily identified by their ^{99}Tc NMR spectra and the characteristic ^1H NMR resonances. The broad and highly shielded ^{99}Tc resonances are observed at -2053 ppm ($\nu_{1/2}$ = 7885 Hz) for the methyl derivative and at -1806 ppm ($\nu_{1/2}$ = 12238 Hz) for the phenyl derivative. This is in the range, where also the signal of the hydrido complex $[TcH(CO)_3(PPh_3)_2]$ (-2208 ppm) and those of $[Tc(L)(CO)_3(PPh_3)_2]^{0/+}$ complexes with other carbon donor ligands (L = CN^-, CO or isonitriles) appear.[65-67]

Both methyl and phenyl complexes of technetium are scarce. Only four methyl complexes have hitherto been characterized by X-ray crystallography. They all contain technetium in its high oxidation states: $[\{(CH_3)_2Tc^{VI}O(\mu\text{-}O)\}_2]$, $[(CH_3)_2Tc^{VI}(NAr)(\mu\text{-}NAr)_2Tc^{VI}(NAr)_2]$, $[\{(CH_3)_2Tc^{VI}N\text{-}Ar(\mu\text{-}NAr)\}_2]$ and $[(CH_3)Tc^{VII}(NAr)_3]$.[55-57] Besides these structurally characterized technetium methyl complexes there exists the iconic $[Tc^{VII}O_3(CH_3)]$, an analog of the widely used catalyst $[Re^{VII}O_3(CH_3)]$, which has been characterized unambiguously by spectroscopic methods.[55] Two of the phenyltechnetium complexes are nitrido complexes with the metal in the formal oxidation state "+5",[48] while with the cyclopentadienyl compound $[Tc(Ph)(Cp)(NO)(PPh_3)]$ also a Tc(I) example is known.[44]

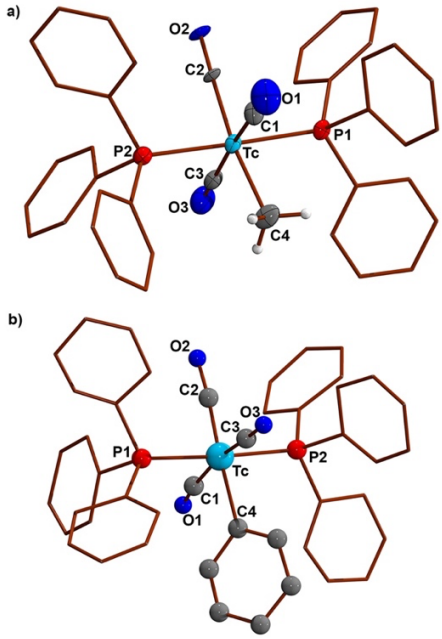

Figure 1. a) Solid-state structure of $[Tc(CH_3)(CO)_3(PPh_3)_2]$ (**3**) (Tc-C1 2.003(3), Tc-C2 1.940(6), Tc-C3 1.988(4), Tc-C4 2.289(8) Å) and b) $[Tc(Ph)(CO)_3(PPh_3)_2]$ (**4**).

Figure 1 depicts the solid-state structures of $[Tc(CH_3)(CO)_3(PPh_3)_2]$ (**3**) and $[Tc(Ph)(CO)_3(PPh_3)_2]$ (**4**). Since the quality of the single crystals of the phenyl complex was low, only a ball and stick drawing is given and no detailed discussion is done on the basis of the obtained data. Fundamental structural aspects of the novel compound and the ligand arrangement, however, can be derived doubtlessly. More details are given as Supporting Information.

The general structures of **3** and **4** are similar to those of other octahedral complexes containing the *mer-trans*-$\{Tc(CO)_3(PPh_3)_2\}^+$ unit.[65-67] Three carbonyl ligands are bound in the equatorial plane, which is completed by the

methyl or phenyl ligands. The axial positions are occupied by two PPh_3 ligands. Thus, two carbonyl ligands are oriented *trans* to each other. This results in a weakening and elongation of the corresponding Tc-C bonds in comparison to the third one, which is in *trans* position to the sixth ligand. The Tc-C4 bond length involving the methyl ligand is 2.288(8) Å and, thus, considerably longer than those in the other structurally characterized methyl complexes of technetium ($[\{Me_2Tc^{VI}O(\mu\text{-}O)\}_2]$: 2.12 Å, $[Me_2Tc^{VI}(NAr)(\mu\text{-}NAr)_2Tc^{VI}(NAr)_2]$: 2.12 and 2.153 Å, $[\{Me_2Tc^{VI}NAr(\mu\text{-}Ar)\}_2]$: 2.13-2.16 Å and $MeTc^{VII}(NAr)_3]$: 2.14 Å .[55-57] The observed elongation of the Tc-methyl bond in compound **3** is likely attributed to the large *trans*-influence of the *trans* oriented carbonyl ligand. Other carbon donors such as carbonyls bind more tightly to technetium. The Tc-C bond lengths in $[Tc(CO)_4(PPh_3)_2]^+$ are ca. 1.94-2.04 Å, while the isonitrile ligands in $[Tc(C{\equiv}N\text{-}R)(CO)_3(PPh_3)_2]^+$ (R = cyclohexyl or $C_6H_2F(C_6H_3(CF_3)_2)_2$) bind with ca. 2.1 Å and the anionic cyanido ligand in $[Tc(CN)(CO)_3(PPh_3)_2]$ binds with 2.14 Å respectively in *trans*-position to a carbonyl ligand.[66,67]

The plane of the phenyl ligand in **4** is twisted against the plane formed by the three carbonyl ligands by 40°. A similar bonding situation has been found in the isostructural pyridine complex $[Tc(py)(CO)_3(PPh_3)_2]^+$, where this angle is 23°.[66]

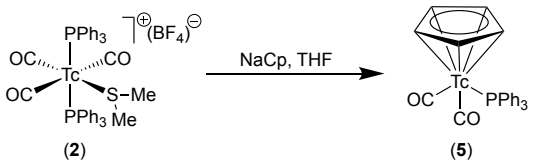

Scheme 3. Synthesis of $[Tc(Cp)(CO)_2(PPh_3)]$ (**5**) from 2.

Another classic C-donating ligand of major importance in the organometallic chemistry not only of technetium is the anionic cyclopentadienyl ligand.[30-44] The piano stool complex $[Tc(cp)(CO)_2(PPh_3)]$ has first been prepared in a low yield by photolysis of $[Tc(cp)(CO)_3]$ in the presence of triphenylphosphine.[40] Later, Jessica Cook successfully prepared the same compound by a thermal reaction starting from the chlorido complex *mer-trans*-$[TcCl(CO)_3(PPh_3)_2]$ with Na(cp). This procedure increased the yield to approximately 50%, but long reaction times and the complete exclusion of moisture and air was required.[68] Given the feasibility of our protocol with methyl and phenyl ligands, we, thus, envisioned a quick and high-yield synthesis of $[Tc(cp)(CO)_2(PPh_3)]$ from a reaction of $[Tc(SMe_2)(CO)_3(PPh_3)_2](BF_4)$ with NaCp, which could provide $[Tc(Cp)(CO)_2(PPh_3)]$ in a scalable amount as a potential starting material for future ligand exchange and organometallic reactions. Indeed, this reaction (Scheme 3) proceeds quantitatively and gives large colorless crystals of $[Tc(Cp)(CO)_2(PPh_3)]$ after evaporation of THF from the crude THF/methanol reaction mixture. Since no positional parameters are available from an early structural study on this compound and no detailed discussion of the structure of **5** was provided,[40] we reinvestigated the solid-state structure of the compound at a lower temperature.

The molecular structure of **5** is depicted in Figure 2. As in other piano stool complexes, the technetium atom is in a pseudo-octahedral coordination environment with a face-occupying Cp^- ligand. The two Tc-CO bond lengths are unexceptional. The large *trans* influence of the carbonyl ligands, however, results in two groups of Tc-C_{Cp} distances in this low-symmetric molecule. The bonds to C3, C6 and C7, which come close to *trans* positions of the two carbonyls, are somewhat longer than those to C4 and C5. The Tc-$C_{centroid}$ distance is 1.9593(3) Å.

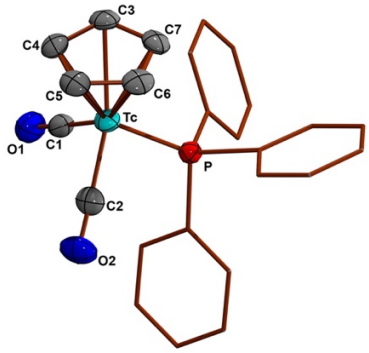

Figure 2. a) Solid-state structure of $[Tc(Cp)(CO)_2(PPh_3)_2]$ (**5**) (Tc-C1 1.881(2), Tc-C2 1.890(2), Tc-C3 2.307(2), Tc-C4 2.282(2), Tc-C5 2.283(2), Tc-C6 2.306(2), Tc-C7 2.308(2), Tc-$C_{centroid}$ 1.959(1) Å).

The ^{99}Tc NMR signal of $[Tc(Cp)(CO)_2(PPh_3)]$ is found at -2420 ppm ($\nu_{1/2}$ = 2036 Hz) which is a surprising downfield value compared to the few hitherto measured cyclopentadienyltechnetium(I) compounds: $[Tc(Cp^*)(CO)_2(PPh_3)]$ (-1782 ppm),[42] $[Tc(Cp)(CO)_3]$ (-1716 ppm),[41] and $[Tc(Cp^*)(CO)_3]$ (-1874 ppm).[41] On the other hand, it matches well with the chemical shift determined for complexes with substituted cyclopentadienyls such as $[Tc(CpC(O)Bz)(CO)_3]$ (-2502 ppm) and $[Tc(CpC(O)PhOMe)(CO)_3]$ (-2478 ppm).[35,39] A reinvestigation of the ^{99}Tc NMR properties of such compounds is therefore envisaged for the future.

Cyclooxycarbene Complexes

The observed reactivity of $[Tc(OH_2)(CO)_3(PPh_3)](BF_4)$ or $[Tc(SMe_2)(CO)_3(PPh_3)](BF_4)$ with neutral or anionic ligands and with classic organometallic reagents challenged us to attempt reactions with molecules containing C≡C triple bonds. Hitherto, all attempts to isolate technetium complexes with side-on or end-on coordinated alkyne ligands were without success. However, in some cases the used alkynes doubtlessly reacted with the Tc precursors and are found as integral parts of the finally formed products (Scheme 4).

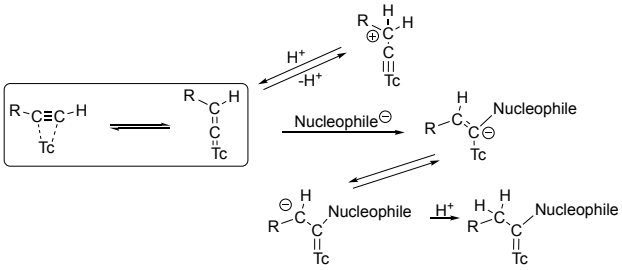

Scheme 4. The formation of vinylidene ligands at technetium and some of their reactions.[54,69]

Thus, the unsaturated 16-electron complex $[Tc(dppe)_2Cl]$ reacts with alkynes under exclusive formation of vinylidene carbene complexes and the protonation of such complexes also did not lead to side-on alkyne complexes but rather to the formation of technetium carbyne complexes containing a Tc≡C triple bond.[54] Also the unexpected formation of phosphonio oxycarbene complexes of the composition $[Tc(=C(OR)CH_2CH_2PPh_3)(Cp)(NO)(PPh_3)]^{2+}$ from reactions of $[TcCl(Cp)(NO)(PPh_3)]$ with $AgPF_6$, $Me_3SiC{\equiv}C\text{-}CH_3$ and alcohols probably proceeds via an alkyne- or vinylidene-coordinated intermediate,[69] as well as the insertion of electron-poor alkynes into the Tc-H bond of $[TcH(CO)_3(PPh_3)_2]$.[70]

In a similar way, hitherto unknown cyclooxycarbene complexes of technetium can be prepared from the highly reactive metallo Lewis acid $\{Tc(CO)_3(PPh_3)_2\}^+$, which is obtained after the dissociation of H_2O or SMe_2 from **1** or **2**. This kind of reactivity is reminiscent of that reported for the unsaturated complex $[Tc(dppe)_2Cl]$, where the formation of a vinylidene intermediate has been proven by X-ray diffraction, but follow-up reactions were performed with electrophiles, i.e. protons (see also Scheme 4).[54] Reactions of $[Tc(SMe_2)(CO)_3(PPh_3)_2](BF_4)$ (**2**) with 1-butyne-4-ol or 1-pentyne-5-ol in THF give yellow, crystalline solids of $[Tc(=\textit{cyclo}\text{-}C(CH_2)_nO)(CO)_3(PPh_3)_2](BF_4)$ (n = 4: **6**; n = 5: **7**) in good yields (Scheme 5). The same products can also be prepared from the aqua complex **1**, but with somewhat lower yields.

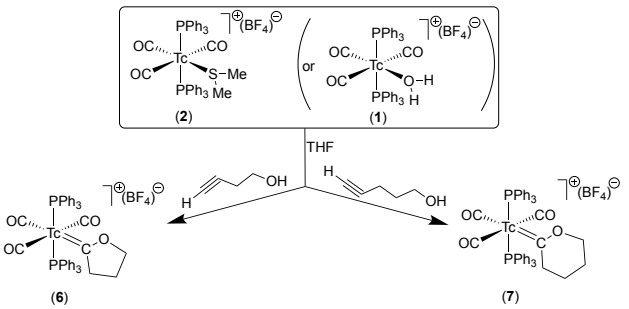

Scheme 5. Reactions between **1** or **2** with ω-alkynols.

Although cyclooxycarbene (mainly cyclooxypentylene) complexes are known for a number of transition metals and many of them have been studied by X-ray crystallography,[71] only some rare examples have been isolated for group 7 metals and up to now no technetium complexes of this type have been prepared.

The commonly accepted mechanism for such reactions starts with a transient side-on coordination of the ω-alkynol, followed by an isomerization to the vinylidene and a nucleophilic attack of the pendant alcohol at the carbenoid carbon atom. A final proton shift from the oxonium intermediate results in the assembly of the cyclooxycarbene. The overall reactions are illustrated in Scheme 6.

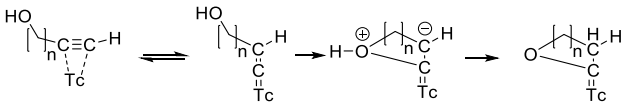

Scheme 6. Proposed mechanism for the formation of cyclooxycarbene complexes of technetium.

The formation of the cyclooxycarbenes is easily identified by their ^1H and ^{99}Tc NMR spectra. The $^1H,^1H$-COSY spectrum of a sample containing both the 2-oxacylcohexylidene ligand and the corresponding 1-pentyne-5-ol exemplifies the differences in the chemical shifts for the methylene groups of the parent alkyne as compared to the cyclooxycarbene as shown in Figure 3. The triplet resonance of the methylene protons neighboring the oxygen atom are most deshielded, followed by the triplet resonance of the protons in α-position to the carbenoid carbon atom. The methylene groups between these two special positions give quintets and are much more shielded. The ring inversion in these complexes is obviously fast as only one resonance is observed for the otherwise non-equivalent ^1H nuclei of the same methylene group.

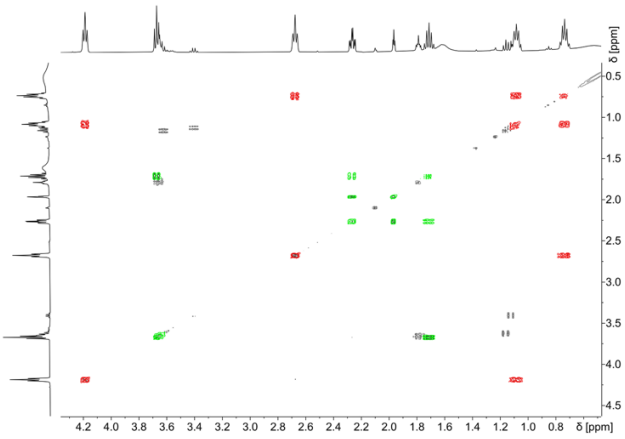

Figure 3. $^1H,^1H$-COSY NMR spectrum of a mixture of $[Tc(=\textit{cyclo}\text{-}C(CH_2)_4O)(CO)_3(PPh_3)_2](BF_4)$ (red) and 1-pentyne-5-ol (green).

Interestingly, the ^{99}Tc NMR chemical shifts of the cyclooxycarbene complexes at -1693 ($\nu_{1/2}$ = 10410 Hz) for compound **6** and -1668 ($\nu_{1/2}$ = 27508 Hz) for **7** are very close to the positions observed for the telluro- and selenoether complex cations $[Tc(L)(CO)_3(PPh_3)_2]^+$ (L = $SeMe_2$, $TeMe_2$, tetrahydroselenophene, tetrahydrotellurophene).[66] The corresponding ^{99}Tc nuclei are much less shielded than in related complexes containing a carbonyl, alkyl, cyanide or isonitrile ligand at the same position. The resonances of the oxycarbenes are among the broadest we observed in complexes with the *mer-trans*-$\{Tc(CO)_3(PPh_3)_2\}^+$ core.

While the cyclooxycarbene complexes are stable in air and against moisture in the solid state, their CH_2Cl_2 solutions undergo a subsequent decomposition at room temperature, e.g. under elimination of the initial ω-alkynols and/or by carbonyl scrambling as was also observed for the starting material $[Tc(OH_2)(CO)_3(PPh_3)_2](BF_4)$.[66]

Although there exist some ways for the preparation of carbene complexes of technetium by nucleophilic attack on coordinated carbonyl ligands,[50-53] detailed structural knowledge of technetium carbene complexes is still scarce. The few complexes, where carbene-type structures have been proven unambiguously, e.g. by X-ray diffraction are $[Tc\{=CPh(OEt)\}(Cp^*)(CO)_2]$,[52] $[Tc[Tc(=C=C(H)Ph)(dppe)_2Cl]$,[54] $[Tc(=C(OMe)CH_2CH_2PPh_3)(Cp)(NO)(PPh_3)](PF_6)_2$,[69] and the isocyanide complex $[Tc(CN^tBu)_4(bpy)](PF_6)$, for which a bent, carbene-like structure has been discussed.[71]

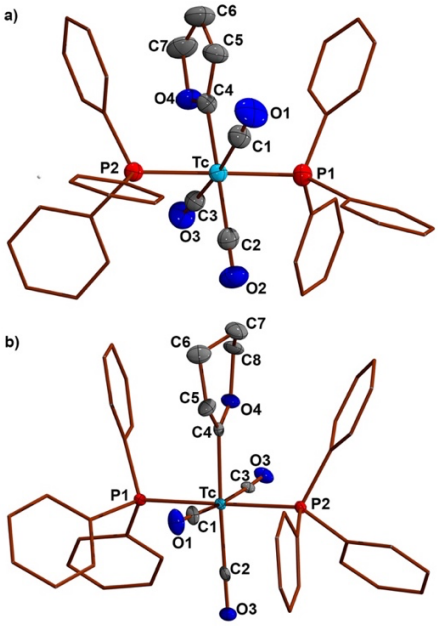

Figure 4. Solid-state structures of a) $[Tc\{=C(CH_2)_3O\}(CO)_3(PPh_3)_2]^+$ (**6**) (Tc-C1 1.964(3), Tc-C2 1.982(3), Tc-C3 1.997(3), Tc-C4 2.098(3), C4-O4 1.300(4), C4-C5 1.495(4) Å) and b) $[Tc\{=C(CH_2)_4O\}(CO)_3(PPh_3)_2]^+$ (**7**) Tc-C1 1.977(3), Tc-C2 1.983(3), Tc-C3 1.992(3), Tc-C4 2.117(3), C4-O4 1.302(4), C4-C5 1.484(5) Å).

The molecular structures of the novel cyclooxycarbene complexes **6** and **7** are shown in Figure 4. The technetium-carbon bond lengths are relatively short with ca. 2.1 Å compared to the methyl and phenyl complexes with Tc-C bond lengths around 2.3 Å. Thus, they are similar to the distances found in the related carbonyl, isocyanide and cyanide complexes.[66,67] This can be understood as a partial double bond character in the technetium carbon bond. The carbon oxygen distance between the carbenoid carbon and its stabilizing oxygen atom suggests the presence of a partial double bond, which is consistent with the interpretation of a partial alkyl character of the carbenoid carbon atom. The other C-C bond lengths and the remaining C-O bond length in the cyclic ligand are in the usual range of single bonds. Interestingly, the oxacyclopentylene moiety is nearly planar, while the oxacyclohexylene ligand is twisted in the hydrocarbon back bone. Reactions of other terminal and internal alkynes in the presence of alcohols did not yield oxycarbenes but resulted in a recovery of the starting materials or a decomposition of the precursors.

Heating a mixture of complex **2** with phenylacetylene, led to the formation of traces of a poorly soluble colorless precipitate and an orange-yellow solution. After filtration, a yellow powder was isolated from the solution by the addition of pentane. The powder contained the remainder of the technetium used in the reaction and showed a shifted ^{99}Tc resonance at -814 ppm. The IR spectrum of this solid shows three intense main bands in the triple bond region: two carbonyl bands at 1956 cm^{-1} and 1931 cm^{-1} and an additional intense band at 1867 cm^{-1}, which fits well with the region of C≡C-bonds in side-on bonded alkyne complexes.

The addition of a base such as triethylamine to a mixture of **1** or **2** and phenylacetylene in THF results in the formation of the same poorly soluble colorless precipitate in a somewhat higher yield. The appearance of a weak IR band at 2095 cm^{-1} is a strong hint for the presence of a C≡C triple bond in addition to the retained *mer-trans*-$\{Tc(CO)_3(PPh_3)_2\}^+$ unit. The absence of BF_4^- is readily verified by IR and NMR spectroscopy. A broad ^{99}Tc NMR resonance at -2056 ($\nu_{1/2}$ = 9638 Hz) indicates the coordination of a carbon donor ligand to technetium. Finally, the recrystallization of the product from CH_2Cl_2/MeOH proved the formation of the first technetium alkyne complex containing the alkyne in an end-on binding mode: $[Tc(C{\equiv}C\text{-}Ph)(CO)_3(PPh_3)_2]$.

Acetylide Complexes and Related Compounds

Although the yield of $[Tc(C{\equiv}C\text{-}Ph)(CO)_3(PPh_3)_2]$ (**8a**) from the above-mentioned reaction between **1** or **2** with phenylacetylene and NEt_3 was unsatisfactorily low, it clearly shows that acetylido complexes of technetium exist and that at least the product **8a** is a stable compound. Thus, the main challenge for a further exploration of technetium acetylides was to find a general and feasible synthetic approach.

Using the findings derived from the synthesis of alkyl and aryl complexes described in the first part of this communication: (i) non-protic precursors improve the yield and (ii) organolithium reagents ensure good yields and should be used instead of Grignard reagents if applicable, we quickly found a suitable protocol for the synthesis of technetium acetylides.

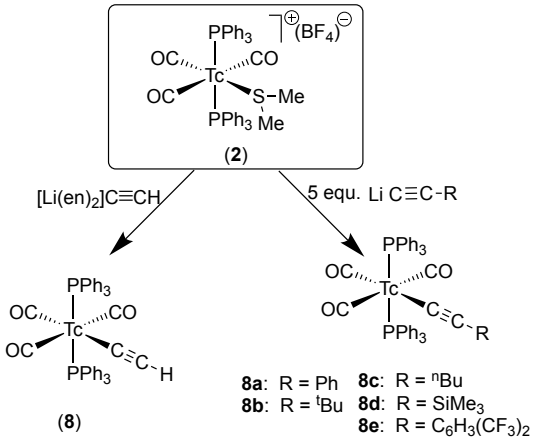

Scheme 7. Synthesis of acetylido complexes of technetium.

A key step was the separation of the deprotonation of the alkyne from the reaction with the technetium precursors by using freshly preparing lithium acetylides. The acetylides were conveniently prepared by a reaction of the corresponding acetylene and *n*-butyllithium. And indeed, freshly prepared solutions of lithium acetylides readily react with the non-protic complex **2** under exchange of the SMe_2 ligand as we have observed for methyllithium or phenyllithium (*vide supra*). Also here, the BF_4^- counter ion was involved in the reaction and consumed four equivalents of the lithium compound. If desired, such a side-reaction can be avoided by the use of another salt of the starting material, but it turned out that this is not necessary since the side-products do not lower the yields and can readily be separated. The general protocol employing fresh lithium alkynyls works with a large number of different alkynes (Scheme 7).

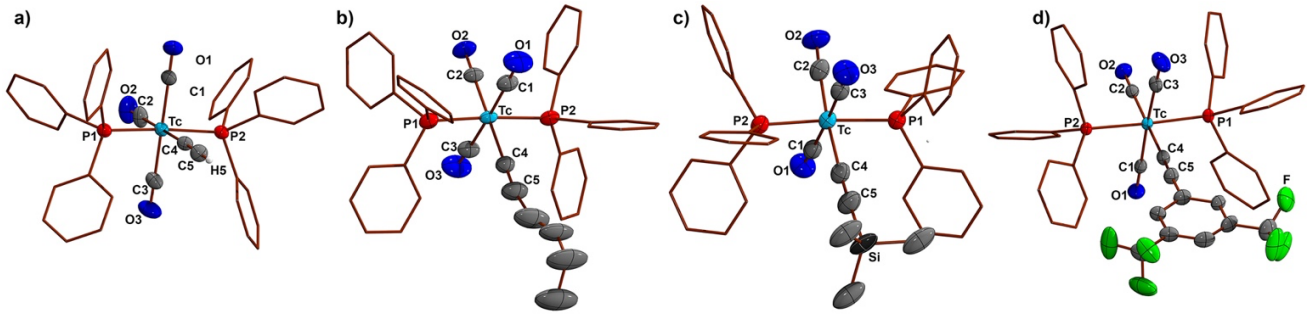

Figure 5. Solid-state structures of a) [Tc(C≡CH)(CO)$_3$(PPh$_3$)$_2$] (**8**), b) [Tc(C≡C-^{n}Bu)(CO)$_3$(PPh$_3$)$_2$] (**8c**), c) [Tc(C≡C-SiMe$_3$)(CO)$_3$(PPh$_3$)$_2$] (**8d**), d) [Tc(C≡C-C$_6$H$_3$(CF$_3$)$_2$)(CO)$_3$(PPh$_3$)$_2$] (**8e**).

Unfortunately, there exist some exceptions, e.g. the synthesis of the parent compound with unsubstituted acetylene, [Tc(C≡C-H)(CO)$_3$(PPh$_3$)$_2$] (**8**), was not attempted in this way as the preparation of mono lithium acetylide solutions imposes an explosion hazard and is less selective. Also, the deprotection of the trimethylsilyl acetylido complex **8d** with fluoride sources such as KF, CsF, NBu$_4$F, HF and HBF$_4$·Et$_2$O did not yield **8**, but resulted in the recovery of the starting material or in a partial decomposition. The unsubstituted parent compound **8** was finally obtained by a reaction of [Tc(SMe$_2$)(CO)$_3$(PPh$_3$)$_2$](BF$_4$) (**2**) with the stabilized reagent [Li(en)$_2$]C≡CH. The success of this reaction was obvious from the IR spectrum of the product, that shows the indicative C≡C-H vibration at 3283 cm^{-1}.

The transmetallation procedures generally give the air- and water-stable technetium alkynyls [Tc(C≡C-R)(CO)$_3$(PPh$_3$)$_2$] (R = H, Ph, C$_6$H$_3$(CF$_3$)$_2$, ^{n}Bu, ^{t}Bu, SiMe$_3$) in excellent yields.

The ^{99}Tc NMR resonances of the products are found between -1914 ppm and -2056 ppm and have half-widths between 8 kHz and 12 kHz. The chemical shifts are similar to those found for the other [Tc(L)(CO)$_3$(PPh$_3$)$_2$]$^{0,+}$ complexes, where L represents a ligand with a carbon donor atom and differ significantly from those of related complexes having ligands with other donor atoms (e.g. nitrogen donor ligands: ca. -1300 to -1500 ppm).[66,67]

Table 1. Selected bond lengths (Å) and angles (°) in [Tc(C≡CH)(CO)$_3$(PPh$_3$)$_2$] (**8**), [Tc(C≡C-^{n}Bu)(CO)$_3$(PPh$_3$)$_2$] (**8c**), [Tc(C≡C-SiMe$_3$)(CO)$_3$(PPh$_3$)$_2$] (**8d**) and [Tc(C≡C-C$_6$H$_3$(CF$_3$)$_2$)(CO)$_3$(PPh$_3$)$_2$] (**8e**). (') symmetry related:-x+1, y, -z+1/2.

	8	8c	8d	8e
C1-Tc	1.977(3)	1.966(3)	1.966(5)	1.974(2)
C2-Tc	1.945(3)	1.922(5)	1.938(5)	1.932(3)
C3-Tc	1.995(3)	1.966(3)'	1.988(5)	1.988(3)
C4-Tc	2.145(3)	2.144(6)	2.126(4)	2.125(2)
C4-C5	1.192(4)	1.207(7)	1.213(6)	1.207(3)
C5-H5	0.79(5)	-	-	-
C5-C6	-	1.440(7)	1.802(5)	1.430(3)
C5-C4-Tc	175.5(3)	180	177.3(4)	176.3(2)
C4-C5-C6	177(4)	168.9(5)	175.5(5)	177.1(3)

Figure 5 depicts the structures of the parent complex [Tc(C≡CH)(CO)$_3$(PPh$_3$)$_2$] (**8**), [Tc(C≡C-^{n}Bu)(CO)$_3$(PPh$_3$)$_2$] (**8c**), [Tc(C≡C-SiMe$_3$)(CO)$_3$(PPh$_3$)$_2$] (**8d**), and [Tc{C≡C-C$_6$H$_3$(CF$_3$)$_2$}(CO)$_3$(PPh$_3$)$_2$] (**8e**). Selected bond lengths and angles are compared in Table 1. The general bonding pattern in the alkynyl complexes [Tc(C≡C-R)(CO)$_3$(PPh$_3$)$_2$] reflects that in the other σ-donor complexes containing the *mer-trans*-{Tc(CO)$_3$(PPh$_3$)$_2$}$^+$ moiety. The carbonyl ligand in *trans* position to the alkynyl is more tightly bound to technetium compared to the two carbonyl ligands in *trans* orientation to each other. The technetium-carbon bond lengths in the alkynyl complexes are 2.12-2.14 Å, which is significantly shorter than those in the pure σ-donor complexes **3** and **4** (2.29 and 2.28 Å), revealing some double-bond character. The alkyne C≡C bonds in **8** and **8d** are almost unchanged compared to the uncoordinated alkynes,[72,73] while no crystallographic data are available for the n-butyl and the bis(trifluoromethyl)phenyl derivatives.

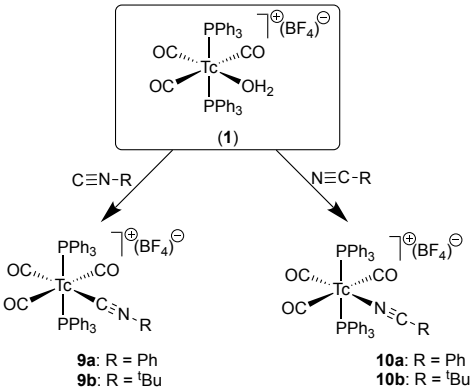

Scheme 8. Synthesis of isonitrile and nitrile complexes of technetium.

For comparison, we synthesized the isonitrile and nitrile analogues of the phenyl and *tert*-butyl substituted acetylide complexes **8a** and **8b**. This could readily be done by ligand exchange procedures starting from the aqua complex **1** (Scheme 8). The cationic complexes were obtained in excellent yields as their BF$_4^-$ salts as colorless (**9b**, **10a**, **10b**) or yellow (**9a**) crystalline products.

The solid-state structures of the isonitrile and nitrile complexes are shown together with those of their alkynido analogs in Figure 6. Selected bond lengths and angles are compared in Table 2.

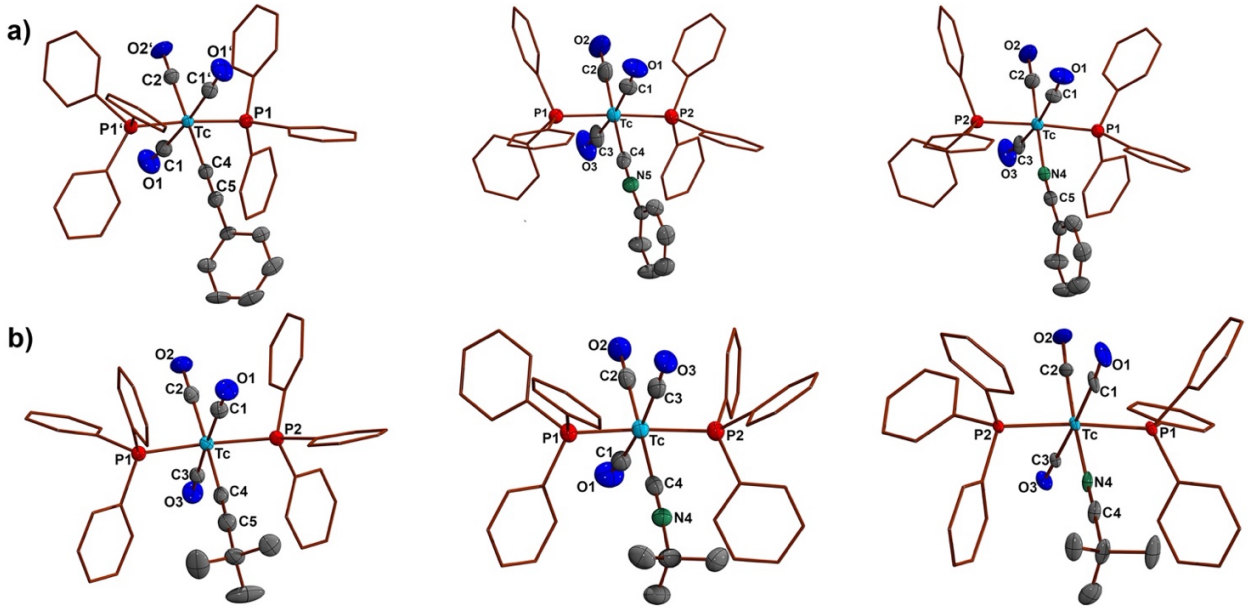

Figure 6. Solid-state structures of a) $[Tc(C{\equiv}C\text{-}Ph)(CO)_3(PPh_3)_2]$ (**8a**), $[Tc(C{\equiv}N\text{-}Ph)(CO)_3(PPh_3)_2]^+$ (**9a**), $[Tc(N{\equiv}C\text{-}Ph)(CO)_3(PPh_3)_2]^+$ (**10a**) and b) $[Tc(C{\equiv}C\text{-}^t Bu)(CO)_3(PPh_3)_2]$ (**8b**), $[Tc(C{\equiv}N\text{-}^t Bu)(CO)_3(PPh_3)_2]^+$ (**9b**), $[Tc(N{\equiv}C\text{-}^t Bu)(CO)_3(PPh_3)_2]^+$ (**10b**), Symmetry operation: 1-x, y, 1/2-z.

Table 2. Selected bond lengths (Å) and angles (°) in $[Tc(C{\equiv}C\text{-}Ph)(CO)_3(PPh_3)_2]$ (**8a**), $[Tc(C{\equiv}C\text{-}^t Bu)(CO)_3(PPh_3)_2]$ (**8b**), $[Tc(C{\equiv}N\text{-}Ph)(CO)_3(PPh_3)_2](BF_4)$ (**9a**), $[Tc(C{\equiv}N\text{-}^t Bu)(CO)_3(PPh_3)_2](BF_4)$ (**9b**), $[Tc(N{\equiv}C\text{-}Ph)(CO)_3(PPh_3)_2](BF_4)$ (**10a**) and $[Tc(N{\equiv}C\text{-}^t Bu)(CO)_3(PPh_3)_2](BF_4)$ (**10b**). Symmetry operation: 1-x, y, 1/2-z.

	8a	**8b**	**9a**	**9b**	**10a**	**10b**
Tc-C1	1.977(5)	1.981(4)	2.004(4)	1.985(7)	2.006(5)	2.024(4)
Tc-C2	1.924(6)	1.924(4)	1.937(4)	1.939(6)	1.878(5)	1.903(4)
Tc-C3	1.977(5)'	1.967(4)	1.992(4)	1.989(7)	1.995(5)	1.967(3)
Tc-C4	2.143(6)	2.144(4)	2.082(4)	2.086(5)	-	-
Tc-N4	-	-	-	-	2.161(4)	2.136(3)
C4-C5	1.191(9)	1.193(6)				
C4-N4			1.148(4)	1.150(7)	1.137(6)	1.140(5)
C5-C6	1.450(9)	1.488(6)	-	-	1.430(7)	1.478(6)
N5-C6	-	-	1.400(4)	1.478(7)	-	-
Tc-C4-C5	180	173.6(4)	-	--	-	-
Tc-C4-N4	-	-	176.4(3)	178.0(5)	-	-
Tc-N4-C4	-	-	-	-	173.2(4)	178.6(3)

Generally, the structural differences between the compounds **8**, **9** and **10** are small. One of the most remarkable difference is the alignment of the aryl rings of the benzonitrile and phenylisonitrile ligands in **9a** and **10a** with the equatorial tricarbonyl plane in comparison to the twisted binding mode found for the acetylide ligand in **8a**. This becomes even more pronounced taking into account that the arylacetylide moiety of $[Tc(C{\equiv}C\text{-}C_6H_3(CF_3)_2)(CO)_3(PPh_3)_2]$ (**8e**) is oriented in a 90° angle to the equatorial plane and aligned with the P-Tc-P axis. Thus, we performed some DFT calculations on the rotational barrier for the three phenyl-substituted compounds in the gas-phase, but neither of the experimentally measured arrangements lies on an energetic minimum and therefore we attribute the found twisting angles to solid-state effects. Details about the calculations are contained in the Supporting Information.

The Tc-C bond lengths in the isocyanide complexes **9** are significantly smaller than the Tc-C bond lengths observed in the acetylide complexes **8** and the Tc-N bond lengths in the nitrile complexes **10**. Parallelly, the *trans*-oriented Tc-C2 bond lengths decrease from **9** to **8** to **10**. Thus, a subtle π-backdonation can be concluded for the carbon donors **8** and **9** in comparison to the nitriles **10**. In comparison, both the asymmetric and the symmetric CO-bands in the IR spectra of the complexes show a red-shift in the order C≡N-R, N≡C-R and C≡C-R with similar wave numbers for the complexes

Table 3. Selected parameters of the NBO analysis, experimental (solid-state) bond lengths [Å], IR stretching frequencies [cm^{-1}], ^{99}Tc NMR chemical shifts [ppm], ^{99}Tc NMR half-widths [Hz].

	NC^{t}Bu	NCPh	CC^{t}Bu	CCPh	CN	CNPh	CN^{t}Bu	CO
$E_{deloc.}$ [kcal/mol]	88	94	182	197	251	261	264	317
$\Delta E_{i,j}$ [a.u.]	0.95	0.96	0.86	0.85	0.79	0.8	0.81	0.77
$F_{i,j}$ [a.u.]	0.257	0.268	0.353	0.365	0.398	0.409	0.412	0.44
Tc-C_{CO} [Å]	1.90	1.88	1.92	1.92	1.95	1.94	1.94	1.90
C≡O [Å]	1.15	1.17	1.17	1.14	1.14	1.15	1.15	1.15
Tc-L [Å]	2.14	2.16	2.14	2.14	2.14	2.08	2.09	2.14
C≡X [Å]	1.14	1.14	1.19	1.19	1.14	1.15	1.15	1.14
$\nu_{c\equiv o,\ sym.}$ [cm^{-1}]	2081	2075	2045	2043	2054	2073	2075	-
$\nu_{c\equiv o,\ asym.}$ [cm^{-1}]	1989	1985	1946	1960	1960	1992	1991	2012
$\nu_{c\equiv o,\ asym.}$ [cm^{-1}]	1936	1954	1925	1929	1935	-	1977	-
$\nu_{c\equiv x}$ [cm^{-1}]	2272	2249	-	2095	2116	2166	2193	2012
δ [ppm]	-1481	-1496	-1956	-2056	-1901	-1880	-1874	-1895
$\nu_{1/2}$ [Hz]	3020	2818	11747	9638	5907	4280	4025	2643

of the types **9** and **10** and much lower wave numbers for the acetylide complexes (red-shift of ca. 30 cm^{-1}). Especially when comparing them with the carbonyl frequencies observed in the cyanido complex $[Tc(CN)(CO)_3(PPh_3)_2]$, where the symmetric stretching vibration was found at 2054 cm^{-1}, and the tetracarbonyl cation $[Tc(CO)_4(PPh_3)_2]^+$, which shows only one carbonyl vibration at 2012 cm^{-1},[66,67] it becomes obvious that the underlying electronic differences are complex and do not follow trivial trends. Similar findings have been reported for a number of isonitrile complexes of technetium and rhenium, where it became evident that isonitriles cannot simply be regarded as electronic surrogates for carbonyl ligands and the related IR frequencies are no simple measures for π back-donation, but the oxidation state of the metal ions and particularly the organic residues of the isocyanides play a critical role.[25,26,74,75]

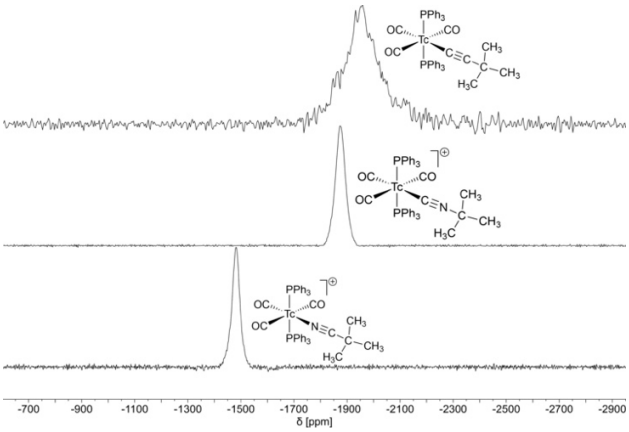

Figure 7. ^{99}Tc NMR spectra of the *tert*-butyl-substituted complexes **8b**, **9b** and **10b**.

In contrast to the subtle differences observed in the IR and X-ray analyses, the ^{99}Tc NMR spectra of the compounds clearly reveal different bonding situations around technetium. The chemical shifts decrease in the order $^-$C≡C-R < C≡N$^-$ < C≡O < C≡N-R << N≡C-R with the acetylide complexes around -2000 ppm, the isonitrile complexes around -1880 ppm, the tetracarbonyl at -1901 ppm,[66] the cyanide at -1895 ppm,[67] and the nitrile complexes around -1500 ppm. The higher shielding of the ^{99}Tc nucleus may be attributed to the stronger σ-donation of the carbon donor atoms compared to the nitrogen donors of the nitrile ligands. The ^{99}Tc NMR spectra of the *tert*.butyl substituted complexes **8b**, **9b** and **10b** are compared in Figure 7.

Given that the spectroscopic behavior of the complexes was not ultimately conclusive, we turned our attention to DFT calculations to improve the understanding of the donor/acceptor differences between the acetylido, isonitrile, nitrile, cyanide and carbon monoxide ligands. An NBO analysis revealed a delocalized three center 4e$^-$ σ-hyperbond between the donor atom of the regarded ligand, technetium and the carbon atom of the *trans*-oriented Tc-C2 bond. A similar 3c/4e$^-$ bond is established between the two *trans*-oriented carbonyl ligands *via* technetium. The latter 3c/4e$^-$ is stabilized by a major donation of one carbonyl carbon atoms lone-pair into the technetium-carbonyl-carbon antibonding orbital of ca. 320 kcal/mol. Therefore, this kind of interactions should somewhat correspond to the donor strength of the corresponding ligand in *trans*-position to the carbonyl, especially when comparing the donation of different ligands into the same antibonding orbital of the Tc-C2 bond. Interestingly, the obtained values strongly differ depending on the substituent and nature of the donor atom. The donation into the three-centered bond is highest for a carbonyl ligand, followed by the isocyanides, the cyanide anion, the acetylide anions and finally the nitrile ligands. In the case of NC^{t}Bu the delocalization energy was only 88 kcal/mol and no hyperbond was concluded from the NBO analysis. Some structural, spectroscopic and calculated parameters are compared in Table 3.

Compound **8b** with the sterically demanding *tert*-butyl group appeared to be a suitable candidate for a further exploration of the reactivity of the novel technetium acetylides. An obvious reaction is to protonate the acetylides as an approach to complexes with side-on coordinated acetylene ligands. Thus, we attempted the protonation of **8b** with $HBF_4{\cdot}Et_2O$ in CD_2Cl_2. The ^{1}H resonance of the *tert*-butyl protons of **8b** rapidly disappears with the parallel formation of a variety of low-intensity ^{1}H resonances (including those of terminal HC≡C protons). A similar reaction pattern is observed by means of the ^{99}Tc NMR spectra. The signal of **8b** at -1971 ppm disappears after the addition of the acid and three new signals are found. Two of them can be assigned to

$[Tc(OH_2)(CO)_3(PPh_3)_2]^+$ (-1229 ppm) and $[Tc(CO)_4(PPh_3)_2]^+$ (-1902 ppm), while a third, very broad ($\nu_{1/2} \approx 26$ kHz) signal appears in the typical range of dicarbonyl complexes with a chemical shift of -1005 ppm. After the addition of a drop *tert*-butylacetylene, only the two latter technetium(I) species remain in this solution. The formation of the $[Tc(CO)_4(PPh_3)_2]^+$ cation is not surprising and has been observed before during reactions of tricarbonyl complexes by ligand scrambling.[66,67] The main-product, a dicarbonyl species is tentatively assigned to a complex with a side-on bonded acetylene ligand. This assumption is supported by the detection of a narrow ^{31}P NMR signal at 6.4 ppm in addition to the broad signal of $[Tc(CO)_4(PPh_3)_2]^+$ at 37 ppm, and ^1H NMR signals for the new species with an integral ratio of 30:9:1 (aromatic/methyl/acetylene). Such a spectral feature might be assigned to either a side-on bonded alkyne species or to an isomeric vinylidene carbene type complex. Based on the knowledge we have so far accumulated on ^{99}Tc resonances of *mer*-tricarbonyl and *cis*-dicarbonyl complexes of technetium, a side-on bonded alkyne complex seems somewhat more likely given that the ^{99}Tc resonance of carbene-type complexes (see the discussion about the cyclooxycarbenes *vide supra*) are found at vastly different chemical shifts. These observations are encouraging and suggest that complexes with acetylene ligands in a side-on binding mode might be prepared by the protonation of technetium acetylide complexes. Related work with other acetylenes is currently in progress, since the described *tert*-butylacetylene compound could hitherto not be isolated in crystalline form.

Conclusions

The bench-stable compounds *mer,trans*-$[Tc(OH_2)(CO)_3(PPh_3)_2](BF_4)$ (**1**) and *mer,trans*-$[Tc(SMe_2)(CO)_3(PPh_3)_2](BF_4)$ (**2**) are valuable synthons for the synthesis of low-valent organotechnetium compounds. They serve as a functional analogues of the unsaturated Lewis acid $\{Tc(CO)_3(PPh_3)_2\}^+$. The aqua complex **1** has been shown to be a suitable starting compound for many ligand exchange procedures with many ligand systems,[66,67] but it is certainly incompatible with sensitive organometallic reagents or procedures. This was overcome by the use of the analogous, non-protic dimethylsulfide complex **2**.

Reactions with lithium alkyls or aryls give the corresponding σ-bonded products, while a reaction with NaCp represents a high-yield approach to $[Tc(Cp)(CO)_2(PPh_3)]$. Hitherto unknown cyclooxycarbene complexes of technetium are formed upon treatment of **1** or **2** with ω-alkynols by an intramolecular attack of the pendent alcohols at the carbenoid carbon atoms of intermediately formed vinylidene ligands.

A feasible approach to technetium complexes with end-on bound alkynyl ligands has been found by the reaction of **2** with freshly prepared lithium acetylides. The alkynyl complexes are stable towards oxygen and moisture in the solid state, but only moderately stable in acidic solutions. The identity of the complexes was proven by X-ray crystallography and spectroscopic methods. ^{99}Tc NMR proved an invaluable tool for the ready identification of such species. The high stability of the alkynides in aqueous media recommends a consideration of corresponding ^{99m}Tc compounds for nuclear medical applications.

Experimental

General Considerations. Unless otherwise stated, reagent-grade starting materials were purchased from commercial sources and either used as received or purified by standard procedures. Solvents were dried and deoxygenated according to standard procedures. $[TcH(CO)_3(PPh_3)_2]$ and $[Tc(OH_2)(CO)_3(PPh_3)_2](BF_4)$ were prepared as previously described.[65,66] The absence of boron, fluorine and lithium containing impurities was verified by the measurement of ^9Li, ^{11}B and ^{19}F NMR spectra.

Physical Measurements: NMR spectra were recorded at 20°C with JEOL 400 MHz multinuclear spectrometers. The values given for the ^{99}Tc chemical shifts are referenced to pertechnetate. IR spectra were recorded with a Shimadzu FTIR 8300 spectrometer as KBr pellets. The following abbreviations were used for the intensities and characteristics of IR absorption bands: vs = very strong, s = strong, m = medium, w = weak, sh = shoulder.

Radiation Precautions. ^{99}Tc is a long-lived weak β^- emitter (E_{max} = 0.292 MeV). Normal glassware provides adequate protection against the weak beta radiation when milligram amounts are used. Secondary X-rays (bremsstrahlung) play a significant role only when larger amounts of ^{99}Tc are handled. All manipulations were done in a laboratory approved for the handling of radioactive materials.

X-Ray Crystallography. The intensities for the X–ray determinations were collected on STOE IPDS II or on Bruker D8 Venture instruments with Mo Kα radiation. The space groups were determined by the detection of systematical absences. Absorption corrections were carried out by multiscan or integration methods.[76,77] Structure solution and refinement were performed with the SHELX program package.[78,79] Hydrogen atoms were derived from the final Fourier maps and refined or placed at calculated positions and treated with the 'riding model' option of SHELXL. The representation of molecular structures was done using the program DIAMOND 4.2.2.[80]

Additional information on the structure determinations is contained in the Supporting Information and has been deposited with the Cambridge Crystallographic Data Centre.

Computational Details. DFT calculations were performed on the high-performance computing systems of the Freie Universität Berlin ZEDAT (Curta)[81] using the program package GAUSSIAN 16.[82] The gas phase geometry optimizations were performed using coordinates derived from the X-ray crystal structures using GAUSSVIEW and Avogadro.[83,84] The calculations were performed with the hybrid density functional B3LYP.[85-87] The double-ζ pseudopotential LANL2DZ basis set with the respective effective core potential (ECP) was applied to N and P.[88] The Stuttgart relativistic small core basis set with the corresponding ECP was applied to Tc.[9,90,] The 6-311+G** basis set was used to model C, H and O atoms.[91,92] All basis sets as well as the ECPs were obtained from the EMSL database.[93] Frequency calculations after the optimizations confirmed the convergence of all non-frozen geometry optimizations with at least two out of four

convergence criteria. No negative frequencies were obtained for these optimized geometries. Several attempts at initial torsion angles were required for the non-rigid *tert*-butyl substituted complexes. Additional calculations for the torsion around the aryl groups of the complexes [Tc(C≡C-Ph)(CO)$_3$(PPh$_3$)$_2$] (**8a**), [Tc(C≡N-Ph)(CO)$_3$(PPh$_3$)$_2$]$^+$ (**9**a) and [Tc(N≡C-Ph)(CO)$_3$(PPh$_3$)$_2$]$^+$ (**10a**) were performed by optimization with a corresponding frozen torsion angle in 10° increments and the experimentally observed values specifically. A solvent model (IEF-PCM; dichloromethane) was tested for the torsion of [Tc(C≡C-Ph)(CO)$_3$(PPh$_3$)$_2$] (**8a**) but the obtained angular-dependence curve is similar to that obtained by the gas-phase calculations. Further analyses were performed with the free multifunctional wavefunction analyzer *Multiwfn*.[94]

Syntheses

*[Tc(SMe$_2$)(CO)$_3$(PPh$_3$)$_2$](BF$_4$) (**2**)*. SMe$_2$ (3 mL) was added to a solution of [Tc(OH$_2$)(CO)$_3$(PPh$_3$)$_2$](BF$_4$) (301 mg, 0.37 mmol) in CH$_2$Cl$_2$ (2 mL) and stirred for 5 min. Addition of diethyl ether (9 mL) and pentane (6 mL) gave a flocculent colorless precipitate. The microcrystals were filtered off, washed with pentane (3x 3 mL) and dried in air. Yield: 311 mg (0.36 mmol, 98%). The analytical data are as described previously.[66]

*[TcMe(CO)$_3$(PPh$_3$)$_2$] (**3**)*. a) A solution of MeLi (0.7 mL, 1 mmol, 1.6 M) was added dropwise to a suspension of [Tc(SMe$_2$)(CO)$_3$(PPh$_3$)$_2$](BF$_4$) (187 mg, 0.22 mmol) in dry, degassed THF(1 mL). The colorless suspension turned to a dark blue-black solution during the first half of the addition. After the complete addition, an orange solution with a voluminous colorless precipitate formed. The mixture was stirred for 45 min. MeOH (11 mL) was added to hydrolyze residual organometallic reagent and precipitate the product as a colorless powder. Caution, excess methyl organometallic reagent react violently with methanol, the addition should be dropwise and slowly in the beginning. After 5 min of stirring, the precipitate was filtered off and washed with MeOH (3 x 2 mL) and pentane (3 mL). After drying in air, a colorless powder was obtained. Yield: 106 mg (0.15 mmol, 67%). b) A solution of MeLi (0.2 mL, 0.3 mmol, 1.6 M) was added dropwise to a suspension of [Tc(OH$_2$)(CO)$_3$(PPh$_3$)$_2$]-(BF$_4$) (41 mg, 0.05 mmol) in dry, degassed THF(1 mL). The colorless suspension turned to a clear red solution. The mixture was stirred for 40 min at room temperature, after which time the color had changed to yellowish-brown. The mixture was evaporated to dryness in vacuum and extracted with toluene (3 x 2 mL). After evaporation of the toluene in vacuum, the colorless residue was triturated with pentane and filtered off. After washing with pentane (2 x 2 mL) and drying in air, a colorless powder was obtained. Yield: 22 mg (0.03 mmol, 61%). Crystals suitable for X-ray diffraction were grown from a saturated CD$_2$Cl$_2$ solution overnight. IR (cm^{-1}): 2019 (w, $\nu_{C\equiv O}$), 1929 (w, $\nu_{C\equiv O}$), 1879 (s, $\nu_{C\equiv O}$). ^{1}H NMR (CD$_2$Cl$_2$, ppm): 7.58+7.40 (30H, m, Ar**H**), -1.17 (2H, t, $^3J_{H,P}$ = Hz, Tc-CH$_3$). ^{31}P NMR (CD$_2$Cl$_2$, ppm): 49 (s, $\nu_{1/2}$ = 799 Hz). ^{99}Tc NMR (CD$_2$Cl$_2$, ppm): -2053 (s, $\nu_{1/2}$ = 7885 Hz).

*[Tc(Ph)(CO)$_3$(PPh$_3$)$_2$] (**4**)*. a) A light yellow solution of phenyllithium (0.05 mL, 0.09 mmol, 1.9 M in Et$_2$O) was added dropwise to a suspension of [Tc(SMe$_2$)(CO)$_3$(PPh$_3$)$_2$](BF$_4$) (20 mg, 0.02 mmol) in dry, degassed THF(0.5 mL). The colorless suspension first turned to a yellowish solution. After the complete addition, the orange-red solution was stirred for 5 min. MeOH (3 mL) was added to hydrolyze residual organometallic reagent. The mixture was opened to the atmosphere and left for evaporation overnight. Colorless needles of **4** formed, which were filtered off and washed with MeOH (2 x 0.5 mL) and pentane (1 mL). After drying in air colorless crystals were obtained. Yield: 8 mg (0.01 mmol, 55%). b) A red solution of phenyllithium (0.24 mL, 0.42 mmol, 1.8 M in Bu$_2$O) was added dropwise to a suspension of [Tc(OH$_2$)(CO)$_3$(PPh$_3$)$_2$](BF$_4$) (68 mg, 0.08 mmol) in dry, degassed THF(1 mL). The colorless suspension turned purple and it was stirred for 45 min. Excess of the organometallic reagent was hydrolyzed by the addition of MeOH (2 drops) and the solvent was evaporated in vacuum to give a brown oil. The residue was extracted with toluene (4 x 2 mL) and the combined reddish yellow extracts was evaporated in vacuum to give a brown oil. Pentane (5 mL) was added and evaporated in vacuum to remove residual toluene. Addition of Et$_2$O (10 mL) resulted in the formation of a colorless precipitate, which was filtered off, washed with Et$_2$O (2 x 2 mL) and pentane (2 x 2 mL) and dried in air. Yield: 11 mg (0.01 mmol, 17%). Crystals suitable for X-ray diffraction were obtained by evaporation of a saturated CH$_2$Cl$_2$ solution. IR (cm^{-1}): 2033 (vw, $\nu_{C\equiv O}$), 1940 (w, $\nu_{C\equiv O}$), 1906 (s, $\nu_{C\equiv O}$), 1906(sh, $\nu_{C\equiv O}$), 1564 (w, $\nu_{Tc\text{-}Ph}$). ^{1}H NMR (CD$_2$Cl$_2$, ppm): 7.35-7.22 (30H, m, Ar**H**), 6.98 (2H, pseudo d, $J_{H,H}$ = 7.17 Hz, Tc-C(C**H**)$_2$(CH)$_2$CH), 6.68 (1H, pseudo t, $J_{H,H}$ = 7.23 Hz, Tc-C(CH)$_2$(CH)$_2$C**H**), 6.53 (2H, pseudo t, $J_{H,H}$ = 7.31 Hz, Tc-C(CH)$_2$(C**H**)$_2$CH). ^{99}Tc NMR (CD$_2$Cl$_2$, ppm): -1806 (s, $\nu_{1/2}$ = 12238 Hz). The ^{31}P resonance was too broad to be observed.

*[Tc(Cp)(CO)$_2$(PPh$_3$)] (**5**)*. A light red solution of Na(Cp) (0.15 mL, 0.25 mmol, 2 M in THF) was added to a frozen suspension of [Tc(SMe$_2$)(CO)$_3$(PPh$_3$)$_2$](BF$_4$) (40 mg, 0.05 mmol) in dry, degassed THF (0.5 mL) in a nitrogen bath. The frozen mixture was allowed to thaw and at ca. 0°C an orange solution had formed. The solution was stirred for 5 min. MeOH (6 mL) was added dropwise to hydrolyze residual organometallic reagent. The mixture was opened to the atmosphere and left for evaporation for three days. Large parallelepipeds of **5** formed, which were filtered off and washed with MeOH (1 mL). After drying in air, beige crystals were obtained. Yield: 22 mg (0.05 mmol, 91%). The crystals were suitable for X-ray diffraction. IR (cm^{-1}): 1938 (vs, $\nu_{C\equiv O}$), 1867 (vs, $\nu_{C\equiv O}$). ^{1}H NMR (CD$_2$Cl$_2$, ppm): 7.39 (15H, m, Ar**H**), 4.91 (5H, s, cp**H**). ^{31}P NMR (CD$_2$Cl$_2$, ppm): 53 (s, $\nu_{1/2}$ = 9888 Hz). ^{99}Tc NMR (CD$_2$Cl$_2$, ppm): -2420 (s, $\nu_{1/2}$ = 2036 Hz).

*[Tc(=CCH$_2$CH$_2$CH$_2$O)(CO)$_3$(PPh$_3$)$_2$](BF$_4$) (**6**)*. 1-Butyne-4-ol (0.1 mL) was added to a suspension of [Tc(SMe$_2$)(CO)$_3$-(PPh$_3$)$_2$](BF$_4$) (40 mg, 0.05 mmol) in dry, degassed THF (2 mL). The colorless suspension was heated to reflux and stirred for 30 min to give a yellow suspension. The flocculent colorless precipitate was filtered off after the addition

of pentane (9 mL). It was washed with isopropanol (2 mL) and pentane (3 mL) and dried in air. Yield: 43 mg (0.05 mmol, 100%). When traces of SMe_2 could not be removed, the formation of $[Tc(SMe_2)(CO)_3(PPh_3)_2](BF_4)$ due to the decomposition of $[Tc(=CCH_2CH_2CH_2O)(CO)_3(PPh_3)_2](BF_4)$ in solution was observed. Crystals suitable for X-ray diffraction were obtained from layered liquid/liquid diffusion of pentane into a CH_2Cl_2 solution at room temperature. IR (cm^{-1}): 2068 (w, $\nu_{C\equiv O}$), 1991 (s, $\nu_{C\equiv O}$), 1969 (vs, $\nu_{C\equiv O}$). ^1H NMR (CD_2Cl_2, ppm): 7.51 (30H, m, Ar**H**), 4.44 (2H, t, $^3J_{H,H}$ = 8.18 Hz, Tc=C-$CH_2CH_2C\mathbf{H_2}O$), 2.42 (2H, t, $^3J_{H,H}$ = 8.06 Hz, Tc=C-$C\mathbf{H_2}CH_2CH_2O$), 1.02 (2H, p, $^3J_{H,H}$ = 8.13 Hz, Tc=C-$CH_2C\mathbf{H_2}CH_2O$). ^{19}F NMR (CD_2Cl_2, ppm): -153.1 (s, $^{10}BF_4$), -153.1 (s, $^{11}BF_4$). ^{11}B NMR (CD_2Cl_2, ppm): -1.1 (s). ^{31}P NMR (CD_2Cl_2, ppm): 37 (s, $\nu_{1/2}$ = 971 Hz). ^{99}Tc NMR (CD_2Cl_2, ppm): -1693 (s, $\nu_{1/2}$ = 10410 Hz).

$[Tc(=CCH_2CH_2CH_2CH_2O)(CO)_3(PPh_3)_2](BF_4)$ ***(7)***. a) 1-Pentyne-5-ol (0.1 mL) was added to a suspension of $[Tc(SMe_2)(CO)_3(PPh_3)_2](BF_4)$ (40 mg, 0.05 mmol) in dry, degassed THF (2 mL). The colorless suspension was heated to reflux and stirred for 30 min to give a yellow suspension. The yellowish precipitate was filtered off after addition of pentane (9 mL). It was washed with isopropanol (2 x 1 mL) and pentane (3 mL) and dried in air. Yield: 35 mg (0.04 mmol, 80%). b) 1-Pentyne-5-ol (0.1 mL) was added to a suspension of $[Tc(OH_2)(CO)_3(PPh_3)_2](BF_4)$ (41 mg, 0.05 mmol) in THF (1 mL). The suspension was heated to reflux and stirred for 5 min to give a yellow solution. The mixture was filtered over a small bed of Na_2SO_4 to remove the released water and traces of brown decomposition products. The Na_2SO_4 was washed with CH_2Cl_2 (0.5 mL) and the combined filtrate and washing solutions were layered with pentane (9 mL). After storage in a refrigerator overnight, yellowish crystals formed. The crystals were filtered off, washed with pentane (3 x 3 mL) and dried in air. Yield: 12 mg (0.01 mmol, 27%). The crystals were suitable for X-ray diffraction. IR (cm^{-1}): 2070 (w, $\nu_{C\equiv O}$), 1960 (vs, $\nu_{C\equiv O}$). ^1H NMR (CD_2Cl_2, ppm): 7.51 (30H, s, Ar**H**), 4.21 (2H, t, $^3J_{H,H}$ = 5.86 Hz, Tc=C-$CH_2CH_2CH_2C\mathbf{H_2}O$), 2.70 (2H, t, $^3J_{H,H}$ = 6.36 Hz, Tc=C-$C\mathbf{H_2}CH_2CH_2CH_2O$), 1.11 (2H, p, $^3J_{H,H}$ = 6.00 Hz, Tc=C-$CH_2CH_2C\mathbf{H_2}CH_2O$), 0.76 (2H, p, $^3J_{H,H}$ = 6.35 Hz, Tc=C-$CH_2C\mathbf{H_2}CH_2CH_2O$). ^{19}F NMR (CD_2Cl_2, ppm): -153.1 (s, $^{10}BF_4$), -153.2 (s, $^{11}BF_4$). ^{11}B NMR (CD_2Cl_2, ppm): -2.1 (s). ^{31}P NMR (CD_2Cl_2, ppm): 39 (s, $\nu_{1/2}$ = 1182 Hz). ^{99}Tc NMR (CD_2Cl_2, ppm): -1668 (s, $\nu_{1/2}$ = 27508 Hz).

$[Tc(C\equiv CH)(CO)_3(PPh_3)_2]$ ***(8)***. Solid $[Li(en)_2](C\equiv CH)$ (23 mg, 0.25 mmol) was added to a suspension of $[Tc(SMe_2)(CO)_3(PPh_3)_2](BF_4)$ (25 mg, 0.03 mmol) in dry, degassed THF(1 mL). The grey suspension was stirred for 1.5 h, after which time a colorless solid precipitated. MeOH (9 mL) was slowly added to hydrolyze residual organometallic reagent and precipitate the product as a colorless powder. The mixture was stored in a refrigerator for 1 h to complete the precipitation. The colorless precipitate was filtered off and washed with MeOH (3 mL) and pentane (1 mL). After drying in air, a colorless powder was obtained. Yield: 16 mg (0.02 mmol, 73%). Crystals suitable for X-ray diffraction were obtained by slow evaporation of a saturated CH_2Cl_2 solution. IR (cm^{-1}): 3283 (w, $\nu_{C\equiv C\text{-}H}$), 2053 (sh, $\nu_{C\equiv C}$), 2050 (w, $\nu_{C\equiv O}$), 1954 (s, $\nu_{C\equiv O}$), 1931 (vs, $\nu_{C\equiv O}$). ^1H NMR (CD_2Cl_2, ppm): 7.81 (11H, s, Ar**H**), 7.42 (18H, s, Ar**H**), 1.89 (1H, s, Tc-C$\equiv$C-**H**). ^{31}P NMR (CD_2Cl_2, ppm): 40 (s, $\nu_{1/2}$ = 885 Hz). ^{99}Tc NMR (CD_2Cl_2, ppm): -1932 (s, $\nu_{1/2}$ = 8110 Hz).

$[Tc(C\equiv C\text{-}Ph)(CO)_3(PPh_3)_2]$ ***(8a)***. a) A solution of Li(C$\equiv$C-Ph) (4 mL, 0.5 M) was freshly prepared by the slow addition of *n*-butyllithium (1.3 mL, 2.1 mmol, 1.6 M in hexane) to a solution of HC$\equiv$C-Ph (204 mg, 0.22 mL, 2 mmol) in dry, degassed THF (2.7 mL) at -78°C followed by warming to room temperature. The thus prepared yellow solution of LiC$\equiv$C-Ph (0.5 mL, 0.25 mmol) was added dropwise to a suspension of $[Tc(SMe_2)(CO)_3(PPh_3)_2](BF_4)$ (43 mg, 0.05 mmol) in dry, degassed THF (1 mL). The resulting yellow suspension was stirred for 30 min. MeOH (7 mL) was added to hydrolyze residual organometallic reagent and precipitate the product as a colorless powder. After storage in a refrigerator for 3 h, the product was filtered off and washed with MeOH (2 mL) and pentane (3 mL). After drying in air, a colorless, sparingly soluble powder was obtained. Yield: 40 mg (0.05 mmol, 99%). b) HC$\equiv$C-Ph (8 drops) and NEt_3 (3 drops) were added to a suspension of $[Tc(OH_2)(CO)_3(PPh_3)_2](BF_4)$ (44 mg, 0.05 mmol) in THF (0.5 mL). Within 10 min, the starting material dissolved and the product started to precipitate. This process was completed after 20 min by the addition of MeOH (9 mL). The light yellow precipitate was filtered off and washed with MeOH (2 mL) and pentane (3 mL). After drying in air, a light yellow, sparingly soluble powder was obtained. Yield: 27 mg (0.03 mmol, 68%). Recrystallization by evaporation of a CH_2Cl_2/MeOH mixture gave crystals suitable for X-ray diffraction. IR (cm^{-1}): 2095 (w, $\nu_{C\equiv C}$), 2043 (m, $\nu_{C\equiv O}$), 1960 (vs, $\nu_{C\equiv O}$), 1929 (vs, $\nu_{C\equiv O}$). 7.67-7.22 (39H, m, Ar**H**), 6.82 (1H, pseudo dd, Tc-C$\equiv$C-C$(CH)_2(CH)_2C\mathbf{H}$, Ar**H**), 6.74 (2H, pseudo dd, Tc-C$\equiv$C-C$(C\mathbf{H})_2(CH)_2CH$), 6.28 (2H, pseudo d, Tc-C$\equiv$C-C$(CH)_2(C\mathbf{H})_2CH$). ^{31}P NMR (CD_2Cl_2, ppm): 39 (s, $\nu_{1/2}$ = 1268 Hz). ^{99}Tc NMR (CD_2Cl_2, ppm): -2056 (s, $\nu_{1/2}$ = 9638 Hz).

$[Tc(C\equiv C\text{-}^tBu)(CO)_3(PPh_3)_2]$ ***(8b)***. A solution of Li(C$\equiv$C-^{t}Bu) (1 mL, 0.5 M) was freshly prepared by the slow addition of *n*-butyllithium (0.32 mL, 0.51 mmol, 1.6 M in hexane) to a solution of HC$\equiv$C-^{t}Bu (41 mg, 0.06 mL, 0.5 mmol) in dry, degassed THF (0.68 mL) at -78°C followed by warming to room temperature. The thus prepared light yellow solution of Li(C$\equiv$C-^{t}Bu) (1 mL, 0.5 mmol) was added dropwise to a suspension of $[Tc(SMe_2)(CO)_3(PPh_3)_2](BF_4)$ (86 mg, 0.1 mmol) in dry, degassed THF (1 mL). The resulting light yellow solution was stirred for 30 min. MeOH (9 mL) was added to hydrolyze residual organometallic reagent and precipitate the product as a colorless powder. After 5 min of stirring, the microcrystals were filtered off and washed with MeOH (2 mL) and pentane (3 mL). After drying in air, a colorless powder was obtained. Slow evaporation of a CH_2Cl_2/MeOH mixture gave pure crystals of **8b** ,which were suitable for X-ray diffraction. Yield: 77 mg (0.1 mmol, 98%). IR (cm^{-1}): 2045 (w, $\nu_{C\equiv O}$), 1946 (s, $\nu_{C\equiv O}$), 1925 (s, $\nu_{C\equiv O}$). ^1H NMR (CD_2Cl_2, ppm): 7.89 (12H, s, Ar**H**), 7.39 (19H, s, Ar**H**), 0.92 (9H, s, Tc-C$\equiv$C-C$(C\mathbf{H_3})_3$). ^{31}P NMR (CD_2Cl_2, ppm): 39 (s, $\nu_{1/2}$ = 1268 Hz). ^{99}Tc NMR (CD_2Cl_2, ppm): -1956 (s, $\nu_{1/2}$ = 11747 Hz).

*[Tc(C≡C-^{n}Bu)(CO)$_3$(PPh$_3$)$_2$] (**8c**)*. A solution of Li(C≡C-^{n}Bu) (2 mL, 0.65 M) was freshly prepared by the slow addition of *n*-butyllithium (0.82 mL, 1.3 mmol, 1.6 M in hexane) to a solution of 1-hexyne (107 mg, 0.15 mL, 1.3 mmol) in dry, degassed THF (1 mL) at -78°C followed by warming to room temperature. The thus prepared light yellow solution of Li(C≡C-^{n}Bu) (0.8 mL, 0.5 mmol) was added dropwise to a suspension of [Tc(SMe$_2$)(CO)$_3$(PPh$_3$)$_2$](BF$_4$) (76 mg, 0.09 mmol) in dry, degassed THF (1 mL). The resulting faint yellow, slightly turbid solution was stirred for 30 min. MeOH (9 mL) was added to hydrolyze residual organometallic reagent and precipitate the product as a colorless powder. After 5 min of stirring, the precipitate was filtered off and washed with MeOH (2 x 2 mL) and pentane (3 mL). After drying in air, a colorless powder was obtained. A minor second crop of the compound was obtained from the combined filtrate and washing solutions. Evaporation of a CH$_2$Cl$_2$/MeOH solution of the complex gave pure crystals of **8c** suitable for x-ray diffraction. Yield: 66 mg (0.08 mmol, 95%). IR (cm^{-1}): 2042 (m, $\nu_{C\equiv O}$), 1948 (vs, $\nu_{C\equiv O}$), 1927 (vs, $\nu_{C\equiv O}$). ^{1}H NMR (CD$_2$Cl$_2$, ppm): 7.85 (12H, s, Ar**H**), 7.40 (18H, s, Ar**H**), 1.99 (2H, s, Tc-C≡C-C**H$_2$**CH$_2$CH$_2$CH$_3$), 1.26 (4H, s, Tc-C≡C-CH$_2$C**H$_2$**C**H$_2$**CH$_3$), 0.82 (3H, s, Tc-C≡C-CH$_2$CH$_2$CH$_2$C**H$_3$**). ^{31}P NMR (CD$_2$Cl$_2$, ppm): 40 (s, $\nu_{1/2}$ = 713 Hz). ^{99}Tc NMR (CD$_2$Cl$_2$, ppm): -1952 (s, $\nu_{1/2}$ = 9690 Hz).

*[Tc(C≡C-SiMe$_3$)(CO)$_3$(PPh$_3$)$_2$] (**8d**)*. A solution of Li(C≡C-SiMe$_3$) (3 mL, 1 M) was freshly prepared by the slow addition of *n*-butyllithium (1.88 mL, 3 mmol, 1.6 M in hexane) to a solution of HC≡C-SiMe$_3$ (294 mg, 0.43 mL, 3 mmol) in dry, degassed THF (0.69 mL) at -78°C followed by warming to room temperature. The thus prepared light yellow solution of Li(C≡C-SiMe$_3$) (1 mL, 1 mmol) was added dropwise to a suspension of [Tc(SMe$_2$)(CO)$_3$(PPh$_3$)$_2$](BF$_4$) (150 mg, 0.2 mmol) in dry, degassed THF (1 mL). The resulting yellow suspension was stirred for 30 min. MeOH (6 mL) was added to hydrolyze residual organometallic reagent and precipitate the product as an off-white solid. After 5 min of stirring, the powder was filtered off and washed with MeOH (3 x 2 mL) and pentane (3 mL). After drying in air, a colorless powder was obtained. Yield: 124 mg (0.15 mmol, 88%). Crystals suitable for X-ray diffraction were obtained by slow evaporation of a CH$_2$Cl$_2$/pentane solution of the complex. IR (cm^{-1}): 2054 (vw, $\nu_{C\equiv C}$), 2023 (w, $\nu_{C\equiv O}$), 1950 (s, $\nu_{C\equiv O}$), 1929 (vs, $\nu_{C\equiv O}$). ^{1}H NMR (CD$_2$Cl$_2$, ppm): 7.83 (15H, s, Ar**H**), 7.39 (20H, s, Ar**H**), -0.15 (9H, s, Tc-C≡C-Si(C**H$_3$**)$_3$). ^{31}P NMR (CD$_2$Cl$_2$, ppm): 38 (s, $\nu_{1/2}$ = 971 Hz). ^{99}Tc NMR (CD$_2$Cl$_2$, ppm): -1939 (s, $\nu_{1/2}$ = 8153 Hz).

*[Tc(C≡C-C$_6$H$_3$(CF$_3$)$_2$}(CO)$_3$(PPh$_3$)$_2$] (**8e**)*. A solution of Li{C≡C-C$_6$H$_3$(CF$_3$)$_2$} (2 mL, 0.5 M) was freshly prepared by the slow addition of *n*-butyllithium (0.65 mL, 1.05 mmol, 1.6 M in hexane) to a solution of HC≡C-C$_6$H$_3$(CF$_3$)$_2$ (238 mg, 0.175 mL, 1 mmol) in dry, degassed THF (1.35 mL) at -78°C followed by warming to room temperature. The thus prepared brown solution of Li{C≡C-C$_6$H$_3$(CF$_3$)$_2$} (0.5 mL, 0.25 mmol) was added dropwise to a suspension of [Tc(SMe$_2$)(CO)$_3$(PPh$_3$)$_2$](BF$_4$) (43 mg, 0.05 mmol) in dry, degassed THF (1 mL). The resulting deep red-brown solution was stirred for 45 min. MeOH (8 mL) was added to hydrolyze residual organometallic reagent. Water (1 mL) was then added to precipitate the product as colorless microcrystals. The microcrystals were filtered off and washed with MeOH (2 mL) and pentane (3 mL). After drying in air, a colorless powder was obtained. Evaporation of a CH$_2$Cl$_2$/MeOH solution gave pure crystals of **8e** suitable for X-ray diffraction. Yield: 48 mg (0.05 mmol, 100%). IR (cm^{-1}): 2091 (w, $\nu_{C\equiv C}$), 2050 (m, $\nu_{C\equiv O}$), 1964 (s, $\nu_{C\equiv O}$), 1919 (vs, $\nu_{C\equiv O}$). ^{1}H NMR (CD$_2$Cl$_2$, ppm): 7.75 (12H, s, Ar**H**), 7.45+7.42 (19H, 2s, Tc-C≡C-C(CH)$_2$(C(CF$_3$))$_2$C**H**, Ar**H**), 2.58 (2H, s, Tc-C≡C-C(C**H**)$_2$(C(CF$_3$))$_2$CH). ^{19}F NMR (CD$_2$Cl$_2$, ppm): -63.2 (s). ^{31}P NMR (CD$_2$Cl$_2$, ppm): 42 (s, $\nu_{1/2}$ = 692 Hz). ^{99}Tc NMR (CD$_2$Cl$_2$, ppm): -1914 (s, $\nu_{1/2}$ = 8739 Hz).

*[Tc(C≡N-Ph)(CO)$_3$(PPh$_3$)$_2$](BF$_4$) (**9a**)*. A solution of C≡N-Ph (2 drops) in CH$_2$Cl$_2$ (0.5 mL) was added to a suspension of [Tc(OH$_2$)(CO)$_3$(PPh$_3$)$_2$](BF$_4$) (41 mg, 0.05 mmol) in CH$_2$Cl$_2$ (1 mL). The resulting orange-red solution was stirred for 10 min and filtered over a small bed of Na$_2$SO$_4$ to remove the released water. The Na$_2$SO$_4$ was washed with CH$_2$Cl$_2$ (0.5 mL) and the combined filtrate and washing solutions were layered with pentane (15 mL). After storage in a refrigerator overnight, large yellow-orange crystals and some orange powder formed. The crystals were filtered off, washed with Et$_2$O (3 mL) and pentane (3 x 3 mL) and dried in air. Yield: 47 mg (0.05 mmol, 100%). The crystals were suitable for X-ray diffraction. IR (cm^{-1}): 2166 (w, $\nu_{C\equiv N}$), 2073 (w, $\nu_{C\equiv O}$), 1992 (s, $\nu_{C\equiv O}$). 7.62-7.49 (30H, m, Ar**H**), 7.46 (2H, m, Tc-C≡N-C(CH)$_2$(C**H**)$_2$CH), 7.32 (1H, pseudo t, Tc-C≡N-C(CH)$_2$(CH)$_2$C**H**), 6.53 (2H, pseudo d, Tc-C≡N-C(C**H**)$_2$(CH)$_2$CH). ^{19}F NMR (CD$_2$Cl$_2$, ppm): -152.7 (s, ^{10}BF$_4$), -152.8 (s, ^{11}BF$_4$). ^{11}B NMR (CD$_2$Cl$_2$, ppm): -2.1 (s). ^{31}P NMR (CD$_2$Cl$_2$, ppm): 37 (s, $\nu_{1/2}$ = 2355 Hz). ^{99}Tc NMR (CD$_2$Cl$_2$, ppm): -1880 (s, $\nu_{1/2}$ = 4280 Hz).

*[Tc(C≡N-^{t}Bu)(CO)$_3$(PPh$_3$)$_2$](BF$_4$) (**9b**)*. C≡N-^{t}Bu (2 drops) was added to a suspension of [Tc(OH$_2$)(CO)$_3$(PPh$_3$)$_2$](BF$_4$) (41 mg, 0.05 mmol) in CH$_2$Cl$_2$ (1 mL). The resulting yellow-orange solution was stirred for 5 min. The clear solution was filtered over a small bed of Na$_2$SO$_4$ to remove the released water. The Na$_2$SO$_4$ was washed with CH$_2$Cl$_2$ (1.5 mL) and the combined filtrate and washing solutions were layered with pentane (12 mL). After storage in a refrigerator overnight, large colorless crystals formed. The crystals were filtered off, washed with and pentane (3 x 3 mL) and dried in air. Yield: 38 mg (0.05 mmol, 92%). Crystals suitable for X-ray diffraction were obtained from CD$_2$Cl$_2$/pentane or CH$_2$Cl$_2$/Et$_2$O by layered liquid/liquid diffusion at room temperature. IR (cm^{-1}): 2193 (m, $\nu_{C\equiv N}$), 2075 (m, $\nu_{C\equiv O}$), 1991 (s, $\nu_{C\equiv O}$), 1977 (s, $\nu_{C\equiv O}$). ^{1}H NMR (CD$_2$Cl$_2$, ppm): 7.52 (30H, s, Ar**H**), 1.01 (9H, s, Tc-C≡N-C(C**H$_3$**)$_3$). ^{19}F NMR (CD$_2$Cl$_2$, ppm): -154.0 (s, ^{10}BF$_4$), -154.0 (s, ^{11}BF$_4$). ^{11}B NMR (CD$_2$Cl$_2$, ppm): -3.1 (s). ^{31}P NMR (CD$_2$Cl$_2$, ppm): 36 (s, $\nu_{1/2}$ = 2957 Hz). ^{99}Tc NMR (CD$_2$Cl$_2$, ppm): -1874 (s, $\nu_{1/2}$ = 4025 Hz).

*[Tc(N≡C-Ph)(CO)$_3$(PPh$_3$)$_2$](BF$_4$) (**10a**)*. N≡C-Ph (2 drops) was added to a suspension of [Tc(OH$_2$)(CO)$_3$(PPh$_3$)$_2$](BF$_4$) (38 mg, 0.05 mmol) in CH$_2$Cl$_2$ (1 mL). The resulting clear,

yellow solution was stirred for 5 min and then filtered over a small bed of Na_2SO_4 to remove the released water. The Na_2SO_4 was washed with CH_2Cl_2 (1.5 mL) and the combined filtrate and washing solutions were layered with pentane (12 mL). After storage in a refrigerator overnight, colorless microcrystals formed. The crystals were filtered off, washed with pentane (3 x 3 mL) and dried in air. Yield: 39 mg (0.04 mmol, 93%). Crystals suitable for X-ray diffraction were grown by evaporation of a saturated CH_2Cl_2 solution. IR (cm^{-1}): 2249 (w, $\nu_{C\equiv N}$), 2075 (m, $\nu_{C\equiv O}$), 1985 (s, $\nu_{C\equiv O}$), 1954 (s, $\nu_{C\equiv O}$). ^1H NMR (CD_2Cl_2, ppm): 7.67-7.46 (31H, 3m, Ar**H**, Tc-N≡C-C(CH)$_2$(CH)$_2$C**H**), 7.46-7.34 (2H, pseudo t, Tc-N≡C-C(CH)$_2$(C**H**)$_2$CH), 6.88-6.65 (2H, pseudo d, Tc-N≡C-C(C**H**)$_2$(CH)$_2$CH). ^{19}F NMR (CD_2Cl_2, ppm): -154.1 (s, $^{10}BF_4$), -154.1 (s, $^{11}BF_4$). ^{11}B NMR (CD_2Cl_2, ppm): -3.1 (s). ^{31}P NMR (CD_2Cl_2, ppm): 37 (s, $^1J_{Tc,P} \approx 360$ Hz, $\nu_{1/2} = 3597$ Hz). ^{99}Tc NMR (CD_2Cl_2, ppm): -1496 (s, $\nu_{1/2} = 2818$ Hz).

[Tc(N≡C-^{t}Bu)(CO)$_3$(PPh$_3$)$_2$](BF$_4$) (***10b***). N≡C-^{t}Bu (4 drops) was added to a suspension of [Tc(OH$_2$)(CO)$_3$(PPh$_3$)$_2$](BF$_4$) (41 mg, 0.05 mmol) in CH_2Cl_2 (1 mL). The resulting yellow-orange solution was stirred for 5 min. The clear solution was filtered over a small bed of Na_2SO_4 to remove the released water. The Na_2SO_4 was washed with CH_2Cl_2 (2 x 0.5 mL) and the combined filtrate and washing solutions were layered with Et_2O (20 mL). After storage in a refrigerator overnight, colorless crystals formed. The crystals were filtered off, washed with and pentane (3 x 3 mL) and dried in air. Yield: 42 mg (0.05 mmol, 96%). Crystals suitable for X-ray diffraction were obtained from CH_2Cl_2/pentane by layered liquid/liquid diffusion at room temperature. IR (cm^{-1}): 2272 (w, $\nu_{C\equiv N}$), 2081 (m, $\nu_{C\equiv O}$), 1989 (vs, $\nu_{C\equiv O}$), 1936 (s, $\nu_{C\equiv O}$). ^1H NMR (CD_2Cl_2, ppm): 7.62-7.42 (30H, m, Ar**H**), 0.84 (9H, s, Tc-N≡C-C(C**H$_3$**)$_3$). ^{19}F NMR (CD_2Cl_2, ppm): -152.8 (s, $^{10}BF_4$), -152.8 (s, $^{11}BF_4$). ^{11}B NMR (CD_2Cl_2, ppm): -2.1 (s). ^{31}P NMR (CD_2Cl_2, ppm): 35 (s, $\nu_{1/2} = 4410$ Hz). ^{99}Tc NMR (CD_2Cl_2, ppm): -1481 (s, $\nu_{1/2} = 3020$ Hz).

ASSOCIATED CONTENT

Supporting Information. This material is available free of charge via the Internet at http://pubs.acs.org.

Crystallographic tables, bond lengths angles and ellipsoid plots; Spectroscopic data (PDF)

Accession Codes. CCDC 2131506-2131521 contain the supplementary crystallographic data for this paper. These data can be obtained free of charge via www.ccdc.cam.ac.uk/data_request/cif, or by emailing data_request@ccdc.cam.ac.uk, or by contacting The Cambridge Crystallographic Data Centre, 12 Union Road, Cambridge CB2 1EZ, UK; fax: +44 1223 336033.

AUTHOR INFORMATION

Corresponding Author

Ulrich Abram – Institute of Chemistry and Biochemistry, Freie Universität Berlin, Fabeckstr. 34/36, 14195 Berlin, Germany; Orcid.org/0000-0002-1747-7927; Email: ulrich.abram@fu-berlin.de

Author

Maximilian Roca Jungfer – Institute of Chemistry and Biochemistry, Freie Universität Berlin, 14195 Berlin, Germany; Orcid.org/0000-0001-7583-9634.

Notes

The authors declare no competing financial interest.

ACKNOWLEDGMENT

Experimental assistance of Laura Elsholz (FU Berlin) is gratefully acknowledged. Additionally we thank for support from the Core Facility 1249 BioSupraMol and the High-Performance Computing (HPC) Centre of the Zentraleinrichtung für Datenverarbeitung (ZEDAT) of the Freie Universität Berlin for computational time and support.

REFERENCES

(1) Mingos, D. M. P.; Crabtree, R. H. *Comprehensive Organometallic Chemistry III, From Fundamentals to Applications*, **2007**, Vol. 1 – 13, Elsevier, and references cited therein.

(2) Samantaray, K. M.; D'Elia, V.; Pump, E.; Falivene, L.; Harb, M.; Chikh, S. O,; Cavallo, L.; Basset, J.-M. The Comparison between Single Atom Catalysis and Surface Organometallic Catalysis. *Chem. Rev.* **2020**, *120*, 734–813.

(3) Zhou, F.; Li, C.-J. *En route* to metal-mediated and metal-catalysed reactions in water. *Chem. Sci.* **2019**, *10*, 34

(4) Vinogradova, E. V. Organometallic chemical biology: an organometallic approach to bioconjugation. *Pure Appl. Chem*. **2017**, *89*, 1619–1640.

(5) Abakumov, G. A.; Piskunov, A. V.; Cherkasov, V. K.; Fedushkin, I. L.; Ananikov, V. P.; Eremin, D. B.; Gordeev, E. G.; Beletskaya, I. P.; Averin, A. D.; Bochkarev, M. N.; Trifonov, A. A.; Dzhemilev, U. M.; D'yakonov, V. A.; Egorov, M. P.; Vereshchagin, A. N.; Syroeshkin, M. A.; Jouikov, V. V.; Muzafarov, A. M.; Anisimov, A. A.; Arzumanyan, A. V.; Kononevich, Y. N.; Temnikov, M. N.; Sinyashin, O. G.; Budnikova, Y. H.; Burilov, A. R.; Karasik, A. A.; Mironov, V. F.; Storozhenko, P. A.; Shcherbakova, G. I.; Trofimov, B. A.; Amosova, S. V.; Gusarova, N. K.; Potapov, V. A.; Shur, V. B.; Burlakov, V. V.; Bogdanov, V. S.; Andreev, M. V. Organoelement chemistry: promising growth areas and challenges. *Russ. Chem. Rev*. **2018**, *87*, 393-507.

(6) Hahn, F. E. Introduction: Carbene Chemistry. *Chem. Rev.* **2018**, *118*, 9455–9456.

(7) Zhang, P.; Sadler, P. J. Advances in the design of organometallic anticancer complexes. *J. Organomet. Chem.* **2017**, *839*, 5-14.

(8) Copéret C.; Fedorov, A.; Zhizhko, P. A. Surface Organometallic Chemistry: Paving the Way Beyond Well-Defined Supported Organometallics and Single-Site Catalysis. *Catal. Lett.* **2017**, *147*, 2247-2259.
(9) Samantaray, M. K.; Pump, E.; Bendjeriou-Sedjerari, A.; D'Elia, V.; Pelletier, J. D. A.; Guidotti, M.; Psaro, R.; Basset, J.-M. Surface organometallic chemistry in heterogeneous catalysis. *Chem. Soc. Rev.*, **2018**, *47*, 8403-8437.
(10) Nelson, D. J.; Nolan, S. P. Hydroxide complexes of the late transition metals: Organometallic chemistry and catalysis. *Coord. Chem. Rev.* **2017**, *353*, 278–294.
(11) Alberto, R. The "Carbonyl Story" and Beyond; Experiences, Lessons and Implications, *ChemMedChem*, **2020**, *21*, 2743-2749.
(12) Duatti, A. Review on ^{99m}Tc radiopharmaceuticals with emphasis on new advancements. *Nucl. Med. Biol.* **2021**, *92*, 202–216.
(13) Alberto, R.; Schibli, R.; Abram, U.; Egli, A.; Knapp, F. F. (Russ); Schubiger, P. A. Potential of the "$[M(CO)_3]^+$" (M = Re, Tc) Moiety for the Labeling of Biomolecules. *Radiochim. Acta* **1997**, *79*, 99-103.
(14) Alberto, R.; Schibli, R.; Egli, A.; Schubiger, A. P. A Novel Organometallic Aqua Complex of Technetium for the Labeling of Biomolecules: Synthesis of $[^{99m}Tc(OH_2)_3(CO)_3]^+$ from $[^{99m}TcO_4]^-$ in Aqueous Solution and Its Reaction with a Bifunctional Ligand. *J. Am. Chem. Soc.* **1998**, *120*, 7987-7988.
(15) Alberto, R.; Schibli, R.; Waibel, R.; Abram, U.; Schubiger, A. P. Basic aqueous chemistry of $[M(OH_2)_3(CO)_3]^+$ (M =Re, Tc) directed towards radiopharmaceutical application. *Coord. Chem. Rev*. **1999**, *190–192*, 901–919.
(16) Alberto, R. The Chemistry of Technetium–Water Complexes within the Manganese Triad: Challenges and Perspectives. *Eur. J. Inorg. Chem.* **2009**, *1*, 21–31.
(17) Grundler, P. V.; Helm, L.; Alberto, R.; Merbach, A. E. Relevance of the Ligand Exchange Rate and Mechanism of *fac*-$[(CO)_3M(H_2O)_3]^+$ (M = Mn, Tc, Re) Complexes for New Radiopharmaceuticals. *Inorg Chem.* **2006**, *45*, 10378-10390.
(18) Alberto, R.; Schibli, R.; Schubiger, P. A. Reactions with the technetium and rhenium carbonyl complexes $(NEt_4)_2[MX_3(CO)_3]$. Synthesis and structure of $[Tc(CN\text{-}Bu^t)_3(CO)_3](NO_3)$ and $(NEt_4)[Tc_2(\mu\text{-}SCH_2CH_2OH)_3(CO)_6]$. *Polyhedron* **1996**, *15*, 1079-1089.
(19) Jones, A. G.; Abrams, M. J.; Davison, A.; Brodack, J. W.; Toothaker, A. K.; Adelstein, S. J.; Kassis, A. I. Biological studies of a new class of technetium complexes: the hexakis(alkylisonitrile)technetium(I) cations. *Int. J. Nucl. Med. Biol*. **1984**, *11*, 225-234.
(20) Kronauge, J. F.; Mindiola, D. J. The Value of Stable Metal-Carbon Bonds in Nuclear Medicine and the Cardiolite Story, *Organometallics* **2016**, *35*, 3432-3435.
(21) Bartholomä, M. D.; Louie, A. S.; Valliant, J. F.; Zubieta, J. Technetium and gallium derived radiopharmaceuticals: comparing and contrasting the chemistry of two important radiometals for the molecular imaging era. *Chem. Rev*. **2010**, *110*, 2903–2920.
(22) Papagiannopoulou, D. Technetium-99m radiochemistry for pharmaceutical applications. *J. Labelled Compd. Radiopharm.* **2017**, *60*, 502–520.
(23) Abram, U.; Alberto, R. Technetium and rhenium – coordination chemistry and nuclear medical applications. *J. Braz. Chem. Soc*. **2006**, *17*, 1486-1500.
(24) Kuntic, V.; Brboric, J.; Vujic, Z.; Uskokovic-Markovic, S. Radioisotopes Used as Radiotracers in vitro and in vivo Diagnostics: A Review. *Asian J. Chem*. **2016**, *28*, 235–411.
(25) Claude, G.; Salsi, F.; Hagenbach, A.; Gembicky, M.; Neville, M.; Chan, C.; Figueroa, J. S.; Abram, U. Structural and Redox Variations in Technetium Complexes Supported by m-Terphenyl Isocyanides. *Organometallics*, **2020**, *39*, 2287–2294.
(26) Salsi, F.; Neville, M.; Drance, M.; Hagenbach, A.; Figueroa, J. S.; Abram, U. $[M^I(CO)X(CNAr^{DArF2}]_4$ (DArF = 3,5-$(CF_3)_2C_6H_3$; M = Re and Tc; X = Br and Cl) Complexes: Convenient Platforms for the Synthesis of Low-Valent Rhenium and Technetium Compounds. *Organometallics*, **2021**, *40*, 1336−1343.
(27) Meola, G.; Braband, H.; Hernández-Valdés, D.; Gotzmann, C.; Fox, T.; Spingler, B.; Alberto, R. A Mixed-Ring Sandwich Complex From Unexpected Ring Contraction in $[Re(\eta^6\text{-}C_6H_5Br)(\eta^6\text{-}C_6R_6)](PF_6)$. *Inorg. Chem*. **2017**, *56*, 6297−6301.
(28) Benz, M.; Braband, H.; Schmutz, P.; Halter, J.; Alberto, R. From Tc^{VII} to Tc^{I}; facile syntheses of bis-arene complexes $[^{99(m)}Tc(arene)_2]^+$ from pertechnetate. *Chem. Sci.* **2015**, *6*, 165-169.
(29) Meola, G.; Braband, H.; Jordi, S.; Fox, T.; Blacque, O.; Spingler, B.; Alberto, R. Structure and reactivities of rhenium and technetium bis-arene sandwich complexes $[M(\eta^6\text{-arene})_2]^+$. *Dalton Trans.* **2017**, *46*, 14631–14637.
(30) Burrell, A. K.; Bryan, J. C. $(\eta^1\text{-Cp})Tc(NAr)_3$: Synthesis and Structure. *Organometallics*, **1992**, *11*, 3501-3503.
(31) Apostolidis, C.; Kanellakopulos, B.; Maier, R.; Rebizant, J.; Ziegler, M. L. Bis(cyclopentadienyl)technetium(III) chlorid und Tris(cyclopentadienyl)technetium(III), neue metallorganische Verbindungen des dreiwertigen Technetiums. *J. Organomet. Chem.* **1990**, *396*, 315-326.
(32) Apostolidis, C.; Kanellakopulos, B.; Maier, R.; Rebizant, J.; Ziegler, M. L. Metallorganische Chemie des Technetiums VII. Röntgenstrukturanalyse von Tris(cyclopentadienyl)technetium(III), $(\eta^5\text{-}C_5H_5)_2Tc(\eta^1\text{-}C_5H_5)$; Dipolmomente und Ladungsverteilung der Spezies $(C_5H_5)_3M$ (M = V, Tc, Re).). *J. Organomet. Chem.* **1991**, *411*, 171-179.
(33) Raptis, K.; Kanellakopoulos, Nuber, B.; Ziegler, M. L. Metallorganische Verbindungen des Technetiums V. Darstellung und Charakterisierung von Photolyseprodukten des $(C_5Me_5)Tc(CO)_3$. Synthese von $(C_5Me_5)_2Tc_2(CO)_5$ und $(C_5Me_5)_2Tc_2(CO)_3$, Röntgenstrukturanalyse von Tri-μ-carbonyl-bis[η^5-pentamethylcyclopentadienyl)technetium] (Tc≡Tc). *J. Organomet. Chem.* **1991**, *405*, 323-331.
(34) Kanellakopulos, B.; Number, B.; Raptis, K.; Ziegler, M. L. A Polymeric Technetium Compound of the Composition $[Tc_2O_3(C_5Me_5)]_n$. *Angew. Chem. Int. Ed. Engl*. **1989**, *28*, 1055.
(35) Bernard, J.; Ortner, K.; Spingler, B.; Pietzsch, H.-J.; Alberto, R. Aqueous Synthesis of Derivatized Cyclopentadienyl Complexes of Technetium and Rhenium Directed toward Radiopharmaceutical Application. *Inorg. Chem*. **2003**, *42*, 1014-1022.
(36) Knight Castro, H. H.; Meetsma, A.; Teuben, J. H.; Vaalburg, W.; Panek, K.; Ensing, G. Synthesis, reactions and structure of $Cp'Tc(CO)_3$ derivatives. *J. Organomet. Chem*. **1991**, *410*, 63-71.
(37) Zobi, F.; Spingler, B.; Alberto, R. Syntheses, Structures and Reactivities of $[CpTc(CO)_3X]^+$ and $[CpRe(CO)_3X]^+$. *Eur. J. Inorg. Chem.* **2008**, *27*, 4205-4214.
(38) Joachim, J. E.; Apostolidis, C.; Kanellakopulos, B.; Meyer, D.; Raptis, K.; Rebizant, J.; Ziegler, M. L. Metallorganische Chemie des Technetiums XI. Synthese, Charakterisierung und Röntgenstrukturanalyse von η^5-Tetramethylazacyclopentadienyltechnetiumtricarbonyl $(Me_4C_4N)Tc(CO)_3{\cdot}HNC_4Me_4$ und seinen Mn- und Re-Homologen. *J. Organomet. Chem*. **1994**, *476*, 77-84.
(39) Masi, S.; Boubekeur, L.; Jaouen, G.; Mundwiler, S.; Spingler, B.; Alberto, R. Direct Synthesis of Tricarbonyl(cyclopentadienyl)rhenium and Tricarbonyl(cyclopentadienyl)technetium Units from Ferrocenyl Moieties - Preparation of 17α-Ethynylestradiol Derivatives Bearing a Tricarbonyl(cyclopentadienyl)technetium Group. *Eur. J. Inorg. Chem.* **2004**, *10*, 2013-2017.
(40) Joachim, J. E.; Apostolidis, C.; Kanellakopulos, B.; Meyer, D.; Number, B.; Raptis, K.; Rebizant, J.; Ziegler, M. L. Metallorganische chemie des technetiums XII. Photolytische CO-substitutionsreaktionen von technetiumtricarbonylverbindungen. Synthesen und Röntgenstrukturanalysen von $(C_5H_5)Tc(CO)_3(PPh_3)$, $(C_5Me_5)Tc(CO)_2(PPh_3)$ und [HB(3,5-

Me_2 Pz)$_3$Tc(CO) $_2$[P(OMe)$_3$] im Vergleich mit seinen Homologen. *J. Organomet. Chem.* **1995**, *492*, 199-210.
(41) Alberto, R.; Schibli, R.; Egli, A.; Abram, U.; Abram, S.; Kaden, T. A.; Schubiger, P. A. Steps towards [(C_5Me_5)TcO_3]: Novel synthesis of [(C_5Me_5)Tc(CO)$_3$] from [{Tc(μ_3−OH)(CO)$_3$}$_4$] and oxidation of [(C_5Me_5)M(CO)$_3$] (M = Tc, Re) with Br_2. *Polyhedron*, **1998**, *17*, 1133-1140.
(42) Alberto, R.; Herrmann, W. A.; Bryan, J. C.; Schubiger, P. A.; Baumgärtner, F.; Mihalios, D. New Organometallic Technetium Complexes in High and Low Oxidation States. *Radiochim. Acta,* **1993**, *63*, 153-161.
(43) Ackermann, J.; Abdulkader, A.; Scholtysik, C.; Roca Jungfer, M.; Hagenbach, A.; Abram, U. [Tc^{I}(NO)X(Cp)(PPh_3)] Complexes (X^- = I^-, I_3^-, SCN^-, $CF_3SO_3^-$, or CF_3COO^-) and Their Reactions. *Organometallics*, **2019**, *38,* 4471−4478.
(44) Ackermann, J.; Hagenbach, A.; Abram, U. {Tc(NO)(Cp)(PPh_3)}$^+$ – a novel technetium(I) core. *Chem. Commun,* **2016**, *52*, 10285-10288.
(45) Braband, H.; Zahn, T. I.; Abram, U. Synthesis and Characterization of Cationic Rhenium(V) and Technetium(V) Dioxo Complexes Containing Four N-Heterocyclic Carbene Ligands. *Inorg. Chem*. **2003**, *42*, 6160-6162.
(46) Braband, H.; Abram, U. Nitridotechnetium(V) Complexes with N-Heterocyclic Carbenes and Unexpected ($OSiMe_2OSiMe_2O$)$^{2-}$ Coligands. *Organometallics* **2005,** *24,* 3362-3364.
(47) Braband, H.; Kückmann, T. I.; Abram, U. Rhenium and Technetium Complexes with N-Heterocyclic Carbenes – A Review. *J. Organomet. Chem*. **2005**, *690*, 5421-5429.
(48) Oehlke, E.; Kong, S.; Arciszewski, P.; Wiebalck, S.; Abram, U. Aryl and NHC Compounds of Technetium and Rhenium*. J. Am. Chem. Soc*. **2012**, *134*, 9118−9121.
(49) Benz, M.; Spingler, B.; Alberto, R.; Braband, H. Toward Organometallic ^{99m}Tc Imaging Agents: Synthesis of Water-Stable ^{99}Tc−NHC Complexes. *J. Am. Chem. Soc*. **2013**, *135*, 17566−17572.
(50) Hieber, W.; Lux, F.; Herget, C. Über Kohlenoxidverbindungen des Technetiums. *Z. Naturforsch.* **1965**, *20b*, 1159-1165.
(51) Fischer, E. O.; Offhaus, E.; Müller, J.; Nöthe, D. Über Methyl(methoxy)- und Phenyl(methoxy)carben-Komplexe des Ditechnetium- und Dirheniumdecacarbonyls, einen Phenyl(methoxy)carben-Komplex des Manganrheniumdecacarbonylsund das Manganpentacarbonyl-Radikal. *Chem. Ber*. **1972**, *105*, 3027-3035.
(52) Fischer, E. O.; Apostolidis, C.; Dornberger, E.; Filippou, A. C.; Kanellakopulos, B.; Lungwitz, B.; Muller, J.; Powietzka, B.; Rebizant, J.; Roth, W. *Z. Naturforsch.* **1995**, *50b*, 1383-1395.
(53) Cook, J.; Davison, A. Nucleophilic attack on coordinated CO in [Tc(CO)$_4$(PPh_3)$_2$]BF_4. *J. Organomet. Chem.* **1996**, *507*, 47-51.
(54) Burrell, A. K.; Bryan, J. C.; Kubas, G. J. Technetium-Carbon Multiple Bonds: Synthesis and Structure of Tc(=C=CHPh)Cl(dppe)$_2$ and [Tc(≡C-CH_2-*t*-Bu)Cl(dppe)$_2$]$^+$. *Organometallics*, **1994**,*13*, 1067-1069.
(55) Herrmann, W. A.; Alberto, R.; Kiprof, P.; Baumgärtner, F. Alkyltechnetium Oxides: First Examples and Reactions. *Angew. Chem. Int. Ed. Engl.* **1990**, *29*, 189-191.
(56) Burrell, A. K.; Bryan, J. C. Methyl Grignard Reactions with Tc_2(NAr)$_4$(μ-NAr)$_2$: The Imido Ligand as a Leaving Group. *Organometallics*, **1993**, *12*, 2426-2428.
(57) Benson, M. T.; Bryan, J. C.; Burrell, A. K.; Cundari, T. R. Bonding and Structure of Heavily π-Loaded Complexes. *Inorg. Chem*. **1995**, *34*, 2348-2355.
(58) Morse, C. A. Synthesis and Reactivity of Rhenium and Technetium Polyaryls. Doctoral thesis, Massachusetts Institute of Technology, **1998**.
(59) Levitskaia, T. G.; Anderson, A.; Chatterjee, S. D.; Cho, H. M.; Rapko, B. M.; Peterson, J. M.; Walter, E. D.; Washton, N. M. U.S. Department of Energy. Speciation and Oxidative Stability of Alkaline Soluble, Non-Pertechnetate Technetium. PNNL-23654; EMSP-RPT-024, Rev. 0, **2014**.
(60) Lukens, W. W.; Shuh, D. K.; Schroeder, N. C.; Ashley, K. R. Behavior of Technetium in Alkaline Solution: Identification of Non-Pertechnetate Species in High-Level Nuclear Waste Tanks at the Hanford Reservation. 11 Sep 2003; 20 p; American Chemical Society Meeting, Fall 2003; New York, NY (United States); 7-11 Sep 2003; AC03-76SF00098; Also available from OSTI as DE00817638; PURL: https://www.osti.gov/servlets/purl/817638-gLf1u2/native/.
(61) McGregor, D.; Burton-Pye, B. P.; Howell, R. C.; Mbomekalle, I. M.; Lukens, W. W. Jr.; Bian, F.; Mausolf, E.; Poineau, F.; Czerwinski, K. R.; Francesconi, L. C. Synthesis, Structure Elucidation, and Redox Properties of ^{99}Tc Complexes of Lacunary Wells-Dawson Polyoxometalates: Insights into Molecular ^{99}Tc-Metal Oxide Interactions. *Inorg. Chem.* **2011**, *50*, 1670-1681.
(62) Lukens, W. W.; Shuh, D. K.; Schroeder, N. C.; Ashley, K. R. Correction to "Identification of the Non-Pertechnetate Species in Hanford Waste Tanks, Tc(I)−Carbonyl Complexes". *Environ. Sci. Technol.* **2004**, *38*, 229−233.
(63) Chatterjee, S.; Holfeltz, V. E.; Hall, G. B.; Johnson, I. E.; Walter, E. D.; Lee, S.; Reinhart, B.; Lukens, W. W.; Machara, N. P.; Levitskaia, T. G. Identification and Quantification of Technetium Species in Hanford Waste Tank AN-102. *Anal. Chem.* **2020**, *92*, 13961-13970.
(64) Heitzmann, M. W.; ; Yang, G. C.; Ford, L. A.; Benson, W. R. Electron Spin Resonance Studies of ^{99}Tc in Aqueous Solutions. Part II. *J. Labelled Compd. Radiopharm*. **1981**, *18*, 535-543.
(65) Roca Jungfer, M.; Elsholz, L.; Abram, U. Technetium Hydrides Revisited: Syntheses, Structures and Reactions of [TcH_3(PPh_3)$_4$] and [TcH(CO)$_3$(PPh_3)$_2$]. *Organometallics* **2021**, *40*, 3095-3112.
(66) Roca Jungfer, M.; Abram, U. [Tc(OH_2)(CO)$_3$(PPh_3)$_2$]$^+$: A Synthon for Tc(I) Complexes and Its Reactions with Neutral Ligands. *Inorg. Chem.* **2021**, *60*, 16734−16753.
(67) Roca Jungfer, M.; Elsholz, L.; Abram, U. Fundamental Technetium Chemistry with Small Inorganic Ligands. *Inorg. Chem.* **2021**, submitted (ic-2021-03919c).
(68) Cook, J. A. *Synthesis and Reactivity of Technetium Hydrides*. Doctoral thesis, Massachusetts Institute of Technology, **1995**.
(69) Abdulkader, A.; Hagenbach, A.; Abram, U. [Tc(NO)Cl(Cp)(PPh_3)] – A Technetium(I) Compound with an Unexpected Synthetic Potential. *Eur. J. Inorg. Chem.* **2021**, *37*, 3812−3818.
(70) Cook, J.; Davison, A.; Davis, W. M.; Jones, A. G. Insertion Chemistry of HTc(CO)$_3$(PPh_3)$_2$. *Organometallics* **1995**, *14*, 650-655.
(71) O'Connel, K. A.; Dewan, J.; Jones, A. G.; Davison, A. Technetium(I) isocyanide complexes with bidentate aromatic amine ligands: structural characterization of [Tc(CN-*tert*-Bu)$_4$(bpy)]PF_6, a complex with "Tc(III) character". *Inorg. Chem*. **1990**, *29*, 3539-3547.
(72) McMullan, R. K.; Kvich, A.; Popelier, P. Structures of Cubic and Orthorhombic phases of Acetylene by Single-Crystal Neutron Diffraction, *Acta Cryst.* **1992**, *B48*, 726-731.
(73) Bond, A. D.; Davies, J. E. (Trimethylsilyl)acetylene. *Acta Cryst.* **2002**, *E58*, 0777-0778.
(74) Salsi, F.; Neville, M.; Drance, M.; Hagenbach, A.; Chan, C; Figueroa, J. S.; Abram, U. A Closed-Shell Monomeric Rhenium(1-) Anion Provided by *m*-Terphenyl Isocyanide Ligation. *Chem. Commun*. **2020**, *56*, 7009-7013.
(75) Figueroa, J. S.; Abram, U. Oxidorhenium(V) and Rhenium(III) Complexes with ***m***-Terphenyl Isocyanides. *Z. Anorg. Allg. Chem.* **2020**, *646*, 909-914.
(76) Sheldrick, G. M. *SADABS*, University of Göttingen, Germany, **1996**.
(77) Coppens, P. The Evaluation of Absorption and Extinction in Single-Crystal Structure Analysis. Crystallographic Computing, Copenhagen, Muksgaard, **1979**.
(78) Sheldrick, G. M. A short history of SHELX. *Acta Cryst.*, **2008**, *A64*, 112−122.

(79) Sheldrick, G. M. Crystal structure refinement with SHELXL. *Acta Cryst.,* **2015**, *C71*, 3-8.
(80) *Diamond - Crystal and Molecular Structure Visualization* Crystal Impact - Dr. H. Putz & Dr. K. Brandenburg GbR, Bonn, Germany.
(81) High performance computing (HPC) system Curta at Freie Universität Berlin. DOI: 10.17169/refubium-26754.
(82) Gaussian 16, Revision B.01, Frisch, M. J.; Trucks, G. W.; Schlegel, H. B.; Scuseria, G. E.; Robb, M. A.; Cheeseman, J. R.; Scalmani, G.; Barone, V.; Petersson, G. A.; Nakatsuji, H.; Li, X.; Caricato, M.; Marenich, A. V.; Bloino, J.; Janesko, B. G.; Gomperts, R.; Mennucci, B.; Hratchian, H. P.; Ortiz, J. V.; Izmaylov, A. F.; Sonnenberg, J. L.; Williams-Young, D.; Ding, F.; Lipparini, F.; Egidi, F.; Goings, J.; Peng, B.; Petrone, A.; Henderson, T.; Ranasinghe, D.; Zakrzewski, V. G.; Gao, J.; Rega, N.; Zheng, G.; Liang, W.; Hada, M.; Ehara, M.; Toyota, K.; Fukuda, R.; Hasegawa, J.; Ishida, M.; Nakajima, T.; Honda, Y.; Kitao, O.; Nakai, H.; Vreven, T.; Throssell, K.; Montgomery, J. A. Jr.; Peralta, J. E.; Ogliaro, F.; Bearpark, M. J.; Heyd, J. J.; Brothers, E. N.; Kudin, K. N.; Staroverov, V. N.; Keith, T. A.; Kobayashi, R.; Normand, J.; Raghavachari, K.; Rendell, A. P.; Burant, J. C.; Iyengar, S. S.; Tomasi, J.; Cossi, M.; Millam, J. M.; Klene, M.; Adamo, C.; Cammi, R.; Ochterski, J. W.; Martin, R. L.; Morokuma, K.; Farkas, O.; Foresman, J. B.; Fox D. J., Gaussian, Inc., Wallingford CT, **2016**.
(83) GaussView, Version 6, Dennington, R.; Keith, T. A.; Millam, J. M. Semichem Inc., Shawnee Mission, KS, **2016**.
(84) Hanwell, M. D.; Curtis, D. E.; Lonie, D. C.; Vandermeersch, C.; Zurek, E.; Hutchison, G. R. Avogadro: An advanced semantic chemical editor, visualization, and analysis platform. *J. Cheminform.* **2012**, *4*:17
(85) Vosko, S. H.; Wilk, L.; Nusair, M. Accurate spin-dependent electron liquid correlation energies for local spin density calculations: a critical analysis. *Can. J. Phys.* **1980**, *58*, 1200–1211.
(86) Becke, A. D. Density-functional thermochemistry. III. The role of exact exchange. *J. Chem. Phys.* **1993**, *98*, 5648-5652
(87) Lee, C.; Yang, W.; Parr, R. G. Development of the Colle-Salvetti correlation-energy formula into a functional of the electron density. *Phys. Rev.* **1988**, *B37*, 785–789.
(88) Wadt, W. R.; Hay, P. J. Ab initio effective core potentials for molecular calculations. Potentials for main group elements Na to Bi. *J. Chem. Phys.* **1985**, *82*, 284-298.
(89) Andrae, D.; Häußermann, U.; Dolg, M.; Stoll, H.; Preuß, H. Energy-adjusted ab initio pseudopotentials for the second and third row transition elements. *Theor. Chim. Acta* **1990**, *77*, 123-141.
(90) Martin, J. M. L.; Sundermann, A. Correlation consistent valence basis sets for use with the Stuttgart-Dresden-Bonn relativistic effective core potentials: The atoms Ga-Kr and In-Xe. *J. Chem. Phys.* **2001**, *114*, 3408-3420.
(91) Krishnan, R.; Binkley, J. S.; Seeger, R.; Pople, J. A. Self-consistent molecular orbital methods. XX. A basis set for correlated wave functions. *J. Chem. Phys*. **1980**, *72*, 650-654.
(92) Clark, T.; Chandrasekhar, J.; Spitznagel; G. W.; Schleyer, P. V. R. Efficient diffuse function-augmented basis sets for anion calculations. III. The 3-21+G basis set for first-row elements, Li-F. *J. Comput. Chem*. **1983**, *4*, 294-301.
(93) Schuchardt, K. L.; Didier, B. T.; Elsethagen, T.; Sun, L.; Gurumoorthi, V.; Chase, J.; Li, J.; Windus, T. L. Basis Set Exchange: A Community Database for Computational Sciences. *J. Chem. Inf. Model.* **2007**, *47*, 1045–1052.
(94) Lu, T.; Chen, F. Multiwfn: A multifunctional wavefunction analyzer. *J. Comput. Chem.*, **2012**, *33*, 580–592.

4.5 $[Tc^{I}(NO)X(cp)(PPh_3)]$ Complexes ($X^- = I^-, I_3^-, SCN^-, CF_3SO_3^-$ or CF_3COO^-) and Their Reactions

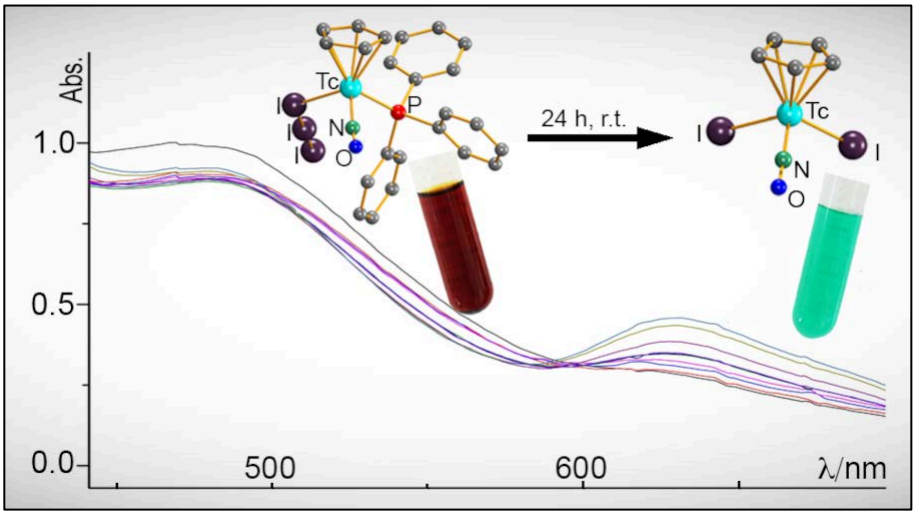

Reproduced with permission from Ackermann, J.; Abdulkader, A.; Roca Jungfer, M.; Hagenbach, A.; Abram, U. *Organometallics*, **2019**, 38, 4471-1178.

DOI: 10.1021/acs.organomet.9b00620

For Supplementary Material see A.5.

Author Contributions:

Janine Ackermann, Abdullah Abdulkader and Ulrich Abram designed the project. Janine Ackermann and Abdullah Abdulkader performed the synthesis and characterization of the compounds. Ulrich Abram and Abdullah Abdulkader wrote the manuscript. Clemens Scholtysik and Adelheid Hagenbach calculated the X-ray structures. Maximilian Roca Jungfer performed DFT calculations on the bond isomerism of the SCN^-/NCS^- complexes, made suggestions and proofed the manuscript. Ulrich Abram supervised the project, provided scientific guidance and suggestions, and corrected the manuscript.

ORGANOMETALLICS
Article
Cite This: Organometallics 2019, 38, 4471−4478
pubs.acs.org/Organometallics

[Tc^{I}(NO)X(Cp)(PPh$_3$)] Complexes (X$^-$ = I$^-$, I$_3^-$, SCN$^-$, CF$_3$SO$_3^-$, or CF$_3$COO$^-$) and Their Reactions

Janine Ackermann, Abdullah Abdulkader, Clemens Scholtysik, Maximilian Roca Jungfer, Adelheid Hagenbach, and Ulrich Abram*

Institute of Chemistry and Biochemistry, Freie Universität Berlin, Fabeckstrasse 34-36, D-14195 Berlin, Germany

Supporting Information

ABSTRACT: Reactions of [Tc(NO)Cl(Cp)(PPh$_3$)] with a series of monodentate ligands X$^-$ (X$^-$ = I$^-$, I$_3^-$, F$_3$CSO$_3^-$, CF$_3$COO$^-$, or SCN$^-$) result in a ready replacement of the chlorido ligand and the formation of complexes of the general composition [Tc(NO)X(Cp)(PPh$_3$)]. Technetium retains its oxidation state "+1" and its pseudotetrahedral coordination environment. [Tc(NO)(SCN)(Cp)(PPh$_3$)] is the first technetium complex with an *S*-coordinated SCN$^-$ ligand. The complexes are stable as solids. In solution, however, a slow isomerization of the thiocyanato compound into the thermodynamically more stable isothiocyanato species is observed, while solutions of [Tc(NO)(I$_3$)(Cp)(PPh$_3$)] undergo an internal oxidation under formation of the technetium(II) complex [Tc(NO)(I)$_2$(Cp)]. All products were characterized by elemental analysis, NMR and IR spectroscopy, and X-ray structure analysis. Particularly, ^{99}Tc NMR spectroscopy proved to be a valuable method for these types of technetium(I) compounds.

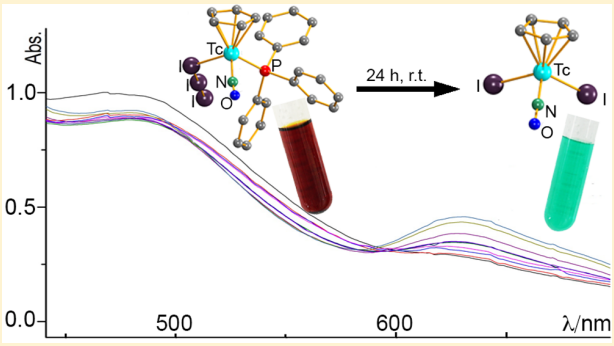

INTRODUCTION

The fascinating chemistry of the chiral {Re(NO)(Cp)(PPh$_3$)}$^+$ core and the derived [Re(NO)(X)(Cp)(PPh$_3$)]$^{0,+1}$ complexes has extensively been explored by John Gladysz and his collaborators since 1979;[1] the related results have been reported in more than 100 papers, and almost 200 crystal structures of such compounds have been published.[2−11]

The chemistry of related technetium complexes is almost unknown. This has mainly to do with the general synthetic routes which are available for the syntheses of the key compounds [M(NO)Cl(Cp)(PPh$_3$)] (M = Re, Tc). The rhenium complex is commonly prepared in a multistep synthesis starting from Re$_2$(CO)$_{10}$ (Scheme 1). Such a synthetic approach, which would start from ditechnetium decacarbonyl, is not appropriate for the synthesis of the corresponding technetium complexes at a large scale because of radiation protection considerations. Tc$_2$(CO)$_{10}$ is volatile, and its handling requires extra safety precautions.[12] The use of [Tc(CO)$_3$(Cp)], which can more readily be synthesized from (NEt$_4$)$_2$[Tc(CO)$_3$Cl$_3$] and a suitable Cp$^-$ source,[12−14] as a starting substance, has not yet been considered for ongoing reactions except for the synthesis and structural characterization of a number of cyclopentadienyl derivatives with the {Tc(CO)$_3$}$^+$ core.[14−17] Thus, the number of well-characterized cyclopentadienyl complexes of ^{99}Tc is still limited. On the other hand, a number of promising results has been reported for ^{99m}Tc complexes, where substituted Cp$^-$ rings have been used for the synthesis of bioconjugates for nuclear medical applications.[17−23] Such results recommend the use of substituted cyclopentadienyls also for other technetium cores.

Scheme 1. Synthesis of [M(NO)Cl(Cp)(PPh$_3$)] Complexes (M = Re, Tc)

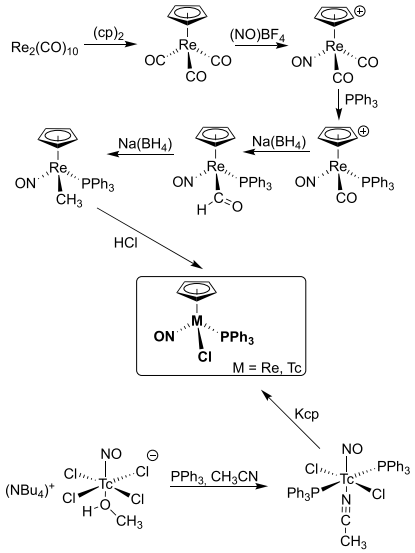

Received: September 11, 2019
Published: November 4, 2019

DOI: 10.1021/acs.organomet.9b00620
Organometallics 2019, 38, 4471−4478

Scheme 2. Synthesis and Reactions of the [Tc(NO)X(Cp)(PPh$_3$)] Complexes of This Study

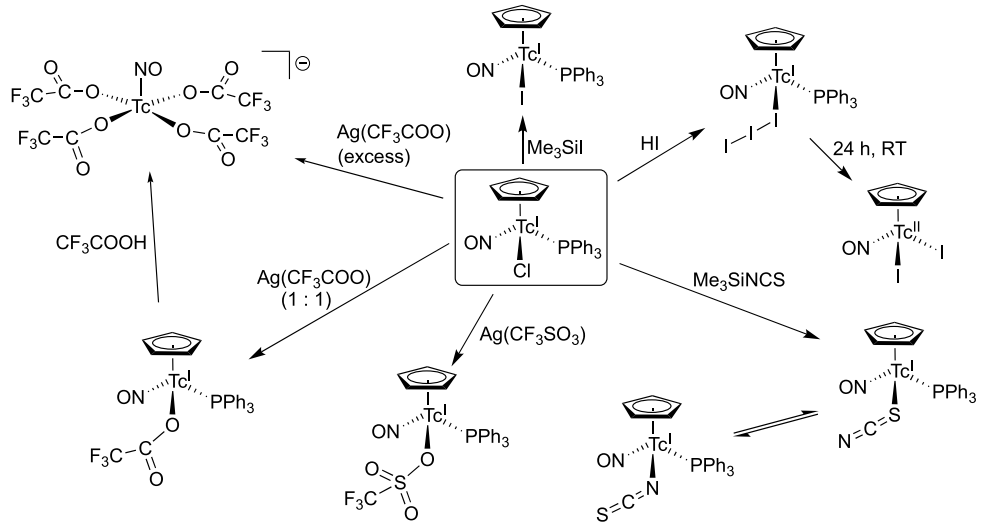

Recently, we published a facile synthesis of [Tc(NO)Cl(Cp)(PPh$_3$)] from [Tc(NO)Cl$_2$(PPh$_3$)$_2$(CH$_3$CN)] and KCp and a few reactions of the novel compound.[24] The ready access to this key compound via a simple, two-step synthesis starting from (NBu$_4$)[Tc(NO)Cl$_4$(MeOH)] (Scheme 1) motivated us for ongoing studies concerning the fundamental coordination chemistry of the novel Tc(I) core.

Here, we describe some ligand exchange reactions of [Tc(NO)Cl(Cp)(PPh$_3$)] with monodentate ligands and the chemical behavior of the formed products.

RESULTS AND DISCUSSION

During reactions of [Tc(NO)Cl(Cp)(PPh$_3$)] with monodentate ligands such as halides, pseudohalides, carboxylates, or related compounds, preferably the chlorido ligand is exchanged. This comes not completely unexpected with regard to the related rhenium chemistry and the previously reported reaction of [Tc(NO)Cl(Cp)(PPh$_3$)] with Me$_3$SiBr or HBr, which both give the corresponding bromido complex in good yields.[24] Nevertheless, some of the products possess remarkable structural features or an unexpected reactivity. Scheme 2 contains a summary of the performed reactions and the obtained products. The chiral complexes crystallize as racemates except (*S*)-[Tc(NO)(F$_3$CSO$_3$)(Cp)(PPh$_3$)] and (*R*)-[Tc(NO)(SCN)(Cp)(PPh$_3$)] (see Supporting Information).

Clean reactions with good yields are observed when [Tc(NO)Cl(Cp)(PPh$_3$)] is mixed with equivalent amounts of Ag(F$_3$CSO$_3$) or Ag(CF$_3$COO) in CH$_2$Cl$_2$. After removal of the precipitated AgCl, the products can be isolated in crystalline form from the resulting solutions by overlayering with *n*-hexane. The IR spectra of the red crystalline substances show NO stretches at 1674 cm^{-1} ([Tc(NO)(F$_3$CSO$_3$)(Cp)(PPh$_3$)]) and 1668 cm^{-1} ([Tc(NO)(CF$_3$COO)(Cp)(PPh$_3$)]). This is in the expected range for technetium(I) nitrosyl complexes.[24−30] The $\nu_{(NO)}$ bands in the analogous rhenium complexes appear at 1680 and 1655 cm^{-1}.[31]

The resonances of the PPh$_3$ ligands in the ^{31}P NMR spectra appear at 49 and 53 ppm, respectively, which corresponds to a downfield shift of about 30 ppm compared with the values in [Re(NO)(F$_3$CSO$_3$)(Cp)(PPh$_3$)] and [Re(NO)(CF$_3$COO)(Cp)(PPh$_3$)], respectively.[31] In contrast to those in the rhenium compounds, the ^{31}P NMR signals of the technetium complexes are very broad. Such a broadening of ^{31}P signals in diamagnetic technetium complexes is not unusual and has been explained by scalar couplings of ^{31}P with the large quadrupole moment of ^{99}Tc ($Q = -0.19 \times 10^{-28}$ m^2).[32,33] The large quadrupole moment is also responsible for a drastic line-widening of the related ^{99}Tc NMR signals, which is frequently observed when ^{99}Tc complexes with low local symmetry are studied.[34] Nevertheless, the ^{99}Tc NMR spectroscopy is a valuable tool for the characterization of the diamagnetic technetium complexes of this study and monitoring of their reactions. The ^{99}Tc nuclide with $I = 9/2$ has a large chemical shift range, spanning from approximately −7000 to +5000 ppm.[30] Moreover, ^{99}Tc NMR chemical shifts are remarkably sensitive to subtle changes in the electronic environment and geometry in which a diamagnetic ^{99}Tc nucleus is found.[30] Thus, ^{99}Tc NMR is expected to be a sensitive and selective spectroscopic probe for the Tc(I) compounds of the present paper. The signals of [Tc(NO)(F$_3$CSO$_3$)(Cp)(PPh$_3$)] (242 ppm) and ([Tc(NO)(CF$_3$COO)(Cp)(PPh$_3$)] (19 ppm) appear at chemical shifts, which can clearly be distinguished from that of the starting compound [Tc(NO)Cl(Cp)(PPh$_3$)] (−231 ppm), and the large line widths of $\nu_{1/2}$ = 7070 and 4690 Hz do not restrict the suitability of the method in the evaluation of reactions and their diamagnetic products.

Single crystals of [Tc(NO)(F$_3$CSO$_3$)(Cp)(PPh$_3$)] and ([Tc(NO)(CF$_3$COO)(Cp)(PPh$_3$)] were obtained from CH$_2$Cl$_2$/*n*-hexane solutions. Figure 1 illustrates the molecular structures of both compounds. They show the expected pseudotetrahedral coordination environment for technetium. The Tc−N═O fragments are linear, which is in agreement with the formal charge of "+1" of the nitrosyl ligand. Trifluoromethylsulfonate and trifluoroacetate are bonded monodentate with Tc−O bond lengths of 2.162(2) and 2.108(2) Å. Similar values have been observed for other nitrosyltechnetium complexes with CF$_3$COO$^-$ ligands.[30] More bond lengths and angles can be found in the Supporting Information.

It is important to perform the reaction between [Tc(NO)Cl(Cp)(PPh$_3$)] and Ag(CF$_3$COO) with a 1:1 ratio of the

DOI: 10.1021/acs.organomet.9b00620
Organometallics 2019, 38, 4471−4478

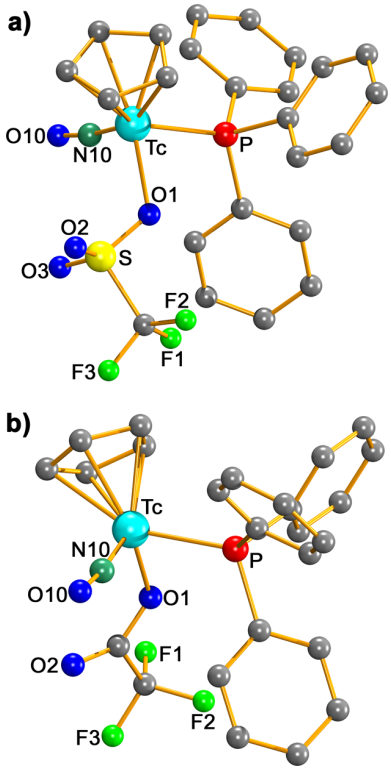

Figure 1. Molecular structures of (a) $[Tc(NO)(F_3CSO_3)(Cp)(PPh_3)]$ and (b) $[Tc(NO)(CF_3COO)(Cp)(PPh_3)]$.

reactants. The use of an excess of trifluoroacetate results in an ongoing reaction, which finally destroys the organometallic $\{Tc(NO)(Cp)(PPh_3)\}^+$ core. On air, oxidation of the metal ion and formation of a technetium(II) complex is observed. The EPR parameters of this compound (g_0 = 1.990, a_0^{Tc} = 185.5 × 10^{-4} cm^{-1}, $g_\parallel$ = 1.910, $g_\perp$ = 2.030, $A_\parallel^{Tc}$ = 295.1 × 10^{-4} cm^{-1}, $A_\perp^{Tc}$ = 123.9 × 10^{-4} cm^{-1}) are very close to the values of $[Tc(NO)F(CF_3COO)_4]^{2-}$ with four equatorially coordinated trifluoroacetato ligands.[30] It should be noted that the coordination position *trans* to the nitrosyl ligand has almost no influence to the EPR parameters of the $4d^5$-low spin complexes under study because the MO of the unpaired electron has preferably "*xy* character".[35] Thus, the spectrum obtained for the reaction of $[Tc(NO)Cl(Cp)(PPh_3)]$ with an excess of $Ag(CF_3COO)$ strongly suggests the formation of a compound of the composition $[Tc(NO)(CF_3COO)_4(solv)]^-$. A similar spectrum is obtained when $[Tc(NO)Cl(Cp)(PPh_3)]$ is heated in neat CF_3COOH.

The reaction of $[Tc(NO)Cl(Cp)(PPh_3)]$ with Me_3SiNCS is straightforward, and the red solid, which is formed after evaporation of the solvent, could be characterized as $[Tc(NO)(SCN)(Cp)(PPh_3)]$. Surprisingly, the SCN^- ligand is *S*-bonded in this complex, while it is *N*-bonded in all other structurally characterized technetium complexes with this ligand.[36−44]

Thus, $[Tc(NO)(SCN)(Cp)(PPh_3)]$ is the first example of a thiocyanato complex of technetium. The molecular structure of the compound is shown in Figure 2. Clearly, the expected bent coordination of the SCN^- ligand with a Tc−S20−C20 angle of 108.5(3)° is seen, which is in contrast to the linearly bonded isothiocyanato ligands.[35−43] As in the other complexes of this study, the nitrosyl ligand is almost linearly coordinated (Tc−N10−O10 angle: 168.4(6)°) and can formally be regarded as NO^+.

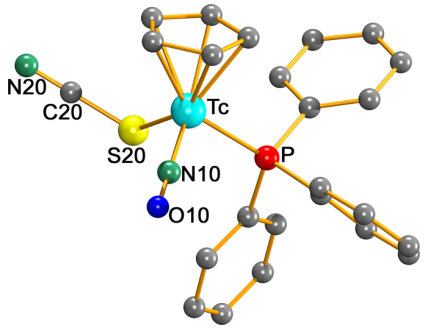

Figure 2. Molecular structure of $[Tc(NO)(SCN)(Cp)(PPh_3)]$.

The formation of coordination isomers with thiocyanato ligands is reported for many metals, including the heavier homologue of technetium, rhenium, and in some cases also isomerization reactions were observed.[45−47] Because the formation of a thiocyanato complex was unexpected and the reason for the preferred formation of the *S*-bonded complex in this particular ligand exchange on $[Tc(NO)Cl(Cp)(PPh_3)]$ is not clear, we performed some DFT calculations on the S- and N-bonded isomers. Indeed, there is a preference in total energy as well as in the Gibb's energy of about 22 kJ/mol for the isothiocyanato complex, and the crystallized thiocyanato species should be regarded as a "kinetic product".

The clear preference of $[Tc(NO)(NCS)(Cp)(PPh_3)]$ encouraged us to study a potential isomerization reaction on $[Tc(NO)(SCN)(Cp)(PPh_3)]$. For this, $[Tc(NO)(SCN)(Cp)(PPh_3)]$ was dissolved in toluene and heated on reflux for a prolonged time. ^{99}Tc NMR proved to be a perfect tool to monitor the course of this reaction. Figure 3 shows the ^{99}Tc NMR spectra obtained from such a solution of $[Tc(NO)(SCN)(Cp)(PPh_3)]$ in boiling toluene. The initially dominating signal at −816 ppm is assigned to the fully characterized S-bonded compound, but a second signal appears at −453 ppm, which we assign to the isothiocyanato species. This compound dominates after a heating period of 6 h. Prolonged heating, however, did not result in the formation of the pure N-bonded complex, but decomposition of the compounds becomes dominating, which goes along with a decrease of the overall intensities of both signals. Nevertheless, from the solution obtained after 6 h reflux in toluene, two different species could be isolated by fractionated crystallization: the red starting

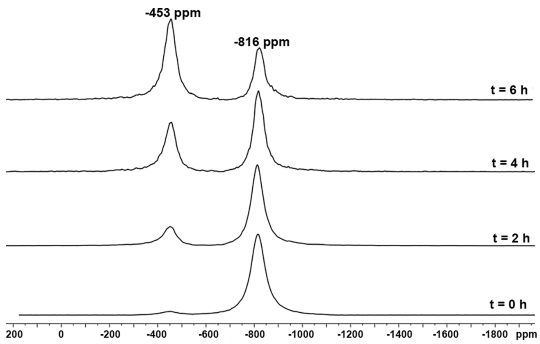

Figure 3. ^{99}Tc NMR spectra obtained from a solution of $[Tc(NO)(SCN)(Cp)(PPh_3)]$ in boiling toluene.

DOI: 10.1021/acs.organomet.9b00620
Organometallics 2019, 38, 4471−4478

material and the orange-red isothiocyanato compound. Unfortunately, we did not obtain single crystals of the orange-red complex suitable for X-ray diffraction, but it shows the expected ^{99}Tc NMR resonance at −453 ppm, and the ν_{CN} stretch in the IR spectrum is shifted by a value of 30 cm^{-1} to higher wavenumbers compared to the value of [Tc(NO)(SCN)(Cp)(PPh_3)].

The exchange of the chlorido ligand in [Tc(NO)Cl(Cp)(PPh_3)] by Br^- is straightforward, and the corresponding bromido complex is readily formed during reactions with HBr or Me_3SiBr.[24] An analogue reaction with HI, however, gives an unexpected result: the formation of the triiodido complex [Tc(NO)(I_3)(Cp)(PPh_3)], the first structurally characterized technetium complex with an I_3^- ligand. The triiodide ion is formed by oxidation of I^- in the reaction mixture and was also observed when carefully purified HI was used. The synthesis of the corresponding [Tc(NO)I(Cp)(PPh_3)] complex succeeded with the use of Me_3SiI as I^- source. Figure 4 illustrates the

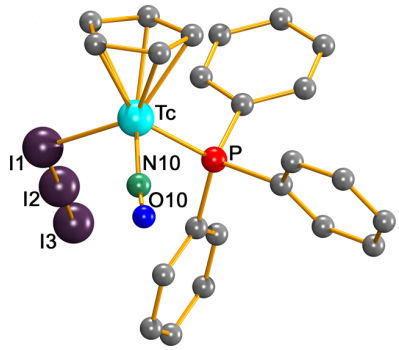

Figure 4. Molecular structure of [Tc(NO)(I_3)(Cp)(PPh_3)].

molecular structure of [Tc(NO)(I_3)(Cp)(PPh_3)] with an almost linear (angle I1−I2−I3:179.59(3)°) triiodido ligand. The I_3^- ligand is bent coordinated with a Tc−I1−I2 angle of 124.38(3)°. The I1−I2 bond of 3.060(1) Å is slightly longer than the I2−I3 bond (2.808(1) Å), which gives a bonding situation similar to that in the rhenium(I) complex [Re(CO)$_3$(I_3)(DPPE)] (DPPE = 1,2-diphenylphosphino ethane).[48] More structural data are summarized in the Supporting Information.

The crystal structure of [Tc(NO)I(Cp)(PPh_3)] is of relatively low quality and could be refined only with isotropic thermal parameters but clearly confirms the nature of the compound as an iodo complex. The Tc−I bond is approximately 2.70 Å, which is close to the value in the triiodo complex (2.704(1) Å). A discussion of more structural parameters of [Tc(NO)I(Cp)(PPh_3)] shall not be done here.

[Tc(NO)(I_3)(Cp)(PPh_3)] is stable as solid, but CH_2Cl_2 solutions of this compound already show at room temperature a gradual change of their color from red to green. In parallel, the intensity of the ^{99}Tc NMR signal decreases and disappears completely after approximately 24 h. A UV/vis monitoring of the decomposition shows an isosbestic point at 594 nm. The loss of the NMR signal and the detected color change are strong hints for a change of the oxidation state of technetium, and indeed, the resulting green solution gives intense, well-resolved EPR spectra, which prove the product is a Tc(II) compound. Figure 5 shows the spectra of the compound in $CHCl_3$ at room temperature and in frozen solution at T = 77 K. In the room-temperature spectrum, no ^{99}Tc hyperfine

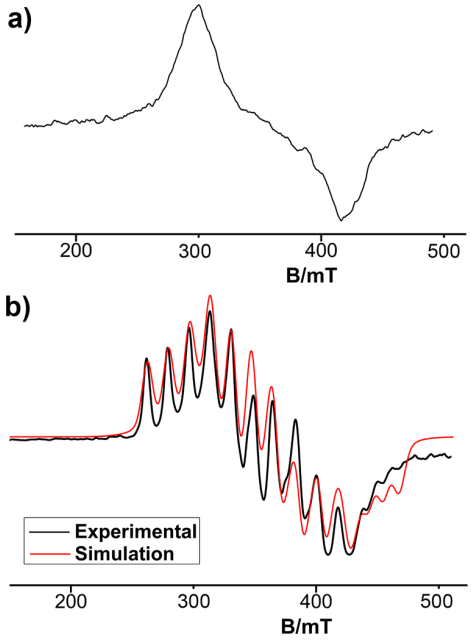

Figure 5. X-band EPR spectra of [Tc(NO)$(I)_2$(Cp)] in $CHCl_3$ (a) at room temperature and (b) at T = 77 K.

interactions are resolved, and also that of a frozen solution has no clear separation of parallel and perpendicular parts as the axially symmetric EPR spectrum of the Tc(II) compound formed as a side-product of the reactions of [Tc(NO)Cl(Cp)(PPh_3)] with an excess of $Ag(CF_3COO)$ or neat CF_3COOH (*vide supra*).

The spectrum of the compound obtained by the decomposition of [Tc(NO)(I_3)(Cp)(PPh_3)] can be described by a rhombic spin-Hamiltonian with the following parameters: g_x = 2.240, g_y = 1.886, g_z = 2.240, $A_x^{Tc} = 50 \times 10^{-4}$ cm^{-1}, $A_y^{Tc} = 70 \times 10^{-4}$ cm^{-1}, $A_z^{Tc} = 136 \times 10^{-4}$ cm^{-1}. No hyperfine interactions with the ^{14}N nucleus of the nitrosyl ligand or ^{127}I are resolved. The EPR parameters suggest that the unpaired electron is not mainly located at the technetium atom, but also populates ligand orbitals to a considerable degree. This conclusion is supported by DFT calculations (see Supporting Information).

The formation of a technetium(II) complex and the "nonaxial" symmetry of the observed EPR spectrum are readily understood by a view to the structure of the green oxidation product: [Tc(NO)$(I)_2$(Cp)]. Single crystals of the compound suitable for X-ray diffraction were obtained by storing a CH_2Cl_2/diethyl ether solution of the complex in a refrigerator.

Figure 6 depicts the molecular structure of the reaction product. It becomes evident that the triiodide is cleaved and the technetium ion is oxidized by the formally released iodine. In parallel, the PPh_3 ligand is replaced by a second iodido ligand. The Tc−I bond lengths of 2.673(3) and 2.677(3) Å are somewhat smaller than those in the triiodo complex. The nitrosyl ligand in the Tc(II) complex is linearly bonded as those in the Tc(I) compounds, but the ν_{NO} stretch in the IR spectrum appears at 1746 cm^{-1}, which is clearly at higher wave numbers than the bands for the Tc(I) complexes, which appear between 1674 and 1690 cm^{-1}. This can be understood by a lower degree of back-donation into antibonding ligand orbitals by the d^5 system compared with the d^6 complexes.

DOI: 10.1021/acs.organomet.9b00620
Organometallics 2019, 38, 4471−4478

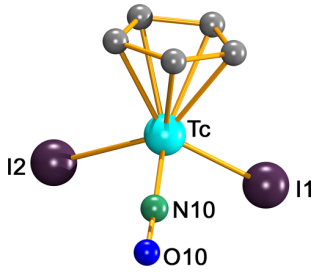

Figure 6. Molecular structure of $[Tc(NO)(I)_2(Cp)]$.

CONCLUSIONS

The "pseudotetrahedral" technetium(I) complex $[Tc(NO)Cl(Cp)(PPh_3)]$ possesses a robust $\{Tc(NO)(Cp)(PPh_3)\}^+$ core, which means that the chlorido ligand can readily be replaced by other monoanionic ligands such as halides, pseudohalides, or carboxylic acids. The products are stable as long as the oxidation state of the transition metal is not changed. Oxidation of the technetium results in the loss of the PPh_3 and/or Cp^- ligands.

EXPERIMENTAL SECTION

Materials. All chemicals used in this study were reagent grade and used without further purification. Solvents were dried and distilled prior to use. ^{99}Tc was purchased as solid ammonium pertechnetate from Oak Ridge National Laboratory (ORNL) and purified as published previously.[28] $[Tc(NO)Cl_2(PPh_3)_2(MeCN)]$, $(NBu_4)[Tc(NO)Cl_4(MeOH)]$, and $[Tc(NO)Cl(Cp)(PPh_3)]$ were prepared as described in the literature.[24,29,49] KCp was obtained following the procedure of Roesky et al.[50]

Physical Measurements. IR spectra were measured from KBr pellets on a Shimadzu FTIR 8300 spectrometer between 400 and 4000 cm^{-1}. NMR spectra were recorded on a JEOL 400 MHz spectrometer, which corresponds to a ^{99}Tc frequency of 90.063 MHz. The ^{99}Tc chemical shifts refer a solution of $NaTcO_4$ in D_2O. Tc values were determined by liquid scintillation counting as has been outlined elsewhere.[51] EPR spectra were measured on a Miniscope MS400 spectrometer (Magnetech).

Radiation Precautions. ^{99}Tc is a long-lived weak β^- emitter (E_{max} = 0.292 MeV). Normal glassware provides adequate protection against the weak beta radiation when milligram amounts are used. Secondary X-rays (bremsstrahlung) play a significant role only when larger amounts of ^{99}Tc are handled. All manipulations were done in a laboratory approved for the handling of radioactive materials.

Computational Chemistry. DFT calculations were performed on the high-performance computing systems of the Freie Universität Berlin ZEDAT (Soroban, Curta) using the program packages GAUSSIAN 09 and GAUSSIAN 16.[52,53] The gas phase geometry optimizations were performed using coordinates derived from the X-ray crystal structures or were modeled with the use of crystal structure fragments using GAUSSVIEW.[54] The calculations were performed by using the hybrid density functional B3LYP (UB3LYP for open shell systems).[55−57] The relativistic small-core basis set Stuttgart RSC 1997 with the respective effective core potential (ECP) was applied to Tc.[58,59] The relativistic large-core basis set Stuttgart RLC with the respective effective core potential (ECP) was applied to I.[60] The double-ζ pseudopotential LANL2DZ basis set with the respective ECP was applied to P and Cl.[61−63] The polarization extended LANL2DZdp basis set was applied to O and S with an ECP in the case of S.[62,64,65] The 6-31++G** basis set was applied for all other atoms.[66−68] All basis sets and ECPs were obtained from the EMSL database.[69,70] The convergence of the optimized geometries was verified by frequency calculations. The absence of negative frequencies indicates that the obtained geometries are reasonable and the derived energies trustworthy.

X-ray Crystallography. The intensities for the X-ray determinations were collected on a Bruker APEX II instrument with Mo Kα radiation. The space groups were determined by the detection of systematical absences. Absorption corrections were carried out by SADABS.[71,72] Structure solutions were performed with the programs SHELXS 97 and SHELXS 2014, and structure refinements were done with the SHELXL 2014 program.[73,74] Hydrogen atoms were placed at calculated positions and treated with the "riding model" option of SHELXL. Details about the measurement and refinement data are summarized in the Supporting Information. The representation of molecular structures was done using the program DIAMOND 4.5.1.[75]

Additional information on the structure determinations is contained in the Supporting Information and has been deposited with the Cambridge Crystallographic Data Centre.

Syntheses of the Complexes. *$[Tc^I(NO)(SO_3CF_3)(Cp)(PPh_3)]$.* $[Tc(NO)Cl(Cp)(PPh_3)]$ (49 mg, 0.1 mmol) was dissolved in 2 mL of CH_2Cl_2. The red solution was mixed with a solution of $AgSO_3CF_3$ (22 mg, 0.1 mmol) in 2 mL of CH_2Cl_2/MeOH (2:1). The reaction mixture was stirred at room temperature for 1 h, and the precipitated AgCl was filtered off. The solvent was removed under vacuum. The residue was redissolved in 1 mL of CH_2Cl_2 and overlayered with 4 mL of *n*-hexane. Red crystals were formed after slow diffusion of the solvents. Yield 37% (23 mg). Elemental analysis Calcd for $C_{24}H_{20}NO_4PSF_3Tc$: Tc 16.3%, Found: Tc 15.9%. IR (KBr, cm^{-1}): 3057 (w), 2961 (w), 2920 (w), 2851 (w), 1674 (vs) NO, 1477 (m), 1435 (s), 1325 (w), 1264 (m), 1232 (w), 1196 (w), 1183 (w), 1161 (w), 1094 (s), 1030 (s), 997 (m), 820 (m), 750 (m), 694 (s), 637 (s), 586 (w), 527 (s), 509 (m), 448 (w). ^1H NMR ($CDCl_3$, ppm): 7.54−7.62 (m, 9H, Ph), 7.40−7.47 (m, 6H, Ph), 5.29 (s, 5H, Cp). ^{13}C NMR ($CDCl_3$, ppm): 137.7 (Ph), 136.5 (Ph), 135.3 (Ph) 133.3 (Ph), 98.1 (Cp). $^{31}P\{^1H\}$ NMR ($CDCl_3$, ppm): 53.1 (very broad). ^{19}F-NMR ($CDCl_3$, ppm): −73. ^{99}Tc-NMR ($CDCl_3$, ppm): 242 ($\nu_{1/2}$ = 7070 Hz).

$[Tc^I(NO)(OOCCF_3)(Cp)(PPh_3)]$. $[Tc(NO)Cl(Cp)(PPh_3)]$ (49 mg, 0.1 mmol) was dissolved in 2 mL of CH_2Cl_2. The red solution was mixed with a solution of $AgOOCCF_3$ (22 mg, 0.1 mmol) in 2 mL of CH_2Cl_2/MeOH (2:1). The reaction mixture was stirred at room temperature for 1 h, and the precipitated AgCl was filtered off. The solvent was removed under vacuum and the residue was redissolved in 1 mL of CH_2Cl_2 and overlayered with 4 mL of *n*-hexane. Red crystals were formed after slow diffusion of the solvents. Yield 42% (25 mg). IR (KBr, cm^{-1}): 3103 (w), 3059 (w), 2920 (w), 1668 (vs) NO, 1479 (m) C = O, 1435 (s), 1396 (w), 1196 (m), 1136 (s), 1074 (w), 997 (m), 841 (m), 816 (m), 783 (m), 746 (m), 725 (m), 692 (s), 586 (m), 527 (m), 501 (m), 447 (w), 424 (w). Elemental analysis Calcd for $C_{25}H_{20}NO_3PF_3Tc$: Tc 17.8%, Found: Tc 17.5%. ^1H NMR (CDCl3, ppm): 7.34−7.47 (Ph), 5.19 (Cp). ^{13}C NMR (CDCl3, ppm): 133.6 (Ph), 132.5 (Ph), 130.8 (Ph), 128.8 (Ph), 93.8 (Cp). $^{31}P\{^1H\}$ NMR ($CDCl_3$, ppm) 48.6 (very broad). ^{19}F NMR (CDCl3, ppm): −75. ^{99}Tc NMR ($CDCl_3$, ppm): 19 ($\nu_{1/2}$ = 4690 Hz).

$[Tc^I(NO)(SCN)(Cp)(PPh_3)]$. $[Tc(NO)Cl(Cp)(PPh_3)]$ (25 mg, 0.05 mmol) was dissolved in 2 mL of CH_2Cl_2. Me_3SiNCS (47 mg, 3.5 mmol) was added. The reaction mixture was heated under reflux for 1 h. The solvent was removed under vacuum, and the residue was redissolved in 0.5 mL of CH_2Cl_2 and overlayered with 2 mL of *n*-hexane. Red crystals were formed after slow diffusion of the solvents. Yield 48% (12 mg). Elemental analysis Calcd for $C_{24}H_{20}N_2OPSTc$: Tc 19.2%, Found: Tc 18.8%. IR (KBr, cm^{-1}): 3121 (w), 3078 (w), 3055 (w), 2918 (w), 2851 (w), 2089 (s) SCN, 1690 (vs) NO, 1477 (m), 1433 (s), 1310 (w), 1244 (m), 1180 (w), 1159 (w), 1092 (s), 997 (m), 835 (w), 816 (m), 748 (m), 694 (s), 578 (m), 546 (m), 525 (s), 500 (m), 446 (w), 424 (w). ^1H NMR (CDCl3, ppm): 7.43−7.45 (m, 9H, Ph), 7.33−7.37 (m, 6H, Ph), 5.23 (s, 5H, Cp) ppm. ^{13}C NMR (CDCl3, ppm): 133.3 (Ph), 132.6 (Ph), 130.93 (Ph) 128.8 (Ph), 125.8 (SCN), 95.7 (Cp). $^{31}P\{^1H\}$ NMR ($CDCl_3$, ppm): 47.5 (very broad). ^{99}Tc-NMR ($CDCl_3$, ppm): −820 ($\nu_{1/2}$ = 6580 Hz).

$[Tc^I(NO)(I_3)(Cp)(PPh_3)]$. $[Tc(NO)Cl(Cp)(PPh_3)]$ (49 mg, 0.1 mmol) was dissolved in 2 mL of CH_2Cl_2 and cooled to 0 °C. HI (0.1 mL) was added to the red solution. The mixture was stirred for 2 h at room temperature and filtered over 2 cm silica gel. The solution

DOI: 10.1021/acs.organomet.9b00620
Organometallics 2019, 38, 4471−4478

was concentrated to 1 mL and covered with a layer of diethyl ether (3 mL). Slow diffusion of the solvents gave brown crystals. Yield 52% (44 mg). IR (KBr, cm^{-1}): 3090 (w), 3050 (w), 2970 (w), 2920 (w), 1682 (vs) NO, 1479 (m), 1431 (s), 1312 (w), 1180 (w), 1157 (w), 1090 (s), 1069 (w), 1026 (w), 999 (m), 918 (w), 837 (m), 804 (m), 746 (m), 694 (s), 617 (w), 581 (m), 525 (s), 494 (m), 447 (w), 428 (w). Elemental analysis. Calcd for $C_{23}H_{20}NOPI_3Tc$: Tc 11.8%, Found: Tc 12.2%. ^1H NMR ($CDCl_3$, ppm): 7.44−7.51 (m, 6H, Ph), 7.39−7.42 (m, 9H, Ph), 5.12 (s, 5H, Cp). ^{13}C NMR ($CDCl_3$, ppm): 131.3 (Ph), 130.1 (Ph), 128.32 (Ph) 126.7 (Ph), 91.7 (Cp). $^{31}P\{^1H\}$ NMR ($CDCl_3$, ppm): 50 (very broad). ^{99}Tc NMR ($CDCl_3$, ppm): −679, ($\nu_{1/2}$ = 6860 Hz).

[Tc^{II}(NO)(I)$_2$(Cp)]. [Tc(NO)(I_3)(Cp)(PPh_3)] (45 mg, 0.1 mmol) was dissolved in 5 mL of CH_2Cl_2 and kept in solution for 2 days. The red-brown solution slowly changed its color to bright green. After concentration of the green solution to 1 mL, diethyl ether (2 mL) was added. Standing overnight in a refrigerator gave green crystals. Yield 60% (20 mg). Elemental analysis Calcd for $C_5H_5NOI_2Tc$: Tc 22.1%, Found: Tc 21.5%. IR (KBr, cm^{-1}): 3447 (w), 2961 (w), 2923 (w), 1746 (m) NO, 1431 (w), 1262 (m), 1161 (w), 1113 (s), 1096 (s), 1022 (m), 802 (s), 721 (m), 691 (m), 538 (s). EPR (CH_2Cl_2, 77 K): $g_x = g_z = 2.240$, $g_y = 1.886$, $A_x^{Tc} = 50 \times 10^{-4}$ cm^{-1}, $A_y^{Tc} = 70 \times 10^{-4}$ cm^{-1}, $A_z^{Tc} = 136 \times 10^{-4}$ cm^{-1}.

[Tc^{I}(NO)I(Cp)(PPh$_3$)]. [Tc(NO)Cl(Cp)(PPh_3)] (49 mg, 0.1 mmol) was dissolved in 2 mL of CH_2Cl_2. Me_3SiI (0.1 mL) was added. The reaction mixture was stirred for 2 h at room temperature. The solvent was removed under vacuum, and the residue was dissolved in 0.5 mL of CH_2Cl_2 and overlayered with 3 mL of diethyl ether. Red-brown microcrystals deposited after slow diffusion of the solvents. Yield 39% (23 mg). IR (KBr, cm^{-1}): 3049 (w), 3050 (w), 2920 (w), 1681 (vs) NO, 1475 (m), 1429 (m), 1311 (w), 1182 (w), 1157 (w), 1089 (s), 999 (m), 918 (w), 833 (m), 806 (m), 746 (m), 696 (s), 617 (w), 582 (m), 522 (s), 493 (m), 441 (w), 428 (w). ^1H NMR (CD_2Cl_2, ppm): 7.33−7.67 (m, 15H, Ph), 5.23 (s, 5H, Cp). ^{13}C NMR (CD2Cl2, ppm): 134.3 (Ph), 132.1 (Ph), 129.72−128.5 (Ph), 94.2 (Cp). $^{31}P\{^1H\}$ NMR (CD_2Cl_2, ppm): 44. ^{99}Tc-NMR (CD_2Cl_2, ppm): −668 ($\nu_{1/2}$ = 4200 Hz). Elemental analysis Calcd for $C_{23}H_{20}NOPITc$: Tc 16.97%, Found: Tc 16.25%.

■ ASSOCIATED CONTENT

Ⓢ Supporting Information

The Supporting Information is available free of charge on the ACS Publications website at DOI: 10.1021/acs.organomet.9b00620.

Crystallographic tables, bond lengths, angles, and ellipsoid plots; coordinates and graphical representations of the optimized structures of [Tc^{I}(NO)(SCN)(Cp)(PPh$_3$)] and [Tc^{I}(NO)(NCS)(Cp)(PPh$_3$)] for the DFT calculations; table of computed energies (PDF)

Structural data file (XYZ)

Accession Codes

CCDC 1951310−1951314 contain the supplementary crystallographic data for this paper. These data can be obtained free of charge via www.ccdc.cam.ac.uk/data_request/cif, by emailing data_request@ccdc.cam.ac.uk, or by contacting The Cambridge Crystallographic Data Centre, 12 Union Road, Cambridge CB2 1EZ, UK; fax: +44 1223 336033.

■ AUTHOR INFORMATION

Corresponding Author

*E-mail ulrich.abram@fu-berlin.de.

ORCID

Ulrich Abram: 0000-0002-1747-7927

Notes

The authors declare no competing financial interest.

■ ACKNOWLEDGMENTS

We gratefully acknowledge financial support from the Deutsche Forschungsgemeinschaft (Graduate School "Fluorine as a key element"). ZEDAT (Freie Universität Berlin) is kindly acknowledged for access to their computing facilities.

■ REFERENCES

(1) Tam, W.; Wong, W. K.; Gladysz, J. A. Neutral metal formyl complexes: generation, reactivity, and models for Fischer−Tropsch catalyst intermediates. *J. Am. Chem. Soc.* **1979**, *101*, 1589−1591.

(2) Agbossou, F.; O'Connor, E. J.; Garner, C. M.; Quiros Mendez, N.; Fernandez, J. M.; Patton, A. T.; Ramsden, J. A.; Gladysz, J. A. Cyclopentadienyl Rhenium Complexes. *Inorg. Synth.* **1992**, *29*, 211−225.

(3) Gladysz, J. A.; Boone, B. J. Chiral Recognition in π Complexes of Alkynes, Aldehydes, and Ketones with Transition Metal Lewis Acids; Development of a General Model for Enatioface Binding Selectivities. *Angew. Chem., Int. Ed. Engl.* **1997**, *36*, 550−583 and references cited therein .

(4) Zhou, Y.; Dewey, M. A.; Gladysz, J. A. Synthesis and Reactivity of Chiral Rhenium Indenyl Complexes of the Formula [(η^5-C_9H_7)Re(NO)(PPh_3)(X)]$^{n+}$. *Organometallics* **1993**, *12*, 3918−3923.

(5) Seidel, S. N.; Prommesberger, M.; Eichenseher, S.; Meyer, O.; Hampel, F.; Gladysz, J. A. Syntheses and structural analyses of chiral rhenium containing amines of the formula (η^5-C_5H_5)Re(NO)(PPh_3)-((CH_2)$_n$NRR′) (n = 0, 1). *Inorg. Chim. Acta* **2010**, *363*, 533−548.

(6) Dembinski, R.; Lis, T.; Szafert, S.; Mayne, C. J.; Bartik, T.; Gladysz, J. A. Appreciably bent sp carbon chains: synthesis, structure, and protonation of organometallic 1,3,5-triynes and 1,3,5,7-tetraynes of the formula (η^5-C_5H_5)Re(NO)(PPh_3) (($C\equiv C$)$_n$-p-C_6H_4Me). *J. Organomet. Chem.* **1999**, *578*, 229.

(7) Quiros Mendez, N.; Arif, A. M.; Gladysz, J. A. Synthesis, structure, and dynamic behavior of rhenium sulfide and sulfoxide complexes of the formula [(η^5-C_5H_5)Re(NO)(L)(XRR')]$^+X'^-$ (X = S, SO). *Organometallics* **1991**, *10*, 2199−2209.

(8) Eichenseher, S.; Delacroix, O.; Kromm, K.; Hampel, F.; Gladysz, J. A. Rhenium-Containing Phosphorus Donor Ligands for Palladium-Catalyzed Suzuki Cross-Coupling Reactions: A New Strategy for High-Activity Systems. *Organometallics* **2005**, *24*, 245−255.

(9) Kromm, K.; Hampel, F.; Gladysz, J. A. A New Family of Chelating Diphosphines with Transition-Metal and Carbon Stereocenters in the Backbone: A Second-Generation Rhenium-Containing System. *Organometallics* **2002**, *21*, 4264−4274.

(10) Legoupy, S.; Crevisy, C.; Guillemin, J.-C.; Gree, R.; Toupet, L. Regio- and Stereoselective Nucleophilic Substitutions of Chiral Allylic Alcohol Rhenium Complexes. *Chem. - Eur. J.* **1998**, *4*, 2162−2172.

(11) *Cambridge Structural Database*, release 5.40; November 2018.

(12) Sattelberger, A. P.; Scott, B. L.; Poineau, F. Technetium Organometallics. In *Comprehensive Organometallic Chemistry III*; Mingos, D. M P., Crabtree, R. H., Eds.; Elsevier: 2007; pp 833−854.

(13) Herrman, W. A.; Alberto, R.; Bryan, J. C.; Sattelberger, A. P. Metal carbonyl syntheses. XX. Simple method for the preparation of technetium tricarbonyl complexes: synthesis, structures, and reactivity of the novel cubane-type cluster Na[$Tc_3(CO)_9(OCH_3)_4$]. *Chem. Ber.* **1991**, *124*, 1107−1111.

(14) Raptis, K.; Kanellakopulos, B.; Nuber, B.; Ziegler, M. L. Metallorganische Verbindungen des Technetiums: V. Darstellung und Charakterisierung von Photolyseprodukten des (C_5Me_5)Tc(CO)$_3$. Synthese von (C_5Me_5)$_2$Tc$_2$(CO)$_5$ und (C_5Me_5)$_2$Tc$_2$(CO)$_3$, Röntgenstrukturanalyse von Tri-μ-carbonyl-bis[η5-pentamethylcyclopentadienyl)technetium] (Tc≡Tc). *J. Organomet. Chem.* **1991**, *405*, 323−331.

(15) Raptis, K.; Dornberger, E.; Kanellakopulos, B.; Nuber, B.; Ziegler, M. L. Metallorganische Verbindungen des Technetiums: VI. Darstellung und Charakterisierung von Verbindungen des Typs LTc(CO)$_3$ (L = C_5Me_5, C_5Me_4Et, C_9H_7); Röntgenstrukturanalysen von (η^5-C_5Me_5)M(CO)$_3$ (M = Tc, Re), (η^5-C_5Me_4Et)Tc(CO)$_3$ sowie (η^5-C_9H_7)Tc(CO)$_3$. *J. Organomet. Chem.* **1991**, *408*, 61−75.

DOI: 10.1021/acs.organomet.9b00620
Organometallics 2019, 38, 4471−4478

(16) Alberto, R.; Schibli, R.; Egli, A.; Abram, U.; Abram, S.; Kaden, T. A.; Schubiger, P. A. Steps towards $[(C_5H_5)TcO_3]$: novel synthesis of $[(C_5H_5)Tc(CO)_3]$ from $[\{Tc(\mu^3\text{-}OH)(CO)3\}4]$ and oxidation of $[(C_5H_5)TcO_3]$ with Br_2. *Polyhedron* **1998**, *17*, 1133−1140.
(17) Bernard, J.; Ortner, K.; Spingler, B.; Pietzsch, H.-J.; Alberto, R. Aqueous Synthesis of Derivatized Cyclopentadienyl Complexes of Technetium and Rhenium Directed toward Radiopharmaceutical Application. *Inorg. Chem.* **2003**, *42*, 1014−1022.
(18) Zobi, F.; Spingler, B.; Alberto, R. Syntheses, Structures and Reactivities of $[CpTc(CO)_3X]^+$ and $[CpRe(CO)_3X]^+$. *Eur. J. Inorg. Chem.* **2008**, *2008*, 4205−4214.
(19) Wald, J.; Alberto, R.; Ortner, K.; Candreia, L. Aqueous one-pot synthesis of derivatized cyclopentadienyl-tricarbonyl complexes of ^{99m}Tc with an in situ CO source: Application to a serotoneric receptor ligand. *Angew. Chem., Int. Ed.* **2001**, *40*, 3062−3066.
(20) Peindy N'Dongo, H. W.; Liu, Y.; Can, D.; Schmutz, P.; Spingler, B.; Alberto, R. Aqueous synthesis of $[(Cp\text{-}R)M(CO)_3]$ type complexes (Cp = cyclopentadienyl, M = Mn, ^{99m}Tc, Re) with bioactive functionalities. *J. Organomet. Chem.* **2009**, *694*, 981−987.
(21) Morais, G. R.; Paulo, A.; Santos, I. Organometallic Complexes for SPECT Imaging and/or Radionuclide Therapy. *Organometallics* **2012**, *31*, 5693−5714.
(22) Frei, A.; Spingler, B.; Alberto, R. Multifunctional Cyclopentadienes as a Scaffold for Combinatorial Bioorganometallics in $[(\eta^5\text{-}C_5H_2R^1R^2R^3)M(CO)_3]$ (M = Re, ^{99m}Tc) Piano-Stool Complexes. *Chem. - Eur. J.* **2018**, *24*, 10156−10164.
(23) Masi, S.; Top, S.; Boubekeur, L.; Jaouen, G.; Mundwiler, S.; Spingler, B.; Alberto, R. Direct Synthesis of Tricarbonyl-(cyclopentadienyl)rhenium and Tricarbonyl(cyclopentadienyl)technetium Units from Ferrocenyl Moieties - Preparation of 17α-Ethynylestradiol Derivatives Bearing a Tricarbonyl-(cyclopentadienyl)technetium Group. *Eur. J. Inorg. Chem.* **2004**, *2004*, 2013−2017.
(24) Ackermann, J.; Hagenbach, A.; Abram, U. $\{Tc(NO)(Cp)(PPh_3)\}^+$ − a novel technetium(I) core. *Chem. Commun.* **2016**, *52*, 10285−10288.
(25) Nicholson, T.; Chun, E.; Mahmood, A.; Mueller, P.; Davison, A.; Jones, A. G. Synthesis, spectroscopy and structural analysis of Technetium and Rhenium nitrosyl complexes *Commun. Inorg. Synth.* **2015**, *3*, 31−39.
(26) Nicholson, T.; Müller, P.; Davison, A.; Jones, A. G. The synthesis and characterization of a cationic technetium nitrosyl complex: The X-ray crystal structure of $[TcCl(NO)(DPPE)_2](PF_6)$ x CH_2Cl_2. *Inorg. Chim. Acta* **2006**, *359*, 1296−1298.
(27) Ackermann, J.; Hagenbach, A.; Abram, U. Nitrosyltechnetium complexes with (2-aminomethylphenyl)diphenylphosphine. *Inorg. Chim. Acta* **2014**, *419*, 59−65.
(28) Balasekaran, S. M.; Spandl, J.; Hagenbach, A.; Köhler, K.; Drees, M.; Abram, U. Fluoridonitrosyl Complexes of Technetium(I) and Technetium(II). Synthesis, Characterization, Reactions, and DFT Calculations. *Inorg. Chem.* **2014**, *53*, 5117−5128.
(29) Ackermann, J.; Noufele, C. N.; Hagenbach, A.; Abram, U. Nitrosyltechnetium(I) Complexes with 2-(Diphenylphosphanyl)-aniline. *Z. Anorg. Allg. Chem.* **2019**, *645*, 8−13.
(30) Balasekaran, S. M.; Hagenbach, A.; Drees, M.; Abram, U. $[Tc^{II}(NO)(trifluoroacetate)_4F]^{2-}$ - synthesis and reactions. *Dalton Trans.* **2017**, *46*, 13544−13553.
(31) Merrifield, J. H.; Fernandez, J. M.; Buhro, W. E.; Gladysz, J. A. Cleavage of the Rhenium-Methyl Bond of $(\eta\text{-}C_5H_5)Re(NO)(PPh_3)(CH_3)$ by Protic and Halogen Electrophiles: Stereochemistry at Rhenium. *Inorg. Chem.* **1984**, *23*, 4022−4029.
(32) Wendlandt, D.; Bauche, J.; Luc, P. Hyperfine structure in Tc I: experiment and theory. *J. Phys. B: At. Mol. Phys.* **1977**, *10*, 1989−2002.
(33) Abram, U.; Lorenz, L.; Kaden, L.; Scheller, D. Nitrido Complexes of Technetium with Tertiary Phosphines and Arsines. *Polyhedron* **1988**, *7*, 285−289.
(34) Mikhalev, V. A. ^{99m}Tc NMR Spectroscopy. *Radiochemistry* **2005**, *47*, 319−333.
(35) Kirmse, R.; Stach, J.; Abram, U.; Marov, I. N. Zu Struktur, Bindung und Ligandaustauschverhalten von Nitrosyltechnetium(II)-Verbindungen. Eine EPR-Untersuchung. *Z. Anorg. Allg. Chem.* **1984**, *518*, 210−226.
(36) Trop, H. S.; Davison, A.; Jones, A. G.; Davis, M. A.; Szalda, D. J.; Lippard, S. J. Synthesis and physical properties of hexakis-(isothiocyanato)technetate(III) and -(IV) complexes. Structure of the $[Tc(NCS)_6]^{3-}$ ion. *Inorg. Chem.* **1980**, *19*, 1105−1010.
(37) Baldas, J.; Bonnyman, J.; Williams, G. A. J. Structural studies of technetium complexes. Part 4. The crystal structure of *trans,trans*-acetonitriledi-isothiocyanato(nitrido)bis(triphenylphosphine)-technetium(V)−acetonitrile (1/0.5). *J. Chem. Soc., Dalton Trans.* **1984**, 833−837.
(38) Bandoli, G.; Mazzi, U.; Ichimura, A.; Libson, K.; Heineman, W. R.; Deutsch, E. An isothiocyanato complex of technetium(II). Spectroelectrochemical and single-crystal x-ray structural studies on trans-$[Tc(DPPE)_2(NCS)_2]^0$, where DPPE = 1,2-bis(diphenylphosphino)ethane. *Inorg. Chem.* **1984**, *23*, 2898−2901.
(39) Williams, G. A.; Bonnyman, J.; Baldas, J. Structural Studies of Technetium Complexes. X. The Crystal-Structure of Tetraphenylarsonium Hexakis(Isothiocyanato)Technetate(IV)-Dichloromethane (1/1). *Aust. J. Chem.* **1987**, *40*, 27−33.
(40) Rochon, F. D.; Melanson, R.; Kong, P.-C. Synthesis of new mixed-ligands Tc complexes containing monodentate phosphine and isothiocyanato ligands: Crystal structures of complexes $Tc(P(C_3H_7)_3)_2(NCS)_4$, $Tc(P(CH_3)_2Ph)_4(NCS)_2$ and $Tc(P(OCH_3)Ph_2)_4(NCS)_2 \cdot 1/2CH_2Cl_2$. *Inorg. Chim. Acta* **2000**, *300*, 43−48.
(41) Hauck, J.; Schwochau, K.; Bucksch, R. Zur Kristallstruktur komplexer Technetiumverbindungen II. $[(CH_3)_4N][Tc^V(NCS)_6]$. *Inorg. Nucl. Chem. Lett.* **1973**, *9*, 927−927.
(42) Roodt, A.; Leipoldt, J. G.; Deutsch, E. A.; Sullivan, J. G. Kinetic and structural studies on the oxotetracyanotechnetate(V) core: protonation and ligation of dioxotetracyanotechnetate(V) ions and crystal structure of 2,2'-bipyridinium trans-oxothiocyanatotetracyanotechnetate(V). *Inorg. Chem.* **1992**, *31*, 1080−1085.
(43) Jurisson, S.; Halihan, M. M.; Lydon, J. D.; Barnes, C. L.; Nowotnik, D. P.; Nunn, A. D. Linkage Isomerization of $MSCN(CDOH)_2(CDO)BMe$ to $MNCS(CDOH)_2(CDO)BMe$ (M = Tc, Re). Crystal Structures of $TcNCS(CDOH)_2(CDO)BMe$, $ReNCS(CDOH)_2(CDO)BMe$, and $ReSCN(CDOH)_2(CDO)BMe$. *Inorg. Chem.* **1998**, *37*, 1922−1928.
(44) Abram, U.; Abram, S.; Dilworth, J. R. Mixed-Ligand Complexes of Technetium. XIV. Structure of trans-$[TcCl_2(NCS)(Me_2PhP)_3]$. *Acta Crystallogr., Sect. C: Cryst. Struct. Commun.* **1996**, *C52*, 605−607.
(45) Homolya, L.; Preetz, W. Kristallstrukturen, Schwingungsspektren und Normalkoordinatenanalyse von cis-$(n\text{-}Bu_4N)_2[ReBr_4(NCS)(SCN)]$, trans-$(n\text{-}Bu_4N)_2[ReBr_4(NCS)(SCN)]$ und trans-$(n\text{-}Bu_4N)_2[ReBr_4(NCSe)(SeCN)]$. *Z. Naturforsch., B: J. Chem. Sci.* **1999**, *B54*, 1009−1014.
(46) Gonzalez, R.; Barboza, N.; Chiozzone, R.; Kremer, C.; Armentano, D.; De Munno, G.; Faus, J. Linkage isomerism in the metal complex hexa(thiocyanato)rhenate(IV): Synthesis and crystal structure of $(NBu_4)_2[Re(NCS)_6]$ and $[Zn(NO_3)(Me_2phen)_2]_2[Re(NCS)_5(SCN)]$. *Inorg. Chim. Acta* **2008**, *361*, 2715−2720.
(47) Gonzalez, R.; Acosta, A.; Chiozzone, R.; Kremer, C.; Armentano, D.; De Munno, G.; Julve, M.; Lloret, F.; Faus, J. New family of thiocyanate-bridged Re(IV)-SCN-M(II) (M = Ni, Co, Fe, and Mn) heterobimetallic compounds: synthesis, crystal structure, and magnetic properties. *Inorg. Chem.* **2012**, *51*, 5737−5747.
(48) Ambrosetti, R.; Baratta, W.; Dell'Amico, D. B.; Calderazzo, F.; Marchetti, F. Adducts of diiodine and other dihalogens with halo metal complexes. I. Reactions with iodo complexes of group 7 metals. Spectroscopic studies, formation constants and crystal and molecular structure of the triiodo complex $Re(I_3)(CO)_3(Me_2PCH_2CH_2PMe_2)$ *Gazz. Chim. Ital.* **1990**, *120*, 511−525.
(49) Blanchard, S. S.; Nicholson, T. L.; Davison, A.; Davis, W. M.; Jones, A. G. The synthesis, characterization and substitution reactions of the mixed ligand technetium(I) nitrosyl complex trans—trans-

DOI: 10.1021/acs.organomet.9b00620
Organometallics 2019, 38, 4471−4478

[(NO)(NCCH$_3$)Cl$_2$(PPh$_3$)$_2$Tc]. *Inorg. Chim. Acta* **1996**, *244*, 121−130.
(50) Panda, T. K.; Gamer, M. T.; Roesky, P. W.; Yoo, H.; Berry, H. H. Sodium and Potassium Cyclopentadienide. *Inorg. Synth.* **2014**, *36*, 35−37.
(51) Nevissi, A. E.; Silverston, M.; Strebin, R. S.; Kaye, J. H. Radiochemical determination of technetium-99. *J. Radioanal. Nucl. Chem.* **1994**, *177*, 91−99.
(52) Frisch, M. J.; Trucks, G. W.; Schlegel, H. B.; Scuseria, G. E.; Robb, M. A.; Cheeseman, J. R.; Scalmani, G.; Barone, V.; Petersson, G. A.; Nakatsuji, H.; Li, X.; Caricato, M.; Marenich, A. V.; Bloino, J.; Janesko, B. G.; Gomperts, R.; Mennucci, B.; Hratchian, H. P.; Ortiz, J. V.; Izmaylov, A. F.; Sonnenberg, J. L.; Williams-Young, D.; Ding, F.; Lipparini, F.; Egidi, F.; Goings, J.; Peng, B.; Petrone, A.; Henderson, T.; Ranasinghe, D.; Zakrzewski, V. G.; Gao, J.; Rega, N.; Zheng, G.; Liang, W.; Hada, M.; Ehara, M.; Toyota, K.; Fukuda, R.; Hasegawa, J.; Ishida, M.; Nakajima, T.; Honda, Y.; Kitao, O.; Nakai, H.; Vreven, T.; Throssell, K.; Montgomery, Jr., J. A.; Peralta, J. E.; Ogliaro, F.; Bearpark, M. J.; Heyd, J. J.; Brothers, E. N.; Kudin, K. N.; Staroverov, V. N.; Keith, T. A.; Kobayashi, R.; Normand, J.; Raghavachari, K.; Rendell, A. P.; Burant, J. C.; Iyengar, S. S.; Tomasi, J.; Cossi, M.; Millam, J. M.; Klene, M.; Adamo, C.; Cammi, R.; Ochterski, J. W.; Martin, R. L.; Morokuma, K.; Farkas, O.; Foresman, J. B.; Fox, D. J. *Gaussian 16*, Revision B.01; Gaussian, Inc.: Wallingford, CT, 2016.
(53) Frisch, M. J.; Trucks, G. W.; Schlegel, H. B.; Scuseria, G. W.; Robb, M. A.; Cheeseman, J. R.; Scalmani, G.; Barone, V.; Petersson, G. A.; Nakatsuji, H.; Li, X.; Caricato, M.; Marenich, A.; Bloino, J.; Janesko, B. G.; Gomperts, R.; Mennucci, B.; Hratchian, H. P.; Ortiz, J. V.; Izmaylov, A. F.; Sonnenberg, J. L.; Williams-Young, D.; Ding, F.; Lipparini, F.; Egidi, F.; Goings, J.; Peng, B.; Petrone, A.; Henderson, T.; Ranasinghe, D.; Zakrzewski, V. G.; Gao, J.; Rega, N.; Zheng, G.; Liang, W.; Hada, M.; Ehara, M.; Toyota, K.; Fukuda, R.; Hasegawa, J.; Ishida, M.; Nakajima, T.; Honda, T.; Kitao, O.; Nakai, H.; Vreven, T.; Throssell, K.; Montgomery, Jr., J. A.; Peralta, J. E.; Ogliaro, F.; Bearpark, M.; Heyd, J. J.; Brothers, E.; Kudin, K. N.; Staroverov, V. N.; Keith, T.; Kobayashi, R.; Normand, J.; Raghavachari, K.; Rendell, A.; Burant, J. C.; Iyengar, S. S.; Tomasi, J.; Cossi, M.; Millam, J. M.; Klene, M.; Adamo, C.; Cammi, R.; Ochterski, J. W.; Martin, R. L.; Morokuma, K.; Farkas, O.; Foresman, J. B.; Fox, D. J. *Gaussian 09*, Revision A.02; Gaussian, Inc.: Wallingford, CT, 2016.
(54) Dennington, R.; Keith, T. A.; Millam, J. M. *GaussView*, Version 6; Semichem Inc.: Shawnee Mission, KS, 2016.
(55) Vosko, S. H.; Wilk, L.; Nusair, M. Accurate spin-dependent electron liquid correlation energies for local spin density calculations: a critical analysis. *Can. J. Phys.* **1980**, *58*, 1200−1211.
(56) Becke, A. D. A new mixing of Hartree−Fock and local density-functional theories. *J. Chem. Phys.* **1993**, *98*, 5648−5652.
(57) Lee, C.; Yang, W.; Parr, R. G. Development of the Colle-Salvetti correlation-energy formula into a functional of the electron density. *Phys. Rev. B: Condens. Matter Mater. Phys.* **1988**, *37*, 785−789.
(58) Andrae, D.; Häußermann, U.; Dolg, M.; Stoll, H.; Preuß, H. Energy-adjustable initio pseudopotentials for the second and third row transition elements. *Theor. Chim. Acta* **1990**, *77*, 123−141.
(59) Martin, J. M. L.; Sundermann, A. Correlation consistent valence basis sets for use with the Stuttgart−Dresden−Bonn relativistic effective core potentials: The atoms Ga−Kr and In−Xe. *J. Chem. Phys.* **2001**, *114*, 3408−3420.
(60) Bergner, A.; Dolg, M.; Küchle, W.; Stoll, H.; Preuß, H. Ab initio energy-adjusted pseudopotentials for elements of groups 13−17. *Mol. Phys.* **1993**, *80*, 1431−1441.
(61) Hay, P. J.; Wadt, W. R. Ab initio effective core potentials for molecular calculations. Potentials for the transition metal atoms Sc to Hg. *J. Chem. Phys.* **1985**, *82*, 270−283.
(62) Wadt, W. R.; Hay, P. J. Ab initio effective core potentials for molecular calculations. Potentials for main group elements Na to Bi. *J. Chem. Phys.* **1985**, *82*, 284−298.
(63) Hay, P. J.; Wadt, W. R. Ab initio effective core potentials for molecular calculations. Potentials for K to Au including the outermost core orbitals. *J. Chem. Phys.* **1985**, *82*, 299−310.
(64) Check, C. E.; Faust, T. O.; Bailey, J. M.; Wright, B. J.; Gilbert, T. M.; Sunderlin, L. S. Addition of Polarization and Diffuse Functions to the LANL2DZ Basis Set for P-Block Elements. *J. Phys. Chem. A* **2001**, *105*, 8111−8116.
(65) Dunning, Jr., T. H. Gaussian Basis Sets for Molecular Calculations. In *Methods of Electronic Structure Theory*; Schaefer, H. F., Ed.; Springer: 1977; pp 1−27.
(66) Krishnan, R.; Binkley, J. S.; Seeger, R.; Pople, J. A. Self-consistent molecular orbital methods. XX. A basis set for correlated wave functions. *J. Chem. Phys.* **1980**, *72*, 650−654.
(67) McLean, A. D.; Chandler, G. S. Contracted Gaussian basis sets for molecular calculations. I. Second row atoms, Z = 11−18. *J. Chem. Phys.* **1980**, *72*, 5639−5648.
(68) Curtiss, L. A.; McGrath, M. P.; Blaudeau, J.-P.; Davis, N. E.; Binning, R. C.; Radom, L. Extension of Gaussian-2 theory to molecules containing third-row atoms Ga−Kr. *J. Chem. Phys.* **1995**, *103*, 6104−6113.
(69) Feller, D. The role of databases in support of computational chemistry calculations. *J. Comput. Chem.* **1996**, *17*, 1571−1586.
(70) Schuchardt, K. L.; Didier, B. T.; Elsethagen, T.; Sun, L.; Gurumoorthi, V.; Chase, J.; Li, J.; Windus, T. L. Basis Set Exchange: A Community Database for Computational Sciences. *J. Chem. Inf. Model.* **2007**, *47*, 1045−1052.
(71) Sheldrick, G. M. *SADABS*; Universität of Göttingen, Germany, 2014.
(72) Spek, A. L. *PLATON: A Multipurpose Crystallographic Tool*; Utrecht University: Utrecht, Netherlands, 1980−2014.
(73) Sheldrick, G. M. A short history of SHELX. *Acta Crystallogr., Sect. A: Found. Crystallogr.* **2008**, *64*, 112−122.
(74) Sheldrick, G. M. Crystal structure refinement with SHELXL. *Acta Crystallogr., Sect. C: Struct. Chem.* **2015**, *71*, 3−8.
(75) Brandenburg, K. *Diamond—Crystal and Molecular Structure Visualization, Crystal impact GbR*, vers. 4.5.1; Bonn, Germany, 2018.

DOI: 10.1021/acs.organomet.9b00620
Organometallics 2019, 38, 4471−4478

4.6 $[\{Tc^{I}(NO)(L^{OMe})(PPh_3)Cl\}_2Ag](PF_6)$ and $[Tc^{II}(NO)(L^{OMe})(PPh_3)Cl](PF_6)$: Two Unusual Technetium Complexes with a "Kläui-type" Ligand

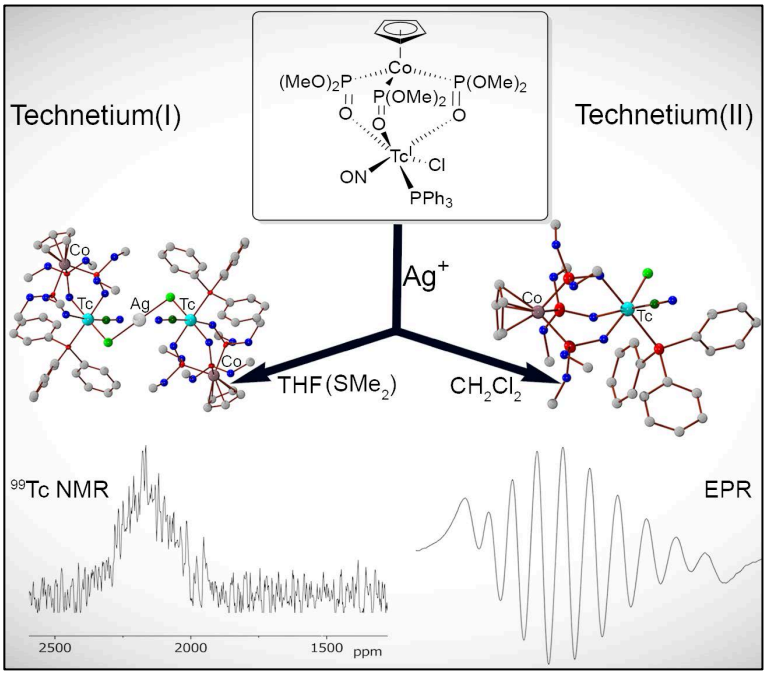

Reproduced with permission from Roca Jungfer, M.; Ernst, M. J.; Hagenbach, A.; Abram, U. *Z. Anorg. Allg. Chem.* **2022**, e202100316.

DOI: 10.1002/zaac.202100316

For Supplementary Material see A.6.

Author Contributions:

Maximilian Roca Jungfer and Ulrich Abram designed the project. Moritz Johannes Ernst performed the synthesis and characterization of the compounds during his research internship under the supervision of Maximilian Roca Jungfer. Maximilian Roca Jungfer, Moritz Johannes Ernst and Ulrich Abram calculated the X-ray structures under the guidance of Adelheid Hagenbach. Ulrich Abram wrote the manuscript. Maximilian Roca Jungfer and Moritz Johannes Ernst corrected the manuscript. Ulrich Abram supervised the project, provided scientific guidance and suggestions and corrected the manuscript.

Journal of Inorganic and General Chemistry
ZAAC
Zeitschrift für anorganische und allgemeine Chemie
www.zaac.wiley-vch.de
ARTICLE

DOI: 10.1002/zaac.202100316

$[\{Tc^{I}(NO)(L^{OMe})(PPh_3)Cl\}_2Ag](PF_6)$ and $[Tc^{II}(NO)(L^{OMe})(PPh_3)Cl](PF_6)$: Two Unusual Technetium Complexes with a "Kläui-type" Ligand

Maximilian Roca Jungfer,[a] Moritz Johannes Ernst,[a] Adelheid Hagenbach,[a] and Ulrich Abram*[a]

The reaction of $[Tc^{I}(NO)(L^{OMe})(PPh_3)Cl]$ ($\{L^{OMe}\}^- = \eta^5$-cyclopentadienyltris(dimethyl phosphito-*P*)cobaltate(III)) with $Ag(PF_6)$ gives two unexpected products: the dimeric technetium(I) complex $[\{Tc(NO)(L^{OMe})(PPh_3)Cl\}_2Ag](PF_6)$ with a central Ag^+ ion and the cationic Tc(II) compound $[Tc(NO)(L^{OMe})(PPh_3)Cl](PF_6)$. The products have been studied spectroscopically and by X-ray diffraction.

Introduction

Technetium complexes are of ongoing interest as potential radiopharmaceuticals. The metastable nuclear isomer ^{99m}Tc is by far the most frequently used nuclide in diagnostic nuclear medicine with some 40 million administrations annually.[1] Since the introduction of a technetium(I) isocyanide complex into the routine myocardial imaging in the 1980's,[2–6] also organometallic approaches found an increasing interest. This includes numerous compounds with the $\{^{99m}Tc(CO)_3\}^+$ core,[7–9] but also bis-arene complexes, and particularly cyclopentadienyl (Cp^-) compounds.[8,10–15]

Recently, we reported a number of technetium complexes having the $\{Tc(NO)(Cp)(PPh_3)\}^+$ core.[16,17] The chlorido ligand of their parent compound $[Tc(NO)(Cp)(PPh_3)Cl]$ (**1**) can readily be replaced by other anionic or neutral ligands. Stimulated by the versatility of this core, we decided to undertake some efforts for the synthesis of similar compounds with ligands, which are isolobal to Cp^-. The classical scorpionate tris(pyrazolyl)borate, but also η^5-cyclopentadienyltris(dialkyl phosphito-*P*)cobaltates(III) ("Kläui-type" ligands) are frequently discussed a surrogates for the 6-electron donor Cp^-.[18–21] A variety of technetium complexes with the "Kläui-type" ligand η^5-cyclopentadienyltris(dimethyl phosphito-*P*)cobaltate(III) ($\{L^{OMe}\}^-$), comprising seven different oxidation states of the transition metal have been introduced recently.[22] The obtained products are of remarkable stability, which recommends them as starting materials for ongoing reactions. One of the isolated technetium(I) complexes, $[Tc(NO)(L^{OMe})(PPh_3)Cl]$ (**2**) in Figure 1, is structurally related to the cyclopentadienyl compound **1**, for which we recently had to note some unexpected behavior.[23] An illustrative example is the reaction of **1** with $Ag(PF_6)$. Not all chlorido ligands are abstracted from technetium in this reaction and the dimeric, chlorido-bridged complex $[\{Tc(NO)(Cp)(PPh_3)\}_2Cl](PF_6)$ is formed instead.

In the present communication, we report about a similar reaction with the corresponding complex containing a "Kläui-type" ligand (**2**) and the structures of the formed products.

Results and Discussion

The starting material $[Tc(NO)(L^{OMe})(PPh_3)Cl]$ (**2**) can be prepared from a simple ligand exchange reaction between $[Tc(NO)Cl_2(PPh_3)_2(CH_3CN)]$ and NaL^{OMe} in reasonable yields and with high purity.[22] No redox processes or the formation of considerable amounts of side-products have been observed during the synthesis. The compound is stable in air, but cyclic voltammetry gave evidence for a quasi-reversible one-electron

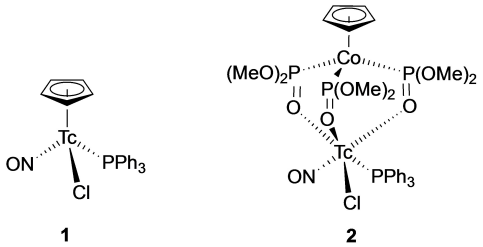

Figure 1. Technetium(I) complexes with (pseudo)tripodal ligands: $[Tc(NO)(Cp)(PPh_3)Cl]$ (**1**) and $[Tc(NO)(L^{OMe})(PPh_3)Cl]$ (**2**).

[a] *M. Roca Jungfer, M. J. Ernst, Dr. A. Hagenbach, Prof. Dr. U. Abram*
Institute of Chemistry and Biochemistry
Freie Universität Berlin
Fabeckstr. 34/36
14195 Berlin, Germany
E-mail: Ulrich.Abram@fu-berlin.de
Homepage: https://www.bcp.fu-berlin.de/chemie/chemie/forschung/InorgChem/agabram/index.html

Supporting information for this article is available on the WWW under https://doi.org/10.1002/zaac.202100316

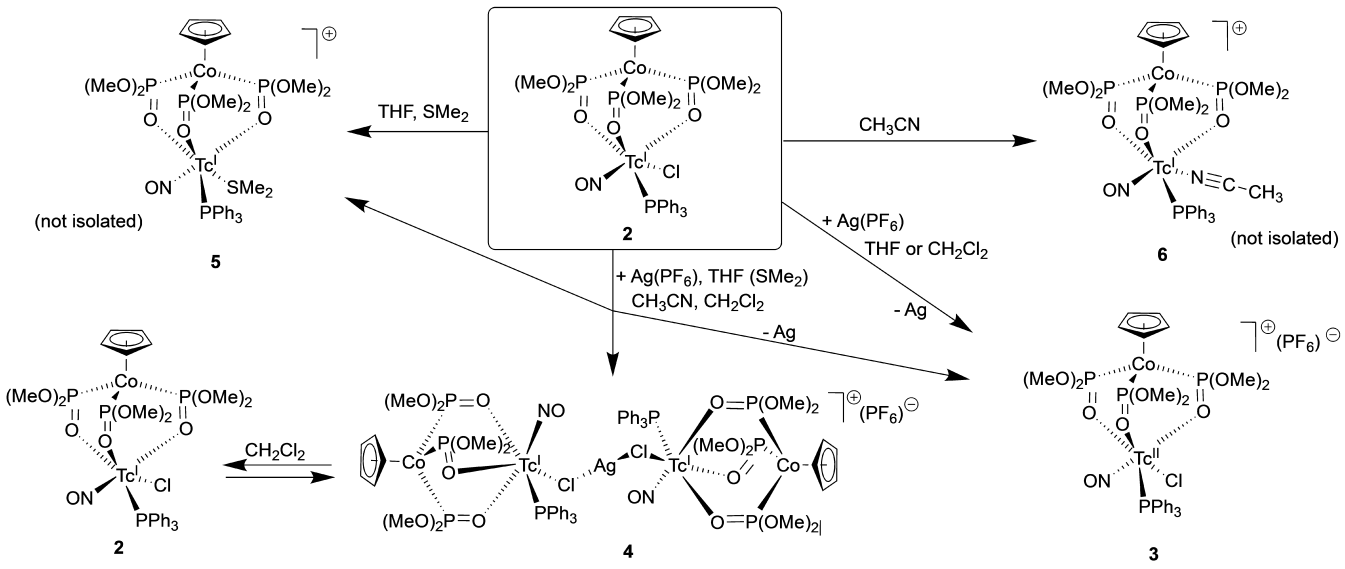

Scheme 1. Reactions of $[Tc^{I}(NO)(L^{OMe})(PPh_3)Cl]$ (**2**) with $Ag(PF_6)$.

oxidation with a half-wave potential of −0.16 V vs. ferrocene.[22] An attempted oxidation of **2** with Cl_2 gave a mixture of various Tc(II) nitrosyl complexes, where one of which could be assigned to the $[Tc(NO)Cl_4(solvent)]^-$ anion on the basis of its EPR data.[24]

A more selective formation of a Tc(II) complex is obtained when solutions of **2** in THF or CH_2Cl_2 are exposed to $Ag(PF_6)$. This reaction results in a rapid dissolution of the sparingly soluble starting material and the deposition of a small amount of a grey solid (elemental silver), which can readily be filtered off. Upon concentration of the resulting solution, the red solid technetium(II) complex $[Tc(NO)(L^{OMe})(PPh_3)Cl](PF_6)$ (**3**) precipitates (Scheme 1). The oxidation state of the product can be derived from the ν_{NO} stretch, which appears as an intense band at 1786 cm^{-1}, the typical range for Tc(II) complexes. The IR spectra of the more electron-rich technetium(I) complexes show their ν_{NO} absorptions at clearly lower frequencies due to a higher degree of back-donation from orbitals of the d^6 Tc(I) ion into antibonding orbitals of the NO ligand.[22,24,25]

The d^5 "low-spin" configuration of Tc(II) allows the detection of resolved EPR spectra. Figure 2 depicts the spectra obtained for compound **3**. At room-temperature, a well resolved 10-line pattern is observed, which is expected from the interaction of the unpaired electron with the nuclear spin of ^{99}Tc (I = 9/2). A frozen solution of the compound shows a more complex, axially symmetric EPR spectrum with two sets of 10-line patterns for the parallel and perpendicular parts as can be described by the following spin Hamiltonian:

$$\hat{\mathcal{H}}_{sp} = \beta_e\left[g_{\|}H_z\hat{S}_z + g_{\perp}\left(H_x\hat{S}_x + H_y\hat{S}_y\right)\right] + A_{\|}^{Tc}\hat{I}_z\hat{S}_z + A_{\perp}^{Tc}\left(\hat{I}_x\hat{S}_x + \hat{I}_y\hat{S}_y\right)$$
$$+A_{\perp}^{Tc}\left(\hat{I}_x\hat{S}_x + \hat{I}_y\hat{S}_y\right) + Q'\left[\hat{I}_z^2 - 1/3I(I+1)\right],$$

where $g_{||}$, $g_{\perp}$, $A_{||}^{Tc}$ and $A_{\perp}^{Tc}$ are the principle values of the $\tilde{g}$ and the ^{99}Tc hyperfine interaction tensors. The ^{99}Tc quadrupole coupling constant Q′ is small and was neglected.

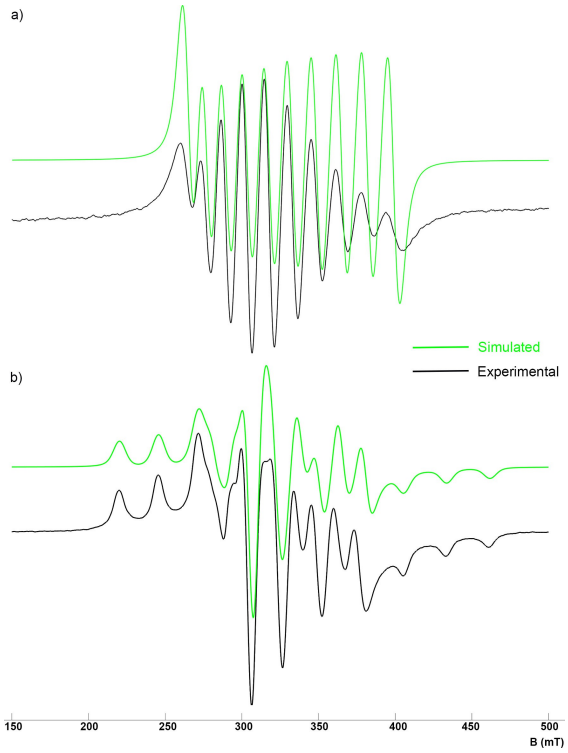

Figure 2. X-Band EPR spectra of $[Tc(NO)(L^{OMe})(PPh_3)Cl](PF_6)$ in CH_2Cl_2 recorded a) in liquid solution at room temperature and b) in frozen solution at 78 K. EPR parameters: $g_0 = 2.0247$, $a_0^{Tc} = 139.5 \cdot 10^{-4}$ cm^{-1}; $g_{||} = 1.972$, $g_{\perp} = 2.015$, $A_{||}^{Tc} = 247 \cdot 10^{-4}$ cm^{-1}, $A_{\perp}^{Tc} = 100 \cdot 10^{-4}$ cm^{-1}, $A_{||}^{P} = 25 \cdot 10^{-4}$ cm^{-1}, $A_{||}^{P} = 20 \cdot 10^{-4}$ cm^{-1}.

The perpendicular part of the spectrum is not fully resolved due to large line widths. They result from superhyperfine interactions of the unpaired electron with the ^{31}P nucleus of PPh_3. Although these interactions are not resolved in the

experimental spectrum, they can be estimated from line-width considerations to have values of approximately $25 \cdot 10^{-4}$ cm^{-1} for the parallel part and $20 \cdot 10^{-4}$ cm^{-1} for the perpendicular part. The obtained values are in the same magnitude as observed for other nitrosyl or thionitrosyl complexes of technetium(II) as $[Tc(NX)Y_3(PMe_2PhP)_2]$ (X = O, S; Y = Cl, Br) complexes or $[Tc(NO)Cl_3\{(2\text{-aminomethylphenyl})diphenylphosphine)]$.[26–28] Unlike the spectra with monodentate phosphines, which have almost isotropic $\tilde{g}$ tensors,[25,26] the spectrum of **3** shows a considerable anisotropy. This is most probably a consequence of the chelate formation and has been observed before for Tc(II) complexes with *P,N*-chelating ligands.[27] Interactions with the nitrosyl ligand have not been observed.

The preservation of the coordination sphere of technetium upon oxidation is proven by an X-ray structure determination. Figure 3 shows the structure of the $[Tc^{II}(NO)(L^{OMe})(PPh_3)Cl]^+$ cation. Selected bond lengths and angles are summarized in Table 1. It is evident that bond lengths and angles around the technetium atoms are not significantly influenced by the oxidation state of the metal. The same holds true for the nitrosyl ligand, which is linearly bound in compounds **2** and compound **3**, and thus, shall be regarded as NO^+. This is not surprising and in accord with all other structurally characterized nitrosyl complexes of technetium.[25]

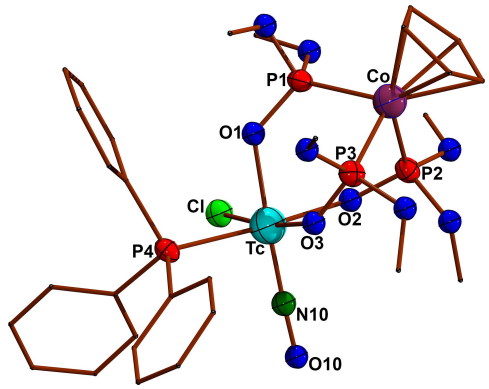

Figure 3. Structure of $[Tc(NO)(L^{OMe})(PPh_3)Cl]^+$. Hydrogen atoms are omitted for clarity.

Table 1. Selected bond lengths (Å) and angles (°) in $[Tc^{I}(NO)(L^{OMe})(PPh_3)Cl]$ (**2**), $[Tc^{II}(NO)(L^{OMe})(PPh_3)Cl](PF_6)$ (**3**) and $[\{Tc^{I}(NO)(L^{OMe})(PPh_3)Cl\}_2Ag](PF_6)$ (**4**).

	2*	3	4**
Tc–N10	1.709(5)	1.734(11)	1.839(8)/1.689(8)
Tc–Cl1	2.361(2)	2.329(5)	2.388(3)/2.424(2)
Tc–O1	2.134(1)	2.051(3)	2.102(3) /2.110(3)
Tc–O2	2.166(1)	2.067(3)	2.162(3)/2.157(3)
Tc–O3	2.124(1)	2.050(3)	2.094(3)/2.076(3)
Tc–P4	2.359(4)	2.481(1)	2.366(1)/2.373(1)
Ag-Cl			2.624(2)/2.490(2)

*Values have been taken from ref. 22 and the atomic labelling scheme has been adopted from Figure 3; **Values for two independent molecules.

$[Tc^{II}(NO)(L^{OMe})(PPh_3)Cl](PF_6)$ is the sole product, when the reaction of **2** with $Ag(PF_6)$ is performed in THF, and there is no evidence for the formation of (intermediate) technetium(I) compounds. This behavior is not unexpected keeping in mind that ether-type ligands such as THF form only very weak bonds to technetium. Up to now, there are only two examples of structurally characterized technetium complexes with monodentate ether ligands,[29,30] and there is experimental evidence that even minor traces of water readily replace dioxane from the coordination sphere of technetium.[31]

A different behavior is observed, when potential ligands such as dimethylsulfide (SMe_2) or acetonitrile are added to the reaction mixture. The addition of a few drops of SMe_2 to a solution of **2** in a CH_2Cl_2/THF/CH_3CN mixture prevents the complete oxidation of the starting material and three additional ^{99}Tc NMR signals are observed. A considerable amount of $[\{Tc^{I}(NO)(L^{OMe})(PPh_3)Cl\}_2Ag](PF_6)$ (**4**) and a minor amount of another technetium(I) complex, which is most probably $[Tc^{I}(NO)(L^{OMe})(PPh_3)(SMe_2)]^+$ (**5**) precipitate directly from the reaction mixture together with the technetium(II) complex **3**, while a small amount of a third Tc(I) complex, $[Tc^{I}(NO)(L^{OMe})(PPh_3)(NCCH_3)]^+$ (**6**), remains in solution. Compounds **5** and **6** have not been isolated in crystalline form and their compositions have been derived on the basis of their ^{99}Tc NMR resonances at 1305 ppm ($\nu_{1/2}$ = 2740 Hz) (**5**) and 1595 ppm ($\nu_{1/2}$ = 1290 Hz) (**6**). The same spectroscopic features are observed for solutions of **2** in a SMe_2/THF mixture or in neat acetonitrile.

The precipitated compounds **3** and **4** can be separated on the basis of their different solubilities in toluene. This allows a separation of compound **4** by subsequent extraction operations with this solvent, while compound **3** remains as a solid. The purity of the compounds in the two fractions can easily be checked by their IR spectra, where the nitrosyl bands appear clearly separated (**3**: 1786 cm^{-1}, **4**: 1705 cm^{-1}). Alternatively, EPR or ^{99}Tc NMR spectroscopy can be used to prove the purity of the samples.

Single crystals of **4** were obtained directly from the slow evaporation of the reaction mixture.

As for all other technetium(I) complexes,[16,17,22–25] the ν_{NO} vibration of compound **3** appears as an intense band at a relatively low frequency. This is readily explained by the high degree of back-donation from orbitals of the d^6 Tc(I) ion into π^* orbitals of the NO ligand. The ^{1}H NMR spectrum of **4** is unexceptional and shows the expected signals for the aromatic and the methyl protons at almost identical positions as in the parent compound **2**. The same holds true for the ^{31}P resonances of the chelate-bonded $\{L^{OMe}\}^-$, which appear as one broad signal at 119.6 ppm. The considerable line broadening of ^{31}P NMR signals is frequently observed for technetium complexes and result from scalar couplings of ^{31}P nuclei with the large quadrupole moment of ^{99}Tc.[26] In many cases (as in those of complex **4**, **5** and **6** of the present study, and their parent compound **2**) such broadenings make the ^{31}P signals of ligands with a Tc–P bond practically invisible.[22,27] The large quadrupole moment of ^{99}Tc ($Q = -0.19 \cdot 10^{-28}$ m^2) is also responsible for a strong line broadening of the related ^{99}Tc NMR signals, which is normally observed when ^{99}Tc complexes with low local

symmetry are studied.[28] Nevertheless, this method is a valuable tool for the characterization of preferably Tc(I) and Tc(VII) complexes. Due to the large chemical shift range of ^{99}Tc NMR from approximately −7000 to +5000 ppm this method is sensitive even to slight changes in the electronic environment and geometry of the ^{99}Tc nuclei in such compounds.[29] The chemical shift of compound **2** appears at 2169 ppm with a line width of approximately 3180 Hz. It is interesting to note that the resonance of the structurally related compound [Tc(NO)(Cp)(PPh_3)Cl] (**1**) is found in a completely different spectral range (−231 ppm),[16] which questions the frequently discussed electronic similarity between Cp^- and $\{L^{OR}\}^-$ (R = alkyl) ligands.

The formation of a cationic complex with a central Ag^+ ion coordinated to the chlorido ligands of two {Tc(NO)(L^{OMe})(PPh_3)Cl} units is proven by a single crystal X-ray structural analysis. The complex cation is shown in Figure 4 and selected bond lengths and angles are contained in Table 1. The most remarkable feature of the compound is the central $\{Tc–Cl–Ag–Cl–Tc\}^+$ unit, which is established between two [Tc(NO)(L^{OMe})(PPh_3)Cl] complexes in the solid state. The Cl–Ag–Cl bridge is linear, while Tc–Cl–Ag angles of 82.88(7) and 86.37(6)° are established for two crystallographically independent species. Weak silver-oxygen interactions (Ag–O2 distance: 2.628 Å) may support the {Cl–Ag–Cl} bridge.

Compounds with (almost) unsupported AgX_2 bridges (X = halogen) are rare and only a few of them have been studied structurally. Three of them, the polymeric $(NBu_4)_x$[Pt(C_6C_5)$_2$$Cl_2$]$_2$Ag]$_x$, [{Pt(N,N′-Schiff base)Cl(Me)}$_2$Ag](BF$_4$) and [{Ru$_2$(anilinopyridine)$_4$}$_2$$AgF_2$](BF$_4$)$_3$ have linear X–Ag–X units,[32–34] while the corresponding angles in [{Re(Tp)(N-p-tol)(Ph)I}$_2$Ag](PF$_6$) and [M((*C,N,N′,P* ligand)(AN)Cl}$_2$Ag](SbF$_6$)$_3$ (M = Rh, Ir) are between 120 and 125°.[35,36] The Ag–Cl bond in all these compounds are around 2.5 Å as we have found for complex **4** of the present work.

The dimeric solid state structure of the [{Tc^{I}(NO)(L^{OMe})(PPh_3)Cl}$_2$Ag]$^+$ cation is not maintained in solution. As mentioned above, the ^{1}H and ^{31}P NMR spectra of **4** in dichloromethane closely resemble those of the starting material **2**, but they are less intense with respect to the lower solubility of the dimer and show broad lines indicating a dynamic behavior. The ^{99}Tc NMR signal of **4** appears approximately at the same chemical shift as that of complex **2**, but an extreme line broadening is observed from 3180 Hz for compound **2** to approximately 23.5 kHz for compound **4** (Figure 5). Hence, we propose a dissociation of **4** in solution according to the equilibrium given in Scheme 1. Another strong hint for the existence of such an equilibrium is the gradual formation of the paramagnetic complex **3** in such solutions. This can evidenced by the detection of its EPR spectrum and understood by the partial oxidation of the Tc(I) complex by the released Ag^+ ions. Such a reaction corresponds to the reaction between **2** and Ag(PF$_6$) described above. It cannot be quantitative in the present case, since only one equivalent of Ag^+ ions per two equivalents of compound **2** is released during the dissociation. It shall be noted that a similar behavior is observed for the Ag^+ bridged rhodium and iridium complexes of ref. 36.

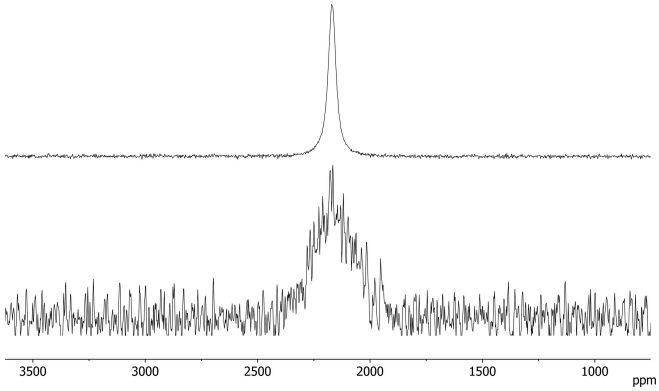

Figure 5. ^{99}Tc NMR spectra of a) compound **2** and b) compound **4** in CH_2Cl_2 with a strong line broadening for **4** indicating a dynamic behavior in solution.

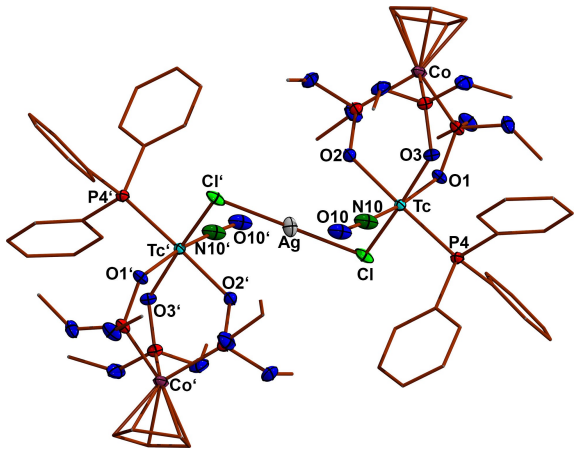

Figure 4. Structure of the [{Tc^{I}(NO)(L^{OMe})(PPh_3)Cl}$_2$Ag]$^+$ cation. Hydrogen atoms are omitted for clarity.

Conclusions

An unexpected oxidation of the technetium(I) complex [Tc(NO)(L^{OMe})(PPh_3)Cl] (**2**) and the formation of the Tc(II) compound [Tc(NO)(L^{OMe})(PPh_3)Cl](PF$_6$) (**3**) are observed during reactions with Ag(PF$_6$) in THF or CH_2Cl_2. The oxidation of the transition metal can partially be suppressed by the addition of SMe_2 in acetonitrile and a considerable amount of the dimeric complex [{Tc^{I}(NO)(L^{OMe})(PPh_3)Cl}$_2$Ag](PF$_6$) (**4**) precipitates from the reaction mixture under such conditions. The dimer contains a central {Cl–Ag–Cl} bridge, which dissociates in solution under re-formation of the starting material.

Experimental Section

Materials. All chemicals were reagent grade and used without further purification. The starting complex [Tc(NO)(L^{OMe})(PPh_3)Cl] has been prepared by a published procedure.[22]

Physical Measurements. The IR spectra of were recorded on a Shimadzu FTIR 8300 spectrometer. NMR spectra were recorded at 298 K on JEOL ECS 400 or JEOL JNM-ECA400II spectrometers. EPR spectra were recorded for CH_2Cl_2 solutions in the X-band at room temperature and at 78 K on a Magnetech Miniscope spectrometer. Simulations were done with Easyspin.[37]

Radiation Precautions. ^{99}Tc is a long-lived β^- emitter (E_{max} = 0.292 MeV). Normal glassware provides adequate protection against the weak beta radiation as long as milligram amounts of the samples are used. Secondary X-rays (bremsstrahlung) play a significant role only when larger amounts of ^{99}Tc are handled. All manipulations were done in a laboratory approved for the handling of radioactive materials.

Syntheses

[Tc(NO)(PPh_3)(L^{OMe})Cl](PF_6) (3). [Tc(NO)(PPh_3)(L^{OMe})Cl] (17 mg, 0.02 mmol) was suspended in CH_2Cl_2 (0.3 mL). Ag(PF_6) (5 mg, 0.02 mmol) was added and the mixture was stirred for 1 h at room temperature. The solvent was removed under vacuum and the residue was washed with toluene (5 mL) and pentane (5 mL). The residue was extracted with CH_2Cl_2 and filtered to remove elemental silver. [Tc(NO)(PPh_3)(L^{OMe})Cl](PF_6) was obtained as a dark red powder after complete evaporation of the solvent. Yield 9 mg (51 %). Single crystals for X-ray diffraction were obtained from a CH_2Cl_2/pentane mixture. IR (KBr, cm**Scheme 1**. Reactions of [Tc^{I}(NO)(L^{OMe})(PPh_3)Cl] (**2**) with Ag(PF_6).

^{1}): 1786 (ν_{NO}). EPR (78 K): $A_{\perp}^{Tc} = 100 \cdot 10^{-4}$ cm^{-1}, $A_{||}^{Tc} = 247 \cdot 10^{-4}$ cm^{-1}, $g_{\perp} = 2.015$, $g_{||} = 1.972$. EPR (RT): $g_0 = 2.0247$, $a_0^{Tc} = 139.5 \cdot 10^{-4}$ cm^{-1}.

[{Tc(NO)(PPh_3)(L^{OMe})Cl}$_2$Ag](PF_6) (4). Ag(PF_6) (25 mg, 0.1 mmol) and SMe_2 (0.5 mL) were added to a suspension of [Tc(NO)(PPh_3)(L^{OMe})Cl] (88 mg, 0.1 mmol) in THF (1.5 mL). Acetonitrile (one drop) and CH_2Cl_2 (two drops) were added after heating at 60 °C for 1 h. The resulting red solution was heated at 60 °C for another 3 h. The colorless precipitate (AgCl) formed upon cooling to room temperature was filtered off. The filtrate was layered with diethyl ether (18 mL) and pentane (15 mL). Orange-red crystals of [{Tc(NO)(PPh_3)(L^{OMe})Cl}$_2$Ag](PF_6) (**4**) and red crystals of [Tc(NO)(PPh_3)(L^{OMe})Cl](PF_6) (**3**) formed after storage of the mixture in a refrigerator for 72 h. The crystals were filtered off and extracted with toluene (2 x 5 ml). The solvent was removed in vacuum to give [{Tc(NO)(PPh_3)(L^{OMe})Cl}$_2$Ag](PF_6) as an orange-red powder. Single crystals of 4 · CH_2Cl_2 were obtained from a CH_2Cl_2/toluene mixture. Yield 35 mg (38 %). IR (KBr, cm^{-1}): 1705 (ν_{NO}). ^{1}H NMR ($CDCl_3$, ppm): 7.65–7.29 (m, 30H, PPh_3), 4.98 (s, 10H, Cp), 3.88 (s, 18H, OCH_3), 3.16 (s, 6H, OCH_3), 2.89 (s, 6H, CH_3). ^{31}P{^{1}H} NMR ($CDCl_3$, ppm): 119.6 (s, $PO(OMe)_2$), −144.3 (sept, $^1J_{P\text{-}F}$ = 715 Hz, PF_6). ^{99}Tc NMR ($CDCl_3$, ppm): 2179 (s, $\nu_{1/2}$ = 23.5 kHz).

X-ray Crystallography. The intensities for the X-ray diffraction studies were recorded on a STOE IPDS T2 (**3**·CH_2Cl_2) and a Bruker D8 Venture instrument (**4**·CH_2Cl_2) with Mo Kα radiation (λ = 0.71073 Å). The space groups were determined from systematic absences. Structure solutions and refinements were performed with the SHELX program package.[38,39] Absorption corrections were done with SADABS.[40] Hydrogen atoms were calculated for the idealized positions and treated with the 'riding model' option of SHELXL. The representation of molecular structures was done by the program DIAMOND 4.[41] More details about the analyses are contained in the Supporting Information.

Deposition Numbers 2105101 (**3**·CH_2Cl_2) and 2105102 (**4**·CH_2Cl_2) contain the supplementary crystallographic data for this paper. These data are provided free of charge by the joint Cambridge Crystallographic Data Centre and Fachinformationszentrum Karlsruhe Access Structures service www.ccdc.cam.ac.uk/structures.

Acknowledgments

This work was done with the assistance of the Core Facility BioSupraMol supported by the DFG. Open Access funding enabled and organized by Projekt DEAL.

Conflict of Interest

The authors declare no conflict of interest.

Data Availability Statement

The data that support the findings of this study are available in the supplementary material of this article.

Keywords: Technetium · nitrosyl complexes · EPR · tripod ligands

[1] World Nuclear Association. Radioisotopes in Medicine: https://www.world-nuclear.org/information-library/non-power-nuclear-applications/radioisotopes-research/radioisotopes-in-medicine.aspx (updated October 2021).
[2] M. J. Abrams, A. Davison, A. G. Jones, C. E. Costello, H. Pang, *Inorg. Chem.* **1983**, *22*, 2798–2800.
[3] a) B. K. Holman, A. G. Jones, J. Lister-James, A. Davison, M. J. Abrams, J. M. Kirshenbaum, S. S. Tumeh, R. J. English, *J. Nucl. Med.* **1984**, *25*, 1350–1355; b) L. I. Delmon-Moingeon, D. Piwnica-Worms, A. D. van den Abbeele, B. L. Holman, A. Davison, A. G. Jones, *Cancer Res.* **1990**, *50*, 2198–2202.
[4] J. F. Kronauge, A. Davison, A. M. Roseberry, C. E. Costello, S. Maleknia, A. G. Jones, *Inorg. Chem.* **1991**, *30*, 4265–4271.
[5] J. F. Kronauge, A. F. Leon, E. S. Verdera, H. S. Balter, E. T. Leon, F. Mut, M. C. Oliveira, F. A. Garcia, B. L. Holman, A. Davison, A. G. Jones, *J. Nucl. Med.* **1992**, *33*, 1949–1957.
[6] J. F. Kronauge, D. J. Mindiola, *Organometallics* **2016**, *35*, 3432–3435.
[7] R. Alberto, R. Schibli, A. P. Schubiger, *J. Am. Chem. Soc.* **1998**, *120*, 7987–7988.
[8] R. Alberto, R. Schibli, R. Waibel, U. Abram, A. P. Schubiger, *Coord. Chem. Rev.* **1999**, *192*, 901–919.
[9] R. Alberto, *ChemBioChem* **2020**, *21*, 1–8 and references cited therein.
[10] J. Wald, R. Alberto, K. Ortner, L. Candreia, *Angew. Chem. Int. Ed.* **2001**, *40*, 3062–3066; *Angew. Chem.* **2001**, *113*, 3152–3156.
[11] S. Masi, S. Top, L. Boubekeur, G. Jaouen, S. Mundwiler, B. Spingler, R. Alberto, *Eur. J. Inorg. Chem.* **2004**, 2013–2017.
[12] F. Zobi, B. Spingler, R. Alberto, *Eur. J. Inorg. Chem.* **2008**, 4205–4214.

[13] S. Ursillo, D. Can, H. W. P. N'Dongo, P. Schnutz, B. Spingler, R. Alberto, *Organometallics* **2014**, *33*, 6945–6952.
[14] A. Frei, B. Spingler, R. Alberto, *Chem. Eur. J.* **2018**, *24*, 10156–10164.
[15] A. Frei, E. Fischer, B. C. Childs, J. P. Holland, R. Alberto, *Dalton Trans.* **2019**, *48*, 14600–14605.
[16] J. Ackermann, A. Hagenbach, U. Abram, *Chem. Commun.* **2016**, *52*, 10285–10288.
[17] J. Ackermann, A. Abdulkader, C. Scholtysik, M. Roca Jungfer, A. Hagenbach, U. Abram, *Organometallics* **2019**, *38*, 4471–4478.
[18] S. Trofimenko, *Chem. Rev.* **1993**, *93*, 943–980.
[19] C. Pettinari, *Eur. J. Inorg. Chem.* **2016**, 2209–2211.
[20] W. Kläui, *Angew. Chem. Int. Ed. Engl.* **1990**, *29*, 627–637.
[21] W.-H. Leung, Q.-F. Zhang, Y.-X. Yi, *Coord. Chem. Rev.* **2007**, *251*, 2266–2279.
[22] A. C. Grunwald, C. Scholtysik, A. Hagenbach, U. Abram, *Inorg. Chem.* **2020**, *59*, 9396–9405.
[23] A. Abdulkader, A. Hagenbach, U. Abram, *Eur. J. Inorg. Chem.* **2021**, 3812–3818.
[24] J. Ackermann, C. Nijki Noufele, A. Hagenbach, U. Abram, *Z. Anorg. Allg. Chem.* **2019**, *645*, 8–13.
[25] T. Nicholson, E. Chun, A. Mahmood, P. Mueller, A. Davison, A. G. Jones, *Commun. Inorg. Chem.* **2015**, *3*, 31–39 and references cited therein.
[26] R. Kirmse, B. Lorenz, K. Schmidt, *Polyhedron* **1983**, *2*, 935–939.
[27] U. Abram, R. Kirmse, K. Köhler, B. Lorenz, L. Kaden, *Inorg. Chim. Acta* **1987**, *129*, 15–20.
[28] J. Ackermann, A. Hagenbach, U. Abram, *Inorg. Chim. Acta* **2014**, *419*, 59–65.
[29] A. Hagenbach, E. Yegen, U. Abram, *Inorg. Chem.* **2006**, *45*, 7331–7338.
[30] E. Oehlke, R. Alberto, U. Abram, *Inorg. Chem.* **2010**, *49*, 3525–3530.
[31] E. Yegen, A. Hagenbach, U. Abram, *Chem. Commun.* **2005**, 5575–5577.
[32] R. Uson, J. Fornies, M. Tomas, J. M. Casas, F. A. Cotton, L. R. Falvello, *Inorg. Chem.* **1986**, *25*, 4519–4525.
[33] V. G. Albano, M. D. Serio, M. Monari, I. Orabona, A. Panunzi, F. Ruffo, *Inorg. Chem.* **2002**, *41*, 2672–2677.
[34] A. R. Corcos, J. F. Berry, *Dalton Trans.* **2016**, *45*, 2386–2389.
[35] W. S. McNeil, D. D. DuMez, Y. Matano, S. Lovell, J. M. Meyer, *Organometallics* **1999**, *18*, 3715–3727.
[36] M. Carmona, L. Tejedor, R. Rodriguez, V. Passarelli, F. J. Lahoz, P. Garcia-Orduna, D. Carmona, *Chem. Eur. J.* **2017**, *23*, 14532–14546.
[37] S. Stoll, A. Schweiger, *J. Magn. Reson.* **2006**, *178*, 42–55.
[38] G. M. Sheldrick, *Acta Crystallogr.* **2008**, *A64*, 112–122.
[39] G. M. Sheldrick, *Acta Crystallogr.* **2015**, *C71*, 3–8.
[40] G. M. Sheldrick, *SADABS*, University of Göttingen, Germany, **1996**.
[41] *Diamond – Crystal and Molecular Structure Visualization*, Crystal Impact – Dr. H. Putz & Dr. K. Brandenburg GbR, Bonn, Germany.

Manuscript received: October 21, 2021
Revised manuscript received: December 11, 2021
Accepted manuscript online: December 13, 2021

ARTICLE

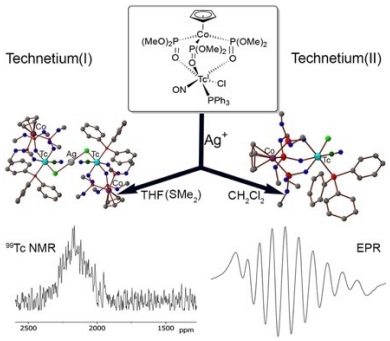

*M. Roca Jungfer, M. J. Ernst, Dr. A. Hagenbach, Prof. Dr. U. Abram**

4.7 Ammonium pertechnetate in mixtures of trifluoromethanesulfonic acid and trifluoromethanesulfonic anhydride

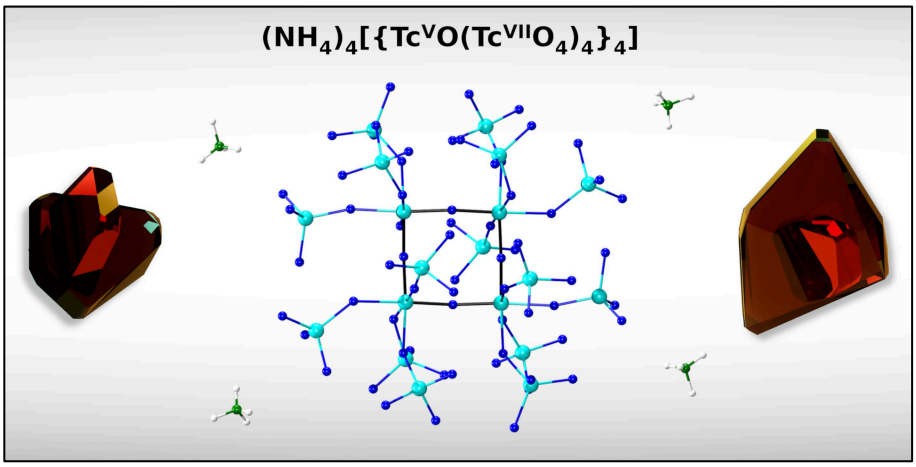

DOI (International Edition): 10.1002/anie.202113777

DOI (German Edition): doi.org/10.1002/ange.20211377

For Supplementary Material see A.7.

Author Contributions:

Markus Zegke, Erik Strub and Mathias S. Wickleder designed the project. Markus Zegke and Erik Strub performed the synthesis and characterization of $(NH_4)[TcO(OTf)_5]$ and $[TcO_3(OTf)]$. Dennis Grödler, Alexander Haseloer, Meike Kreuter, Jörg M. Neudörfl, Axel Klein, Martin Breugst, Thomas Sittel, Christopher M. James, Jörg Rothe and Marcus Altmeier assisted in some of the spectroscopic characterizations. Markus Zegke and Erik Strub wrote the manuscript and corrected the manuscript. Maximilian Roca Jungfer performed the synthesis an characterization of the ammonium polyoxotechnetate salt $(NH_4)_4[\{TcO(TcO_4)_4\}_4]$. Maximilian Roca Jungfer and Ulrich Abram completed and verified the characterization of some of the compounds and corrected the manuscript.

Technetium Hot Paper

How to cite: *Angew. Chem. Int. Ed.* **2022**, *61*, e202113777
International Edition: doi.org/10.1002/anie.202113777
German Edition: doi.org/10.1002/ange.202113777

Ammonium Pertechnetate in Mixtures of Trifluoromethanesulfonic Acid and Trifluoromethanesulfonic Anhydride

Markus Zegke[+], Dennis Grödler, Maximilian Roca Jungfer, Alexander Haseloer, Meike Kreuter, Jörg M. Neudörfl, Thomas Sittel, Christopher M. James, Jörg Rothe, Marcus Altmaier, Axel Klein, Martin Breugst,* Ulrich Abram, Erik Strub[+],* and Mathias S. Wickleder**

Dedicated to Uwe Otto on the occasion of his retirement

Abstract: *Ammonium pertechnetate reacts in mixtures of trifluoromethanesulfonic anhydride and trifluoromethanesulfonic acid under final formation of ammonium pentakis(trifluoromethanesulfonato)oxidotechnetate(V), $(NH_4)_2[TcO(OTf)_5]$. The reaction proceeds only at exact concentrations and under the exclusion of air and moisture via pertechnetyl trifluoromethanesulfonate, $[TcO_3(OTf)]$, and intermediate Tc^{VI} species. ^{99}Tc nuclear magnetic resonance (NMR) has been used to study the Tc^{VII} compound and electron paramagnetic resonance (EPR), ^{99}Tc NMR and X-ray absorption near-edge structure (XANES) experiments indicate the presence of the reduced technetium species. In moist air, $(NH_4)_2[TcO(OTf)_5]$ slowly hydrolyses under formation of the tetrameric oxidotechnetate(V) $(NH_4)_4[\{TcO(TcO_4)_4\}_4]\cdot 10\,H_2O$. Single-crystal X-ray crystallography was used to determine the solid-state structures. Additionally, UV/Vis absorption and IR spectra as well as quantum chemical calculations confirm the identity of the species.*

Introduction

Even though metal trifluoromethanesulfonates (triflates, $^-$OTf) see wide applications as catalysts[1,2] or leaving groups in both organic[3–6] and inorganic chemistry,[7–9] their solid-state chemistry has not seen much attention. Homoleptic triflates are crystallographically poorly investigated, even though these weakly coordinating anions (WCAs)[10,11] are, amongst others, widely used in organic reactions,[12–15] and have been proposed for novel applications such as the recycling of thoria in thorium-based nuclear fuels.[16] There may be a variety of reasons for this, as triflates generally crystallise rather poorly, and they are readily displaced by stronger donors such as water. In addition, the chemistry in anhydrous superacids (HOTf: $pK_{a(H_2O)} = -14$) often demands skilled techniques such as working in flame-sealed ampoules and the use of inert gas systems with corrosion-resistant equipment. Less than 24 of homoleptic p-, f- and d-block metal triflates have been reported with structural data so far (Conquest search v. 5.42, Nov. 2020). High triflate coordination has been observed with actinides, such as in $(H_5O_2)[Th(H_2O)_6(OTf)_3][Th(H_2O)_3(OTf)_6]$[17] as well as with lanthanides such as in $(NO)_5[Eu(OTf)_8]^{5-}$.[18] However, high oxidation state triflates are rare.[19,20] Of these, antimony complexes show the highest valency of +5 at the metal centre in the complexes $[SbCl_4(OTf)]_2$[21] and $[Sb(C_6F_5)_4(OTf)]$.[22] Particularly interesting in this regard is the chemistry of the group 7 metals Mn, Tc and Re, as their position in the periodic table makes them prone to unique chemistry. However, a systematic

[*] Dr. M. Zegke,[+] D. Grödler, A. Haseloer, C. M. James, Prof. Dr. A. Klein, Prof. Dr. M. S. Wickleder
University of Cologne, Department of Chemistry
Institute for Inorganic Chemistry
Greinstrasse 4–6, 50939 Cologne (Germany)
E-mail: m.zegke@uni-koeln.de
mathias.wickleder@uni-koeln.de

M. Kreuter, Priv.-Doz. Dr. E. Strub[+]
University of Cologne, Department of Chemistry
Division of Nuclear Chemistry
Zülpicher Strasse 45, 50674 Cologne (Germany)
E-mail: erik.strub@uni-koeln.de

Dr. J. M. Neudörfl, Priv.-Doz. Dr. M. Breugst
University of Cologne, Department of Chemistry
Institute for Organic Chemistry
Greinstrasse 4–6, 50939 Cologne (Germany)
E-mail: mbreugst@uni-koeln.de

T. Sittel, Dr. J. Rothe, Dr. M. Altmaier
Karlsruhe Institute of Technology
Institute for Nuclear Waste Disposal
Hermann-von-Helmholtz-Platz 1, 76344 Eggenstein-Leopoldshafen (Germany)

M. Roca Jungfer, Prof. Dr. U. Abram
Freie Universität Berlin
Institute for Chemistry and Biochemistry
Inorganic Chemistry
Fabeckstrasse 34–36, 14195 Berlin (Germany)

[+] These authors contributed equally to this work.

Supporting information and the ORCID identification number(s) for the author(s) of this article can be found under: https://doi.org/10.1002/anie.202113777.

approach is hampered by the fact that Tc is a radioelement (^{99}Tc, β^- emitter, $t_{1/2} = 210000$ years). Although its radiological properties do not require much shielding, a radionuclide laboratory is needed for open handling of milligram amounts. The unique differences between the group 7 elements can be seen in the properties of their oxides in oxidation state +7. Mn_2O_7 is a shock-sensitive, violet oil that solidifies at 5.9 °C with a bent structure of corner-sharing MnO_4 tetrahedra.[23] In contrast, Tc_2O_7 is a volatile compound crystallising in thin, pale yellow, hygroscopic plates with a unique linear arrangement[24] and Re_2O_7 is made up of regular corner-sharing ReO_4 tetrahedra which form polymeric double layers.[25] Their corresponding acids also behave very differently from each other, as $HMnO_4$ is not existent, and the only material represented in the literature is known as "*feste Permangansäure*" ("solid permanganic acid") with the composition $Mn_2O_7{\cdot}2H_2O$.[26] In contrast, concentrated $HTcO_4$ is dark-yellow and forms a dark-red solid upon further evaporation.[27] A hypothetic "$HReO_4$" does not exist and must be described as a hydrated rhenium oxide $Re_2O_7(OH_2)_2$.[28] In addition, the chemistry of oxocations ("metalyl" ions) of oxidation states +7 or higher are limited to a few compounds, such as rare group 8 complexes of the perosmyl(VIII) trioxo dication OsO_3^{2+} or the perosmyl(VIII) dioxo tetracation OsO_2^{4+}.[29,30] The osmyl(VII) pentacation $Os^{VII}O^{5+}$ is a rare example of a cation with an overall charge of +5.[31] Oxo cations of ruthenium have only been known in oxidation state +6 in $RuOF_4$.[32] In contrast, rhenium forms in oxidation state +7 stable compounds with the ReO^{5+},[31,33] ReO_2^{3+}[33,34] and ReO_3^+ cores. The latter has been most prominently known from organometallic complexes such as the classic methyl trioxorhenium.[35] Its respective halide salts (F, Cl, Br), are all highly reactive and only moderately stable at ambient conditions. $[ReO_3]^+[I]^-$ cannot be isolated due to the oxidation potential of Re^{VII}.[36,37] Of the lighter homologues, MnO_3^+ is known in the solid state, however, there is no indication that a free and unsolvated cation of this type can be generated, while the radioactive pertechnetyl cation TcO_3^+ has been made in the form of the fluoride[38] and fluorosulfate.[39] Inspired by the work of Seppelt, who notes that *"the best candidate for a largely unsolvated MO_3^+ cation is TcO_3^+"*, we have investigated the chemistry of NH_4TcO_4 in triflic acid (HOTf) and triflic anhydride (Tf_2O). TcO_3^+ has previously been stabilised in the 1,4,7-triazacyclononane (tacn) complex $[TcO_3(tacn)]^+Br^-$.[40] TcO_4^- also reacts in the presence of benzoyl chloride and stabilising coordinating ligands such as 1,10-phenanthroline or 2,2′-bipyridine to $[TcO_3Cl(phen)]$ and $[TcO_3Cl(bipy)]$, respectively.[41] The volatile pertechnetyl fluorosulfate $[TcO_3]^+[SO_3F]^-$ has been isolated by treating $KTcO_4$ with fluorosulfuric acid that contained SO_3, followed by sublimation at room temperature and cooling to −78 °C.[40] Pertechnetyl fluoride $[TcO_3]^+[F]^-$ can be isolated from a reaction of TcO_2 with F_2 or after treatment of $KTcO_4$ with BiF_5 and anhydrous HF followed by sublimation at −78 °C.[39,42]

Results and Discussion

In our reinvestigation of the Tc chemistry in superacids, following up on the work by Poineau et al.[43] and Denden et al.,[44,45] we have been able to isolate pertechnetyl triflate $[TcO_3(OTf)]$ for the first time and have observed that TcO_4^- in such systems undergoes a spontaneous reduction to ammonium pentakis(trifluoromethanesulfonato)oxotechnetate(V) without the presence of an obvious reducing agent (see SI for proposed mechanism). We were interested in a more straightforward way of targeting a pertechnetyl cation with a weakly coordinating anion, and have hypothesised that the formation of the trioxotechnetium monocation may indeed follow a protonation–dehydration process as proposed by Poineau and co-workers.[43] Using a suitable strong acid such as triflic acid with its corresponding anhydride thus results in the formation of the TcO_3^+ core (Scheme 1).[43]

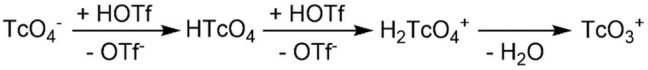

Scheme 1. Formation of TcO_3^+ in triflic acid.

In our hands, the treatment of NH_4TcO_4 (2 mg, 11 μmol, 0.693 MBq; dry, as an evaporated residue from an aqueous stock solution) with 581 μL Tf_2O and 19 μL HOTf under Ar atmosphere and subsequent heating to 60 °C for 30 min yields a colourless solution. Upon cooling to room temperature this shows a tinge of purple and microcrystalline yellow $[TcO_3(OTf)]$ in nearly quantitative yield according to liquid scintillation counting (LSC, see SI).

A ^{99}Tc NMR spectrum of the anhydrous reaction mixture (without any added d-solvent) shows a very narrow signal at $\delta = 209$ ppm ($\nu_{1/2} = 350$ Hz), which can be assigned to $[TcO_3(OTf)]$. It shall be noted that the same signal is obtained from a reaction of NBu_4TcO_4 and neat fuming triflic acid under strictly dry conditions and also appears as a side-product when solid ammonium or alkaline pertechnetates react with HOTf without the addition of Tf_2O. When such reaction mixtures are exposed to moist air, quickly another, much broader signal can be detected at $\delta = 273$ ppm ($\nu_{1/2} =$ approx. 8300 Hz). This can be assigned to the formation of a compound with lower local symmetry and/or fast ligand exchange reactions in solution.[46] A similar spectrum is observed for a solution of pertechnetate in sulfuric acid. The spectra and more details are given in the Supporting Information. With regard to previous XAFS and spectroscopic studies,[44,45,47,48] the species with the broad ^{99}Tc NMR signals can be assigned to pseudo-octahedral $[TcO_3(OH)(OH_2)_2]$ or $[TcO_3(L)(OH_2)_2]$ species ($L = OTf^-$ or HSO_4^-).

If the amount of acid, the time or the temperature is increased, the formation of the purple colour becomes more and more intense at room temperature, and the yield of pertechnetyl triflate is decreased to as low as 44 % (see SI for synthetic details, UV/Vis absorption spectra and yields). As the reaction proceeds, small amounts of gas can be seen evolving. As no additional reductant was present, we propose

that in the redox reaction, molecular O_2 might form in the presence of HOTf (see video in supplement). An attempt to analyse the gas evolution in the head space of the reaction using mass spectrometry was rendered impossible due to the highly corrosive nature of the HOTf.

Interestingly, as long as purple material is present in the solution, the mixture shows thermochromic properties. Cooling to −15 °C intensifies the purple colour, while heating to 100 °C results in a colourless solution within less than a minute (see videos). We have not been able to fully identify the nature of the purple solution. But previous research has also noted the observation of red and/or purple compounds when experiments on pertechnetic acid have been performed. They have been attributed to reduced species, for example, Tc^{VI} compounds.[47–50] The purple solutions obtained during our experiments are indeed EPR-active, and indicate the presence of transient Tc^{VI} species, but with relatively low concentrations (see SI). The spectral parameters are close to those of nitridotechnetium(VI) complexes with OTf^- ligands.[51,52] The EPR signal disappears with the purple colour. In parallel, the purple solution shows a strong ^{99}Tc NMR resonance at $\delta = +209$ ppm, which correlates well with other hexacoordinate compounds containing TcO_3^+.[40,53,54] In addition, in some of the recorded spectra a small resonance at $\delta = -817$ ppm is visible, which could not yet be assigned unambiguously.

To fully address the varying degrees at which the pertechnetyl cation forms under synthetic conditions, we have undertaken a range of synthetic studies with varying ratios of acid to anhydride, and at different temperatures and concentrations. We can state that the exact ratio of NH_4TcO_4:HOTf:Tf_2O is paramount to the successful synthesis. While NH_4TcO_4 does not react with Tf_2O alone, varying amounts of HOTf have a strong effect on the stability of the colour of the solution (see SI for details). However, we have been able to isolate bright yellow crystals of $[TcO_3(OTf)]$ from a purple solution after careful crystallisation at −15 °C. The material is air-sensitive, but can be handled under Fomblin-Y® oil for several minutes without decomposition. Figure 1 shows the yellow crystals under Fomblin-Y® oil with residual purple mother liquor floating on top (left), and isolated crystals as seen through a microscope (right).

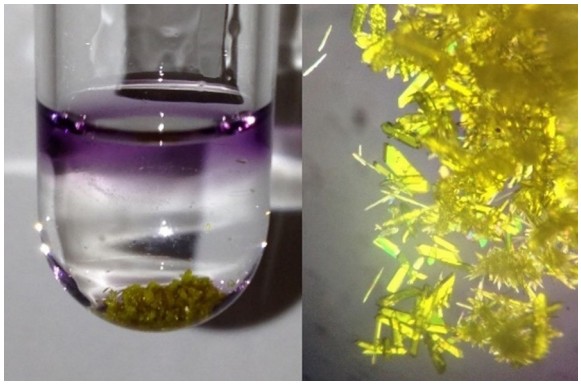

Figure 1. Yellow crystals of $[TcO_3(OTf)]$ under Fomblin-Y® oil with residual purple mother liquor floating on top (left), and isolated crystals as seen through a microscope (right) (field of view ca. 5 mm).

The material was isolated easily by removing the supernatant via syringe or pipette. It was possible to dry the yellow product under vacuum and to store it for several months under Ar at room temperature. The solid-state structure (CCDC 2114965) of the material can be seen in Figure 2.

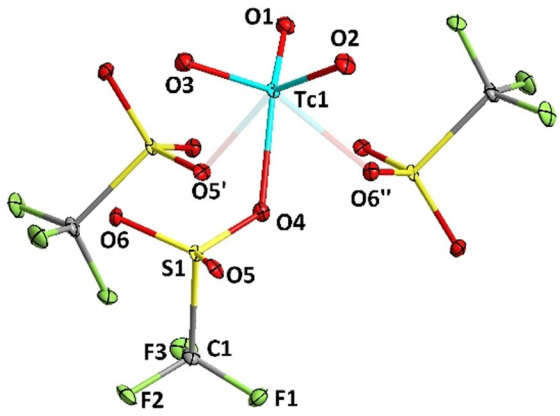

Figure 2. ORTEP representation of the coordination of $[TcO_3(OTf)]$. Ellipsoids are drawn at the 50% probability level. Selected bond lengths [Å] and angles [°]: Tc1–O1 1.690(3), Tc1–O2 1.683(2), Tc1–O3 1.682(3), Tc1–O4 2.221(3), Tc1–O5′ 2.272(2) Tc1–O6″ 2.275(2); O1-Tc1-O4 155.4(1), O1-Tc1-O2 105.5(1), O1-Tc1-O3 104.5(1), O1-Tc1-O5′ 86.7(1), O1-Tc1-O6″ 88.0(1), O4-Tc1-O2 89.9(1), O4-Tc1-O3 89.4(1), O4-Tc1-O5 73.20(9), O5′-Tc1-O6″ 73.78(8).

The Tc atom is coordinated pseudo-octahedrally, and the Tc=O double bond lengths (Tc1−O1 1.690(3) Å, Tc1−O2 1.683(2) Å, Tc1−O3 1.682(3) Å) are consistent with Tc^{VII} in other TcO_3^+ complexes. The distance to one triflate oxygen atom (Tc1−O4 2.221(3) Å) is slightly shorter than to the two other triflate oxygen atoms (Tc1−O5′ 2.272(2) Å and Tc1−O6″ 2.275(2) Å) coming from the neighbouring molecules.

The coordination in the solid state is represented in Figure 3. Separated layers of bridged pertechnetyl triflate units run along the crystallographic *b*- and *c*-axes. One SO_3 moiety of the triflate anion, thus, binds to one technetium atom and coordinates two other adjacent TcO_3 moieties to form a two-dimensional network.

We have attempted to obtain PXRD of this material, however, finely grained crystals of the sample are unstable on the PXRD film and decompose within five minutes. In contrast, suspending $[TcO_3(OTf)]$ in Tf_2O gives a pale yellow suspension. After letting the material settle for five minutes, a UV/Vis absorption spectrum was measured with a distinct

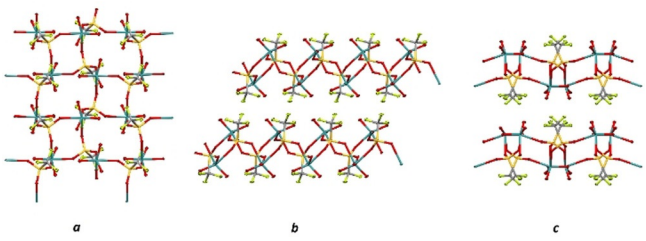

Figure 3. Crystal packing of pertechnetyl triflate $[TcO_3(OTf)]$ in the direction of the crystallographic *a*-axis (a), *b*-axis (b) and *c*-axis (c).

absorption at 350 nm. Dissolving the material in water gives a pale yellow solution with a similar absorption spectrum. This corresponds well with quantum mechanical calculations that predict a λ_{max} at 335 and 370 nm, respectively. UV/Vis absorption spectra were calculated at the ωB2GP-PLYP/def2-TZVP/SMD//PBE-D3BJ/def2-TZVP/SMD level of theories (see SI for details).[54–60]

From the purple solution, green needle-like crystals were grown at −15 °C over the course of two weeks, which were suitable for X-ray diffraction (Figure 4).

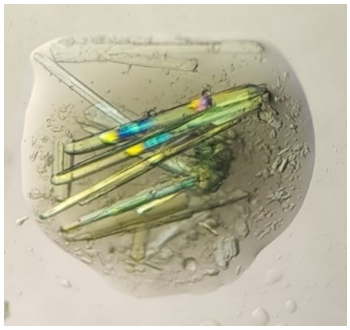

Figure 4. Green crystals of $(NH_4)_2[TcO(OTf)_5]\cdot HOTf$ (field of view ca. 1 mm).

The solid state structure (CCDC 2114967) of the hitherto unknown ammonium pentakis(trifluoromethanesulfonato)-oxidotechnetate(V), $(NH_4)_2[TcO(OTf)_5]$ can be seen in Figure 5. The structure consists of pseudo-octahedrally coordinated Tc atoms, with one apex occupied by an oxido ligand with a Tc1=O1 bond length of 1.612(2) Å, while the other five

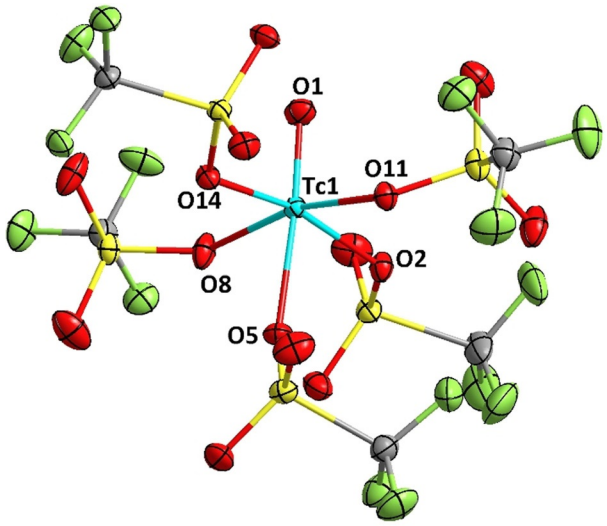

Figure 5. ORTEP representation of the $[TcO(OTf)_5]^{2-}$ anion. One molecule of coordinated HOTf and the two NH_4^+ cations are omitted for clarity. Ellipsoids are drawn at the 50% probability level. Selected bond lengths [Å] and angles [°]: Tc1–O1 1.612(2), Tc1–O2 2.010(2), Tc1–O5 2.130(2), Tc1–O8 2.025(2), Tc1–O11 2.013(2), Tc1–O14 2.046(2); O1-Tc1-O5 175.66(8), O1-Tc1-O2 99.85(8), O1-Tc1-O8 96.10(8), O1-Tc1-O11 98.40(8), O1-Tc1-O14 94.98(8), O5-Tc1-O2 82.70(7), O5-Tc1-O8 80.48(7), O5-Tc1-O11 85.11(7), O5-Tc1-O14 82.65(6).

coordination sites are occupied by κ^1-*O* coordinating triflate anions. The triflate *trans* to the Tc=O moiety has, due to the *trans*-influence,[61] a significantly longer bond length of 2.130-(2) Å compared to the triflate groups in the equatorial positions, which range between 2.010(2)–2.046(2) Å. The O=Tc-OTf(*trans*) axis is nearly linear (175.66(8)°), while the equatorial ligands are slightly bent downwards in an umbrella-type fashion (94.98(8)–99.85(8)°), which is the typical motif for Tc^VO complexes. The network is held together by hydrogen bonds, most prominently those of the NH_4^+ cations, which coordinate two adjacent $[TcO(OTf)_5]^{2-}$ moieties (Figure 6). Two protons of the NH_4^+ ion are connected to one equatorial OTf^- ligand and the *trans* triflate group of one $[TcO(OTf)_5]^{2-}$ moiety and at the same time to an equatorial triflate group of a neighbouring $[TcO(OTf)_5]^{2-}$ complex.

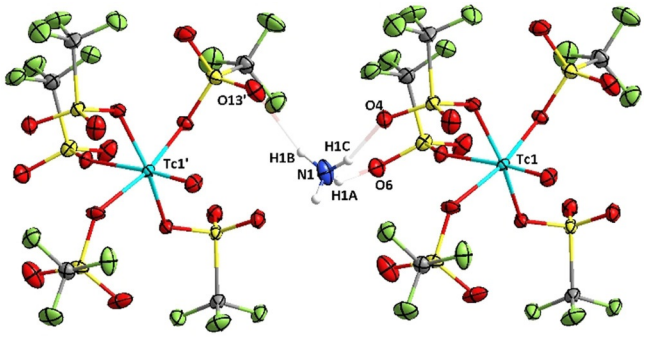

Figure 6. Hydrogen interactions of the NH_4^+ linking two adjacent $[TcO(OTf)_5]^{2-}$ moieties.

A XANES spectrum of $(NH_4)_2[TcO(OTf)_5]$ is in accord with the Tc +5 oxidation state. We were also able to record a ^{99}Tc NMR spectrum of the technetium(V) complex. Expectedly, it is characterised by an extremely broad line at $\delta =$ 6600 ppm ($\nu_{1/2} \approx 18$ kHz). The chemical shift and the line width are in accord with the ^{99}Tc NMR spectrum of (NBu_4)-$[TcOCl_4]$, one of the few Tc^V complexes which have been studied by ^{99}Tc NMR before.[62] The spectra of both compounds are shown in the SI.

$(NH_4)_2[TcO(OTf)_5]$ is sensitive against moisture and exposure to air results in a slow decomposition. Hydrolysis and disproportionation finally give TcO_2 and TcO_4^-. When the hydrolysis is performed under controlled conditions, green-red dichroic crystals of $(NH_4)_4[\{TcO$-$(OTcO_3)_4\}_4]\cdot 10H_2O$ can be isolated in approximately 30% yield. They have a melting point of about 30 °C, but can be stored at lower temperature and dry conditions without decomposition. The compound consists of a central $\{Tc_4O_4\}^{12+}$ unit with four pertechnetato ligands coordinated to each of the central technetium atoms. Figure 7 shows the structure of the resulting $(NH_4)_4[\{TcO(OTcO_3)_4\}_4]$ salt (CCDC 2114966). A similar compound with the same anionic unit and four $(H_7O_3)^+$ cations has been reported very recently as the product of a not yet fully understood auto reduction of $HTcO_4$.[63]

$(NH_4)_4[\{TcO(OTcO_3)_4\}_4]$ partially dissolves in HOTf. The orange-red solution displays very broad ^{99}Tc NMR signals

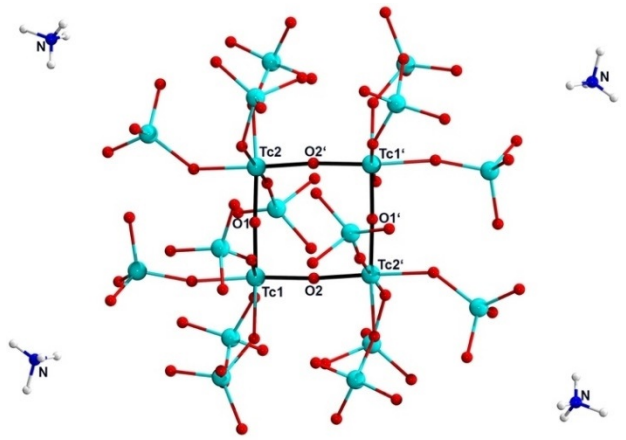

Figure 7. ORTEP representation of $(NH_4)_4[\{TcO(OTcO_3)_4\}_4]$. A ball and stick model has been chosen for clarity, an ellipsoid plot is depicted in the SI. Selected bond lengths [Å] and angles [°]: Tc1–O1 1.804(7), Tc1–O2 1.822(8), Tc2–O1 1.822(7), Tc2–O2′ 1.805(8); Tc1-O1-Tc2 177.8(5) Tc1-O2-Tc2′ 172.6(5).

($\nu_{1/2}$ approximately 50 kHz) in the region between those of $[TcOCl_4]^-$ ($\delta = 4950$ ppm) and $[TcO(OTf)_5]^{2-}$ ($\delta = 6600$ ppm) together with a broadened pertechnetate signal ($\nu_{1/2} =$ 400 Hz), see SI.

Denden et al. have investigated the reduction of technetium(VII) in triflic acid under α irradiation at a dose rate of 66 ± 7 kGy h^{-1}.[45] Under these conditions, they observe higher reaction kinetics between 4 and 8 M HOTf, while forming the same Tc^V oxopolymeric species as without irradiation.[44] At higher concentrations (> 11 M) they observe the formation of a yellow solution, which is attributed to $[Tc^{VII}O_3(H_2O)_2(OH)]$.[43] They further describe the formation of a green solution upon irradiation, with UV/Vis absorptions at 400 and 750 nm, assigning this to a reduced species comparable to $[Tc^VO(HSO_4)_2(OH)(H_2O)_2]$. The authors hypothesise that the reduction is due to thermal decomposition and hydrolysis processes, caused by the exothermic hydration reaction of triflic acid in water. Using XAFS and DFT, they further identified $[Tc^VO(OTf)_2(OH)(H_2O)]$ to be the most probable compound to form, but no crystal structure was determined at that point. We consider that behaviour very similar to our observations. It is remarkable that the amount of energy deposited due to the α irradiation is comparable to the energy provided by heating the sample by 90 K as applied during our experiment (see SI for details).

Interestingly, an attempt to isolate the $[TcO(OTf)_5]^{2-}$ moiety from the Tc^V precursor $(NBu_4)[TcOCl_4]$[64] by simply dissolving it in triflic acid did not yield the desired product but resulted in a blue solution that quickly decomposed.

Conclusion

We have identified a straightforward reaction pathway to synthesise pertechnetyl triflate in near-quantitative yield from NH_4TcO_4 without needing to use sublimation techniques or any unusual or hazardous precursors. The material crystallises as yellow crystals or microcrystals from triflic anhydride upon addition of triflic acid at 60 °C and can be readily isolated by syringing off the mother liquor. UV/Vis absorption and LSC spectra show that the exact concentration, ratio and temperature are imperative for the successful synthesis. Pertechnetyl triflate may thus become a versatile starting material for future investigations on high-valency pertechnetyl compounds. From these solutions, pentakis(triflato)-oxidotechnetate(V) salts form spontaneously without addition of a reducing agent, indicating that a spontaneous auto reduction of pertechnetate is possible in nuclear waste materials.

Acknowledgements

MZ sincerely thanks Lars Hemmersbach and Prof. Dr. Hans-Günther Schmalz for attempting to measure the O_2 evolution using their MS equipment and essentially ruining it with the highly corrosive triflic acid. MB thanks the Fonds der Chemischen Industrie and the Regional Computing Centre of the University of Cologne (RRZK) for providing computing time on the DFG-funded (Funding number: INST 216/512/1FUGG) High Performance Computing (HPC) system CHEOPS as well as for their support. The authors acknowledge the KIT synchrotron light source and the Institute for Beam Physics and Technology (KIT-IBPT) for operation of the Karlsruhe Research Accelerator (KARA). AH and AK thank Prof. Dr. Bernd Neumaier, Department of Chemistry, Division of Nuclear Chemistry, Cologne University Clinics, Institute of Radiochemistry, and Forschungszentrum Jülich for financial support. Open Access funding enabled and organized by Projekt DEAL.

Conflict of Interest

The authors declare no conflict of interest.

Keywords: anhydride · pertechnetate · reduction · super acid · trifluoromethanesulfonic acid

[1] K. Ishihara, M. Kubota, H. Kurihara, H. Yamamoto, *J. Am. Chem. Soc.* **1995**, *117*, 4413 – 4414.
[2] L. Coulombel, M. Rajzmann, J.-M. Pons, S. Olivero, E. Duñach, *Chem. Eur. J.* **2006**, *12*, 6356 – 6365.
[3] P. J. Stang, M. Hanack, L. R. Subramanian, *Synthesis* **1982**, 85 – 126.
[4] D. L. Comins, A. Dehghani, *Tetrahedron Lett.* **1992**, *33*, 6299 – 6302.
[5] T. Gramstad, R. N. Haszeldine, *J. Chem. Soc.* **1957**, 4069 – 4079.
[6] B. Dhakal, L. Bohé, D. Crich, *J. Org. Chem.* **2017**, *82*, 9263 – 9269.
[7] D. Veghini, H. Berke, *Inorg. Chem.* **1996**, *35*, 4770 – 4778.
[8] S. Schlecht, J. Magull, D. Fenske, K. Dehnicke, *Angew. Chem. Int. Ed. Engl.* **1997**, *36*, 1994 – 1995; *Angew. Chem.* **1997**, *109*, 2087 – 2089.
[9] J. Bonnamour, C. Bolm, *Org. Lett.* **2011**, *13*, 2012 – 2014.
[10] I. Krossing, *Chem. Eur. J.* **2001**, *7*, 490 – 502.
[11] A. Martens, P. Weis, M. C. Krummer, M. Kreuzer, A. Meierhöfer, S. C. Meier, J. Bohnenberger, H. Scherer, I. Riddlestone, I. Krossing, *Chem. Sci.* **2018**, *9*, 7058 – 7068.

[12] S. Kobayashi, *Eur. J. Org. Chem.* **1999**, 15 – 27.
[13] S. Kobayashi, M. Sugiura, H. Kitagawa, W. W.-L. Lam, *Chem. Rev.* **2002**, *102*, 2227 – 2302.
[14] R. D. Howells, J. D. Mc Cown, *Chem. Rev.* **1977**, *77*, 69 – 92.
[15] J. Keskiväli, A. Parviainen, K. Lagerblom, T. Repo, *RSC Adv.* **2018**, *8*, 15111 – 15118.
[16] S. Cagno, L. Gijsemans, V. Tyrpekl, T. Cardinaels, M. Verwerft, K. Binnemans, *J. Sustain. Metall.* **2017**, *3*, 659 – 667.
[17] N. Torapava, I. Persson, L. Eriksson, D. Lundberg, *Inorg. Chem.* **2009**, *48*, 11712 – 11723.
[18] J. Bruns, S. Krüger, M. Adlung, C. Wickleder, O. Niehaus, R. Pöttgen, T. Klüner, J. Kräuter, M. S. Wickleder, *Chem. Eur. J.* **2015**, *21*, 12389 – 12395.
[19] K. Neuschulz, M. Penning, L. Groß, T. Klüner, M. S. Wickleder, *Dalton Trans.* **2012**, *41*, 4685 – 4691.
[20] C. Logemann, T. Klüner, M. S. Wickleder, *Z. Anorg. Allg. Chem.* **2013**, *639*, 485 – 492.
[21] A. Burchardt, K.-W. Klinkhammer, G. Lang, M. Lauster, A. Rihm, A. Schmidt, *Main Group Met. Chem.* **1998**, *21*, 543 – 552.
[22] B. Pan, F. P. Gabbaï, *J. Am. Chem. Soc.* **2014**, *136*, 9564 – 9567.
[23] A. Simon, R. Dronskowski, B. Krebs, B. Hettich, *Angew. Chem. Int. Ed. Engl.* **1987**, *26*, 139 – 140; *Angew. Chem.* **1987**, *99*, 160 – 161.
[24] B. Krebs, *Angew. Chem. Int. Ed. Engl.* **1969**, *8*, 381 – 382; *Angew. Chem.* **1969**, *81*, 395 – 395.
[25] B. Krebs, A. Mueller, H. H. Beyer, *Inorg. Chem.* **1969**, *8*, 436 – 443.
[26] B. Krebs, K.-D. Hasse, *Z. Naturforsch. B* **1973**, *28*, 218 – 219.
[27] C. Soderquist, J. Weaver, H. Cho, B. McNamara, S. Sinkov, J. McCloy, *Inorg. Chem.* **2019**, *58*, 14015 – 14023.
[28] H. Beyer, O. Glemser, B. Krebs, G. Wagner, *Z. Anorg. Allg. Chem.* **1970**, *376*, 87 – 100.
[29] R. Bougon, B. Buu, K. Seppelt, *Chem. Ber.* **1993**, *126*, 1331 – 1336.
[30] M. A. Hepworth, P. L. Robinson, *J. Inorg. Nucl. Chem.* **1957**, *4*, 24 – 29.
[31] J. H. Holloway, H. Selig, H. H. Claassen, *J. Chem. Phys.* **1971**, *54*, 4305 – 4311.
[32] H. Shorafa, K. Seppelt, *Z. Anorg. Allg. Chem.* **2007**, *633*, 543 – 547.
[33] E. E. Aynsley, R. D. Peacock, P. L. Robinson, *J. Chem. Soc.* **1950**, 1622 – 1624.
[34] R. D. Peacock, *J. Chem. Soc.* **1955**, 602 – 603.
[35] W. A. Herrmann, P. Kiprof, K. Rypdal, J. Tremmel, R. Blom, R. Alberto, J. Behm, R. W. Albach, H. Bock, *J. Am. Chem. Soc.* **1991**, *113*, 6527 – 6537.
[36] C. C. Romão, F. E. Kühn, W. A. Herrmann, *Chem. Rev.* **1997**, *97*, 3197 – 3246.
[37] A. Engelbrecht, A. V. Grosse, *J. Am. Chem. Soc.* **1954**, *76*, 2042 – 2045.
[38] J. Supeł, U. Abram, A. Hagenbach, K. Seppelt, *Inorg. Chem.* **2007**, *46*, 5591 – 5595.
[39] J. Supeł, A. Hagenbach, U. Abram, K. Seppelt, *Z. Anorg. Allg. Chem.* **2008**, *634*, 646 – 648.
[40] H. Braband, U. Abram, *Inorg. Chem.* **2006**, *45*, 6589 – 6591.
[41] Y. Tooyama, H. Braband, B. Spingler, U. Abram, R. Alberto, *Inorg. Chem.* **2008**, *47*, 257 – 264.
[42] H. Selig, J. G. Malm, *J. Inorg. Nucl. Chem.* **1963**, *25*, 349 – 351.
[43] F. Poineau, P. F. Weck, K. German, A. Maruk, G. Kirakosyan, W. Lukens, D. B. Rego, A. P. Sattelberger, K. R. Czerwinski, *Dalton Trans.* **2010**, *39*, 8616 – 8619.
[44] I. Denden, R. Essehli, M. Fattahi, *J. Radioanal. Nucl. Chem.* **2013**, *296*, 149 – 155.
[45] I. Denden, J. Roques, F. Poineau, P. L. Solari, M. L. Schlegel, G. Blain, M. Fattahi, *Radiochim. Acta* **2017**, *105*, 135 – 140.
[46] A. D. Bain, G. J. Duns, *Can. J. Chem.* **1996**, *74*, 819 – 824.
[47] G. E. Boyd, J. W. Cobble, C. M. Nelson, W. T. Smith, *J. Am. Chem. Soc.* **1952**, *74*, 556 – 557.
[48] C. L. Rulfs, R. A. Pacer, R. F. Hirsch, *J. Inorg. Nucl. Chem.* **1967**, *29*, 681 – 691.
[49] B. C. Childs, K. V. Lawler, H. Braband, D. S. Mast, L. Bigler, U. Stalder, D. R. Peterson, A. Jansen, P. M. Forster, K. R. Czerwinski, R. Alberto, A. P. Sattelberger, F. Poineau, *Eur. J. Inorg. Chem.* **2018**, 1137 – 1144.
[50] K. V. Lawler, B. C. Childs, K. R. Czerwinski, A. P. Sattelberger, F. Poineau, P. M. Forster, *Chem. Commun.* **2018**, *54*, 1261 – 1264.
[51] J. Baldas in *Technetium and Rhenium Their Chemistry and Its Applications* (Eds.: K. Yoshihara, T. Omori), Springer, Berlin, **1996**, pp. 37 – 76.
[52] U. Abram, R. Kirmse, *Radiochim. Acta* **1993**, *63*, 139 – 144.
[53] K. J. Franklin, C. J. L. Lock, B. G. Sayer, G. J. Schrobilgen, *J. Am. Chem. Soc.* **1982**, *104*, 5303 – 5306.
[54] J. A. Thomas, A. Davison, *Inorg. Chem.* **1992**, *31*, 1976 – 1978.
[55] J. P. Perdew, K. Burke, M. Ernzerhof, *Phys. Rev. Lett.* **1997**, *78*, 1396.
[56] J. P. Perdew, K. Burke, M. Ernzerhof, *Phys. Rev. Lett.* **1996**, *77*, 3865 – 3868.
[57] F. Weigend, R. Ahlrichs, *Phys. Chem. Chem. Phys.* **2005**, *7*, 3297 – 3305.
[58] S. Grimme, S. Ehrlich, L. Goerigk, *J. Comput. Chem.* **2011**, *32*, 1456 – 1465.
[59] A. V. Marenich, C. J. Cramer, D. G. Truhlar, *J. Phys. Chem. B* **2009**, *113*, 6378 – 6396.
[60] L. Goerigk, M. Casanova-Paéz, *Aust. J. Chem.* **2021**, *74*, 3 – 15.
[61] B. J. Coe, S. J. Glenwright, *Coord. Chem. Rev.* **2000**, *203*, 5 – 80.
[62] L. A. O'Connell, R. M. Pearlstein, A. Davison, J. R. Thornback, J. F. Kronauge, A. G. Jones, *Inorg. Chim. Acta* **1989**, *161*, 39 – 43.
[63] K. E. German, A. M. Fedoseev, M. S. Grigoriev, G. A. Kirakosyan, T. Dumas, C. Den Auwer, P. Moisy, K. V. Lawler, P. M. Forster, F. Poineau, *Chem. Eur. J.* **2021**, *27*, 13624 – 13631.
[64] A. Davison, H. S. Trop, B. V. Depamphilis, A. G. Jones, R. W. Thomas, S. S. Jurisson, *Inorganic Syntheses*, Wiley, Hoboken, **1982**, pp. 160 – 162.

Manuscript received: October 11, 2021
Accepted manuscript online: November 9, 2021
Version of record online: December 3, 2021

4.8 Rhenium(V) Complexes with Selenolato- and Tellurolato-substituted Schiff Bases – Released PPh_3 as a Facile Reductant

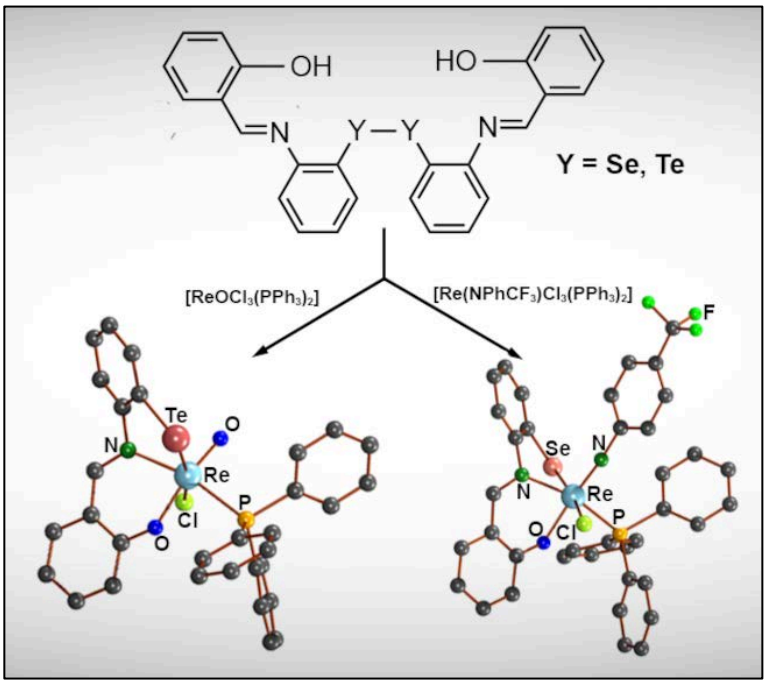

Reproduced with permission from Roca Jungfer, M.; Hagenbach, A.; Schulz Lang, E.; Abram U. *Eur. J. Inorg. Chem.* **2019**, 4974–4984.

DOI: 10.1002/ejic.201901092

For Supplementary Material see A.8.

Author Contributions:

Maximilian Roca Jungfer, Ulrich Abram and Ernesto Schulz Lang designed the project. Maximilian Roca Jungfer performed the synthesis and characterization of the compounds, performed DFT calculations and wrote a draft of the manuscript. Ernesto Schulz Lang provided guidance and the laboratory space to perform some of the experiments in Brazil. Maximilian Roca Jungfer calculated the X-ray structures under guidance of Adelheid Hagenbach. Ulrich Abram supervised the project, provided scientific guidance and suggestions, and corrected the manuscript.

ChemPubSoc Europe

DOI: 10.1002/ejic.201901092

EurJIC European Journal of Inorganic Chemistry

Full Paper

Rhenium Complexes

Rhenium(V) Complexes with Selenolato- and Tellurolato-Substituted Schiff Bases – Released PPh_3 as a Facile Reductant

Maximilian Roca Jungfer,[a] Adelheid Hagenbach,[a] Ernesto Schulz Lang,[b] and Ulrich Abram*[a]

Abstract: The salicylidene Schiff bases of bis(2-aminophenyl)-diselenide and -ditelluride react with $[ReOCl_3(PPh_3)_2]$ or the arylimidorhenium(V) compounds $[Re(NPhR)Cl_3(PPh_3)_2]$ (R = H, F, CF_3) with formation of rhenium(V) complexes with tridentate {O,N,Se/Te} chalcogenolato ligands. The ligands adopt a *facial* coordination mode with the oxygen donors *trans* to the multiply bonded O^{2-} or $NPhR^{2-}$ ligands. The reduction of the dichalcogenides and the formation of the chalcogenolato ligands occurs *in situ* by released PPh_3 ligands. The absence of additional reducing agents provides good yields of products with rhenium in the high formal oxidation state "+5". A mechanism for the dichalcogenide reduction is proposed on the basis of the experimental results. In accordance with the proposed mechanism, best yields are obtained with a strict exclusion of oxygen, but in the presence of water.

Introduction

In contrast to the large number of alcoholato or thiolato complexes, organoselenolato and -tellurolato complexes of rhenium are rare. Only a few of such compounds have been characterized crystallographically.[1] The majority of them contains the metal in low oxidation states and tricarbonylrhenium(I) species dominate.[2–14] Organoselenolato and -tellurolato complexes with rhenium in higher oxidation states are even more scarce despite their proposed potentially beneficial catalytic properties.[15–17] They mainly contain simple, unsubstituted phenylselenolato ligands.[18–21] A few more rhenium(V) complexes with special ligands such as acylselenoureas, a diselenolenate, and pyridine-2-selenolate have been reported.[22–24] The rarity of these reports may result from the more complicated syntheses of heavier organochalcogenolato ligands. For some organochalcogenolates, such as alkynylselenolates, exist some special synthetic routes.[25,26] But commonly, the corresponding selenols and tellurols are unstable and prepared by reduction of the corresponding diorganodichalcogenides directly before the complex formation. The reaction conditions of such procedures must be controlled carefully in order to avoid the parallel reduction of the transition metal ions. This problem has been described in detail for the synthesis of complexes of the composition $(NBu_4)[M^VO(arylselenolate)_4]$ (M = Tc, Re), where the use of $Li(BH_4)$ in THF proved to be a suitable and easy to control reductant.[27,28] Recently, an oxidorhenium(V) complex with pyridylselenolato ligands was prepared by the reaction of the corresponding diselenide with $[ReOCl_3(PPh_3)_2]$ without the addition of a reducing agent. Obviously, the released PPh_3 acted as a selective reducing agent for dipyridyldiselenide, while the oxidation state of rhenium was retained.[24]

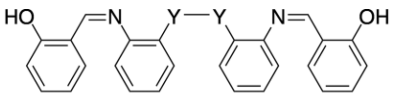

Y = Se: $\{HL^{Se}\}_2$
Y = Te: $\{HL^{Te}\}_2$

In the present work, we demonstrate that the assumed reaction pathway can be extended to other diorganodiselenides and -ditellurides. Thereto, we performed reactions of $[ReOCl_3(PPh_3)_2]$ and $[Re(NPhR)Cl_3(PPh_3)_2]$ (R = 4-H, 4-F or 4-CF_3) with the Schiff bases prepared from salicylaldehyde and bis(2-aminophenyl)diselenide ($\{HL^{Se}\}_2$) and -ditelluride ($\{HL^{Te}\}_2$).

Results and Discussion

The salicylidene Schiff base of bis(2-aminophenyl)diselenide $\{HL^{Se}\}_2$ was prepared by a reaction of di(2-aminophenyl)diselenide with two equivalents of salicylaldehyde in boiling ethanol. For the synthesis of $\{HL^{Te}\}_2$, an excess of the aldehyde (about 3:1) was used to obtain good yields. The products precipitated as yellow-orange ($\{HL^{Se}\}_2$) or orange-red ($\{HL^{Te}\}_2$) solids and were recrystallized from $CHCl_3$/EtOH. The synthetic route is simi-

[a] *Institute of Chemistry and Biochemistry, Freie Universität Berlin, Fabeckstr. 34/36, 14195 Berlin, Germany*
E-mail: Ulrich.Abram@fu-berlin.de
https://www.bcp.fu-berlin.de/chemie/chemie/forschung/InorgChem/agabram/index.html
[b] *Universidade Federal de Santa Maria, Laboratorio de Materiais Inorganicos,*
Santa Maria/RS, Brazil
https://www.ufsm.br/cursos/pos-graduacao/santa-maria/ppgq/
Supporting information and ORCID(s) from the author(s) for this article are available on the WWW under https://doi.org/10.1002/ejic.201901092.

lar to previous reports,[29,30] but the optimized conditions described in the Experimental Part give better yields and pure products. The purity of the dichalcogenides can readily be checked by their ^{77}Se and ^{125}Te NMR spectra giving resonances at 363 ppm ($\{HL^{Se}\}_2$) and 228 ppm ($\{HL^{Te}\}_2$). The other spectral features match the previously reported data.

Single crystals of $\{HL^{Se}\}_2$ and $\{HL^{Te}\}_2$ suitable for X-ray diffraction were grown from $CHCl_3$/EtOH mixtures. Figure 1a shows an ellipsoid representation of the selenium compound with the atomic labelling scheme, which has also been applied for $\{HL^{Te}\}_2$. A unit cell of the latter compound is shown in Figure 1b. It clearly illustrates that the ditelluride crystallizes in the present tetragonal polymorph with well-separated molecules. This is in contrast to the situation in the previously studied orthorhombic polymorph, in which each two molecules are connected by Te···Te interactions of 4.054 Å. In the compound under study, the shortest intermolecular Te–Te distances are larger than 6.5 Å.

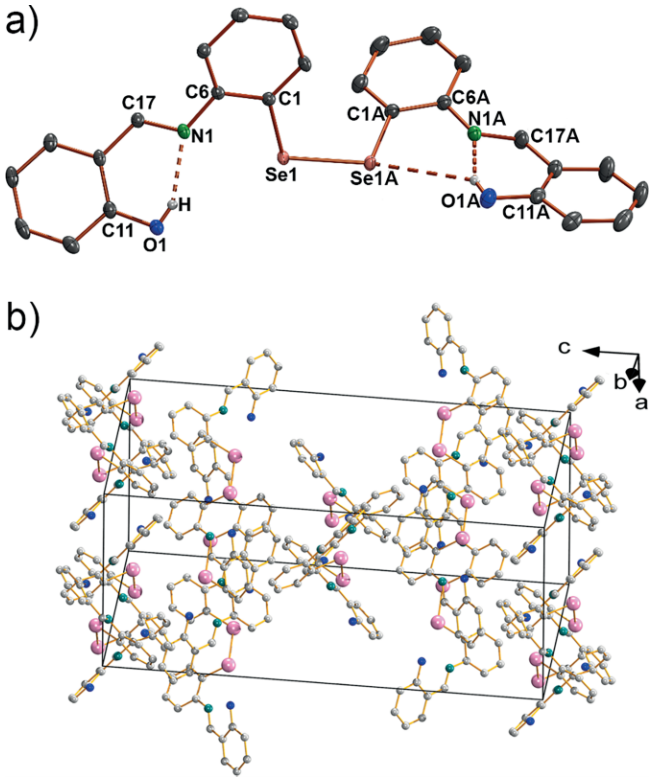

Figure 1. (a) Molecular structure of $\{HL^{Se}\}_2$. Ellipsoids represent 50 % probability. Hydrogen atoms bonded to carbon atoms are omitted for clarity. (b) Unit cell plot of $\{HL^{Te}\}_2$ illustrating the absence of intermolecular Te···Te interactions.

Some fundamental bond lengths of the dichalcogenides are compared with those in the rhenium complexes in Table 1 and Table 2. Some more details are summarized in the Supporting Information.

Reactions of the two functionalized dichalcogenides with oxido- and arylimidorhenium(V) complexes show that they are reduced during such procedures and form tridentate selenolato and tellurolato ligands, which bind tridentate to the $\{ReO\}^{3+}$ or $\{Re(NPhR)\}^{3+}$ cores. A summary of the performed reactions and obtained products is shown in Scheme 1. Although all reactions worked at room temperature and without the addition of a supporting base, they are slow and the yields of the products are in many cases unsatisfactorily low. This comes, however, not completely unexpected with regard to the low solubility of most of the starting materials used. But surprisingly, also the use of the better soluble, fluorinated starting complex $[Re(NPhF)Cl_3(PPh_3)]$ does not necessarily improve the yields. This means that the conditions for the individual reactions had to be optimized in terms of solvent, temperature and reaction time. Generally, we found that the presence of traces of water and the absence of oxygen are mandatory for good yields.

Reactions of $[ReOCl_3(PPh_3)_2]$ with $\{HL^{Se}\}_2$ give yields of $[ReO(L^{Se})Cl(PPh_3)]$ in the range of 70 %, when the reaction is performed at room temperature in moist CH_2Cl_2 under inert conditions. Interestingly, the yields are significantly lower (only about 20 %) when the reaction is done in dry solvent or on air. Since such a behavior suggests a sophisticated mechanism, we followed the course of the reaction by ^{31}P NMR spectroscopy. And indeed we found evidence for the formation of various phosphorus-containing species depending on the reaction time and the reaction conditions (presence of air and/or water). These experiments allow to propose a potential mechanism for the formation of $[ReO(L^{Se})Cl(PPh_3)]$, which is given in Scheme 2).

Initially, some phosphine (most probably together with one Cl^- ligand) dissociates from $[ReOCl_3(PPh_3)_2]$ under replacement by a diselenide. The phosphine attacks the coordinated diselenide with formation of an intermediate, which may be assigned to $\{Ph_3PSe(C_6H_4)\text{-}2\text{-}N{=}CH(C_6H_4)\text{-}2\text{-}OH\}^+Cl^-$, and the liberation of a $\{L^{Se}\}^{2-}$ ligand. The recorded chemical shift of 30 ppm of this potential intermediate is in the range where also the ^{31}P resonances of the related organoseleno-phosphonium species $\{Ph_3PSePh\}Br$ (37 ppm),[31] $\{Bu_3PSeMe\}I$ (50 ppm),[32] $\{Ph_3PSePh\}[GaCl_4]$ (38 ppm)[33] and $\{Ph_3PSeMe\}(BF_4)$ (36 ppm)[34] are found. The reduction of disulfides and diselenides with phosphines with formation of phosphonium-chalcogenolate ion pairs or bis(organochalcogen)phosphoranes has been observed before.[34–37] In the reactions of the present study, the phosphonium species seems to have a remarkably high formation probability and is also found as a fragment of high intensity in the ESI+ mass spectra taken from CH_2Cl_2 solutions of $[ReO(L^{Se})Cl(PPh_3)]$. Therefore, we consider the formation of an intermediate phosphonium species as highly probable, although an reaction pathway via a coordinated phosphorane cannot completely be excluded.

The intermediate can either decompose slowly in the anhydrous pathway with formation of triphenylphosphine selenide or it can quickly hydrolyze and give triphenylphosphine oxide and the respective selenol. The highly air-sensitive selenol is quickly re-oxidized to the diselenide in air. Thus, for the formation of the rhenium chalcogenolato complex, the exclusion of air is required and the presence of water supports the formation of $OPPh_3$ instead of $SePPh_3$. Both reactions, which lead to $OPPh_3$ or $SePPh_3$ can be understood as nucleophilic attacks of H_2O or RSe^- on the phosphorus atom of the $\{Ph_3PSe(C_6H_4)\text{-}2\text{-}N{=}CH(C_6H_4)\text{-}2\text{-}OH\}^+$ ion. In the case of water, the resulting pentacoordinate phosphorus species

Table 1. Selected bond lengths [Å] and angles (°) in $\{HL^{Se}\}_2$, $[ReO(L^{Se})Cl(PPh_3)]$, $[Re(NPhF)(L^{Se})Cl(PPh_3)]$ and $[Re(NPhCF_3)(L^{Se})Cl(PPh_3)]$.

	$\{HL^{Se}\}_2$	$[ReO(L^{Se})Cl(PPh_3)]$	$[Re(NPhF)(L^{Se})Cl(PPh_3)]$[a]	$[Re(NPhCF_3)(L^{Se})Cl(PPh_3)]$
Se1–C1	1.929(2)/1.933(2)	1.924(8)	1.923(2)	1.936(5)
O1–C11	1.356(2)/1.349(2)	1.332(9)	1.332(2)	1.341(5)
N1–C6	1.415(2)/1.415(2)	1.45(1)	1.443(3)	1.445(6)
N1–C17	1.287(2)/1.283(2)	1.302(9)	1.305(3)	1.299(6)
Re1–O10/N10	–	1.688(5)	1.728(2)	1.723(4)
Re1–O1	–	1.992(5)	2.020(2)	2.006(3)
Re1–P1	–	2.461(2)	2.4471(7)	2.430(1)
Re1–Cl1	–	2.537(2)	2.4967(7)	2.483(1)
Re1–N1	–	2.104(6)	2.117(2)	2.111(4)
Re1–Se1	–	2.439(1)	2.4923(5)	2.5003(6)
O1–Re1–O10/N10	–	161.3(3)	171.53(7)	172.3(2)
Re1–N10–C51	–	–	176.8(2)	174.1(4)
C1–Se1–Re1	–	92.9(3)	91.22(7)	90.4(1)

[a] Values taken from $[Re(NPhF)(L^{Se})Cl(PPh_3)]\cdot CH_3CN$.

Table 2. Selected bond lengths [Å] and angles (°) in $\{HL^{Te}\}_2$, $[ReO(L^{Te})Cl(PPh_3)]$, $[Re(NPh)(L^{Te})Cl(PPh_3)]$ and $[Re(NPhF)(L^{Te})Cl(PPh_3)]$.

Bond lengths/Å	$\{HL^{Te}\}_2$	$[ReO(L^{Te})Cl(PPh_3)]$[a]	$[Re(NPh)(L^{Te})Cl(PPh_3)]$	$[Re(NPhF)(L^{Te})Cl(PPh_3)]$
Te1–C1	2.127(2)	2.119(8)/2.123(8)	2.132(3)	2.128(4)
O1–C11	1.356(3)	1.33(1)/1.325(9)	1.332(4)	1.328(4)
N1–C6	1.415(3)	1.45(1)/1.44(1)	1.447(4)	1.449(5)
N1–C17	1.287(3)	1.30(1)/1.30(1)	1.296(4)	1.299(5)
Re1–O10/N10	–	1.699(6)/1.695(6)	1.726(3)	1.720(3)
Re1–O1	–	1.962(6)/1.985(6)	1.994(2)	1.990(2)
Re1–P1	–	2.469(2)/2.458(2)	2.4422(8)	2.4437(9)
Re1–Cl1	–	2.539(2)/2.527(2)	2.5045(9)	2.498(1)
Re1–N1	–	2.120(6)/2.105(7)	2.115(3)	2.107(3)
Re1–Te1	–	2.6416(6)/2.6469(6)	2.6899(3)	2.6869(3)
O1–Re1–O10/N10	–	166.4(3)/164.1(3)	169.6(1)	172.2(1)
Re1–N10–C51	–	–	168.1(3)	172.3(3)
C1–Te1–Re1	–	86.1(2)/85.7(2)	86.2(1)	85.7(1)

[a] Values for two independent species.

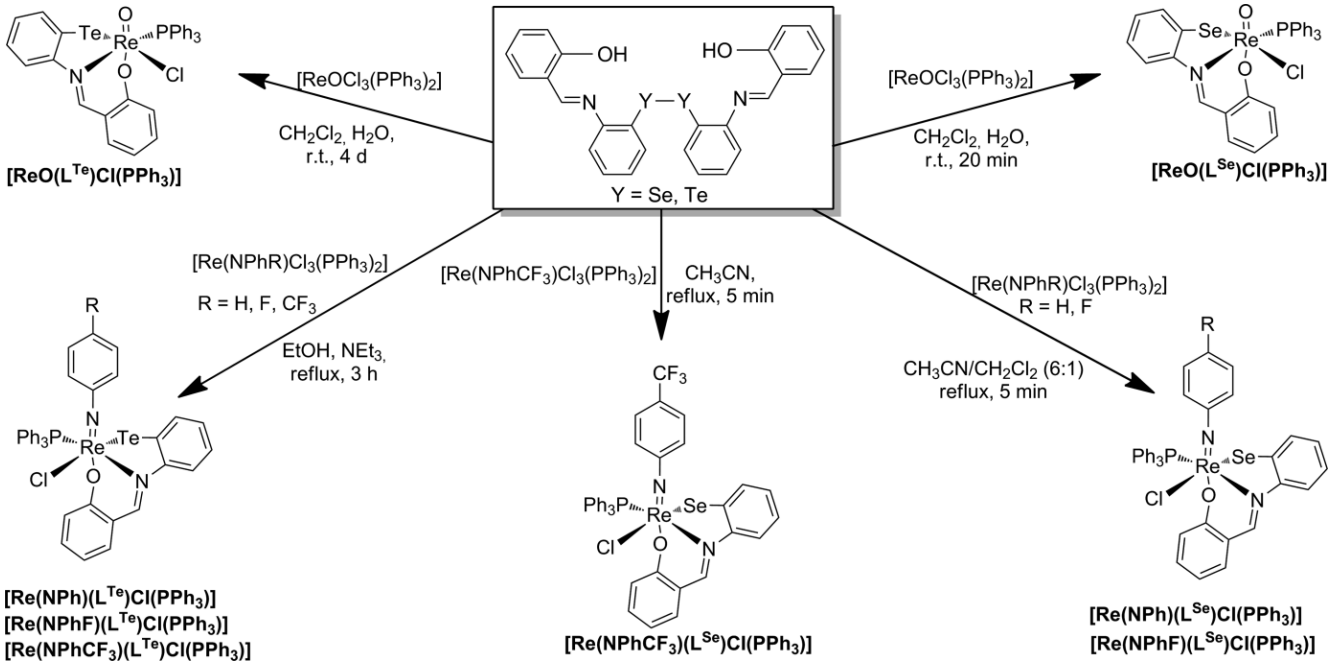

Scheme 1. Synthesis of the rhenium(V) selenolato and tellurolato complexes (all reactions were performed under argon).

$\{Ph_3P(OH_2)(Se(C_6H_4)\text{-}2\text{-}N{=}CH(C_6H_4)\text{-}2\text{-}OH)\}^+$ eliminates the free selenol (H_2L^{Se}), HCl and $OPPh_3$ as a consequence of the formation of the very stable P=O bond. The analogous $Ph_3P(Se{-}R)(Se(C_6H_4)\text{-}2\text{-}N{=}CH(C_6H_4)\text{-}2\text{-}OH)$ probably follows the same path-

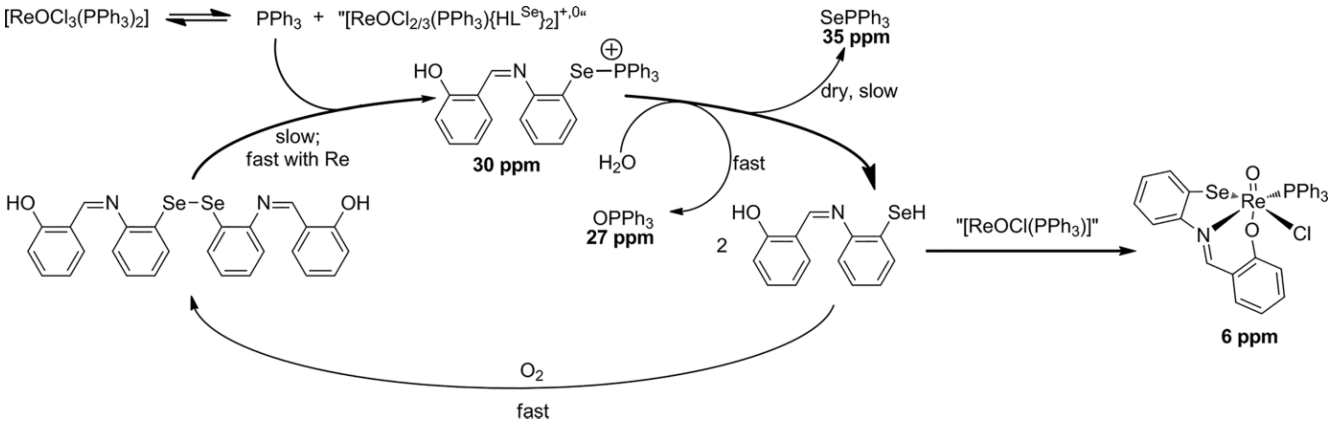

Scheme 2. Proposed mechanism for the reaction between $[ReOCl_3(PPh_3)_2]$ and $\{HLSe\}_2$ in CH_2Cl_2. Chemical shifts refer to ^{31}P.

way with formation of $Se\{(C_6H_4)\text{-}2\text{-}N{=}CH(C_6H_4)\text{-}2\text{-}OH)\}_2$ and $SePPh_3$. The formation of such chalcogenoethers from organo-chalcogeno-phosphonium starting materials with formation of a formal phosphorus-chalcogen double bond is well-established.[34–37]

It should be noted that the relative rates of the described reactions are only valid in the presence of the rhenium complex. Reactions of $\{HL^{Se}\}_2$ with pure PPh_3 are very slow and form under the same conditions considerable amounts of $OPPh_3$ only within days or weeks.

The same general course of the reaction as outlined in Scheme 2 can also be assumed for the phenylimido starting complexes and also for reactions with $\{HL^{Te}\}_2$. It should be mentioned that the reaction times may significantly differ and particularly the used solvent plays a crucial role. While $[ReOCl_3(PPh_3)_2]$ and $[Re(NPh)Cl_3(PPh_3)_2]$ are sparingly soluble in most solvents, it proved to be favorable to reduce the solubility of the fluorinated phenylimido complexes for the reactions under study. For example, $[Re(NPhF)(L^{Se})Cl(PPh_3)]$ is formed only in low yields from reactions in CH_2Cl_2, in which the starting complex $[Re(NPhF)Cl_3(PPh_3)_2]$ is readily soluble. Higher yields are obtained in a CH_2Cl_2/CH_3CN (1:6) mixture, in which the starting material is less soluble.

The red to brown complexes are stable as solids. In solution, however, they show gradual decomposition, which is normally higher in non-degassed solvents and can be understood by the re-formation of the dichalcogenides on air. The instability of some of the products and (in some cases) their low solubility prevent from the measurement of ^{13}C, ^{77}Se and ^{125}Te NMR spectra of sufficient quality. $[ReO(L^{Se})Cl(PPh_3)]$ is the most unstable compound of our series and in the related NMR spectra appear signals of decomposition products directly after dissolution, even when measured in dry, degassed CD_2Cl_2. In turn, the related tellurium complex is stable in solution for several hours. The highest stability was found for $[Re(NPhCF_3)(L^{Se})Cl(PPh_3)]$, which shows no decomposition after several days in wet, non-degassed solvents.

The ^{77}Se signals of the coordinated selenolato ligands appear between 360 and 395 ppm and the corresponding ^{125}Te resonances are found between 378 and 695 ppm. In the spectra of the well-soluble fluorinated complexes $[Re(NPhF)(L^{Se})Cl(PPh_3)]$ and $[Re(NPhCF_3)(L^{Se})Cl(PPh_3)]$, the ^{77}Se resonances are observed as doublets at 360 ppm ($^2J_{Se,P}$ = 22 Hz) and 395 ppm ($^2J_{Se,P}$ = 24 Hz). The coupling constants are within the magnitude of couplings, which have previously been observed for mixed selenolato/phosphine complexes of platinum.[38,39] The ^{125}Te NMR spectra show signals with a $^2J_{Te,P}$ coupling of 50–60 Hz, which is also in accord with the situation in similar Pt(II) compounds.[38] The ^{77}Se and ^{125}Te couplings could not be observed in the respective ^{31}P NMR spectra.

A key feature in the proton NMR spectra of Schiff base complexes is the resonance of their unique imine proton. It is well-separated from the remaining aromatic resonances. The imine protons in the selenolato complexes are more deshielded compared to those in the tellurolato complexes, which is similar to the situation in the corresponding dichalcogenides $\{HL^{Se}\}_2$ and $\{HL^{Te}\}_2$. Additionally, the imine protons are more deshielded in the oxido complexes compared to the phenylimido complexes. These observations can be attributed to the better donor abilities of the phenylimido ligands as compared to oxido ligands. In complexes with imine and phosphine ligands, the imine protons often couple to the ^{31}P nuclei. This is also the case in the reported complexes with coupling constants of about 8 Hz and allows an *in situ* control of the complex formation. The ^{31}P chemical shifts observed for the rhenium complexes are correlated to the donor strength of the rhenium multiple bonded cores. It is highest for the oxido complexes and decreases by 5 ppm to the phenylimido complexes. ESI+ mass spectra of the rhenium complexes under study show intense signals of their $[M - Cl]^+$ ions. Typically, fragment peaks are observed, which correspond to ions with chalcogen–phosphorus bonds, such as $\{Ph_3PSe(C_6H_4)\text{-}2\text{-}N{=}CHC_6H_4\text{-}2\text{-}OH\}^+$ (m/z = 538.0818) or $\{Ph_3PSe(C_6H_4)\text{-}2\text{-}NH_2\}^+$ (m/z = 343.0556). The number and the intensities of such fragments depend on the stability of the complexes in solution.

Crystallographic studies on single-crystals of $[ReO(L^{Se})Cl(PPh_3)]$, $[Re(NPhF)(L^{Se})Cl(PPh_3)]\cdot CH_3CN$, $[Re(NPhF)(L^{Se})Cl(PPh_3)]\cdot 0.5CH_2Cl_2$, $[Re(NPhCF_3)(L^{Se})Cl(PPh_3)]$, $[ReO(L^{Te})Cl(PPh_3)]\cdot CH_2Cl_2$, $[Re(NPh)(L^{Te})Cl(PPh_3)]\cdot CHCl_3$ and $[Re(NPhF)(L^{Te})Cl(PPh_3)]$ have been undertaken. All complexes show the same general structure with facially bonded tridentate ligands. The hydroxylic group of the organic tridentate ligand is in *trans* position to the oxido or

phenylimido ligand in all compounds. PPh_3 and Cl^- ligands complete the equatorial coordination spheres of rhenium with the latter ligand being arranged *trans* to the selenium or tellurium atoms of the Schiff base. The molecular structures of $[ReO(L^{Te})Cl(PPh_3)]$ and $[Re(NPhCF_3)(L^{Se})Cl(PPh_3)]$ are shown in Figure 2 and Figure 3 as representatives for the complexes with the selenium- and tellurium-containing ligands. Since the general features of the other oxido and phenylimido complexes with the tridentate ligands are similar, their structures are not shown here. They can be found in the Supplementary Information. Selected bond lengths and angles of all complexes and the corresponding dichalcogenides are summarized in Table 1 (selenium compounds) and Table 2 (tellurium compounds).

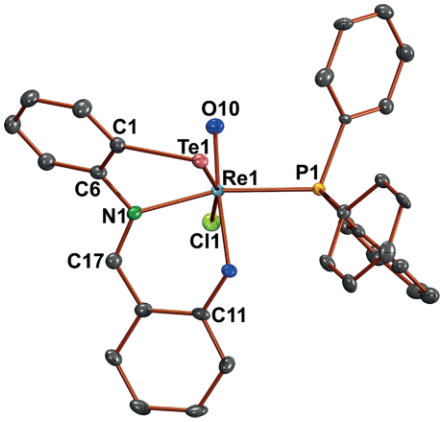

Figure 2. Molecular structure of $[ReO(L^{Te})Cl(PPh_3)]$. Ellipsoids are depicted at 50 % probability. Hydrogen atoms are omitted for clarity.

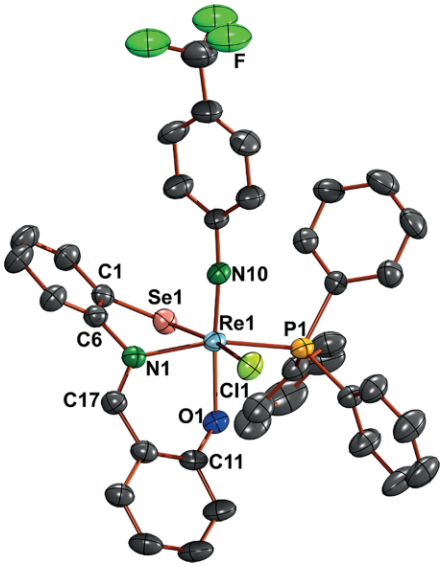

Figure 3. Molecular structure of $[Re(NPhCF_3)(L^{Se})Cl(PPh_3)]$. Ellipsoids are depicted at 50 % probability. Hydrogen atoms are omitted for clarity.

The rhenium atoms in the complexes have distorted octahedral coordination environments. Main distortions come from the restrictions caused by the facially coordinated tridentate ligands. The N1–Re1–Se1/Te1 angles are between 79.1 and 80.6° and the N1–Re1–O1 angles are between 82.2 and 83.6°. The angles between the axially bonded atoms O10 or N10 and the donor atoms of the tridentate ligands in the equatorial coordination sphere are all larger the 90°. This is a consequence of the steric demand of the double bonds, which are established between rhenium and the oxido and arylimido ligands.

Similar results have been found in a series of related complexes before.[40–43] The corresponding Re1–O10 (1.688(5)-1.699(5) Å) and Re1–N10 bonds (1.720(3)-1.728(3) Å) are in the usual ranges and the imido ligands are linear.[40] It is interesting to note that all Re1–O1 bonds are in the range or smaller than 2 Å. Such values are somewhat smaller than expected for Re–O single bonds, but not unusual for oxido or arylimido complexes of rhenium(V), since similar features are found with about 50 per cent of the crystallographically studied compounds of these types.[1] The effect is commonly explained by a partial transfer of electron density from the Re–O/N double bonds to the *trans* Re–O bond.[40,44–46]

The Re–Se bonds between 2.439(1) and 2.5003(6) Å are relatively short and similar bond lengths have hitherto only been found in some rare examples of Re(V) complexes with terminal phenylselenolato complexes,[19,21,28] while in the majority of their rhenium complexes such ligands bridge two low-valent rhenium atoms and the related Re–Se bond are in the range of 2.6 Å or longer.[1] Short Re–Se bonds are also established in binuclear rhenium compounds with Re–Re bonds or diselenolene complexes.[18,23] Most of the few rhenium complexes with tellurolato ligands are carbonyl compounds of Re(I) and they have Re–Te bond lengths between 2.760 and 2.811 Å.[3,6,8,11–14] Very recently, a series of $[Re^{V}O(aryltellurolate)_4]^-$ and $[Re^{III}(aryltellurolate)_3(PPh_3)(CH_3CN)]$ complexes was prepared and structurally characterized.[28] The Re–Te bond lengths in the Re(V) complexes are very similar to the values for the compounds of the present study.

An interesting feature is the bond length distribution in the six-membered chelate rings of the $[ReO(L^{Y})Cl(PPh_3)]$ and $[Re(NPhR)(L^{Y})Cl(PPh_3)]$ complexes (Y = Se, Te; R = H, F, CF_3). The N1–C17 bonds are only slightly lengthened compared to the related bonds in $\{HL^{Se}\}_2$ and $\{HL^{Te}\}_2$. This means that the imine double bonds remain mainly localized and no significant delocalization of π-electron density is observed in this chelate ring. A similar bonding situation is observed in analogous oxidorhenium(V) complexes with the salicylidene Schiff bases derived from 2-aminophenol ($\{L^{O}\}^{2-}$) or 2-aminothiophenol ($\{L^{S}\}^{2-}$),[47,48] despite the fact that the tridentate *O,N,O* and *O,N,S* ligands are both coordinated in a *meridional* arrangement.

Since all hitherto structurally studied Re(V) complexes with the $\{L^{O}\}^{2-}$ and $\{L^{S}\}^{2-}$ show a *mer*-arrangement of these ligands,[47–55] and the complexes with their selenium and tellurium analogues of the present study contain the tridentate ligand exclusively in a *facial* coordination mode, we undertook a series of DFT calculations on the B3LYP level for both isomers of the $[ReO(L^{Y})Cl(PPh_3)]$ (Y = O, S, Se, Te) complexes. Frequency calculations after the optimizations showed convergence of at least two out of four criteria in all cases and full convergence on the experimentally expected isomers. No negative frequencies were obtained. The calculated bonding parameters for the facial isomers with $\{L^{Se}\}^{2-}$ and $\{L^{Te}\}^{2-}$ match the determined crystal structures of *fac*-$[ReO(L^{Se})Cl(PPh_3)]$ and *fac*-$[ReO(L^{Te})$-

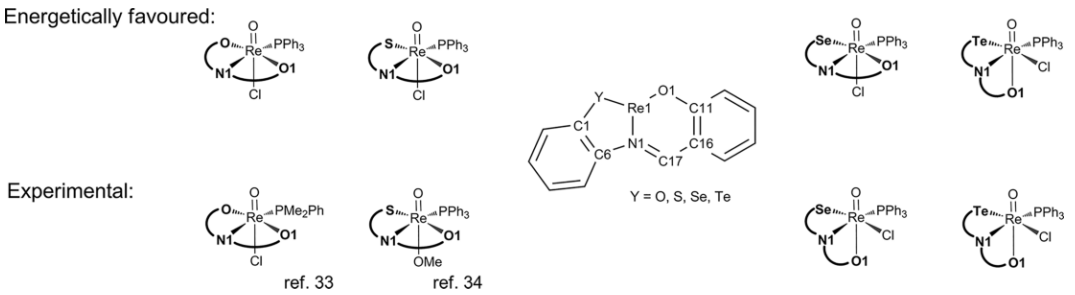

Scheme 3. Calculated and experimentally isolated isomers for [ReO(L^{Y})X(PR$_3$)] complexes (Y = O, S, Se, Te; X = Cl or OMe).

Cl(PPh$_3$)] on average within 0.037 Å. The deviations are highest with an average of 0.053 Å for the coordination sphere of rhenium, which is expected for a gas phase calculation.

Table 3 contains a comparison of the calculated over-all energies for the respective isomers and Scheme 3 visualizes the results. It becomes evident that the meridional isomers are more stable for the complexes with the phenolato, thiophenolato and selenophenolato ligands, while the *fac* compound is preferred for the tellurolato complex. But it is also clear that the calculated energy differences are small and are only suitable for the justification of the preferred formation of the *mer* complex in the case of [ReO(L^{O})Cl(PPh$_3$)]. Nevertheless, the trend found in the experiments, namely that the stability of the *facial* isomers increases for the heavier chalcogens, is well reflected by the computational results, even when the crystallized products for the Se-containing complexes show *fac* and not *mer* coordination.

Table 3. Energies for the *mer* and *fac* isomers the [ReO(L^{Y})Cl(PPh$_3$)] complexes (Y = O, S, Se, Te). The energies of the most stable geometries are in bold.

	E_{mer}/Hartree	E_{fac}/Hartree	ΔE/kJ mol^{-1}
Y = O	**–1577.20576**	–1577.19178	36.8
Y = S	**–1512.08892**	–1512.08631	6.7
Y = Se	**–1511.20096**	–1511.19872	5.9
Y = Te	–1510.00999	**–1510.01209**	–5.4

A possible reason for this result might be given by the well-known labilization of the coordination positions *trans* to the multiple-bonded oxido or arylimido ligands. It is generally accepted, that ligand exchange reactions at complexes with the {ReO/NAr}$^{3+}$ cores start with the substitution of the *trans*-ligand. Therefore, complexes with the *fac*-coordinated ligands should be the initial products in such reactions. As the reactions with the oxido complexes were performed under mild conditions, which means under kinetic control, a rationale for the observation of the *fac* complexes is given. Obviously, the formation of such intermediates at room temperature is faster than their subsequent isomerization. As the complexes tend to decompose at prolonged times of higher temperatures an isomerization to the *mer*-isomers could not be observed.

It would be interesting to study similar reactions with corresponding technetium compounds, where the kinetics of ligand exchange reactions is commonly faster. Unfortunately, there exists no oxidotechnetium(V) analogue to [ReOCl$_3$(PPh$_3$)$_2$] and the phenylimido complex [Tc(NPh)Cl$_3$(PPh$_3$)$_2$] is almost insoluble. But recently the synthesis of two fluorinated arylimidotechnetium(V) complexes, [Tc(NPh-4-F)Cl$_3$(PPh$_3$)$_2$] and [Tc(NPh-4-CF$_3$)-Cl$_3$(PPh$_3$)$_2$], has been reported.[43] Reactions between these novel precursors and dichalcogenides are planned for the future and their results may give a deeper insight into the mechanism of such reactions.

Conclusions

Rhenium(V) complexes with tridentate selenolato- and tellurolato-substituted Schiff base ligands are formed during reactions of the corresponding dichalcogenides {HL^{Se}}$_2$ or {HL^{Te}}$_2$ with phosphine-containing rhenium(V) complexes such as [ReOCl$_3$-(PPh$_3$)] or [Re(NAr)Cl$_3$(PPh$_3$)$_2$] (Ar = Ph, PhF, PhCF$_3$). The resulting [ReO(L^{Y})Cl(PPh$_3$)$_2$] or [Re(NAr)(L^{Y})Cl(PPh$_3$)] complexes (Y = Se, Te) contain the tridentate ligands in a *facial* arrangement.

A mechanism for such reactions has been deduced, in which released PPh$_3$ acts as reducing agent for the dichalcogenides. Optimal yields are obtained in the presence of water and under strict exclusion of dioxygen. The method is well-suited for the synthesis of high-valent rhenium complexes.

Experimental Section

(NBu$_4$)[ReOCl$_4$],[56] [ReOCl$_3$(PPh$_3$)$_2$],[57] [Re(NPh)Cl$_3$(PPh$_3$)$_2$],[58] [Re(NPhF)Cl$_3$(PPh$_3$)$_2$],[42] bis(2-aminophenyl)diselenide and bis(2-aminophenyl)ditelluride were prepared according to literature procedures.[59–61] All other chemicals were reagent grade and used as received. Reactions involving oxygen- or water-sensitive compounds were performed with standard Schlenk technique.

NMR spectra were recorded at 25 °C on JEOL 400 MHz ECS-400 or JNM-ECA400II spectrometers. Chemical shifts (δ) are given relative to the signals of external standards (tetramethylsilane, (^{1}H, ^{13}C), ClCF$_3$ (^{19}F), 85 % phosphoric acid (^{31}P), dimethylselenide (^{77}Se) and dimethyltelluride (^{125}Te)).

IR-Spectra were recorded with an FT-IR spectrometer (Nicolet iS10, Thermo Scientific). Intensities are classified as vs. = very strong, s = strong, m = medium, w = weak, vw = very weak, sh = shoulder.

Electrospray ionization mass spectrometry (ESI MS) was carried out with the ESI MSD TOF unit of an Agilent 6210 TOF LC/MS system. The measurements were performed in CHCl$_3$, CDCl$_3$, CH$_2$Cl$_2$, MeOH or mixtures of them.

Elemental analyses were performed using a vario EL III CHN elemental analyzer (Elementar Analysensysteme GmbH) or a vario MICRO cube CHNS elemental analyzer.

Single crystal X-ray diffraction data were collected on a Bruker D8 Venture or a STOE IPDS II T. Absorption corrections were carried out by the multiscan (Bruker D8 Venture) or integration methods (STOE IPDS II T).[62,63] Structure solutions and refinements were done with the SHELX-2008 program packages.[64,65] Hydrogen atom positions at heteroatoms or the imino carbon atoms were taken from the Fourier maps when possible or placed at calculated positions and refined by a riding model. All other hydrogen atoms were placed at calculated positions and refined by a riding model. The visualization of the molecular structures was done using the program DIAMOND 4.2.2.[66]

CCDC 1956176–1956184 (see Supporting Information for the reference number of each compound) contain the supplementary crystallographic data for this paper. These data can be obtained free of charge from The Cambridge Crystallographic Data Centre.

DFT calculations were performed on the high-performance computing systems of the Freie Universität Berlin ZEDAT (Soroban, Curta) using the program packages GAUSSIAN 09 and GAUSSIAN 16.[67,68] The gas phase geometry optimizations were performed using coordinates derived from the X-ray crystal structures or have been modelled with the use of crystal structure fragments using GAUSSVIEW.[69] The calculations were performed with the hybrid density functional B3LYP.[70–72] The double-ζ pseudopotential LANL2DZ basis set with the respective effective core potential (ECP) was applied to Re as well as S, Se and Te.[73] The 6-311G**basis set was applied for all other atoms.[74–76] The LANL2DZ and 6-311G** basis sets as well as the ECPs were obtained from the EMSL database.[77]

{HL^{Se}}$_2$. Salicylaldehyde (0.12 mL, 1.16 mmol) was added to a stirred suspension of bis(2-aminophenyl)diselenide (200 mg, 0.58 mmol) in 18 mL of EtOH. The mixture was heated under reflux for 4 h. A yellow solid precipitated over this period. After cooling to room temperature, the solid was filtered off. Before crystallization from EtOH/$CHCl_3$, traces of elemental selenium must be removed by filtration of the hot solution. Orange-yellow crystals. Yield: 172 mg (53 %).

Alternatively, if no precipitate is observed after one hour, the addition of dry $MgSO_4$ starts the reaction. The procedure is followed as described above. The precipitate is extracted with CH_2Cl_2 until the extract is colorless, the solvent is removed in vacuo and the residue recrystallized from EtOH/$CHCl_3$.

Elemental analysis: Calculated for $C_{26}H_{20}N_2O_2Se_2$: C 56.7, H 3.7, N 5.1 %; Found C 56.6, H 3.7, N 5.1 %. IR: 1608 (s) C=N, 1579 (m), 1562 (s), 1490 (m), 1461 (s), 1437 (m), 1362 (m), 1275 (s), 1226 (m), 1183 (s), 1147 (s), 1110 (w), 1044 (w), 1029 (m), 970 (m), 936 (w), 907 (s), 862 (w), 843 (m), 781 (m), 746 (vs), 706 (s), 672 (m), 641 (m), 601 (w), 576 (w), 569 (w), 553 cm^{-1} (s). ESI+ MS (*m*/*z*): 552.9959 (calc. 552.9937) $[M + H]^+$, 574.9786 (calc. 574.9757) $[M + Na]^+$, 590.9524 (calc. 590.9496) $[M + K]^+$, 1124.9671 (calc. 1124.9640) $[2M+Na]^+$, 1140.9407 (calc. 1140.9379) $[2M+K]^+$. ESI-MS (*m*/*z*): 550.9759 (calc. 550.9781) $[M - H]^-$. ^{1}H NMR ($CDCl_3$, ppm): 12.74 (2H, br, O**H**), 8.60 (2H, s, **H**CR=NR), 7.75–7.69 (2H, m, *o*-Se-*m*-NR-Ar**H**), 7.45–7.38 (4H, m, *o*-CNR-*m*-OH-Ar**H**; *p*-CNR-*m*-OH-Ar**H**), 7.29–7.38 (2H, m, *p*-Se-*m*-NR-Ar**H**), 7.17–7.09 (4H, m, *m*-Se-*p*-NR-Ar**H**; *m*-CNR-*p*-OH-Ar**H**), 7.08–7.04 (2H, m, *m*-CNR-*o*-OH-Ar**H**), 6.99–6.93 (2H, m, *m*-Se-*o*-NR-Ar**H**). ^{13}C NMR ($CDCl_3$, ppm): 163.2 (s, H**C**R=NR), 161.2 (s, $R_2\mathbf{C_{Ar}}$-OH), 147.5 (s, NR-$\mathbf{C_{Ar}}R_2$), 133.9 (s, *m*-NC-*o*-Se-$R_2\mathbf{C_{Ar}}$), 132.8 (s, *m*-OH-*p*-CN-$R_2\mathbf{C_{Ar}}$), 131.0 (s, *m*-OH-*o*-CN-$R_2\mathbf{C_{Ar}}$), 128.4 (s, *p*-NC-*m*-Se-$R_2\mathbf{C_{Ar}}$), 128.2 (s, *m*-NC-*p*-Se-$R_2\mathbf{C_{Ar}}$), 126.8 (s, $R_2\mathbf{C_{Ar}}$-Se), 119.4 (s, *o*-NC-*m*-Se-$R_2\mathbf{C_{Ar}}$), 119.2 (s, *p*-OH-*m*-CN-$R_2\mathbf{C_{Ar}}$), 117.7 (s, *o*-OH-$R_2\mathbf{C_{Ar}}$-CNR), 117.6 (s, *o*-OH-*m*-CN-$R_2\mathbf{C_{Ar}}$). ^{77}Se NMR ($CDCl_3$, ppm): 363 (s).

{HL^{Te}}$_2$. Salicylaldehyde (0.15 mL, 1.41 mmol) was added to a suspension of bis(2-aminophenyl)ditelluride (200 mg, 0.46 mmol) in dry, degassed MeOH (9 mL) whilst stirring. It was heated under reflux for 3 h. An orange-red solid precipitated over this period. After cooling to room temperature, the pure product was filtered off and dried in vacuo. The product can be recrystallized from hot EtOH/$CHCl_3$. Orange-red crystals. Yield: 240 mg (0.44 mmol, 96 %).

Alternatively, if no precipitate is observed after one hour, the addition of dry $MgSO_4$ starts the reaction. The procedure is followed as described above. The precipitate is extracted with CH_2Cl_2 until the extract is colorless, the solvent is removed in vacuo and the residue recrystallized from EtOH/$CHCl_3$.

Elemental analysis: Calculated for $C_{26}H_{20}N_2O_2Te_2$: C 48.2, H 3.1, N 4.3 %; Found C 48.1, H 3.2, N 4.3 %. IR (cm^{-1}): $\tilde{\nu}$ = 1605 (s) C=N, 1578 (m), 1558 (m), 1492 (m), 1457 (m), 1435 (m), 1384 (m), 1361 (m), 1274 (s), 1239 (w), 1225 (m), 1179 (m), 1154 (m), 1146 (m), 1108 (m), 1034 (m), 1018 (m), 975 (w), 937 (w), 905 (m), 853 (m), 841 (m), 779 (m), 747 (vs), 732 (sh), 708 (s), 666 (m), 638 (m), 575 (m), 551 (s). ESI+ MS (*m*/*z*): 648.9699 (calc. 648.9701) $[M + H]^+$, 670.9532 (calc. 670.9521) $[M + Na]^+$, 686.9269 (calc. 686.9259) $[M + K]^+$, 1318.9152 (calc. 1318.9147) $[2M+Na]^+$, 1334.8862 (calc. 1334.8885) $[2M+K]^+$. ESI- MS (*m*/*z*): 646.9514 (calc. 646.9545) $[M - H]^-$. ^{1}H NMR ($CDCl_3$, ppm): 12.53 (2H, s, O**H**), 8.55 (2H, s, **H**CR=NR), 7.94–7.85 (2H, m, *o*-Te-*m*-NR-Ar**H**), 7.47–7.38 (4H, m, *o*-CNR-*m*-OH-Ar**H**; *p*-CNR-*m*-OH-Ar**H**), 7.34–7.27 (2H, m, *p*-Te-*m*-NR-Ar**H**) 7.12–6.93 (8H, m, *m*-Te-*p*-NR-Ar**H**; *m*-CNR-*p*-OH-Ar**H**, *m*-CNR-*o*-OH-Ar**H**, *m*-Te-*o*-NR-Ar**H**). ^{13}C NMR ($CDCl_3$, ppm): 163.7 (s, H**C**R=NR), 161.0 (s, $R_2\mathbf{C_{Ar}}$-OH), 150.6 (s, NR-$\mathbf{C_{Ar}}R_2$), 138.3 (s, *m*-NC-*o*-Te-$R_2\mathbf{C_{Ar}}$), 134.0 (s, *m*-OH-*p*-CN-$R_2\mathbf{C_{Ar}}$), 133.0 (s, *m*-OH-*o*-CN-$R_2\mathbf{C_{Ar}}$), 129.4 (s, *p*-NC-*m*-Te-$R_2\mathbf{C_{Ar}}$), 128.5 (s, *m*-NC-*p*-Te-$R_2\mathbf{C_{Ar}}$), 119.6 (s, *o*-NC-*m*-Te-$R_2\mathbf{C_{Ar}}$), 119.1 (s, *p*-OH-*m*-CN-$R_2\mathbf{C_{Ar}}$), 117.6 (s, *o*-OH-$R_2\mathbf{C_{Ar}}$-CNR), 117.1 (s, *o*-OH-*m*-CN-$R_2\mathbf{C_{Ar}}$), 107.5 (s, $R_2\mathbf{C_{Ar}}$-Te). ^{125}Te NMR ($CDCl_3$, ppm): 228 (s).

[ReO(L^{Se})Cl(PPh$_3$)]. {HL^{Se}}$_2$ (44 mg, 0.08 mmol) was dissolved in a degassed mixture of CH_2Cl_2 (6 mL) and water (1 drop). [$ReOCl_3$-$(PPh_3)_2$] (88 mg, 0.1 mmol) was added whilst stirring. The color changed from light yellow to dark brown and after 20 min of stirring at room temperature, the suspension became a clear brown solution. The mixture was overlayered with degassed diethyl ether (12 mL) and left in the freezer for slow diffusion. The formed crystals of [ReO(L^{Se})Cl(PPh_3)] were filtered off and washed with diethyl ether. Red-brown plates. Yield: 50 mg (68 %).

Elemental analysis: Calculated for $C_{31}H_{24}ClNO_2PReSe$: C 48.1, H 3.1, N 1.8 %; Found C 48.0, H 3.2, N 1.5 %. IR (cm^{-1}): $\tilde{\nu}$ = 3046 (w), 1601 (m) C=N, 1582 (m), 1567 (m), 1532 (m), 1481 (m), 1454 (m), 1432 (m), 1373 (m), 1283 (m), 1230 (w), 1175 (m), 1157 (m), 1148 (m), 1119 (m), 1094 (s), 1027 (m), 998 (m), 967 (sh), 955 (s) Re=O, 926 (m), 858 (m), 804 (m), 746 (vs), 718 (sh), 707 (sh), 690 (vs), 615 (s), 595 (m), 559 (s), 544 (m). ESI+ MS (*m*/*z*): 740.0224 (calc. 740.0267) $[M - Cl]^+$. ^{1}H NMR (CD_2Cl_2, ppm): 8.69 (1H, s, **H**CR=NR), 8.00–6.96 (23H, m, Ar**H**). ^{31}P NMR (CD_2Cl_2, ppm): 6.1 (s).

[ReO(L^{Te})Cl(PPh$_3$)]. {HL^{Te}}$_2$ (64 mg, 0.1 mmol) was added to a suspension of [$ReOCl_3(PPh_3)_2$] (88 mg, 0.1 mmol) in a degassed mixture of CH_2Cl_2 (10 mL) and water (1 drop) whilst stirring. The color changed from light yellow to brown-yellow over a period of 2 h. The mixture was stirred at room temperature for 3 days. During this time, an orange-red powder precipitated. The volume was reduced to 2 mL and the orange-red precipitate was filtered off. Diethyl ether (12 mL) was added to the mixture and the solvent was reduced in a stream of dry argon to approximately 8 mL. An additional amount of degassed diethyl ether (12 mL) was added. The procedure was repeated four times. Finally, dark red crystals were formed. They were filtered off and washed subsequently with diethyl ether and hexane. Dark red plates. Yield: 15 mg (20 %).

Elemental analysis: Calculated for $C_{32}H_{26}Cl_3NO_2PReTe$: C 44.7, H 3.1, N 1.6 %; Found C 45.1, H 3.1, N 1.6 %. IR (cm^{-1}): $\tilde{\nu}$ = 3054 (w), 1602 (s) C=N, 1583 (s), 1566 (m), 1537 (s), 1481 (m), 1452 (m), 1432 (s), 1373 (m), 1341 (w), 1289 (s), 1263 (m), 1231 (w), 1189 (w), 1177 (w), 1160 (w), 1148 (m), 1121 (w), 1094 (s), 1072 (sh), 1028 (m), 998 (m), 961 (s) Re=O, 944 (s), 927 (m), 892 (w), 862 (m), 806 (m), 749 (vs), 732 (vs), 704 (sh), 690 (vs), 641 (w), 617 (s), 598 (m),574 (w), 559 (m), 544 (vs). ESI+ MS (*m/z*): 788.0143 (calc. 788.0147) $[M - Cl]^+$. ^1H NMR ($CDCl_3$, ppm): 8.60 (1H, d, $^4J_{H,P}$ = 7.71 Hz, **H**CR=NR), 8.10–7.31 (25H, m, Ar**H**), 7.20–7.09 (1H, m, ^{L}Ar**H**), 7.07–7.03 (1H, m, ^{L}Ar**H**), 6.18–6.00 (1H, m, ^{L}Ar**H**). ^{13}C NMR ($CDCl_3$, ppm): 169.8 (s, R_2**C**$_{ar}$-O), 162.2 (s, R**C**-NR), 160.8 (s, R_2**C**$_{ar}$-NCR), 137.7 (s, *p*-CN-*m*-O-**C**$_{ar}$), 136.4 (R_2**C**$_{ar}$-Te), 135.7 (s, ^{L}**C**$_{ar}$), 134.9 (d, $^3J_{C,P}$ = 10 Hz, *m*-P-**C**$_{ar}$), 132.8 (s, ^{L}**C**$_{ar}$), 132.2 (s, ^{L}**C**$_{ar}$), 131.3 (d, $^4J_{C,P}$ = 0 Hz, *p*-P-**C**$_{ar}$), 128.7, (d, $^2J_{C,P}$ = 11 Hz, *o*-P-**C**$_{ar}$), 128.6 (s, ^{L}**C**$_{ar}$), 128.1 (s, ^{L}**C**$_{ar}$), 127.1 (s, ^{L}**C**$_{ar}$), 122.4, (s, ^{L}**C**$_{ar}$), 119.5 (d, $^1J_{C,P}$ = 12 Hz, P-**C**$_{ar}$), 119.3 (s, ^{L}**C**$_{ar}$). ^{31}P NMR ($CDCl_3$, ppm): 6.3 (s). ^{125}Te NMR ($CDCl_3$, ppm): 695 (d, $^2J_{Te,P}$ = 59 Hz).

[Re(NPh)(L^{Se})Cl(PPh$_3$)]. $[Re(NPh)Cl_3(PPh_3)_2]$ (88 mg, 0.1 mmol) was suspended in a degassed mixture of CH_3CN (6 mL) and water (1 drop). $\{HL^{Se}\}_2$ (44 mg, 0.08 mmol) was added as a solid after heating this mixture to reflux. The color changed from dark green to red-violet immediately and a red-brown solid precipitated together with unreacted $\{HL^{Se}\}_2$. After 3 min, CH_2Cl_2 (1 mL) was added, which dissolved the remaining diselenide. The CH_2Cl_2 was removed in a stream of argon. The mixture was cooled to room temperature and the product was filtered off as a brown powder. After washing with diethyl ether (10 mL) to remove potentially remaining $\{HL^{Se}\}_2$, a brown-violet powder was obtained. Yield: 44 mg (54 %).

Elemental analysis: Calculated for $C_{37}H_{29}ClN_2OPReSe$: C 52.3, H 3.4, N 3.3 %; Found C 50.7, H 3.5, N 3.4 %. IR (cm^{-1}): $\tilde{\nu}$ = 3043 (w), 1599 (m) C=N, 1586 (m), 1570 (m), 1534 (m), 1478 (m), 1456 (m), 1435 (s), 1380 (m), 1334 (m), 1291 (s), 1246 (w), 1234 (w), 1223 (w), 1188 (m), 1179 (m), 1158 (m), 1148 (m), 1120 (m), 1095 (s), 1066 (m), 1025 (m), 1011 (w), 991 (w), 965 (m), 947 (w), 925 (m), 859 (m), 804 (m), 770 (s), 762 (sh), 753 (vs), 743 (vs), 720 (m), 703 (sh), 693 (vs), 683 (vs), 625 (w), 613 (s), 604 (m), 567 (w), 556 (s), 544 (m). ESI+ MS (*m/z*): 815.0793 (calc. 815.0741) $[M - Cl]^+$, 833.0700 (calc. 833.0847) $[M - Cl+H_2O]^+$. ^1H NMR (CD_2Cl_2, ppm): 8.34 (1H, d, $^4J_{H,P}$ = 8.02 Hz, **H**CR=NR), 7.89–7.80 (6H, m, *m*-P-Ar**H**), 7.67–7.60 (1H, m, ^{L}Ar**H**), 7.60–7.51 (2H, m, 2 ^{L}Ar**H**), 7.44–7.30 (10H, m, *o,p*-P-Ar**H**, ^{NPh}Ar**H**), 7.30–7.20 (2H, m, 2 ^{L}Ar**H**), 7.13–7.05 (1H, m, ^{L}Ar**H**), 7.05–6.94 (1H, m, ^{L}Ar**H**), 6.97–6.78 (2H, m, ^{NPh}Ar**H**), 6.44–6.39 (1H, m, ^{L}Ar**H**), 6.39–6.32 (2H, m, ^{NPh}Ar**H**). ^{13}C NMR (CD_2Cl_2, ppm): 166.7 (s, R_2**C**$_{ar}$-O), 164.1 (s, R**C**-NR), 160.2 (s, R_2**C**$_{ar}$-NCR), 149.8 (s, ^{L}**C**$_{ar}$), 136.8 (s, R_2**C**$_{ar}$-Se), 135.1 (br, ^{NPh}**C**$_{ar}$), 135.1 (d, $^3J_{C,P}$ = 10 Hz, *m*-P-**C**$_{ar}$), 134.2 (s, ^{L}**C**$_{ar}$), 133.7 (s, ^{L}**C**$_{ar}$), 131.3 (s, *p*-P-**C**$_{ar}$), 129.0 (s, ^{L}**C**$_{ar}$), 128.7 (d, $^2J_{C,P}$ = 10 Hz, *o*-P-**C**$_{ar}$), 128.6 (s, ^{L}**C**$_{ar}$), 128.5 (s, ^{NPh}**C**$_{ar}$), 125.9 (s, ^{NPh}**C**$_{ar}$), 124.8 (m, P-**C**$_{ar}$), 123.0 (s, ^{L}**C**$_{ar}$), 120.3 (s, ^{L}**C**$_{ar}$), 118.5 (s, ^{L}**C**$_{ar}$), 118.2 (s, ^{L}**C**$_{ar}$), 97.7 (s, ^{NPh}**C**$_{ar}$). ^{31}P NMR ($CDCl_3$, ppm): 2.4 (s).

[Re(NPh)(L^{Te})Cl(PPh$_3$)]. A mixture of $[Re(NPh)Cl_3(PPh_3)_2]$ (91 mg, 0.1 mmol), $\{HL^{Te}\}_2$ (52 mg, 0.08 mmol), water (1 drop) and NEt_3 (1 drop) was suspended in degassed EtOH (3 mL) and heated to reflux whilst stirring. Degassed CH_2Cl_2 (2 mL) was added. The mixture was heated for 5 h under reflux. The grey-brown precipitate formed was separated by filtration. This mixture of $[Re(NPh)Cl_3(PPh_3)_2]$ and $[Re(NPh)(L^{Te})Cl(PPh_3)]$ (approximate ratio: 1:2) was washed with EtOH, diethyl ether and hexane. After drying, it was charged on a column of neutral alumina (d = 1 cm, h = 12 cm) and eluted with CH_2Cl_2 containing 0.1 % MeOH. A brown band was collected and the solvent was evaporated in vacuo. The residue was re-dissolved in a minimum amount of CH_2Cl_2 and a mixture of diethyl ether and EtOH (1:1) was added. After evaporation, $[Re(NPh)(L^{Te})Cl(PPh_3)]$ precipitated as a red powder from the remaining EtOH. It was filtered off, washed with EtOH, diethyl ether and hexane and dried in vacuo. Red-brown powder. Recrystallization can be done from CH_2Cl_2/hexane or CH_2Cl_2/diethyl ether. Yield: 24 mg (27 %).

Elemental analysis: Calculated for $C_{37}H_{29}ClN_2OPReTe$: C 49.5, H 3.3, N 3.1 %; Found C 50.7, H 3,4, N 2.8 %. IR (cm^{-1}): $\tilde{\nu}$ = 3051 (w), 1600 (m) C=N, 1584 (m), 1567 (m), 1538 (m), 1483 (m), 1474 (m), 1451 (m), 1434 (s), 1372 (m), 1335 (m), 1312 (w), 1293 (s), 1262 (w), 1220 (w), 1188 (m), 1177 (m), 1161 (m), 1148 (m), 1122 (m), 1095 (s), 1066 (m), 1024 (m), 990 (w), 968 (w), 936 (sh), 926 (s), 859 (m), 804 (s), 768 (s), 758 (s), 743 (s), 718 (w), 706 (m), 689 (vs), 625 (w), 615 (s), 603 (s), 572 (w), 560 (s), 545 (s). ESI+ MS (*m/z*): 863.0679 (calc. 863.0621) $[M - Cl]^+$. ^1H NMR (CD_2Cl_2, ppm): 8.28 (1H, d, $^4J_{H,P}$ = 8.20 Hz, **H**CR=NR), 7.91–7.83 (6H, m, *m*-P-Ar**H**), 7.72–7.64 (1H, m, ^{L}Ar**H**), 7.52–7.45 (2H, m, 2 ^{L}Ar**H**), 7.40–7.21 (11H, m, integral corrected for $CHCl_3$, *o,p*-P-Ar**H**, ^{NPh}Ar**H**, ^{L}Ar**H**), 7.15–7.05 (2H, m, 2 ^{L}Ar**H**), 7.02–6.95 (1H, m, ^{L}Ar**H**), 6.79–6.70 (2H, m, ^{NPh}Ar**H**), 6.51–6.44 (1H, m, ^{L}Ar**H**), 6.44–6.33 (2H, m, ^{NPh}Ar**H**). ^{13}C NMR ($CDCl_3$, ppm): 171.1 (s, ^{NPh}**C**$_{ar}$), 166.8 (s, R_2**C**$_{ar}$-O), 163.2 (s, R**C**-NR), 162.2 (m, ^{L}**C**$_{ar}$), 156.0 (s, R_2**C**$_{ar}$-NCR), 136.4 (s, R_2**C**$_{ar}$-Te), 136.2 (s, ^{L}**C**$_{ar}$), 135.3 (s, ^{NPh}**C**$_{ar}$), 134.8 (s, ^{NPh}**C**$_{ar}$), 134.4 (d, $^3J_{C,P}$ = 10 Hz, *m*-P-**C**$_{ar}$), 134.4 (s, ^{L}**C**$_{ar}$), 130.6 ($^4J_{C,P}$ = 2 Hz, *p*-P-**C**$_{ar}$), 128.2 (d, $^2J_{C,P}$ = 10 Hz, *o*-P-**C**$_{ar}$), 127.7 (d, *J* = 3 Hz, ^{L}**C**$_{ar}$), 126.5 (s, P-**C**$_{ar}$), 124.8 (s, ^{L}**C**$_{ar}$), 124.0 (d, *J* = 2 Hz, ^{L}**C**$_{ar}$), 122.0 (s, ^{L}**C**$_{ar}$), 119.9 (s, ^{L}**C**$_{ar}$), 118.6 (s, ^{NPh}**C**$_{ar}$), 118.1 (s, ^{L}**C**$_{ar}$). ^{31}P NMR ($CDCl_3$, ppm): 1.5 (s). ^{125}Te NMR ($CDCl_3$, ppm): 378 (d, $^2J_{Te,P}$ = 50 Hz).

[Re(NPhF)(L^{Se})Cl(PPh$_3$)]. A mixture of $[Re(NPhF)Cl_3(PPh_3)_2]$ (92 mg, 0.1 mmol) and $\{HL^{Se}\}_2$ (45 mg, 0.08 mmol) was suspended in a mixture of CH_3CN (3 mL) and CH_2Cl_2 (0.5 mL) and heated under reflux for 10 min. After cooling to room temperature, the mixture was overlayered with diethyl ether (6 mL) and left in the freezer for slow diffusion. The formed crystals of $[Re(NPhF)(L^{Se})Cl(PPh_3)]\cdot CH_3CN$ were filtered off, washed with diethyl ether and dried. From the combined filtrates and washing solutions, a second crop of crystals was obtained by slow evaporation. Red-brown plates. Yield: 73 mg (83 %).

Elemental analysis: Calculated for $C_{37}H_{28}ClFN_2OPReSe$: C 51.2, H 3.3, N 3.2 %; Found C 50.7, H 3.7, N 3.2 %. IR (cm^{-1}): $\tilde{\nu}$ = 3056 (w), 2973 (w), 1599 (m) C=N, 1584 (m), 1569 (m), 1536 (m), 1507 (m), 1481 (m), 1455 (m), 1434 (s), 1377 (m), 1334 (w), 1312 (w), 1285 (m), 1265 (sh), 1228 (s), 1179 (m), 1146 (s), 1119 (m), 1093 (s), 1070 (w), 1045 (w), 1027 (m), 1006 (m), 997 (m), 963 (m), 935 (w), 925 (m), 859 (m), 845 (s), 803 (m), 749 (vs). 740 (sh), 721 (m), 711 (sh), 692 (vs), 647 (m), 612 (s), 603 (s), 584 (sh), 576 (w), 556 (s), 540 (s), 527 (vs). ESI+ MS (*m/z*): 833.0675 (calc. 833.0647) $[M - Cl]^+$. ^1H NMR (CD_2Cl_2, ppm): 8.34 (1H, d, $^4J_{H,P}$ = 8.14 Hz, **H**CR=NR), 7.90–6.31 (27H, m, Ar**H**). ^{13}C NMR (CD_2Cl_2, ppm): 166.7 (s, R_2**C**$_{ar}$-O), 164.2 (s, R**C**-NR), 161.5 (d, $^1J_{C,F}$ = 256 Hz, ^{NPhF}**C**$_{ar}$-F), 158.6 (s, R_2**C**$_{ar}$-NCR), 153.3 (s, ^{NPhF}**C**$_{ar}$), 136.9 (s, ^{L}**C**$_{ar}$), 135.5 (R_2**C**$_{ar}$-Se), 135.1 (d, $^3J_{C,P}$ = 10 Hz, *m*-P-**C**$_{ar}$), 134.2 (s, ^{L}**C**$_{ar}$), 133.7 (s, ^{L}**C**$_{ar}$), 132.6 (s, ^{L}**C**$_{ar}$), 132.5 (s, ^{L}**C**$_{ar}$), 131.3 (s, *p*-P-**C**$_{ar}$), 129.1 (d, $^3J_{C,F}$ = 12 Hz, ^{NPhF}**C**$_{ar}$), 128.7, (d, $^2J_{C,P}$ = 10 Hz, P-**C**$_{ar}$), 126.9 (d, $^3J_{C,P}$ = 8 Hz, *o*-P-**C**$_{ar}$), 125.9 (s, ^{L}**C**$_{ar}$), 120.4 (s, ^{L}**C**$_{ar}$), 118.6 (s, ^{L}**C**$_{ar}$), 118.2 (s, ^{L}**C**$_{ar}$), 116.3 (d, $^2J_{C,F}$ = 23.9 Hz, ^{NPhF}**C**$_{ar}$). ^{19}F NMR (CD_2Cl_2, ppm): –107.7 (s). ^{31}P NMR (CD_2Cl_2, ppm): 1.8 (s). ^{77}Se NMR (CD_2Cl_2, ppm): 360 (d, $^2J_{Se,P}$ = 22 Hz).

[Re(NPhF)(L^{Te})Cl(PPh$_3$)]. A mixture of $[Re(NPhF)Cl_3(PPh_3)_2]$ (92 mg, 0.1 mmol), $\{HL^{Te}\}_2$ (52 mg, 0.08 mmol), water (1 drop) and NEt_3 (1 drop) was suspended in degassed EtOH (3 mL). Degassed CH_2Cl_2 (2 mL) was added. The mixture was heated under reflux for 6 h. The formed grey-brown solid consisting of a mixture of $[Re(NPhF)Cl_3(PPh_3)_2]$ and $[Re(NPhF)(L^{Te})Cl(PPh_3)]$ (1:1) was filtered

off, washed with EtOH, diethyl ether and hexane and charged on a column of neutral alumina (d = 1 cm, h = 9.5 cm). Elution with CH_2Cl_2 containing 2.5 % MeOH gave a brown band of [Re(NPhF)(L^{Te})Cl(PPh_3)]. The solvent was evaporated in vacuo, the residue was re-dissolved in a minimum amount of CH_2Cl_2 and a large excess of diethyl ether was added. The precipitated [Re(NPhF)(L^{Te})Cl(PPh_3)] was filtered off, washed with diethyl ether and hexane and dried on air. Red-brown powder. Yield: 18.6 mg (20 %). Recrystallization can be done from CH_2Cl_2/hexane or CH_2Cl_2/diethyl ether mixtures.

Elemental analysis: Calculated for $C_{37}H_{28}ClFN_2OPReTe$: C 48.5, H 3.1, N 3.1 %; Found C 47.4, H 3.1, N 2.9 %. IR (cm^{-1}): $\tilde{\nu}$ = 3051 (w), 1599 (m) C=N, 1583 (m), 1566 (m), 1538 (m), 1485 (m), 1450 (m), 1434 (s), 1369 (m), 1334 (w), 1314 (w), 1290 (s), 1262 (sh), 1228 (s), 1188 (w), 1177 (m), 1162 (m), 1141 (s), 1121 (m), 1095 (s), 1028 (w), 1008 (m), 998 (m), 968 (m), 945 (w), 937 (w), 926 (m), 860 (m), 839 (s), 803 (s), 761 (s), 742 (s). 718 (m), 706 (m), 690 (vs), 648 (m), 616 (s), 603 (s), 558 (s), 546 (s). ESI+ MS (*m/z*): 881.0556 (calc. 881.0527) [M – Cl]$^+$. ^{1}H NMR ($CDCl_3$, ppm): 8.29 (1H, d, $^4J_{H,P}$ = 8.24 Hz, **H**CR=NR), 7.97–7.80 (6H, m, *m*-P-Ar**H**), 7.71–7.63 (1H, m, ^{L}Ar**H**), 7.51–7.23 (12H, m, integral corrected for $CHCl_3$, 3 ^{L}Ar**H**; *o,p*-P-Ar**H**), 7.17–7.04 (2H, m, ^{NPhF}Ar**H**), 7.04–6.96 (1H, m, ^{L}Ar**H**), 6.54–6.46 (1H, m, ^{L}Ar**H**), 6.46–6.35 (4H, m, 2 ^{L}Ar**H**; ^{NPhF}Ar**H**). ^{13}C NMR ($CDCl_3$, ppm): 166.9 (s, R_2**C$_{ar}$**-O), 163.2 (s, R**C**-NR), 162.2 (d, $^1J_{C,F}$ = 156 Hz, ^{NPhF}**C$_{ar}$**-F), 160.6 (m, ^{L}**C$_{ar}$**), 153.9 (s, R_2**C$_{ar}$**-NCR), 136.6 (s, R_2**C$_{ar}$**-Te), 136.3 (s, ^{L}**C$_{ar}$**), 135.5 (s, ^{NPhF}**C$_{ar}$**), 134.5 (d, $^3J_{C,P}$ = 10 Hz, *m*-P-**C$_{ar}$**), 130.8 ($^4J_{C,P}$ = 2 Hz, *p*-P-**C$_{ar}$**), 128.4 (d, $^2J_{C,P}$ = 10 Hz, *o*-P-**C$_{ar}$**), 127.9 (s, ^{L}**C$_{ar}$**), 126.6 (s, ^{NPhF}**C$_{ar}$**), 126.0 (m, P-**C$_{ar}$**), 124.9 (s, ^{L}**C$_{ar}$**), 124.9 (s, ^{L}**C$_{ar}$**), 120.0 (s, ^{L}**C$_{ar}$**), 118.8 (s, ^{L}**C$_{ar}$**), 118.4 (s, ^{NPhF}**C$_{ar}$**), 116.0 (s, ^{L}**C$_{ar}$**), 115.8 (s, ^{L}**C$_{ar}$**). ^{19}F NMR ($CDCl_3$, ppm): –106.8 ppm (pseudo-ddd). ^{19}F{^{31}P} NMR ($CDCl_3$, decoupled at 1.1 ppm): –106.8 (pseudo-p, $^2J_{F,H}$ = $^3J_{F,H}$ = 7.16 Hz). ^{31}P NMR ($CDCl_3$, ppm): 1.1 (s). ^{125}Te NMR ($CDCl_3$, ppm): 383 (d, $^2J_{Te,P}$ = 59 Hz).

[Re(NPhCF$_3$)Cl$_3$(PPh$_3$)$_2$]. [$ReOCl_3(PPh_3)_2$] (500 mg, 0.59 mmol), 4-(trifluoromethyl)aniline (0.08 mL, 0.59 mmol) and PPh_3 (309 mg, 1.18 mmol) were suspended in toluene (15 mL). The mixture was heated under reflux for 4 h and filtered while hot. EtOH (10 mL) and hexane (200 mL) were added after the mixture reached room temperature. The product crystallized in the freezer overnight.

The crystals were filtered off and washed with EtOH, diethyl ether and hexane. The combined filtrates and washing solutions were left to evaporate for two days at room temperature. The remaining solvent (ca. 15 mL) was diluted with acetone. A second crop of crystals was filtered off and washed with acetone, hexane and diethyl ether. Olive-green crystals. Yield: 242 mg (42 %).

Elemental analysis: Calculated for $C_{43}H_{34}Cl_3F_3NP_2Re$: C 52.9, H 3.5, N 1.4 %; Found C 53.5, H 3.9, N 1.3 %. IR (cm^{-1}): $\tilde{\nu}$ = 3059 (w),1602 (vw), 1586 (vw), 1572 (vw), 1482 (w), 1434 (m), 1406 (w), 1338 (w), 1315 (m), 1178 (m), 1122 (m), 1104 (m), 1090 (m), 1062 (m), 1029 (w), 1008 (m), 998 (w), 912 (w), 849 (m), 745 (s). 704 (sh), 691 (vs), 618 (w), 599 (w), 561 (w). ESI+ MS (*m/z*): 940.1029 (calc. 940.1038) [M – Cl]$^+$. ^{1}H NMR ($CDCl_3$, ppm): 7.85–7.77 (12H, m, *m*-P-Ar**H**), 7.35–7.20 (18H, m, integral corrected for $CHCl_3$, *o,p*-P-Ar**H**), 7.03–6.83 (4H, m ^{NPhCF3}Ar**H**). ^{13}C NMR ($CDCl_3$, ppm): 158.0 (m, R_2C_{ar}-**CF$_3$**), 135.2 (s, R_2**C$_{ar}$**-N=Re), 134.2 (t, $^3J_{C,P}$ = 5 Hz, *m*-P-**C$_{ar}$**), 131.4 (t, $^1J_{C,P}$ = 24 Hz, P-**C$_{ar}$**), 130.6 (s, *o*-CF_3-*m*-N=Re-**C$_{ar}$**), 130.3 (s, *p*-P-**C$_{ar}$**), 127.9 (t, $^2J_{C,P}$ = 5 Hz, *o*-P-**C$_{ar}$**), 125.9 (m, R_2**C$_{ar}$**-CF_3), 121.3 (s, *m*-CF_3-*o*-N=Re-**C$_{ar}$**). ^{19}F NMR ($CDCl_3$, ppm): –63.1 (s). ^{31}P NMR ($CDCl_3$, ppm): –23.3 (s).

[Re(NPhCF$_3$)(L^{Se})Cl(PPh$_3$)]. A mixture of [$Re(NPhCF_3)Cl_3(PPh_3)_2$] (96 mg, 0.1 mmol) and {HL^{Se}}$_2$ (44 mg, 0.08 mmol) was suspended in CH_3CN (12 mL) and heated under reflux for 5 min. The resulting clear, dark red solution was filtered through cotton. Diethyl ether (24 mL) and hexane (52 mL) were added and the mixture was left for slow evaporation at ambient temperature for three days. The formed single crystals of [Re(NPhCF$_3$)(L^{Se})Cl(PPh_3)] were filtered off, washed with hexane and dried in vacuo. Red-brown cubes. Yield: 50 mg (57 %).

Elemental analysis: Calculated for $C_{38}H_{28}ClF_3N_2OPReSe$: C 49.8, H 3.1, N 3.1 %; Found C 49.7, H 3.6, N 2.5 %. IR (cm^{-1}): $\tilde{\nu}$ = 3052 (w), 1600 (s) C=N, 1583 (m), 1569 (m), 1533 (m), 1497 (w), 1482 (m), 1454 (m), 1434 (s), 1407 (w), 1372 (sh), 1361 (m), 1335 (w), 1317 (vs), 1292 (s), 1248 (w), 1230 (w), 1177 (sh), 1159 (s), 1133 (s), 1095 (s), 1063 (s), 1029 (m), 1011 (m), 1000 (m), 962 (m), 925 (m), 847 (s), 807 (m), 752 (s). 744 (s), 719 (m), 707 (s), 690 (vs), 645 (m), 618 (m), 597 (m), 562 (m), 540 (m), 529 (vs). ESI+ MS (*m/z*): 883.0608 (calc. 883.0615) [M – Cl]$^+$. ^{1}H NMR ($CDCl_3$, ppm): 8.36 (1H, d, $^4J_{H,P}$ = 8.05 Hz, **H**CR=NR), 7.90–7.82 (6H, m, *m*-P-Ar**H**), 7.66–7.62 (1H, m, ^{L}Ar**H**), 7.58–7.50 (2H, m, 2 ^{L}Ar**H**), 7.45–7.34 (9H, m, *o,p*-P-Ar**H**), 7.30–7.20 (2H, m, integral corrected for $CHCl_3$, 2 ^{L}Ar**H**), 7.12–7.06 (1H, m, ^{L}Ar**H**), 7.04–6.98 (3H, m, ^{L}Ar**H**; ^{NPhCF3}Ar**H**), 6.46–6.40 (1H, m, ^{L}Ar**H**), 6.46–6.40 (2H, m, ^{NPhCF3}Ar**H**). ^{13}C NMR ($CDCl_3$, ppm): 166.7 (s, R_2**C$_{ar}$**-O), 163.5 (s, R**C**-NR), 158.6 (s, R_2**C$_{ar}$**-NCR), 158.1 (m, ^{NPhCF3}**C$_{ar}$**), 149.8 (s, ^{L}**C$_{ar}$**), 136.8 (s, R_2**C$_{ar}$**-Se), 135.2 (m, ^{NPhCF3}**C$_{ar}$**), 134.6 (d, $^3J_{C,P}$ = 10 Hz, *m*-P-**C$_{ar}$**), 133.9 (s, ^{L}**C$_{ar}$**), 133.4 (s, ^{L}**C$_{ar}$**), 131.0 (d, $^4J_{C,P}$ = 2 Hz, *p*-P-**C$_{ar}$**), 131.0 (s, ^{L}**C$_{ar}$**), 128.4 (d, $^2J_{C,P}$ = 10 Hz, *o*-P-**C$_{ar}$**), 128.2 (s, ^{L}**C$_{ar}$**), 128.1 (m, ^{NPhCF3}**C$_{ar}$**), 125.7 (m, P-**C$_{ar}$**), 124.4 (d, *J* = 2 Hz, ^{L}**C$_{ar}$**), 122.3 (s, ^{NPhCF3}**C$_{ar}$**), 120.0 (s, ^{L}**C$_{ar}$**), 118.7 (s, ^{L}**C$_{ar}$**), 118.3 (s, ^{L}**C$_{ar}$**) 117.9 (s, ^{NPhCF3}**C$_{ar}$**). ^{19}F NMR ($CDCl_3$, ppm): –63.0 (s). ^{31}P NMR ($CDCl_3$, ppm): 0.6 (s). ^{77}Se NMR ($CDCl_3$, ppm): 395 (d, $^2J_{Se,P}$ = 24 Hz).

[Re(NPhCF$_3$)(L^{Te})Cl(PPh$_3$)]. A mixture of [$Re(NPhCF_3)Cl_3(PPh_3)_2$] (96 mg, 0.1 mmol), {HL^{Te}}$_2$ (104 mg, 0.16 mmol), water (1 drop) and NEt_3 (1 drop) was suspended in degassed EtOH (3 mL). Degassed CH_2Cl_2 (2 mL) was added. The mixture was heated under reflux for 2.5 h. The solvents were evaporated in vacuo. The residue was re-dissolved in CH_2Cl_2 and charged on a column of neutral alumina (d = 1 cm, h = 15 cm). Elution with CH_2Cl_2 containing 0.1 % MeOH gave a brown band of the product. The solvent was evaporated in vacuo and the residue re-dissolved in a minimum amount of CH_2Cl_2 and filtered. After removal of the solvent in vacuo, a sticky product remained, which was solidified by the addition of *n*-hexane and vigorous stirring. It was filtered off, washed with hexane and dried on air. Brown powder. Yield: 16.0 mg (17 %).

Elemental analysis: Calculated for $C_{38}H_{28}ClF_3N_2OPReTe$: C 47.3, H 2.9, N 2.9 %; Found C 45.5, H 3.1, N 3.0 %. IR (cm^{-1}): $\tilde{\nu}$ = 3051 (w), 2923 (w), 2867 (w), 1600 (s) C=N, 1586 (sh), 1567 (sh), 1541 (m), 1481 (w), 1469 (m), 1452 (m), 1434 (s), 1407 (w), 1362 (m), 1381 (vs), 1287 (s), 1261 (sh), 1168 (m), 1121 (s), 1103 (s), 1063 (vs), 1029 (m), 1010 (m), 960 (w), 925 (m), 861 (sh), 845 (s), 803 (m), 744 (vs), 717 (m), 692 (vs), 645 (m), 617 (m), 603 (m), 558 (m), 541 (s). ESI+ MS (*m/z*): 931.0582 (calc. 931.0495) [M – Cl]$^+$. ^{1}H NMR ($CDCl_3$, ppm): 8.33 (1H, d, $^4J_{H,P}$ = 8.24 Hz, **H**CR=NR), 7.97–7.31 (20H, 4m, *m,o,p*-P-Ar**H**; 4 ^{L}Ar**H**), 7.21–6.93 (5H, 2m, 3 ^{L}Ar**H**; 2 ^{NPhCF3}Ar**H**), 6.49–6.43 (1H, m, ^{L}Ar**H**), 6.40–6.33 (2H, m, ^{NPhCF3}Ar**H**). ^{13}C NMR ($CDCl_3$, ppm): 167.3 (s, R_2**C$_{ar}$**-O), 164.1 (m, ^{NPhCF3}**C$_{ar}$**), 163.0 (s, R**C**-NR), 162.2 (m, ^{L}**C$_{ar}$**), 158.4 (s, R_2**C$_{ar}$**-NCR), 136.9 (s, R_2**C$_{ar}$**-Te), 136.4 (s, ^{L}**C$_{ar}$**), 135.6 (m, ^{NPhCF3}**C$_{ar}$**), 134.6 (d, $^3J_{C,P}$ = 10 Hz, *m*-P-**C$_{ar}$**), 132.3 (s, ^{L}**C$_{ar}$**), 132.2 (s, ^{L}**C$_{ar}$**), 131.1 (s, *p*-P-**C$_{ar}$**), 130.8 (s, ^{L}**C$_{ar}$**), 128.5 (d, $^2J_{C,P}$ = 10 Hz, *o*-P-**C$_{ar}$**), 128.2 (m, ^{NPhCF3}**C$_{ar}$**), 128.1 (s, ^{L}**C$_{ar}$**), 125.9 (m, P-**C$_{ar}$**), 125.5 (s, ^{NPhCF3}**C$_{ar}$**), 122.8 (d, *J* = 2 Hz, ^{L}**C$_{ar}$**), 119.8 (s, ^{L}**C$_{ar}$**), 118.8 (s, ^{L}**C$_{ar}$**), 118.7 (s, ^{NPhCF3}**C$_{ar}$**). ^{19}F NMR ($CDCl_3$, ppm): –63.1 (s). ^{31}P NMR ($CDCl_3$, ppm): 0.3 (s). ^{125}Te NMR ($CDCl_3$, ppm): 486 (d, $^2J_{Te,P}$ = 67 Hz).

Acknowledgments

This work was generously supported by the German Academic Exchange Service (DAAD, Germany) and the Coordenadoria de Aperfeiçoamento de Pessoal de Nível Superior (CAPES, Brazil). We also gratefully acknowledge the assistance of the Core Facility BioSupraMol supported by the DFG and the High-Performance-Computing (HPC) Centre of the Zentraleinrichtung für Datenverarbeitung (ZEDAT) of the Freie Universität Berlin for computational time and support.

Keywords: Rhenium · Selenolates · Tellurolates · Schiff bases · Reduction

[1] *Cambridge Structural Database*, Release 5.40, November **2018**.
[2] W.-F. Liaw, Y.-C. Horng, D.-S. Ou, C.-Y. Chuang, C.-K. Lee, G.-H. Lee, S.-M. Peng, *J. Chin. Chem. Soc.* **1995**, *42*, 59–65.
[3] H. Egold, U. Flörke, *Z. Anorg. Allg. Chem.* **2001**, *627*, 2295–2305.
[4] B. Manimaran, A. Vanitha, M. Karthikeyan, B. Ramakrishna, S. M. Mobin, *Organometallics* **2014**, *33*, 465–472.
[5] R. Nagarajaprakash, C. A. Kumar, S. M. Mobin, B. Manimaran, *Organometallics* **2015**, *34*, 724–730.
[6] H. Egold, S. Klose, U. Flörke, *Z. Anorg. Allg. Chem.* **2001**, *627*, 164–171.
[7] A. Vanitha, S. M. Mobin, B. Manimaran, *J. Organomet. Chem.* **2011**, *696*, 1609–1617.
[8] L. Veronese, E. Q. Procopio, D. Maggioni, P. Mercandelli, M. Panigati, *New J. Chem.* **2017**, *41*, 11268–11279.
[9] A. Meltzer, R. Cargnelutti, A. Hagenbach, E. Schulz Lang, U. Abram, *Z. Anorg. Allg. Chem.* **2015**, *641*, 2617–2623.
[10] A. A. Pasynskii, Y. V. Torubaev, A. V. Pavlova, I. V. Skabitsky, G. L. Denisov, V. A. Grinberg, *J. Cluster Sci.* **2015**, *26*, 247–260.
[11] A. A. Pasynsky, Y. V. Torubaev, A. V. Pavlova, S. S. Shapovalov, I. V. Skabitsky, G. L. Denisov, *Russ. J. Coord. Chem.* **2014**, *40*, 611–616.
[12] A. A. Pasynskii, S. S. Shapovalov, I. V. Skabitsky, O. G. Tikhonova, T. A. Krishtop, *Russ. J. Coord. Chem.* **2015**, *41*, 76–79.
[13] A. Vanitha, J. Muthukumaran, R. Krishna, B. Manimaran, *Acta Crystallogr., Sect. E. Struct. Rep. Online* **2010**, *66*, m518–m519.
[14] J. Muthukumaran, M. Kannan, A. Vanitha, B. Manimaran, R. Krishna, *Acta Crystallogr., Sect. E: Struct. Rep. Online* **2010**, *66*, m558–m559.
[15] J. S. Jones, F. P. Gabbaï, *Chem. Lett.* **2016**, *45*, 376–384.
[16] M. Godoi, M. W. Paixão, A. L. Braga, *Dalton Trans.* **2011**, *40*, 11347–11355.
[17] Q. Yao, E. P. Kinney, C. Zheng, *Org. Lett.* **2004**, *6*, 2997–2999.
[18] F. A. Cotton, K. R. Dunbar, *Inorg. Chem.* **1987**, *26*, 1305–1309.
[19] T. Fietz, H. Spies, P. Leibnitz, D. Scheller, *J. Coord. Chem.* **1996**, *38*, 227–235.
[20] T.-F. Wang, C.-C. Hwu, C.-W. Tsai, Y.-S. Wen, *Organometallics* **1998**, *17*, 131–138.
[21] F. De Montigny, L. Guy, G. Pliet, N. Vanthuyne, C. Ruossel, R. Lombardi, T. B. Freedman, L. A. Nafie, J. Crassous, *Chem. Commun.* **2009**, 4841–4843.
[22] V. D. Schwade, A. Hagenbach, E. Schulz Lang, K. Klauke, F. Mohr, U. Abram, *Eur. J. Inorg. Chem.* **2014**, *2014*, 1949–1954.
[23] M. Herberhold, C.-X. Jin, W. Millius, *Z. Anorg. Allg. Chem.* **1994**, *620*, 1295–1300.
[24] R. Cargnelutti, E. S. Lang, P. Piquini, U. Abram, *Inorg. Chem. Commun.* **2014**, *45*, 48–50.
[25] R. Pietschnig, K. Merz, S. Schäfer, *Heteroat. Chem.* **2005**, *16*, 169–174.
[26] L. M. Caldwell, A. F. Hill, A. G. Hulkes, C. M. A. McQueen, A. J. P. White, D. J. Williams, *Organometallics* **2010**, *29*, 6350–6358.
[27] B. Noschang Cabral, L. Kirsten, A. Hagenbach, P. C. Piquini, M. Patzschke, E. S. Lang, U. Abram, *Dalton Trans.* **2017**, *46*, 9280–9286.
[28] B. Noschang Cabral, *Doctoral* Thesis, Universidade Federal Santa Maria, **2017**.
[29] E. Labisbal, J. Romero, M. L. Durán, J. A. García-Vázquez, A. Sousa, U. Russo, R. Pritchard, M. Renson, *J. Chem. Soc., Dalton Trans.* **1993**, 755–758.
[30] I. S. Vasil'chenko, I. G. Borodkina, A. S. Burlov, N. V. Karpova, G. M. Abakarov, K. A. Lyssenko, G. S. Borodkin, I. E. Uflyand, A. D. Garnovskii, V. I. Minkin, *Russ. Chem. Bull.* **2013**, *62*, 1809–1814.
[31] N. A. Barnes, S. M. Godfrey, R. T. A. Halton, I. Mushtaq, R. G. Pritchard, S. Sarwar, *Dalton Trans.* **2006**, 1517–1523.
[32] R. Pietschnig, S. Spirk, G. N. Rechberger, K. Merz, *Inorg. Chim. Acta* **2008**, *361*, 1958–1964.
[33] L. C. Forfar, M. Green, M. F. Haddow, S. Hussein, J. M. Lynam, J. M. Slattery, C. A. Russell, *Dalton Trans.* **2015**, *44*, 110–118.
[34] R. K. Haynes, C. Indorato, *Aust. J. Chem.* **1984**, *37*, 1183–1194.
[35] H. Ohmori, H. Maeda, K. Konomoto, K. Sakai, M. Masui, *Chem. Pharm. Bull.* **1987**, *35*, 4473–4481.
[36] M. Sakakibara, Y. Watanabe, T. Toru, Y. Ueno, *J. Chem. Soc., Perkin Trans. 1* **1991**, 1231–1234.
[37] I. Nakagawa, T. Hata, *Tetrahedron Lett.* **1975**, *17*, 1409–1412.
[38] S. Ford, C. P. Morley, M. Di Vaira, *Inorg. Chem.* **2004**, *43*, 7101–7110.
[39] M. Risto, E. M. Jahr, M. S. Hannu-Kuure, R. Oilunkaniemi, R. S. Laitinen, *J. Organomet. Chem.* **2007**, *692*, 2193–2204.
[40] U. Abram, *Rhenium*, in Comprehensive Coordination Chemistry II, From Biology to Nanotechnology (Eds.: J. A. McCleverty, T. J. Meyer), Elsevier **2005**, pp. 271–402.
[41] B. Kuhn, U. Abram, *Z. Anorg. Allg. Chem.* **2010**, *637*, 242–245.
[42] C. Scholtysik, M. Roca Jungfer, A. Hagenbach, U. Abram, *Z. Anorg. Allg. Chem.* **2018**, *644*, 1451–1455.
[43] C. Scholtysik, C. Njiki Noufeele, A. Hagenbach, U. Abram, *Inorg. Chem.* **2019**, *58*, 5241–5252.
[44] S. Abram, U. Abram, E. Schulz Lang, J. Strähle, *Acta Crystallogr., Sect. C* **1995**, *51*, 1078–1080.
[45] H. H. Nguyen, U. Abram, *Inorg. Chem.* **2007**, *46*, 5310–5319.
[46] H. H. Nguyen, C. T. Pham, A. Rodenstein, R. Kirmse, U. Abram, *Inorg. Chem.* **2011**, *50*, 590–596.
[47] U. Mazzi, F. Refosco, G. Bandoli, M. Nicolini, *Transition Met. Chem.* **1985**, *10*, 121–127.
[48] X. Chen, F. J. Femia, J. W. Babich, J. Zubieta, *Inorg. Chim. Acta* **2000**, *307*, 149–153.
[49] J.-Y. Kim, Y.-J. Ji, H.-J. Ha, H.-K. Chae, *Bull. Korean Chem. Soc.* **2003**, *24*, 504–506.
[50] C. Bolzati, M. Porchia, G. Bandoli, A. Boschi, E. Malago, *Inorg. Chim. Acta* **2001**, *315*, 205–212.
[51] P. Mayer, K. C. Potgieter, T. I. A. Gerber, *Polyhedron* **2010**, *29*, 1423–1430.
[52] F. J. Femia, X. Chen, J. W. Babich, J. Zubieta, *Inorg. Chim. Acta* **2001**, *316*, 145–148.
[53] X. Chen, F. J. Femia, J. W. Babich, J. Zubieta, *Inorg. Chim. Acta* **2000**, *308*, 80–90.
[54] F. J. Femia, X. Chen, J. W. Babich, J. Zubieta, *Inorg. Chim. Acta* **2000**, *300*, 517–524.
[55] X. Chen, F. J. Femia, J. W. Babich, J. Zubieta, *Inorg. Chim. Acta* **2001**, *316*, 33–40.
[56] R. Alberto, R. Schibli, R. Egli, P. A. Schubiger, W. A. Herrmann, G. Artus, U. Abram, T. A. Kaden, *J. Organomet. Chem.* **1995**, *493*, 119–127.
[57] N. P. Johnson, C. J. L. Lock, G. Wilkinson, *J. Chem. Soc.* **1964**, 1054–1066.
[58] J. Chatt, G. A. Rowe, *J. Chem. Soc.* **1964**, 1012–1020.
[59] C. S. Radatz, D. Alves, P. H. Schneider, *Tetrahedron* **2013**, *69*, 1316–1321.
[60] L. Engman, D. Stern, I. A. Cotgreave, C. M. Andersson, *J. Am. Chem. Soc.* **1992**, *114*, 9737–9743.
[61] A. M. Deobald, L. R. S. de Camargo, G. Tabarelli, M. Hörner, O. E. D. Rodrigues, D. Alves, A. L. Braga, *Tetrahedron Lett.* **2010**, *51*, 3364–3367.
[62] G. M. Sheldrick, *SADABS*, University of Göttingen, Germany, **1996**.
[63] P. Coppens, *The Evaluation of Absorption and Extinction in Single-Crystal Structure Analysis. Crystallographic Computing*, Copenhagen, Muksgaard, **1979**.
[64] G. M. Sheldrick, *Acta Crystallogr., Sect. A* **2008**, *64*, 112–122.
[65] G. M. Sheldrick, *Acta Crystallogr., Sect. C* **2015**, *71*, 3–8.
[66] *Diamond - Crystal and Molecular Structure Visualization* Crystal Impact - Dr. H. Putz & Dr. K. Brandenburg GbR, Bonn, Germany.
[67] M. J. Frisch, G. W. Trucks, H. B. Schlegel, G. E. Scuseria, M. A. Robb, J. R. Cheeseman, G. Scalmani, V. Barone, B. Mennucci, G. A. Petersson, H. Nakatsuji, M. Caricato, X. Li, H. P. Hratchian, A. F. Izmaylov, J. Bloino, G. Zheng, J. L. Sonnenberg, M. Hada, M. Ehara, K. Toyota, R. Fukuda, J. Hasegawa, M. Ishida, T. Nakajima, Y. Honda, O. Kitao, H. Nakai, T. Vreven, J. A.

Montgomery Jr., J. E. Peralta, F. Ogliaro, M. Bearpark, J. J. Heyd, E. Brothers, K. N. Kudin, V. N. Staroverov, R. Kobayashi, J. Normand, K. Raghavachari, A. Rendell, J. C. Burant, S. S. Iyengar, J. Tomasi, M. Cossi, N. Rega, J. M. Millam, M. Klene, J. E. Knox, J. B. Cross, V. Bakken, C. Adamo, J. Jaramillo, R. Gomperts, R. E. Stratmann, O. Yazyev, A. J. Austin, R. Cammi, C. Pomelli, J. W. Ochterski, R. L. Martin, K. Morokuma, V. G. Zakrzewski, G. A. Voth, P. Salvador, J. J. Dannenberg, S. Dapprich, A. D. Daniels, Ö. Farkas, J. B. Foresman, J. V. Ortiz, J. Cioslowski, D. J. Fox, *Gaussian 09, Revision B.01*, Gaussian, Inc., Wallingford CT, **2016**.

[68] M. J. Frisch, G. W. Trucks, H. B. Schlegel, G. E. Scuseria, M. A. Robb, J. R. Cheeseman, G. Scalmani, V. Barone, G. A. Petersson, H. Nakatsuji, X. Li, M. Caricato, A. Marenich, J. Bloino, B. G. Janesko, R. Gomperts, B. Mennucci, H. P. Hratchian, J. V. Ortiz, A. F. Izmaylov, J. L. Sonnenberg, D. Williams-Young, F. Ding, F. Lipparini, F. Egidi, J. Goings, B. Peng, A. Petrone, T. Henderson, D. Ranasinghe, V. G. Zakrzewski, J. Gao, N. Rega, G. Zheng, W. Liang, M. Hada, M. Ehara, K. Toyota, R. Fukuda, J. Hasegawa, M. Ishida, T. Nakajima, Y. Honda, O. Kitao, H. Nakai, T. Vreven, K. Throssell, J. A. Montgomery Jr., J. E. Peralta, F. Ogliaro, M. Bearpark, J. J. Heyd, E. Brothers, K. N. Kudin, V. N. Staroverov, T. Keith, R. Kobayashi, J. Normand, K. Raghavachari, A. Rendell, J. C. Burant, S. S. Iyengar, J. Tomasi, M. Cossi, J. M. Millam, M. Klene, C. Adamo, R. Cammi, J. W. Ochterski, R. L. Martin, K. Morokuma, O. Farkas, J. B. Foresman, D. J. Fox, *Gaussian 09, Revision A.02*, Gaussian, Inc., Wallingford CT, **2016**.

[69] *GaussView*, Version 6, Roy Dennington, Todd A. Keith, and John M. Millam, Semichem Inc., Shawnee Mission, KS, **2016**.

[70] S. H. Vosko, L. Wilk, M. Nusair, *Can. J. Phys.* **1980**, *58*, 1200–1211.

[71] A. D. Becke, *J. Chem. Phys.* **1993**, *98*, 5648–5652.

[72] C. Lee, W. Yang, R. G. Parr, *Phys. Rev. B* **1988**, *37*, 785–789.

[73] P. J. Hay, W. R. Wadt, *J. Chem. Phys.* **1985**, *82*, 270; P. J. Hay, W. R. Wadt, *J. Chem. Phys.* **1985**, *82*, 284; P. J. Hay, W. R. Wadt, *J. Chem. Phys.* **1985**, *82*, 299.

[74] R. Krishnan, J. S. Binkley, R. Seeger, J. A. Pople, *J. Chem. Phys.* **1980**, *72*, 650–654.

[75] A. D. McLean, G. S. Chandler, *J. Chem. Phys.* **1980**, *72*, 5639–5648.

[76] L. A. Curtiss, M. P. McGrath, J.-P. Blandeau, N. E. Davis, R. C. Binning, J. L. Radom, *J. Chem. Phys.* **1995**, *103*, 6104–6113.

[77] K. L. Schuchardt, B. T. Didier, T. Elsethagen, L. Sun, V. Gurumoorthi, J. Chase, J. Li, T. L. Windus, *J. Chem. Inf. Model.* **2007**, *47*, 1045–1052.

Received: October 10, 2019

4.9 Reactions of Schiff Base-Substituted Diselenides and -tellurides with Ni(II), Pd(II) and Pt(II) Phosphine Complexes

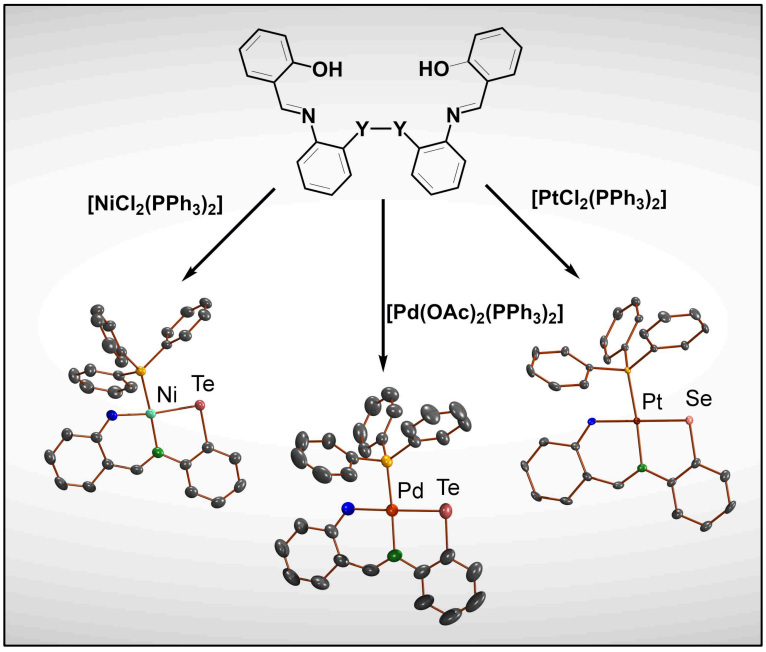

Reproduced with permission from Roca Jungfer, M.; Schulz Lang, E.; Abram U. *Eur. J. Inorg. Chem.* **2020**, 4303–4312.

DOI: 10.1002/ejic.202000750

For Supplementary Material see A.9.

Author Contributions:

Maximilian Roca Jungfer designed the project. Maximilian Roca Jungfer performed the synthesis and characterization of the compounds, performed DFT calculations, calculated the X-ray structures and wrote a draft of the manuscript. Ernesto Schulz Lang provided guidance and the laboratory space to perform some of the experiments in Brazil. Ulrich Abram supervised the project, provided scientific guidance and suggestions, and corrected the manuscript.

EurJIC
European Journal of Inorganic Chemistry

Full Paper
doi.org/10.1002/ejic.202000750

Chemistry Europe
European Chemical Societies Publishing

Rhenium Complexes

Reactions of Schiff Base-Substituted Diselenides and -tellurides with Ni(II), Pd(II) and Pt(II) Phosphine Complexes

Maximilian Roca Jungfer,[a] Ernesto Schulz Lang,[b] and Ulrich Abram*[a]

Abstract: The salicylidene Schiff bases of bis(2-aminophenyl)diselenide and -ditelluride react with $[M^{II}Cl_2(PPh_3)_2]$ (M = Ni, Pt) or $[Pd^{II}(OAc)_2(PPh_3)_2]$ with formation of square-planar complexes with the general formulae $[M^{II}(L^Y)(PPh_3)]$ (M = Ni, Pd, Pt, Y = Se, Te). The ligands coordinate to the metals as tridentate {O,N,Se/Te} chelates. The reduction of the dichalcogenides and the formation of the chalcogenolato ligands occurs in situ by released PPh_3 ligands. A mechanism for such reactions has been derived from the experimental data with the aid of DFT calculations. It suggests a higher polarization of the dichalcogenide bond with partial charge separation upon coordination to a metal centre, which therefore facilitates the cleavage of the dichalcogenide bond with PPh_3. In accordance with the proposed mechanism, best yields are obtained with a strict exclusion of oxygen, but in the presence of water.

Introduction

The interest in the chemistry of the nickel, palladium and platinum triad is fueled by the manifold of catalytic properties of their complexes and their biological activities. Many easily accessible chelating ligand systems were exhaustively investigated in this regard. Until today, tri- and tetradentate Schiff bases are common ligands for nickel, palladium and platinum, as they yield stable, flexible and easily tunable complexes due to the modularity of the Schiff base preparation.[1–15] Hundreds of such compounds have been characterized crystallographically.[16] The introduction of additional chalcogen donor atoms in the form of arylchalcogenolato units is a common motif to modulate the properties of the resulting complexes.[1,4–15] However, only a few of such complexes with aryltellurolato ligands have been structurally characterized up to now.[16] More complexes are known with arylselenolato ligands, albeit mainly derived from simple diphenyldiselenide and still with very limited accessibility compared to their sulfur and oxygen analogs. The synthesis of the arylselenolato and -tellurolato ligands is commonly complicated in contrast to the corresponding phenolato and thiophenolato ligands because the respective selenols and tellurols are unstable. They are commonly prepared by the reduction of the corresponding diorganodichalcogenides directly before the complex formation. The reaction conditions of such procedures must be controlled carefully in order to avoid the parallel reduction of the transition metal ions.[17,18] Occasionally, nickel, palladium and platinum complexes with organochalcogenolato ligands have been prepared from the dichalcogenides via an oxidative addition to a low-valent metal species.[19–23] In the case of palladium, organochalcogenolato complexes are also accessible via an oxidative addition to Pd^{II} with formation of Pd^{IV} species. But often complex mixtures and mainly polynuclear complexes are obtained following such procedures.[24–29] Overall, the methods for the preparation of complexes with heavier chalcogenolates as ligands remain limited.

Recently, we reported an alternative method for the preparation of rhenium selenolato and tellurolato complexes with the metal in the high formal oxidation state "+5". The reduction of the salicylidene Schiff bases of bis(2-aminophenyl)diselenide and –telluride was performed in situ by released PPh_3 ligands from the oxido- and arylimidorhenium(V) starting materials.[30,31] This methods represents a considerable progress over the hitherto occasionally use of metal(0) species.[32]

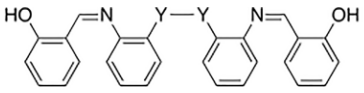

Y = Se: $\{HL^{Se}\}_2$
Y = Te: $\{HL^{Te}\}_2$

In the present work, we demonstrate that the method used for high-valent rhenium complexes can be extended to the metals nickel, palladium and platinum. Thereto, we performed reactions of $[M^{II}Cl_2(PPh_3)_2]$ (M = Ni, Pt) and $[Pd^{II}(OAc)_2(PPh_3)_2]$ with the Schiff bases prepared from salicylaldehyde and bis-(2-aminophenyl)diselenide ($\{HL^{Se}\}_2$) and -ditelluride ($\{HL^{Te}\}_2$).

[a] M. Roca Jungfer, Prof. Dr. U. Abram
Institute of Chemistry and Biochemistry, Freie Universität Berlin,
Fabeckstr. 34/36, 14195 Berlin, Germany
E-mail: Ulrich.Abram@fu-berlin.de
https://www.bcp.fu-berlin.de/chemie/chemie/forschung/InorgChem/agabram/index.html
[b] Prof. Dr. E. S. Lang
Universidade Federal de Santa Maria,
Laboratorio de Materiais Inorganicos, Santa Maria/RS, Brazil
https://www.ufsm.br/cursos/pos-graduacao/santa-maria/ppgq/
Supporting information and ORCID(s) from the author(s) for this article are available on the WWW under https://doi.org/10.1002/ejic.202000750.

Results and Discussion

Reactions of the two dichalcogenide Schiff bases with $[NiCl_2(PPh_3)_2]$, $[PtCl_2(PPh_3)_2]$ or $[Pd(OAc)_2(PPh_3)_2]$ show that they are reduced and form tridentate selenolato and tellurolato ligands. A summary of the performed reactions and obtained products is shown in Scheme 1. The red-orange or red-brown complexes are stable as solids and in solution. Even their solutions can be heated in the air without considerable decomposition. At room temperature, no decomposition or dichalcogenide formation is noticeable even after several days in non-degassed, wet solutions of chlorinated solvents. This is in contrast to the instability of rhenium(V) complexes with the same ligands we reported earlier.[30] Similarly to the reported rhenium complexes, the ^{77}Se signals of the selenolato ligands appear between 197 and 326 ppm and the corresponding ^{125}Te resonances are found between 300 and 477 ppm. The shielding of the chalcogen atoms decreases in the order Pd > Ni > Pt, which has been observed in Schiff base selenolato complexes before.[23] Unfortunately, we could not correlate this shielding trend in the chalcogen chemical shift with any common rationale such as the electronegativity of the involved elements or the solid state geometry of the complexes. The selenium-phosphorus coupling constants are in the range of 21 to 77 Hz. This is within the range of couplings, which have previously been observed for mixed selenolato/phosphine complexes of platinum.[33,34] The ^{125}Te NMR spectra of the analogous tellurolato complexes show doublets with $^2J_{Te,P}$ couplings of 58–194 Hz, which is also in accordance with the situation in previously reported Pt(II) compounds.[33] Unexpectedly, the chalcogen-phosphorus couplings in the nickel complexes are between 77 Hz and 194 Hz, which is four times larger than those of the platinum and palladium complexes. When observed, the ^{77}Se and ^{125}Te couplings in the respective ^{31}P NMR spectra confirm the coupling constants in the ^{77}Se and ^{125}Te spectra. A key feature in the proton NMR spectra of Schiff base complexes is the resonance of their unique aldiminic proton. It is well-separated from the remaining aromatic resonances. As we reported for the rhenium complexes of these ligands, the aldiminic protons in the selenolato complexes are more deshielded compared to those in the tellurolato complexes. The chemical shift of the sulfur analogous nickel complex $[Ni^{II}(L^S)(PPh_3)]$[12] follows the same trend: the aldiminic proton of this compound is more deshielded than that of the selenolato complex $[Ni^{II}(L^{Se})(PPh_3)]$. Additionally, the aldiminic protons are more deshielded along the series nickel-palladium-platinum. In complexes with aldiminic and phosphine ligands, the aldiminic protons often couple to the ^{31}P nuclei. This is also the case in the complexes of the present study with coupling constants in the range of 9–15 Hz. This allows an in situ monitoring of the complex formation. The coupling constants of the selenolato complexes are larger than those of the tellurolato complexes. The platinum NMR resonances of the platinum complexes are observed around –3700 ppm with a $^1J_{Pt,P}$ coupling of ca. 3700 Hz. The $^1J_{Pt,P}$ coupling constants are in the expected range for a phosphine in *trans*-position to a stronger σ-donor with weaker π-accepting abilities.[35] The resonance of $[Pt^{II}(L^{Se})(PPh_3)]$ is more shielded than that of $[Pt^{II}(L^{Te})(PPh_3)]$ and shows a larger coupling to the phosphorus.

Single crystal structure determinations show that the six metal complexes of this study have the same general structure with square-planar coordination spheres of the metal ions bound to tridentate chalcogenolato ligands. The molecular structures of $[Ni(L^{Te})(PPh_3)]$, $[Pd(L^{Te})(PPh_3)]$ and $[Pt(L^{Se})(PPh_3)]$ are shown in Figure 1 as representatives for the complexes with the selenium- and tellurium-containing ligands. Since the general bonding features of the other complexes are similar, their structures are not shown here. They can be found in the Supporting Information. Selected bond lengths and angles of all complexes and the corresponding dichalcogenides[30] are compared in Table 1.

Main distortions of the square-planar coordination environments of the transition metal ions come from the restrictions caused by the size of the chalcogen atoms, the size of the metal ions and the rigidity of the C17–N1 bonds. The two *trans*-spanning angles N1–M1–P1 and O1–M1–Se1/Te1 range from 174.8° to 176.5° and from 172.2° to 179.5° respectively. The N1–M1–Se1/Te1 angles are between 86.8° and 91.0°, while the N1–M1–O1 angles are between 93.3° and 96.8°. The *cis* Se1/Te1–M1–P1 angles are between 91.2° and 96.6°.

In general, the bonding features of the selenium- and tellurium-containing complexes are very similar to the corresponding compounds with the analogous sulfur-containing ligand $\{L^S\}^{2-}$, while the respective complexes with a second phenolato unit, $\{L^O\}^{2-}$, behave differently.[7,9,10,12,15]

The structurally similar complexes of the ligands L^S, L^{Se} and L^{Te} all crystallize in two similar triclinic unit cells. The packing

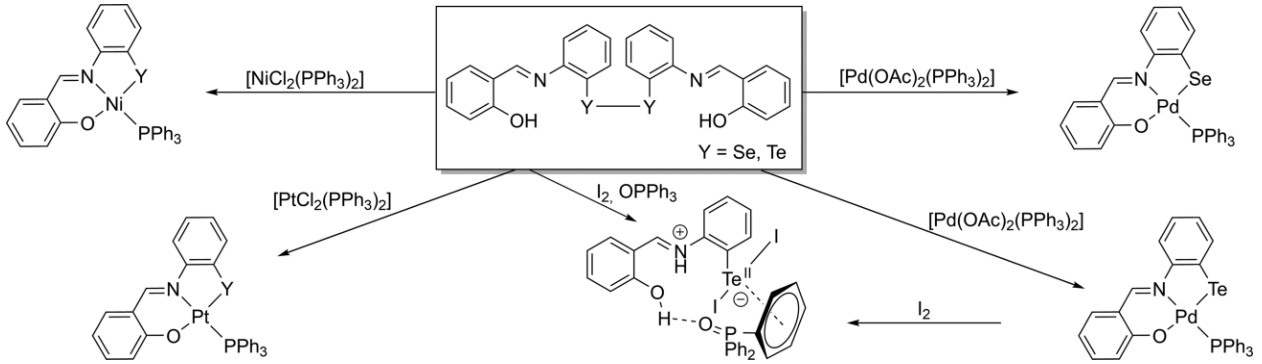

Scheme 1. Performed reactions and their products.

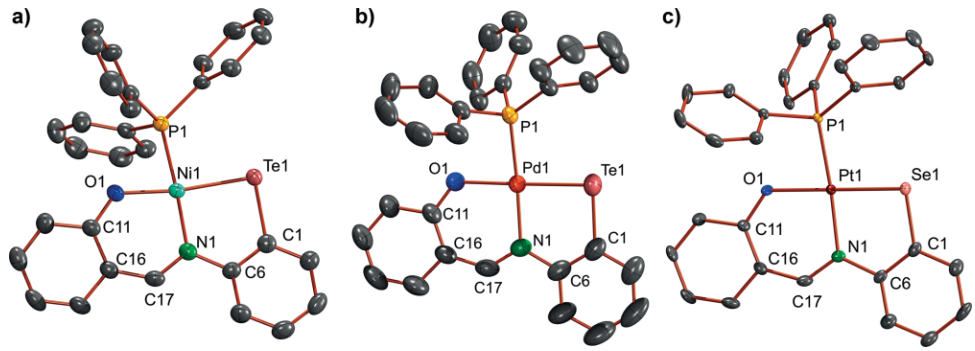

Figure 1. Molecular structures of a) [Ni(L^{Te})(PPh_3)], b) [Pd(L^{Te})(PPh_3)] and c) [Pt(L^{Se})(PPh_3)]. Ellipsoids are depicted at 50 % probability. Hydrogen atoms are omitted for clarity.

Table 1. Selected bond lengths [Å] and angles (°) in the dichalcogenides $\{HL^Y\}_2$[30] and their nickel, palladium and platinum complexes [M(L^Y)(PPh_3)] (Y = Se, Te).

	$\{HL^{Se}\}_2$	[Ni(L^{Se})(PPh_3)]	[Pd(L^{Se})(PPh_3)]	[Pt(L^{Se})(PPh_3)]	$\{HL^{Te}\}_2$	[Ni(L^{Te})(PPh_3)]	[Pd(L^{Te})(PPh_3)]	[Pt(L^{Te})(PPh_3)]
Y1–C1	1.929(2)/1.933(2)	1.900(1)	1.904(3)	1.896(4)	2.127(2)	2.096(3)	2.099(3)	2.11(1)
O1–C11	1.356(2)/1.349(2)	1.303(2)	1.288(3)	1.314(4)	1.356(3)	1.304(4)	1.292(3)	1.31(1)
N1–C6	1.415(2)/1.415(2)	1.438(2)	1.433(3)	1.435(4)	1.415(3)	1.448(4)	1.440(3)	1.40(2)
N1–C17	1.287(2)/1.283(2)	1.310(2)	1.292(3)	1.303(5)	1.287(3)	1.312(4)	1.289(3)	1.28(2)
M1–N1	–	1.915(1)	2.056(2)	2.061(3)	–	1.865(2)	2.041(2)	2.022(8)
M1–O1	–	1.856(1)	2.031(2)	2.031(2)	–	1.933(3)	2.073(2)	2.07(1)
M1–P1	–	2.1900(4)	2.2636(6)	2.2464(9)	–	2.1874(9)	2.2588(6)	2.238(3)
M1–Y1	–	2.2440(3)	2.3402(3)	2.3526(4)	–	2.4050(5)	2.4825(2)	2.502(1)
O1–M1–N1	–	96.46(5)	93.35(7)	93.3(1)	–	96.8(1)	93.29(8)	94.2(4)
O1–M1–P1	–	80.75(3)	84.13(5)	83.34(7)	–	81.01(8)	84.50(5)	81.9(3)
O1–M1–Y1	–	172.88(3)	179.14(7)	179.48(9)	–	172.18(7)	178.85(5)	177.7(2)
N1–M1–P1	–	174.79(4)	176.49(6)	175.71(9)	–	175.01(9)	176.22(6)	174.8(4)
N1–M1–Y1	–	90.63(4)	87.20(5)	86.75(8)	–	91.02(8)	87.82(6)	88.1(3)
Y1–M1–P1	–	92.14(1)	95.35(2)	96.63(2)	–	91.18(3)	94.40(2)	95.85(9)
C1–Y1–M1	–	94.35(4)	95.09(8)	95.3(1)	–	89.48(9)	90.66(8)	89.9(4)

of the [Ni(L^{Se})(PPh_3)], [Ni(L^{Te})(PPh_3)] and [Pt(L^{Te})(PPh_3)] in their unit cells is more compact than that of the other complexes. For most of the structural parameters, a linear dependence with the size of the chalcogen or the size of the metal is observed along the series [M(L^S)(PPh_3)] – [M(L^{Se})(PPh_3)] – [M(L^{Te})(PPh_3)]. The Pd1–Te1 and Pt1–Te1 bonds of 2.4825(2) and 2.502(1) Å are similar to the shortest bond lengths reported in previous studies of palladium[21,25–29,34,36–38] and platinum[39–52] phenyltellurolato complexes. Remarkably and probably as a result of the strain in the five-membered Te1–Ni1–N1 chelate ring, the Ni1–Te1 bond length in [Ni(L^{Te})(PPh_3)] is only 2.4050(5) Å. Compared to the nickel-tellurium bond lengths in the five to date structurally characterized aryltellurolato complexes of nickel, which vary between 2.45 and 2.51 Å, this is surprisingly short. The Ni–Te bonds in [Ni(TePh)Cp(PPh_3)],[53] Ni(TeMes)Cp(PEt_3),[54] [W(CO)$_5$-μ-(TePh)NiCp(PPh_3)][55] and [W(CO)$_4$-μ-{(TePh)NiCp-(PPh_3)}$_2$][55] are relatively long with 2.48 to 2.51 Å, while the shortest known Ni-aryltellurolato bond length reported to date was found in [Ni(NH-C_6H_4-Te)$_2$][56] with 2.4441(6) Å. Of all ca. 40 structurally characterized compounds with a Ni–Te bond, [Ni(NH-C_6H_4-Te)$_2$] as well as [(NiCp*i*Pr^4)$_2$-μ$_2$-(Te$_2$)] (2.440(2) Å),[57] [(NiCp*i*Pr^4)$_2$-μ-(Te)$_2$] (2.44–2.45 Å),[58] [CpFe(C_5H_4)-Te(I)$_2$-Ni(NHC)Cp] (2.4407(8) Å)[59] and (μ$_4$-telluro)-hexakis(μ$_3$-telluro)-bis(μ$_2$-bis(diphenylphosphino)methane)-bis(η$_5$-*tert*-butylcyclopentadienyl)-pentanickeldiniobium (2.436(5) Å)[60] show the overall shortest Ni–Te bond lengths. The Ni–Te bond in [Ni(L^{Te})(PPh_3)] is therefore not only the shortest so far crystallographically determined Ni–Te bond length for an aryltellurolato ligand, but also the shortest Ni–Te distance observed in any compound with a Ni–Te bond.

A more detailed structural comparison of the (almost) full series of [M(L^Y)(PPh_3)] complexes (M = Ni, Pd, Pt; Y = O, S, Se Te) can be found in the Supporting information.

ESI$^+$ mass spectra of the complexes under study clearly show the signals of their molecular ions $[M]^+$ or $[M + H]^+$ ions. In many of the spectra also high-intensity peaks for adducts of the type [2M + cation]$^+$ or ions, which contain protonated, oxidized ligands and reduced metals such as $[(MH)_2 + H]^+$, are observed. Additional signals for ions of the composition $[M + L^Y + H]^+$ with an intact, deprotonated dichalcogenide coordinating to one or two metal ions can also be observed. The formation of adducts, the oxidation of the ligands to the dichalcogenides and the reduction of the metal ions occurs mainly for the tellurolato complexes. The presence of such species in the ESI$^+$ mass spectra indicates that compounds such as $[M^{II}\{L^Y\}_2]$, $[M^{II}{}_2(L^Y)_2]$ and $[M^0{}_2\{HL^Y\}_2]$ with reformed dichalcogenides can formed from [M^{II}(L^Y)(PPh_3)]. In some of the complexes, a fragment of the phosphonium-species $\{Ph_3PSe(C_6H_4)$-2-N=CHC_6H_4-2-OH$\}^+$ (*m/z* = 538.0818) can be observed. This is not unexpected, since such species are also present in the fragmentation patterns of the rhenium complexes, we have studied recently.[30]

The yields reported in the Experimental Section are in the range between 55 and 80 per cent and refer to the isolated pure compounds. But it should be mentioned that the reaction

conditions had to be optimized for parameters such as solvent, temperature and reaction time for each individual complex. This is in analogy to the syntheses of the rhenium(V) complexes with the same ligands,[30] and is explained by a number of relevant, competing side-reactions. Thus, the availability of the precursor molecules in the solution, the release of PPh_3, its favored oxidation to $OPPh_3$ instead of taking part in undesired side-reactions etc. must be controlled carefully. An illustrative example of the requirement for an individual optimization is the reaction of $[Ni^{II}Cl_2(PPh_3)_2]$ with $\{HL^{Se}\}_2$. This reaction generally works at room and elevated temperatures and without the addition of a supporting base in CH_2Cl_2, where it is well soluble. However, under these conditions it is slow and gives unsatisfactorily low yields of $[Ni^{II}(L^{Se})(PPh_3)]$ (ca. 15 %). With regard to our earlier observations, that the yield of such reactions is frequently low when the starting materials are highly soluble in the solvent used for the reaction, we changed the solvent and used boiling acetonitrile, in which the starting materials are insoluble. Upon the addition of a small amount of CH_2Cl_2 to this mixture, a gradual dissolution of the starting materials was observed and the deposition of microcrystalline $[Ni^{II}(L^{Se})(PPh_3)]$ proceeded within minutes with yields of 80 %.

Generally, we found that the presence of traces of water and the absence of oxygen are necessary for good yields. This observation is consistent with the mechanism for the dichalcogenide reduction we proposed for the formation of the related rhenium(V) complexes.[30] Therefore, we believe the mechanism is generally applicable to the reaction of transition metal phosphine complexes with dichalcogenides as is shown in Scheme 2.

Interestingly, an exception to the strict necessity of water are the reactions of $[Pd^{II}(OAc)_2(PPh_3)_2]$ with $\{HL^{Y}\}_2$ (Y = Se, Te), which work slowly at room temperature and without the addition of a supporting base in dry, degassed solvents (yield of $[Pd^{II}(L^{Y})(PPh_3)]$ ca. 50 %). However, also the yield of $[Pd^{II}(L^{Y})(PPh_3)]$ increased to the range of 80 % by the addition of water to the reaction mixture.

To give some rational explanations for the mechanism of the reduction of $\{HL^{Se}\}_2$ with PPh_3 and to the point that it does not proceed without the presence of metal ions,[30] we performed a series of DFT calculations on the B3LYP level for the reactions of free $\{HL^{Se}\}_2$ and metal-bound $\{HL^{Se}\}_2$, in the form of $[Pd\{L^{Se}–HL^{Se}\}(PPh_3)]^+(OAc)^-$, with PPh_3 and H_2O in CH_2Cl_2 solution. Both, a di(organoseleno)phosphorane and an organoselenophosphonium-organoselenolate ion pair were considered as possible intermediates in these reactions. However, the phosphorane intermediates, which were stable intermediates in the gas-phase, did not converge with the solvation model. Therefore, we assume that the ion-pair structures resemble the intermediates in solution better. The summed relative free energies of the respective starting materials, products and intermediates are shown in Scheme 3. Apparently, the release of the phosphonium species is favored for the metal-bound reaction, while it is energetically disfavored for the reaction of free $\{HL^{Se}\}_2$. This is probably due to the stabilization of the complementarily released $\{HL^{Se}\}^-$ anion by the coordination to the metal ion. Furthermore, the energy surface in the metal-bound reaction is much smoother, resulting in better accessible reaction intermediates compared to the reaction of the non-coordinated dichalcogenide.

To get further information about such reactions and possible reasons for the increased reactivity upon coordination, we performed gas-phase calculations on a series of diaryldiselenides R-Se-Se-R (R = Ph, Ph-2-NMe_2, Ph-2-$NCMe_2$, 2-Py, 3-Py-2-NMe_2, 3-Py-2-$NCMe_2$) and their Pd(II) complexes $[PdCl_2(PR'_3)$-η^1-{R-Se-Se-R}] (R'= Ph, Me, CF_3), where we also considered the respective chelated $[PdCl(PR'_3)$-η^2-{R-Se-Se-R}]$^+$ cations. Generally, we found an increase in the intensity and/or size of the σ-hole of the Se-Se bond upon coordination to the metal. This results in an increased polarization of the Se-Se bond and a positive partial charge on the exposed surface of the non-coordinating selenium atom, which bears the majority of the σ*(Se-Se) or σ-hole. For all regarded examples, we then additionally calculated interactions with PPh_3. PPh_3 acts in all (sterically accessible) cases on the metal-bound diselenides as a donor into the σ*(Se-Se) orbitals at the non-coordinated selenium atoms with formation of $[PdCl_2(PR'_3)$-η^1-{R-Se-Se(R)←:PPh_3}]-type donor-acceptor complexes (R'=Me). They show elongated Se-Se bonds (delocalization energy in second order perturbation analysis: 20–60 kcal/mol). In some cases, an inversion of the bonding situation is observed, where the Se-Se bond is broken and a Se–P bond is formed. The resulting selenylphosphonium ions are stabilized in many cases by donation of the liberated selenolato ligands into the σ*-Se-P orbitals: $[PdCl_2(PR'_3)$-η^1-R-

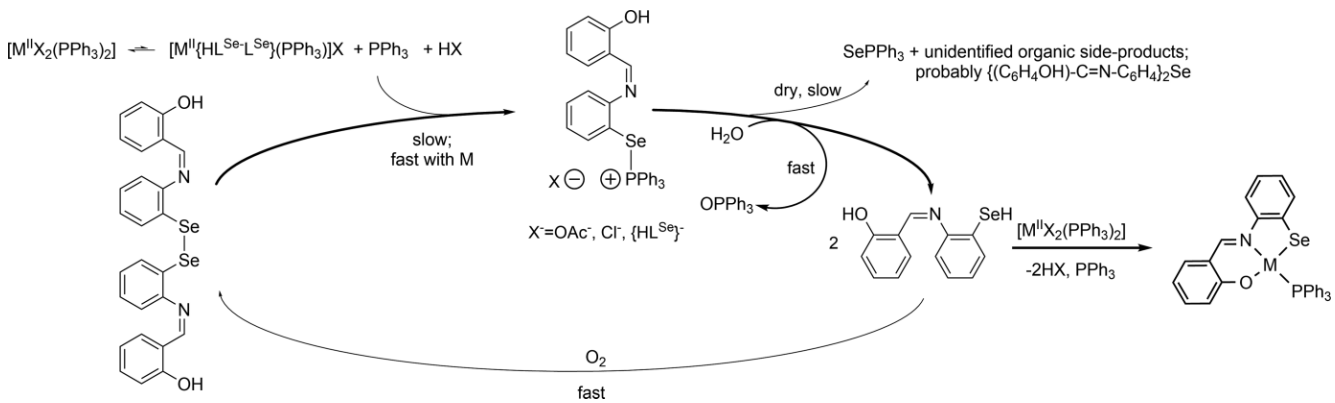

Scheme 2. Proposed mechanism for the reaction between $[MX_2(PPh_3)_2]$ (M = Ni,Pd,Pt) with $\{HL^{Se}\}_2$.

Full Paper
doi.org/10.1002/ejic.202000750

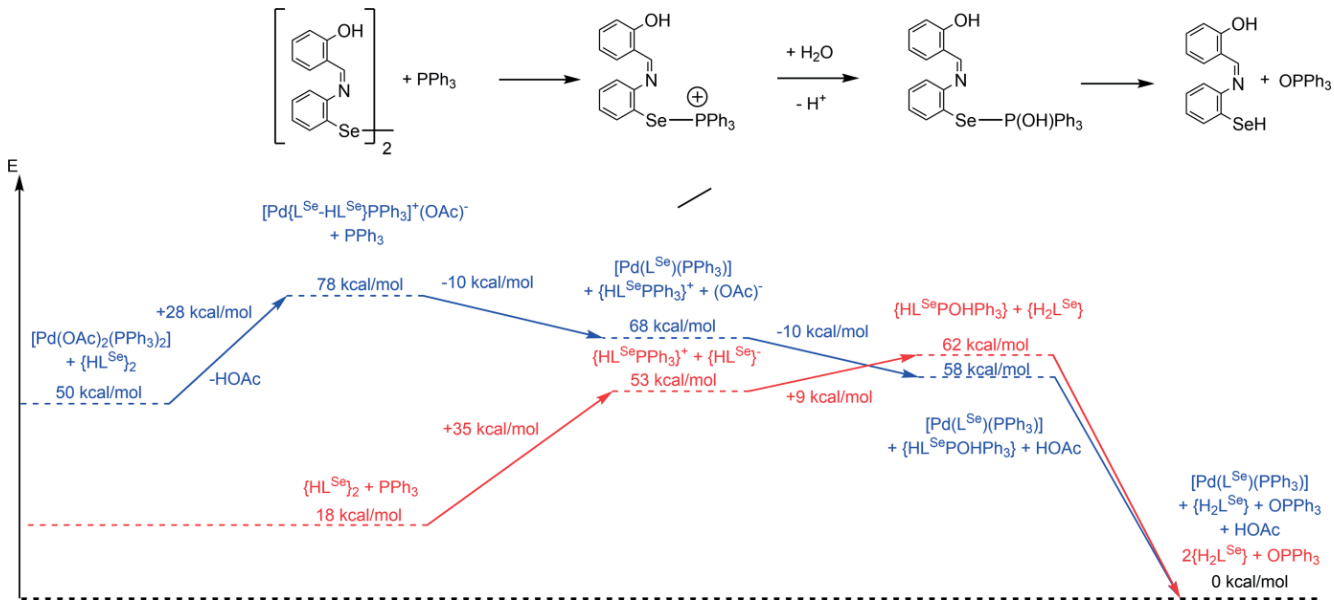

Scheme 3. Differences in free energy between starting materials, products and intermediates suggested for the reaction between free (red) and metal-bound (blue) $\{HL^{Se}\}_2$ with PPh_3 in the presence of water in CH_2Cl_2 solution. The energy values were corrected by the quasi-harmonic method of Grimme.

Se:→Se(R)PPh_3] (R'=Me). The likely reason for the metal-induced reduction is therefore not only the stabilization of the released selenolato anion, but also an increased polarization of the Se-Se bond upon coordination. A positive charge on the metal-diselenide complex further polarizes the non-coordinated selenium atom positively and leads to an even stronger interaction with the phosphine. This commonly results in a cleavage of the Se-Se bond.

In contrast, the donation of PPh_3 to the uncoordinated diselenides is very weak – no formation of donor-acceptor complexes could be concluded and no break of a Se-Se bond is found (maximum delocalization energy in second order perturbation analysis: 2 kcal/mol).

The electrostatic potential maps of the phenyl diselenide model with some further electronic information are shown in Figure 2. Further information on the calculations can be found in the Supporting Information.

Attempted oxidations of the metal(II) complexes with elemental iodine did not result in the formation of defined metal(IV) complexes, but gave intractable, poorly soluble products. Only from the reaction between $[Pd^{II}(L^{Te})(PPh_3)]$ and I_2, which also yields an insoluble dark red powder with low carbon content, a small amount (approximately 10 %) of a crystalline product could be isolated from the remaining solution. It is the zwitterionic compound $[(HO)C_6H_4\text{-}(CHN^+H)\text{-}C_6H_4\text{-}Te^{II}I_2]$, which is associated with one molecule $OPPh_3$ giving a dark purple solid. The same products can be prepared by a direct reaction between $\{L^{Te}\}_2$, I_2 and $OPPh_3$ with somewhat higher yields.

The formation of zwitterionic compounds upon oxidation of diaryldiorganotellurides by I_2 is not without precedent and has been observed before e.g. during the reaction of bis(pyridyl)ditelluride with iodine.[61] The stabilization of such zwitterions by long-range interactions with other building blocks is frequently observed and has extensively been studied in a recent work

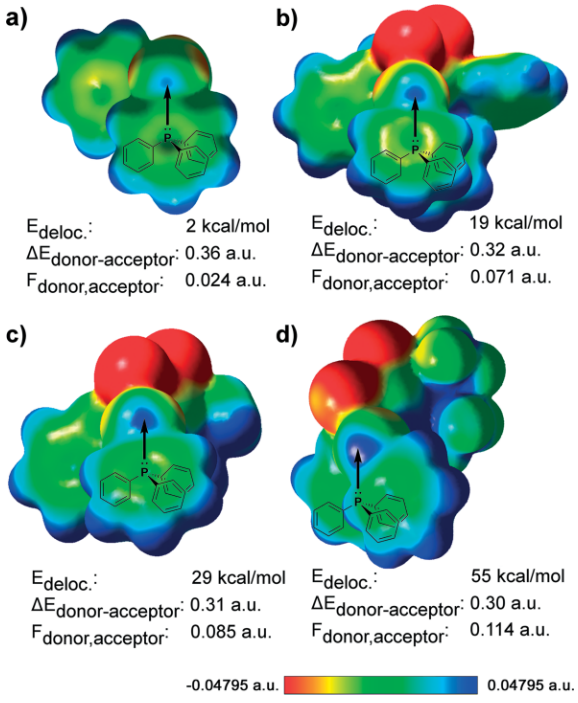

Figure 2. 3D Electrostatic potential maps at the ρ = 0.004 level of the gas-phase calculated model compounds a) $(PhSe)_2$, b) $[PdCl_2(PhSe)_2(PPh_3)]$, c) $[PdCl_2(PhSe)_2(PMe_3)]$ and d) $[PdCl_2(PhSe)_2(P(CF_3)_3)]$. Orientation along the Se-Se bonds with the non-metal-bonded selenium atom and its σ-hole pointing towards the viewer (blue = positive; red = negative; color normalized to the potential of free $(PhSe)_2$). Donation of the PPh_3 lone-pair to the σ-hole on the Se-Se axis centered at the non-coordinating selenium atom is indicated. The estimated second order perturbation energy gain from the donation ($E_{deloc.}$), the energy difference between donor and acceptor orbitals ($\Delta E_{donor-acceptor}$) and the overlap factor ($F_{donor,acceptor}$) are given besides the graphs.

dealing with pyridyltellurium(II) chlorides, bromides and iodides.[62] Long-range interactions play also a role in the solid-state structure of {[(HO)C_6H_4-(CHN$^+$H)-C_6H_4-TeI_2]•$OPPh_3$}. The structure of the compound is shown in Figure 3 and selected bond lengths and angles are summarized in Table 2. The Te1–I1 and Te2–I2 distances are approximately equal and they are bound linearly. One of the phenyl rings in the triphenylphosphine oxide shows a tellurium-centroid distance of 3.771(1) Å and the corresponding Te–centroid contact aligns linearly with the C-Te axis. The individual C=C···Te distances are between 3.569(1) Å (C22–C23 centroid) and 4.306(1) Å (C25–C26 centroid) and do not align with the C-Te axis. Therefore, it cannot be finally concluded if the observed long range interaction should be attributed to individual C=C···Te interactions, Ph···Te interactions or a mixture of both. The infrared spectrum of the zwitterion confirms the protonation of the aldiminic nitrogen atom. A sharp N-H stretch of medium intensity is observed at 3050 cm^{-1}. The intense band for the O-H stretch is very broad and centered at 2324 cm^{-1}. The ESI$^+$ mass spectrum of {[(HO)C_6H_4-(CHN$^+$H)-C_6H_4-TeI_2]•$OPPh_3$} is less instructive and mainly contains peaks, which are related to triphenylphosphine oxide.

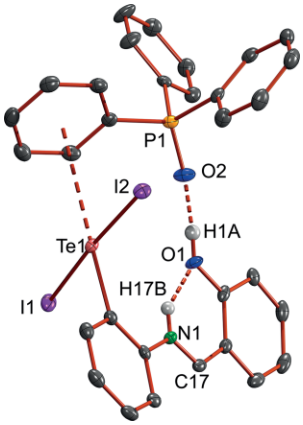

Figure 3. Structure of {[(HO)C_6H_4-(CHN$^+$H)-C_6H_4-TeI_2]•$OPPh_3$}. Ellipsoids are depicted at 50 % probability. Hydrogen atoms bonded to carbon atoms are omitted for clarity.

Table 2. Selected bond lengths [Å] and angles (°) in {[(HO)C_6H_4-(CHN$^+$H)-C_6H_4-$Te^{II}I_2$]•$OPPh_3$}.

Te1–I1	2.9466(9)	N1–C17	1.303(4)	
Te1–I2	2.969(1)	P1–O2	1.497(2)	
Te–Centroid	3.771(1)			
C-Te1–I1	88.36(8)	C-Te1–I2	89.90(8)	
I1–Te1–I2	176.181(9)	C-Te–centroid	179.32(8)	
I1–Te1-centroid	91.84(1)	I2–Te1-centroid	89.86(1)	
D–H···A	d(D–H)	d(H···A)	d(D···A)	<(DHA)
N1–H17B···O1	0.80(3)	1.95(3)	2.604(3)	138(3)
O1–H1···O2	0.81(4)	1.70(4)	2.506(3)	171(4)

Conclusions

In the present communication, we extended the recently reported method, in which released PPh_3 acts as reducing agent for metal-bound dichalcogenides to nickel, palladium and platinum. All three group 10 elements form stable complexes with the tridentate selenolato- and tellurolato-substituted Schiff base ligands {HL^{Se}}$^{2-}$ and {HL^{Te}}$^{2-}$, respectively. The resulting [M(L^Y)(PPh_3)] complexes (Y = Se, Te) have a square-planar coordination geometry. Optimum yields are obtained in the presence of water and under strict exclusion of dioxygen. The intermediates of the reactions of [$Pd(OAc)_2(PPh_3)_2$] and {HL^{Se}}$_2$ as well as {HL^{Se}}$_2$ with PPh_3 were evaluated via DFT calculations. Calculations about the coordination of several model diselenides to a palladium(II) center reveal an increased polarization of the Se-Se bonds upon coordination, which facilitates the nucleophilic attack of PPh_3. The stabilization of the {L^{Se}}$^{2-}$ anion by coordination to a metal ion results in the stabilization of an intermediate {L^{Se}-PPh_3}$^+$ phosphonium salt, which is less stable without the presence of a metal. Therefore, the reduction does not (or only very slowly) proceed without the presence of metal ions.

Experimental Section

[$NiCl_2(PPh_3)_2$],[63] [$Pd(OAc)_2$],[64] [$Pd(OAc)_2(PPh_3)_2$],[64] [$PtCl_2(PPh_3)_2$],[65–67] {HL^{Se}}$_2$,[30] {HL^{Te}}$_2$,[30] bis(2-aminophenyl) diselenide and bis-(2-aminophenyl)ditelluride were prepared according to literature procedures.[68–70] All other chemicals were reagent grade and used as received. Reactions involving oxygen- or water-sensitive compounds were performed with standard Schlenk technique. Large amounts of solvents were degassed using three freeze-pump-thaw cycles with Ar as the filling gas. Small amounts of solvents were alternatively degassed by bubbling a strong stream of argon through the solvent for 15–30 min immediately before use.

NMR spectra were recorded at 25 °C on JEOL 400 MHz ECS-400 or JNM-ECA400II spectrometers. Reported chemical shifts (δ) are referenced according to the IUPAC recommendations of 2008.[71] External reference standards: tetramethylsilane, (^{1}H, ^{13}C), $ClCF_3$ (^{19}F), 85 % phosphoric acid (^{31}P), dimethylselenide (^{77}Se), dimethyltelluride (^{125}Te) and 1.2 M $Na_2[PtCl_4]$ in D_2O (^{195}Pt).

IR-Spectra were recorded with an FT IR spectrometer (Nicolet iS10, Thermo Scientific). Intensities are classified as vs. = very strong, s = strong, m = medium, w = weak, vw = very weak, sh = shoulder.

Electrospray ionization mass spectrometry (ESI MS) was carried out with the ESI MSD TOF unit of an Agilent 6210 TOF LC/MS system. The measurements were performed in $CHCl_3$, CH_2Cl_2, MeOH, DMSO or mixtures of them.

Elemental analyses were performed using a vario EL III CHN elemental analyzer (Elementar Analysensysteme GmbH) or a vario MICRO cube CHNS elemental analyzer. Some of the determined carbon values of the metal complexes show slightly too low contents. This is a systematic finding on our analyzers and might have to do with the formation of carbides.

Single crystal X-ray diffraction data were collected on a Bruker D8 Venture or a STOE IPDS II T. Absorption corrections were carried out by the multiscan (Bruker D8 Venture) or integration methods (STOE IPDS II T).[72,73] Structure solutions and refinements were done with the SHELX-2008, SHELX-2014 and SHELX-2016 program packages.[74,75] Hydrogen atom positions at heteroatoms or the aldiminic carbon atoms were taken from the Fourier maps when possible or placed at calculated positions and refined by a riding model. All other hydrogen atoms were placed at calculated posi-

tions and refined by a riding model. The visualization of the molecular structures was done using the program DIAMOND 4.2.2.[76]

CCDC 2021656 (for [Ni(L^{Se})(PPh_3)]), 2021657 (for [Ni(L^{Te})(PPh_3)]), 2021658 (for [Pd(L^{Se})(PPh_3)]), 2021659 (for [Pd(L^{Te})(PPh_3)]), 2021660 (for [Pt(L^{Se})(PPh_3)]), 2021661(for [Pt(L^{Te})(PPh_3)]) and 2021662 (for {[(HO)C_6H_4-(CHN^+H)-C_6H_4-TeI$_2$]·$OPPh_3$}) contain the supplementary crystallographic data for this paper. These data can be obtained free of charge from The Cambridge Crystallographic Data Centre.

DFT calculations were performed on the high-performance computing systems of the Freie Universität Berlin ZEDAT (Curta) using the program packages GAUSSIAN 09 and GAUSSIAN 16.[77,78] The gas phase and solution geometry optimizations were performed using coordinates derived from the X-ray crystal structures using GAUSSVIEW.[79] The polarizable continuum model (PCM) with the integral equation formalism variant (IEFPCM) was used to implicitly simulate the solvent dichloromethane. The calculations were performed with the hybrid density functional B3LYP.[80–82] The double-ζ pseudopotential LANL2DZ basis set with the respective effective core potential (ECP) was applied to Ni, Pd and Pt.[83] The Stuttgart relativistic large core basis set RLC with the corresponding ECP was applied to I.[84] The Stuttgart relativistic large core basis set RLC with the corresponding ECP and an extension by STO-3G* polarization functions was applied to Te.[84,85] The 6-31G* basis set was applied for all other atoms excluding H.[86–90] For H, the 6-31G basis set was applied.[91] All basis sets as well as the ECPs were obtained from the EMSL database.[92] Frequency calculations after the optimizations confirmed the convergence. No negative frequencies were obtained for the given optimized geometries of all compounds. The entropic contribution to the free energy was corrected for low-energy modes using the quasi-harmonic approximation of Grimme[93] as implemented in the freely accessible python code *GoodVibes* of Funes-Ardoiz and Paton with a cut-off at 500 cm^{-1}.[94] Further analysis of orbitals, charges, 2D ESP mapping, QTAIM, etc. was performed with the free multifunctional wavefunction analyzer *Multiwfn*.[95] Vizualisation of the electrostatic potential maps was done with GAUSSVIEW.[79] To verify the suitability of the employed methods, the structures of all [M(L^Y)(PPh_3)] (M = Ni, Pd, Pt; Y = O, S, Se, Te) were calculated in the gas-phase. The calculated bonding parameters match the determined crystal structures, where they were available, on average within 0.036 Å. The deviations are highest with an average elongation of 0.054 Å for the coordination sphere of the metals, which is expected for a gas phase calculation. The latter is most prominent in the metal tellurium distances with an average elongation of 0.115 Å compared to the solid-state structures.

[Ni(L^{Se})(PPh_3)]. [$NiCl_2(PPh_3)_2$] (66 mg, 0.1 mmol) and {HL^{Se}}$_2$ (22 mg, 0.04 mmol) were suspended in degassed CH_3CN (6 mL). and heated to reflux. CH_2Cl_2 (1 mL) was added and the color of the suspension changed from dark green to dark brown. After 5 min, the solution was cooled to room temperature. Diethyl ether (24 mL) was added to the yellow solution with a brown precipitate. The mixture was left in the freezer overnight to finish the precipitation. The brown-red microcrystals were filtered off, washed with diethyl ether and dried in vacuo. A second crop of crystals was obtained by evaporation of the combined filtrates and washing solutions. The product can be recrystallized from CH_2Cl_2/diethyl ether or CH_2Cl_2/EtOH. Brown-red microcrystals or red-green dichroic cubes. Yield: 36 mg (76 %).

Elemental analysis: Calculated for $C_{31}H_{24}NNiOPSe$: C 62.6, H 4.1, N 2.4 %; Found C 62.0, H 4.1, N 2.3 %. IR (cm^{-1}): $\tilde{\nu}$ = 3058 (w), 1605 (m) C=N, 1580 (m), 1564 (m), 1523 (m), 1478 (m), 1455 (m), 1431 (s), 1377 (m), 1366 (m), 1332 (m), 1307 (w), 1262 (m), 1248 (m), 1225 (m), 1169 (m), 1157 (m), 1145 (m), 1123 (m), 1100 (sh), 1092 (s), 1038 (m), 1025 (m), 997 (m), 976 (vw), 950 (w), 926 (m), 841 (m), 806 (m), 756 (sh), 744 (vs), 715 (sh), 702 (sh), 690 (vs), 618 (w), 609 (m), 555 (s), 548 (m). ESI^+ MS (*m/z*): 538.0856 (calc. 538.0843) [HL^{Se} + PPh_3]$^+$, 596.0193 (calc. 596.0191) [M + H]$^+$, 618.0017 (calc. 618.0010) [M + Na]$^+$, 633.9753 (calc. 633.9750) [M + K]$^+$. ^{1}H NMR (CD_2Cl_2, ppm): 8.86 (1H, d, $^4J_{H,P}$ = 9.29 Hz, **H17**CR=NR), 7.96–7.79 (6H, m, *m*-P-Ar**H**), 7.62 (1H, d, $^3J_{H15,H14}$ = 8.31 Hz, ^{L}Ar**H15**), 7.56–7.48 (3H, m, *p*-P-Ar**H**), 7.56–7.48 (8H, m, 6 *o*-P-Ar**H**, ^{L}Ar**H2** [ca. 7.44], ^{L}Ar**H12** [ca. 7.41]), 7.17 (1H, m, ^{L}Ar**H4**), 7.09 (1H, m, ^{L}Ar**H14**), 6.98 (1H, m, ^{L}Ar**H13**), 6.64 (1H, m, ^{L}Ar**H3**), 6.33 (1H, d, $^3J_{H5,H4}$ = 8.31 Hz, ^{L}Ar**H5**). ^{13}C NMR (CD_2Cl_2, ppm): 164.4 (d, $^3J_{C,P}$ = 1 Hz, ^{L}**C$_{Ar}$6**), 157.1 (s, H**C17**R=NR), 152.5 (d, $^3J_{C,P}$ = 10 Hz, ^{L}**C$_{Ar}$11**), 135.7 (d, $^4J_{C,P}$ = 14 Hz, ^{L}**C$_{Ar}$16**), 134.9 (d, $^3J_{C,P}$ = 10 Hz, *m*-P-**C$_{Ar}$**), 134.7 (s, ^{L}**C$_{Ar}$2**), 134.6 (s, ^{L}**C$_{Ar}$4**), 130.9 (d, $^4J_{C,P}$ = 3 Hz, *p*-P-**C$_{Ar}$**), 130.6 (d, $^3J_{C,P}$ = 2 Hz, ^{L}**C$_{Ar}$1**-Se), 129.8 (d, $^1J_{C,P}$ = 46 Hz, P-**C$_{Ar}$**), 128.4 (d, $^2J_{C,P}$ = 10 Hz, *o*-P-**C$_{Ar}$**), 127.0 (s, ^{L}**C$_{Ar}$13**), 123.5 (s, ^{L}**C$_{Ar}$14**), 121.6 (d, $^4J_{C,P}$ = 1 Hz, ^{L}**C$_{Ar}$5**), 119.8 (s, ^{L}**C$_{Ar}$12**), 116.5 (s, ^{L}**C$_{Ar}$15**), 115.7 (s, ^{L}**C$_{Ar}$3**). ^{31}P NMR (CD_2Cl_2, ppm): 22.1 (s). ^{77}Se NMR (CD_2Cl_2, ppm): 233.0 (d, $^2J_{Se,P}$ = 77 Hz).

[Ni(L^{Te})(PPh_3)]. [$NiCl_2(PPh_3)_2$] (66 mg, 0.1 mmol) and {HL^{Te}}$_2$ (22 mg, 0.08 mmol) were suspended in degassed EtOH (2 mL). and heated to reflux. NEt_3 (3 drops) was added and the mixture was heated under reflux for further 15 min. After cooling to room temperature, the dark precipitate was filtered off and washed with water, diethyl ether and hexane. It was dried in vacuo. A second crop of crystals was obtained by layering the combined filtrate and washing solutions with hexane. Brown-red microcrystals or red-green dichroic cubes. Yield: 40 mg (59 %).

Elemental analysis: Calculated for $C_{31}H_{24}NNiOPTe$: C 57.8, H 3.8, N 2.2 %; Found C 57.5, H 3.8, N 2.1 %. IR (cm^{-1}): $\tilde{\nu}$ = 3060 (w), 1606 (m) C=N, 1581 (m), 1563 (m), 1522 (m), 1479 (m), 1453 (m), 1431 (s), 1381 (m), 1365 (m), 1337 (m), 1259 (m), 1247 (m), 1222 (m), 1169 (m), 1156 (m), 1146 (s), 1126 (m), 1101 (s), 1091 (s), 1044 (w), 1028 (m), 997 (m), 952 (w), 926 (m), 841 (m), 805 (m), 758 (sh), 744 (vs), 715 (sh), 701 (sh), 690 (vs), 618 (w), 604 (m), 555 (s), 546 (m), 528 (s). ESI^+ MS (*m/z*): 706.8907 (calc. 706.8890) [Ni{HL^{Te}}$_2$ + H], 728.8723 (calc. 728.8709) [Ni{HL^{Te}}$_2$ + Na], 744.8459 (calc. 744.8447) [Ni{HL^{Te}}$_2$ + K], 1410.7711 (calc. 1410.7700) [2Ni{HL^{Te}}$_2$ + H], 1432.7522 (calc. 1432.7519) [2Ni{HL^{Te}}$_2$ + Na], 1448.7282 (calc. 1448.7257) [2Ni{HL^{Te}}$_2$ + K], 1526.7746 (calc. 1526.7091) [2Ni{HL^{Te}}$_2$ + Ni(OAc)]. ^{1}H NMR ($CDCl_3$, ppm): 8.47 (1H, d, $^4J_{H,P}$ = 8.23 Hz, **H17**CR=NR), 7.87–7.66 (6H, m, *m*-P-Ar**H**), 7.46 (1H, d, $^3J_{H15,H14}$ = 7.58 Hz, ^{L}Ar**H15**), 7.40–7.09 (11H corrected for $CHCl_3$, m, *p*-P-Ar**H**, *o*-P-Ar**H**, ^{L}Ar**H2**, ^{L}Ar**H12**), 6.99 (2H, m, ^{L}Ar**H4**, ^{L}Ar**H14**), 6.79 (1H, m, ^{L}Ar**H13**), 6.45 (1H, m, ^{L}Ar**H3**), 6.10 (1H, d, $^3J_{H5,H4}$ = 8.58 Hz, ^{L}Ar**H5**). ^{13}C NMR ($CDCl_3$, ppm): 164.8 (s, ^{L}**C$_{Ar}$6**), 159.9 (s, H**C17**R=NR), 158.6 (s, ^{L}**C$_{Ar}$11**), 135.3 (s, ^{L}**C$_{Ar}$2**), 134.8 (s, ^{L}**C$_{Ar}$4**), 134.7 (d, $^3J_{C,P}$ = 6 Hz, *m*-P-**C$_{Ar}$**), 134.7 (overlapped s (in the middle of the d for *m*-P-C_{Ar}), ^{L}**C$_{Ar}$16**), 132.2 (d, $^4J_{C,P}$ = 10 Hz, ^{L}**C$_{Ar}$16**), 130.6 (s, *p*-P-**C$_{Ar}$**), 130.6 (d, $^1J_{C,P}$ = 48 Hz, P-**C$_{Ar}$**), 128.2 (d, $^2J_{C,P}$ = 10 Hz, *o*-P-**C$_{Ar}$**), 126.6 (s, ^{L}**C$_{Ar}$13**), 125.2 (s, ^{L}**C$_{Ar}$14**), 121.9 (s, ^{L}**C$_{Ar}$5**), 120.1 (s, ^{L}**C$_{Ar}$12**), 118.1 (s, ^{L}**C$_{Ar}$15**), 115.3 (s, ^{L}**C$_{Ar}$3**), 112.4 (d, $^3J_{C,P}$ = 11 Hz, ^{L}**C$_{Ar}$1**-Te). ^{31}P NMR ($CDCl_3$, ppm): 25.6 (s), 25.5 (d, $^2J_{P,Te}$ = 191 Hz, P-Ni-^{125}Te). ^{125}Te NMR ($CDCl_3$, ppm): 338.6 (d, $^2J_{Te,P}$ = 194 Hz).

[Pd(L^{Se})(PPh_3)]. [$Pd(OAc)_2(PPh_3)_2$] (112 mg, 0.15 mmol) was dissolved in a degassed mixture of CH_2Cl_2 (3 mL) and water (3 drops). {HL^{Se}}$_2$ (83 mg, 0.15 mmol) was added as a solid. The color of the solution turned from yellow to red immediately and the mixture was stirred vigorously for 3 h. It was layered with diethyl ether (18 mL) and left in the freezer. After 3 days, large red crystals had formed, which were filtered off, washed with diethyl ether and dried in vacuo. A second crop of crystals was obtained by evaporation

of the combined filtrate and washing solutions. Orange-red plates. Yield: 76 mg (78 %).

Elemental analysis: Calculated for $C_{31}H_{24}NOPPdSe$: C 57.9, H 3.8, N 2.1 %; Found C 56.8, H 3.9, N 2.1 %. IR (cm^{-1}): $\tilde{\nu}$ = 3047 (w), 3015 (w), 1967 (w), 1911 (w), 1605 (m) C=N, 1587 (m), 1571 (m), 1522 (m), 1482 (m), 1457 (m), 1433 (s), 1387 (m), 1364 (m), 1332 (m), 1308 (w), 1306 (w), 1263 (w), 1250 (w), 1219 (w), 1191 (m) 1171 (m), 1148 (s), 1125 (m), 1098 (s), 1037 (sh), 1028 (m), 997 (m), 948 (w), 929 (m), 850 (w), 838 (w), 800 (w), 748 (sh), 736 (vs), 709 (sh), 693 (vs), 642 (w), 616 (w), 607 (m), 577 (vw), 565 (w), 551 (s), 531 (s). ESI^+ MS (*m/z*): 643.9895 (calc. 643.9888) $[M + H]^+$, 665.9718 (calc. 665.9707) $[M + Na]^+$, 681.9452 (calc. 681.9446) $[M + K]^+$, 944.0577 (calc. 944.00364) $[M + PPh_3 + K]^+$, 1308.9532 (calc. 1308.9536) $[2M + Na]^+$, 1324.9274 (calc. 1324.9274) $[2M + K]^+$. ^1H NMR (CD_2Cl_2, ppm): 8.94 (1H, d, $^4J_{H,P}$ = 14.98 Hz, **H17**CR=NR), 7.85–7.73 (6H, m, *m*-P-Ar**H**), 7.69 (1H, d, $^3J_{H15,H14}$ = 7.89 Hz, ^{L}Ar**H15**), 7.60–7.41 (11H corrected for $CHCl_3$, m, *p*-P-Ar**H**, *o*-P-Ar**H**, ^{L}Ar**H2** [ca. 7.48], ^{L}Ar**H12** [ca. 7.44]), 7.32 (1H, m, ^{L}Ar**H4**), 7.14 (1H, m, ^{L}Ar**H13**), 7.03 (1H, m, ^{L}Ar**H12**), 6.70–6.62 (2H, m, ^{L}Ar**H3** [ca. 6.64], ^{L}Ar**H5** [ca. 6.62]). ^{13}C NMR (CD_2Cl_2, ppm): 165.6 (s, ^{L}**C$_{Ar}$6**), 156.3 (s, H**C17**R=NR), 151.2 (d, $^3J_{C,P}$ = 2 Hz, ^{L}**C$_{Ar}$11**), 136.6 (s, ^{L}**C$_{Ar}$2**), 135.8 (s, ^{L}**C$_{Ar}$4**), 135.0 (d, $^3J_{C,P}$ = 11 Hz, *m*-P-**C$_{Ar}$**), 134.9 (s, ^{L}**C$_{Ar}$16**), 131.3 (d, $^4J_{C,P}$ = 3 Hz, *p*-P-**C$_{Ar}$**), 131.3 (d, $^3J_{C,P}$ = 1 Hz, ^{L}**C$_{Ar}$1**-Se), 129.8 (d, $^1J_{C,P}$ = 51 Hz, P-**C$_{Ar}$**), 128.5 (d, $^2J_{C,P}$ = 11 Hz, *o*-P-**C$_{Ar}$**), 127.3 (s, ^{L}**C$_{Ar}$13**), 123.8 (s, ^{L}**C$_{Ar}$14**), 122.0 (d, $^4J_{C,P}$ = 2 Hz, ^{L}**C$_{Ar}$5**), 119.7 (s, ^{L}**C$_{Ar}$12**), 116.9 (d, $^5J_{C,P}$ = 1 Hz, ^{L}**C$_{Ar}$15**), 115.1 (s, ^{L}**C$_{Ar}$3**). ^{31}P NMR (CD_2Cl_2, ppm): 25.6 (s). ^{77}Se NMR (CD_2Cl_2, ppm): 326.4 (dd, $^2J_{Se,P}$ = 21 Hz, *J* = 6 Hz).

[Pd(L^{Te})(PPh$_3$)]. $[Pd(OAc)_2(PPh_3)_2]$ (72 mg, 0.1 mmol) was dissolved in a degassed mixture of CH_2Cl_2 (1 mL) and water (1 drop). $\{HL^{Te}\}_2$ (64 mg, 0.1 mmol) was added as a solid. The color of the solution turned immediately from yellow to brown. The mixture was stirred vigorously for 3 h. It was layered with diethyl ether (18 mL) and left in the freezer overnight. The large deep red crystals, which formed, were filtered off. They were washed with diethyl ether and hexane and dried in vacuo. A second crop of crystals was obtained by evaporation of the combined filtrate and washing solutions. Dark red blocks. Yield: 52 mg (75 %).

Elemental analysis: Calculated for $C_{31}H_{24}NOPPdTe$: C 53.8, H 3.5, N 2.0 %; Found C 53.6, H 3.6, N 2.0 %. IR (cm^{-1}): $\tilde{\nu}$ = 3048 (w), 1605 (m) C=N, 1582 (m), 1566 (sh), 1558 (m), 1518 (m), 1505 (sh), 1480 (m), 1450 (m), 1431 (s), 1390 (m), 1368 (m), 1335 (m), 1308 (w), 1287 (vw), 1259 (m), 1244 (m), 1215 (w), 1182 (m), 1164 (m), 1157 (sh), 1146 (s), 1128 (m), 1102 (s), 1093 (sh), 1069 (w), 1044 (w), 1027 (m), 997 (m), 969 (w), 953 (w), 926 (m), 841 (m), 794 (w), 757 (sh), 743 (vs), 716 (m), 716 (sh), 703 (vs), 637 (vw), 618 (w), 602 (m), 573 (vw), 550 (m), 530 (s). ESI^+ MS (*m/z*): 693.9772 (calc. 693.9771) $[M + H]^+$, 715.9657 (calc. 715.9591) $[M + Na]^+$, 731.9346 (calc. 731.9328) $[M + K]^+$, 944.0577 (calc. 944.00364) $[M + PPh_3 + K]^+$, 1152.8675 (calc. 1152.8998) $[\{Pd^0(PPh_3)(HL^{Te})\text{-}(HL^{Te})Pd^0H_2\} + Na]^+$. ^1H NMR (CD_2Cl_2, ppm): 8.72 (1H, d, $^4J_{H,P}$ = 14.09 Hz, **H17**CR=NR), 7.83–7.72 (6H, m, *m*-P-Ar**H**), 7.46 (1H, dd, $^3J_{H15,H14}$ = 7.64 Hz, $^4J_{H15,H12}$ = 1.32 Hz, ^{L}Ar**H15**), 7.56–7.48 (3H, m, *p*-P-Ar**H**), 7.48–7.39 (8H, m, 6 *o*-P-Ar**H**, ^{L}Ar**H2**, ^{L}Ar**H12**), 7.29 (1H, ddd, $^3J_{H4,H5}$ = 8.64 Hz, $^3J_{H4,H3}$ = 6.78 Hz, $^4J_{H4,H2}$ = 1.88 Hz, ^{L}Ar**H4**), 7.20 (1H, m, ^{L}ArH**14**), 6.96 (1H, m, ^{L}Ar**H13**), 6.61 (1H, ddd, $^3J_{H3,H2}$ = 7.95 Hz, $^3J_{H3,H4}$ = 6.78 Hz, $^4J_{H3,H5}$ = 1.14 Hz, ^{L}Ar**H3**), 6.54 (1H, d, $^3J_{H5,H4}$ = 8.64 Hz, ^{L}Ar**H5**). ^{13}C NMR (CD_2Cl_2, ppm): 166.6 (s, ^{L}**C$_{Ar}$6**), 159.6 (s, H**C17**R=NR), 157.3 (d, $^3J_{C,P}$ = 2 Hz, ^{L}**C$_{Ar}$11**), 137.2 (s, ^{L}**C$_{Ar}$2**), 136.4 (s, ^{L}**C$_{Ar}$4**), 136.1 (d, $^4J_{C,P}$ = 1 Hz, ^{L}**C$_{Ar}$16**), 135.2 (d, $^3J_{C,P}$ = 11 Hz, *m*-P-**C$_{Ar}$**), 131.5 (d, $^4J_{C,P}$ = 3 Hz, *p*-P-**C$_{Ar}$**), 131.0 (d, $^1J_{C,P}$ = 52 Hz, P-**C$_{Ar}$**), 128.8 (d, $^2J_{C,P}$ = 11 Hz, *o*-P-**C$_{Ar}$**), 127.3 (s, ^{L}**C$_{Ar}$13**), 125.7 (s, ^{L}**C$_{Ar}$14**), 122.2 (d, $^4J_{C,P}$ = 2 Hz, ^{L}**C$_{Ar}$5**), 120.1 (s, ^{L}**C$_{Ar}$12**), 118.9 (d, $^5J_{C,P}$ = 1 Hz, ^{L}**C$_{Ar}$15**), 115.1 (s, ^{L}**C$_{Ar}$3**), 112.1 (d, $^3J_{C,P}$ = 6 Hz, ^{L}**C$_{Ar}$1**-Te). ^{31}P NMR (CD_2Cl_2, ppm): 21.7 (s), 21.7 (d, $^2J_{P,Te}$ = 53 Hz, P-Pd-^{125}Te). ^{125}Te NMR (CD_2Cl_2, ppm): 476.5 (d, $^2J_{Te,P}$ = 61 Hz).

[Pt(L^{Se})(PPh$_3$)]. $[PtCl_2(PPh_3)_2]$ (80 mg, 0.1 mmol) and $\{HL^{Se}\}_2$ (44 mg, 0.08 mmol) were suspended in a degassed mixture of EtOH (1 mL) and CH_2Cl_2 (1 mL). The yellow-beige solution was heated to reflux and NEt_3 (3 drops) was added, which resulted in a color change to orange-red. After 30 min, the mixture was cooled to room temperature, the bright orange precipitate was filtered off and washed with diethyl ether and hexane. It was dried in vacuo. The product can be recrystallized by slow diffusion of diethyl ether into a CH_2Cl_2 solution. Bright orange-red powder or orange-red needles. Yield: 55 mg (75 %).

Elemental analysis: Calculated for $C_{31}H_{24}NOPPtSe$: C 50.9, H 3.3, N 1.9 %; Found C 50.8, H 3.4, N 1.9 %. IR (cm^{-1}): $\tilde{\nu}$ = 3047 (w), 1605 (m) C=N, 1587 (m), 1573 (m), 1524 (m), 1482 (m), 1459 (m), 1434 (s), 1387 (m), 1366 (m), 1329 (m), 1297 (w), 1264 (w), 1250 (w), 1221 (w), 1191 (w), 1172 (m), 1149 (m), 1126 (m), 1099 (s), 1049 (w), 1038 (w), 1028 (m), 996 (w), 960 (vw), 945 (vw), 931 (sh), 921 (w), 867 (w), 850 (w), 837 (w), 804 (w), 749 (sh), 735 (vs), 709 (sh), 694 (vs), 644 (vw), 616 (m), 585 (w), 567 (vw), 556 (m), 538 (vs), 526 (s). ESI^+ MS (*m/z*): 754.0342 (calc. 754.0304) $[M + Na]^+$, 770.0092 (calc. 770.0043) $[M + K]^+$, 1486.0782 (calc. 1486.0738) $[2M + Na]^+$, 1503.0516 (calc. 1503.0476) $[2M + K]^+$. ^1H NMR ($CDCl_3$, ppm): 9.20 (1H, d, $^4J_{H,P}$ = 13.29 Hz, **H17**CR=NR), 9.20 (dd, $^3J_{H,Pt}$ = 42.98 Hz, $^4J_{H,P}$ = 11.08 Hz, **H17**CR=NR), 9.20 (dd, $^1J_{C17,H17}$ = 161.48 Hz, $^4J_{H,P}$ = 12.69 Hz, **H17**CR=NR), 7.85–7.75 (6H, m, *m*-P-Ar**H**), 7.70 (1H, dd, $^3J_{H15,H14}$ = 7.72 Hz, $^4J_{H15,H13}$ = 1.48 Hz, ^{L}Ar**H15**), 7.57 (1H, dd, $^3J_{H12,H13}$ = 8.01 Hz, $^4J_{H12,H14}$ = 1.83 Hz, ^{L}Ar**H12**), 7.53–7.38 (11H, m, *p*-P-Ar**H**, *o*-P-Ar**H**, ^{L}Ar**H2**, ^{L}Ar**H14**), 7.09 (1H, ddd, $^3J_{H13,H12}$ = 8.38 Hz, $^4J_{H13,H14}$ = 6.81 Hz, $^4J_{H13,H15}$ = 1.53 Hz, ^{L}Ar**H13**), 7.02 (1H, ddd, $^3J_{H4,H3}$ = 8.08 Hz, $^4J_{H4,H5}$ = 7.04 Hz, $^4J_{H4,H2}$ = 1.18 Hz, ^{L}Ar**H4**), 6.75–6.90 (2H, m + ddd, $^3J_{H3,H4}$ = 7.93 Hz, $^3J_{H3,H2}$ = 6.77 Hz, $^3J_{H3,H5}$ = 1.15 Hz, ^{L}Ar**H5**, ^{L}Ar**H3**). ^{13}C NMR ($CDCl_3$, ppm): 163.1 (s, ^{L}**C$_{Ar}$6**), 153.3 (s, H**C17**R=NR), 150.8 (d, $^3J_{C,P}$ = 1 Hz, ^{L}**C$_{Ar}$11**), 135.3 (s, ^{L}**C$_{Ar}$2**), 135.0 (s, ^{L}**C$_{Ar}$4**), 134.6 (d, $^3J_{C,P}$ = 11 Hz, *m*-P-**C$_{Ar}$**), 133.3 (d, $^4J_{C,P}$ = 7 Hz, ^{L}**C$_{Ar}$16**), 131.0 (d, $^3J_{C,P}$ = 1 Hz, ^{L}**C$_{Ar}$1**-Se), 130.8 (d, $^4J_{C,P}$ = 3 Hz, *p*-P-**C$_{Ar}$**), 129.2 (d, $^1J_{C,P}$ = 61 Hz, P-**C$_{Ar}$**), 127.9 (d, $^2J_{C,P}$ = 11 Hz, *o*-P-**C$_{Ar}$**), 126.6 (s, ^{L}**C$_{Ar}$13**), 123.1 (s, ^{L}**C$_{Ar}$14**), 122.0 (d, $^4J_{C,P}$ = 1 Hz, ^{L}**C$_{Ar}$5**), 119.3 (s, ^{L}**C$_{Ar}$12**), 116.7 ($^5J_{C,P}$ = 1 Hz, ^{L}**C$_{Ar}$15**), 115.6 (s, ^{L}**C$_{Ar}$3**). ^{31}P NMR ($CDCl_3$, ppm): 8.1 (s), 8.2 (d, $^1J_{P,Pt}$ = 3719 Hz, P^{195}Pt). ^{77}Se NMR ($CDCl_3$, ppm): 196.8 (d, $^2J_{Se,P}$ = 31 Hz). ^{195}Pt NMR ($CDCl_3$, ppm): –3675 (d, $^1J_{Pt,P}$ = 3772 Hz).

[Pt(L^{Te})(PPh$_3$)]. $[PtCl_2(PPh_3)_2]$ (80 mg, 0.1 mmol) and $\{HL^{Te}\}_2$ (52 mg, 0.08 mmol) were suspended in a degassed mixture of EtOH (1 mL) and CH_2Cl_2 (3 mL). The clear orange-red solution was heated to reflux and NEt_3 (1 drop) was added, which resulted in a color-change to dark red-brown. The heating was continued for 3 days. Then, the CH_2Cl_2 was distilled off and the remaining solution was cooled to room temperature. The addition of an excess of a 1:1 mixture of EtOH and hexane (ca. 60 mL) induced precipitation. The light red precipitate was filtered off and washed with EtOH, diethyl ether and hexane. The dark red powder was dried in vacuo. The product can be recrystallized by slow evaporation of a CH_2Cl_2/diethyl ether mixture. Dark red powder or orange-red needles. Yield: 43 mg (55 %).

Elemental analysis: Calculated for $C_{31}H_{24}NOPPtTe$: C 47.7, H 3.1, N 1.8 %; Found C 47.5, H 3.2, N 1.8 %. IR (cm^{-1}): $\tilde{\nu}$ = 3048 (w), 1605 (m) C=N, 1584 (m), 1569 (m), 1523 (m), 1482 (m), 1455 (m), 1435 (s), 1390 (m), 1366 (m), 1331 (m), 1263 (w), 1248 (w), 1216 (w), 1191 (w), 1170 (m), 1148 (s), 1127 (m), 1099 (s), 1047 (w), 1028 (m), 997 (w), 951 (vw), 931 (w), 839 (w), 801 (w), 738 (vs), 709 (sh), 693 (vs),

617 (sh), 610 (m), 580 (w), 556 (m), 538 (vs). ESI$^+$ MS (*m*/*z*): 781.0349 (calc. 798.0324) $[M]^+$, 798.0332 (calc. 798.0324) $[M + OH]^+$, 812.0551 (calc. 812.0481) $[M + OMe]^+$. ^{1}H NMR ($CDCl_3$, ppm): 8.9 (1H, d, $^4J_{H,P}$ = 12.65 Hz, **H17**CR=NR), 8.9 (dd, $^3J_{H,Pt}$ = 43.94 Hz, $^4J_{H,P}$ not determined due to overlap with the main signal of the aldiminic proton, **H17**CR=NR), 7.86–7.73 (7H, m, *m*-P-Ar**H**, ^{L}Ar**H15**), 7.54–7.39 (11H, m, 6 *o*-P-Ar**H**, 3 *p*-P-Ar**H**, ^{L}Ar**H2**, ^{L}Ar**H12**), 7.16–7.10 (2H, m, ^{L}Ar**H4**, ^{L}ArH**14**), 6.92 (1H, m, ^{L}Ar**H13**), 6.71–6.58 (2H, m, ^{L}Ar**H3**, ^{L}Ar**H5**). ^{13}C NMR ($CDCl_3$, ppm): 168.6 (s, ^{L}**C$_{Ar}$6**), 164.2 (s, H**C17**R=NR), 157.4 (d, $^3J_{C,P}$ = 4 Hz, ^{L}**C$_{Ar}$11**), 136.3 (s, ^{L}**C$_{Ar}$2**), 136.2 (s, ^{L}**C$_{Ar}$4**), 136.2 (d, $^4J_{C,P}$ = 1 Hz, ^{L}**C$_{Ar}$16**), 135.1 (d, $^3J_{C,P}$ = 11 Hz, *m*-P-**C$_{Ar}$**), 131.4 (d, $^4J_{C,P}$ = 3 Hz, *p*-P-**C$_{Ar}$**), 130.8 (d, $^1J_{C,P}$ = 62 Hz, P-**C$_{Ar}$**), 128.5 (d, $^2J_{C,P}$ = 11 Hz, *o*-P-**C$_{Ar}$**), 127.1 (s, ^{L}**C$_{Ar}$13**), 125.2 (s, ^{L}**C$_{Ar}$14**), 122.3 (d, $^4J_{C,P}$ = 1 Hz, ^{L}**C$_{Ar}$5**), 120.2 (s, ^{L}**C$_{Ar}$12**), 119.4 (d, $^5J_{C,P}$ = 1 Hz, ^{L}**C$_{Ar}$15**), 116.1 (s, ^{L}**C$_{Ar}$3**), 110.6 (d, $^3J_{C,P}$ = 6 Hz, ^{L}**C$_{Ar}$1**-Te). ^{31}P NMR ($CDCl_3$, ppm): 4.8 (s), 4.8 (d, $^1J_{P,Pt}$ = 3712 Hz, $P^{\hat{1}95}$Pt), 4.5 (d, *J* = 1559 Hz). ^{125}Te NMR ($CDCl_3$, ppm): 300.1 (d, $^2J_{Te,P}$ = 58 Hz). ^{195}Pt NMR ($CDCl_3$, ppm): –3895 (d, $^1J_{Pt,P}$ = 3651 Hz).

{[(HO)C$_6$H$_4$-(CHN$^+$H)-C$_6$H$_4$-TeI$_2$]·OPPh$_3$}. A solution of elemental iodine (25 mg, 0.1 mmol) in CH_2Cl_2 (2 mL) was added dropwise to a dry, degassed solution of $OPPh_3$ (28 mg, 0.1 mmol) and $\{HL^{Te}\}_2$ (32 mg, 0.05 mmol) in CH_2Cl_2 (4 mL). A red precipitate formed from the green-brown solution immediately. The mixture was stirred at room temperature for 3 h. The precipitate was filtered off and extracted with CH_2Cl_2 (3 × 4 mL), diethyl ether (10 mL) and hexane (10 mL). The combined filtrates and extract solutions were slowly evaporated. The formed black-violet crystals were filtered off, washed with diethyl ether and dried in vacuo. Black-violet blocks. Yield: 19 mg (22 %).

Elemental analysis: Calculated for $C_{31}H_{26}I_2NO_2PTe$: C 43.5, H 2.9, N 1.6 %; Found C 42.8, H 3.1, N 1.6 %. IR (cm^{-1}): $\tilde{\nu}$ = 3050 (m) N-H, 2324 (br) O-H, 1737 (br), 1624 (s) C=N, 1606 (s), 1584 (s), 1571 (s), 1502 (w), 1476 (w), 1434 (s), 1380 (m), 1360 (m), 1294 (w), 1242 (m), 1185 (m), 1160 (sh), 1141 (vs), 1120 (vs), 1086 (vs), 1069 (s), 1026 (m), 995 (vs), 944 (w), 905 (m), 876 (m), 852 (m), 784 (vw), 748 (vs), 722 (vs), 691 (vs), 632 (vw), 616 (w), 573 (w), 557 (m), 538 (vs). ESI$^+$ MS (*m*/*z*): 301.0600 (calc. 301.0758) $[OPPh_3 + Na]^+$, 579.1396 (calc. 579.1619) $[(OPPh_3)_2 + Na]^+$, 666.0842 (calc. 666.0695) $[M – 2HI – H + CH_3CN + Na]^+$, 857.2221 (calc. 857.2479) $[(OPPh_3)_3 + Na]^+$. ^{1}H NMR (CD_2Cl_2, ppm): 8.76 (1H, s, **H17**CR=NR), 8.38 (d, $^2J_{H,P}$ = 7.79 Hz, RO-**H1**···$OPPh_3$), 7.79–7.69 (21H, m, 6 *m*-P-Ar**H**, ^{L}Ar**H15**, 3 *p*-P-Ar**H**, 6 *o*-P-Ar**H**, ^{L}Ar**H2**, ^{L}Ar**H12**, ^{L}Ar**H5**, ^{L}ArH**14**, ^{L}Ar**H15**), 7.37 (1H, m, ^{L}Ar**H3**), 7.28 (1H, m, ^{L}Ar**H4**), 7.09 (1H, m, ^{L}Ar**H13**). ^{31}P NMR (CD_2Cl_2, ppm): 32.6 (s).

Deposition Numbers 2021656, 2021657, 2021658, 2021659, 2021660, 2021661 and 2021662 contain the supplementary crystallographic data for this paper. These data are provided free of charge by the joint Cambridge Crystallographic Data Centre and Fachinformationszentrum Karlsruhe Access Structures service www.ccdc.cam.ac.uk/structures.

Acknowledgments

This work was generously supported by the German Academic Exchange Service (DAAD, Germany) and the Coordenação de Aperfeiçoamento de Pessoal de Nível Superior (CAPES, Brazil). We also gratefully acknowledge the assistance of the Core Facility BioSupraMol supported by the DFG and the High-Performance-Computing (HPC) Centre of the Zentraleinrichtung für Datenverarbeitung (ZEDAT) of the Freie Universität Berlin for computational time and support. Open access funding enabled and organized by Projekt DEAL.

Keywords: Nickel · Palladium · Platinum · Selenolate · Tellurolate · Schiff bases · Reduction

[1] W. H. Hegazy, A. E.-D. M. Gaafar, *Am. Chem. Sci. J.* **2012**, *2*, 86–99.
[2] Z. H. Chohan, H. Pervez, A. Rauf, A. Scozzafava, C. T. Supuran, *J. Enzyme Inhib. Med. Chem.* **2002**, *17*, 117–122.
[3] N. I. al-Salim, W. R. McWhinnie, *Polyhedron* **1989**, *8*, 2769–2776.
[4] M. A. Arafath, F. Adam, M. R. Razali, L. E. A. Hassan, M. B. K. Ahamed, A. M. S. A. Majid, *J. Mol. Struct.* **2017**, *1130*, 791–798.
[5] E. A. Elzahany, K. H. Hegab, S. K. H. Khalil, N. S. Youssef, *Aust. J. Basic Appl. Sci.* **2008**, *2*, 210–220.
[6] P.-Y. Shi, Y.-H. Liu, S.-M. Peng, S.-T. Liu, *Organometallics* **2002**, *21*, 3203–3207.
[7] H. Motschi, C. Nusaumer, P. S. Pregosin, *Helv. Chim. Acta* **1980**, *63*, 2071–2086.
[8] N. Roy, S. Sproules, E. Bothe, T. Weyhermüller, K. Wieghardt, *Eur. J. Inorg. Chem.* **2009**, *2009*, 2655–2663.
[9] M. M. Tamizh, B. F. T. Cooper, C. L. B. Macdonald, R. Karvembu, *Inorg. Chim. Acta* **2013**, *394*, 391–400.
[10] M. Shabbir, Z. Akhter, I. Ahmad, S. Ahmed, M. Shafiq, B. Mirza, V. McKee, K. S. Munawar, A. R. Ashraf, *J. Mol. Struct.* **2016**, *1118*, 250–258.
[11] M. Shabbir, Z. Akhter, A. R. Ashraf, H. Ismail, A. Habib, B. Mirza, *J. Mol. Struct.* **2017**, *1149*, 720–726.
[12] M. M. Tamizh, K. Mereiter, K. Kirchner, B. R. Bhat, R. Karvembu, *Polyhedron* **2009**, *28*, 2157–2164.
[13] C. Manzur, C. Bustos, R. Schrebler, D. Carrillo, *Polyhedron* **1989**, *8*, 2321–2330.
[14] P. Raj, A. Singh, K. Kaur, T. Aree, A. Singh, N. Singh, *Inorg. Chem.* **2016**, *55*, 4874–4883.
[15] V. Kuchtanin, L. Kleščíková, M. Šoral, R. Fischer, Z. Růžičková, E. Rakovský, J. Moncol', P. Segl'a, *Polyhedron* **2016**, *117*, 90–96.
[16] *Cambridge Structural Database*, Release 5.40, November **2018**.
[17] B. Noschang Cabral, L. Kirsten, A. Hagenbach, P. C. Piquini, M. Patzschke, E. S. Lang, U. Abram, *Dalton Trans.* **2017**, *46*, 9280–9286.
[18] B. Noschang Cabral, *Doctoral* Thesis, Universidade Federal Santa Maria, **2017**.
[19] V. P. Ananikov, I. P. Beletskaya, G. G. Aleksandrov, I. L. Eremenko, *Organometallics* **2003**, *22*, 1414–1421.
[20] Gysling, H. J., *Ligand properties of organic selenium and tellurium compounds, in Organic Selenium and Tellurium Compounds: Volume 1*, 679–855, **1986**, (Eds.: S. Patai, Z. Rappoport), John Wiley & Sons, Inc., Chichester, UK. DOI: https://doi.org/https://doi.org/10.1002/9780470771761.ch18.
[21] R. Oilunkaniemi, R. S. Laitinen, M. Ahlgrén, *J. Organomet. Chem.* **2001**, *623*, 168–175.
[22] T. Chakraborty, K. Srivastava, H. B. Singh, R. J. Butcher, *J. Organomet. Chem.* **2011**, *696*, 2782–2788.
[23] P. K. Dutta, A. K. Asatkar, S. S. Zade, S. Panda, *Dalton Trans.* **2014**, *43*, 1736–1743.
[24] N. Ghavale, A. Wadawale, S. Dey, V. K. Jain, *Ind. J. Chem.* **2009**, *48A*, 1510–1514.
[25] B. Tirloni, C. N. Cechin, G. F. Razera, M. B. Pereira, G. M. de Oliveira, E. S. Lang, *Z. Anorg. Allg. Chem.* **2016**, *642*, 239–245.
[26] R. Kaur, S. C. Menon, S. Panda, H. B. Singh, R. P. Patel, R. J. Butcher, *Organometallics* **2009**, *28*, 2363–2371.
[27] D. Back, G. M. de Oliveira, E. S. Lang, *Polyhedron* **2015**, *85*, 565–569.
[28] B. Tirloni, E. S. Lang, G. M. de Oliveira, P. Piquini, M. Horner, *New J. Chem.* **2014**, *38*, 2394–2399.
[29] S. Kolay, M. Kumar, A. Wadawale, D. Das, V. K. Jain, *Dalton Trans.* **2014**, *43*, 16056–16065.
[30] M. Roca Jungfer, A. Hagenbach, E. S. Lang, U. Abram, *Eur. J. Inorg. Chem.* **2019**, *2019*, 4974–4984.
[31] R. Cargnelutti, E. S. Lang, P. Piquini, U. Abram, *Inorg. Chem. Commun.* **2014**, *45*, 48–50.
[32] C. Amatore, A. Jutand, M. A. M'Barki, *Organometallics* **1992**, *11*, 3009–3013.
[33] S. Ford, C. P. Morley, M. Di Vaira, *Inorg. Chem.* **2004**, *43*, 7101–7110.
[34] M. Risto, E. M. Jahr, M. S. Hannu-Kuure, R. Oilunkaniemi, R. S. Laitinen, *J. Organomet. Chem.* **2007**, *692*, 2193–2204.

[35] T. G. Appleton, M. A. Bennett, *Inorg. Chem.* **1978**, *17*, 738–747.
[36] R. J. Butcher, T. Chakravorty, H. B. Singh, *Acta Crystallogr., Sect. E.* **2012**, *68*, m141.
[37] M. Risto, R. Oilunkaniemi, R. S. Laitinen, M. Ahlgren, *Acta Crystallogr., Sect. E.* **2010**, *66*, m147.
[38] L. Kirsten, V. D. Schwade, L. Selter, A. Hagenbach, P. C. Piquini, E. S. Lang, U. Abram, *Eur. J. Inorg. Chem.* **2015**, *2015*, 3748–3757.
[39] L.-B. Han, F. Mirzaei, S. Shimada, *Heteroat. Chem.* **2018**, *29:e21463*, 1–4.
[40] R. Singh Chauhan, G. Kedarnath, A. Wadawale, D. K. Maity, J. A. Golen, A. L. Rheingold, V. K. Jain, *J. Organomet. Chem.* **2013**, *737*, 40–46.
[41] S. Kolay, A. Wadawale, S. Nigam, M. Kumar, C. Majumder, D. Das, V. K. Jain, *Inorg. Chem.* **2015**, *54*, 11741–11750.
[42] L.-B. Han, N. Choi, M. Tanaka, *J. Am. Chem. Soc.* **1997**, *119*, 1795–1796.
[43] L.-B. Han, S. Shimada, M. Tanaka, *J. Am. Chem. Soc.* **1997**, *119*, 8133–8134.
[44] P. J. Bonasia, J. Arnold, *J. Organomet. Chem.* **1993**, *449*, 147–157.
[45] R. G. Fortney-Zirker, W. Henderson, E. R. T. Tiekink, *Inorg. Chim. Acta* **2017**, *462*, 83–96.
[46] V. K. Jain, S. Kannan, R. Bohra, *Polyhedron* **1992**, *11*, 1551–1557.
[47] A. A. Pasynsky, Y. V. Torubaev, A. V. Pavlova, S. S. Shapovalov, I. V. Skabitsky, G. L. Denisov, *Russ. J. Coord. Chem.* **2014**, *40*, 527.
[48] T. Nakagawa, H. Seino, Y. Mizobe, *J. Organomet. Chem.* **2010**, *695*, 137–144.
[49] T. Nakagawa, H. Seino, S. Nagao, Y. Mizobe, *Angew. Chem. Int. Ed.* **2006**, *118*, 7922–7926; *Angew. Chem.* **2006**, *118*, 7922.
[50] M. M. Karjalainen, T. Wiegand, J. Mikko Rautiainen, A. Wagner, H. Gorls, W. Weigand, R. Oilunkaniemi, R. S. Laitinen, *J. Organomet. Chem.* **2007**, *836–837*, 17.
[51] D. M. Giolando, T. B. Rauchfuss, A. L. Rheingold, *Inorg. Chem.* **1987**, *26*, 1636–1638.
[52] S. A. Batten, J. C. Jeffery, L. H. Rees, M. D. Rudd, F. G. A. Stone, *J. Chem. Soc., Dalton Trans.* **1998**, 2839.
[53] C.-K. Hsieh, F.-C. Lo, G.-H. Lee, S.-M. Peng, W.-F. Liaw, *J. Chin. Chem. Soc.* **2000**, *47*, 103–107.
[54] J. J. Schneider, J. Kuhnigkh, C. Kruger, *Inorg. Chim. Acta* **1997**, *266*, 109–112.
[55] A. A. Pasynskii, S. S. Shapovalov, I. V. Skabitskii, O. G. Tikhonova, *Russ. J. Coord. Chem.* **2017**, *43*, 837–842.
[56] C.-H. Hsieh, I.-J. Hsu, C.-M. Lee, S.-C. Ke, T.-Y. Wang, G.-H. Lee, Y. Wang, J.-M. Chen, J.-F. Lee, W.-F. Liaw, *Inorg. Chem.* **2003**, *42*, 3925–3933.
[57] S. A. Yao, V. Martin-Diaconescu, I. Infante, K. M. Lancaster, A. W. Götz, S. DeBeer, J. F. Berry, *J. Am. Chem. Soc.* **2015**, *137*, 4993–5011.
[58] H. Sitzmann, D. Saurenz, G. Wolmershäuser, A. Klein, R. Boese, *Organometallics* **2001**, *20*, 700–705.
[59] S. S. Shapovalov, A. A. Pasynskii, I. V. Skabitskii, O. G. Tikhonova, A. V. Kolos, M. O. Grigor'eva, *Russ. J. Coord. Chem.* **2018**, *44*, 647–652.
[60] M. Brandl, A. Ebner, M. M. Kubicki, Y. Mugnier, J. Wachter, E. Vigier-Juteau, M. Zabel, *Eur. J. Inorg. Chem.* **2007**, *2007*, 994–1003.
[61] S. dos Santos, B. N. Cabral, U. Abram, E. S. Lang, *J. Organomet. Chem.* **2013**, *723*, 115–121.
[62] A. J. Londero, N. Ramirez, P. C. Piquini, U. Abram, E. S. Lang, *J. Organomet. Chem.* submitted.
[63] L. M. Venanzi, *J. Chem. Soc.* **1958**, 719–724.
[64] T. A. Stephenson, S. M. Morehouse, A. R. Powell, J. P. Heffer, G. Wilkinson, *J. Chem. Soc.* **1965**, 3632–3640.
[65] K. A. Jensen, *Z. Anorg. Allg. Chem.* **1936**, *229*, 242–251.
[66] A. A. Grinberg, Z. A. Razumova, *Zh. Prikl. Khim.* **1954**, *27*, 105.
[67] J. C. Bailar Jr., H. Itatani, *Inorg. Chem.* **1965**, *4*, 1618–1620.
[68] C. S. Radatz, D. Alves, P. H. Schneider, *Tetrahedron* **2013**, *69*, 1316–1321.
[69] L. Engman, D. Stern, I. A. Cotgreave, C. M. Andersson, *J. Am. Chem. Soc.* **1992**, *114*, 9737–9743.
[70] A. M. Deobald, L. R. S. de Camargo, G. Tabarelli, M. Hörner, O. E. D. Rodrigues, D. Alves, A. L. Braga, *Tetrahedron Lett.* **2010**, *51*, 3364–3367.
[71] R. K. Harris, E. D. Becker, S. M. Cabral de Menezes, P. Granger, R. E. Hoffman, K. W. Zilm, *Magn. Reson. Chem.* **2008**, *46*, 582–598.
[72] G. M. Sheldrick, *SADABS*, University of Göttingen, Germany, **1996**.
[73] P. Coppens, *The Evaluation of Absorption and Extinction in Single-Crystal Structure Analysis*, Crystallographic Computing, Copenhagen, Muksgaard, **1979**.
[74] G. M. Sheldrick, *Acta Crystallogr., Sect. A* **2008**, *64*, 112–122.
[75] G. M. Sheldrick, *Acta Crystallogr., Sect. C* **2015**, *71*, 3–8.
[76] *Diamond - Crystal and Molecular Structure Visualization* Crystal Impact - Dr. H. Putz & Dr. K. Brandenburg GbR, Bonn, Germany.
[77] M. J. Frisch, G. W. Trucks, H. B. Schlegel, G. E. Scuseria, M. A. Robb, J. R. Cheeseman, G. Scalmani, V. Barone, B. Mennucci, G. A. Petersson, H. Nakatsuji, M. Caricato, X. Li, H. P. Hratchian, A. F. Izmaylov, J. Bloino, G. Zheng, J. L. Sonnenberg, M. Hada, M. Ehara, K. Toyota, R. Fukuda, J. Hasegawa, M. Ishida, T. Nakajima, Y. Honda, O. Kitao, H. Nakai, T. Vreven, J. A. Montgomery Jr., J. E. Peralta, F. Ogliaro, M. Bearpark, J. J. Heyd, E. Brothers, K. N. Kudin, V. N. Staroverov, R. Kobayashi, J. Normand, K. Raghavachari, A. Rendell, J. C. Burant, S. S. Iyengar, J. Tomasi, M. Cossi, N. Rega, J. M. Millam, M. Klene, J. E. Knox, J. B. Cross, V. Bakken, C. Adamo, J. Jaramillo, R. Gomperts, R. E. Stratmann, O. Yazyev, A. J. Austin, R. Cammi, C. Pomelli, J. W. Ochterski, R. L. Martin, K. Morokuma, V. G. Zakrzewski, G. A. Voth, P. Salvador, J. J. Dannenberg, S. Dapprich, A. D. Daniels, Ö. Farkas, J. B. Foresman, J. V. Ortiz, J. Cioslowski, D. J. Fox, *Gaussian 09, Revision B.01*, Gaussian, Inc., Wallingford CT, **2016**.
[78] M. J. Frisch, G. W. Trucks, H. B. Schlegel, G. E. Scuseria, M. A. Robb, J. R. Cheeseman, G. Scalmani, V. Barone, G. A. Petersson, H. Nakatsuji, X. Li, M. Caricato, A. Marenich, J. Bloino, B. G. Janesko, R. Gomperts, B. Mennucci, H. P. Hratchian, J. V. Ortiz, A. F. Izmaylov, J. L. Sonnenberg, D. Williams-Young, F. Ding, F. Lipparini, F. Egidi, J. Goings, B. Peng, A. Petrone, T. Henderson, D. Ranasinghe, V. G. Zakrzewski, J. Gao, N. Rega, G. Zheng, W. Liang, M. Hada, M. Ehara, K. Toyota, R. Fukuda, J. Hasegawa, M. Ishida, T. Nakajima, Y. Honda, O. Kitao, H. Nakai, T. Vreven, K. Throssell, J. A. Montgomery Jr., J. E. Peralta, F. Ogliaro, M. Bearpark, J. J. Heyd, E. Brothers, K. N. Kudin, V. N. Staroverov, T. Keith, R. Kobayashi, J. Normand, K. Raghavachari, A. Rendell, J. C. Burant, S. S. Iyengar, J. Tomasi, M. Cossi, J. M. Millam, M. Klene, C. Adamo, R. Cammi, J. W. Ochterski, R. L. Martin, K. Morokuma, O. Farkas, J. B. Foresman, and D. J. Fox, *Gaussian 09*, *Revision A.02*, Gaussian, Inc., Wallingford CT, **2016**.
[79] *GaussView*, Version 6, Roy Dennington, Todd A. Keith, and John M. Millam, Semichem Inc., Shawnee Mission, KS, **2016**.
[80] S. H. Vosko, L. Wilk, M. Nusair, *Can. J. Phys.* **1980**, *58*, 1200–1211.
[81] A. D. Becke, *J. Chem. Phys.* **1993**, *98*, 5648–5652.
[82] C. Lee, W. Yang, R. G. Parr, *Phys. Rev. B* **1988**, *37*, 785–789.
[83] P. J. Hay, W. R. Wadt, R. Willard, *J. Chem. Phys.* **1985**, *82*, 299–310.
[84] A. Bergner, M. Dolg, W. Küchle, H. Stoll, H. Preuß, *Mol. Phys.* **1993**, *80*, 1431–1441.
[85] W. J. Pietro, E. S. Blurock, R. F. Hout, W. J. Hehre, D. J. DeFrees, R. F. Stewart, *Inorg. Chem.* **1981**, *20*, 3650–3654.
[86] M. M. Francl, W. J. Pietro, W. J. Hehre, J. S. Binkley, M. S. Gordon, D. J. DeFrees, J. A. Pople, *J. Chem. Phys.* **1982**, *77*, 3654–3665.
[87] M. S. Gordon, J. S. Binkley, J. A. Pople, W. J. Pietro, W. J. Hehre, *J. Am. Chem. Soc.* **1982**, *104*, 2797–2803.
[88] P. C. Hariharan, J. A. Pople, *Theor. Chim. Acta* **1973**, *28*, 213–222.
[89] W. J. Hehre, R. Ditchfield, J. A. Pople, *J. Chem. Phys.* **1972**, *56*, 2257–2261.
[90] V. A. Rassolov, M. A. Ratner, J. A. Pople, P. C. Redfern, L. A. Curtiss, *J. Comput. Chem.* **2001**, *22*, 976–984.
[91] R. Ditchfield, W. J. Hehre, J. A. Pople, *J. Chem. Phys.* **1971**, *54*, 724–728.
[92] K. L. Schuchardt, B. T. Didier, T. Elsethagen, L. Sun, V. Gurumoorthi, J. Chase, J. Li, T. L. Windus, *J. Chem. Inf. Model.* **2007**, *47*, 1045–1052.
[93] S. Grimme, *Chem. Eur. J.* **2012**, *18*, 9955–9964. (DOI: https://doi.org/10.1002/chem.201200497).
[94] R. Paton, I. Funes-Ardoiz; https://zenodo.org/badge/latestdoi/16266/bobbypaton/GoodVibes; DOI: https://doi.org/10.5281/zenodo.3346166.
[95] T. Lu, F. Chen, *J. Comput. Chem.* **2012**, *33*, 580–592. (http://sobereva.com/multiwfn).

Received: August 6, 2020

4.10 Solvents and Ligands Matter: Structurally Variable Palladium and Nickel Clusters Assembled by Tridentate Selenium- and Tellurium-Containing Schiff Bases

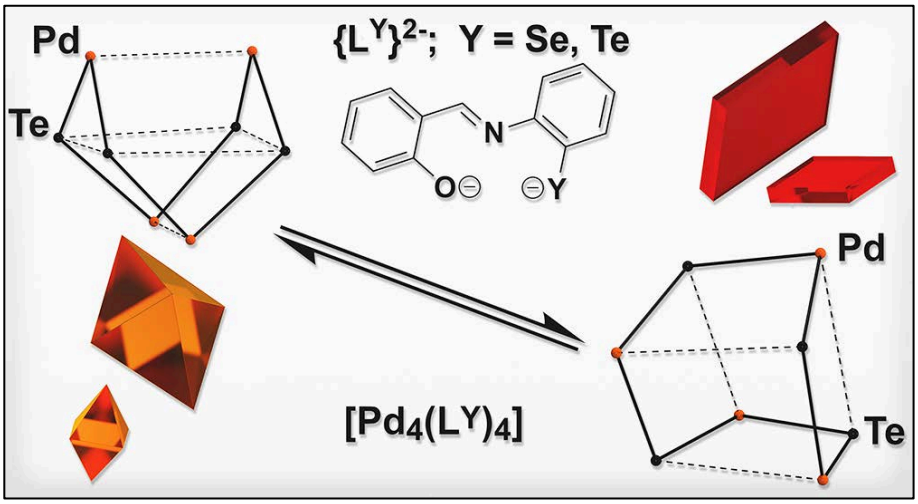

Reproduced with permission from Roca Jungfer, M.; Schulz Lang, E.; Abram, U. *Inorg. Chem*. **2022**, *61*, 3785–3800.

DOI: 10.1021/acs.inorgchem.2c00076

For Supplementary Material see A.10.

Author Contributions:

Maximilian Roca Jungfer designed the project. Maximilian Roca Jungfer performed the synthesis and characterization of the compounds, performed DFT calculations, calculated the X-ray structures and wrote a draft of the manuscript. Ernesto Schulz Lang provided scientific guidance and suggestions. Ulrich Abram supervised the project, provided scientific guidance and suggestions and corrected the manuscript.

Inorganic Chemistry

pubs.acs.org/IC Article

Solvents and Ligands Matter: Structurally Variable Palladium and Nickel Clusters Assembled by Tridentate Selenium- and Tellurium-Containing Schiff Bases

Maximilian Roca Jungfer, Ernesto Schulz Lang, and Ulrich Abram*

Cite This: *Inorg. Chem.* 2022, 61, 3785−3800 Read Online

ACCESS | Metrics & More | Article Recommendations | Supporting Information

ABSTRACT: Structurally variable organochalcogen clusters containing palladium(II) and nickel(II) ions were assembled starting from the salicylidene-substituted dichalcogenides (Y−C_6H_4−N═CH−C_6H_4−OH)$_2$ ({HL^Y}$_2$, where Y = Se or Te), and palladium or nickel acetate. The tetrameric palladium clusters contain reduced chalcogenolato ligands {Y−C_6H_4−N═CH−C_6H_4−O)}$^{2-}$ ({L'^Y}$^{2-}$, where Y = Se or Te), while the initially formed trimeric nickel clusters contain the intact, coordinated dichalcogenides. The palladium clusters have a general formula of [$Pd_4(L'^Y)_4$] and represent the first examples of palladium complexes where both a gyrobifastigial and a pseudocubane arrangement of the central Pd_4Y_4 unit could be established with the same ligand, only depending on the solvents used for crystallization. Reduced density gradient (RDG) considerations based on density functional theory calculations suggest that the commonly referred to stabilizing chalcogen−palladium or palladium−palladium interactions for the two geometric arrangements are weak van der Waals contacts resulting from the contact of two nonbinding lone pairs. In the case of the pseudocubane arrangement, a repulsive steric effect, which is indicated by RDG analysis, is clearly supported by the cuplike distortions detected in the solid-state structure of the compound. In contrast to the reactions with palladium acetate, where the dichalcogenides were cleaved, during similar reactions with nickel acetate, the dichalcogenides remained intact and trimeric clusters of the composition [Ni-μ^2-κ^2-(Ni{κ^5-L^Y}$_2$)$_2$-μ^2-(OAc)$_2$] (Y = Se, Te) were formed. Air oxidation and hydrolysis of [Ni-μ^2-κ^2-(Ni{κ^5-L^{Te}}$_2$)$_2$-μ^2-(OAc)$_2$] gave a rare example of a hexanuclear nickel cluster of the composition [Ni_2-κ^5-(Ni_4-κ^6-μ^6-{($L'^{Te}{}_2O_3$)($L'^{Te}O_2$)$_2$}$_2$)-μ^2-(H_2O)$_2$], which is composed of a well-defined framework consisting of tellurinic anhydride and tellurinate units, which proves the comparably higher oxidation sensitivity of the trinickel dichalcogenide complexes. Electron spray ionization mass spectrometry spectra of both the palladium and nickel clusters indicate that they show fluctional behavior with varying nuclearity in solution and can adopt multiple charge states especially because of the noninnocence of the chalcogen-based ligands. The complexes were fully characterized by spectroscopic methods, elemental analyses, and X-ray diffraction.

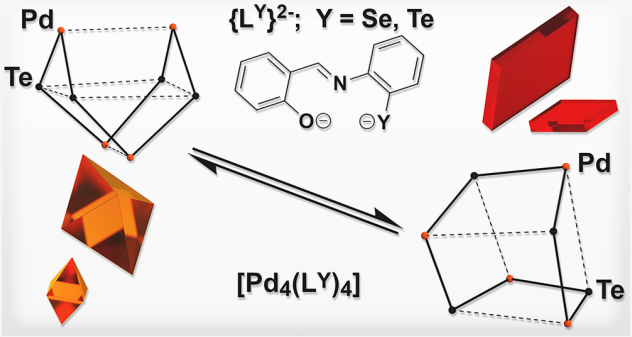

INTRODUCTION

The ongoing development of the coordination chemistry of nickel, palladium, and platinum triads with chalcogen-containing ligands is frequently stimulated by the catalytic activity,[1−3] structural flexibility, and bioactivity of the obtained products.[4,5] This also includes the cluster chemistry of these metals.[6−9] The nuclearity and bonding modes inside such multinuclear units are frequently controlled by the nature and size of the organic ligands used. A widespread class of ligands that bind well to many metals are Schiff bases. Their modular synthesis can be used to easily tune the properties of the resulting complexes.[10−24] Organochalcogen units are often used as the building blocks of such ligands because of the potentially promising optoelectronic, supramolecular, or redox properties of their metal complexes. The latter holds especially true for the heavier chalcogen elements sulfur, selenium, and tellurium. A complete listing of the hitherto known structurally characterized Schiff base complexes with disulfide units, together with their corresponding references, is given in the Supporting Information (SI) of this paper. Although the synthesis of such complexes has been steadily developed, methods for the preparation of defined species are still limited, and the resultant supramolecular aggregates are poorly controlled. Exemplarily, organochalcogenolato complexes of palladium are accessible via an oxidative addition to

Received: January 9, 2022
Published: February 15, 2022

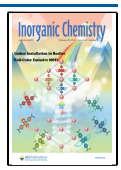

palladium(II) species, resulting in (commonly transient) palladium(IV) species, which are easily reduced back to palladium(II). However, often complex mixtures and mainly several different polynuclear complexes are obtained in such reactions.[25−30]

Recently, we developed a reliable method for the preparation of defined monomeric organochalcogenolato complexes from dichalcogenides via a reduction by intrinsically released phosphine ligands of nickel, palladium, platinum and rhenium starting materials.[31−33]

In the present study, we report the reactivity of the diselenide- and ditelluride-tethered Schiff bases ($\{HL^{Y}\}_2$, where Y = Se or Te) shown in Scheme 1 toward nickel(II) and palladium(II) acetates. Because of the absence of the intrinsic reductant PPh_3, a completely different course of reaction can be expected.

Scheme 1. Syntheses of Monomeric Transition-Metal Selenolato and Tellurolato Complexes by the Controlled Reduction of Dichalcogenides by Release of the PPh_3 Ligand[32,33]

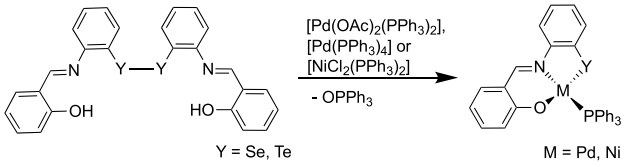

EXPERIMENTAL SECTION

Materials. Palladium acetate $[Pd(OAc)_2]$,[34] the Schiff bases derived from salicylaldehyde and bis(2-aminophenyl)diselenide ($\{HL^{Se}\}_2$) and ditelluride ($\{HL^{Te}\}_2$),[35] bis(2-aminophenyl)diselenide, and bis(2-aminophenyl)ditelluride were prepared according to literature procedures.[36−38] All other chemicals were reagent-grade and were used as received. Reactions involving oxygen- or water-sensitive compounds were performed with standard Schlenk techniques.

Physical Measurements. NMR spectra were recorded at 25 °C on a JEOL 400 MHz ECS-400 or a JNM-ECA400II spectrometer. Reported chemical shifts (δ) are referenced to the Ξ values given in the 2008 IUPAC recommendations using the ^{2}H signal of the deuterated solvent as the internal reference.[39] IR spectra were recorded with an Fourier transform infrared (FT-IR) spectrometer (Nicolet iS10, Thermo Scientific). The intensities are classified as vs = very strong, s = strong, m = medium, w = weak, vw = very weak, and sh = shoulder. Electrospray ionization mass spectrometry (ESI MS) was carried out with the ESI MSD time-of-flight (TOF) unit of an Agilent 6210 TOF liquid chromatography/mass spectrometry system. The measurements were performed in trichloromethane ($CHCl_3$), dichloromethane (CH_2Cl_2), and methanol (MeOH) or mixtures of them. The original data of a 1 min scan were converted to .mzXML files using the *MSConvert* program of the freely distributed *ProteoWizard* package.[40] The spectra were then averaged and smoothed with a Gaussian model (three cycles) to enable a better interpretation of the data because the observed peaks are rather broad as a result of largely overlapping isotopic distributions. The freely distributed executable *mmass* was used for this processing and simulation of the isotopic distributions.[41] Especially in the ESI$^-$ MS spectra, a lot of unidentified low-molecular-weight organic noise was observed up to ca. m/z 800 as very intense signals (no isotopic patterns of the chalcogen or metal atoms). Elemental analyses were performed using a Vario EL III CHN elemental analyzer (Elementar Analysensysteme GmbH) or a Vario MICRO cube CHNS elemental analyzer. Analyses were performed on finely powdered and carefully dried (vacuum) samples because the crystalline products undergo a subsequent loss of incorporated solvents. Systematically low carbon values are attributed to carbide and/or nitride formation due to incomplete combustion of some of the metal-rich cluster compounds.

X-ray Crystallography. Single-crystal X-ray diffraction data were collected on a Bruker D8 Venture or a STOE IPDS II T diffractometer. Absorption corrections were carried out by the multiscan (Bruker D8 Venture) or integration (STOE IPDS II T) methods.[42,43] Structure solutions and refinements were done with the *SHELX-2008*, *SHELX-2014*, and *SHELX-2016* program packages.[44,45] The hydrogen-atom positions at heteroatoms or imino carbon atoms were taken from the final Fourier maps when possible or placed at calculated positions and refined by a riding model. Other hydrogen atoms were placed at calculated positions and refined by a riding model. Visualization of the molecular structures was done using the program *DIAMOND 4.2.2*.[46]

In addition to the structures of the cluster compounds, the SI contains the crystal structure of the tetragonal polymorph $\{HL^{Se}\}_2$. Deep-red crystals of this compound were isolated from the filtrate obtained during the synthesis of $[Pd_4(L'^{Se})_4]$. The crystals are isomorphous to the tetragonal polymorph $\{HL^{Te}\}_2$ reported by us.[32]

Computational Details. Density functional theory (DFT) calculations were performed on the high-performance computing systems of Freie Universität Berlin ZEDAT (Curta)[47] using the program packages *Gaussian 09* and *Gaussian 16*.[48,49] The gas- and solution-phase geometry optimizations were performed using coordinates derived from the X-ray crystal structures by *GaussView*.[50] The polarizable continuum model with the integral equation formalism variant was used to implicitly simulate the solvents CH_2Cl_2 and EtOH. Calculations were performed with the hybrid density functional B3LYP.[51−53] The double-ζ pseudopotential LANL2DZ basis set with the respective effective core potential (ECP) was applied to nickel, palladium, and platinum.[54] The Stuttgart relativistic large-core basis set RLC with the corresponding ECP and an extension by STO-3G* polarization functions was applied to tellurium.[55,56] The 6-31G* basis set was applied for all other atoms except hydrogen.[57−61] For hydrogen atoms, the 6-31G basis set was applied.[62] All basis sets as well as the ECPs were obtained from the EMSL database.[63] Frequency calculations after the optimizations confirmed the convergence. No negative frequencies were obtained for the given optimized geometries of all compounds, except for the cuboid structure of $[Pd_4(L'^{Te})_4]$ with the CAM-B3LYP functional, where a full convergence was not reached after numerous attempts, as indicated by a residual minor negative frequency. Further analysis of the obtained wave functions was performed with the free multifunctional wave function analyzer *Multiwfn*.[64] The reduced density gradient (RDG) method was used as implemented in *Multiwfn* and visualized using the *VMD* package.[65,66]

Synthetic Procedures. *$[Pd_4(L'^{Se})_4]$.* $Pd(OAc)_2$ (45 mg, 0.2 mmol) and $\{HL^{Se}\}_2$ (55 mg, 0.1 mmol) were suspended in EtOH (6 mL). After the addition of $CHCl_3$ (3 mL) and NEt_3 (4 drops), the mixture was heated to reflux. The yellow-brown suspension turned bright orange-red over the course of the reaction. It was heated to reflux for 3.5 h, and after cooling to room temperature, the bright-orange-red precipitate was filtered off. It was then washed with EtOH to remove traces of $HNEt_3^+$ salts and a large amount of hexane to remove traces of unreacted $\{HL^{Se}\}_2$. After drying, the thus-obtained mixture of $[Pd_4(L'^{Se})_4]$ and $Pd(OAc)_2$ was suspended in CH_2Cl_2 and loaded onto a bed of Celite to retain $Pd(OAc)_2$. It was extracted with 5 mL portions of CH_2Cl_2 and then $CHCl_3$ until the filtrate became colorless. The extracts were evaporated to dryness and the orange-red solid was redissolved in warm $CHCl_3$. The volume of the combined extracts was carefully reduced to approximately 1 mL, at which point deep-red microcrystals formed. The solution was layered with hexane and stored in a refrigerator overnight. Deep-orange-red crystals and an orange-yellow powder precipitated. The orange-red crystals were collected on a fritted glass filter, with a suitable pore size to hold back the crystals but not the orange-yellow powder, and copiously washed with hexane. The combined filtrate and washing solutions were evaporated to dryness, and the resulting orange-yellow residue was redissolved in warm $CHCl_3$. The volume was reduced for

https://doi.org/10.1021/acs.inorgchem.2c00076
Inorg. Chem. 2022, 61, 3785−3800

crystallization. The deep-orange-red crystalline product was washed with hexane and dried in air at room temperature to give pure $[Pd_4(L'^{Se})_4]$. Recrystallization could also be achieved by slow evaporation of CH_2Cl_2 solutions or by diffusion of EtOH into CH_2Cl_2 solutions at low temperature. In all of the crystallization attempts, it is imperative to add the antisolvents slowly and to evaporate the solvents carefully to avoid precipitation of the less soluble orange-yellow material, which is most probably polymeric $[Pd(L'^{Se})]_x$. Yield: 24.5 mg (0.016 mmol, 32% based on $\{HL^{Se}\}_2$) of deep-red microcrystals. Elem anal. Calcd for $C_{52}H_{36}N_4O_4Pd_4Se_4$: C, 41.0; H, 2.4; N, 3.7. Found: C, 40.6; H, 2.8; N, 3.1. Selected IR bands (cm^{-1}): 1601 (s, $\nu_{C=N}$), 1585 (s, $\nu_{C=C}$), 1567 (s, $\nu_{C=C}$). ^1H NMR (CD_2Cl_2): δ 7.98 (1H, s, **H17**CR=NR), 7.89 (1H, dd, $^3J_{H15,H14}$ = 7.79 Hz, $^4J_{H15,H13}$ = 1.39 Hz, ^{L}Ar**H15**), 7.57 (1H, dd, $^3J_{H12,H13}$ = 8.69 Hz, $^4J_{H12,H14}$ = 1.08 Hz, ^{L}Ar**H12**), 7.41 (2H, m, ^{L}Ar**H4**, ^{L}Ar**H13**), 7.15 (1H, ddd, $^3J_{H14,H15}$ = 7.91 Hz, $^3J_{H14,H13}$ = 7.00 Hz, $^4J_{H14,H12}$ = 1.04 Hz, ^{L}Ar**H14**), 6.77 (1H, dd, $^4J_{H5,H3}$ = 8.07 Hz, $^3J_{H5,H2}$ = 1.86 Hz, ^{L}Ar**H5**), 6.67 (1H, d, $^4J_{H2,H4}$ = 8.56 Hz, ^{L}Ar**H2**), 6.48 (1H, ddd, $^4J_{H3,H5}$ = 7.92 Hz, $^3J_{H3,H4}$ = 6.77 Hz, $^3J_{H3,H2}$ = 1.11 Hz, ^{L}Ar**H3**). ^1H NMR (CD_2Cl_2 + $CDCl_3$): δ 7.95 (1H, s, **H17**CR=NR), 7.93 (1H, s, ^{L}Ar**H15**), 7.55 (1H, m, ^{L}Ar**H12**), 7.41 (2H, m, ^{L}Ar**H4**, ^{L}Ar**H13**), 7.15 (1H, m, ^{L}Ar**H14**), 6.75 (2H, m, ^{L}Ar**H5**, ^{L}Ar**H2**), 6.51 (1H, m, ^{L}Ar**H3**). ^{13}C NMR (CD_2Cl_2 + $CDCl_3$): δ 205.5 (s, ^{L}**C$_{Ar}$6**), 164.9 (s, H**C17**R=NR), 155.2 (s, ^{L}**C$_{Ar}$11**), 152.3 (s, ^{L}**C$_{Ar}$2**), 137.8 (s, ^{L}**C$_{Ar}$4**), 136.3 (s, ^{L}**C$_{Ar}$16**), 135.9, (s, ^{L}**C$_{Ar}$13**), 128.6 (s, ^{L}**C$_{Ar}$14**), 128.4 (s, ^{L}**C$_{Ar}$5**), 122.4 (s, ^{L}**C$_{Ar}$12**), 120.9 (s, ^{L}**C$_{Ar}$1**-Se), 117.6 (s, ^{L}**C$_{Ar}$15**), 115.8 (s, ^{L}**C$_{Ar}$3**). ^{77}Se NMR (CD_2Cl_2 + $CDCl_3$): δ 329 (s). Selected (>5%; for the full spectrum and assignment, see the SI). ESI^+ MS (*m*/*z*): 762.7863 ($[(Pd(L'^{Se}))_2 + H]^+$; calcd 762.7902, 6%), 784.7683 ($[(Pd(L'^{Se}))_2 + Na]^+$; calcd 784.7722, 6%), 801.6509 ($[(Pd(L'^{Se}))_2 + K + H]^+$; calcd 801.7489, 6%), 1544.5488 ($[(Pd(L'^{Se}))_4 + Na]^+$; calcd 1544.5525, 23%). The ESI^- MS spectra are less intense (see the SI).

$[Pd_4(L'^{Te})_4]$. $Pd(OAc)_2$ (45 mg, 0.2 mmol) and $\{HL^{Te}\}_2$ (65 mg, 0.1 mmol) were suspended in EtOH (6 mL). After the addition of CH_2Cl_2 (2 mL) and triethylamine (NEt_3; 4 drops), the mixture was heated to reflux. The orange-brown suspension turned red over the course of the reaction. It was heated to reflux for 2 h, and after cooling to room temperature, the microcrystalline precipitate was filtered off. It was washed with EtOH to remove traces of $HNEt_3^+$ salts and with a small volume of diethyl ether (Et_2O) to remove traces of unreacted $\{HL^{Te}\}_2$ (***Caution!****the product itself is slightly soluble in* Et_2O) and a large amount of hexane. After drying, the thus-obtained mixture of $[Pd_4(L'^{Te})_4]$ and $Pd(OAc)_2$ (75 mg, 45:55) was suspended in CH_2Cl_2 and loaded onto a bed of Celite to retain $Pd(OAc)_2$. It was extracted with 5 mL portions of CH_2Cl_2 and $CHCl_3$ until no more color was observed in the filtrate. The extracts were evaporated to dryness and redissolved in warm $CHCl_3$. The volume of the solution was carefully reduced to 2 mL, at which point deep-red microcrystals formed. After the addition of 6 mL of Et_2O and layering of 120 mL of hexane on top of the solution, the product was stored in the refrigerator overnight. The obtained crystals were filtered off and washed with hexane, a small volume of Et_2O, and pentane. A second crop of crystals was obtained from the combined filtrate and washing solutions by evaporation of the solvent mixture and recrystallization from $CHCl_3$/hexane. After drying in air at room temperature, pure $[Pd_4(L'^{Te})_4]$ was obtained. Recrystallization could also be achieved by slow evaporation of CH_2Cl_2 solutions or by diffusion of EtOH or Et_2O into CH_2Cl_2 solutions at low temperature. In all recrystallization attempts, care must be taken not to precipitate the sparingly soluble orange-yellow polymer $[Pd(L'^{Te})]_x$ by a fast addition of the antisolvents or a too fast evaporation of the solvents. Yield: 34.0 mg (0.020 mmol, 40% based on $\{HL^{Te}\}_2$) of deep-red microcrystals. Elem anal. Calcd for $C_{52}H_{36}N_4O_4Pd_4Te_4$: C, 36.4; H, 2.1; N, 3.3. Found: C, 35.3; H, 2.3; N, 2.9. Selected IR bands (cm^{-1}): 1602 (s, $\nu_{C=N}$), 1586 (s, $\nu_{C=C}$), 1565 (s, $\nu_{C=C}$). ^1H NMR (CD_2Cl_2): δ 8.16 (1H, s, **H17**CR=NR), 7.84 (1H, dd, $^3J_{H15,H14}$ = 7.61 Hz, $^4J_{H15,H13}$ = 1.41 Hz, ^{L}Ar**H15**), 7.60 (1H, d, $^3J_{H12,H13}$ = 8.3 Hz, ^{L}Ar**H12**), 7.48 (1H, ddd, $^4J_{H13,H12}$ = 8.26 Hz, $^3J_{H13,H14}$ = 7.00 Hz, $^3J_{H13,H15}$ = 1.46 Hz, ^{L}Ar**H13**), 7.37 (1H, ddd, $^4J_{H4,H2}$ = 8.59 Hz, $^3J_{H4,H3}$ = 6.82 Hz, $^3J_{H4,H5}$ = 1.87 Hz, ^{L}Ar**H4**), 7.10 (1H, ddd, $^3J_{H14,H15}$ = 7.95 Hz, $^3J_{H14,H13}$ = 7.00 Hz, $^4J_{H14,H12}$ = 1.07 Hz, ^{L}Ar**H14**), 6.78 (1H, dd, $^4J_{H5,H3}$ = 8.09 Hz, $^3J_{H5,H2}$ = 1.87 Hz, ^{L}Ar**H5**), 6.69 (1H, dd, $^4J_{H2,H4}$ = 8.25 Hz, $^3J_{H2,H3}$ = 0.99 Hz, ^{L}Ar**H2**), 6.41 (1H, ddd, $^4J_{H3,H5}$ = 8.01 Hz, $^3J_{H3,H4}$ = 6.81 Hz, $^3J_{H3,H2}$ = 1.14 Hz, ^{L}Ar**H3**). Selected (>5%; for the full spectrum and assignment, see the SI) ESI^+ MS (*m*/*z*): 1718.5037 ($[(Pd(L'^{Te}))_4 + H]^+$; calcd 1718.5191, 9%), 1740.4933 ($[Pd(L'^{Te}))_4 + Na]^+$; calcd 1740.5011, 26%), 1756.4750 ($Pd(L'^{Te}))_4 + K]^+$; calcd 1756.4749, 9%). The ESI^- MS spectra are less intense (see the SI).

[Ni-μ^2-κ^2-(Ni{κ^5-L^{Se}}$_2$)$_2$-μ^2-(OAc)$_2$]. $Ni(OAc)_2{\cdot}4H_2O$ (50 mg, 0.2 mmol) and $\{HL^{Se}\}_2$ (55 mg, 0.1 mmol) were suspended in EtOH (6 mL). After the addition of CH_2Cl_2 (1.5 mL) and NEt_3 (5 drops), the mixture was heated to reflux for 20 min. Additional EtOH (10 mL) was added after cooling, and the mixture was stored in a refrigerator for 3 h. The brown-green precipitate formed was filtered off and washed with EtOH to remove traces of salts and with Et_2O to remove traces of unreacted $\{HL^{Se}\}_2$. After drying in air at room temperature, pure $[Ni\text{-}\mu^2\text{-}\kappa^2\text{-}(Ni\{\kappa^5\text{-}L^{Se}\}_2)_2\text{-}\mu^2\text{-}(OAc)_2]$ was obtained. Recrystallization can be achieved by evaporation of CH_2Cl_2 solutions or by diffusion of EtOH into CH_2Cl_2 solutions at low temperature. Yield: 59.6 mg (0.043 mmol, 85% based on $\{HL^{Se}\}_2$) of light-green-brown microcrystals. Elem anal. Calcd for $C_{56}H_{44}N_4Ni_3O_8Se_4$: C, 48.4; H, 3.0; N, 4.0. Found: C, 47.0; H, 3.4; N, 3.6. Selected IR bands (cm^{-1}) 1605 (s, $\nu_{C=N}$), 1569 (s, $\nu_{C=C}$), 1537 (s, $\nu_{C=C}$), 1457 (s, $\nu_{C=O,acetate}$). Selected (>5%; for the full spectrum and assignment, see the SI) ESI^+ MS (*m*/*z*): 608.9156 ($[Ni\{L^{Se}\}_2 + H]^+$; calcd 608.9117, 22%), 630.9089 ($[Ni\{L^{Se}\}_2 + Na]^+$; calcd 630.8945, 20%), 646.8740 ($[Ni\{L^{Se}\}_2 + K]^+$; calcd 646.8676, 11%), 1214.8171 ($[Ni_2\{(L^{Se})_2\}_2 + H]^+$; calcd 1214.8215, 100%), 1236.8109 ($[Ni_2\{(L^{Se})_2\}_2 + Na]^+$; calcd 1236.8034, 33%), 1252.7694 ($[Ni_2\{(L^{Se})_2\}_2+K]^+$; calcd 1252.7774, 13%), 1844.7071 ($[Ni_3\{(L^{Se})_2\}_3 + Na]^+$; calcd 1844.7047, 33%), 1860.6810 ($[Ni_3\{(L^{Se})_2\}_3 + K]^+$; calcd 1860.6858, 7%). ESI^- MS (*m*/*z*): 666.9196 ($[Ni\{L^{Se}\}_2 + OAc^-]^-$; calcd 666.9172, 100%), 696.9285 ($[Ni\{L^{Se}\}_2 + OCH_2 + OAc^-]^-$; calcd 696.9187, 32%), 863.1067 ($[Ni\{L^{Se}\}_2 + 8MeOH - H^+]^-$; calcd 863.0948, 22%), 1232.7831 ($[Ni_2\{(L^{Se})_2\}_2 + H_2O + H^-]^-$; calcd 1232.8301, 3%), 1250.7832 ($[Ni_2\{(L^{Se})_2\}_2 + Cl^-]^-$; calcd 1250.7784, 5%).

[Ni-μ^2-κ^2-(Ni{κ^5-L^{Te}}$_2$)$_2$-μ^2-(OAc)$_2$]. $Ni(OAc)_2{\cdot}4H_2O$ (50 mg, 0.2 mmol), $\{HL^{Te}\}_2$ (65 mg, 0.1 mmol), and NEt_3 (2 drops) were suspended in EtOH (6 mL) under an atmosphere of argon and heated to reflux. CH_2Cl_2 (1.5 mL) was added to the boiling solution to complete the dissolution of $\{HL^{Te}\}_2$. After heating for 30 min and cooling to room temperature, the brown-red precipitate formed was filtered off. It was washed with EtOH and Et_2O. After drying in air at room temperature, pure $[Ni\text{-}\mu^2\text{-}\kappa^2\text{-}(Ni\{\kappa^5\text{-}L^{Te}\}_2)_2\text{-}\mu^2\text{-}(OAc)_2]$ was obtained. Recrystallization could be achieved by evaporation of CH_2Cl_2 solutions or by diffusion of EtOH or Et_2O into CH_2Cl_2 solutions at low temperature. The compound is insoluble in $CHCl_3$, acetone, and ethyl acetate but well-soluble in CH_2Cl_2. Yield: 73.0 mg (0.046 mmol, 92% based on $\{HL^{Te}\}_2$) of light-brown-red microcrystals. Elem anal. Calcd for $C_{56}H_{44}N_4Ni_3O_8Te_4$: C, 42.4; H, 2.7; N, 3.5. Found: C, 41.2; H, 2.8; N, 3.2. Selected IR bands (cm^{-1}): 1603 (s, $\nu_{C=N}$), 1566 (s, $\nu_{C=C}$), 1537 (s, $\nu_{C=C}$), 1454 (s, $\nu_{C=O,acetate}$). ^1H NMR ($CDCl_3$): δ 14.29 (br, s), 13.81 (br, s), 13.53 (br, s, overlapped), 13.10 (br, s, overlapped), 12.96 (br, s), 12.52 (br, s), 12.41 (br, s), 11.81 (br, s), 10.59 (br, s), 9.73 (br, s), 9.44 (br, s), 9.10 (br, s), 8.88 (br, s), 8.56 (br, s), 8.39 (br, s), 8.30 (br, s), 7.89 (br, s), 7.43 (br, s), 7.07 (br, s), 6.99 (br, sh, s), 5.30 (br, s), 4.98 (br, s), 4.13 (br, s), 3.75 (br, s), 3.49 (br, s), 2.42 (br, s), 2.23 (br, s), 2.05 (br, s), 1.26 (br, s), 0.87 (br, s), 0.08 (br, s), −1.59 (br, s), −2.45 (br, s), −3.39 (br, s), −3.95 (br, s), −4.28 (br, sh, s), −5.39 (br, s), −6.49 (br, s, overlapped), −6.65 (br, s, overlapped), −7.22 (br, s), −7.96 (br, s). Selected (>5%; for the full spectrum and assignment, see the SI) ESI^+ MS (*m*/*z*): 706.8956 ($[Ni\{L^{Te}\}_2 + H]^+$; calcd 706.8911, 34%), 726.8692 ($[Ni\{L^{Te}\}_2 + Na]^+$; calcd 728.8731, 25%), 744.8606 ($[Ni\{L^{Te}\}_2 + K]^+$; calcd 744.8470, 6%), 1076.8102 ($[Ni_3\{(L^{Te})_2\}_3 + H + K]^{2+}$; calcd 1076.8073, 10%), 1410.7641 ($[Ni_2\{(L^{Te})_2\}_2 + H]^+$; calcd 1410.7713, 100%), 1432.7605 ($[Ni_2\{(L^{Te})_2\}_2 + Na]^+$; calcd 1432.7521, 38%), 1450.7208 ($[Ni_2\{(L^{Te})_2\}_2 + K]^+$; calcd 1450.7271,

https://doi.org/10.1021/acs.inorgchem.2c00076
Inorg. Chem. 2022, 61, 3785−3800

Scheme 2. Synthesis of the $[Pd_4(L'^{Y})_4]$ Clusters (Y = Se, Te)

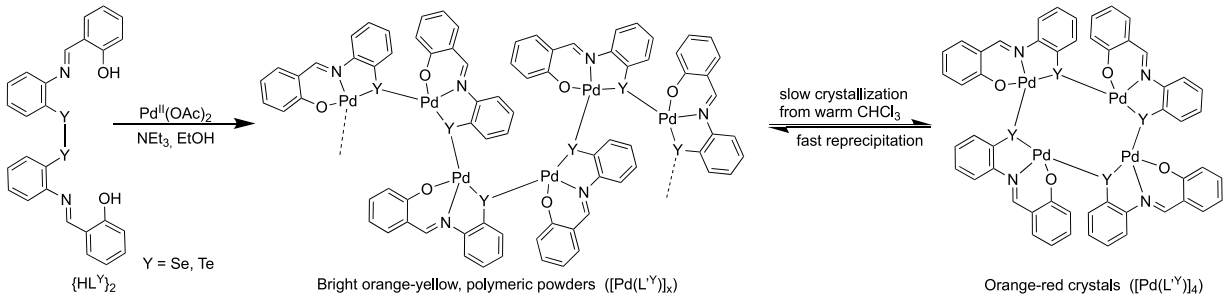

7%), 2136.6394 ($[Ni_3\{(L^{Te})_2\}_3 + Na]^+$; calcd 2136.6327, 30%), 2152.6091 ($[Ni_3\{(L^{Te})_2\}_3 + K]^+$; calcd 2152.6077, 5%). Selected (>5%; for the full spectrum and assignment, see the SI) ESI^- MS (*m*/*z*): 722.8859 ($[Ni\{L^{Te}\}_2 + OH_2 + H^-]^-$; calcd 722.8989, 22%), 740.8506 ($[Ni\{L^{Te}\}_2 + Cl^-]^-$; calcd 740.8490, 53%), 764.9030 ($[Ni\{L^{Te}\}_2 + OAc^-]^-$; calcd 764.8945, 68%), 794.9012 ($[Ni\{L^{Te}\}_2 + H_2CO + OAc^-]^-$; calcd 794.9051, 17%), 832.8042 ($[Ni\{L^{Te}\}_2 + MeOH + HCl + OAc^-]^-$; calcd 832.8965, 8%), 959.1075 ($[Ni\{L^{Te}\}_2 + 7MeOH - H^+]^-$; calcd 959.0826, 16%), 987.1337 ($[Ni\{L^{Te}\}_2 + 7MeOH + OAc^-]^-$; calcd 987.0775, 11%), 1428.7545 ($[Ni_2\{(L^{Te})_2\}_4 + OH_2 + H^-]^-$; calcd 1428.7805, 10%), 1550.7666 ($[Ni_2\{(L^{Te})_2\}_2 + Na^+ + 2OAc^-]^-$; calcd 1550.7787, 7%).

$[Ni_2$-κ^5-$(Ni_4$-κ^6-μ^6-$\{(L'^{Te}{}_2O_3)(L'^{Te}O_2)_2\}_2)$-$\mu^2$-$(H_2O)_2]$. A solution of $[Ni$-μ^2-κ^2-$(Ni\{\kappa^5$-$L^{Te}\}_2)_2$-μ^2-$(OAc)_2]$ in CH_2Cl_2 (0.5 mL) was layered with wet EtOH (2 mL) or wet Et_2O (2 mL) in air. After the initial formation of red plates consisting of $[Ni$-μ^2-κ^2-$(Ni\{\kappa^5$-$L^{Te}\}_2)_2$-μ^2-$(OAc)_2]$, a very fine yellow powder deposited over the course of several weeks. After 4 months, even the red crystals of $[Ni$-μ^2-κ^2-$(Ni\{\kappa^5$-$L^{Te}\}_2)_2$-μ^2-$(OAc)_2]$ had turned yellow, and the reaction was complete. From the EtOH solution, yellow crystals of $[Ni_2$-κ^5-$(Ni_4$-κ^6-μ^6-$\{(L'^{Te}{}_2O_3)(L'^{Te}O_2)_2\}_2)$-$\mu^2$-$(H_2O)_2]$ grew, while a very fine yellow powder was obtained from Et_2O. The compound is insoluble in common solvents (alcohols, acetone, ethers, chlorinated solvents, and ethyl acetate) and can be isolated quantitatively by suspension in Et_2O, CH_2Cl_2, or $CHCl_3$ followed by filtration through a fine fritted glass filter. Selected IR bands (cm^{-1}): 1606 (s, $\nu_{C=N}$), 1573 (m, $\nu_{C=C}$), 1527 (m, $\nu_{C=C}$). The compositions of the yellow powder and crystalline material are identical. For a comparison of the IR spectra of the yellow powder and single crystals, see the SI.

RESULTS AND DISCUSSION

Palladium Compounds. Reactions of the tridentate Schiff bases $\{HL^Y\}_2$ (Y = Se, Te) with $Pd(OAc)_2$ and NEt_3 in EtOH result in the formation of bright-orange-yellow to orange-red solids. The yields of these reactions are between 30 and 50% and did not increase upon a further increase of the reaction times or by alteration of the palladium/dichalcogenide ratio. This is most probably due to the fact that $Pd(OAc)_2$ has a low solubility under the required reaction conditions and precipitates together with the cluster compounds. Thus, part of the unreacted starting material can be recovered unchanged.

Remarkably, the solubilities of the obtained products differ depending on the method of isolation. Bright-orange-yellow powders precipitate when the reactions are performed in boiling $EtOH/CHCl_3$ or $EtOH/CH_2Cl_2$ mixtures upon cooling. The powders are sparingly soluble even in cold chlorinated solvents but slowly dissolve in warm $CHCl_3$. Red-orange crystals of the products are obtained from such solutions after slow concentration. The almost insoluble yellow-orange and more soluble red-orange crystalline materials possess identical analytical data. We believe that the orange-yellow powders are polymeric compounds of the composition $[Pd(L'^Y)]_x$ containing the corresponding chalcogenato ligands $\{L^Y\}^{2-}$ (Y = Se, Te). They are preferably formed during a quick precipitation, while well-defined tetrameric cluster compounds deposit when the crystallization conditions allow molecular self-organization. The yellow and red solids are freely interconvertible by dissolution and reprecipitation (red to yellow) or slow recrystallization (yellow to red) (Scheme 2).

The IR spectra of the crystalline materials clearly indicate the presence of Schiff bases by the prominent and characteristic three-band pattern of the C=N and C=C stretches around 1600 cm^{-1}. Furthermore, the absence of O−H stretching bands indicates deprotonated ligands. The presence of the organic ligands and deprotonation of the phenol group are further confirmed by the ^1H NMR spectra. A comparison of the ^1H NMR spectra of the clusters with those of the uncoordinated ligands and the previously reported $[Pd(L'^Y)(PPh_3)]$ complexes revealed two remarkable features: (i) the respective imine proton resonances are more shielded in the clusters and (ii) the other proton resonances are spread over a wider range because of less homogeneous delocalization (or a higher polarization) of the aromatic systems. As a result, the protons of the phenyl rings attached to the selenium and tellurium atoms are more deshielded than those of the phenolate ring. This is most likely caused by the presence of a stronger π and/or σ donor in the trans position to the imine compared to the phosphine in the corresponding $[Pd(L'^Y)(PPh_3)]$ complexes.[33] Therefore, a considerable degree of back-donation into the π^* orbital of the Schiff bases or less σ donation of the Schiff base nitrogen atoms can be assumed. Generally, we already observed a similar donor atom dependence of the imine chemical shifts in octahedral rhenium complexes of $\{L'^Y\}^{2-}$, where the donor ability of the respective cis-axial ligand had a reasonable influence on the shielding of the imine proton.[32] The ^{77}Se NMR resonance of the $[Pd(L'^{Se})]_4$ cluster is found at 329 ppm, which is much closer to that of $[Pd(L'^{Se})(PPh_3)]$ (326 ppm) than to that of $\{HL^{Se}\}_2$ (363 ppm).[32,33] Unfortunately, the low solubility of the tellurium compound prohibited the measurement of ^{125}Te and ^{13}C NMR spectra of sufficient quality. A comparison of the corresponding ^1H and ^{77}Se NMR spectra is shown in the SI.

ESI^+ MS spectra of the products support the formation of tetrameric $[Pd_4(L'^Y)_4]$ cluster compounds by the detection of dominant peaks for $[\{Pd(L'^Y)\}_4 + H]^+$, $[\{Pd(L'^Y)\}_4 + Na]^+$, and $[\{Pd(L'^Y)\}_4 + K]^+$ ions for the selenium- and tellurium-containing products with a somewhat higher probability for the $[Pd_4(L'^{Te})_4]$ cluster. The ESI^+ MS spectra of $[Pd_4(L'^{Se})_4]$ give evidence for the formation of clusters with lower and higher nuclearity under the conditions in the mass spectrometer because additionally $[Pd(L'^{Se})]_x$ fragments with x = 2−5 and 8

https://doi.org/10.1021/acs.inorgchem.2c00076
Inorg. Chem. 2022, 61, 3785−3800

are observed. ESI$^-$ MS spectra are less indicative for the compounds under study. More details about the MS spectra are contained in the SI.

Orange-red octahedral crystals of both compounds were grown by slow evaporation of CH_2Cl_2/EtOH solutions. They were suitable for X-ray diffraction and finally confirmed the tetrameric nature of the two compounds. $[Pd_4(L'^{Se})_4]\cdot 4EtOH$ and $[Pd_4(L'^{Te})_4]\cdot 4EtOH$ both crystallize in the tetragonal space group $I4_1/a$, with each having one $\{Pd(L'^{Y})\}$ unit and a molecule of EtOH per asymmetric unit. The central motif of the products is a nearly ideal gyrobifastigial Pd_4Y_4 cluster, which is generated by the space group symmetry from the monomeric $\{Pd(L'^{Y})\}$ units. Figure 1 shows the structure of

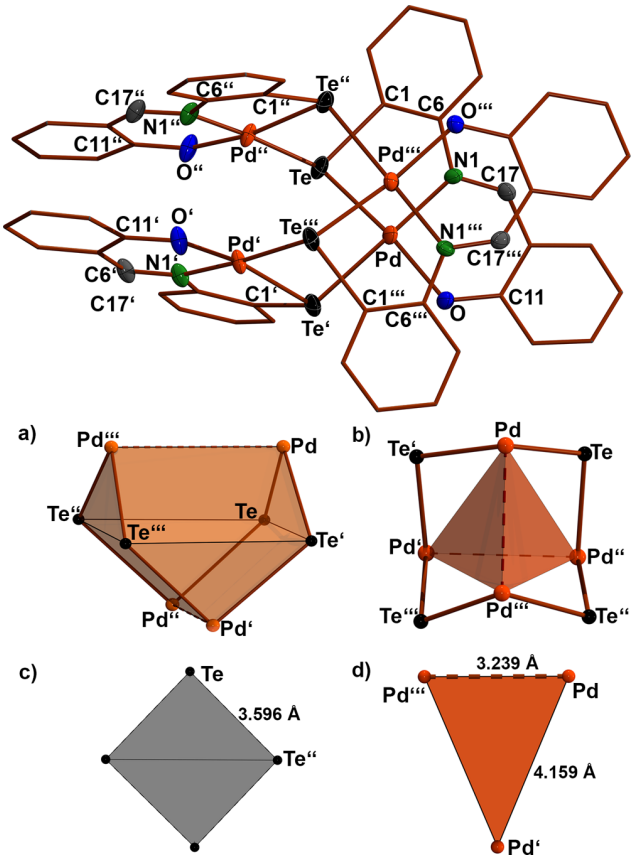

Figure 1. Structure of the gyrobifastigial $[Pd(L'^{Te})_4]$ cluster together with some structural fragments for an illustration of the bonding situation. Symmetry operations: (′) $-{}^1/_4 + y, {}^5/_4 - x, {}^5/_4 - z$; (″) ${}^5/_4 - y, {}^1/_4 + x, {}^5/_4 - z$; (‴) $1 - x, {}^3/_2 - y, z$. (a) Gyrobifastigial geometry of the central $\{Pd_4Te_4\}$ unit, (b) distorted Pd_4 tetrahedron, (c) equilateral Te_4 square plane, and (d) one of the four identical isosceles triangles comprising the distorted Pd_4 tetrahedron.

the corresponding tellurium-containing compound. The structure of the analogous gyrobifastigial $[Pd_4(L'^{Se})_4]\cdot 4EtOH$ is virtually identical, and an ellipsoid representation is given in the SI. Selected bond lengths and angles for both compounds are summarized in Table 1.

Gyrobifastigium is the common geometry adopted by such tetrameric palladium compounds with four bridging chalcogen donors.[67] Nevertheless, such compounds are rare, especially with chelating or functionalized chalcogenolates, because a higher denticity or substituents with varying electronic parameters of the ligands frequently lead to smaller clusters.[3,8,9] Generally, two of the neighboring ligand backbones point to the same side, while the two remaining ligands point to the opposite direction. The four palladium atoms essentially span a compressed tetragonal bisphenoid (a nonregular tetrahedron), which is intersected by the square plane of the chalcogen atoms. This description is equivalent to a combination of two trigonal prisms each spun by two palladium and four chalcogen atoms, which are combined at their square bases with a shift angle of 90° between them.

The central palladium atoms in the $[Pd_4(L'^{Y})_4]$ (Y = Se, Te) complexes are four-coordinate in a distorted square-planar coordination environment. The coordination sphere formed by the tridentate Schiff bases is completed by a symmetry-generated chalcogen donor from the adjacent $\{Pd(L'^{Y})\}$ unit, resulting in an {O, N, Y, Y} donor set. Compared to the values found in the corresponding mononuclear $[Pd(L'^{Se})(PPh_3)]$ complexes,[33] the Pd−N bond length of 2.044(4) Å is shorter by 0.01 Å, while the Pd1−O1 bond length of 2.042(3) Å is longer by 0.01 Å. On the contrary, the Pd−N bond length of 2.071(4) Å in $[Pd_4(L'^{Te})_4]$ is 0.03 Å longer and the Pd−O bond length of 2.063(3) Å is 0.01 Å shorter compared to those in $[Pd(L'^{Te})(PPh_3)]$. Each oxygen atom is stacked with the adjacent nitrogen atom of the neighboring ligand. The Pd−Se/Te bond lengths of 2.3416(7) and 2.4782(4) Å are only slightly elongated compared to those in the corresponding $[Pd(L'^{Y})(PPh_3)]$ complexes.[33] Interestingly, the Pd−Y bonds to the symmetry-generated chalcogenolato ligands are each elongated by approximately 0.06 Å compared to the values found in the chelates. This difference is clearly a result of chelate formation with the tridentate ligands and represents a special situation in such clusters, where usually a more symmetric environment around the bridging chalcogenolates is found.[8,9] The relative elongation of the Pd−Te bond is ca. 2%, while that of the Pd−Se bond is 3%. Hence, in agreement with the MS spectra, $[Pd_4(L'^{Se})_4]$ is concluded to be more prone to dissociation into $\{Pd(L'^{Y})\}_x$ units than $[Pd_4(L'^{Te})_4]$. The chalcogenolato donors form square planes within the gyrobifastigial Pd_4Y_4 core (Figure 1c). The sides of the Se_4 square are 3.46 Å, while those of the Te_4 square are 3.60 Å. These short contacts may indicate weak Se···Se or Te···Te interactions because they are smaller than the sum of the respective van der Waals radii [$r_{cryst.}$(Se) = 1.90 Å; $r_{cryst.}$(Te) = 2.1 Å].[68]

Additionally, each palladium atom has a short axial Pd···Pd contact (3.1900(8) Å in $[Pd_4(L'^{Se})_4]$ and 3.2394(7) Å in $[Pd_4(L'^{Te})_4]$; Figure 1a,d). Both contacts are significantly smaller than the sum of their van der Waals radii [$r_{cryst.}$(Pd) = 2.05 Å].[69] Frequently, such short contacts are discussed as constructive Pd···Pd interactions or even as Pd−Pd bonds.[3,8,9,68] They represent the short sides of a distorted Pd_4 tetrahedron formed by isosceles triangles, as is shown in Figure 1d. The isosceles sides of the triangles are ca. 3.94 Å in $[Pd_4(L'^{Se})_4]$ and ca. 4.16 Å in $[Pd_4(L'^{Te})_4]$, and, hence, the Pd_4 polyhedron in both structures is compressed in the direction of the short Pd−Pd contacts.

Surprisingly, the oxygen and nitrogen donor atoms of the $\{L^Y\}^{2-}$ ligands are slightly bent away from the short axial Pd···Pd contacts, resulting in trans angles around the palladium atoms between 168.2(1) and 177.4(1)°. In comparison, the trans angles in the related $[Pd(L'^{Y})(PPh_3)]$ complexes are 176.22(6)−179.14(7)°.[33] The Pd−Se−Pd or Pd−Te−Pd angles are approximately 112°. The deviation from the ideal

https://doi.org/10.1021/acs.inorgchem.2c00076
Inorg. Chem. 2022, 61, 3785−3800

Table 1. Selected Bond Lengths (Å) and Angles (deg) in the $[Pd_4(L'^{Y})_4]$ (Y = Se, Te) Clusters[a]

	$[Pd_4(L'^{Te})_4]$ gyrobifastigium	$[Pd_4(L'^{Te})_4]$ cuboid range	$[Pd_4(L'^{Te})_4]$ cuboid mean	$[Pd_4(L'^{Se})_4]$ gyrobifastigium
Pd−Te/Se	2.478(1)	2.4807(8)−2.4961(8)	2.488(8)	2.3416(7)
Pd−O	2.063(3)	2.039(6)−2.07(2)	2.05(1)	2.042(3)
Pd−N	2.071(4)	2.061(7)−2.070(7)	2.065(4)	2.044(4)
Pd−Te/Se[b]	2.535(1)″	2.5409(9)−2.5635(8)	2.55(1)	2.4020(6)[IV]
Pd···Pd[b]	3.239(1)‴	3.414−3.589	3.53(8)	3.1900(8)[V]
Te/Se−C1	2.121(5)	2.131(9)−2.149(9)	2.138(8)	1.927(5)
C1−O1	1.307(5)	1.29(1)−1.31(1)	1.30(1)	1.312(6)
N1−C6	1.429(6)	1.43(1)−1.45(1)	1.44(1)	1.421(7)
N1−C17	1.303(6)	1.30(1)−1.31(1)	1.305(7)	1.305(6)
Te/Se−Pd−O1	168.2(1)	166.6(8)−176.2(6)	173(4)	170.8(1)
Te/Se−Pd−N1	89.0(1)	89.1(2)−90.0(2)	89.5(4)	87.6(1)
O1−Pd−N1	94.8(1)	93.8(5)−95.5(7)	94.5(7)	94.9(2)
Te/Se−Pd−Te/Se[b]	91.67(1)″	89.50(3)−92.95(3)	91(2)	93.62(2)[IV]
Pd−Te/Se−Pd[b]	112.10(2)′	110.39(3)−112.83(3)	112(1)	112.49(3)[VI]
Te/Se−Pd···Pd[b]	96.11(1)‴	84.16−88.08	86(2)	93.99(2)[V]

[a]Short Pd···Pd and Pd···Te contacts (Å) are also given. [b]Symmetry operations: (′) $-{}^{1}/_{4} + y, {}^{5}/_{4} - x, {}^{5}/_{4} - z$; (″) ${}^{5}/_{4} - y, {}^{1}/_{4} + x, {}^{5}/_{4} - z$; (‴) $1 - x, {}^{3}/_{2} - y, z$; ([IV]) $ {}^{3}/_{4} - y, -{}^{1}/_{4} + x, {}^{3}/_{4} - z$; ([V]) $1 - x, {}^{1}/_{2} - y, z$; ([VI]) $ {}^{1}/_{4} + y, {}^{3}/_{4} - x, {}^{3}/_{4} - z$.

value of 90° for pure p-orbital contributions suggests a significant s character of the chalcogen donor orbitals.

In the backbones of the ligand, the C1−Se/Te bonds of 1.927(5) and 2.121(5) Å are elongated compared to those in $[Pd(L'^{Y})(PPh_3)]$, whereas the N1−C6 bonds of 1.421(7) and 1.429(6) Å are shorter. The N1−C17 and O1−C11 bonds are less influenced. Overall, the bond lengths in the ligand backbone are between those in the uncoordinated dichalcogenides $\{HL^{Y}\}_2$ and the $[Pd(L'^{Y})(PPh_3)]$ complexes.[33] The electron density distribution in the ligands based on the structural parameters is more localized than that in the related $[Pd(L'^{Y})(PPh_3)]$ complexes but more delocalized than those in $\{HL^{Se}\}_2$ and $\{HL^{Te}\}_2$. A more localized electronic structure also results in higher partial charges on the ligand backbone, which favors an intermolecular stacking.

In addition to the potentially constructive intramolecular Pd···Pd and Y···Y contacts, there are several intermolecular interactions, which may stabilize the conformation of the clusters. For example, each nitrogen atom is additionally located over the center of a phenolato ring of the adjacent cluster. The most important intermolecular interactions are due to a hydrogen-bonding network established around the solvent EtOH. This is depicted in Figure 2. In $[Pd_4(L'^{Se})_4]\cdot 4EtOH$, the selenolato donors also contribute to the hydrogen bonding, whereas in $[Pd_4(L'^{Te})_4]\cdot 4EtOH$, the potential H90−Te interactions are only weak. Nonclassical C−H···O(H)Et bonds are in the acceptable range for such interactions, albeit weak.

A competing geometrical arrangement for the $\{Pd_4Y_4\}$ core and the predominant structural motif in many other tetrameric metal complexes is a distorted cube, cuboid, or square frustum.[70] In this arrangement, the metal and chalcogen atoms alternate on the corners of a cuboid. However, such arrangements are scarce for palladium and the gyrobifastigium dominates. Only six reports about cuboid-like structures are known to date: three with a central Pd_4O_4 unit, two with a central Pd_4S_4 unit, and one with a Pd_4Se_4 core.[3,71−75] Commonly, constructive interactions between the chalcogen and palladium atoms on opposite sides of the cuboid are formulated as stabilizing forces for the Pd_4O_4 and Pd_4S_4 complexes, which results in a cubic array of delocalized electron density. Unfortunately, up to now, no plausible and general information about structural factors that influence the clear preference of one of the arrangements is available.

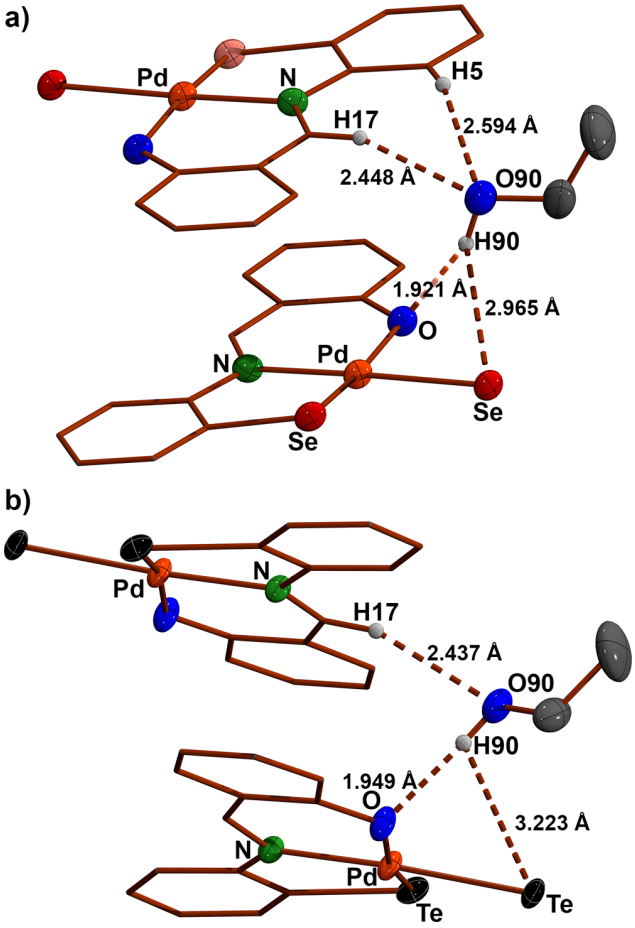

Figure 2. Hydrogen bonds in (a) $[Pd_4(L'^{Se})_4]\cdot 4EtOH$ and (b) $[Pd_4(L'^{Te})_4]\cdot 4EtOH$. Hydrogen atoms that are not involved in hydrogen bonding and further labels are omitted for clarity.

https://doi.org/10.1021/acs.inorgchem.2c00076
Inorg. Chem. 2022, 61, 3785−3800

So far, there is no example where both structures are accessible with one single ligand; therefore, there are also no reports about possible interconversions between the gyrobifastigial and cuboid-like forms of Pd_4Y_4 (Y = chalcogen) clusters. In that respect, it is presumed that the clear preference heavily depends on the exact structures of the ligands used, such as their steric demand, their donor atom constellation (when chelating ligands are involved), and the nature of the potential coligands that are used to construct the clusters.[3,71−75] To the best of our knowledge, there is only one case that remotely resembles this description, that is, a (dimethylaminoalkyl)selenolatopalladium(II) complex, where both isomers were observed when different ancillary ligands were employed, i.e., the additional coordination of three water molecules and one triflato ligand versus the coordination of four carboxylato ligands.[3] Thus, it was unexpected that, by slow evaporation of CH_2Cl_2 solutions of the $[Pd_4(L'^{Y})_4]$ clusters or by layering of such solutions with nonpolar antisolvents such as Et_2O or hexane, a second isomer for each of the compounds could be isolated. Both complexes crystallize as thin red trapezoidal plates. Thus, they could easily be distinguished optically from those of the gyrobifastigial forms of the compound discussed above, which were obtained as orange-red octahedra. Elemental analysis, IR, and MS data of the products are equal to those of the gyrobifastigial isomers.

The red plates of both compounds crystallize in the triclinic system. Those of the selenium compound were unfortunately not suitable for X-ray diffraction because they rapidly lost solvent during measurement at room temperature and a phase transition between 100 and 200 K precluded a low-temperature measurement. The crystals of the tellurium compound were stable enough for X-ray structure analysis. It turned out that this second isomer is one of the extremely rare examples of Pd_4Te_4 clusters with a cuboid-like core structure and the first compound in which a reversible interconversion between a cuboid-like and a gyrobifastigial form is possible. This can be induced by respective crystallization from polar solvents such as EtOH, which results in the gyrobifastigial isomer, or nonpolar solvents such as CH_2Cl_2 or $CHCl_3$, from which the cuboid-like isomer is obtained (Scheme 3).

The structure of the cuboid-like form of $[Pd_4(L'^{Te})_4]$ contains four crystallographically independent $\{Pd(L'^{Te})\}$ moieties and one molecule of Et_2O per asymmetric unit. The palladium atoms form an almost regular tetrahedron,

Scheme 3. Interconversion of the Gyrobifastigial and Cuboid-like $[Pd(L'^{Y})]_4$ Clusters

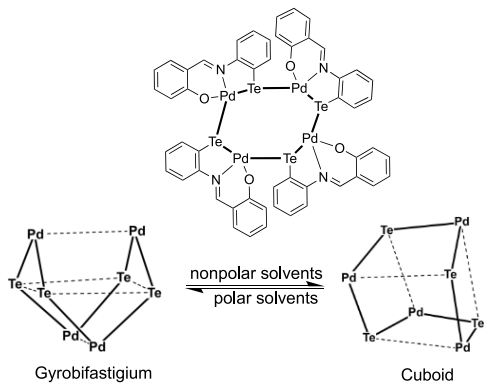

which is intersected by a flattened tetragonal bisphenoid formed by the four chalcogen atoms (Figure 3). In contrast to

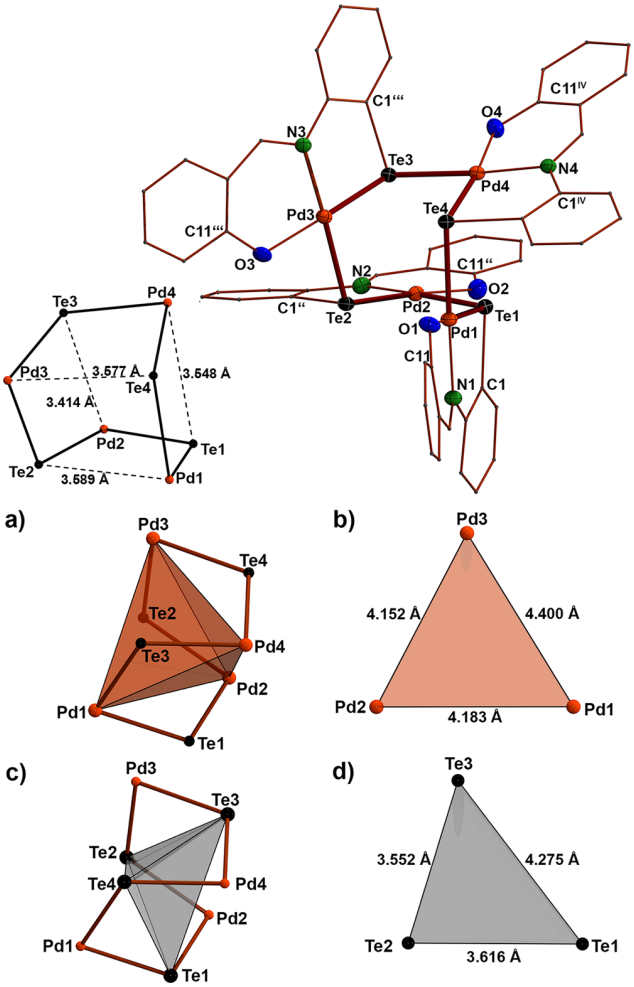

Figure 3. Structure of the cuboid-like $[Pd_4(L'^{Te})_4]$ cluster together with some structural fragments for an illustration of the bonding situation: (a) the distorted Pd_4 tetrahedron within the $\{Pd_4Te_4\}$ unit, (b) one of the four nonregular triangles comprising the Pd_4 tetrahedron within the $\{Pd_4Te_4\}$ unit, (c) the Te_4 tetragonal bisphenoid within the $\{Pd_4Te_4\}$ unit, and (d) one of the four nonregular triangles comprising the Te_4 tetragonal bisphenoid within the $\{Pd_4Te_4\}$ unit.

the Pd_4 tetrahedron of the gyrobifastigial isomer, where a compression along one Pd···Pd axis is observed and may give some indications for metal−metal interactions, the corresponding Pd···Pd distances in the cuboid-like form are prohibitively elongated and correspond to the diagonals on a face of the cuboid.

The sides of the triangles forming the Pd_4 tetrahedron in this structure are all longer than twice the van der Waals radius of palladium. While two of them are in the range between 4.16 and 4.18 Å, which comes close to the values observed in the gyrobifastigial isomer, the third side of 4.4 Å is significantly longer (Figure 3b). This means that the main difference between the two distorted Pd_4 tetrahedra in the isomers of $[Pd_4(L'^{Te})_4]$ is the lack of short Pd···Pd contacts in the cuboid-like structure. The intersecting tetragonal bisphenoid spun by the tellurium atoms has three different sides (Figure 3d). The neighboring Te···Te distances, where the tellurium atoms are

https://doi.org/10.1021/acs.inorgchem.2c00076
Inorg. Chem. 2022, 61, 3785−3800

connected to the same palladium atom, are similar to those found in the square of the gyrobifastigial isomer. However, the distances between the two nonneighboring tellurium atoms are clearly too long for Te···Te interactions. The main distortions in the cube formed by the two intersecting tetrahedra result from the different Te···Pd distances: one of them is with 3.41 Å significantly shorter than the others, which are between 3.55 and 3.59 Å. The contacts are smaller than the sum of the van der Waals radii of the involved atoms [$r_{cryst.}$(Te) = 2.1 Å; $r_{cryst.}$(Pd) = 2.05 Å] and therefore may suggest some weak interactions.[68] However, the angles observed within the cuboid actually rather suggest repulsive interactions between the opposite corners of the cube rather than attractive ones. The resulting mean value for the Pd···Te−Pd angles of 86(2)° is closer to the ideal cubic angle of 90° compared to the mean value for the Te···Pd−Te angle of 71.1(9)°. The cuboid-like structure results in an alternating or "paddle-wheel" arrangement of the aromatic ligand backbones compared to the stacked arrangement in the gyrobifastigial isomer.

The average value for the Pd−Te bonds of the chelate-bonded tellurium atoms is 2.49 Å, while that to the neighboring unit is 2.55 Å. They are elongated compared to those of the gyrobifastigial isomer by approximately 0.01 Å. The average cis and trans angles for the coordination sphere of the palladium atoms in this isomer are closer to the ideal square-planar geometry. The cis angles range from 85(2)° to 94.5(7)°, and the trans angles range from 173(4)° to 177(2)°. The situation in the ligand backbone is similar to that found for the gyrobifastigial isomer with the exception of the Te−C bonds. The Te−C bond lengths are between 2.131(9) and 2.149(9) Å, where the longest ones are even longer than those in the corresponding ditelluride. Overall, the electron distribution in the cuboid-like structure appears to be more localized than that in the gyrobifastigial structure.

With regard to the intermolecular arrangement, strong interactions such as hydrogen bonds are absent and mainly N···Ph or T-shaped Ph···Ph stacking is observed. The solvent Et_2O does not participate in any intermolecular interactions with the palladium species because the oxygen donors of the Et_2O moieties point toward the CH_2CH_3 groups of the second Et_2O moiety in the unit cell. Additionally, the structure contains large, empty voids.

In previous communications, frequently positive (binding) interactions between the metal and chalcogen atoms forming the skeleton of the cuboid were formulated as the prevalent reason for stabilization of the cuboid-like isomers.[3,71−75] Unfortunately, the results of such a consideration could not be compared with the real situation in the respective (gyrobifastigial) isomers of the same composition because such couples of compounds did not exist. With the isolation and structural characterization of the two forms of $[Pd_4(L'^{Y})_4]$, such evaluations of the electronic structures in structurally related complexes are now possible. Thus, we performed some DFT calculations for the $[Pd_4(L'^{Y})_4]$ (Y = O, S, Se, Te) complexes on the B3LYP level in the gas phase and for some of them in an implicit solvent model for CH_2Cl_2 and EtOH. The complexes in both solvent models fulfilled two out of four convergence criteria, with a residual predicted energy change in the magnitude of 10^{-4}−10^{-6} hartree. Additional calculations with the long-range-corrected function CAM-B3LYP in an implicit solvent model for CH_2Cl_2 also fulfilled two out of four convergence criteria, with a residual predicted energy change in the magnitude of 10^{-4}−10^{-6} hartree. Even after several attempts, the cuboid-like structure of $[Pd_4(L'^{Te})_4]$ did not converge and showed a single miniscule negative frequency. For the complexes of the smaller chalcogens with oxygen and sulfur, $[Pd_4(L'^{Y})_4]$ (Y = O, S), calculations starting from either the cuboid-like or gyrobifastigial arrangement of the cluster quickly converged into the gyrobifastigial isomer. For the selenium cluster $[Pd_4(L'^{Se})_4]$, a cubically distorted gyrobifastigial geometry resulted from either starting geometry, suggesting a free fluxionality between the two isomers in solution for the selenium-containing cluster. Interestingly, for $[Pd_4(L'^{Te})_4]$, both isomers were located as minima with minor distortions from the experimental geometry. The dispersion effects of the large systems, however, prohibited a quantitative analysis of the thermochemistry output of the calculations.

Although we located "bond" critical points (+3, −1) on the edges of the pseudocuboid (Pd···Te contacts) as on the Pd···Pd contacts of the gyrobifastigial isomer, they are not related to "bonding" interactions. The (+3, −1) critical points result from the close contact of two nonbinding lone pairs in each case. The absence of constructive orbital interactions in a second-order perturbation analysis of natural bonding orbitals supports this interpretation. This finding is additionally verified by a RDG analysis for the visualization of weak interactions, which allows classification of the interactions as a combination of van der Waals interactions with some minor steric repulsion component.[65,66] The RDG analyses based on the electron densities of the (not entirely converged) CAM-B3LYP calculations showed the same distribution with the same features as those based on the B3LYP calculations.[66] Because the RDG analysis is largely independent of the basis functions as well as the functional, the corresponding structures with the highest conversion rate on the B3LYP level were chosen for the RDG analyses of $[Pd_4(L'^{Te})_4]$. Similar grid spacing and isodensity ensure the comparability of the results, while the isodensity was additionally chosen to ensure that artifacts (i.e., from ionic bonds) do not hinder the visualization. An additional feature in the two topological analyses is the presence of a "cage" critical point (+3, +3) located in the respective center of the Pd_4Te_4 unit, which indicates that the center of the respective clusters is entirely shielded by the electron density of the surrounding Pd_4Te_4 unit. The RDG maps of both structures are shown in Figure 4.

In general, a conclusion of constructive Pd···Te or Pd···Pd interactions from the close contacts found in the two isomers is not supported. This means that other stabilizing effects such as π-stacking, hydrogen-bonding, and/or secondary interactions with the solvent should be considered as the main reason for the preference of one isomer over the other. Even when the interconversion between the two $[Pd_4(L'^{Y})_4]$ isomers of the present study is mainly based on external factors such as solvents, additional influences of internal supramolecular factors such as ligand substitution patterns, which may result in steric, electronic, or electrostatic effects, are not excluded. More (systematic) studies are required to derive a rationale for the general design and structural control of defined tetrameric palladium clusters on the basis of chalcogen-containing ligands.

Nickel Compounds. In contrast to the reactions of $Pd(OAc)_2$ with the dichalcogenides $\{HL^{Y}\}_2$, the corresponding reactions of nickel(II) acetate with the dichalcogenides did not result in cleavage of the Se−Se or Te−Te bonds. This is not completely surprising because the analogous disulfide $\{HL^{S}\}_2$ forms monomeric complexes of the type $[Ni\{\kappa^5\text{-}L^{S}\}_2(solvent)]$ or dimeric complexes of the type $[(Ni\{\kappa^5\text{-}L^{S}\}_2)_2]$, where the

https://doi.org/10.1021/acs.inorgchem.2c00076
Inorg. Chem. 2022, 61, 3785−3800

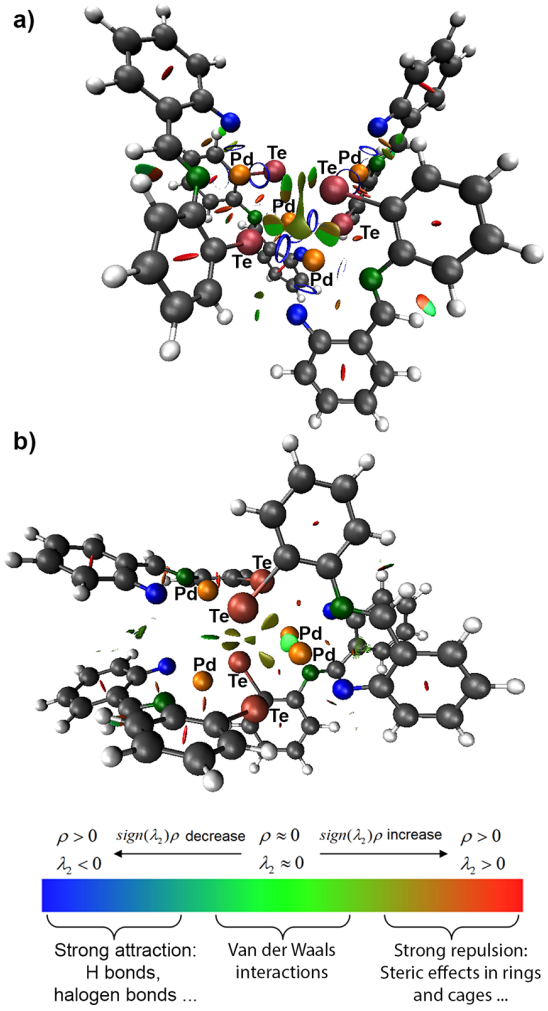

Figure 4. RDG plots (a) of the gas-phase structure of the cuboid-like $[Pd_4(L'^{Te})_4]$ cluster at an isodensity of 0.3 with a grid spacing of 0.05 bohr and (b) of the CH_2Cl_2 solution structure of the gyrobifastigial $[Pd_4(L'^{Te})_4]$ at an isodensity of 0.20 with a grid spacing of 0.05 bohr.

disulfide moiety coordinates but remains intact.[76,77] Similarly, other disulfides have been observed to coordinate through one of the disulfide sulfur atoms to nickel.[78−89] Only one example of a ditelluride coordinating to nickel has been claimed but was not proven unambiguously, e.g., by X-ray diffraction.[90]

The reactions of $Ni(OAc)_2{\cdot}4H_2O$ with $\{HL^{Se}\}_2$ or $\{HL^{Te}\}_2$ and NEt_3 as a supporting base in boiling $EtOH/CH_2Cl_2$ mixtures give brown-green (Y = Se) or red-brown (Y = Te) solids of trinuclear complexes of the composition $[Ni\text{-}\mu^2\text{-}\kappa^2\text{-}(Ni\{\kappa^5\text{-}L^Y\}_2)_2\text{-}\mu^2\text{-}(OAc)_2]$ (Scheme 4). The products are slightly soluble in CH_2Cl_2 and can be recrystallized from this solvent. Their ^1H NMR spectra show broad signals spread over a large chemical shift range, as is typical for paramagnetic nickel(II) complexes. The presence of remaining acetate in the products is indicated by corresponding IR bands, which did not disappear after recrystallization.

Single crystals of the two products were grown from CH_2Cl_2/Et_2O or hexane mixtures, revealing them as trinuclear nickel clusters of the composition $[Ni\text{-}\mu^2\text{-}\kappa^2\text{-}(Ni\{\kappa^5\text{-}L^Y\}_2)_2\text{-}\mu^2\text{-}(OAc)_2]$. $[Ni\text{-}\mu^2\text{-}\kappa^2\text{-}(Ni\{\kappa^5\text{-}L^{Se}\}_2)_2\text{-}\mu^2\text{-}(OAc)_2]{\cdot}0.5CH_2Cl_2$ crystallizes in the monoclinic space group $P2_1/n$, while $[Ni\text{-}\mu^2\text{-}\kappa^2\text{-}(Ni\{\kappa^5\text{-}L^{Te}\}_2)_2\text{-}\mu^2\text{-}(OAc)_2]{\cdot}CH_2Cl_2$ crystallizes in the

Scheme 4. Reactions of $Ni(OAc)_2{\cdot}4H_2O$ with $\{HL^Y\}_2$ (Y = Se, Te)

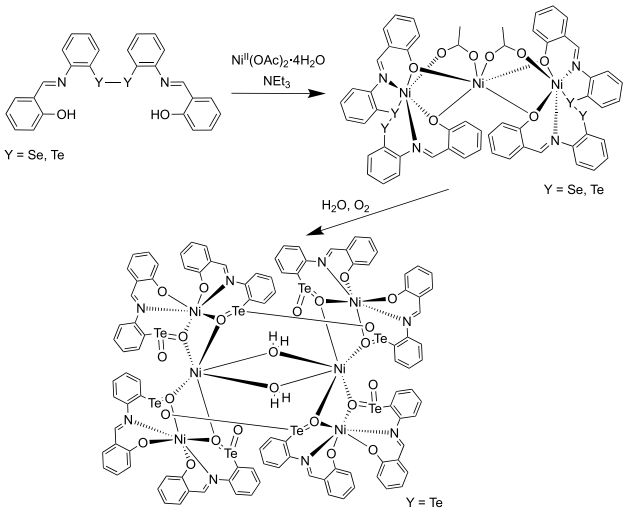

triclinic space group $P\bar{1}$ with two molecules in the asymmetric unit. The structure of the selenium compound is shown in Figure 5, and the selected bond lengths and angles are given in

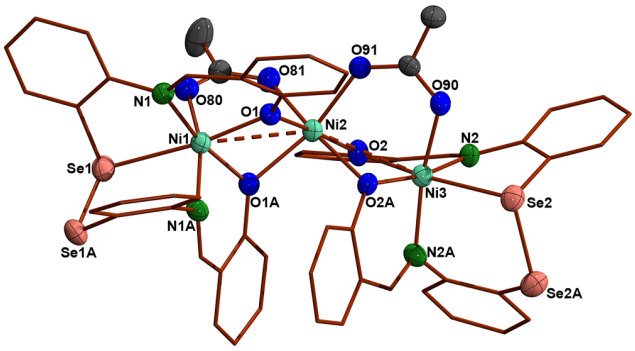

Figure 5. Structure of $[Ni\text{-}\mu^2\text{-}\kappa^2\text{-}(Ni\{\kappa^5\text{-}L^{Se}\}_2)_2\text{-}\mu^2\text{-}(OAc)_2]$.

Table 2. The single crystals obtained for the corresponding complex with the ditelluride were of limited quality but sufficient to derive the structure of the cluster unequivocally, which well resembles that of the acetato-bridged diselenide complex. Details about this compound are given in the SI.

The clusters contain two intact dichalcogenide moieties. Each $\{L^Y\}_2^{2-}$ unit is wrapped around one nickel ion in a pentadentate fashion with an O,N,Y,N,O-donor set. The coordination sphere of the two $\{Ni\{\kappa^5\text{-}L^Y\}_2\}$ units is completed by a bridging acetato ligand. The second oxygen atoms of the acetato ligands respectively coordinate to a third nickel(II) ion. This additional nickel(II) ion is also bridged in a $\mu_2\text{-}\kappa_2$ fashion by the two phenolato groups of each $\{Ni\{\kappa^5\text{-}L^Y\}_2\}$ subunit. The resulting arrangement of nickel ions is slightly bent with a Ni1···Ni2···Ni3 angle of 150.56°. The Ni−Ni distances are 3.078(1) and 3.066(1) Å. These are smaller than the sum of the van der Waals radii (2 × 1.63 Å).[68] Therefore, weak interactions between the three nickel atoms cannot be excluded in the solid-state structures of the diselenide and ditelluride clusters because the bonding situation between the Ni(II) ions is practically identical for both compounds and independent of the dichalcogenide. Similar weak Ni···Ni contacts have been found for trinuclear,

https://doi.org/10.1021/acs.inorgchem.2c00076
Inorg. Chem. 2022, 61, 3785−3800

Table 2. Selected Bond Lengths (Å) in $[Ni\text{-}\mu^2\text{-}\kappa^2\text{-}(Ni\{\kappa^5\text{-}L^{Se}\}_2)_2\text{-}\mu^2\text{-}(OAc)_2]$[a]

Ni1−Se1	2.632(1)	Ni2−O1	2.079(4)	Ni3−Se2	2.606(1)
Ni1−N1	2.057(6)	Ni2−O1A	2.104(5)	Ni3−N2	2.041(5)
Ni1−N1A	2.056(6)	Ni2−O2	2.075(4)	Ni3−N2A	2.061(6)
Ni1−O1	1.987(5)	Ni2−O2A	2.133(5)	Ni3−O2	2.010(5)
Ni1−O1A	2.030(5)	Ni2−O81	2.026(5)	Ni3−O2A	2.028(4)
Ni1−O80	2.019(5)	Ni2−O91	2.027(5)	Ni3−O90	2.043(5)
Ni1···Ni2	3.078(1)	N12···Ni3	3.066(1)	Ni1···Ni2···Ni3	150.56(1)

[a]Short Ni···Ni (Å) contacts and angles (deg) are also given.

oxygen-bridged nickel complexes with other chelating ligands.[91−96] The bond lengths in the dichalcogenides are similar to those in the noncoordinated ligands.[32]

$[Ni\text{-}\mu^2\text{-}\kappa^2\text{-}(Ni\{\kappa^5\text{-}L^{Se}\}_2)_2\text{-}\mu^2\text{-}(OAc)_2]$ is stable in solution and does not undergo redox reactions or ligand scrambling under ambient conditions. The compound can be recrystallized in air without special precautions. Cleavage of the trinuclear compound and partial re-formation of (other) clusters is observed by mass spectrometry. ESI^+ and ESI^- MS studies clearly show the formation of fragments of the trinuclear compound but also acetate-free clusters as products of an assembly of such fragments to larger aggregates. Figure 6 illustrates ESI+ overview spectra of the two $[Ni\text{-}\mu^2\text{-}\kappa^2\text{-}(Ni\{\kappa^5\text{-}L^Y\}_2)_2\text{-}\mu^2\text{-}(OAc)_2]$ clusters, in which the fragmentation and reassembly of a fragment is clearly seen for both compounds. It is evident that the signals of the original trinuclear compounds are not prevalent in either of the spectra.

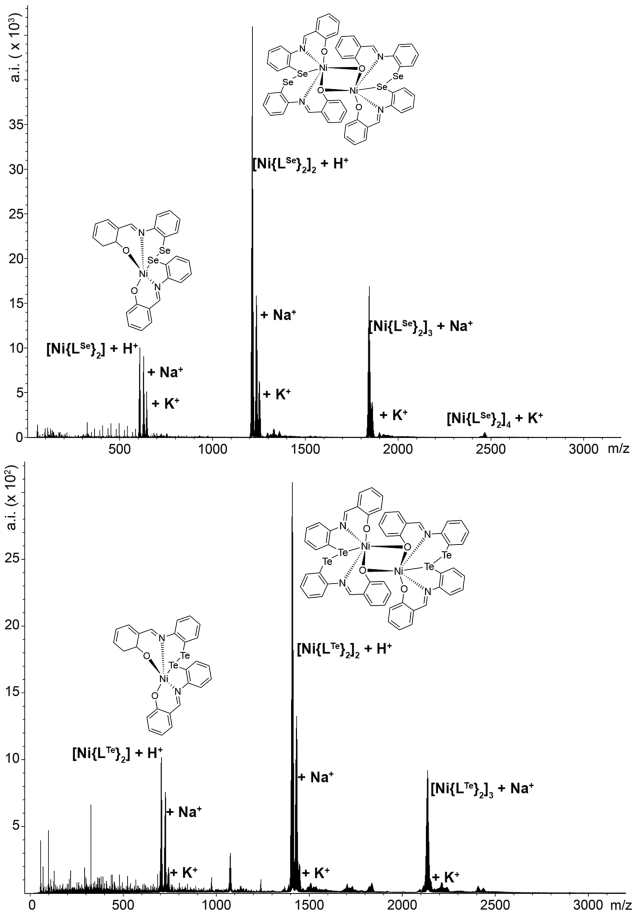

Figure 6. ESI^+ MS spectra of $[Ni\text{-}\mu^2\text{-}\kappa^2\text{-}(Ni\{\kappa^5\text{-}L^{Se}\}_2)_2\text{-}\mu^2\text{-}(OAc)_2]$ and $[Ni\text{-}\mu^2\text{-}\kappa^2\text{-}(Ni\{\kappa^5\text{-}L^{Te}\}_2)_2\text{-}\mu^2\text{-}(OAc)_2]$.

The signal group with the highest intensity in the ESI^+ spectrum of $[Ni\text{-}\mu^2\text{-}\kappa^2\text{-}(Ni\{\kappa^5\text{-}L^Y\}_2)_2\text{-}\mu^2\text{-}(OAc)_2]$ is found at m/z 1214.8171 and corresponds to the proton adduct of the dimeric $[Ni\{L^{Se}\}_2]_2$ unit. Expectedly, also the neighboring signal group of the sodium and the potassium adduct of the dimer are observed around the main peaks at m/z 1236.8109 and 1252.7694, respectively. The formation of the dimeric species can be understood as a simple substitution of the bridging $\{Ni(OAc)_2\}$ unit for a proton, a sodium, or a potassium ion and suggests that the central $\{Ni(OAc)_2\}$ is only weakly bound in the original cluster. Three intense peak groups around the maxima at m/z 608.9156, 630.9089, and 646.8740 correspond to the proton, sodium, and potassium adducts of the monomeric $[Ni\{L^{Se}\}_2]$ unit and represent the expected fragmentation pattern of the dimeric ions. Interestingly, two intense peak groups around m/z 1844.7071 and 1860.6810 indicate the formation of trimeric aggregates $[Ni\{L^{Se}\}_2]_3$ that are bridged by sodium and potassium ions, but no proton adducts are evident. A chemically sensitive explanation for the absence of the proton adduct is a favorable coordination of sodium and potassium by six oxygen donor atoms of three $[Ni\{L^{Se}\}_2]$ subunits compared to the smaller protons, with the latter preferentially binding the dimer through a hydrogen bond ($\{[Ni\{L^{Se}\}_2]\text{-}H\text{-}[Ni\{L^{Se}\}_2]\}^+$).

Higher aggregates such as the tetrameric $[Ni\{L^{Se}\}_2]_4$ also assemble around sodium and potassium but not around protons, as shown by the peak groups around m/z 2450.6000 and 2466.5854, respectively. These main features are analogously found in the respective spectrum of the tellurium compound. The minor signals in both compounds, however, indicate a stepwise mechanism for the loss of the central $\{Ni(OAc)_2\}$ unit through the presence of peak groups corresponding to $[Ni\text{-}\mu^2\text{-}\kappa^2\text{-}(Ni\{\kappa^5\text{-}L^Y\}_2)_2\text{-}\mu^2\text{-}(OAc)]^+$, which forms through the loss of acetate. While the assignment of the low-intensity peak groups in the spectrum of the selenium compound are relatively straightforward, for the tellurium compound, much more diverse adducts are found. They include doubly charged adducts based on the trimeric $[Ni\{L^{Te}\}_2]_3$ unit but also a permutation of trimeric adducts with all possible cations and anions. Additionally, cluster cations of higher nuclearity such as $\{[Ni\{L^{Te}\}_2]_3Ni_2(OAc)_3\}^+$ can be identified. The exact assignment of the lower-intensity peak groups for the tellurium-based compounds is further hindered by the sheer number of possible adducts that are present in the spectrum. Some of them involve seemingly random additions of single oxygen atoms, water molecules, cations, or hydroxide, methoxide, chloride, and acetate anions. Similar observations were made in the ESI^- MS spectra. The observed behavior might be attributed to an instability of the initial cluster and some sort of reactivity under ambient

https://doi.org/10.1021/acs.inorgchem.2c00076
Inorg. Chem. 2022, 61, 3785−3800

conditions. Further insights on the peak group assignment and MS spectra are provided in the SI. These considerations also contain simulated patterns for prominent peak groups.

As was already suspected from the MS spectra, solutions of the ditelluride cluster [Ni-μ^2-κ^2-(Ni{κ^5-L^{Te}}$_2$)$_2$-μ^2-(OAc)$_2$] are not stable in air or in a wet solvent over prolonged times. This means that exposure to ambient conditions during recrystallization of the complex must be minimized by a fast crystallization at low temperatures or it must be done in dry solvents in an inert atmosphere. When CH_2Cl_2/EtOH or CH_2Cl_2/Et_2O solutions are stored in the open atmosphere for prolonged times at room temperature, the red-orange color of the trinickel cluster continuously fades to bright yellow and an insoluble yellow solid precipitates. The IR spectrum of the deposited solid clearly shows the presence of a Schiff base ligand and a very broad, low-intensity water band, while no acetate bands are observed. The product is completely insoluble, which prevents the measurement of NMR or MS spectra of reasonable quality. Finally, single crystals of the yellow compound could be grown by a very slow (4 months) evaporation after the diffusion of wet EtOH into a CH_2Cl_2 solution of [Ni-μ^2-κ^2-(Ni{κ^5-L^{Te}}$_2$)$_2$-μ^2-(OAc)$_2$]. The identity of the composition of the thus-obtained single crystals with the yellow powder, which deposited from a corresponding CH_2Cl_2/Et_2O solution, was checked by IR spectroscopy.

Single-crystal X-ray diffraction revealed the formation of a hexanuclear cluster of the composition [Ni_2-κ^5-(Ni_4-κ^6-μ^6-{($L'^{Te}{}_2O_3$)($L'^{Te}O_2$)$_2$}$_2$)-μ^2-(H_2O)$_2$] (Figure 7). Thus, the yellow substance can be regarded as a hydrolysis/oxidation product of the trinuclear starting material [Ni-μ^2-κ^2-(Ni{κ^5-L^{Te}}$_2$)$_2$-μ^2-(OAc)$_2$]. The structure of the decomposition product easily explains the instability of the parent ditelluride complex by oxidation and hydrolysis at the tellurium and acetate moieties, respectively. All tellurium atoms of the starting material have been oxidized to tellurium(IV). The beginning formation of a telluroxane framework is indicated, and the central nickel acetate unit has been hydrolyzed, resulting in the formation of a central di(aqua)dinickel unit. Each of the equivalent telluroxane subunits contains the tetrameric oxygen-bridged fragment {$OTe^{IV}O\cdots Te^{IV}(O)-O-Te^{IV}(O)\cdots OTe^{IV}O$}, which connects all six nickel atoms. The electron density along the telluroxane backbone is delocalized in the tellurinic anhydride fragment {$Te^{IV}(O)-O-Te^{IV}(O)$} and the tellurinato units {$OTe^{IV}O$} but not between them. Such an interpretation is supported by consideration of the corresponding bond lengths, which are summarized in Table 3.

The coordination environment around all nickel(II) ions is octahedral, with four of them being coordinated by two cis-oriented nitrogen atoms of the Schiff base fragments, two trans-oriented phenolato oxygen donor atoms, and two cis-oriented Te=O oxygen donor atoms. Consequently, each oxidized ligand system coordinates the nickel ions in a facial arrangement. Four of the tellurium atoms are four-coordinate with a slightly distorted seesaw configuration, while the remaining four tellurium atoms are three-coordinate in a distorted trivacant *fac*-octahedral arrangement with X−Te−X angles between 85° and 102°. The substructure of the oxidized Schiff base and that of the contained tellurinate backbone are illustrated in Figure 7a,b. The flexible Schiff base ligand backbone twists to accommodate the requirements of the nickel and tellurium atoms. This is seen in the twist boat conformation of the six-membered O,N-chelate rings as well as the envelope conformation of the five-membered O,N-chelate

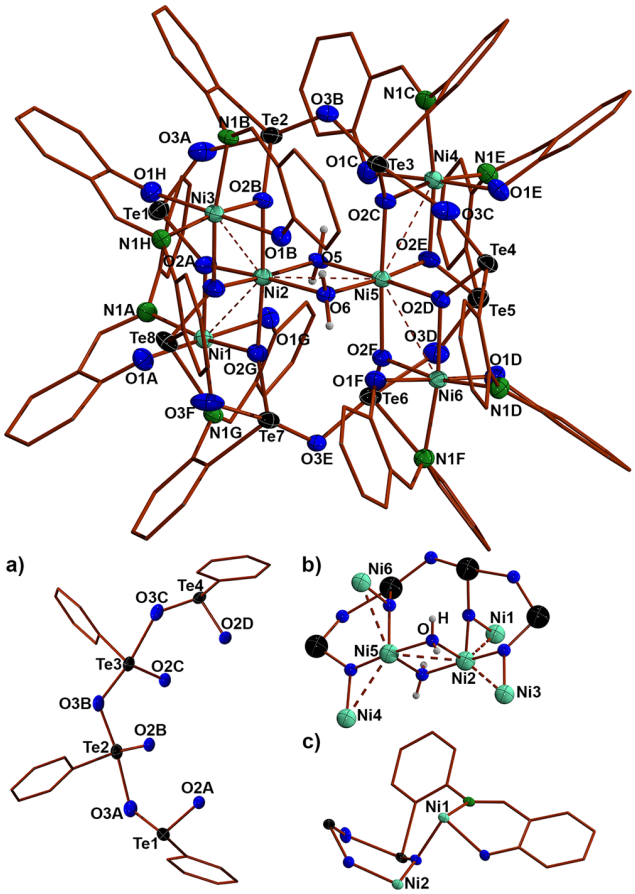

Figure 7. Structure of the hexanuclear [Ni_2-κ^5-(Ni_4-κ^6-μ^6-{($L'^{Te}{}_2O_3$)($L'^{Te}O_2$)$_2$}$_2$)-μ^2-(H_2O)$_2$] cluster together with some structural fragments for an illustration of the bonding situation: (a) the backbone of the formed tellurinate, (b) the coordination environment of the central nickel(II) ions, and (c) the conformations of the chelate rings.

Table 3. Selected Distances (Å) in [Ni_2-κ^5-(Ni_4-κ^6-μ^6-{($L'^{Te}{}_2O_3$)($L'^{Te}O_2$)$_2$}$_2$)-μ^2-(H_2O)$_2$]

Ni1/3/4/6−Ni5	3.042(2), 3.044(1), 3.034(2), 3.057(2)
Ni2−Ni5	2.998(1)
C−Te	2.150(8), 2.122(8), 2.131(7), 2.144(7), 2.144(7), 2.146(7), 2.142(7), 2.129(8)
Te−O2	1.845(6), 1.854(5), 1.864(5), 1.831(5), 1.859(5), 1.843(5), 1.857(5), 1.852(5), 1.853(6), 1.855(5), 1.847(6)
Te−O3−Te	1.961(6), 1.986(6), 1.981(5), 1.990(5)
Te···O2=Te	2.253(6), 2.278(6), 2.252(5), 2.285(6)
Ni−N	2.075(6), 2.071(6), 2.084(6), 2.087(6), 2.042(6), 2.081(6), 2.076(6), 2.080(6)
Ni1/3/4/6−O1	2.024(5), 2.029(5), 2.009(5), 2.040(5), 2.025(5), 2.039(5), 1.999(5), 2.041(5)
Ni1/3/4/6−O2	2.031(5), 2.061(5), 2.040(5), 2.065(5), 2.036(5), 2.062(5), 2.036(5), 2.058(5)
Ni2/5−O2	1.959(5), 1.983(5), 2.031(5), 2.036(5), 1.982(5), 1.983(5), 2.018(5), 2.040(5)
Ni2/5−O5/6	2.108(5), 2.129(4), 2.105(5), 2.125(5)

rings, as shown in Figure 7c. Weak chalcogen bonding stabilizes the cluster given that the σ^*_{CAr-Te} orbitals of the corresponding tellurinato ($Ar-TeO_2$) units align rather linearly with the neighboring oxygen atoms of the phenolato groups with distances of 2.8−2.9 Å. In contrast, the chalcogen

https://doi.org/10.1021/acs.inorgchem.2c00076
Inorg. Chem. 2022, 61, 3785−3800

bonds formed between the oxygen atoms of the phenolato groups and the $\sigma^*_{Te=O}$ orbitals of the O=Te bonds are much longer, with 3.7−3.9 Å. Finally, the chalcogen bonds with donation of the phenolato oxygen atoms into the σ^*_{CAr-Te} orbitals of the tellurinic anhydride units ($C_{Ar}-Te_2O_5$) are indicated by linear distances of around 3.3−3.5 Å.

Consequently, the two remaining nickel ions are coordinated by four cis-oriented Te=O oxygen donor atoms and two additional bridging cis-oriented water oxygen atoms (Figure 7b). The water oxygen atoms are fixed in place by hydrogen bonds to the phenolato oxygen atoms of the neighboring Schiff bases. Because the exact placement of the hydrogen atoms was ambiguous, the hydrogen-bonding situation is not discussed here in detail, but the corresponding parameters are provided in the SI. The donor−acceptor distances are between 2.6 and 2.7 Å. Interestingly, the six-membered chelate rings formed by the bridging $\{OTe^{IV}O\}$ and $\{Te^{IV}(O)-O-Te^{IV}(O)\}$ units of $[Ni_2\text{-}\kappa^5\text{-}(Ni_4\text{-}\kappa^6\text{-}\mu^6\text{-}\{(L'^{Te}{}_2O_3)(L'^{Te}O_2)_2\}_2)\text{-}\mu^2\text{-}(H_2O)_2]$ are in a boat conformation, as is shown in Figure 7c.

Commonly, the isolation of defined telluroxane species is prohibited by the amorphous and ill-defined nature of tellurinic acid and tellurinic anhydride compounds.[97−103] The few reported molecular aryltellurinic compounds include aryltellurinic and aryltellurinic anhydrides, as well as sodium or stannous salts.[97−103] Very recently, the formation of defined tellurinate and tellurinic anhydride units was observed in the self-assembly of large bowl-shaped telluroxane frameworks by the controlled hydrolysis of $PhTe^{IV}I_3$.[103] The resulting telluroxane network was proven to act as a ligand and coordinate metal ions in a crown-ether-like fashion.[103]

$[Ni_2\text{-}\kappa^5\text{-}(Ni_4\text{-}\kappa^6\text{-}\mu^6\text{-}\{(L'^{Te}{}_2O_3)(L'^{Te}O_2)_2\}_2)\text{-}\mu^2\text{-}(H_2O)_2]$ is only the second example of a transition-metal complex containing defined organotellurinato ligands and the first example of a transition-metal complex containing a defined organotellurinic anhydride ligand coordinating via the oxygen atoms.[67] The only other transition-metal complex containing an aryltellurinato ligand that coordinates through its oxygen atoms is a dimeric zinc β-diketimine complex, with the ligand in a bridging mode, resulting in the formation of an eight-membered $\{\cdots Zn\text{-}OTe^{IV}O-Zn-OTe^{IV}O\}$ ring that adopts a chair conformation.[97]

Compared to the triangular nickel core in the dichalcogenide-based trinickel clusters, the triangular arrangement of each trinickel subunit in the telluroxane-based hexanuclear cluster is strongly contracted and the resulting Ni−Ni distances are around 3.04 Å. This value is smaller than the sum of the van der Waals radii.[67] Additionally, there is an even shorter contact of 2.99 Å between the two central nickel atoms in the hexanuclear cluster that connects the two trinickel subunits through the bridging water molecules.

CONCLUSIONS

The polarity of the solvents used for recrystallization (and cocrystallization) and the nature of the chelating coligands are important factors for the structural assembly of tetranuclear palladium clusters with selenium- and tellurium-containing ligands. Using a tridentate Schiff base, interconversion between the gyrobifastigial and cuboid-like isomeric forms of such clusters becomes possible.

Dichalcogenide-based Schiff bases are reduced during reaction with $Pd(OAc)_2$ and bind in the clusters as chalcogenolato building blocks, while the same ligands remain intact during reactions with nickel acetate. They form trinuclear nickel clusters with coordinated diselenides and ditellurides. The nickel cluster with the selenium-containing ligand is air-stable as a solid, while its tellurium analogue undergoes a slow air oxidation of the tellurium building blocks, which results in the formation of a hexanuclear nickel(II) cluster with an unprecedented, well-defined backbone consisting of tellurinic anhydride and tellurinate units.

Future studies may show whether the nickel diselenide and ditelluride clusters of the present study have potentials similar to those of their disulfide analogues, which show an interesting and selective supramolecular sensing of the highly toxic wood preservatives chlorpyrifos and phosmet through increased fluorescence emission by the mono- and dimeric complexes, respectively, down to nanomolar concentrations of the toxin.[22,23]

ASSOCIATED CONTENT

Supporting Information

The Supporting Information is available free of charge at https://pubs.acs.org/doi/10.1021/acs.inorgchem.2c00076.

Crystallographic tables, bond lengths and angles, ellipsoid plots, and spectroscopic data (PDF)

Accession Codes

CCDC 2133215−2133221 contain the supplementary crystallographic data for this paper. These data can be obtained free of charge via www.ccdc.cam.ac.uk/data_request/cif, or by emailing data_request@ccdc.cam.ac.uk, or by contacting The Cambridge Crystallographic Data Centre, 12 Union Road, Cambridge CB2 1EZ, UK; fax: +44 1223 336033.

AUTHOR INFORMATION

Corresponding Author

Ulrich Abram − *Institute of Chemistry and Biochemistry, Freie Universität Berlin, Berlin 14195, Germany*; orcid.org/0000-0002-1747-7927; Email: Ulrich.Abram@fu-berlin.de; https://www.bcp.fu-berlin.de/chemie/chemie/forschung/InorgChem/agabram/index.html

Authors

Maximilian Roca Jungfer − *Institute of Chemistry and Biochemistry, Freie Universität Berlin, Berlin 14195, Germany*

Ernesto Schulz Lang − *Departamento de Química, Universidade Federal de Santa Maria, Santa Maria, Rio Grande do Sul 97105-900, Brazil*

Complete contact information is available at: https://pubs.acs.org/10.1021/acs.inorgchem.2c00076

Funding

Deutsche Forschungsgemeinschaft (DFG, Germany), Deutscher Akademischer Austauschdienst (DAAD, Germany), and Coordenação de Aperfeicoamento de Pessoal de Nível Superior (Brazil).

Notes

The authors declare no competing financial interest.

ACKNOWLEDGMENTS

We gratefully acknowledge support from the Core Facility BioSupraMol 1249 supported by DFG and the High-Performance Computing Centre of the Zentraleinrichtung für Datenverarbeitung of the Freie Universität Berlin for computa-

tional time. The authors are grateful for travel grants from DAAD (Project 57390729) and CAPES (Project 88881.144118/2017-01) because they only made this collaborative work possible.

REFERENCES

(1) Cargnelutti, R.; Schumacher, R. F.; Belladona, A. L.; Kazmierczak, J. C. Coordination chemistry and synthetic approaches of pyridyl-selenium ligands: A decade update. *Coord. Chem. Rev.* **2021**, *426*, 213537.
(2) Dubey, P.; Gupta, S.; Singh, A. K. Complexes of Pd(II), η^6-C_6H_6Ru(II), and η^5-Cp*Rh(III) with Chalcogenated Schiff Bases of Anthracene-9-carbaldehyde and Base-Free Catalytic Transfer Hydrogenation of Aldehydes/Ketones and N-Alkylation of Amines. *Organometallics* **2019**, *38*, 944−961.
(3) Paluru, D. K.; Dey, S.; Wadawale, A.; Maity, D. K.; Bhuvanesh, N.; Jain, V. K. Coordination Polymers of Palladium Bridged by Carboxylate and Dimethylaminoalkylselenolate Ligands. *Eur. J. Inorg. Chem.* **2015**, *2015*, 397−410.
(4) Jain, V. K.; Chauhan, R. S. New vistas in the chemistry of platinum group metals with tellurium ligands. *Coord. Chem. Rev.* **2016**, *306*, 270−301.
(5) Bugarcic, Z. M.; Divac, V. M.; Kostic, M. D.; Jankovic, N. Z.; Heinemann, F. W.; Radulovic, N. S.; Stojanovic-Radic, Z. Z. Synthesis, crystal and solution structures and antimicrobial screening of palladium(II) complexes with 2-(phenylselanylmethyl)oxolane and 2-(phenylselanylmethyl)oxane as ligands. *J. Inorg. Biochem.* **2015**, *143*, 9−19.
(6) Jain, V. K.; Jain, L. The chemistry of tri- and high-nuclearity palladium(II) and platinum(II) complexes. *Coord. Chem. Rev.* **2010**, *254*, 2848−2903.
(7) Kedarnath, G.; Jain, V. K. Pyridyl and pyrimidyl chalcogen (Se and Te) compounds: A family of multi utility molecules. *Coord. Chem. Rev.* **2013**, *257*, 1409−1435.
(8) Cechin, C. N.; Paz, A. V.; Piquini, P. C.; Bevilacqua, A. C.; Pineda, N. R.; Fagundes, N. V.; Abram, U.; Lang, E. S.; Tirloni, B. Intermolecular metallophilic interactions in palladium(II) chalcogenolate compounds − An experimental and theoretical study. *Polyhedron* **2020**, *177*, 114315.
(9) Cechin, C. N.; Cabral, B. N.; Bublitz, F.; Bortolotto, T.; da Silveira, G. D.; de Carvalho, L. M.; Cargnelutti, R.; Abram, U.; Nakagaki, S.; Lang, E. S.; Tirloni, B. Nuclearity growth of new PdII complexes induced by the electronic effect of selenium-containing ligands. *New J. Chem.* **2021**, *45*, 19255−19263.
(10) Hegazy, W. H.; Gaafar, A. E.-D. M. Synthesis, Characterization and Antibacterial Activities of New Pd(II) And Pt(IV) Complexes of Some Unsymmetrical Tetradentate Schiff Bases. *Am. Chem. Sci. J.* **2012**, *2*, 86−99.
(11) Chohan, Z. H.; Pervez, H.; Rauf, A.; Scozzafava, A.; Supuran, C. T. Antibacterial Co(II), Cu(II), Ni(II) and Zn(II) Complexes of Thiadiazole Derived Furanyl, Thiophenyl and Pyrrolyl Schiff Bases. *J. Enzyme Inhib. Med. Chem.* **2002**, *17*, 117−122.
(12) Al-Salim, N. I.; McWhinnie, W. R. Complexes of palladium, platinum and rhodium with potentially tetradentate ligands containing nitrogen and tellurium donor atoms (N2Te2). *Polyhedron* **1989**, *8*, 2769−2776.
(13) Arafath, M. A.; Adam, F.; Razali, M. R.; Ahmed Hassan, L. E.; Ahamed, M. B. K.; Majid, A. M. S. A. Synthesis, characterization and anticancer studies of Ni(II), Pd(II) and Pt(II) complexes with Schiff base derived from N-methylhydrazinecarbothioamide and 2-hydroxy-5-methoxy-3-nitrobenzaldehyde. *J. Mol. Struct.* **2017**, *1130*, 791−798.
(14) Elzahany, E. A.; Hegab, K. H.; Khalil, S. K. H.; Youssef, N. S. Synthesis, Characterization and Biological Activity of Some Transition Metal. Complexes with Schiff Bases Derived from 2-Formylindole, Salicyladehyde, and N-amino Rhodanine. *Aust. J. Basic Appl. Sci.* **2008**, *2*, 210−220.
(15) Shi, P.-Y.; Liu, Y.-H.; Peng, S.-M.; Liu, S.-T. Palladium(II) Complexes Containing P ∼ N∼O Donors. Ligand Effect of Tridentate versus Bidentate Coordination on the Oligomerization of Ethylene. *Organometallics* **2002**, *21*, 3203−3207.
(16) Motschi, H.; Nussbaumer, C.; Pregosin, P. S.; Bachechi, F.; Mura, P.; Zambonelli, L. The trans-Influence in Platinum (II) Complexes. ^{1}H- and ^{13}C-NMR. and X-ray structural studies of tridentate Schiff's base complexes of platinum (II). *Helv. Chim. Acta* **1980**, *63*, 2071−2086.
(17) Roy, N.; Sproules, S.; Bothe, E.; Weyhermüller, T.; Wieghardt, K. Polynuclear Complexes Containing the Redox Noninnocent Schiff Base Ligand 2-[(E)-2-Mercaptophenylimino]methyl-4,6-di-tert-butylphenolate(2-). *Eur. J. Inorg. Chem.* **2009**, *2009*, 2655−2663.
(18) Muthu Tamizh, M.; Cooper, B. F. T.; Macdonald, C. L. B.; Karvembu, R. Palladium(II) complexes with salicylideneimine based tridentate ligand and triphenylphosphine: Synthesis, structure and catalytic activity in Suzuki−Miyaura cross coupling reactions. *Inorg. Chim. Acta* **2013**, *394*, 391−400.
(19) Shabbir, M.; Akhter, Z.; Ahmad, I.; Ahmed, S.; Shafiq, M.; Mirza, B.; McKee, V.; Munawar, K. S.; Ashraf, A. R. J. Schiff base triphenylphosphine palladium (II) complexes: Synthesis, structural elucidation, electrochemical and biological evaluation. *J. Mol. Struct.* **2016**, *1118*, 250−258.
(20) Shabbir, M.; Akhter, Z.; Ashraf, A. R.; Ismail, H.; Habib, A.; Mirza, B. Nickel(II) and palladium(II) triphenylphosphine complexes incorporating tridentate Schiff base ligands: Synthesis, characterization and biocidal activities. *J. Mol. Struct.* **2017**, *1149*, 720−726.
(21) Muthu Tamizh, M.; Mereiter, K.; Kirchner, K.; Ramachandra Bhat, B.; Karvembu, R. Synthesis, crystal structures and spectral studies of square planar nickel(II) complexes containing an ONS donor Schiff base and triphenylphosphine. *Polyhedron* **2009**, *28*, 2157−2164.
(22) Manzur, C.; Bustos, C.; Schrebler, R.; Carrillo, D.; Knobler, C. B.; Gouzerh, P.; Jeannin, Y. Synthesis, characterization and electrochemistry of nickel(II) complexes of Schiff base ligands containing a disulphide group. Crystal structure of $[Ni\{(o\text{-}OC_6H_4CHNC_6H_4)_2S_2\}(MeOH)] \cdot MeOH$. *Polyhedron* **1989**, *8*, 2321−2330.
(23) Raj, P.; Singh, A.; Kaur, K.; Aree, T.; Singh, A.; Singh, N. Fluorescent Chemosensors for Selective and Sensitive Detection of Phosmet/Chlorpyrifos with Octahedral Ni^{2+} Complexes. *Inorg. Chem.* **2016**, *55*, 4874−4883.
(24) Kuchtanin, V.; Kleščikova, L.; Šoral, M.; Fischer, R.; Ružičkova, Z.; Rakovský, E.; Moncol, J.; Segla, P. Nickel(II) Schiff base complexes: Synthesis, characterization and catalytic activity in Kumada−Corriu cross-coupling reactions. *Polyhedron* **2016**, *117*, 90−96.
(25) Dutta, P. K.; Asatkar, A. K.; Zade, S. S.; Panda, S. Oxidative addition of disulfide/diselenide to group 10 metal(0) and *in situ* functionalization to form neutral thiasalen/selenasalen group 10 metal(ii) complexes. *Dalton Trans.* **2014**, *43*, 1736−1743.
(26) Ghavale, N.; Wadawale, A.; Dey, S.; Jain, V. K. Palladium assisted formation of arylselenoacetone from diaryldiselenides in methanol-acetone. *Indian J. Chem.* **2009**, *48A*, 1510−1514.
(27) Tirloni, B.; Nunes Cechin, C.; Ferro Razera, G.; Barbalho Pereira, M.; Manzoni de Oliveira, G.; Schulz Lang, E. Exploring Te−Te Bond Cleavage with Palladium(II): Synthesis, X-ray Structural Characterization, and Optical Features of Tellurolate and Telluro-Ether Complexes of Palladium(II). *Z. Anorg. Allg. Chem.* **2016**, *642*, 239−245.
(28) Kaur, R.; Menon, S. C.; Panda, S.; Singh, H. B.; Patel, R. P.; Butcher, R. J. Facile Cleavage of Organochalcogen Hybrid (NEEN, NEN, EN, where E = Se or Te) Ligand C−E and E−E Bonds by Pd(II). *Organometallics* **2009**, *28*, 2363−2371.
(29) Back, D.; Manzoni de Oliveira, G.; Schulz Lang, E. Synthesis and structural characterization of dinuclear tellurolate palladium(II) complexes. *Polyhedron* **2015**, *85*, 565−569.
(30) Tirloni, B.; Lang, E. S.; de Oliveira, G. M.; Piquini, P. C.; Hörner, M. Synthesis, crystal structure, and optical characteristics of $[Pd_2Hg_4Cl_6\{Te(DMB)\}_6]\cdot 2DMF$, $[HgClTe(DMB)]_4$, and the ring-forming cluster $[Pd_{12}(TePh)_{24}]\cdot 2DMF$. *New J. Chem.* **2014**, *38*, 2394−2399.

https://doi.org/10.1021/acs.inorgchem.2c00076
Inorg. Chem. 2022, 61, 3785−3800

(31) Cargnelutti, R.; Lang, E. S.; Piquini, P. C.; Abram, U. Synthesis and structure of [ReOSe(2-Se-py)3]: A rhenium(V) complex with selenium(0) as a ligand. *Inorg. Chem. Commun.* **2014**, *45*, 48−50.
(32) Roca Jungfer, M.; Hagenbach, A.; Schulz Lang, E.; Abram, U. Rhenium(V) complexes with selenolato- and tellurolato-substituted Schiff bases − Released PPh_3 as a facile reductant. *Eur. J. Inorg. Chem.* **2019**, *2019*, 4974−4984.
(33) Roca Jungfer, M.; Lang, E. S.; Abram, U. Reactions of Schiff Base-Substituted Diselenides and -tellurides with Ni(II), Pd(II) and Pt(II) Phosphine Complexes. *Eur. J. Inorg. Chem.* **2020**, *2020*, 4303−4312.
(34) Stephenson, T. A.; Morehouse, S. M.; Powell, A. R.; Heffer, J. P.; Wilkinson, G. Carboxylates of palladium, platinum, and rhodium, and their adducts. *J. Chem. Soc.* **1965**, 3632−3640.
(35) Kolay, S.; Kumar, M.; Wadawale, A.; Das, D.; Jain, V. K. Cyclopalladation of telluroether ligands: synthesis, reactivity and structural characterization. *Dalton Trans.* **2014**, *43*, 16056−16065.
(36) Butcher, R. J.; Chakravorty, T.; Singh, H. B. Bis{μ-2-[(dimethylamino)methyl]benzenetellurolato}bis[chloridopalladium-(II)] dichloromethane hemisolvate. *Acta Crystallogr., Sect. E* **2012**, *68*, m141.
(37) Risto, M.; Oilunkaniemi, R.; Laitinen, R. S.; Ahlgren, M. Bis(μ-2-phenyltellurolato)bis(phenyltellurolato)tetra-μ-3-tellurido-hexakis-(triphenylphosphine)hexapalladium(II) benzene nonasolvate. *Acta Crystallogr., Sect. E* **2010**, *66*, m147.
(38) Kirsten, L.; Schwade, V. D.; Selter, L.; Hagenbach, A.; Piquini, P. C.; Schulz Lang, E.; Abram, U. Pt, Pd and Hg Complexes with Potentially Tridentate Telluroether Ligands. *Eur. J. Inorg. Chem.* **2015**, *2015*, 3748−3757.
(39) Harris, R. K.; Becker, E. D.; Cabral de Menezes, S. M.; Granger, P.; Hoffman, R. E.; Zilm, K. W. Further Conventions For NMR Shielding and Chemical Shifts (IUPAC Recommendations 2008). *Magn. Reson. Chem.* **2008**, *46*, 582−598.
(40) Chambers, M. C.; Maclean, B.; Burke, R.; Amodei, D.; Ruderman, D. L.; Neumann, S.; Gatto, L.; Fischer, B.; Pratt, B.; Egertson, J.; Hoff, K.; Kessner, D.; Tasman, N.; Shulman, N.; Frewen, B.; Baker, T. A.; Brusniak, M.-Y.; Paulse, C.; Creasy, D.; Flashner, L.; Kani, K.; Moulding, C.; Seymour, S. L.; Nuwaysir, L. M.; Lefebvre, B.; Kuhlmann, F.; Roark, J.; Rainer, P.; Detlev, S.; Hemenway, T.; Huhmer, A.; Langridge, J.; Connolly, B.; Chadick, T.; Holly, K.; Eckels, J.; Deutsch, E. W.; Moritz, R. L.; Katz, J. E.; Agus, D. B.; MacCoss, M.; Tabb, D. L.; Mallick, P. A cross-platform toolkit for mass spectrometry and proteomics. *Nat. Biotechnol.* **2012**, *30*, 918−920.
(41) Strohalm, M.; Hassman, M.; Košata, B.; Kodicek, M. mMass data miner; an open source alternative for mass spectrometric data analysis. *Rapid Commun. Mass Spectrom.* **2008**, *22*, 905−908.
(42) Sheldrick, G. M. *SADABS*; University of Göttingen: Göttingen, Germany, 1996.
(43) Coppens, P. *The Evaluation of Absorption and Extinction in Single-Crystal Structure Analysis*; Crystallographic Computing: Muksgaard, Copenhagen, 1979.
(44) Sheldrick, G. M. A short history of SHELX. *Acta Crystallogr.* **2008**, *A64*, 112−122.
(45) Sheldrick, G. M. Crystal structure refinement with SHELXL. *Acta Crystallogr.* **2015**, *C71*, 3−8.
(46) *Diamond - Crystal and Molecular Structure Visualization, Crystal Impact*; Dr. H. Putz & Dr. K. Brandenburg GbR: Bonn, Germany.
(47) *High performance computing (HPC) system Curta*, Freie Universität Berlin; DOI: 10.17169/refubium-26754.
(48) Frisch, M. J.; Trucks, G. W.; Schlegel, H. B.; Scuseria, G. E.; Robb, M. A.; Cheeseman, J. R.; Scalmani, G.; Barone, V.; Mennucci, B.; Petersson, G. A.; Nakatsuji, H.; Caricato, M.; Li, X.; Hratchian, H. P.; Izmaylov, A. F.; Bloino, J.; Zheng, G.; Sonnenberg, J. L.; Hada, M.; Ehara, M.; Toyota, K.; Fukuda, R.; Hasegawa, J.; Ishida, M.; Nakajima, T.; Honda, Y.; Kitao, O.; Nakai, H.; Vreven, T.; Montgomery, J. A., Jr.; Peralta, J. E.; Ogliaro, F.; Bearpark, M. J.; Heyd, J. J.; Brothers, E. N.; Kudin, K. N.; Staroverov, V. N.; Kobayashi, R.; Normand, J.; Raghavachari, K.; Rendell, A. P.; Burant, J. C.; Iyengar, S. S.; Tomasi, J.; Cossi, M.; Rega, N.; Millam, J. M.; Klene, M.; Adamo, J.; Gomperts, R.; Stratmann, R. E.; Yazyev, O.; Austin, A. J.; Cammi, R.; Pomelli, C.; Ochterski, J. W.; Martin, R. L.; Morokuma, K.; Zakrzewski, V. G.; Voth, G. A.; Salvador, P.; Dannenberg, J. J.; Dapprich, S.; Daniels, A. D.; Farkas, O.; Foresman, J. B.; Ortiz, J. V.; Ciolowski, J.; Fox, D. J. *Gaussian 09*, revision B.01; Gaussian, Inc.: Wallingford, CT, 2016.
(49) Frisch, M. J.; Trucks, G. W.; Schlegel, H. B.; Scuseria, G. E.; Robb, M. A.; Cheeseman, J. R.; Scalmani, G.; Barone, V.; Petersson, G. A.; Nakatsuji, H.; Li, X.; Caricato, M.; Marenich, A. V.; Bloino, J.; Janesko, B. G.; Gomperts, R.; Mennucci, B.; Hratchian, H. P.; Ortiz, J. V.; Izmaylov, A. F.; Sonnenberg, J. L.; Williams-Young, D.; Ding, F.; Lipparini, F.; Egidi, F.; Goings, J.; Peng, B.; Petrone, A.; Henderson, T.; Ranasinghe, D.; Zakrzewski, V. G.; Gao, J.; Rega, N.; Zheng, G.; Liang, W.; Hada, M.; Ehara, M.; Toyota, K.; Fukuda, R.; Hasegawa, J.; Ishida, M.; Nakajima, T.; Honda, Y.; Kitao, O.; Nakai, H.; Vreven, T.; Throssell, K.; Montgomery, J. A., Jr.; Peralta, J. E.; Ogliaro, F.; Bearpark, M. J.; Heyd, J. J.; Brothers, E. N.; Kudin, K. N.; Staroverov, V. N.; Keith, T. A.; Kobayashi, R.; Normand, J.; Raghavachari, K.; Rendell, A. P.; Burant, J. C.; Iyengar, S. S.; Tomasi, J.; Cossi, M.; Millam, J. M.; Klene, M.; Adamo, C.; Cammi, R.; Ochterski, J. W.; Martin, R. L.; Morokuma, K.; Farkas, O.; Foresman, J. B.; Fox, D. J. *Gaussian 16*, revision A.02; Gaussian, Inc.: Wallingford, CT, 2016.
(50) Dennington, R.; Keith, T. A.; Millam, J. M. *GaussView*, version 6; Semichem Inc.: Shawnee Mission, KS, 2016.
(51) Vosko, S. H.; Wilk, L.; Nusair, M. Accurate spin-dependent electron liquid correlation energies for local spin density calculations: a critical analysis. *Can. J. Phys.* **1980**, *58*, 1200−1211.
(52) Becke, A. D. Density-functional thermochemistry. III. The role of exact exchange. *J. Chem. Phys.* **1993**, *98*, 5648−5652.
(53) Lee, C.; Yang, W.; Parr, R. G. Development of the Colle-Salvetti correlation-energy formula into a functional of the electron density. *Phys. Rev.* **1988**, *B37*, 785−789.
(54) Wadt, W. R.; Hay, P. J. Ab initio effective core potentials for molecular calculations. Potentials for main group elements Na to Bi. *J. Chem. Phys.* **1985**, *82*, 284−298.
(55) Bergner, A.; Dolg, M.; Küchle, W.; Stoll, H.; Preuß, H. Ab initio energy-adjusted pseudopotentials for elements of groups 13−17. *Mol. Phys.* **1993**, *80*, 1431−1441.
(56) Pietro, W. J.; Blurock, E. S.; Hout, R. F.; Hehre, W. J.; DeFrees, D. J.; Stewart, R. F. Molecular orbital theory of the properties of inorganic and organometallic compounds. 2. STO-NG basis sets for fourth-row main-group elements. *Inorg. Chem.* **1981**, *20*, 3650−3654.
(57) Francl, M. M.; Pietro, W. J.; Hehre, W. J.; Binkley, J. S.; Gordon, M. S.; DeFrees, D. J.; Pople, J. A. Self-consistent molecular orbital methods. XXIII. A polarization-type basis set for second-row elements. *J. Chem. Phys.* **1982**, *77*, 3654−3665.
(58) Gordon, M. S.; Binkley, J. S.; Pople, J. A.; Pietro, W. J.; Hehre, W. J. Self-consistent molecular-orbital methods. 22. Small split-valence basis sets for second-row elements. *J. Am. Chem. Soc.* **1982**, *104*, 2797−2803.
(59) Hariharan, P. C.; Pople, J. A. The influence of polarization functions on molecular orbital hydrogenation energies. *Theor. Chim. Acta* **1973**, *28*, 213−222.
(60) Hehre, W. J.; Ditchfield, R.; Pople, J. A. Self—Consistent Molecular Orbital Methods. XII. Further Extensions of Gaussian—Type Basis Sets for Use in Molecular Orbital Studies of Organic Molecules. *J. Chem. Phys.* **1972**, *56*, 2257−2261.
(61) Rassolov, V. A.; Ratner, M. A.; Pople, J. A.; Redfern, P. C.; Curtiss, L. A. 6-31G* basis set for third-row atoms. *J. Comput. Chem.* **2001**, *22*, 976−984.
(62) Ditchfield, R.; Hehre, W. J.; Pople, J. A. Self-Consistent Molecular-Orbital Methods. IX. An Extended Gaussian-Type Basis for Molecular-Orbital Studies of Organic Molecules. *J. Chem. Phys.* **1971**, *54*, 724−728.
(63) Schuchardt, K. L.; Didier, B. T.; Elsethagen, T.; Sun, L.; Gurumoorthi, V.; Chase, J.; Li, J.; Windus, T. L. Basis Set Exchange: A Community Database for Computational Sciences. *J. Chem. Inf. Model.* **2007**, *47*, 1045−1052.

(64) Lu, T.; Chen, F. Multiwfn: A multifunctional wavefunction analyzer. *J. Comput. Chem.* **2012**, *33*, 580−592.
(65) Johnson, E. R.; Keinan, S.; Mori-Sánchez, P.; Contreras-García, J.; Cohen, A. J.; Yang, W. Revealing Noncovalent Interactions. *J. Am. Chem. Soc.* **2010**, *132*, 6498−6506.
(66) Humphrey, W.; Dalke, A.; Schulten, K. VMD - Visual Molecular Dynamics. *J. Mol. Graphics* **1996**, *14*, 33−38.
(67) *Cambridge Structural Database*, Release 5.42; updated May 2021.
(68) Batsanov, S. S. Van der Waaals Radii of Elements. *Inorg. Mater.* **2001**, *37*, 871−885.
(69) Nayek, H. P.; Niedermeyer, P. N.; Dehnen, S. Synthesis and properties of the tetranuclear palladium chalcogenolato-acetato complex $[Pd(SePh)(OOCCH_3)]_4$ with Pd−Pd bonding: an experimental and theoretical study. *Dalton Trans.* **2009**, 4208−4212.
(70) Alvarez, S. The Gyrobifastigium, not an Uncommon Shape in Chemistry. *Coord. Chem. Rev.* **2017**, *350*, 3−13.
(71) Vicente, J.; Abad, J.-A.; Förtsch, W.; Jones, P. G.; Fischer, A. K. Synthesis of Ortho-Palladated Phenol Derivatives. Study of Their Reactivity with Carbon Monoxide and Isonitriles. *Organometallics* **2001**, *20*, 2704−2715.
(72) Sembiring, S. B.; Colbran, S. B.; Craig, D. C.; Scudder, M. L. Palladium(II) 2-Diphenylphosphinohydroquinone (H_2pphq) Complexes: Preparation and Structures of a Novel Cluster, $[\{PdBr(Hpphq)\}_4]\bullet 2H_2O$, and a Phosphine Phosphinite Complex, cis-$[PdBr_2\{C_6H_3(OH)\text{-}1,PPh_2\text{-}3,PPh_2O\text{-}4\}]\bullet 2H_2O$. *J. Chem. Soc., Dalton Trans.* **1995**, 3731−3741.
(73) Yang, H.; Khan, M. A.; Nicholas, K. M. Formation of a Novel Pd_4 Cluster from the Acetolysis of Bis[(*R*)-*N*-*α*-methylbenzylsalicylideneaminato-*N*,*O*]palladium(II). *J. Chem. Soc., Chem. Commun.* **1992**, 210−212.
(74) Kawahashi, T.; Mikuriya, M.; Nukada, R.; Lim, J.-W. Synthesis and Structural Characterization of Thiolato-Bridged Tetranuclear Palladium(II) Complexes with *N,N,S*-Tridentate Ligands. *Bull. Chem. Soc. Jpn.* **2001**, *74*, 323−329.
(75) Kawahashi, T.; Tsutsumi, H.; Mikuriya, M. A novel tetranuclear palladium(II) complex with 2-[(3-aminopropyl)amino]ethanethiol. *Polyhedron* **1996**, *15*, 169−171.
(76) Manzur, C.; Bustos, C.; Schrebler, R.; Carrillo, D.; Knobler, C. B.; Gouzerh, P.; Jeannin, Y. Synthesis, characterization and electrochemistry of nickel(II) complexes of Schiff base ligands containing a disulphide group. Crystal structure of $[Ni\{(o\text{-}OC_6H_4CH = NC_6H_4)_2S_2\}(MeOH)]\bullet MeOH$. *Polyhedron* **1989**, *8* (18), 2321−2330.
(77) Raj, P.; Singh, A.; Kaur, K.; Aree, T.; Singh, A.; Singh, N. Fluorescent Chemosensors for Selective and Sensitive Detection of Phosmet/Chlorpyrifos with Octahedral Ni^{2+} Complexes. *Inorg. Chem.* **2016**, *55*, 4874−4883.
(78) Pandey, R. N.; Nag, A. K.; Pande, P.; Singh, S. K. Spectral studies on cobalt (II) and nickel (II) complexes of bis(1-phenyl tetrazoline)-5,5′-disulphide. *Orient. J. Chem.* **2010**, *26*, 109−112.
(79) Fox, S.; Stibrany, R. T.; Potenza, J. A.; Knapp, S.; Schugar, H. J. Copper(II) and Nickel(II) Complexes of Binucleating Macrocyclic Bis(disulfide)tetramine Ligands. *Inorg. Chem.* **2000**, *39*, 4950−4961.
(80) Lai, C.-H.; Reibenspies, J. H.; Darensbourg, M. Y. Nickel mediated sulfur−selenium and sulfur−sulfur bond formation. *Chem. Commun.* **1999**, 2473−2474.
(81) Kumar, M.; Day, R. O.; Colpas, G. J.; Maroney, M. J. Ligand Oxidation in a Nickel Thiolate Complex. *J. Am. Chem. Soc.* **1989**, *111*, 5974−5976.
(82) Bloodworth, B. C.; Demetriou, B.; Grzeskowiak, R. Cobalt and Nickel Complexes of some Thioethers and Mercaptothioethers. *Transition Met. Chem.* **1979**, *4*, 187−190.
(83) Anacona, J. R.; Gomez, J. Transition metal bis(2-bromophenyl)disulfide complexes. *J. Chil. Chem. Soc.* **2008**, *53*, 1694−1696.
(84) Yuan, N.; Tian, C.; Sheng, T.; Hu, S.; Wu, X. A new coordination polymer incorporating an unprecedented $[Ni_9S_{10}]$ cluster as secondary building unit. *Inorg. Chem. Commun.* **2017**, *81*, 33−36.
(85) Beloglazkina, E. K.; Moiseeva, A. A.; Churakov, A. V.; Orlov, I. S.; Zyk, N. V.; Howard, J. A. K.; Butin, K. P. Redox properties of N_2S_2-type nickel complexes with aromatic ligands. Crystal structure of $[1,2\text{-}C_6H_4(SMe)NH_2]_2Ni^{2+}(MeCN)_2 \bullet 2ClO_4^-$. *Russ. Chem. Bull.* **2002**, *51*, 467−475.
(86) Wright, A. M.; Zaman, H. T.; Wu, G.; Hayton, T. W. Nitric Oxide Release from a Nickel Nitrosyl Complex Induced by One-Electron Oxidation. *Inorg. Chem.* **2013**, *52*, 3207−3216.
(87) Belle, C.; Bougault, C.; Averbuch, M.-T.; Durif, A.; Pierre, J.-L.; Latour, J.-M.; Le Pape, L. Paramagnetic NMR Investigations of High-Spin Nickel(II) Complexes. Controlled Synthesis, Structural, Electronic, and Magnetic Properties of Dinuclear vs Mononuclear Species. *J. Am. Chem. Soc.* **2001**, *123*, 8053−8066.
(88) Beloglazkina, E. K.; Moiseeva, A. A.; Chizhevskii, A. A.; Tarasevich, B. N.; Zyk, N. V.; Butin, K. P. Synthesis and properties of nickel(II) diiminodithiolate and diiminodisulfide N_2S_2-type complexes. New complexes with non-innocent ligands. *Russ. Chem. Bull.* **2003**, *52*, 1990−2004.
(89) Livingstone, S. E.; Nolan, J. D. Sulphur-nitrogen chelating agents X.* Metal complexes of the tridentate ligand 2,2'-dithiodianiline and the quinquedentate *α,α'*-[dithiobis(*o*-phenylenenitrilo)]di-2-picoline. *Aust. J. Chem.* **1973**, *26*, 961−970.
(90) Kuhn, N.; Winter, M. Synthese und Reaktivität von Dienylmetall-Verbindungen XVII*. Zur Chemie von $[C_5H_5Ni(RTeTeR)][BF_4]$. *J. Organomet. Chem.* **1983**, *252*, C86−C88.
(91) Soldatov, D. V.; Henegouwen, A. T.; Enright, G. D.; Ratcliffe, C. I.; Ripmeester, J. A. Nickel(II) and Zinc(II) Dibenzoylmethanates: Molecular and Crystal Structure, Polymorphism, and Guest- or Temperature-Induced Oligomerization. *Inorg. Chem.* **2001**, *40*, 1626−1636.
(92) Chandrasekhar, V.; Azhakar, R.; Murugesapandian, B.; Senapati, T.; Bag, P.; Pandey, M. D.; Maurya, S. K.; Goswami, D. Synthesis, Structure, and Two-Photon Absorption Studies of a Phosphorus-Based Tris Hydrazone Ligand (*S*)P[N(Me)N = CH-C_6H_3-2-OH-4-$N(CH_2CH_3)_2]_3$ and Its Metal Complexes. *Inorg. Chem.* **2010**, *49*, 4008−4016.
(93) Albrecht, M.; Fiege, M.; Kögerler, P.; Speldrich, M.; Fröhlich, R.; Engeser, M. Magnetic Coupling in Enantiomerically Pure Trinuclear Helicate-Type Complexes Formed by Hierarchical Self-Assembly. *Chem. Eur. J.* **2010**, *16*, 8797−8804.
(94) Reglinski, J.; Morris, S.; Stevenson, D. E. Supporting conformational change at metal centres. Part 1: octahedral systems. *Polyhedron* **2002**, *21*, 2167−2174.
(95) Chandrasekhar, V.; Azhakar, R.; Senthil Andavan, G. T.; Krishnan, V.; Zacchini, S.; Bickley, J. F.; Steiner, A.; Butcher, R. J.; Kögerler, P. A Phosphorus Supported Multisite Coordinating Tris Hydrazone P(S)[N(Me)N = CH-C_6H_4-*o*-OH$]_3$ as an Efficient Ligand for the Assembly of Trinuclear Metal Complexes: Synthesis, Structure, and Magnetism. *Inorg. Chem.* **2003**, *42*, 5989−5998.
(96) Tang, G.; Jin, G.-X. Polymerization of methyl methacrylate catalyzed by nickel complexes with hydroxyindanone-imine ligands. *Dalton Trans.* **2007**, 3840−3846.
(97) Gondzik, S.; Schulz, S.; Bläser, D.; Wölper, C. Reaction of L_2Zn_2 with Ph_2E_2 − synthesis of LZnEPh and reactions with oxygen and H-acidic substrates. *Chem. Commun.* **2014**, *50*, 1189−1191.
(98) Srivastava, K.; Panda, A.; Sharma, S.; Singh, H. Telluroxanes: Synthesis, structure and applications. *J. Organomet. Chem.* **2018**, *861*, 174−206.
(99) Beckmann, J.; Bolsinger, J.; Duthie, A. Intramolecularly Coordinated Telluroxane Clusters and Polymers. *Chem. Eur. J.* **2011**, *17*, 930−940.
(100) Oba, M.; Nishiyama, K.; Koguchi, S.; Shimada, S.; Ando, W. Synthesis and Properties of Tellurinic Anhydride−Tellurone Adducts. *Organometallics* **2013**, *32*, 6620−6623.
(101) Chakraborty, T.; Sharma, S.; Singh, H. B.; Butcher, R. J. Reactions of Di-o-tolyl Telluride and Selenide with Palladium Acetate: Isolation of a Novel Palladium Complex of a Tellurenic

https://doi.org/10.1021/acs.inorgchem.2c00076
Inorg. Chem. 2022, 61, 3785−3800

Acid Anhydride and Related Trinuclear and Tetranuclear Palladium Complexes. *Organometallics* **2011**, *30*, 2525−2530.
(102) Beckmann, J.; Bolsinger, J.; Hesse, M. Molecular Stannatelluroxanes. *Organometallics* **2009**, *28*, 4225−4228.
(103) Kirsten, L.; Fonseca Rodrigues, J.; Hagenbach, A.; Springer, A.; Pineda, N. R.; Piquini, P. C.; Roca Jungfer, M.; Schulz Lang, E.; Abram, U. Large Telluroxane Bowls Connected by a Layer of Iodine Ions. *Angew. Chem., Int. Ed.* **2021**, *60*, 15517−15523.

https://doi.org/10.1021/acs.inorgchem.2c00076
Inorg. Chem. 2022, 61, 3785−3800

4.11 Large Telluroxane Bowls Connected by a Layer of Iodine Ions

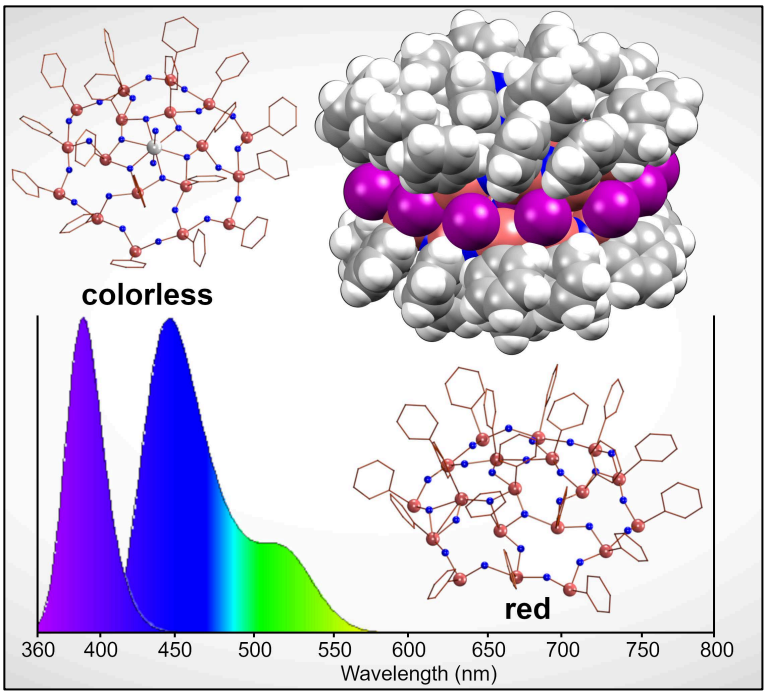

Reproduced with permission from Kirsten, L.; Fonseca Rodrigues, J.; Hagenbach, A.; Springer, A.; Pineda, N. R.; Piquini, P. C.; Roca Jungfer, M.; Schulz Lang, E.; Abram U. *Angew. Chem. Int. Ed.* **2021**, 60, *28*, 15517–15523.

DOI (International Edition): 10.1002/anie.202103700

DOI (German Edition): 10.1002/ange.20210370

For Supplementary Material see A.11.

Author Contributions:

Lars Kirsten, Ulrich Abram and Ernesto Schulz Lang designed the project. Lars Kirsten and Jessica Fonseca Rodrigues performed the synthesis and characterization of the compounds. Andreas Springer measured, simulated and interpreted the mass spectral data. Adelheid Hagenbach, Ulrich Abram and Jessica Fonseca Rodrigues calculated the X-ray structures. Maximilian Roca Jungfer, Nahum Ramirez Pineda and Paulo Cesar Piquini performed DFT calculations on the large telluroxane bowls. Ulrich Abram and Jessica Fonseca Rodrigues wrote the manuscript. Maximilian Roca Jungfer, Adelheid Hagenbach, Andreas Springer, Ernesto Schulz Lang and Ulrich Abram corrected the manuscript. Ernesto Schulz Lang and Ulrich Abram supervised the project, provided scientific guidance and suggestions and corrected the manuscript.

How to cite: *Angew. Chem. Int. Ed.* **2021**, *60*, 15517–15523
International Edition: doi.org/10.1002/anie.202103700
German Edition: doi.org/10.1002/ange.202103700

Clusters

Large Telluroxane Bowls Connected by a Layer of Iodine Ions

Lars Kirsten, Jessica Fonseca Rodrigues, Adelheid Hagenbach, Andreas Springer, Nahum R. Pineda, Paulo C. Piquini, Maximilian Roca Jungfer, Ernesto Schulz Lang, and Ulrich Abram**

Abstract: *Phenyltelluroxane clusters of the composition [{(PhTe)$_{19}$O$_{24}$}$_2$I$_{18}$(solv)] (**1**) are formed during the hydrolysis of [PhTeI$_3$]$_2$ or the oxidation of various phenyltellurium(II) compounds with iodine under hydrolytic conditions. The compounds consist of two half-spheres with a {(PhTe)$_{19}$O$_{24}$}$^{9+}$ network, which are connected by 18 iodine atoms. The spherical clusters can accommodate solvent molecules such as pyridine or methanol in the center of two rings formed by iodine atoms. The presence of other metal ions during the cluster formation results in a selective replacement of the central {PhTe}$^{3+}$ units of each half-sphere as has been demonstrated with the isolation of [{(PhTe)$_{18}$({Ca(H$_2$O)$_2$}O$_{24}$}$_2$I$_{16}$] (**2**) and [{(PhTe)$_{18}$({Y(NO$_3$)(H$_2$O)}O$_{24}$}$_2$I$_{16}$] (**3**). A crownether-like coordination by six oxygen atoms of the telluroxane network is found for the {Ca(H$_2$O)$_2$}$^{2+}$ and {Y(NO$_3$)(H$_2$O)}$^{2+}$ building blocks. Mass spectrometric studies show that considerable amounts of the intact clusters are transferred to the gas phase without dissociation.*

Introduction

Organotellurium oxides or telluroxanes represent a class of compounds, which has attracted an increasing interest during the recent years. Two excellent reviews comprise synthetic routes, general structural patterns and applications of this class of compounds having at least one covalent tellurium-oxygen bond.[1,2] But these recent summaries make also obvious that hitherto relatively little is known about the structural chemistry particularly of larger telluroxanes. Telluroxanes are commonly prepared by hydrolysis of organotellurium(IV) halides and a strict control of the reaction conditions is required for the preparation of defined molecular products and to avoid polymerization. This means that frequently starting materials with sterically hindered organic residues or additional oxygen or nitrogen donor atoms have been used. Following such an approach, well defined dimeric, trimeric, hexameric, heptameric or octameric units have been isolated and characterized by crystallography.[2–8] Some examples are shown in Scheme 1.

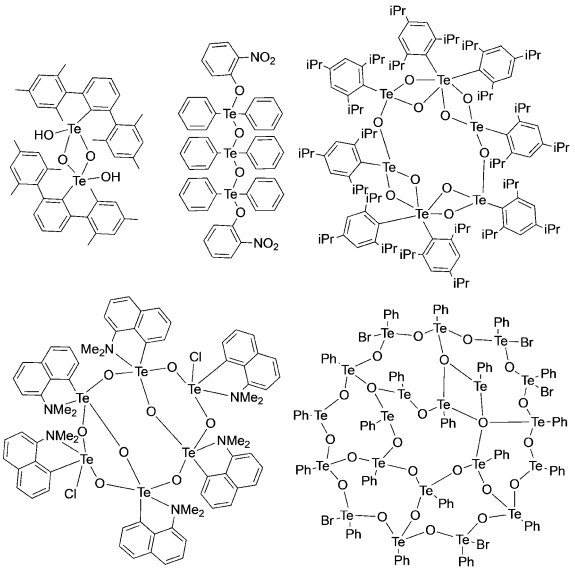

Scheme 1. Examples of well-defined molecular telluroxanes stabilized by bulky substituents or additional donor atoms.[3,5,6,7,10]

Two larger, well-defined telluroxanes comprising twelve and nineteen tellurium atoms have been serendipitously obtained from unintended reactions. The anionic cluster compound [{(^{i}PrTe)$_{12}$O$_{16}$Br$_4$}{Li(THF)Br}$_4$}Br]$^-$ is formed by a reaction of lithium hex-1-ynyl tellurolate with isopropyl bromide in THF by partial air oxidation and hydrolysis,[9] while a bowl-shaped cluster described as [(PhTe)$_{19}$O$_{24}$Br$_5$]$^{4+}$ is formed by the disproportionation of the selone adduct [(1,3-dibutylbenzimidazolin-2-selone)TePh](PhTeBr$_2$) in acetonitrile with subsequent hydrolysis.[10] Even when the used

[*] Dr. L. Kirsten, Dr. A. Hagenbach, M. Sc. M. Roca Jungfer, Prof. Dr. U. Abram
Institute of Chemistry and Biochemistry, Freie Universität Berlin
Fabeckstr. 34/36, 14195 Berlin (Germany)
E-mail: ulrich.abram@fu-berlin.de
M. Sc. J. Fonseca Rodrigues, M. Sc. N. R. Pineda, Prof. Dr. E. Schulz Lang
Laboratory of Inorganic Materials, Universidade Federal Santa Maria
97105-900 Santa Maria, RS (Brazil)
E-mail: eslang@ufsm.br
Dr. A. Springer
Institute of Chemistry and Biochemistry, Core Facility BioSupraMol, Freie Universität Berlin
Takustr. 3, 14195 Berlin (Germany)
Prof. Dr. P. C. Piquini
Department of Physics, Universidade Federal Santa Maria
97105-900 Santa Maria, RS (Brazil)
Supporting information and the ORCID identification number(s) for the author(s) of this article can be found under: https://doi.org/10.1002/anie.202103700.

starting materials and the intended reactions applied for the formation of the two large tellurium clusters are completely different, there is a striking similarity: both mixtures finally contain organotellurium(IV) bromides and traces of water as a starting point for a controlled hydrolysis and the self-assembly of defined, charged $\{Te^{IV}_xO_y\}$ networks, and they contain bromide ions, which seem to play a role in the stabilization of the established 3-dimensional structures. A third example of such reactions, the accidental formation of the spherical compound $[\{(PhTe)_{19}O_{24}\}_2I_{18}(pyridine)]$ (**1a**) from a reaction of *N*-{3-(phenyltellanyl)propyl}picolinamide (**I**) with elemental iodine in CH_2Cl_2,[11] lead us to more detailed studies about the essential compounds and a rational synthetic approach to such clusters (Scheme 2).

Results and Discussion

In the context of our studies on transition metal complexes with tellurium-containing ligands,[12–15] we synthesized some telluroethers such as *N*-{3-(phenyltellanyl)propyl}picolinamide (**I**) or 3-(phenyltellanyl)propylamine (**II**) as building blocks for chelating ligands. The oxidation of compound **I** with elemental iodine did not yield the expected tellurium(IV) diiodide, but gave a red-brown, crystalline substance of the composition $[\{(PhTe)_{19}O_{24}\}_2I_{18}(pyridine)]$ (**1a**). Single crystals of the product were obtained from a $CH_2Cl_2/CHCl_3$/MeOH (3:8:3) mixture. They consist of large, spherical clusters with an almost planar layer of eighteen iodine atoms between two half-shells each composed from a $\{(PhTe)_{19}O_{24}\}^{9+}$ network (Figure 1). The phenyltellurium units of the $\{(PhTe)_{19}O_{24}\}^{9+}$ subunits establish two concentric oxygen-bridged ring systems comprising twelve and six $\{PhTe\}^{3+}$ building blocks with the remaining subunit in its center. Also the iodine atoms are arranged in two rings comprising twelve and six members, respectively.

The iodine atoms of the outer ring establish electrostatic interactions with the tellurium atoms of the outer ring systems of both half-shells. Te–I distances between 3.093 and 3.795 Å are found between the iodine atoms I1 to I12 and their adjacent tellurium atoms in both half spheres, which corresponds to "normalized contacts" N_C of 0.76 and 0.94 ($N_C = D_{TeI}/(r_{Te} + r_I)$, D_{TeI} is the experimentally determined distance between the tellurium and iodine atoms and r_{Te} and r_I correspond to the van der Waals radii of the elements). N_C is a useful indicator to estimate the strength of contacts in compounds with "long-range interactions" and has been applied for the evaluation of compounds with halogen bonds by Metrangolo and Resnati.[16] Unlike the absolute values of the bond lengths, this parameter allows a direct comparison

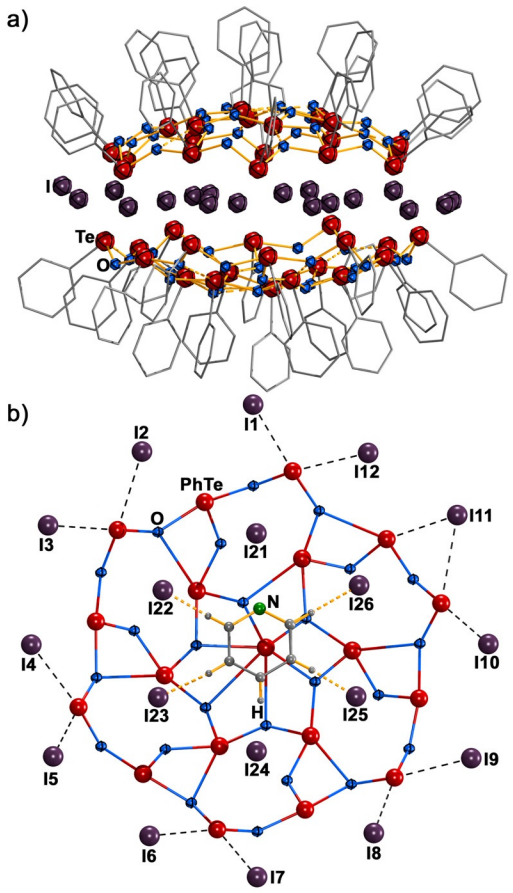

Figure 1. a) Structure of **1a** (the central pyridine ring is omitted for clarity) and b) top-view to one $\{(PhTe)_{19}O_{24}\}^{9+}$ half-shell of **1a** with the central layer of iodine atoms and the central pyridine ring.[36]

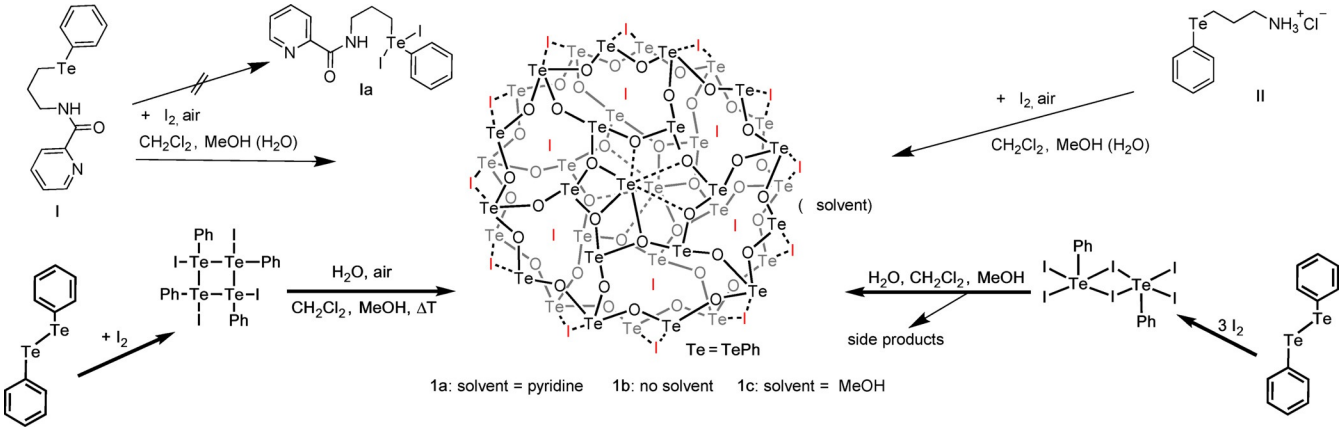

Scheme 2. Formation of the $[\{(PhTe)_{19}O_{24}\}_2I_{18}]$ telluroxane clusters.

between "long-range" interactions with donor-acceptor pairs. This means for the compounds under study that the bonding forces for the "outer-sphere" Te–I bonds are in the magnitude of those of the iodine atoms in the triiodide ions in $(Me_3NC_6H_{12}NMe_3)I_3$.[17] But also many Te–I bonds fall into this range, for example, those in $[PhTeI_3]_2$, $[TeI(thiourea)]_2$ or $[Me_2PhTeI]_2$.[18–21] Due to the spherical structure of the cluster, the distances of the inner, six-membered ring of iodine atoms to their adjacent tellurium atoms are clearly longer (3.808–4.150 Å), but most of them are still within the sum of the van der Waals radii of tellurium and iodine.[22] DFT calculations confirm the mainly electrostatic nature of these interactions. Average energies of $-13\,kJ\,mol^{-1}$ ($Te–I_{outer\ ring}$) and $-8\,kJ\,mol^{-1}$ ($Te–I_{inner\ ring}$) have been derived for the tellurium-iodine interactions. Additionally, some hydrogen bonds between ortho H atoms of outer-sphere phenyl rings and iodine atoms support the formation of the cluster. They are evident from a detailed inspection of the solid-state structures, but are also reflected by the appearance of bond critical points in the DFT calculations. Details are discussed in the Supporting information.

The center of the sphere of compound **1a** is occupied by a molecule of pyridine. It clearly comes from the decomposition of the starting material **I** and is located in the center of the inner ring of iodine atoms. Hydrogen bonds are established between the pyridine and the inner ring of iodine atoms (Figure 1b), which allows the unambiguous assignment of the nitrogen atom since the detected N···I distance is clearly longer than the C(H)···I ones. It is interesting to note that the incorporation of pyridine into the spheres of $[\{(PhTe)_{19}O_{24}\}_2I_{18}]$ only succeeds when the cluster is prepared by the decomposition of **I**. All our attempts to prepare **1a** via the more rational approaches starting from $[PhTeI]_4$ or $[PhTeI_3]_2$ (vide infra) with the addition of small amounts of pyridine only resulted in co-crystallization of the solvent in the voids between the large clusters.

With respect to the ready and reproducible formation of **1a** from the telluroether **I**, it is not surprising that a similar reaction of 3-(phenyltellanyl)propylamine (**II**) with iodine results in the related cluster **1b**. All basic structural features discussed above for **1a** also apply for **1b**, with the exception that of course no pyridine is embedded in the central layer of iodine atoms.

It is evident that the synthesis of such large, but well-defined cluster compounds from less defined degradation reactions of particular organotellurium compounds is not satisfactory. Thus, we tested more rational and reliable approaches to the compounds of type **1**. Having in mind that for the assembly of the $\{(PhTe)_{19}O_{24}\}^{9+}$ half-shells only $\{PhTe\}^{3+}$ building blocks and water are required, we performed reactions starting from diphenylditelluride with water and different amounts of iodine. It is known that Ph_2Te_2 reacts with one equivalent of I_2 under formation of $[PhTeI]_4$,[23,24] while a similar reaction with three equivalents of iodine gives $[PhTeI_3]_2$.[18] The subsequent addition of water (and in the case of $[PhTeI]_4$ exposure to air) gave the clusters **1** as red-brown crystalline solids. It turned out that the direct hydrolysis of previously isolated (or by the oxidation of diphenyl ditelluride with 3 equivalents of I_2 in situ-produced) $[PhTeI_3]_2$ is less favorable. It forms the cluster compounds **1b** and **1c**, but with a number of side-products and the required purification operations lower the yields. Best results and yields of about 50% of the pure clusters are obtained, when diphenyl ditelluride is reacted with only one equivalent iodine and the in situ-produced $[PhTeI]_4$ is subsequently heated in a $CH_2Cl_2/MeOH/H_2O$ mixture on air. Pure crystalline products of **1b** and **1c** are obtained, when the obtained red-brown solid is crystallized from a $CH_2Cl_2/CHCl_3/MeOH$ (3:8:3) mixture. The incorporation of MeOH in the void between the iodine atoms is observed when the reaction is performed in $MeOH/H_2O$ without the addition of CH_2Cl_2.

As in the cluster **1a**, iodine-tellurium interactions and hydrogen bonds connect the two half-spheres of **1b** and **1c**.

To prove the existence of the cluster after dissolving in CH_2Cl_2 and the ionization process, the $[\{(PhTe)_{19}O_{24}\}_2I_{18}]$ cluster (**1b**) was studied by ESI mass spectrometry. Ions of the intact $[\{(PhTe)_{19}O_{24}\}_2I_{18}]$ cluster are present in a CH_2Cl_2 solution of the compound and are transferred into the gas phase without decomposition.

The (+)-ESI mass spectrum is dominated by a peak group with a charge state of +3 with an m/z range of approximately 3400 to 3520, showing the $[M-3I]^{3+}$ ion as the major peak. Not only the organic residues, but mainly the 38 tellurium atoms of the two half-shells lead to a theoretical isotopic pattern with more than 80 single peaks of significant abundance (>1%). This results in an impressively peak-rich mass spectrum. Figure 2 shows the "+3" charge state region

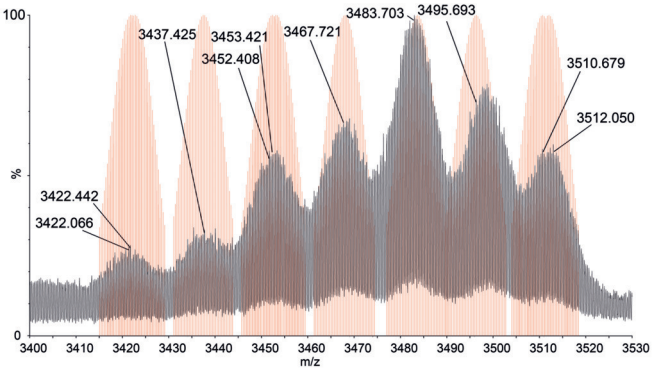

Figure 2. ESI-MS spectrum of the "+3" charge state region of **1b**. Black: experimental data, red: simulations.[26] For assignment see Table 1.

of the spectrum and the assignment of the peaks as well as a comparison with calculated isotopic patterns is summarized in Table 1. The situation is complicated by the fact that a few I^- ions are exchanged by Br^- (presumably coming from a minor impurity of the used I_2) or Cl^- (abstracted from the solvents used). Up to three exchanges in total, max. 2 exchanges for Br^- and max. one for Cl^- are observed. A second group of peaks of slightly lower abundance is found between m/z 5150 and 5350, showing the $[M-2I]^{2+}$ ion and the derivatives formed by exchange of I^- by Br^- or Cl^- (see Supporting information). In both charge states, addition of CH_2Cl_2 can be observed, presumably located in the inner void of the cluster.

Table 1: Comparison of the experimental and calculated isotopic patterns of the "+3" ion region in the mass spectra of **1b**.

Ion	Chemical Formula	m/z_{exp}	m/z_{calc}	$\Delta\, m/z$ [ppm]
$[M-3\,I]^{3+}$	$(C_{228}H_{190}O_{48}I_{15}Te_{38})^{3+}$	3483.703	3483.733	8.6
$[M-4\,I+Br]^{3+}$	$(C_{228}H_{190}O_{48}I_{14}Te_{38}Br)^{3+}$	3467.721	3467.737	4.6
$[M-4\,I+Cl]^{3+}$	$(C_{228}H_{190}O_{48}I_{14}Te_{38}Cl)^{3+}$	3453.421	3453.393	8.1
$[M-5\,I+2\,Br]^{3+}$	$(C_{228}H_{190}O_{48}I_{13}Te_{38}Br_2)^{3+}$	3452.408	3452.367	11.9
$[M-5\,I+Br+Cl]^{3+}$	$(C_{228}H_{190}O_{48}I_{13}Te_{38}BrCl)^{3+}$	3437.425	3437.379	13.3
$[M-6\,I+2\,Br+Cl]^{3+}$	$(C_{228}H_{190}O_{48}I_{12}Te_{38}Br_2Cl)^{3+}$	3422.066	3422.096	8.8
$[M-5\,I+2\,Cl]^{3+}$	$(C_{228}H_{190}O_{48}I_{13}Te_{38}Cl_2)^{3+}$	3422.442	3422.398	12.8
$[M-3\,I+(CH_2Cl_2)]^{3+}$	$(C_{229}H_{192}O_{48}I_{15}Te_{38}Cl_2)^{3+}$	3512.050	3511.998	14.8
$[M-3\,I+H+Br]^{3+}$	$(C_{228}H_{191}O_{48}I_{15}Te_{38}Br)^{3+}$	3510.679	3510.708	8.3
$[M-4\,I+Br+(CH_2Cl_2)]^{3+}$	$(C_{229}H_{192}O_{48}I_{14}Te_{38}BrCl_2)^{3+}$	3495.693	3495.721	7.8

Another hint for the stability of the clusters **1** in solution is given with their NMR spectra. ^{1}H spectra show the expected variety of aromatic protons in the range between 6.5 and 8.2 ppm due to the slightly varying environments of the PhTe groups inside the telluroxane network. All our attempts to measure well-resolved ^{125}Te NMR spectra failed. This comes not completely unexpected with regard to the limited solubility of the cluster compounds and the low natural abundance (≈7%) and less favorable NMR properties of ^{125}Te (≈0.2% receptivity relative to ^{1}H). A comparison with the behavior of the related bromide cluster $[(PhTe)_{19}O_{24}Br_5]^{4+}$, however, let us interpret this finding as another proof of the stability of the compounds **1** in solution. For $[(PhTe)_{19}O_{24}Br_5]Br_4$, one single, intense ^{125}Te NMR signal has been observed at 1516 ppm, which has been described as a proof of the rapid decomposition of $[(PhTe)_{19}O_{24}Br_5]Br_4$ in solution.[10]

The obviously higher stability of the clusters **1** compared to the related bromide compound of ref. [10] is not related to the composition of the tellurium-oxygen networks in both compounds. The arrangement of the tellurium atoms, the Te–O bond lengths and the connectivity patterns are almost identical in both compounds. Figure 3 shows the Te–O network of one half-shell of cluster **1b**. It is evident that, with the exception of Te31, all tellurium atoms undergo additional bonding interactions with the atoms of the central layer of iodine atoms as has been discussed before for **1a**. The phenyltellurium unit of Te31 is bonded in the center of six oxygen atoms, the arrangement of which reminds of the crown ether 18-crown-6. The related Te–O distances vary within a large range (1.926(9)–3.343(9) Å), but their arrangement (two short, two medium and two long bonds) is similar to the situation in the only other crown-ether complex with a Te^{IV} ion, $[(18\text{-crown-6})Te(Cl)(\mu\text{-}O)_2Te(Cl)(18\text{-crown-6})][SbCl_6]_2$, where the $Te{-}O_{(crown\ ether)}$ distances are 2.549/2.582, 2.651/2.751 and 2.886, 4.164 Å.[26]

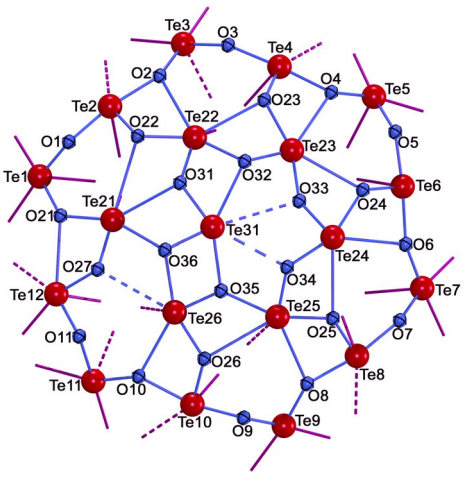

Figure 3. Te–O network of **1b** with designation of Te–I interactions with the central layer of iodine atoms. Dotted lines indicate Te–O (blue) and Te·I (purple) interactions larger than 3.220 Å and 3.636 Å, respectively (90% of the sum of the van der Waals radii). Solid lines represent shorter bonds.[36]

The unique bonding situation of the "PhTe31 groups" in the cluster is also reflected by its reactivity. Unlike all other phenyltellurium building blocks in compound **1b**, this central unit can be replaced by metal ions and, thus, "functionalized" telluroxane clusters can be formed. The introduction of Ca^{2+} ions in the central positions of the half-shells is readily possible by exposing the $(PhTe)_2/I_2/H_2O$ reaction mixture to a Ca^{2+} source such as CaO. The color of the solution becomes brighter and finally colorless crystals of the composition $[\{(PhTe)_{18}\{Ca(H_2O)_2\}O_{24}\}_2I_{16}]$ (**2**) can be isolated. The molecular structure of the compound is shown in Figure 4.

Unlike the atom Te31 and its expression in the second half-sphere in the compounds **1a**–**1c**, which are non-centrically embedded between the six oxygen atoms of the central ring (Figure 3), the Ca^{2+} ions in the $[\{(PhTe)_{18}\{Ca(H_2O)_2\}O_{24}\}_2I_{16}]$ networks are located on a twofold axis and show very similar Ca–O bonds between 2.479(7) and 2.538(3) Å. These values are somewhat shorter than in 18-crown-6 complexes with Ca^{2+} ions (2.538–2.684 Å), where the metal ions are nine-coordinate with three additional water ligands.[27–30] The calcium ions in **2** are eight-coordinate with only two axial H_2O ligands in a hexagonal-bipyramidal coordination environment. Due to the formal replacement of two $\{PhTe\}^{3+}$ groups by two $\{Ca(H_2O)_2\}^{2+}$ units, the charge of the cluster is reduced. Charge compensation is done by an only partial occupation of the positions of the iodine atoms of the inner ring (see Figure 4b).

An unexpected feature of compound **2** is the fact that it is nearly colourless, particularly in contrast to the brown compounds of type **1** with a central $PhTe^{3+}$ unit. DFT calculations show that main contributions within the near UV-Visible/absorption region of both complexes can be attributed to charge-transfer bands of iodine-centered p-orbitals into Te–O anti-bonding or Te-centered empty p-orbitals. Both compounds show a large degree of delocalization in their HOMO and LUMO orbitals. The degree of delocalization of the ground state LUMO is similar in both compounds. However, the ground state HOMO of $[\{(PhTe)_{19}O_{24}\}_2I_{18}]$ (**1b**) is delocalized over the whole layer of iodine atoms. Contrarily, the HOMO of $[\{(PhTe)_{18}\{Ca(H_2O)_2\}O_{24}\}_2I_{16}]$ (**2**) is rather concentrated on the outer iodide ring, while the LUMO is still centered on the inner telluroxane ring. The overall more prominent delocalization

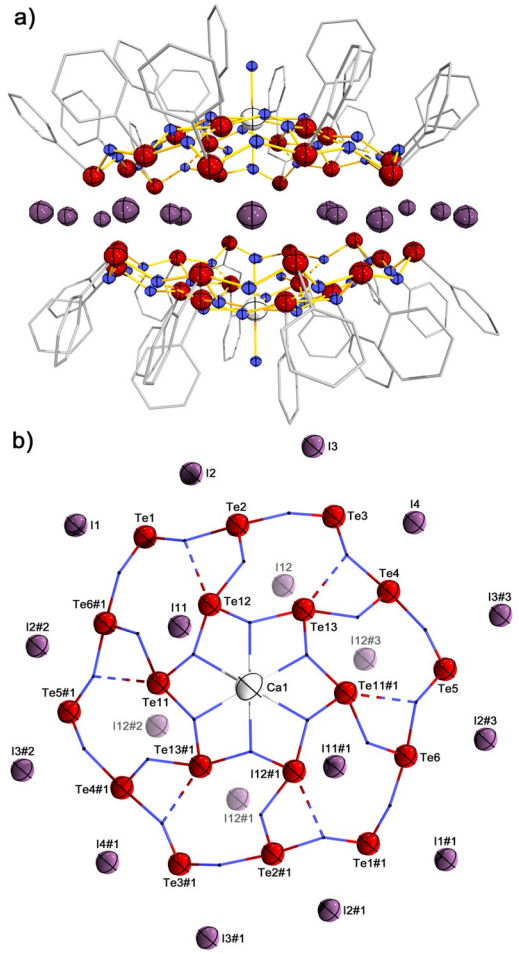

Figure 4. a) Structure of **2** and b) top-view to one $\{(PhTe)_{18}\{Ca(H_2O)_2\}O_{24}\}^{8+}$ half-shell with the central layer of iodine atoms (the atom I12 and its symmetry related positions possess an occupancy of 0.5.).[36]

of the electron density in $[\{(PhTe)_{19}O_{24}\}_2I_{18}]$ (**1b**) results in smaller HOMO–LUMO gaps between the ground-state and the excited states compared to $[\{(PhTe)_{18}\{Ca(H_2O)_2\}O_{24}\}_2I_{16}]$ (**2**). Consequently, the HOMO and LUMO geometric arrangement and energy difference in **1b** are much more favorable for a charge transfer compared to $[\{(PhTe)_{18}\{Ca(H_2O)_2\}O_{24}\}_2I_{16}]$ (**2**). This results in a shift of the corresponding absorption from the visible part of the spectrum into the near UV range, and can explain the fact that compound **2** appears almost colorless, while the compounds **1** with phenyltellurium-centered half-shells have a brownish color. More details are outlined in the Supporting Information.

All telluroxanes under study form highly porous structures with large voids between the cluster units. Figure 5 depicts the channel structure inside compound **2**. The peripheral phenyl substituents enclose hydrophobic voids with a mean diameter of 7.4 Å. They are filled with diffuse solvent molecules. The remaining percentage of the voids is 11% in **2**. This is somewhat more than in the previously discussed $[\{(PhTe)_{19}O_{24}\}_2I_{18}]$ compounds (approximately 9%).[31]

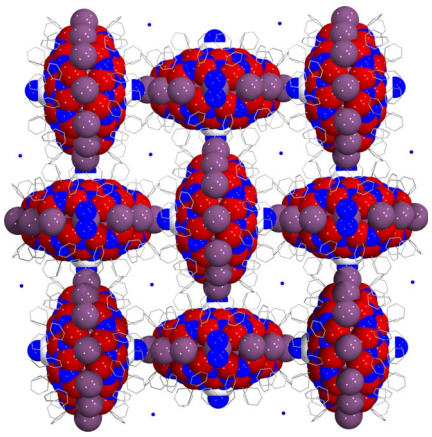

Figure 5. View along the crystallographic *c*-axis of compound **2** depicting large hydrophobic voids between the cluster units.[36]

Mass spectrometric studies confirm that also the calcium modified telluroxane cluster is stable in solution and can be transferred into the gas phase. The regions of the "+3" and "+2" ions are dominated by the $[\{(PhTe)_{18}\{Ca(H_2O)\}O_{24}\}_2I_{13}]^{3+}$ (i.e. $[M-3I-2H_2O]^{3+}$) and $[\{(PhTe)_{18}\{Ca(H_2O)\}O_{24}\}_2I_{14}]^{2+}$ (i.e. $[M-2I-2H_2O]^{2+}$) ions as well as by the corresponding ions with one water molecule more or less and/or partial addition of the solvent used, CH_2Cl_2. This clearly shows that the integrity of the clusters is preserved after dissolving in dichloromethane and ionization by electrospray. Species with minor abundance can be attributed to an exchange of one I^- ion by Cl^- (coming from the solvent). More details are given in the Supporting Information.

The concept for the synthesis of compound **2** can be extended to other metal ions such as lanthanides or "group 3" elements. Addition of M^{3+} nitrates to the above described $(PhTe)_2/I_2/H_2O$ reaction mixture gives telluroxane clusters with two central $\{M^{III}(NO_3)(H_2O)\}^{2+}$ units. Their aqua ligands point to the center of the cluster, while the bidentate bonded nitrato ligands are located in their outer sphere. Charge balance is done as in the case of compound **2** by the partial occupation of the central layer of iodine atoms giving a composition of $[\{(PhTe)_{18}\{M^{III}(NO_3)(H_2O)\}O_{24}\}_2I_{16}]$.

Figure 6 illustrates the structure of $[\{(PhTe)_{18}\{Y(NO_3)(H_2O)\}O_{24}\}_2I_{16}]$ (**3**) with two peripheral nitrato ligands. The Y^{3+} ions are nine-coordinate with $Y{-}O_{(network)}$ bonds all being between 2.387(9) and 2.456(9) Å. These values perfectly fit with the corresponding $Y{-}O_{(crown\ ether)}$ bond lengths in $[Y(Cl)(H_2O)_2(18\text{-crown-}6)]^{2+}$.[32] But unlike the situation in the crown ether, the oxygen donors in **3** are embedded in the telluroxane networks. Thus, they form an almost planar hexagonal plane (maximum deviation from a mean-least-square plane: 0.056 Å). The Y^{3+} ion is situated 0.242 Å above this plane.

As already described for the compounds **1** and **2**, also the intact cluster $[\{(PhTe)_{18}\{Y(NO_3)(H_2O)\}O_{24}\}_2I_{16}]$ is transferred to the gas phase during the mass spectrometric ionization procedure. The spectra are dominated by doubly charged ions with *m*/*z* values between 5100 and 5400. The following molecular compositions have been assigned with changing intensities: $[M-2I]^{2+}$, $[M-I+H]^{2+}$, $[M+2H]^{2+}$. Additionally,

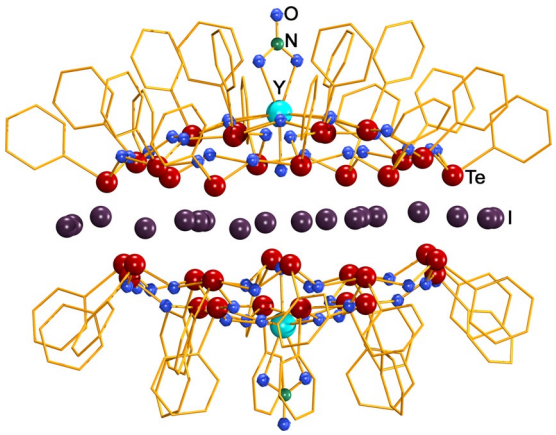

Figure 6. Molecular structure of $[\{(PhTe)_{18}\{Y(NO_3)(H_2O)\}O_{24}\}_2I_{16}]$ (**3**).[36]

corresponding complexes with up to two molecules of dioxane and/or $CHCl_3$ are visible: $[M-2I+(C_4H_8O)]^{2+}$, $[M-2I+(C_4H_8O)_2]^{2+}$, $[M-I+H+(C_4H_8O)]^{2+}$, $[M-I+H+(C_4H_8O)_2]^{2+}$, $[M+2H+(C_4H_8O)]^{2+}$ and $[M+2H+(C_4H_8O)_2]^{2+}$ as well as $[M-3I-H_2O+Cl+CCl_3H]^{2+}$, $[M-3I+Cl+CCl_3H]^{2+}$,. $[M-2I-H_2O+CCl_3H]^{2+}$, $[M-2I+CCl_3H]^{2+}$, $[M-I+H+C_4H_8O_2+CCl_3H]^{2+}$ and $[M-I+H+C_4H_8O_2+CCl_3H-H_2O]^{2+}$. Dioxane has been used for recrystallization and has also been detected crystallographically as co-crystallized solvent. Its binding mode in the mass-spectrometrically detected ions, however, is not yet clear. It could be additionally coordinated to the Y^{3+} ions or incorporated in the central void of the cluster as has been observed for compounds **1a** and **1c**, but the detection of cluster species with two dioxane molecules makes the first option more probable. Chloroform was used to dissolve the sample before the analysis and presumably is filling the void between the telluroxane bowls. Additionally, peaks of ions formed by the loss of one water molecule are seen. A more detailed discussion of the mass spectrometric study on **3a** is found in the Supporting Information.

More examples of $[\{(PhTe)_{18}\{M^{III}(NO_3)(H_2O)\}O_{24}\}_2I_{16}]$ clusters have been prepared with La^{3+}(**4**), Eu^{3+} (**5**) and Lu^{3+} (**6**) instead of Y^{3+} by using the corresponding lanthanide nitrates during the synthesis. This covers M^{3+} ions with effective ionic radii between 1.075 and 1.216 Å.[33] It should be mentioned that a corresponding reaction with the addition of $Sc(NO_3)_3$ did not succeed and resulted in the formation of compound **1b** only. This might be due to the small ionic radius of Sc^{3+} ions, which can obviously not be stabilized in the rigid, 18-crown-6-like coordination environment of the Te–O skeleton. Similar findings have been reported for the coordination chemistry of scandium with crown ethers, where the complexation with 15-crown-5 is preferred and in complexes with 18-crown-6 only five oxygen donors are used for the coordination of the Sc^{3+} ions.[34,35]

Conclusion

Large telluroxane clusters of the composition $[\{(PhTe)_{19}O_{24}\}_2I_{18}(solv)]$ with overall dimensions of approximately 22 × 20 × 18 Å can be prepared by a facile synthesis from diphenylditelluride and iodine in a CH_2Cl_2/methanol/water mixture. Two of the contained $\{PhTe\}^{3+}$ building blocks can readily be replaced by $\{Ca(H_2O)_2\}^{2+}$ or $\{M^{III}(NO_3)(H_2O)\}^{2+}$ (M = Y, La, Eu, Lu) units giving well-defined, "metal-decorated" large inorganic clusters.

Acknowledgements

This work was generously supported by the German Academic Exchange Service (DAAD, Germany) and the Coordenadoria de Aperfeiçoamento de Pessoal de Nível Superior (CAPES, Brazil). We gratefully appreciate the experimental help of Bernhard Loll (FU Berlin), Karine Sparta (Helmholtz-Zentrum Berlin), Manfred S. Weiss (Helmholtz-Zentrum Berlin) and Uwe Müller (Helmholtz-Zentrum Berlin). Additionally, we would like to acknowledge the assistance of the Core Facility BioSupraMol supported by the DFG and High-Performance-Computing (HPC) Centre of the Zentraleinrichtung für Datenverarbeitung (ZEDAT) of the Freie Universität Berlin for computational time and support. Open access funding enabled and organized by Projekt DEAL.

Conflict of interest

The authors declare no conflict of interest.

Keywords: clusters · mass spectrometry · tellurium · telluroxanes · X-ray diffraction

[1] J. Beckmann, P. Finke in *Selenium and Tellurium Chemistry: from Small Molecules to Biomolecules and Materials* (Eds.: J. D. Woollins, R. Laitinen), Springer, Berlin, **2011**, pp. 151–177.
[2] K. Srivastava, A. Panda, S. Sharma, H. B. Singh, *J. Organomet. Chem.* **2018**, *861*, 174–206, and references therein.
[3] J. Beckmann, P. Finke, M. Hesse, B. Wettig, *Angew. Chem. Int. Ed.* **2008**, *47*, 9982–9984; *Angew. Chem.* **2008**, *120*, 10130–10133.
[4] K. V. Domasevitch, V. V. Skopenko, E. B. Rusanov, *Z. Naturforsch. B* **1996**, *51*, 832–837.
[5] J. Beckmann, J. Bolsinger, A. Duthie, *Aust. J. Chem.* **2008**, *61*, 172–182.
[6] J. Beckmann, J. Bolsinger, A. Duthie, *Chem. Eur. J.* **2011**, *17*, 930–940.
[7] M. Oba, K. Nishiyama, S. Koguchi, S. Shimada, W. Ando, *Organometallics* **2013**, *32*, 6620–6623.
[8] K. Srivastava, S. Sharma, H. B. Singh, U. B. Singh, R. J. Butcher, *Chem. Commun.* **2010**, *46*, 1130–1132.
[9] H. Citeau, K. Kirschbaum, O. Conrad, D. M. Giolando, *Chem. Commun.* **2001**, 2006–2007.
[10] S. Yadav, H. B. Singh, M. Zeller, R. J. Butcher, *Organometallics* **2017**, *36*, 2067–2071.
[11] L. Kirsten, Dissertation, Freie Universität Berlin, **2016**.
[12] B. Tirloni, A. Hagenbach, E. Schulz Lang, U. Abram, *Polyhedron* **2014**, *79*, 284–290.

[13] L. Kirsten, V. D. Schwade, L. Selters, A. Hagenbach, P. C. Piquini, E. Schulz Lang, U. Abram, *Eur. J. Inorg. Chem.* **2015**, 3748 – 3757.
[14] L. Kirsten, L. Selter, A. Hagenbach, E. Schulz Lang, U. Abram, *Polyhedron* **2015**, *101*, 146 – 151.
[15] B. Noschang Cabral, L. Kirsten, A. Hagenbach, P. C. Piquini, M. Patzschke, E. Schulz Lang, U. Abram, *Dalton Trans.* **2017**, *46*, 9280 – 9286.
[16] G. Cavallo, P. Metrangolo, R. Milani, T. Pilati, A. Priimagi, G. Resnati, G. Terraneo, *Chem. Rev.* **2016**, *116*, 2478 – 2601.
[17] A. Abate, M. Brischetto, G. Cavallo, M. Lahtinen, P. Metrangolo, T. Pilati, S. Radice, G. Resnati, K. Rissanen, G. Terraneo, *Chem. Commun.* **2010**, *46*, 2724 – 2726.
[18] N. W. Alcock, W. D. Harrison, *J. Chem. Soc. Dalton Trans.* **1984**, 869 – 875.
[19] O. Foss, K. Maartmann-Moe, *Acta Chem. Scand.* **1987**, *41*, 121 – 129.
[20] N. J. Hill, W. Levason, G. Reid, A. J. Ward, *J. Organomet. Chem.* **2002**, *642*, 186 – 190.
[21] A. J. Z. Londero, N. R. Pineda, V. Matos, P. C. Piquini, U. Abram, E. S. Lang, *J. Organomet. Chem.* **2020**, *929*, 121553.
[22] A. Bondi, *J. Phys. Chem.* **1964**, *68*, 441 – 451.
[23] E. S. Lang, R. M. Fernandez, Jr., E. T. Silveira, U. Abram, E. M. Vazquez-Lopez, *Z. Anorg. Allg. Chem.* **1999**, *625*, 1401 – 1404.
[24] P. D. Boyle, W. I. Cross, S. M. Godfrey, C. A. McAuliffe, R. G. Pritchard, S. Sarwar, J. M. Sheffield, *Angew. Chem. Int. Ed.* **2000**, *39*, 1796 – 1798; *Angew. Chem.* **2000**, *112*, 1866 – 1868.
[25] Note that the program used for simulation incorporated in the software for data evaluation (MassLynx Vs. 4.1 SCN 941, by Waters Co., MA, USA) generates isotopic pattern which are significantly narrower than the found isotopic pattern due to data reduction, more precise calculations are found in the Supporting Information.
[26] G. R. Willey, M. P. Spry, W. Errington, *Polyhedron* **2000**, *19*, 1799 – 1802.
[27] P. G. Junk, J. W. Steed, *J. Coord. Chem.* **2007**, *60*, 1017 – 1028.
[28] A. Nurtaeva, E. M. Holt, *J. Chem. Crystallogr.* **2002**, *32*, 337 – 346.
[29] X. Liu, G.-C. Guo, *Acta Crystallogr. Sect. E* **2007**, *63*, m365 – m366.
[30] A. N. Chekhlov, *Russ. J. Coord. Chem.* **2006**, *32*, 474 – 480.
[31] A. L. Spek, *Acta Crystallogr. Sect. D* **2009**, *65*, 148 – 155.
[32] R. D. Rogers, L. K. Kurihara, E. J. Voss, *Inorg. Chem.* **1987**, *26*, 2360 – 2365.
[33] R. D. Shannon, *Acta Crystallogr. Sect. A* **1976**, *32*, 751 – 767.
[34] G. R. Willey, M. T. Lakin, N. W. Alcock, *J. Chem. Soc. Chem. Commun.* **1992**, 1619 – 1620.
[35] M. D. Brown, W. Levason, D. C. Murray, M. C. Popham, G. Reid, M. Webster, *Dalton Trans.* **2003**, 857 – 865.
[36] Deposition Number(s) 1938243 (for **3**), 1938244 (for **1c**), 1938245 (for **1a**), 1938246 (for **2**) and 1938247 (for **1b**) contain(s) the supplementary crystallographic data for this paper. These data are provided free of charge by the joint Cambridge Crystallographic Data Centre and Fachinformationszentrum Karlsruhe Access Structures service www.ccdc.cam.ac.uk/structures.

Manuscript received: March 15, 2021
Accepted manuscript online: May 3, 2021
Version of record online: June 7, 2021

5 List of all publications (ORCID iD: 0000-0001-7583-9634)

1. Scholtysik, C.; Roca Jungfer, M.; Hagenbach, A.; Abram, U. "**Reactions of [$ReOCl_3(PPh_3)_2$] with 4-Fluoroaniline**", *Z. Anorg. Allg. Chem.* **2018**, *644*, 1451-1455.

2. Salsi, F.; Portapilla, G. B.; Schutjajew, K.; Roca Jungfer, M.; Goulart, A.; Hagenbach, A.; de Albuquerque, S.; Abram, U. "**Organometallic Gold(III) Complexes with Tridentate Halogen-Substituted Thiosemicarbazones: Effects of Halogenation on Cytotoxicity and Anti-Parasitic Activity**", *Eur. J. Inorg. Chem.* **2019**, *41*, 4455-4462.

3. Salsi, F.; Portapilla, G. B.; Simon, S.; Roca Jungfer, M.; Hagenbach, A.; de Albuquerque, S.; Abram, U. "**Effect of Fluorination on the Structure and Anti-*Trypanosoma cruzy* Activity of Oxorhenium(V) Complexes with *S*,*N*,*S*-Tridentate Thiosemicarbazones and Benzoylthioureas. Synthesis and Structures of Technetium(V) Analogues**", *Inorg. Chem.* **2019**, *58*(*15*), 10129-10138.

4. Roca Jungfer, M.; Hagenbach, A.; Schulz Lang, E.; Abram, U. "**Rhenium(V) Complexes with Selenolato- and Tellurolato-substituted Schiff' Bases – Released PPh_3 as a Facile Reductant**", *Eur. J. Inorg. Chem.* **2019**, *47*, 4974–4984.

5. Ackermann, J.; Abdulkader, A.; Scholtysik, C.; Roca Jungfer, M.; Hagenbach, A.; Abram, U. "**[$Tc^{I}(NO)X(cp)(PPh_3)$] Complexes (X^- = I^-, I_3^-, SCN^-, $CF_3SO_3^-$ or CF_3COO^-) and Their Reactions**", *Organometallics*, **2019**, *38*, 4471-1178.

6. Salsi, F.; Roca Jungfer, M.; Hagenbach, A.; Abram, U. "**Trigonal-Bipyramidal vs. Octahedral Coordination in Indium(III) Complexes with Potentially *S*,*N*,*S*-Tridentate Thiosemicarbazones**", *Eur. J. Inorg. Chem.* **2020**, *13*, 1222-1229.

7. Thang Pham, C.; Roca Jungfer, M.; Abram, U. "**Indium(III) {2}-Metallacryptates Assembled from 2,6-Dipicolinoyl-bis(*N*,*N*-diethylthiourea)**", *New J. Chem.* **2020**, 44, 3672-3680.

8. Roca Jungfer, M.; Schulz Lang, E.; Abram, U. "**Reactions of Schiff Base-Substituted Diselenides and -tellurides with Ni(II), Pd(II) and Pt(II) Phosphine Complexes",** *Eur. J. Inorg. Chem.* **2020**, *45*, 4303–4312.

9. Kirsten, L.; Fonseca Rodrigues, J.; Hagenbach, A.; Springer, A.; Pineda, N. R.; Piquini, P. C.; Roca Jungfer, M.; Schulz Lang, E.; Abram, U. "**Large Telluroxane Bowls Connected by a Layer of Iodine Ions**", *Angew. Chem. Int. Ed.* **2021**, *60*, 15517–15523.

10. Roca Jungfer, M.; Elsholz, L.; Abram, U. "**Technetium Hydrides Revisited: Syntheses, Structures, and Reactions of [$TcH_3(PPh_3)_4$] and [$TcH(CO)_3(PPh_3)_2$]**", *Organometallics*, **2021**, *40*, 3095–3112. Featured on the cover of volume 40 issue 18 (published 09/2021).

11. Roca Jungfer, M.; Abram, U. **"[$Tc(OH_2)(CO)_3(PPh_3)_2]^+$: A Synthon for Tc(I) Complexes and its Reactions with Neutral Ligands"**, *Inorg. Chem.* **2021**, *60*, 16734-16753.

12. Roca Jungfer, M.; Ernst, M. J.; Hagenbach, A.; Abram, U. **"[{$Tc^{I}(NO)(L^{OMe})(PPh_3)Cl$}$_2$Ag]($PF_6$) and [$Tc^{II}(NO)(L^{OMe})(PPh_3)Cl$]($PF_6$): Two Unusual Technetium Complexes with a "Kläui-type" Ligand"**, *Z. Anorg. Allg. Chem.* **2022***,* e202100316.

13. Zegke, M.; Grödler, D.; Roca Jungfer, M.; Haseloer, A.; Kreuter, M.; Neudörfl, J. M.; Sittel, T.; James, C. M.; Rothe, J.; Altmaier, M.; Klein, A.; Breugst, M.; Abram, U.; Strub, E.; Wickleder, M. S. **"Ammonium pertechnetate in mixtures of trifluoromethanesulfonic acid and trifluoromethanesulfonic anhydride"**, *Angew. Chem. Int. Ed.* **2021***, 61,* e202113777*.*

14. Bohl, M.; Claude, C.; Roca Jungfer, M.; Abram, U.; Sathiyendiran, M. **"Calix[4]arene-Analogous Technetium Supramolecules"**, *Inorg. Chem.* in revision.

15. Roca Jungfer, M.; Elsholz, L.; Abram, U. **"Technetium(I) Carbonyl Chemistry with Small Inorganic Ligands"**, *Inorg. Chem.* **2022**, *61*, 2980-2997.

16. Roca Jungfer, M.; Abram, **Technetium and the C≡C triple bond: Unlocking air- and waterstable technetium acetylides and other organometallic complexes"**, *Inorg. Chem.* submitted.

17. Roca Jungfer, M.; Schulz Lang, E.; Abram, U. "**Solvents and Ligands Matter: Structurally Variable Palladium and Nickel Clusters Assembled by Tridentate Selenium- and Tellurium-Containing Schiff Bases",** *Inorg. Chem.* **2022**, *61*, 3785–3800.

6 References

1) Kenna, D. T. The Search for Technetium in Nature. *J. Chem. Educ.* **1962**, *39*(*9*), 436-442.

2) Lieser, K. H. Technetium in the Nuclear Fuel Cycle, in Medicine and in the Environment. *Radiochim. Acta*, **1993**, *63*, 5-8.

3) Ali, S. A.; Ache, H. J. Production Techniques of Fission Molybdenum-99. *Radiochim. Acta*, **1987**, *41*, 65-72.

4) Zolle, I. *Technetium-99m Pharmaceuticals. Preparation and Quality Control in Nuclear Medicine*, **2007**, (eds U. Heilmann and W. McHugh), Springer, Heidelberg, DE. ISBN-10 3-540-33989-2; ISBN-13 978-3-540-33989-2.

5) Nuclear Energy Agency (NEA). *Nuclear Development. The Supply of Medical Radioisotopes. Policy Options for Ensuring Long-term Supply Security of Molybdenum-99 and/or Technetium-99m Produced Without Highly Enriched Uranium Targets.* **2012** (www.oecd-nea.org).

6) Kuwert, T.; Grünwald, F.; Haberkorn, U.; Krause, T. *Nuklearmedizin*. Ed. 4, **2008**, Thieme, Stuttgart, DE. doi: 10.1055/b-003-125780

7) Taylor, A. T. Lipowska, M.; Hansen, L.; Malveaux, E.; Marzilli, L. G. 99mTc-MAEC Complexes: New Renal Radiopharmaceuticals Combining Characteristics of 99mTc-MAG3 and 99mTc-EC. *J. Nucl. Med.* **2004**, *45*(*5*), 885-886.

8) Morse, E. C. *Analytical Methods for Nonproliferation, Advanced Sciences and Technologies for Security. The Nuclear Fuel Cycle*. **2016**, Springer International Publishing AG, Basel, CH. doi: 10.1007/978-3-319-29731-6_5

9) Ewing, R. C. Long-term storage of spent nuclear fuel. *Nat. Mater.* **2015**, *14*, 252-257.

10) Settle, F. A. Uranium to Electricity: The Chemistry of the Nuclear Fuel Cycle. *J. Chem. Educ.* **2009**, *86*(*3*), 316-323.

11) Baisden, P. A.; Choppin, G. R. *Radiochemistry and nuclear chemistry. Encyclopedia of life support systems. Nuclear waste management and the nuclear fuel cycle.* Vol. 2, **2009**, (ed. Nagy, S.) Eolss Publishers Co Ltd, Oxford, EN.

12) Schulte, E. H.; Scoppa, P. Sources and behavior of technetium in the environment. *Sci. Total Environ*. **1987**, *64*, 163-179.

13) Mitchell, P. I.; Vintró, L. L. *What is the environmental impact of Sellafield?* Proc. Royal Irish Academy Conference - Making Sense of Sellafield, **2002**, Academy House, Dublin, IE. Published by the Royal Irish Academy, pp. 5-11. Available online at https://www.researchgate.net/publication/289375344_What_is_the_environmental_impact_of_Sellafield (last accessed, Jan. 2022).

14) Vintró, L. L.; Smith, K. J.; Lucey, J. A.; Mitchell, P. I. The environmental impact of the Sellafield discharges. *SCOPE-RADSIDE*, **2000**, 1-27. Available online at https://www.researchgate.net/publication/237631215_The_environmental_impact_of_the_Sellafield_discharges (last accessed, Jan. 2022).

15) Sellafield Ltd. *Discharges and Environmental Monitoring Annual Report 2019*. **2020**. Corporate report. Available online at https://www.gov.uk/government/publications/discharges-and-environmental-monitoring-annual-report-2019/discharges-and-environmental-monitoring-annual-report-2019 (last accessed, Jan. 2022).

16) Clearance and Exemptions Working Group. *The UK Nuclear Industry Guide To: Clearance and Radiological Sentencing: Principles, Process and Practices*. Revision 2.01. 2017, Nuclear Industry Safety Directors Forum (SDF). Available online at https://www.nuclearinst.com/write/MediaUploads/SDF%20documents/CEWG/Clearance_and_Exemption_GPG_2.01.pdf (last accessed, Jan. 2022).

17) Pegg, I. L. Behavior of technetium in nuclear waste vitrification processes. *J. Radioanal. Nucl. Chem.* **2015**, *305*, 287–292.

18) Allan, C. J.; Nuttall, K. How to cope with the hazards of nuclear fuel waste. *Nucl. Eng. Des*. **1997**, *176*, 51-66.

19) Tananaev, I. G.; Myasoedov, B. F. Problems of the Nuclear Fuel Cycle. *Russ. J. Gen. Chem*. **2011**, *81*(*9*), 1925-1927.

20) Meena, A. H.; Arai, Y. Environmental geochemistry of technetium. *Environ. Chem. Lett.* **2017**, *15*, 241-263.

21) Levitskaia, T. G.; Anderson, A.; Chatterjee, S. D.; Cho, H. M.; Rapko, B. M.; Peterson, J. M.; Walter, E. D.; Washton, N. M. U.S. Department of Energy. Speciation and Oxidative Stability of *23654; EMSP-RPT-024, Rev. 0*, **2014**.

22) Lukens, W. W.; Shuh, D. K.; Schroeder, N. C.; Ashley, K. R. Behavior of Technetium in Alkaline Solution: Identification of Non-Pertechnetate Species in High-Level Nuclear Waste Tanks at the Hanford Reservation. 11 Sep 2003; 20 p; American Chemical Society Meeting, Fall 2003; New York, NY (United States); 7-11 Sep 2003;

AC03-76SF00098; Also available from OSTI as DE00817638; PURL: https://www.osti.gov/servlets/purl/817638-gLf1u2/native/.

23) McGregor, D.; Burton-Pye, B. P.; Howell, R. C.; Mbomekalle, I. M.; Lukens, W. W. Jr.; Bian, F.; Mausolf, E.; Poineau, F.; Czerwinski, K. R.; Francesconi, L. C. Synthesis, Structure Elucidation, and Redox Properties of ^{99}Tc Complexes of Lacunary Wells-Dawson Polyoxometalates: Insights into Molecular ^{99}Tc-Metal Oxide Interactions. *Inorg. Chem.* **2011**, *50*, 1670-1681.

24) Lukens, W. W.; Shuh, D. K.; Schroeder, N. C.; Ashley, K. R. Correction to "Identification of the Non-Pertechnetate Species in Hanford Waste Tanks, Tc(I)−Carbonyl Complexes". *Environ. Sci. Technol.* **2004**, *38*, 1, 229−233.

25) Chatterjee, S.; Holfeltz, V. E.; Hall, G. B.; Johnson, I. E.; Walter, E. D.; Lee, S.; Reinhart, B.; Lukens, W. W.; Machara, N. P.; Levitskaia, T. G. Identification and Quantification of Technetium Species in Hanford Waste Tank AN-102. *Anal. Chem.* **2020**, *92*, 13961-13970.

26) Uchida, S.; Tagami, K.; Wirth, E.; Rühm, W. Concentration levels of technetium-99 in forest soils collected within the 30-km zone around the Chernobyl reactor. *Environ. Pollut.* **1999**, *105*, 75-77.

27) Ackermann, J.; Hagenbach, A.; Abram, U. $\{Tc(NO)(Cp)(PPh_3)\}^+$ – a novel technetium(I) core.

28) Abdulkader, A.; Hagenbach, A.; Abram, U. $[Tc(NO)Cl(Cp)(PPh_3)]$ – A Technetium(I) Compound with an Unexpected Synthetic Potential. *Eur. J. Inorg. Chem.* **2021**, 37, 3812–3818.

29) Cargnelutti, R.; Schumacher, R. F.; Belladona, A. L.; Kazmierczak, J. C. Coordination chemistry and synthetic approaches of pyridyl-selenium ligands: A decade update. *Coord. Chem. Rev.* **2021**, *426*, 213537.

30) Dubey, P.; Gupta S.; Singh, A. K. Complexes of Pd(II), η^6-C_6H_6Ru(II), and η^5-Cp*Rh(III) with Chalcogenated Schiff Bases of Anthracene-9-carbaldehyde and Base-Free Catalytic Transfer Hydrogenation of Aldehydes/Ketones and N-Alkylation of Amines. *Organometallics*, **2019**, *38*, 944-961.

31) Paluru, D. K.; Dey, S.; Wadawale, A.; Maity, D. K.; Bhuvanesh N.; Jain, V. K. Coordination Polymers of Palladium Bridged by Carboxylate and Dimethylaminoalkylselenolate Ligands. *Eur. J. Inorg. Chem*. **2015**, 397-410.

32) Hegazy, W. H.; Gaafar, A. E.-D M. Synthesis, Characterization and Antibacterial Activities of New Pd(II) And Pt(IV) Complexes of Some Unsymmetrical Tetradentate Schiff Bases, *Am. Chem. Sci. J.* **2012**, *2*, 86-99.

33) Arafath, M. A.; Adam, F.; Razali, M. R.; Hassan, L. E. A.; Ahamed, M. B. K.; Majid, A. M. S.A. Synthesis, characterization and anticancer studies of Ni(II), Pd(II) and Pt(II) complexes with Schiff base derived from N-methylhydrazinecarbothioamide and 2-hydroxy-5-methoxy-3-nitrobenzaldehyde. *J. Mol. Struct.* **2017**, *1130*, 791-798.

34) Elzahany, E. A.; Hegab, K. H.; Khalil, S. K. H.; Youssef, N. S. Synthesis, Characterization and Biological Activity of Some Transition Metal Complexes with Schiff Bases Derived from 2-Formylindole, Salicyladehyde, and N-amino Rhodanine. *Aust. J. Basic Appl. Sci.* **2008**, *2*, 210-220.

35) Shi, P.-Y.; Liu, Y.-H.; Peng, S.-M.; Liu, S.-T. Palladium(II) Complexes Containing P∼N∼O Donors. Ligand Effect of Tridentate versus Bidentate Coordination on the Oligomerization of Ethylene. *Organometallics*, **2002**, *21*, 3203-3207.

36) Motschi, H.; Nussbaumer, C.; Pregosin, P. S. The *trans*-Influence in Platinum (II) Complexes. ^{1}H- and ^{13}C-NMR. and X-ray structural studies of tridentate *Schiff*'s base complexes of platinum (II). *Helv. Chim. Acta*, **1980**, *63*, 2071-2086.

37) Roy, N.; Sproules, S.; Bothe, E.; Weyhermüller, T.; Wieghardt, K.; Polynuclear Complexes Containing the Redox Noninnocent Schiff Base Ligand 2-[(*E*)-2-Mercaptophenylimino]methyl-4,6-di-*tert*-butylphenolate(2–). *Eur. J. Inorg. Chem.* **2009**, 2655–2663.

38) Tamizh, M. M.; Cooper, B. F. T.; Macdonald, C. L. B.; Karvembu, R. Palladium(II) complexes with salicylideneimine based tridentate ligand and triphenylphosphine: Synthesis, structure and catalytic activity in Suzuki–Miyaura cross coupling reactions**.** *Inorg. Chim. Acta*, **2013**, *394*, 391–400.

39) Shabbir, M.; Akhter, Z.; Ahmad, I.; Ahmed, S.; Shafiq, M.; Mirza, B.; McKee, V.; Munawar, K. S.; Ashraf, A. R. Schiff base triphenylphosphine palladium (II) complexes: Synthesis, structural elucidation, electrochemical and biological evaluation. *J. Mol. Struct.* **2016**, *1118*, 250-258.

40) Shabbir, M.; Akhter, Z.; Ashraf, A. R.; Ismail, H.; Habib, A.; Mirza, B. Nickel(II) and palladium(II) triphenylphosphine complexes incorporating tridentate Schiff base ligands: Synthesis, characterization and biocidal activities. *J. Mol. Struct.* **2017**, *1149*, 720-726.

41) Tamizh, M. M.; Mereiter, K.; Kirchner, K.; Bhat, B. R.; Karvembu, R. Synthesis, crystal structures and spectral studies of square planar nickel(II) complexes containing an ONS donor Schiff base and triphenylphosphine. *Polyhedron*, **2009**, *28*, 2157-2164.

42) Manzur, C.; Bustos, C.; Schrebler, R.; Carrillo, D. Synthesis, characterization and electrochemistry of nickel(II)

complexes of Schiff base ligands containing a disulphide group. Crystal structure of [Ni{(*o*-$OC_6H_4CH=NC_6H_4)_2S_2$}(MeOH)] · MeOH, *Polyhedron*, **1989**, *8*, 2321-2330.

43) Raj, P.; Kaur, K.; Aree, T.; Singh, A. Singh, N. Fluorescent Chemosensors for Selective and Sensitive Detection of Phosmet/Chlorpyrifos with Octahedral Ni^{2+} Complexes. *Inorg. Chem.* **2016**, *55*, 4874−4883.

44) Kuchtanin, V.; Kleščíková, L.; Šoral, M.; Fischer, R.; Růžičková, Z.; Rakovský, E.; Moncol', J.; Segl'a, P. Nickel(II) Schiff base complexes: Synthesis, characterization and catalytic activity in Kumada–Corriu cross-coupling reactions, *Polyhedron*, **2016**, *117*, 90-96.

45) Noschang Cabral, B.; Kirsten, L.; Hagenbach, A.; Piquini, P. C.; Patzschke, M.; Lang, E. S.; Abram, U. Technetium complexes with arylselenolato and aryltellurolato ligands, *Dalton Trans.* **2017**, *46*, 9280–9286.

46) Noschang Cabral, B. *Doctoral Thesis*, Universidade Federal Santa Maria, **2017**.

47) Ananikov, V. P.; Beletskaya, I. P.; Aleksandrov, G. G.; Eremenko, I. L. Mechanistic Investigation and New Catalyst Design in Palladium- and Platinum-Catalyzed Se−Se Bond Addition to Alkynes. *Organometallics*, **2003**, *22*, 1414-1421.

48) Gysling, H. J. *Ligand properties of organic selenium and tellurium compounds, in Organic Selenium and Tellurium Compounds: Volume 1*, 679-855, **1986**, (eds S. Patai and Z. Rappoport), John Wiley & Sons, Inc. Chichester, UK. doi: 10.1002/9780470771761.ch18

49) Oilunkaniemi, R.; Laitinen, R. S.; Ahlgrén, M. The oxidative addition of diphenyl diselenide and ditelluride to tetrakis(triphenylphosphine)palladium. *J. Organomet. Chem.* **2001**, *623*, 168-175.

50) Chakraborty, T.; Srivastava, K.; Singh, H. B.; Butcher R. J. Palladium selenolates via oxidative addition of organylselenenyl halides to palladium(0) precursor and via cleavage reaction of diselenides: Synthesis, structure and spectroscopic investigation. *J. Organomet. Chem.* **2011**, *696*, 2782-2788.

51) Ghavale, N.; Wadawale, A.; Dey, S.; Jain, V. K. Palladium assisted formation of arylselenoacetone from diaryldiselenides in methanol-acetone *Ind. J. Chem.* **2009**, *48A*, 1510-1514.

52) Tirloni, B.; Cechin, C. N.; Razera, G. F.; Pereira, M. P.; de Oliveira, G. M.; Lang, E. S. Exploring Te–Te Bond Cleavage with Palladium(II): Synthesis, X-ray Structural Characterization, and Optical Features of Tellurolate and Telluro-Ether Complexes of Palladium(II). *Z. Anorg. Allg. Chem*. **2016**, *642*, 239-245.

53) Kaur, R.; Menon, S. C.; Panda, S. Singh, H. B.; Patel, R. P.; Butcher, R. J. Facile Cleavage of Organochalcogen Hybrid (NEEN, NEN, EN, where E = Se or Te) Ligand C−E and E−E Bonds by Pd(II). *Organometallics*, **2009**, *28*, 2363-2371.

54) Back, D.; de Oliveira, G. M.; Lang, E. S. Synthesis and structural characterization of dinuclear tellurolate palladium(II) complexes. *Polyhedron* **2015**, *85*, 565-569.

55) Tirloni, B.; Lang, E. S.; de Oliveira, G. M.;. Piquini, P. C.; Hörner, M. Synthesis, crystal structure, and optical characteristics of $[Pd_2Hg_4Cl_6\{Te(DMB)\}_6]$·2DMF, $[HgClTe(DMB)]_4$, and the ring-forming cluster $[Pd_{12}(TePh)_{24}]$·2DMF. *New J. Chem*. **2014**, *38*, 2394-2399.S. Kolay, M. Kumar, A. Wadawale, D. Das, V. K. Jain, *Dalton Trans.* **2014**, *43*, 16056-16065.

56) Jain, V. K.; Chauhan, R. S. New vistas in the chemistry of platinum group metals with tellurium ligands. *Coord. Chem. Rev*. **2016**, *306*, 270-301.

57) Bugarcic, Z. M.; Divac, V. M.; Kosti, M. D.; Jankovi, N. Z.; Heinemann, F. W.; Radulovi, N. S.; Stojanovi, Z. Z. Synthesis, crystal and solution structures and antimicrobial screening of palladium(II) complexes with 2-(phenylselanylmethyl)oxolane and 2-(phenylselanylmethyl)oxane as ligands. *J. Inorg. Biochem.* **2015**, *143*, 9-19.

58) R. Cargnelutti, E. S. Lang, P. Piquini, U. Abram, Synthesis and structure of $[ReOSe(2\text{-}Se\text{-}py)_3]$: A rhenium(V) complex with selenium(0) as a ligand. *Inorg. Chem. Commun.* **2014**, *45*, 48–50.

59) Dutta, P. K.; Asatkar, A. K.; Zade, S. S.; Panda, S. Oxidative addition of disulfide/diselenide to group 10 metal(0) and *in situ* functionalization to form neutral thiasalen/selenasalen group 10 metal(ii) complexes. *Dalton Trans*. **2014**, *43*, 1736-1743.

A Appendix: Supporting Information of Publications

A.1 Technetium Hydrides Revisited: Syntheses, Structures, and Reactions of $[TcH_3(PPh_3)_4]$ and $[TcH(CO)_3(PPh_3)_2]$

Authors	M. Roca Jungfer, L. Elsholz, U. Abram
Journal	*Organometallics*, **2021**, *40*, 3095–3112
DOI	10.1021/acs.organomet.1c00274
Link	https://pubs.acs.org/doi/abs/10.1021/acs.organomet.1c00274
Detailed scientific contribution	Maximilian Roca Jungfer and Ulrich Abram designed the project. Maximilian Roca Jungfer performed the synthesis and characterization of the compounds, performed DFT calculations, calculated the X-ray structures and wrote a draft of the manuscript. Laura Elsholz performed some of the experiments and DFT calculations during a research internship under the supervision of Maximilian Roca Jungfer. Ulrich Abram supervised the project, provided scientific guidance and suggestions and corrected the manuscript. Maximilian Roca Jungfer and Ulrich Abram designed the cover picture of the issue.
Estimated own contribution	80%

Return to publication 4.1.

Supporting information for the paper entitled:

Technetium Hydrides Revisited: Syntheses, Structures and Reactions of $[TcH_3(PPh_3)_4]$ and $[TcH(CO)_3(PPh_3)_2]$

Maximilian Roca Jungfer, Laura Elsholz and Ulrich Abram*

Freie Universität Berlin, Institute of Chemistry and Biochemistry, Fabeckstr. 34–36, 14195 Berlin, Germany

E-mail: ulrich.abram@fu-berlin.de

Table of Contents

Part 1: Crystallographic data

Table S1. Crystal data and structure determination parameters.

	$[TcH_3(PPh_3)_4] \cdot 2$ toluene	α-$[TcH(CO)_3(PPh_3)_2]$	$[TcBr(CO)_3(PPh_3)_2]$
Empirical formula	$C_{86}H_{79}P_4Tc$	$C_{39}H_{31}O_3P_2Tc$	$C_{39}H_{30}BrO_3P_2Tc$
Formula weight	1334.37	707.58	786.48
Temperature/K	230(2)	240(2)	250(2)
Crystal system	triclinic	monoclinic	triclinic
Space group	$P\bar{1}$	$P2_1/c$	$P\bar{1}$
a/Å	13.2510(7)	19.2611(9)	10.3013(8)
b/Å	15.7303(9)	10.5406(5)	12.5297(8)
c/Å	17.3877(12)	17.7709(7)	14.5795(9)
α/°	74.273(5)	90	96.929(5)
β/°	88.512(5)	111.859(3)	104.749(5)
γ/°	89.107(4)	90	105.959(5)
Volume/Å^3	3487.3(4)	3348.5(3)	1712.5(2)
Z	2	4	2
ρ_{calc}g/cm^3	1.271	1.404	1.525
μ/mm^{-1}	0.344	0.562	1.717
F(000)	1396.0	1448.0	792.0
Crystal size/mm^3	0.34 × 0.23 × 0.05	0.170 × 0.140 × 0.063	0.510 × 0.240 × 0.030
Radiation	MoKα (λ = 0.71073)	MoKα (λ = 0.71073)	MoKα (λ = 0.71073)
2Θ range for data collection/°	6.564 to 52	6.584 to 54	6.884 to 58.414
Index ranges	-16 ≤ h ≤ 16, -19 ≤ k ≤ 19, -21 ≤ l ≤ 21	-24 ≤ h ≤ 24, -13 ≤ k ≤ 13, -22 ≤ l ≤ 22	-14 ≤ h ≤ 14, -17 ≤ k ≤ 17, -19 ≤ l ≤ 19
Reflections collected	31296	29212	20215
Independent reflections	13666 [R_{int} = 0.0863, R_{sigma} = 0.1821]	7302 [R_{int} = 0.1057, R_{sigma} = 0.1158]	9177 [R_{int} = 0.0620, R_{sigma} = 0.0838]
Data/restraints/parameters	13666/858/939	7302/0/410	9177/648/467
Goodness-of-fit on F^2	0.697	0.786	0.840
Final R indexes [I>=2σ (I)]	R_1 = 0.0434, wR_2 = 0.0513	R_1 = 0.0396, wR_2 = 0.0541	R_1 = 0.0376, wR_2 = 0.0729
Final R indexes [all data]	R_1 = 0.1106, wR_2 = 0.0615	R_1 = 0.0902, wR_2 = 0.0615	R_1 = 0.0744, wR_2 = 0.0799
Largest diff. peak/hole / e Å^{-3}	0.32/-0.46	0.30/-0.44	0.51/-1.13
CCDC access code	2081313	2081314	2081315

Table S1. Crystal data and structure determination parameters (continued).

	$[TcI(CO)_3(PPh_3)_2]$	$[Tc(\eta^1\text{-}O(CH)O)(CO)_3(PPh_3)_2]$	$[Tc(\eta^1\text{-}OC(CF_3)O)(CO)_3(PPh_3)_2] \cdot 0.5$ toluene
Empirical formula	$C_{39}H_{30}IO_3P_2Tc$	$C_{40}H_{31}O_5P_2Tc$	$C_{44.5}H_{34}F_3O_5P_2Tc$
Formula weight	833.47	751.59	865.65
Temperature/K	293(2)	230(2)	230(2)
Crystal system	monoclinic	triclinic	triclinic
Space group	$P2_1/c$	$P\bar{1}$	$P\bar{1}$
a/Å	14.0578(9)	9.9928(11)	11.0443(6)
b/Å	13.8081(6)	10.4225(12)	12.2708(6)
c/Å	18.7262(13)	18.853(3)	18.1810(11)
α/°	90	93.755(10)	109.690(4)
β/°	108.754(5)	103.764(9)	93.562(5)
γ/°	90	112.475(8)	106.981(4)
Volume/Å^3	3442.0(4)	1735.3(4)	2183.2(2)
Z	4	2	2
ρ_{calc}g/cm^3	1.608	1.438	1.317
μ/mm^{-1}	1.445	0.551	0.457
F(000)	1656.0	768.0	882.0
Crystal size/mm^3	0.260 × 0.230 × 0.200	0.092 × 0.064 × 0.010	0.980 × 0.670 × 0.450
Radiation	MoKα (λ = 0.71073)	MoKα (λ = 0.71073)	MoKα (λ = 0.71073)
2Θ range for data collection/°	7.214 to 58.482	6.756 to 51.992	6.896 to 51.996
Index ranges	-19 ≤ h ≤ 19, -18 ≤ k ≤ 18, -25 ≤ l ≤ 25	-12 ≤ h ≤ 12, -12 ≤ k ≤ 12, -23 ≤ l ≤ 21	-13 ≤ h ≤ 12, -15 ≤ k ≤ 15, -22 ≤ l ≤ 22
Reflections collected	25944	15202	17446
Independent reflections	9247 [R_{int} = 0.0365, R_{sigma} = 0.0392]	6782 [R_{int} = 0.1316, R_{sigma} = 0.2741]	8486 [R_{int} = 0.0536, R_{sigma} = 0.0462]
Data/restraints/parameters	9247/0/415	6782/0/437	8486/795/551
Goodness-of-fit on F^2	0.958	0.659	1.029
Final R indexes [I>=2σ (I)]	R_1 = 0.0341, wR_2 = 0.0822	R_1 = 0.0490, wR_2 = 0.0591	R_1 = 0.0490, wR_2 = 0.1395
Final R indexes [all data]	R_1 = 0.0552, wR_2 = 0.0878	R_1 = 0.1621, wR_2 = 0.0836	R_1 = 0.0551, wR_2 = 0.1441
Largest diff. peak/hole / e Å^{-3}	0.57/-1.20	0.53/-0.68	1.11/-1.09
CCDC access code	2081316	2081317	2081318

Table S1. Crystal data and structure determination parameters (continued).

	$[Tc(\eta^2\text{-}O(CH)O)(CO)_2(PPh_3)_2] \cdot MeOH$	$[Tc(\eta^2\text{-}OC(CH_3)O)(CO)_2(PPh_3)_2]$	$[Tc(\eta^2\text{-}OC(Ph)O)(CO)_2(PPh_3)_2]$
Empirical formula	$C_{40}H_{35}O_5P_2Tc$	$C_{40}H_{33}O_4P_2Tc$	$C_{45}H_{35}O_4P_2Tc$
Formula weight	755.62	737.60	799.67
Temperature/K	293(2)	230(2)	293(2)
Crystal system	triclinic	monoclinic	triclinic
Space group	$P\bar{1}$	$P2_1/c$	$P\bar{1}$
a/Å	10.0895(12)	17.5550(7)	10.1509(12)
b/Å	11.1139(13)	9.7210(2)	10.6112(14)
c/Å	18.190(2)	20.9453(8)	19.917(2)
α/°	93.559(9)	90	78.829(10)
β/°	103.416(9)	104.485(3)	80.302(9)
γ/°	115.836(8)	90	68.034(9)
Volume/Å^3	1754.4(4)	3460.7(2)	1941.0(4)
Z	2	4	2
ρ_{calc}g/cm^3	1.430	1.416	1.368
μ/mm^{-1}	0.545	0.549	0.496
F(000)	776.0	1512.0	820.0
Crystal size/mm^3	0.280 × 0.100 × 0.090	0.421 × 0.375 × 0.375	0.220 × 0.080 × 0.070
Radiation	MoKα (λ = 0.71073)	MoKα (λ = 0.71073)	MoKα (λ = 0.71073)
2Θ range for data collection/°	6.812 to 51.99	6.984 to 58.438	7.022 to 53.998
Index ranges	-11 ≤ h ≤ 12, -13 ≤ k ≤ 13, -22 ≤ l ≤ 22	-24 ≤ h ≤ 24, -10 ≤ k ≤ 13, -28 ≤ l ≤ 28	-12 ≤ h ≤ 12, -13 ≤ k ≤ 13, -19 ≤ l ≤ 25
Reflections collected	14600	37804	17402
Independent reflections	6861 [R_{int} = 0.0778, R_{sigma} = 0.1076]	9315 [R_{int} = 0.0439, R_{sigma} = 0.0332]	8429 [R_{int} = 0.0551, R_{sigma} = 0.0800]
Data/restraints/parameters	6861/0/440	9315/625/468	8429/0/469
Goodness-of-fit on F^2	0.880	0.942	0.821
Final R indexes [I>=2σ (I)]	R_1 = 0.0500, wR_2 = 0.1125	R_1 = 0.0273, wR_2 = 0.0628	R_1 = 0.0412, wR_2 = 0.0852
Final R indexes [all data]	R_1 = 0.0966, wR_2 = 0.1262	R_1 = 0.0420, wR_2 = 0.0660	R_1 = 0.0937, wR_2 = 0.0977
Largest diff. peak/hole / e Å^{-3}	0.66/-0.81	0.44/-0.70	0.82/-0.87
CCDC access code	2081319	2081320	2081321

Table S1. Crystal data and structure determination parameters (continued).

	$[Tc(btuNEt_2)(CO)_2(PPh_3)_2]$	$[\{Tc(CO)_3\}_3(PhSeOO)_3(OH)\{Tc(CO)_3\}] \cdot OPPh_3 \cdot 0.25$ pentane	$[Tc_2(\mu^2\text{-}\eta^2\text{-ox})(CO)_6(OPPh_3)_2]$
Empirical formula	$C_{50}H_{45}N_2O_3P_2STc$	$C_{49.25}H_{34}O_{20}PSe_3Tc_4$	$C_{44}H_{30}O_{12}P_2Tc_2$
Formula weight	913.88	1605.61	1008.62
Temperature/K	230(2)	100(2)	293(2)
Crystal system	monoclinic	monoclinic	triclinic
Space group	$P2_1/n$	$P2/c$	$P\bar{1}$
a/Å	11.3803(11)	18.362(6)	9.9066(11)
b/Å	18.016(2)	17.668(7)	10.6962(11)
c/Å	21.461(2)	19.038(8)	11.0189(12)
α/°	90	90	88.275(9)
β/°	100.987(8)	105.836(9)	88.561(9)
γ/°	90	90	68.328(8)
Volume/Å^3	4319.4(8)	5942(4)	1084.4(2)
Z	4	4	1
ρ_{calc}g/cm^3	1.405	1.795	1.544
μ/mm^{-1}	0.501	2.845	0.772
F(000)	1888.0	3114.0	506.0
Crystal size/mm^3	0.452 × 0.045 × 0.043	0.287 × 0.268 × 0.040	0.280 × 0.260 × 0.130
Radiation	MoKα (λ = 0.71073)	MoKα (λ = 0.71073)	MoKα (λ = 0.71073)
2Θ range for data collection/°	6.34 to 51.998	4.416 to 57.736	7.056 to 51.994
Index ranges	-14 ≤ h ≤ 13, -22 ≤ k ≤ 22, -26 ≤ l ≤ 26	-24 ≤ h ≤ 24, -23 ≤ k ≤ 23, -23 ≤ l ≤ 24	-12 ≤ h ≤ 12, -12 ≤ k ≤ 13, -13 ≤ l ≤ 13
Reflections collected	31266	74356	8623
Independent reflections	8478 [R_{int} = 0.1657, R_{sigma} = 0.2253]	14014 [R_{int} = 0.0441, R_{sigma} = 0.0308]	4238 [R_{int} = 0.0384, R_{sigma} = 0.0414]
Data/restraints/parameters	8478/660/532	14014/12/713	4238/0/272
Goodness-of-fit on F^2	0.767	1.024	0.921
Final R indexes [I>=2σ (I)]	R_1 = 0.0520, wR_2 = 0.0753	R_1 = 0.0259, wR_2 = 0.0626	R_1 = 0.0373, wR_2 = 0.0920
Final R indexes [all data]	R_1 = 0.1625, wR_2 = 0.0984	R_1 = 0.0360, wR_2 = 0.0675	R_1 = 0.0501, wR_2 = 0.0979
Largest diff. peak/hole / e Å^{-3}	0.59/-1.26	1.32/-0.59	0.38/-0.50
CCDC access code	2081322	2081323	2081324

Table S1. Crystal data and structure determination parameters (continued).

	$[Tc(\eta^2\text{-oxH})(CO)_2(PPh_3)_2]\cdot 0.25CH_2Cl_2$	$[Tc(\eta^2\text{-ox})(CO)_2(PPh_3)_2]HNEt_3$	$[TcCl_3(PMe_3)_3] \cdot OPPh_3$
Empirical formula	$C_{40.25}H_{31.5}Cl_{0.5}O_6P_2Tc$	$C_{46}H_{46}NO_6P_2Tc$	$C_{27}H_{42}Cl_3OP_4Tc$
Formula weight	788.82	868.78	710.83
Temperature/K	230(2)	230(2)	230(2)
Crystal system	monoclinic	triclinic	triclinic
Space group	$P2_1/n$	$P\bar{1}$	$P\bar{1}$
a/Å	10.2030(8)	9.1340(16)	9.3259(10)
b/Å	29.770(2)	10.635(2)	13.1564(13)
c/Å	12.7848(9)	22.486(4)	14.4435(16)
α/°	90	80.065(16)	82.503(9)
β/°	108.693(6)	84.711(14)	75.739(9)
γ/°	90	80.839(15)	83.350(8)
Volume/Å^3	3678.4(5)	2119.5(7)	1696.4(3)
Z	4	2	2
ρ_{calc}g/cm^3	1.424	1.361	1.392
μ/mm^{-1}	0.561	0.464	0.868
F(000)	1610.0	900.0	732.0
Crystal size/mm^3	0.160 × 0.130 × 0.060	0.390 × 0.187 × 0.050	0.320 × 0.220 × 0.110
Radiation	MoKα (λ = 0.71073)	MoKα (λ = 0.71073)	MoKα (λ = 0.71073)
2Θ range for data collection/°	6.426 to 54.022	6.766 to 52.068	6.504 to 52
Index ranges	-13 ≤ h ≤ 12, -38 ≤ k ≤ 38, -7 ≤ l ≤ 16	-11 ≤ h ≤ 11, -13 ≤ k ≤ 13, -27 ≤ l ≤ 27	-11 ≤ h ≤ 11, -16 ≤ k ≤ 16, -17 ≤ l ≤ 17
Reflections collected	8060	8237	13764
Independent reflections	8060 [R_{sigma} = 0.1441]	8237 [R_{sigma} = 0.2198]	6641 [R_{int} = 0.0484, R_{sigma} = 0.0820]
Data/restraints/parameters	8060/20/471	8237/608/495	6641/0/325
Goodness-of-fit on F^2	0.958	1.071	0.819
Final R indexes [I>=2σ (I)]	R_1 = 0.0722, wR_2 = 0.1529	R_1 = 0.1398, wR_2 = 0.3683	R_1 = 0.0359, wR_2 = 0.0708
Final R indexes [all data]	R_1 = 0.1456, wR_2 = 0.1900	R_1 = 0.2345, wR_2 = 0.4100	R_1 = 0.0697, wR_2 = 0.0764
Largest diff. peak/hole / e Å^{-3}	0.96/-0.55	3.03/-2.06	0.79/-0.43
CCDC access code	2081325	2081326	2081327

Table S1. Crystal data and structure determination parameters (continued).

	$[TcH(CO)_3(PPh_3)_2]$, triclinic	β-$[TcH(CO)_3(PPh_3)_2]$, monoclinic
Empirical formula	$C_{39}H_{31}O_3P_2Tc$	$C_{39}H_{31}O_3P_2Tc$
Formula weight	707.58	707.58
Temperature/K	100(2)	293(2)
Crystal system	triclinic	monoclinic
Space group	$P\bar{1}$	$P2_1/c$
a/Å	9.8450(4)	13.6700(13)
b/Å	10.5678(5)	13.9234(10)
c/Å	17.9662(6)	17.9506(15)
α/°	75.816(2)	90
β/°	77.711(2)	104.899(7)
γ/°	65.441(2)	90
Volume/Å^3	1635.16(12)	3301.7(5)
Z	2	4
ρ_{calc}g/cm^3	1.437	1.423
μ/mm^{-1}	4.794	0.570
F(000)	724.0	1448.0
Crystal size/mm^3	0.15 × 0.12 × 0.07	0.15 × 0.13 × 0.08
Radiation	CuKα (λ = 1.54178)	MoKα (λ = 0.71073)
2Θ range for data collection/°	5.114 to 149.43	9.092 to 52
Index ranges	-12 ≤ h ≤ 12, -13 ≤ k ≤ 13, -21 ≤ l ≤ 22	-16 ≤ h ≤ 16, -16 ≤ k ≤ 17, -21 ≤ l ≤ 21
Reflections collected	33207	23859
Independent reflections	6673 [R_{int} = 0.0653, R_{sigma} = 0.0445]	6407 [R_{int} = 0.1240, R_{sigma} = 0.1723]
Data/restraints/parameters	6673/750/557	6407/0/409
Goodness-of-fit on F^2	1.029	0.754
Final R indexes [I>=2σ (I)]	R_1 = 0.0368, wR_2 = 0.0814	R_1 = 0.0462, wR_2 = 0.0632
Final R indexes [all data]	R_1 = 0.0574, wR_2 = 0.0905	R_1 = 0.1245, wR_2 = 0.0765
Largest diff. peak/hole / e Å^{-3}	0.49/-0.50	0.46/-0.88
CCDC access code	2081328	2081329

Figure S1. Ellipsoid representation (50% probability) of $[TcH_3(PPh_3)_4] \cdot 2$ toluene. Hydrogen atoms bonded to carbon atoms are omitted for clarity. The co-crystallized solvent toluene molecules are disordered over two positions respectively.

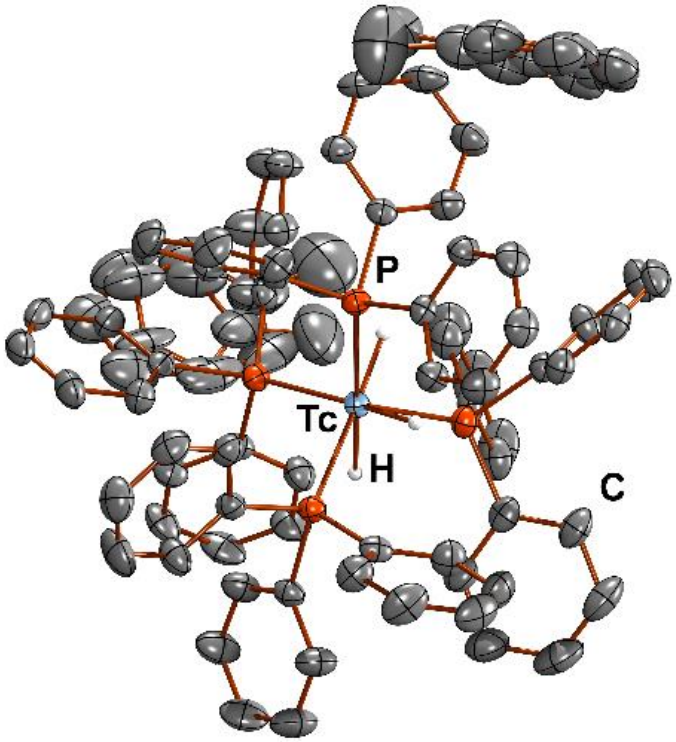

Figure S2. Ellipsoid representation (50% probability) of α-monoclinic $[TcH(CO)_3(PPh_3)_2]$. Hydrogen atoms bonded to carbon atoms are omitted for clarity.

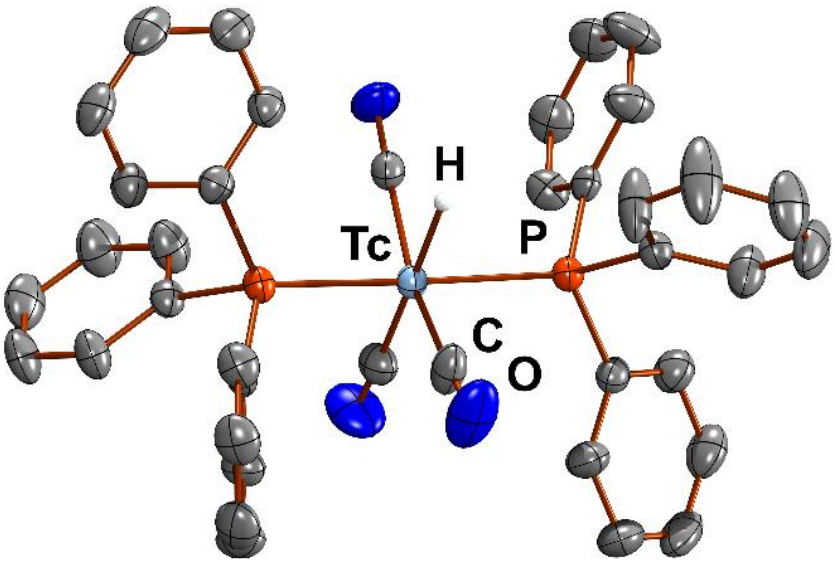

Figure S3. Ellipsoid representation (50% probability) of $[TcBr(CO)_3(PPh_3)_2]$. Hydrogen atoms are omitted for clarity. The three carbonyl ligands and the bromido ligand are disordered over two cis-orientations with a contribution of the minor component of the disorder of ca. 15%.

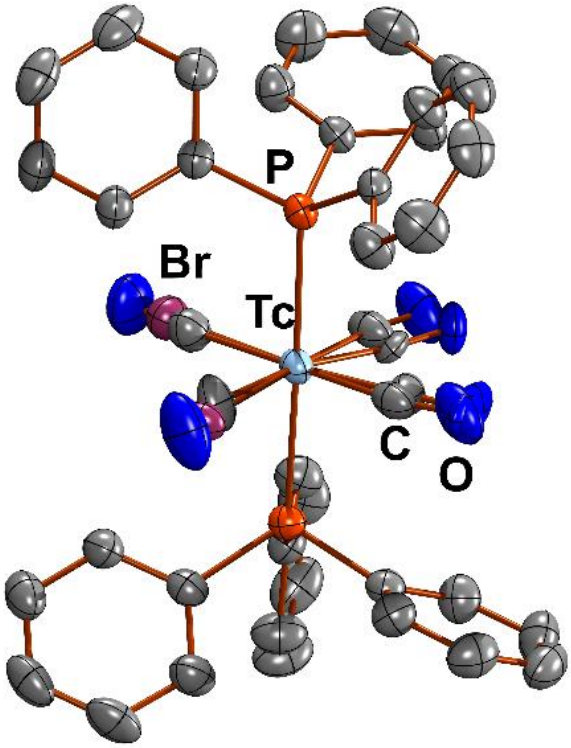

Figure S4. Ellipsoid representation (50% probability) of the structure of $[TcI(CO)_3(PPh_3)_2]$. Hydrogen atoms are omitted for clarity.

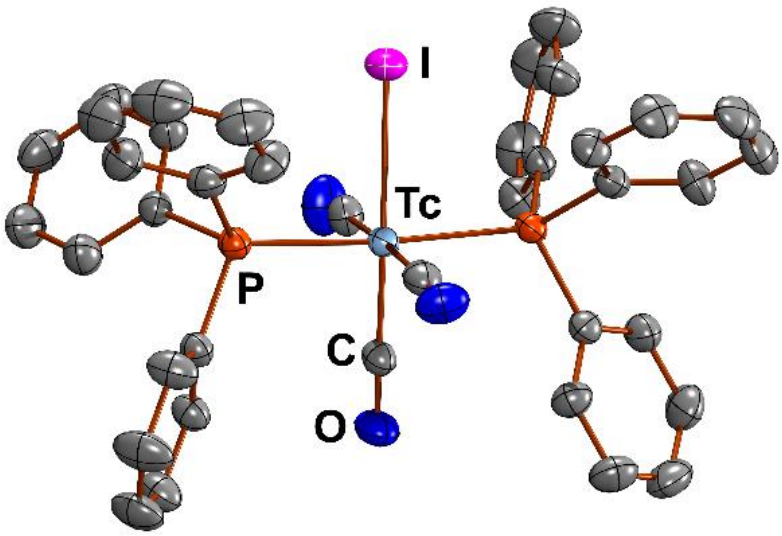

Figure S5. Ellipsoid representation (50% probability) of [Tc(η^1-O(CCF$_3$)O)(CO)$_3$(PPh$_3$)$_2$] · 0.5 toluene. Hydrogen atoms are omitted for clarity. The co-crystallized 0.25 solvent toluene molecules are disordered over two positions respectively. The CF_3 group is expectedly disordered over two positions due to unhindered rotation around the adjacent C-C bond.

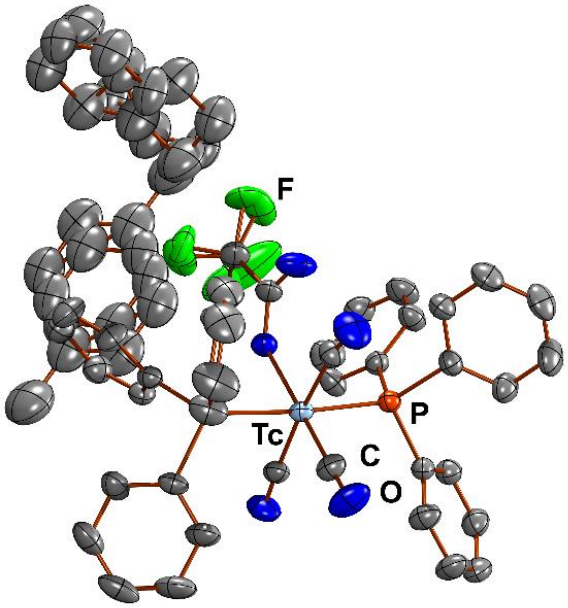

Figure S6. Ellipsoid representation (50% probability) of [Tc(η^1-O(CH)O)(CO)$_3$(PPh$_3$)$_2$] · 0.5 toluene. Hydrogen atoms are omitted for clarity.

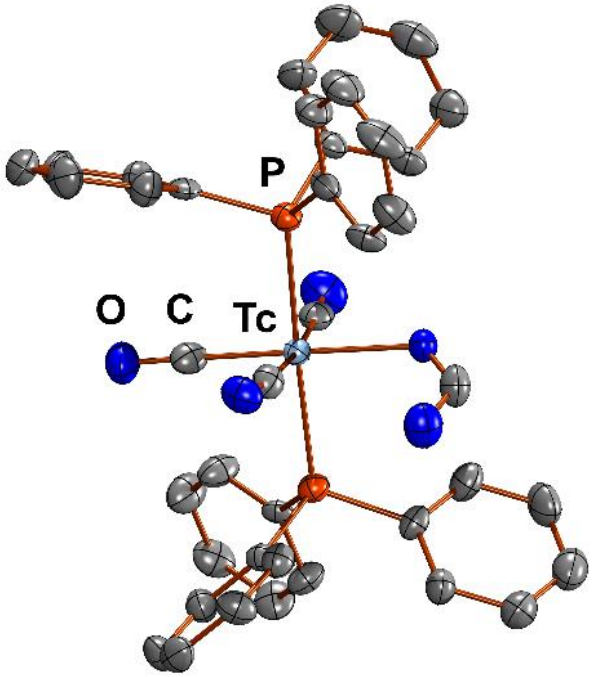

Figure S7. Ellipsoid representation (50% probability) of [Tc(η^2-OO(CH))$(CO)_2(PPh_3)_2$] · MeOH. Hydrogen atoms are omitted for clarity. The co-crystallized solvent methanol is somewhat ill-defined as it lies very close to the space-group symmetry and its methyl hydrogen atoms show a short contact to the symmetry generated methanol molecule as a possible artefact of unresolvable disorder.

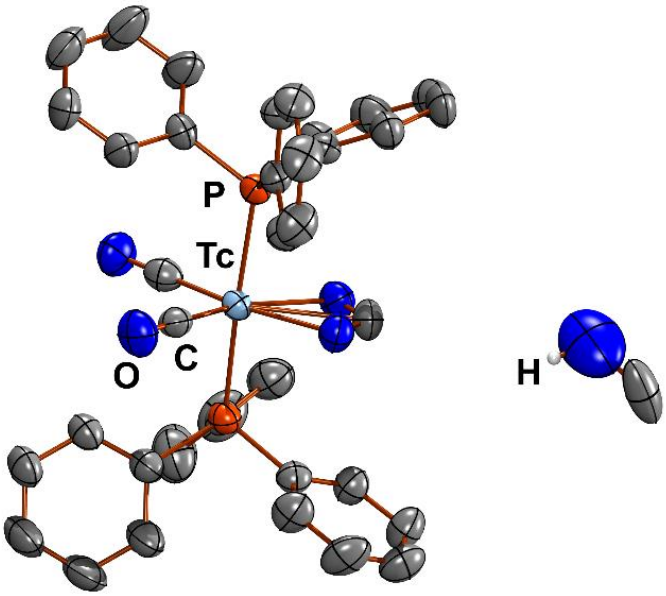

Figure S8. Ellipsoid representation (50% probability) of [Tc(η^2-OO(CCH_3))$(CO)_2(PPh_3)_2$]. Hydrogen atoms are omitted for clarity. One of the phenyl rings in one of the PPh_3 ligands is disordered over two positions.

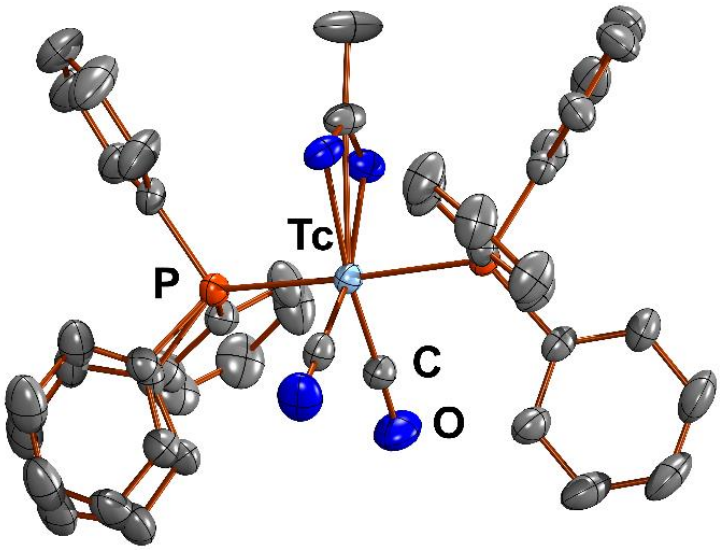

Figure S9. Ellipsoid representation (50% probability) of [Tc(η^2-OO(CPh))$(CO)_2(PPh_3)_2$]. Hydrogen atoms are omitted for clarity.

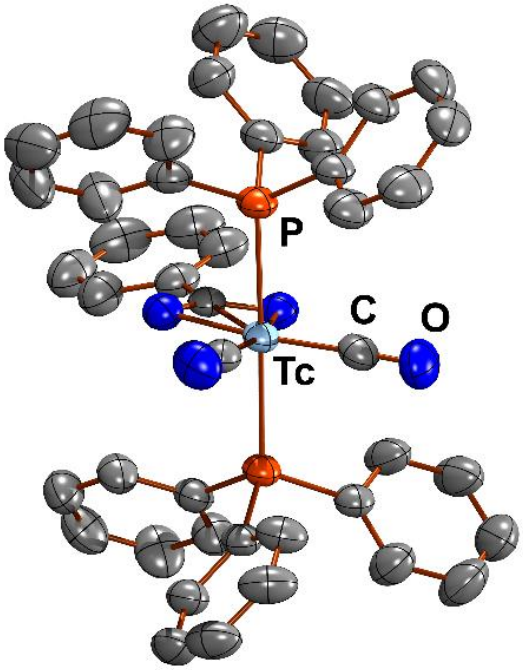

Figure S10. Ellipsoid representation (50% probability) of [Tc(η^2-Et_2btu)$(CO)_2(PPh_3)_2$]. Hydrogen atoms are omitted for clarity.

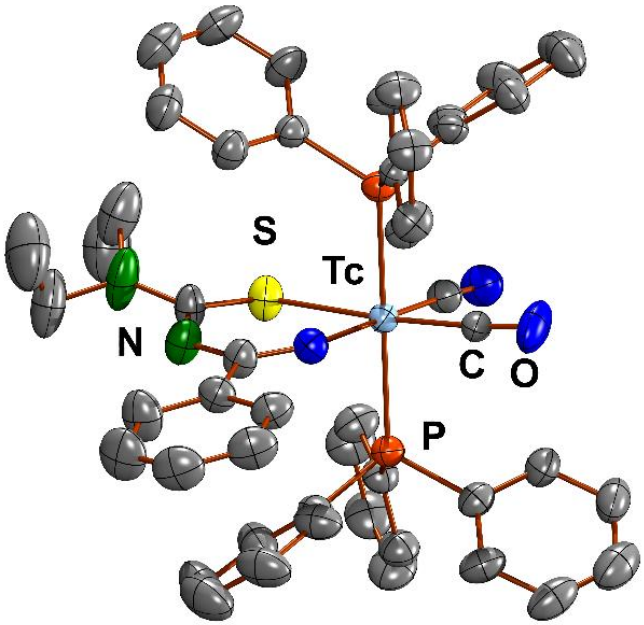

Figure S11. Ellipsoid representation (50% probability) of [Tc(η^2-oxH)$(CO)_2(PPh_3)_2$]. Hydrogen atoms are omitted for clarity. The hydrogen atom on the hydrogenoxalato ligand is disordered over the two oxygen atoms and respectively forms hydrogen bonds to the adjacent non-protonated oxygen atom of the next hydrogenoxalato ligand of the neighbouring molecule. However, the hydrogen atom positions were not found in the density map and placed in accordance with possible hydrogen bonds. Therefore, the hydrogen bonds are arbitrary and their parameters are not discussed. The structure was refined as a twin.

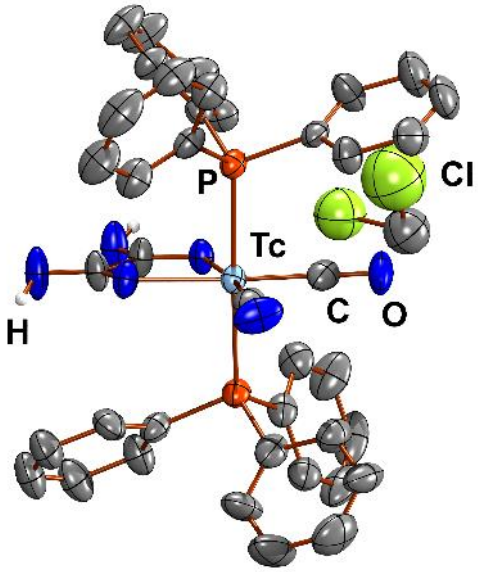

Figure S12. Ellipsoid representation (50% probability) of $HNEt_3$[Tc(η^2-ox)$(CO)_2(PPh_3)_2$]. Hydrogen atoms are omitted for clarity. A hydrogen bond is formed between the contact ion pair. However, the relevant hydrogen atom was placed on the nitrogen atom at a calculated position as it was not located in the density map. Thus, the parameters in this hydrogen bond are rather arbitrary and not discussed further. The structure was refined as a twin.

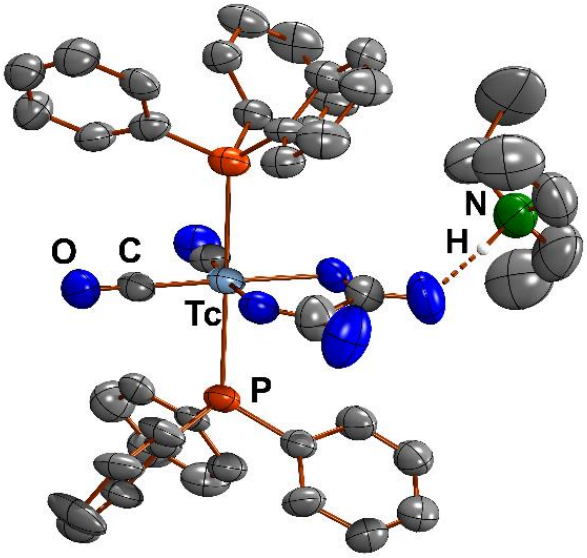

Figure S13. Ellipsoid representation (50% probability) of $[Tc_2(\mu^2\text{-}\eta^2\text{-ox})(CO)_6(OPPh_3)_2]$. Hydrogen atoms are omitted for clarity. Symmetry code for the generation of equivalent atoms: 1-x, 1-y, -z. The molecule is symmetric to inversion and lies on the crystallographic space group symmetry.

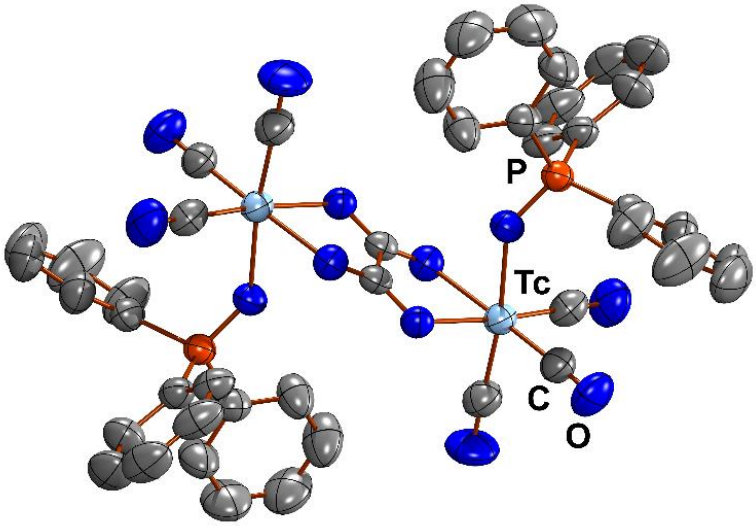

Figure S14. Ellipsoid representation (50% probability) of $[\{Tc(CO)_3\}_3(\mu^3\text{-OH})(\mu^2\text{-O(SePh)O})_3\{Tc(CO)_3\}] \cdot (OPPh_3) \cdot 0.25(\text{pentane})$. Hydrogen atoms are omitted for clarity. Symmetry code for the generation of equivalent atoms: -x+1, y, -z+3/2. The co-crystallized solvent pentane lies on the crystallographic space group symmetry. A hydrogen bond is established between the phosphine oxide moiety and the hydroxido group of the cluster. The hydroxido hydrogen atom was located in the density map and refined freely. Hydrogen bond parameters: O31—H31···O41 Å, O31-H 0.74(4) Å, H…O41 1.84(4) Å, O31…O41 2.575(3) Å, O31-H…O41 177.4°.

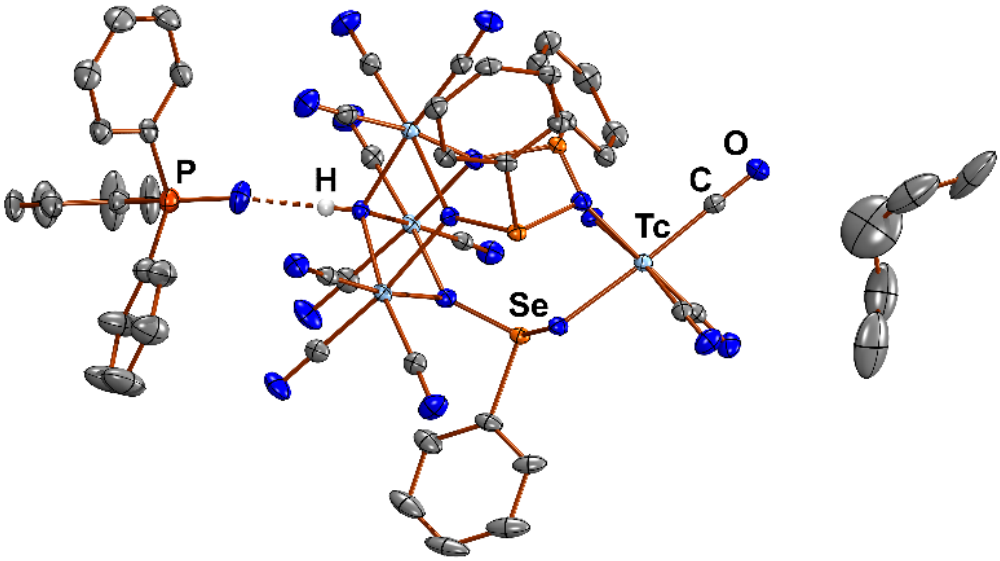

Figure S15. Ellipsoid representation (50% probability) of $[TcCl_3(PMe_3)_3] \cdot OPPh_3$. Hydrogen atoms are omitted for clarity. Selected bond lengths [Å]: P1—Tc 12.472(1), P2—Tc1 2.451(1), P3—Tc1 2.394(1), Cl1—Tc1 2.333(1), Cl2—Tc1 2.475(1), Cl3—Tc1 2.346(1).

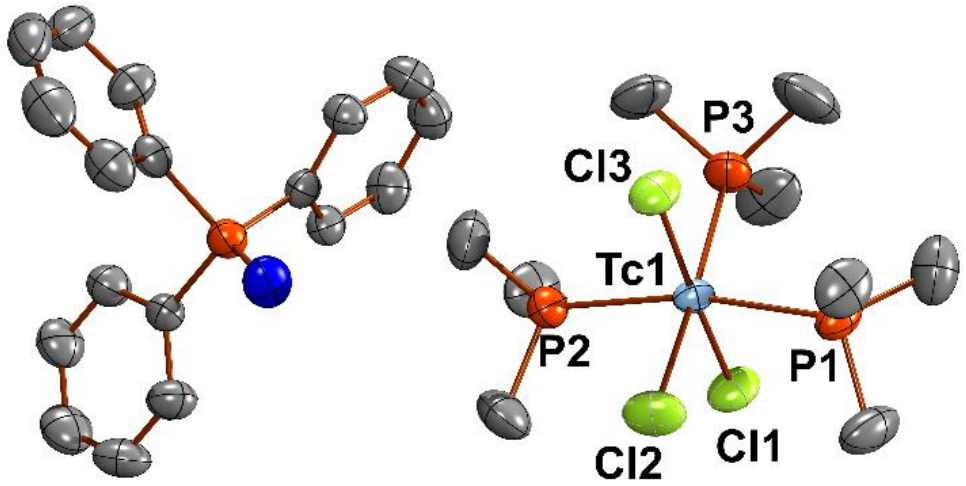

Figure S16. Ellipsoid representation (50% probability) of β-monoclinic $[TcH(CO)_3(PPh_3)_2]$. Hydrogen atoms bonded to carbon atoms are omitted for clarity.

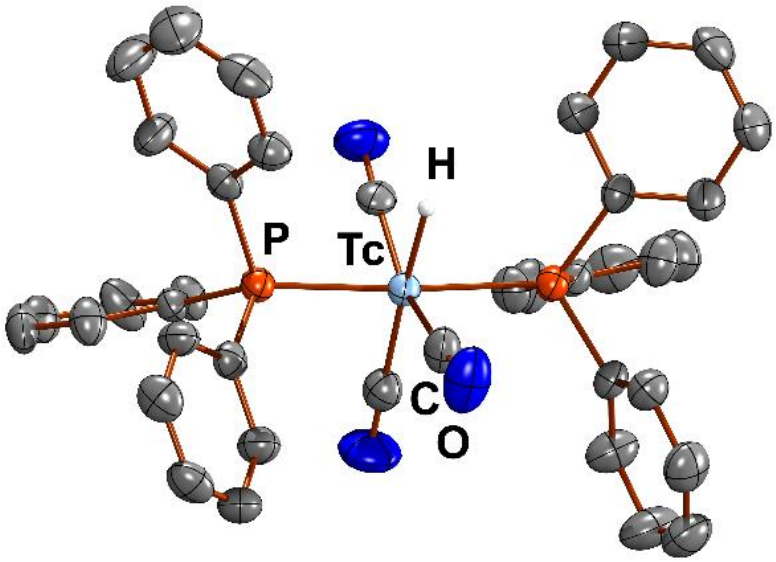

Figure S17. Ellipsoid representation (50% probability) of triclinic $[TcH(CO)_3(PPh_3)_2]$. Hydrogen atoms bonded to carbon atoms are omitted for clarity. All phenyl rings in one of the PPh_3 ligands are disordered. In addition, the central Tc atom is disordered. Also, the three carbonyl ligands and the hydrido ligand are disordered over two *cis*-orientations. The hydrido ligand was not taken from the density map but placed at a fixed distance to the technetium atom. The thermal displacement parameter of the hydrido ligand was set to a fixed value.

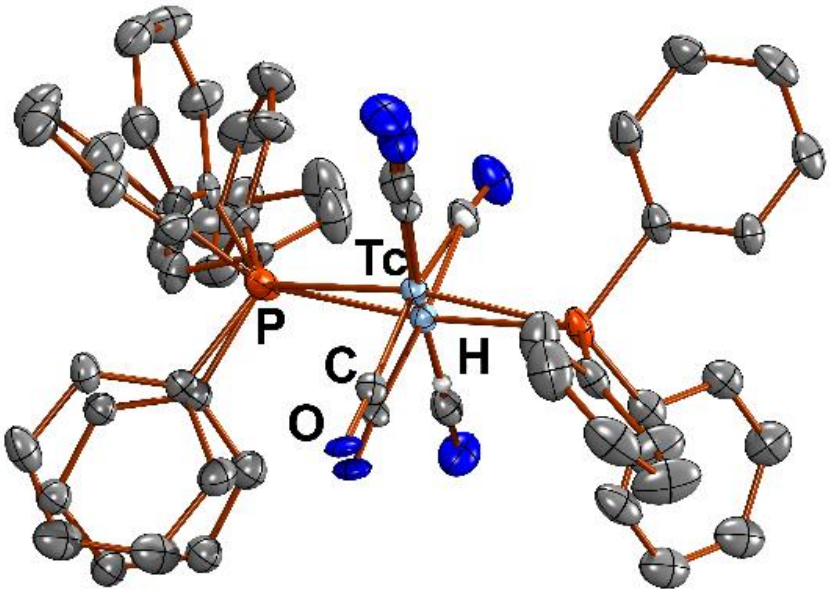

Part 2: Computational data

DFT calculations were performed on the high-performance computing systems of the Freie Universität Berlin ZEDAT (Curta)[1] using the program package GAUSSIAN 16.[2] The gas phase and solution geometry optimizations were performed using coordinates derived from the X-ray crystal structures using GAUSSVIEW and Avogadro.[3,4] The polarizable continuum model (PCM) with the integral equation formalism variant (IEFPCM) was used to implicitly simulate the solvent dichloromethane. The calculations were performed with the hybrid density functional B3LYP.[5-7] The double-ζ pseudopotential LANL2DZ basis set with the respective effective core potential (ECP) was applied to P.[8] The Stuttgart relativistic small core basis set with the corresponding ECP was applied to Tc.[9,10] The 6-311+G** basis set was used to model all other atoms in the calculations regarding the carbonyl complexes.[11,12] The 6-311G** basis set was applied for C and H in the calculation of the trihydrido complexes.[11] Only for the assessment of the energetic differences in $[TcH_3(PMe_3)_4]$ isomers, the all-electron basis set x2c-TZVPPall-s was employed for all atoms.[13] The system size of the other complexes quickly became prohibitive for the use of all-electron basis sets. All basis sets as well as the ECPs were obtained from the EMSL database.[14] Frequency calculations after the optimizations confirmed the convergence. No negative frequencies were obtained for the given optimized geometries of all compounds. The entropic contribution to the free energy was corrected for low-energy modes using the quasi-harmonic approximation of Grimme[15] as implemented in the freely accessible python code *GoodVibes* of Funes-Ardoiz and Paton with a cut-off at 300 cm^{-1}.[16] Further analysis of orbitals, charges, electron localization function (ELF), etc. was performed with the free multifunctional wavefunction analyzer *Multiwfn*.[17] Visualization of the electrostatic potential maps was done with GAUSSVIEW.[3]

Figure S18. Electron localization function maps of trihydrides. ELF of $[TcH_3(PPh_3)_4]$ (**A**), $[TcH_3(PMe_3)_4]$-COC (**B**) and $[TcH_3(PMe_3)_4]$-PBP (**C**) on ECP-calculation level as well as the all-electron calculation for $[TcH_3(PMe_3)_4]$-PBP (**D**) with topological features; sections are provided through the H,H,H plane. It is evident from the green density hills, that albeit no real H-H bonds are observed, the electron density is somewhat shared between the hydrido ligands. In the capped octahedral structures, some delocalization between all three hydrido ligands over the Tc-P anti-bonding orbitals (see pictures below) is observed as also indicated by NBO and ADNDP checks. COC = capped octahedron; PBP = pentagonal bipyramid

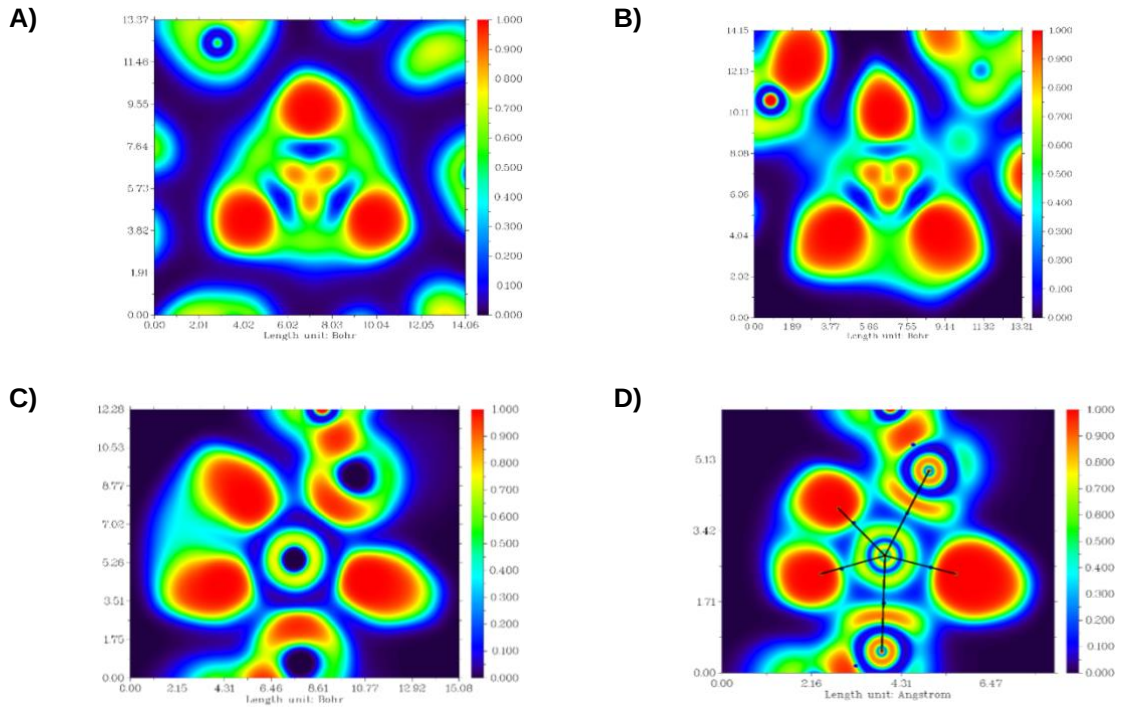

Figure S19. ELF of the all-electron calculation for $[TcH_3(PMe_3)_4]$-PBP with topological features; cutting through the close contact of two hydrido ligands and the one remaining hydrido ligands. The green area on the opposite site of the isolated hydrido ligand indicates some interaction between the two remaining hydrido ligands. PBP = pentagonal bipyramid.

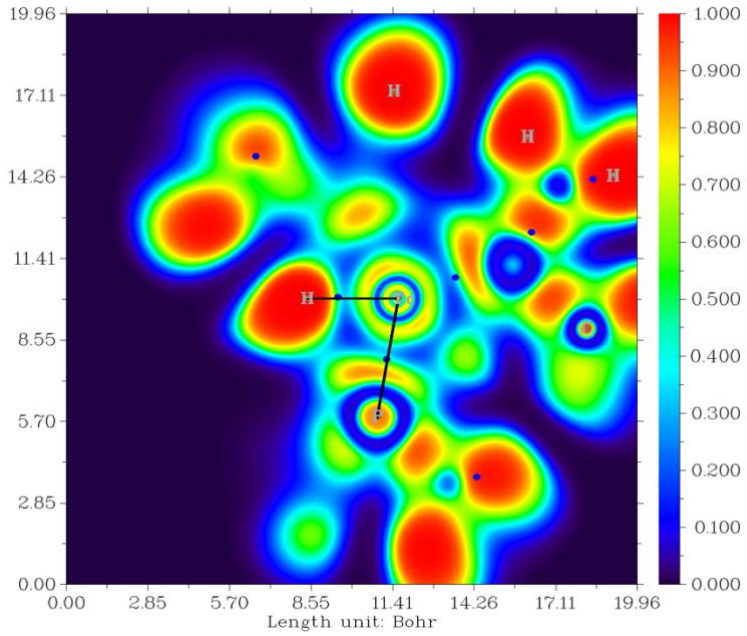

Figure S20. ELF of the all-electron calculation for $[TcH_3(PMe_3)_4]$-PBP with topological features; cutting through a Tc,P,H plane. It is evident that electron density is not only shared between the hydrido ligands but also with the adjacent phosphorus donors. PBP = pentagonal bipyramid.

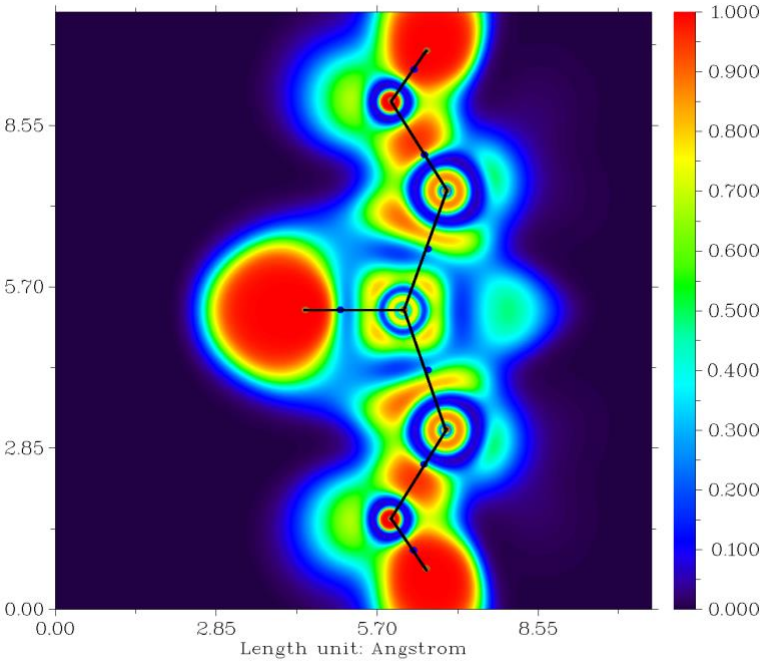

Figure S21. ELF of $[TcH_3(PMe_3)_4]$-COC on ECP-level; cut through the Tc,H,H planes. COC = capped octahedron

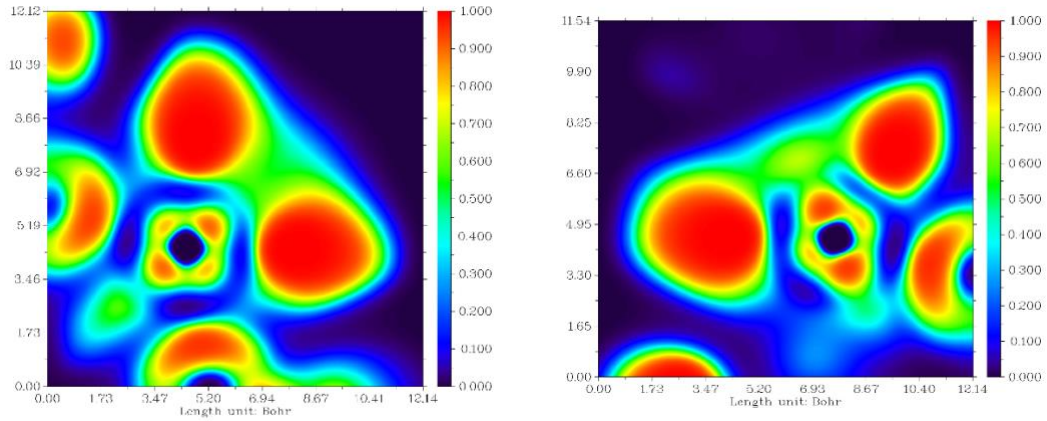

Table S2. Calculated free energies and free energy differences between the two isomers of $[TcH_3(PMe_3)_4]$.

	x2c-TZVPPall-s	Stuttgart1997, lanl2dz, 6-311G**
Δ*G*(COC)	-6004.26753	-587.338368
Δ*G*(PBP)	-6004.27998	-587.333548
ΔΔ*G*	0.012457	-0.00482
ΔΔ*G* [kJ/mol]	7.81688584	-3.02459579

COC = capped octrahedron, PBP = pentagonal bipyramid

Figure S22. Theoretical IR spectrum of $[TcH_3(PPh_3)_2(PMe_3)_2]$.Line-broadening: 30 cm^{-1}; broadening function: Pseudo-Voigt. Individual transitions are indicated by lines.

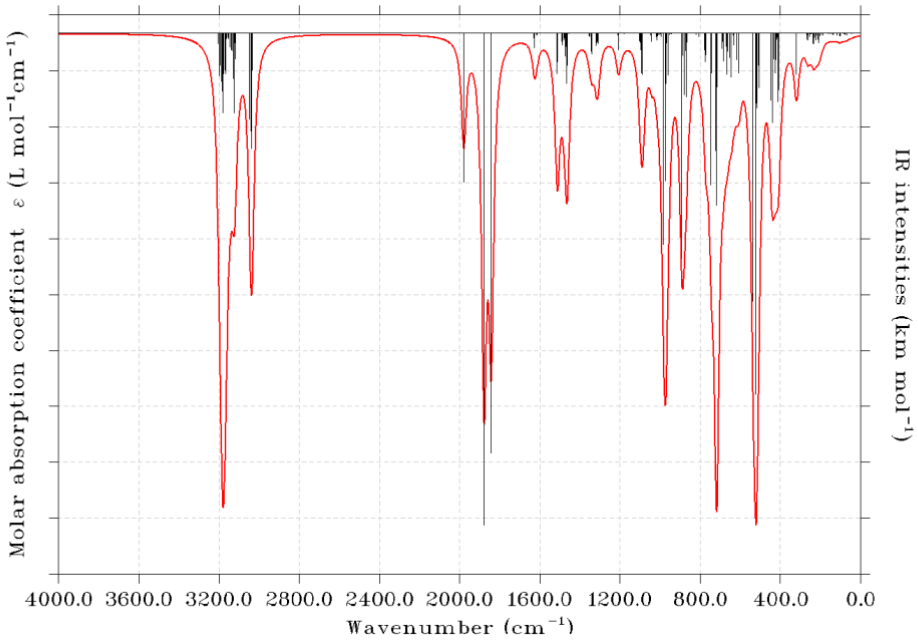

Table S3. Calculated free energies and free energy differences before Grimme-type correction values given are in a.u. unless stated otherwise.

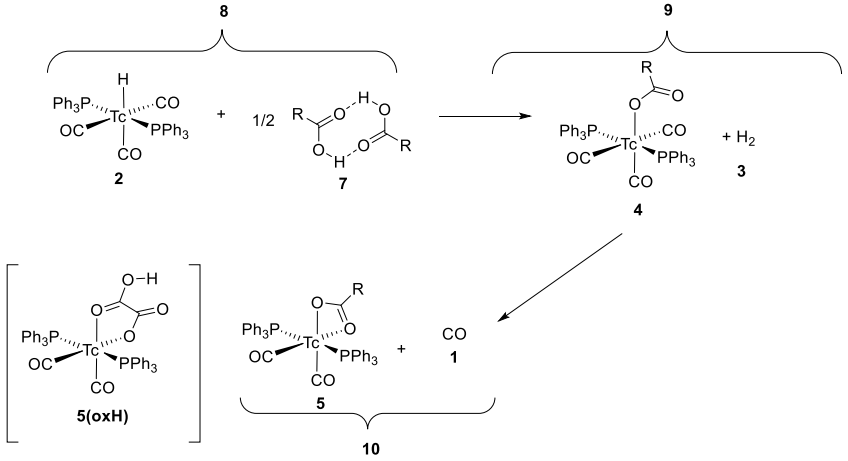

ΔG(CO); **1**	-113.363793	ΔG([TcH(CO)$_3$(PPh$_3$)$_2$]); **2**	-1824.38274	ΔG(H$_2$); **3**	-1.181137
	H	CH_3	CF_3	CO_2	Ph
ΔG([Tc(η^1-O(CR)O)(CO)$_3$(PPh$_3$)$_2$]); **4**	-2013.03122	-2052.33755	-2350.18462	-2201.65582	-2244.0736
ΔG([Tc(η^2-OO(CR))(CO)$_2$(PPh$_3$)$_2$]) ; **5**	-1899.66644	-1938.97837	-2236.81462	-2088.28925	-2130.71427
ΔG({O(CR)OH}$_2$); **6**	-379.647761	-458.273791	-1053.92757	-756.88204	-841.744723
1/2·**6**; **7**	-189.823881	-229.136896	-526.963783	-378.44102	-420.872362
7+**2**; **8**	-2014.20662	-2053.51963	-2351.34652	-2202.82376	-2245.2551
4+**3**; **9**	-2014.21235	-2053.51869	-2351.36576	-2202.83696	-2245.25474
$\Delta\Delta G$(**9**-**8**)	-0.0057365	0.0009475	-0.019238	-0.013201	0.0003585
$\Delta\Delta G$(**9**-**8**) [kcal/mol]	-3.5997081	0.59456523	-12.0720273	-8.28375257	0.22496215
$\Delta\Delta G$(**9**-**8**) [kJ/mol]	-15.0611787	2.48766091	-50.5093621	-34.6592207	0.94124162
5+**1**; **10**	-2013.03023	-2052.34216	-2350.17841	-2201.65304	-2244.07806
$\Delta\Delta G$(**10**-**4**)	0.000988	-0.004616	0.006208	0.002783	-0.004455
$\Delta\Delta G$(**10**-**4**) [kcal/mol]	0.61997936	-2.89658373	3.89557881	1.74635887	-2.79555471
$\Delta\Delta G$(**10**-**4**) [kJ/mol]	2.59399364	-12.1193063	16.2991018	7.3067655	-11.6966009
ΔG([Tc(η^2-O(CO)(CO)O)(CO)$_2$(PPh$_3$)$_2$]) ; **5(oxH)**				-2088.29448	
$\Delta\Delta G$(**5**-**5(oxH)**)				-0.005234	
$\Delta\Delta G$(**5**-**5(oxH)**) [kcal/mol]				-3.28438459	
$\Delta\Delta G$(**5**-**5(oxH)**) [kJ/mol]				-13.7418651	
5(oxH)+**1**; **10(oxH)**				-2201.65827	
$\Delta\Delta G$(**10(oxH)**-**4**)				-0.002451	
$\Delta\Delta G$(**10(oxH)**-**4**) [kcal/mol]				-1.53802572	
$\Delta\Delta G$(**10(oxH)**-**4**) [kJ/mol]				-6.43509962	

Figure S23. Free energy differences before Grimme-type correction.

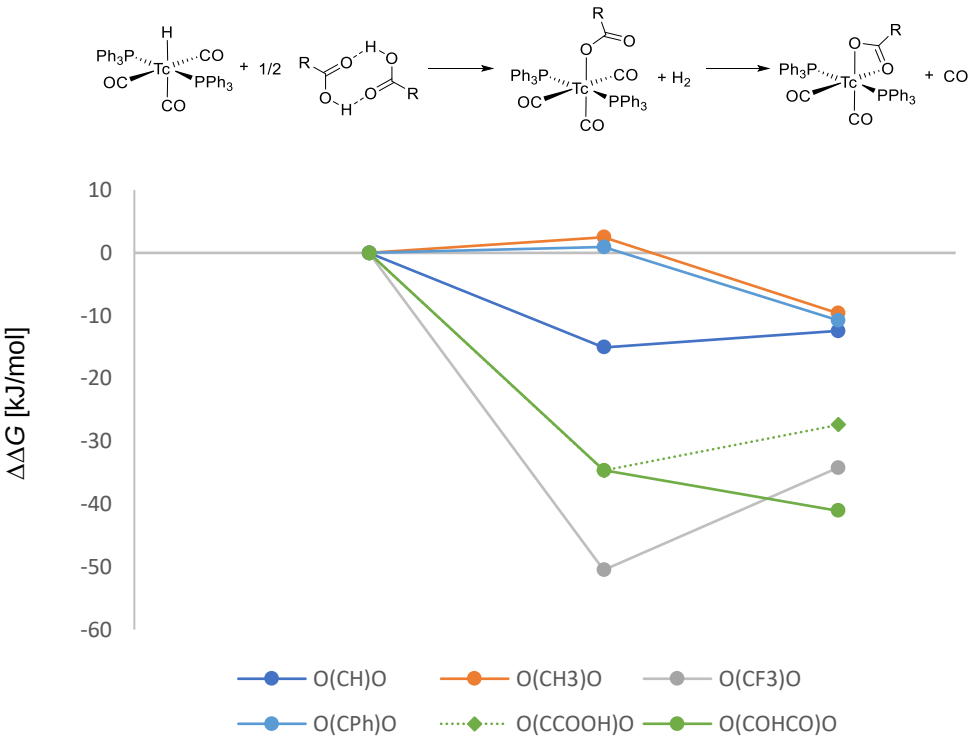

Table S4. Calculated free energies and free energy differences after Grimme-type correction values given are in a.u. unless stated otherwise.

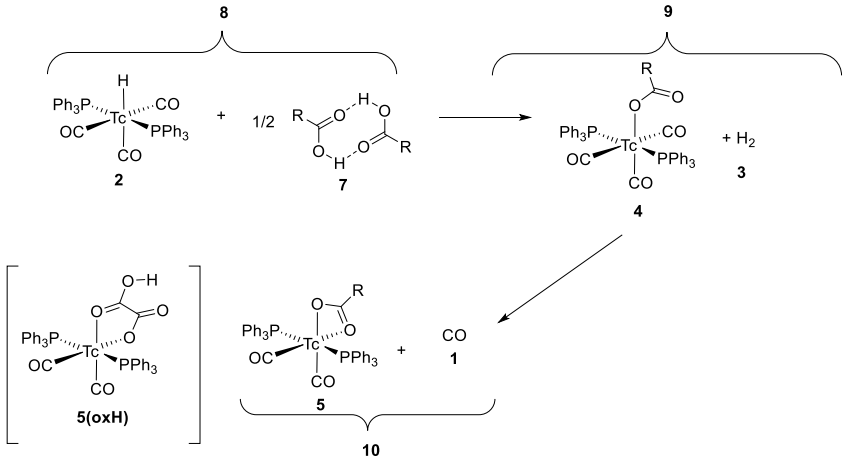

ΔG(CO); **1**	-113.363793	ΔG([TcH(CO)$_3$(PPh$_3$)$_2$]); **2**	-1824.36942	ΔG(H$_2$); **3**	-1.181137
	H	CH_3	CF_3	CO_2	Ph
ΔG([Tc(η^1-O(CR)O)(CO)$_3$(PPh$_3$)$_2$]); **4**	-2013.01801	-2052.32398	-2350.1695	-2201.64111	-2244.05845
ΔG([Tc(η^2-OO(CR))(CO)$_2$(PPh$_3$)$_2$]) ; **5**	-1899.65344	-1938.96433	-2236.7997	-2088.27462	-2130.69905
ΔG({O(CR)OH}$_2$); **6**	-379.647301	-458.271435	-1053.92364	-756.878495	-841.740635
1/2·**6**; **7**	-189.823651	-229.135718	-526.961821	-378.439248	-420.870318
7+**2**; **8**	-2014.19307	-2053.50514	-2351.33124	-2202.80867	-2245.23974
4+**3**; **9**	-2014.19915	-2053.50511	-2351.35064	-2202.82224	-2245.23959
ΔG(**9**-**8**)	0.0060735	-2.75E-05	0.019396	0.0135745	-0.0001535
ΔG(**9**-**8**) [kcal/mol]	3.81117879	-0.01725651	12.1711738	8.51812735	-0.0963227
ΔG(**9**-**8**) [kJ/mol]	15.9459721	-0.07220124	50.924191	35.6398449	-0.40301419
5+**1**; **10**	-2013.01723	-2052.32813	-2350.16349	-2201.63841	-2244.06285
$\Delta\Delta G$(**10**-**4**)	0.000777	-0.004152	0.006011	0.002698	-0.004398
$\Delta\Delta G$(**10**-**4**) [kcal/mol]	0.48757486	-2.60541934	3.77195945	1.69302056	-2.75978667
$\Delta\Delta G$(**10**-**4**) [kJ/mol]	2.04001322	-10.9010745	15.7818783	7.08359803	-11.5469474
ΔG([Tc(η^2-O(CO)(CO)O)(CO)$_2$(PPh$_3$)$_2$]) ; **5(oxH)**				-2088.281	
$\Delta\Delta G$(**5**-**5(oxH)**)				-0.006386	
$\Delta\Delta G$(**5**-**5(oxH)**) [kcal/mol]				-4.0072755	
$\Delta\Delta G$(**5**-**5(oxH)**) [kJ/mol]				-16.7664407	
5(oxH)+**1**; **10(oxH)**				-2201.6448	
$\Delta\Delta G$(**10(oxH)**-**4**)				-0.003688	
$\Delta\Delta G$(**10(oxH)**-**4**) [kcal/mol]				-2.31425494	
$\Delta\Delta G$(**10(oxH)**-**4**) [kJ/mol]				-9.68284267	

Figure S24. Free energy differences after Grimme-type correction.

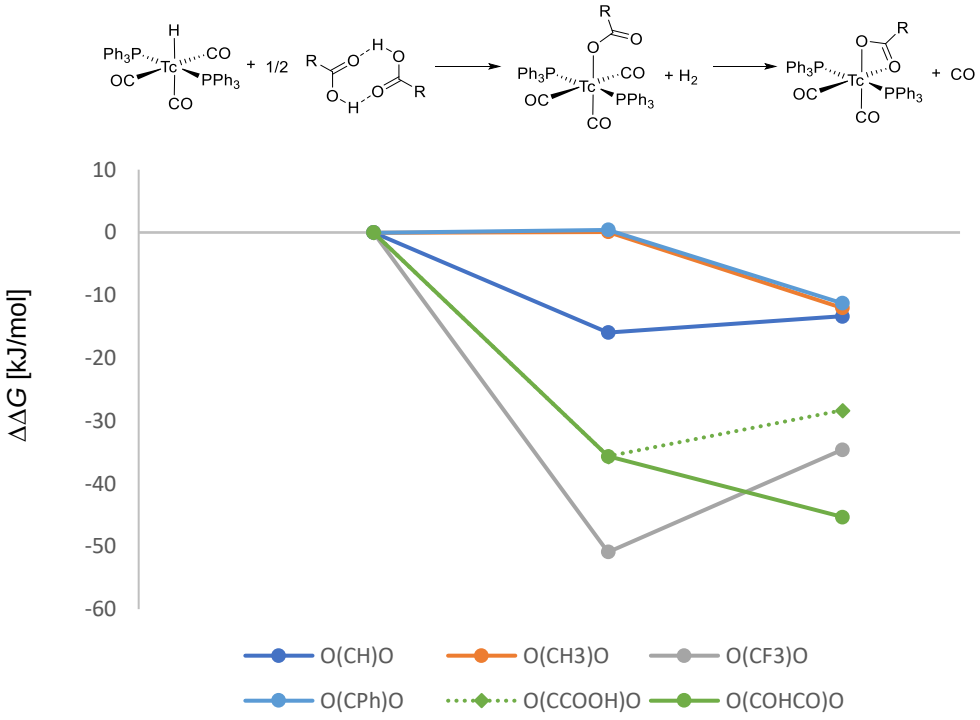

Part 3: Spectral data

Spectragryph 1.2.8 was used to visualize the IR spectra.[18]

Figure S25. Hydride part of the ^{1}H NMR spectrum of $[TcH_3(PPh_3)_4]$.

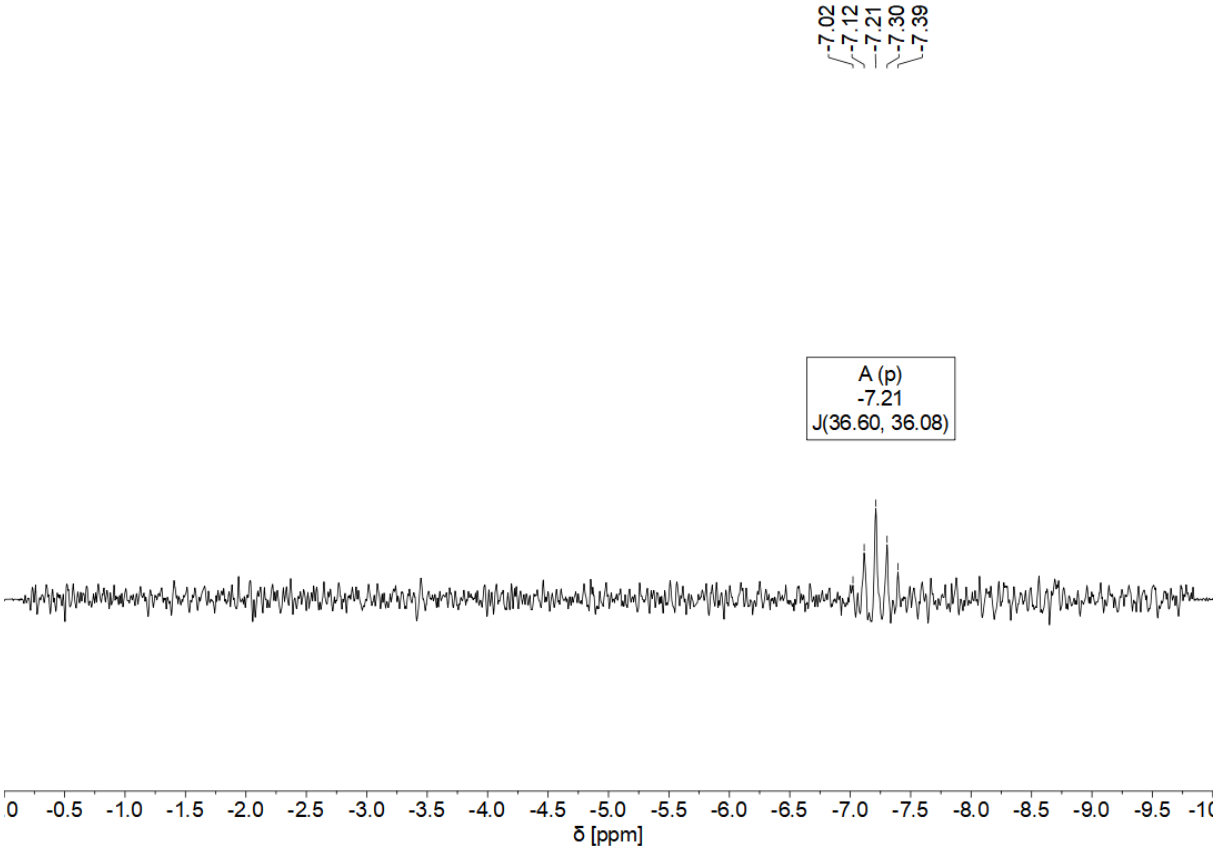

Figure S25. IR spectrum of $[TcH_3(PPh_3)_4]$.

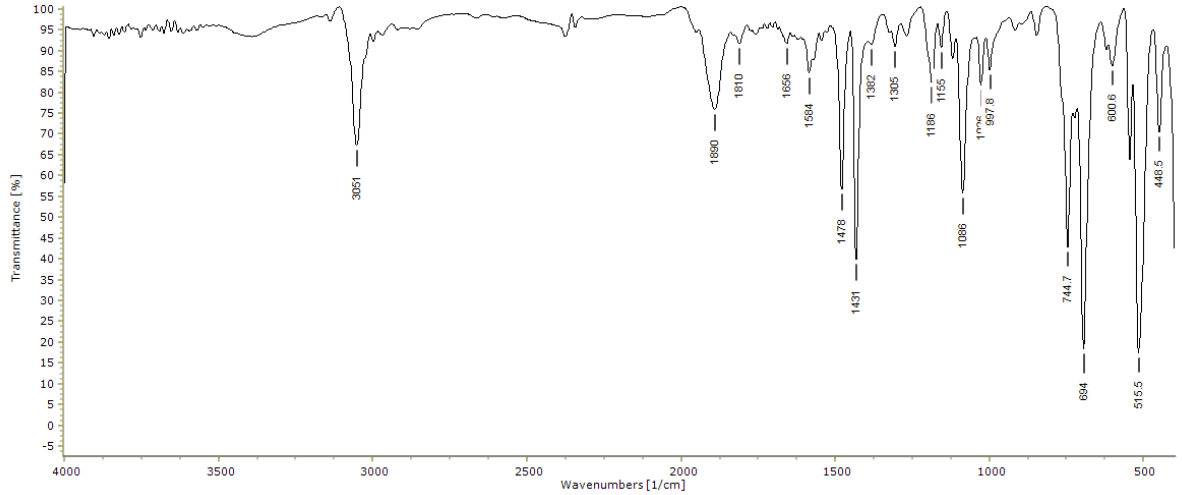

Figure S26. ^{1}H NMR spectrum of $[TcH_3(PPh_3)_2(PMe_3)_2]$.

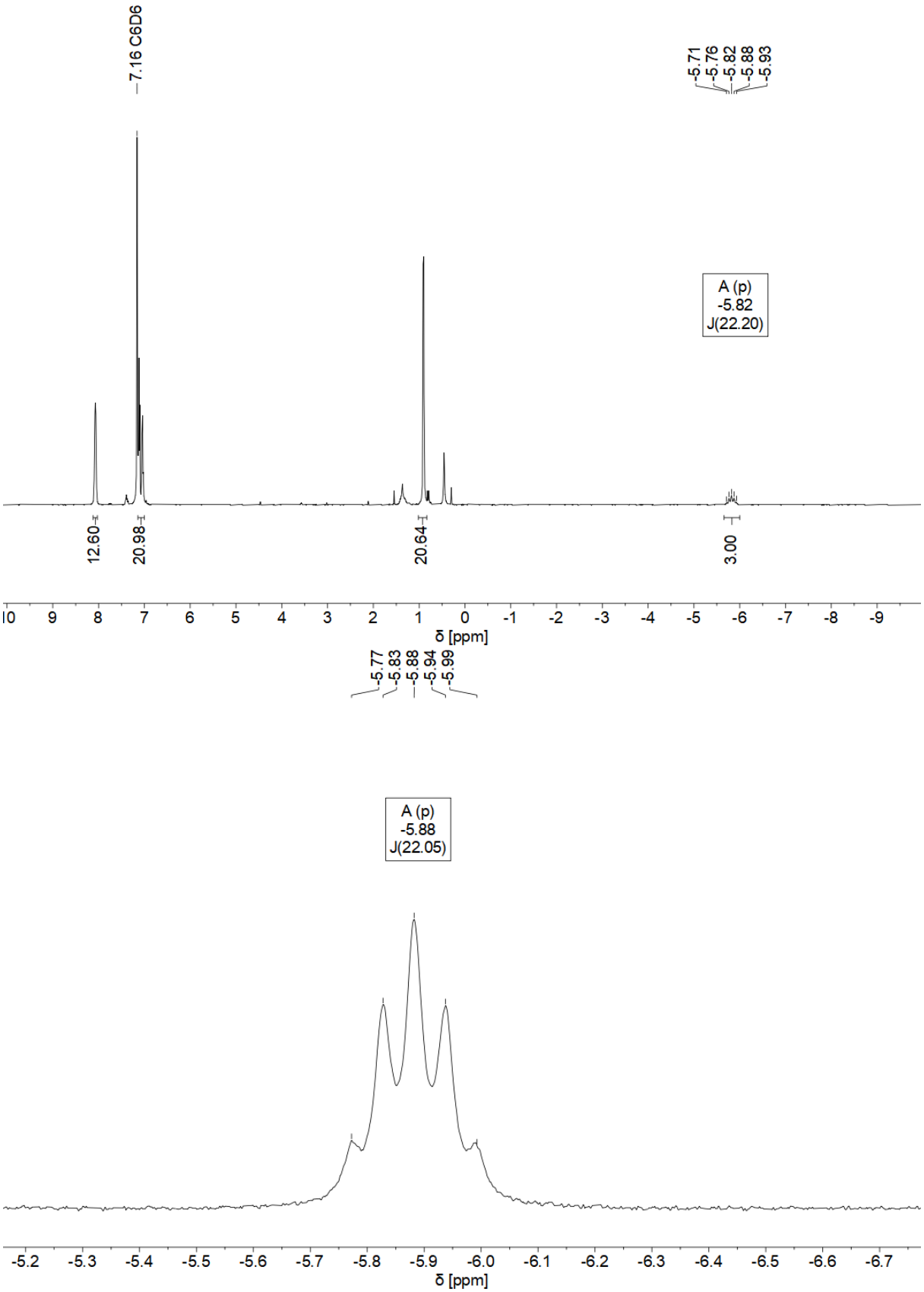

Figure S27. ^{99}Tc NMR spectrum of $[TcH_3(PPh_3)_2(PMe_3)_2]$.

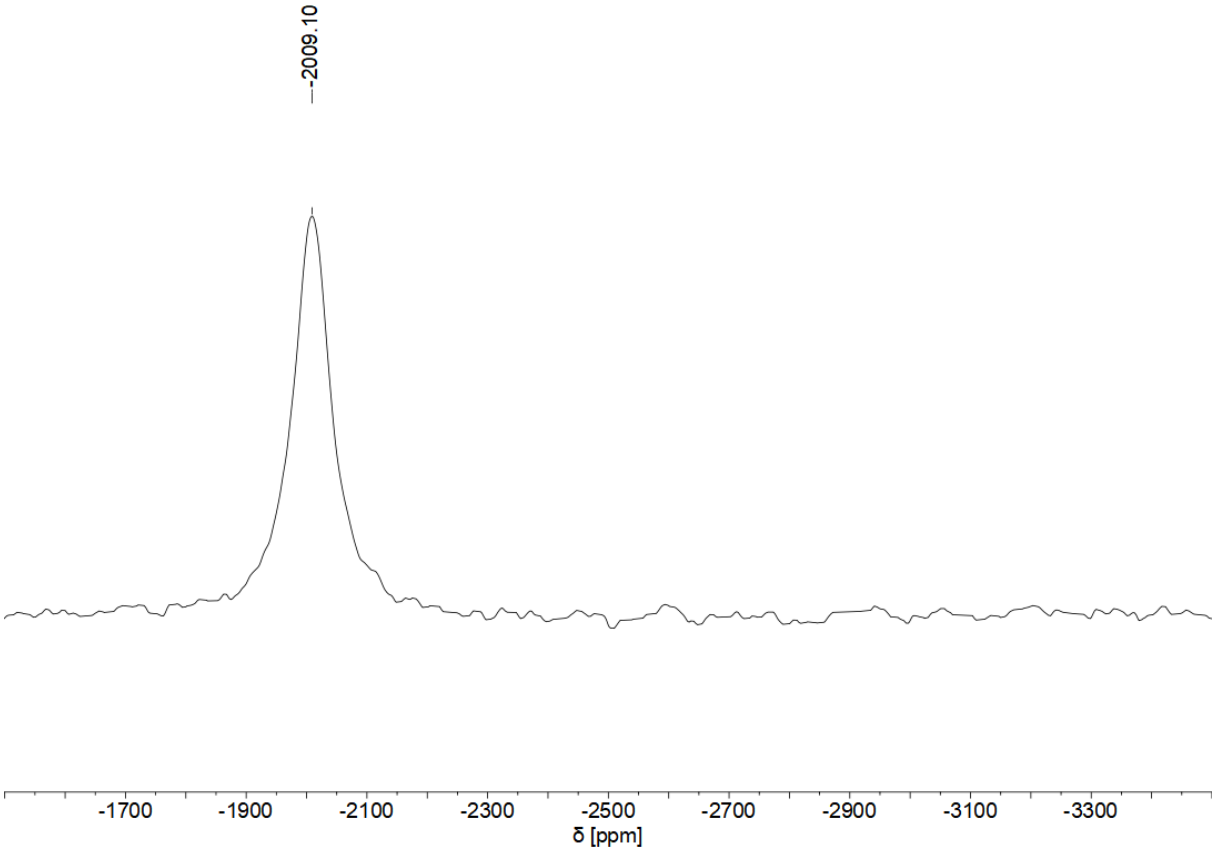

Figure S28. IR spectrum of $[TcH_3(PPh_3)_2(PMe_3)_2]$.

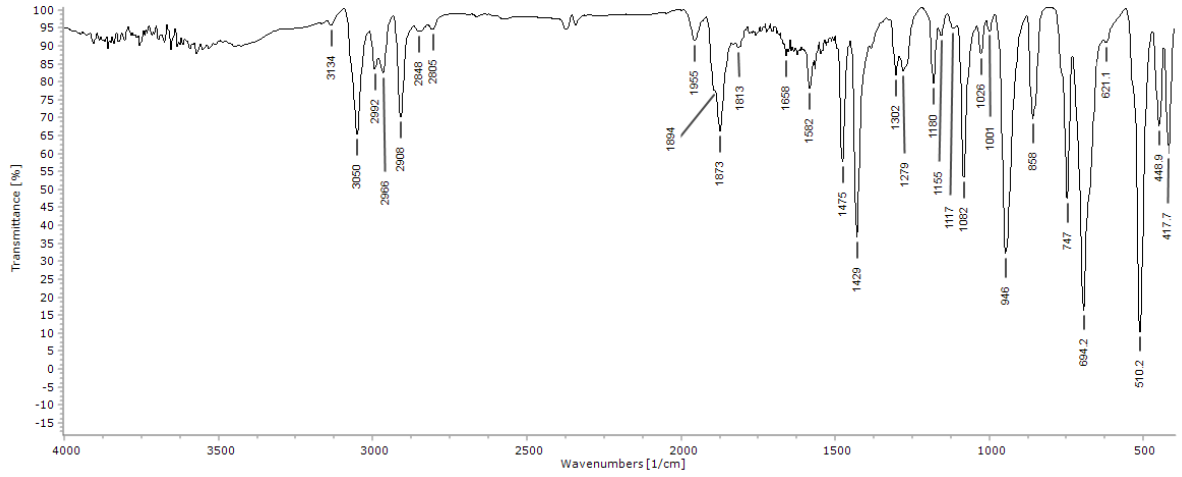

Figure S29. ^{1}H NMR spectrum of $[TcH(CO)_3(PPh_3)_2]$.

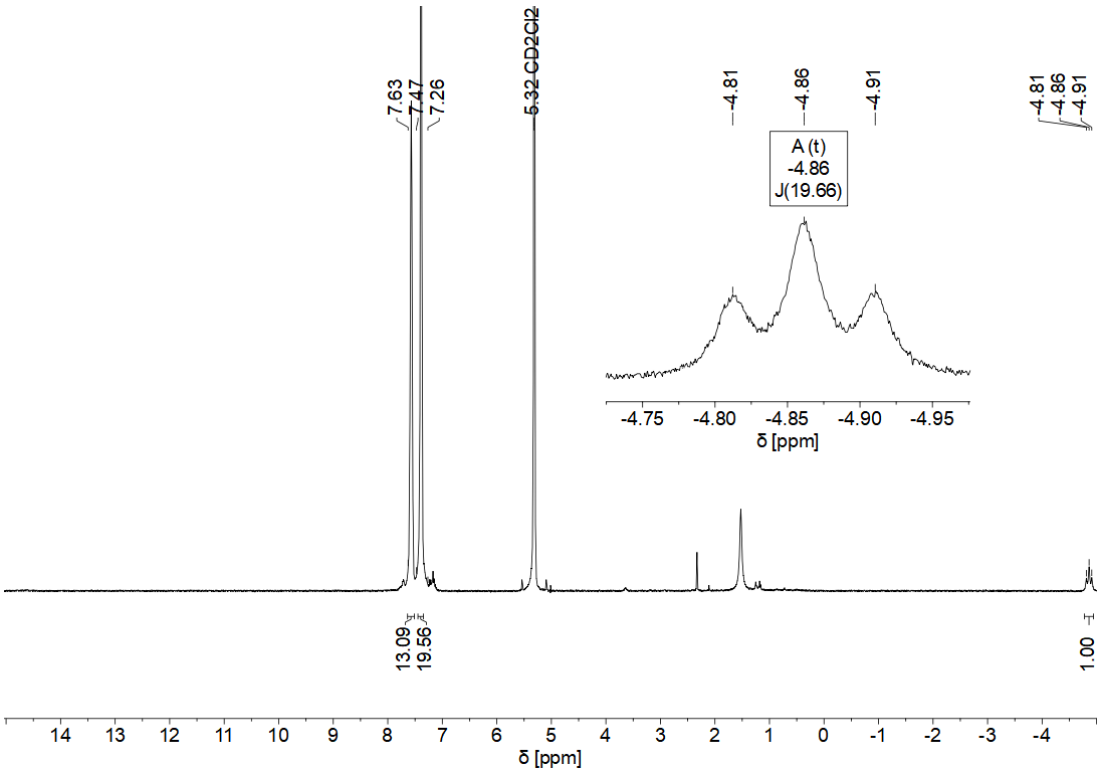

Figure S30. $^{1}H\{^{31}P\}$ NMR spectrum of $[TcH(CO)_3(PPh_3)_2]$.

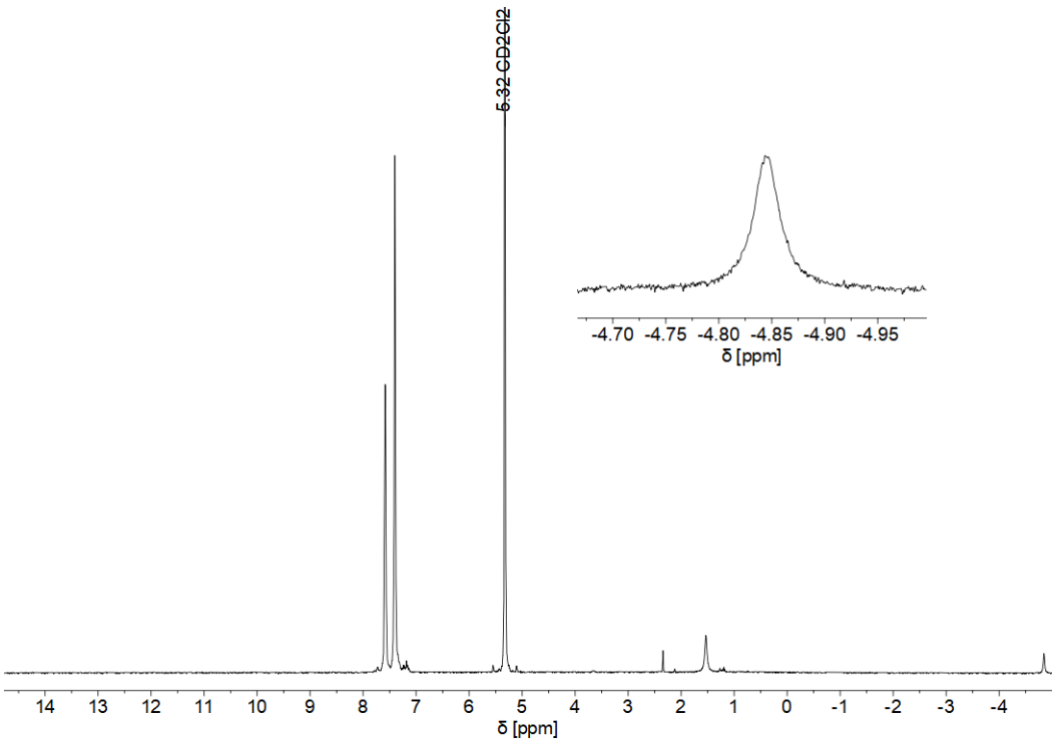

Figure S31. ^{99}Tc NMR spectrum of $[TcH(CO)_3(PPh_3)_2]$.

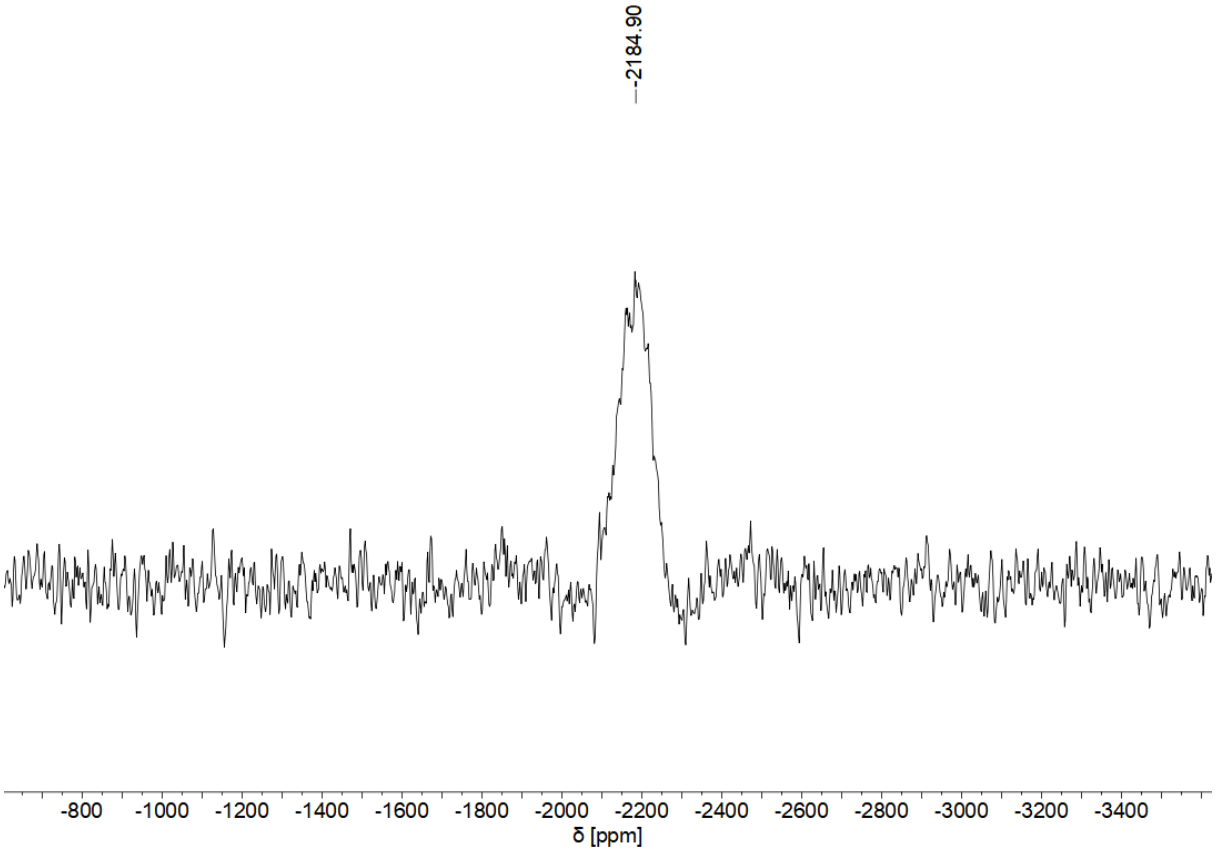

Figure S32. IR spectrum of $[TcH(CO)_3(PPh_3)_2]$.

IR

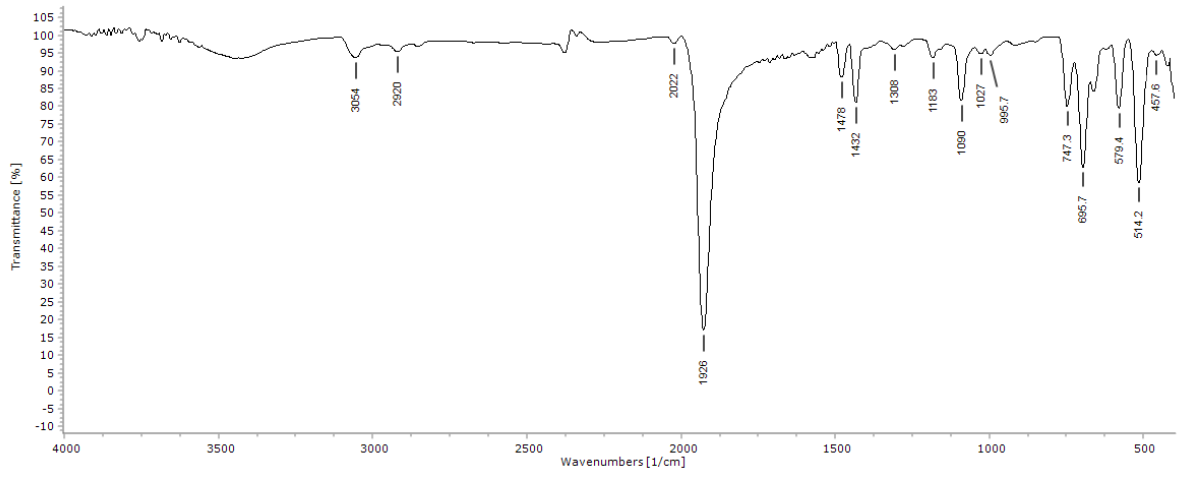

Figure S33. ^{1}H NMR spectrum of $[TcCl(CO)_3(PPh_3)_2]$.

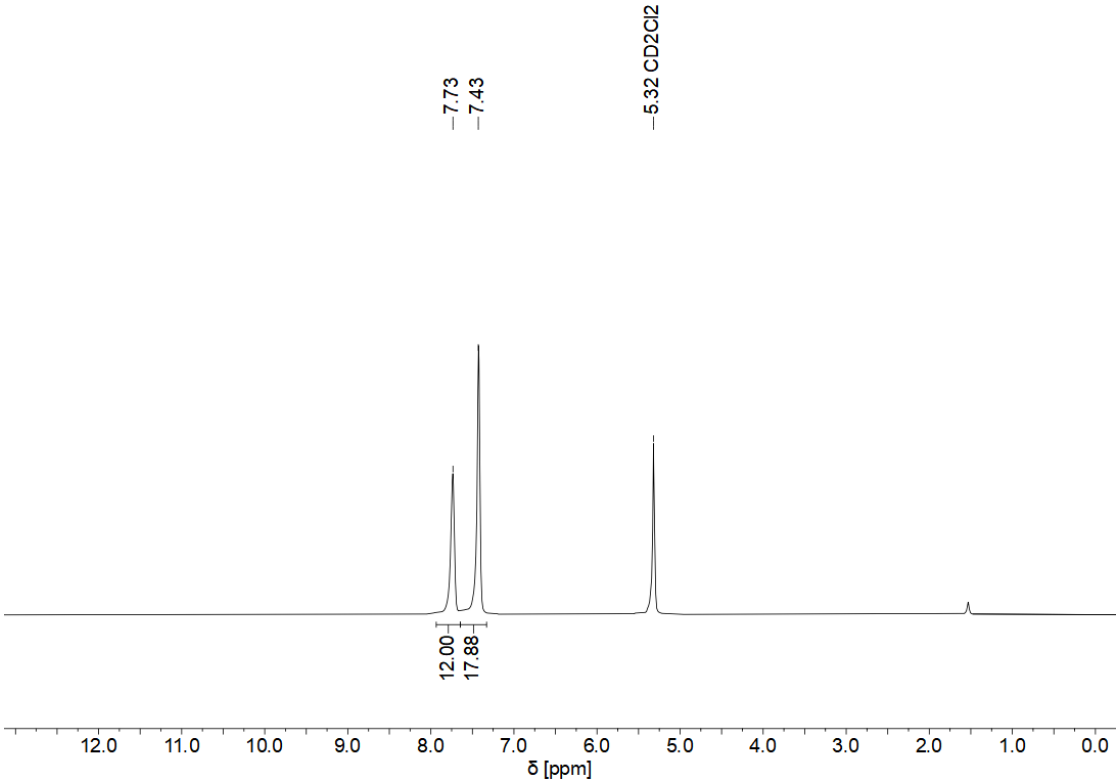

Figure S34. ^{31}P NMR spectrum of $[TcCl(CO)_3(PPh_3)_2]$.

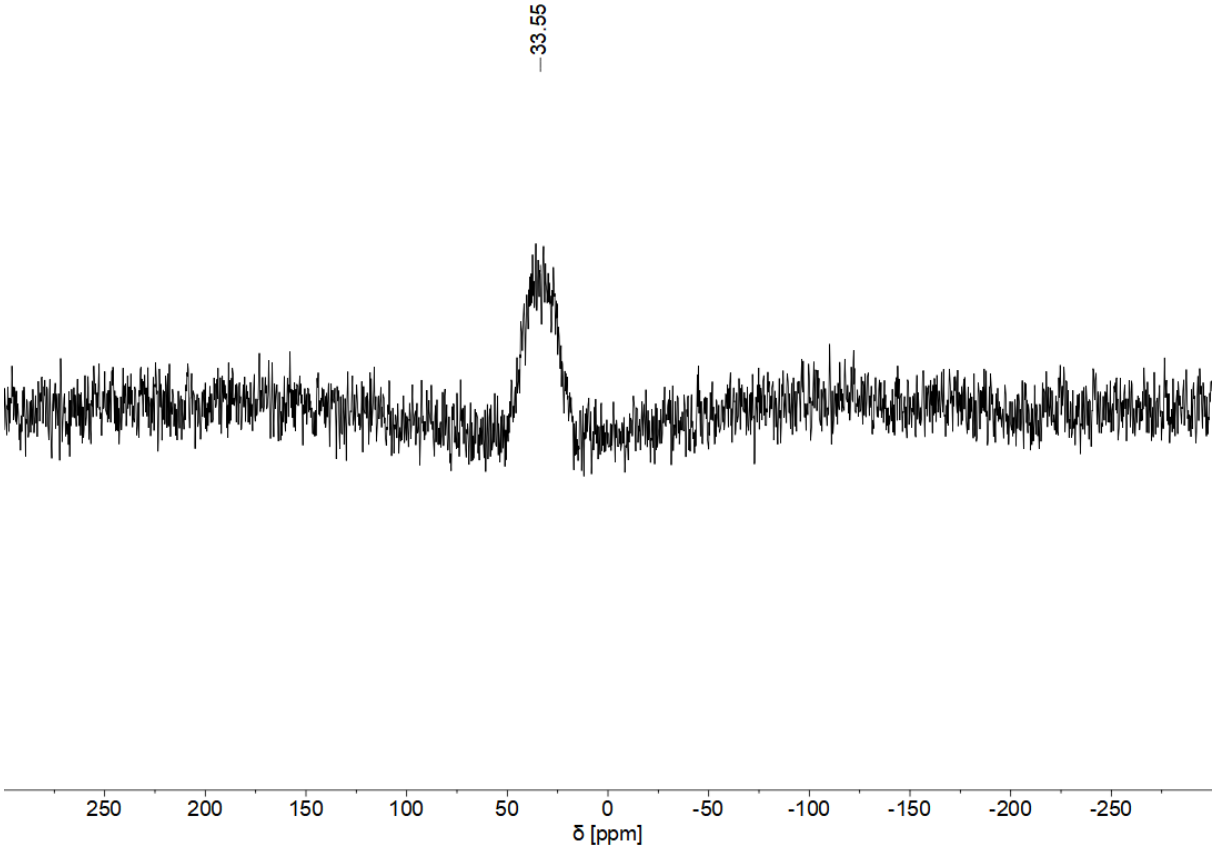

Figure S35. ^{99}Tc NMR spectrum of $[TcCl(CO)_3(PPh_3)_2]$.

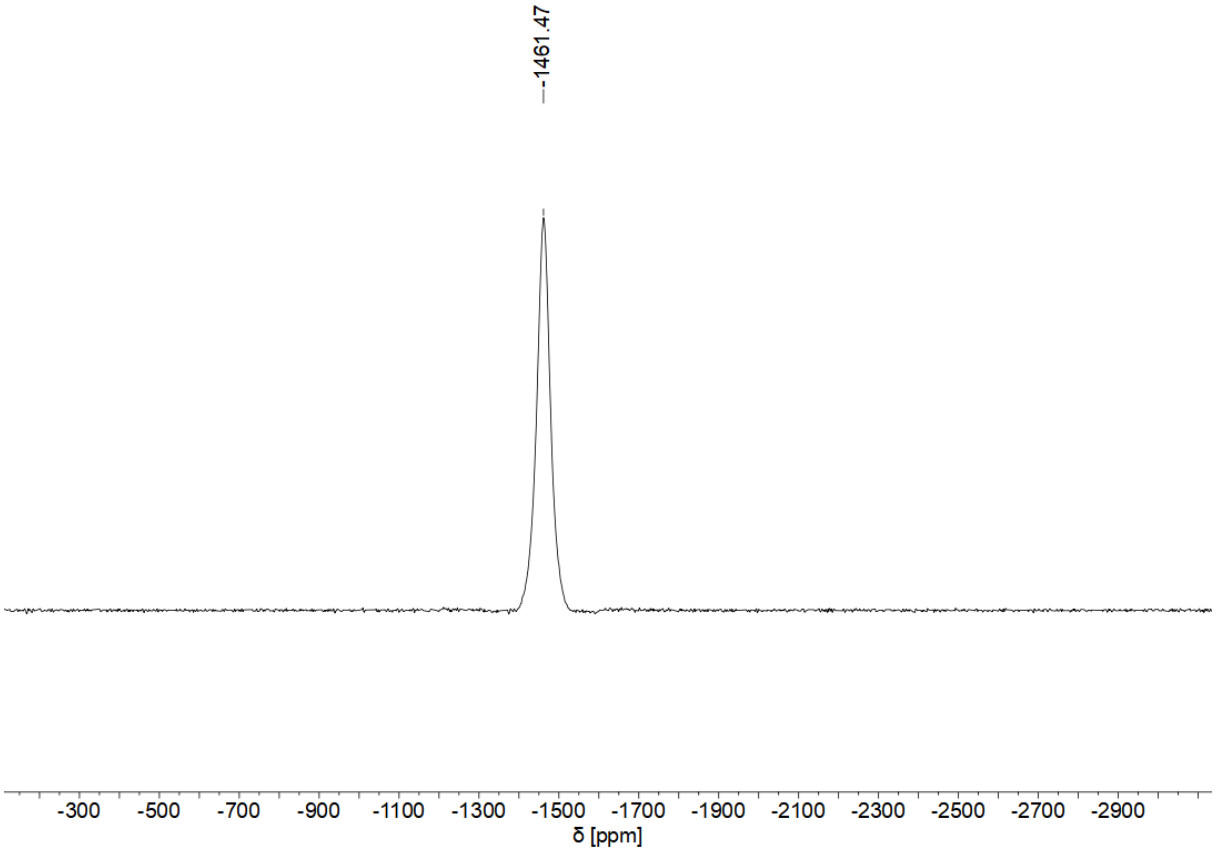

Figure S36. IR spectrum of $[TcCl(CO)_3(PPh_3)_2]$.

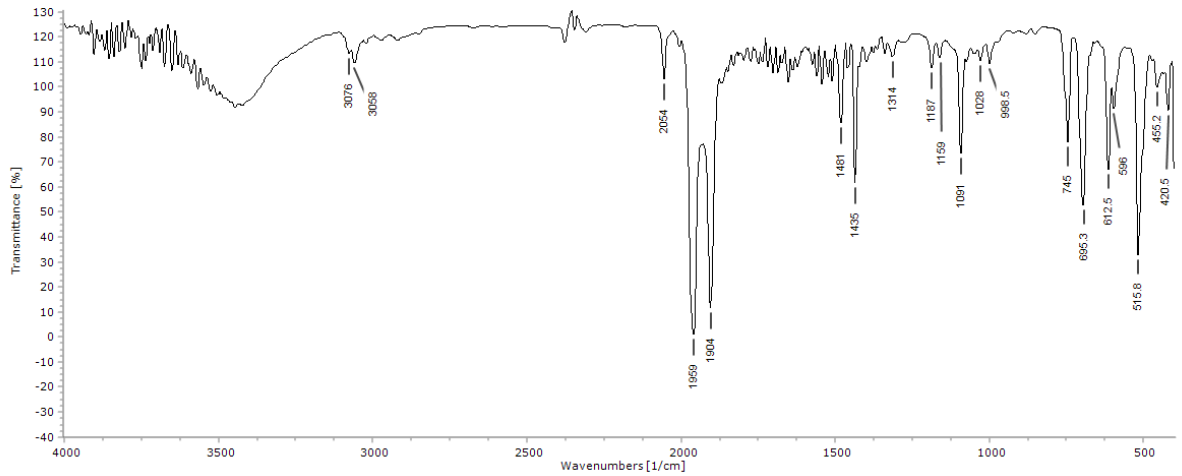

Figure S37. ^{1}H NMR spectrum of $[TcBr(CO)_3(PPh_3)_2]$.

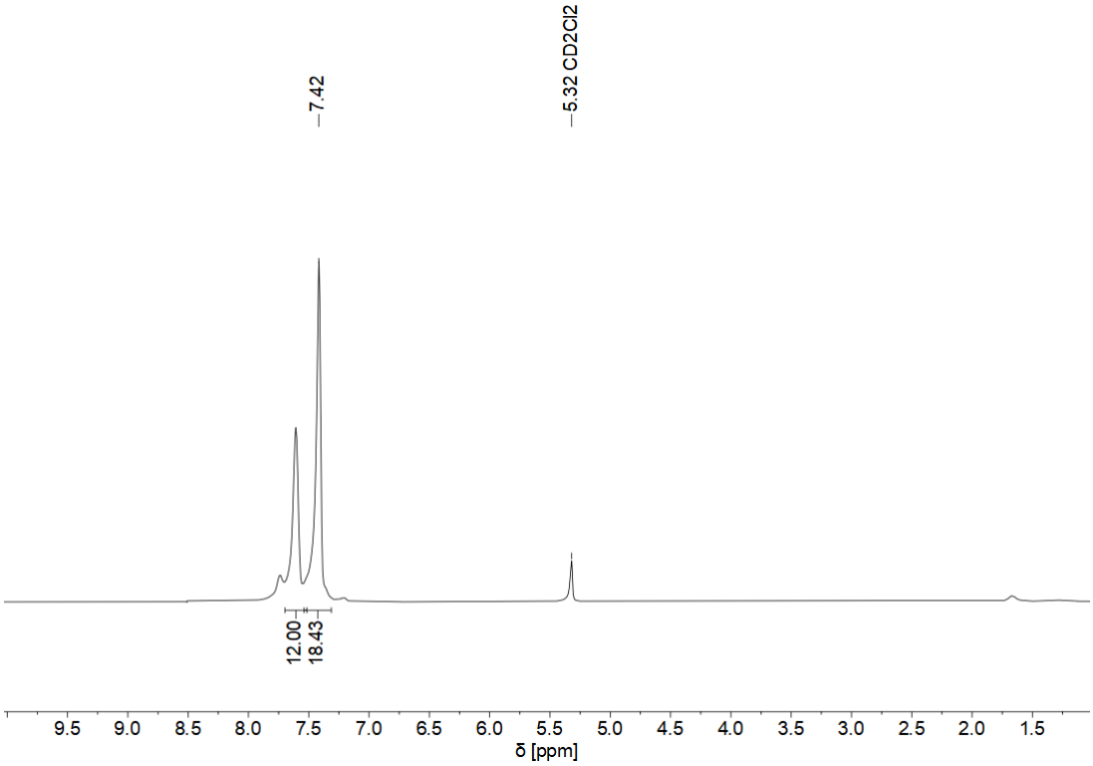

Figure S38. ^{31}P NMR spectrum of $[TcBr(CO)_3(PPh_3)_2]$.

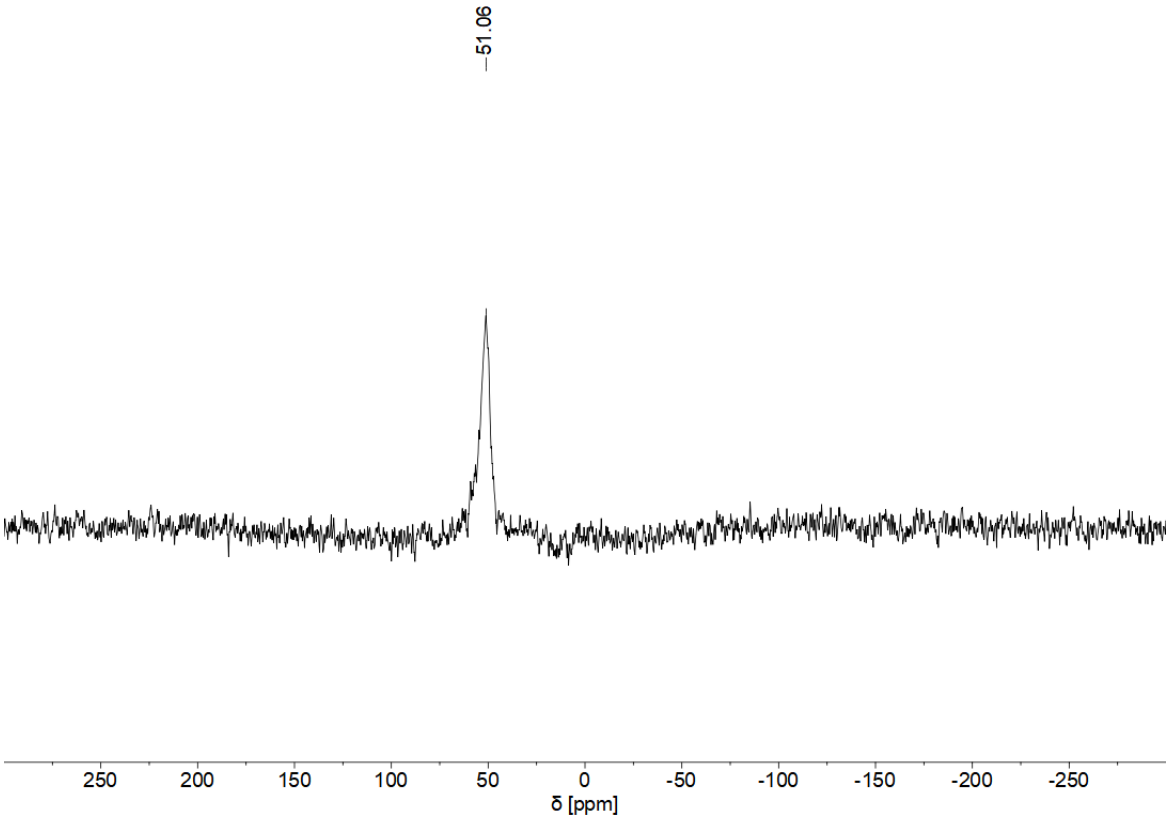

Figure S39. ^{99}Tc NMR spectrum of $[TcBr(CO)_3(PPh_3)_2]$.

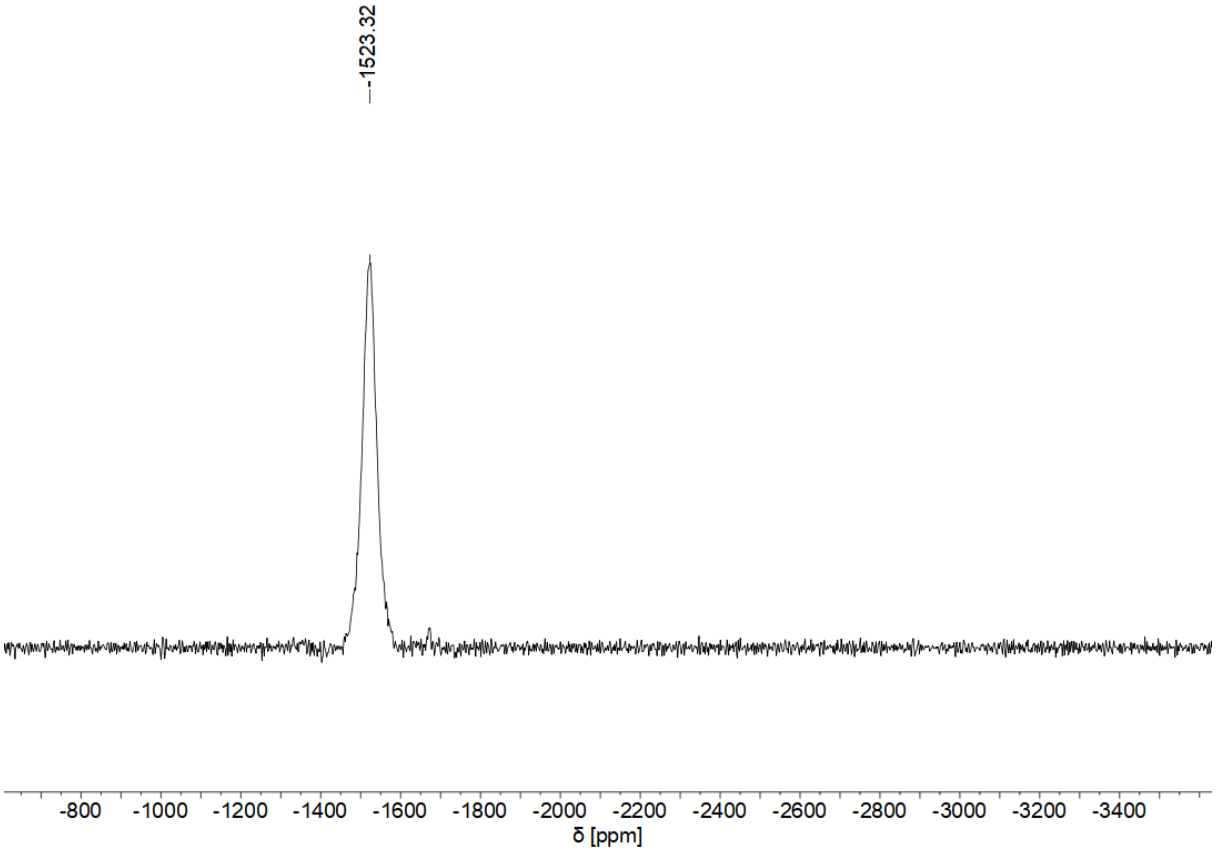

Figure S40. IR spectrum of $[TcBr(CO)_3(PPh_3)_2]$.

IR

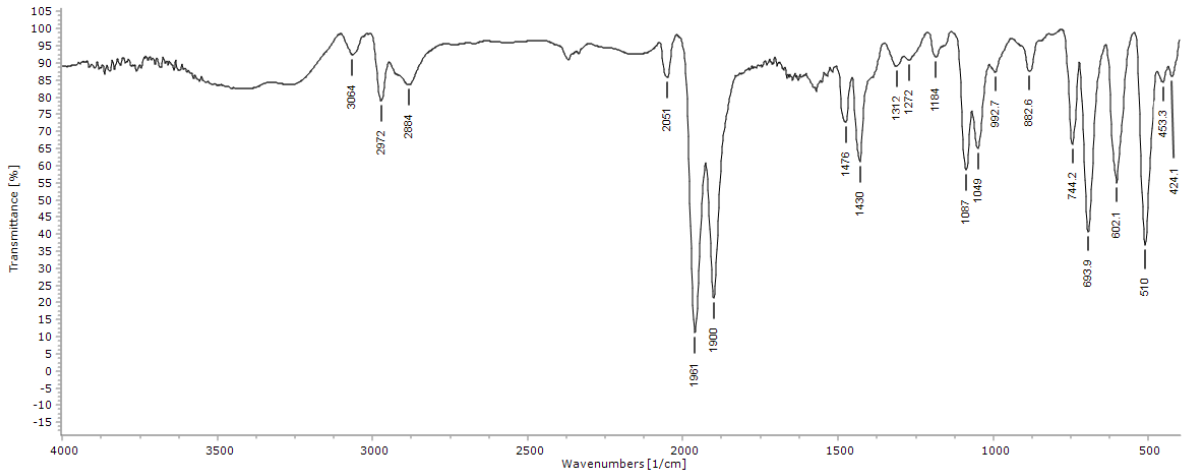

Figure S41. ^{1}H NMR spectrum of $[TcI(CO)_3(PPh_3)_2]$.

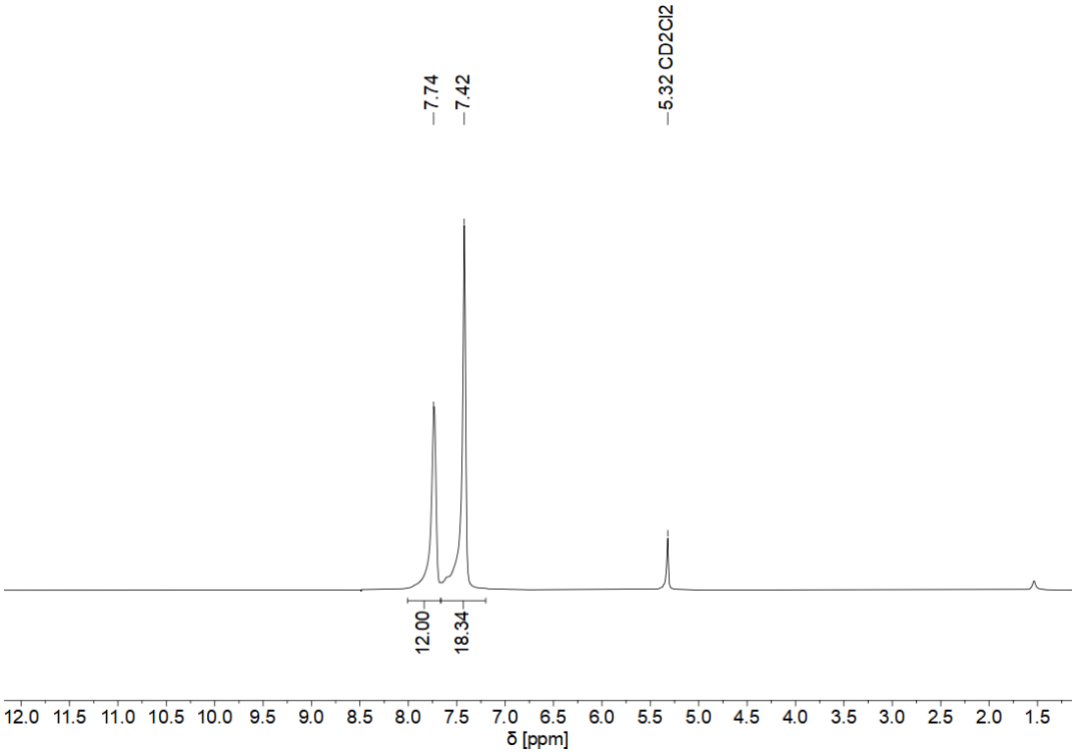

Figure S42. ^{31}P NMR spectrum of $[TcI(CO)_3(PPh_3)_2]$.

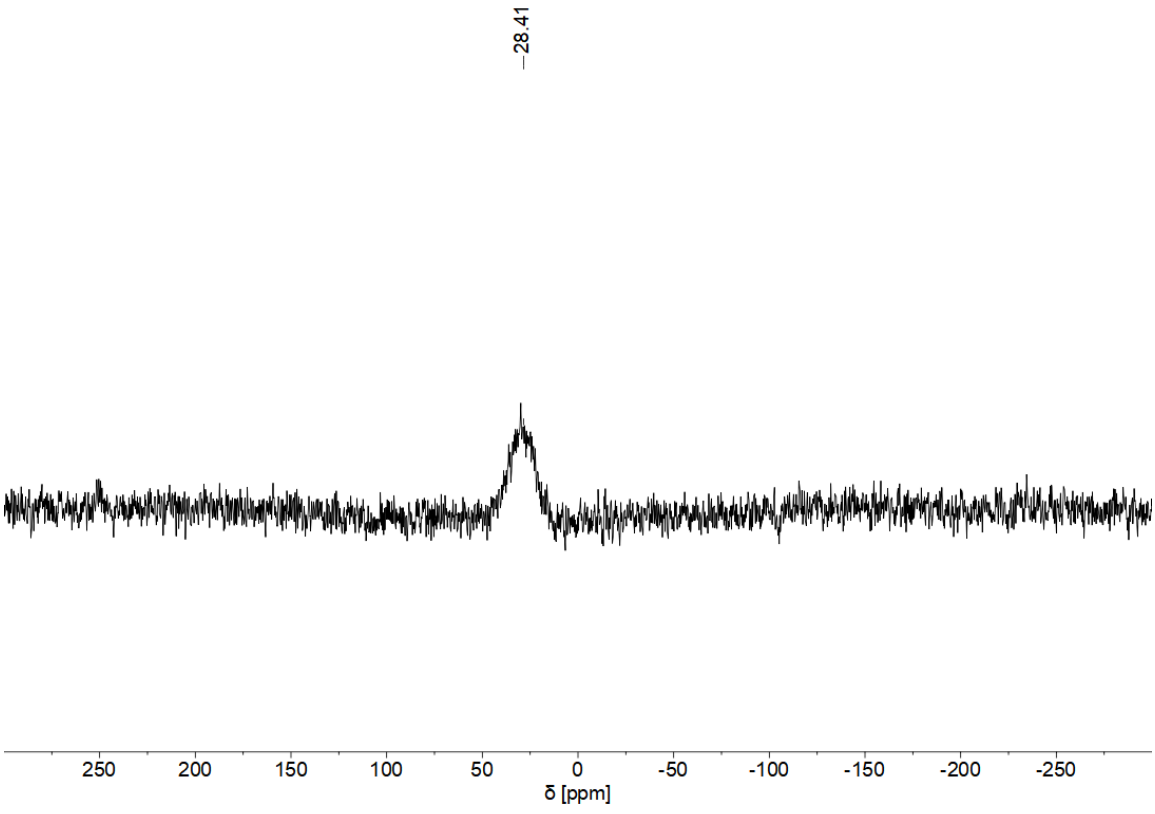

Figure S43. ^{99}Tc NMR spectrum of $[TcI(CO)_3(PPh_3)_2]$.

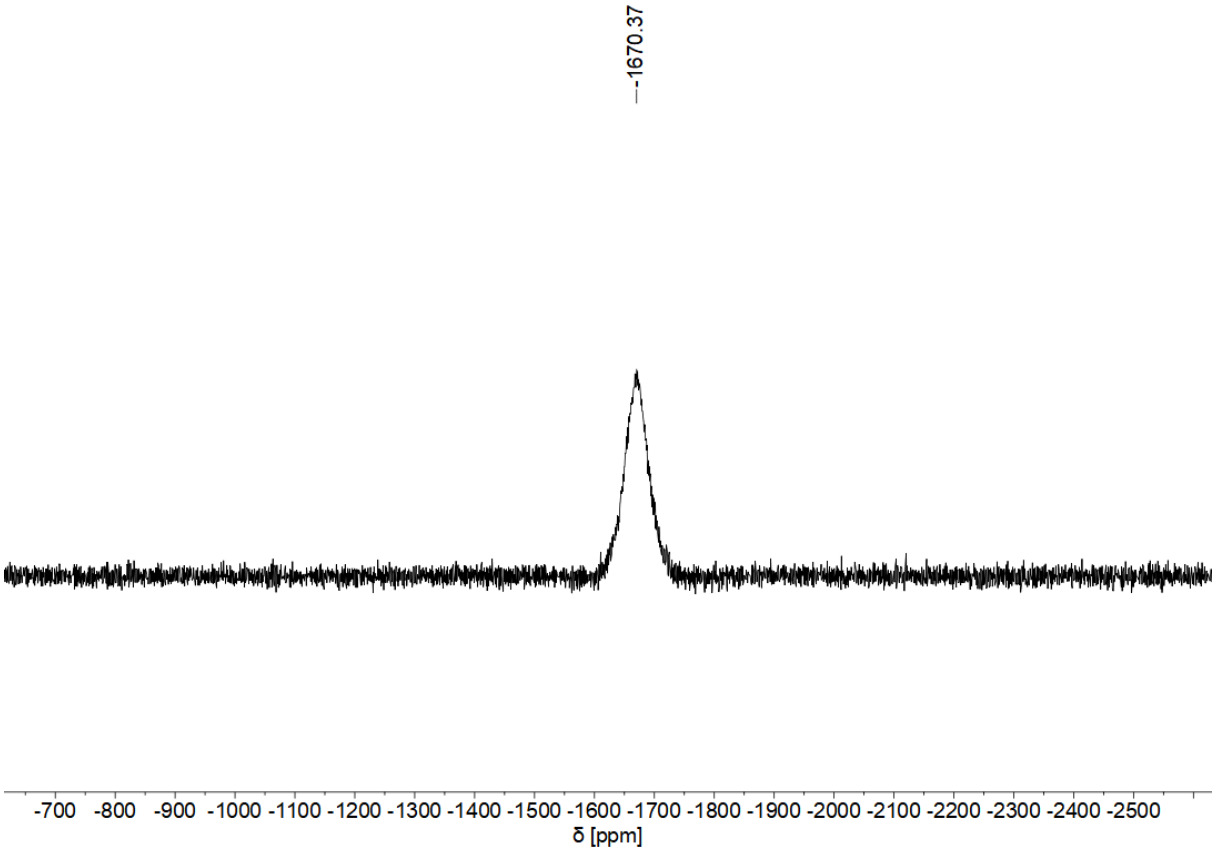

Figure S44. IR spectrum of $[TcI(CO)_3(PPh_3)_2]$.

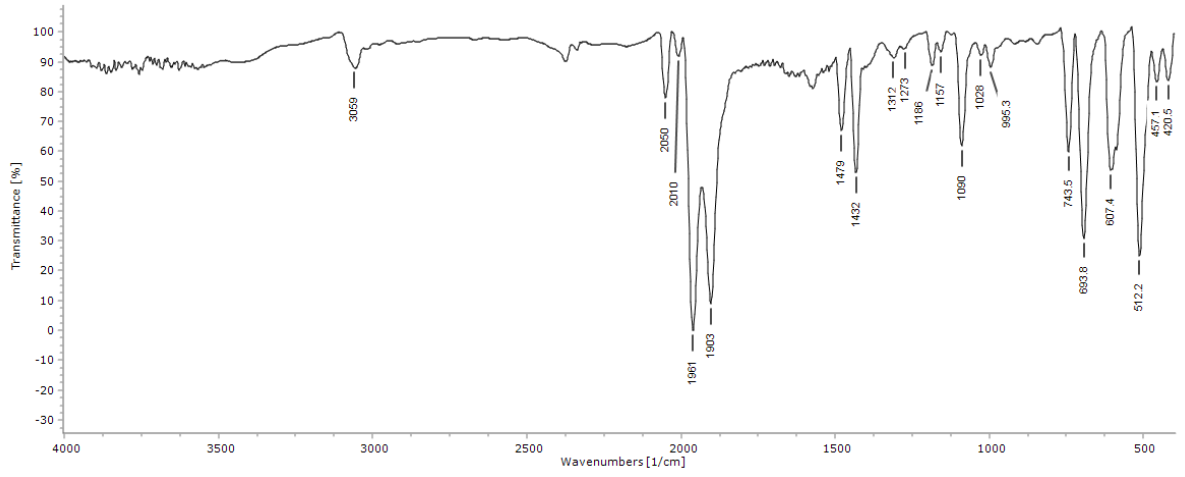

Figure S45. ^{1}H NMR spectrum of [Tc(η^{1}-O(CH)O)(CO)$_3$(PPh$_3$)$_2$].

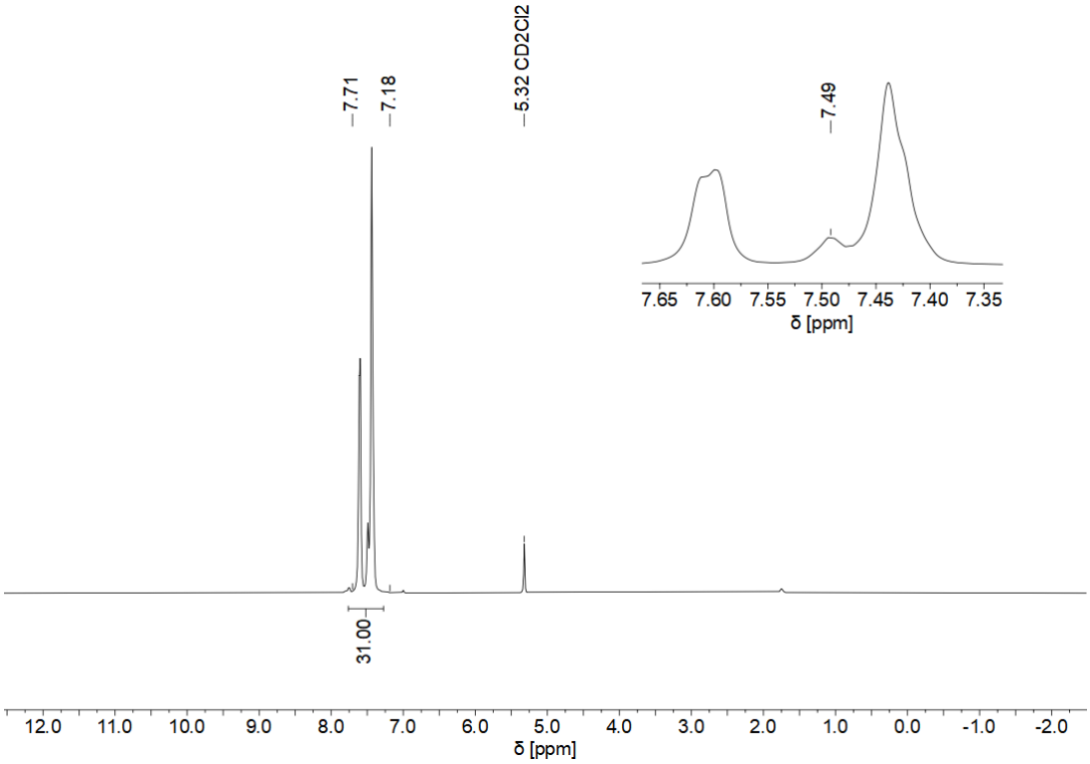

Figure S46. ^{31}P NMR spectrum of [Tc(η^{1}-O(CH)O)(CO)$_3$(PPh$_3$)$_2$].

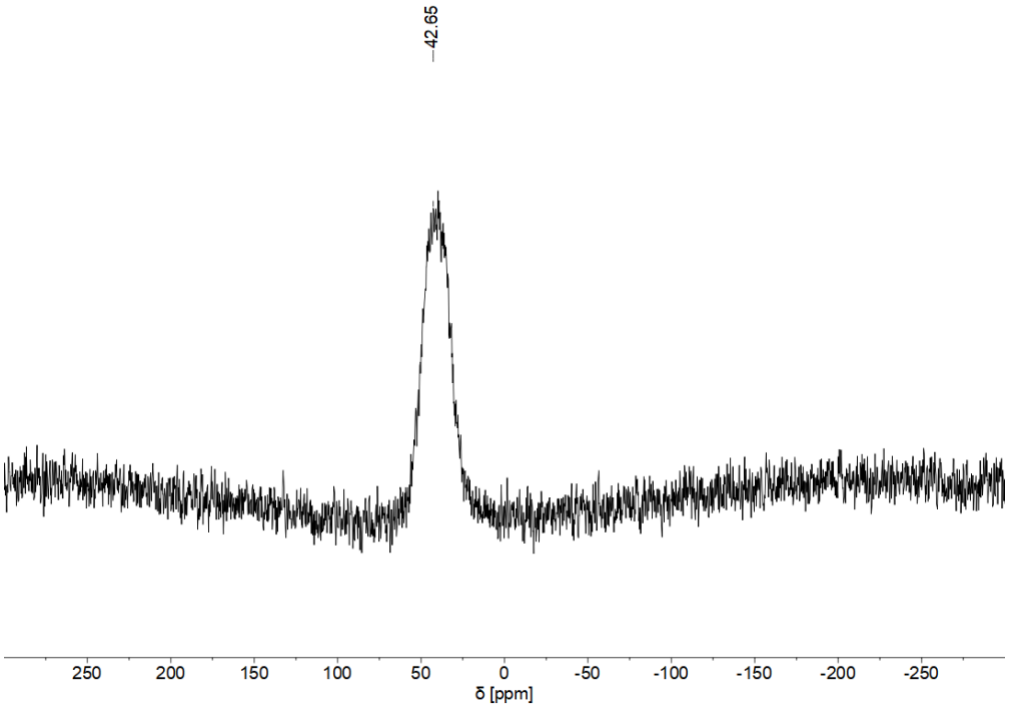

Figure S47. ^{99}Tc NMR spectra of [Tc(η^1-O(CH)O)(CO)$_3$(PPh$_3$)$_2$].

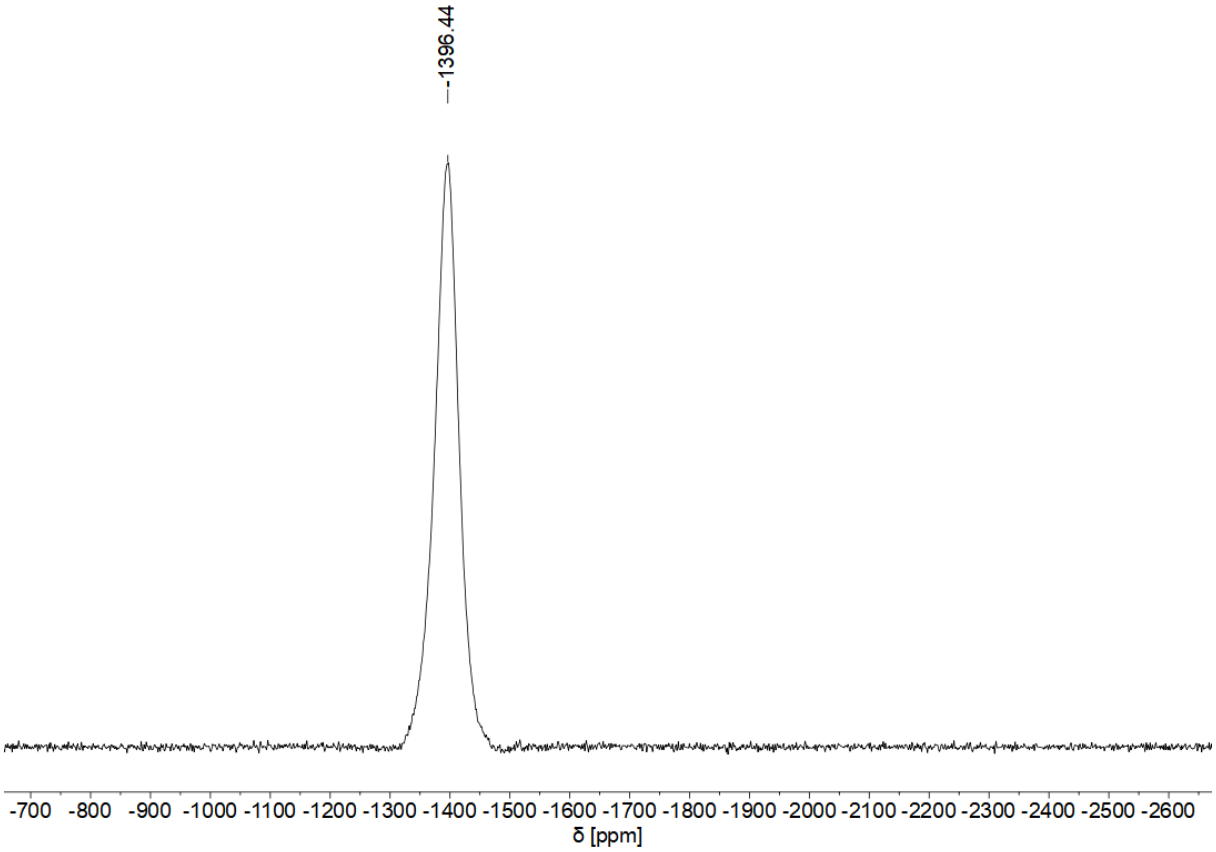

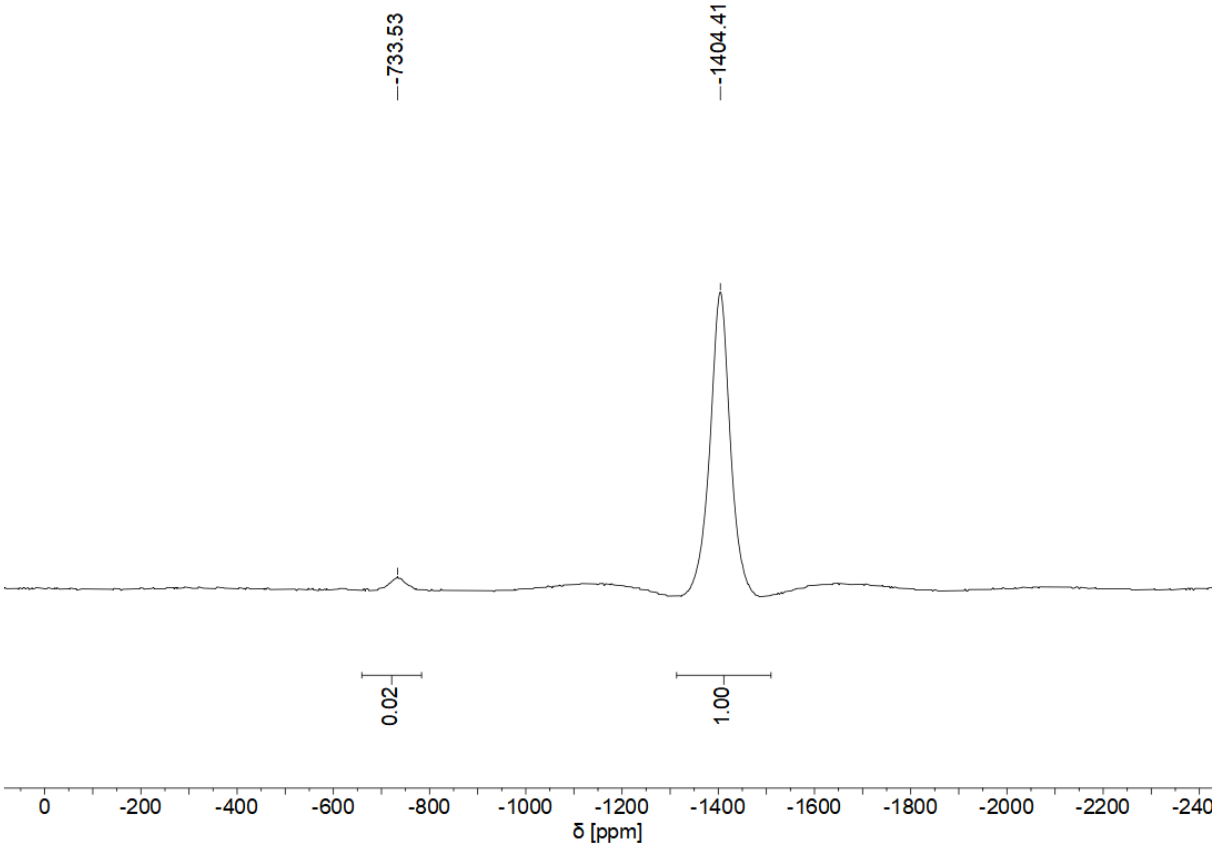

Figure S48. IR spectrum of [Tc(η^1-O(CH)O)$(CO)_3(PPh_3)_2$].

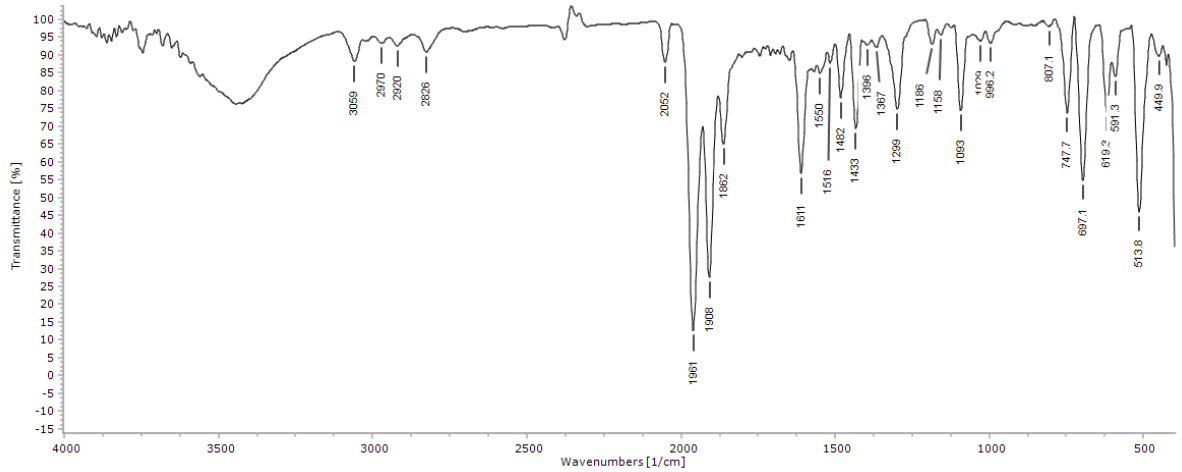

Figure S49. ^{1}H NMR spectrum of [Tc(η^1-O(CCF_3)O)$(CO)_3(PPh_3)_2$] · 0.5 toluene.

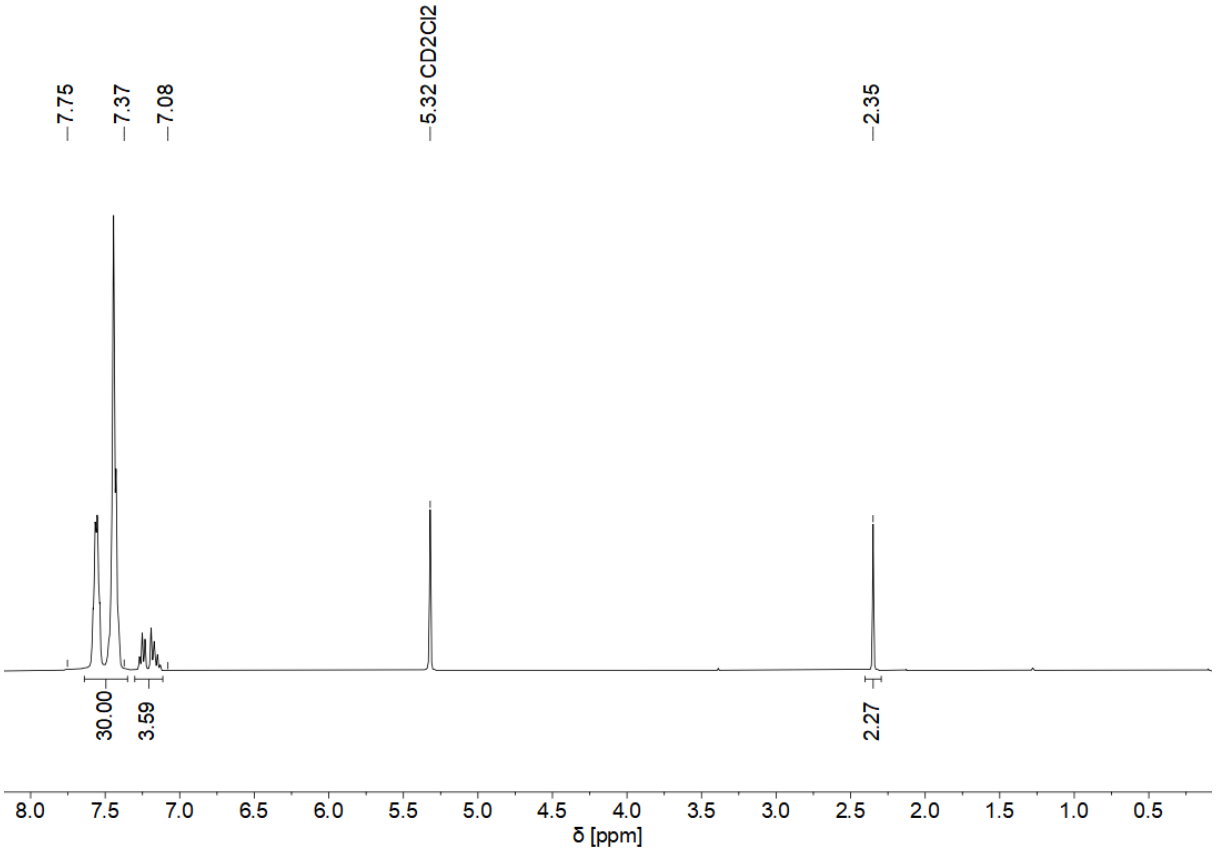

Figure S50. ^{31}P NMR spectrum of [Tc(η^1-O(CCF$_3$)O)(CO)$_3$(PPh$_3$)$_2$] · 0.5 toluene.

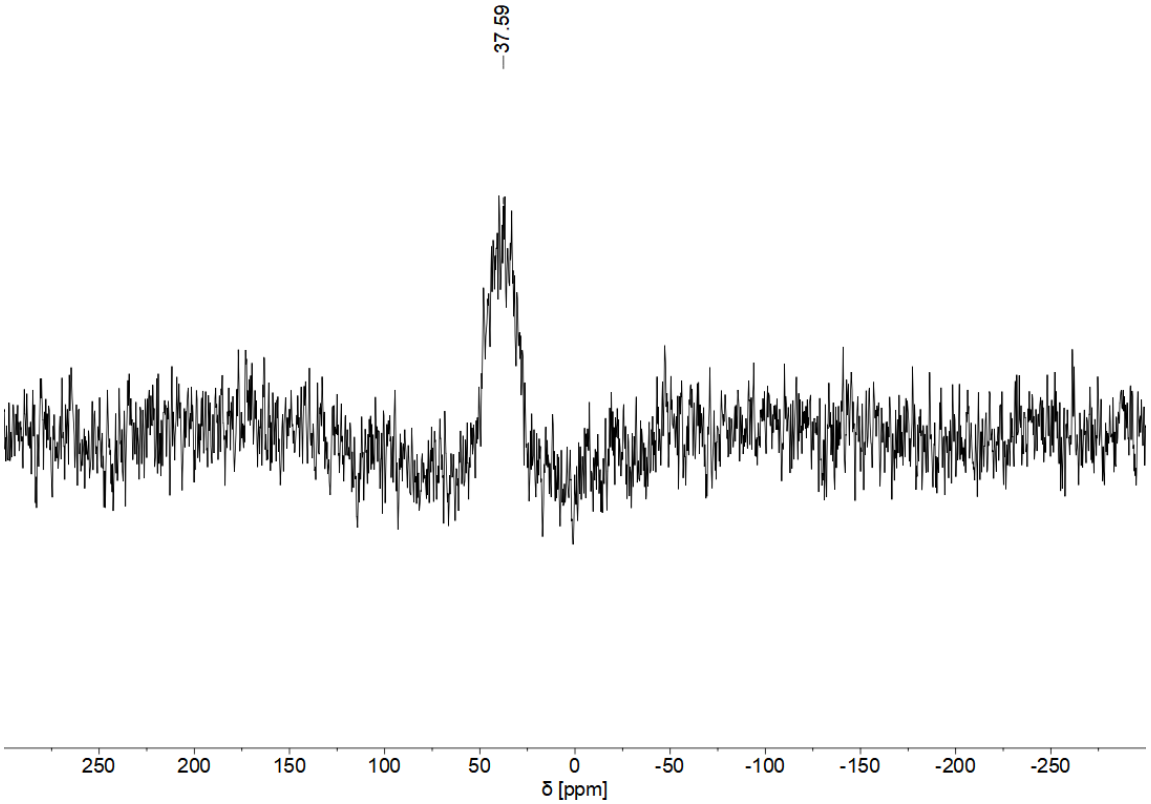

Figure S51. ^{19}F NMR spectrum of [Tc(η^1-O(CCF$_3$)O)(CO)$_3$(PPh$_3$)$_2$] · 0.5 toluene.

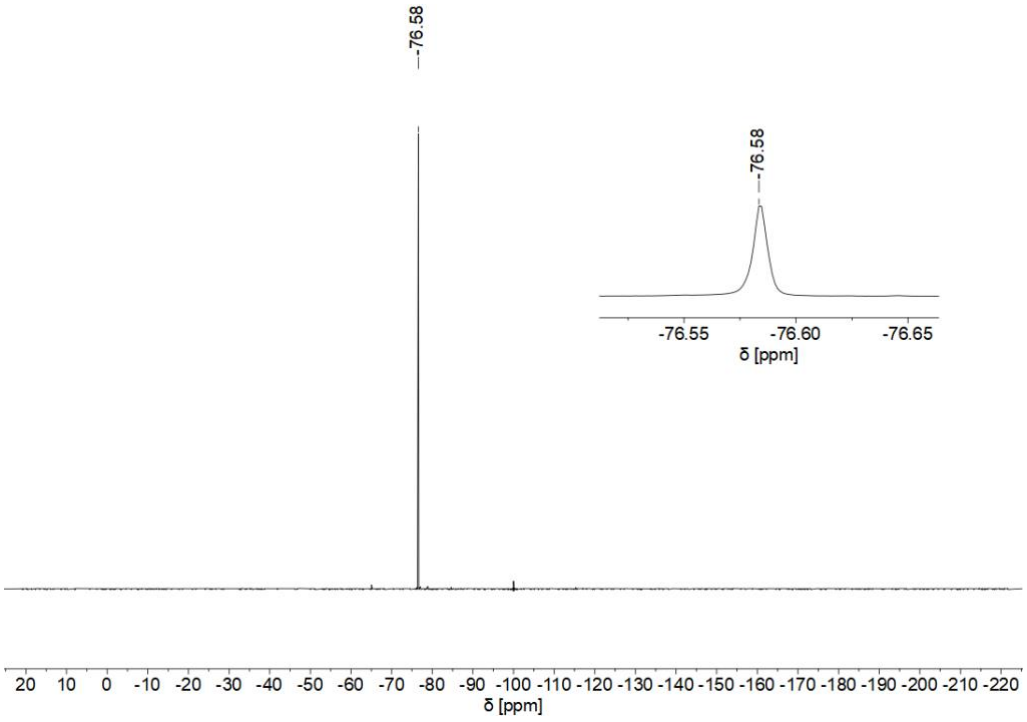

Figure S52. ^{99}Tc NMR spectra of [Tc(η^1-O(CCF$_3$)O)(CO)$_3$(PPh$_3$)$_2$] · 0.5 toluene.

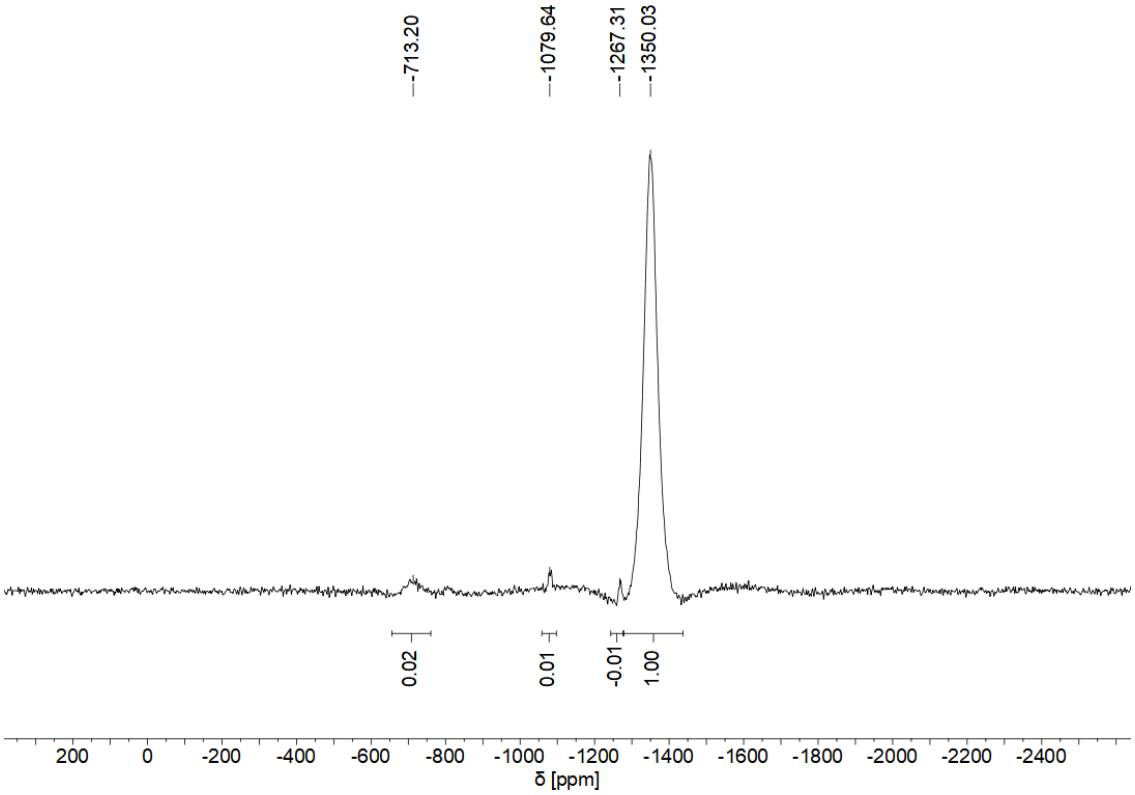

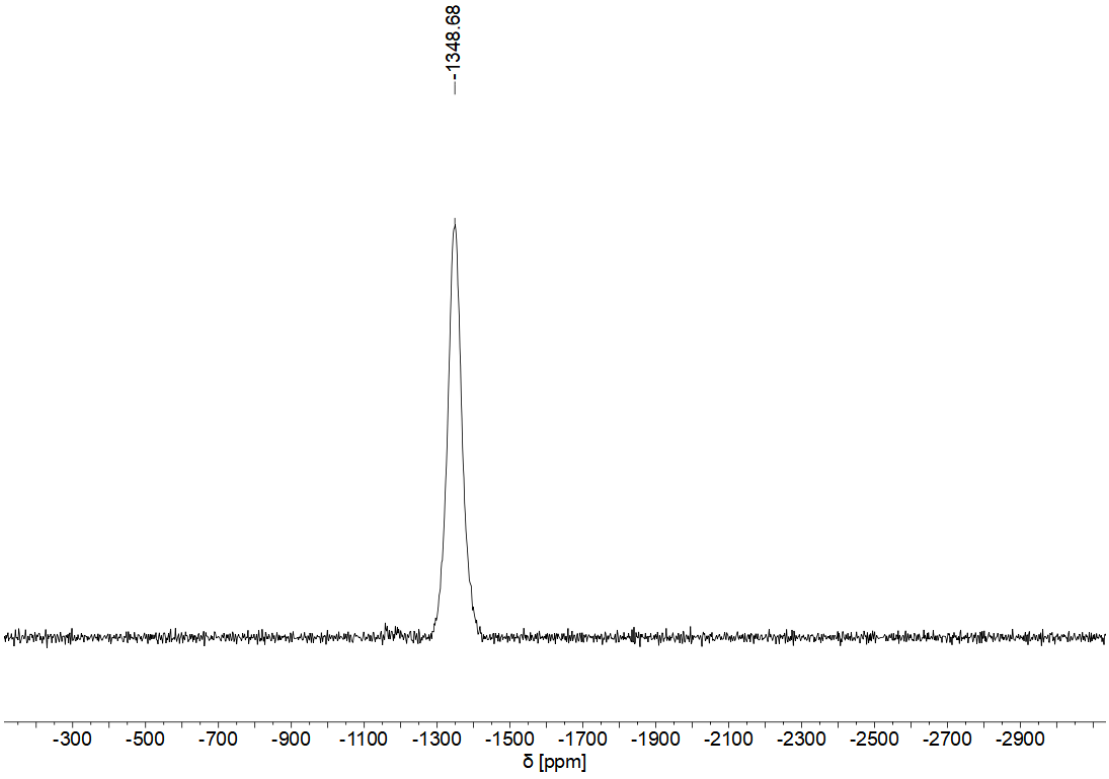

Figure S53. IR spectrum of [Tc(η^1-O(CCF$_3$)O)(CO)$_3$(PPh$_3$)$_2$] · 0.5 toluene.

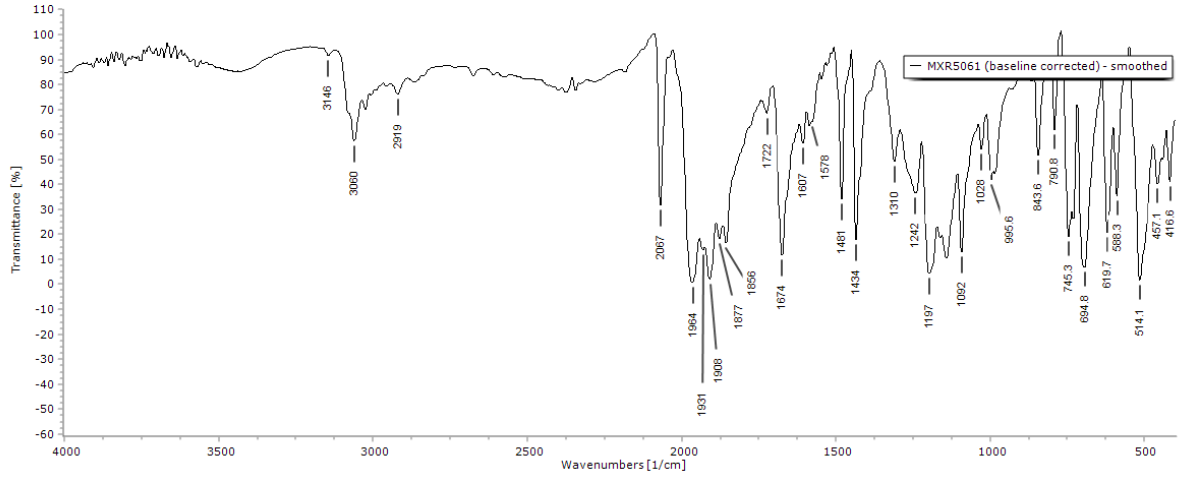

Figure S54. ^{1}H NMR spectrum of [Tc(η^2-OO(CH))(CO)$_2$(PPh$_3$)$_2$].

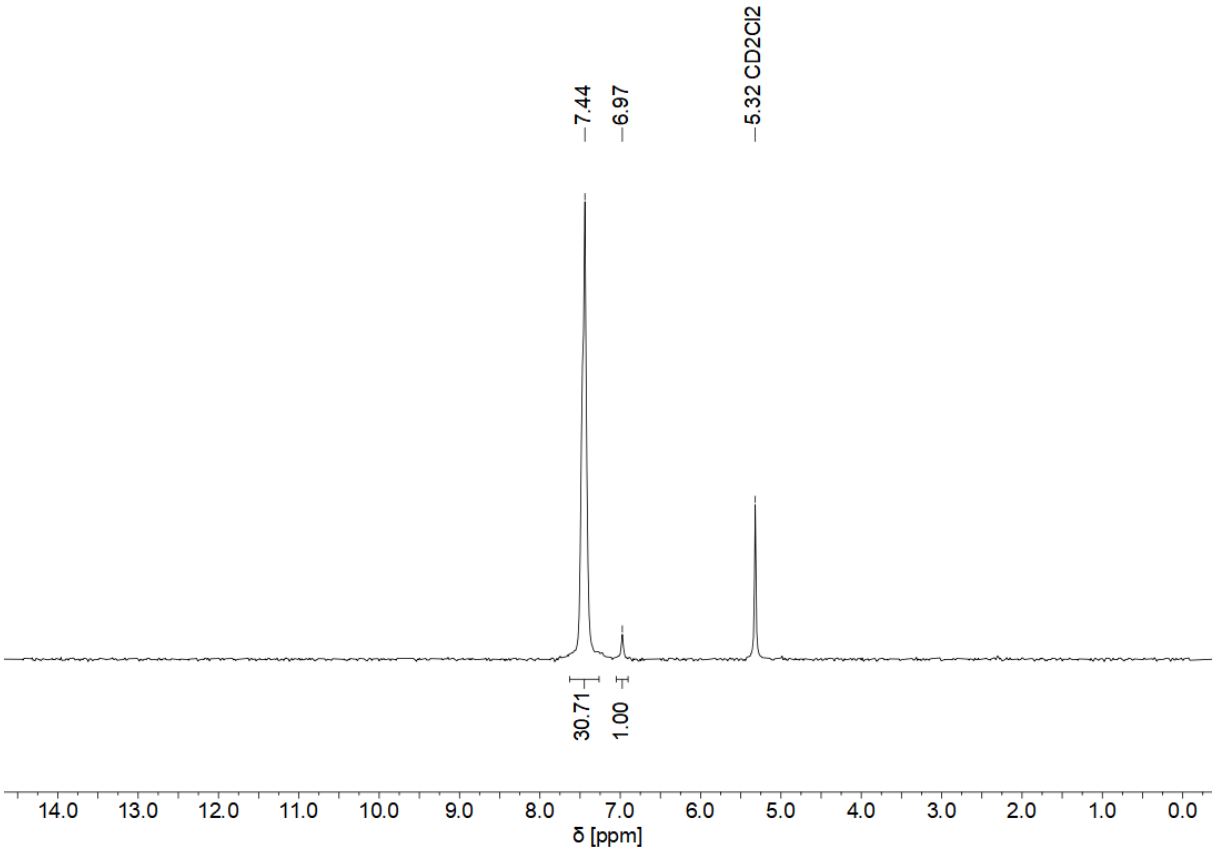

Figure S55. ^{1}H NMR spectrum of [Tc(η^2-OO(CH))(CO)$_2$(PPh$_3$)$_2$].

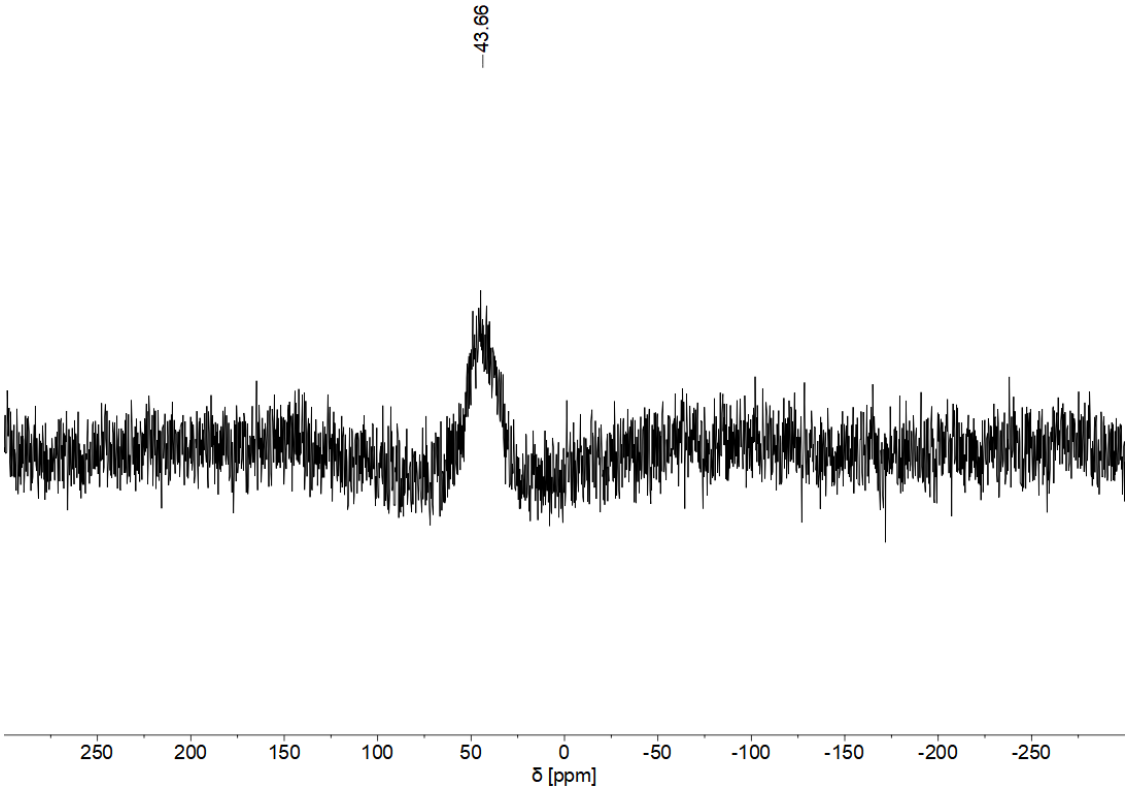

Figure S56. ^{1}H NMR spectrum of [Tc(η^2-OO(CH))(CO)$_2$(PPh$_3$)$_2$].

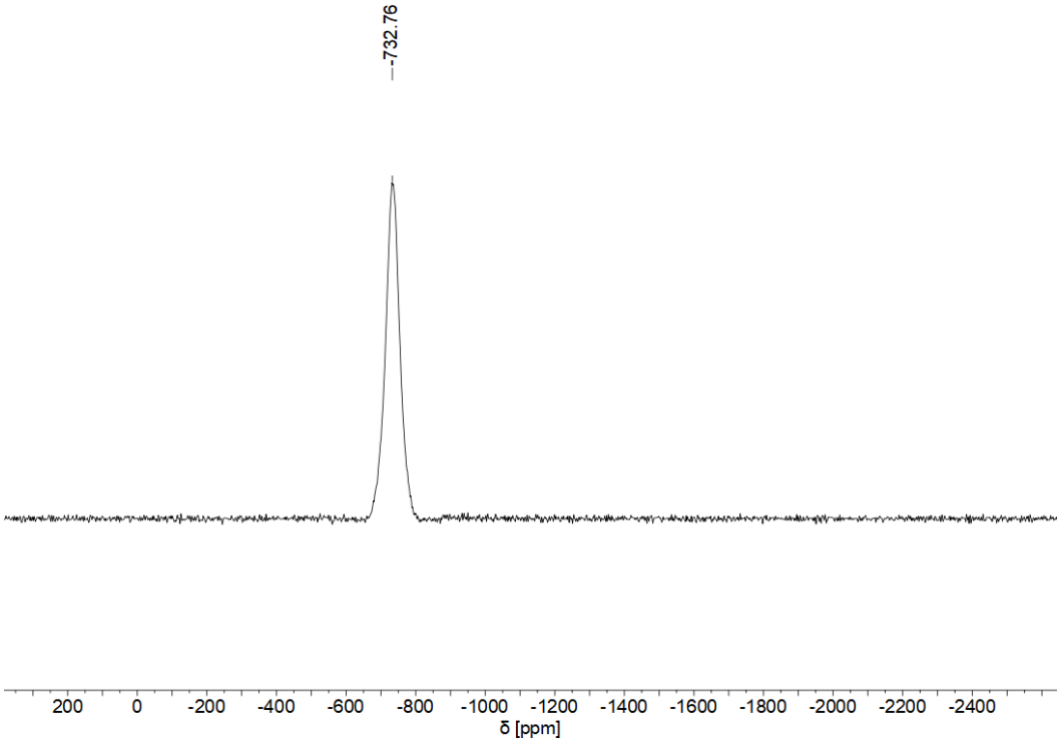

Figure S57. IR spectrum of [Tc(η^2-OO(CH))$(CO)_2(PPh_3)_2$].

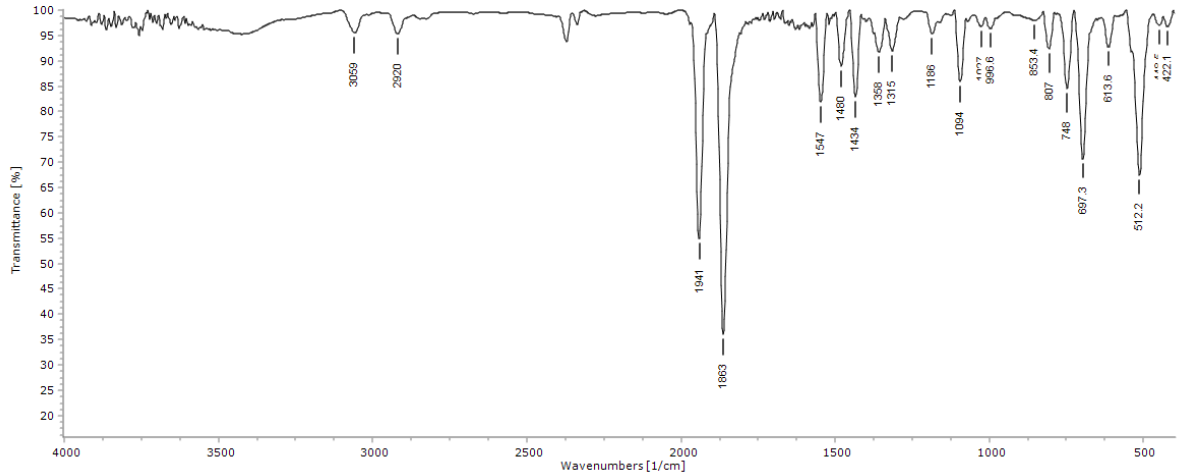

Figure S58. ^{1}H NMR spectrum of [Tc(η^2-OO(CCH_3))$(CO)_2(PPh_3)_2$].

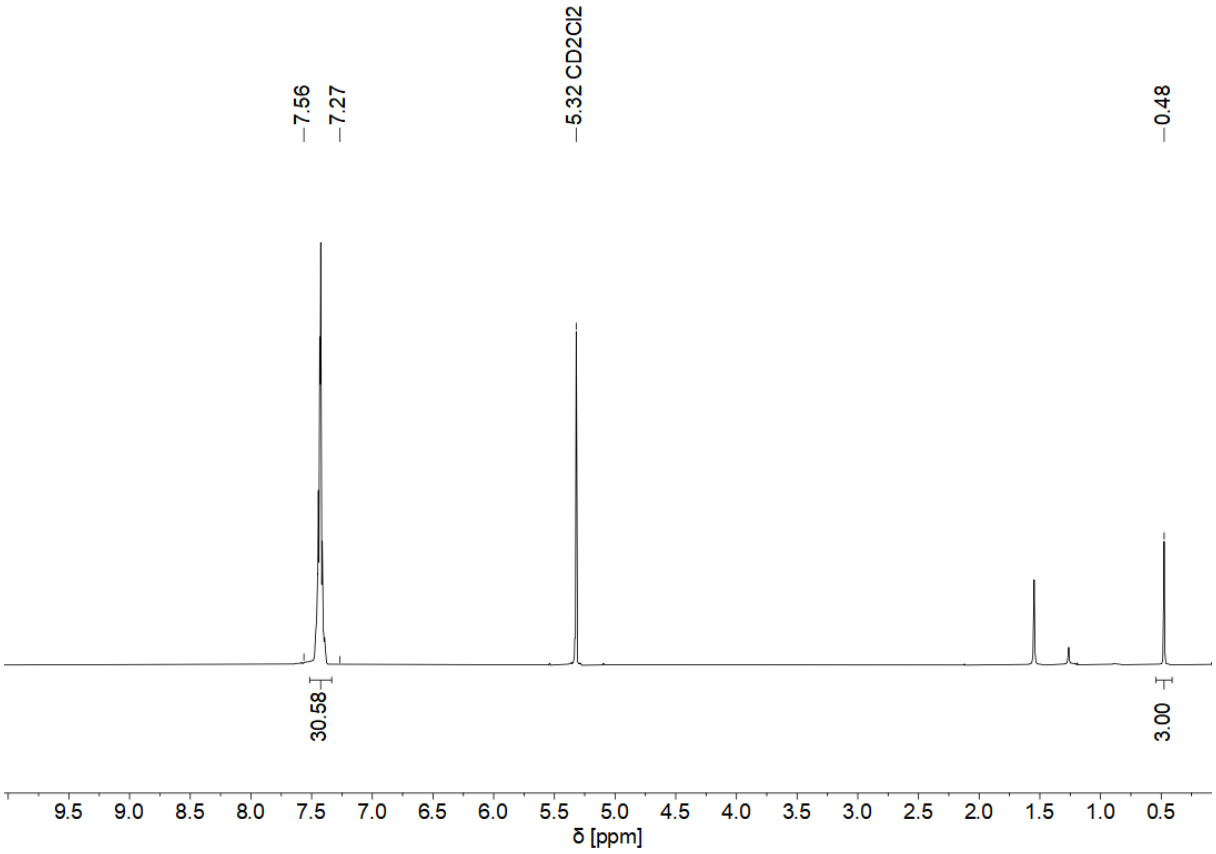

Figure S59. ^{31}P NMR spectrum of [Tc(η^2-OO(CCH$_3$))(CO)$_2$(PPh$_3$)$_2$].

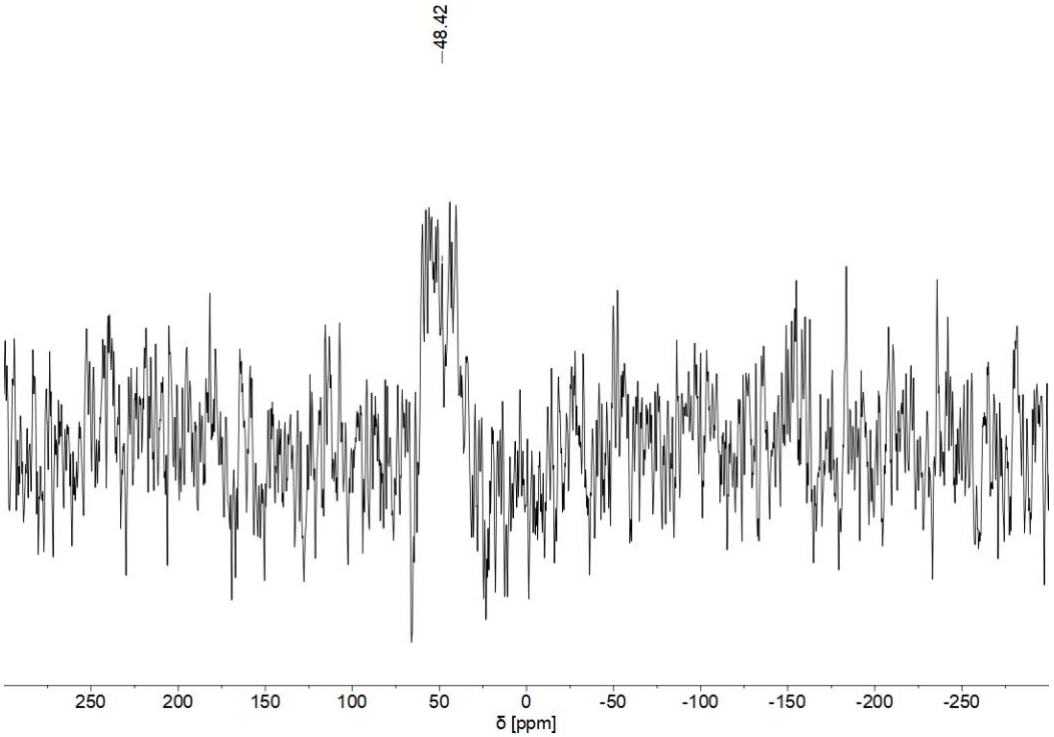

Figure S60. ^{99}Tc NMR spectrum of [Tc(η^2-OO(CCH$_3$))(CO)$_2$(PPh$_3$)$_2$].

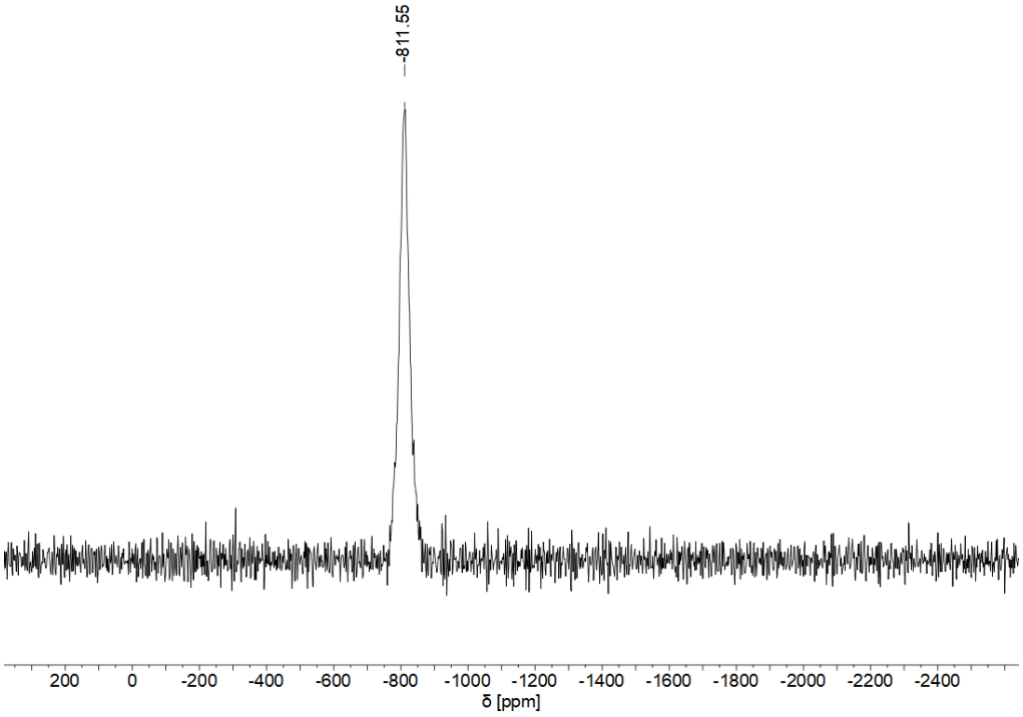

Figure S61. IR spectrum of [Tc(η^2-OO(CCH$_3$))(CO)$_2$(PPh$_3$)$_2$].

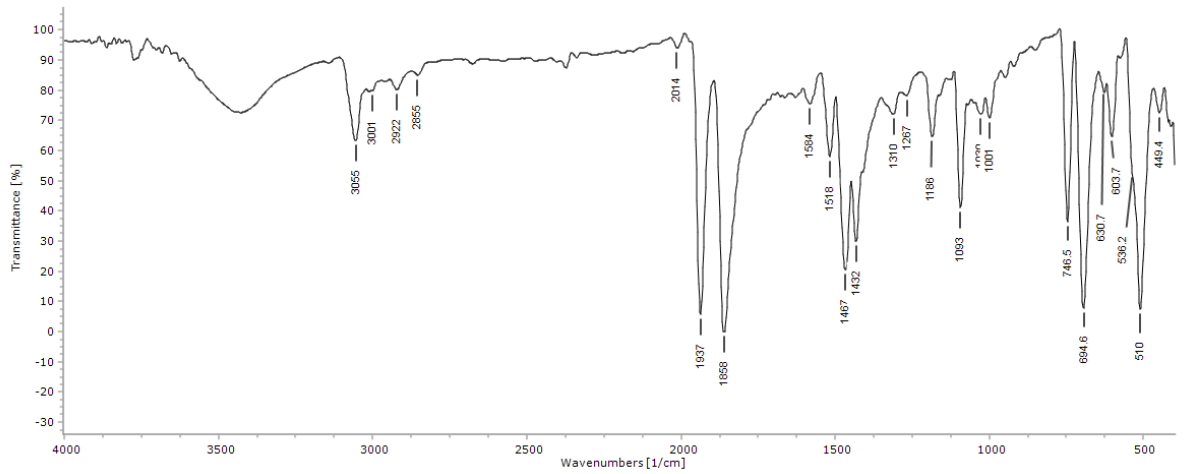

Figure S62. ^{1}H NMR spectrum of [Tc(η^2-OO(CPh))(CO)$_2$(PPh$_3$)$_2$].

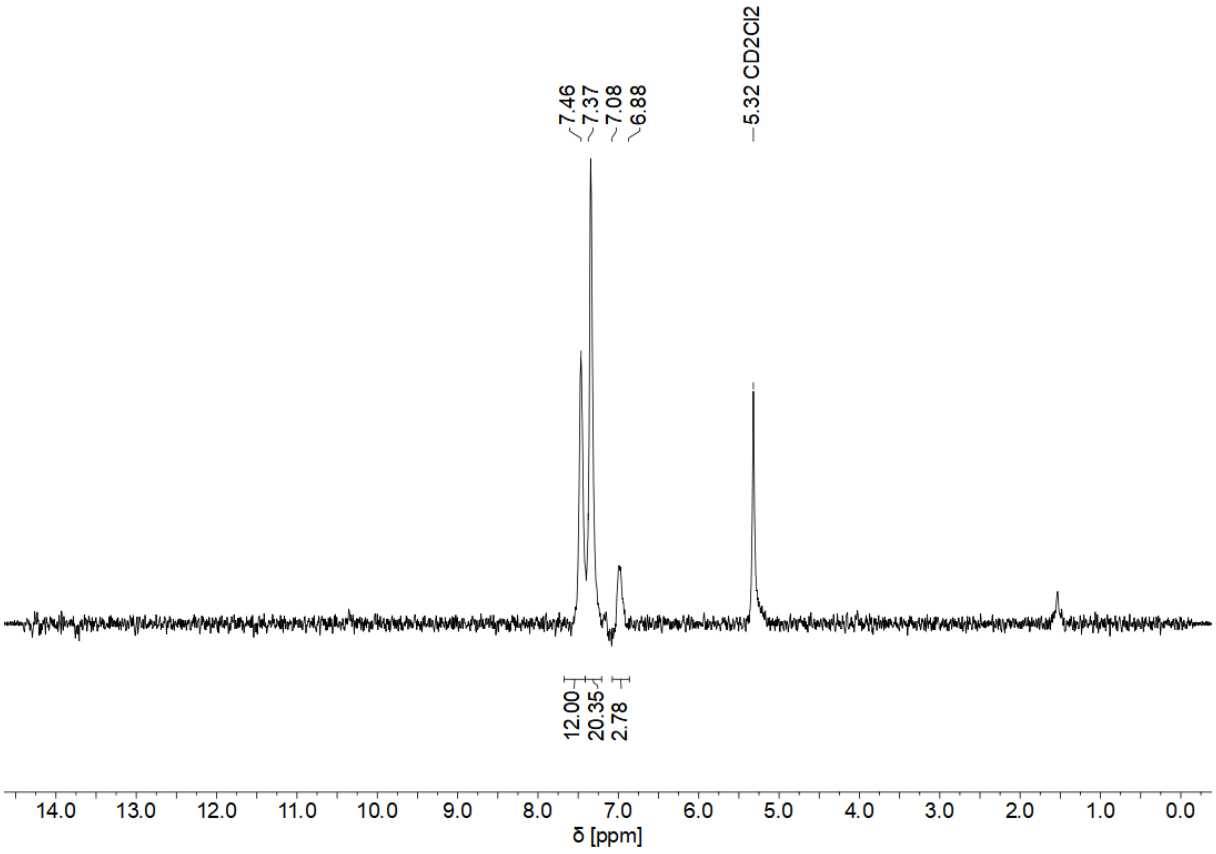

Figure S62. ^{31}P NMR spectrum of [Tc(η^2-OO(CPh))$(CO)_2(PPh_3)_2$].

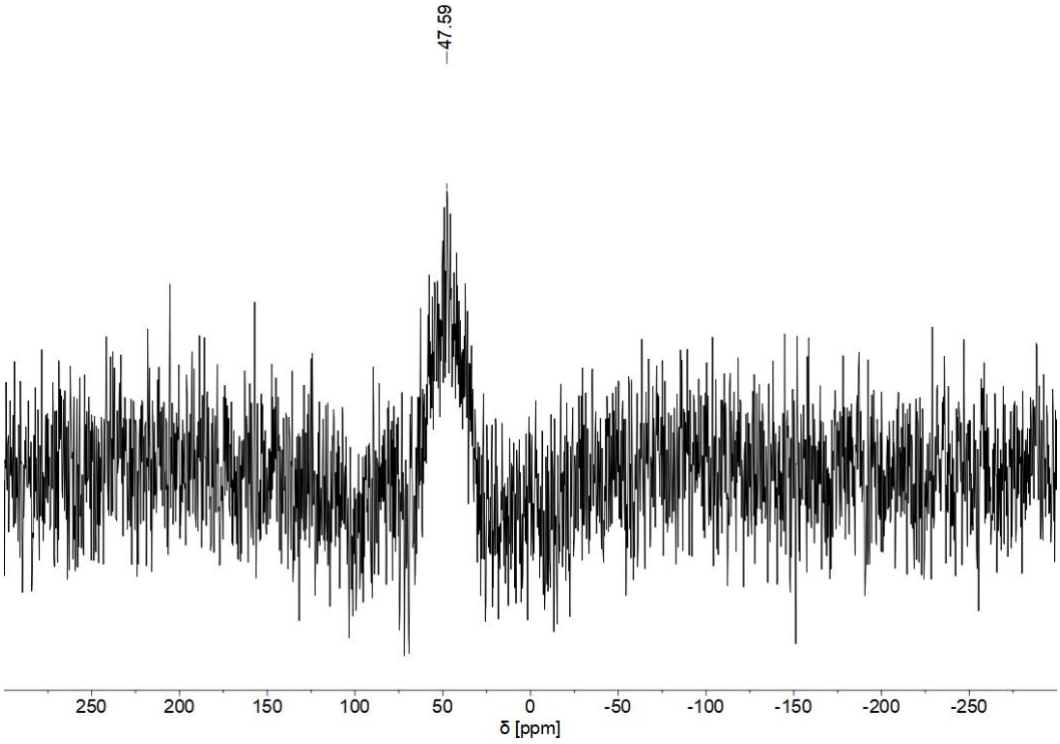

Figure S63. ^{99}Tc NMR spectrum of [Tc(η^2-OO(CPh))$(CO)_2(PPh_3)_2$].

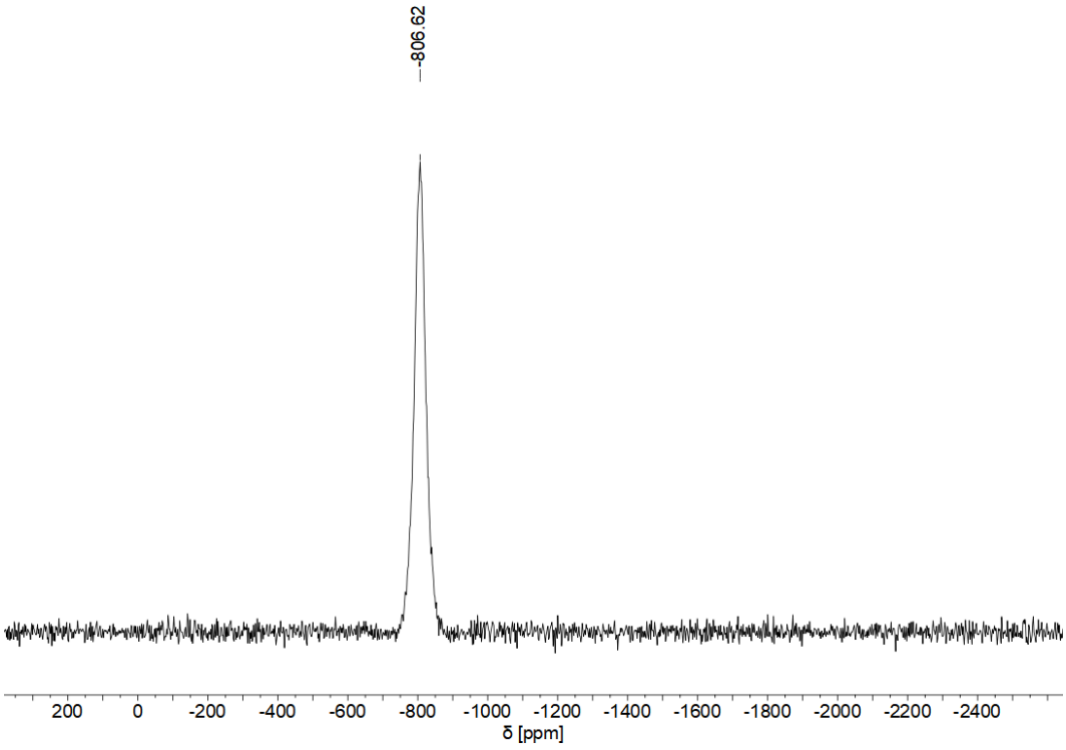

Figure S64. IR spectrum of [Tc(η^2-OO(CPh))$(CO)_2(PPh_3)_2$].

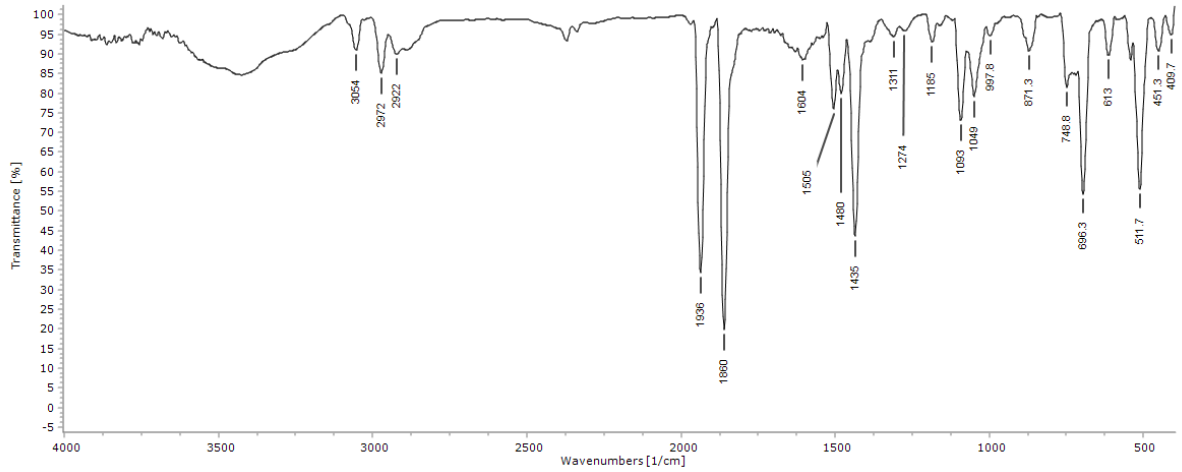

Figure S65. ^{1}H NMR spectrum of [Tc(η^2-Et_2btu)$(CO)_2(PPh_3)_2$].

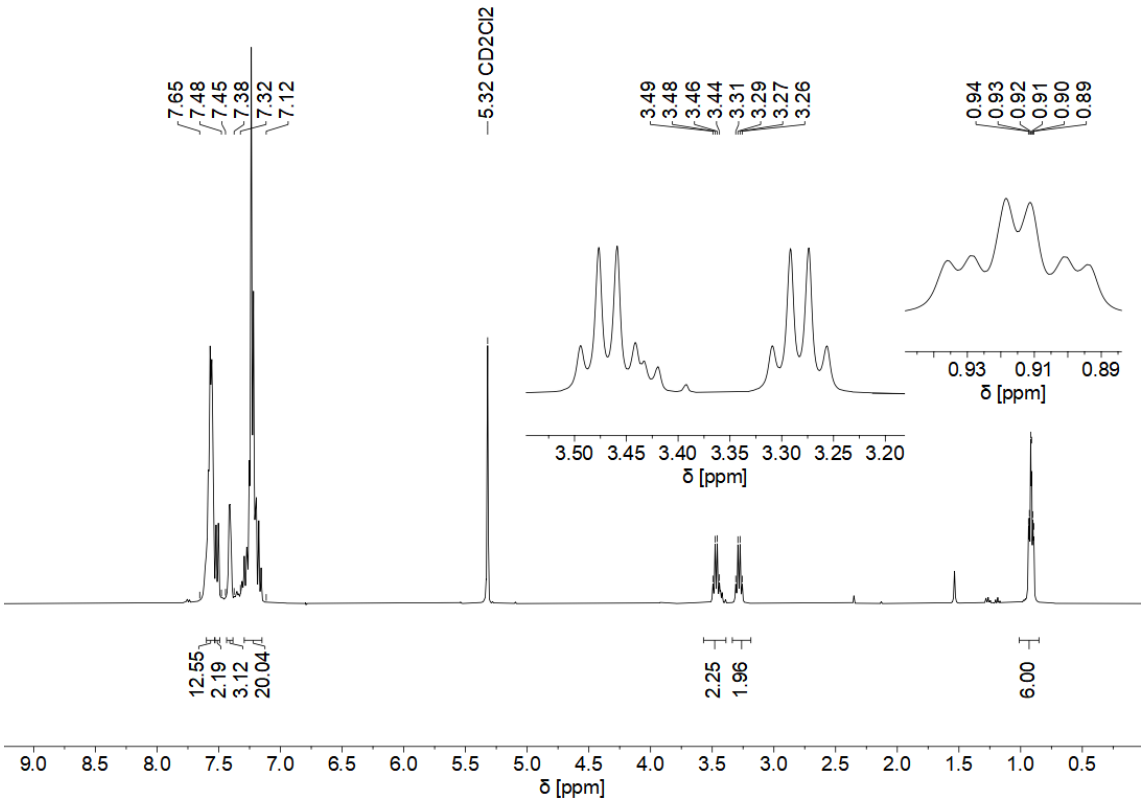

Figure S66. ^{99}Tc NMR spectra of [Tc(η^2-Et$_2$btu)(CO)$_2$(PPh$_3$)$_2$].

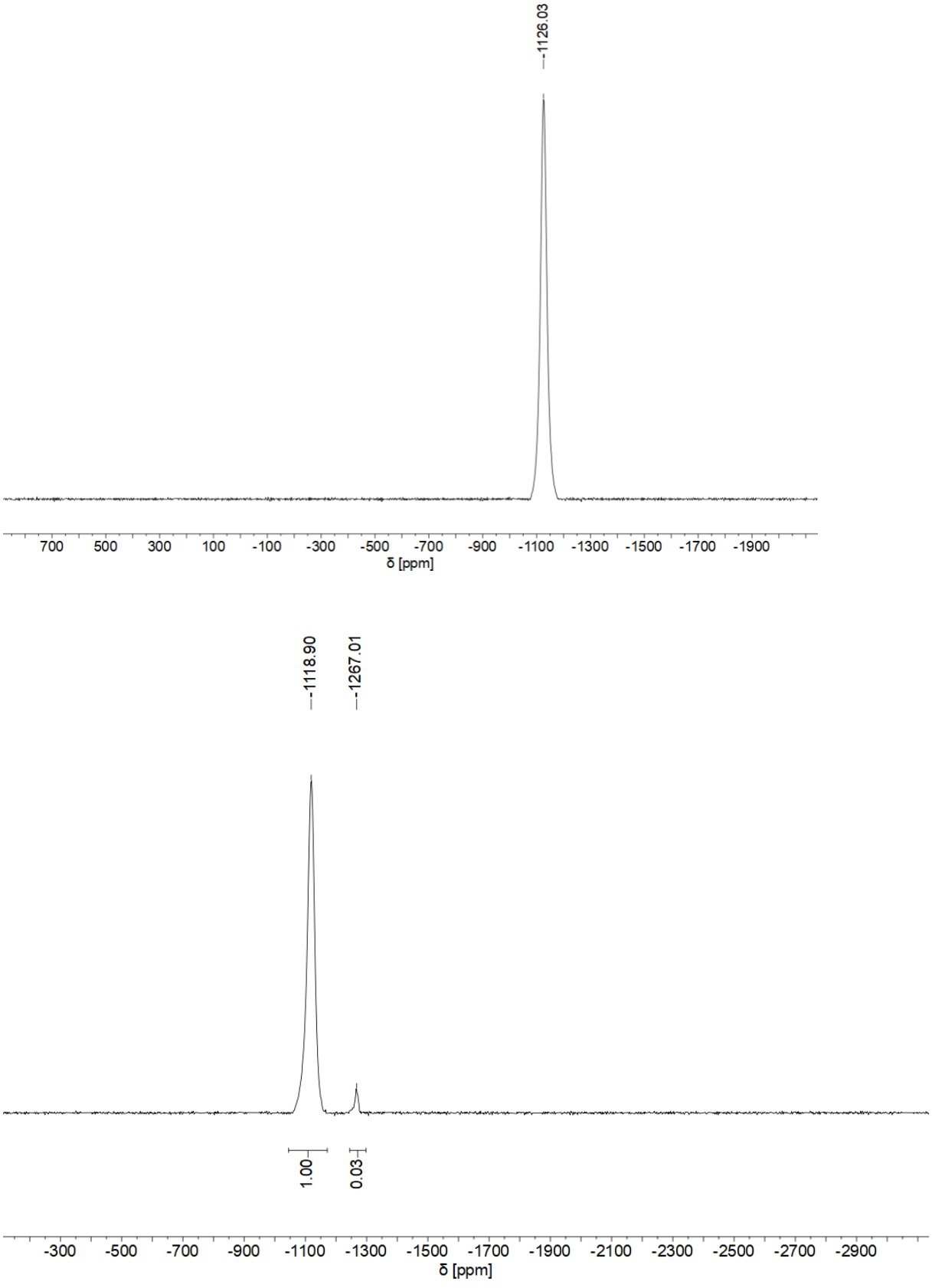

Figure S67. ^{31}P NMR spectrum of [Tc(η^2-Et$_2$btu)(CO)$_2$(PPh$_3$)$_2$].

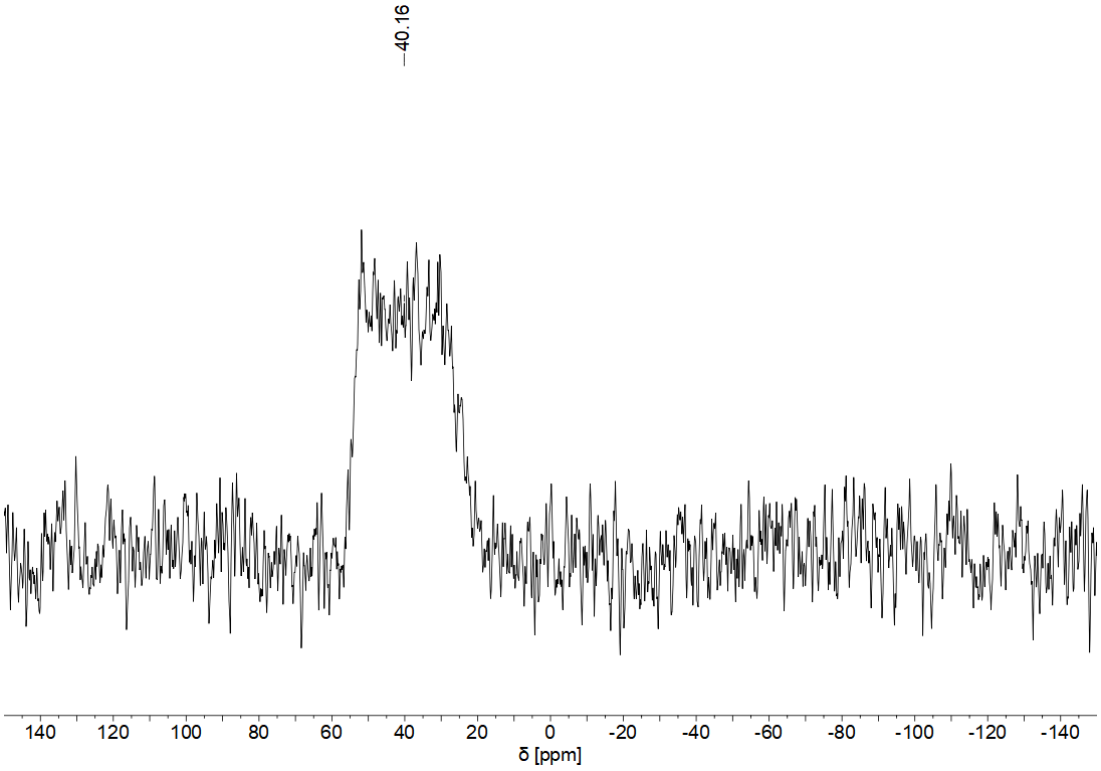

Figure S68. IR spectrum of [Tc(η^2-Et$_2$btu)(CO)$_2$(PPh$_3$)$_2$].

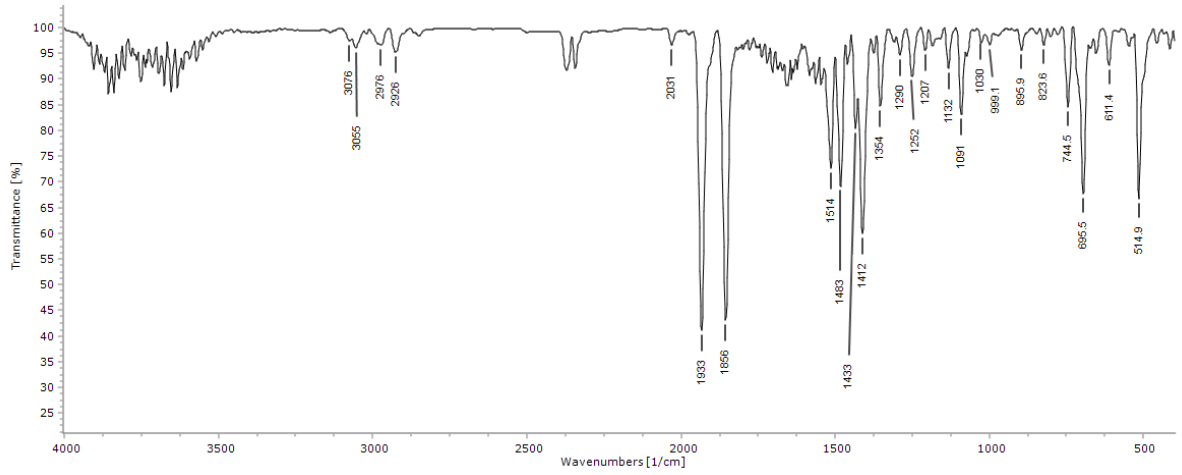

Figure S69. ^{1}H NMR spectrum of [Tc(η^2-oxH)(CO)$_2$(PPh$_3$)$_2$].

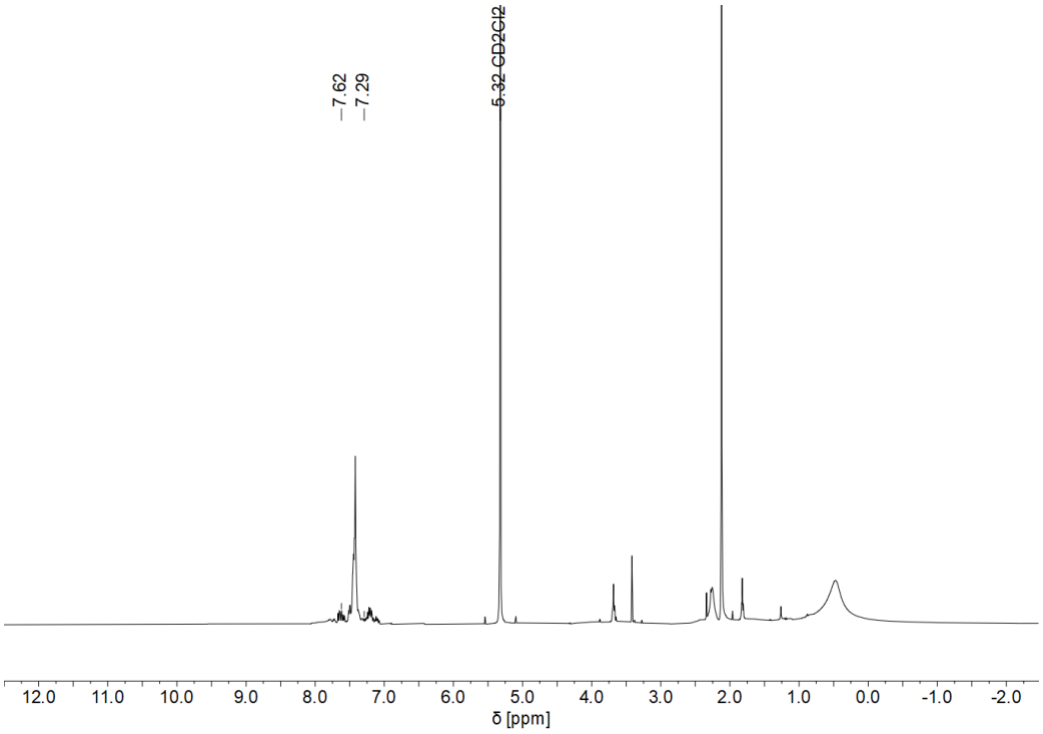

Figure S70. ^{99}Tc NMR spectrum of [Tc(η^2-oxH)(CO)$_2$(PPh$_3$)$_2$].

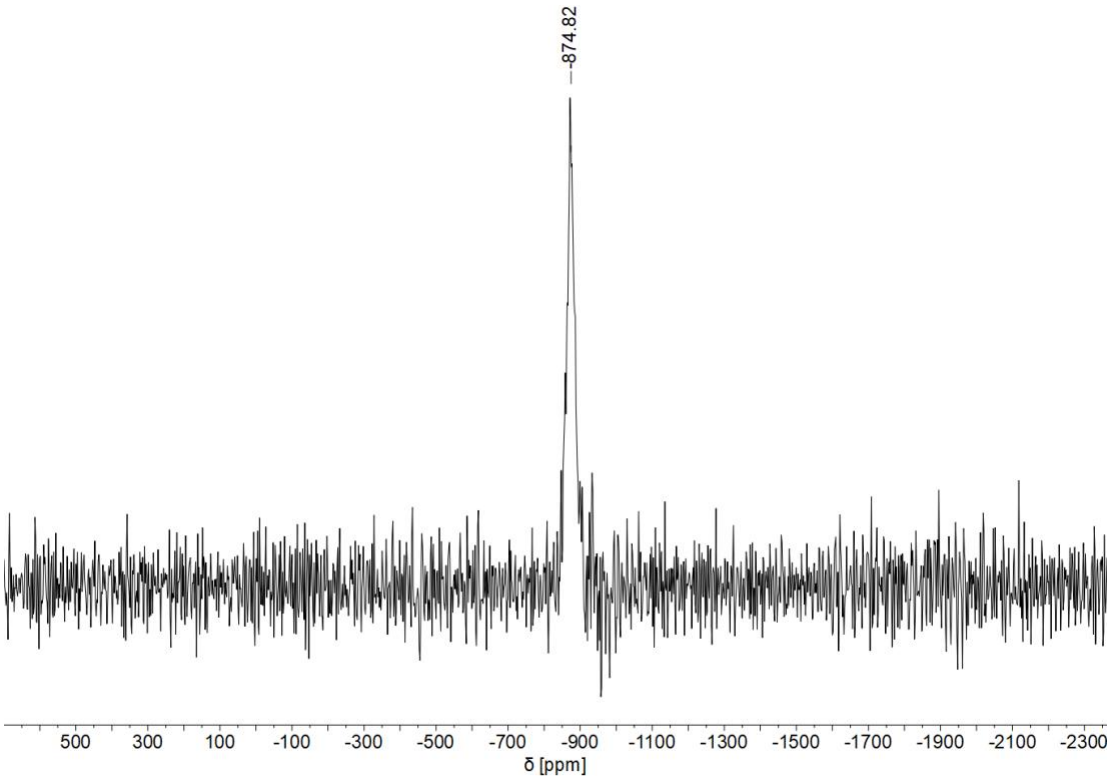

Figure S71. IR spectrum of [Tc(η^2-oxH)$(CO)_2(PPh_3)_2$].

IR

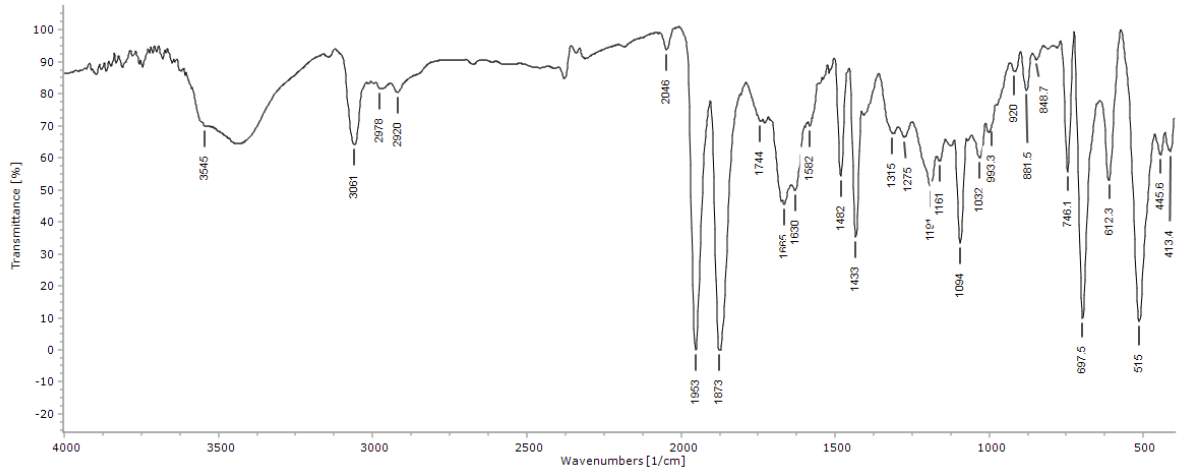

Figure S72. ^{1}H NMR spectrum of $(HNEt_3)$[Tc(η^2-ox)$(CO)_2(PPh_3)_2$].

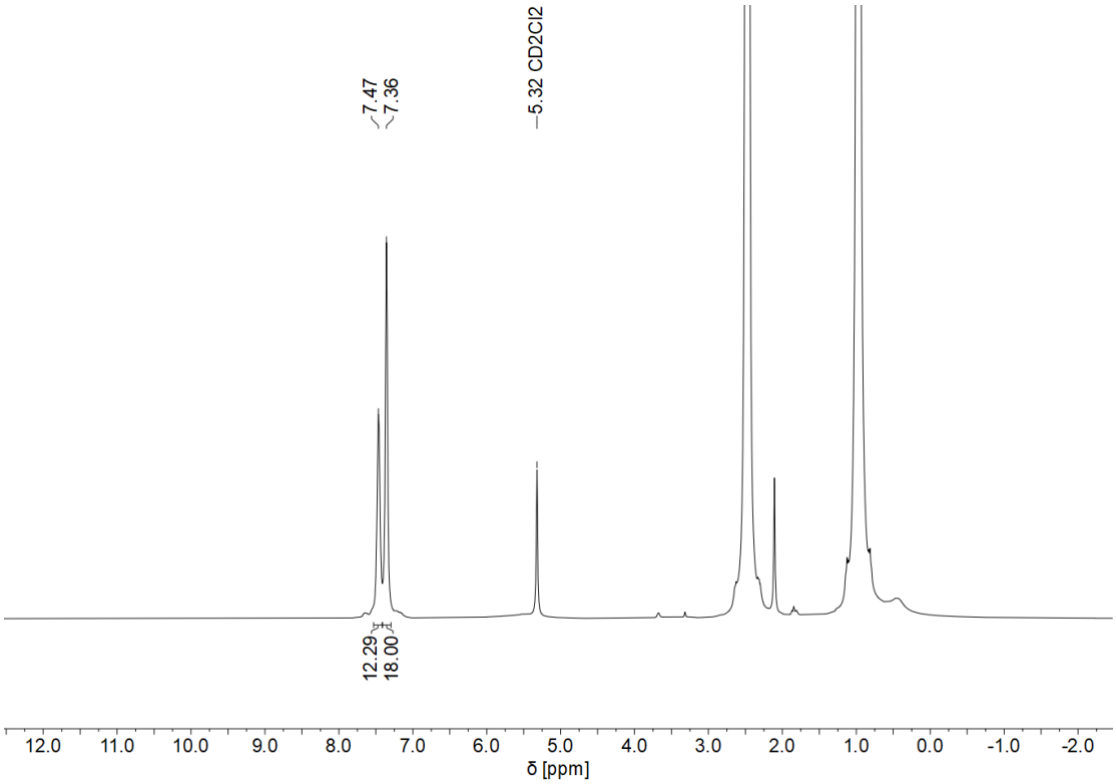

Figure S73. ^{31}P NMR spectrum of $(HNEt_3)[Tc(\eta^2\text{-ox})(CO)_2(PPh_3)_2]$.

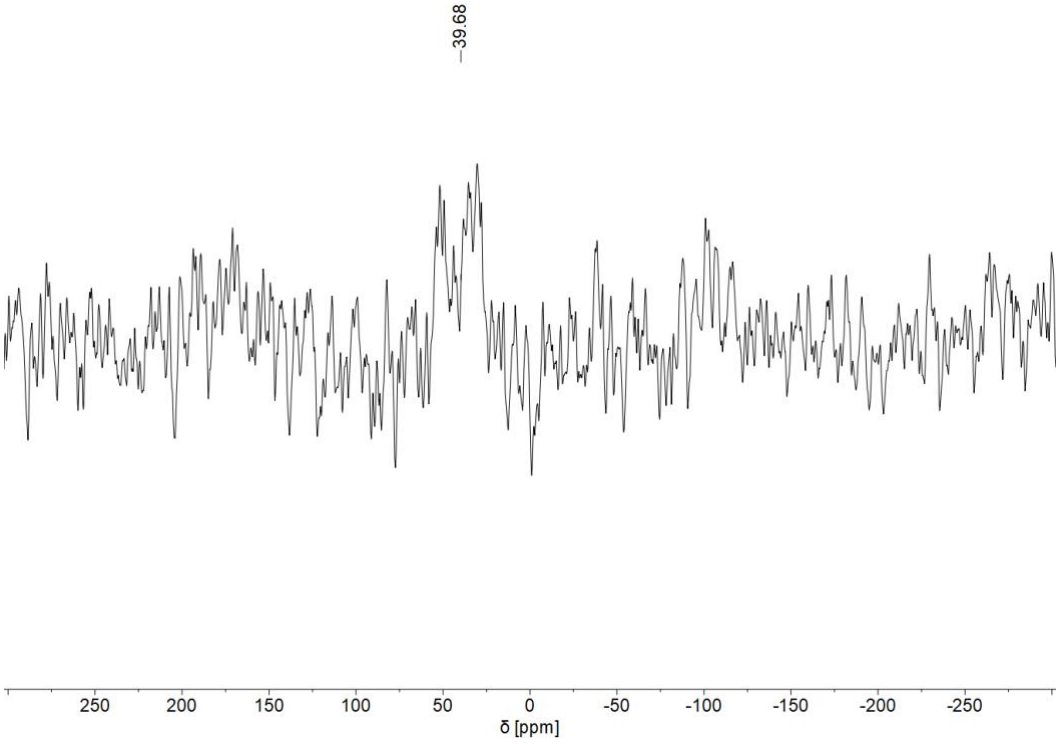

Figure S74. ^{99}Tc NMR spectrum of $(HNEt_3)[Tc(\eta^2\text{-ox})(CO)_2(PPh_3)_2]$.

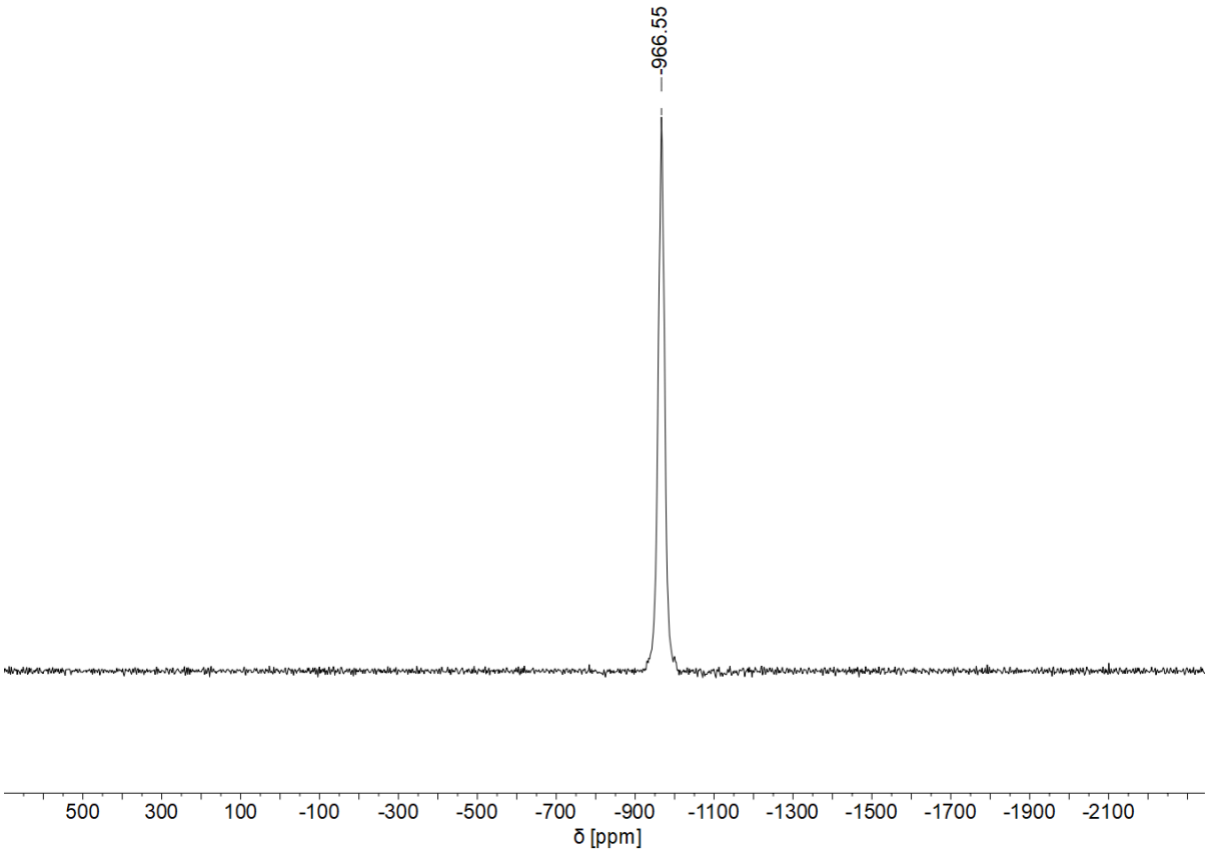

Figure S75. IR spectrum of $(HNEt_3)[Tc(\eta^2\text{-ox})(CO)_2(PPh_3)_2]$.

IR

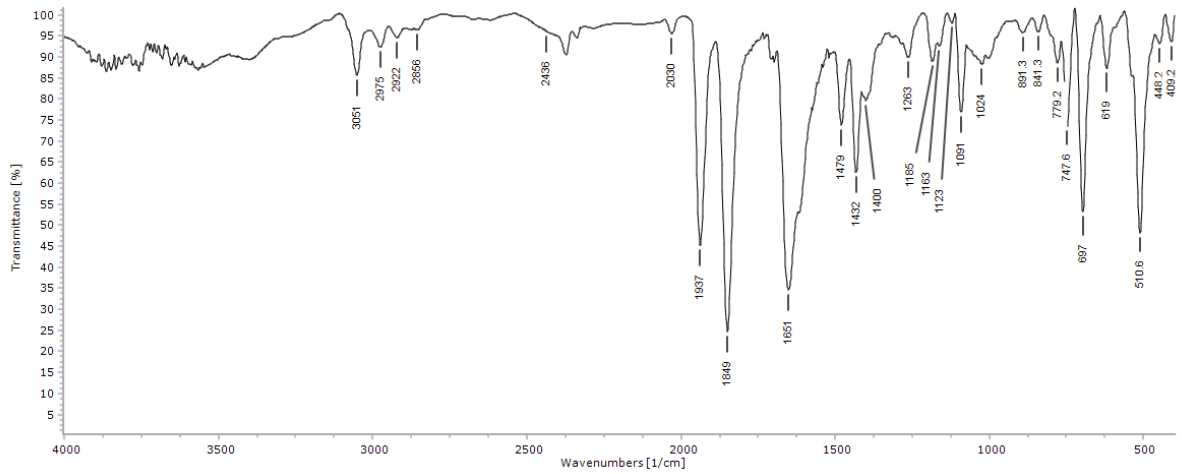

Figure S76. ^1H NMR spectrum of $[Tc_2(\mu^2\text{-}\eta^2\text{-ox})(CO)_6(OPPh_3)_2]$.

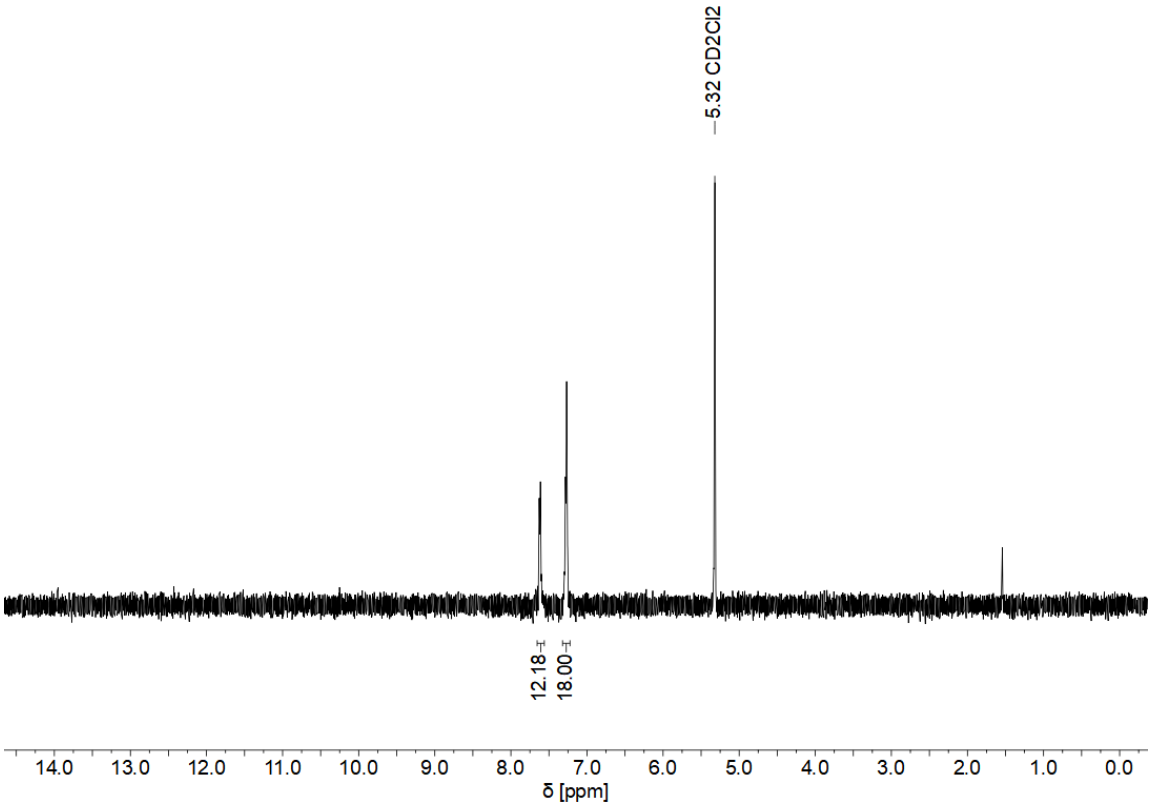

Figure S77. ^{31}P NMR spectrum of $[Tc_2(\mu^2\text{-}\eta^2\text{-ox})(CO)_6(OPPh_3)_2]$.

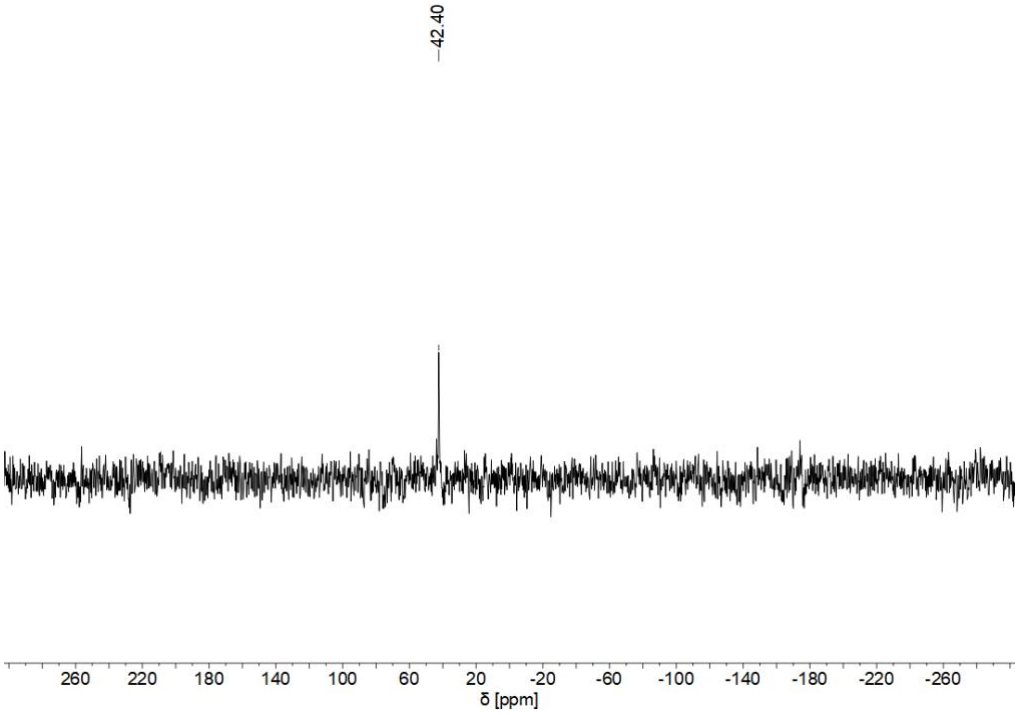

Figure S78. ^{99}Tc NMR spectrum of $[Tc_2(\mu^2\text{-}\eta^2\text{-ox})(CO)_6(OPPh_3)_2]$.

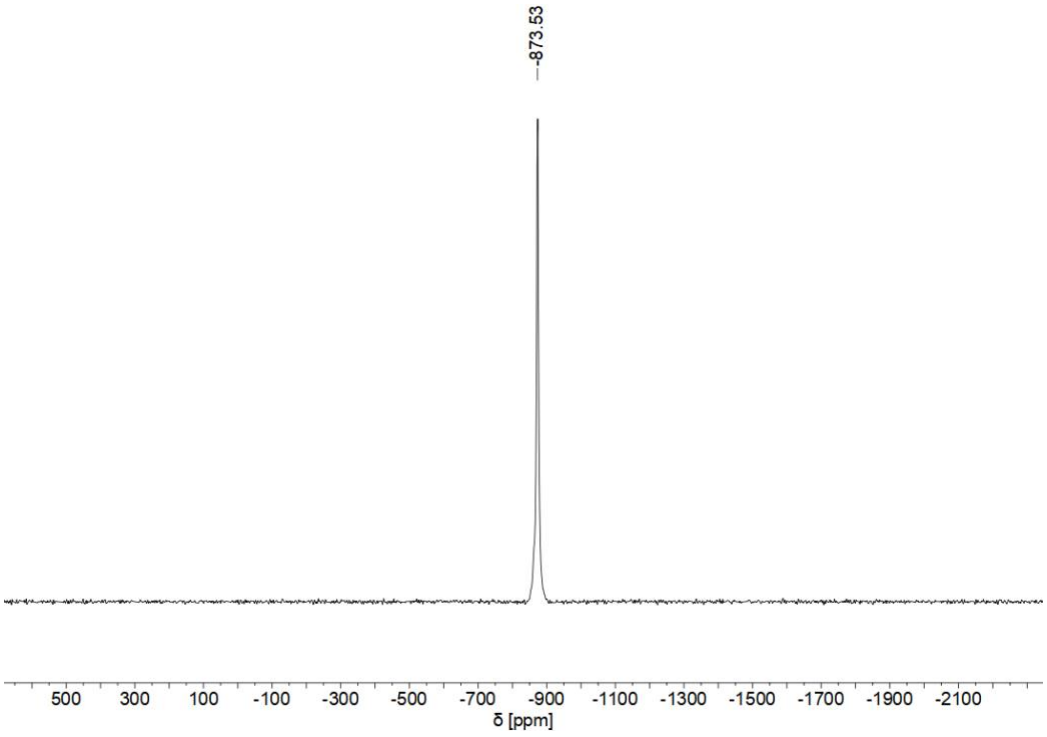

Figure S79. IR spectrum of $[Tc_2(\mu^2\text{-}\eta^2\text{-ox})(CO)_6(OPPh_3)_2]$.

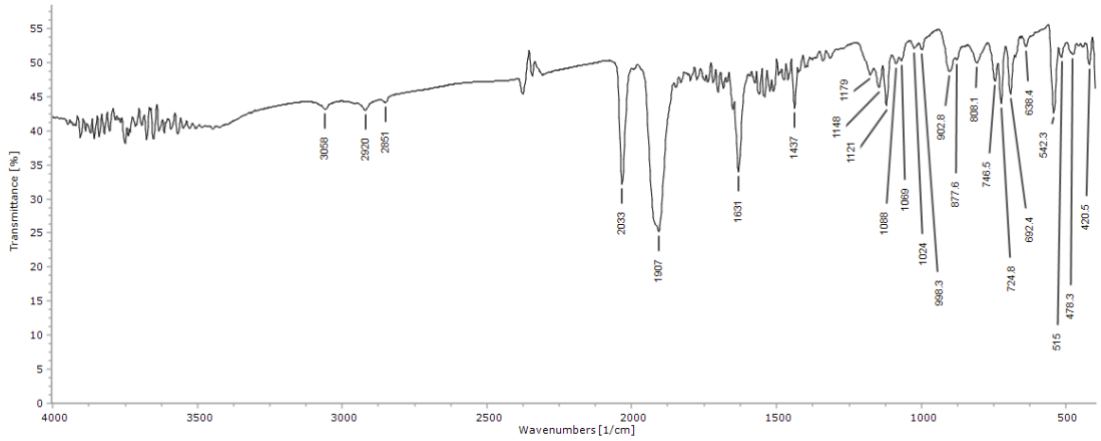

Figure S80. ^{1}H NMR spectrum of $[\{Tc(CO)_3\}_3(\mu^3\text{-}OH)(\mu^2\text{-}O(SePh)O)_3\{Tc(CO)_3\}] \cdot (OPPh_3)$.

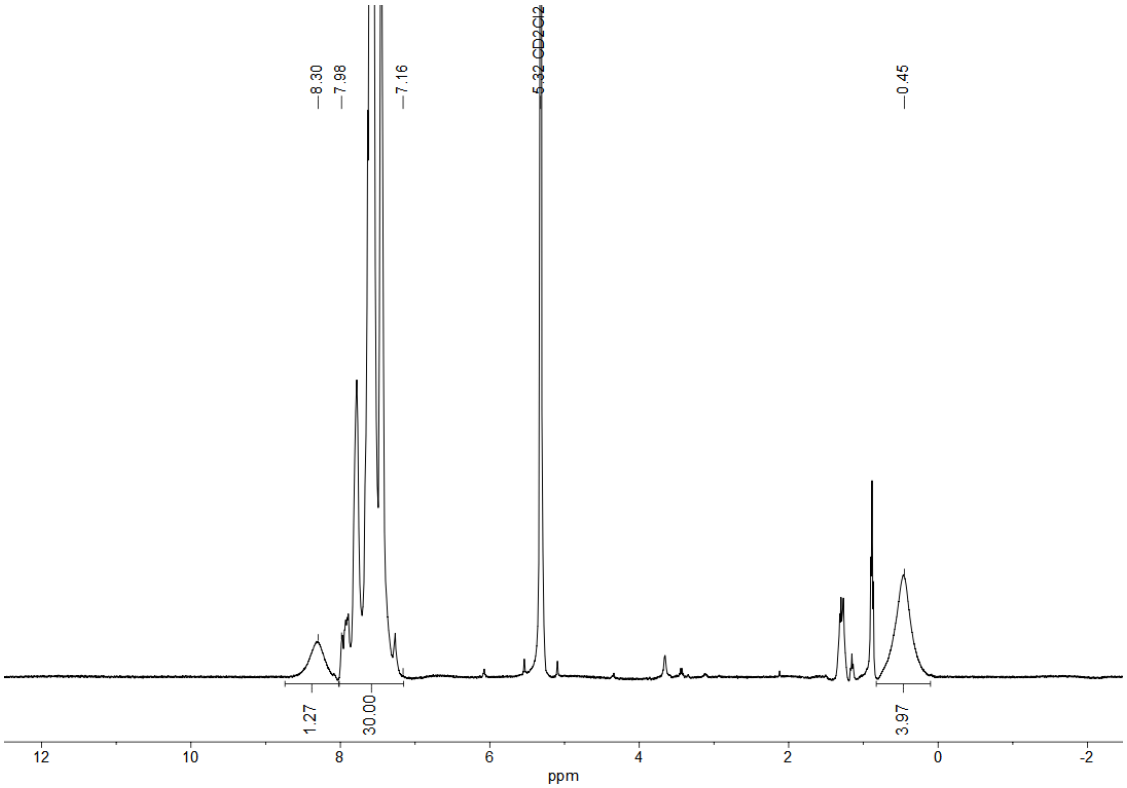

Figure S81. ^{31}P NMR spectrum of [{$Tc(CO)_3$}$_3$(μ^3-OH)(μ^2-O(SePh)O)$_3${$Tc(CO)_3$}] · ($OPPh_3$).

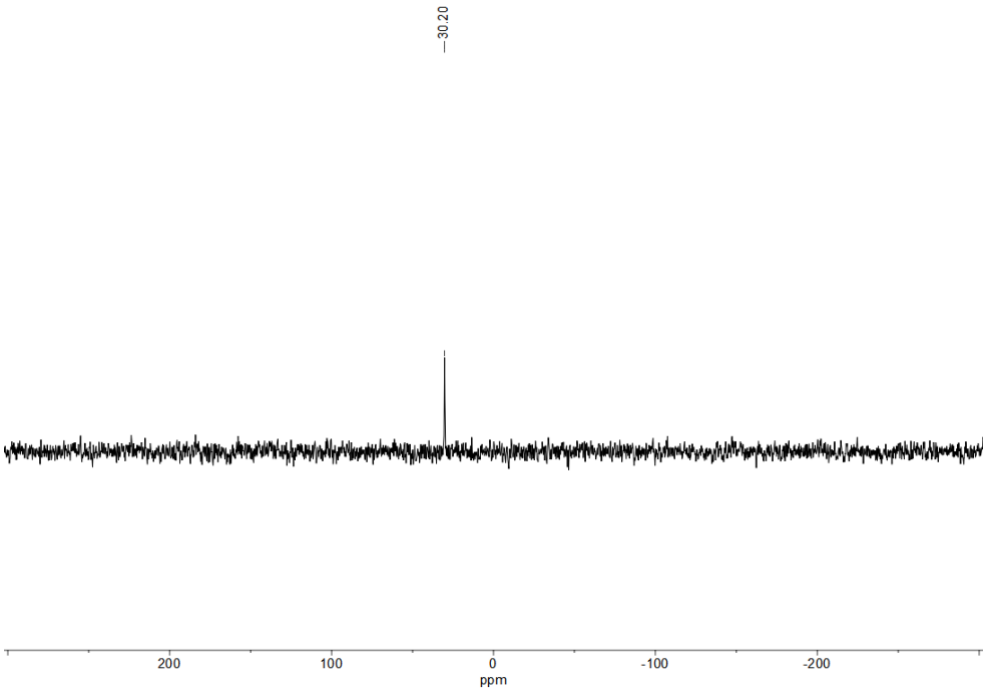

Figure S82. IR spectrum of [{$Tc(CO)_3$}$_3$(μ^3-OH)(μ^2-O(SePh)O)$_3${$Tc(CO)_3$}] · ($OPPh_3$).

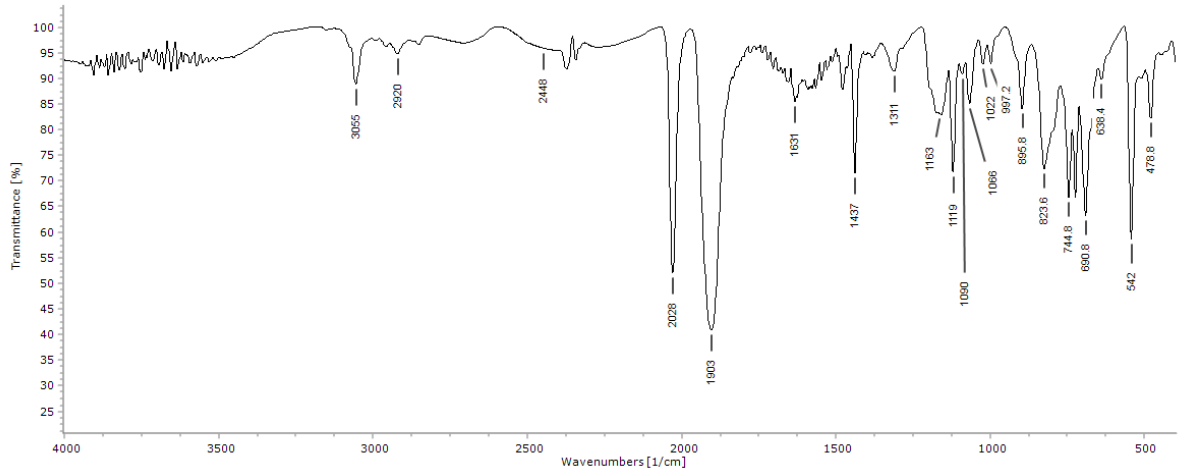

Figure S83. ^{99}Tc NMR spectra of [{Tc(CO)$_3$}$_3$(μ^3-OH)(μ^2-O(SePh)O)$_3${Tc(CO)$_3$}] · (OPPh$_3$)

(focussed on the -580 ppm signal

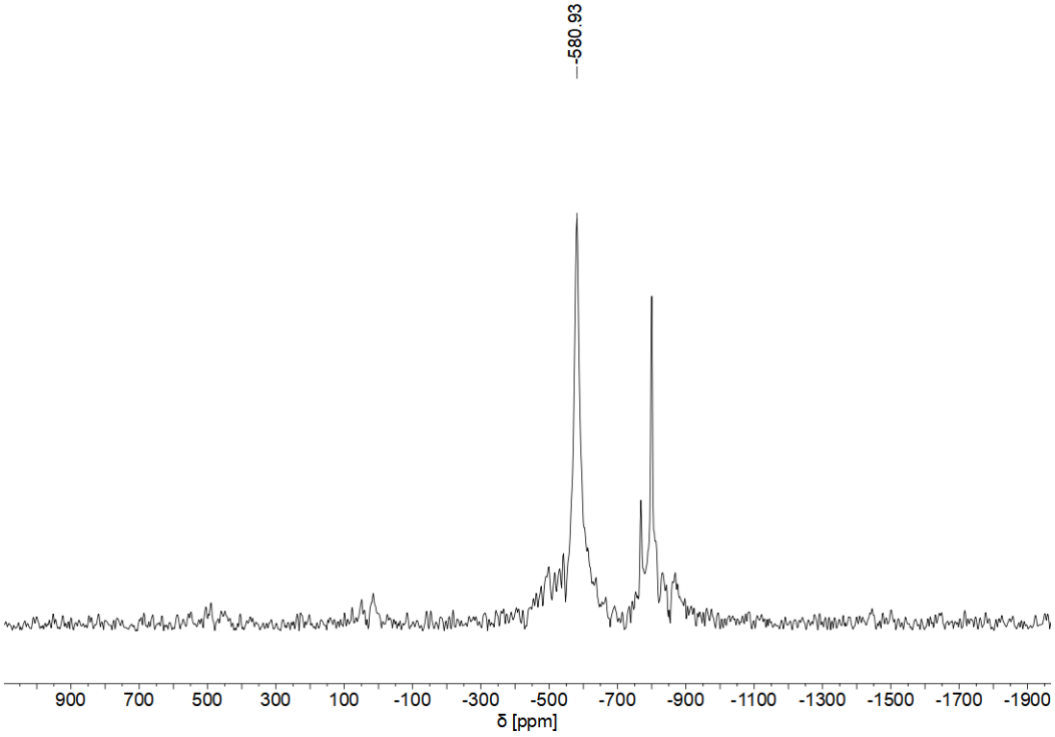

Focussed on the -764 ppm to -860 ppm signals

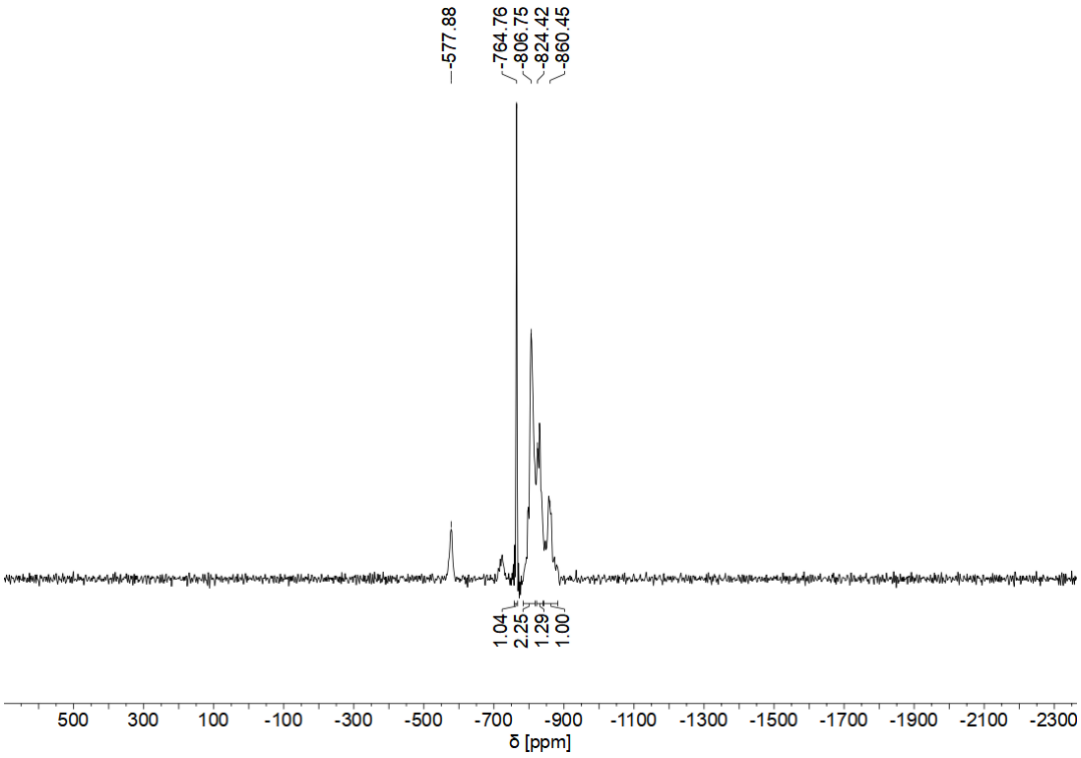

Figure S84. *In-situ* NMR spectra of the reaction between $[TcH(CO)_3(PPh_3)_2]$ and PhSeOOH with and without HCOOH.
Stacking of all relevant spectra in the reaction of $[TcH(CO)_3(PPh_3)_2]$ with PhSeOOH in toluene followed by addition of methanol/H_2O/Et_2O.

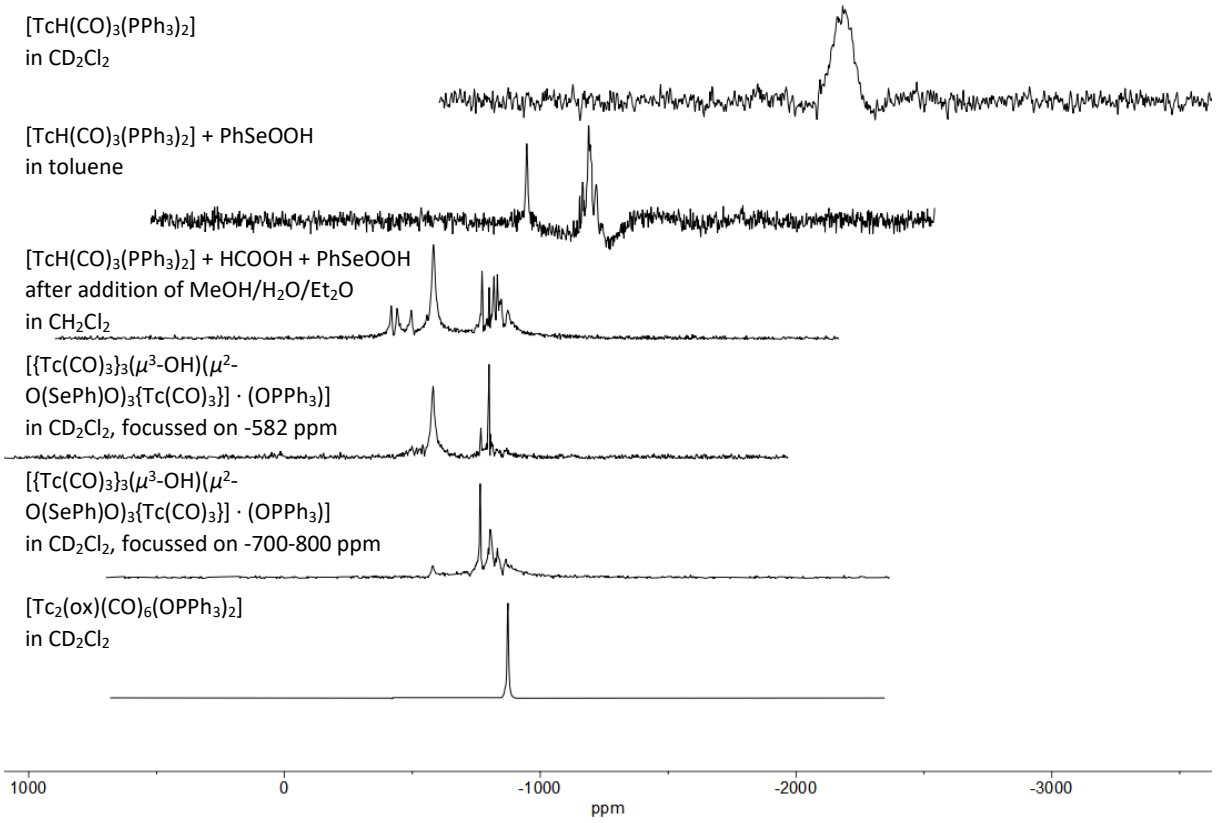

Figure S85. Stacking of all relevant spectra in the reaction of $[TcH(CO)_3(PPh_3)_2]$ with HCOOH and PhSeOOH in toluene followed by addition of methanol/H_2O/Et_2O.

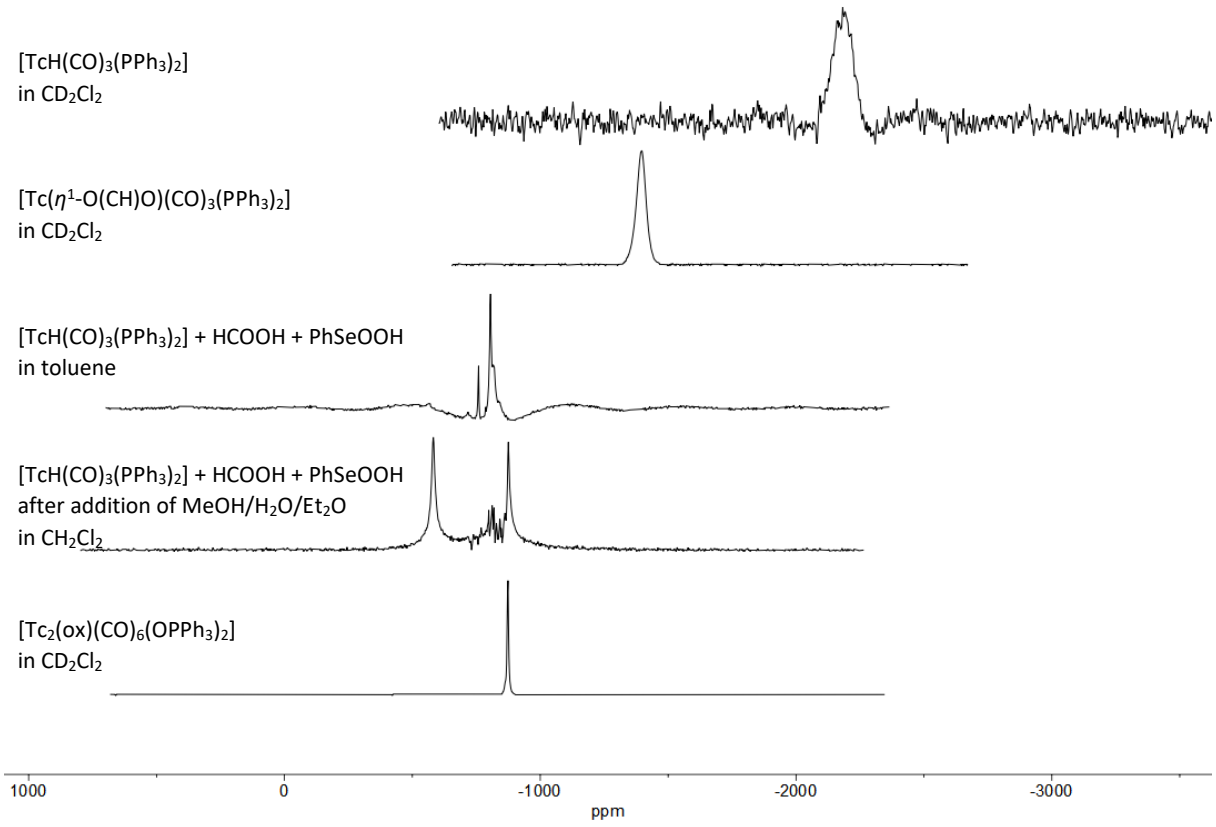

Figure S86. Stacking of the spectra of all relevant reaction mixtures and isolated species.

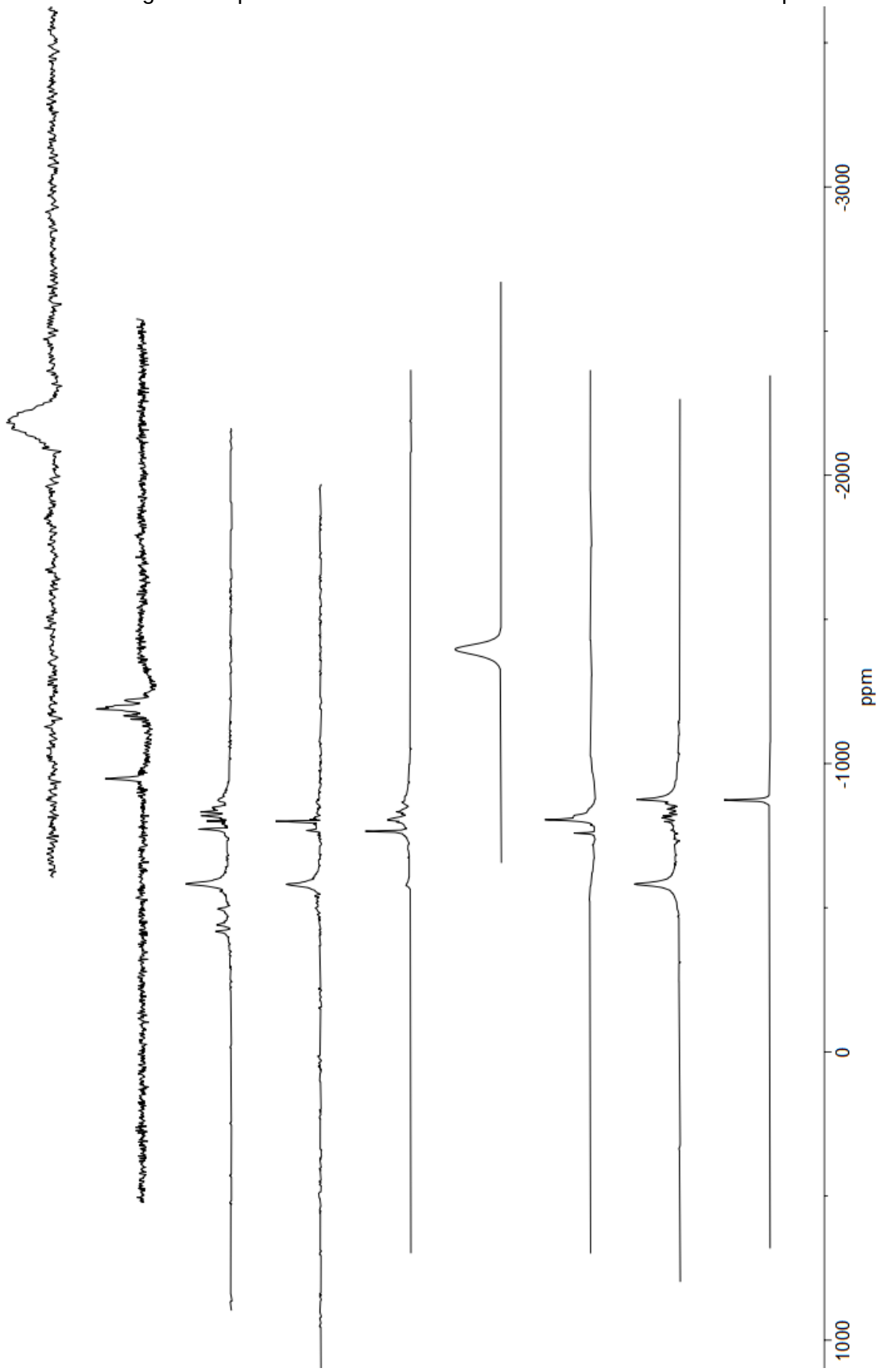

Figure S87. Potential mechanism for the formation of $[Tc_2(\mu^2\text{-}\eta^2\text{-ox})(CO)_6(OPPh_3)_2]$ from $[TcH(CO)_3(PPh_3)_2]$, MeOH and PhSeOOH.

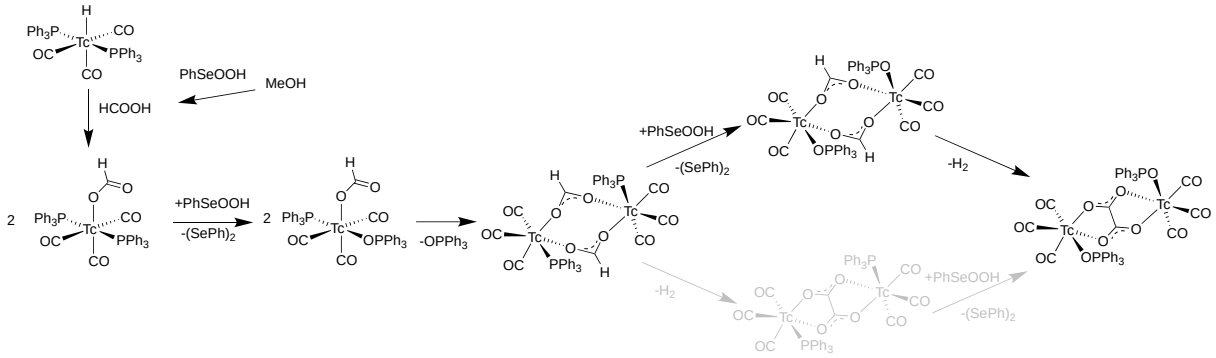

Part 4: Attempted reaction of $[TcH(CO)_3(PPh_3)_2]$ with HF·py.

HF·py (3 drops) was added to a suspension of $[TcH(CO)_3(PPh_3)_2]$ (35 mg, 0.05 mmol) in THF (1 mL). Gas evolution was imminent, but the starting material did not dissolve. Heating for 5 min resulted in the formation of a clear yellow solution, from which the starting material was recovered upon layering MeOH (5 ml) and storage in the fridge overnight.

References

(1) High performance computing (HPC) system Curta at Freie Universität Berlin. DOI: 10.17169/refubium-26754.

(2) Gaussian 16, Revision B.01, Frisch, M. J.; Trucks, G. W.; Schlegel, H. B.; Scuseria, G. E.; Robb, M. A.; Cheeseman, J. R.; Scalmani, G.; Barone, V.; Petersson, G. A.; Nakatsuji, H.; Li, X.; Caricato, M.; Marenich, A. V.; Bloino, J.; Janesko, B. G.; Gomperts, R.; Mennucci, B.; Hratchian, H. P.; Ortiz, J. V.; Izmaylov, A. F.; Sonnenberg, J. L.; Williams-Young, D.; Ding, F.; Lipparini, F.; Egidi, F.; Goings, J.; Peng, B.; Petrone, A.; Henderson, T.; Ranasinghe, D.; Zakrzewski, V. G.; Gao, J.; Rega, N.; Zheng, G.; Liang, W.; Hada, M.; Ehara, M.; Toyota, K.; Fukuda, R.; Hasegawa, J.; Ishida, M.; Nakajima, T.; Honda, Y.; Kitao, O.; Nakai, H.; Vreven, T.; Throssell, K.; Montgomery, J. A. Jr.; Peralta, J. E.; Ogliaro, F.; Bearpark, M. J.; Heyd, J. J.; Brothers, E. N.; Kudin, K. N.; Staroverov, V. N.; Keith, T. A.; Kobayashi, R.; Normand, J.; Raghavachari, K.; Rendell, A. P.; Burant, J. C.; Iyengar, S. S.; Tomasi, J.; Cossi, M.; Millam, J. M.; Klene, M.; Adamo, C.; Cammi, R.; Ochterski, J. W.; Martin, R. L.; Morokuma, K.; Farkas, O.; Foresman, J. B.; Fox D. J., Gaussian, Inc., Wallingford CT, **2016**.

(3) GaussView, Version 6, Dennington, R.; Keith, T. A.; Millam, J. M. Semichem Inc., Shawnee Mission, KS, **2016**.

(4) Hanwell, M. D.; Curtis, D. E.; Lonie, D. C.; Vandermeersch, C.; Zurek, E.; Hutchison, G. R. Avogadro: An advanced semantic chemical editor, visualization, and analysis platform. *J. Cheminform.* **2012**, *4*:17

(5) Vosko, S. H.; Wilk, L.; Nusair, M. Accurate spin-dependent electron liquid correlation energies for local spin density calculations: a critical analysis. *Can. J. Phys.* **1980**, *58*, 1200–1211.

(6) Becke, A. D. Density-functional thermochemistry. III. The role of exact exchange. *J. Chem. Phys.* **1993**, *98*, 5648-5652

(7) Lee, C.; Yang, W.; Parr, R. G. Development of the Colle-Salvetti correlation-energy formula into a functional of the electron density. *Phys. Rev.* **1988**, *B37*, 785–789.

(8) Wadt, W. R.; Hay, P. J. Ab initio effective core potentials for molecular calculations. Potentials for main group elements Na to Bi. *J. Chem. Phys.* **1985**, *82*, 284-298.

(9) Andrae, D.; Häußermann, U.; Dolg, M.; Stoll, H.; Preuß, H. Energy-adjusted ab initio pseudopotentials for the second and third row transition elements. *Theor. Chim. Acta* **1990**, *77*, 123-141.

(10) Martin, J. M. L.; Sundermann, A. Correlation consistent valence basis sets for use with the Stuttgart-Dresden-Bonn relativistic effective core potentials: The atoms Ga-Kr and In-Xe. *J. Chem. Phys.* **2001**, *114*, 3408-3420.

(11) Krishnan, R.; Binkley, J. S.; Seeger, R.; Pople, J. A. Self-consistent molecular orbital methods. XX. A basis set for correlated wave functions. *J. Chem. Phys*. **1980**, *72*, 650-654.

(12) Clark, T.; Chandrasekhar, J.; Spitznagel; G. W.; Schleyer, P. V. R. Efficient diffuse function-augmented basis sets for anion calculations. III. The 3-21+G basis set for first-row elements, Li-F. *J. Comput. Chem*. **1983**, *4*, 294-301.

(13) Franzke, Y. J.; Treß, R.; Pazdera, T. M.; Weigend, F. Error-consistent segmented contracted all-electron relativistic basis sets of double- and triple-zeta quality for NMR shielding constants. *Phys. Chem. Chem. Phys*. **2019**, *21*, 16658-16664.

(14) Schuchardt, K. L.; Didier, B. T.; Elsethagen, T.; Sun, L.; Gurumoorthi, V.; Chase, J.; Li, J.; Windus, T. L. Basis Set Exchange: A Community Database for Computational Sciences. *J. Chem. Inf. Model.* **2007**, *47*, 1045–1052.

(15) Grimme, S. Supramolecular Binding Thermodynamics by Dispersion-Corrected Density Functional Theory. *Chem. Eur. J*., **2012**, *18*, 9955–9964.

(16) Paton, R.; Funes-Ardoiz, I. ; https://zenodo.org/badge/latestdoi/16266/bobbypaton/GoodVibes; DOI: 10.5281/zenodo.3346166.

(17) Lu, T.; Chen, F. Multiwfn: A multifunctional wavefunction analyzer. *J. Comput. Chem.*, **2012**, *33*, 580–592.

(18) Menges, F. Spectragryph, Software for Optical Spectroscopy, Version 1.2.8, 2016–2020.

A.2 $[Tc(OH_2)(CO)_3(PPh_3)_2]^+$: A Synthon for Tc(I) Complexes and its Reactions with Neutral Ligands

Authors	M. Roca Jungfer, U. Abram
Journal	*Inorg. Chem.* **2021***, 60*, 16734–16753
DOI	10.1021/acs.inorgchem.1c02599
Link	https://pubs.acs.org/doi/10.1021/acs.inorgchem.1c02599
Detailed scientific contribution	Maximilian Roca Jungfer and Ulrich Abram designed the project. Maximilian Roca Jungfer performed the synthesis and characterization of the compounds, calculated the X-ray structures and wrote a draft of the manuscript. Ulrich Abram supervised the project, provided scientific guidance and suggestions and corrected the manuscript.
Estimated own contribution	90%

Return to publication 4.2.

Supporting information for the paper entitled:

$[Tc(OH_2)(CO)_3(PPh_3)_2]^+$: A Synthon for the Tc(I) Complexes and its Reactions with Neutral Ligands.

Maximilian Roca Jungfer, Ulrich Abram*

[a]*Freie Universität Berlin, Institute of Chemistry and Biochemistry, Fabeckstr. 34–36, 14195 Berlin, Germany*

E-mail: ulrich.abram@fu-berlin.de

Table of Contents

Part 1: Crystallographic data

Table S1. Crystal data and structure determination parameters.

	$[Tc(OH_2)(CO)_3(PPh_3)_2][BArF_{24}]\cdot 0.5CH_2Cl_2$	α-$[Tc(OH_2)(CO)_3(PPh_3)_2][BF_4]$	β-$[Tc(OH_2)(CO)_3(PPh_3)_2][BF_4]$
Number code	**1a**·$0.5CH_2Cl_2$	**1b**	**1b**
Empirical formula	$C_{143}H_{90}B_2Cl_2F_{48}O_8P_4Tc_2$	$C_{39}H_{32}BF_4O_4P_2Tc$	$C_{39}H_{32}BF_4O_4P_2Tc$
Formula weight	3260.54	811.39	811.39
Temperature/K	293(2)	230(2)	230(2)
Crystal system	Triclinic	Triclinic	Monoclinic
Space group	$P\bar{1}$	$P\bar{1}$	$P2_1/n$
a/Å	13.5169(8)	11.3147(9)	12.8320(12)
b/Å	18.2894(12)	12.3699(10)	14.5283(7)
c/Å	18.3875(12)	14.5560(10)	19.8885(17)
α/°	107.396(5)	96.276(6)	90
β/°	110.446(5)	92.001(6)	97.541(7)
γ/°	104.856(5)	112.876(6)	90
Volume/$Å^3$	3718.8(4)	1859.1(3)	3675.7(5)
Z	1	2	4
$\rho_{calc}g/cm^3$	1.456	1.449	1.466
μ/mm^{-1}	0.379	0.533	0.539
F(000)	1634	824	1648
Crystal size/mm^3	0.52 x 0.48 x 0.45	0.320 x 0.100 x 0.035	0.411 x 0.150 x 0.051
Radiation	0.71073 Å	0.71073 Å	0.71073 Å
2Θ range for data collection/°	3.273 to 26.999	3.445 to 28.998	3.203 to 26.249
Index ranges	-17<=h<=16, -23<=k<=23, -19<=l<=23	-11<=h<=15, -16<=k<=16, -19<=l<=19	-15<=h<=15, -18<=k<=16, -24<=l<=24
Reflections collected	33664	20308	21035
Independent reflections	16105 [R(int) = 0.0436]	9813 [R(int) = 0.0606]	7378 [R(int) = 0.0717]
Data/restraints/parameters	16105 / 1480 / 1209	9813 / 0 / 468	7378 / 0 / 460
Goodness-of-fit on F^2	0.961	0.738	0.812
Final R indexes [I>=2σ (I)]	R1 = 0.0425, wR2 = 0.1121	R1 = 0.0363, wR2 = 0.0581	R1 = 0.0433, wR2 = 0.0776
Final R indexes [all data]	R1 = 0.0606, wR2 = 0.1215	R1 = 0.0818, wR2 = 0.0642	R1 = 0.1017, wR2 = 0.0894
Largest diff. peak/hole / e $Å^{-3}$	0.558 and -0.558	0.427 and -0.598	0.411 and -0.655
CCDC access code	2103082	2103086	2103102

Table S1. Crystal data and structure determination parameters (continued).

	$[Tc(OH_2)(CO)_3(PPh_3)_2][BF_4]\cdot Et_2O$	$[Tc(OH_2)(CO)_3(PPh_3)_2][OTf]$	$[Tc(DMSO)_2(CO)_2(PPh_3)_2][BF_4]$ ·toluene
Number code	**1b**·Et_2O	**1c**	**3**·toluene
Empirical formula	$C_{43}H_{42}BF_4O_5P_2Tc$	$C_{40}H_{32}F_3O_7P_2STc$	$C_{49}H_{50}BF_4O_4P_2S_2Tc$
Formula weight	885.51	873.65	1013.76
Temperature/K	230(2)	230(2)	293(2)
Crystal system	Triclinic	Triclinic	Orthorhombic
Space group	$P\bar{1}$	$P\bar{1}$	$Pca2_1$
a/Å	12.316(5)	11.2597(5)	24.369(5)
b/Å	13.473(3)	12.3145(5)	10.077(3)
c/Å	14.130(5)	15.3704(7)	20.012(5)
α/°	87.28(2)	97.262(4)	90
β/°	65.32(3)	94.663(4)	90
γ/°	83.89(3)	111.302(3)	90
Volume/$Å^3$	2118.5(13)	1950.94(15)	4914(2)
Z	2	2	4
$\rho_{calc}g/cm^3$	1.388	1.487	1.37
μ/mm^{-1}	0.475	0.567	0.5
F(000)	908	888	2088
Crystal size/mm^3	0.20 x 0.18 x 0.15	0.820 x 0.450 x 0.440	0.440 x 0.320 x 0.130
Radiation	0.71073 Å	0.71073 Å	0.71073 Å
2Θ range for data collection/°	3.332 to 25.007	3.389 to 29.162	3.321 to 28.996
Index ranges	-14<=h<=14, -15<=k<=16, -15<=l<=16	-15<=h<=14, -13<=k<=16, -21<=l<=21	-33<=h<=33, -13<=k<=13, -27<=l<=27
Reflections collected	15973	21698	50910
Independent reflections	7412 [R(int) = 0.0976]	10443 [R(int) = 0.0368]	13019 [R(int) = 0.0485]
Data/restraints/parameters	7412 / 650 / 541	10443 / 0 / 495	13019 / 203 / 646
Goodness-of-fit on F^2	0.605	1.03	0.989
Final R indexes [I>=2σ (I)]	R1 = 0.0438, wR2 = 0.0554	R1 = 0.0346, wR2 = 0.0959	R1 = 0.0394, wR2 = 0.0866
Final R indexes [all data]	R1 = 0.1325, wR2 = 0.0700	R1 = 0.0400, wR2 = 0.0986	R1 = 0.0544, wR2 = 0.0914
Largest diff. peak/hole / e $Å^{-3}$	0.445 and -0.277	0.968 and -0.954	0.918 and -0.533
Absolute structure parameter	-	-	-0.01(1)
CCDC access code	2103103	2103091	2103087

Table S1. Crystal data and structure determination parameters (continued).

	$[Tc(DMF)(CO)_3(PPh_3)_2][BF_4]$	$[Tc(DMF)(CO)_3(PPh_3)_2][BF_4]$ ·0.5pentane	$[Tc(DMF)_2(CO)_2(PPh_3)_2][BF_4]$ ·toluene
Number code	**4**	**4**·0.5pentane	**5**·toluene
Empirical formula	$C_{42}H_{37}BF_4NO_4P_2Tc$	$C_{44.50}H_{43}BF_4NO_4P_2Tc$	$C_{51}H_{52}BF_4N_2O_4P_2Tc$
Formula weight	866.47	902.55	1003.69
Temperature/K	293(2)	293(2)	100(2)
Crystal system	Monoclinic	Triclinic	Triclinic
Space group	$P2_1/n$	$P\bar{1}$	$P\bar{1}$
a/Å	9.5175(13)	9.6528(7)	12.0819(7)
b/Å	19.298(3)	10.8387(7)	14.1249(10)
c/Å	22.926(3)	22.4838(15)	14.8289(9)
α/°	90	100.764(5)	89.271(2)
β/°	100.310(11)	100.362(6)	78.836(2)
γ/°	90	94.075(5)	75.176(2)
Volume/Å^3	4142.9(10)	2259.9(3)	2398.3(3)
Z	4	2	2
ρ_{calc}g/cm^3	1.389	1.326	1.390
μ/mm^{-1}	0.484	0.446	0.429
F(000)	1768	926	1036
Crystal size/mm^3	0.61 x 0.05 x 0.05	0.230 x 0.130 x 0.060	0.15 x 0.07 x 0.04
Radiation	0.71073 Å	0.71073 Å	0.71073 Å
2Θ range for data collection/°	3.157 to 26.055	3.298 to 29.270	2.005 to 27.329
Index ranges	-11<=h<=11, -23<=k<=23, -6<=l<=28	-12<=h<=13, -14<=k<=14, -24<=l<=30	-15<=h<=15, -18<=k<=18, -18<=l<=19
Reflections collected	8145	24325	45079
Independent reflections	8145	11953 [R(int) = 0.0478]	10606 [R(int) = 0.0674]
Data/restraints/parameters	8145 / 598 / 429	11953 / 627 / 521	10606 / 1063 / 786
Goodness-of-fit on F^2	1.171	0.992	1.066
Final R indexes [I>=2σ (I)]	R1 = 0.1627, wR2 = 0.4631	R1 = 0.0688, wR2 = 0.1951	R1 = 0.0564, wR2 = 0.1232
Final R indexes [all data]	R1 = 0.2849, wR2 = 0.4991	R1 = 0.0988, wR2 = 0.2141	R1 = 0.0718, wR2 = 0.1305
Largest diff. peak/hole / e Å^{-3}	1.021 and -1.400	2.537 and -1.376	1.589 and -0.998
CCDC access code	2103104	2103088	2104393

Table S1. Crystal data and structure determination parameters (continued).

	$[Tc(CO)_4(PPh_3)_2][BArF_{24}]$ $\cdot 0.25CH_2Cl_2$	$[Tc(CO)_4(PPh_3)_2][BF_4]$	$2[Tc(CO)_4(PPh_3)_2][OTf]$ $\cdot HOTf$
Number Code	**6a**$\cdot 0.25CH_2Cl_2$	**6b**	**6c**$\cdot$HOTf
Empirical formula	$C_{144.50}H_{85}B_2ClF_{48}O_8P_4Tc_2$	$C_{40}H_{30}BF_4O_4P_2Tc$	$C_{83}H_{61}F_9O_{17}P_4S_3Tc_2$
Formula weight	3238.07	821.39	1917.37
Temperature/K	293(2)	230(2)	273(2)
Crystal system	Triclinic	Orthorhombic	Triclinic
Space group	$P\bar{1}$	$P2_12_12$	$P\bar{1}$
a/Å	13.4491(7)	11.6077(12)	9.132(4)
b/Å	18.2663(11)	14.856(2)	13.069(11)
c/Å	18.2745(10)	10.7450(13)	37.18(3)
α/°	107.049(4)	90	92.091(12)
β/°	110.826(4)	90	95.232(14)
γ/°	104.653(4)	90	109.036(14)
Volume/Å^3	3677.2(4)	1852.8(4)	4167(5)
Z	1	2	2
ρ_{calc}g/cm^3	1.462	1.472	1.528
μ/mm^{-1}	0.365	0.536	0.57
F(000)	1621	832	1940
Crystal size/mm^3	0.46 x 0.32 x 0.24	0.210 x 0.162 x 0.075	0.15 x 0.02 x 0.01
Radiation	0.71073 Å	0.71073 Å	0.71073 Å
2Θ range for data collection/°	3.325 to 29.318	3.256 to 25.982	1.921 to 27.515
Index ranges	-18<=h<=15, -25<=k<=25, -25<=l<=25	-14<=h<=13, -18<=k<=18, -12<=l<=13	-11<=h<=11, -16<=k<=16, -47<=l<=47
Reflections collected	40522	13570	18439
Independent reflections	19708 [R(int) = 0.0491]	3621 [R(int) = 0.1294]	18439
Data/restraints/parameters	19708 / 283 / 1160	3621 / 257 / 237	18439 / 1954 / 1052
Goodness-of-fit on F^2	0.895	0.827	1.114
Final R indexes [I>=2σ (I)]	R1 = 0.0477, wR2 = 0.1193	R1 = 0.0534, wR2 = 0.0769	R1 = 0.2337, wR2 = 0.5366
Final R indexes [all data]	R1 = 0.0782, wR2 = 0.1315	R1 = 0.1197, wR2 = 0.0914	R1 = 0.2443, wR2 = 0.5417
Largest diff. peak/hole / e Å^{-3}	0.902 and -1.130	0.418 and -0.687	7.164 and -7.584
Absolute structure parameter	-	0.37(5)	-
CCDC access code	2103090	2103101	-

Table S1. Crystal data and structure determination parameters (continued).

	$[Tc(SS(CPPh_3))(CO)_2(PPh_3)_2][BF_4]\cdot CH_2Cl_2$	$[Tc(CO)_3(CNCy)(PPh_3)_2][BF_4]$	$[Tc(NH_3)_2(CO)_2(PPh_3)_2][BF_4]$ ·pentane
Number code	**7**·CH_2Cl_2	**8**	**10**·pentane
Empirical formula	$C_{58}H_{47}BCl_2F_4O_2P_3S_2Tc$	$C_{46}H_{41}BF_4NO_3P_2Tc$	$C_{43}H_{48}BF_4N_2O_2P_2Tc$
Formula weight	1188.69	902.55	871.58
Temperature/K	230(2)	230(2)	230(2)
Crystal system	Triclinic	Triclinic	Triclinic
Space group	$P\bar{1}$	$P\bar{1}$	$P\bar{1}$
a/Å	10.0106(8)	8.9739(7)	12.2253(10)
b/Å	12.9606(10)	12.2598(9)	13.5547(14)
c/Å	22.8048(16)	21.1783(17)	14.3662(13)
α/°	102.134(6)	73.443(6)	89.987(8)
β/°	102.370(6)	79.837(6)	82.082(7)
γ/°	99.592(6)	71.491(6)	64.069(7)
Volume/$Å^3$	2755.2(4)	2108.4(3)	2115.7(4)
Z	2	2	2
$\rho_{calc}g/cm^3$	1.433	1.422	1.368
μ/mm^{-1}	0.577	0.477	0.471
F(000)	1212	924	900
Crystal size/mm^3	0.330 x 0.170 x 0.150	0.420 x 0.177 x 0.020	0.240 x 0.100 x 0.040
Radiation	0.71073 Å	0.71073 Å	0.71073 Å
2Θ range for data collection/°	3.190 to 26.499	3.281 to 29.301	3.284 to 25.999
Index ranges	-12<=h<=12, -16<=k<=16, -28<=l<=28	-12<=h<=12, -16<=k<=14, -29<=l<=29	-15<=h<=14, -16<=k<=16, -17<=l<=17
Reflections collected	24176	32730	18602
Independent reflections	11209 [R(int) = 0.0617]	11271 [R(int) = 0.0977]	8272 [R(int) = 0.0502]
Data/restraints/parameters	11209 / 824 / 687	11271 / 0 / 523	8272 / 862 / 643
Goodness-of-fit on F^2	0.9	1.014	0.884
Final R indexes [I>=2σ (I)]	R1 = 0.0529, wR2 = 0.1258	R1 = 0.0659, wR2 = 0.1725	R1 = 0.0445, wR2 = 0.0906
Final R indexes [all data]	R1 = 0.0931, wR2 = 0.1415	R1 = 0.1018, wR2 = 0.1870	R1 = 0.0899, wR2 = 0.0999
Largest diff. peak/hole / e $Å^{-3}$	0.629 and -0.739	1.569 and -1.356	0.430 and -0.680
CCDC access code	2103105	2103089	2103098

Table S1. Crystal data and structure determination parameters (continued).

	$[Tc(py)(CO)_3(PPh_3)_2][BF_4]$ $\cdot 3CH_2Cl_2$	$[Tc(py)(CO)_3(PPh_3)_2][BF_4]$ $\cdot$pyridine	$[Tc(NCCH_3)(CO)_3(PPh_3)_2][BF_4]$ $\cdot CH_2Cl_2$
Number code	**11**$\cdot 3CH_2Cl_2$	**11**$\cdot$pyridine	**12**$\cdot CH_2Cl_2$
Empirical formula	$C_{47}H_{41}BCl_6F_4NO_3P_2Tc$	$C_{49}H_{40}BF_4N_2O_3P_2Tc$	$C_{42}H_{35}BCl_2F_4NO_3P_2Tc$
Formula weight	1127.26	951.58	919.36
Temperature/K	233(2)	100(2)	293(2)
Crystal system	Monoclinic	Monoclinic	Monoclinic
Space group	$P2_1$	$P2_1/c$	$P2_1/c$
a/Å	10.2800(6)	11.3235(7)	11.9819(11)
b/Å	19.3028(10)	19.8639(12)	25.979(3)
c/Å	12.5830(7)	19.4647(14)	13.9322(13)
α/°	90	90	90
β/°	93.976(5)	96.838(3)	106.794(7)
γ/°	90	90	90
Volume/$Å^3$	2490.9(2)	4347.0(5)	4151.9(7)
Z	2	4	4
$\rho_{calc}g/cm^3$	1.503	1.454	1.471
μ/mm^{-1}	0.731	0.467	0.61
F(000)	1140	1944	1864
Crystal size/mm^3	0.370 x 0.227 x 0.060	0.08 x 0.08 x 0.08	1.200 x 0.130 x 0.120
Radiation	0.71073 Å	0.71073 Å	0.71073 Å
2Θ range for data collection/°	3.413 to 29.287	2.050 to 27.126	3.434 to 29.334
Index ranges	-12<=h<=14, -26<=k<=26, -17<=l<=17	-14<=h<=14, -25<=k<=22, -24<=l<=24	-16<=h<=16, -34<=k<=35, -19<=l<=18
Reflections collected	18633	39568	28489
Independent reflections	13071 [R(int) = 0.0452]	9605 [R(int) = 0.1215]	11047 [R(int) = 0.1480]
Data/restraints/parameters	13071 / 1 / 586	9605 / 142 / 590	11047 / 670 / 553
Goodness-of-fit on F^2	0.9	1.111	1.625
Final R indexes [I>=2σ (I)]	R1 = 0.0458, wR2 = 0.1010	R1 = 0.0773, wR2 = 0.1586	R1 = 0.1986, wR2 = 0.5285
Final R indexes [all data]	R1 = 0.0678, wR2 = 0.1069	R1 = 0.1087, wR2 = 0.1728	R1 = 0.2753, wR2 = 0.5497
Largest diff. peak/hole / e $Å^{-3}$	0.441 and -0.881	1.338 and -1.268	4.582 and -1.546
Absolute structure parameter	0.01(3)	-	-
CCDC access code	2103092	2103094	2103093

Table S1. Crystal data and structure determination parameters (continued).

	[{Tc(*N,O*-C_5H_4N-COO)$(CO)_2(PPh_3)_2$}$_2$H][BF_4]	[Tc(bpy^{COOMe2})$(CO)_2(PPh_3)_2$][BF_4] ·$2CH_2Cl_2$·acetone	[Tc$(SMe_2)(CO)_3(PPh_3)_2$][BF_4]
Number code	**14**	**15**·$2CH_2Cl_2$·acetone	**16**
Empirical formula	$C_{88}H_{69}BF_4N_2O_8P_4Tc_2$	$C_{57}H_{52}BCl_4F_4N_2O_7P_2Tc$	$C_{41}H_{36}BF_4O_3P_2STc$
Formula weight	1689.14	1265.55	855.51
Temperature/K	100(2)	100(2)	100(2)
Crystal system	Monoclinic	Monoclinic	Monoclinic
Space group	*C*2$_1$/*c*	*P*2$_1$/*n*	*P*2$_1$/*n*
a/Å	26.7386(10)	16.8419(15)	12.926(4)
b/Å	13.2553(5)	14.9254(11)	14.767(5)
c/Å	24.4190(9)	23.5969(19)	19.859(4)
α/°	90	90	90
β/°	114.8080(10)	109.465(3)	92.908(10)
γ/°	90	90	90
Volume/Å^3	7856.1(5)	5592.6(8)	3785.8(19)
Z	4	4	4
ρ_{calc}g/cm^3	1.428	1.503	1.501
μ/mm^{-1}	0.501	0.574	0.579
F(000)	3448	2584	1744
Crystal size/mm^3	0.21 x 0.16 x 0.04	0.10 x 0.04 x 0.03	0.204 x 0.171 x 0.002
Radiation	0.71073 Å	0.71073 Å	0.71073 Å
2Θ range for data collection/°	2.134 to 27.898	2.264 to 27.220	1.925 to 27.912
Index ranges	-35<=h<=33, -17<=k<=17, -31<=l<=31	-21<=h<=20, -19<=k<=19, -30<=l<=30	-17<=h<=17, -19<=k<=19, -26<=l<=26
Reflections collected	102912	12357	110544
Independent reflections	9386 [R(int) = 0.1443]	12357	9050 [R(int) = 0.0484]
Data/restraints/parameters	9386 / 40 / 491	12357 / 1303 / 710	9050 / 0 / 480
Goodness-of-fit on F^2	1.257	1.107	1.045
Final R indexes [I>=2σ (I)]	R1 = 0.1144, wR2 = 0.2391	R1 = 0.1366, wR2 = 0.2991	R1 = 0.0274, wR2 = 0.0633
Final R indexes [all data]	R1 = 0.1373, wR2 = 0.2497	R1 = 0.1605, wR2 = 0.3121	R1 = 0.0343, wR2 = 0.0678
Largest diff. peak/hole / e Å^{-3}	9.427 and -2.342	2.306 and -3.104	1.556 and -0.754
CCDC access code	2103100	2103095	2103096

Table S1. Crystal data and structure determination parameters (continued).

	$[Tc(SEt_2)(CO)_3(PPh_3)_2][BF_4]$	$[Tc(tht)(CO)_3(PPh_3)_2][BF_4]$	$[Tc(SeMe_2)(CO)_3(PPh_3)_2][BF_4]\cdot 2CH_2Cl_2$
Number code	**17**	**18**	**19**·$2CH_2Cl_2$
Empirical formula	$C_{43}H_{40}BF_4O_3P_2STc$	$C_{43}H_{38}BF_4O_3P_2STc$	$C_{43}H_{40}BCl_4F_4O_3P_2SeTc$
Formula weight	883.56	881.54	1072.26
Temperature/K	230(2)	100(2)	100(2)
Crystal system	Monoclinic	Monoclinic	Monoclinic
Space group	$P2_1/n$	$P2_1/n$	$P2_1$
a/Å	13.1209(7)	13.0525(9)	9.1825(5)
b/Å	15.2983(7)	14.9605(10)	19.7992(10)
c/Å	19.9492(9)	19.8022(13)	12.3717(6)
α/°	90	90	90
β/°	93.964(4)	93.642(2)	90.956(2)
γ/°	90	90	90
Volume/$Å^3$	3994.8(3)	3859.0(4)	2248.9(2)
Z	4	4	2
$\rho_{calc}g/cm^3$	1.469	1.517	1.583
μ/mm^{-1}	0.551	0.57	1.493
F(000)	1808	1800	1076
Crystal size/mm^3	0.280 x 0.190 x 0.070	0.110 x 0.080 x 0.020	0.340 x 0.280 x 0.220
Radiation	0.71073 Å	0.71073 Å	0.71073 Å
2Θ range for data collection/°	3.284 to 29.299	2.061 to 27.965	2.218 to 28.322
Index ranges	-17<=h<=17, -20<=k<=21, -27<=l<=21	-17<=h<=17, -19<=k<=19, -26<=l<=26	-12<=h<=12, -26<=k<=26, -16<=l<=16
Reflections collected	29822	53000	90211
Independent reflections	10755 [R(int) = 0.0545]	9221 [R(int) = 0.1246]	11171 [R(int) = 0.0577]
Data/restraints/parameters	10755 / 80 / 533	9221 / 0 / 496	11171 / 1 / 535
Goodness-of-fit on F^2	0.872	1.14	1.013
Final R indexes [I>=2σ (I)]	R1 = 0.0391, wR2 = 0.0781	R1 = 0.0885, wR2 = 0.1811	R1 = 0.0337, wR2 = 0.0751
Final R indexes [all data]	R1 = 0.0781, wR2 = 0.0863	R1 = 0.1292, wR2 = 0.1970	R1 = 0.0396, wR2 = 0.0769
Largest diff. peak/hole / e $Å^{-3}$	0.525 and -0.951	1.838 and -1.197	1.079 and -0.865
Absolute structure parameter	-	-	0.016(9)
CCDC access code	2103097	2103107	2103099

Table S1. Crystal data and structure determination parameters (continued).

	$[Tc(thse)(CO)_3(PPh_3)_2][BF_4]\cdot CH_2Cl_2$	$[Tc(tu)(CO)_3(PPh_3)_2][BF_4]\cdot 2CH_2Cl_2$	$[Tc(seu)(CO)_3(PPh_3)_2][BF_4]\cdot 0.75CH_2Cl_2$
Number code	**20**$\cdot CH_2Cl_2$	**23**$\cdot 2CH_2Cl_2$	**24**$\cdot 0.75CH_2Cl_2$
Empirical formula	$C_{44}H_{40}BCl_2F_4O_3P_2SeTc$	$C_{42}H_{38}BCl_4F_4N_2O_3P_2STc$	$C_{40.75}H_{35.50}BCl_{1.50}F_4N_2O_3P_2SeTc$
Formula weight	1013.37	1039.35	980.09
Temperature/K	230(2)	100(2)	230(2)
Crystal system	Monoclinic	Triclinic	Triclinic
Space group	$P2_1/n$	$P\bar{1}$	$P\bar{1}$
a/Å	13.3231(4)	12.3703(9)	12.4261(14)
b/Å	15.4219(5)	12.8048(9)	13.0893(14)
c/Å	21.3214(7)	15.0097(10)	15.1477(16)
α/°	90	75.410(2)	75.580(8)
β/°	92.079(3)	76.203(2)	75.961(9)
γ/°	90	88.412(3)	88.509(9)
Volume/Å^3	4378.0(2)	2233.1(3)	2313.3(5)
Z	4	2	2
ρ_{calc}g/cm^3	1.537	1.546	1.407
μ/mm^{-1}	1.411	0.738	1.306
F(000)	2040	1052	983
Crystal size/mm^3	0.320 x 0.230 x 0.130	0.480 x 0.160 x 0.040	0.190 x 0.080 x 0.030
Radiation	0.71073 Å	0.71073 Å	0.71073 Å
2Θ range for data collection/°	3.216 to 28.998	2.322 to 27.137	3.167 to 26.000
Index ranges	-18<=h<=18, -21<=k<=21, -28<=l<=29	-15<=h<=15, -16<=k<=16, -19<=l<=19	-15<=h<=15, -15<=k<=16, -17<=l<=18
Reflections collected	48616	50468	18748
Independent reflections	11602 [R(int) = 0.0801]	9867 [R(int) = 0.1149]	9027 [R(int) = 0.0668]
Data/restraints/parameters	11602 / 0 / 523	9867 / 40 / 607	9027 / 611 / 553
Goodness-of-fit on F^2	0.901	1.109	0.93
Final R indexes [I>=2σ (I)]	R1 = 0.0425, wR2 = 0.0888	R1 = 0.0766, wR2 = 0.1795	R1 = 0.0725, wR2 = 0.1879
Final R indexes [all data]	R1 = 0.0804, wR2 = 0.0979	R1 = 0.0932, wR2 = 0.1881	R1 = 0.1390, wR2 = 0.2187
Largest diff. peak/hole / e Å^{-3}	0.552 and -0.789	1.576 and -1.573	0.842 and -1.934
CCDC access code	2103106	2103109	2103108

Figure S1. Ellipsoid representation (50% probability) of $[Tc(OH_2)(CO)_3(PPh_3)_2][BArF_{24}]$ (**1a**) · $0.5CH_2Cl_2$. Hydrogen atoms bonded to carbon atoms are omitted for clarity. The water hydrogen atom positions were taken from the density map, however they could not be refined freely and were therefore not refined. The CF_3 groups as well as the co-crystallized solvent dichloromethane are disordered over two positions respectively. Restraints were used to model the disorder components accurately.

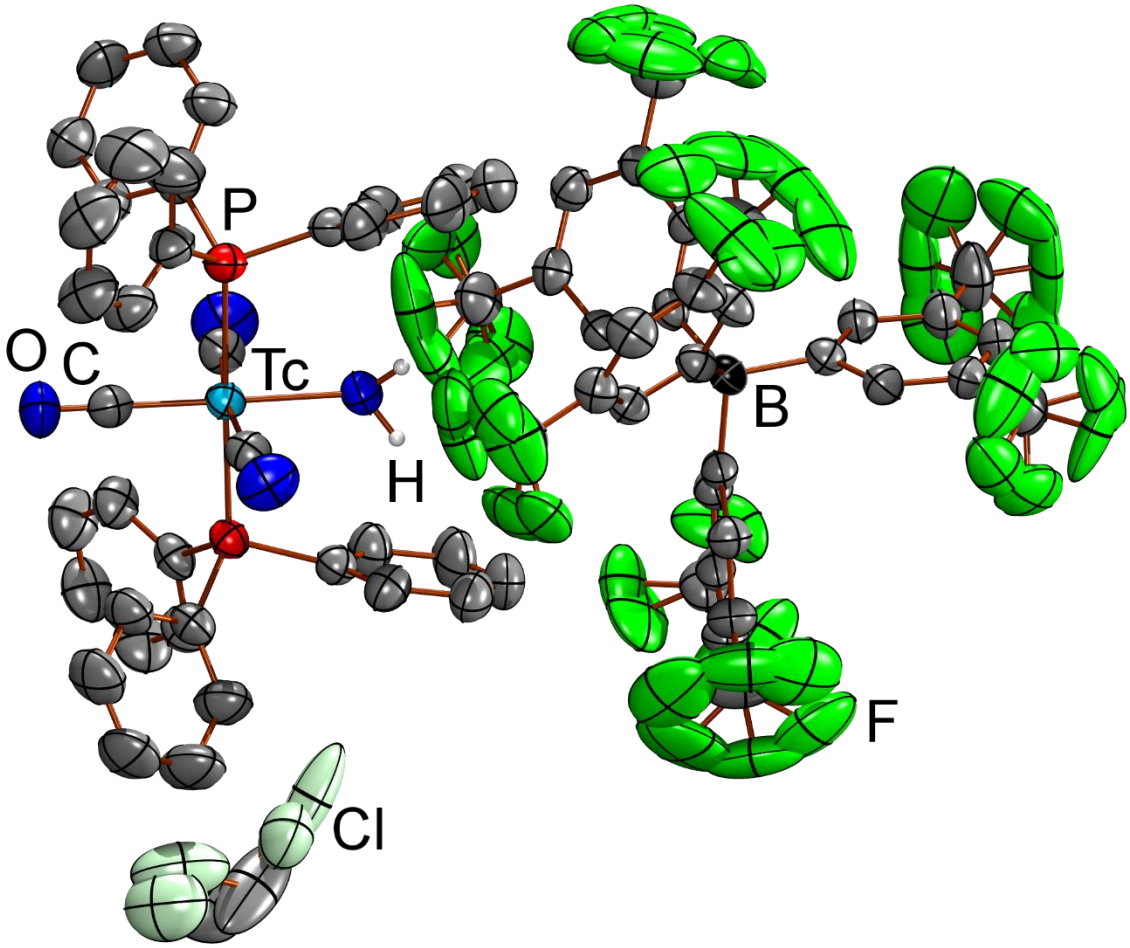

Figure S2. Ellipsoid representation (50% probability) of α-[Tc(OH_2)($CO)_3$($PPh_3)_2$][BF_4] (**1b**). Hydrogen atoms bonded to carbon atoms are omitted for clarity. The water hydrogen atoms were located in the density map and refined freely.

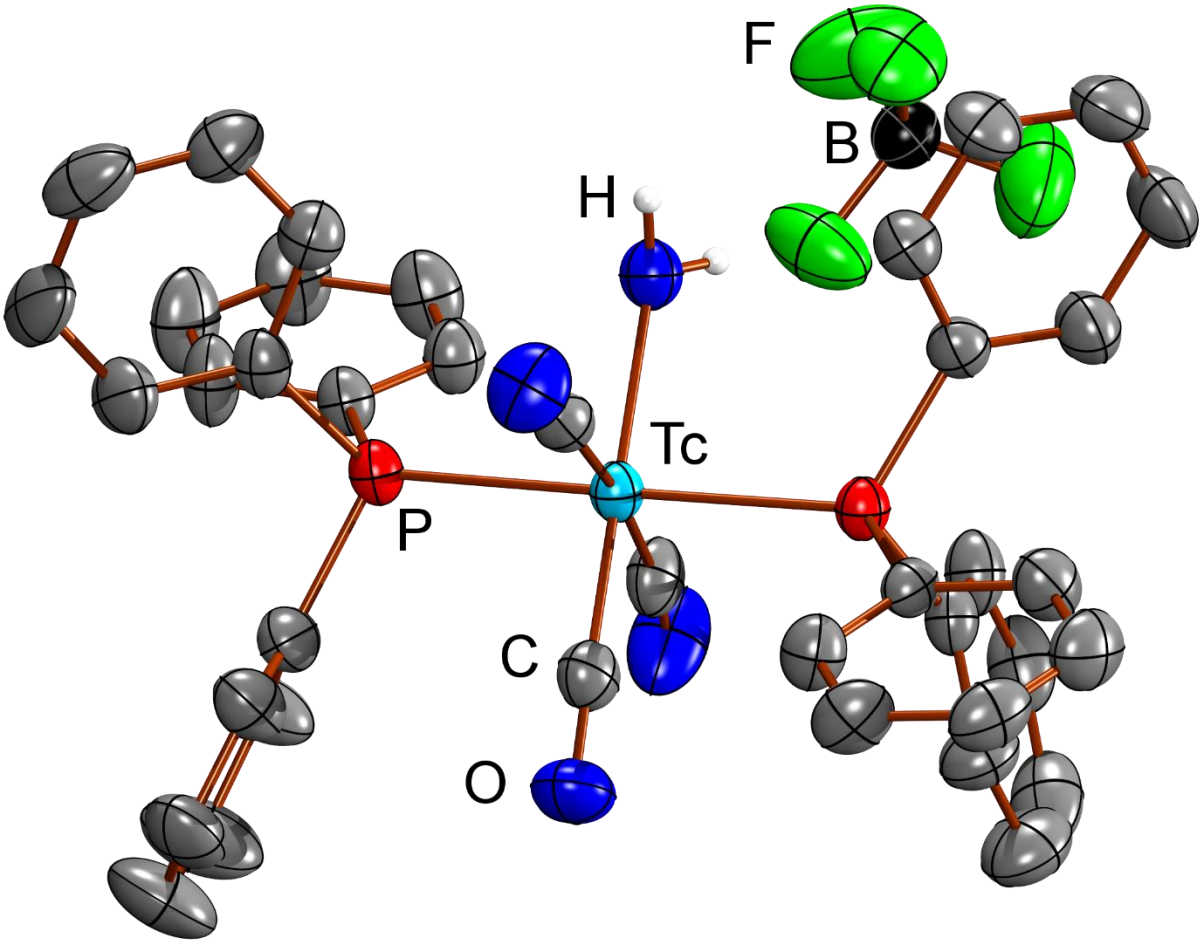

Figure S3. Ellipsoid representation (50% probability) of β-[Tc(OH_2)(CO)$_3$(PPh_3)$_2$][BF_4] (**1b**). Hydrogen atoms bonded to carbon atoms are omitted for clarity. The water hydrogen atom positions were not located in the density map. They were placed and fixed at calculated positions using the CALC-OH functionality with fixed thermal parameters. Restraints were mainly used to improve the thermal motion of the BF_4 anion. The GOOF is somewhat low and could not be improved with a variation of the weighting scheme.

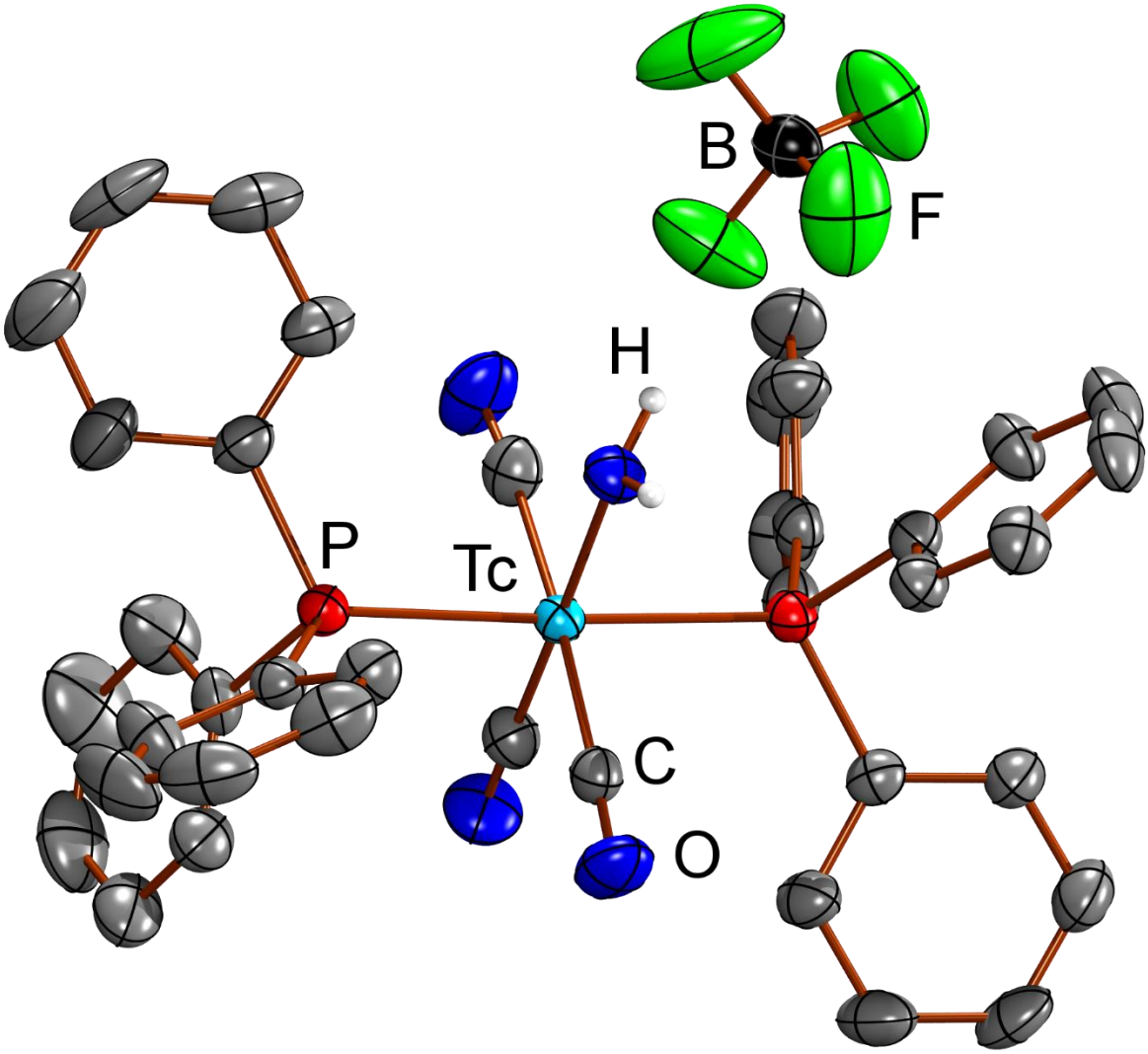

Figure S4. Ellipsoid representation (50% probability) of $[Tc(OH_2)(CO)_3(PPh_3)_2][BF_4]$ (**1b**) · diethyl ether. Hydrogen atoms bonded to carbon atoms are omitted for clarity. The water hydrogen atom positions were taken from the density map and refined freely. The $[BF_4]^-$ counter-ion is disordered over two positions. Restraints were mainly used to improve the thermal motion of the disordered BF_4 anion and the diethyl ether moiety. The GOOF is somewhat low and could not be improved with a variation of the weighting scheme.

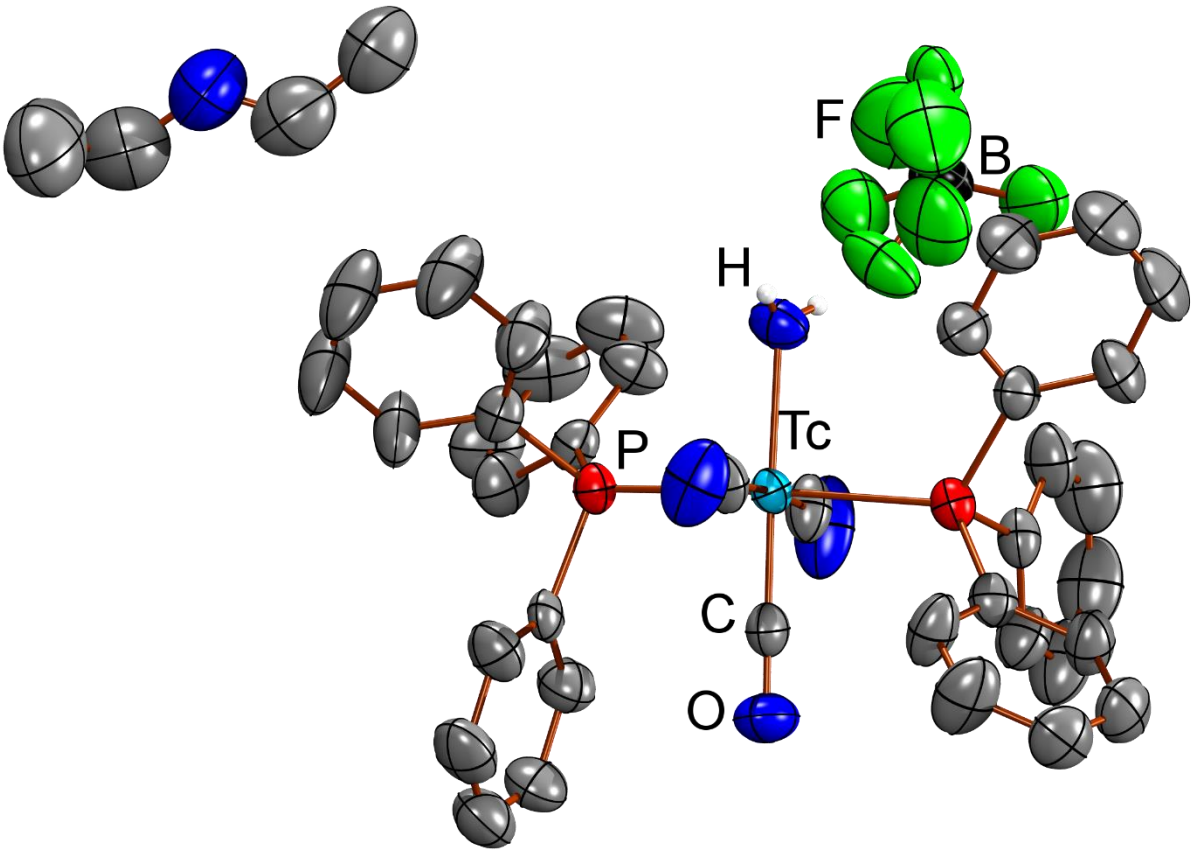

Figure S5. Ellipsoid representation (50% probability) of $[Tc(OH_2)(CO)_3(PPh_3)_2][OTf]$ (**1c**). Hydrogen atoms bonded to carbon atoms are omitted for clarity.

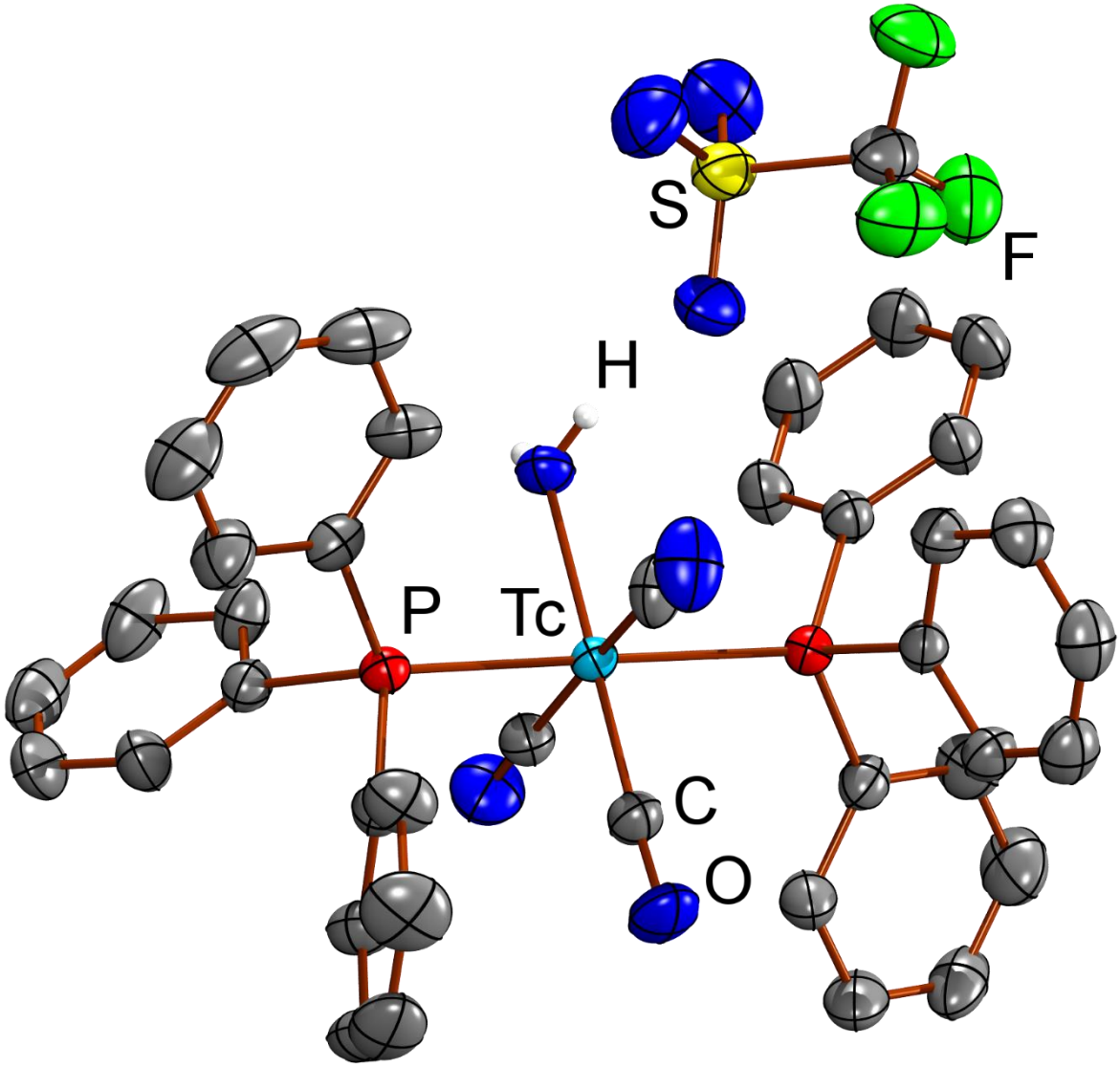

Figure S6. Ellipsoid representation (50% probability) of $[Tc(DMSO)_2(CO)_2(PPh_3)_2][BF_4]$ (**3**) · toluene. Hydrogen atoms are omitted for clarity. The DMSO ligands are disordered through the inversion of the sulfur atom, giving two sets of orientations with a ratio of ca. 45:55. The co-crystallized solvent toluene is ill-defined and was modelled with a two-fold disorder using appropriate constraints and restraints. The Flack parameter indicates that the correct absolute structure has been assigned to the crystal.

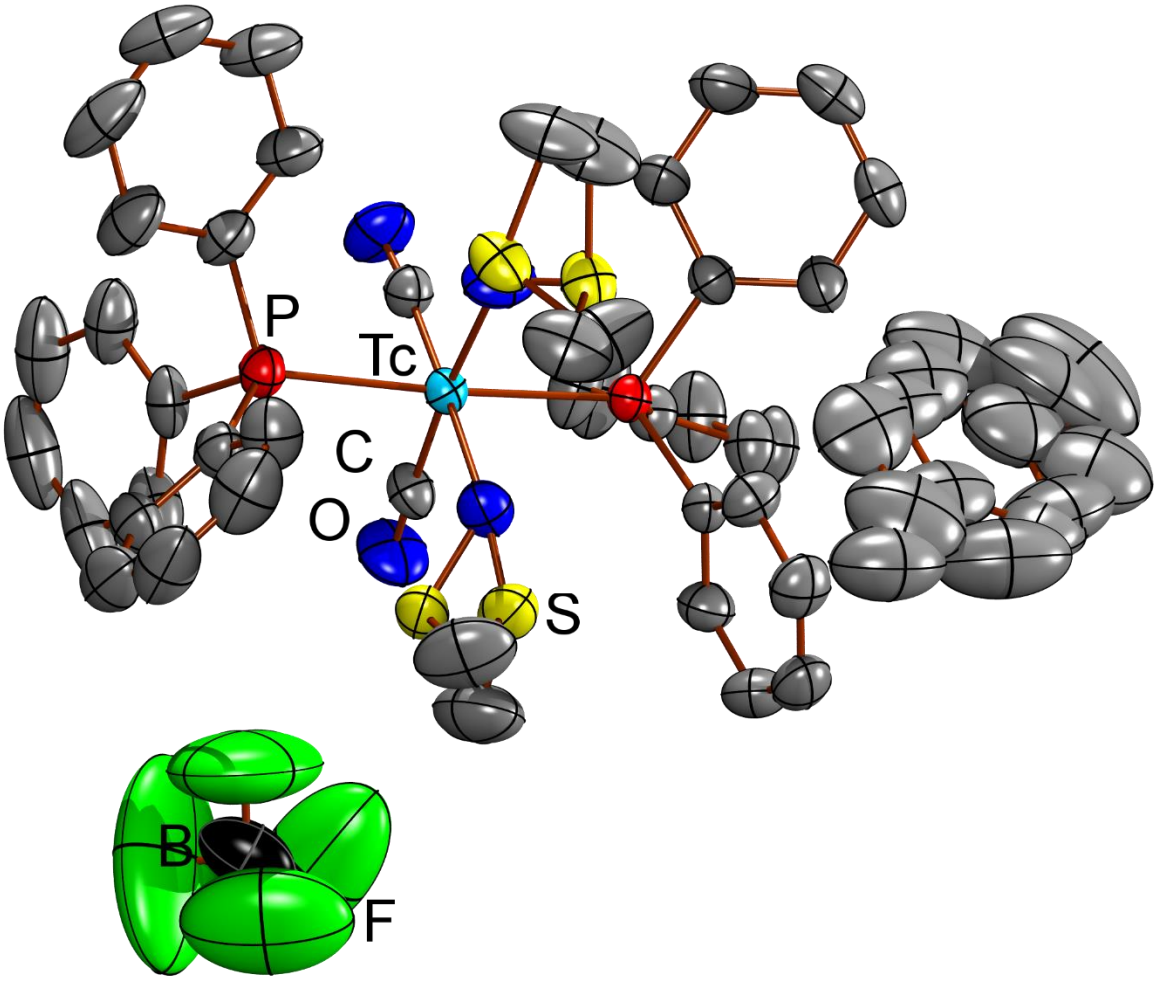

Figure S7. Ellipsoid representation (50% probability) of $[Tc(DMF)(CO)_3(PPh_3)_2][BF_4]$ (**4**) · 0.5pentane. Hydrogen atoms are omitted for clarity. The co-crystallized solvent pentane was ill-defined and modelled using appropriate constraints and restraints. Restraints were mainly used to improve the thermal motion of the BF_4 anion and to model the ill-defined solvent pentane.

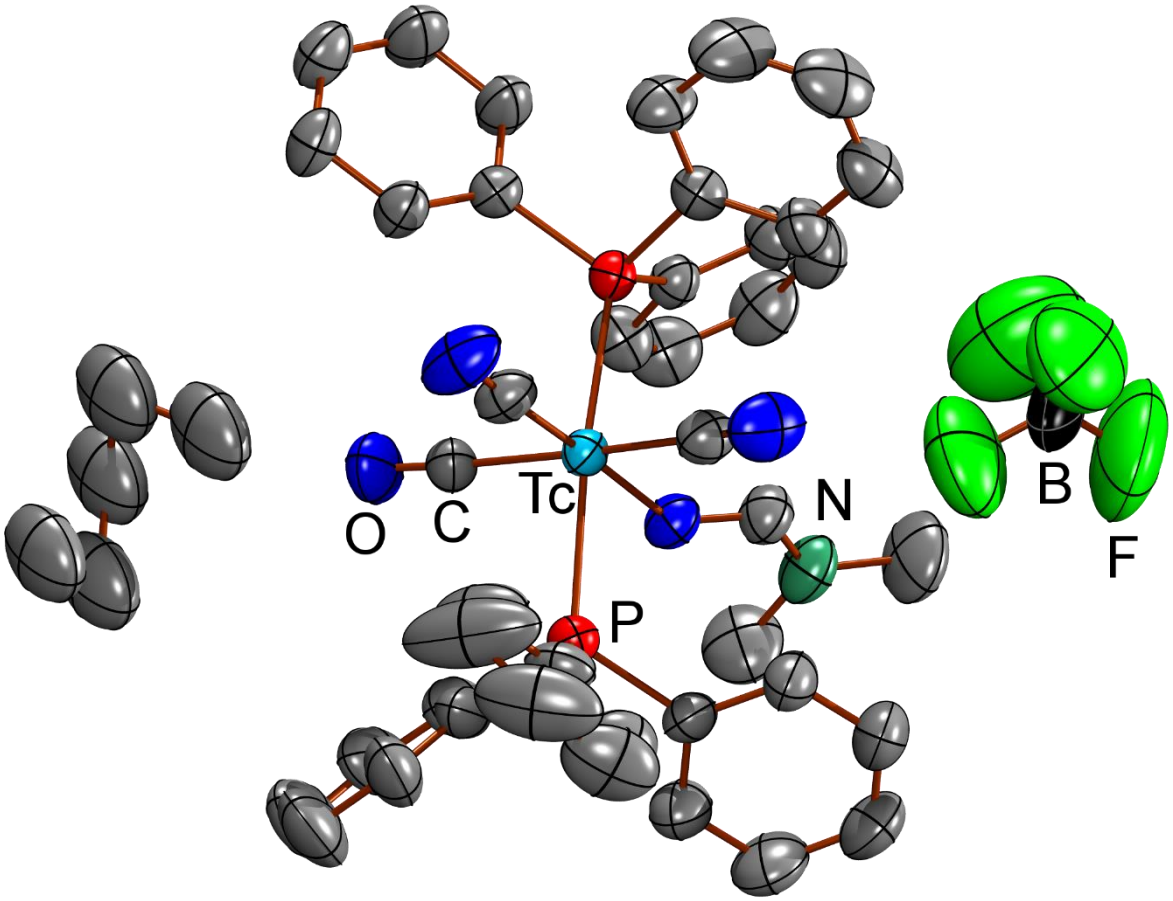

Figure S8. Ellipsoid representation (50% probability) of $[Tc(DMF)(CO)_3(PPh_3)_2][BF_4]$ (**4**). Hydrogen atoms are omitted for clarity. The $[BF_4]^-$ counter-ion is somewhat ill-defined and modelled using appropriate constraints and restraints. The crystal was treated as a three-component twin. The overall quality of this structure is low. Restraints were mainly used to improve the thermal motion of the BF_4 anion.

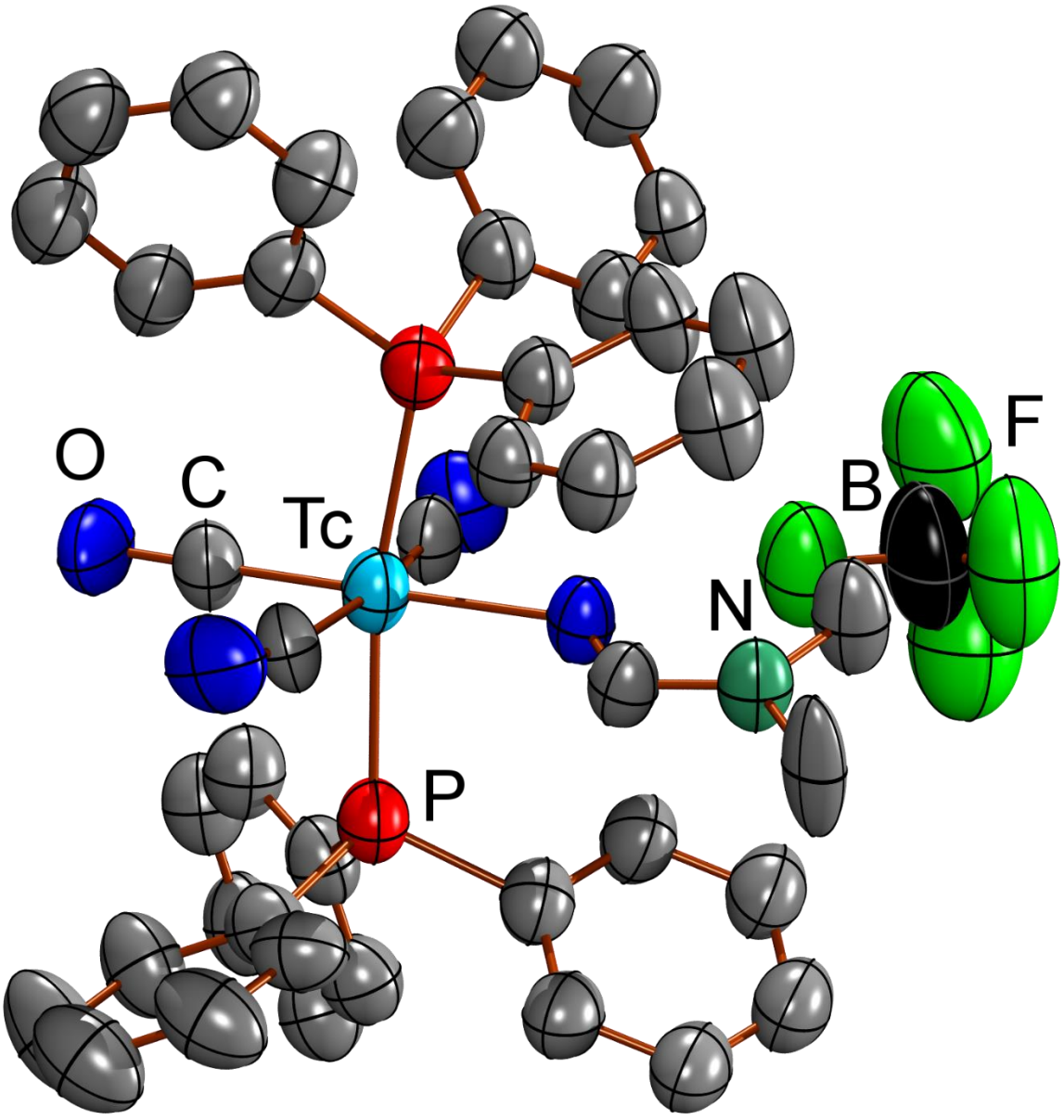

Figure S9. Ellipsoid representation (50% probability) of $[Tc(DMF)_2(CO)_2(PPh_3)_2][BF_4]$ (**5**) · toluene. Hydrogen atoms are omitted for clarity. The co-crystallized solvent toluene is ill-defined and was modelled using appropriate constraints and restraints. One of the DMF ligands is disordered over two positions, which is coupled to a disorder in three phenyl rings of the two triphenylphosphine co-ligands. Restraints were mainly used to improve the thermal motion of the BF_4 anion and to model the disordered solvent toluene.

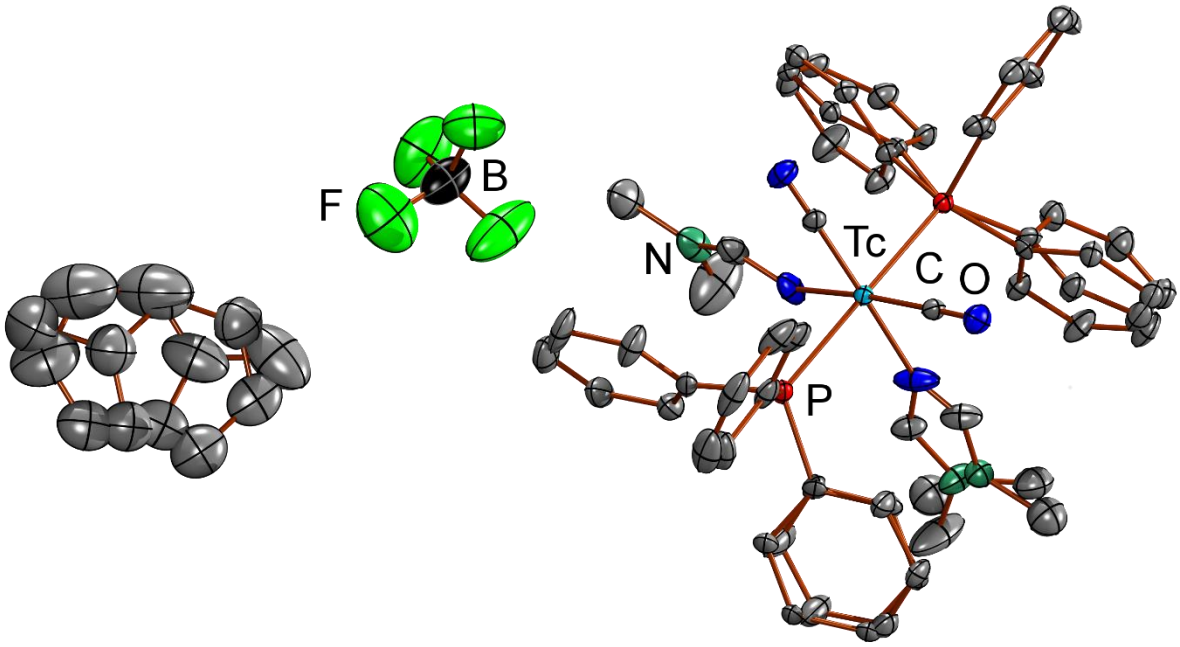

Figure S10. Ellipsoid representation (50% probability) of $[Tc(CO)_4(PPh_3)_2][BArF_{24}]$ (**6a**) · $0.25CH_2Cl_2$. Hydrogen atoms are omitted for clarity. Most of the CF_3-groups are expectedly disordered over two positions. Restraints were mainly used to model the disordered CF_3 groups.

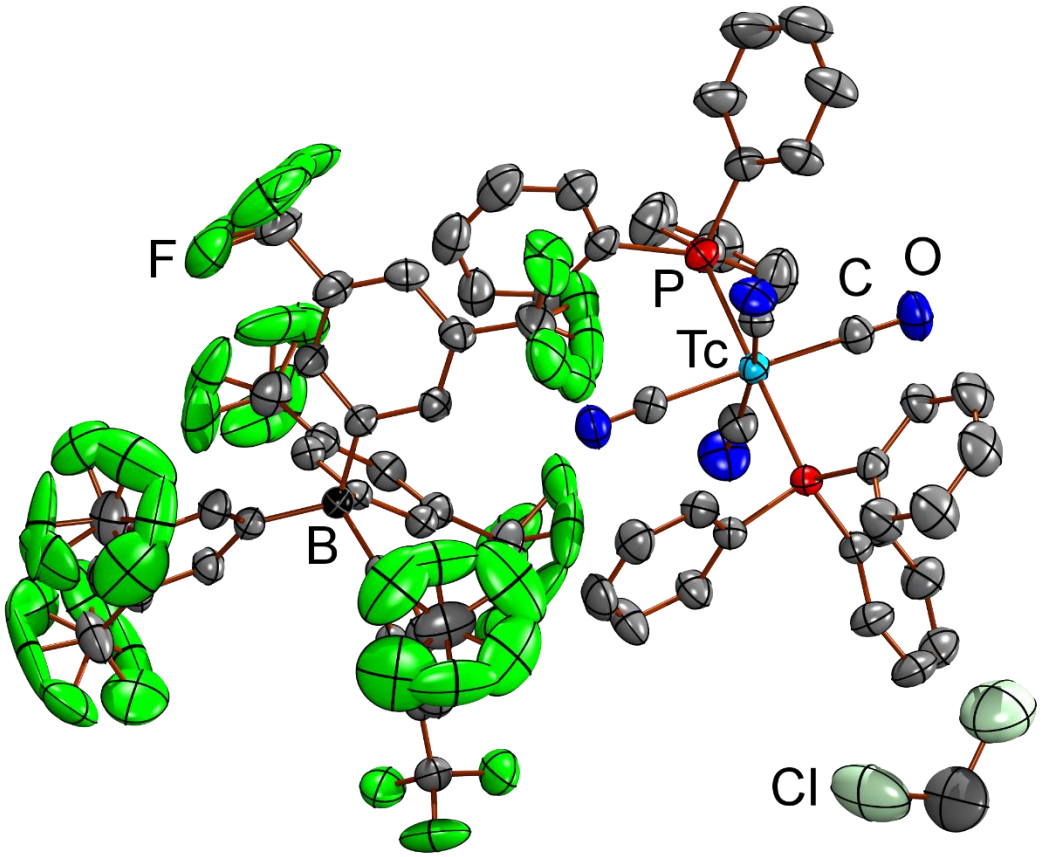

Figure S11. Ellipsoid representation (50% probability) of $[Tc(CO)_4(PPh_3)_2][BF_4]$ (**6b**). Hydrogen atoms are omitted for clarity. Symmetry code for the generation of equivalent atoms: -*x*+1, -*y*+1, *z*. The *trans*-CO ligands are generated by the space-group symmetry from two *cis*-CO ligands. One PPh_3 ligand is symmetry related to the second PPh_3 ligand. The Flack parameter regarding the absolute structure of the crystal is not conclusive. Restraints were mainly used to improve the thermal motion of the BF_4 anion and to model the disordered solvent toluene.

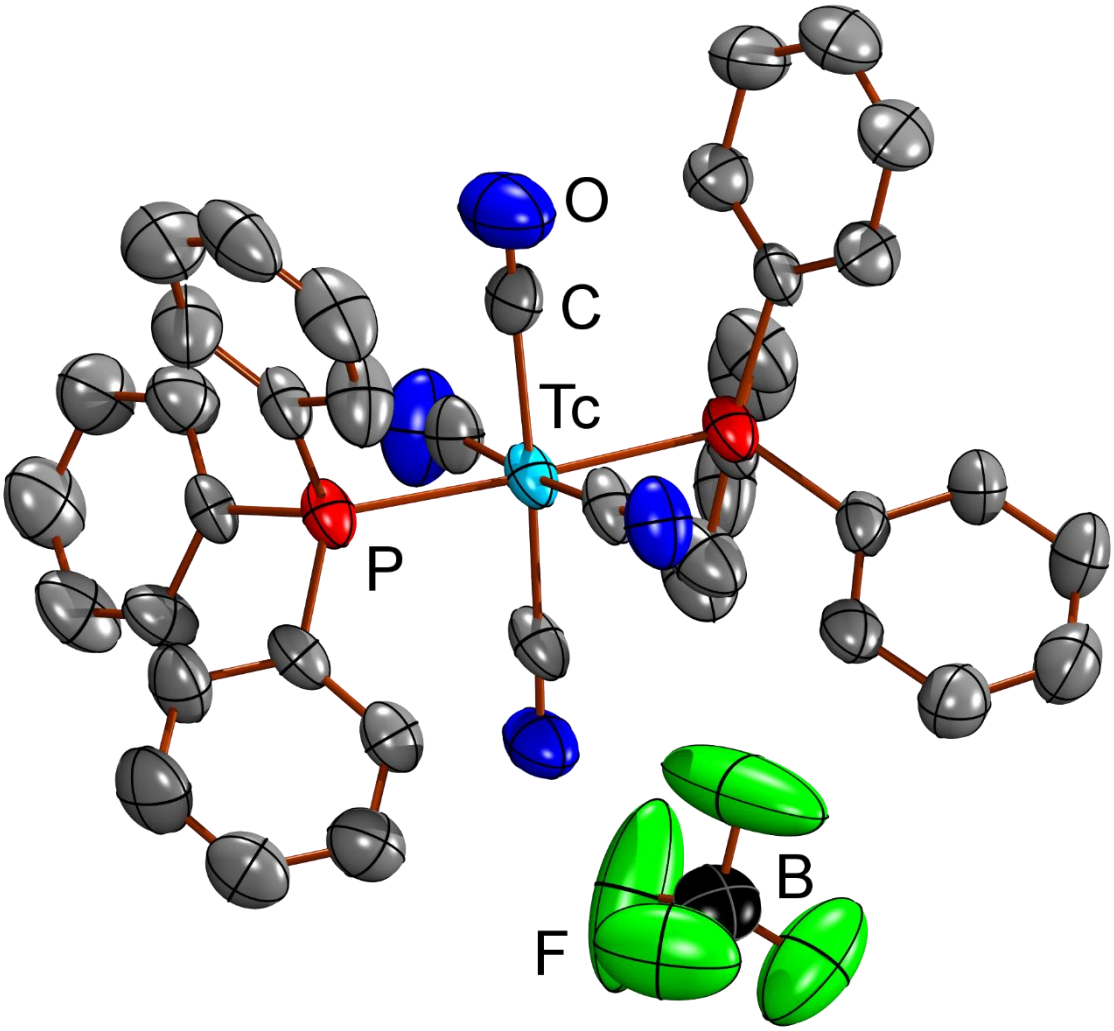

Figure S12. Ellipsoid representation (50% probability) of 2[Tc(CO)$_4$(PPh$_3$)$_2$][OTf] (**6c**) · HOTf. Hydrogen atoms bonded to carbon atoms are omitted for clarity. Symmetry codes for the generation of equivalent atoms: -*x*+2, -*y*, -*z*+2; -*x*+2, -*y*+1, -*z*+1. The two outer complex cations are symmetric regarding the space-group symmetry: the two corresponding *trans*-CO ligands are generated from two *cis*-CO ligands. The acidic HOTf proton was not located and was placed on a calculated position based on the assumption that the closest OTf···OTf contact may indicate a long hydrogen bond. The position of the acidic hydrogen atom was not refined. The crystal was treated as a five-component twin. The overall quality of the structure is (too) low and was originally provided for an additional structural verification. Restraints were mainly used to improve the thermal motion of the OTf moieties, the hydrogen bond and to improve the thermal motion of the ligands.

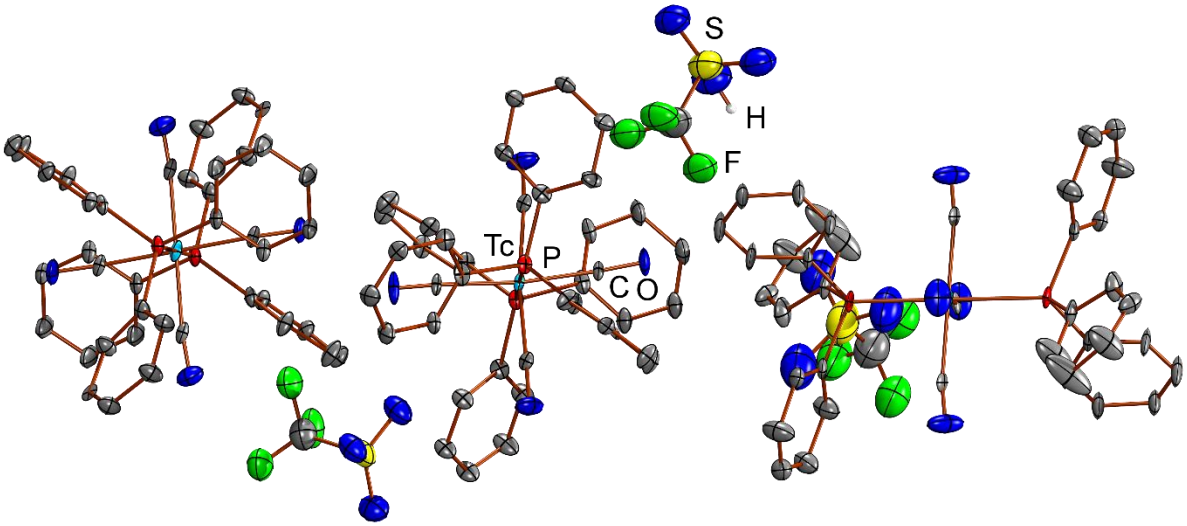

Figure S13. Ellipsoid representation (50% probability) of $[Tc(SS(CPPh_3))(CO)_2(PPh_3)_2][BF_4]$ (**7**) · CH_2Cl_2. Hydrogen atoms are omitted for clarity. The $[BF_4]^-$ counter-ion is disordered over two positions. Restraints were mainly used to model the disordered BF_4.

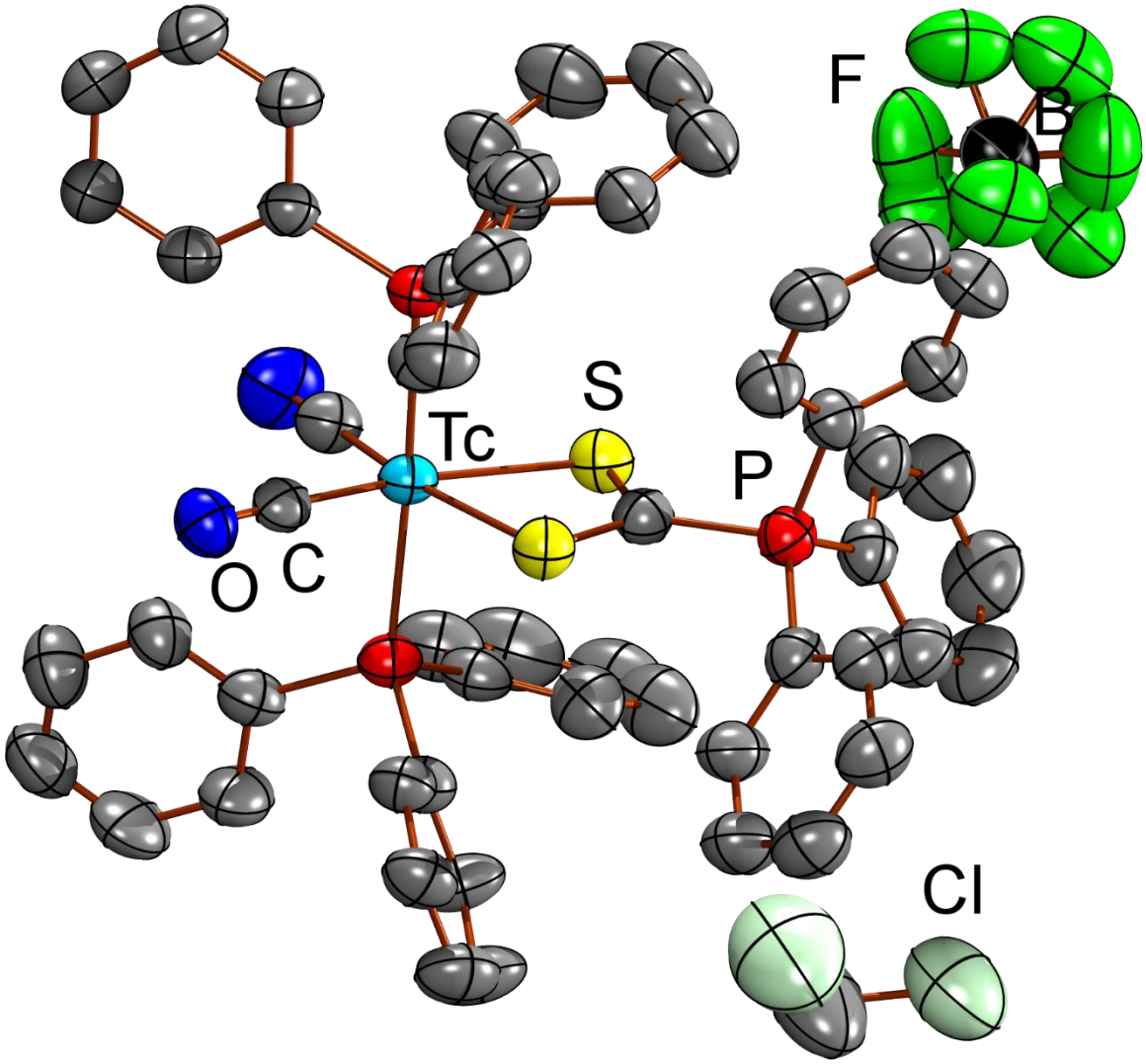

Figure S14. Ellipsoid representation (50% probability) of $[Tc(CNCy)(CO)_3(PPh_3)_2][BF_4]$ (**8**). Hydrogen atoms are omitted for clarity.

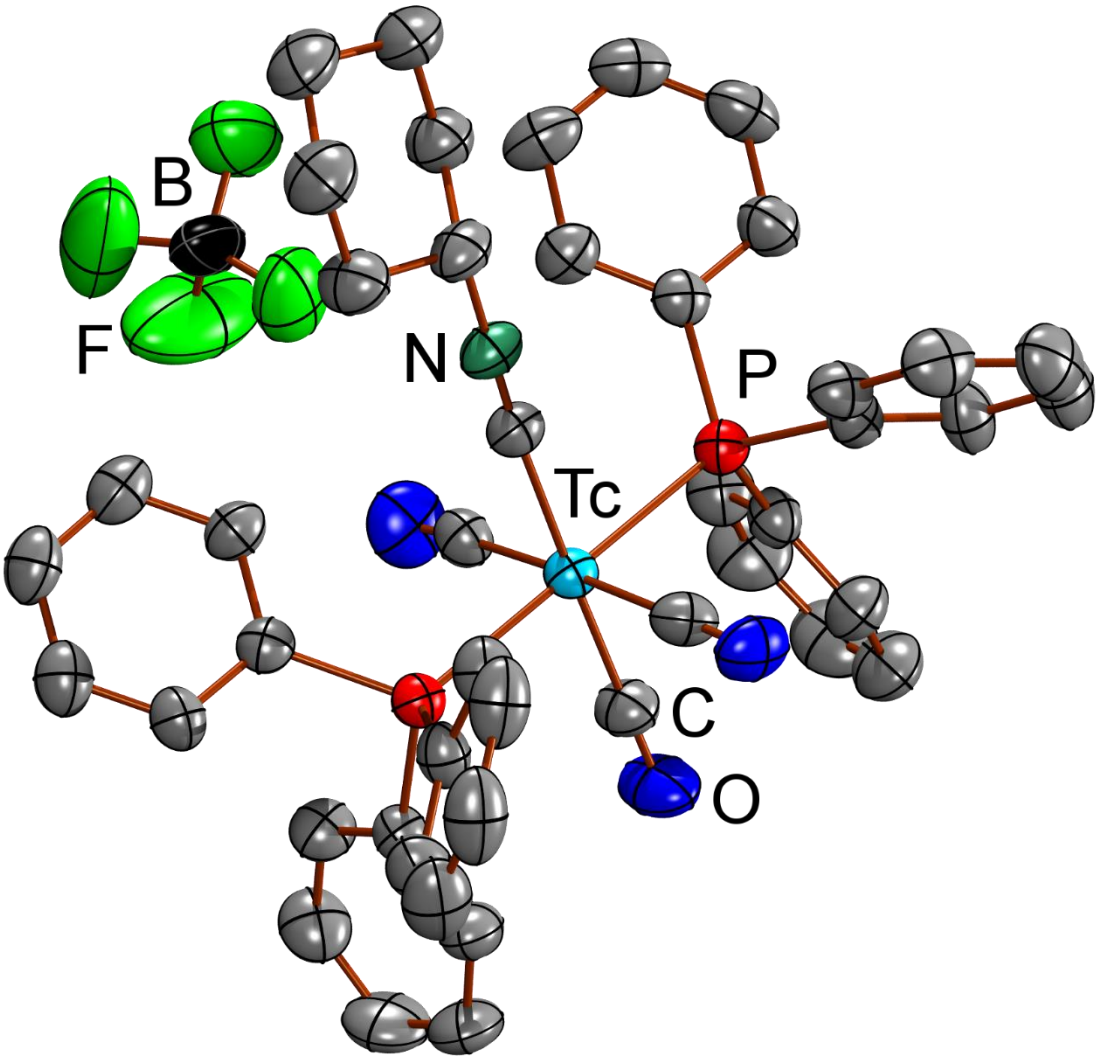

Figure S15. Ellipsoid representation (50% probability) of $[Tc(NH_3)_2(CO)_2(PPh_3)_2][BF_4]$ (**10**) · pentane. Hydrogen atoms bonded to carbon atoms are omitted for clarity. The $[BF_4]^-$ counter-ion is disordered over two positions. With approximately the same occupational factors, the second ammine ligand is disordered with one of the carbonyl ligands. The co-crystallized solvent pentane is ill-defined and was modelled as a two-fold disorder using restraints and constraints. The hydrogen atom positions were taken from the density map, however, those of the second part of the disorder had their thermal parameter modelled as a portion of the thermal parameter of the parent nitrogen atom. Restraints were mainly used to model the disordered BF_4 anion and the disordered ammonia/carbonyl sites.

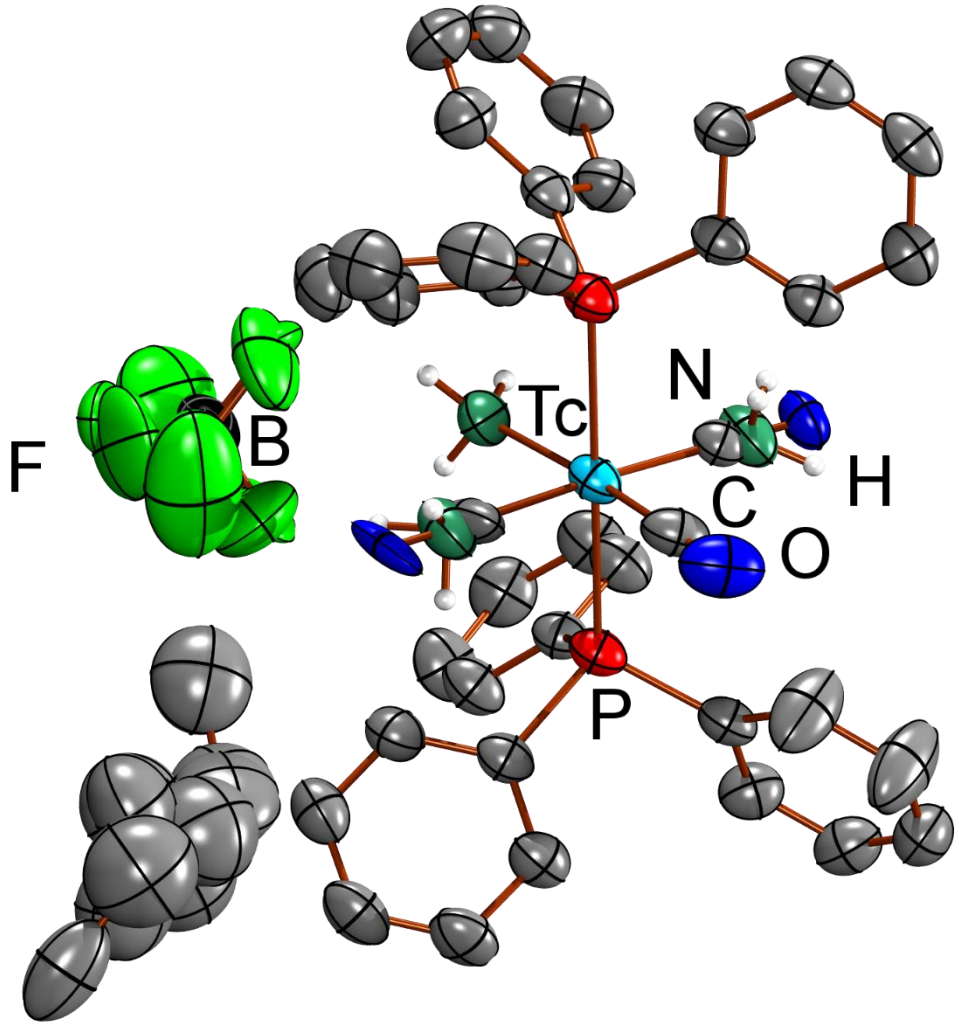

Figure S16. Ellipsoid representation (50% probability) of $[Tc(py)(CO)_3(PPh_3)_2][BF_4]$ (**11**) · $3CH_2Cl_2$. Hydrogen atoms are omitted for clarity. The Flack parameter indicates that the correct absolute structure has been assigned to the crystal.

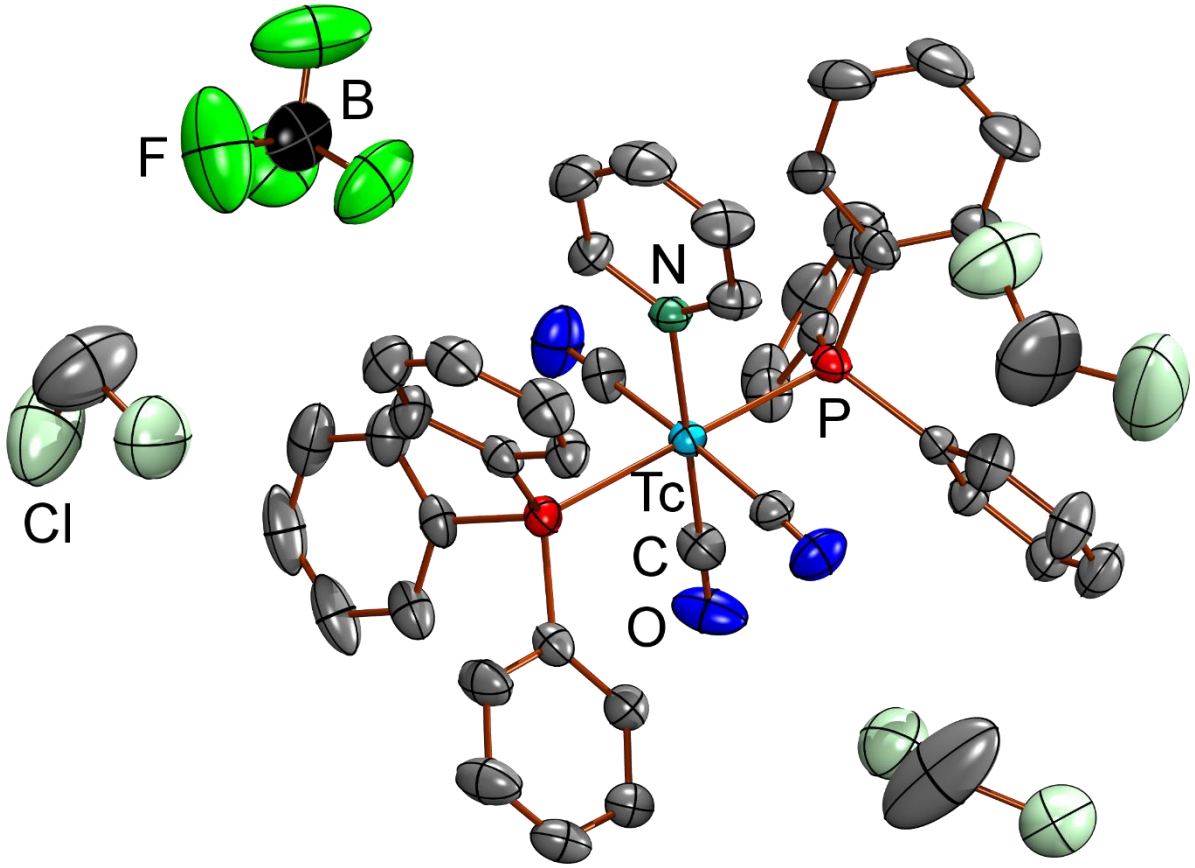

Figure S17. Ellipsoid representation (50% probability) of $[Tc(py)(CO)_3(PPh_3)_2][BF_4]$ (**11**) · pyridine. Hydrogen atoms are omitted for clarity. The co-crystallized solvent pyridine is disordered over two positions and was modelled using constraints and restraints.

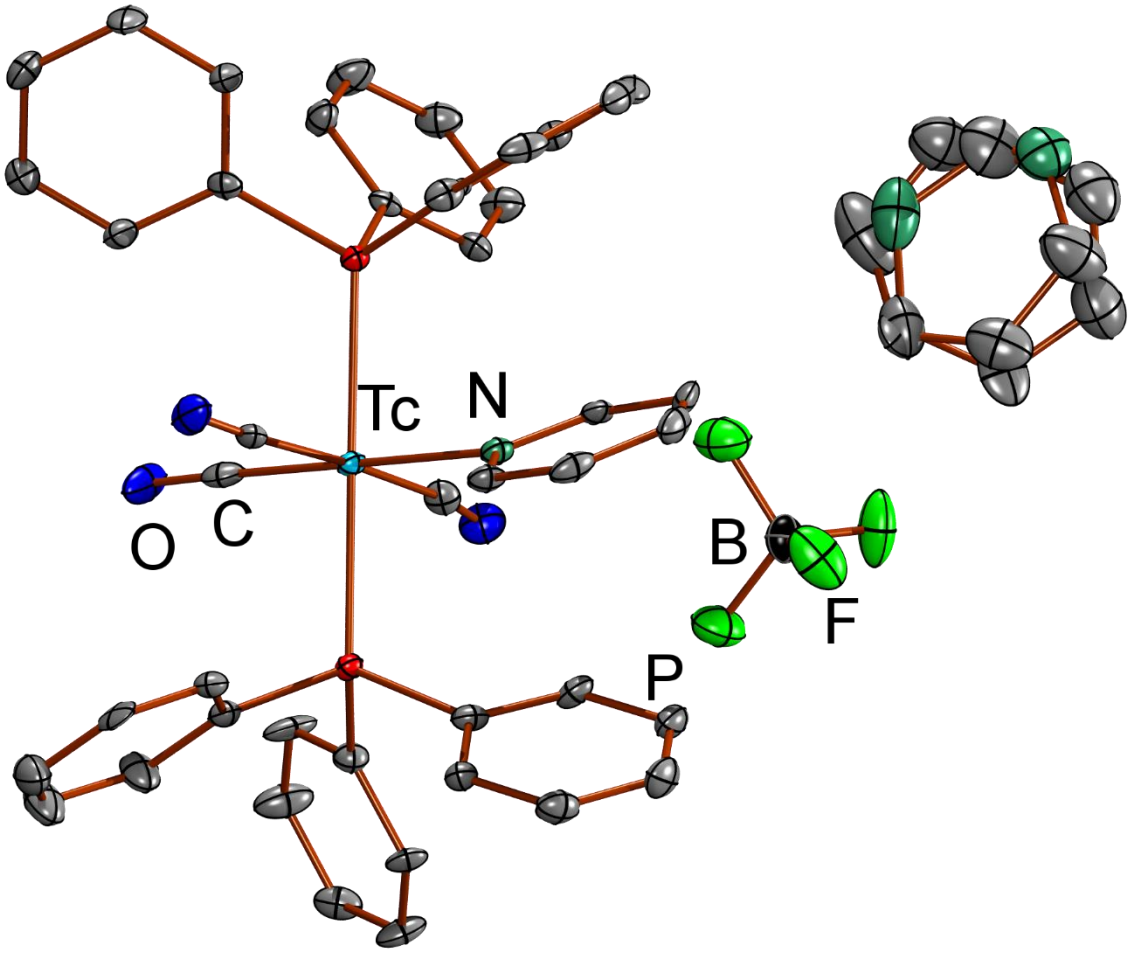

Figure S18. Ellipsoid representation (50% probability) of $[Tc(NCCH_3)(CO)_3(PPh_3)_2][BF_4]$ (**12**) · CH_2Cl_2. Hydrogen atoms are omitted for clarity. The $[BF_4]^-$ counter-ion is disordered over two positions. The crystal was treated as a two-component twin. The overall quality of the structure is (too) low and was originally provided for an additional structural verification. Restraints were mainly used to improve the thermal motion of the disordered BF_4 anion.

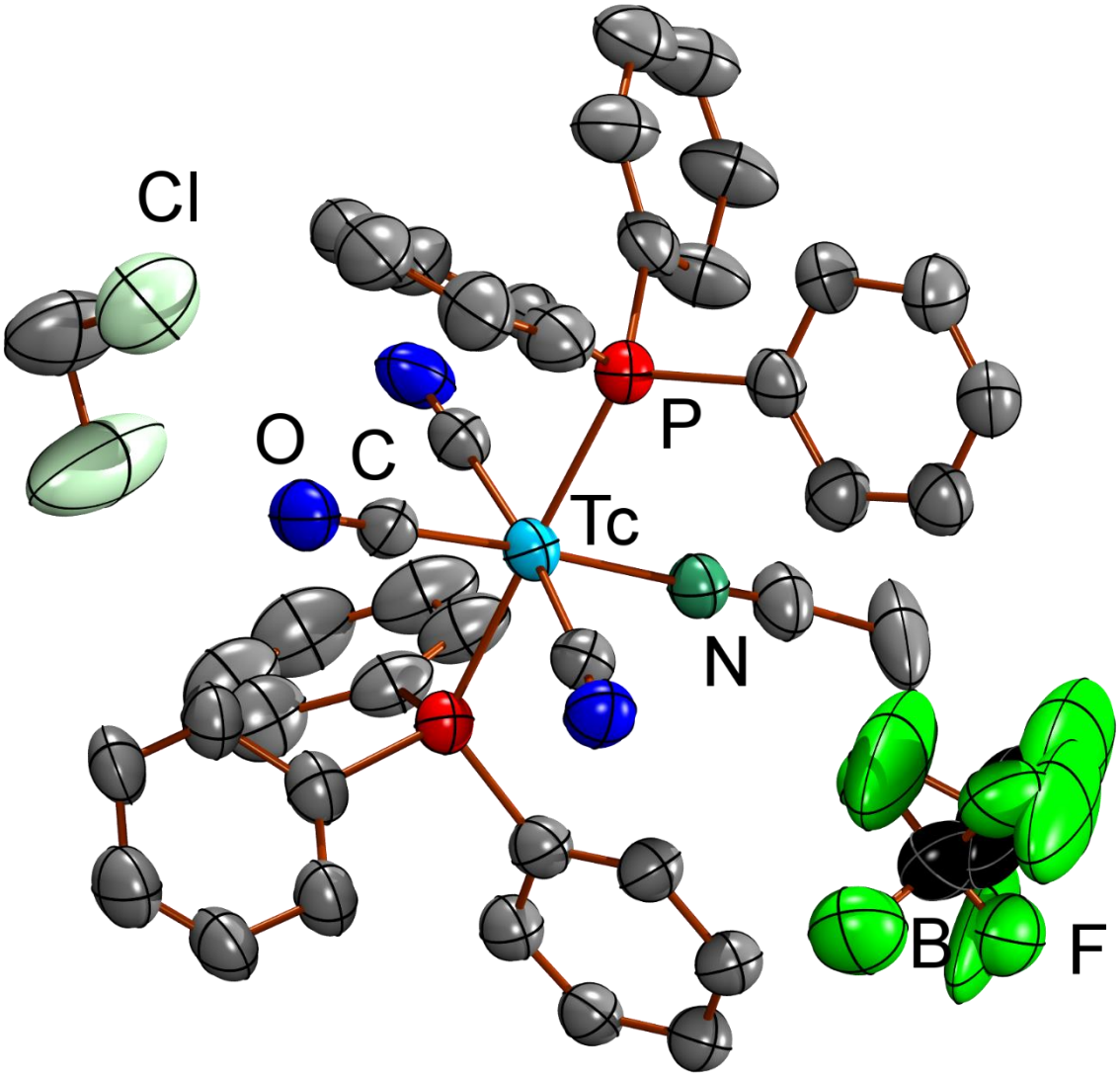

Figure S19. Ellipsoid representation (50% probability) of [{Tc(N,O-C_5H_4N-COO)$(CO)_2(PPh_3)_2$}$_2$H][BF_4] (**14**). Hydrogen atoms bonded to carbon atoms are omitted for clarity. The $[BF_4]^-$ counter-ion is disordered over two positions involving the space-group symmetry. A large portion of residual density lies on the symmetry generated second position of the boron atom and probably results as an artefact of the proximity to the space-group origin. The bridging proton was found in the density map lying on the space-group symmetry. It was refined freely, however, the proximity to the space-group symmetry leaves ambiguity about the ingenuity of this position and a distinction between symmetric and asymmetric hydrogen bridge cannot be finally concluded from the present data.

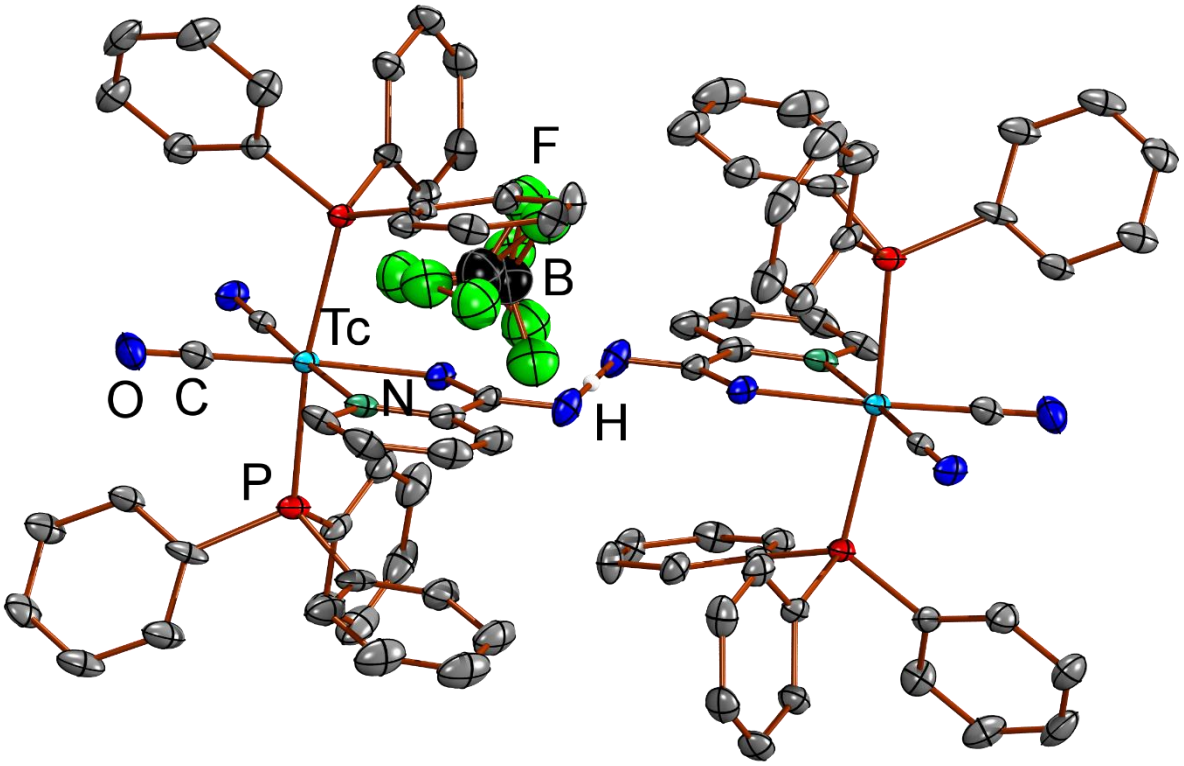

Figure S20. Ellipsoid representation (50% probability) of [Tc(bpy^{COOMe2})(CO)$_2$(PPh$_3$)$_2$][BF$_4$] (**15**) · acetone · 2CH$_2$Cl$_2$. Hydrogen atoms are omitted for clarity. Three of the four fluorine atoms of the [BF$_4$]$^-$ counter-ion are disordered over two positions. The co-crystallized solvent acetone is disordered over two positions. The thermal parameters were restrained with a strong ISOR command to give more reasonable thermal ellipsoids. The crystal was treated as a two-component twin. Restraints were mainly used to model the disordered BF4 moiety, the co-crystallized solvent dichloromethane, the ill-defined solvent acetone and additionally a rigorous isotropic restraint was obviously applied to all atoms due to some anomalies in thermal parameters that could not be modelled as a disorder.

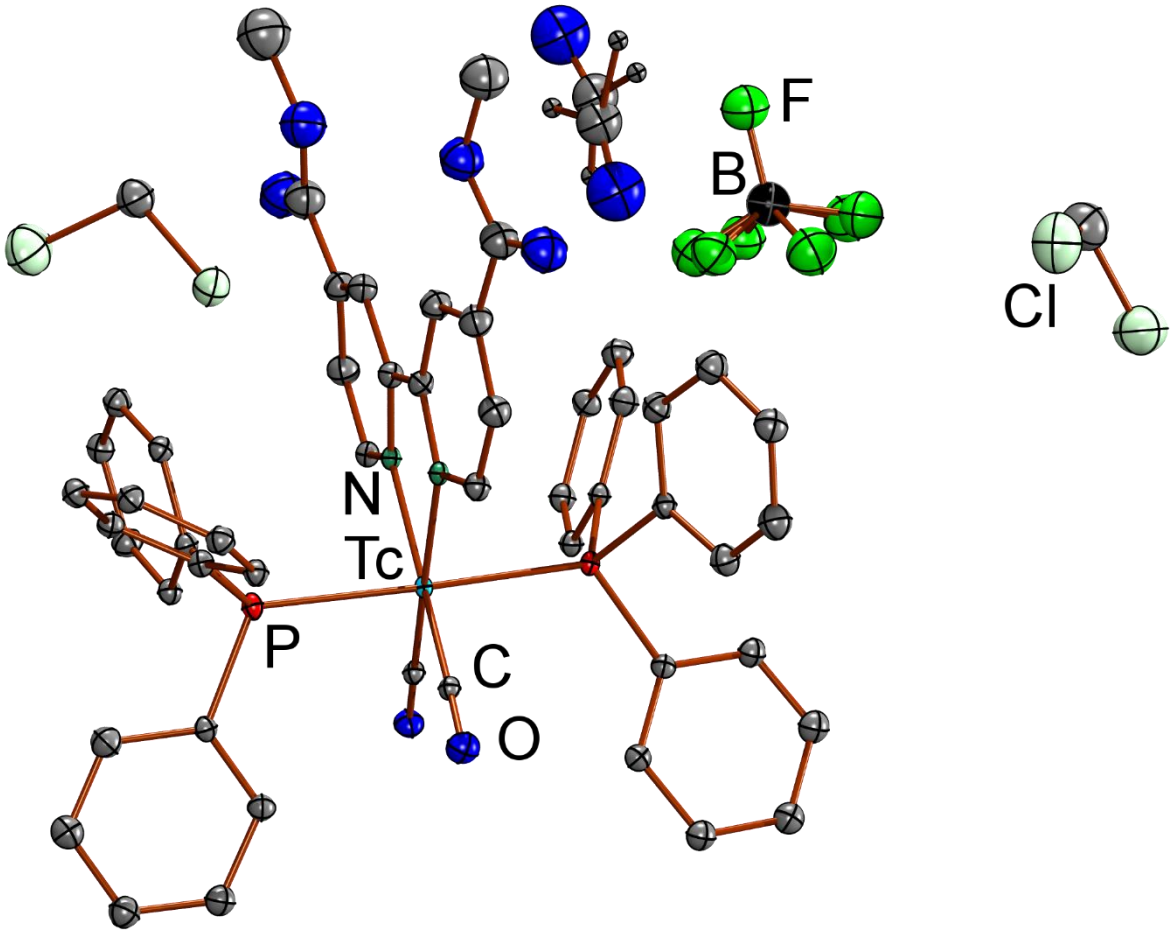

Figure S21. Ellipsoid representation (50% probability) of $[Tc(SMe_2)(CO)_3(PPh_3)_2][BF_4]$ (**16**). Hydrogen atoms are omitted for clarity.

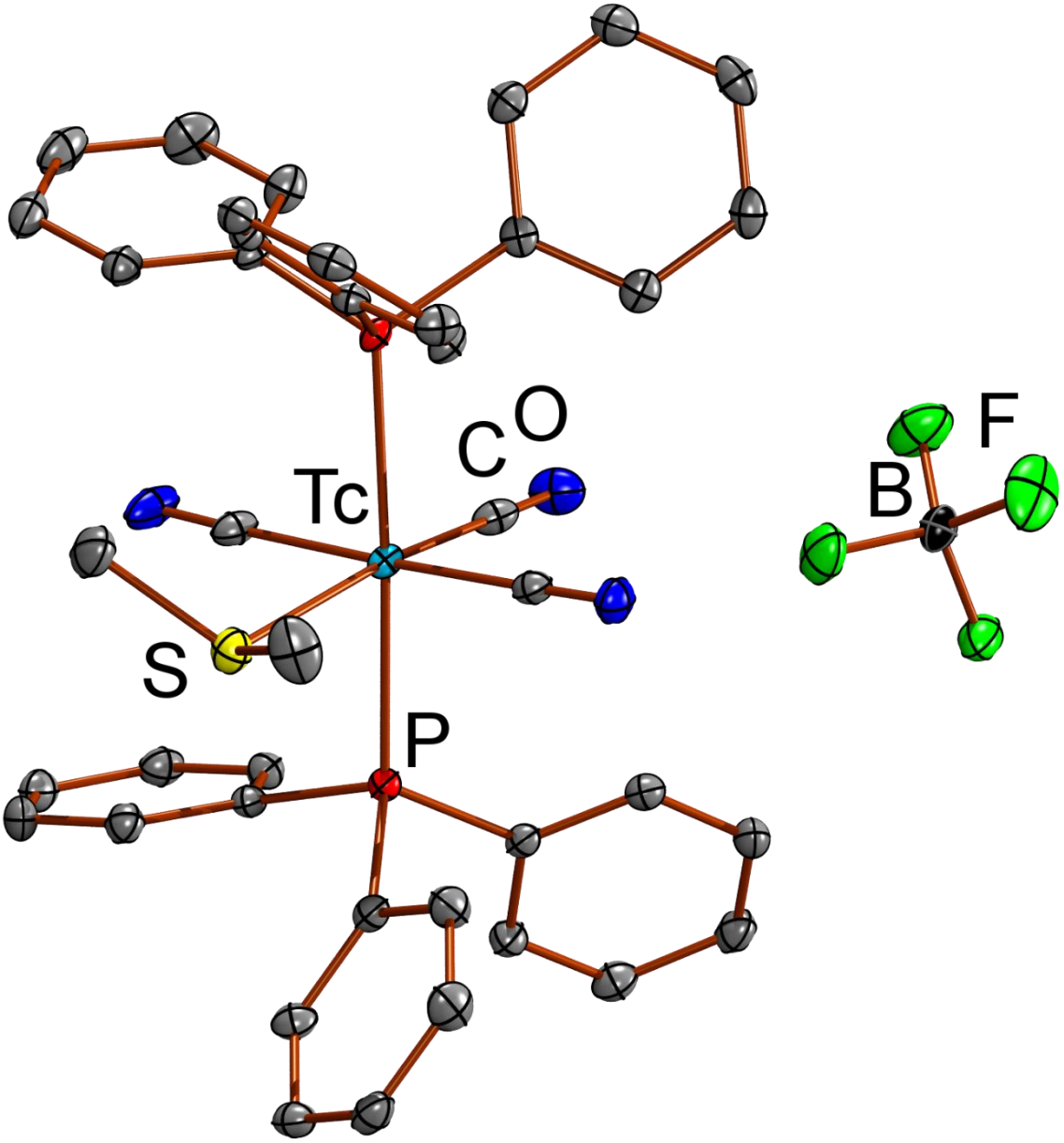

Figure S22. Ellipsoid representation (50% probability) of $[Tc(SEt_2)(CO)_3(PPh_3)_2][BF_4]$ (**17**). Hydrogen atoms are omitted for clarity. The $[BF_4]^-$ counter-ion is disordered over two positions.

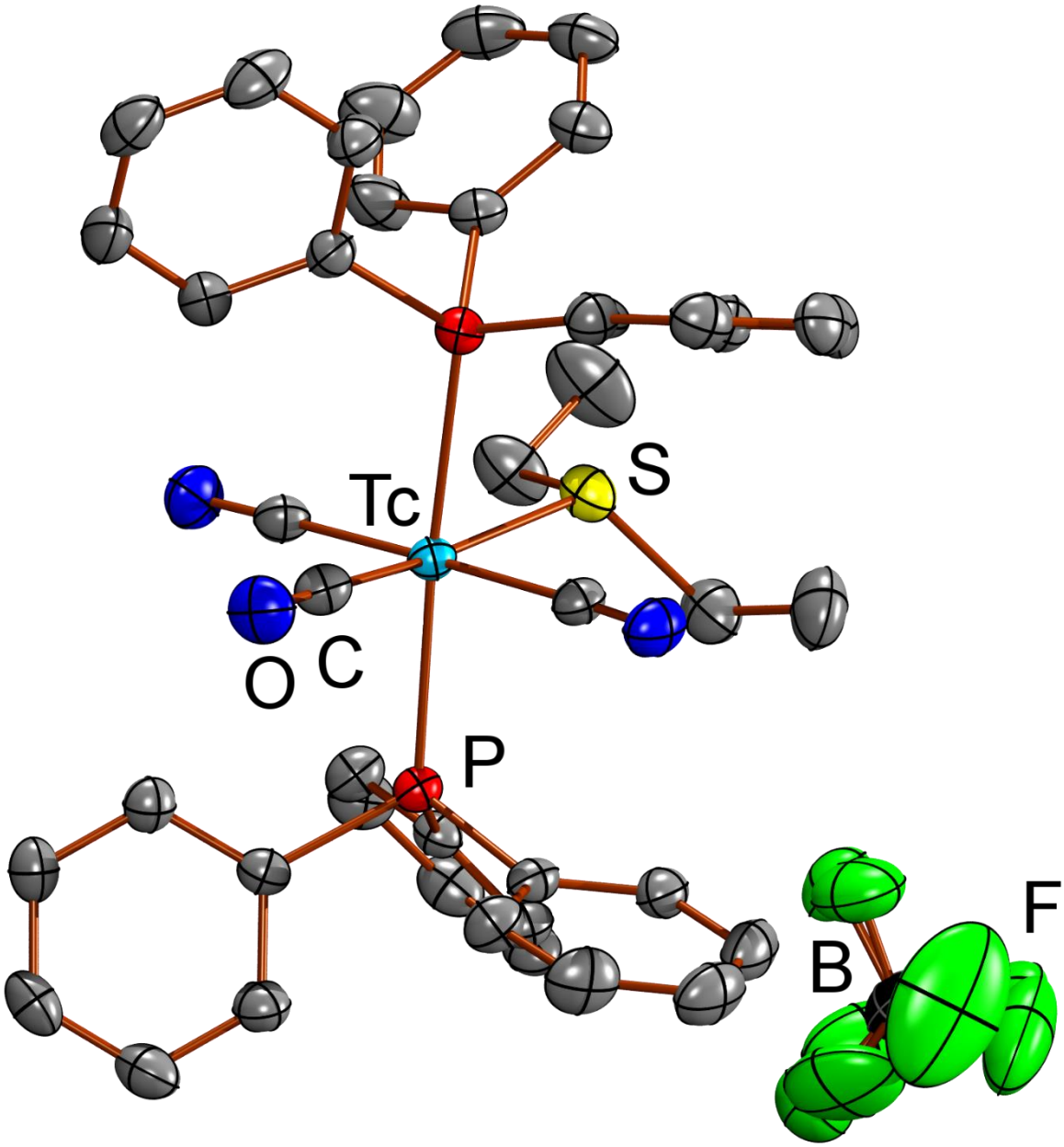

Figure S23. Ellipsoid representation (50% probability) of $[Tc(tht)(CO)_3(PPh_3)_2][BF_4]$ (**18**). Hydrogen atoms are omitted for clarity.

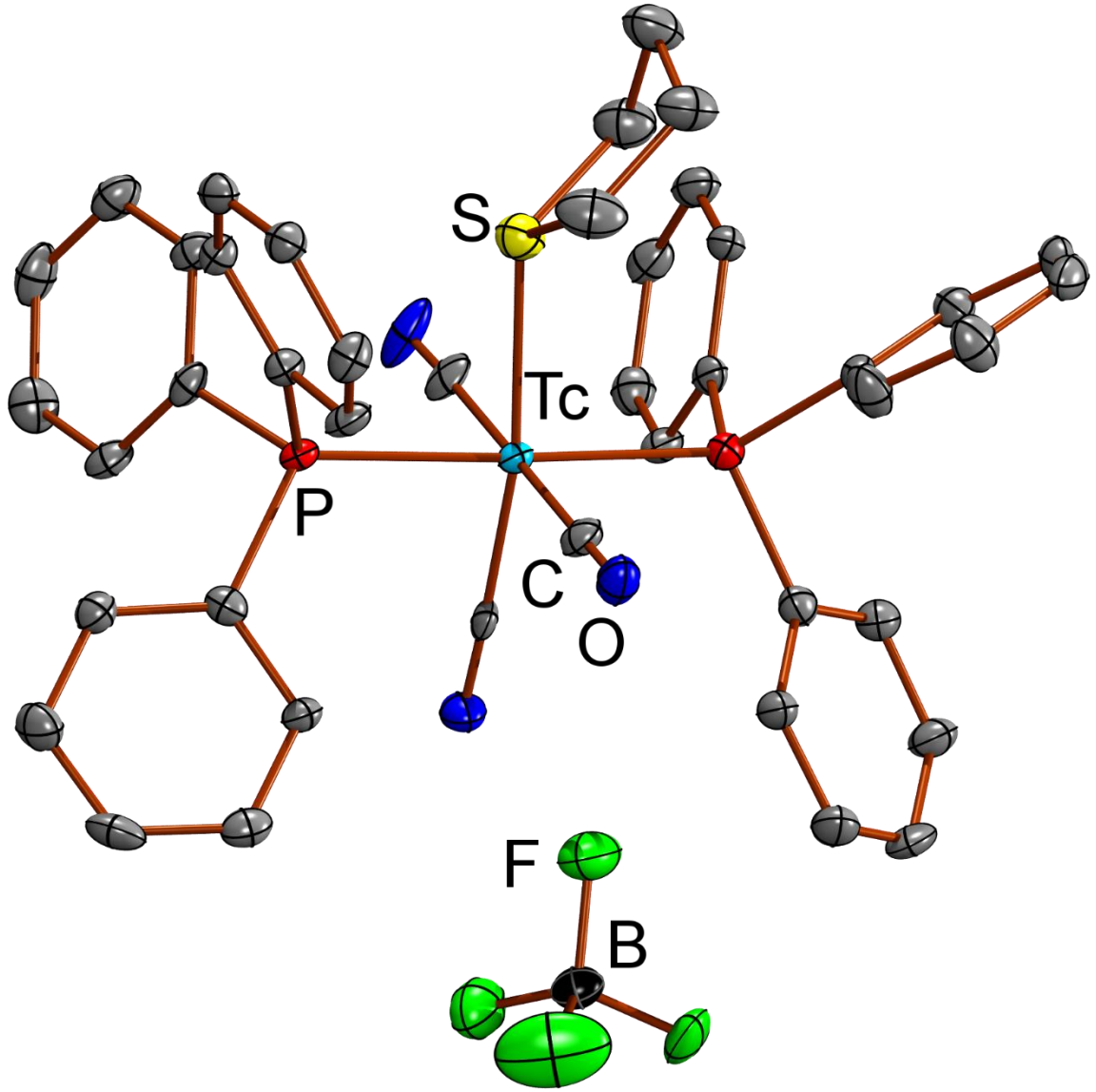

Figure S24. Ellipsoid representation (50% probability) of $[Tc(SeMe_2)(CO)_3(PPh_3)_2][BF_4]$ (**19**) · $2CH_2Cl_2$. Hydrogen atoms are omitted for clarity. The Flack parameter indicates that the correct absolute structure has been assigned to the crystal.

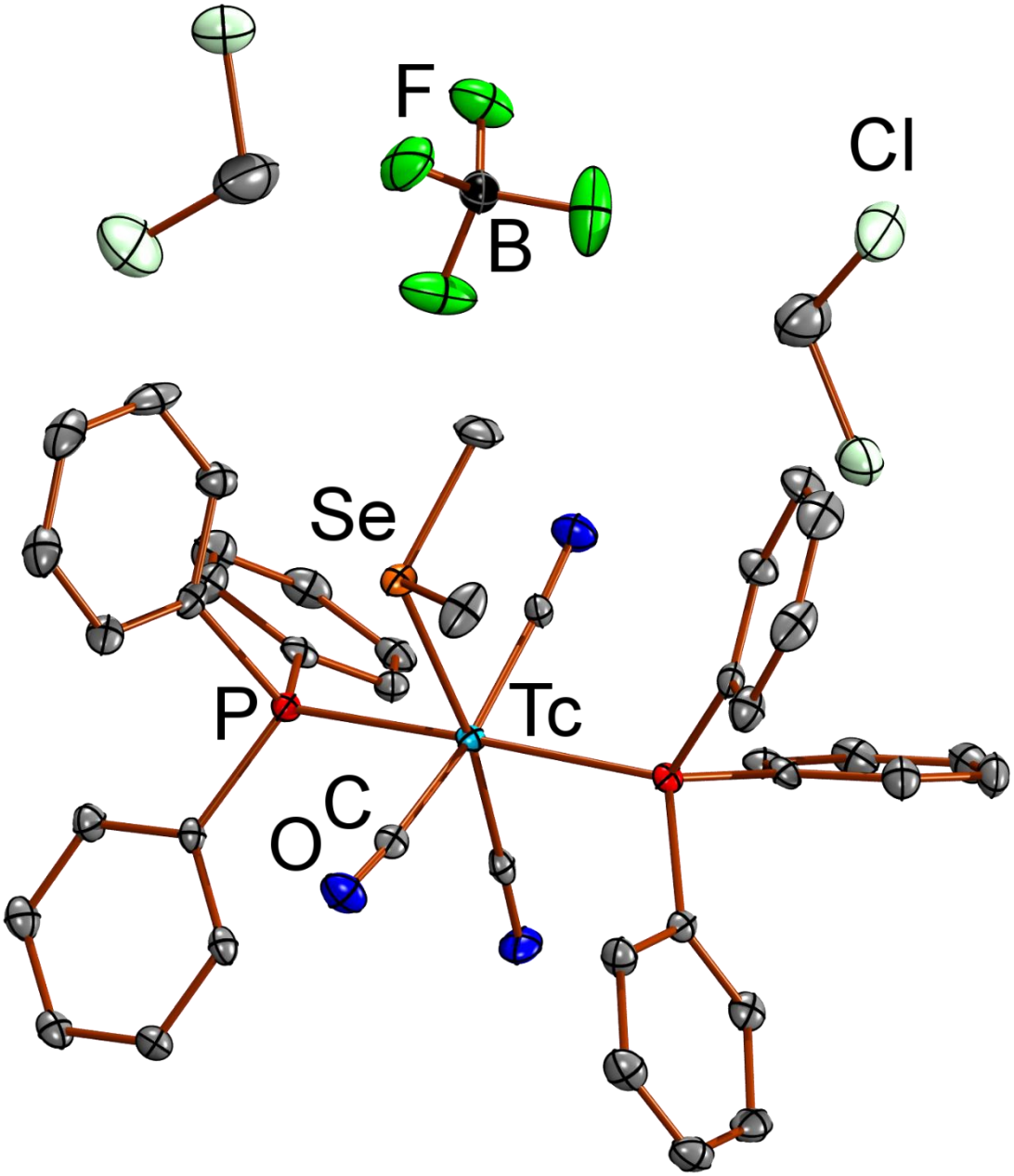

Figure S25. Ellipsoid representation (50% probability) of $[Tc(thse)(CO)_3(PPh_3)_2][BF_4]$ (**20**) · CH_2Cl_2. Hydrogen atoms are omitted for clarity.

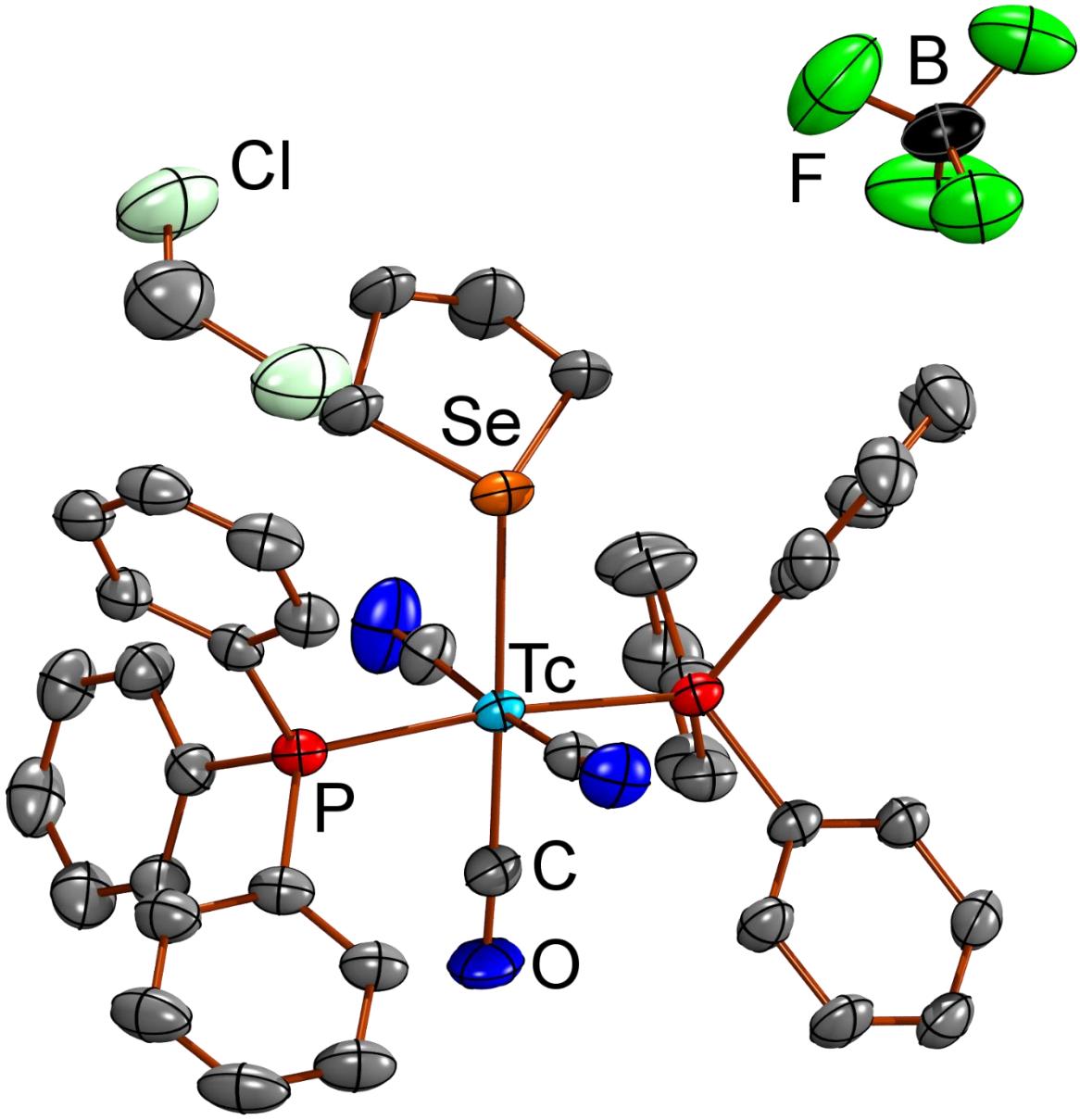

Figure S26. Ellipsoid representation (50% probability) of $[Tc(NCCH_3)(CO)_3(PPh_3)_2][BF_4]$ (**23**) · $2CH_2Cl_2$. Hydrogen atoms bonded to carbon atoms are omitted for clarity. The amine hydrogen atom positions were taken from the density map and refined freely using a SADI constraint. One of the co-crystallized solvent CH_2Cl_2 molecules is disordered over two positions.

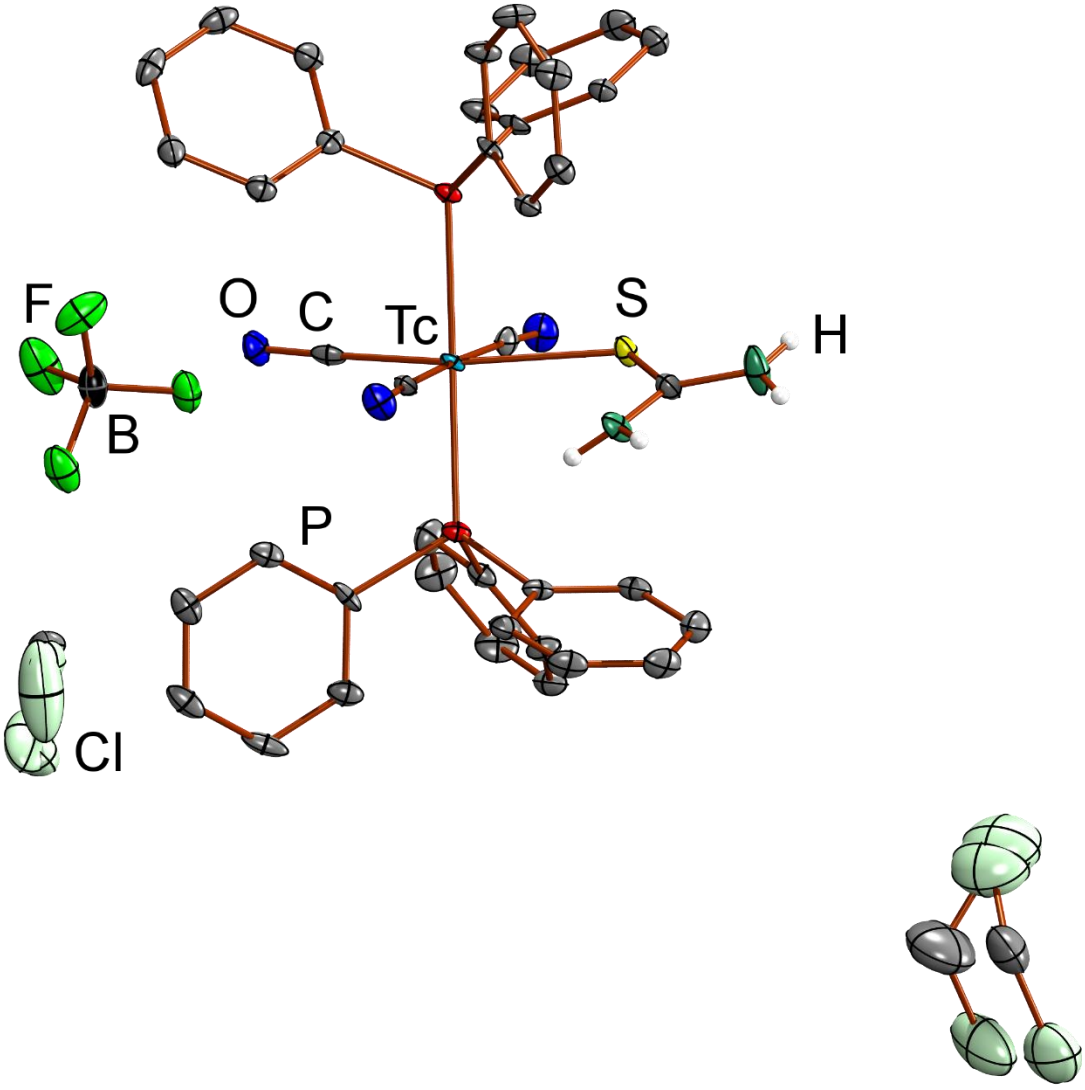

Figure S27. Ellipsoid representation (50% probability) of $[Tc(Se\text{-}urea)(CO)_3(PPh_3)_2][BF_4]$ (**24**) · $0.75CH_2Cl_2$. Hydrogen atoms are omitted for clarity. The hydrogen atom positions on the selenourea ligand were taken from the electron density map. All but one were refined freely, while one had its thermal and positional parameters fixed. The selenourea moiety showed large thermal motion with regard to the technetium, selenium and carbon atoms involved. A hard DELU and RIGU restraint was applied to technetium and selenium. Restraints were mainly used to improve the hydrogen bond contacts as well as to model the thermal motion of the BF_4 anion and the dichloromethane moieties.

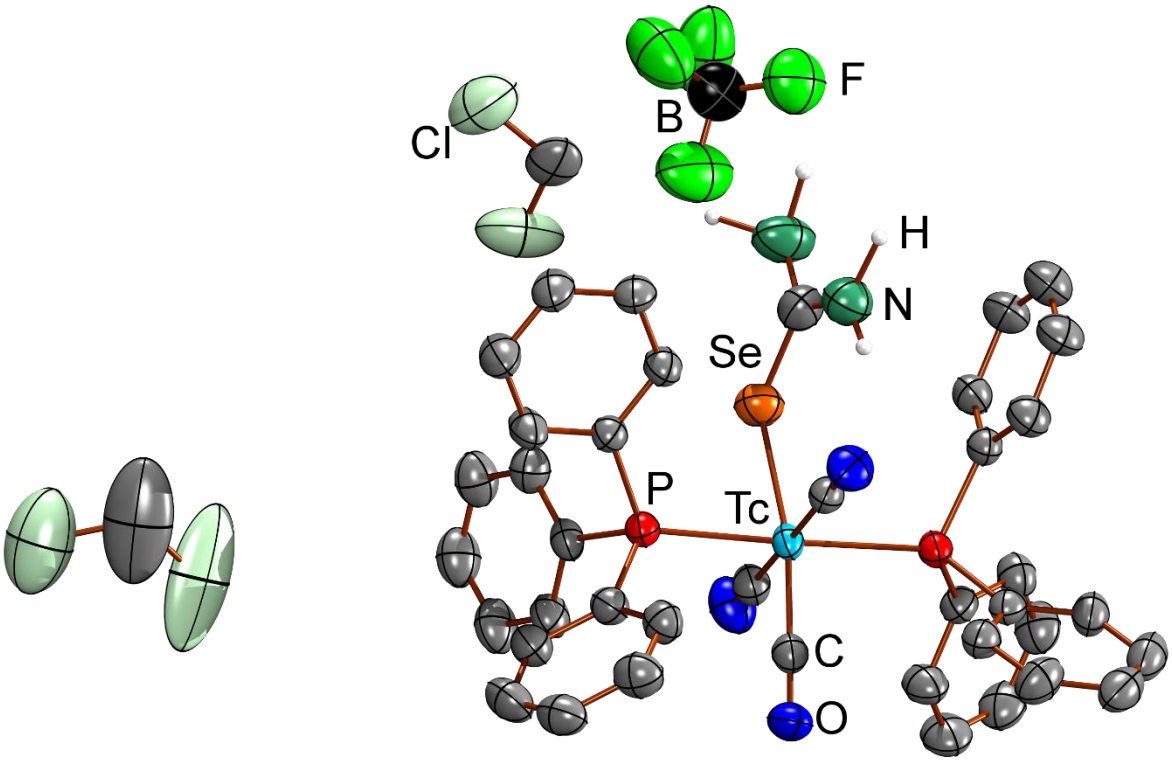

Part 2: Spectral data

Spectragryph 1.2.8 was used to visualize the IR spectra.[1]

Figure S28. ^{1}H NMR spectrum of $[Tc(OH_2)(CO)_3(PPh_3)_2][BArF_{24}]$.

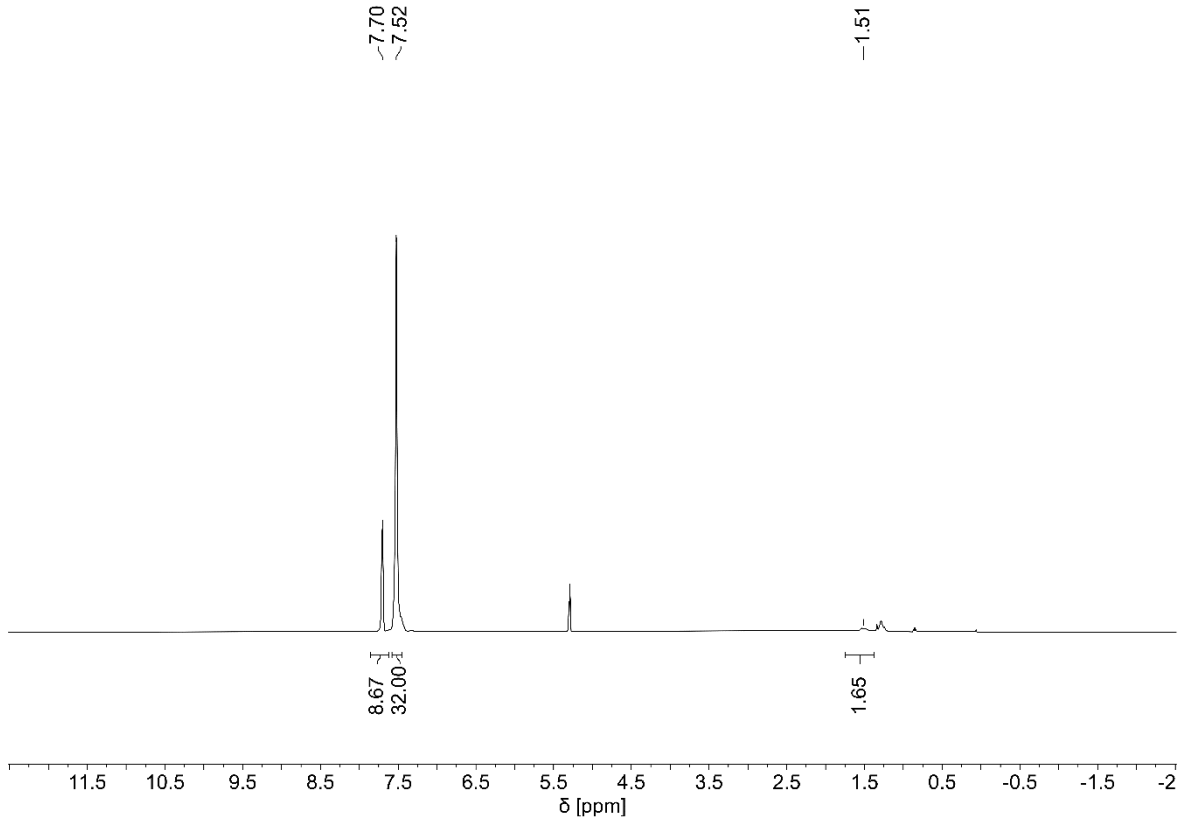

Figure S29. ^{99}Tc NMR spectrum of $[Tc(OH_2)(CO)_3(PPh_3)_2][BArF_{24}]$.

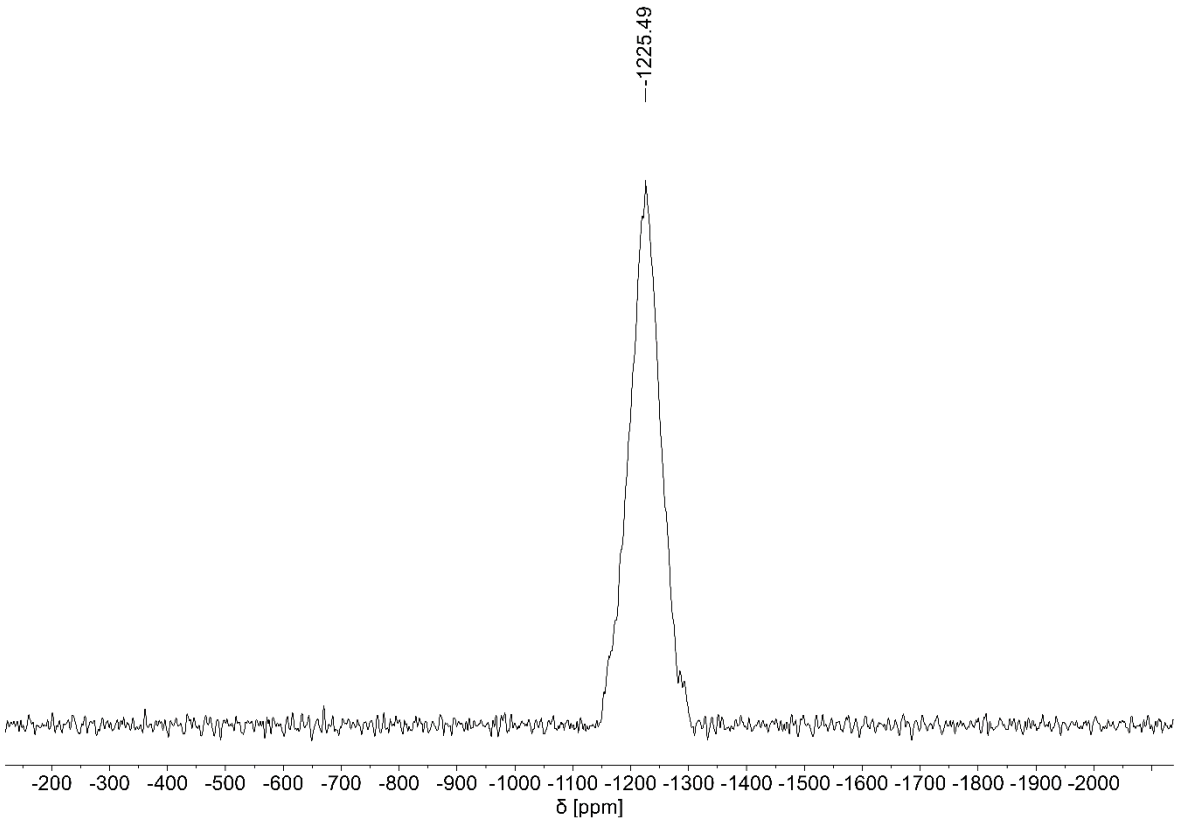

Figure S30. $^{31}P\{^1H\}$ NMR spectrum of $[Tc(OH_2)(CO)_3(PPh_3)_2][BArF_{24}]$.

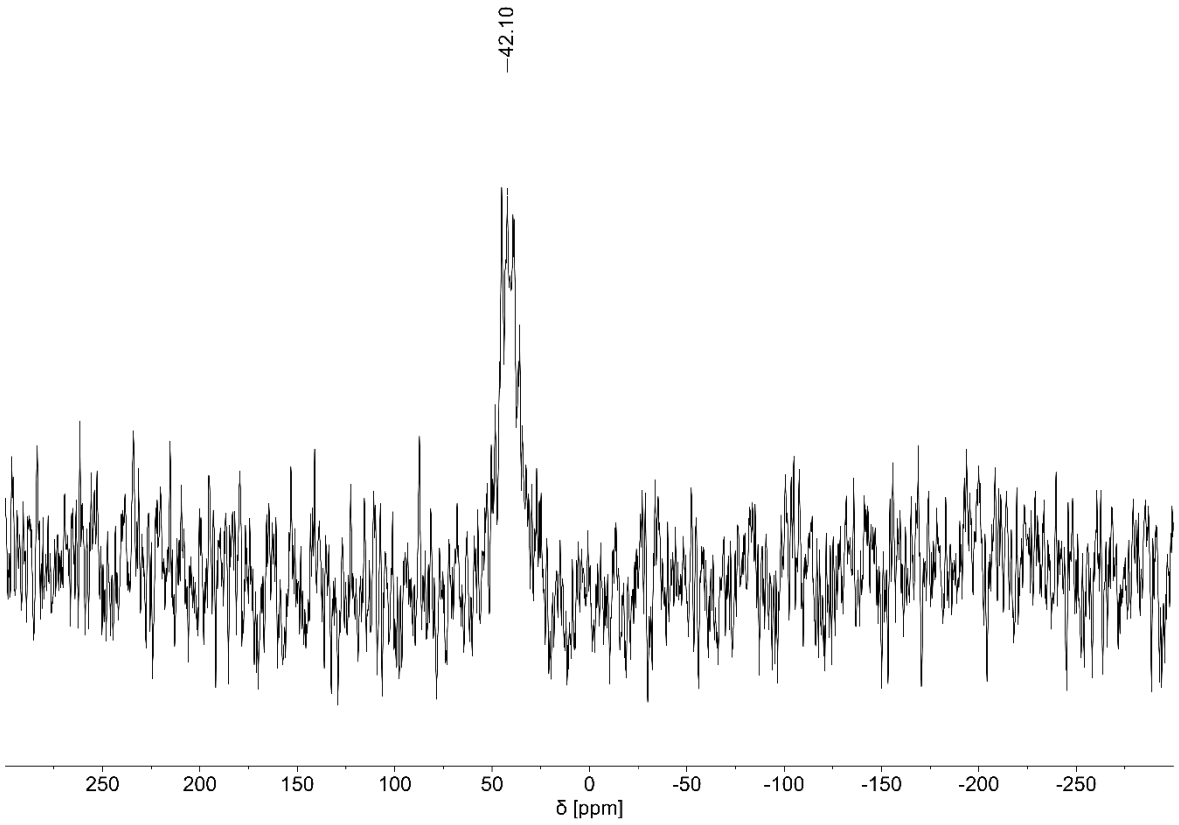

Figure S31. ^{19}F NMR spectrum of $[Tc(OH_2)(CO)_3(PPh_3)_2][BArF_{24}]$.

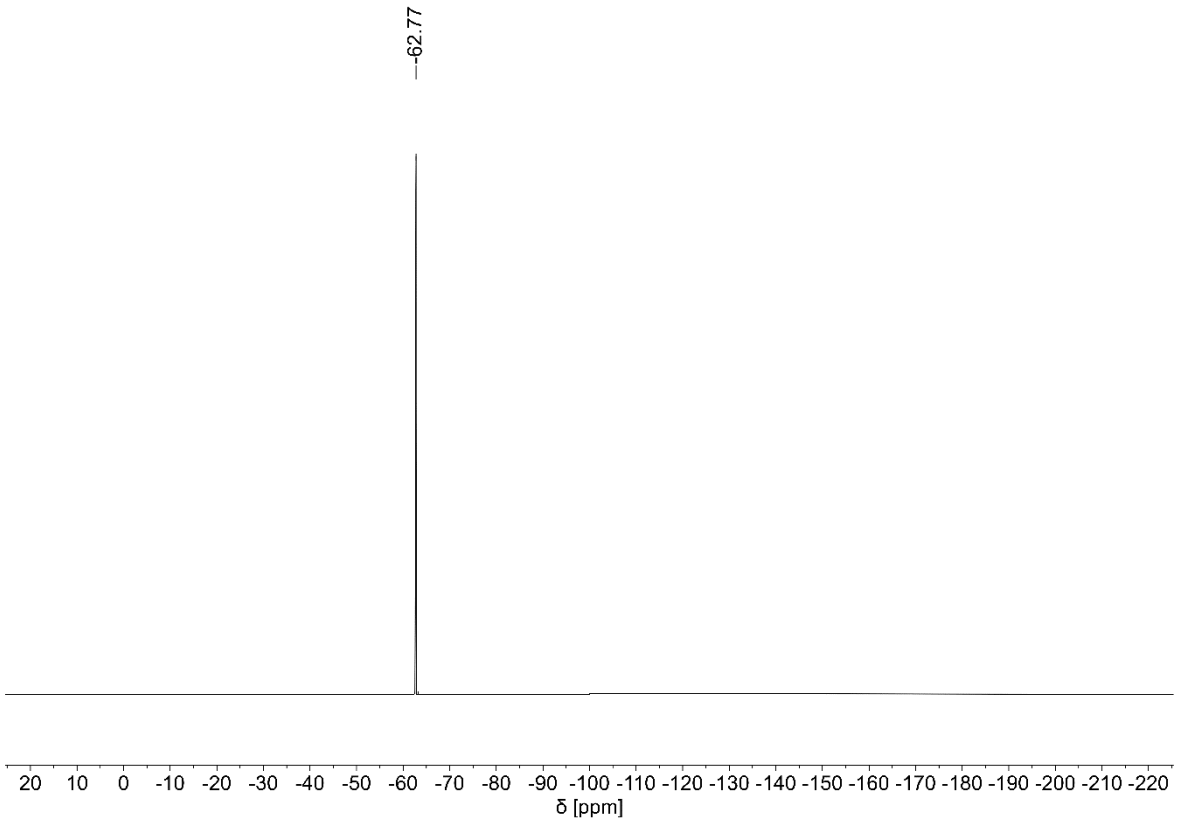

Figure S32. ^{11}B NMR spectrum of $[Tc(OH_2)(CO)_3(PPh_3)_2][BArF_{24}]$.

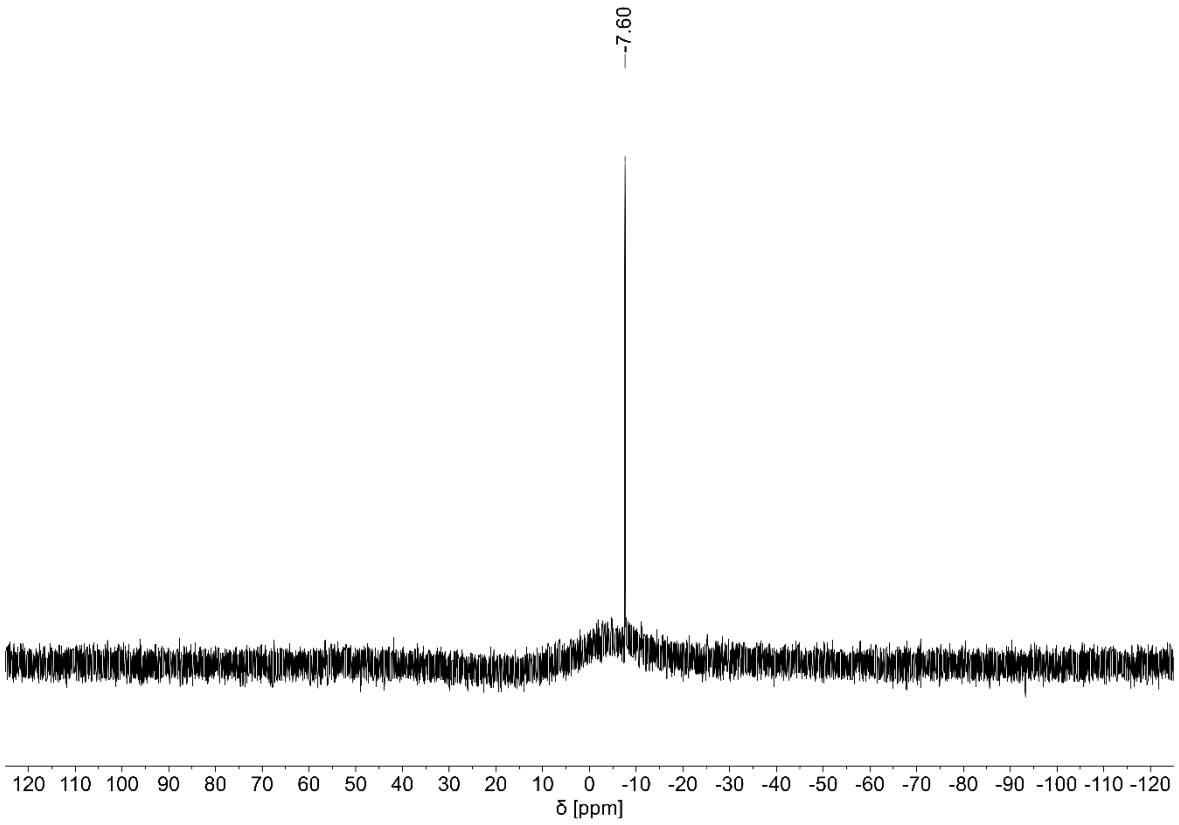

Figure S33. IR spectrum of $[Tc(OH_2)(CO)_3(PPh_3)_2][BArF_{24}]$.

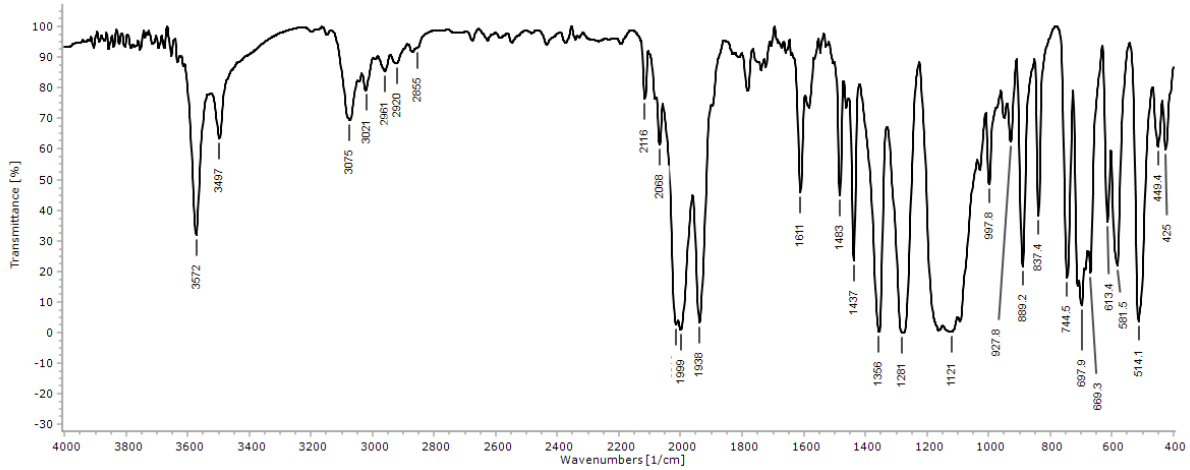

Figure S34. ^{1}H NMR spectrum of $[Tc(OH_2)(CO)_3(PPh_3)_2][BF_4]$.

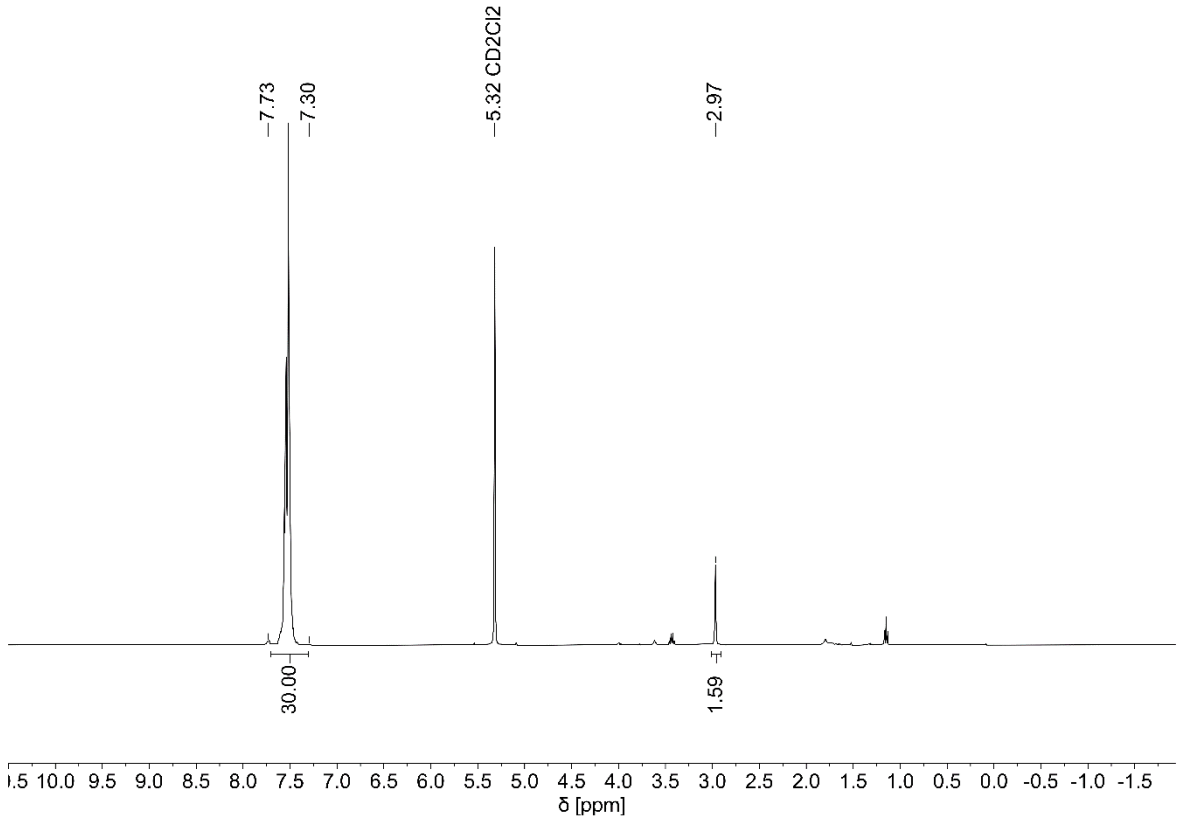

Figure S35. ^{99}Tc NMR spectrum of $[Tc(OH_2)(CO)_3(PPh_3)_2][BF_4]$.

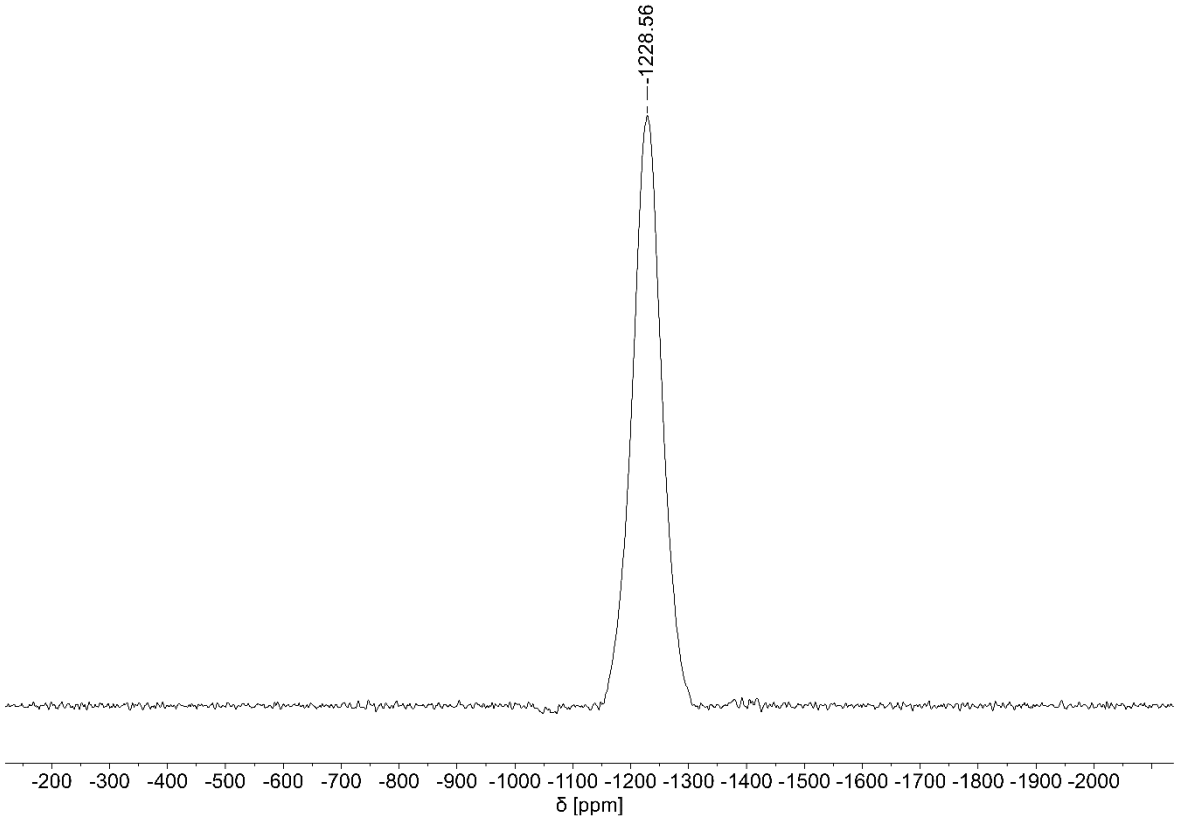

Figure S36. $^{31}P\{^1H\}$ NMR spectrum of $[Tc(OH_2)(CO)_3(PPh_3)_2][BF_4]$.

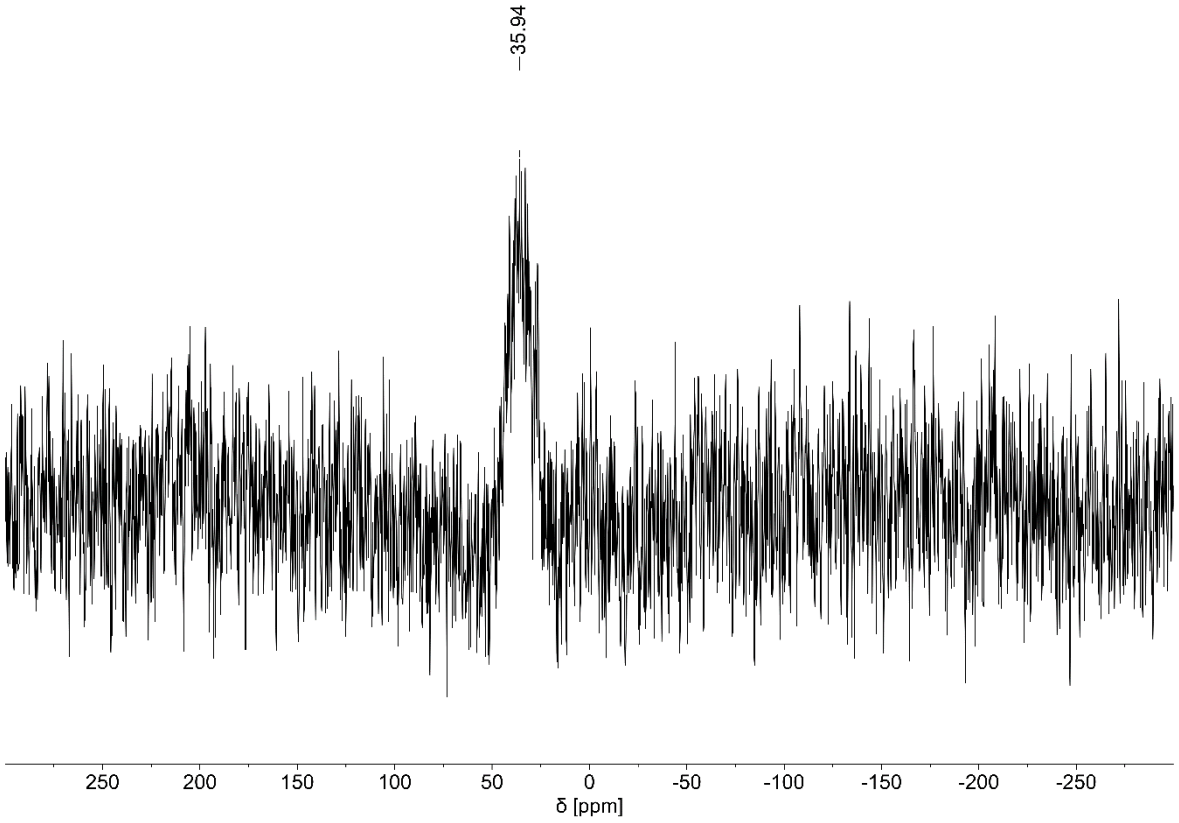

Figure S37. ^{19}F NMR spectrum of $[Tc(OH_2)(CO)_3(PPh_3)_2][BF_4]$.

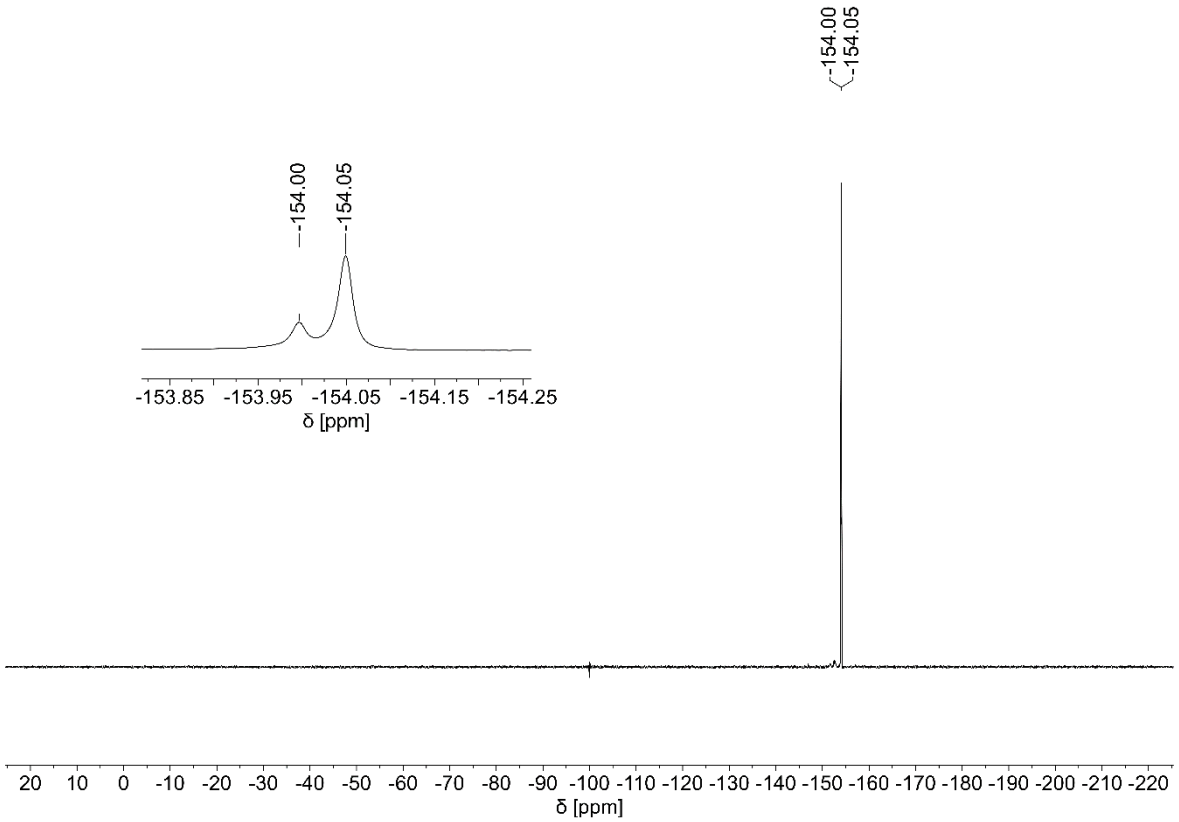

Figure S38. ^{11}B NMR spectrum of $[Tc(OH_2)(CO)_3(PPh_3)_2][BF_4]$.

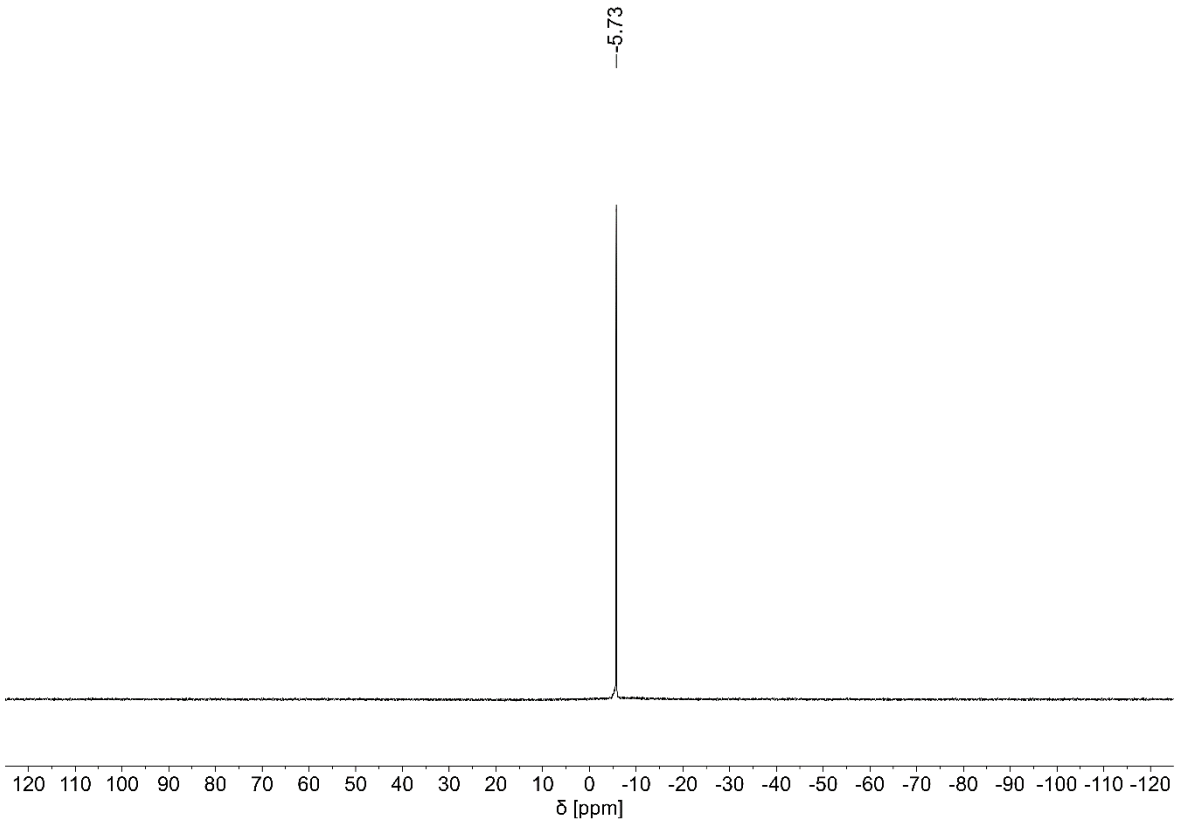

Figure S39. IR spectrum of $[Tc(OH_2)(CO)_3(PPh_3)_2][BF_4]$.

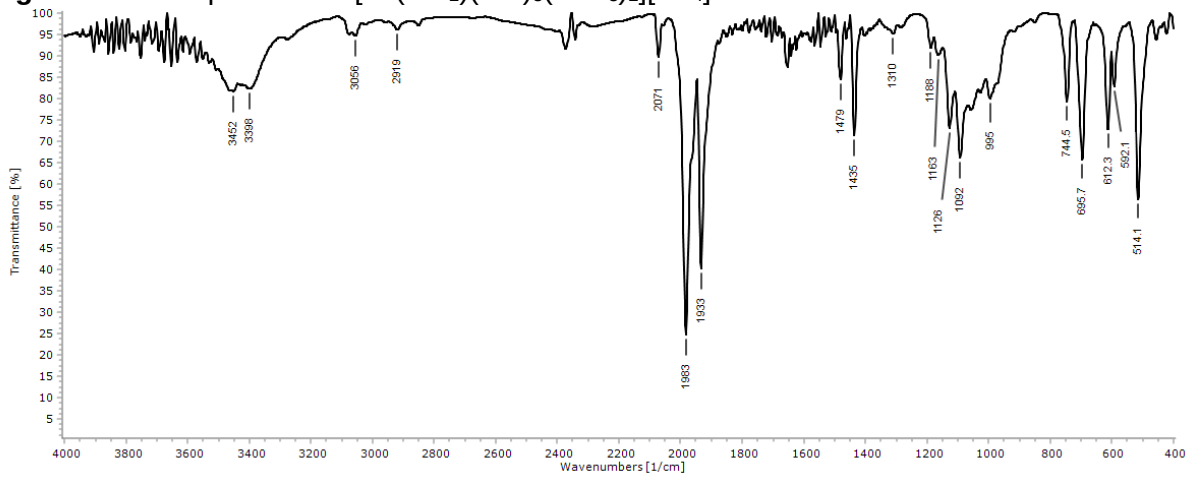

Figure S40. ^{1}H NMR spectrum of $[Tc(OH_2)(CO)_3(PPh_3)_2][OTf]$.

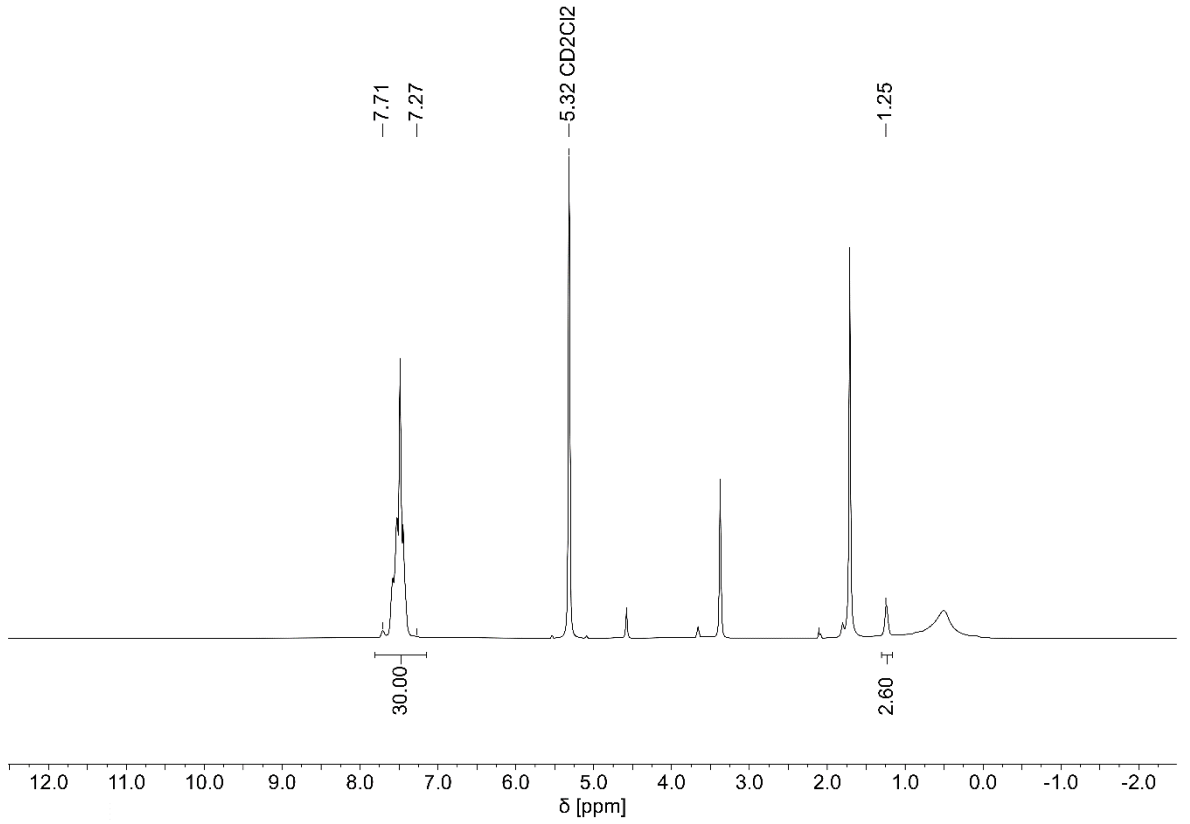

Figure S41. ^{99}Tc NMR spectrum of $[Tc(OH_2)(CO)_3(PPh_3)_2][OTf]$.

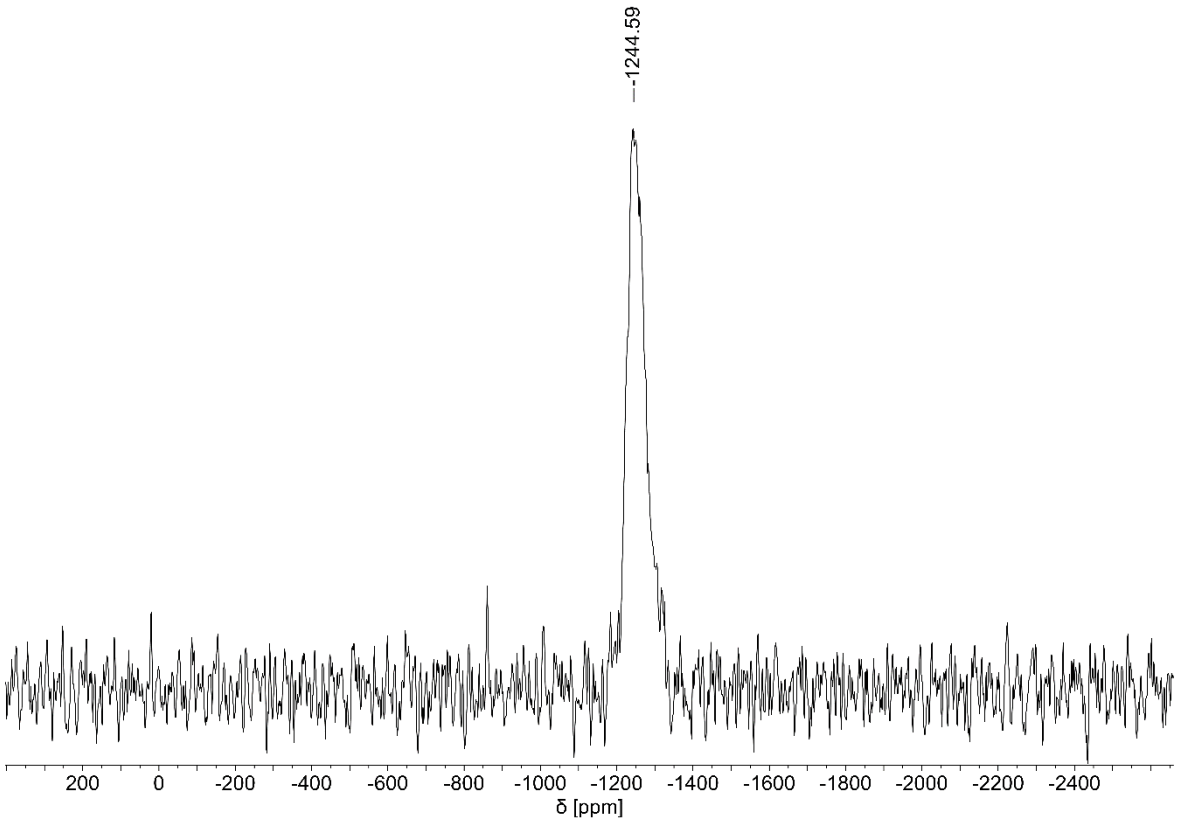

Figure S42. ^{19}F NMR spectrum of $[Tc(OH_2)(CO)_3(PPh_3)_2][OTf]$.

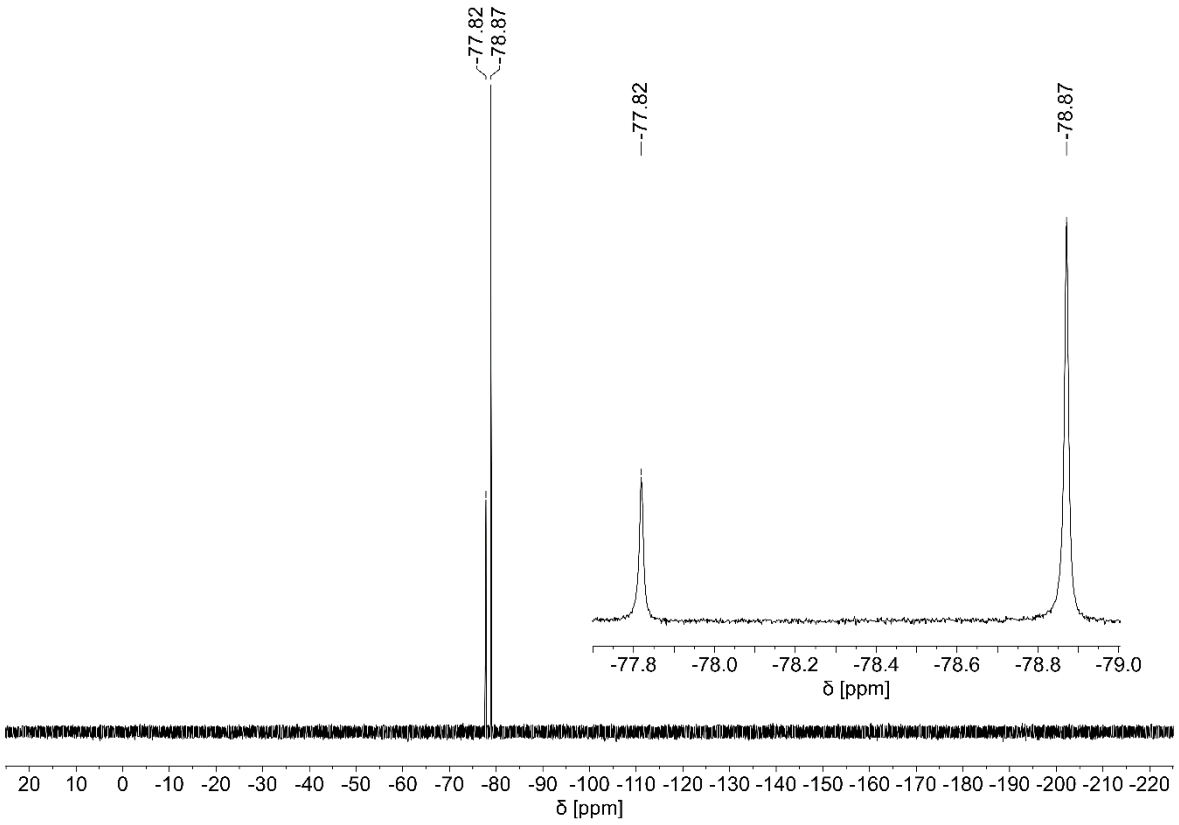

Figure S43. IR spectrum of $[Tc(OH_2)(CO)_3(PPh_3)_2][OTf]$.

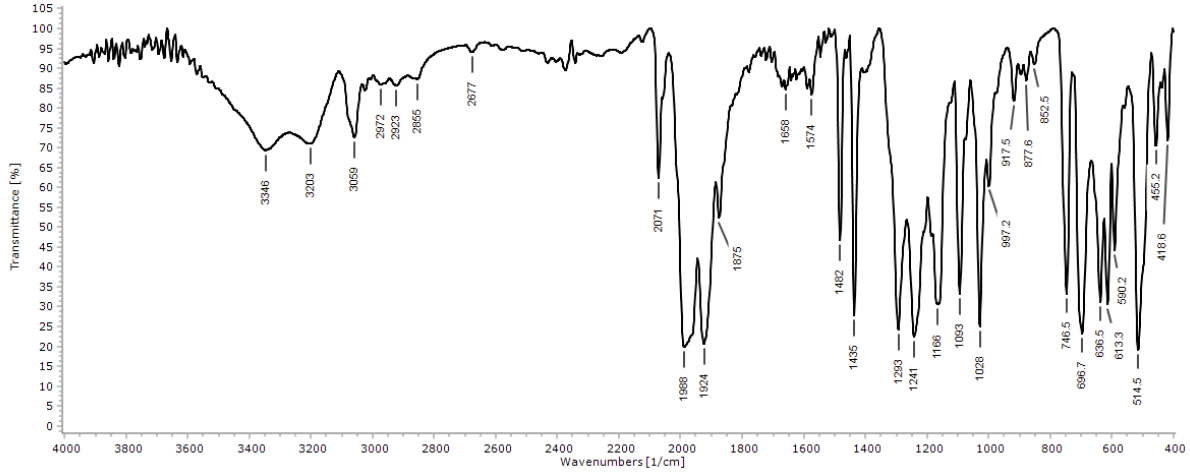

Figure S44. IR spectrum of $[Tc(DMSO)(CO)_3(PPh_3)_2][BF_4]$ + $[Tc(DMSO)_2(CO)_2(PPh_3)_2][BF_4]$.

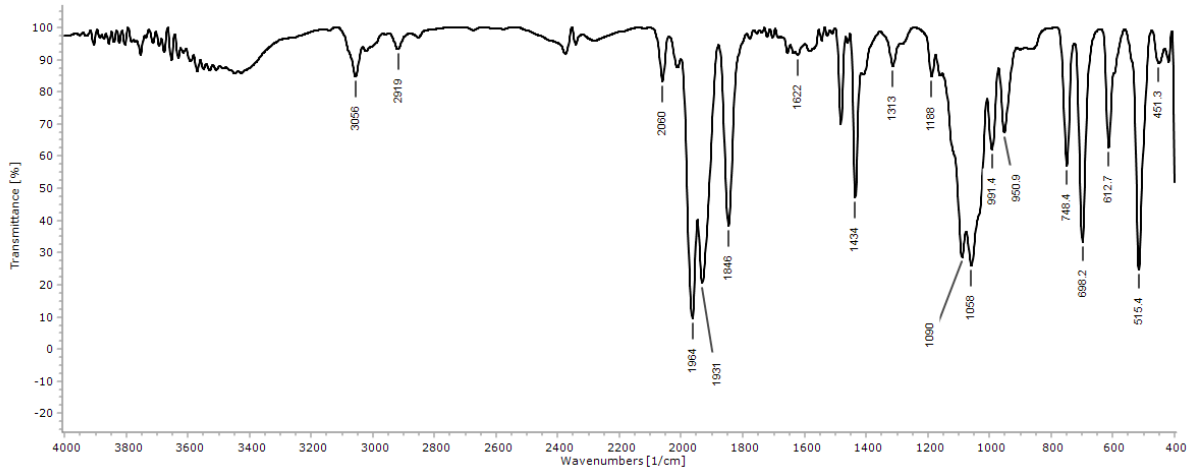

Figure S45. ^{1}H NMR spectrum of $[Tc(DMSO)_2(CO)_2(PPh_3)_2][BF_4]$.

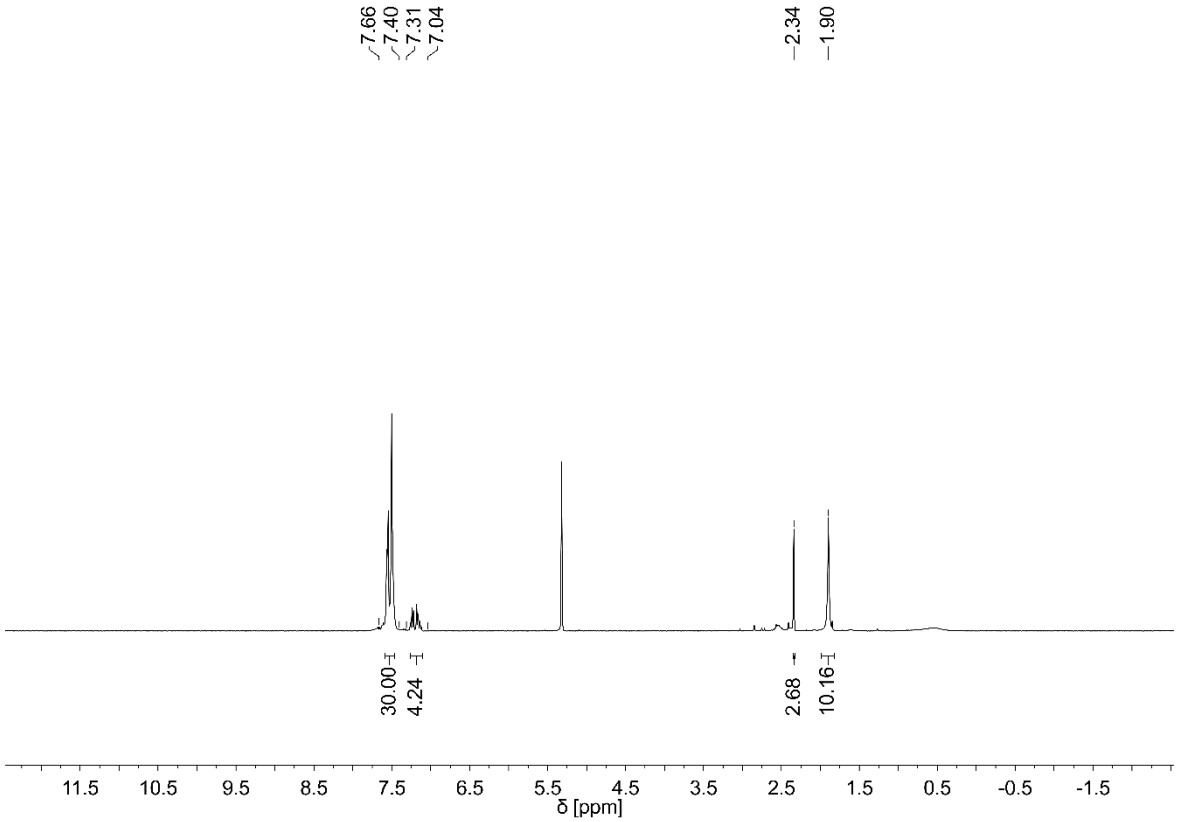

Figure S46. ^{99}Tc NMR spectrum of $[Tc(DMSO)_2(CO)_2(PPh_3)_2][BF_4]$.

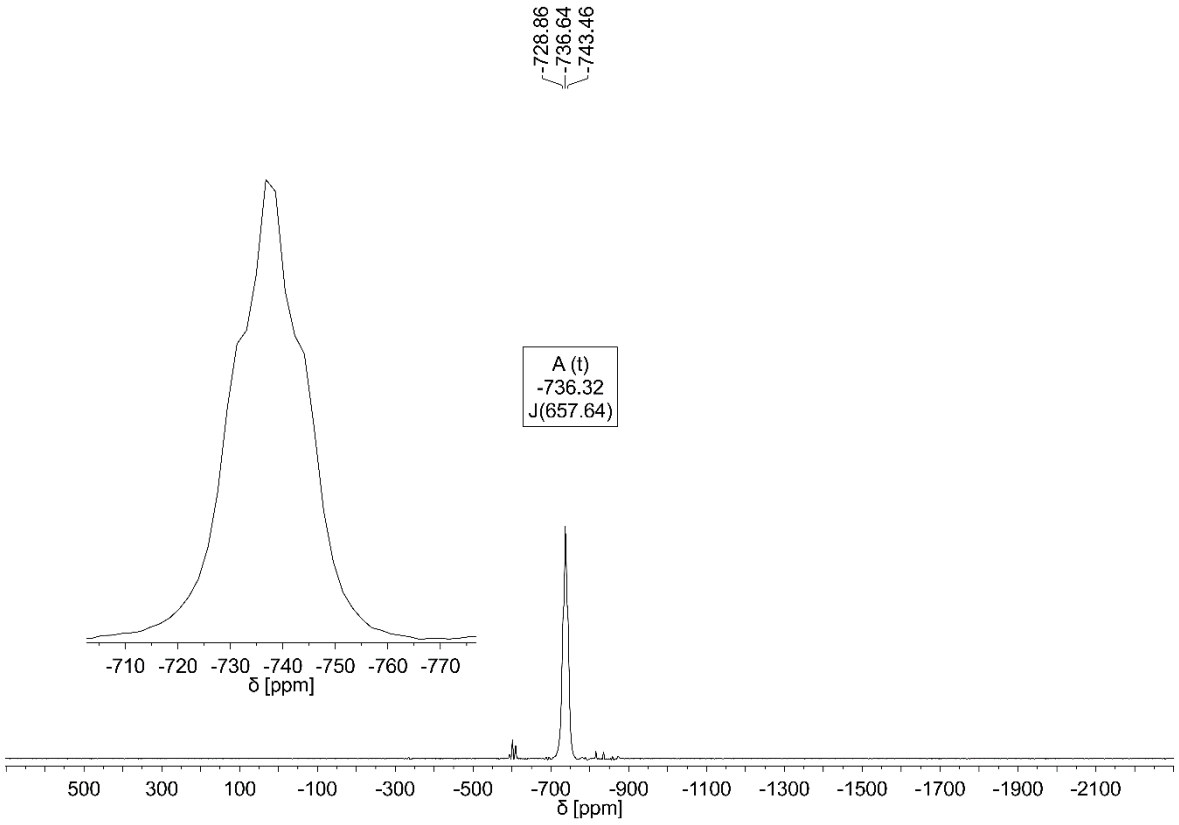

Figure S47. ^{19}F NMR spectrum of $[Tc(DMSO)_2(CO)_2(PPh_3)_2][BF_4]$.

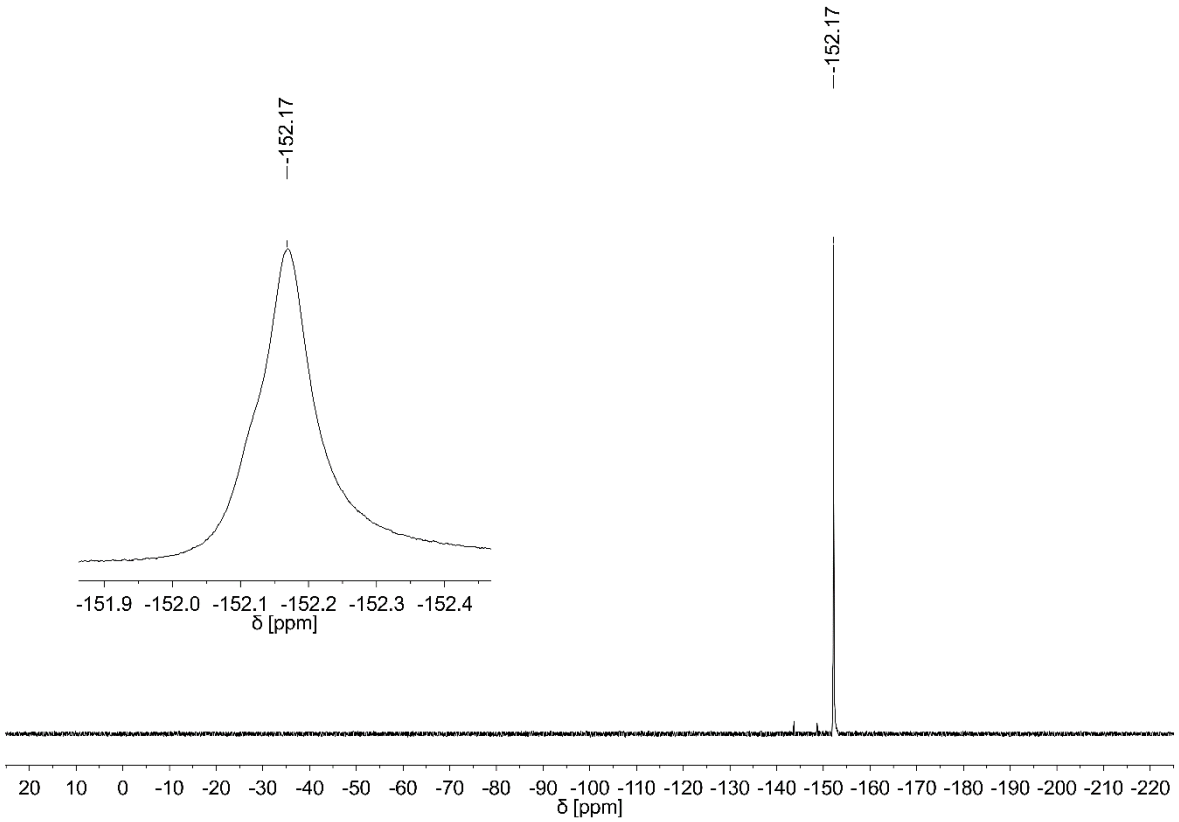

Figure S48. ^{11}B NMR spectrum of $[Tc(DMSO)_2(CO)_2(PPh_3)_2][BF_4]$.

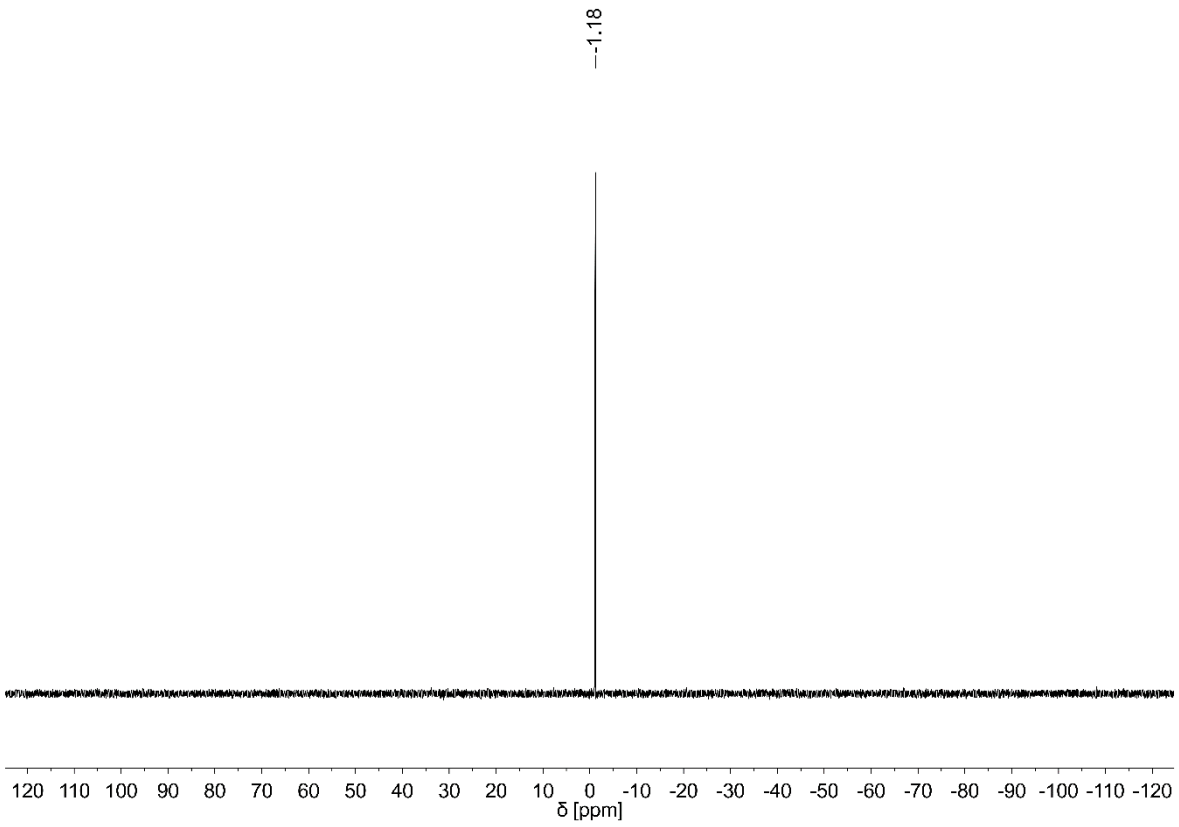

Figure S49. IR spectrum of $[Tc(DMSO)_2(CO)_2(PPh_3)_2][BF_4]$.

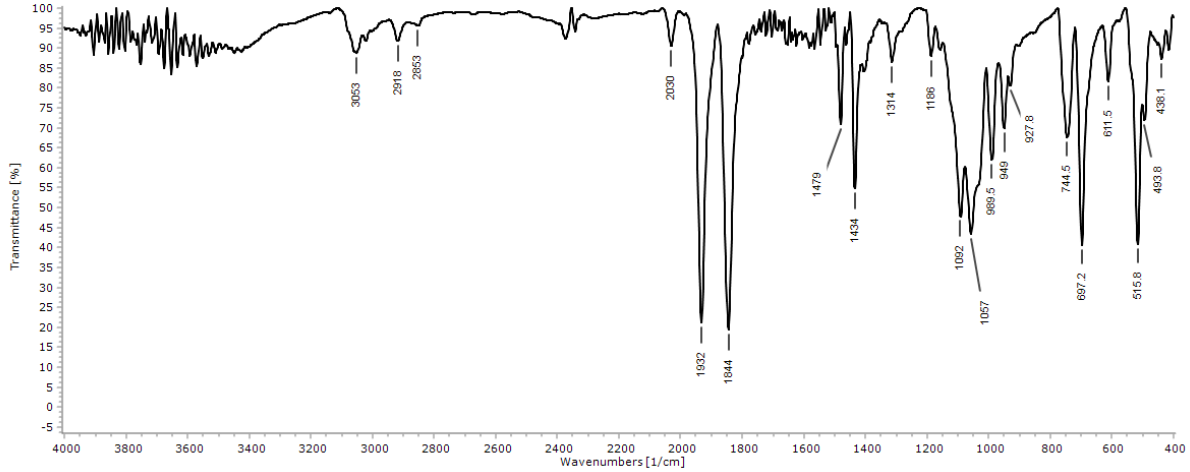

Figure S50. ^1H NMR spectrum of $[Tc(DMF)(CO)_3(PPh_3)_2][BF_4]$.

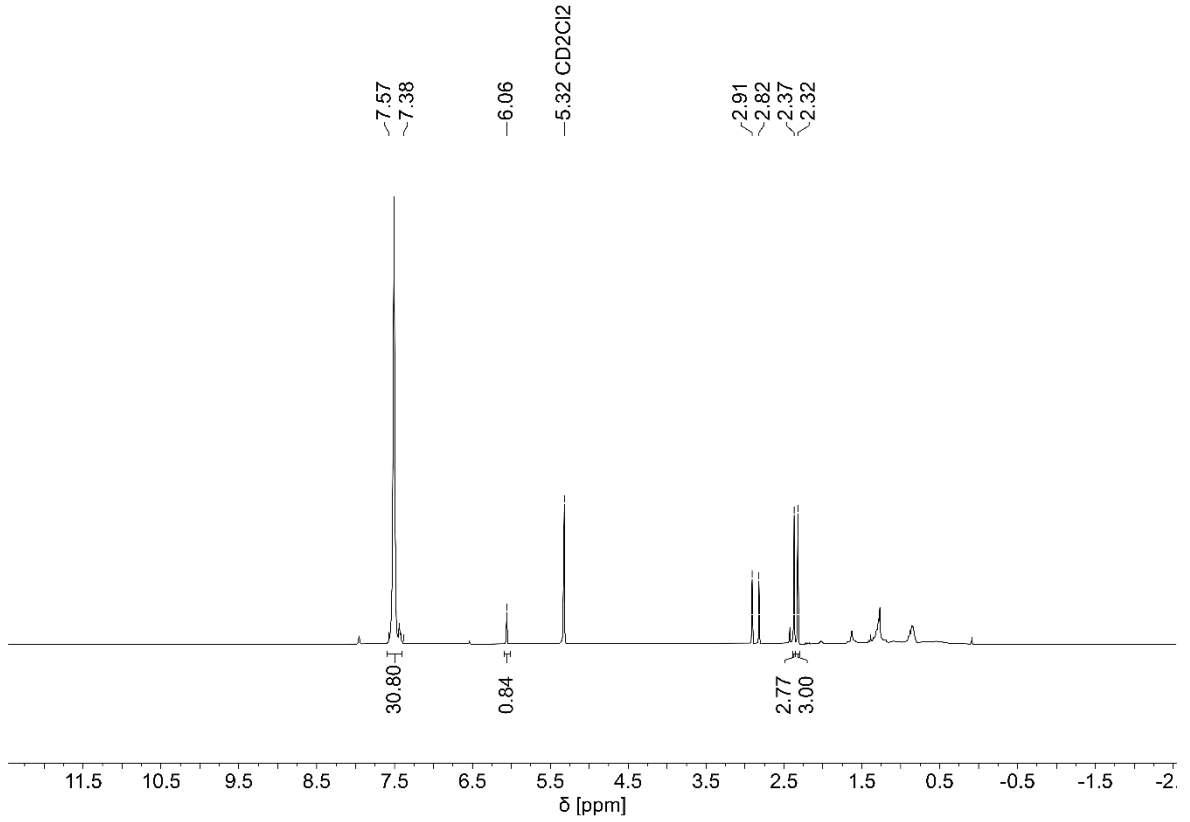

Figure S51. ^{99}Tc NMR spectrum of [Tc(DMF)(CO)$_3$(PPh$_3$)$_2$][BF$_4$].

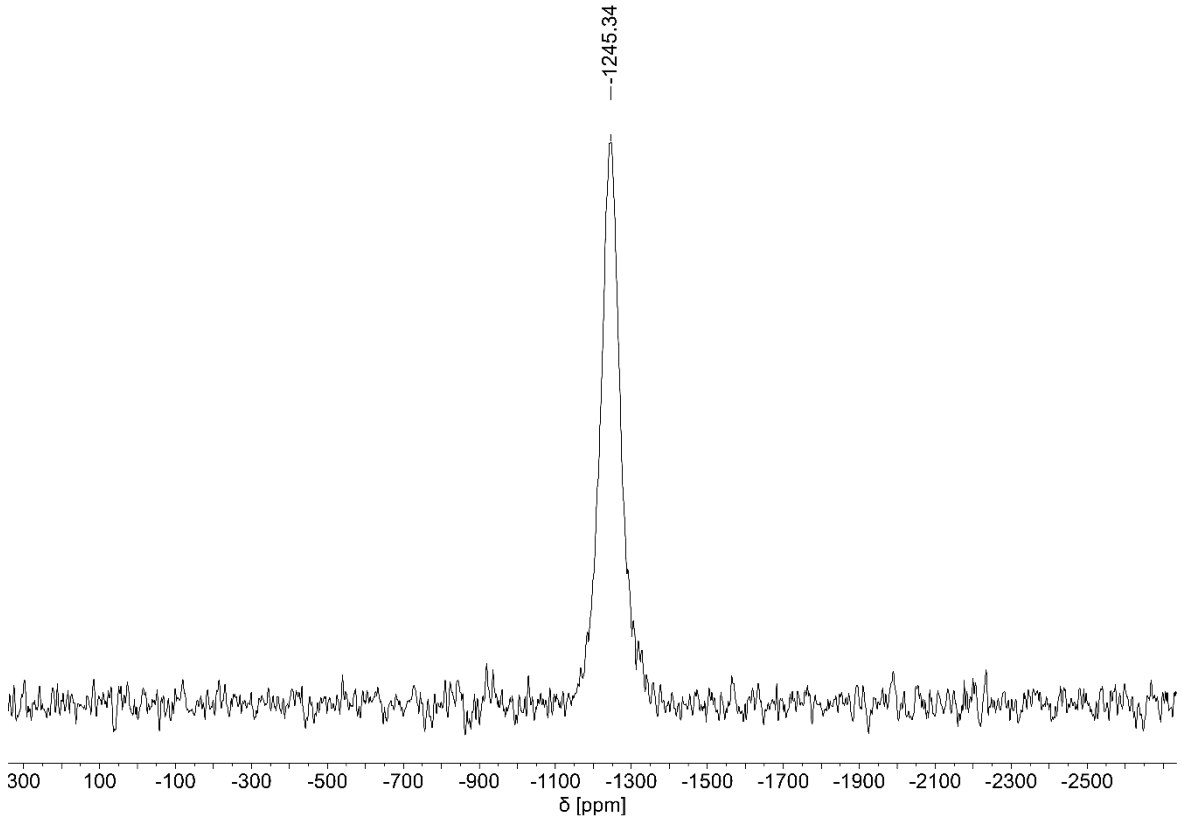

Figure S52. ^{31}P{^{1}H} NMR spectrum of [Tc(DMF)(CO)$_3$(PPh$_3$)$_2$][BF$_4$].

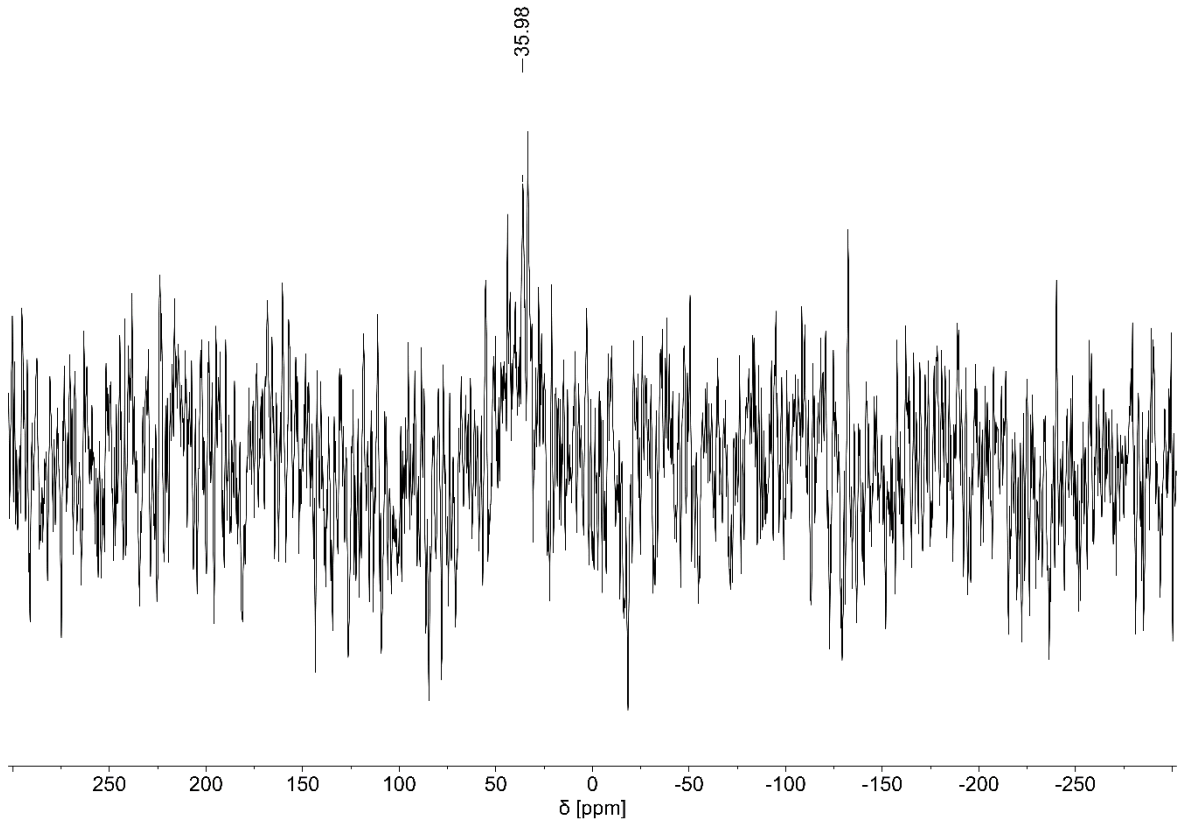

Figure S53. ^{19}F NMR spectrum of $[Tc(DMF)(CO)_3(PPh_3)_2][BF_4]$.

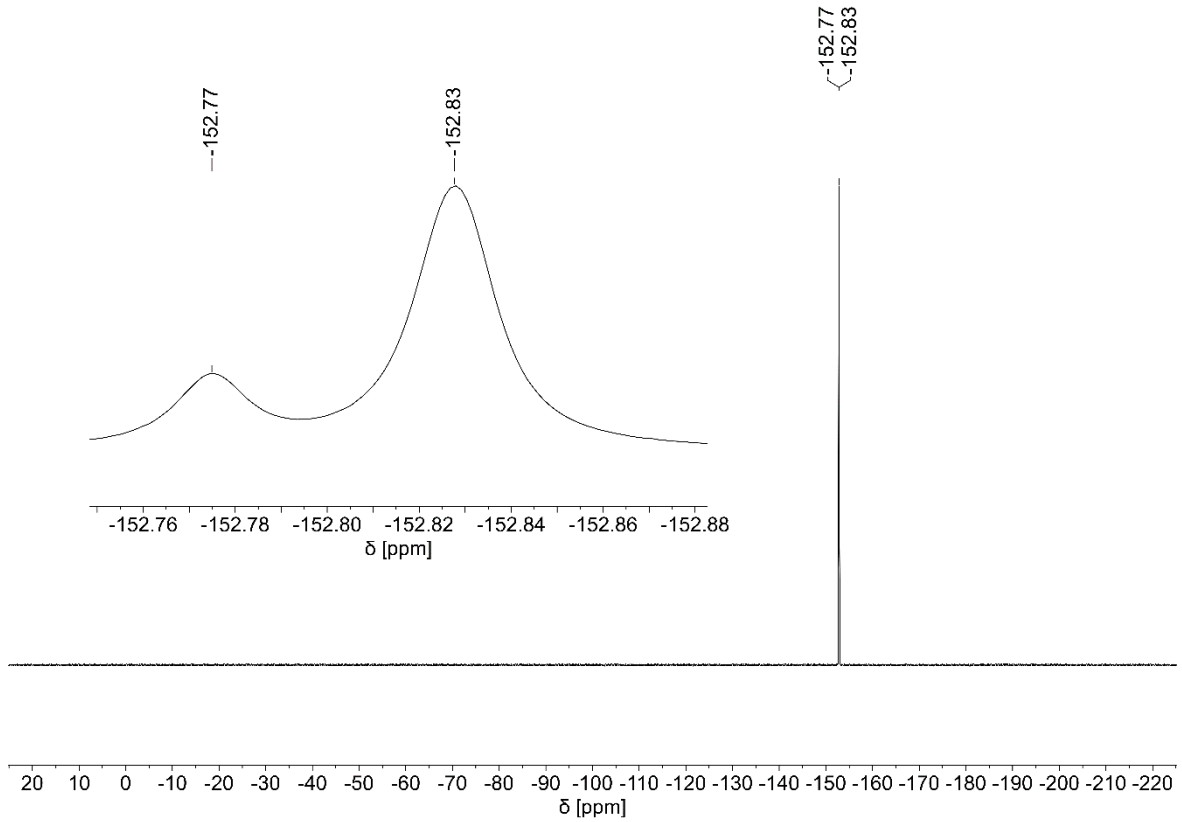

Figure S54. ^{11}B NMR spectrum of $[Tc(DMF)(CO)_3(PPh_3)_2][BF_4]$.

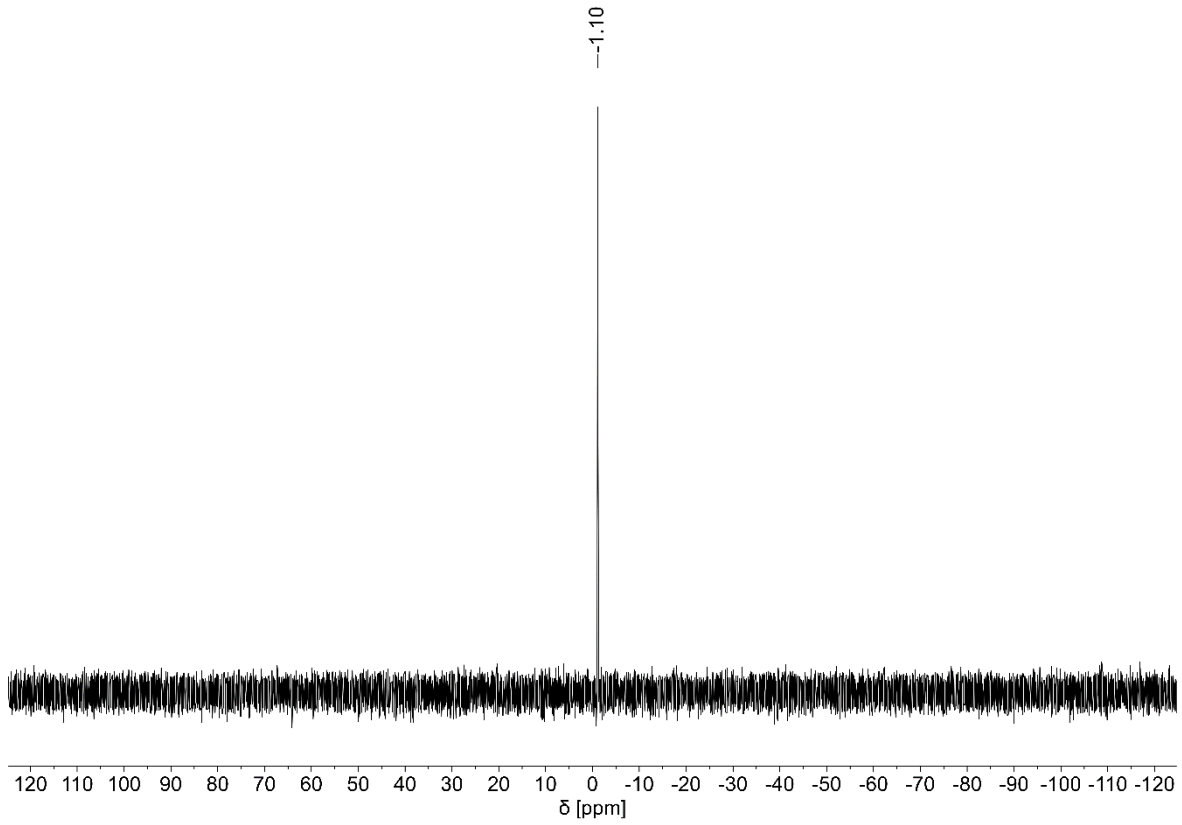

Figure S55. IR spectrum of $[Tc(DMF)(CO)_3(PPh_3)_2][BF_4]$.

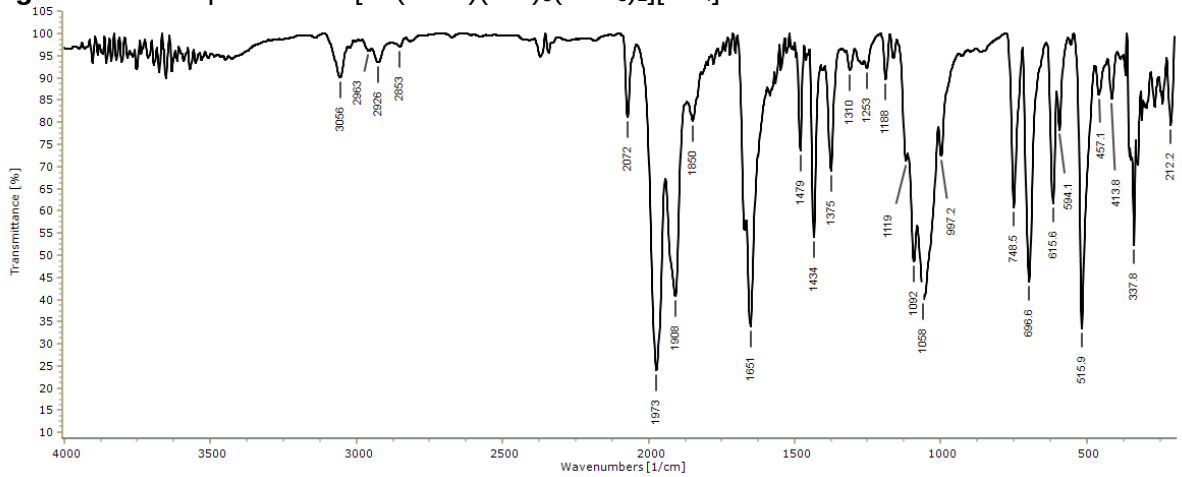

Figure S56. ^1H NMR spectrum of $[Tc(DMF)_2(CO)_2(PPh_3)_2][BF_4]$.

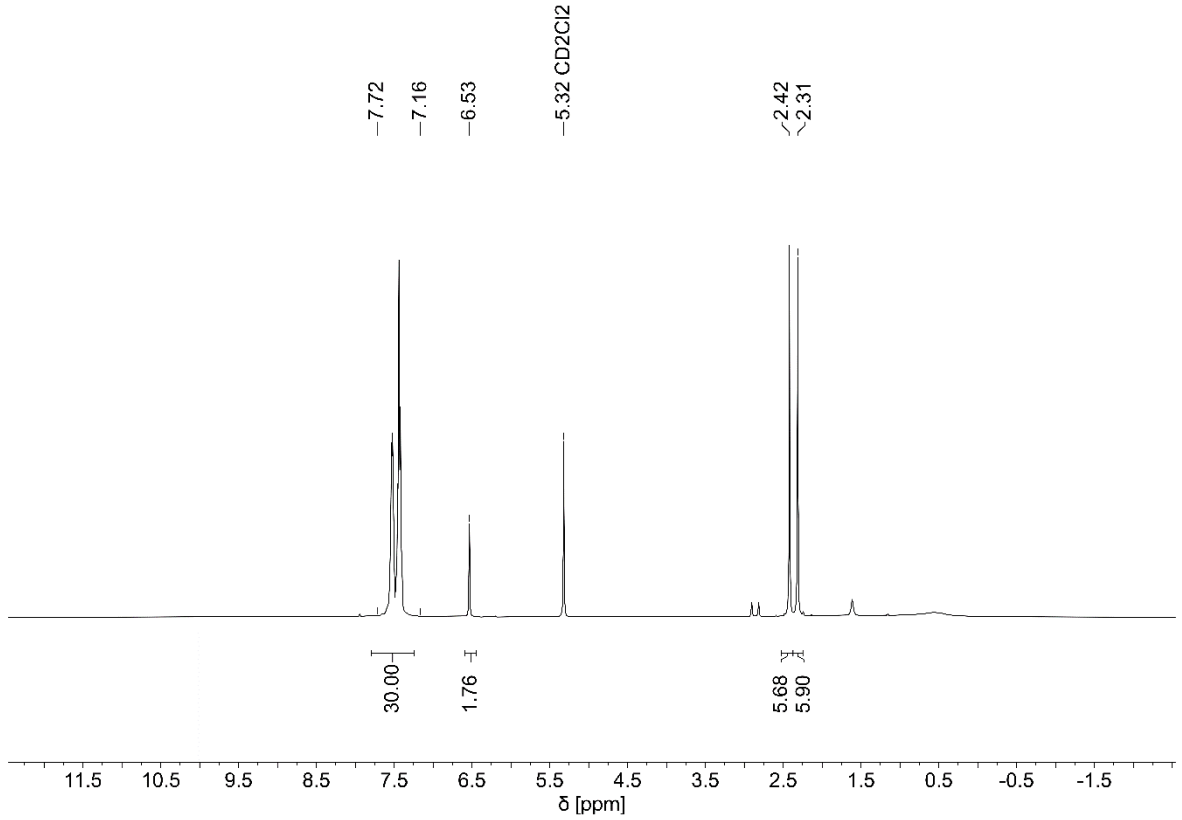

Figure S57. ^{99}Tc NMR spectrum of $[Tc(DMF)_2(CO)_2(PPh_3)_2][BF_4]$.

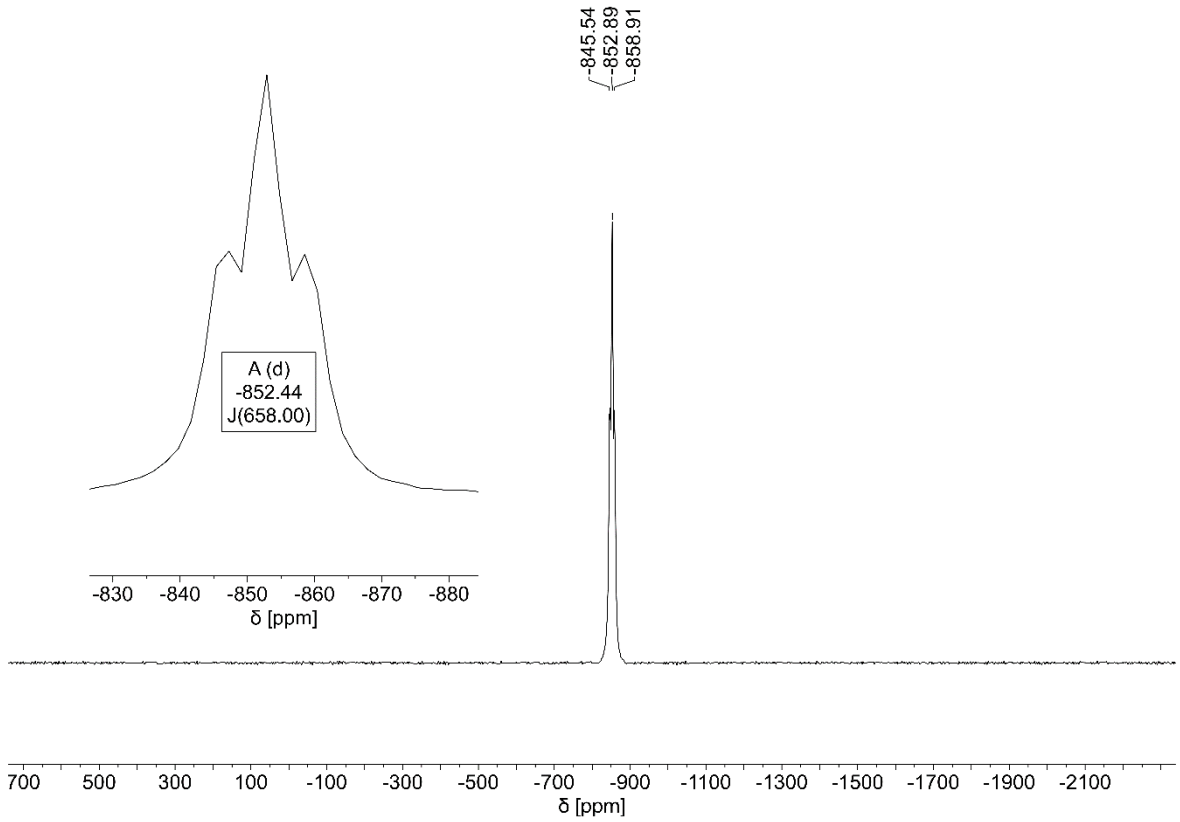

Figure S58. ^{19}F NMR spectrum of $[Tc(DMF)_2(CO)_2(PPh_3)_2][BF_4]$.

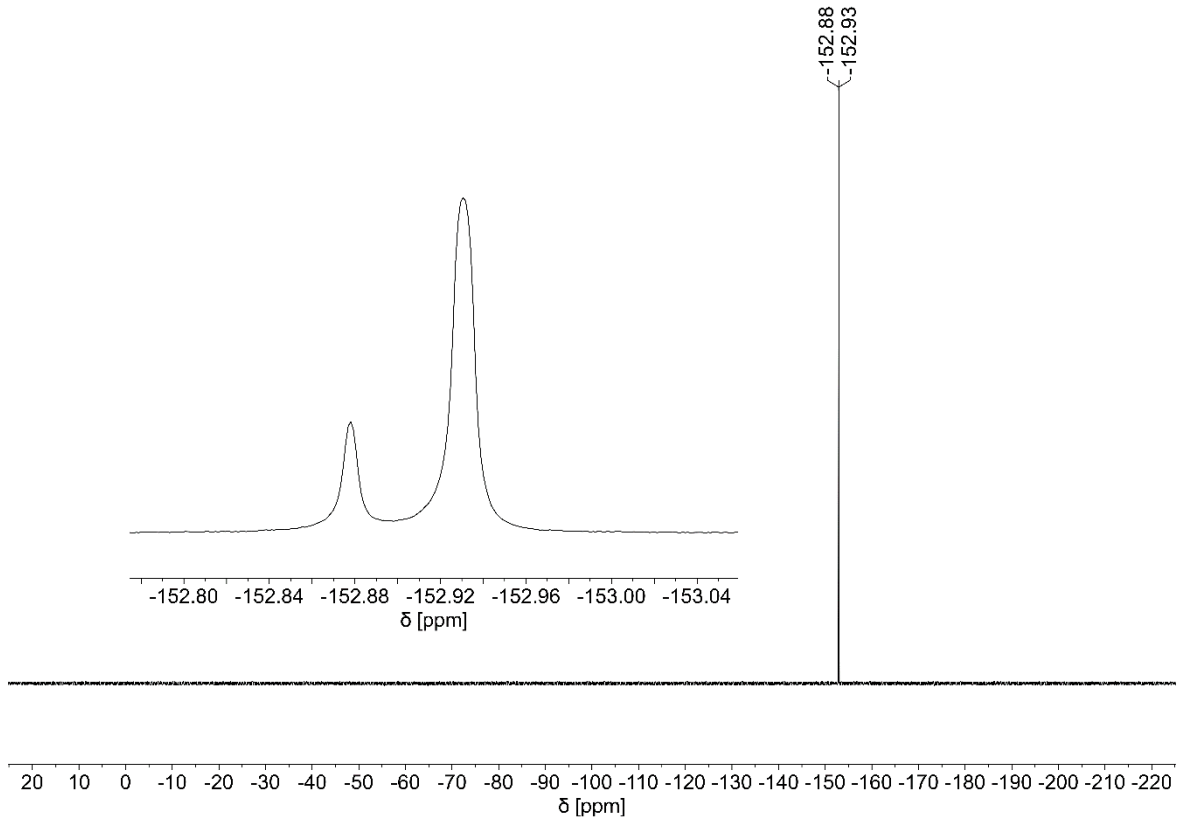

Figure S59. ^{11}B NMR spectrum of $[Tc(DMF)_2(CO)_2(PPh_3)_2][BF_4]$.

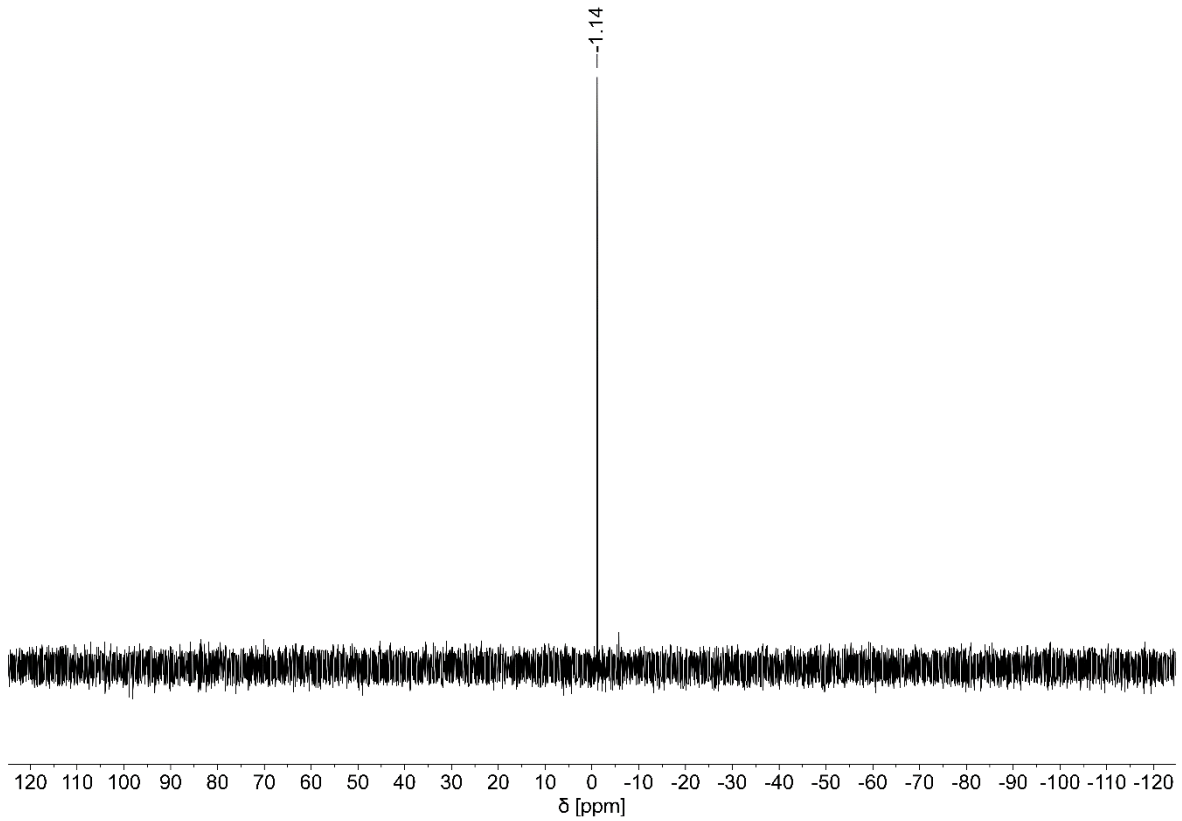

Figure S60. IR spectrum of $[Tc(DMF)_2(CO)_2(PPh_3)_2][BF_4]$.

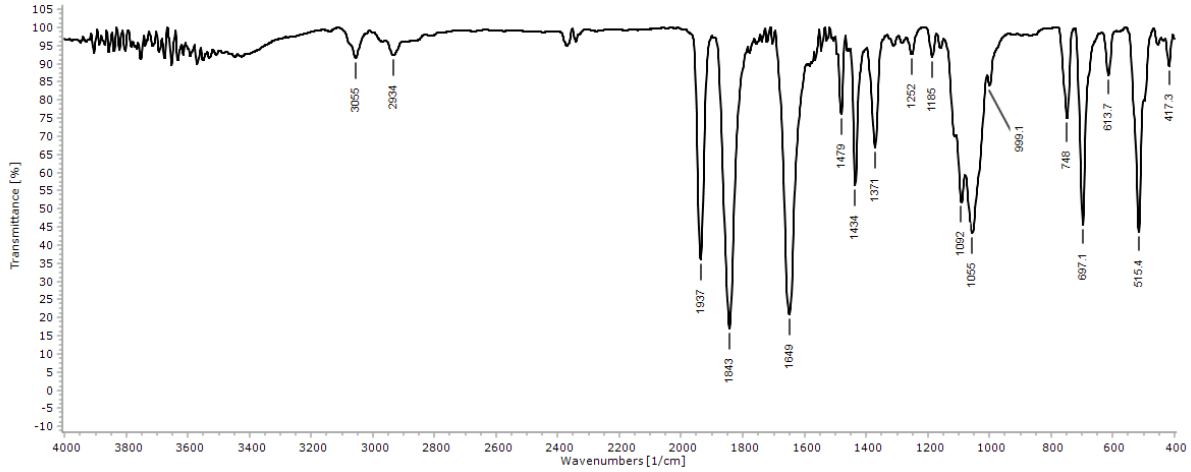

Figure S61. ^{1}H NMR spectrum of $[Tc(CO)_4(PPh_3)_2][BArF_{24}]$.

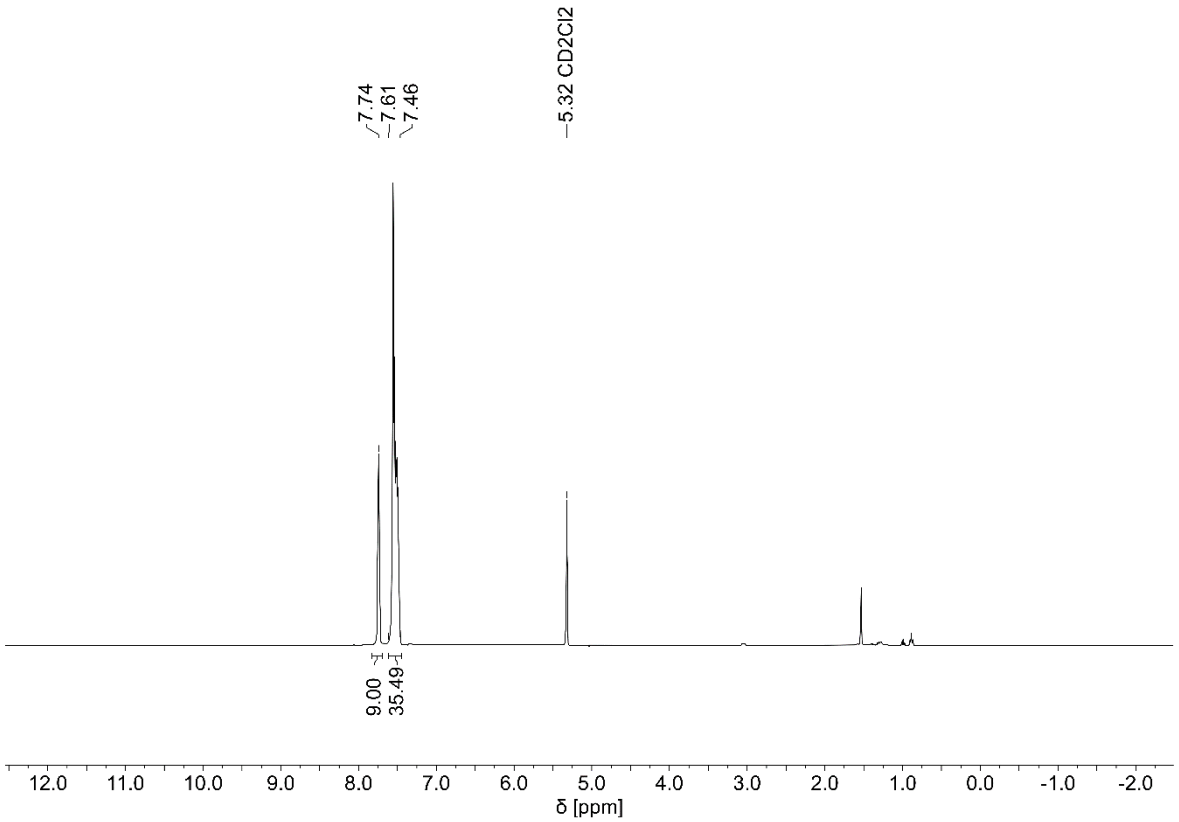

Figure S62. ^{99}Tc NMR spectrum of $[Tc(CO)_4(PPh_3)_2][BArF_{24}]$.

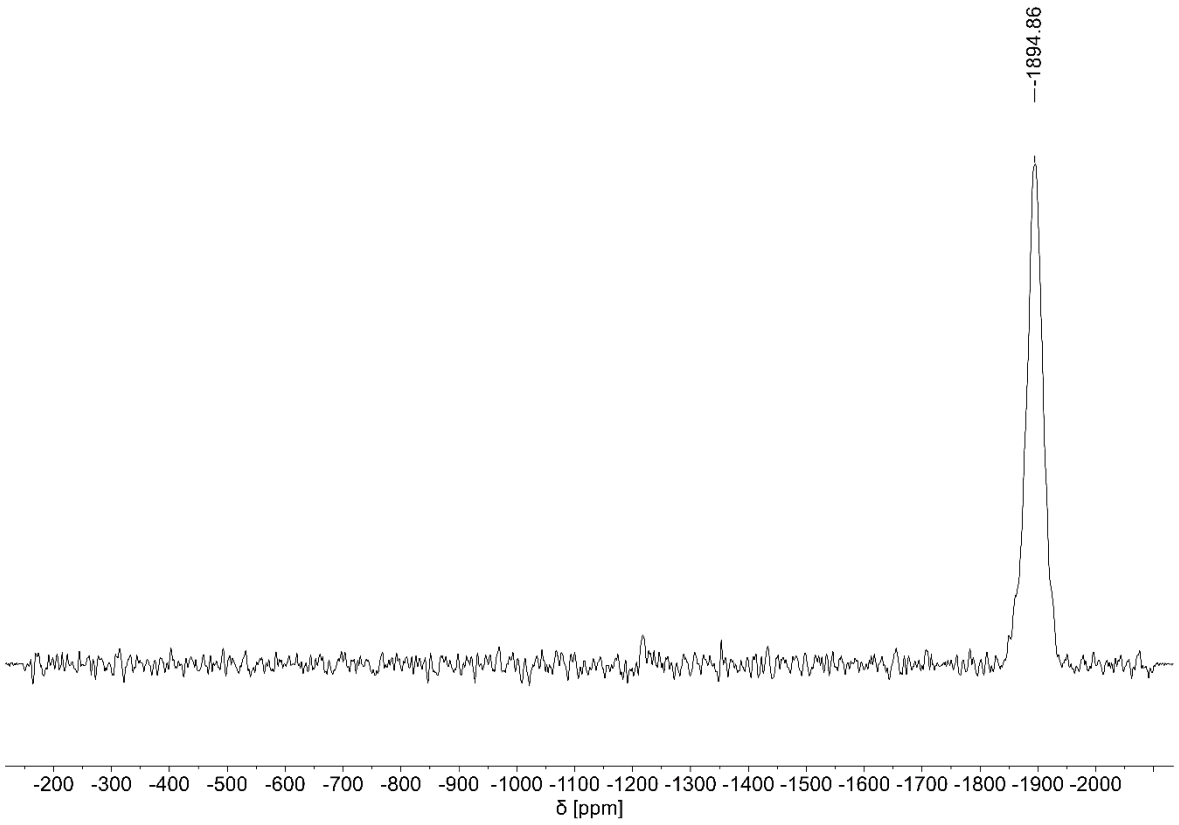

Figure S63. $^{31}P\{^{1}H\}$ NMR spectrum of $[Tc(CO)_4(PPh_3)_2][BArF_{24}]$.

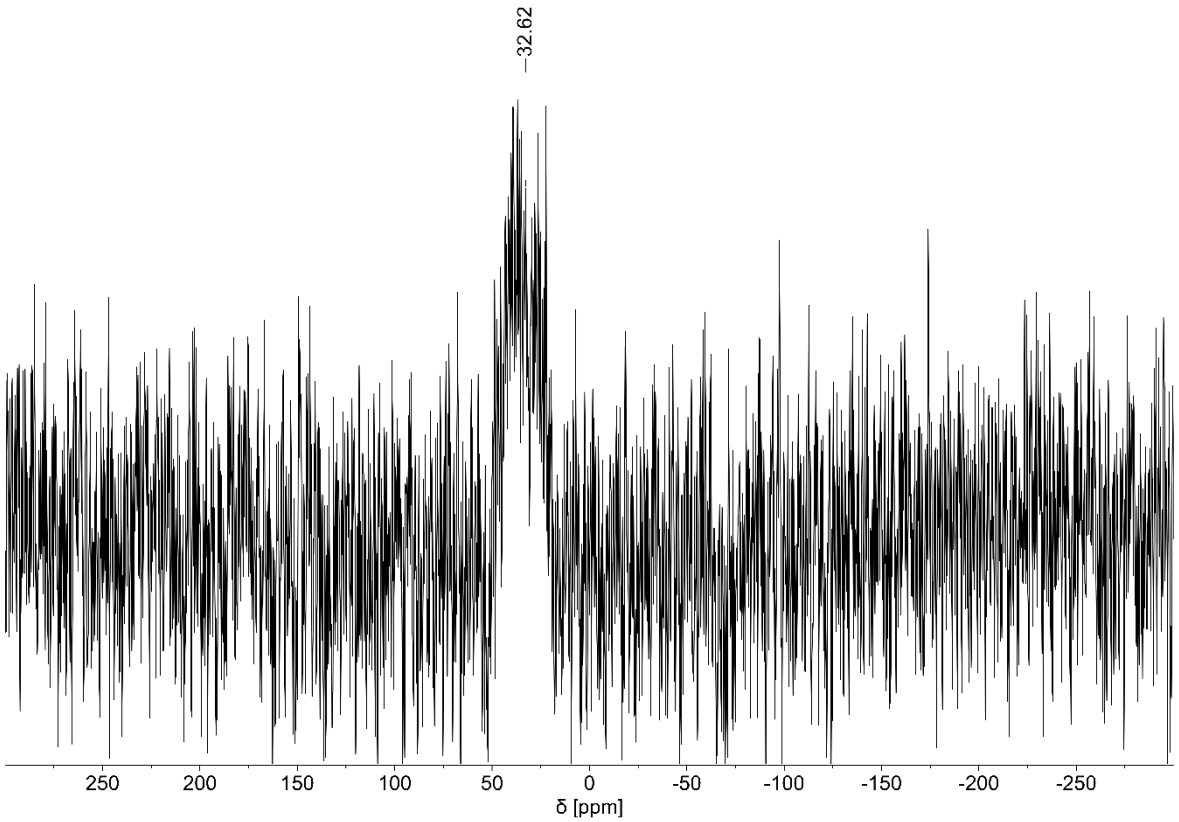

Figure S64. ^{19}F NMR spectrum of $[Tc(CO)_4(PPh_3)_2][BArF_{24}]$.

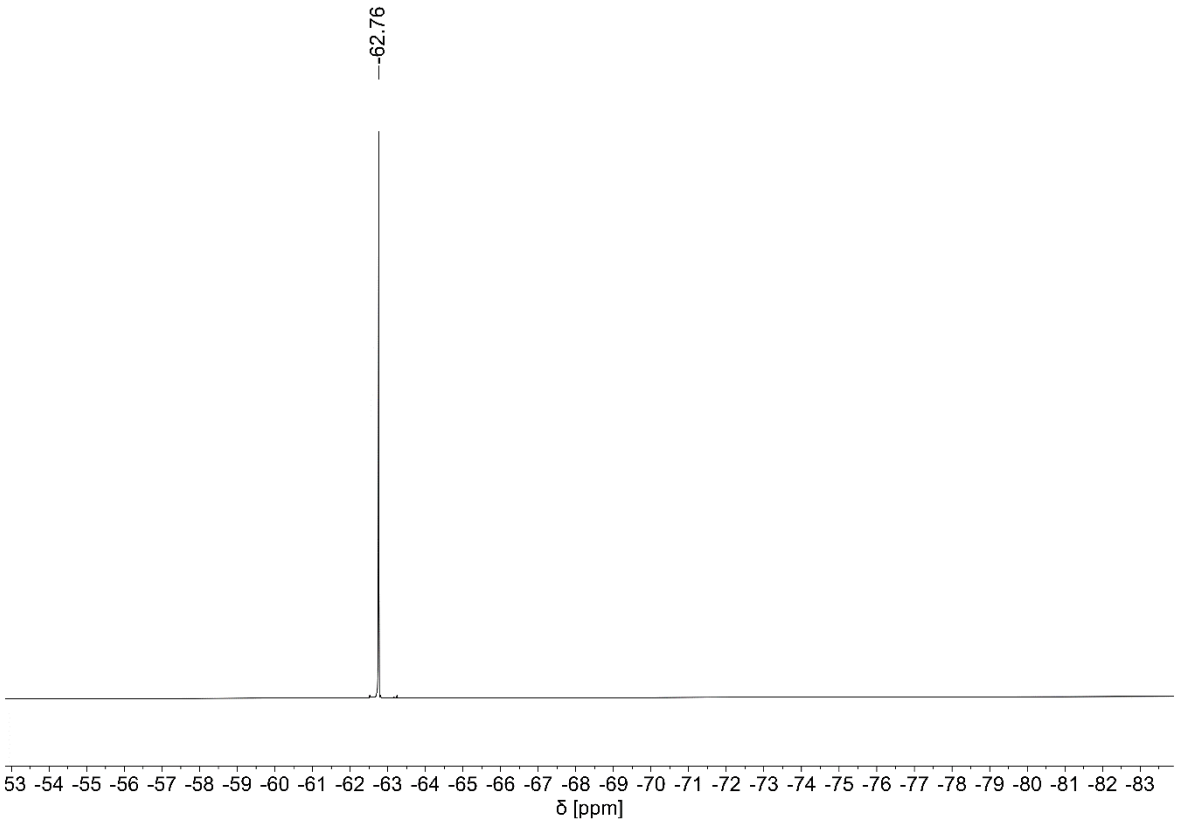

Figure S65. ^{11}B NMR spectrum of $[Tc(CO)_4(PPh_3)_2][BArF_{24}]$.

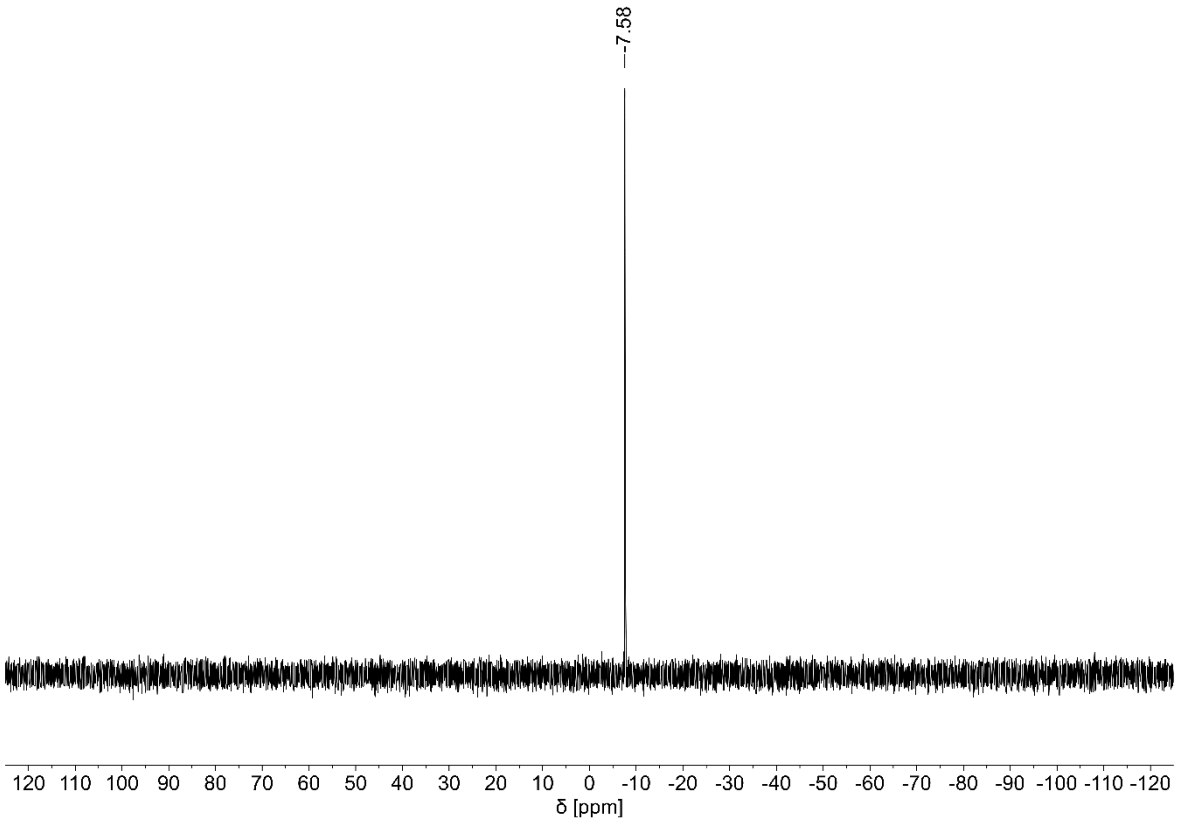

Figure S66. IR spectrum of $[Tc(CO)_4(PPh_3)_2][BArF_{24}]$.

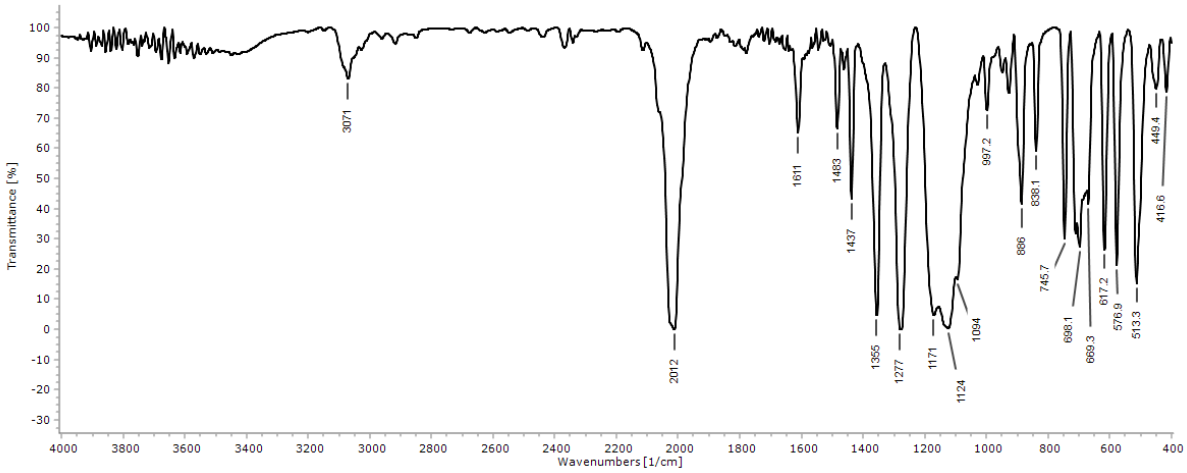

Figure S67. ^{99}Tc NMR spectrum of $[Tc(CO)_4(PPh_3)_2][BF_4]$.

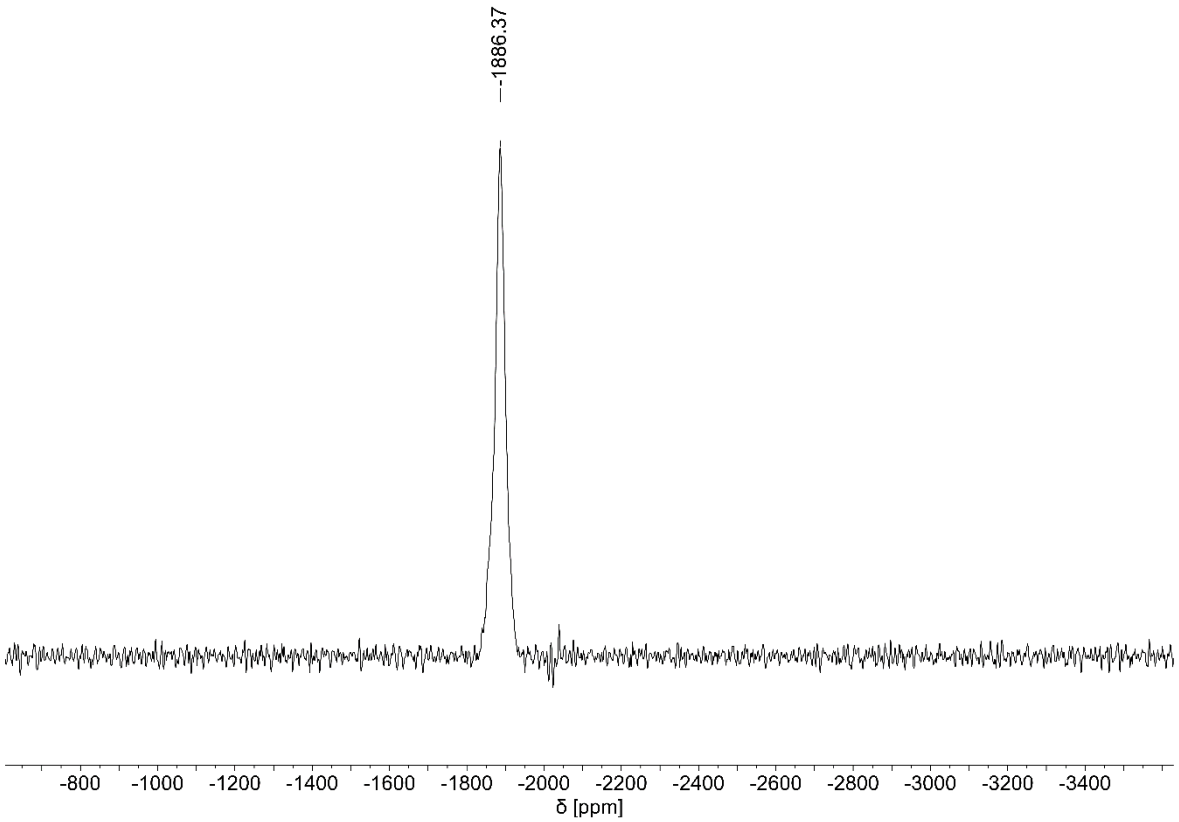

Figure S68. ^{1}H NMR spectrum of $[Tc(S_2CPPh_3)(CO)_2(PPh_3)_2][BF_4]$.

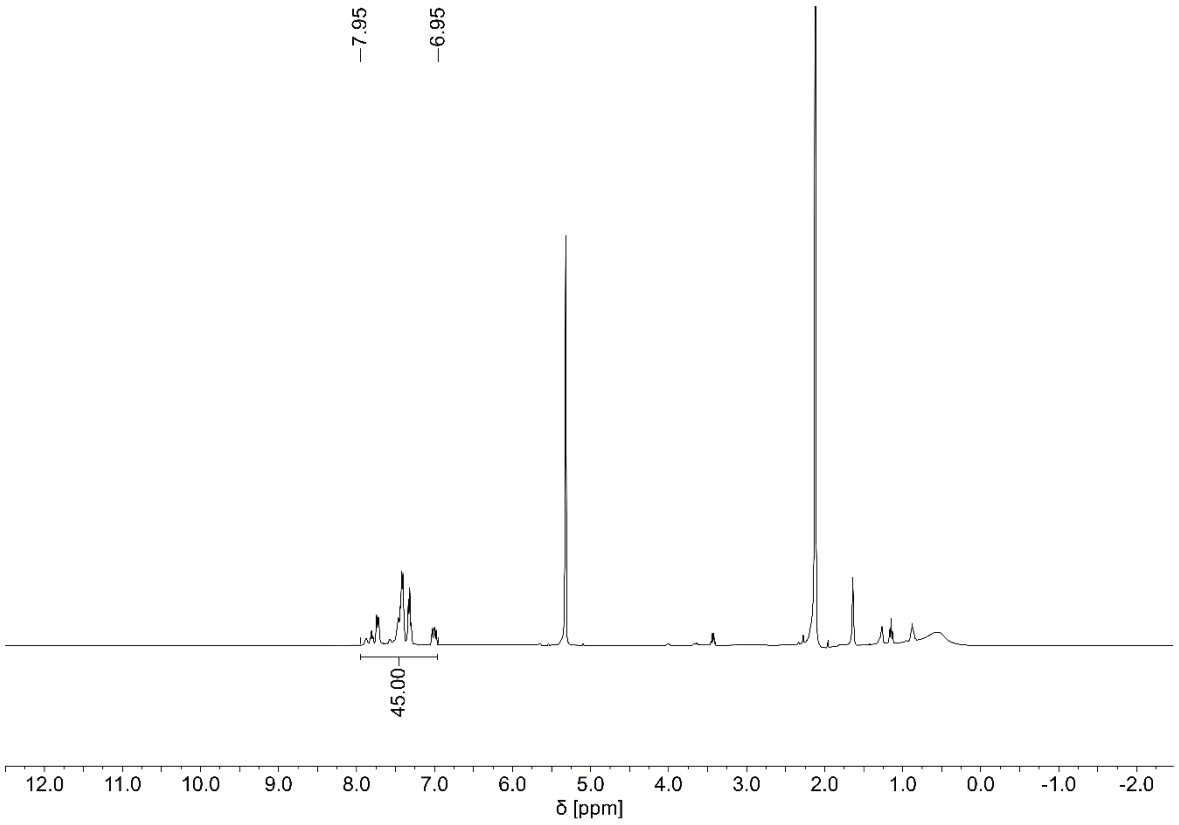

Figure S69. ^{99}Tc NMR spectrum of $[Tc(S_2CPPh_3)(CO)_2(PPh_3)_2][BF_4]$.

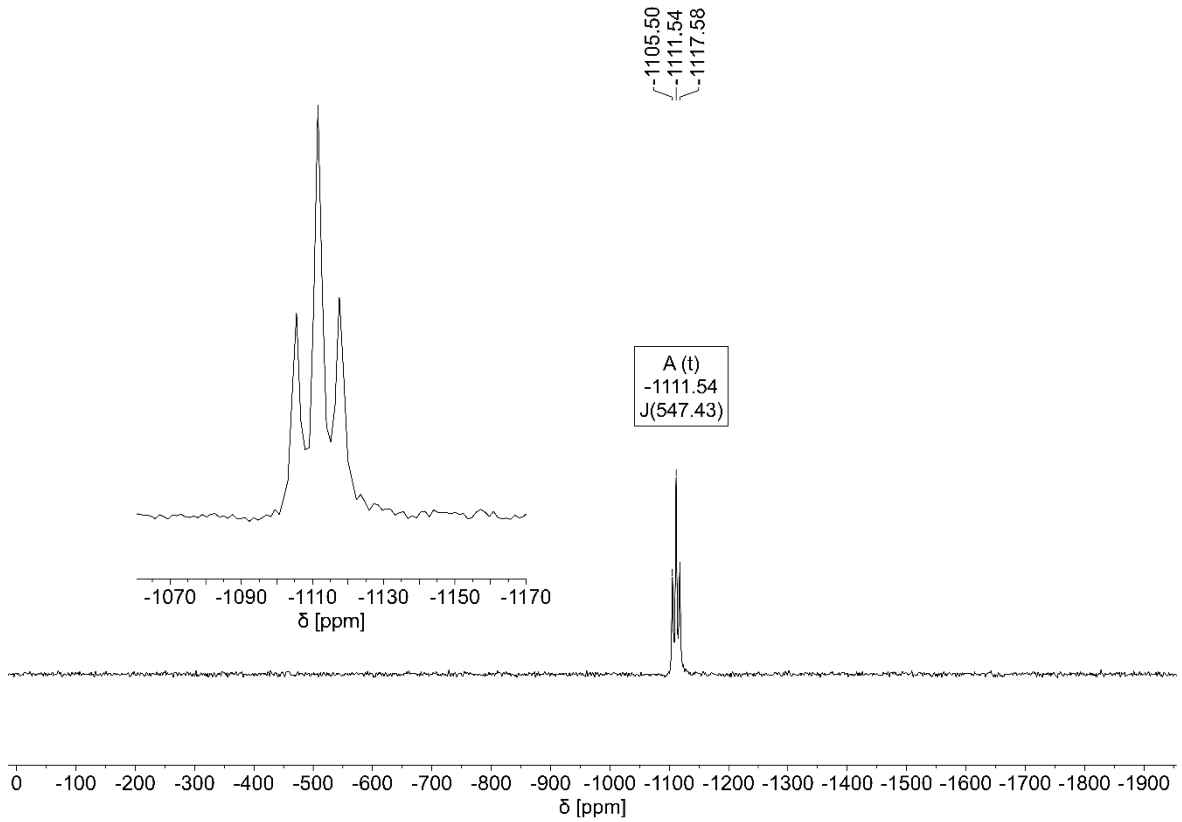

Figure S70. $^{31}P\{^1H\}$ NMR spectrum of $[Tc(S_2CPPh_3)(CO)_2(PPh_3)_2][BF_4]$.

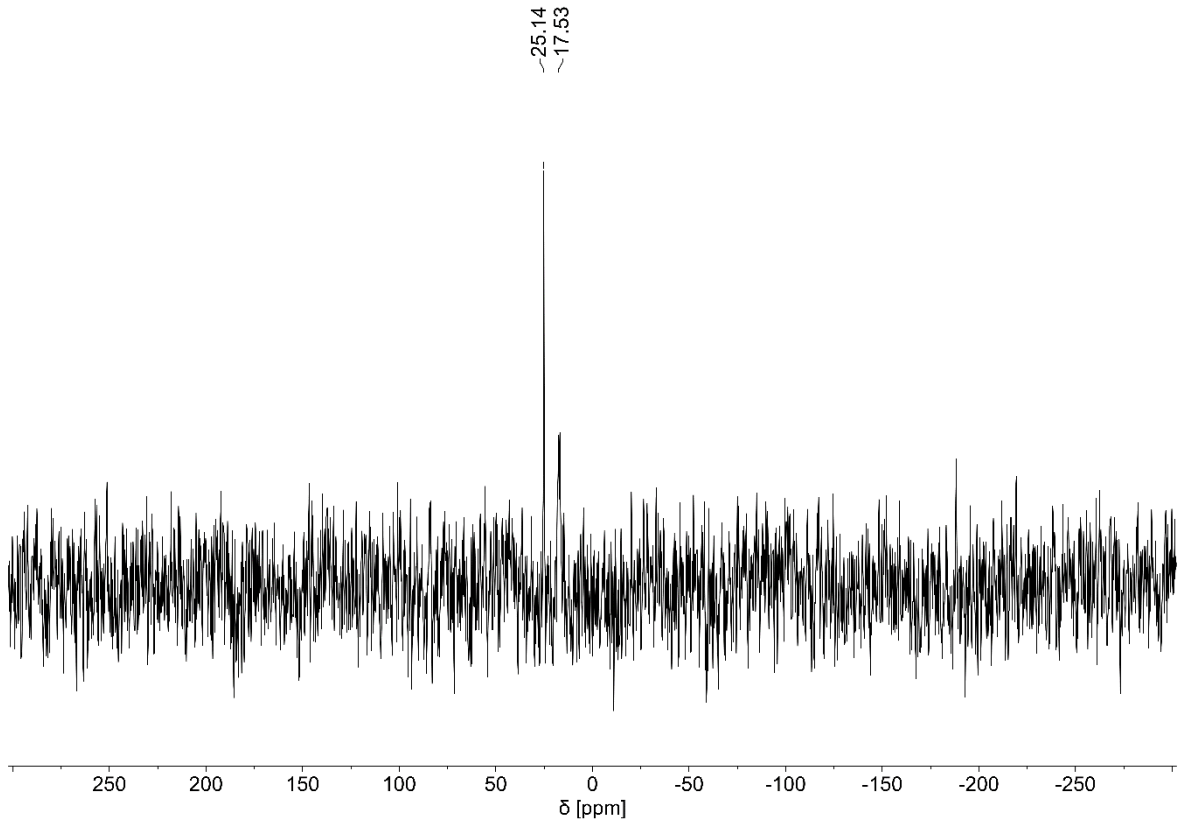

Figure S71. ^{19}F NMR spectrum of $[Tc(S_2CPPh_3)(CO)_2(PPh_3)_2][BF_4]$.

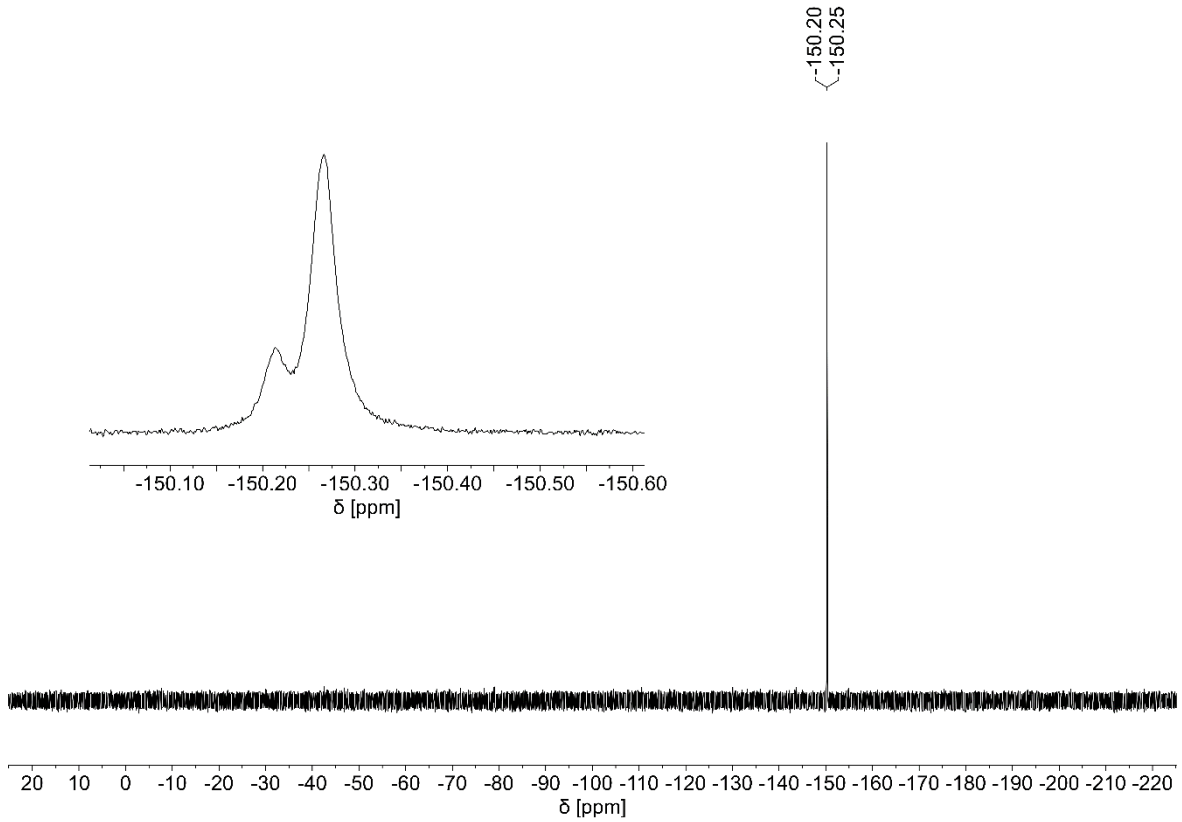

Figure S72. ^{11}B NMR spectrum of $[Tc(S_2CPPh_3)(CO)_2(PPh_3)_2][BF_4]$.

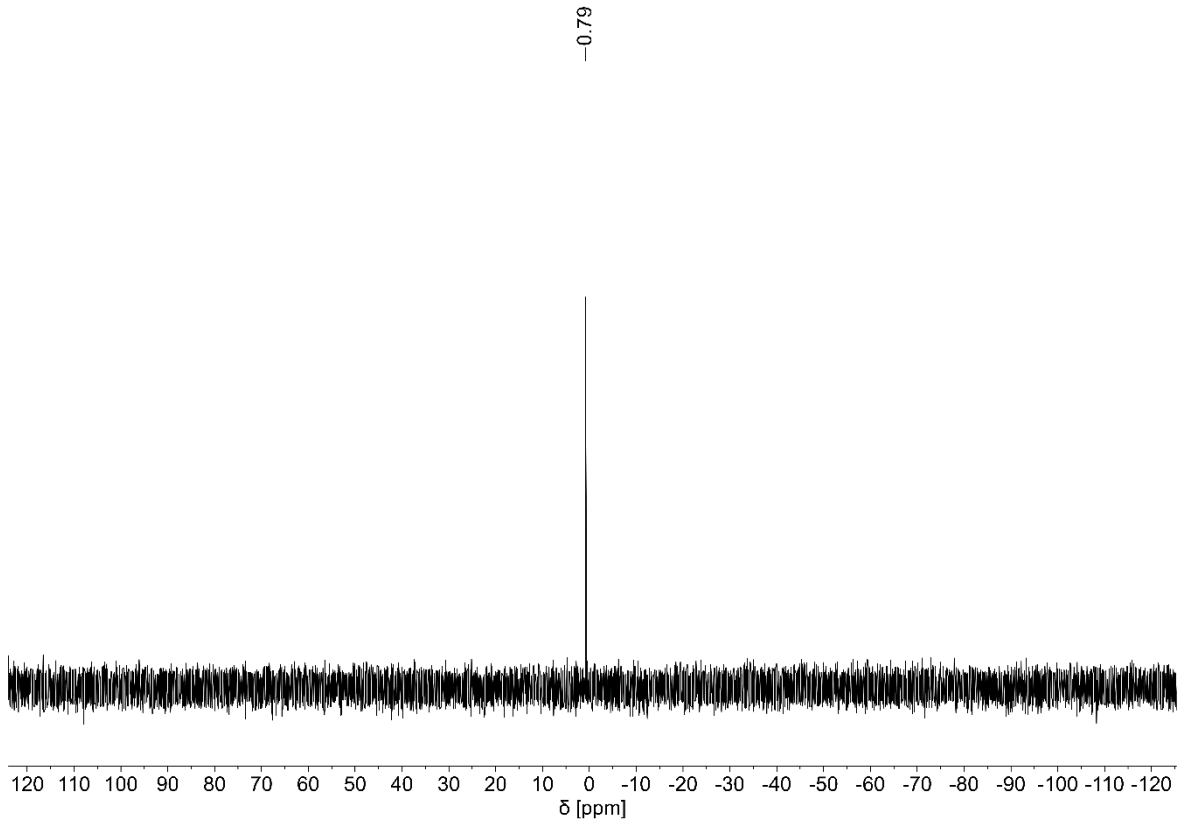

Figure S73. IR spectrum of $[Tc(S_2CPPh_3)(CO)_2(PPh_3)_2][BF_4]$.

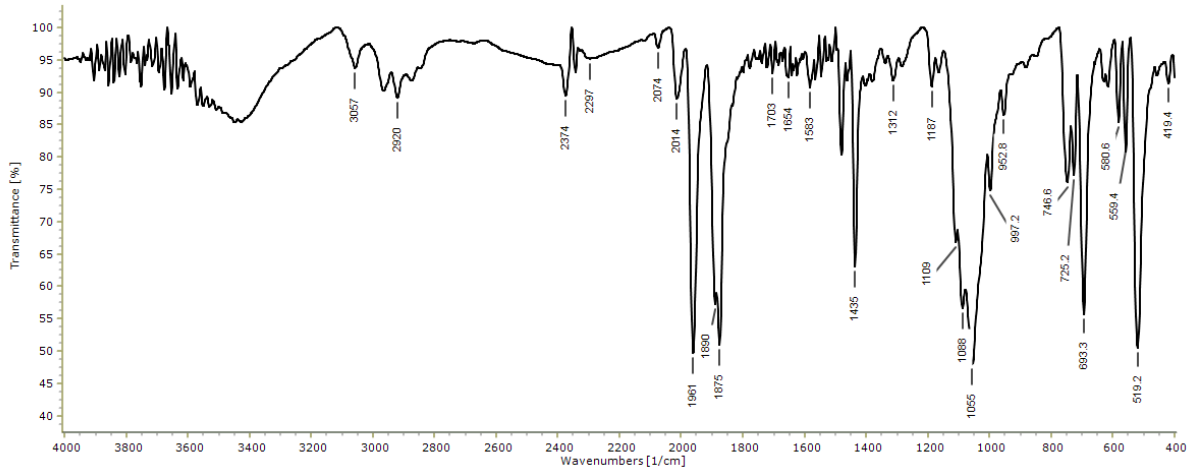

Figure S74. ^1H NMR spectrum of $[Tc(CNCy)(CO)_3(PPh_3)_2][BF_4]$.

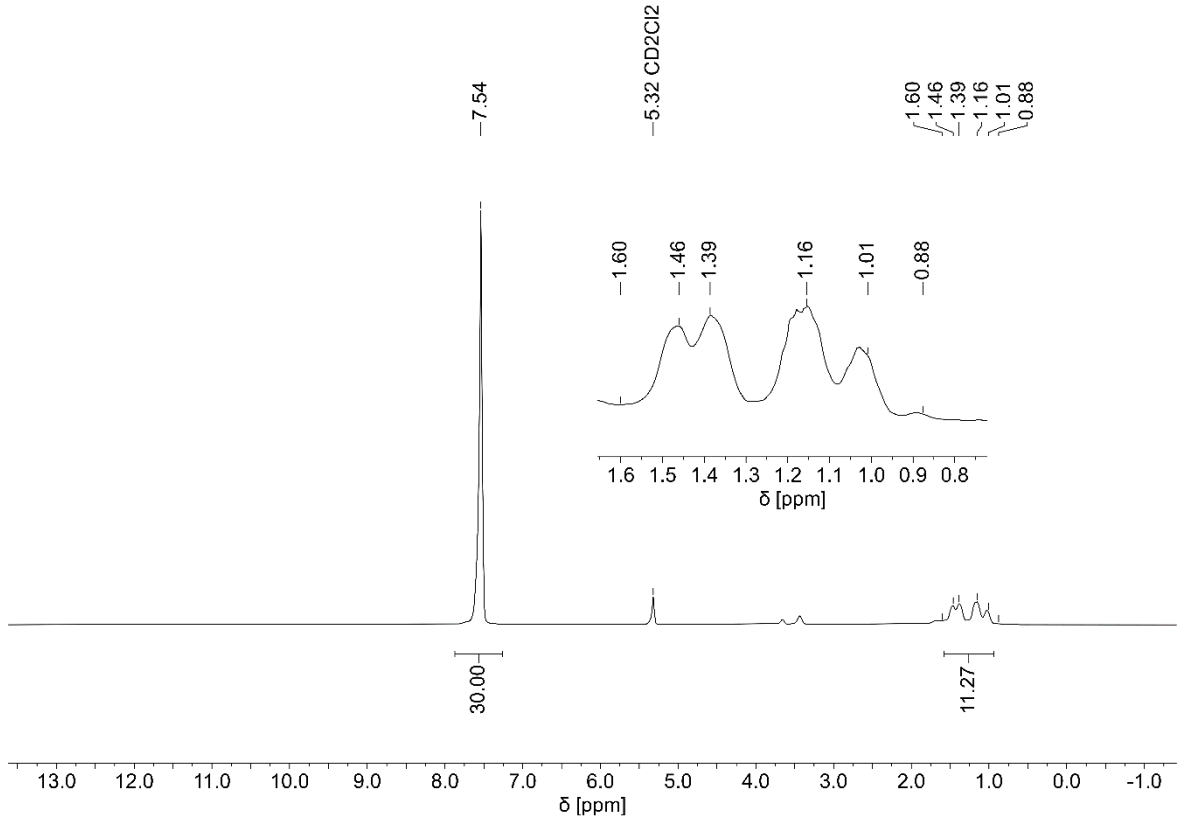

Figure S75. ^{99}Tc NMR spectrum of [Tc(CNCy)(CO)$_3$(PPh$_3$)$_2$][BF$_4$].

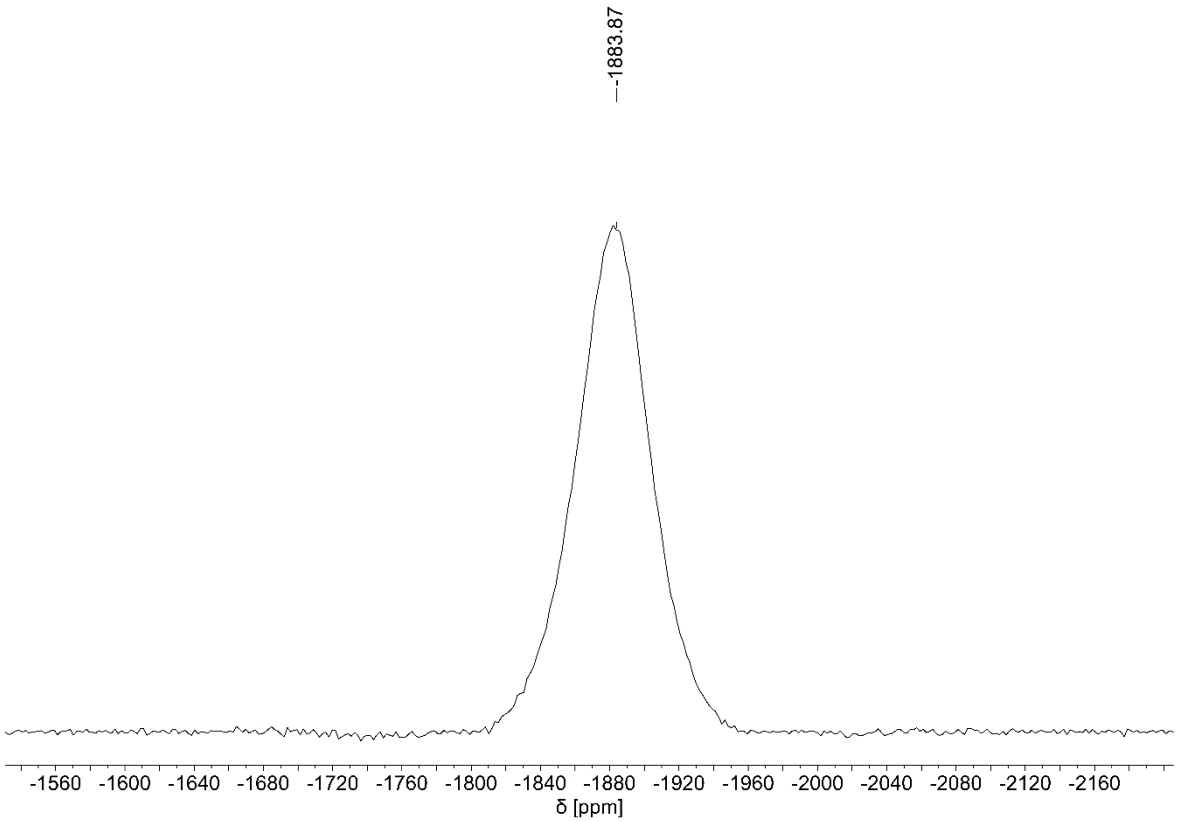

Figure S76. ^{31}P{^{1}H} NMR spectrum of [Tc(CNCy)(CO)$_3$(PPh$_3$)$_2$][BF$_4$].

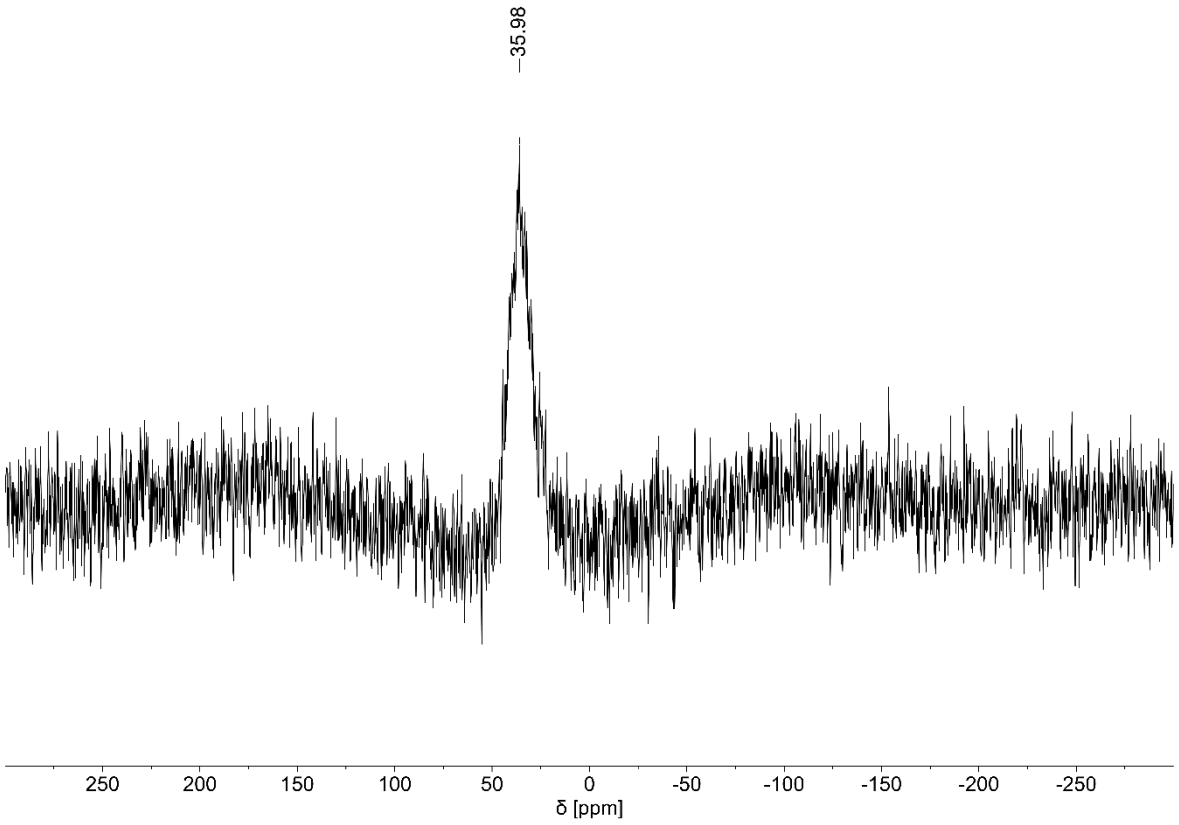

Figure S77. ^{19}F NMR spectrum of $[Tc(CNCy)(CO)_3(PPh_3)_2][BF_4]$.

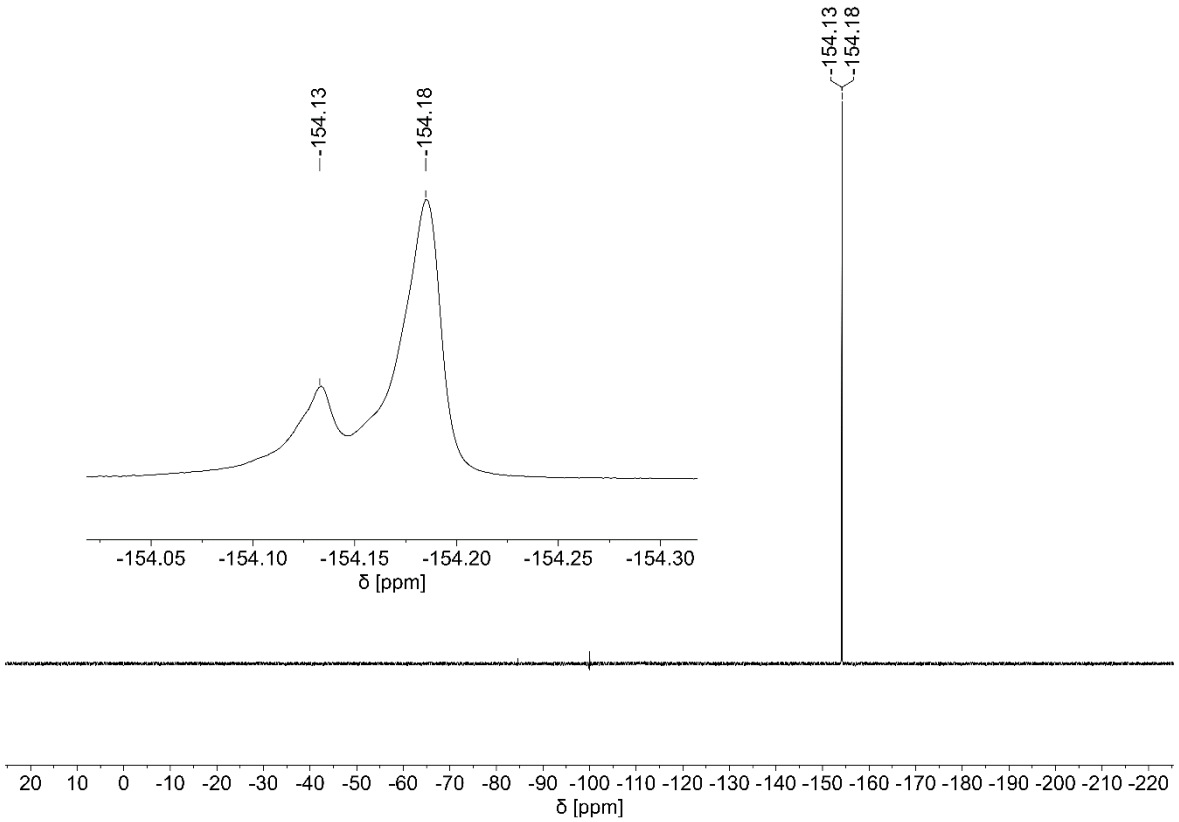

Figure S78. ^{11}B NMR spectrum of $[Tc(CNCy)(CO)_3(PPh_3)_2][BF_4]$.

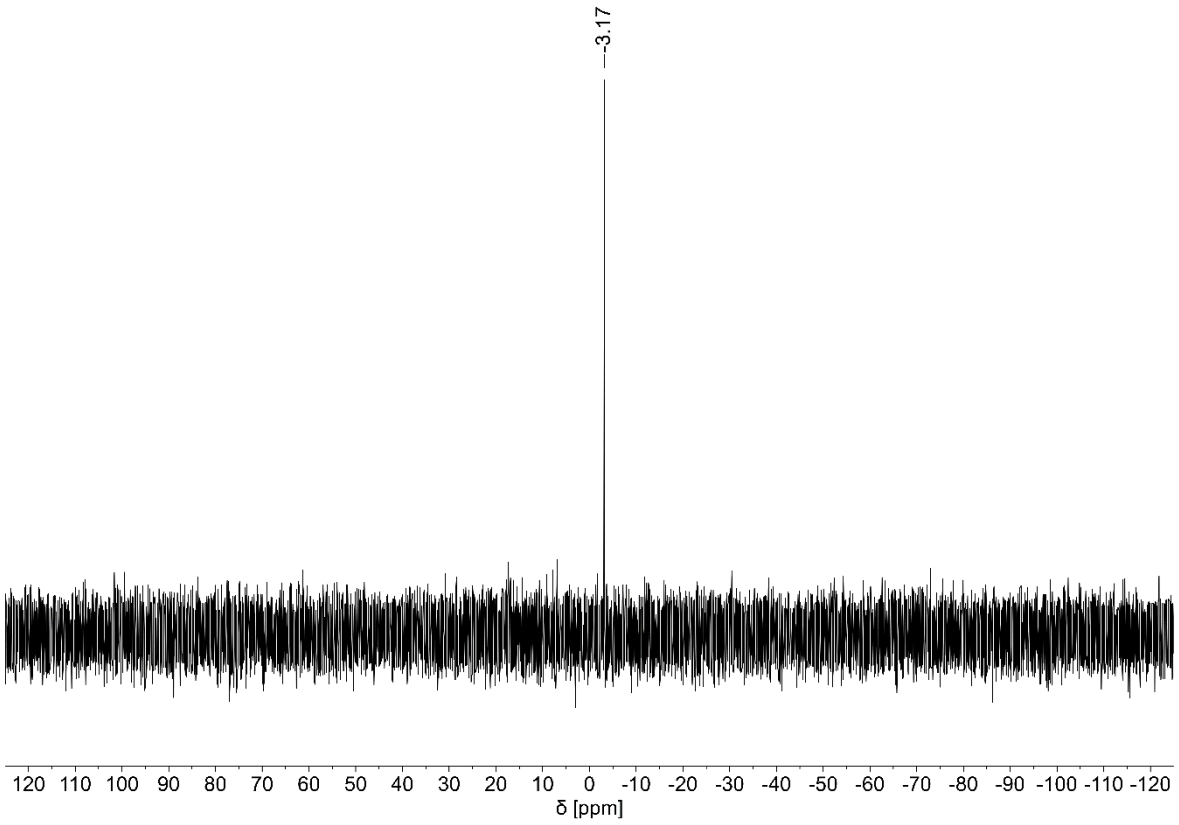

Figure S79. IR spectrum of $[Tc(CNCy)(CO)_3(PPh_3)_2][BF_4]$.

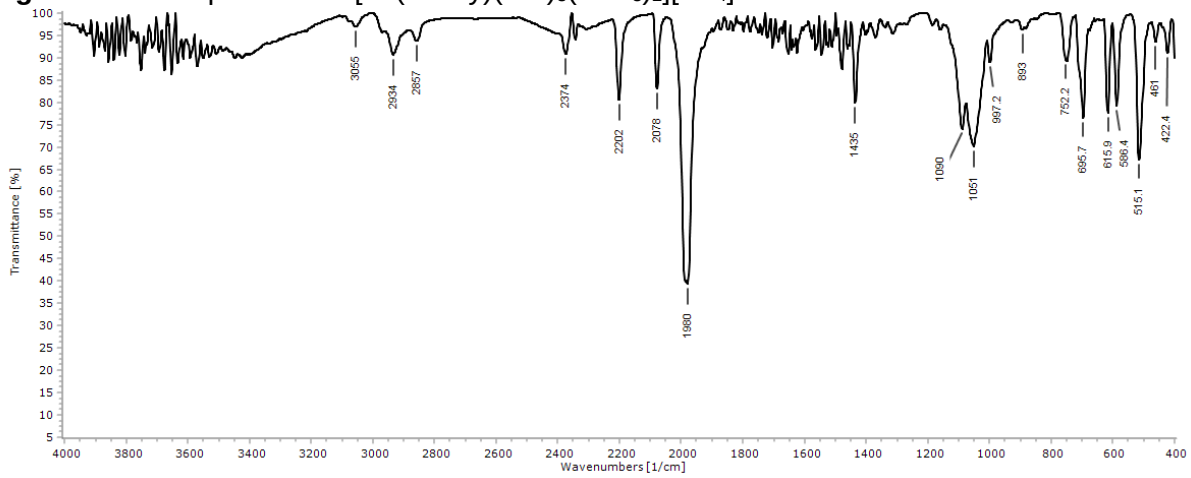

Figure S80. ^1H NMR spectrum of $[Tc(CNDArF2)(CO)_3(PPh_3)_2][BArF_{24}]$.

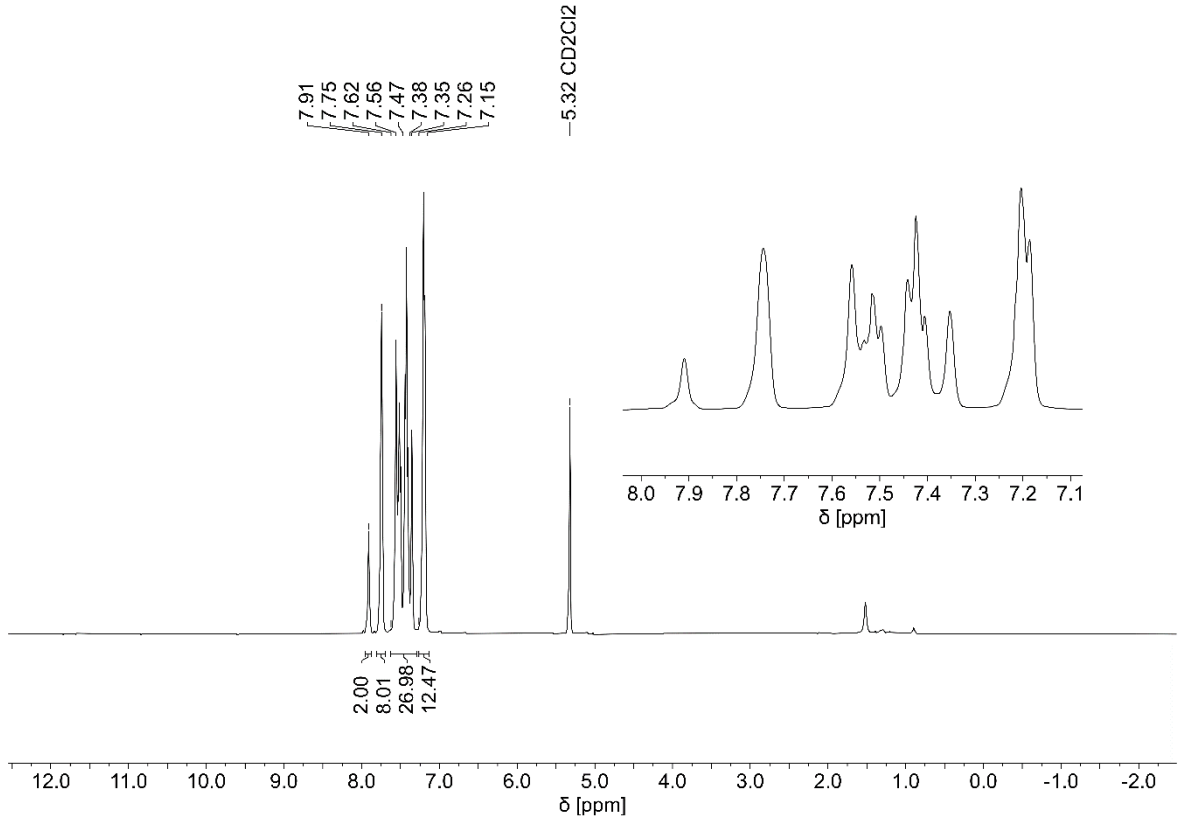

Figure S81. $^{1}H\{^{31}P\}$ NMR spectrum (aromatic region) of $[Tc(CNDArF2)(CO)_3(PPh_3)_2][BArF_{24}]$.

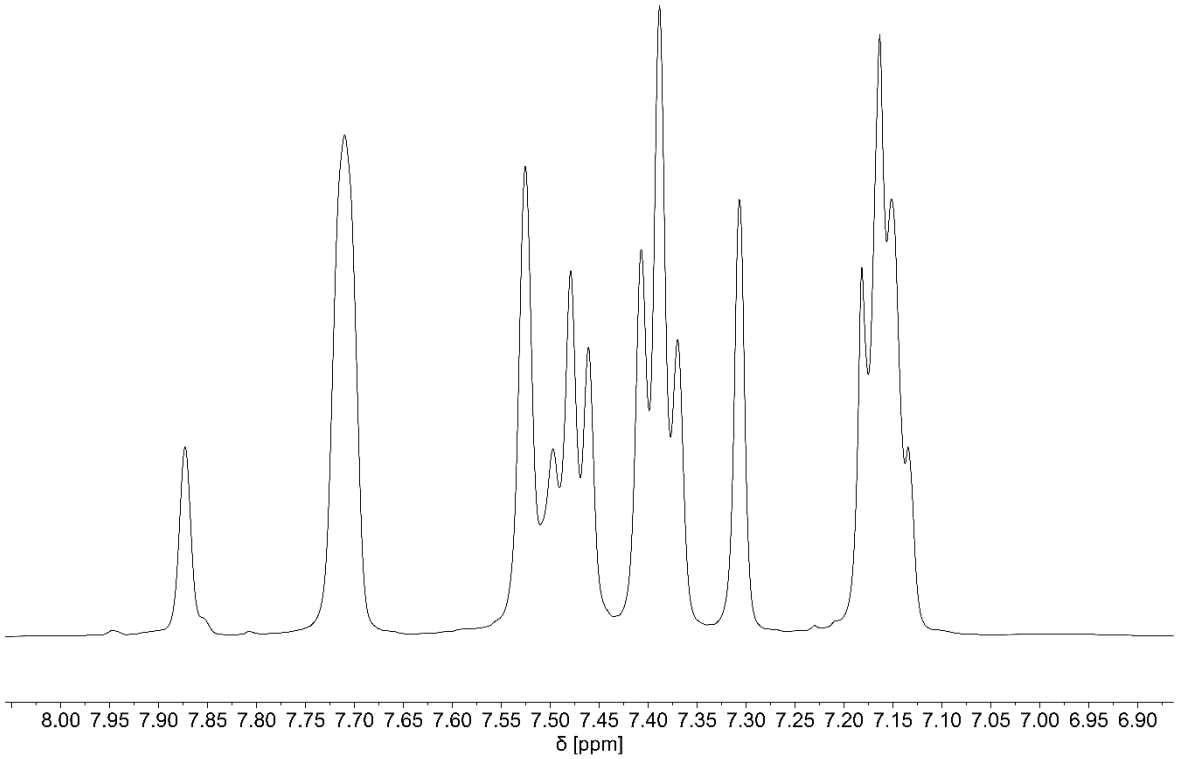

Figure S82. ^{99}Tc NMR spectrum of $[Tc(CNDArF2)(CO)_3(PPh_3)_2][BArF_{24}]$.

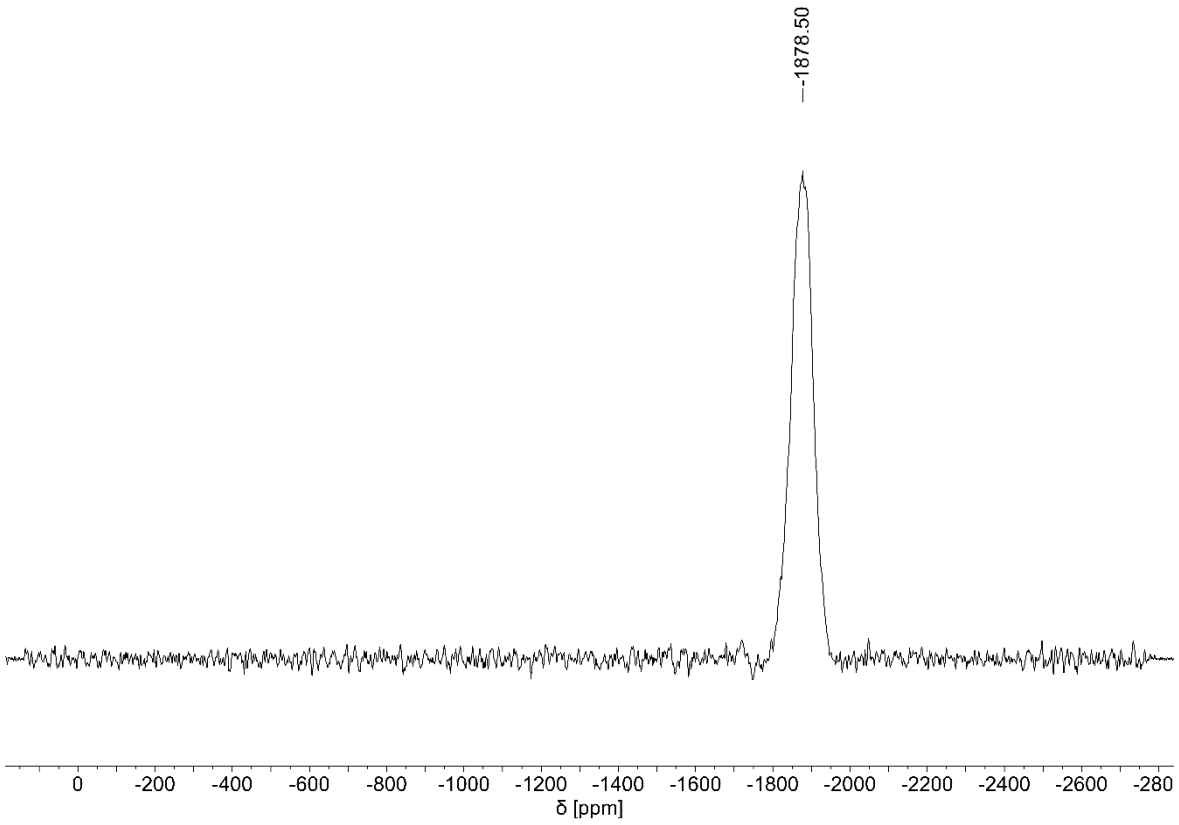

Figure S83. $^{31}P\{^{1}H\}$ NMR spectrum of $[Tc(CNDArF2)(CO)_3(PPh_3)_2][BArF_{24}]$.

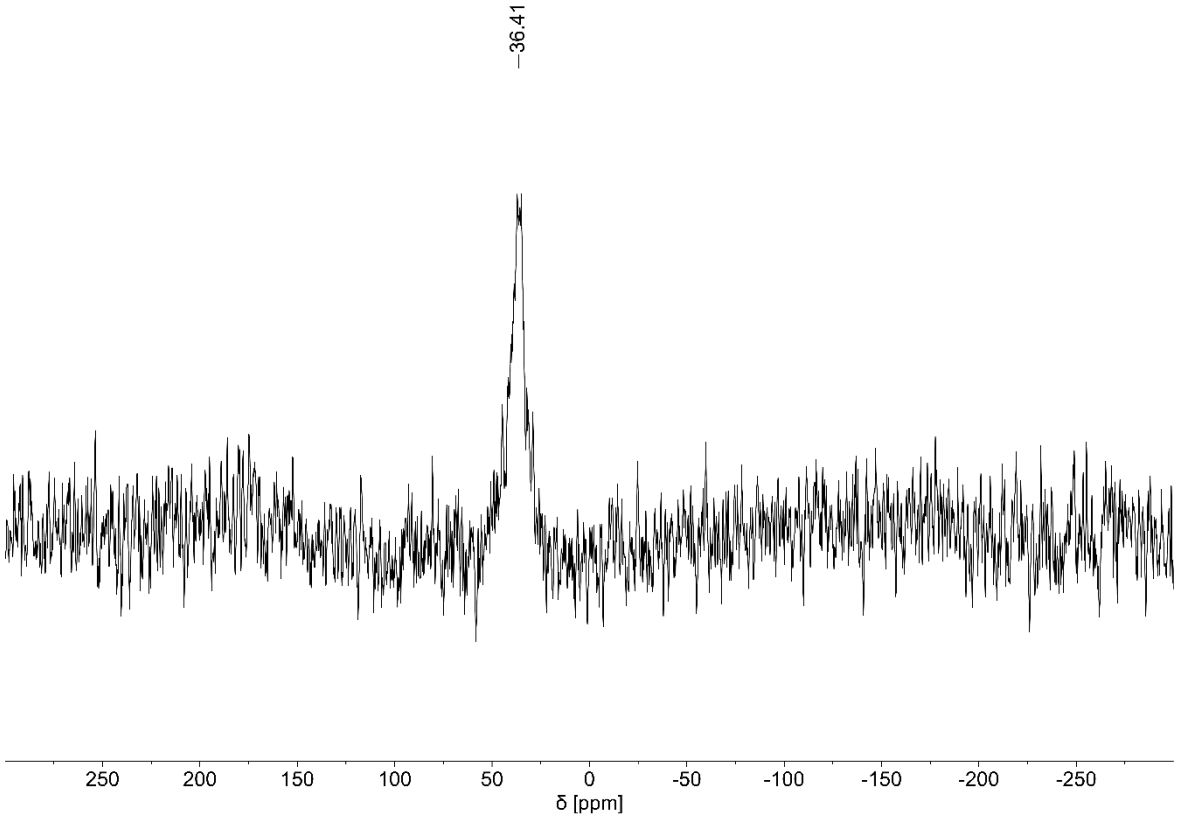

Figure S84. ^{19}F NMR spectrum of $[Tc(CNDArF2)(CO)_3(PPh_3)_2][BArF_{24}]$.

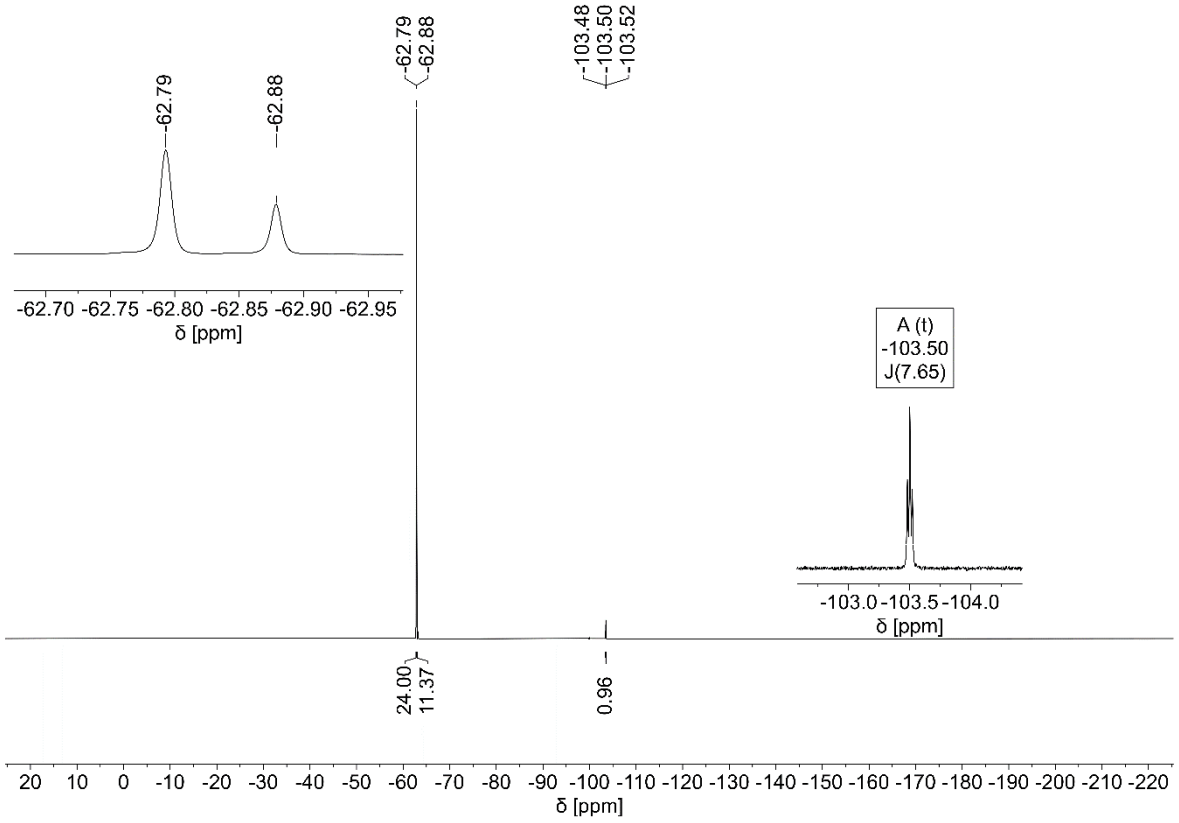

Figure S85. ^{11}B NMR spectrum of $[Tc(CNDArF2)(CO)_3(PPh_3)_2][BArF_{24}]$.

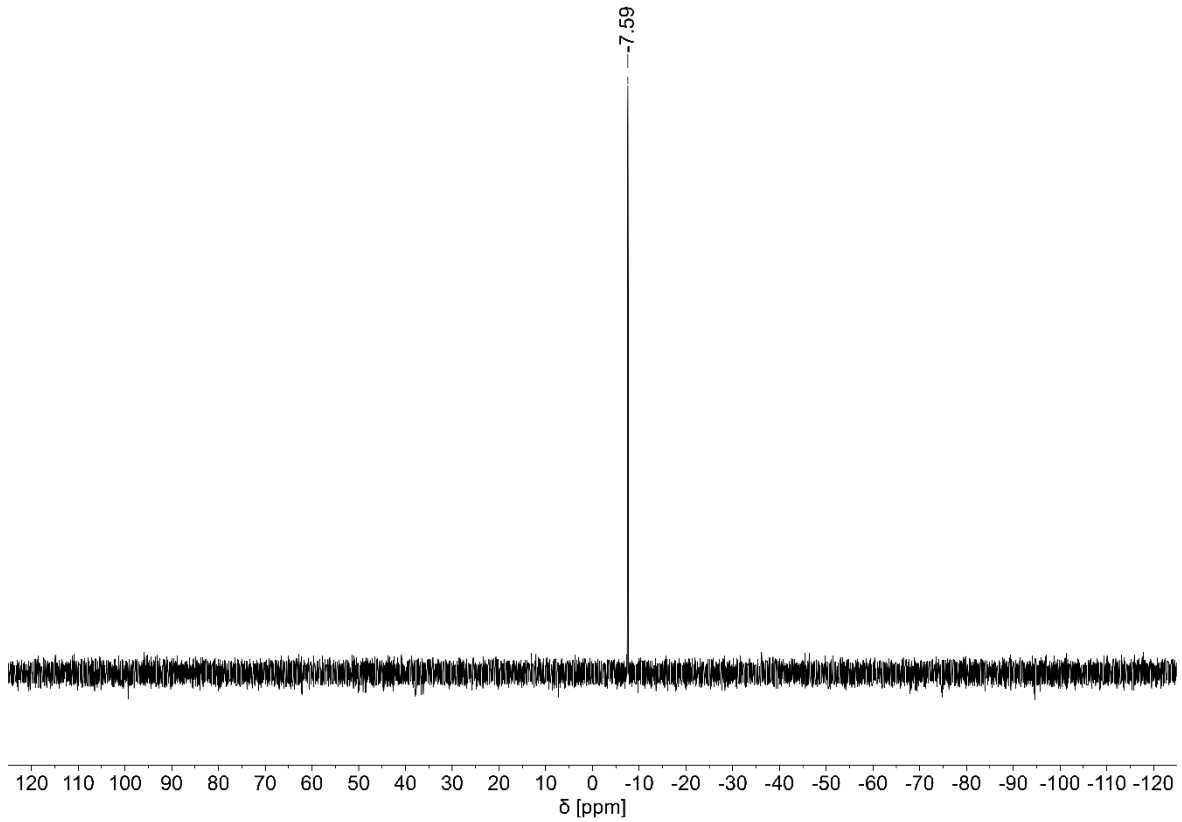

Figure S86. IR spectrum of $[Tc(CNDArF2)(CO)_3(PPh_3)_2][BArF_{24}]$.

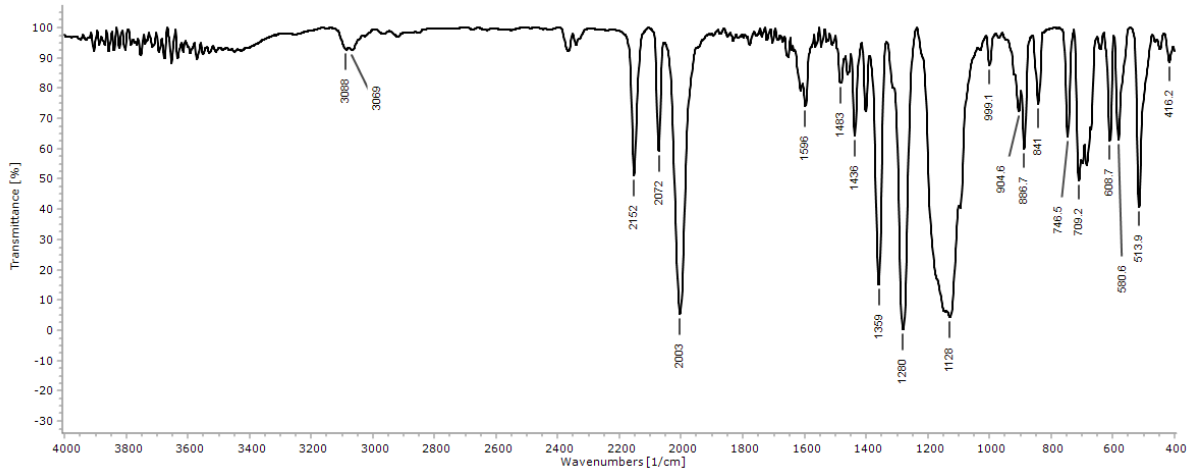

Figure S87. ^{1}H NMR spectrum of $[Tc(CNDArF2)(CO)_3(PPh_3)_2][BF_4]$.

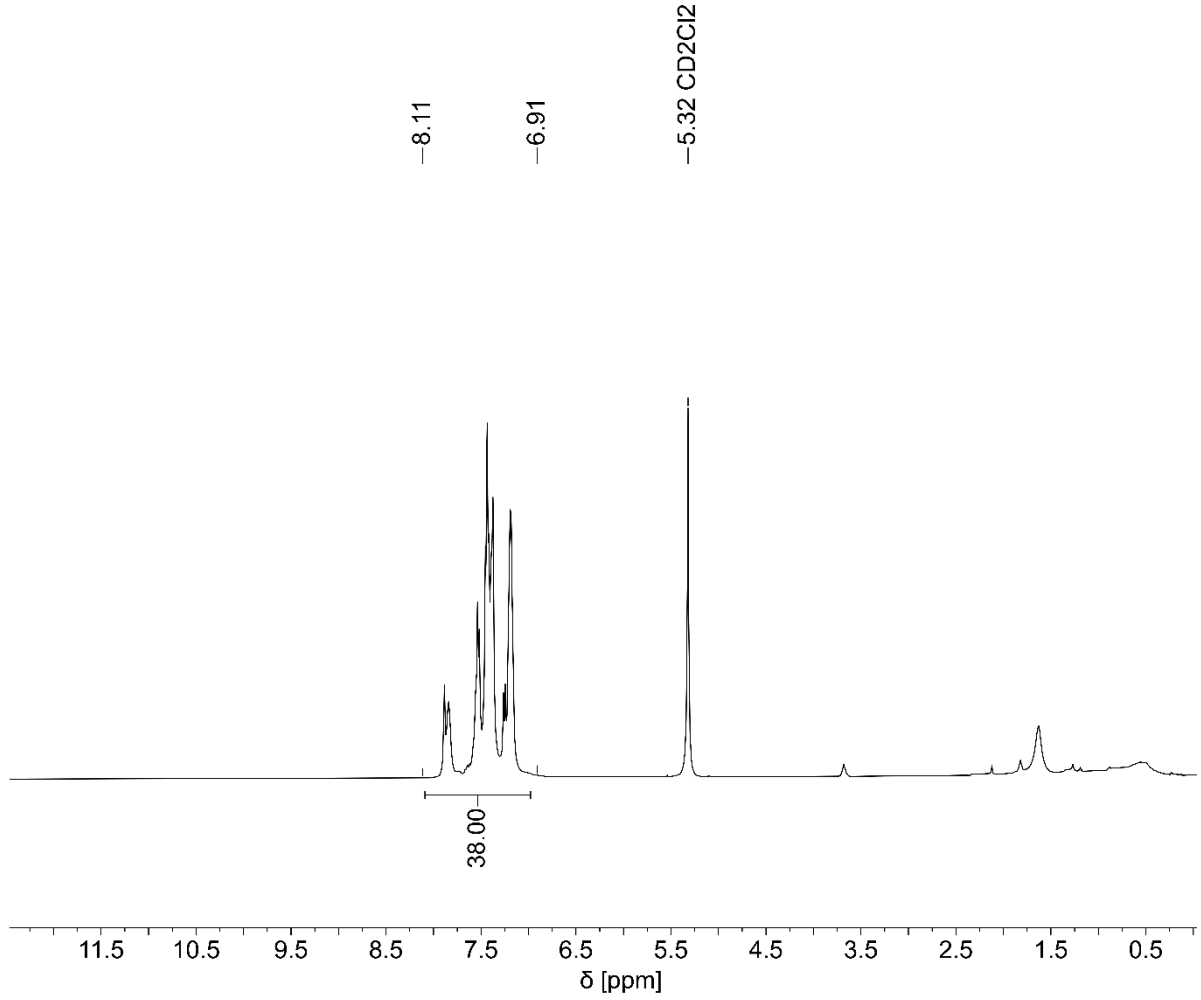

Figure S88. ^{99}Tc NMR spectrum of [Tc(CNDArF2)(CO)$_3$(PPh$_3$)$_2$][BF$_4$].

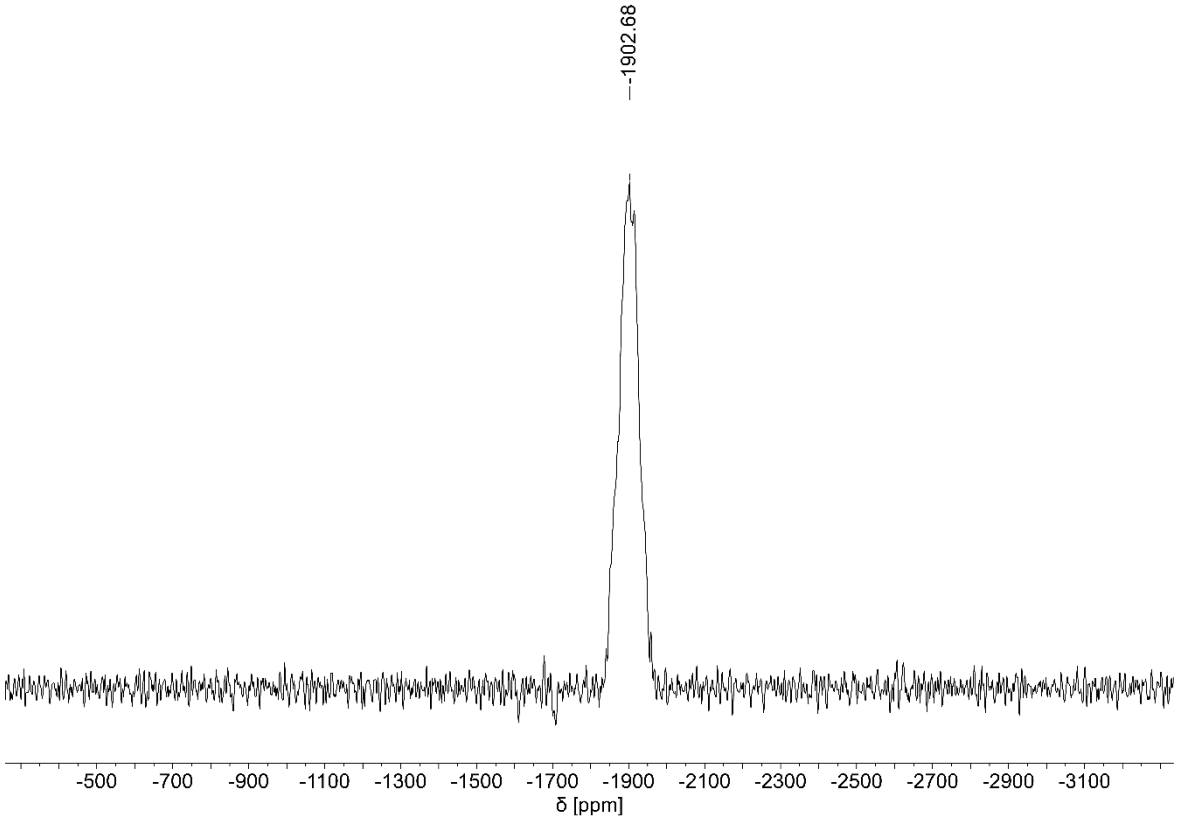

Figure S89. ^{31}P{^{1}H} NMR spectrum of [Tc(CNDArF2)(CO)$_3$(PPh$_3$)$_2$][BF$_4$].

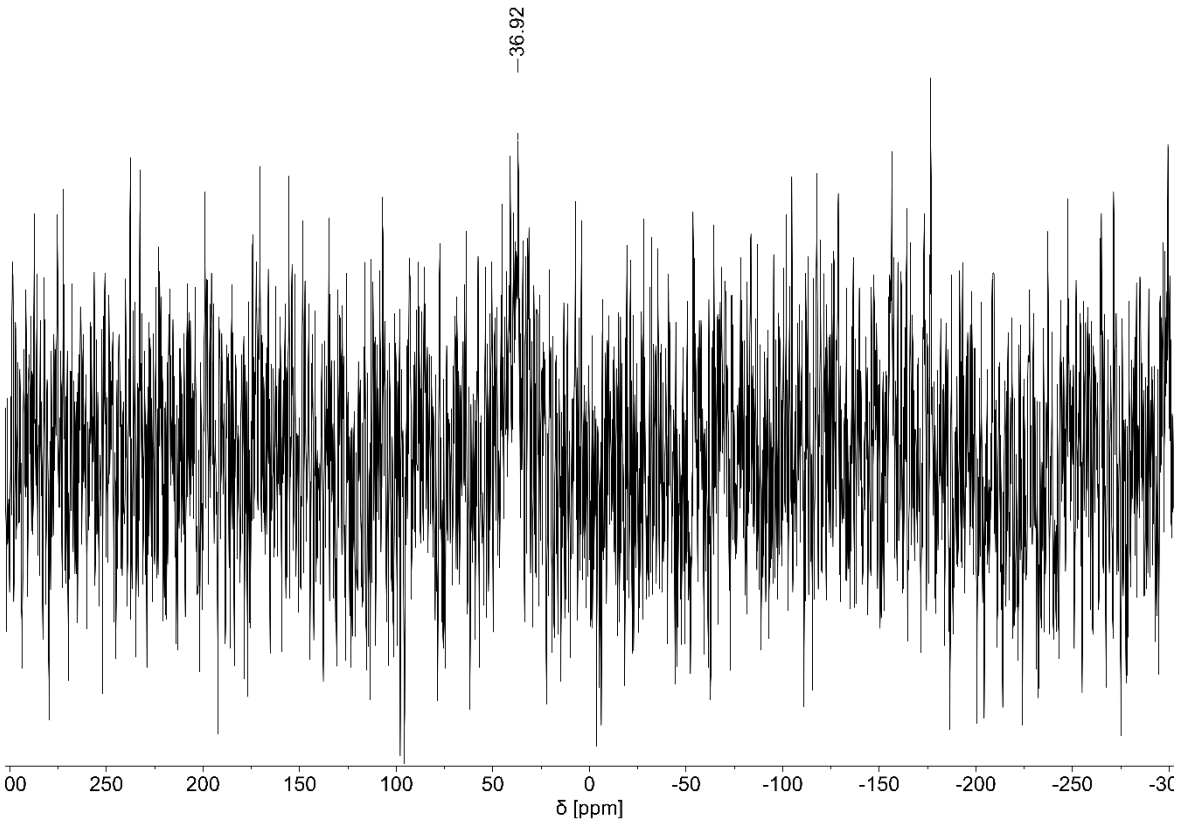

Figure S90. ^{19}F NMR spectrum of $[Tc(CNDArF2)(CO)_3(PPh_3)_2][BF_4]$.

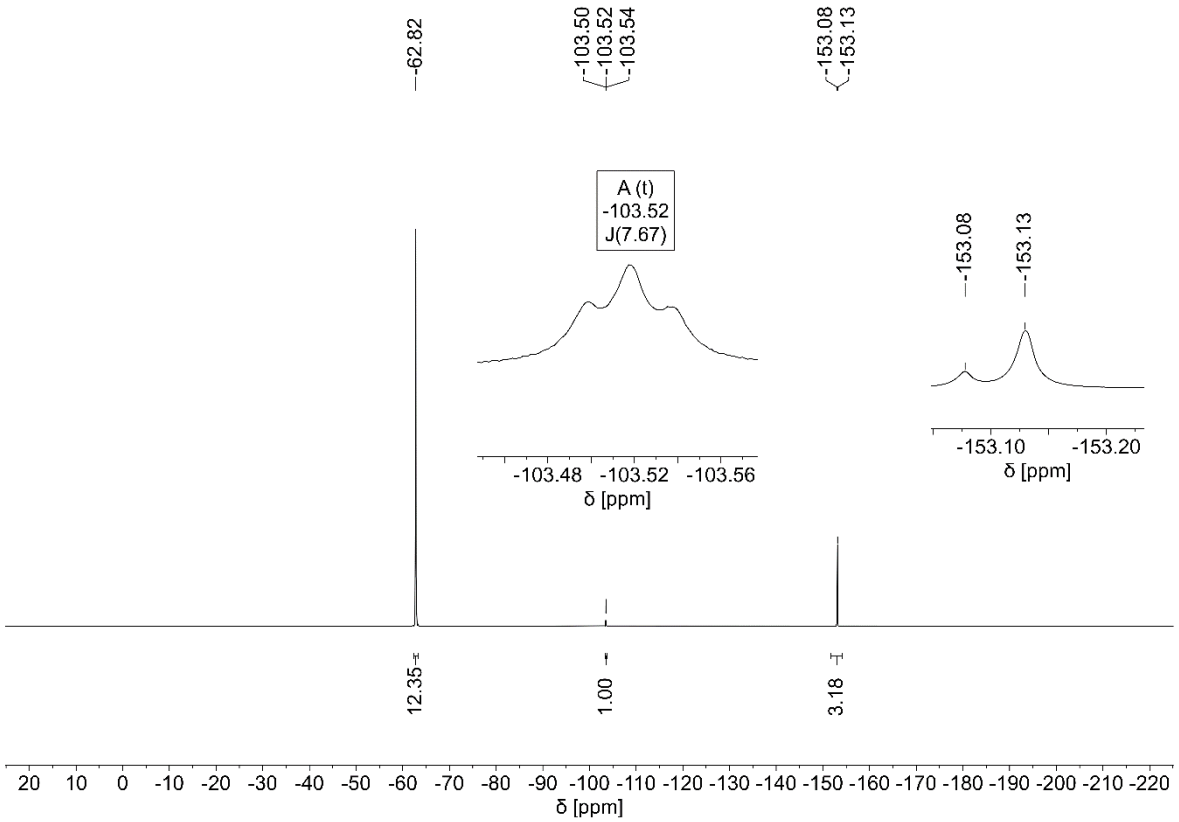

Figure S91. ^{11}B NMR spectrum of $[Tc(CNDArF2)(CO)_3(PPh_3)_2][BF_4]$.

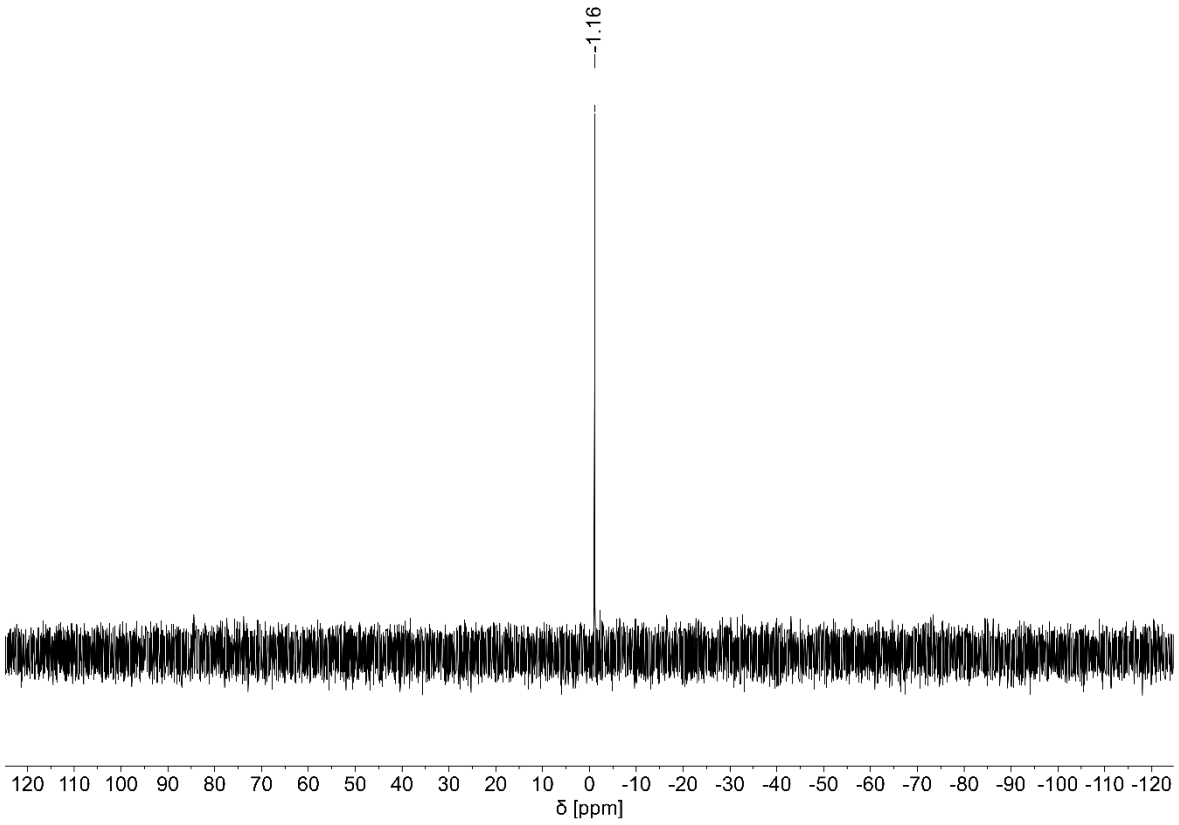

Figure S92. IR spectrum of $[Tc(CNDArF2)(CO)_3(PPh_3)_2][BF_4]$.

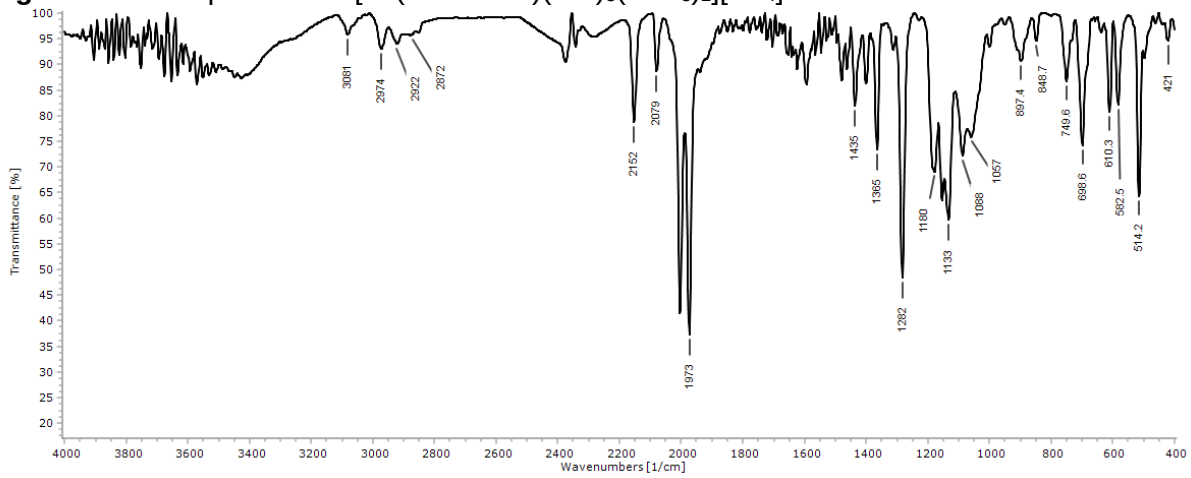

Figure S93. ^1H NMR spectrum of $[Tc(NH_3)_2(CO)_2(PPh_3)_2][BF_4]$.

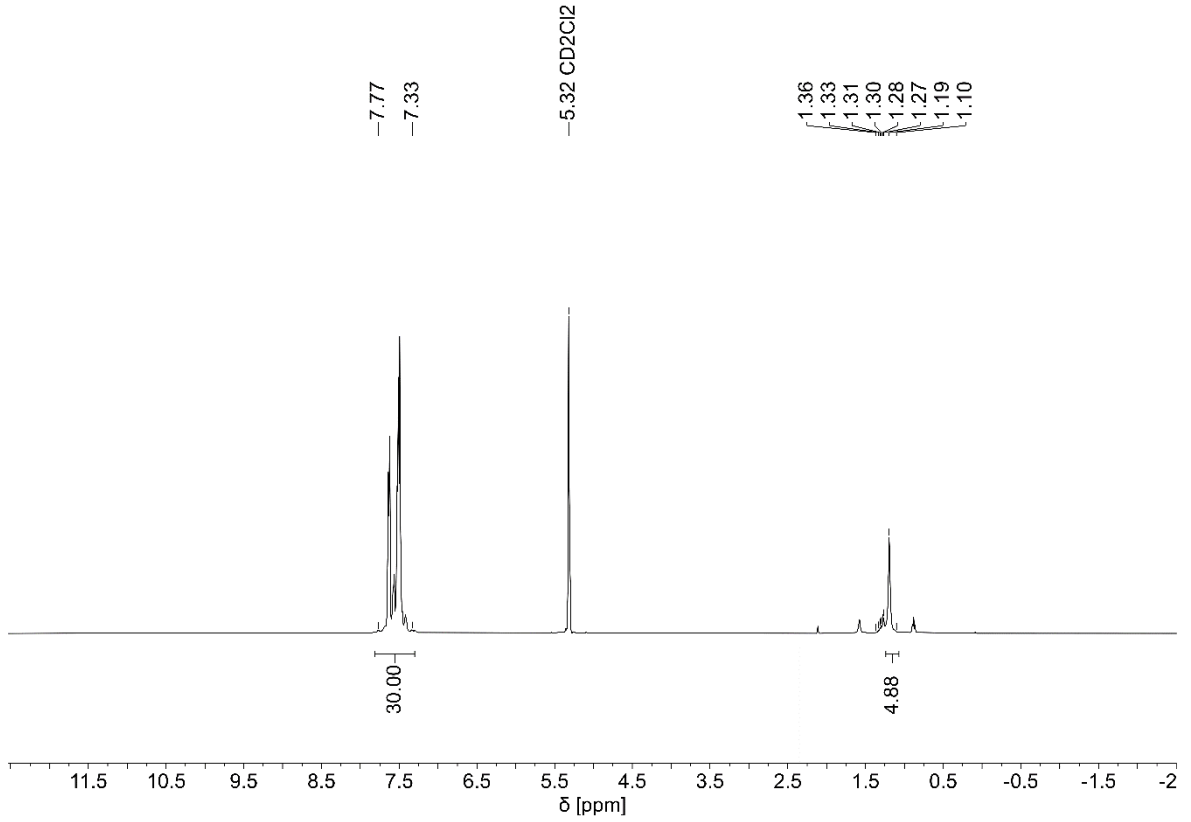

Figure S94. ^{99}Tc NMR spectrum of $[Tc(NH_3)_2(CO)_2(PPh_3)_2][BF_4]$.

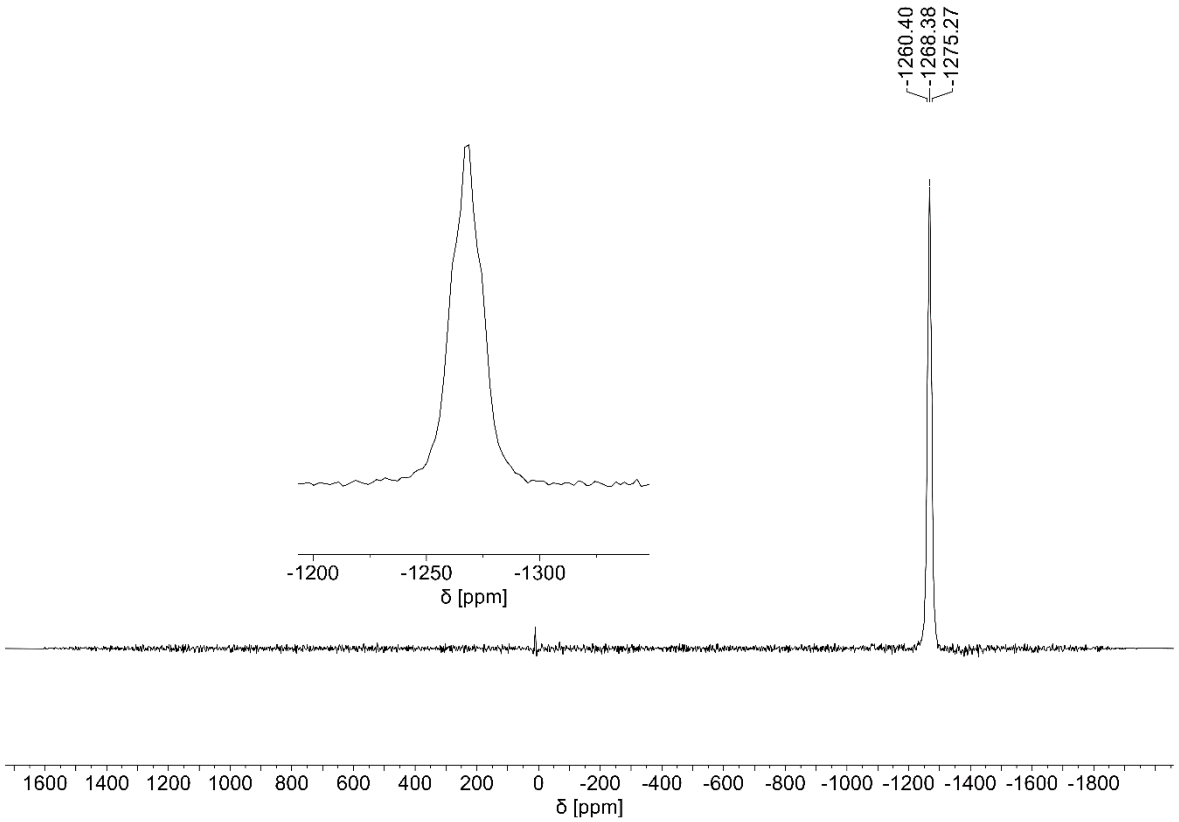

Figure S95. $^{31}P\{^1H\}$ NMR spectrum of $[Tc(NH_3)_2(CO)_2(PPh_3)_2][BF_4]$.

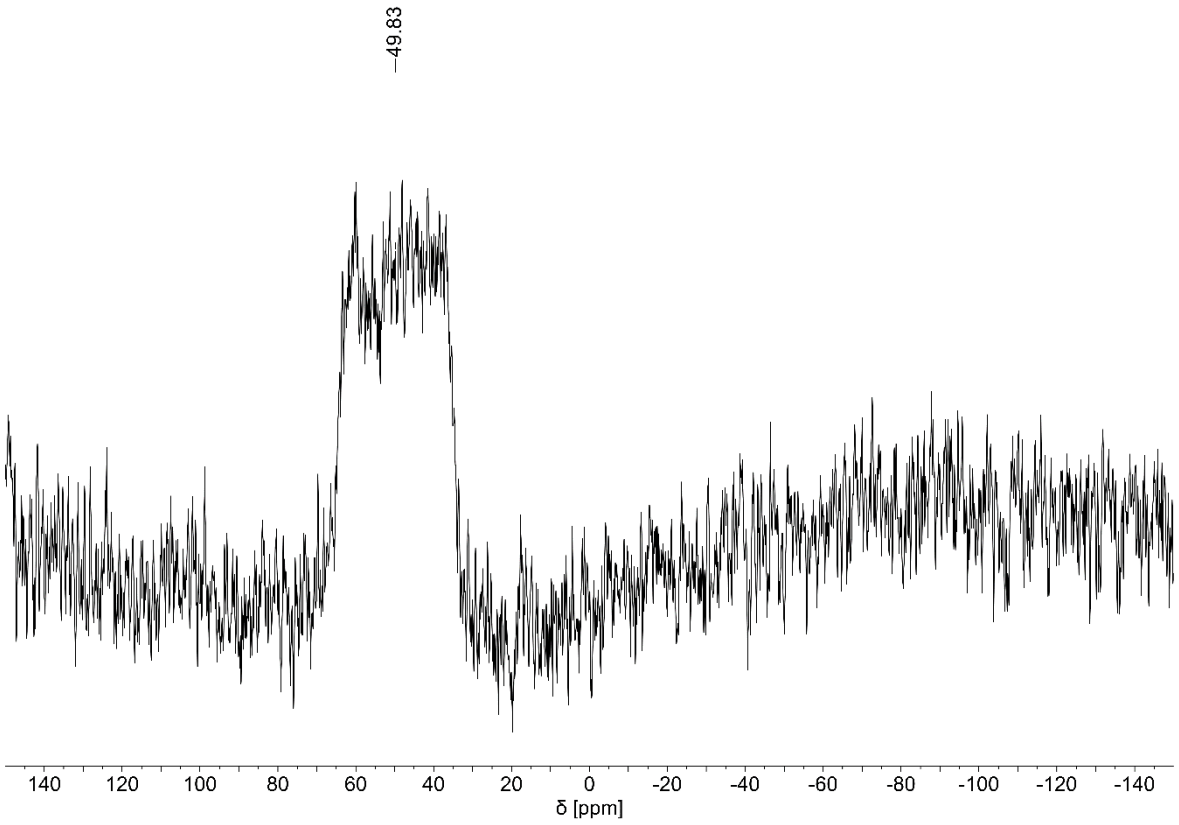

Figure S96. ^{19}F NMR spectrum of $[Tc(NH_3)_2(CO)_2(PPh_3)_2][BF_4]$.

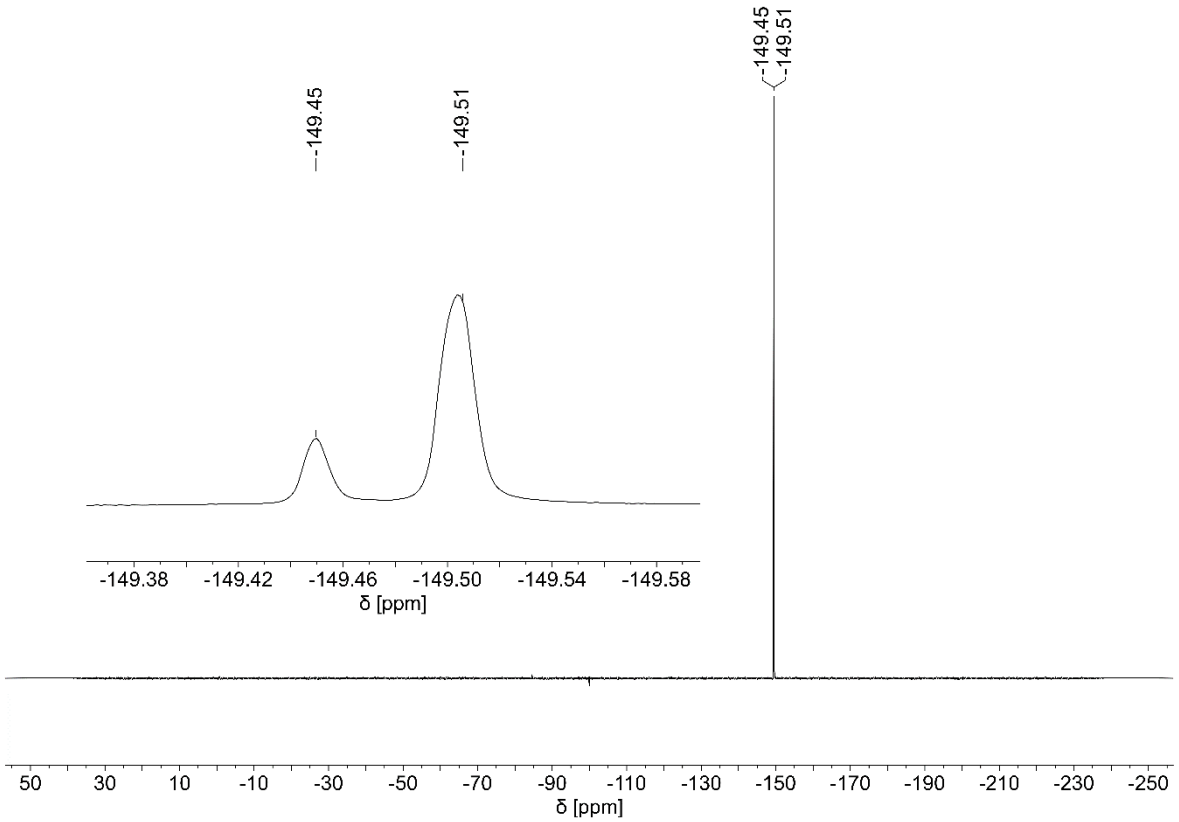

Figure S97. ^{11}B NMR spectrum of $[Tc(NH_3)_2(CO)_2(PPh_3)_2][BF_4]$.

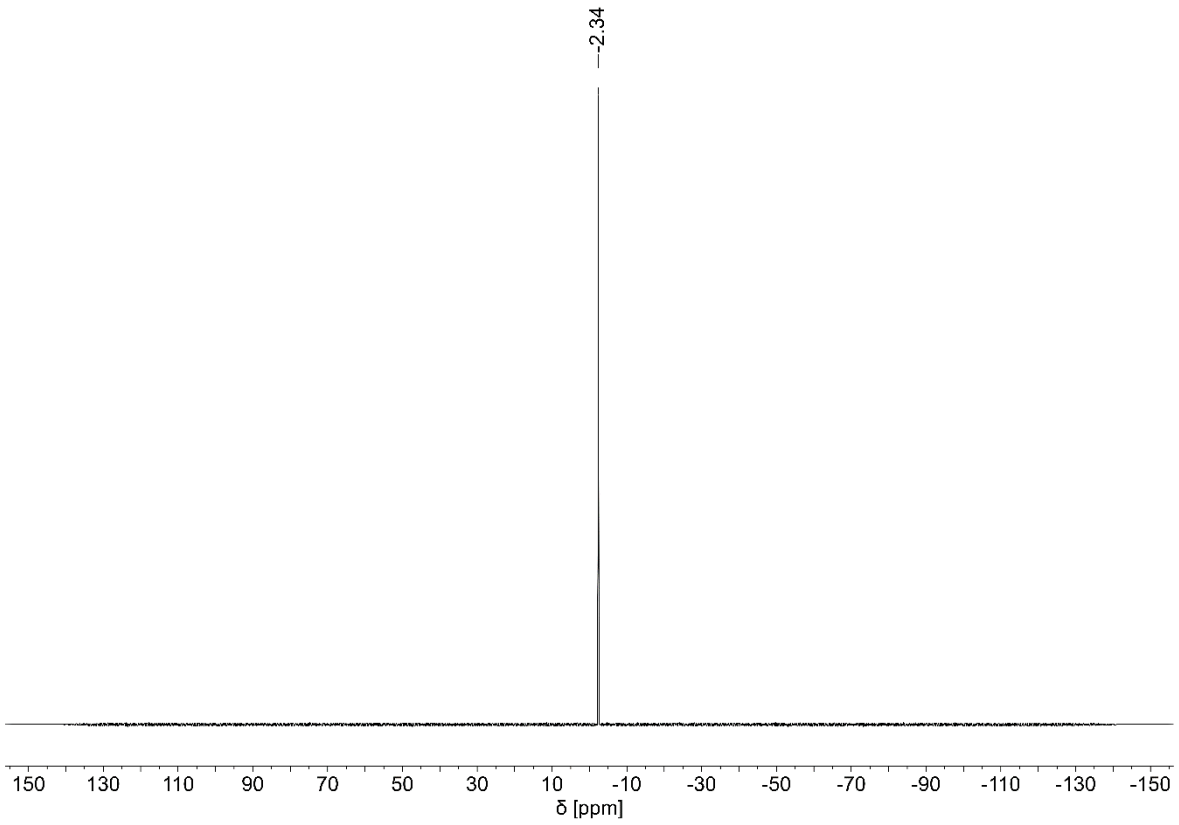

Figure S98. IR spectrum of $[Tc(NH_3)_2(CO)_2(PPh_3)_2][BF_4]$.

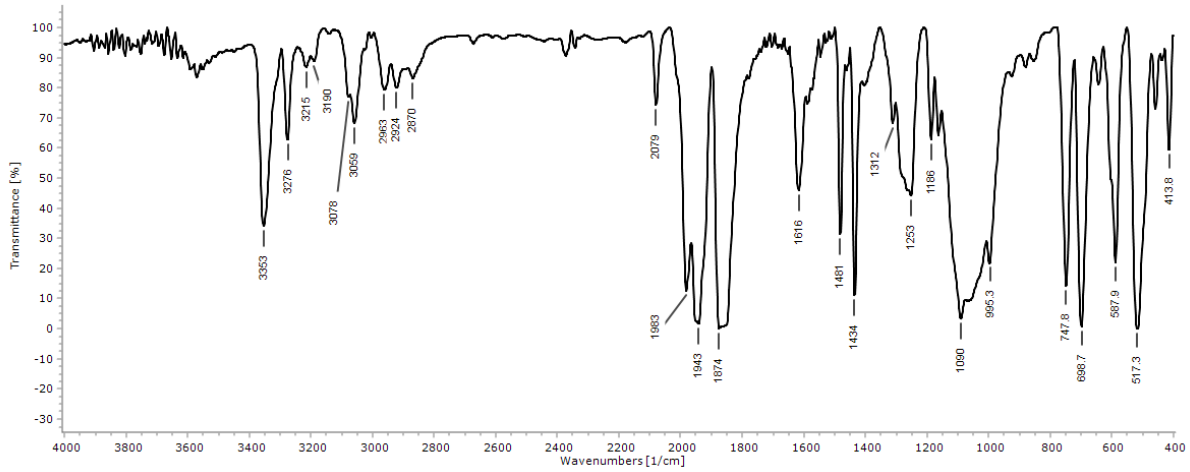

Figure S99. ^{1}H NMR spectrum of $[Tc(^{15}NH_3)_2(CO)_2(PPh_3)_2][BF_4]$.

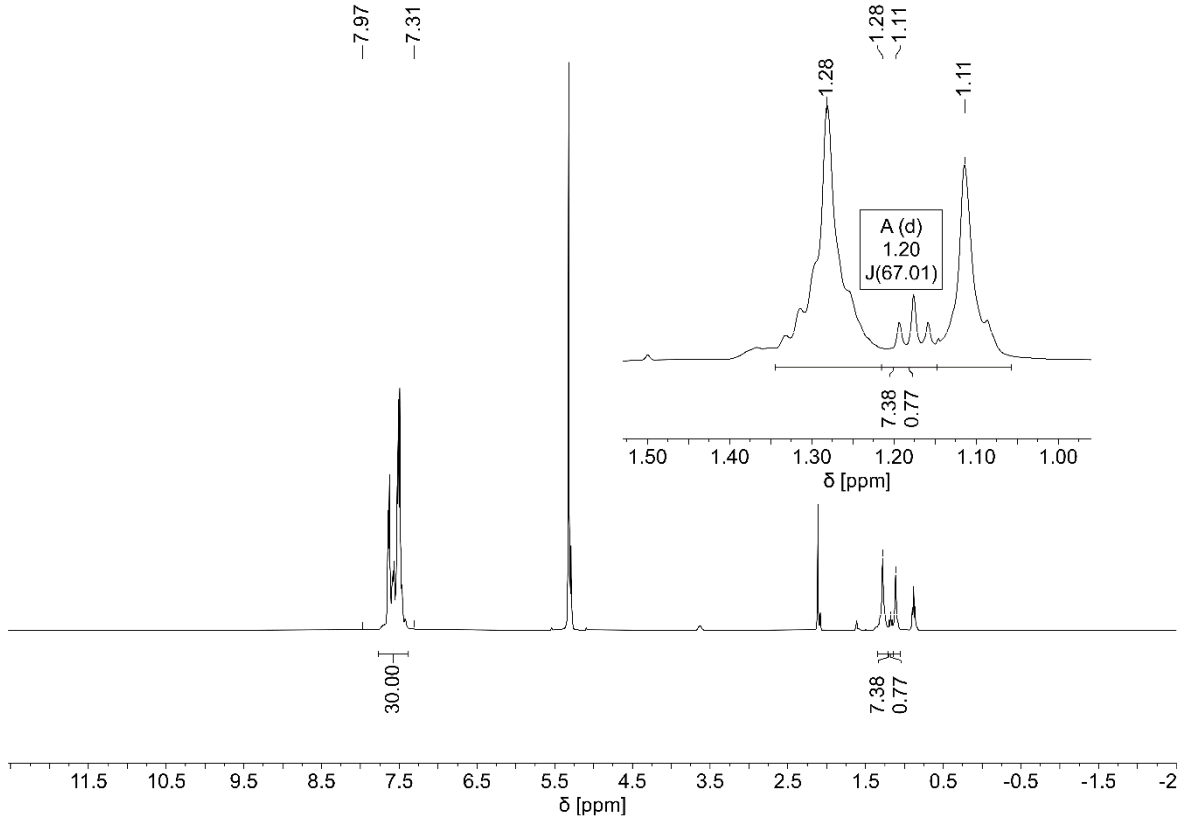

Figure S100. ^{99}Tc NMR spectrum of [Tc(^{15}NH$_3$)$_2$(CO)$_2$(PPh$_3$)$_2$][BF$_4$].

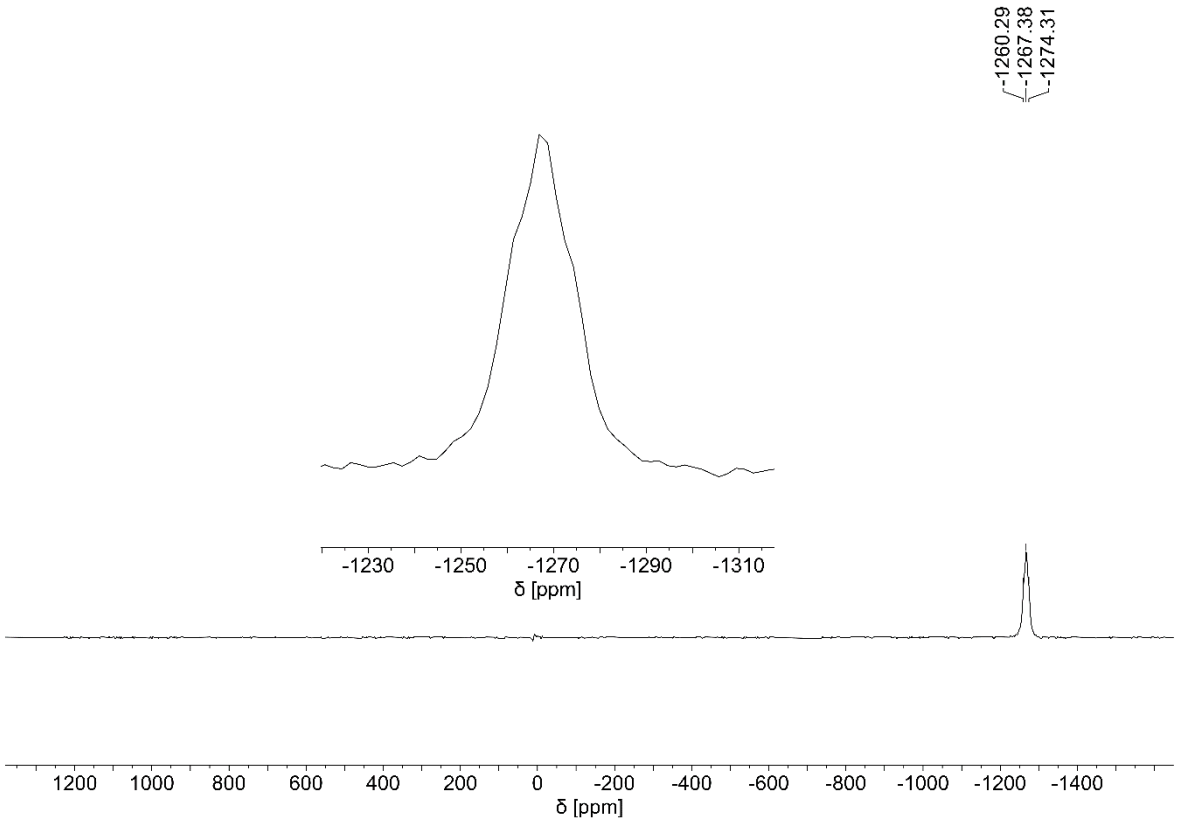

Figure S101. ^{31}P{^{1}H} NMR spectrum of [Tc(^{15}NH$_3$)$_2$(CO)$_2$(PPh$_3$)$_2$][BF$_4$].

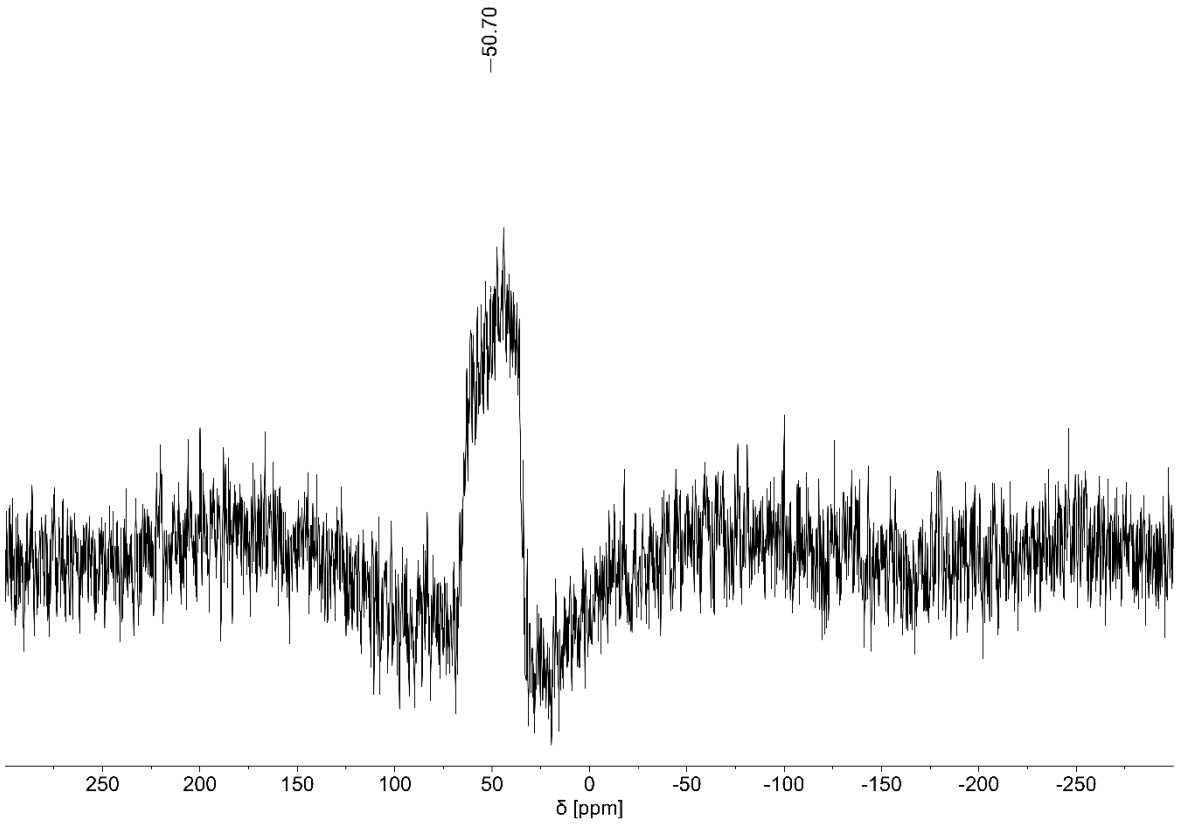

Figure S102. ^{19}F NMR spectrum of $[Tc(^{15}NH_3)_2(CO)_2(PPh_3)_2][BF_4]$.

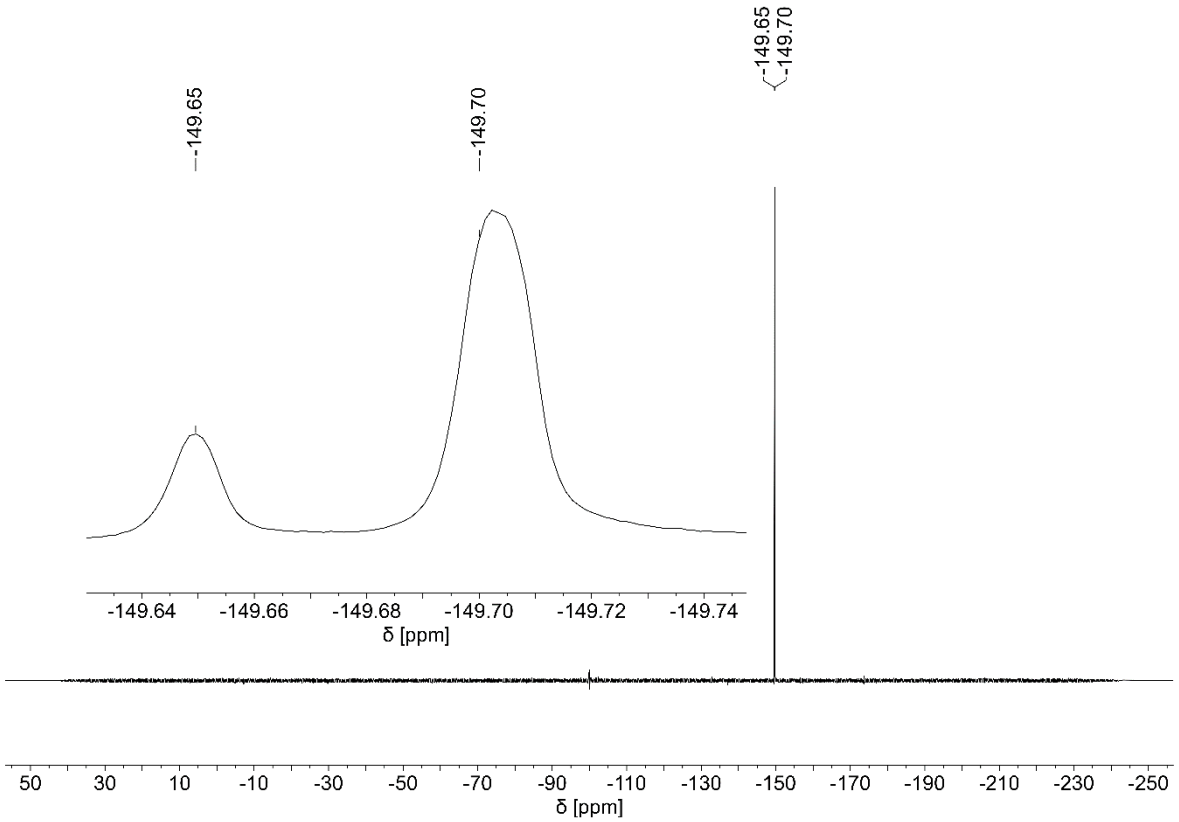

Figure S103. ^{11}B NMR spectrum of $[Tc(^{15}NH_3)_2(CO)_2(PPh_3)_2][BF_4]$.

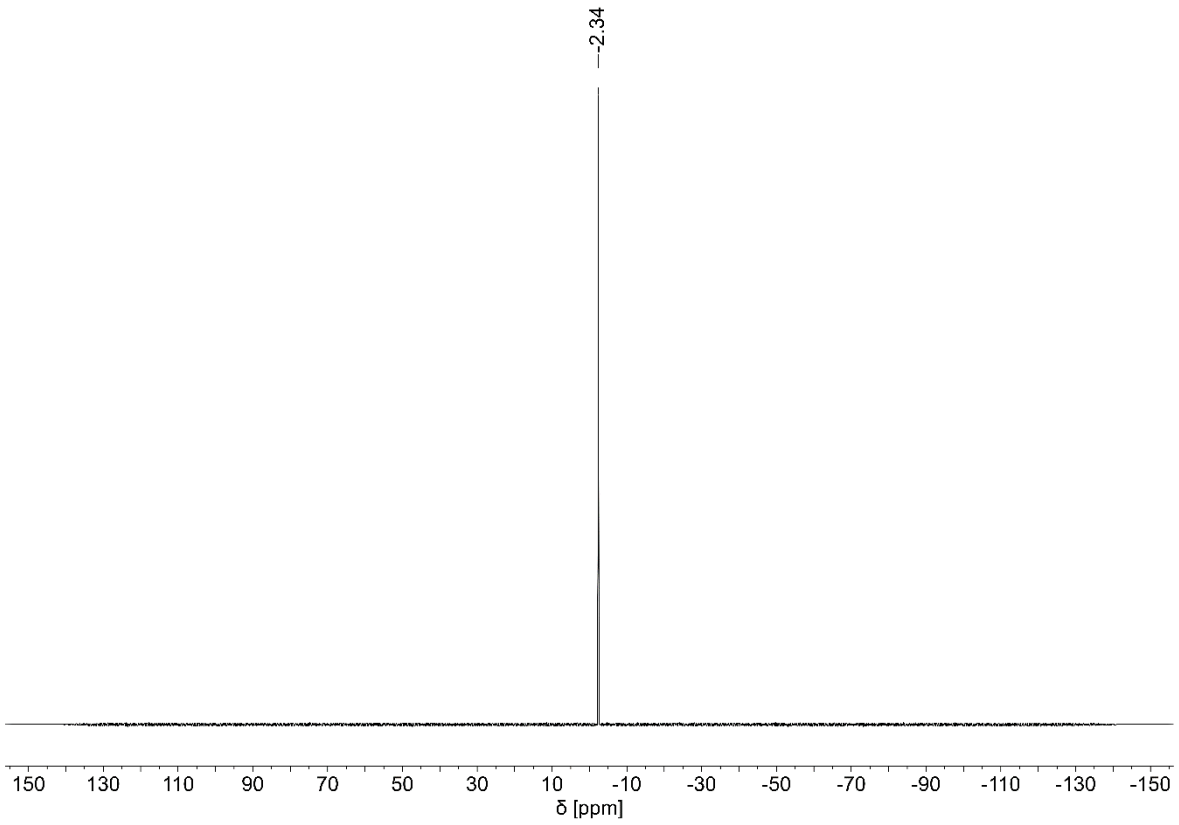

Figure S104. IR spectrum of $[Tc(^{15}NH_3)_2(CO)_2(PPh_3)_2][BF_4]$.

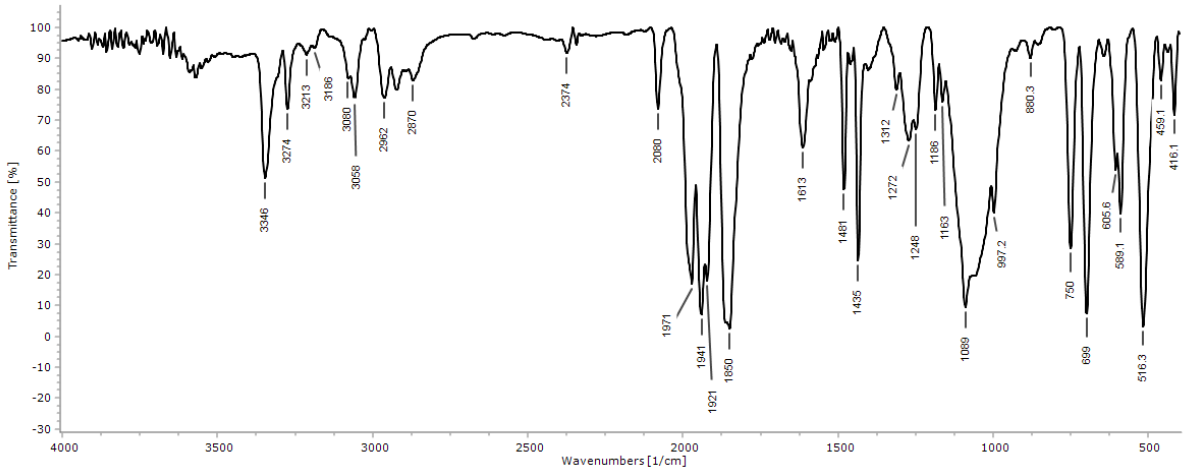

Figure S105. ^{1}H NMR spectrum of $[Tc(py)(CO)_3(PPh_3)_2][BF_4]$.

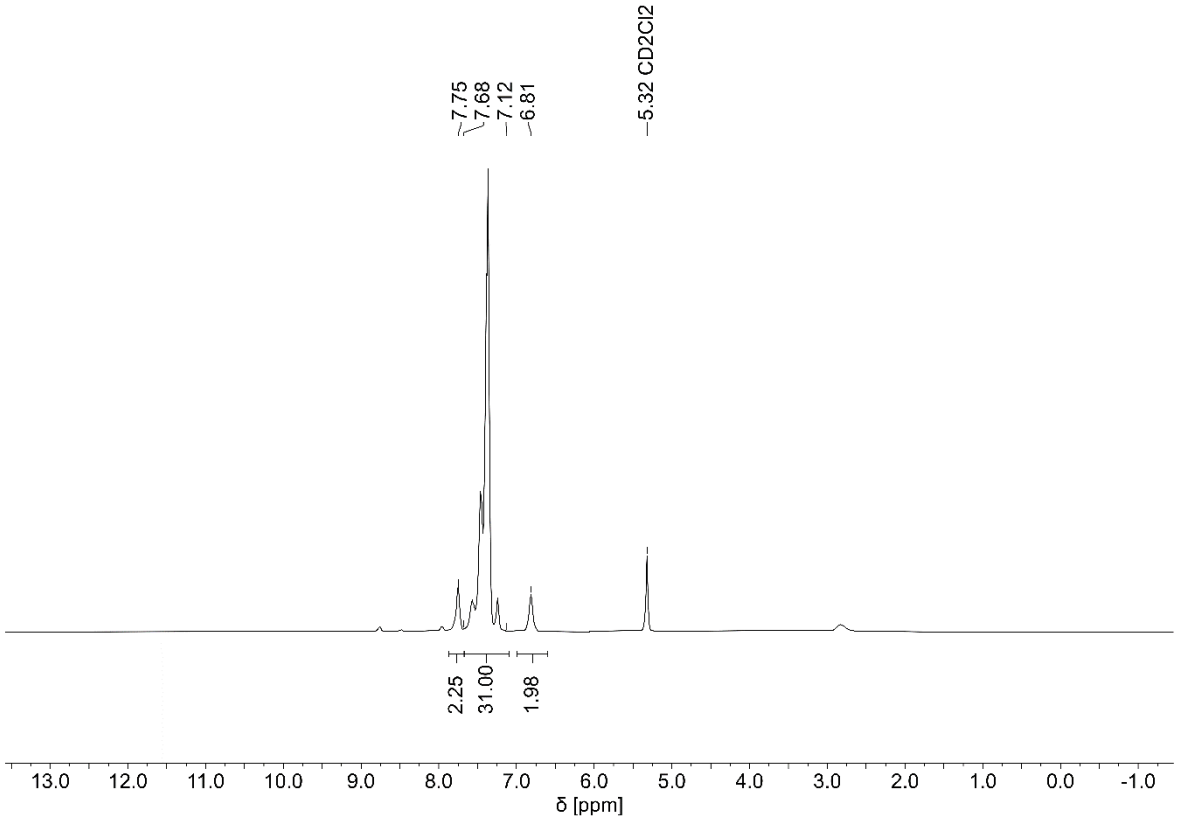

Figure S106. ^{99}Tc NMR spectrum of [Tc(py)(CO)$_3$(PPh$_3$)$_2$][BF$_4$].

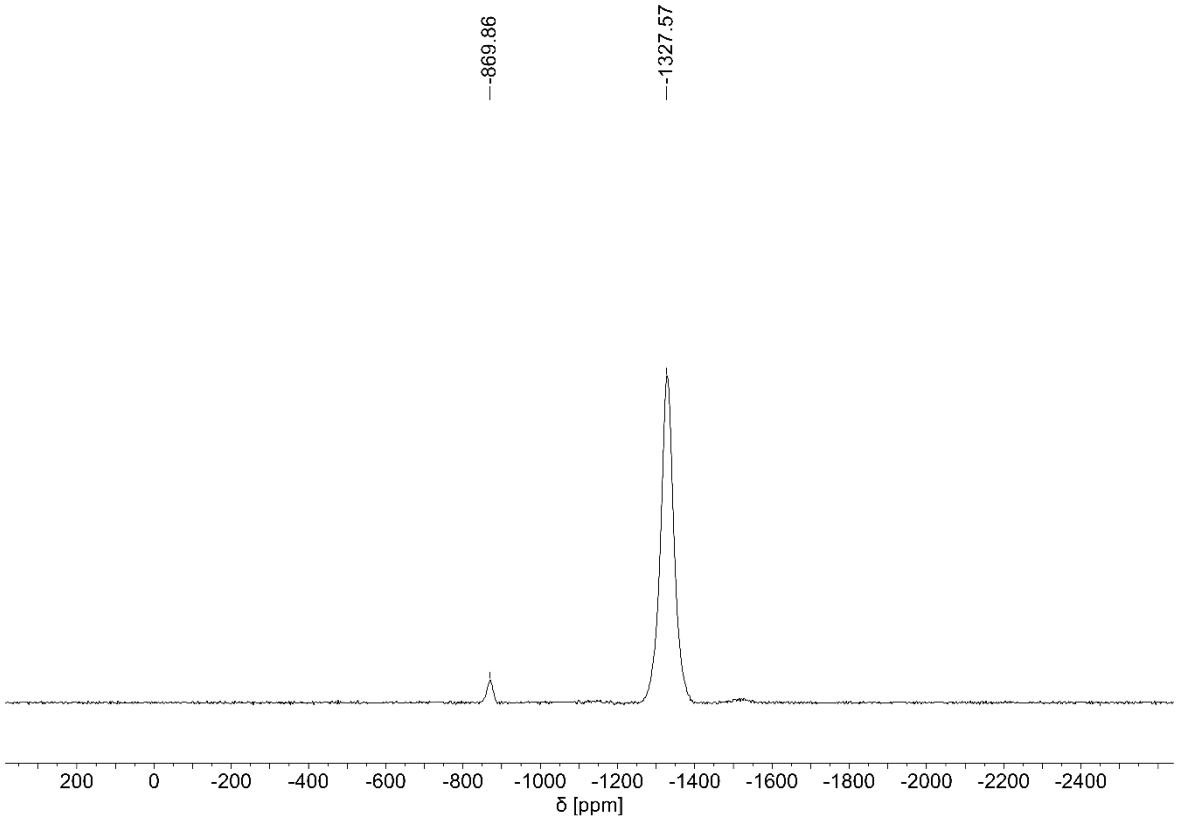

Figure S107. ^{31}P{^{1}H} NMR spectrum of [Tc(py)(CO)$_3$(PPh$_3$)$_2$][BF$_4$].

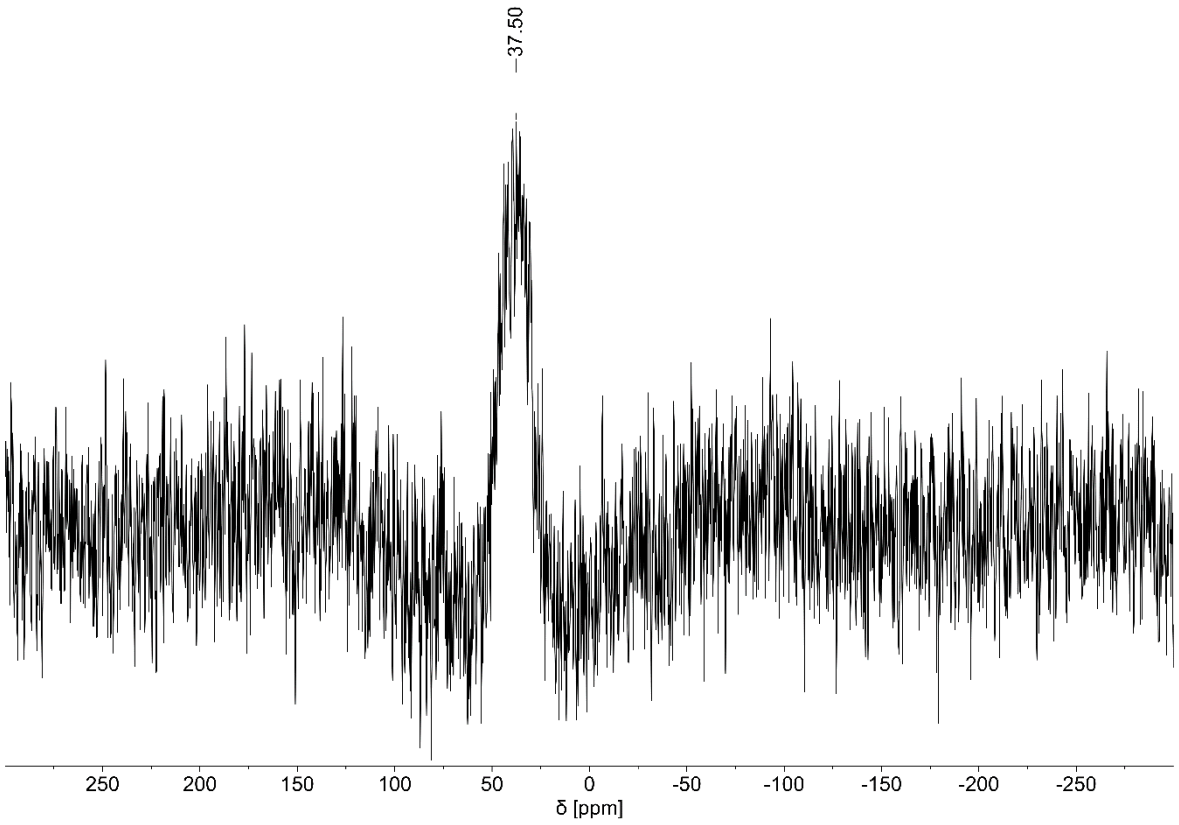

Figure S108. ^{19}F NMR spectrum of $[Tc(py)(CO)_3(PPh_3)_2][BF_4]$.

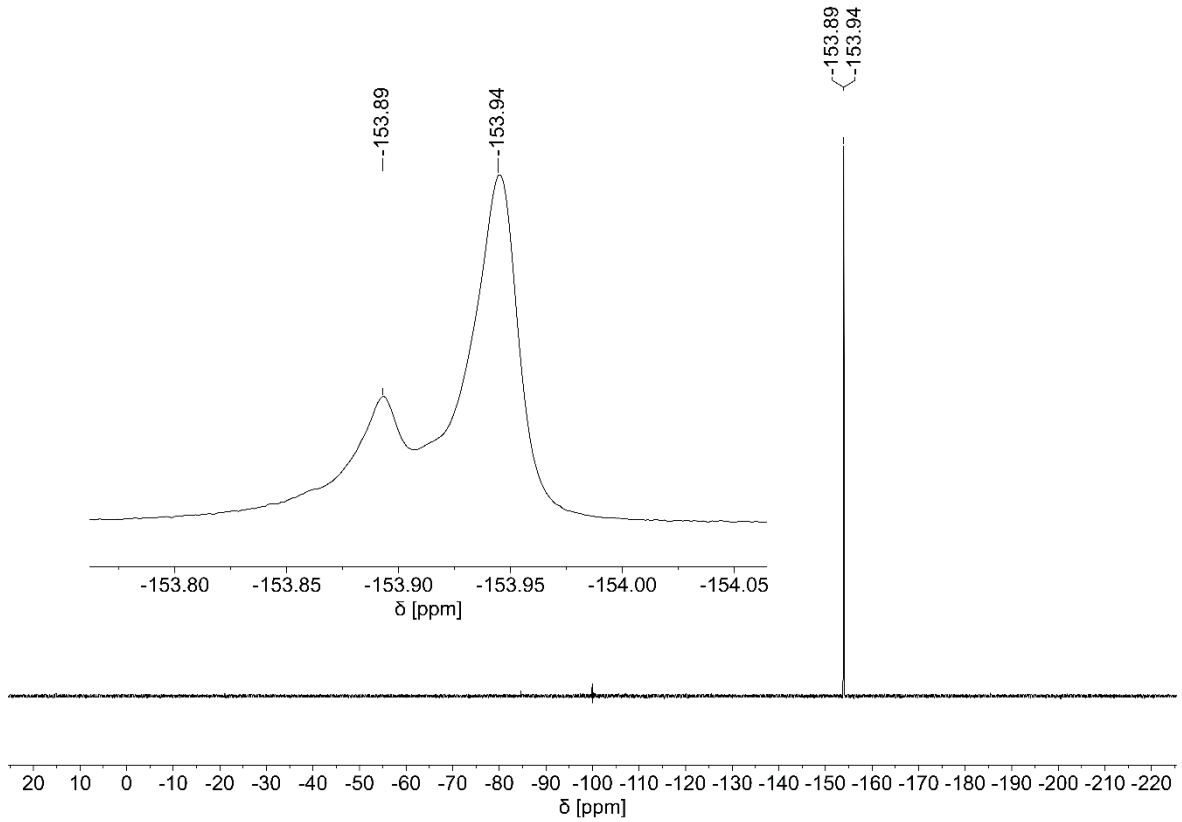

Figure S109. ^{11}B NMR spectrum of $[Tc(py)(CO)_3(PPh_3)_2][BF_4]$.

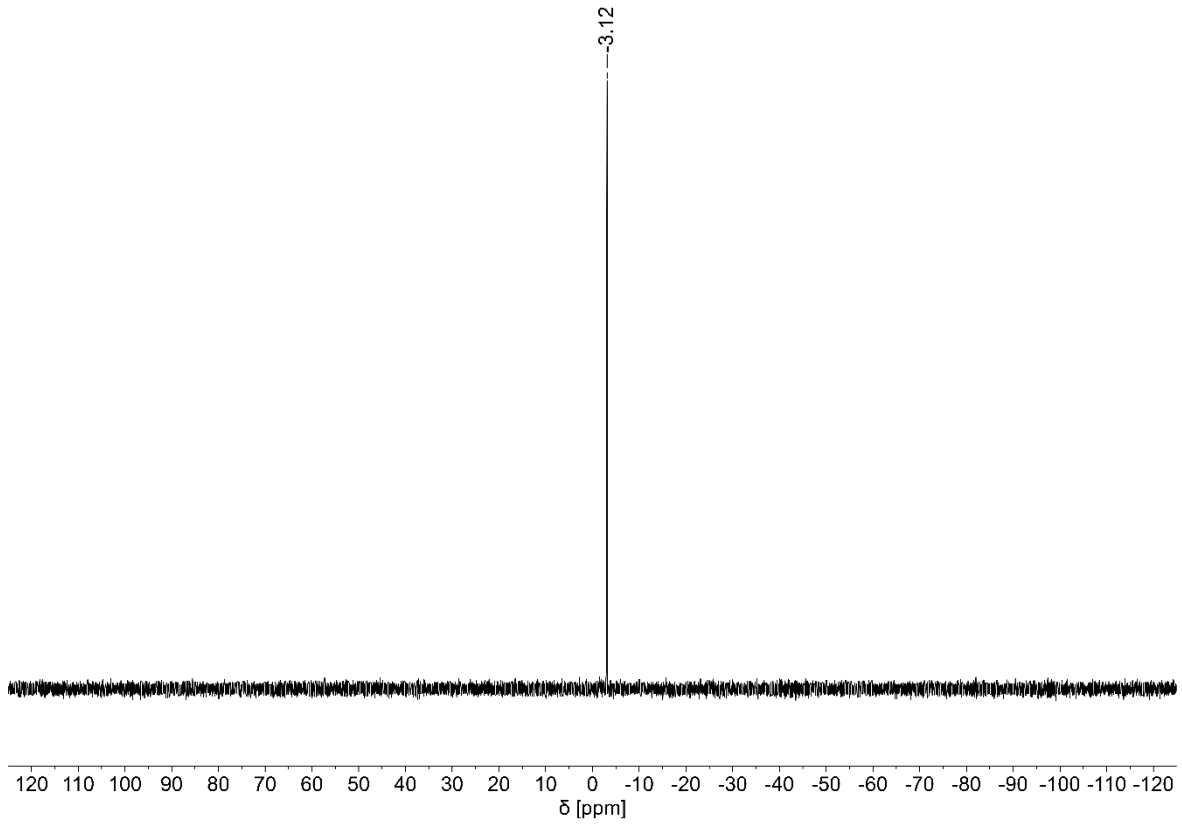

Figure S110. IR spectrum of $[Tc(py)(CO)_3(PPh_3)_2][BF_4]$.

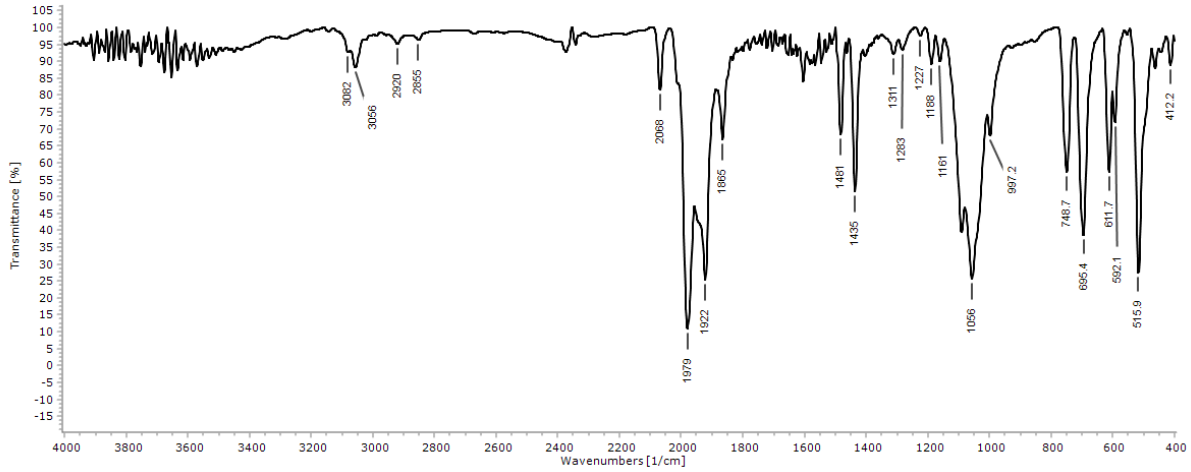

Figure S111. ^1H NMR spectrum of $[Tc(NCCH_3)(CO)_3(PPh_3)_2][BF_4]$.

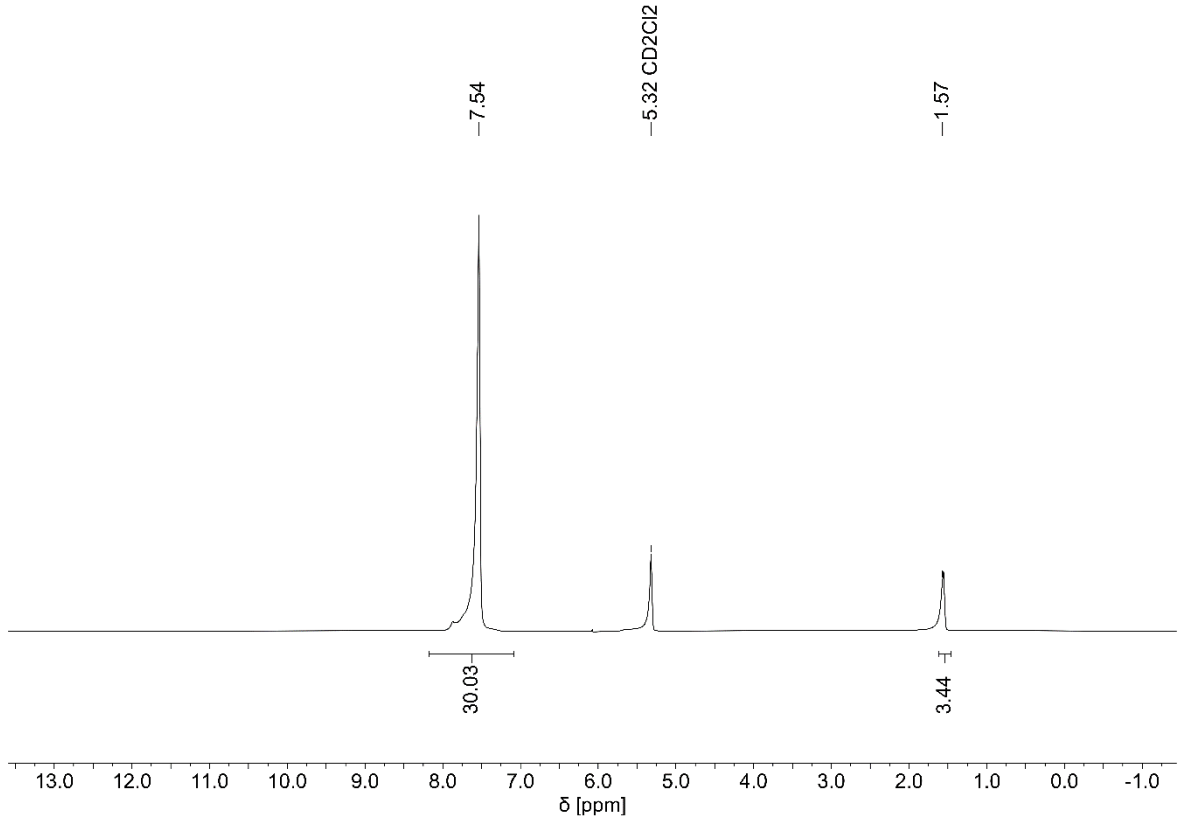

Figure S112. ^{99}Tc NMR spectrum of [Tc(NCCH$_3$)(CO)$_3$(PPh$_3$)$_2$][BF$_4$].

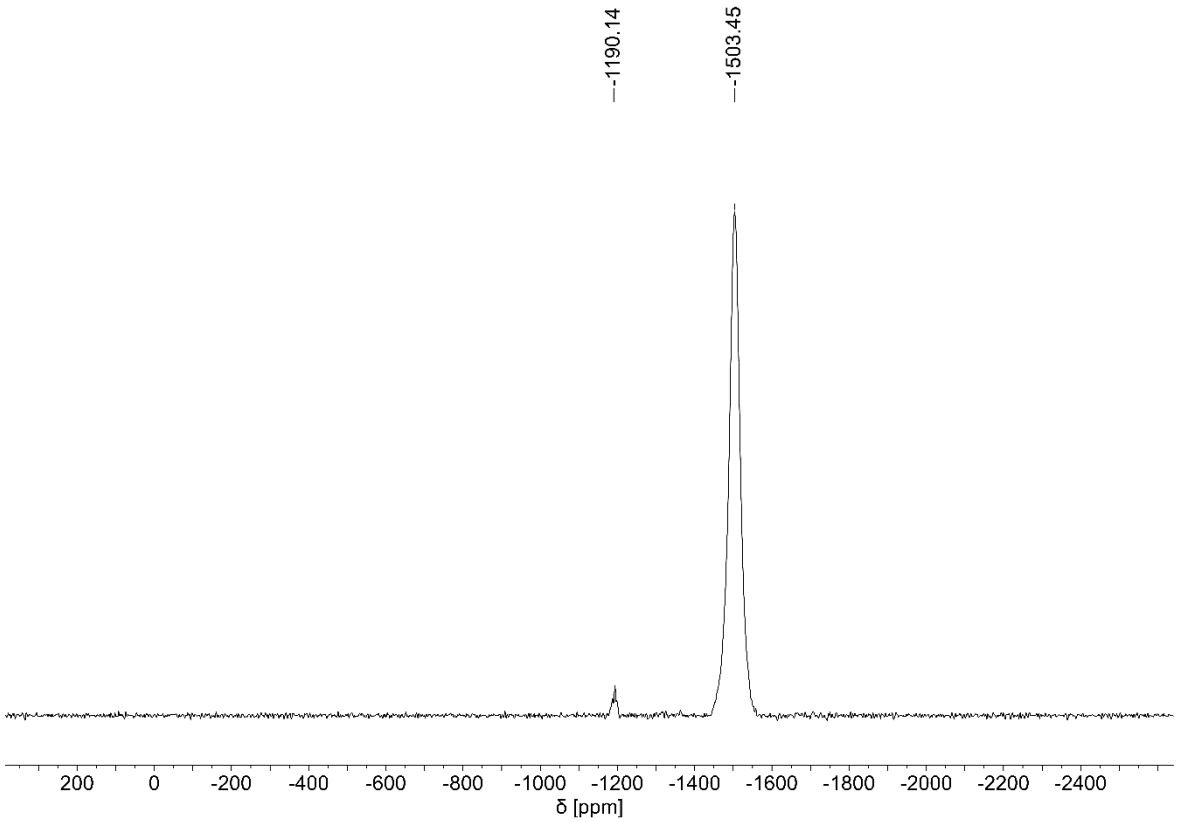

Figure S113. ^{31}P{^{1}H} NMR spectrum of [Tc(NCCH$_3$)(CO)$_3$(PPh$_3$)$_2$][BF$_4$].

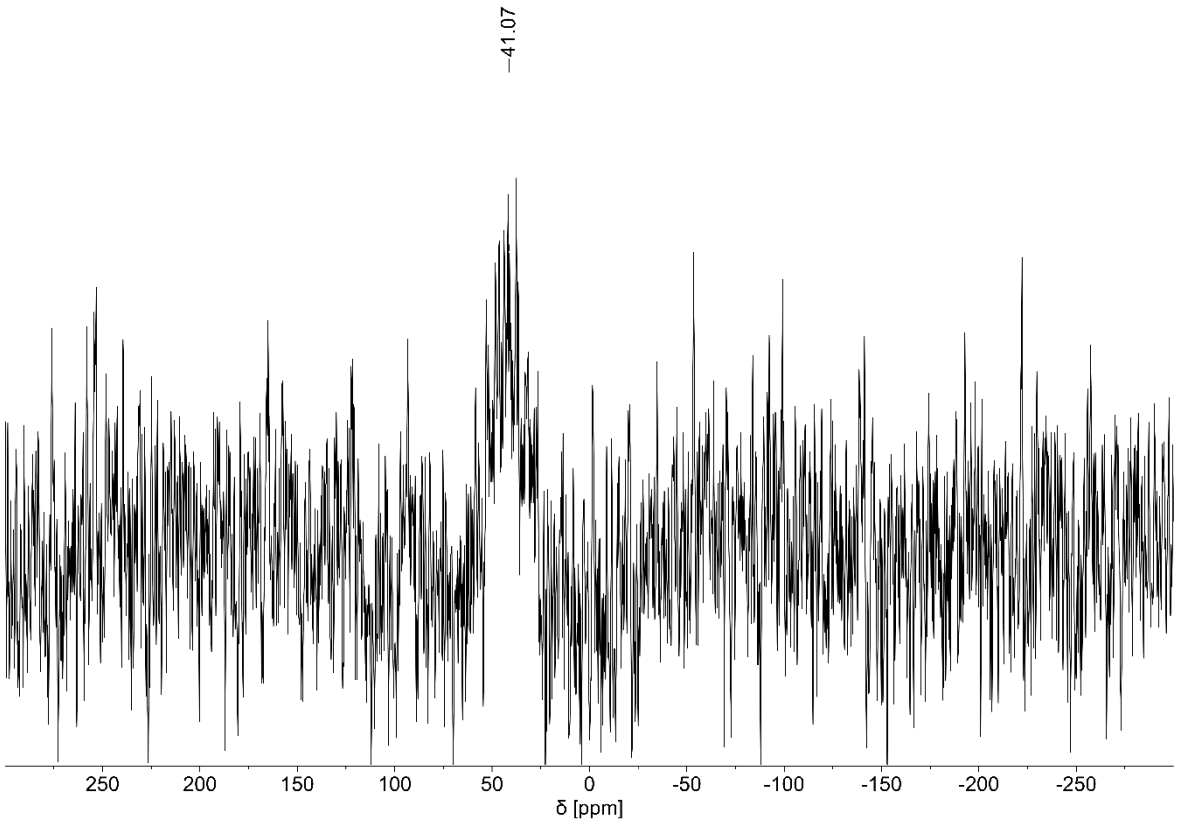

Figure S114. ^{19}F NMR spectrum of $[Tc(NCCH_3)(CO)_3(PPh_3)_2][BF_4]$.

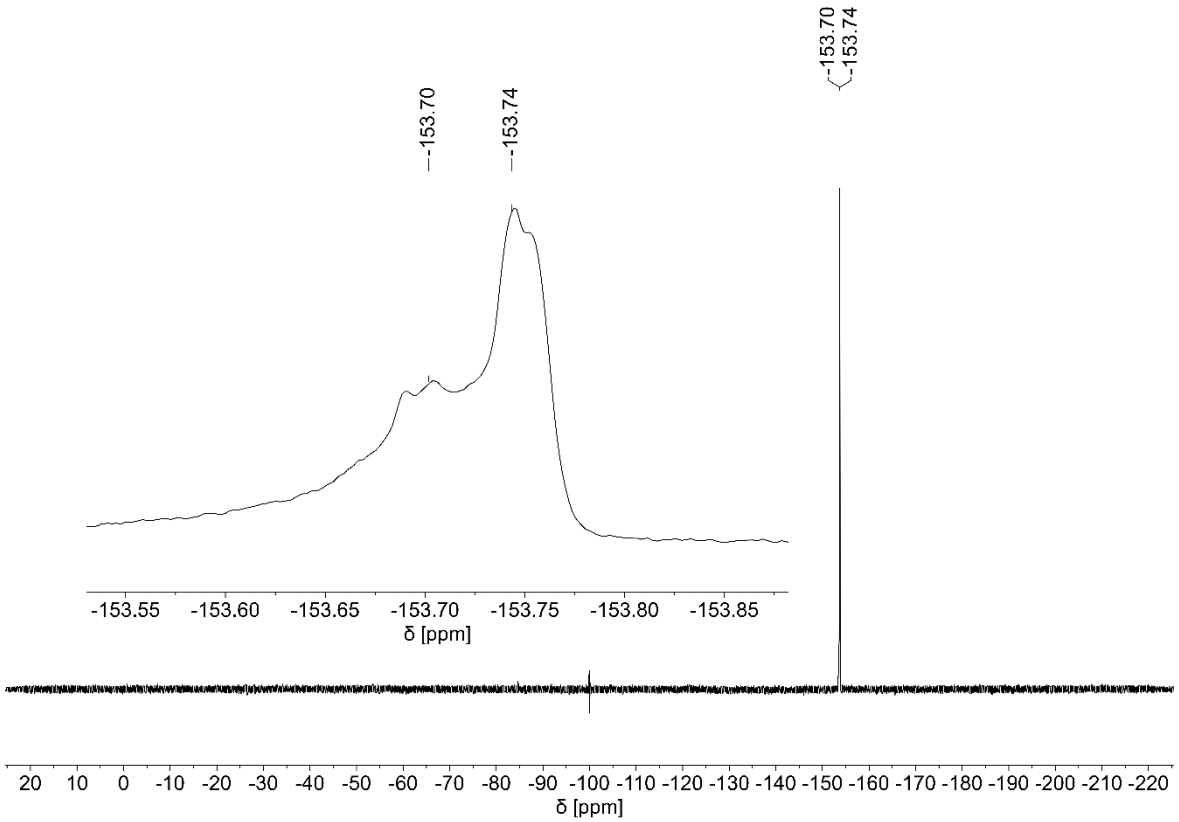

Figure S115. ^{11}B NMR spectrum of $[Tc(NCCH_3)(CO)_3(PPh_3)_2][BF_4]$.

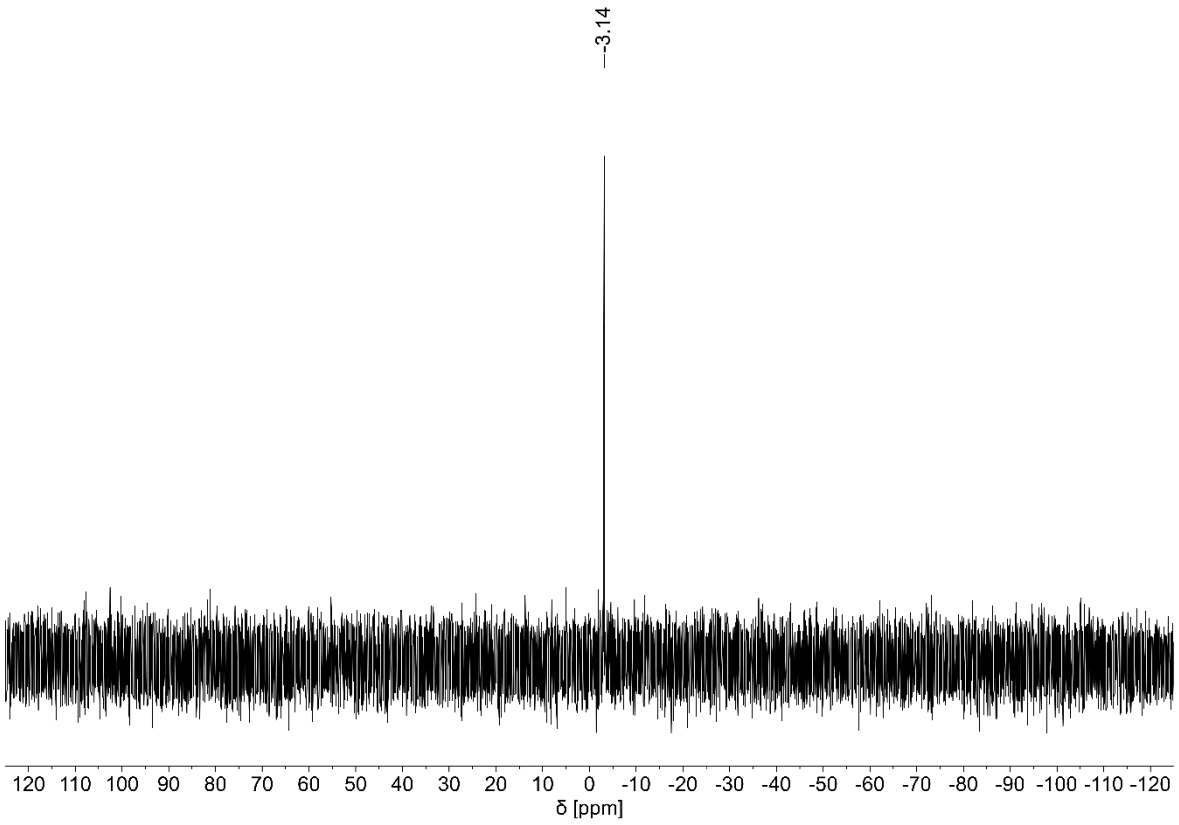

Figure S116. IR spectrum of $[Tc(NCCH_3)(CO)_3(PPh_3)_2][BF_4]$.

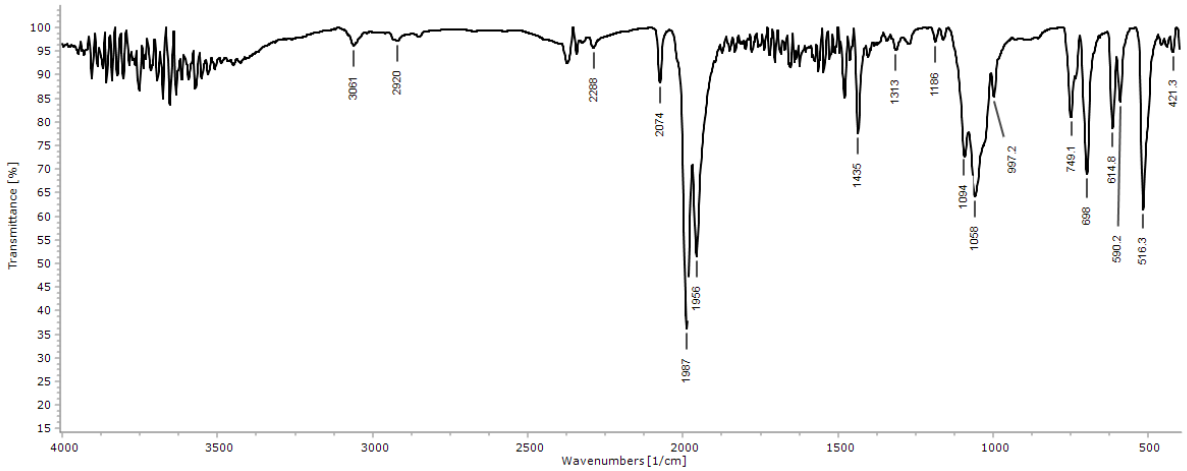

Figure S117. ^1H NMR spectrum of $[Tc(bpy)(CO)_2(PPh_2)_2][BF_4]$.

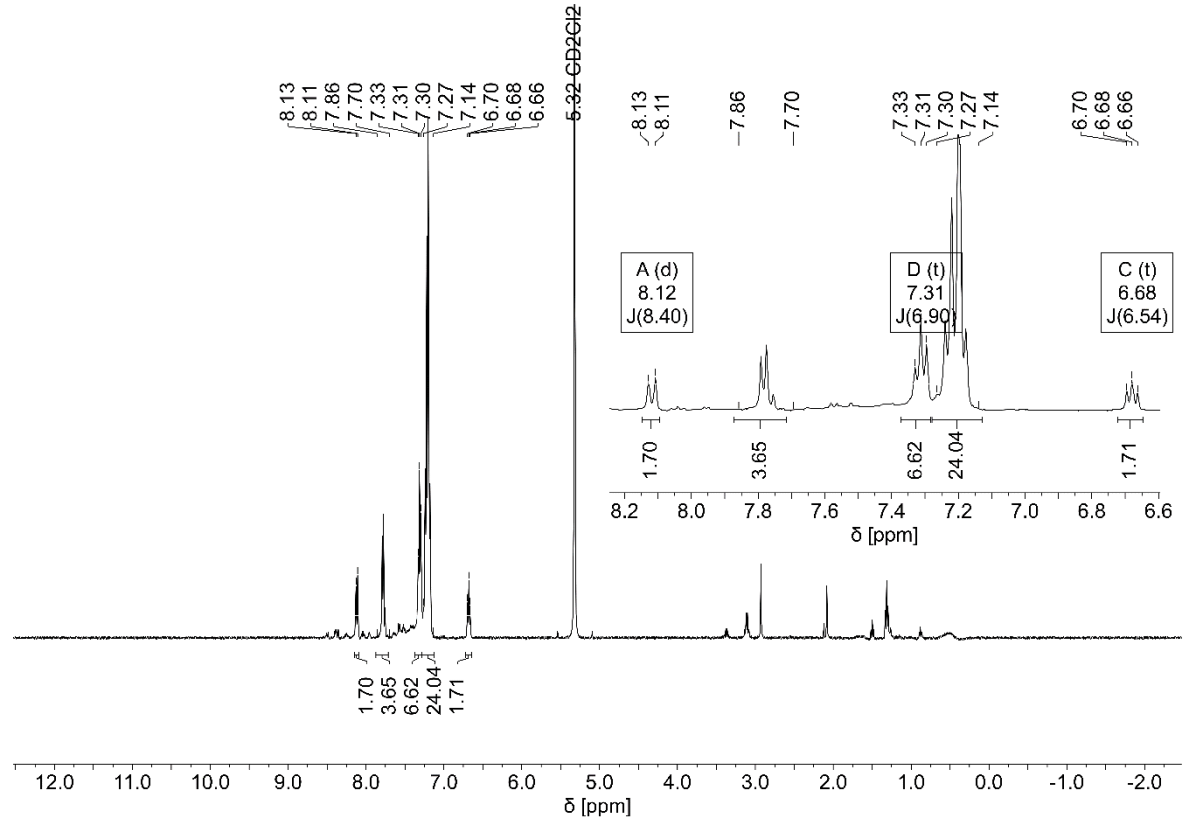

Figure S118. ^{99}Tc NMR spectrum of [Tc(bpy)(CO)$_2$(PPh$_2$)$_2$][BF$_4$].

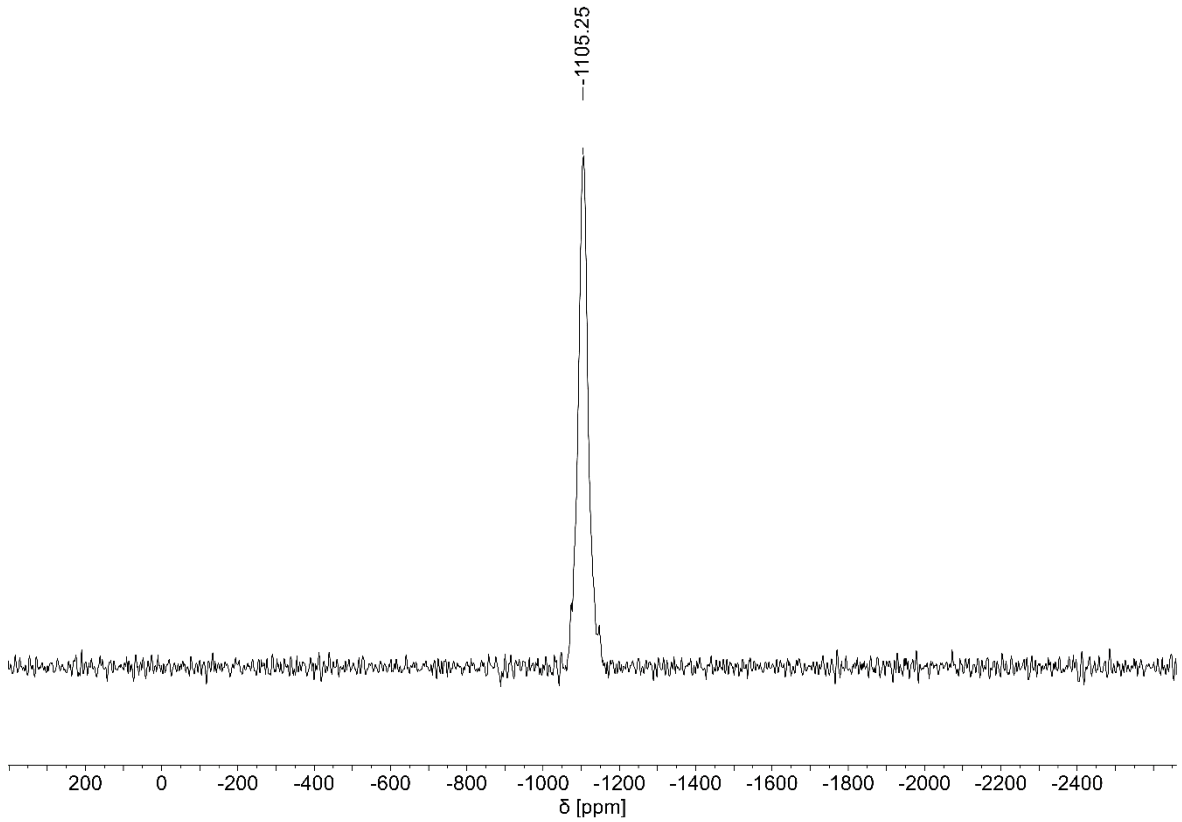

Figure S119. ^{31}P{^{1}H} NMR spectrum of [Tc(bpy)(CO)$_2$(PPh$_2$)$_2$][BF$_4$].

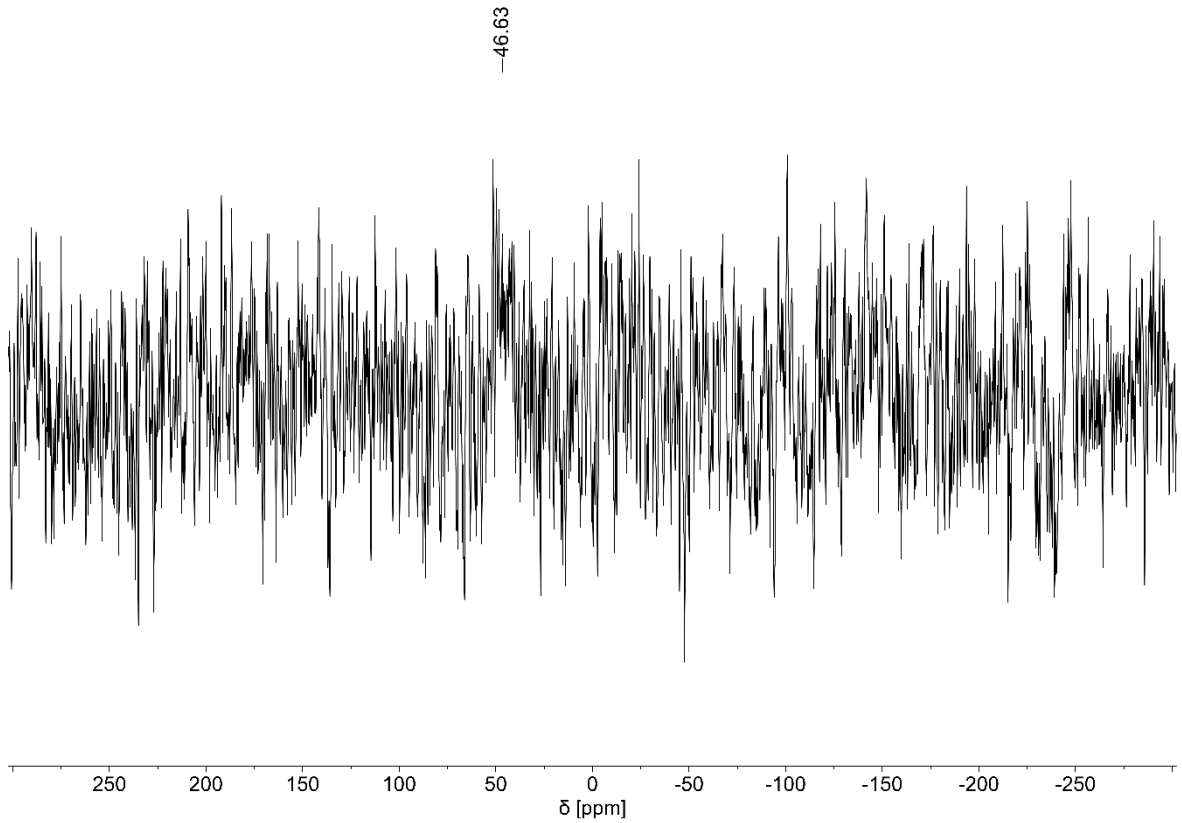

Figure S120. ^{19}F NMR spectrum of $[Tc(bpy)(CO)_2(PPh_2)_2][BF_4]$.

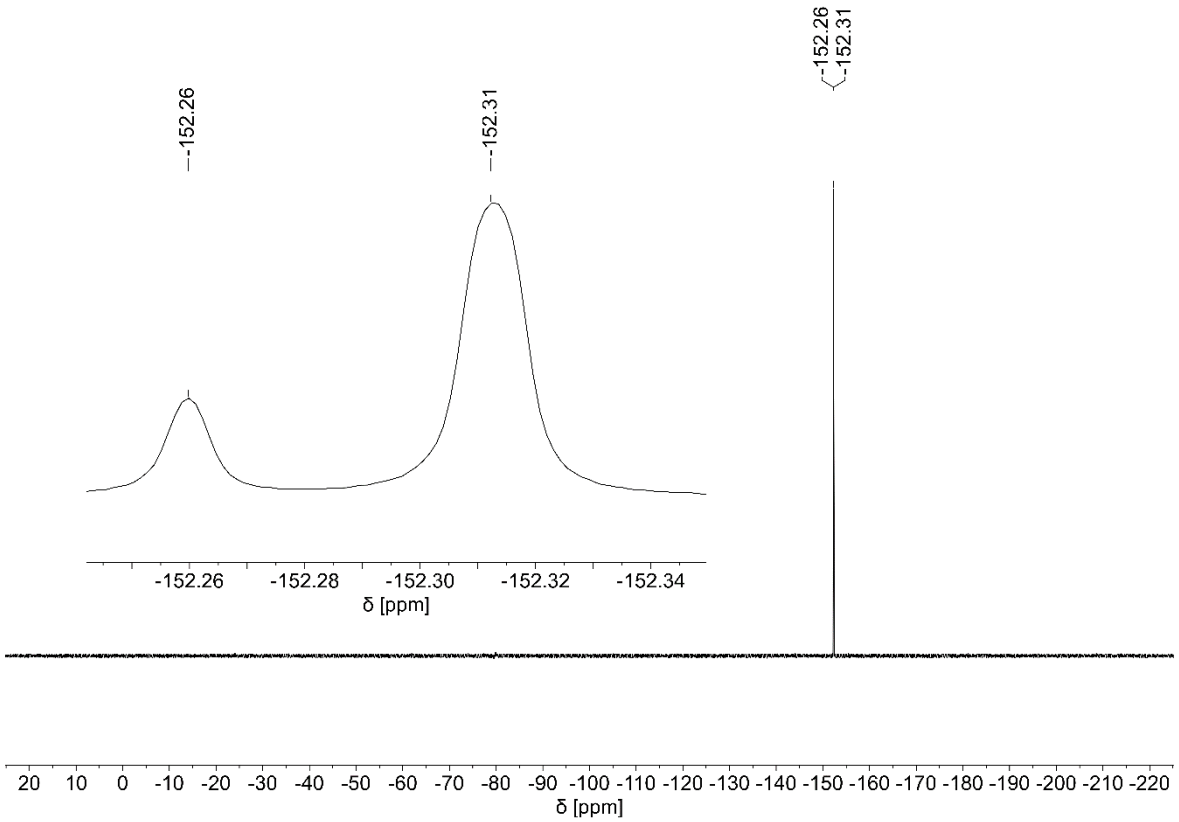

Figure S121. ^{11}B NMR spectrum of $[Tc(bpy)(CO)_2(PPh_2)_2][BF_4]$.

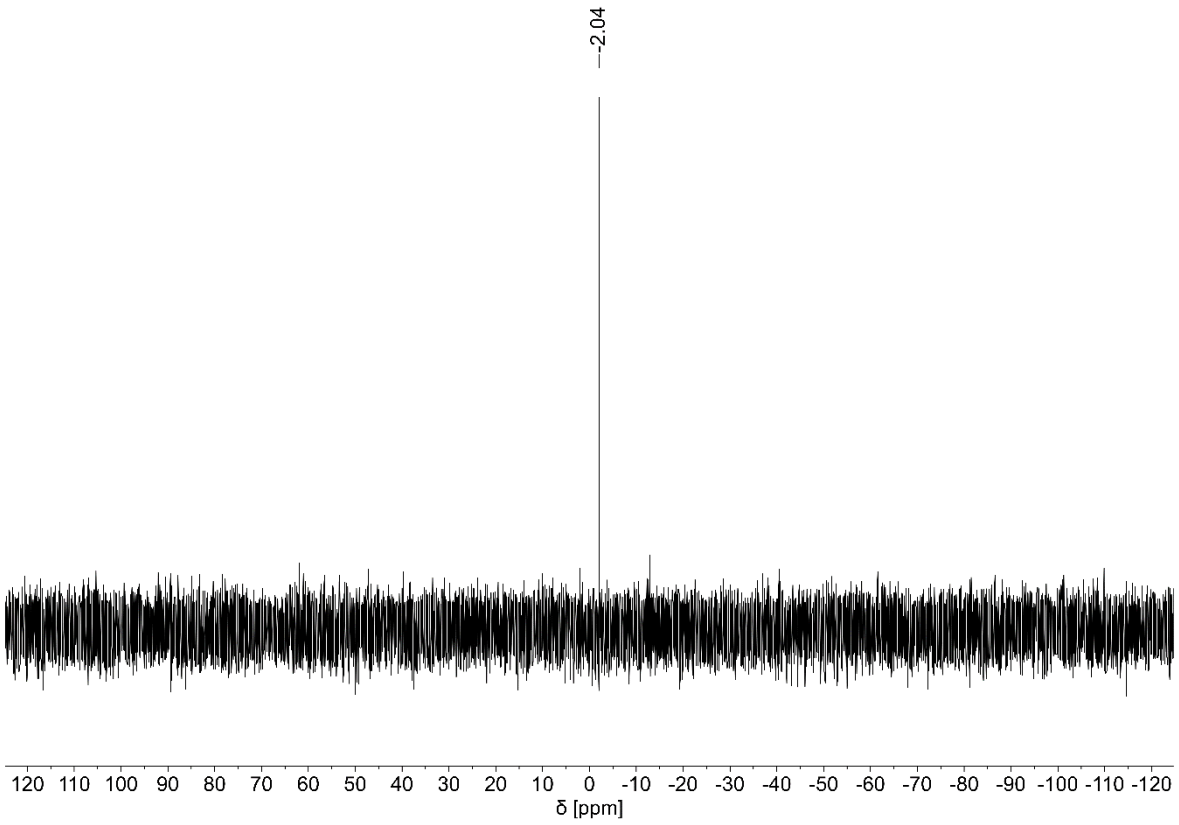

Figure S122. IR spectrum of $[Tc(bpy)(CO)_2(PPh_2)_2][BF_4]$.

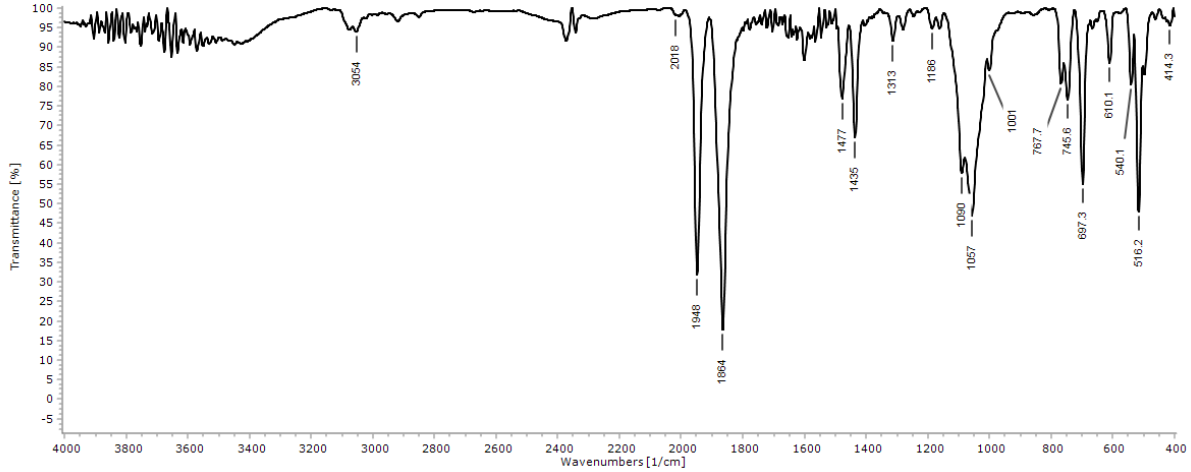

Figure S123. ^1H NMR spectrum of $[\{Tc(N,O\text{-}C_5H_4N\text{-}COO)(CO)_2(PPh_3)_2\}_2H][BF_4]$.

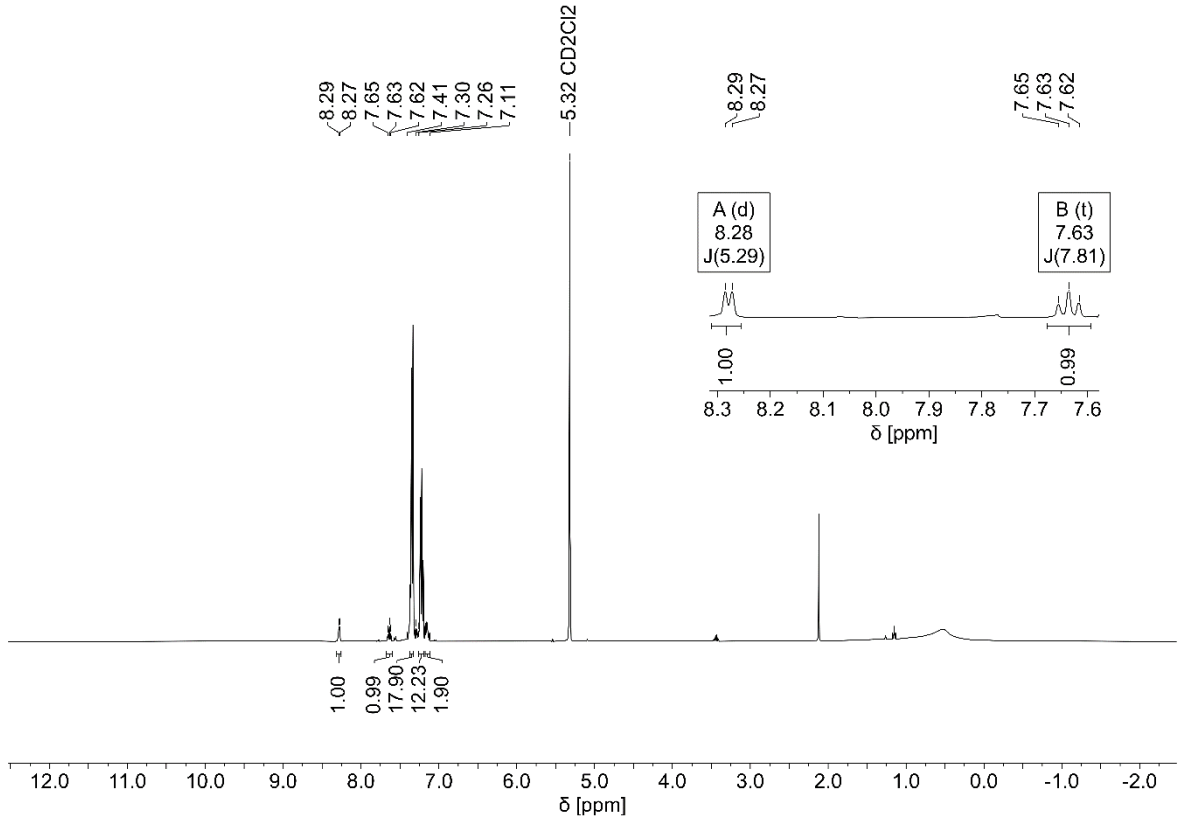

Figure S124. ^{99}Tc NMR spectrum of [{Tc(*N*,*O*-C_5H_4N-COO)$(CO)_2(PPh_3)_2$}$_2$H][BF_4].

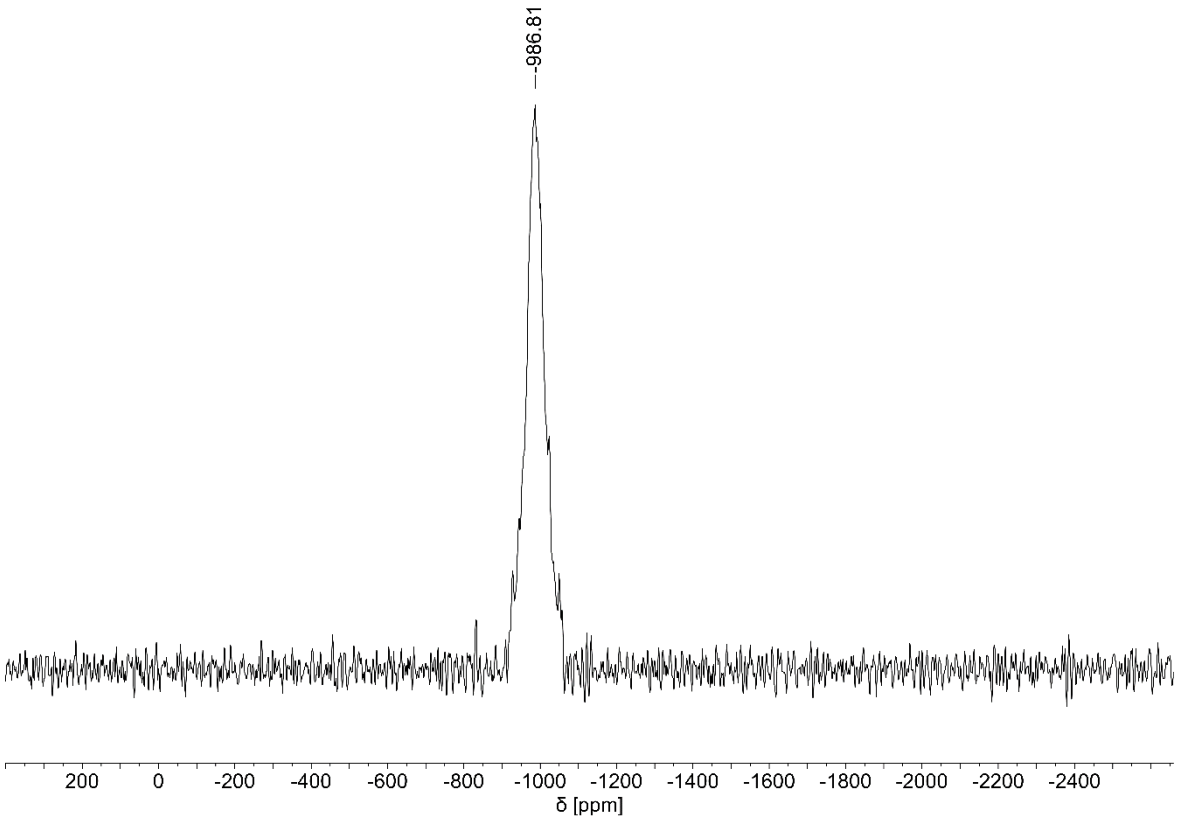

Figure S125. ^{19}F NMR spectrum of [{Tc(*N*,*O*-C_5H_4N-COO)$(CO)_2(PPh_3)_2$}$_2$H][BF_4].

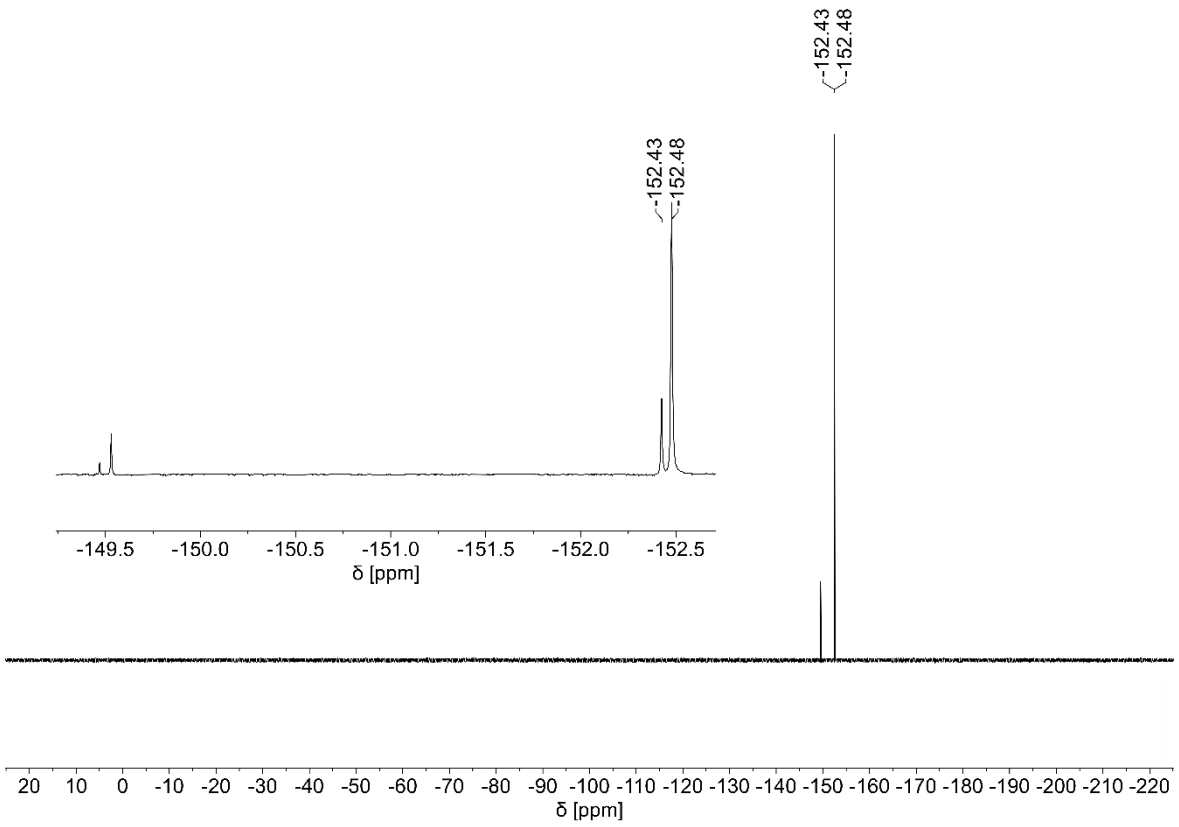

Figure S126. ^{11}B NMR spectrum of [{Tc(*N*,*O*-C_5H_4N-COO)$(CO)_2(PPh_3)_2$}$_2$H][BF_4].

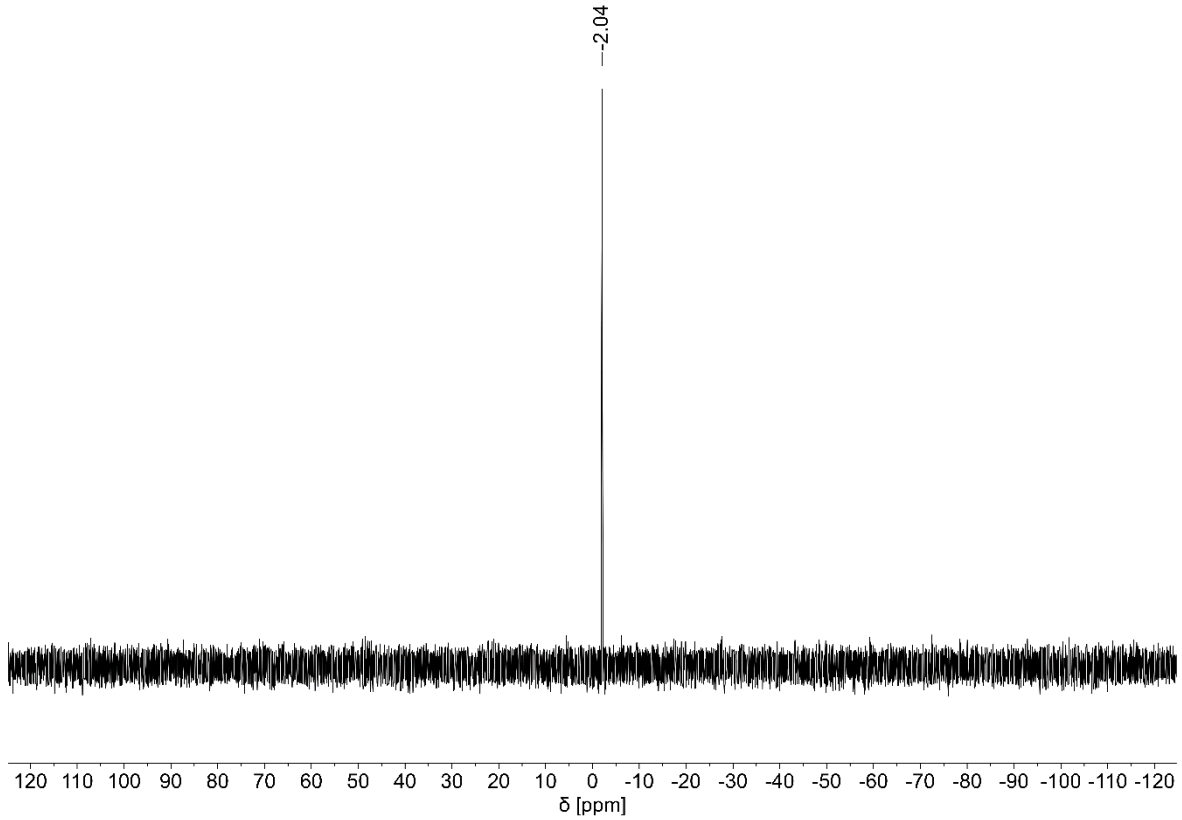

Figure S127. IR spectrum of [{Tc(*N*,*O*-C_5H_4N-COO)$(CO)_2(PPh_3)_2$}$_2$H][BF_4].

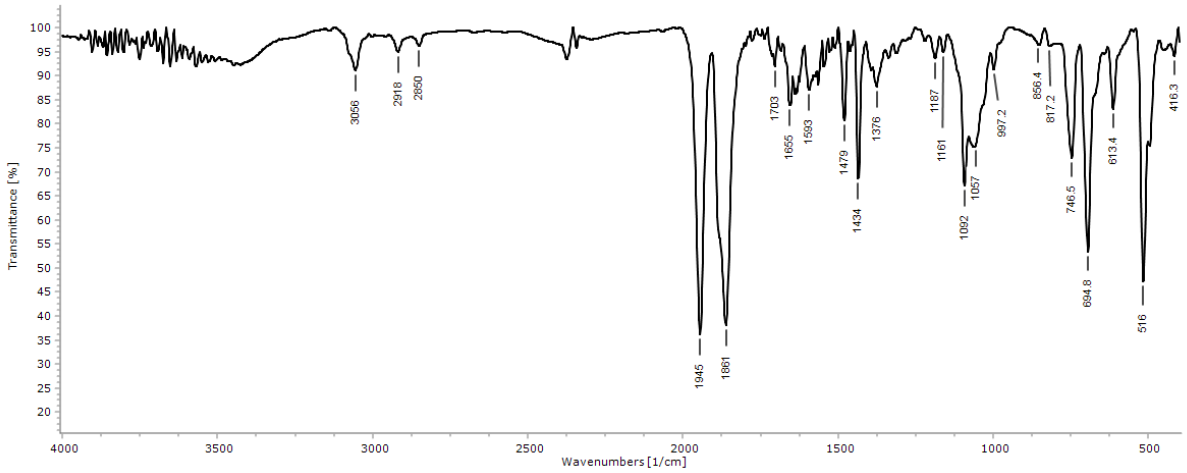

Figure S128. ^{1}H NMR spectrum of $[Tc(bpy^{COOMe2})(CO)_2(PPh_2)_2][BF_4]$.

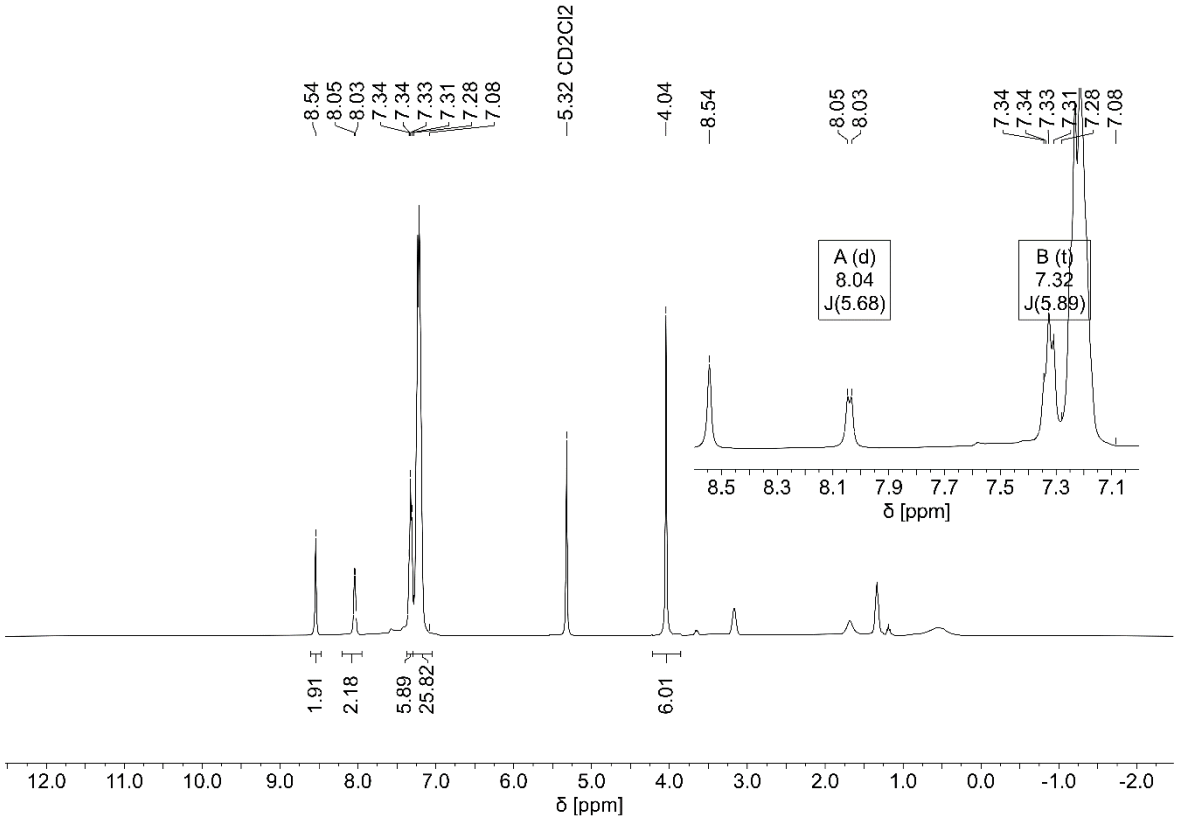

Figure S129. ^{99}Tc NMR spectrum of $[Tc(bpy^{COOMe2})(CO)_2(PPh_2)_2][BF_4]$.

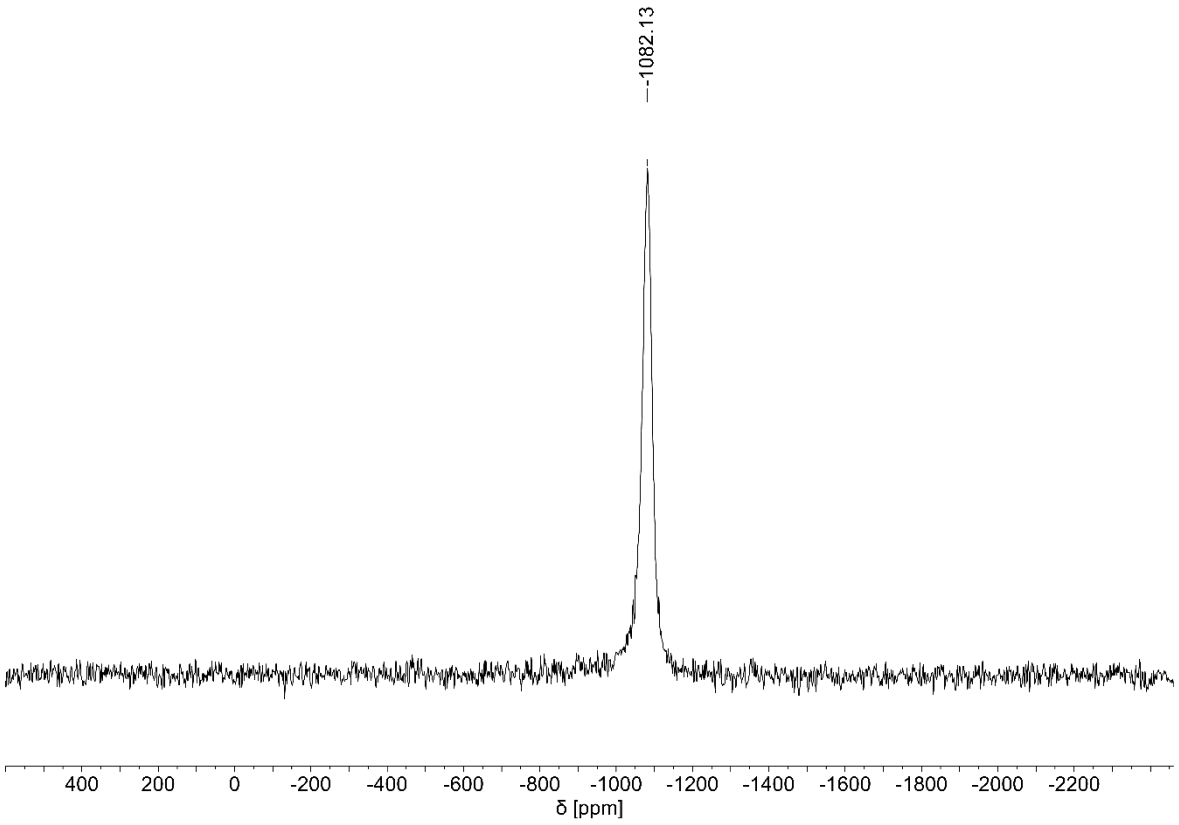

Figure S130. $^{31}P\{^{1}H\}$ NMR spectrum of $[Tc(bpy^{COOMe2})(CO)_2(PPh_2)_2][BF_4]$.

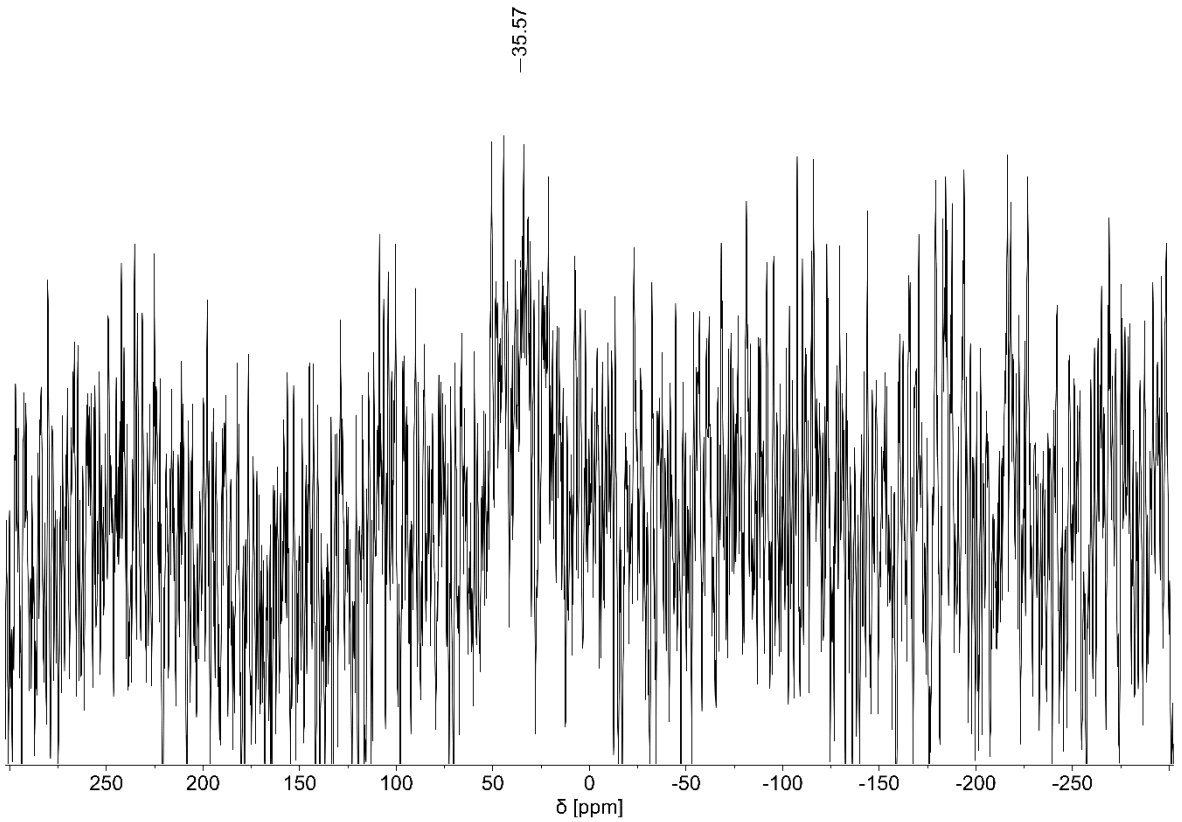

Figure S131. ^{19}F NMR spectrum of $[Tc(bpy^{COOMe2})(CO)_2(PPh_2)_2][BF_4]$.

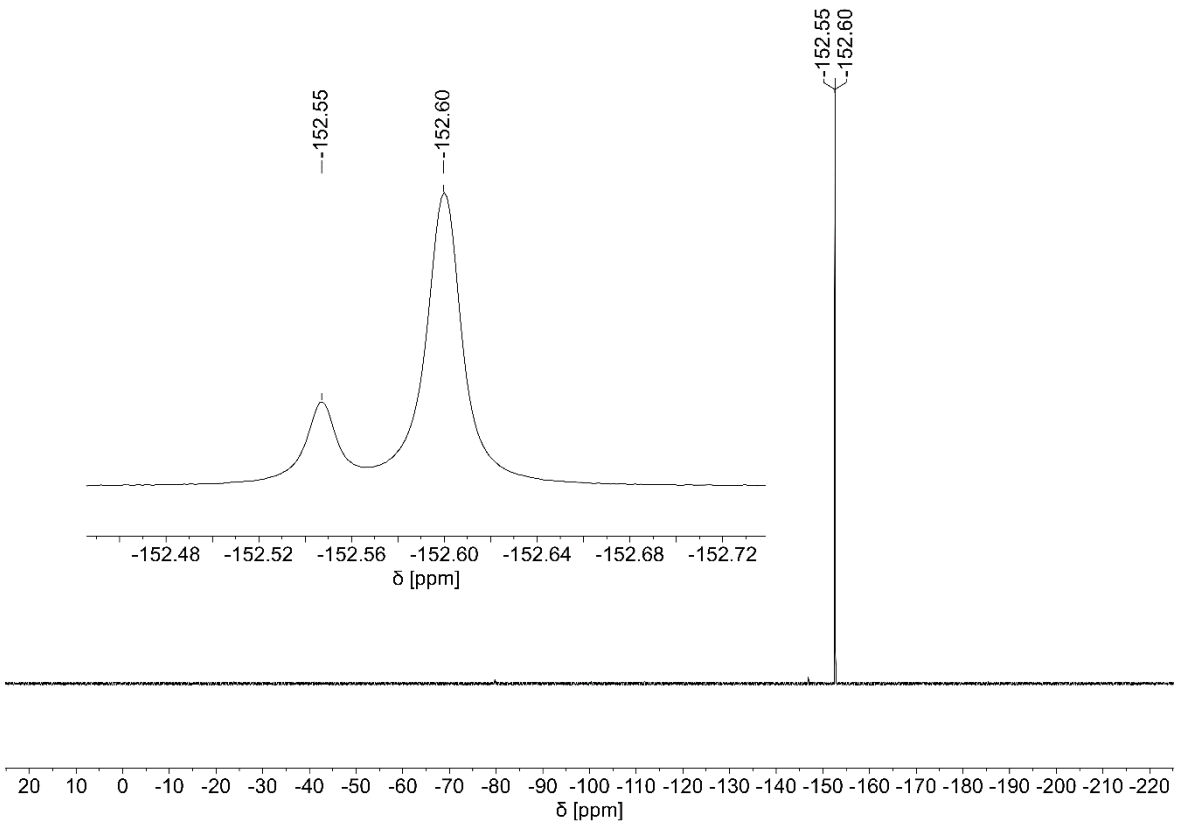

Figure S132. ^{11}B NMR spectrum of $[Tc(bpy^{COOMe2})(CO)_2(PPh_2)_2][BF_4]$.

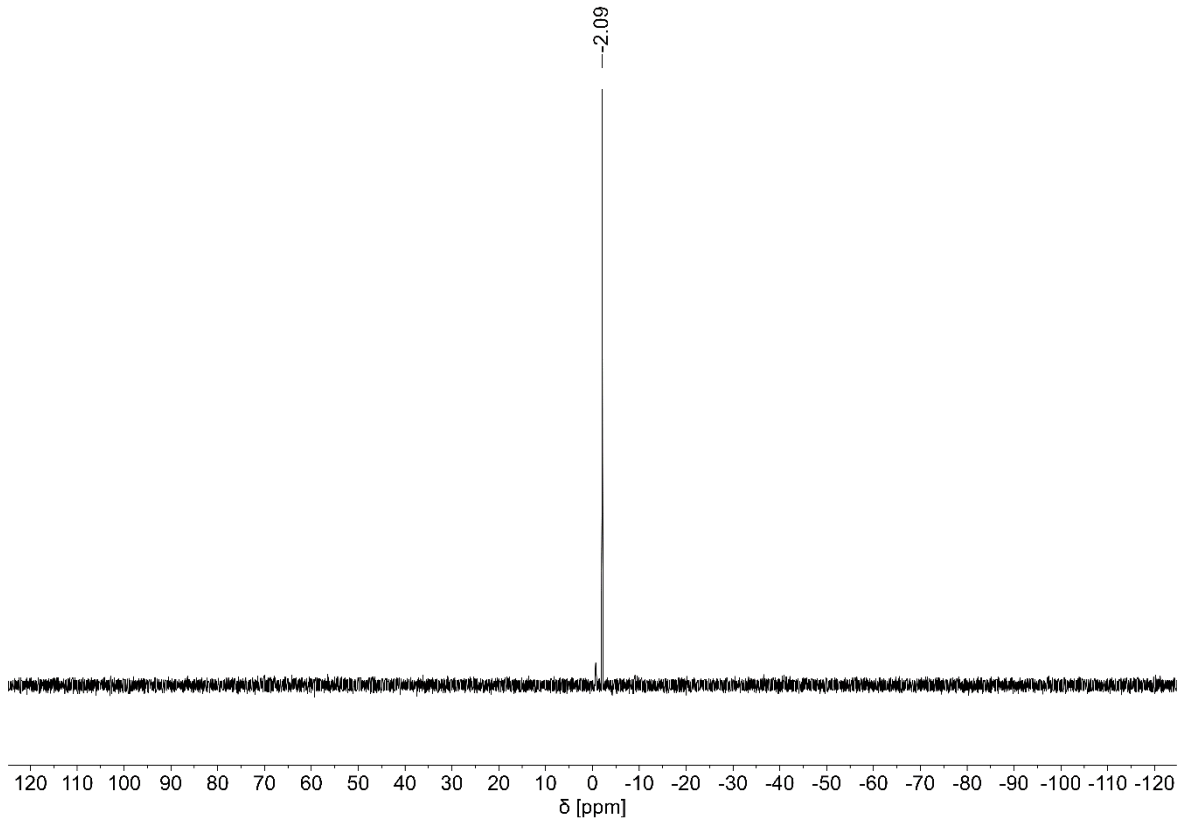

Figure S133. IR spectrum of $[Tc(bpy^{COOMe2})(CO)_2(PPh_2)_2][BF_4]$.

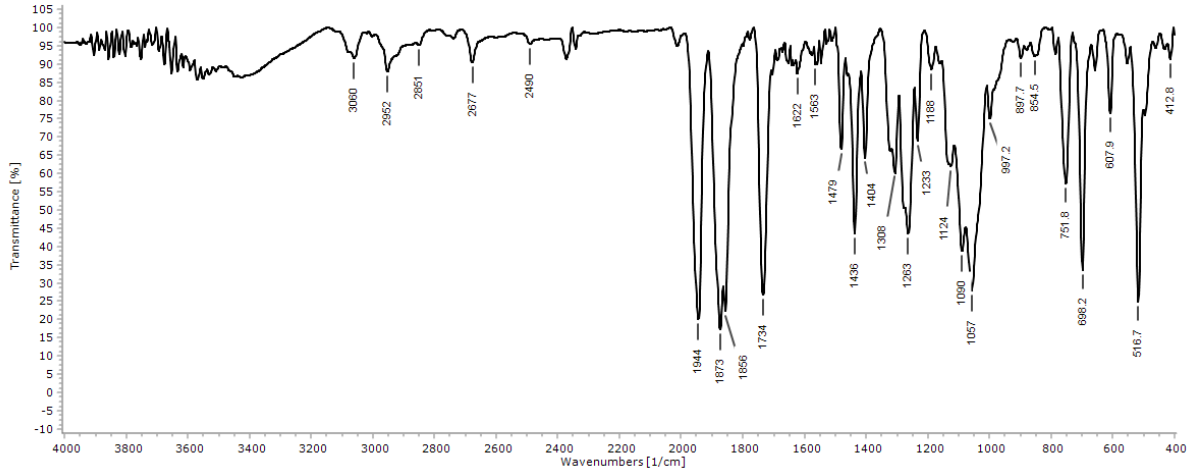

Figure S134. ^{1}H NMR spectrum of $[Tc(SMe_2)(CO)_3(PPh_3)_2][BF_4]$.

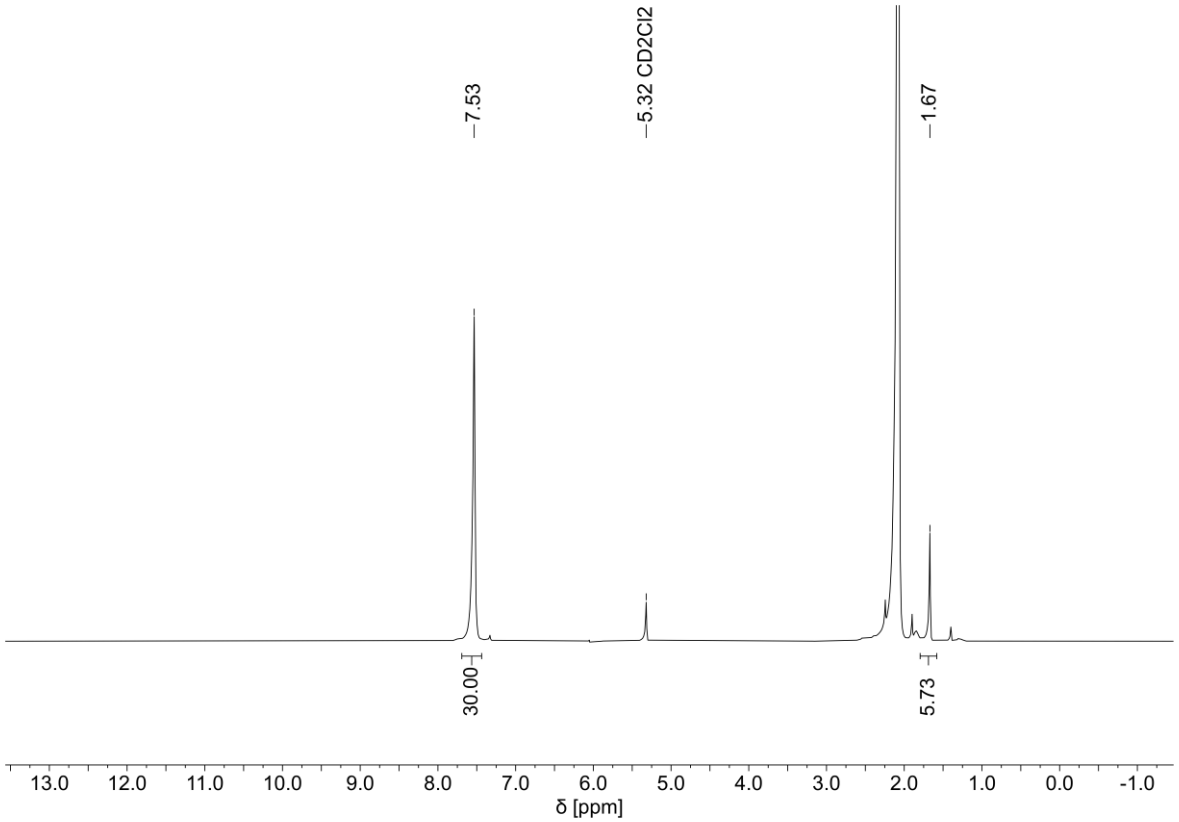

Figure S135. ^{1}H NMR spectrum of $[Tc(SMe_2)(CO)_3(PPh_3)_2][BF_4]$ before and after addition of excess SMe_2.

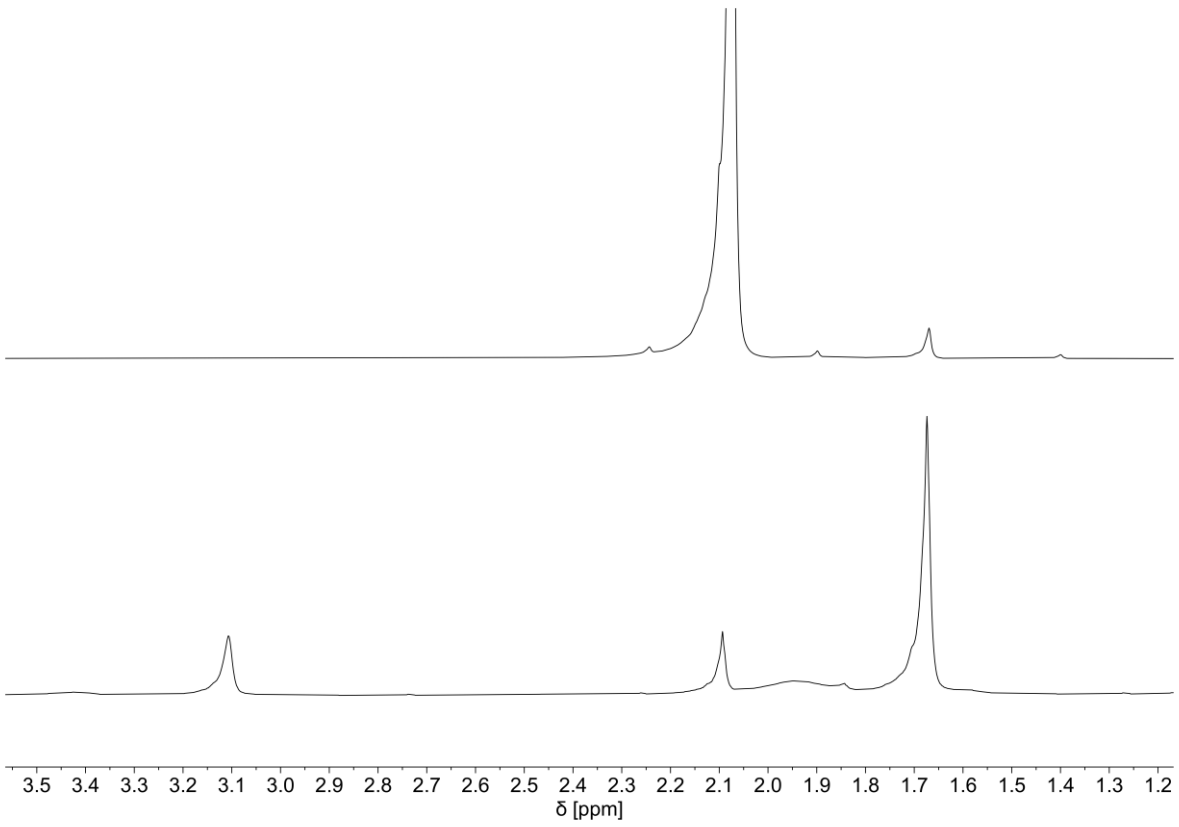

Figure S136. ^{99}Tc NMR spectrum of $[Tc(SMe_2)(CO)_3(PPh_3)_2][BF_4]$.

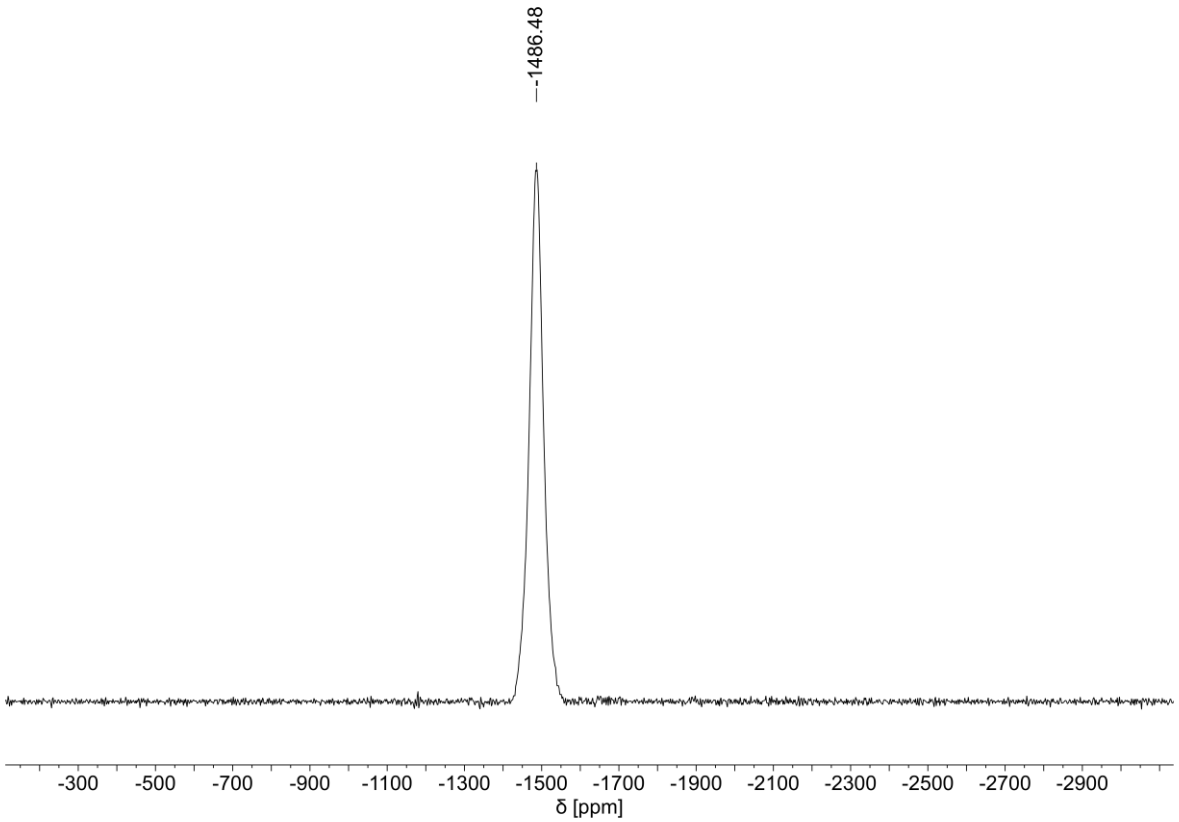

Figure S137. ^{99}Tc NMR spectrum of $[Tc(SMe_2)(CO)_3(PPh_3)_2][BF_4]$ before and after addition of excess SMe_2.

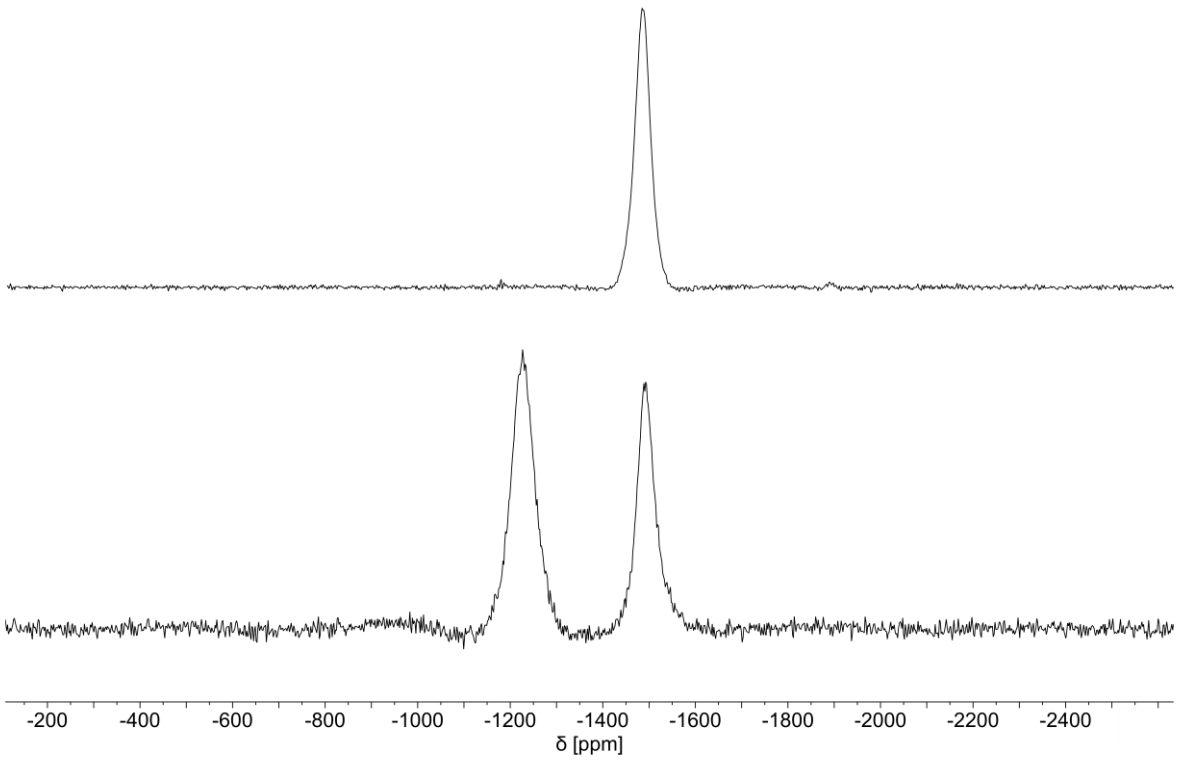

Figure S138. $^{31}P\{^{1}H\}$ NMR spectrum of $[Tc(SMe_2)(CO)_3(PPh_3)_2][BF_4]$.

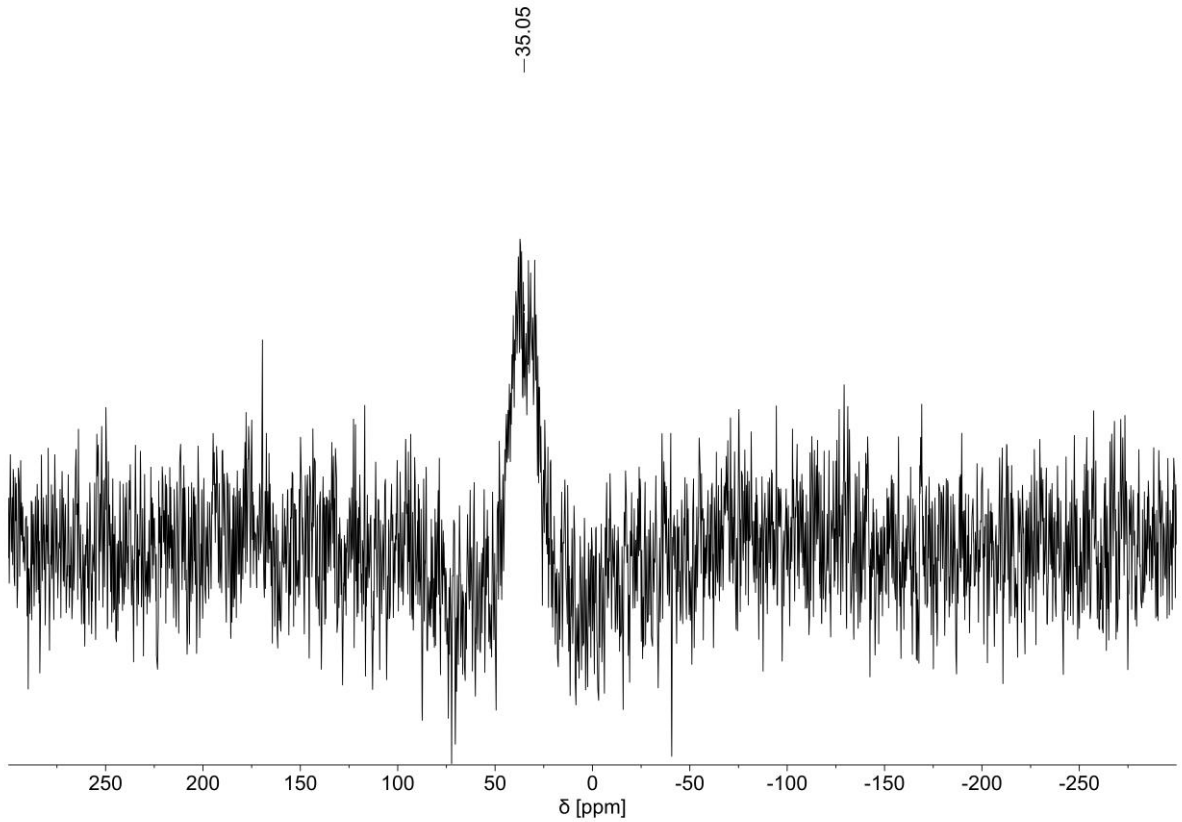

Figure S139. ^{19}F NMR spectrum of $[Tc(SMe_2)(CO)_3(PPh_3)_2][BF_4]$.

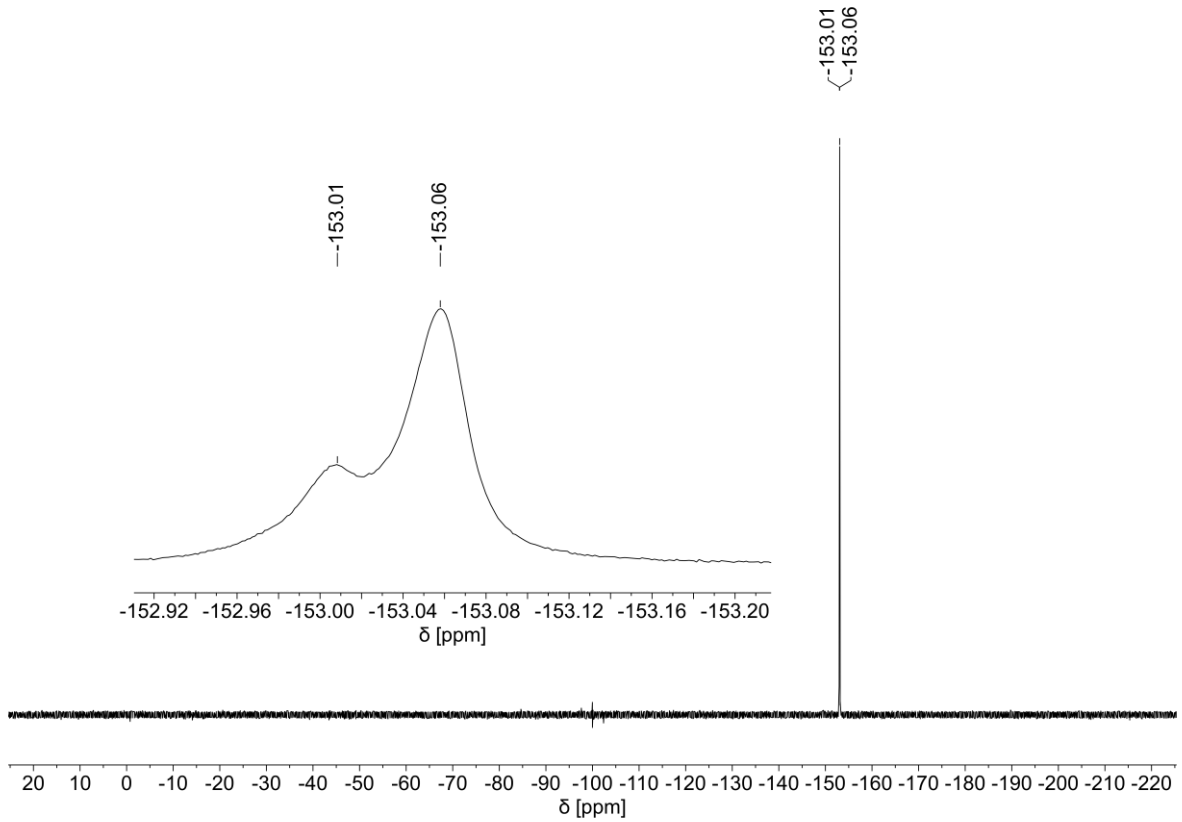

Figure S140. ^{11}B NMR spectrum of $[Tc(SMe_2)(CO)_3(PPh_3)_2][BF_4]$.

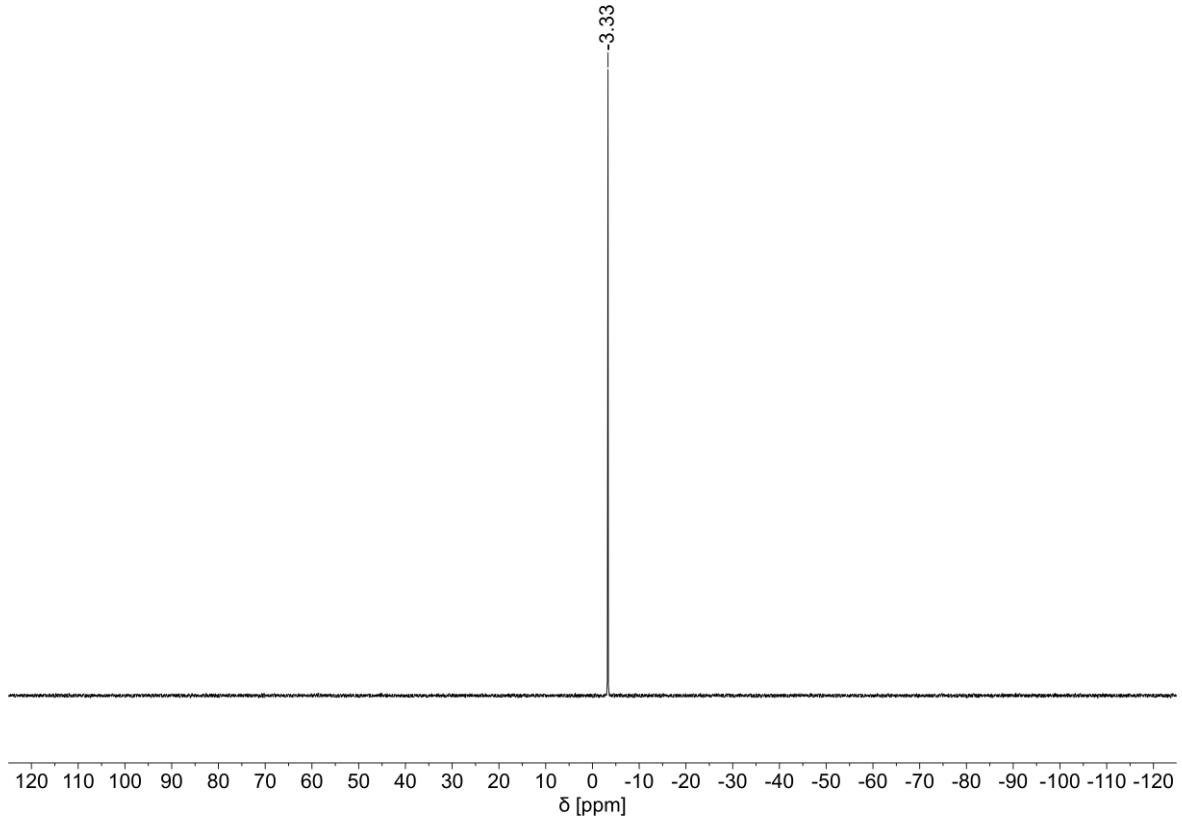

Figure S141. IR spectrum of $[Tc(SMe_2)(CO)_3(PPh_3)_2][BF_4]$.

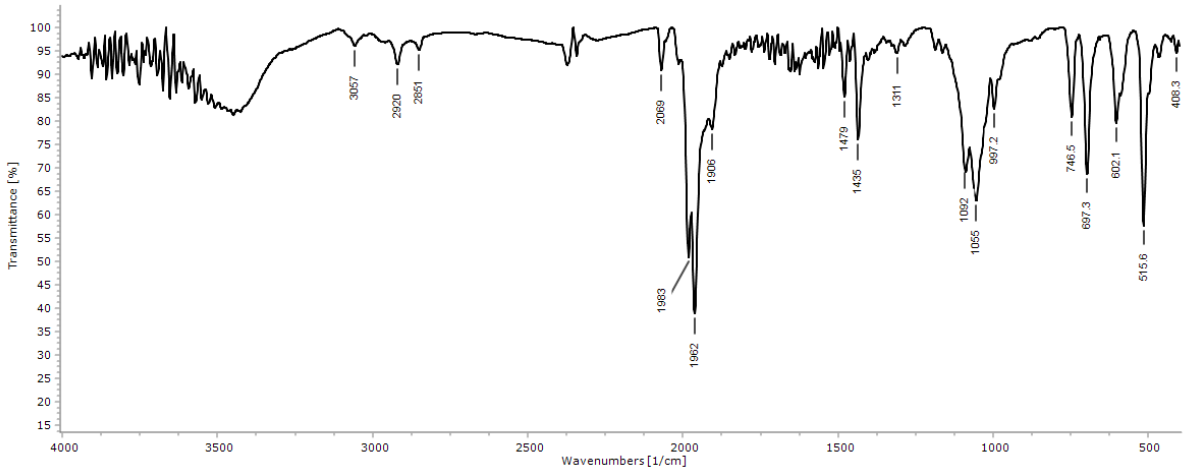

Figure S142. ^{1}H NMR spectrum of $[Tc(SEt_2)(CO)_3(PPh_3)_2][BF_4]$ before the addition of excess SEt_2.

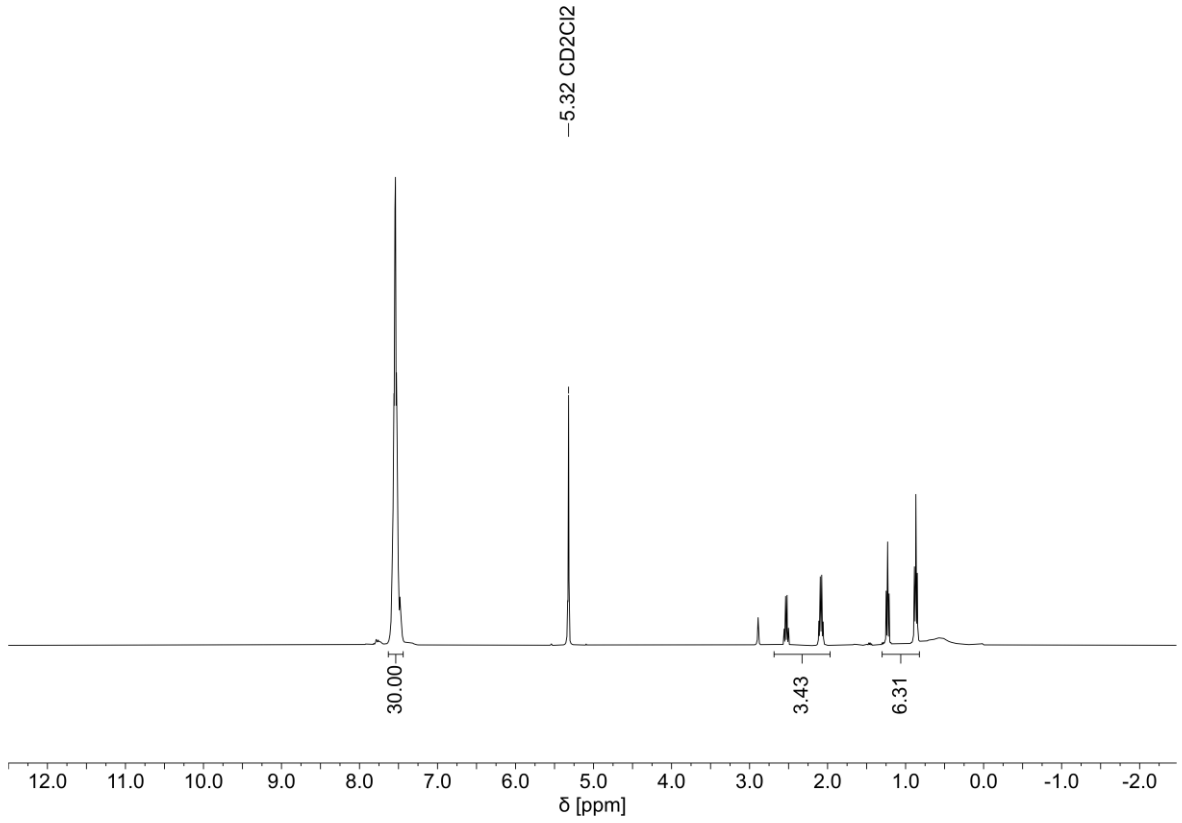

Figure S143. ^{1}H NMR spectrum of $[Tc(SEt_2)(CO)_3(PPh_3)_2][BF_4]$ after the addition of excess SEt_2.

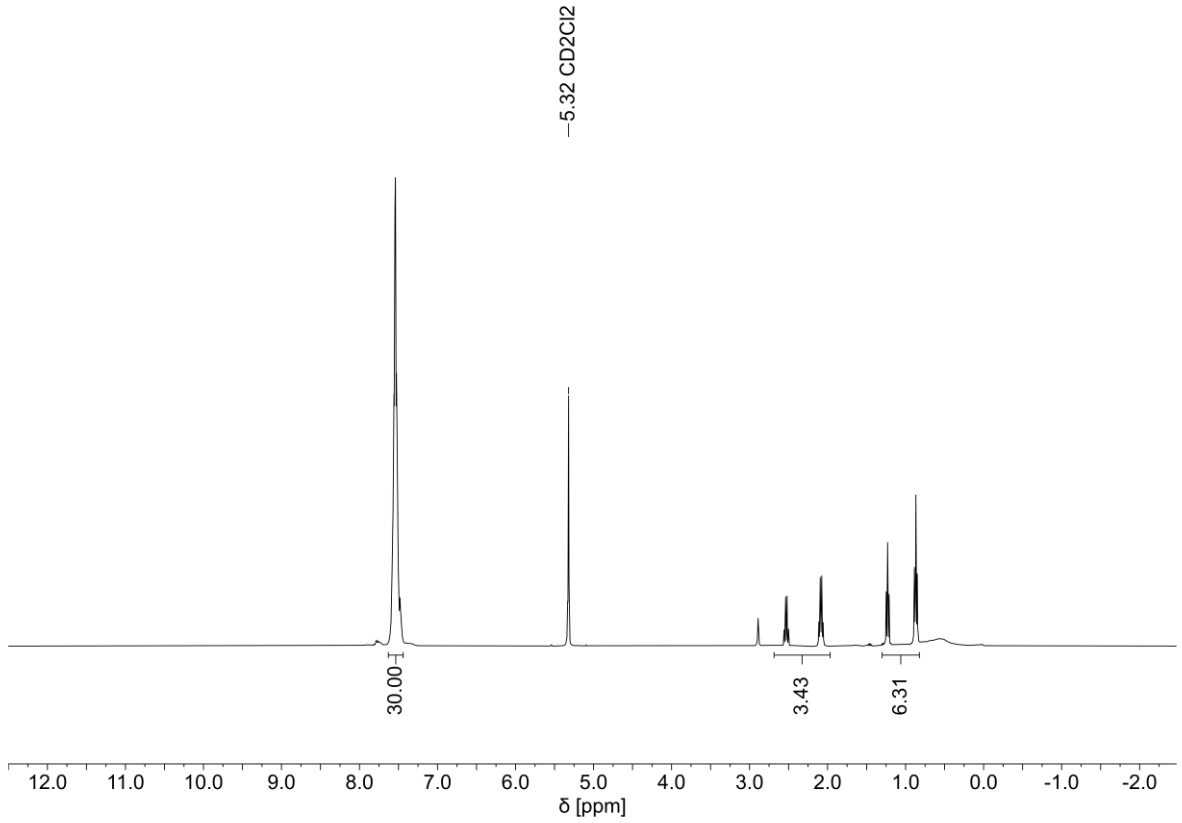

Figure S144. ^{99}Tc NMR spectrum of $[Tc(SEt_2)(CO)_3(PPh_3)_2][BF_4]$.

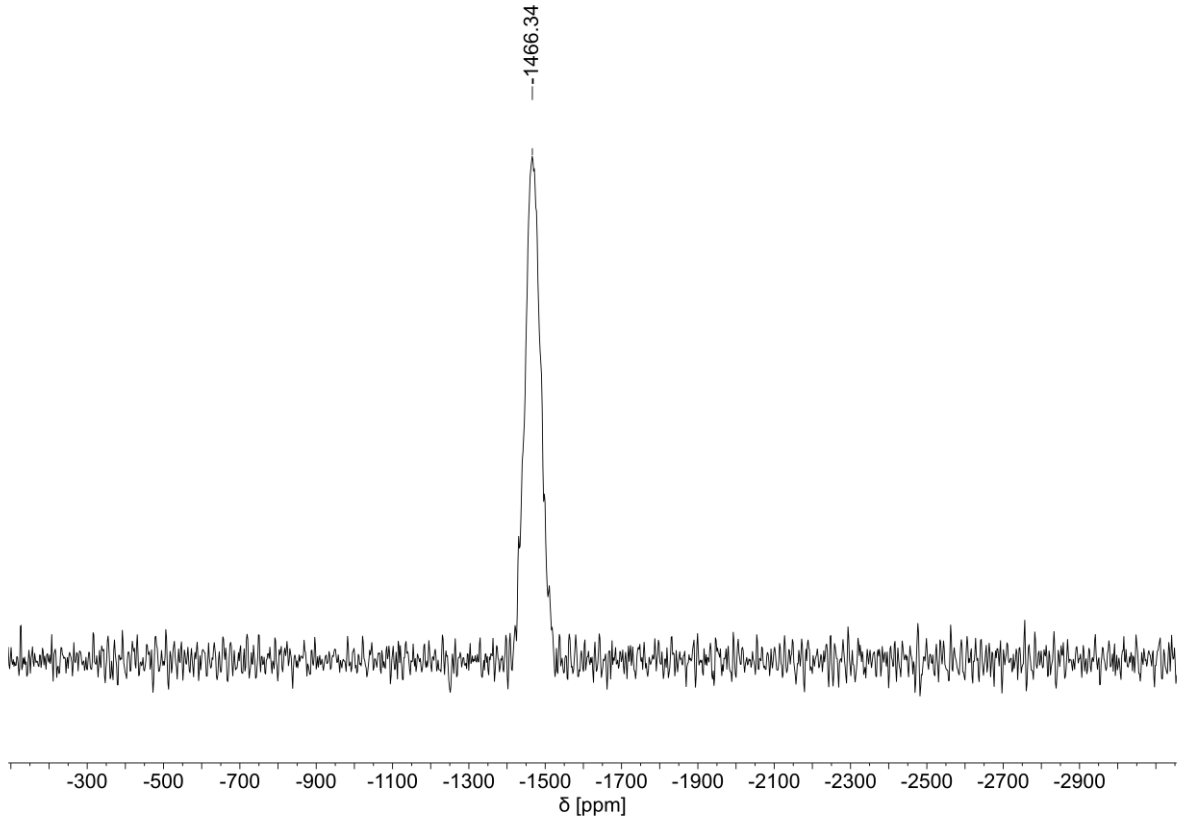

Figure S145. $^{31}P\{^1H\}$ NMR spectrum of $[Tc(SEt_2)(CO)_3(PPh_3)_2][BF_4]$.

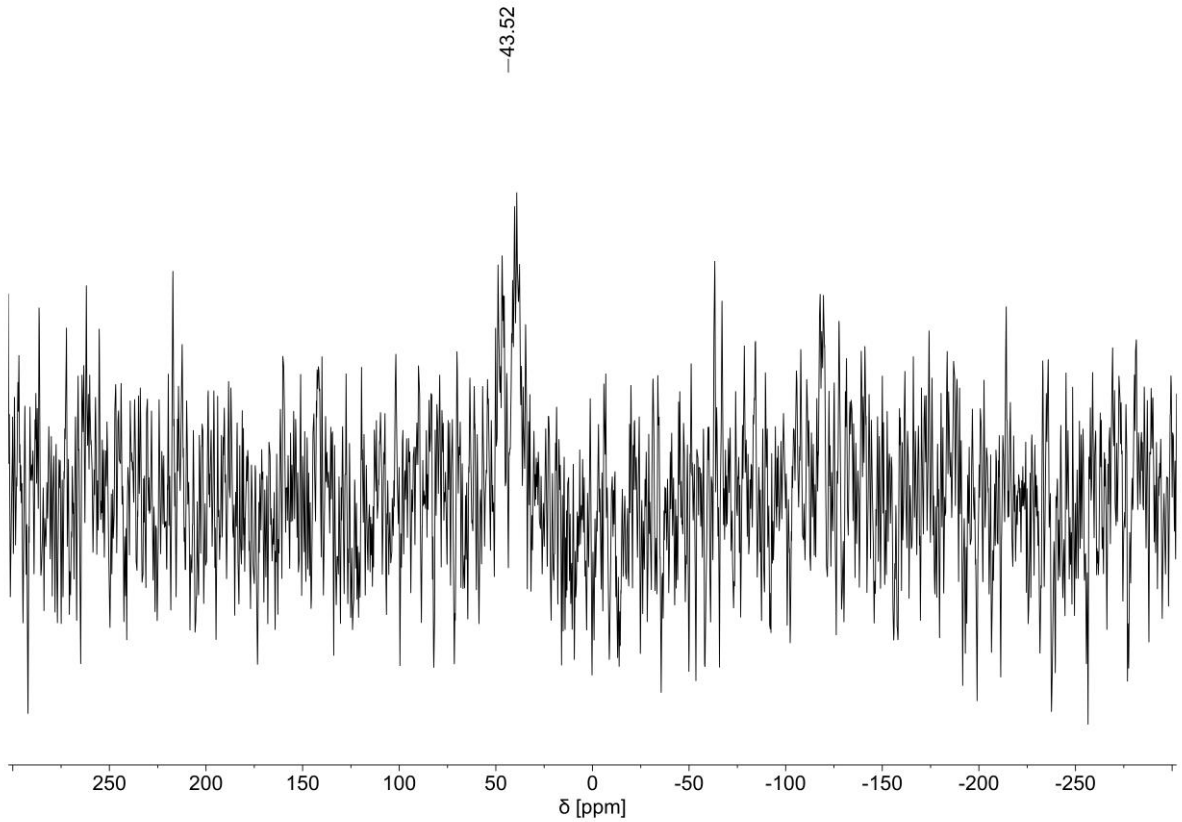

Figure S146. ^{19}F NMR spectrum of $[Tc(SEt_2)(CO)_3(PPh_3)_2][BF_4]$.

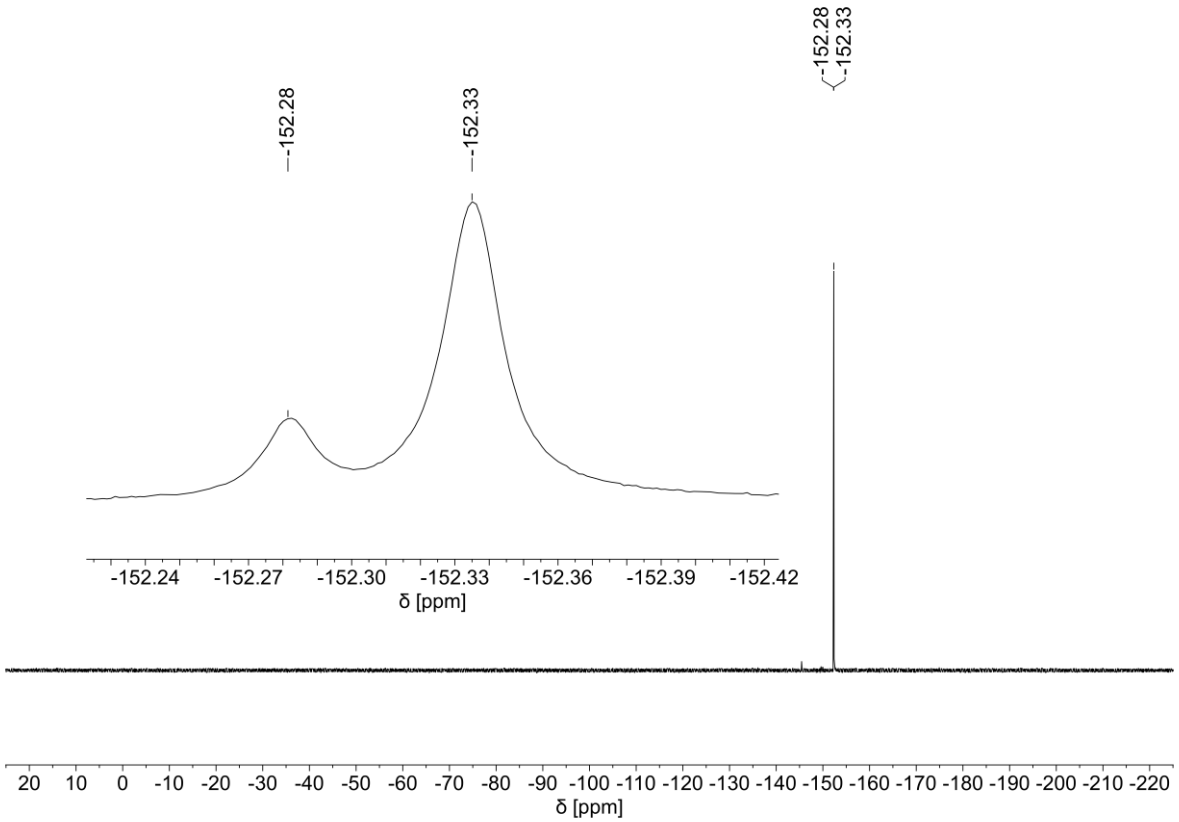

Figure S147. ^{11}B NMR spectrum of $[Tc(SEt_2)(CO)_3(PPh_3)_2][BF_4]$.

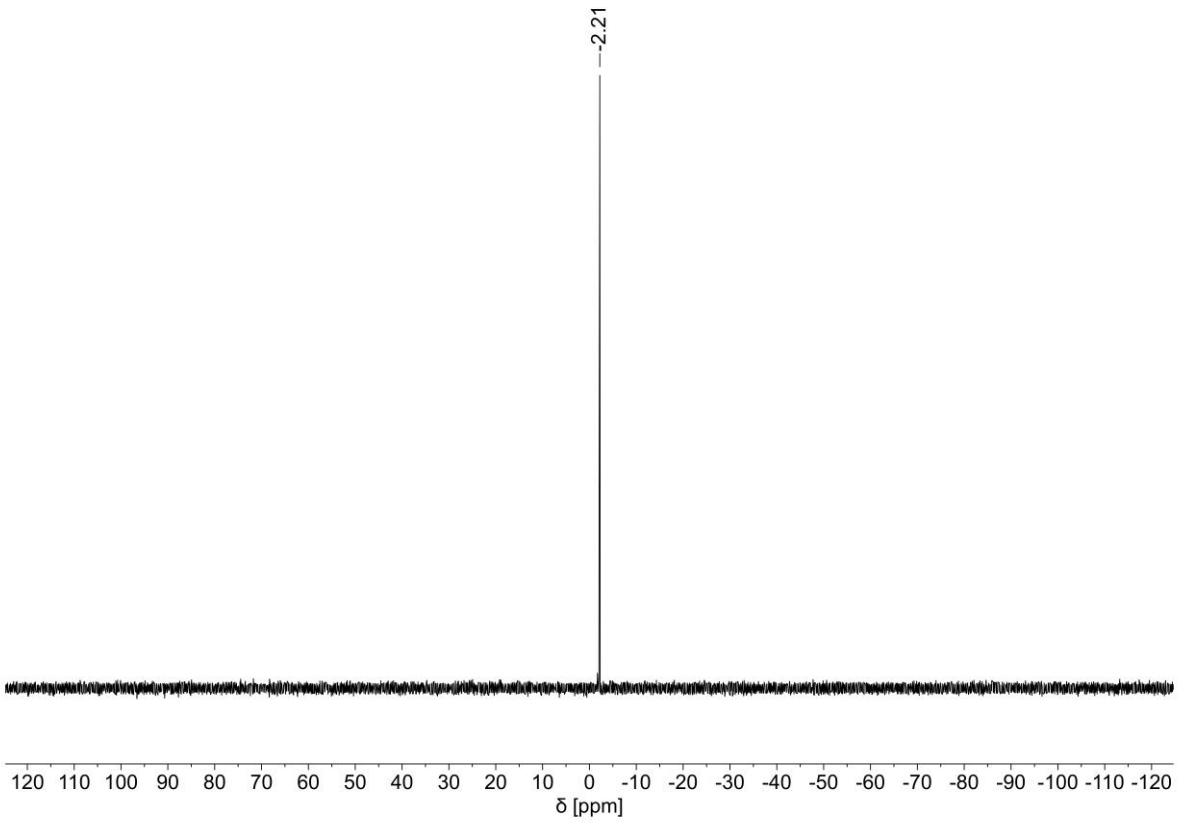

Figure S148. IR spectrum of $[Tc(SEt_2)(CO)_3(PPh_3)_2][BF_4]$.

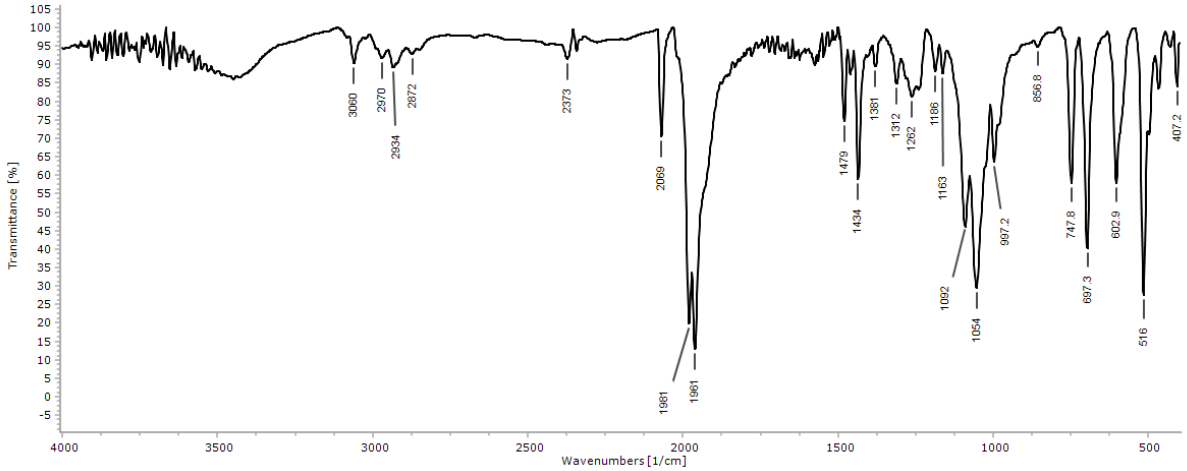

Figure S149. ^1H NMR spectrum of $[Tc(tht)(CO)_3(PPh_3)_2][BF_4]$.

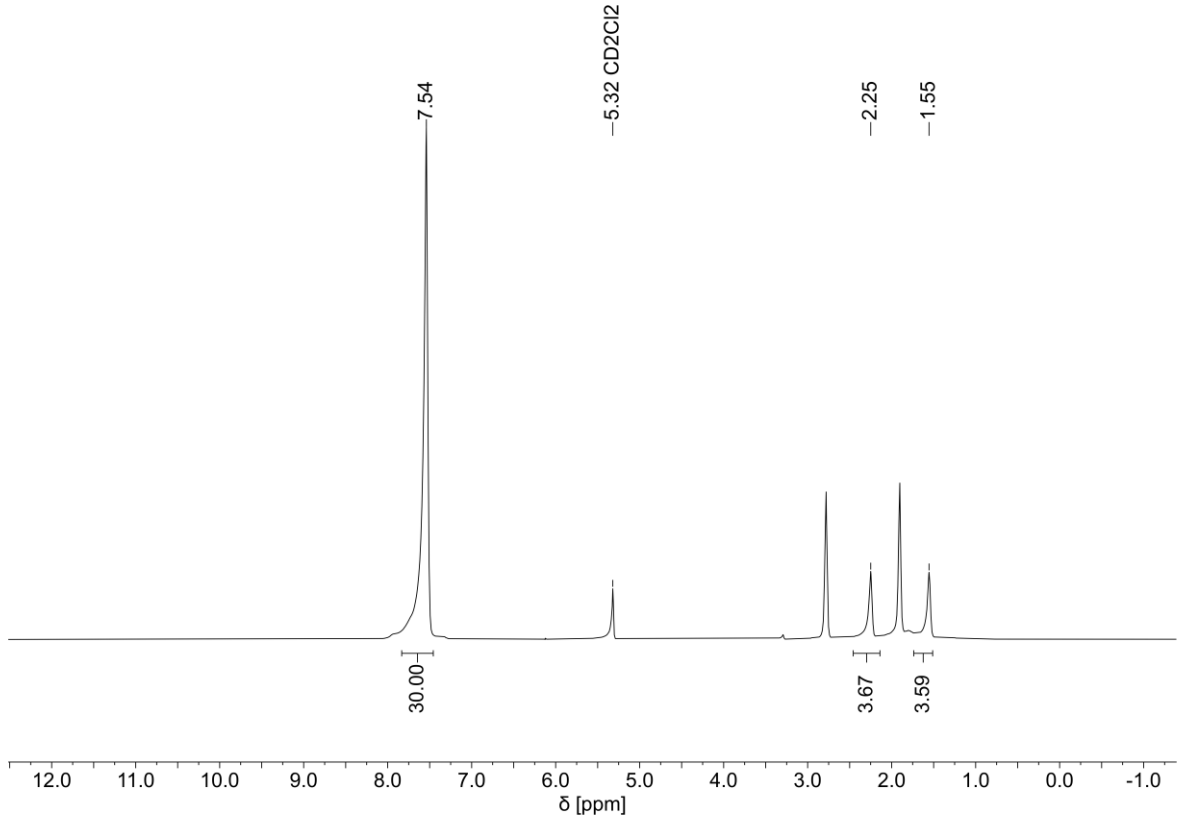

Figure S150. ^{99}Tc NMR spectrum of [Tc(tht)(CO)$_3$(PPh$_3$)$_2$][BF$_4$].

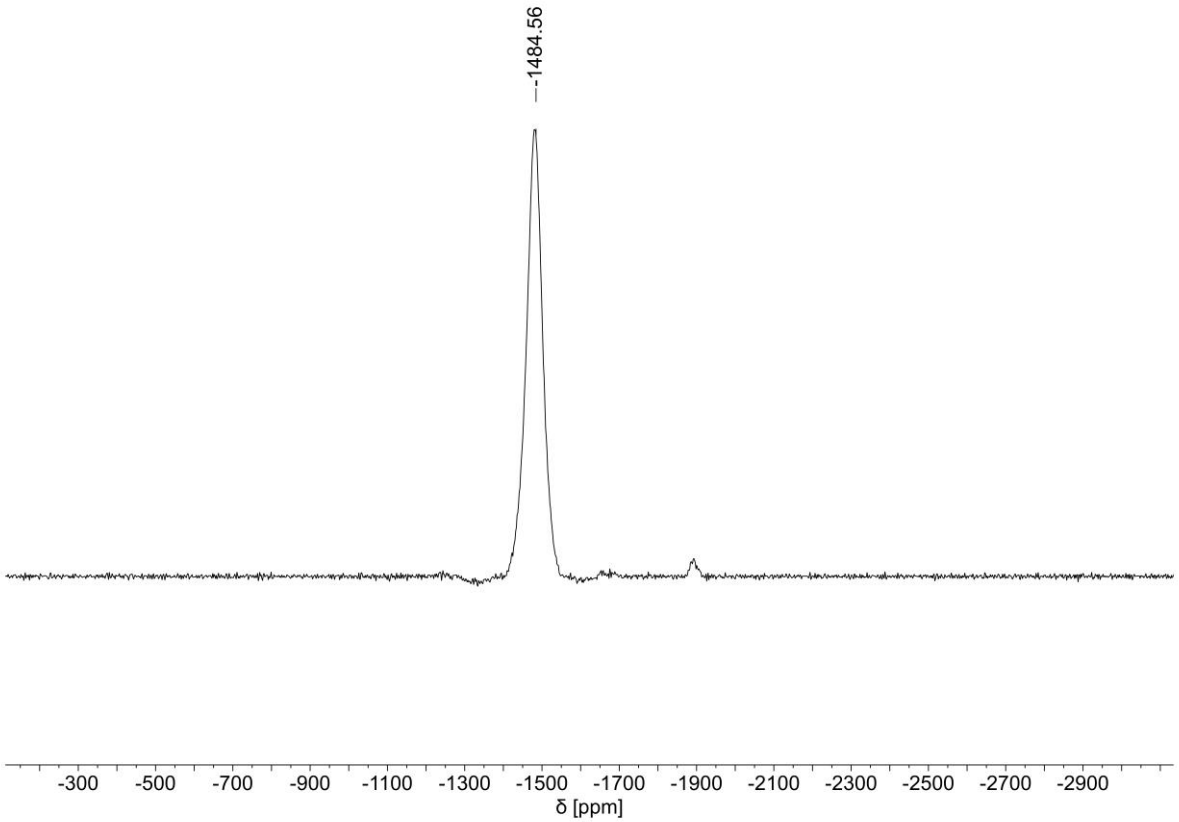

Figure S151. ^{31}P{^{1}H} NMR spectrum of [Tc(tht)(CO)$_3$(PPh$_3$)$_2$][BF$_4$].

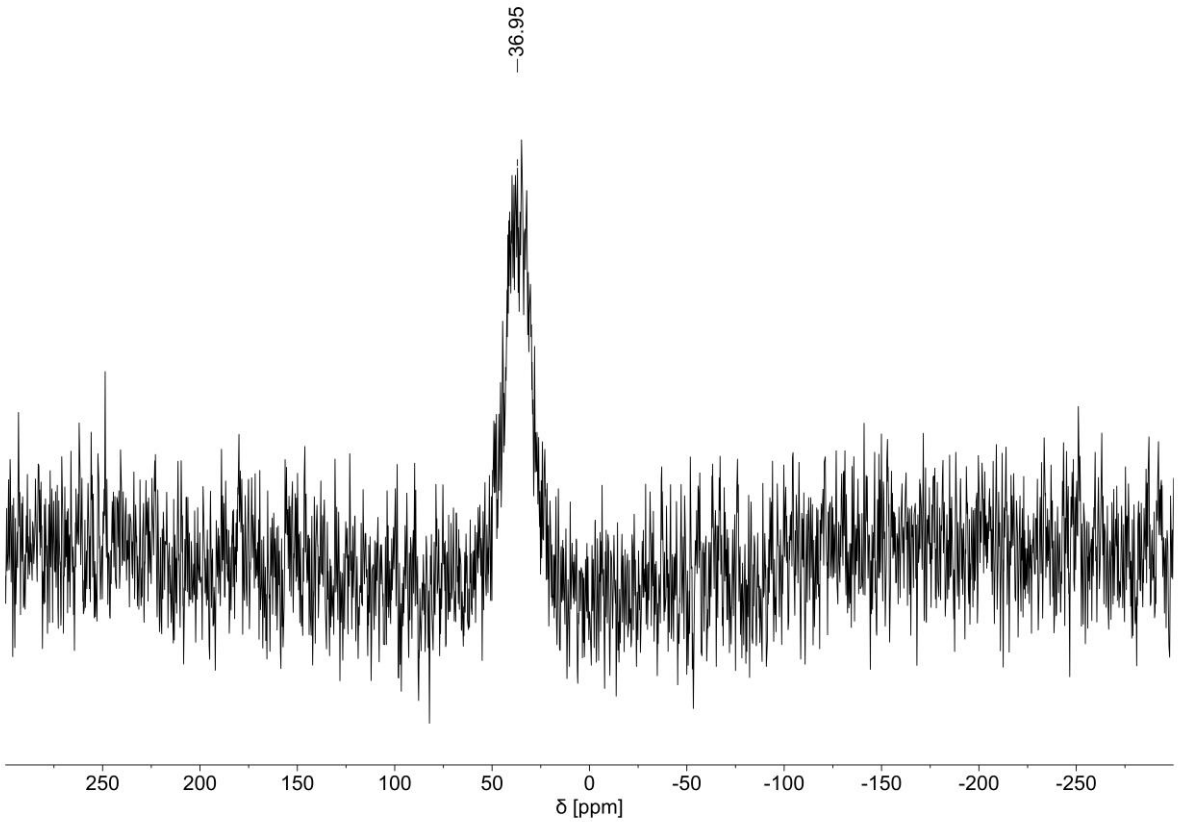

Figure S152. ^{19}F NMR spectrum of $[Tc(tht)(CO)_3(PPh_3)_2][BF_4]$.

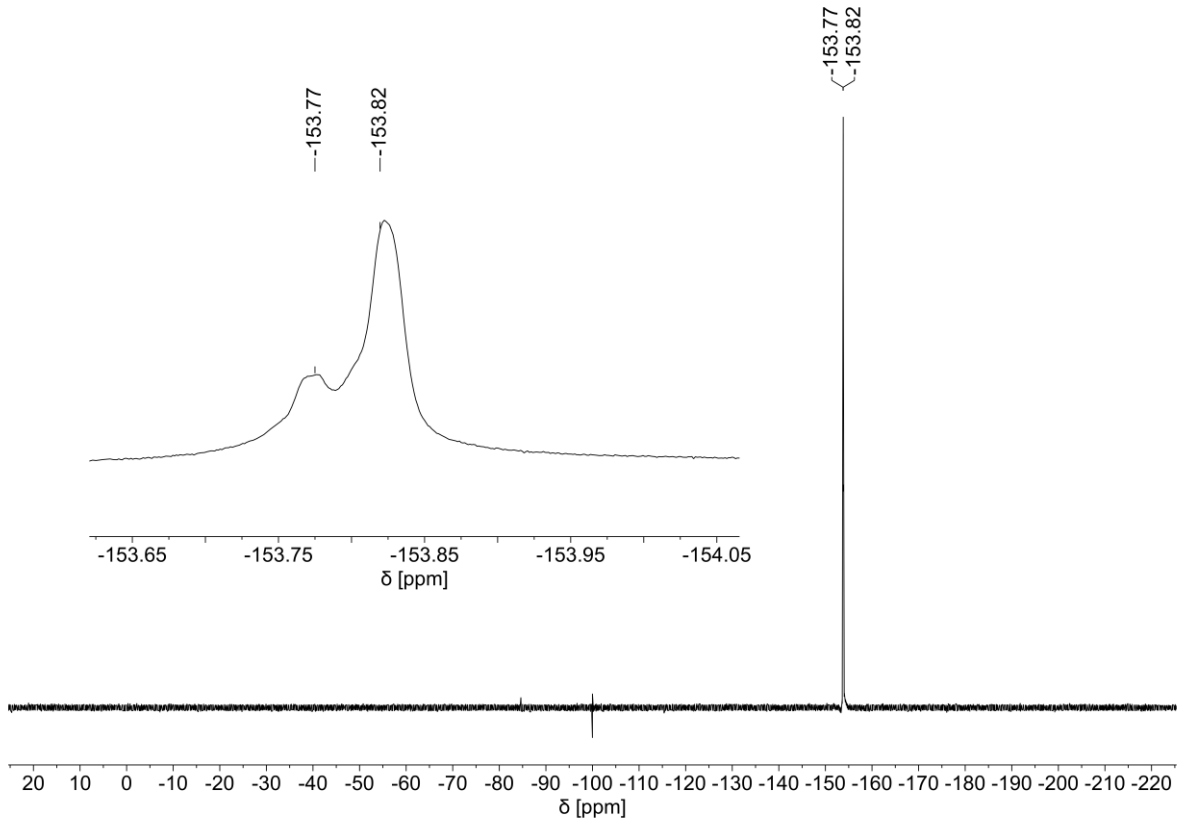

Figure S153. ^{11}B NMR spectrum of $[Tc(tht)(CO)_3(PPh_3)_2][BF_4]$.

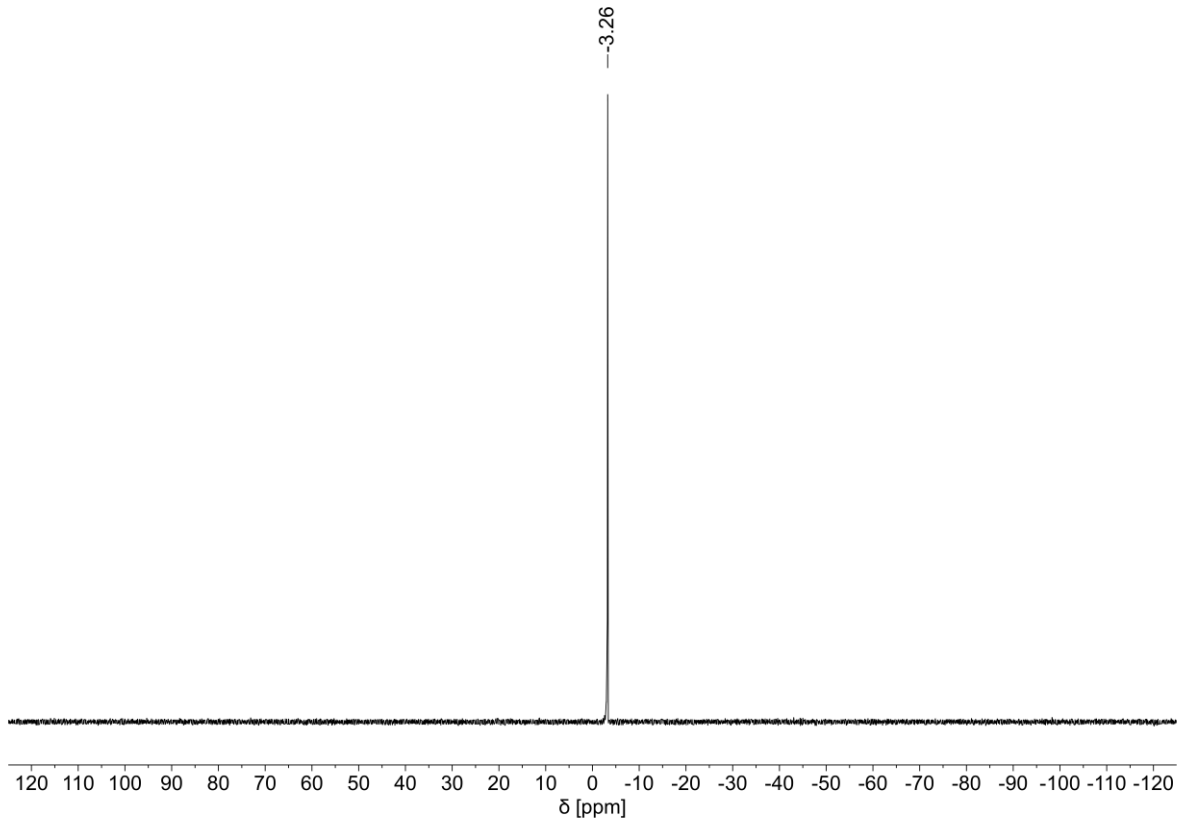

Figure S154. IR spectrum of $[Tc(tht)(CO)_3(PPh_3)_2][BF_4]$.

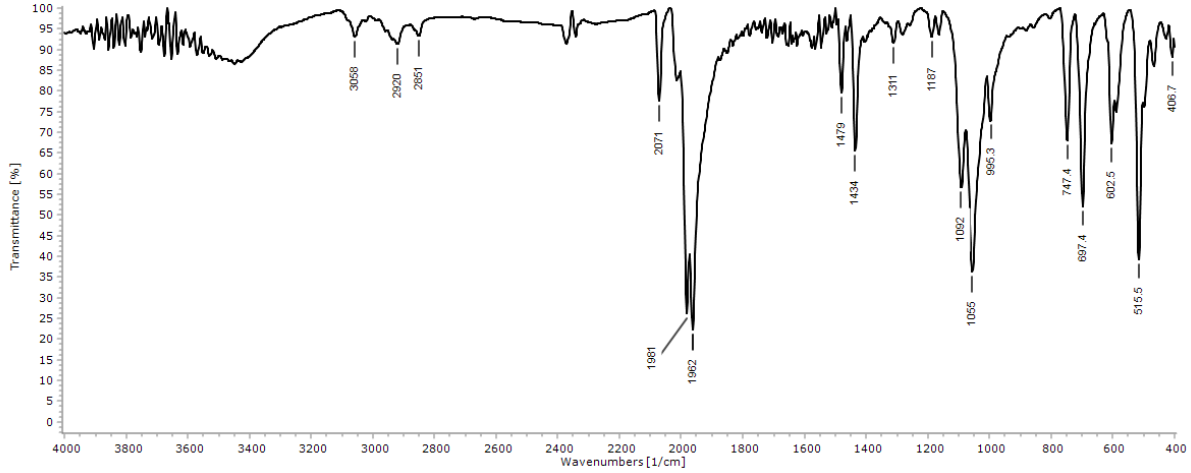

Figure S155. ^1H NMR spectrum of $[Tc(SeMe_2)(CO)_3(PPh_3)_2][BF_4]$.

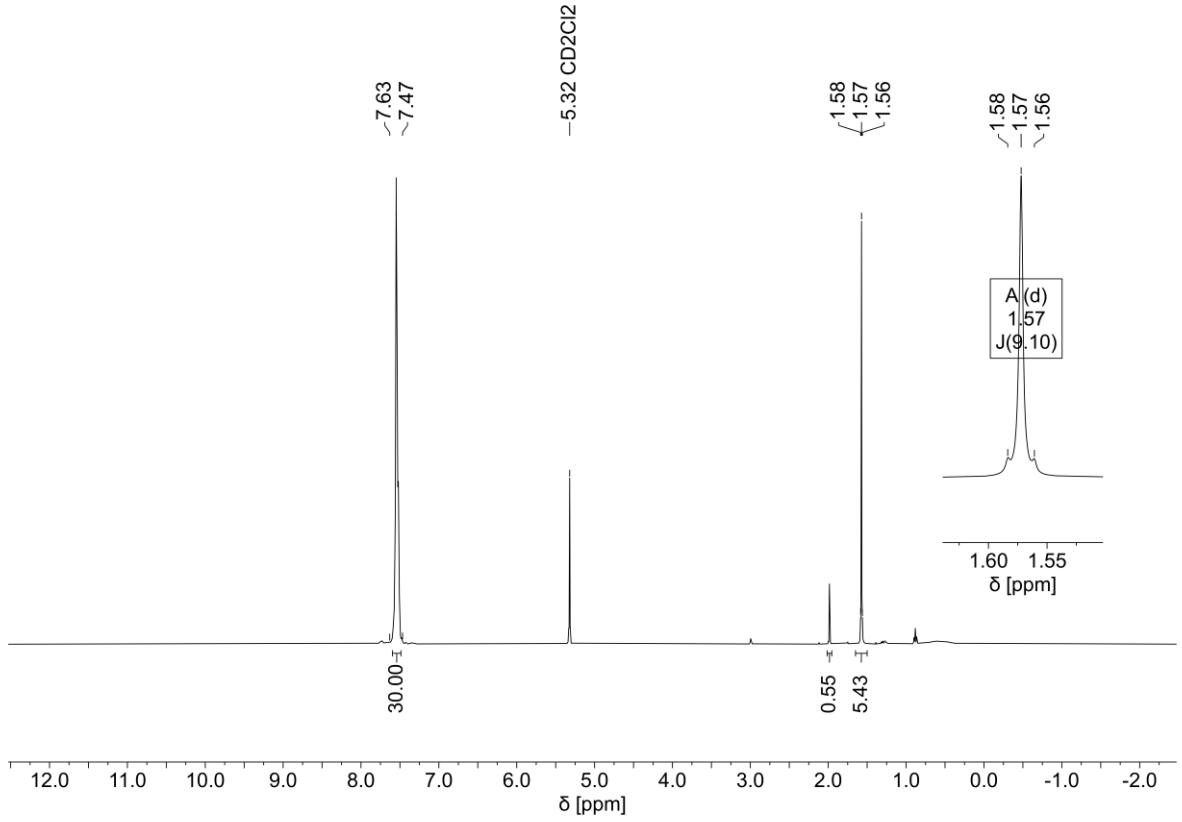

Figure S156. ^{99}Tc NMR spectrum of [Tc(SeMe$_2$)(CO)$_3$(PPh$_3$)$_2$][BF$_4$].

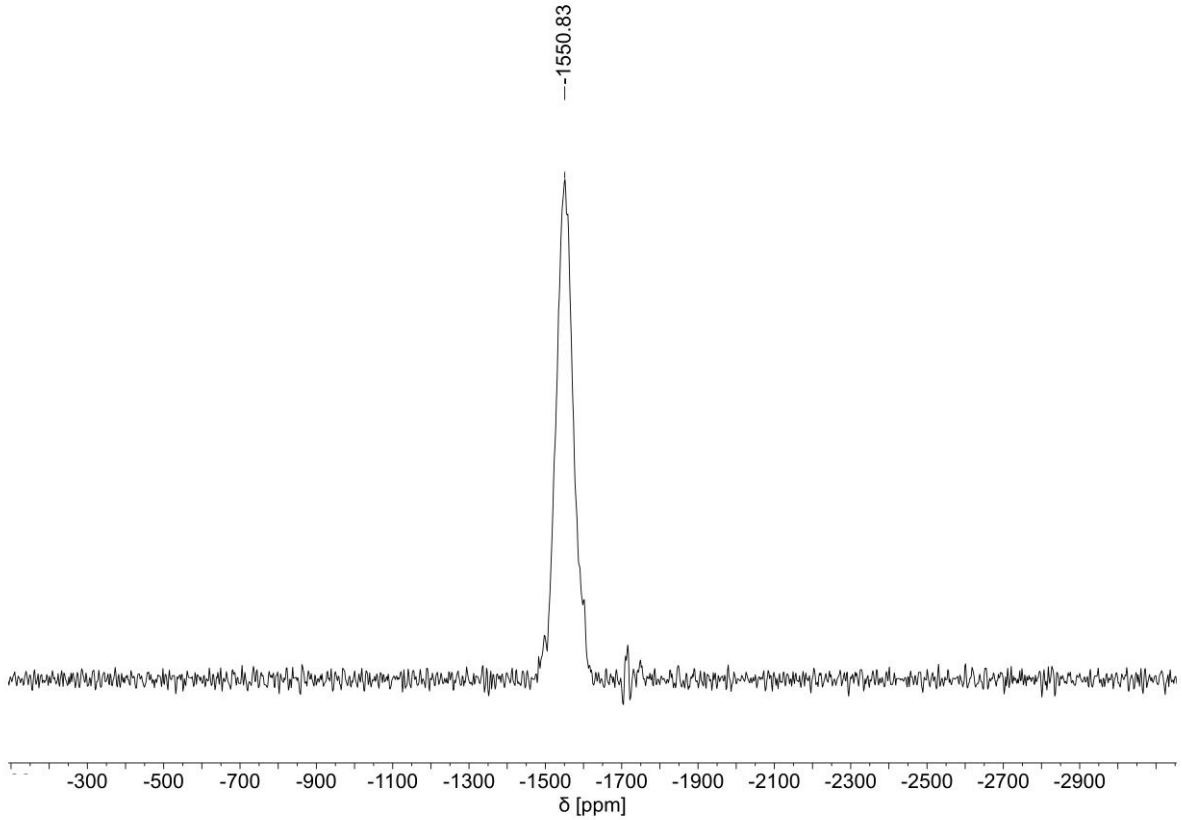

Figure S157. ^{31}P{^{1}H} NMR spectrum of [Tc(SeMe$_2$)(CO)$_3$(PPh$_3$)$_2$][BF$_4$].

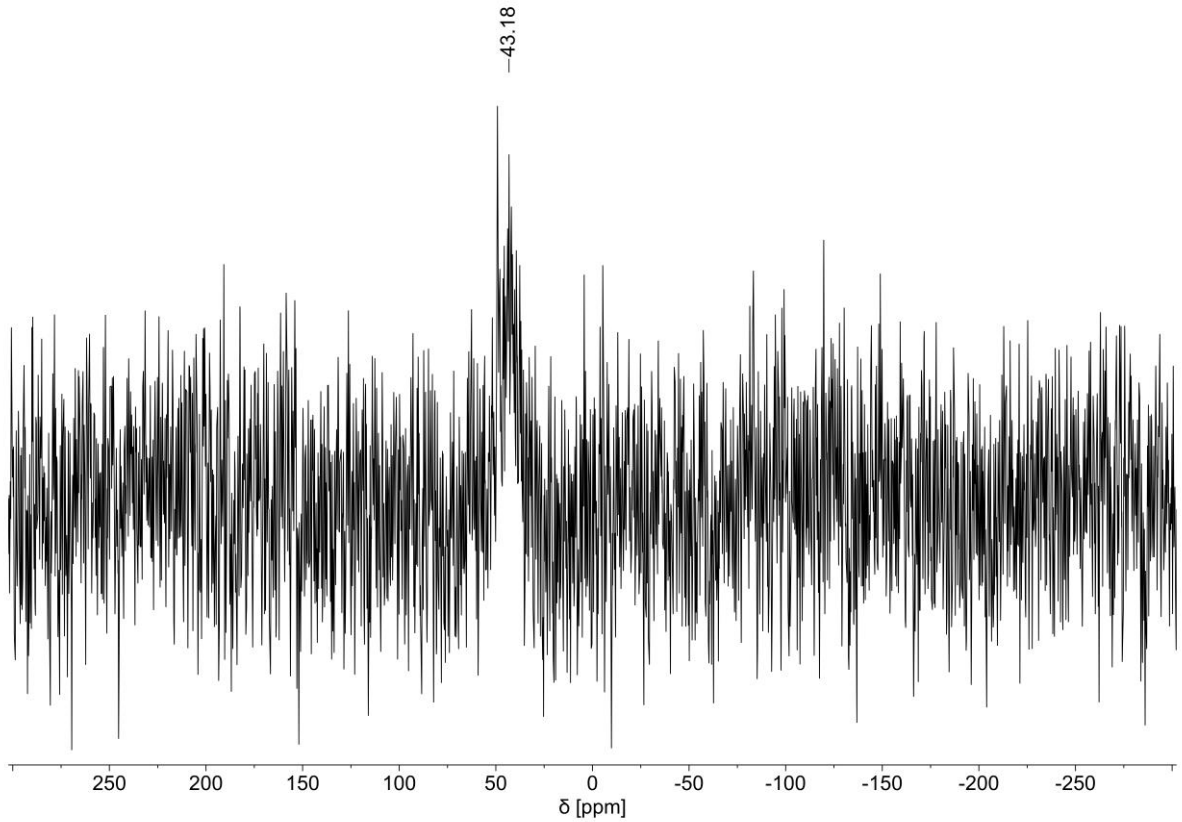

Figure S158. ^{19}F NMR spectrum of $[Tc(SeMe_2)(CO)_3(PPh_3)_2][BF_4]$.

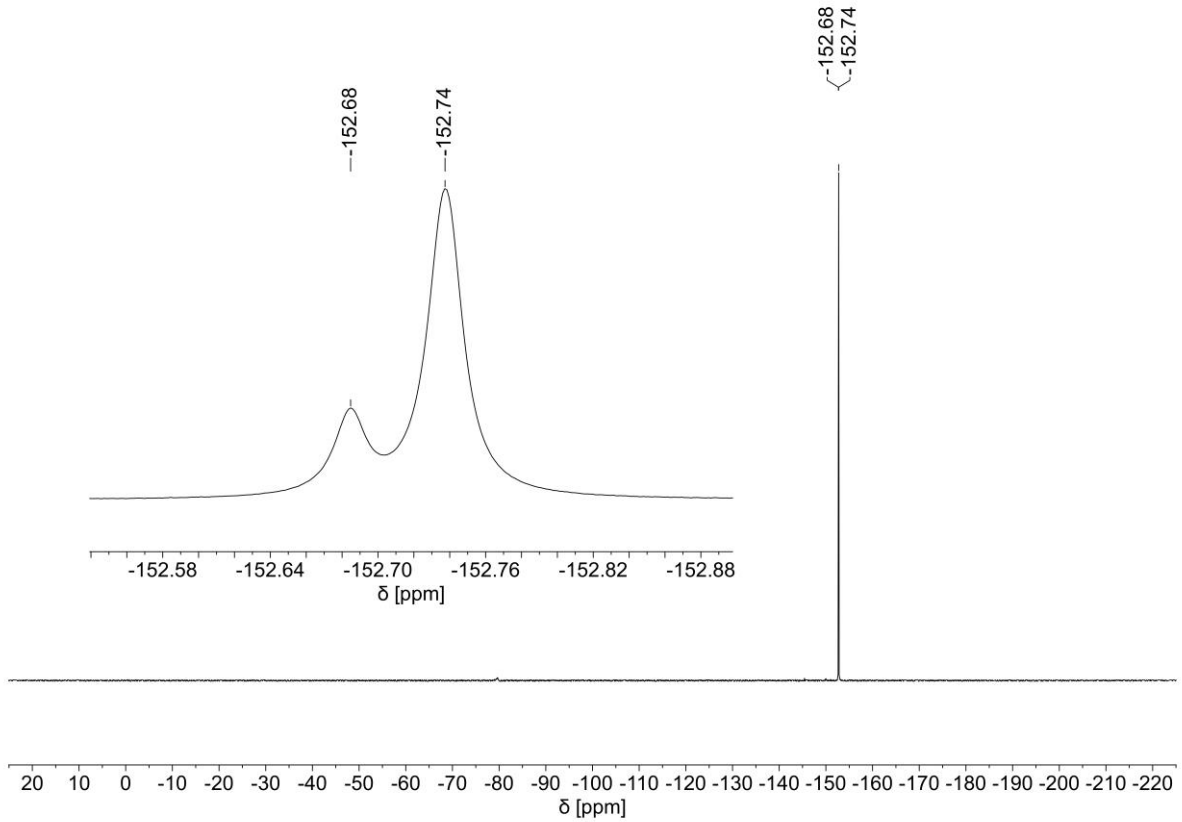

Figure S159. ^{11}B NMR spectrum of $[Tc(SeMe_2)(CO)_3(PPh_3)_2][BF_4]$.

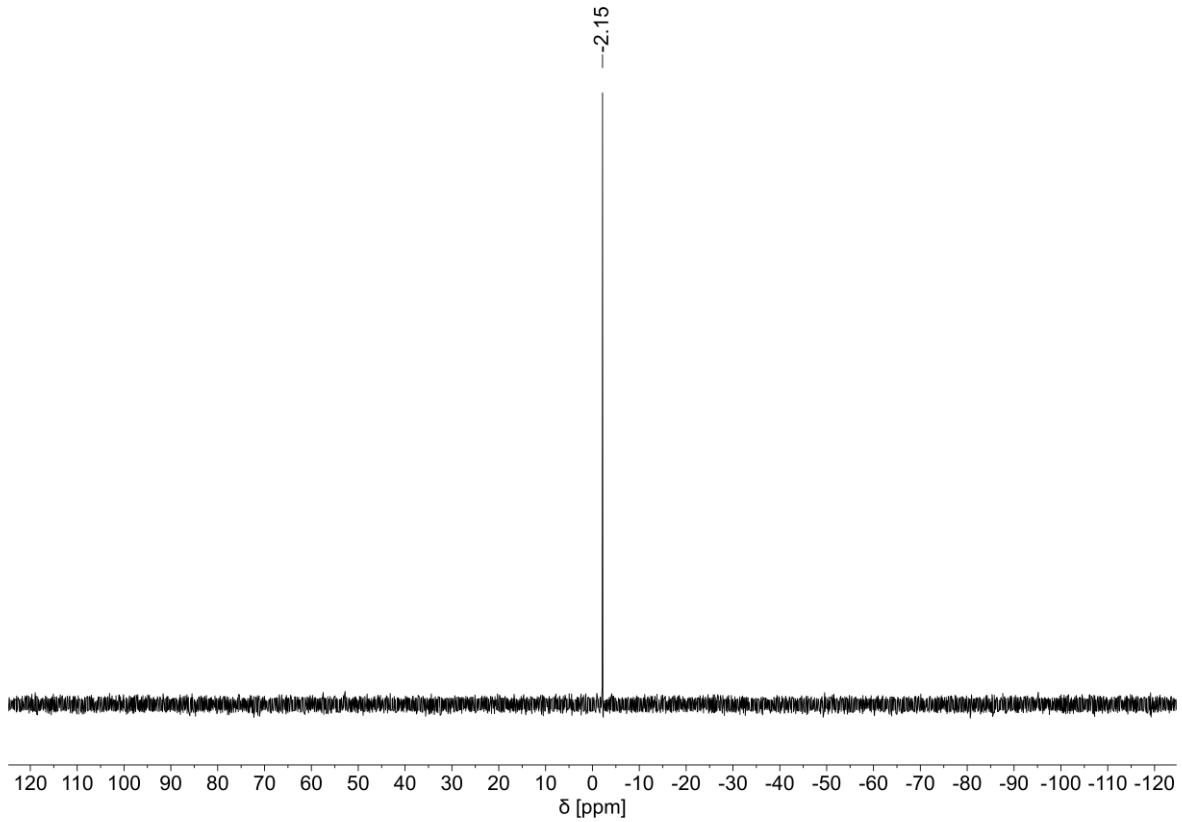

Figure S160. IR spectrum of $[Tc(SeMe_2)(CO)_3(PPh_3)_2][BF_4]$.

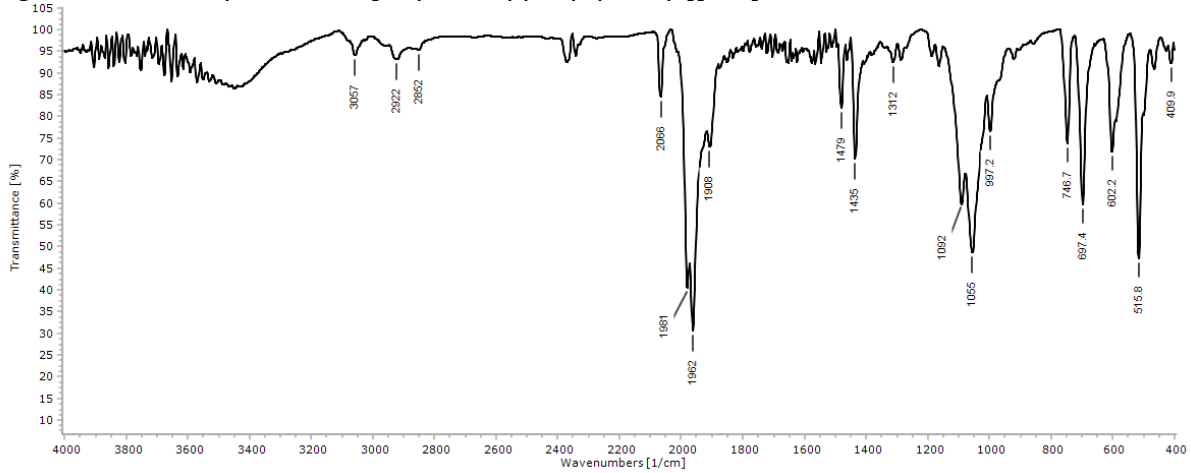

Figure S161. ^1H NMR spectrum of $[Tc(thse)(CO)_3(PPh_3)_2][BF_4]$.

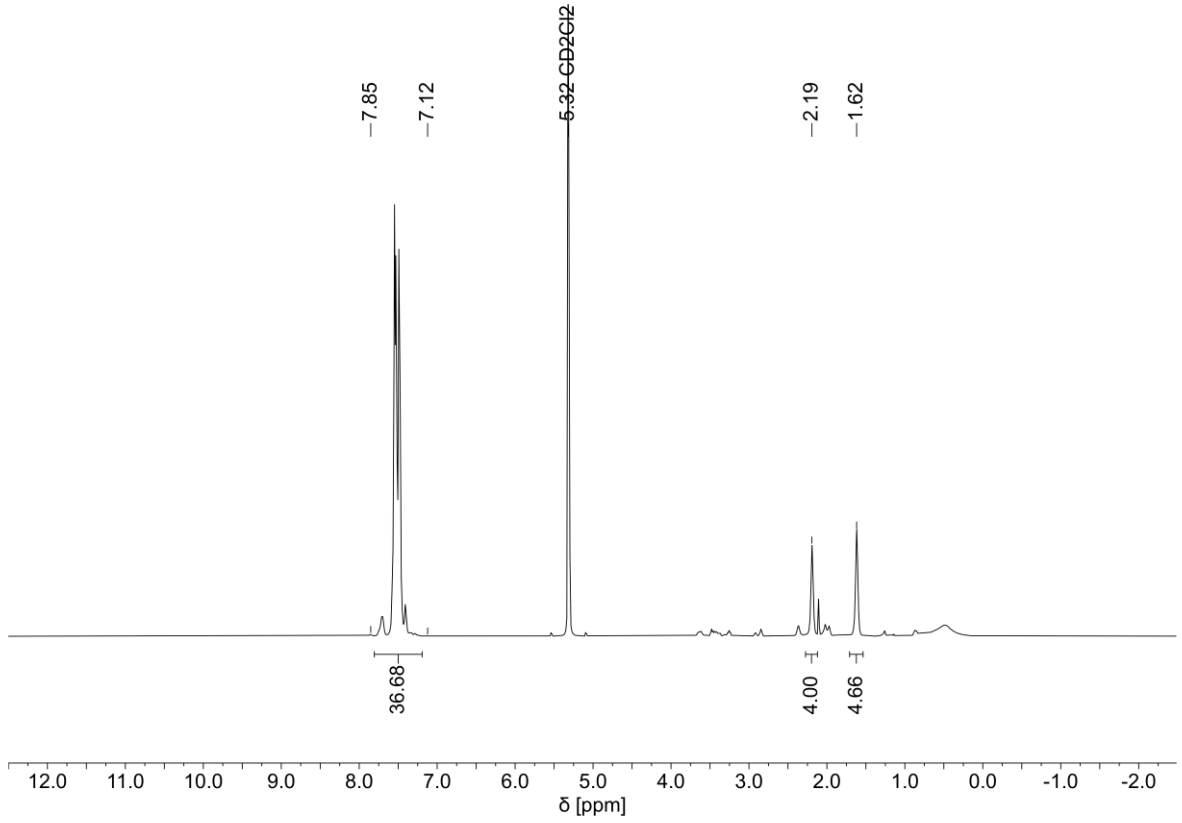

Figure S162. ^{99}Tc NMR spectrum of [Tc(thse)(CO)$_3$(PPh$_3$)$_2$][BF$_4$].

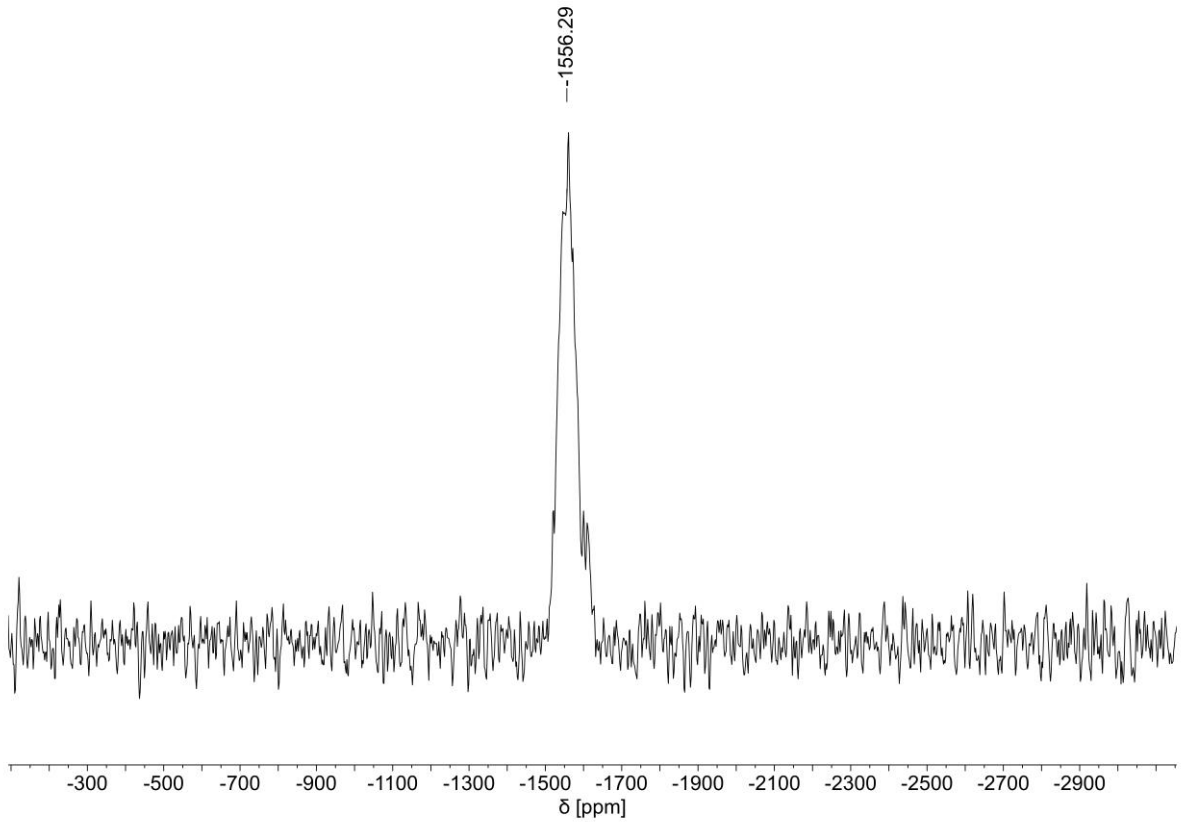

Figure S163. ^{31}P{^{1}H} NMR spectrum of [Tc(thse)(CO)$_3$(PPh$_3$)$_2$][BF$_4$].

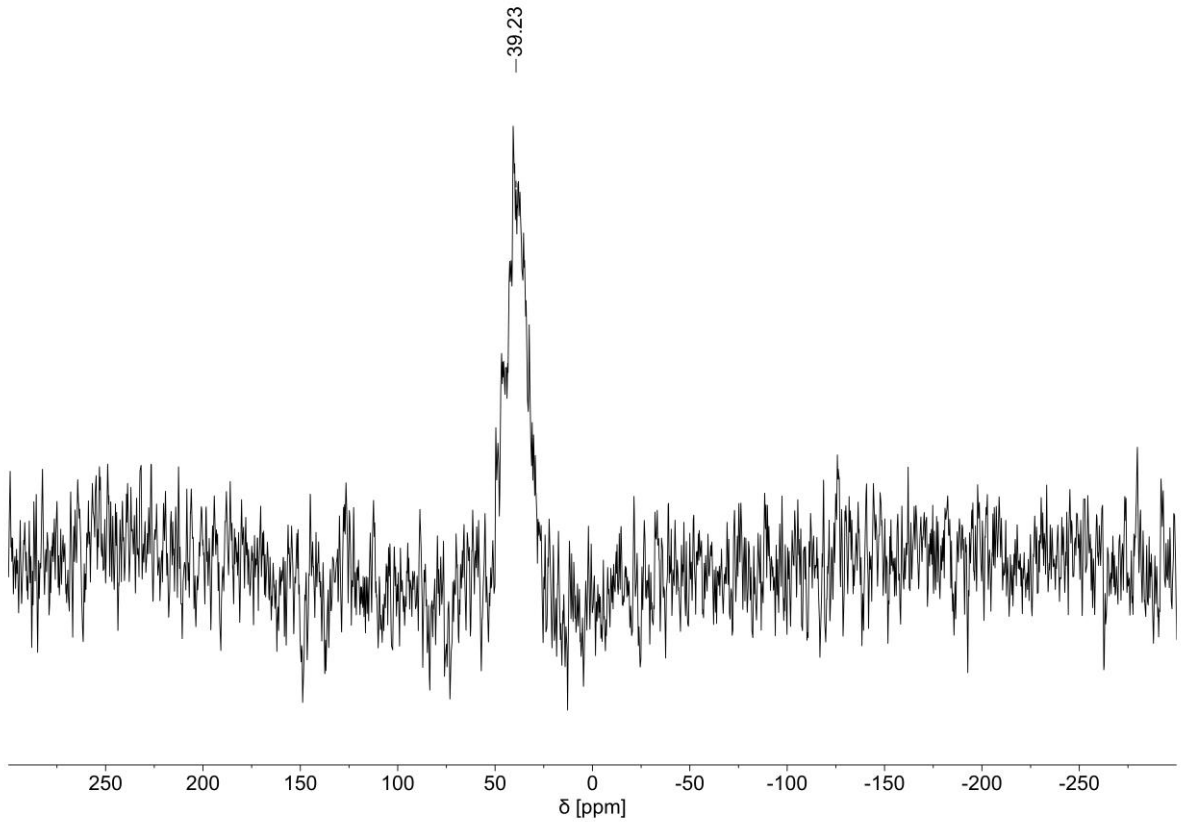

Figure S164. ^{19}F NMR spectrum of $[Tc(thse)(CO)_3(PPh_3)_2][BF_4]$.

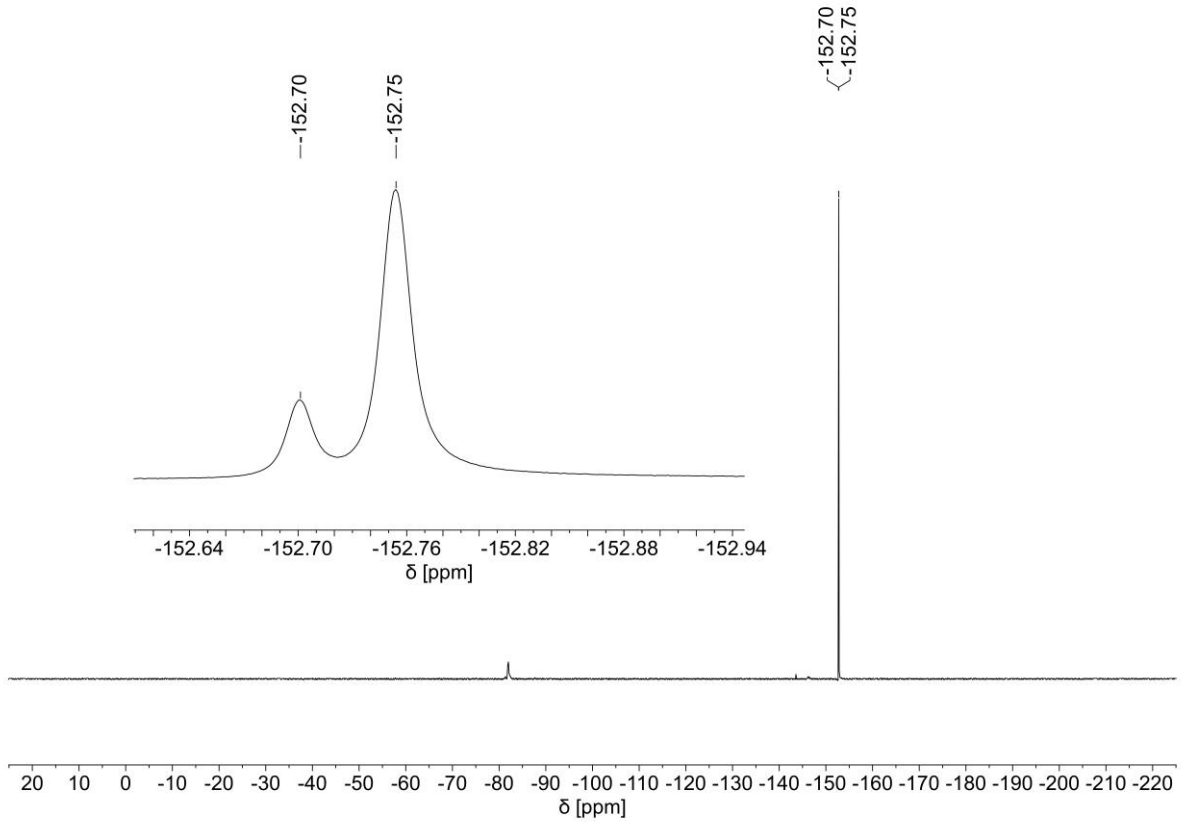

Figure S165. ^{11}B NMR spectrum of $[Tc(thse)(CO)_3(PPh_3)_2][BF_4]$.

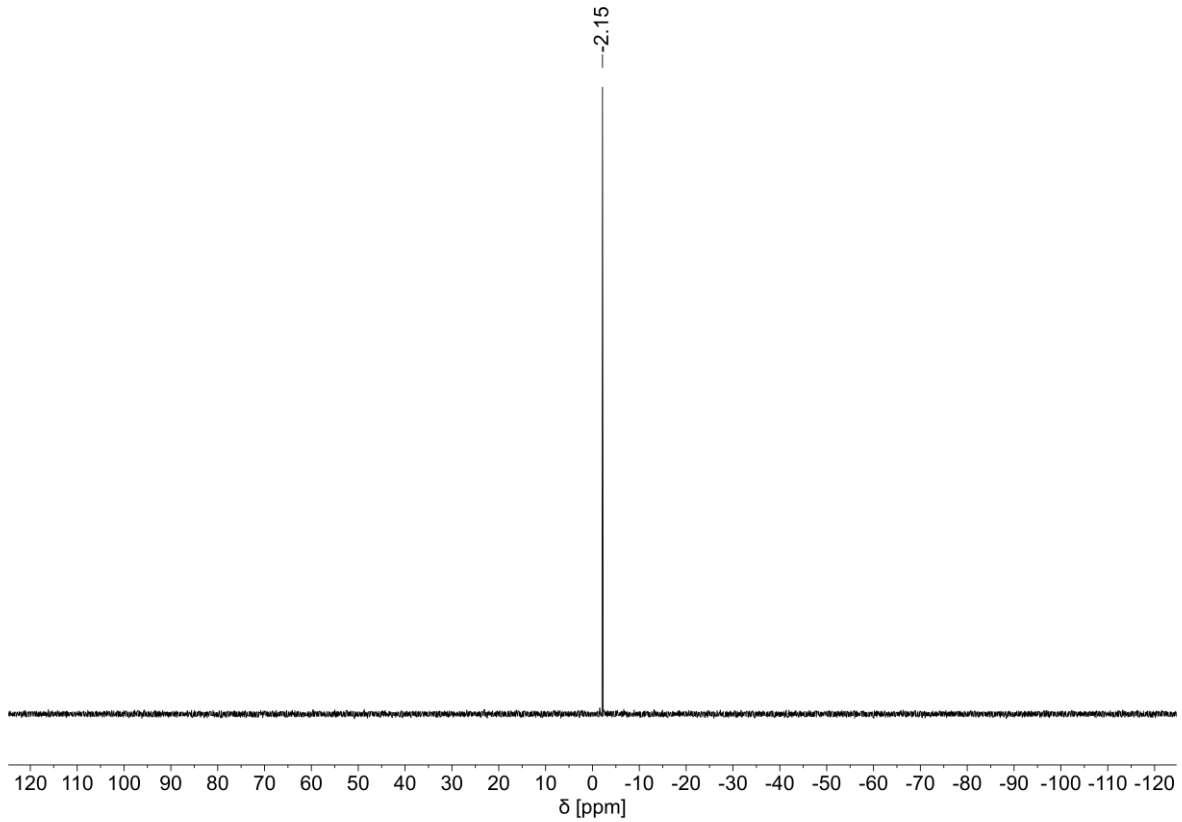

Figure S166. IR spectrum of $[Tc(thse)(CO)_3(PPh_3)_2][BF_4]$.

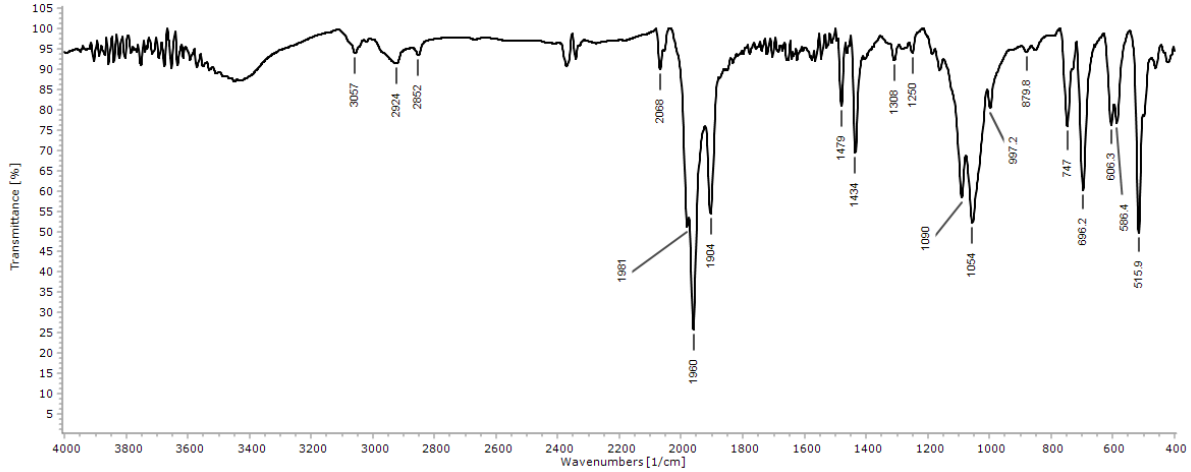

Figure S167. ^1H NMR spectrum of $[Tc(TeMe_2)(CO)_3(PPh_3)_2][BF_4]$.

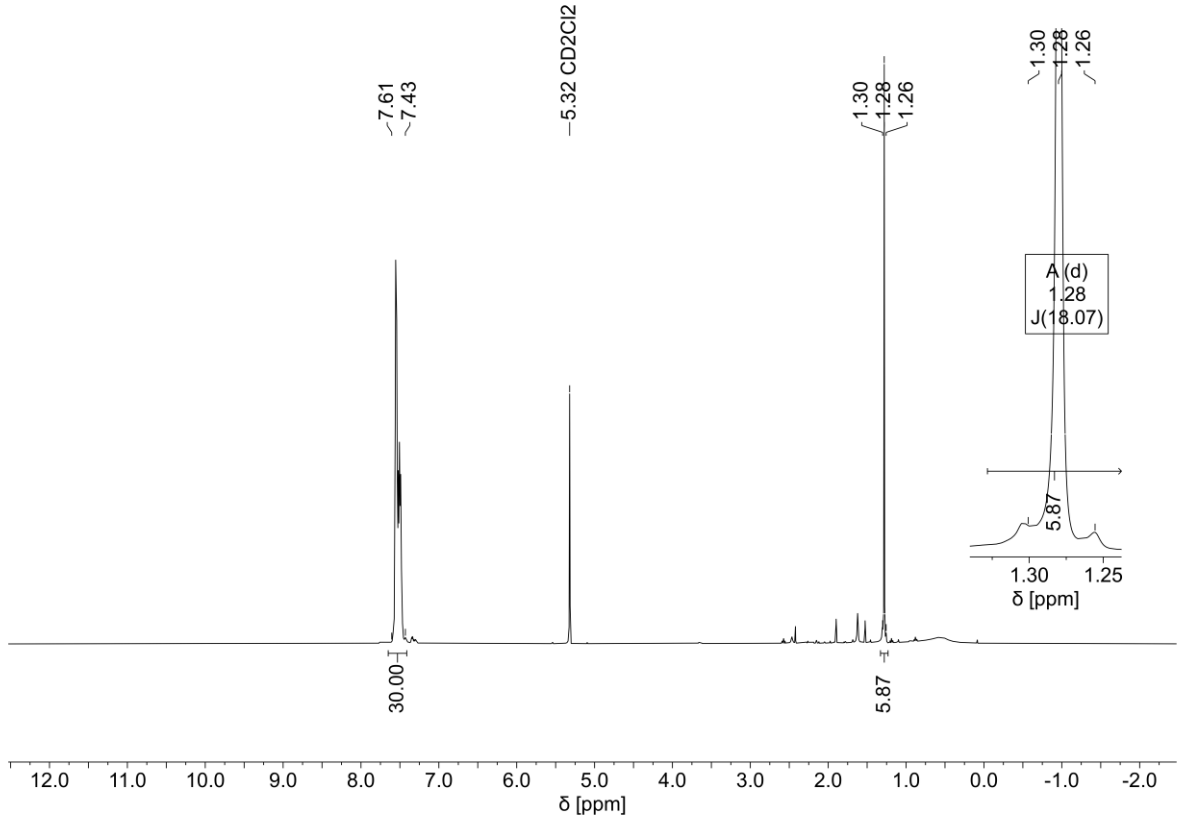

Figure S168. ^{99}Tc NMR spectrum of $[Tc(TeMe_2)(CO)_3(PPh_3)_2][BF_4]$.

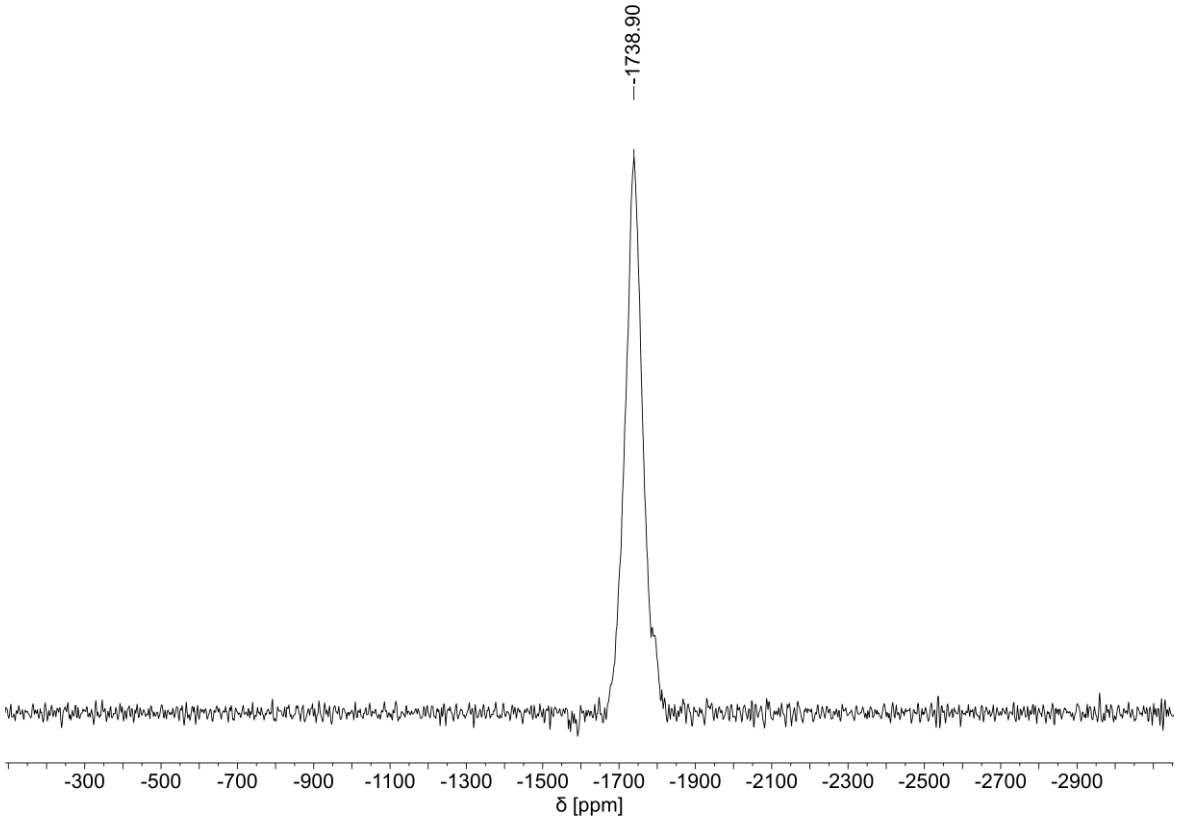

Figure S169. $^{31}P\{^1H\}$ NMR spectrum of $[Tc(TeMe_2)(CO)_3(PPh_3)_2][BF_4]$.

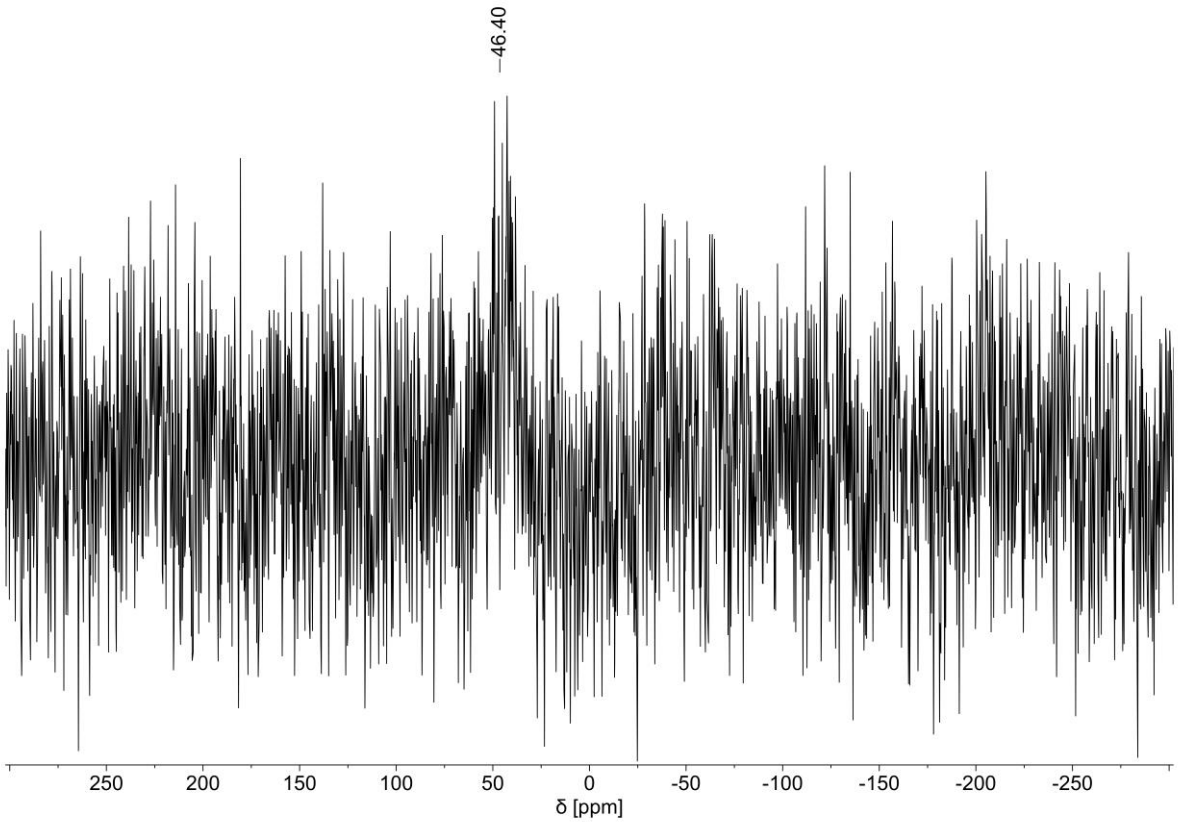

Figure S170. ^{19}F NMR spectrum of $[Tc(TeMe_2)(CO)_3(PPh_3)_2][BF_4]$.

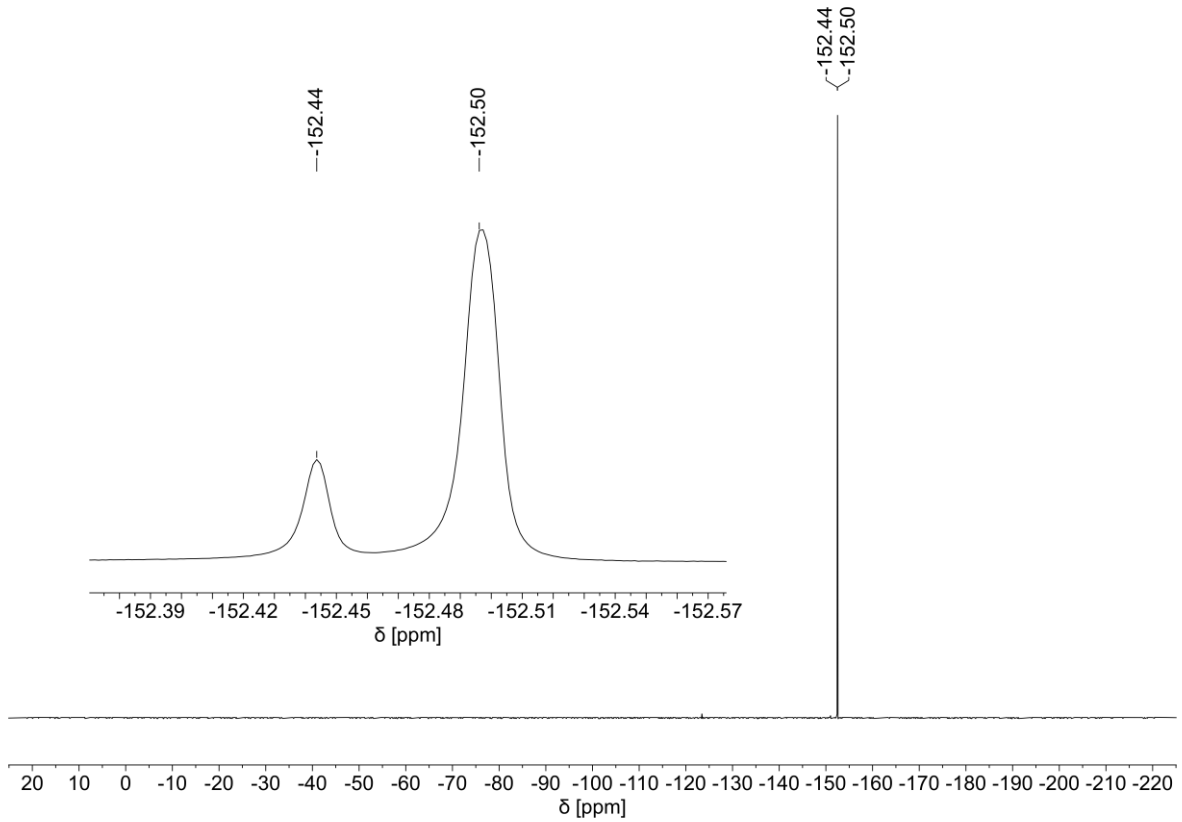

Figure S171. ^{11}B NMR spectrum of $[Tc(TeMe_2)(CO)_3(PPh_3)_2][BF_4]$.

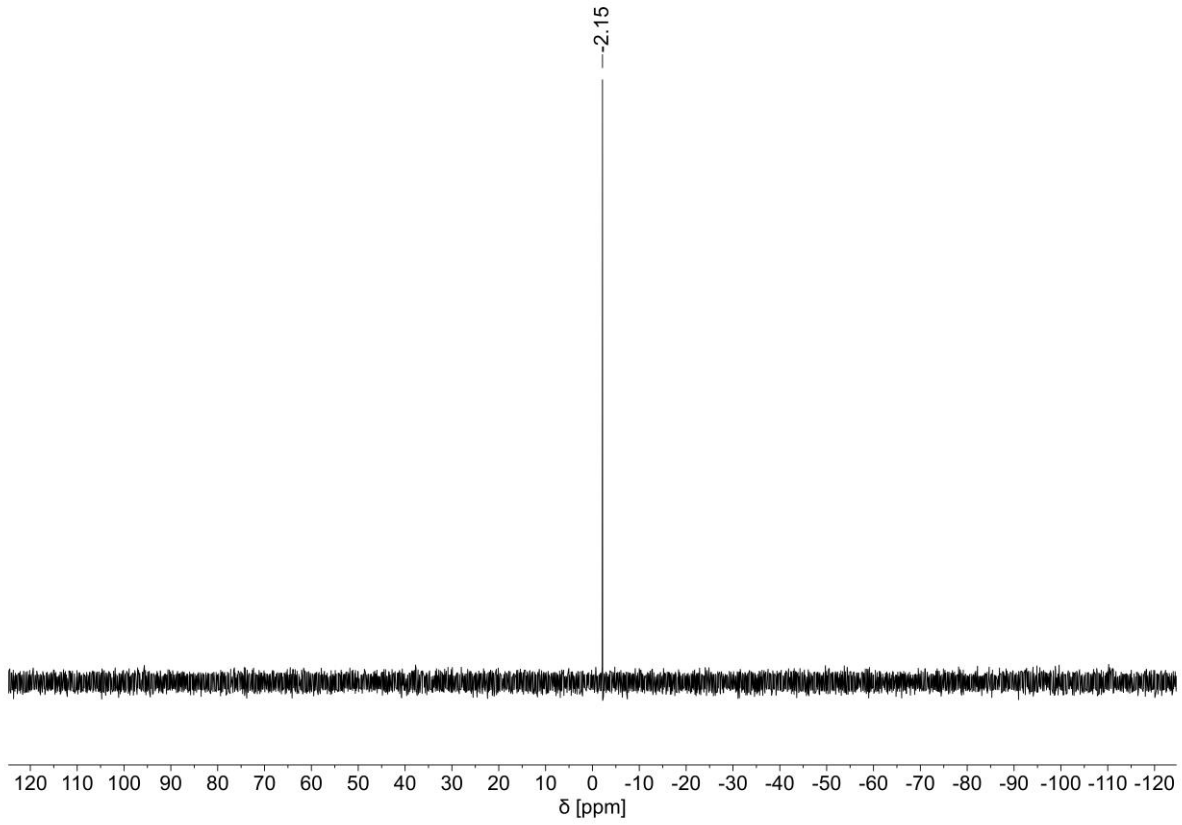

Figure S172. IR spectrum of $[Tc(TeMe_2)(CO)_3(PPh_3)_2][BF_4]$.

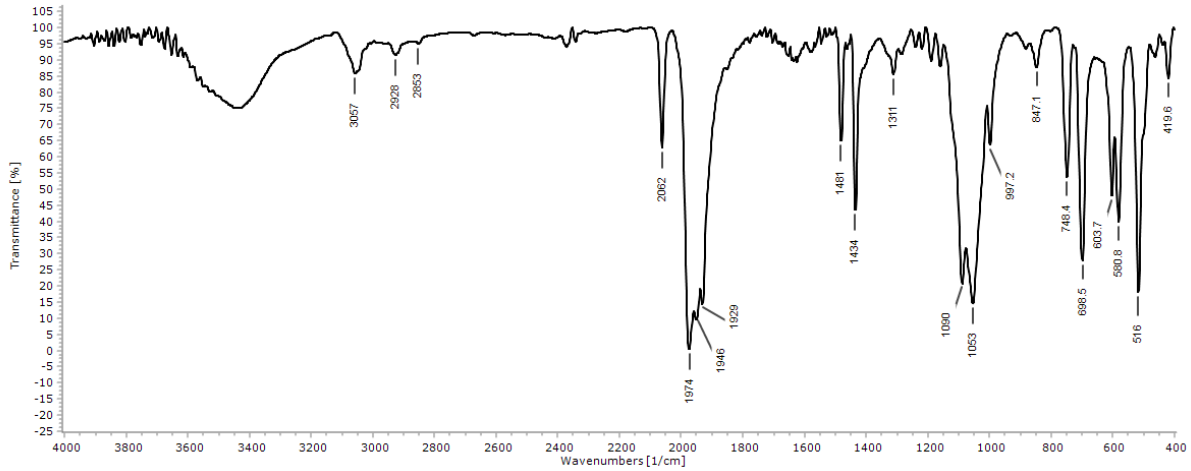

Figure S173. ^1H NMR spectrum of $[Tc(thte)(CO)_3(PPh_3)_2][BF_4]$.

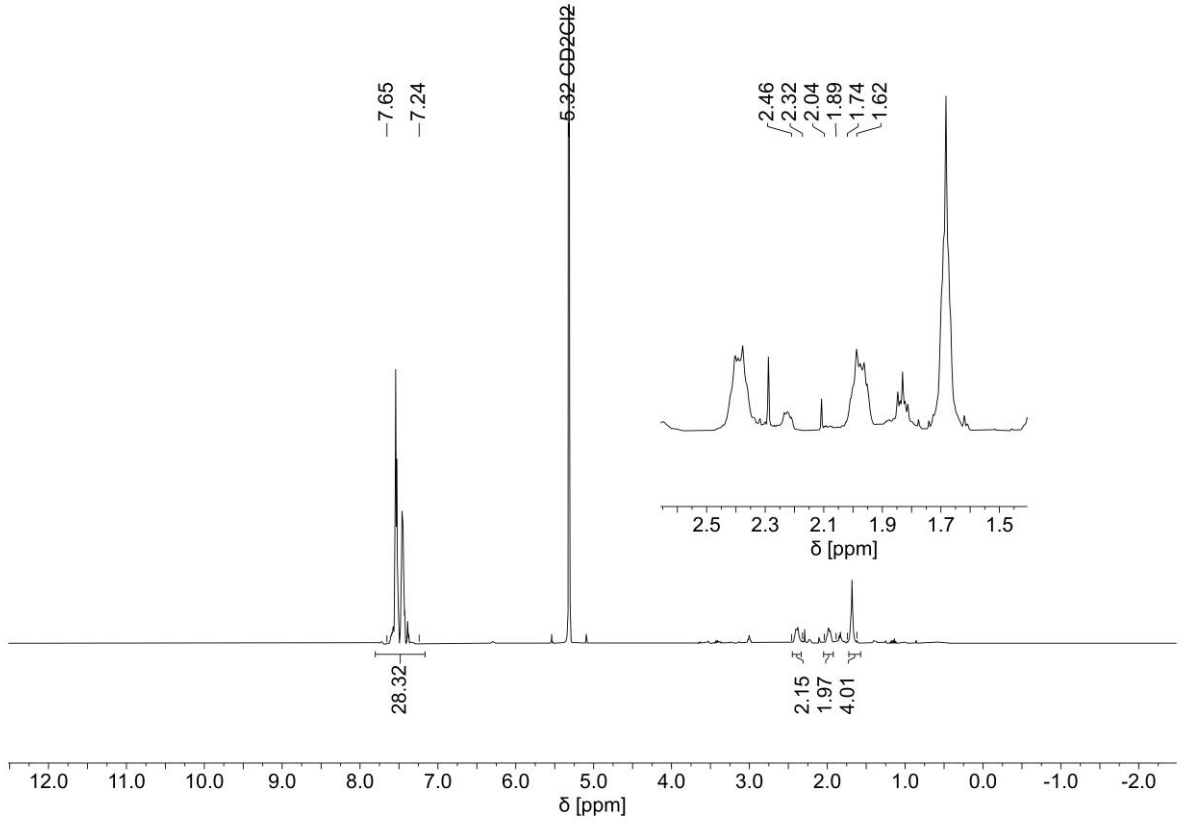

Figure S174. $^{1}H,^{1}H$-NOESY NMR spectrum of $[Tc(thte)(CO)_3(PPh_3)_2][BF_4]$.

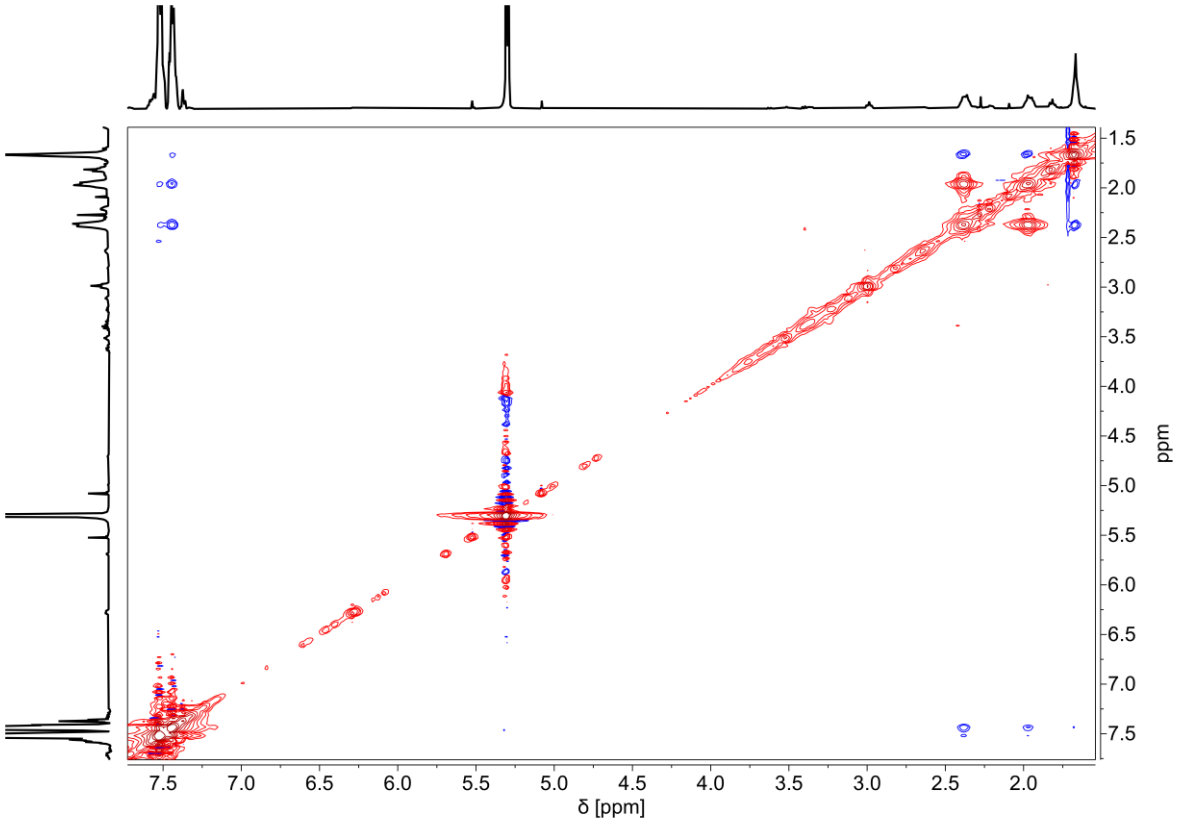

Figure S175. ^{99}Tc NMR spectrum of $[Tc(thte)(CO)_3(PPh_3)_2][BF_4]$.

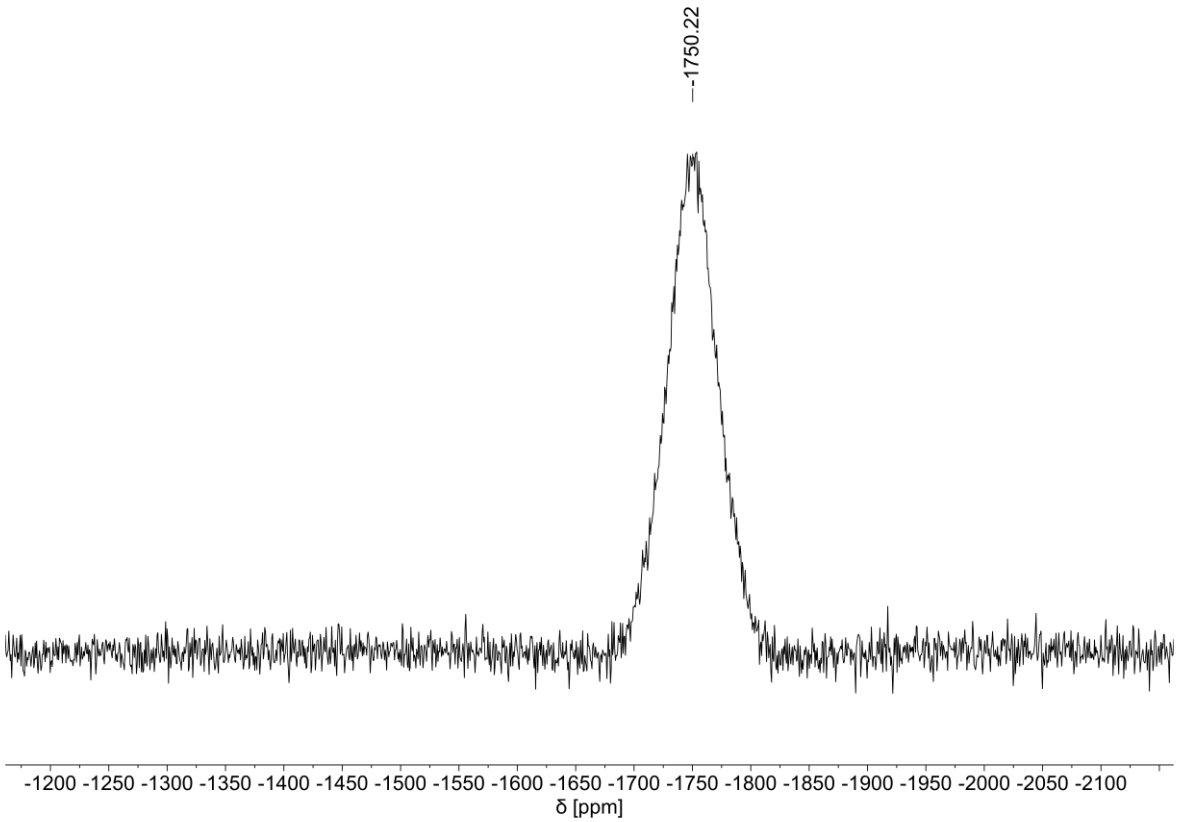

Figure S176. $^{31}P\{^{1}H\}$ NMR spectrum of $[Tc(thte)(CO)_3(PPh_3)_2][BF_4]$.

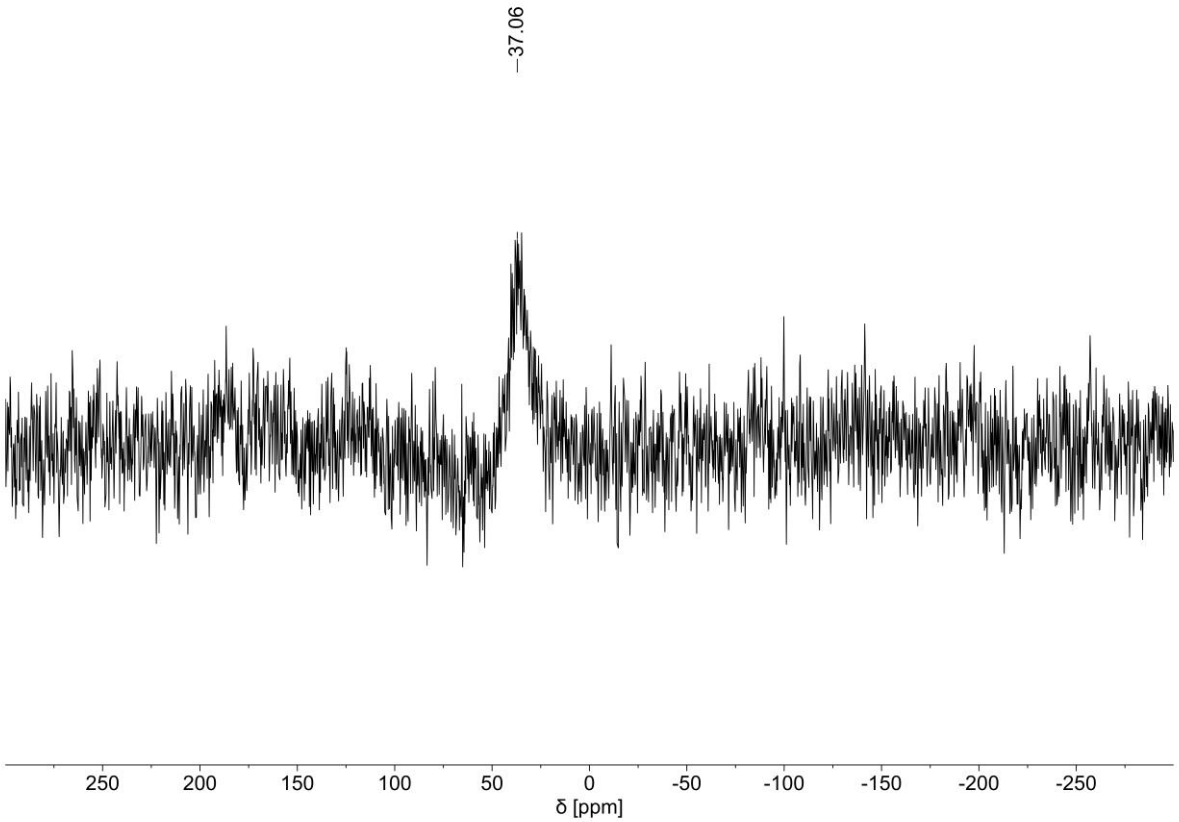

Figure S177. ^{19}F NMR spectrum of $[Tc(thte)(CO)_3(PPh_3)_2][BF_4]$.

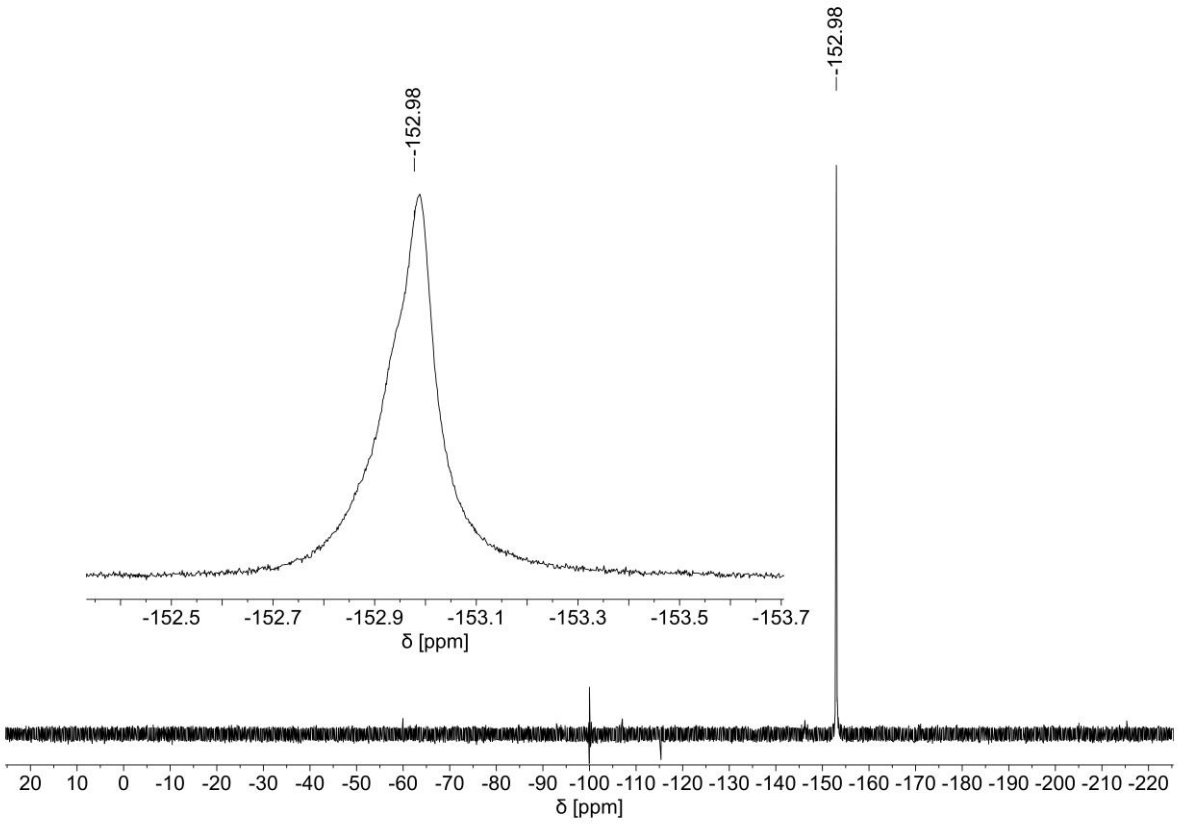

Figure S178. ^{11}B NMR spectrum of $[Tc(thte)(CO)_3(PPh_3)_2][BF_4]$.

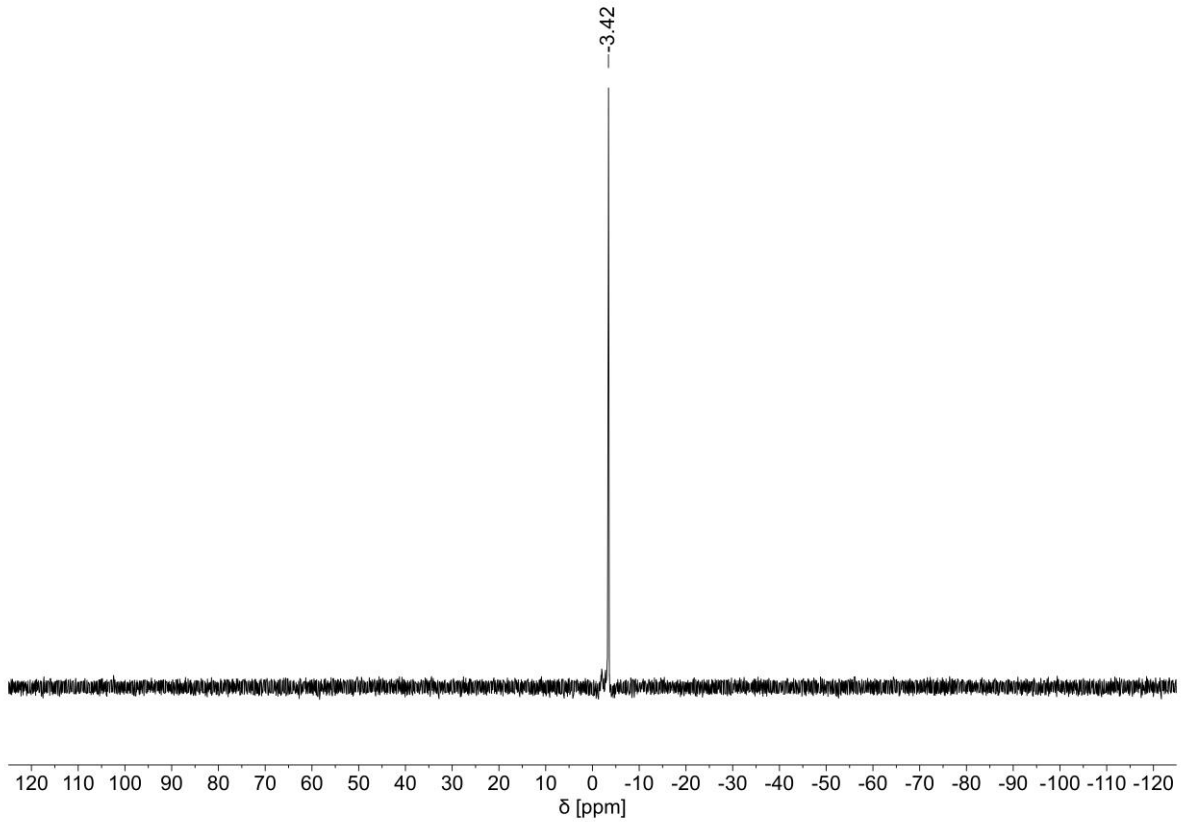

Figure S179. IR spectrum of $[Tc(thte)(CO)_3(PPh_3)_2][BF_4]$.

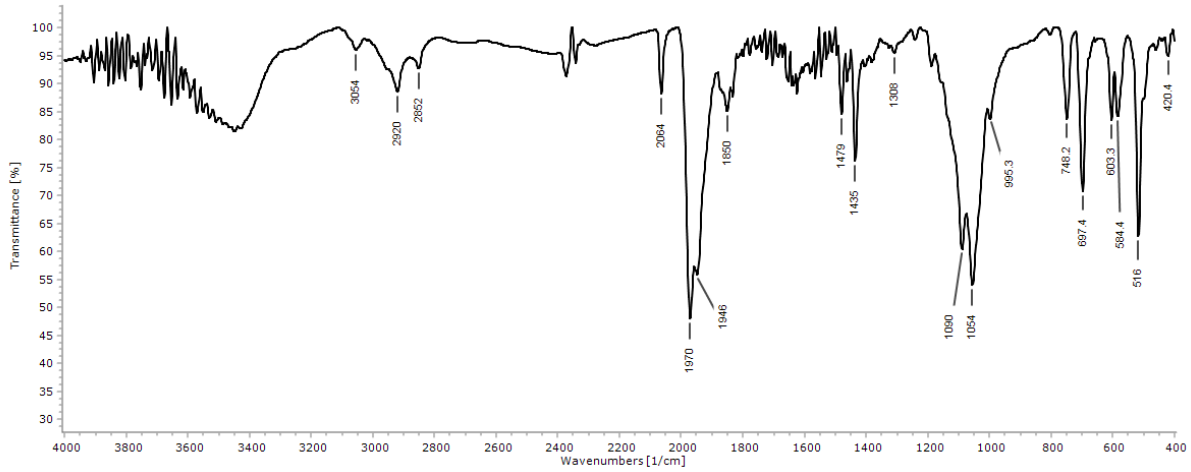

Figure S180. ^{1}H NMR spectrum of $[Tc(tu)(CO)_3(PPh_3)_2][BF_4]$.

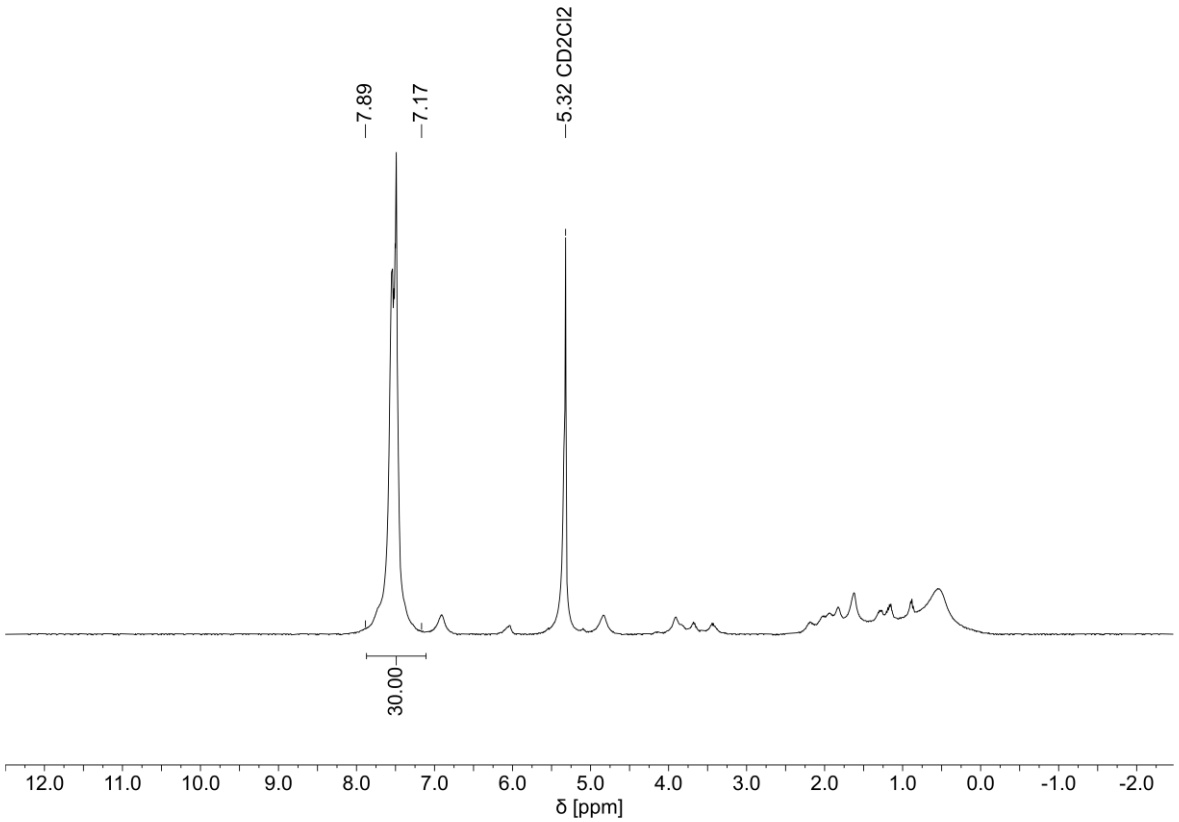

Figure S181. ^{99}Tc NMR spectrum of $[Tc(tu)(CO)_3(PPh_3)_2][BF_4]$.

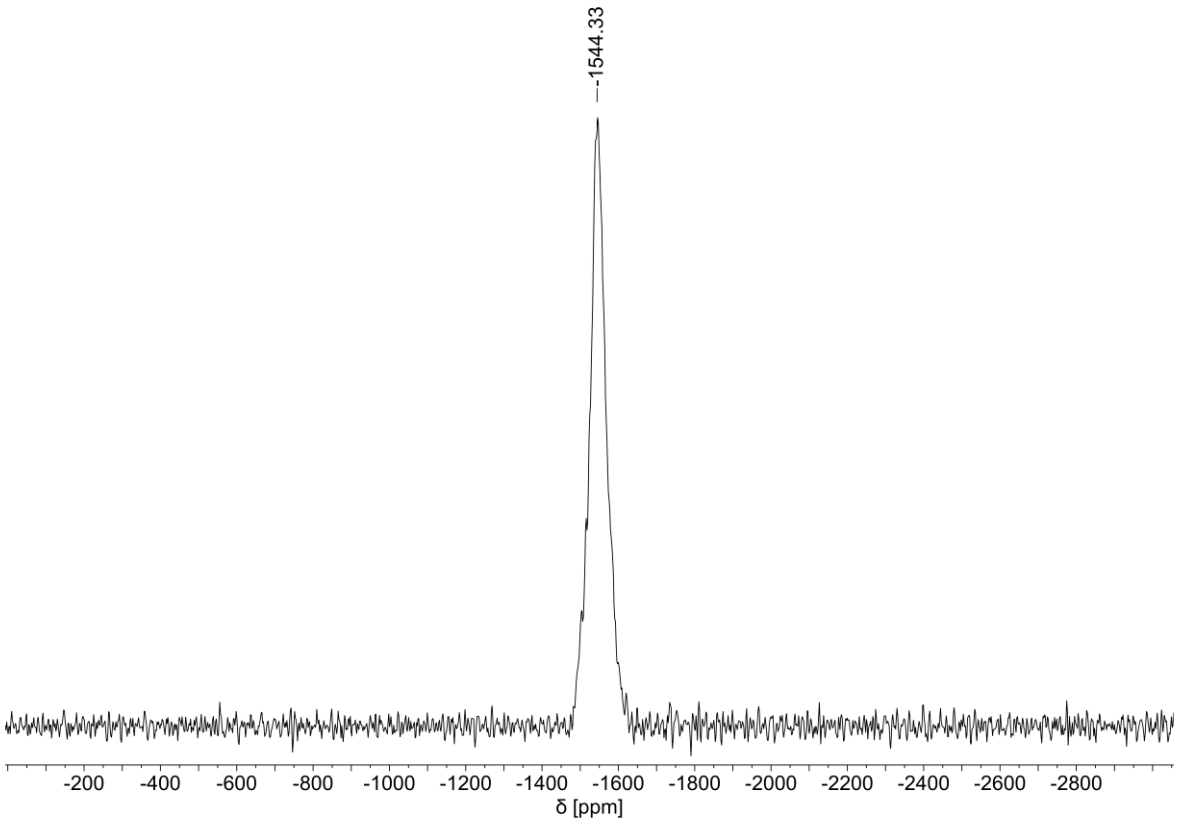

Figure S182. ^{19}F NMR spectrum of $[Tc(tu)(CO)_3(PPh_3)_2][BF_4]$.

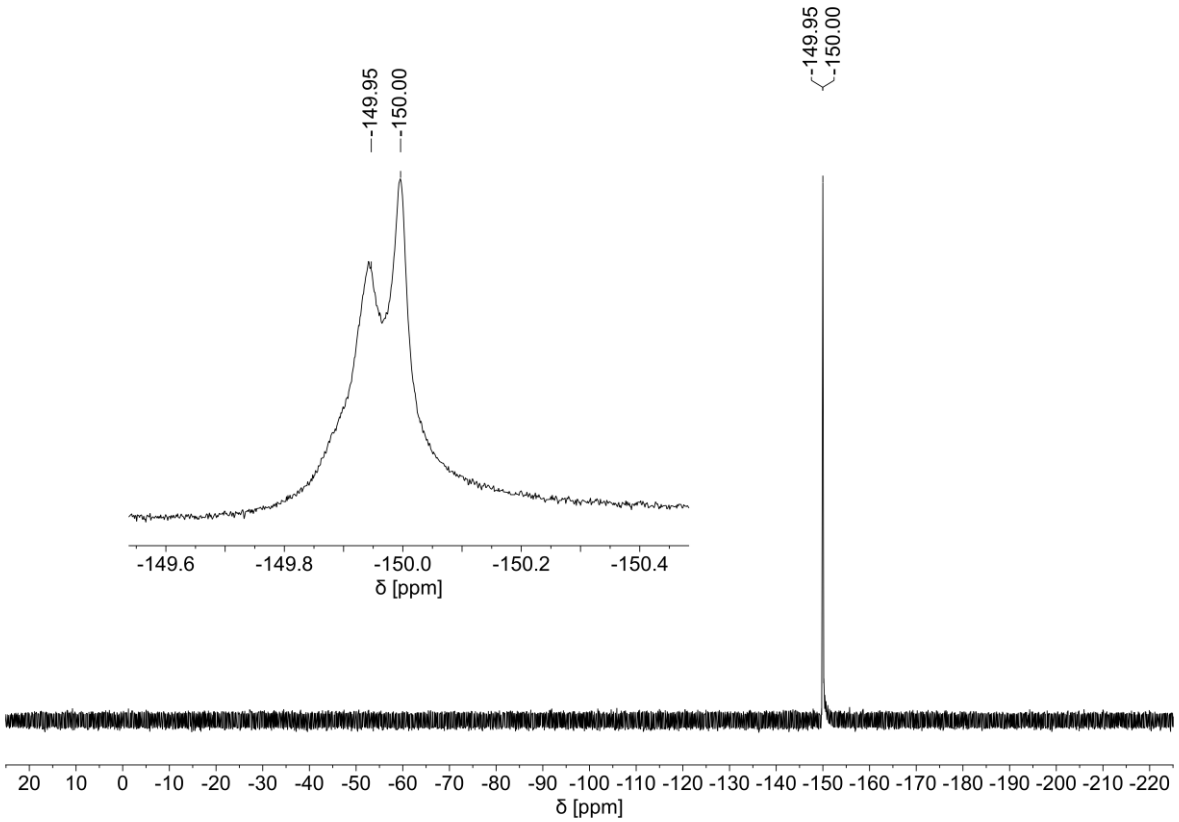

Figure S183. ^{11}B NMR spectrum of $[Tc(tu)(CO)_3(PPh_3)_2][BF_4]$.

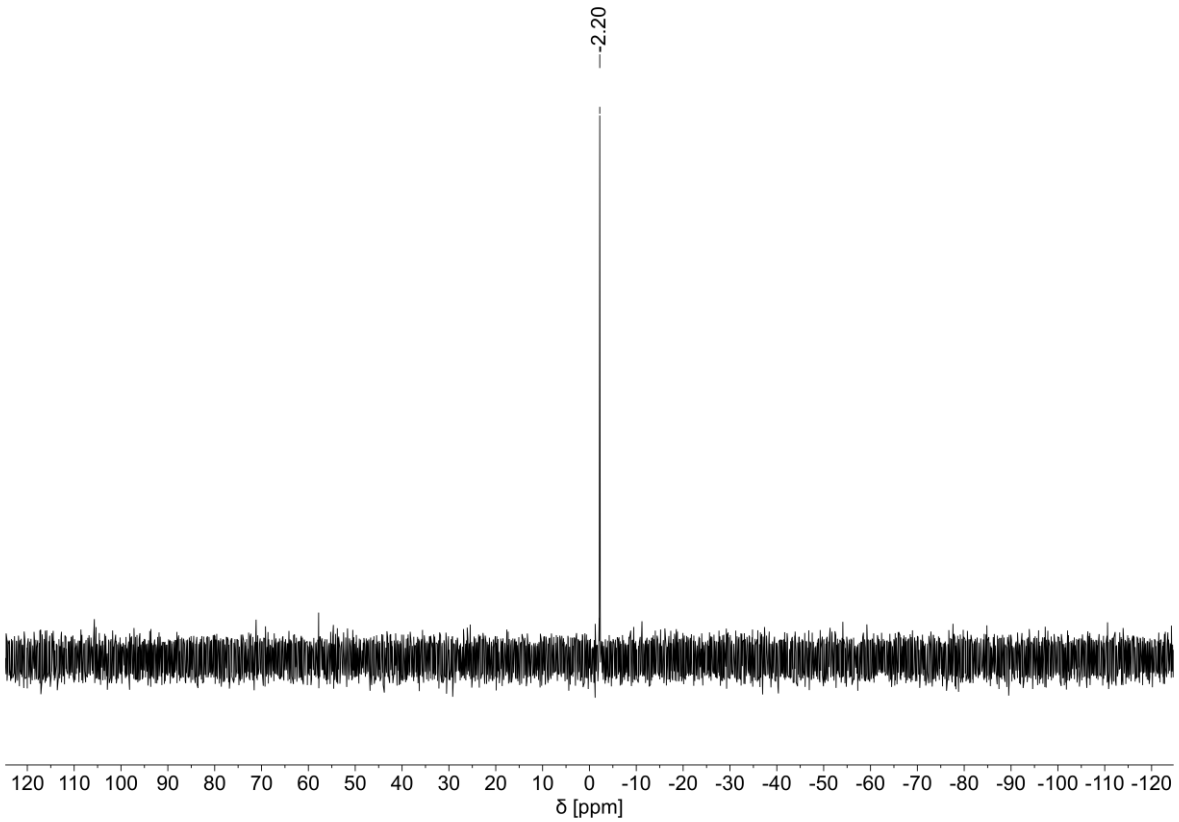

Figure S184. IR spectrum of $[Tc(tu)(CO)_3(PPh_3)_2][BF_4]$.

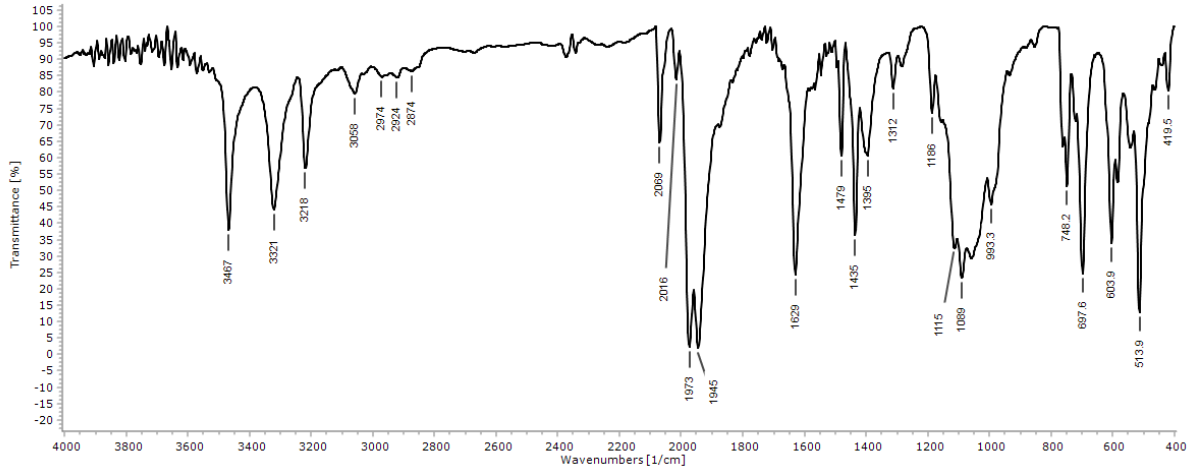

Figure S185. ^1H NMR spectrum of $[Tc(seu)(CO)_3(PPh_3)_2][BF_4]$.

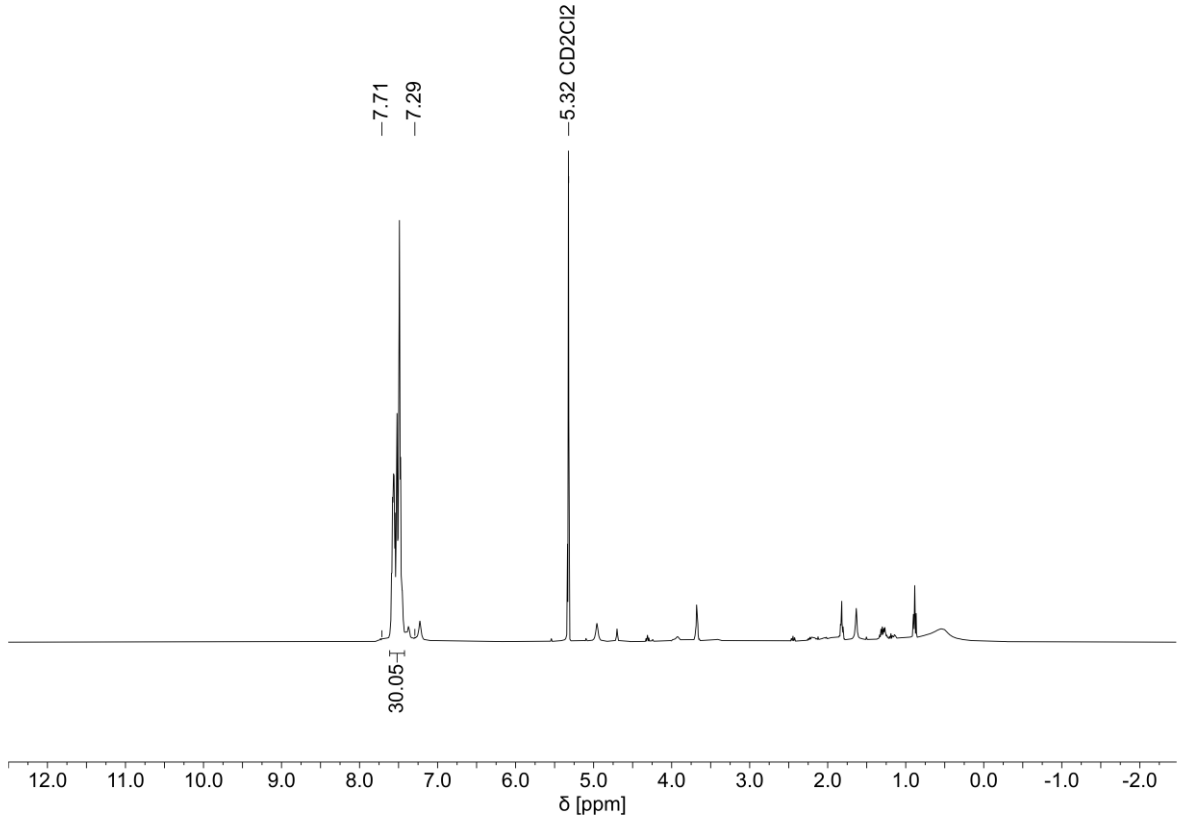

Figure S186. ^{99}Tc NMR spectrum of [Tc(seu)(CO)$_3$(PPh$_3$)$_2$][BF$_4$].

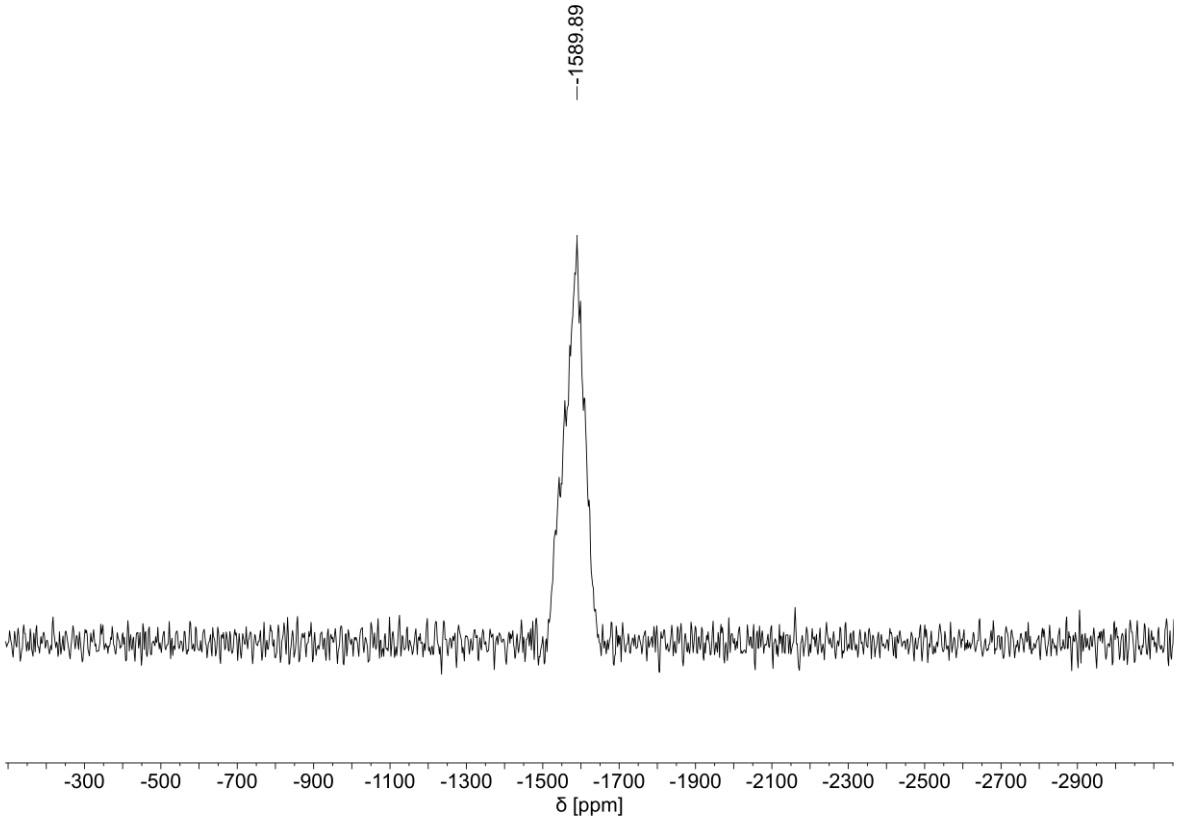

Figure S187. ^{19}F NMR spectrum of [Tc(seu)(CO)$_3$(PPh$_3$)$_2$][BF$_4$].

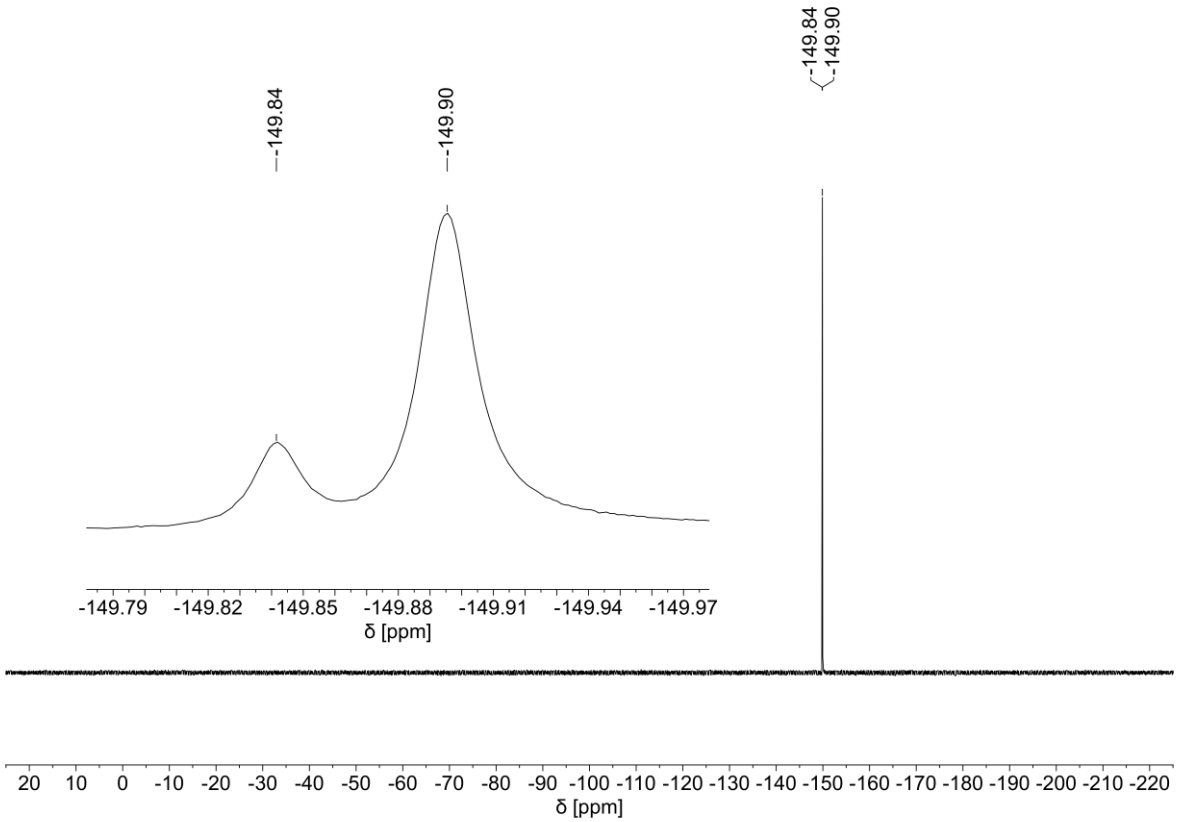

Figure S188. ^{11}B NMR spectrum of $[Tc(seu)(CO)_3(PPh_3)_2][BF_4]$.

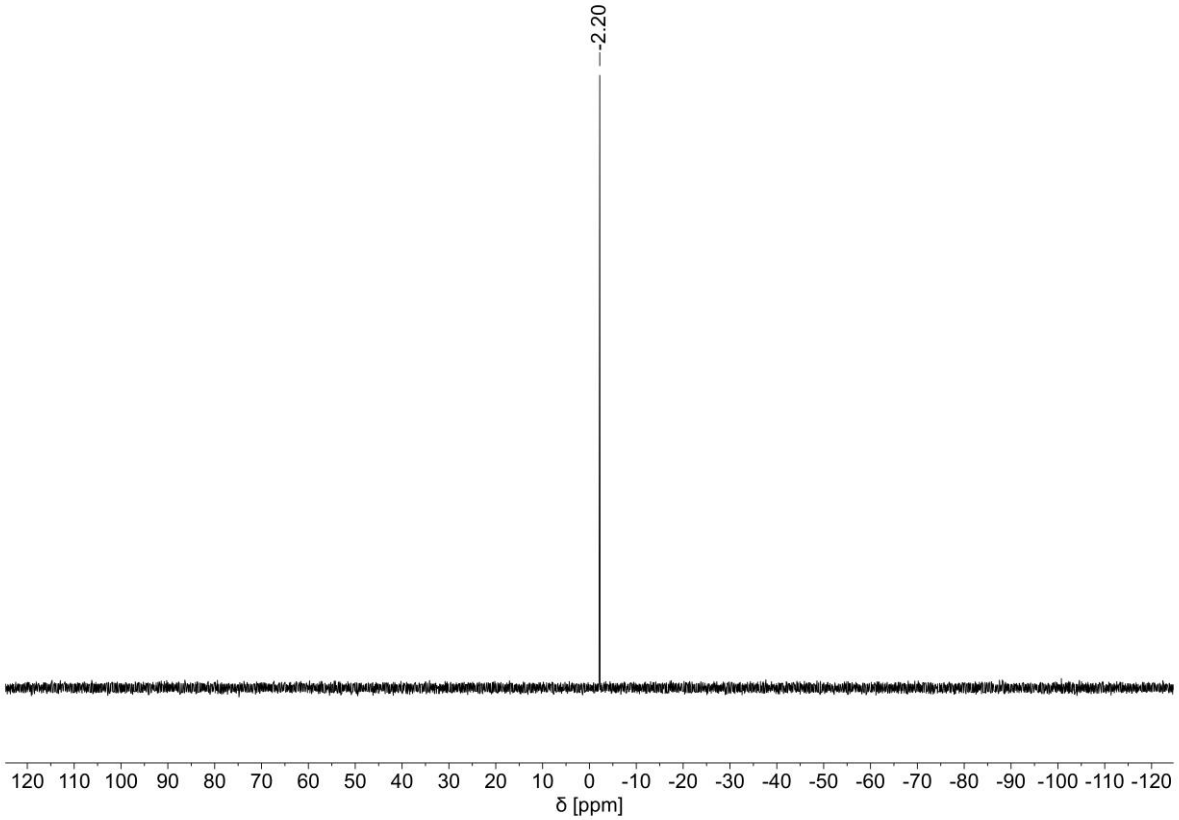

Figure S189. IR spectrum of $[Tc(seu)(CO)_3(PPh_3)_2][BF_4]$.

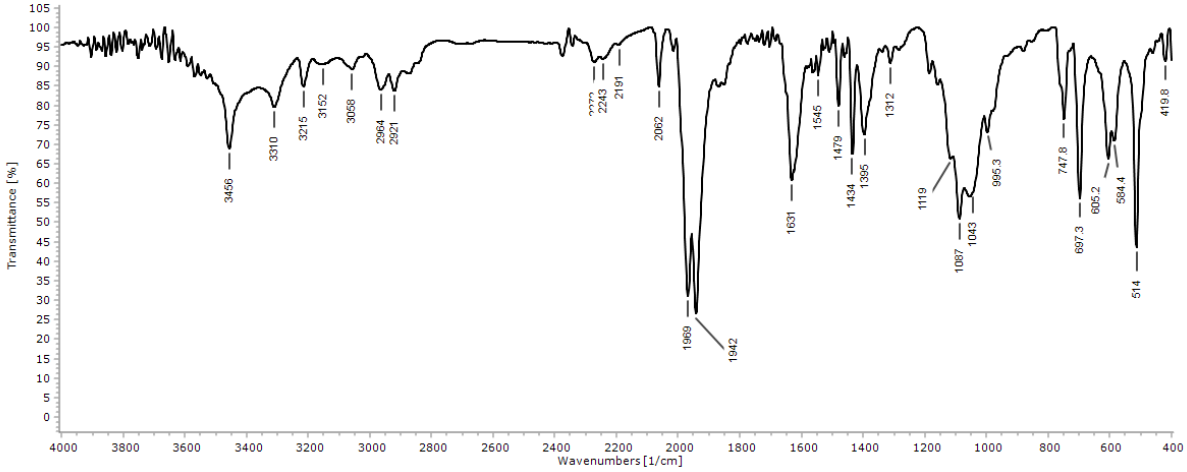

Figure S190. Proposed mechanism for the reaction between $[TcH(CO)_3(PPh_3)_2]$ and $[H(OEt_2)_2][BArF_{24}]$.

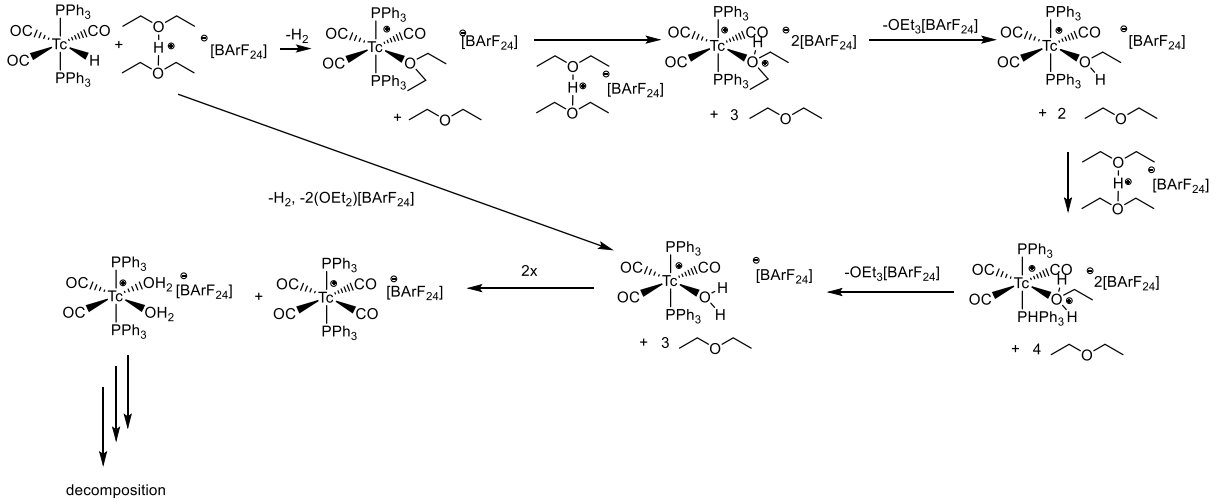

Figure S191. Proposed metal-mediated equilibrium between proton and ethylium groups in $[H(OEt_2)_2][BArF_{24}]$ and $[(OEt_2)_3][BArF_{24}]$.

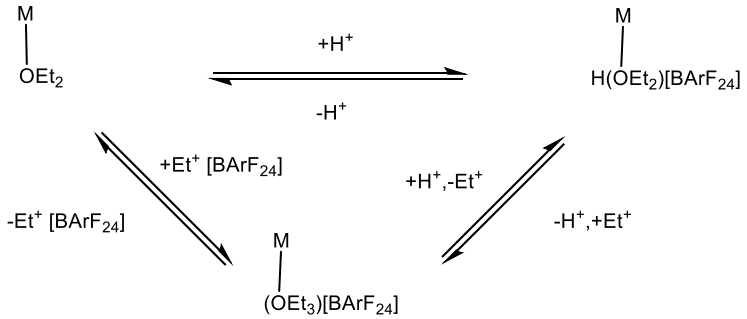

Figure S192. ^{99}Tc NMR spectrum (overlay between all relevant spectral regions) for the reaction between $[TcH(CO)_3(PPh_3)_2]$ and $[H(OEt_2)_2][BArF_{24}]$ in dry, degassed CD_2Cl_2 under Ar; addition of solvent performed at 100 K. Time: initial reaction after thawing.

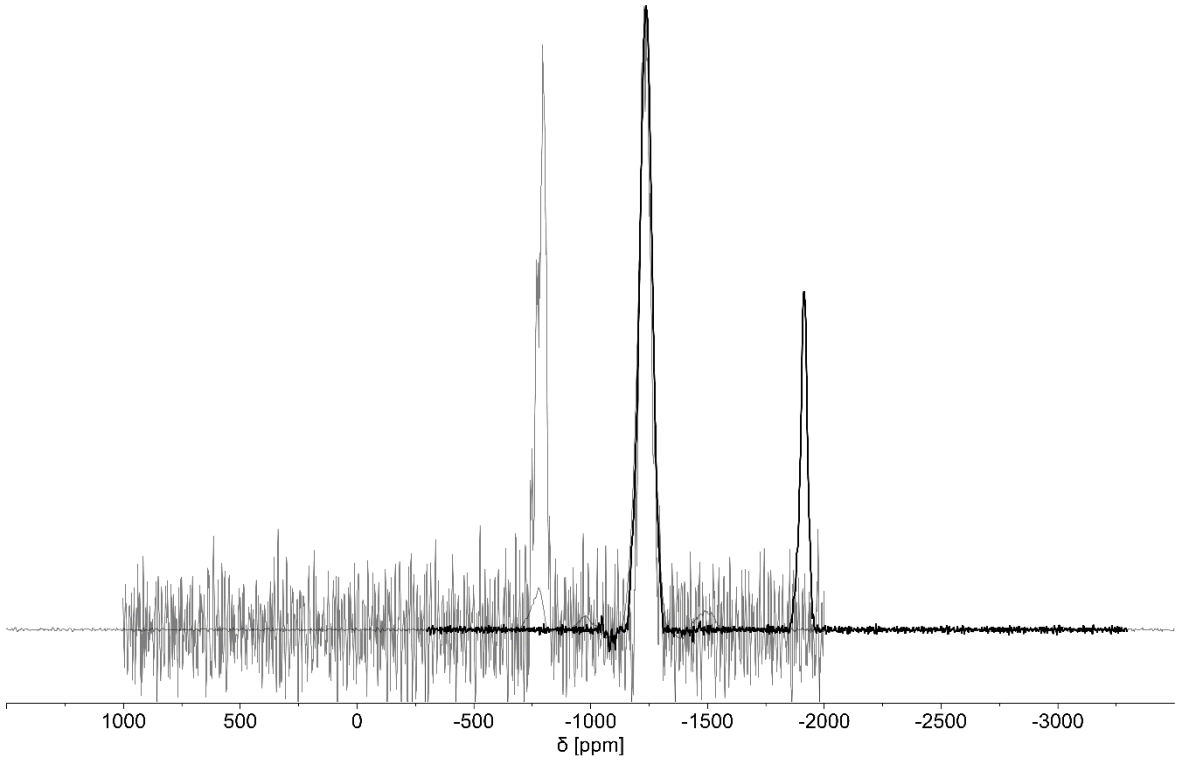

Figure S193. ^{99}Tc NMR spectrum (overlay between all relevant spectral regions) for the reaction between $[TcH(CO)_3(PPh_3)_2]$ and $[H(OEt_2)_2][BArF_{24}]$ in dry, degassed CD_2Cl_2 under Ar; addition of solvent performed at 100 K. Time: 2.5 h.

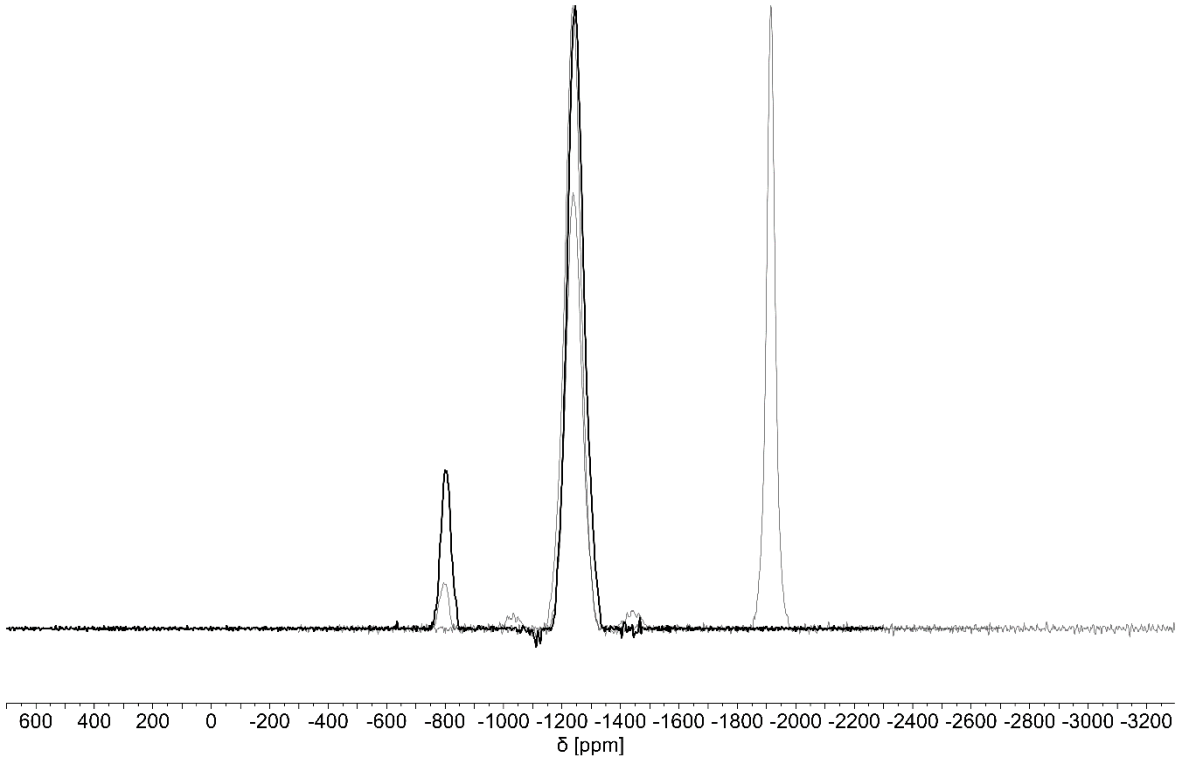

Figure S194. ^{99}Tc NMR spectrum (overlay between all relevant spectral regions) for the reaction between $[TcH(CO)_3(PPh_3)_2]$ and $[H(OEt_2)_2][BArF_{24}]$ in dry, degassed CD_2Cl_2 under Ar; addition of solvent performed at 100 K. Time: 21 h.

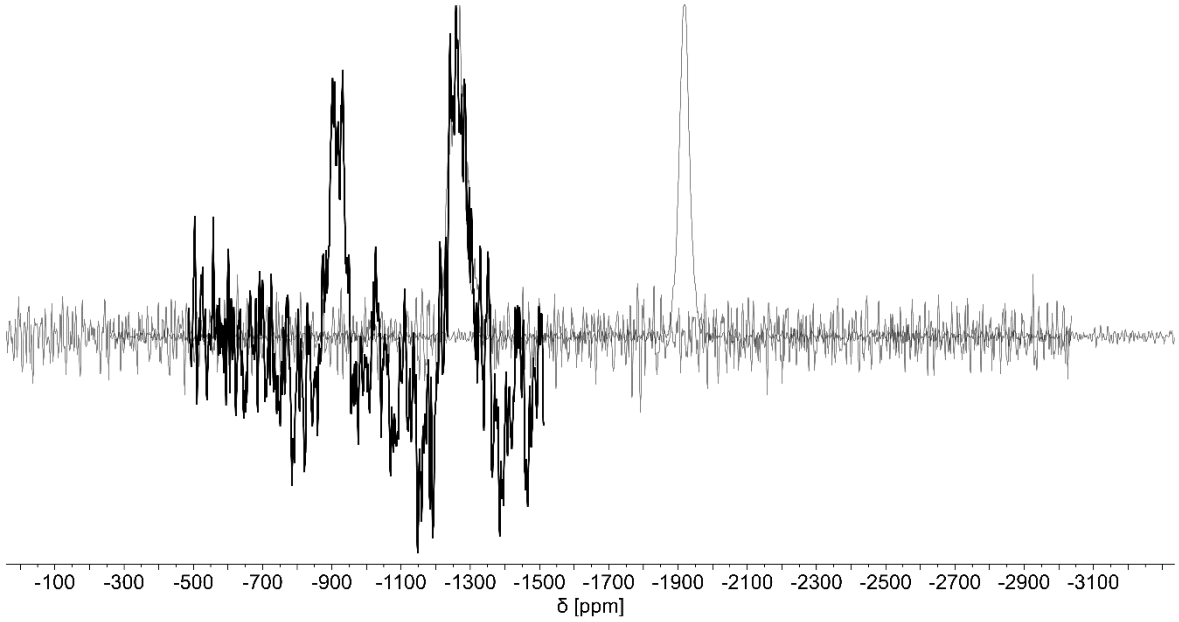

Figure S195. ^{99}Tc NMR spectrum (overlay between all relevant spectral regions) for the reaction between $[TcH(CO)_3(PPh_3)_2]$ and $[H(OEt_2)_2][BArF_{24}]$ in dry, degassed CD_2Cl_2 under Ar; addition of solvent performed at 100 K. Time: 3 d.

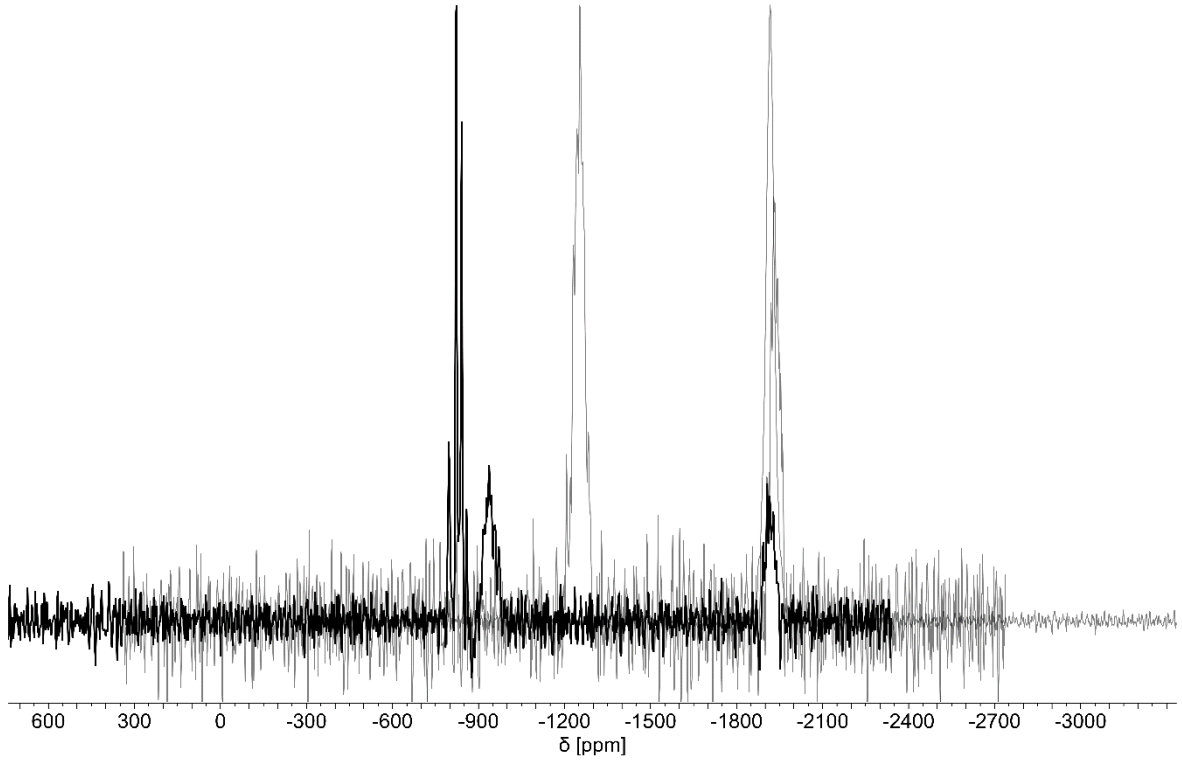

Figure S196. ^{99}Tc NMR spectra (stacked) for the reaction between $[TcH(CO)_3(PPh_3)_2]$ and $[H(OEt_2)_2][BArF_{24}]$ in dry, degassed CD_2Cl_2 under Ar; addition of solvent performed at 100 K.

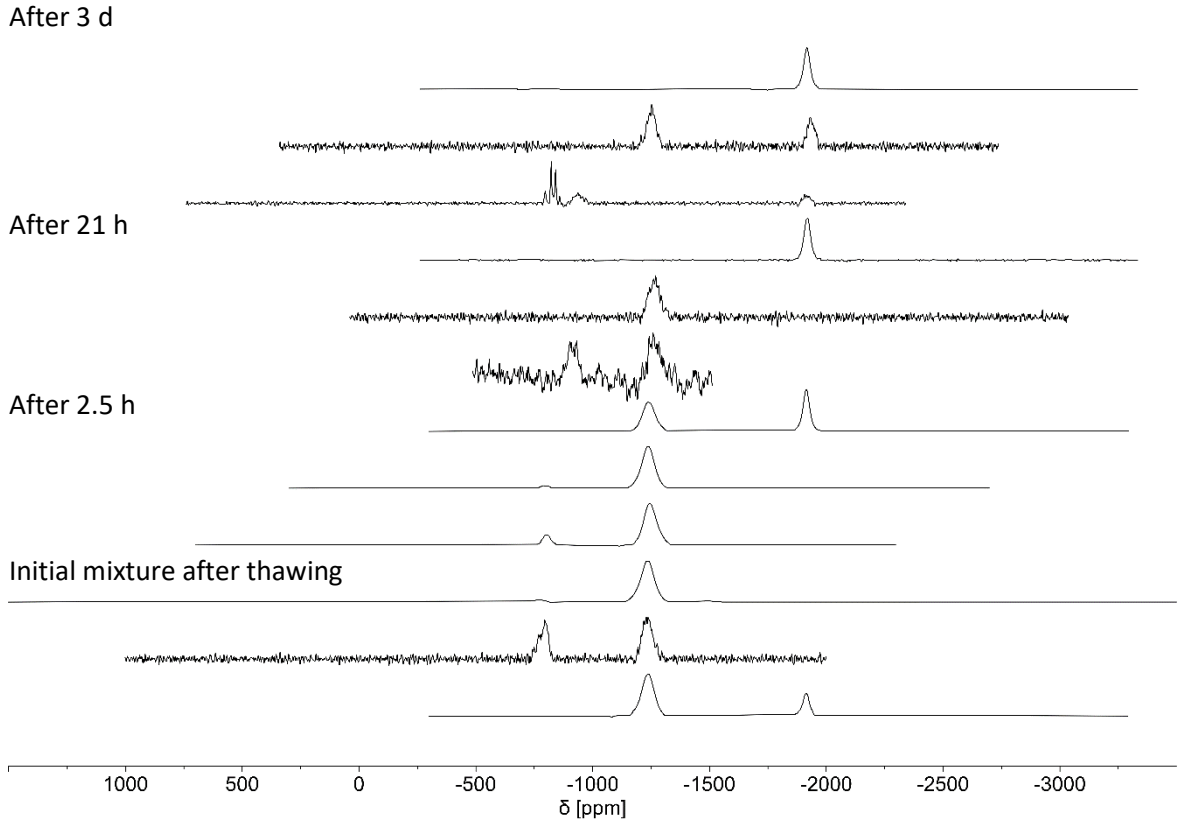

Figure S197. ^{1}H NMR spectra (stacked) for the reaction between $[TcH(CO)_3(PPh_3)_2]$ and $[H(OEt_2)_2][BArF_{24}]$ in dry, degassed CD_2Cl_2 under Ar; addition of solvent performed at 100 K.

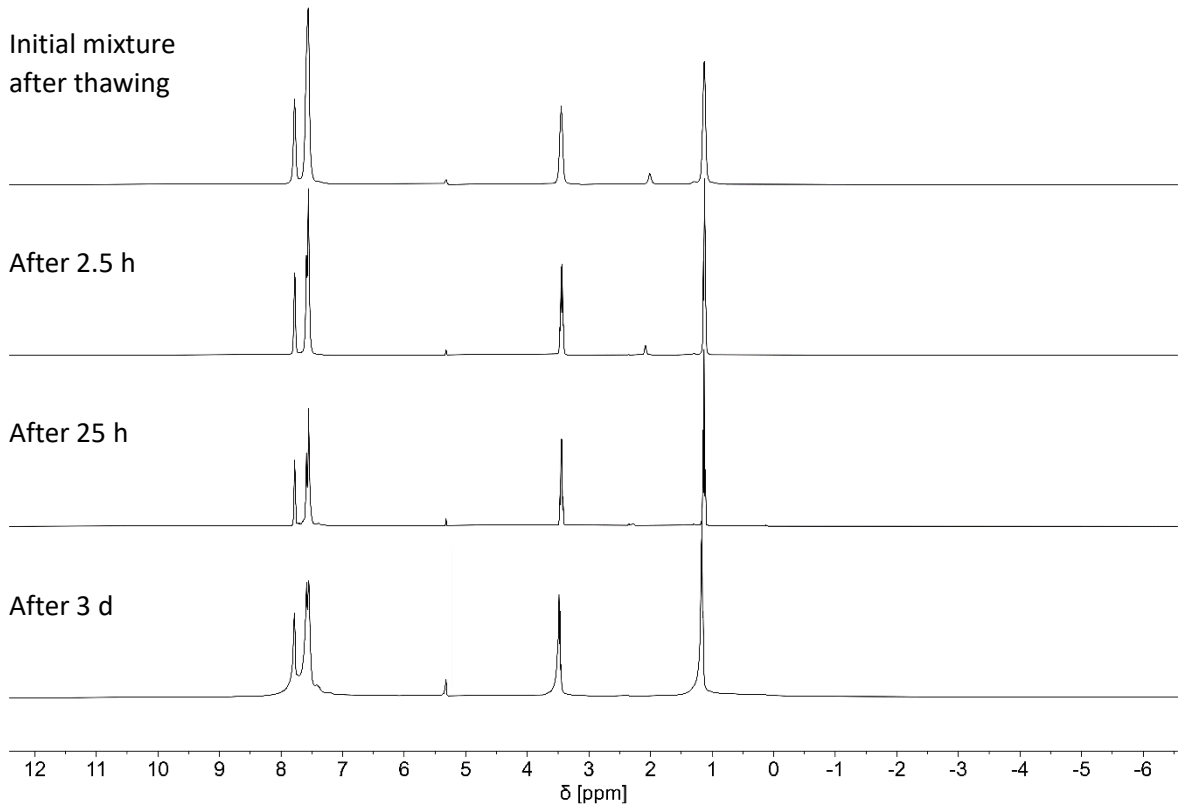

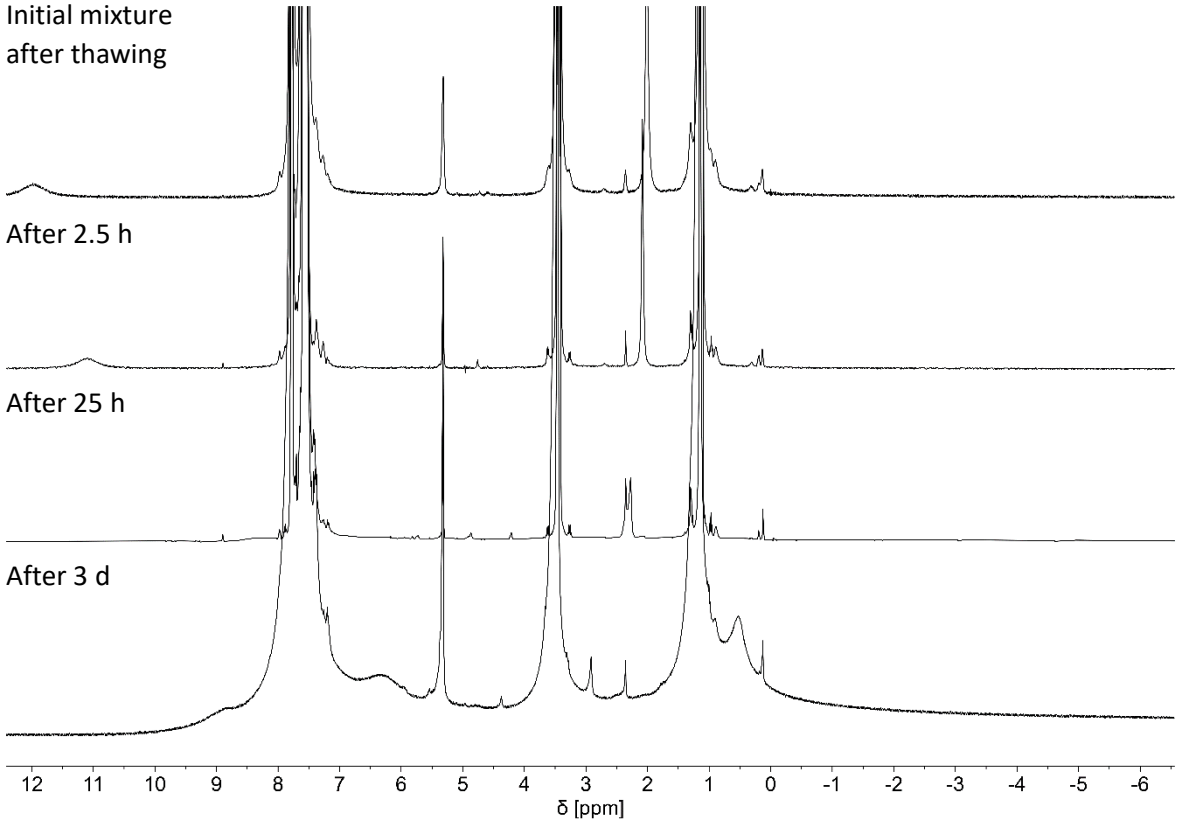
Initial mixture
after thawing
After 2.5 h
After 25 h
After 3 d
12
11
10
9
8
7
6
5
4
3
2
1
0
-1
-2
-3
-4
-5
-6
δ [ppm]

Figure S198. ^{1}H NMR spectra (stacked) for the reaction between $[TcH(CO)_3(PPh_3)_2]$ and $[H(OEt_2)_2][BArF_{24}]$ in dry, degassed thf-d8 under Ar; addition of solvent performed at 100 K.

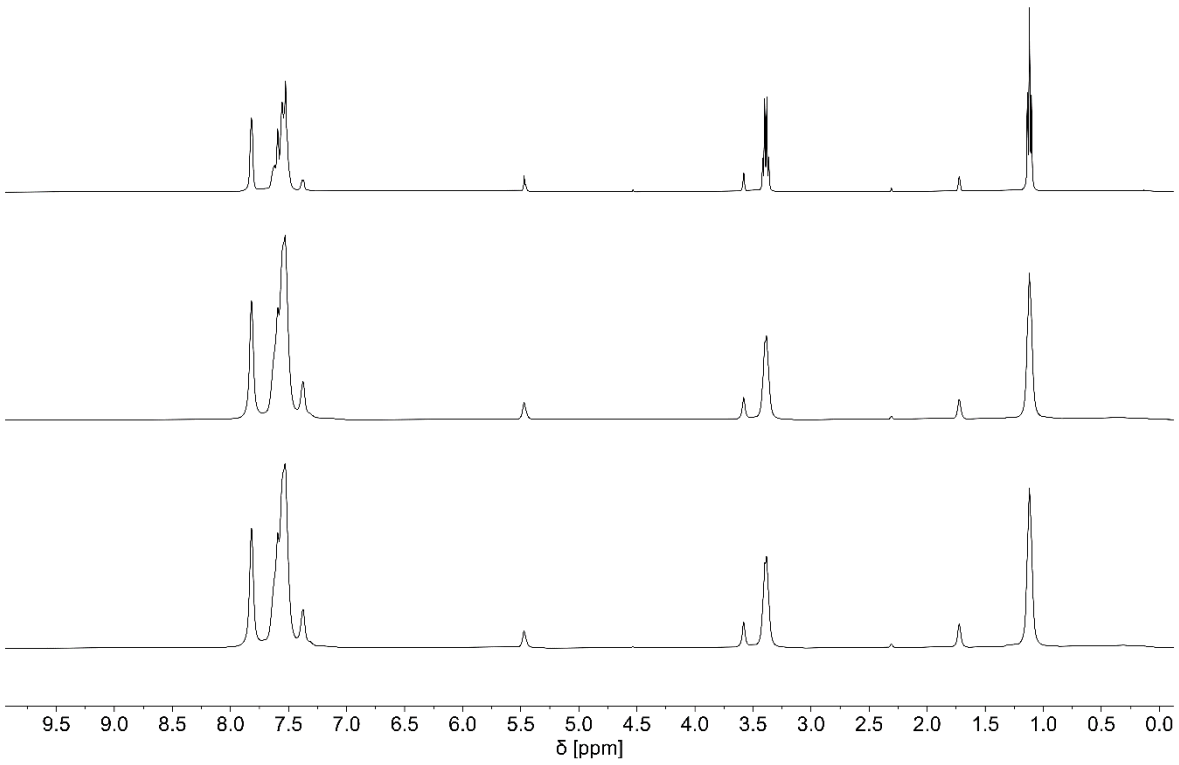

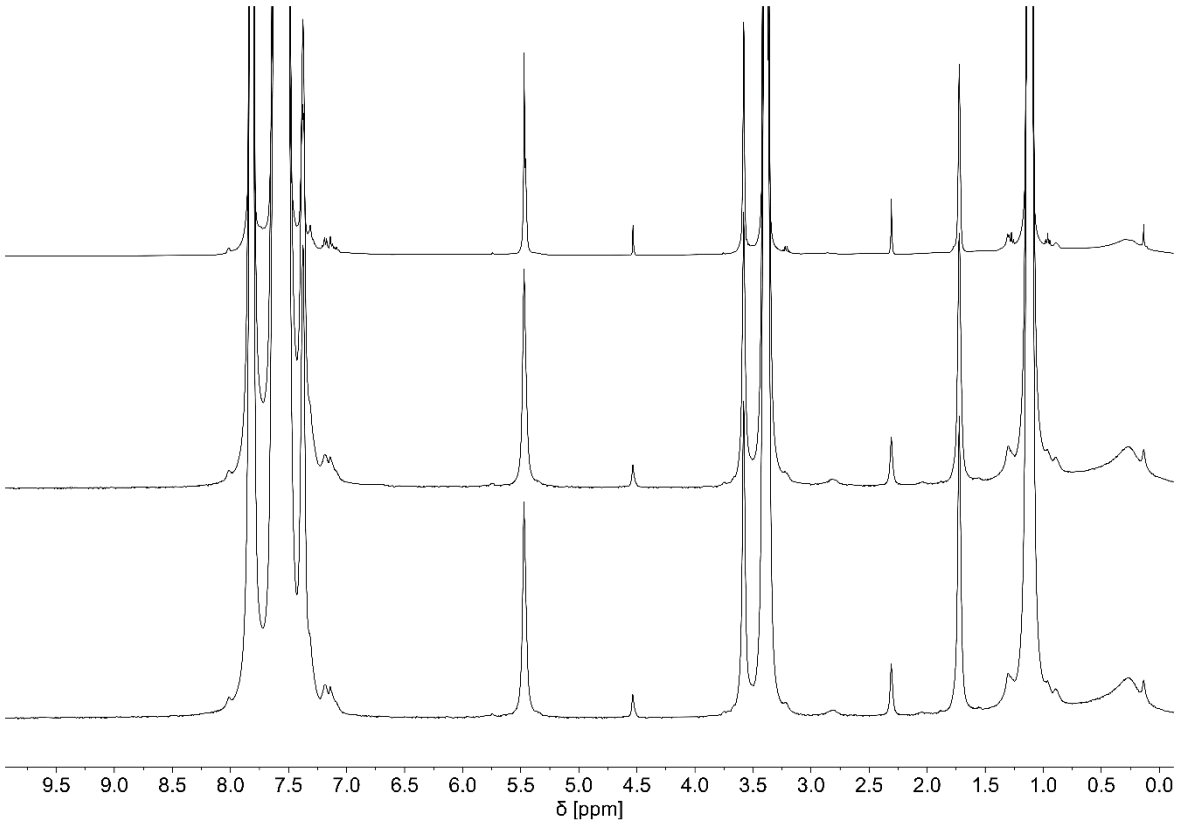

Figure S199. Proposed mechanism for the reaction between $[Tc(OH_2)(CO)_3(PPh_3)_2]^+$ and DMSO.

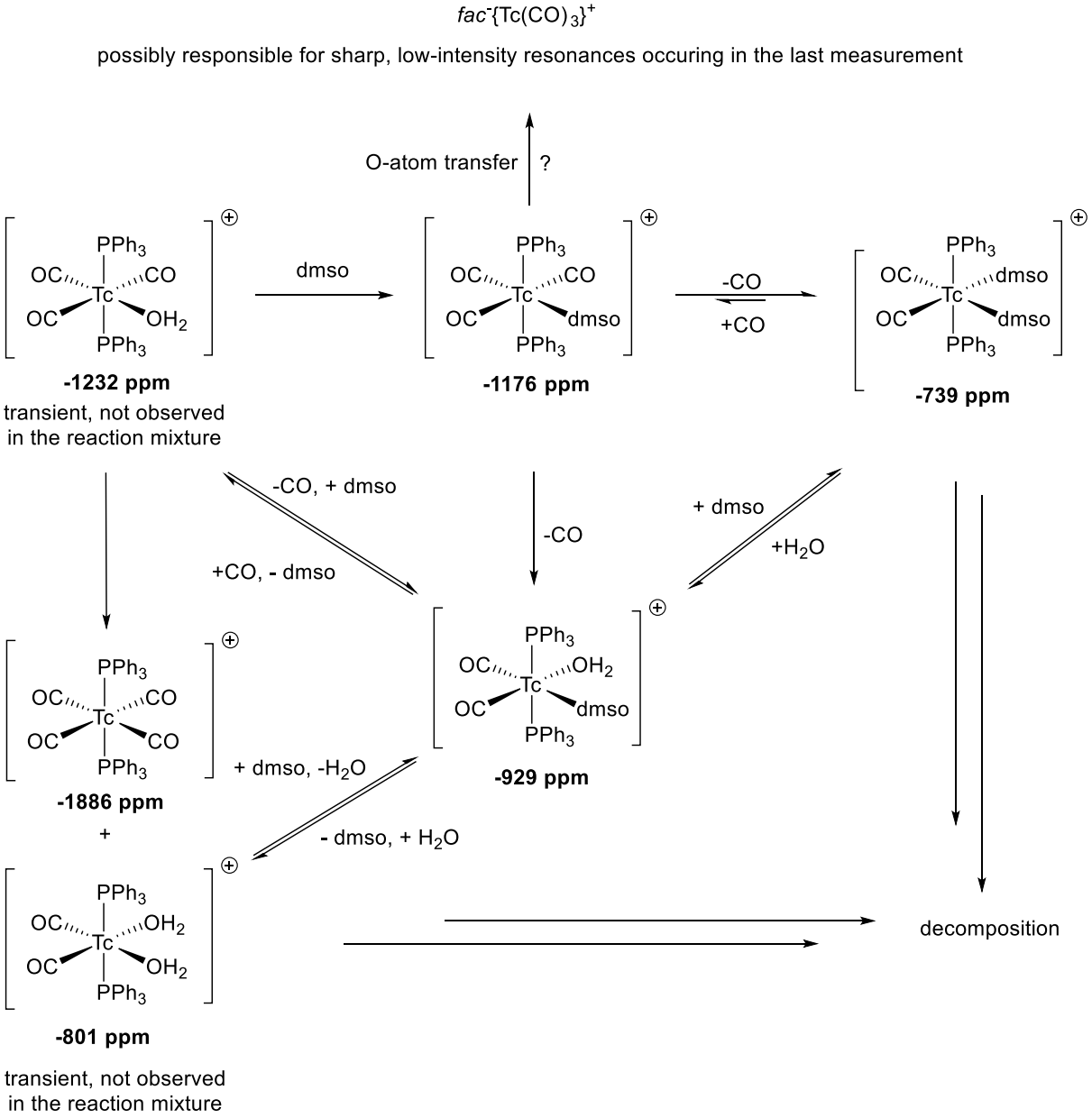

Figure S200. Estimated speciation of the reaction between $[Tc(OH_2)(CO)_3(PPh_3)_2]^+$ and DMSO based on (relative) ^{99}Tc NMR integrals.

The spectra were recorded on the same machine using the same measurement parameters such as offset, spectral width (3 ppt), scan number (10000 scans) and relaxation delay (0.01 µs). All spectra were processed the same: manual phase-correction, apodization (300 Hz, exponential), base-line correction by Whittaker Smoother algorithm with optimized parameters for optimal individual noise-suppression, simultaneous integration of the same regions in all spectra to ensure comparability. Given the large spectral range, the integrals are not valid as absolutes and do not allow for the determination of rate constants or accurate speciation estimates given the strong distortion along the gaussian-shaped pulse profile. The shown speciation is thus a rough, relative estimation.

Color-code: grey: $[Tc(DMSO)(CO)_3(PPh_3)_2]^+$, blue: $[Tc(DMSO)_2(CO)_2(PPh_3)_2]^+$, orange: proposed species $[Tc(DMSO)(OH_2)(CO)_2(PPh_3)_2]^+$, green: $[Tc(CO)_4(PPh_3)_2]^+$.

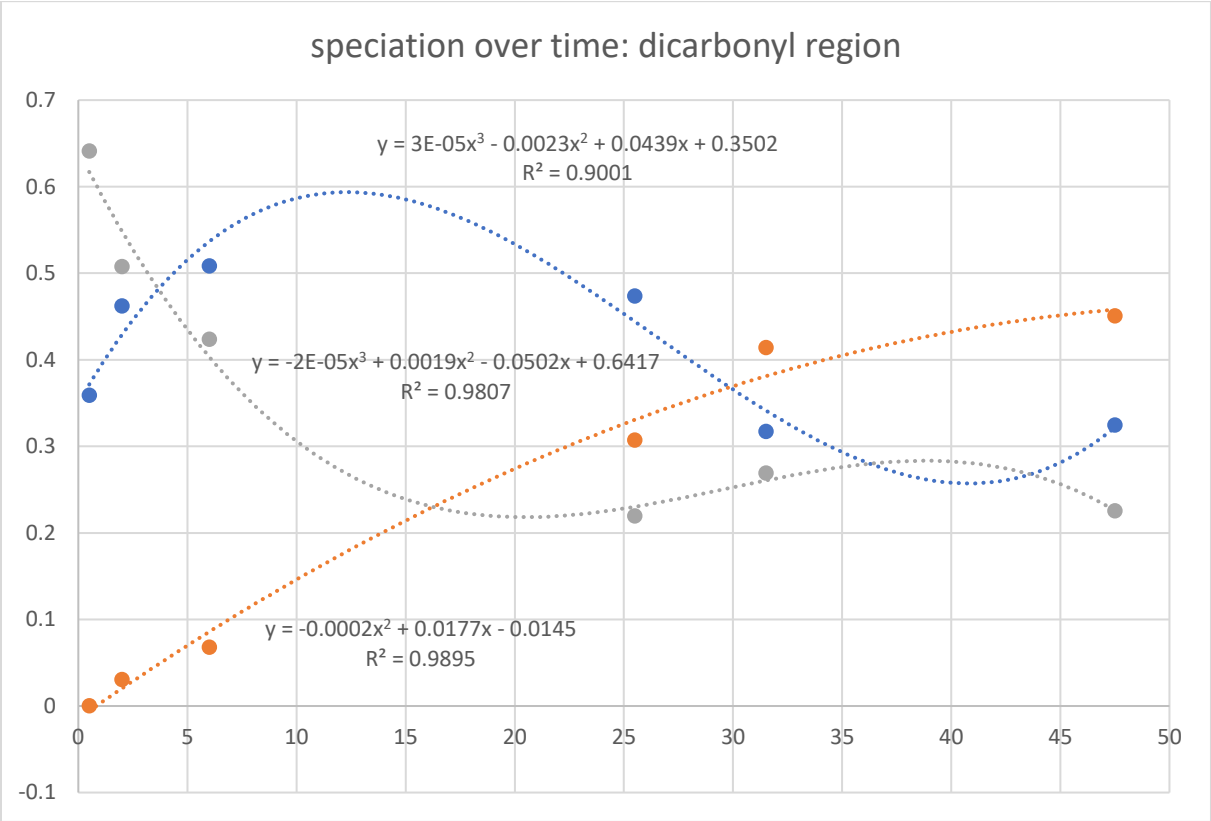

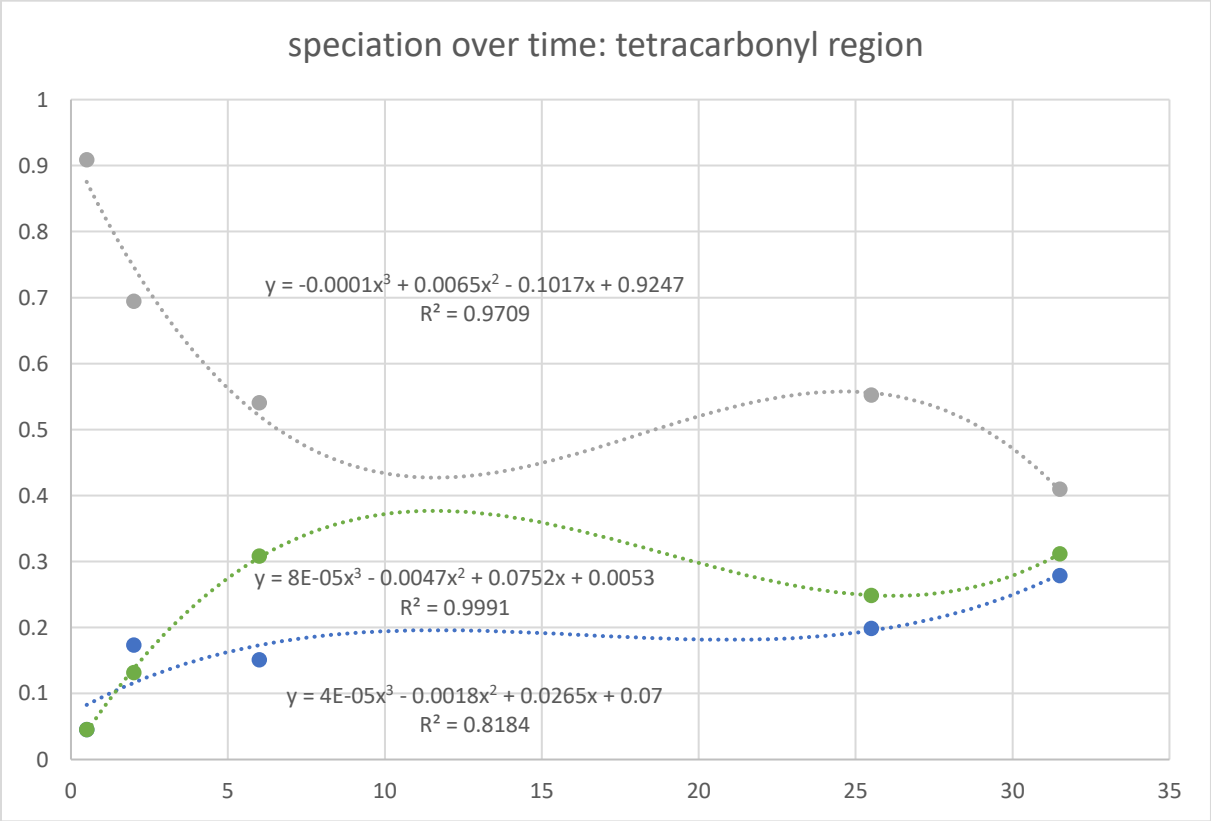

Figure S201. Initial ^{1}H NMR spectrum for the reaction between $[Tc(OH_2)(CO)_3(PPh_3)_2]^+$ and DMSO.

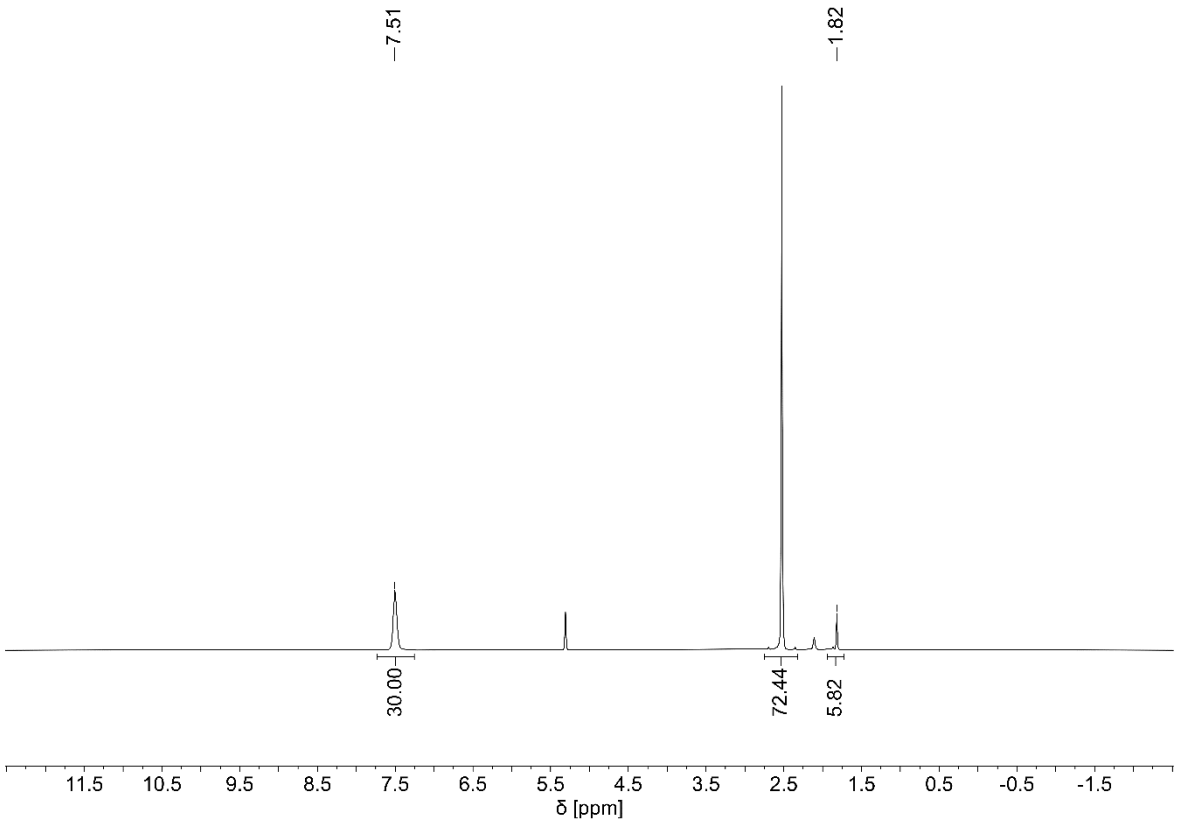

Figure S202. *In-situ* NMR spectrum of the reaction between $[Tc(OH_2)(CO)_3(PPh_3)_2]^+$ and DMSO. ^{99}Tc NMR spectrum focussed on the region around -1000 ppm after ca. 48 h.

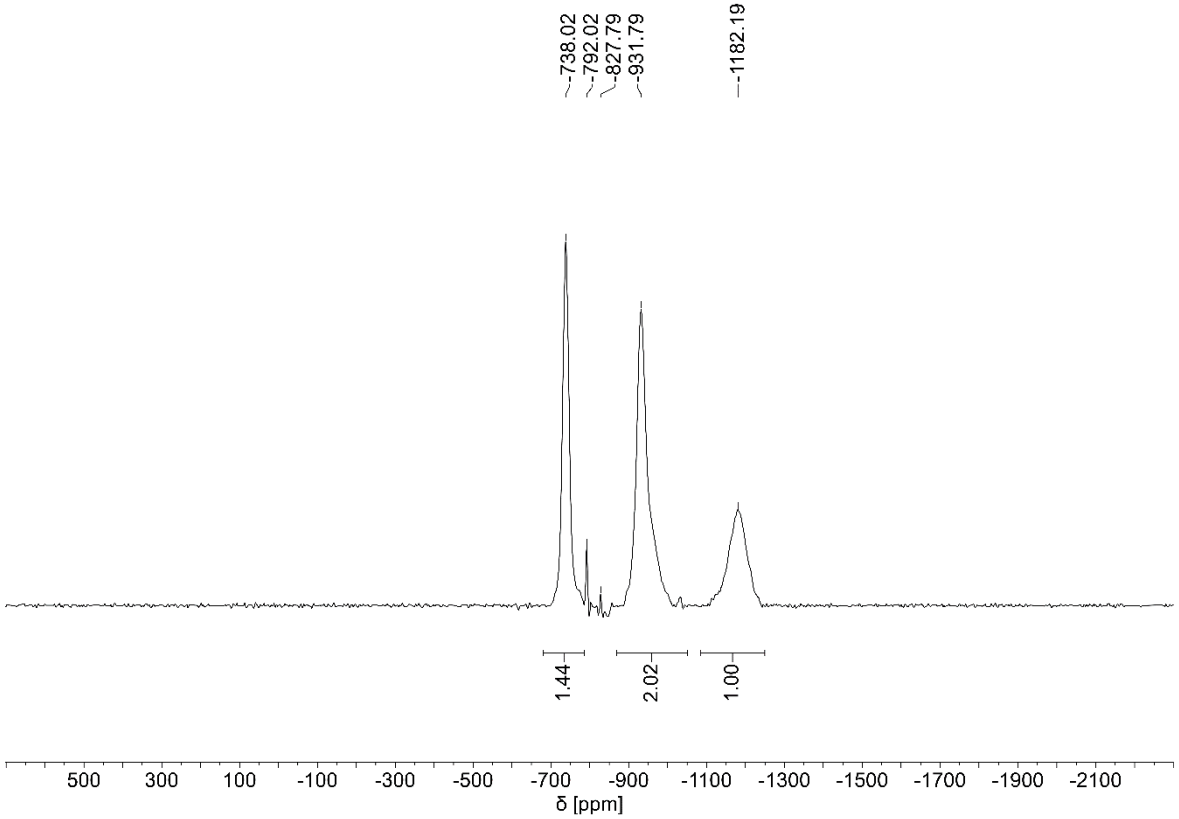

Figure S203. *In-situ* NMR spectrum of the reaction between $[Tc(OH_2)(CO)_3(PPh_3)_2]^+$ and DMSO. Stacking of ^{99}Tc-spectra focussed on the region around -1000 ppm.

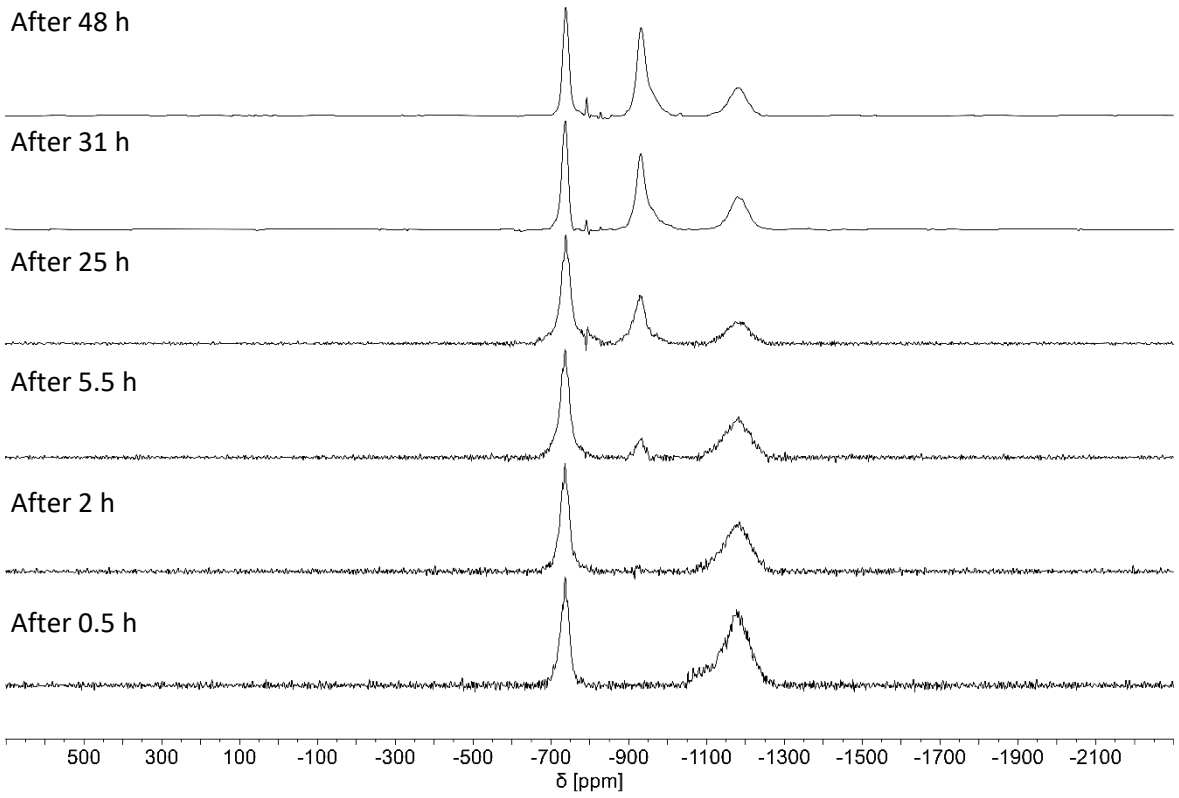

Figure S204. *In-situ* NMR spectrum of the reaction between $[Tc(OH_2)(CO)_3(PPh_3)_2]^+$ and DMSO. ^{99}Tc NMR spectrum focussed on the region around -1500 ppm after ca. 48 h.

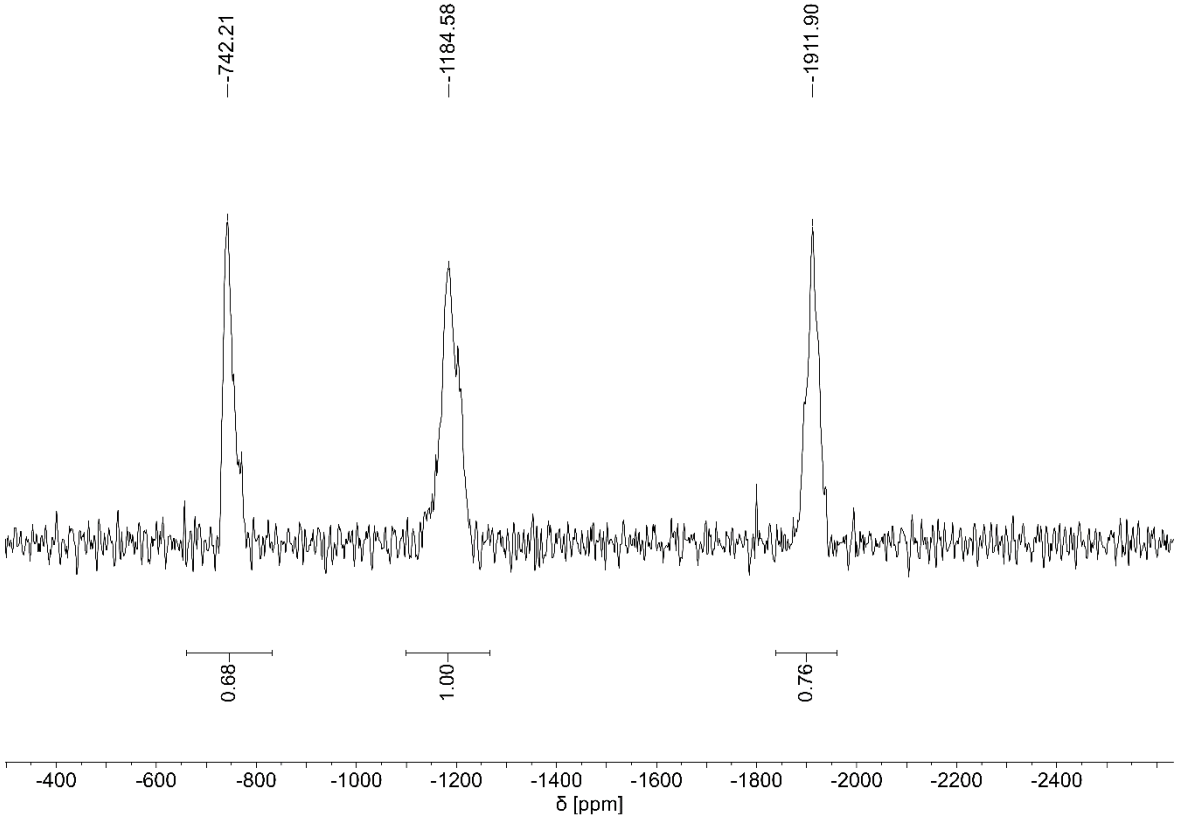

Figure S205. *In-situ* NMR spectra of the reaction between $[Tc(OH_2)(CO)_3(PPh_3)_2]^+$ and DMSO. Stacking of ^{99}Tc-spectra focussed on the region around -1000 ppm.

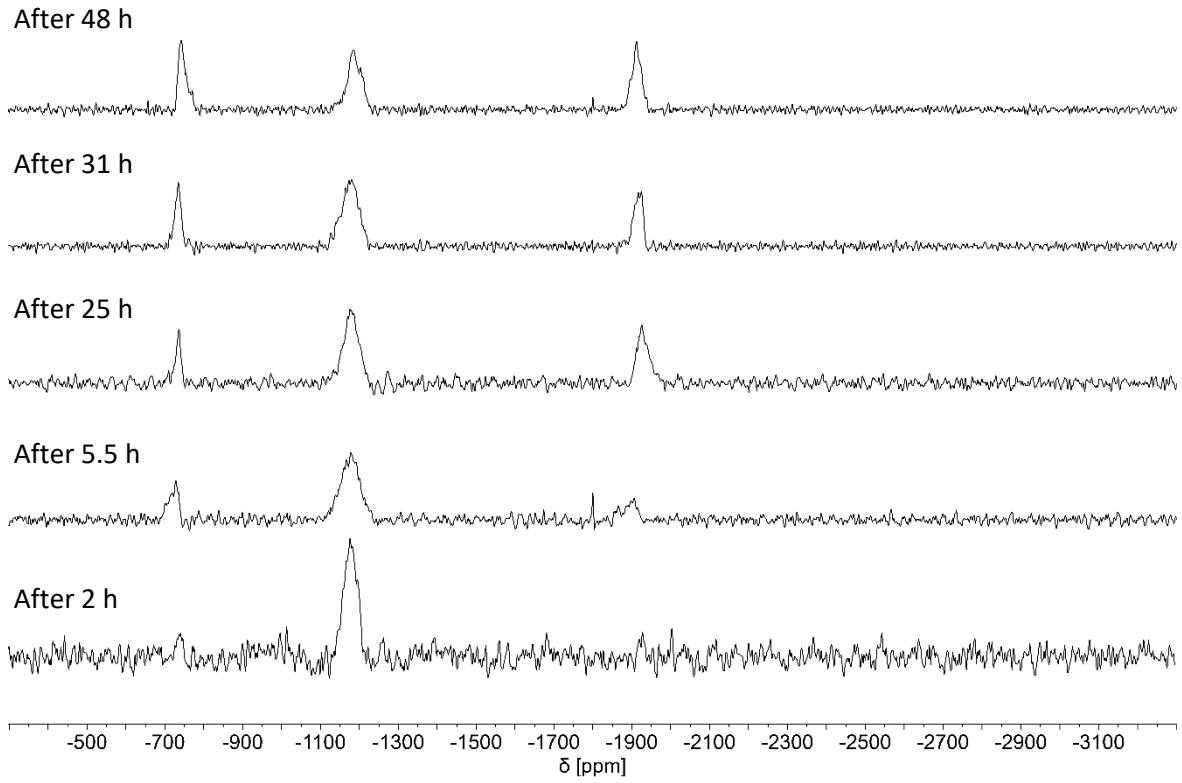

Figure S206. *In-situ* NMR spectra of the reaction between $[Tc(OH_2)(CO)_3(PPh_3)_2]^+$ and bpy without the addition of a base. Stacking of ^{99}Tc-spectra.

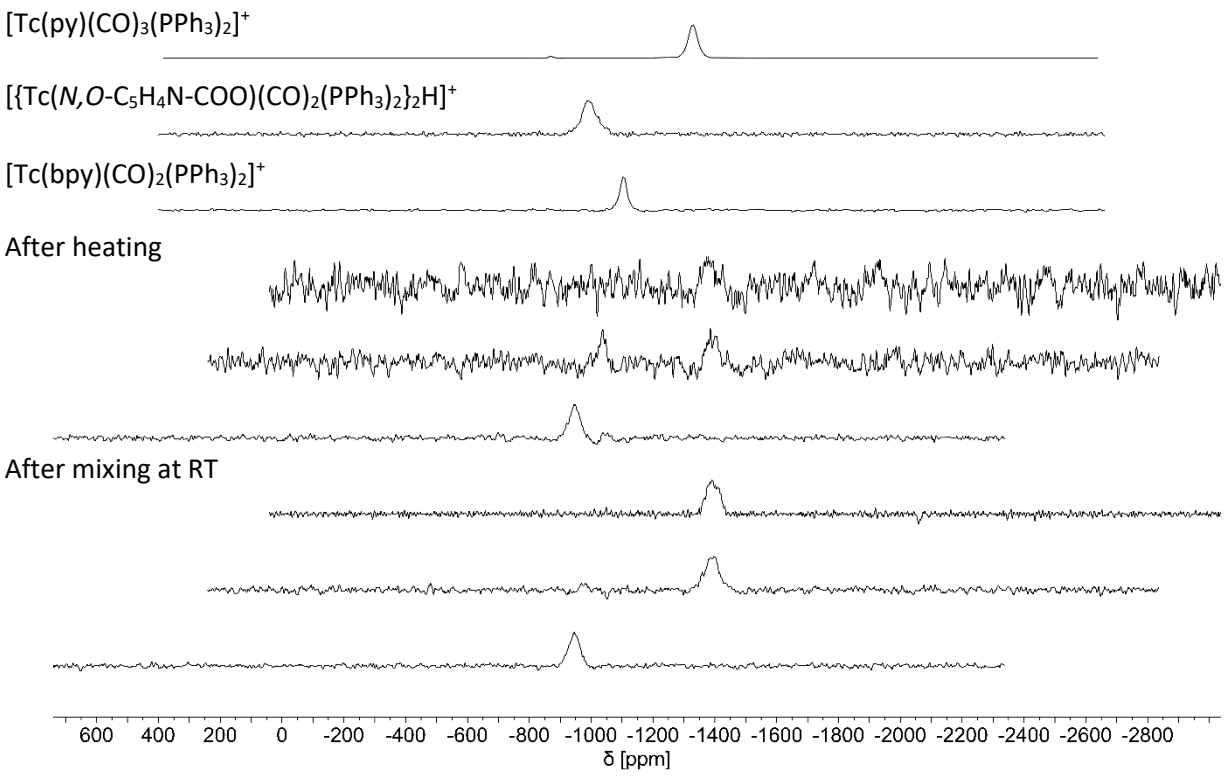

Part 3: Reference

(1) Menges, F. Spectragryph, Software for Optical Spectroscopy,Version 1.2.8, 2016–2020.

A.3 Technetium(I) Carbonyl Chemistry With Small Inorganic Ligands

Authors	M. Roca Jungfer, L. Elsholz, U. Abram
Journal	*Inorg. Chem.* **2022,** *61*, 2980-2997
DOI	10.1021/acs.inorgchem.1c03919
Link	https://pubs.acs.org/doi/abs/10.1021/acs.inorgchem.1c03919
Detailed scientific contribution	Maximilian Roca Jungfer and Ulrich Abram designed the project. Maximilian Roca Jungfer performed the synthesis and characterization of the compounds, performed DFT calculations, calculated the X-ray structures and wrote a draft of the manuscript. Laura Elsholz performed some of the experiments and DFT calculations during a research internship under the supervision of Maximilian Roca Jungfer. Ulrich Abram supervised the project, provided scientific guidance and suggestions and corrected the manuscript.
Estimated own contribution	80%

Return to publication 4.3.

Supporting information for the paper entitled:

Carbonyltechnetium(I) Chemistry with Small Inorganic Ligands.

Maximilian Roca Jungfer, Laura Elsholz, Ulrich Abram*

[a]*Freie Universität Berlin, Institute of Chemistry and Biochemistry, Fabeckstr. 34–36, 14195 Berlin, Germany*

E-mail: ulrich.abram@fu-berlin.de

Table of Contents

Part 1: Crystallographic data

Table S1. Crystal data and structure determination parameters.

	$[Tc(NCO)(OH_2)(CO)_2(PPh_3)_2]$	$[Tc(N_3)(CO)_3(PPh_3)_2]$	$[Tc(NCO)(CO)_3(PPh_3)_2]$
Number code	**4**	**5**	**6**
Empirical formula	$C_{39}H_{32}NO_4P_2Tc$	$C_{39}H_{30}N_3O_3P_2Tc$	$C_{40}H_{30}NO_4P_2Tc$
Formula weight	738.59	748.60	748.59
Temperature/K	240(2)	273(2)	100(2)
Crystal system	Monoclinic	Monoclinic	Triclinic
Space group	$P2_1/n$	$P2_1/n$	$P\bar{1}$
a/Å	12.2546(14)	12.2179(14)	9.2366(4)
b/Å	17.196(2)	16.9936(13)	10.1622(4)
c/Å	17.482(3)	17.879(2)	10.8215(4)
α/°	90	90	63.7160(10)
β/°	108.479(11)	108.405(9)	67.5400(10)
γ/°	90	90	82.407(2)
Volume/$Å^3$	3494.0(9)3	3522.2(7)3	840.81(6)3
Z	4	4	1
$\rho_{calc}g/cm^3$	1.404	1.412	1.478
μ/mm^{-1}	0.545	0.541	0.567
F(000)	1512	1528	382
Crystal size/mm^3	0.410 x 0.187 x 0.070	0.340 x 0.101 x 0.070	0.272 x 0.176 x 0.035
Radiation	0.71073	0.71073	0.71073
2Θ range for data collection/°	3.400 to 25.985	3.394 to 29.359	2.237 to 27.906
Index ranges	-15<=h<=15, -21<=k<=21, -16<=l<=21	-14<=h<=16, -23<=k<=20, -24<=l<=24	-12<=h<=12, -13<=k<=13, -14<=l<=13
Reflections collected	18105	26815	19199
Independent reflections	6807 [R(int) = 0.0858]	9492 [R(int) = 0.1432]	4012 [R(int) = 0.0599]
Data/restraints/parameters	6807 / 580 / 452	9492 / 81 / 473	4012 / 198 / 241
Goodness-of-fit on F^2	0.848	0.981	1.082
Final R indexes [I>=2σ (I)]	R1 = 0.0541, wR2 = 0.0832	R1 = 0.0815, wR2 = 0.1639	R1 = 0.0344, wR2 = 0.0819
Final R indexes [all data]	R1 = 0.1594, wR2 = 0.1051	R1 = 0.1781, wR2 = 0.2013	R1 = 0.0399, wR2 = 0.0851
Largest diff. peak/hole / e^{-3}	0.324 and -0.327	1.137 and -1.079	0.897 and -1.023
CCDC access code	2127177	2127178	2127179

Table S1. Crystal data and structure determination parameters (continued).

	$[Tc(NCS)(CO)_3(PPh_3)_2]$ triclinic	$[Tc(NCS)(CO)_3(PPh_3)_2]$ monoclinic	$[Tc(CN)(CO)_3(PPh_3)_2]$
Number code	**7**	**7**	**9**
Empirical formula	$C_{40}H_{30}NO_3P_2STc$	$C_{40}H_{30}NO_3P_2STc$	$C_{40}H_{30}NO_3P_2Tc$
Formula weight	764.65	764.65	732.59
Temperature/K	230(2)	230(2)	230(2)
Crystal system	Triclinic	Monoclinic	Triclinic
Space group	$P\bar{1}$	$P2_1/c$	$P\bar{1}$
a/Å	10.2662(8)	19.4399(8)	10.2496(10)
b/Å	10.6455(7)	9.9074(3)	10.6673(11)
c/Å	17.4705(13)	20.9425(8)	25.710(3)
α/°	76.961(6)	90	88.181(8)
β/°	78.921(6)	117.450(3)	84.192(8)
γ/°	71.139(6)	90	65.324(8)
Volume/Å^3	1745.4(2)	3579.4(2)	2541.0(5)
Z	2	4	3
ρ_{calc}g/cm^3	1.455	1.419	1.436
μ/mm^{-1}	0.604	0.589	0.559
F(000)	780	1560	1122
Crystal size/mm^3	0.15 x 0.13 x 0.07	0.330 x 0.183 x 0.110	0.240 x 0.127 x 0.061
Radiation	0.71073	0.71073	0.71073
2Θ range for data collection/°	3.409 to 29.265	3.543 to 29.274	3.400 to 28.000
Index ranges	-14<=h<=14, -14<=k<=14, -21<=l<=23	-26<=h<=24, -13<=k<=13, -28<=l<=28	-13<=h<=13, -14<=k<=14, -33<=l<=33
Reflections collected	20393	42071	25232
Independent reflections	9370 [R(int) = 0.0580]	9653 [R(int) = 0.0384]	11890 [R(int) = 0.1180]
Data/restraints/parameters	9370 / 0 / 433	9653 / 0 / 433	11890 / 0 / 637
Goodness-of-fit on F^2	0.834	0.945	0.852
Final R indexes [I>=2σ (I)]	R1 = 0.0360, wR2 = 0.0667	R1 = 0.0262, wR2 = 0.0603	R1 = 0.0605, wR2 = 0.1188
Final R indexes [all data]	R1 = 0.0682, wR2 = 0.0725	R1 = 0.0388, wR2 = 0.0629	R1 = 0.1472, wR2 = 0.1444
Largest diff. peak/hole / e^{-3}	0.365 and -0.873	0.350 and -0.581	0.962 and -1.185
CCDC access code	2127180	2127181	2127182

Table S1. Crystal data and structure determination parameters (continued).

	$[Tc(CN)(CO)_3(PPh_3)_2] \cdot MeOH$	$[Tc(\eta^2\text{-}OON)(CO)_2(PPh_3)_2]$	$[Tc(\eta^1\text{-}NO_2)(CO)_3(PPh_3)_2]$/ $[Tc(\eta^1\text{-}ONO)(CO)_3(PPh_3)_2]$
Number code	**9** · MeOH	**10**	**11a/11b**
Empirical formula	$C_{41}H_{34}NO_4P_2Tc$	$C_{38}H_{30}NO_4P_2Tc$	$C_{39}H_{30}NO_5P_2Tc$
Formula weight	764.63	724.57	752.58
Temperature/K	230(2)	200(2)	200(2)
Crystal system	Triclinic	Triclinic	Triclinic
Space group	$P\bar{1}$	$P\bar{1}$	$P\bar{1}$
a/Å	10.5113(5)	10.2339(11)	10.1042(10)
b/Å	12.5923(6)	10.6602(12)	10.5710(10)
c/Å	15.7943(7)	18.386(2)	18.315(2)
α/°	96.311(4)	73.243(9)	77.442(8)
β/°	105.040(3)	74.618(8)	75.403(8)
γ/°	111.858(3)	61.997(8)	66.521(7)
Volume/$Å^3$	1823.37(15)	1675.6(4)	1721.2(3)
Z	2	2	2
$\rho_{calc}g/cm^3$	1.393	1.436	1.452
μ/mm^{-1}	0.525	0.566	0.557
F(000)	784	740	768
Crystal size/mm^3	0.820 x 0.420 x 0.310	0.390 x 0.110 x 0.010	0.300 x 0.160 x 0.060
Radiation	0.71073	0.71073	0.71073
2Θ range for data collection/°	3.529 to 29.152	3.513 to 26.000	3.342 to 26.996
Index ranges	-14<=h<=14, -17<=k<=14, -21<=l<=21	-12<=h<=12, -13<=k<=13, -22<=l<=22	-12<=h<=12, -13<=k<=13, -23<=l<=22
Reflections collected	21119	14568	15707
Independent reflections	9732 [R(int) = 0.0552]	6563 [R(int) = 0.0892]	7464 [R(int) = 0.0794]
Data/restraints/parameters	9732 / 8 / 493	6563 / 0 / 415	7464 / 14 / 455
Goodness-of-fit on F^2	1.020	1.015	0.896
Final R indexes [I>=2σ (I)]	R1 = 0.0338, wR2 = 0.0910	R1 = 0.0622, wR2 = 0.1349	R1 = 0.0470, wR2 = 0.1049
Final R indexes [all data]	R1 = 0.0402, wR2 = 0.0939	R1 = 0.1213, wR2 = 0.1464	R1 = 0.0885, wR2 = 0.1189
Largest diff. peak/hole / e^{-3}	0.660 and -1.085	0.769 and -0.760	0.516 and -0.994
CCDC access code	2127183	2127185	2127184

Table S1. Crystal data and structure determination parameters (continued).

	[Tc(η^2-OONO)(CO)$_2$(PPh$_3$)$_2$]	[Tc(η^2-HHBH$_2$)(CO)$_2$(PPh$_3$)$_2$]	[Tc(η^2-SSCCH$_3$)(CO)$_2$(PPh$_3$)$_2$]/ [Tc(η^2-SSCSCH$_3$)(CO)$_3$(PPh$_3$)$_2$]
Number Code	**12**	**15**	**17/18a**
Empirical formula	$C_{38}H_{30}NO_5P_2Tc$	$C_{38}H_{34}BO_2P_2Tc$	$C_{40}H_{33}O_2P_2S_{2.54}Tc$
Formula weight	740.57	693.40	787.05
Temperature/K	100(2)	100(2)	100(2)
Crystal system	Orthorhombic	Monoclinic	Triclinic
Space group	*Pbcn*	*I*2/*a*	$P\bar{1}$
a/Å	19.1642(5)	15.8758(9)	9.0253(4)
b/Å	10.8834(3)	9.5516(5)	11.1374(5)
c/Å	15.6788(3)	22.6354(16)	18.9056(9)
α/°	90	90	100.1920(10)
β/°	90	105.060(2)	94.479(2)
γ/°	90	90	104.7360(10)
Volume/Å^3	3270.15(14)	3314.5(3)	1793.66(14)
Z	4	4	2
ρ_{calc}g/cm^3	1.504	1.390	1.457
μ/mm^{-1}	0.584	0.564	0.673
F(000)	1512	1424	805
Crystal size/mm^3	0.160 x 0.110 x 0.070	0.08 x 0.07 x 0.01	0.210 x 0.130 x 0.010
Radiation	0.71073	0.71073	0.71073
2Θ range for data collection/°	2.125 to 27.888	2.327 to 26.386	2.208 to 27.910
Index ranges	-25<=h<=23, -14<=k<=14, -20<=l<=19	-19<=h<=19, -11<=k<=11, -28<=l<=28	-11<=h<=11, -14<=k<=14, -24<=l<=24
Reflections collected	48812	50795	49373
Independent reflections	3911 [R(int) = 0.0488]	3395 [R(int) = 0.0382]	8561 [R(int) = 0.0890]
Data/restraints/parameters	3911 / 0 / 214	3395 / 9 / 234	8561 / 0 / 470
Goodness-of-fit on F^2	1.081	1.059	1.182
Final R indexes [I>=2σ (I)]	R1 = 0.0700, wR2 = 0.1698	R1 = 0.0276, wR2 = 0.0695	R1 = 0.0610, wR2 = 0.1086
Final R indexes [all data]	R1 = 0.0759, wR2 = 0.1744	R1 = 0.0297, wR2 = 0.0708	R1 = 0.0789, wR2 = 0.1144
Largest diff. peak/hole / e^{-3}	3.180 and -1.571	1.069 and -0.502	0.818 and -1.759
CCDC access code	2127186	2127187	2127188

Table S1. Crystal data and structure determination parameters (continued).

	[Tc(SSCH)(CO)$_2$(PPh$_3$)$_2$]	[Tc(η^1-OTcO$_3$)(CO)$_3$(PPh$_3$)$_2$]	[Tc(η^1-OTcO$_3$)(CO)$_3$(PPh$_3$)$_2$] ·benzene
Number code	**20**	**21**	**21·benzene**
Empirical formula	$C_{39}H_{31}O_2P_2S_2Tc$	$C_{39}H_{30}O_7P_2Tc_2$	$C_{45}H_{36}O_7P_2Tc_2$
Formula weight	755.70	868.57	946.68
Temperature/K	200(2)	100(2)	200(2)
Crystal system	Triclinic	Monoclinic	Triclinic
Space group	$P\bar{1}$	$P2_1/n$	$P\bar{1}$
a/Å	10.2100(12)	10.111(3)	12.3055(15)
b/Å	12.8433(17)	27.243(5)	12.8227(17)
c/Å	14.484(2)	13.129(4)	14.7115(19)
α/°	69.523(10)	90	92.223(11)
β/°	74.934(10)	97.675(8)	99.914(10)
γ/°	81.285(10)	90	114.031(9)
Volume/Å^3	1714.3(4)	3583.9(17)	2073.1(5)
Z	2	4	2
ρ_{calc}g/cm^3	1.464	1.610	1.517
μ/mm^{-1}	0.669	0.910	0.794
F(000)	772	1744	956
Crystal size/mm^3	0.190 x 0.060 x 0.055	0.300 x 0.050 x 0.020	0.230 x 0.120 x 0.060
Radiation	0.71073	0.71073	0.71073
2Θ range for data collection/°	1.884 to 25.999	2.165 to 27.888	3.292 to 25.998
Index ranges	-12<=h<=12, -15<=k<=15, -17<=l<=17	-13<=h<=13, -32<=k<=35, -17<=l<=17	-14<=h<=15, -15<=k<=14, -18<=l<=18
Reflections collected	14766	59160	17941
Independent reflections	6731 [R(int) = 0.0842]	8558 [R(int) = 0.1027]	8092 [R(int) = 0.0743]
Data/restraints/parameters	6731 / 0 / 460	8558 / 0 / 451	8092 / 608 / 493
Goodness-of-fit on F^2	0.806	1.036	0.821
Final R indexes [I>=2σ (I)]	R1 = 0.0428, wR2 = 0.0737	R1 = 0.0458, wR2 = 0.1075	R1 = 0.0456, wR2 = 0.0729
Final R indexes [all data]	R1 = 0.1067, wR2 = 0.0878	R1 = 0.0596, wR2 = 0.1153	R1 = 0.1137, wR2 = 0.0868
Largest diff. peak/hole / e^{-3}	0.363 and -1.069	0.984 and -1.578	0.522 and -0.589
CCDC access code	2127189	2127190	2127191

Table S1. Crystal data and structure determination parameters (continued).

	[Tc(η^1-OTcO$_3$)(acetone)(CO)$_2$(PPh$_3$)$_2$] ·acetone
Number code	**23c·acetone**
Empirical formula	$C_{44}H_{42}O_8P_2Tc_2$
Formula weight	956.71
Temperature/K	200(2)
Crystal system	Triclinic
Space group	$P\bar{1}$
a/Å	12.439(2)
b/Å	12.970(2)
c/Å	15.233(2)
α/°	79.022(13)
β/°	79.243(13)
γ/°	62.793(12)
Volume/Å^3	2131.7(6)
Z	2
ρ_{calc}g/cm^3	1.490
μ/mm^{-1}	0.774
F(000)	972
Crystal size/mm^3	0.140 x 0.100 x 0.030
Radiation	0.71073
2Θ range for data collection/°	3.214 to 25.998
Index ranges	-15<=h<=13, -15<=k<=15, -18<=l<=18
Reflections collected	18151
Independent reflections	8301 [R(int) = 0.1712]
Data/restraints/parameters	8301 / 608 / 505
Goodness-of-fit on F^2	0.809
Final R indexes [I>=2σ (I)]	R1 = 0.0768, wR2 = 0.1565
Final R indexes [all data]	R1 = 0.2365, wR2 = 0.2017
Largest diff. peak/hole / e^{-3}	1.140 and -0.668
CCDC access code	2127192

Figure S1. Ellipsoid representation (50% probability) of [Tc(NCO)(OH_2)$(CO)_2(PPh_3)_2$] (**4**). Hydrogen atoms bonded to carbon atoms are omitted for clarity. The water hydrogen atom positions were taken from the density map; however they could not be refined freely and were therefore not refined. The aqua ligand and one carbonyl group are disordered with an occupancy of 80% for the major component.

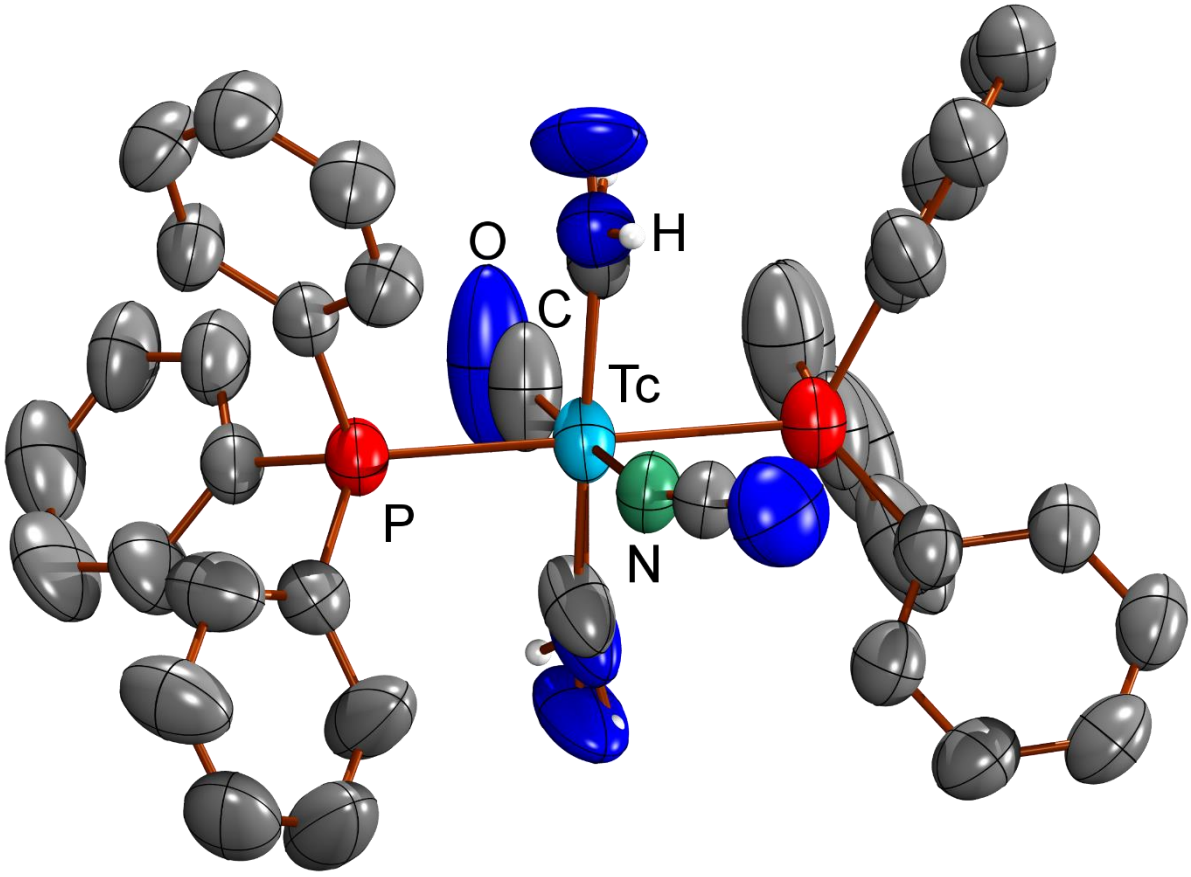

Figure S2. Representation of the dimeric structure of [Tc(NCO)(OH_2)$(CO)_2(PPh_3)_2$] (**4**) resulting from solid-state interactions with a molecule in a neighboring unit cell (symmetry code: -x. -y+1, -z).

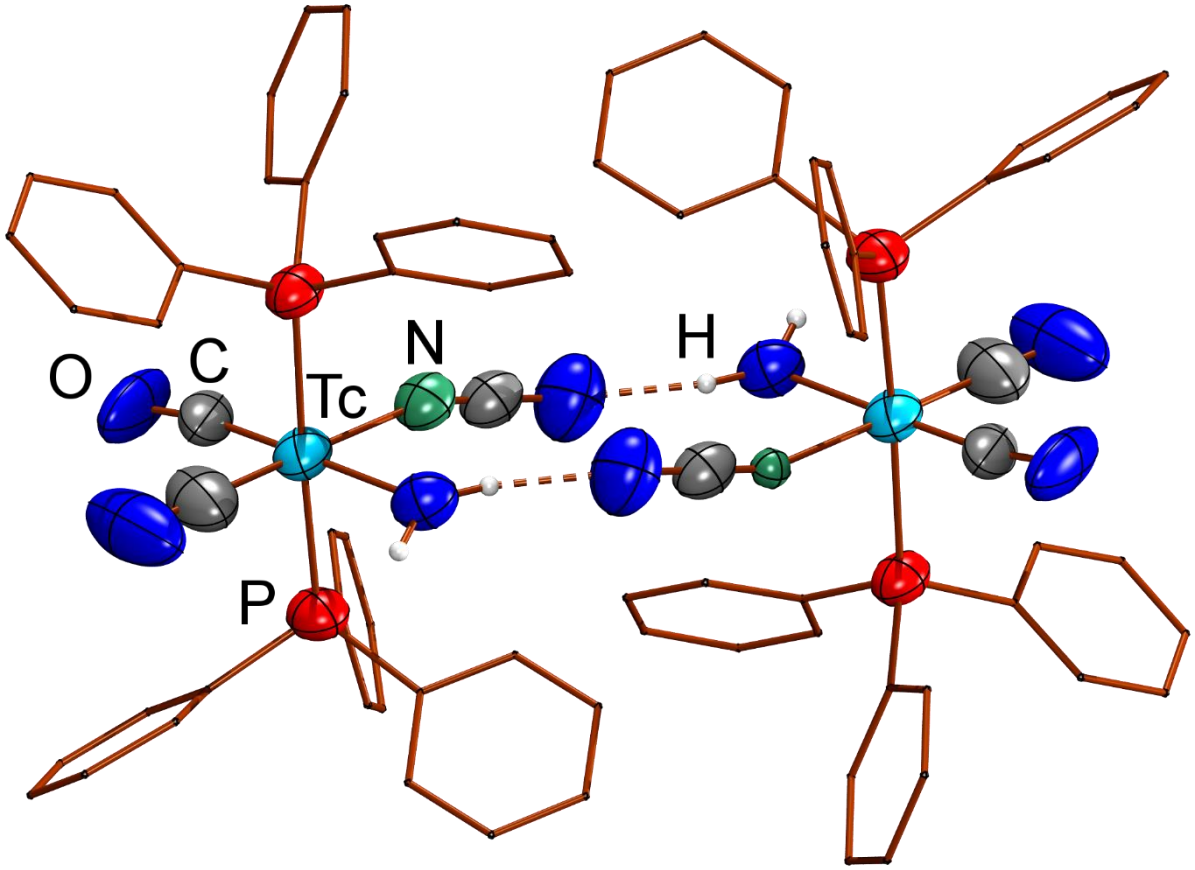

Figure S3. Ellipsoid representation (50% probability) of $[Tc(N_3)(CO)_3(PPh_3)_2]$ (**5**). Hydrogen atoms are omitted for clarity. The azido ligand is disordered with one of the carbonyl ligands. The major component of the disorder accounts for ca. 70% occupancy.

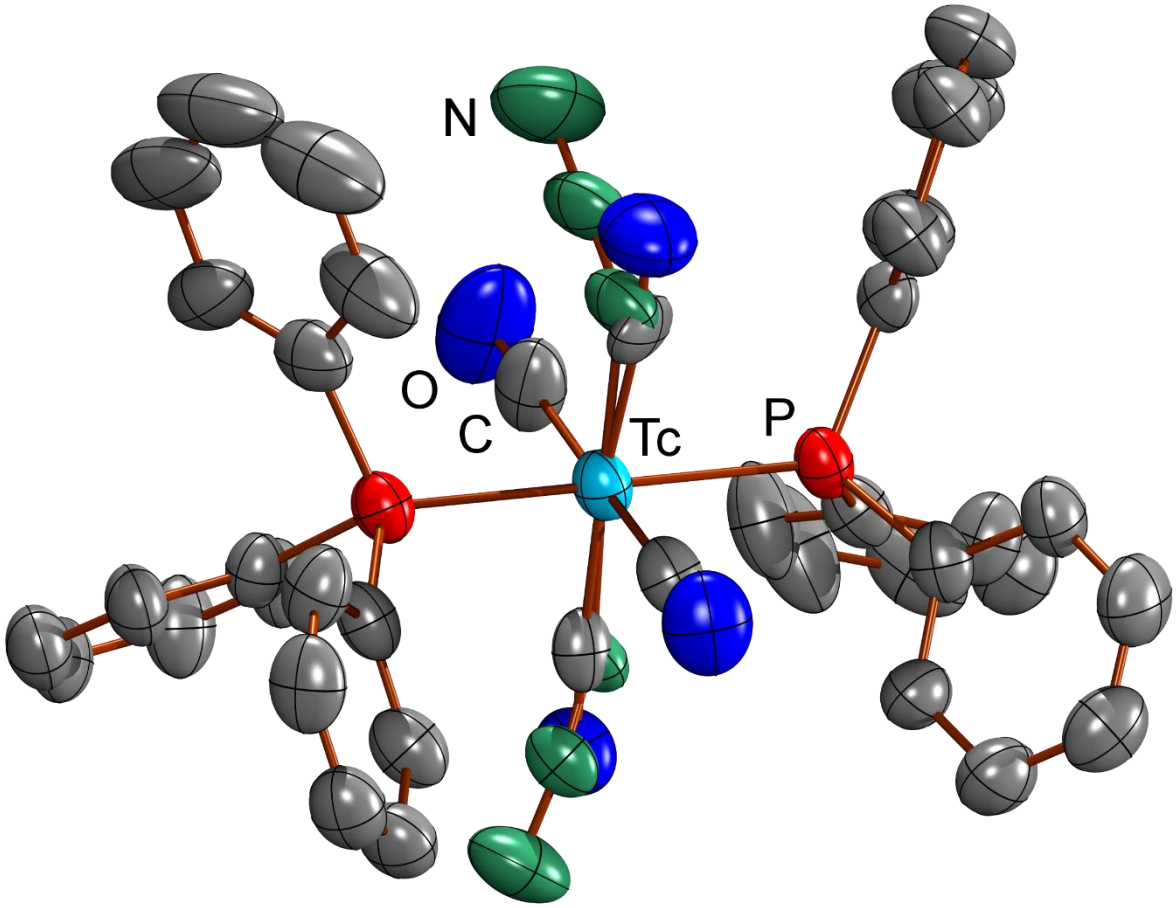

Figure S4. Ellipsoid representation (50% probability) of [Tc(NCO)$(CO)_3(PPh_3)_2$] (**6**). Hydrogen atoms are omitted for clarity. Half of the molecule is generated via the space-group symmetry. The isocyanato ligand is disordered with one of the carbonyl ligands through the space-group symmetry (50% occupancy each). DELU and RIGU instructions with 'smaller than usual' standard uncertainties of 0.001 were used due to proximity of the disordered NCO and CO moieties to the space group symmetry.

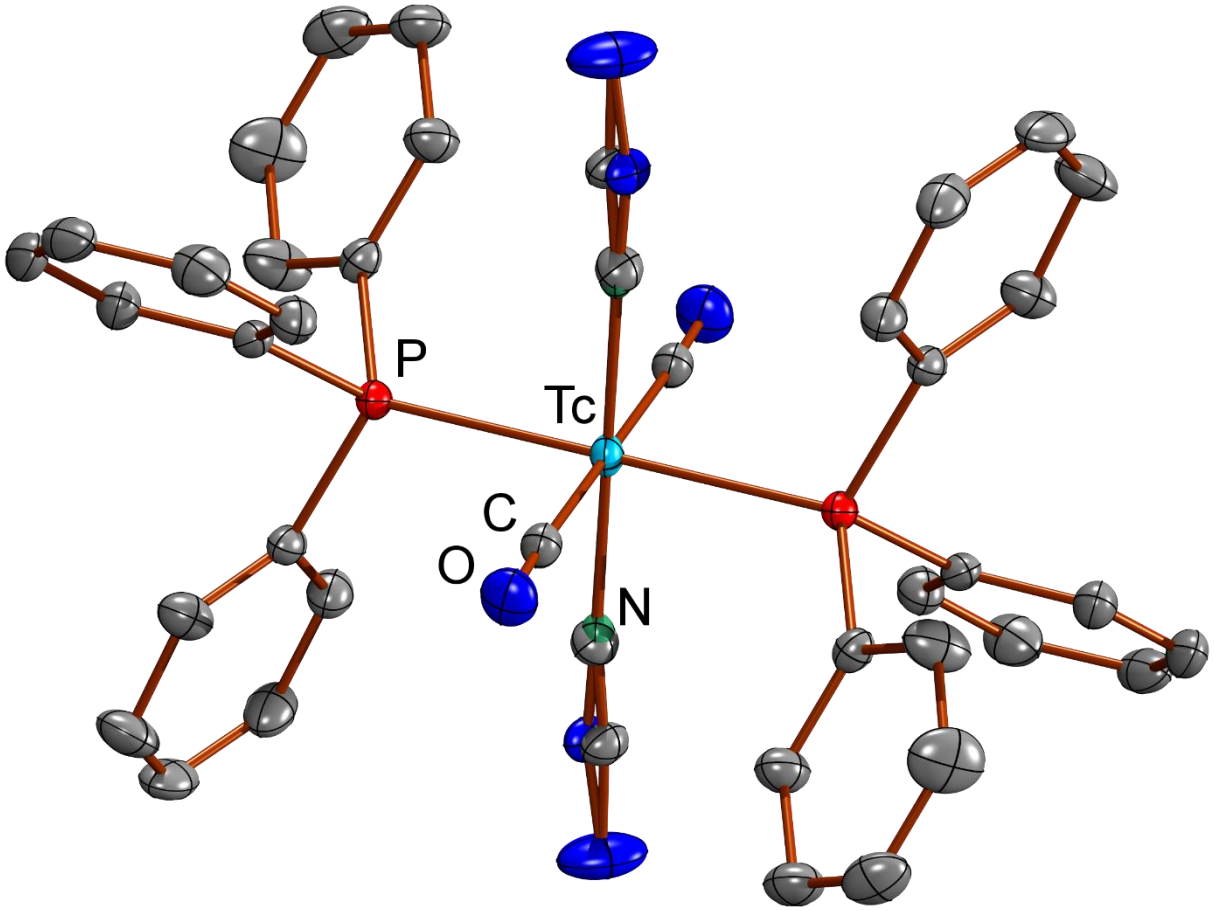

Figure S5. Ellipsoid representation (50% probability) of [Tc(NCS)$(CO)_3(PPh_3)_2$] (**7**) in the triclinic polymorph of the compound. Hydrogen atoms are omitted for clarity.

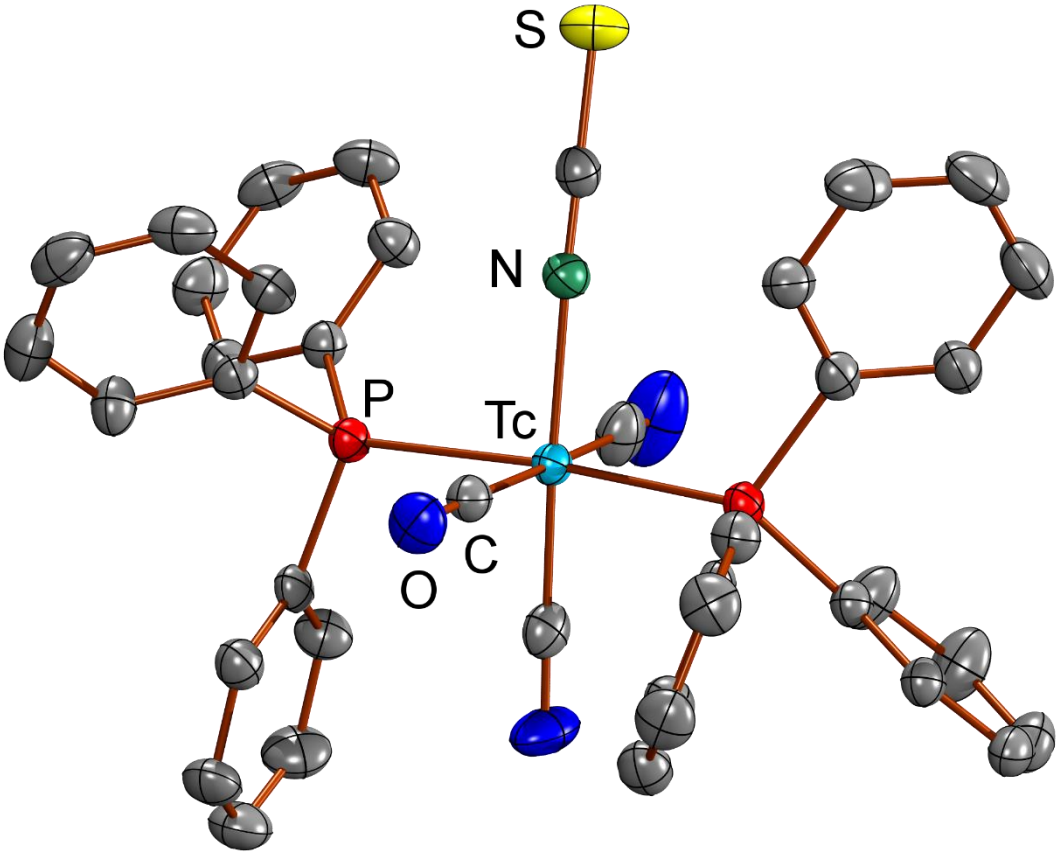

Figure S6. Ellipsoid representation (50% probability) of [Tc(NCS)$(CO)_3(PPh_3)_2$] (**7**) in the monoclinic polymorph of the compound. Hydrogen atoms are omitted for clarity.

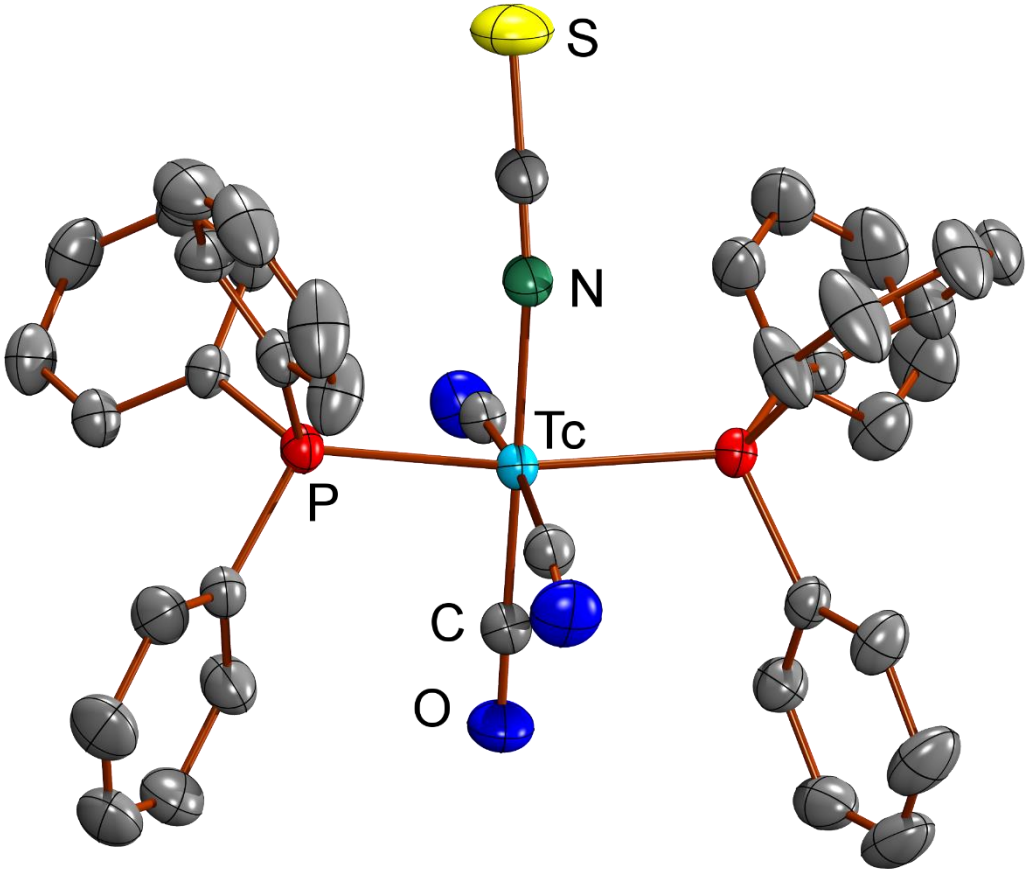

Figure S7. Ellipsoid representation (50% probability) of [Tc(CN)$(CO)_3(PPh_3)_2$] (**9**) in the triclinic polymorph of the compound. Hydrogen atoms are omitted for clarity. The three carbonyl and one cyanido ligands are indistinguishably disordered over the four equatorial ligand sites with an occupational ratio of 75:25 for each position.

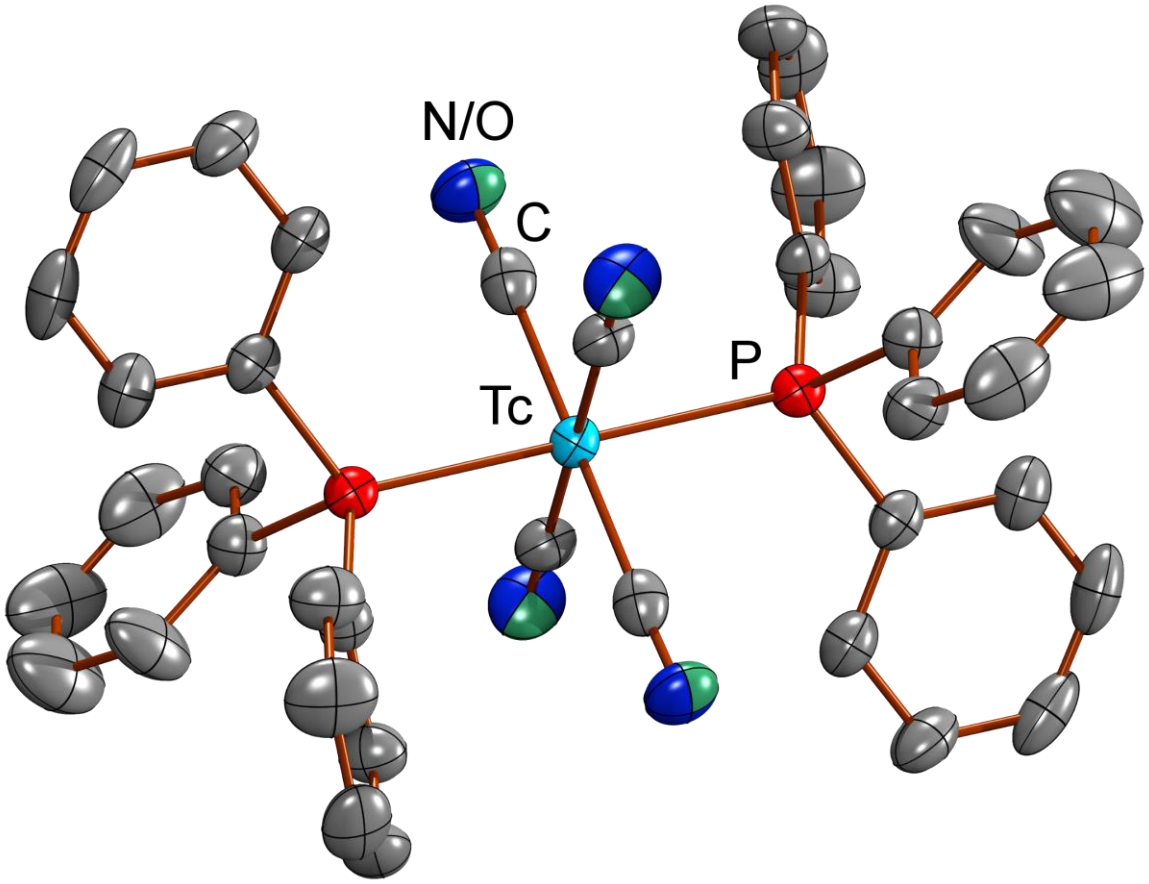

Figure S8. Ellipsoid representation (50% probability) of [Tc(CN)(CO)$_3$(PPh$_3$)$_2$] (**9**) · MeOH. Hydrogen atoms bonded to carbon atoms are omitted for clarity. The hydrogen atom of the co-crystallized solvent methanol was localized in the density map and refined freely. One of the phenyl rings in one triphenylphosphine moiety is disordered with 80% occupancy for the major component.

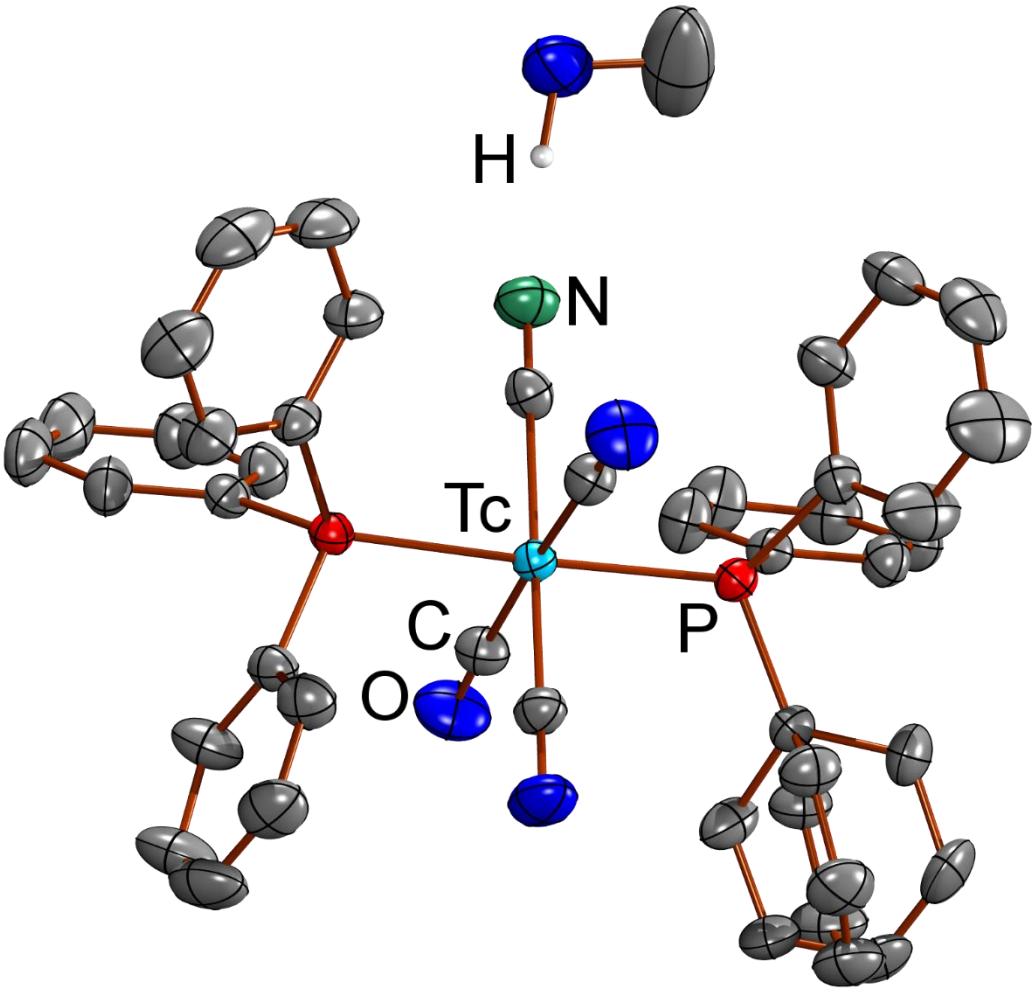

Figure S9. Ellipsoid representation (50% probability) of [Tc(η^2-OON)$(CO)_2(PPh_3)_2$] (**10**). Hydrogen atoms are omitted for clarity.

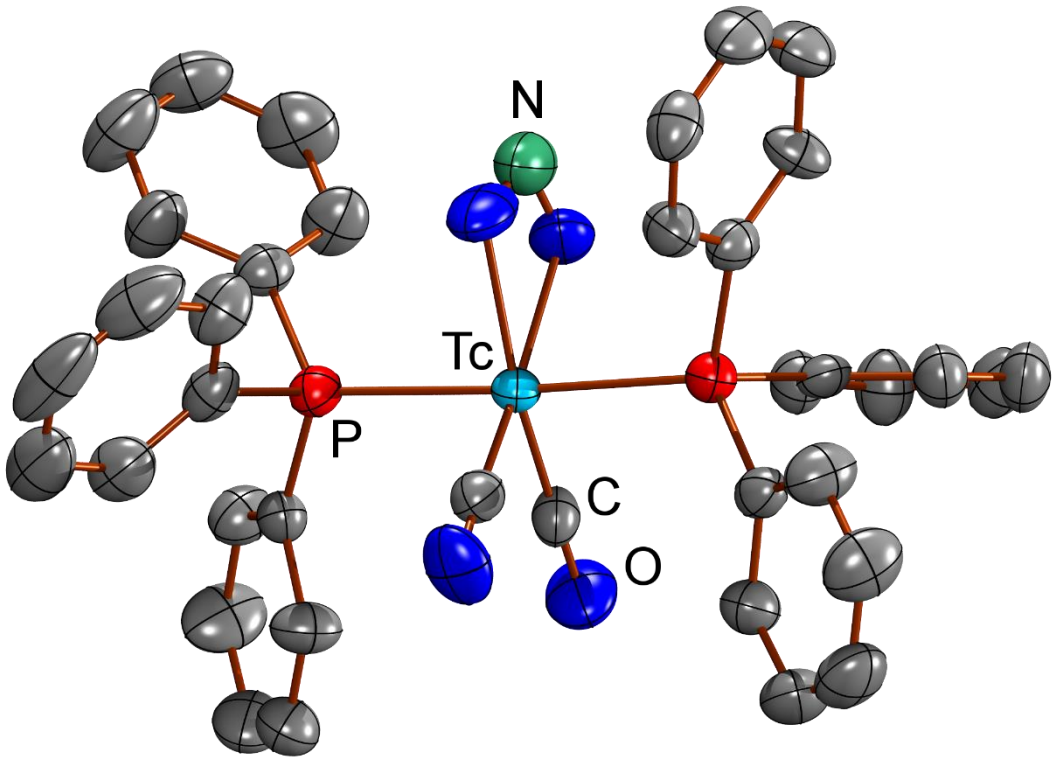

Figure S10. Ellipsoid representation (50% probability) of [Tc(η^1-ONO)$(CO)_3(PPh_3)_2$]/[Tc(η^1-NO_2)$(CO)_3(PPh_3)_2$] (**11a/11b**). Hydrogen atoms are omitted for clarity. The nitrito and nitro isomers of the compound are disordered over the same position with a ratio of 60:40 in favor of the nitrito complex **11a**. The angular distance in the minor nitro isomer was restraint to 2.0 Å and the N-O distances in the nitro isomer were restrained to be similar.

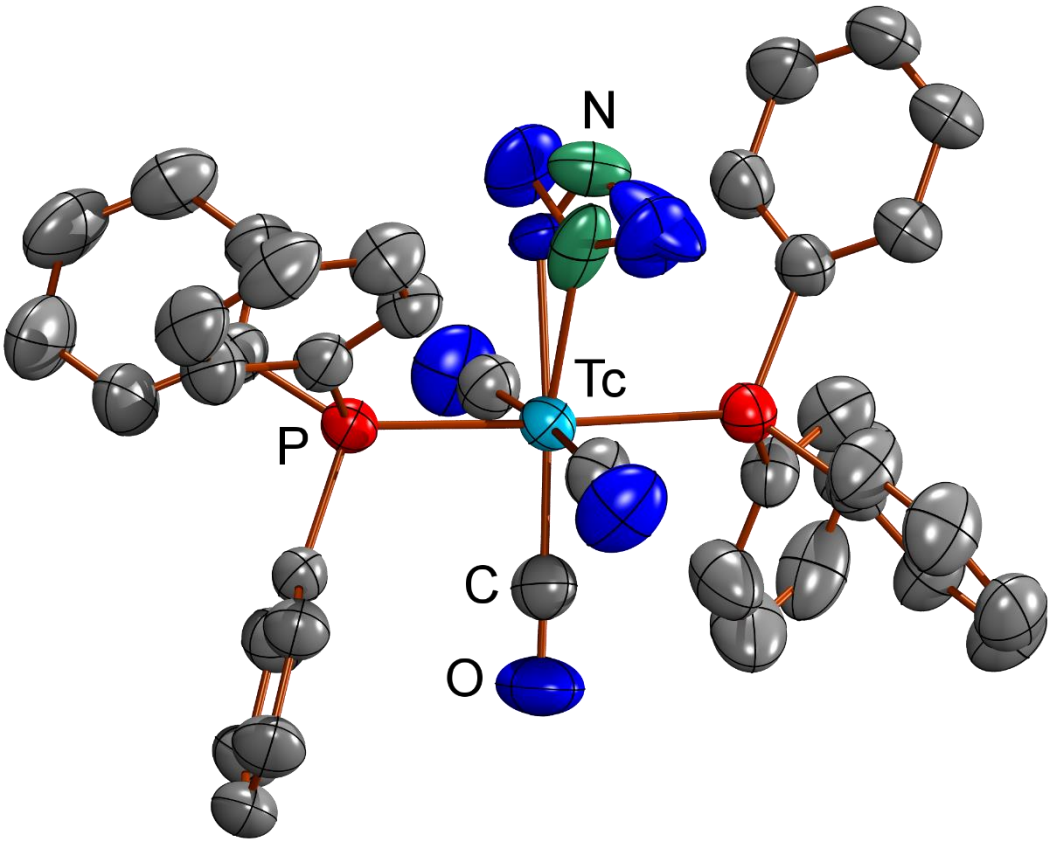

Figure S11. Ellipsoid representation (50% probability) of [Tc(η^2-OONO)$(CO)_2(PPh_3)_2$] (**12**). Hydrogen atoms are omitted for clarity. The second half of the molecule is generated by symmetry. The ellipsoid shape (and the remaining electron density) suggests an unresolvable, underlying disorder along the P-Tc-P axis. The disorder also persists in lower-symmetry solutions and is therefore attributed to a systematic artifact of the crystal itself rather than an artifact of inappropriately high symmetry of the space group.

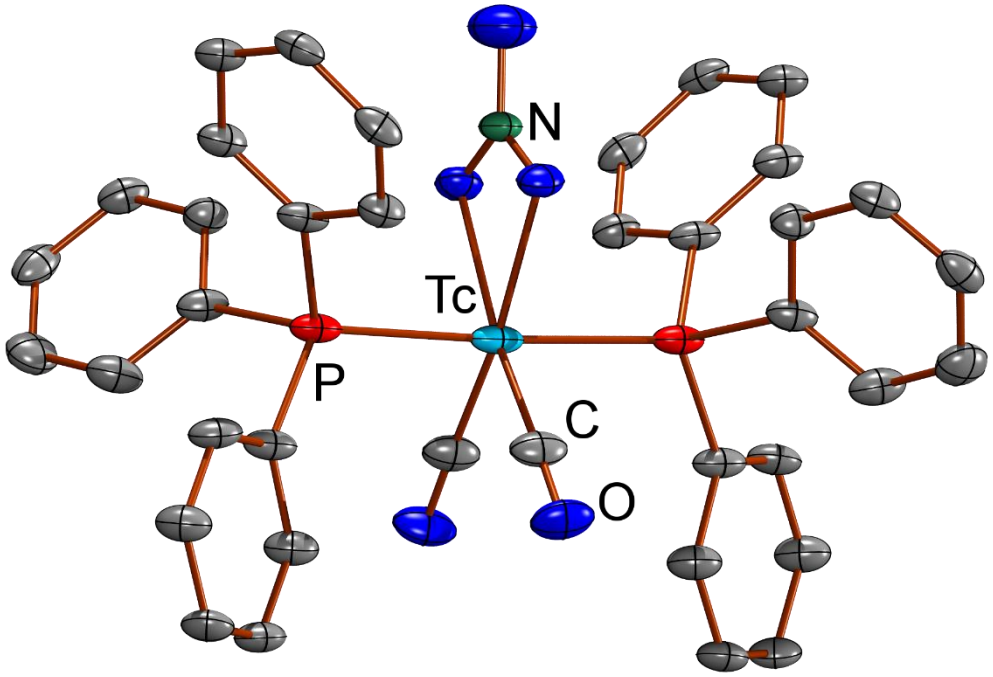

Figure S12. Ellipsoid representation (50% probability) of [Tc(η^2-HHBH$_2$)(CO)$_2$(PPh$_3$)$_2$] (**15**). Hydrogen atoms bonded to carbon atoms are omitted for clarity. Half of the molecule is generated via the space group symmetry and the equatorial plane is disordered over the space-group symmetry. The elusive hydrogen atoms of the tetrahydridoborato ligand were located in the electron density maps and restrained to fixed distances of 1.14 Å to boron. A FLAT restraint was used to generate a reasonable tetrahedral geometry around boron and ultimately, the electronic parameters of the hydrogen atoms were modelled based on the thermal displacement parameter of boron with a shelx factor of -1.2.

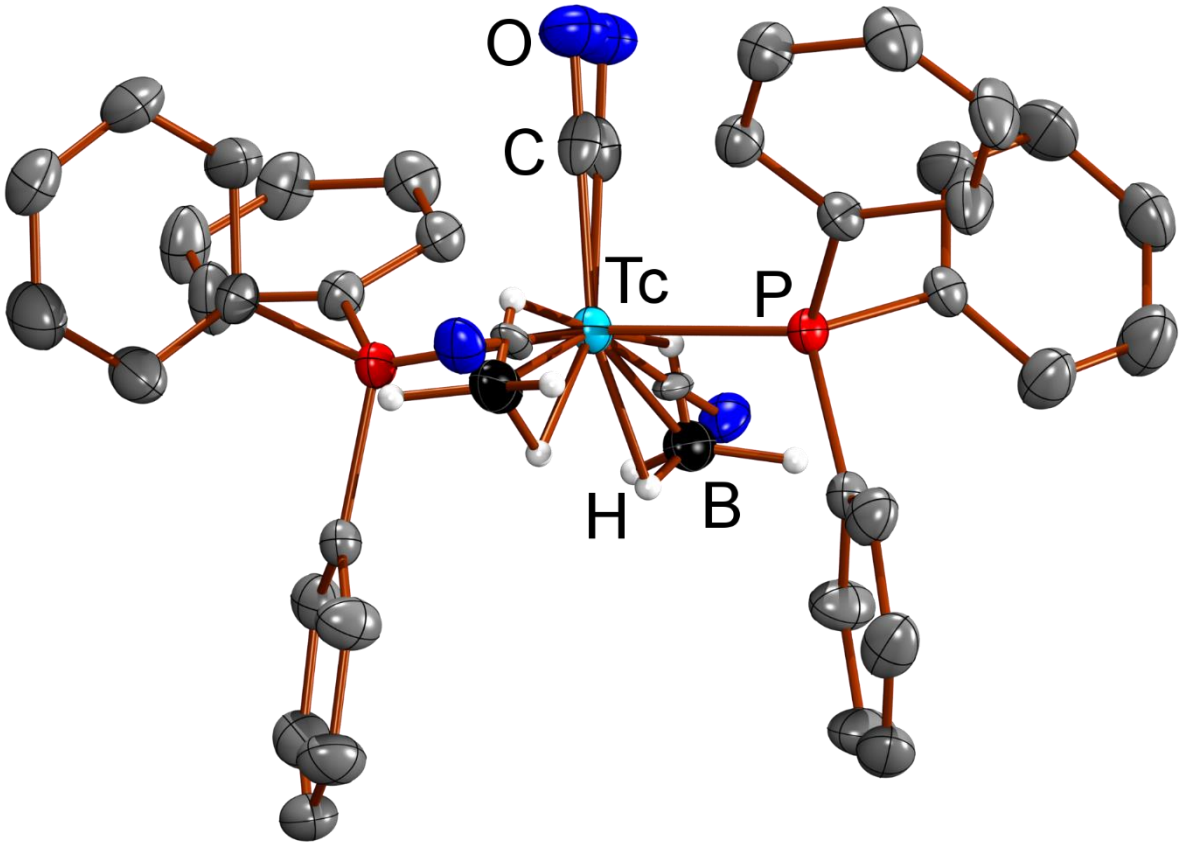

Figure S13. Ellipsoid representation (50% probability) of [Tc(η^2-SSCMe)$(CO)_2(PPh_3)_2$]/[Tc(η^2-SSCSMe)$(CO)_2(PPh_3)_2$] (**17/18a**). Hydrogen atoms are omitted for clarity. The dithioacetato and methyltrithiocarbonato isomers of the compound are disordered over the same position with a ratio of 55:45 in favor of the methyltrithiocarbonato complex **18a**.

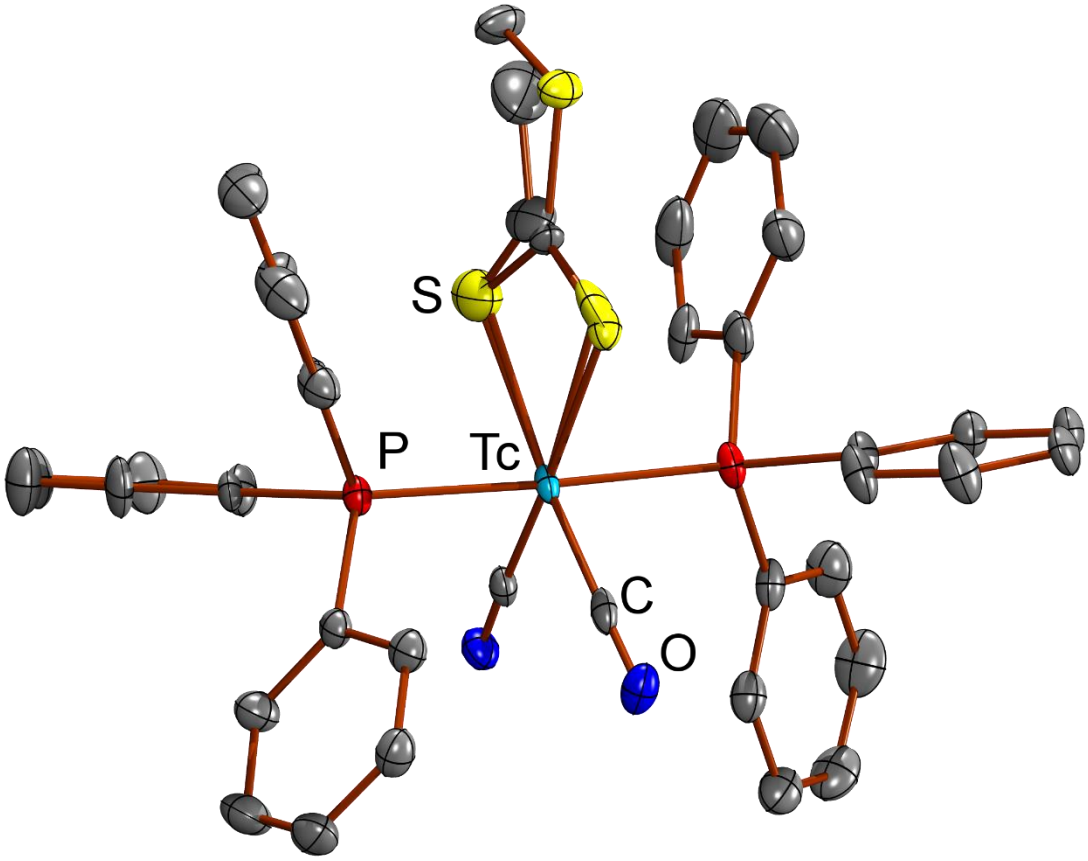

Figure S14. Ellipsoid representation (50% probability) of [Tc(η^2-SSCH)$(CO)_2(PPh_3)_2$] (**20**). Hydrogen atoms are omitted for clarity. The dithioformato ligand is disordered with a carbonyl ligand over two positions respectively. The ratio of the disorder is 55:45. Negative part instructions were included to avoid a short H···H contact generation between the two disordered components through the space-group symmetry.

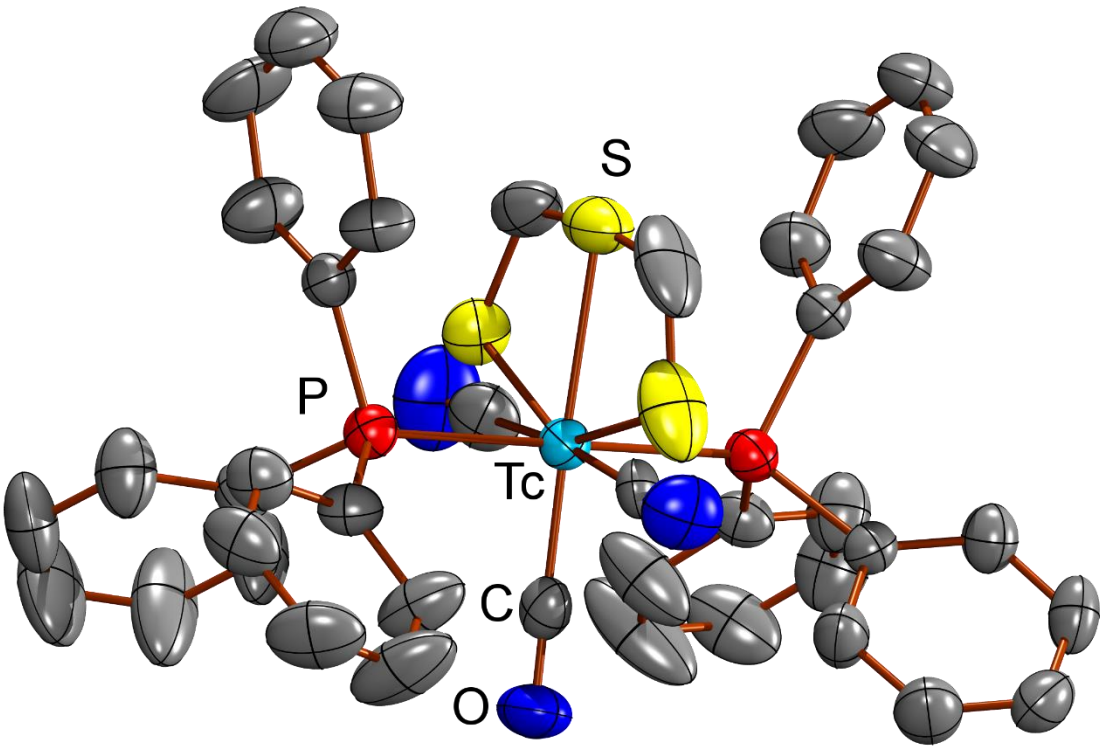

Figure S15. Ellipsoid representation (50% probability) of [Tc(η^1-OTcO$_3$)(CO)$_3$(PPh$_3$)$_2$] (**21**). Hydrogen atoms are omitted for clarity.

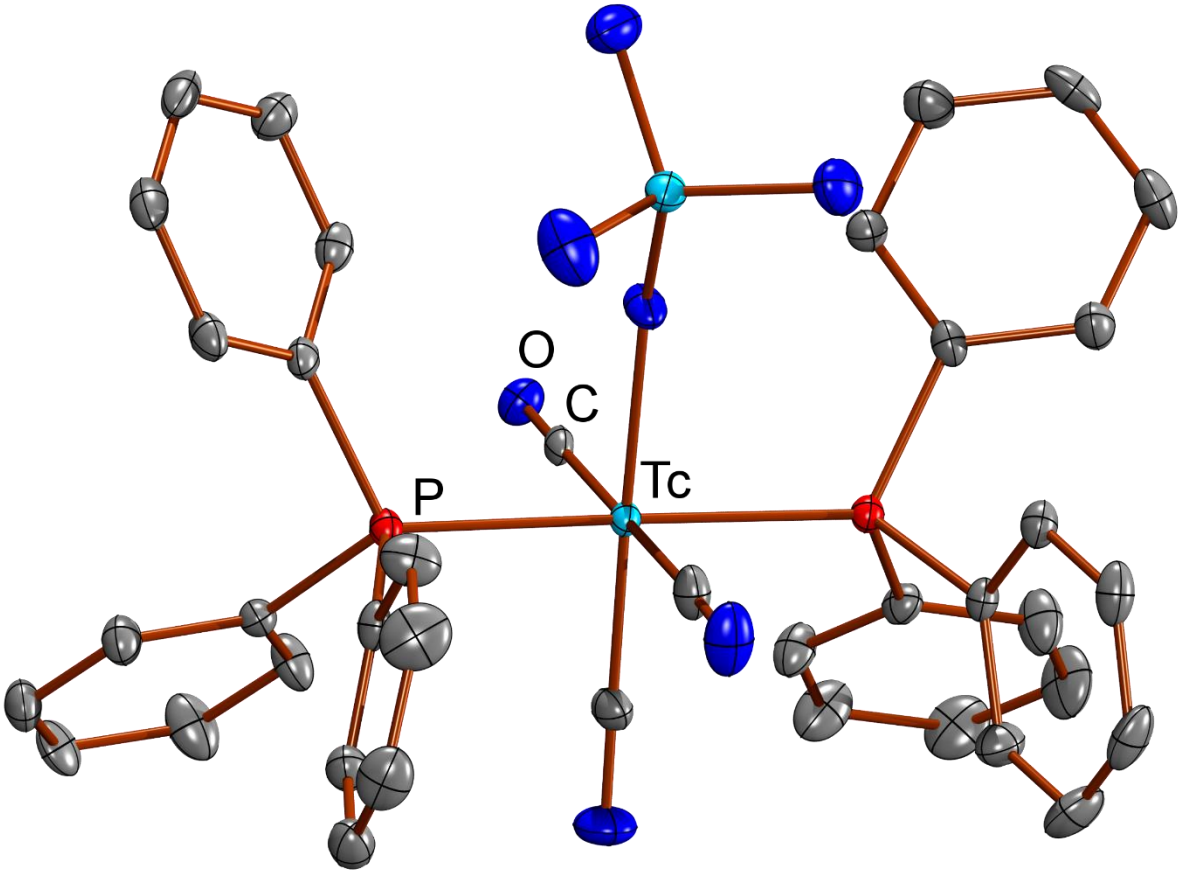

Figure S16. Ellipsoid representation (50% probability) of [Tc(η^1-OTcO$_3$)(CO)$_3$(PPh$_3$)$_2$] (**21**) · benzene. Hydrogen atoms are omitted for clarity.

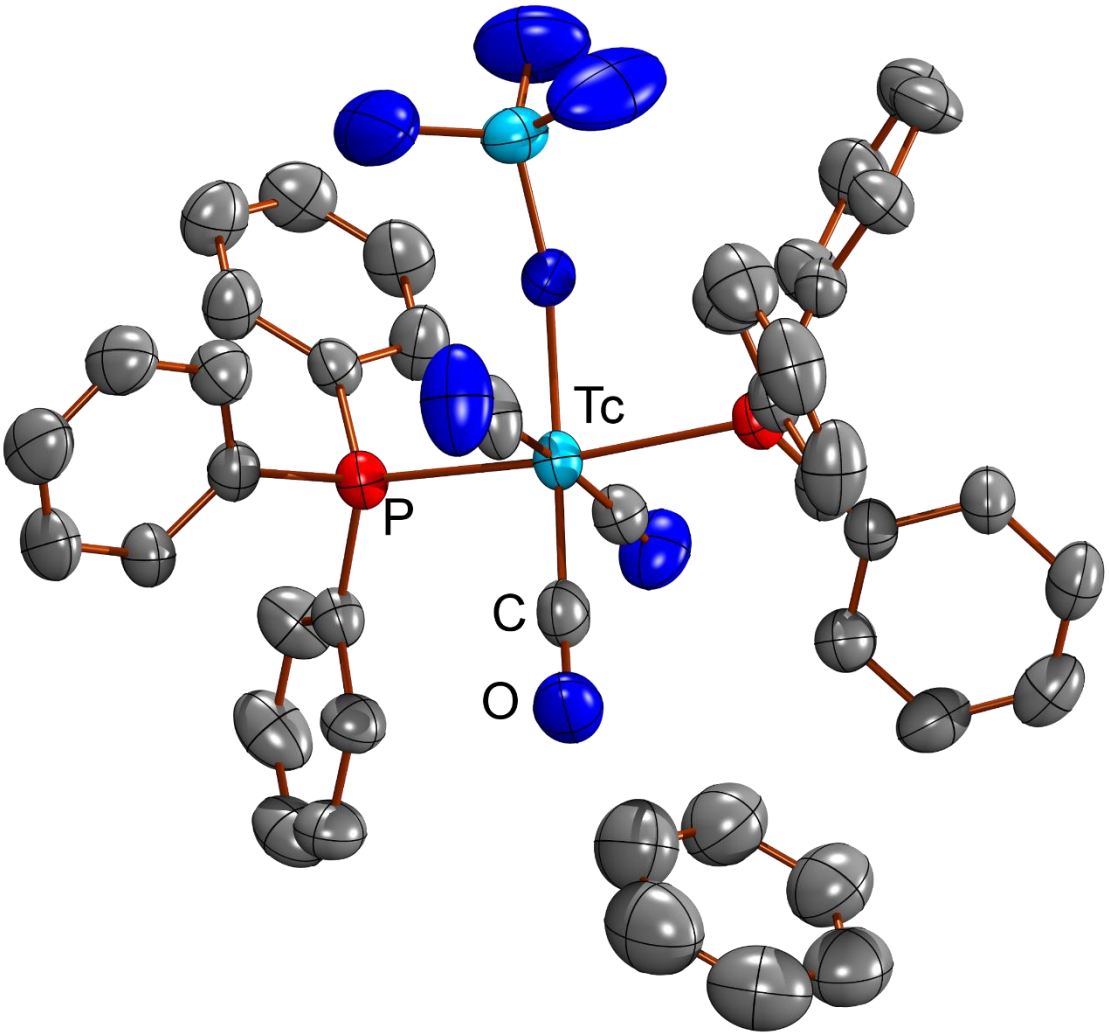

Figure S17. Ellipsoid representation (50% probability) of [Tc(η^1-$OTcO_3$)(acetone)$(CO)_2(PPh_3)_2$] · acetone (**23c**). Hydrogen atoms are omitted for clarity. The ill-defined co-crystallized solvent acetone was modelled by appropriate restraints and constraints into a reasonable geometry since it has been proven by other spectroscopic methods.

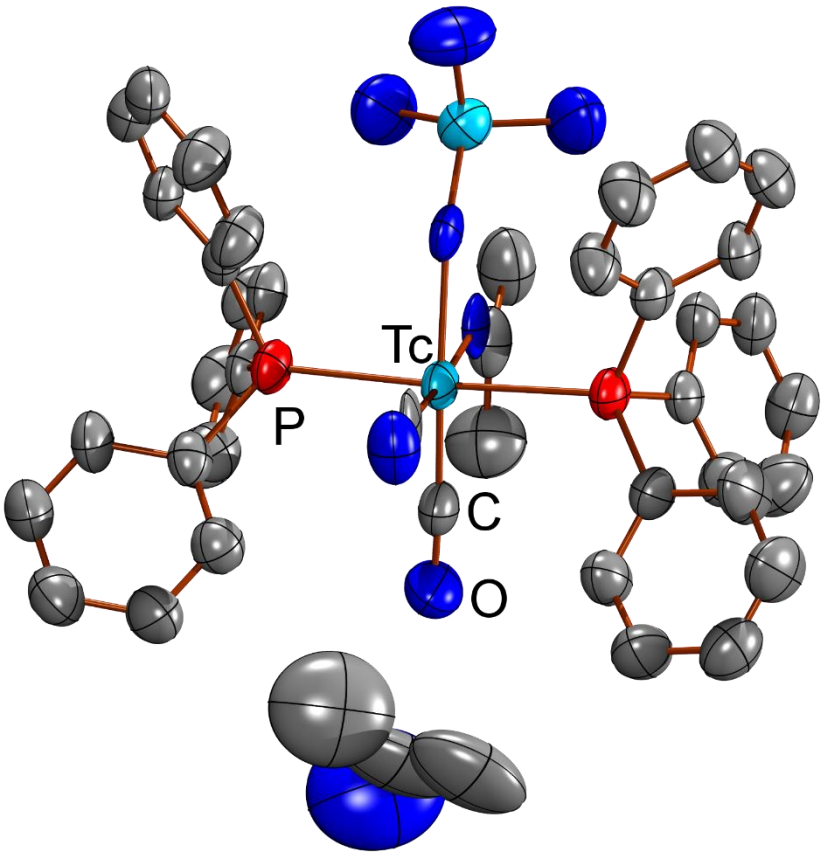

Part 2: Spectral data

Spectragryph 1.2.8 was used to visualize the IR spectra.[1]

Figure S18. ^{1}H NMR spectrum of $[Tc(OH)(OH_2)(CO)_2(PPh_3)_2]$ (**3**).

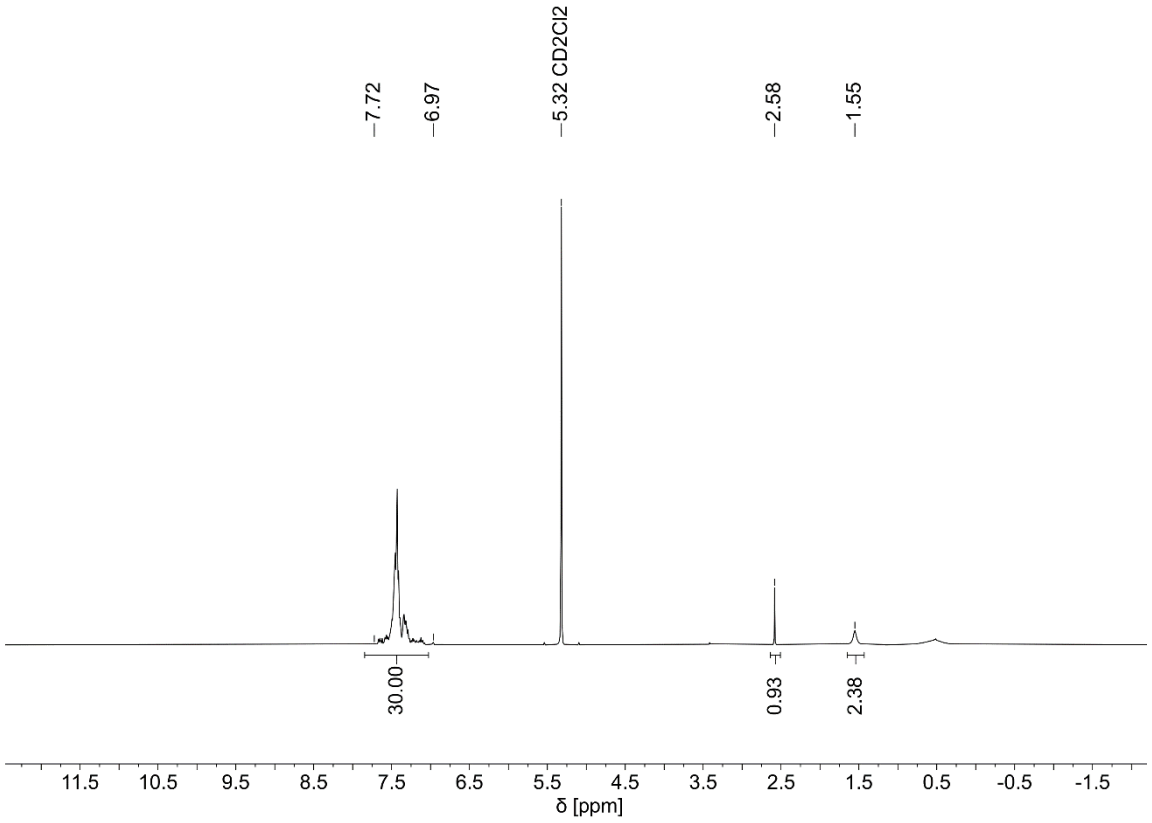

Figure S19. ^{99}Tc NMR spectrum of [Tc(OH)(OH_2)$(CO)_2(PPh_3)_2$] (**3**).

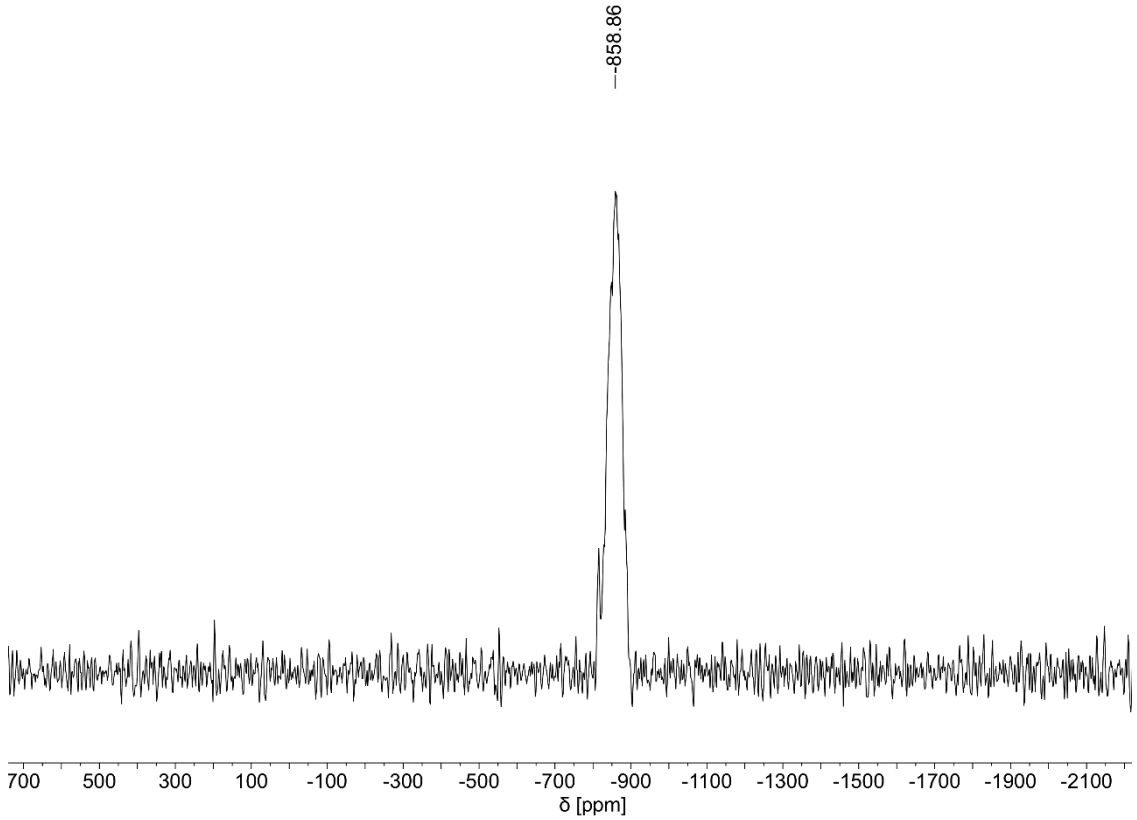

Figure S20. $^{31}P\{^1H\}$ NMR spectrum of [Tc(OH)(OH_2)$(CO)_2(PPh_3)_2$] (**3**).

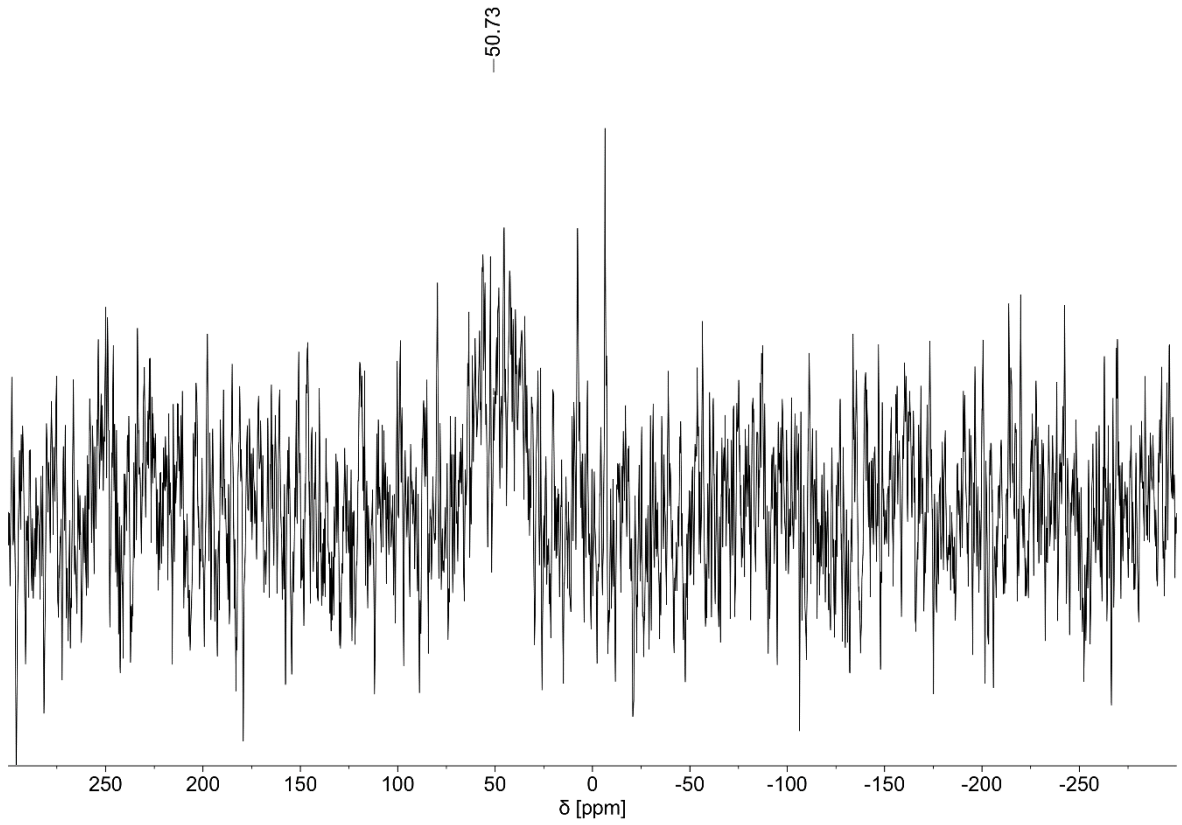

Figure S21. IR spectrum of $[Tc(OH)(OH_2)(CO)_2(PPh_3)_2]$ (**3**).

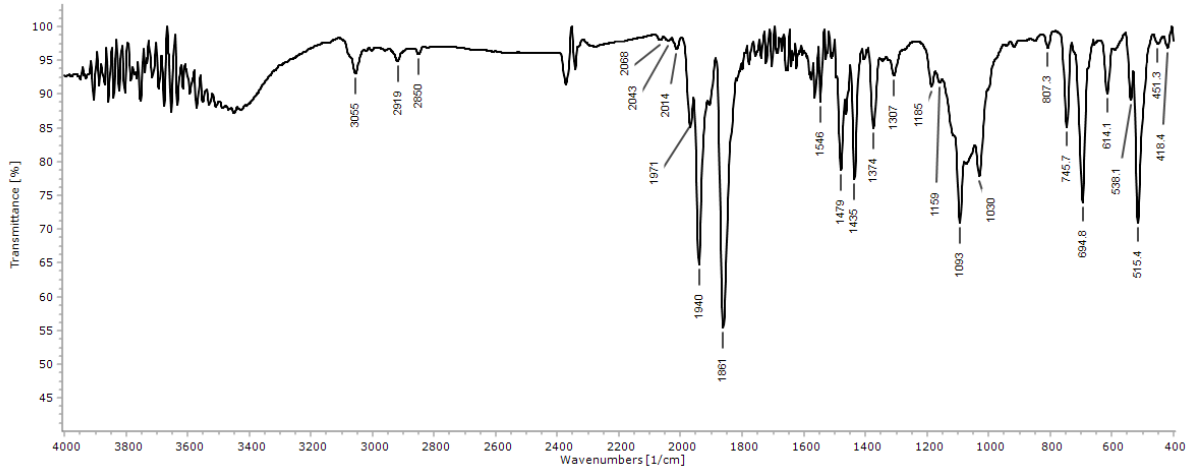

Figure S22. ^1H NMR spectrum of $[Tc(NCO)(OH_2)(CO)_2(PPh_3)_2]$ (**4**).

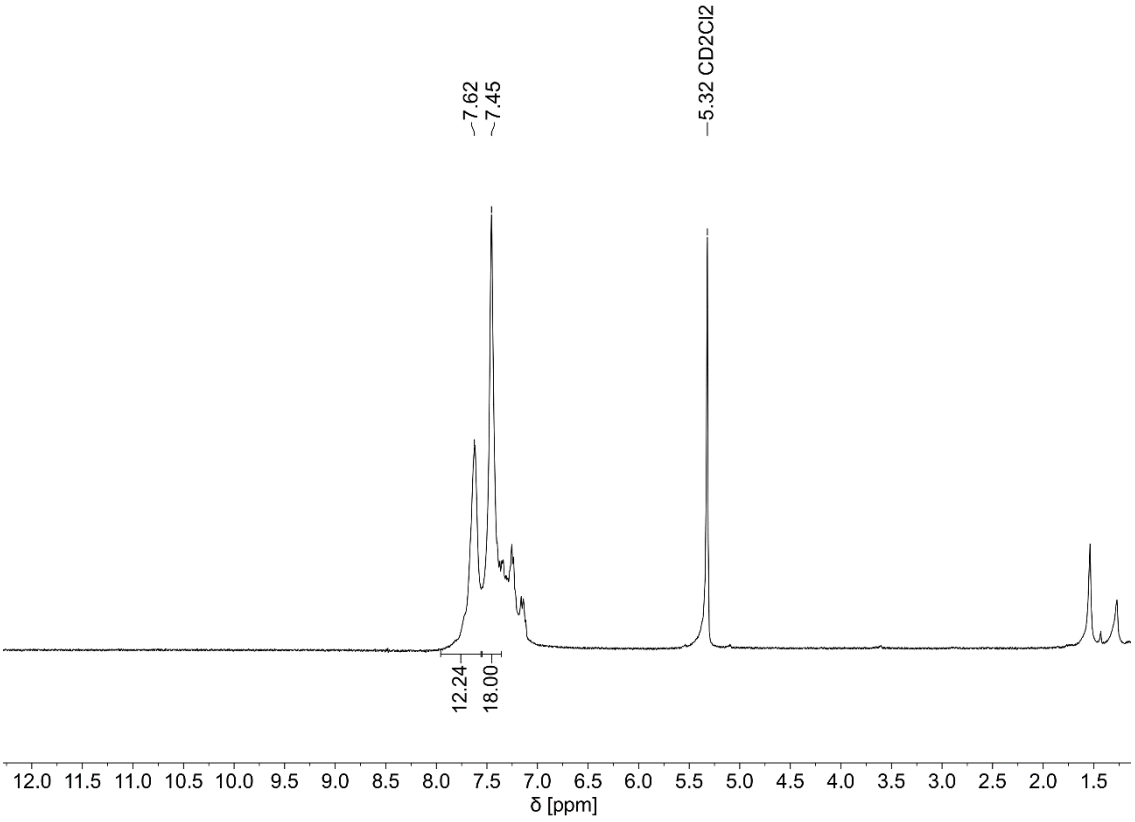

Figure S23. ^{99}Tc NMR spectrum of [Tc(NCO)(OH_2)($CO)_2$($PPh_3)_2$] (**4**). Minor resonances resemble the azide and an unknown impurity.

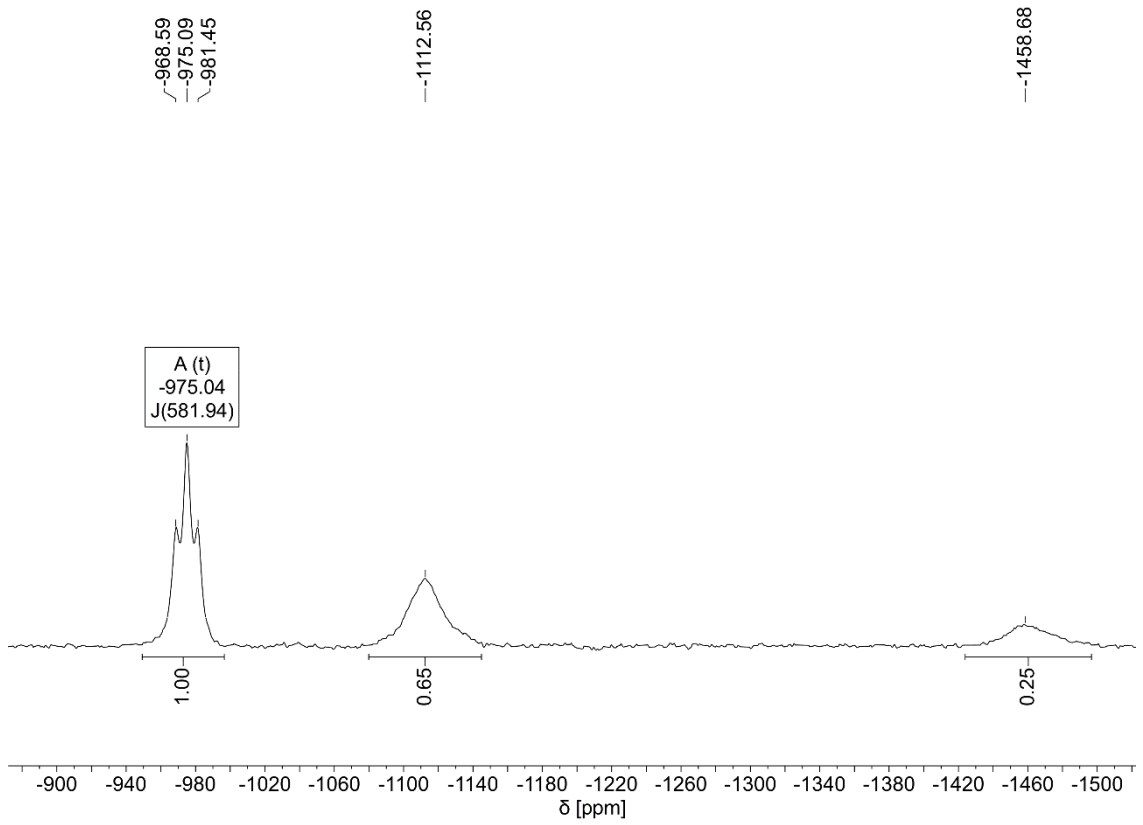

Figure S24. IR spectrum of [Tc(NCO)(OH_2)($CO)_2$($PPh_3)_2$] (**4**).

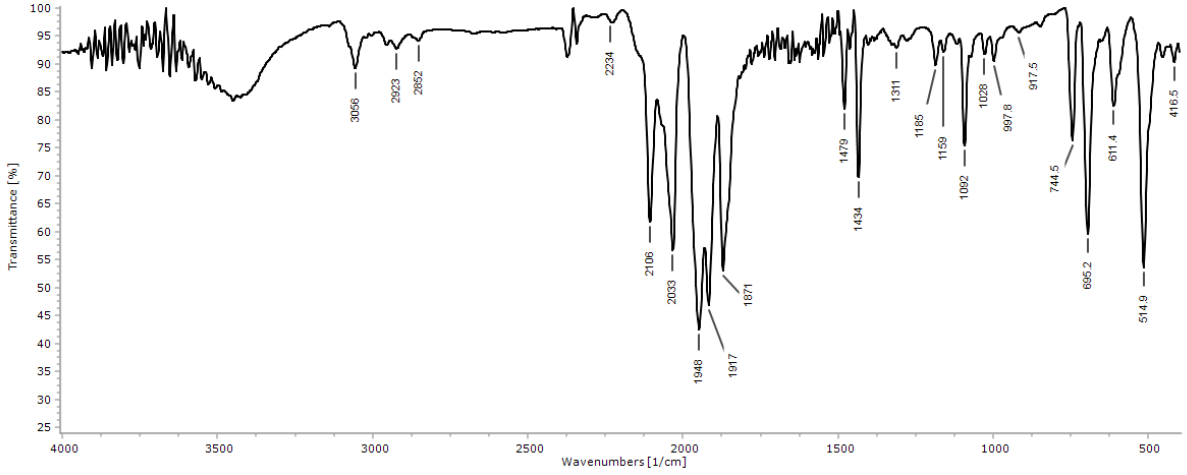

Figure S25. ^{1}H NMR spectrum of [Tc(N$_3$)(CO)$_3$(PPh$_3$)$_2$] (**5**).

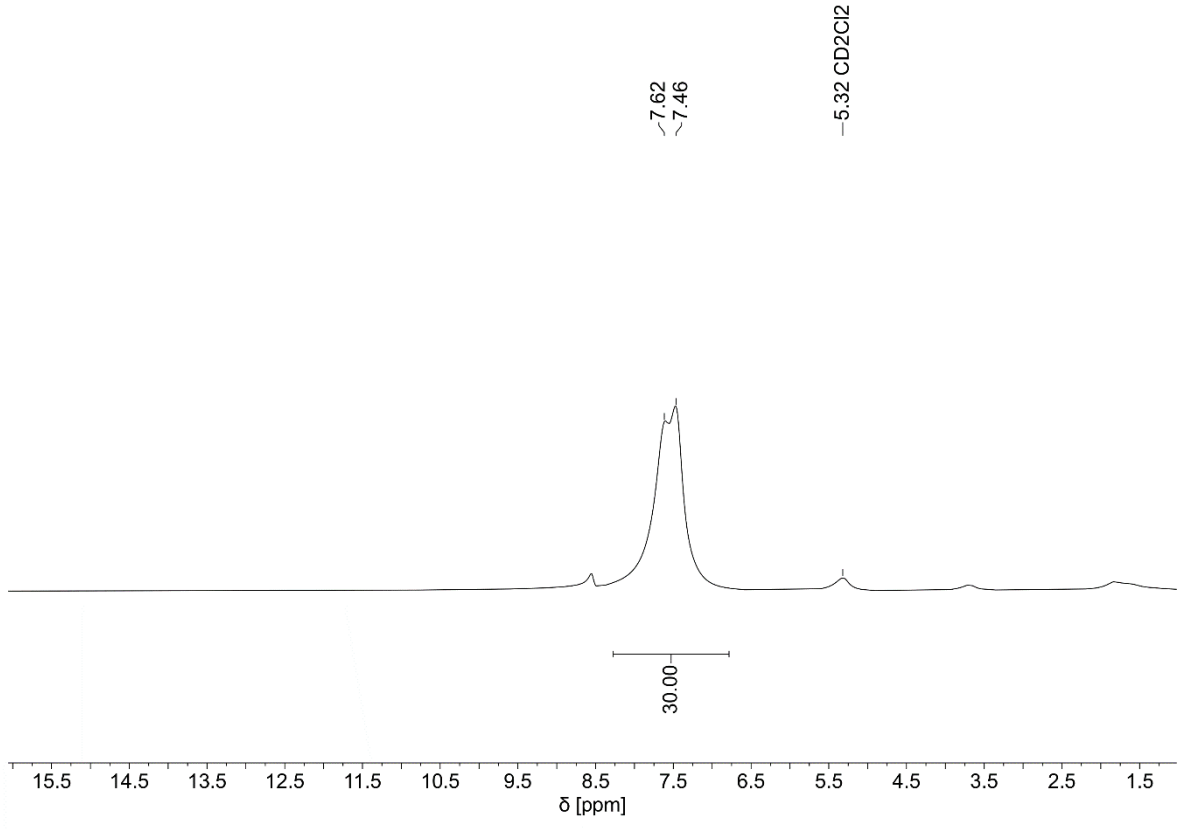

Figure S26. ^{99}Tc NMR spectrum of [Tc(N$_3$)(CO)$_3$(PPh$_3$)$_2$] (**5**).

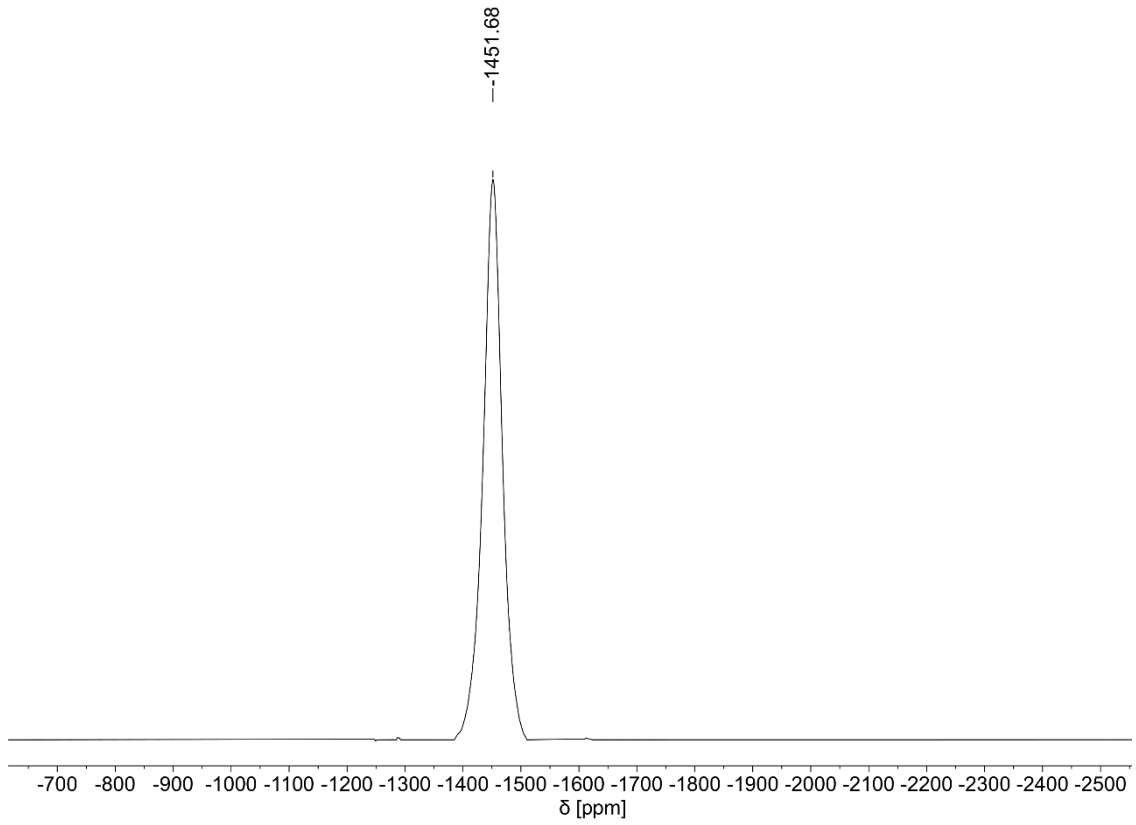

Figure S27. $^{31}P\{^{1}H\}$ NMR spectrum of $[Tc(N_3)(CO)_3(PPh_3)_2]$ (**5**).

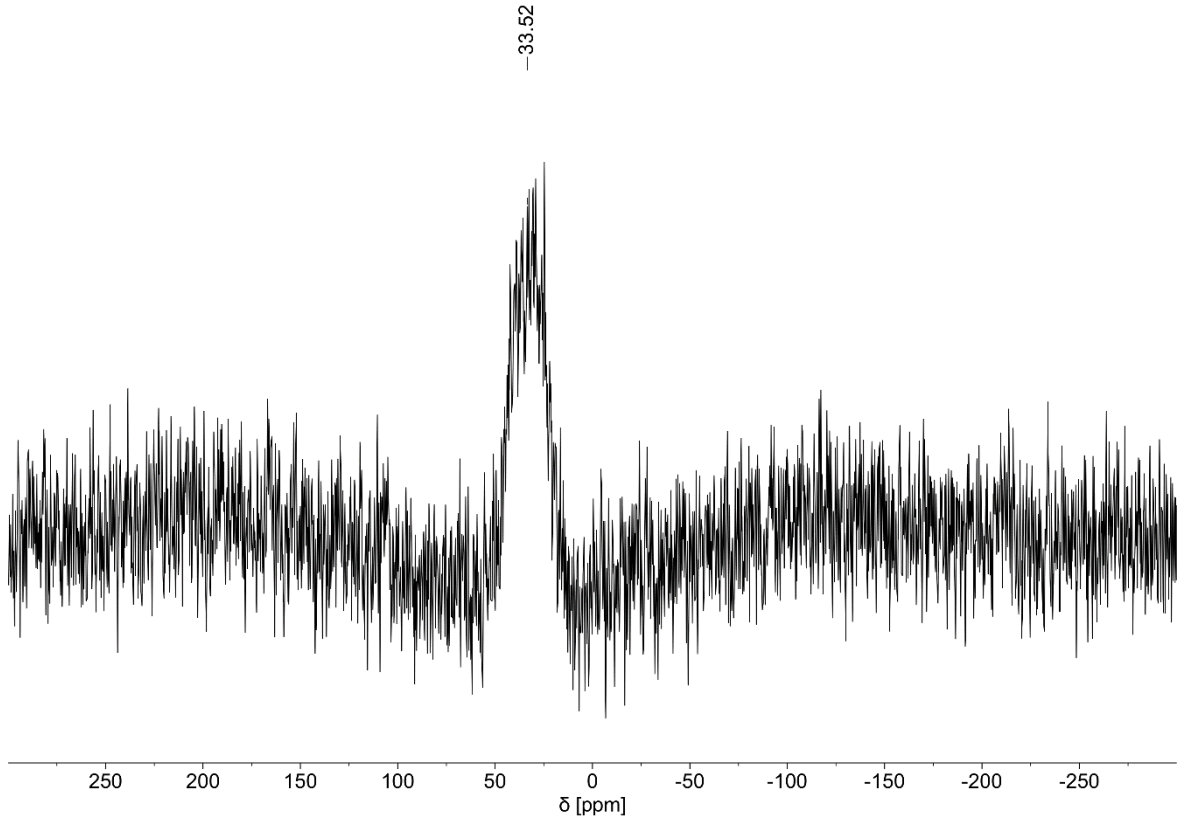

Figure S28. IR spectrum of $[Tc(N_3)(CO)_3(PPh_3)_2]$ (**5**).

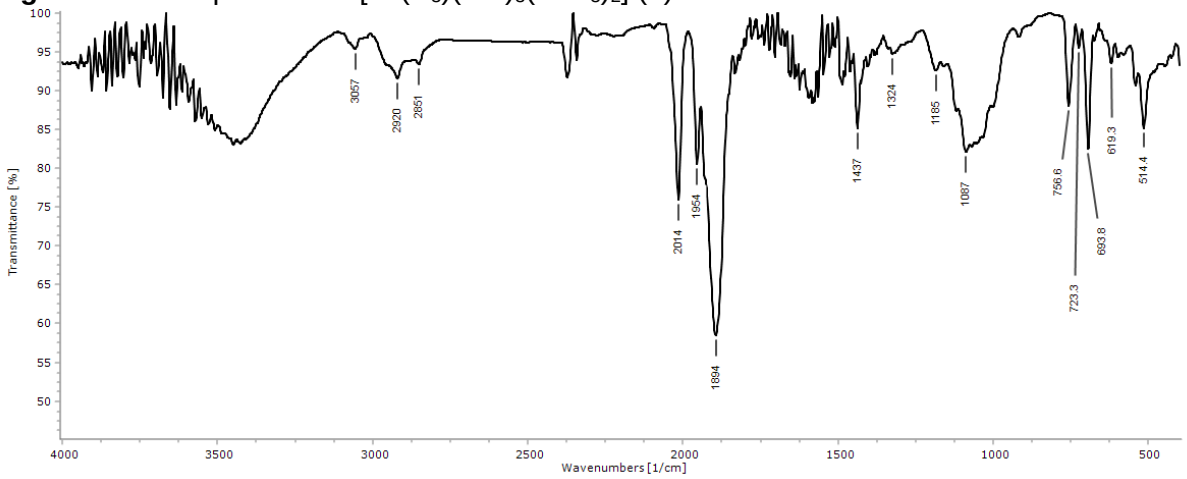

Figure S29. ^{1}H NMR spectrum of [Tc(NCO)(CO)$_3$(PPh$_3$)$_2$] (**6**).

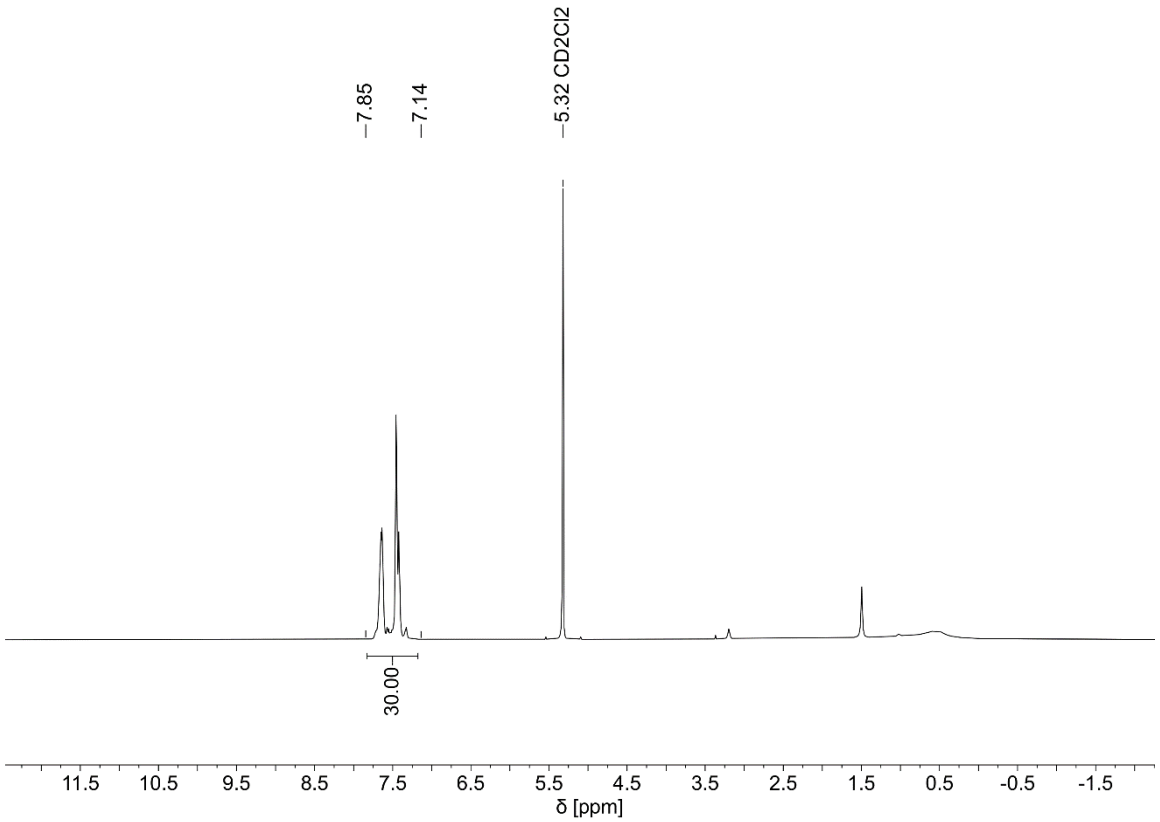

Figure S30. ^{99}Tc NMR spectrum of [Tc(NCO)(CO)$_3$(PPh$_3$)$_2$] (**6**).

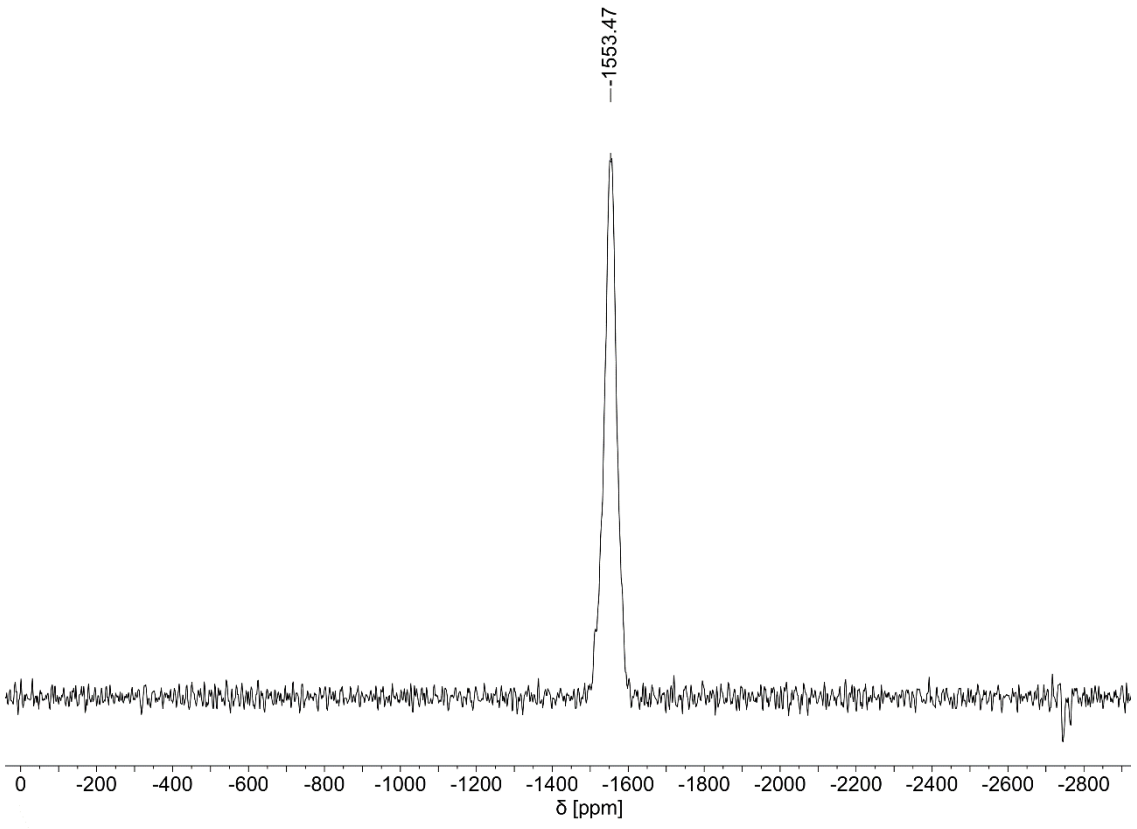

Figure S31. $^{31}P\{^{1}H\}$ NMR spectrum of $[Tc(NCO)(CO)_3(PPh_3)_2]$ (**6**).

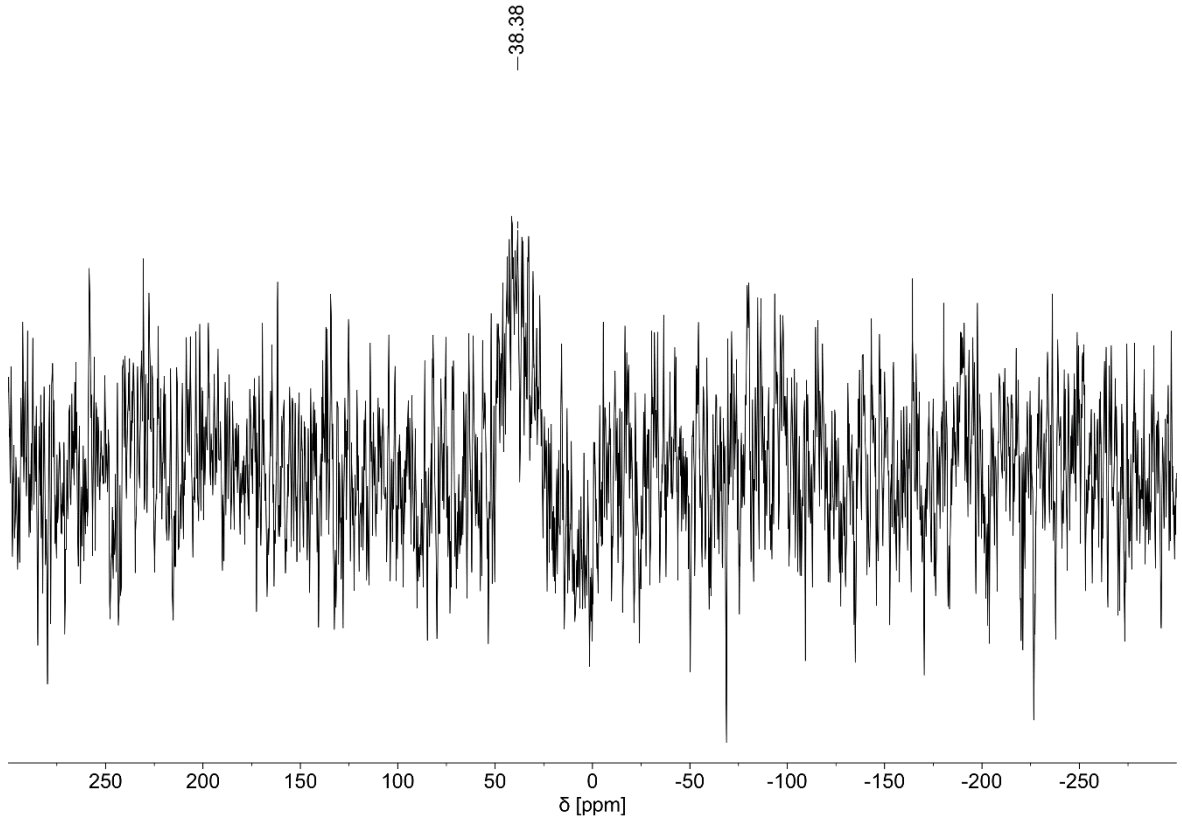

Figure S32. IR spectrum of $[Tc(NCO)(CO)_3(PPh_3)_2]$ (**6**).

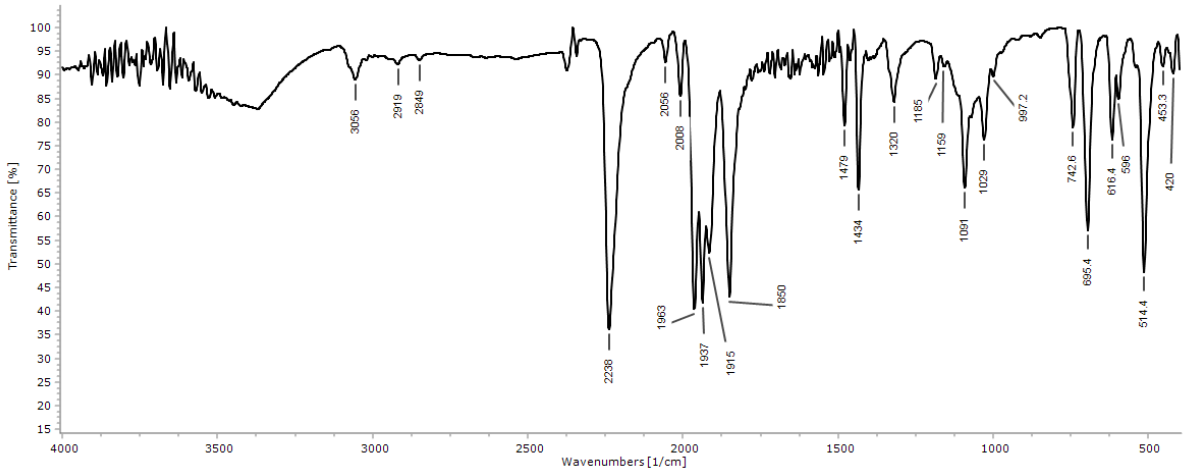

Figure S33. ^{1}H NMR spectrum of [Tc(NCS)(CO)$_3$(PPh$_3$)$_2$] (**7**).

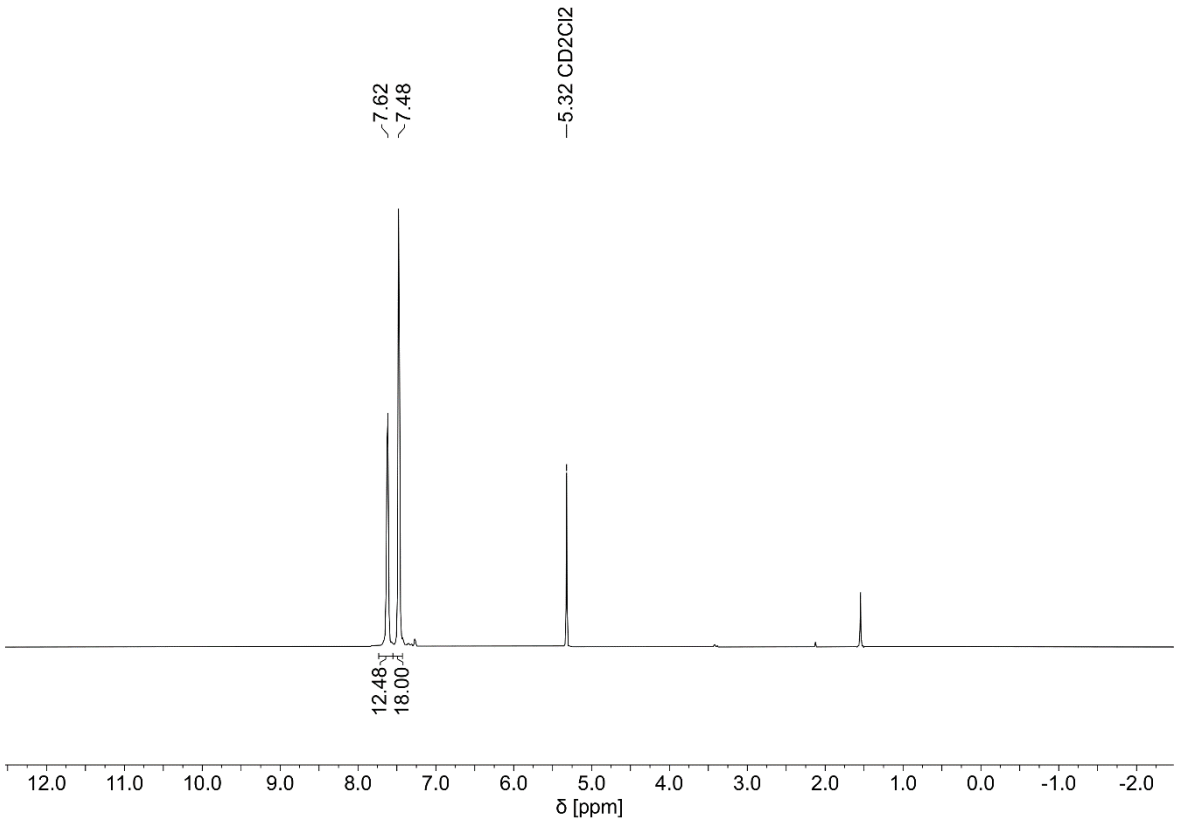

Figure S34. ^{99}Tc NMR spectrum of [Tc(NCS)(CO)$_3$(PPh$_3$)$_2$] (**7**).

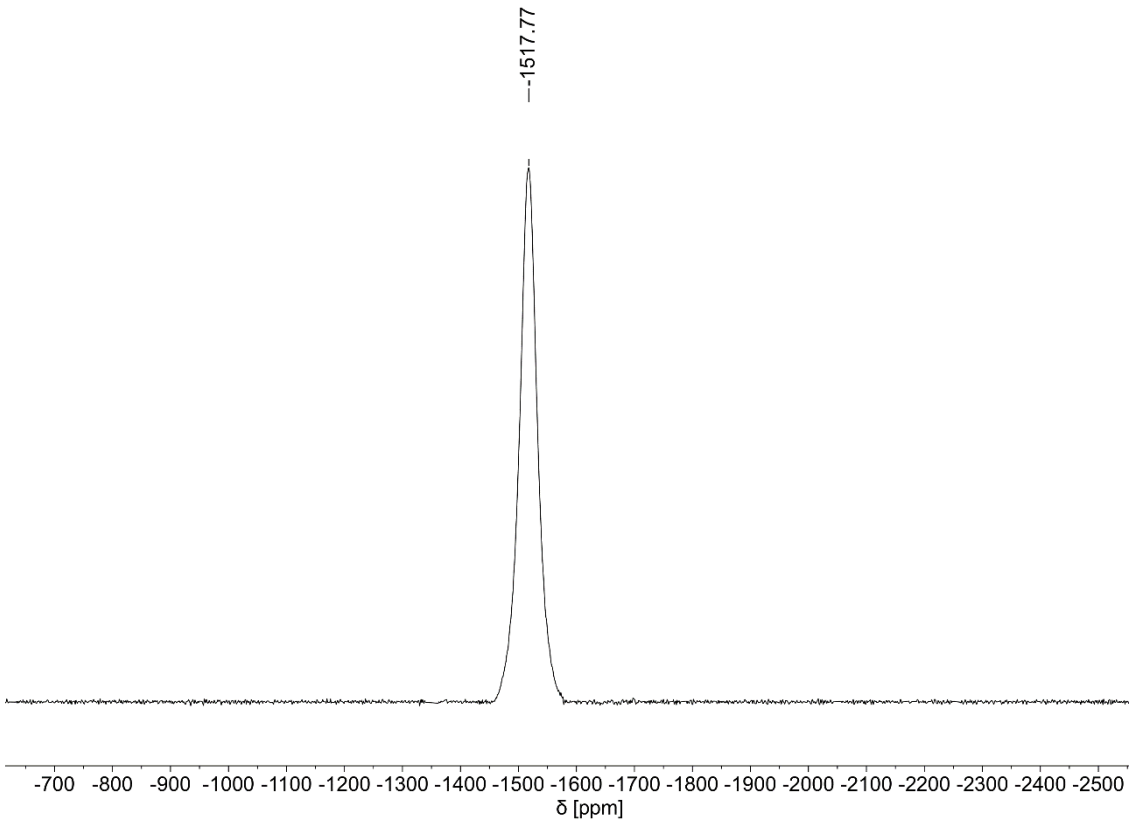

Figure S35. $^{31}P\{^{1}H\}$ NMR spectrum of $[Tc(NCS)(CO)_3(PPh_3)_2]$ (**7**).

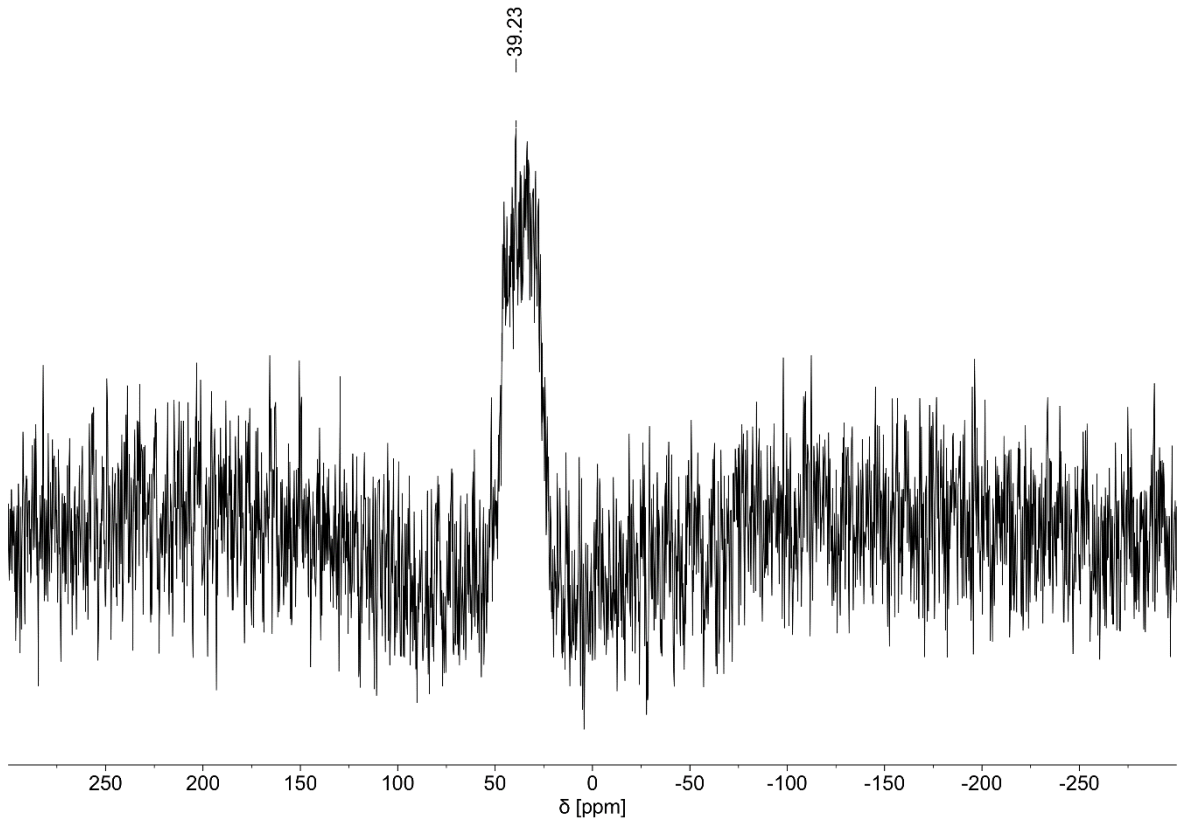

Figure S36. IR spectrum of $[Tc(NCS)(CO)_3(PPh_3)_2]$ (**7**).

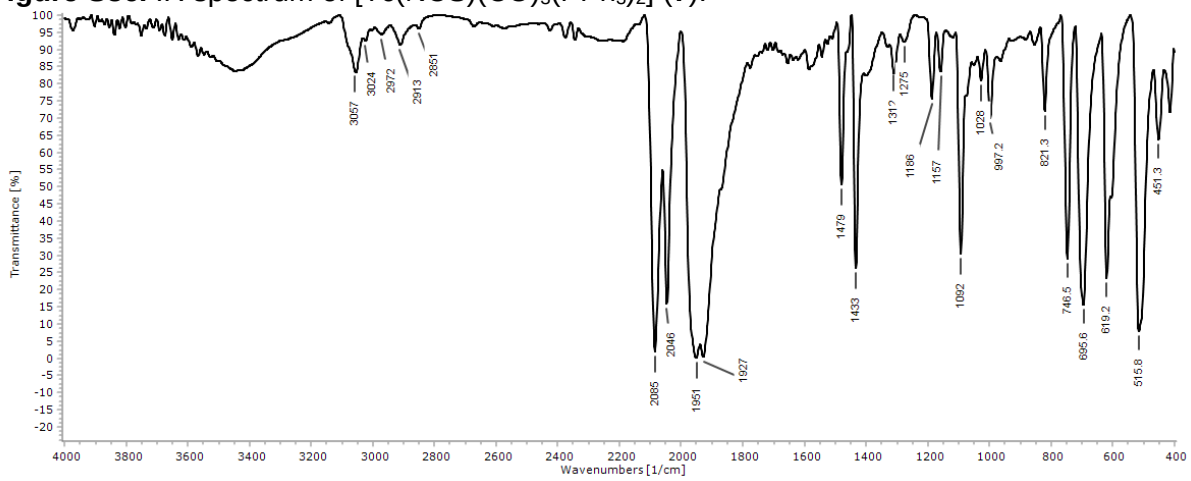

Figure S37. ^{1}H NMR spectrum of [Tc(SeCN)(CO)$_3$(PPh$_3$)$_2$]/[Tc(NCSe)(CO)$_3$(PPh$_3$)$_2$] (**8a**)/(**8b**).

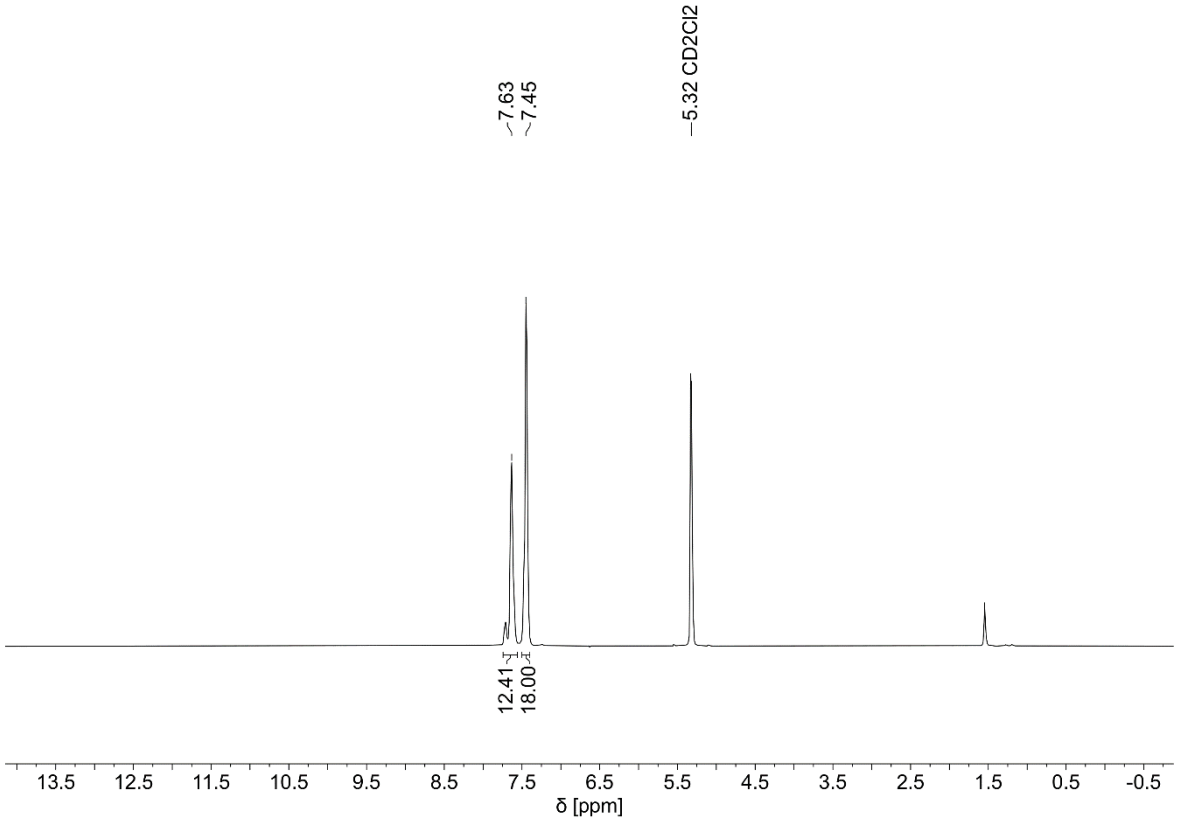

Figure S38. ^{99}Tc NMR spectrum of [Tc(SeCN)(CO)$_3$(PPh$_3$)$_2$]/[Tc(NCSe)(CO)$_3$(PPh$_3$)$_2$] (**8a**)/(**8b**).

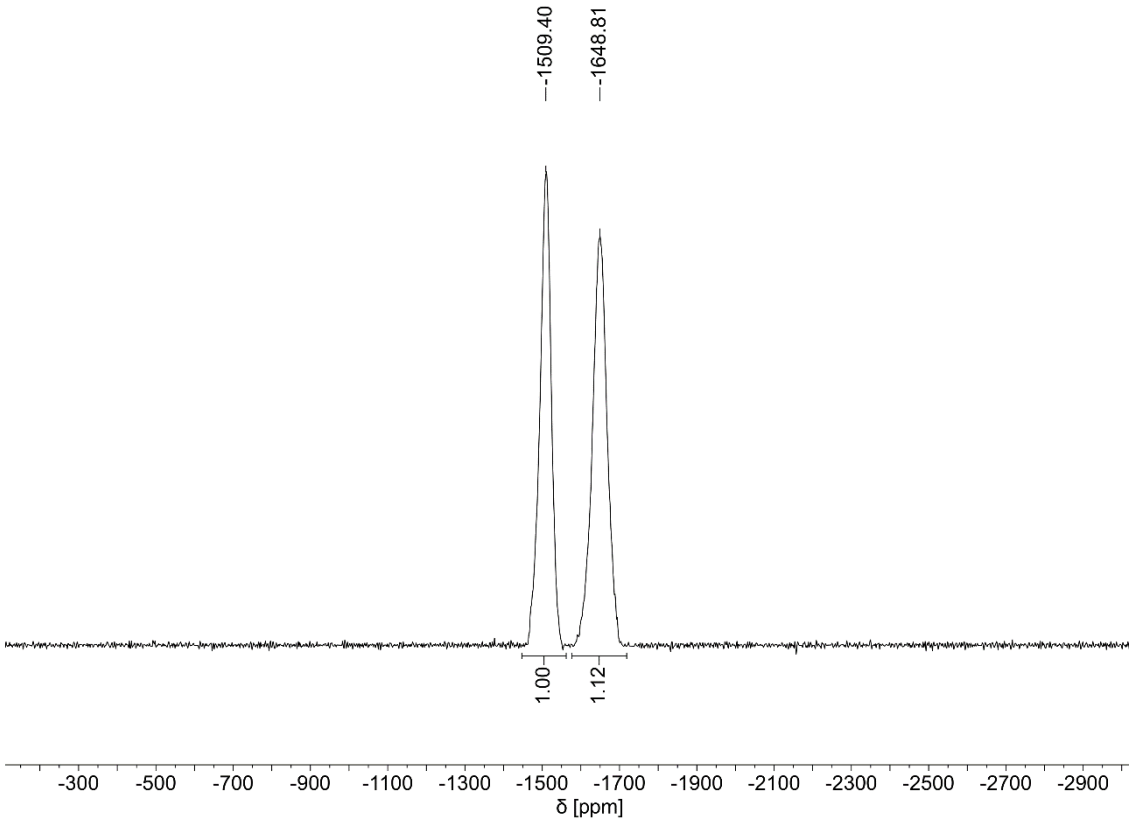

Figure S39. ^{99}Tc NMR spectrum of in-situ generated [Tc(^{15}NCSe)(CO)$_3$(PPh$_3$)$_2$] (**8b**) from a reaction of [Tc(OH$_2$)(CO)$_3$(PPh$_3$)$_2$]BF$_4$ and PPNSeC^{15}N.

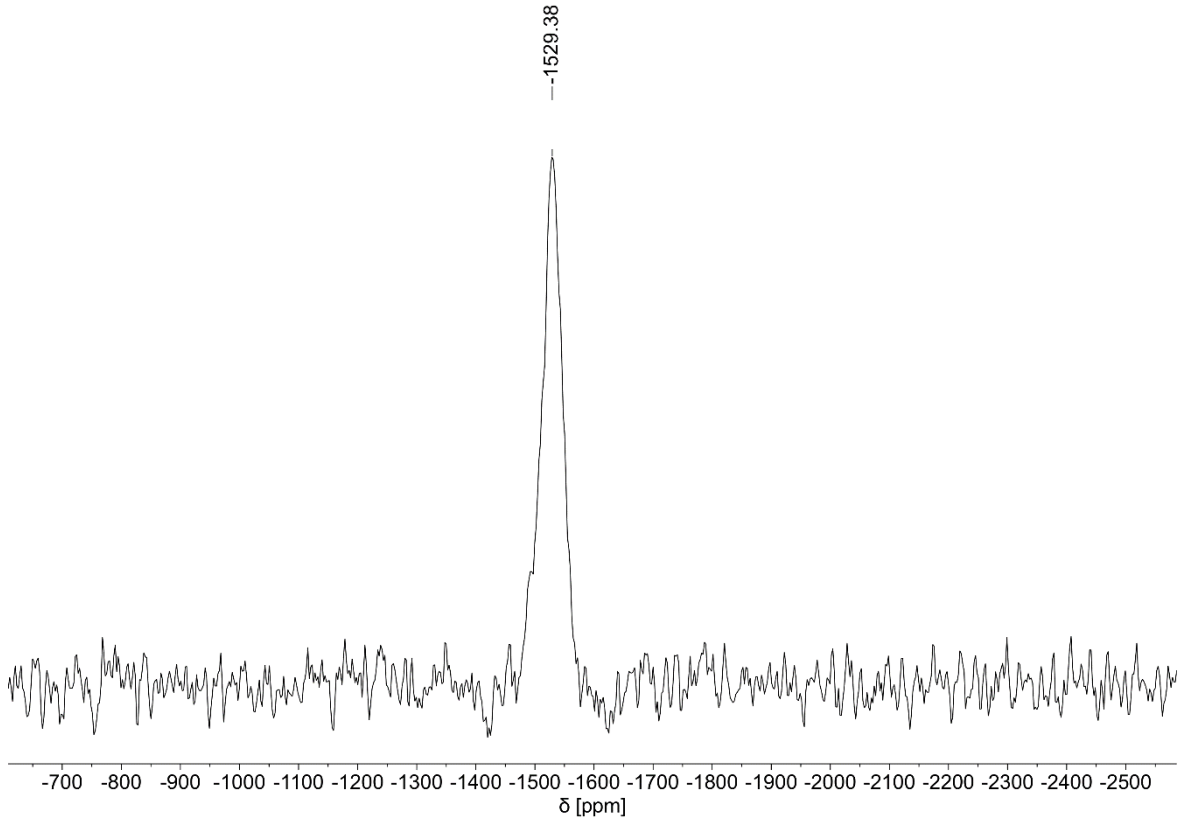

Figure S40. ^{31}P{^{1}H} NMR spectrum of [Tc(SeCN)(CO)$_3$(PPh$_3$)$_2$]/[Tc(NCSe)(CO)$_3$(PPh$_3$)$_2$] (**8a**)/(**8b**).

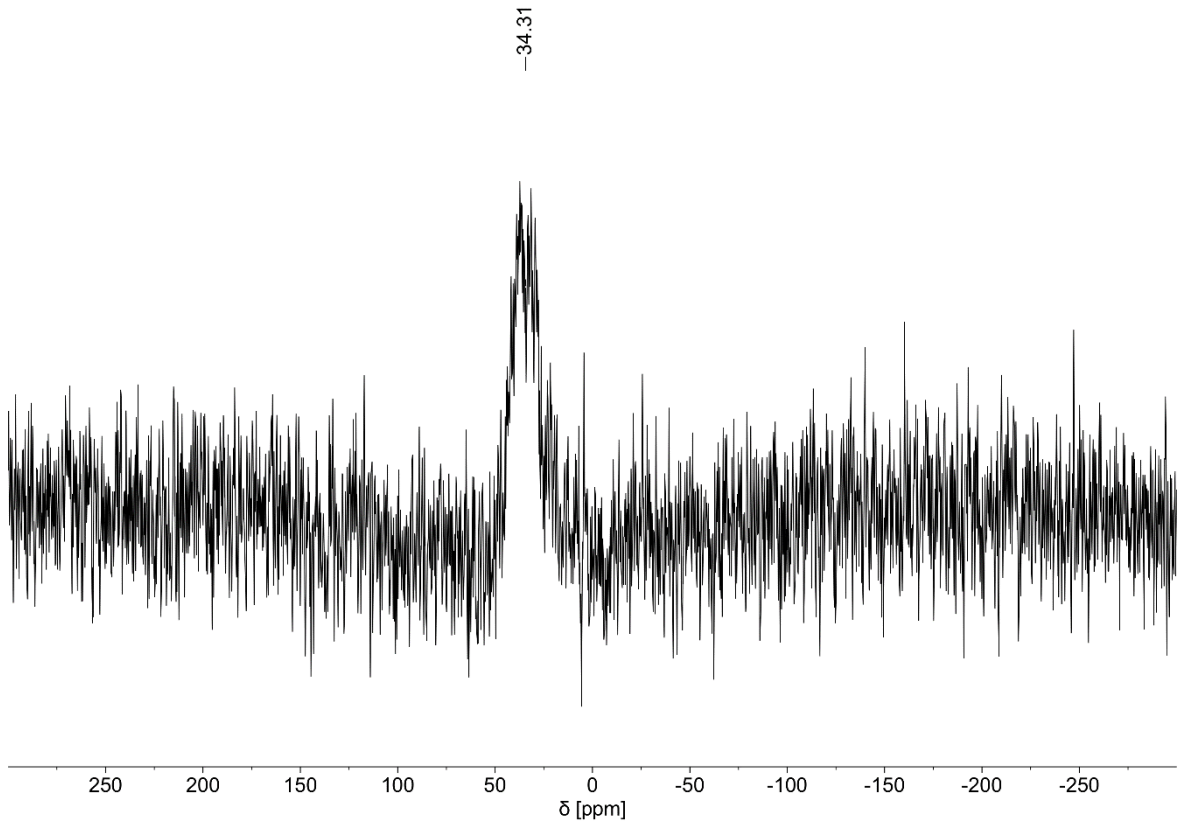

Figure S41. IR spectrum of [Tc(SeCN)(CO)$_3$(PPh$_3$)$_2$]/[Tc(NCSe)(CO)$_3$(PPh$_3$)$_2$] (**8a**)/(**8b**).

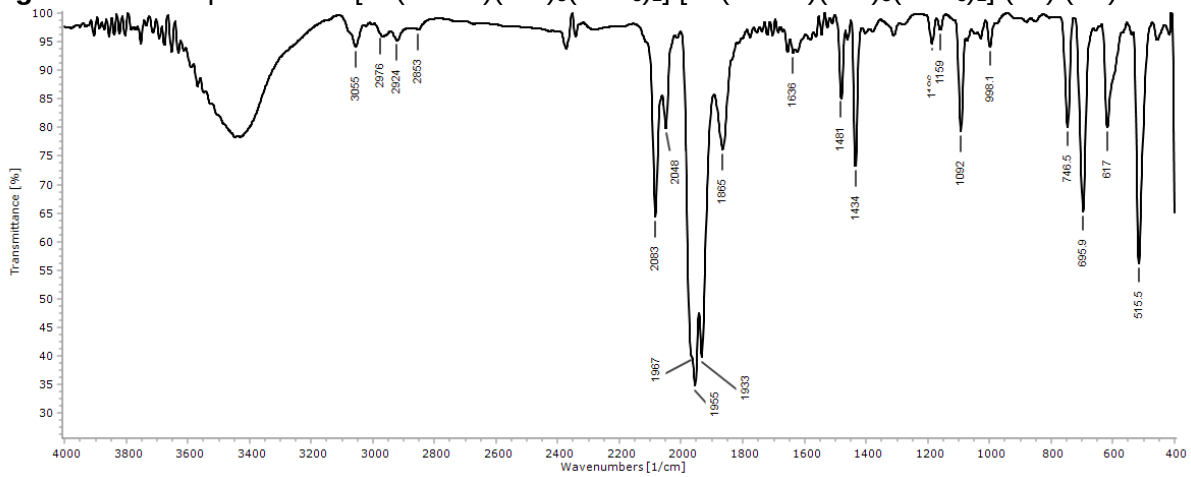

Figure S42. ^{1}H NMR spectrum of [Tc(CN)(CO)$_3$(PPh$_3$)$_2$] (**9**).

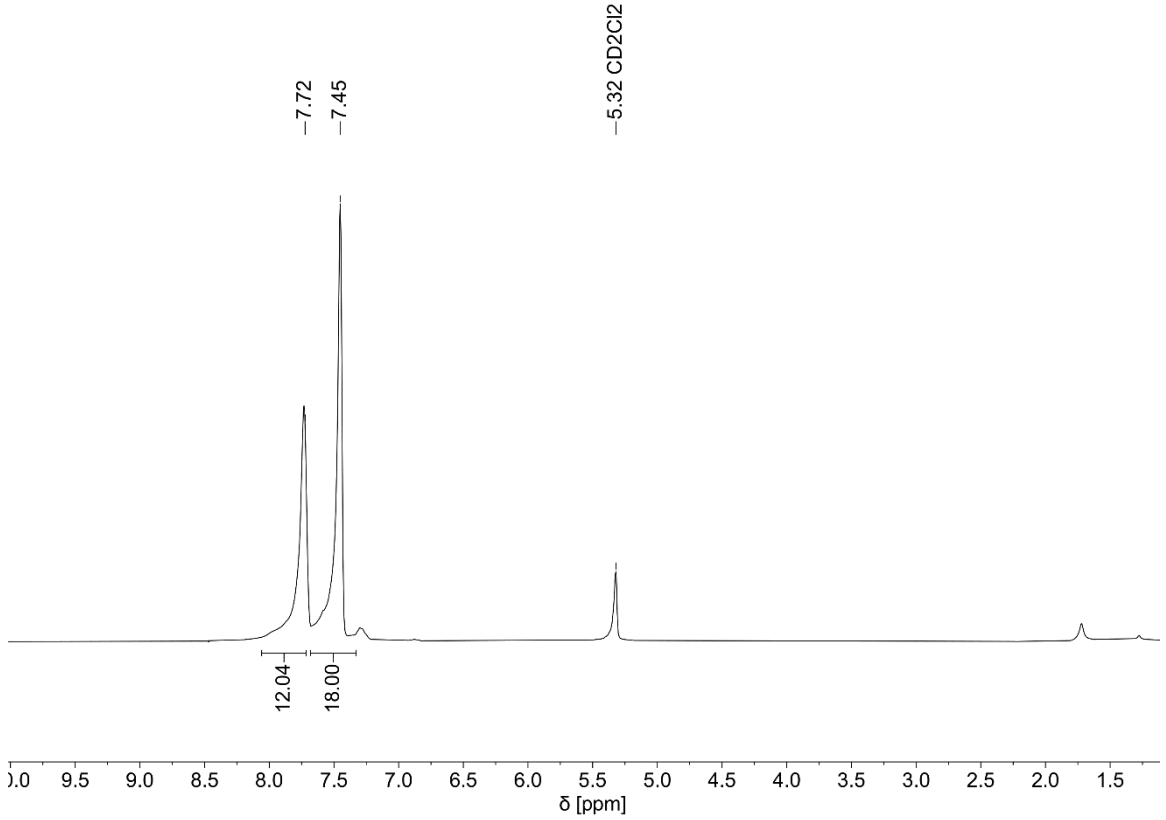

Figure S43. ^{99}Tc NMR spectrum of [Tc(CN)(CO)$_3$(PPh$_3$)$_2$] (**9**).

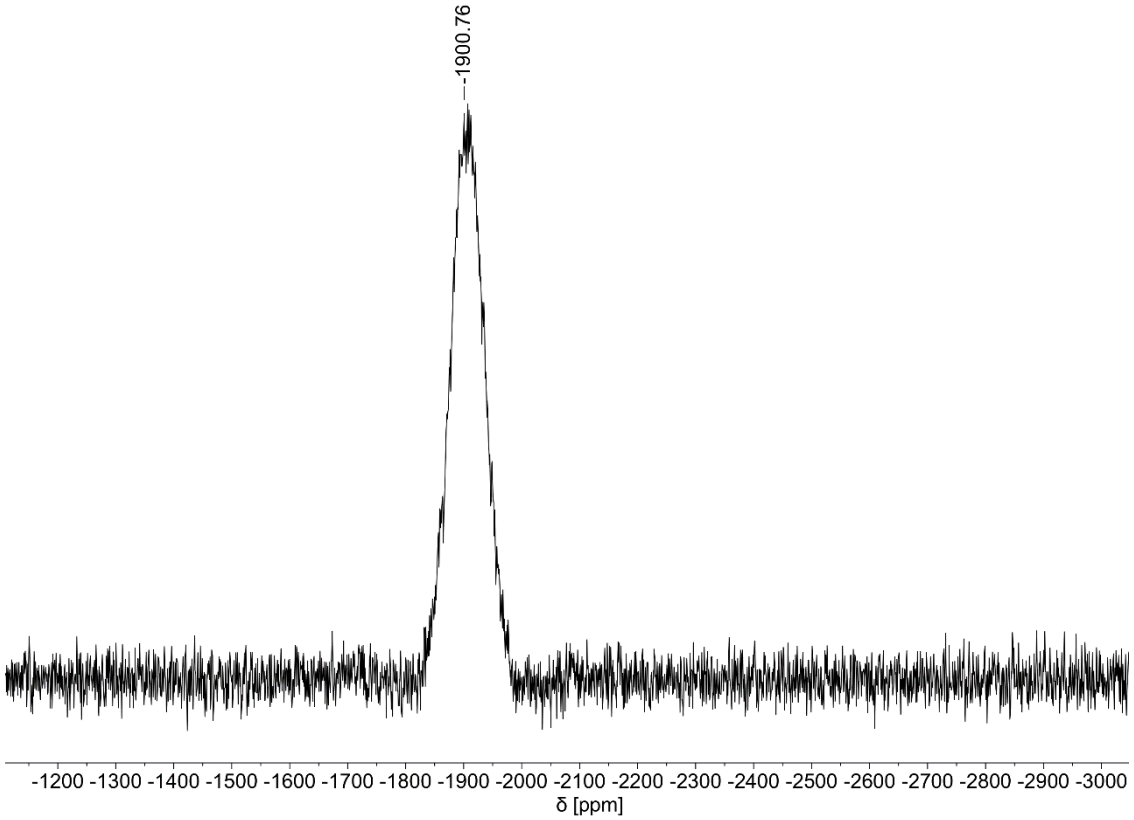

Figure S44. ^{31}P{^{1}H} NMR spectrum of [Tc(CN)(CO)$_3$(PPh$_3$)$_2$] (**9**).

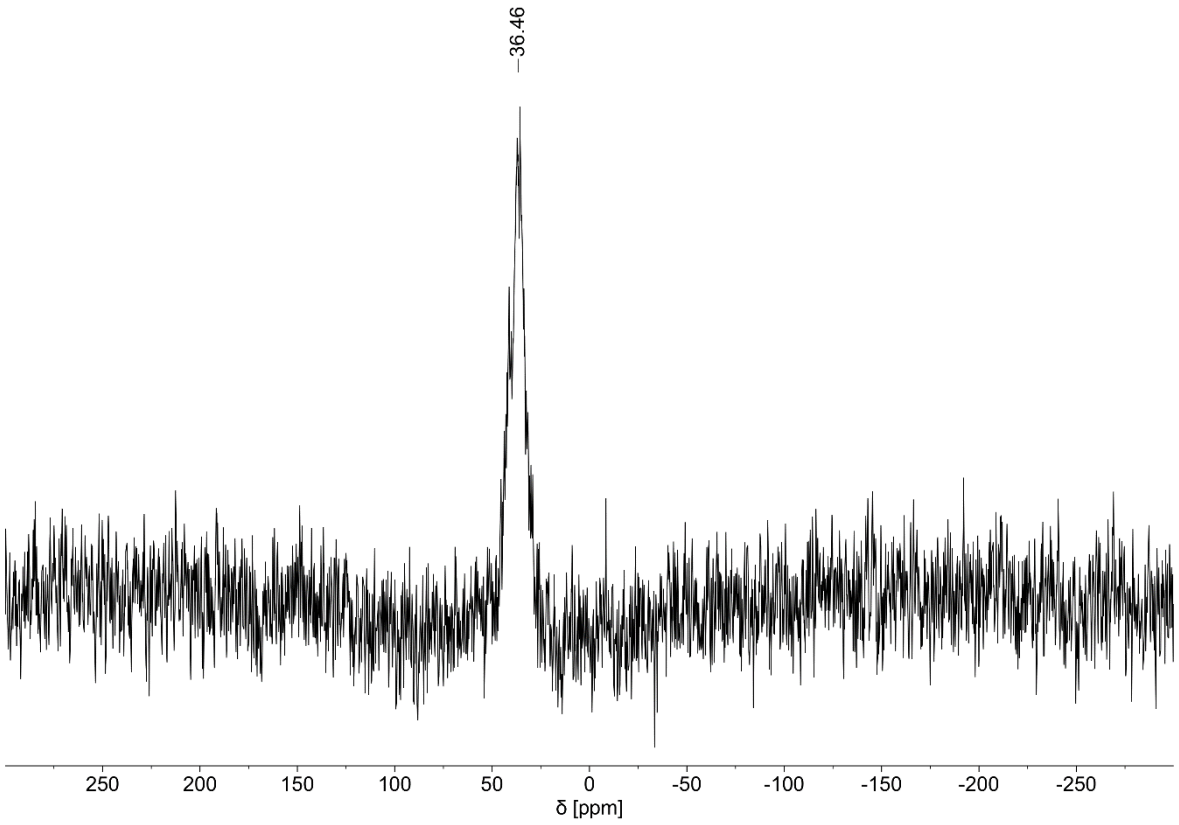

Figure S45. IR spectrum of $[Tc(CN)(CO)_3(PPh_3)_2]$ (**9**).

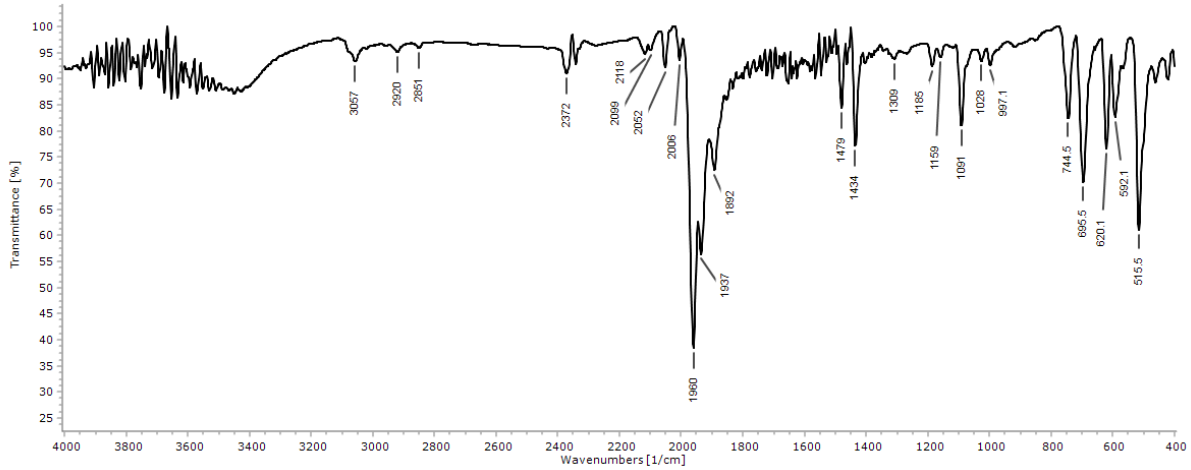

Figure S46. IR spectrum of $[Tc(CN)(CO)_3(PPh_3)_2]$ (**9**) · MeOH.

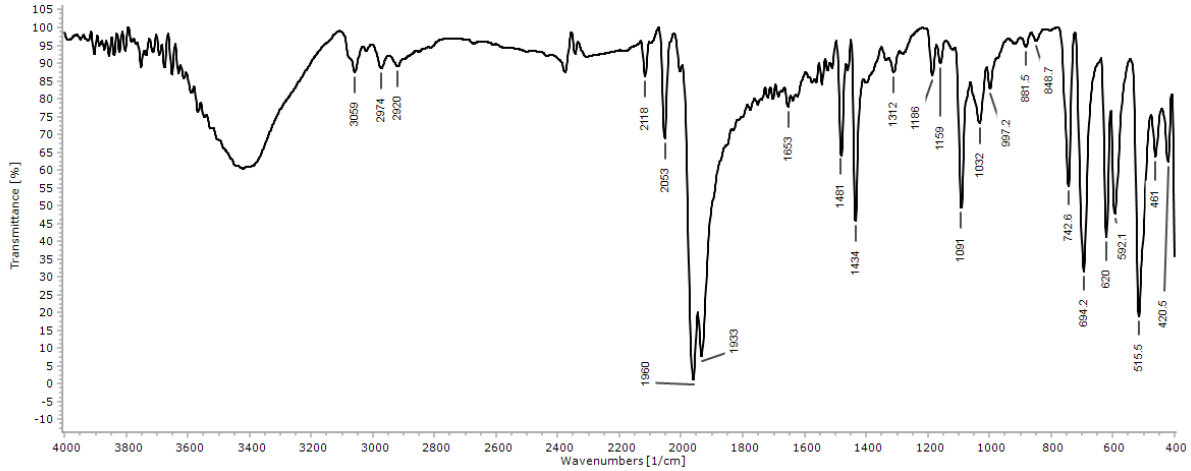

Figure S47. ^{1}H NMR spectrum of [Tc(η^2-OON)(CO)$_2$(PPh$_3$)$_2$] (**10**).

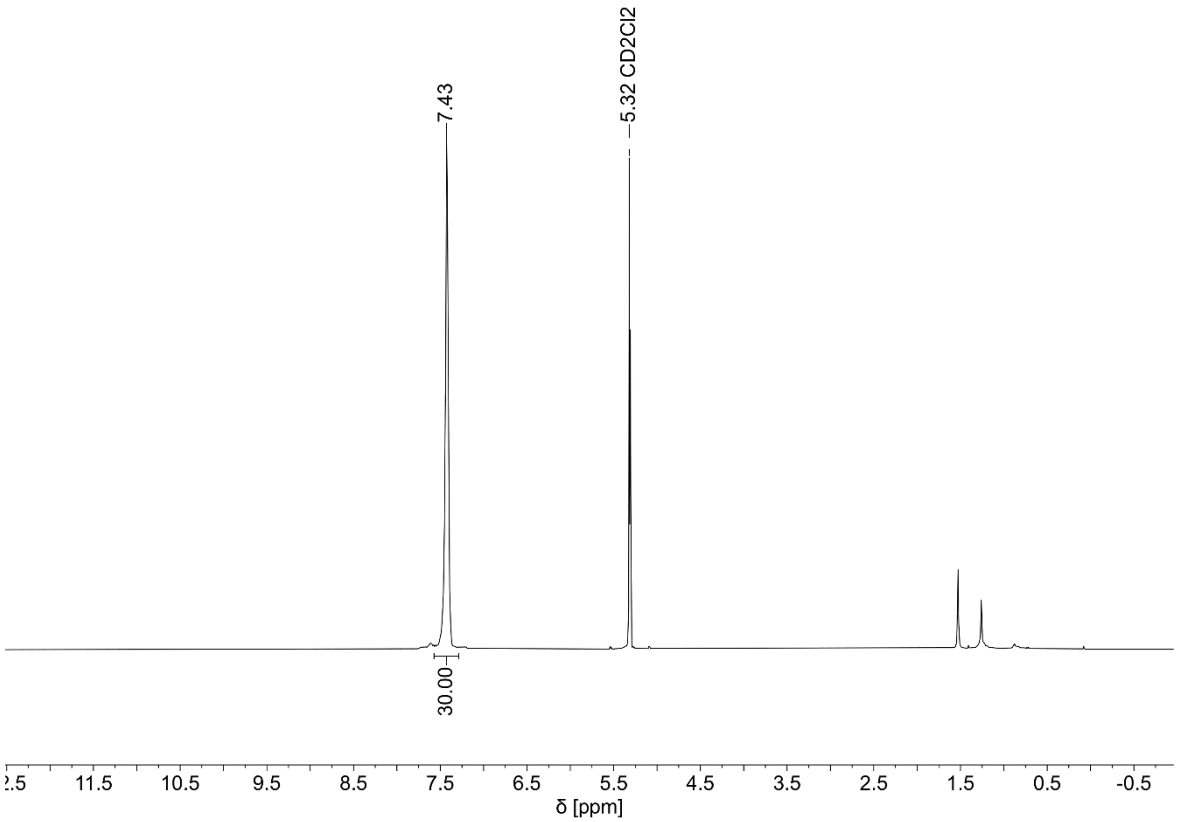

Figure S48. ^{99}Tc NMR spectrum of [Tc(η^2-OON)(CO)$_2$(PPh$_3$)$_2$] (**10**).

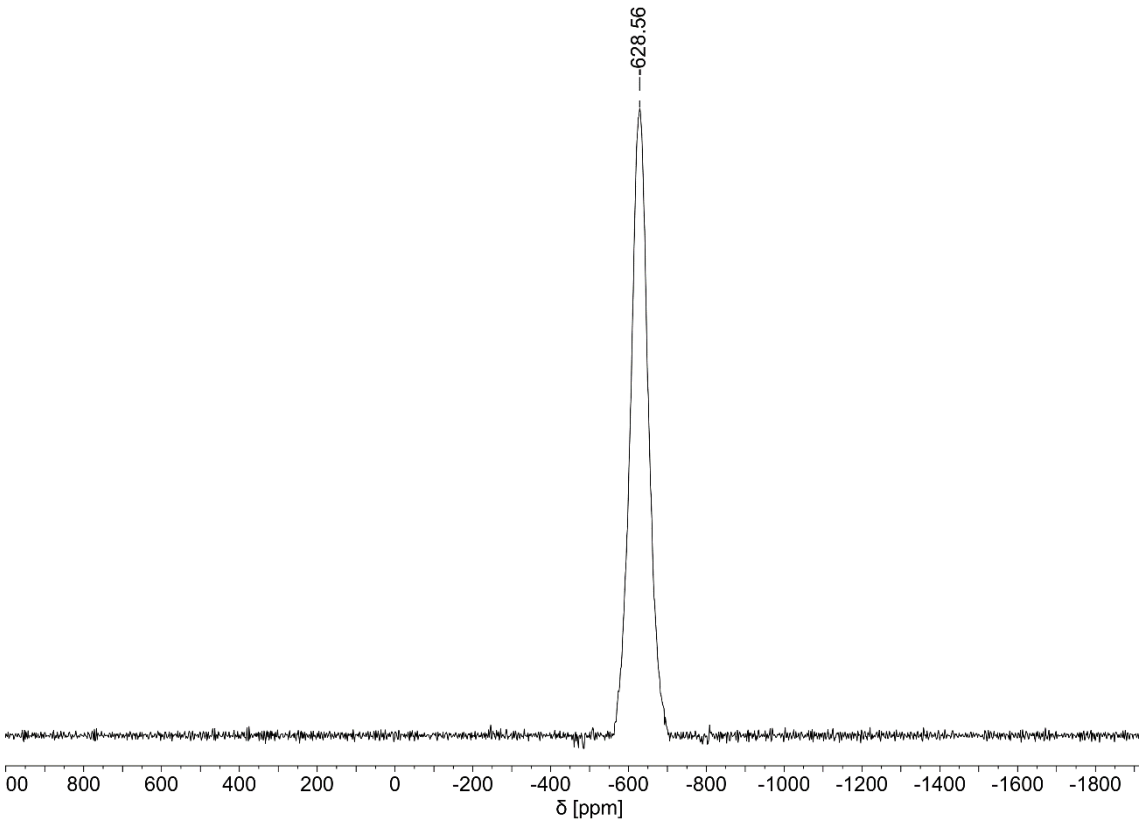

Figure S49. $^{31}P\{^{1}H\}$ NMR spectrum of [Tc(η^2-OON)(CO)$_2$(PPh$_3$)$_2$] (**10**).

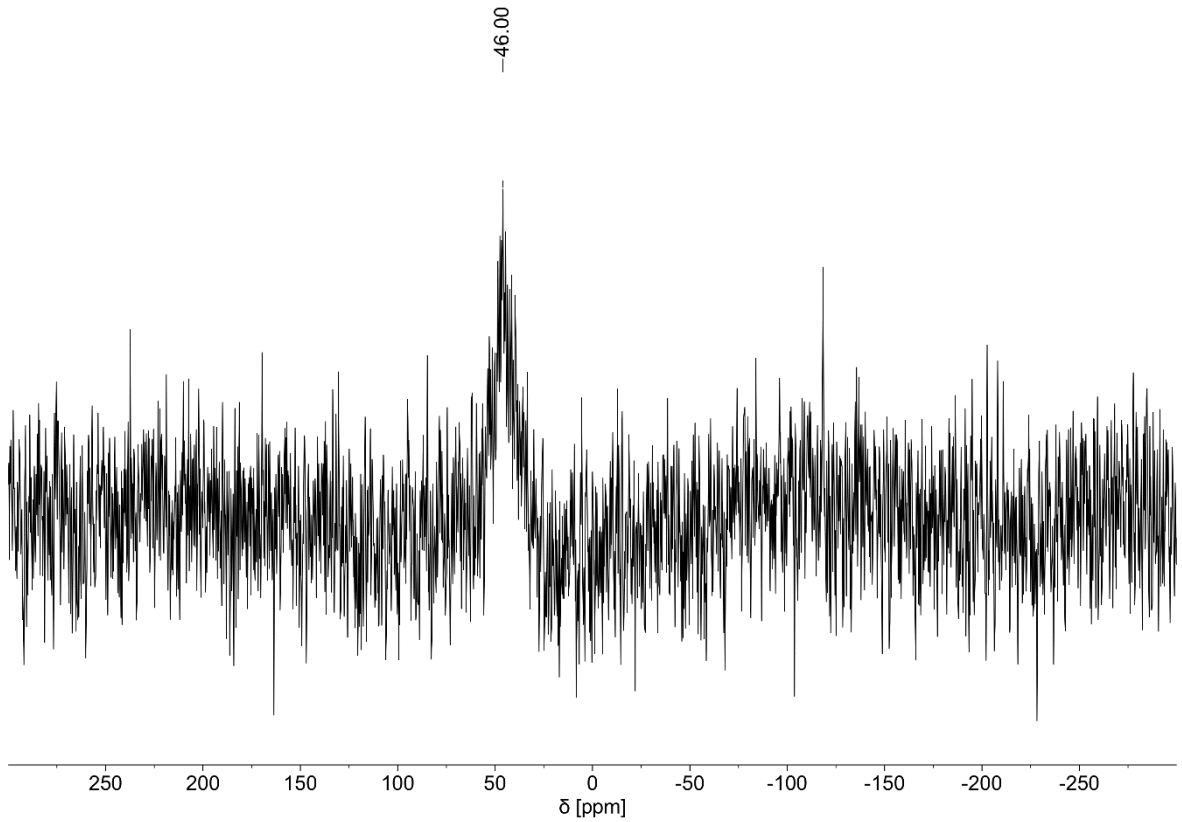

Figure S50. IR spectrum of [Tc(η^2-OON)(CO)$_2$(PPh$_3$)$_2$] (**10**).

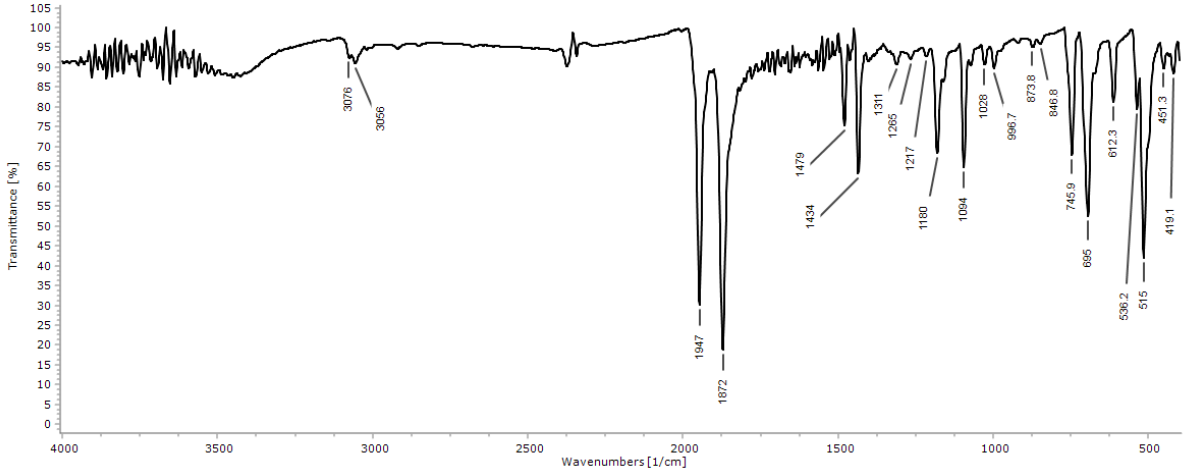

Figure S51. ^{99}Tc NMR spectrum of [Tc(η^1-NO_2)$(CO)_3(PPh_3)_2$]/[Tc(η^1-ONO)$(CO)_3(PPh_3)_2$] (**11a/11b**).

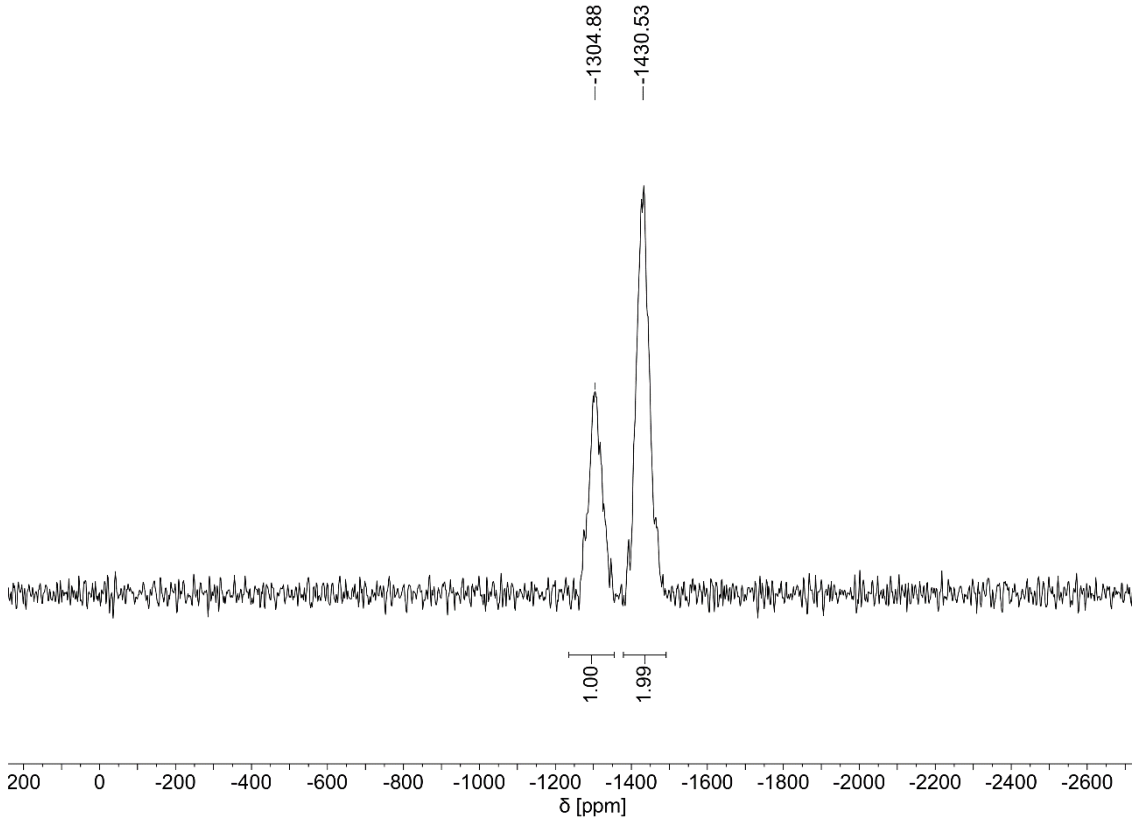

Figure S52. IR spectrum of [Tc(η^1-NO_2)$(CO)_3(PPh_3)_2$]/[Tc(η^1-ONO)$(CO)_3(PPh_3)_2$] (**11a**)/(**11b**).

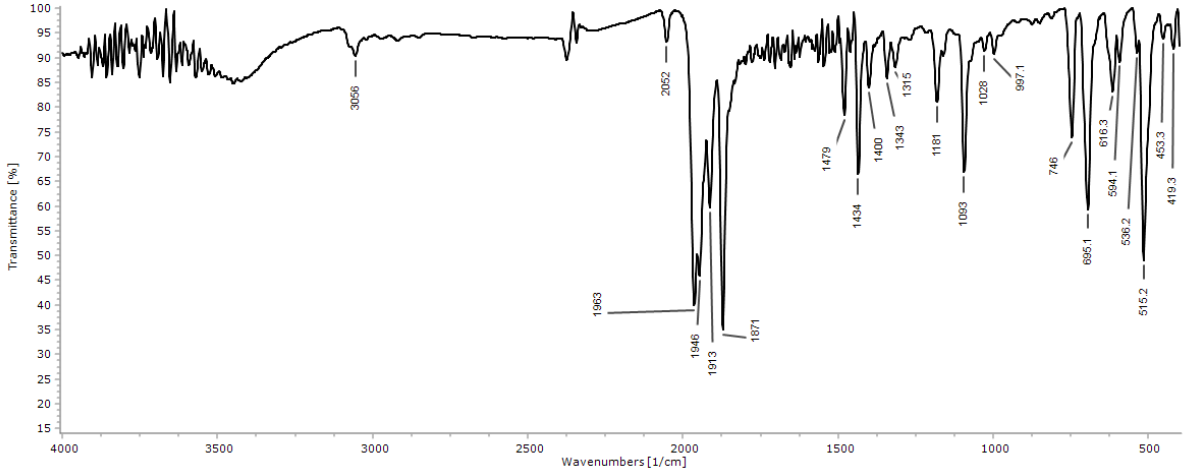

Figure S53. ^{1}H NMR spectrum of [Tc(η^2-OONO)(CO)$_2$(PPh$_3$)$_2$] (**12**).

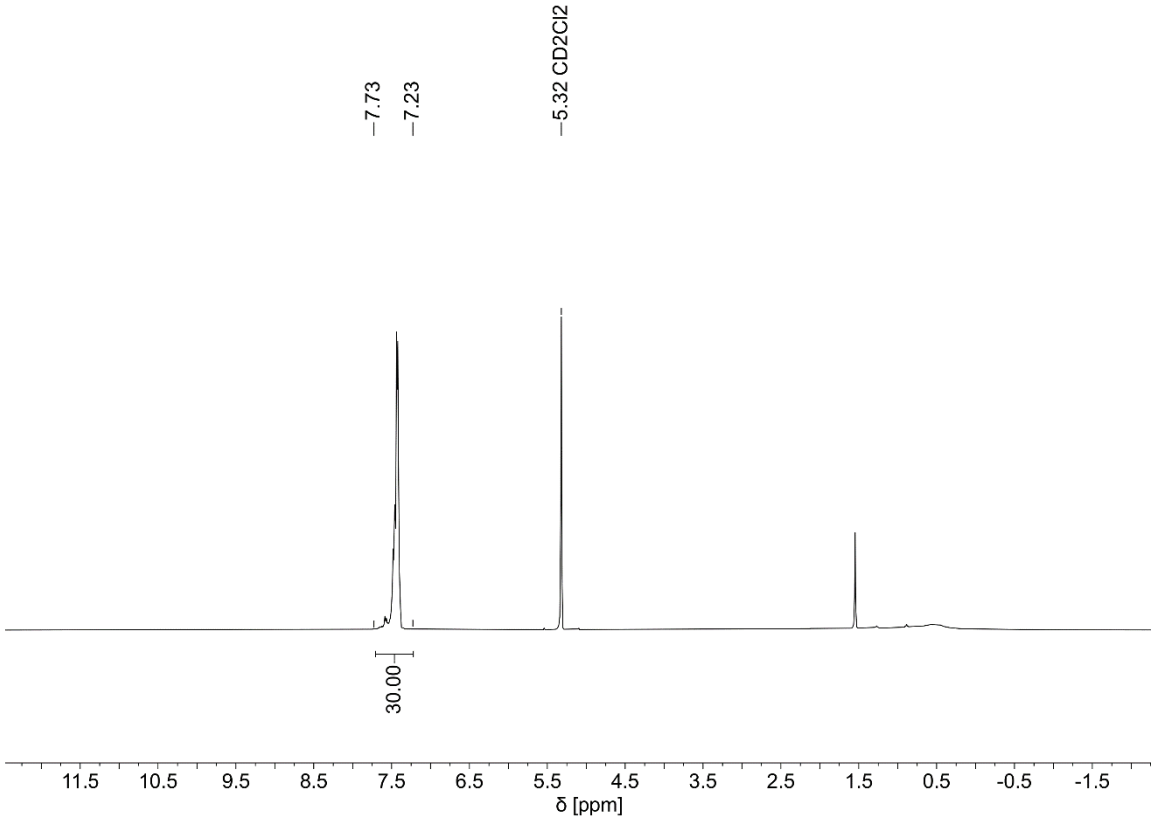

Figure S54. ^{99}Tc NMR spectrum of [Tc(η^2-OONO)(CO)$_2$(PPh$_3$)$_2$] (**12**).

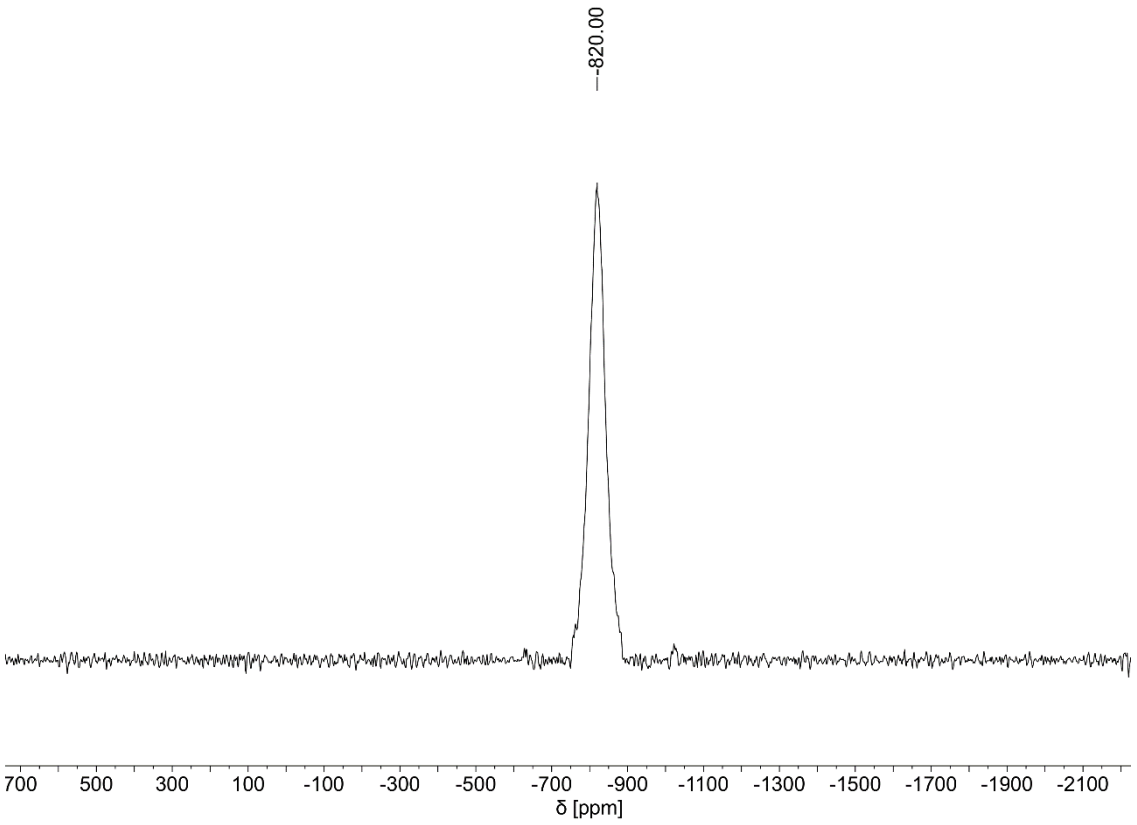

Figure S55. IR spectrum of [Tc(η^2-OONO)(CO)$_2$(PPh$_3$)$_2$] (**12**).

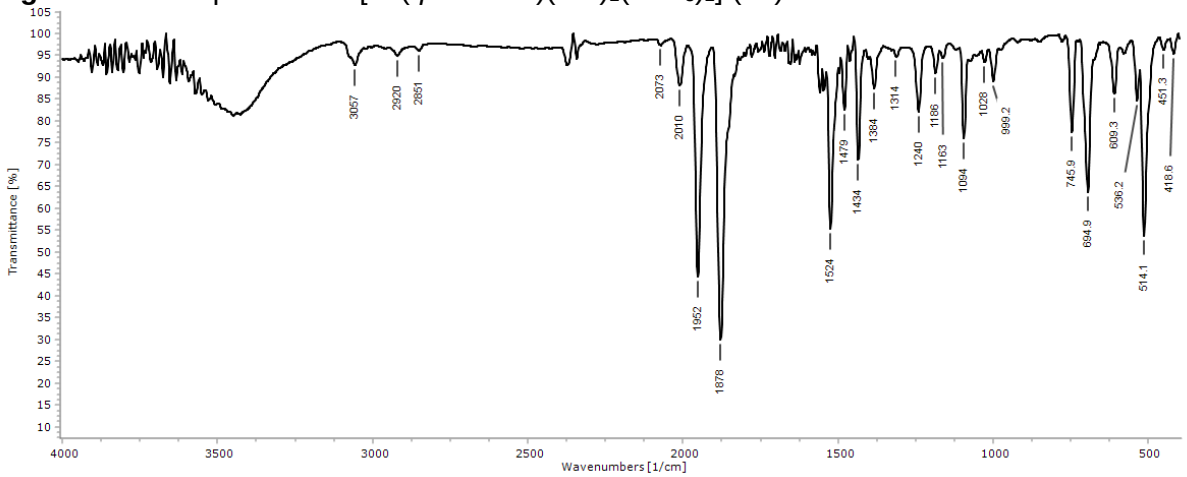

Figure S56. ^{99}Tc NMR spectrum of [Tc(η^1-ONO$_2$)(CO)$_3$(PPh$_3$)$_2$] (**13**).

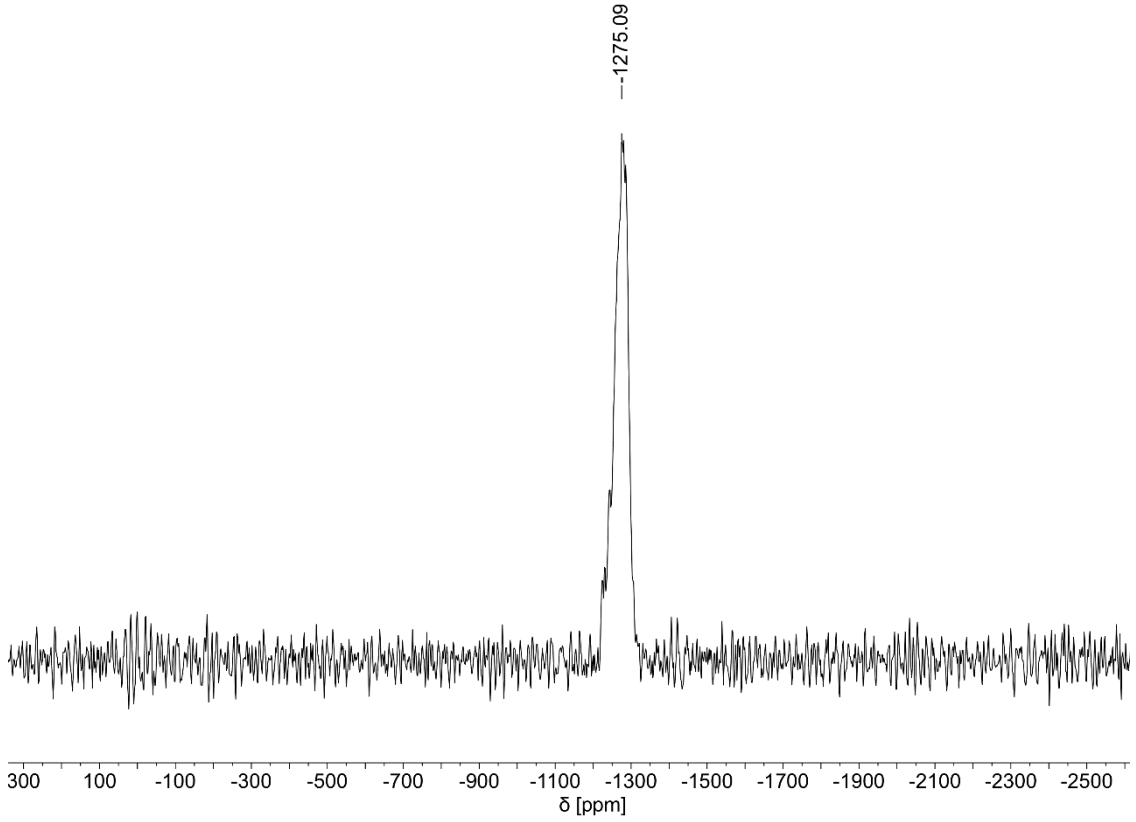

Figure S57. $^{31}P\{^{1}H\}$ NMR spectrum of $[Tc(\eta^{1}\text{-}ONO_2)(CO)_2(PPh_3)_2]$ (**13**).

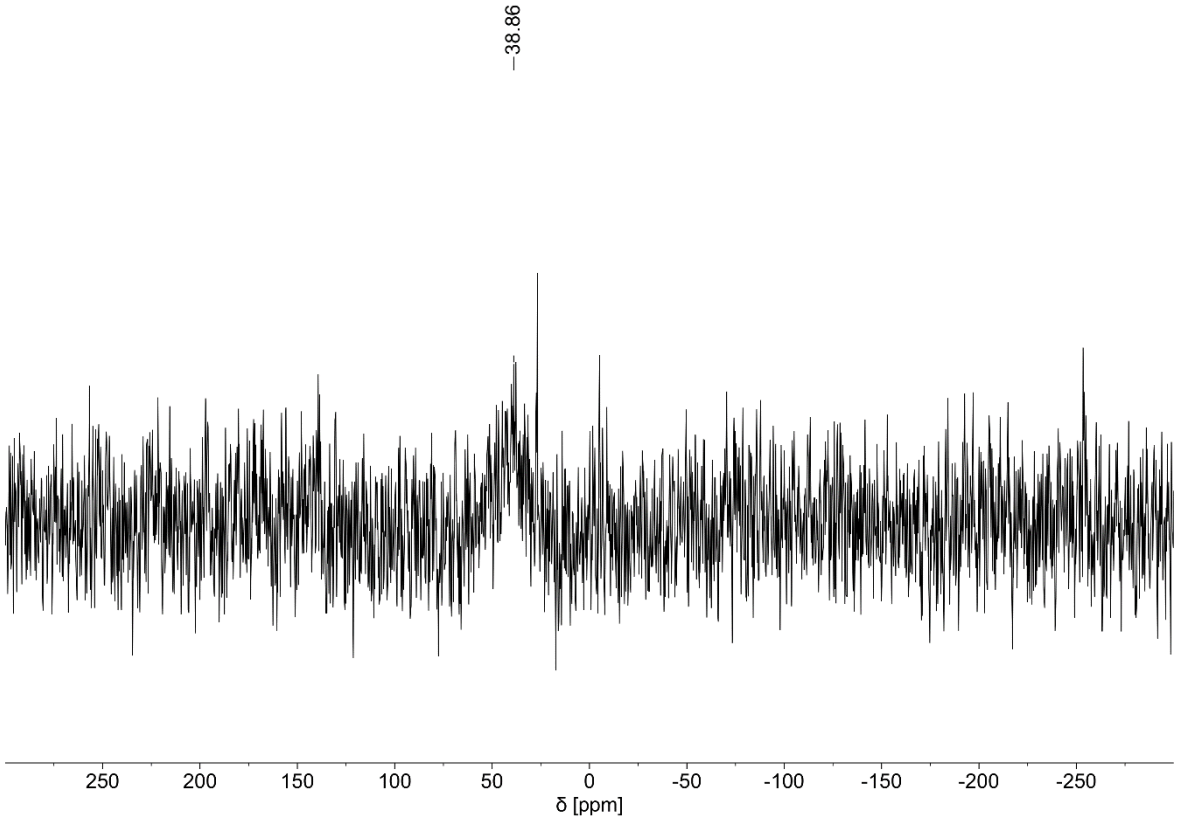

Figure S58. ^{1}H NMR spectrum of $[TcH(CO)_3(PPh_3)_2]$/$[Tc(\eta^{2}\text{-}HHBH_2)(CO)_2(PPh_3)_2]$ (**14**)/(**15**) in the hydride region.

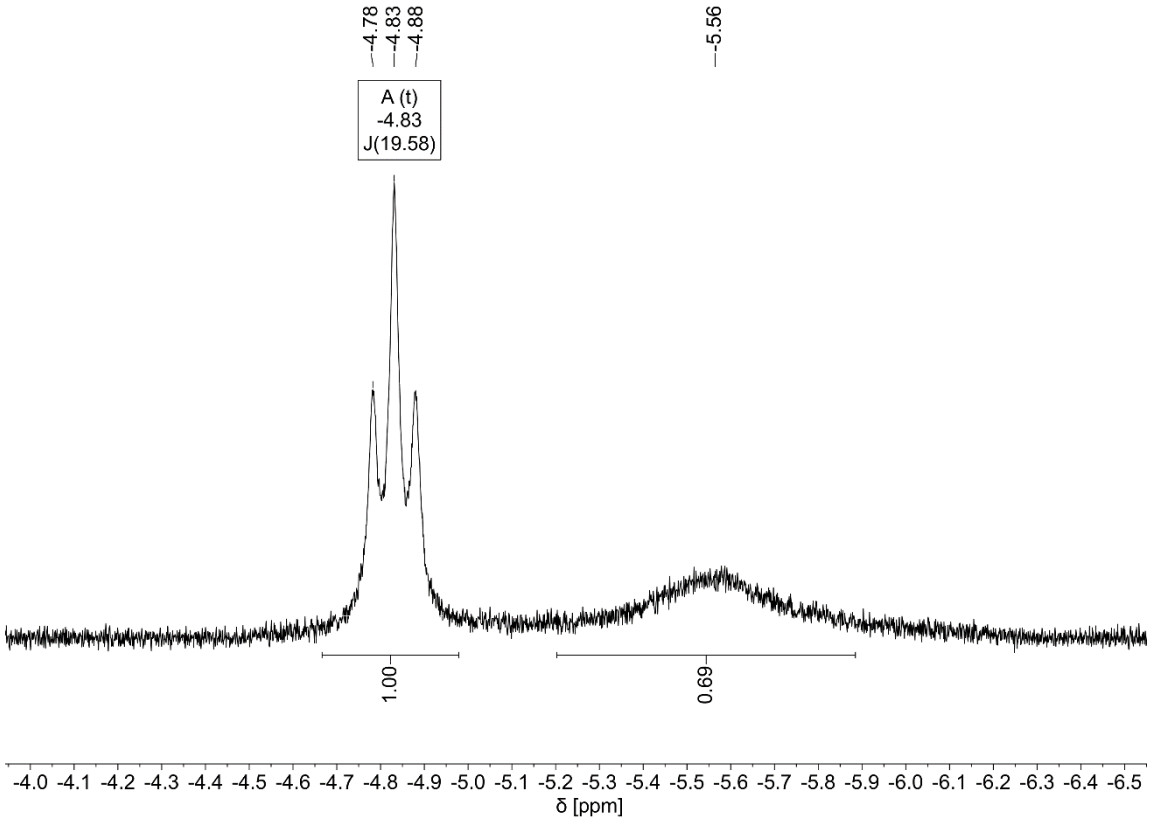

Figure S59. ^{1}H NMR spectrum of [TcH(CO)$_3$(PPh$_3$)$_2$]/[Tc(η^2-HHBH$_2$)(CO)$_2$(PPh$_3$)$_2$] (**14**)/(**15**); complete spectrum.

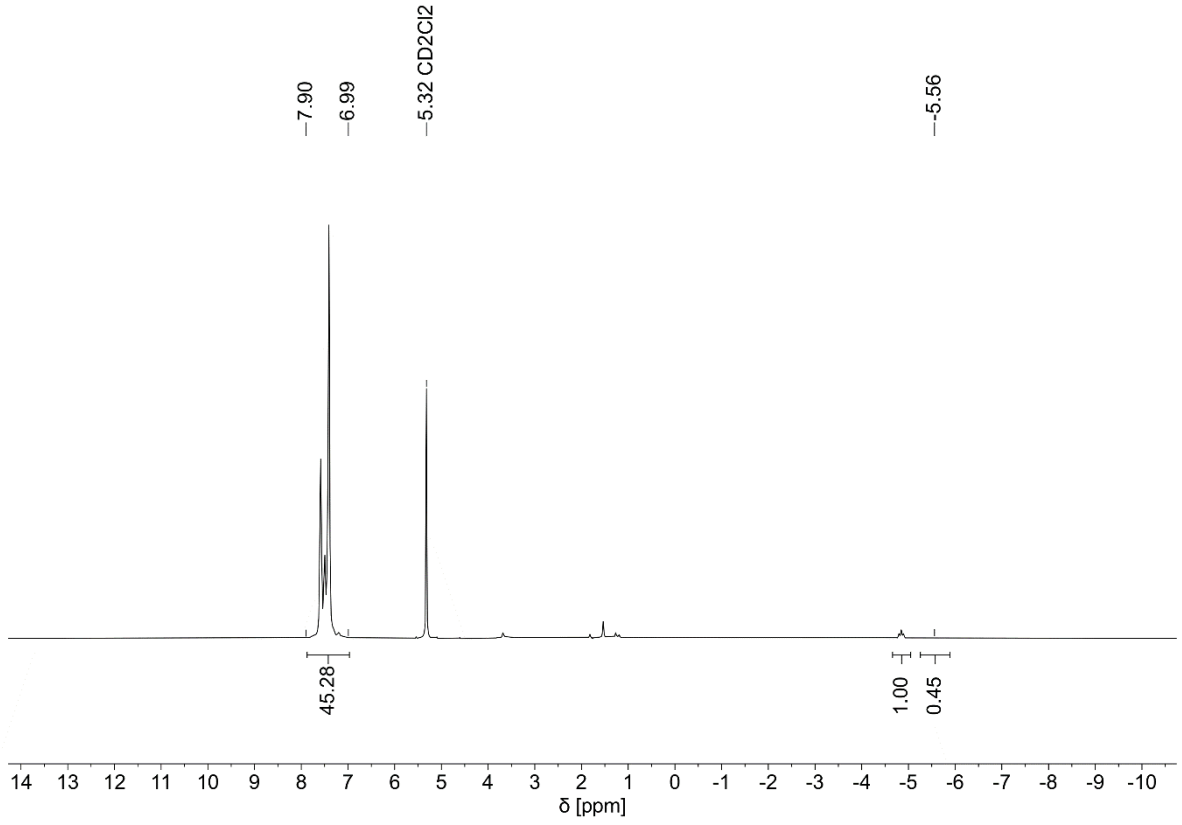

Figure S60. ^{99}Tc NMR spectrum of [TcH(CO)$_3$(PPh$_3$)$_2$]/[Tc(η^2-HHBH$_2$)(CO)$_2$(PPh$_3$)$_2$] (**14**)/(**15**) focused on the dicarbonyl region.

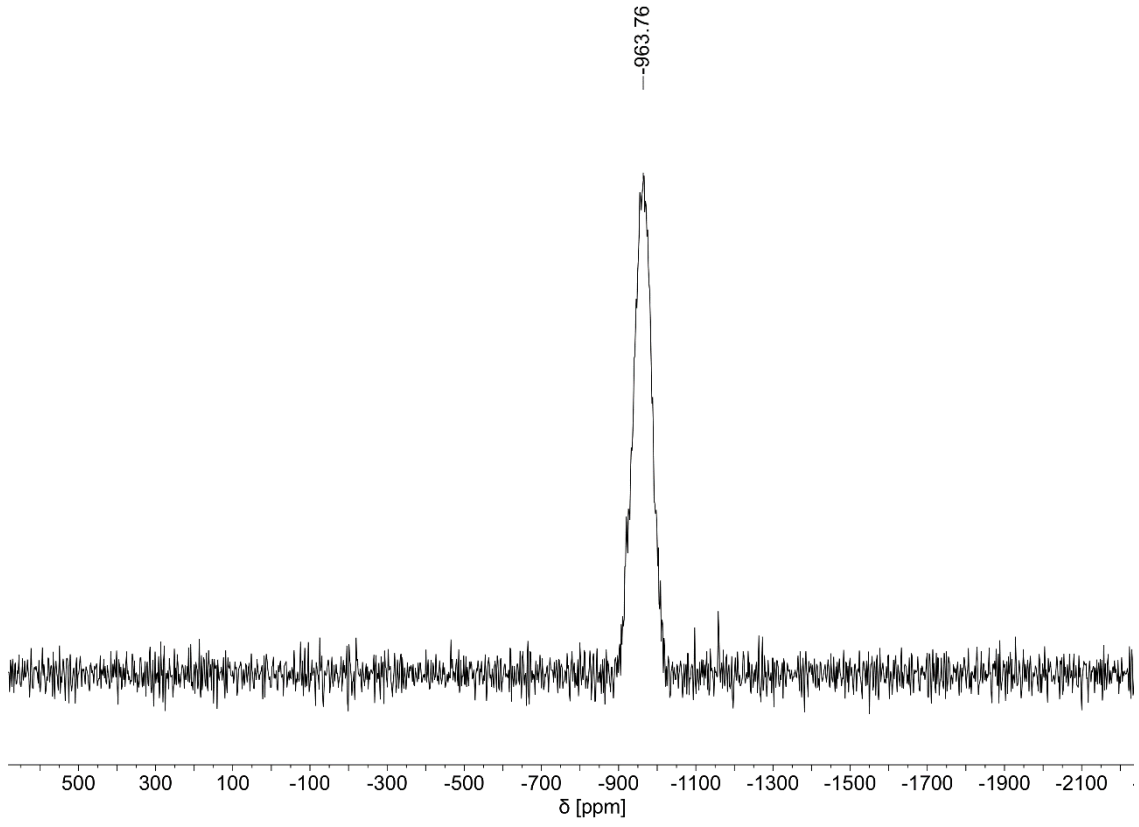

Figure S61. ^{99}Tc NMR spectrum of [TcH(CO)$_3$(PPh$_3$)$_2$]/[Tc(η^2-HHBH$_2$)(CO)$_2$(PPh$_3$)$_2$] (**14**)/(**15**), stacking of the spectra recorded with focus to the dicarbonyl and the monohydride regions.

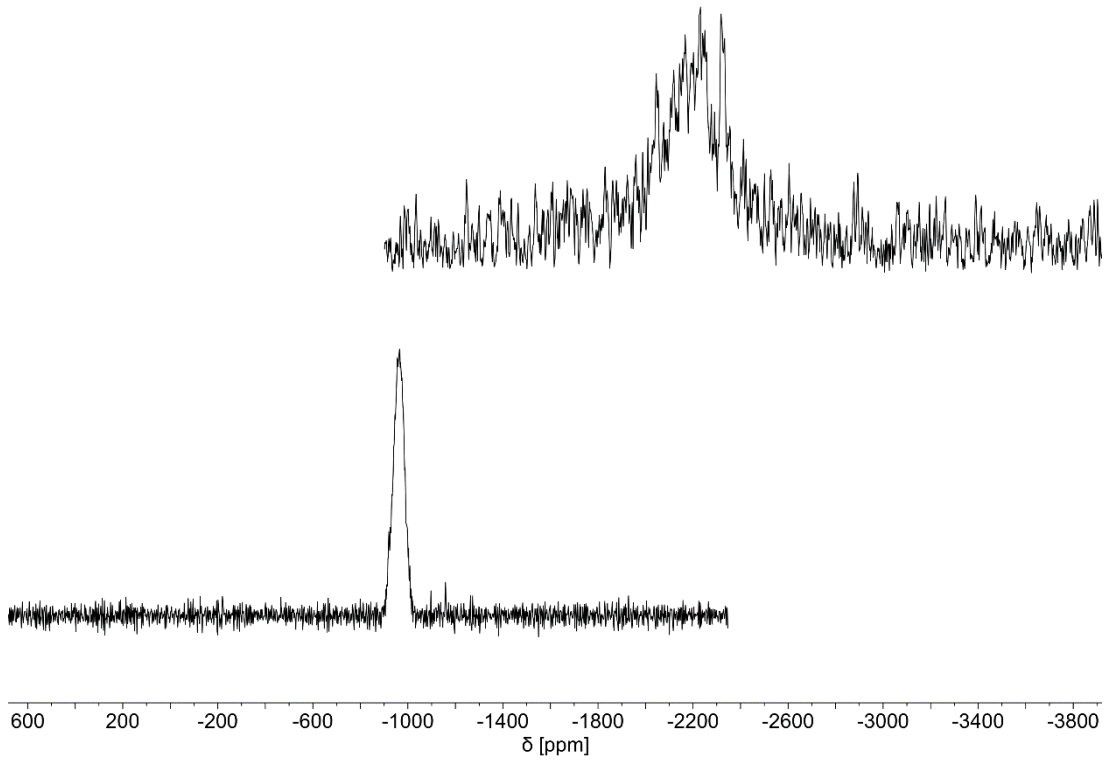

Figure S62. ^{11}B NMR spectrum of [TcH(CO)$_3$(PPh$_3$)$_2$]/[Tc(η^2-HHBH$_2$)(CO)$_2$(PPh$_3$)$_2$] (**14**)/(**15**).

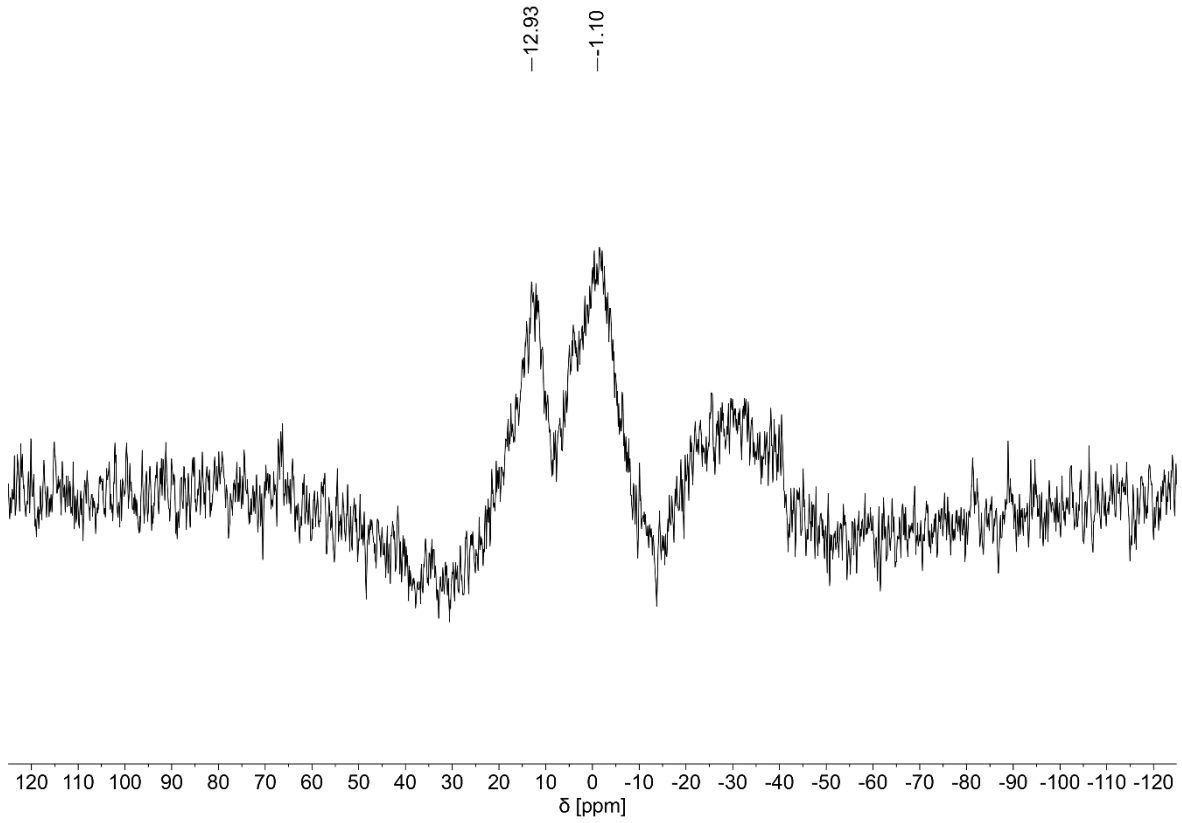

Figure S63. IR spectrum of [TcH(CO)$_3$(PPh$_3$)$_2$]/[Tc(η^2-HHBH$_2$)(CO)$_2$(PPh$_3$)$_2$] (**14**)/(**15**).

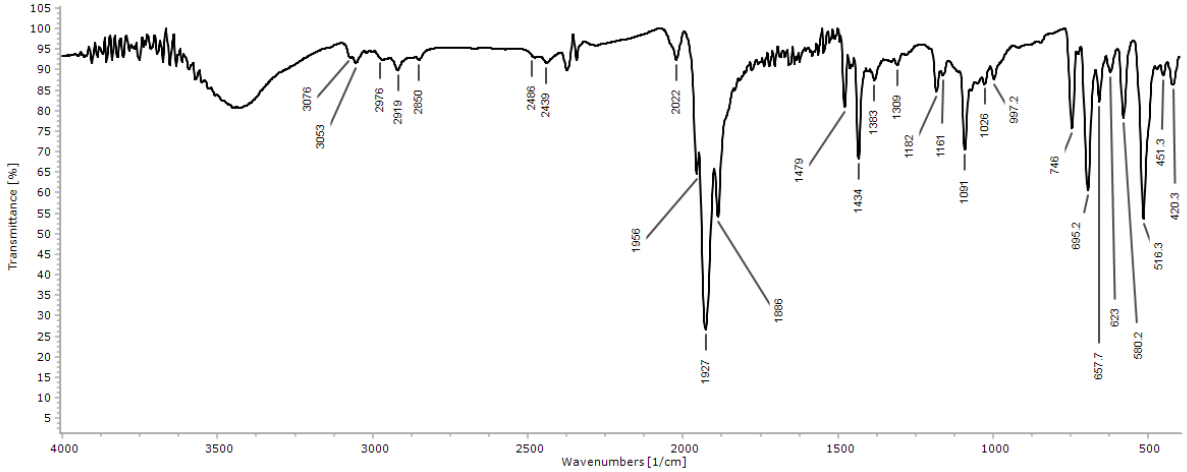

Figure S64. ^{1}H NMR spectrum of [Tc(η^2-SSCMe)(CO)$_2$(PPh$_3$)$_2$]/[Tc(η^2-SSCSMe)(CO)$_2$(PPh$_3$)$_2$]/[Tc(η^2-SSCOMe)(CO)$_2$(PPh$_3$)$_2$] (**17**)/(**18a**)/(**18b**).

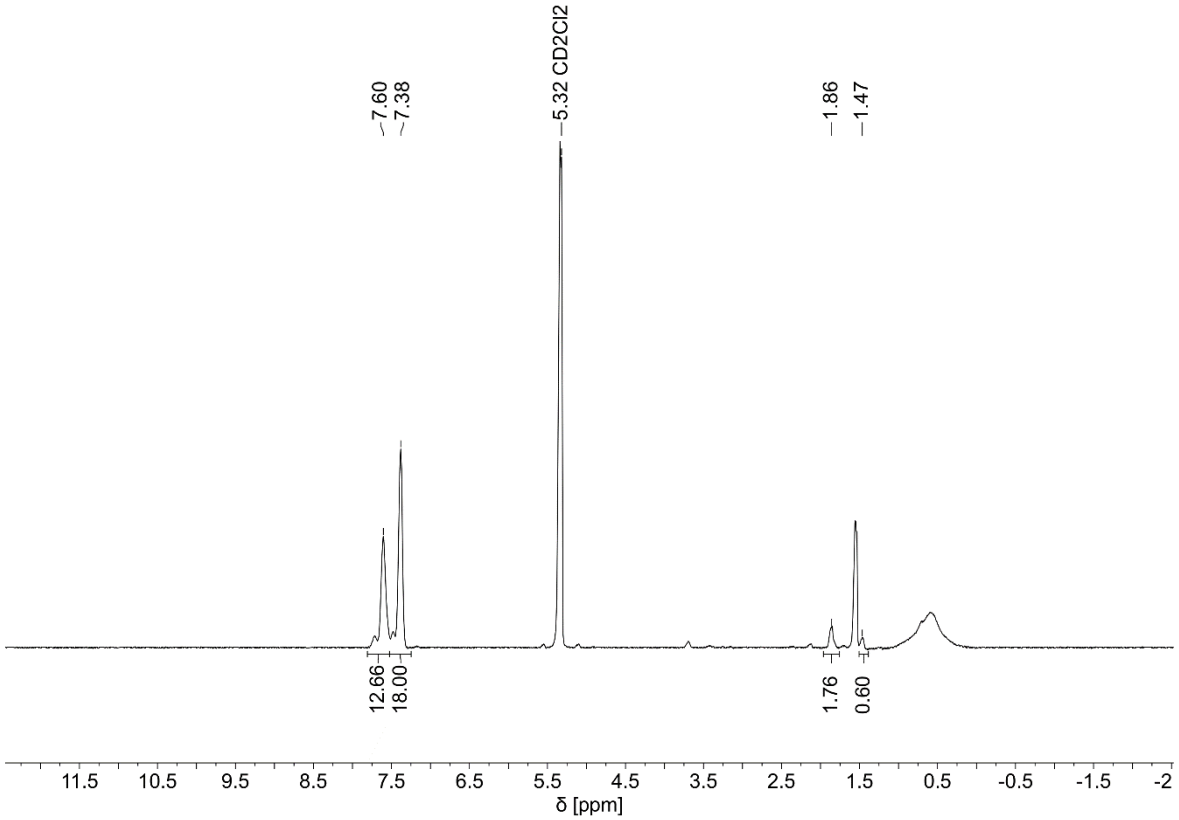

Figure S65. ^{99}Tc NMR spectrum of [Tc(η^2-SSCMe)(CO)$_2$(PPh$_3$)$_2$]/[Tc(η^2-SSCSMe)(CO)$_2$(PPh$_3$)$_2$]/[Tc(η^2-SSCOMe)(CO)$_2$(PPh$_3$)$_2$] (**17**)/(**18a**)/(**18b**).

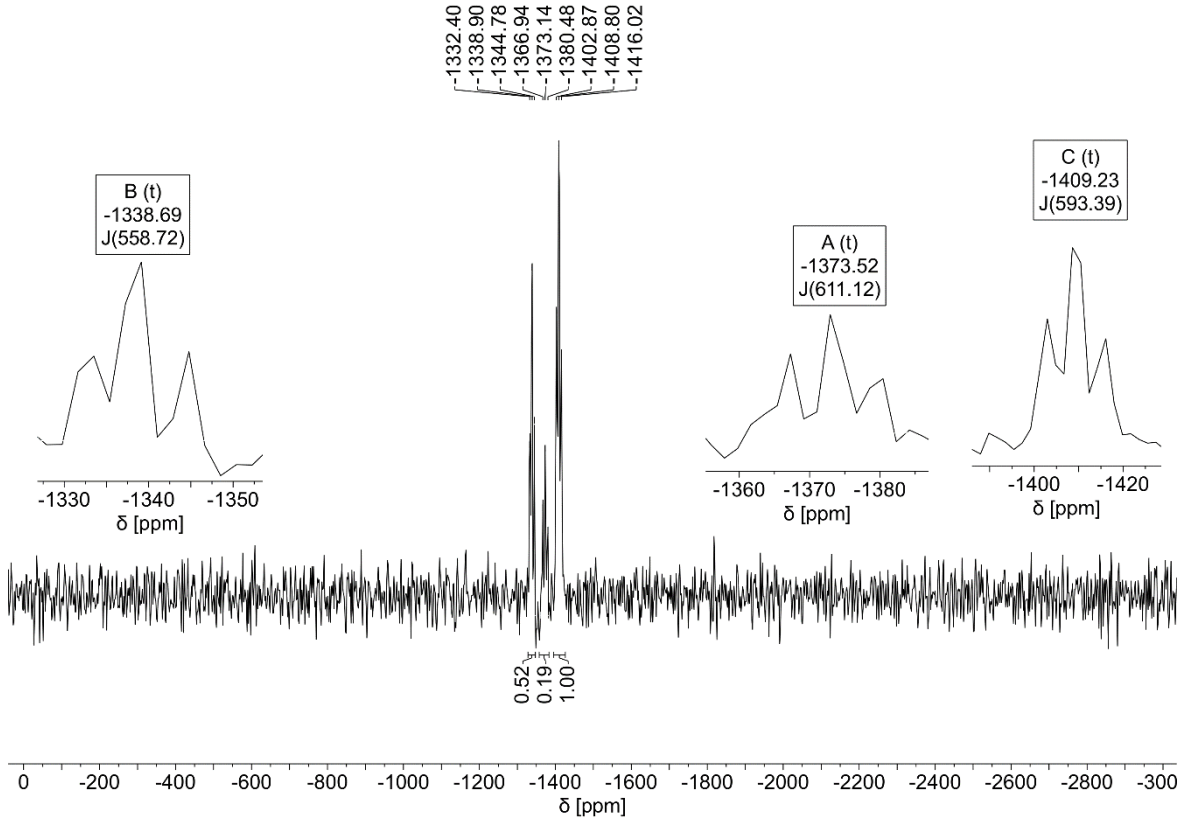

Figure S66. IR spectrum of [Tc(η^2-SSCMe)(CO)$_2$(PPh$_3$)$_2$]/[Tc(η^2-SSCSMe)(CO)$_2$(PPh$_3$)$_2$]/[Tc(η^2-SSCOMe)(CO)$_2$(PPh$_3$)$_2$] (**17**)/(**18a**)/(**18b**).

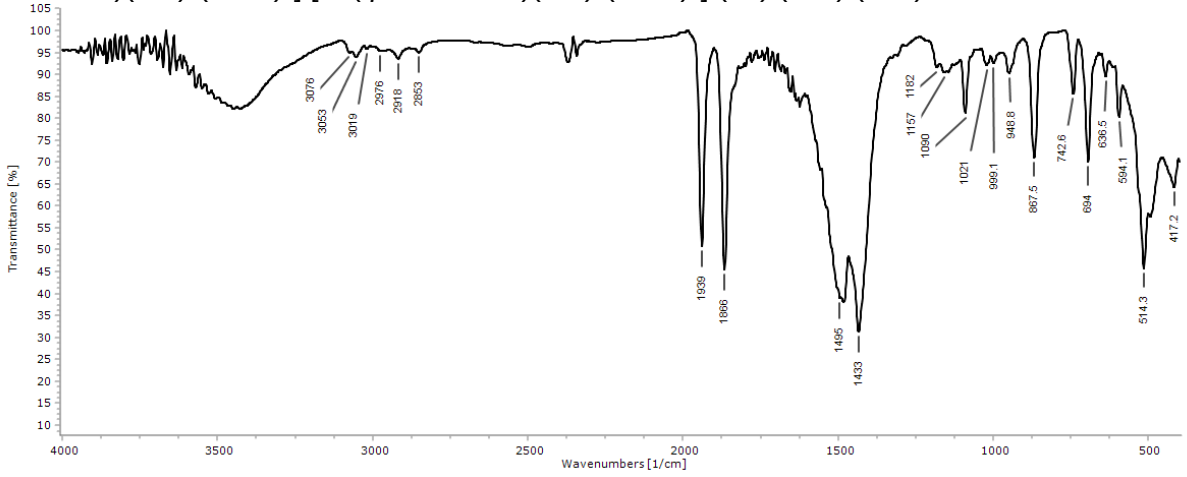

Figure S67. ^{1}H NMR spectrum of [Tc(η^1-SCHS)(CO)$_3$(PPh$_3$)$_2$]/[Tc(η^2-SSCH)(CO)$_2$(PPh$_3$)$_2$] (**19**)/(**20**).

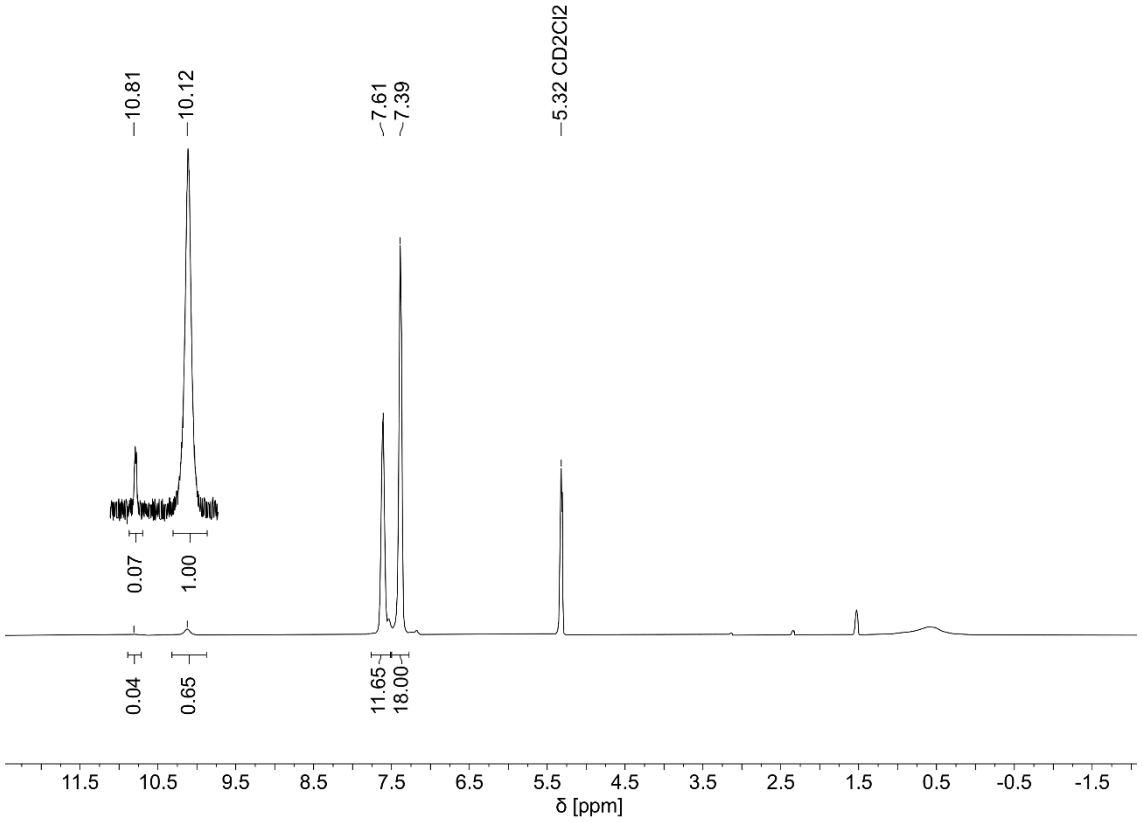

Figure S68. ^{99}Tc NMR spectrum of [Tc(η^1-SCHS)(CO)$_3$(PPh$_3$)$_2$]/[Tc(η^2-SSCH)(CO)$_2$(PPh$_3$)$_2$] (**19**)/(**20**).

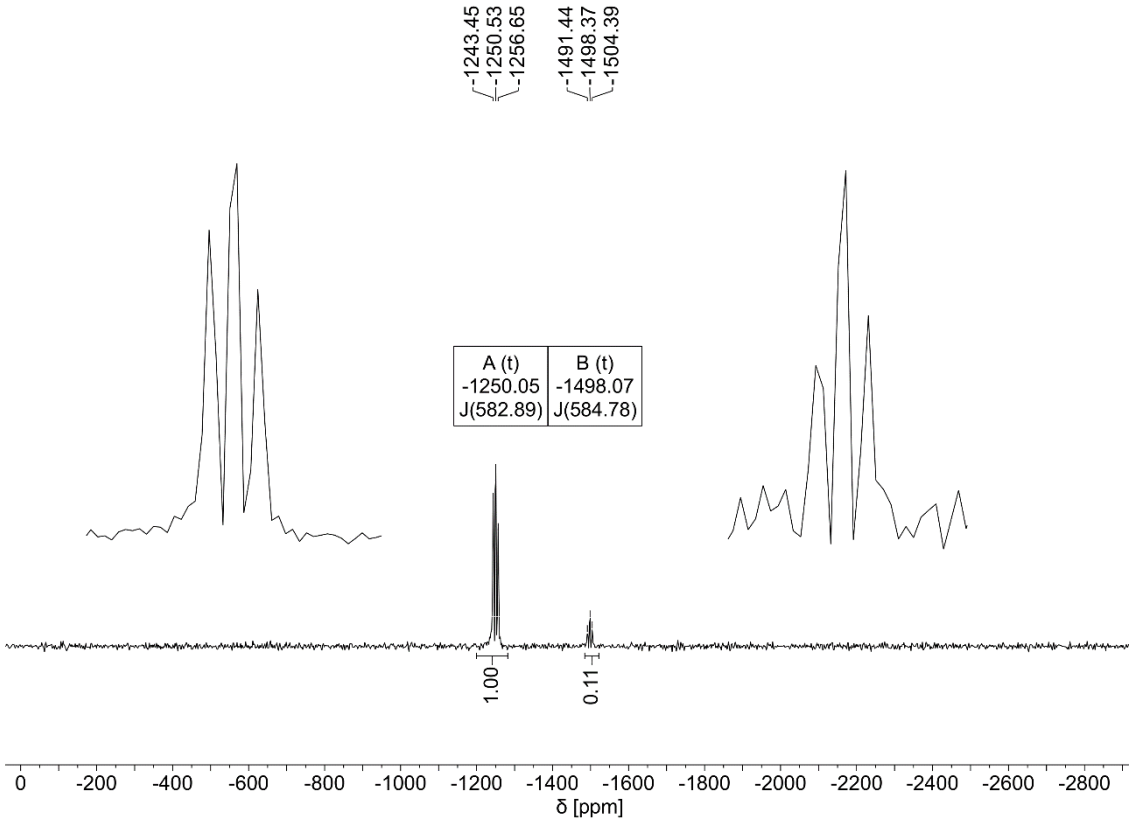

Figure S69. IR spectrum of [Tc(η^1-SCHS)(CO)$_3$(PPh$_3$)$_2$]/[Tc(η^2-SSCH)(CO)$_2$(PPh$_3$)$_2$] (**19**)/(**20**).

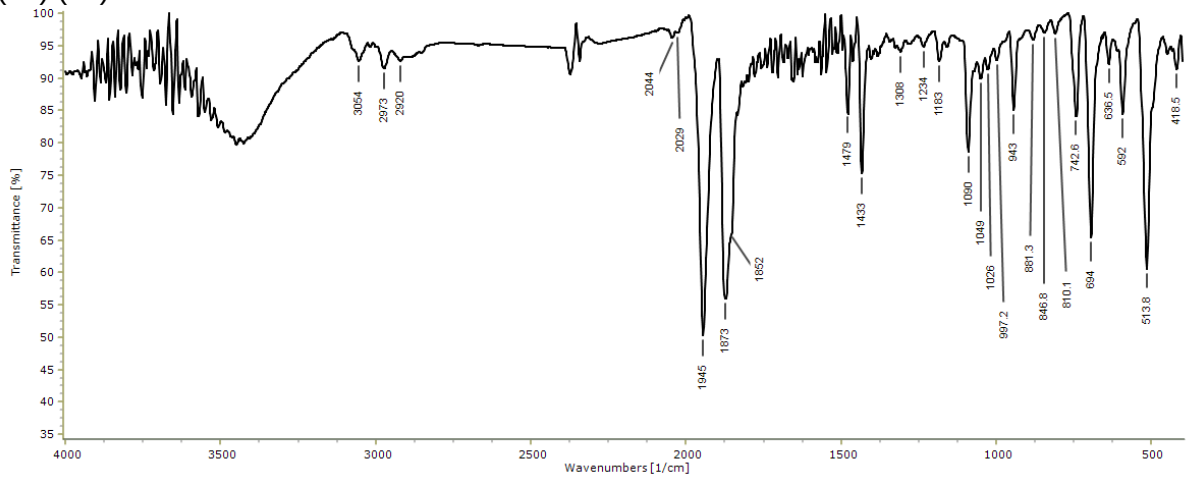

Figure S70. ^{1}H NMR spectrum of [Tc(η^1-OTcO$_3$)(CO)$_3$(PPh$_3$)$_2$] (**21**).

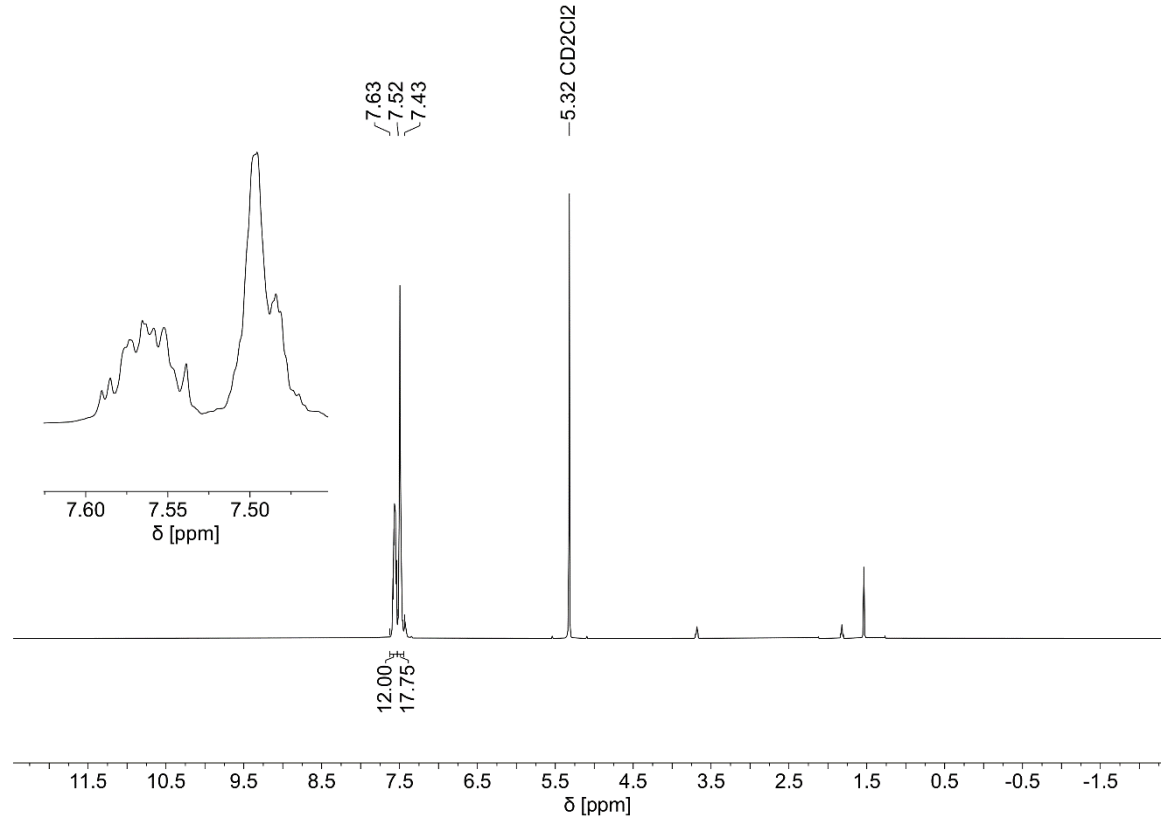

Figure S71. ^{99}Tc NMR spectrum of [Tc(η^1-OTcO$_3$)(CO)$_3$(PPh$_3$)$_2$] (**21**) focused on the pertechnetate region.

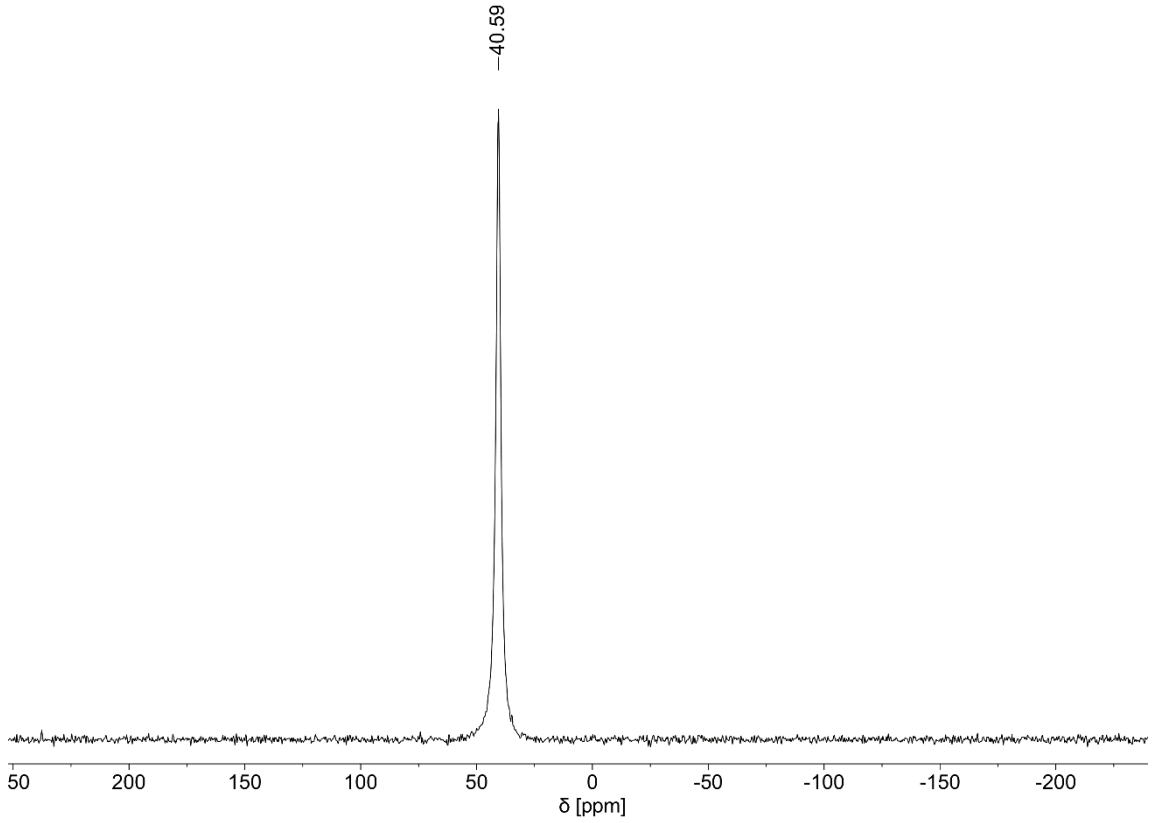

Figure S72. ^{99}Tc NMR spectrum of [Tc(η^1-OTcO$_3$)(CO)$_3$(PPh$_3$)$_2$] (**21**) focused on the tricarbonyl region.

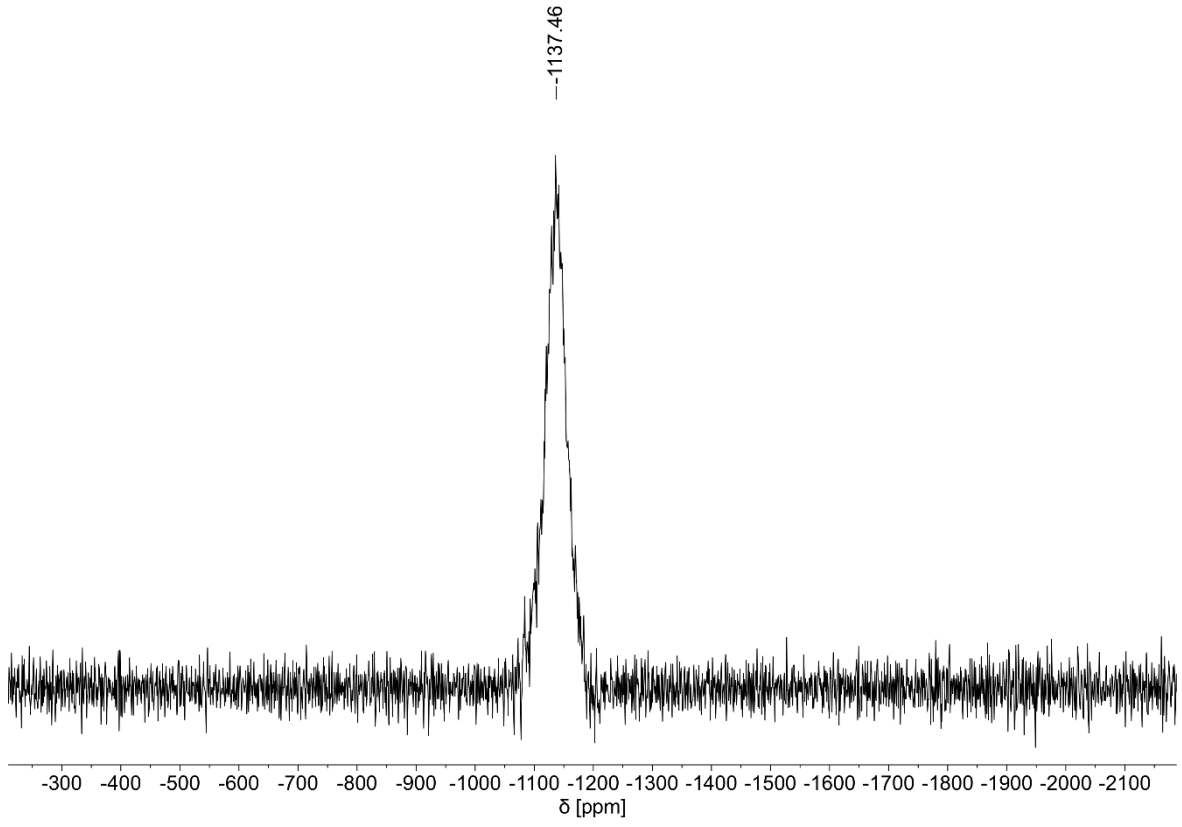

Figure S73. $^{31}P\{^{1}H\}$ NMR spectrum of $[Tc(\eta^1\text{-}OTcO_3)(CO)_3(PPh_3)_2]$ (**21**).

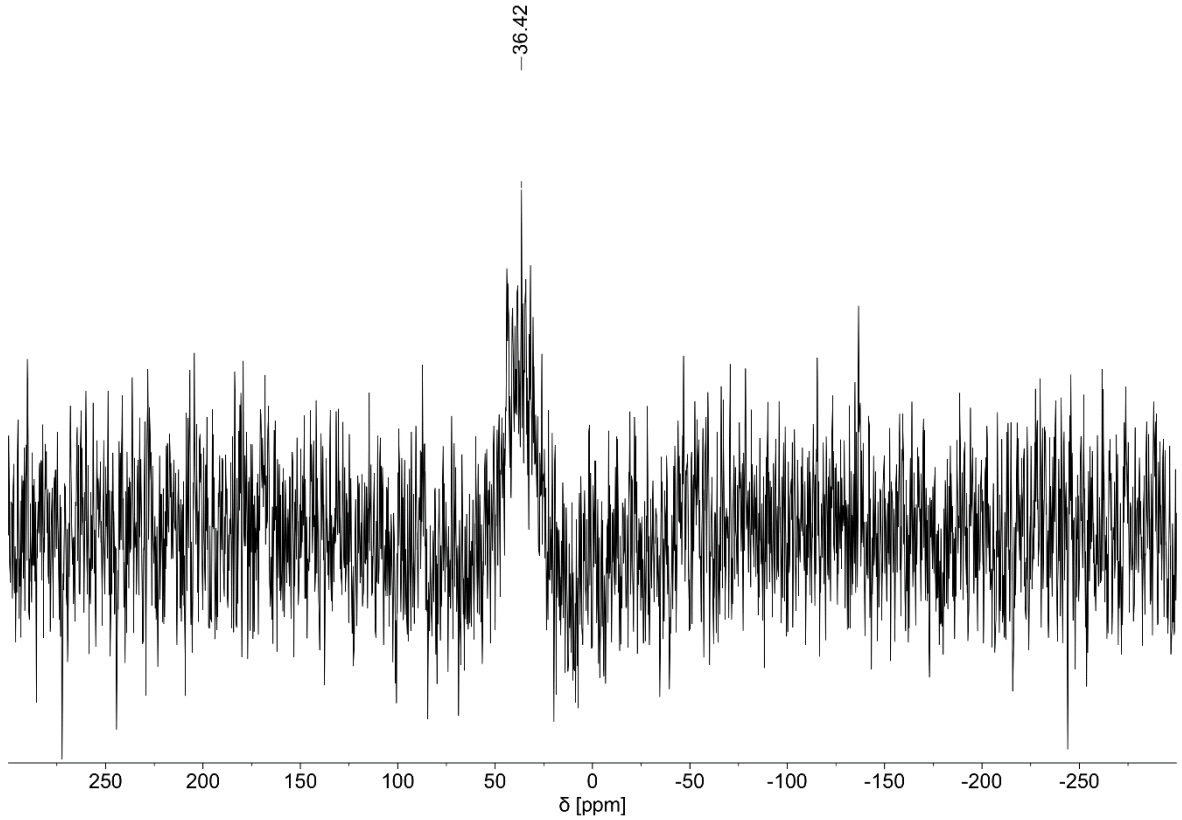

Figure S74. IR spectrum of $[Tc(\eta^1\text{-}OTcO_3)(CO)_3(PPh_3)_2]$ (**21**).

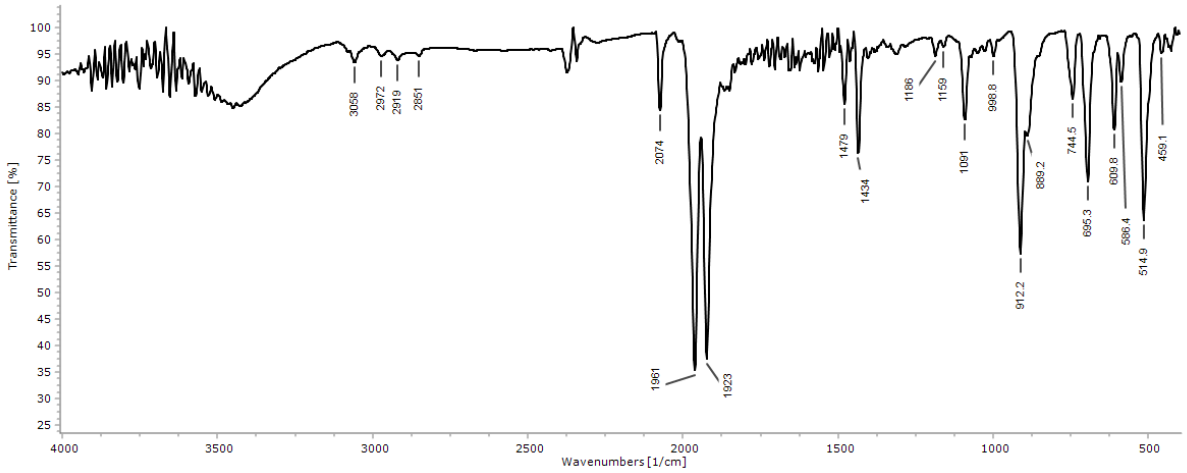

Figure S75. ^{1}H NMR spectrum of [Tc(η^{1}-OReO$_3$)(CO)$_3$(PPh$_3$)$_2$] (**22**).

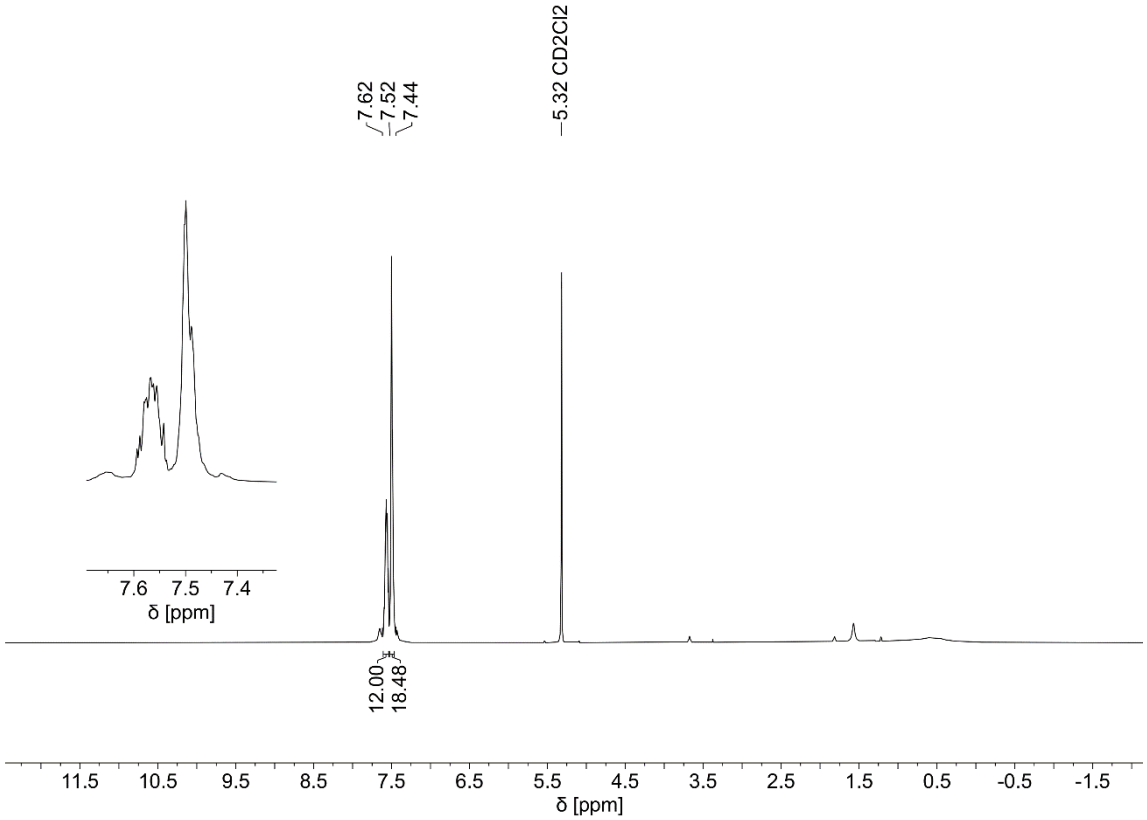

Figure S76. ^{99}Tc NMR spectrum of [Tc(η^{1}-OReO$_3$)(CO)$_3$(PPh$_3$)$_2$] (**22**).

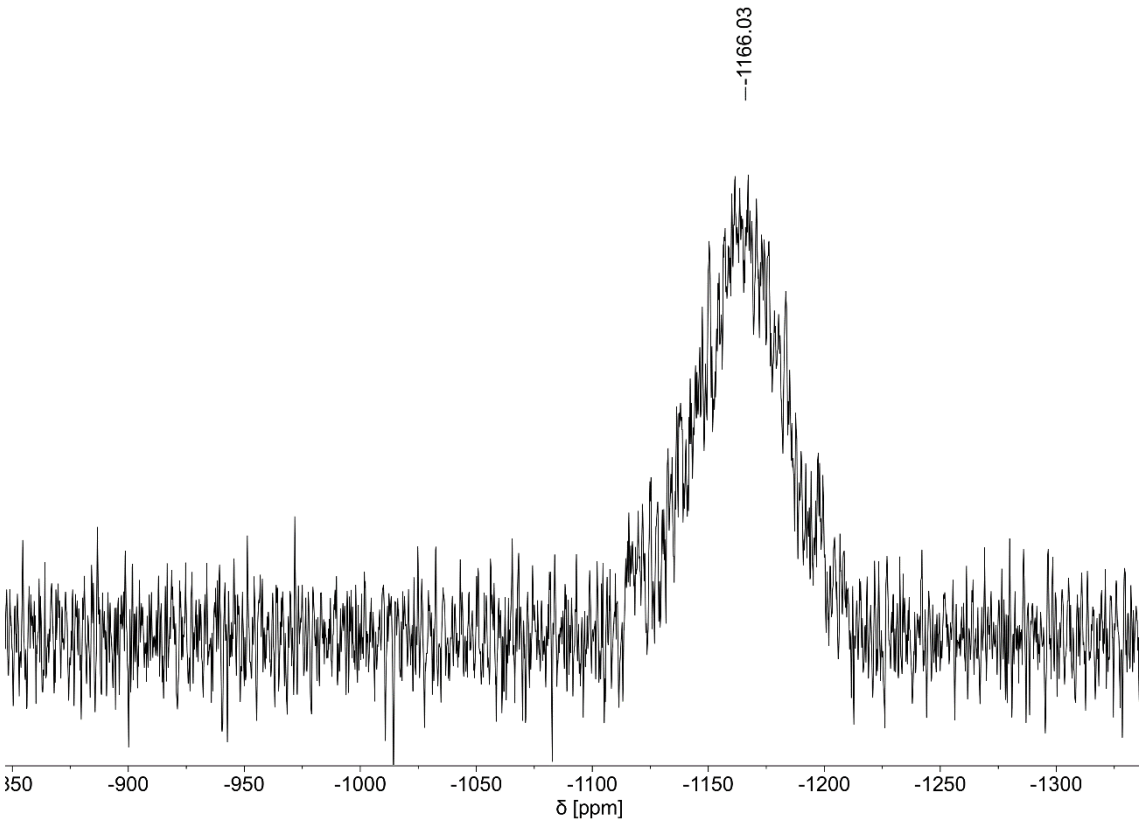

Figure S77. $^{31}P\{^{1}H\}$ NMR spectrum of [Tc(η^1-OReO$_3$)(CO)$_3$(PPh$_3$)$_2$] (**22**).

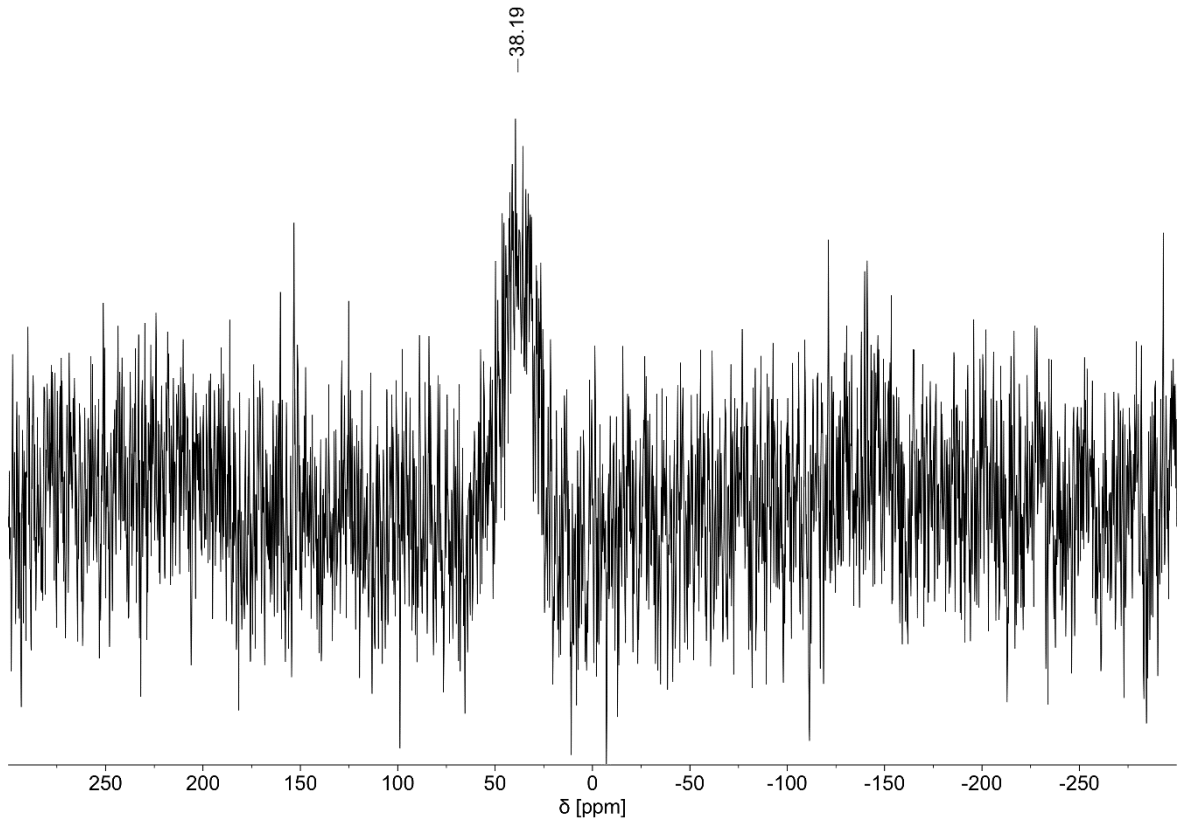

Figure S78. IR spectrum of [Tc(η^1-OReO$_3$)(CO)$_3$(PPh$_3$)$_2$] (**22**).

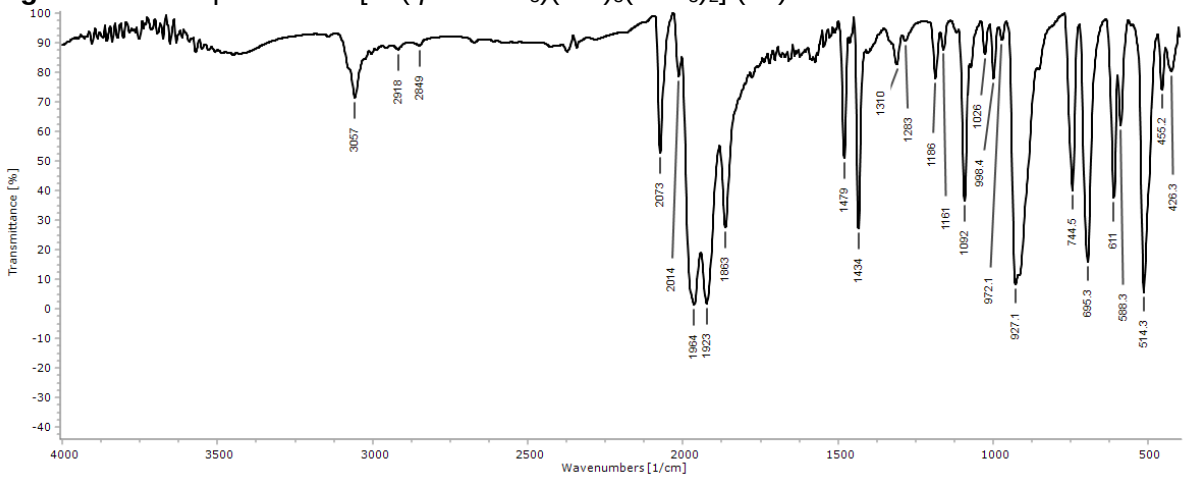

Figure S79. ^{1}H NMR spectrum of [Tc(η^{1}-OTcO$_3$)(acetone)(CO)$_2$(PPh$_3$)$_2$] · acetone (**23c**).

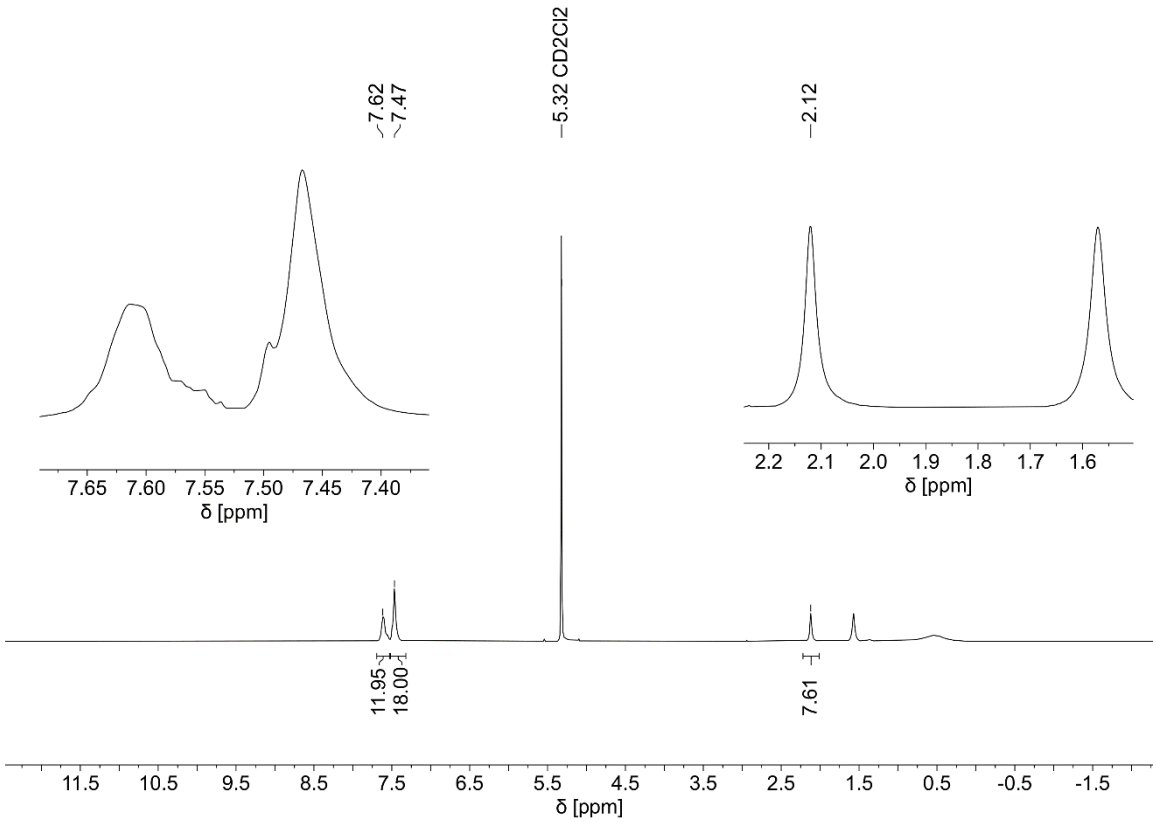

Figure S80. ^{99}Tc NMR spectrum of [Tc(η^{1}-OTcO$_3$)(acetone)(CO)$_2$(PPh$_3$)$_2$] · acetone (**23c**) focused on the pertechnetate region.

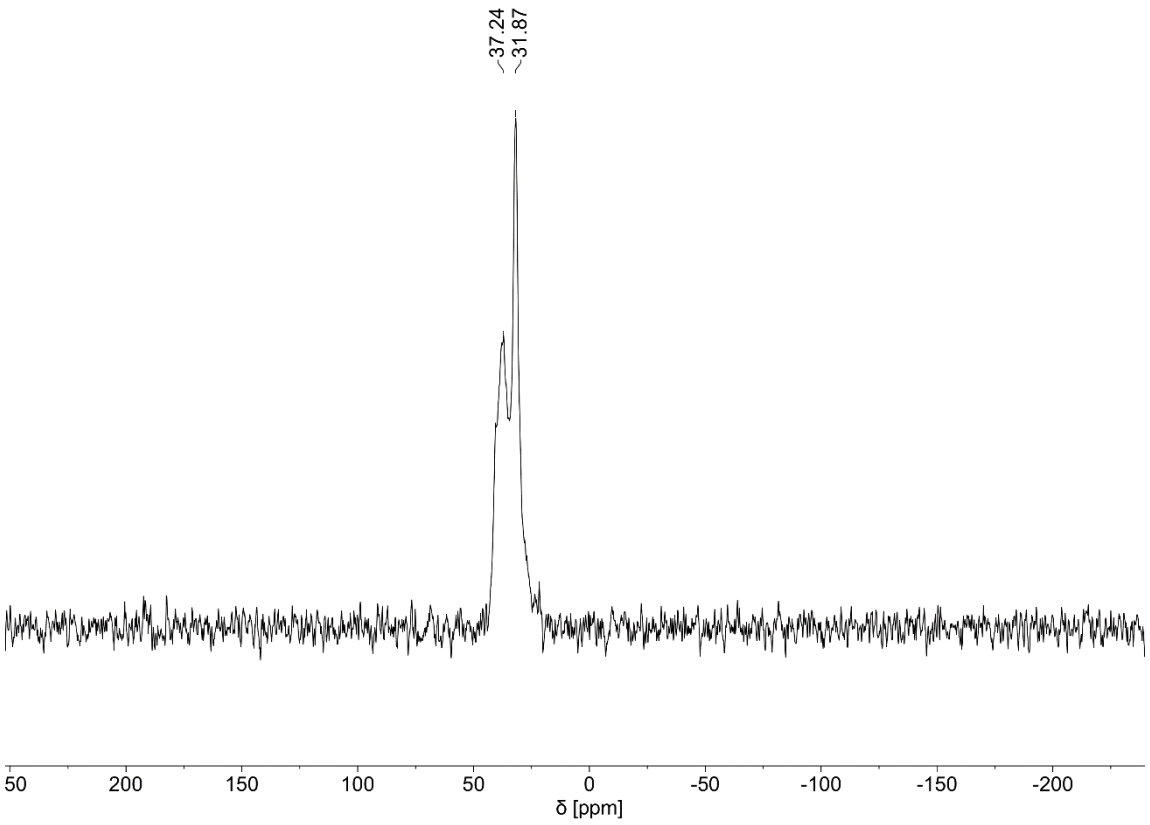

Figure S81. ^{99}Tc NMR spectrum of [Tc(η^1-OTcO$_3$)(acetone)(CO)$_2$(PPh$_3$)$_2$] · acetone (**23c**) focused on the dicarbonyl region.

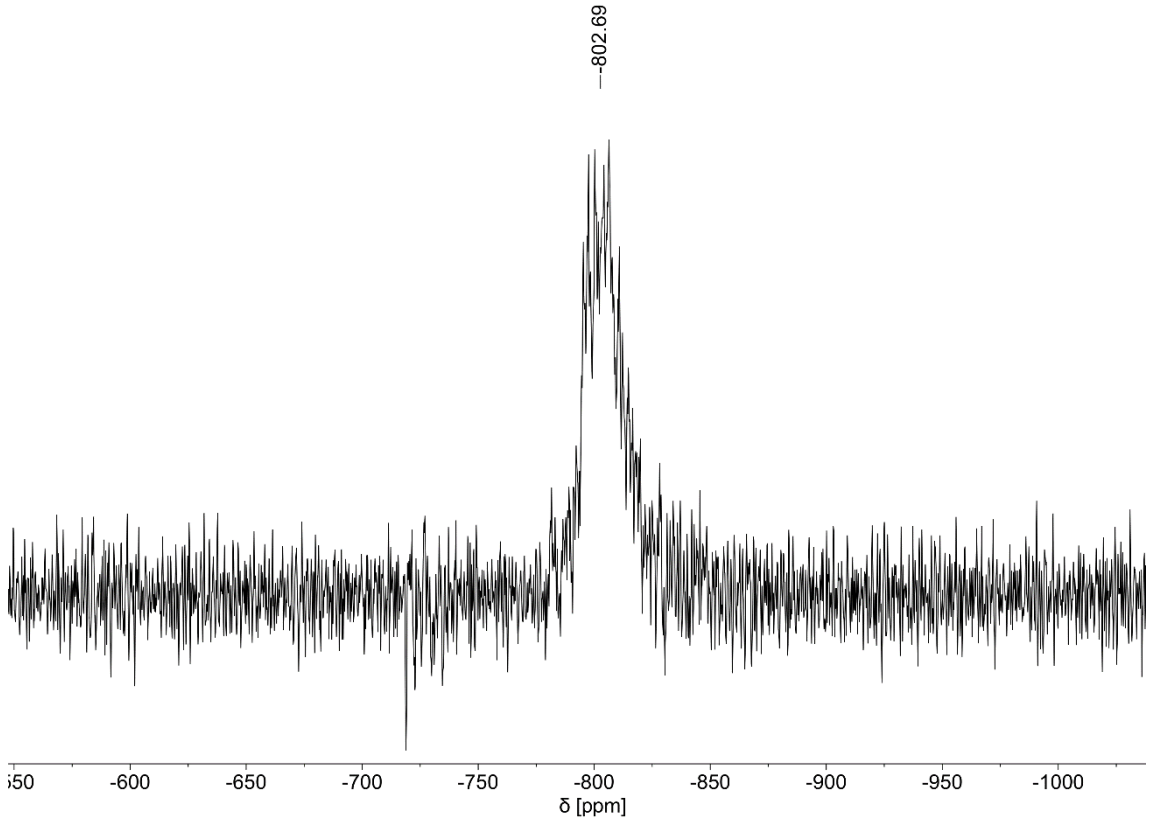

Figure S82. IR spectrum of [Tc(η^1-OTcO$_3$)(acetone)(CO)$_2$(PPh$_3$)$_2$] · acetone (**23c**).

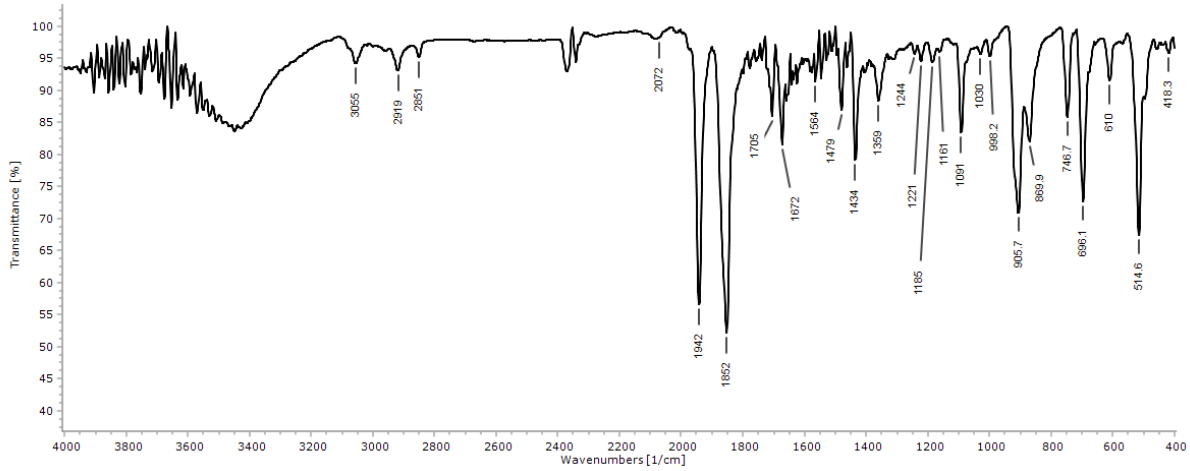

Figure S83. *In-situ* ^{99}Tc NMR spectra of the reaction between $[Tc(OH_2)(CO)_3(PPh_3)_2]^+$ and 10 eq. NBu_4Cl, NBu_4Br and NBu_4I in CH_2Cl_2. Spectra vary in focused region.

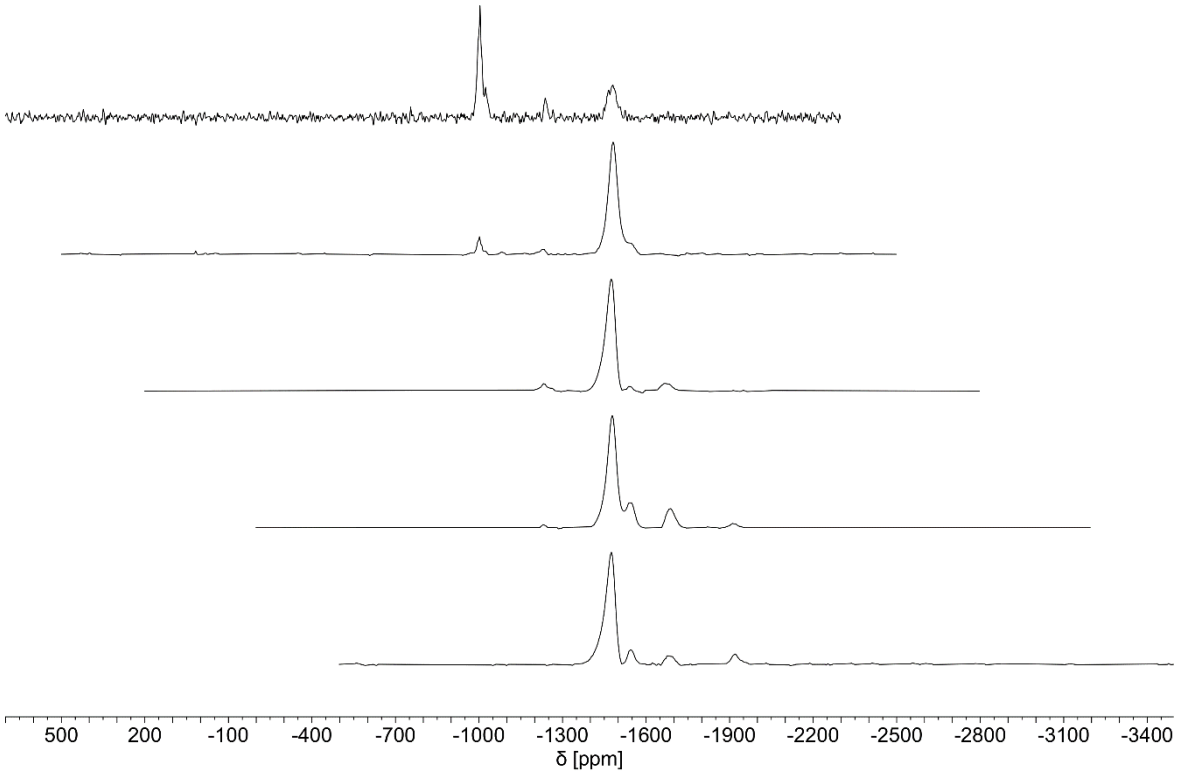

Figure S84. *In-situ* ^{99}Tc NMR spectra of the reaction between $[Tc(OH_2)(CO)_3(PPh_3)_2]^+$ and 10 eq. NBu_4Cl, NBu_4Br and NBu_4I in CH_2Cl_2 after one day. Spectra vary in focused region.

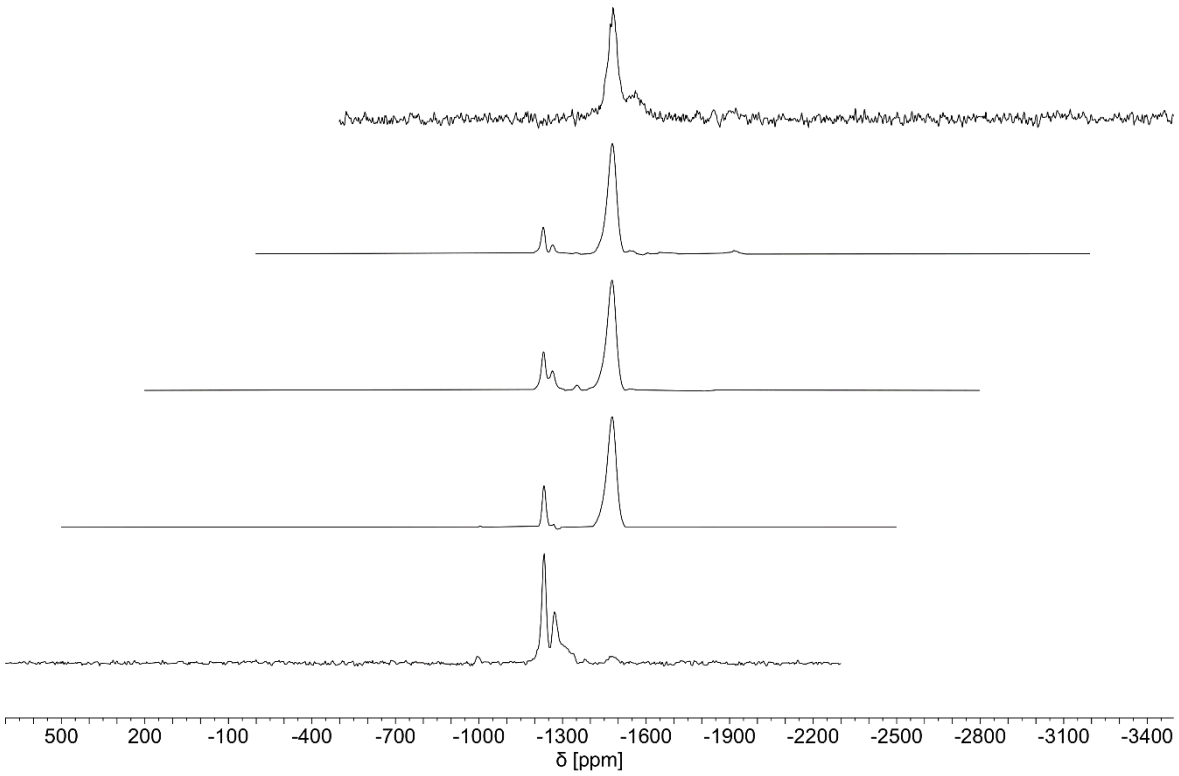

Figure S85. *In-situ* ^{99}Tc NMR spectra of the reaction between $[Tc(OH_2)(CO)_3(PPh_3)_2]^+$ and 10 eq. NBu_4F, NBu_4Cl, NBu_4Br and NBu_4I in CH_2Cl_2. Spectra vary in focused region.

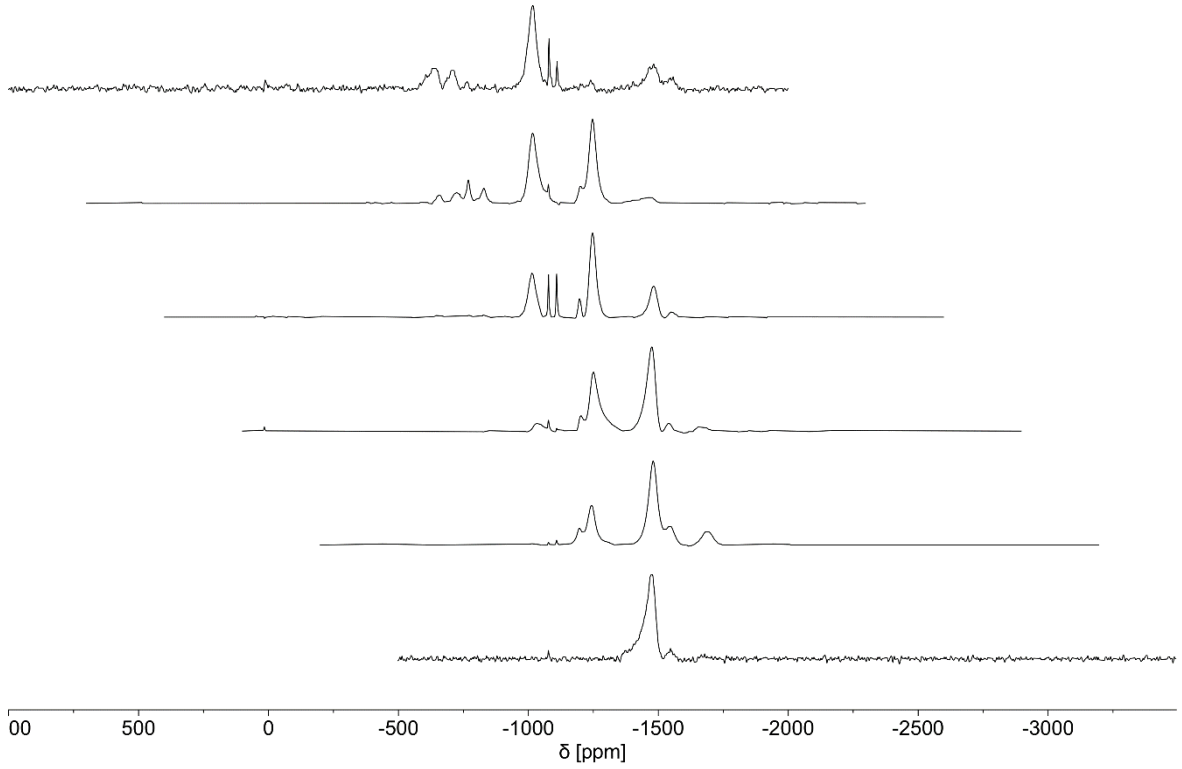

Figure S86. *In-situ* ^{99}Tc NMR spectra of the reaction between $[Tc(OH_2)(CO)_3(PPh_3)_2]^+$ and 10 eq. NBu_4F, NBu_4Cl, NBu_4Br and NBu_4I in CH_2Cl_2 after one hour. Spectra vary in focused region.

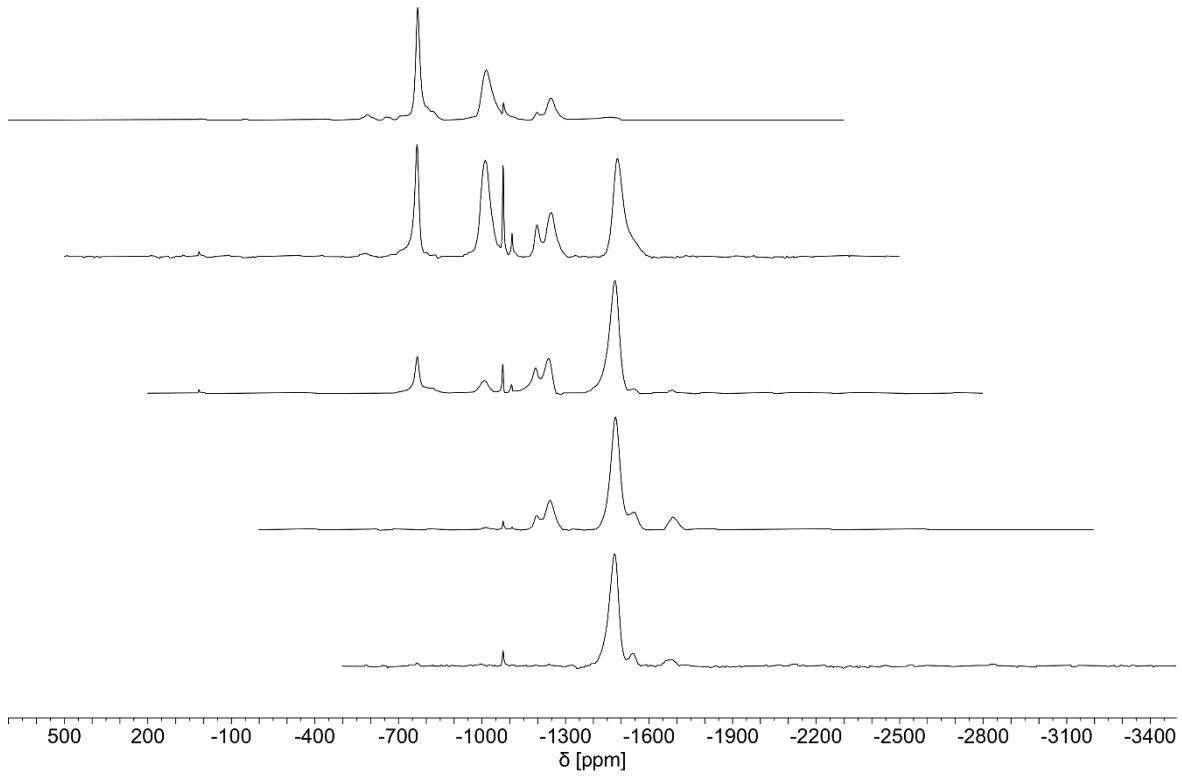

Figure S87. *In-situ* ^{99}Tc NMR spectra of the reaction between $[Tc(OH_2)(CO)_3(PPh_3)_2]^+$ and 10 eq. NBu_4F, NBu_4Cl, NBu_4Br and NBu_4I in CH_2Cl_2 after one day. Spectra vary in focused region.

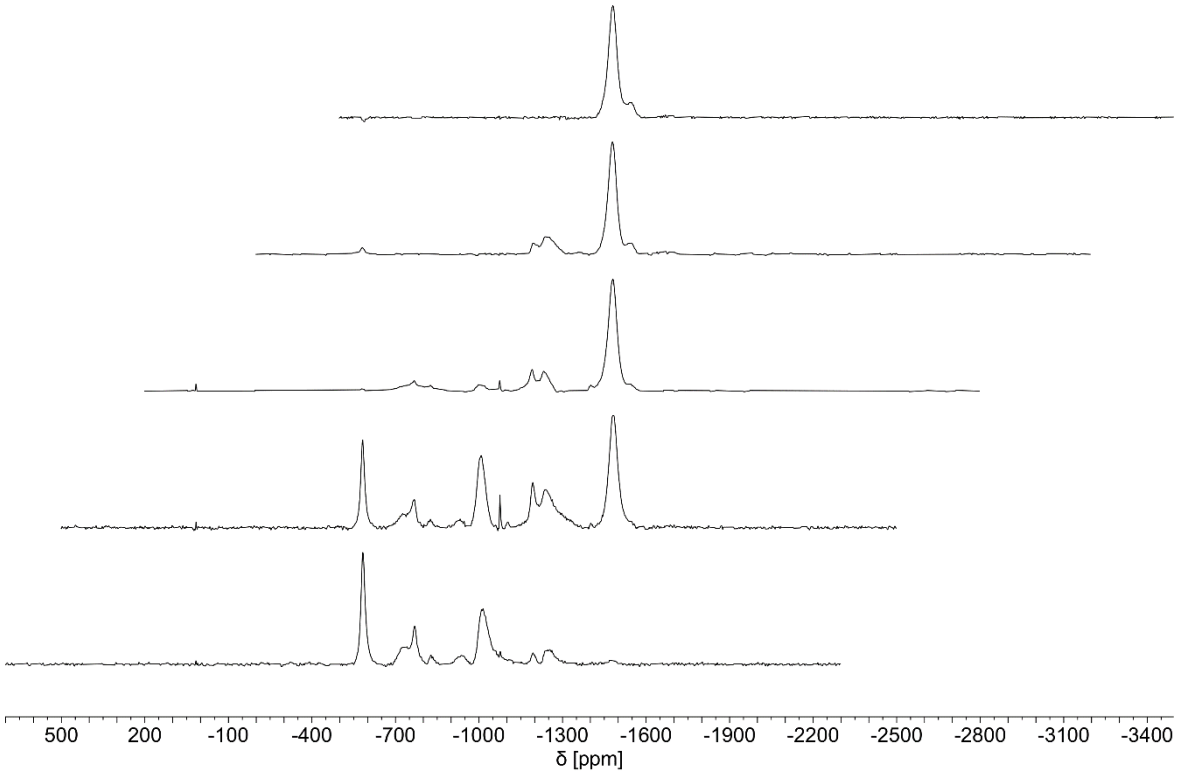

Figure S88. *In-situ* ^{99}Tc NMR spectra of the organic phase (CH_2Cl_2) in the two-phase reaction between $[Tc(OH_2)(CO)_3(PPh_3)_2]^+$ and KF after 5 min. Spectra vary in focused region.

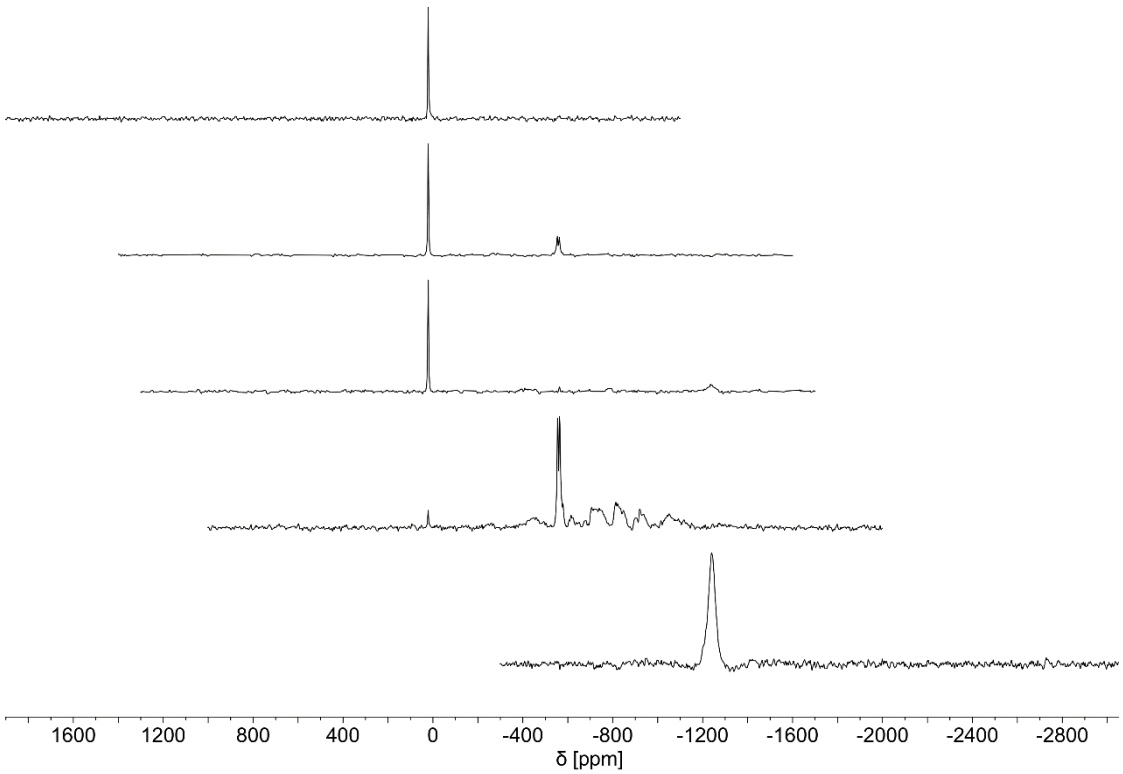

Figure S89. *In-situ* ^{19}F NMR spectrum of the organic phase (CH_2Cl_2) in the two-phase reaction between $[Tc(OH_2)(CO)_3(PPh_3)_2]^+$ and KF after 5 min. Spectra vary in focused region.

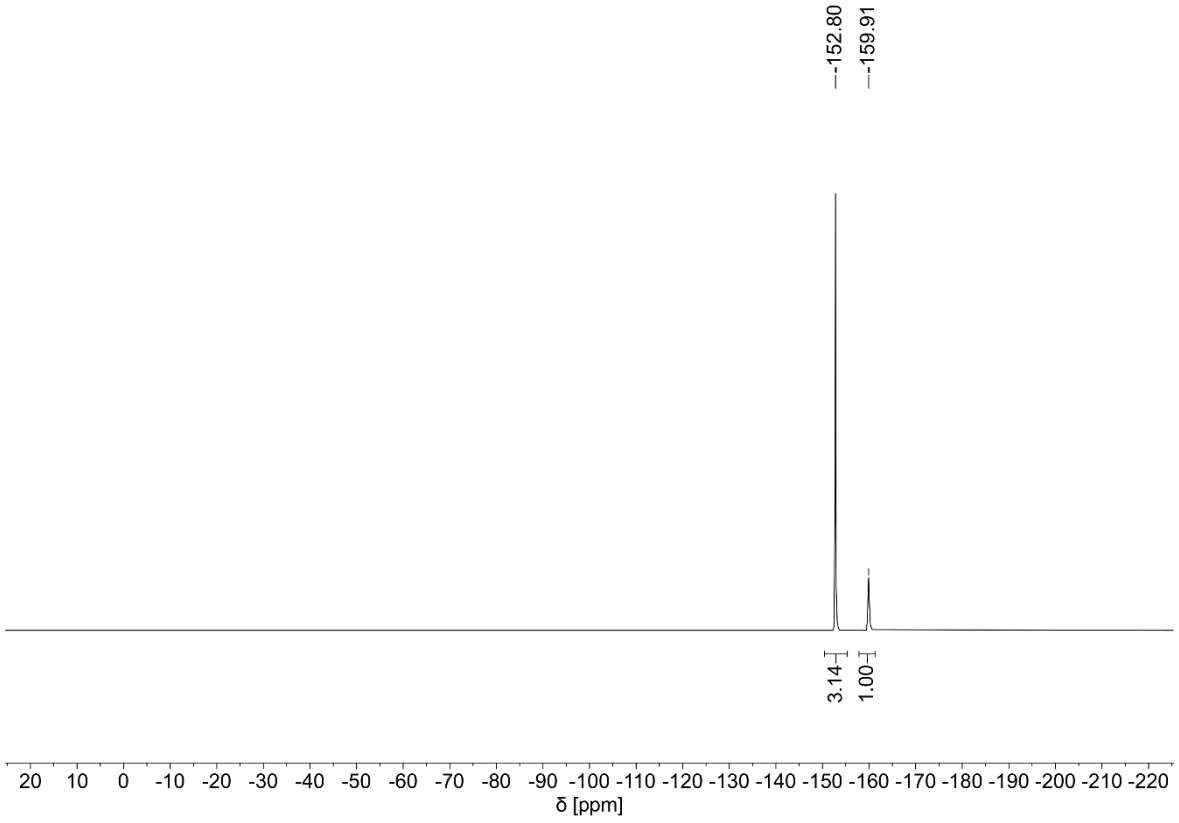

Figure S90. *In-situ* ^{31}P NMR spectra of the organic phase (CH_2Cl_2) in the two-phase reaction between $[Tc(OH_2)(CO)_3(PPh_3)_2]^+$ and KF after 5 min. Spectra vary in focused region.

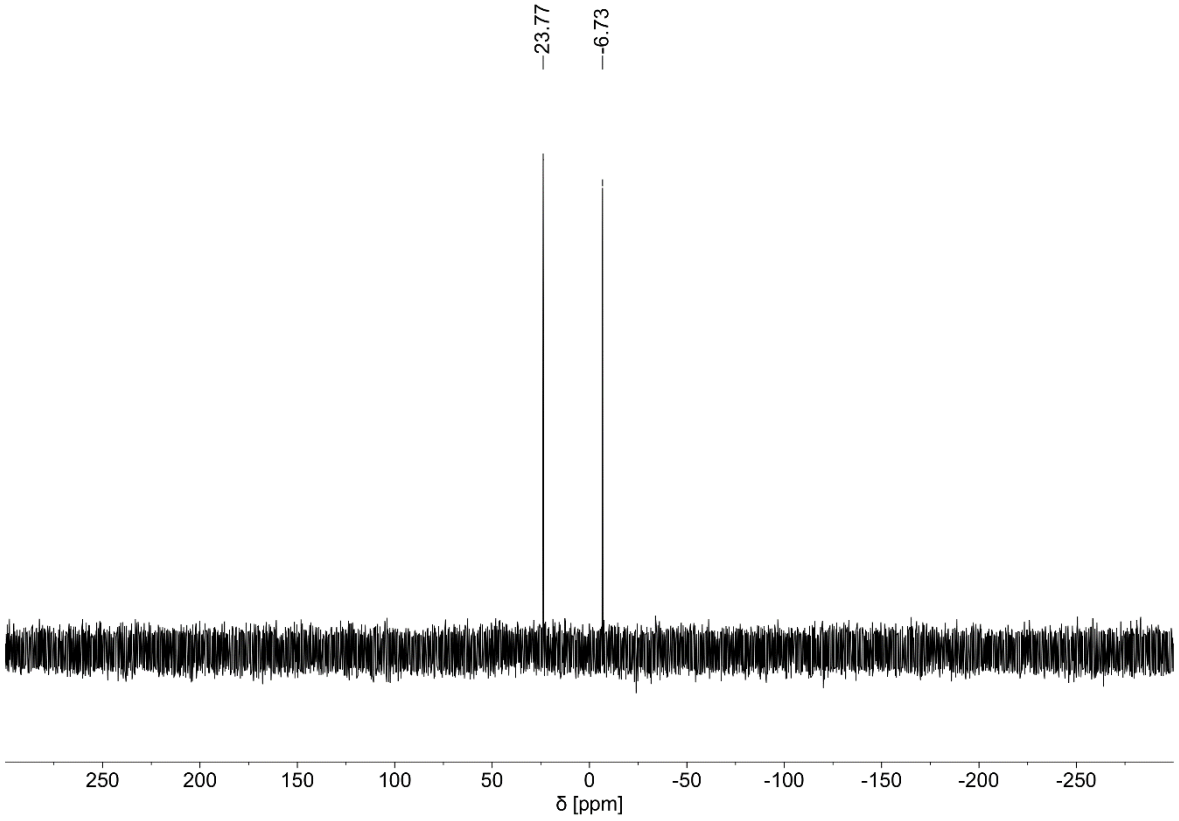

Figure S91. *In-situ* ^{99}Tc NMR spectra of the organic phase (CH_2Cl_2) in the two-phase reaction between $[Tc(OH_2)(CO)_3(PPh_3)_2]^+$ and $NaHCO_3$. Spectra vary in focused region.

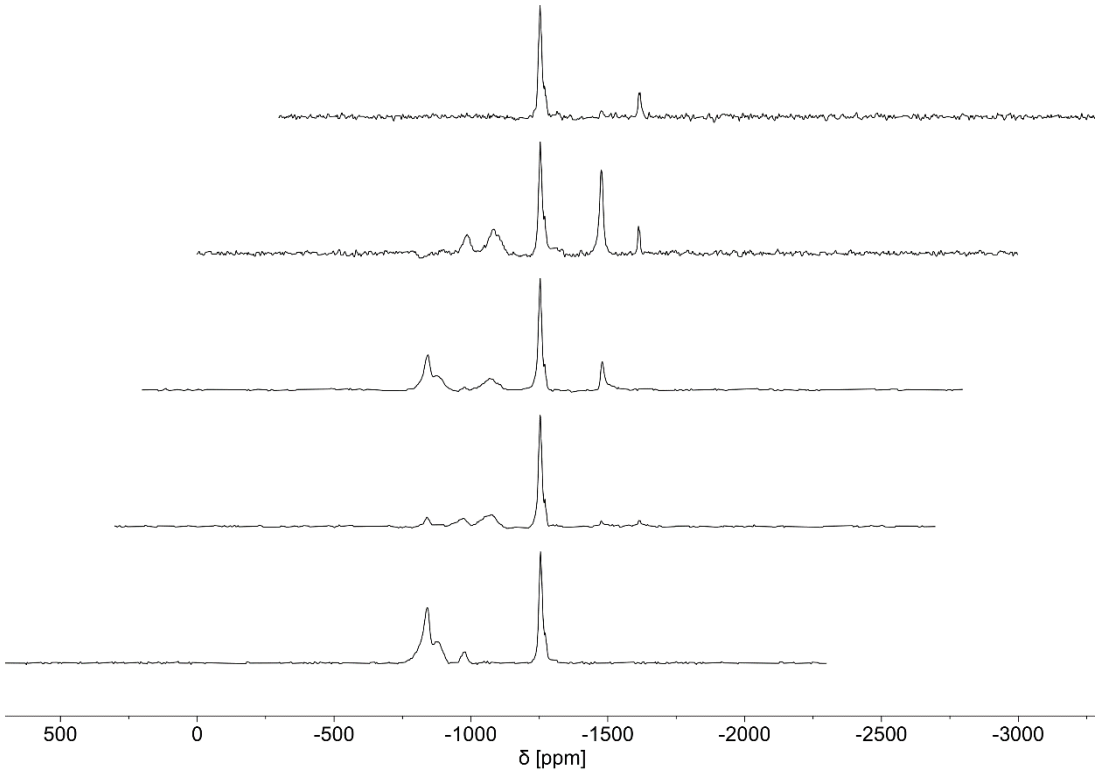

Figure S92. *In-situ* ^{31}P NMR spectra of the organic phase (CH_2Cl_2) in the two-phase reaction between $[Tc(OH_2)(CO)_3(PPh_3)_2]^+$ and $NaHCO_3$. Spectra vary in focused region.

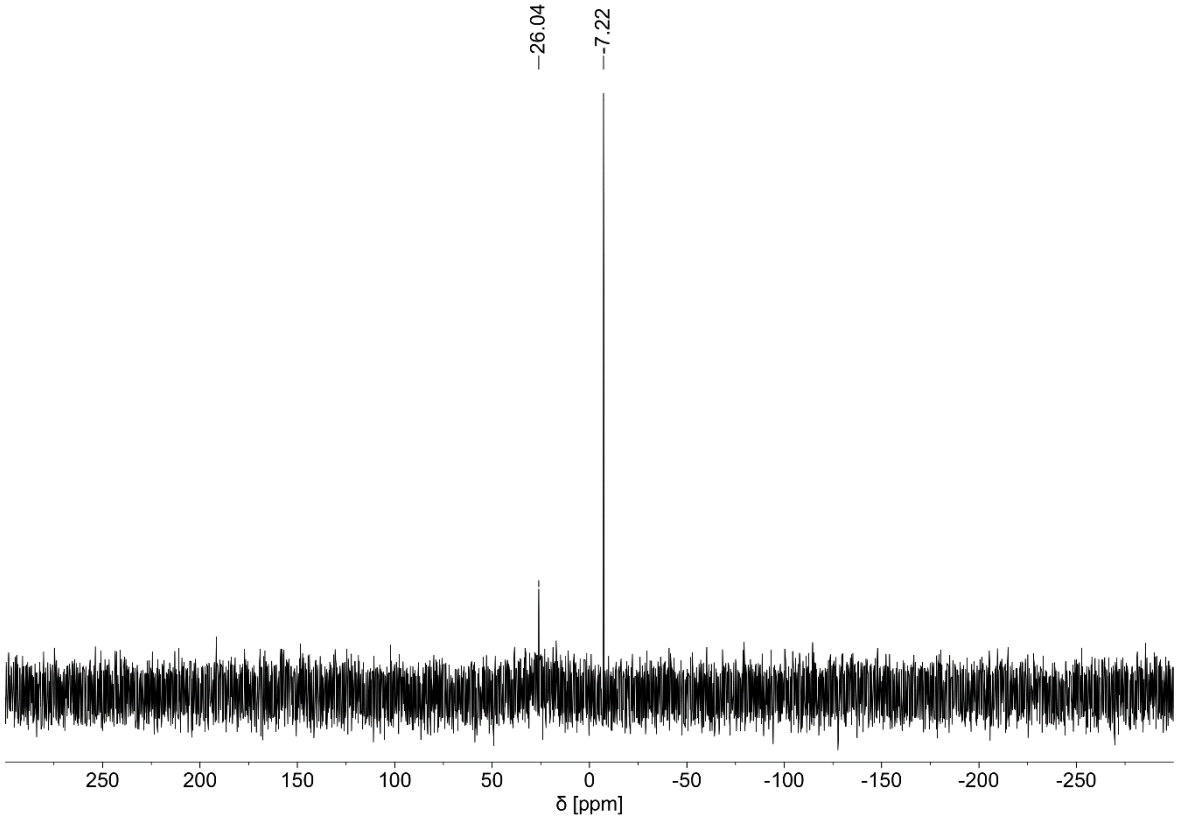

Figure S93. ^{99}Tc NMR spectra of the isolated solid obtained by heating [Tc(η^1-$OTcO_3$)$(CO)_3(PPh_3)_2$] in wet thf and evaporation. Solvent = CH_2Cl_2. Spectra vary in focused region.

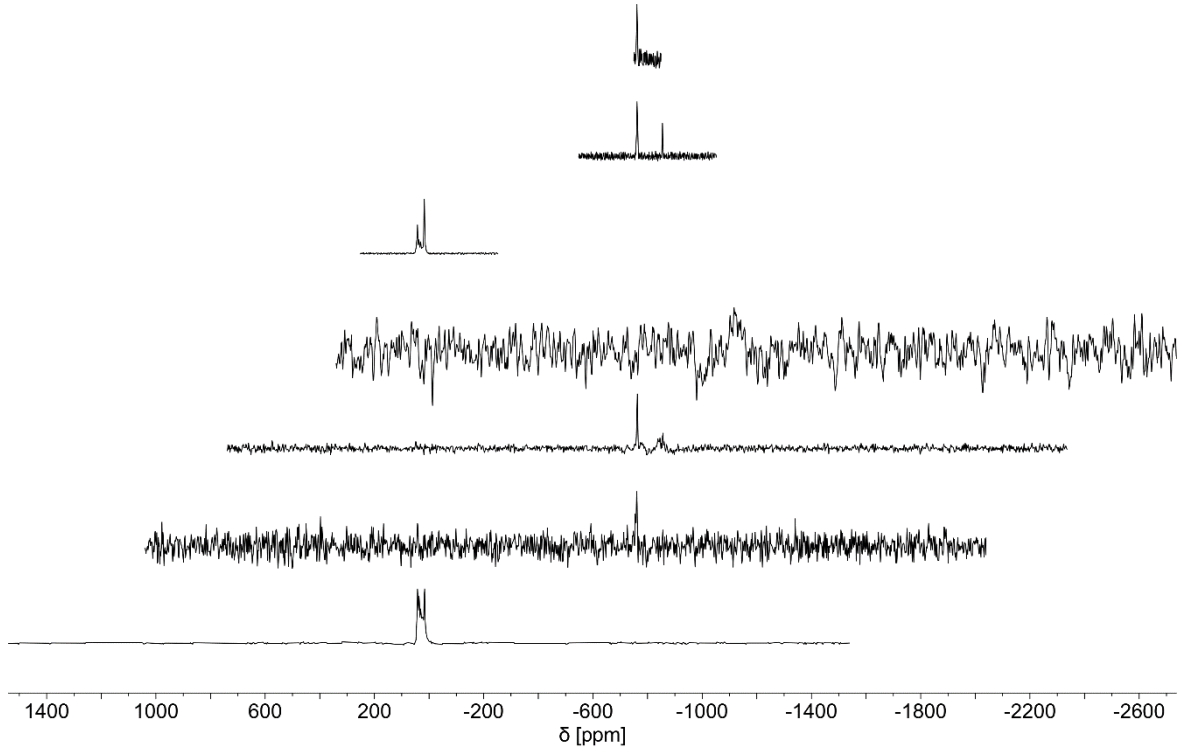

Figure S94. ^{99}Tc NMR spectrum of the isolated solid obtained by heating [Tc(η^1-$OTcO_3$)$(CO)_3(PPh_3)_2$] in wet thf and evaporation focused on the pertechnetate region. Solvent = CH_2Cl_2.

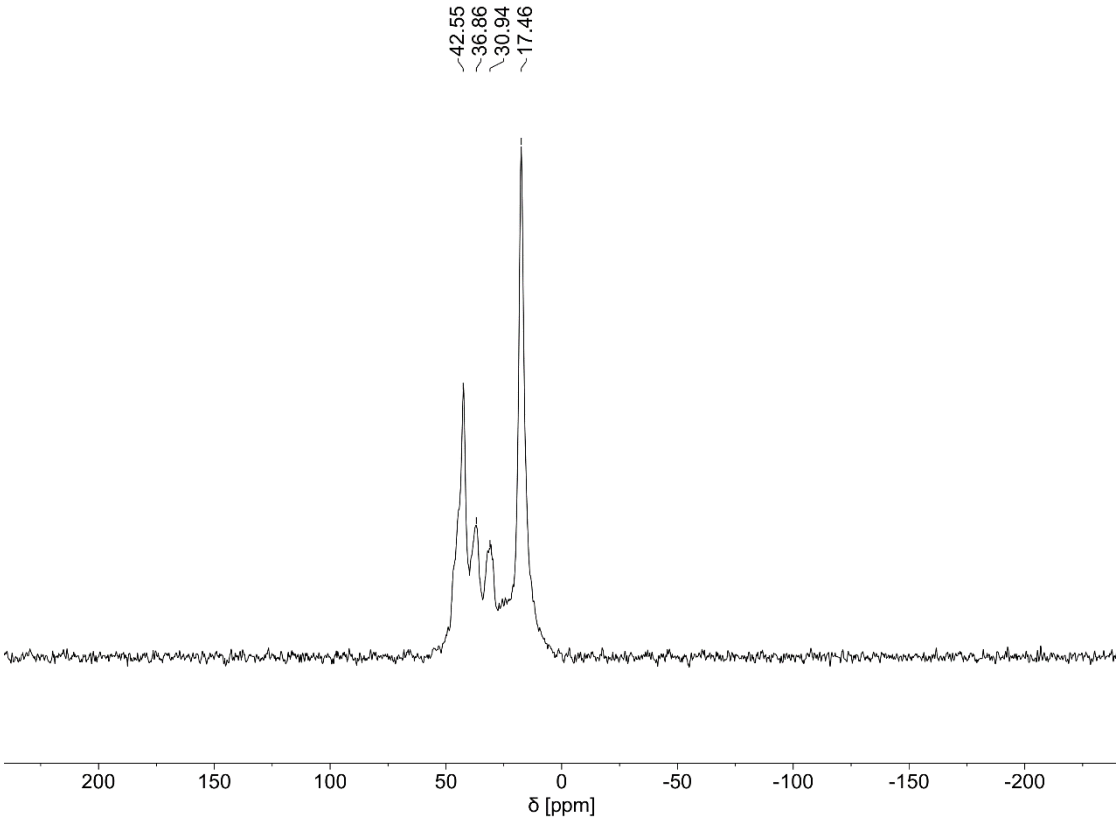

Figure S95. ^{99}Tc NMR spectra of the isolated solid obtained by heating [Tc(η^1-$OTcO_3$)$(CO)_3(PPh_3)_2$] in wet thf and evaporation focused on the dicarbonyl region. Solvent = CH_2Cl_2.

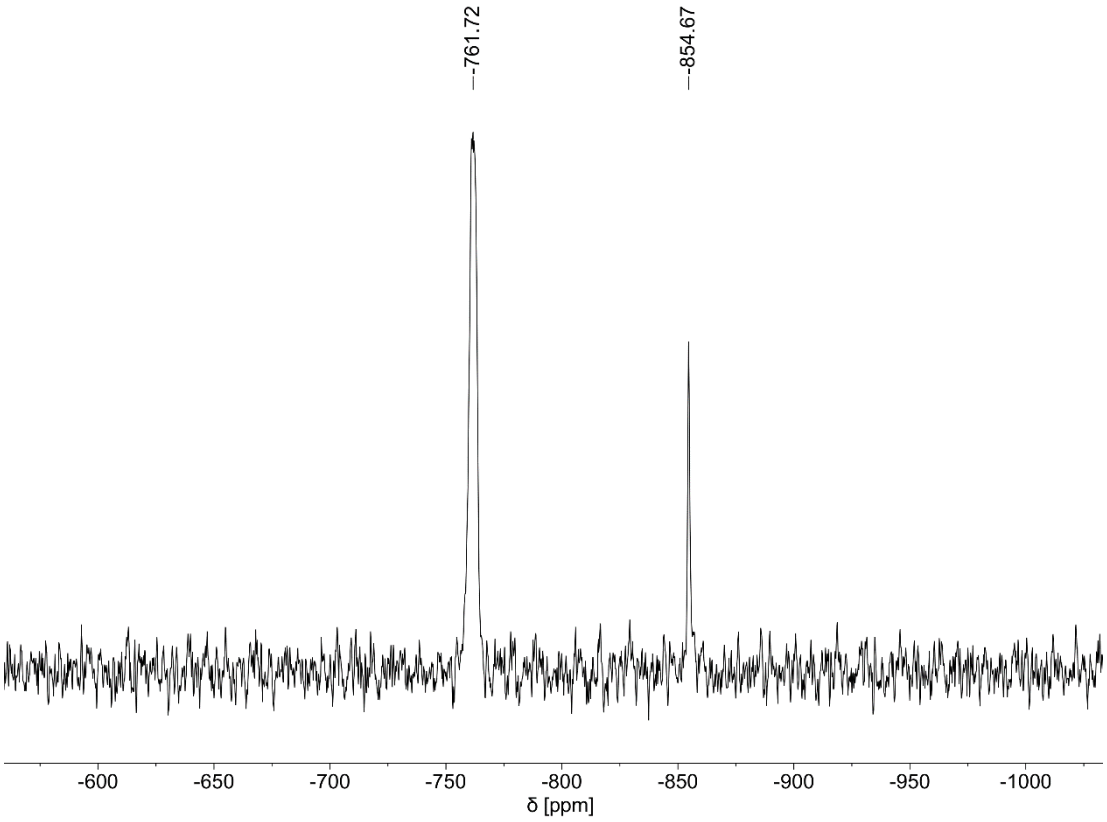

Figure S96. ^{31}P NMR spectra of the isolated solid obtained by heating [Tc(η^1-$OTcO_3$)$(CO)_3(PPh_3)_2$] in wet thf and evaporation focused on the dicarbonyl region. Solvent = CH_2Cl_2.

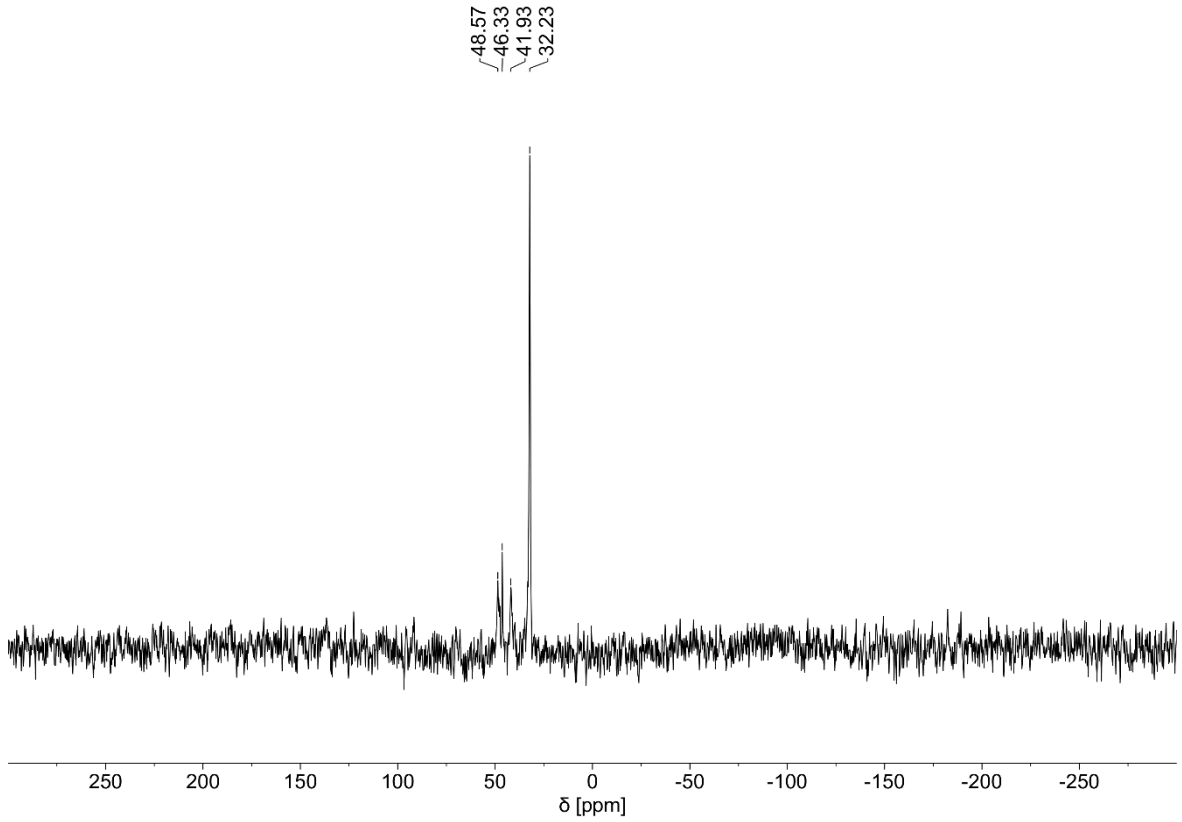

Figure S97. *In-situ* ^{99}Tc NMR spectra of [Tc(η^1-OTcO$_3$)(CO)$_3$(PPh$_3$)$_2$] heated in xylene. Spectra vary in focused region.

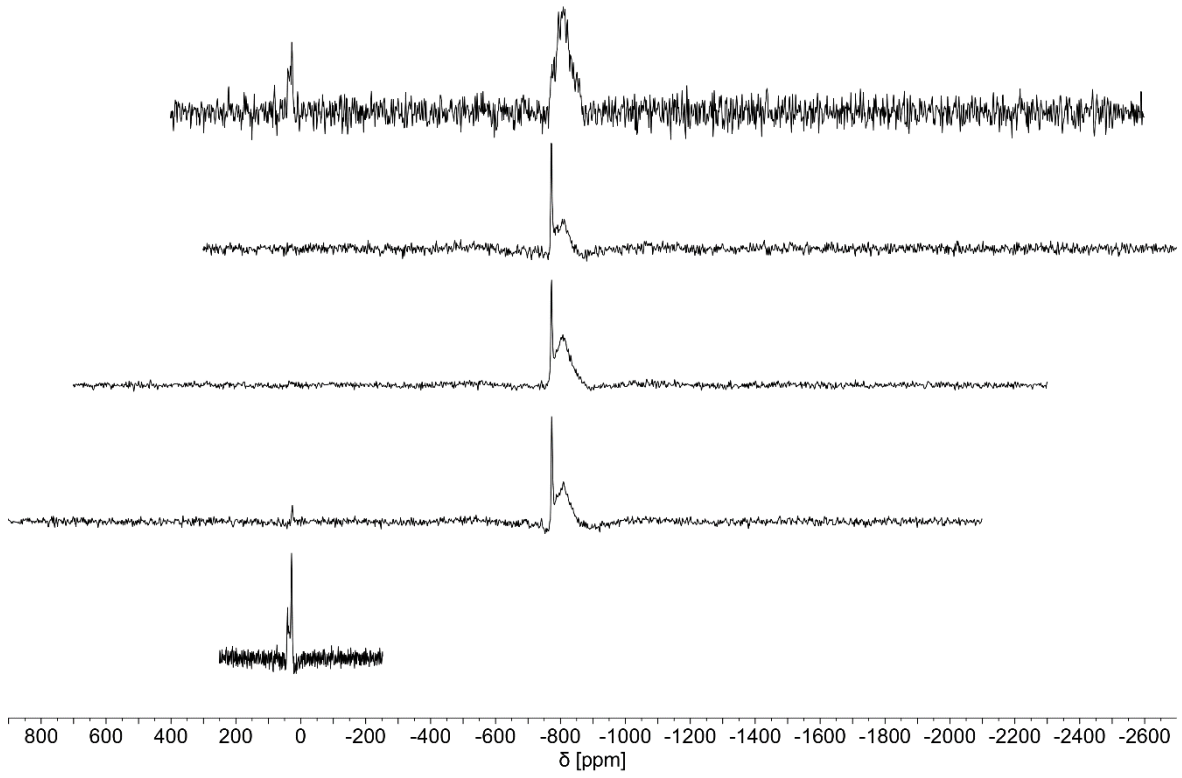

Figure S98. *In-situ* ^{99}Tc NMR spectrum of [Tc(η^1-OTcO$_3$)(CO)$_3$(PPh$_3$)$_2$] heated in xylene focused on the pertechnetate region.

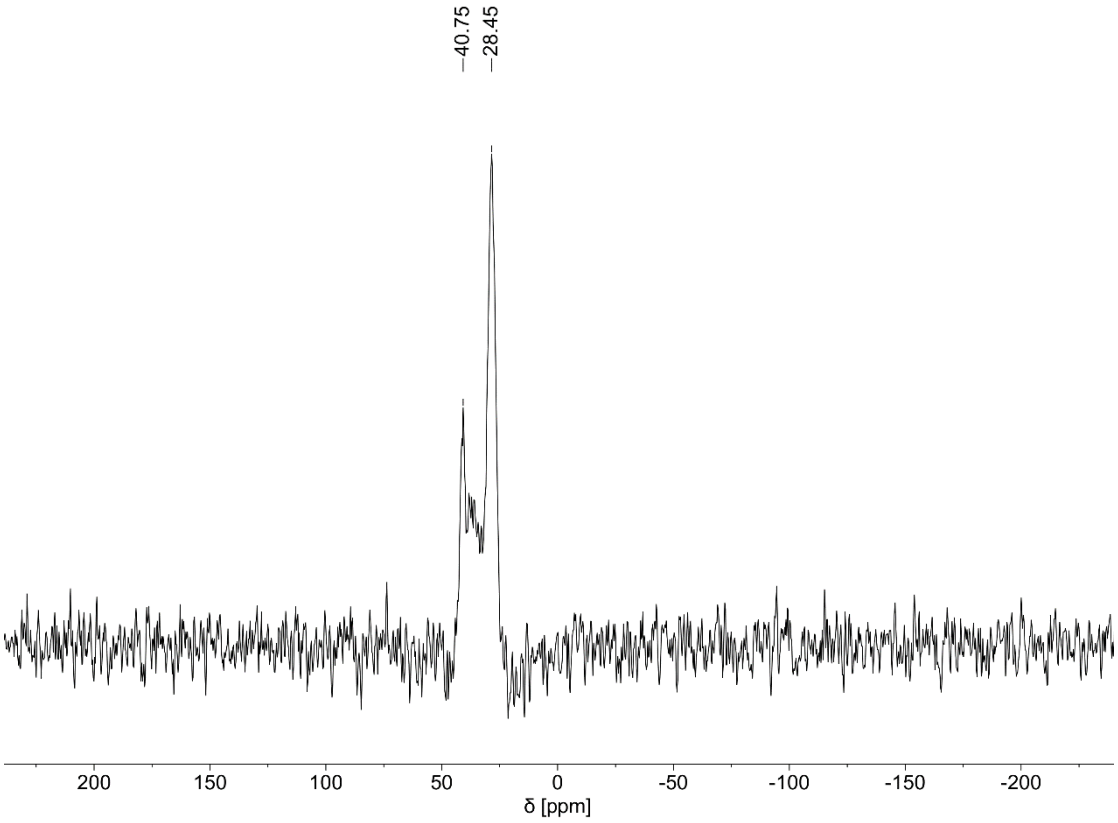

Figure S99. *In-situ* ^{99}Tc NMR spectrum of [Tc(η^1-OTcO$_3$)(CO)$_3$(PPh$_3$)$_2$] heated in xylene focused on the dicarbonyl region.

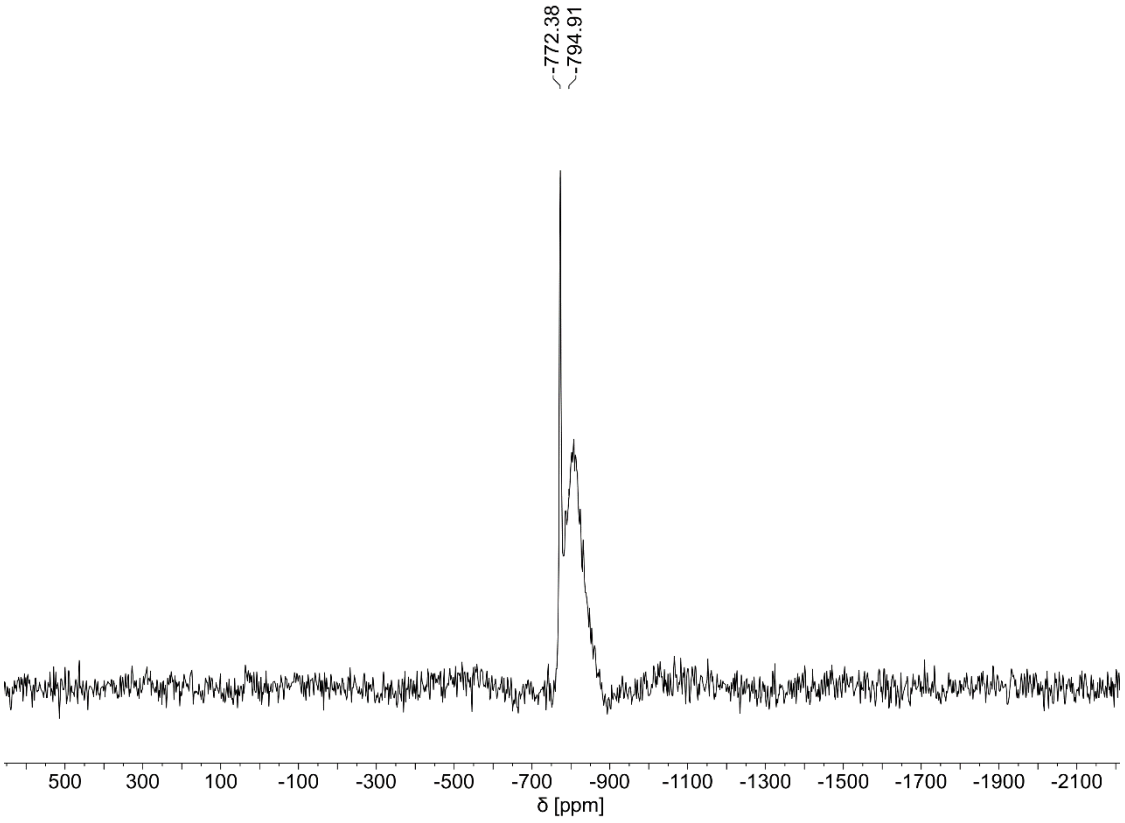

Figure S100. *In-situ* ^{31}P NMR spectrum of [Tc(η^1-OTcO$_3$)(CO)$_3$(PPh$_3$)$_2$] heated in xylene focused on the pertechnetate region.

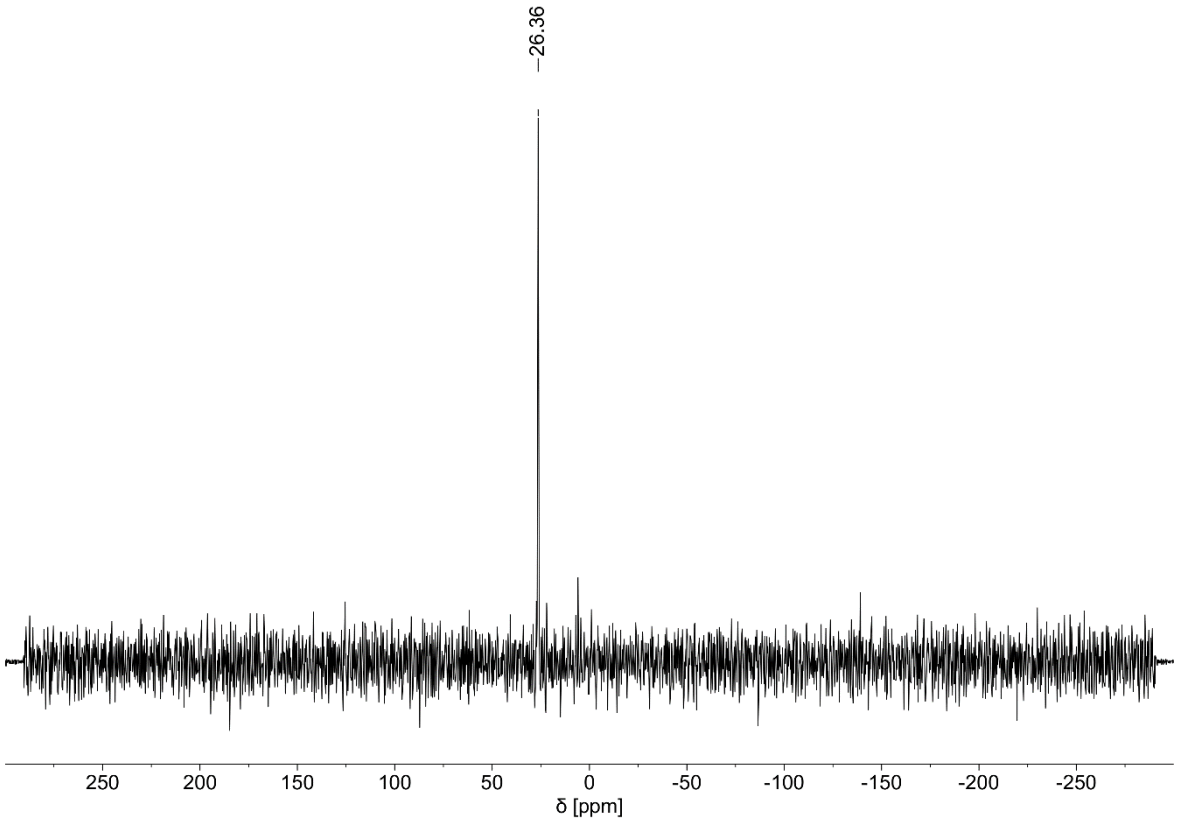

Figure S101. *In-situ* ^{99}Tc NMR spectrum of [Tc(η^1-OTcO$_3$)(CO)$_3$(PPh$_3$)$_2$] heated in dry toluene focused on the pertechnetate region.

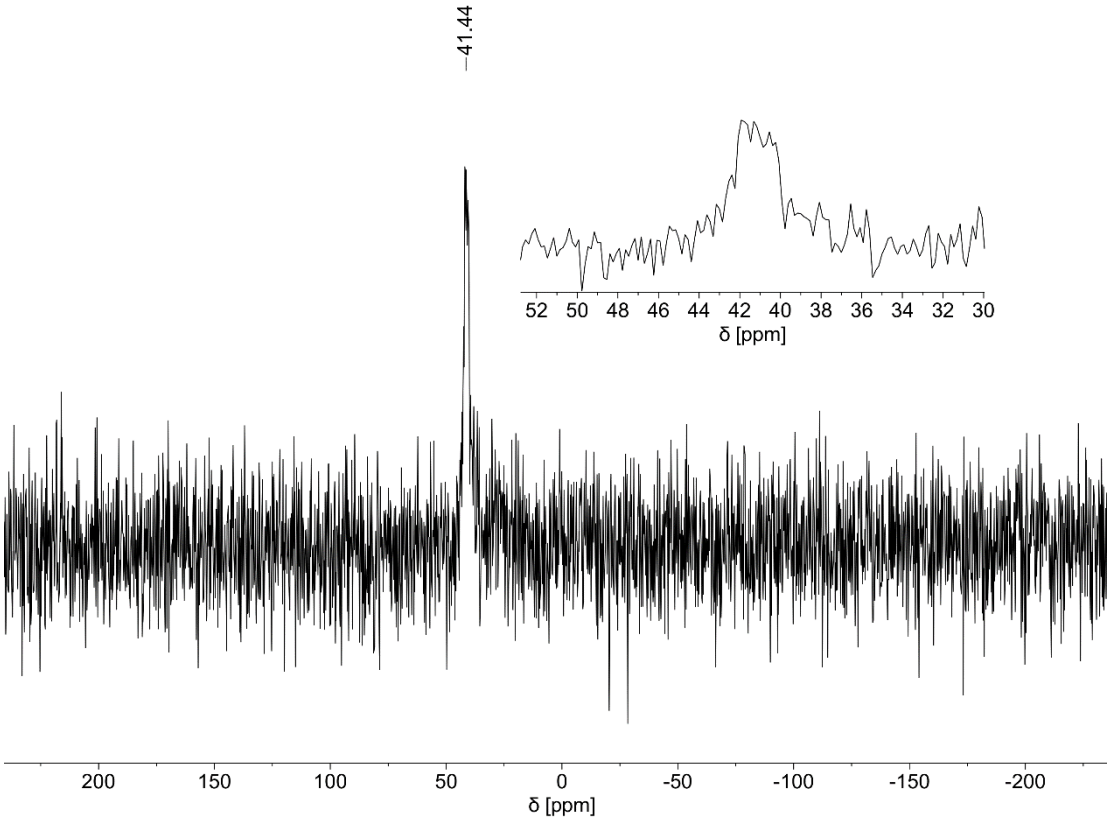

Figure S102. *In-situ* ^{99}Tc NMR spectrum of [Tc(η^1-OTcO$_3$)(CO)$_3$(PPh$_3$)$_2$] heated in dry toluene focused on the dicarbonyl region.

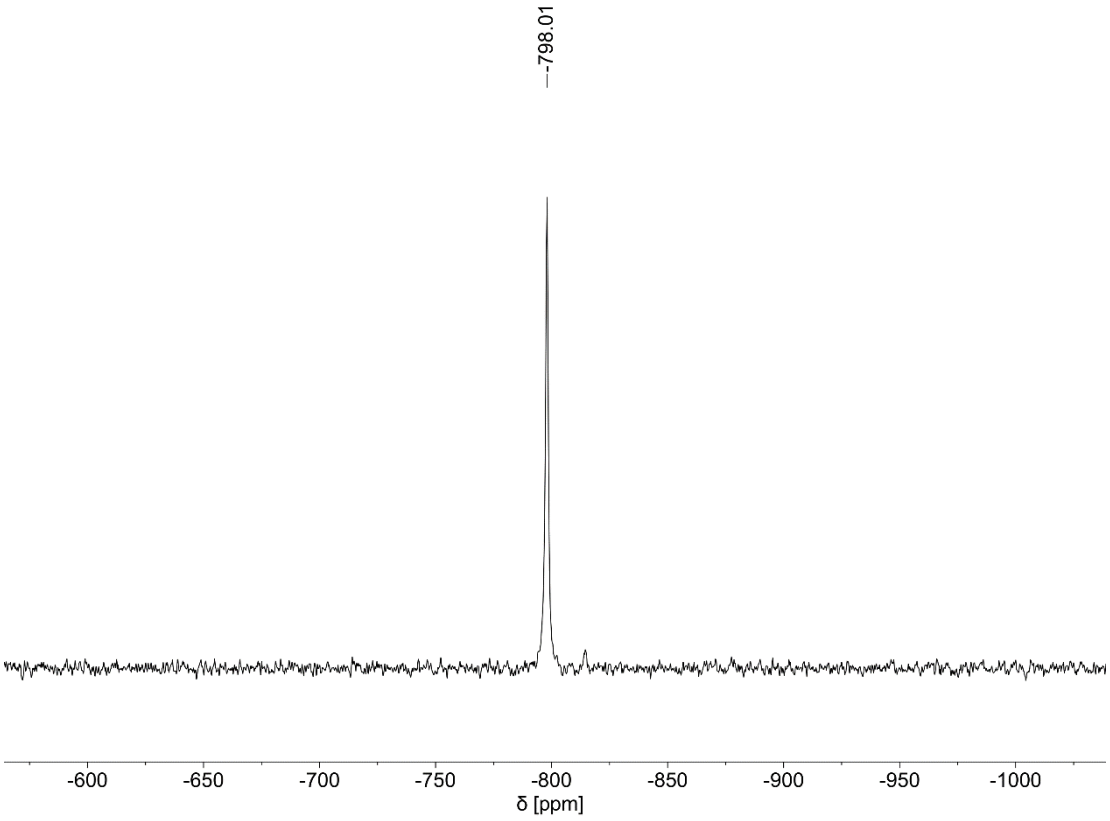

Figure S103. Stacking of ^{99}Tc NMR spectra of the isolated solid obtained from heating [Tc(η^1-$OTcO_3$)$(CO)_3(PPh_3)_2$] in acetone followed by evaporation of the solvent (bottom two spectra) and its subsequent reaction with thf (middle two spectra) and water (top two spectra). Spectra are focused on different spectral regions. Solvent = CH_2Cl_2.

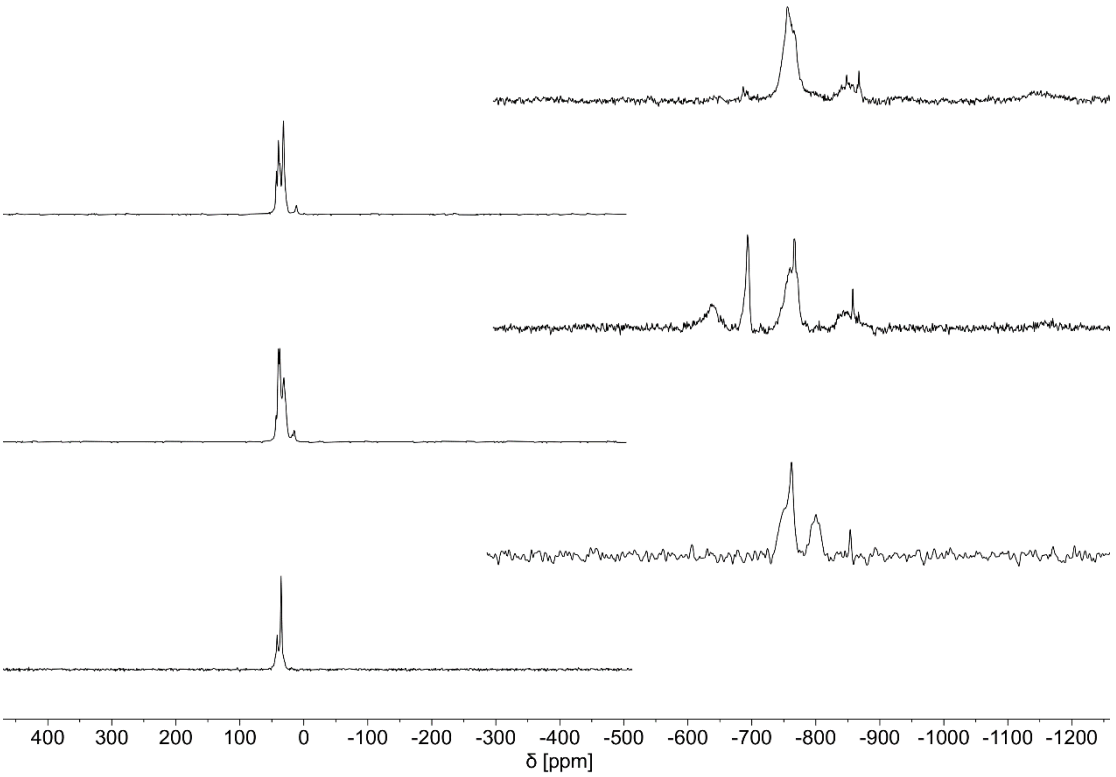

Figure S104. ^{99}Tc NMR spectrum of the isolated solid obtained from heating [Tc(η^1-$OTcO_3$)$(CO)_3(PPh_3)_2$] in acetone followed by evaporation of the solvent, focused on the pertechnetate region. Solvent = CH_2Cl_2.

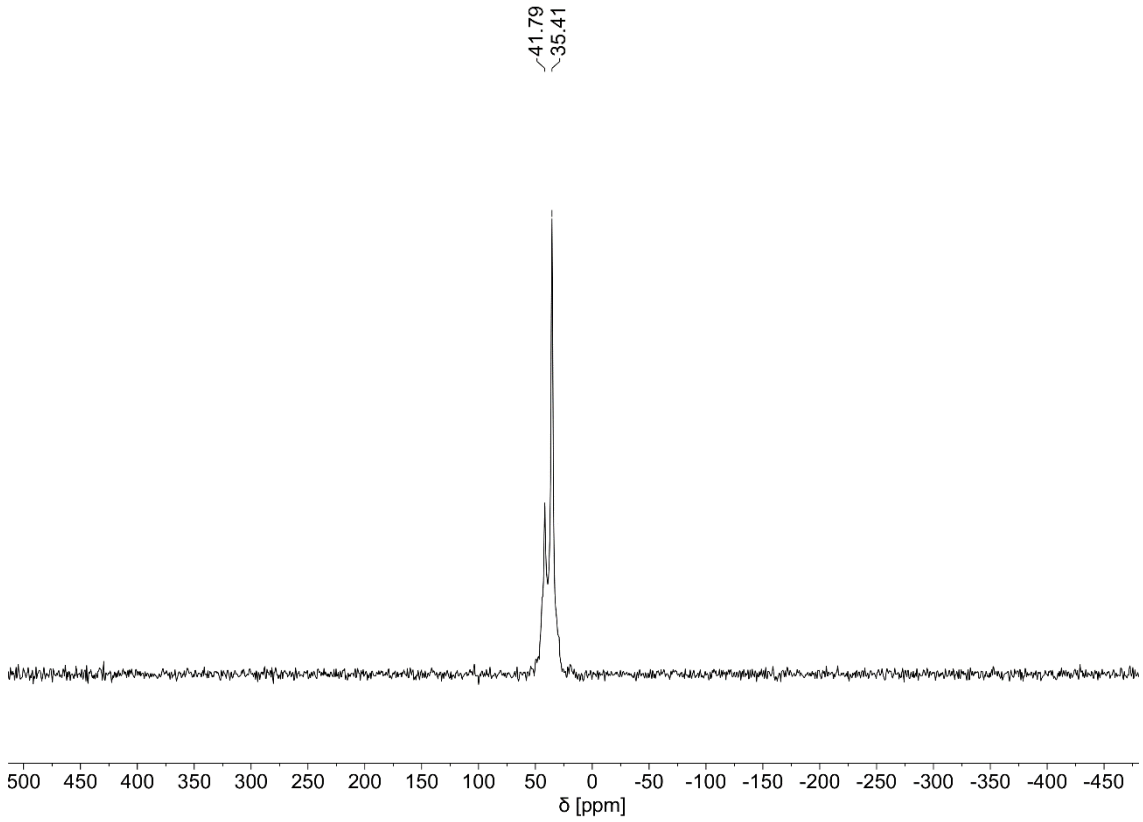

Figure S105. ^{99}Tc NMR spectrum of the isolated solid obtained from heating [Tc(η^1-$OTcO_3$)$(CO)_3(PPh_3)_2$] in acetone followed by evaporation of the solvent, focused on the dicarbonyl region. Solvent = CH_2Cl_2.

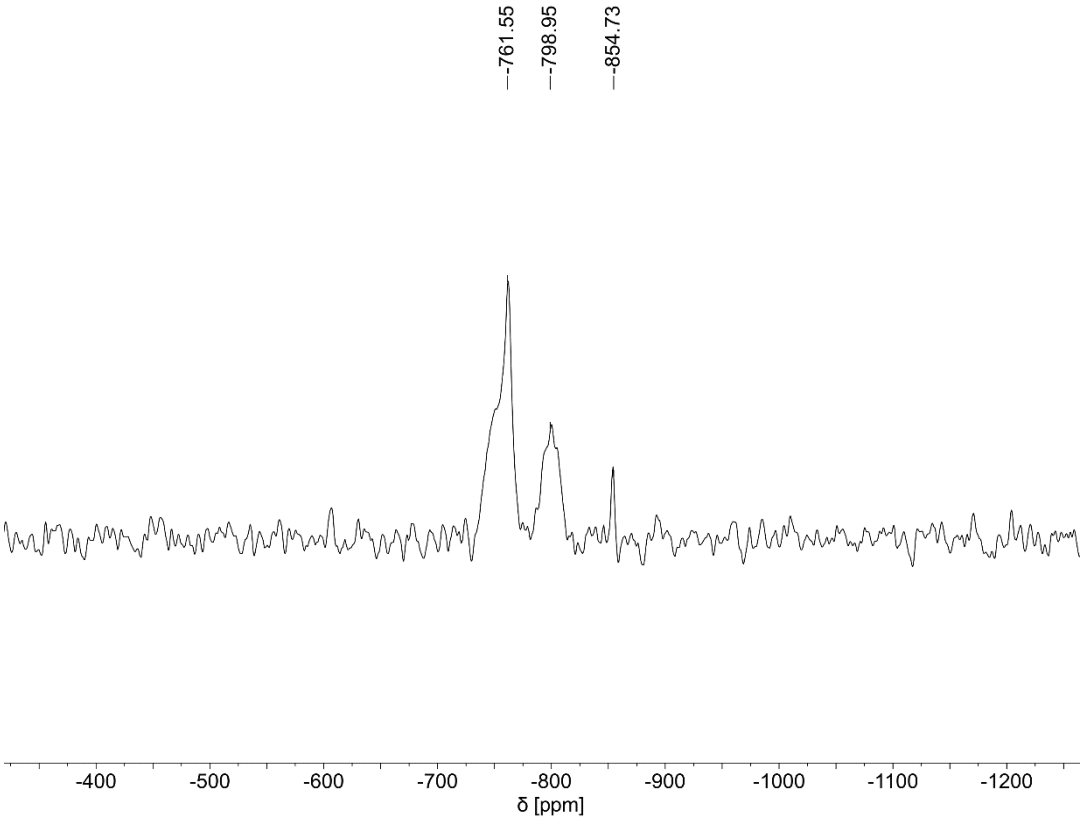

Figure S106. ^{99}Tc NMR spectrum of the isolated solid obtained from heating [Tc(η^1-$OTcO_3$)$(CO)_3(PPh_3)_2$] in acetone followed by evaporation of the solvent and addition of thf, focused on the pertechnetate region. Solvent = CH_2Cl_2.

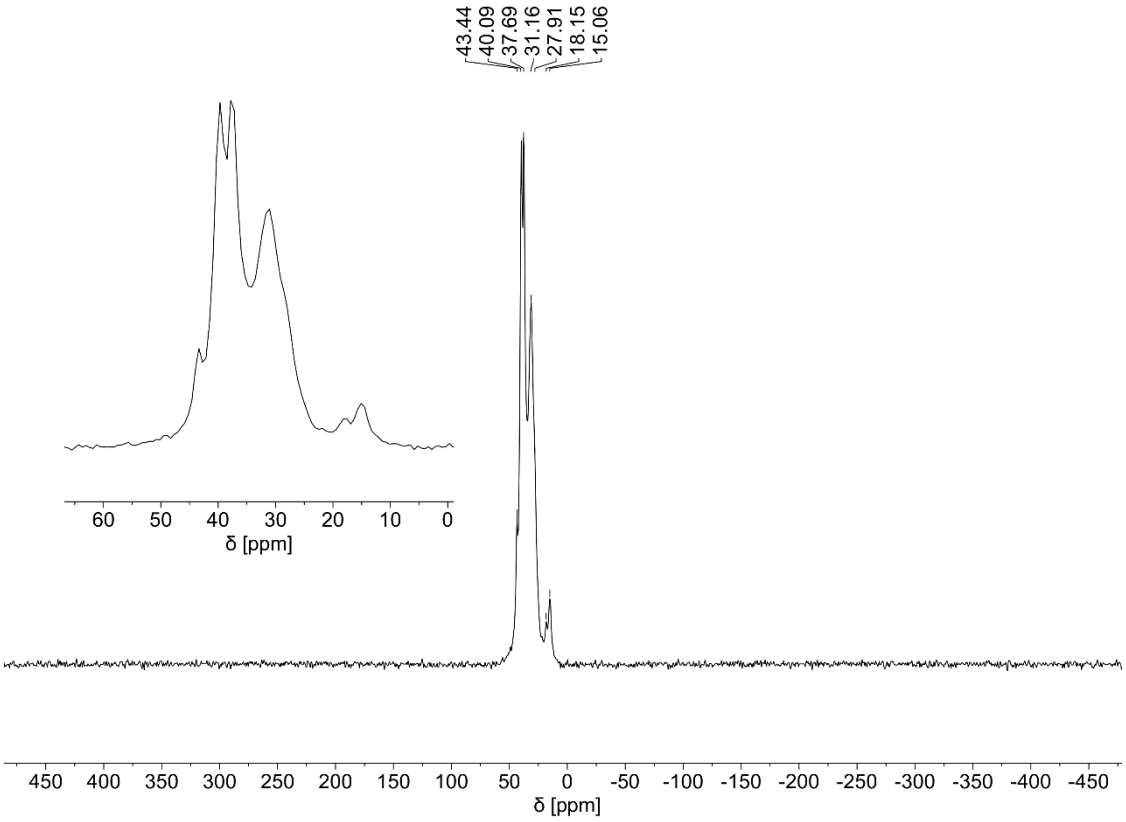

Figure S107. ^{99}Tc NMR spectrum of the isolated solid obtained from heating [Tc(η^1-$OTcO_3$)$(CO)_3(PPh_3)_2$] in acetone followed by evaporation of the solvent and addition of thf, focused on the dicarbonyl region. Solvent = CH_2Cl_2.

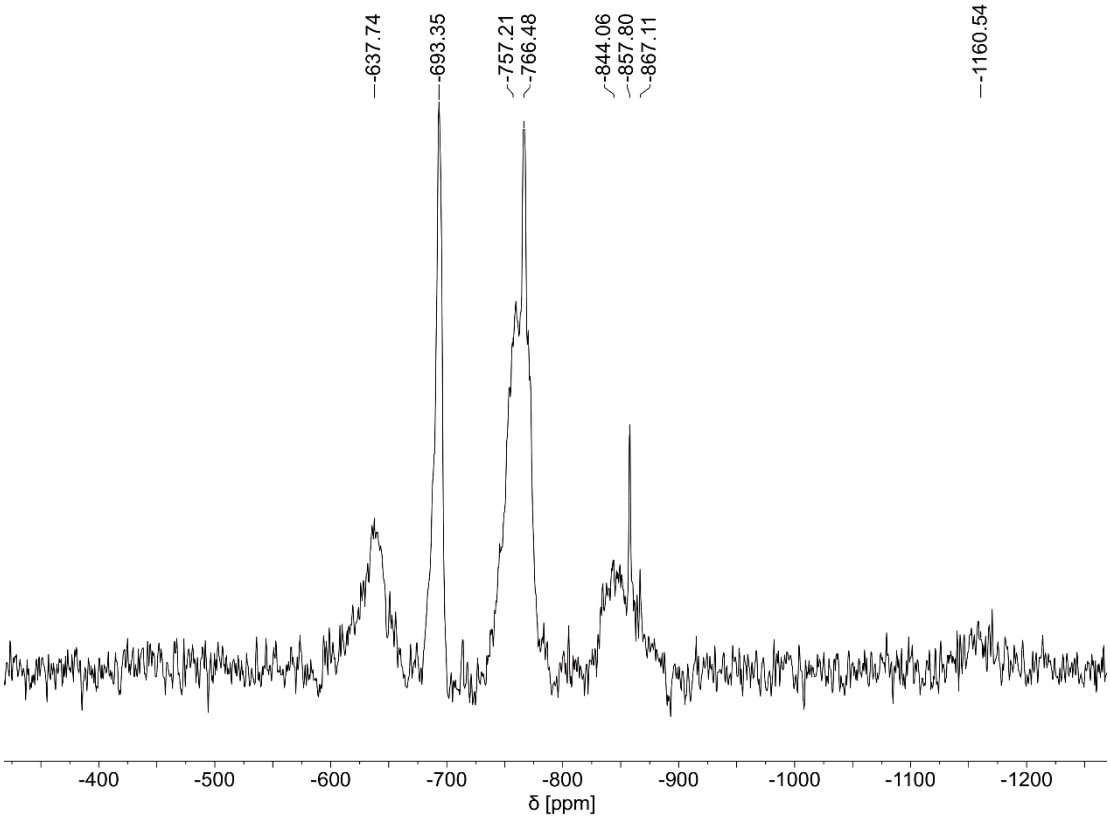

Figure S108. ^{99}Tc NMR spectrum of the isolated solid obtained from heating [Tc(η^1-$OTcO_3$)$(CO)_3(PPh_3)_2$] in acetone followed by evaporation of the solvent and addition of thf/H_2O, focused on the pertechnetate region. Solvent = CH_2Cl_2.

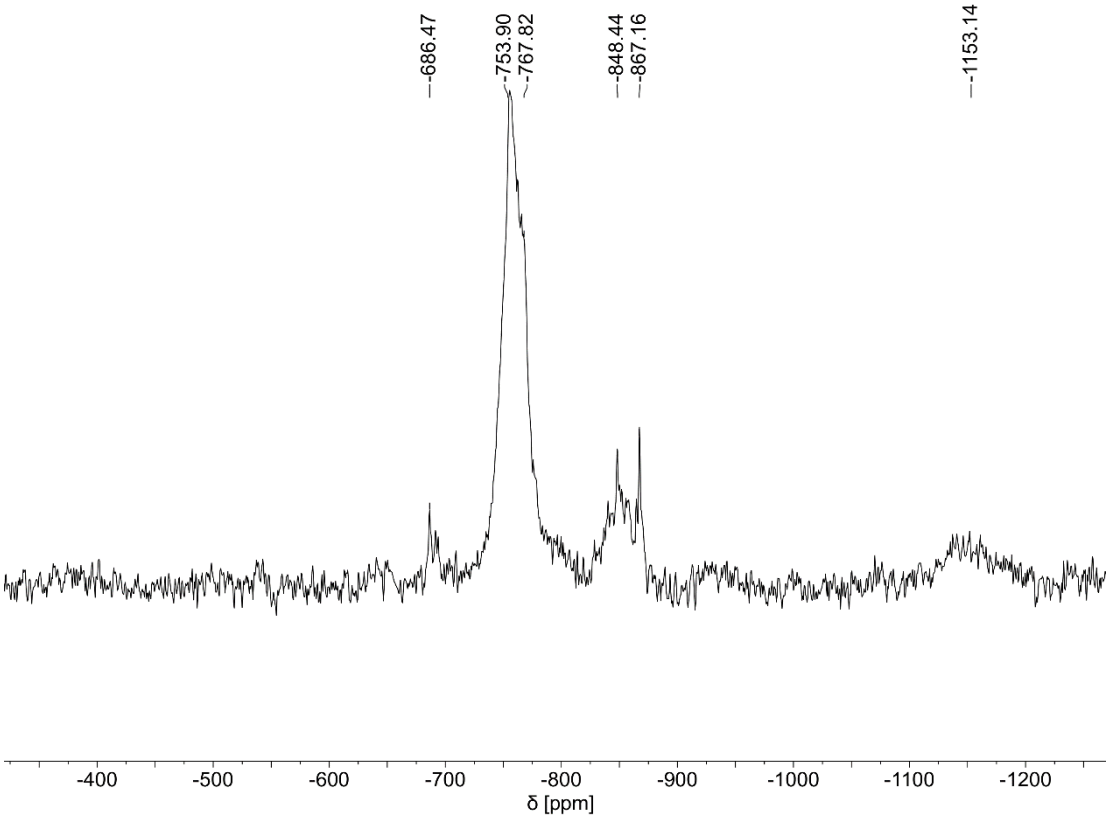

Figure S109. ^{99}Tc NMR spectrum of the isolated solid obtained from heating [Tc(η^1-$OTcO_3$)$(CO)_3(PPh_3)_2$] in acetone followed by evaporation of the solvent and addition of thf/H_2O, focused on the dicarbonyl region. Solvent = CH_2Cl_2.

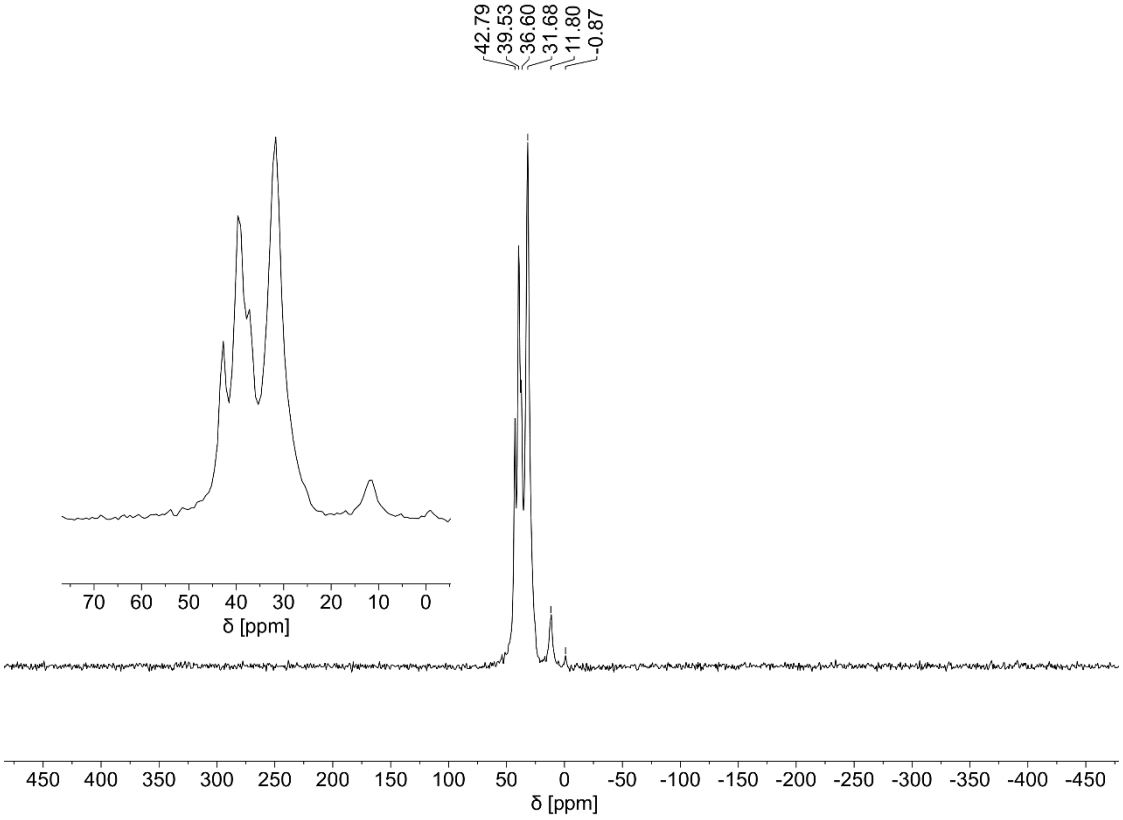

Part 3: Computational chemistry

Initial structural models were derived from X-ray structures and/or modelled with the program packages Avogadro and GaussView. The structures were optimized at the B3LYP level of theory. In some cases, only two out of four internal gaussian convergence criteria were fulfilled but the differences on the other two criteria were neglectable. The convergence of all structures was verified by the absence of negative frequencies (or exactly one negative frequency along the bond path for transition states). In the case of the chalcogenocyanates only a PMe_3 model converged within a reasonable time. In the case of the nitrite and nitrate containing complexes, only the PMe_3 model converged for all compounds including transition states, while for the PPh_3-compound the nitrato-complexes transition state was not located within a reasonable amount of time. A local minimum was obvious from the energy pathway during the transition state optimization, but it collapsed to either starting materials or products in all attempts given there was only a minor energy barrier for the collapse to either side. In most cases the transition states were successfully localized after an initial restraint calculation to obtain a reasonable starting geometry (i.e. with elongated Tc-O and/or Tc-C bond lengths in the direction of the potential reaction). Interestingly, the differences in free energy majorly decreased for the PPh_3 complexes in comparison to the PMe_3 model complexes and thus the energies derived from a much less costly PMe_3 model may be considered overestimated. For all model reactions where a transition state was considered, the free energies were not corrected for rotation for comparability with the transition states. A transition state was not located for the pertechnetato complex, while both the η^1 and η^2 structures readily converged. The energies of the two pertechnetato complexes did not change significantly when a Grimme-type correction for rotation was applied as implemented in the postprocessing code GoodVibes. References for the employed program packages are provided in the main publication.

Table S2. Gibbs free energies for the isomerization reaction of $[Tc(YCN)(CO)_3(PMe_3)_2]$ & $[Tc(NCY)(CO)_3(PMe_3)_2]$ model complexes in dichloromethane.

Y	$[Tc(YCN)(CO)_3(PPh_3)_2]$	$[Tc(NCY)(CO)_3(PPh_3)_2]$	$[Tc(YCN)(CO)_3(PPh_3)_2]$-$[Tc(NCY)(CO)_3(PPh_3)_2]$	
	ΔG	ΔG	$\Delta\Delta G$	
	[Hartree]	[Hartree]	[Hartree]	[kJ/mol]
O	-841,596364	-841,576856	-0,019508	-51,3368421
S	-776,456204	-776,444485	-0,011719	-30,8394737
Se	-775,574352	-775,566158	-0,008194	-21,5631579
Te	-774,395591	-774,390194	-0,005397	-14,2026316

Table S3. Gibbs free energies for the transition states of the isomerization reaction of $[Tc(YCN)(CO)_3(PMe_3)_2]$ & $[Tc(NCY)(CO)_3(PMe_3)_2]$ model complexes in dichloromethane.

Y	$\Delta G(TS_{YCN\rightarrow NCY})$	$\Delta G(TS_{YCN\rightarrow NCY}$- $[Tc(NCY)(CO)_3(PPh_3)_2])$		$\Delta G(TS_{YCN\rightarrow NCY}$-$[Tc(YCN)(CO)_3(PPh_3)_2])$	
		[Hartree]	[kJ/mol]	[Hartree]	[kJ/mol]
O	-841,549342	-0,047022	-123,742105	-0,027514	-72,4052632
S	-776,413327	-0,042877	-112,834211	-0,031158	-81,9947368
Se	-775,533641	-0,040711	-107,134211	-0,032517	-85,5710526
Te	-774,354573	-0,041018	-107,942105	-0,035621	-93,7394737

Table S4. Gibbs free energies for the carbonylation and decarbonylation of [Tc(η^1-ONO_2)$(CO)_3(PMe_3)_2$] & [Tc(η^2-OONO)$(CO)_2(PMe_3)_2$] model complexes in dichloromethane.

	[Tc(OONO)$(CO)_2(PMe_3)_2$]	[Tc(ONO_2)$(CO)_3(PMe_3)_2$]	CO	[Tc(OONO)$(CO)_2(PMe_3)_2$] +CO
Δ*G* [Hartree]	-840.47352	-953.845916	-113.363793	-953.837313

ΔΔ*G*([Tc(ONO_2)$(CO)_3(PMe_3)_2$]-[Tc(OONO)$(CO)_2(PMe_3)_2$])	
[Hartree]	[kJ/mol]
-0.008603	-22.6394737

Table S5. Gibbs free energies of the transition state for the carbonylation and decarbonylation of [Tc(η^1-ONO_2)$(CO)_3(PMe_3)_2$] & [Tc(η^2-OONO)$(CO)_2(PMe_3)_2$] model complexes in dichloromethane.

Δ*G*($TS_{ONO\rightarrow OON+CO}$)	ΔΔ*G*([Tc(ONO_2)$(CO)_3(PMe_3)_2$]-$TS_{ONO_2\rightarrow OONO+CO}$)		ΔΔ*G*([Tc(OONO)$(CO)_2(PMe_3)_2$]+CO-$TS_{ONO_2\rightarrow OONO+CO}$)	
[Hartree]	[Hartree]	[kJ/mol]	[Hartree]	[kJ/mol]
-953.81203	-0.033886	-89.1736842	-0.025283	-66.5342105

Table S6. Gibbs free energies for the carbonylation/decarbonylation and isomerization of [Tc(η^1-NO_2)$(CO)_3(PMe_3)_2$], [Tc(η^1-ONO)$(CO)_3(PMe_3)_2$] & [Tc(η^2-OON)$(CO)_2(PMe_3)_2$] model complexes in dichloromethane.

	[Tc(OON)$(CO)_2$ $(PMe_3)_2$]	[Tc(ONO)$(CO)_3(PMe_3)_2$]	[Tc(NO_2)$(CO)_3(PMe_3)_2$]	[Tc(OON)$(CO)_2(PMe_3)_2$] +CO
Δ*G* [Hartree]	-765.260565	-878.634379	-878.635423	-878.624358

ΔΔ*G*([Tc(ONO)$(CO)_3(PMe_3)_2$]-[Tc(NO_2)$(CO)_3(PMe_3)_2$])		ΔΔ*G*([Tc(ONO)$(CO)_3(PMe_3)_2$]-[Tc(OON)$(CO)_2(PMe_3)_2$])	
[Hartree]	[kJ/mol]	[Hartree]	[kJ/mol]
-0.001044	-2.74736842	-0.010021	-26.3710526

Table S7. Gibbs free energies for the transition states in the carbonylation/decarbonylation and isomerization of [Tc(η^1-NO_2)$(CO)_3(PMe_3)_2$], [Tc(η^1-ONO)$(CO)_3(PMe_3)_2$] & [Tc(η^2-OON)$(CO)_2(PMe_3)_2$] model complexes in dichloromethane.

Δ*G*($TS_{ONO\rightarrow OON+CO}$)	ΔΔ*G*([Tc(ONO)$(CO)_3(PMe_3)_2$]-$TS_{ONO\rightarrow OON+CO}$)		ΔΔ*G*([Tc(OON)$(CO)_2(PMe_3)_2$]+CO-$TS_{ONO\rightarrow OON+CO}$)	
[Hartree]	[Hartree]	[kJ/mol]	[Hartree]	[kJ/mol]
-878.599077	-0.035302	-92.9	-0.025281	-66.5289474

Δ*G*($TS_{NO2\rightarrow ONO}$)	ΔΔ*G*([Tc(NO_2)$(CO)_3(PMe_3)_2$]-$TS_{NO2\rightarrow ONO}$)		ΔΔ*G*([Tc(ONO)$(CO)_3(PMe_3)_2$]-$TS_{NO2\rightarrow ONO}$)	
[Hartree]	[Hartree]	[kJ/mol]	[Hartree]	[kJ/mol]
-878.607942	-0.027481	-72.3184211	-0.026437	-69.5710526

Table S8. Gibbs free energies for the carbonylation and decarbonylation of [Tc(η^1-ONO_2)$(CO)_3(PPh_3)_2$] & [Tc(η^2-OONO)$(CO)_2(PPh_3)_2$] in dichloromethane.

	[Tc(OONO)$(CO)_2(PPh_3)_2$]	[Tc(ONO_2)$(CO)_3(PPh_3)_2$]	CO	[Tc(OONO)$(CO)_2(PPh_3)_2$] +CO
Δ*G* [Hartree]	-1990.84386	-2104.20643	-113.363793	-2104.20766

ΔΔ*G*([Tc(ONO)$(CO)_3(PPh_3)_2$]-[Tc(OON)$(CO)_2(PPh_3)_2$])	
[Hartree]	[kJ/mol]
0.001224	3.22105263

Table S9. Gibbs free energies for the carbonylation/decarbonylation and isomerization of [Tc(η^1-NO_2)$(CO)_3(PPh_3)_2$], [Tc(η^1-ONO)$(CO)_3(PPh_3)_2$] & [Tc(η^2-OON)$(CO)_2(PPh_3)_2$] in dichloromethane.

	[Tc(OON)$(CO)_2(PPh_3)_2$]	[Tc(ONO)$(CO)_3(PPh_3)_2$]	[Tc(NO_2)$(CO)_3(PPh_3)_2$]	[Tc(OON)$(CO)_2(PPh_3)_2$] +CO
Δ*G* [Hartree]	-1915.62931	-2028.99322	-2028.99282	-2028.99311

ΔΔ*G*([Tc(ONO)$(CO)_3(PPh_3)_2$]-[Tc(NO_2)$(CO)_3(PPh_3)_2$])		ΔΔ*G*([Tc(ONO)$(CO)_3(PPh_3)_2$]-[Tc(OON)$(CO)_2(PPh_3)_2$])	
[Hartree]	[kJ/mol]	[Hartree]	[kJ/mol]
-0.000114	-0.3	0.000398	1.04736842

Table S10. Gibbs free energies for the transition states in the carbonylation/decarbonylation and isomerization of [Tc(η^1-NO_2)$(CO)_3(PPh_3)_2$], [Tc(η^1-ONO)$(CO)_3(PPh_3)_2$] & [Tc(η^2-OON)$(CO)_2(PPh_3)_2$] in dichloromethane.

Δ*G*($TS_{ONO→OON+CO}$)	ΔΔ*G*([Tc(ONO)$(CO)_3(PPh_3)_2$]-$TS_{ONO→OON+CO}$)		ΔΔ*G*([Tc(OON)$(CO)_2(PPh_3)_2$]+CO-$TS_{ONO→OON+CO}$)	
[Hartree]	[Hartree]	[kJ/mol]	[Hartree]	[kJ/mol]
-2028.9612	-0.032024	-84.2736842	-0.03191	-83.9736842

Δ*G*($TS_{NO2→ONO}$)	ΔΔ*G*([Tc(NO_2)$(CO)_3(PPh_3)_2$]-$TS_{NO2→ONO}$)		ΔΔ*G*([Tc(ONO)$(CO)_3(PPh_3)_2$]-$TS_{NO2→ONO}$)	
[Hartree]	[Hartree]	[kJ/mol]	[Hartree]	[kJ/mol]
-2028.96645	-0.02637	-69.3947368	-0.026768	-70.4421053

Table S11. Gibbs free energies for the carbonylation and decarbonylation of [Tc(η^1-$OTcO_3$)$(CO)_3(PPh_3)_2$] & [Tc(η^2-$OOTcO_2$)$(CO)_2(PPh_3)_2$] in dichloromethane.

	ΔG [Hartree]	$\Delta G_{Grimme\text{-}corrected}$ [Hartree]
[Tc(η^1-$OTcO_3$)$(CO)_2(PPh_3)_2$]	-2205.69823	-2205.68485
[Tc(η^2-$OOTcO_2$)$(CO)_2(PPh_3)_2$]	-2092.31601	-2092.30363
CO	-113.363793	-113.363793
[Tc(η^2-$OOTcO_2$)$(CO)_2(PPh_3)_2$]+CO	-2205.6798	-2205.66742
$\Delta\Delta G$ [Hartree]	-0.018428	-0.017427
$\Delta\Delta G$ [kJ/mol]	-48.4947368	-45.8605263

Part 4: Reference

(1) Menges, F. Spectragryph, Software for Optical Spectroscopy,Version 1.2.8, 2016–2020.

A.4 Technetium and the C≡C triple bond: Unlocking air- and water-stable technetium acetylides and other organometallic complexes

Authors	M. Roca Jungfer, U. Abram
Journal	*Inorg. Chem.* submitted
DOI	-
Link	-
Detailed scientific contribution	Maximilian Roca Jungfer and Ulrich Abram designed the project. Maximilian Roca Jungfer performed the synthesis and characterization of the compounds, calculated the X-ray structures and wrote a draft of the manuscript. Ulrich Abram supervised the project, provided scientific guidance and suggestions and corrected the manuscript.
Estimated own contribution	90%

Return to publication 4.4.

Supporting information for the paper entitled:

Technetium and the C≡C triple bond: Unlocking air- and water-stable technetium acetylides and other organometallic complexes.

Maximilian Roca Jungfer, Ulrich Abram*

[a]*Freie Universität Berlin, Institute of Chemistry and Biochemistry, Fabeckstr. 34–36, 14195 Berlin, Germany*

E-mail: ulrich.abram@fu-berlin.de

Table of Contents

Part 1: Crystallographic data

Table S1. Crystal data and structure determination parameters.

	$[Tc(Me)(CO)_3(PPh_3)_2]$	$[Tc(Ph)(CO)_3(PPh_3)_2]$ (· XCH_2Cl_2)*	$[Tc(cp)(CO)_2(PPh_3)]$
Number code	**3**	**4***	**5**
Empirical formula	$C_{40}H_{33}O_3P_2Tc$	$C_{45}H_{35}O_3P_2Tc$	$C_{25}H_{20}O_2PTc$
Formula weight	721.6	784.58	481.38
Temperature/K	100(2)	200(2)	200(2)
Crystal system	Triclinic	Orthorhombic	Triclinic
Space group	$P\bar{1}$	$Pca2_1$	$P\bar{1}$
a/Å	10.155(2)	13.0040(14)	9.4334(8)
b/Å	10.4983(19)	34.470(4)	10.6395(9)
c/Å	17.826(4)	17.9241(16)	11.6572(9)
α/°	75.995(12)	90	75.999(6)
β/°	77.805(15)	90	75.823(6)
γ/°	65.404(9)	90	77.342(7)
Volume/$Å^3$	1663.4(6)	8034.5(14)	1084.65(16)
Z	2	4	2
ρ_{calc} / g/cm^3	1.441	0.649	1.474
μ/mm^{-1}	0.567	0.238	0.755
F(000)	740	1608	488
Crystal size/mm^3	0.15 x 0.04 x 0.02	0.480 x 0.070 x 0.050	0.770 x 0.310 x 0.160
Radiation	MoKα (λ = 0.71073)	MoKα (λ = 0.71073)	MoKα (λ = 0.71073)
2Θ range for data collection/°	2.223 to 27.195	3.188 to 26.019	3.679 to 29.164
Index ranges	-13<=h<=13, -13<=k<=11, -22<=l<=22	-16<=h<=16, -42<=k<=42, -21<=l<=22	-12<=h<=12, -14<=k<=14, -15<=l<=15
Reflections collected	38801	49216	12994
Independent reflections	7362 [R(int) = 0.0400]	15733 [R(int) = 0.2794]	5802 [R(int) = 0.0606]
Data/restraints/parameters	7362 / 597 / 433	15733 / 573 / 449	5802 / 40 / 262
Goodness-of-fit on F^2	1.138	0.53(9)	1.004
Final R indexes [I>=2σ (I)]	R1 = 0.0437, wR2 = 0.1022	R1 = 0.0674, wR2 = 0.1254	R1 = 0.0303, wR2 = 0.0818
Final R indexes [all data]	R1 = 0.0512, wR2 = 0.1058	R1 = 0.2225, wR2 = 0.1628	R1 = 0.0367, wR2 = 0.0848
Absorption correction	Semi-empirical from equivalents	none	Integration
T_{max} and T_{min}	0.7455 and 0.7029	-	0.8589 and 0.6916
Largest diff. peak/hole / e^{-3}	0.784 and -0.592	0.655 and -0.546	0.718 and -0.817
CCDC access code	2131506	*	2131507

*The data quality of the crystal of $[Tc(Ph)(CO)_3(PPh_3)_2]$ (**4**) was very low. Although the connectivity derived from other analytical data was verified, no detailed structural parameters were derived and the crystallographic data was not deposited with the CCDC. The data given in Table S1 are for a dataset that has been treated with the SQUEEZE procedure to remove large regions of diffuse electron density situated in the voids of the structure corresponding to ca. 40 CH_2Cl_2 molecules per unit cell.

Table S1. Crystal data and structure determination parameters (continued).

	[Tc(=*cyclo*-$C(CH_2)_3O$)$(CO)_3(PPh_3)_2$](BF_4) · $2CH_2Cl_2$	[Tc(=*cyclo*-$C(CH_2)_4O$)$(CO)_3(PPh_3)_2$](BF_4)	[Tc(CCH)$(CO)_3(PPh_3)_2$] · CH_2Cl_2
Number code	**6** · $2CH_2Cl_2$	**7**	**8** · CH_2Cl_2
Empirical formula	$C_{45}H_{40}BCl_4F_4O_4P_2Tc$	$C_{44}H_{38}BF_4O_4P_2Tc$	$C_{42}H_{33}Cl_2O_3P_2Tc$
Formula weight	1033.32	877.49	816.52
Temperature/K	200(2)	100(2)	230(2)
Crystal system	Monoclinic	Monoclinic	Triclinic
Space group	$P2_1/c$	$P2_1/n$	$P\bar{1}$
a/Å	15.7452(7)	14.6840(5)	12.3447(7)
b/Å	14.8348(5)	12.2314(4)	13.6153(8)
c/Å	20.7936(9)	22.3126(8)	13.8619(8)
α/°	90	90	98.502(5)
β/°	103.241(4)	102.9410(10)	109.472(4)
γ/°	90	90	114.770(4)
Volume/Å^3	4727.8(3)	3905.7(2)	1878.7(2)
Z	4	4	2
ρ_{calc} / g/cm^3	1.452	1.492	1.443
μ/mm^{-1}	0.655	0.513	0.649
F(000)	2096	1792	832
Crystal size/mm^3	0.400 x 0.210 x 0.040	0.120 x 0.120 x 0.020	0.620 x 0.229 x 0.094
Radiation	MoKα (λ = 0.71073)	MoKα (λ = 0.71073)	MoKα (λ = 0.71073)
2Θ range for data collection/°	3.249 to 27.998	2.190 to 27.123	3.310 to 29.220
Index ranges	-20<=h<=20, -18<=k<=19, -27<=l<=27	-18<=h<=18, -15<=k<=15, -28<=l<=28	-16<=h<=16, -18<=k<=16, -18<=l<=18
Reflections collected	48357	65278	21771
Independent reflections	11401 [R(int) = 0.0615]	8627 [R(int) = 0.0777]	10054 [R(int) = 0.0978]
Data/restraints/parameters	11401 / 729 / 609	8627 / 0 / 505	10054 / 0 / 456
Goodness-of-fit on F^2	0.866	1.083	0.936
Final R indexes [I>=2σ (I)]	R1 = 0.0433, wR2 = 0.0924	R1 = 0.0479, wR2 = 0.0972	R1 = 0.0530, wR2 = 0.1307
Final R indexes [all data]	R1 = 0.0779, wR2 = 0.0997	R1 = 0.0607, wR2 = 0.1028	R1 = 0.0654, wR2 = 0.1358
Absorption correction	Integration	Semi-empirical from equivalents	Integration
T_{max} and T_{min}	0.9442 and 0.7792	0.7455 and 0.6920	0.9873 and 0.8549
Largest diff. peak/hole / e·Å^{-3}	0.693 and -0.708	1.005 and -0.890	1.333 and -1.834
CCDC access code	2131508	2131509	2131510

Table S1. Crystal data and structure determination parameters (continued).

	[Tc(CCPh)(CO)$_3$(PPh$_3$)$_2$]	[Tc(CC^{t}Bu)(CO)$_3$(PPh$_3$)$_2$]	[Tc(CC^{n}Bu)(CO)$_3$(PPh$_3$)$_2$]
Number Code	**8a**	**8b**	**8c**
Empirical formula	$C_{47}H_{35}O_3P_2Tc$	$C_{45}H_{39}O_3P_2Tc$	$C_{45}H_{39}O_3P_2Tc$
Formula weight	807.69	787.7	787.7
Temperature/K	247(2)	230(2)	293(2)
Crystal system	Monoclinic	Monoclinic	Monoclinic
Space group	*C*2/*c*	*P*2$_1$/*n*	*C*2/*c*
a/Å	14.7544(11)	9.9771(7)	14.2081(18)
b/Å	13.9569(11)	19.3245(9)	14.3173(12)
c/Å	19.0921(19)	20.1796(16)	19.268(2)
α/°	90	90	90
β/°	94.562(7)	93.803(6)	97.444(10)
γ/°	90	90	90
Volume/Å^3	3919.1(6)	3882.1(4)	3886.5(7)
Z	4	4	4
ρ_{calc} / g/cm^3	1.369	1.348	1.346
μ/mm^{-1}	0.49	0.492	0.492
F(000)	1656	1624	1624
Crystal size/mm^3	0.200 x 0.135 x 0.084	0.225 x 0.107 x 0.039	0.530 x 0.207 x 0.040
Radiation	MoKα (λ = 0.71073)	MoKα (λ = 0.71073)	MoKα (λ = 0.71073)
2Θ range for data collection/°	3.364 to 29.224	3.213 to 26.998	3.364 to 29.304
Index ranges	-20<=h<=20, -19<=k<=19, -26<=l<=22	-11<=h<=12, -22<=k<=24, -25<=l<=25	-19<=h<=19, -19<=k<=19, -22<=l<=25
Reflections collected	14596	32991	16147
Independent reflections	5259 [R(int) = 0.1051]	8414 [R(int) = 0.1089]	5100 [R(int) = 0.1241]
Data/restraints/parameters	5259 / 0 / 243	8414 / 634 / 494	5100 / 383 / 311
Goodness-of-fit on F^2	0.922	0.817	0.737
Final R indexes [I>=2σ (I)]	R1 = 0.0610, wR2 = 0.1225	R1 = 0.0453, wR2 = 0.0775	R1 = 0.0481, wR2 = 0.0726
Final R indexes [all data]	R1 = 0.1133, wR2 = 0.1382	R1 = 0.1020, wR2 = 0.0896	R1 = 0.1488, wR2 = 0.0929
Absorption correction	None	None	None
Largest diff. peak/hole / e·Å^{-3}	1.001 and -1.383	0.488 and -0.748	0.550 and -1.214
CCDC access code	2131514	2131515	2131511

Table S1. Crystal data and structure determination parameters (continued).

	$[Tc(CCSiMe_3)(CO)_3(PPh_3)_2]$	$[Tc\{CC(C_6H_3(CF_3)_2)\}(CO)_3(PPh_3)_2]$	$[Tc(CNPh)(CO)_3(PPh_3)_2](BF_4)$
Number code	**8d**	**8e**	**9a**
Empirical formula	$C_{44}H_{39}O_3P_2SiTc$	$C_{49}H_{33}F_6O_3P_2Tc$	$C_{46}H_{35}BF_4NO_3P_2Tc$
Formula weight	803.78	943.69	896.5
Temperature/K	293(2)	230(2)	293(2)
Crystal system	Monoclinic	Triclinic	Monoclinic
Space group	$P2_1/n$	$P\bar{1}$	$P2_1/n$
a/Å	10.0918(6)	10.4013(6)	9.3770(7)
b/Å	19.7389(11)	10.5086(6)	18.2055(8)
c/Å	20.1172(12)	21.2263(12)	24.6248(16)
α/°	90	79.763(4)	90
β/°	94.552(5)	81.710(5)	96.465(6)
γ/°	90	72.338(4)	90
Volume/$Å^3$	3994.7(4)	2165.4(2)	4177.0(5)
Z	4	2	4
ρ_{calc} / g/cm^3	1.336	1.447	1.426
μ/mm^{-1}	0.508	0.474	0.481
F(000)	1656	956	1824
Crystal size/mm^3	0.273 x 0.103 x 0.076	0.290 x 0.220 x 0.070	0.220 x 0.110 x 0.030
Radiation	MoKα (λ = 0.71073)	MoKα (λ = 0.71073)	MoKα (λ = 0.71073)
2Θ range for data collection/°	3.154 to 25.998	3.303 to 29.251	3.300 to 29.272
Index ranges	-12<=h<=12, -24<=k<=23, -24<=l<=24	-14<=h<=14, -14<=k<=14, -29<=l<=29	-12<=h<=11, -24<=k<=24, -33<=l<=33
Reflections collected	33985	27325	32352
Independent reflections	7856 [R(int) = 0.0839]	11611 [R(int) = 0.0583]	11221 [R(int) = 0.0860]
Data/restraints/parameters	7856 / 30 / 464	11611 / 132 / 606	11221 / 30 / 551
Goodness-of-fit on F^2	0.866	0.841	0.793
Final R indexes [I>=2σ (I)]	R1 = 0.0463, wR2 = 0.1025	R1 = 0.0363, wR2 = 0.0747	R1 = 0.0454, wR2 = 0.0814
Final R indexes [all data]	R1 = 0.0865, wR2 = 0.1128	R1 = 0.0661, wR2 = 0.0808	R1 = 0.1213, wR2 = 0.0971
Absorption correction	None	Integration	None
T_{max} and T_{min}		0.9353 and 0.8925	
Largest diff. peak/hole / $e \cdot Å^{-3}$	0.569 and -0.935	0.591 and -1.085	0.528 and -1.005
CCDC access code	2131512	2131513	2131516

Table S1. Crystal data and structure determination parameters (continued).

	$[Tc(CN^tBu)(CO)_3(PPh_3)_2](BF_4) \cdot CH_2Cl_2$	$[Tc(CN^tBu)(CO)_3(PPh_3)_2](BF_4) \cdot CH_3CN$	$[Tc(NCPh)(CO)_3(PPh_3)_2](BF_4)$
Number code	**9b** · CH_2Cl_2	**9b** · CH_3CN	**10a**
Empirical formula	$C_{45}H_{41}BCl_2F_4NO_3P_2Tc$	$C_{46}H_{42}BF_4N_2O_3P_2Tc$	$C_{46}H_{35}BF_4NO_3P_2Tc$
Formula weight	961.44	917.56	896.5
Temperature/K	230(2)	230(2)	263(2)
Crystal system	Monoclinic	Monoclinic	Monoclinic
Space group	$P2_1/n$	$P2_1/n$	$P2_1/n$
a/Å	9.4927(7)	13.2202(7)	9.2931(9)
b/Å	25.1522(18)	15.0053(6)	18.2489(11)
c/Å	18.8124(14)	22.1130(12)	24.548(2)
α/°	90	90	90
β/°	90.707(6)	90.774(4)	96.143(8)
γ/°	90	90	90
Volume/Å^3	4491.3(6)	4386.2(4)	4139.2(6)
Z	4	4	4
ρ_{calc} / g/cm^3	1.422	1.389	1.439
μ/mm^{-1}	0.567	0.46	0.485
F(000)	1960	1880	1824
Crystal size/mm^3	0.280 x 0.100 x 0.075	0.42 x 0.32 x 0.20	0.230 x 0.120 x 0.060
Radiation	MoKα (λ = 0.71073)	MoKα (λ = 0.71073)	MoKα (λ = 0.71073)
2Θ range for data collection/°	3.240 to 26.999	3.368 to 29.208	3.307 to 27.999
Index ranges	-12<=h<=12, -32<=k<=28, -24<=l<=24	-17<=h<=18, -20<=k<=20, -30<=l<=30	-12<=h<=12, -24<=k<=24, -27<=l<=32
Reflections collected	26936	34700	28204
Independent reflections	9389 [R(int) = 0.1233]	11807 [R(int) = 0.0856]	9961 [R(int) = 0.1513]
Data/restraints/parameters	9389 / 3 / 531	11807 / 0 / 536	9961 / 694 / 551
Goodness-of-fit on F^2	0.991	0.851	0.621
Final R indexes [I>=2σ (I)]	R1 = 0.0688, wR2 = 0.1663	R1 = 0.0447, wR2 = 0.1020	R1 = 0.0466, wR2 = 0.0573
Final R indexes [all data]	R1 = 0.1101, wR2 = 0.1837	R1 = 0.0778, wR2 = 0.1093	R1 = 0.1726, wR2 = 0.0806
Absorption correction	None	None	None
Largest diff. peak/hole / e·Å^{-3}	1.046 and -1.161	0.905 and -2.069	0.432 and -0.641
CCDC access code	2131517	2131518	2131519

Table S1. Crystal data and structure determination parameters (continued).

	$[Tc(CN^tBu)(CO)_3(PPh_3)_2](BF_4)$	$[Tc(CO)_4(PPh_3)_2](PF_6)$
Number code	**10b**	
Empirical formula	$C_{45}H_{41}BCl_2F_4NO_3P_2Tc$	$C_{40}H_{30}F_6O_4P_3Tc$
Formula weight	961.44	879.55
Temperature/K	100(2)	250(2)
Crystal system	Monoclinic	Monoclinic
Space group	$P2_1/n$	$P2_1/c$
a/Å	12.2369(4)	19.8444(19)
b/Å	25.0985(8)	15.444(2)
c/Å	14.3938(4)	12.6337(11)
α/°	90	90
β/°	97.3980(10)	96.468(7)
γ/°	90	90
Volume/Å^3	4383.9(2)	3847.4(7)
Z	4	4
ρ_{calc} / g/cm^3	1.457	1.518
μ/mm^{-1}	0.581	0.568
F(000)	1960	1776
Crystal size/mm^3	0.280 x 0.180 x 0.020	0.890 x 0.370 x 0.090
Radiation	MoKα (λ = 0.71073)	MoKα (λ = 0.71073)
2Θ range for data collection/°	2.058 to 27.123	3.246 to 25.998
Index ranges	-15<=h<=15, -32<=k<=32, -18<=l<=18	-20<=h<=24, -19<=k<=19, -15<=l<=15
Reflections collected	69221	31724
Independent reflections	9680 [R(int) = 0.0667]	7538 [R(int) = 0.1565]
Data/restraints/parameters	9680 / 666 / 577	7538 / 0 / 490
Goodness-of-fit on F^2	1.087	0.772
Final R indexes [I>=2σ (I)]	R1 = 0.0553, wR2 = 0.1234	R1 = 0.0476, wR2 = 0.0915
Final R indexes [all data]	R1 = 0.0679, wR2 = 0.1297	R1 = 0.1149, wR2 = 0.1052
Absorption correction	Semi-empirical from equivalents	Integration
T_{max} and T_{min}	0.7455 and 0.6436	0.9675 and 0.8300
Largest diff. peak/hole / e·Å^{-3}	1.299 and -1.023	0.645 and -0.989
CCDC access code	2131520	2131521

Figure S1. Ellipsoid representation (50% probability) of [Tc(CH_3)($CO)_3$(PPh_3)$_2$] (**3**). Hydrogen atoms bonded to aromatic carbon atoms are omitted for clarity. The methyl hydrogen atom positions were placed at calculated positions and refined using a riding model. The methyl ligand and one carbonyl group are disordered with an occupancy of ca. 60% for the major component. The disorder was treated using appropriate distance and thermal ellipsoid restraints.

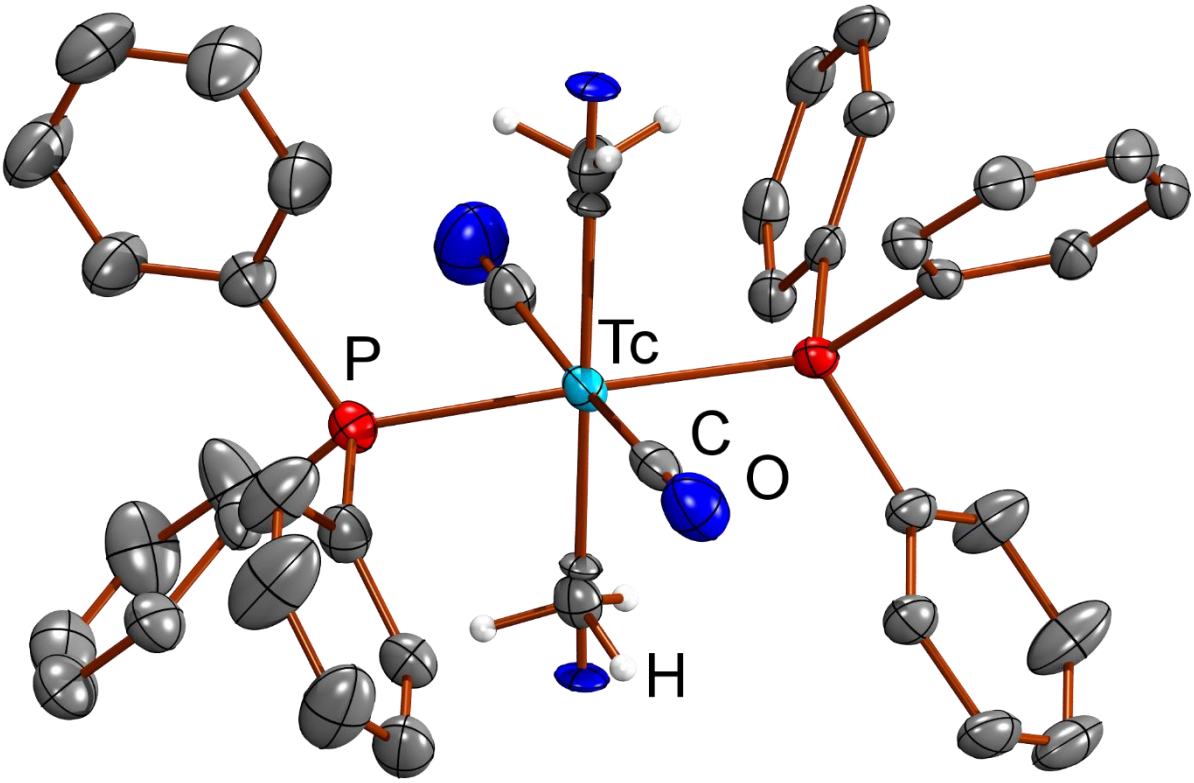

Figure S2. Ellipsoid representation (50% probability) of [Tc(Ph)$(CO)_3(PPh_3)_2$] (**4**). Hydrogen atoms are omitted for clarity. The structure was not deposited with the CCDC repository as only the connectivity was assigned unambiguously and high, diffuse electron density remained. Despite several attempts we were unable to model these regions properly, which can be accounted to a high mosaicity (i.e. several randomly oriented domains) and thus low quality of the crystal combined with the high lattice solvent content. The dataset was treated with the SQUEEZE routine of platon to obtain somewhat more reliable Tc-X bond lengths but overall the data quality was too low to be interpreted quantitatively. The removed electron density accounts for 1669.3 electrons in 4643.0 Å^3 of solvent accessible voids. This roughly matches the electron density of 40 CH_2Cl_2 molecules (48 electrons each; 10 CH_2Cl_2 molecules per asymmetric unit). This roughly matches with the dichloromethane moieties we assigned during our initial modelling attempts. Additionally, the structure was refined as an inversion twin (ratio ca. 0.5) and thus the obtained Flack-parameter of ca. 0.5 is meaningless.

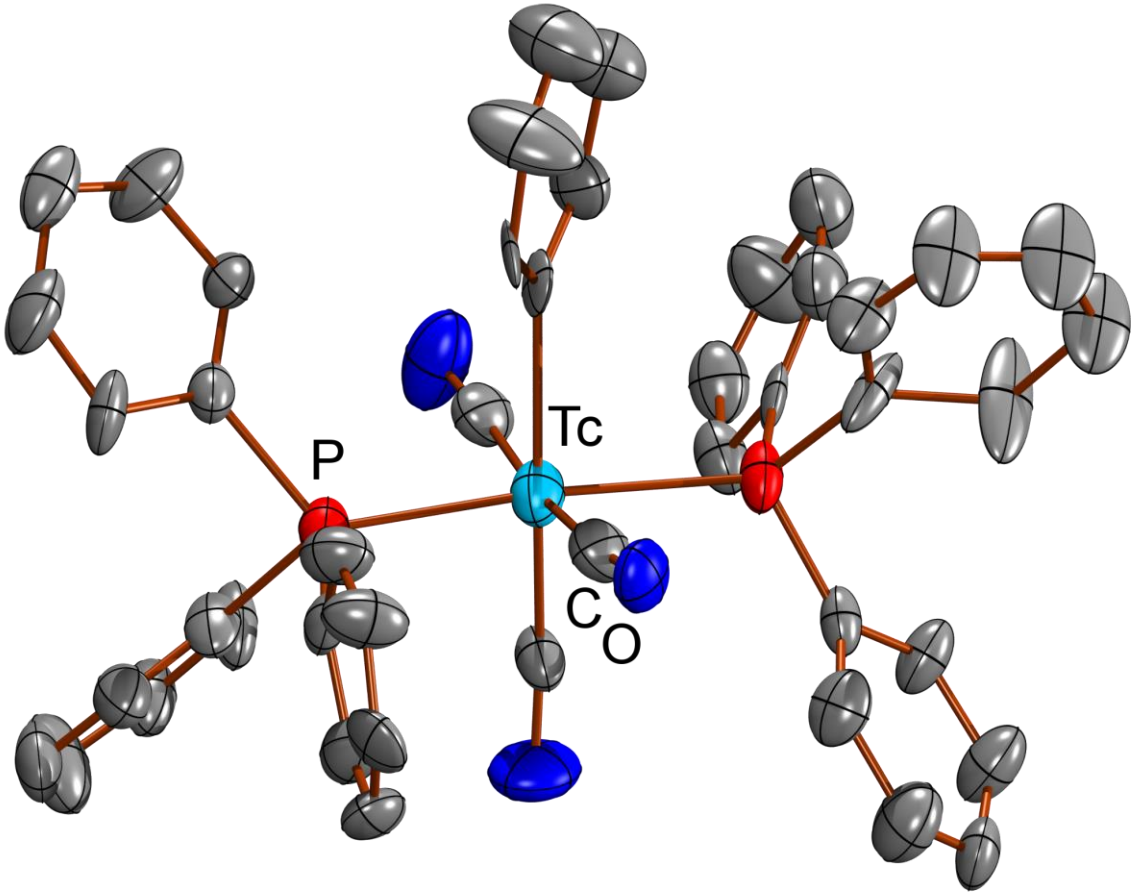

Figure S3. Ellipsoid representation (50% probability) of [Tc(cp)$(CO)_2(PPh_3)$] (**5**). Hydrogen atoms are omitted for clarity.

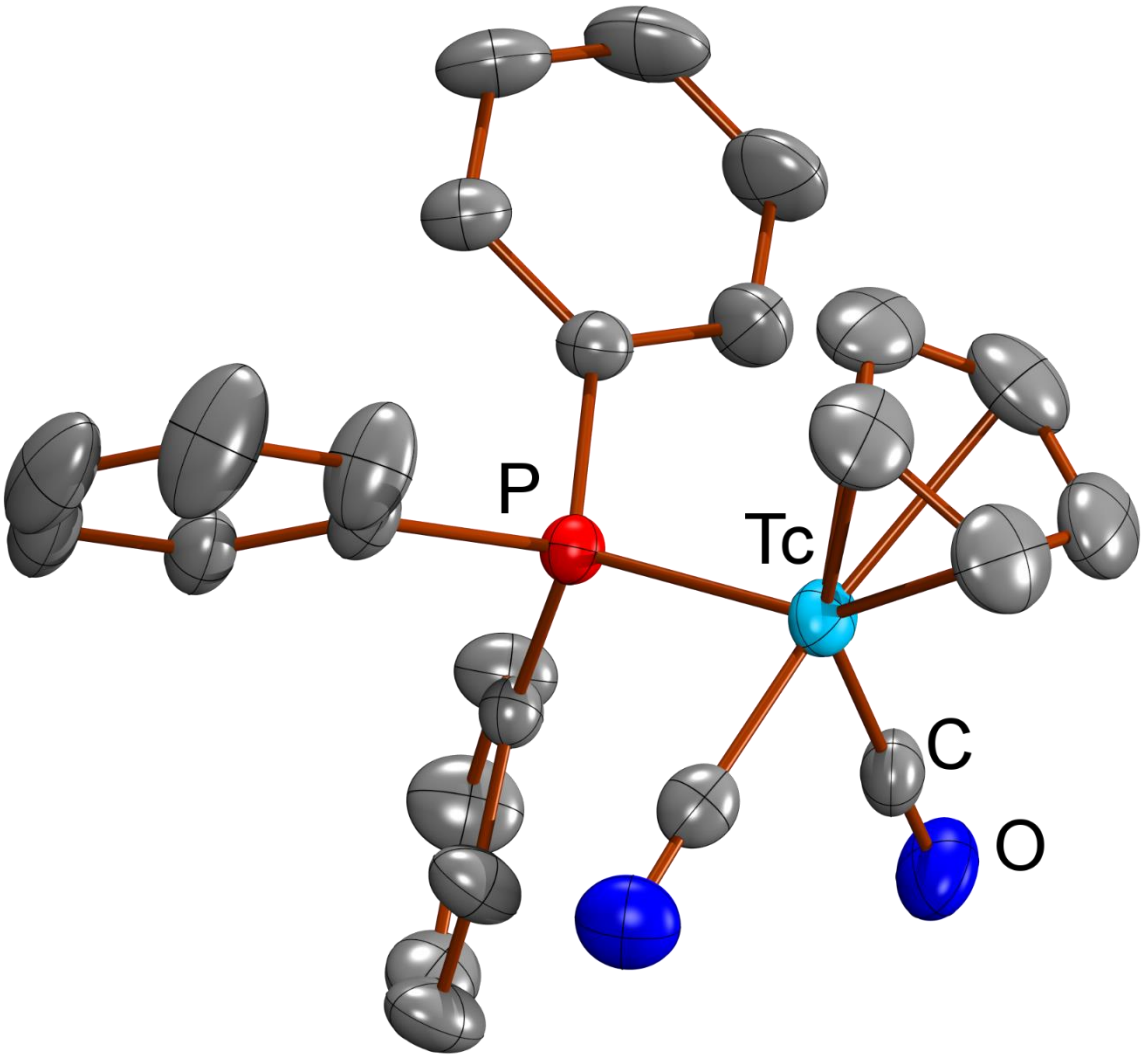

Figure S4. Ellipsoid representation (50% probability) of [Tc(=*cyclo*-$C(CH_2)_3O)(CO)_3(PPh_3)_2](BF_4)$ (**6**) · 2 CH_2Cl_2. Hydrogen atoms are omitted for clarity. The BF_4^- anion is disordered over two positions in a ratio of ca. 50:50 and was modelled using appropriate constraints and restraints. The second co-crystallized solvent dichloromethane molecule is disordered over four positions (ca. 50:10:20:20) and was modelled using appropriate constraints and restraints.

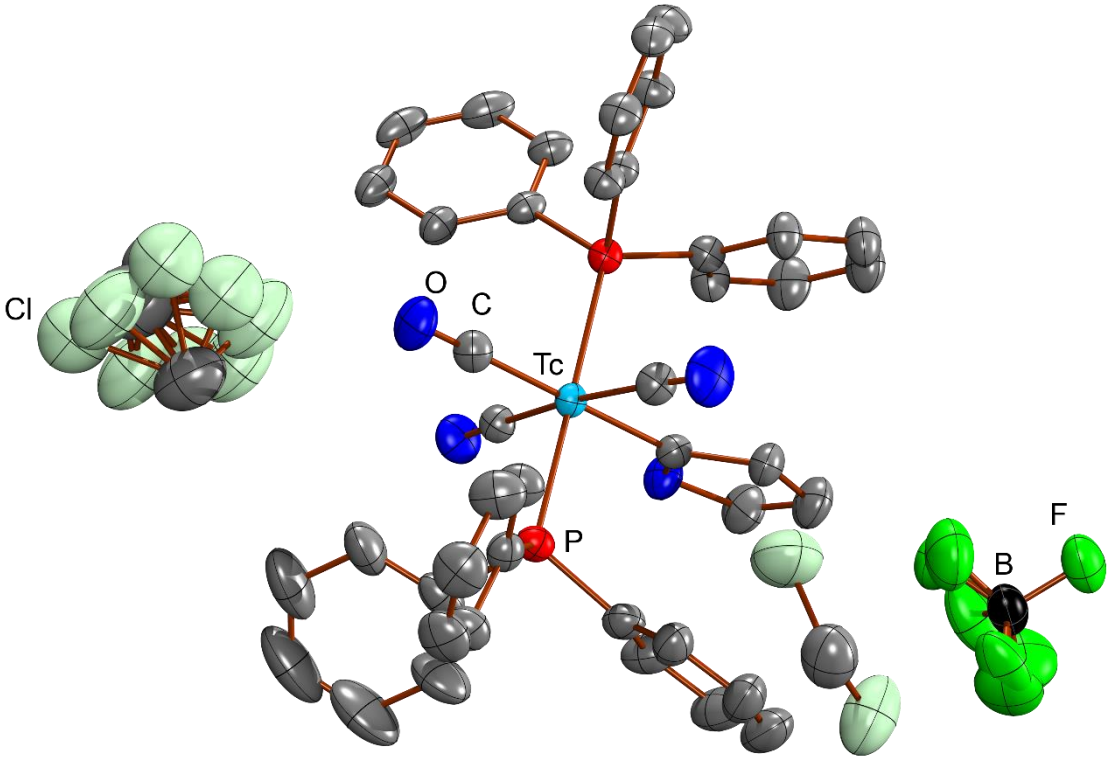

Figure S5. Ellipsoid representation (50% probability) of [Tc(=*cyclo*-$C(CH_2)_4O)(CO)_3(PPh_3)_2$]($BF_4$) (**7**). Hydrogen atoms are omitted for clarity.

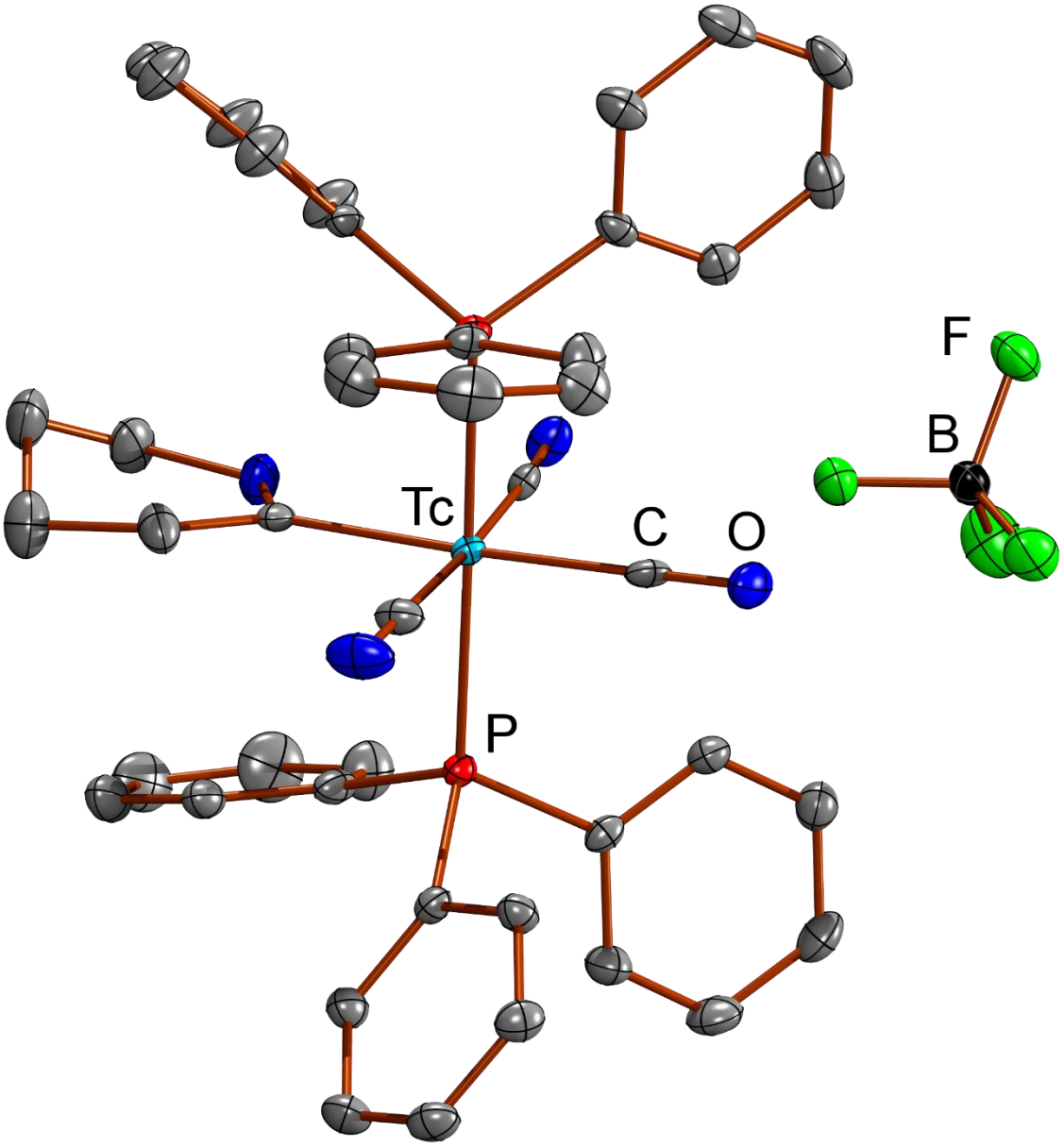

Figure S6. Ellipsoid representation (50% probability) of [Tc(CCH)$(CO)_3(PPh_3)_2$] (**8**) · CH_2Cl_2. Hydrogen atoms bonded to aromatic carbon atoms are omitted for clarity.

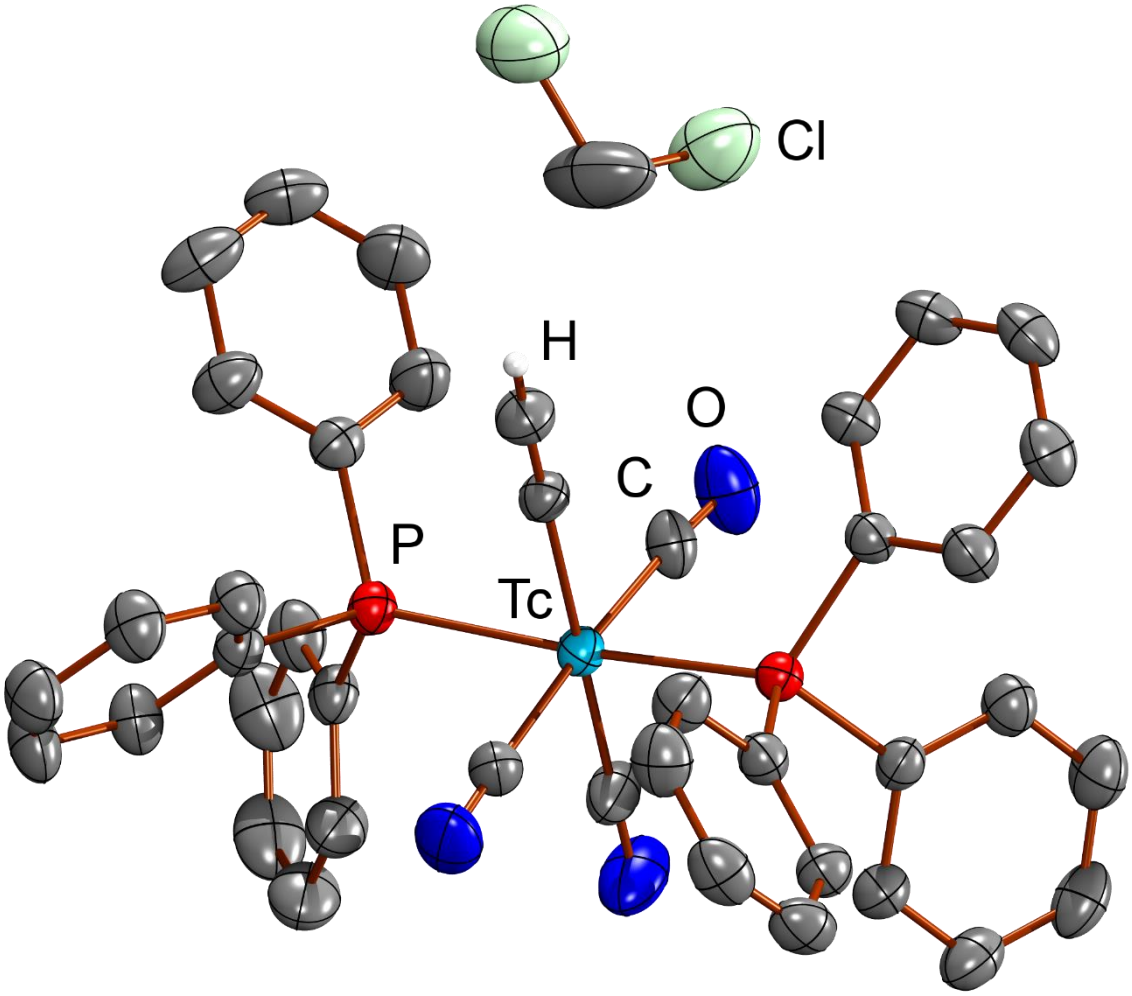

Figure S7. Ellipsoid representation (50% probability) of [Tc(CCPh)$(CO)_3(PPh_3)_2$] (**8a**). Hydrogen atoms are omitted for clarity.

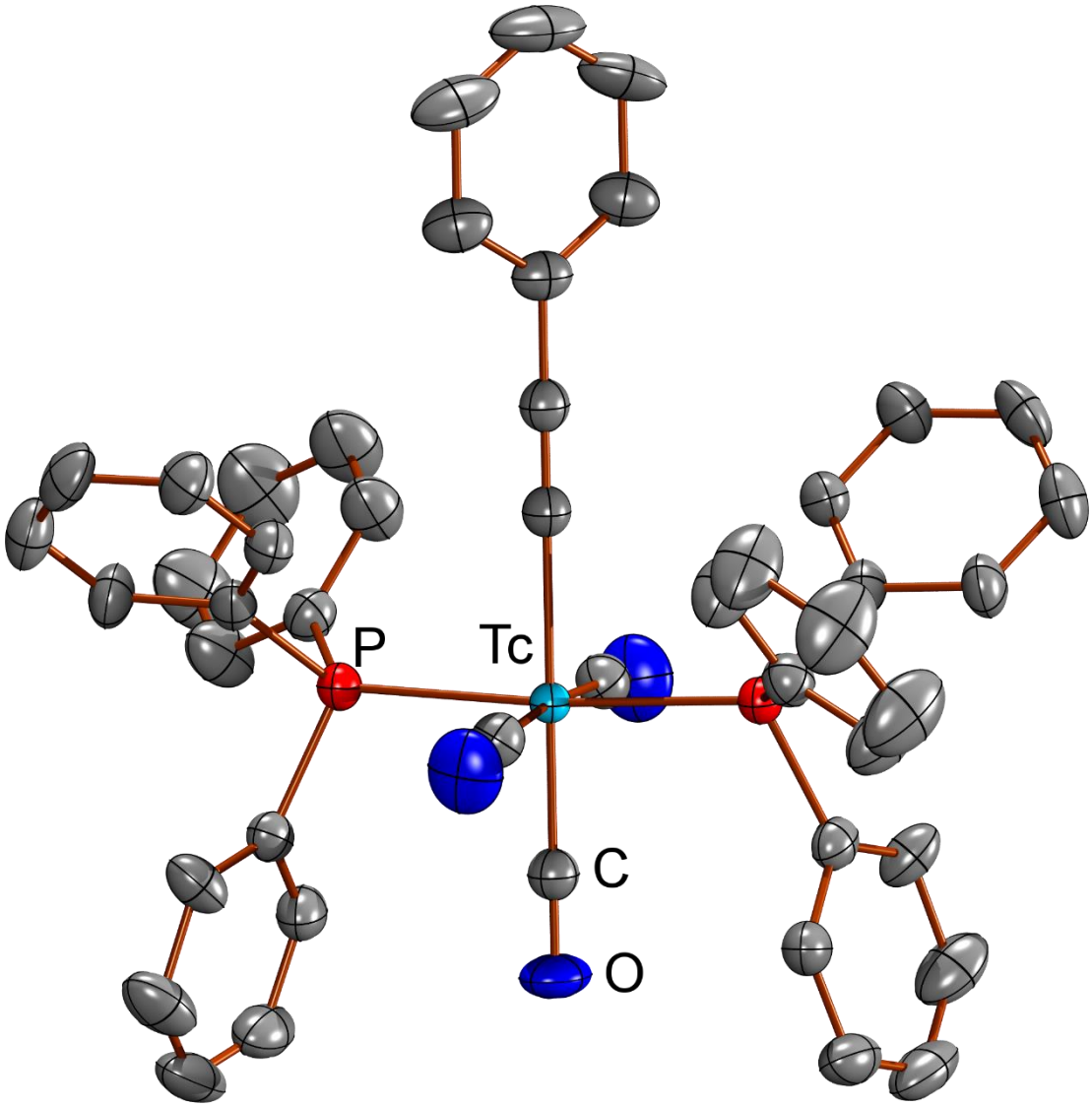

Figure S8. Ellipsoid representation (50% probability) of [Tc(CC^{t}Bu)(CO)$_3$(PPh$_3$)$_2$] (**8b**). Hydrogen atoms are omitted for clarity. The *tert*-butyl group is disordered over two positions with maximum contribution of 80% for the major component and has been modelled using appropriate restraints.

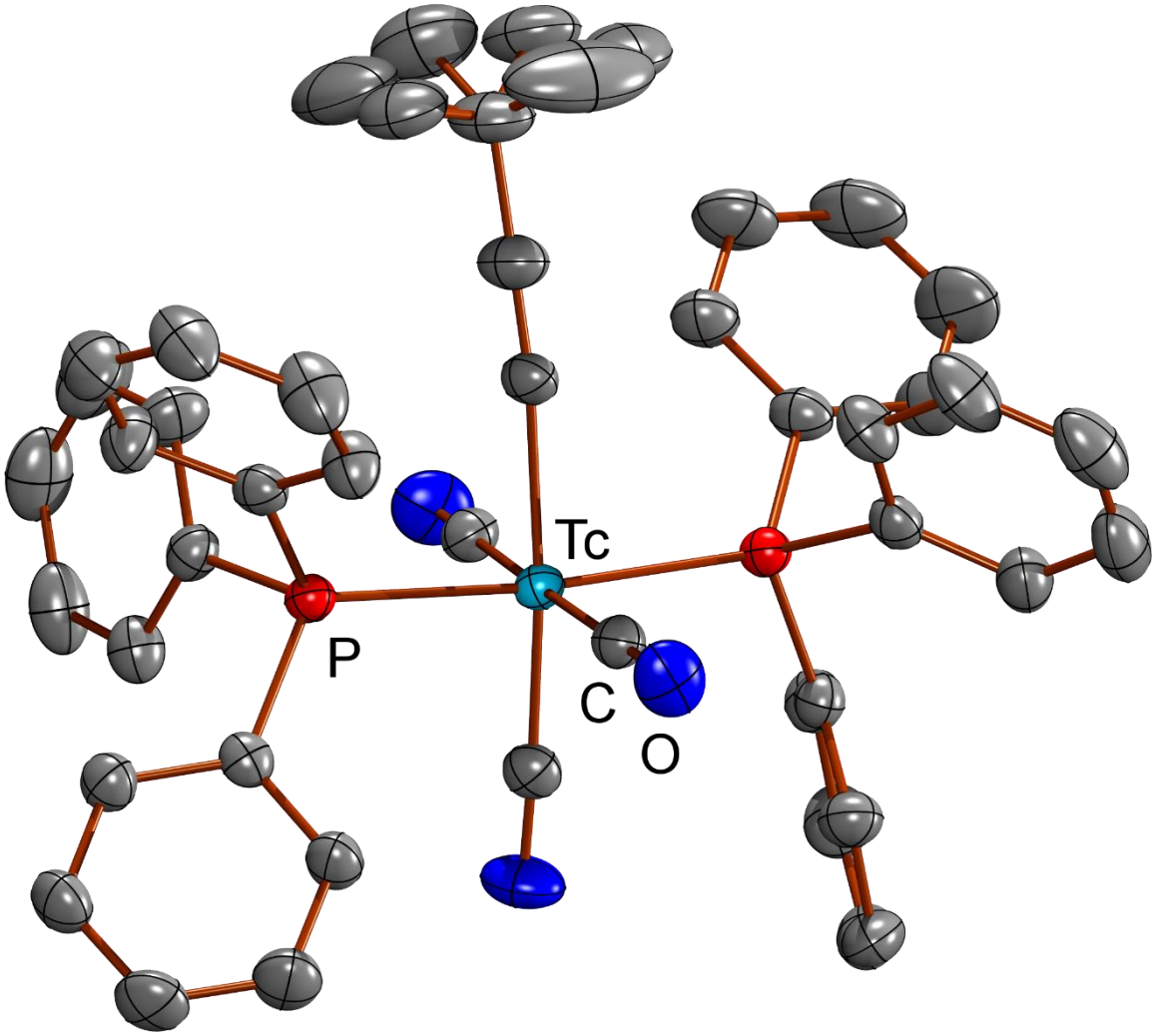

Figure S9. Ellipsoid representation (50% probability) of [Tc(CC^{n}Bu)(CO)$_3$(PPh$_3$)$_2$] (**8c**). Hydrogen atoms are omitted for clarity. Half of the molecule is generated through the space-group symmetry (-x+1, y, -z+1/2). The butyl residue is disordered over a total of four positions around the monoclinic space-group symmetry and was modelled using appropriate restraints and constraints. Additionally, one of the phenyl rings in one of the triphenylphosphine ligands is disordered over two positions with the major component accounting for 70% of the occupancy.

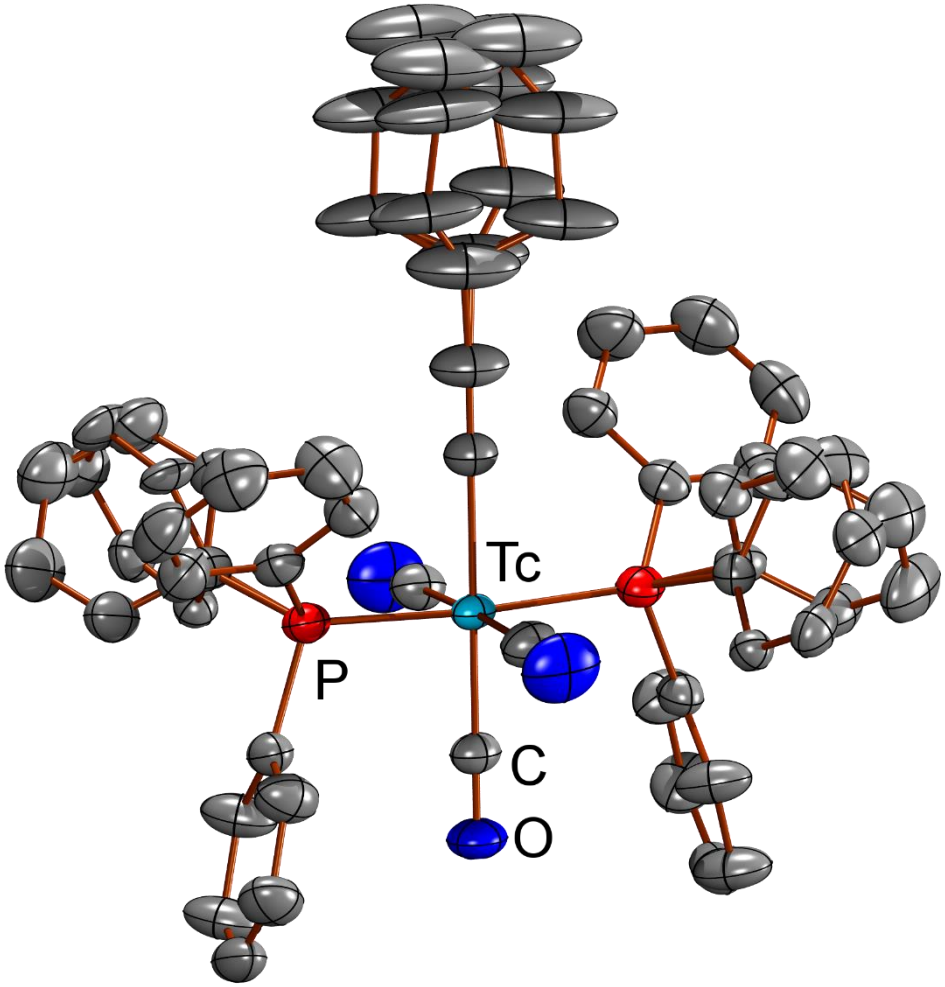

Figure S10. Ellipsoid representation (50% probability) of [Tc(CCSiMe$_3$)(CO)$_3$(PPh$_3$)$_2$] (**8d**). Hydrogen atoms are omitted for clarity. The trimethylsilyl group is disordered over two positions with maximum contribution of ca. 65% for the major component and has been modelled using appropriate restraints.

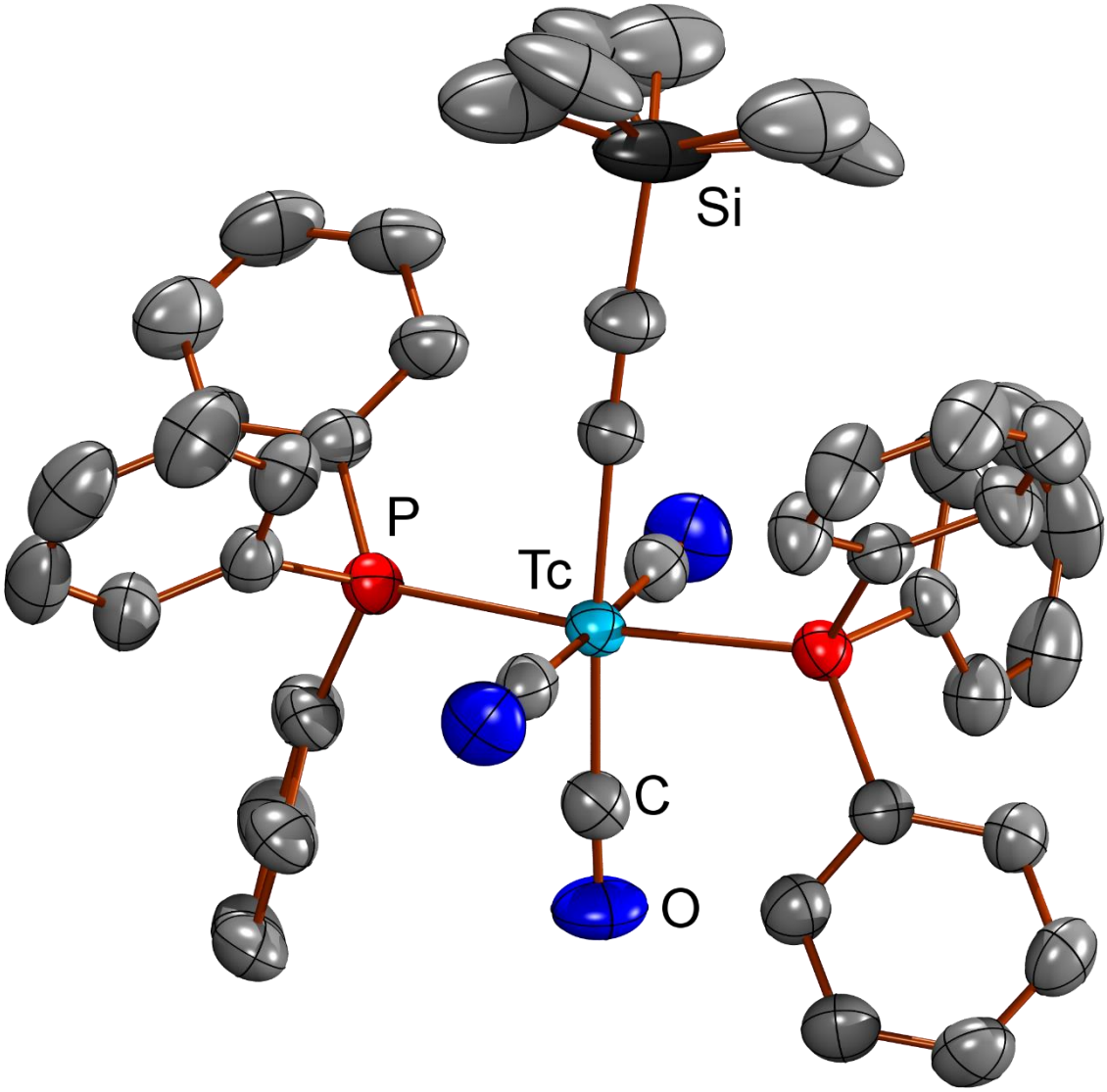

Figure S11. Ellipsoid representation (50% probability) of [Tc{CC($C_6H_3(CF_3)_2$)}$(CO)_3(PPh_3)_2$] (**8e**). Hydrogen atoms are omitted for clarity. The trifluoromethyl groups are disordered over two positions in a ratio of ca. 50:50 respectively and have been modelled using appropriate restraints.

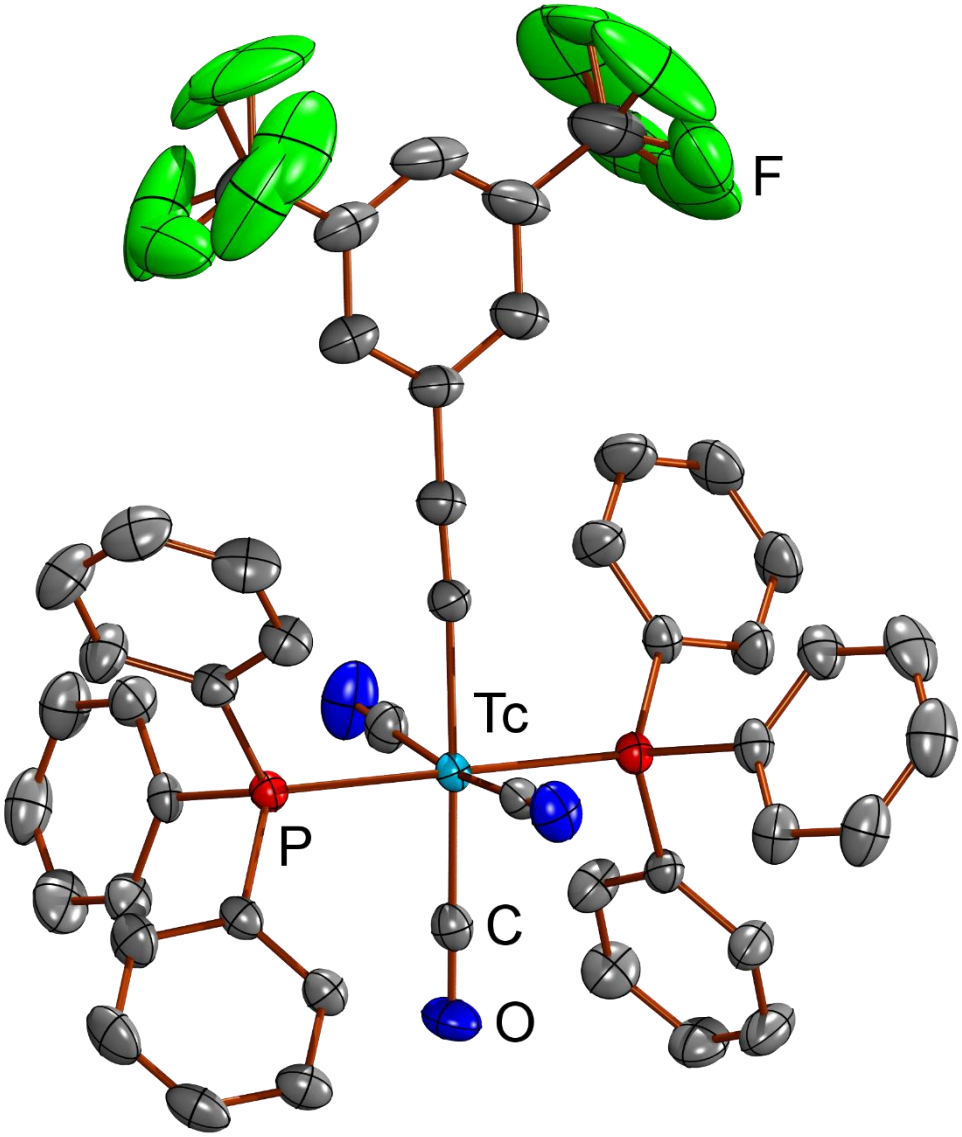

Figure S12. Ellipsoid representation (50% probability) of $[Tc(CNPh)(CO)_3(PPh_3)_2](BF_4)$ (**9a**). Hydrogen atoms are omitted for clarity. The BF_4^- anion is disordered over two positions in a ratio of ca. 50:50 and was modelled using appropriate constraints and restraints.

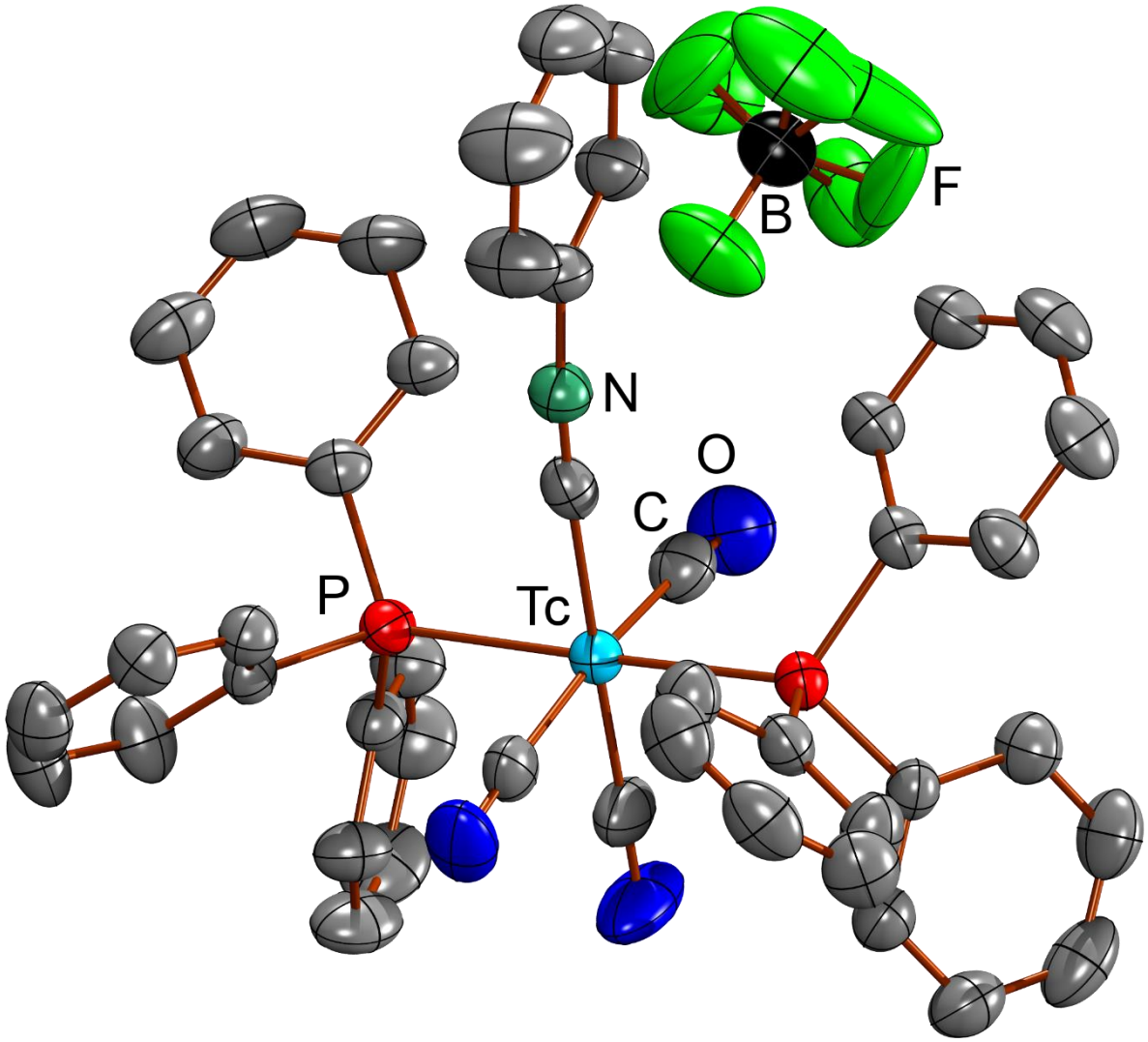

Figure S13. Ellipsoid representation (50% probability) of $[Tc(CN^tBu)(CO)_3(PPh_3)_2](BF_4)$ (**9b**) · CH_2Cl_2. Hydrogen atoms are omitted for clarity. The dichloromethane solvent molecule is disordered over two orientations.

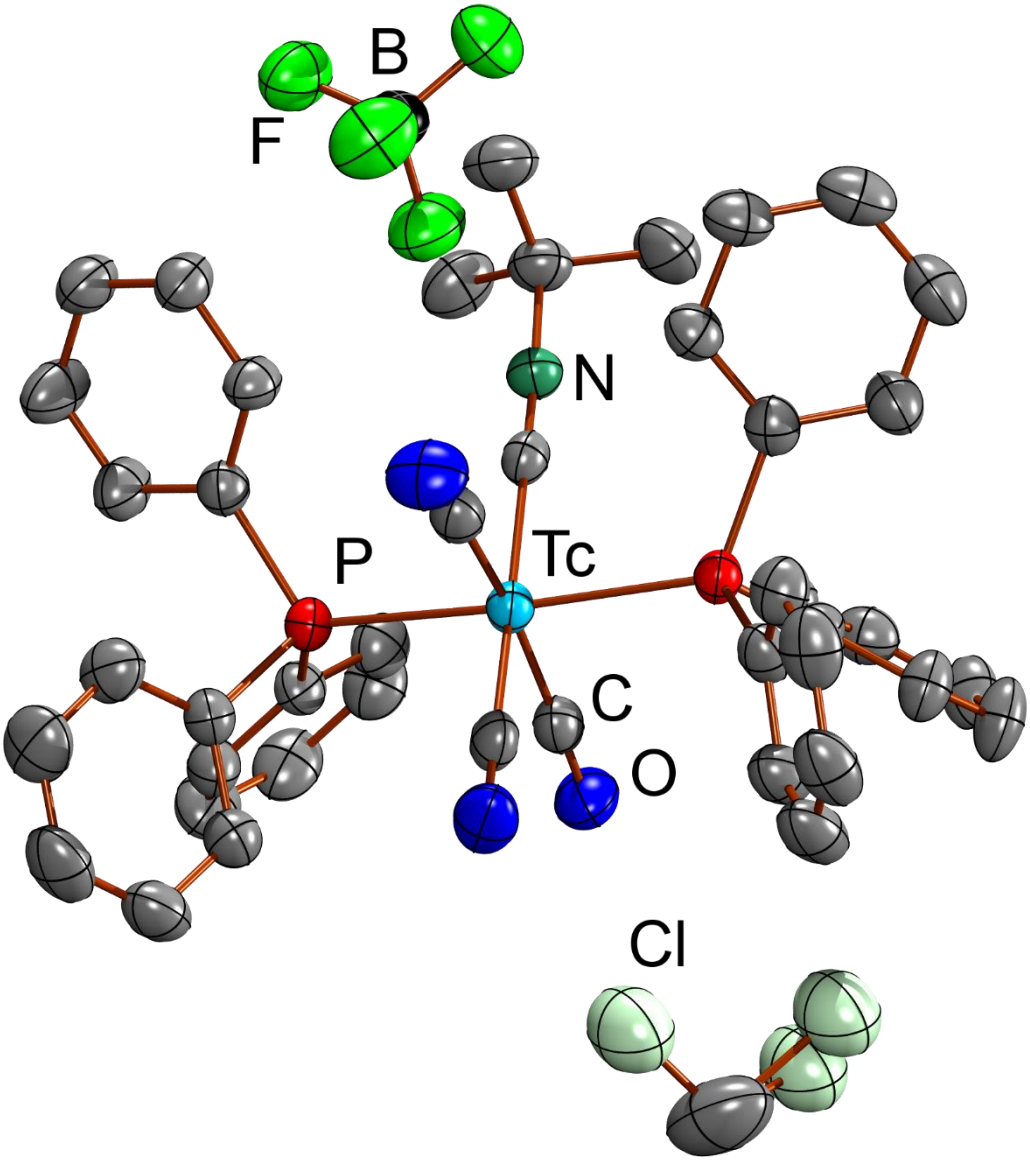

Figure S14. Ellipsoid representation (50% probability) of $[Tc(CN^tBu)(CO)_3(PPh_3)_2](BF_4)$ (**9b**) · CH_3CN. Hydrogen atoms are omitted for clarity.

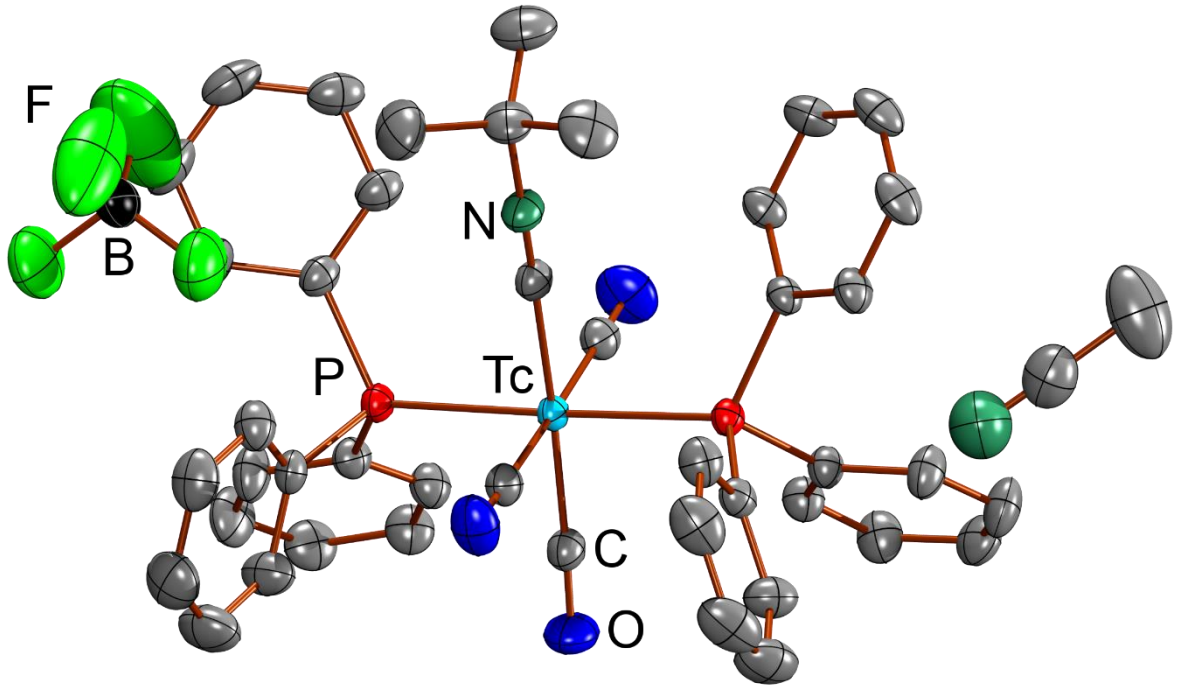

Figure S15. Ellipsoid representation (50% probability) of $[Tc(NCPh)(CO)_3(PPh_3)_2](BF_4)$ (**10a**) · CH_2Cl_2. Hydrogen atoms are omitted for clarity. The BF_4^- anion is disordered over two positions in a ratio of ca. 60:40 and was modelled using appropriate constraints and restraints.

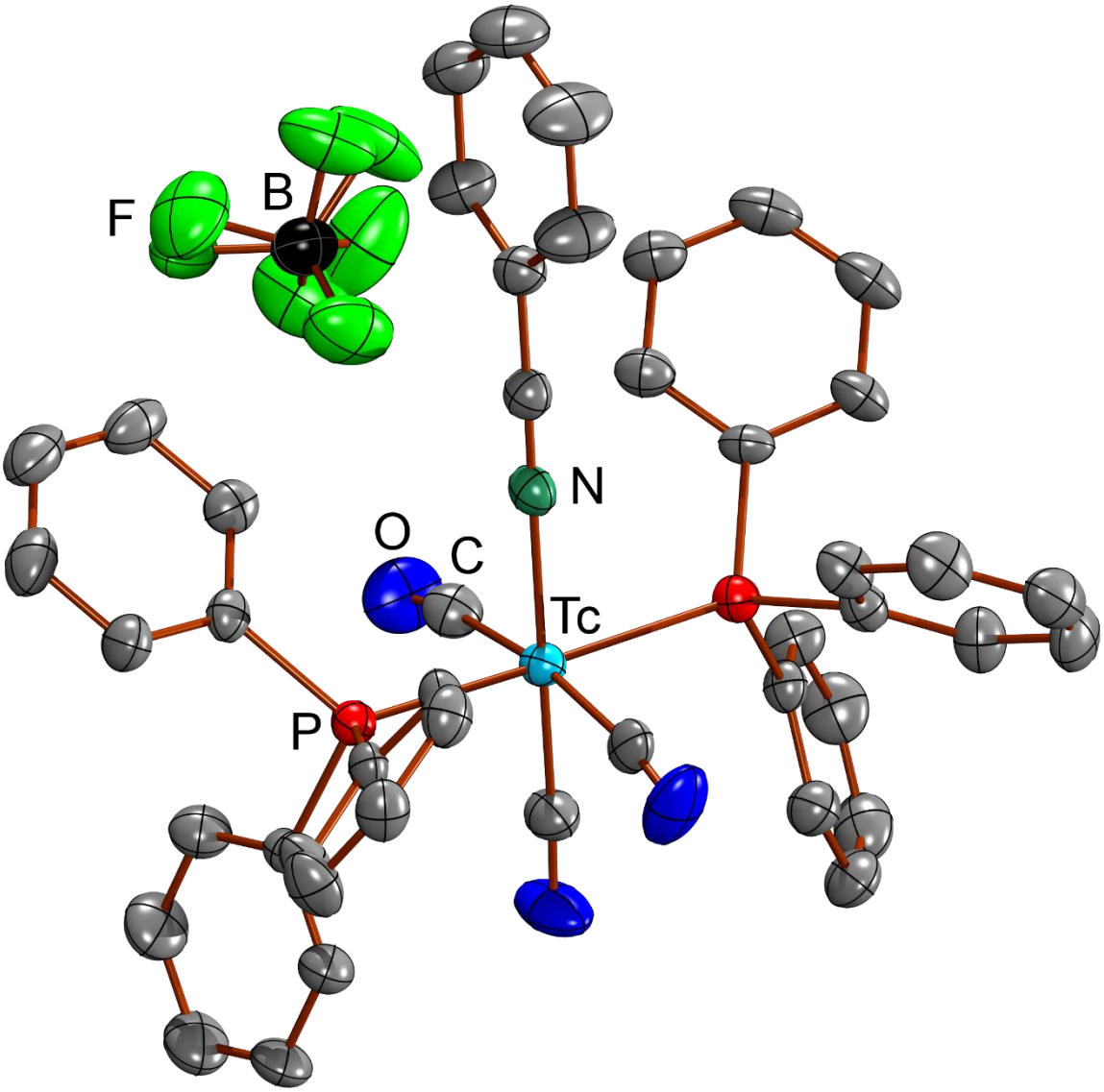

Figure S16. Ellipsoid representation (50% probability) of $[Tc(NC^tBu)(CO)_3(PPh_3)_2](BF_4)$ (**10b**) · CH_2Cl_2. Hydrogen atoms are omitted for clarity. The co-crystallized solvent dichloromethane molecule is disordered over 3 positions with a ratio of 30:30:40.

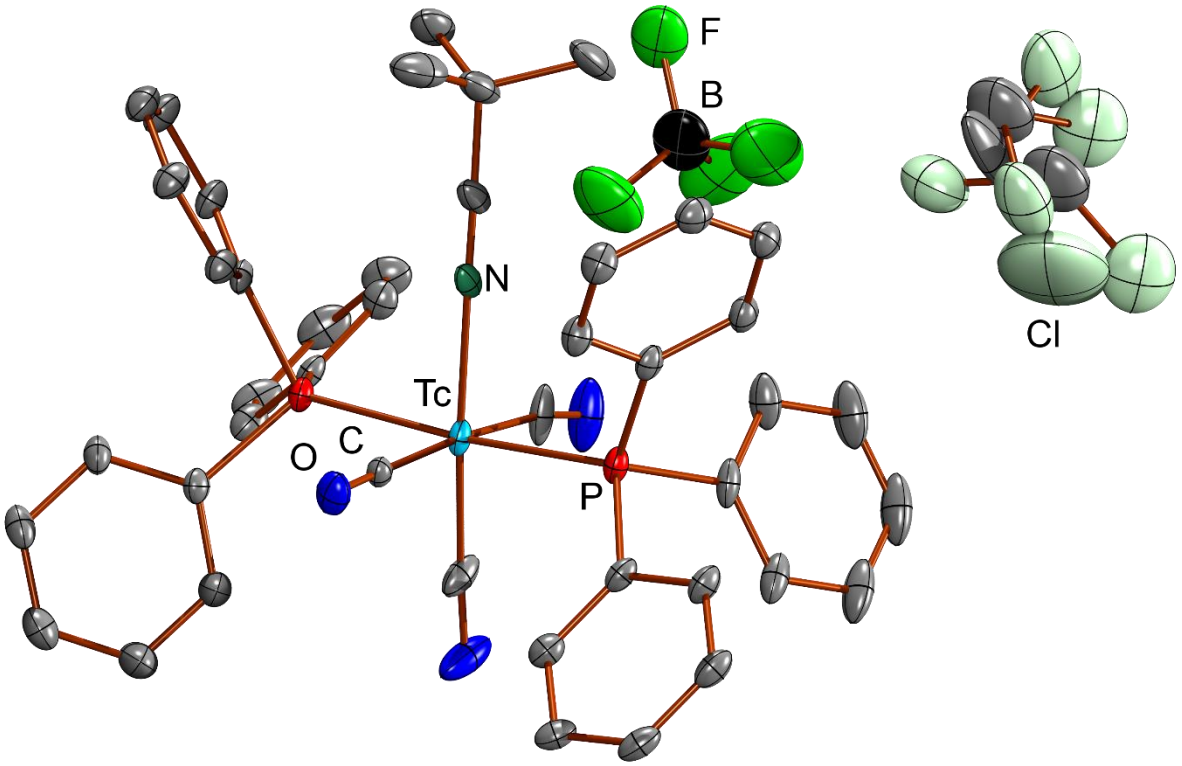

Figure S17. Ellipsoid representation (50% probability) of $[Tc(CO)_4(PPh_3)_2](PF_6)$. The two $[Tc(CO)_4(PPh_3)_2]^+$ cations are completed via the space-group symmetry as their central technetium atom lies on the symmetry center respectively (*via* -x+1, -y+1, -z and -x+2, -y+1, -z+1). The additional PF_6^- anion is entirely generated via translational symmetry and thus omitted. Average Tc-P bond length: 2.462 Å; average Tc-C bond length: 1.985 Å.

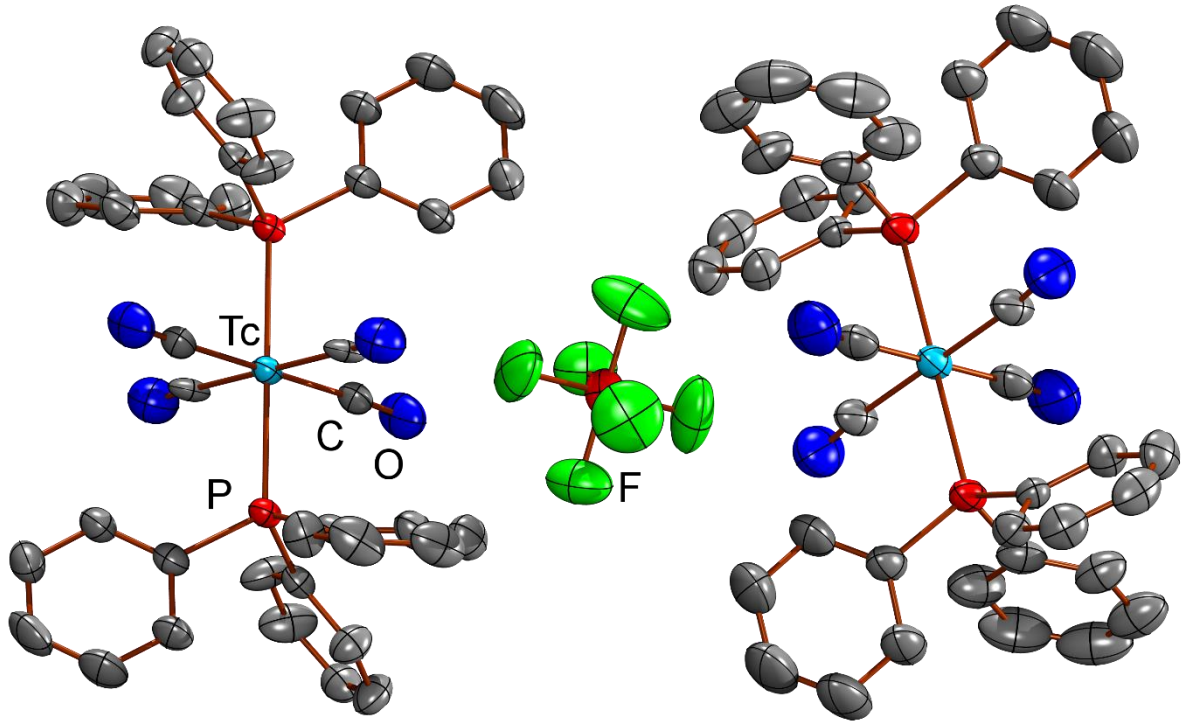

Part 2: Spectral data

Spectragryph 1.2.8 was used to visualize the IR spectra. (Menges, F. Spectragryph, Software for Optical Spectroscopy,Version 1.2.8, 2016–2020.)

Figure S18. ^{1}H NMR spectrum of [Tc(CH$_3$)(CO)$_3$(PPh$_3$)$_2$] (**3**).

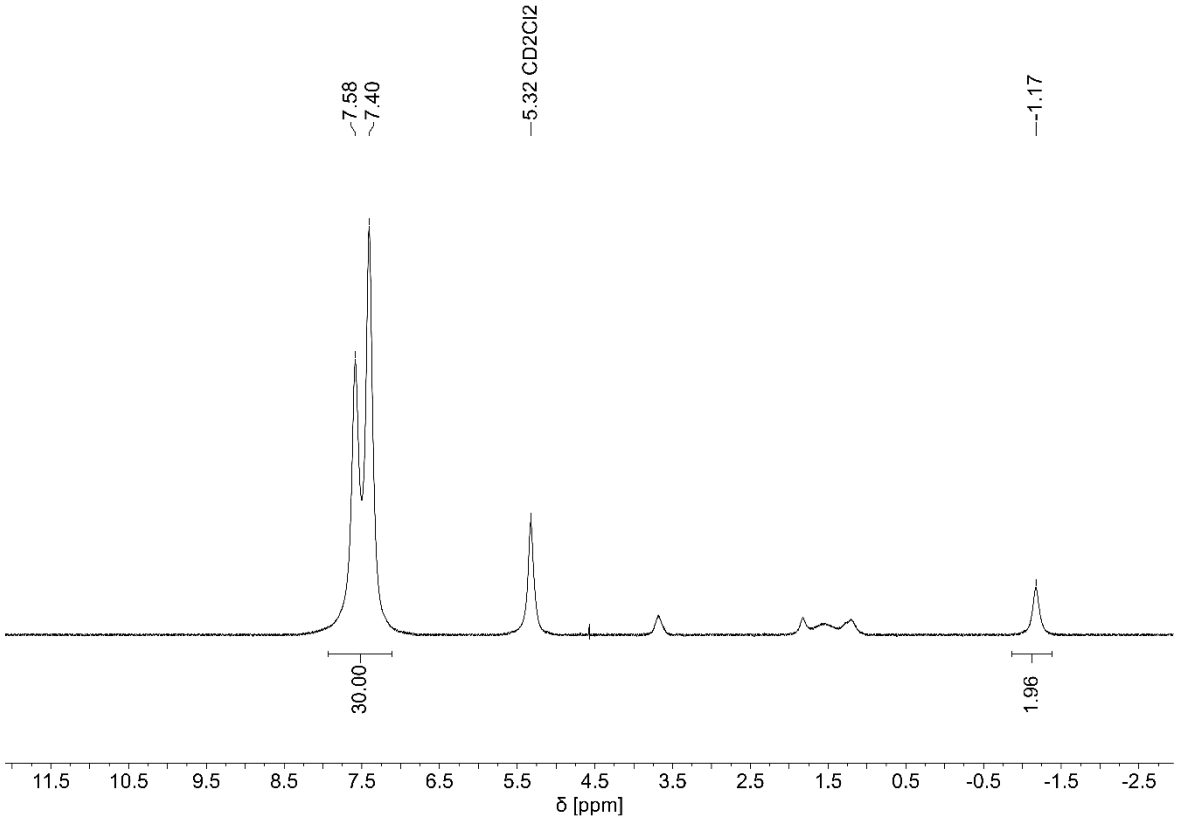

Figure S19. ^{1}H NMR spectrum of $[Tc(CH_3)(CO)_3(PPh_3)_2]$ (**3**); focused on the CH_3 resonance.

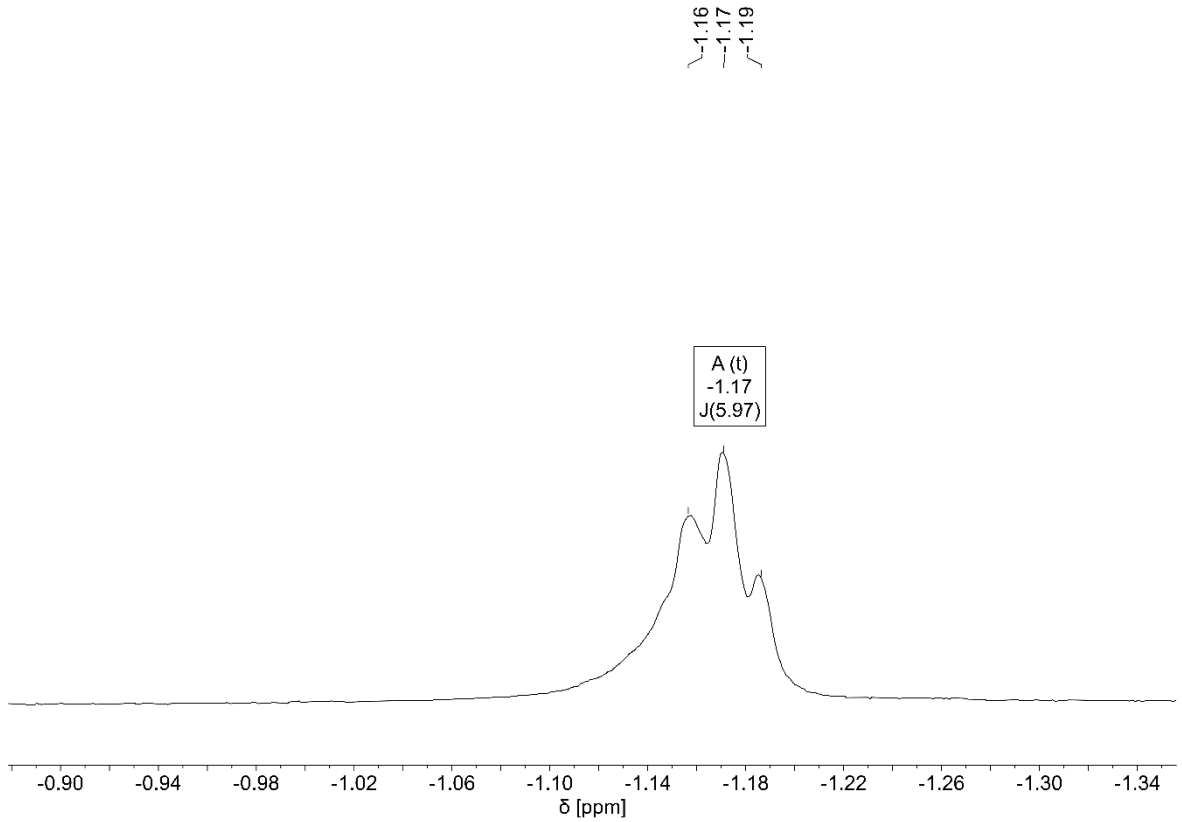

Figure S20. ^{99}Tc NMR spectrum of $[Tc(CH_3)(CO)_3(PPh_3)_2]$ (**3**).

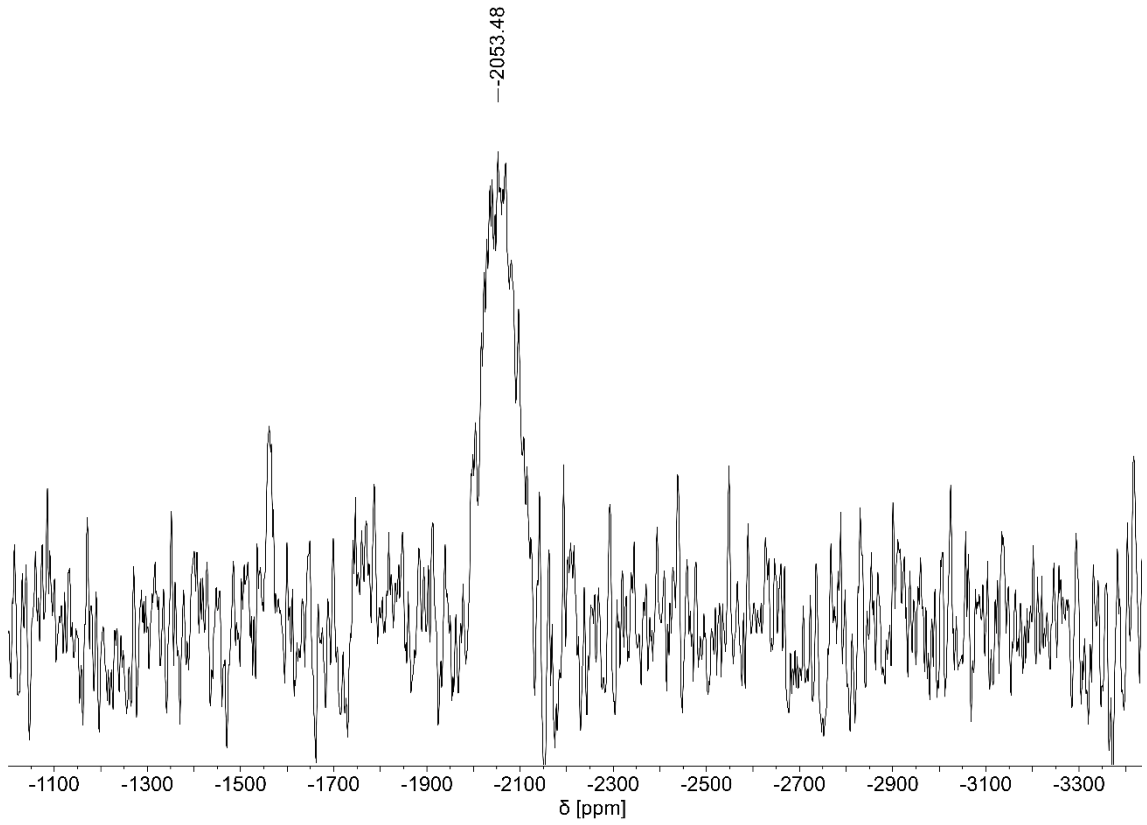

Figure S21. $^{31}P\{^{1}H\}$ NMR spectrum of $[Tc(CH_3)(CO)_3(PPh_3)_2]$ (**3**).

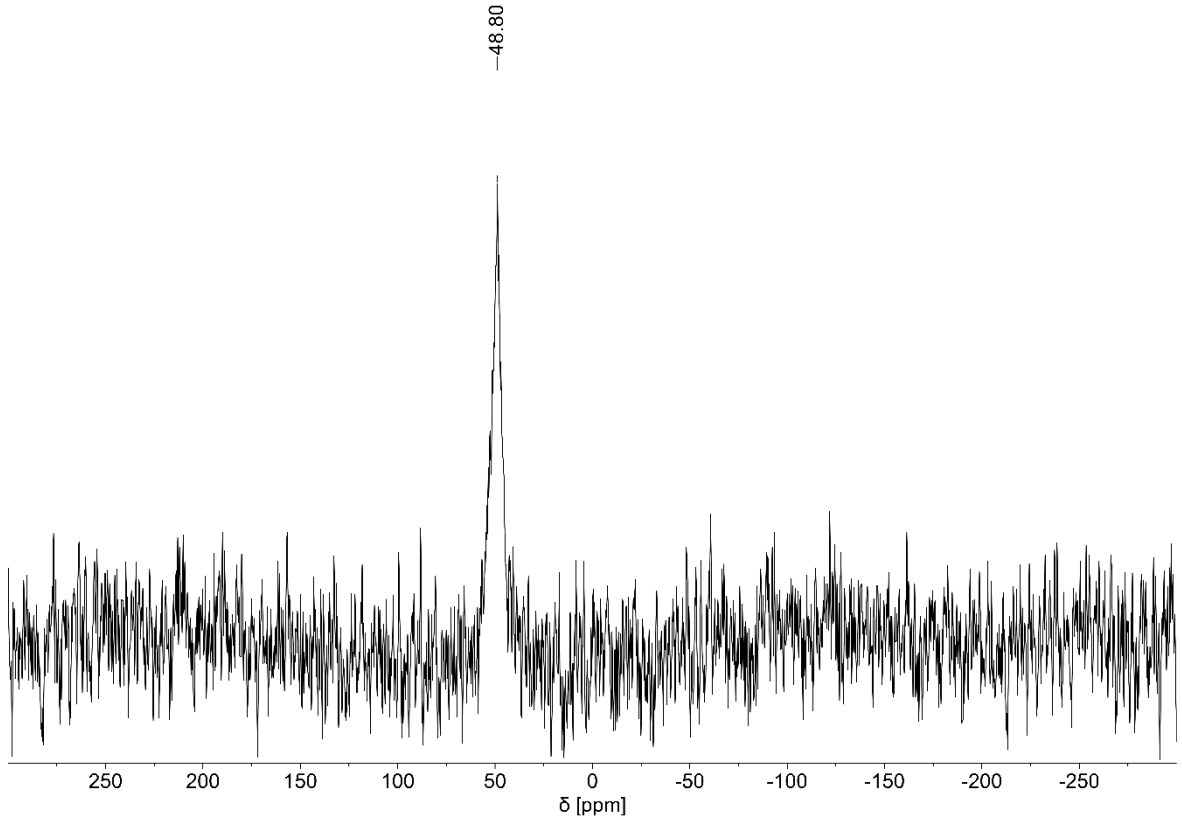

Figure S22. IR spectrum of $[Tc(CH_3)(CO)_3(PPh_3)_2]$ (**3**).

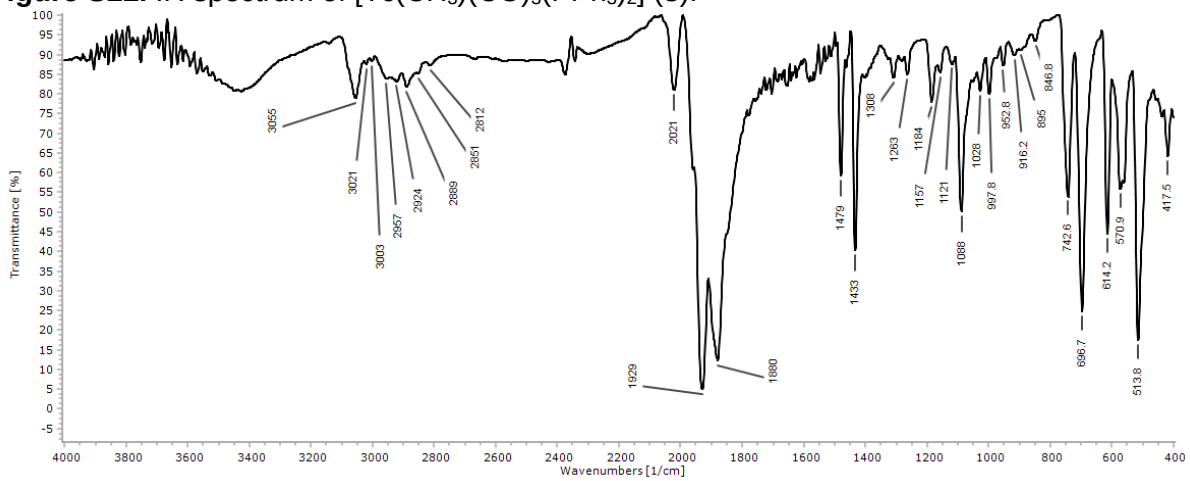

Figure S23. ^{1}H NMR spectrum of $[Tc(Ph)(CO)_3(PPh_3)_2]$ (**4**).

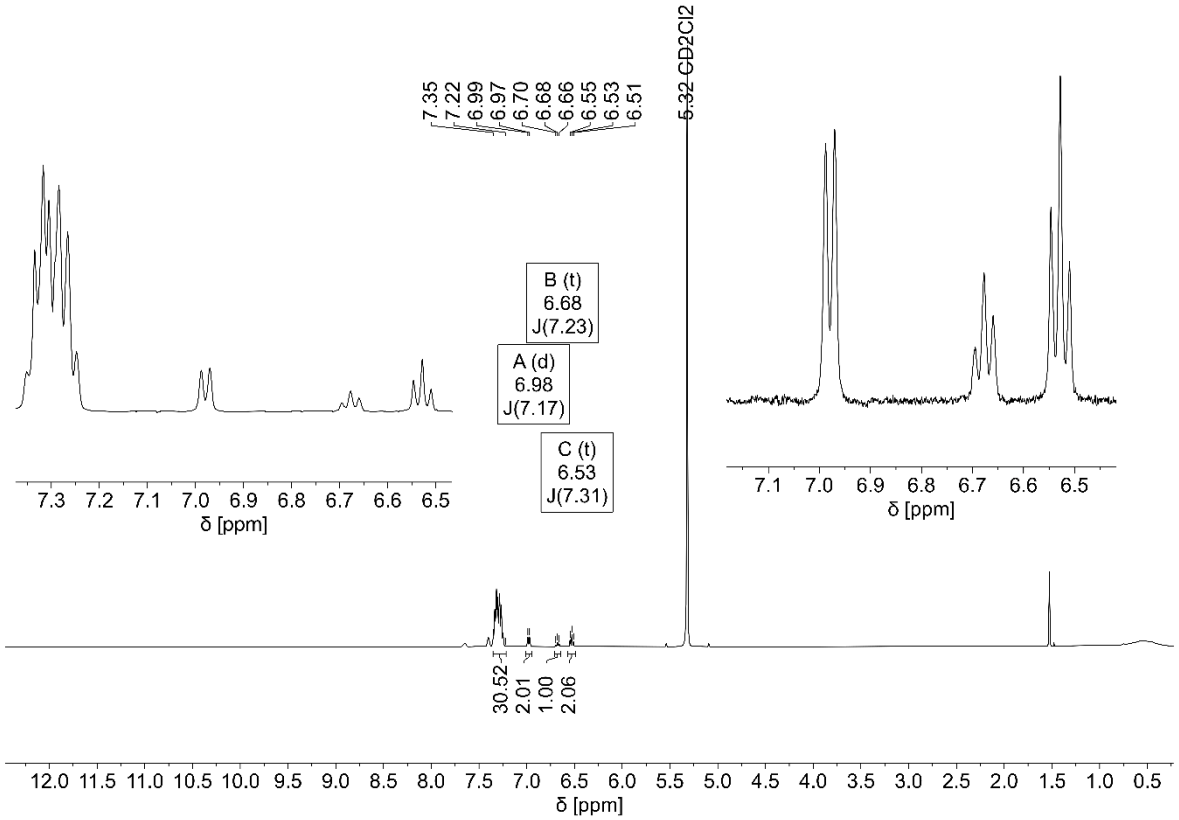

Figure S24. ^{99}Tc NMR spectrum of $[Tc(Ph)(CO)_3(PPh_3)_2]$ (**4**).

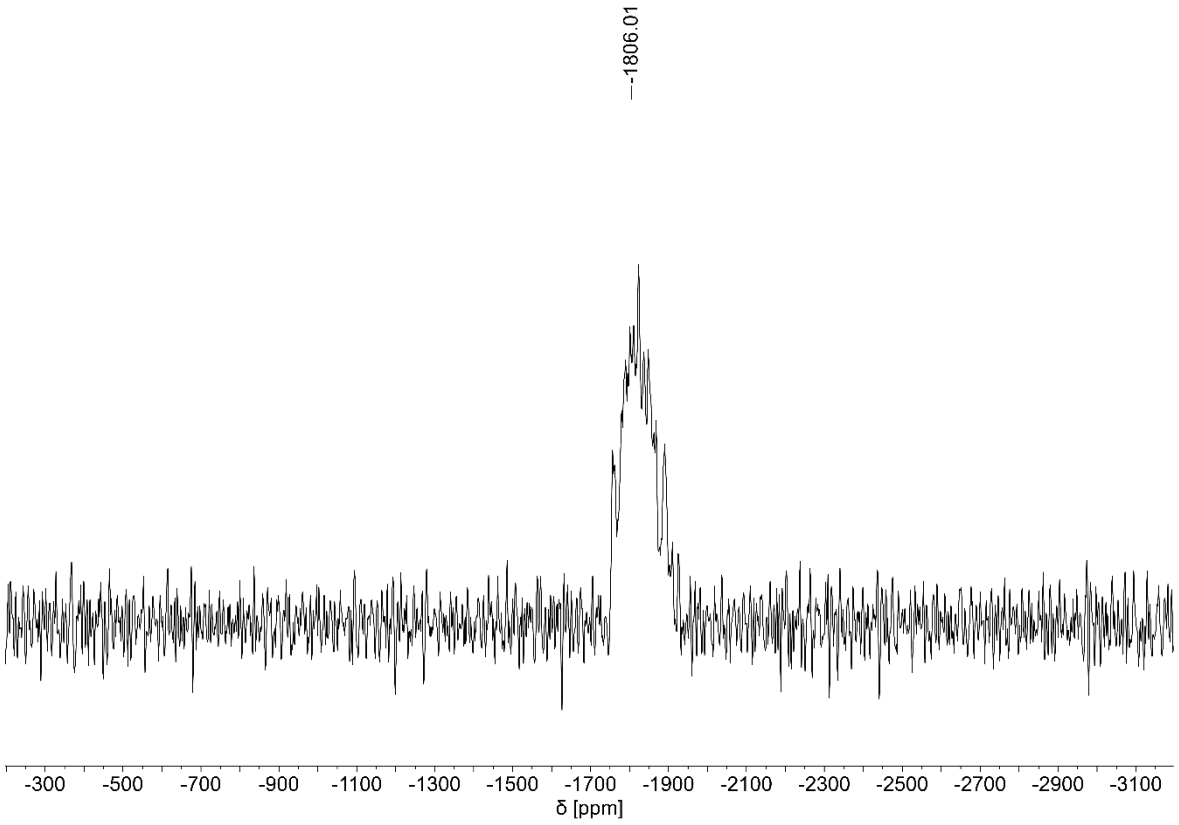

Figure S25. IR spectrum of $[Tc(Ph)(CO)_3(PPh_3)_2]$ (**4**).

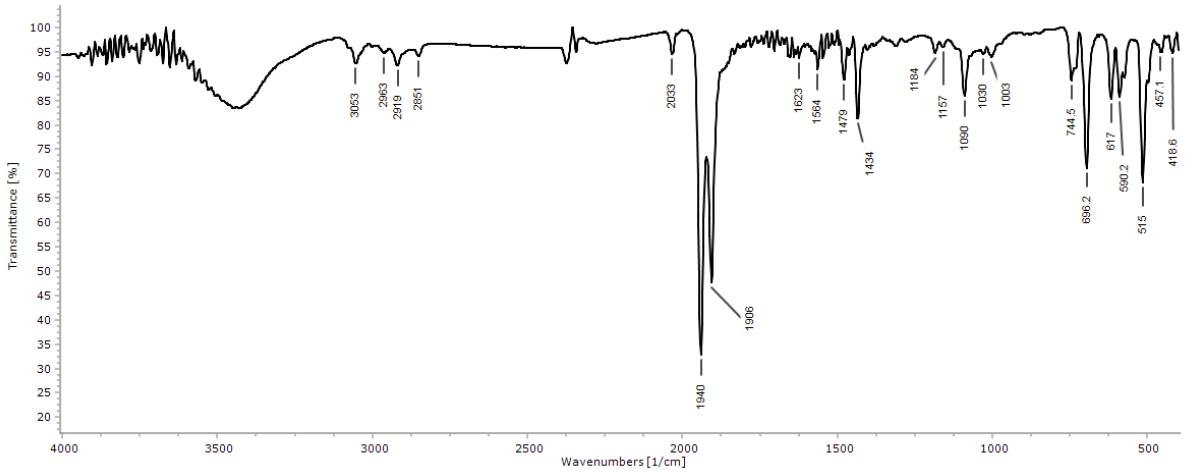

Figure S26. ^1H NMR spectrum of $[Tc(cp)(CO)_2(PPh_3)]$ (**5**).

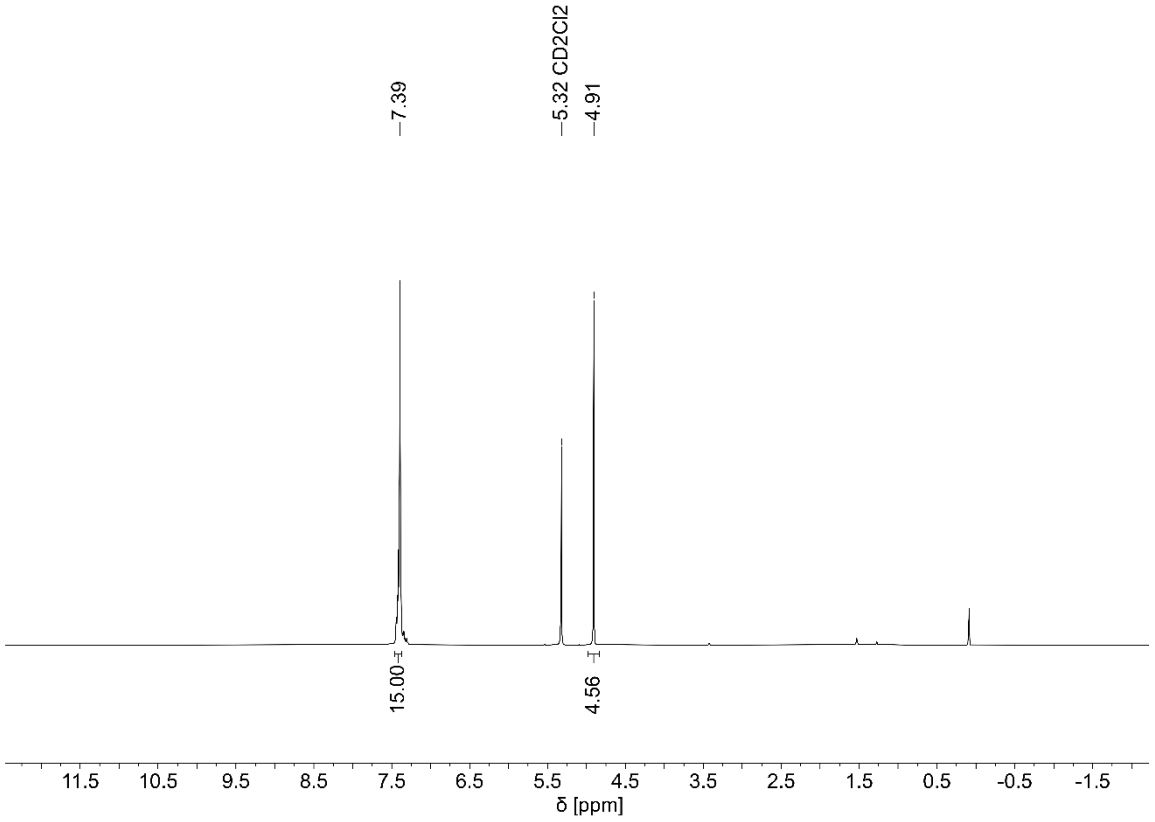

Figure S27. ^{99}Tc NMR spectrum of [Tc(cp)(CO)$_2$(PPh$_3$)] (**5**).

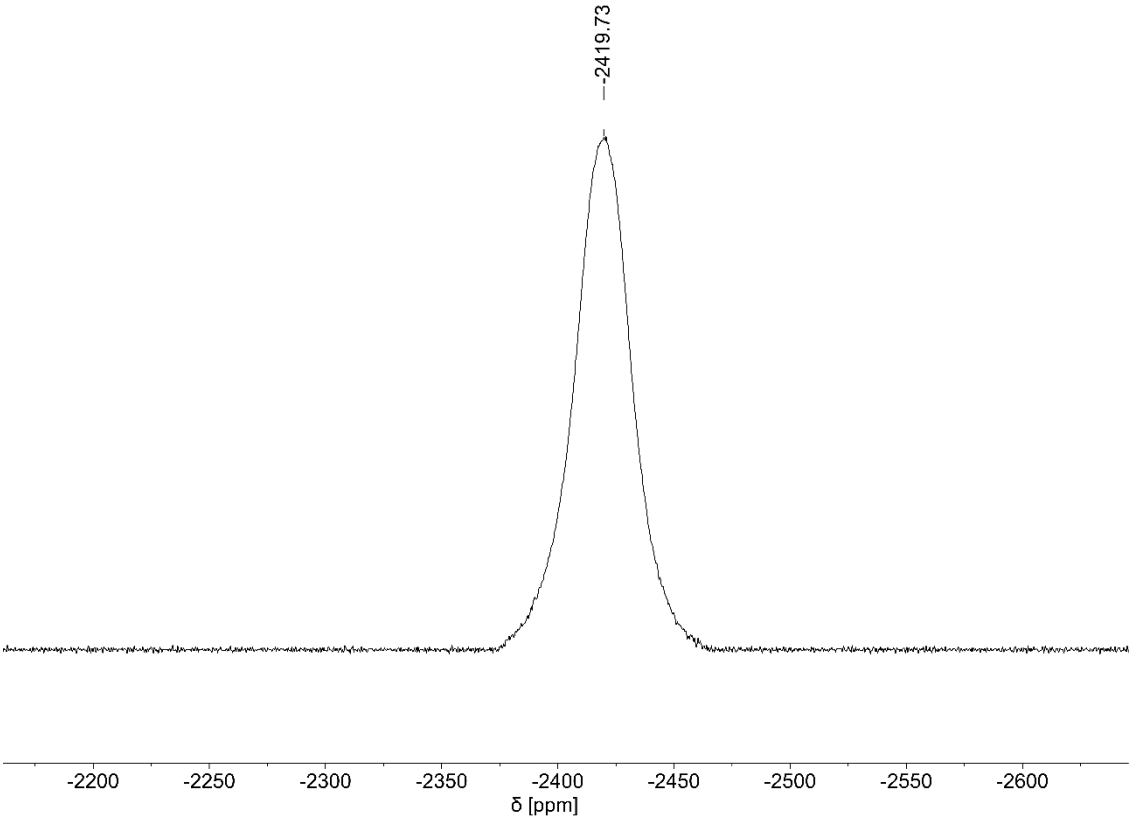

Figure S28. ^{31}P{^{1}H} NMR spectrum of [Tc(cp)(CO)$_2$(PPh$_3$)] (**5**).

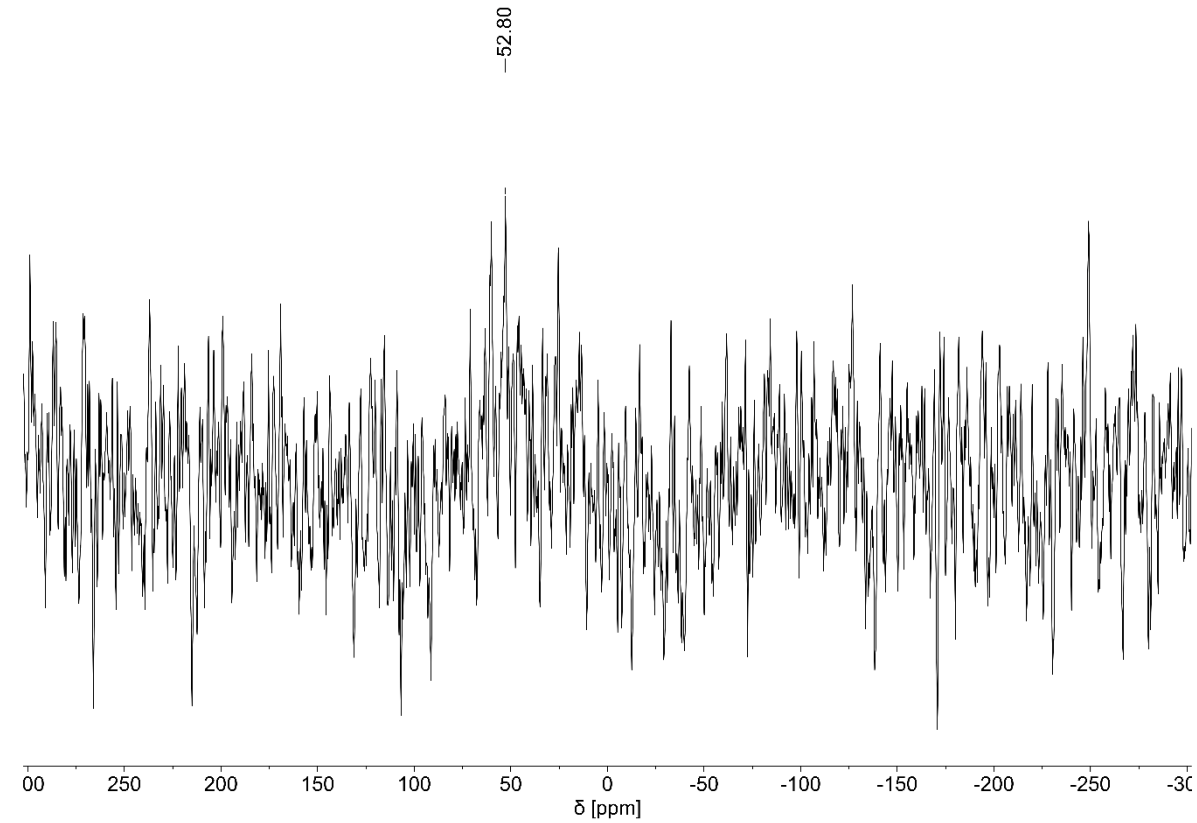

Figure S29. IR spectrum of [Tc(cp)$(CO)_2(PPh_3)$] (**5**).

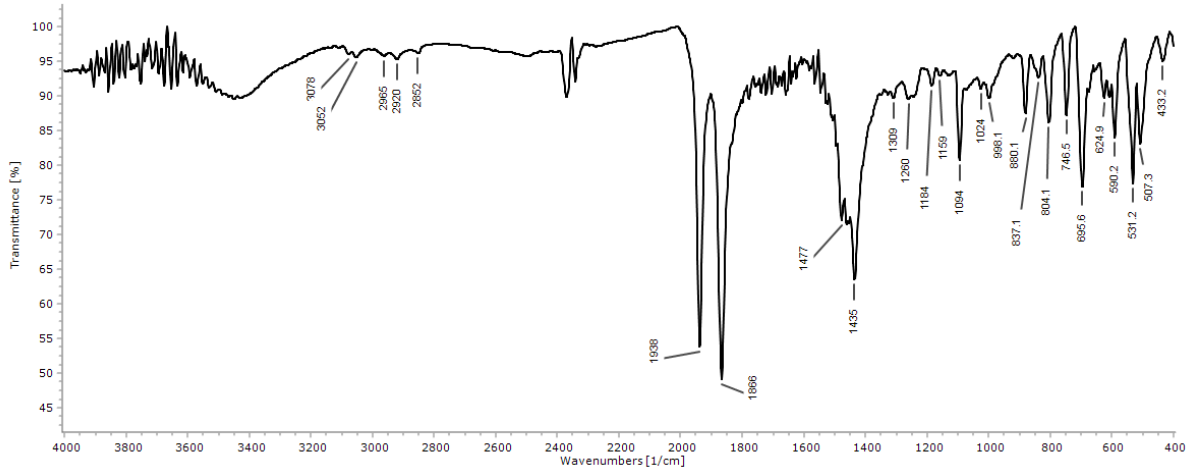

Figure S30. ^{1}H NMR spectrum of [Tc(=*cyclo*-$C(CH_2)_3O$)$(CO)_3(PPh_3)_2$](BF_4) (**6**).

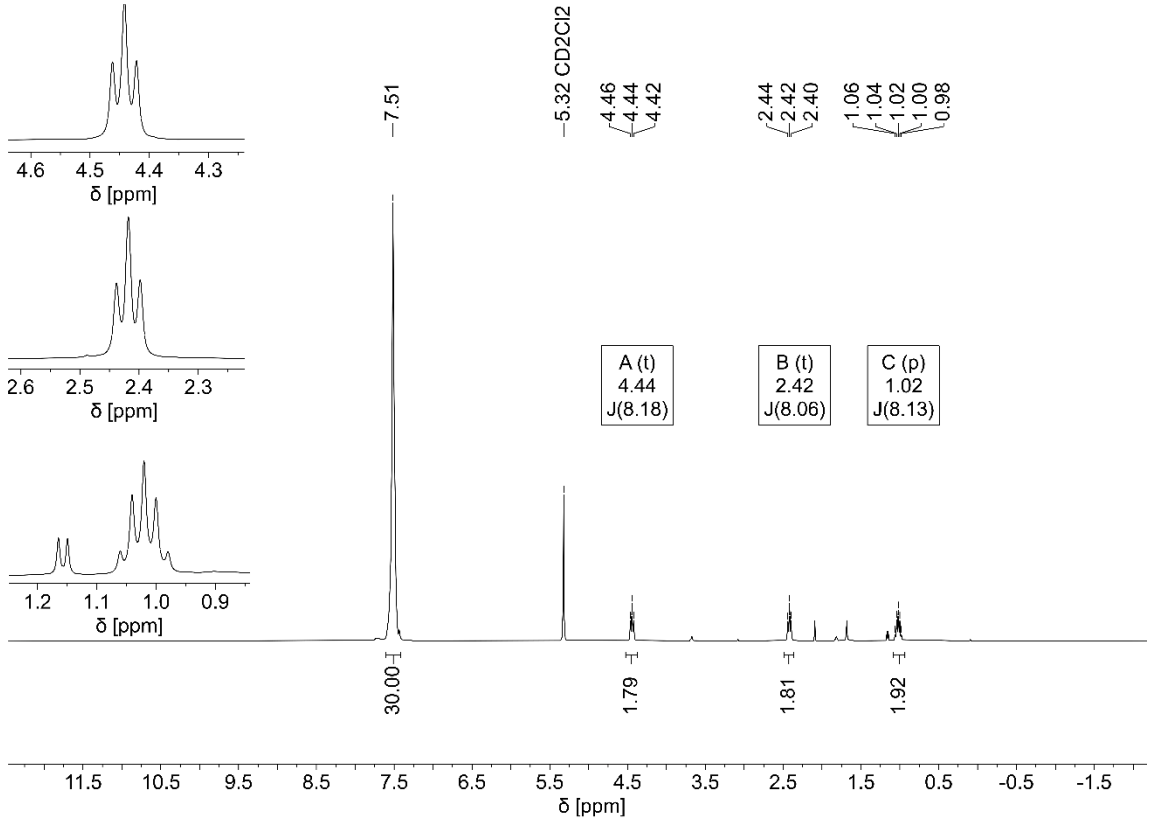

Figure S31. $^{1}H,^{1}H$-COSY NMR spectrum of [Tc(=*cyclo*-$C(CH_2)_3O)(CO)_3(PPh_3)_2$]($BF_4$) (**6**).

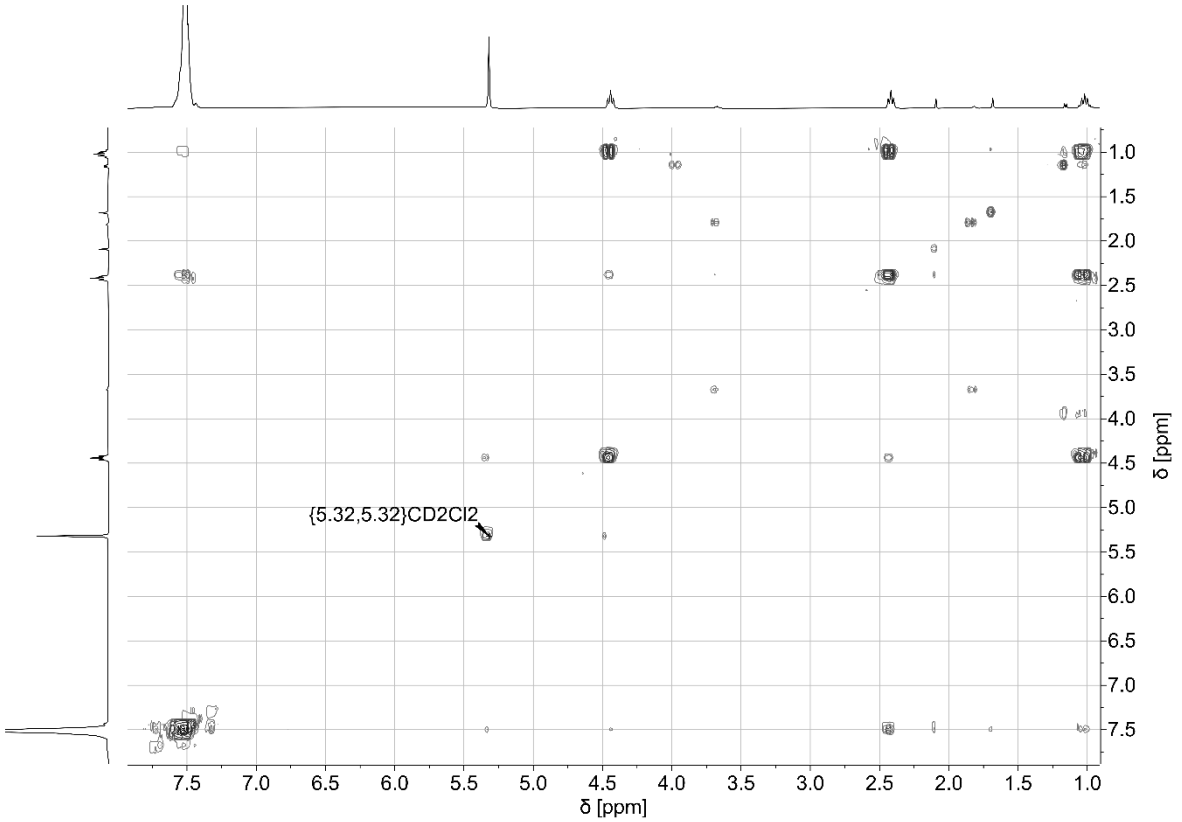

Figure S32. ^{99}Tc NMR spectrum of [Tc(=*cyclo*-$C(CH_2)_3O)(CO)_3(PPh_3)_2$]($BF_4$) (**6**).

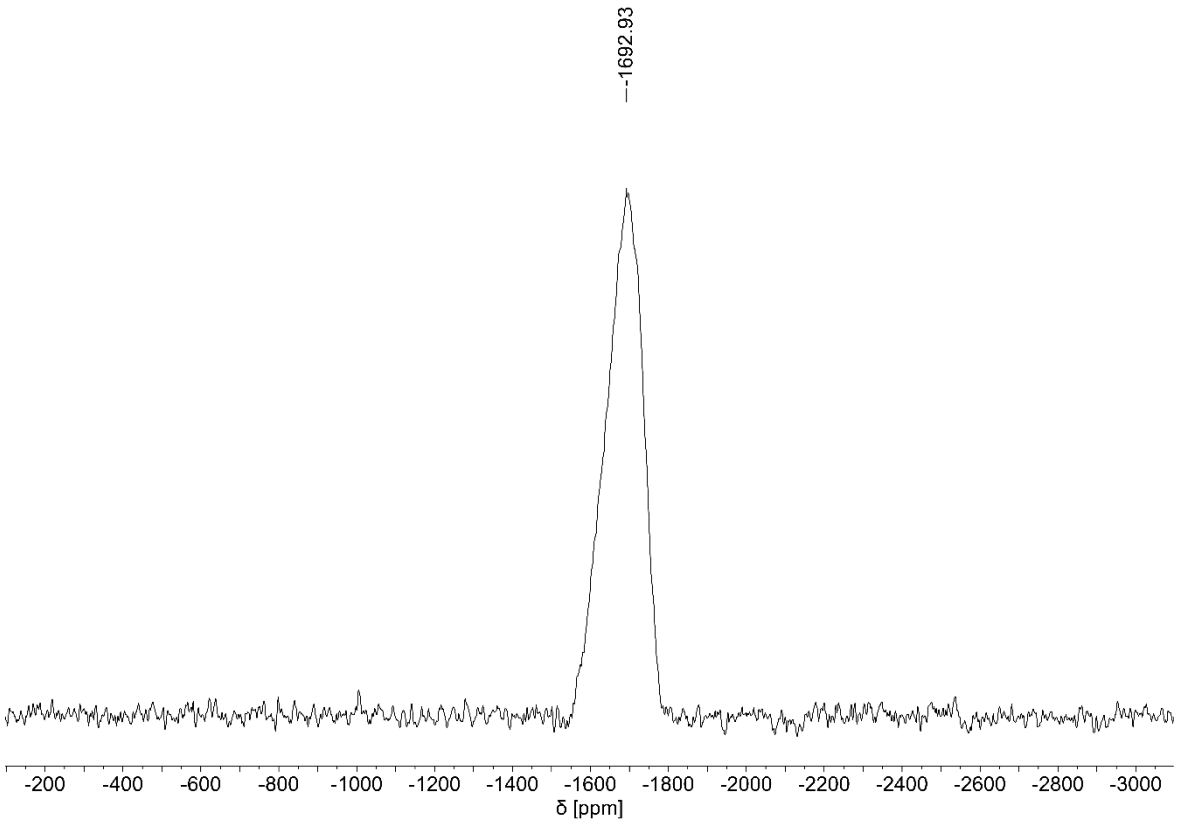

Figure S33. $^{31}P\{^{1}H\}$ NMR spectrum of [Tc(=*cyclo*-$C(CH_2)_3O$)$(CO)_3(PPh_3)_2$](BF_4) (**6**).

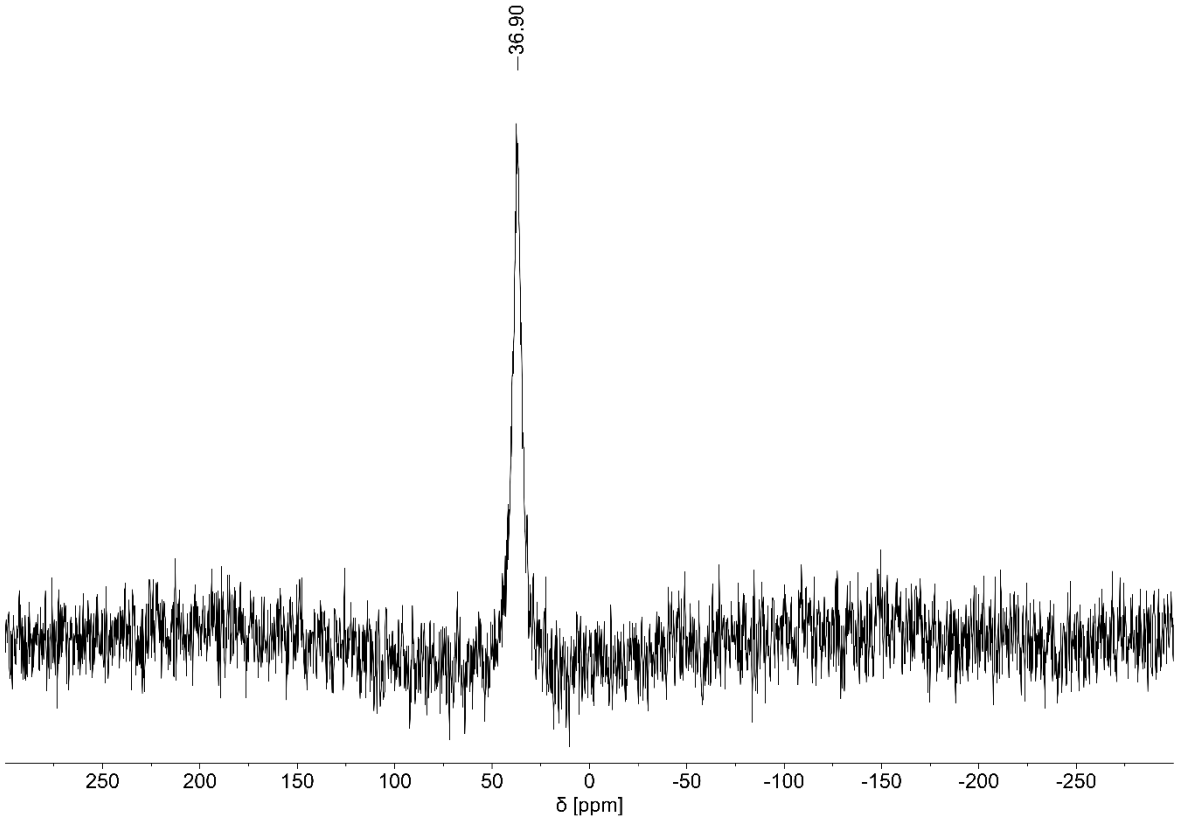

Figure S34. ^{11}B NMR spectrum of [Tc(=*cyclo*-$C(CH_2)_3O$)$(CO)_3(PPh_3)_2$](BF_4) (**6**).

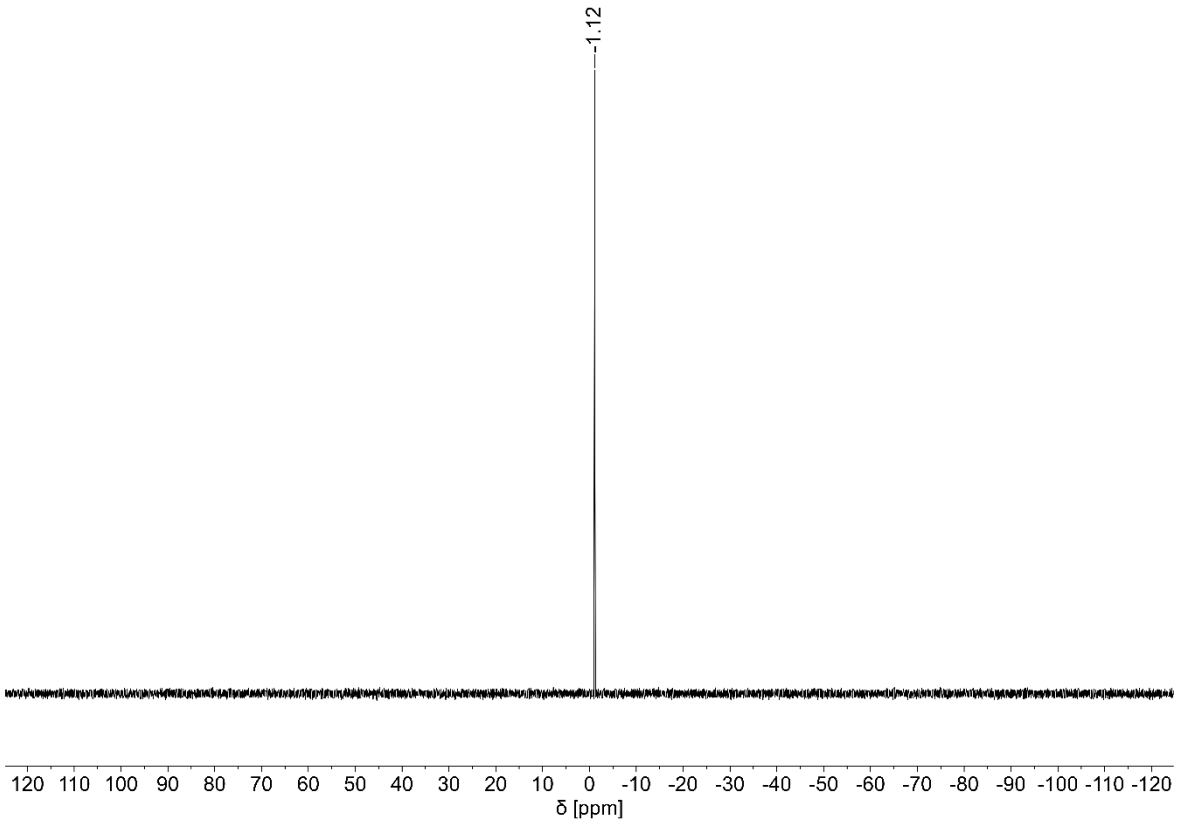

Figure S35. ^{19}F NMR spectrum of [Tc(=*cyclo*-$C(CH_2)_3O$)$(CO)_3(PPh_3)_2$](BF_4) (**6**).

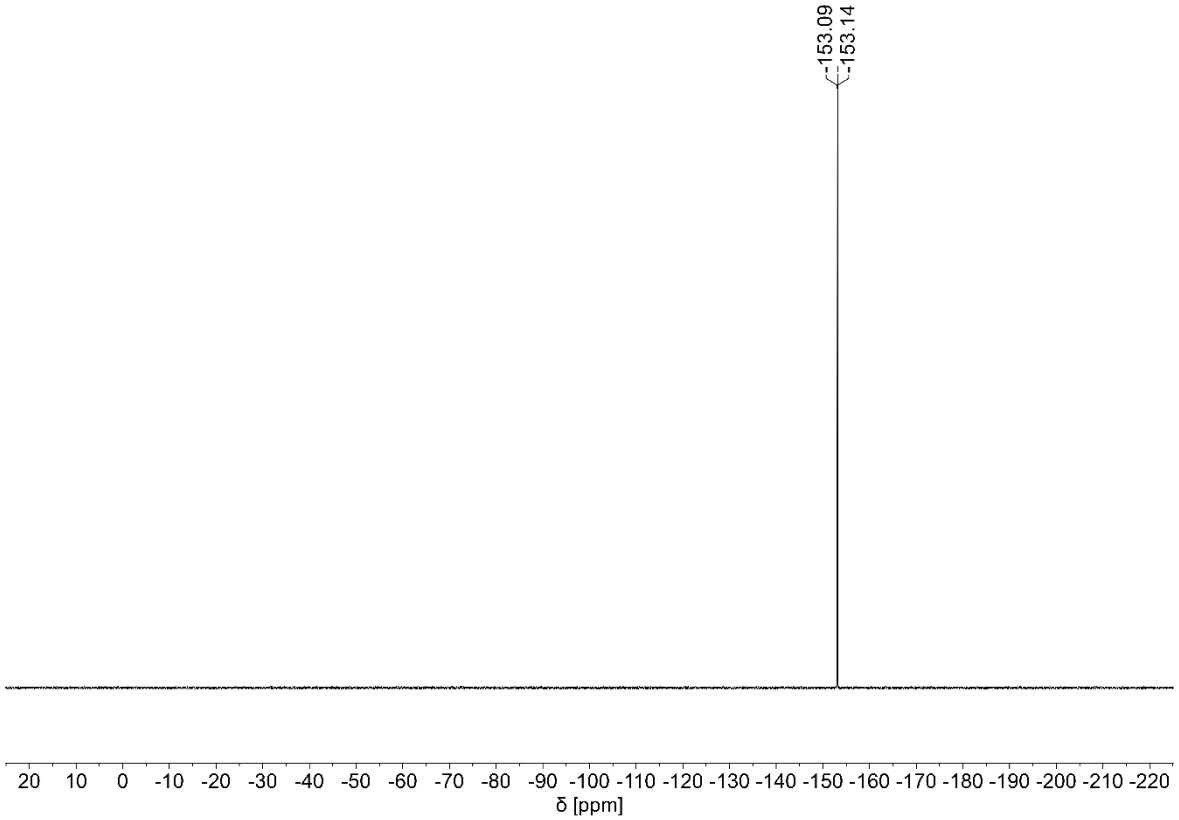

Figure S36. IR spectrum of [Tc(=*cyclo*-$C(CH_2)_3O$)$(CO)_3(PPh_3)_2$](BF_4) (**6**).

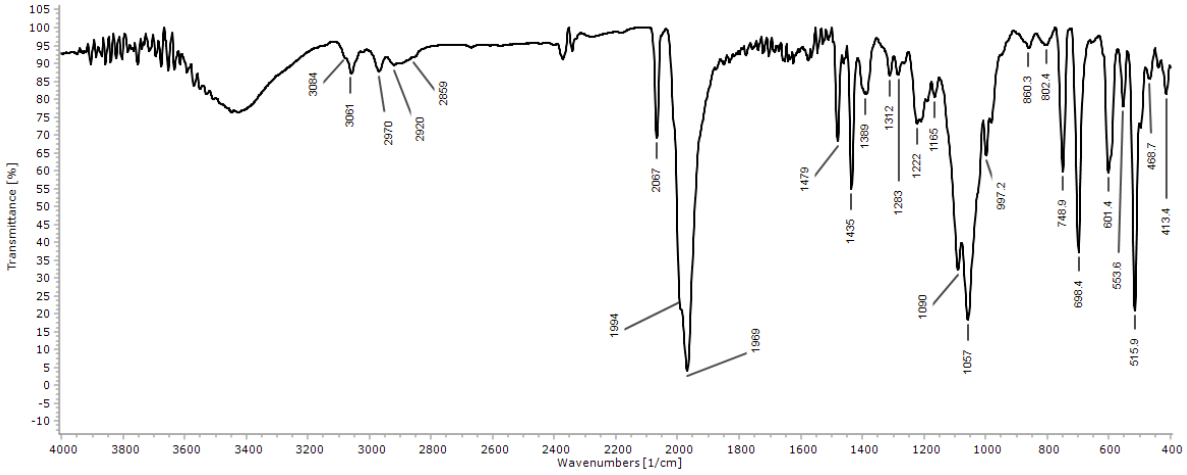

Figure S37. ^{1}H NMR spectrum of [Tc(=*cyclo*-C$(CH_2)_4$O)$(CO)_3(PPh_3)_2$](BF_4) (**7**).

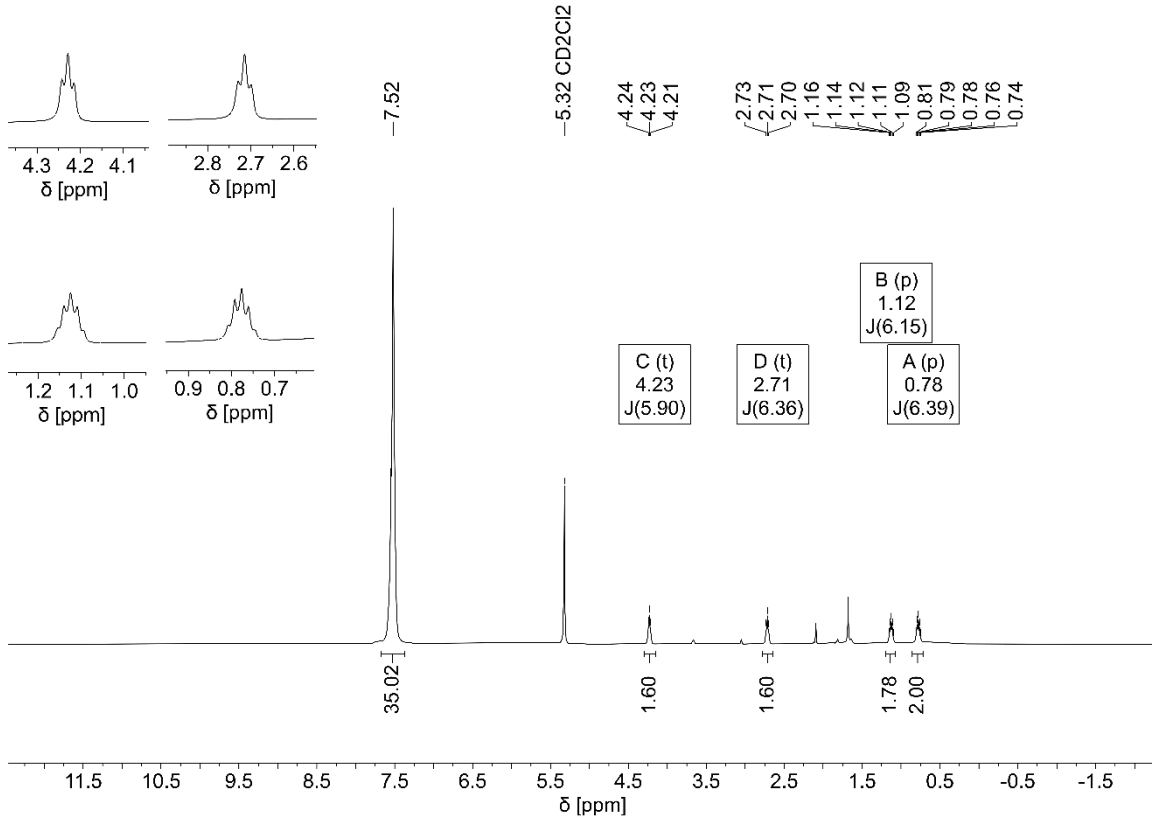

Figure S38. ^{1}H NMR spectrum of [Tc(=*cyclo*-C$(CH_2)_4$O)$(CO)_3(PPh_3)_2$](BF_4) (**7**) and ω-pentynol.

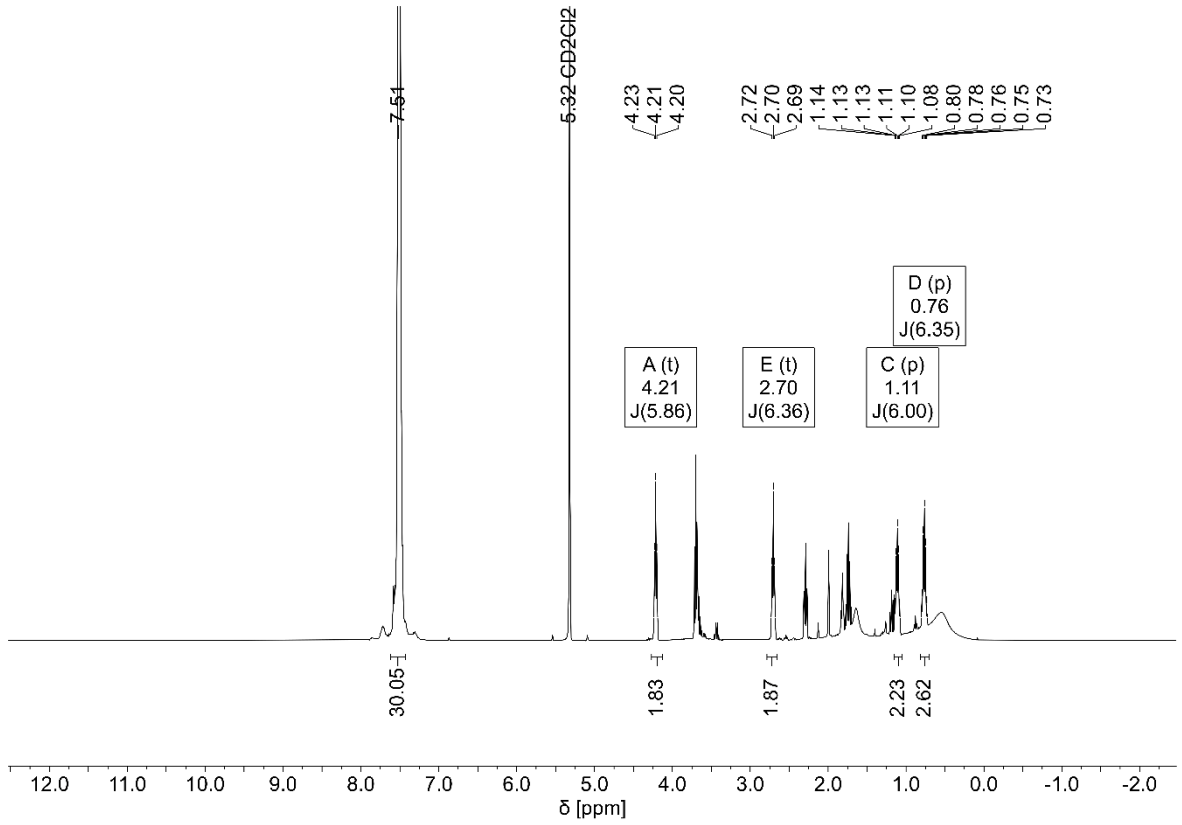

Figure S39. $^{1}H,^{1}H$-COSY NMR spectrum of [Tc(=*cyclo*-$C(CH_2)_4O$)$(CO)_3(PPh_3)_2$](BF_4) (**7**).

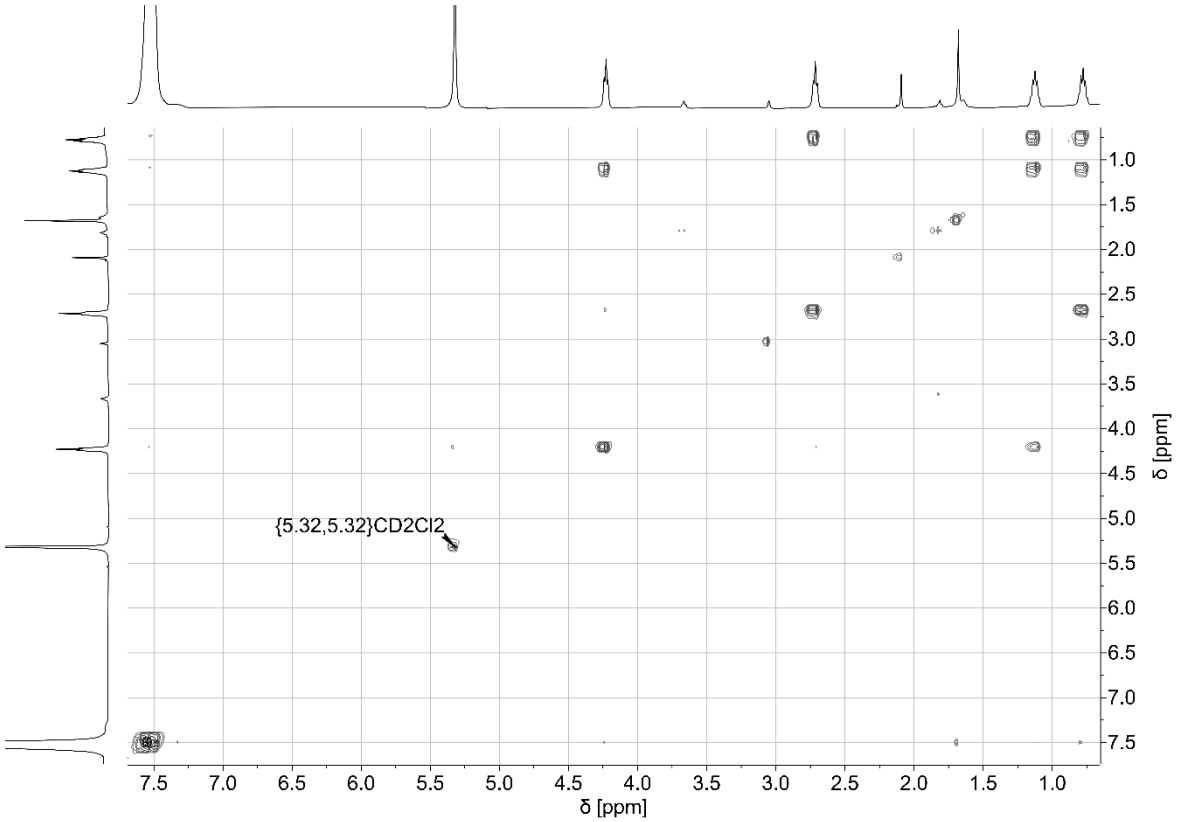

Figure S40. $^{1}H,^{1}H$-COSY NMR spectrum of [Tc(=*cyclo*-$C(CH_2)_4O$)$(CO)_3(PPh_3)_2$](BF_4) (**7**) and ω-pentynol.

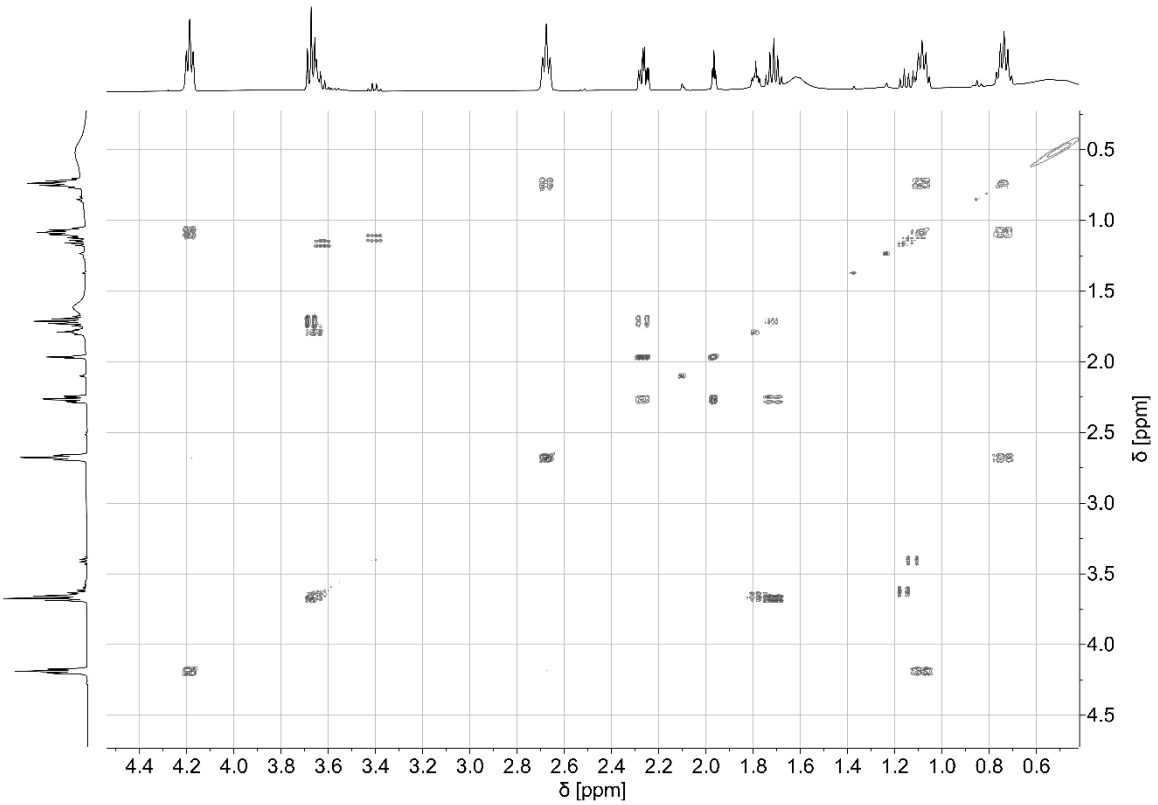

Figure S41. ^{99}Tc NMR spectrum of [Tc(=*cyclo*-C$(CH_2)_4$O)$(CO)_3(PPh_3)_2$](BF_4) (**7**).

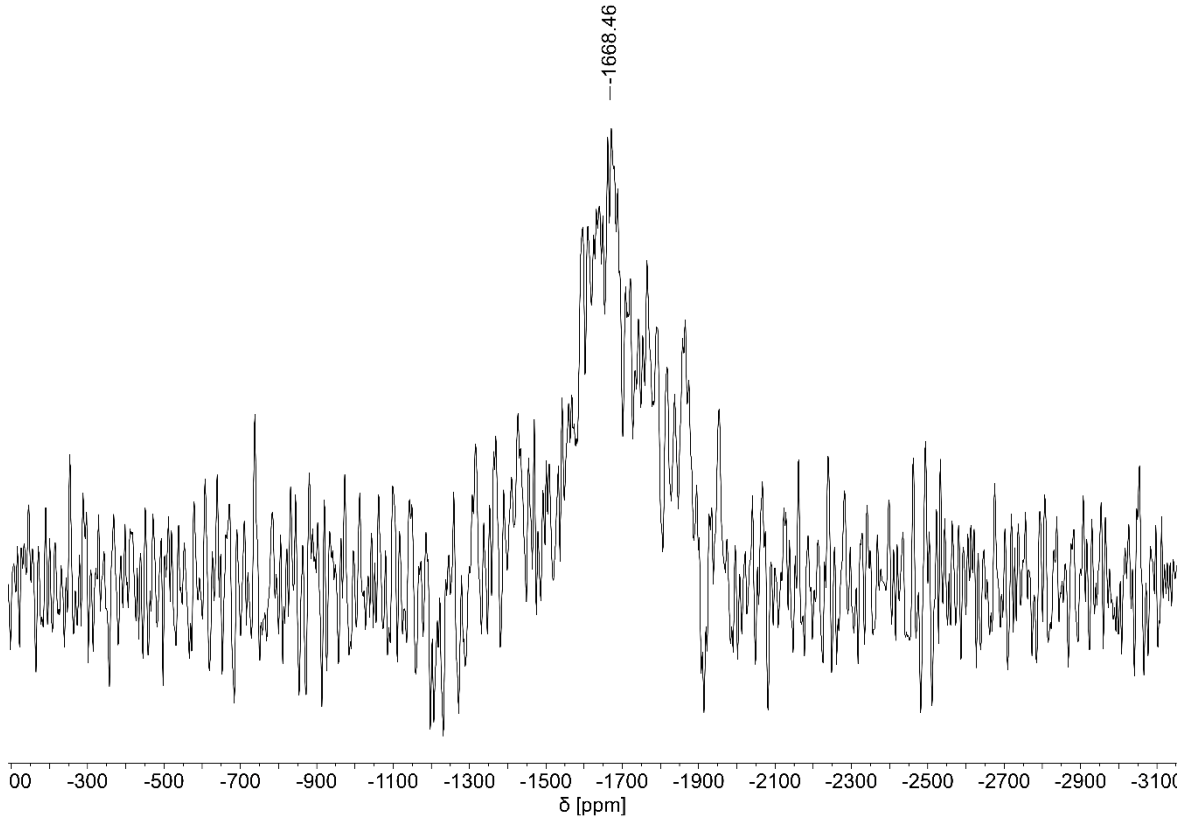

Figure S42. ^{31}P{^{1}H} NMR spectrum of [Tc(=*cyclo*-C$(CH_2)_4$O)$(CO)_3(PPh_3)_2$](BF_4) (**7**).

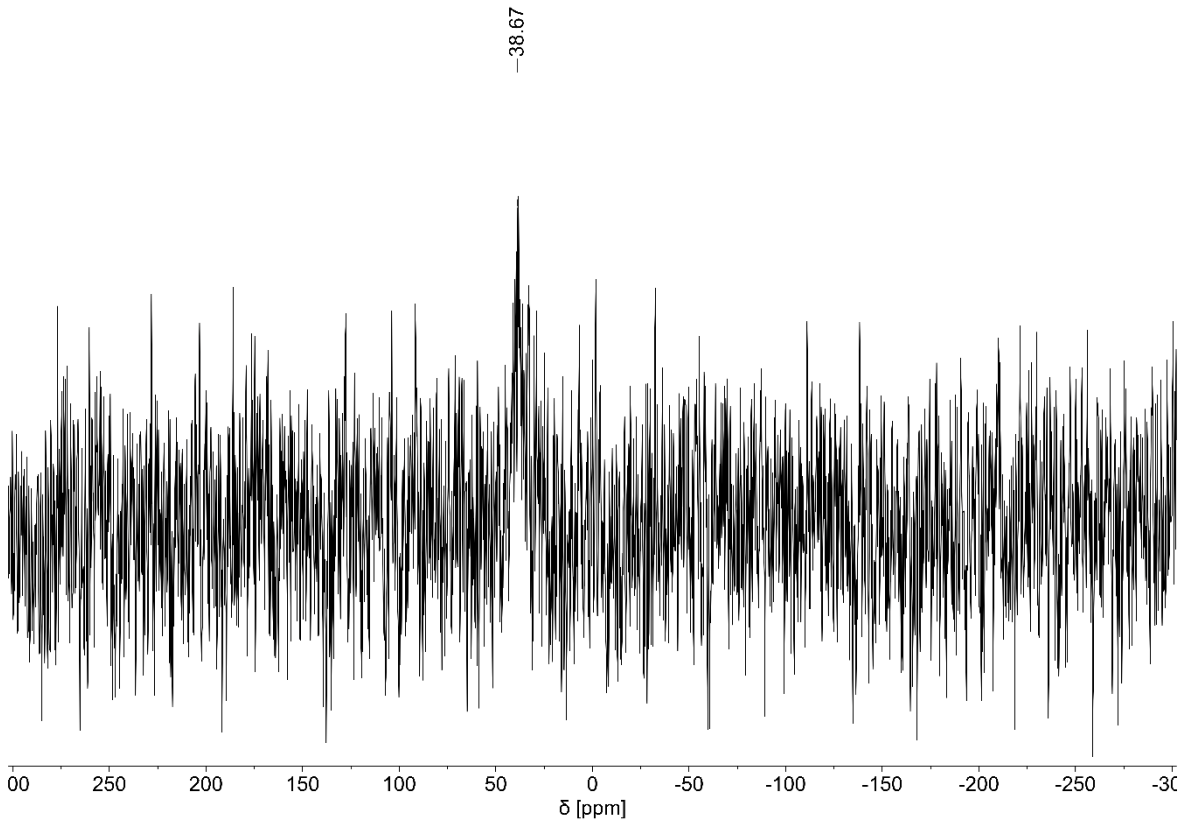

Figure S43. ^{11}B NMR spectrum of [Tc(=*cyclo*-$C(CH_2)_4O$)$(CO)_3(PPh_3)_2$](BF_4) (**7**).

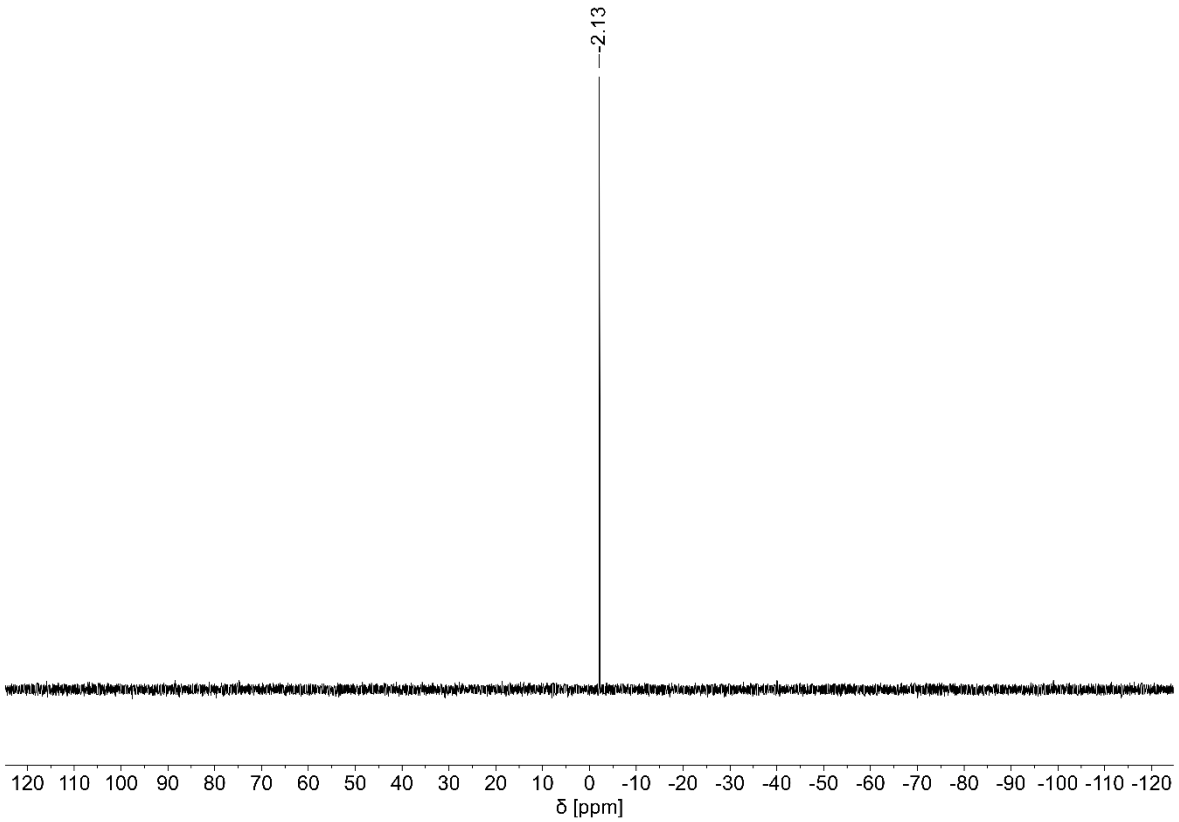

Figure S44. ^{19}F NMR spectrum of [Tc(=*cyclo*-$C(CH_2)_4O$)$(CO)_3(PPh_3)_2$](BF_4) (**7**).

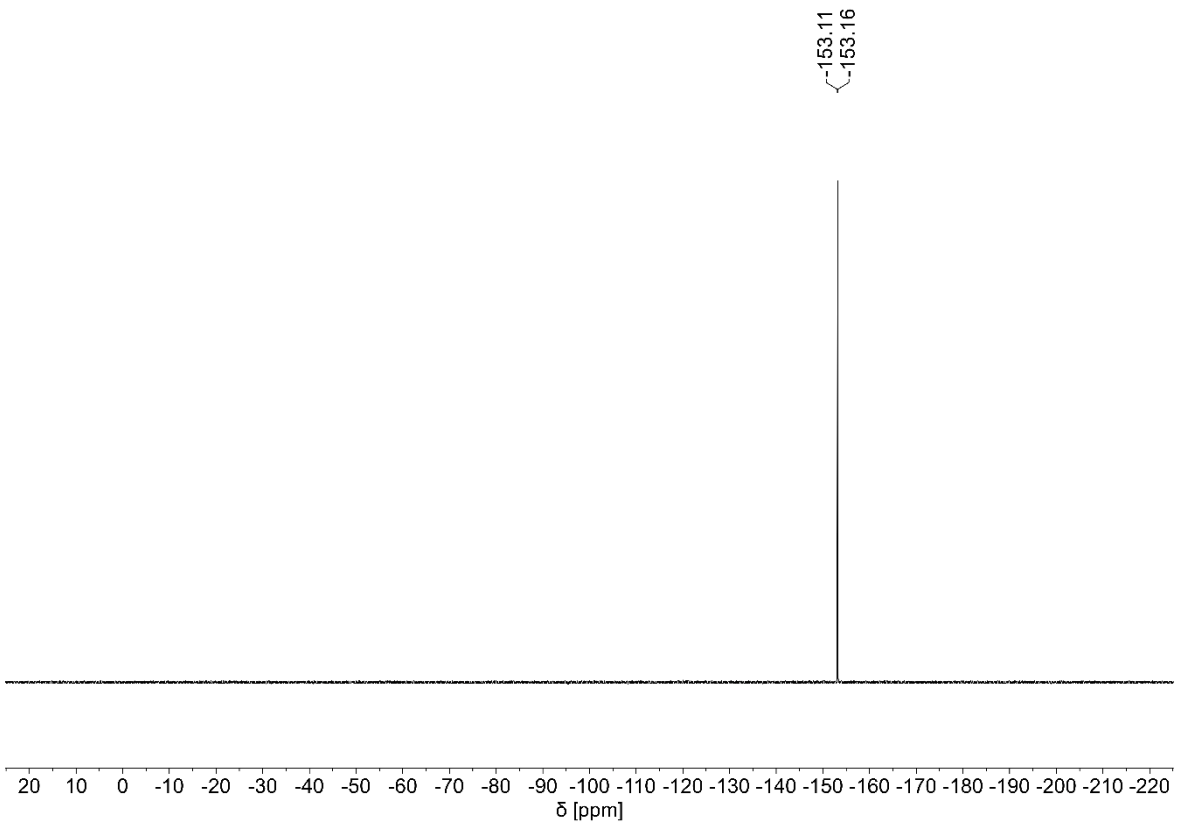

Figure S45. IR spectrum of [Tc(=*cyclo*-C$(CH_2)_4$O)$(CO)_3(PPh_3)_2$](BF_4) (**7**).

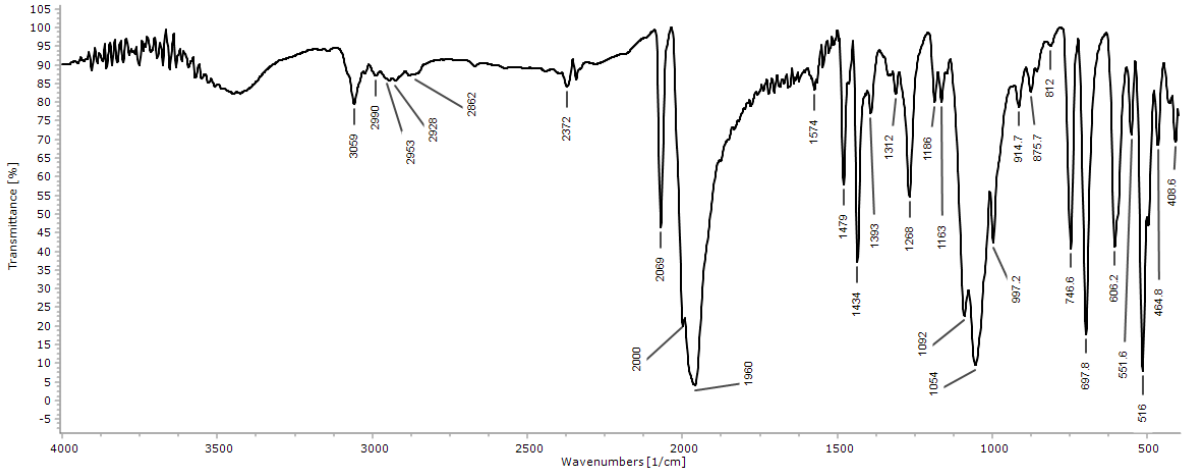

Figure S46. ^{1}H NMR spectrum of [Tc(CCH)$(CO)_3(PPh_3)_2$] (**8**).

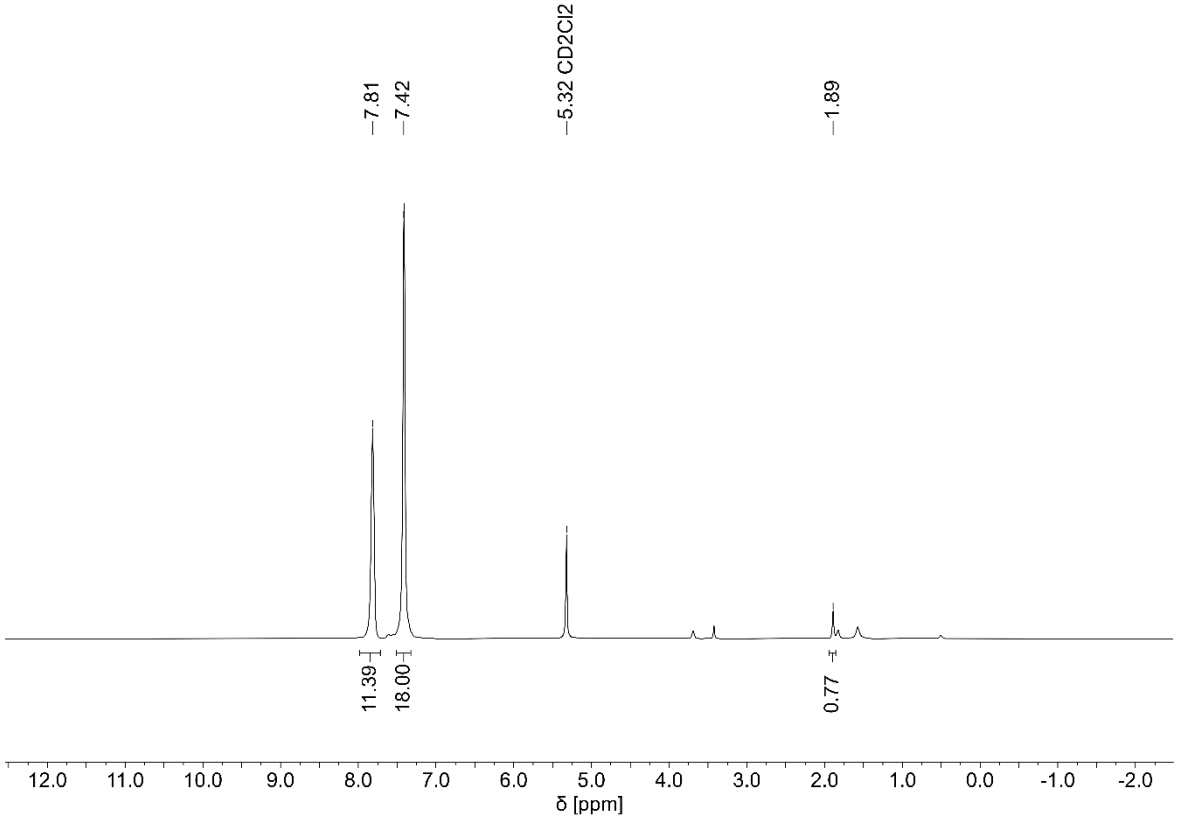

Figure S47. ^{99}Tc NMR spectrum of [Tc(CCH)(CO)$_3$(PPh$_3$)$_2$] (**8**).

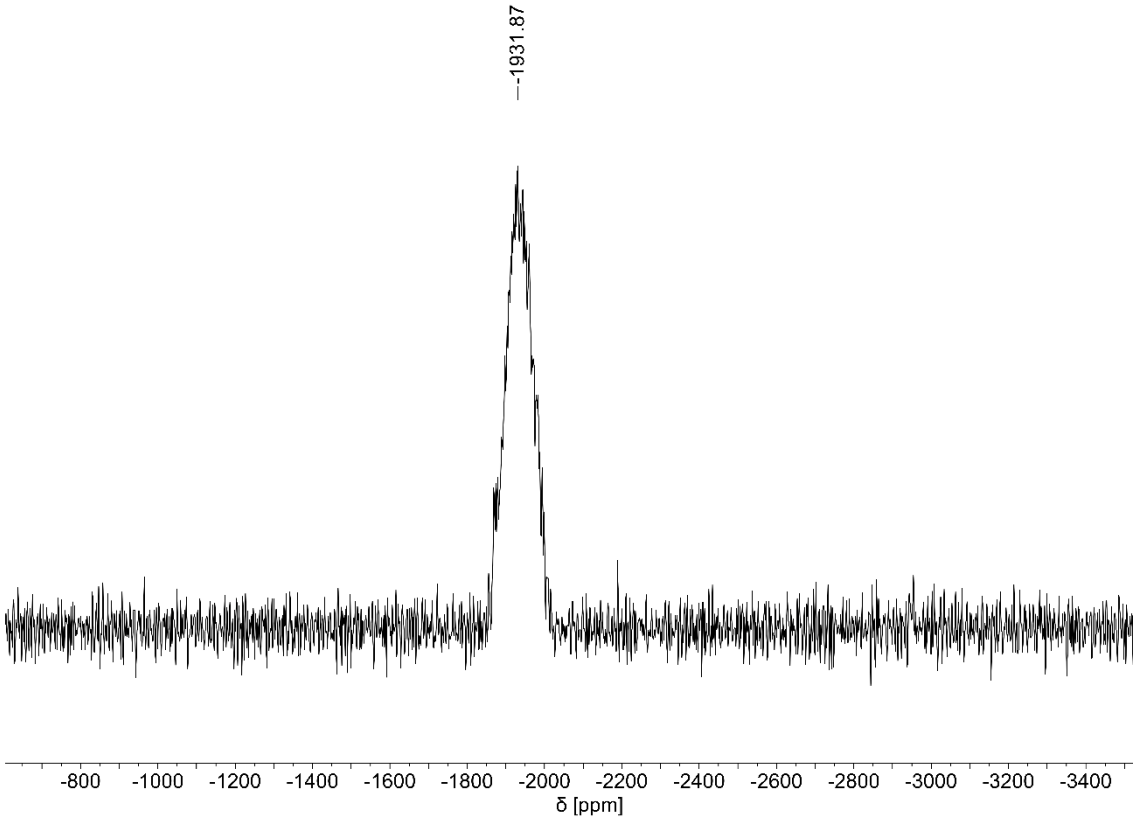

Figure S48. ^{31}P{^{1}H} NMR spectrum of [Tc(CCH)(CO)$_3$(PPh$_3$)$_2$] (**8**).

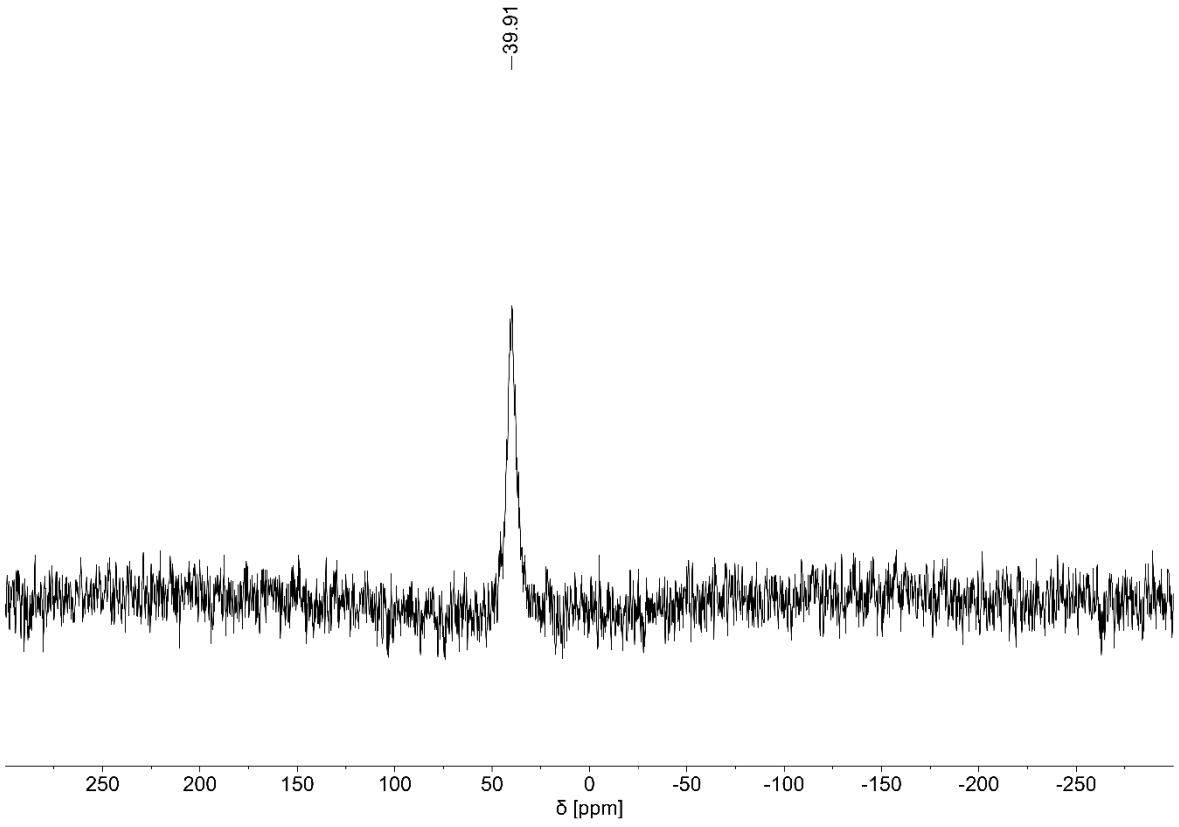

Figure S49. IR spectrum of [Tc(CCH)(CO)$_3$(PPh$_3$)$_2$] (**8**).

Figure S50. ^{1}H NMR spectrum of [Tc(CCPh)(CO)$_3$(PPh$_3$)$_2$] (**8a**).

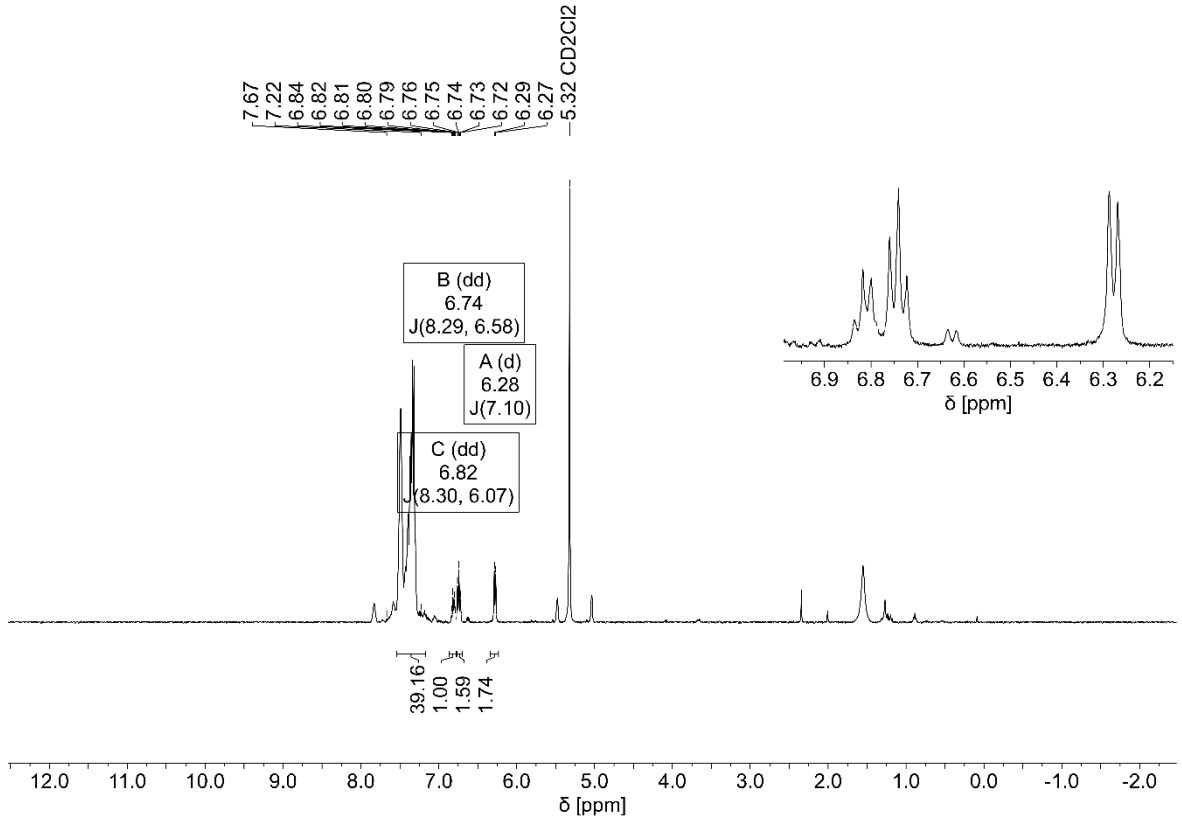

Figure S51. ^{99}Tc NMR spectrum of [Tc(CCPh)(CO)$_3$(PPh$_3$)$_2$] (**8a**).

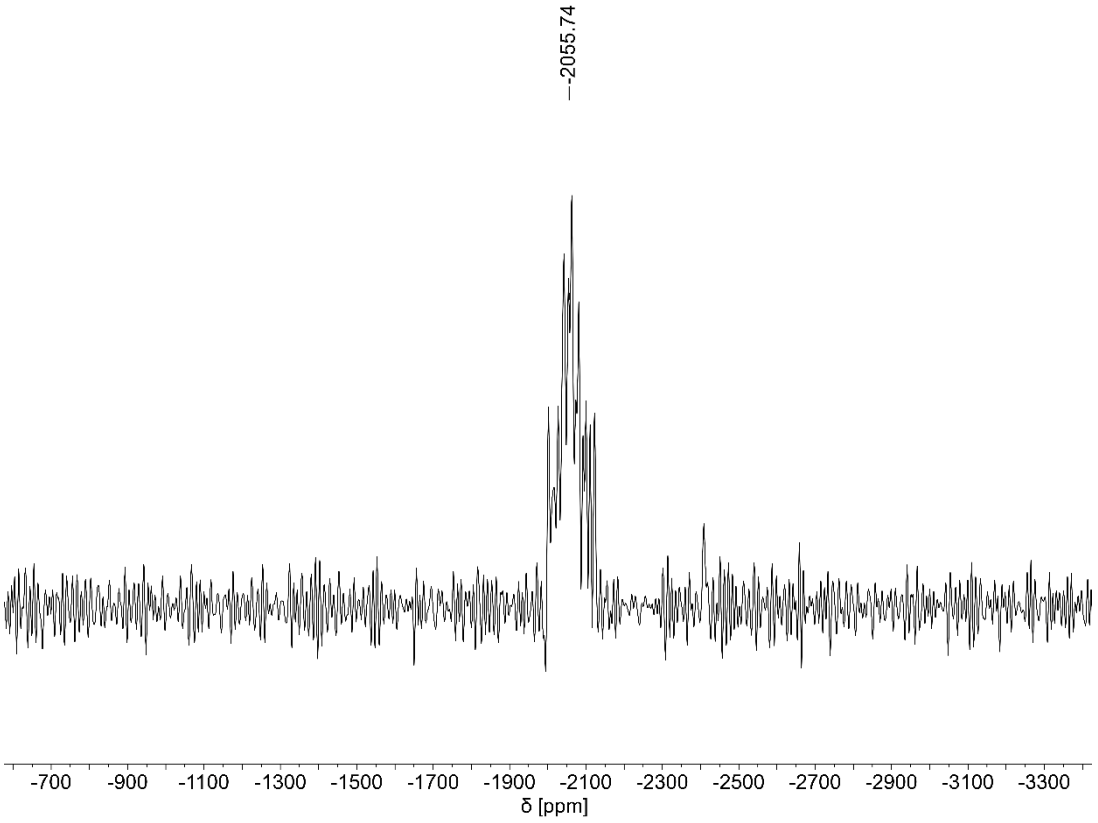

Figure S52. $^{31}P\{^{1}H\}$ NMR spectrum of $[Tc(CCPh)(CO)_3(PPh_3)_2]$ (**8a**).

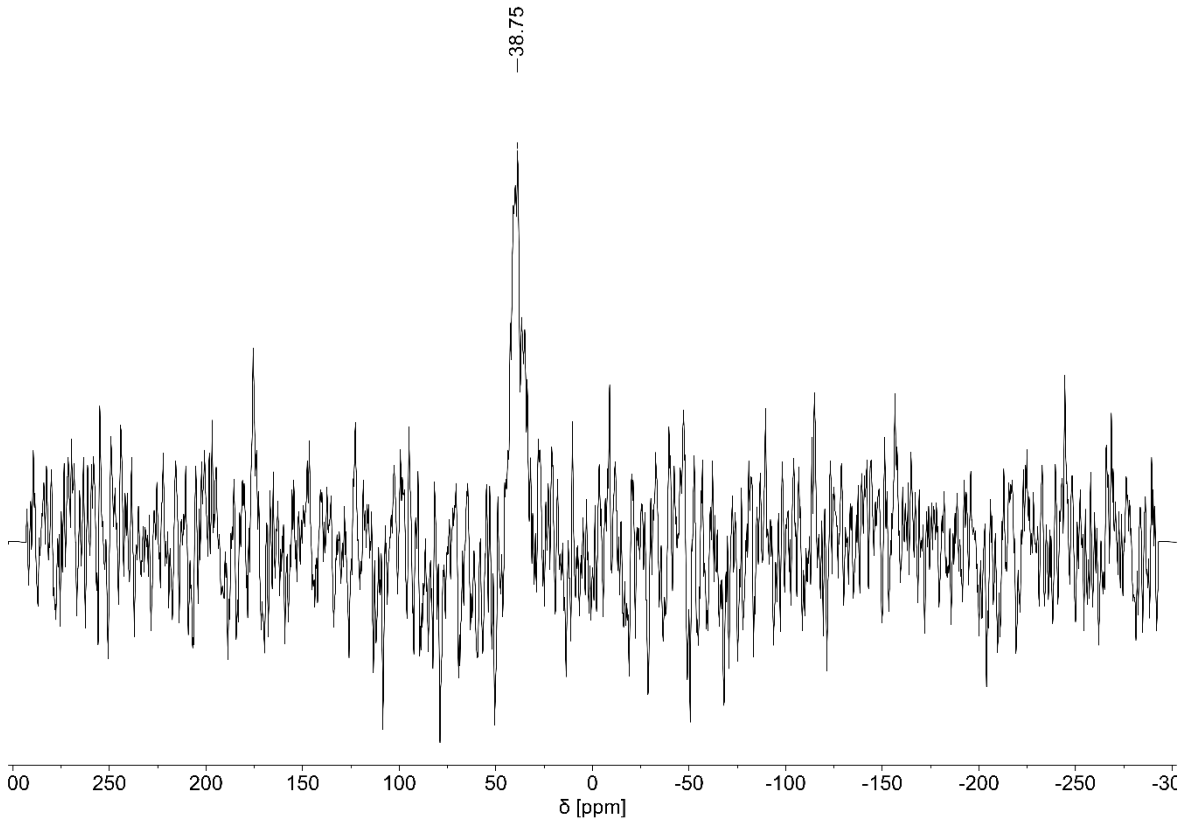

Figure S53. IR spectrum of $[Tc(CCPh)(CO)_3(PPh_3)_2]$ (**8a**).

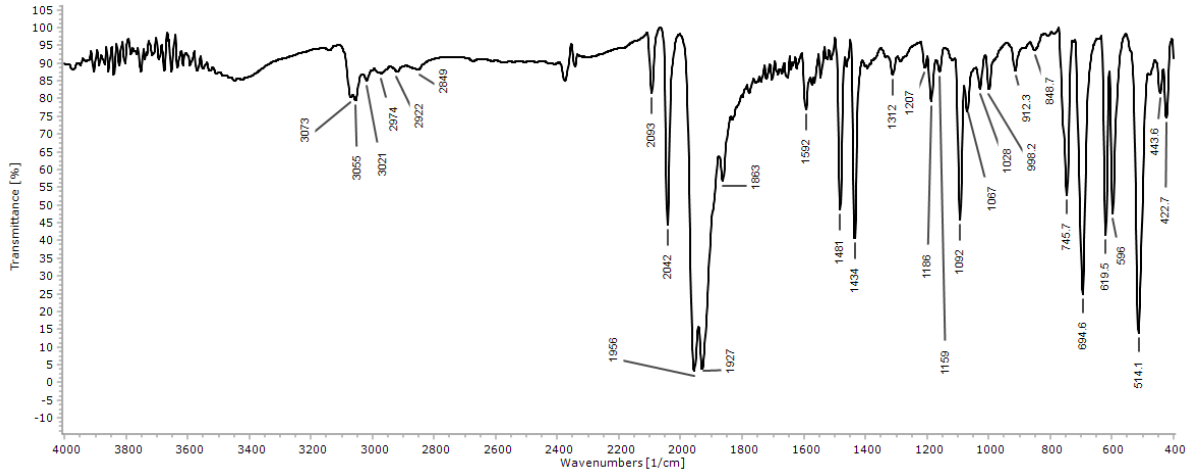

Figure S54. ^{1}H NMR spectrum of [Tc(CC^{t}Bu)(CO)$_3$(PPh$_3$)$_2$] (**8b**).

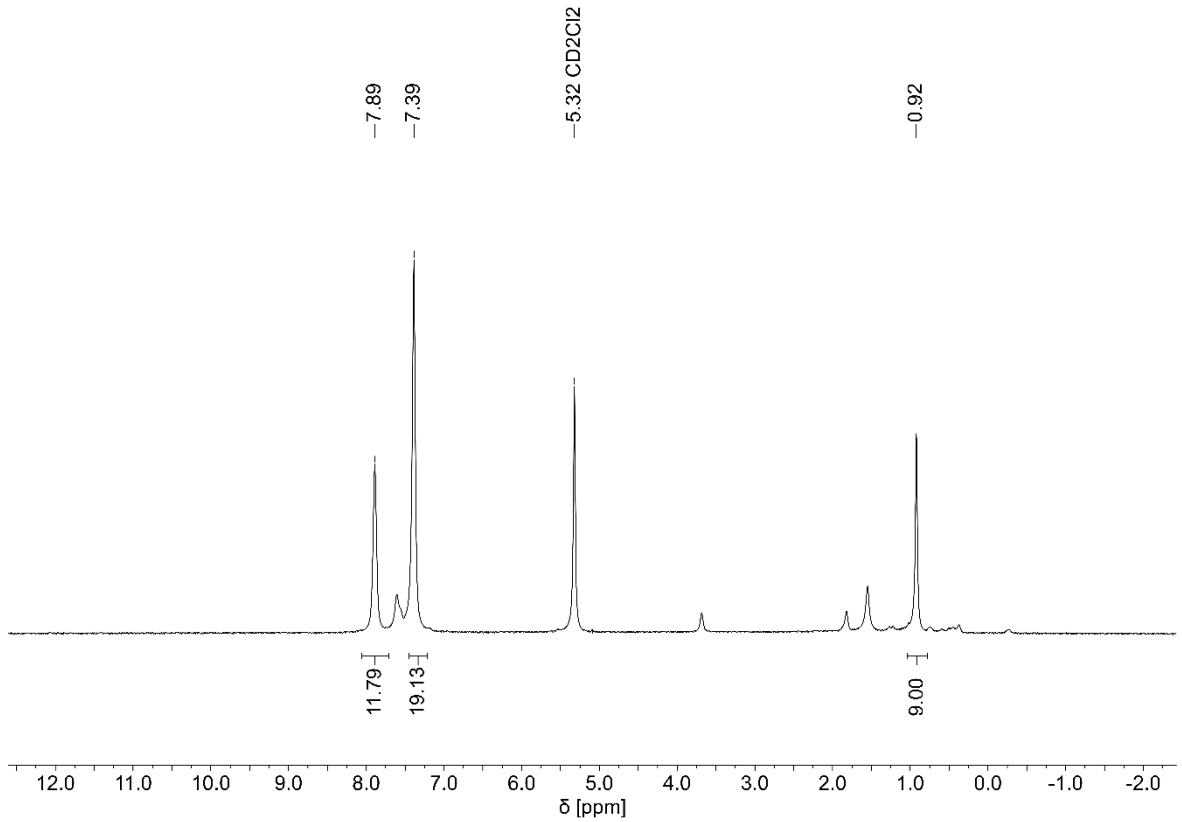

Figure S55. ^{99}Tc NMR spectrum of [Tc(CC^{t}Bu)(CO)$_3$(PPh$_3$)$_2$] (**8b**).

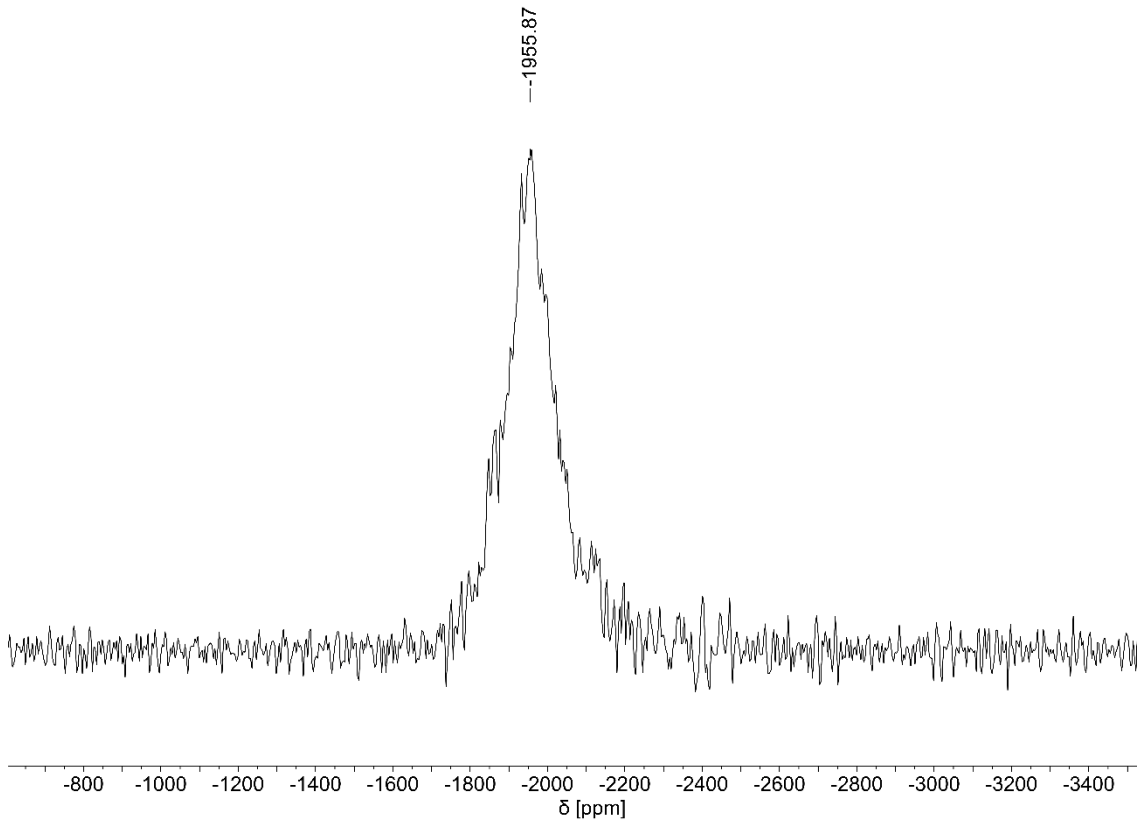

Figure S56. $^{31}P\{^{1}H\}$ NMR spectrum of $[Tc(CC^{t}Bu)(CO)_3(PPh_3)_2]$ (**8b**).

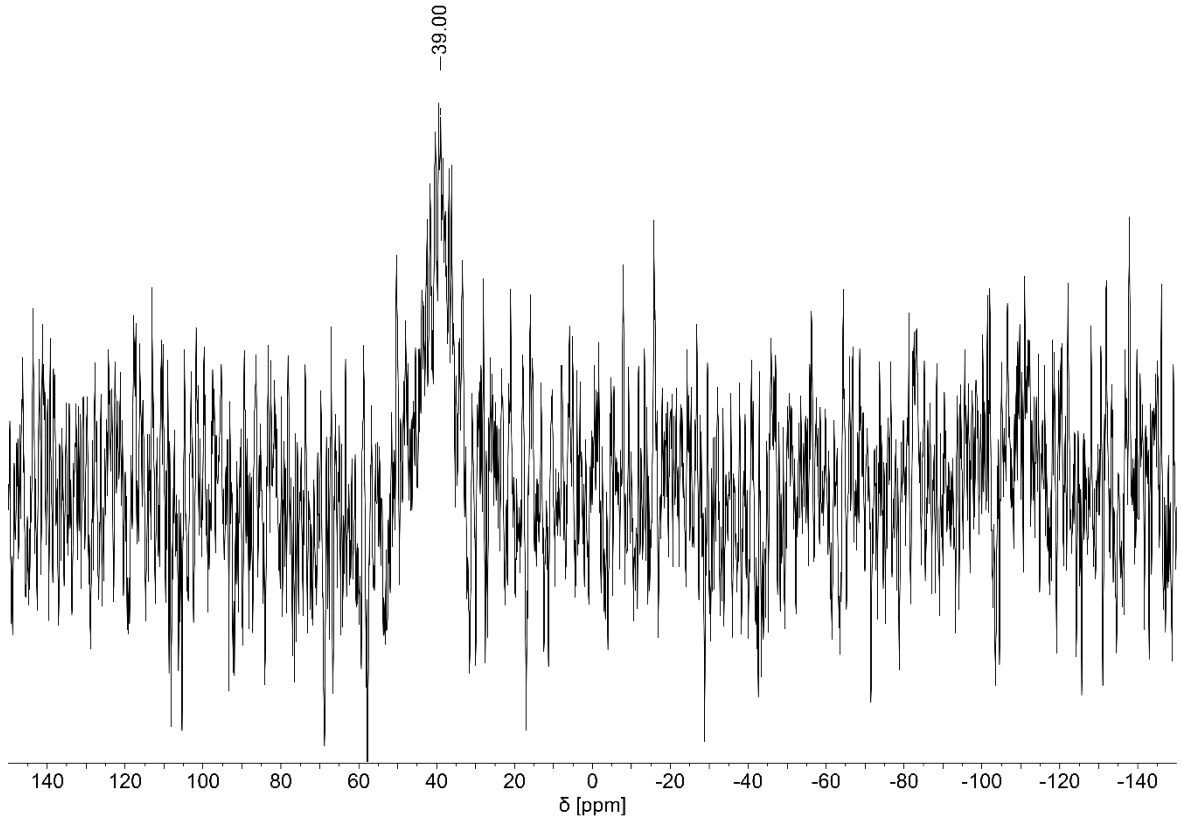

Figure S57. IR spectrum of $[Tc(CC^{t}Bu)(CO)_3(PPh_3)_2]$ (**8b**).

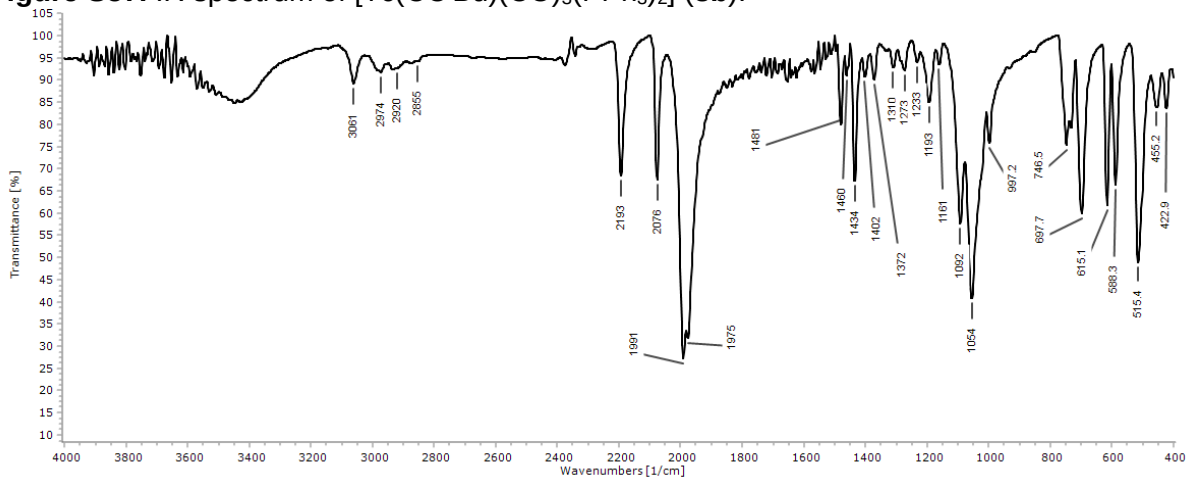

Figure S58. ^{1}H NMR spectrum of [Tc(CC^{n}Bu)(CO)$_3$(PPh$_3$)$_2$] (**8c**).

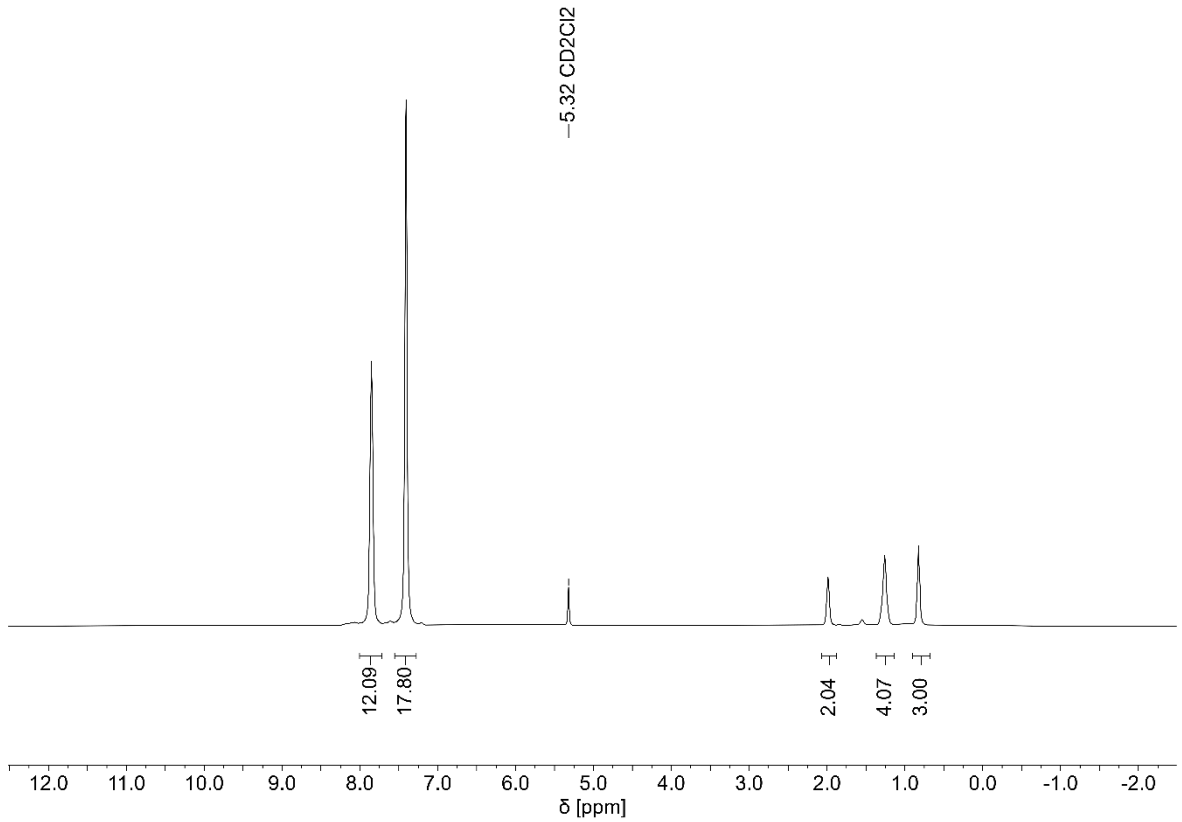

Figure S59. ^{99}Tc NMR spectrum of [Tc(CC^{n}Bu)(CO)$_3$(PPh$_3$)$_2$] (**8c**).

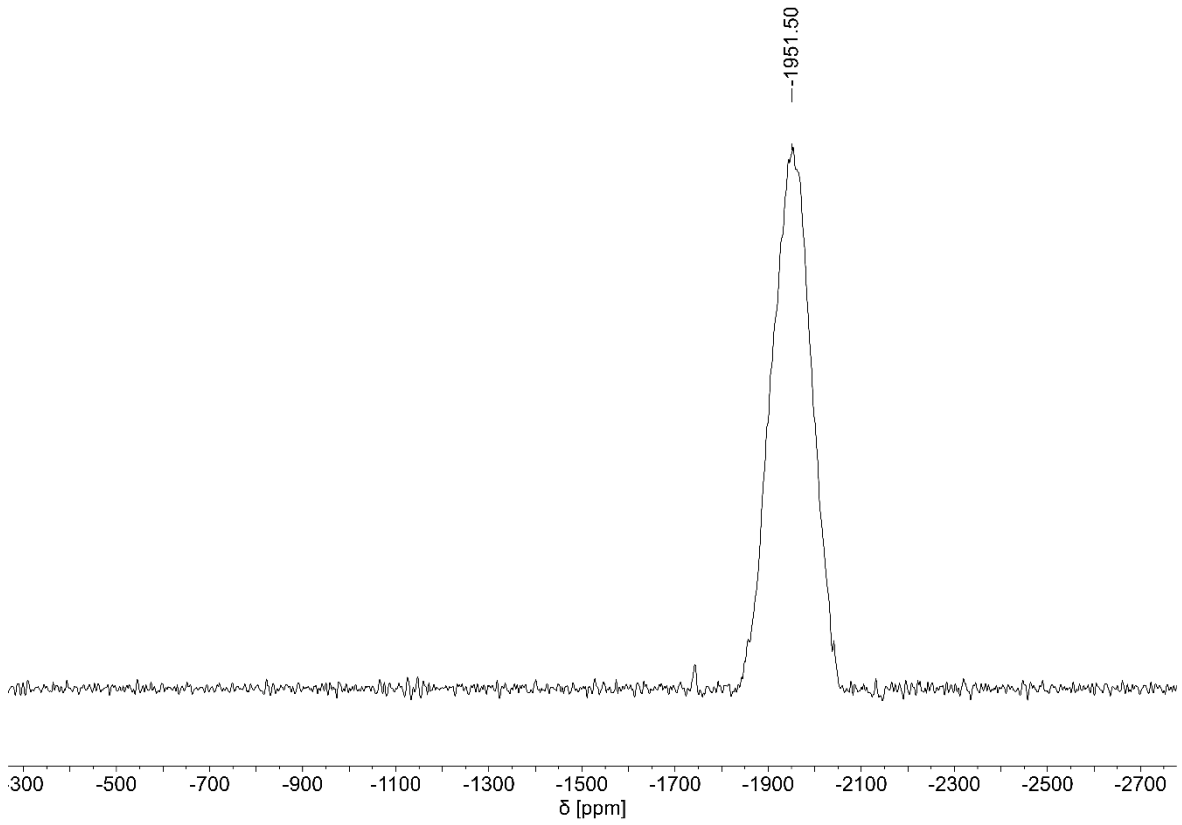

Figure S60. $^{31}P\{^{1}H\}$ NMR spectrum of $[Tc(CC^{n}Bu)(CO)_3(PPh_3)_2]$ (**8c**).

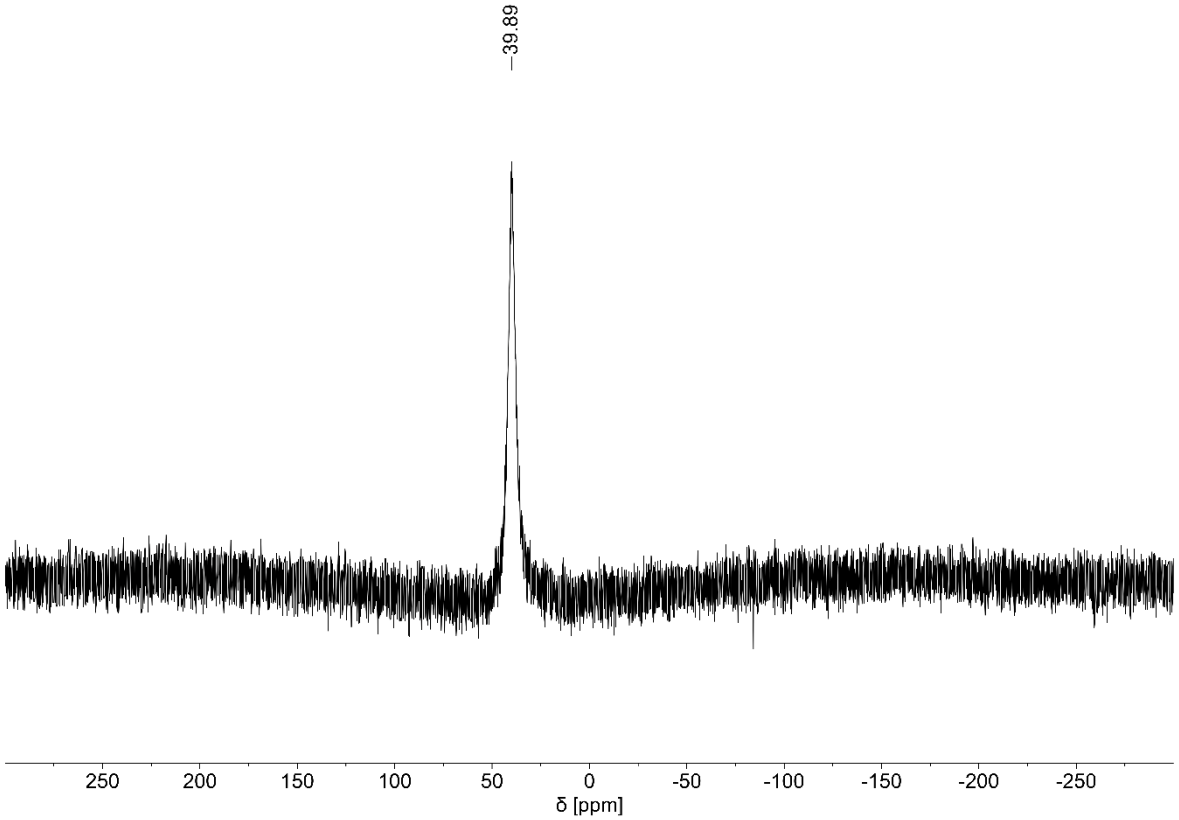

Figure S61. IR spectrum of $[Tc(CC^{n}Bu)(CO)_3(PPh_3)_2]$ (**8c**).

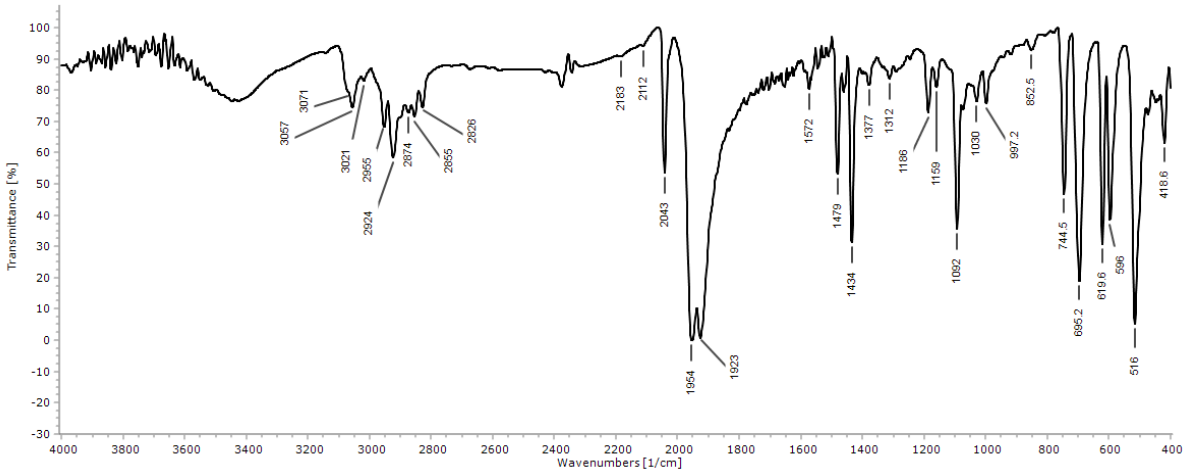

Figure S62. ^{1}H NMR spectrum of [Tc(CCSiMe$_3$)(CO)$_3$(PPh$_3$)$_2$] (**8d**).

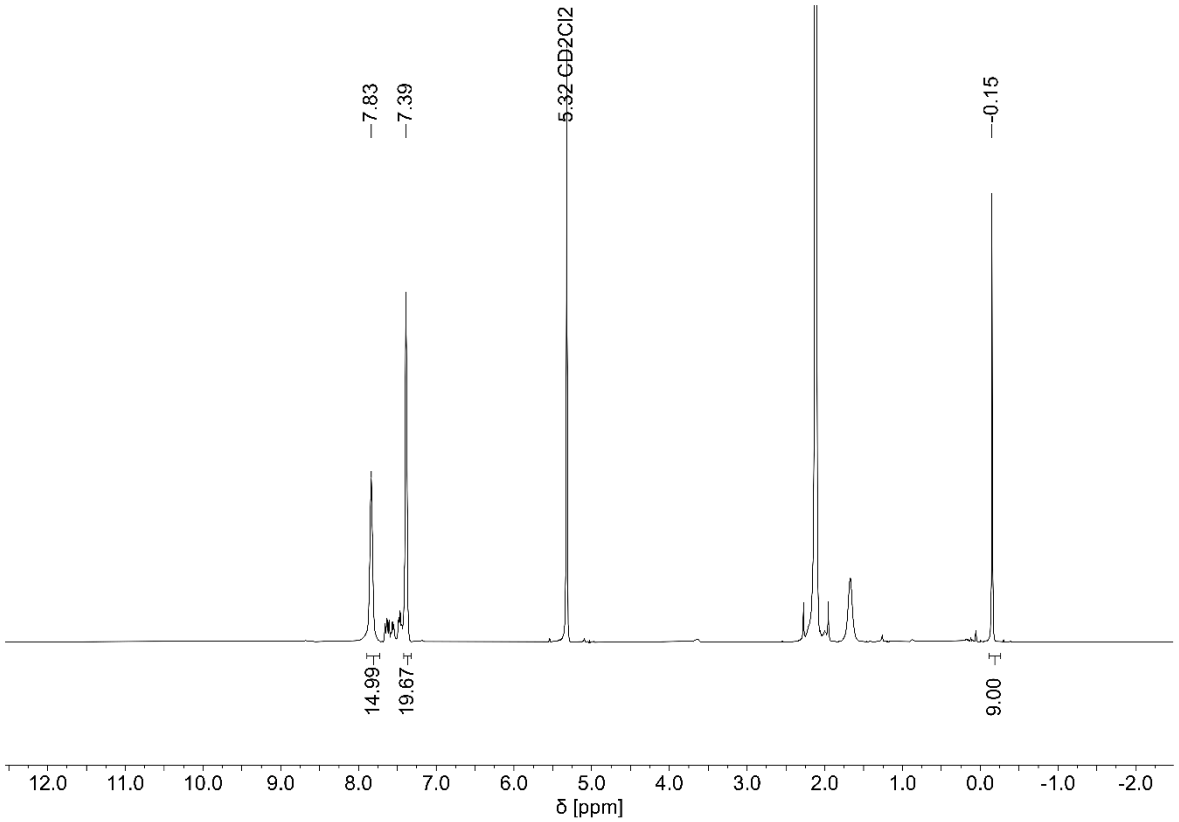

Figure S63. ^{99}Tc NMR spectrum of [Tc(CCSiMe$_3$)(CO)$_3$(PPh$_3$)$_2$] (**8d**).

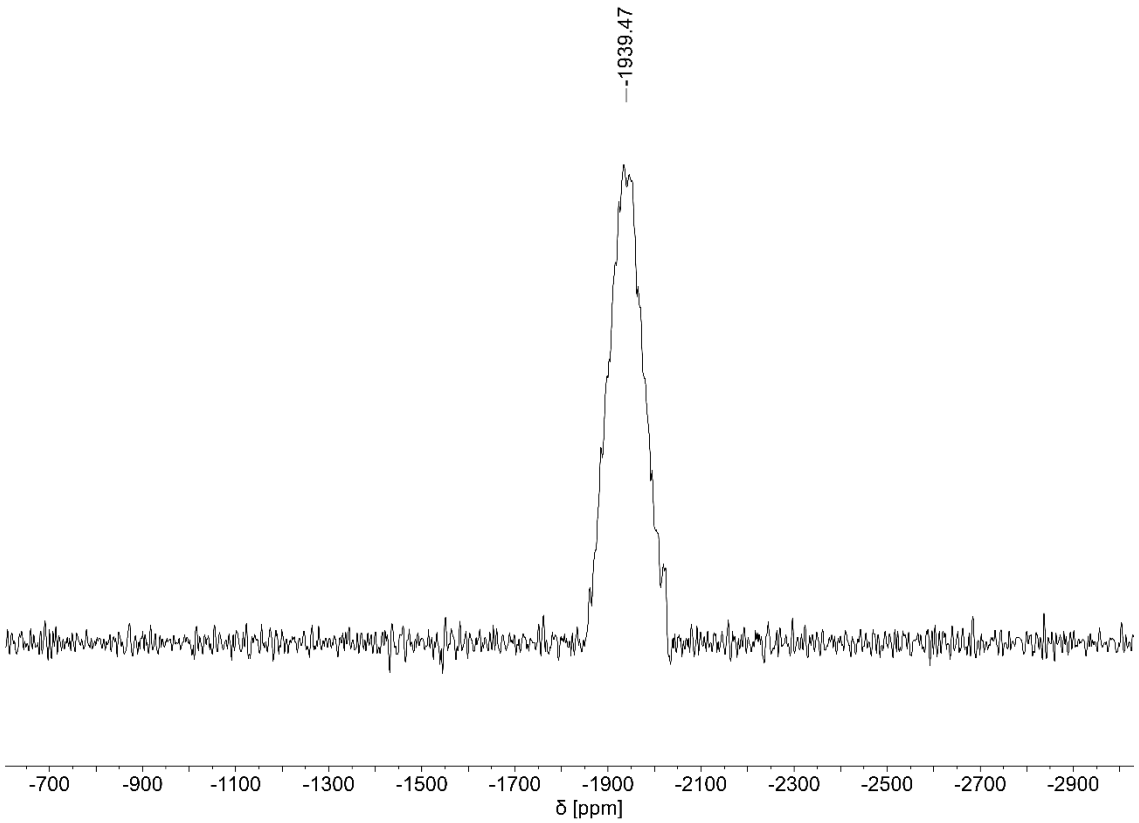

Figure S64. $^{31}P\{^{1}H\}$ NMR spectrum of $[Tc(CCSiMe_3)(CO)_3(PPh_3)_2]$ (**8d**). Minor traces of triphenylphosphine oxide are visible (resonance at ca. 28 ppm).

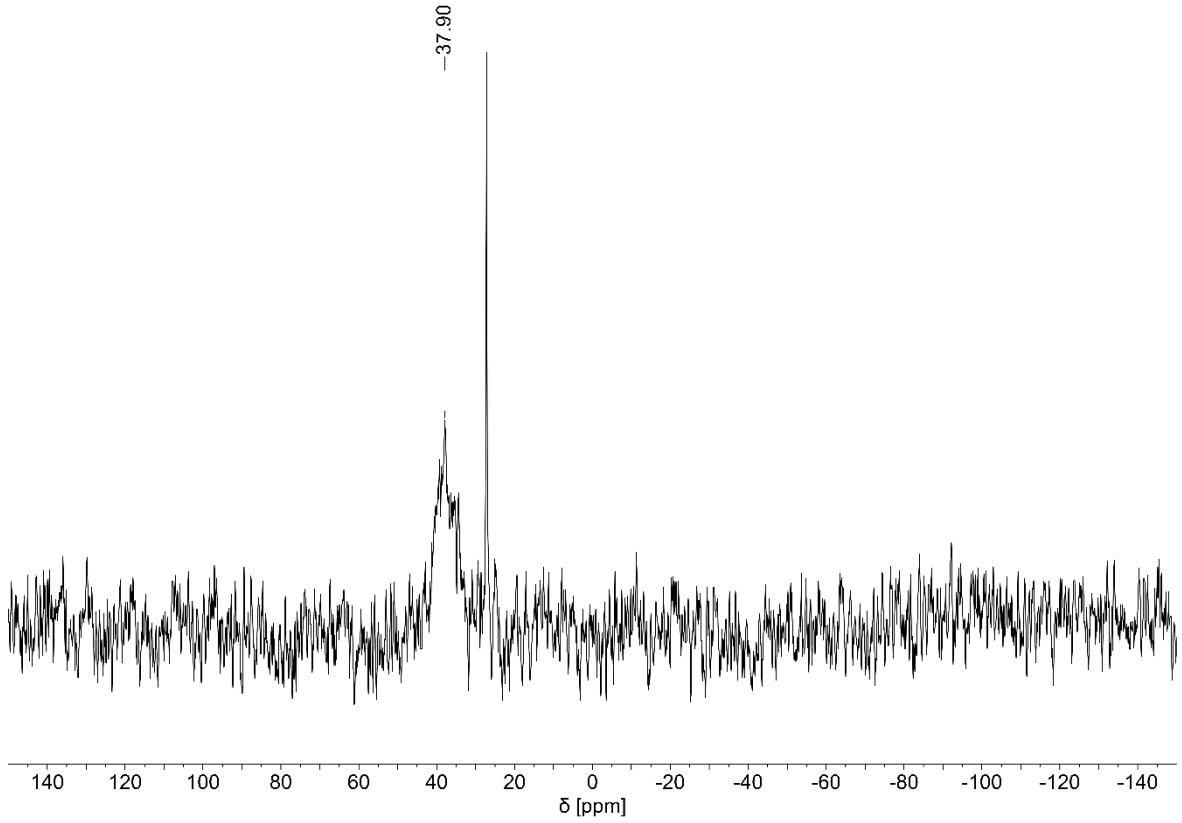

Figure S65. IR spectrum of $[Tc(CCSiMe_3)(CO)_3(PPh_3)_2]$ (**8d**).

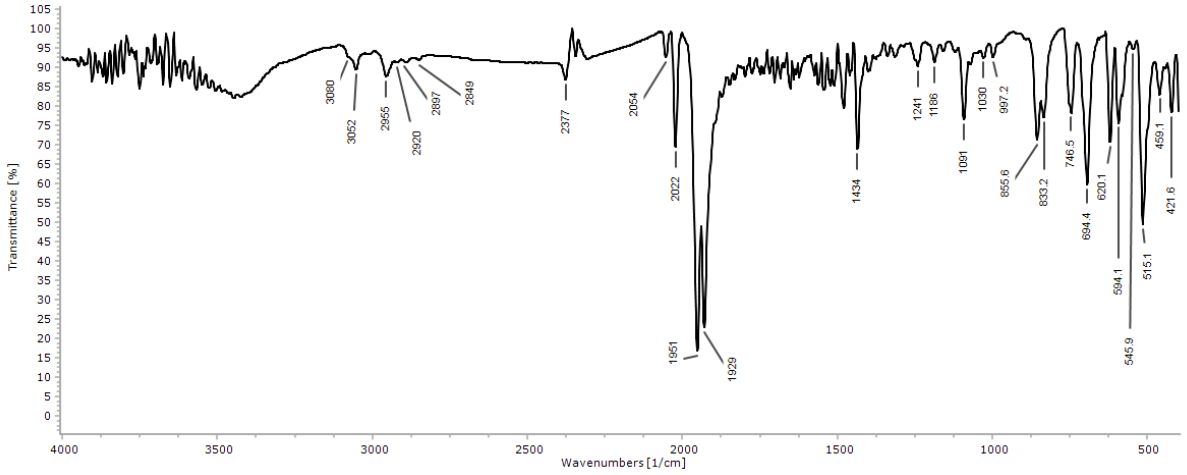

Figure S66. ^{1}H NMR spectrum of [Tc{CC($C_6H_3(CF_3)_2$)}$(CO)_3(PPh_3)_2$] (**8e**).

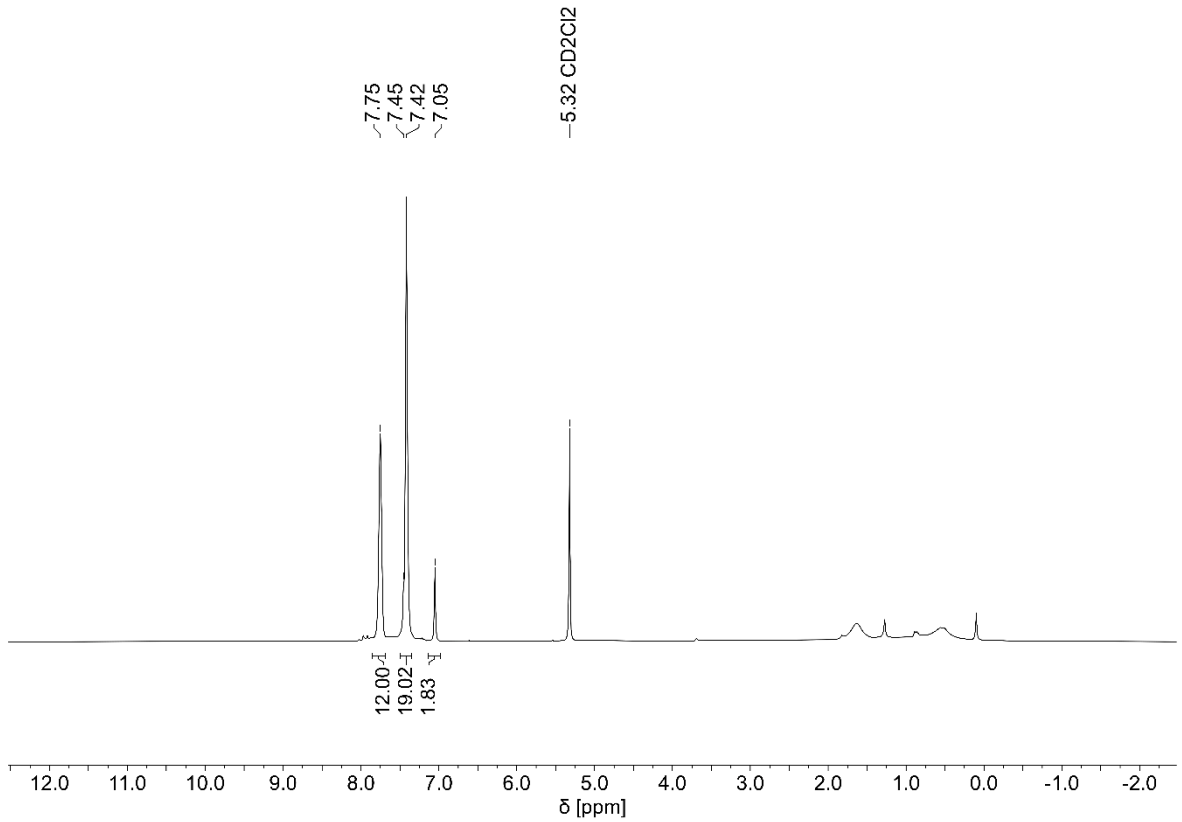

Figure S67. ^{99}Tc NMR spectrum of [Tc{CC($C_6H_3(CF_3)_2$)}$(CO)_3(PPh_3)_2$] (**8e**).

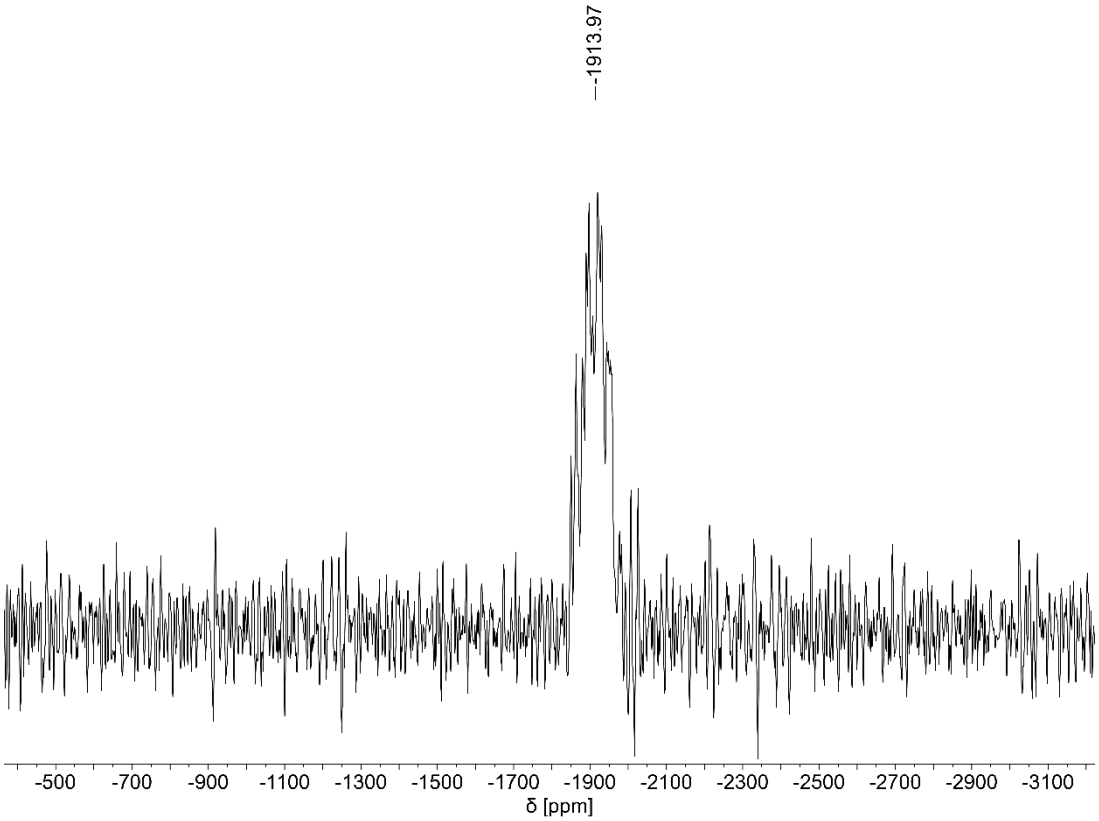

Figure S68. $^{31}P\{^{1}H\}$ NMR spectrum of $[Tc\{CC(C_6H_3(CF_3)_2)\}(CO)_3(PPh_3)_2]$ (**8e**).

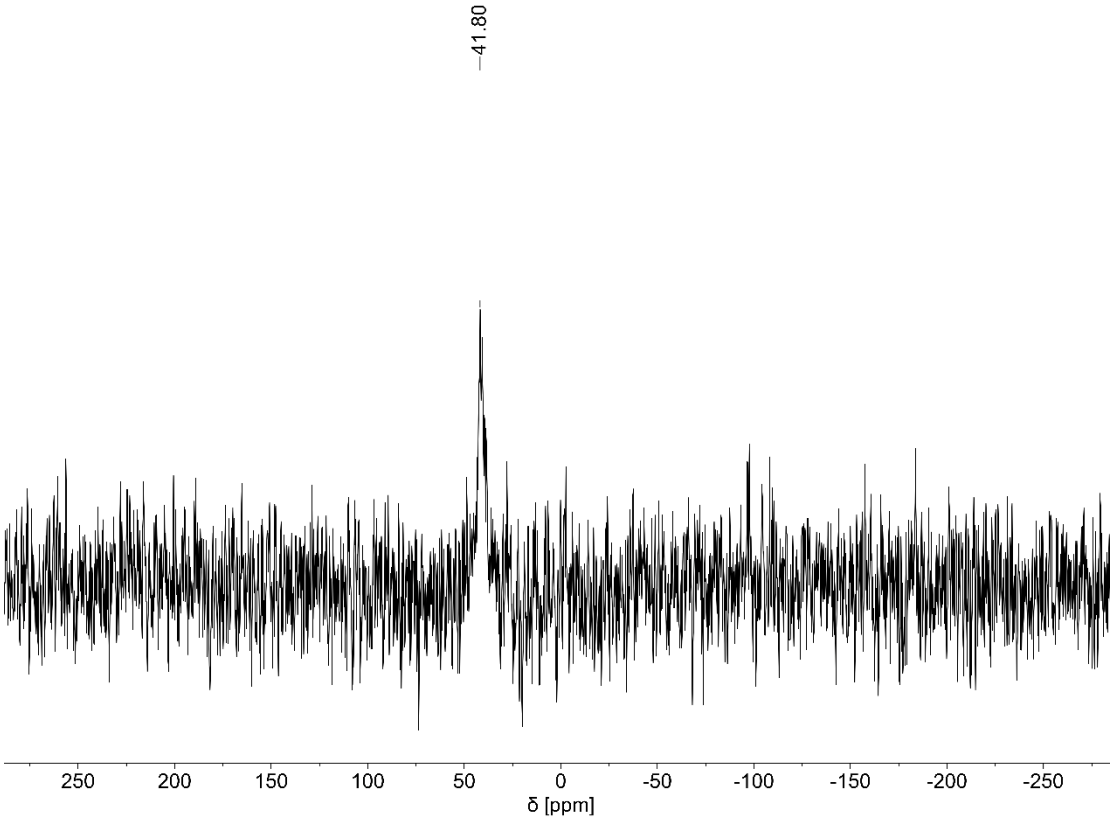

Figure S69. ^{19}F NMR spectrum of $[Tc\{CC(C_6H_3(CF_3)_2)\}(CO)_3(PPh_3)_2]$ (**8e**).

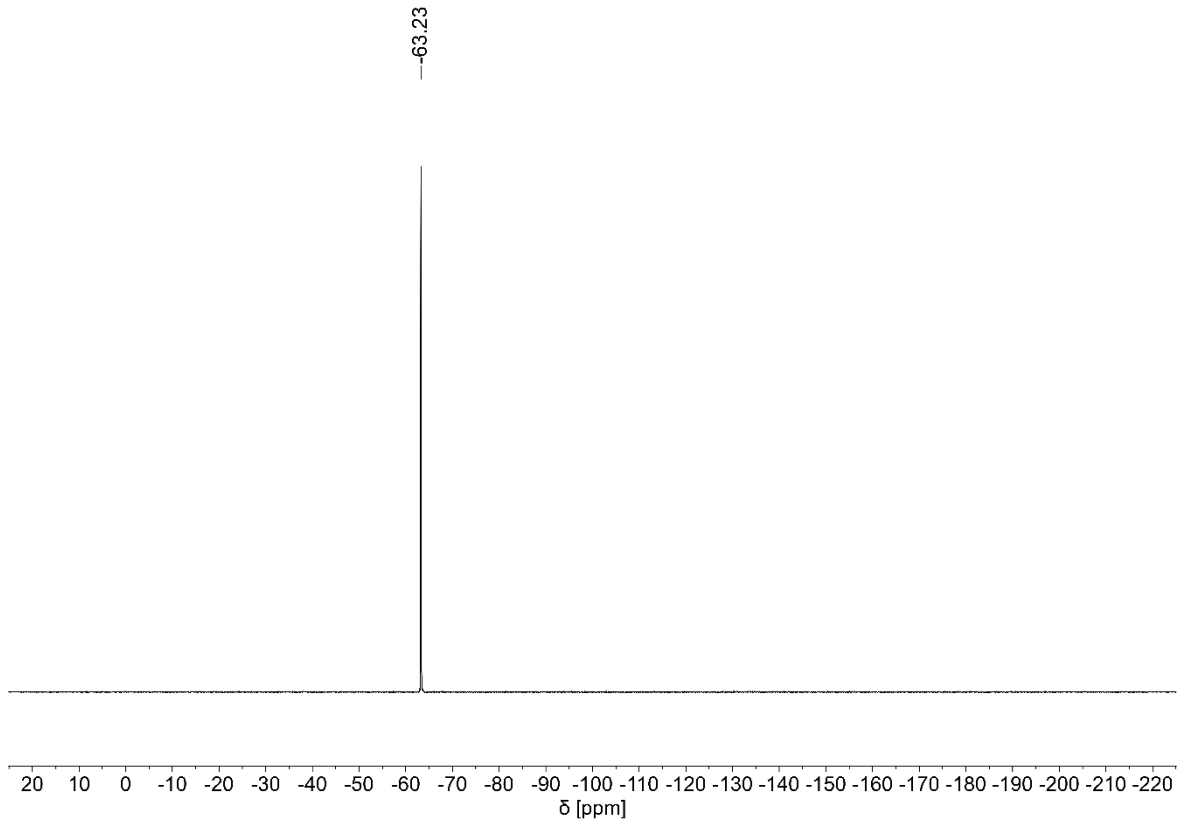

Figure S70. IR spectrum of [Tc{CC($C_6H_3(CF_3)_2$)}$(CO)_3(PPh_3)_2$] (**8e**).

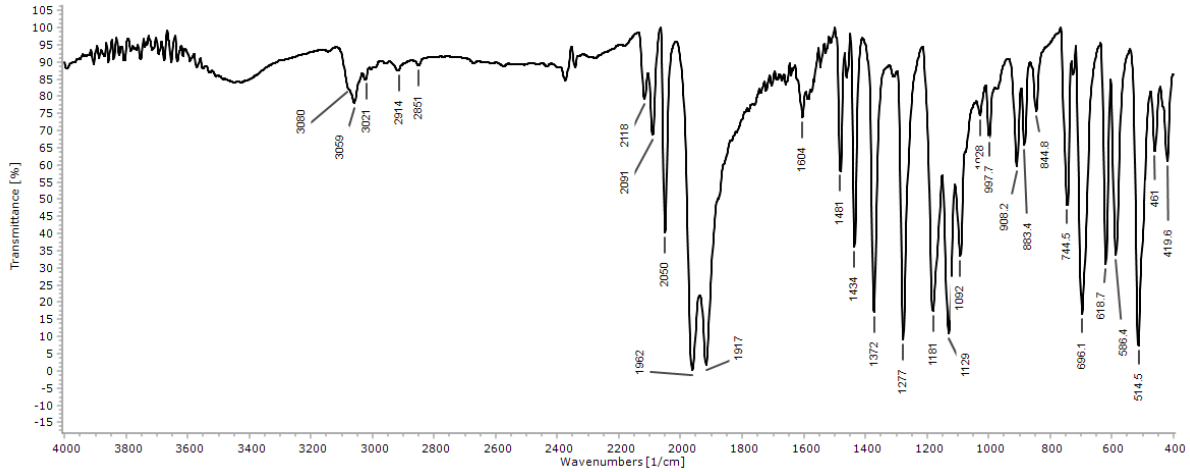

Figure S71. ^{1}H NMR spectrum of [Tc(CNPh)$(CO)_3(PPh_3)_2$](BF_4) (**9a**).

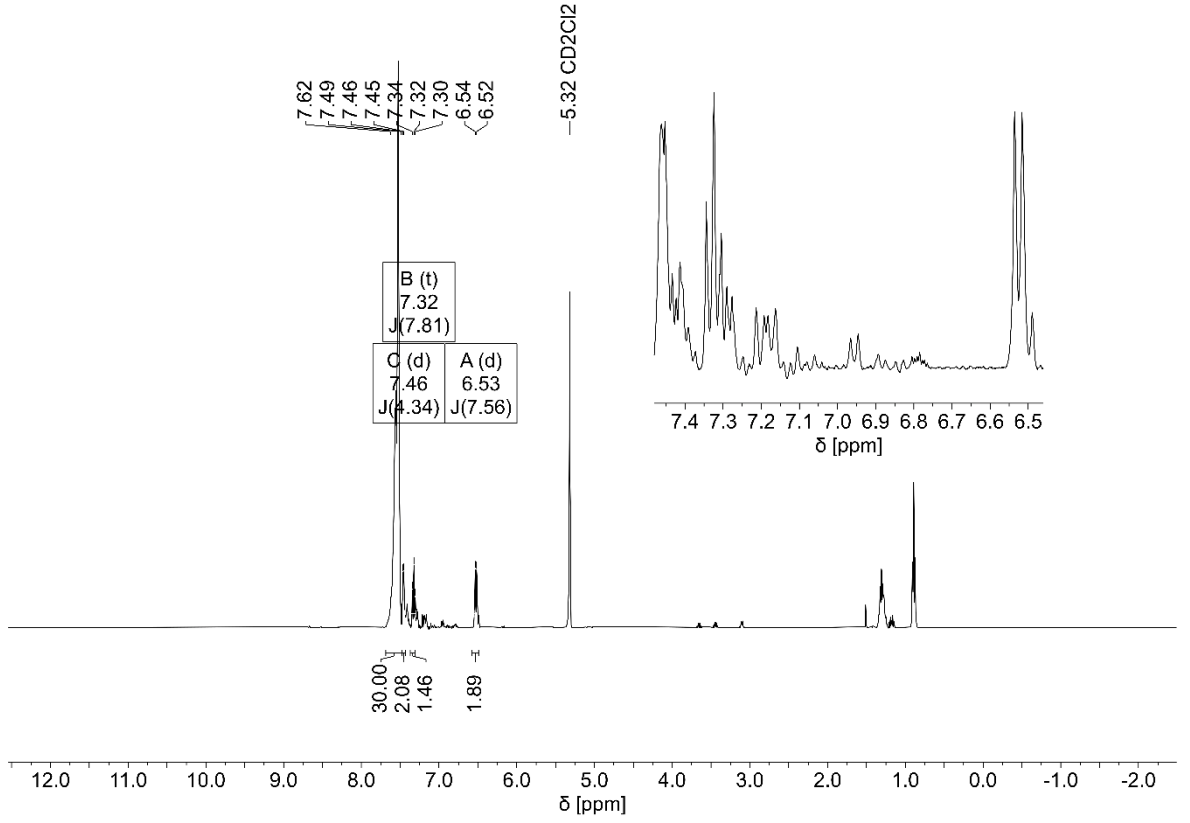

Figure S72. ^{99}Tc NMR spectrum of [Tc(CNPh)(CO)$_3$(PPh$_3$)$_2$](BF$_4$) (**9a**).

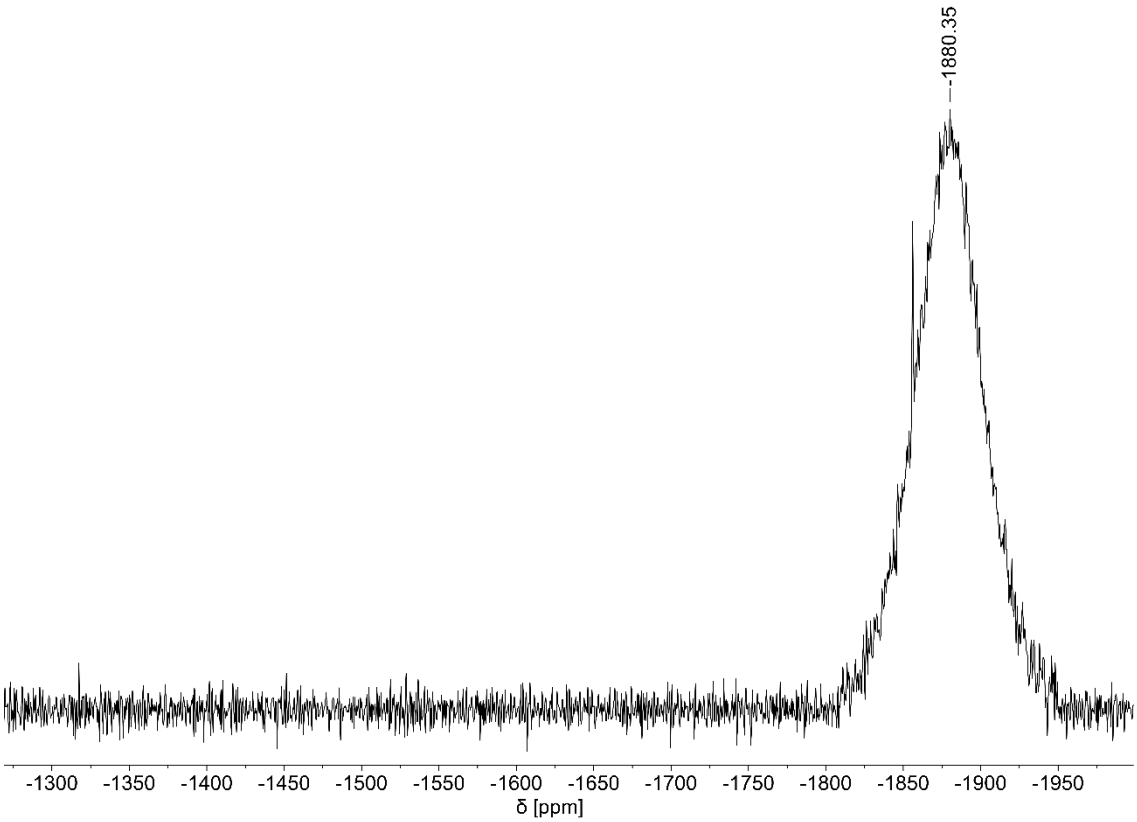

Figure S73. ^{31}P{^{1}H} NMR spectrum of [Tc(CNPh)(CO)$_3$(PPh$_3$)$_2$](BF$_4$) (**9a**).

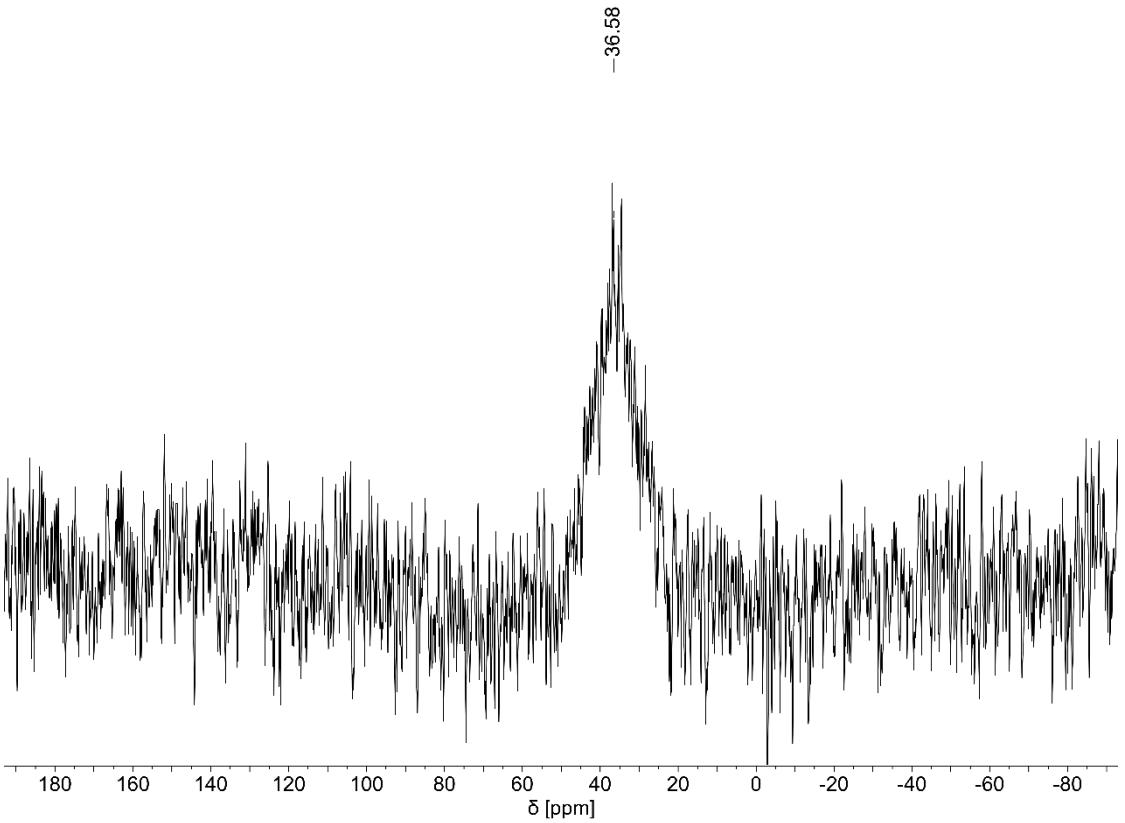

Figure S74. ^{11}B NMR spectrum of $[Tc(CNPh)(CO)_3(PPh_3)_2](BF_4)$ (**9a**).

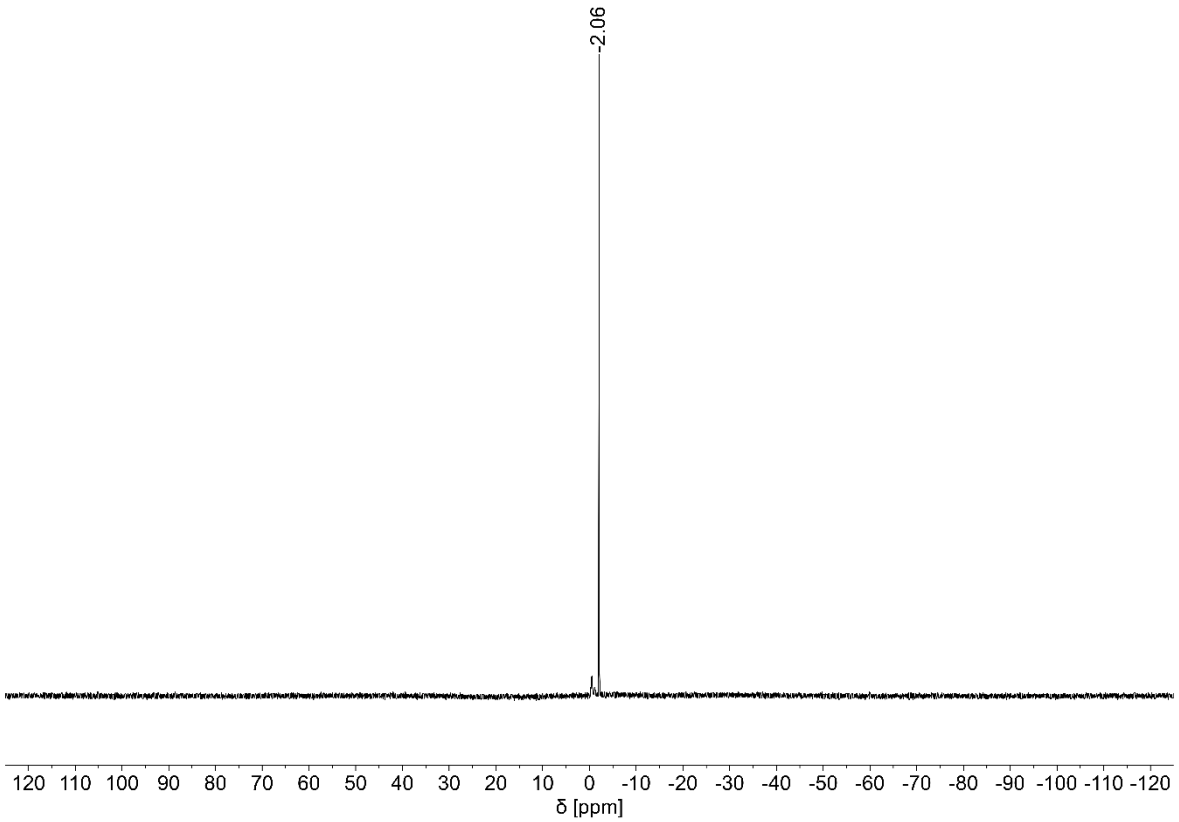

Figure S75. ^{19}F NMR spectrum of $[Tc(CNPh)(CO)_3(PPh_3)_2](BF_4)$ (**9a**).

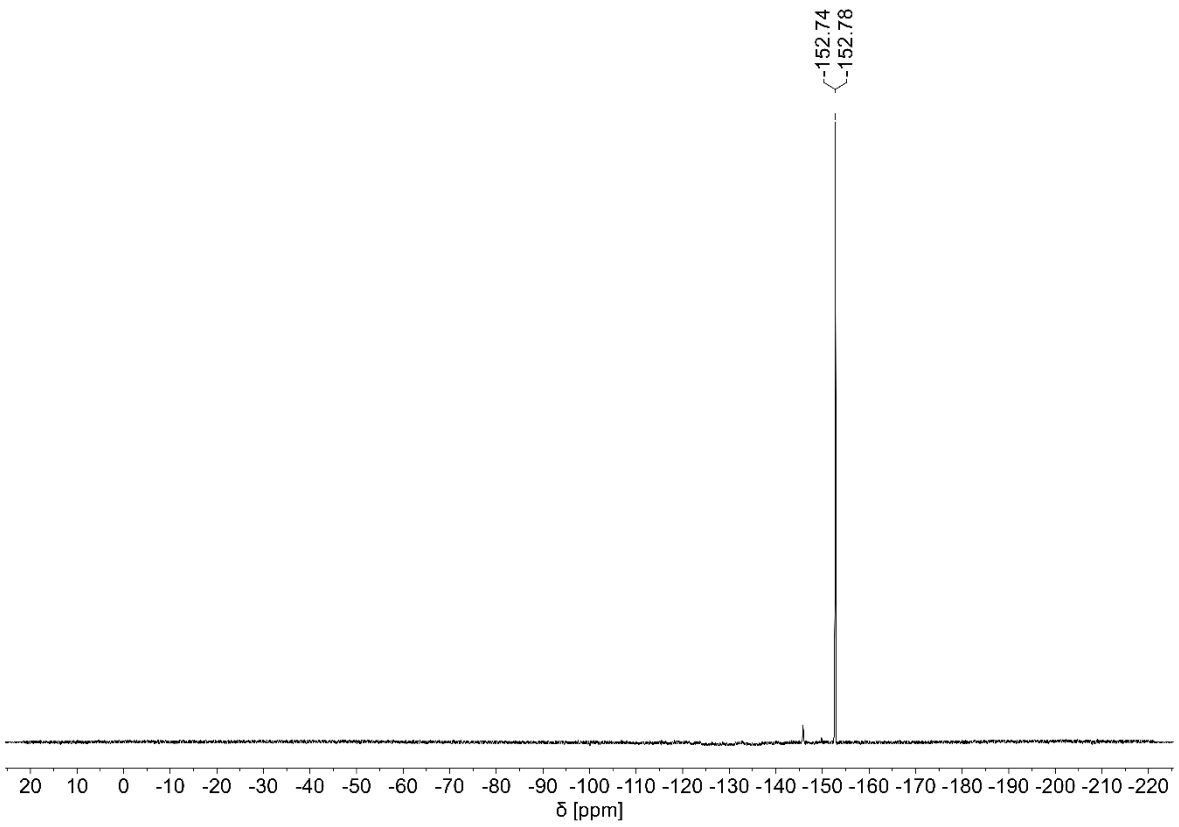

Figure S76. IR spectrum of $[Tc(CNPh)(CO)_3(PPh_3)_2](BF_4)$ (**9a**).

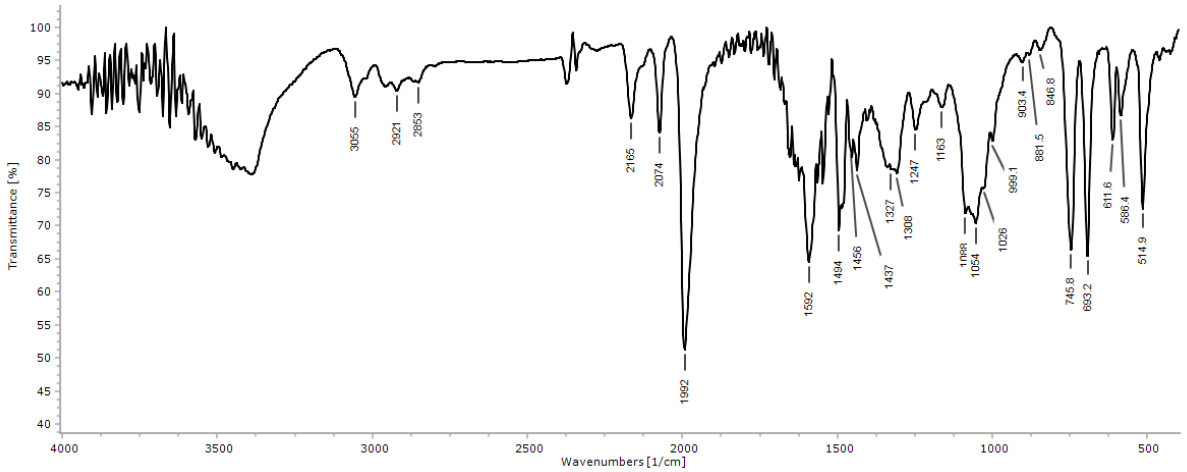

Figure S77. ^1H NMR spectrum of $[Tc(CN^tBu)(CO)_3(PPh_3)_2](BF_4)$ (**9b**).

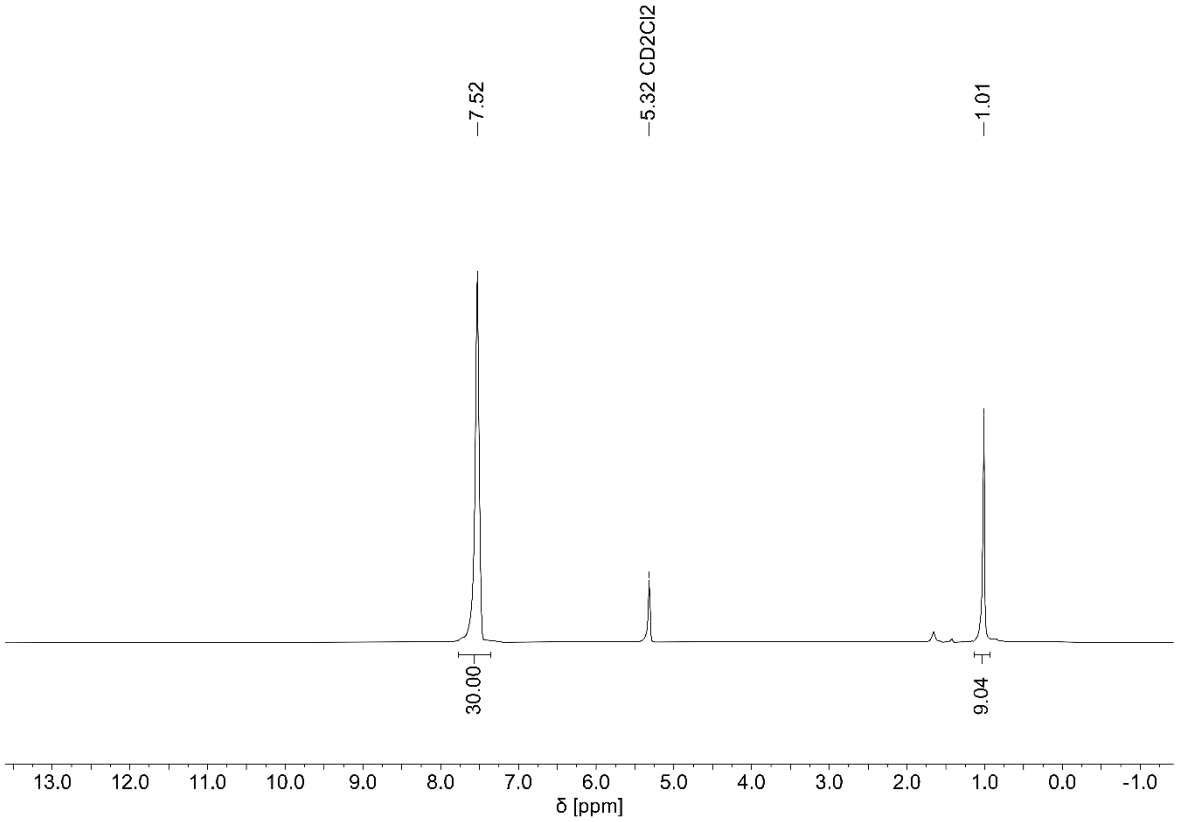

Figure S78. ^{99}Tc NMR spectrum of [Tc(CN^{t}Bu)(CO)$_3$(PPh$_3$)$_2$](BF$_4$) (**9b**).

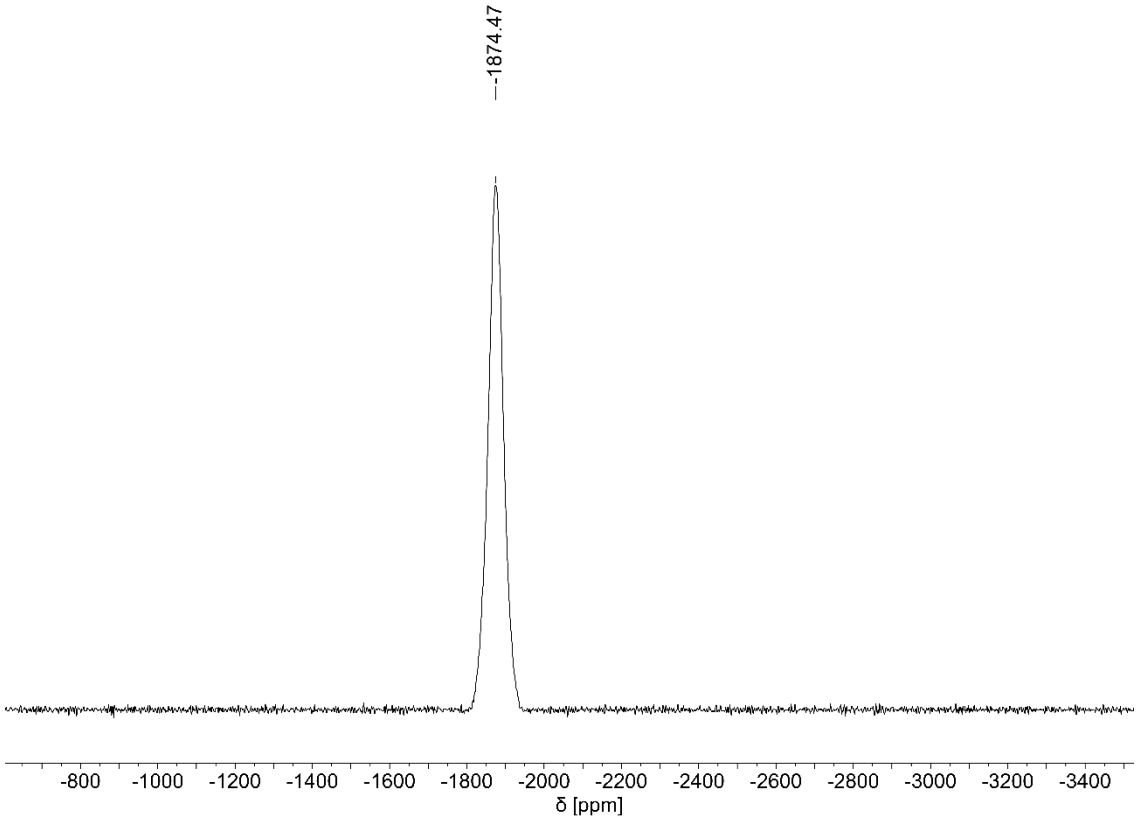

Figure S79. ^{31}P{^{1}H} NMR spectrum of [Tc(CN^{t}Bu)(CO)$_3$(PPh$_3$)$_2$](BF$_4$) (**9b**).

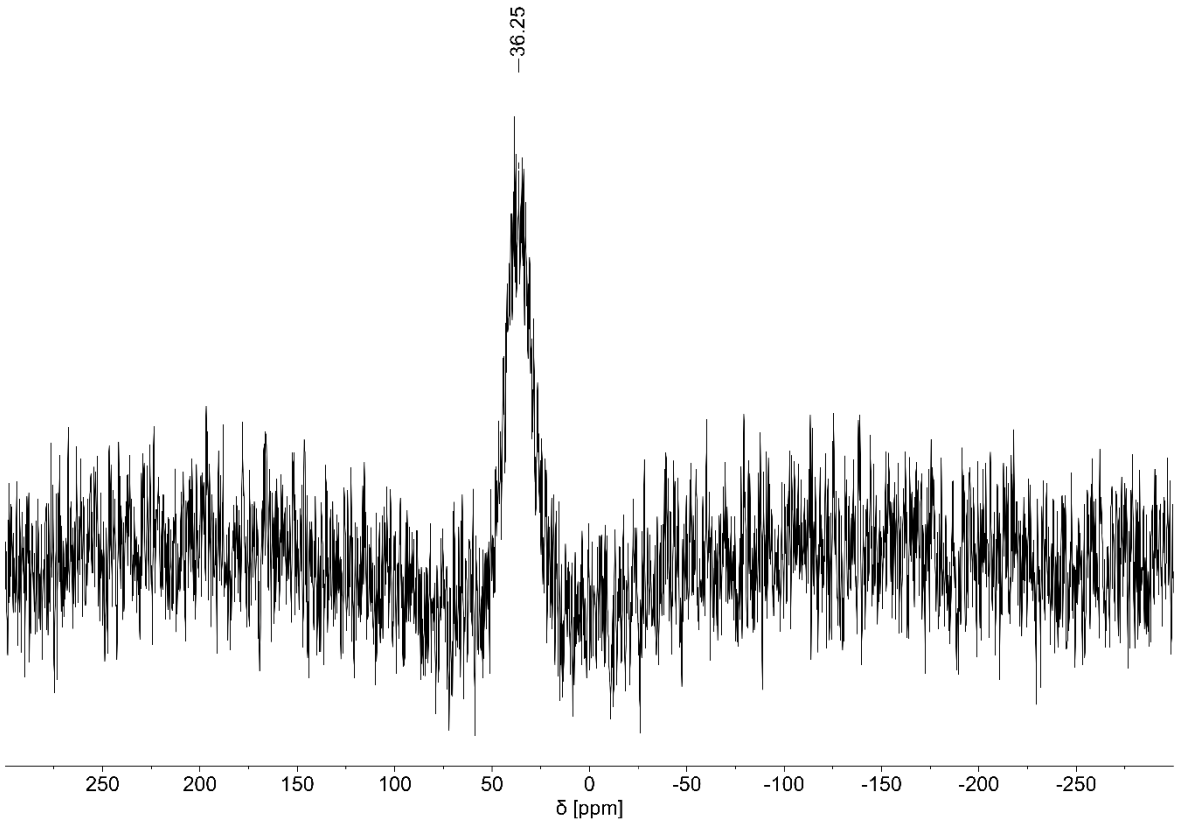

Figure S80. ^{11}B NMR spectrum of $[Tc(CN^tBu)(CO)_3(PPh_3)_2](BF_4)$ (**9b**).

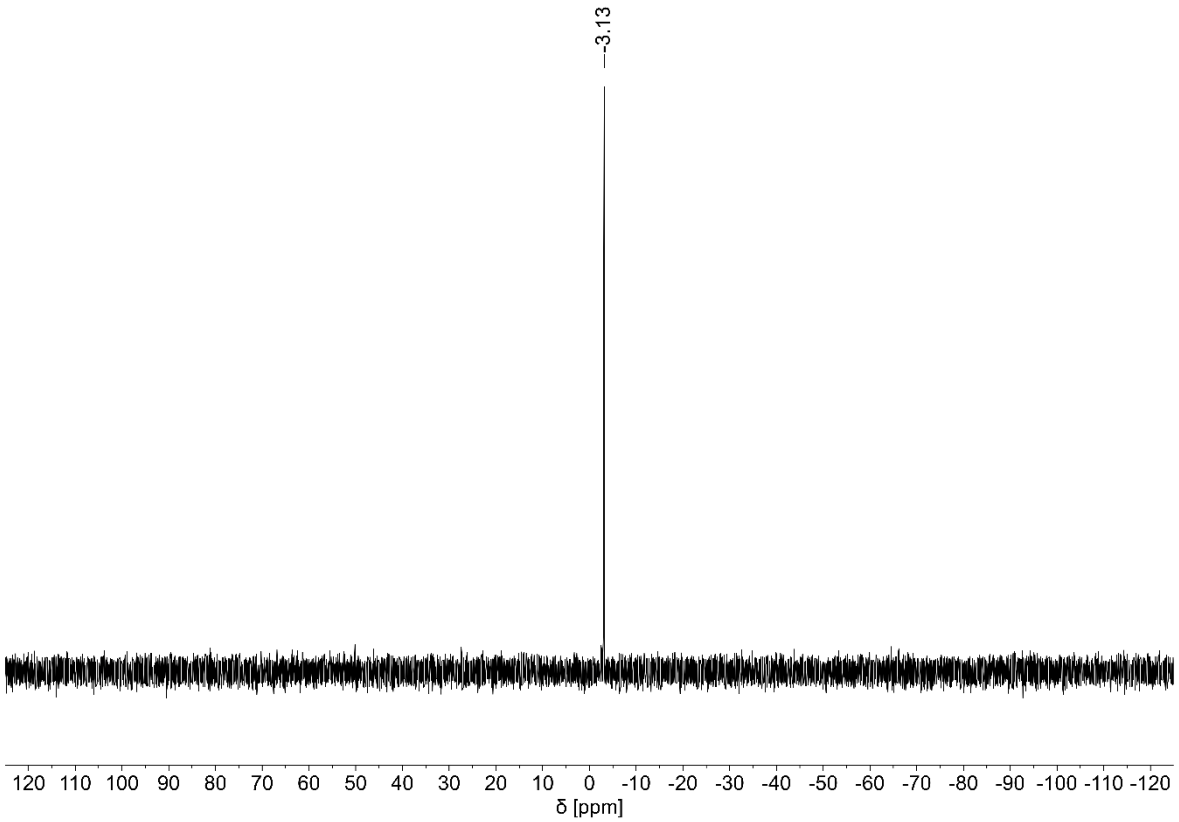

Figure S81. ^{19}F NMR spectrum of $[Tc(CN^tBu)(CO)_3(PPh_3)_2](BF_4)$ (**9b**).

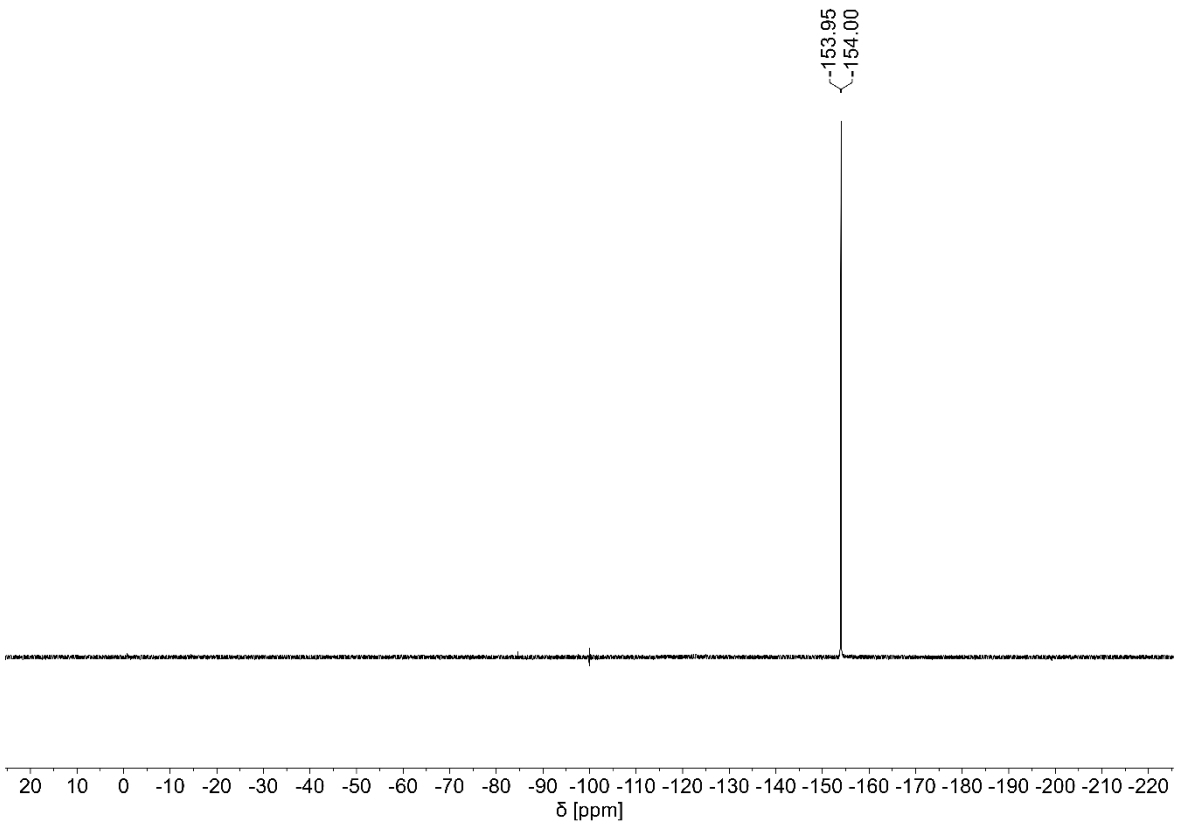

Figure S82. IR spectrum of [Tc(CN^{t}Bu)(CO)$_3$(PPh$_3$)$_2$](BF$_4$) (**9b**).

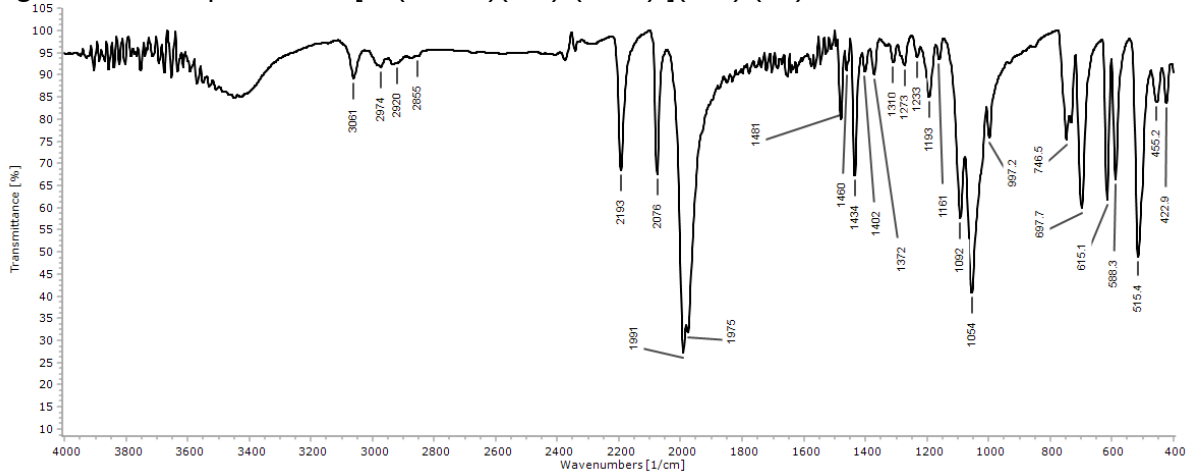

Figure S83. ^{1}H NMR spectrum of [Tc(NCPh)(CO)$_3$(PPh$_3$)$_2$](BF$_4$) (**10a**).

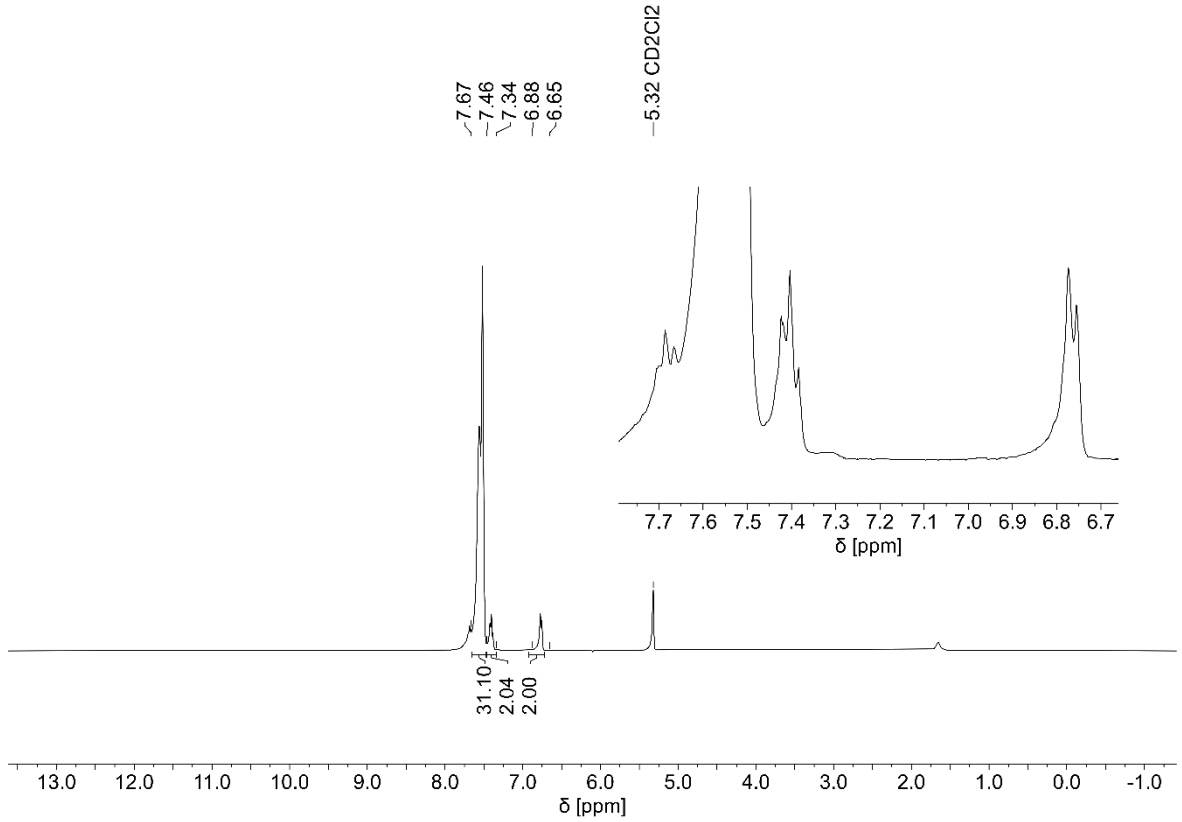

Figure S84. ^{99}Tc NMR spectrum of [Tc(NCPh)(CO)$_3$(PPh$_3$)$_2$](BF$_4$) (**10a**).

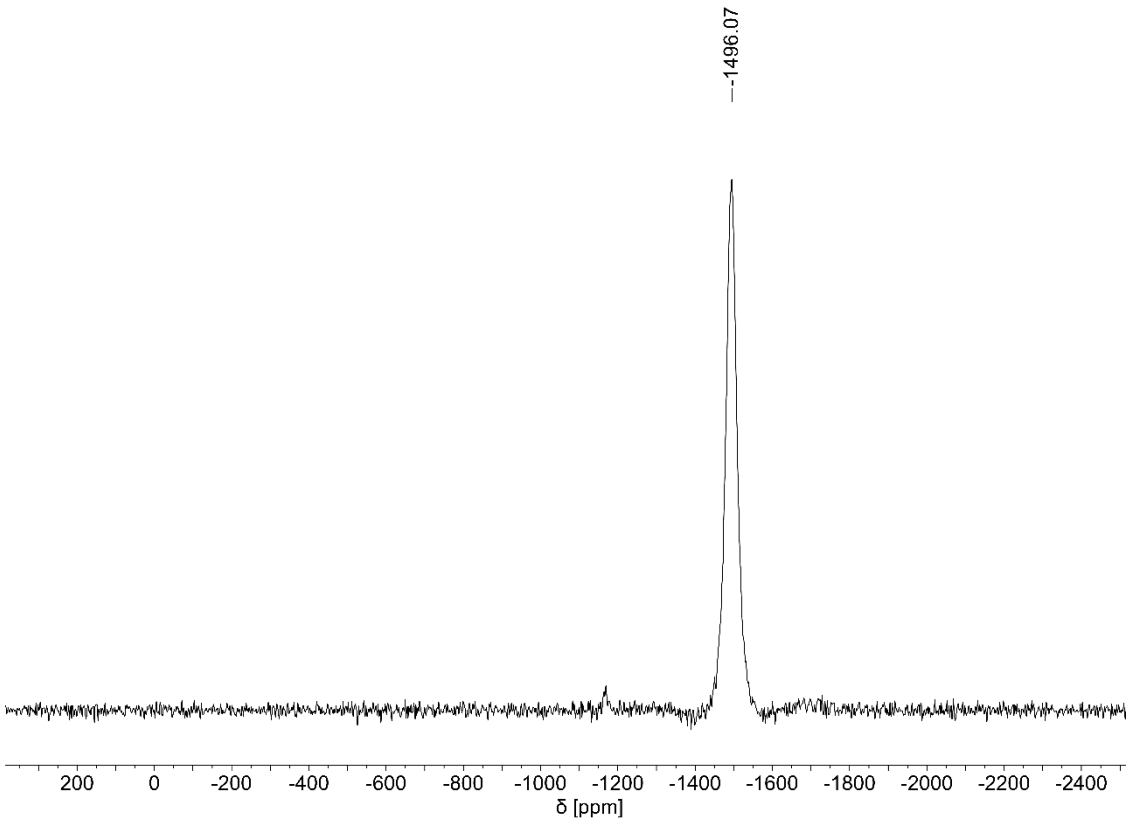

Figure S85. ^{31}P{^{1}H} NMR spectrum of [Tc(NCPh)(CO)$_3$(PPh$_3$)$_2$](BF$_4$) (**10a**).

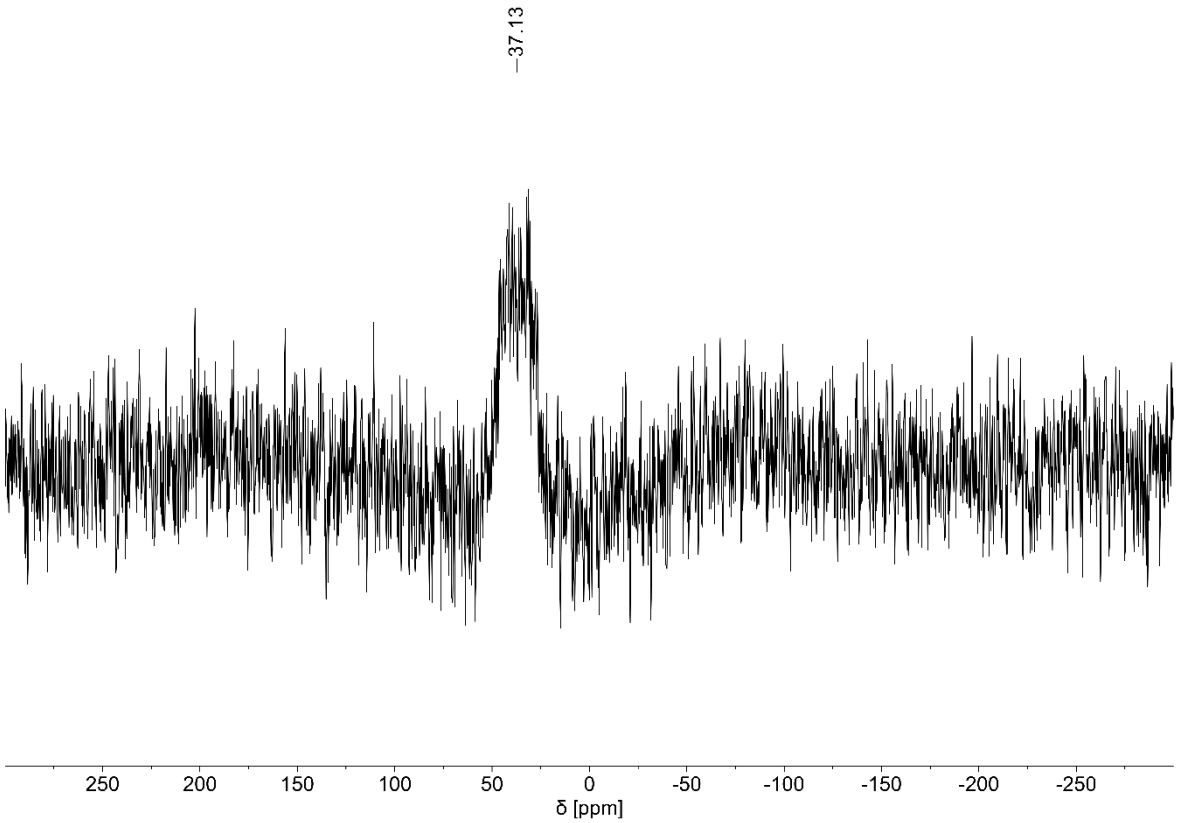

Figure S86. ^{11}B NMR spectrum of $[Tc(NCPh)(CO)_3(PPh_3)_2](BF_4)$ (**10a**).

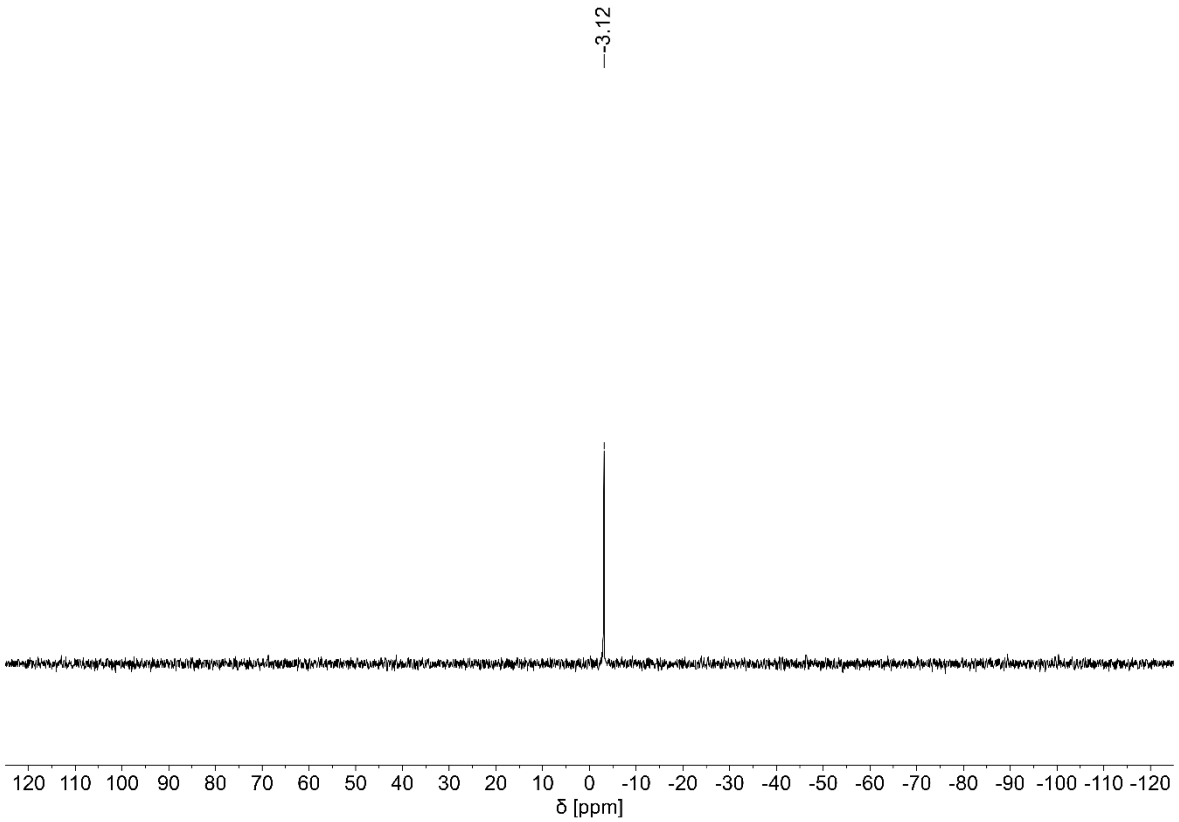

Figure S87. ^{19}F NMR spectrum of $[Tc(NCPh)(CO)_3(PPh_3)_2](BF_4)$ (**10a**).

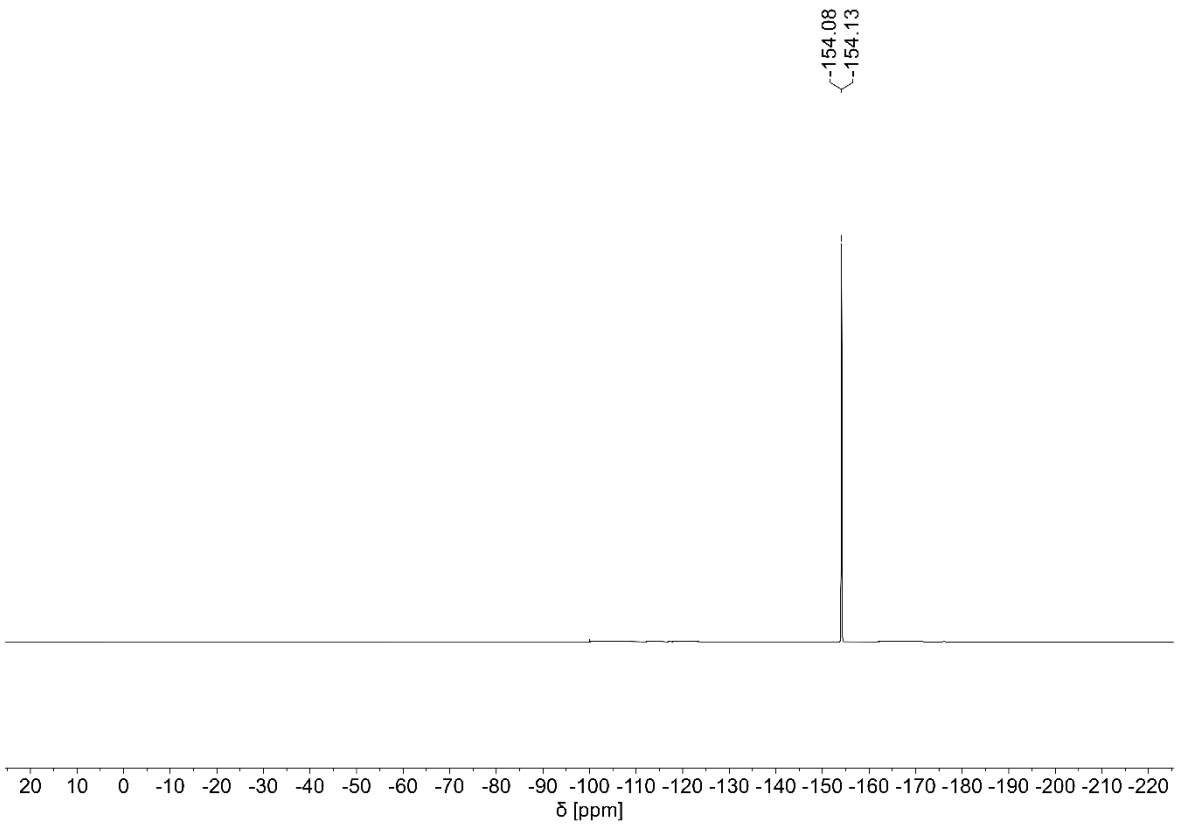

Figure S88. IR spectrum of $[Tc(NCPh)(CO)_3(PPh_3)_2](BF_4)$ (**10a**).

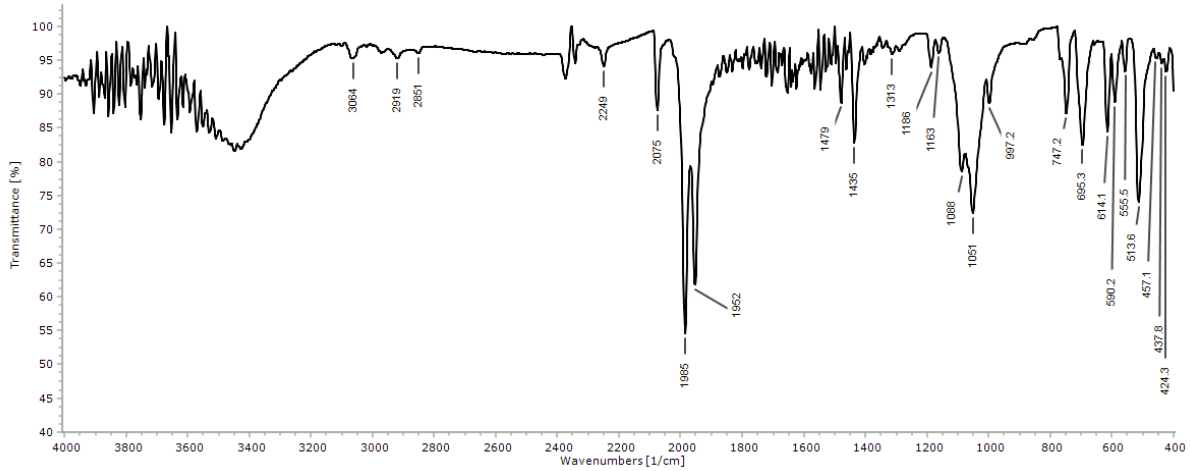

Figure S89. ^1H NMR spectrum of $[Tc(NC^tBu)(CO)_3(PPh_3)_2](BF_4)$ (**10b**).

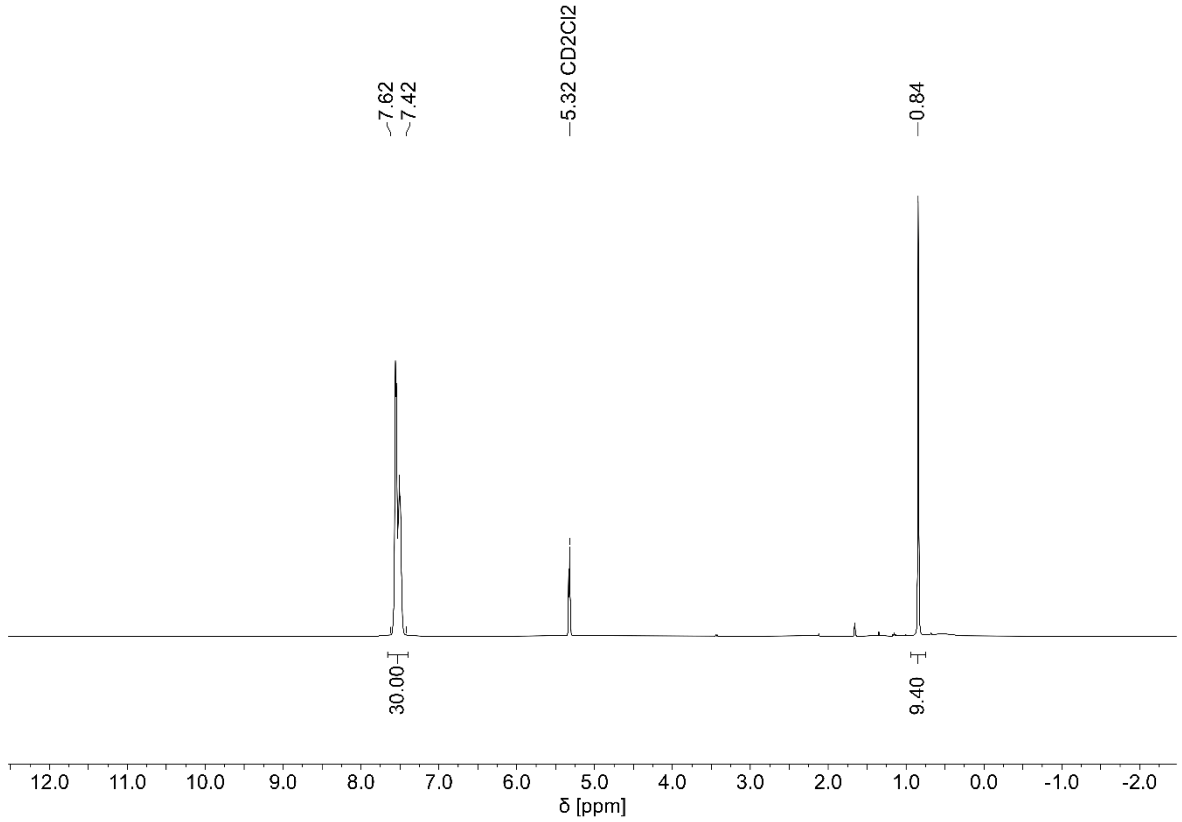

Figure S90. ^{99}Tc NMR spectrum of [Tc(NC^{t}Bu)(CO)$_3$(PPh$_3$)$_2$](BF$_4$) (**10b**).

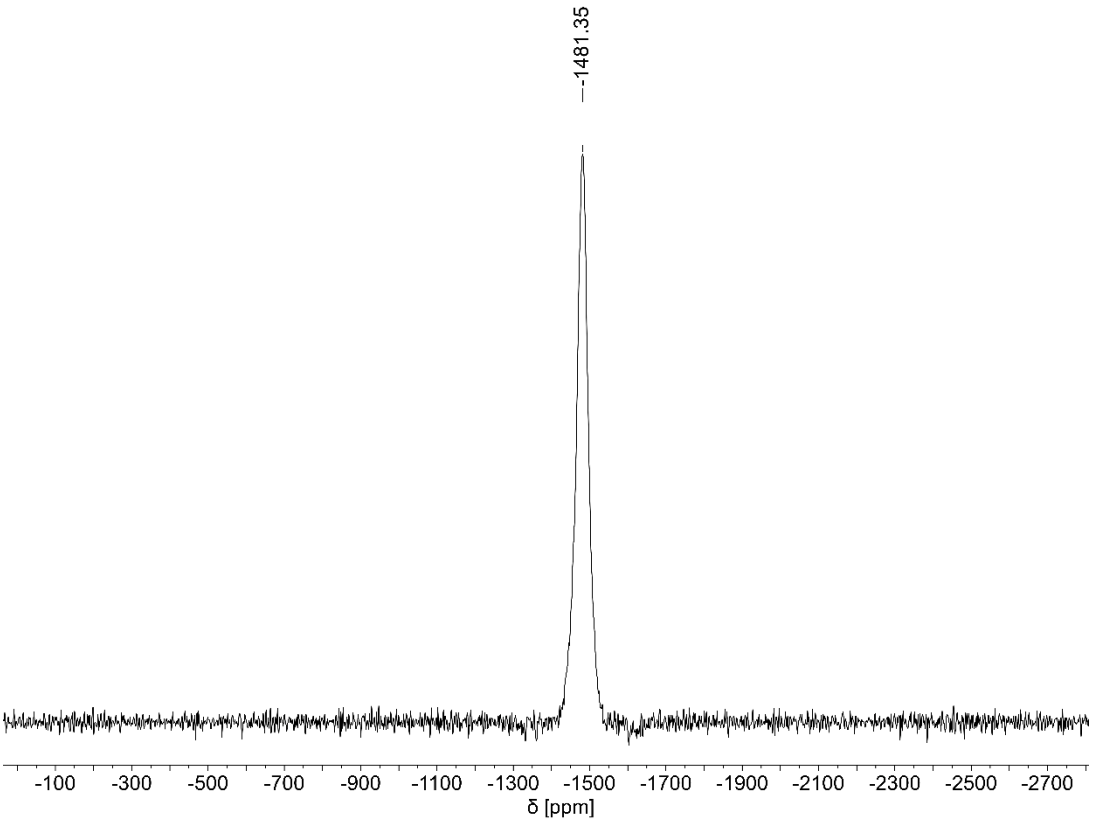

Figure S91. ^{31}P{^{1}H} NMR spectrum of [Tc(NC^{t}Bu)(CO)$_3$(PPh$_3$)$_2$](BF$_4$) (**10b**).

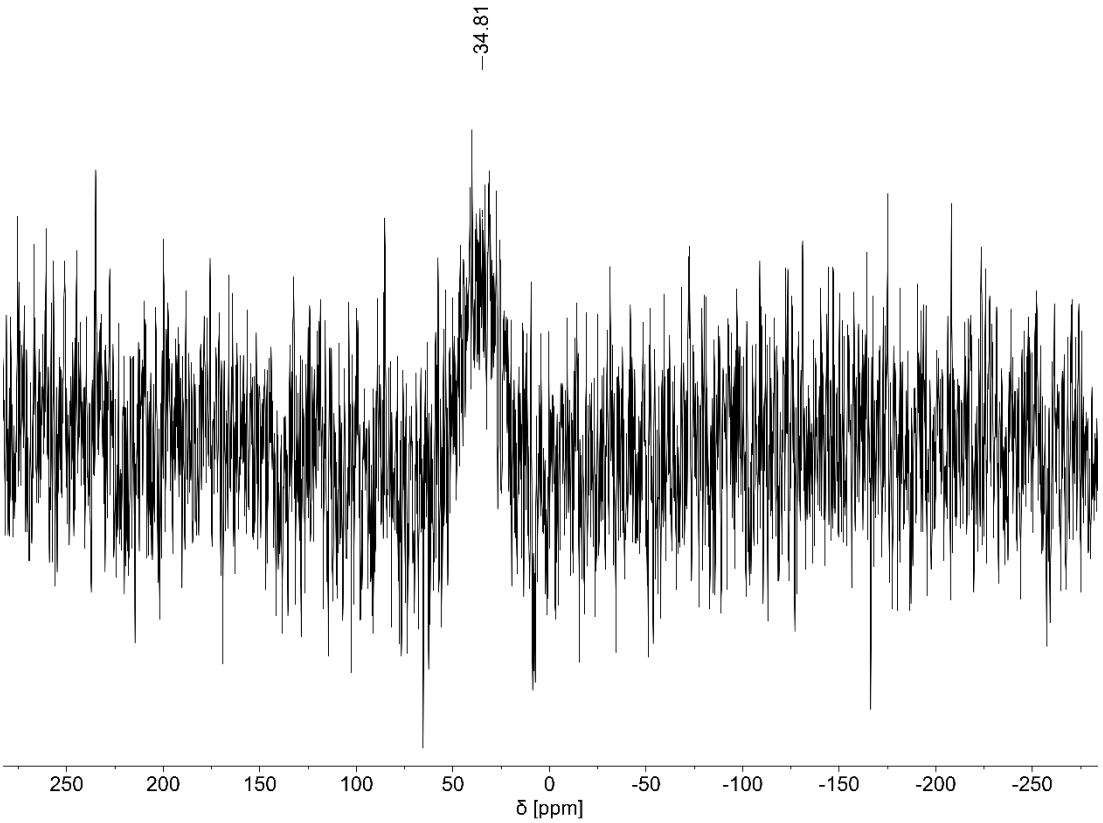

Figure S92. ^{11}B NMR spectrum of $[Tc(NC^tBu)(CO)_3(PPh_3)_2](BF_4)$ (**10b**).

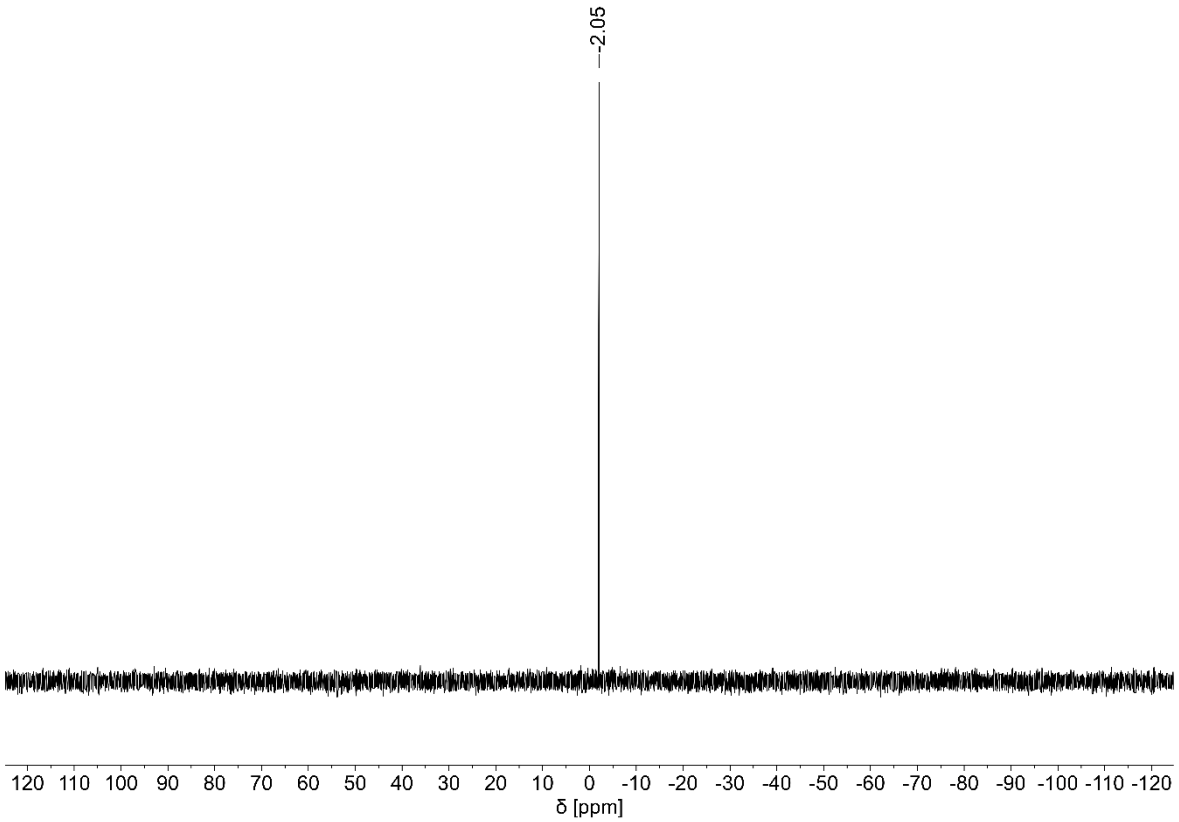

Figure S93. ^{19}F NMR spectrum of $[Tc(NC^tBu)(CO)_3(PPh_3)_2](BF_4)$ (**10b**).

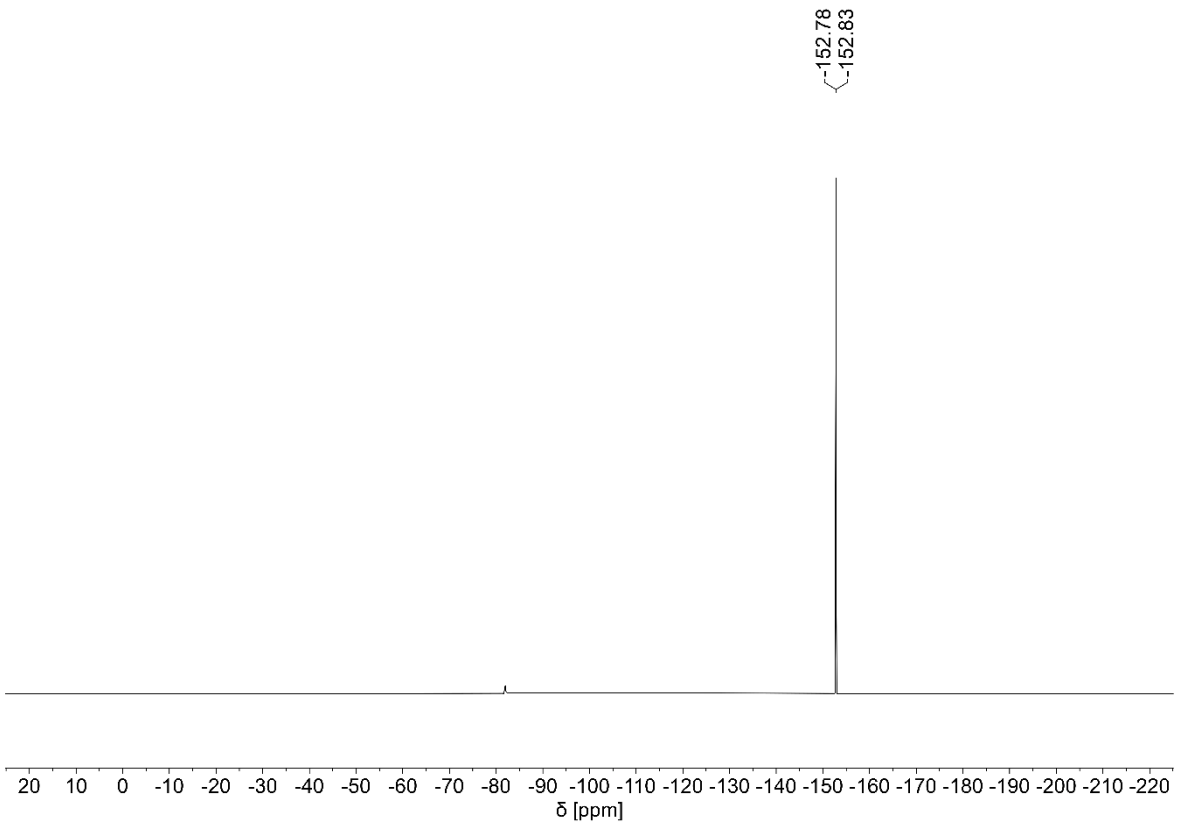

Figure S94. IR spectrum of $[Tc(NC^tBu)(CO)_3(PPh_3)_2](BF_4)$ (**10b**).

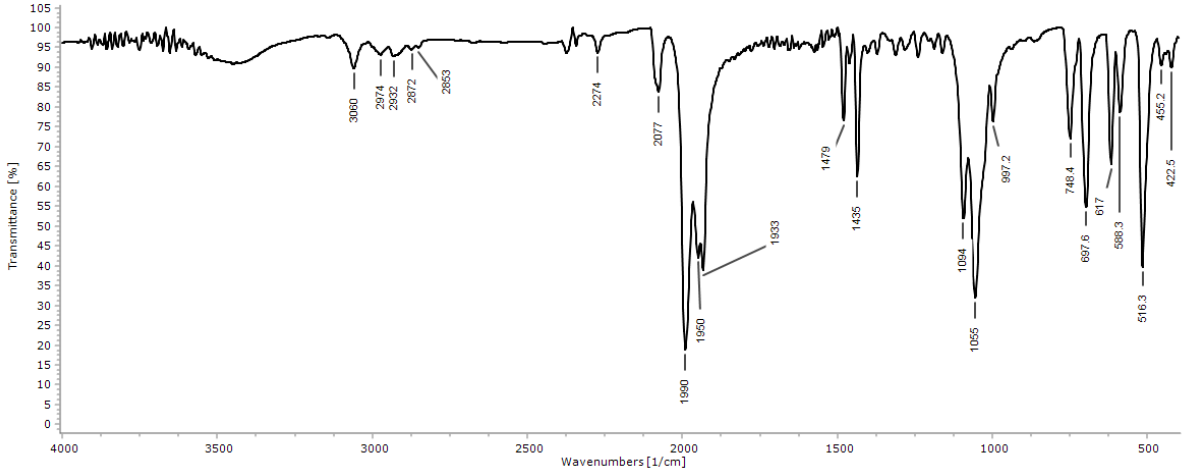

Figure S95. IR spectrum of the product obtained by heating $[Tc(OH_2)(CO)_3(PPh_3)_2](BF_4)$ (**1**) with HCCPh.

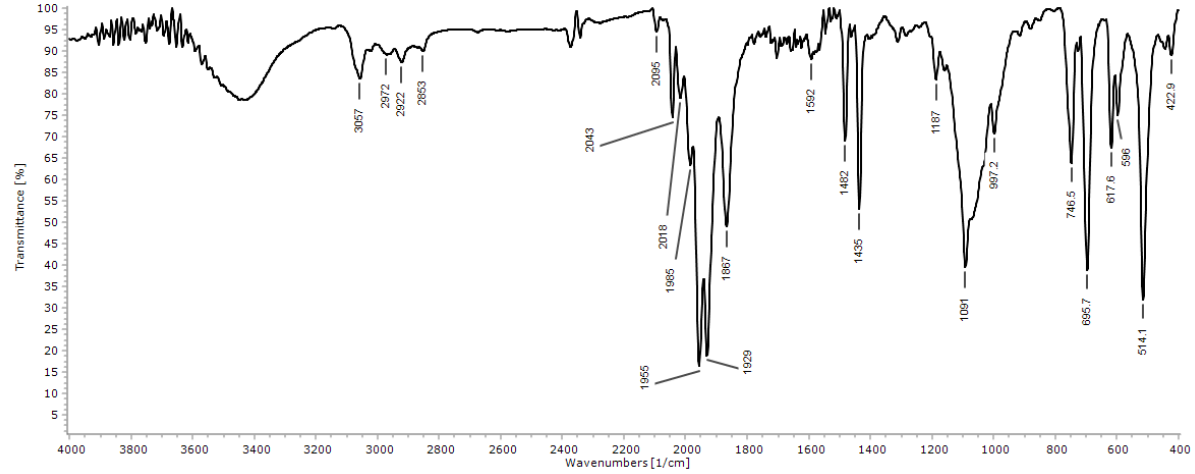

Figure S96. IR spectrum of the protonation/deprotection attempt of $[Tc(CCSiMe_3)(CO)_3(PPh_3)_2]$ (**8d**) with HBF_4.

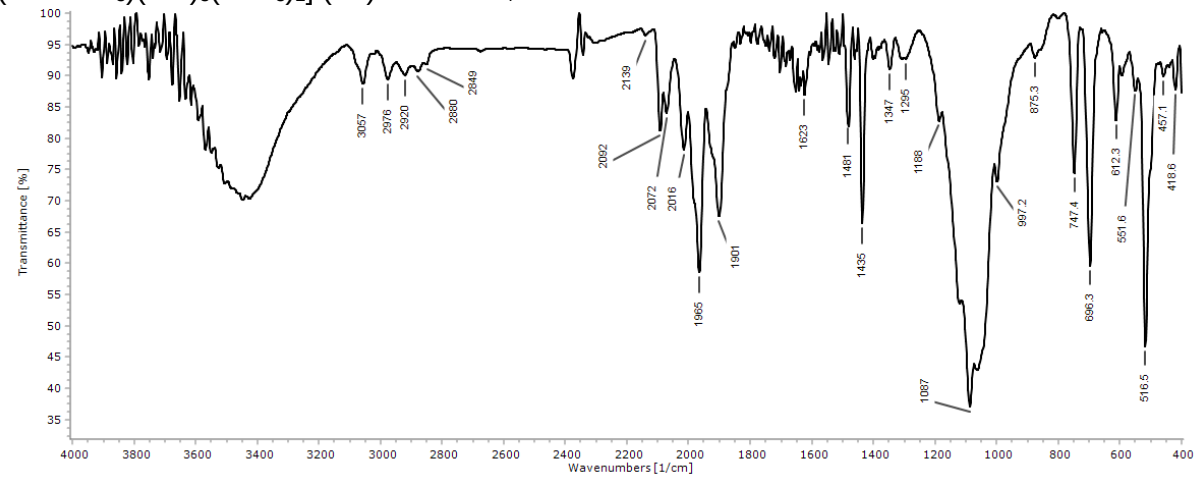

Part 4: Computational chemistry

Initial structural models were derived from X-ray structures and/or modelled with the program packages Avogadro and GaussView. The structures were optimized at the B3LYP level of theory. In some cases, only two out of four internal gaussian convergence criteria were fulfilled but the differences on the other two criteria were neglectable. The convergence of all structures was verified by the absence of negative frequencies.

Table S2. Angular energy dependence of **8a**, **9a** and **10a** in the gas-phase; values are given in Hartree, angles are given in °.

P-Tc-Aryl torsion	**8a**	$\Delta E_{rel.\ to\ min.}$	**9a**	$\Delta E_{rel.\ to\ min.}$	**10a**	$\Delta E_{rel.\ to\ min.}$
90	-2132.15955	0.00103457	-2148.67265	0.00158137		
85	-2132.15938	0.00119875	-2148.67235	0.00188828		
84	-2132.15933	0.00124874				
80	-2132.1596	0.00098626	-2148.67285	0.00138324	-2147.97232	0.00142896
70	-2132.15968	0.0008975	-2148.67316	0.00107348	-2147.97261	0.00114197
60	-2132.1598	0.00078154	-2148.67351	0.0007266	-2147.97292	0.00083132
56	-2132.15988	0.00070462	-2148.67364	0.00059078	-2147.97309	0.00066042
50	-2132.16002	0.00056168	-2148.67384	0.00039811	-2147.97334	0.00041183
40	-2132.16027	0.00031022	-2148.67408	0.00015809	-2147.97342	0.00032338
30	-2132.16049	9.422E-05	-2148.6742	2.949E-05	-2147.97363	0.00011465
20	-2132.16058	0	-2148.67423	0	-2147.97375	0
10	-2132.16057	1.175E-05	-2148.67417	6.225E-05	-2147.97374	4.61E-06
0	-2132.16042	0.00015947	-2148.67398	0.00025135	-2147.97356	0.00018636

Figure S97. Angular energy dependence of **8a**, **9a** and **10a** in the gas-phase; energy values are given in Hartree, angles are given in °.

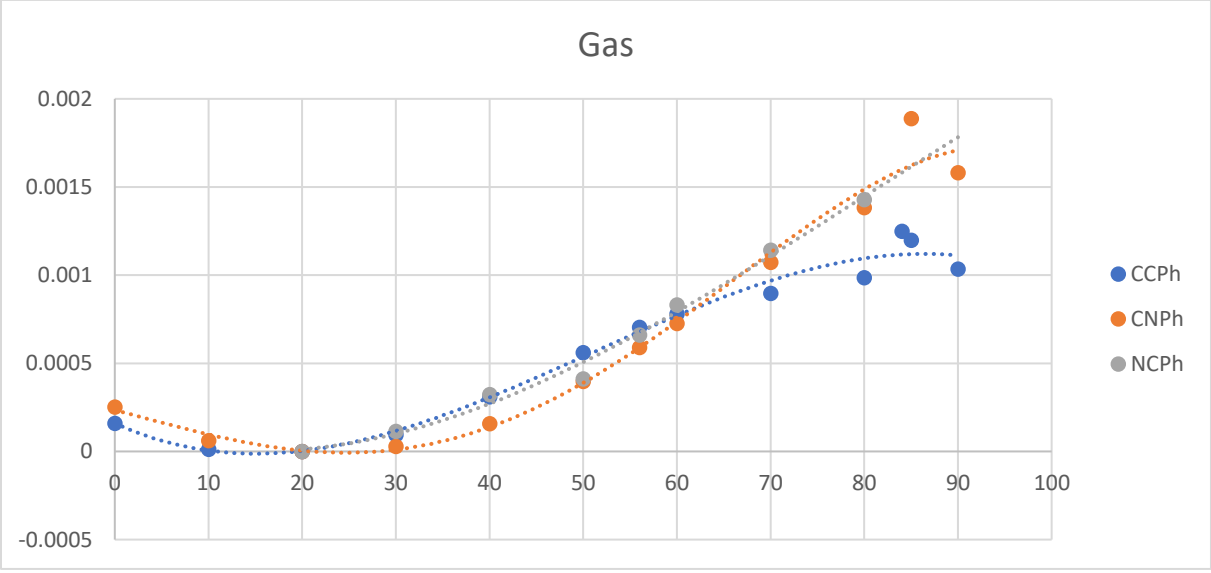

Table S3. Angular energy dependence of **8a** in dichloromethane solution; values are given in Hartree, angles are given in °.

P-Tc-Aryl torsion	**8a**	$\Delta E_{\text{rel. to min.}}$
90	-2132.175309	9.42E-05
85	-2132.175113	0.00029058
84	-2132.174847	0.00055637
80	-2132.175289	0.00011493
70	-2132.175128	0.00027539
60		
56	-2132.175065	0.00033885
50	-2132.175059	0.00034506
40	-2132.175115	0.00028825
30	-2132.175219	0.00018507
20	-2132.175306	9.787E-05
10	-2132.175389	1.411E-05
0	-2132.175404	0

Figure S98. Angular energy dependence of **8a** in dichloromethane solution; energy values are given in Hartree, angles are given in °.

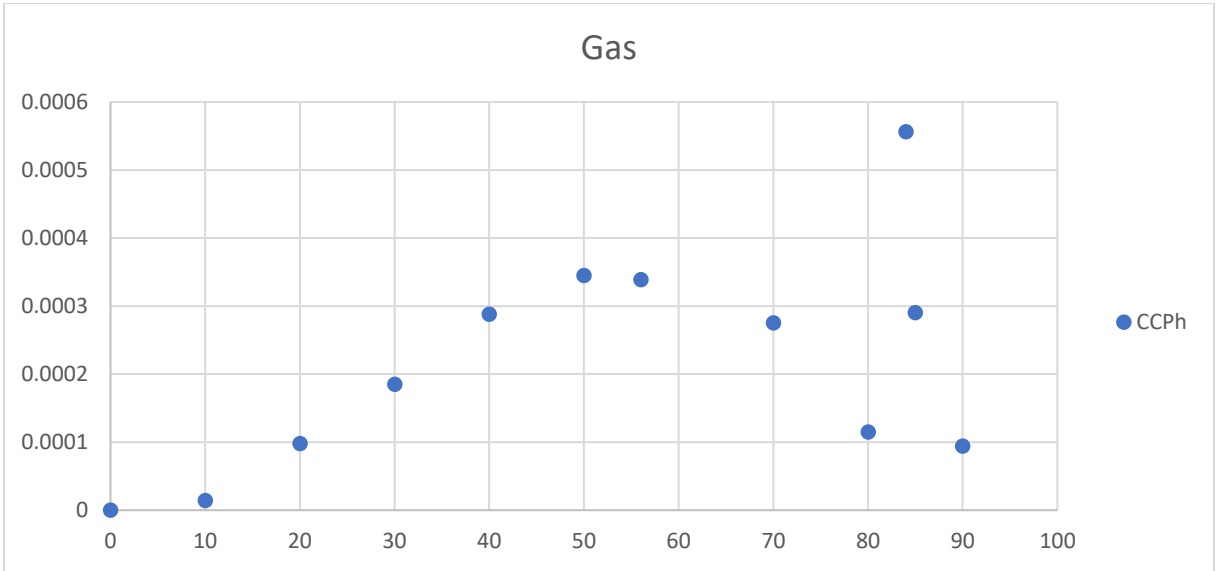

Table S4. Selected NBO and second order perturbation analyses of **8a/8b**, **9a/9b**, **10a/10b**, $[Tc(CN)(CO)_3(PPh_3)_2]$ and $[Tc(CO)_4(PPh_3)_2]^+$ in the gas-phase compared to spectroscopic and solid-state parameters. The first parameters describe the L-Tc-C2 3c/4e$^-$ bond concerning the additional ligand and its *trans*-CO ligand, while the second given parameters describe the C1-Tc-C3 3c/4e$^-$ bond concerning the two *trans*-CO ligands respectively.

	10b	**10a**	**8b**	**8a**	**$[Tc(CN)(CO)_3(PPh3)_2]$**	**9a**	**9b**	**$[Tc(CO)_4(PPh_3)_2]^+$**
$E_{deloc.}$ [kcal/mol]	88	94	182	197	251	261	264	317
$\Delta E_{i,j}$ [Hartree]	0.95	0.96	0.86	0.85	0.79	0.8	0.81	0.77
$F_{i,j}$ [a.u.]	0.257	0.268	0.353	0.365	0.398	0.409	0.412	0.44
Occ. [e$^-$]	-	3.94	3.84	3.85	3.88	3.90	3.89	3.91
%C_{CO}-Tc	-	66.4	51.4	51.5	51.9	52.9	52.9	49.9
%Tc-L	-	33.6	48.6	48.5	48.1	47.1	47.1	50.1
Tc-C_{CO} [Å]	1.90	1.88	1.92	1.92	1.95	1.94	1.94	1.985
C≡O [Å]	1.15	1.17	1.17	1.14	1.14	1.15	1.15	1.133
Tc-L [Å]	2.14	2.16	2.14	2.14	2.14	2.08	2.09	1.985
C≡X [Å]	1.14	1.14	1.19	1.19	1.14	1.15	1.15	1.133
$\nu_{c\equiv o,\ sym.}$ [cm^{-1}]	2081	2075	2045	2043	2054	2073	2075	
$\nu_{c\equiv o,\ asym.}$ [cm^{-1}]	1989	1985	1946	1960	1960	1992	1991	2012
$\nu_{c\equiv o,\ asym.}$ [cm^{-1}]	1936	1954	1925	1929	1935		1977	
$\nu_{c\equiv x}$ [cm^{-1}]	2272	2249		2095	2116	2166	2193	2012
δ [ppm]	-1481	-1496	-1956	-2056	-1901	-1880	-1874	-1895
$\nu_{1/2}$ [Hz]	3020	2818	11747	9638	5907	4280	4025	2643
$E_{deloc.}$ [kcal/mol]	329	323	326	314	307	310	313	317
$\Delta E_{i,j}$ [Hartree]	0.83	0.84	0.83	0.81	0.82	0.79	0.78	0.76
$F_{i,j}$ [a.u.]	0.466	0.466	0.463	0.451	0.448	0.442	0.442	0.44
Occ. [e$^-$]	3.91	3.91	3.91	3.90	3.90	3.92	3.93	3.91
%C_{CO}-Tc	49.9	49.9	50	49.9	49.8	49.7	49.7	49.9
%Tc-C_{CO}	50.1	50.1	50	50.1	50.2	50.3	50.3	50.1

Figure S99. Mapping of the Laplacian of the electron density ($\nabla^2\rho$) of **A)** $[Tc(CCPh)(CO)_3(PPh_3)_2]$, **B)** $[Tc(CNPh)(CO)_3(PPh_3)_2]^+$, **C)** $[Tc(CO)_4(PPh_3)_2]^+$, **D)** $[Tc(CN)(CO)_3(PPh_3)_2]$ and **E)** $[Tc(NCPh)(CO)_3(PPh_3)_2]^+$ in the P/L/*trans*-CO plane. Negative values correspond to an accumulation of electron density (dashed black lines), while positive values correspond to a charge depletion (solid black lines). A gradient color-scheme (red-white-blue; positive → negative) has been applied to the Laplacian iso-contours. Electron density gradient lines are additionally shown (grey lines). Atom labels are in red, chemical bonds are shown as bold, black lines between the atoms.

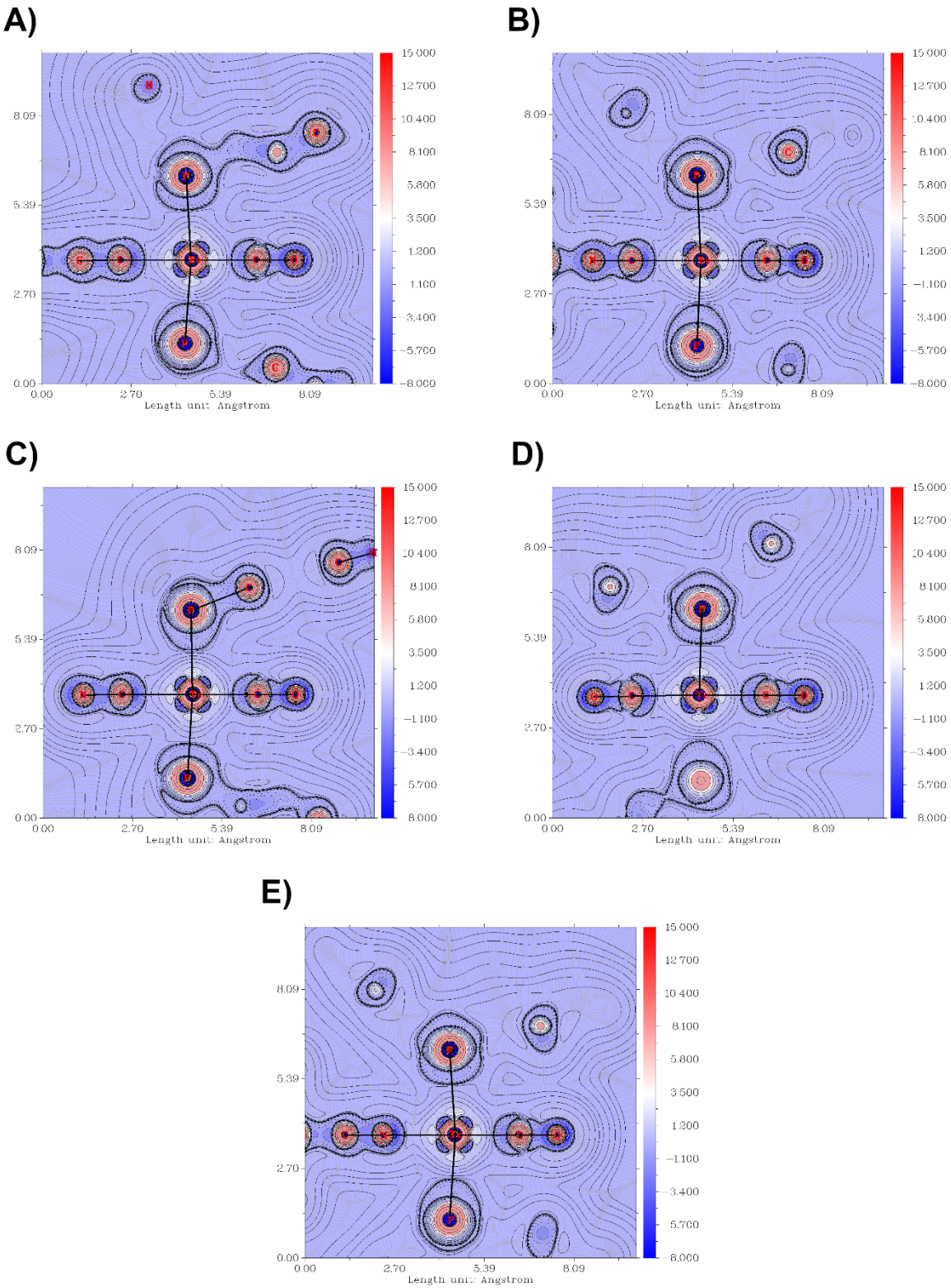

Figure S100. Mapping of the Laplacian of the electron density ($\nabla^2\rho$) of **A)** $[Tc(CCPh)(CO)_3(PPh_3)_2]$, **B)** $[Tc(CNPh)(CO)_3(PPh_3)_2]^+$, **C)** $[Tc(CO)_4(PPh_3)_2]^+$, **D)** $[Tc(CN)(CO)_3(PPh_3)_2]$ and **E)** $[Tc(NCPh)(CO)_3(PPh_3)_2]^+$ in the *cis*-CO/L/*trans*-CO plane. Negative values correspond to an accumulation of electron density (dashed black lines), while positive values correspond to a charge depletion (solid black lines). A gradient color-scheme (red-white-blue; positive → negative) has been applied to the Laplacian iso-contours. Electron density gradient lines are additionally shown (grey lines). Atom labels are in red, chemical bonds are shown as bold, black lines between the atoms.

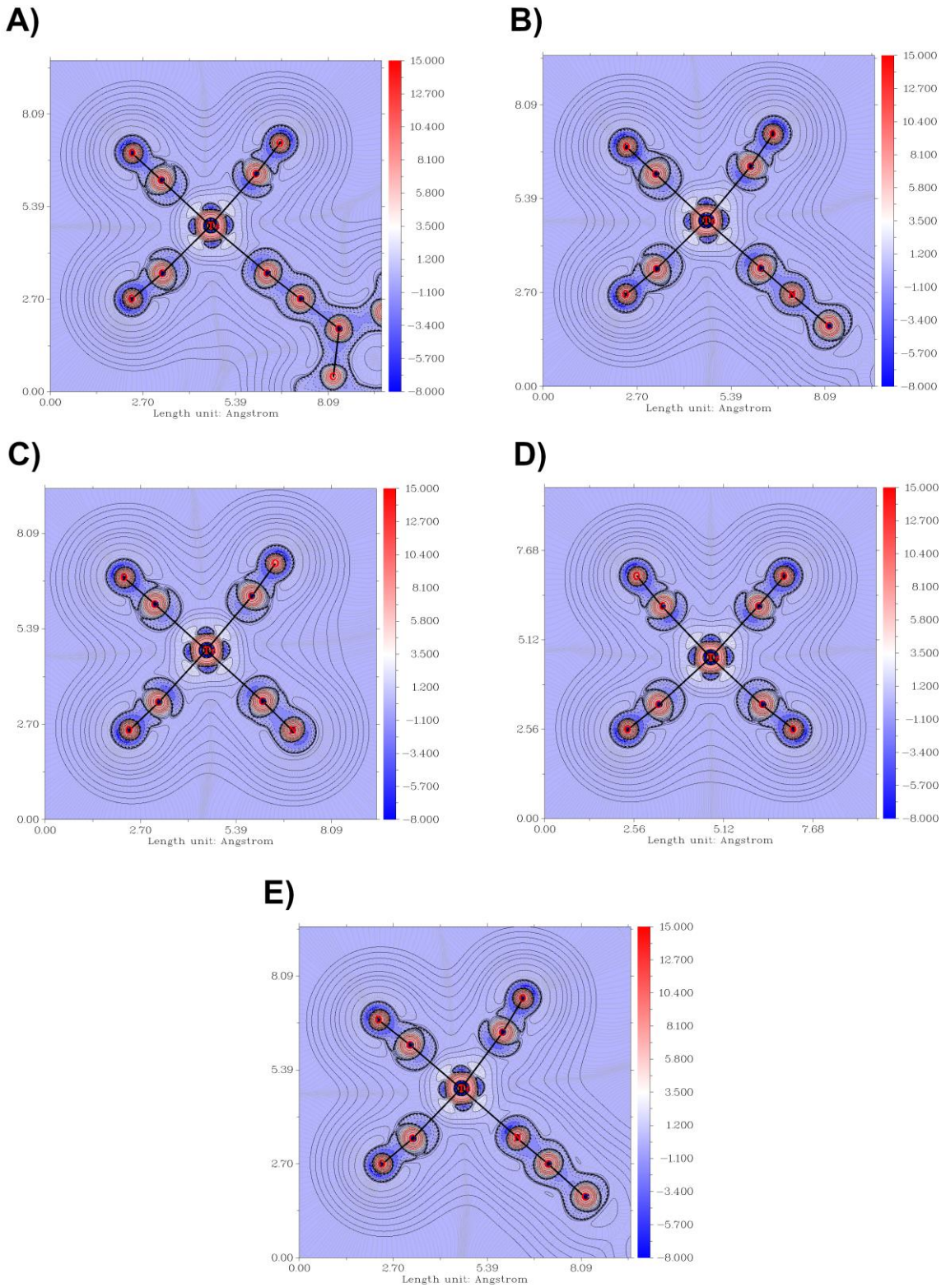

A.5 $[Tc^{I}(NO)X(cp)(PPh_3)]$ Complexes ($X^- = I^-, I_3^-, SCN^-, CF_3SO_3^-$ or CF_3COO^-) and Their Reactions

Authors	J. Ackermann, A. Abdulkader, C. Scholtysik, M. Roca Jungfer, A. Hagenbach, U. Abram
Journal	*Organometallics*, **2019**, *38*, 4471-1178
DOI	10.1021/acs.organomet.9b00620
Link	https://pubs.acs.org/doi/abs/10.1021/acs.organomet.9b00620
Detailed scientific contribution	Janine Ackermann, Abdullah Abdulkader and Ulrich Abram designed the project. Janine Ackermann and Abdullah Abdulkader performed the synthesis and characterization of the compounds. Ulrich Abram and Abdullah Abdulkader wrote the manuscript. Clemens Scholtysik and Adelheid Hagenbach calculated the X-ray structures. Maximilian Roca Jungfer performed DFT calculations on the bond isomerism of the SCN^-/NCS^- complexes, made suggestions and proofed the manuscript. Ulrich Abram supervised the project, provided scientific guidance and suggestions and corrected the manuscript.
Estimated own contribution	10%

Return to publication 4.5.

$[Tc^{I}(NO)X(cp)(PPh_3)]$ Complexes ($X^- = I^-$, I_3^-, SCN^-, $CF_3SO_3^-$ or CF_3COO^-) and Their Reactions

*Janine Ackermann, Abdullah Abdulkader, Clemens Scholtysik, Maximilian Roca Jungfer, Adelheid Hagenbach, Ulrich Abram**

Freie Universität Berlin, Institute of Chemistry and Biochemistry, Fabeckstr. 34-36, D-14195 Berlin, Germany

Table of Contents

Part 1 Crystallographic data

Part 2 DFT calculations

Part 1 Crystallographic data

Table S1. Crystal data and Structure determination parameters

	[Tc(NO)(SO_3CF_3)(Cp)(PPh_3)]	[Tc(NO)($OOCCF_3$)(Cp)(PPh_3)]
Formula	$C_{24}H_{20}NO_4PF_3STc$	$C_{25}H_{20}NO_3PF_3Tc$
Mw	604.44	568.41
Crystal system	monoclinic	orthorhombic
a/Å	9.283(1)	15.314(1)
b/Å	18.844(1)	9.187(1)
c/Å	14.129(1)	16.233(1)
β/°	104.94(1)°	90°
V/Å^3	2388.0(3)	2283.8(3)
Space group	$P2_1/n$	$Pca2_1$
Z	4	4
No. reflect.	60204	27454
No. indep.	5268	4925
R_{int}	0.0489	0.0396
No. param.	316	307
R1/ wR2	0.0294/0.0541	0.0243/0.0472
GOF	1.046	1.025
CCDC	1951310	1951311

	[Tc(NO)(SCN)(Cp)(PPh_3)]	[Tc(NO)(I_3)(Cp)(PPh_3)]	[Tc(NO)(I_2)(Cp)]
Formula	$C_{24}H_{20}N_2OPSTc$	$C_{23}H_{20}NOPI_3Tc$	$C_5H_5NOI_2Tc$
Mw	513.45	863.11	446.90
Crystal system	monoclinic	monoclinic	triclinic
a/Å	9.317(1)	17.257(1)	7.147(8)
b/Å	13.621(1)	8.025(1)	7.159(0)
c/Å	9.750(1)	18.359(1)	10.393(6)
α/°	90	90	74.839(2)
β/°	117.63(1)	104.29(9)	88.069(2)
γ/°	90	90	66.956(2)
V/Å^3	1096.3(2)	2463.8(4)	470.96(6)
Space group	$P2_1$	$P2_1/n$	P -1
Z	2	4	2
No. reflect.	59801	77830	15238
No. indep.	4511	5455	2269
R_{int}	0.0542	0.0874	0.0304
No. param.	271	248	91
R1/ wR2	0.0386/0.0977	0.0516/0.1312	0.0206/0.0544
GOF	1.040	1.111	1.407
CCDC	1951312	1951313	1951314

Fig. S1. Ellipsoid plot of [Tc(NO)(SO_3CF_3)(Cp)(PPh_3)]

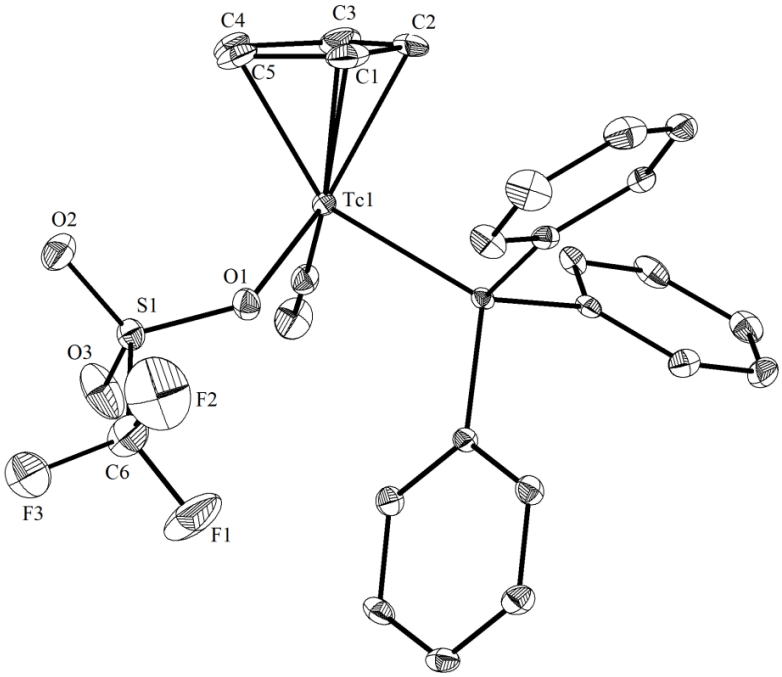

Table S2. Selected bond lengths and angles in [Tc(NO)(SO_3CF_3)(Cp)(PPh_3)]

Bond lengths (Å)			
Tc1-C1	2.259(2)	Tc1-N10	1.766(2)
Tc1-C2	2.240(2)	Tc1-O1	2.162(1)
Tc1-C3	2.254(1)	N10-O10	1.1848(1)
Tc1-C4	2.313(2)	Tc1-Cp(centroid)	
Tc1-C5	2.300(2)	Tc1-P1	2.3746(5)
Angles (˚)			
Tc1-N10-O10	172.1(2)	N10-Tc1-O1	102.18(6)
N10-Tc1-P1	93.87(5)		

Fig. S2. Ellipsoid plot of [Tc(NO)(OOCCF$_3$)(Cp)(PPh$_3$)]

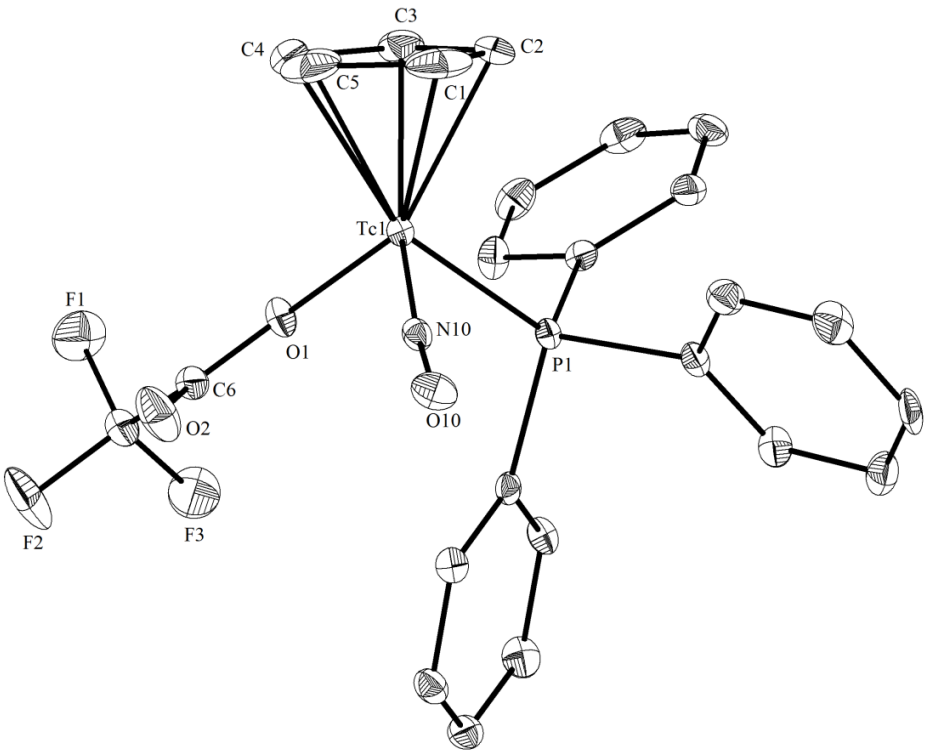

Table S3. Selected bond lengths and angles in [Tc(NO)(OOCCF$_3$)(Cp)(PPh$_3$)]

Bond lengths (Å)			
Tc1-C1	2.247(3)	Tc1-P1	2.3702(1)
Tc1-C2	2.275(3)	Tc1-N10	1.763(3)
Tc1-C3	2.304(3)	Tc1-O1	2.108(2)
Tc1-C4	2.305(3)	N10-O10	1.182(3)
Tc1-C5	2.247(3)	Tc1-Cp(centroid)	1.9339(1)
Angles (˚)			
Tc1-N10-O10	171.6(2)	N10-Tc1-O1	1053(1)
N10-Tc1-P1	92.22(8)		

Fig. S3. Ellipsoid plot of [Tc(NO)(SCN)(Cp)(PPh_3)]

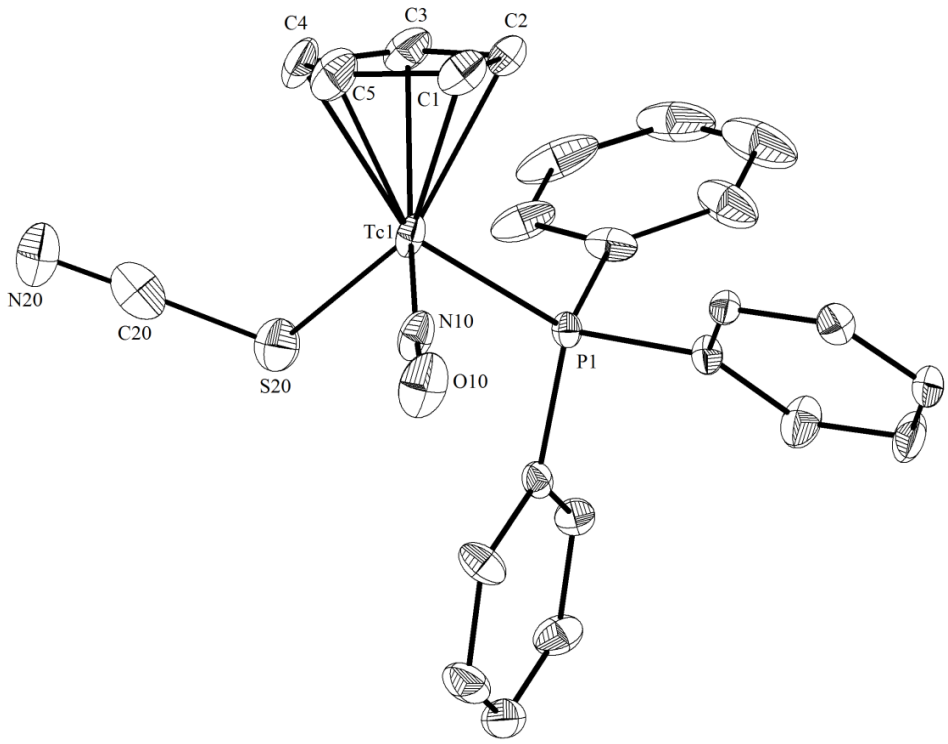

Table S4. Selected bond lengths and angles in [Tc(NO)(SCN)(Cp)(PPh_3)]

Bond lengths (Å)			
Tc1-C1	2.279(7)	Tc1-P1	2.371(2)
Tc1-C2	2.315(7)	Tc1-S20	2.469(2)
Tc1-C3	2.280(6)	N10-O10	1.179(8)
Tc1-C4	2.266(6)	S20-C20	1.664(9)
Tc1-C5	2.264(7)	C20-N20	1.18(1)
Tc1-Cp(centroid)	1.9330(2)		
Angles (˚)			
Tc1-N10-O10	168.4(6)	Tc1-S20-C20	108.5(3)
S20-C20-N20	176.6(7)		

Fig. S4. Ellipsoid plot of [Tc(NO)(I_3)(Cp)(PPh_3)]

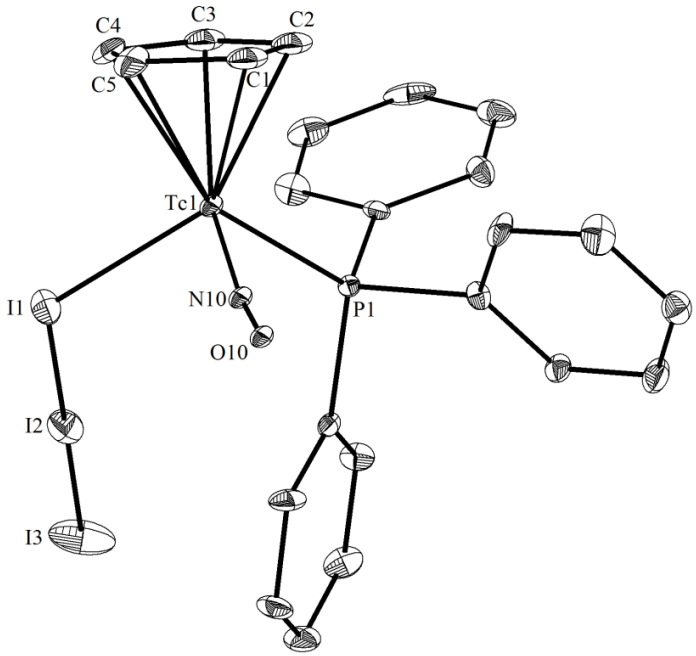

Table S5. Selected bond lengths and angles in [Tc(NO)(I_3)(Cp)(PPh_3)]

Bond lengths (Å)			
Tc1-C1	2.245(9)	Tc1-P1	2.375(2)
Tc1-C2	2.243(8)	Tc1-N10	1.819(6)
Tc1-C3	2.317(8)	N10-O10	0.958(8)
Tc1-C4	2.302(8)	Tc1-I1	2.7037(9)
Tc1-C5	2.283(9)	I1-I2	3.0597(9)
Tc1-Cp(centroid)	1.9373(2)	I2-I3	2.8077(9)
Angles (˚)			
Tc1-N10-O10	170.8(7)	Tc1-I1-I2	124.38(3)
I1-I2-I3	179.59(3)		

Fig. S5. Ellipsoid plot of $[Tc(NO)(I)_2(Cp)]$.

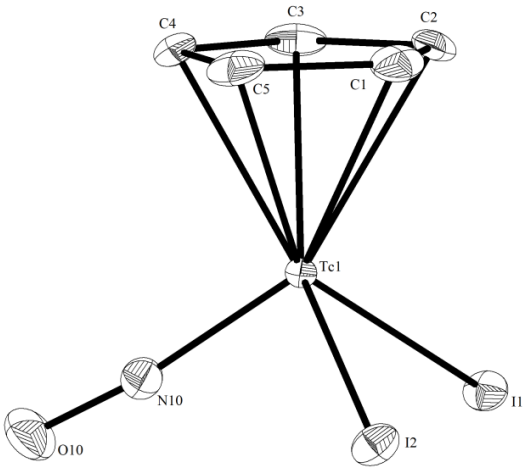

Table S6. Selected bond lengths and angles in $[Tc(NO)(I)_2(Cp)]$.

Bond lengths (Å)			
Tc1-C1	2.328(3)	Tc1-Cp(centroid)	1.9504(1)
Tc1-C2	2.332(3)	Tc1-N10	1.763(3)
Tc1-C3	2.265(3)	N10-O10	1.159(4)
Tc1-C4	2.259(3)	Tc1-I1	2.6774(3)
Tc1-C5	2.272(3)	Tc1-I2	2.6731(3)
Angles (˚)			
Tc1-N10-O10	173.2(3)	I2-Tc1-I1	100.22(1)

Part 2 DFT calculations

Table S7: Calculated Energies for the optimized **S**CN and **N**CS geometries.

	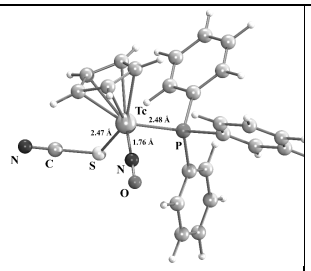 **S**CN	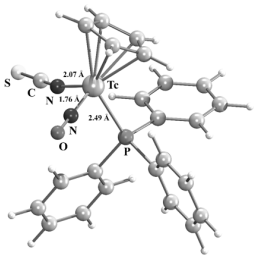 **N**CS	Δ	
	[Hartree]	[Hartree]	[Hartree]	[kcal/mol]
$E_{elec.}$	-1209.063896	-1209.072190	0.008294	5.20456
$\Sigma(E_{elec.}+E_{ZP})$	-1208.686549	-1208.694517	0.007968	4.99999
$\Sigma(E_{elec.}+E_{therm.})$	-1208.657944	-1208.666038	0.008094	5.07906
$\Sigma(E_{elec.}+\Delta H)$	-1208.657000	-1208.665094	0.008094	5.07906
$\Sigma(E_{elec.}+\Delta G)$	-1208.750147	-1208.758741	0.008594	5.39282

Figure S6. Representations of the orbital of the unpaired electron, illustrating significant contribution of Tc and Cp^- orbitals in $[Tc(NO)(I)_2(Cp)]$.

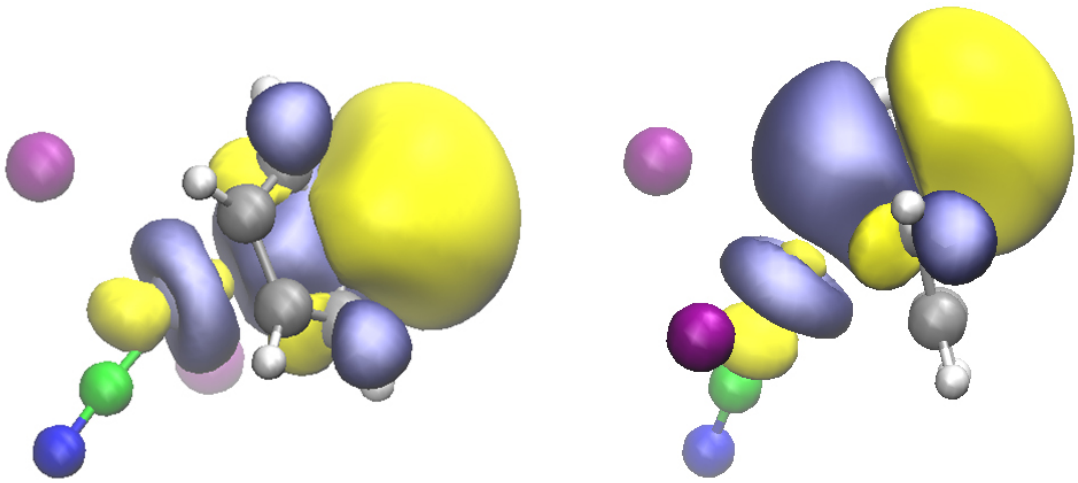

A.6 $[\{Tc^{I}(NO)(L^{OMe})(PPh_3)Cl\}_2Ag](PF_6)$ and $[Tc^{II}(NO)(L^{OMe})(PPh_3)Cl](PF_6)$: Two Unusual Technetium Complexes with a "Kläui-type" Ligand

Authors	M. Roca Jungfer, M. J. Ernst, A. Hagenbach, U. Abram
Journal	*Z. Anorg. Allg. Chem.* **2022**, e202100316.
DOI	10.1002/zaac.202100316
Link	https://onlinelibrary.wiley.com/doi/10.1002/zaac.202100316
Detailed scientific contribution	Maximilian Roca Jungfer and Ulrich Abram designed the project. Moritz Johannes Ernst performed the synthesis and characterization of the compounds during his research internship under the supervision of Maximilian Roca Jungfer. Maximilian Roca Jungfer, Moritz Johannes Ernst and Ulrich Abram calculated the X-ray structures under the guidance of Adelheid Hagenbach. Ulrich Abram wrote the manuscript. Maximilian Roca Jungfer and Moritz Johannes Ernst corrected the manuscript. Ulrich Abram supervised the project, provided scientific guidance and suggestions and corrected the manuscript.
Estimated own contribution	50%

Return to publication 4.6.

Zeitschrift für anorganische und allgemeine Chemie

Supporting Information

$[\{Tc^{I}(NO)(L^{OMe})(PPh_3)Cl\}_2Ag](PF_6)$ and $[Tc^{II}(NO)(L^{OMe})(PPh_3)Cl](PF_6)$: Two Unusual Technetium Complexes with a "Kläui-type" Ligand

Maximilian Roca Jungfer, Moritz Johannes Ernst, Adelheid Hagenbach, and Ulrich Abram*

Supporting Information to the paper

$[\{Tc^{I}(NO)(L^{OMe})(PPh_3)Cl\}_2Ag](PF_6)$ and $[Tc^{II}(NO)(L^{OMe})(PPh_3)Cl](PF_6)$: Two Unusual Technetium Complexes with a "Kläui-type" Ligand

Maximilian Roca Jungfer, Moritz Johannes Ernst, Adelheid Hagenbach and Ulrich Abram

Freie Universität Berlin, Institute of Chemistry and Biochemistry, Fabeckstr. 34/36, 14195 Berlin

Table S1. Crystal data and structure determination parameters of and [Tc(NO)(L^{MeO})Cl(PPh_3)](PF_6) · CH_2Cl_2 (**3** · CH_2Cl_2) and [{Tc(NO)(L^{OMe})Cl(PPh_3)}$_2$Ag](PF_6) · CH_2Cl_2 (**4** · CH_2Cl_2)

	3 · CH_2Cl_2	**4** · CH_2Cl_2
Formula	$C_{30}H_{40}Cl_3CoF_6NO_{10}P_5Tc$	$C_{59}H_{78}AgCl_4Co_2F_6N_2O_{20}P_9Tc_2$
M_w	1106.76	2091.49
a/Å	9.5746(9)	10.4038(5)
b/Å	13.761(1)	13.7776(6)
c/Å	17.483(1)	27.435(1)
α/°	87.831(7)	91.959(2)
β/°	81.238(7)	93.382(2)
γ/°	73.170(7)	92.053(2)
V/ Å^3	2179.1(3)	3920.6(3)
Crystal system	Triclinic	Triclinic
Space group	$P\bar{1}$	$P\bar{1}$
Z	2	2
D_{calc} g/cm^{-3}	1.687	1.772
μ/mm^{-1}	1.142	1.405
No. reflect.	20981	85177
No. indep.	9457	17327
R_{int}	0.069	0.0831
No. param.	547	955
R_1/wR_2 [I>2σ(I)]	0.0500/0.0965	0.0574/0.1220
GOF	0.852	1.059
CSD	2105101	2105102

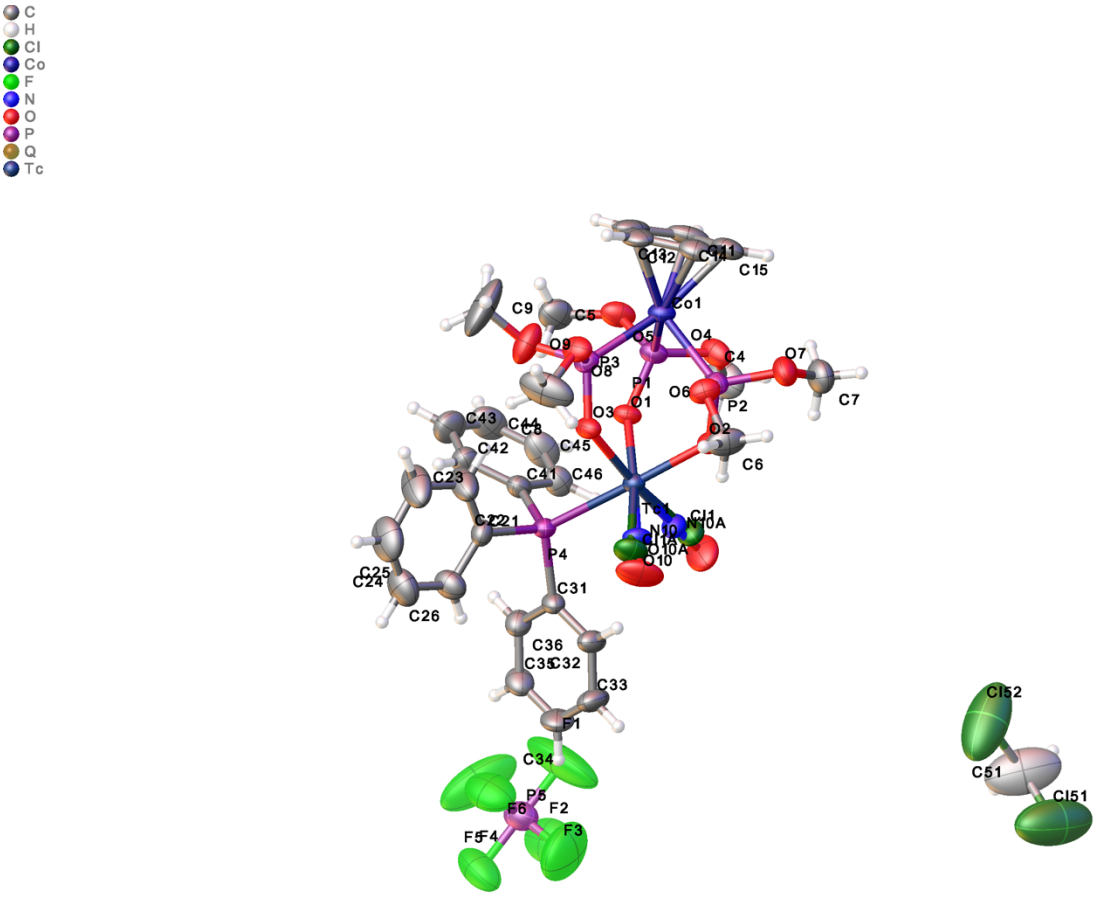

Figure S1. Ellipsoid representation of [Tc(NO)(L^{MeO})Cl(PPh_3)](PF_6) · CH_2Cl_2 (**3** · CH_2Cl_2) including disordered atoms.

Table S2. Selected bond lengths (Å) and angle (°) in [Tc(NO)(L^{MeO})Cl(PPh_3)](PF_6) · CH_2Cl_2 (**3** · CH_2Cl_2).

Tc1-N10*	1.73(1)	Tc1-O3	2.050(3)
Tc1-Cl1*	2.329(5)	Tc1-P4	2.481(1)
Tc1-O1	2.051(3)	N10-O10*	1.19(1)
Tc1-O2	2.067(3)		
N10-Tc1-Cl1*	95.9(4)	N10-Tc1-O3*	91.6(4)
N10-Tc1-O1*	175.5(4)	N10-Tc1-P4*	90.6(4)
N10-Tc1-O2*	92.5(4)	Tc1-N10-O10*	177.9(14)

*Disorder. Values refer to the main component.

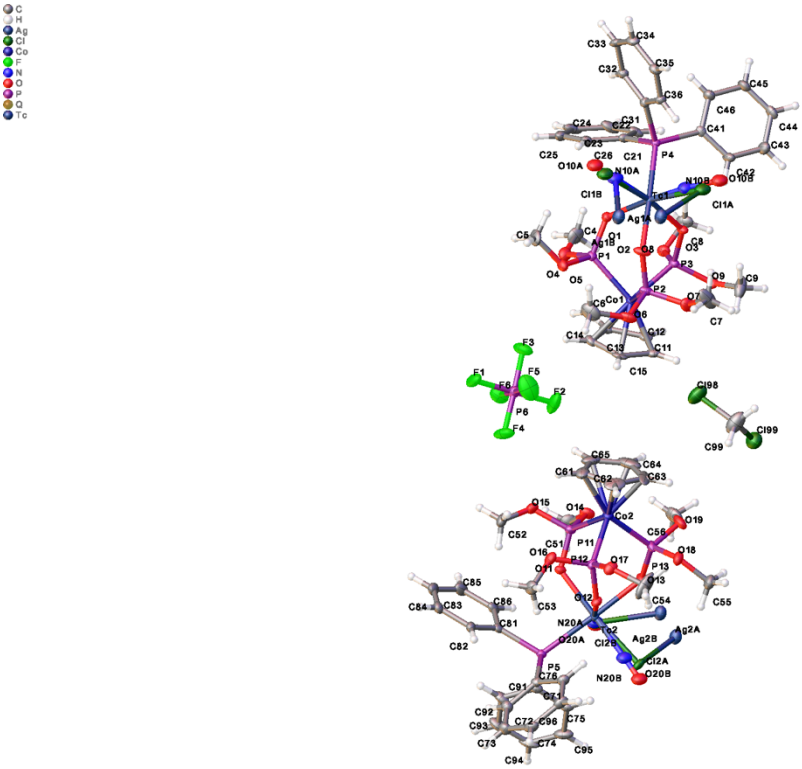

Figure S2. Ellipsoid representation of the asymmetric unit of [{Tc(NO)(L^{OMe})Cl(PPh_3)}$_2$Ag](PF_6) · CH_2Cl_2 (**4** · CH_2Cl_2) including disordered atoms. Thermal ellipsoids represent 50 per cent probability.

Table S3. Selected bond lengths (Å) and angles (°) in [{Tc(NO)(L^{OMe})Cl(PPh_3)}$_2$Ag](PF_6) · CH_2Cl_2 (**4** · CH_2Cl_2).

Tc1-N10 / Tc2-N20*	1.839(8) / 1.689(8)	Tc1-O3 / Tc2-O13	2.102(3) / 2.157(3)
Tc1-Cl1 / Tc2-Cl2*	2.388(3) / 2.424(2)	Tc1-P4 / Tc2-P5	2.366(1) / 2.373(1)
Tc1-O1 / Tc2-O11	2.094(3) / 2.076(3)	N10-O10 / N20-O20*	1.025(8) / 1.257(9)
Tc1-O2 / Tc2-O12	2.162(3) / 2.110(3)	Cl1-Ag1 / Cl2-Ag2*	2.624(2) / 2.490(2)
N10-Tc1-Cl1 / N20-Tc2-Cl2*	97.7(2) / 94.1(3)	N10-Tc1-O3 / N20-Tc2-O13*	172.(2) / 173.1(3)
N10-Tc1-O1 / N20-Tc2-O11*	90.4(3) / 92.6(2)	N10-Tc1-P4 / N20-Tc2-P5*	89.2(2) / 90.7(3)
N10-Tc1-O2 / N20-Tc2-O12*	90.1(3) / 89.4(3)	Cl1-Tc1-Cl1' / Cl2-Tc2-Cl2'*	180 / 180
Tc1-Cl1-Ag1 / Tc2-Cl2-Ag2*	82.88(7) / 86.37(6)	Tc1-N10-O10 / Tc2-N20-O20*	174.0(8) / 186.8(6)

(') 1-x,-y.-z

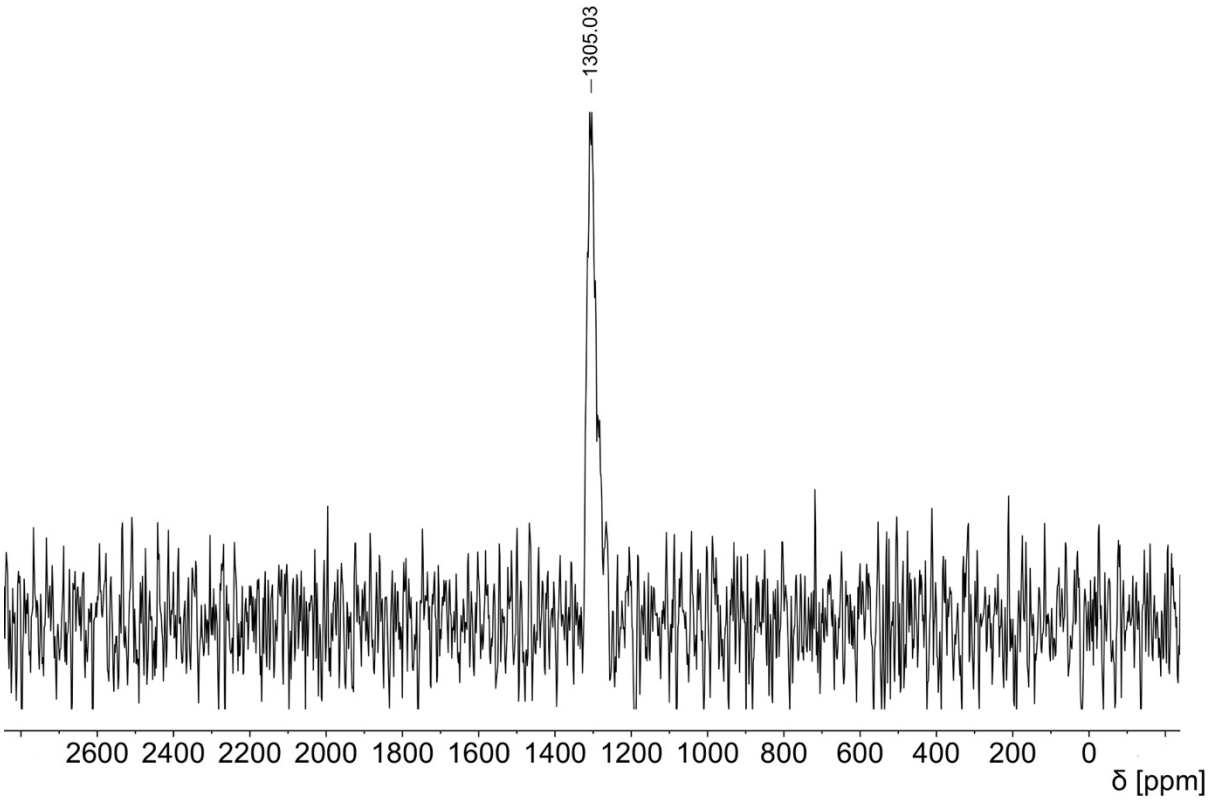

Figure S3. ^{99}Tc NMR spectrum of $[Tc^{I}(NO)(L^{OMe})(PPh_3)(SMe_2)]^+$ (**5**) in SMe2/THF.

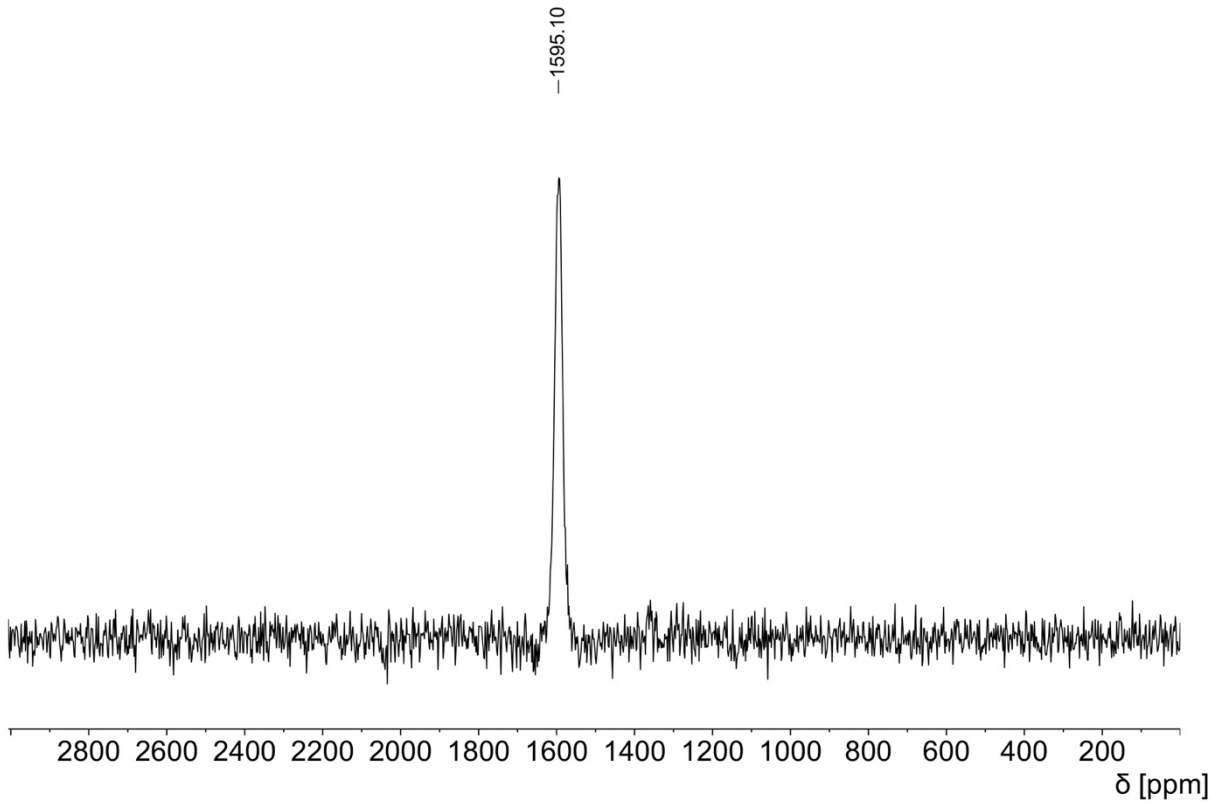

Figure S4. ^{99}Tc NMR spectrum of $[Tc^{I}(NO)(L^{OMe})(PPh_3)(CH_3CN)]^+$ (**6**) in CH_3CN.

A.7 Ammonium pertechnetate in mixtures of trifluoromethanesulfonic acid and trifluoromethanesulfonic anhydride

Authors	M. Zegke, D. Grödler, M. Roca Jungfer, A. Haseloer, M. Kreuter, J. M. Neudörfl, T. Sittel, C. M. James, J. Rothe, M. Altmaier, A. Klein, M. Breugst, U. Abram, E. Strub, M. S. Wickleder
Journal	*Angew. Chem. Int. Ed.* **2021**, *61*, e202113777
DOI	10.1002/anie.202113777 10.1002/ange.202113777
Link	https://onlinelibrary.wiley.com/doi/abs/10.1002/anie.202113777
Detailed scientific contribution	Markus Zegke, Erik Strub and Mathias S. Wickleder designed the project. Markus Zegke and Erik Strub performed the synthesis and characterization of $(NH_4)[TcO(OTf)_5]$ and $[TcO_3(OTf)]$. Dennis Grödler, Alexander Haseloer, Meike Kreuter, Jörg M. Neudörfl, Axel Klein, Martin Breugst, Thomas Sittel, Christopher M. James, Jörg Rothe and Marcus Altmeier assisted in some of the spectroscopic characterizations. Markus Zegke and Erik Strub wrote the manuscript and corrected the manuscript. Maximilian Roca Jungfer performed the synthesis an characterization of the ammonium polyoxotechnetate salt $(NH_4)_4[\{TcO(TcO_4)_4\}_4]$. Maximilian Roca Jungfer and Ulrich Abram completed and verified the characterization of some of the compounds and corrected the manuscript.
Estimated own contribution	30%

Return to publication 4.7.

Angewandte Chemie
Eine Zeitschrift der Gesellschaft Deutscher Chemiker

Supporting Information

Ammonium Pertechnetate in Mixtures of Trifluoromethanesulfonic Acid and Trifluoromethanesulfonic Anhydride

Markus Zegke[+], Dennis Grödler, Maximilian Roca Jungfer, Alexander Haseloer, Meike Kreuter, Jörg M. Neudörfl, Thomas Sittel, Christopher M. James, Jörg Rothe, Marcus Altmaier, Axel Klein, Martin Breugst,* Ulrich Abram, Erik Strub[+],* and Mathias S. Wickleder**

anie_202113777_sm_miscellaneous_information.pdf
anie_202113777_sm_cif.zip
anie_202113777_sm_Movie_O2_evol.mp4

Supporting Information

Table of Contents

General information

Chemicals

Trifluoromethanesulfonic acid (HOTf) and trifluoromethanesulfonic anhydride (Tf_2O) were purchased from ABCR and used as received without further purification.

^{99}Tc was provided as an aqueous solution of 2 g NH_4TcO_4 in ca. 20 ml of water. The sample is a stock solution dated 1965 and produced at the Oak Ridge National Laboratories, USA.

General procedure

All reactions and analyses were performed using standard Schlenk techniques under Ar (4.6 (99.996%)), using 10 ml DURAN® culture tubes with a PTFE lined DIN thread and PBT screw cap. All glassware was oven dried at 150 °C overnight or using an external heat gun at 550 °C for several minutes.

Prior to the experiment, 20 µl (2 mg, 11.0 µmol, 0.693 MBq) of an aqueous NH_4TcO_4 solution were added to a 10 ml DURAN® culture tube inside a Schlenk flask and evacuated to dryness overnight. To the colourless solid HOTf and Tf_2O were added (as detailed in the respective experiments below) using oven dried FORTUNA® pipettes flushed with Ar or Eppendorf microliter pipettes.

Precautions and safety

The work was carried out at the certified radiochemical laboratories of the University of Cologne and Freie Universität Berlin and the Institute for Nuclear Waste Disposal at the Karlsruhe Institute of Technology.

To reduce contamination, all work was monitored with appropriate detectors. All surfaces were wiped clean before and after use. Standard PPE was worn at all times. NMR samples were measured in double containment technique with the sample inside a PTFE inlay within the actual NMR tube. Even closed samples containing triflic acid of triflic anhydride have been handled in a double containment system, e.g. placing the vial in a beaker, in order to avoid contamination by leakages due to occasional gas evolution. After the experiments, residual triflic acid was carefully diluted in acetone and neutralised with organic bases.

Instrumentation

UV-vis absorption

UV-vis spectra were recorded using a VWR UV-1600PC spectrophotometer. The spectrometer was equipped with a cuvette holder that was connected to a thermostat to cool or heat the samples. These DURAN® vials were directly used as reaction vessels and cuvettes in the spectrometer. Because the vials are taller than the standard cuvettes, an additional lid was added to the spectrometer to ensure a lightproof cover of the vials during measurement. A vial filled with HOTf was used as a blank before the experiment commenced.

As the control program did not allow automated measurements to obtain timed series, repeated spectra were obtained using the GS Auto Clicker program. In analogy to a scene from a popular TV series, we refer to this automation technique as "Simpsons Woodpecker Spectroscopy" (SWS).

Liquid Scintillation Counting (LSC)

LSC measurements were performed using a HIDEX SL-300 TDCR counter. For yield control, typically 20 µL aliquots of supernatant were taken and diluted with 10 mL H_2O to obtain a suitable pH value for LSC: Of this dilutions, again 20 µL aliquots were pipetted into 20 mL LSC PP vial containing 5 mL H_2O and 10 mL scintillation cocktail (Perkin Elmer Ultima Gold). Using this procedure resulted in samples with typical count rates of several hundred to several thousand cpm (counts per minute). Samples were measured for 5-10 minutes.

XRD

Single crystal data of $[TcO_3(OTf)]$, $(NH_4)_2[TcO(OTf)_5] \cdot (HOTf)$ and $Na_2[TcO(OTf)_5] \cdot 2\,(HOTf)$ were collected at 100 K with a Bruker D8 Venture diffractometer (Cu-$K_{\alpha1}$ radiation, λ = 1.5406 Å) equipped with a Bruker APEX-II CCD detector. A suitable single crystal was selected and immersed in an inert oil. The crystal was then mounted on a MicroLoop. The crystal was cooled to 100 K by an Oxford Cryostream low temperature device.[1] The single crystal data of $(NH_4)_4[\{TcO(OTcO_3)_4\}_4] \cdot 10\ H_2O$ were collected on a Bruker D8 Venture instrument with Mo Kα radiation. The crystal was stored in liquid N_2 until it was directly mounted into the diffractometers cryostream. The full data set was recorded and the images processed using APEX3.[2] Structure solution by direct methods or intrinsic phasing[3] was achieved through the use of SHELXS programs,[4] and the structural model refined by full matrix least squares on F^2 using SHELXL-2014.[5] Semi-empirical absorption correction form equivalents (multiscan) was executed using SADABS-2016/2.[6] Molecular graphics were plotted using Mercury.[7] Editing of CIFs and construction of tables and bond lengths and angles was achieved using WC[8] and PLATON,[9] or Olex2 program.[10] All non-hydrogen atoms were refined anisotropically. Where possible, hydrogen atoms were placed according to residual electron density peaks, otherwise placed using idealised geometric positions and allowed to move in a "riding model" along with the atoms to which they are attached, and refined isotropically.

Powder X-ray diffraction was attempted to be measured on a P-XRD Stoe Stadi-P equipped with a Mythen 1 K detector and measured from 3 to 60° in 3° steps and 60 s exposure time in transmission using Mo-Kα radiation. The sample was prepared using Scotch tape and cling film, with traces of Fomblin® oil but decomposed to NH_4TcO_4 on the tape (Figure S 1). Another sample was attempted to be measured between two microscope slide cover glasses, and visually the yellow material did not decompose. However, the absorption of the glass was too strong and no reflections attributable to the complex were observed. Due to the very small amount of material, the low stability and the radioactive nature of the compound, we could not measure the material inside a sealed glass capillary.

Figure S 1. Pertechnetyl triflate immediately after preparation on Scotch tape (left) and five minutes after inserting into mounting disk (right). Only reflections of NH_4TcO_4 were observed. The brown material is attributed to TcO_2.

NMR

NMR samples of the Tf_2O/HOTf reactions were flame-sealed under vacuum with a C_6D_6 insert and measured on a Bruker Avance III 400 spectrometer operating at 400.18 MHz for ^{1}H and 90.07 MHz for ^{99}Tc at 300 K. The spectrometer was equipped with a broadband observe probe (BBFOplus) with direct x-magnetisation detection for proton and heteronuclear detection experiments. Chemical shifts are referenced internally to TMS (δ(TMS) = 0 ppm) for ^{1}H and to $Na^{99}TcO_4$ with $\delta(Na^{99}TcO_4)$ = 0 ppm for ^{99}Tc. For all spectra, standard Bruker pulse sequences were used. 1D spectra of ^{1}H and ^{99}Tc were recorded with 32k data points and were zero filled to 64k data points.

The ^{99}Tc NMR spectra of the reactions in neat HOTf and other acids without the addition of Tf_2O and that of $[TcOCl_4]^-$ were measured on a Jeol JNM-ECA400II **(**400 MHz ECA II) spectrometer and referenced internally to TcO_4^-.

XANES

Tc K-edge X-ray absorption near-edge structure (XANES) spectra were collected from the same flame-sealed solutions as used for the NMR (see above) at the INE-Beamline, KIT synchrotron source (KARA storage ring, KIT Campus North), using the conventional fluorescence yield XAS setup.[11] The Tc Kα-line was detected by combining the signal of a 4-pixel and a single-pixel SDD (Vortex) detector (Hitachi, USA), using an Ar-filled ionisation chamber at ambient pressure as I_0 monitor. The double crystal monochromator was equipped with a pair of Ge<422> crystals. The energy scale was calibrated by assigning the first inflection point in the rising K-edge absorption of a Mo metal foil (20 µm) to the 1s-energy (E_{1s} (Mo^0): 20000.0 eV).

MS

Head space gas chromatography for O_2 detection was attempted by using a Trace 1300 Chromatograph equipped with a TriPlus RSH auto sampler from Thermo Scientific with a thermal conductivity detector. The capillary column used was a Shin carbon ST 100/120 1.0 mm x 2 m 1/16'' OD silico. The carrier gas was helium. An attempt at calibrating the equipment with HOTf and Tf_2O resulted in a blockage and malfunctioning of the device, rendering the O_2 detection impossible.

EPR

EPR spectra were recorded on glassy frozen solutions in HOTf at 78 K in the X-band on a Miniscope MS400 spectrometer (Magnetech). Simulations have been done with Easyspin.[12]

IR

IR spectra were measured from KBr pellets on a Shimadzu Affinity-1 FTIR spectrometer and verified by a direct measurement on a Nicolet iS10 FT-IR.

Experiments

1. Reactions in Tf_2O or Tf_2O/HOTf mixtures

1.1. NH_4TcO_4 with Tf_2O

2.0 mg NH_4TcO_4 (0.011 mmol, 1.0 eq.) were treated with 1.5 ml (1237.6 mg, 8.92 mmol, 810.6 eq) Tf_2O. The material does not dissolve, and the mixture does not change colour, even after repeated heating for a total of 5 hours at 80 °C with freezing periods in between.

1.2. NH_4TcO_4 with 1.5 ml Tf_2O and 200 µl HOTf

2.0 mg NH_4TcO_4 (0.011 mmol, 1.0 eq.) were treated with 1.5 ml (1237.6 mg, 8.92 mmol, 810.6 eq) Tf_2O, followed by the addition of 200 µl (372 mg, 2.6 mmol, 234 eq.) HOTf. After one hour of heating to 80 °C a green solution was obtained.

1.3. NH_4TcO_4 with 1.5 ml Tf_2O and 10 µl HOTf

A suspension of 2.0 mg NH_4TcO_4 (0.011 mmol, 1.0 eq.) in 1.5 ml (1237.6 mg, 8.92 mmol, 810.6 eq) Tf_2O was treated with 10 µl (18.6 mg, 0.13 mmol, 11.7 eq.) of HOTf. After one hour of heating to 80 °C a deep purple solution was obtained. The colour intensified over the course of 3 hours. After 5 d at -15 °C green needles suitable for X-ray crystallography could be isolated.

1.4. NH_4TcO_4 with 1.5 ml Tf_2O and 20 µl HOTf

A suspension of NH_4TcO_4 in 1.5 ml (1237.6 mg, 8.92 mmol, 810.6 eq) Tf_2O was treated with 20 µl (37.2 mg, 0.26 mmol, 23.4 eq.) HOTf. After one hour of heating to 80 °C a dark purple solution was obtained. From this solution green crystals of $(NH_4)_2[TcO(OTf)_5]$ could be isolated.

1.5. NH_4TcO_4 with 1.5 ml Tf_2O and 40 µl HOTf

A suspension of NH_4TcO_4 in 1.5 ml (1237.6 mg, 8.92 mmol, 810.6 eq) Tf_2O was treated with 40 µl (74.4 mg, 0.52 mmol, 46.8 eq.) of HOTf. After one hour of heating to 80 °C a dark purple solution was obtained. The solution was kept at -15 °C for one night. Yellow crystals of $[TcO_3(OTf)]$ suitable for X-ray crystallography were isolated.

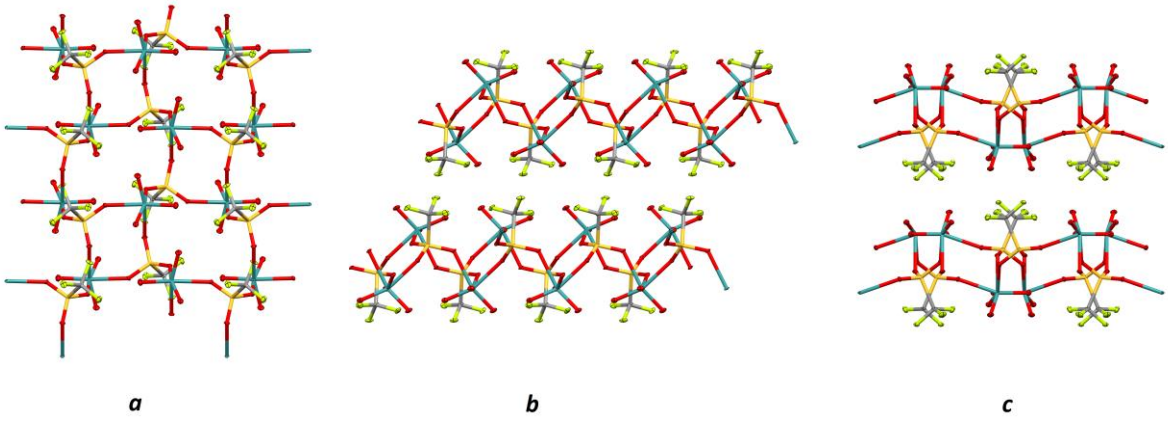

Figure S 2 High resolution image of the packing of $[TcO_3(OTf)]$.

1.6. NH_4TcO_4 with 3.62 µl Tf_2O and 0.38 µl HOTf in 16 µl Et_2O

A solution of 0.38 µl HOTf (0.65 mg, 0.004 mmol, 0.4 eq.) and 3.62 µl (6.07 mg, 0.022 mmol, 2.0 eq.) Tf_2O in 16.0 µl Et_2O were added to 2.0 mg NH_4TcO_4 (0.011 mmol, 1.0 eq.) and was heated for 4 h at 60 °C. All volatiles were removed under reduced pressure for 18 h leaving a brown solid as a residue, supposedly TcO_2.

1.7. NH_4TcO_4 with 90.5 µl Tf_2O and 8.5 µl HOTf

A solution of 8.5 µl (15.8 mg, 0.11 mmol, 10.0 eq.) HOTf and 90.5 µl (151.77 mg, 0.54 mmol, 49.1 eq.) Tf_2O were added to 2.0 mg NH_4TcO_4 (0.011 mmol, 1.0 eq.) and was heated for 3 h at 60 °C. The reaction mixture started to turn purple after 10 min and remained deep purple after 3 h of heating. After 3 d at –15 °C no crystallisation of $[TcO_3(OTf)]$ was observed.

1.8. NH_4TcO_4 with 290.5 µl Tf_2O and 8.5 µl HOTf

A solution of 8.5 µl (15.8 mg, 0.11 mmol, 10.0 eq.) HOTf and 290.5 µl (487.2 mg, 1.73 mmol, 118.2 eq.) Tf_2O were added to 2.0 mg NH_4TcO_4 (0.011 mmol, 1.0 eq.) and was heated for 3 h at 60 °C. The reaction mixture started to turn purple after 30 min and remained deep purple after 3 h of heating. After 3 d at –15 °C no crystallisation of $[TcO_3(OTf)]$ was observed.

1.9. NH_4TcO_4 with 590.5 µl Tf_2O and 8.5 µl HOTf

A solution of 8.5 µl HOTf (15.8 mg, 0.11 mmol, 10.0 eq.) and 590.5 µl (487.2 mg, 3.51 mmol, 319.1 eq.) Tf_2O were added to 2.0 mg NH_4TcO_4 (0.011 mmol, 1.0 eq.) and was heated for 2 h at 60 °C. The NH_4TcO_4 reacted under formation of yellow oily droplets, which dissolved after 30 min. The reaction mixture stayed colourless at 60 °C but darkened to purple at room temperature. After additional 3 h of heating at 60 °C the mixture stayed purple at given temperature. After 3 d at –15 °C no crystallisation of $[TcO_3(OTf)]$ was observed.

1.10. NH_4TcO_4 with 890 µl Tf_2O and 10 µl HOTf

A solution of 10.0 µl HOTf (17.1 mg, 0.114 mmol, 10.4 eq.) and 890 µl (1.492 g, 5.29 mmol, 480.9 eq.) Tf_2O were added to 2.0 mg NH_4TcO_4 (0.011 mmol, 1.0 eq.) and was heated for 2 h at 60 °C. The NH_4TcO_4 reacted under formation of yellow oily droplets, which dissolved after 30 min. The reaction mixture stayed colourless at 60 °C but darkened to purple at room temperature. After additional 5 h of heating at 60 °C, the mixture stayed purple at the given temperature. After 3 d at –15 °C no crystallisation of $[TcO_3(OTf)]$ was observed.

1.11. NH_4TcO_4 with 581 µl Tf_2O and 19 µl HOTf at 60 °C for 0.5, 1, 2 and 4 h

Four solutions of 19.0 µl HOTf (32.5 mg, 0.216 mmol, 19.6 eq.) and 581 µl (974 mg, 3.45 mmol, 313.9 eq.) Tf_2O were added to 2.0 mg NH_4TcO_4 (0.011 mmol, 1.0 eq.) respectively and were heated for 0.5 h (**11a**), 1 h (**11b**)**,** 2 h (**11c**) and 4 h (**11d**) at 60 °C. The reaction supernatant was analysed by UV-Vis spectroscopy at room temperature to monitor the reaction process. After 3 d at –15 °C crystallisation of $[TcO_3(OTf)]$ was observed in all batches but in different yields.

Yields (wrt $[TcO_3(OTf)]$): **11a**: 97%; **11b**: 81%; **11c**: 48%; **11d**: 44%

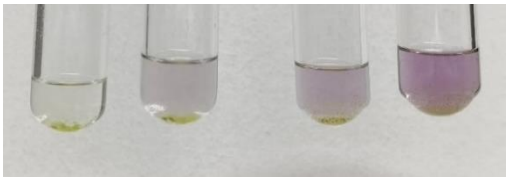

Figure S 3. Reaction vials of **11a**, **11b**, **11c** and **11d**.

1.12. NH_4TcO_4 with 1162 µl Tf_2O and 38 µl HOTf at 60 °C for 0.5, 1, 2 and 4 h

Four solutions of 38.0 µl HOTf (65.0 mg, 0.432 mmol, 39.2 eq.) and 1162 µl (1.948 g, 6.90 mmol, 627.3 eq.) Tf_2O were added to 2.0 mg NH_4TcO_4 (0.011 mmol, 1.0 eq.) respectively and were heated for 0.5 h (**12a**), 1 h (**12b**), 2 h (**12c**) and 4 h (**12d**) at 60 °C. The reaction supernatant was analysed by UV-Vis spectroscopy at room temperature to monitor the reaction process. After 3 d at –15 °C crystallisation of $[TcO_3(OTf)]$ was observed in moderate yields (LSC).

Yields (wrt $[TcO_3(OTf)]$): **12a**: 47%; **12b**: 42%; **12c**: 49%; **12d**: 37%

Figure S 4. Reaction vials of **12a**, **12b**, **12c** and **12d**.

1.13. NH_4TcO_4 with 581 µl Tf_2O and 10, 19, 38 and 76 µl HOTf at 60 °C for 0.5 h

Four solutions of either 10.0 µl (17.1 mg, 0.114 mmol, 10.4 eq.) (**13a**), 19.0 µl (32.5 mg, 0.217 mmol, 19.7 eq.) (**13b**), 38.0 µl (65.0 mg, 0.432 mmol, 39.2 eq.) (**13c**) or 76.0 µl (130.0 mg, 0.866 mmol, 78.7 eq.) (**13d**) HOTf in 581 µl (974 mg, 3.45 mmol, 313.7 eq.) Tf_2O were added to 2.0 mg NH_4TcO_4 (0.011 mmol, 1.0 eq.), respectively, and were heated for 0.5 h at 60 °C. The reaction supernatant was analysed by UV-Vis spectroscopy at room temperature to monitor the reaction process. After 3 d at -15 °C crystallisation of $[TcO_3(OTf)]$ was observed in the first two batches in different yields (LSC).

Yields (wrt $[TcO_3(OTf)]$): **13a**: 82%; **13b**: 68%; **13c**: 44%; **13d**: 11%

Figure S 5. Reaction vials of **13a**, **13b**, **13c** and **13d**.

1.14. NH_4TcO_4 with 581 µl Tf_2O and 19 µl HOTf at 80 °C for 0.5 h

A solution of 19.0 µl HOTf (32.5 mg, 0.216 mmol, 19.6 eq.) and 581 µl (974 mg, 3.45 mmol, 313.9 eq.) Tf_2O were added to 2.0 mg NH_4TcO_4 (0.011 mmol, 1.0 eq.) and was heated for 0.5 h at 80 °C. The reaction supernatant was analysed by UV-Vis spectroscopy at room temperature to monitor the reaction process. After 3 d at –15 °C crystallisation of $[TcO_3(OTf)]$ was observed in a yield of 71%.

1.15. NH_4TcO_4 with 581 µl Tf_2O and 19 µl HOTf at 100 °C for 10 min

A solution of 19.0 µl HOTf (32.5 mg, 0.216 mmol, 19.6 eq.) and 581 µl (974 mg, 3.45 mmol, 313.9 eq.) Tf_2O were added to 2.0 mg NH_4TcO_4 (0.011 mmol, 1.0 eq.) and was heated for 10 min at 100 °C. The reaction supernatant was analysed by UV-Vis spectroscopy at room temperature to monitor the reaction process. After 3 d at –15 °C crystallisation of $[TcO_3(OTf)]$ was observed in a yield of 97%.

1.16. NH_4TcO_4 with 19 µl Tf_2O and 581 µl HOTf at r.t.

A solution containing 581 µl HOTf (993 mg, 6.6 mmol, 600 eq.) and 19 µl (31 mg, 0.11 mmol, 10 eq.) Tf_2O was added to 2.0 mg NH_4TcO_4 (0.011 mmol, 1.0 eq.). The mixture was left standing at room temperature. The solid turned yellow, and the supernatant turned purple within 30 min. After three days, the solution showed a pale green colour.

2. Reactions in neat HOTf

$K[TcO_4]$, $Cs[TcO_4]$, $Ag[TcO_4]$ and $NBu_4[TcO_4]$ were prepared by salt metathesis between $NH_4[TcO_4]$ in a minimum amount of water with KOH, Cs_2CO_3, $AgNO_3$ and NBu_4Cl following standard procedures.

2.1. Reactions of ammonium and alkaline pertechnetates at room temperature

NH_4TcO_4, $KTcO_4$, $AgTcO_4$ and $CsTcO_4$ (0.07 mmol) react with neat, fuming triflic acid (0.5 ml) at room temperature (20 – 30°C) under a colour change to yellow and the formation of a purple solution. The purple solution contained a transient, paramagnetic Tc(VI) species. After storage overnight, pure, yellow $[TcO_3(OTf)]$ crystallises from such solutions as verified by X-ray diffraction. This material is highly reactive towards an open atmosphere due to the hygroscopic nature of the adhered residual HOTf on the surface of the crystals.

Under strictly anhydrous conditions, the yellow crystals of $[TcO_3(OTf)]$ gradually dissolve under intensification of the purple colour, but ultimately form bright green solutions of $[TcO(OTf)_5]^{2-}$. Such solutions turn reddish-orange when partially exposed to the atmosphere, forming the polyoxometallate $[\{TcO(OTcO_3)_4\}_4]^{4-}$.

2.2. Reactions of ammonium and alkaline pertechnetates at low temperatures

NH_4TcO_4, $KTcO_4$, $AgTcO_4$ and $CsTcO_4$ (0.07 mmol) react with neat, fuming triflic acid (0.5 ml) between -20° and +5°C under a colour change to yellow and the formation of a yellow solution. After storage overnight, the formation of yellow crystals of $[TcO_3(OTf)]$ was observed in all cases. No dissolution of the crystals and formation of a purple or green solution was observed. Exposure to the atmosphere, however, resulted in a change of colour to the orange-red of the polyoxometallate $[\{TcO(OTcO_3)_4\}_4]^{4-}$, which crystallises after prolonged time.

2.3. Reaction of tetrabutylammonium pertechnetate at room temperature

NBu_4TcO_4 (0.07 mmol) dissolved in neat, fuming HOTf (0.5 ml) at room temperature in a violent reaction. The initially yellow solution heated to boiling before changing its colour to purple through red and finally yellow within seconds. No formation of solid $[TcO_3(OTf)]$ was observed.

2.4. Reaction of tetrabutylammonium pertechnetate at low temperature

NBu_4TcO_4 (0.07 mmol) was dissolved in neat, fuming HOTf (0.5 ml) to give a yellow solution.

2.5. Reaction of ammonium pertechnetate with aqueous HBF_4

NH_4TcO_4 (0.07 mmol) was dissolved in aqueous BF_4 (0.5 ml, 45-50%) giving a colourless solution.

2.6. Reaction of ammonium pertechnetate with conc. H_2SO_4

NH_4TcO_4 (0.07 mmol) was dissolved in conc. H_2SO_4 (0.5 ml) giving a yellow solution.

2.7. Hydrolysis of $(NH_4)_2[TcO(OTf)_5]$ and $[TcO_3(OTf)]$: formation of solid $(NH_4)_4[\{TcO(OTcO_3)_4\}_4] \cdot 10H_2O$

NH_4TcO_4 (12 mg, 0.07 mmol) was added to neat, fuming triflic acid (0.5 ml) at room temperature in a screw-lid glass vial. The vial was closed and carefully shaken resulting in a purple solution with yellow sediment. Overnight, large yellow crystals of $[TcO_3(OTf)]$ formed. The crystals dissolved within one week and during this time a colourless liquid condensed on the sides of the vial above the solution. The condensed liquid turned reddish-purple and red-green dichroic and highly hygroscopic crystals of $(NH_4)_4[\{TcO(OTcO_3)_4\}_4] \cdot 10H_2O$ slowly formed upon slow exposure to the atmosphere. After three weeks, the bottom solution had turned orange and crystals of $(NH_4)_4[\{TcO(OTcO_3)_4\}_4] \cdot 10H_2O$ deposited. The vial was opened under Ar and the crystals were filtered off via a reverse frit under Ar. They were washed with dry, degassed pentane and diethyl ether. They were then transferred to an Ar-filled, tared screw-lid vial as a suspension in dry diethyl ether. The diethyl ether was evaporated in vacuum. The thus obtained green-red dichroic crystals of $(NH_4)_4[\{TcO(OTcO_3)_4\}_4] \cdot 10H_2O$ were stored under Ar.

Yield: 3.2 mg (1 µmol, 31%). Melting point: ca. 30°C. FT-IR: 3493 (broad, ν_{OH_2}), 3211 (broad, ν_{NH_4}), 2961 (m, ν_{NH_4}), 2916 (w, ν_{NH_4}), 2849 (w, ν_{NH_4}), 1618 (w, ν_{NH_4}/ν_{OH_2}), 1402 (m, ν_{NH_4}), 1259 (m, ν_{TcO}), 1089 (m, ν_{TcO}), 1026 (m, ν_{TcO}), 910 (vs, ν_{TcO}), 788 (broad, ν_{TcO}).

The highly hygroscopic crystals form a deep brown-red oil upon exposure to moisture, while dilute solutions in acetone, ethanol or water show a range of colours from red-brown via orange to yellow depending on the concentration. Crystals suitable for X-ray diffraction were obtained by slow hydrolysis of the initial purple solution and some of the $[TcO_3(OTf)]$ crystals on a glass plate. Due to the highly hygroscopic nature and the low melting point, the crystals were stored in liquid nitrogen until the measurement.

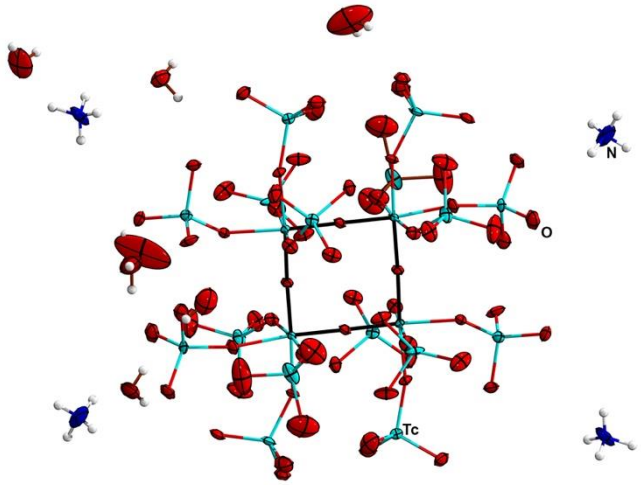

Figure S 6. Ellipsoid plot of $(NH_4)_4[\{TcO(OTcO_3)_4\}_4] \cdot 10\ H_2O$ including the partially disordered solvent water molecules.

Spectra

UV-vis spectra

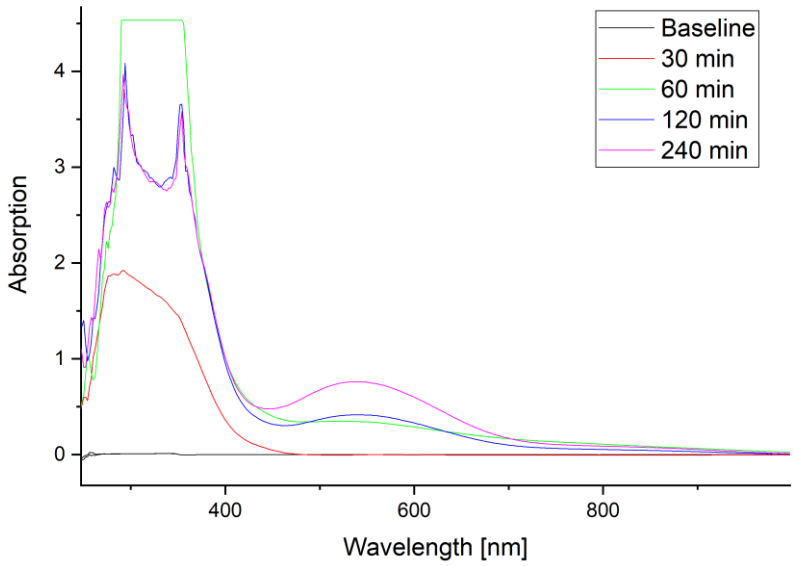

Figure S 7. Absorption spectrum of experiment 1.11.

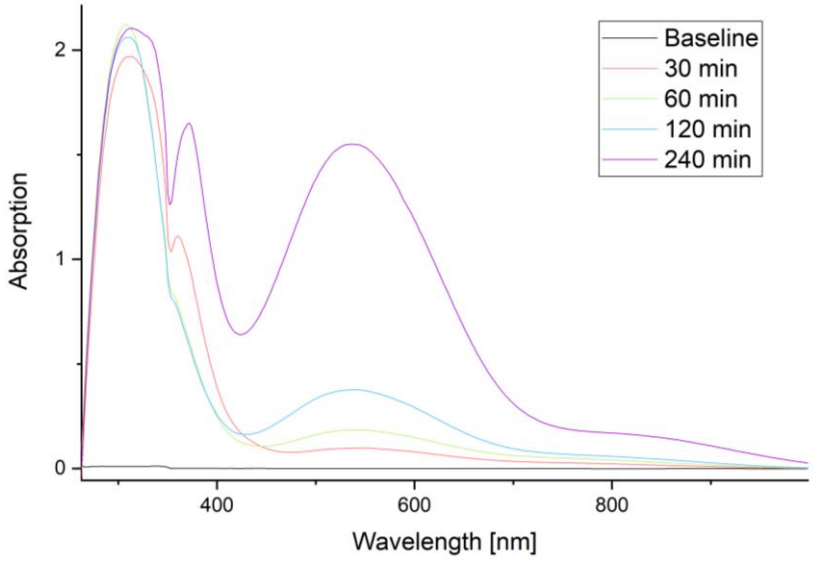

Figure S 8. Absorption spectrum of experiment 1.12.

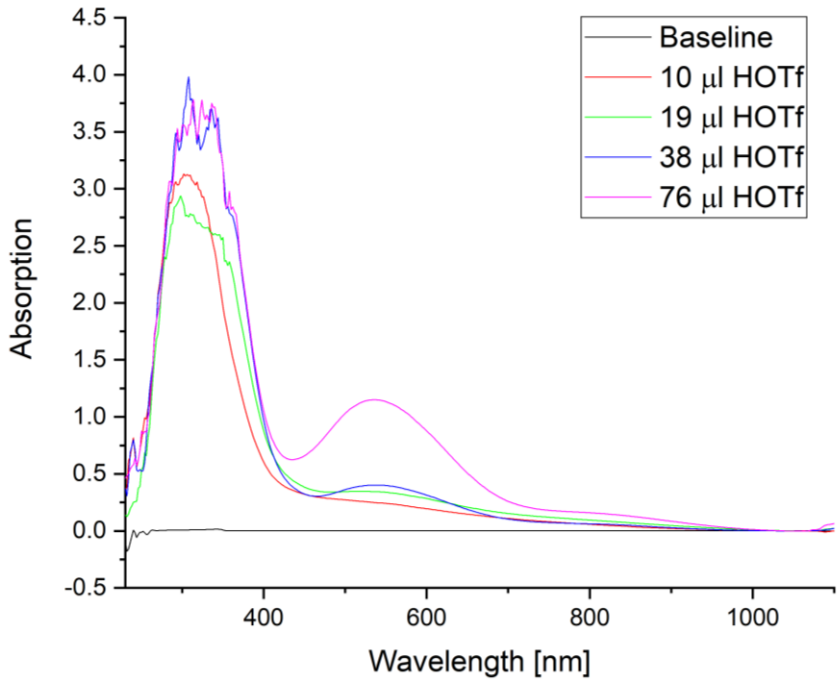

Figure S 9. Absorption spectrum of experiment 1.13.

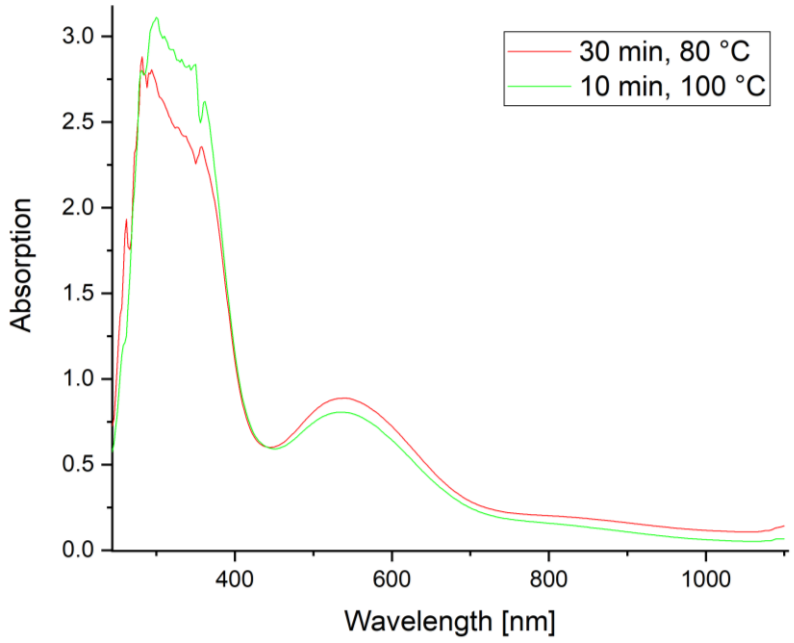

Figure S 10. Absorption spectra of experiments 1.14 and 1.15.

Powder XRD

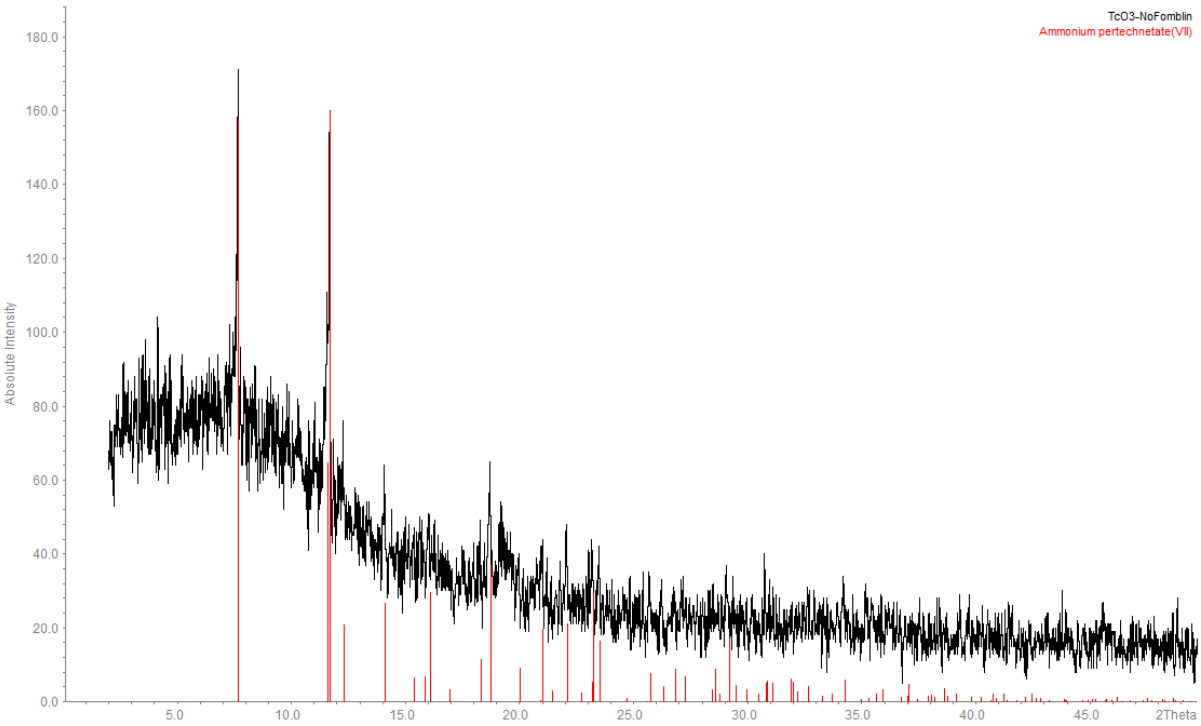

Figure S 11. Powder diffractogram of the brown material, which formed when pertechnetyl triflate was mounted onto Scotch tape (*cf*. Fig S 1). The observed reflections can only be attributed to NH_4TcO_4.

Single crystal XRD

Table S 1. Crystal data and refinement parameters.

Complex	$(NH_4)_2[TcO(OTf)_5] \cdot HOTf$	$[TcO_3(OTf)]$	$(NH_4)_4[\{TcO(OTcO_3)_4\}_4] \cdot 10\ H_2O$
CCDC Number	2114967	2114965	2114966
Empirical formula	$C_6H_9F_{18}N_2O_{19}S_6Tc$	$C_2F_6O_{12}S_2Tc_2$	$H_{36}N_4O_{78}Tc_{20}$
Formula weight	1045.51	590.14	3300.33
Temperature/K	100.0	100.0	100.0
Crystal system	orthorhombic	monoclinic	triclinic
Space group	Pbca	$P2_1/c$	P-1
a/Å	9.4625(2)	8.7221(5)	11.328(2)
b/Å	24.2120(5)	8.8945(6)	12.833(2)
c/Å	26.4840(6)	9.1632(6)	13.987(2)
α/°	90	90	71.842(6)
β/°	90	115.3430(10)	69.144(6)
γ/°	90	90	74.378(6)
Volume/Å³	6067.6(2)	642.46(7)	1776.5(5)
Z	8	2	1
ρ_{calc}g/cm³	2.289	3.051	3.085
μ/mm⁻¹	9.552	22.027	3.886
F(000)	4096.0	560.0	1548
Crystal size/mm³	0.207 × 0.124 × 0.06	0.1 × 0.1 × 0.1	0.09 x 0.03 x 0.02
Radiation	CuKα (λ = 1.54178)	CuKα (λ = 1.54178)	MoKα (λ = 0.71073)
2Θ range for data collection/°	6.674 to 144.25	11.224 to 143.854	2.35 to 25.94
Index ranges	-10 ≤ h ≤ 11, -29 ≤ k ≤ 29, -32 ≤ l ≤ 32	-10 ≤ h ≤ 10, -10 ≤ k ≤ 10, -11 ≤ l ≤ 11	-13 ≤ h ≤ 13, -15 ≤ k ≤ 15, -17 ≤ l ≤ 17
Reflections collected	94865	14565	45155
Independent reflections	5971 [R_{int} = 0.0945, R_{sigma} = 0.0263]	1262 [R_{int} = 0.0559, R_{sigma} = 0.0243]	6745 [R_{int} = 0.0559, R_{sigma} = 0.0243]
Data/restraints/parameters	5971/9/505	1262/0/109	645/720/643
Goodness-of-fit on F²	1.040	1.234	1.085
Final R indexes [I>=2σ (I)]	R_1 = 0.0255, wR_2 = 0.0651	R_1 = 0.0235, wR_2 = 0.0585	R_1 = 0.0588, wR_2 = 0.1263
Final R indexes [all data]	R_1 = 0.0291, wR_2 = 0.0662	R_1 = 0.0242, wR_2 = 0.0588	R_1 = 0.0701, wR_2 = 0.1312
Largest diff. peak/hole/e Å⁻³	2.08/-0.84	0.52/-0.99	2.01/-1.27

NMR Spectra

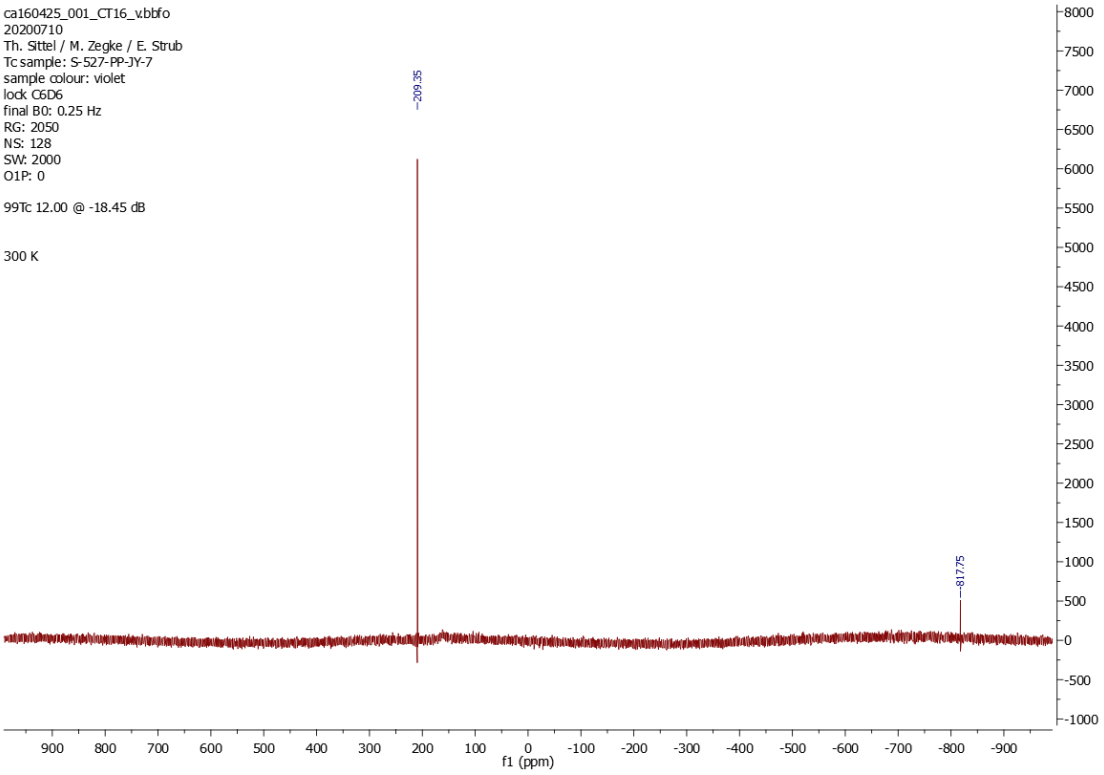

Figure S 12. ^{99}Tc-NMR of purple sample obtained from experiment 1.5.

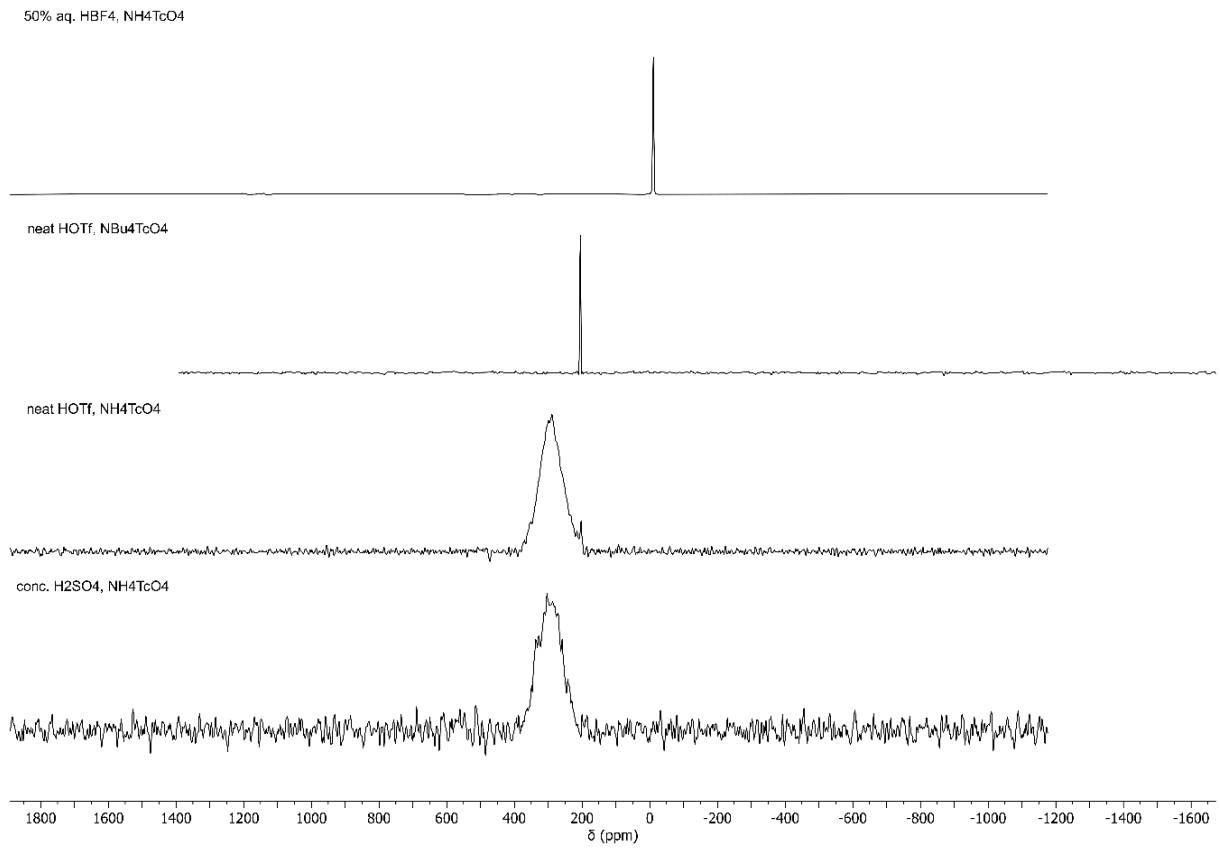

Figure S 13. ^{99}Tc-NMR spectra of NH_4TcO_4 and NBu_4TcO_4 in different, highly acidic media. Pertechnetate did not react with HBF_4 (experiment *2.5*): the ^{99}Tc NMR spectrum shows only the resonance of TcO_4^-. It is assumed that the dissolution of pertechnetate in H_2SO_4 (experiment *2.6*) gives probably the water adduct $[TcO_3(OSO_3H)(OH_2)_2]$ (δ = 273 ppm, $\nu_{1/2}$ = 8316 Hz). When water-free TcO_4^- is dissolved in triflic acid (experiments *2.1* and *2.4*), the narrow resonance of $[TcO_3(OTf)]$ is observed (δ = 204 ppm, $\nu_{1/2}$ = 350 Hz). When such solutions are exposed to moisture or moisture is present in the starting materials, a resonance similar to that of $[TcO_3(OSO_3H)(OH_2)_2]$ was observed. It can be attributed to $[TcO_3(OSO_2CF_3)(OH_2)_2]$ (δ = 269 ppm, $\nu_{1/2}$ = 6565 Hz) and the intensity of the resonance of $[TcO_3(OTf)]$ eventually vanishes.

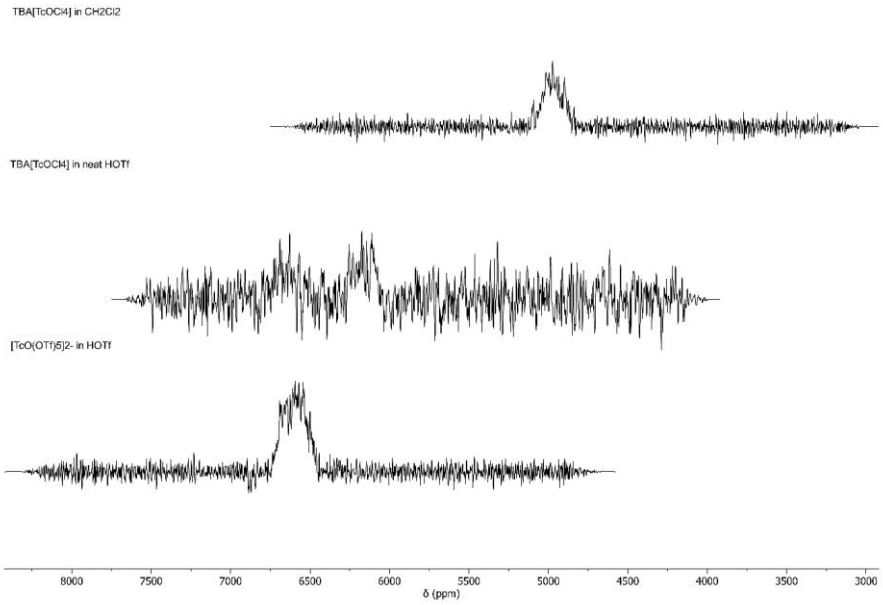

Figure S 14. ^{99}Tc-NMR spectra of $NBu_4[TcOCl_4]$ (δ = 4951 ppm, $\nu_{1/2}$ = 12.1 kHz) in CH_2Cl_2 and neat HOTf compared to *an in situ* sample of $[TcO(OTf)_5]^{2-}$ (δ = 6601 ppm, $\nu_{1/2}$ = 17.8 kHz).

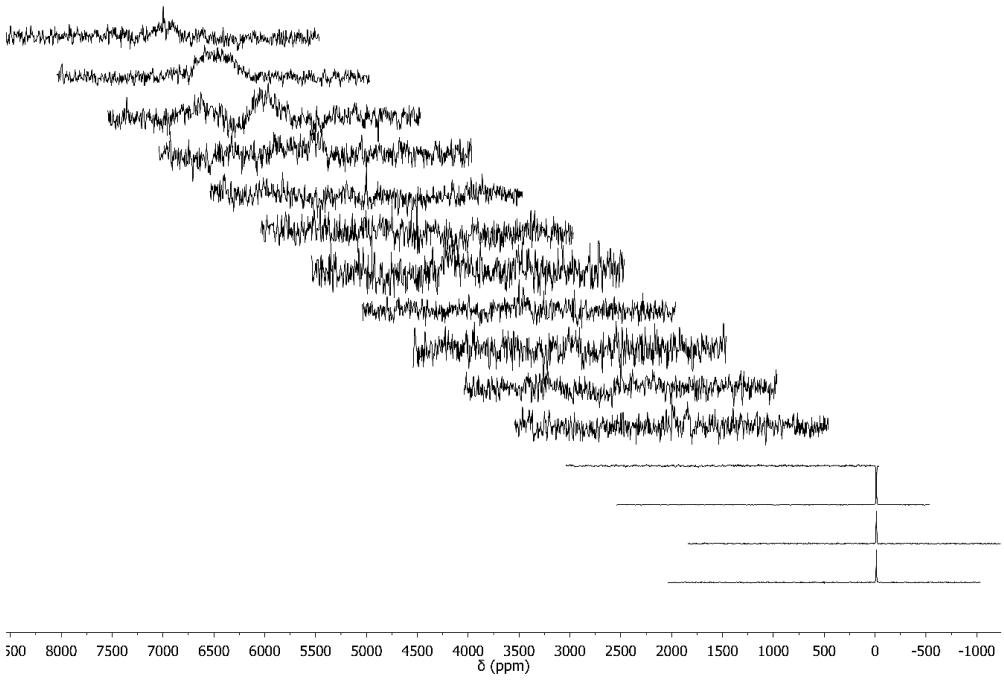

Figure S 15. ^{99}Tc-NMR spectra of a red-orange solution of $(NH_4)_4[\{TcO(OTcO_3)_4\}_4] \cdot 10H_2O$ in triflic acid (experiment *2.7*). The solvent fuming HOTf had turned into non-fuming (dilute/aqueous) HOTf over the course of the storage. After dissolution of $[\{TcO(OTcO_3)_4\}_4]^{4-}$ several low-intensity Tc(V) resonances are observed with chemical shifts between those observed for the reference compounds $[TcOCl_4]^-$ and $[TcO(OTf)_5]^{2-}$. In addition, a considerably broadened TcO_4^- resonance ($\nu_{1/2}$ = 400 Hz) was observed. The main Tc(V) species in the sample gives an extremely broad resonance at δ = 6530 ppm with $\nu_{1/2}$ = 48 kHz. The presence of several technetium(V) species suggests that different substitution equilibria under exchange of the pertechnetato ligands play a role upon dissolution of the tetrameric polyoxotechnetate anion.

EPR Spectra

Purple reaction solutions between NH_4TcO_4 and neat fuming HOTf allow the detection of EPR spectra. The concentrations of the paramagnetic species are generally low and reach a maximum with the intensity of the purple colour. The course of the reaction (reduction of the Tc(VII) complex $[TcO_3(OTf)]$) depends on the ratio of the starting materials and the moisture, which was allowed to enter the reaction vessel. Generally, the appearance of intermediate Tc(VI) species was observed for all reactions performed, but the intensity of the observed spectra were highest, when small amounts of moisture were present. In such cases, also the signals of more than one Tc(VI) species appeared in the EPR spectra. However, one species, which we assume to be the triflato complex $[Tc^{VI}O(OTf)_5]^-$ dominates in all measured spectra.

Figure S 16 depicts the X-band EPR spectrum of $[Tc^{VI}O(OTf)_5]^-$ (S = 1/2) recorded for a frozen-glass sample of the complex in HOTf at 78 K. The spectrum shows an axial symmetry with well resolved ^{99}Tc hyperfine interactions in parallel and perpendicular parts. In the centre of the spectrum, some signals of a second species are visible. The formation of a minor second species has also been found during reactions of $TcNCl_4^-$ with HOTf and CH_3SO_3H.[13,14]

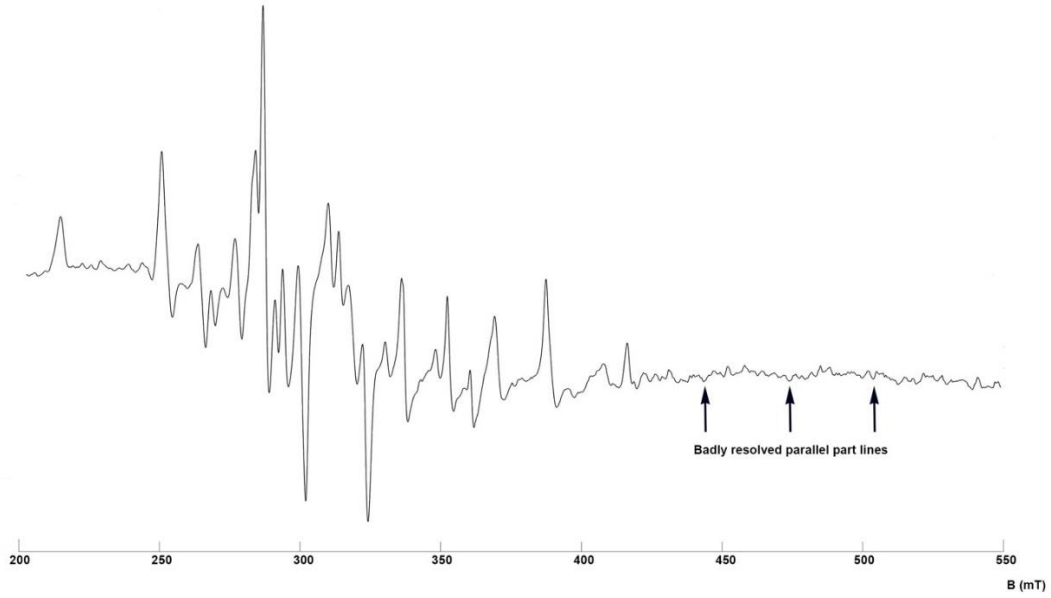

Figure S 16. Frozen solution X-band EPR spectrum of $[Tc^{VI}O(OTf)_5]^-$ in HOTf, T = 78 K.

The spectral parameters of $[Tc^{VI}O(OTf)_5]^-$ are close to those of the previously studied nitrido complexes $[TcN(OTf)_5]^{2-}$ and $[TcN(CH_3SO_3)_5]^{2-}$.[14] They are compared in Table S 2. It is evident that the ^{99}Tc couplings are generally smaller for the oxido complexes. This effect is also observed for corresponding chloride complexes and the corresponding spectral parameters are contained in Table S 2.

Table S 2. EPR parameters of $[Tc^{VI}O(OTf)_5]^-$ and related compounds

	$g_{\parallel}$	$g_{\perp}$	$A_{\parallel}^{Tc}$ (10^{-4} cm^{-1})	$A_{\perp}^{Tc}$ (10^{-4} cm^{-1})	Ref.
$[TcO(OTf)_5]^-$	1.712	1.950	312	155	This work.
$[TcN(OTf)_5]^{2-}$	1.895	1.995	360	174	[13]
$[TcN(CH_3SO_3)_5]^{2-}$	1.900	1.985	352	165	[13]
$[TcOCl_5]^-$	2.057	1.938	230	96	[14]
$[TcNCl_4]^-$	2.016	2.003	295	137	[15]

XANES spectra

Six consecutive measurements (scans) were taken of the “green” compound, and eight consecutive measurements (scans) of the “purple” compound, both in triflic acid solution. In all measurements, a Mo foil was measured as a reference. The raw spectra of the purple compound showed only a very low absorption in the X-ray range (underlining the strong absorption in the visible range), which made a correct determination of the exact edge energy for this sample impossible.

All raw spectra were loaded into the XASviewer program of the Larch package. Larch is distributed under an open-source license that is nearly identical to the BSD license. It is under active and open development centered at the GeoScoilEnviroCARS sector of Center for Advanced Radiation Sources at the University of Chicago.

All Mo XANES spectra were plotted as normalised μ(E) and then recalibrated by auto aligning the Mo K edges to the edge of the first scan. The spectra of the six scans were summed up. The turning point of the resulting K edge was found at 20002.8 eV. The Tc XANES spectra were plotted as normalised μ(E). The energy shifts determined from the Mo K edges were applied manually to the respective spectrum (0 eV, 0.440 eV, 0.408 eV, 0.647 eV, 0.977 eV, and 2.551 eV, respectively). The Tc spectra 1-6 were summed up to obtain a single XANES spectrum of the green solution.

Reference spectra of Tc(VII) and Tc(IV) were obtained from a previous measurement in which the turning point of the Mo K edge had been fixed at 20000.0 eV. Hence, to enable a comparison, the sum spectrum of the green solution was again shifted by -2.8 eV. All 3 spectra are plotted in Figure S 17.

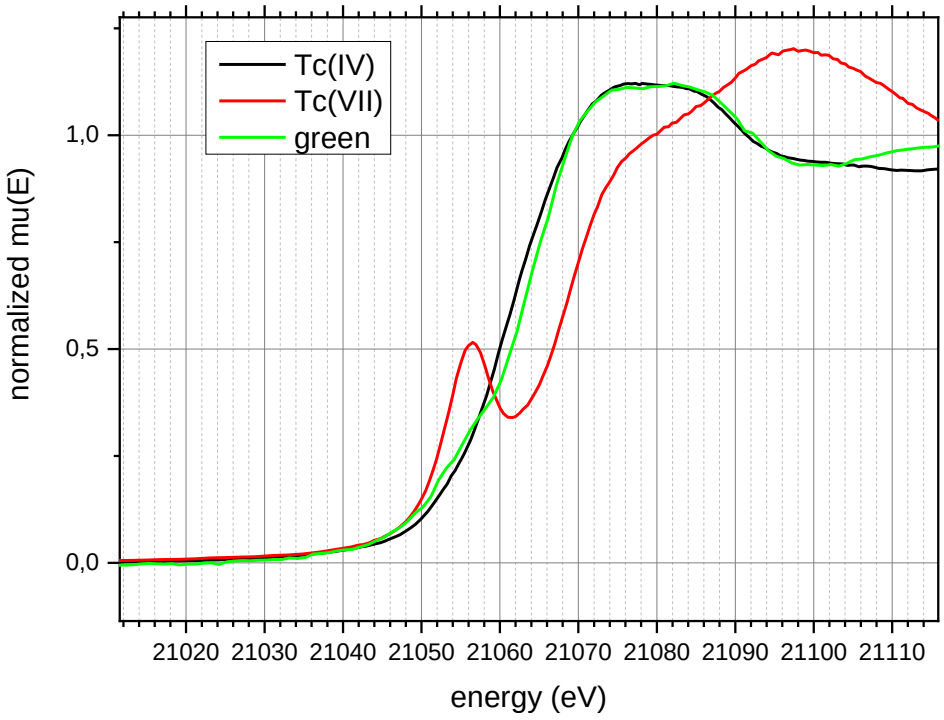

Figure S 17. XANES spectra of Tc(IV), Tc(VII) and the unknown compound (“green” solution).

From the data it can be seen that the green sample is exhibiting an oxidation state well below +VII, indicating the presence of a reduced Tc species. The absorption is clearly in between the edges of the

Tc(IV) and the Tc(VII). A closer look at an enlarged section (Figure S 18) shows a difference of +1.4 eV between the Tc(IV) reference and the green solution and of -5.2 eV with respect to the Tc(VII) reference. We conclude that the most probable oxidation state of the green solution is Tc(V), although the shift is slightly below the average value of 2.2 eV per oxidation state.

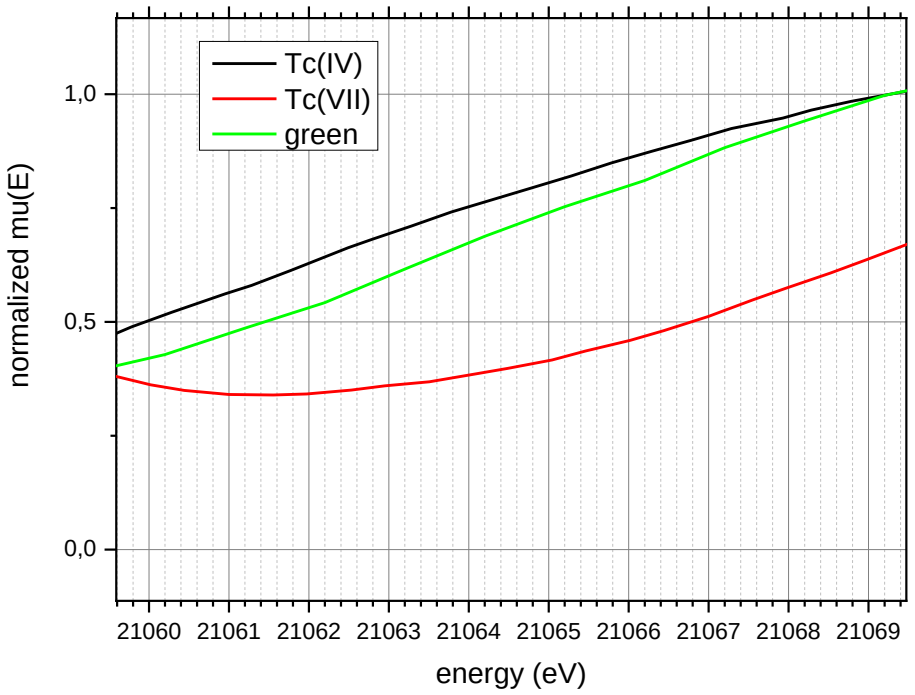

Figure S 18 Enlarged XANES spectra from 21060 to 21069 eV.

Computations

Computational Details

All Tc complexes were optimised employing the GGA functional PBE,[16,17] the triple-ζ basis set def2-TZVP with the corresponding pseudopotential for Tc,[18] Grimme's D3 correction with Becke-Johnson damping,[19] and the SMD continuum model for water.[20] As the solvent mixture of trifluoromethanesulfonic acid and trifluoromethanesulfonic anhydride cannot be adequately modelled within Gaussian, water was chosen as the closest alternative. Density fitting was used to accelerate the calculations and an extremely fine grid with 99 radial shells per atom and 974 angular points per shell for numerical integration of the density. Subsequently, electronic energies were obtained from single point calculations with different methods (e.g., B3LYP-D3BJ, CAM-B3LYP-D3BJ, DLPNO-CCSD(T), M06-L-D3, (RI)-MP2, PBE-D3BJ, TPSSh,-D3BJ ωB97X-D3BJ, ωB2PLYP), the def2-QZVP or def2-QZVPP basis set, and the SMD model for water. UV-Vis spectra were obtained from the PBE-optimised structures relying on either time-dependent DFT (B3LYP-D3BJ, CAM-B3LYP-D3BJ, ωB97XX-D3BJ, ωB2PLP, ωB2GPPLYP) or STEOM-DLPNO-CCSD calculations, the def2-TZVP basis set, and the SMD model for water. Control reactions indicated that neither the basis set nor the number of transitions (30–100) had a significant influence on the observed spectra. All theoretical spectra were simulated by overlapping Gaussian functions for each transition and a value of σ = 0.4 eV (3226 cm^{-1}) was chosen for the width of the absorption band at a height of 1/e.

Control Calculations

As shown in Figure S 19 for the $[TcO_3]^+$ system for the ωB2GP-PLYP functional (a very reliable functional to calculate the UV-Vis spectra for organic compounds[21]) different parameters had no significant effect on the resulting spectra.

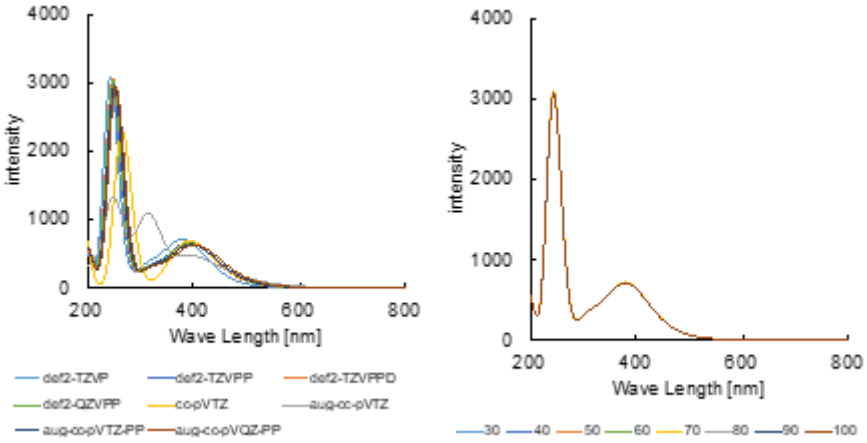

Figure S 19 Calculated UV-Vis-spectra for the $[TcO_3]^+$ system (ωB2GP-PLYP): left: different basis sets, right: different transition numbers.

Calculated Spectra

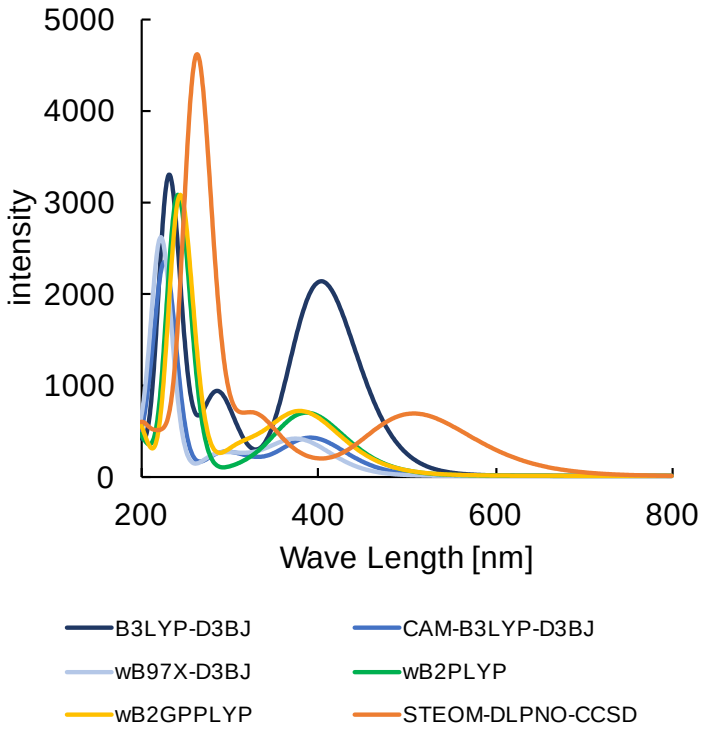

Figure S 20 Calculated UV-Vis-spectra for the $[TcO_3]^+$ system (ωB2GP-PLYP): left: different basis sets, right: different transition numbers.

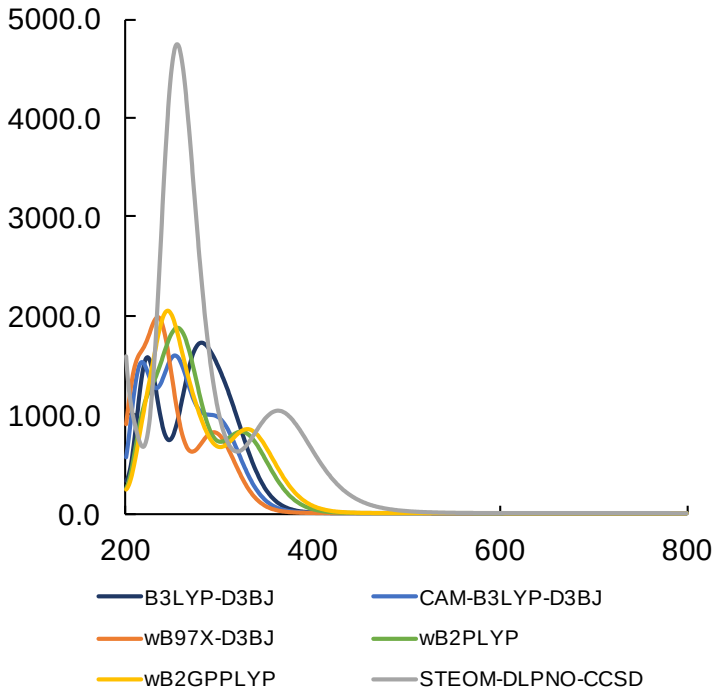

Figure S 21 Calculated UV-Vis-spectra for the $[TcO_3Cl]$ system.

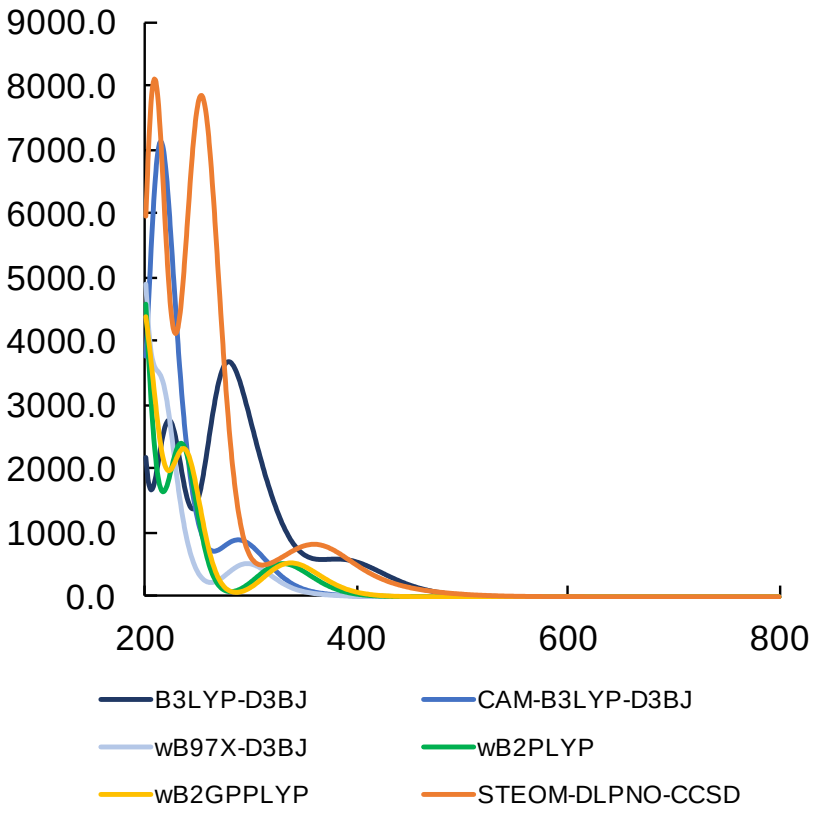

Figure S 22 Calculated UV-Vis-spectra for the [TcO_3OTf] system.

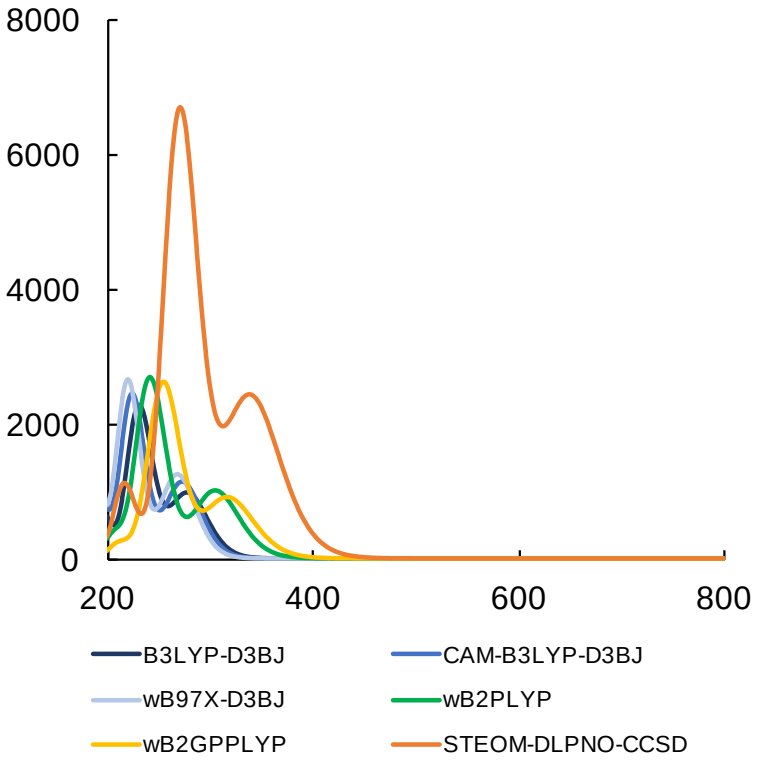

Figure S 23 Calculated UV-Vis-spectra for the $[TcO_4]^-$ system.

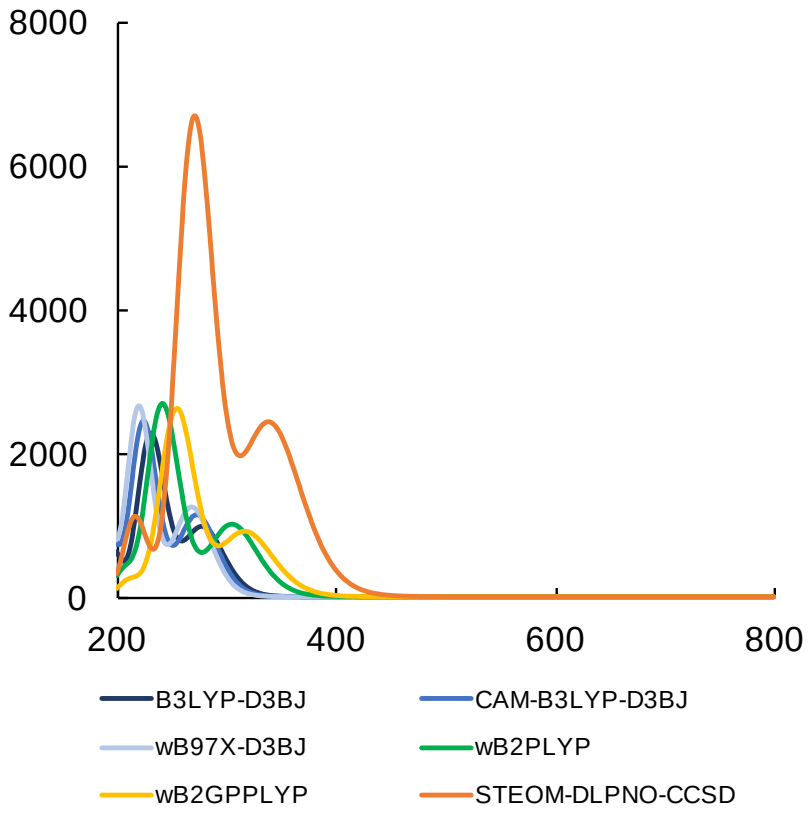

Figure S 24 Calculated UV-Vis-spectra for the $[TcO_4]^{2-}$ system.

Coordinates of Different Tc Complexes

$[TcO_3]^+$

Tc	-0.37626	1.51746	6.25390
O	-0.94044	1.09815	4.72395
O	-1.56775	1.00303	7.33387
O	-0.36687	3.19543	6.33042

$[TcO_3]Cl$

Tc	-0.47295	1.69790	6.04491
O	-1.34545	1.25381	4.65373
O	-0.52691	0.46407	7.21880
O	-0.98487	3.20637	6.63001
Cl	1.72154	1.88455	5.41748

$[TcO_3]OTf$

Tc	-0.67160	1.68673	6.01049
O	-1.03537	0.64471	4.72503
O	-1.63253	1.22669	7.33046
O	-1.18072	3.23280	5.54974
O	1.35812	1.71362	6.26980
S	2.50778	2.30386	7.10756
O	2.19237	3.60821	7.65861
O	3.10033	1.29306	7.96216
C	3.74081	2.59312	5.72369
F	4.00355	1.44454	5.08292
F	3.25803	3.48876	4.84961
F	4.87641	3.06818	6.26192

Pertechnetate Anion $[TcO_4]^-$

Tc	-1.01079	0.19607	0.01562
O	-0.41967	1.01414	1.43989
O	-0.42735	1.02374	-1.40633
O	-2.74469	0.21863	0.02237
O	-0.41380	-1.43299	0.00985

Technetate Anion $[TcO_4]^{2-}$

Tc	-1.01301	0.20838	0.00559
O	-0.45469	1.12735	1.44066
O	-0.29575	1.03190	-1.41614
O	-2.79874	0.14621	0.12047
O	-0.45410	-1.49426	-0.06918

Proposed reduction mechanism for the reduction

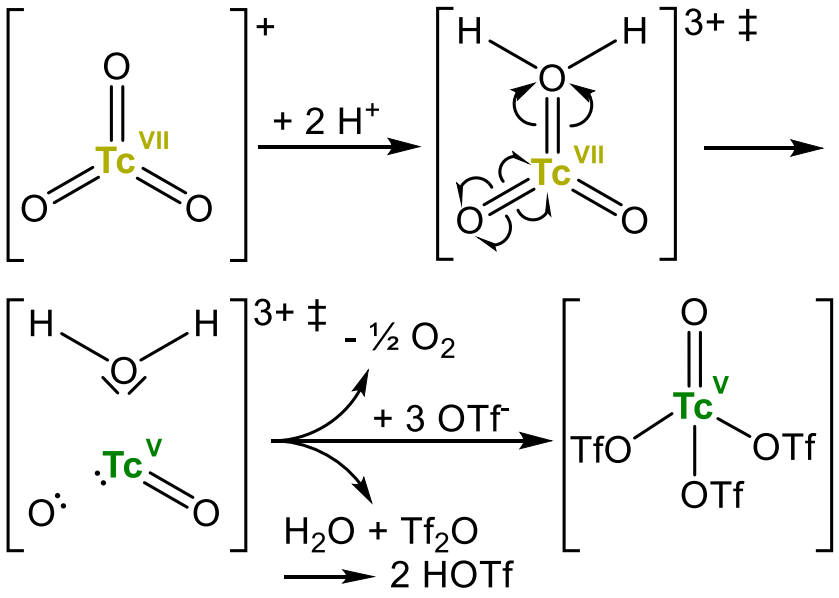

Scheme S 1 Proposed reduction mechanism for the reduction of the pertechnetyl cation TcO^{3+} to the Tc(V) complex.

Heat energy calculation

In comparison to the work by Denden et al.[22,23] we would like to address the fact that the applied dose of irradiation may very well correspond to the energy applied by us during simple heating from freezing at -18 °C to +60 °C or from room temperature to 80 °C or 100 °C (average ΔT of ca. 60 – 80 K).

The applied dose corresponds to a heating of around 90K (see calculation below):

$$1\ \text{Gy} = 1\ \text{J/kg}$$

Applied dose H:

$$H = 360\ \text{kGy} = 360\ \text{kJ/kg} = 360\ \text{J/g}$$

Heat capacity C_p of liquid water is more or less constant at $C_p = 4\ \text{J/(K*g)}$, therefore:

$$\Delta T = H / C_p$$
$$= (360\ \text{J/g})/(4\ \text{J/(K*g)})$$
$$= 360/4\ \text{K}$$
$$\underline{= 90\ \text{K}}$$

References

[1] J. Cosier, A. M. Glazer, *J. Appl. Crystallogr.* **1986**, *19*, 105–107.
[2] Bruker, *APEX2*, Madison, Wisconsin, USA, **2012**.
[3] G. M. Sheldrick, *Acta Crystallogr. Sect. Found. Adv.* **2015**, *71*, 3–8.
[4] G. Sheldrick, *Acta Crystallogr. Sect. A* **2008**, *64*, 112–122.
[5] G. M. Sheldrick, *Acta Crystallogr. Sect. C Struct. Chem.* **2015**, *71*, 3–8.
[6] G. M. Sheldrick, *SADABS* **1996**.
[7] C. F. Macrae, I. J. Bruno, J. A. Chisholm, P. R. Edgington, P. McCabe, E. Pidcock, L. Rodriguez-Monge, R. Taylor, J. van de Streek, P. A. Wood, *J. Appl. Crystallogr.* **2008**, *41*, 466–470.
[8] M. Thornton-Pett, *WC-A Windown CIF Processor*, **2000**.
[9] A. Spek, *J. Appl. Crystallogr.* **2003**, *36*, 7–13.
[10] O. V. Dolomanov, L. J. Bourhis, R. J. Gildea, J. A. K. Howard, H. Puschmann, *J. Appl. Crystallogr.* **2009**, *42*, 339–341.
[11] J. Rothe, S. Butorin, K. Dardenne, M. A. Denecke, B. Kienzler, M. Löble, V. Metz, A. Seibert, M. Steppert, T. Vitova, C. Walther, H. Geckeis, Rev. Sci. Instrum. 2012, 83, 043105.
[12] S. Stoll, A. Schweiger, J. Magn. Reson. 2006, 178, 42-55.
[13] J. Baldas, J.F. Boas, Z. Ivanov, B.D. James, Inorg. Chim. Acta 1993, 204, 199-212.
[14] R. Kirmse, J. Stach, U. Abram, Inorg. Chem. 1985, 24, 2196-2198.
[15] J. Baldas, J. F. Boas, G. A. Williams, *Appl. Magn. Reson.* **1996**, *11*, 499–508.
[16] J. P. Perdew, K. Burke, M. Ernzerhof, *Phys. Rev. Lett.* **1996**, *77*, 3865–3868.
[17] J. P. Perdew, K. Burke, M. Ernzerhof, *Phys. Rev. Lett.* **1997**, *78*, 1396.
[18] F. Weigend, R. Ahlrichs, *Phys. Chem. Chem. Phys.* **2005**, *7*, 3297–3305.
[19] S. Grimme, S. Ehrlich, L. Goerigk, *J. Comput. Chem.* **2011**, *32*, 1456–1465.
[20] A. V. Marenich, C. J. Cramer, D. G. Truhlar, *J. Phys. Chem. B* **2009**, *113*, 6378–6396.
[21] L. Goerigk, M. Casanova-Paéz, *Aust. J. Chem.* **2020**, *74*, 3–15.
[22] I. Denden, R. Essehli, M. Fattahi, *J. Radioanal. Nucl. Chem.* **2013**, *296*, 149–155.
[23] I. Denden, J. Roques, F. Poineau, P. L. Solari, M. L. Schlegel, G. Blain, M. Fattahi, *Radiochim. Acta* **2017**, *105*, 135–140.

A.8 Rhenium(V) Complexes with Selenolato- and Tellurolato-substituted Schiff Bases – Released PPh_3 as a Facile Reductant

Authors	M. Roca Jungfer, A. Hagenbach, E. Schulz Lang, U. Abram
Journal	*Eur. J. Inorg. Chem.* **2019**, 4974–4984
DOI	10.1002/ejic.201901092
Link	https://chemistry-europe.onlinelibrary.wiley.com/doi/10.1002/ejic.201901092
Detailed scientific contribution	Maximilian Roca Jungfer, Ulrich Abram and Ernesto Schulz Lang designed the project. Maximilian Roca Jungfer performed the synthesis and characterization of the compounds, performed DFT calculations and wrote a draft of the manuscript. Ernesto Schulz Lang provided guidance and the laboratory space to perform some of the experiments in Brazil. Maximilian Roca Jungfer calculated the X-ray structures under guidance of Adelheid Hagenbach. Ulrich Abram supervised the project, provided scientific guidance and suggestions and corrected the manuscript.
Estimated own contribution	80%

Return to publication 4.8.

Supporting Information

Rhenium(V) Complexes with Selenolato- and Tellurolato-Substituted Schiff Bases – Released PPh_3 as a Facile Reductant

Maximilian Roca Jungfer, Adelheid Hagenbach, Ernesto Schulz Lang, and Ulrich Abram*

ejic201901092-sup-0001-SupMat.pdf

Table of Contents

Part 1: Crystallographic data

Table S1.1 Crystal data and structure determination parameters of the selenium-containing compounds.

	$\{HL^{Se}\}_2$	$[ReO(L^{Se})Cl(PPh_3)]$	$[Re(NPhF)(L^{Se})Cl(PPh_3)]\cdot CH_3CN$	2 $[Re(NPhF)(L^{Se})Cl(PPh_3)]\cdot CH_2Cl_2$	$[Re(NPhCF_3)(L^{Se})Cl(PPh_3)]$
Formula	$C_{26}H_{20}N_2O_2Se_2$	$C_{31}H_{24}ClNO_2PReSe$	$C_{39}H_{31}ClFN_3OPReSe$	$C_{75}H_{58}Cl_4F_2N_6O_2P_2Re_2Se_2$	$C_{38}H_{28}ClF_3N_2OPReSe$
Mw/g·mol^{-1}	550.36	774.09	908.25	1819.31	917.20
Crystal system	Triclinic	Monoclinic	Triclinic	Triclinic	Triclinic
a/Å	8.1196(4)	17.1976(9)	11.035(2)	11.2071(4)	10.0736(8)
b/Å	12.2560(7)	10.3765(5)	13.152(3)	13.8498(5)	13.605(1)
c/Å	12.6479(6)	16.8027(9)	13.973(2)	23.0619(9)	13.9047(9)
α/°	72.350(2)	90	74.722(6)	74.868(2)	75.536(5)
β/°	73.849(1)	113.562(3)	68.181(6)	81.765(2)°	76.540(6)
γ/°	70.714(1)	90	85.734(6)	85.587(2)	81.618(6)
V/Å^3	1109.7(1)	2748.5(3)	1815.6(6)	3416.9(2)	1786.8(2)
Space group	$P\bar{1}$	$P2_1/c$	$P\bar{1}$	$P\bar{1}$	$P\bar{1}$
Z	2	4	2	2	2
$\rho_{calc.}$/g·cm^{-3}	1.647	1.871	1.661	1.768	1.705
μ/mm^{-1}	4.380	11.847	4.506	10.372	4.587
No. reflect.	28855	47170	86180	91688	16546
No. indep.	4516	5103	8686	13967	7768
R_{int}.	0.0343	0.1682	0.0433	0.0591	0.0644
No. param.	297	343	437	838	435
GOOF	1.040	1.044	1.076	1.029	0.918
R_1/wR_2	0.0240/0.0544	0.0604/0.0843	0.0195/0.0468	0.0382/0.0719	0.0497/0.0749
CCDC	1956176	1956178	1956180	1956179	1956181

Table S1.2 Crystal data and structure determination parameters of the tellurium-containing compounds.

	$\{HL^{Te}\}_2$	$[ReO(L^{Te})Cl(PPh_3)]\cdot CH_2Cl_2$	$[Re(NPh)(L^{Te})Cl(PPh_3)]\cdot CHCl_3$	$[Re(NPhF)(L^{Te})Cl(PPh_3)]$
Formula	$C_{26}H_{20}N_2O_2Te_2$	$C_{32}H_{26}Cl_3NO_2PReTe$	$C_{38}H_{30}Cl_4N_2OPReTe$	$C_{37}H_{28}ClFN_2OPReTe$
Mw/g·mol^{-1}	647.64	907.66	1017.21	915.83
Crystal system	Tetragonal	Triclinic	Monoclinic	Monoclinic
a/Å	12.974(1)	9.3520(5)	18.2528(1)	13.8928(7)
b/Å	12.974(1)	16.754(1)	10.0360(7)	15.1644(6)
c/Å	27.646(3)	21.351(1)	20.1066(1)	16.6086(9)
α/°	90	76.142(2)	90	90
β/°	90	82.971(2)	90.511(2)	109.552(4)
γ/°	90	84.198(2)	90	90
V/Å^3	4653(1)	3214.7(3)	3671.8(4)	3297.3(3)
Space group	$I4_1/a$	$P\bar{1}$	$P2_1/c$	$P2_1/n$
Z	8	4	4	4
$\rho_{calc.}$/g·cm^{-3}	1.849	1.875	1.840	1.845
μ/mm^{-1}	2.533	4.999	4.457	4.721
No. reflect.	37168	95870	33800	19226
No. indep.	2783	14357	8140	6456
R_{int}.	0.0458	0.0470	0.0396	0.0398
No. param.	149	782	402	410
GOOF	1.179	0.968	1.098	0.872
R_1/wR_2	0.0251/0.0474	0.0561/0.1560	0.0370/0.0496	0.0406/0.0467
CCDC	1956177	1956182	1956183	1956184

Figure S1.3 Ellipsoid representations (50% probability) of $\{HL^{Se}\}_2$. Hydrogen atoms bonded to carbon atoms are omitted for clarity. Hydrogen-acceptor contacts are represented by dashed bonds.

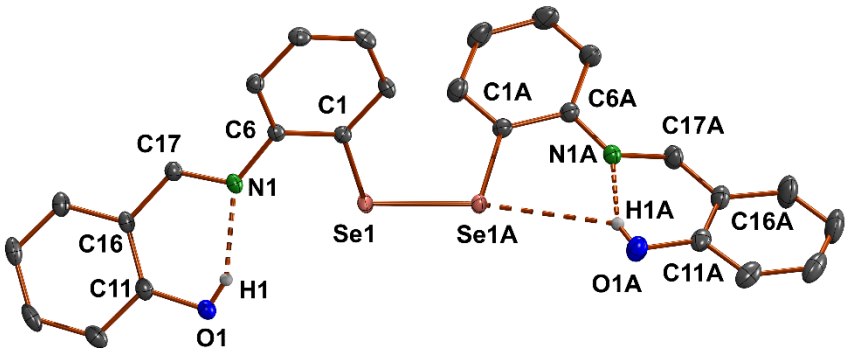

Table S1.3 Hydrogen bonds for $\{HL^{Se}\}_2$ (Å and °).

D-H···A	d(D-H)	d(H···A)	d(D···A)	<(DHA)
O1A-H1A···Se1A	0.77(3)	3.01(3)	3.624(2)	139(2)
O1A-H1A···N1A	0.77(3)	1.95(3)	2.657(2)	152(3)
O1-H1···N1	0.74(3)	1.97(3)	2.651(2)	153(3)

Figure S1.4 Ellipsoid representations (50% probability) of [ReO(L^{Se})Cl(PPh_3)]. Hydrogen atoms are omitted for clarity.

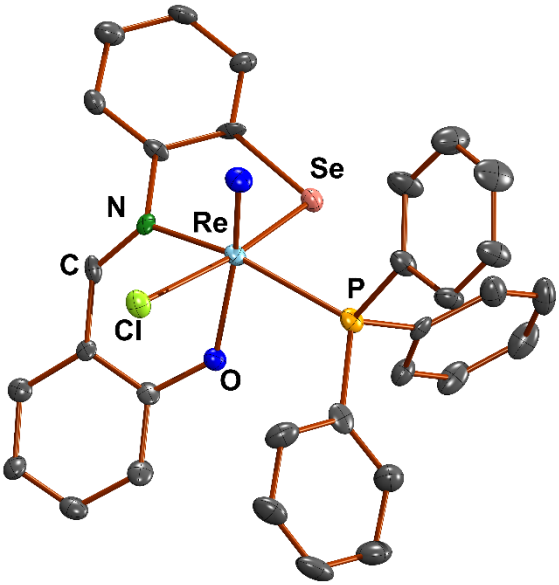

Figure S1.5 Ellipsoid representations (50% probability) of [Re(NPhF)(L^{Se})Cl-(PPh_3)]·CH_3CN. The disordered solvent acetonitrile was calculated isotropically and shown in both orientations. Hydrogen atoms are omitted for clarity.

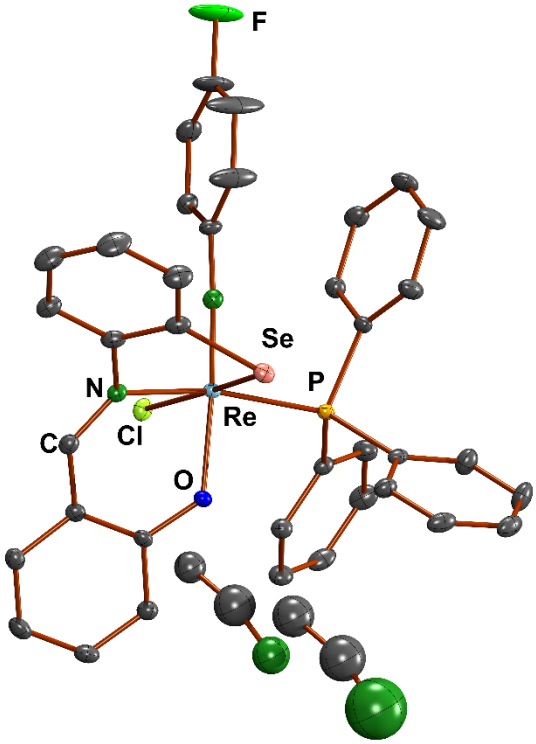

Figure S1.6 Ellipsoid representations (50% probability) of 2 [Re(NPhF)(L^{Se})Cl-(PPh_3)]·CH_2Cl_2. Both molecules in the asymmetric unit of [Re(NPhF)(L^{Se})Cl-(PPh_3)] and the solvent methylene chloride are shown. Hydrogen atoms are omitted for clarity.

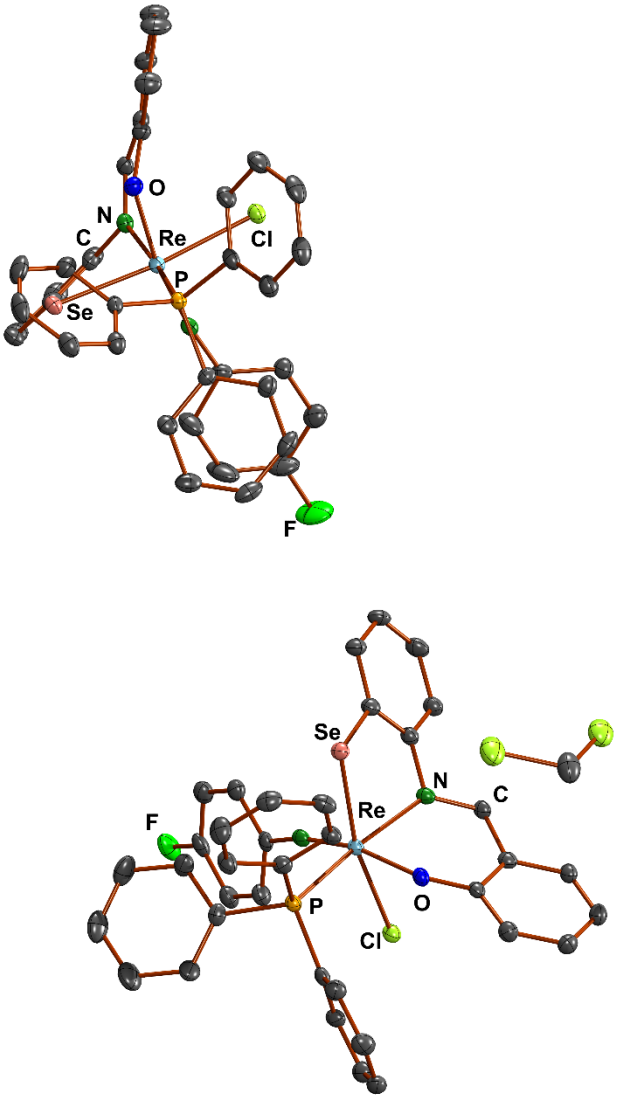

Figure S1.7 Ellipsoid representations (50% probability) of [Re(NPhCF$_3$)(L^{Se})Cl-(PPh$_3$)]. The fluorine atoms of the disordered CF$_3$ group (ca. 85:15) are shown in both orientations. Hydrogen atoms are omitted for clarity.

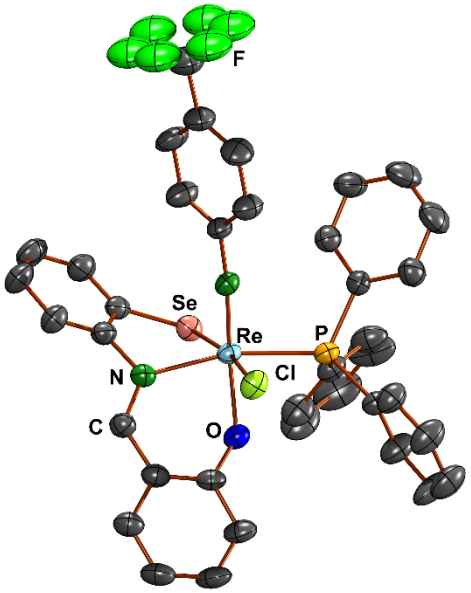

Figure S1.8 Ellipsoid representations (50% probability) of {HL^{Te}}$_2$. The symmetry-generated part of the molecule is also shown. Hydrogen atoms bonded to carbon atoms are omitted for clarity. Hydrogen-acceptor contacts are represented by dashed bonds.

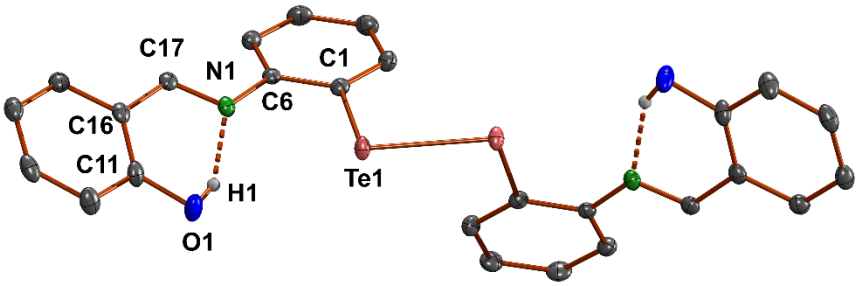

Table S1.8 Hydrogen bonds for {HL^{Te}}$_2$ (Å and °).

D-H···A	d(D-H)	d(H···A)	d(D···A)	<(DHA)
O1-H1···N1	0.78(3)	1.91(3)	2.638(3)	155(3)

Figure S1.9 Ellipsoid representations (50% probability) of [ReO(L^{Te})Cl-(PPh_3)]·CH_2Cl_2. Both molecules of the asymmetric unit and all positions of the disordered solvent methylene chloride are shown. Hydrogen atoms are omitted for clarity.

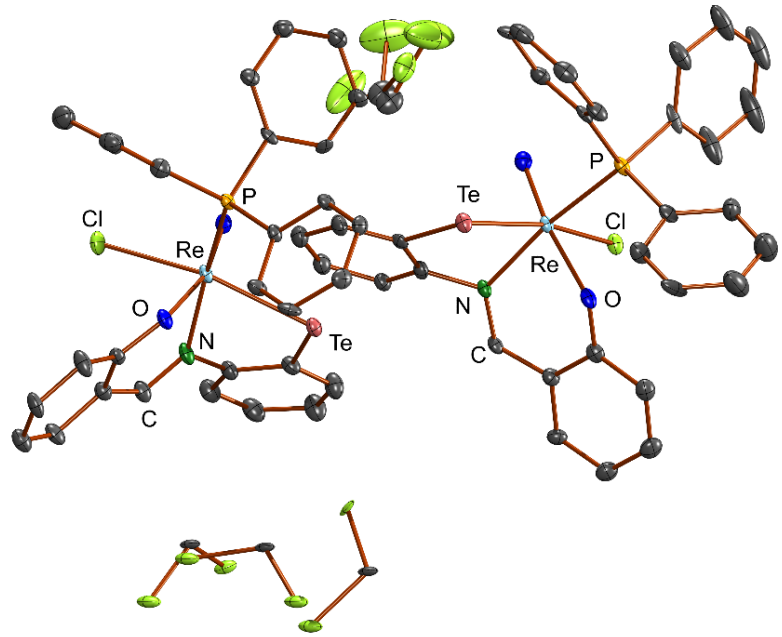

Figure S1.10 Ellipsoid representations (50% probability) of [Re(NPh)(L^{Te})Cl-(PPh_3)]·$CHCl_3$. Both positions of the disordered phenylimido ring (ca. 40:60) and the solvent chloroform are shown. Hydrogen atoms are omitted for clarity.

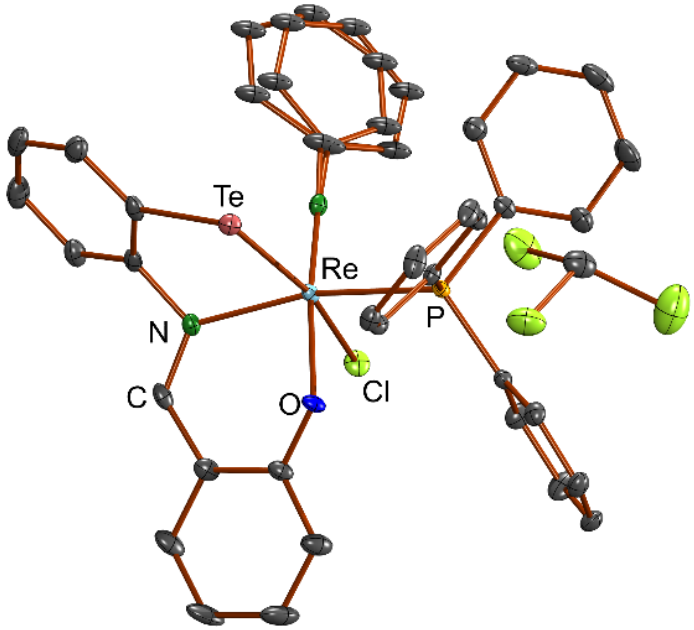

Figure S1.11 Ellipsoid representations (50% probability) of [Re(NPhF)(L^{Te})Cl-(PPh_3)]. Hydrogen atoms are omitted for clarity.

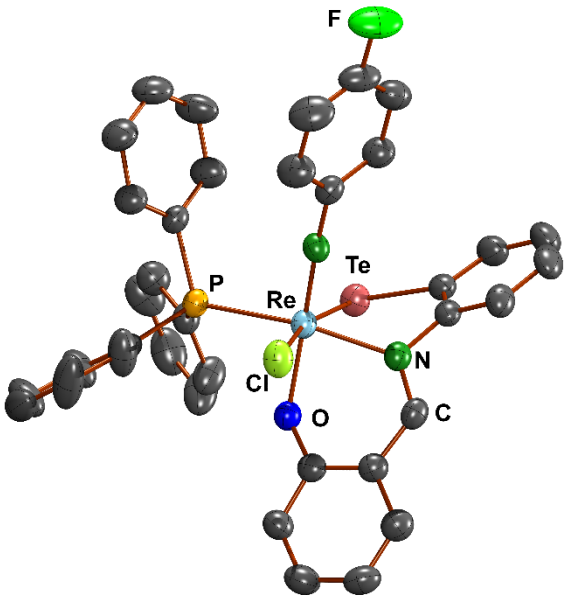

Part 2: Computational data

Figure S2.1 Optimized structure of *fac*-[ReO(L^O)Cl(PPh_3)].

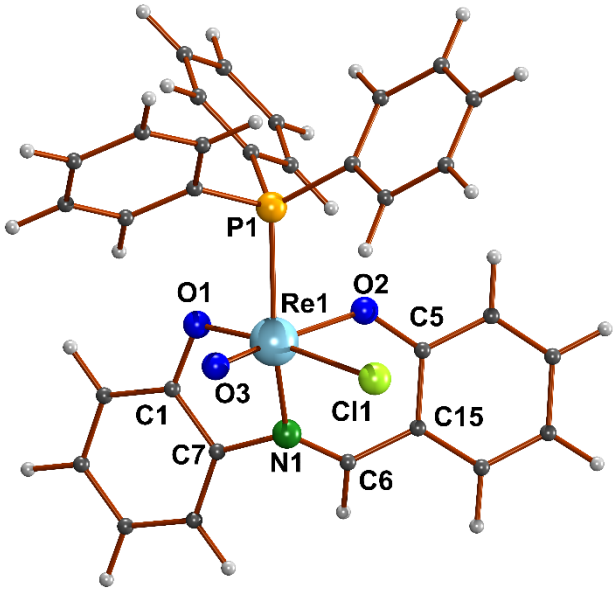

Table S2.1 Final coordinates of the gas-phase optimized structure for *fac*-[ReO-(L^O)Cl(PPh_3)].

	x	y	z
C1	-21,216	-23,825	0.5208
C2	25,169	15,746	-0.1367
C3	18,789	-0.4567	18,647
C4	26,952	-12,826	-0.8031
C5	-18,626	22,598	0.5900
C6	-35,981	0.6867	-0.1983
C7	-31,656	-16,669	-0.1132
C8	-23,684	-36,857	0.9685
C9	24,271	22,244	-13,793
C10	32,716	21,554	0.8945
C11	10,221	0.1153	28,199
C12	29,046	-13,135	22,924
C13	22,402	-26,121	-0.8361
C14	39,067	-0.9512	-14,231
C15	-31,847	20,177	0.0889
C16	-15,612	35,450	10,961
C17	-44,119	-22,495	-0.3374
C18	-36,182	-42,642	0.7475
C19	30,934	34,328	-15,832
C20	39,299	33,682	0.6837
C21	11,917	-0.1701	41,746
C22	30,669	-15,972	36,499
C23	29,933	-35,916	-14,799
C24	46,525	-19,376	-20,739
C25	-41,410	30,642	0.1125
C26	-25,074	45,528	10,688
C27	-46,345	-35,590	0.0912
C28	38,437	40,070	-0.5545
C29	22,113	-10,277	45,933
C30	41,988	-32,560	-21,033
C31	-38,088	43,206	0.5728
Cl1	-0.7846	16,390	-23,087
H1	-46,626	0.4602	-0.1109
H2	-15,710	-42,268	14,681
H3	18,149	18,032	-21,692
H4	33,473	16,654	18,592
H5	0.2241	0.7755	24,995

H6	35,769	-17,636	15,701
H7	13,006	-28,743	-0.3584
H8	42,671	0.0717	-14,063
H9	-0.5578	37,182	14,711
H10	-51,910	-16,968	-0.8556
H11	-37,995	-52,828	10,797
H12	30,124	39,306	-25,454
H13	45,100	38,111	14,888
H14	0.5203	0.2759	49,034
H15	38,630	-22,659	39,663
H16	26,336	-46,165	-15,028
H17	55,873	-16,699	-25,588
H18	-51,450	28,595	-0.2523
H19	-22,447	55,409	14,381
H20	-55,953	-40,300	-0.0931
H21	43,558	49,519	-0.7160
H22	23,374	-12,512	56,494
H23	47,794	-40,206	-26,124
H24	-45,412	51,217	0.5651
N1	-27,832	-0.3223	-0.3973
O1	-0.9265	-17,751	0.6747
O2	-0.9583	13,084	0.6476
O3	-0.3812	-12,538	-19,927
P1	16,703	-0.0374	0.0798
Re1	-0.7106	-0.2732	-0.6591

Figure S2.2 Optimized structure of *fac*-[ReO(L^S)Cl(PPh_3)].

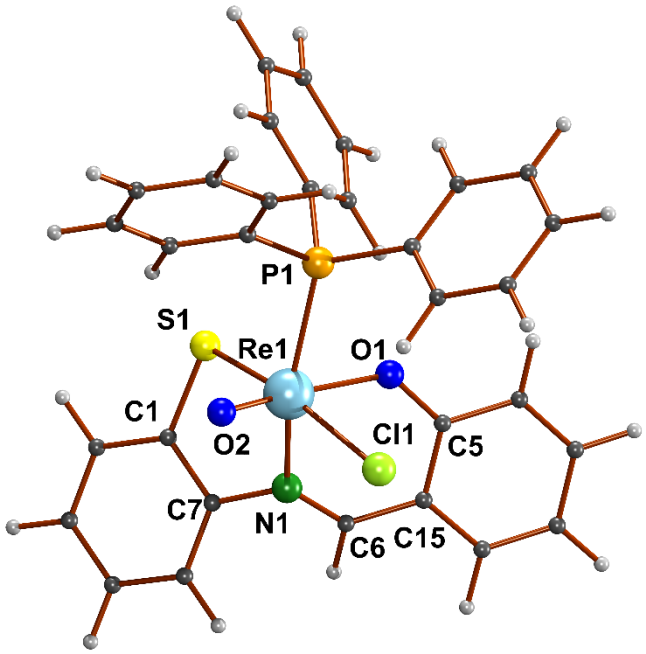

Table S2.2 Final coordinates of the gas-phase optimized structure for *fac*-[ReO-(L^S)Cl(PPh_3)].

	x	y	z
C1	-2.845815	-2.166228	0.652486
C2	2.661124	1.351378	-0.308265
C3	2.062592	-0.553874	1.813395
C4	2.63958	-1.528632	-0.873006
C5	-1.42623	2.496221	0.573095
C6	-3.400033	1.169972	-0.133928
C7	-3.498664	-1.197052	-0.137294
C8	-3.524081	-3.353239	0.95208
C9	2.553584	1.941346	-1.579013
C10	3.490632	1.941723	0.658122
C11	1.332554	0.141034	2.793245
C12	3.03671	-1.48072	2.213795
C13	2.102601	-2.827327	-0.875739
C14	3.848446	-1.282853	-1.538593
C15	-2.783335	2.42879	0.126534
C16	-0.919521	3.739809	1.011424
C17	-4.772739	-1.429676	-0.658162
C18	-4.804827	-3.580508	0.446552
C19	3.272747	3.099672	-1.87365
C20	4.202065	3.104645	0.356898
C21	1.576323	-0.092581	4.146387
C22	3.272364	-1.712772	3.570543
C23	2.771339	-3.859722	-1.530756
C24	4.509137	-2.320838	-2.200269
C25	-3.577923	3.601529	0.139111
C26	-1.712329	4.873047	0.976561
C27	-5.425258	-2.627858	-0.366663
C28	4.095791	3.684072	-0.908431
C29	2.543639	-1.020791	4.538373
C30	3.973742	-3.608603	-2.197197
C31	-3.051563	4.813495	0.53687
Cl1	-0.704269	1.514418	-2.355243
H1	-4.488384	1.131586	-0.061437
H2	-3.035462	-4.102843	1.567694
H3	1.889361	1.514441	-2.321992
H4	3.58453	1.498214	1.64327
H5	0.578299	0.859145	2.48987
H6	3.609767	-2.025525	1.47135
H7	1.162366	-3.029244	-0.371415
H8	4.27389	-0.285322	-1.547504

H9	0.112468	3.77835	1.344686
H10	-5.236706	-0.6901	-1.304806
H11	-5.312388	-4.514241	0.67238
H12	3.176596	3.550675	-2.857191
H13	4.839878	3.554228	1.113248
H14	1.00349	0.448122	4.894784
H15	4.025673	-2.437472	3.867427
H16	2.346204	-4.859484	-1.528381
H17	5.441793	-2.117136	-2.719189
H18	-4.613905	3.532385	-0.184945
H19	-1.296298	5.82501	1.296446
H20	-6.409289	-2.819988	-0.783781
H21	4.649627	4.589994	-1.140573
H22	2.726924	-1.204763	5.593623
H23	4.487917	-4.41392	-2.714822
H24	-3.662182	5.710771	0.521322
N1	-2.781315	0.029391	-0.316227
O1	-0.673736	1.421184	0.641451
O2	-0.52413	-1.379943	-1.779847
P1	1.741468	-0.201106	0.030947
Re1	-0.709671	-0.264822	-0.526311
S1	-1.183879	-1.834761	1.21762

Figure S2.3 Optimized structure of *fac*-[ReO(L^{Se})Cl(PPh_3)].

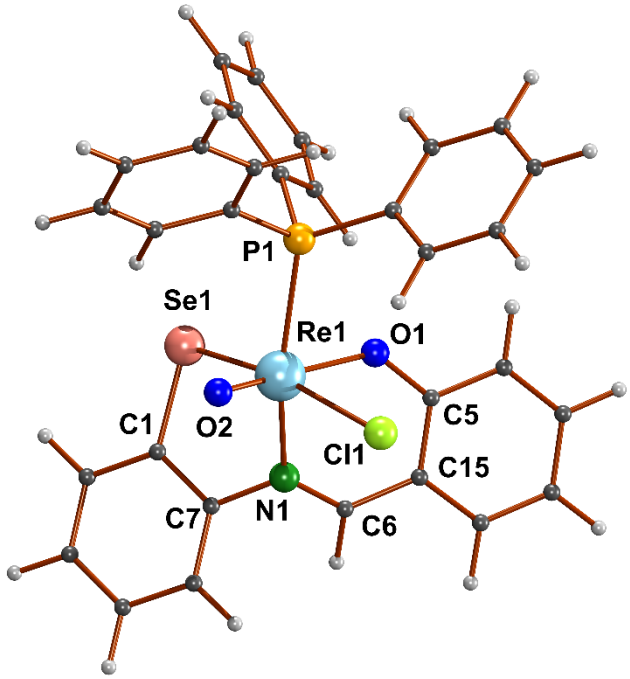

Table S2.3 Final coordinates of the gas-phase optimized structure for *fac*-[ReO-(L^{Se})Cl(PPh_3)].

	x	y	z
C1	-3.049917	-1.931771	0.474327
C2	2.802603	1.292561	-0.311872
C3	2.112404	-0.653187	1.741661
C4	2.635043	-1.558779	-0.980404
C5	-1.190911	2.64009	0.612834
C6	-3.24157	1.470618	-0.161221
C7	-3.535552	-0.869069	-0.311062
C8	-3.857922	-3.057328	0.657565
C9	2.727862	1.930014	-1.561867
C10	3.659216	1.807223	0.673929
C11	1.425142	0.048832	2.74756
C12	3.034122	-1.645847	2.106864
C13	2.033	-2.827278	-1.037651
C14	3.858961	-1.349362	-1.631243
C15	-2.546382	2.674595	0.161038
C16	-0.608333	3.831452	1.098087
C17	-4.778844	-0.952059	-0.942291
C18	-5.109645	-3.135143	0.043093
C19	3.504899	3.059991	-1.816874
C20	4.428925	2.942429	0.412595
C21	1.658881	-0.243038	4.091327
C22	3.259599	-1.935875	3.45424
C23	2.652151	-3.86583	-1.730743
C24	4.469898	-2.392593	-2.331227
C25	-3.265544	3.893298	0.216065
C26	-1.32841	5.013228	1.105255
C27	-5.565578	-2.090697	-0.765131
C28	4.354381	3.569253	-0.832193
C29	2.573475	-1.236745	4.447828
C30	3.869723	-3.65048	-2.381772
C31	-2.666291	5.054468	0.661129
Cl1	-0.542661	1.692551	-2.360274
H1	-4.331133	1.506959	-0.110306
H2	-3.498748	-3.880828	1.268044
H3	2.045115	1.562251	-2.31947
H4	3.729379	1.326461	1.643423
H5	0.712581	0.818661	2.470805
H6	3.57382	-2.196804	1.344192
H7	1.080499	-3.001567	-0.546355
H8	4.335157	-0.375592	-1.598535

H9	0.422535	3.792313	1.434811
H10	-5.11314	-0.142766	-1.585496
H11	-5.720788	-4.022981	0.180288
H12	3.433626	3.548146	-2.784672
H13	5.087245	3.333159	1.183922
H14	1.1195	0.303946	4.859712
H15	3.971571	-2.711301	3.723671
H16	2.176388	-4.841729	-1.769893
H17	5.414838	-2.216275	-2.837808
H18	-4.302154	3.901963	-0.113277
H19	-0.854793	5.92419	1.462308
H20	-6.525384	-2.164726	-1.267759
H21	4.953564	4.453475	-1.033284
H22	2.748852	-1.46588	5.495531
H23	4.345326	-4.459865	-2.929077
H24	-3.219792	5.98803	0.678402
N1	-2.704398	0.297584	-0.386185
O1	-0.50857	1.516879	0.641066
O2	-0.527729	-1.22996	-1.846687
P1	1.80374	-0.222132	-0.026353
Re1	-0.650756	-0.128117	-0.57456
Se1	-1.272921	-1.770239	1.225058

Figure S2.4 Optimized structure of *fac*-[ReO(L^{Te})Cl(PPh_3)].

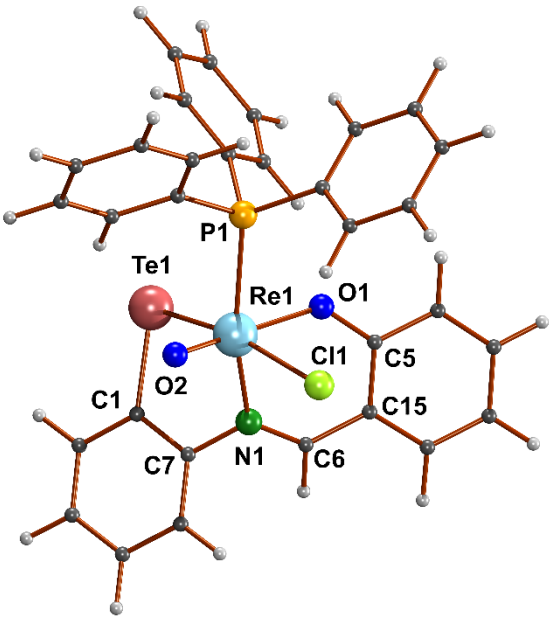

Table S2.4 Final coordinates of the gas-phase optimized structure for *fac*-[ReO-(L^{Te})Cl(PPh_3)].

	x	y	z
C1	-3.286623	-1.649436	0.246016
C2	2.956964	1.211985	-0.327287
C3	2.179743	-0.774559	1.649862
C4	2.631237	-1.593785	-1.112626
C5	-0.918242	2.764704	0.679844
C6	-3.045272	1.77713	-0.154798
C7	-3.54714	-0.496522	-0.518031
C8	-4.240101	-2.672491	0.24826
C9	2.91816	1.89785	-1.553048
C10	3.838542	1.644847	0.675662
C11	1.545792	-0.073181	2.690915
C12	3.045196	-1.832682	1.964987
C13	1.956494	-2.820393	-1.235158
C14	3.870955	-1.426426	-1.746235
C15	-2.269209	2.910068	0.244063
C16	-0.25162	3.886521	1.215983
C17	-4.703466	-0.390746	-1.296644
C18	-5.40783	-2.563038	-0.511198
C19	3.753623	2.994037	-1.76727
C20	4.667174	2.746953	0.455557
C21	1.775319	-0.430818	4.019751
C22	3.265686	-2.189378	3.297324
C23	2.518933	-3.858989	-1.975292
C24	4.425128	-2.468794	-2.492951
C25	-2.904178	4.168717	0.365978
C26	-0.891263	5.112541	1.290981
C27	-5.63505	-1.428663	-1.292844
C28	4.627372	3.422004	-0.765259
C29	2.632055	-1.491057	4.326034
C30	3.752312	-3.68503	-2.608402
C31	-2.225582	5.26416	0.864153
Cl1	-0.358232	1.858302	-2.356436
H1	-4.129616	1.896261	-0.125812
H2	-4.063707	-3.570482	0.83422
H3	2.218651	1.594282	-2.323519
H4	3.883001	1.126273	1.626935
H5	0.878389	0.748741	2.453333
H6	3.54419	-2.383222	1.174798
H7	0.991258	-2.962434	-0.759088
H8	4.40369	-0.485487	-1.663711

H9	0.776608	3.761435	1.539616
H10	-4.854078	0.487406	-1.918373
H11	-6.129765	-3.375229	-0.507402
H12	3.709581	3.519907	-2.716763
H13	5.344254	3.073768	1.240262
H14	1.278485	0.117533	4.815352
H15	3.933095	-3.015373	3.527598
H16	1.986238	-4.801549	-2.064806
H17	5.382971	-2.324318	-2.985183
H18	-3.939665	4.263611	0.046873
H19	-0.355284	5.970396	1.68895
H20	-6.526446	-1.354421	-1.908833
H21	5.272498	4.280197	-0.934344
H22	2.804104	-1.771239	5.361761
H23	4.183826	-4.493587	-3.192234
H24	-2.716052	6.229963	0.933941
N1	-2.598256	0.58196	-0.4424
O1	-0.314302	1.595272	0.642862
O2	-0.534783	-1.082115	-1.895252
P1	1.876703	-0.256609	-0.096566
Re1	-0.573878	0.014483	-0.615268
Te1	-1.425503	-1.755246	1.295296

Figure S2.5 Optimized structure of *mer*-[ReO(L^O)Cl(PPh_3)].

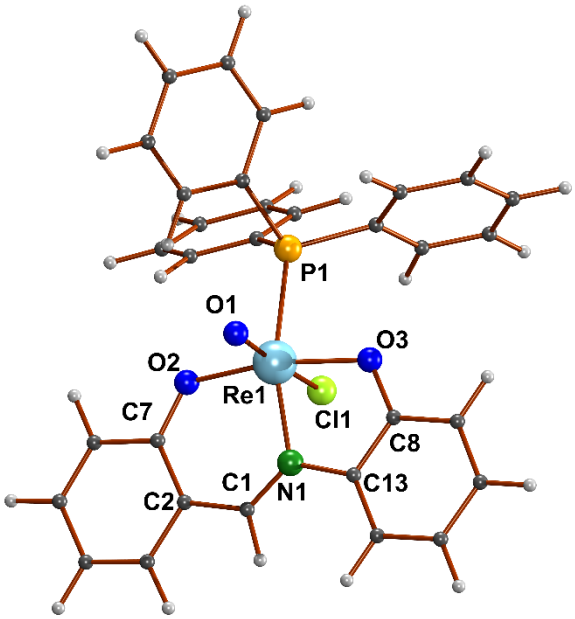

Table S2.5 Final coordinates of the gas-phase optimized structure for *mer*-[ReO(L^O)Cl(PPh_3)].

	x	y	z
C1	3.660146	-0.421042	0.102477
C2	3.47683	-1.834547	0.062166
C3	4.661788	-2.614734	-0.055359
C4	4.631489	-3.990576	-0.103918
C5	3.383058	-4.64314	-0.035321
C6	2.209107	-3.92372	0.076345
C7	2.204372	-2.505726	0.12449
C8	1.835567	2.688806	0.164196
C9	1.935739	4.083835	0.124156
C10	3.193256	4.683622	0.100597
C11	4.356667	3.904928	0.111273
C12	4.266855	2.513581	0.142848
C13	3.009284	1.904252	0.168685
C14	-2.83034	-0.486734	1.390273
C15	-2.335089	-1.267306	2.443381
C16	-3.180184	-1.676481	3.477943
C17	-4.524787	-1.307179	3.476819
C18	-5.028107	-0.532356	2.429004
C19	-4.189867	-0.128063	1.390985
C20	-2.251373	-1.294896	-1.265939
C21	-3.018666	-1.029445	-2.406861
C22	-1.857329	-2.615528	-0.99792
C23	-3.380237	-2.067465	-3.268883
C24	-2.222189	-3.647165	-1.860145
C25	-2.981671	-3.376224	-3.000858
C26	-2.322691	1.635069	-0.574175
C27	-2.767905	2.555157	0.389547
C28	-2.144402	2.073599	-1.896829
C29	-3.103826	3.858315	0.02318
C30	-2.486128	3.377291	-2.258675
C31	-2.979632	4.268648	-1.305227
Cl1	0.72213	0.020092	-2.077863
H1	4.694817	-0.08484	0.031106
H2	5.614049	-2.091606	-0.109737
H3	5.549346	-4.562091	-0.196307
H4	3.340634	-5.728791	-0.074983
H5	1.245883	-4.42151	0.11815
H6	1.021433	4.668226	0.109207
H7	3.269418	5.767182	0.071571
H8	5.333209	4.379248	0.093728
H9	5.177118	1.921546	0.151135
H10	-1.286382	-1.533857	2.476482

H11	-2.779032	-2.278818	4.288381
H12	-5.178509	-1.6204	4.286419
H13	-6.075404	-0.24257	2.41695
H14	-4.600201	0.45523	0.572897
H15	-3.362593	-0.024351	-2.619456
H16	-1.241356	-2.831939	-0.131912
H17	-3.975866	-1.846604	-4.150587
H18	-1.906963	-4.664325	-1.64354
H19	-3.261583	-4.181497	-3.674733
H20	-2.847583	2.261184	1.430877
H21	-1.683137	1.421951	-2.629256
H22	-3.455665	4.553458	0.780659
H23	-2.347058	3.698418	-3.28728
H24	-3.247744	5.282236	-1.591284
N1	2.739554	0.505042	0.208673
O1	0.497838	-0.030494	2.131027
O2	1.038686	-1.91629	0.218998
O3	0.63851	2.072549	0.182136
P1	-1.741515	-0.02133	-0.035044
Re1	0.719388	0.107105	0.458711

Figure S2.6 Optimized structure of *mer*-[ReO(L^S)Cl(PPh_3)].

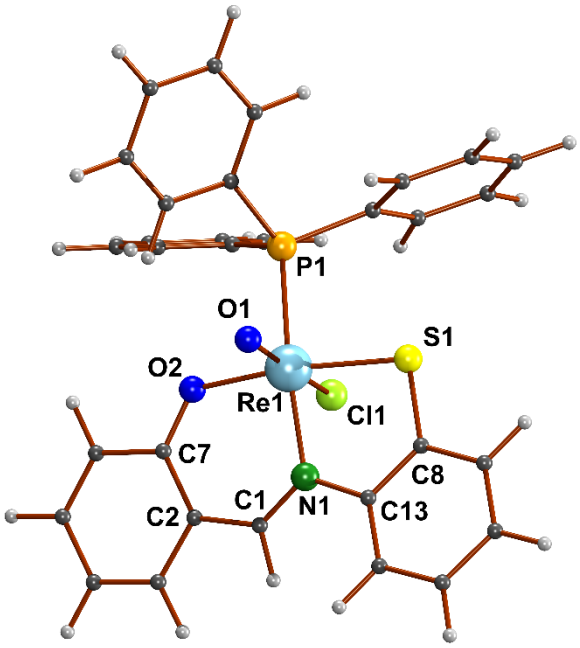

Table S2.6 Final coordinates of the gas-phase optimized structure for *mer*-[ReO(L^S)Cl(PPh_3)].

	x	y	z
C1	-3.335485	1.219069	0.075066
C2	-2.773992	2.524773	0.050721
C3	-3.697091	3.596808	-0.128354
C4	-3.294251	4.91173	-0.146425
C5	-1.923181	5.204364	0.030171
C6	-0.995493	4.198019	0.20211
C7	-1.376185	2.828375	0.197182
C8	-2.851479	-2.37173	0.080457
C9	-3.56541	-3.576403	0.0547
C10	-4.952376	-3.584396	0.173338
C11	-5.639666	-2.378114	0.325524
C12	-4.941194	-1.172739	0.344304
C13	-3.544633	-1.154006	0.210025
C14	2.868969	-0.165323	1.436219
C15	2.535128	0.78739	2.416684
C16	3.263742	0.87504	3.602484
C17	4.334595	0.011145	3.836532
C18	4.665554	-0.946472	2.878647
C19	3.936711	-1.039435	1.690977
C20	2.505149	1.198927	-1.082861
C21	2.810709	1.169437	-2.45129
C22	2.692973	2.411953	-0.39714
C23	3.296789	2.302499	-3.105815
C24	3.175314	3.543796	-1.052298
C25	3.48236	3.49571	-2.411827
C26	2.197265	-1.883996	-0.875968
C27	2.266808	-2.988294	-0.003062
C28	2.224821	-2.136437	-2.256184
C29	2.453134	-4.280421	-0.491609
C30	2.409438	-3.432101	-2.742195
C31	2.546341	-4.506162	-1.865075
Cl1	-0.607313	0.249441	-2.131428
H1	-4.416906	1.21028	-0.043299
H2	-4.749747	3.351059	-0.250748
H3	-4.013453	5.710246	-0.297047
H4	-1.591486	6.239884	0.027257
H5	0.05966	4.415291	0.329578
H6	-3.016671	-4.507639	-0.053314
H7	-5.494095	-4.525829	0.151543
H8	-6.720006	-2.369889	0.436398
H9	-5.505979	-0.25724	0.482196
H10	1.670657	1.428049	2.282802

H11	2.977293	1.607404	4.352141
H12	4.905087	0.0836	4.758462
H13	5.496221	-1.626154	3.048704
H14	4.23761	-1.768838	0.948487
H15	2.67914	0.27329	-3.034139
H16	2.463746	2.491184	0.655502
H17	3.524823	2.243505	-4.166452
H18	3.310981	4.465027	-0.491889
H19	3.859244	4.377345	-2.92302
H20	2.137723	-2.849285	1.064573
H21	2.041961	-1.348838	-2.970268
H22	2.50778	-5.111055	0.206521
H23	2.42628	-3.596687	-3.8159
H24	2.689052	-5.513022	-2.247616
N1	-2.751606	0.047254	0.206409
O1	-0.41979	-0.177286	2.05555
O2	-0.436197	1.938657	0.320122
P1	1.833998	-0.240813	-0.108715
Re1	-0.665041	-0.125162	0.382415
S1	-1.083096	-2.378913	-0.080441

Figure S2.7 Optimized structure of *mer*-[ReO(L^{Se})Cl(PPh_3)].

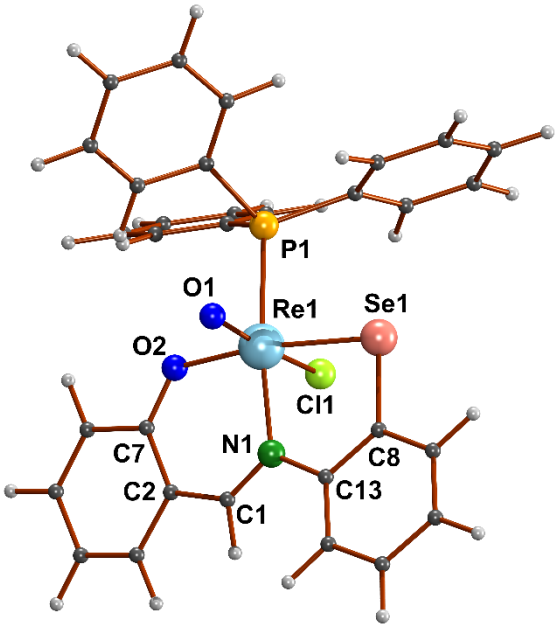

Table S2.7 Final coordinates of the gas-phase optimized structure for *mer*-[ReO(L^{Se})Cl(PPh_3)].

	x	y	z
C1	-3.133105	1.645037	0.117164
C2	-2.460423	2.895163	0.035037
C3	-3.291768	4.039881	-0.140309
C4	-2.775377	5.31223	-0.220586
C5	-1.379056	5.487215	-0.096916
C6	-0.538441	4.407122	0.075429
C7	-1.038182	3.077028	0.115113
C8	-3.108503	-1.991008	0.112593
C9	-3.985477	-3.082367	0.116203
C10	-5.35835	-2.896903	0.245152
C11	-5.861095	-1.60223	0.386513
C12	-4.997218	-0.510626	0.380032
C13	-3.608866	-0.682938	0.232744
C14	2.88183	-0.31667	1.557468
C15	2.688688	0.811714	2.376507
C16	3.297707	0.914232	3.625756
C17	4.12975	-0.103969	4.090273
C18	4.311313	-1.238179	3.303203
C19	3.684747	-1.352634	2.058539
C20	2.74683	1.05524	-1.066295
C21	3.197035	0.936793	-2.388529
C22	2.886864	2.306575	-0.442613
C23	3.779269	2.018526	-3.053334
C24	3.464573	3.386629	-1.109041
C25	3.919316	3.24964	-2.41934
C26	2.12291	-2.011123	-0.86656
C27	2.136648	-3.136175	-0.021732
C28	2.076257	-2.243511	-2.251854
C29	2.209082	-4.43129	-0.536135
C30	2.146164	-3.540814	-2.763383
C31	2.237473	-4.640683	-1.91317
Cl1	-0.462715	0.375841	-2.180633
H1	-4.213821	1.753656	0.078071
H2	-4.366239	3.885809	-0.212363
H3	-3.426515	6.16567	-0.378647
H4	-0.958271	6.488936	-0.136596
H5	0.533751	4.534422	0.178926
H6	-3.57775	-4.084667	0.020004
H7	-6.02855	-3.751731	0.235155
H8	-6.927369	-1.434773	0.507092
H9	-5.438549	0.471522	0.503439
H10	2.011933	1.599097	2.076019

H11	3.101224	1.788098	4.240627
H12	4.624821	-0.015846	5.053214
H13	4.944556	-2.050751	3.648707
H14	3.887428	-2.247248	1.488824
H15	3.129861	0.012243	-2.932694
H16	2.521591	2.474985	0.556953
H17	4.120748	1.883715	-4.075848
H18	3.550197	4.339644	-0.593769
H19	4.369515	4.090869	-2.93887
H20	2.046723	-3.02178	1.046905
H21	1.918209	-1.447137	-2.958646
H22	2.22299	-5.272881	0.150666
H23	2.107208	-3.681407	-3.839845
H24	2.287811	-5.647629	-2.31755
N1	-2.670683	0.415578	0.202349
O1	-0.327524	-0.006364	2.010753
O2	-0.180496	2.108264	0.240566
P1	1.930989	-0.328149	-0.072776
Re1	-0.5786	0.048114	0.340825
Se1	-1.225583	-2.300122	-0.101583

Figure S2.8 Optimized structure of *mer*-[ReO(L^{Te})Cl(PPh_3)].

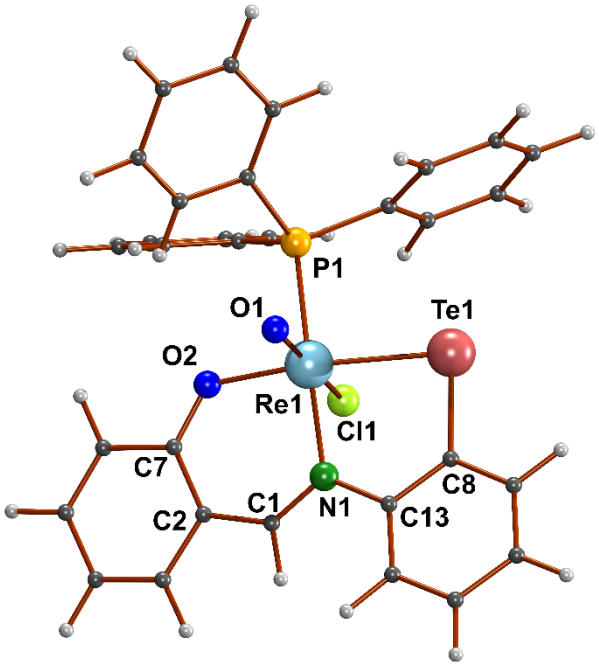

Table S2.8 Final coordinates of the gas-phase optimized structure for *mer*-[ReO(L^{Te})Cl(PPh_3)].

	x	y	z
C1	-2.755177	2.183846	0.045933
C2	-1.871397	3.296822	-0.052608
C3	-2.491683	4.560095	-0.278069
C4	-1.764514	5.724178	-0.380162
C5	-0.362799	5.664405	-0.221732
C6	0.277076	4.461617	-0.000315
C7	-0.444279	3.239721	0.05344
C8	-3.478475	-1.38947	0.116646
C9	-4.582196	-2.253996	0.132287
C10	-5.882476	-1.771694	0.23451
C11	-6.086697	-0.396273	0.344082
C12	-5.001407	0.474002	0.328382
C13	-3.680591	-0.000035	0.203656
C14	2.795566	-0.502387	1.626409
C15	2.716009	0.668691	2.406059
C16	3.323706	0.749276	3.657449
C17	4.044297	-0.333449	4.162908
C18	4.104416	-1.510542	3.420418
C19	3.477704	-1.599155	2.174773
C20	2.968284	0.737272	-0.999201
C21	3.3151	0.49047	-2.334095
C22	3.406714	1.946178	-0.43224
C23	4.07221	1.395888	-3.076629
C24	4.163662	2.854705	-1.172096
C25	4.502927	2.587566	-2.498379
C26	1.970005	-2.144709	-0.79901
C27	1.884234	-3.270607	0.043113
C28	1.961659	-2.377326	-2.186906
C29	1.870253	-4.568114	-0.470944
C30	1.943195	-3.675747	-2.698488
C31	1.915128	-4.779365	-1.847637
Cl1	-0.331928	0.482078	-2.182353
H1	-3.794143	2.49017	-0.017428
H2	-3.574966	4.591665	-0.371675
H3	-2.257618	6.66972	-0.580378
H4	0.223275	6.578672	-0.272924
H5	1.352111	4.409644	0.134591
H6	-4.41318	-3.325761	0.064019
H7	-6.724646	-2.457925	0.228082
H8	-7.089907	0.007025	0.446729
H9	-5.221399	1.529784	0.427212
H10	2.126235	1.514177	2.072369

H11	3.212937	1.657912	4.242484
H12	4.544328	-0.262653	5.124656
H13	4.641598	-2.374018	3.802893
H14	3.562831	-2.52863	1.631222
H15	3.001297	-0.430669	-2.790186
H16	3.162563	2.21715	0.582217
H17	4.320709	1.159371	-4.10727
H18	4.483793	3.779935	-0.700539
H19	5.091776	3.298679	-3.070865
H20	1.795723	-3.147038	1.113455
H21	1.927806	-1.563335	-2.896422
H22	1.808191	-5.408995	0.214045
H23	1.938138	-3.814692	-3.775771
H24	1.898609	-5.787257	-2.252185
N1	-2.530077	0.893029	0.168053
O1	-0.319374	0.146241	2.030358
O2	0.23146	2.139508	0.218637
P1	1.913639	-0.441837	-0.010445
Re1	-0.512673	0.218686	0.355007
Te1	-1.539929	-2.193856	-0.092208

Part 3: Spectra

S3.1 Spectra of $\{HL^{Se}\}_2$.

^1H

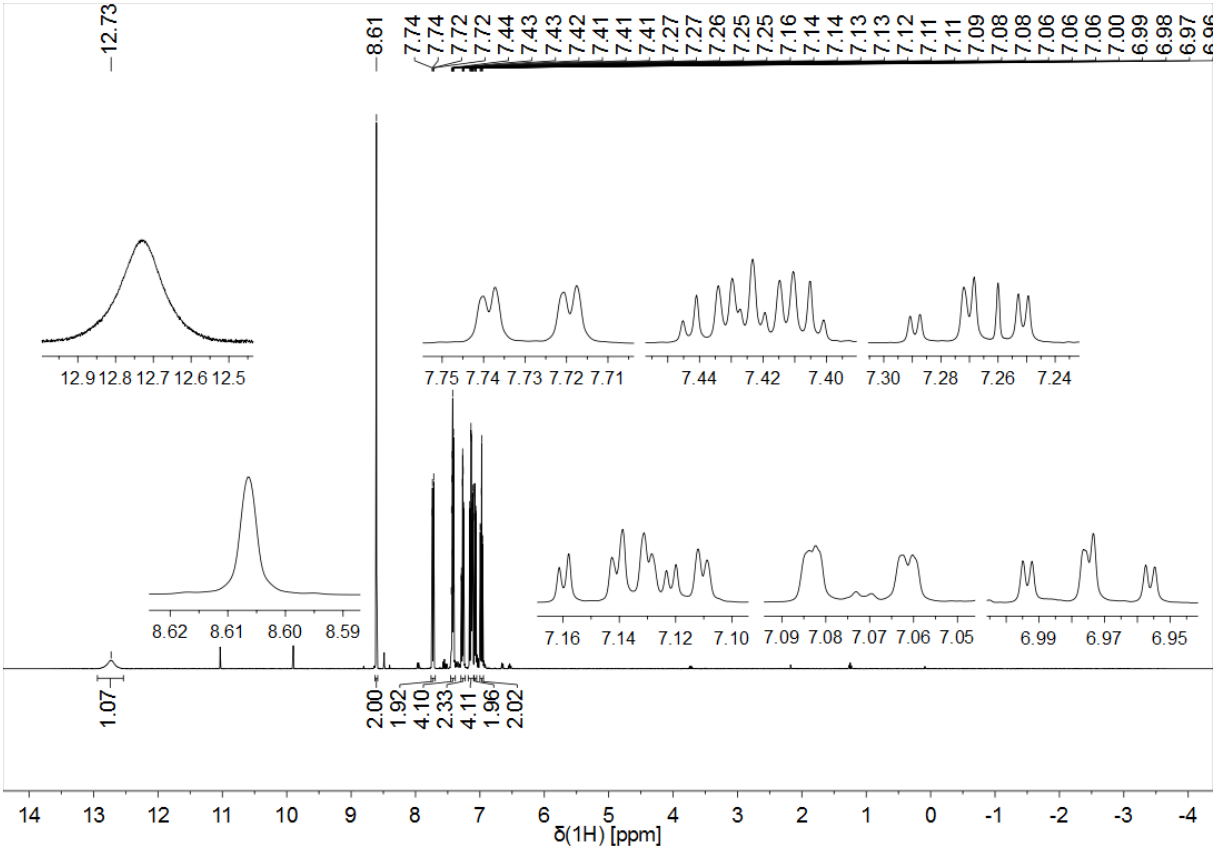

^{13}C

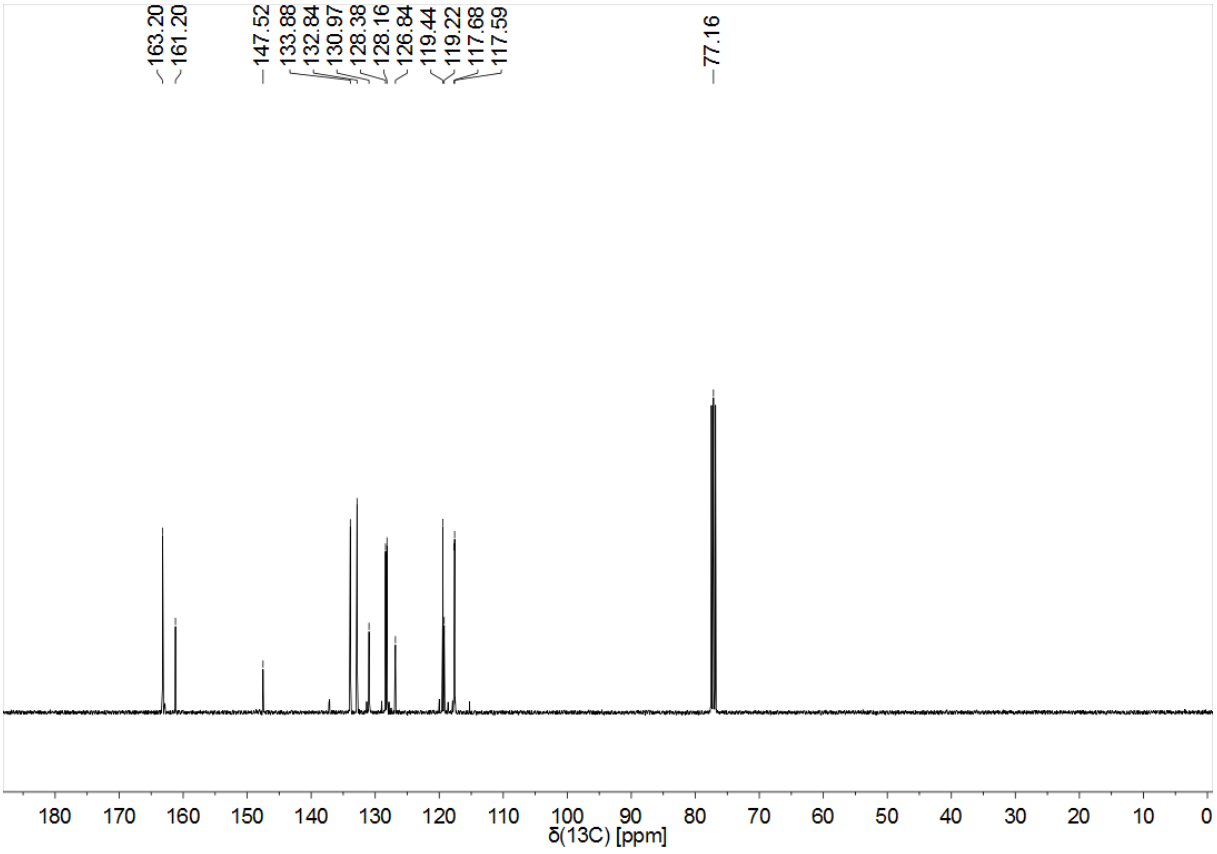

^{77}Se

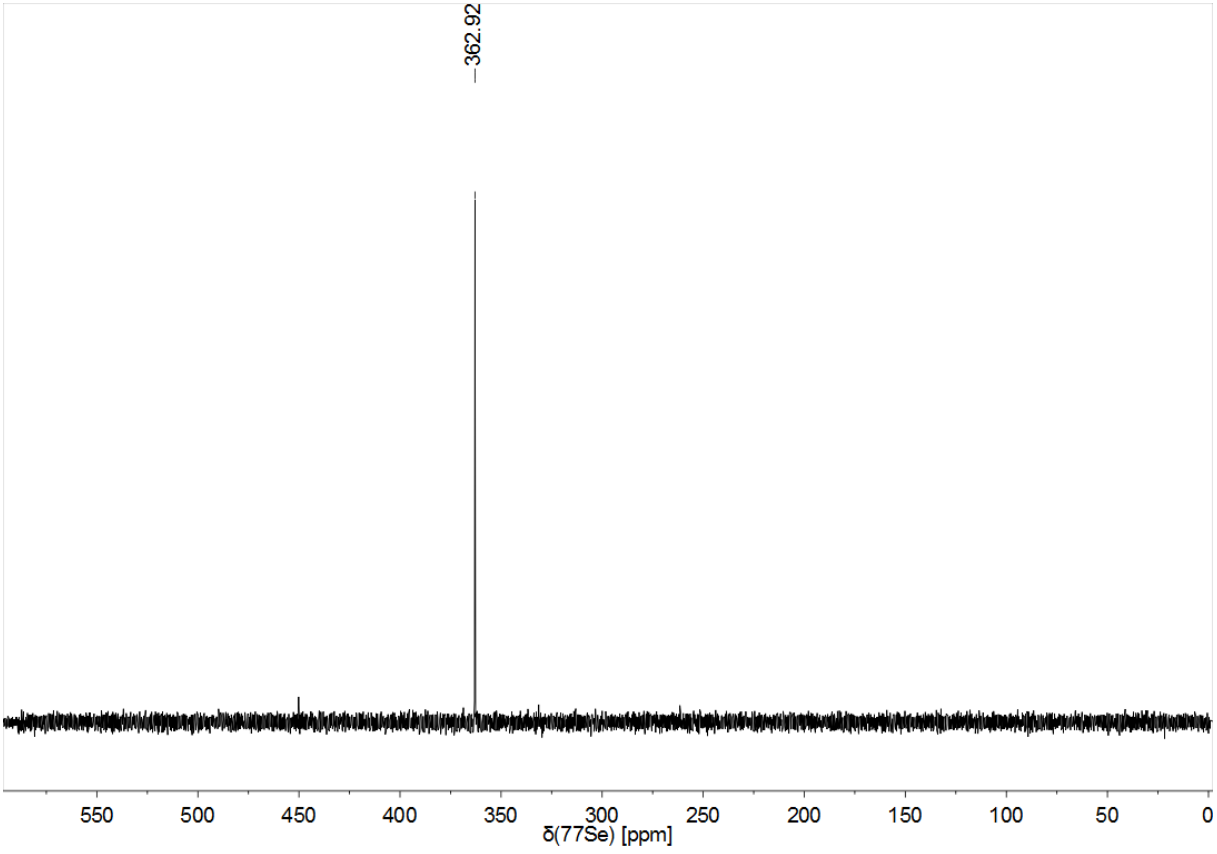
362.92
550
500
450
400
350
300
250
200
150
100
50
0
δ(77Se) [ppm]

IR

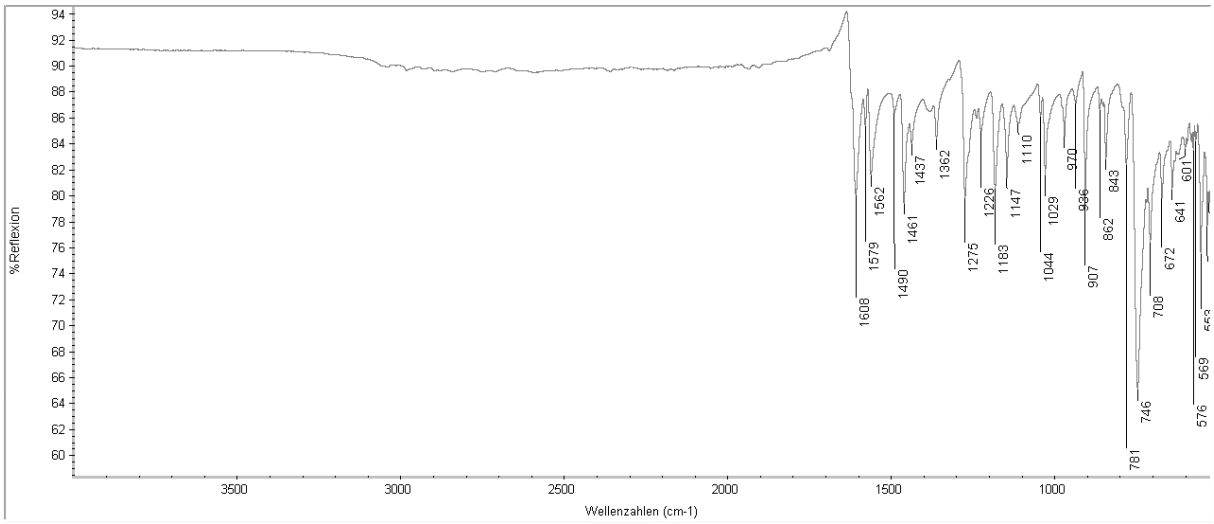
%Reflexion
Wellenzahlen (cm-1)
3500
3000
2500
2000
1500
1000
1608
1579
1562
1490
1461
1437
1362
1275
1226
1183
1147
1110
1044
1029
970
936
907
862
843
781
746
708
672
641
601
576
569

ESI+

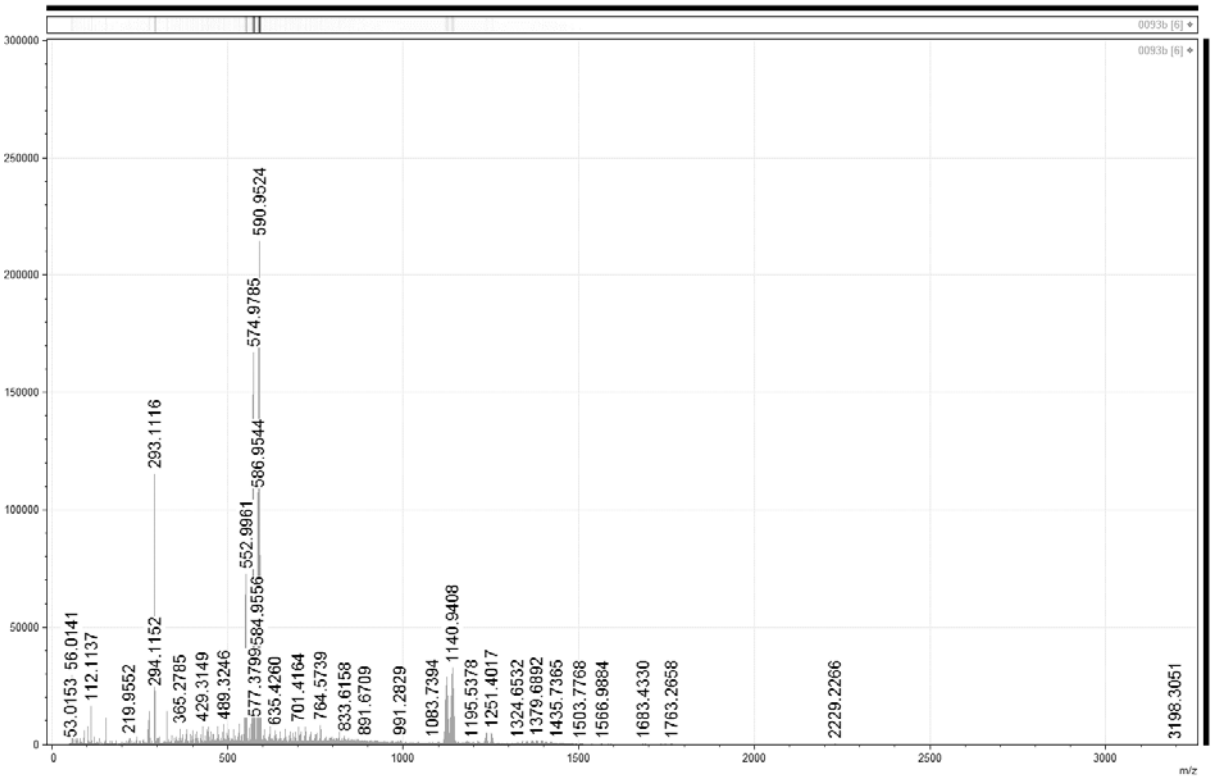

S3.2 Spectra of $\{HL^{Te}\}_2$.

^1H

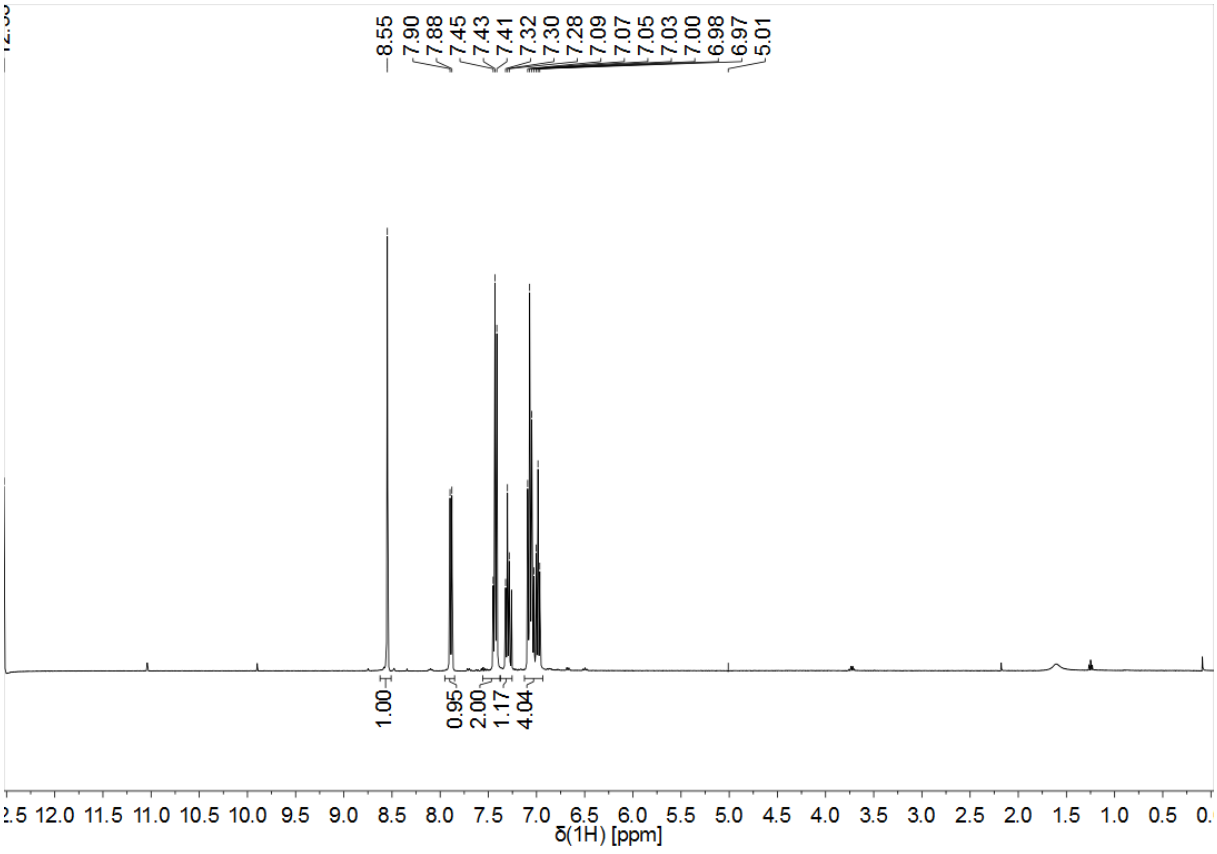

^{13}C

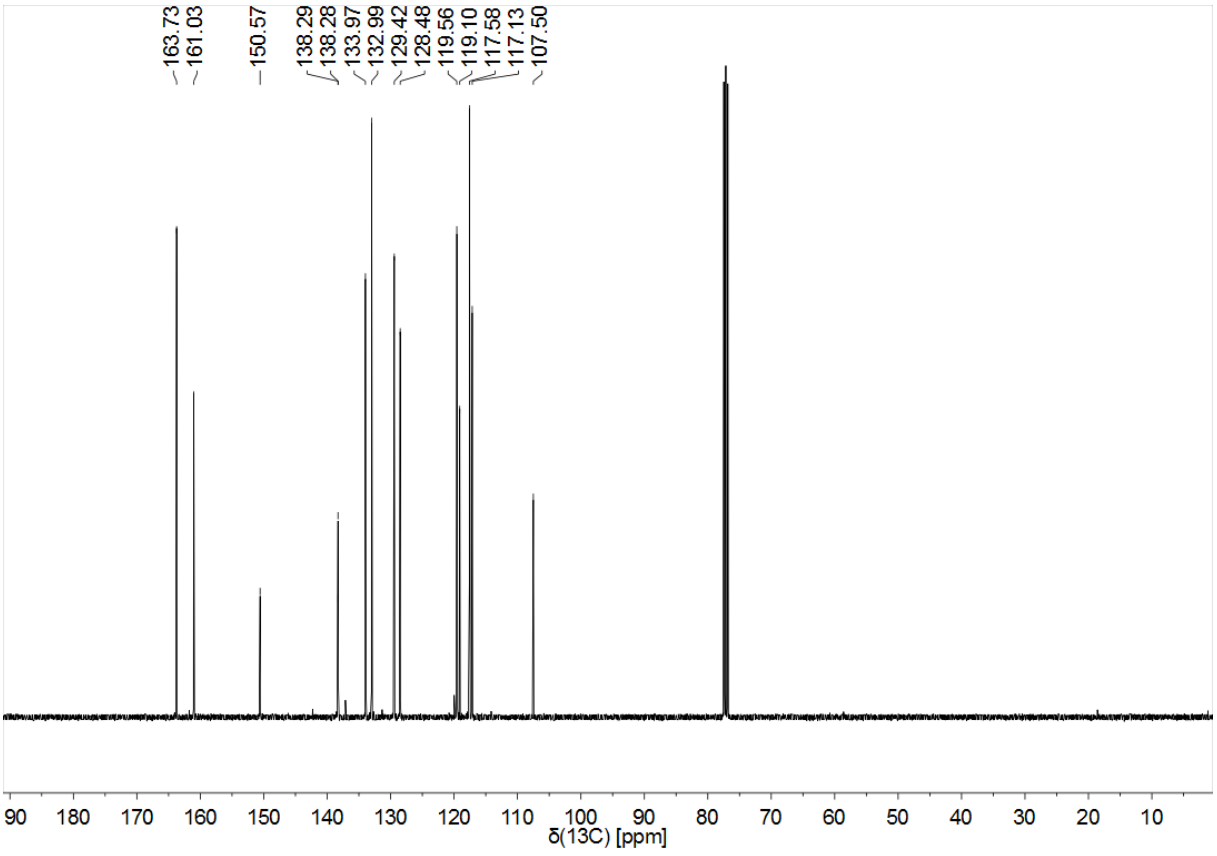
163.73
161.03
150.57
138.29
138.28
133.97
132.99
129.42
128.48
119.56
119.10
117.58
117.13
107.50
90 180 170 160 150 140 130 120 110 100 90 80 70 60 50 40 30 20 10
δ(13C) [ppm]

^{125}Te

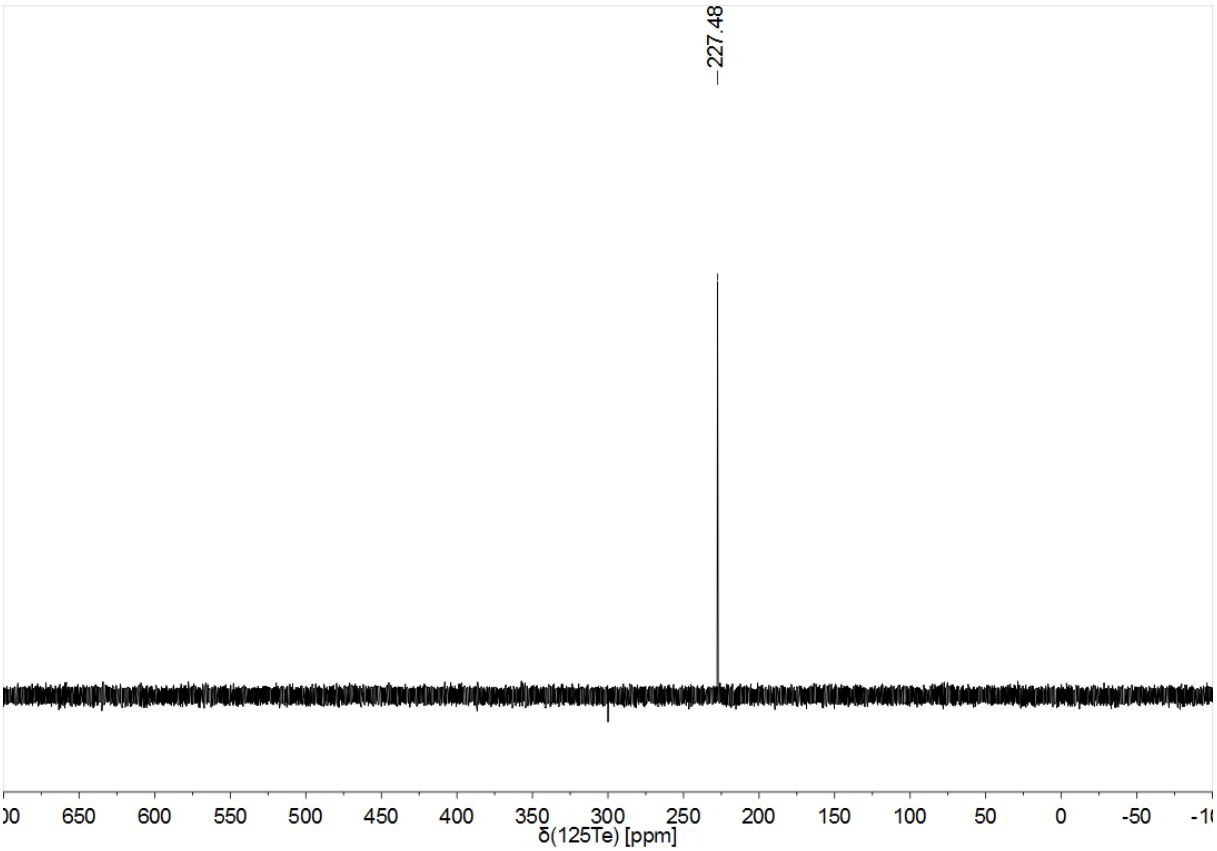
227.48
650 600 550 500 450 400 350 300 250 200 150 100 50 0 -50
δ(125Te) [ppm]

IR

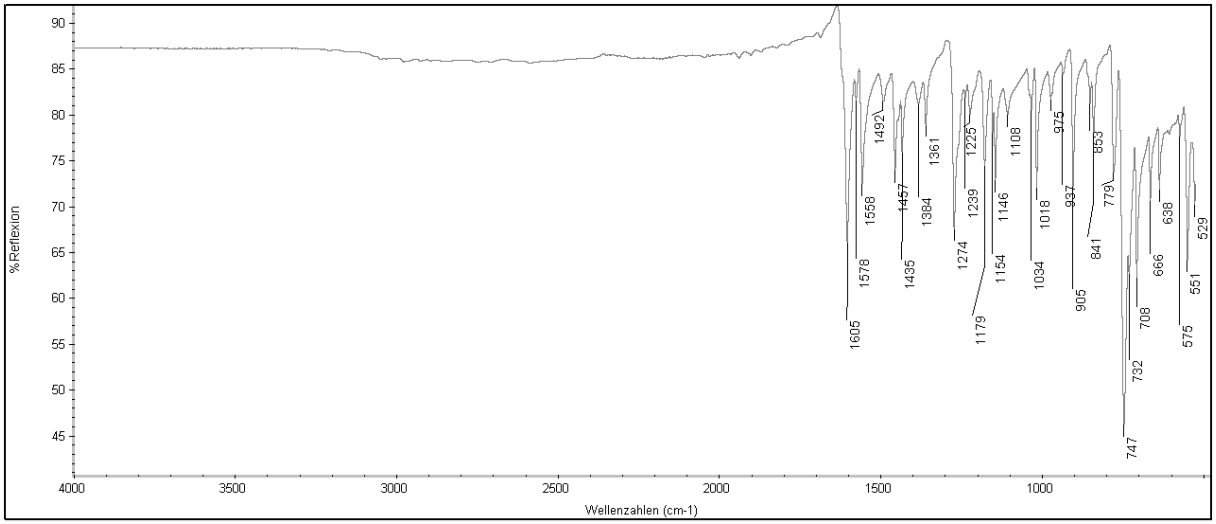
%Reflexion
Wellenzahlen (cm-1)
4000
3500
3000
2500
2000
1500
1000
1605
1578
1558
1492
1457
1435
1384
1361
1274
1239
1225
1179
1154
1146
1108
1034
1018
975
937
905
853
841
779
747
732
708
666
638
575
551
529

ESI+

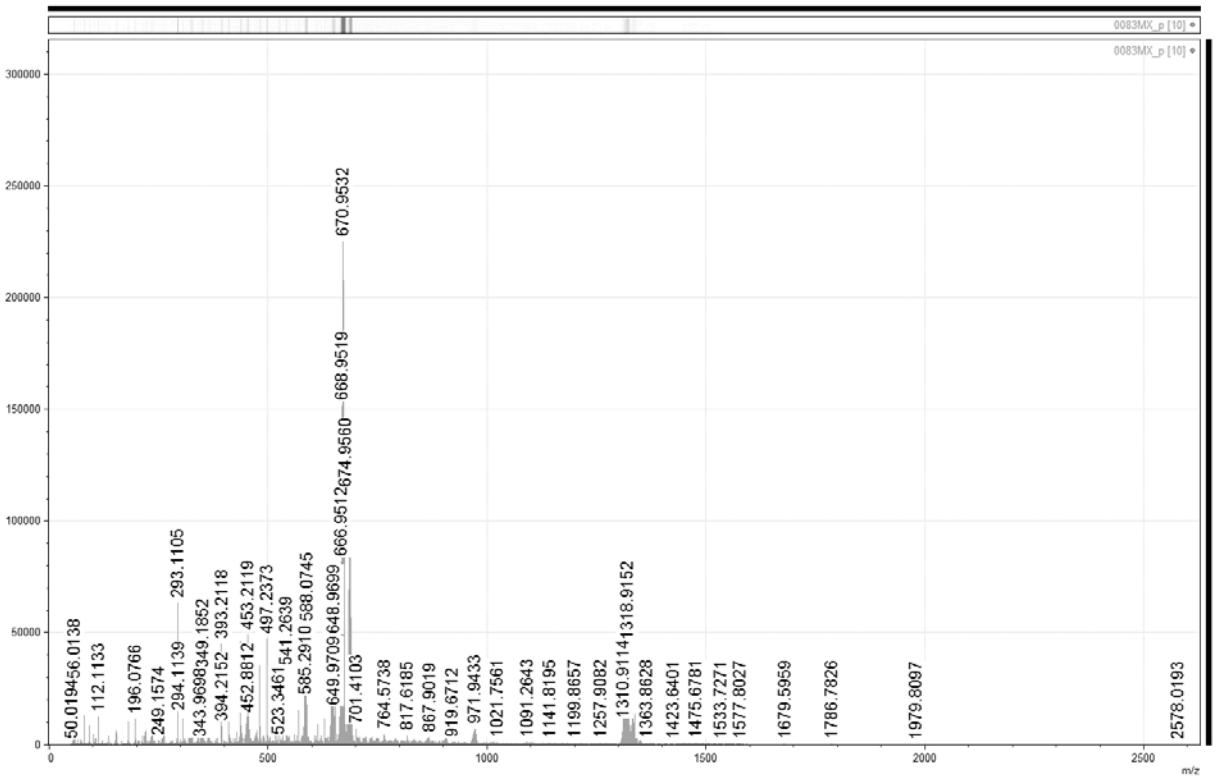
0083MX_p [10]
m/z
50.0194
56.0138
112.1133
196.0766
249.1574
294.1139
293.1105
343.9698
349.1852
394.2152
393.2118
452.8812
453.2119
497.2373
523.3461
541.2639
585.2910
588.0745
649.9709
648.9699
666.9512
674.9560
668.9519
670.9532
701.4103
764.5738
817.6185
867.9019
919.6712
971.9433
1021.7561
1091.2643
1141.8195
1199.8657
1257.9082
1310.9114
1318.9152
1363.8628
1423.6401
1475.6781
1533.7271
1577.8027
1679.5959
1786.7826
1979.8097
2578.0193

S3.3 Spectra of [ReO(L^{Se})Cl(PPh_3)].

^1H

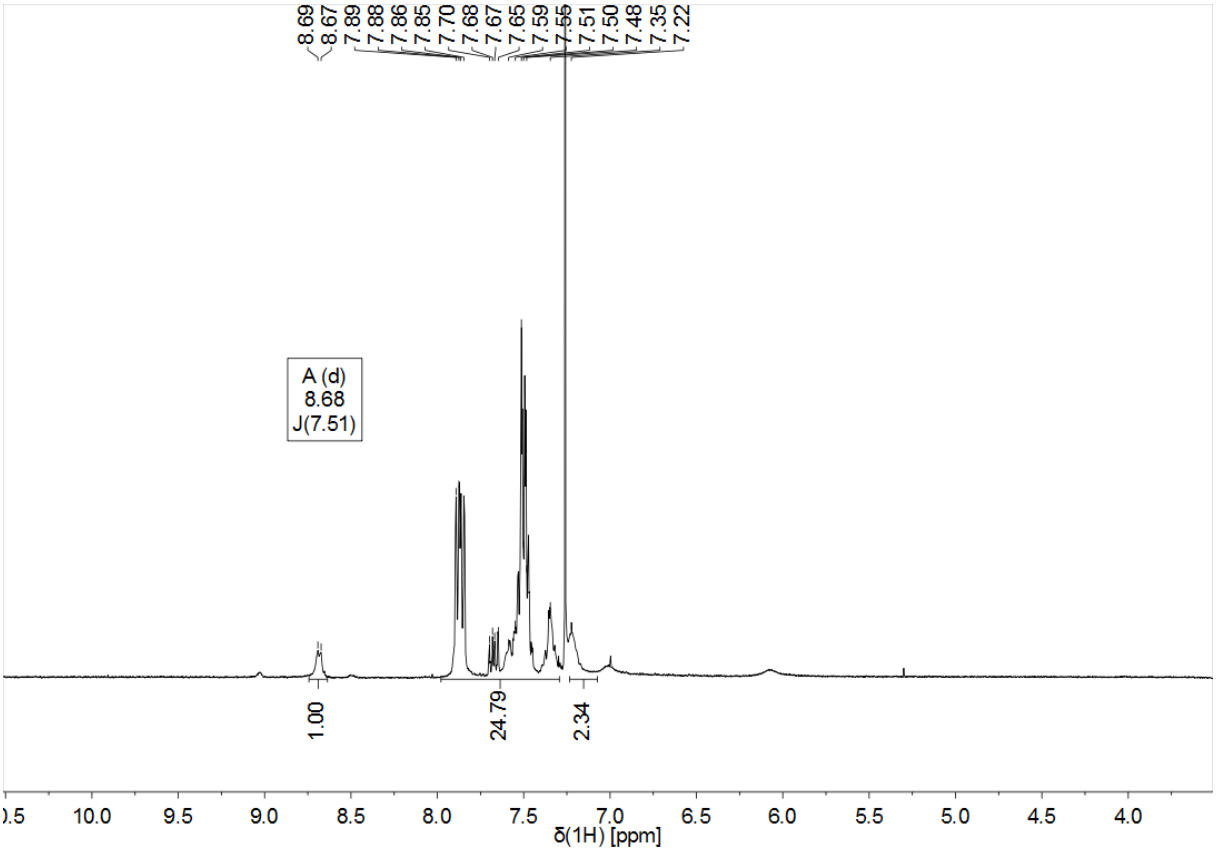

^{31}P

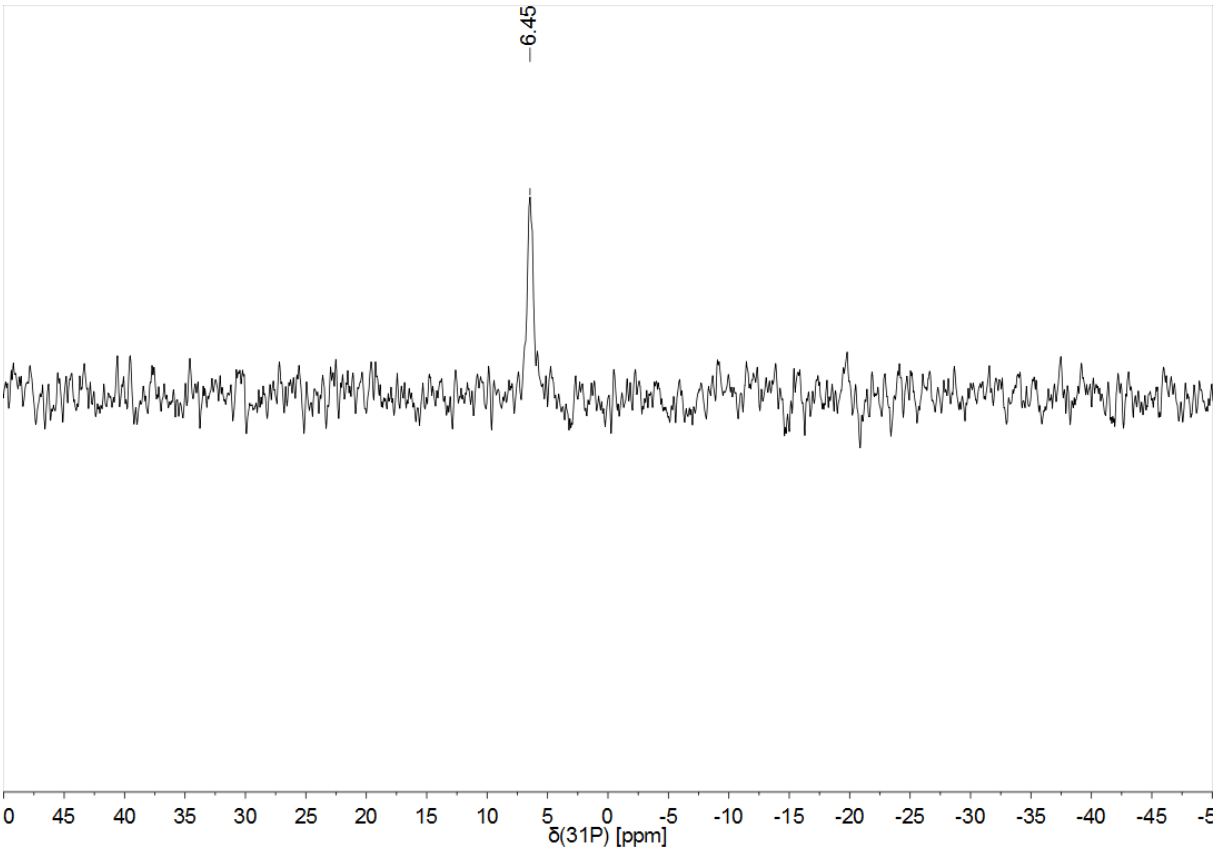

^{1}H-^{31}P-HMBC

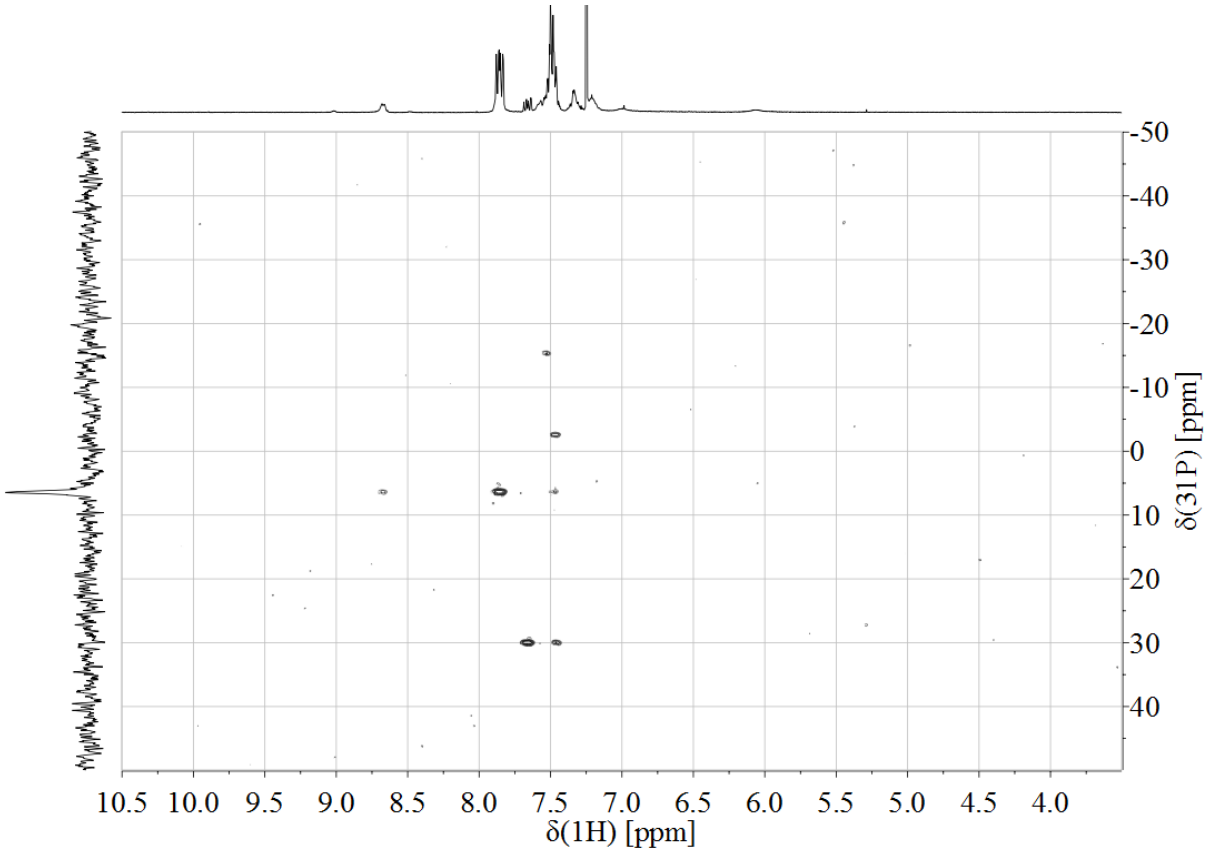

IR

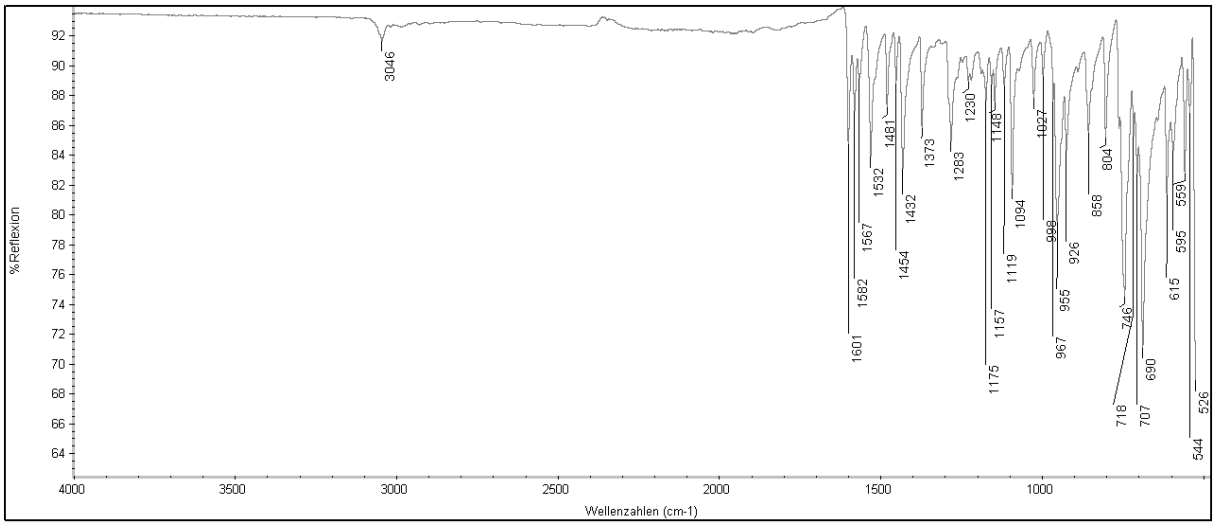

ESI+

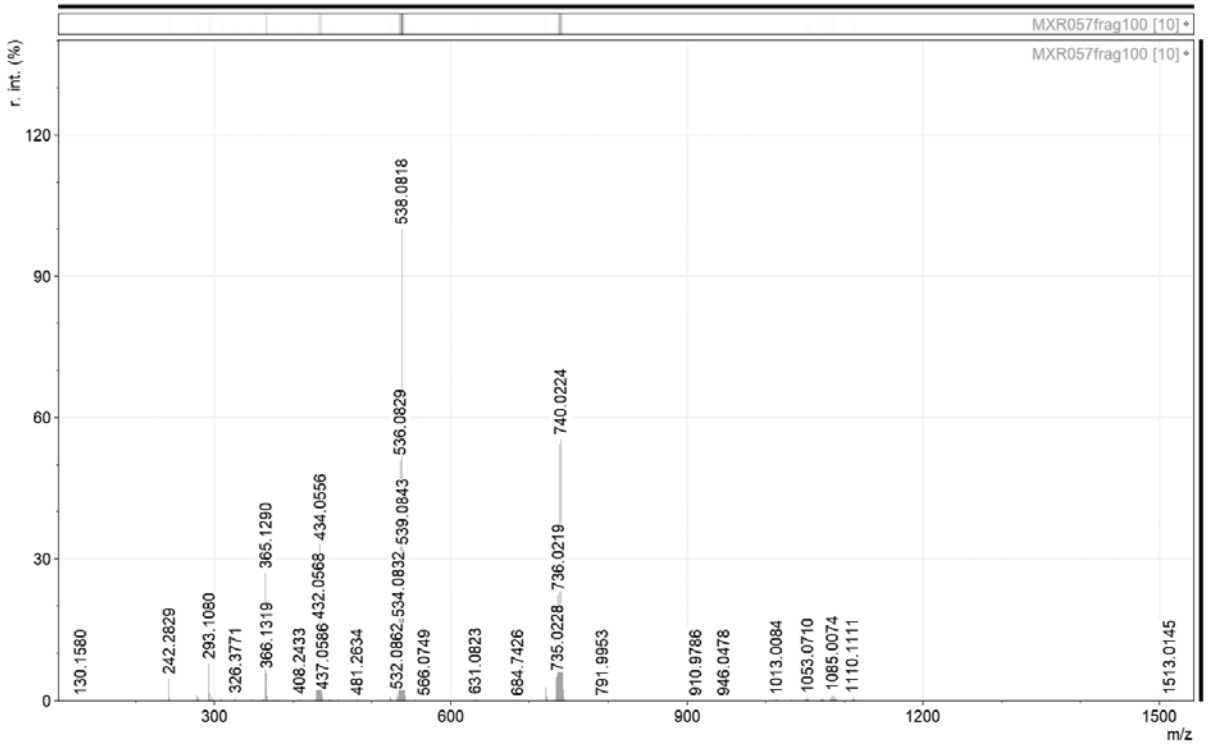
MXR057frag100 [10] •
MXR057frag100 [10] •
r. int. (%)
120
90
60
30
0
538.0818
740.0224
536.0829
539.0843
434.0556
365.1290
736.0219
130.1580
242.2829
293.1080
326.3771
366.1319
408.2433
437.0586
432.0568
481.2634
532.0862
534.0832
566.0749
631.0823
684.7426
735.0228
791.9953
910.9786
946.0478
1013.0084
1053.0710
1085.0074
1110.1111
1513.0145
300
600
900
1200
1500
m/z

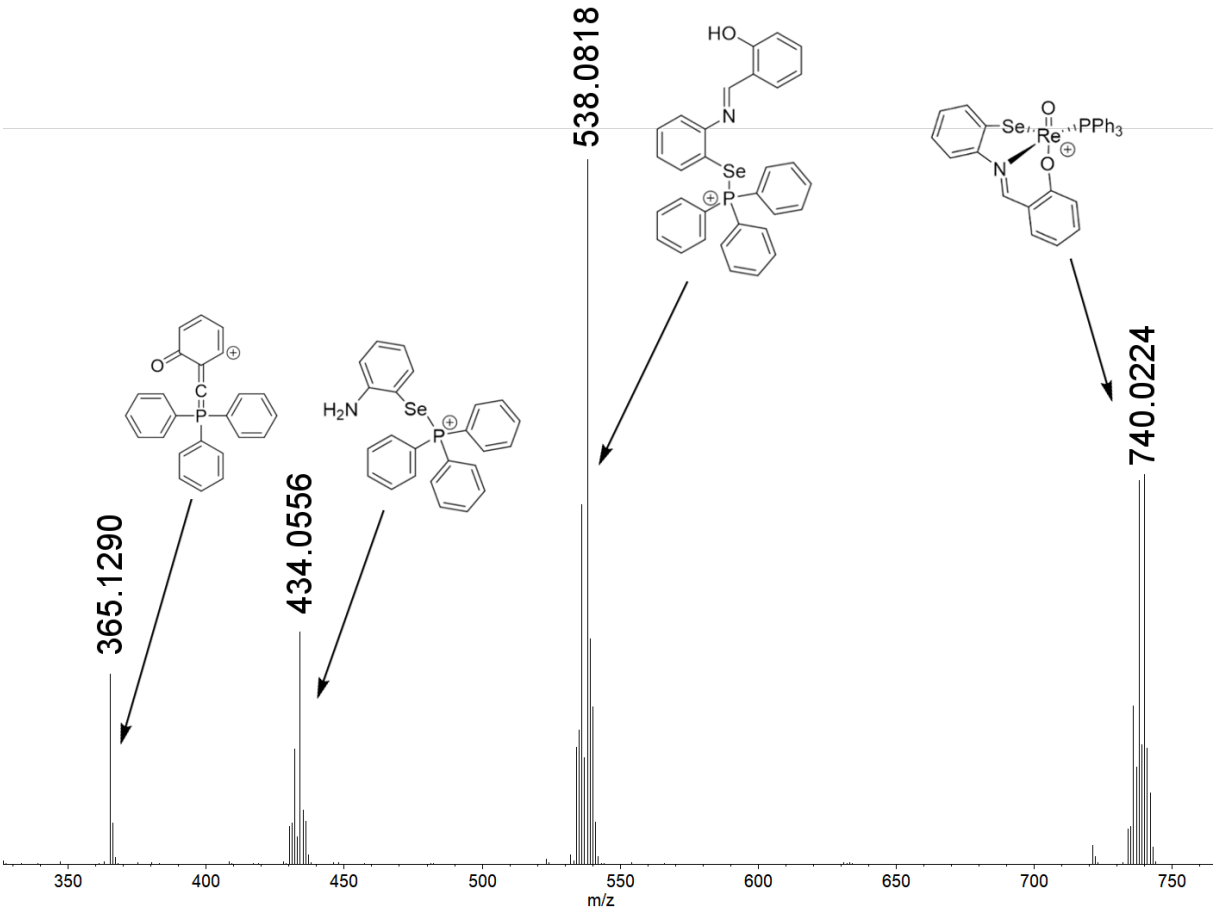
538.0818
740.0224
365.1290
434.0556
HO
N
Se
P
O
C
H2N
Se
P
Se
Re
PPh3
O
N
O
350
400
450
500
550
600
650
700
750
m/z

S3.4 Spectra of [ReO(L^{Te})Cl(PPh_3)].

^1H

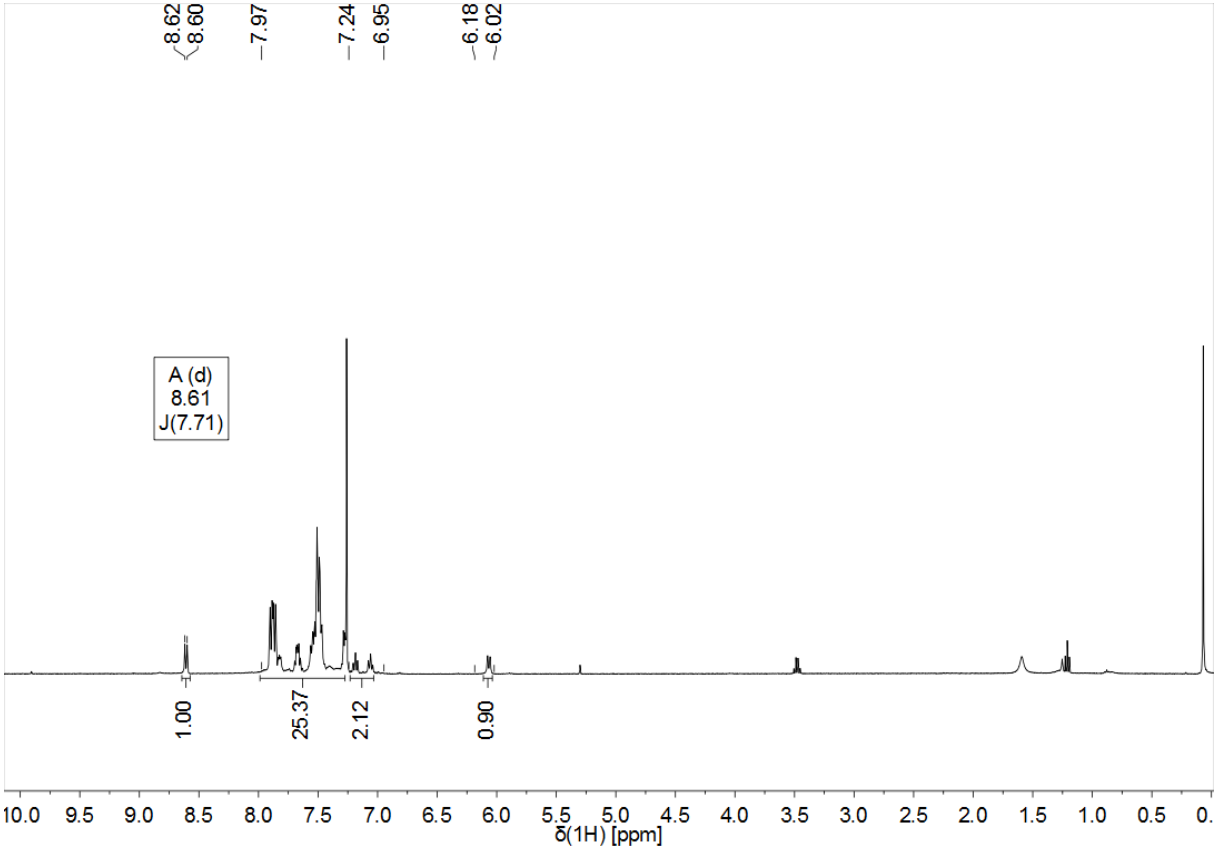

$^1H\{^{31}P\}$

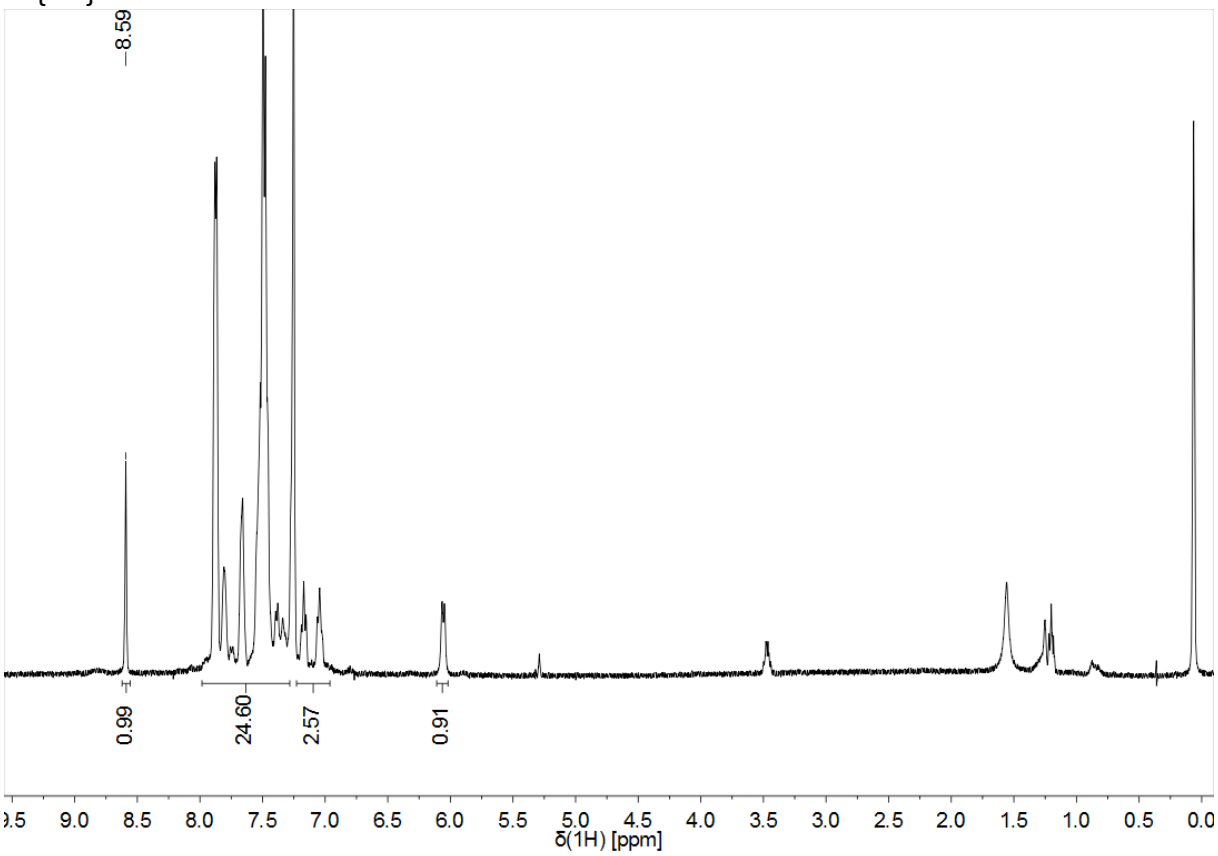

^{31}P

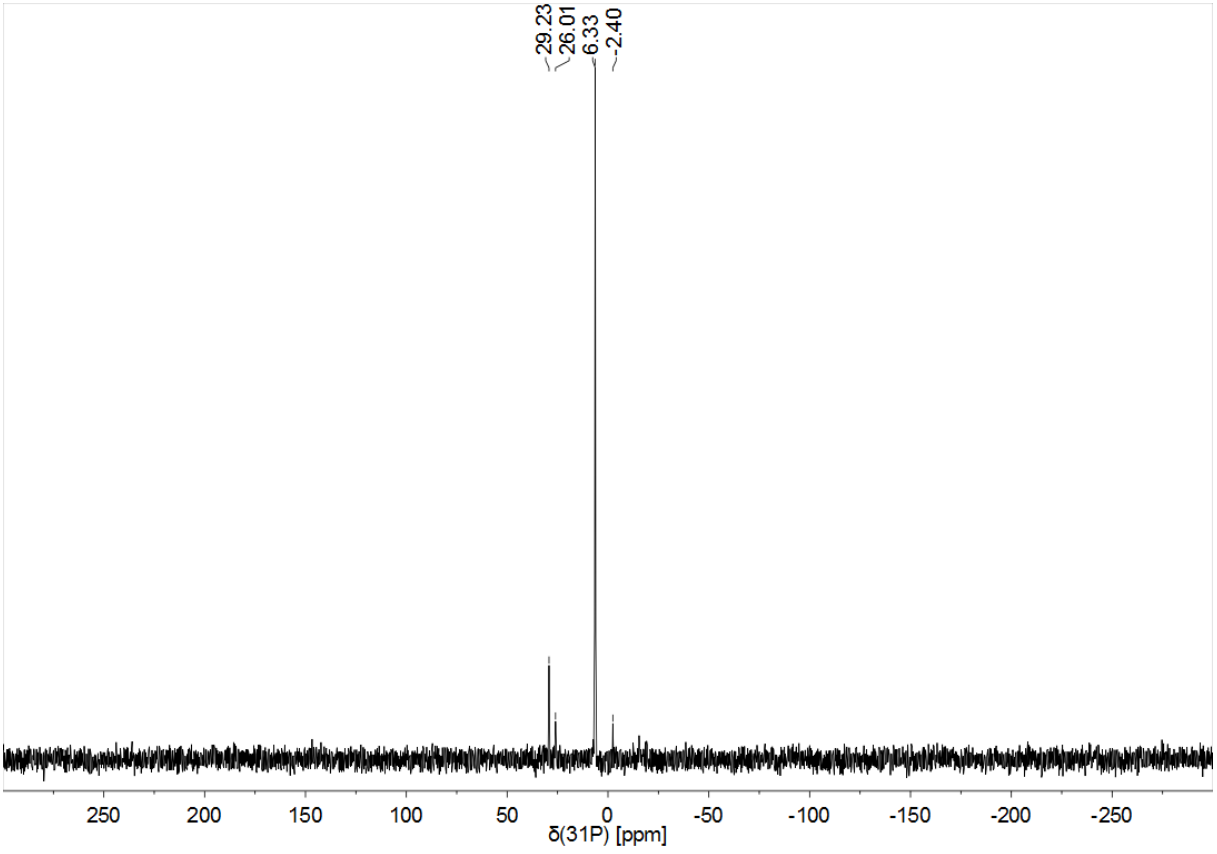

^{1}H-^{31}P-HMBC

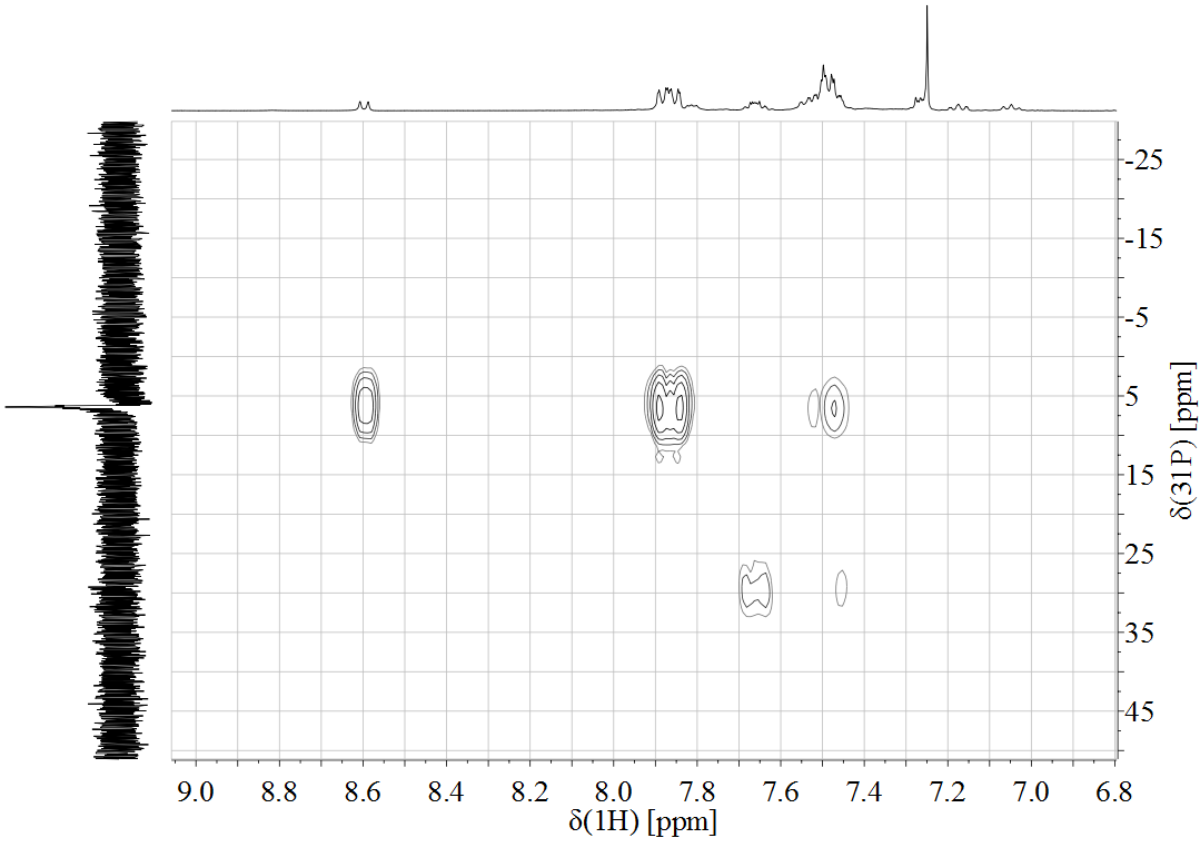

^{13}C

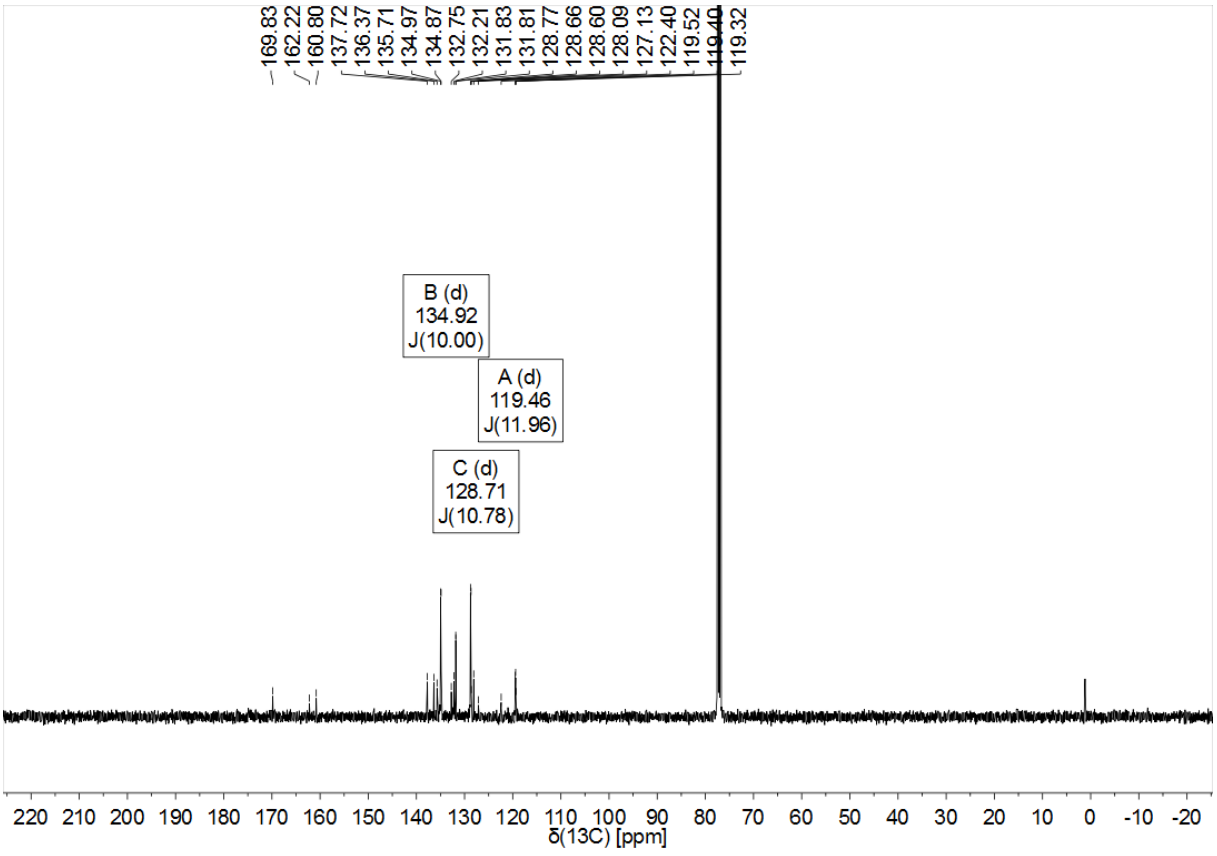
169.83
162.22
160.80
137.72
136.37
135.71
134.97
134.87
132.75
132.21
131.83
131.81
128.77
128.66
128.60
128.09
127.13
122.40
119.52
119.40
119.32
B (d)
134.92
J(10.00)
A (d)
119.46
J(11.96)
C (d)
128.71
J(10.78)
220 210 200 190 180 170 160 150 140 130 120 110 100 90 80 70 60 50 40 30 20 10 0 -10 -20
δ(13C) [ppm]

^{77}Se

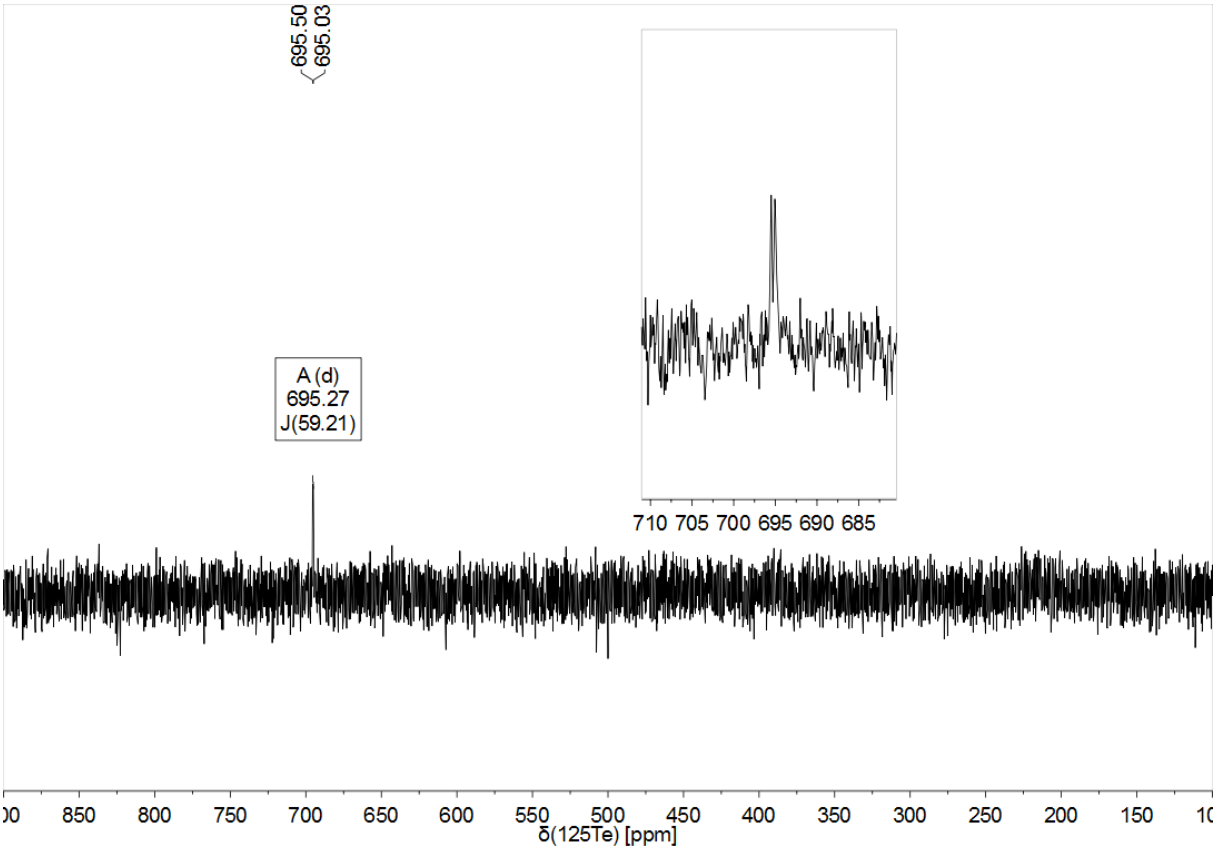
695.50
695.03
A (d)
695.27
J(59.21)
710 705 700 695 690 685
850 800 750 700 650 600 550 500 450 400 350 300 250 200 150
δ(125Te) [ppm]

IR

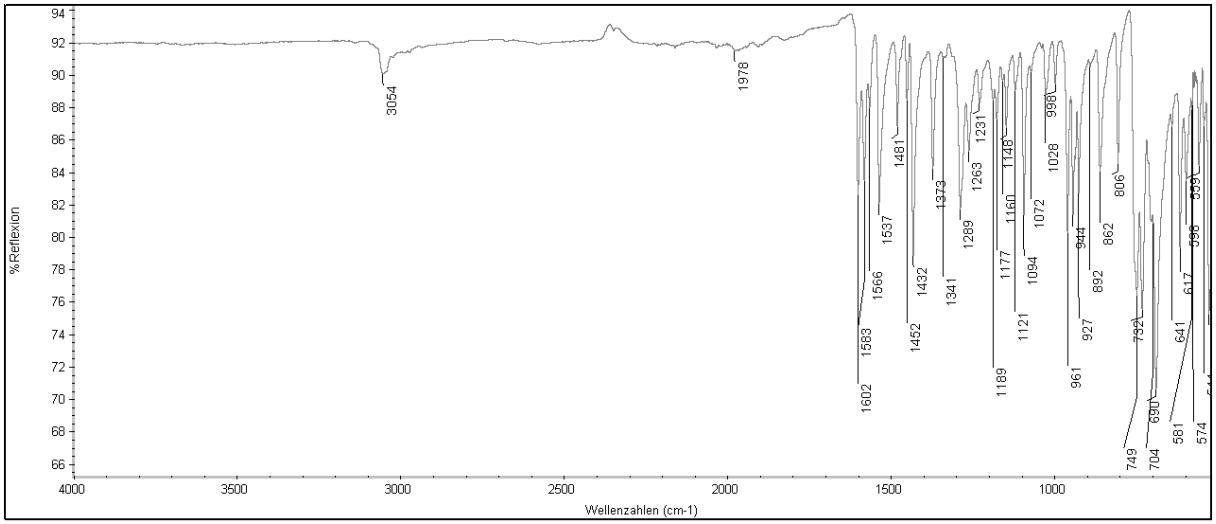
%Reflexion
Wellenzahlen (cm-1)
3054
1978
1602
1583
1566
1537
1481
1452
1432
1373
1341
1289
1263
1231
1189
1177
1160
1148
1121
1094
1072
1028
998
961
944
927
892
862
806
749
704
690
641
617
596
581
574

ESI+

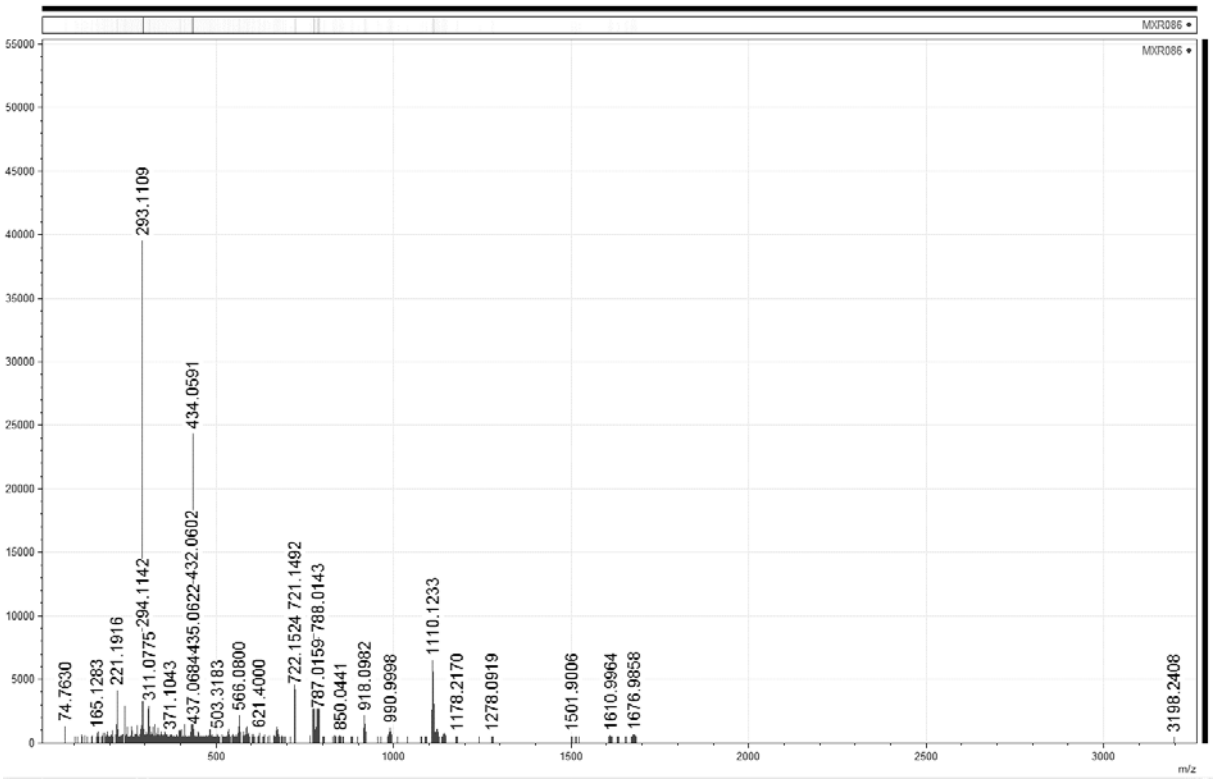
MXR086
m/z
74.7630
165.1283
221.1916
293.1109
294.1142
311.0775
371.1043
434.0591
435.0622
437.0684
503.3183
566.0800
621.4000
722.1524
721.1492
787.0159
788.0143
850.0441
918.0982
990.9998
1110.1233
1178.2170
1278.0919
1501.9006
1610.9964
1676.9858
3198.2408

S3.5 Spectra of [Re(NPh)(L^{Se})Cl(PPh_3)].

^1H

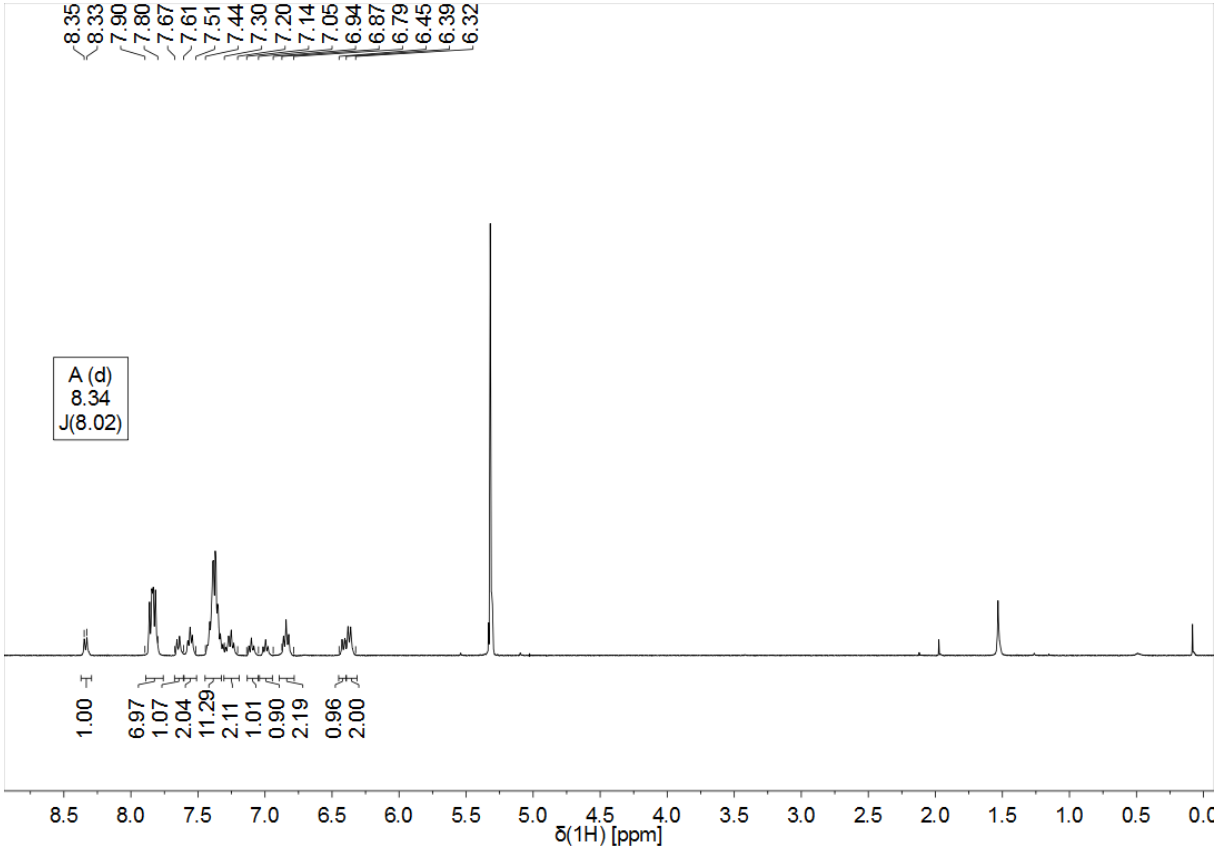

$^1H\{^{31}P\}$

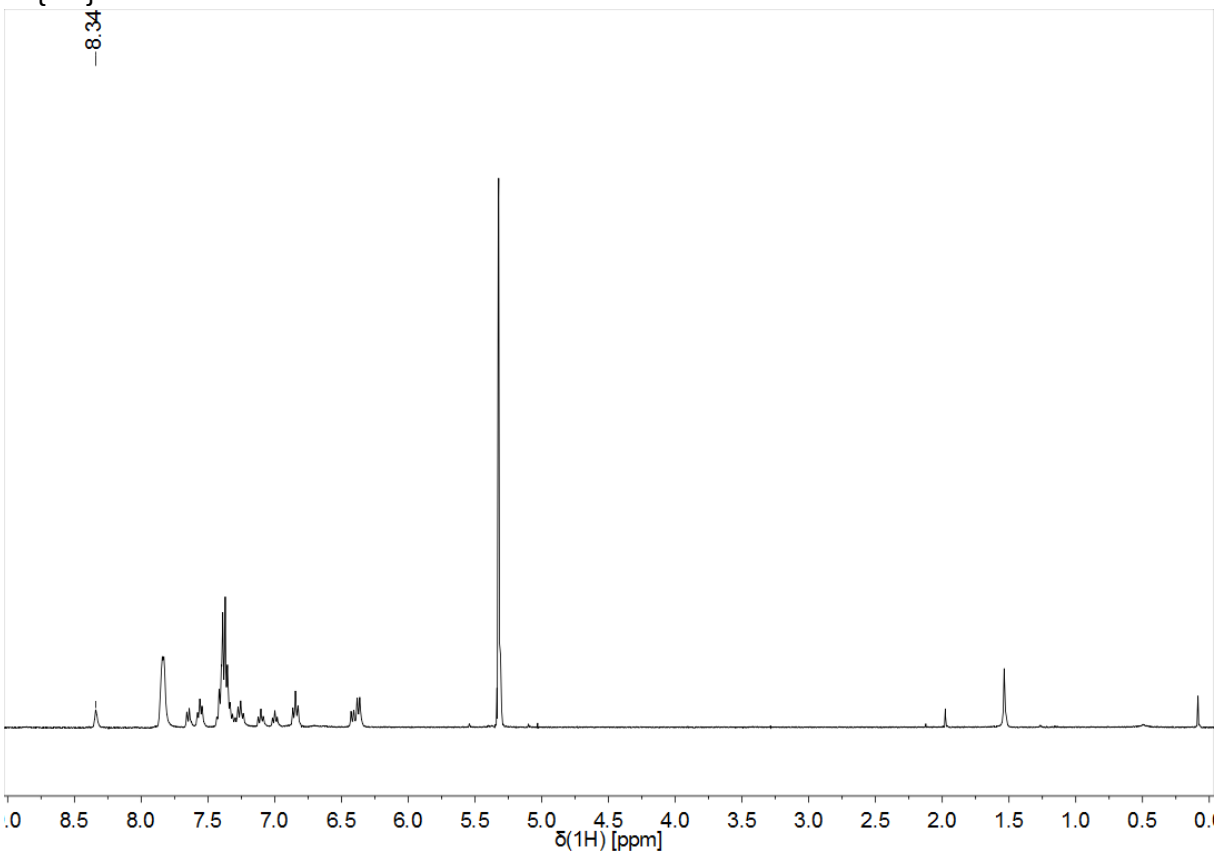

^{31}P

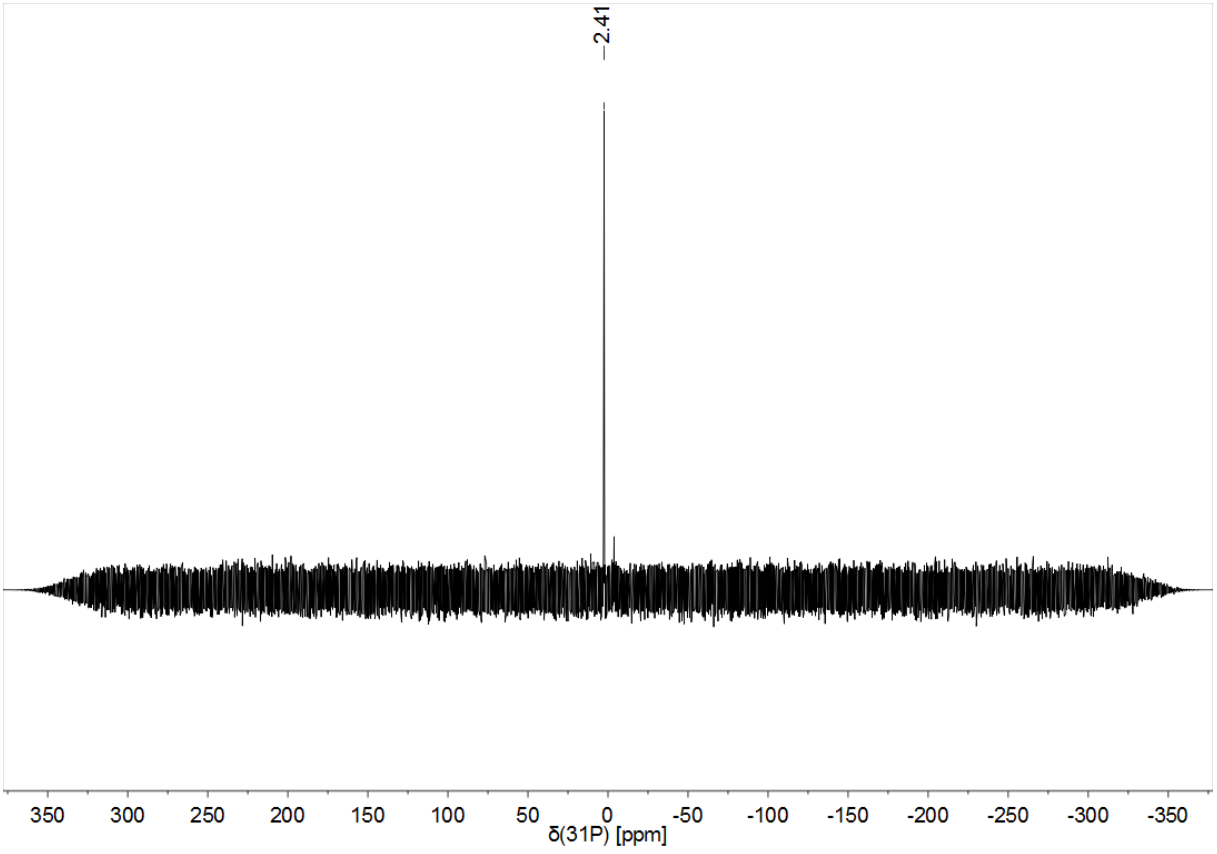

^{1}H-^{31}P-HMBC

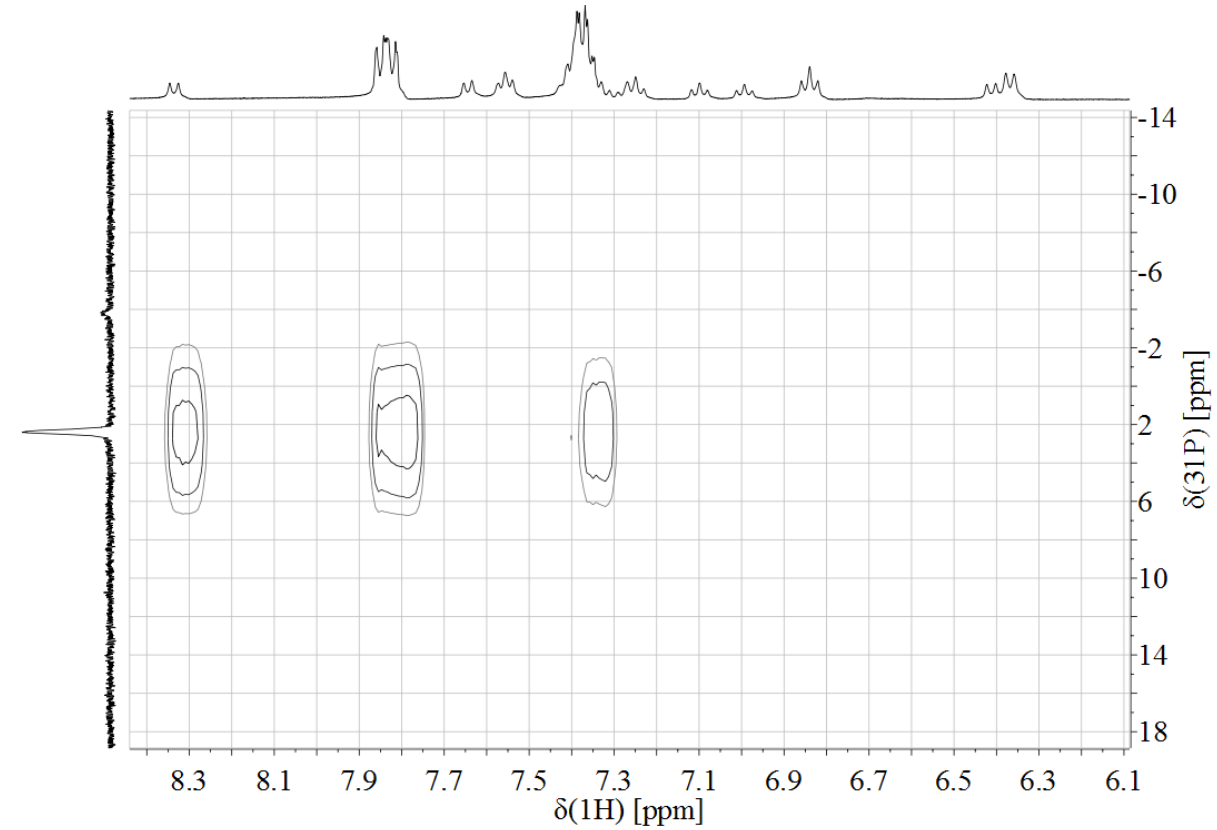

^{13}C

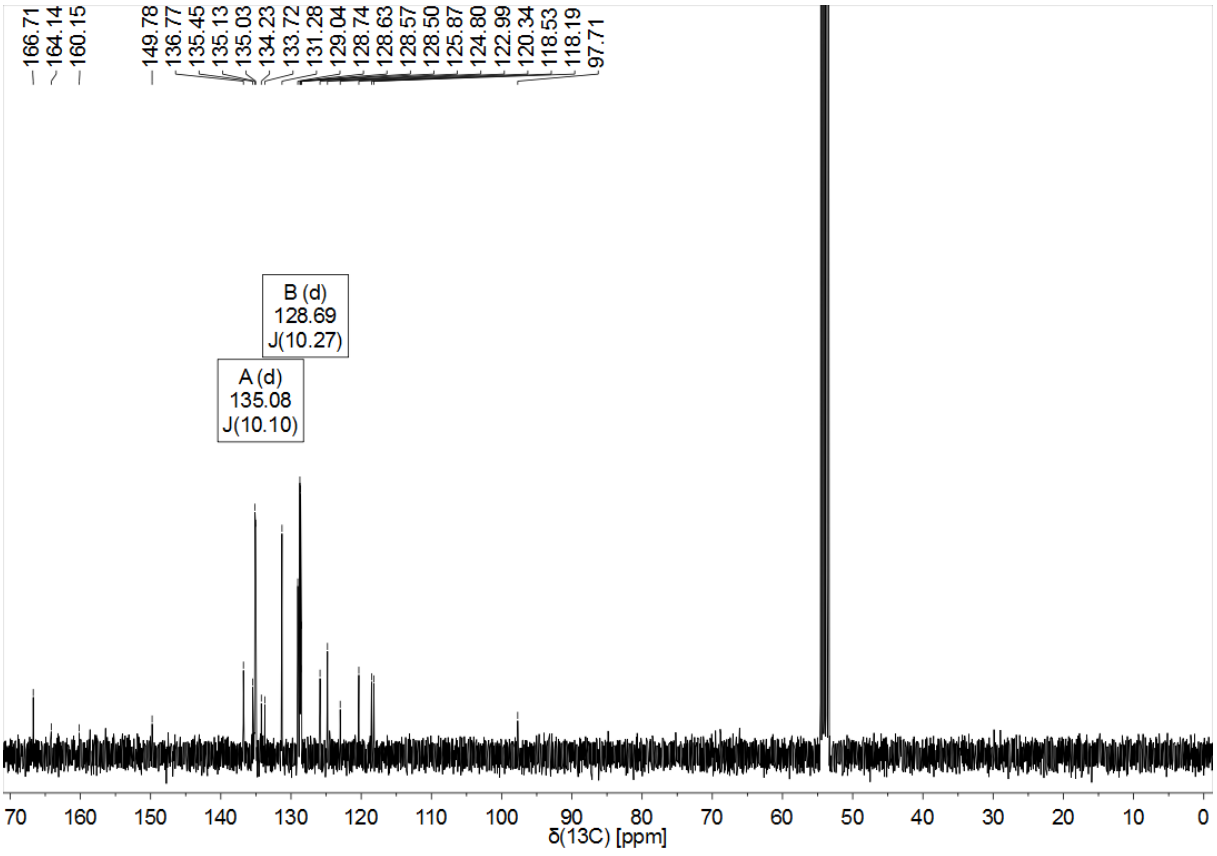
166.71
164.14
160.15
149.78
136.77
135.45
135.13
135.03
134.23
133.72
131.28
129.04
128.74
128.63
128.57
128.50
125.87
124.80
122.99
120.34
118.53
118.19
97.71
B (d)
128.69
J(10.27)
A (d)
135.08
J(10.10)
70 160 150 140 130 120 110 100 90 80 70 60 50 40 30 20 10 0
δ(13C) [ppm]

IR

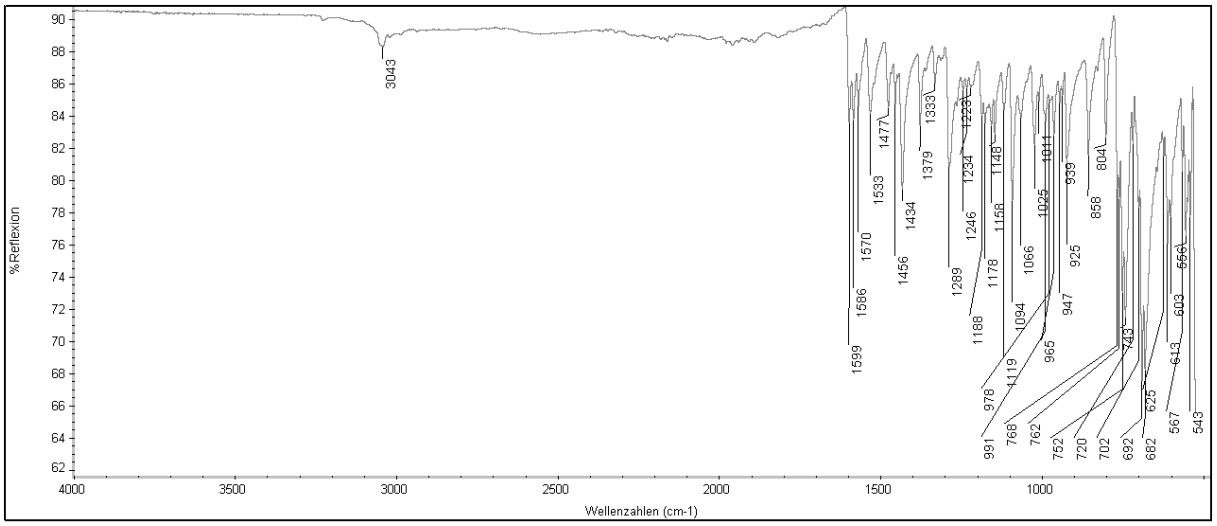
%Reflexion
90 88 86 84 82 80 78 76 74 72 70 68 66 64 62
4000 3500 3000 2500 2000 1500 1000
Wellenzahlen (cm-1)
3043
1599 1586 1570 1533 1477 1456 1434 1379 1333 1289 1246 1234 1223 1188 1178 1158 1148 1119 1094 1066 1025 1011 978 965 947 939 925 858 804 768 762 752 743 720 702 692 682 625 613 603 567 566 543 991

ESI+

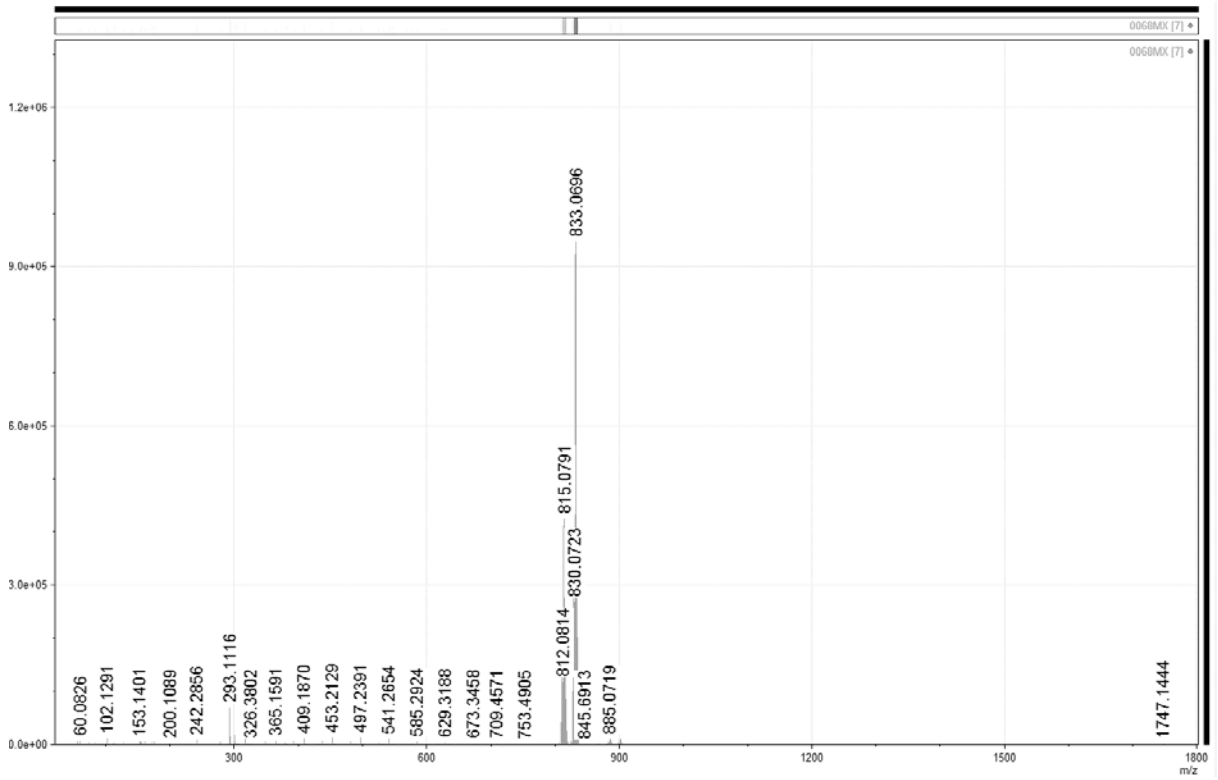

S3.6 Spectra of [Re(NPh)(L^{Te})Cl(PPh_3)].

^{1}H

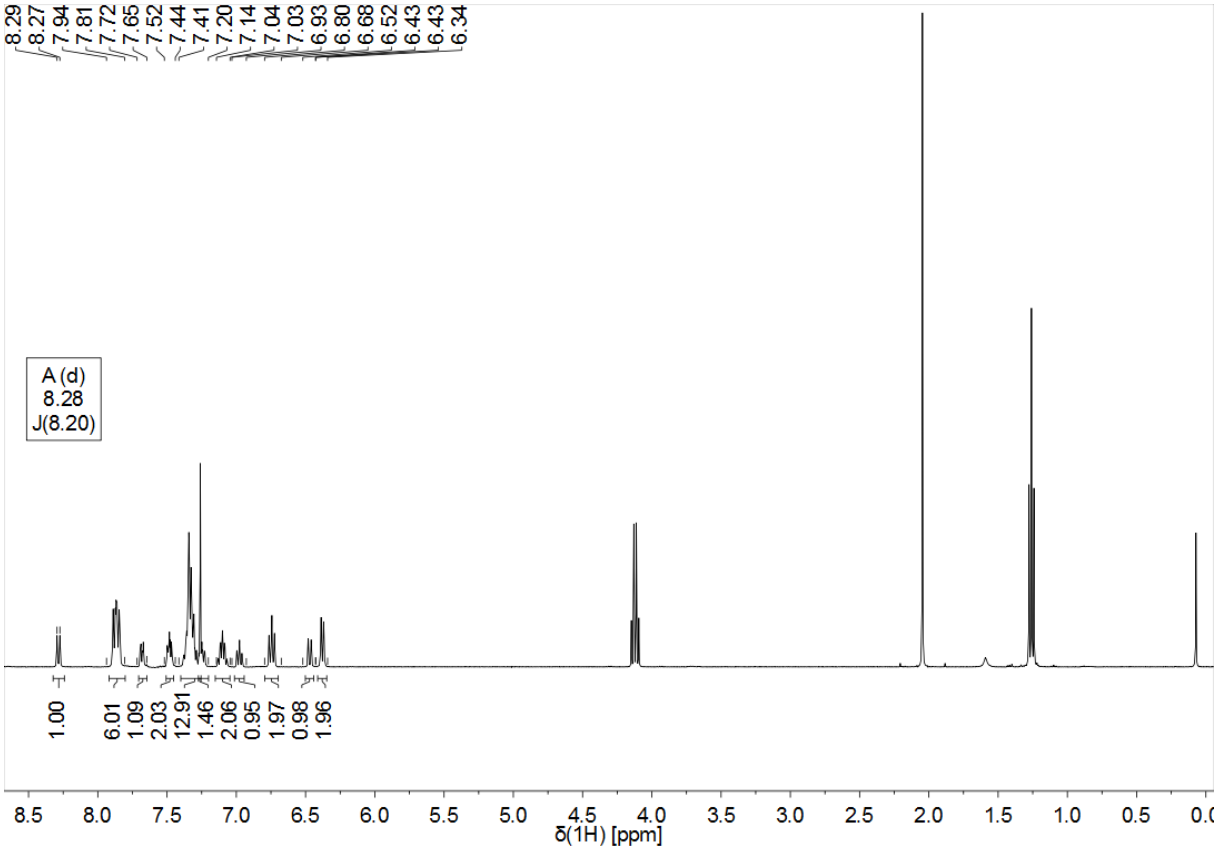

^{1}H-^{1}H-COSY

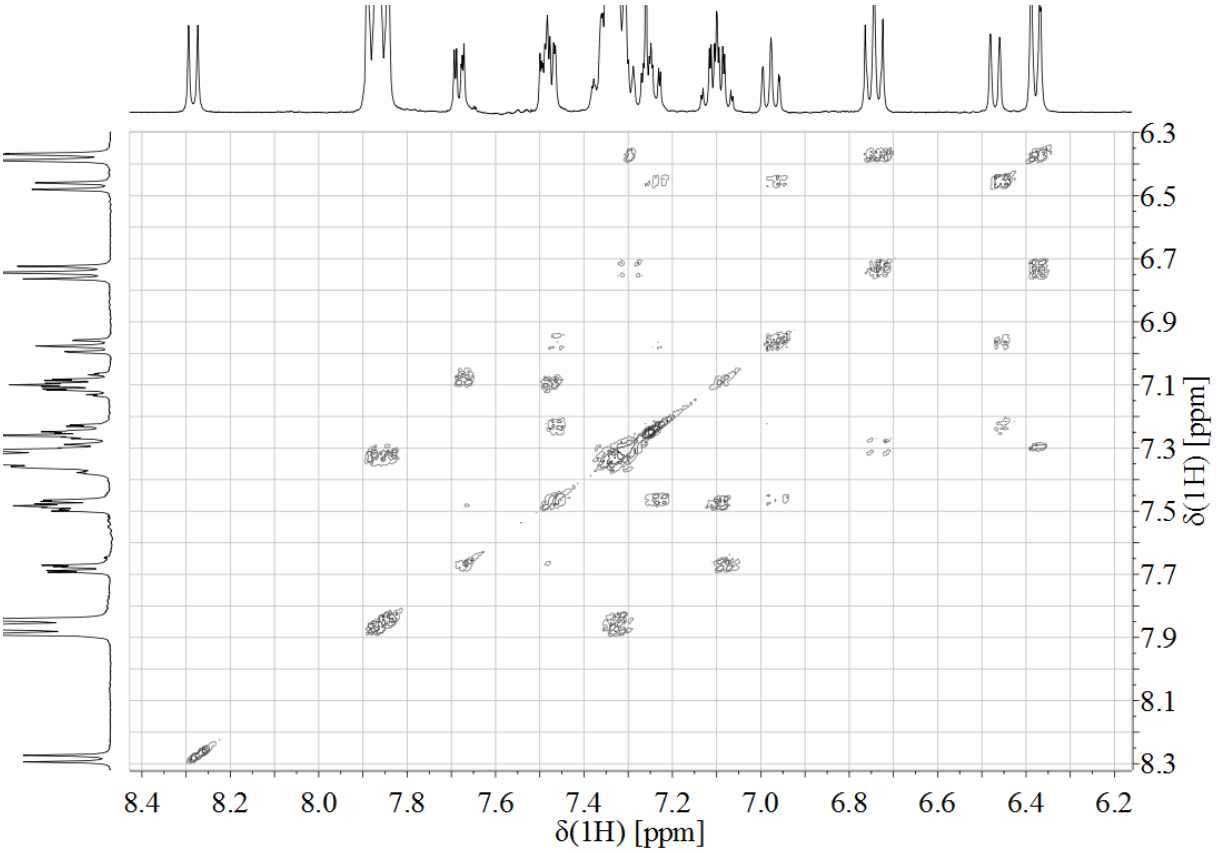

^{31}P

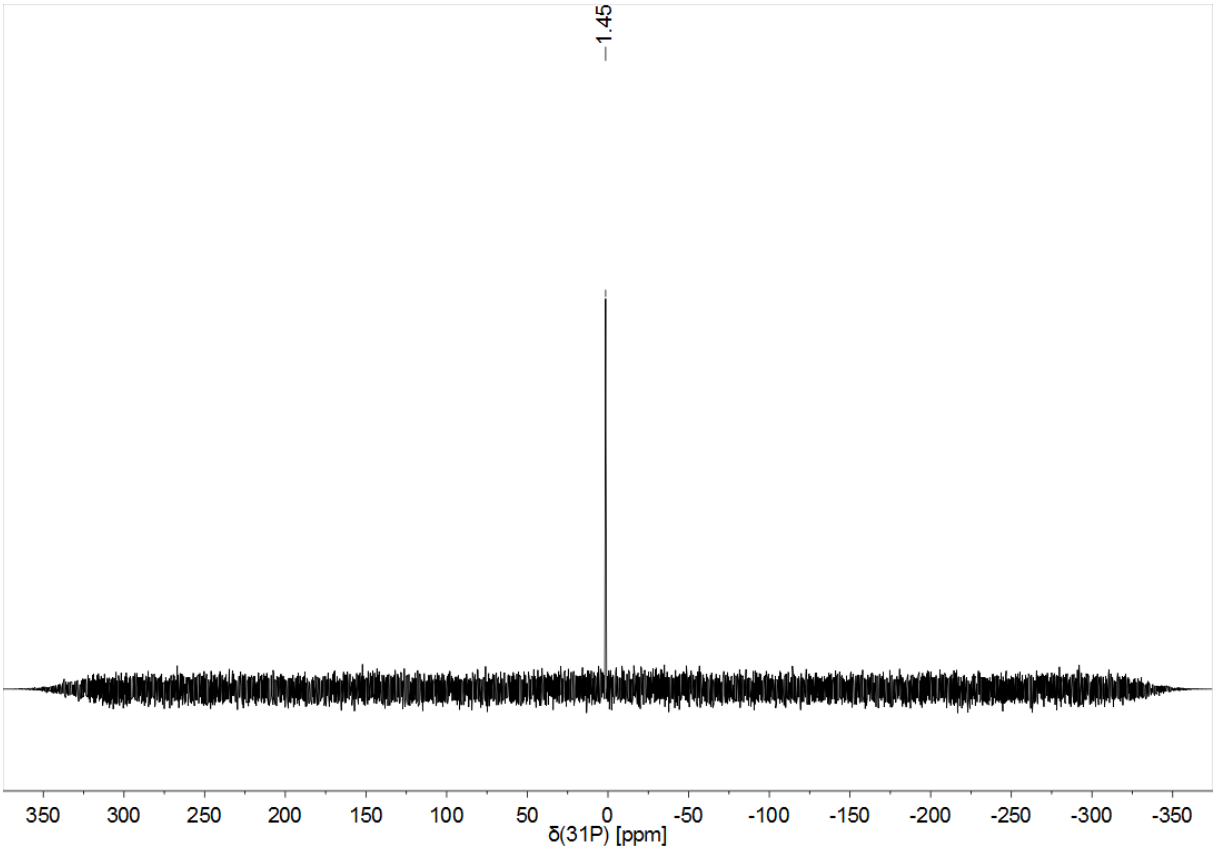

^{1}H-^{31}P-HMBC

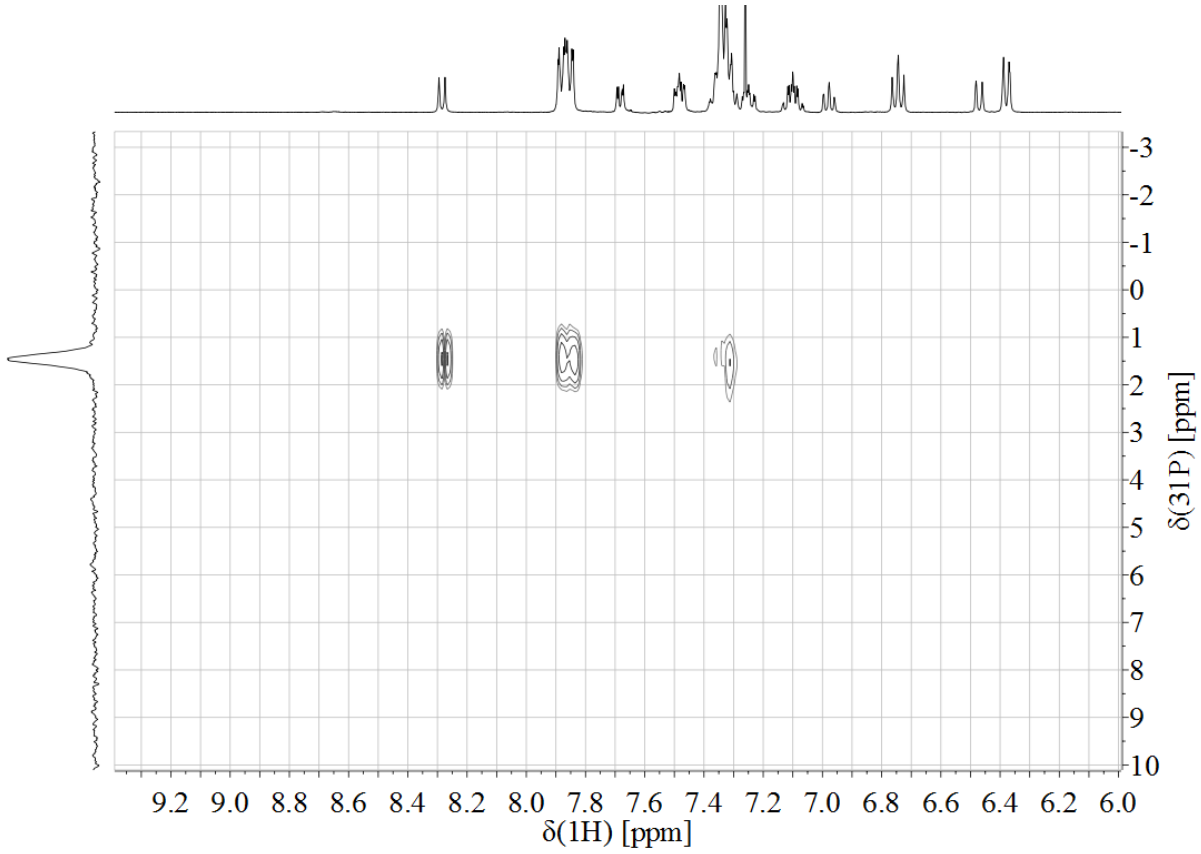

^{13}C

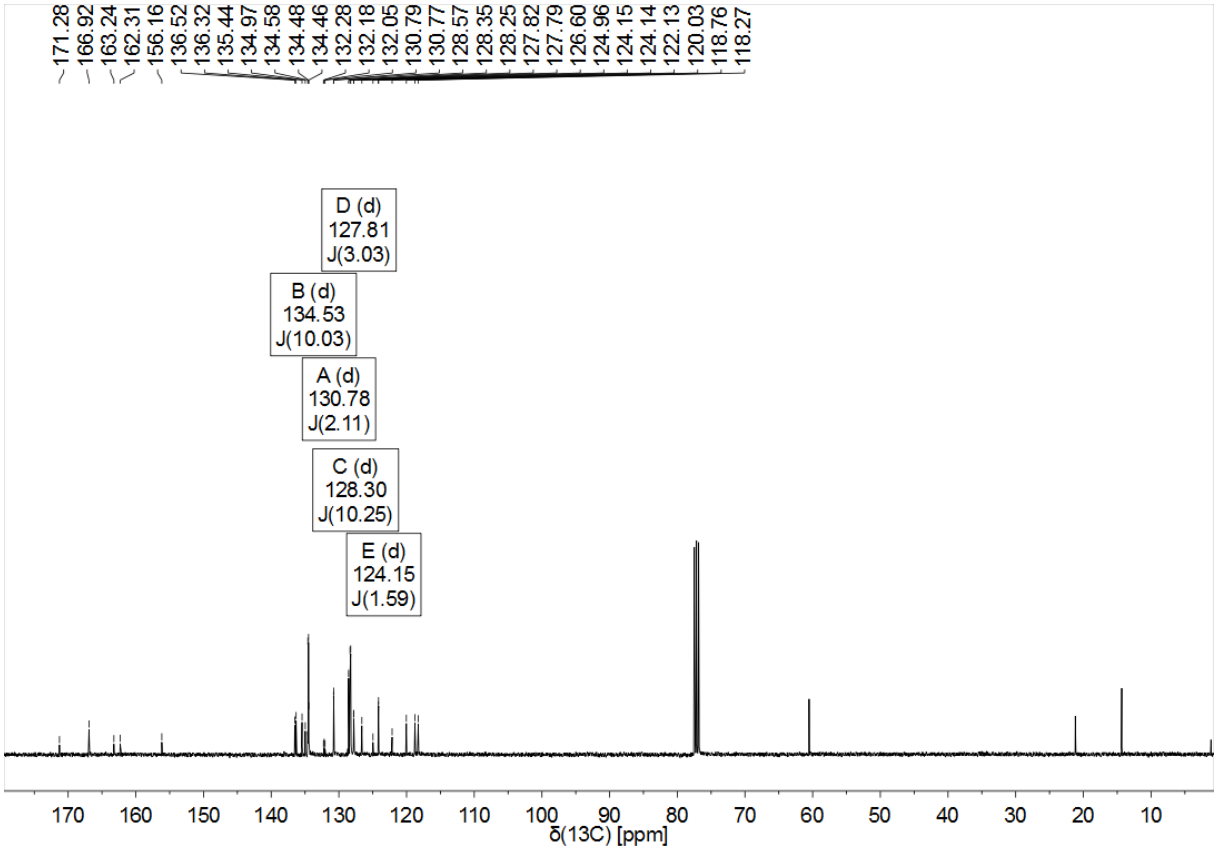

^{1}H-^{13}C-HMBC

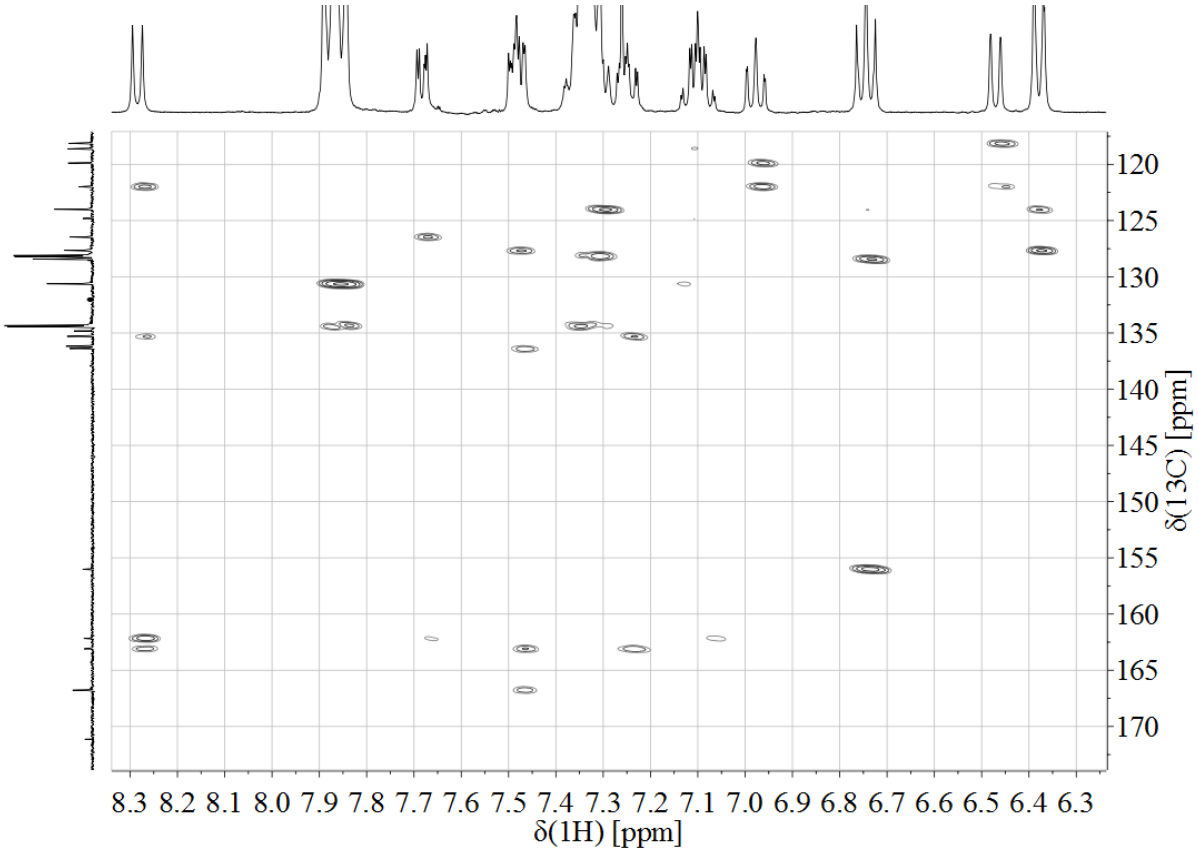

^{125}Te

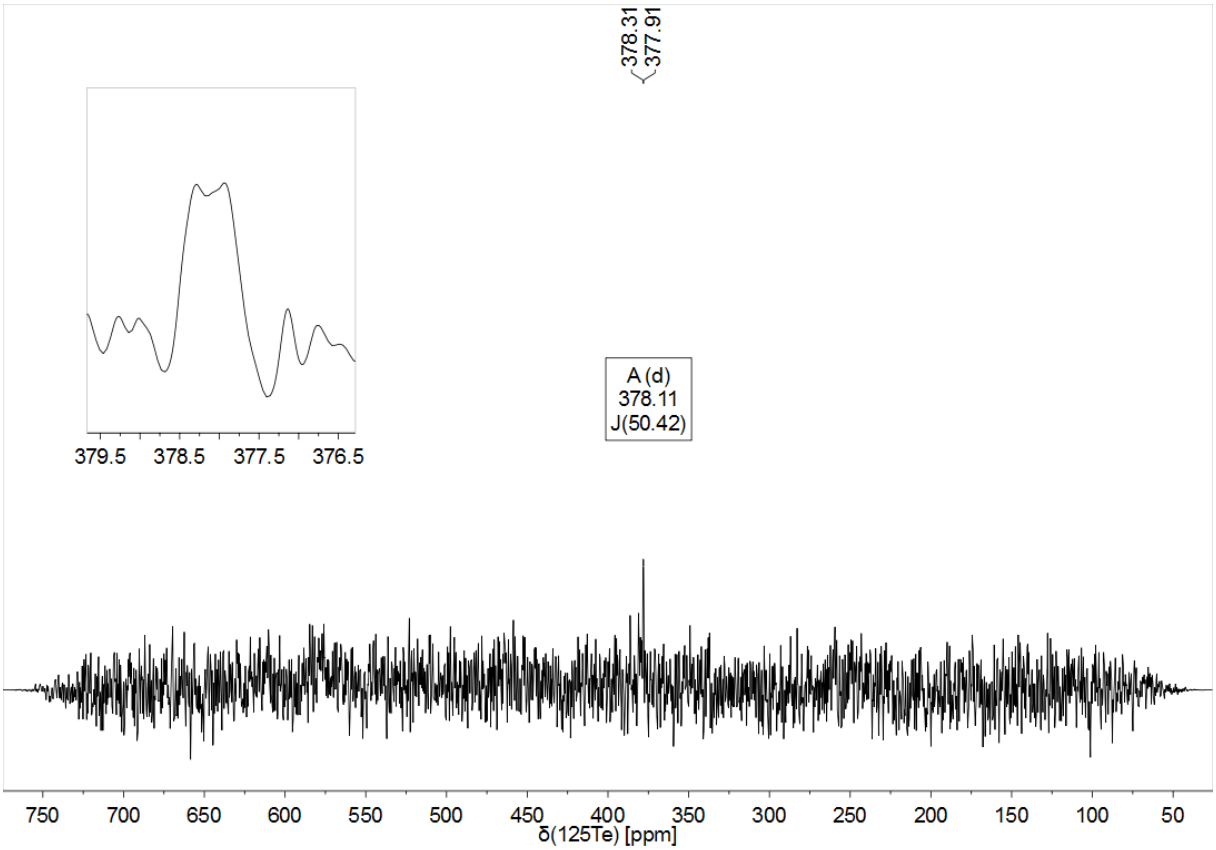

IR

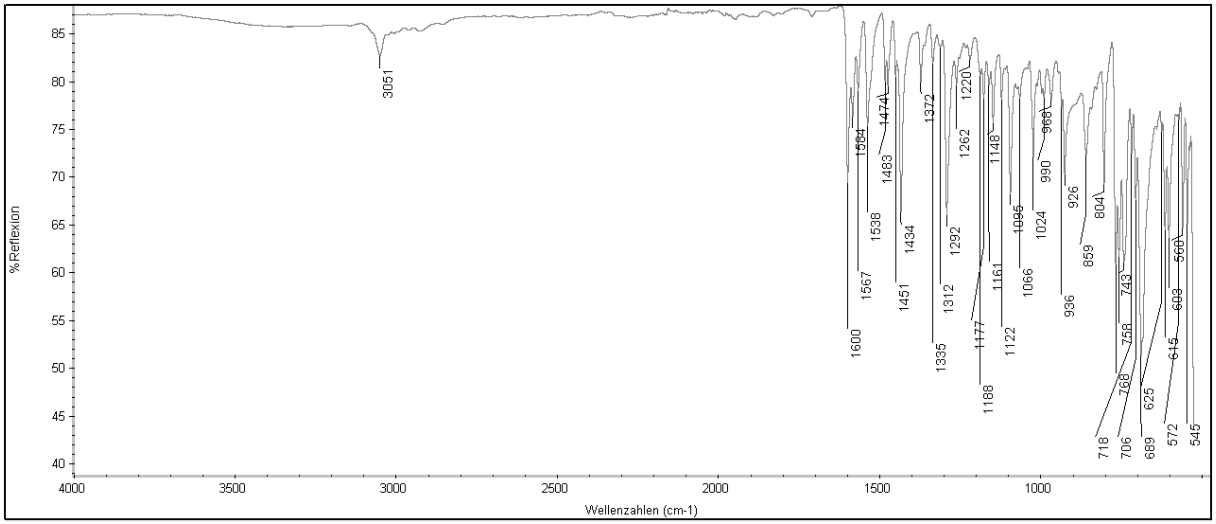
%Reflexion
Wellenzahlen (cm-1)
3051
1600
1567
1538
1494
1483
1474
1451
1434
1372
1335
1312
1292
1262
1220
1188
1177
1161
1148
1122
1096
1066
1024
990
968
936
926
859
804
758
743
718
706
689
625
615
603
572
560
545

ESI+

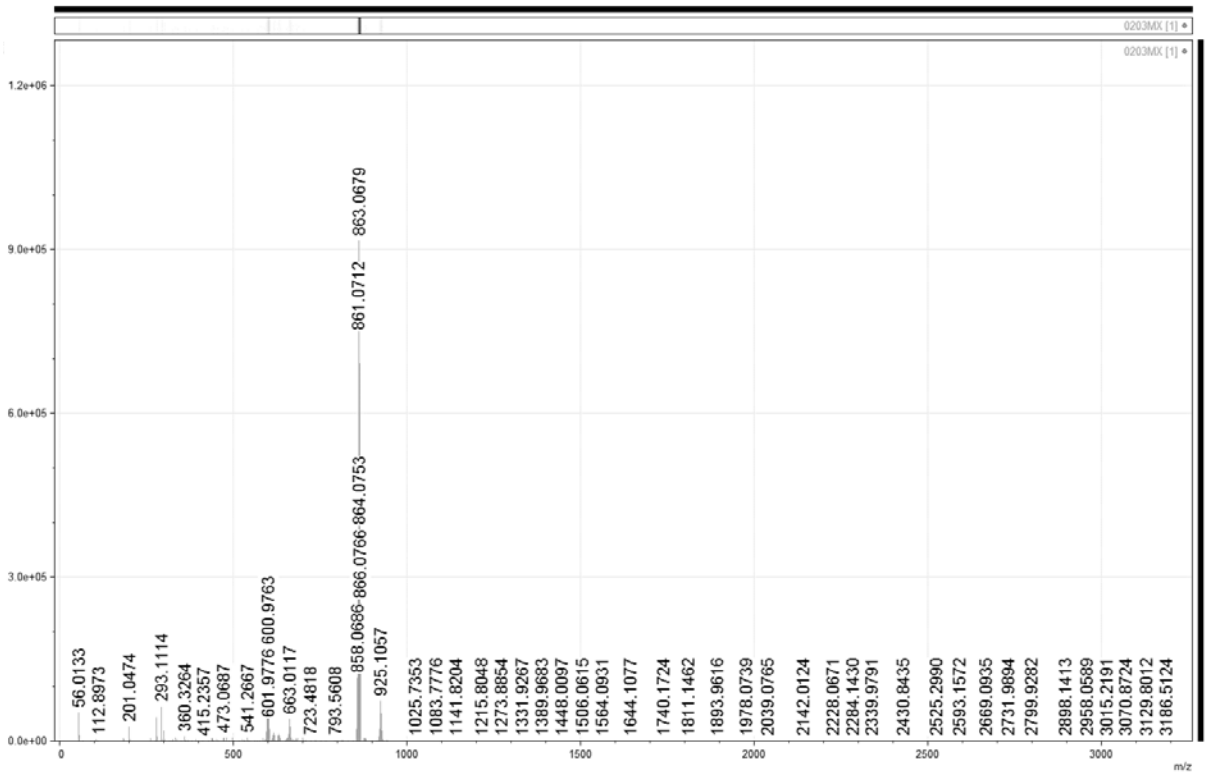
0203MX [1]
0203MX [1]
1.2e+06
9.0e+05
6.0e+05
3.0e+05
0.0e+00
0
500
1000
1500
2000
2500
3000
m/z
863.0679
861.0712
864.0753
866.0766
858.0686
601.9776
600.9763
56.0133
112.8973
201.0474
293.1114
360.3264
415.2357
473.0687
541.2667
663.0117
723.4818
793.5608
925.1057
1025.7353
1083.7776
1141.8204
1215.8048
1273.8854
1331.9267
1389.9683
1448.0097
1506.0615
1564.0931
1644.1077
1740.1724
1811.1462
1893.9616
1978.0739
2039.0765
2142.0124
2228.0671
2284.1430
2339.9791
2430.8435
2525.2990
2593.1572
2669.0935
2731.9894
2799.9282
2898.1413
2958.0589
3015.2191
3070.8724
3129.8012
3186.5124

S3.7 Spectra of [Re(NPhF)(L^{Se})Cl(PPh_3)].

^1H $CDCl_3$

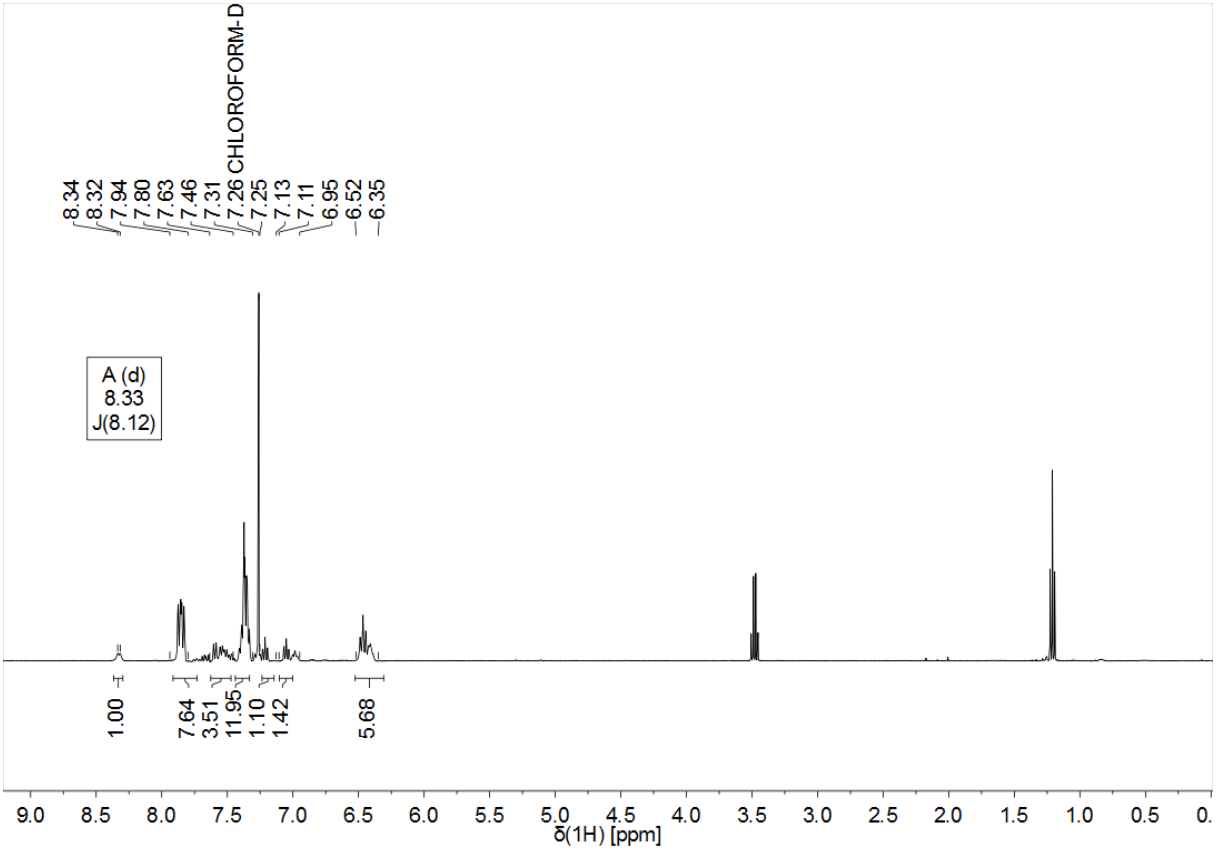

$^1H\{^{31}P\}$ $CDCl_3$

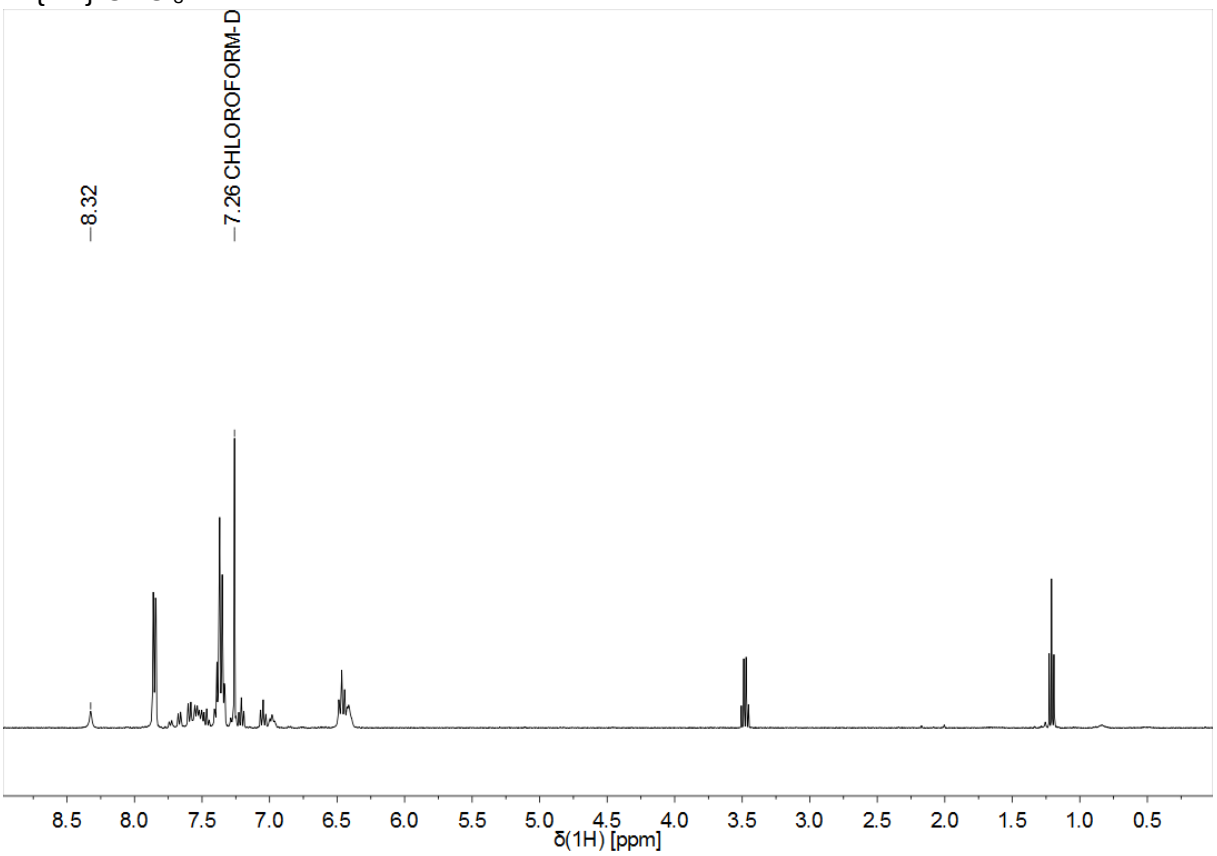

^{31}P $CDCl_3$

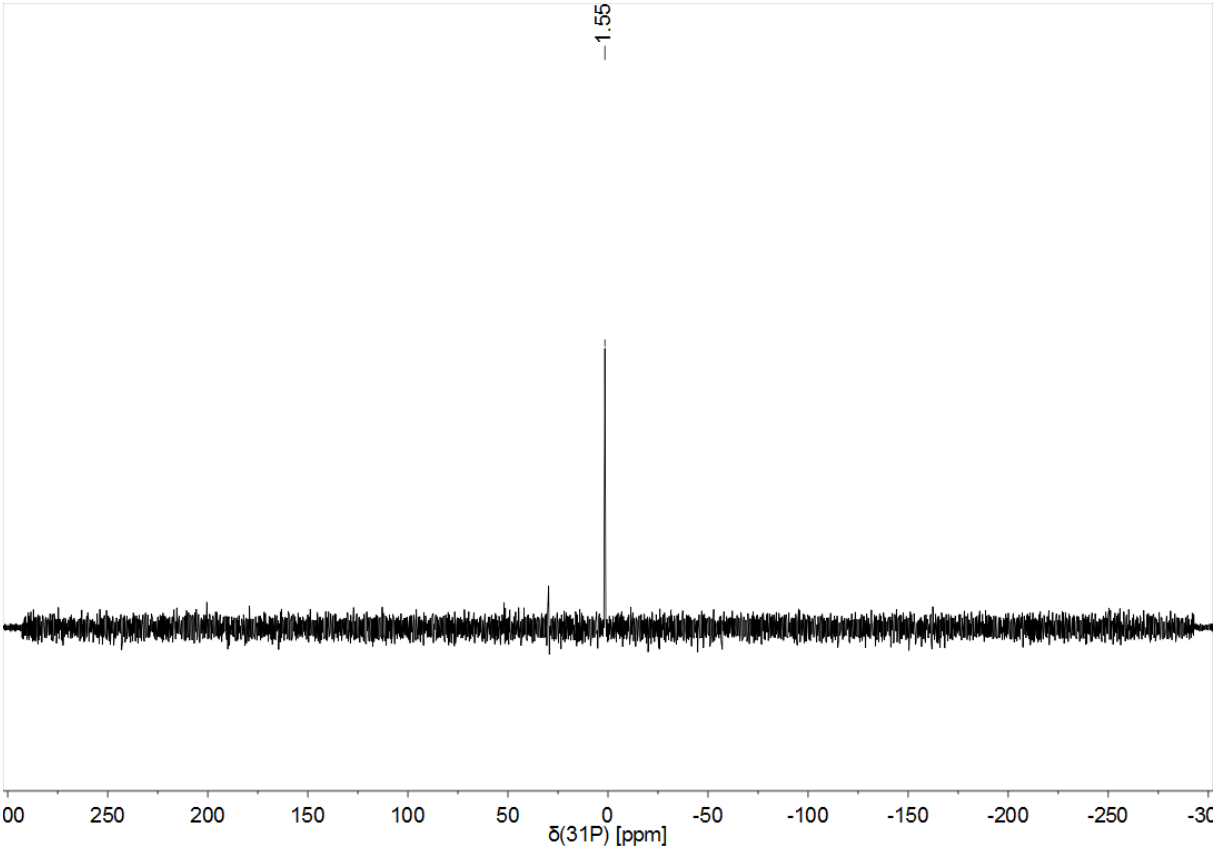

^{19}F $CDCl_3$

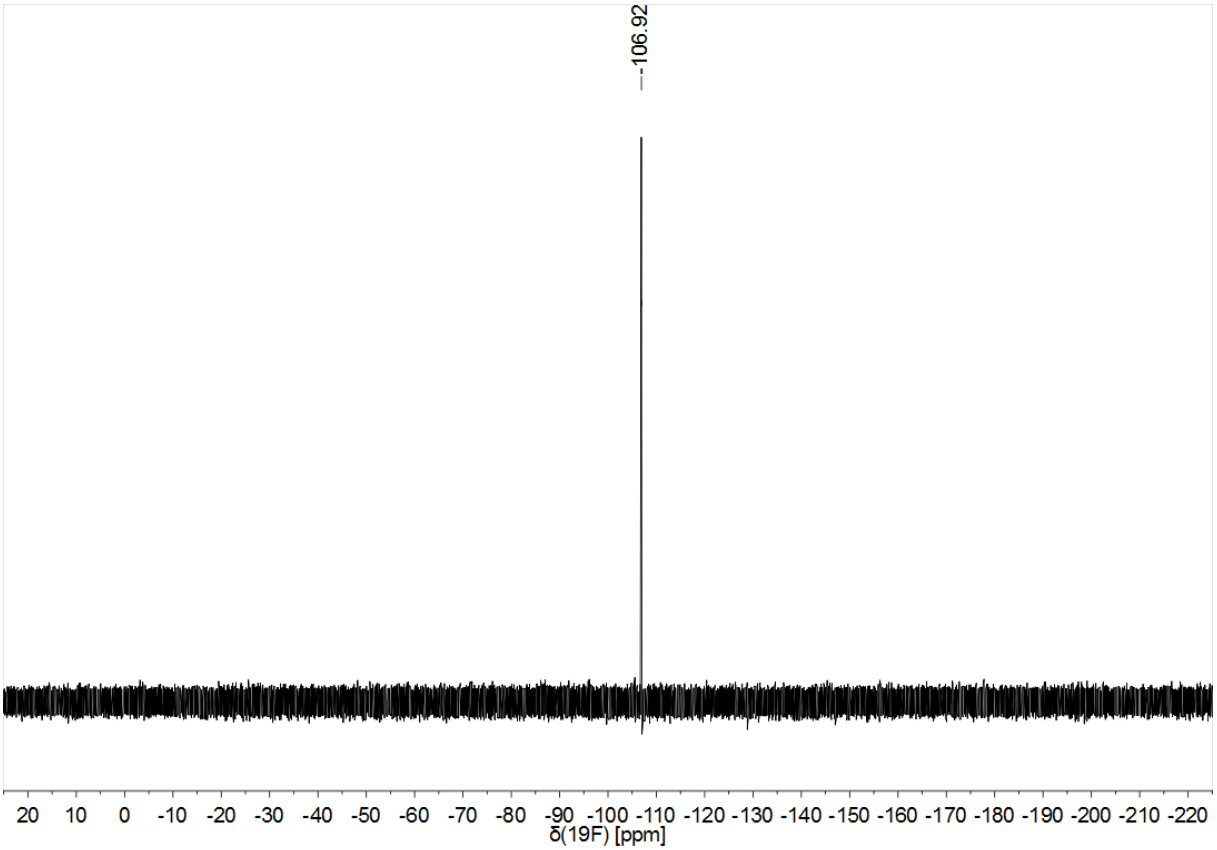

^{1}H CD_2Cl_2

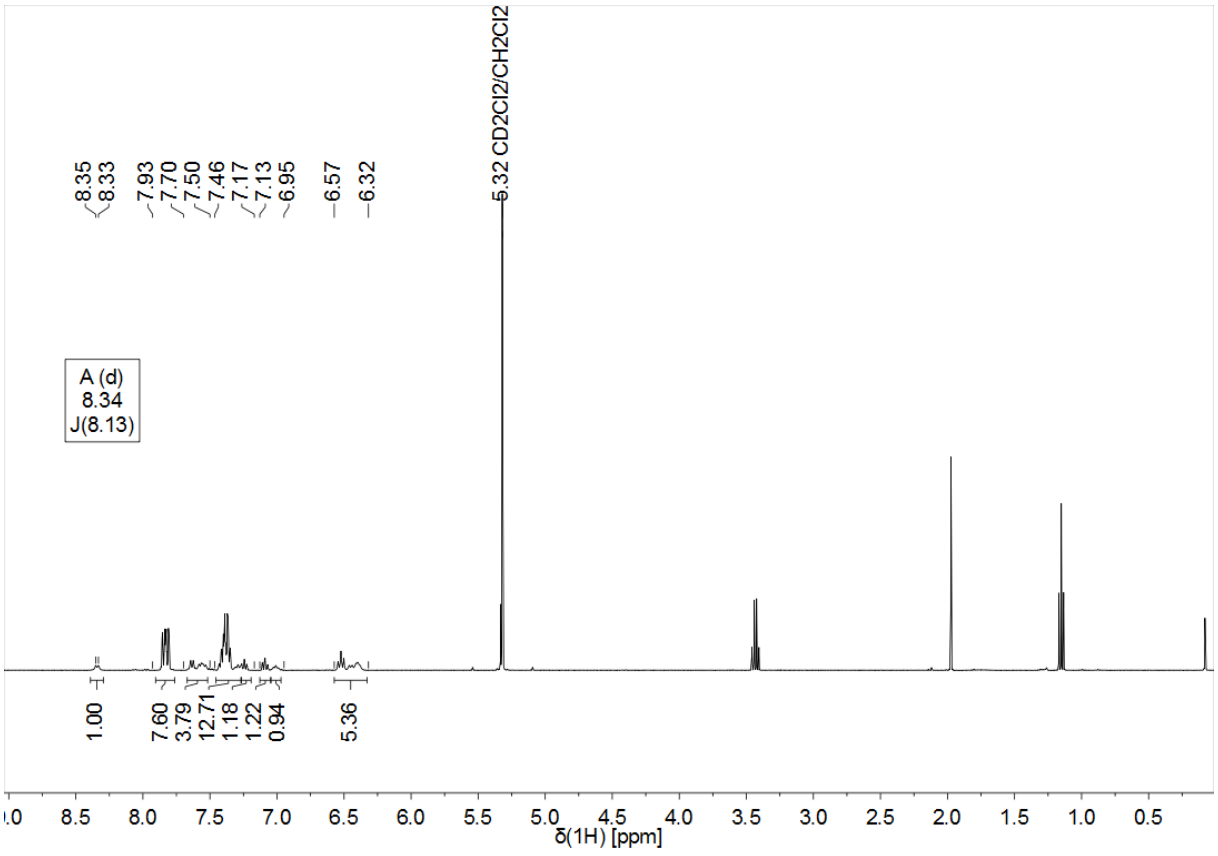

^{31}P CD_2Cl_2

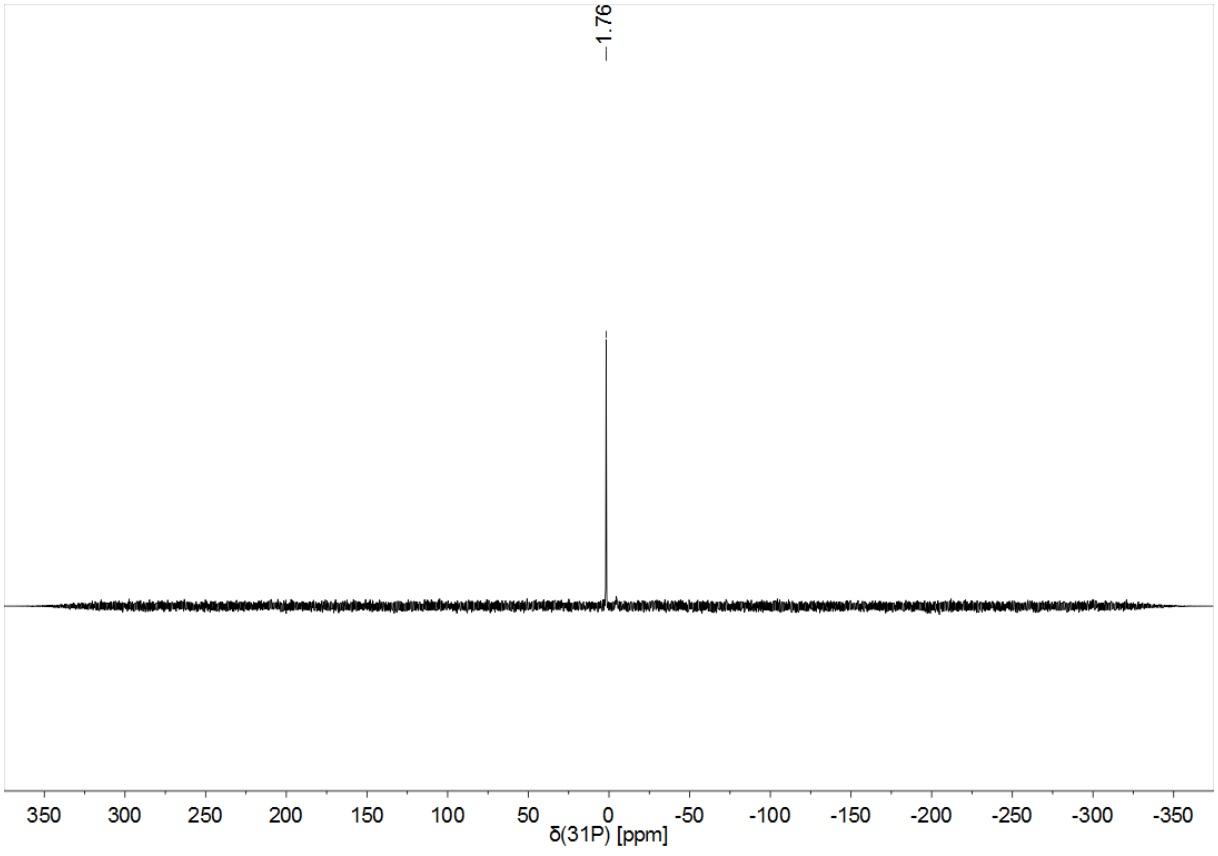

^{19}F CD_2Cl_2

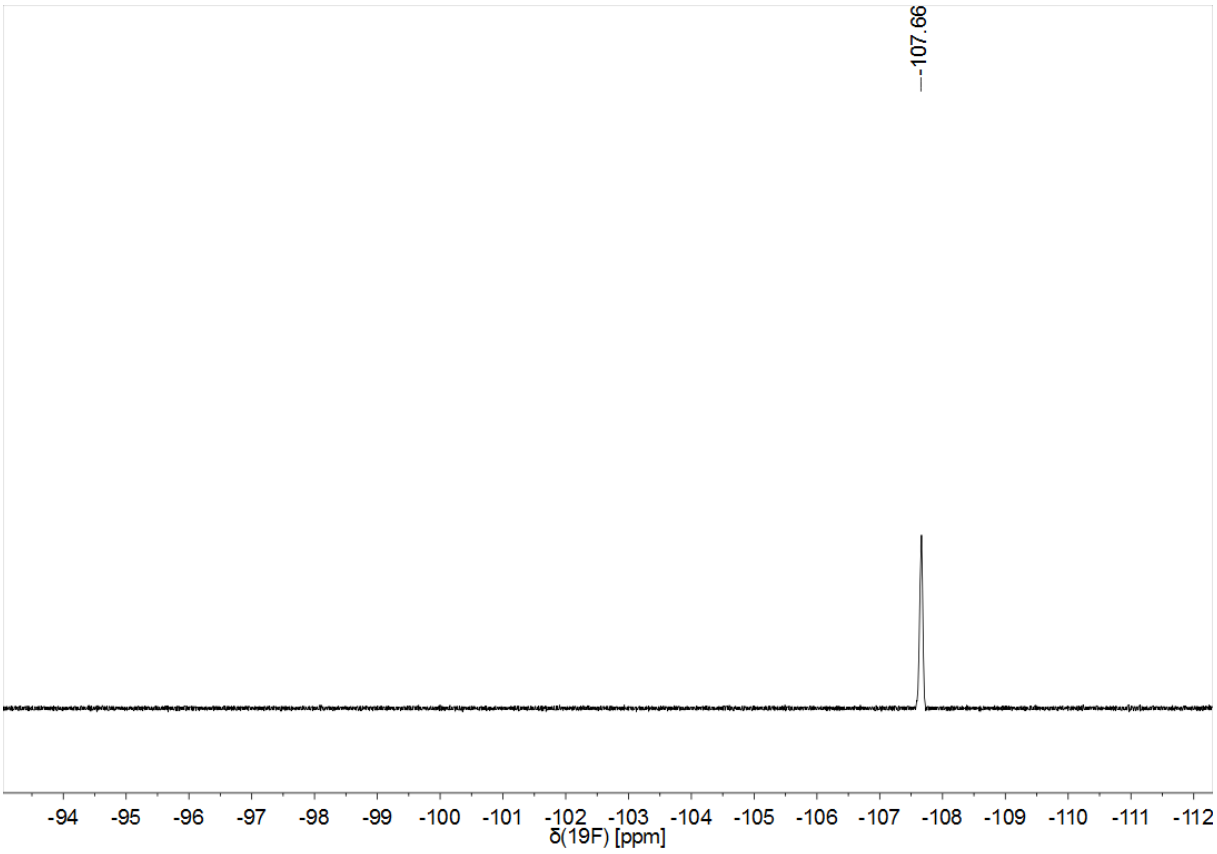

^{13}C CD_2Cl_2

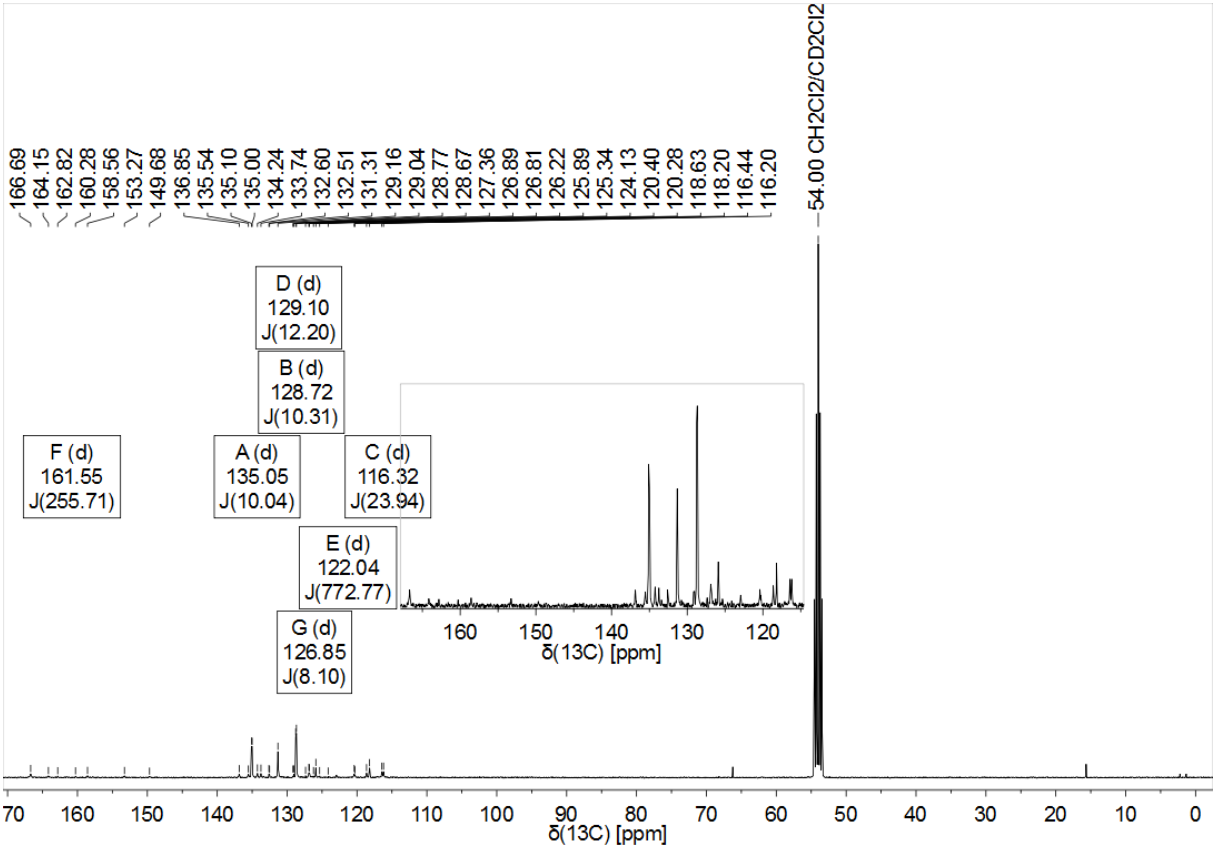

^{77}Se CD_2Cl_2

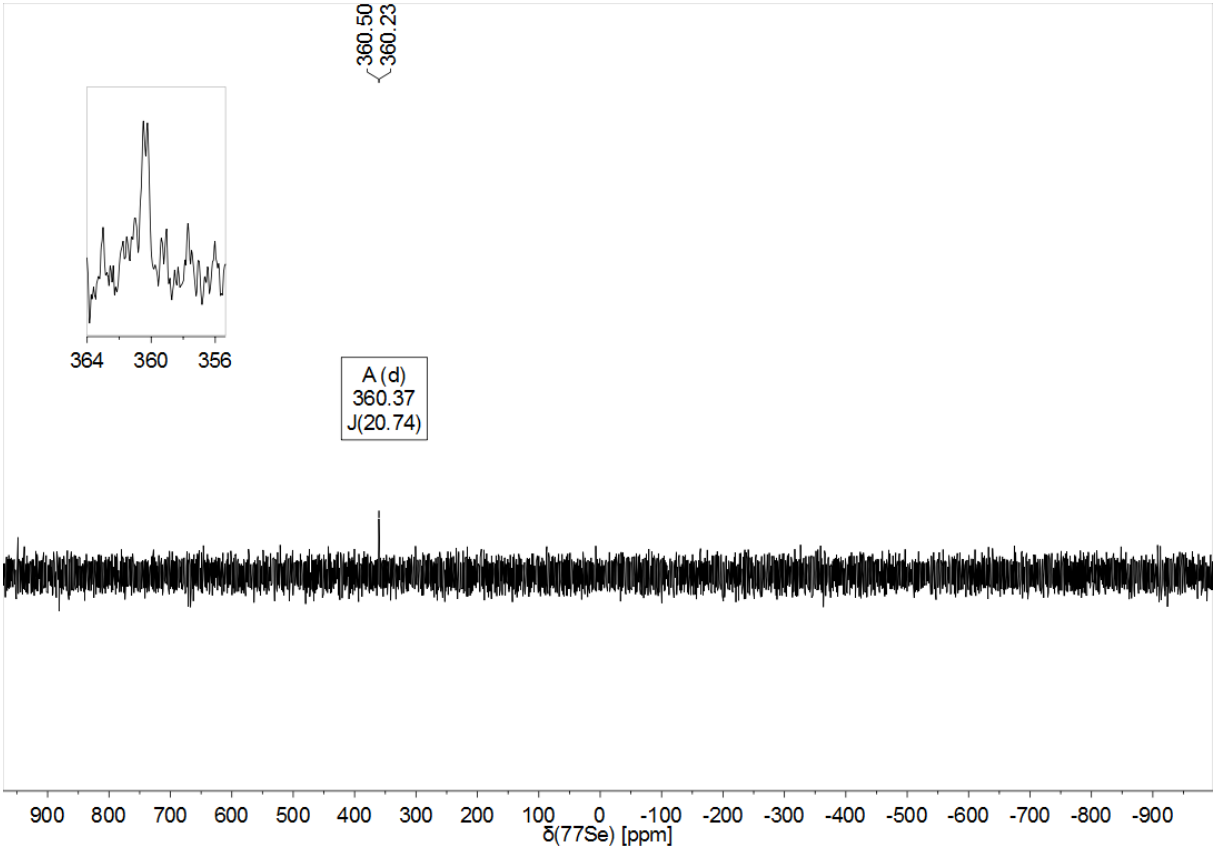

IR

Powder:

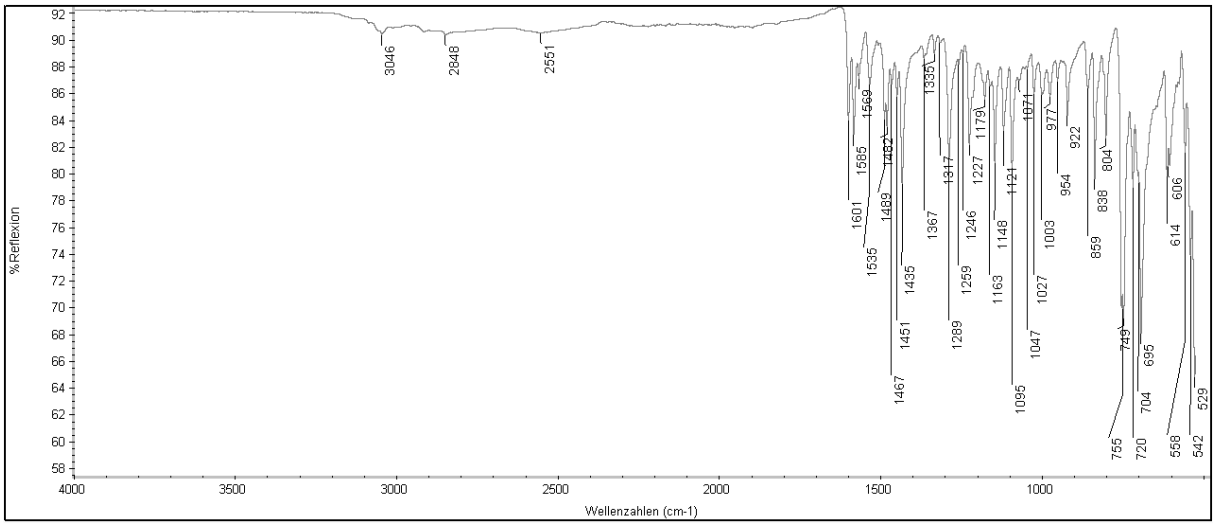

Crystals with cocrystallized CH_2Cl_2:

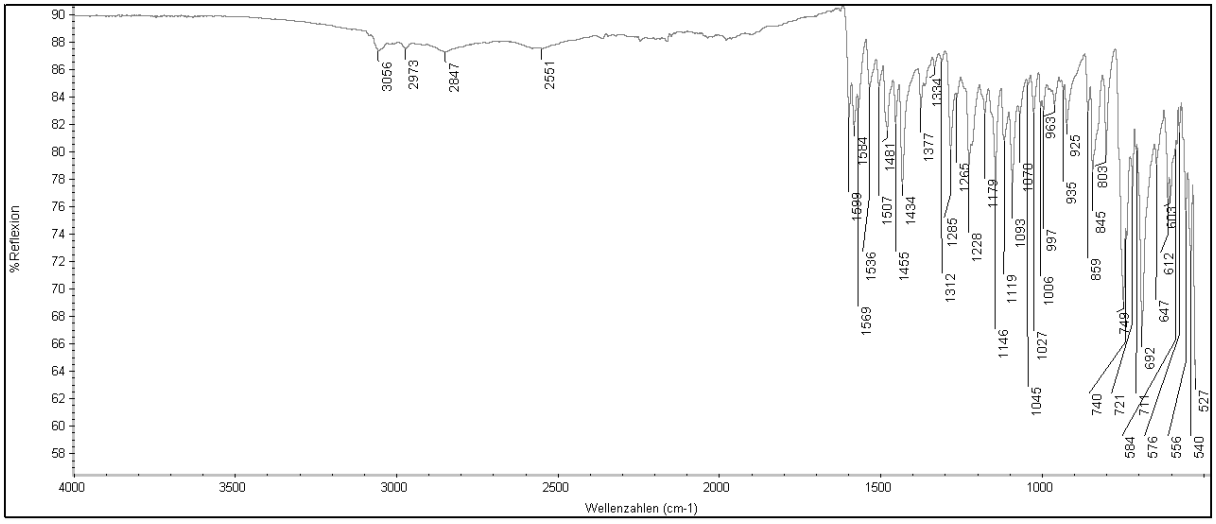

Crystals with cocrystallized CH_3CN:

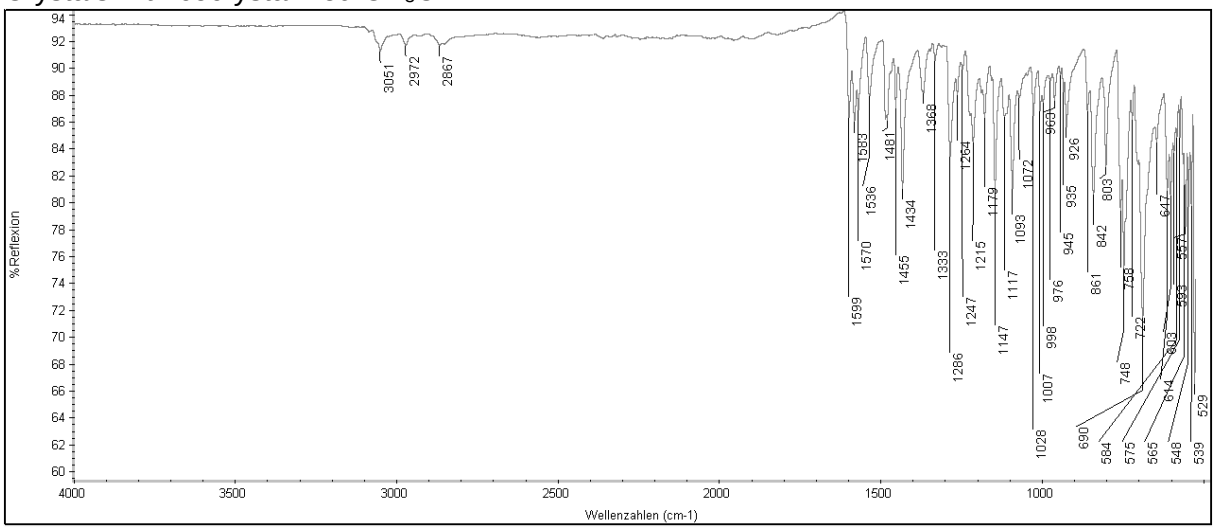

ESI+

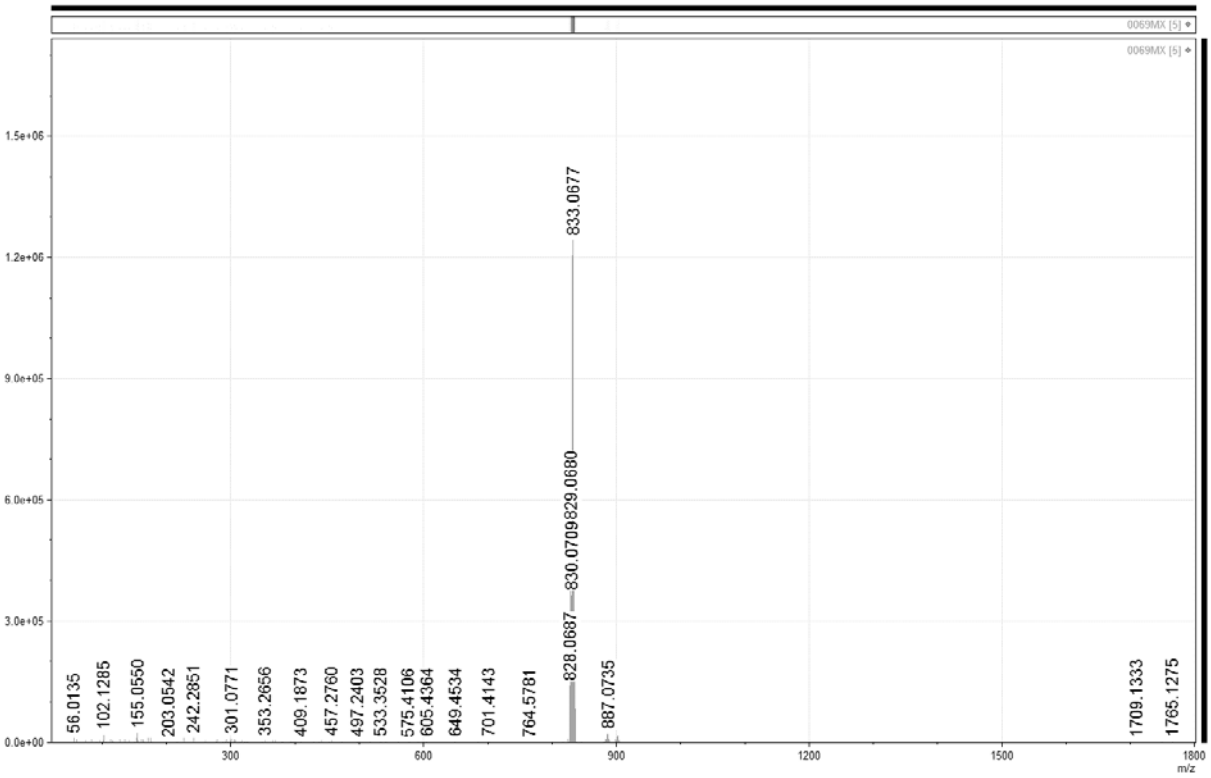

Measured isotopic distribution of $[Re(NPhF)(L^{Se})(PPh_3)]^+$

Simulated isotopic distribution of $[Re(NPhF)(L^{Se})(PPh_3)]^+$

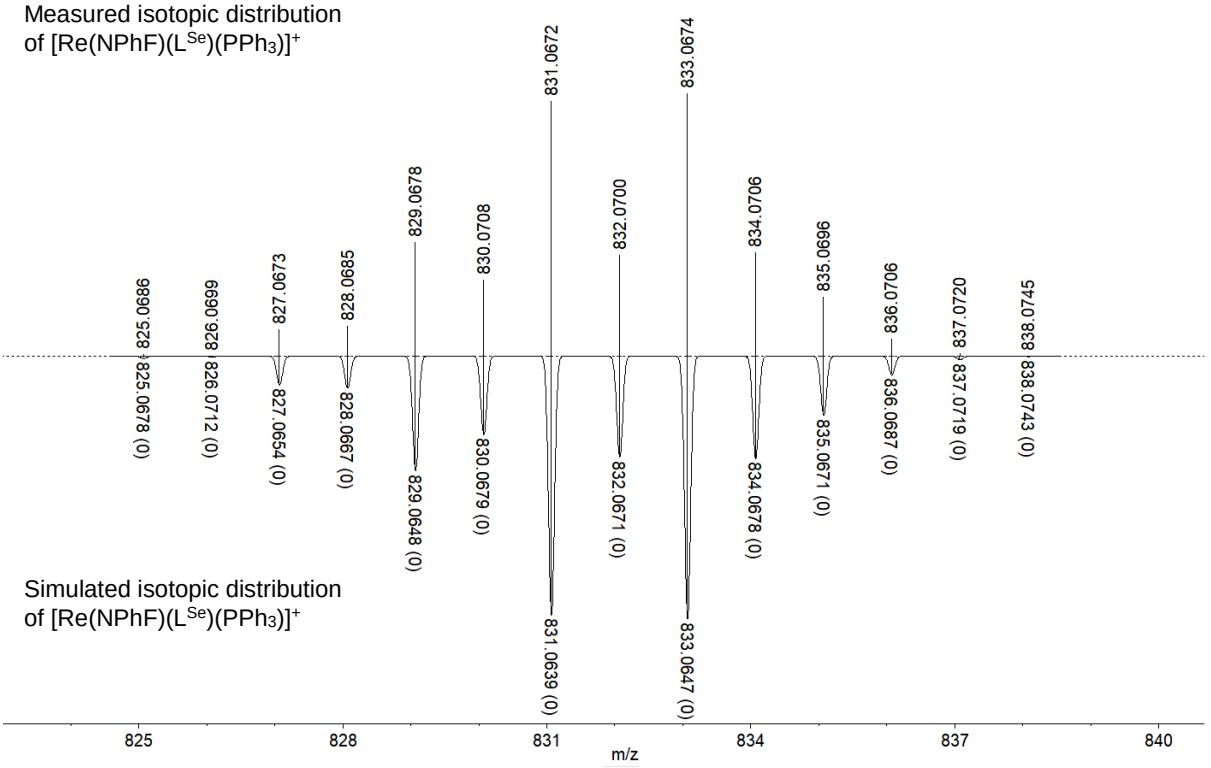

S3.8 Spectra of [Re(NPhF)(L^{Te})Cl(PPh_3)].

^{1}H

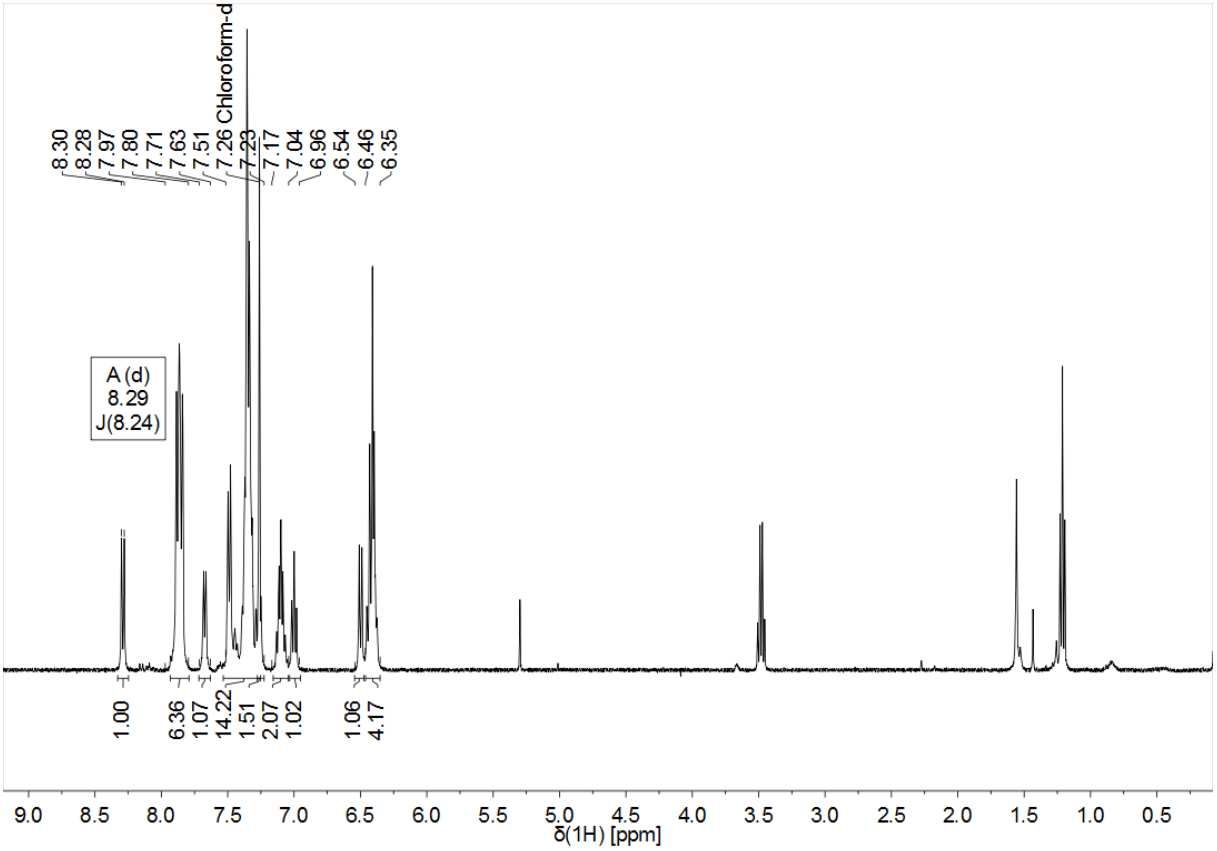

^{31}P

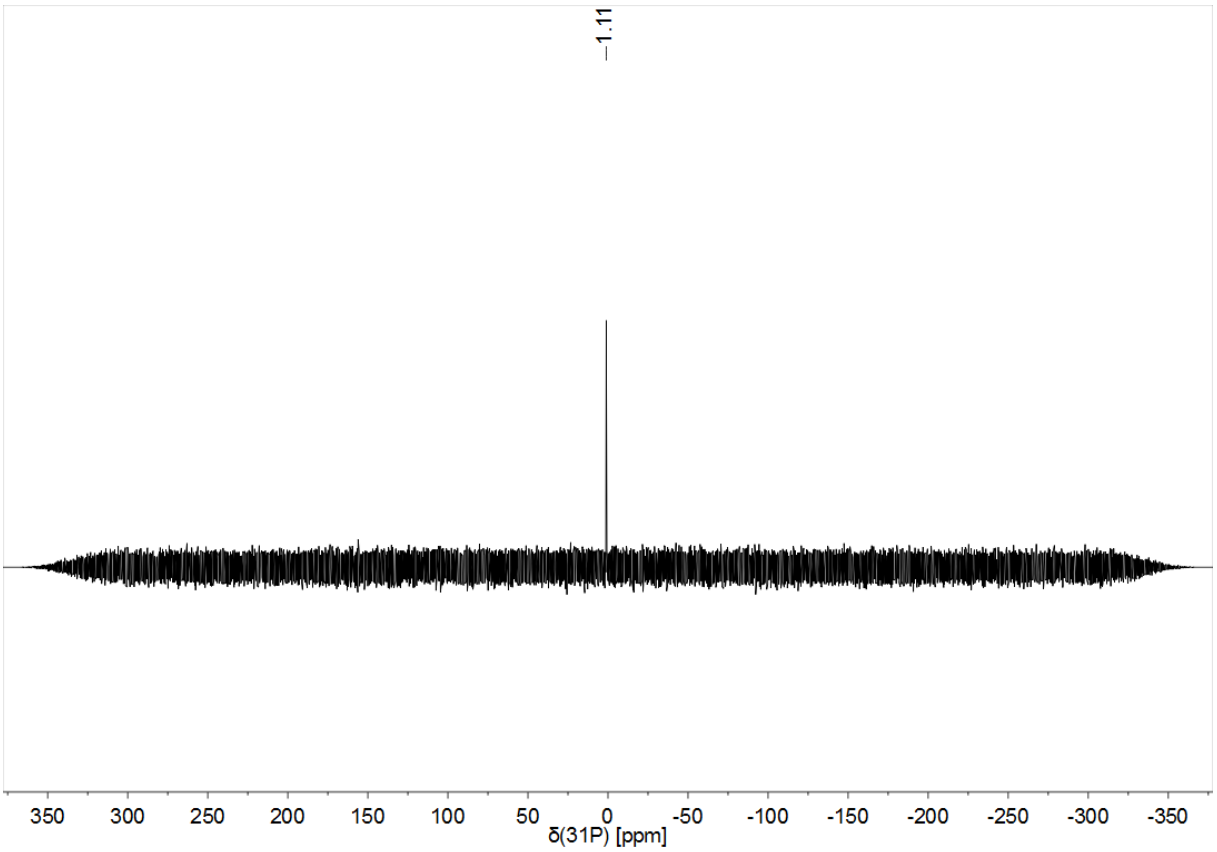

^{19}F

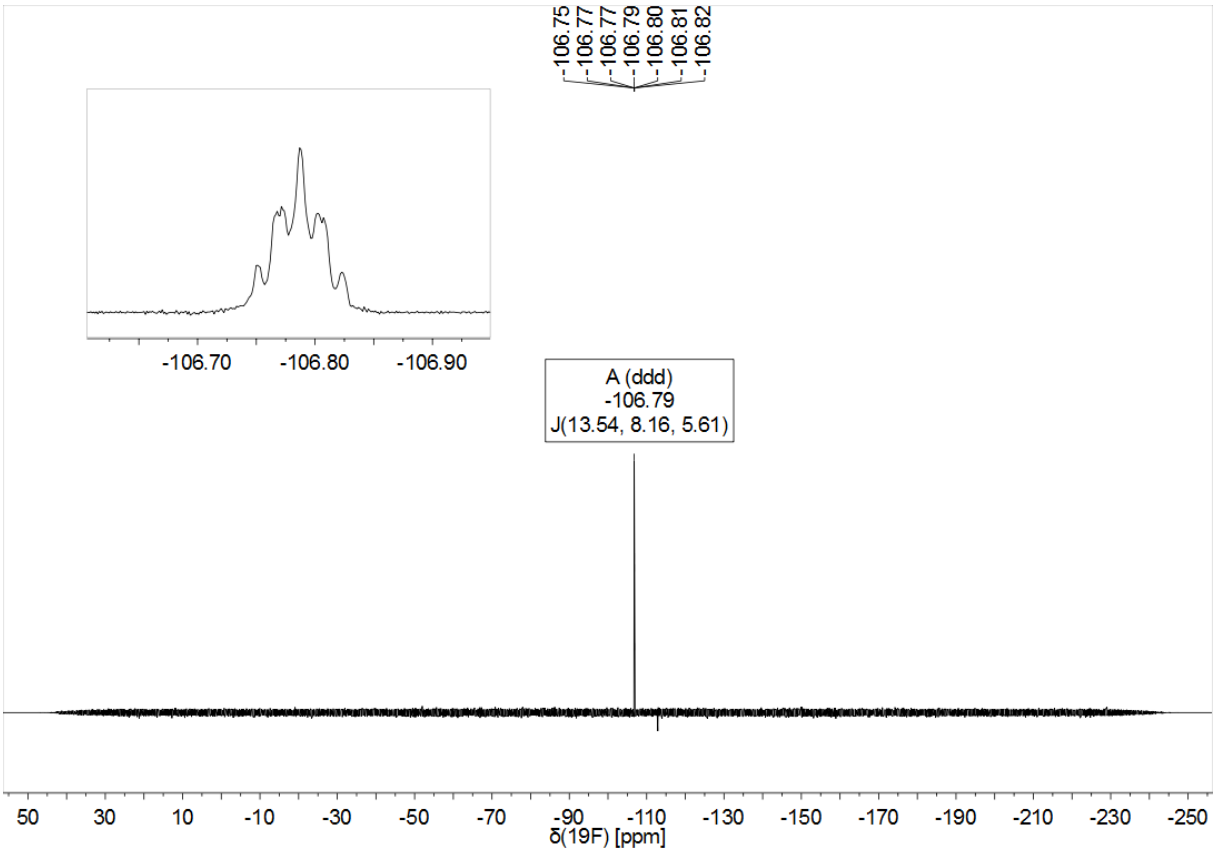
106.75
106.77
106.77
106.79
106.80
106.81
106.82
-106.70
-106.80
-106.90
A (ddd)
-106.79
J(13.54, 8.16, 5.61)
50 30 10 -10 -30 -50 -70 -90 -110 -130 -150 -170 -190 -210 -230 -250
δ(19F) [ppm]

$^{19}F\{^{31}P\}$

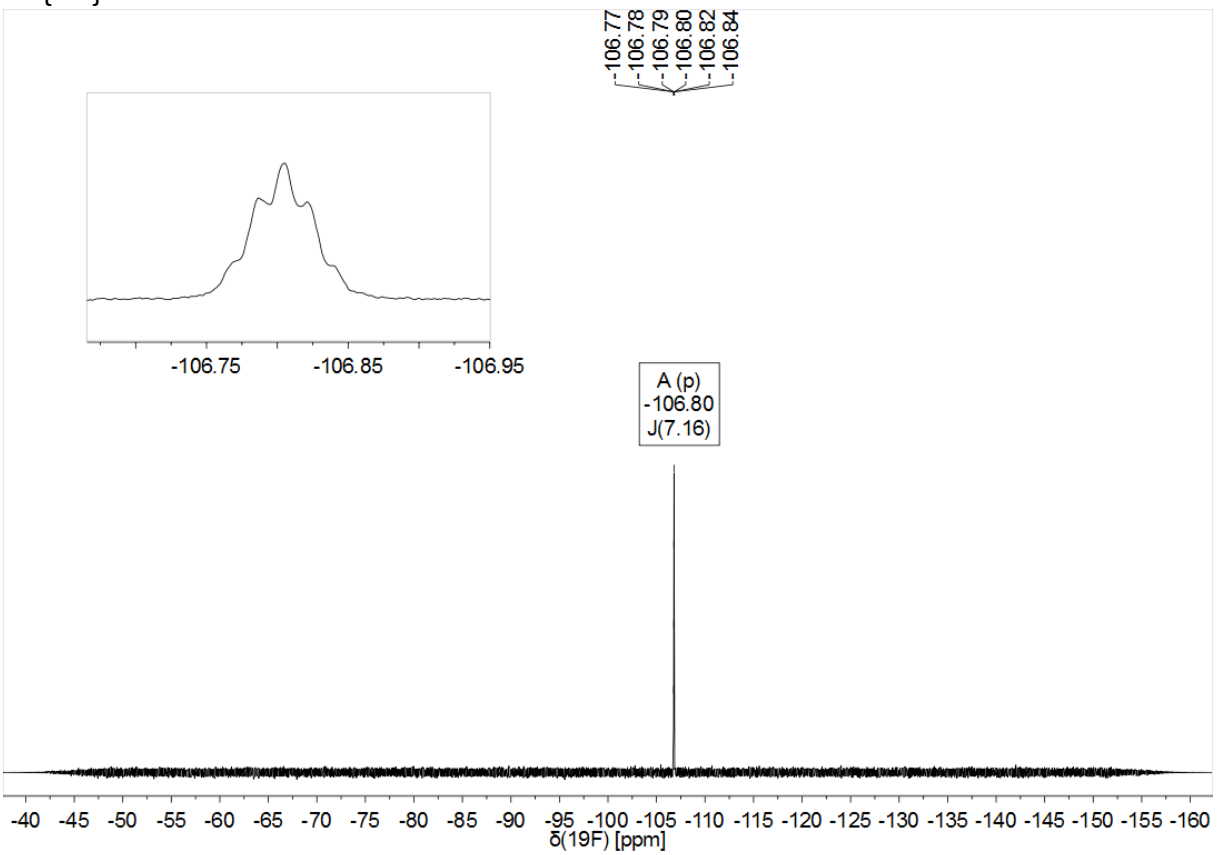
106.77
106.78
106.79
106.80
106.82
106.84
-106.75
-106.85
-106.95
A (p)
-106.80
J(7.16)
-40 -45 -50 -55 -60 -65 -70 -75 -80 -85 -90 -95 -100 -105 -110 -115 -120 -125 -130 -135 -140 -145 -150 -155 -160
δ(19F) [ppm]

^{13}C

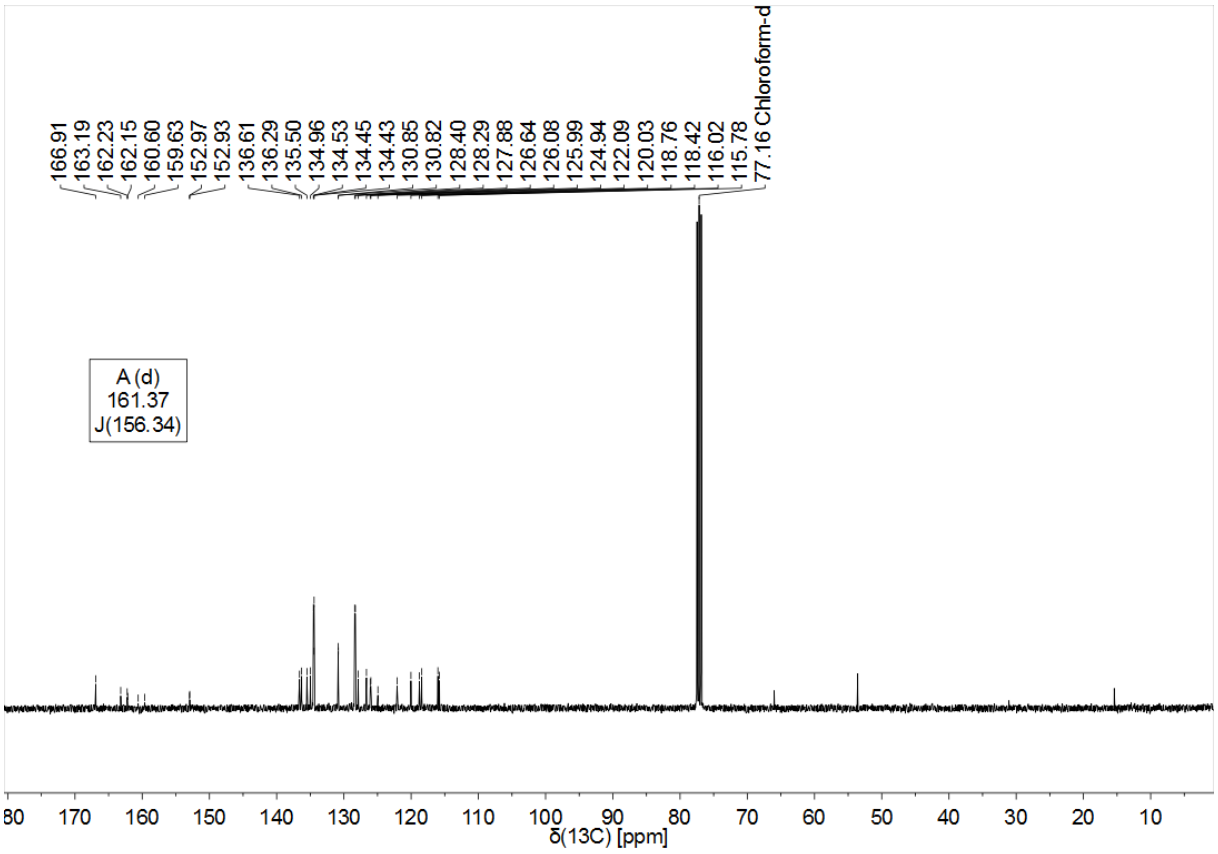

$^{13}C\{^{19}F$(decoupled at -106 ppm),$^{1}H\}$

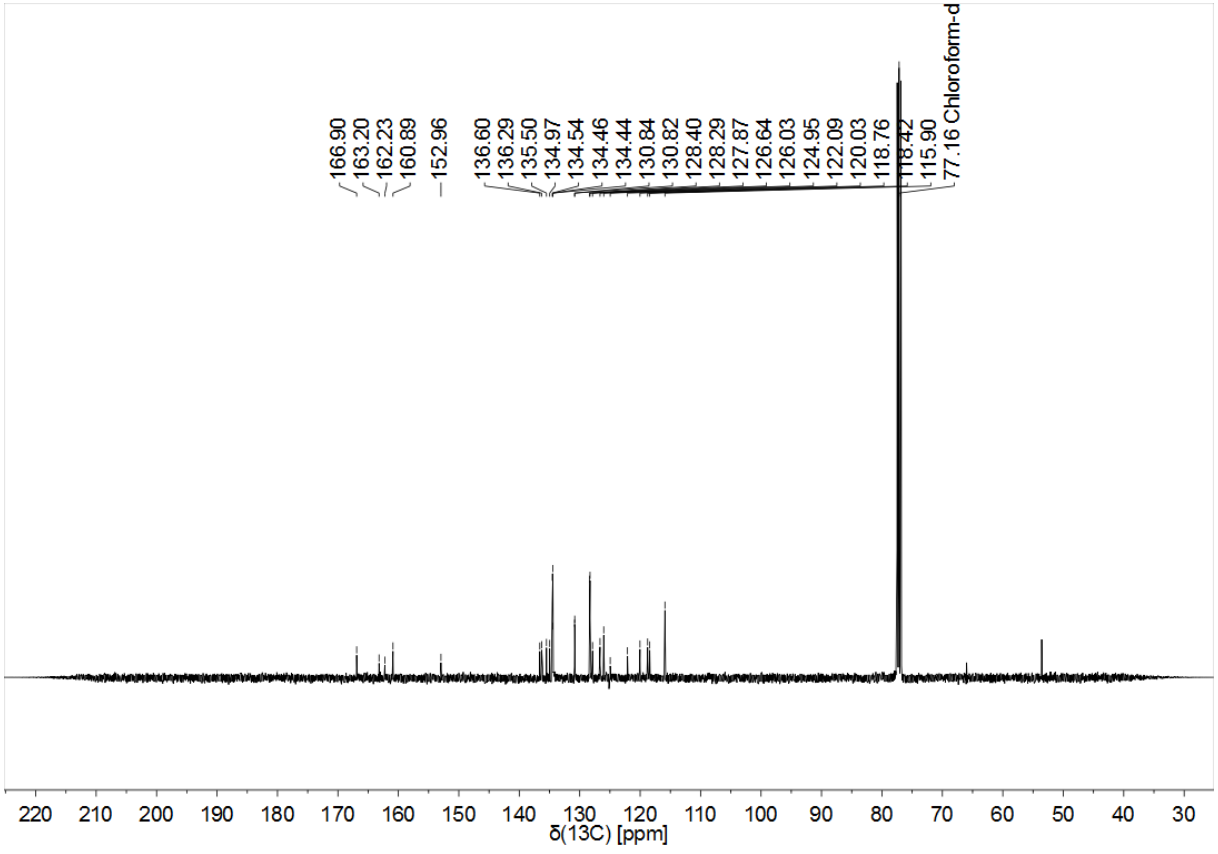

^{125}Te

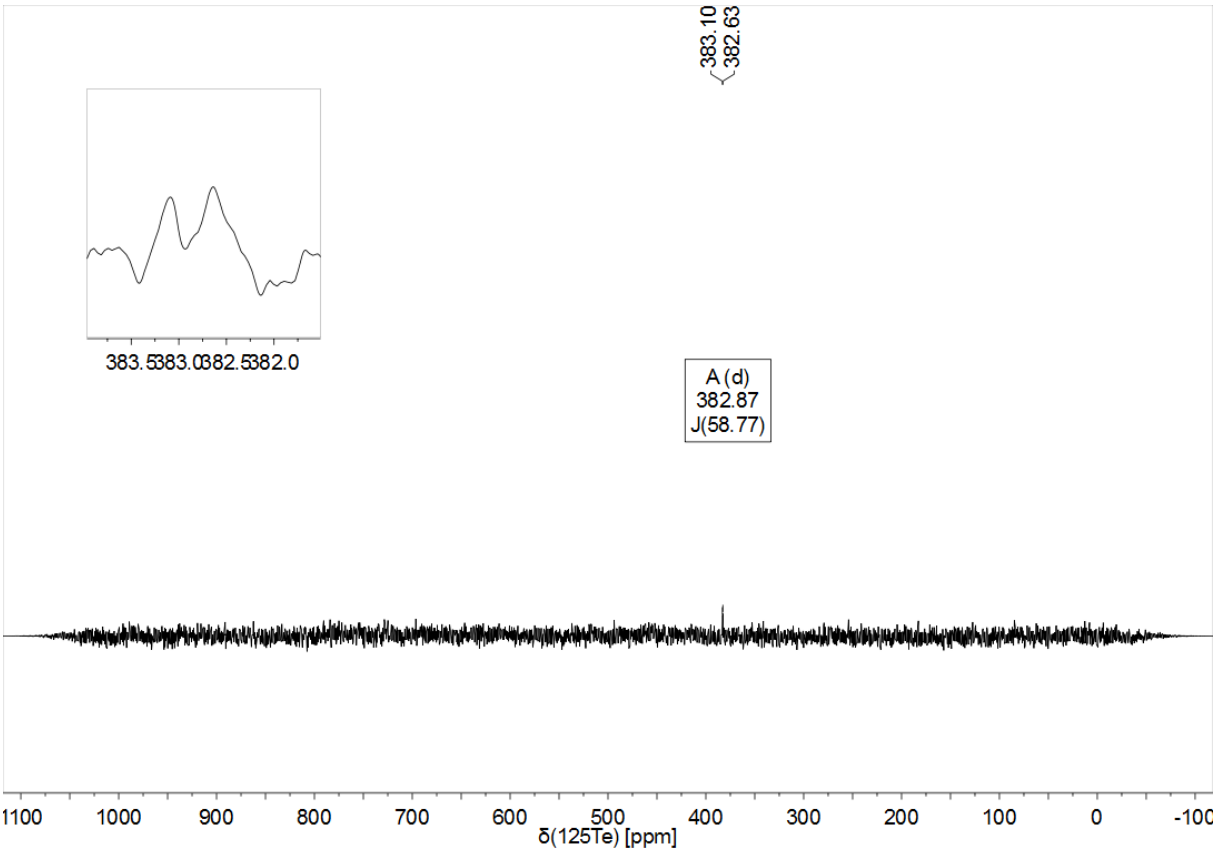
383.10
382.63
383.5383.0382.5382.0
A (d)
382.87
J(58.77)
1100
1000
900
800
700
600
500
400
300
200
100
0
-100
δ(125Te) [ppm]

IR

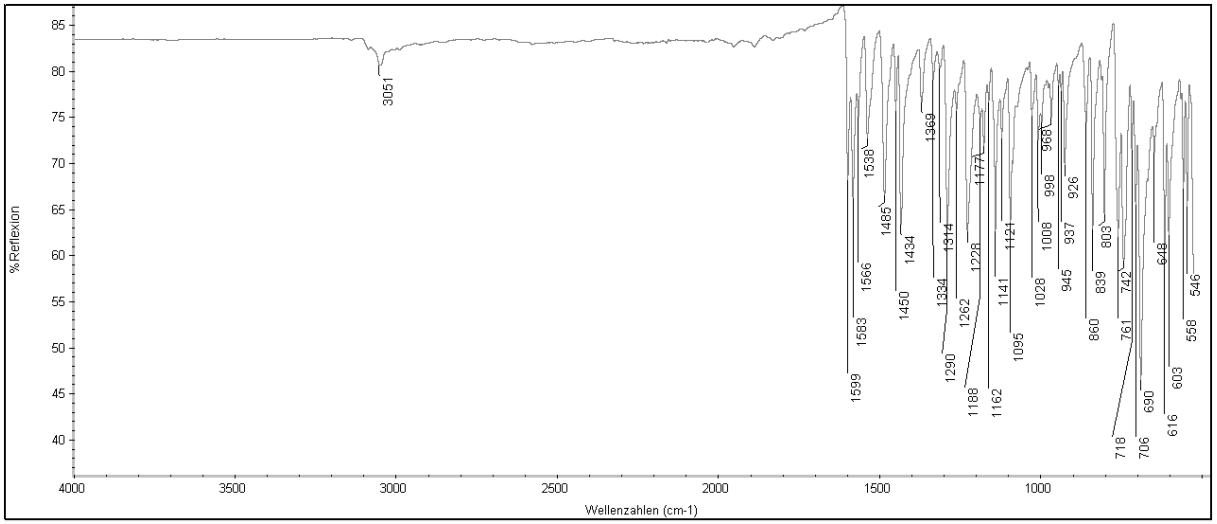
%Reflexion
Wellenzahlen (cm-1)
4000
3500
3000
2500
2000
1500
1000
3051
1599
1583
1566
1538
1485
1450
1434
1369
1334
1314
1290
1262
1228
1188
1177
1162
1141
1121
1095
1028
1008
998
968
945
937
926
860
839
803
761
742
718
706
690
648
616
603
558
546

ESI+

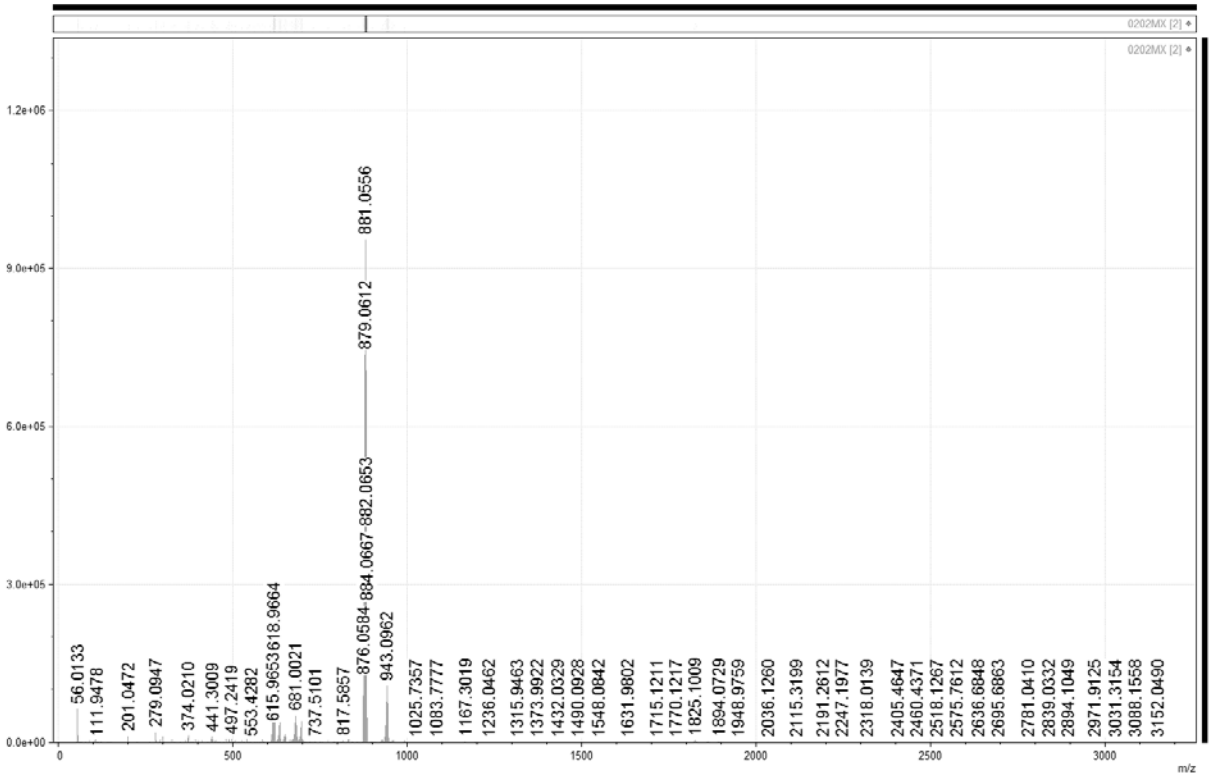

S3.9 Spectra of $[Re(NPhCF_3)Cl_3(PPh_3)_2]$.

^1H

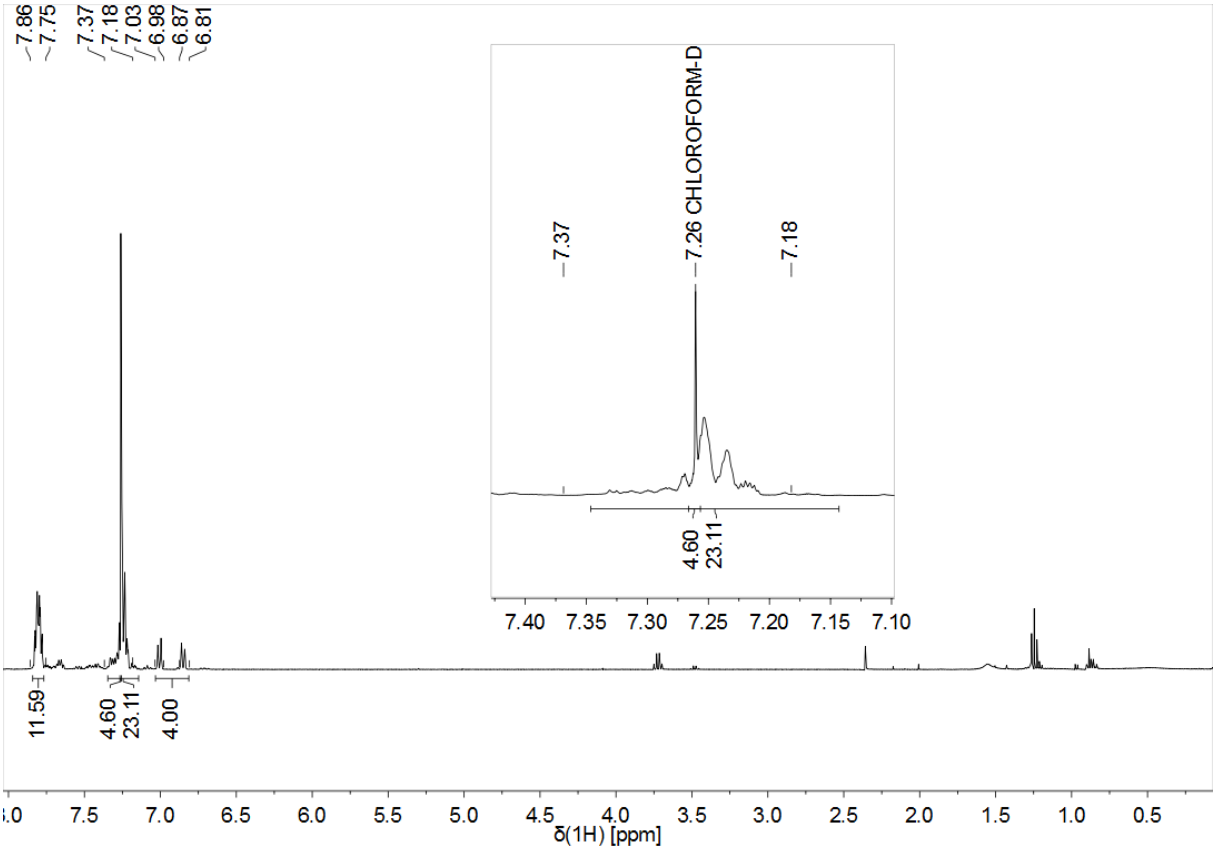

^{31}P

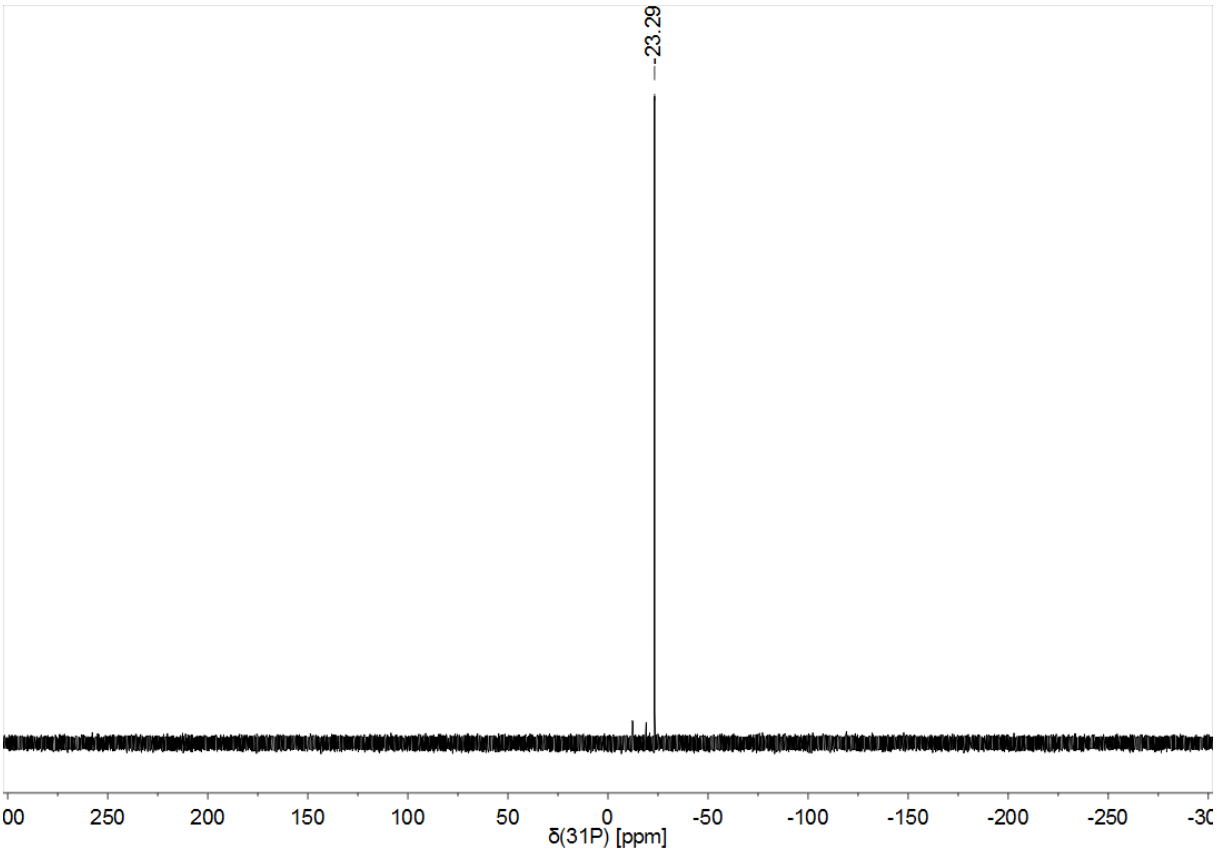

^{19}F

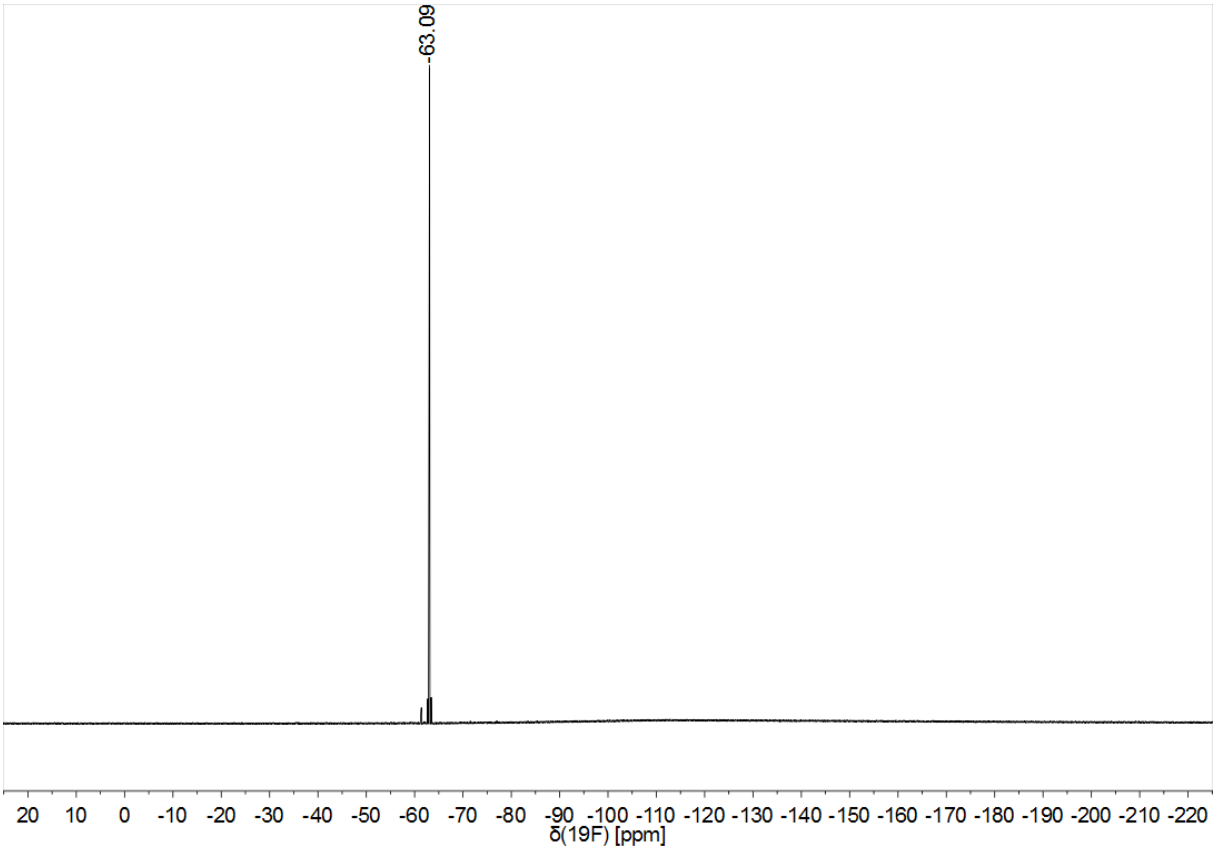

^{13}C

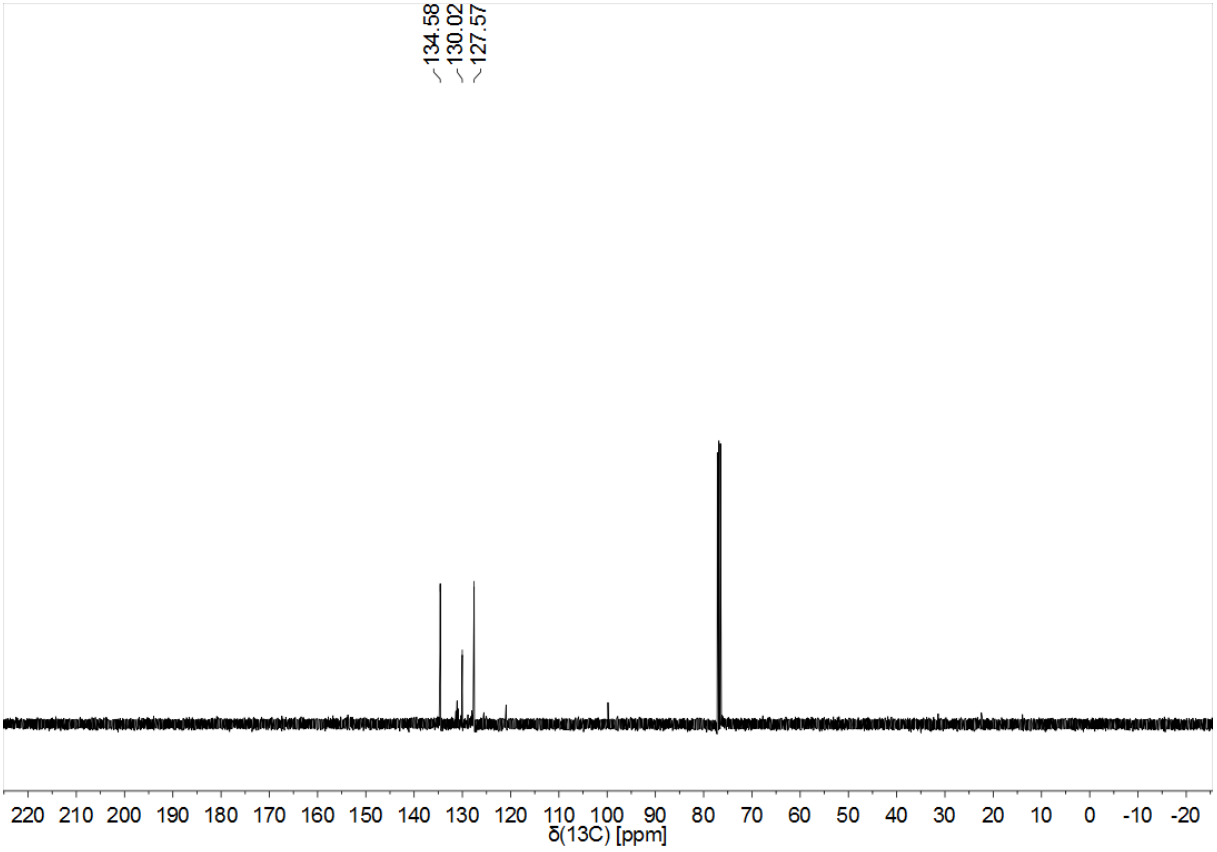

IR

Powder:

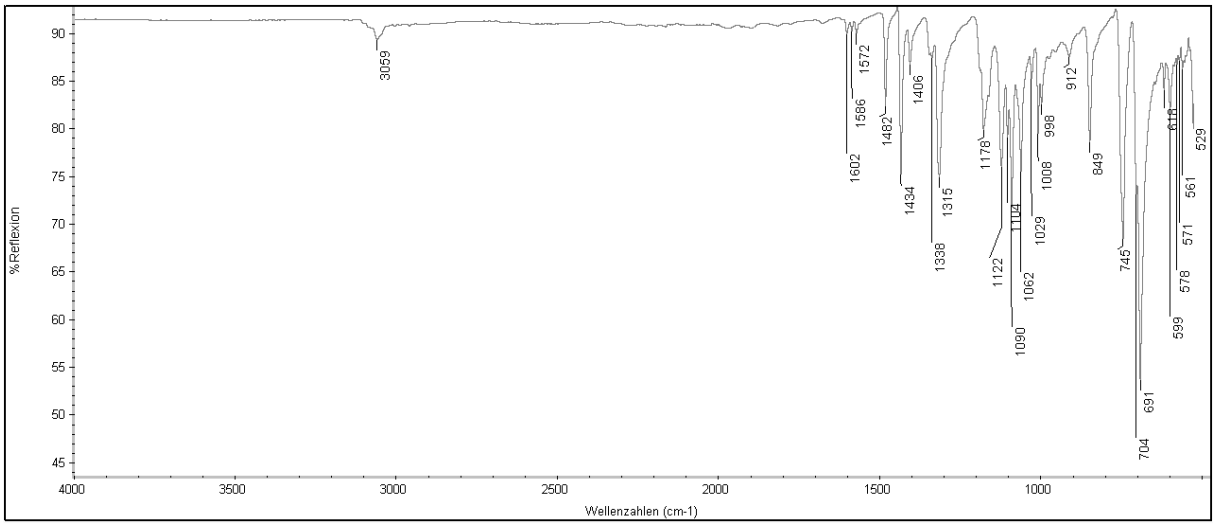

Crystals:

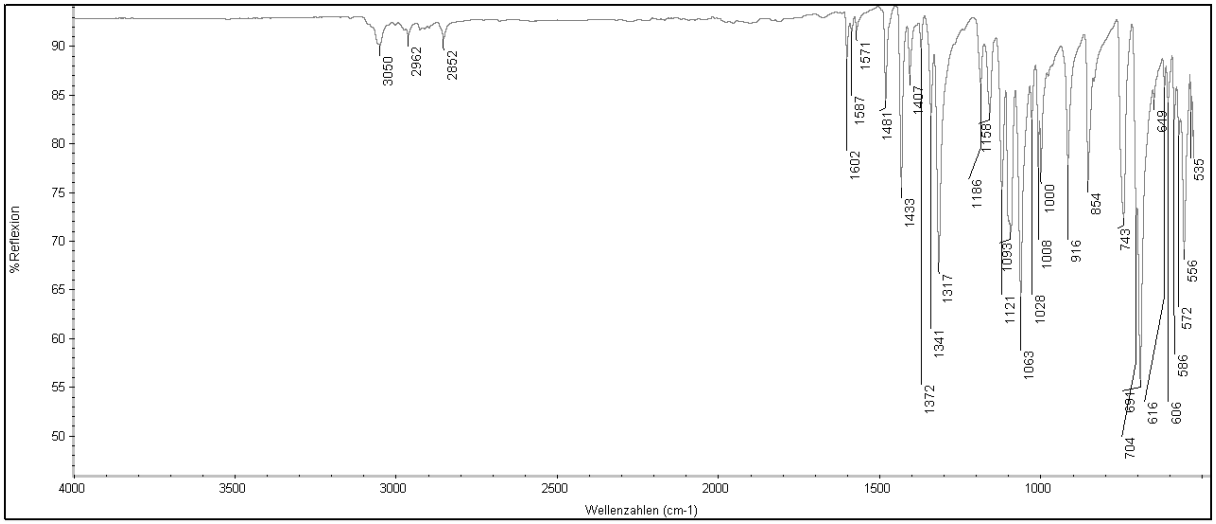

ESI+

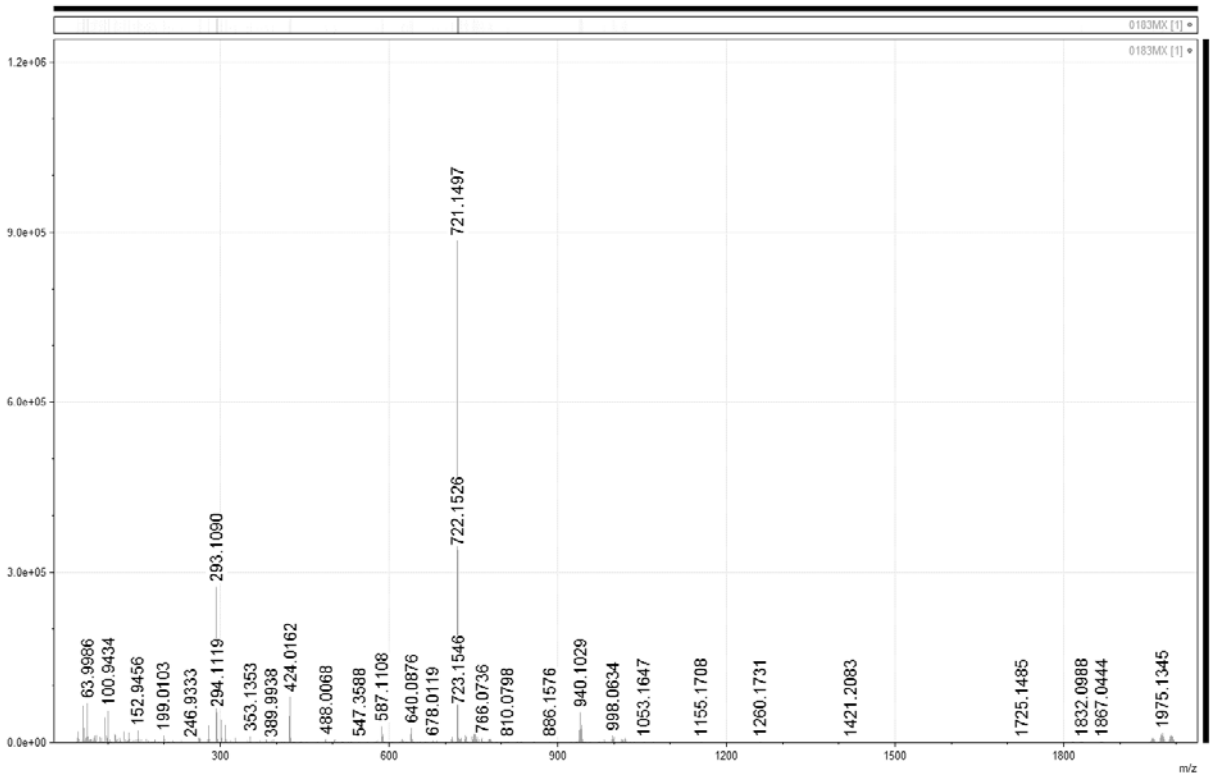

S3.10 Spectra of [Re(NPhCF$_3$)(L^{Se})Cl(PPh$_3$)].

^{1}H

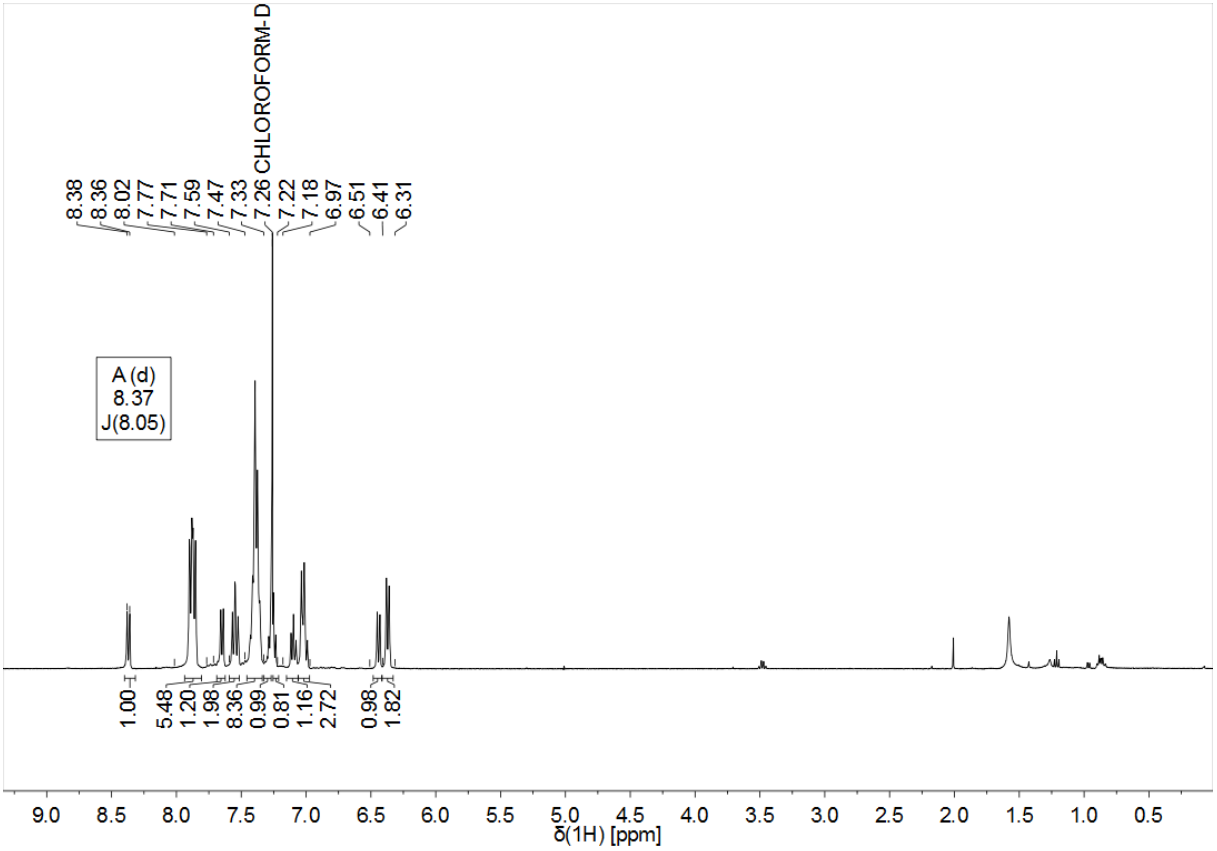

^{1}H{^{31}P}

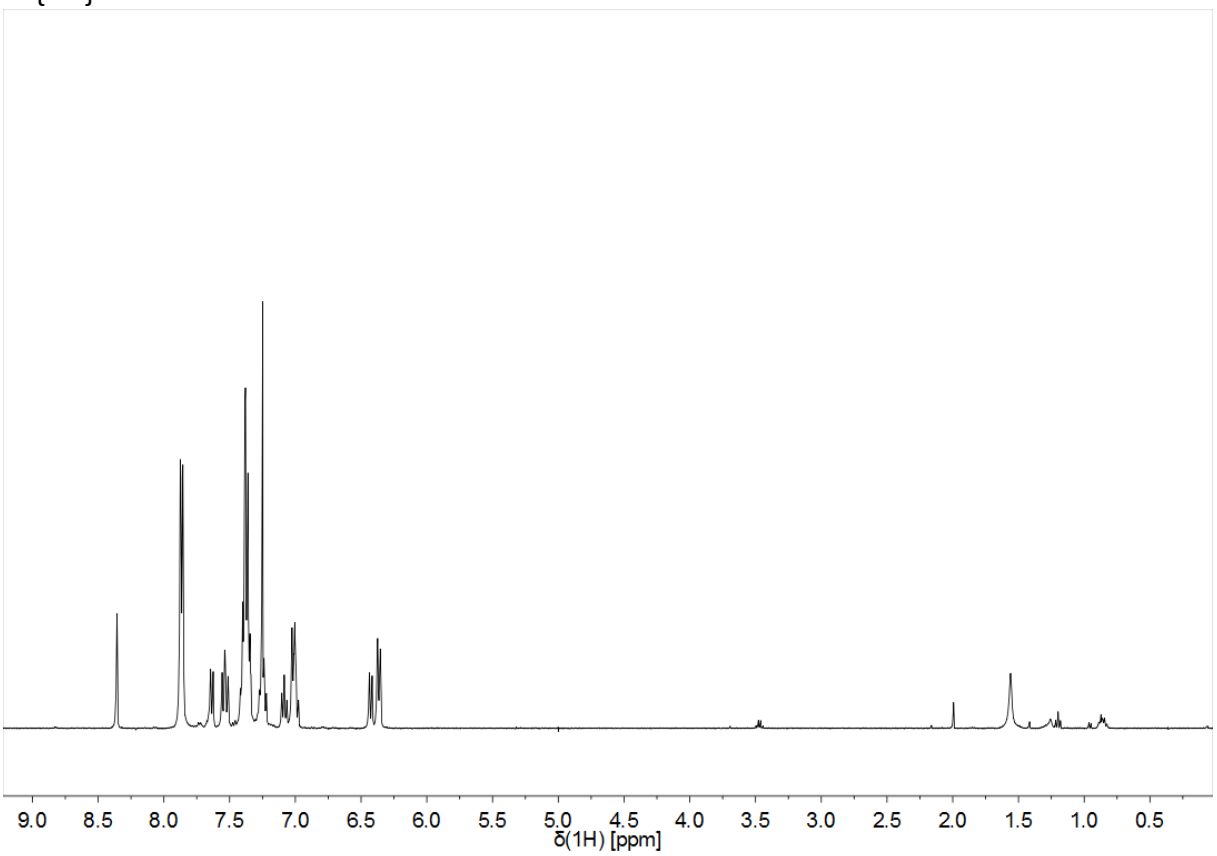

^{31}P

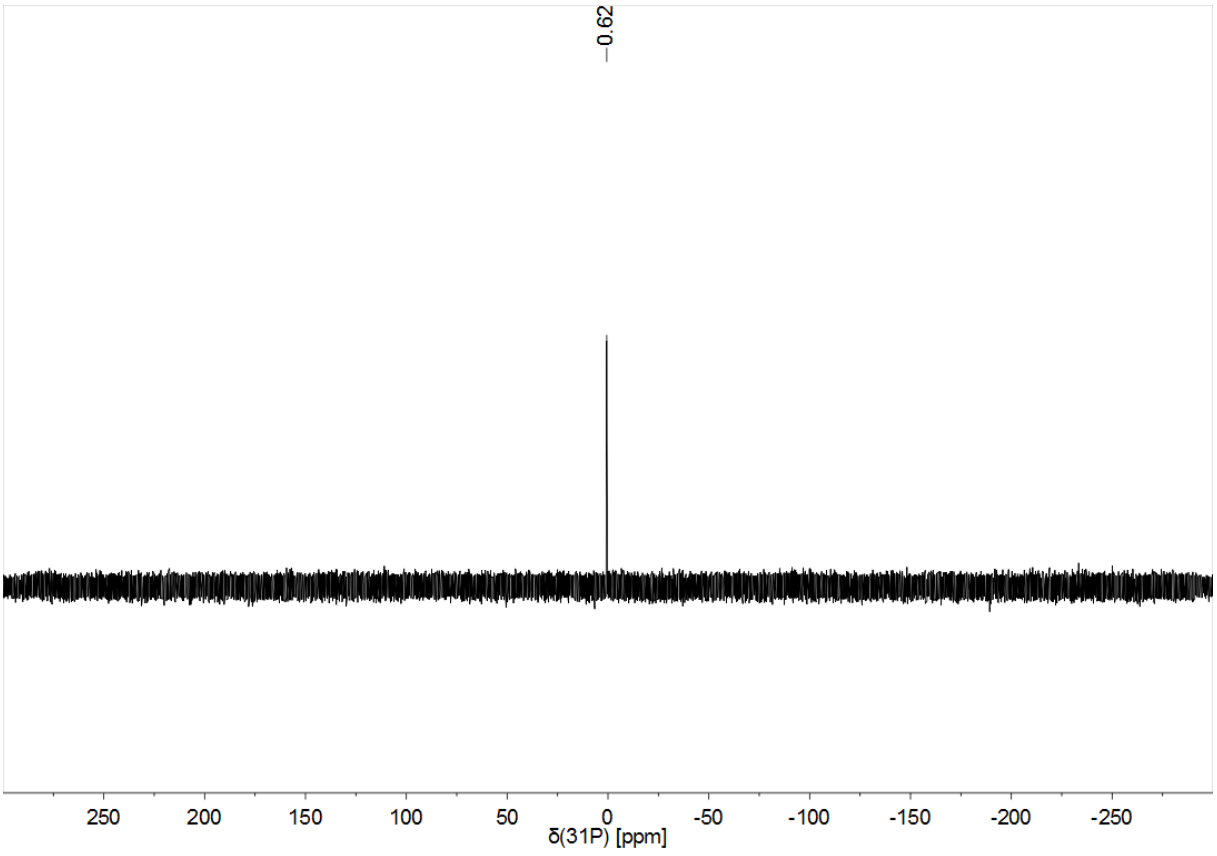
0.62
250
200
150
100
50
0
-50
-100
-150
-200
-250
δ(31P) [ppm]

^{13}C

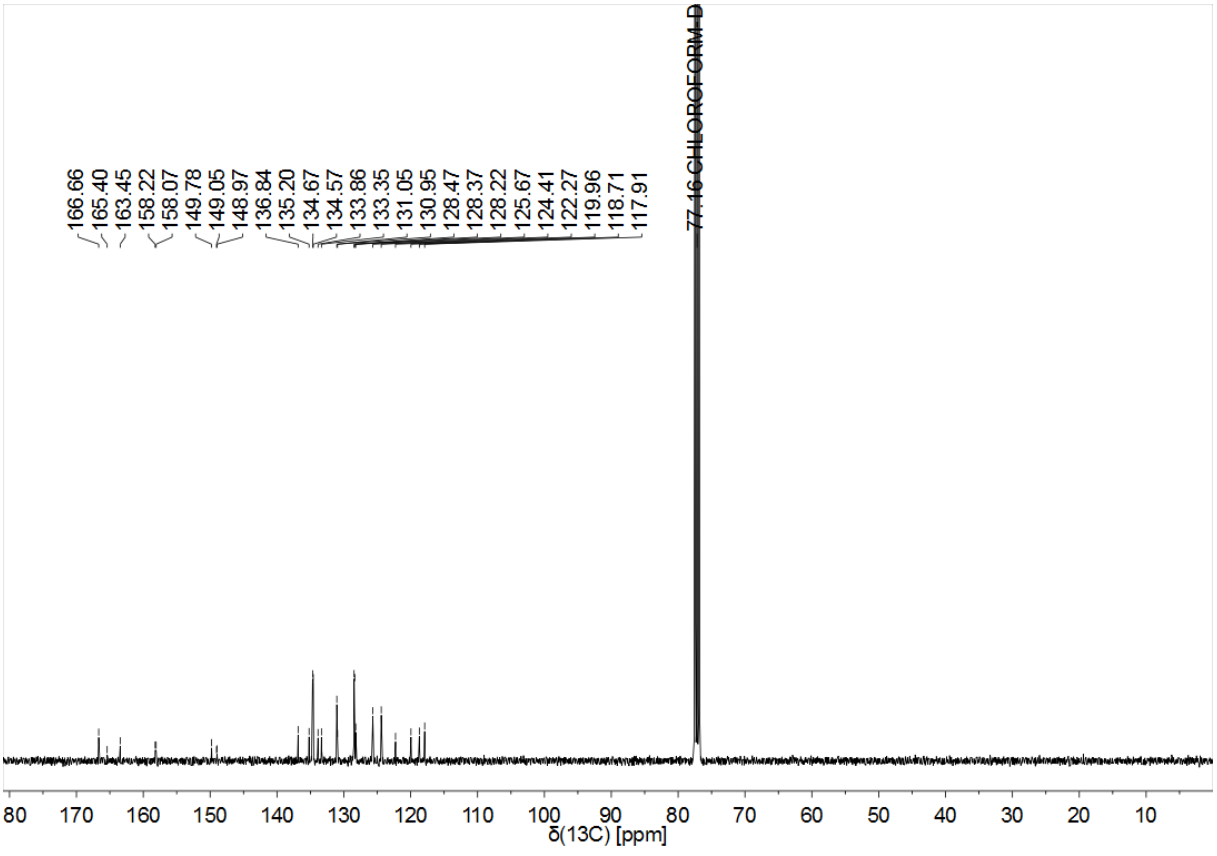
166.66
165.40
163.45
158.22
158.07
149.78
149.05
148.97
136.84
135.20
134.67
134.57
133.86
133.35
131.05
130.95
128.47
128.37
128.22
125.67
124.41
122.27
119.96
118.71
117.91
77.16 CHLOROFORM-D
80
170
160
150
140
130
120
110
100
90
80
70
60
50
40
30
20
10
δ(13C) [ppm]

^{77}Se

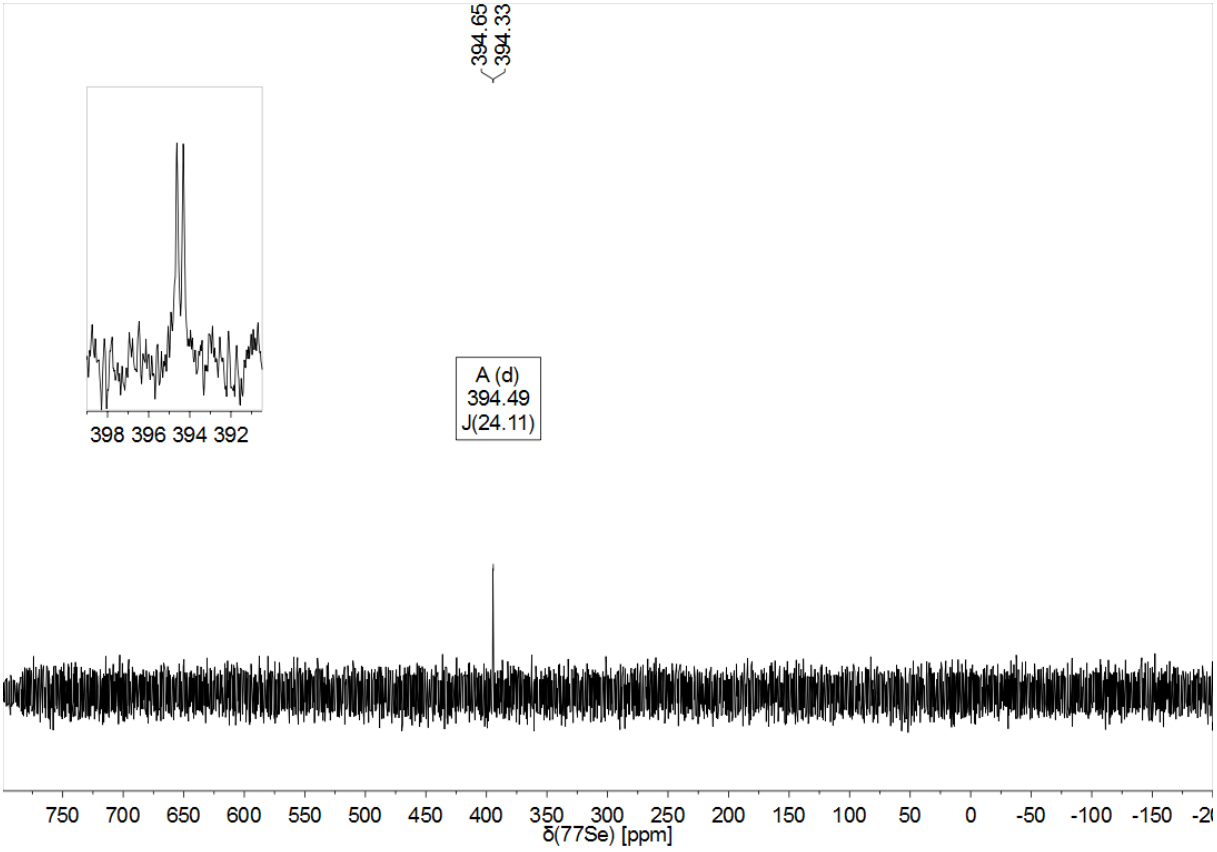
394.65
394.33
398 396 394 392
A (d)
394.49
J(24.11)
750 700 650 600 550 500 450 400 350 300 250 200 150 100 50 0 -50 -100 -150
δ(77Se) [ppm]

IR

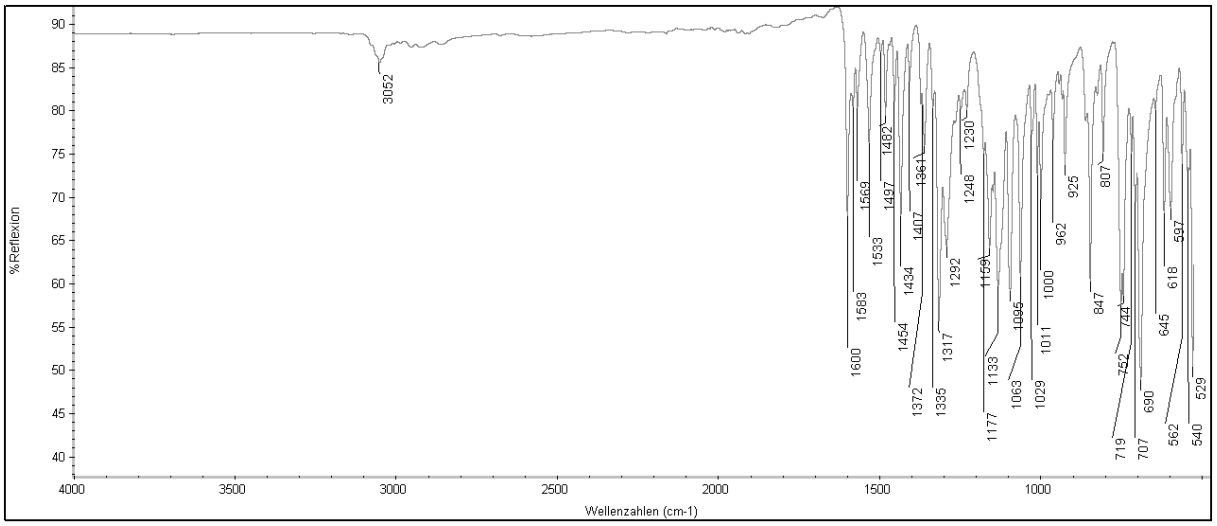
%Reflexion
Wellenzahlen (cm-1)
4000 3500 3000 2500 2000 1500 1000
3052
1600 1583 1569 1533 1497 1482 1454 1434 1407 1361 1335 1317 1292 1248 1230 1177 1159 1133 1095 1063 1029 1011 1000 962 925 847 807 752 744 719 707 690 645 618 597 562 540 529

ESI+

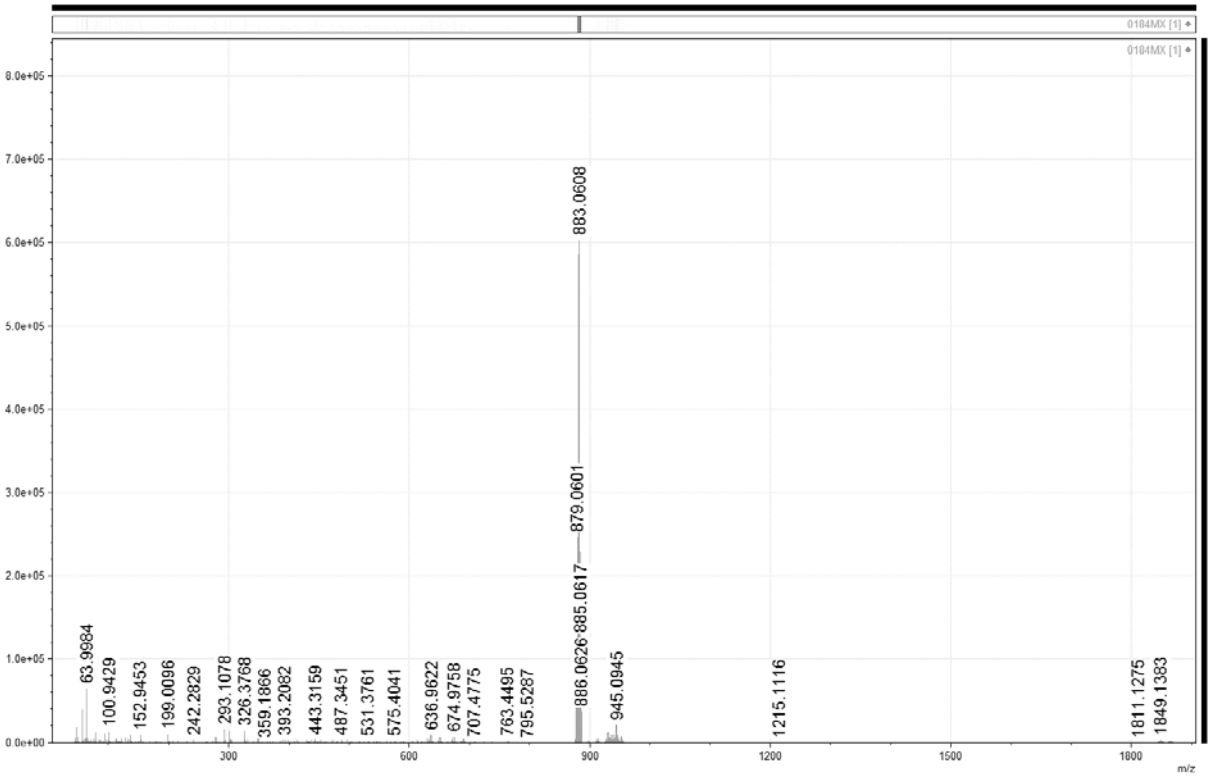

S3.11 Spectra of [Re(NPhCF$_3$)(L^{Te})Cl(PPh$_3$)].

^{1}H

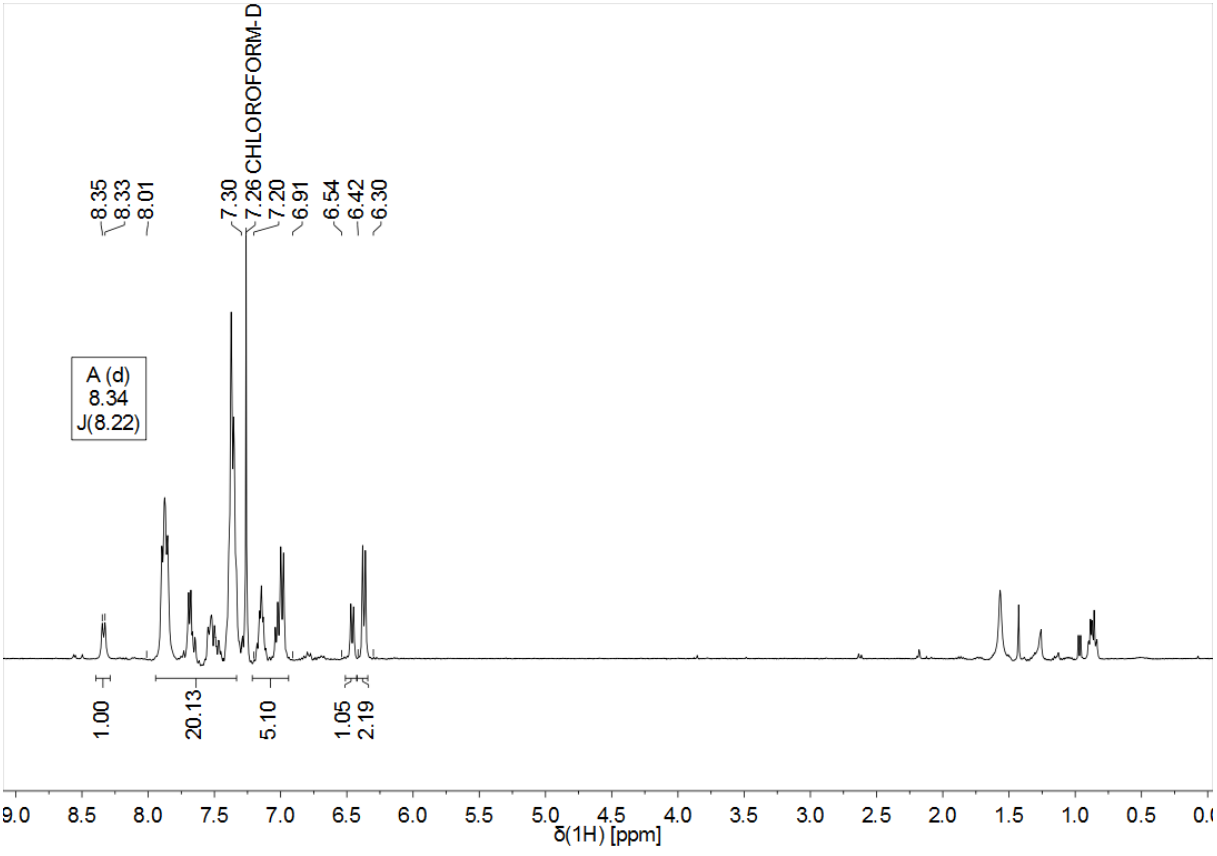

^{1}H-^{1}H-COSY

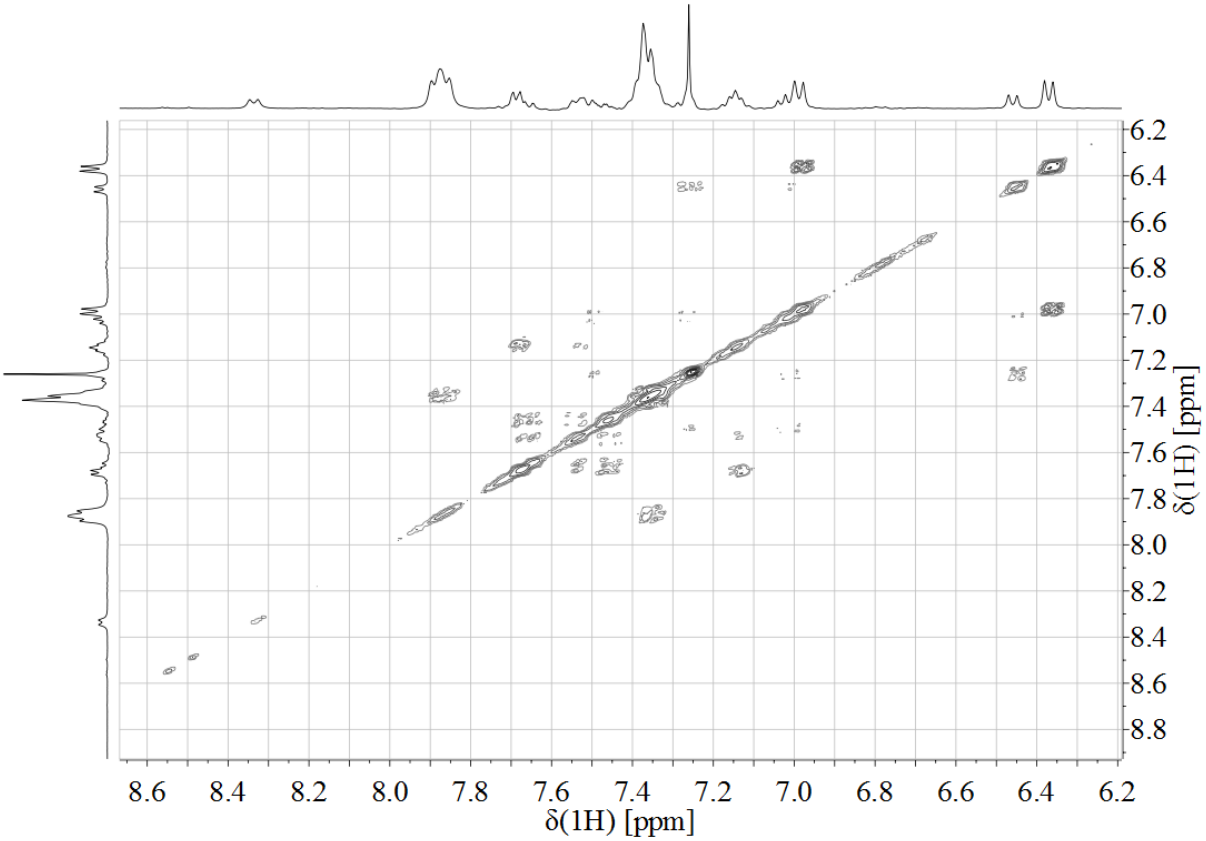

$^{1}H\{^{31}P\}$

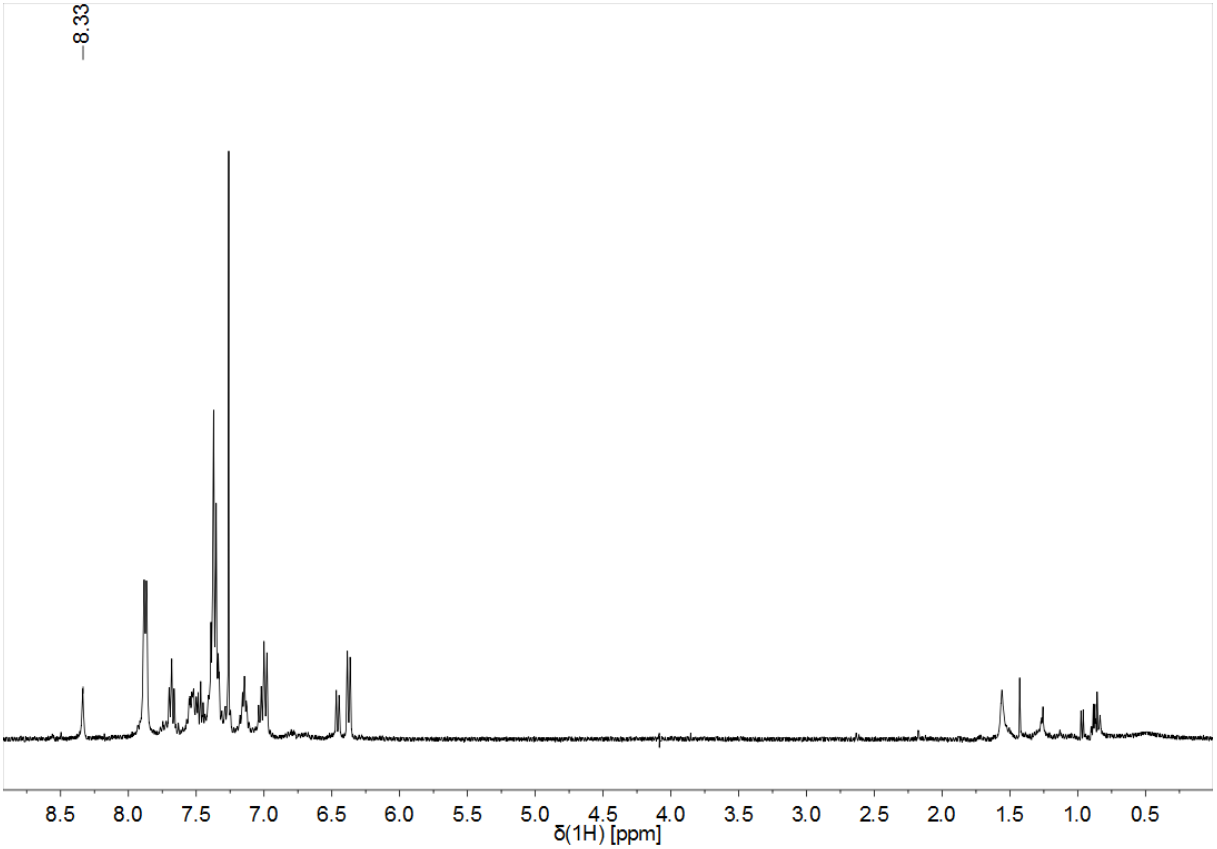

^{31}P

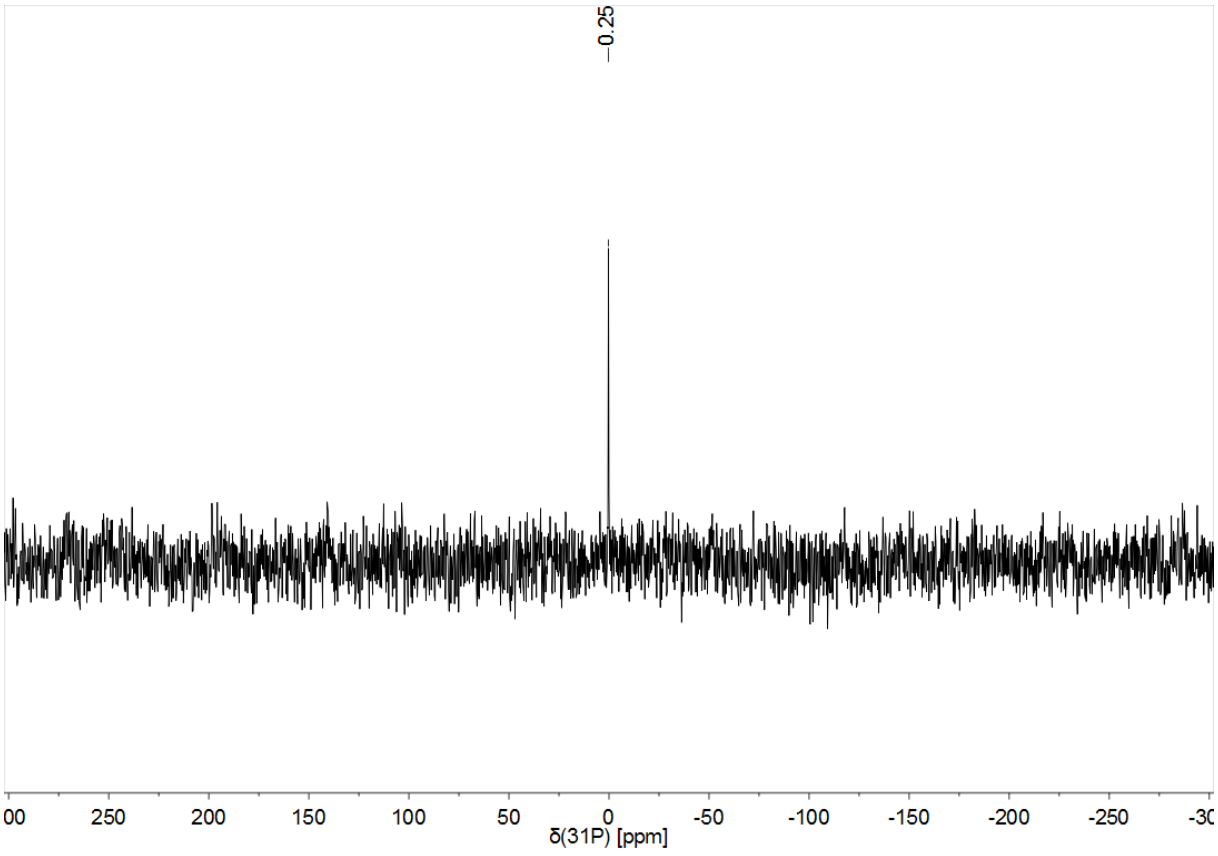
0.25
00
250
200
150
100
50
0
-50
-100
-150
-200
-250
-30
δ(31P) [ppm]

^{19}F

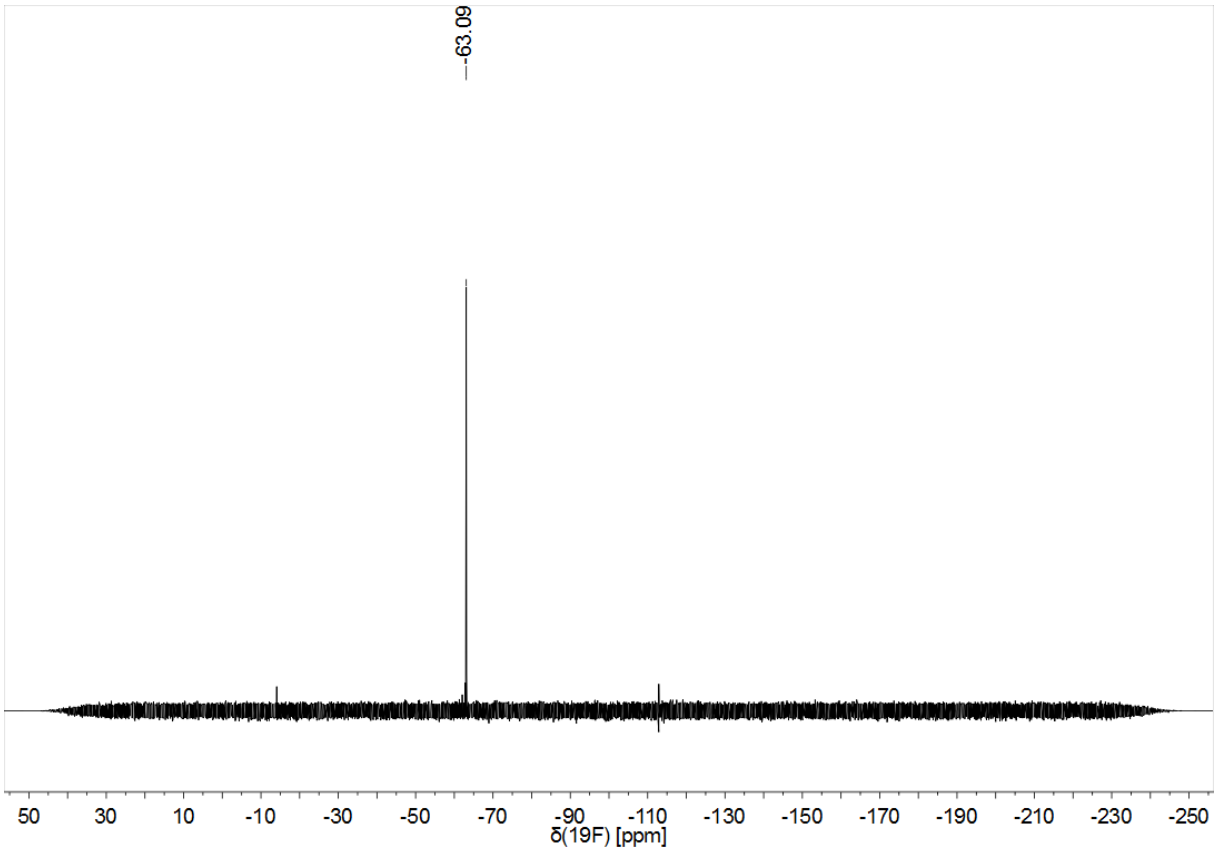
-63.09
50
30
10
-10
-30
-50
-70
-90
-110
-130
-150
-170
-190
-210
-230
-250
δ(19F) [ppm]

^{13}C

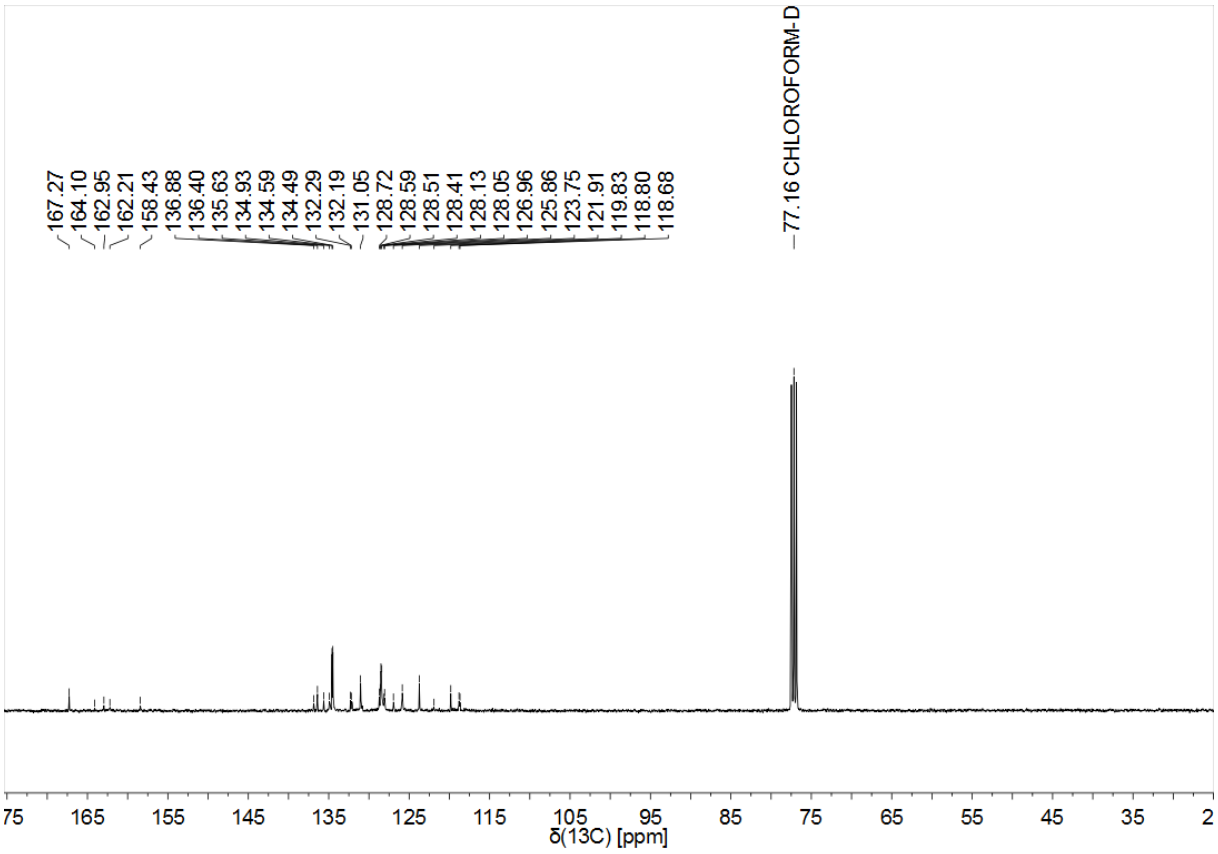

^{1}H-^{13}C-HMQC

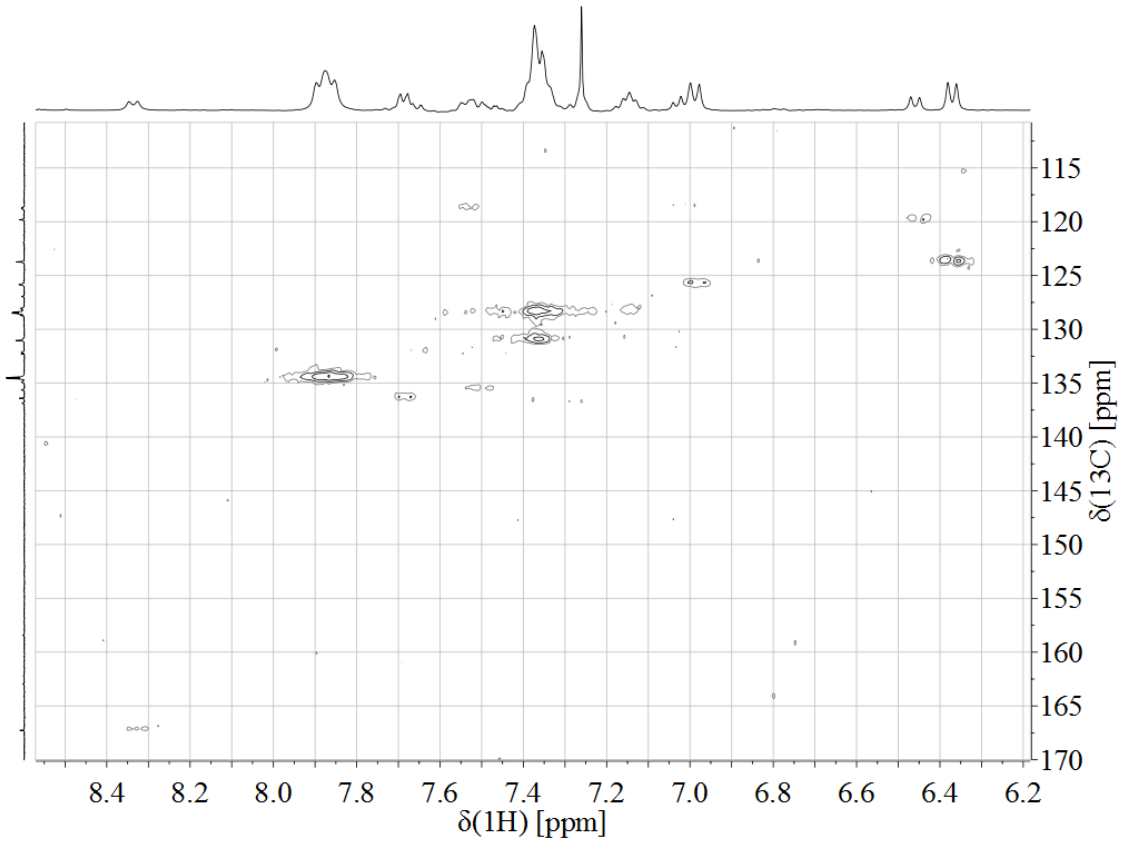

^{1}H-^{13}C-HMBC

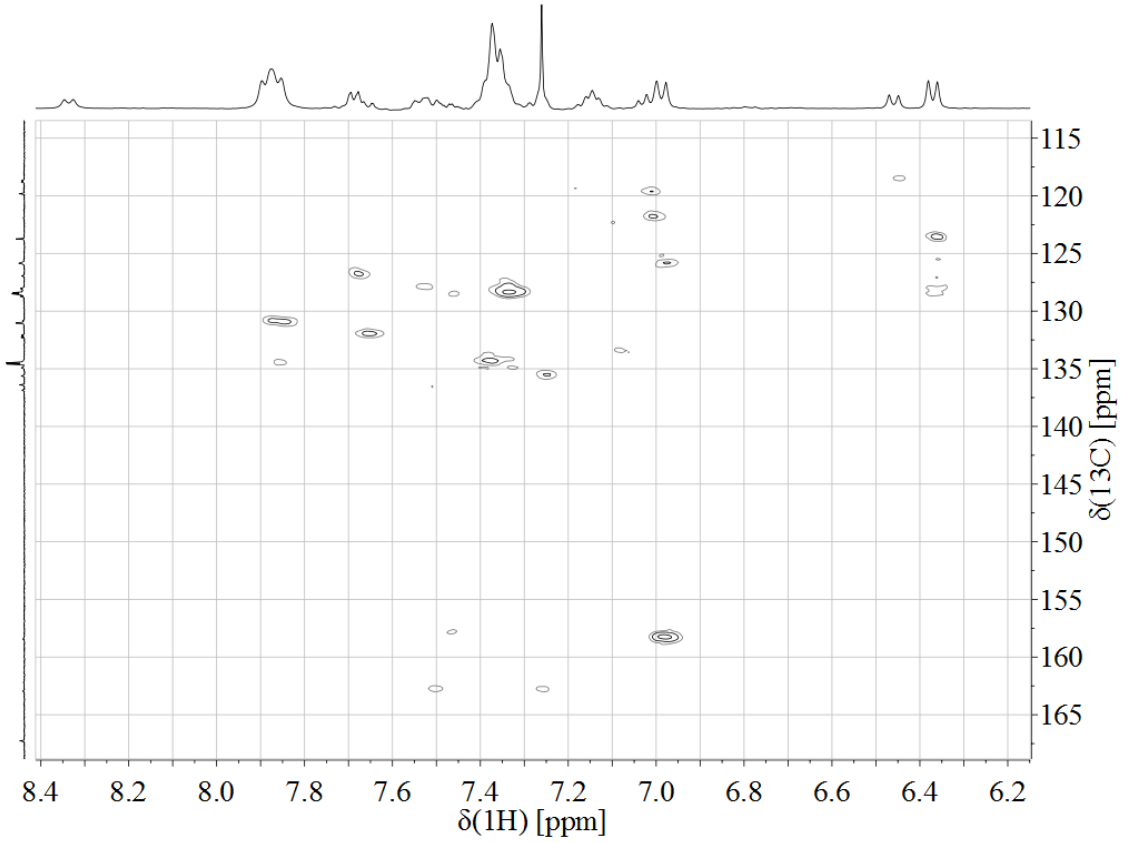

IR

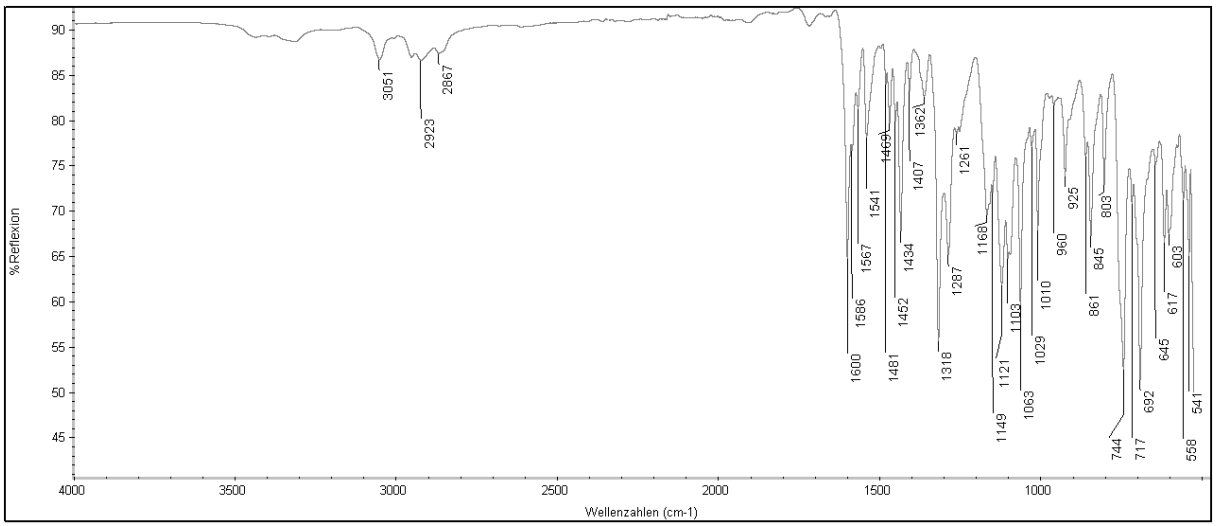

ESI+

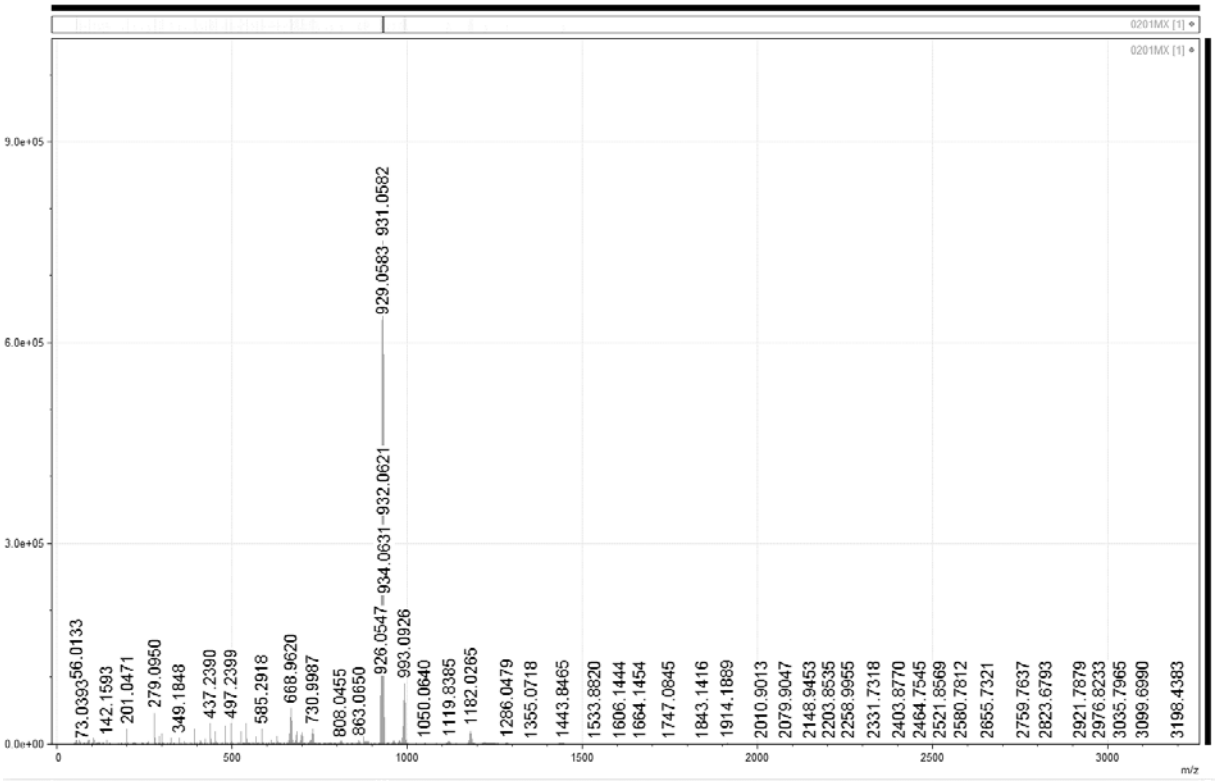
0201MX [1]
0201MX [1]
9.0e+05
6.0e+05
3.0e+05
0.0e+00
0
500
1000
1500
2000
2500
3000
m/z
929.0583
931.0582
932.0621
934.0631
926.0547
993.0926
73.0393
56.0133
142.1593
201.0471
279.0950
349.1848
437.2390
497.2399
585.2918
668.9620
730.9987
808.0455
863.0650
1050.0640
1119.8385
1182.0265
1286.0479
1355.0718
1443.8465
1533.8820
1606.1444
1664.1454
1747.0845
1843.1416
1914.1889
2010.9013
2079.9047
2148.9453
2203.8535
2258.9955
2331.7318
2403.8770
2464.7545
2521.8569
2580.7812
2655.7321
2759.7637
2823.6793
2921.7879
2976.8233
3035.7965
3099.6990
3198.4383

A.9 Reactions of Schiff Base-Substituted Diselenides and -tellurides with Ni(II), Pd(II) and Pt(II) Phosphine Complexes

Authors	M. Roca Jungfer, E. Schulz Lang, U. Abram
Journal	*Eur. J. Inorg. Chem.* **2020**, 4303–4312
DOI	10.1002/ejic.202000750
Link	https://chemistry-europe.onlinelibrary.wiley.com/doi/full/10.1002/ejic.202000750
Detailed scientific contribution	Maximilian Roca Jungfer designed the project. Maximilian Roca Jungfer performed the synthesis and characterization of the compounds, performed DFT calculations, calculated the X-ray structures and wrote a draft of the manuscript. Ernesto Schulz Lang provided guidance and the laboratory space to perform some of the experiments in Brazil. Ulrich Abram supervised the project, provided scientific guidance and suggestions and corrected the manuscript.
Estimated own contribution	80%

Return to publication 4.9.

European Journal of Inorganic Chemistry

Supporting Information

Reactions of Schiff Base-Substituted Diselenides and -tellurides with Ni(II), Pd(II) and Pt(II) Phosphine Complexes

Maximilian Roca Jungfer, Ernesto Schulz Lang, Ulrich Abram*

Table of Contents

Part 1: Crystallographic data

Table S1.1 Crystal data and structure determination parameters of the metal-containing compounds.

	[Ni(L^{Se})(PPh_3)]	[Ni(L^{Te})(PPh_3)]	[Pd(L^{Se})(PPh_3)]	[Pd(L^{Te})(PPh_3)]	[Pt(L^{Se})(PPh_3)]	[Pt(L^{Te})(PPh_3)]
Formula	$C_{31}H_{24}NNiOPSe$	$C_{31}H_{24}NNiOPTe$	$C_{31}H_{24}NOPPdSe$	$C_{31}H_{24}NOPPdTe$	$C_{31}H_{24}NOPPtSe$	$C_{31}H_{24}NOPPtTe$
Mw/g·mol^{-1}	595.15	643.79	642.84	691.48	731.53	780.17
Crystal system	Triclinic	Triclinic	Triclinic	Triclinic	Triclinic	Triclinic
a/Å	10.1784(8)	10.2299(7)	8.9709(3)	9.0114(3)	8.8500(4)	10.2046(10)
b/Å	11.1667(10)	11.4728(9)	10.1658(4)	10.4780(4)	10.1196(5)	11.7555(10)
c/Å	11.6562(10)	11.8807(9)	14.6310(6)	14.6345(5)	14.5352(7)	11.8136(13)
α/°	105.184(3)	105.048(6)	101.0730(10)	100.8770(10)	101.290(2)	106.026(8)
β/°	91.121(3)	91.346(6)	92.1640(10)	93.3130(10)	92.701(2)	91.708(8)
γ/°	103.802(2)	103.536(6)	96.479(2)	96.5050(10)	96.332(2)	103.324(7)
V/Å^3	1236.90(18)	1303.88(17)	1298.67(9)	1343.80(8)	1265.61(10)	1318.8(2)
Space group	$P\bar{1}$	$P\bar{1}$	$P\bar{1}$	$P\bar{1}$	$P\bar{1}$	$P\bar{1}$
Z	2	2	2	2	2	2
$\rho_{calc.}$/g·cm^{-3}	1.598	1.640	1.644	1.709	1.920	1.965
μ/mm^{-1}	2.347	1.927	2.203	1.839	7.071	6.490
No. reflect.	39444	11354	22348	35500	14769	11559
No. indep.	5488	5630	7908	8214	5558	5163
$R_{int.}$	0.0341	0.0415	0.0307	0.0340	0.0373	0.1152
No. param.	325	329	329	329	317	319
GOOF	1.055	0.669	1.008	0.998	1.060	0.615
R_1/wR_2	0.0205/0.0527	0.0300/0.0657	0.0329/0.0732	0.0329/0.0624	0.0258/0.0461	0.0463/0.0679
CCDC	2021656	2021657	2021658	2021659	2021660	2021661

Table S1.2 Crystal data and structure determination parameters of {[(HO)C_6H_4-(CHN$^+$H)-C_6H_4-TeI_2] · $OPPh_3$}.

Formula	$C_{31}H_{26}I_2NO_2PTe$
Mw/g·mol^{-1}	856.90
Crystal system	Triclinic
a/Å	9.426(3)
b/Å	10.262(4)
c/Å	16.160(5)
α/°	87.835(10)
β/°	79.045(16)
γ/°	81.366(10)
V/Å^3	1517.3(9)
Space group	$P\bar{1}$
Z	2
$\rho_{calc.}$/g·cm^{-3}	1.876
μ/mm^{-1}	3.096
No. reflect.	23561
No. indep.	6658
$R_{int.}$	0.0392
No. param.	353
GOOF	1.042
R_1/wR_2	0.0259/0.0471
CCDC	2021662

Figure S1.3 Ellipsoid representations (50% probability) of [Ni(L^{Se})(PPh_3)]. Hydrogen atoms are omitted for clarity.

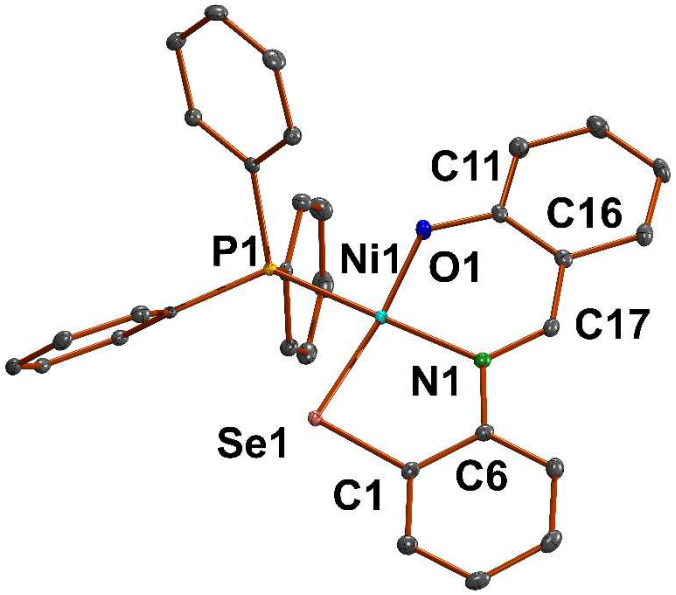

Figure S1.4 Ellipsoid representations (50% probability) of [Ni(L^{Te})(PPh_3)]. Hydrogen atoms are omitted for clarity.

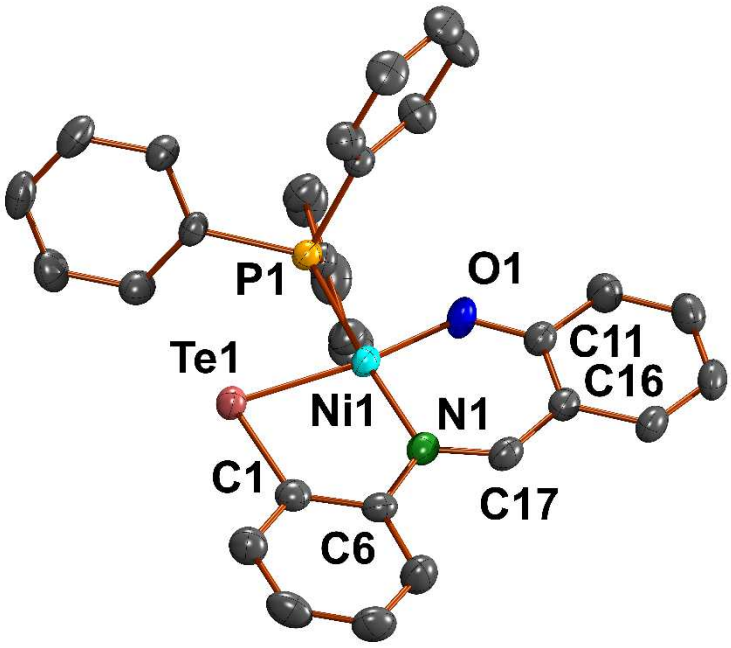

Figure S1.5 Ellipsoid representations (50% probability) of [Pd(L^{Se})(PPh_3)]. Hydrogen atoms are omitted for clarity.

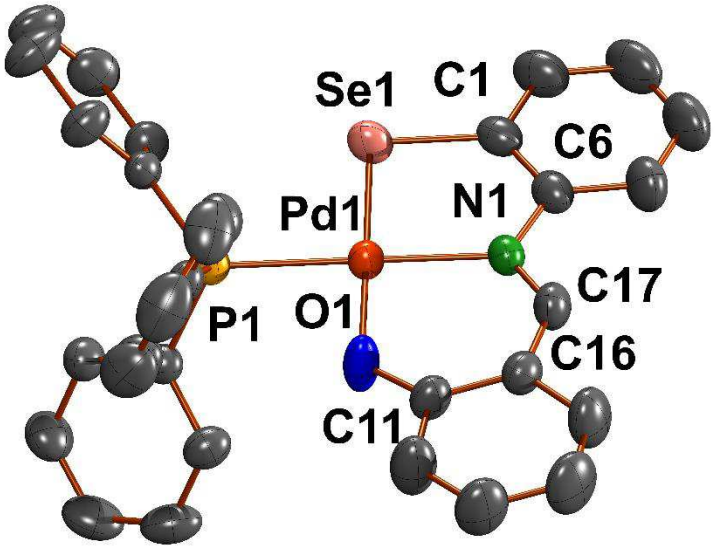

Figure S1.6 Ellipsoid representations (50% probability) of [Pd(L^{Te})(PPh_3)]. Hydrogen atoms are omitted for clarity.

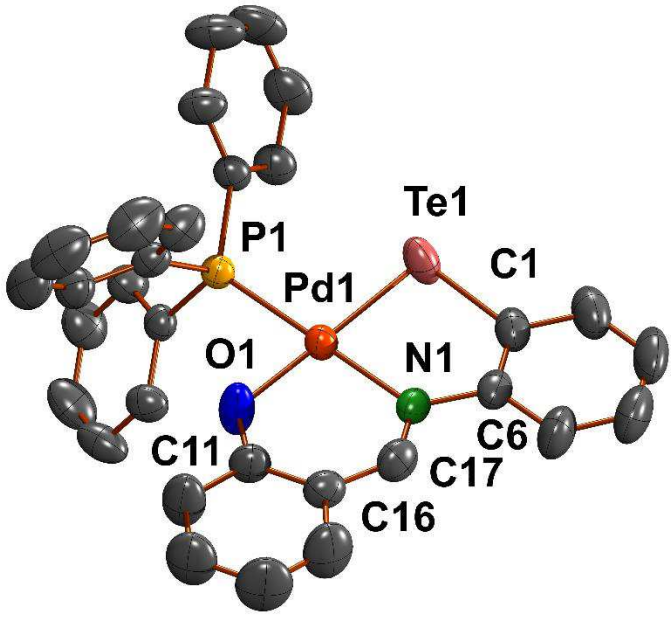

Figure S1.7 Ellipsoid representations (50% probability) of [Pt(L^{Se})(PPh_3)]. Hydrogen atoms are omitted for clarity.

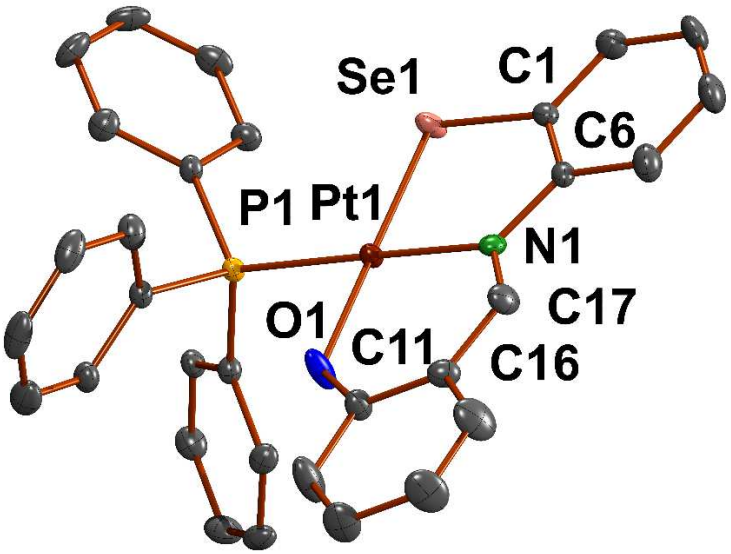

Figure S1.8 Ellipsoid representations (50% probability) of [Pt(L^{Te})(PPh_3)]. Hydrogen atoms are omitted for clarity.

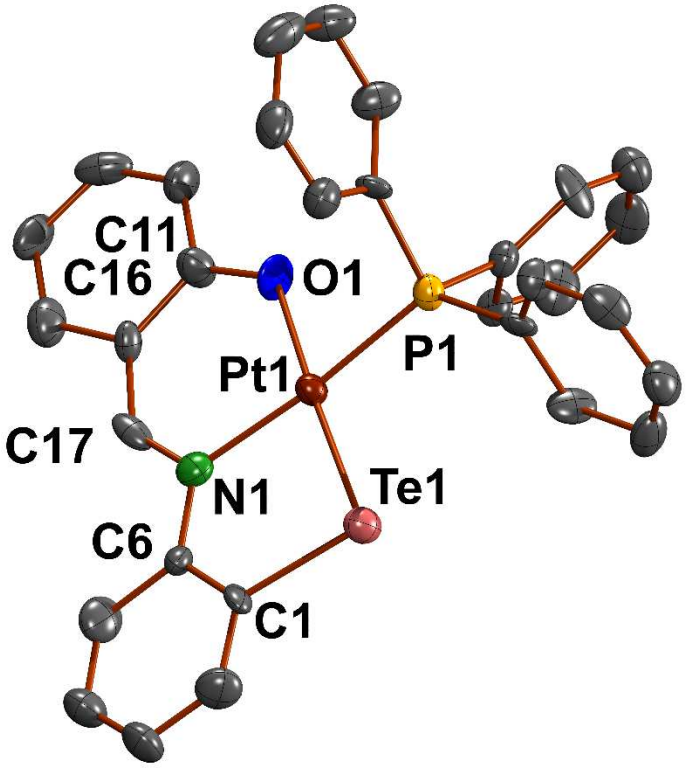

Table S1.9 Data on literature known [M(L^Y)(PPh_3)] (M = Ni, Pd, Pt; Y = O, S) complexes with exception of the non-existing [Pt(L^S)(PPh_3)], which is used in the following comparisons.[1-5]

	NiO	NiS	PdO	PdS	PtO
V		1242.95(9)	2486.4(3)	1317.0(4)	
spgrp	P21/n	P-1	P21/n	P-1	P21/n
a	15.3470(9)	8.9703(4)	15.486(1)	9.041(2)	15.721(4)
b	9.1090(3)	9.9644(4)	9.0872(7)	10.125(2)	9.106(2)
c	18.246(1)	14.3335(6)	18.350(1)	14.7840(2)	18.500(5)
alpha	90	99.836(1)	90	101.249(2)	90
beta	105.959(7)	94.904(1)	105.655(1)	92.357(2)	106.05(2)
gamma	90	97.785(1)	90	96.148(2)	90
Y1-C1	1.322	1.751(1)		1.789(4)	1.31(1)
O1-C11	1.3129	1.300(1)		1.326(4)	1.32(2)
N1-C6	1.4036	1.427(1)		1.447(5)	1.49(2)
N1-C17	1.2925	1.305(1)		1.317(5)	1.19(2)
M1-O1	1.8225	1.8496(9)	1.948(3)	2.046(3)	1.964(9)
M1-N1	1.8783	1.910(1)	2.006(4)	2.078(3)	2.06(1)
M1-P1	2.2496	2.2164(3)	2.298(1)	2.3056(9)	2.248(3)
M1-Y1	1.8487	2.1359(3)	2.019(3)	2.277(1)	2.005(9)
O1-M1-N1	95.513	95.37(4)	83.7(1)	93.6(1)	94.8(4)
O1-M1-P1	90.981	82.58(3)	91.55(7)	83.67(8)	91.5(2)
O1-M1-Y1	174.646	173.98(3)	176.6(1)	179.03(9)	176.1(4)
N1-M1-P1	171.513	174.75(3)	174.5(1)	176.44(8)	172.4(3)
N1-M1-Y1	86.731	89.32(3)	95.1(1)	86.47(8)	82.4(4)
Y1-M1-P1	87.273	93.06(1)	89.85(9)	96.35(4)	91.5(2)
C1-Y1-M1	111.9	98.64(4)		98.7(1)	113.5(7)

Analysis S1.10 Comparison of bond angles in [M(L^Y)(PPh_3)] (M = Ni, Pd, Pt; Y = O, S, Se, Te) complexes with exception of the non-existing [Pt(L^S)(PPh_3)].

Comparison of the metal-centered angles sorted by metal:

	O	S	Se	Te
O1-Ni1-N1	95.513	95.37	96.46	96.8
O1-Ni1-P1	90.981	82.58	80.75	81.01
O1-Ni1-Y1	174.646	173.98	172.88	172.18
N1-Ni1-P1	171.513	174.75	174.79	175.01
N1-Ni1-Y1	86.731	89.32	90.63	91.02
Y1-Ni1-P1	87.273	93.06	92.14	91.18
O1-Pd1-N1	83.7	93.6	93.35	93.29
O1-Pd1-P1	91.55	83.67	84.13	84.5
O1-Pd1-Y1	176.6	179.03	179.14	178.85
N1-Pd1-P1	174.5	176.44	176.49	176.22
N1-Pd1-Y1	95.1	86.47	87.2	87.82
Y1-Pd1-P1	89.85	96.35	95.35	94.4
O1-Pt1-N1	94.8		93.3	94.2
O1-Pt1-P1	91.5		83.34	81.9
O1-Pt1-Y1	176.1		179.48	177.7
N1-Pt1-P1	172.4		175.71	174.8
N1-Pt1-Y1	82.4		86.75	88.1
Y1-Pt1-P1	91.5		96.63	95.85

Graphical representation of the metal-centered angles sorted by metal (1 = O, 2 = S, 3 = Se, 4 = Te):

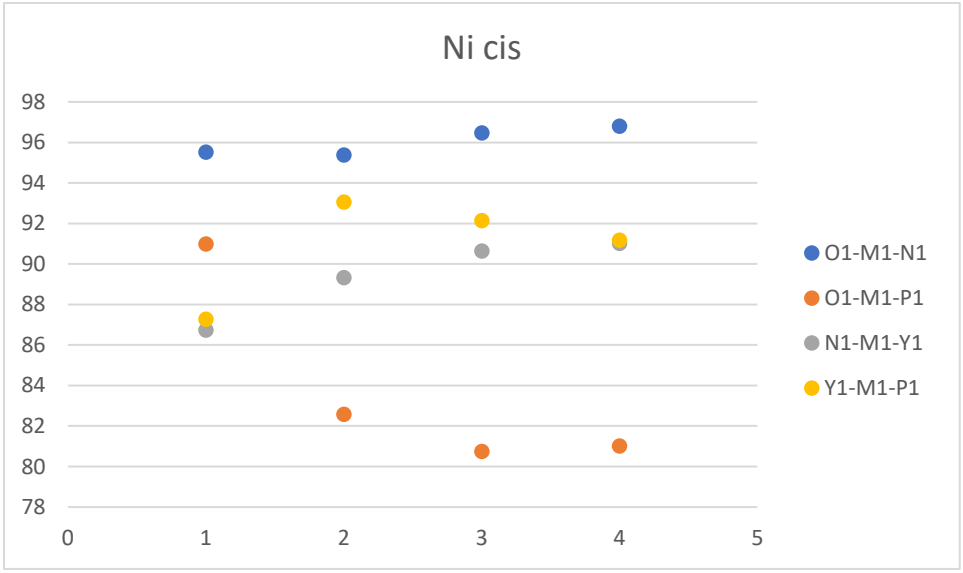

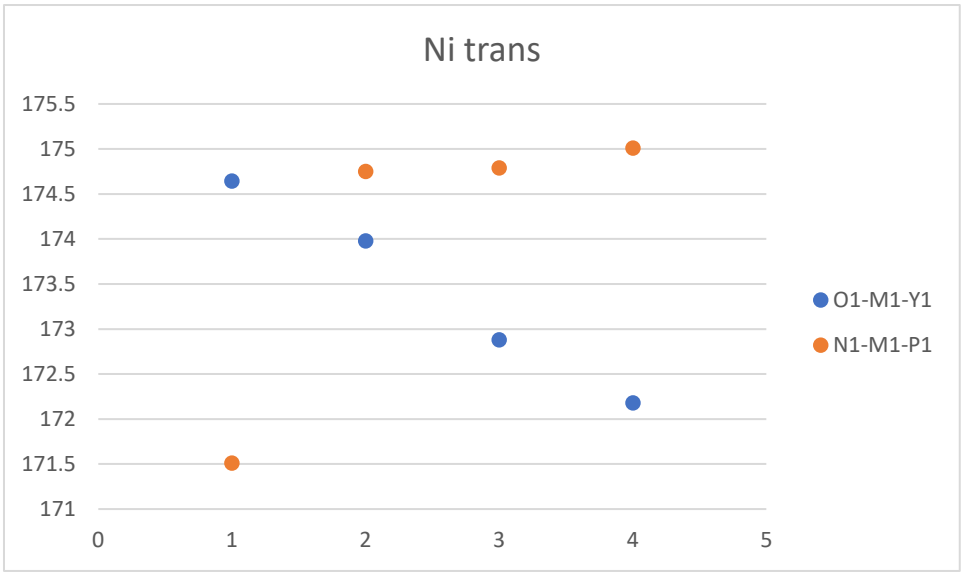
Ni trans
175.5
175
174.5
174
173.5
173
172.5
172
171.5
171
0
1
2
3
4
5
O1-M1-Y1
N1-M1-P1

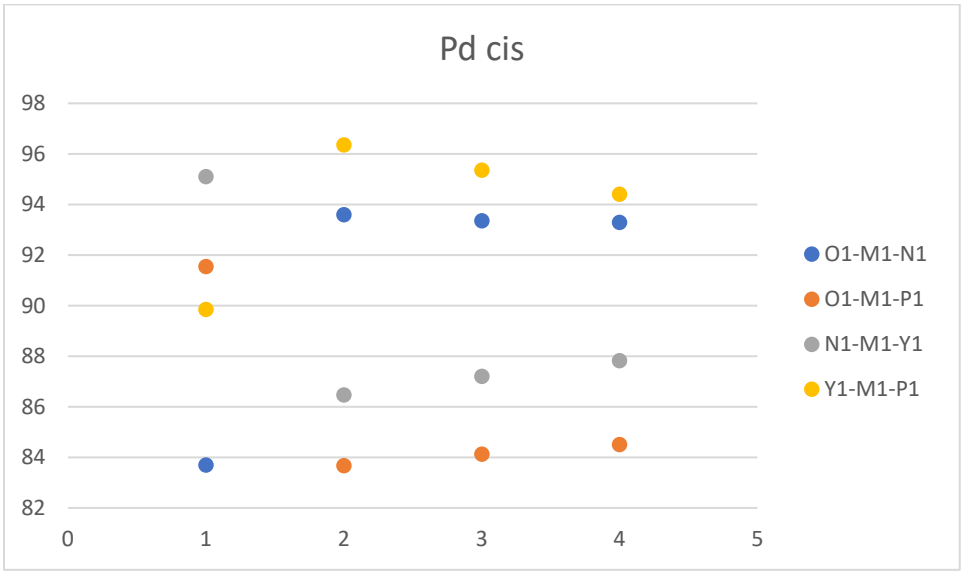
Pd cis
98
96
94
92
90
88
86
84
82
0
1
2
3
4
5
O1-M1-N1
O1-M1-P1
N1-M1-Y1
Y1-M1-P1

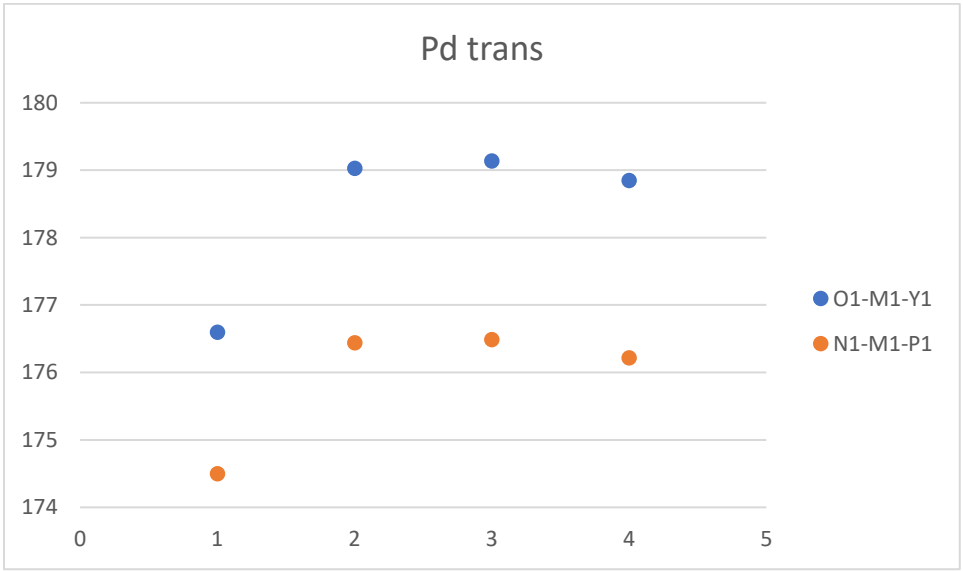
Pd trans
180
179
178
177
176
175
174
0
1
2
3
4
5
O1-M1-Y1
N1-M1-P1

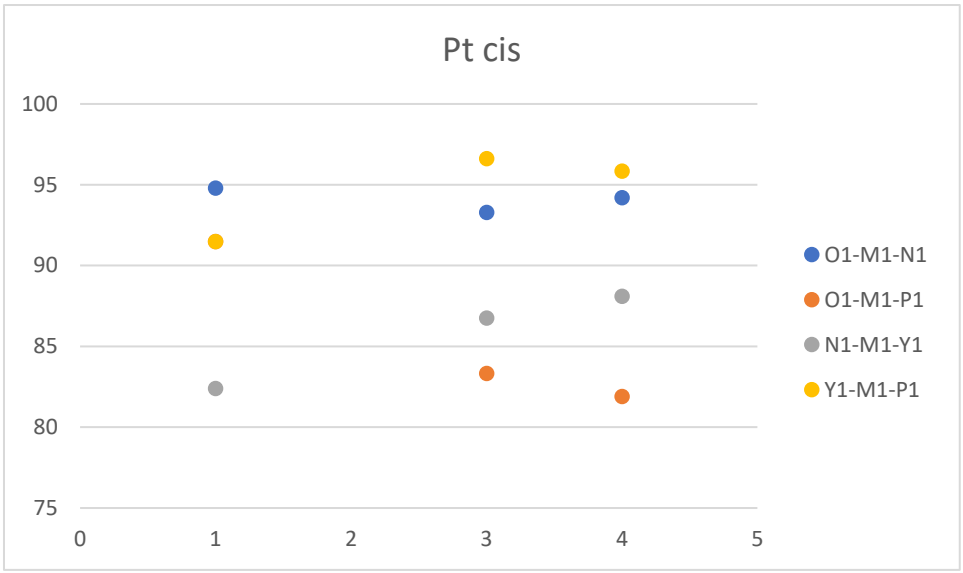

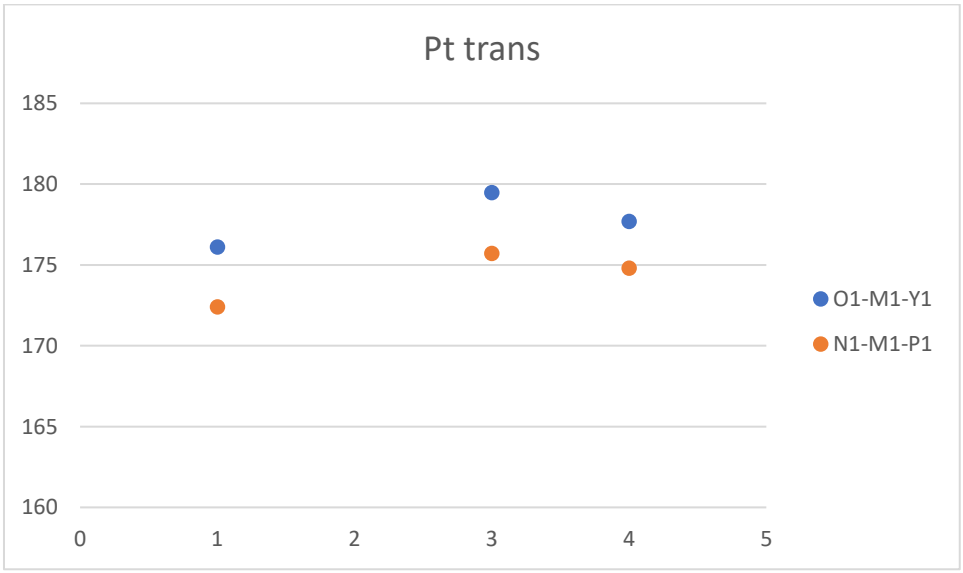

Comparison of the metal-centered angles sorted by chalcogen:

	O	S	Se	Te
O1-Ni1-N1	95.513	95.37	96.46	96.8
O1-Pd1-N1	83.7	93.6	93.35	93.29
O1-Pt1-N1	94.8		93.3	94.2
O1-Ni1-P1	90.981	82.58	80.75	81.01
O1-Pd1-P1	91.55	83.67	84.13	84.5
O1-Pt1-P1	91.5		83.34	81.9
O1-Ni1-Y1	174.646	173.98	172.88	172.18
O1-Pd1-Y1	176.6	179.03	179.14	178.85
O1-Pt1-Y1	176.1		179.48	177.7
N1-Ni1-P1	171.513	174.75	174.79	175.01
N1-Pd1-P1	174.5	176.44	176.49	176.22
N1-Pt1-P1	172.4		175.71	174.8
N1-Ni1-Y1	86.731	89.32	90.63	91.02
N1-Pd1-Y1	95.1	86.47	87.2	87.82

710

N1-Pt1-Y1	82.4		86.75	88.1
Y1-Ni1-P1	87.273	93.06	92.14	91.18
Y1-Pd1-P1	89.85	96.35	95.35	94.4
Y1-Pt1-P1	91.5		96.63	95.85

Graphical representation of the metal-centered angles sorted by chalcogen (1 = Ni, 2 = Pd, 3 = Pt):

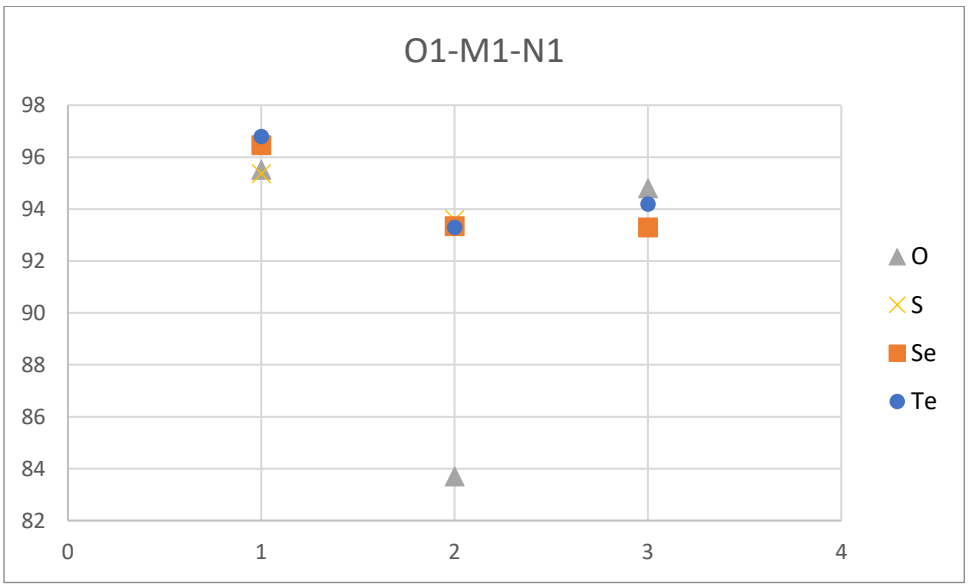

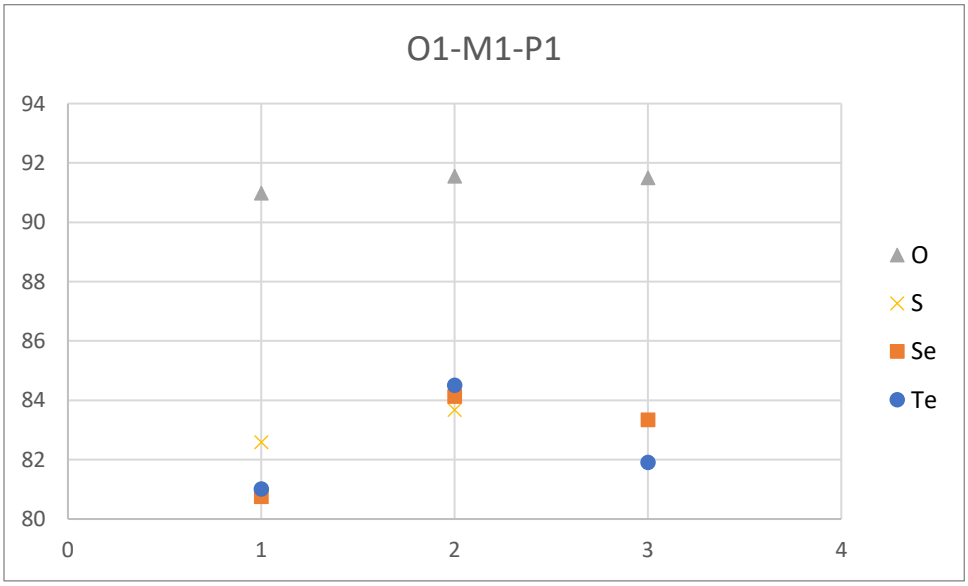

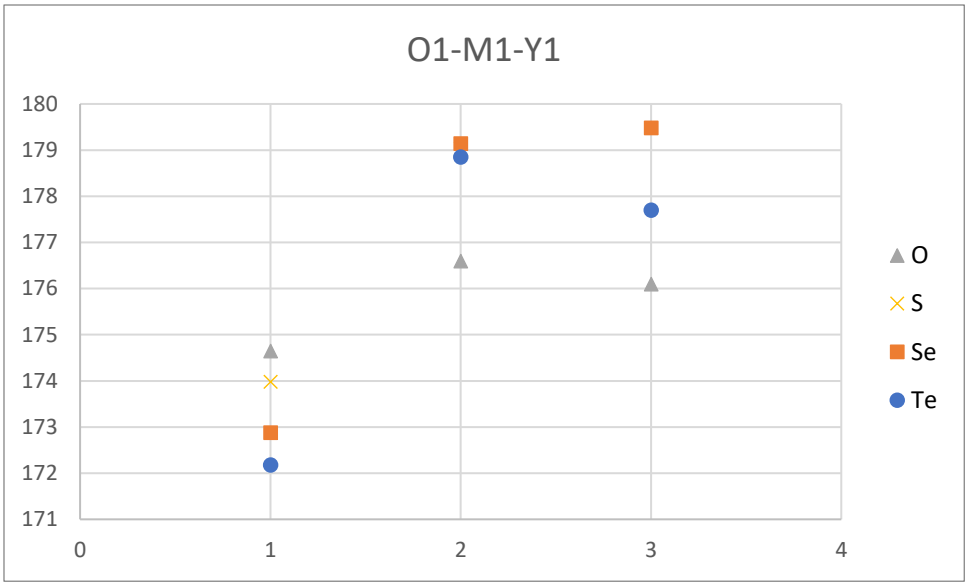
O1-M1-Y1
180
179
178
177
176
175
174
173
172
171
0
1
2
3
4
O
S
Se
Te

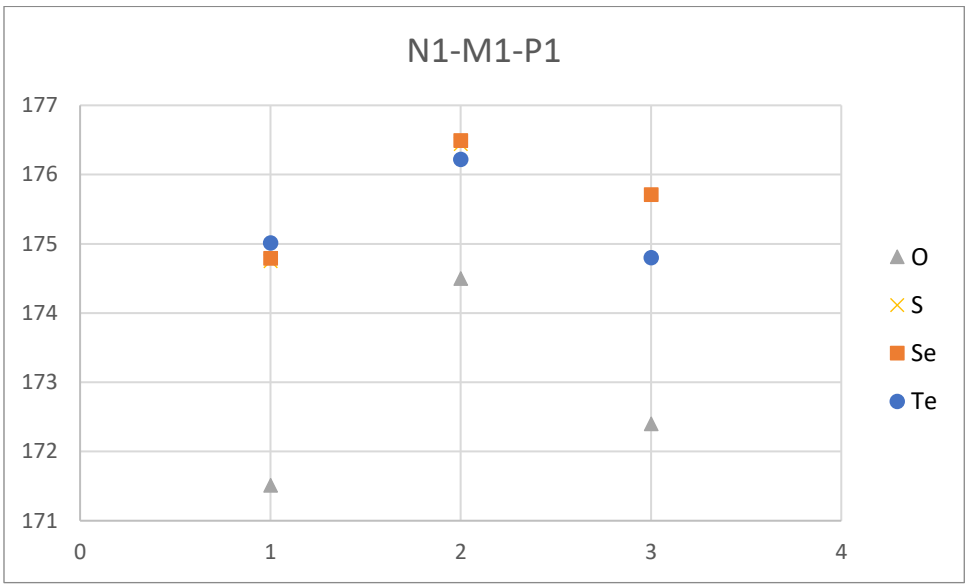
N1-M1-P1
177
176
175
174
173
172
171
0
1
2
3
4
O
S
Se
Te

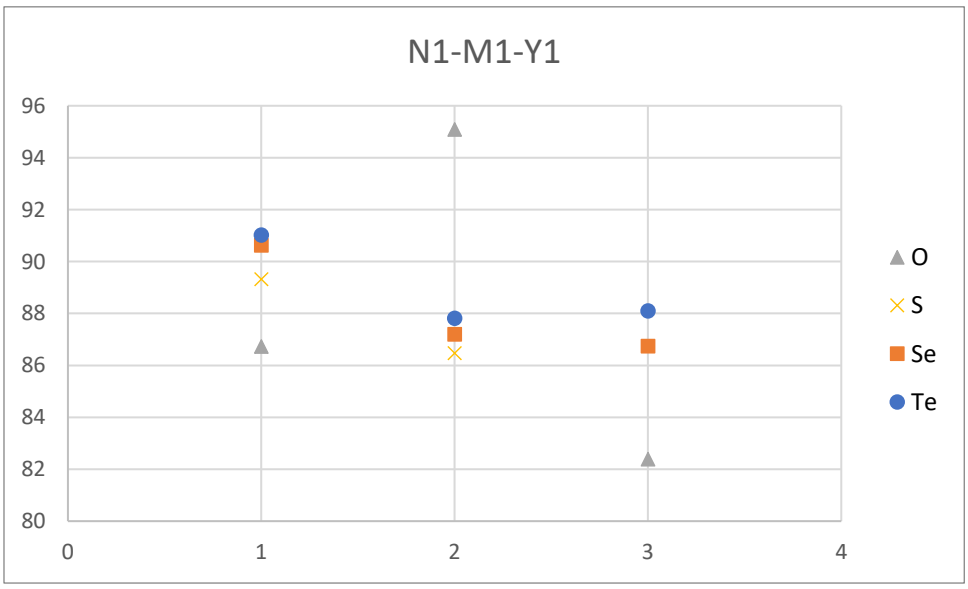
N1-M1-Y1
96
94
92
90
88
86
84
82
80
0
1
2
3
4
O
S
Se
Te

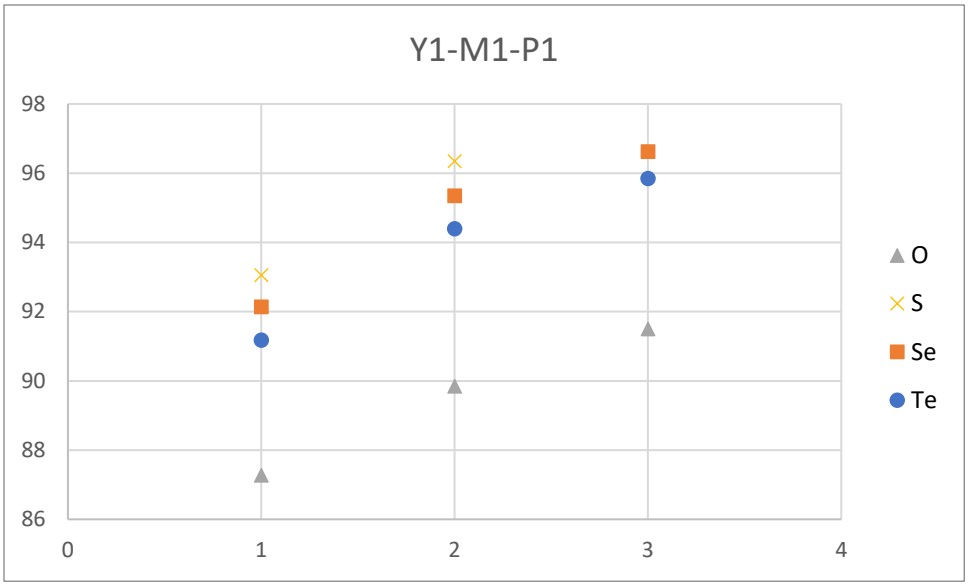

Table S1.11 Comparison of cell parameters in [M(L^Y)(PPh_3)] (M = Ni, Pd, Pt; Y = O, S, Se, Te) complexes with exception of the non-existing [Pt(L^S)(PPh_3)].

M	Y	a	b	c	α	β	γ	spacegroup
Ni	O	15.3470(9)	9.1090(3)	18.246(1)	90	105.959(7)	90	P21/n
Ni	S	8.9703(4)	9.9644(4)	14.3335(6)	99.836(1)	94.904(1)	97.785(1)	P-1
Ni	Se	10.1784(8)	11.1667(10)	11.6562(10)	105.184(3)	91.121(3)	103.802(2)	P-1
Ni	Te	10.2299(7)	11.4728(9)	11.8807(9)	105.048(6)	91.346(6)	103.536(6)	P-1
Pd	O	15.486(1)	9.0872(7)	18.350(1)	90	105.655(1)	90	P21/n
Pd	S	9.041(2)	10.125(2)	14.7840(2)	101.249(2)	92.357(2)	96.148(2)	P-1
Pd	Se	8.9709(3)	10.1658(4)	14.6310(6)	101.0730(10)	92.1640(10)	96.479(2)	P-1
Pd	Te	9.0114(3)	10.4780(4)	14.6345(5)	100.8770(10)	93.3130(10)	96.5050(10)	P-1
Pt	O	15.721(4)	9.106(2)	18.500(5)	90	106.05(2)	90	P21/n
Pt	S							
Pt	Se	8.8500(4)	10.1196(5)	14.5352(7)	101.290(2)	92.701(2)	96.332(2)	P-1
Pt	Te	10.2046(10)	11.7555(10)	11.8136(13)	106.026(8)	91.708(8)	103.324(7)	P-1

Figure S1.12 Ellipsoid representations (50% probability) of $\{H_2L^{Te}I_2\}\cdots OPPh_3$. Hydrogen atoms bonded to carbon atoms are omitted for clarity. Hydrogen-acceptor contacts are represented by dashed bonds and their lengths in Å are given.

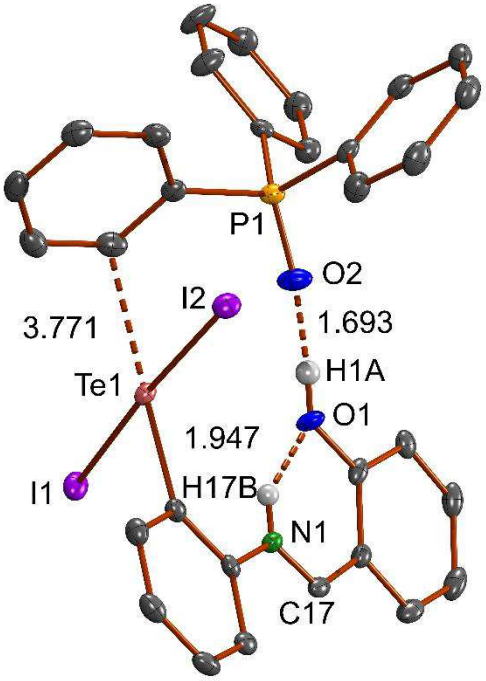

Table S1.13 Hydrogen bonds for $\{H_2L^{Te}I_2\}\cdots OPPh_3$ (Å and °).

D-H···A	d(D-H)	d(H···A)	d(D···A)	<(DHA)
N1—H17B···O1	0.80(3)	1.95(3)	2.604(3)	138(3)
O1—H1···O2	0.81(4)	1.70(4)	2.506(3)	171(4)

Part 2: Computational data on mechanism in CH_2Cl_2 solution

To give a further rationale on the reduction mechanism and why the reduction of $\{HL^{Se}\}_2$ with PPh_3 without the presence of metal ions is neglectable as we observed earlier,[6] we performed a series of DFT calculations on the B3LYP level for the reactions of free $\{HL^{Se}\}_2$ and metal-bound $\{HL^{Se}\}_2$, in the form of $[Pd\{L^{Se}\text{-}HL^{Se}\}(PPh_3)]^+(OAc)^-$, with PPh_3 and H_2O in CH_2Cl_2 solution. Both, a di(organoseleno)phosphorane and an organoselenophosphonium-organoselenolate ion pair were considered as possible intermediates in these reactions. However, the phosphorane intermediates, which were stable intermediates in the gas-phase, did not converge with the solvation model. Therefore, we assume that the ion-pair structures resemble the intermediates in solution better. Apparently, the release of the phosphonium species is favored for the metal-bound reaction, while it is energetically disfavored for the reaction of free $\{HL^{Se}\}_2$. This is probably due to the stabilization of the complementarily released $\{HL^{Se}\}^-$ anion by the coordination to the metal-ion. Furthermore, the energy surface in the metal-bound reaction is probably much smoother, resulting in more accessible reaction intermediates compared to the reaction of free dichalcogenide. Additionally, the polarization in the Se-Se bond increases by the metal coordination and leads to an increased electrophilicity of the selenium atoms. This charge is rather concentrated on the σ-hole of the Se-Se bond and significantly more accessible on the surface of the non-metal-bound selenium atom. Therefore, the nucleophilic attack on the coordinated diselenide is much more probable than that on the free diselenide.

Energy values are in Hartree if not specified otherwise.

Overall electronic and free energies:

	PPh_3	$OPPh_3$	H_2O	$\{HL^{Se}\text{-}PPh_3\}^+$	$\{HL^{Se}\}^-$	$\{HL^{Se}\}_2$	H_2L^{Se}	$\{HL^{Se}\text{-}P(OH)Ph_3\}$ + H_2L^{Se}
	1	**2**	**3**	**4**	**5**	**6**	**7**	**8**
E	-1036.28689	-1111.54394	-76.413245	-4068.78777	-3032.78994	-6065.34317	-3033.26011	-7178.004932
ΔG	-1036.05793	-1111.31043	-76.409818	-4068.37424	-3032.63479	-6065.00692	-3033.09653	-7177.404105
	HOAc	OAc^-	*trans*-$Pd(OAc)_2(PPh_3)_2$	$\{HL^{Se}\text{-}P(OH)Ph_3\}$	$[Pd(L^{Se})(PPh_3)]$	$[Pd\{L^{Se}\text{-}HL^{Se}\}(PPh_3)]^+$	$[Pd\{L^{Se}\}_2(PPh_3)]$	$\{HL^{Se}\text{-}P(OH)Ph_3\}$ + HOAc
	9	**10**	**11**	**12**	**13**	**14**	**15**	**16**
E	-229.015909	-228.586077	-2656.38053	-4144.75123	-4195.19556	-7227.67869	-7227.1985	-4373.838793
ΔG	-229.048706	-228.563805	-2655.80188	-4144.32742	-4194.79429	-7227.09479	-7226.6276	-4373.363277

Sums of free energies for starting materials, intermediates and products without metal:

	1+6	4+5	8	2+2x7
	A	**B**	**C**	**D**
ΣE	-7178.043302	-7177.99095	-7178.004932	-7178.06416
ΣΔG	-7177.474669	-7177.41885	-7177.404105	-7177.50349
	A-D	**A-B**	**B-C**	**C-D**
ΔΔG	0.028819	-0.055816	-0.014748	0.099383
ΔΔG [kcal/mol]	18.08419553	-35.0250688	-9.254509723	62.36377405
		B-D	**C-D**	
ΔΔG [kcal/mol]		53.1092643	62.36377405	

Sums of free energies for starting materials, intermediates and products with metal:

	3+6+11	1+3+2x9+15	1+3+9+10+14	1+3+10+14	3+4+10+13	13+16	2+7+9+13
	E	**F**	**G**	**H**	**I**	**J**	**K**
ΣE	-8798.13694	-8797.930448	-8797.98081	-8568.964901	-8568.982647	-8569.034351	-8569.01552
ΣΔG	-8797.21862	-8797.192757	-8797.175045	-8568.126339	-8568.142159	-8568.15757	-8568.24996
		E-F	**F-G**		**I-H**	**H-J**	**J-K**
ΔΔG		-0.025864	-0.017712		0.01582	0.015411	0.079539
ΔΔG [kcal/mol]		-16.22990504	-11.1144478		9.927199879	9.670548503	49.9114761
				H+9			K+9
				L			**M**
ΣΔG				-8797.175045			-8797.29867
	E-M	**F-M**	**G-M**	**E-L**	**I-K**		
ΔΔG	0.080044	0.105908	0.12362	-0.043576	0.1078		
ΔΔG [kcal/mol]	50.2283683	66.45827337	77.57272117	-27.34435284	67.6455213		

Free energies of transition state estimates:

	$[Pd[\{L^{Se}\text{-}HL^{Se}\}\cdots PPh_3](PPh_3)]^{+\ddagger}$	$[\{HL^{Se}\}_2\cdots PPh_3]^{\ddagger}$
	N	**O**
ΔG	-8263.130639	-7100.991872
	N+3+10	O+3
	P	**Q**
ΣΔG	-8568.104262	-7177.40169
	P-H	**O-A**
ΔΔG	-0.022077	-0.072979
ΔΔG [kcal/mol]	-13.85352666	-45.7950139
	P-I	**O-B**
ΔΔG	-0.037897	-0.017163
ΔΔG [kcal/mol]	-23.78072654	-10.7699451
	P-K	**O-D**
ΔΔG	-0.145697	-0.101798
ΔΔG [kcal/mol]	-91.42624783	-63.87920943

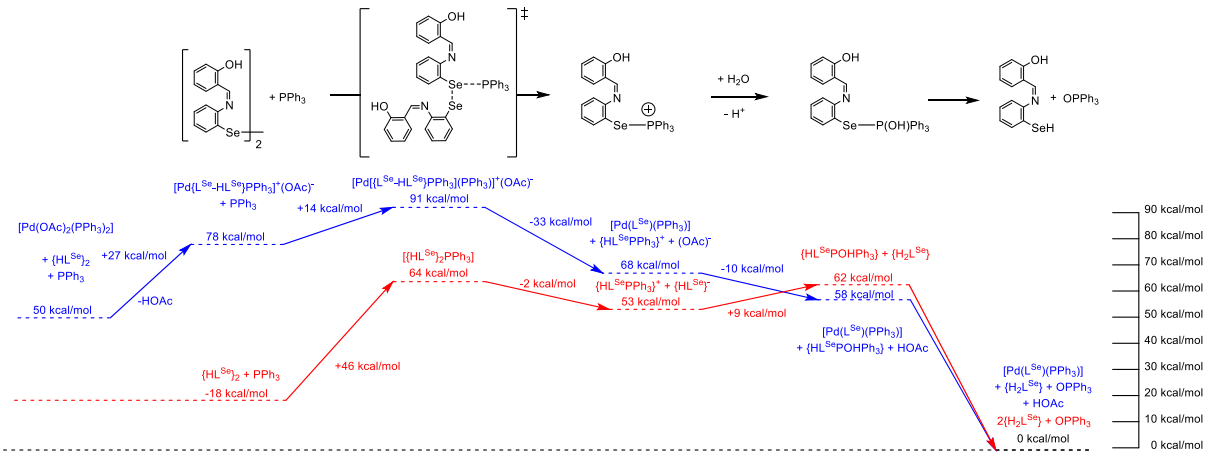

A free optimization of the transition states was not successful as the transition state structure, while visible in the scan, was not converging to a stable transition state but rather the starting materials or products. However, a scan along the reaction coordinate and subsequent optimization of the structures with frozen Se-Se-P distances corresponding to the observed maximum energy allowed for an estimation of the energy of the corresponding transition states. These estimated transition state structures show exactly one imaginary frequency along the bond path and an internal reaction coordinate scan (IRC) results in formation of either products or starting materials from these estimates. The difficulties likely arise from the functional and/or basis set, however also more sophisticated functionals (e.g. CAM-B3LYP) or larger basis sets on the heavy atoms (e.g. def2-TZVPPD) did not improve the convergence problem on the free coordinates. Alternative functionals and bigger basis sets in this system quickly became prohibitive due to the size of the system, which lead us to the estimation using an optimization with frozen Se-Se-P distances. Those possess exactly one negative frequency along the bond path and correspond to maxima on the potential energy curve between reactants and products, however only represent a rough estimate on the transition structure.

Coordinates are given in .XYZ with first energies in Hartree.

Structure S2.1. Optimized structure of $\{HL^{Se}\}_2$.
Energy: -6065.34316658

52

C	-1.68549	0.83165	1.23025
C	-0.79041	1.62784	1.94201
C	-3.05668	0.83254	1.56084
Se	-1.19432	-0.28146	-0.29608
H	0.26099	1.63675	1.67384
C	-1.24330	2.40527	3.01134
C	-3.49512	1.61001	2.64610
N	-3.91327	0.00897	0.80898
Se	1.15351	-0.38866	-0.14891
H	-0.53576	3.01215	3.56884
C	-2.59426	2.39225	3.36611
H	-4.53972	1.56857	2.94044
C	-5.12858	0.36778	0.54253
C	1.74531	1.22471	-1.07934
H	-2.94564	2.98155	4.20799
C	-6.05591	-0.48522	-0.17327
H	-5.50393	1.35235	0.84560
C	0.89663	2.13365	-1.70657
C	3.14235	1.41590	-1.11322

C	-5.69207	-1.79232	-0.60300
C	-7.35628	-0.01449	-0.45276
H	-0.17685	1.97314	-1.68988
C	1.42636	3.25354	-2.35400
C	3.65969	2.55186	-1.75760
N	3.94845	0.47490	-0.44714
C	-6.62788	-2.58072	-1.28849
O	-4.46908	-2.30614	-0.37147
C	-8.27606	-0.79877	-1.13287
H	-7.62794	0.98504	-0.12148
H	0.75568	3.96300	-2.83010
C	2.80674	3.46443	-2.37615
H	4.73089	2.73059	-1.73935
C	5.10663	0.13277	-0.91482
H	-6.33148	-3.57525	-1.60687
C	-7.90139	-2.08648	-1.54905
H	-3.94643	-1.62238	0.12970
H	-9.27264	-0.42255	-1.34059
H	3.21960	4.34310	-2.86297
C	5.99044	-0.78321	-0.22247
H	5.46238	0.52418	-1.87517
H	-8.61371	-2.70993	-2.08255
C	5.64984	-1.34111	1.04171
C	7.22443	-1.13324	-0.81031
C	6.54194	-2.21976	1.67347
O	4.48997	-1.05064	1.66135
C	8.10113	-2.00429	-0.18093
H	7.47886	-0.70335	-1.77619
H	6.26397	-2.63413	2.63748
C	7.74993	-2.54547	1.06632
H	3.99240	-0.41277	1.08093
H	9.04658	-2.26441	-0.64602
H	8.42895	-3.22913	1.56855

718

Structure S2.2. Optimized structure of PPh_3.
Energy: -1036.28688998

34

P	-0.00012	-0.00012	-1.19801
C	-1.55167	-0.62499	-0.40063
C	0.23459	1.65613	-0.40090
C	1.31709	-1.03124	-0.40090
C	-2.11217	-0.09616	0.77302
C	-2.21727	-1.68223	-1.04571
C	-0.35036	2.76084	-1.04466
C	0.97471	1.87750	0.77156
C	1.13900	-1.78305	0.77153
C	2.56616	-1.07699	-1.04493
H	-1.62154	0.72680	1.28389
C	-3.30059	-0.61726	1.29163
C	-3.39866	-2.21022	-0.52245
H	-1.80935	-2.09235	-1.96688
H	-0.91119	2.61235	-1.96473
C	-0.21711	4.04790	-0.52131
C	1.11746	3.16728	1.29015
H	1.44362	1.04135	1.28142
H	0.18060	-1.77106	1.28174
C	2.18472	-2.55162	1.28987
C	3.61429	-1.83588	-0.52177
H	2.71783	-0.51716	-1.96510
H	-3.72194	-0.19494	2.20023
C	-3.94477	-1.67649	0.64795
H	-3.89701	-3.02983	-1.03327
H	-0.67949	4.88902	-1.03098
C	0.52018	4.25436	0.64776
H	1.69532	3.32132	2.19777
H	2.02937	-3.12918	2.19746
C	3.42471	-2.57771	0.64730

H	4.57378	-1.85596	-1.03169
H	-4.86944	-2.07953	1.05208
H	0.63323	5.25667	1.05198
H	4.23632	-3.17680	1.05127

Structure S2.3. Optimized structure of H_2O.
Energy: -76.4132446651

3

O	0.00000	-0.00000	0.12030
H	0.00000	0.76028	-0.48121
H	-0.00000	-0.76028	-0.48121

Structure S2.4. Optimized structure of *trans*-$[Pd(OAc)_2(PPh_3)_2]$.
Energy: -2656.38052618

83

P	-2.41203	0.04050	0.06349
C	-3.05848	1.56169	-0.74896
C	-3.06508	0.09792	1.78220
C	-3.32839	-1.32542	-0.77256
C	-4.20167	2.22634	-0.27729
C	-2.41388	2.04079	-1.90041
C	-2.26728	0.68717	2.77824
C	-4.33653	-0.39186	2.12404
C	-3.86659	-1.14836	-2.05748
C	-3.46162	-2.57794	-0.14766
H	-4.70904	1.87510	0.61532
C	-4.69319	3.34583	-0.95093
C	-2.91404	3.15582	-2.57624
H	-1.50900	1.55838	-2.25434
H	-1.29395	1.08996	2.51821
C	-2.73406	0.77736	4.09064
C	-4.79676	-0.30044	3.43941
H	-4.96775	-0.85010	1.36993
H	-3.78121	-0.19090	-2.55970
C	-4.52603	-2.19788	-2.70104

720

C	-4.12987	-3.62056	-0.79163
H	-3.03038	-2.74598	0.83243
H	-5.57639	3.85424	-0.57413
C	-4.05344	3.81008	-2.10302
H	-2.40507	3.51764	-3.46512
H	-2.10792	1.23340	4.85253
C	-3.99634	0.28100	4.42505
H	-5.78082	-0.68582	3.69130
H	-4.93756	-2.04179	-3.69434
C	-4.66328	-3.43503	-2.06975
H	-4.23150	-4.57972	-0.29137
H	-4.43785	4.68171	-2.62551
H	-4.35500	0.34717	5.44848
H	-5.18137	-4.24909	-2.56899
Pd	0.00830	-0.04449	0.04104
P	2.41348	-0.09244	-0.02317
C	3.25149	-1.27208	1.11566
C	3.29240	1.47675	0.36942
C	2.90755	-0.54613	-1.73188
C	4.65674	-1.30125	1.19253
C	2.50243	-2.10901	1.95435
C	3.05360	2.06311	1.62410
C	4.21799	2.07169	-0.49870
C	3.70517	-1.66048	-2.02822
C	2.39634	0.23696	-2.78369
H	5.25206	-0.64169	0.56781
C	5.29659	-2.16859	2.07661
C	3.14995	-2.97258	2.84379
H	1.41820	-2.09487	1.91687
H	2.33104	1.61996	2.30265
C	3.73425	3.22037	2.00221
C	4.89472	3.23364	-0.11758
H	4.41390	1.63405	-1.47186

H	4.09589	-2.28338	-1.23090
C	4.00095	-1.97903	-3.35650
C	2.70418	-0.08189	-4.10635
H	1.75945	1.08804	-2.55656
H	6.38186	-2.18448	2.12429
C	4.54314	-3.00711	2.90460
H	2.55857	-3.61592	3.48940
H	3.54359	3.66277	2.97612
C	4.65603	3.80930	1.13116
H	5.61018	3.68492	-0.79946
H	4.61896	-2.84560	-3.57472
C	3.50564	-1.19045	-4.39612
H	2.31093	0.53208	-4.91203
H	5.04308	-3.67845	3.59738
H	5.18431	4.71176	1.42587
H	3.73786	-1.44043	-5.42770
O	0.07793	-1.96670	-0.69874
C	-0.25695	-2.94993	0.08458
O	-0.62187	-2.83466	1.26269
O	-0.04521	1.89443	0.73199
C	0.26700	2.84937	-0.10174
O	0.65260	2.69157	-1.26450
C	-0.18734	-4.31511	-0.59000
H	-0.13169	-5.10362	0.16391
H	-1.09609	-4.46406	-1.18481
H	0.66976	-4.37807	-1.26573
C	0.11994	4.23938	0.50620
H	0.85120	4.36669	1.31164
H	0.28612	5.00424	-0.25493
H	-0.87698	4.36015	0.94179

Structure S2.5. Optimized structure of $[Pd\{L^{Se}\text{-}HL^{Se}\}(PPh_3)]^+$.
Energy: -7227.67868942

86

722

Pd	1.26227	0.86217	-0.48059
N	-0.19730	2.31737	-0.83467
O	2.64175	2.26661	0.07354
P	2.99633	-0.69755	-0.07229
Se	-0.48878	-0.74362	-1.06544
C	-1.35222	1.97330	-1.58650
C	-0.07894	3.51598	-0.32049
C	2.33568	3.47630	0.46654
C	3.65775	-0.41951	1.61093
C	4.38369	-0.50384	-1.25777
C	2.54652	-2.47517	-0.16947
C	-1.68200	0.61523	-1.74694
C	-2.17072	2.92569	-2.21840
C	1.04547	4.09692	0.33796
H	-0.94248	4.17634	-0.40100
C	3.37762	4.24205	1.05980
C	5.03421	-0.45509	1.87833
C	2.75397	-0.17657	2.65928
C	4.61338	0.74033	-1.86873
C	5.23491	-1.58462	-1.54833
C	2.57548	-3.30939	0.95756
C	2.16001	-3.01011	-1.41244
C	-2.81837	0.21593	-2.45337
C	-3.30635	2.52805	-2.92204
H	-1.91018	3.97784	-2.19199
C	0.86360	5.42310	0.82944
H	4.35212	3.77194	1.14519
C	3.15754	5.52345	1.52556
H	5.74395	-0.63353	1.07730
C	5.49780	-0.25658	3.18054
C	3.22281	0.01420	3.95891
H	1.68652	-0.13377	2.45951
H	3.97112	1.58185	-1.63384

C	5.67747	0.89592	-2.75844
C	6.29898	-1.41892	-2.43596
H	5.06926	-2.55365	-1.08913
H	2.87282	-2.91548	1.92319
C	2.23063	-4.65881	0.84093
C	1.81945	-4.35765	-1.52313
H	2.14066	-2.38177	-2.29891
H	-3.04681	-0.83988	-2.55901
C	-3.64418	1.17730	-3.03482
H	-3.92074	3.28368	-3.40184
C	1.88698	6.13020	1.41883
H	-0.11812	5.87776	0.72165
H	3.97803	6.06977	1.98359
H	6.56525	-0.28234	3.37929
C	4.59541	-0.02375	4.22043
H	2.51758	0.19900	4.76388
H	5.84607	1.86045	-3.22864
C	6.51970	-0.18099	-3.04447
H	6.95152	-2.25946	-2.65343
H	2.26410	-5.29710	1.71900
C	1.85447	-5.18494	-0.39629
H	1.53057	-4.76122	-2.48905
H	-4.52424	0.87327	-3.59204
H	1.72409	7.13740	1.78769
H	4.96002	0.13181	5.23171
H	7.34521	-0.05693	-3.73952
H	1.59267	-6.23530	-0.48475
N	-4.43036	-1.28165	0.90590
Se	-1.30677	-1.18676	1.17600
C	-3.84952	-2.53812	0.71674
C	-5.39598	-0.90945	0.14359
C	-6.02869	1.26868	1.32569
C	-2.44448	-2.70223	0.82651

724

C	-4.63151	-3.69306	0.51431
C	-6.17110	0.32055	0.27935
H	-5.70101	-1.53066	-0.71192
C	-6.84344	2.40871	1.34681
C	-1.86365	-3.97292	0.71375
C	-4.04428	-4.95134	0.40171
H	-5.71214	-3.59316	0.47952
C	-7.14656	0.56966	-0.70876
H	-6.72572	3.12763	2.15486
C	-7.79445	2.62383	0.35255
H	-0.78671	-4.07582	0.79795
C	-2.65766	-5.09834	0.49707
H	-4.67516	-5.82268	0.24974
C	-7.95256	1.70067	-0.68650
H	-7.26187	-0.15773	-1.50856
H	-8.41410	3.51511	0.39287
H	-2.19974	-6.07954	0.41889
H	-8.69422	1.86286	-1.46195
O	-5.10468	1.05080	2.29384
H	-5.14287	1.78262	2.93305

Structure S2.6. Optimized structure of [Pd{L^{Se}}$_2$(PPh_3)].
Energy: -7227.19849506

85

Pd	-1.39609	0.92673	0.24562
N	-0.57644	2.82368	-0.04868
O	-3.30678	1.63192	-0.00784
P	-2.44047	-1.16192	0.63677
Se	0.92258	0.16746	0.37080
C	0.76992	3.05708	0.34159
C	-1.26909	3.77189	-0.62574
C	-3.59806	2.75615	-0.60846
C	-3.56633	-1.52507	-0.76108
C	-3.45426	-1.14705	2.16991

C	-1.36072	-2.63505	0.82266
C	1.63257	1.95879	0.51088
C	1.28094	4.34078	0.59748
C	-2.65771	3.78519	-0.95984
H	-0.73323	4.68436	-0.88878
C	-4.96659	2.98053	-0.92904
C	-4.85143	-2.05014	-0.56202
C	-3.11500	-1.27463	-2.06829
C	-4.00143	0.05971	2.63722
C	-3.70320	-2.33651	2.87676
C	-1.42901	-3.72308	-0.05971
C	-0.44930	-2.67409	1.89381
C	2.97895	2.12867	0.83434
C	2.62324	4.51168	0.93399
H	0.62960	5.20690	0.56048
C	-3.12751	4.95305	-1.62812
H	-5.67380	2.20486	-0.65254
C	-5.37957	4.12666	-1.57964
H	-5.21531	-2.24167	0.44218
C	-5.67148	-2.32577	-1.65845
C	-3.93612	-1.55824	-3.15957
H	-2.12481	-0.85723	-2.23227
H	-3.82819	0.97733	2.08618
C	-4.78135	0.07220	3.79474
C	-4.48730	-2.31592	4.03124
H	-3.28496	-3.27687	2.53347
H	-2.12914	-3.71288	-0.88796
C	-0.60063	-4.83224	0.12889
C	0.37321	-3.78474	2.07784
H	-0.39113	-1.84620	2.59522
H	3.63166	1.26808	0.92593
C	3.48041	3.41428	1.03777
H	2.99546	5.51354	1.12616

726

C	-4.45617	5.13067	-1.94341
H	-2.40215	5.72109	-1.88541
H	-6.43319	4.25304	-1.81562
H	-6.66681	-2.72914	-1.49582
C	-5.21612	-2.08187	-2.95575
H	-3.57903	-1.36348	-4.16666
H	-5.19744	1.01057	4.15027
C	-5.02425	-1.11235	4.49395
H	-4.67318	-3.24082	4.56961
H	-0.66398	-5.67037	-0.55888
C	0.29967	-4.86558	1.19450
H	1.07031	-3.80500	2.91033
H	4.52713	3.54531	1.29259
H	-4.78918	6.02780	-2.45480
H	-5.85737	-2.29543	-3.80614
H	-5.62867	-1.09813	5.39650
H	0.94251	-5.72918	1.33771
N	4.30860	-0.90445	-0.88948
Se	1.38906	-0.33010	-1.98451
C	3.68847	-2.03469	-1.37189
C	5.13809	-1.00574	0.11703
C	6.29521	1.26977	-0.05552
C	2.35473	-1.97541	-1.87537
C	4.34833	-3.28725	-1.46756
C	6.02221	-0.00547	0.62754
H	5.15757	-1.95174	0.68386
C	7.21650	2.15171	0.64934
C	1.72277	-3.12108	-2.38815
C	3.72066	-4.40569	-2.00183
H	5.38333	-3.35052	-1.14575
C	6.68414	-0.30919	1.85107
H	7.42699	3.10472	0.16821
C	7.81360	1.81369	1.84046

H	0.69718	-3.04786	-2.73545
C	2.40087	-4.33364	-2.46698
H	4.26643	-5.34399	-2.06332
C	7.55879	0.56239	2.46315
H	6.47533	-1.27353	2.31528
H	8.50093	2.51344	2.31475
H	1.91193	-5.20743	-2.88679
H	8.04409	0.30273	3.39960
O	5.79594	1.60004	-1.16063

Structure S2.7. Optimized structure of $\{HL^{Se}\text{-}PPh_3\}^+$.
Energy: -4068.78776738

60

N	2.46676	1.01987	-0.14872
Se	-0.22887	0.30788	-1.55533
C	1.62246	2.13259	-0.23662
C	3.70680	1.15582	-0.46584
C	4.58193	-1.16099	0.18004
C	0.31824	1.99828	-0.76881
C	2.00160	3.39735	0.25574
C	4.74952	0.14073	-0.35757
H	4.06550	2.10889	-0.87931
C	5.67011	-2.04120	0.22946
C	-0.53777	3.10171	-0.85987
C	1.13307	4.48428	0.19475
H	2.97971	3.50680	0.71384
C	6.03129	0.50031	-0.82591
H	5.52773	-3.03598	0.64552
C	6.92079	-1.65316	-0.24463
H	-1.51626	2.98891	-1.31289
C	-0.13754	4.34439	-0.36860
H	1.45253	5.44552	0.58704
C	7.10945	-0.37360	-0.77740
H	6.16492	1.49779	-1.23681

728

H	7.74917	-2.35399	-0.19556
H	-0.81304	5.19202	-0.42691
H	8.08242	-0.06668	-1.14698
O	3.36049	-1.53106	0.64226
H	3.40754	-2.44771	0.96334
P	-1.74578	-0.43269	-0.02852
C	-0.99234	-0.97939	1.53249
C	-2.50138	-1.87345	-0.84068
C	-2.99249	0.84210	0.29303
C	-1.82906	-1.58786	2.48881
C	0.38178	-0.84764	1.77243
C	-1.65575	-2.87662	-1.34930
C	-3.89500	-2.02388	-0.91856
C	-3.10937	1.42438	1.56489
C	-3.80541	1.29269	-0.76501
H	-2.89211	-1.71006	2.30319
C	-1.28601	-2.04346	3.68769
C	0.91119	-1.31299	2.97916
H	1.04856	-0.40523	1.03810
H	-0.57623	-2.78273	-1.27793
C	-2.20636	-4.00949	-1.94482
C	-4.43419	-3.16689	-1.51112
H	-4.55799	-1.26468	-0.51968
H	-2.47728	1.09695	2.38236
C	-4.04988	2.43341	1.77965
C	-4.74272	2.29719	-0.53764
H	-3.70644	0.86531	-1.75818
H	-1.93113	-2.51129	4.42497
C	0.08409	-1.90423	3.93431
H	1.97706	-1.21276	3.15861
H	-1.55093	-4.77881	-2.34088
C	-3.59425	-4.15497	-2.02737
H	-5.51228	-3.28063	-1.56813

H	-4.13902	2.87981	2.76506
C	-4.86617	2.86702	0.73426
H	-5.37324	2.63728	-1.35313
H	0.50359	-2.26367	4.86947
H	-4.01936	-5.04018	-2.49078
H	-5.59610	3.65236	0.90617

Structure S2.8. Optimized structure of $\{HL^{Se}\}^-$.
Energy: -3032.78993904

26

C	2.34023	-0.04289	-0.01774
C	3.65093	0.47846	-0.00888
C	1.27863	0.89003	0.15379
H	4.47754	-0.21392	-0.14199
C	3.91569	1.83590	0.16220
C	1.55487	2.25959	0.33420
N	-0.04566	0.41835	0.20261
H	4.94516	2.18731	0.16900
C	2.86158	2.73929	0.33814
H	0.72846	2.94325	0.51233
C	-1.02979	1.08815	-0.29552
H	3.05472	3.79745	0.49380
C	-2.40547	0.62726	-0.17812
H	-0.86913	2.02741	-0.84109
C	-2.71509	-0.61347	0.44782
C	-3.45703	1.40790	-0.69499
C	-4.05511	-1.02074	0.54519
O	-1.75957	-1.41731	0.94655
C	-4.78113	0.99788	-0.59635
H	-3.21209	2.35207	-1.17703
H	-4.27111	-1.96988	1.02666
C	-5.07251	-0.22322	0.02975
H	-0.87191	-0.97401	0.77416
H	-5.57912	1.61410	-0.99932

730

H	-6.10380	-0.55640	0.11345
Se	2.04655	-1.92183	-0.30111

Structure S2.9. Optimized structure of [{HL^{Se}}$_2$···PPh_3]‡. With frozen Se-Se-P distances (2.72 Å and 3.11 Å).
Energy: -7101.58393029

86

N	2.80837	-2.19359	-1.12528
Se	1.87688	0.02096	-3.20482
C	3.67421	-1.09397	-1.17418
C	2.36712	-2.59193	0.01131
C	1.24029	-4.77169	-0.72599
C	3.42803	-0.02267	-2.06760
C	4.85060	-1.07342	-0.40056
C	1.55472	-3.78841	0.24692
H	2.57255	-2.00999	0.92191
C	0.46724	-5.88487	-0.36690
C	4.35122	1.02988	-2.15150
C	5.77065	-0.03279	-0.51618
H	5.05126	-1.90955	0.26336
C	1.07091	-3.98108	1.55658
H	0.23742	-6.63373	-1.12192
C	0.00213	-6.04089	0.93737
H	4.14383	1.85756	-2.82307
C	5.52494	1.02366	-1.39627
H	6.67713	-0.04833	0.08286
C	0.30196	-5.08359	1.91157
H	1.31349	-3.23066	2.30509
H	-0.59161	-6.91481	1.19047
H	6.23675	1.83865	-1.49261
H	-0.05644	-5.19916	2.92950
N	1.21370	2.24753	0.58240
Se	-0.20506	0.27085	-1.47235
C	0.47420	2.92123	-0.40195

C	2.38892	2.67796	0.87056
C	2.97269	1.12383	2.82558
C	-0.25755	2.20065	-1.37866
C	0.37460	4.32690	-0.39324
C	3.26540	2.18707	1.93505
H	2.83349	3.49793	0.28759
C	3.90026	0.76182	3.81109
C	-1.03233	2.89558	-2.31711
C	-0.40639	5.00231	-1.32895
H	0.89455	4.88255	0.38169
C	4.50411	2.84392	2.08335
H	3.66122	-0.05619	4.48720
C	5.11362	1.43536	3.93038
H	-1.57769	2.33240	-3.06722
C	-1.11216	4.28841	-2.29939
H	-0.46750	6.08671	-1.29332
C	5.42382	2.48621	3.06195
H	4.73475	3.65874	1.40162
H	5.81554	1.13600	4.70358
H	-1.72685	4.80693	-3.02930
H	6.36738	3.01552	3.14869
O	1.78818	0.47000	2.70554
H	1.73418	-0.21946	3.38873
P	-2.79731	0.17942	0.24805
C	-2.70082	0.32233	2.08516
C	-3.59781	-1.46317	-0.01354
C	-4.08214	1.39727	-0.26004
C	-3.73111	-0.10519	2.94130
C	-1.52953	0.86152	2.63960
C	-2.75482	-2.58798	-0.03720
C	-4.97880	-1.64890	-0.18872
C	-4.59955	2.37234	0.60662
C	-4.48175	1.41420	-1.61007

732

H	-4.63686	-0.53969	2.52776
C	-3.59666	0.01871	4.32434
C	-1.39881	0.98327	4.02661
H	-0.71066	1.17257	1.99629
H	-1.68165	-2.46450	0.08596
C	-3.28109	-3.86810	-0.21669
C	-5.50289	-2.93036	-0.37566
H	-5.64705	-0.79353	-0.18443
H	-4.29995	2.38616	1.64943
C	-5.50620	3.32820	0.13976
C	-5.39474	2.36208	-2.07078
H	-4.08210	0.67814	-2.30317
H	-4.39965	-0.31400	4.97676
C	-2.42989	0.56538	4.86937
H	-0.48413	1.39765	4.44139
H	-2.61333	-4.72489	-0.22987
C	-4.65695	-4.04180	-0.38843
H	-6.57377	-3.05842	-0.50979
H	-5.89891	4.07399	0.82581
C	-5.90951	3.32436	-1.19643
H	-5.69943	2.35315	-3.11383
H	-2.32583	0.65790	5.94724
H	-5.06715	-5.03720	-0.53574
H	-6.61624	4.06689	-1.55656
O	1.70633	-4.62242	-1.99104
H	1.40976	-5.37845	-2.52559

Structure S2.10. Optimized structure of [Pd[{L^{Se}-HL^{Se}}⋯PPh_3](PPh_3)]$^{+\ ‡}$. With frozen Se-Se-P distances (2.72 Å and 3.11 Å).
Energy: -8263.97148561

120

Pd	2.59241	0.15773	-0.50442
N	2.50903	2.23454	-0.72460
O	3.91152	0.29653	1.06527

P	2.75262	-2.17888	-0.20756
Se	0.98732	0.08932	-2.33391
C	1.93304	2.79036	-1.89823
C	2.88898	3.01981	0.25227
C	4.10637	1.37987	1.76703
C	2.56178	-2.60583	1.56485
C	4.39926	-2.80049	-0.73104
C	1.52954	-3.21291	-1.10577
C	1.12761	1.97040	-2.71145
C	2.15976	4.11566	-2.30957
C	3.59755	2.68644	1.44609
H	2.64555	4.07827	0.15772
C	4.89168	1.25414	2.94861
C	3.21309	-3.71693	2.12242
C	1.72672	-1.81751	2.37224
C	5.51384	-1.95125	-0.62097
C	4.57371	-4.11020	-1.20932
C	0.49028	-3.86804	-0.42847
C	1.60579	-3.31230	-2.50736
C	0.49516	2.48320	-3.84865
C	1.53531	4.62101	-3.44914
H	2.84702	4.74953	-1.76048
C	3.86274	3.76984	2.33434
H	5.28520	0.26907	3.17909
C	5.12808	2.33113	3.77952
H	3.87104	-4.32913	1.51382
C	3.02244	-4.03789	3.46751
C	1.53702	-2.14395	3.71624
H	1.23530	-0.94463	1.95291
H	5.38729	-0.94470	-0.23600
C	6.78039	-2.40861	-0.98702
C	5.84449	-4.56024	-1.57250
H	3.72378	-4.77766	-1.30559

734

H	0.41153	-3.80320	0.65094
C	-0.45357	-4.61298	-1.13947
C	0.66395	-4.06266	-3.21137
H	2.40712	-2.81857	-3.04968
H	-0.13005	1.83628	-4.45586
C	0.68734	3.81553	-4.21349
H	1.72972	5.64644	-3.74880
C	4.60570	3.60917	3.48235
H	3.46017	4.74761	2.08132
H	5.72295	2.18837	4.67818
H	3.53278	-4.89771	3.89172
C	2.18485	-3.25416	4.26516
H	0.89324	-1.52534	4.33481
H	7.63602	-1.74497	-0.90060
C	6.94783	-3.71081	-1.46471
H	5.96887	-5.57396	-1.94217
H	-1.25170	-5.11517	-0.60057
C	-0.36834	-4.71302	-2.52901
H	0.73830	-4.13889	-4.29221
H	0.20536	4.20963	-5.10259
H	4.79390	4.44920	4.14295
H	2.04362	-3.50270	5.31314
H	7.93444	-4.06253	-1.75272
H	-1.10095	-5.29599	-3.07970
N	-1.88440	2.89350	-0.43442
Se	-1.29540	-0.18470	-0.88046
C	-2.48718	2.38920	-1.59350
C	-1.27883	4.02588	-0.49680
C	-0.64686	4.32184	1.96855
C	-2.35645	1.01851	-1.93855
C	-3.30650	3.20198	-2.40191
C	-0.66702	4.74972	0.61652
H	-1.16751	4.53770	-1.46325

C	-0.02893	5.11557	2.94382
C	-3.00222	0.51745	-3.07949
C	-3.94968	2.68742	-3.52519
H	-3.45536	4.23954	-2.11842
C	-0.04702	5.97870	0.30639
H	-0.02401	4.77547	3.97693
C	0.57184	6.32472	2.60190
H	-2.88117	-0.52980	-3.33541
C	-3.79583	1.34293	-3.87425
H	-4.57773	3.33887	-4.12652
C	0.56786	6.76467	1.27372
H	-0.05932	6.31054	-0.72854
H	1.04179	6.92360	3.37675
H	-4.29910	0.93770	-4.74670
H	1.03190	7.70736	1.00217
O	-1.22925	3.14046	2.29203
H	-1.13242	2.98731	3.24736
P	-3.78931	-1.07469	0.75545
C	-4.35200	-0.03712	2.16296
C	-3.45100	-2.72267	1.49944
C	-5.24974	-1.30564	-0.33025
C	-5.15069	-0.55234	3.19951
C	-3.95543	1.30867	2.20069
C	-2.25217	-2.86776	2.22059
C	-4.30489	-3.82919	1.37114
C	-6.46450	-0.63508	-0.11913
C	-5.11196	-2.12408	-1.46740
H	-5.45192	-1.59578	3.18854
C	-5.55719	0.27255	4.24833
C	-4.36639	2.12983	3.25470
H	-3.31451	1.71642	1.42384
H	-1.57387	-2.02433	2.32309
C	-1.92155	-4.08760	2.81067

736

C	-3.96670	-5.05270	1.95608
H	-5.23300	-3.74051	0.81622
H	-6.58847	0.00790	0.74588
C	-7.52376	-0.79478	-1.01596
C	-6.17576	-2.28981	-2.35338
H	-4.17314	-2.63822	-1.65657
H	-6.17542	-0.13290	5.04452
C	-5.16686	1.61543	4.27618
H	-4.04888	3.16838	3.27643
H	-0.99369	-4.18063	3.36822
C	-2.77761	-5.18518	2.67607
H	-4.63788	-5.90063	1.85086
H	-8.45946	-0.27200	-0.83818
C	-7.38469	-1.62346	-2.13069
H	-6.05852	-2.93307	-3.22104
H	-5.48203	2.25474	5.09636
H	-2.51824	-6.13753	3.12988
H	-8.21105	-1.74748	-2.82486

Structure S2.11. Optimized structure of H_2L^{Se}.
Energy: -3033.26011178

27

C	2.35336	-0.03262	-0.03371
C	3.68116	0.40083	-0.06829
C	1.31255	0.89578	0.17419
H	4.48272	-0.31072	-0.24148
C	3.98491	1.75005	0.12622
C	1.63523	2.24814	0.37902
N	-0.00516	0.40692	0.21836
H	5.02194	2.07265	0.11002
C	2.96173	2.67383	0.35328
H	0.83958	2.95600	0.59239
C	-0.99418	1.09973	-0.24861
H	3.19543	3.72079	0.52270

C	-2.37033	0.65336	-0.15921
H	-0.82281	2.06117	-0.74693
C	-2.71955	-0.57008	0.47868
C	-3.39524	1.44766	-0.71497
C	-4.06622	-0.95707	0.54278
O	-1.79338	-1.37719	1.02993
C	-4.72485	1.05803	-0.64948
H	-3.12179	2.38146	-1.20066
H	-4.31229	-1.89322	1.03419
C	-5.05258	-0.15152	-0.01607
H	-0.90516	-0.94406	0.89976
H	-5.50214	1.67985	-1.08201
H	-6.09087	-0.46690	0.04110
Se	1.84469	-1.87718	-0.30353
H	3.24308	-2.36047	-0.36018

Structure S2.12. Optimized structure of {HL^{Se}-$P(OH)Ph_3$}.
Free {HL^{Se}-$P(OH)Ph_3$}: Refined to {HL^{Se}}$^-$ + {$HOPPh_3$}$^+$; final coordinates below.

Energy: -4144.75122850

62

N	3.03831	0.69435	-0.09323
Se	0.71591	0.69221	-2.31831
C	2.23953	1.85694	-0.07186
C	4.31213	0.82778	-0.15918
C	5.04983	-1.60678	0.20715
C	1.11528	1.97423	-0.93631
C	2.51689	2.86958	0.86712
C	5.31083	-0.24652	-0.09443
H	4.75658	1.82537	-0.29862
C	6.10050	-2.53338	0.22864
C	0.30837	3.11883	-0.78387
C	1.69969	3.99259	0.98929
H	3.36754	2.74077	1.53218

738

C	6.64747	0.11879	-0.35015
H	5.88213	-3.57391	0.46047
C	7.40944	-2.13772	-0.03924
H	-0.55707	3.22305	-1.43254
C	0.58464	4.11265	0.15582
H	1.92623	4.75384	1.73157
C	7.69116	-0.80042	-0.33009
H	6.85538	1.16187	-0.57639
H	8.20571	-2.87652	-0.01745
H	-0.07284	4.97539	0.23736
H	8.70777	-0.48108	-0.53753
O	3.77567	-1.99427	0.48485
H	3.77056	-2.95093	0.65661
C	-1.78398	-1.24863	1.68437
C	-3.70962	-1.70056	-0.56102
C	-3.47081	0.98785	0.72791
C	-1.76212	-2.05449	2.83593
C	-0.58272	-0.82304	1.08932
C	-2.67039	-2.16183	-1.38624
C	-5.05212	-1.93518	-0.91343
C	-2.98011	1.83340	1.73931
C	-4.06884	1.52917	-0.42182
H	-2.68519	-2.36707	3.31272
C	-0.53807	-2.44016	3.38025
C	0.63642	-1.22762	1.63512
H	-0.57366	-0.19129	0.20279
H	-1.63252	-1.98341	-1.12704
C	-2.97878	-2.85216	-2.55777
C	-5.34587	-2.63121	-2.08462
H	-5.85970	-1.58298	-0.27925
H	-2.50153	1.41966	2.62140
C	-3.10453	3.21357	1.60112
C	-4.18338	2.91262	-0.55044

H	-4.43318	0.88116	-1.21154
H	-0.51926	-3.05689	4.27376
C	0.65545	-2.03264	2.77743
H	1.56068	-0.91218	1.15883
H	-2.17557	-3.20635	-3.19594
C	-4.31103	-3.08833	-2.90525
H	-6.38105	-2.81620	-2.35402
H	-2.72631	3.86800	2.37998
C	-3.70482	3.75161	0.45870
H	-4.64015	3.33299	-1.44078
H	1.60679	-2.34061	3.20236
H	-4.54403	-3.63057	-3.81683
H	-3.79360	4.82874	0.35229
P	-3.35943	-0.78843	0.95247
O	-4.54715	-1.13130	2.00305
H	-4.77226	-2.07898	2.05992

{HL^{Se}-$P(OH)Ph_3$}···HOAc. Coordinates below.

Energy: -4373.8387931

70

N	3.20126	0.98647	-0.23363
Se	0.39086	0.12674	-1.34905
C	2.36599	2.09468	-0.45897
C	4.40851	1.02135	-0.66643
C	5.28834	-1.17386	0.32942
C	1.03352	1.90052	-0.90410
C	2.81660	3.40205	-0.18959
C	5.43743	-0.00015	-0.45180
H	4.75640	1.86945	-1.27579
C	6.35651	-2.07148	0.45379
C	0.21777	3.02383	-1.10081
C	1.97954	4.50257	-0.36368
H	3.82495	3.53939	0.19117

740

C	6.68196	0.21475	-1.07761
H	6.22557	-2.96723	1.05723
C	7.57211	-1.82823	-0.18185
H	-0.78919	2.88246	-1.47765
C	0.67622	4.31474	-0.82759
H	2.34651	5.50060	-0.13868
C	7.74209	-0.67640	-0.95507
H	6.80284	1.11405	-1.67668
H	8.38447	-2.54073	-0.06984
H	0.01645	5.16544	-0.97620
H	8.68596	-0.47848	-1.45316
O	4.10394	-1.41146	0.95449
H	4.17071	-2.25044	1.44131
C	-0.44334	-0.31301	1.92738
C	-1.42802	-2.13837	-0.47981
C	-2.45134	0.92492	-0.16664
C	-1.09189	-0.12022	3.16526
C	0.95903	-0.34851	1.89868
C	-0.25045	-2.90260	-0.50480
C	-2.58986	-2.62349	-1.10532
C	-2.65604	1.99581	0.71211
C	-3.01520	0.95832	-1.44974
H	-2.17272	-0.10079	3.21211
C	-0.35102	0.03972	4.33611
C	1.69143	-0.21736	3.08067
H	1.49663	-0.45461	0.96447
H	0.64735	-2.54624	-0.01312
C	-0.23551	-4.13690	-1.15685
C	-2.55169	-3.84439	-1.78175
H	-3.52391	-2.07231	-1.05157
H	-2.22531	1.98402	1.70797
C	-3.41074	3.09948	0.30329
C	-3.78128	2.05470	-1.84368

H	-2.84966	0.14159	-2.14363
H	-0.86972	0.20043	5.27707
C	1.04376	-0.01683	4.29967
H	2.77467	-0.26300	3.02778
H	0.67504	-4.72909	-1.15830
C	-1.37934	-4.60331	-1.80806
H	-3.44821	-4.20660	-2.27706
H	-3.55318	3.93159	0.98700
C	-3.97707	3.13055	-0.97095
H	-4.22039	2.07002	-2.83714
H	1.61900	0.09793	5.21445
H	-1.35942	-5.55795	-2.32624
H	-4.56670	3.98689	-1.28581
P	-1.49701	-0.53148	0.41821
O	-2.93194	-1.02270	1.31227
H	-2.83112	-1.91345	1.69238
C	-6.23466	-0.70705	0.10347
O	-5.73277	-1.34765	-0.80646
C	-7.68249	-0.27815	0.14347
H	-7.74394	0.81539	0.15538
H	-8.21028	-0.66589	-0.72843
H	-8.15835	-0.64166	1.06003
O	-5.56211	-0.29813	1.18507
H	-4.60959	-0.57986	1.11868

{HL^{Se}-$P(OH)Ph_3$}···H_2L^{Se}. Coordinates below.

Energy: -7178.004932

89

N	-5.91371	0.53896	-0.17246
Se	-3.37788	-0.00271	1.62172
C	-5.35985	1.72922	0.33393
C	-7.17918	0.35481	-0.07053
C	-7.41195	-1.82186	-1.40966

C	-4.17584	1.68571	1.11458
C	-5.93553	2.97635	0.02156
C	-7.93929	-0.77693	-0.60993
H	-7.80318	1.07637	0.47891
C	-8.25056	-2.84947	-1.86034
C	-3.63341	2.89507	1.57495
C	-5.36527	4.16641	0.47049
H	-6.82003	3.00026	-0.60937
C	-9.31443	-0.81876	-0.30415
H	-7.82973	-3.64423	-2.47284
C	-9.60515	-2.86095	-1.53462
H	-2.74579	2.86653	2.19803
C	-4.21134	4.12600	1.25546
H	-5.82109	5.11728	0.20674
C	-10.14730	-1.83868	-0.75080
H	-9.72532	-0.01860	0.30672
H	-10.23389	-3.66972	-1.89616
H	-3.75927	5.04580	1.61756
H	-11.20174	-1.83873	-0.49322
O	-6.09134	-1.80855	-1.73523
H	-5.89722	-2.58871	-2.28190
C	-1.61587	-0.06793	-1.38910
C	-1.02298	-1.90079	1.11224
C	-0.45558	1.27654	1.19727
C	-0.72056	0.27618	-2.42398
C	-2.97082	-0.25810	-1.70161
C	-2.02670	-2.81747	0.76293
C	-0.03749	-2.27083	2.04365
C	-0.27645	2.45089	0.45521
C	-0.21400	1.28076	2.57855
H	0.32964	0.42356	-2.20691
C	-1.17659	0.42882	-3.73318
C	-3.41227	-0.12842	-3.02011

H	-3.69408	-0.48582	-0.92775
H	-2.78527	-2.54962	0.03696
C	-2.04459	-4.08515	1.34680
C	-0.08295	-3.52886	2.64549
H	0.76708	-1.58732	2.29265
H	-0.46467	2.46319	-0.61356
C	0.13689	3.62381	1.09472
C	0.21146	2.45075	3.20560
H	-0.37417	0.38443	3.16758
H	-0.47343	0.70505	-4.51383
C	-2.52310	0.21953	-4.03734
H	-4.46339	-0.29436	-3.23384
H	-2.81671	-4.79340	1.06081
C	-1.08370	-4.43884	2.29652
H	0.67259	-3.79980	3.37727
H	0.26226	4.53286	0.51332
C	0.38566	3.62634	2.46704
H	0.40121	2.44466	4.27516
H	-2.87529	0.33063	-5.05934
H	-1.11046	-5.42182	2.75792
H	0.71070	4.53718	2.96164
P	-0.90510	-0.25747	0.30589
O	0.73172	-0.46020	-0.16288
H	0.86284	-1.30333	-0.63329
C	4.68639	0.88751	-0.71284
C	3.64851	1.75927	-1.05483
C	5.99370	1.12521	-1.18526
H	2.64571	1.58308	-0.67842
C	3.89767	2.85440	-1.88500
C	6.22492	2.22579	-2.02868
N	7.00054	0.21050	-0.82915
H	3.08111	3.51865	-2.15355
C	5.18545	3.08627	-2.37529

744

H	7.21943	2.38029	-2.43705
C	8.21620	0.59850	-0.61200
H	5.37867	3.92693	-3.03527
C	9.28738	-0.33029	-0.30842
H	8.48276	1.66169	-0.63969
C	9.06449	-1.73496	-0.25310
C	10.58580	0.16272	-0.06192
C	10.13374	-2.59390	0.04080
O	7.85088	-2.27398	-0.47606
C	11.63839	-0.69248	0.22984
H	10.74955	1.23694	-0.10580
H	9.94362	-3.66204	0.07761
C	11.40211	-2.07562	0.27943
H	7.22400	-1.52377	-0.67461
H	12.63190	-0.29776	0.41719
H	12.21897	-2.75509	0.50711
Se	4.41812	-0.63942	0.44066
H	2.94678	-0.47058	0.48223

Structure S2.13. Optimized structure of OAc^-.
Energy: -228.586093185

7

C	-0.20281	0.00034	-0.00742
O	-0.71236	1.15444	0.00158
C	1.35285	-0.04410	-0.00239
H	1.74040	-1.04995	-0.19760
H	1.76118	0.65185	-0.74594
H	1.72886	0.28530	0.97629
O	-0.80398	-1.10752	0.00169

Structure S2.14. Optimized structure of HOAc.
Energy: -229.083268606

8

C	-0.09208	0.12246	0.00000
O	-0.64427	1.20396	-0.00000

C	1.39674	-0.11102	0.00000
H	1.68435	-0.69194	-0.88243
H	1.91938	0.84568	0.00002
H	1.68435	-0.69198	0.88240
O	-0.77918	-1.04356	-0.00000
H	-1.72845	-0.81358	0.00000

Structure S2.15. Optimized structure of $OPPh_3$.
Energy: -1111.54393666

35

C	-1.02764	-1.34621	0.22363
C	1.68033	-0.21758	0.22338
C	-0.65086	1.56189	0.22199
C	-0.77068	-1.95640	-1.01376
C	-2.12410	-1.77551	0.98831
C	2.60392	-0.94384	0.99188
C	2.07719	0.30487	-1.01720
C	-1.29816	1.64450	-1.02037
C	-0.48690	2.72469	0.99163
H	0.08696	-1.65338	-1.60723
C	-1.60813	-2.97019	-1.48469
C	-2.95684	-2.79090	0.51662
H	-2.31164	-1.32110	1.95655
H	2.30658	-1.32883	1.96269
C	3.90015	-1.15468	0.52033
C	3.37444	0.08933	-1.48785
H	1.38268	0.88970	-1.61316
H	-1.45469	0.75086	-1.61754
C	-1.76004	2.87555	-1.49158
C	-0.95211	3.95249	0.51940
H	-0.00767	2.65972	1.96380
H	-1.40125	-3.43848	-2.44290
C	-2.70164	-3.38676	-0.72160
H	-3.80130	-3.11910	1.11615

746

H	4.60952	-1.71535	1.12259
C	4.28552	-0.64119	-0.72113
H	3.67428	0.49871	-2.44845
H	-2.26171	2.93056	-2.45364
C	-1.58625	4.02956	-0.72375
H	-0.82371	4.84694	1.12251
H	-3.34950	-4.17835	-1.08784
H	5.29557	-0.80395	-1.08691
H	-1.95009	4.98555	-1.09009
P	0.00076	-0.00051	0.91422
O	0.00067	0.00080	2.42484

Structure S2.16. Optimized structure of [Pd(L^{Se})(PPh_3)].
Energy: -4195.19555794

60

Pd	0.69172	-0.02709	0.08917
N	2.78163	0.07418	0.08072
O	0.50098	2.02791	0.34751
P	-1.65587	-0.09314	0.02455
Se	0.97146	-2.40889	-0.25003
C	3.54964	-1.12643	0.13334
C	3.37811	1.22477	-0.10440
C	1.46265	2.88635	0.17390
C	-2.26742	1.11830	-1.21378
C	-2.42366	0.37629	1.63012
C	-2.46067	-1.68698	-0.41953
C	2.88310	-2.35163	-0.06084
C	4.93345	-1.14016	0.39879
C	2.83737	2.54967	-0.08801
H	4.45146	1.19683	-0.29267
C	1.13006	4.27242	0.24245
C	-3.45207	1.84475	-1.02044
C	-1.53322	1.30268	-2.39683
C	-1.72333	1.22730	2.50151

C	-3.70281	-0.07827	1.99398
C	-3.11801	-1.86764	-1.64550
C	-2.38488	-2.76455	0.48150
C	3.61612	-3.54682	-0.07781
C	5.64790	-2.33427	0.39405
H	5.45702	-0.22144	0.64035
C	3.77531	3.60123	-0.30205
H	0.09369	4.52046	0.45155
C	2.07210	5.25883	0.03269
H	-4.02679	1.72116	-0.10818
C	-3.89607	2.73699	-1.99835
C	-1.98475	2.18955	-3.37521
H	-0.60687	0.75581	-2.54882
H	-0.74295	1.59537	2.21776
C	-2.29517	1.61268	3.71526
C	-4.26890	0.31192	3.20914
H	-4.25616	-0.74087	1.33654
H	-3.18718	-1.04957	-2.35440
C	-3.69276	-3.10094	-1.96201
C	-2.96574	-3.99224	0.16297
H	-1.88018	-2.64490	1.43548
H	3.09638	-4.48667	-0.24388
C	4.99167	-3.54308	0.13844
H	6.71324	-2.32070	0.60473
C	3.41645	4.93024	-0.25007
H	4.80913	3.32938	-0.50393
H	1.77157	6.30271	0.08293
H	-4.81227	3.29801	-1.83700
C	-3.16560	2.90951	-3.17631
H	-1.40972	2.32319	-4.28704
H	-1.74426	2.26911	4.38303
C	-3.56577	1.15525	4.07245
H	-5.25766	-0.04720	3.48038

748

H	-4.20073	-3.22604	-2.91409
C	-3.61998	-4.16361	-1.05994
H	-2.90432	-4.81425	0.87038
H	5.54384	-4.47865	0.13363
H	4.15282	5.71009	-0.41604
H	-3.51262	3.60573	-3.93468
H	-4.00608	1.45331	5.01991
H	-4.07000	-5.12091	-1.30734

Tables S2.17. Atomic charges and Fukui functions.

Atomic Charges and Bader size (N+1e corresponds to molecule plus 1 electron; N-1e corresponds to molecule minus 1 electron; charges correspond to integrals of the electron density ρ(r) within the boundaries of the van der Waals or Bader atoms in [eÅ^{-3}]):

	Bader charge	Size [Bohr^2]	Hirshfeld charges	ADCH** charges	Hirshfeld charges	ADCH** charges	Hirshfeld charges	ADCH** charges
$\{HL^{Se}\}_2$			N		N+1e(-1charge)		N-1e(+1charge)	
Se9	0.04	220.07	0	-0.4	0.01	-0.39	0.11	-0.12
Se4	0.07	217.97	0	0.1	-0.01	0.2	0.12	0.3
$[Pd\{L^{Se}\text{-}HL^{Se}\}Ph_3]^+$								
Se62	0.18	220.1	0.06	0.07	-0.02	-0.06	0.07	0.1
Se5*	0.29	179.44	0.21	0.21	0.03	0.05	0.13	0.14
$[Pd\{L^{Se}\}_2Ph_3]$								
Se62	0.23	215.86	0.04	0.01	-0.02	-0.07	0.15	0.06
Se5*	0.42	166.49	0.28	0.3	0.1	0.16	0.05	0.17

* connected to Pd

** dipole corrected Hirshfeld charges

Fukui functions:

		From Hirshfeld charges				From ADCH** charges			
		f^-	f^+	$f^\pm$	f^0	f^-	f^+	$f^\pm$	f^0
$\{HL^{Se}\}_2$	Se9	0.11	-0.01	-0.12	0.05	0.27	-0.01	-0.28	0.13
	Se4	0.12	0.00	-0.12	0.06	0.20	-0.10	-0.30	0.05
$[Pd\{L^{Se}\text{-}HL^{Se}\}Ph_3]^+$	Se62	0.01	0.08	0.07	0.05	0.03	0.13	0.10	0.08
	Se5*	-0.08	0.18	0.27	0.05	-0.07	0.17	0.23	0.05
$[Pd\{L^{Se}\}_2Ph_3]$	Se62	0.11	0.06	-0.05	0.08	0.05	0.08	0.03	0.06
	Se5*	-0.22	0.18	0.40	-0.02	-0.13	0.14	0.27	0.00

f^-: electrophilic attack (large = prone to electrophilic attack; small = prone to nucleophilic attack); $f^- = \rho_N(r)-\rho_{N-1}(r)$

f^+: nucleophilic attack (large = prone to nucleophilic attack; small = prone to electrophilic attack); $f^+ = \rho_{N+1}(r)-\rho_N(r)$

$f^{\pm}$: condensed dual descriptor (positive: prone to nucleophilic attack; negative = prone to electrophilic attack) $f^{\pm} = f^{+} - f^{-}$

f^{0}: radical attack (large = prone to radical attack; small = not prone to radical attack); $f^{0} = 1(2(\rho_{N+1}(r)-\rho_{N-1}(r))$

* connected to Pd

** dipole corrected Hirshfeld charges

σ-Hole parameters of the electrostatic potential on the van der Waals surface:

		Surface area oft he atom			Average potential			Potential	
		Positive	Negative	Overall	Positive	Negative	Overall	maximum	minimum
		[Bohr²]			[kcal/mol]			[kcal/mol]	
$\{HL^{Se}\}_2$	Se9	13.91	4.26	18.17	16.85	-1.49	12.55	1604.36	-12.46
	Se4	13.60	2.72	16.33	3.29	-0.97	2.58	102.28	-7.62
$[Pd\{L^{Se}\text{-}HL^{Se}\}Ph_3]^+$	Se62	58.05	0.00	58.05	41.14	0.00	41.14	2142.61	22.67
	Se5*	6.74	0.00	6.74	40.02	0.00	40.02	825.03	22.86
$[Pd\{L^{Se}\}_2Ph_3]$	Se62	17.54	1.14	18.66	16.28	-1.21	15.21	4747.83	-9.18
	Se5*	3.07	0.15	3.22	14.47	-0.96	13.77	1076.17	-6.74

* connected to Pd

Overall, the charge/polarization increases, which results in a tendency towards easier nucleophilic attacks as seen by the positive values of $f^{\pm}$, the increase in f^{+} and the decrease in f^{-} upon coordination to the metal. Additionally, the exposed surface area has a larger average and maximum positive charge as well as an overall increase of accessible surface area for the non-coordinated selenium atom compared to the metal-bound selenium atom. Overall, the nucleophilic attack is therefore much more probable at the exposed non-metal-bound selenium atom.

Part 3: Computational data on model systems

To further increase our knowledge on these reactions and possible reasons for the increased reactivity upon coordination, we performed gas-phase calculations on a series of aryl diselenides R-Se-Se-R (R = Ph, Ph-2-NMe_2, Ph-2-$NCMe_2$, 2-Py, 3-Py-2-NMe_2, 3-Py-2-$NCMe_2$) and their Pd(II) complexes [$PdCl_2(PMe_3)$-η^1-{R-Se-Se-R}]. We choose PMe_3 as a co-ligand, as we observed some steric hinderance with other phosphines such as PPh_3 and $P(CF_3)_3$ in the case of the 2-NMe_2 substituted compounds. For R = Ph-2-NMe_2 and Ph-2-$NCMe_2$ we also considered the respective chelated $[PdCl(PMe_3)$-η^2-{R-Se-Se-R}$]^+$ cations. For all examples we additionally calculated their interactions with PPh_3. We found in all cases an increase in the intensity and/or size of the σ-hole of the Se-Se bond upon coordination to the metal. This increased polarization (localization of σ/σ* in free diselenide 49/51 changes to σ/σ*: 54/46 for metal-bound Se atom and σ/σ*: 46/54 for non-metal-bound Se atom) is also reflected in the calculated Bader charges of the two selenium atoms and was even stronger, when additional chelation leads to a metal cation. The PPh_3 acted in all (sterically accessible) cases on the metal-bound diselenides as a donor into the σ*(Se-Se) orbital at the non-coordinated selenium atom. They essentially yielded donor-acceptor complexes (stabilization energy in second order perturbation analysis: 20-60 kcal/mol) of the type [$PdCl_2(PMe_3)$-η^1-{R-Se-Se(R)←:PPh_3}] with elongated Se-Se bonds. In some cases, an inversion of the bonding situation was observed, where essentially the Se-Se bond was broken and a coordinated selenolato ligand was released, that donated to a selenylphosphonium ion: [$PdCl_2(PMe_3)$-η^1-R-Se:→Se(R)PPh_3]. In

contrast, the donation to the uncoordinated diselenides was very weak and no donor-acceptor complex formation could be concluded; no break of a Se-Se bond was found (maximum stabilization energy in second order perturbation analysis: 2 kcal/mol). We conclude therefore, that the most likely reason for the metal-induced reduction is the increased polarization of the Se-Se bond upon coordination and therefore the more intense (stronger interaction) and larger σ-hole (better overlap) on the non-coordinated selenium atom. Additionally, electron withdrawing substituents on either the metal or the diselenide increase the σ-hole and therefore also assist in the reduction by PPh_3. A positive charge on the metal-diselenide complex further polarizes the non-coordinated selenium atom positively and leads to an even stronger interaction with the phosphine.

Structure S3.1a. Optimized structure of $\{SePh\}_2$.
Energy: -5265.87888219

24

Se	-0.79661	-1.35227	0.88677
C	-3.12028	-0.22779	-0.45365
C	-2.01053	0.06250	0.35066
C	-4.01278	0.78823	-0.79906
C	-1.80107	1.36939	0.81088
C	-3.80264	2.09218	-0.34325
H	-4.87279	0.56057	-1.42329
H	-0.94230	1.59008	1.43689
C	-2.69794	2.38108	0.46101
H	-4.49997	2.88088	-0.61274
H	-2.53373	3.39401	0.81915
Se	0.79662	-1.35229	-0.88677
C	1.80113	1.36937	-0.81096
C	2.01052	0.06250	-0.35068
C	2.69797	2.38108	-0.46104
C	3.12024	-0.22778	0.45369
C	3.80263	2.09218	0.34328
H	2.53377	3.39400	-0.81920
H	3.28030	-1.24163	0.80692
C	4.01274	0.78823	0.79911
H	4.49995	2.88088	0.61280
H	4.87270	0.56057	1.42338
H	-3.28036	-1.24165	-0.80685

H	0.94239	1.59008	-1.43703

Structure S3.1b. Optimized structure of $\{SePh\}_2\cdots PPh_3$.
Energy: -6302.16235609

58

Se	-3.72603	0.66808	-1.54849
C	-5.10390	2.00093	0.64337
C	-4.85133	0.76710	0.02954
C	-5.94795	2.06638	1.75303
C	-5.45213	-0.39690	0.52717
C	-6.54538	0.90537	2.25063
H	-6.14086	3.02514	2.22722
H	-5.25729	-1.35116	0.04798
C	-6.29765	-0.32418	1.63665
H	-7.20400	0.95976	3.11336
H	-6.76268	-1.22889	2.01964
Se	-1.53384	0.50716	-0.60598
C	-1.88802	-1.91542	0.95897
C	-1.41102	-1.39830	-0.25275
C	-1.77094	-3.28130	1.22642
C	-0.80860	-2.24938	-1.18825
C	-1.17165	-4.13084	0.29289
H	-2.14405	-3.67973	2.16638
H	-0.42998	-1.84565	-2.12168
C	-0.68903	-3.61307	-0.91183
H	-1.07955	-5.19297	0.50406
H	-0.21847	-4.26980	-1.63871
H	-4.63965	2.90163	0.25408
H	-2.34673	-1.25245	1.68550
P	2.18418	0.34820	0.20830
C	3.05555	1.96049	0.47365
C	4.21800	2.35813	-0.20522
C	2.48182	2.84787	1.40037
C	4.79573	3.60506	0.04492

752

H	4.67149	1.69395	-0.93481
C	3.06501	4.08861	1.65829
H	1.56787	2.56507	1.91767
C	4.22383	4.47119	0.97870
H	5.69458	3.89894	-0.49136
H	2.60870	4.76054	2.38060
H	4.67419	5.44155	1.17071
C	2.90683	-0.24997	-1.38921
C	4.02972	-1.08606	-1.48884
C	2.25450	0.14386	-2.57092
C	4.49342	-1.50810	-2.73730
H	4.54185	-1.41216	-0.58860
C	2.72418	-0.26983	-3.81807
H	1.36901	0.77227	-2.51065
C	3.84497	-1.09927	-3.90409
H	5.36372	-2.15699	-2.79666
H	2.20941	0.04797	-4.72115
H	4.20697	-1.42936	-4.87434
C	2.97935	-0.76270	1.45906
C	4.16286	-0.46044	2.15057
C	2.32018	-1.97052	1.74798
C	4.67873	-1.34766	3.09831
H	4.68220	0.47213	1.95162
C	2.84250	-2.86062	2.68664
H	1.39098	-2.21276	1.23835
C	4.02278	-2.55048	3.36634
H	5.59531	-1.09735	3.62671
H	2.32085	-3.79134	2.89444
H	4.42518	-3.23903	4.10486

Structure S3.2a. Optimized structure of [$PdCl_2$-η1-{SePh}$_2$(PPh_3)].
Energy: -7349.40678571

61

Se	1.36073	0.08187	-0.01578

C	1.61639	2.93026	-0.69961
C	1.81549	1.95365	0.28253
C	1.95576	4.25335	-0.41224
C	2.34997	2.28335	1.53365
C	2.48386	4.59626	0.83600
H	1.80598	5.01753	-1.16985
H	2.50249	1.51427	2.28489
C	2.68174	3.61283	1.80692
H	2.74275	5.62960	1.05031
H	3.09563	3.87588	2.77670
Se	3.10416	-0.63491	-1.51596
C	5.29448	-0.31880	0.37212
C	4.34809	-1.21764	-0.14137
C	6.23162	-0.75435	1.31090
C	4.35161	-2.55322	0.28587
C	6.23162	-2.08490	1.73639
H	6.96446	-0.05546	1.70537
H	3.62287	-3.24966	-0.11744
C	5.29284	-2.98312	1.22260
H	6.96491	-2.42264	2.46382
H	5.29421	-4.01968	1.54907
Pd	-0.68363	0.17185	-1.45892
H	1.22036	2.65262	-1.67166
H	5.29713	0.71283	0.03408
Cl	-2.60045	0.16349	-2.84927
Cl	0.69585	0.64178	-3.35515
P	-2.18066	-0.26128	0.30736
C	-1.36762	-0.64010	1.92215
C	-1.21736	-1.95877	2.37554
C	-0.81532	0.40651	2.68217
C	-0.54103	-2.22349	3.56861
H	-1.63420	-2.78104	1.80322
C	-0.14669	0.13800	3.87678

754

H	-0.91866	1.43530	2.34879
C	-0.00768	-1.17816	4.32344
H	-0.43828	-3.25019	3.90917
H	0.26286	0.95931	4.45867
H	0.51316	-1.38673	5.25388
C	-3.21893	-1.73931	-0.02597
C	-4.48025	-1.91038	0.56234
C	-2.70717	-2.74319	-0.86218
C	-5.21195	-3.07473	0.32539
H	-4.90236	-1.13308	1.19081
C	-3.43792	-3.90989	-1.08762
H	-1.75172	-2.59736	-1.35707
C	-4.69081	-4.07729	-0.49474
H	-6.19273	-3.19386	0.77768
H	-3.03465	-4.67743	-1.74203
H	-5.26460	-4.98121	-0.68045
C	-3.30158	1.13771	0.72771
C	-3.91760	1.20824	1.99111
C	-3.55402	2.14800	-0.21302
C	-4.77777	2.26196	2.29925
H	-3.71719	0.44945	2.74111
C	-4.41179	3.20302	0.10498
H	-3.09805	2.09455	-1.19513
C	-5.02568	3.26226	1.35641
H	-5.24859	2.30288	3.27778
H	-4.59820	3.97815	-0.63293
H	-5.69242	4.08537	1.59922

Structure S3.2b. Optimized structure of $[PdCl_2\text{-}\eta1\text{-}\{SePh\}_2(PPh_3)]\cdots PPh_3$.
Energy: -8385.69438732

95

Se	0.87022	-1.11535	0.11484
C	0.89795	-2.31302	-2.57412
C	0.97873	-2.55070	-1.19716

C	0.98967	-3.39232	-3.45476
C	1.14177	-3.85071	-0.70232
C	1.15830	-4.69295	-2.97092
H	0.92771	-3.21235	-4.52462
H	1.19995	-4.02424	0.36809
C	1.23234	-4.92127	-1.59575
H	1.23032	-5.52627	-3.66478
H	1.36027	-5.93098	-1.21422
Se	-1.52189	-0.44324	-0.00375
C	-2.40881	-3.09542	0.80230
C	-2.10241	-1.80619	1.26212
C	-2.84214	-4.07334	1.70100
C	-2.23764	-1.50495	2.62385
C	-2.97822	-3.76888	3.05754
H	-3.07524	-5.07165	1.33957
H	-2.00525	-0.50674	2.98053
C	-2.67737	-2.48446	3.51647
H	-3.31963	-4.52966	3.75450
H	-2.78596	-2.24243	4.57038
Pd	2.04301	0.82688	-0.95003
H	0.75304	-1.30239	-2.94296
H	-2.30620	-3.32933	-0.25277
Cl	3.09946	2.75870	-1.84743
Cl	0.15121	1.21432	-2.37751
P	4.01025	0.55641	0.30841
C	3.95904	-0.76801	1.59519
C	3.77335	-0.46890	2.95233
C	4.04119	-2.11555	1.20189
C	3.68482	-1.49438	3.89692
H	3.70489	0.56410	3.27704
C	3.95972	-3.13603	2.14881
H	4.17942	-2.37007	0.15487
C	3.78131	-2.82816	3.49980

H	3.54631	-1.24563	4.94562
H	4.03631	-4.17183	1.82920
H	3.71729	-3.62372	4.23714
C	4.42573	2.07482	1.25690
C	5.74250	2.39224	1.61878
C	3.37864	2.91462	1.66556
C	6.00444	3.52723	2.38748
H	6.56683	1.76779	1.29031
C	3.64404	4.04206	2.44284
H	2.36192	2.69872	1.35107
C	4.95687	4.35035	2.80465
H	7.02946	3.77017	2.65423
H	2.82583	4.68826	2.74808
H	5.16420	5.23541	3.40015
C	5.48823	0.09270	-0.68949
C	6.60311	-0.51225	-0.07992
C	5.51531	0.33858	-2.07080
C	7.72519	-0.85019	-0.83624
H	6.59265	-0.73323	0.98281
C	6.63970	-0.00844	-2.82273
H	4.66881	0.81897	-2.54814
C	7.74497	-0.59962	-2.21018
H	8.57994	-1.31464	-0.35183
H	6.64626	0.18747	-3.89127
H	8.61764	-0.86809	-2.79968
P	-4.41743	0.63302	-0.11014
C	-4.37269	2.31317	-0.86218
C	-5.37028	3.27802	-0.63577
C	-3.28013	2.63929	-1.68149
C	-5.27934	4.53759	-1.22793
H	-6.21322	3.04579	0.00887
C	-3.19262	3.90228	-2.27193
H	-2.48184	1.92290	-1.85348

C	-4.19067	4.85106	-2.04725
H	-6.05599	5.27617	-1.04585
H	-2.33409	4.13869	-2.89386
H	-4.11867	5.83589	-2.50160
C	-5.28820	0.91439	1.49428
C	-6.56161	0.41067	1.79628
C	-4.59584	1.63691	2.48322
C	-7.13129	0.63080	3.05335
H	-7.11305	-0.15225	1.05007
C	-5.17021	1.86355	3.73267
H	-3.60540	2.03137	2.26819
C	-6.44064	1.35787	4.02307
H	-8.12065	0.23589	3.26996
H	-4.62462	2.43175	4.48167
H	-6.88696	1.52955	4.99898
C	-5.62474	-0.32133	-1.12645
C	-6.38605	0.24449	-2.16010
C	-5.73423	-1.70246	-0.88307
C	-7.24619	-0.54941	-2.92209
H	-6.30552	1.30546	-2.37319
C	-6.60407	-2.49010	-1.63676
H	-5.13288	-2.16335	-0.10331
C	-7.36140	-1.91539	-2.66057
H	-7.82712	-0.09656	-3.72136
H	-6.68140	-3.55485	-1.43237
H	-8.03149	-2.53068	-3.25514

Structure S3.3a. Optimized structure of [$PdCl_2$-η1-{SePh}$_2$(PMe_3)].
Energy: -6774.22761887

40

Se	0.42078	0.00267	0.40430
C	0.12172	2.61939	-0.89570
C	0.66482	1.92360	0.19035
C	0.31804	3.99885	-0.97585

758

C	1.39909	2.58457	1.18204
C	1.04192	4.67219	0.01299
H	-0.09859	4.54737	-1.81594
H	1.82440	2.03065	2.01396
C	1.58239	3.96667	1.08954
H	1.18628	5.74680	-0.05771
H	2.14898	4.48685	1.85704
Se	1.86536	-0.92580	-1.28300
C	4.35447	-0.00202	-0.09464
C	3.44803	-1.07009	-0.16658
C	5.52487	-0.13164	0.65516
C	3.72488	-2.26756	0.50885
C	5.79744	-1.32466	1.32906
H	6.22592	0.69704	0.70787
H	3.02622	-3.09622	0.44543
C	4.89862	-2.39172	1.25388
H	6.71144	-1.42457	1.90823
H	5.11181	-3.32211	1.77333
Pd	-1.88339	-0.38294	-0.46169
H	-0.42905	2.08598	-1.66473
H	4.14434	0.92074	-0.62649
Cl	-4.10412	-0.74626	-1.21958
Cl	-1.06099	-0.31023	-2.70474
P	-2.86644	-0.47898	1.64825
C	-1.78798	-0.24409	3.13037
H	-1.00525	-1.00761	3.15740
H	-1.30986	0.73985	3.09768
H	-2.38477	-0.31480	4.04668
C	-4.17581	0.78999	1.88294
H	-4.67265	0.66101	2.85120
H	-3.72832	1.78746	1.83541
H	-4.89868	0.69293	1.07021
C	-3.68239	-2.09432	1.97011

H	-4.20448	-2.08265	2.93360
H	-4.38829	-2.28911	1.15974
H	-2.92922	-2.88812	1.97538

Structure S3.3b. Optimized structure of [$PdCl_2$-η1-{$SePh$}$_2$(PMe_3)]···PPh_3.
Energy: -7810.51637437

74

Se	-2.03199	-1.12883	-0.35119
C	-2.42370	-1.35209	2.55076
C	-2.41430	-2.03443	1.32835
C	-2.71476	-2.05817	3.71941
C	-2.68404	-3.40736	1.27277
C	-2.99167	-3.42758	3.67287
H	-2.72443	-1.53176	4.67004
H	-2.66758	-3.93060	0.32090
C	-2.97399	-4.10123	2.45025
H	-3.21944	-3.96801	4.58776
H	-3.18565	-5.16647	2.40842
Se	0.42489	-0.60474	-0.17309
C	1.31391	-3.36596	-0.51267
C	0.97438	-2.18203	-1.18074
C	1.72306	-4.48703	-1.23860
C	1.04704	-2.13066	-2.58035
C	1.79394	-4.43321	-2.63229
H	1.98715	-5.40161	-0.71412
H	0.78475	-1.21308	-3.09857
C	1.45487	-3.25462	-3.30220
H	2.11227	-5.30666	-3.19515
H	1.50732	-3.20918	-4.38698
Pd	-3.06081	1.12871	-0.05706
H	-2.19529	-0.29109	2.58232
H	1.25707	-3.40813	0.57061
Cl	-4.08786	3.27689	0.11993
Cl	-1.19412	1.85944	1.27310

760

P	-4.97004	0.59365	-1.26366
C	-5.15849	-1.11941	-1.92831
H	-4.34072	-1.35362	-2.61538
H	-5.13569	-1.84515	-1.10995
H	-6.11198	-1.21305	-2.46054
C	-6.50445	0.82142	-0.27535
H	-7.39405	0.64387	-0.89047
H	-6.50041	0.12165	0.56600
H	-6.51208	1.84017	0.11796
C	-5.19032	1.64831	-2.75410
H	-6.14597	1.43479	-3.24643
H	-5.15042	2.69405	-2.44151
H	-4.37174	1.46142	-3.45590
P	3.16874	0.45819	0.07677
C	3.18331	2.04653	-0.85191
C	4.25993	2.46336	-1.64965
C	2.03236	2.85274	-0.77463
C	4.19025	3.66849	-2.35242
H	5.15283	1.85036	-1.72309
C	1.97427	4.05982	-1.47107
H	1.17901	2.54690	-0.17329
C	3.05015	4.46890	-2.26340
H	5.03064	3.98095	-2.96717
H	1.08094	4.67369	-1.39677
H	2.99862	5.40639	-2.81098
C	4.73781	-0.38972	-0.39271
C	5.91352	-0.31195	0.37065
C	4.73627	-1.17535	-1.55821
C	7.06362	-0.99396	-0.03123
H	5.93096	0.28148	1.27930
C	5.88962	-1.84830	-1.96176
H	3.82761	-1.26861	-2.14662
C	7.05588	-1.76032	-1.19828

H	7.96693	-0.92420	0.56928
H	5.87287	-2.45026	-2.86641
H	7.95224	-2.29105	-1.50813
C	3.41829	0.95033	1.83264
C	3.96842	2.18473	2.21250
C	3.02873	0.04237	2.83052
C	4.13602	2.49625	3.56279
H	4.25753	2.90506	1.45351
C	3.20339	0.35363	4.17896
H	2.57350	-0.90364	2.55000
C	3.75683	1.58160	4.54735
H	4.55837	3.45710	3.84472
H	2.89353	-0.35631	4.94102
H	3.88242	1.82935	5.59797

Structure S3.4a. Optimized structure of [$PdCl_2$-η1-{SePh}$_2$($P(CF_3)_3$)].
Energy: -7667.30579358

40

Se	1.18136	0.00490	0.13714
C	1.38971	2.92582	-0.12441
C	1.55205	1.82394	0.72230
C	1.66125	4.20048	0.37406
C	1.98140	1.97856	2.04516
C	2.08461	4.37033	1.69580
H	1.53742	5.06293	-0.27464
H	2.10513	1.11400	2.69035
C	2.24444	3.26226	2.52948
H	2.28963	5.36753	2.07510
H	2.57418	3.39158	3.55649
Se	2.90347	-0.43575	-1.48363
C	5.11951	-0.36955	0.39345
C	4.17718	-1.19713	-0.23467
C	6.07784	-0.92827	1.24062
C	4.20220	-2.58213	-0.01561

762

C	6.10067	-2.30785	1.45990
H	6.80842	-0.28652	1.72545
H	3.47551	-3.22050	-0.50846
C	5.16473	-3.13324	0.83130
H	6.84984	-2.74023	2.11745
H	5.18443	-4.20664	0.99838
Pd	-0.90495	0.27731	-1.22298
H	1.06471	2.78594	-1.15051
H	5.10301	0.70110	0.21515
Cl	-2.90821	0.47651	-2.47538
Cl	0.37186	1.00288	-3.06290
P	-2.41961	-0.40061	0.38118
C	-1.75190	-1.04056	2.05290
C	-3.54440	-1.87601	-0.09454
C	-3.67114	0.86340	1.07875
F	-2.91190	-2.63181	-0.99534
F	-3.81300	-2.64151	0.97944
F	-4.70108	-1.44770	-0.59979
F	-2.68996	-1.23846	2.98479
F	-1.10648	-2.19999	1.83708
F	-0.86663	-0.14980	2.54361
F	-4.67109	0.23754	1.72096
F	-3.00541	1.62492	1.97057
F	-4.18613	1.65156	0.14746

Structure S3.4b. Optimized structure of [$PdCl_2$-η1-{SePh}$_2$($P(CF_3)_3$)]···PPh_3.
Energy: -8703.59545358

74

Se	-1.05907	-1.16846	-0.16859
C	-0.95811	-2.12389	2.61004
C	-1.18844	-2.46558	1.27208
C	-1.05973	-3.11169	3.59087
C	-1.51086	-3.78106	0.91590
C	-1.38260	-4.42690	3.24468

H	-0.88751	-2.84805	4.63095
H	-1.69146	-4.03752	-0.12370
C	-1.60634	-4.76004	1.90770
H	-1.46209	-5.18871	4.01553
H	-1.85978	-5.78029	1.63210
Se	1.42458	-0.38672	-0.08404
C	2.31710	-3.09392	-0.67935
C	1.98126	-1.85398	-1.24017
C	2.70229	-4.15253	-1.50477
C	2.02506	-1.68495	-2.63022
C	2.75299	-3.97900	-2.88952
H	2.96018	-5.11229	-1.06495
H	1.74915	-0.72939	-3.06488
C	2.41284	-2.74590	-3.45045
H	3.05341	-4.80353	-3.53035
H	2.44637	-2.60907	-4.52797
Pd	-2.26412	0.84098	0.71130
H	-0.70643	-1.10204	2.87479
H	2.26435	-3.23186	0.39635
Cl	-3.43171	2.81155	1.39562
Cl	-0.40307	1.43266	2.05548
P	-4.22148	0.51647	-0.44676
C	-4.38865	-0.95759	-1.65458
C	-4.72823	1.93876	-1.62737
C	-5.83461	0.20479	0.53051
F	-3.63652	2.58828	-2.01908
F	-5.34006	1.47439	-2.72544
F	-5.55497	2.78795	-1.03263
F	-5.62237	-1.12291	-2.14406
F	-3.54840	-0.76406	-2.68250
F	-4.04589	-2.09499	-1.03333
F	-6.91063	0.41356	-0.23385
F	-5.83371	-1.08455	0.89941

764

F	-5.94283	0.94287	1.61174
P	3.98145	0.67114	0.00503
C	4.83103	0.26409	1.58298
C	5.60997	1.19809	2.28382
C	4.67764	-1.02971	2.10702
C	6.23181	0.83783	3.47990
H	5.72349	2.20718	1.90051
C	5.30860	-1.38890	3.29856
H	4.05714	-1.75298	1.58562
C	6.08503	-0.45493	3.98744
H	6.82834	1.57006	4.01721
H	5.18198	-2.39269	3.69463
H	6.56733	-0.73088	4.92122
C	3.82390	2.49889	-0.02143
C	4.81764	3.33650	-0.55737
C	2.66525	3.07193	0.52943
C	4.65395	4.72209	-0.53660
H	5.71416	2.90826	-0.99495
C	2.51007	4.45892	0.54970
H	1.87438	2.45082	0.94076
C	3.50107	5.28488	0.01652
H	5.42767	5.36094	-0.95428
H	1.60664	4.88498	0.97619
H	3.37467	6.36416	0.02745
C	5.17804	0.26290	-1.32608
C	6.33293	-0.49854	-1.09182
C	4.87858	0.65799	-2.64279
C	7.17676	-0.84395	-2.14953
H	6.57892	-0.81647	-0.08391
C	5.72832	0.31794	-3.69367
H	3.98610	1.24422	-2.84434
C	6.87964	-0.43599	-3.45030
H	8.07099	-1.42907	-1.95215

H	5.48961	0.63935	-4.70391
H	7.53962	-0.70377	-4.27084

Structure S3.5a. Optimized structure of {Se(2-NMe_2)Ph}$_2$.
Energy: -5533.80199052

40

Se	1.08426	-1.10521	-0.48304
C	3.36006	0.42186	0.20425
C	1.99535	0.30552	0.50873
C	4.11929	1.42127	0.82198
C	1.39959	1.17173	1.42536
C	3.52566	2.29597	1.73405
H	5.17682	1.51327	0.58774
H	0.34374	1.07553	1.65836
C	2.16877	2.16561	2.03549
H	4.12012	3.07233	2.20790
H	1.70033	2.84304	2.74470
Se	-1.08427	-1.10522	0.48304
C	-3.36005	0.42186	-0.20426
C	-1.99534	0.30555	-0.50871
C	-4.11929	1.42125	-0.82201
C	-1.39956	1.17180	-1.42529
C	-3.52565	2.29600	-1.73404
H	-5.17683	1.51322	-0.58780
H	-0.34370	1.07563	-1.65827
C	-2.16875	2.16567	-2.03543
H	-4.12011	3.07235	-2.20789
H	-1.70029	2.84314	-2.74460
N	-3.90301	-0.51882	0.74180
N	3.90299	-0.51880	-0.74185
C	4.61333	0.08731	-1.86513
H	5.58369	0.53566	-1.58523
H	4.80641	-0.68271	-2.62042
H	3.98985	0.86430	-2.31575

766

C	4.66910	-1.59488	-0.10963
H	4.89647	-2.36227	-0.85799
H	5.62104	-1.24408	0.32790
H	4.07052	-2.05319	0.68204
C	-4.66918	-1.59483	0.10955
H	-4.89675	-2.36214	0.85793
H	-5.62102	-1.24393	-0.32811
H	-4.07056	-2.05328	-0.68201
C	-4.61329	0.08728	1.86513
H	-4.80628	-0.68273	2.62046
H	-3.98979	0.86431	2.31568
H	-5.58368	0.53560	1.58530

Structure S3.5b. Optimized structure of $\{Se(2\text{-}NMe_2)Ph\}_2\cdots PPh_3$.
No complex formation.

Energy: -6570.08558876

74

Se	-2.95950	-1.14484	-1.09993
C	-2.20231	-3.41481	0.39039
C	-2.84833	-2.18058	0.54781
C	-2.05609	-4.26175	1.49386
C	-3.33753	-1.79240	1.79529
C	-2.54723	-3.88048	2.74390
H	-1.55640	-5.21966	1.37181
H	-3.83807	-0.83597	1.91056
C	-3.18491	-2.64664	2.88993
H	-2.43167	-4.54171	3.59841
H	-3.56794	-2.34318	3.86083
Se	-4.16085	0.78860	-0.42207
C	-3.17620	3.21008	0.66200
C	-2.75751	1.91083	0.33742
C	-2.26710	4.09708	1.24929
C	-1.44737	1.50649	0.59520
C	-0.95652	3.69450	1.51296

H	-2.58836	5.10492	1.49999
H	-1.12885	0.49879	0.34798
C	-0.54821	2.40050	1.18325
H	-0.25772	4.38837	1.97233
H	0.46895	2.07441	1.38582
N	-4.54174	3.55614	0.36171
N	-1.71808	-3.73481	-0.92898
C	-0.25806	-3.77561	-1.02371
H	0.18719	-4.63223	-0.48620
H	0.03227	-3.84476	-2.07738
H	0.16259	-2.85219	-0.61780
C	-2.35475	-4.90834	-1.52462
H	-2.06851	-4.97256	-2.58040
H	-2.06914	-5.85734	-1.03569
H	-3.44157	-4.80261	-1.46752
C	-4.67947	4.34844	-0.86190
H	-5.74052	4.42236	-1.12560
H	-4.27553	5.37164	-0.75793
H	-4.15576	3.84924	-1.68140
C	-5.28883	4.12416	1.48058
H	-6.35221	4.15639	1.21769
H	-5.16985	3.48702	2.36115
H	-4.97709	5.15041	1.74676
P	3.26387	0.55618	0.42005
C	4.39055	-0.67531	1.22495
C	5.78586	-0.69522	1.07332
C	3.79283	-1.62979	2.06587
C	6.55962	-1.65072	1.73653
H	6.27055	0.04057	0.43866
C	4.56431	-2.59067	2.71971
H	2.71516	-1.61523	2.21272
C	5.95171	-2.60209	2.55771
H	7.63937	-1.65086	1.60990

768

H	4.08384	-3.32266	3.36378
H	6.55566	-3.34371	3.07394
C	4.44107	1.87311	-0.13985
C	4.98986	1.95645	-1.42859
C	4.76548	2.87345	0.79329
C	5.84686	3.00575	-1.77024
H	4.74540	1.20198	-2.16995
C	5.63070	3.91402	0.45628
H	4.33326	2.83704	1.79089
C	6.17252	3.98406	-0.82955
H	6.26072	3.05646	-2.77423
H	5.87324	4.67541	1.19314
H	6.83882	4.79972	-1.09775
C	2.80468	-0.29002	-1.16320
C	3.53245	-1.34302	-1.74083
C	1.63365	0.14956	-1.80454
C	3.10717	-1.92957	-2.93486
H	4.43227	-1.70827	-1.25476
C	1.21233	-0.43216	-3.00145
H	1.04314	0.94768	-1.36112
C	1.94942	-1.47351	-3.56969
H	3.68245	-2.74327	-3.36961
H	0.30305	-0.07994	-3.48057
H	1.62023	-1.93093	-4.49913

Structure S3.6a. Optimized structure of [$PdCl_2$-η1-{Se(2-NMe_2)Ph}$_2$(PMe_3)].
Energy: -7042.14255334

56

Se	0.32899	-0.07119	0.33505
C	0.19505	1.87423	0.32062
C	1.04752	2.50057	1.24210
C	-0.04026	4.60685	0.84905
H	1.78320	1.90481	1.77365
C	0.93950	3.86493	1.50816

H	-0.14886	5.66965	1.04930
H	1.60110	4.33300	2.23090
Se	1.82053	-0.66158	-1.47091
C	4.01363	1.11315	-0.97396
C	3.43727	-0.09267	-0.55327
C	5.16371	1.61865	-0.36620
C	5.73451	0.91190	0.68994
H	5.59219	2.55791	-0.70344
H	6.62591	1.28988	1.18415
Pd	-1.94025	-0.91126	-0.27316
H	3.53764	1.66789	-1.77653
Cl	-4.14316	-1.67965	-0.75857
Cl	-1.14340	-1.72243	-2.37568
P	-2.85419	-0.43984	1.82188
C	-1.77838	0.31376	3.12266
H	-0.91539	-0.33050	3.31628
H	-1.41265	1.29161	2.79673
H	-2.34274	0.43708	4.05394
C	-4.31054	0.68283	1.79062
H	-4.77921	0.73780	2.77977
H	-3.99167	1.68480	1.48876
H	-5.02328	0.30087	1.05653
C	-3.45459	-1.97888	2.63134
H	-3.93526	-1.75357	3.59028
H	-4.16177	-2.46858	1.95845
H	-2.60925	-2.65324	2.79874
C	-0.76838	2.62978	-0.40169
C	4.03333	-0.83713	0.50227
N	-1.59931	2.02935	-1.37015
N	3.46044	-2.05152	0.95718
C	-2.91682	2.62140	-1.57434
H	-3.38895	2.83479	-0.61147
H	-2.89293	3.55202	-2.16926

770

H	-3.53698	1.89430	-2.10687
C	-0.94554	1.73834	-2.65551
H	-1.54151	1.00809	-3.20636
H	-0.83328	2.65894	-3.25516
H	0.04061	1.30553	-2.49308
C	3.59773	-3.20498	0.06084
H	4.61911	-3.62384	0.08805
H	2.89344	-3.98515	0.36805
H	3.35841	-2.92585	-0.96437
C	3.72857	-2.42273	2.33960
H	3.02688	-3.21322	2.62725
H	4.75001	-2.80984	2.50970
H	3.56803	-1.56361	2.99703
C	5.17845	-0.29602	1.11342
H	5.65618	-0.83936	1.92178
C	-0.87296	3.99885	-0.08868
H	-1.60568	4.60138	-0.61521

Structure S3.6b. Optimized structure of [$PdCl_2$-η1-{Se(2-NMe_2)Ph}$_2$(PMe_3)]···PPh_3.
No complex formation.

Energy: -8078.42662276

90

Se	2.65927	0.52057	0.14847
C	1.74980	-1.19683	0.32342
C	0.65640	-1.16140	1.20096
C	0.52172	-3.56074	1.16361
H	0.31178	-0.20424	1.58038
C	0.03464	-2.33662	1.62284
H	0.06385	-4.49008	1.49300
H	-0.80227	-2.29275	2.31332
Se	1.82818	1.55776	-1.86764
C	-1.01465	1.38373	-1.57955
C	0.11276	2.07446	-1.11528

C	-2.29209	1.67291	-1.09643
C	-2.43573	2.64974	-0.11261
H	-3.15921	1.13519	-1.46955
H	-3.41846	2.87348	0.29401
Pd	5.05775	-0.04716	-0.24147
H	-0.88019	0.59857	-2.31736
Cl	7.35171	-0.63784	-0.51138
Cl	4.95119	0.75543	-2.49010
P	5.44803	-0.62571	1.98571
C	4.06557	-0.49564	3.20613
H	3.68148	0.52863	3.23058
H	3.24610	-1.16483	2.92902
H	4.42064	-0.76350	4.20773
C	6.05808	-2.34260	2.23669
H	6.36313	-2.49824	3.27774
H	5.26290	-3.05107	1.98629
H	6.90492	-2.50786	1.56710
C	6.74196	0.45469	2.72258
H	6.96802	0.14769	3.75022
H	7.63815	0.39161	2.10172
H	6.39059	1.49102	2.72245
C	2.21397	-2.43355	-0.20363
C	-0.03197	3.10510	-0.14624
N	3.27428	-2.48582	-1.12951
N	1.09655	3.81695	0.33858
C	4.09679	-3.69028	-1.13616
H	4.35018	-3.98111	-0.11310
H	3.61489	-4.54807	-1.63859
H	5.02594	-3.46349	-1.66712
C	2.93058	-2.07052	-2.49830
H	3.84536	-1.82624	-3.04166
H	2.38438	-2.87300	-3.02465
H	2.30700	-1.17778	-2.48150

772

C	1.68765	4.78413	-0.59311
H	1.07111	5.69595	-0.68252
H	2.68108	5.07030	-0.23186
H	1.80738	4.34079	-1.58095
C	0.98780	4.37414	1.67954
H	1.99031	4.65712	2.01888
H	0.35184	5.27639	1.74031
H	0.59030	3.62213	2.36706
C	-1.32323	3.35394	0.35049
H	-1.46509	4.12757	1.09785
C	1.58566	-3.60419	0.26416
H	1.92466	-4.56502	-0.10854
P	-6.09675	-0.03059	-0.53804
C	-7.86205	-0.28591	-1.03619
C	-8.95801	-0.16881	-0.16674
C	-8.10476	-0.59062	-2.38641
C	-10.25991	-0.36121	-0.63461
H	-8.79481	0.07797	0.87809
C	-9.40438	-0.79333	-2.85149
H	-7.26872	-0.66409	-3.07817
C	-10.48618	-0.67686	-1.97576
H	-11.09803	-0.26452	0.05094
H	-9.57275	-1.03122	-3.89854
H	-11.50007	-0.82475	-2.33808
C	-6.26114	0.87312	1.07182
C	-6.20370	0.26637	2.33544
C	-6.41172	2.27018	1.00486
C	-6.30147	1.03444	3.49886
H	-6.08079	-0.80961	2.41241
C	-6.52056	3.03563	2.16608
H	-6.44650	2.76036	0.03416
C	-6.46273	2.41839	3.41839
H	-6.25412	0.54759	4.46975

H	-6.64416	4.11312	2.09354
H	-6.53921	3.01347	4.32454
C	-5.56743	-1.72628	-0.01188
C	-6.44965	-2.77788	0.28202
C	-4.18477	-1.97182	0.05060
C	-5.96139	-4.03778	0.63570
H	-7.52178	-2.61470	0.22797
C	-3.69685	-3.22836	0.41107
H	-3.48445	-1.17510	-0.18978
C	-4.58553	-4.26578	0.70262
H	-6.65832	-4.84226	0.85676
H	-2.62383	-3.39687	0.44863
H	-4.20845	-5.24886	0.97253

Structure S3.7a. Optimized structure of [PdCl-η2-{Se(2-NMe_2)Ph}$_2$(PPh_3)]$^+$. No complex formation.

Energy: -7156.93309412

76

Se	-0.92181	0.18823	-0.96597
C	-1.74515	2.94145	-0.47369
C	-2.08299	1.72873	-1.08260
C	-2.64260	4.01119	-0.58385
C	-3.27532	1.58616	-1.80429
C	-3.83372	3.87355	-1.29627
H	-2.41582	4.96370	-0.11697
H	-3.51112	0.63734	-2.27610
C	-4.15217	2.66273	-1.91350
H	-4.50908	4.72020	-1.37325
H	-5.07274	2.55810	-2.47934
Se	-1.81837	-0.95633	0.99066
C	-4.65250	-1.40341	0.41608
C	-3.31990	-1.82652	0.15262
C	-5.67506	-1.98773	-0.35709
C	-3.05884	-2.84428	-0.77860

C	-5.39984	-2.96257	-1.31312
H	-6.70437	-1.69222	-0.18696
H	-2.03522	-3.17049	-0.93466
C	-4.09210	-3.40927	-1.52015
H	-6.21902	-3.39570	-1.88037
H	-3.88120	-4.18604	-2.24851
Pd	0.92538	1.32548	0.16192
Cl	2.57061	2.46005	1.43540
P	2.49150	-0.41444	-0.02968
N	-4.92638	-0.42540	1.39113
N	-0.48554	3.10277	0.27074
C	0.28769	4.25986	-0.27922
H	-0.26393	5.19818	-0.15222
H	1.23687	4.32428	0.25121
H	0.47039	4.09137	-1.34273
C	-0.77735	3.32101	1.72169
H	0.16953	3.39575	2.25745
H	-1.35698	4.24091	1.86648
H	-1.35012	2.47169	2.09996
C	-4.68758	-0.79199	2.79257
H	-4.50777	0.11114	3.38502
H	-5.55086	-1.32652	3.22308
H	-3.81430	-1.43948	2.88260
C	-6.16327	0.33399	1.24606
H	-6.10687	1.21282	1.89662
H	-6.27269	0.67878	0.21464
H	-7.06571	-0.23328	1.53118
C	3.19083	-0.86899	1.59513
C	2.34254	-0.92479	2.71280
C	4.54809	-1.19011	1.73675
C	2.84430	-1.31623	3.95247
H	1.29625	-0.64778	2.61779
C	5.04542	-1.57347	2.98356

H	5.21889	-1.13289	0.88620
C	4.19693	-1.63991	4.08929
H	2.18357	-1.35520	4.81349
H	6.09923	-1.81382	3.08867
H	4.58903	-1.93490	5.05820
C	1.79664	-1.96791	-0.73011
C	1.61061	-3.11201	0.06031
C	1.44911	-2.01116	-2.09346
C	1.09468	-4.28033	-0.50572
H	1.87833	-3.10038	1.11100
C	0.93599	-3.18035	-2.65317
H	1.60384	-1.14114	-2.72587
C	0.75853	-4.31820	-1.85981
H	0.96617	-5.16296	0.11394
H	0.68505	-3.20557	-3.70961
H	0.36914	-5.23216	-2.29921
C	3.85779	0.01532	-1.17306
C	4.20755	1.35277	-1.41829
C	4.58946	-1.01475	-1.79519
C	5.27068	1.65208	-2.27156
H	3.66659	2.15326	-0.92814
C	5.65520	-0.70580	-2.63933
H	4.32994	-2.05457	-1.62514
C	5.99515	0.62734	-2.88176
H	5.53258	2.69000	-2.45458
H	6.21639	-1.50781	-3.10986
H	6.82221	0.86490	-3.54453

Structure S3.7b. Optimized structure of [PdCl-η2-{Se(2-NMe_2)Ph}$_2$(PPh_3)]$^+$···PPh_3.
Energy: -8193.22905547

110

Se	1.74055	-1.66746	-1.05069
C	0.64328	-1.04563	-3.67992

776

C	1.00919	-2.06665	-2.79972
C	0.14242	-1.40005	-4.94107
C	0.88536	-3.41281	-3.16805
C	0.01371	-2.73724	-5.30926
H	-0.15330	-0.62916	-5.64463
H	1.17356	-4.19257	-2.46981
C	0.38564	-3.74972	-4.42241
H	-0.37572	-2.98598	-6.29174
H	0.29064	-4.79337	-4.70590
Se	-0.24532	-2.05298	0.38466
C	-0.83378	-4.29202	1.77452
C	0.20538	-3.85873	0.95106
C	-0.81415	-5.56894	2.33193
C	1.29387	-4.68198	0.67626
C	0.26963	-6.40843	2.05459
H	-1.62531	-5.90700	2.97088
H	2.11859	-4.34848	0.05486
C	1.31260	-5.96471	1.23752
H	0.30084	-7.40757	2.47836
H	2.15321	-6.62152	1.03204
Pd	1.67592	0.76611	-1.27442
Cl	1.48667	3.11950	-1.56891
P	2.79607	1.24532	0.73670
N	-1.85477	-3.28523	1.95672
N	0.77412	0.37506	-3.31434
C	1.69467	1.05938	-4.27541
H	1.29395	1.02091	-5.29509
H	1.80550	2.09881	-3.96771
H	2.66690	0.56203	-4.25373
C	-0.56981	1.03191	-3.33551
H	-0.45161	2.06786	-3.01887
H	-0.99979	1.00457	-4.34372
H	-1.23739	0.50936	-2.64911

C	-1.92788	-2.75316	3.32639
H	-2.58572	-1.87973	3.33441
H	-2.32152	-3.49830	4.03467
H	-0.92827	-2.45162	3.64888
C	-3.17416	-3.65135	1.42016
H	-3.82182	-2.77004	1.43476
H	-3.06332	-3.99636	0.38932
H	-3.65206	-4.44741	2.01137
C	1.91793	2.48882	1.74912
C	0.51459	2.48126	1.78292
C	2.62798	3.42135	2.51945
C	-0.16718	3.38976	2.59198
H	-0.04814	1.78552	1.16642
C	1.93775	4.32938	3.32377
H	3.71197	3.45117	2.48696
C	0.54277	4.31351	3.36308
H	-1.25295	3.39262	2.59655
H	2.49325	5.05373	3.91234
H	0.00861	5.02712	3.98386
C	3.02798	-0.20711	1.84193
C	2.30012	-0.33925	3.03401
C	3.95068	-1.20923	1.48788
C	2.49827	-1.44856	3.85919
H	1.59014	0.42640	3.32662
C	4.14378	-2.31420	2.31620
H	4.53974	-1.11465	0.57994
C	3.41695	-2.43663	3.50341
H	1.94010	-1.53146	4.78752
H	4.86904	-3.07368	2.03866
H	3.57229	-3.29529	4.15006
C	4.50232	1.84350	0.42188
C	4.82766	2.48969	-0.78157
C	5.49449	1.68605	1.40833

778

C	6.12204	2.96719	-0.99236
H	4.06730	2.63761	-1.53921
C	6.78343	2.17226	1.19166
H	5.26635	1.18319	2.34235
C	7.10044	2.81026	-0.00971
H	6.36181	3.46551	-1.92711
H	7.53957	2.04846	1.96150
H	8.10665	3.18324	-0.17787
P	-3.21380	1.16181	0.17320
C	-3.53867	2.98250	0.18308
C	-4.71713	3.56726	0.67693
C	-2.53165	3.81906	-0.32907
C	-4.88690	4.95258	0.64752
H	-5.50226	2.93981	1.08844
C	-2.70685	5.20394	-0.36486
H	-1.60013	3.39155	-0.69291
C	-3.88443	5.77288	0.12379
H	-5.80331	5.39118	1.03337
H	-1.91829	5.83540	-0.76474
H	-4.01904	6.85086	0.10270
C	-4.33252	0.54833	1.51855
C	-5.55656	-0.10161	1.29688
C	-3.89679	0.72091	2.84535
C	-6.32526	-0.55947	2.37197
H	-5.91751	-0.24511	0.28323
C	-4.67146	0.27842	3.91818
H	-2.94626	1.21369	3.04027
C	-5.88870	-0.36803	3.68343
H	-7.27286	-1.05620	2.18081
H	-4.32586	0.43695	4.93647
H	-6.49171	-0.71676	4.51713
C	-4.06560	0.58096	-1.36625
C	-4.94277	1.36837	-2.12814

C	-3.77691	-0.72287	-1.80930
C	-5.52241	0.86169	-3.29404
H	-5.17482	2.38040	-1.81195
C	-4.36595	-1.23274	-2.96728
H	-3.08512	-1.34287	-1.24239
C	-5.23992	-0.43923	-3.71457
H	-6.19957	1.48526	-3.87164
H	-4.13798	-2.24567	-3.28908
H	-5.69571	-0.83139	-4.61960

Structure S3.8a. Optimized structure of [PdCl-η2-{Se(2-NMe_2)Ph}$_2$(PMe_3)]$^+$.
Energy: -6581.74941307

55

Se	0.00054	-0.23060	-1.04739
C	0.18229	2.61043	-0.42569
C	-0.58805	1.60922	-1.02660
C	-0.30979	3.92168	-0.44196
C	-1.80846	1.90353	-1.64850
C	-1.52733	4.22060	-1.05292
H	0.25869	4.72271	0.01842
H	-2.38192	1.11032	-2.11784
C	-2.27862	3.21426	-1.66258
H	-1.88264	5.24648	-1.05805
H	-3.21961	3.44814	-2.15065
Se	-1.11463	-1.19537	0.90337
C	-3.96462	-0.68397	0.48660
C	-2.85346	-1.50580	0.14091
C	-5.15356	-0.87680	-0.24544
C	-2.98204	-2.51963	-0.82326
C	-5.25314	-1.85395	-1.23249
H	-6.02297	-0.27160	-0.01464
H	-2.12969	-3.15609	-1.03967
C	-4.17369	-2.69517	-1.51795
H	-6.19336	-1.97802	-1.76241

780

H	-4.26039	-3.47362	-2.26920
Pd	2.16171	0.18089	0.00323
Cl	4.21047	0.60293	1.12550
P	3.00285	-1.97291	-0.21532
C	1.93374	-3.16976	-1.11599
H	0.98126	-3.29468	-0.59275
H	1.74134	-2.81966	-2.13440
H	2.43753	-4.14135	-1.16820
C	4.58506	-1.98929	-1.14171
H	4.96473	-3.01488	-1.20934
H	4.42574	-1.59839	-2.15101
H	5.30958	-1.35474	-0.62771
C	3.31823	-2.76381	1.40752
H	3.75113	-3.75947	1.25999
H	4.00490	-2.13919	1.98246
H	2.37811	-2.85898	1.95876
N	-3.86633	0.29148	1.49332
N	1.47848	2.31379	0.20702
C	2.55507	3.14502	-0.42071
H	2.36959	4.21279	-0.25981
H	3.50978	2.87191	0.02742
H	2.58127	2.94186	-1.49330
C	1.40484	2.59026	1.67661
H	2.36283	2.32799	2.12647
H	1.18935	3.64922	1.86191
H	0.61241	1.97942	2.11398
C	-3.66419	-0.17220	2.87269
H	-3.14000	0.59640	3.45003
H	-4.62582	-0.38652	3.36709
H	-3.06685	-1.08431	2.89410
C	-4.80574	1.40664	1.44218
H	-4.43812	2.19727	2.10414
H	-4.85822	1.80790	0.42689

H	-5.82311	1.14032	1.77483

Structure S3.8b. Optimized structure of [PdCl-η2-{Se(2-NMe_2)Ph}$_2$(PMe_3)]$^+$···PPh_3.
Energy: -7618.06023069

89

Se	2.08336	-0.10666	-1.58581
C	2.38960	2.71695	-0.91195
C	1.90361	1.79305	-1.84338
C	2.21245	4.08788	-1.14752
C	1.24741	2.25210	-2.99700
C	1.56212	4.53845	-2.29388
H	2.59124	4.81450	-0.43567
H	0.88023	1.52957	-3.72020
C	1.07799	3.61497	-3.22405
H	1.44578	5.60473	-2.46336
H	0.58078	3.95496	-4.12829
Se	-0.80702	-0.04120	-0.36827
C	-1.04107	-2.62250	-1.76624
C	-0.98656	-1.97593	-0.50258
C	-1.01830	-4.03166	-1.76285
C	-0.93041	-2.72219	0.68215
C	-0.96907	-4.76793	-0.58049
H	-1.05762	-4.55943	-2.70948
H	-0.86415	-2.20563	1.63383
C	-0.93565	-4.11752	0.65308
H	-0.96393	-5.85339	-0.62773
H	-0.89428	-4.68218	1.57965
Pd	3.33436	0.05432	0.48373
Cl	4.46468	0.21113	2.62022
P	3.77502	-2.20043	0.61582
C	3.17963	-3.27867	-0.75383
H	2.08764	-3.25031	-0.81189
H	3.59107	-2.93383	-1.70665

782

H	3.49909	-4.31222	-0.57965
C	5.58601	-2.50268	0.65985
H	5.79324	-3.57352	0.76578
H	6.03955	-2.13740	-0.26631
H	6.01366	-1.95209	1.50067
C	3.10045	-2.99839	2.12661
H	3.44533	-4.03623	2.19577
H	3.43359	-2.43374	3.00006
H	2.00734	-2.98561	2.08567
N	-1.05053	-1.89420	-2.97929
N	3.09734	2.26768	0.30212
C	4.49758	2.79396	0.30123
H	4.50295	3.89081	0.32081
H	5.01467	2.40928	1.18086
H	5.00341	2.44884	-0.60271
C	2.37941	2.73235	1.52455
H	2.89929	2.34358	2.40086
H	2.34754	3.82818	1.57086
H	1.35870	2.34425	1.50062
C	-2.30570	-1.22502	-3.32784
H	-2.11457	-0.50183	-4.12771
H	-3.07089	-1.93749	-3.68081
H	-2.70684	-0.68680	-2.47035
C	-0.45667	-2.55209	-4.13979
H	-0.27472	-1.79463	-4.90892
H	0.50301	-2.99799	-3.86729
H	-1.09857	-3.33142	-4.58622
P	-2.89808	0.40453	0.62153
C	-3.00134	2.22200	0.55187
C	-3.49842	2.94691	1.64811
C	-2.58820	2.90533	-0.60634
C	-3.58828	4.33695	1.57965
H	-3.81154	2.43185	2.55013

C	-2.67812	4.29605	-0.66240
H	-2.19190	2.35996	-1.45721
C	-3.17841	5.01180	0.42760
H	-3.97483	4.89182	2.42924
H	-2.34998	4.81763	-1.55626
H	-3.24581	6.09478	0.38085
C	-2.95095	-0.09162	2.37524
C	-4.14189	-0.54319	2.96837
C	-1.79134	0.04614	3.15900
C	-4.16621	-0.85501	4.32892
H	-5.04487	-0.65112	2.37707
C	-1.82631	-0.26552	4.51714
H	-0.86458	0.38925	2.70834
C	-3.01224	-0.71822	5.10255
H	-5.08916	-1.20487	4.78170
H	-0.92707	-0.15737	5.11623
H	-3.03576	-0.96382	6.16018
C	-4.33768	-0.32070	-0.22070
C	-5.21677	0.48613	-0.96232
C	-4.54146	-1.71322	-0.17124
C	-6.29189	-0.09395	-1.63644
H	-5.07002	1.55997	-1.00737
C	-5.62019	-2.28079	-0.84689
H	-3.86690	-2.34961	0.39266
C	-6.49531	-1.47399	-1.57967
H	-6.97286	0.53579	-2.20112
H	-5.77676	-3.35438	-0.80072
H	-7.33492	-1.92097	-2.10381

Structure S3.9a. Optimized structure of [PdCl-η2-{Se(2-NMe_2)Ph}$_2$($P(CF_3)_3$)]$^+$.
Energy: -7474.81406169

55

Se	-0.99755	0.51497	-0.63863
C	-1.02080	3.37945	-0.12649

784

C	-1.76593	2.28566	-0.57083
C	-1.62735	4.64269	-0.13015
C	-3.08506	2.43470	-1.01590
C	-2.93914	4.79881	-0.57485
H	-1.08235	5.51418	0.21568
H	-3.63956	1.55934	-1.33839
C	-3.67202	3.69659	-1.02053
H	-3.38747	5.78742	-0.57110
H	-4.69234	3.82001	-1.36956
Se	-1.85982	-0.44268	1.43057
C	-3.84285	-2.07213	-0.02909
C	-2.64512	-2.05281	0.73978
C	-4.28576	-3.32531	-0.48286
C	-1.96667	-3.24356	1.04912
C	-3.60608	-4.50315	-0.17008
H	-5.19238	-3.38716	-1.07373
H	-1.04889	-3.19499	1.62514
C	-2.44973	-4.47243	0.60900
H	-3.99449	-5.45080	-0.53201
H	-1.92146	-5.38748	0.85670
Pd	1.22303	1.21458	0.11922
Cl	3.31286	1.86704	1.04978
P	2.36763	-0.76721	-0.21563
C	1.53843	-2.07344	-1.33219
C	4.06784	-0.61408	-1.09379
C	2.73596	-1.83639	1.32254
N	-4.53208	-0.87394	-0.35910
N	0.36800	3.23090	0.35386
C	1.27837	4.13500	-0.42767
H	0.99986	5.18282	-0.27690
H	2.30110	3.98021	-0.08725
H	1.19873	3.88801	-1.48800
C	0.43489	3.56699	1.81543

H	1.45812	3.42233	2.16117
H	0.13271	4.60714	1.97883
H	-0.23843	2.90607	2.36455
C	-5.28540	-0.27219	0.75611
H	-5.57978	0.74615	0.48255
H	-6.19545	-0.84830	0.98718
H	-4.66897	-0.21735	1.65305
C	-5.35880	-0.92736	-1.56722
H	-5.64615	0.09475	-1.83566
H	-4.78793	-1.35517	-2.39526
H	-6.28901	-1.50486	-1.43984
F	1.53442	-1.60710	-2.58857
F	0.26195	-2.25108	-0.94042
F	2.15355	-3.25364	-1.29691
F	4.03616	0.44605	-1.90370
F	4.30523	-1.70856	-1.82796
F	5.03948	-0.47833	-0.19780
F	3.67931	-2.74186	1.05224
F	3.11327	-1.09464	2.35337
F	1.59352	-2.47792	1.63816

Structure S3.9b. Optimized structure of [PdCl-η2-{Se(2-NMe_2)Ph}$_2$($P(CF_3)_3$)]$^+$···PPh_3.
No complex formation.

Energy: -8511.10610897

89

Se	1.51725	1.39963	1.08165
C	0.19896	0.64857	3.56486
C	0.58703	1.70970	2.74603
C	-0.45860	0.94250	4.76724
C	0.33867	3.03872	3.10921
C	-0.70845	2.26310	5.13539
H	-0.78199	0.14283	5.42455
H	0.64393	3.83721	2.44090

C	-0.30839	3.31601	4.30955
H	-1.21753	2.46670	6.07231
H	-0.49944	4.34462	4.59881
Se	-0.34853	1.59692	-0.48623
C	0.76847	4.15260	-1.45753
C	0.48130	2.79012	-1.74654
C	1.39928	4.90021	-2.46526
C	0.79045	2.24144	-3.00124
C	1.70236	4.34662	-3.70980
H	1.64013	5.94153	-2.28360
H	0.57430	1.19473	-3.18775
C	1.38783	3.01759	-3.99121
H	2.17925	4.96609	-4.46406
H	1.62060	2.58430	-4.95879
Pd	1.64149	-1.02888	1.35996
Cl	1.60469	-3.40731	1.54421
P	3.06918	-1.52251	-0.39005
C	4.02741	-0.07095	-1.17483
C	4.53249	-2.68655	0.04262
C	2.32293	-2.30180	-1.96386
N	0.46753	4.71757	-0.18711
N	0.46420	-0.75655	3.19652
C	1.27642	-1.41528	4.27480
H	0.71834	-1.43247	5.21659
H	1.50134	-2.43595	3.96869
H	2.20385	-0.85630	4.41404
C	-0.83231	-1.48972	3.00375
H	-0.60840	-2.52101	2.73204
H	-1.41410	-1.47245	3.93198
H	-1.40878	-1.01960	2.20420
C	-0.96077	5.01373	0.02180
H	-1.13419	5.21710	1.08375
H	-1.27794	5.89686	-0.55655

H	-1.58105	4.16612	-0.26847
C	1.29613	5.85586	0.21467
H	1.12747	6.04936	1.27942
H	2.35374	5.62106	0.06969
H	1.06061	6.78677	-0.32731
F	4.91021	0.38175	-0.27291
F	3.16778	0.92310	-1.46584
F	4.66871	-0.40816	-2.29264
F	4.84018	-2.52627	1.33153
F	5.60569	-2.37335	-0.69578
F	4.20369	-3.95229	-0.19581
F	3.27994	-2.81609	-2.74098
F	1.43949	-3.24993	-1.66916
F	1.69728	-1.31721	-2.63603
P	-3.60358	-1.02472	-0.07256
C	-5.29430	-1.55462	0.45713
C	-6.49354	-1.02154	-0.04430
C	-5.36285	-2.57709	1.41800
C	-7.72544	-1.50493	0.40040
H	-6.46826	-0.22051	-0.77699
C	-6.59428	-3.06700	1.85490
H	-4.44464	-2.99478	1.82478
C	-7.77888	-2.52985	1.34759
H	-8.64444	-1.08187	0.00372
H	-6.62854	-3.86204	2.59473
H	-8.73885	-2.90501	1.69098
C	-3.88664	0.68159	-0.73577
C	-4.48429	1.64722	0.09449
C	-3.40900	1.09017	-1.99369
C	-4.63014	2.96783	-0.33071
H	-4.85962	1.36019	1.07359
C	-3.54235	2.41918	-2.41320
H	-2.95956	0.36223	-2.66216

788

C	-4.15901	3.36041	-1.58730
H	-5.11806	3.69048	0.31818
H	-3.18172	2.70941	-3.39656
H	-4.28114	4.38676	-1.92212
C	-3.30271	-2.02316	-1.60202
C	-2.00513	-2.51450	-1.81385
C	-4.29995	-2.32400	-2.54489
C	-1.70484	-3.27486	-2.94694
H	-1.22796	-2.31310	-1.08052
C	-4.00199	-3.08746	-3.67326
H	-5.31534	-1.97126	-2.39134
C	-2.70320	-3.56216	-3.87788
H	-0.69615	-3.64957	-3.09260
H	-4.78451	-3.31641	-4.39153
H	-2.47487	-4.16096	-4.75528

Structure S3.10a. Optimized structure of $\{Se(2\text{-}NCMe_2)Ph\}_2$.
Energy: -5610.02735733

42

Se	-0.41730	-0.93558	1.78514
C	-2.68702	0.17328	0.28386
C	-1.63879	0.44309	1.19436
C	-3.60408	1.20192	-0.00489
C	-1.52987	1.71096	1.77903
C	-3.49413	2.45428	0.59625
H	-4.42426	0.98928	-0.68488
H	-0.71537	1.90207	2.47173
C	-2.45705	2.71558	1.49526
H	-4.22420	3.22535	0.36393
H	-2.37210	3.68711	1.97412
Se	0.73025	-1.66146	-0.17564
C	2.56184	0.56595	-0.75583
C	2.41285	-0.70331	-0.14960
C	3.84697	1.14030	-0.79290

C	3.52292	-1.34065	0.41969
C	4.94420	0.48930	-0.23408
H	3.97308	2.09852	-1.28898
H	3.38572	-2.30912	0.89058
C	4.78761	-0.75434	0.38085
H	5.92415	0.95744	-0.28038
H	5.63953	-1.26599	0.81920
N	-2.88557	-1.12022	-0.20634
C	-2.80626	-1.44771	-1.43997
C	-3.12494	-2.87586	-1.81036
H	-2.25227	-3.35356	-2.27451
H	-3.41480	-3.44151	-0.92283
H	-3.93715	-2.91314	-2.54823
C	-2.37946	-0.54933	-2.58003
H	-1.47984	-0.96444	-3.05052
H	-3.15915	-0.51226	-3.35159
H	-2.15666	0.46558	-2.24852
N	1.49106	1.17720	-1.41981
C	1.03217	2.33021	-1.10899
C	-0.06406	2.91157	-1.96791
H	-0.25686	2.26367	-2.82539
H	-0.98547	3.02347	-1.38178
H	0.21161	3.91291	-2.32435
C	1.45984	3.18230	0.06811
H	0.57278	3.50295	0.62616
H	2.13494	2.65315	0.74306
H	1.96108	4.09368	-0.28385

Structure S3.10b. Optimized structure of $\{Se(2\text{-}NCMe_2)Ph\}_2\cdots PPh_3$.
No complex formation.

Energy: -6646.31268901

76

Se	-3.54709	0.33149	-1.99301
C	-3.12508	2.80201	-0.46100

C	-3.94879	1.66735	-0.65318
C	-3.54995	3.78667	0.45271
C	-5.14724	1.54268	0.06031
C	-4.75204	3.65799	1.14538
H	-2.93478	4.67244	0.58347
H	-5.76327	0.66215	-0.09719
C	-5.56062	2.53532	0.95097
H	-5.05910	4.44067	1.83444
H	-6.50413	2.43486	1.48032
Se	-1.49990	-0.67961	-1.30400
C	-2.24198	-2.33119	1.01525
C	-2.05604	-2.29480	-0.38589
C	-2.55052	-3.56459	1.61845
C	-2.20328	-3.46718	-1.13820
C	-2.68654	-4.72381	0.85810
H	-2.66253	-3.60161	2.69853
H	-2.06252	-3.41944	-2.21350
C	-2.51754	-4.68060	-0.52697
H	-2.92393	-5.66263	1.35188
H	-2.62085	-5.58145	-1.12495
N	-1.99931	3.00162	-1.26201
C	-0.80695	3.14310	-0.81869
C	0.28405	3.45323	-1.81309
H	1.06318	2.68120	-1.77306
H	-0.12750	3.51301	-2.82261
H	0.77161	4.40525	-1.56294
C	-0.35945	2.99931	0.61938
H	0.47565	2.29063	0.67053
H	0.01625	3.95940	0.99801
H	-1.16185	2.65437	1.27332
N	-1.99671	-1.19694	1.80549
C	-2.89192	-0.63803	2.52978
C	-2.48293	0.53483	3.38659

H	-1.40537	0.69893	3.32208
H	-3.00848	1.44098	3.05780
H	-2.76371	0.36761	4.43487
C	-4.35552	-1.01923	2.60013
H	-4.97242	-0.12381	2.46577
H	-4.63063	-1.75932	1.84664
H	-4.59300	-1.42551	3.59231
P	3.17952	0.54351	-0.09063
C	4.90130	1.22455	-0.01116
C	6.04711	0.54537	-0.45326
C	5.04864	2.52779	0.49479
C	7.30456	1.14987	-0.38206
H	5.95755	-0.45811	-0.85784
C	6.30543	3.12714	0.57771
H	4.16945	3.07778	0.82319
C	7.43815	2.43911	0.13620
H	8.18107	0.61011	-0.73173
H	6.39914	4.13406	0.97635
H	8.41732	2.90768	0.19005
C	3.36656	-0.92814	-1.19915
C	3.72376	-2.21139	-0.75535
C	3.10850	-0.73760	-2.56699
C	3.83099	-3.27096	-1.65852
H	3.91199	-2.38406	0.30009
C	3.22381	-1.79434	-3.47097
H	2.80802	0.24451	-2.92447
C	3.58475	-3.06475	-3.01757
H	4.10545	-4.25938	-1.29864
H	3.02003	-1.62801	-4.52548
H	3.66559	-3.89161	-3.71833
C	2.96565	-0.23311	1.57712
C	4.00363	-0.42246	2.50276
C	1.66343	-0.62508	1.93502

792

C	3.74668	-0.99692	3.75032
H	5.01559	-0.11979	2.25122
C	1.41116	-1.21199	3.17516
H	0.83348	-0.47611	1.24807
C	2.45240	-1.39656	4.08811
H	4.56184	-1.13454	4.45659
H	0.39664	-1.51560	3.41659
H	2.25632	-1.84582	5.05846

Structure S3.11a. Optimized structure of [$PdCl_2$-η1-{Se(2-$NCMe_2$)Ph}$_2$(PMe_3)].
Energy: -7118.37912512

58

Se	0.35296	0.45126	0.58689
C	-0.48649	2.20383	0.53058
C	-0.38280	2.97368	1.69596
C	-1.67701	4.72312	0.66808
H	0.18006	2.58797	2.54134
C	-0.98076	4.23152	1.77462
H	-2.14492	5.70316	0.70939
H	-0.88958	4.82218	2.68118
Se	2.00545	0.68194	-1.14850
C	4.38921	1.73577	0.06251
C	3.55755	0.60844	-0.00432
C	5.59984	1.68886	0.75161
C	5.97018	0.50877	1.40211
H	6.23989	2.56547	0.78912
H	6.90885	0.45885	1.94789
Pd	-1.47157	-1.13660	-0.07630
H	4.08096	2.64830	-0.43893
Cl	-3.36078	-2.47063	-0.67873
Cl	-0.38002	-1.75175	-2.10601
P	-2.59440	-0.94215	1.96767
C	-1.83428	0.02132	3.34778

H	-0.82655	-0.35029	3.55707
H	-1.76868	1.07976	3.08310
H	-2.44412	-0.08006	4.25261
C	-4.28677	-0.23236	1.84694
H	-4.80263	-0.29139	2.81196
H	-4.22082	0.81515	1.53760
H	-4.84145	-0.79131	1.09009
C	-2.81937	-2.60513	2.72297
H	-3.39816	-2.53262	3.65088
H	-3.33221	-3.24871	2.00549
H	-1.83816	-3.03722	2.94229
C	-1.17406	2.69648	-0.60353
C	3.92481	-0.58797	0.65953
N	-1.11759	2.03945	-1.82818
N	3.05647	-1.68266	0.75756
C	-2.12080	1.55806	-2.46382
C	-3.53509	1.46288	-1.93808
H	-4.23781	1.92649	-2.64126
H	-3.80946	0.40297	-1.85726
H	-3.64956	1.93354	-0.95921
C	-1.88793	0.98094	-3.83346
H	-2.01409	-0.10751	-3.79519
H	-2.61635	1.38233	-4.54938
H	-0.87388	1.19880	-4.17264
C	2.98920	-2.63020	-0.10134
C	1.98890	-3.73275	0.12511
H	1.18716	-3.64972	-0.62041
H	2.45619	-4.71797	0.00548
H	1.55214	-3.65266	1.12317
C	3.79973	-2.71874	-1.37276
H	4.26096	-3.70888	-1.46717
H	3.12259	-2.59352	-2.22723
H	4.57720	-1.95345	-1.42414

C	-1.76518	3.97267	-0.50115
H	-2.27356	4.37261	-1.37360
C	5.13895	-0.60826	1.36857
H	5.41287	-1.51824	1.89457

Structure S3.11b. Optimized structure of [$PdCl_2$-η1-{Se(2-$NCMe_2$)Ph}$_2$(PMe_3)]···PPh_3.
Energy: -8154.66645714

92

Se	-1.87768	0.70789	-1.00196
C	-2.31131	-0.73261	-2.23700
C	-2.84035	-0.34275	-3.47418
C	-3.04857	-2.64717	-4.13567
H	-2.94744	0.71552	-3.69543
C	-3.21522	-1.29154	-4.42599
H	-3.33240	-3.40144	-4.86496
H	-3.61814	-0.97338	-5.38297
Se	0.53161	0.33935	-0.72212
C	1.79512	1.94615	-2.76625
C	1.03259	1.99671	-1.59248
C	2.26212	3.11587	-3.36745
C	1.94473	4.35132	-2.79863
H	2.85593	3.06073	-4.27527
H	2.29488	5.27137	-3.25975
Pd	-3.13166	0.12177	1.09407
H	2.02553	0.97973	-3.20346
Cl	-4.45349	-0.58376	2.96557
Cl	-1.13738	-0.26025	2.36497
P	-5.20150	0.71585	0.19384
C	-5.29637	1.49601	-1.47674
H	-4.64919	2.37706	-1.51905
H	-4.97263	0.78921	-2.24480
H	-6.32798	1.80079	-1.68640
C	-6.41092	-0.66516	0.07351

H	-7.39671	-0.29270	-0.22738
H	-6.06055	-1.39236	-0.66521
H	-6.47497	-1.15279	1.04867
C	-6.01458	1.97415	1.26347
H	-7.01434	2.21561	0.88449
H	-6.07889	1.57979	2.27950
H	-5.40488	2.88279	1.27785
C	-2.11962	-2.10257	-1.94004
C	0.70838	3.24705	-1.01298
N	-1.41620	-2.51397	-0.81085
N	-0.17894	3.33285	0.06831
C	-1.89714	-3.21046	0.15104
C	-3.35194	-3.58214	0.32906
H	-3.45778	-4.66581	0.46236
H	-3.72761	-3.10466	1.24359
H	-3.96974	-3.26576	-0.51415
C	-0.96374	-3.66203	1.24151
H	-1.16426	-3.07989	2.14913
H	-1.12487	-4.72185	1.47522
H	0.07507	-3.50054	0.94801
C	0.18359	3.52649	1.28059
C	-0.88163	3.57756	2.34481
H	-0.89604	2.62027	2.88275
H	-0.68182	4.37325	3.07224
H	-1.86552	3.72569	1.89417
C	1.61118	3.65166	1.76001
H	1.74460	4.58840	2.31523
H	1.83468	2.83289	2.45491
H	2.33011	3.61876	0.93917
C	-2.50397	-3.04370	-2.91734
H	-2.33966	-4.09642	-2.70583
C	1.16943	4.41660	-1.64233
H	0.90127	5.37665	-1.21031

796

P	3.57311	-0.46008	0.09482
C	3.86168	0.01286	1.85746
C	5.10959	0.39521	2.37304
C	2.74456	0.00541	2.71293
C	5.24026	0.75332	3.71741
H	5.98145	0.41504	1.72622
C	2.88219	0.35233	4.05777
H	1.76140	-0.26369	2.33339
C	4.12972	0.72960	4.56271
H	6.21316	1.04842	4.10266
H	2.00916	0.33293	4.70453
H	4.23420	1.00681	5.60853
C	5.16793	-0.04238	-0.74255
C	6.21506	-0.95466	-0.94640
C	5.30991	1.26753	-1.23338
C	7.37878	-0.56217	-1.61160
H	6.12159	-1.97471	-0.58698
C	6.47734	1.66109	-1.88785
H	4.49751	1.97954	-1.11202
C	7.51499	0.74593	-2.07995
H	8.18013	-1.28109	-1.76239
H	6.57117	2.67892	-2.25741
H	8.42141	1.04877	-2.59761
C	3.57543	-2.30677	0.15656
C	4.21893	-3.05157	1.15850
C	2.87624	-2.99106	-0.85137
C	4.17817	-4.44672	1.14114
H	4.74616	-2.53908	1.95771
C	2.84032	-4.38671	-0.87007
H	2.34460	-2.42858	-1.61423
C	3.49211	-5.11697	0.12558
H	4.67927	-5.01013	1.92411
H	2.29327	-4.90088	-1.65579

H	3.45819	-6.20331	0.11622

Structure S3.12a. Optimized structure of [PdCl-η2-{Se(2-NCMe$_2$)Ph}$_2$(PPh$_3$)]$^+$.
Energy: -7233.16613453

78

Se	-0.93226	0.07118	0.66658
C	-1.39542	-2.76421	0.32450
C	-1.72595	-1.64664	1.11209
C	-1.79795	-4.03446	0.74848
C	-2.49495	-1.78369	2.26707
C	-2.55454	-4.17474	1.91536
H	-1.49716	-4.91045	0.18340
H	-2.73966	-0.91140	2.86567
C	-2.91489	-3.05618	2.66820
H	-2.85166	-5.16725	2.24009
H	-3.49407	-3.17252	3.57910
Se	-2.04499	0.81842	-1.35194
C	-4.64662	1.69961	-0.38116
C	-3.31861	2.09177	-0.68978
C	-5.56890	2.71320	-0.05568
C	-2.93583	3.44075	-0.62074
C	-5.18277	4.04994	-0.00669
H	-6.60137	2.43670	0.13409
H	-1.90940	3.71179	-0.84621
C	-3.86262	4.42159	-0.27928
H	-5.91956	4.80748	0.24547
H	-3.56453	5.46463	-0.24095
Pd	1.02174	-1.13479	-0.31907
Cl	2.73669	-2.60803	-0.98869
P	2.68164	0.42658	0.20078
N	-0.59096	-2.53866	-0.83033
C	-0.90480	-2.98141	-2.00538
C	-0.02913	-2.68296	-3.18646
H	-0.52126	-1.91802	-3.80345

H	0.96224	-2.34041	-2.89325
H	0.06990	-3.57620	-3.81371
C	-2.15900	-3.75878	-2.32063
H	-2.54493	-3.43371	-3.29213
H	-1.91997	-4.82571	-2.41802
H	-2.93879	-3.64600	-1.56663
N	-5.04587	0.37278	-0.53978
C	-5.63282	-0.32326	0.36147
C	-6.09852	-1.70825	-0.01170
H	-5.91222	-1.90048	-1.06999
H	-5.57883	-2.46209	0.59452
H	-7.17048	-1.82350	0.19344
C	-5.89415	0.09359	1.79379
H	-5.58458	-0.70804	2.47468
H	-5.37948	1.01733	2.06577
H	-6.97002	0.23864	1.95592
C	1.99165	2.09814	0.54399
C	1.39983	2.35877	1.79418
C	2.01488	3.11291	-0.42496
C	0.85484	3.61222	2.06907
H	1.38693	1.59203	2.56357
C	1.46379	4.36557	-0.14502
H	2.47622	2.93773	-1.39059
C	0.88489	4.61843	1.09948
H	0.41407	3.80475	3.04290
H	1.50181	5.14649	-0.89907
H	0.46724	5.59700	1.31817
C	3.65277	0.00041	1.69108
C	4.35040	1.00652	2.38637
C	3.73499	-1.32960	2.13334
C	5.12092	0.68011	3.50156
H	4.29094	2.04104	2.06314
C	4.50413	-1.64519	3.25456

H	3.21879	-2.11425	1.59195
C	5.19667	-0.64495	3.93838
H	5.65890	1.46183	4.02985
H	4.56253	-2.67668	3.58918
H	5.79458	-0.89532	4.80997
C	3.82179	0.63746	-1.21217
C	5.20279	0.78020	-1.02004
C	3.29410	0.67811	-2.51338
C	6.04208	0.97373	-2.11884
H	5.62754	0.73029	-0.02324
C	4.13649	0.88087	-3.60475
H	2.22806	0.53952	-2.67333
C	5.51233	1.02769	-3.40844
H	7.11197	1.07665	-1.96348
H	3.72163	0.91147	-4.60802
H	6.16946	1.17561	-4.26041

Structure S3.12b. Optimized structure of [PdCl-η2-{Se(2-$NCMe_2$)Ph}$_2$(PPh_3)]$^+$⋯PPh_3.
Energy: -8269.46865119

112

Se	-1.04456	1.62099	0.97439
C	-1.19023	3.46990	-1.24390
C	-1.04886	3.37262	0.15245
C	-1.37131	4.72079	-1.84263
C	-1.00089	4.53853	0.92067
C	-1.34627	5.88027	-1.06368
H	-1.55875	4.78380	-2.90988
H	-0.89741	4.46603	1.99943
C	-1.14075	5.79065	0.31335
H	-1.50126	6.84650	-1.53403
H	-1.12751	6.68928	0.92351
Se	1.55486	0.10354	0.22186
C	3.22141	1.47316	2.18519

800

C	2.29480	0.42675	1.98355
C	3.72867	1.65996	3.48478
C	1.85522	-0.35820	3.05602
C	3.30388	0.86303	4.54494
H	4.47151	2.43556	3.64576
H	1.11219	-1.13016	2.88314
C	2.35706	-0.14309	4.33896
H	3.70993	1.03554	5.53783
H	2.01327	-0.75625	5.16642
Pd	-2.38480	0.74572	-0.92030
Cl	-3.81551	0.27744	-2.78782
P	-3.56184	-0.83526	0.32453
N	-1.20869	2.24345	-1.98238
C	-0.46457	2.04911	-3.02097
C	-0.49003	0.73461	-3.74770
H	0.43065	0.18214	-3.51179
H	-1.36315	0.13763	-3.48798
H	-0.48474	0.90655	-4.83052
C	0.52813	3.04786	-3.57030
H	1.42861	2.51099	-3.88807
H	0.11751	3.53557	-4.46356
H	0.79953	3.82255	-2.85222
N	3.71720	2.22255	1.10594
C	3.57489	3.49448	1.02060
C	4.23284	4.20758	-0.13496
H	4.84824	3.51881	-0.71758
H	3.47453	4.66054	-0.78709
H	4.86372	5.02857	0.22790
C	2.77078	4.37389	1.95168
H	2.02074	4.92581	1.37168
H	2.26241	3.80714	2.73286
H	3.41887	5.12276	2.42400
P	3.34881	-1.29431	-0.51897

C	2.79052	-3.02833	-0.64820
C	3.73167	-4.07274	-0.70240
C	1.42195	-3.32373	-0.74920
C	3.30217	-5.39028	-0.86041
H	4.79268	-3.86061	-0.61530
C	1.00062	-4.64426	-0.90933
H	0.68566	-2.52896	-0.68455
C	1.93859	-5.67702	-0.96515
H	4.03351	-6.19222	-0.89854
H	-0.06109	-4.86095	-0.98545
H	1.60890	-6.70493	-1.08550
C	4.84625	-1.29359	0.51235
C	6.00545	-0.60396	0.12445
C	4.81860	-1.97483	1.74292
C	7.12743	-0.61070	0.95306
H	6.03955	-0.07417	-0.82081
C	5.94334	-1.97293	2.56451
H	3.92636	-2.50707	2.05655
C	7.09868	-1.29231	2.17088
H	8.02540	-0.08474	0.64273
H	5.91744	-2.50350	3.51158
H	7.97514	-1.29516	2.81237
C	3.76594	-0.70613	-2.19407
C	3.86540	-1.58845	-3.28122
C	3.98860	0.66969	-2.38661
C	4.19664	-1.09913	-4.54598
H	3.68635	-2.64977	-3.14558
C	4.33137	1.14611	-3.65218
H	3.89694	1.35353	-1.54706
C	4.43311	0.26402	-4.73220
H	4.27056	-1.78547	-5.38428
H	4.51804	2.20670	-3.79549
H	4.69473	0.63958	-5.71724

802

C	-5.23947	-0.26947	0.80758
C	-5.89441	0.70332	0.03548
C	-5.89408	-0.81772	1.92585
C	-7.18311	1.11589	0.37793
H	-5.40527	1.11923	-0.83840
C	-7.18320	-0.40197	2.25868
H	-5.39845	-1.56017	2.54322
C	-7.82884	0.56633	1.48638
H	-7.68051	1.86882	-0.22653
H	-7.67986	-0.83228	3.12373
H	-8.83128	0.89168	1.75005
C	-2.77096	-1.33706	1.91438
C	-2.09419	-2.56020	2.03740
C	-2.82098	-0.47262	3.02291
C	-1.49153	-2.91724	3.24594
H	-2.05251	-3.24610	1.19807
C	-2.22177	-0.83523	4.22926
H	-3.34144	0.47657	2.95045
C	-1.55724	-2.05857	4.34496
H	-0.98734	-3.87615	3.33063
H	-2.28032	-0.16224	5.07983
H	-1.10320	-2.34501	5.28976
C	-3.75112	-2.41909	-0.58896
C	-4.83607	-3.27500	-0.35265
C	-2.76578	-2.79936	-1.51251
C	-4.92625	-4.49628	-1.02308
H	-5.61960	-2.98769	0.34088
C	-2.85577	-4.02349	-2.17600
H	-1.94818	-2.11983	-1.73347
C	-3.93671	-4.87436	-1.93166
H	-5.77631	-5.14717	-0.83983
H	-2.09754	-4.29943	-2.90404
H	-4.01475	-5.82125	-2.45844

Structure S3.13a. Optimized structure of [PdCl-η2-{Se(2-NCMe$_2$)Ph}$_2$(PMe$_3$)]$^+$.
Energy: -6657.98230092

57

Se	0.04769	-0.49412	0.83926
C	-0.38702	2.32039	0.32765
C	0.30456	1.40853	1.14590
C	-0.35799	3.67873	0.65773
C	1.05866	1.84336	2.23473
C	0.38268	4.11548	1.75989
H	-0.93654	4.38661	0.07367
H	1.58437	1.12542	2.85694
C	1.09894	3.20762	2.54119
H	0.38611	5.17126	2.01290
H	1.66298	3.55171	3.40261
Se	1.20007	-1.03693	-1.22839
C	4.00140	-0.94506	-0.43578
C	2.86491	-1.77314	-0.63025
C	5.23096	-1.57753	-0.16623
C	2.96562	-3.16864	-0.50549
C	5.32181	-2.96271	-0.06106
H	6.12126	-0.96473	-0.06620
H	2.08045	-3.77908	-0.65263
C	4.18905	-3.76722	-0.22155
H	6.28602	-3.41813	0.14631
H	4.26291	-4.84704	-0.14133
Pd	-2.22738	0.01889	-0.04136
Cl	-4.37672	0.79771	-0.63304
P	-3.33561	-1.86004	0.72642
C	-2.25934	-3.17835	1.42783
H	-1.53718	-3.51379	0.67741
H	-1.71529	-2.80491	2.29995
H	-2.87249	-4.03319	1.73382

804

C	-4.53757	-1.47129	2.05431
H	-5.07277	-2.37831	2.35629
H	-4.01167	-1.05810	2.92004
H	-5.24501	-0.72593	1.68417
C	-4.27408	-2.69411	-0.60961
H	-4.80818	-3.56195	-0.20704
H	-4.98422	-1.98598	-1.04169
H	-3.58593	-3.02679	-1.39233
N	-1.15484	1.78802	-0.74990
C	-1.06679	2.22381	-1.96604
C	-1.88725	1.59737	-3.05414
H	-1.22737	0.98382	-3.68325
H	-2.69837	0.98370	-2.66455
H	-2.30452	2.37574	-3.70315
C	-0.13125	3.31733	-2.41749
H	0.26856	3.05981	-3.40344
H	-0.68788	4.25559	-2.53933
H	0.69505	3.49171	-1.72734
N	3.91637	0.42879	-0.65269
C	4.32422	1.32542	0.16717
C	4.27228	2.76390	-0.28218
H	3.93647	2.82747	-1.31895
H	3.59361	3.34115	0.35955
H	5.26166	3.23060	-0.19416
C	4.84194	1.09428	1.57129
H	4.36016	1.79491	2.26333
H	4.67885	0.07247	1.91990
H	5.91805	1.30559	1.61802

Structure S3.13b. Optimized structure of [PdCl-η2-{Se(2-$NCMe_2$)Ph}$_2$(PMe_3)]$^+$···PPh_3.
Energy: -7694.28978591

91

Se	2.28328	0.83910	-1.40300

C	3.69019	1.49897	1.03958
C	3.44919	1.90214	-0.28732
C	4.67214	2.15022	1.79450
C	4.11928	3.01698	-0.79922
C	5.35782	3.24616	1.26555
H	4.91847	1.78266	2.78550
H	3.93600	3.32751	-1.82379
C	5.06355	3.69463	-0.02182
H	6.12602	3.73544	1.85648
H	5.59403	4.54524	-0.43998
Se	-0.92861	0.31128	-0.44997
C	-1.82753	3.00239	-1.16462
C	-1.77128	1.65126	-1.57391
C	-2.40240	3.93571	-2.04783
C	-2.21903	1.27472	-2.84712
C	-2.87351	3.54760	-3.29888
H	-2.48160	4.97036	-1.72793
H	-2.12852	0.23997	-3.15874
C	-2.77836	2.21548	-3.70882
H	-3.30824	4.29198	-3.95996
H	-3.13187	1.91224	-4.68931
Pd	2.79486	-1.15562	-0.04088
Cl	3.41392	-3.09167	1.27856
P	2.83573	-2.58460	-1.84437
C	2.25578	-1.94808	-3.47200
C	1.88131	-4.14119	-1.63404
N	2.95352	0.37384	1.53935
C	2.36170	0.40796	2.68872
C	1.60753	-0.78561	3.19936
H	0.53024	-0.57081	3.16916
H	1.83084	-1.68719	2.63065
H	1.86024	-0.96003	4.25238
C	2.30701	1.60973	3.60560

806

H	1.31297	1.65927	4.06309
H	3.02500	1.49483	4.42741
H	2.52213	2.55002	3.09684
N	-1.43993	3.38482	0.12674
C	-0.47750	4.19929	0.36191
C	-0.22224	4.60038	1.79281
H	-0.91733	4.09781	2.46834
H	0.80739	4.35575	2.08202
H	-0.33051	5.68636	1.90940
C	0.46377	4.78990	-0.66206
H	1.49546	4.52083	-0.40358
H	0.25577	4.44561	-1.67600
H	0.40871	5.88555	-0.64117
P	-2.83086	-0.71487	0.43045
C	-2.33852	-2.44056	0.74012
C	-3.29109	-3.47431	0.71505
C	-1.00560	-2.73371	1.07407
C	-2.90748	-4.77980	1.02622
H	-4.32276	-3.26729	0.44858
C	-0.62909	-4.04106	1.38144
H	-0.24788	-1.95653	1.09261
C	-1.58109	-5.06369	1.35961
H	-3.64743	-5.57439	1.00442
H	0.40834	-4.24804	1.62909
H	-1.28877	-6.08181	1.59950
C	-4.23488	-0.70222	-0.71764
C	-5.31625	0.16780	-0.50807
C	-4.21147	-1.53003	-1.85534
C	-6.36978	0.19715	-1.42242
H	-5.34118	0.81145	0.36489
C	-5.27110	-1.49701	-2.75880
H	-3.37743	-2.20432	-2.02637
C	-6.34985	-0.63349	-2.54386

H	-7.20740	0.86708	-1.25370
H	-5.25654	-2.14579	-3.62955
H	-7.17425	-0.61082	-3.25049
C	-3.35288	0.02345	2.01405
C	-3.96465	-0.78697	2.98710
C	-3.18426	1.39806	2.24640
C	-4.41505	-0.21983	4.17817
H	-4.08261	-1.85329	2.82410
C	-3.64632	1.95287	3.44165
H	-2.68392	2.03496	1.51964
C	-4.25969	1.14998	4.40516
H	-4.88302	-0.84939	4.92909
H	-3.51998	3.01710	3.61895
H	-4.61158	1.58825	5.33465
C	4.56598	-3.11705	-2.15257
H	4.60897	-3.83186	-2.98202
H	5.17808	-2.24354	-2.39524
H	4.95658	-3.57754	-1.24179
H	2.23758	-4.65156	-0.73726
H	2.01239	-4.78524	-2.51081
H	0.81917	-3.91160	-1.50971
H	1.20061	-1.66541	-3.40777
H	2.83223	-1.06454	-3.75611
H	2.37205	-2.72264	-4.23819

Structure S3.14a. Optimized structure of [PdCl-η2-{Se(2-$NCMe_2$)Ph}$_2$($P(CF_3)_3$)]$^+$.
Energy: -7551.04720527

57

Se	0.78513	-0.07562	0.59306
C	0.83165	2.79831	0.31590
C	1.33545	1.72620	1.07343
C	1.05784	4.10619	0.75071
C	2.10792	1.95026	2.21092

808

C	1.81871	4.33240	1.90198
H	0.61918	4.93955	0.21249
H	2.48617	1.11325	2.78983
C	2.35314	3.26471	2.62355
H	1.98007	5.35130	2.23973
H	2.93292	3.44847	3.52265
Se	1.97824	-0.61321	-1.45345
C	4.45008	-1.70830	-0.37737
C	3.15687	-2.00621	-0.88276
C	5.32029	-2.79015	-0.13955
C	2.75037	-3.33664	-1.08302
C	4.91424	-4.10334	-0.35996
H	6.33073	-2.58194	0.19769
H	1.75151	-3.53581	-1.45756
C	3.62520	-4.38643	-0.82478
H	5.61097	-4.91414	-0.16706
H	3.31268	-5.41156	-0.99540
Pd	-1.32372	0.92143	-0.30435
Cl	-3.23904	2.16940	-0.88353
P	-2.82950	-0.71306	0.28759
C	-2.10710	-2.24288	1.16532
C	-4.20275	-0.19371	1.51406
C	-3.78419	-1.56630	-1.12730
N	0.04328	2.46853	-0.83104
C	0.24234	2.96412	-2.01206
C	-0.59548	2.52919	-3.17617
H	0.03195	1.93760	-3.85676
H	-1.46626	1.94681	-2.87970
H	-0.92998	3.40713	-3.74099
C	1.33343	3.95192	-2.33793
H	1.72916	3.73354	-3.33440
H	0.91182	4.96460	-2.38073
H	2.14939	3.94771	-1.61420

N	4.87401	-0.38688	-0.26702
C	5.39855	0.13100	0.78171
C	5.92197	1.54140	0.68120
H	5.83538	1.90883	-0.34286
H	5.36543	2.20691	1.35436
H	6.97282	1.58449	0.99430
C	5.53139	-0.52753	2.13884
H	5.20072	0.16397	2.92322
H	4.96533	-1.45806	2.21573
H	6.58550	-0.74821	2.35102
F	-2.91615	-2.38369	-1.74835
F	-4.25500	-0.68647	-1.99998
F	-4.79380	-2.29215	-0.63811
F	-1.04548	-2.68650	0.46702
F	-2.97961	-3.23995	1.28703
F	-1.68786	-1.86686	2.38415
F	-4.57999	-1.23856	2.26158
F	-3.71968	0.75755	2.31675
F	-5.25723	0.26658	0.84706

Structure S3.14b. Optimized structure of [PdCl-η2-{Se(2-$NCMe_2$)Ph}$_2$($P(CF_3)_3$)]$^+$···PPh_3.
Energy: -8587.36939233

91

Se	-4.40365	1.99245	-0.76196
C	-7.05135	0.85928	-0.76657
C	-6.32150	2.03582	-0.52743
C	-8.42118	0.80912	-0.49960
C	-6.99402	3.18320	-0.10627
C	-9.08314	1.95684	-0.05460
H	-8.96090	-0.12568	-0.61313
H	-6.43851	4.09845	0.07513
C	-8.37394	3.14479	0.12007
H	-10.14550	1.91331	0.16440

H	-8.88484	4.03894	0.46540
Se	3.77298	0.90140	-1.20429
C	5.30809	3.05041	0.04880
C	4.14295	2.25346	0.13575
C	5.48225	4.06675	1.00624
C	3.16199	2.52257	1.10095
C	4.52212	4.30365	1.98621
H	6.39044	4.66080	0.97196
H	2.24608	1.94285	1.11525
C	3.35282	3.54052	2.03256
H	4.68304	5.09819	2.70923
H	2.59409	3.73779	2.78319
Pd	-4.44228	-0.41934	-0.22485
Cl	-4.68299	-2.70724	0.55223
P	-2.48238	-0.49665	0.90505
C	-1.40138	1.07310	1.06969
C	-2.58666	-0.99018	2.75472
C	-1.11904	-1.67785	0.26954
N	-6.30198	-0.27111	-1.23972
C	-6.64430	-0.95951	-2.27970
C	-5.78825	-2.09395	-2.76454
H	-5.22326	-1.75558	-3.64437
H	-5.09610	-2.44825	-2.00114
H	-6.42066	-2.92683	-3.09221
C	-7.85769	-0.67019	-3.12985
H	-7.60774	-0.85824	-4.17920
H	-8.67220	-1.35836	-2.87012
H	-8.22296	0.35134	-3.01878
N	6.31343	2.76104	-0.88298
C	6.67685	3.57093	-1.80936
C	7.82814	3.16762	-2.69460
H	8.22893	2.19702	-2.39650
H	7.50634	3.11793	-3.74244

H	8.62759	3.91793	-2.64757
C	6.03949	4.90463	-2.12651
H	5.78617	4.94670	-3.19258
H	5.14054	5.09639	-1.53852
H	6.75477	5.71705	-1.94572
F	-0.36818	-1.00486	-0.63142
F	-1.60773	-2.75898	-0.32373
F	-0.29608	-2.07760	1.26526
F	-1.26837	1.66305	-0.12372
F	-0.15053	0.80943	1.52870
F	-1.97858	1.92281	1.92187
F	-1.56868	-0.44377	3.45955
F	-3.73049	-0.53192	3.25973
F	-2.52371	-2.31166	2.90196
P	4.39839	-1.06865	-0.22531
C	3.49520	-2.28796	-1.22563
C	2.36246	-2.95954	-0.74045
C	3.92389	-2.49947	-2.54969
C	1.66499	-3.83279	-1.57549
H	2.02311	-2.81237	0.27743
C	3.22025	-3.37540	-3.37377
H	4.80561	-1.99315	-2.93194
C	2.09025	-4.03982	-2.88890
H	0.78505	-4.34390	-1.19677
H	3.55501	-3.53890	-4.39358
H	1.54330	-4.72014	-3.53489
C	3.89656	-1.11884	1.51398
C	4.82979	-1.43890	2.51386
C	2.56248	-0.84208	1.86030
C	4.41806	-1.49974	3.84548
H	5.86409	-1.64143	2.25920
C	2.15879	-0.91894	3.19119
H	1.84166	-0.57459	1.09722

812

C	3.08711	-1.24675	4.18349
H	5.13993	-1.74745	4.61769
H	1.12226	-0.72304	3.44533
H	2.77260	-1.30190	5.22151
C	6.16749	-1.45704	-0.35875
C	6.55414	-2.81054	-0.30951
C	7.13557	-0.44617	-0.44729
C	7.90698	-3.14297	-0.34142
H	5.80892	-3.59815	-0.25271
C	8.48705	-0.79643	-0.47842
H	6.85176	0.60204	-0.51463
C	8.87356	-2.13658	-0.42478
H	8.20449	-4.18666	-0.30675
H	9.23811	-0.01506	-0.54852
H	9.92691	-2.39995	-0.45285

Structure S3.15a. Optimized structure of {Se-2-Py}$_2$.
Energy: -5297.95326108

22

Se	-0.90581	-1.29038	0.80249
C	-2.10027	0.11671	0.14997
C	-2.39103	2.18714	-0.77058
C	-3.47984	-0.07694	0.29989
C	-3.77878	2.10861	-0.65624
H	-1.91684	3.06776	-1.19983
H	-3.87115	-1.00483	0.70470
C	-4.32991	0.95054	-0.10461
H	-4.40553	2.92816	-0.99357
H	-5.40653	0.84034	-0.00561
Se	0.82288	-1.26726	-0.78421
C	1.78081	1.05717	0.82089
C	2.07792	0.07149	-0.12424
C	2.80143	1.94202	1.16129
C	4.04940	1.82279	0.54402

H	2.62044	2.72350	1.89486
C	4.22153	0.81368	-0.40153
H	4.86614	2.49615	0.78474
H	5.17113	0.68642	-0.91789
H	0.79097	1.13408	1.25330
N	-1.56087	1.21693	-0.36429
N	3.25566	-0.05564	-0.72938

Structure S3.15b. Optimized structure of $\{Se\text{-}2\text{-}Py\}_2\cdots PPh_3$.
No complex formation.

Energy: -6334.23859268

56

Se	-4.85354	-1.44567	0.44239
C	-5.98996	0.00216	-0.22089
C	-6.41301	2.23955	-0.43265
C	-7.19481	-0.34353	-0.84629
C	-7.64154	2.00923	-1.05220
H	-6.05964	3.25407	-0.25832
H	-7.45149	-1.38385	-1.01689
C	-8.03894	0.68728	-1.25682
H	-8.26269	2.84202	-1.36680
H	-8.98321	0.46014	-1.74439
Se	-2.71351	-0.81968	-0.30596
C	-2.76313	1.07250	1.97935
C	-1.98726	0.24347	1.16401
C	-2.09951	1.79296	2.97035
C	-0.71220	1.68048	3.08935
H	-2.66012	2.44682	3.63362
C	-0.03683	0.84978	2.19664
H	-0.16437	2.22957	3.84904
H	1.04561	0.74229	2.22699
H	-3.83042	1.16645	1.81577
N	-5.60485	1.25858	-0.00968
N	-0.66450	0.12949	1.25325

P	3.62393	0.16102	0.49218
C	3.54145	1.45633	-0.83092
C	3.46716	1.18325	-2.20516
C	3.51464	2.79785	-0.41175
C	3.37864	2.22358	-3.13356
H	3.47470	0.15454	-2.55177
C	3.43852	3.83710	-1.33872
H	3.55086	3.02848	0.65077
C	3.36779	3.55169	-2.70448
H	3.31871	1.99346	-4.19440
H	3.42331	4.86827	-0.99501
H	3.29784	4.35950	-3.42830
C	3.24584	-1.40026	-0.42795
C	4.21333	-2.18825	-1.07263
C	1.90391	-1.81931	-0.45140
C	3.84674	-3.36230	-1.73349
H	5.25658	-1.88707	-1.05453
C	1.54006	-2.98885	-1.12184
H	1.13720	-1.23756	0.05746
C	2.50929	-3.76342	-1.76240
H	4.60728	-3.96362	-2.22564
H	0.49778	-3.29725	-1.13195
H	2.22580	-4.67856	-2.27614
C	5.44628	0.02266	0.80147
C	6.43825	0.56720	-0.02891
C	5.84551	-0.65007	1.96927
C	7.79054	0.43416	0.29579
H	6.15381	1.09906	-0.93177
C	7.19604	-0.79324	2.28784
H	5.09095	-1.06132	2.63576
C	8.17340	-0.24833	1.45169
H	8.54542	0.86378	-0.35815
H	7.48472	-1.32077	3.19339

H	9.22597	-0.35023	1.70282

Structure S3.16a. Optimized structure of [$PdCl_2$-η1-{Se-2-Py}$_2$(PMe_3)].
Energy: -6806.30334917

38

Se	0.46558	0.09560	0.46916
C	0.45865	1.80253	-0.51306
C	-0.04647	4.01447	-0.30356
C	0.82313	1.92030	-1.85283
C	0.30916	4.26357	-1.62767
H	-0.40230	4.81416	0.34217
H	1.12416	1.05396	-2.42973
C	0.74558	3.19426	-2.41366
H	0.23666	5.26769	-2.03335
H	1.01332	3.34572	-3.45553
Se	1.97896	-1.27219	-0.74063
C	4.62211	-1.67496	0.34659
C	3.55984	-0.76132	0.29718
C	5.78224	-1.29189	1.01527
C	5.83284	-0.03499	1.62234
H	6.62875	-1.97080	1.07300
C	4.71121	0.78686	1.52692
H	6.71495	0.29868	2.15954
H	4.70027	1.77093	1.99156
Pd	-1.76944	-0.68857	-0.28831
H	4.53773	-2.65464	-0.11390
Cl	-3.94536	-1.36714	-0.95606
Cl	-0.80285	-1.52398	-2.31368
P	-2.87181	0.12650	1.59560
C	-1.86713	0.96594	2.89705
H	-1.14476	0.26621	3.32834
H	-1.31817	1.80626	2.46016
H	-2.52075	1.33549	3.69548
C	-4.13298	1.38952	1.15705

816

H	-4.69395	1.70302	2.04485
H	-3.63279	2.25839	0.71889
H	-4.80835	0.96064	0.41372
C	-3.77737	-1.18048	2.51753
H	-4.35303	-0.74614	3.34276
H	-4.44282	-1.69512	1.82099
H	-3.06181	-1.90520	2.91773
N	0.02850	2.79580	0.25450
N	3.59653	0.44100	0.86731

Structure S3.16b. Optimized structure of $[PdCl_2\text{-}\eta1\text{-}\{Se\text{-}2\text{-}Py\}_2(PMe_3)]\cdots PPh_3$.
Energy: -7842.59144727

72

Se	-2.16337	-1.00571	-0.50022
C	-2.61421	-1.80268	1.23942
C	-4.21459	-3.00154	2.33497
C	-1.80435	-1.68965	2.36816
C	-3.48744	-2.96883	3.52323
H	-5.17665	-3.50650	2.28036
H	-0.87449	-1.13484	2.33463
C	-2.26327	-2.29612	3.53618
H	-3.87512	-3.45108	4.41510
H	-1.67432	-2.23498	4.44708
Se	0.19604	-0.55712	-0.38922
C	1.82124	-2.38658	-1.97575
C	0.69462	-2.30024	-1.14564
C	2.19159	-3.64469	-2.44751
C	1.42070	-4.75597	-2.10154
H	3.06341	-3.74947	-3.08769
C	0.30753	-4.55401	-1.28680
H	1.67038	-5.75149	-2.45521
H	-0.33019	-5.38747	-0.99787
Pd	-3.17815	1.23307	-0.09525
H	2.38523	-1.50104	-2.24441

Cl	-4.21938	3.35015	0.22673
Cl	-1.26430	1.89620	1.19848
P	-5.15054	0.70184	-1.20382
C	-5.32922	-0.99596	-1.90438
H	-4.57884	-1.16737	-2.68189
H	-5.18329	-1.73858	-1.11355
H	-6.32716	-1.11837	-2.34088
C	-6.60805	0.84999	-0.09358
H	-7.53703	0.66767	-0.64590
H	-6.51718	0.11802	0.71457
H	-6.61384	1.85260	0.33911
C	-5.50097	1.80640	-2.63084
H	-6.48295	1.58412	-3.06382
H	-5.46633	2.84059	-2.28122
H	-4.72943	1.66900	-3.39458
N	-3.78590	-2.42747	1.20011
N	-0.04559	-3.35524	-0.80366
P	3.45083	0.47363	0.02123
C	3.49840	2.31228	0.15600
C	4.65268	3.07884	-0.08176
C	2.30532	2.96669	0.50402
C	4.61370	4.46854	0.03741
H	5.57969	2.58988	-0.36740
C	2.27159	4.35749	0.62675
H	1.39234	2.40180	0.67283
C	3.42379	5.10963	0.39354
H	5.51237	5.05092	-0.15027
H	1.33787	4.84413	0.89384
H	3.39521	6.19267	0.48160
C	4.80420	0.11440	-1.19038
C	5.97392	-0.59240	-0.87472
C	4.59779	0.50815	-2.52618
C	6.91419	-0.89044	-1.86511

818

H	6.15557	-0.90876	0.14752
C	5.54068	0.21746	-3.51129
H	3.69745	1.05751	-2.79332
C	6.70300	-0.48658	-3.18370
H	7.81672	-1.43568	-1.60044
H	5.36708	0.53884	-4.53507
H	7.43672	-0.71768	-3.95133
C	4.13744	-0.12996	1.62763
C	4.83755	0.67861	2.53588
C	3.90464	-1.47514	1.96229
C	5.30293	0.15073	3.74197
H	5.01330	1.72438	2.30416
C	4.38156	-2.00519	3.16161
H	3.34171	-2.10910	1.28111
C	5.08072	-1.19144	4.05591
H	5.83938	0.79113	4.43738
H	4.19606	-3.04869	3.40271
H	5.44331	-1.59926	4.99582

Structure S3.17a. Optimized structure of $[PdCl\text{-}\eta2\text{-}\{Se\text{-}2\text{-}Py\}_2(PMe_3)]^+$.
Energy: -6345.89468478

37

Se	0.57203	0.01384	0.86111
C	0.43004	1.89615	0.33334
C	-1.20168	3.36241	-0.42043
C	1.42329	2.86126	0.34850
C	-0.27191	4.40377	-0.43202
H	-2.23967	3.48395	-0.71259
H	2.43552	2.60413	0.63861
C	1.04692	4.15055	-0.04897
H	-0.58272	5.39567	-0.74185
H	1.78178	4.94996	-0.05751
Se	1.64164	-0.93613	-1.03646
C	4.39596	-1.77473	-0.77807

C	3.47085	-0.82385	-0.34054
C	5.70904	-1.64361	-0.32450
C	6.02458	-0.60558	0.55336
H	6.46739	-2.35373	-0.64060
C	5.01046	0.26986	0.93929
H	7.03142	-0.47820	0.93656
H	5.20924	1.08384	1.63198
Pd	-1.83319	0.23246	0.07010
H	4.10601	-2.58873	-1.43445
Cl	-3.92047	0.97603	-0.66670
P	-2.77903	-1.86180	0.25359
C	-1.61682	-3.14786	0.86794
H	-0.75739	-3.23405	0.19648
H	-1.26060	-2.88518	1.86857
H	-2.12518	-4.11720	0.91922
C	-4.19246	-1.88408	1.41904
H	-4.62734	-2.88863	1.46525
H	-3.85466	-1.59111	2.41734
H	-4.94403	-1.16778	1.07931
C	-3.40467	-2.48766	-1.35064
H	-3.87187	-3.46962	-1.21718
H	-4.13556	-1.77857	-1.74641
H	-2.57919	-2.57511	-2.06298
N	-0.83500	2.13113	-0.03946
N	3.74937	0.17598	0.48659

Structure S3.17b. Optimized structure of [PdCl-η2-{Se-2-Py}$_2$(PMe$_3$)]$^+$···PPh$_3$.
Energy: -7382.21637495

71

Se	-3.92391	1.39584	0.96545
C	-3.37371	2.17286	-0.70565
C	-2.33610	1.48737	-2.68937
C	-3.53546	3.47459	-1.18257
C	-2.45780	2.76307	-3.23153

820

H	-1.89060	0.65358	-3.22282
H	-4.02557	4.22563	-0.57225
C	-3.06511	3.76346	-2.46271
H	-2.09400	2.96495	-4.23307
H	-3.17978	4.76581	-2.86619
Se	0.68199	0.27314	0.28482
C	-0.03622	2.57552	1.82977
C	1.00770	2.03733	1.06921
C	0.16173	3.84330	2.37479
C	1.37551	4.49979	2.15917
H	-0.62269	4.30579	2.96683
C	2.34347	3.86193	1.38775
H	1.56749	5.48313	2.57548
H	3.30354	4.33277	1.19055
Pd	-2.99751	-0.54773	-0.29011
H	-0.96874	2.03841	1.97785
Cl	-1.93714	-2.09499	-1.80575
P	-3.54115	-2.29245	1.09603
C	-4.44523	-1.86234	2.64008
H	-3.82975	-1.20424	3.26069
H	-5.36976	-1.33444	2.38910
H	-4.69033	-2.76572	3.20951
C	-4.63060	-3.49662	0.23785
H	-4.85342	-4.35246	0.88482
H	-5.56588	-3.00454	-0.04479
H	-4.12883	-3.83495	-0.67224
C	-2.09552	-3.27360	1.66757
H	-2.42039	-4.14848	2.24171
H	-1.52401	-3.59305	0.79276
H	-1.45395	-2.64883	2.29615
N	-2.78016	1.22131	-1.45283
N	2.16187	2.64942	0.83760
P	2.81045	-0.43374	-0.12110

C	2.60831	-2.23457	-0.23310
C	3.54092	-3.08609	0.38299
C	1.53937	-2.77232	-0.97191
C	3.40280	-4.46835	0.25395
H	4.36607	-2.67883	0.95752
C	1.40934	-4.15585	-1.08553
H	0.79516	-2.14020	-1.44958
C	2.33968	-5.00285	-0.47732
H	4.12539	-5.12533	0.72861
H	0.57500	-4.56125	-1.64943
H	2.23555	-6.07988	-0.57172
C	3.92910	-0.03984	1.24990
C	5.19329	0.51412	0.99840
C	3.53836	-0.34230	2.56570
C	6.06305	0.75713	2.06244
H	5.49729	0.75460	-0.01448
C	4.41411	-0.09363	3.61962
H	2.55809	-0.76556	2.76442
C	5.67548	0.45594	3.36903
H	7.04224	1.18377	1.86732
H	4.11224	-0.32642	4.63627
H	6.35487	0.64918	4.19398
C	3.47647	0.17653	-1.69683
C	3.95774	-0.74313	-2.64455
C	3.51814	1.55625	-1.96602
C	4.48503	-0.27928	-3.85012
H	3.92152	-1.80906	-2.44953
C	4.04700	2.00414	-3.17464
H	3.13963	2.25894	-1.23028
C	4.52962	1.09004	-4.11603
H	4.85576	-0.99125	-4.58118
H	4.07848	3.06928	-3.38397
H	4.93697	1.44581	-5.05790

Structure S3.18a. Optimized structure of {Se(2-NCMe$_2$)-3-Py}$_2$.
Energy: -5642.10815586

40

Se	0.55322	-0.54836	-1.05428
C	1.94233	0.76314	-0.75023
C	1.84595	2.01918	-1.34815
C	3.98379	2.55274	-0.42884
H	0.96443	2.26911	-1.93099
C	2.88201	2.94192	-1.18583
H	4.81968	3.23479	-0.27821
H	2.83345	3.93028	-1.63227
Se	-0.55330	-0.54844	1.05408
C	-1.84596	2.01913	1.34821
C	-1.94236	0.76315	0.75018
C	-2.88202	2.94189	1.18601
C	-3.98386	2.55276	0.42905
H	-2.83343	3.93022	1.63251
H	-4.81974	3.23483	0.27852
H	-0.96442	2.26900	1.93104
C	3.10564	0.46655	0.00574
C	-3.10566	0.46665	-0.00582
N	-4.10597	1.35275	-0.15165
N	4.10590	1.35266	0.15172
N	3.17664	-0.72613	0.72465
N	-3.17672	-0.72594	-0.72488
C	4.16133	-1.53928	0.65665
C	5.34173	-1.44139	-0.28492
H	6.23438	-1.13314	0.27387
H	5.55577	-2.42424	-0.72144
H	5.18170	-0.71446	-1.08209
C	4.15725	-2.72888	1.58419
H	4.11781	-3.66359	1.00943
H	5.08286	-2.75875	2.17400

H	3.29898	-2.68393	2.25708
C	-4.16122	-1.53928	-0.65658
C	-4.15731	-2.72876	-1.58428
H	-4.11763	-3.66355	-1.00968
H	-5.08308	-2.75861	-2.17382
H	-3.29925	-2.68363	-2.25743
C	-5.34125	-1.44172	0.28551
H	-6.23431	-1.13409	-0.27298
H	-5.55462	-2.42455	0.72241
H	-5.18123	-0.71448	1.08239

Structure S3.18b. Optimized structure of $\{Se(2\text{-}NCMe_2)\text{-}3\text{-}Py\}_2\cdots PPh_3$.
No complex formation.

Energy: -6678.39482336

74

Se	2.60109	0.37969	-1.16456
C	2.06498	1.91397	-0.11698
C	0.78213	1.95258	0.42978
C	1.25488	4.15623	1.21508
H	0.12136	1.09756	0.31991
C	0.35986	3.09455	1.11448
H	0.97111	5.07013	1.73564
H	-0.63300	3.15405	1.54902
Se	4.15418	-0.69669	0.28191
C	2.84233	-1.55949	2.70015
C	3.00956	-1.84023	1.34413
C	2.09232	-2.42590	3.49879
C	1.53823	-3.54954	2.89321
H	1.94031	-2.23040	4.55565
H	0.94755	-4.25694	3.47333
H	3.29509	-0.66705	3.12177
C	2.90035	3.04929	0.04116
C	2.39965	-3.00975	0.82386
N	1.68135	-3.84425	1.59436

N	2.48965	4.14829	0.69656
N	4.22766	2.99676	-0.38555
N	2.42298	-3.25746	-0.55018
C	4.76602	3.88448	-1.13251
C	4.06285	5.05376	-1.78693
H	4.32136	5.98103	-1.26027
H	4.40200	5.16343	-2.82384
H	2.97700	4.95311	-1.76609
C	6.24305	3.76427	-1.41520
H	6.41779	3.61365	-2.48870
H	6.76354	4.69016	-1.13690
H	6.66978	2.92689	-0.86004
C	2.87403	-4.33627	-1.06795
C	2.73455	-4.51830	-2.55852
H	3.72358	-4.58840	-3.02985
H	2.20908	-5.45563	-2.78311
H	2.18659	-3.68177	-2.99596
C	3.56269	-5.46043	-0.32631
H	2.90706	-6.33993	-0.29812
H	4.47520	-5.75566	-0.85788
H	3.81045	-5.19348	0.70175
P	-4.27115	0.51416	-1.16582
C	-6.00010	-0.10979	-0.92366
C	-6.75995	0.07219	0.24228
C	-6.58822	-0.78339	-2.00825
C	-8.06700	-0.41458	0.32350
H	-6.33161	0.59882	1.08974
C	-7.88898	-1.27978	-1.92343
H	-6.02192	-0.91542	-2.92746
C	-8.63356	-1.09422	-0.75613
H	-8.64194	-0.26268	1.23366
H	-8.32464	-1.80171	-2.77157
H	-9.65077	-1.47154	-0.69126

C	-4.07726	1.70444	0.24451
C	-3.54143	1.37297	1.49885
C	-4.46478	3.03573	0.01292
C	-3.40859	2.34363	2.49611
H	-3.22766	0.35285	1.69864
C	-4.34150	4.00326	1.01027
H	-4.86200	3.31574	-0.96015
C	-3.81060	3.65971	2.25619
H	-2.99623	2.06780	3.46368
H	-4.65104	5.02625	0.81240
H	-3.70893	4.41270	3.03342
C	-3.24010	-0.92453	-0.62348
C	-3.70408	-1.98242	0.17407
C	-1.90390	-0.94860	-1.06059
C	-2.84760	-3.02451	0.53827
H	-4.73688	-1.99323	0.51005
C	-1.04420	-1.98320	-0.68708
H	-1.53627	-0.15159	-1.70362
C	-1.51637	-3.02501	0.11613
H	-3.22289	-3.83605	1.15729
H	-0.01062	-1.98364	-1.02248
H	-0.84154	-3.82353	0.41191

Structure S3.19a. Optimized structure of [$PdCl_2$-η1-{Se(2-$NCMe_2$)-3-Py}$_2$(PMe_3)].
Energy: -7150.45629133

56

Se	0.32267	-0.03320	0.48736
C	-0.15788	1.81795	0.83353
C	0.27716	2.34777	2.04892
C	-0.88313	4.35856	1.50825
H	0.89342	1.74681	2.71223
C	-0.08439	3.64886	2.40293
H	-1.21326	5.36895	1.74644

H	0.24163	4.09182	3.33835
Se	1.78092	0.11807	-1.41876
C	3.76445	2.01382	-0.50000
C	3.32684	0.69171	-0.40370
C	4.94507	2.39743	0.13966
C	5.64331	1.42397	0.84998
H	5.31077	3.41802	0.08647
H	6.57470	1.67253	1.35708
Pd	-1.80597	-1.07503	-0.28783
H	3.18371	2.73010	-1.07364
Cl	-3.93369	-1.90502	-0.97717
Cl	-0.93752	-1.34634	-2.48893
P	-2.75616	-1.15821	1.84722
C	-1.74993	-0.62578	3.30222
H	-0.81336	-1.19033	3.34065
H	-1.51196	0.43917	3.23095
H	-2.30724	-0.80168	4.22915
C	-4.31166	-0.19718	2.04295
H	-4.76121	-0.38334	3.02483
H	-4.09762	0.87091	1.94145
H	-5.00217	-0.49547	1.25113
C	-3.20345	-2.89121	2.27231
H	-3.69903	-2.93616	3.24881
H	-3.86407	-3.27941	1.49419
H	-2.29691	-3.50360	2.29778
C	-0.92965	2.63755	-0.03746
C	4.10731	-0.21953	0.35636
N	5.24788	0.14950	0.96300
N	-1.29351	3.88325	0.32887
N	-1.18530	2.24321	-1.33195
N	3.62674	-1.50621	0.59533
C	-2.33299	2.13675	-1.88884
C	-3.66226	2.22882	-1.17825

H	-4.31313	2.94829	-1.68887
H	-4.15559	1.24933	-1.22844
H	-3.55681	2.53410	-0.13588
C	-2.38653	1.82912	-3.35952
H	-2.77471	0.81376	-3.50478
H	-3.06197	2.52550	-3.87205
H	-1.38939	1.88173	-3.79839
C	4.26741	-2.57363	0.30257
C	3.66463	-3.89486	0.70812
H	3.41031	-4.48527	-0.18166
H	4.38499	-4.48611	1.28801
H	2.76129	-3.73706	1.30033
C	5.57845	-2.64798	-0.44705
H	6.37219	-2.98710	0.23051
H	5.50513	-3.38817	-1.25280
H	5.87906	-1.68583	-0.86320

Structure S3.19b. Optimized structure of [$PdCl_2$-η1-{Se(2-$NCMe_2$)-3-Py}$_2$(PMe_3)]···PPh_3.
Energy: -8186.74601361

90

Se	1.80274	-0.58453	-1.11896
C	2.24280	1.01482	-2.13409
C	2.70592	0.84256	-3.43813
C	2.97204	3.20777	-3.59025
H	2.77103	-0.15630	-3.86125
C	3.07665	1.95718	-4.19412
H	3.26942	4.10735	-4.12780
H	3.43322	1.85493	-5.21415
Se	-0.60786	-0.14349	-0.72672
C	-1.96788	-1.57963	-2.85393
C	-1.16602	-1.70993	-1.72097
C	-2.44306	-2.72583	-3.49677
C	-2.08759	-3.96272	-2.96579

828

H	-3.06979	-2.65669	-4.38037
H	-2.44545	-4.88435	-3.42317
Pd	3.12327	-0.30235	1.00265
H	-2.22190	-0.59111	-3.22357
Cl	4.50205	0.12613	2.91440
Cl	1.17110	-0.08275	2.37555
P	5.16259	-0.77017	-0.03043
C	5.20556	-1.30796	-1.79654
H	4.55089	-2.17195	-1.94394
H	4.86723	-0.49896	-2.44864
H	6.22866	-1.58363	-2.07632
C	6.37384	0.61378	0.00992
H	7.34745	0.29009	-0.37525
H	6.00170	1.44149	-0.60140
H	6.47218	0.95410	1.04302
C	5.99975	-2.16814	0.82579
H	6.98866	-2.35192	0.39027
H	6.09148	-1.92319	1.88577
H	5.38829	-3.07023	0.72579
C	2.12552	2.33572	-1.62489
C	-0.84157	-3.01863	-1.27495
N	-1.30592	-4.11845	-1.88953
N	2.50993	3.40296	-2.35079
N	1.46455	2.57026	-0.43038
N	0.09999	-3.18621	-0.26083
C	1.95497	3.17710	0.58595
C	3.40094	3.57875	0.75355
H	3.47024	4.64449	1.00190
H	3.82515	3.01764	1.59659
H	3.99379	3.39109	-0.14276
C	1.05109	3.46018	1.75399
H	1.28399	2.75734	2.56360
H	1.21099	4.47793	2.12989

H	0.00491	3.32692	1.47326
C	-0.14691	-3.70847	0.88072
C	0.98757	-3.84875	1.86118
H	0.94244	-3.02330	2.58379
H	0.92159	-4.79275	2.41432
H	1.94881	-3.78446	1.34685
C	-1.50888	-4.14214	1.36959
H	-1.48585	-5.20336	1.64574
H	-1.76697	-3.57765	2.27424
H	-2.28874	-3.99458	0.62165
P	-3.49386	0.49142	0.15320
C	-3.79807	-0.28878	1.79719
C	-5.06631	-0.68819	2.24839
C	-2.68241	-0.48749	2.63022
C	-5.21663	-1.26871	3.50988
H	-5.93718	-0.54979	1.61493
C	-2.84034	-1.05719	3.89480
H	-1.68659	-0.20452	2.29719
C	-4.10605	-1.45182	4.33608
H	-6.20397	-1.57465	3.84657
H	-1.96853	-1.19383	4.52888
H	-4.22596	-1.90165	5.31827
C	-5.05789	0.20606	-0.78379
C	-5.94062	1.23374	-1.14933
C	-5.33085	-1.10406	-1.21884
C	-7.07348	0.95571	-1.91832
H	-5.74690	2.25285	-0.83074
C	-6.46828	-1.38066	-1.97587
H	-4.64999	-1.91182	-0.96313
C	-7.34298	-0.34985	-2.33027
H	-7.74775	1.76351	-2.19102
H	-6.66725	-2.40014	-2.29580
H	-8.22597	-0.56374	-2.92657

830

C	-3.50053	2.29924	0.51862
C	-4.23318	2.86666	1.57426
C	-2.72305	3.13763	-0.29685
C	-4.19925	4.24332	1.79801
H	-4.82405	2.22986	2.22595
C	-2.69306	4.51604	-0.07287
H	-2.12654	2.71023	-1.09807
C	-3.43155	5.07042	0.97384
H	-4.76872	4.66986	2.61966
H	-2.08296	5.15108	-0.70930
H	-3.40274	6.14191	1.15345

Structure S3.20a. Optimized structure of [PdCl-η2-{Se(2-NCMe$_2$)-3-Py}$_2$(PMe$_3$)]$^+$.
Energy: -6690.05829309

55

Se	-0.05545	-0.53966	-0.80472
C	0.37304	2.29754	-0.34889
C	-0.32516	1.35611	-1.13000
C	-1.11782	1.80340	-2.18354
C	-0.41729	4.02749	-1.62805
H	-1.66985	1.10104	-2.80096
C	-1.16127	3.17543	-2.44428
H	-0.40908	5.09996	-1.80609
H	-1.74290	3.57050	-3.27062
Se	-1.18140	-1.01940	1.28644
C	-3.97655	-0.93638	0.40940
C	-2.85266	-1.75712	0.70504
C	-3.00559	-3.14893	0.68469
C	-5.30479	-2.80870	0.14491
H	-2.15754	-3.78983	0.90473
C	-4.25530	-3.69330	0.40530
H	-6.30222	-3.18713	-0.07125
H	-4.41638	-4.76603	0.39740

Pd	2.23273	0.00403	0.01661
Cl	4.39637	0.80232	0.50754
P	3.33647	-1.88693	-0.73378
C	2.24701	-3.22923	-1.36682
H	1.54937	-3.54839	-0.58665
H	1.67600	-2.88327	-2.23308
H	2.85603	-4.08893	-1.66737
C	4.49429	-1.52905	-2.10851
H	5.02587	-2.44153	-2.40026
H	3.93934	-1.14468	-2.96936
H	5.20768	-0.76910	-1.78232
C	4.31772	-2.68032	0.59604
H	4.84299	-3.55702	0.20115
H	5.03767	-1.95845	0.98705
H	3.65477	-2.99394	1.40784
N	1.19140	1.80366	0.70690
C	1.23790	2.36509	1.87550
C	2.10190	1.78688	2.95353
H	1.45721	1.44793	3.77559
H	2.72623	0.96631	2.60527
H	2.74672	2.57248	3.36632
C	0.43667	3.57802	2.27457
H	0.31194	3.59520	3.36033
H	0.97725	4.48352	1.97647
H	-0.54142	3.61532	1.79178
N	-3.86280	0.44130	0.51796
C	-4.46959	1.28140	-0.24205
C	-4.39475	2.73737	0.13734
H	-3.87492	2.86232	1.08893
H	-3.87774	3.31241	-0.64222
H	-5.40506	3.15872	0.21765
C	-5.25599	0.96806	-1.49420
H	-5.14293	1.77660	-2.22474

H	-4.97186	0.01587	-1.94526
H	-6.32171	0.89730	-1.24478
N	0.32831	3.60280	-0.59763
N	-5.17755	-1.47955	0.13860

Structure S3.20b. Optimized structure of [PdCl-η2-{Se(2-NCMe$_2$)-3-Py}$_2$(PMe$_3$)]$^+$···PPh$_3$.
Energy: -7726.36909619

89

Se	-1.95510	-0.23314	-1.47597
C	-3.26125	-2.14089	0.28791
C	-2.69331	-1.94658	-0.98941
C	-2.74034	-3.01624	-1.88481
C	-3.92959	-4.27456	-0.22674
H	-2.31899	-2.91123	-2.88030
C	-3.37028	-4.20227	-1.50073
H	-4.45366	-5.16749	0.10585
H	-3.44480	-5.04195	-2.18467
Se	1.05688	0.21606	-0.33029
C	1.79734	-2.55625	-0.93842
C	1.63596	-1.24791	-1.46260
C	1.82979	-1.03491	-2.82768
C	2.34426	-3.35673	-3.03610
H	1.69292	-0.04401	-3.24829
C	2.20155	-2.10712	-3.63906
H	2.62910	-4.22515	-3.62774
H	2.37032	-1.97802	-4.70304
Pd	-3.48942	0.84023	0.13713
Cl	-5.24520	1.67218	1.55523
P	-3.84580	2.74891	-1.09425
C	-2.74923	3.03779	-2.54669
H	-1.70888	3.12008	-2.21735
H	-2.82680	2.20053	-3.24514
H	-3.03569	3.96398	-3.05718

C	-5.54093	2.78022	-1.79733
H	-5.71826	3.71687	-2.33759
H	-5.66599	1.93701	-2.48300
H	-6.25809	2.67634	-0.97980
C	-3.68336	4.29420	-0.11335
H	-3.93753	5.16561	-0.72712
H	-4.35215	4.23285	0.74773
H	-2.65488	4.39480	0.24662
N	-3.20246	-1.04262	1.20458
C	-2.99356	-1.20369	2.47164
C	-2.89184	-0.01209	3.37852
H	-1.90490	-0.02009	3.86092
H	-3.05001	0.92993	2.85768
H	-3.63560	-0.09527	4.18085
C	-2.80475	-2.53471	3.16142
H	-2.26619	-2.38824	4.10232
H	-3.78220	-2.97361	3.38786
H	-2.27727	-3.25925	2.53860
N	1.72651	-2.76496	0.43439
C	1.13485	-3.76784	0.97401
C	1.29155	-3.94803	2.46206
H	1.98672	-3.21095	2.86829
H	0.32074	-3.85225	2.96593
H	1.65925	-4.95795	2.68502
C	0.28163	-4.79702	0.26971
H	-0.54211	-5.11455	0.91820
H	-0.12206	-4.43133	-0.67545
H	0.88778	-5.68407	0.04842
N	-3.86892	-3.26647	0.65474
N	2.14743	-3.58370	-1.73376
P	3.18994	0.91264	0.32056
C	4.30044	-0.40445	0.89262
C	4.54914	-0.59200	2.26149

834

C	4.88100	-1.27251	-0.04980
C	5.37631	-1.63434	2.67940
H	4.11235	0.07509	2.99673
C	5.70381	-2.31154	0.37891
H	4.69631	-1.13803	-1.11090
C	5.95132	-2.49451	1.74184
H	5.57554	-1.76885	3.73842
H	6.14994	-2.97921	-0.35185
H	6.59494	-3.30469	2.07179
C	2.84163	2.07120	1.68065
C	3.48079	3.32053	1.73536
C	1.92526	1.71057	2.68582
C	3.21028	4.19387	2.78892
H	4.18343	3.61220	0.96205
C	1.66285	2.59135	3.73479
H	1.42084	0.74958	2.64940
C	2.30341	3.83184	3.78699
H	3.70739	5.15849	2.82682
H	0.95533	2.30976	4.50890
H	2.09378	4.51619	4.60377
C	4.03764	1.82182	-1.01331
C	5.44197	1.85306	-1.07673
C	3.28331	2.55548	-1.94438
C	6.07691	2.60825	-2.06343
H	6.03740	1.29175	-0.36459
C	3.92689	3.30769	-2.92606
H	2.19871	2.53323	-1.90243
C	5.32243	3.33346	-2.98794
H	7.16169	2.62715	-2.10860
H	3.33853	3.87085	-3.64436
H	5.82106	3.91722	-3.75611

Structure S3.21a. Optimized structure of {Se(2-NMe_2)-3-Py}$_2$.
Energy: -5565.88430891

38

Se	-0.63953	-0.80937	1.07528
C	-1.90673	0.53251	0.48721
C	-1.53468	1.86504	0.69553
C	-3.77901	2.52463	0.28822
H	-0.51435	2.08342	0.99438
C	-2.46702	2.89418	0.57237
H	-4.56905	3.27410	0.24488
H	-2.19550	3.93168	0.73753
Se	0.77674	-1.23693	-0.81641
C	1.48486	1.45224	-1.45989
C	1.94392	0.30973	-0.79743
C	2.15163	2.66960	-1.32532
C	3.25418	2.69357	-0.47424
H	1.80587	3.56736	-1.82716
H	3.77742	3.62774	-0.27138
H	0.57596	1.38674	-2.05013
C	-3.25849	0.27106	0.08846
C	3.15969	0.41515	-0.04888
N	-3.74966	-0.98564	-0.20556
N	3.78080	-0.65148	0.56759
C	-5.19481	-1.17109	-0.24762
H	-5.67038	-0.61794	0.56212
H	-5.63531	-0.83121	-1.19700
H	-5.40422	-2.23964	-0.12641
C	-3.01033	-1.93411	-1.03293
H	-2.84360	-2.88477	-0.51214
H	-3.58075	-2.13637	-1.95143
H	-2.04626	-1.52377	-1.32810
C	3.87844	-1.96672	-0.05801
H	4.93622	-2.25926	-0.11018
H	3.33017	-2.73541	0.49868
H	3.49134	-1.94087	-1.07761

836

C	4.82283	-0.37781	1.55047
H	4.92447	-1.25711	2.19552
H	5.79634	-0.16813	1.08262
H	4.54811	0.48344	2.15862
N	3.75172	1.61452	0.12812
N	-4.16265	1.27205	0.04528

Structure S3.21b. Optimized structure of $\{Se(2\text{-}NMe_2)\text{-}3\text{-}Py\}_2\cdots PPh_3$.
No complex formation. No full conversion.

Energy: -6602.16650123

72

Se	4.96380	-0.03155	0.46066
C	4.01216	-1.64453	0.95561
C	3.12143	-1.53086	2.02839
C	3.04398	-3.89949	2.17607
H	2.87305	-0.54225	2.40118
C	2.59784	-2.66663	2.64434
H	2.72517	-4.82374	2.65759
H	1.91061	-2.59502	3.48096
Se	3.59771	1.04596	-1.19438
C	1.11623	1.02124	0.20634
C	2.20183	1.83413	-0.10558
C	0.18011	1.42821	1.14738
C	0.40956	2.65039	1.77345
H	-0.66743	0.80496	1.41447
H	-0.24884	2.99670	2.56827
H	1.03340	0.04733	-0.26571
C	4.31915	-2.96095	0.47885
C	2.26464	3.12063	0.51065
N	5.13662	-3.22045	-0.60442
N	3.21015	4.06418	0.22855
C	5.65589	-4.57226	-0.76891
H	5.95121	-4.98360	0.19625
H	4.91919	-5.25475	-1.21899

H	6.53310	-4.52222	-1.42349
C	5.01827	-2.48142	-1.85776
H	5.97246	-2.02870	-2.15333
H	4.69684	-3.16685	-2.65608
H	4.26917	-1.69596	-1.77728
C	3.67459	4.32482	-1.13011
H	3.52131	5.38795	-1.36229
H	4.73691	4.08812	-1.25980
H	3.10338	3.74226	-1.85429
C	3.35141	5.19077	1.14108
H	4.35170	5.61603	1.00821
H	2.60517	5.97796	0.95509
H	3.23811	4.85444	2.17207
N	1.39737	3.47039	1.45936
N	3.85991	-4.04790	1.13297
P	-4.07540	-0.34175	0.37651
C	-5.67166	-0.95452	1.09040
C	-6.63304	-1.68741	0.37720
C	-5.90610	-0.68464	2.44970
C	-7.80037	-2.12883	1.00485
H	-6.46813	-1.91787	-0.67098
C	-7.07683	-1.11556	3.07388
H	-5.16226	-0.13608	3.02319
C	-8.02708	-1.84169	2.35213
H	-8.53363	-2.69749	0.43844
H	-7.24216	-0.89392	4.12507
H	-8.93545	-2.18701	2.83877
C	-3.93584	-1.31051	-1.19679
C	-4.40522	-0.87287	-2.44498
C	-3.28131	-2.55231	-1.12357
C	-4.23305	-1.66092	-3.58554
H	-4.90328	0.08840	-2.52776
C	-3.11928	-3.34450	-2.26024

838

H	-2.89219	-2.89791	-0.16841
C	-3.59374	-2.89874	-3.49614
H	-4.60032	-1.30579	-4.54515
H	-2.61357	-4.30352	-2.18310
H	-3.45974	-3.50967	-4.38497
C	-4.52115	1.35345	-0.22378
C	-5.83289	1.82272	-0.39340
C	-3.45360	2.22906	-0.48671
C	-6.06807	3.13089	-0.82352
H	-6.67321	1.16745	-0.18443
C	-3.68811	3.53228	-0.92492
H	-2.43400	1.88215	-0.33753
C	-4.99828	3.98693	-1.09266
H	-7.08983	3.48087	-0.94778
H	-2.84958	4.19447	-1.12400
H	-5.18447	5.00501	-1.42455

Structure S3.22a. Optimized structure of [$PdCl_2$-η1-{Se(2-NMe_2)-3-Py}$_2$(PMe_3)].
Energy: -7074.23125142

54

Se	0.30067	-0.04009	0.34745
C	0.14209	1.88128	0.07721
C	0.95984	2.62467	0.93676
C	-0.34708	4.54648	0.45228
H	1.73546	2.11843	1.50355
C	0.74622	3.99051	1.11367
H	-0.62552	5.58663	0.61848
H	1.36731	4.58157	1.77820
Se	1.86271	-0.88913	-1.32313
C	3.76527	1.22134	-1.02192
C	3.43218	-0.05709	-0.55455
C	4.76719	1.97026	-0.40967
C	5.37139	1.41022	0.71549

H	5.03595	2.96083	-0.76107
H	6.10902	1.97463	1.28577
Pd	-1.92735	-1.07261	-0.11084
H	3.20440	1.63445	-1.85493
Cl	-4.05509	-2.07292	-0.45828
Cl	-1.02921	-2.26625	-1.97559
P	-2.97340	-0.13703	1.75750
C	-2.00947	0.97495	2.87523
H	-1.12214	0.45649	3.25116
H	-1.68647	1.87113	2.33933
H	-2.62955	1.27495	3.72758
C	-4.45482	0.86958	1.34473
H	-4.97232	1.19040	2.25588
H	-4.14635	1.75079	0.77482
H	-5.12037	0.26468	0.72528
C	-3.57280	-1.44248	2.90644
H	-4.12563	-0.99891	3.74240
H	-4.21460	-2.12746	2.34862
H	-2.71753	-2.00351	3.29543
C	-0.85224	2.58150	-0.68370
C	4.21125	-0.59129	0.52699
N	-1.63499	1.99208	-1.65197
N	4.08294	-1.86951	1.01831
C	-2.82443	2.71231	-2.09932
H	-3.35190	3.14288	-1.24768
H	-2.57936	3.52861	-2.79431
H	-3.47630	1.99554	-2.60746
C	-1.01736	1.20956	-2.72943
H	-1.63743	0.34809	-2.98430
H	-0.89092	1.84800	-3.61807
H	-0.03760	0.84237	-2.43398
C	3.79030	-3.02235	0.16758
H	4.49552	-3.82459	0.41641

840

H	2.76965	-3.39719	0.29908
H	3.92981	-2.77256	-0.88592
C	4.72154	-2.19954	2.28916
H	4.21311	-3.07246	2.71080
H	5.78926	-2.43405	2.17028
H	4.63609	-1.36303	2.98178
N	5.11775	0.18325	1.16400
N	-1.10697	3.87967	-0.41517

Structure S3.22b. Optimized structure of [$PdCl_2$-η1-{Se(2-NMe_2)-3-Py}$_2$(PMe_3)]···PPh_3.
Energy: -8110.51850043

88

Se	-1.95371	-0.71200	-0.60520
C	-2.52821	-1.74341	0.94609
C	-2.55396	-3.12221	0.71081
C	-3.85582	-3.39793	2.67702
H	-2.10206	-3.51584	-0.19481
C	-3.19969	-3.98302	1.59762
H	-4.44893	-4.00337	3.36173
H	-3.23159	-5.05394	1.42715
Se	0.47521	-0.30113	-0.32444
C	1.07987	-2.86070	0.79274
C	0.92303	-2.18818	-0.42443
C	1.22072	-4.24772	0.83400
C	1.13030	-4.92454	-0.37988
H	1.34226	-4.78090	1.77112
H	1.15730	-6.01378	-0.41046
Pd	-3.10947	1.50386	-0.55515
H	1.06083	-2.28559	1.71319
Cl	-4.25817	3.59040	-0.59332
Cl	-1.00834	2.63665	-0.32642
P	-5.23391	0.62808	-0.93954
C	-5.45014	-1.19970	-1.09571

H	-4.80907	-1.58918	-1.89219
H	-5.18135	-1.69822	-0.16109
H	-6.49399	-1.43131	-1.33616
C	-6.46380	1.08516	0.34766
H	-7.46532	0.73969	0.06715
H	-6.17685	0.63000	1.29984
H	-6.45595	2.17131	0.46047
C	-5.93145	1.25363	-2.52289
H	-6.95849	0.89696	-2.66186
H	-5.90846	2.34516	-2.50426
H	-5.31180	0.90489	-3.35474
C	-3.10458	-1.25753	2.16497
C	0.97087	-2.97173	-1.62583
N	-3.05497	0.06436	2.56661
N	0.91342	-2.44323	-2.89663
C	-3.95988	0.47684	3.63620
H	-4.95864	0.07206	3.46828
H	-3.62026	0.13669	4.62566
H	-4.00420	1.57016	3.63227
C	-1.76302	0.75746	2.63857
H	-1.88207	1.81226	2.38259
H	-1.35331	0.67195	3.65806
H	-1.04530	0.32480	1.94635
C	1.60290	-1.20814	-3.26703
H	2.25178	-1.41274	-4.12876
H	0.90437	-0.40699	-3.53475
H	2.23459	-0.85607	-2.45262
C	0.65506	-3.34293	-4.01519
H	0.27803	-2.74615	-4.85235
H	1.56009	-3.87667	-4.34079
H	-0.09205	-4.08615	-3.73773
N	1.01648	-4.32091	-1.56217
N	-3.80312	-2.09594	2.95809

842

P	3.69058	0.60535	0.16726
C	3.78532	2.43306	0.39702
C	5.00068	3.14077	0.40180
C	2.58411	3.14112	0.55521
C	5.01030	4.52466	0.57276
H	5.93786	2.60877	0.26401
C	2.59694	4.52793	0.72579
H	1.63035	2.62205	0.52785
C	3.80802	5.22007	0.73600
H	5.95555	5.06162	0.57337
H	1.65570	5.05895	0.83504
H	3.81783	6.29970	0.86167
C	5.08152	0.28380	-1.01276
C	6.25504	-0.41248	-0.68877
C	4.91068	0.73504	-2.33464
C	7.23224	-0.64816	-1.65993
H	6.41189	-0.77061	0.32357
C	5.89067	0.50751	-3.29941
H	4.00887	1.27928	-2.60630
C	7.05517	-0.18945	-2.96536
H	8.13660	-1.18762	-1.38990
H	5.74388	0.87162	-4.31296
H	7.81728	-0.37292	-3.71800
C	4.29143	-0.09746	1.76689
C	4.66035	0.68810	2.86919
C	4.29649	-1.49773	1.90794
C	5.03695	0.08970	4.07417
H	4.65354	1.77008	2.78865
C	4.68669	-2.09348	3.10720
H	3.99265	-2.12639	1.07478
C	5.05645	-1.30010	4.19631
H	5.31836	0.71476	4.91775
H	4.69322	-3.17706	3.19318

H	5.35211	-1.76280	5.13416

Structure S3.23a. Optimized structure of [PdCl-η2-{Se(2-NMe_2)-3-Py}$_2$(PMe_3)]$^+$.
Energy: -6613.83435573

53

Se	-0.01329	-0.24149	-1.02097
C	0.23115	2.59972	-0.42079
C	-0.57044	1.60490	-0.98861
C	-1.79645	1.97080	-1.55907
C	-1.31377	4.22495	-0.92181
H	-2.43579	1.22246	-2.01752
C	-2.17722	3.30852	-1.52677
H	-1.56799	5.28064	-0.86714
H	-3.11599	3.63534	-1.96140
Se	-1.16575	-1.18184	0.97036
C	-4.03600	-0.66067	0.40027
C	-2.89634	-1.53051	0.25608
C	-3.02758	-2.63748	-0.60720
C	-5.13299	-1.79191	-1.30472
H	-2.20422	-3.34121	-0.68372
C	-4.16516	-2.80498	-1.37815
H	-5.99725	-1.80624	-1.96702
H	-4.28458	-3.64875	-2.04842
Pd	2.17625	0.16861	-0.00483
Cl	4.25279	0.59507	1.05415
P	2.99378	-2.00027	-0.19212
C	1.88976	-3.20866	-1.03447
H	0.95071	-3.31210	-0.48291
H	1.67268	-2.88116	-2.05553
H	2.38232	-4.18641	-1.07751
C	4.55013	-2.05587	-1.16000
H	4.92010	-3.08596	-1.21053
H	4.36717	-1.68993	-2.17465

H	5.29319	-1.41425	-0.68243
C	3.34739	-2.75721	1.43934
H	3.76916	-3.75929	1.30366
H	4.05402	-2.12484	1.98072
H	2.42248	-2.83205	2.01875
N	-4.16873	0.30533	1.35612
N	1.54409	2.30015	0.16885
C	2.58512	3.12817	-0.52730
H	2.34347	4.18970	-0.42363
H	3.55296	2.90757	-0.07902
H	2.60393	2.85815	-1.58595
C	1.51465	2.65188	1.62630
H	2.49399	2.43116	2.05048
H	1.27325	3.71243	1.74701
H	0.75611	2.04261	2.12374
C	-3.50593	0.25594	2.65601
H	-2.65769	0.94566	2.72265
H	-4.23571	0.52500	3.42705
H	-3.15178	-0.75625	2.86961
C	-5.29397	1.24185	1.28150
H	-5.00557	2.16492	1.79251
H	-5.53627	1.45619	0.24245
H	-6.19035	0.83242	1.76475
N	-0.14026	3.87542	-0.38637
N	-5.07949	-0.77767	-0.45366

Structure S3.23b. Optimized structure of [PdCl-η2-{Se(2-NMe_2)-3-Py}$_2$(PMe_3)]$^+$···PPh_3.
Energy: -7650.14535697

87

Se	-2.43610	0.87714	1.53879
C	-3.41449	1.99231	-0.97215
C	-2.96068	2.26391	0.32400
C	-2.90464	3.61246	0.70932

C	-3.69963	4.21528	-1.46885
H	-2.57577	3.87514	1.71075
C	-3.28121	4.60202	-0.19340
H	-4.00042	4.95132	-2.21082
H	-3.25791	5.65088	0.08589
Se	0.93008	0.21373	0.56747
C	1.60207	3.14691	0.92935
C	1.78769	1.77985	1.33959
C	2.50894	1.53402	2.51829
C	2.77877	3.86566	2.81713
H	2.63407	0.50983	2.85256
C	3.04215	2.57244	3.27032
H	3.13232	4.73222	3.37450
H	3.60308	2.39049	4.18019
Pd	-3.01814	-0.94474	0.03543
Cl	-3.42167	-2.76870	-1.52223
P	-2.74563	-2.57316	1.64381
C	-2.27399	-2.04147	3.34311
H	-1.29970	-1.54376	3.32607
H	-3.01359	-1.33705	3.73355
H	-2.21993	-2.91030	4.00836
C	-4.32256	-3.48469	1.88250
H	-4.19608	-4.28850	2.61645
H	-5.09430	-2.79367	2.23419
H	-4.63572	-3.90083	0.92199
C	-1.50296	-3.86263	1.22955
H	-1.49334	-4.64462	1.99714
H	-1.75747	-4.29360	0.25909
H	-0.50944	-3.40997	1.16192
N	0.92319	3.59636	-0.17177
N	-3.56250	0.60442	-1.45027
C	-5.01036	0.35491	-1.74968
H	-5.35748	1.06149	-2.51058

H	-5.11891	-0.67226	-2.09899
H	-5.58909	0.49239	-0.83329
C	-2.76366	0.41689	-2.69697
H	-2.89687	-0.60980	-3.03826
H	-3.09248	1.12598	-3.46320
H	-1.70898	0.59229	-2.46848
C	0.67799	2.81747	-1.37833
H	-0.28591	2.29568	-1.35011
H	0.67274	3.50274	-2.23082
H	1.47180	2.09028	-1.54786
C	0.62586	5.02702	-0.28598
H	-0.26221	5.13969	-0.91334
H	0.42953	5.45303	0.69600
H	1.45912	5.58238	-0.73689
N	-3.76415	2.93503	-1.84370
N	2.10149	4.13676	1.71009
P	2.76127	-0.77988	-0.46516
C	3.56776	0.32148	-1.65944
C	3.40935	0.10505	-3.03862
C	4.29922	1.43562	-1.20323
C	3.99123	0.98669	-3.94998
H	2.84370	-0.74793	-3.39872
C	4.87540	2.30906	-2.12399
H	4.42104	1.61836	-0.14035
C	4.72322	2.08549	-3.49549
H	3.87425	0.81093	-5.01504
H	5.44290	3.16416	-1.76946
H	5.17582	2.76796	-4.20876
C	2.07057	-2.23382	-1.31009
C	2.87892	-3.37028	-1.49582
C	0.74686	-2.23290	-1.78375
C	2.36563	-4.48315	-2.15980
H	3.89782	-3.38908	-1.12236

C	0.23601	-3.35897	-2.43078
H	0.10359	-1.36978	-1.64399
C	1.04682	-4.47975	-2.62302
H	2.99387	-5.35685	-2.30533
H	-0.80004	-3.35640	-2.75560
H	0.64831	-5.35496	-3.12780
C	4.00155	-1.36351	0.73324
C	5.37795	-1.23481	0.48504
C	3.56161	-2.02439	1.89436
C	6.29972	-1.75779	1.39435
H	5.73275	-0.73555	-0.40984
C	4.48889	-2.54405	2.79451
H	2.49887	-2.12852	2.09364
C	5.85852	-2.40897	2.54688
H	7.36261	-1.65466	1.19789
H	4.14392	-3.05281	3.68963
H	6.57925	-2.81227	3.25198

Figure S3.24. 3D electrostatic potential maps of $\{SePh\}_2$, $\{Se(2\text{-}NMe_2)Ph\}_2$ and $\{Se(2\text{-}N{=}CMe_2)Ph\}_2$ at ρ=0.004 level (red = negative, blue = positive, color-normalized to potential of $\{SePh\}_2$ at $-4.795e^{-2}$).

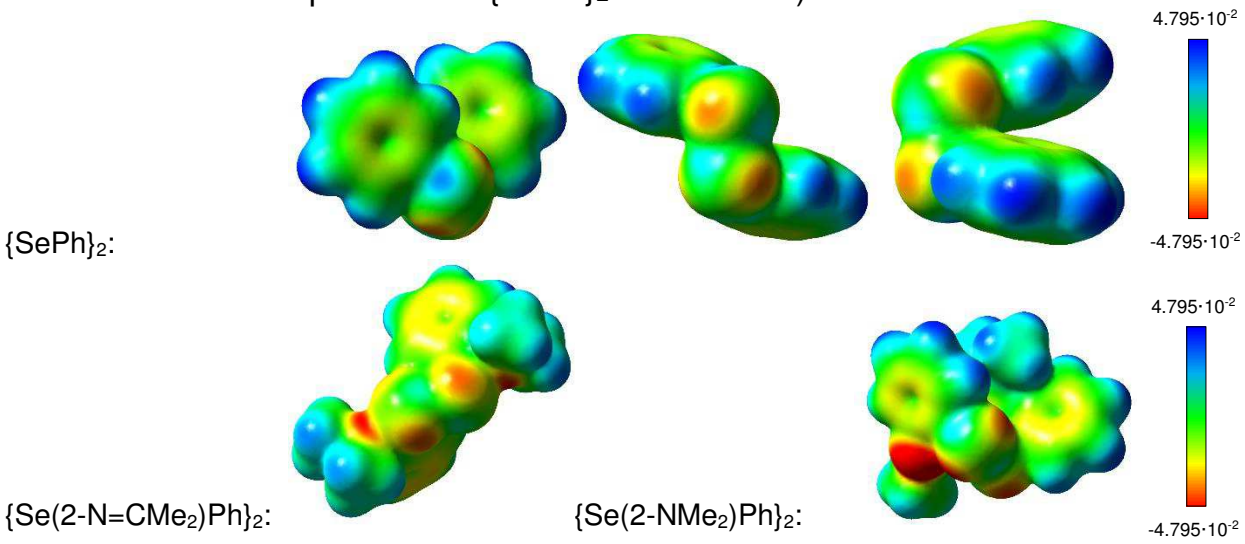

Figure S3.25. 2D electrostatic potential maps of $\{SePh\}_2$, $[PdCl_2\text{-}\eta1\text{-}\{SePh\}_2(PPh_3)]$, $[PdCl_2\text{-}\eta1\text{-}\{SePh\}_2(PMe_3)]$ and $[PdCl_2\text{-}\eta1\text{-}\{SePh\}_2(P(CF_3)_3)]$ with iso lines. The bold line resembles the van der Waals radii; red = positive; blue = negative. The numbers given on the selenium atoms are the Bader atomic charge (upper number) and the Bader size (lower number). The viewer looks on a cross-section of the C-Se-Se-Pd plane.

Ph2Se2:

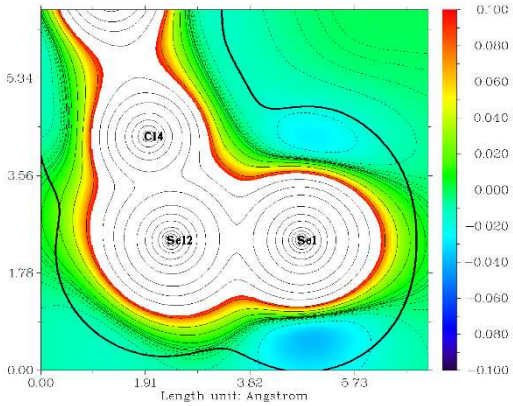

PdPhSe2Cl2PMe3

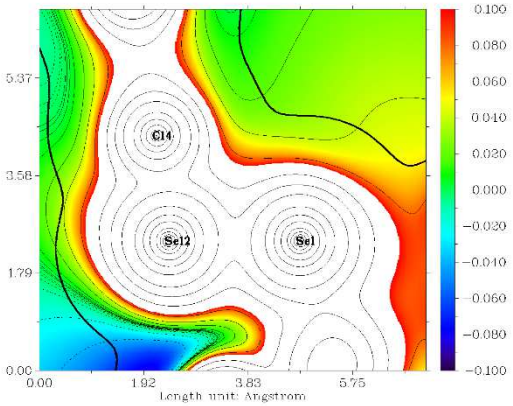

PdPhSe2Cl2PPh3:

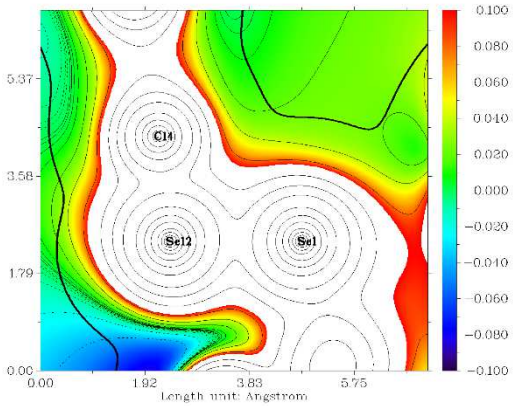

PdPhSe2Cl2P(CF3)3

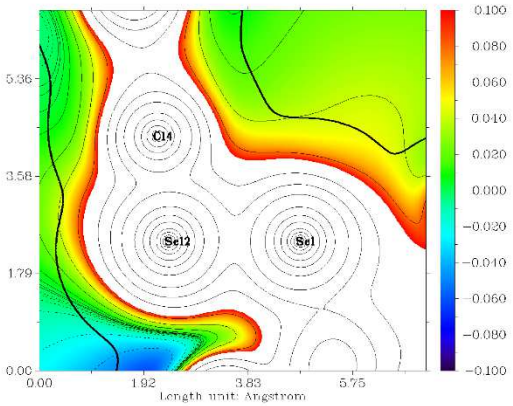

Figure S3.26. 3D electrostatic potential maps of $\{SePh\}_2$, $[PdCl_2\text{-}\eta1\text{-}\{SePh\}_2(PPh_3)]$, $[PdCl_2\text{-}\eta1\text{-}\{SePh\}_2(PMe_3)]$ and $[PdCl_2\text{-}\eta1\text{-}\{SePh\}_2(P(CF_3)_3)]$ at ρ=0.004 level (red = negative, blue = positive, color-normalized to potential of $\{SePh\}_2$ at $-4.795\cdot10^{-2}$ to $4.795\cdot10^{-2}$).

$\{SePh\}_2$:

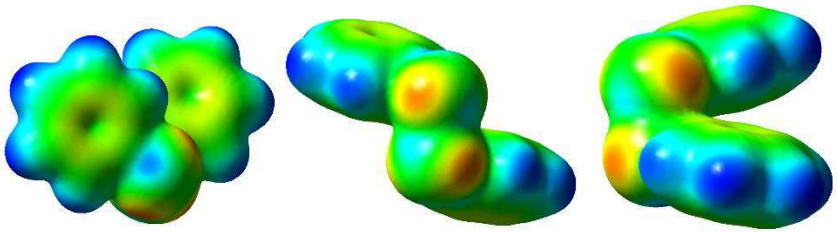

$[PdCl_2\text{-}\eta1\text{-}\{SePh\}_2(PPh_3)]$:

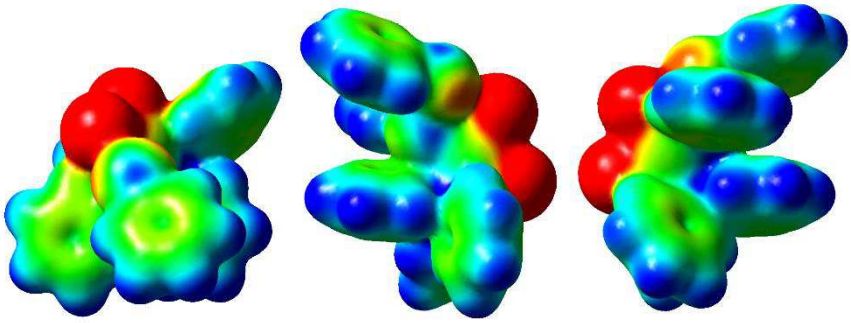

$[PdCl_2\text{-}\eta1\text{-}\{SePh\}_2(PMe_3)]$:

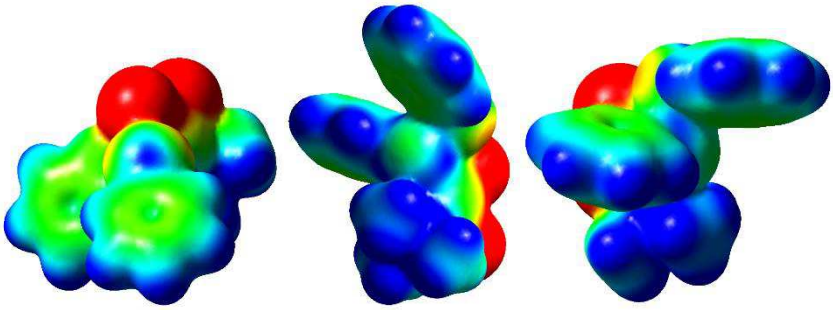

$[PdCl_2\text{-}\eta1\text{-}\{SePh\}_2(P(CF_3)_3)]$:

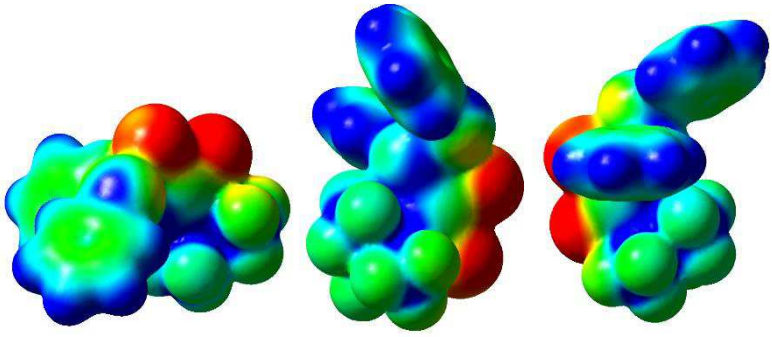

$[PdCl_2\text{-}\eta1\text{-}\{Se(2\text{-}NMe_2)Ph\}_2(PMe_3)]$:

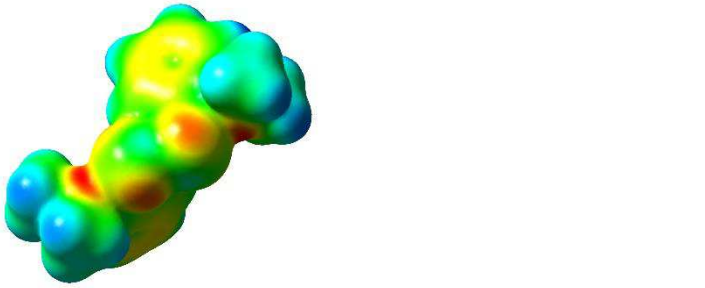

850

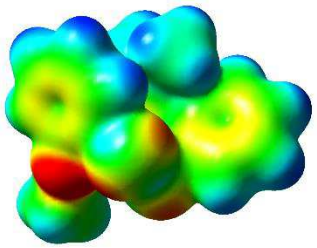

[$PdCl_2$-η1-{Se(2-$NCMe_2$)Ph}$_2$(PMe_3)]:

Figure S3.27. 3D electrostatic potential maps of {Se-2-Py}$_2$, {Se(2-$NCMe_2$)-3-Py}$_2$, {Se(2-NMe_2)-3-Py}$_2$, [$PdCl_2$-η1-{Se-2-Py}$_2$(PMe_3)] and [$PdCl_2$-η1-{Se(2-$NCMe_2$)-3-Py}$_2$(PMe_3)] at ρ=0.004 level (red = negative, blue = positive; , color-normalized to potential of {SePh}$_2$ at $-4.795\cdot10^{-2}$ to $4.795\cdot10^{-2}$).

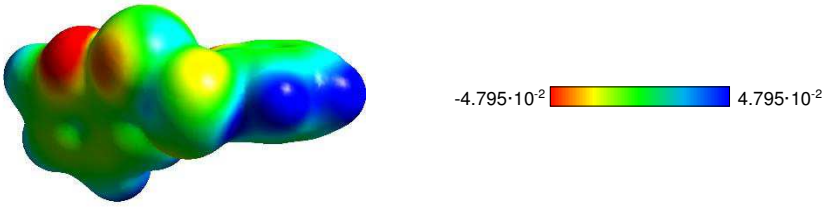

{Se-2-Py}$_2$:

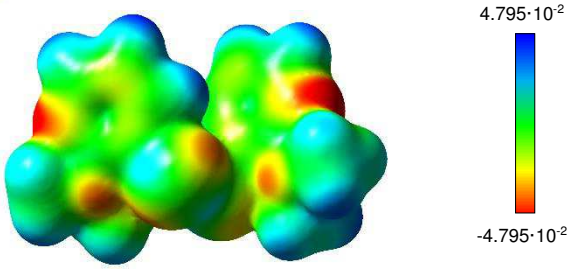

{Se(2-$NCMe_2$)-3-Py}$_2$

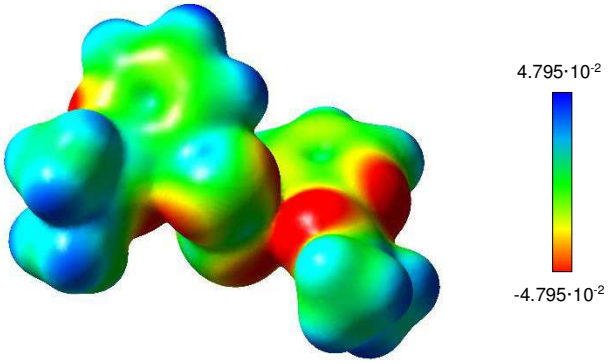

{Se(2-$NCMe_2$)-3-Py}$_2$

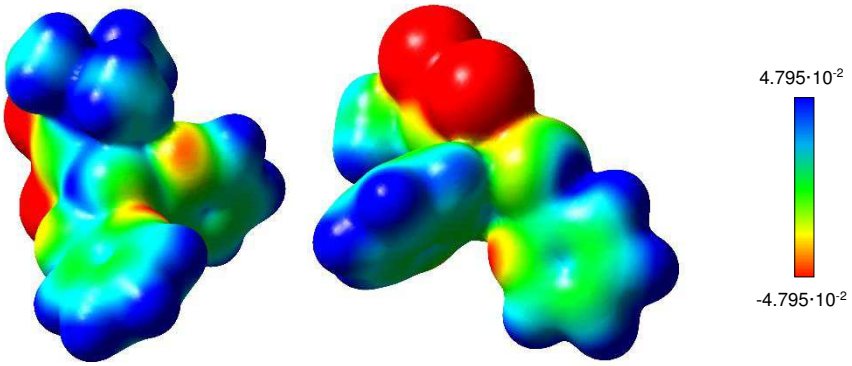

[$PdCl_2$-η1-{Se-2-Py}$_2$(PMe_3)]:

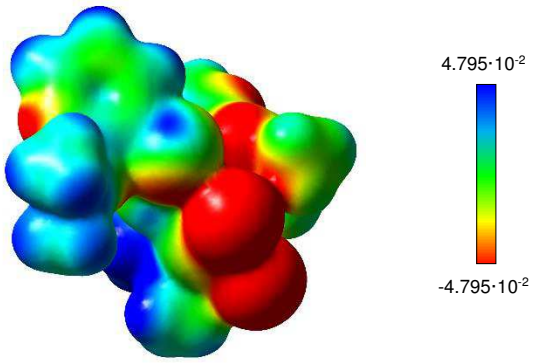

[PdCl$_2$-η1-{Se(2-NCMe$_2$)-3-Py}$_2$(PMe$_3$)]:

Analysis S3.28. Analysis of the binding in the Se-Se and Se-P bonds in {SePh}$_2$, [PdCl-η2-{SePh}$_2$(PPh$_3$)]$^+$, [PdCl-η2-{SePh}$_2$(PMe$_3$)]$^+$ and [PdCl-η2-{SePh}$_2$(P(CF$_3$)$_3$)]$^+$ with and without presence of PPh$_3$.

Analysis of the bond length variation:

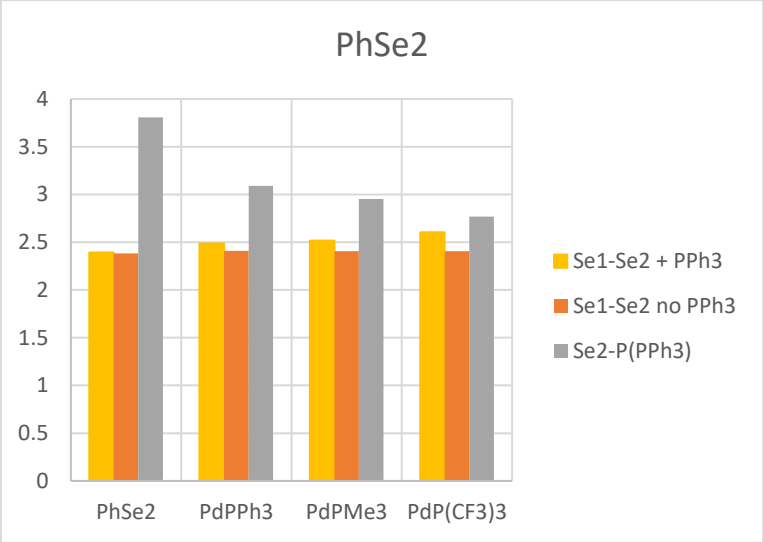

Second order perturbation analysis of Ph-Se-Se(Ph)-PPh$_3$ adducts: P donates into Se-Se antibond.

{SePh}$_2$: 144. LP (1) P 25 /478. BD*(1)Se 1 -Se 12 1.99 0.36 0.024
[PdCl-η2-{SePh}$_2$(PPh$_3$)]: 240. LP (1) P 62 /787. BD*(1)Se 1 -Se 12 19.31 0.32 0.071
[PdCl-η2-{SePh}$_2$(PMe$_3$)]: 192. LP (1) P 41 /598. BD*(1)Se 1 -Se 12 28.95 0.31 0.085
[PdCl-η2-{SePh}$_2$(P(CF$_3$)$_3$)]: 228. LP (1) P 41 /706. BD*(1)Se 1 -Se 12 54.57 0.30 0.114

Bader charges and atom sizes of the two selenium atoms:

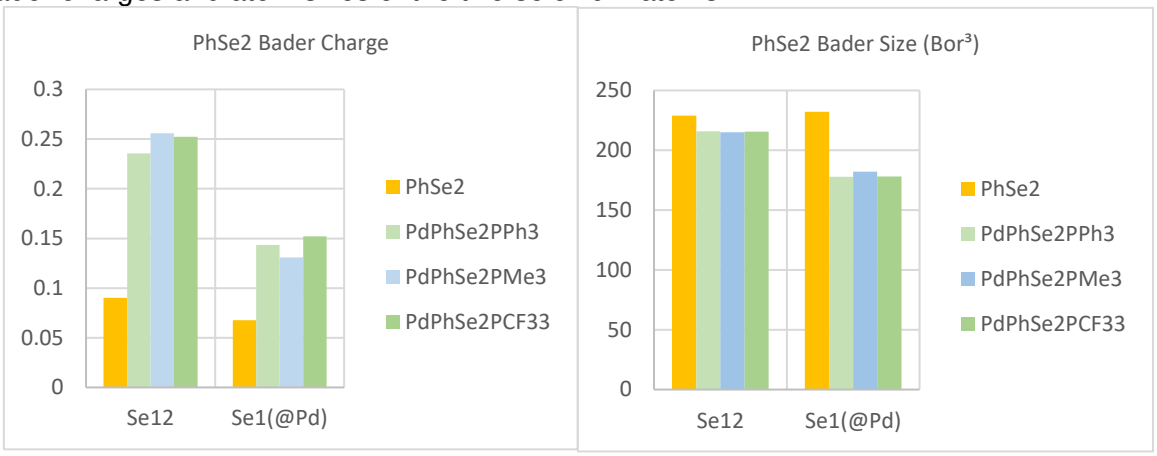

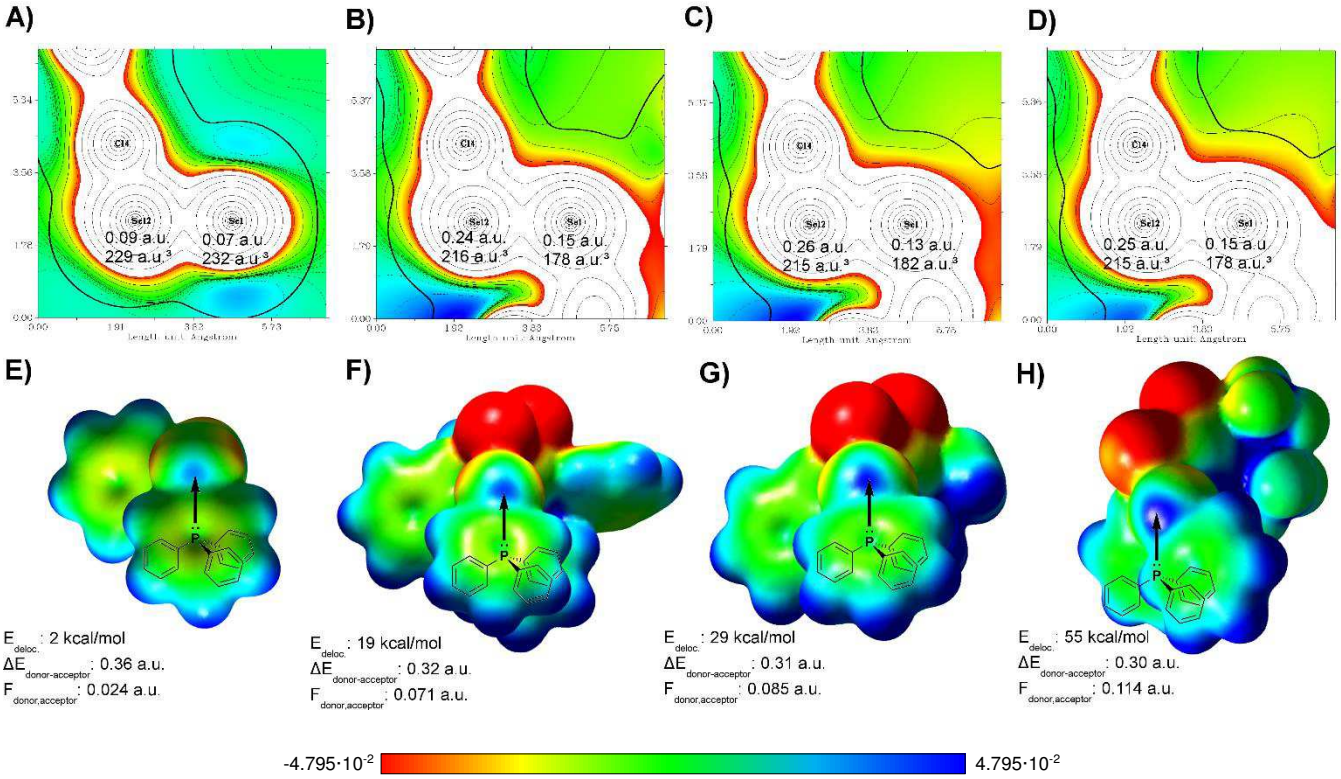

Electrostatic potential maps of the gas-phase calculated model compounds from left to right: $(PhSe)_2$, $[PdCl_2(PhSe)_2(PPh_3)]$, $[PdCl_2(PhSe)_2(PMe_3)]$, $[PdCl_2(PhSe)_2(P(CF_3)_3)]$. Top (A-D): 2D electrostatic potential maps with iso lines and bold line resembling van der Waals radius; red = positive; blue = negative. The numbers given on the selenium atoms are the Bader atomic charge (upper number) and the Bader size (lower number). The viewer looks on a cross-section of the C-Se-Se-Pd plane. Bottom (E-H): 3D electrostatic potential maps oriented along the Se-Se bonds with the non-metal-bonded selenium atom pointing to the viewer; blue = positive; red = negative. Donation of the PPh_3 lone-pair to the σ-hole on the Se-Se axis centered at Se12 is indicated. The estimated second order perturbation energy gain from the donation ($E_{deloc.}$), the energy difference between donor and acceptor orbitals ($\Delta E_{donor\text{-}acceptor}$) and the overlap factor ($F_{donor,acceptor}$) are given besides the graphs.

Bonding and anti-bonding character of the Se-Se bond in free and the coordinated $\{SePh\}_2$:

Dichalcogenide: Complexes:

σ(Se1-Se12):	49% Se12 51% Se1	44% Se12 56% Se1
σ*(Se1-Se12):	51% Se12 49% Se1	56% Se12 44% Se1

Approximate Lewis-description of the compounds:

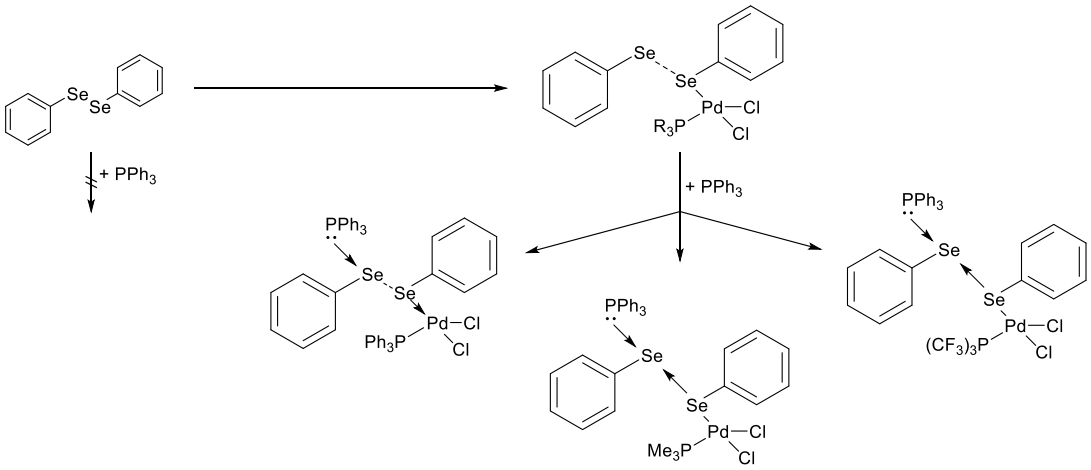

Analysis S3.29. Analysis of the binding in the Se-Se and Se-P bonds in {Se(2-N=CMe$_2$)Ph}$_2$, [PdCl-η2-{Se(2-N=CMe$_2$)Ph}$_2$(PPh$_3$)]$^+$, [PdCl-η2-{Se(2-N=CMe$_2$)Ph}$_2$(PMe$_3$)]$^+$ and [PdCl-η2-{Se(2-N=CMe$_2$)Ph}$_2$(P(CF$_3$)$_3$)]$^+$ with and without presence of PPh$_3$.

Analysis of the bond length variation:

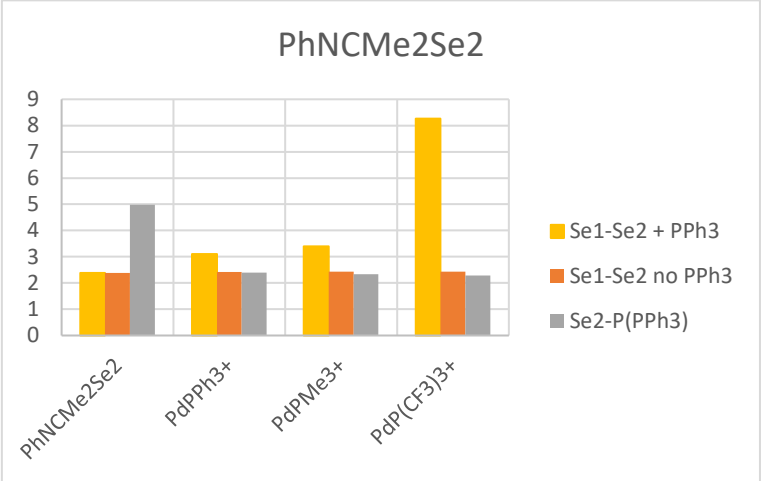

Second order perturbation analysis of Ph-Se-Se(Ph)-PPh$_3$ adducts:

{Se(2-N=CMe$_2$)Ph}$_2$: no interaction with phosphine; dichalcogenide intact.

[PdCl-η2-{Se(2-N=CMe$_2$)Ph}$_2$(PPh$_3$)]$^+$: Se-Se bond broken and Se-P bond formed; Se donates into Se-P anti-bond.

318. (1.93260) BD (1)Se 12 - P 46 (44%;56%)

248. LP (1)Se 1 /898. BD*(1)Se 12 - P 46 2.00 0.69 0.035

249. LP (2)Se 1 /898. BD*(1)Se 12 - P 46 22.19 0.22 0.062

[PdCl-η2-{Se(2-N=CMe$_2$)Ph}$_2$(PMe$_3$)]$^+$: Se-Se bond broken and Se-P bond formed; Se donates into Se-P anti-bond.

18. (1.94167) BD (1)Se 12 - P 48 (46%;54%)

199. LP (1)Se 1 /710. BD*(1)Se 12 - P 48 0.69 0.70 0.020

200. LP (2)Se 1 /710. BD*(1)Se 12 - P 48 8.59 0.22 0.039

[PdCl-η2-{Se(2-N=CMe$_2$)Ph}$_2$(P(CF$_3$)$_3$)]$^+$: Se-Se bond broken and Se-P bond formed; no donation of Se into Se-P anti-bond.

18. (1.94451) BD (1)Se 12 - P 58 (48%;52%)

Approximate Lewis-description of the compounds:

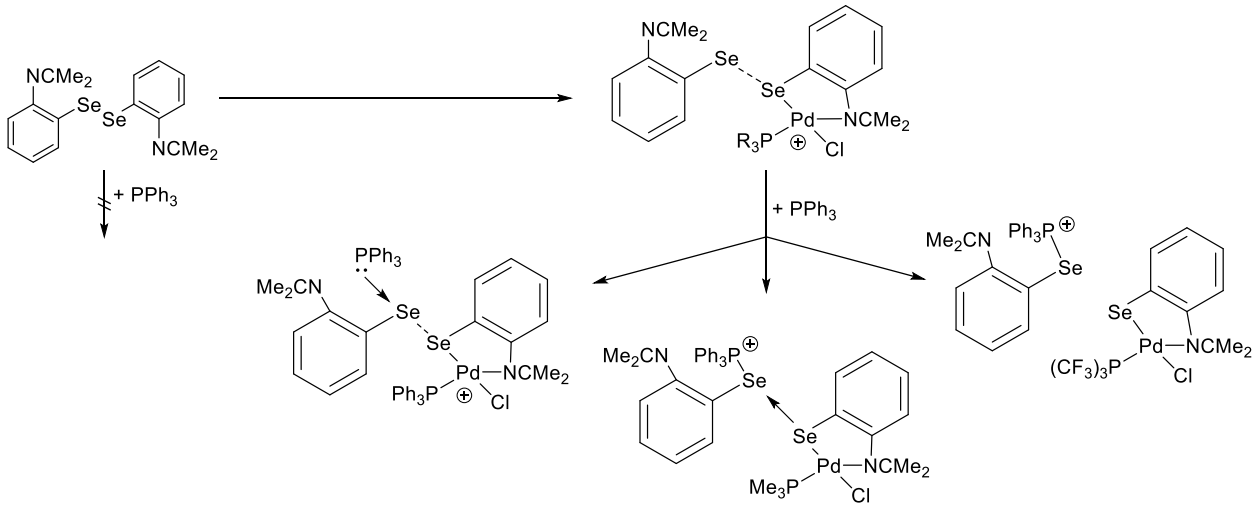

Analysis S3.30. Analysis of the binding in the Se-Se and Se-P bonds in {Se(2-NMe_2)Ph}$_2$, [PdCl-η2-{Se(2-NMe_2)Ph}$_2$(PPh_3)]$^+$, [PdCl-η2-{Se(2-NMe_2)Ph}$_2$(PMe_3)]$^+$ and [PdCl-η2-{Se(2-NMe_2)Ph}$_2$($P(CF_3)_3$)]$^+$ with and without presence of PPh_3.

Analysis of the bond length variation:

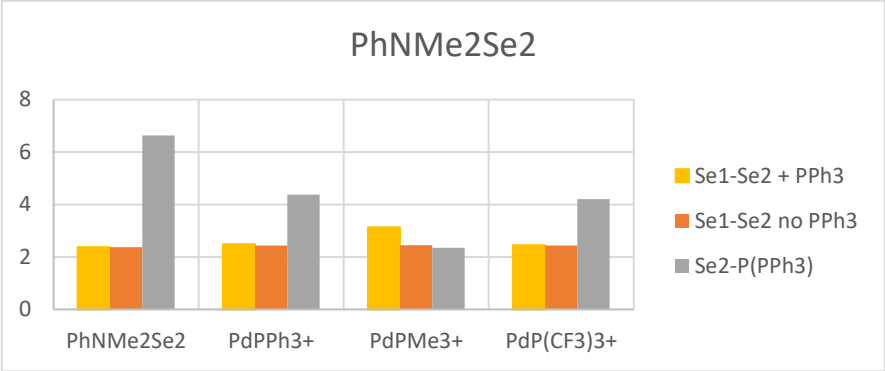

Approximate Lewis-description of the compounds:

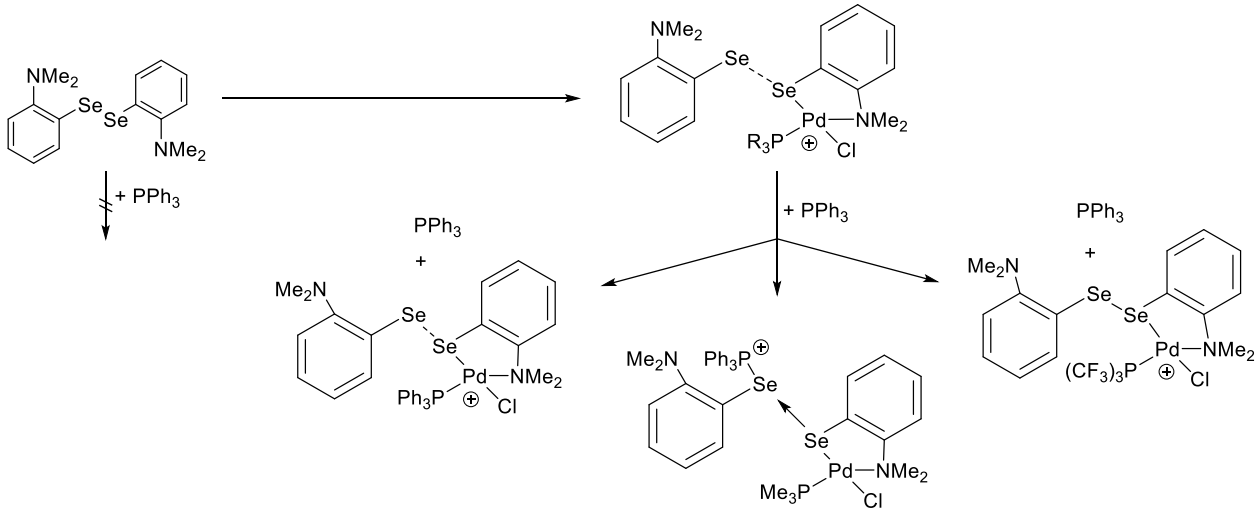

Steric bulk limits the attack of the phosphine at the selenium (only accessible for PMe_3, where it successfully cleaves the bond).

Analysis S3.31. Analysis of the bond lengths in the Se-Se and Se-P bonds in all model dichalcogenides, their neutral [$PdCl_2$-η1-{SeR}$_2$(PMe_3)] model complexes and their cationic [PdCl-η2-{SeR}$_2$(PMe_3)]$^+$ complex with and without presence of PPh_3.

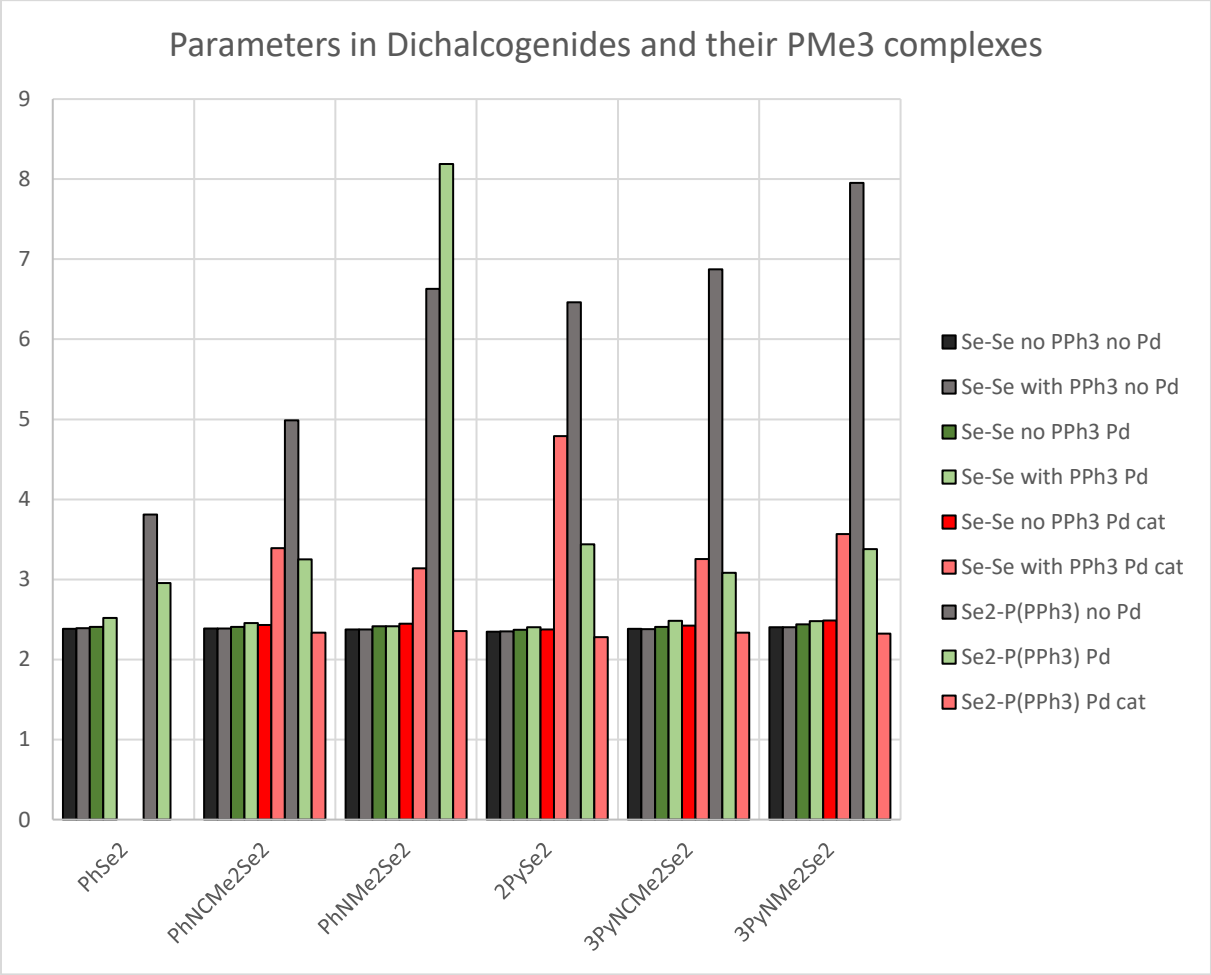

Overall, a combination of metal and phosphine is required for the observation of the resulting Se-Se cleavage and Se-P formation. The accessibility of cationic species greatly enhances the donation of PPh_3 into the Se-Se bond resulting in eventual cleavage and formation of a Se-P bond. The formation of σ-hole phosphine complexes is enhances by the coordination of the diselenide to a metal center such as Pd, resulting in shorter Se-P distances and longer Se-Se distances.

Part 4: Computational data on products and oxidation reactions

Structure S4.1. Optimized structure of [Ni(L^O)(PPh_3)].
Energy: -1911.68019974

60

Ni	-0.92619	-0.16091	0.00302
O	-1.11045	1.66808	-0.02625
N	-2.78708	-0.54017	0.02263
O	-0.65497	-1.99352	0.01218
P	1.37339	0.04949	-0.00384
C	-2.22400	2.35405	-0.02569
C	-3.73266	0.35809	0.03249
C	-3.01264	-1.93667	0.03298
C	-1.80056	-2.66653	0.02714
C	2.13883	-0.96627	-1.32963
C	2.15403	-0.52747	1.56296
C	2.03936	1.74446	-0.24686
C	-2.13582	3.77264	-0.06391
C	-3.53306	1.77131	0.00924
H	-4.76991	0.01833	0.05618
C	-4.24779	-2.59813	0.04384
C	-1.85195	-4.07325	0.03520
C	1.41067	-1.18517	-2.50884
C	3.42493	-1.51325	-1.20737
C	1.58561	-1.62737	2.22797
C	3.29564	0.08662	2.10247
C	1.64377	2.75323	0.64875
C	2.90820	2.06959	-1.29776
H	-1.14207	4.20792	-0.10020
C	-3.26905	4.56318	-0.05966
C	-4.67349	2.61574	0.01349
H	-5.17976	-2.03978	0.04577
C	-4.28233	-3.99007	0.05189

858

C	-3.08347	-4.71986	0.04765
H	-0.91847	-4.62816	0.02730
H	0.40470	-0.78634	-2.60255
C	1.96537	-1.92511	-3.55350
C	3.97502	-2.25802	-2.25169
H	3.99409	-1.36436	-0.29467
H	0.70542	-2.10368	1.80678
C	2.15601	-2.10157	3.40972
C	3.85960	-0.39271	3.28652
H	3.74103	0.94243	1.60535
H	0.95280	2.52197	1.45234
C	2.12518	4.05332	0.50346
C	3.37895	3.37682	-1.44691
H	3.22171	1.30523	-2.00107
H	-5.65740	2.15128	0.04161
H	-3.16372	5.64522	-0.08986
C	-4.55766	3.98964	-0.01897
H	-5.23753	-4.50666	0.06086
H	-3.11597	-5.80658	0.05272
H	1.39099	-2.09011	-4.46089
C	3.24754	-2.46327	-3.42601
H	4.97044	-2.68094	-2.14538
H	1.70807	-2.95169	3.91731
C	3.29107	-1.48610	3.94218
H	4.74193	0.09191	3.69621
H	1.81739	4.82215	1.20721
C	2.99211	4.36918	-0.54660
H	4.05144	3.61456	-2.26680
H	-5.44151	4.61998	-0.01566
H	3.67619	-3.04656	-4.23662
H	3.72947	-1.85517	4.86567
H	3.36156	5.38472	-0.66171

Structure S4.2. Optimized structure of [Ni(L^S)(PPh_3)].
Energy: -2234.65039753

60

Ni	-0.86062	-0.22459	0.07730
S	-0.87649	-2.40587	-0.24772
P	1.43493	-0.14902	0.01439
O	-0.71264	1.62948	0.30950
N	-2.78784	-0.25269	0.07194
C	-2.61472	-2.64081	-0.08881
C	2.39054	-1.67607	-0.36954
C	2.20246	0.43734	1.58641
C	1.93836	1.05168	-1.28439
C	-1.65223	2.52286	0.18735
C	-3.49223	0.84364	-0.05894
C	-3.44139	-1.51755	0.10273
C	-3.19077	-3.92069	-0.12678
C	2.34663	-2.74528	0.54230
C	3.14356	-1.81439	-1.54417
C	3.54152	0.14127	1.89463
C	1.44378	1.19253	2.49501
C	3.01420	1.93597	-1.12719
C	1.21095	1.06370	-2.48541
C	-3.02761	2.19106	-0.02811
C	-1.30680	3.90038	0.26719
H	-4.56740	0.73621	-0.20606
C	-4.81666	-1.69853	0.33003
H	-2.54841	-4.78135	-0.29017
C	-4.55887	-4.08698	0.06093
H	1.75767	-2.66186	1.45039
C	3.05102	-3.92050	0.28600
C	3.84334	-2.99602	-1.79918
H	3.18890	-1.00201	-2.26159
H	4.13878	-0.45327	1.21053

860

C	4.10990	0.59644	3.08510
C	2.01679	1.64100	3.68628
H	0.41516	1.43620	2.25516
H	3.57916	1.94675	-0.20048
C	3.35947	2.81353	-2.15711
C	1.56400	1.93537	-3.51553
H	0.36417	0.39344	-2.60907
C	-3.98181	3.23239	-0.17739
H	-0.26202	4.14425	0.43340
C	-2.26321	4.88577	0.11936
C	-5.37242	-2.97388	0.30379
H	-5.45799	-0.85329	0.55834
H	-4.99031	-5.08424	0.04003
H	3.00707	-4.73856	0.99965
C	3.80057	-4.04931	-0.88565
H	4.42338	-3.08857	-2.71347
H	5.14622	0.35971	3.31104
C	3.34799	1.34523	3.98432
H	1.41779	2.22099	4.38321
H	4.19217	3.49881	-2.02264
C	2.63801	2.81349	-3.35209
H	0.99375	1.93494	-4.44040
C	-3.61846	4.56043	-0.10907
H	-5.02223	2.95899	-0.34289
H	-1.96533	5.93018	0.17665
H	-6.43572	-3.09982	0.48669
H	4.34602	-4.96769	-1.08569
H	3.78970	1.69332	4.91431
H	2.90770	3.49867	-4.15131
H	-4.36044	5.34433	-0.22453

Structure S4.3. Optimized structure of [Ni(L^{Se})(PPh_3)].
Energy: -4237.75094083

60

Ni	-0.79572	-0.02831	-0.11868
N	-2.72484	0.12068	-0.10596
O	-0.48777	1.81071	-0.41045
P	1.49084	-0.13440	-0.03894
Se	-1.00609	-2.29515	0.30830
C	-3.53422	-1.05123	-0.17421
C	-3.30698	1.27951	0.08431
C	-1.33002	2.78477	-0.22384
C	2.06977	1.05205	1.24196
C	2.33302	-1.71807	0.38713
C	2.31392	0.35779	-1.61518
C	-2.89963	-2.28237	0.06399
C	-4.90473	-1.03336	-0.48959
C	-2.71596	2.57678	0.06791
H	-4.38165	1.27262	0.27111
C	-0.86505	4.12674	-0.30889
C	3.20605	1.85576	1.07786
C	1.33597	1.13819	2.43615
C	3.02342	-1.89892	1.59419
C	2.25766	-2.78878	-0.52151
C	3.63889	-0.02297	-1.89026
C	1.61361	1.12355	-2.56093
C	-3.65560	-3.46151	0.07623
C	-5.64419	-2.21287	-0.48973
H	-5.39457	-0.10654	-0.77100
C	-3.55896	3.69779	0.29147
H	0.18574	4.27753	-0.53634
C	-1.71534	5.19203	-0.08647
H	3.77689	1.81054	0.15583
C	3.60458	2.72615	2.09453
C	1.74213	2.00204	3.45331
H	0.44299	0.53168	2.56450
H	3.09226	-1.08653	2.30968

C	3.62994	-3.12305	1.88456
C	2.86869	-4.00745	-0.22914
H	1.72056	-2.67142	-1.45769
H	4.19073	-0.62762	-1.17745
C	4.25096	0.35979	-3.08446
C	2.22982	1.49879	-3.75605
H	0.59770	1.43469	-2.34661
H	-3.16069	-4.40760	0.27701
C	-5.02234	-3.42913	-0.18907
H	-6.70053	-2.18337	-0.74144
C	-3.07850	4.98801	0.22230
H	-4.60900	3.51758	0.51418
H	-1.32601	6.20578	-0.14681
H	4.48420	3.34886	1.95451
C	2.87652	2.79916	3.28324
H	1.16638	2.05908	4.37300
H	4.16207	-3.24770	2.82381
C	3.55566	-4.17804	0.97486
H	2.80134	-4.82538	-0.94108
H	5.27573	0.05811	-3.28421
C	3.54667	1.11939	-4.02087
H	1.67559	2.08782	-4.48183
H	-5.59624	-4.35199	-0.18884
H	-3.73595	5.83420	0.39566
H	3.18803	3.47857	4.07211
H	4.02841	-5.12960	1.20275
H	4.02189	1.41094	-4.95378

Structure S4.4. Optimized structure of [Ni(L^{Te})(PPh_3)].
Energy: -1844.53114879

60

Te	1.24043	-2.22196	0.40774
Ni	0.70204	0.16688	-0.16915
C	3.26852	-1.78500	0.01782

P	-1.55498	-0.17419	-0.07863
O	0.18966	1.94813	-0.54704
N	2.60753	0.55578	-0.13590
C	3.61164	-0.45291	-0.26840
C	4.25845	-2.77375	-0.03208
C	-2.41555	0.16520	-1.67475
C	-2.24843	1.00482	1.15217
C	-2.25188	-1.80953	0.42001
C	0.87201	3.01695	-0.25625
C	3.00890	1.77504	0.13473
C	4.91677	-0.15377	-0.70138
H	3.99911	-3.80257	0.20446
C	5.56468	-2.46129	-0.40668
C	-3.71009	-0.32634	-1.91781
C	-1.77438	0.92027	-2.66964
C	-1.52767	1.21377	2.33920
C	-3.45789	1.68554	0.95786
C	-2.11890	-2.89973	-0.45885
C	-2.88187	-2.00858	1.65721
C	2.24493	2.97950	0.14720
C	0.24189	4.28947	-0.34263
H	4.06806	1.90591	0.36251
H	5.16726	0.85066	-1.02862
C	5.88811	-1.14943	-0.76190
H	6.31774	-3.24355	-0.45236
H	-4.21484	-0.92597	-1.16676
C	-4.35116	-0.06177	-3.12860
H	-0.78391	1.31804	-2.48178
C	-2.41889	1.17654	-3.88127
H	-0.57935	0.70423	2.49063
C	-2.01788	2.07585	3.32037
H	-4.02055	1.54606	0.04033
C	-3.94092	2.55497	1.93805

H	-1.63220	-2.76819	-1.42043
C	-2.61405	-4.15550	-0.10772
H	-2.99513	-1.18185	2.35018
C	-3.37084	-3.26925	2.00694
C	2.90945	4.18882	0.48209
H	-0.79605	4.31298	-0.65991
C	0.92024	5.44502	-0.00693
H	6.88896	-0.90267	-1.10499
H	-5.35188	-0.44799	-3.30293
C	-3.70550	0.68818	-4.11386
H	-1.91023	1.75867	-4.64497
H	-1.45140	2.22787	4.23499
C	-3.22505	2.74951	3.12046
H	-4.87725	3.08185	1.77440
C	-3.23967	-4.34394	1.12676
H	-2.50553	-4.98682	-0.79875
H	-3.85682	-3.40707	2.96902
C	2.26680	5.40699	0.41738
H	3.95317	4.13744	0.78648
H	0.40518	6.40105	-0.06762
H	-4.20259	0.88754	-5.05953
H	-3.60276	3.42775	3.88088
H	-3.62213	-5.32355	1.40031
H	2.78754	6.32299	0.67828

Structure S4.5. Optimized structure of [Pd(L^{O})(PPh_3)].
Energy: -1869.09228465

60

O	-1.04994	1.85368	-0.01452
C	-2.20669	2.46578	-0.01359
C	-2.16857	3.88934	-0.04185
H	-1.18616	4.35040	-0.06820
C	-3.31977	4.65071	-0.03853
H	-3.24221	5.73527	-0.06090

C	-4.59028	4.03962	-0.00817
H	-5.49411	4.64086	-0.00544
C	-4.66137	2.66357	0.01610
H	-5.63296	2.17387	0.03757
C	-3.50206	1.83984	0.01283
Pd	-0.82512	-0.14578	0.01109
C	-3.72880	0.42371	0.03302
H	-4.77821	0.12360	0.05324
N	-2.82782	-0.51538	0.02624
C	-3.08574	-1.90917	0.03714
C	-4.35713	-2.50415	0.04692
H	-5.25314	-1.89032	0.04541
C	-4.48125	-3.88883	0.05847
H	-5.46732	-4.34361	0.06657
C	-3.32914	-4.69057	0.05911
H	-3.42505	-5.77349	0.06717
C	-2.06463	-4.11673	0.04768
H	-1.16540	-4.72553	0.04368
C	-1.91602	-2.71386	0.03581
O	-0.70420	-2.16431	0.01983
P	1.52752	0.04229	-0.00225
C	2.25660	-0.86511	-1.42251
C	1.51185	-0.96743	-2.60748
H	0.51367	-0.54085	-2.65290
C	2.04104	-1.62726	-3.71704
H	1.45445	-1.70352	-4.62831
C	3.31325	-2.19887	-3.65038
H	3.72168	-2.71969	-4.51229
C	4.05672	-2.10898	-2.47143
H	5.04396	-2.55935	-2.41308
C	3.53247	-1.44628	-1.36081
H	4.11257	-1.38859	-0.44470
C	2.31669	-0.67930	1.49496

866

C	1.76051	-1.84694	2.04536
H	0.87714	-2.28574	1.58889
C	2.34410	-2.43288	3.16906
H	1.90752	-3.33445	3.59030
C	3.47629	-1.86257	3.75578
H	3.92358	-2.31937	4.63468
C	4.03016	-0.70161	3.21360
H	4.90916	-0.25166	3.66747
C	3.45477	-0.10981	2.08728
H	3.88800	0.79692	1.67706
C	2.18664	1.75150	-0.10774
C	3.11788	2.14041	-1.08121
H	3.47570	1.42159	-1.81102
C	3.59233	3.45374	-1.11722
H	4.31349	3.74336	-1.87677
C	3.14500	4.38713	-0.18183
H	3.51638	5.40808	-0.21014
C	2.21444	4.00709	0.78908
H	1.85780	4.73119	1.51660
C	1.72966	2.70050	0.82280
H	0.98662	2.41981	1.56137

Structure S4.6. Optimized structure of [Pd(L^S)(PPh_3)].
Energy: -2192.07843937

60

C	1.74531	2.62897	0.14444
C	1.51377	4.03545	0.20104
H	0.48634	4.35665	0.34244
C	2.53864	4.94797	0.06500
H	2.31543	6.01167	0.10649
C	3.86979	4.51978	-0.13132
H	4.67286	5.24205	-0.23932
C	4.12859	3.16827	-0.17812
H	5.14981	2.81983	-0.32001

C	3.10327	2.18968	-0.03815
C	3.53439	0.82555	-0.06247
H	4.60973	0.71022	-0.20363
C	3.45904	-1.55026	0.08342
C	4.83865	-1.74178	0.28564
H	5.48757	-0.89809	0.49612
C	5.39069	-3.01717	0.25625
H	6.45695	-3.14474	0.41948
C	4.56900	-4.12854	0.03381
H	4.99452	-5.12813	0.00900
C	3.19988	-3.95523	-0.12904
H	2.55214	-4.81498	-0.27641
C	2.62365	-2.67382	-0.08646
C	-2.50093	-1.67165	-0.35515
C	-2.37222	-2.75380	0.53311
H	-1.74075	-2.66463	1.41172
C	-3.04632	-3.94931	0.28823
H	-2.93782	-4.77783	0.98252
C	-3.84638	-4.08477	-0.84872
H	-4.36674	-5.01928	-1.04049
C	-3.97102	-3.01843	-1.73969
H	-4.58962	-3.11747	-2.62758
C	-3.30372	-1.81616	-1.49578
H	-3.41149	-0.99319	-2.19424
C	-2.32603	0.48020	1.58724
C	-3.59142	0.05105	2.02014
H	-4.15414	-0.66823	1.43397
C	-4.12952	0.53742	3.21306
H	-5.10812	0.19572	3.53959
C	-3.41164	1.45297	3.98440
H	-3.82981	1.82620	4.91551
C	-2.15408	1.88489	3.55761
H	-1.59035	2.59643	4.15490

868

C	-1.60916	1.40344	2.36673
H	-0.63630	1.74544	2.02839
C	-2.13494	1.07386	-1.27933
C	-3.29134	1.85381	-1.13119
H	-3.88139	1.78596	-0.22243
C	-3.68377	2.72752	-2.14643
H	-4.57853	3.33124	-2.02043
C	-2.92804	2.82925	-3.31625
H	-3.23391	3.51275	-4.10381
C	-1.77443	2.05717	-3.46916
H	-1.17798	2.13838	-4.37361
C	-1.37520	1.18747	-2.45397
H	-0.46729	0.60111	-2.56492
N	2.83417	-0.27133	0.06106
O	0.71240	1.84692	0.25681
P	-1.58817	-0.11765	0.00806
S	0.86933	-2.50411	-0.22106
Pd	0.76014	-0.20990	0.05930

Structure S4.7. Optimized structure of [Pd(L^{Se})(PPh_3)].
Energy: -4195.18189592

60

Pd	0.69884	-0.03126	0.09809
N	2.78281	0.06639	0.09517
O	0.51131	2.02689	0.35237
P	-1.64476	-0.09343	0.02934
Se	0.97298	-2.40480	-0.27862
C	3.54546	-1.13579	0.15214
C	3.38160	1.21516	-0.08871
C	1.47239	2.88260	0.17658
C	-2.25095	1.07688	-1.25173
C	-2.43563	0.43684	1.60739
C	-2.46334	-1.69430	-0.36261
C	2.87661	-2.35553	-0.06388

C	4.92366	-1.15485	0.44065
C	2.84733	2.54210	-0.07858
H	4.45637	1.18056	-0.27310
C	1.14170	4.26964	0.23491
C	-3.45443	1.78287	-1.10835
C	-1.48795	1.24914	-2.41718
C	-1.77356	1.36993	2.42264
C	-3.69112	-0.05331	2.00362
C	-3.20608	-1.88381	-1.53683
C	-2.31675	-2.76726	0.53458
C	3.60903	-3.55090	-0.08486
C	5.63586	-2.34954	0.43394
H	5.44122	-0.23888	0.70640
C	3.78679	3.59089	-0.29402
H	0.10374	4.51695	0.43555
C	2.08583	5.25215	0.02429
H	-4.04833	1.66964	-0.20671
C	-3.88941	2.64164	-2.11894
C	-1.92974	2.10325	-3.42806
H	-0.54482	0.72034	-2.52425
H	-0.81068	1.76225	2.11182
C	-2.36189	1.79992	3.61274
C	-4.27302	0.38230	3.19547
H	-4.21202	-0.78082	1.38956
H	-3.32720	-1.06886	-2.24244
C	-3.79584	-3.12080	-1.80581
C	-2.91331	-3.99825	0.26400
H	-1.73539	-2.64201	1.44303
H	3.08870	-4.48681	-0.26977
C	4.98018	-3.55244	0.15221
H	6.69734	-2.34237	0.66466
C	3.43089	4.92014	-0.25005
H	4.82129	3.31628	-0.49122

870

H	1.78725	6.29721	0.06671
H	-4.82063	3.18822	-1.99633
C	-3.12988	2.80171	-3.27974
H	-1.33043	2.23007	-4.32535
H	-1.84016	2.51959	4.23780
C	-3.60886	1.30733	4.00289
H	-5.24331	-0.00634	3.49301
H	-4.36820	-3.25395	-2.71983
C	-3.65323	-4.17823	-0.90693
H	-2.79209	-4.81842	0.96606
H	5.53050	-4.48940	0.14516
H	4.16954	5.69786	-0.41674
H	-3.46927	3.47345	-4.06368
H	-4.06072	1.64095	4.93331
H	-4.11323	-5.13973	-1.11835

Structure S4.8. Optimized structure of [Pd(L^{Te})(PPh_3)].
Energy: -1801.96545473

60

Pd	0.61335	0.14088	0.14514
Te	1.16799	-2.34934	-0.37205
P	-1.70778	-0.12007	0.06488
N	2.69046	0.45799	0.13209
O	0.23356	2.17287	0.46791
C	3.21498	-1.92793	-0.02126
C	-2.39874	1.04015	-1.18273
C	-2.54069	0.29600	1.65583
C	-2.41124	-1.76309	-0.38403
C	3.13968	1.66138	-0.12390
C	3.63029	-0.61086	0.24814
C	1.07679	3.12114	0.19603
C	4.15849	-2.96321	0.01145
C	-1.64753	1.30938	-2.33746
C	-3.65505	1.64345	-1.02476

C	-3.76820	-0.28409	2.01750
C	-1.94296	1.23148	2.51672
C	-2.22950	-2.84466	0.49665
C	-3.09680	-1.97394	-1.58910
C	2.45980	2.91993	-0.14741
H	4.20590	1.73994	-0.34362
C	4.95956	-0.38225	0.65516
C	0.60268	4.46671	0.23906
H	3.84390	-3.97937	-0.21399
C	5.48618	-2.71842	0.35632
H	-0.66481	0.86099	-2.45524
C	-2.15219	2.15743	-3.32383
H	-4.24154	1.45520	-0.13090
C	-4.15310	2.49677	-2.01055
H	-4.24009	-1.01433	1.36809
C	-4.38515	0.06462	3.22015
H	-1.00515	1.69704	2.23217
C	-2.56582	1.57383	3.71775
H	-1.69653	-2.70236	1.43197
C	-2.73447	-4.10542	0.17893
H	-3.24522	-1.15281	-2.28214
C	-3.59344	-3.24028	-1.90597
C	3.26206	4.05247	-0.46695
H	5.26773	0.60828	0.97433
C	5.88110	-1.42355	0.70072
H	-0.43831	4.61050	0.51173
C	1.41650	5.53423	-0.07646
H	6.19874	-3.53824	0.38885
C	-3.40457	2.75342	-3.16107
H	-1.56158	2.35961	-4.21303
H	-5.12521	2.96365	-1.87647
H	-5.33310	-0.39312	3.49012
C	-3.78398	0.99157	4.07346

H	-2.09350	2.29631	4.37786
H	-2.58940	-4.93068	0.87046
C	-3.41577	-4.30675	-1.02394
H	-4.12140	-3.38915	-2.84393
H	4.30457	3.88184	-0.72880
C	2.76618	5.33678	-0.44280
H	6.89933	-1.22514	1.02340
H	1.00957	6.54252	-0.04553
H	-3.79341	3.42068	-3.92561
H	-4.26257	1.25736	5.01232
H	-3.80452	-5.29065	-1.27186
H	3.40102	6.18145	-0.69123

Structure S4.9. Optimized structure of [Pt(L^O)(PPh_3)].
Energy: -1861.52740698

60

Pt	0.73237	-0.13339	0.01306
P	-1.58868	0.02867	-0.00518
O	0.92242	1.87859	-0.01259
O	0.66915	-2.16538	0.02310
N	2.74285	-0.46961	0.02739
C	-2.32088	-0.85097	-1.44261
C	-2.25509	1.73830	-0.07441
C	-2.38372	-0.72269	1.47532
C	2.07346	2.50745	-0.01422
C	1.89336	-2.69093	0.03503
C	3.62844	0.48948	0.02983
C	3.04021	-1.85580	0.03682
C	-3.60442	-1.41617	-1.39136
C	-1.57615	-0.94454	-2.62845
C	-1.83702	2.65723	0.90314
C	-3.15487	2.15440	-1.06503
C	-3.54064	-0.17857	2.05457
C	-1.82005	-1.88861	2.02085

C	2.00892	3.92870	-0.04150
C	3.37573	1.89880	0.00943
C	2.07248	-4.08842	0.04355
C	4.32562	-2.41865	0.04607
C	-4.13605	-2.05547	-2.51203
C	-2.11269	-1.58195	-3.74781
C	-2.32735	3.96193	0.89609
C	-3.63596	3.46614	-1.07385
C	-4.12640	-0.79249	3.16362
C	-2.41351	-2.49700	3.12739
C	3.14686	4.70866	-0.04111
C	4.52188	2.74308	0.00933
C	3.35071	-4.63063	0.05392
C	4.48243	-3.79989	0.05519
C	-3.39217	-2.13802	-3.69127
C	-3.22629	4.36983	-0.09357
C	-3.56402	-1.95125	3.70152
C	4.42751	4.11689	-0.01459
H	4.68093	0.20510	0.04573
H	-4.18512	-1.36551	-0.47529
H	-0.57327	-0.52884	-2.66461
H	-1.12139	2.35349	1.65987
H	-3.48288	1.45870	-1.83029
H	-3.98041	0.72695	1.64864
H	-0.92278	-2.30931	1.57537
H	1.01840	4.37215	-0.06404
H	1.18795	-4.71824	0.03872
H	5.20686	-1.78406	0.04617
H	-5.12900	-2.49402	-2.46105
H	-1.52610	-1.65194	-4.65961
H	-2.00085	4.66281	1.65961
H	-4.33230	3.77731	-1.84787
H	-5.01948	-0.36096	3.60778

H	-1.97027	-3.39691	3.54518
H	3.05229	5.79174	-0.06255
H	5.50140	2.26947	0.02826
H	3.47395	-5.71066	0.05997
H	5.47935	-4.23031	0.06261
H	-3.80626	-2.64072	-4.56125
H	-3.60272	5.38931	-0.10044
H	-4.01894	-2.42538	4.56724
H	5.32143	4.73279	-0.01437

Structure S4.10. Optimized structure of [Pt(L^S)(PPh_3)].
Energy: -2184.51344882

60

C	2.61748	-2.60185	-0.08926
C	3.23374	-3.86532	-0.12674
C	3.41713	-1.45015	0.06509
H	2.61117	-4.74563	-0.26077
C	4.60806	-3.99405	0.02203
C	4.80467	-1.59750	0.25244
N	2.75297	-0.18876	0.04291
Pt	0.68003	-0.18201	0.04124
H	5.06545	-4.97948	-0.00019
C	5.39624	-2.85426	0.22636
H	5.43176	-0.73459	0.44932
C	3.43008	0.92861	-0.06281
O	0.58224	1.88444	0.21771
P	-1.64068	-0.11594	0.00295
H	6.46783	-2.94594	0.37809
C	2.96875	2.28058	-0.03648
H	4.50777	0.83668	-0.18897
C	1.60179	2.69104	0.12373
C	-2.39424	0.46092	1.58328
C	-2.24253	1.05025	-1.28447
C	-2.50042	-1.70352	-0.34577

C	3.97363	3.28424	-0.15491
C	1.33194	4.08883	0.17932
C	-1.69439	1.38242	2.37926
C	-3.66088	0.01812	1.99822
C	-3.43551	1.77269	-1.13487
C	-1.49191	1.19954	-2.46116
C	-3.27446	-1.89356	-1.49887
C	-2.35922	-2.76260	0.56764
C	3.68133	4.62837	-0.10823
H	5.00504	2.96049	-0.27984
H	0.29429	4.38326	0.30242
C	2.33688	5.02578	0.06469
H	-0.71996	1.73372	2.05692
C	-2.25639	1.84888	3.56827
C	-4.21696	0.48935	3.18894
H	-4.21046	-0.70158	1.40004
H	-4.01961	1.67793	-0.22478
C	-3.87278	2.62524	-2.14970
C	-1.93574	2.04840	-3.47570
H	-0.55733	0.65711	-2.57180
H	-3.39088	-1.08802	-2.21600
C	-3.90072	-3.11997	-1.73214
C	-2.99142	-3.98265	0.33288
H	-1.75053	-2.63567	1.45765
H	4.46895	5.36974	-0.19924
H	2.08840	6.08374	0.10486
H	-1.70487	2.55891	4.17860
C	-3.51527	1.40353	3.97663
H	-5.19607	0.13625	3.50145
H	-4.79565	3.18460	-2.02178
C	-3.12542	2.76317	-3.32116
H	-1.34610	2.15768	-4.38170
H	-4.49695	-3.25514	-2.63048

C	-3.76290	-4.16425	-0.81750
H	-2.87345	-4.79376	1.04593
H	-3.94685	1.76486	4.90632
H	-3.46631	3.43001	-4.10868
H	-4.25125	-5.11757	-1.00078
S	0.86258	-2.48488	-0.21086

Structure S4.11. Optimized structure of [Pt(L^{Se})(PPh_3)].
Energy: -4187.61626109

60

C	2.86347	-2.30130	-0.07595
C	3.63114	-3.47533	-0.09185
C	3.49685	-1.06084	0.12912
Se	0.96584	-2.40202	-0.27865
H	3.13647	-4.42680	-0.26781
C	5.00176	-3.43589	0.13754
C	4.87662	-1.03903	0.41187
N	2.70191	0.12347	0.06892
Pt	0.62425	-0.02418	0.07128
H	5.57958	-4.35613	0.13337
C	5.62312	-2.21175	0.40906
H	5.37072	-0.10907	0.67263
C	3.28196	1.28779	-0.10106
O	0.39345	2.04137	0.30672
P	-1.69129	-0.10104	0.02184
H	6.68466	-2.17162	0.63581
C	2.72462	2.60291	-0.08590
H	4.35708	1.27145	-0.27550
C	1.34340	2.91795	0.15132
C	-2.49094	0.41015	1.60246
C	-2.35194	1.04055	-1.25984
C	-2.45867	-1.73174	-0.35132
C	3.64671	3.67208	-0.28015
C	0.98035	4.29462	0.21525

C	-1.83926	1.33532	2.43406
C	-3.74845	-0.08746	1.98252
C	-3.58242	1.69702	-1.11069
C	-1.60596	1.23788	-2.43258
C	-3.17256	-1.96440	-1.53508
C	-2.30072	-2.78109	0.57107
C	3.26303	4.99293	-0.23076
H	4.68904	3.41937	-0.46446
H	-0.06555	4.51808	0.40154
C	1.90757	5.29726	0.02614
H	-0.87368	1.73117	2.13824
C	-2.43914	1.75093	3.62363
C	-4.34276	0.33347	3.17345
H	-4.26103	-0.81101	1.35668
H	-4.16416	1.56534	-0.20378
C	-4.06072	2.53190	-2.12171
C	-2.09089	2.06837	-3.44358
H	-0.64313	0.74703	-2.54270
H	-3.30138	-1.16702	-2.25918
C	-3.72225	-3.22268	-1.79040
C	-2.85621	-4.03385	0.31357
H	-1.74244	-2.61996	1.48829
H	3.98837	5.78647	-0.38049
H	1.58810	6.33581	0.07175
H	-1.92449	2.46434	4.26159
C	-3.68838	1.25140	3.99688
H	-5.31421	-0.06168	3.45832
H	-5.01258	3.04037	-1.99378
C	-3.31765	2.71746	-3.28928
H	-1.50452	2.21495	-4.34644
H	-4.27224	-3.39018	-2.71245
C	-3.56734	-4.25757	-0.86776
H	-2.72631	-4.83637	1.03422

H	-4.14938	1.57356	4.92686
H	-3.69082	3.37039	-4.07380
H	-3.99604	-5.23574	-1.06836

Structure S4.12. Optimized structure of [Pt(L^{Te})(PPh_3)].
Energy: -1794.39773656

60

C	-3.19956	-1.88501	0.04081
C	-4.17331	-2.89251	-0.00294
C	-3.57590	-0.55526	-0.22344
Te	-1.17006	-2.36320	0.39071
H	-3.88805	-3.91824	0.21823
C	-5.49108	-2.60896	-0.35216
C	-4.89585	-0.28791	-0.63800
N	-2.61112	0.49470	-0.09703
Pt	-0.54654	0.12845	-0.10524
H	-6.22673	-3.40776	-0.39216
C	-5.84656	-1.30140	-0.69352
H	-5.17470	0.71062	-0.95862
C	-3.04618	1.70828	0.15033
O	-0.12895	2.16675	-0.41276
P	1.74683	-0.13740	-0.05638
H	-6.85608	-1.07219	-1.02287
C	-2.34930	2.95543	0.16894
H	-4.11142	1.79981	0.36196
C	-0.96310	3.13298	-0.16117
C	2.39874	-1.80378	0.38311
C	2.50109	1.00059	1.17680
C	2.57464	0.24822	-1.65839
C	-3.13599	4.10460	0.46917
C	-0.46229	4.46617	-0.21531
C	2.19862	-2.87066	-0.51105
C	3.06338	-2.04419	1.59397
C	1.77042	1.32279	2.33128

C	3.78796	1.53271	1.00859
C	1.98523	1.18003	-2.52829
C	3.79412	-0.34968	-2.01764
C	-2.61737	5.37938	0.43554
H	-4.18364	3.95411	0.72227
H	0.58411	4.58741	-0.47752
C	-1.26086	5.55080	0.08044
H	1.68210	-2.70351	-1.45138
C	2.66427	-4.14797	-0.19926
C	3.52116	-3.32666	1.90464
H	3.22520	-1.23355	2.29635
H	0.76575	0.92873	2.45534
C	2.32482	2.15333	3.30604
C	4.33623	2.36792	1.98306
H	4.35993	1.30454	0.11470
H	1.05176	1.65597	-2.24812
C	2.60787	1.50212	-3.73508
C	4.41158	-0.02176	-3.22590
H	4.25913	-1.07910	-1.36214
H	-3.23999	6.23745	0.66836
H	-0.83678	6.55160	0.04307
H	2.50561	-4.96245	-0.90053
C	3.32481	-4.37920	1.00990
H	4.03300	-3.49912	2.84746
H	1.74962	2.39711	4.19496
C	3.60727	2.67801	3.13303
H	5.33183	2.77944	1.84025
H	2.14118	2.22172	-4.40228
C	3.81844	0.90252	-4.08768
H	5.35292	-0.49405	-3.49392
H	3.68371	-5.37572	1.25253
H	4.03520	3.33101	3.88902
H	4.29700	1.15222	-5.03096

880

Structure S4.13. Optimized structure of [{$H_2L^{Te}I_2$}$OPPh_3$].
Energy: -1774.48766547

64

Te	2.15040	-0.90207	-0.89033
I	1.40561	-3.57247	0.53774
I	2.83854	1.83737	-2.25475
C	3.67419	-0.55767	0.56980
C	3.58176	0.47434	1.52092
C	4.82148	-1.36017	0.58318
N	2.42830	1.30783	1.53711
C	4.59803	0.68889	2.46153
H	4.91325	-2.15935	-0.14428
C	5.84251	-1.14439	1.50865
C	2.42605	2.59279	1.79929
H	1.53701	0.89142	1.24134
H	4.48199	1.45421	3.22345
C	5.73146	-0.11722	2.44835
H	6.72180	-1.78168	1.49788
C	1.28979	3.44957	1.86194
H	3.40150	3.03723	1.97878
H	6.51507	0.04514	3.18228
C	-0.04642	2.99611	1.64148
C	1.51400	4.82219	2.14346
O	-0.23200	1.70366	1.37812
C	-1.10549	3.91831	1.71028
H	2.53494	5.15961	2.30291
C	0.46609	5.71757	2.20840
H	-1.20798	1.48332	1.17314
H	-2.11393	3.56152	1.53220
C	-0.84425	5.25257	1.98761
H	0.64831	6.76552	2.42145
H	-1.67416	5.95279	2.03235
P	-3.44506	0.15153	0.13034

O	-2.70539	1.29695	0.82572
C	-2.62094	-0.34377	-1.41115
C	-5.13175	0.71075	-0.28359
C	-3.60086	-1.33742	1.16188
C	-2.82037	-1.60247	-2.00214
C	-1.76808	0.58435	-2.02772
C	-5.65425	1.81156	0.41082
C	-5.91283	0.07465	-1.26020
C	-4.78634	-1.61908	1.85969
C	-2.48098	-2.16909	1.33652
H	-3.44899	-2.34373	-1.51710
C	-2.18192	-1.91920	-3.20131
H	-1.59123	1.54774	-1.56033
C	-1.12431	0.25994	-3.22266
H	-5.04045	2.31082	1.15371
C	-6.94577	2.26444	0.13658
C	-7.20252	0.53081	-1.53147
H	-5.51250	-0.76574	-1.81961
H	-5.65788	-0.98406	1.73422
C	-4.84981	-2.71923	2.71533
H	-1.55308	-1.97908	0.80449
C	-2.55013	-3.26708	2.19285
H	-2.33151	-2.89741	-3.64916
C	-1.33519	-0.98948	-3.81086
H	-0.44547	0.97445	-3.67818
C	-7.72052	1.62420	-0.83246
H	-7.34431	3.11898	0.67647
H	-7.80026	0.03693	-2.29240
H	-5.77153	-2.93363	3.24929
C	-3.73395	-3.54263	2.88157
H	-1.67570	-3.90030	2.31011
H	-0.82905	-1.24334	-4.73808
H	-8.72467	1.97932	-1.04765

H -3.78740 -4.40055 3.54649

Table S4.14. Character of the LUMO+1, LUMO, HOMO and HOMO-1 of the [M(L^Y)(PPh_3)] (M = Ni, Pd, Pt; Y = O, S, Se, Te) complexes.

		O	S	Se	Te
Ni	LUMO+1	Ligand, π*/p_z(C_{Ph}=O)	Ligand, π*(C=N)	Ligand, π*(C=N)	Ligand, π*(C=N)
	LUMO	Ligand, π*/p_z(C_{Ph}=O)	Ligand, π*/p_z(**C**$_{Ph}$=O)	Ligand, π*/p_z(**C**$_{Ph}$=O)	Ligand, π*/p_z(**C**$_{Ph}$=O)
	HOMO	Ligand, π(C_{Ph}=C_{Ph})	Ligand, π*/p_z(**C**$_{Ph}$-CN)	Ligand, π*/p_z(**C**$_{Ph}$-CN)	Ligand, π*/p_z(**C**$_{Ph}$-CN)
	HOMO-1	Ligand, π(C_{Ph}=C_{Ph})	Ligand, p_z(**S**)	Ligand, p_z(**Se**)	Ligand, p_z(**Te**)
Pd	LUMO+1	Ligand, π*(C=N)	PPh_3, π*(C_{Ph}=C_{Ph})	PPh_3, π*(C_{Ph}=C_{Ph})	PPh_3, π*(C_{Ph}=C_{Ph})
	LUMO	Pd, σ*/$d_{x^2-y^2}$(**Pd**)	Ligand, π*(C=N)	Ligand, π*(C=N)	Ligand, π*(C=N)
	HOMO	Ligand, π(C_{Ph}=C_{Ph})	Ligand, p_z(**S**)	Ligand, p_z(**Se**)	Ligand, p_z(**Te**)
	HOMO-1	Ligand, π(C_{Ph}=C_{Ph})	Ligand, π(C_{Ph}=C_{Ph})	Ligand, π(C_{Ph}=C_{Ph})	Ligand, π(C_{Ph}=C_{Ph})
Pt	LUMO+1	Pt, σ*/$d_{x^2-y^2}$(**Pt**)	PPh_3, π*(C_{Ph}=C_{Ph})	PPh_3, π*(C_{Ph}=C_{Ph})	PPh_3, π*(C_{Ph}=C_{Ph})
	LUMO	Ligand, π*/p_z(**C**$_{Ph}$=O)	Ligand, π*(C=N)	Ligand, π*(C=N)	Ligand, π*(C=N)
	HOMO	Ligand, π*/p_z(**C**$_{Ph}$-CN)	Ligand, p_z(**S**)	Ligand, p_z(**Se**)	Ligand, p_z(**Te**)
	HOMO-1	Ligand, π(C_{Ph}=C_{Ph})	Ligand, π(C_{Ph}=C_{Ph})	Ligand, π(C_{Ph}=C_{Ph})	Ligand, π(C_{Ph}=C_{Ph})

Tables S4.15. Comparison of selected bond lengths in calculated structures with the crystal structures of [M(L^Y)(PPh_3)] (M = Ni, Pd, Pt; Y = O, S, Se, Te with exception of M = Pt; Y = S) in Å. Distinctions were made between the organic ligand backbone and the coordination sphere of the metal ions. Distances are given in Å.

Differences in O/S compounds[1-5]:

	XRD	Calc	delta	XRD	Calc	delta	XRD	Calc	delta	XRD	Calc	delta	XRD	Calc	delta
	NiO			NiS			PdO			PdS			PtO		
Y1-C1	1.32	1.31	0.01	1.75	1.76	0.01		*	*	1.79	1.77	0.02	1.31	1.33	0.02
O1-C11	1.31	1.33	0.02	1.30	1.30	0.00		*	*	1.33	1.30	0.03	1.32	1.31	0.01
N1-C6	1.40	1.41	0.01	1.43	1.43	0.00		*	*	1.45	1.42	0.02	1.49	1.42	0.07
N1-C17	1.29	1.30	0.01	1.31	1.31	0.00		*	*	1.32	1.31	0.01	1.19	1.31	0.12
M1-O1	1.82	1.84	0.02	1.85	1.87	0.02	1.95	2.01	0.06	2.05	2.07	0.02	1.96	2.04	0.07
M1-N1	1.88	1.90	0.02	1.91	1.93	0.02	2.01	2.04	0.03	2.08	2.07	0.00	2.06	2.02	0.04
M1-P1	2.25	2.31	0.06	2.22	2.30	0.08	2.30	2.36	0.06	2.31	2.35	0.05	2.25	2.33	0.08
M1-Y1	1.85	1.85	0.00	2.14	2.21	0.07	2.02	2.02	0.00	2.28	2.31	0.04	2.01	2.03	0.03
avg org			0.01			0.00			*			0.02			0.05
avg metal			0.03			0.05			0.04			0.03			0.06

* for the organic backbone in M = Pd; Y = O there was no information given, which does not allow for a comparison between model and theory.

Differences in Se/Te compounds:

	XRD	Calc	delta	XRD	Calc	delta	XRD	Calc	delta	XRD	Calc	delta	XRD	Calc	delta	XRD	Calc	delta
	NiSe			PdSe			PtSe			NiTe			PdTe			PtTe		
Y1-C1	1.90	1.90	0.00	1.90	1.92	0.01	1.90	1.91	0.02	2.10	2.11	0.01	2.10	2.12	0.02	2.11	2.11	0.00
O1-C11	1.30	1.30	0.00	1.29	1.30	0.01	1.31	1.30	0.01	1.30	1.30	0.00	1.29	1.30	0.01	1.31	1.30	0.01
N1-C6	1.44	1.43	0.01	1.43	1.42	0.01	1.44	1.43	0.01	1.45	1.43	0.02	1.44	1.43	0.01	1.40	1.43	0.03
N1-C17	1.31	1.31	0.00	1.29	1.31	0.02	1.30	1.31	0.01	1.31	1.31	0.00	1.29	1.31	0.02	1.28	1.31	0.03
M1-N1	1.92	1.93	0.02	2.06	2.09	0.03	2.06	2.08	0.02	1.87	1.95	0.08	2.04	2.10	0.06	2.02	2.10	0.07
M1-O1	1.86	1.89	0.03	2.03	2.08	0.05	2.03	2.09	0.06	1.93	1.89	0.04	2.07	2.09	0.02	2.07	2.10	0.03
M1-P1	2.19	2.29	0.10	2.26	2.35	0.08	2.25	2.32	0.07	2.19	2.28	0.10	2.26	2.34	0.08	2.24	2.31	0.07
M1-Y1	2.24	2.32	0.07	2.34	2.42	0.08	2.35	2.43	0.08	2.41	2.52	0.11	2.48	2.60	0.12	2.50	2.62	0.11
avg org			0.00			0.01			0.01			0.01			0.01			0.02
avg metal			0.06			0.06			0.06			0.08			0.07			0.07

Overall differences:

average Te	0.12
overall average org	0.02
overall average metal	0.05
total average of all bonds	0.04

Literature

[1] H. Motschi, C. Nusaumer, P. S. Pregosin, *Helv. Chim. Acta*, **1980**, *63*, 2071-2086.

[2] M. M. Tamizh, B. F. T. Cooper, C. L. B. Macdonald, R. Karvembu, *Inorg. Chim. Acta*, **2013**, *394*, 391–400.

[3] M. Shabbir, Z. Akhter, I. Ahmad, S. Ahmed, M. Shafiq, B. Mirza, V. McKee, K. S. Munawar, A. R. Ashraf, *J. Mol. Struct.*, **2016**, *1118*, 250-258.

[4] M. M. Tamizh, K. Mereiter, K. Kirchner, B. R. Bhat, R. Karvembu, *Polyhedron*, **2009**, *28*, 2157-2164.

[5] V. Kuchtanin, L. Kleščíková, M. Šoral, R. Fischer, Z. Růžičková, Erik Rakovský, J. Moncol', Peter Segl'a, *Polyhedron*, **2016**, *117*, 90-96.

[6] M. Roca Jungfer, A. Hagenbach, E. S. Lang, U. Abram, *Eur. J. Inorg. Chem.*, **2019**, 4974–4984.

A.10 Solvents and Ligands Matter: Structurally Variable Palladium and Nickel Clusters Assembled by Tridentate Selenium- and Tellurium-Containing Schiff Bases

Authors	M. Roca Jungfer, E. Schulz Lang, U. Abram
Journal	*Inorg. Chem.* **2022**, *61*, 3785–3800
DOI	10.1021/acs.inorgchem.2c00076
Link	https://pubs.acs.org/doi/abs/10.1021/acs.inorgchem.2c00076
Detailed scientific contribution	Maximilian Roca Jungfer designed the project. Maximilian Roca Jungfer performed the synthesis and characterization of the compounds, performed DFT calculations, calculated the X-ray structures and wrote a draft of the manuscript. Ernesto Schulz Lang provided scientific guidance and suggestions. Ulrich Abram supervised the project, provided scientific guidance and suggestions and corrected the manuscript.
Estimated own contribution	80%

Return to publication 4.10.

Supporting information for the paper entitled:

Solvents and Ligands Matter: Structurally Variable Palladium and Nickel Clusters Assembled by Tridentate Se- and Te-Containing Schiff' Bases

*Maximilian Roca Jungfer,[§] Ernesto Schulz Lang,[#] and Ulrich Abram[§]**

[§] Institute of Chemistry and Biochemistry, Freie Universität Berlin, Fabeckstr. 34/36, 14195 Berlin, Germany,

[#] Universidade Federal de Santa Maria Departamento de Química: Santa Maria, Rio Grande do Sul, Brazil

Corresponding Author:

E-mail: ulrich.abram@fu-berlin.de

Table of Contents

Part 1: Crystallographic data

Table S1. Crystal data and structure determination parameters.

	$H_2\{L^{Se}\}_2$	GBF-$[Pd_4(L^{Se})_4]$·4EtOH	GBF-$[Pd_4(L^{Te})_4]$·4EtOH
Empirical formula	$C_{26}H_{20}N_2O_2Se_2$	$C_{60}H_{60}N_4O_8Pd_4Se_4$	$C_{60}H_{60}N_4O_8Pd_4Te_4$
Formula weight	550.36	1706.56	1901.12
Temperature/K	293(2)	156(2)	100(2)
Crystal system	Tetragonal	Tetragonal	Tetragonal
Space group	*I*4$_1$/*a*	*I*4$_1$/*a*	*I*4$_1$/*a*
a/Å	12.6652(13)	12.7025(6)	12.8977(3)
b/Å	12.6652(13)	12.7025(6)	12.8977(3)
c/Å	28.608(4)	36.145(2)	36.8311(17)
α/°	90	90	90
β/°	90	90	90
γ/°	90	90	90
Volume/Å^3	4588.9(12)	5832.2(6)	6126.9(4)
Z	8	4	4
ρ_{calc} g/cm^3	1.593	1.944	2.061
μ/mm^{-1}	3.249	13.124	24.506
F(000)	2192	3328	3616
Crystal size/mm^3	0.400 x 0.383 x 0.350	0.25 x 0.1 x 0.1	0.12 x 0.06 x 0.03
Radiation	0.71073	1.5418	1.5418
2Θ range for data collection/°	3.518 to 26.797	3.688 to 72.276	3.631 to 74.579
Index ranges	-14<=h<=16, -11<=k<=16, -31<=l<=36	-15<=h<=15, -14<=k<=12, -44<=l<=25	-13<=h<=16, -15<=k<=8, -45<=l<=45
Reflections collected	7473	14319	20385
Independent reflections	2433 [R(int) = 0.0845]	2642 [R(int) = 0.0509]	3134 [R(int) = 0.0537]
Absorption correction	Integration	Multi Scan	Multi Scan
$T_{max.}$ and $T_{min.}$	0.5676 and 0.4289	0.7536 and 0.5920	0.7538 and 0.5476
Data/restraints/parameters	2433 / 0 / 153	2642 / 0 / 190	3134 / 0 / 186
Goodness-of-fit on F^2	1.039	1.321	1.061
Final R indexes [I>=2σ (I)]	R1 = 0.0647, wR2 = 0.1295	R1 = 0.0399, wR2 = 0.0733	R1 = 0.0296, wR2 = 0.0648
Final R indexes [all data]	R1 = 0.1173, wR2 = 0.1480	R1 = 0.0547, wR2 = 0.0799	R1 = 0.0395, wR2 = 0.0695
Largest diff. peak/hole / e^{-3}	0.746 and -0.449	0.746 and -0.449	0.602 and -0.473
CCDC access code	2133215	2133216	2133217

Table S1. Crystal data and structure determination parameters (continued).

	cuboid-$[Pd_4(L^{Se})_4]\cdot Et_2O$	$[Ni\text{-}\mu_2\text{-}\kappa_2\text{-}(Ni\{\kappa_5\text{-}L^{Se}\}_2)_2\text{-}\mu_2\text{-}(OAc)_2]\cdot 0.5CH_2Cl_2$	$[Ni\text{-}\mu_2\text{-}\kappa_2\text{-}(Ni\{\kappa_5\text{-}L^{Te}\}_2)_2\text{-}\mu_2\text{-}(OAc)_2]\cdot CH_2Cl_2$
Empirical formula	$C_{56}H_{46}N_4O_5Pd_4Te_4$	$C_{56.50}H_{43}ClN_4Ni_3O_8Se_4$	$C_{57}H_{44}Cl_2N_4Ni_3O_8Te_4$
Formula weight	1790.97	1433.37	1670.39
Temperature/K	100(2)	273(2)	230(2)
Crystal system	Triclinic	Monoclinic	Triclinic
Space group	$P\bar{1}$	$P2_1/n$	$P\bar{1}$
a/Å	13.2285(5)	10.6160(7)	12.8500(15)
b/Å	14.5854(5)	26.2845(16)	22.023(2)
c/Å	15.2255(5)	20.1484(12)	22.545(3)
α/°	79.9090(10)	90	75.916(9)
β/°	78.0170(10)	96.767(5)	87.165(10)
γ/°	66.9710(10)	90	87.274(9)
Volume/Å^3	2630.18(16)	5583.0(6)	6176.6(13)
Z	2	4	4
ρ_{calc} g/cm^3	2.261	1.705	1.796
μ/mm^{-1}	3.573	3.714	2.897
F(000)	1684	2844	3216
Crystal size/mm^3	0.31 x 0.22 x 0.06	0.220 x 0.137 x 0.040	0.290 x 0.180 x 0.020
Radiation	0.71073	0.71073	0.71073
2Θ range for data collection/°	2.007 to 27.167	3.151 to 26.000	3.162 to 28.099
Index ranges	-16<=h<=16, -18<=k<=18, -19<=l<=19	-13<=h<=11, -32<=k<=32, -24<=l<=24	-17<=h<=17, -28<=k<=28, -29<=l<=29
Reflections collected	50176	27487	29392
Independent reflections	11641 [R(int) = 0.0930]	10735 [R(int) = 0.1005]	29392
Absorption correction	Multi Scan	Integration	Integration
$T_{max.}$ and $T_{min.}$	0.7455 and 0.6259	0.7604 and 0.6130	0.7314 and 0.2413
Data/restraints/parameters	11641 / 988 / 704	10735 / 1090 / 718	29392 / 2112 / 1217
Goodness-of-fit on F^2	1.077	0.891	0.930
Final R indexes [I>=2σ (I)]	R1 = 0.0447, wR2 = 0.0966	R1 = 0.0566, wR2 = 0.0710	R1 = 0.1278, wR2 = 0.3196
Final R indexes [all data]	R1 = 0.0879, wR2 = 0.1217	R1 = 0.1644, wR2 = 0.0854	R1 = 0.3187, wR2 = 0.3748
Largest diff. peak/hole / e^{-3}	1.487 and -1.736	0.884 and -0.646	2.503 and -1.753
CCDC access code	2133218	2133219	2133220

Table S1. Crystal data and structure determination parameters (continued).

	[Ni_2-κ_5-(Ni_4-κ_6-μ_6-{($L^{Te}_2O_3$)($L^{Te}O_2$)$_2$}$_2$)-μ_2-(H_2O)$_2$]
Empirical formula	$C_{104}H_{76}N_8Ni_6O_{24}Te_8$
Formula weight	3194.78
Temperature/K	100(2)
Crystal system	Triclinic
Space group	$P\bar{1}$
a/Å	16.325(3)
b/Å	16.984(3)
c/Å	22.694(6)
α/°	95.523(8)
β/°	92.294(7)
γ/°	112.975(6)
Volume/Å^3	5746(2)
Z	2
ρ_{calc} g/cm^3	1.847
μ/mm^{-1}	3.024
F(000)	3064
Crystal size/mm^3	0.12 x 0.09 x 0.08
Radiation	0.71073
2Θ range for data collection/°	2.102 to 27.161
Index ranges	-20<=h<=20, -21<=k<=21, -29<=l<=29
Reflections collected	98545
Independent reflections	25393 [R(int) = 0.0844]
Absorption correction	Semi-empirical from equivalents
$T_{max.}$ and $T_{min.}$	0.7455 and 0.6500
Data/restraints/parameters	25393 / 0 / 1351
Goodness-of-fit on F^2	1.006
Final R indexes [I>=2σ (I)]	R1 = 0.0521, wR2 = 0.1250
Final R indexes [all data]	R1 = 0.0876, wR2 = 0.1451
Largest diff. peak/hole / e^{-3}	1.298 and -1.695
CCDC access code	2133221

Figure S1. Ellipsoid representation (50% probability) of tetragonal $\{HL^{Se}\}_2$. Hydrogen atoms bonded to carbon atoms are omitted for clarity. The positions for the hydrogen atom at the imino carbon and the hydrogen atom participating in the hydrogen bond were taken from the density map and refined freely. Hydrogen-bonding is established between oxygen and nitrogen but also oxygen and selenium. The structural parameters are similar to those found in the previously characterized polymorphs of $\{HL^{Se}\}_2$. The second half of the molecule is generated through the tetragonal space group symmetry (symmetry code: 1-x, 1/2-y, +z).

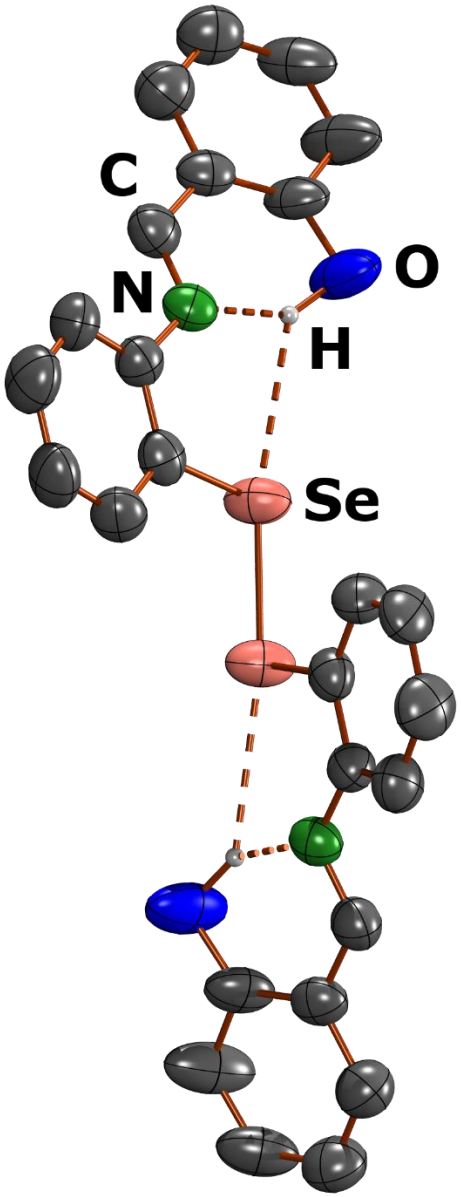

Figure S2. Ellipsoid representation (50% probability) of gyrobifastigial $[Pd_4(L'^{Se})_4]\cdot 4EtOH$. Hydrogen atoms bonded to carbon atoms are omitted for clarity. The positions for the hydrogen atom at the imino carbon and the hydrogen atom participating in the hydrogen bond were taken from the density map and refined freely. The molecule is completed by the tetragonal space group symmetry (symmetry codes: -1/4+x, 3/4-y, 3/4-z; 3/4-x, 1/4+y, 3/4-z; 1-x, 1/2-y, +z).

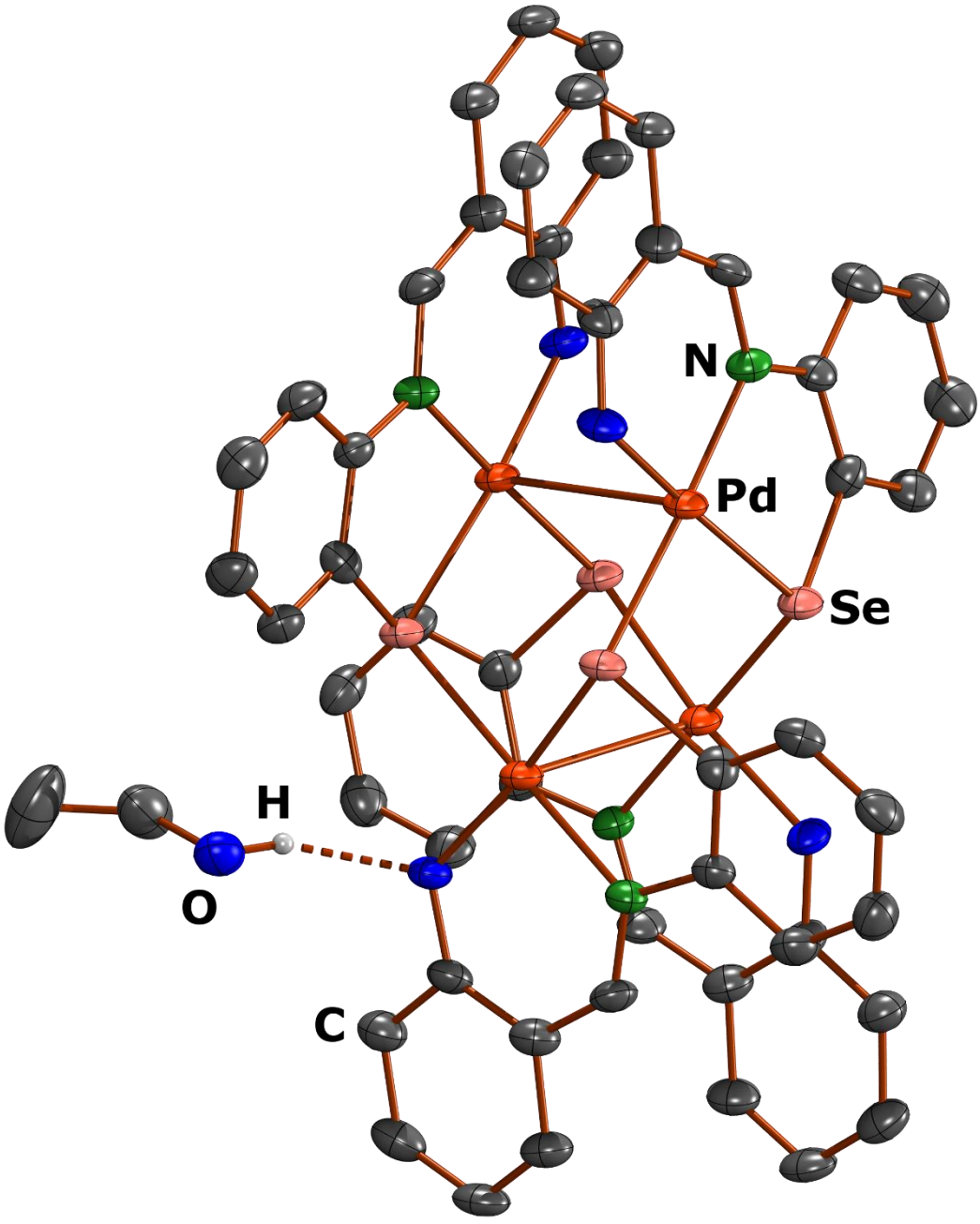

Figure S3. Ellipsoid representation (50% probability) of gyrobifastigial $[Pd_4(L'^{Te})_4]\cdot 4EtOH$. Hydrogen atoms bonded to carbon atoms are omitted for clarity. The position of the hydrogen atom participating in the hydrogen bond was taken from the density map and refined freely. The molecule is completed by the tetragonal space group symmetry (symmetry codes: 1/4+x, 5/4-y, 5/4-z; 5/4-x, -1/4+y, 5/4-z; 1-x, 3/2-y, +z).

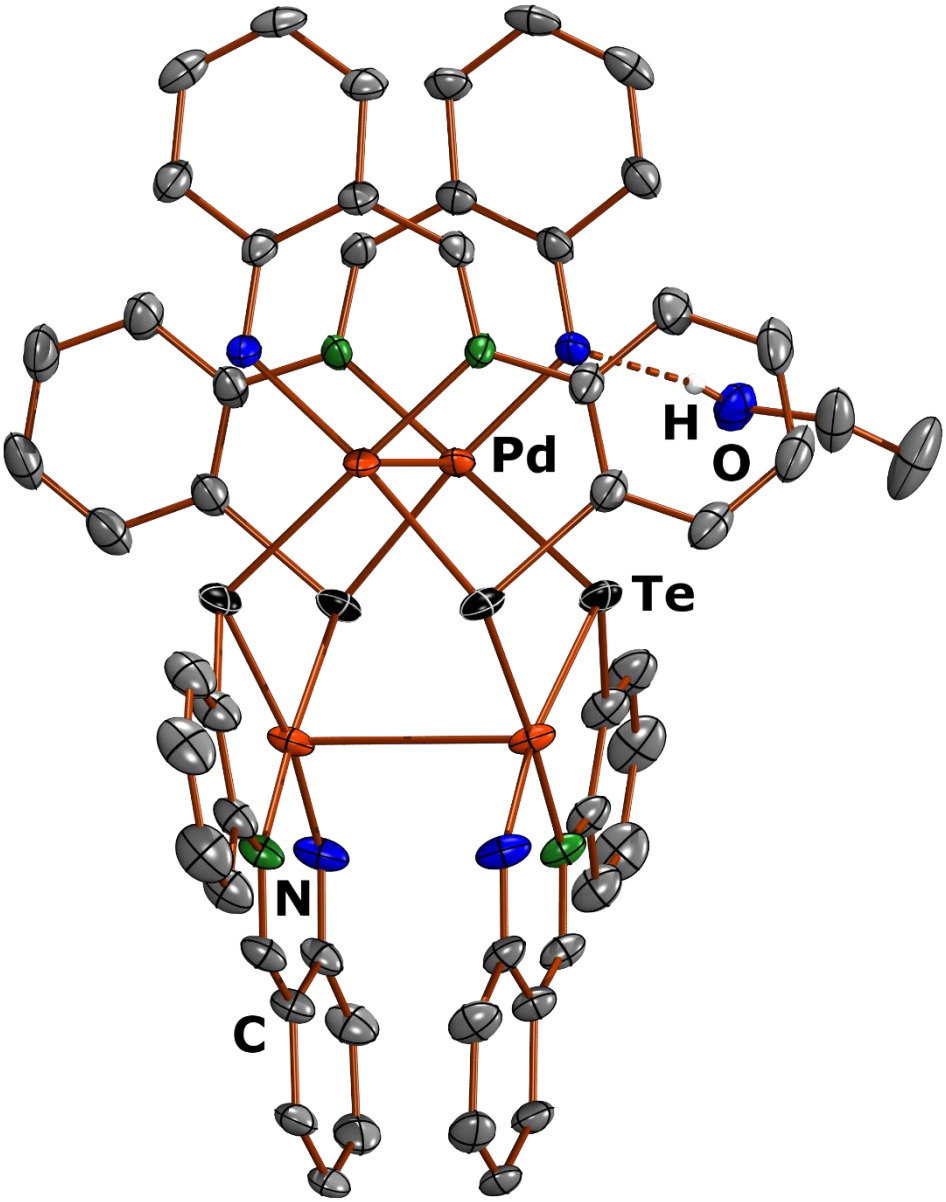

Figure S4. Ellipsoid representation (50% probability) of cuboidal $[Pd_4(L'^{Te})_4]\cdot Et_2O$. Hydrogen atoms are omitted for clarity. One of the phenolato groups is disordered over two positions with a ratio of ca. 45:55.

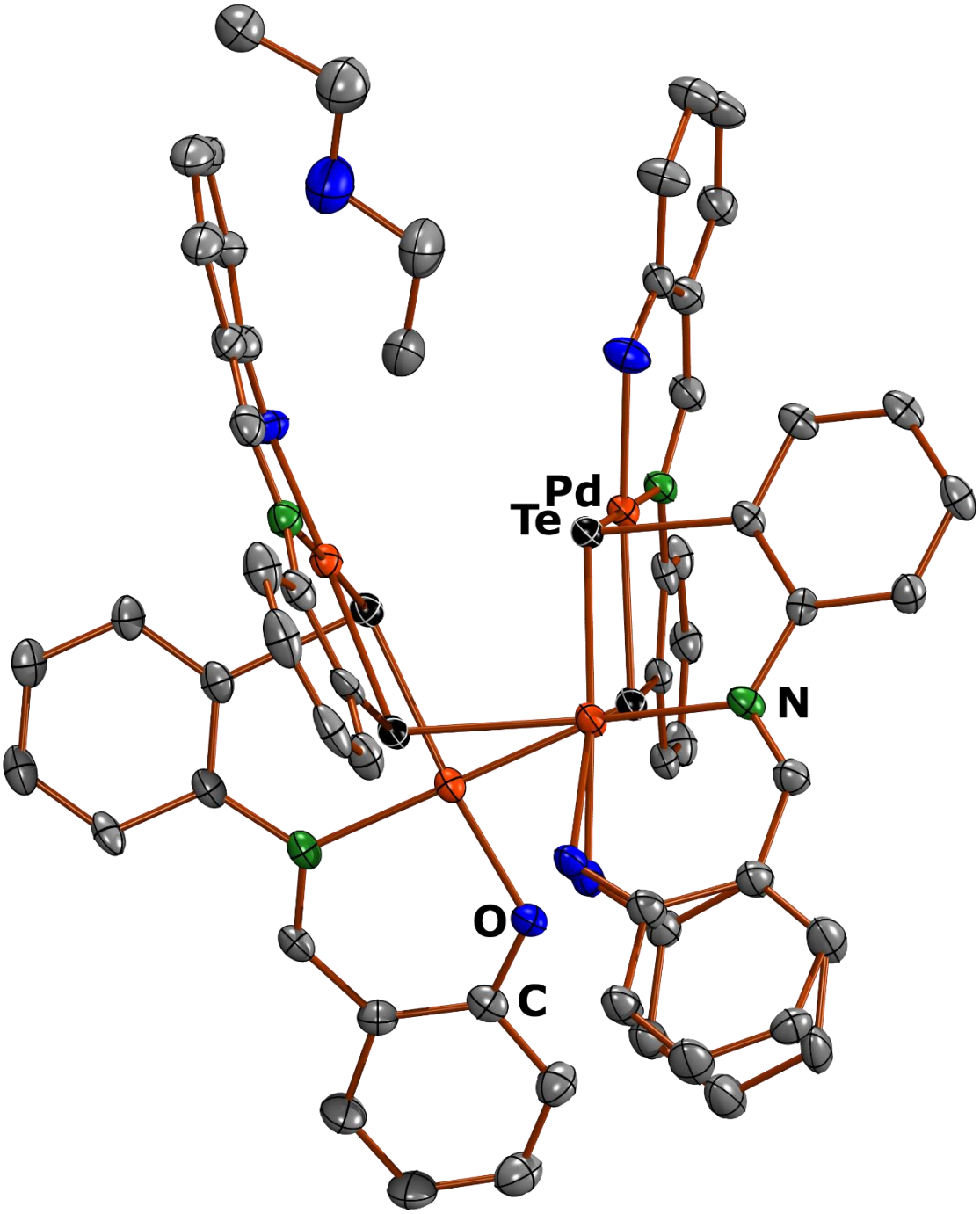

Figure S5. Ellipsoid representation (50% probability) of [Ni-μ_2-κ_2-(Ni{κ_5-L^{Se}}$_2$)$_2$-μ_2-(OAc)$_2$]·0.5CH_2Cl_2. Hydrogen atoms are omitted for clarity. The ill-defined co-crystallized solvent dichloromethane was modelled using appropriate restraints and constraints as it is disordered over three positions (ratio 15:20:15) with a total set occupancy of 0.5 by a SUMP instruction. Due to the algorithm of the internal SHELX calculation, the ESD of the SUMP must differ from 0 and therefore the internally calculated occupancy (0.501) does not match the reported value (0.5) exactly.

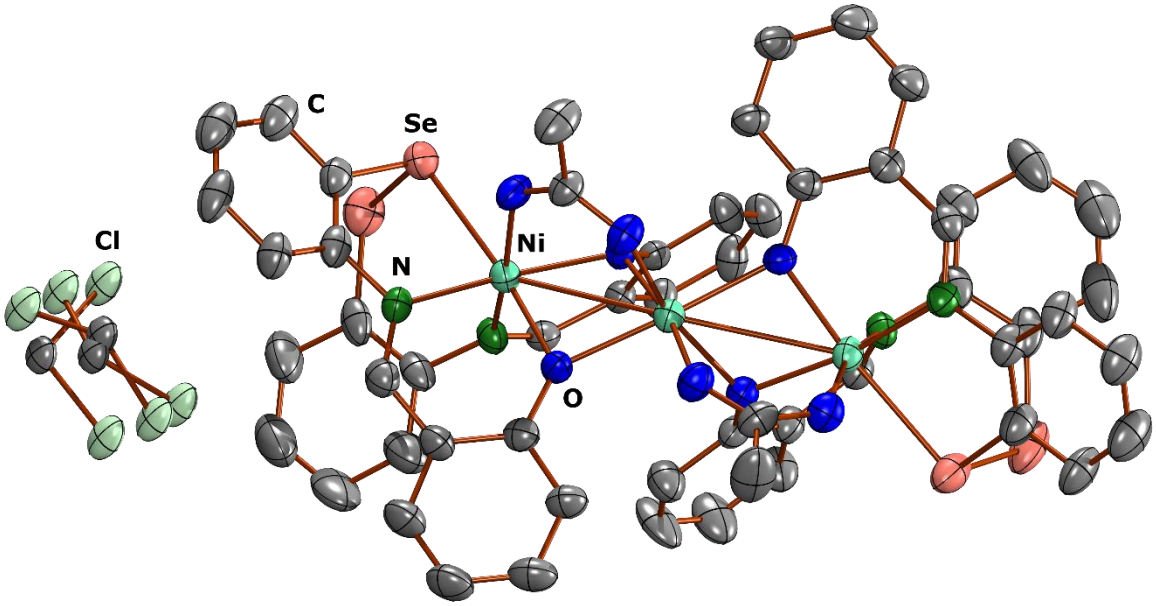

Figure S6. Ellipsoid representation (50% probability) of [Ni-μ_2-κ_2-(Ni{κ_5-L^{Te}}$_2$)$_2$-μ_2-(OAc)$_2$]·CH_2Cl_2. Hydrogen atoms are omitted for clarity. The two co-crystallized solvent dichloromethane molecules broke the higher space-group symmetries and therefore two [Ni-μ_2-κ_2-(Ni{κ_5-L^{Te}}$_2$)$_2$-μ_2-(OAc)$_2$] moieties are present in the asymmetric unit. The crystal quality was low and the size was small. Thus, the diffraction data was very weak and and the crystal was refined as a five-component twin. As a results the six-membered phenyl rings in the structure showed varying degrees of deformity and were set to a regular hexagonal geometry using AFIX 66 to improve the model around tellurium and nickel. Obviously, the C-C bond precision is consequently low. The structural parameters should therefore not be overvalued. Nevertheless, the connectivity has been verified doubtlessly.

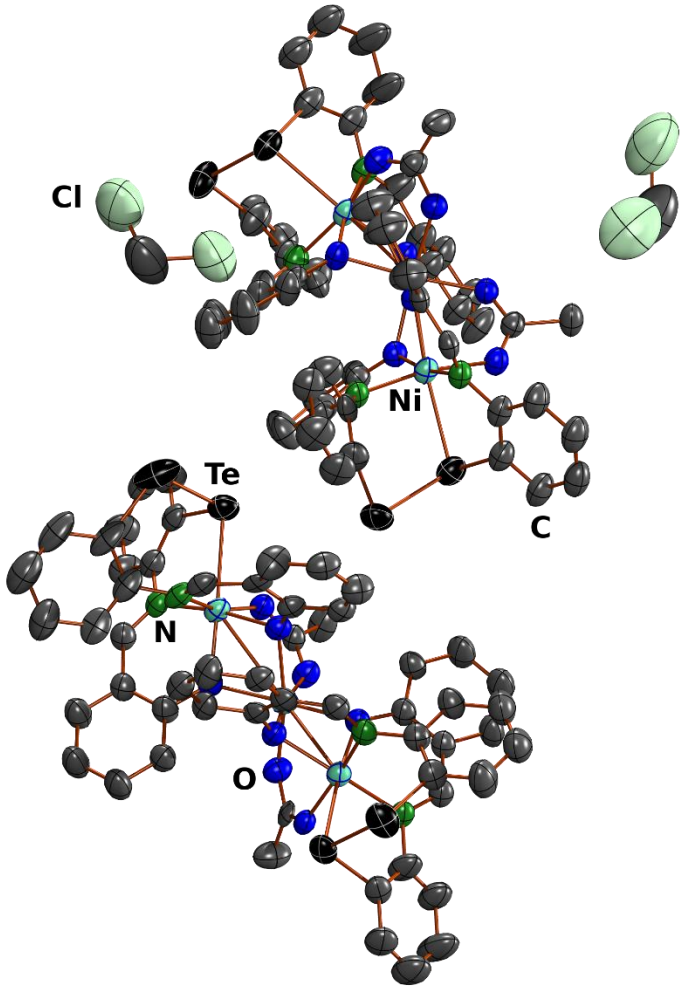

Table S2. Comparison of the bond lengths (Å) and bond angles (°) in [Ni-μ_2-κ_2-(Ni{κ_5-L^{Se}}$_2$)$_2$-μ_2-(OAc)$_2$] and [Ni-μ_2-κ_2-(Ni{κ_5-L^{Te}}$_2$)$_2$-μ_2-(OAc)$_2$].

	[Ni-μ_2-κ_2-(Ni{κ_5-L^{Se}}$_2$)$_2$-μ_2-(OAc)$_2$]	[Ni-μ_2-κ_2-(Ni{κ_5-L^{Te}}$_2$)$_2$-μ_2-(OAc)$_2$][a)]
Ni-N	2.057(6). 2.055(6), 2.041(5), 2.062(6)	2.06(2), 2.05(2), 2.01(2), 2.08(1) [2.05(2), 2.08(2), 2.03(2), 2.05(2)]
Ni1/Ni3-O$^{(phenol)}$	1.987(5), 2.030(4), 2.010(5), 2.028(4)	2.06(2), 1.99(2), 1.98(2), 2.02(2) [1.99(2), 2.02(2), 2.04(2), 2.04(2)]
Ni2-O$^{(phenol)}$	2.080(4), 2.104(5), 2.075(4), 2.134(5)	2.12(2), 2.10(2), 2.10(2), 2.09(2) [2.09(2), 2.11(2), 2.12(2), 2.08(2)]
Ni1/Ni3-O$^{(acetate)}$	2.019(5), 2.043(5)	2.05(2), 1.99(2) [2.03(2), 2.01(2)]
Ni2-O$^{(acetate)}$	2.026(5), 2.027(5)	2.03(2), 2.01(2) [2.04(2), 2.02(2)]
Ni-Y	2.632(1), 2.606(1)	2.777(4), 2.747(4) [2.764(4), 2.769(4)]
Y-Y	2.351(1), 2.335(1)	2.728(3), 2.717(3) [2.703(3), 2.710(3)]
Ni···Ni	3.078(1), 3.066(1)	3.075(4), 3.062(4) [3.076(4), 3.067(4)]
Ni-Y-C	90.6(3), 91.4(3)	84.9(5), 85.9(6) [85.5(5), 86.2(5)]
Ni-Y-Y	106.81(5), 106.88(5)	102.6(1), 102.4(1) [102.5(1), 102.4(1)]
C-Y$^{(Ni)}$-Y	102.8(2), 100.7(2)	99.4(5), 95.4(6) [98.4(5), 96.8(6)]
C-Y-Y$^{(Ni)}$	98.9(2), 104.3(3)	100.0(5), 96.9(5) [98.3(5), 99.2(5)]

Figures S7 and S8. Ellipsoid representation (50% probability) of [Ni_2-κ_5-(Ni_4-κ_6-μ_6-{($L'^{Te}{}_2O_3$)-($L'^{Te}O_2$)$_2$}$_2$)-μ_2-(H_2O)$_2$]. Hydrogen atoms bonded to carbon atoms are omitted for clarity. The hydrogen atom positions for the water hydrogen atoms were calculated in optimized positions for hydrogen bonding using the CALC-OH algorithm and then fixed in place. Additionally, their thermal parameters were linked to the parenting oxygen atom. The structure contains diffuse, apolar solvent molecules that we attempted to refined as several dichloromethane moieties. However, there was clearly a large spread of the dichloromethane over several occupied positions and therefore we applied the SQUEEZE procedure of PLATON on the distant, diffuse electron density for the final refinement. Electron density corresponding to 270 electrons per unit cell (ca. 6.5 CH_2Cl_2 or Et_2O molecules) was removed leaving solvent accessible voids of 1246.1 Å^3.

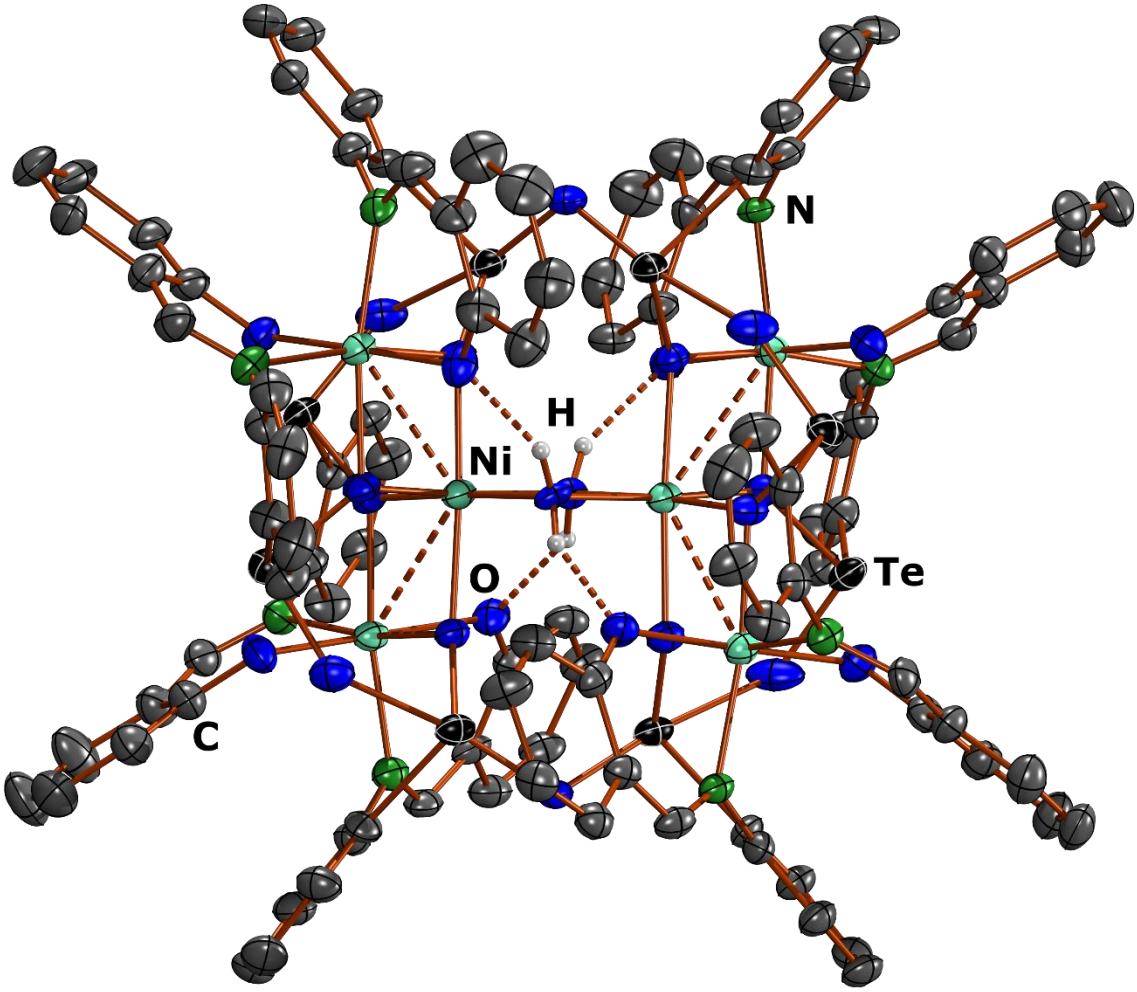

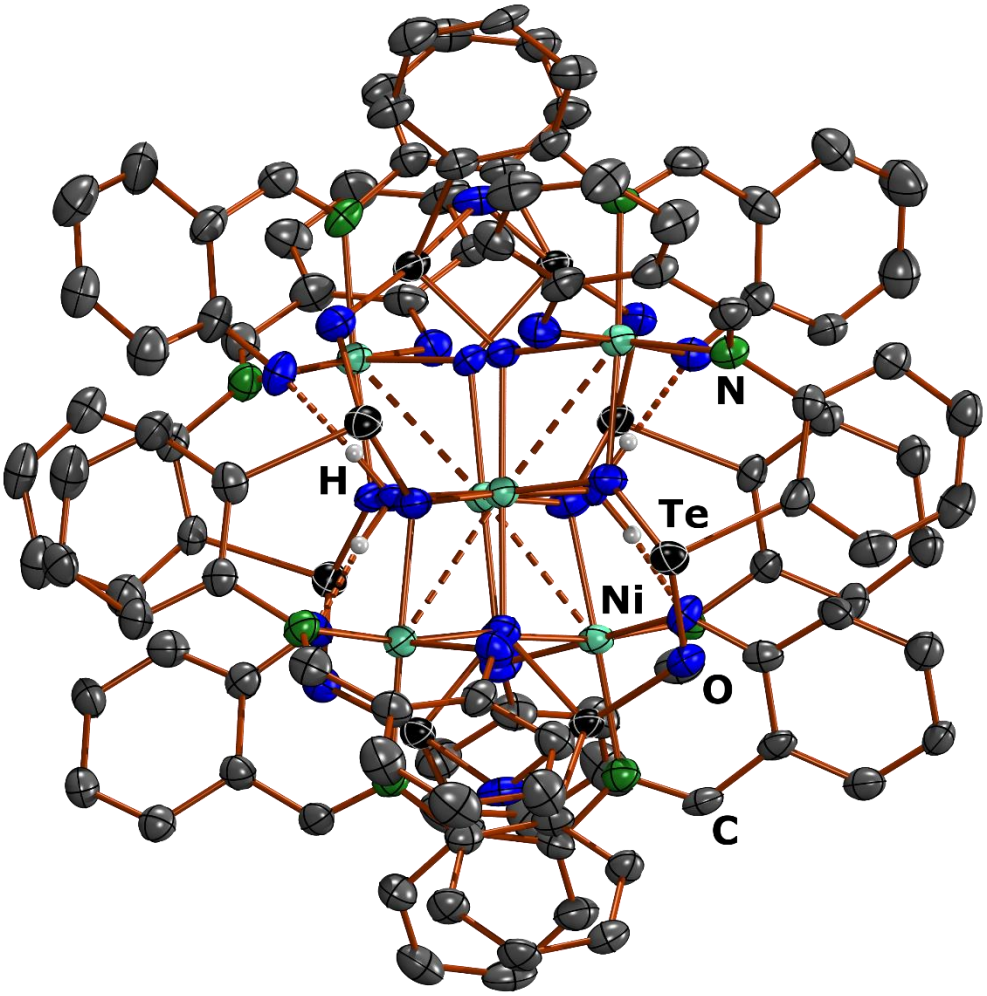

Table S3. Hydrogen bond parameters in [Ni_2-κ_5-(Ni_4-κ_6-μ_6-{($L'^{Te}_2O_3$)($L'^{Te}O_2$)$_2$}$_2$)-μ_2-(H_2O)$_2$]. Note that the hydrogen atom positions were taken from the density map but not refined due to their elusive nature in this heavy-atom-containing structure.

D—H···*A*	*D*—H (Å)	H···*A* (Å)	*D*···*A* (Å)	*D*—H···*A* (°)
O5—H1O5···O1C	0.86	1.92	2.711 (7)	153.8
O5—H2O5···O1G	0.86	1.78	2.568 (6)	151.9
O6—H1O6···O1B	0.86	1.89	2.677 (7)	152.5
O6—H2O6···O1F	0.86	1.84	2.602 (7)	146.8
O5—H1O5···O1C	0.86	1.92	2.711 (7)	153.8
O5—H2O5···O1G	0.86	1.78	2.568 (6)	151.9
O6—H1O6···O1B	0.86	1.89	2.677 (7)	152.5
O6—H2O6···O1F	0.86	1.84	2.602 (7)	146.8

Part 2: Spectroscopic data

Figure S9. ^{1}H NMR spectrum of $[Pd_4(L'^{Se})_4]$ in CD_2Cl_2 focused on the aromatic region.

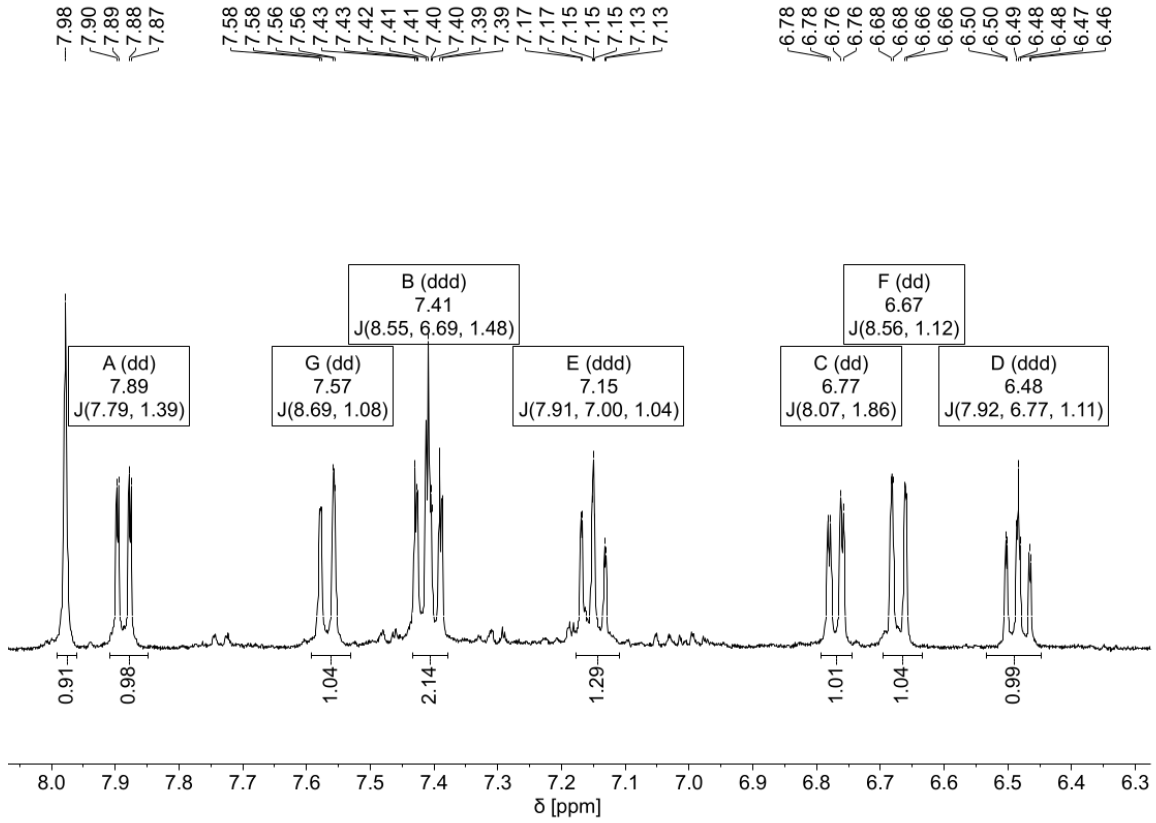

Figure S10. $^{1}H,^{1}H$-COSY NMR spectrum of $[Pd_4(L'^{Se})_4]$ in CD_2Cl_2 focused on the aromatic region.

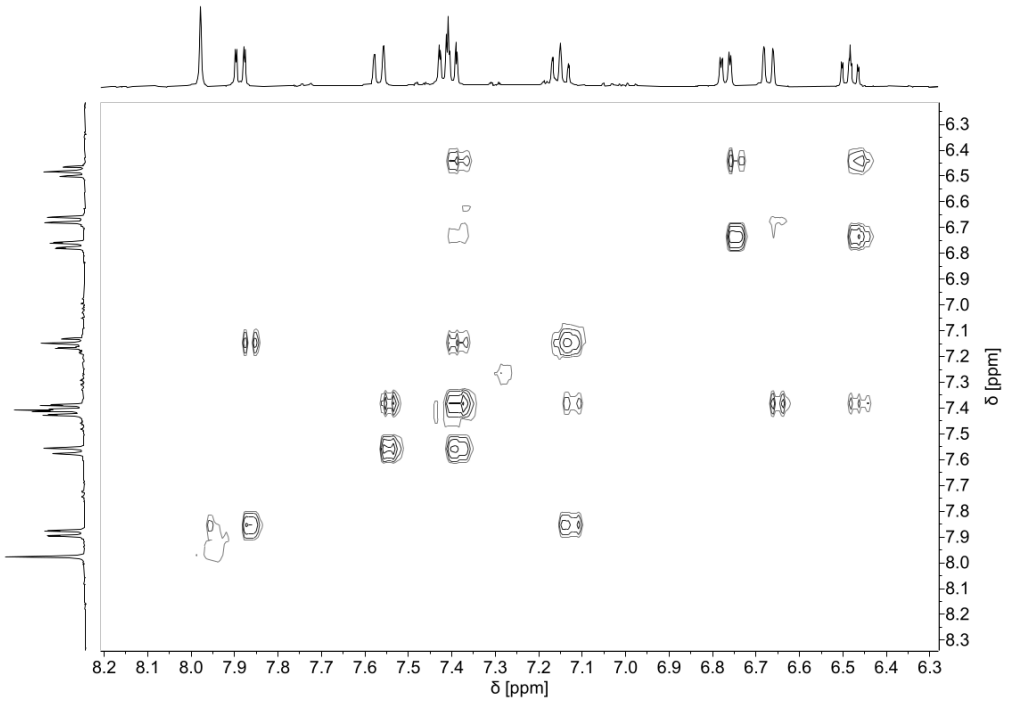

Figure S11. Stacked ^{1}H NMR spectra of [Pd(L'^{Se})(PPh$_3$)], {HL^{Se}}$_2$ and [Pd$_4$(L'^{Se})$_4$] in CD_2Cl_2.

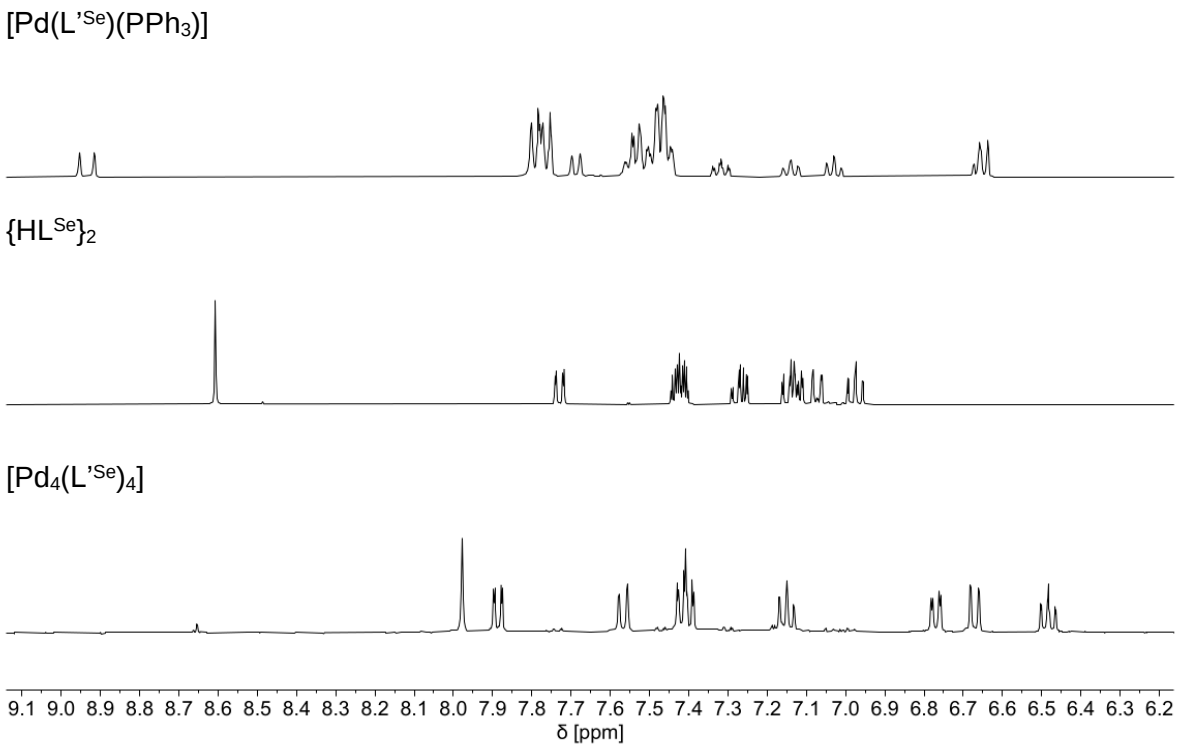

Figure S12. Full ^{1}H NMR spectrum of [Pd$_4$(L'^{Se})$_4$] in CD_2Cl_2. The low intensity is a result of the low solubility of the cluster.

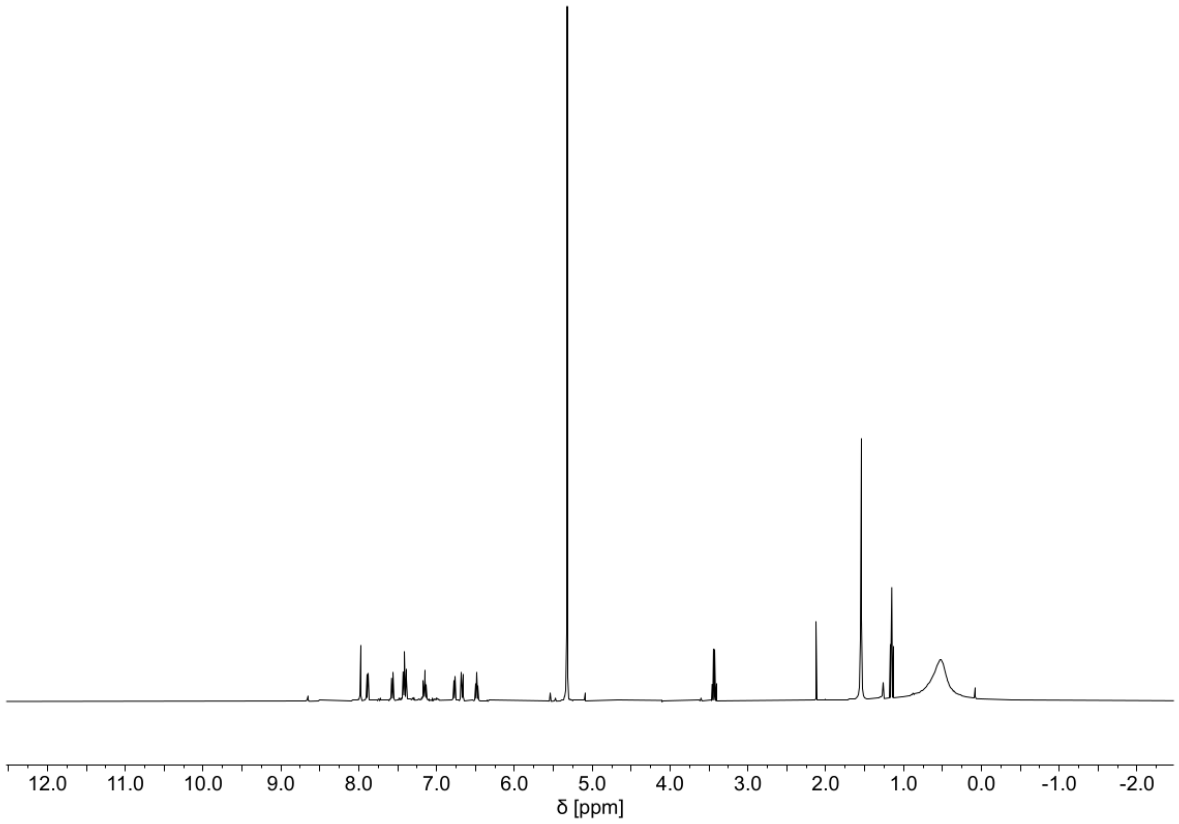

Figure S13. ^{1}H NMR spectrum of $[Pd_4(L'^{Se})_4]$ in a mixture of $CDCl_3/CD_2Cl_2$ focused on the aromatic region.

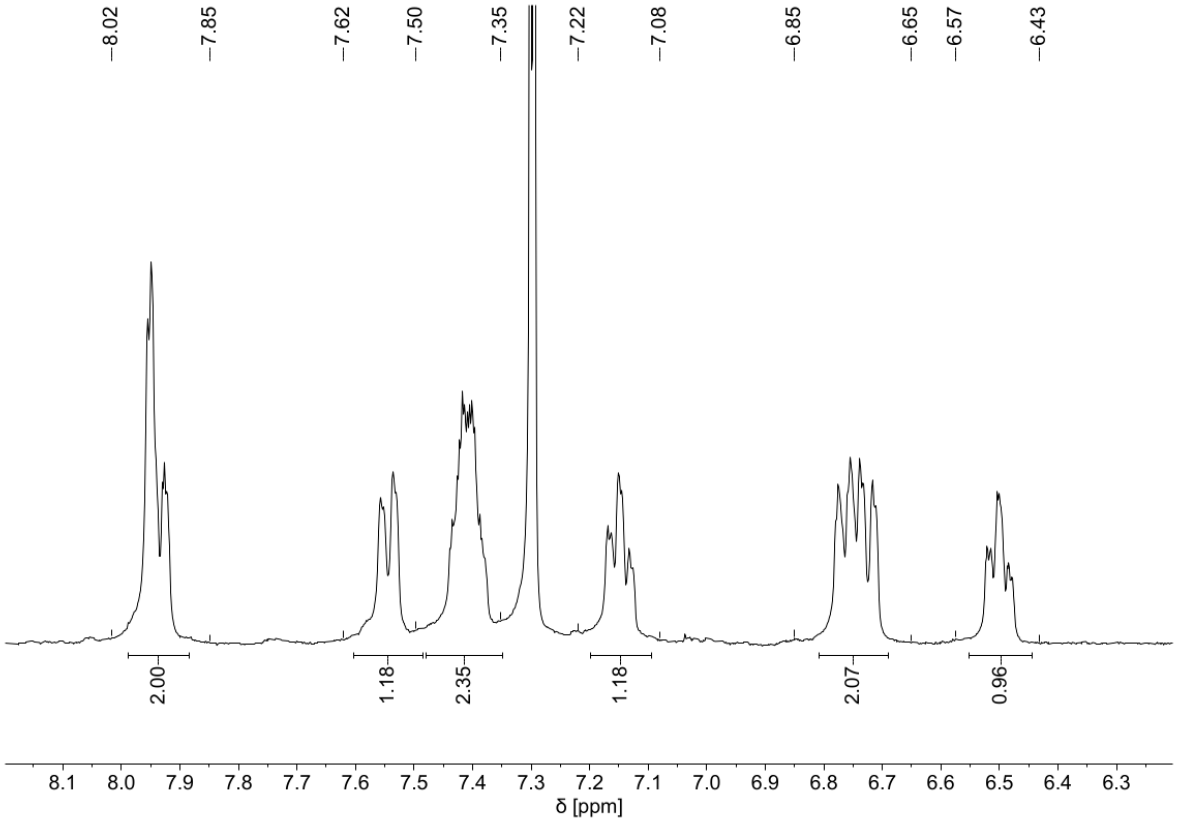

Figure S14. ^{1}H NMR spectrum of $[Pd_4(L'^{Se})_4]$ in a mixture of $CDCl_3/CD_2Cl_2$.

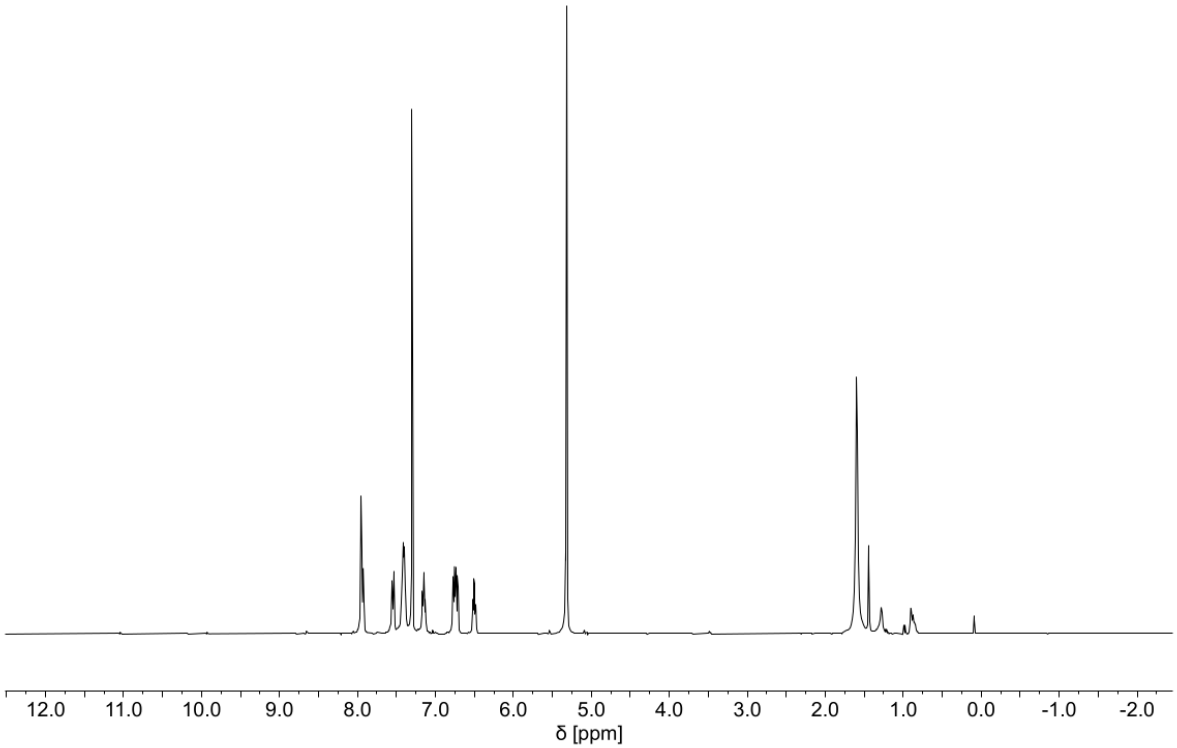

Figure S15. $^{13}C\{^{1}H\}$ NMR spectrum of $[Pd_4(L'^{Se})_4]$ in a mixture of $CDCl_3/CD_2Cl_2$.

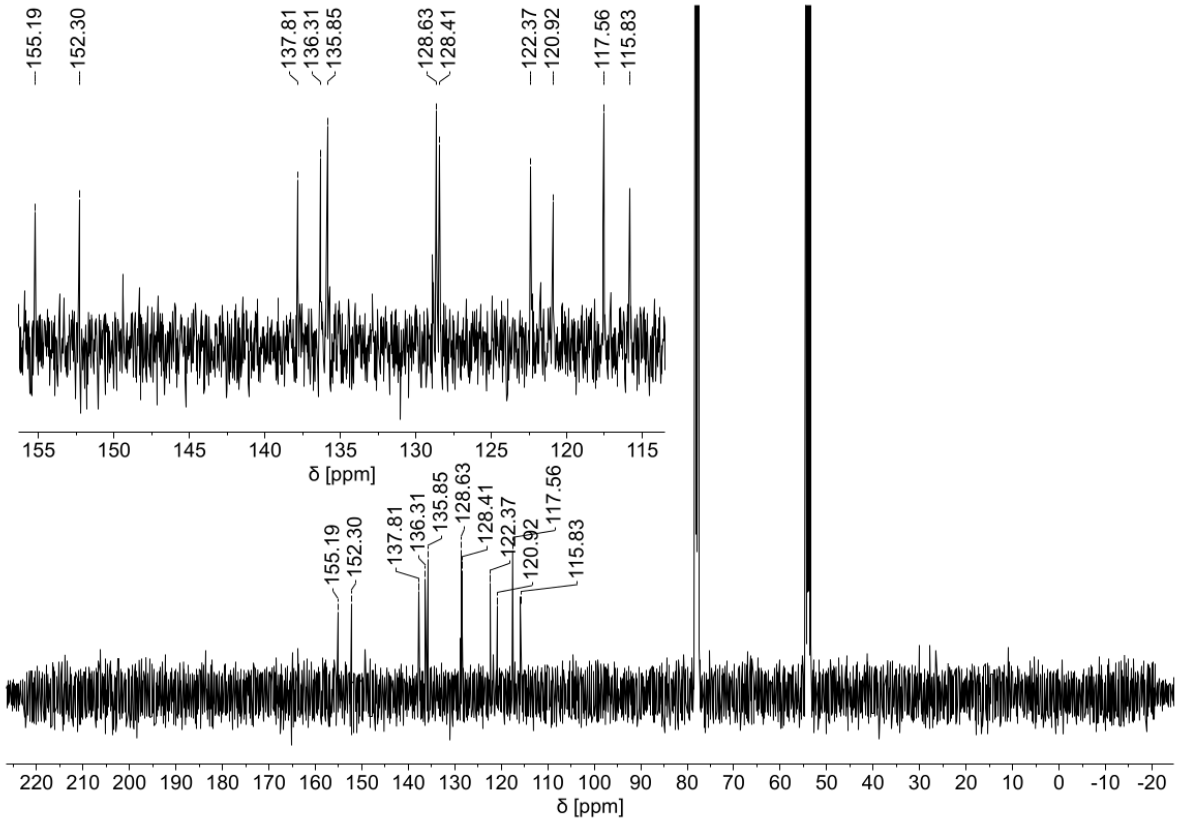

Figure S16. $^{13}C\{^{1}H\}$ APT-NMR spectrum of $[Pd_4(L'^{Se})_4]$ in a mixture of $CDCl_3/CD_2Cl_2$.

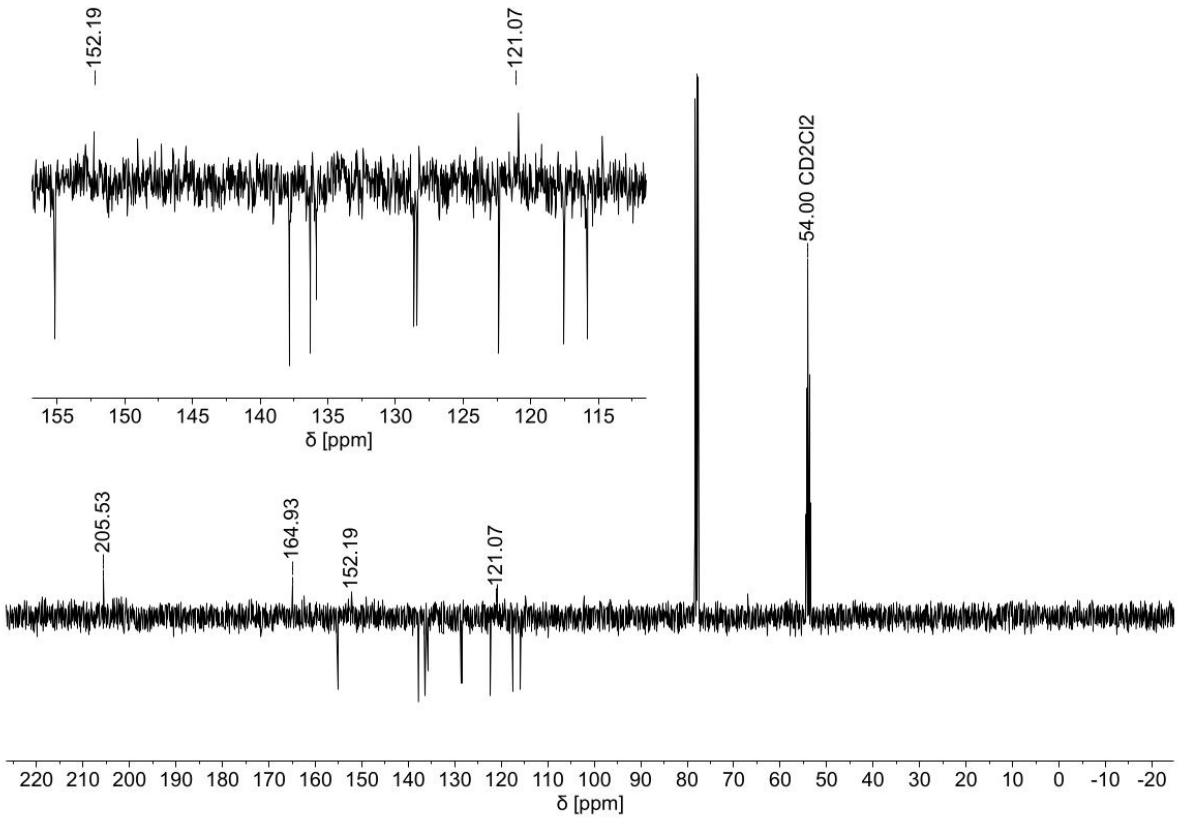

Figure S17. Stacked $^{13}C\{^{1}H\}$ NMR and APT-NMR spectra of $[Pd_4(L'^{Se})_4]$ in a mixture of $CDCl_3/CD_2Cl_2$.

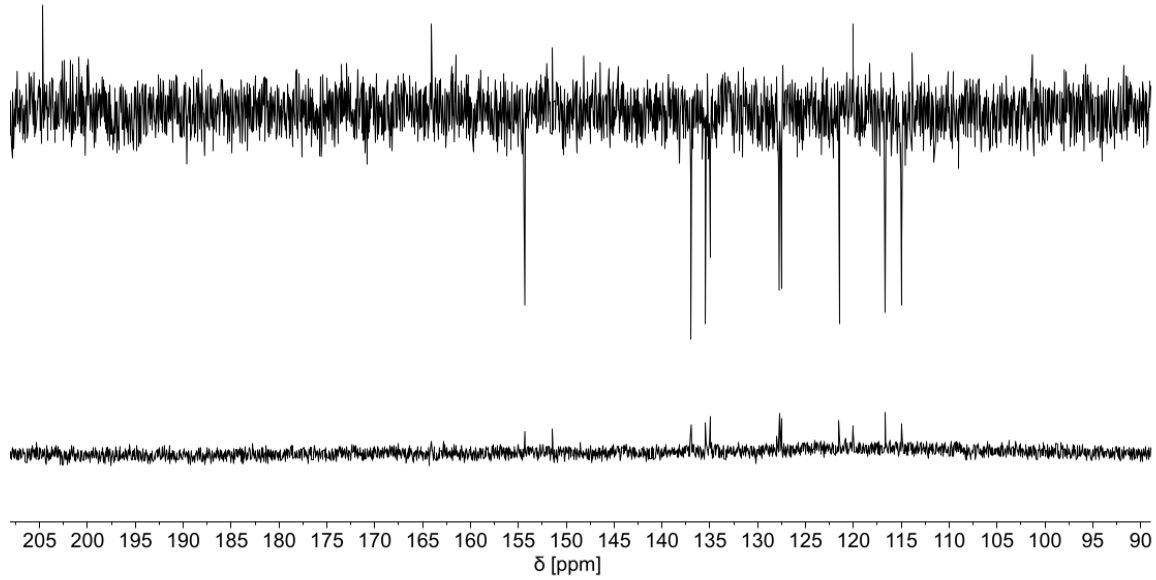

Figure S18. ^{77}Se NMR spectrum of $[Pd_4(L'^{Se})_4]$ in a mixture of $CDCl_3/CD_2Cl_2$. The feature around 500 ppm is an artifact of the measurement and independent of the sample.

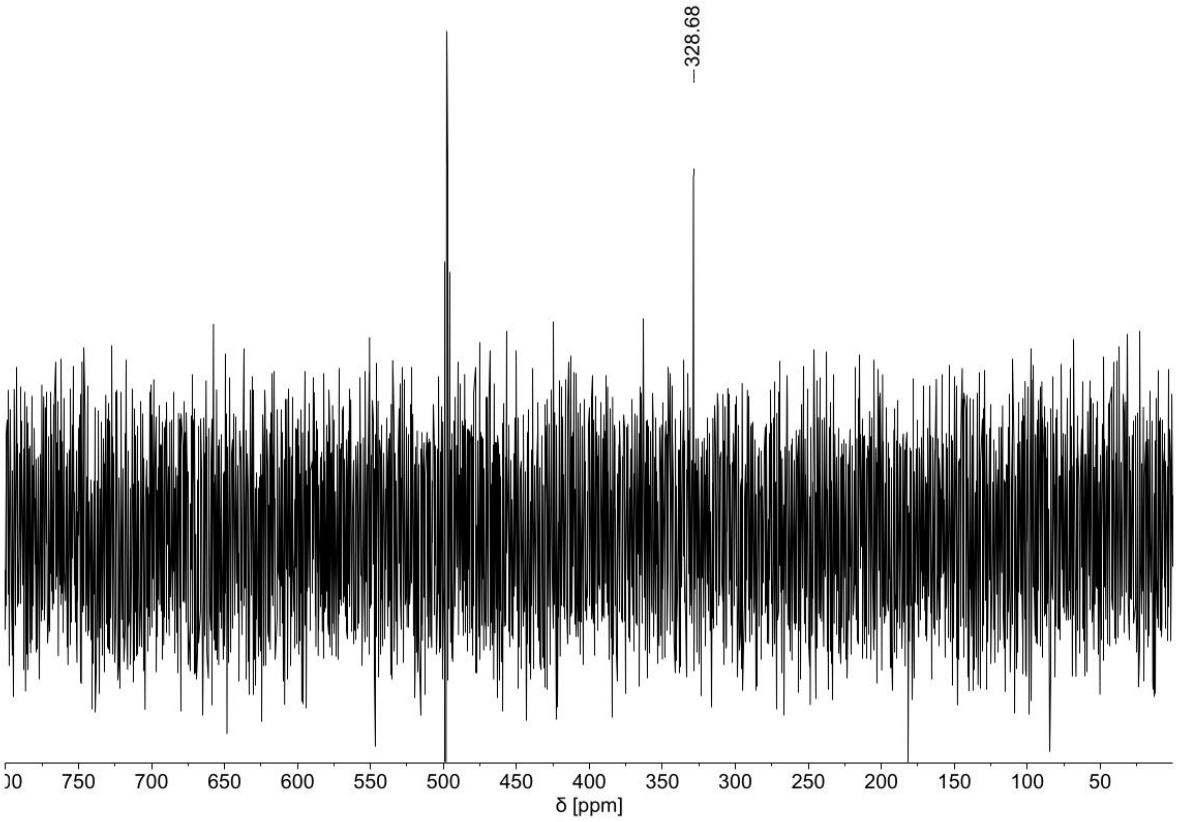

Figure S19. Stacked ^{77}Se NMR spectra of [Pd(L'^{Se})(PPh$_3$)] in CD_2Cl_2, {HL^{Se}}$_2$ in $CDCl_3$ and [Pd$_4$(L'^{Se})$_4$] in a mixture of $CDCl_3$/CD_2Cl_2.

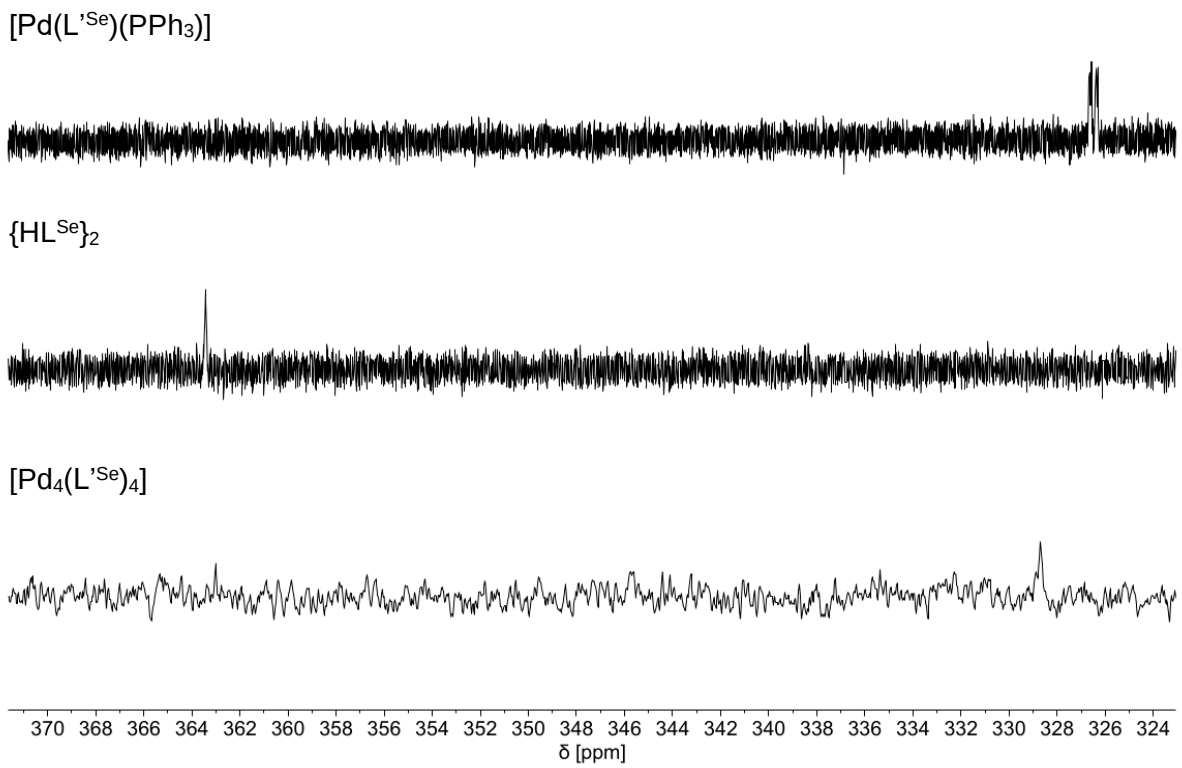

Figure S20. IR spectrum of crude [Pd$_4$(L'^{Se})$_4$]/Pd(OAc)$_2$.

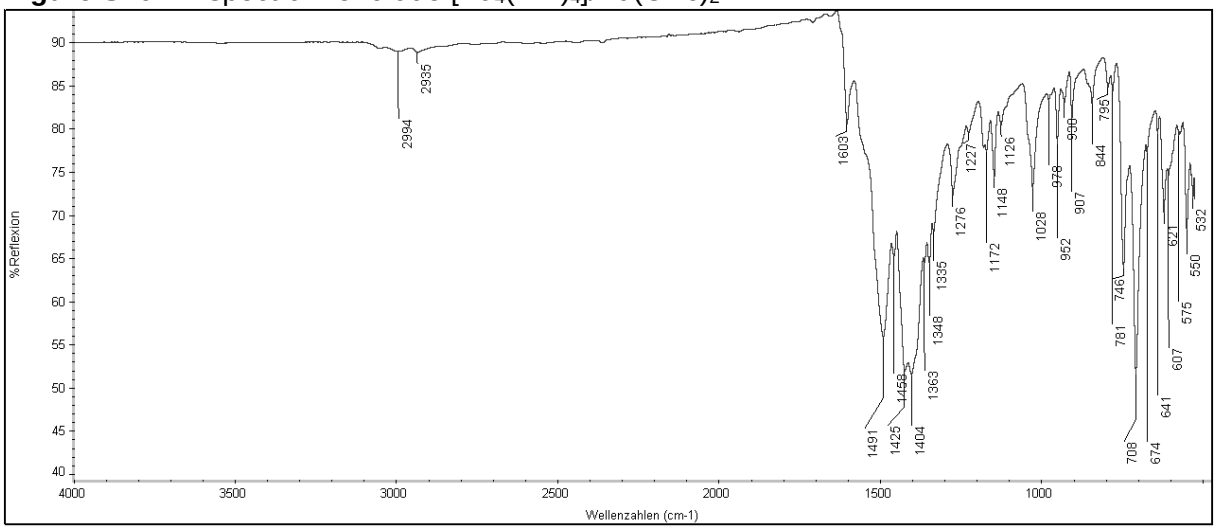

Figure S21. IR spectrum of $[Pd_4(L'^{Se})_4]$.

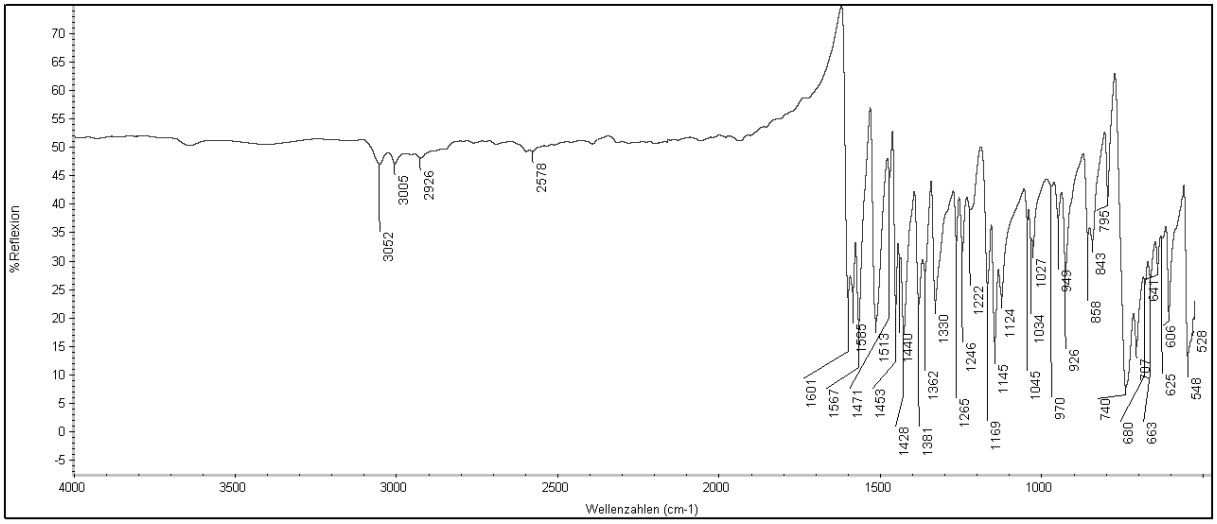

Figure S22. Full ESI^+ mass spectrum of $[Pd_4(L'^{Se})_4]$ with a list of the assigned species.

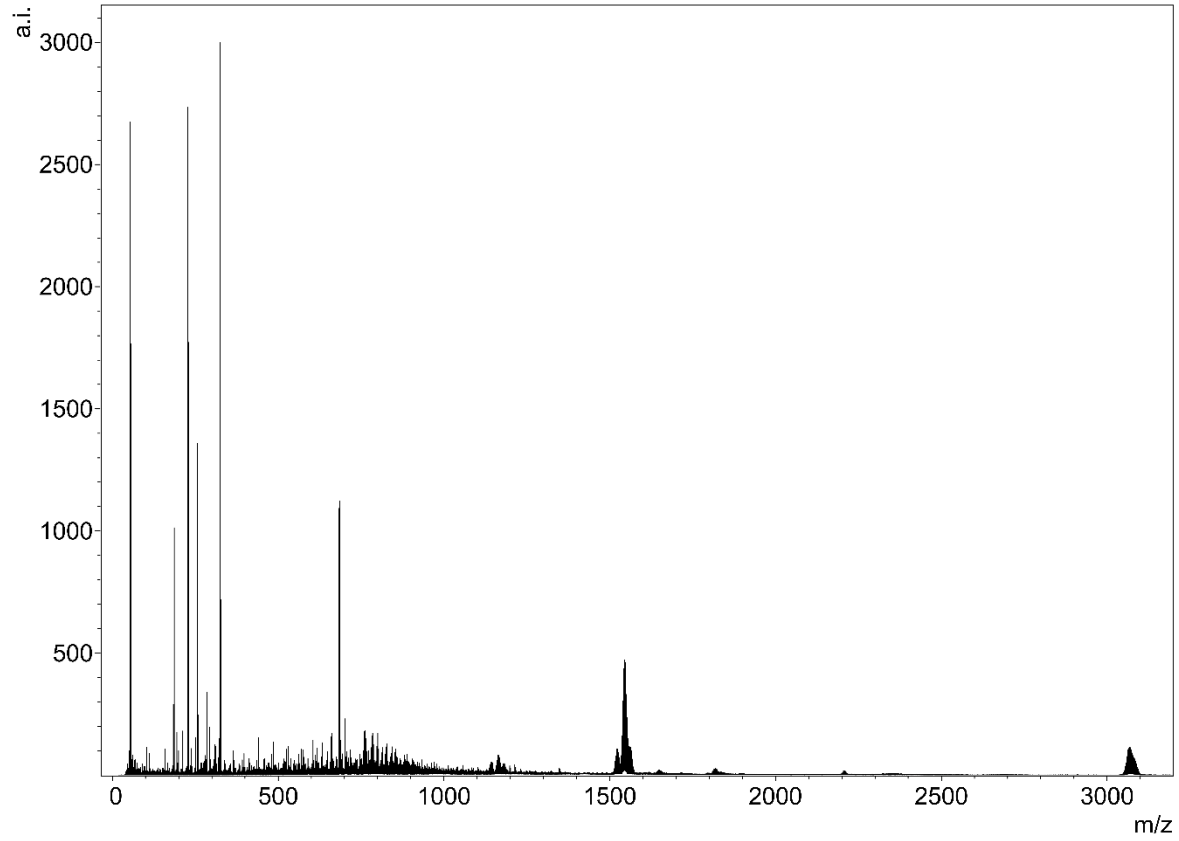

ESI^+ MS (m/z): 762.7863 ($[(Pd(L^{Se}))_2+H]^+$ Calcd 762.7902, 6%), 784.7683 ($[(Pd(L^{Se}))_2+Na]^+$ Calcd 784.7722, 6%), 801.6509 ($[(Pd(L^{Se}))_2+K+H]^+$ Calcd 801.7489, 6%), 815.6902 ($[(Pd(L^{Se}))_2+Na+OMe]^+$ Calcd 815.7906, 4%), 1141.7140 ($[(Pd(L^{Se}))_3+H]^+$ Calcd 1141.6807, 2%), 1165.6667 ($[(Pd(L^{Se}))_3+Na]^+$ Calcd 1165.6616, 3%), 1179.6405 ($[(Pd(L^{Se}))_3+K]^+$ Calcd 1179.6366, 2%), 1522.5593 ($[(Pd(L^{Se}))_4+H]^+$ Calcd 1522.5669, 4%), 1542.0429 ($[(Pd(L^{Se}))_4+K]^{2+}$ Calcd 1542.0425, 1%), 1544.5488 ($[(Pd(L^{Se}))_4+Na]^+$ Calcd 1544.5525, 23%), 1560.5143 ($[(Pd(L^{Se}))_4+K]^+$ Calcd 1560.5278, 4%), 1820.5720 ($[(Pd(L^{Se}))_5+H+Na]^+$ Calcd 1820.5436, 1%), 2207.0002 (no unambiguous assignment), 3068.0991 ($[2(Pd(L^{Se}))_4+Na]^+$ Calcd 3068.1124, 4%), 3084.0691 ($[2(Pd(L^{Se}))_4+Na]^+$ Calcd 3084.0863, 2%).

Figures S23-S29. Zoomed ESI$^+$ mass spectrum of $[Pd_4(L'^{Se})_4]$ for selected regions. For the assignments see Figure S22 on the previous page.

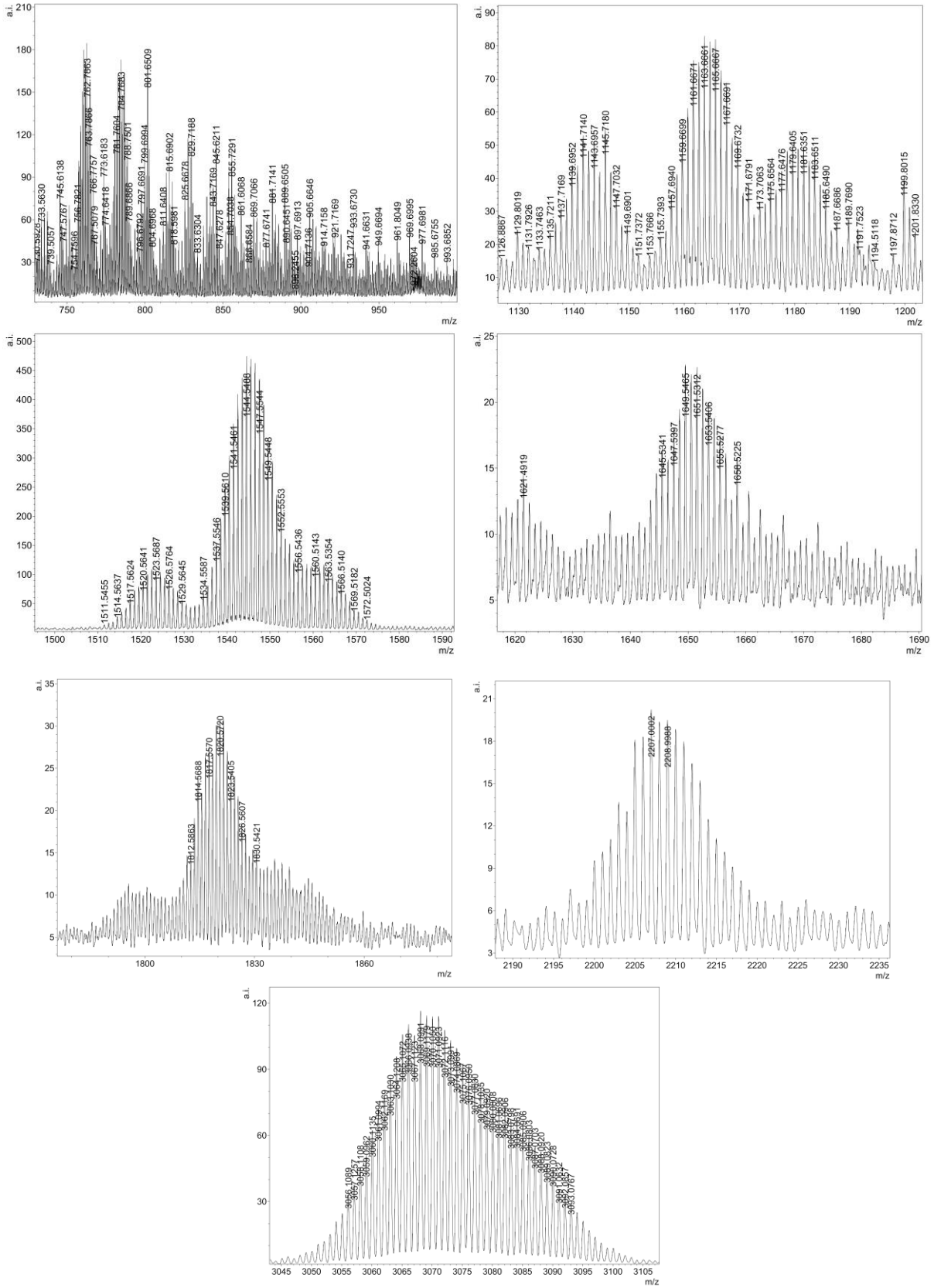

Figures S30-S34. Predicted (down) vs. experimental (up) isotope patterns of main species in the ESI$^+$ mass spectrum of $[Pd_4(L'^{Se})_4]$. For the assignments see Figure 22 on page S25.

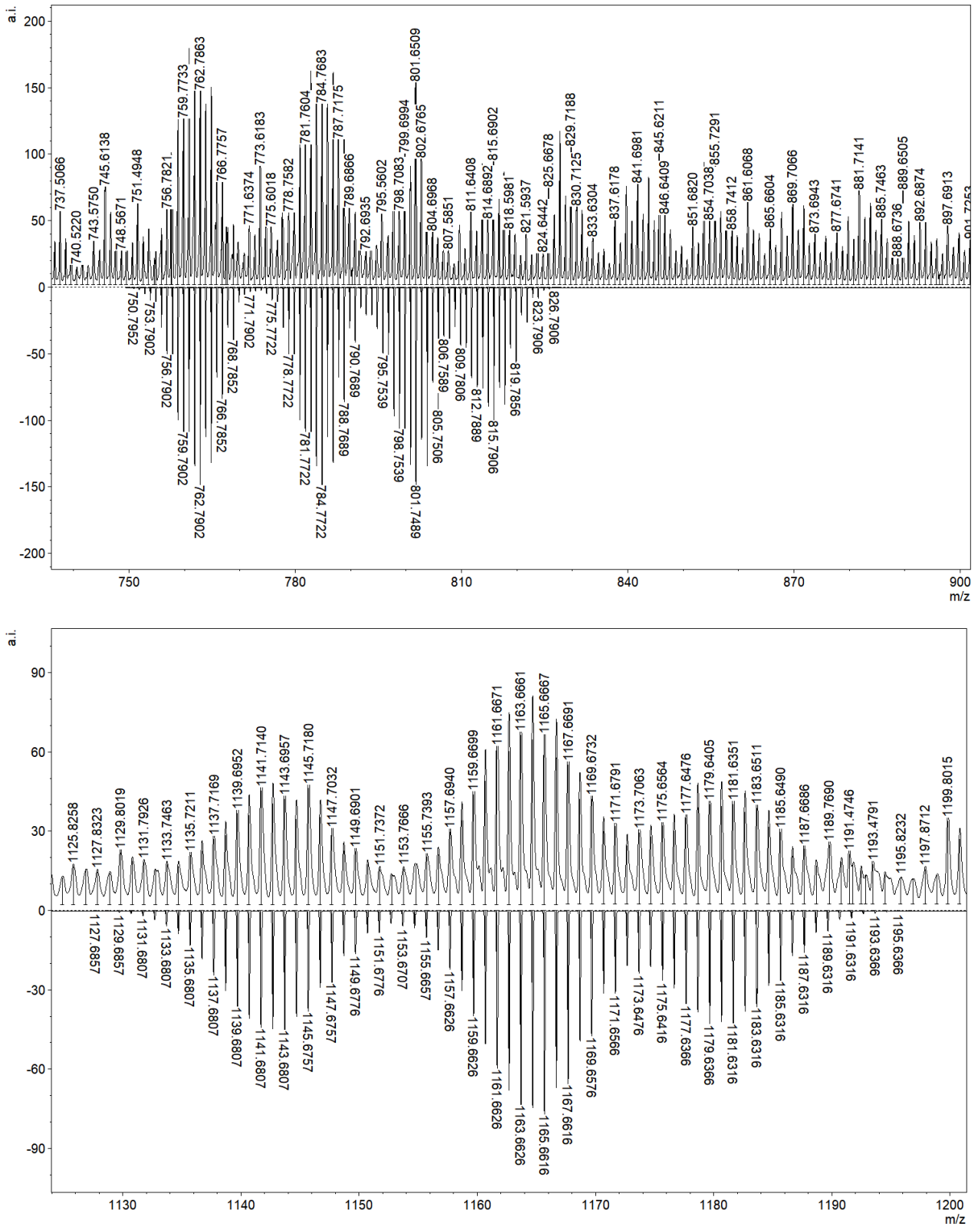

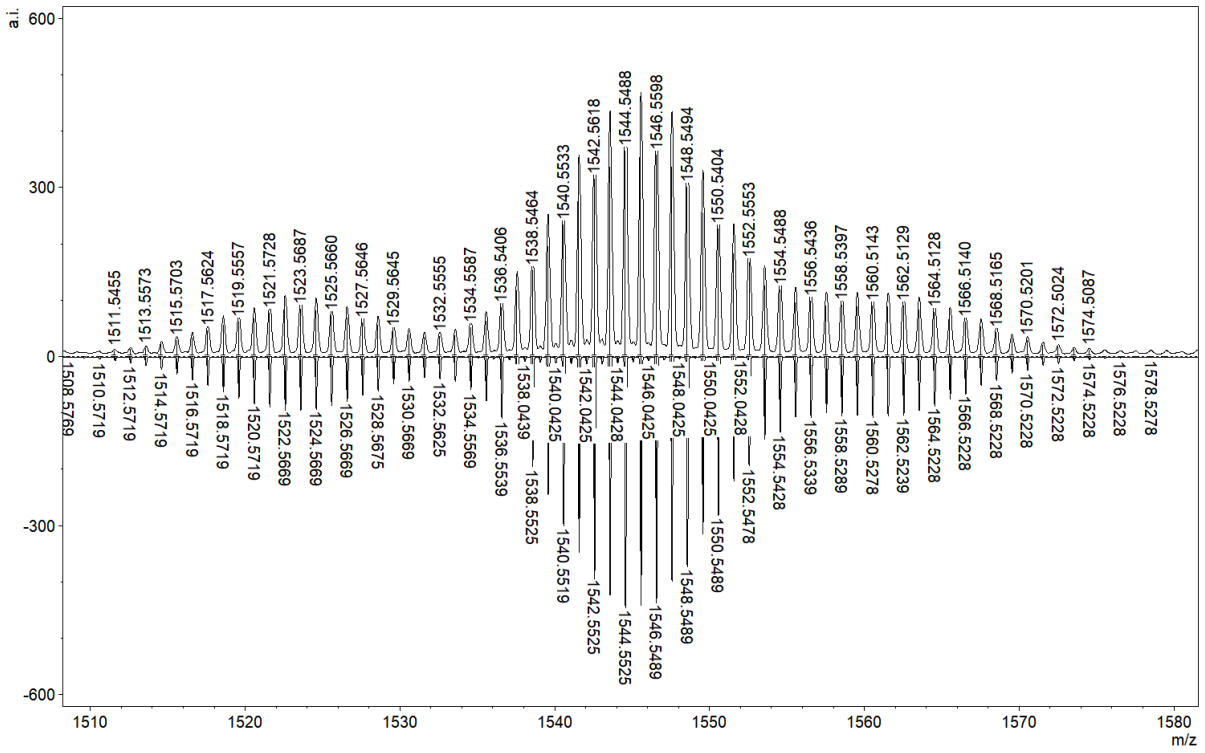
a.i.
600
300
0
-300
-600
1510
1520
1530
1540
1550
1560
1570
1580
m/z
1508.5769
1510.5719
1511.5455
1512.5719
1513.5573
1514.5719
1515.5703
1516.5719
1517.5624
1518.5719
1519.5557
1520.5719
1521.5728
1522.5669
1523.5687
1524.5669
1525.5660
1526.5669
1527.5646
1528.5675
1529.5645
1530.5669
1532.5555
1532.5625
1534.5587
1534.5569
1536.5406
1536.5539
1538.5464
1538.0439
1538.5525
1540.5533
1540.0425
1540.5519
1542.5618
1542.0425
1542.5525
1544.5488
1544.0428
1544.5525
1546.5568
1546.0425
1546.5489
1548.5494
1548.0425
1548.5489
1550.5404
1550.0425
1550.5489
1552.5553
1552.0428
1552.5478
1554.5488
1554.5428
1556.5436
1556.5339
1558.5397
1558.5289
1560.5143
1560.5278
1562.5129
1562.5239
1564.5128
1564.5228
1566.5140
1566.5228
1568.5165
1568.5228
1570.5201
1570.5228
1572.5024
1572.5228
1574.5087
1574.5228
1576.5228
1578.5278

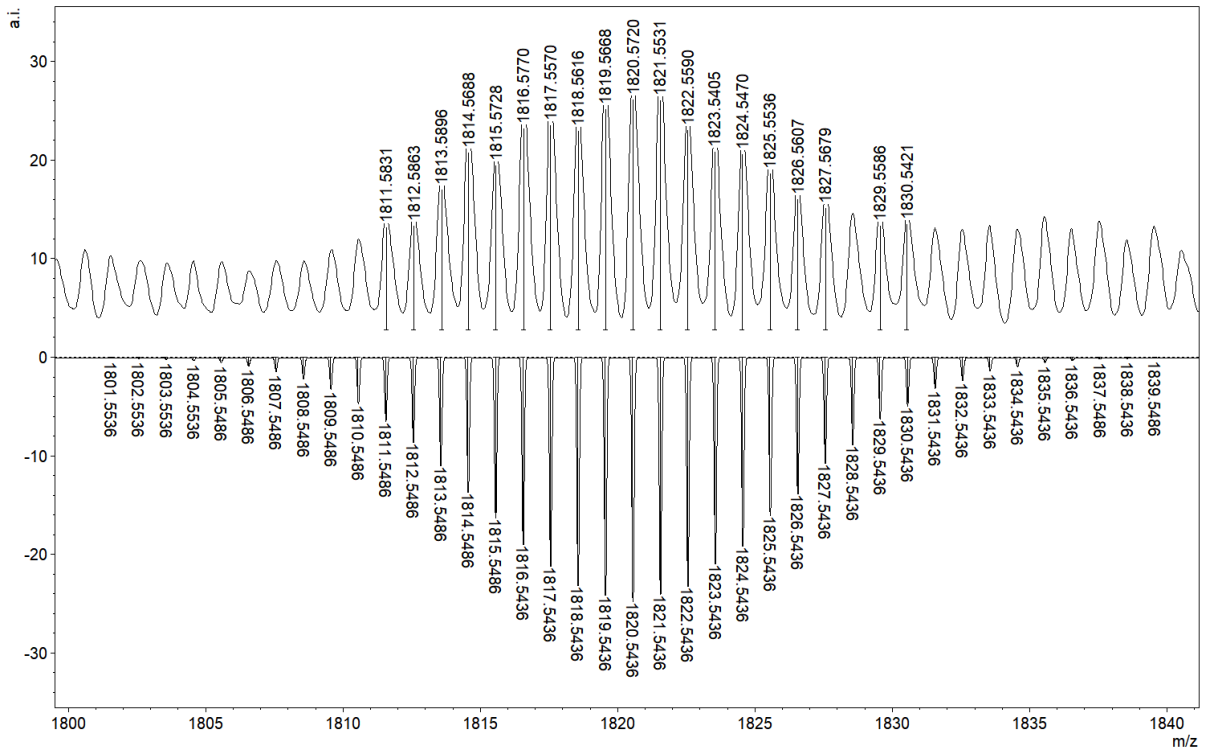
a.i.
30
20
10
0
-10
-20
-30
1800
1805
1810
1815
1820
1825
1830
1835
1840
m/z
1801.5536
1802.5536
1803.5536
1804.5536
1805.5486
1806.5486
1807.5486
1808.5486
1809.5486
1810.5486
1811.5486
1812.5486
1813.5486
1814.5486
1815.5486
1816.5436
1817.5436
1818.5436
1819.5436
1820.5436
1821.5436
1822.5436
1823.5436
1824.5436
1825.5436
1826.5436
1827.5436
1828.5436
1829.5436
1830.5436
1831.5436
1832.5436
1833.5436
1834.5436
1835.5436
1836.5436
1837.5486
1838.5436
1839.5486
1811.5831
1812.5863
1813.5896
1814.5688
1815.5728
1816.5770
1817.5570
1818.5616
1819.5668
1820.5720
1821.5531
1822.5590
1823.5405
1824.5470
1825.5536
1826.5607
1827.5679
1829.5589
1830.5421

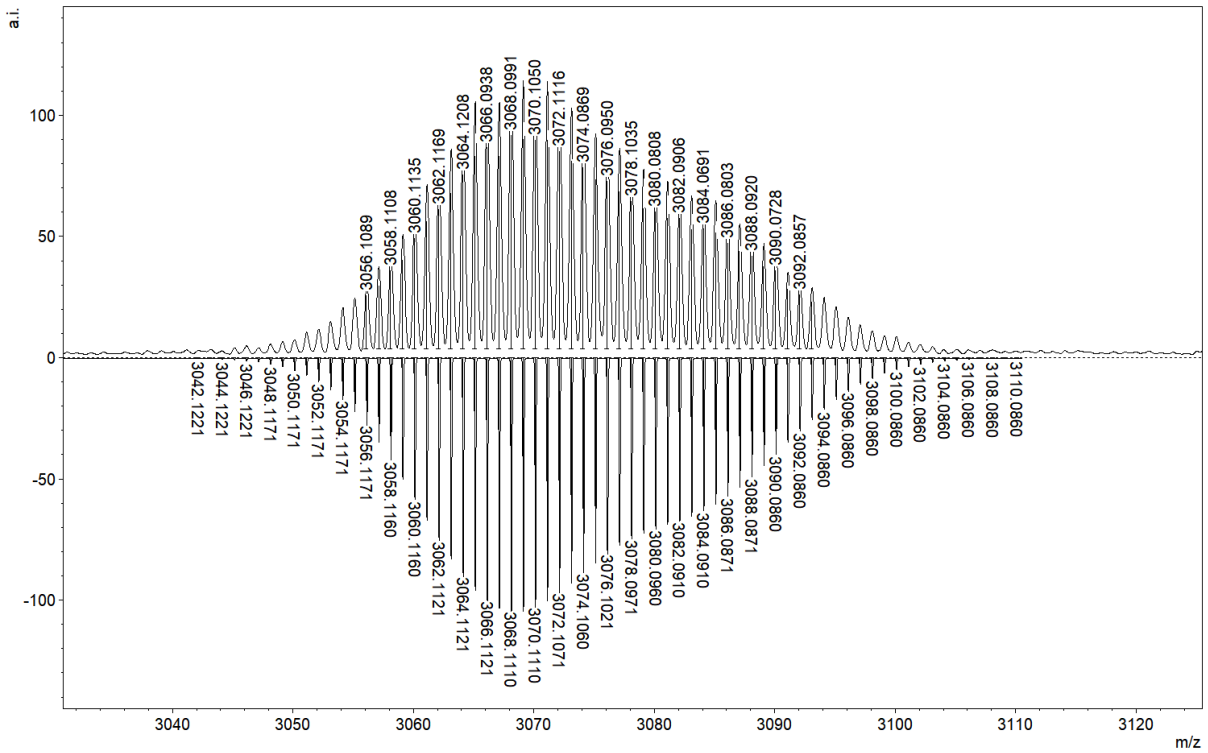

Figure S35. Full ESI$^-$ mass spectrum of $[Pd_4(L'^{Se})_4]$ with a list of the assigned species.

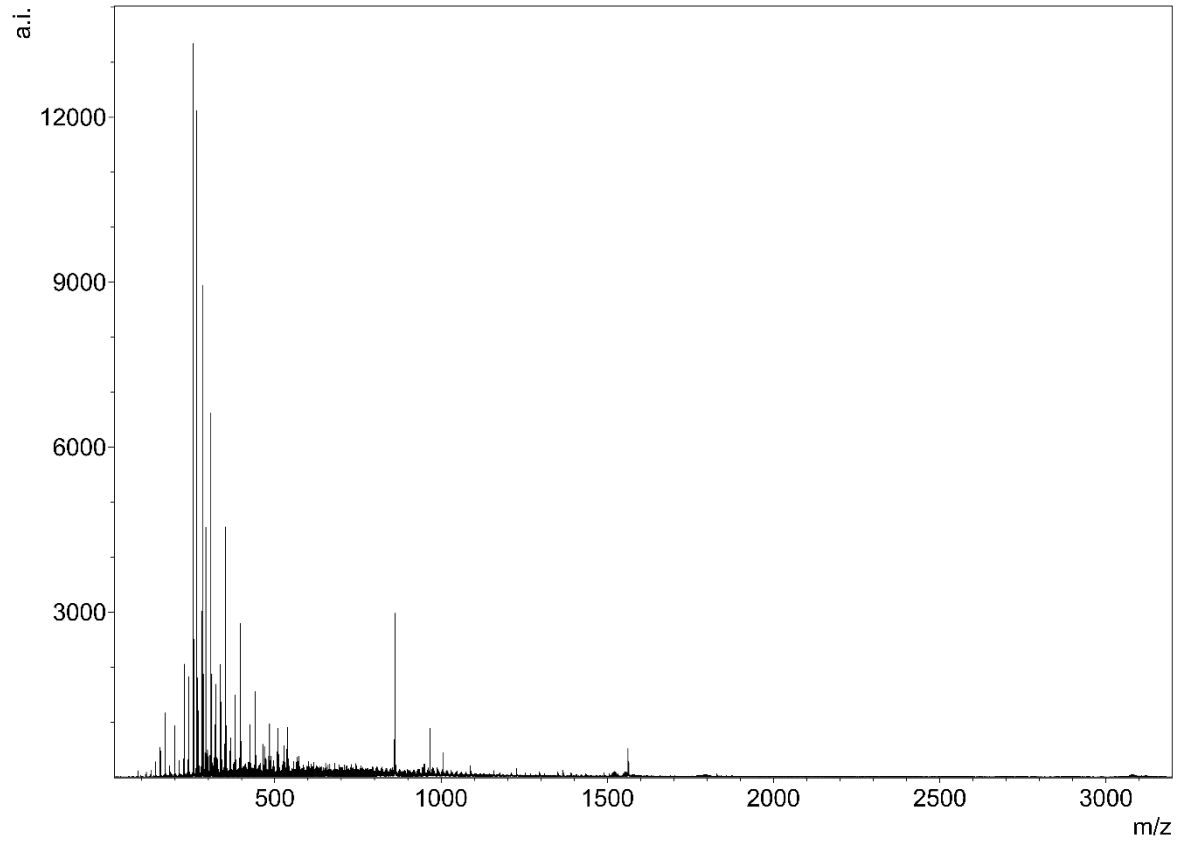

ESI$^-$ MS (m/z): 1520.5341 ($[(Pd(L^{Se}))_4\text{-}H^-]^-$ Calcd 1520.5534, ca. 0.3%), 1521.5422 ($[(Pd(L^{Se}))_4]^-$ Calcd 1521.5612, ca. 0.3%), 1552.5543 ($[(Pd(L^{Se}))_4+CH_3O]^-$ Calcd 1552.5797, ca. 0.4%), 1557.5380 ($[(Pd(L^{Se}))_4+Cl]^-$ Calcd 1557.5293, ca. 0.4%).

Figures S36-S38. Zoomed ESI$^-$ mass spectrum of $[Pd_4(L'^{Se})_4]$ for selected regions. For the assignments see Figure S35 on the previous page.

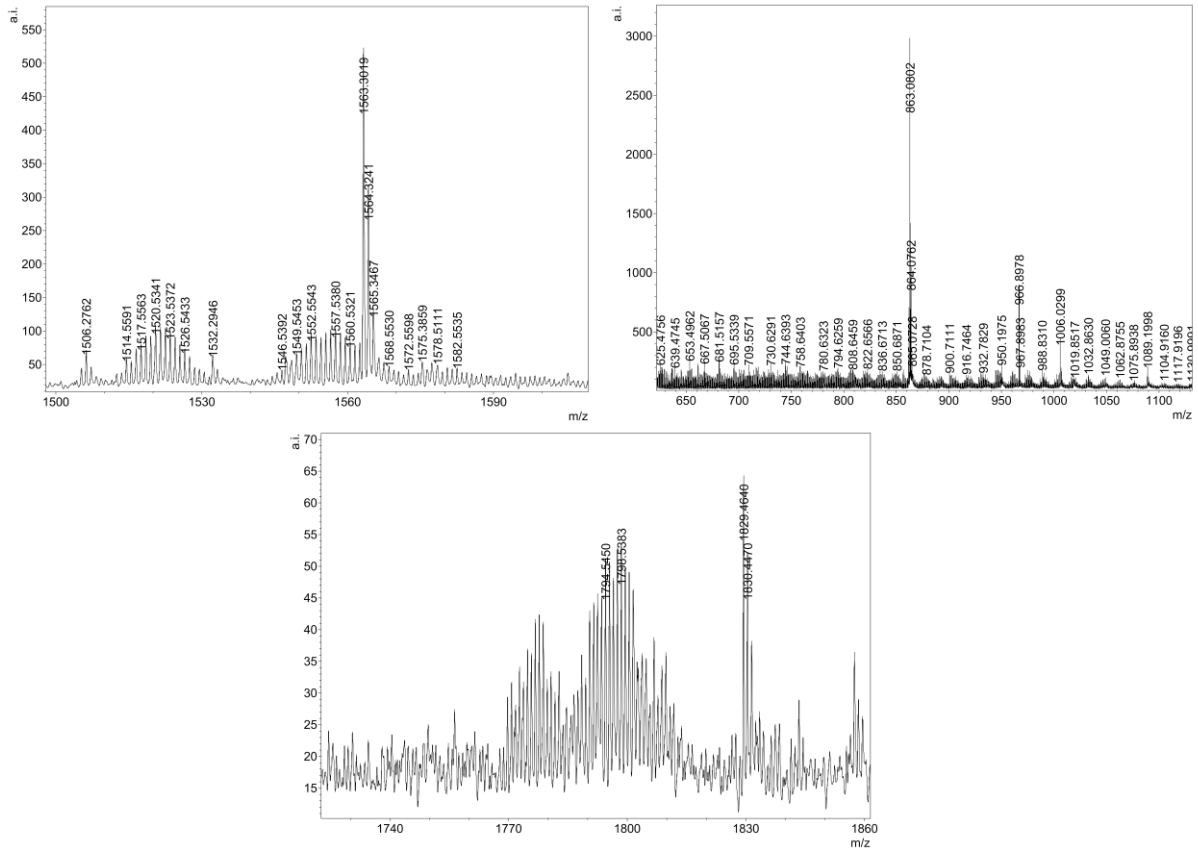

Figures S39. Predicted (down) vs. experimental (up) isotope patterns of main species in the ESI$^-$ mass spectrum of $[Pd_4(L'^{Se})_4]$. For the assignments see Figure S35 on page S29.

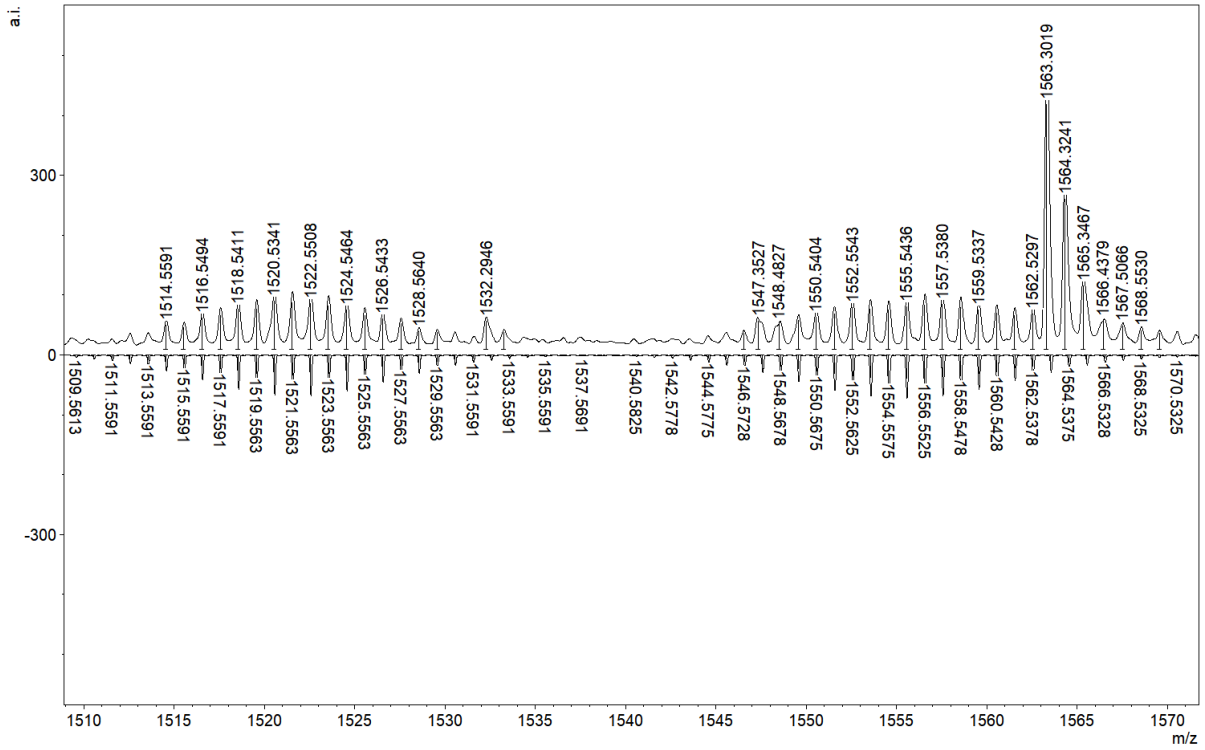

Figure S40. ^{1}H NMR spectrum of $[Pd_4(L'^{Te})_4]$ in CD_2Cl_2 focused on the aromatic region.

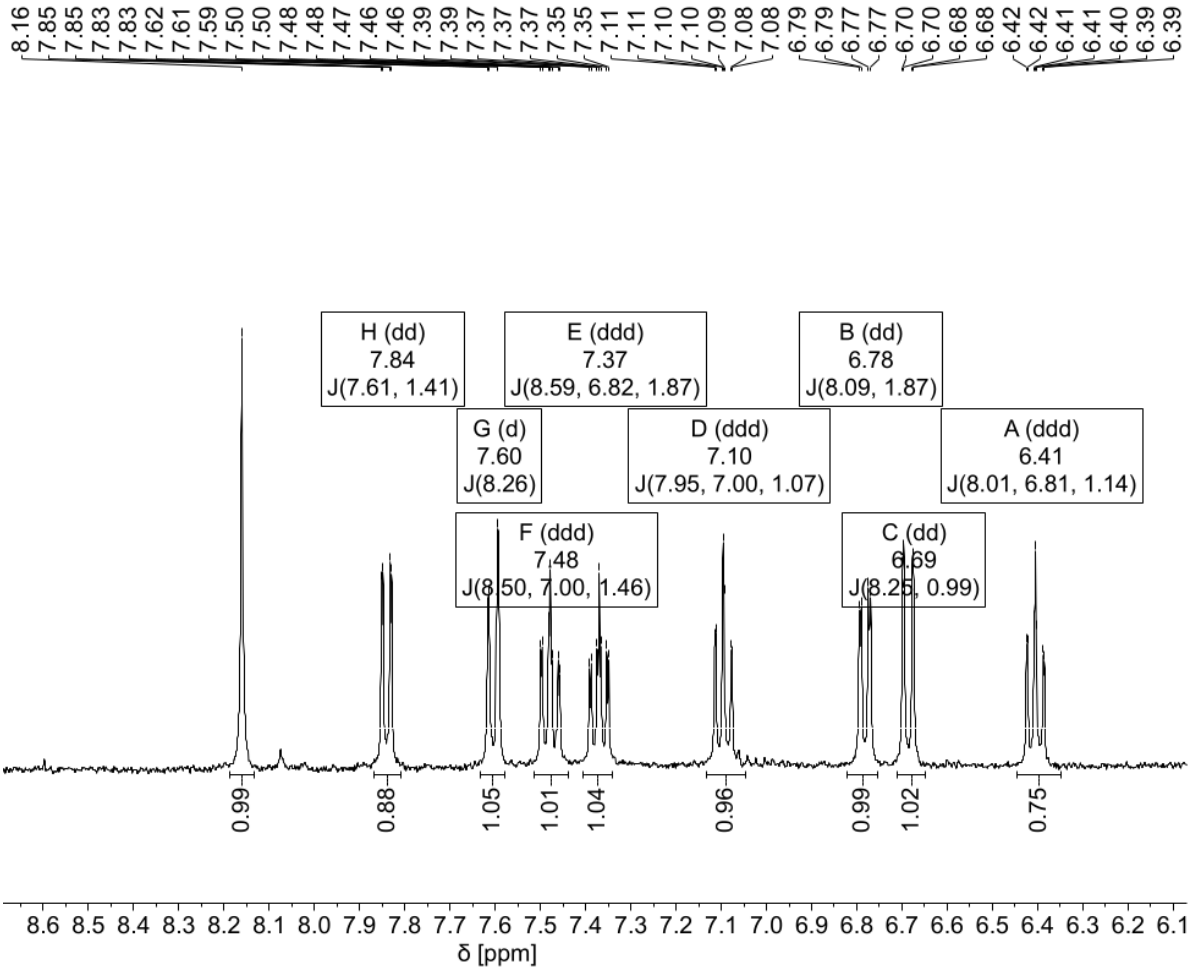

Figure S41. $^{1}H,^{1}H$-COSY NMR spectrum of $[Pd_4(L'^{Te})_4]$ in CD_2Cl_2 focused on the aromatic region.

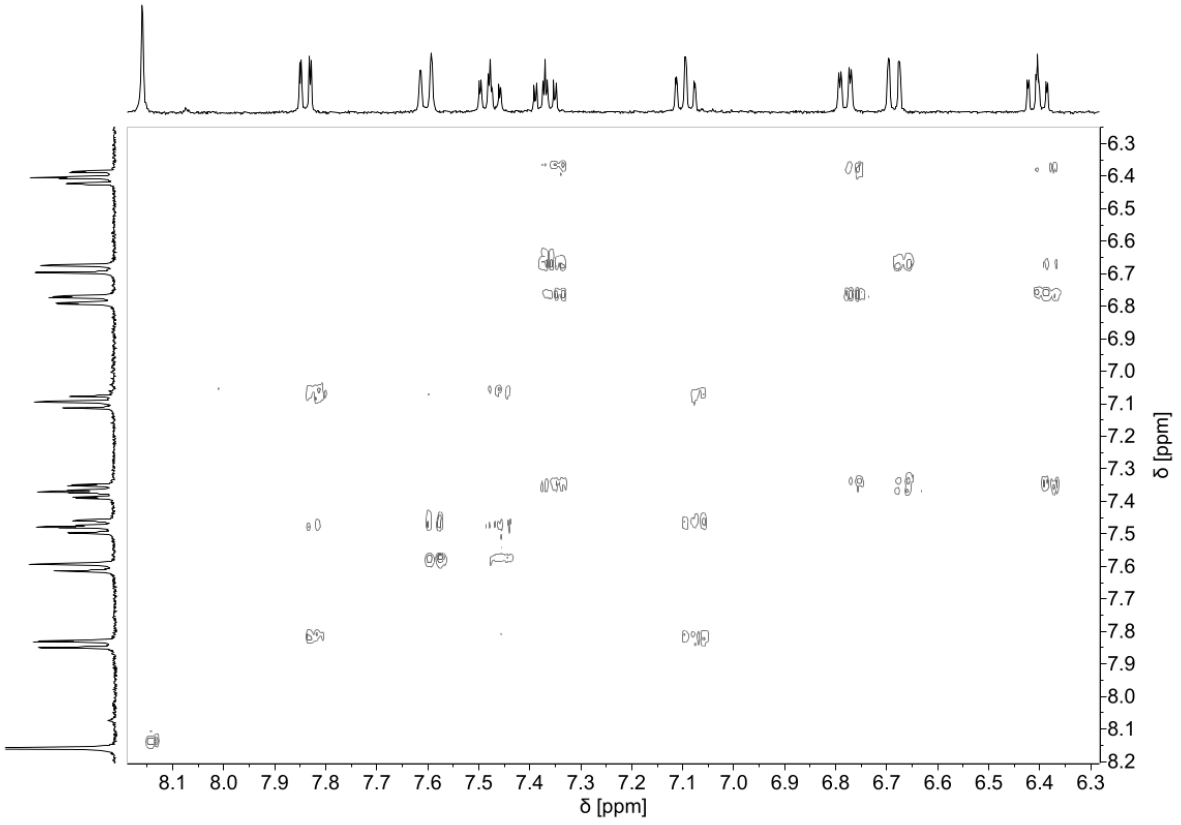

Figure S42. Stacked ^{1}H NMR spectra of $[Pd(L'^{Te})(PPh_3)]$, $\{HL^{Te}\}_2$ and $[Pd_4(L'^{Te})_4]$ in CD_2Cl_2.

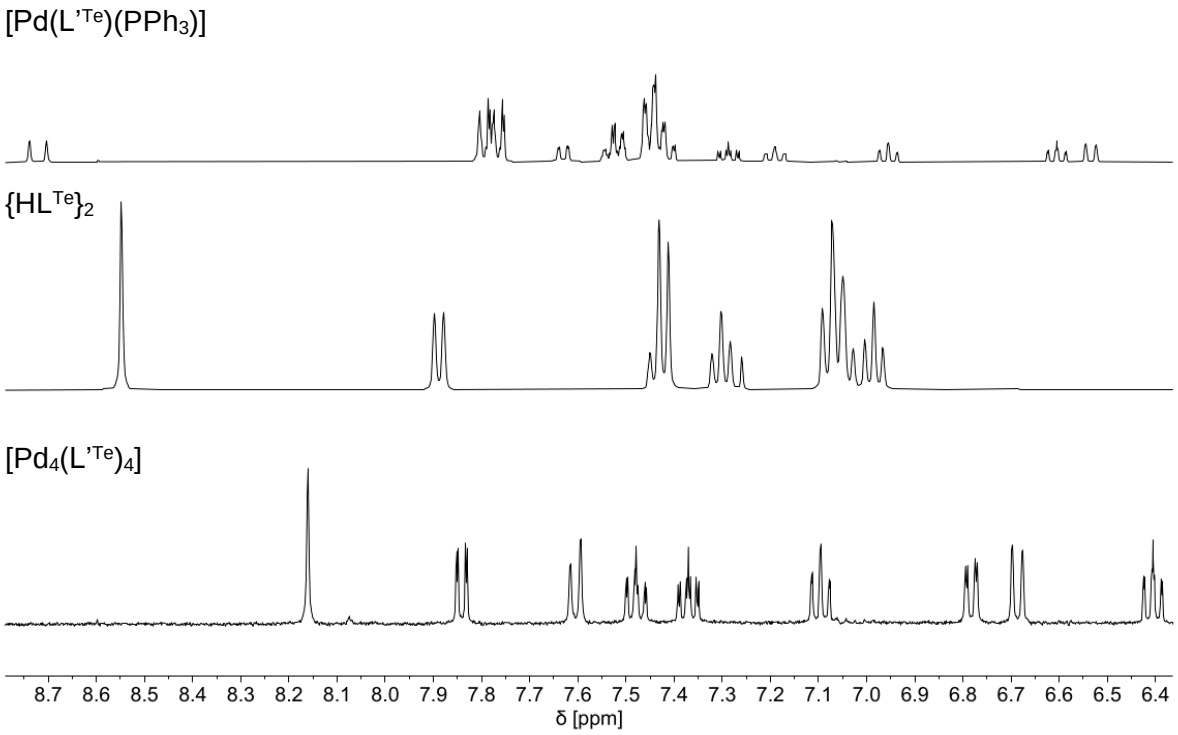

Figure S43. Full ^{1}H NMR spectrum of $[Pd_4(L'^{Te})_4]$ in CD_2Cl_2. The low intensity is a result of the low solubility of the cluster.

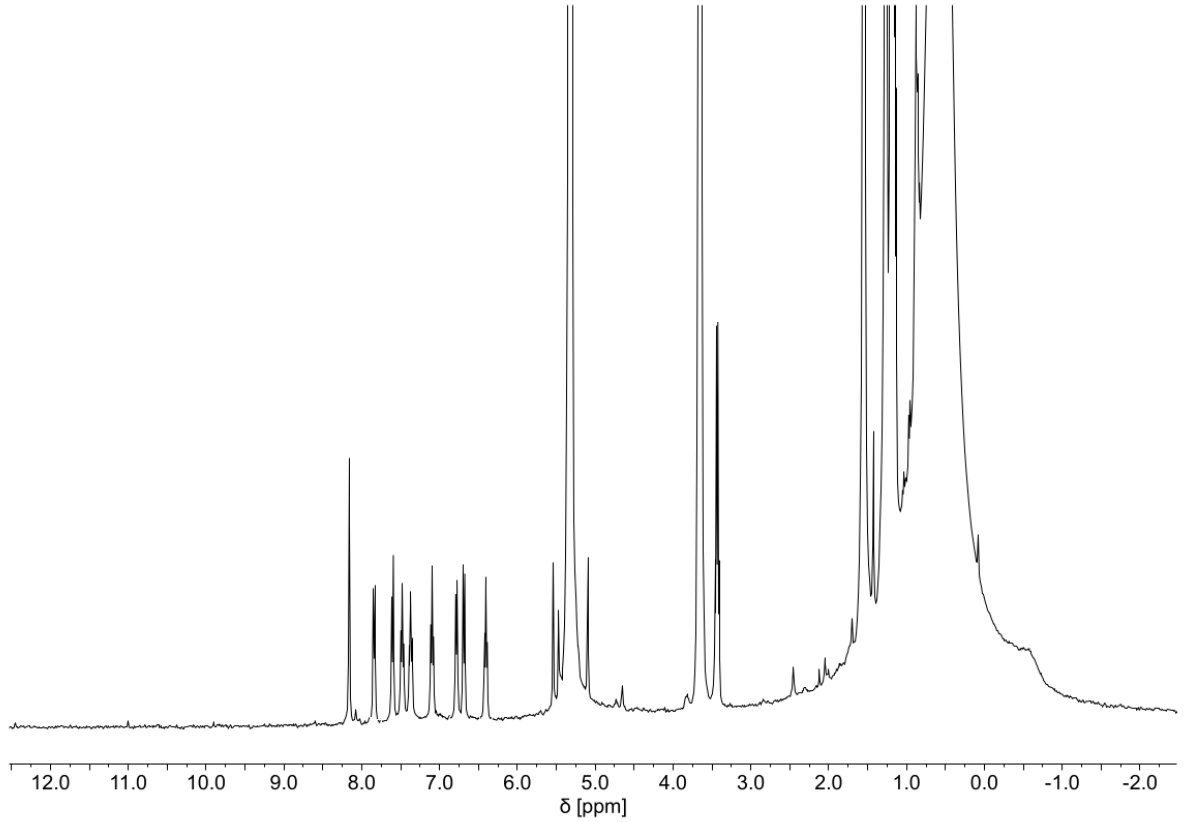

Figure S44. IR spectrum of crude $[Pd_4(L'^{Te})_4]/Pd(OAc)_2$.

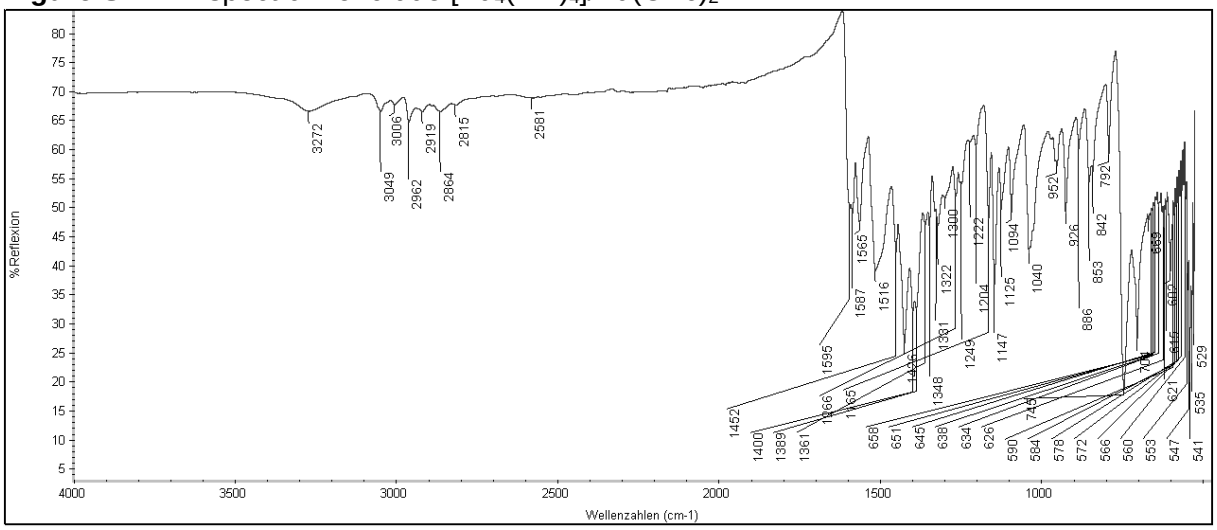

Figure S45. IR spectrum of $[Pd_4(L'^{Te})_4]$.

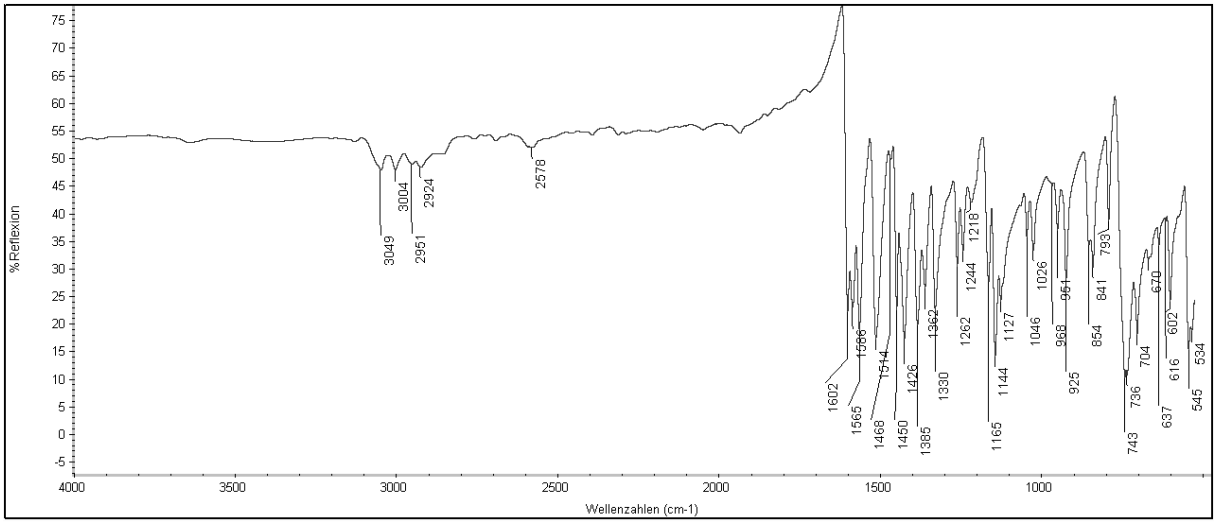

Figure S46. Full ESI^+ mass spectrum of $[Pd_4(L'^{Te})_4]$ with a list of the assigned species.

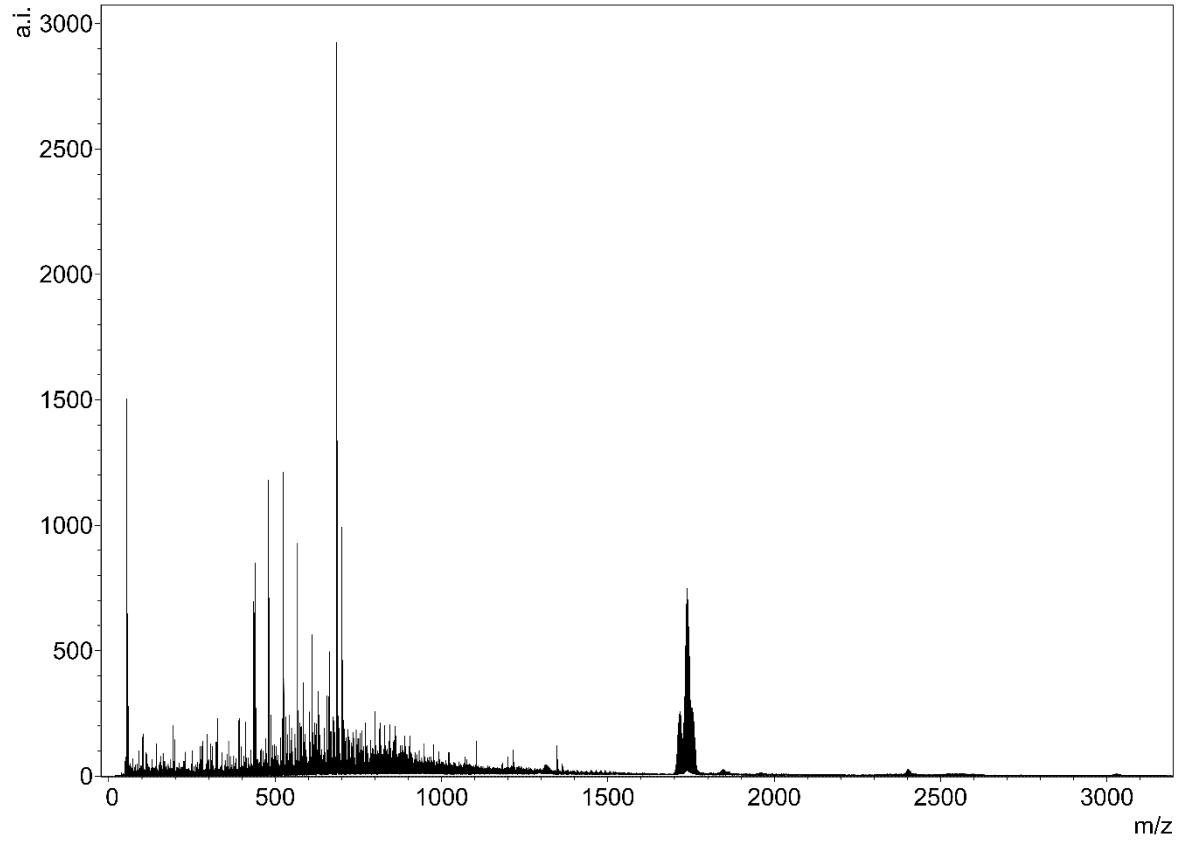

ESI^+ MS (m/z): 1718.5037 ($[(Pd(L^{Te}))_4+H]^+$ Calcd 1718.5191, 9%), 1740.4933 ($[Pd(L^{Te}))_4+Na]^+$ Calcd 1740.5011, 26%), 1756.4750 $(Pd(L^{Te}))_4+K]^+$ Calcd 1756.4749, 9%).

Figures S47-S50. Zoomed ESI⁺ mass spectrum of $[Pd_4(L'^{Te})_4]$ for selected regions. For the assignments see Figure S46 on the previous page.

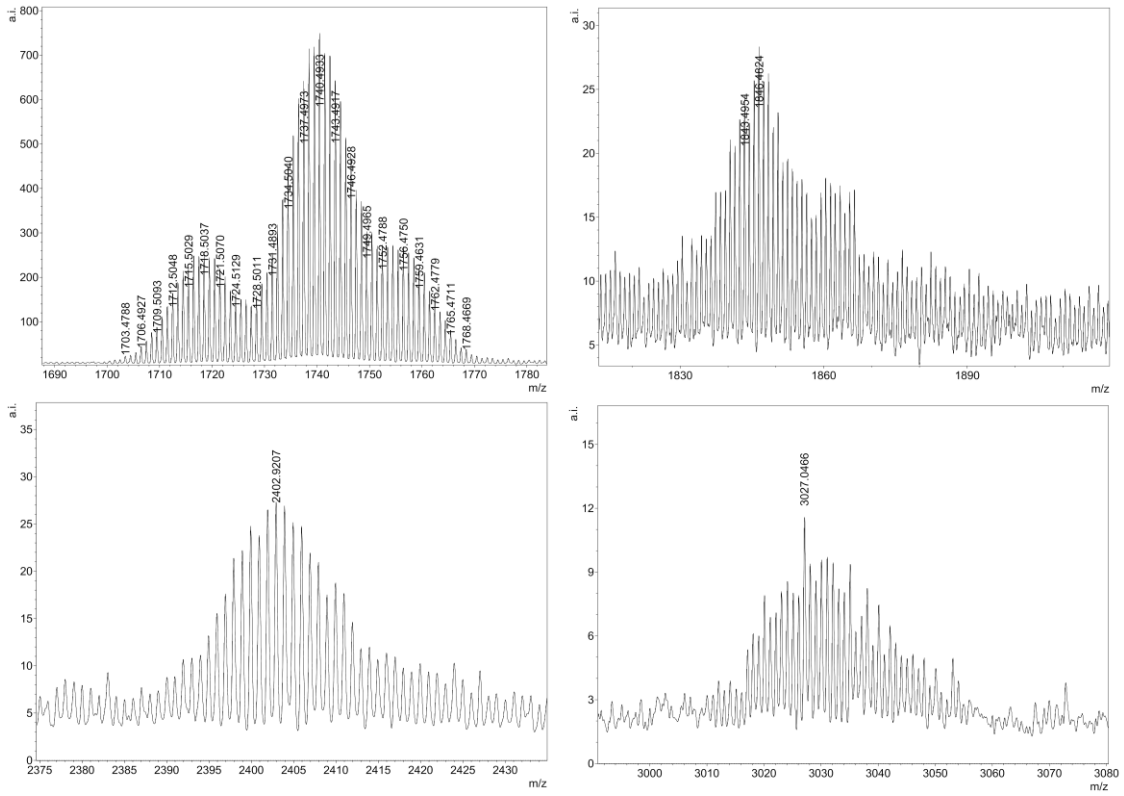

Figures S51. Predicted (down) vs. experimental (up) isotope patterns of main species in the ESI⁺ mass spectrum of $[Pd_4(L'^{Te})_4]$. For the assignments see Figure S46 on page S34.

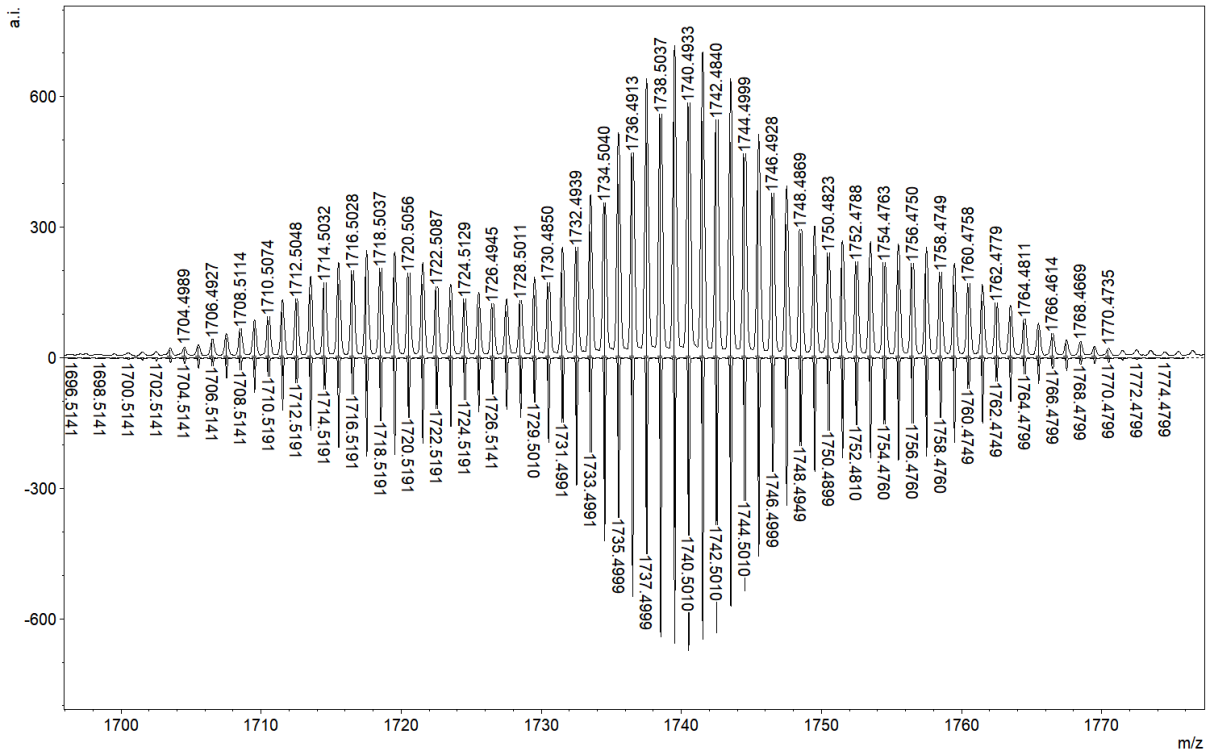

Figure S52. Full ESI$^-$ mass spectrum of $[Pd_4(L'^{Te})_4]$ with a list of the assigned species.

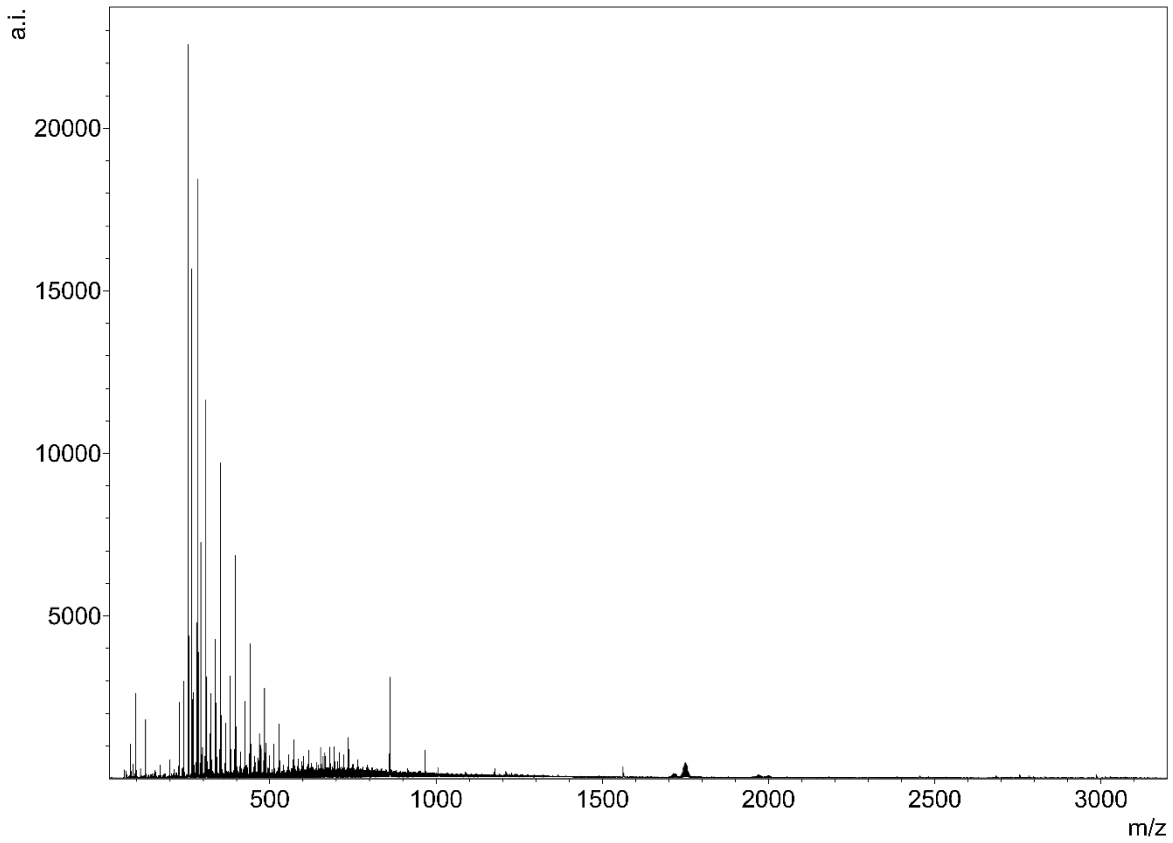

ESI$^-$ MS (m/z): 1716.4503 ($[(Pd(L^{Te}))_4\text{-}H^-]^-$ Calcd 1716.5035, ca. 0.5%), 1717.4501 ($[(Pd(L^{Te}))_4]^-$ Calcd 1717.5113, ca. 0.5%), 1748.4429 ($[(Pd(L^{Te}))_4+CH_3O]^-$ Calcd 1748.5297, ca. 1%), 1752.4326 ($[(Pd(L^{Te}))_4+Cl]^-$ Calcd 1752.4795, ca. 2%).

Figures S53 and S54. Zoomed ESI$^-$ mass spectrum of $[Pd_4(L'^{Te})_4]$ for selected regions. For the assignments see Figure S52.

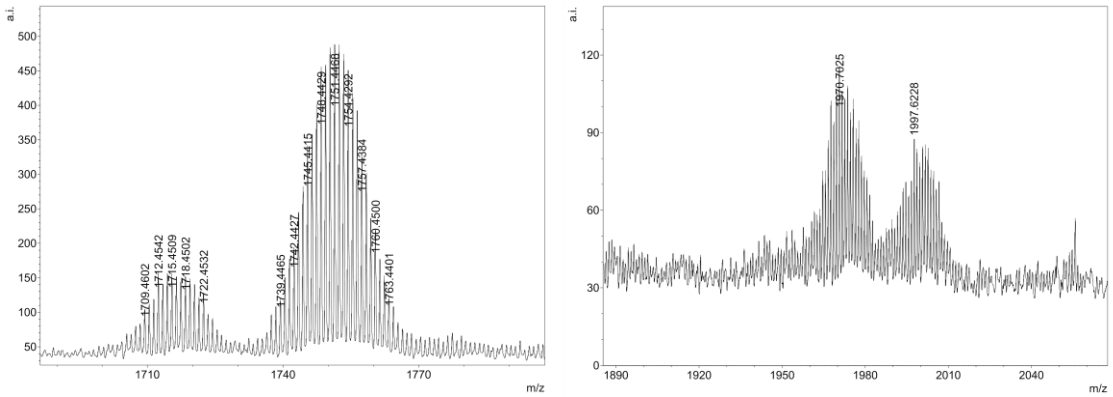

Figure S55. Predicted (down) vs. experimental (up) isotope patterns of main species in the ESI$^-$ mass spectrum of [$Pd_4(L'^{Te})_4$]. For the assignments see Figure S52 on S36.

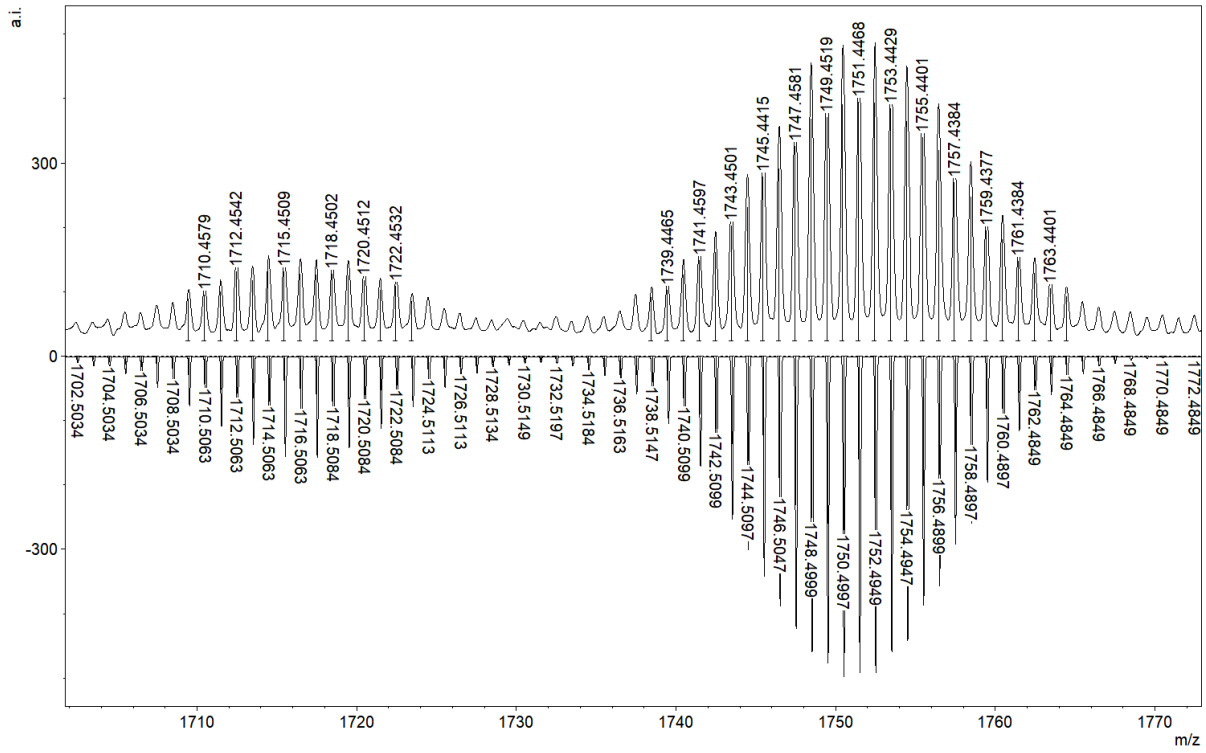

Figure S56. IR spectrum of [Ni-μ_2-κ_2-(Ni{κ_5-L^{Se}}$_2$)$_2$-μ_2-(OAc)$_2$].

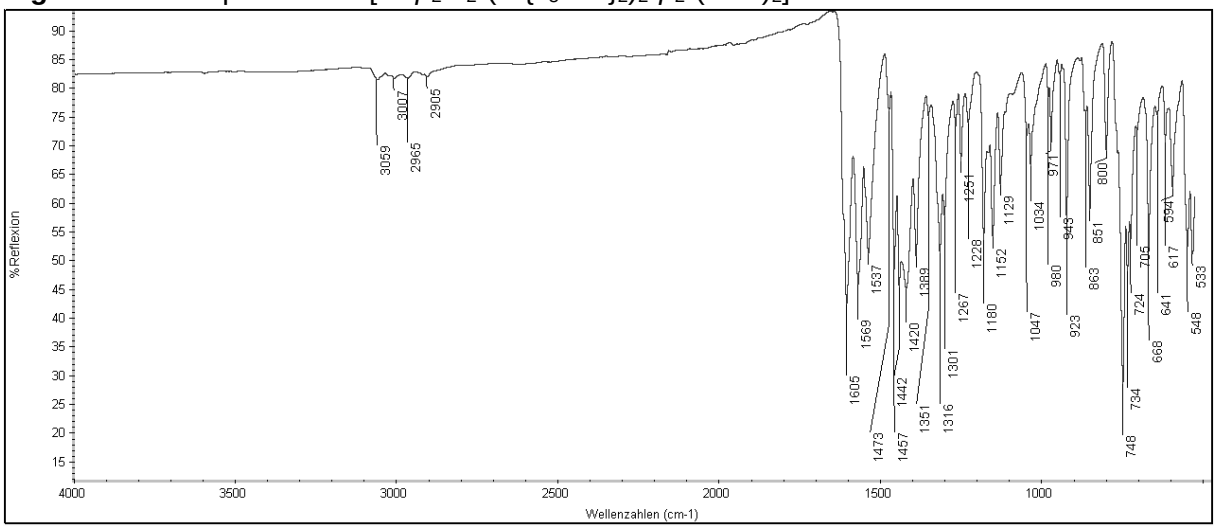

Figure S57. Full ESI$^+$ mass spectrum of [Ni-μ_2-κ_2-(Ni{κ_5-L^{Se}}$_2$)$_2$-μ_2-(OAc)$_2$] with a list of the assigned species.

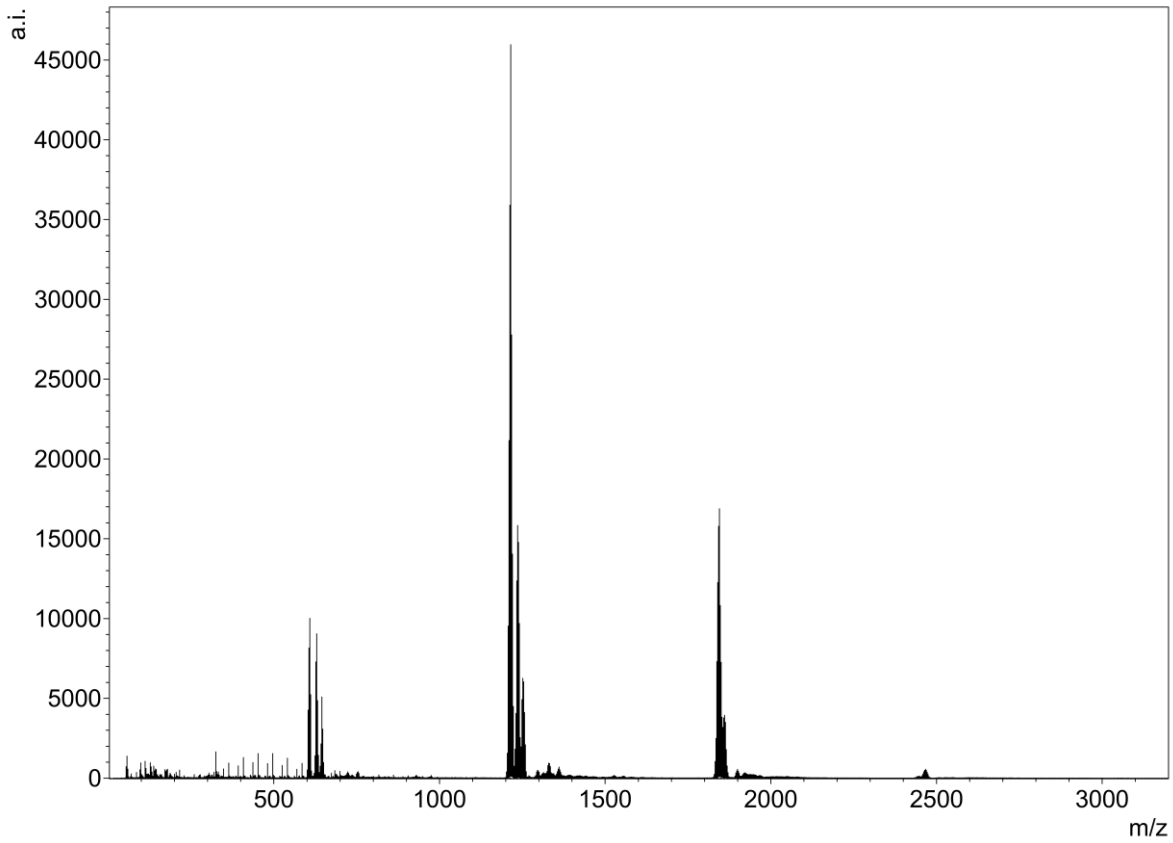

ESI$^+$ MS (m/z): 608.9156 ([Ni{L^{Se}}$_2$+H]$^+$ Calcd 608.9117, 22%), 630.9089 ([Ni{L^{Se}}$_2$+Na]$^+$ Calcd 630.8945, 20%), 646.8740 ([Ni{L^{Se}}$_2$+K]$^+$ Calcd 646.8676, 11%), 1214.8171 ([Ni$_2${L^{Se}}$_4$+H]$^+$ Calcd 1214.8215, 100%), 1236.8109 ([Ni$_2${L^{Se}}$_4$+Na]$^+$ Calcd 1236.8034, 33%), 1252.7694 ([Ni$_2${L^{Se}}$_4$+K]$^+$ Calcd 1252.7774, 13%), 1330.7606 ([Ni$_3${L^{Se}}$_4$+OAc$^-$]$^+$ Calcd 1330.7595, 1.3%), 1350.7954 ([Ni$_3${L^{Se}}$_4$+OAc$^-$+H$_2$O]$^+$ Calcd 1350.7684, ca. 0.3%), 1363.7540 ([Ni$_3${L^{Se}}$_4$+OAc$^-$+MeO$^-$]$^+$ Calcd 1363.7763, ca. 0.3%), 1364.7729 ([Ni$_3${L^{Se}}$_4$+OAc$^-$+MeOH]$^+$ Calcd 1364.7841, ca. 0.5%), 1844.7071 ([Ni$_3${L^{Se}}$_6$+Na]$^+$ Calcd 1844.7047, 33%), 1860.6810 ([Ni$_3${L^{Se}}$_6$+K]$^+$ Calcd 1860.6858, 7%), 2450.6000 ([Ni$_4${L^{Se}}$_8$+Na]$^+$ Calcd 2450.6144, 0.4%), 2466.5854 ([[Ni$_4${L^{Se}}$_8$+K]$^+$ Calcd 2466.5883, 1.3%).

Figures S58-S63. Zoomed ESI⁺ mass spectrum of [Ni-μ_2-κ_2-(Ni{κ_5-L^{Se}}$_2$)$_2$-μ_2-(OAc)$_2$] for selected regions. For the assignments see Figure S57 on the previous page.

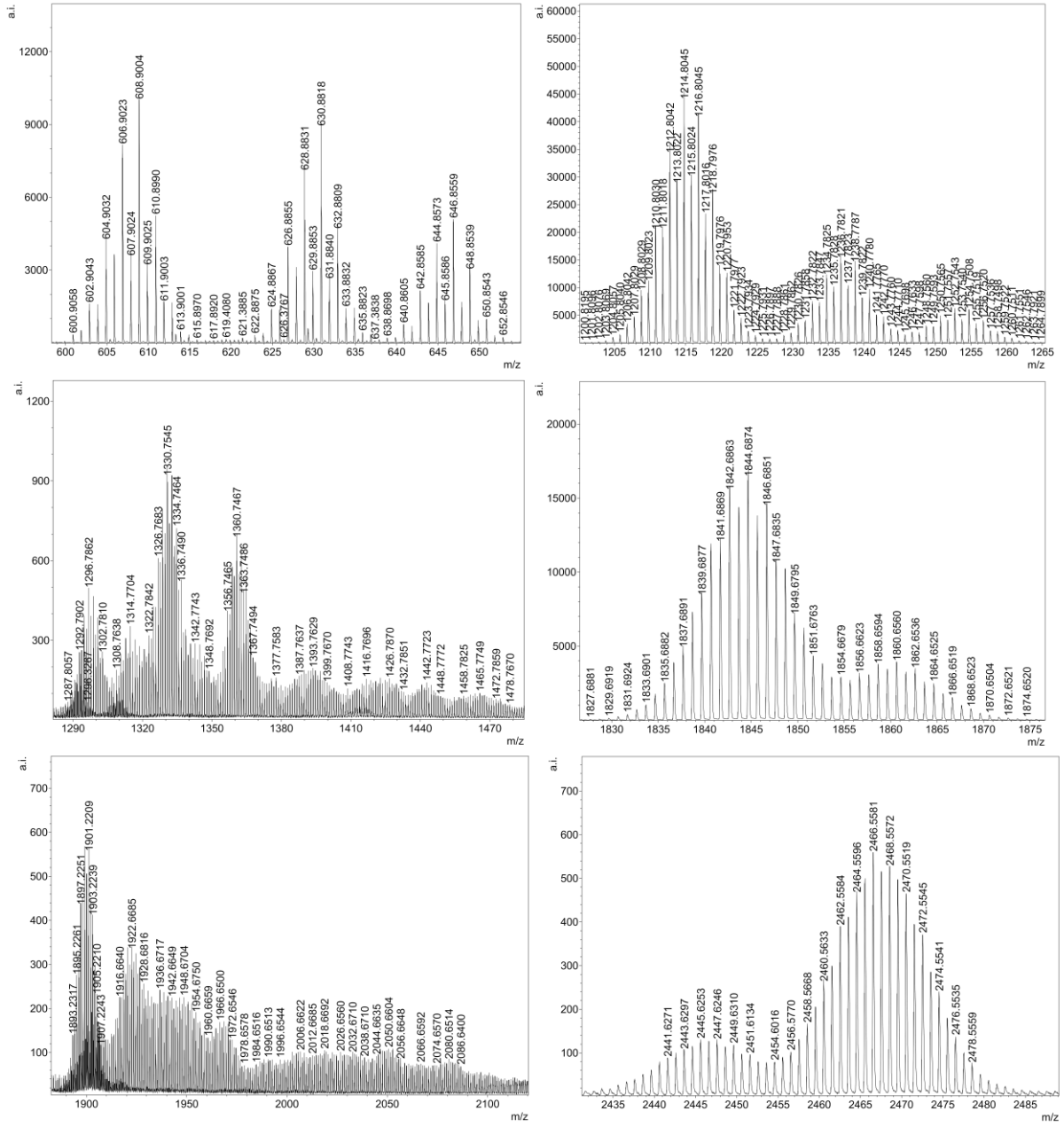

Figures S64-S68. Predicted (down) vs. experimental (up) isotope patterns of main species in the ESI$^+$ mass spectrum of [Ni-μ_2-κ_2-(Ni{κ_5-L^{Se}}$_2$)$_2$-μ_2-(OAc)$_2$]. For the assignments see Figure S57 on page S38.

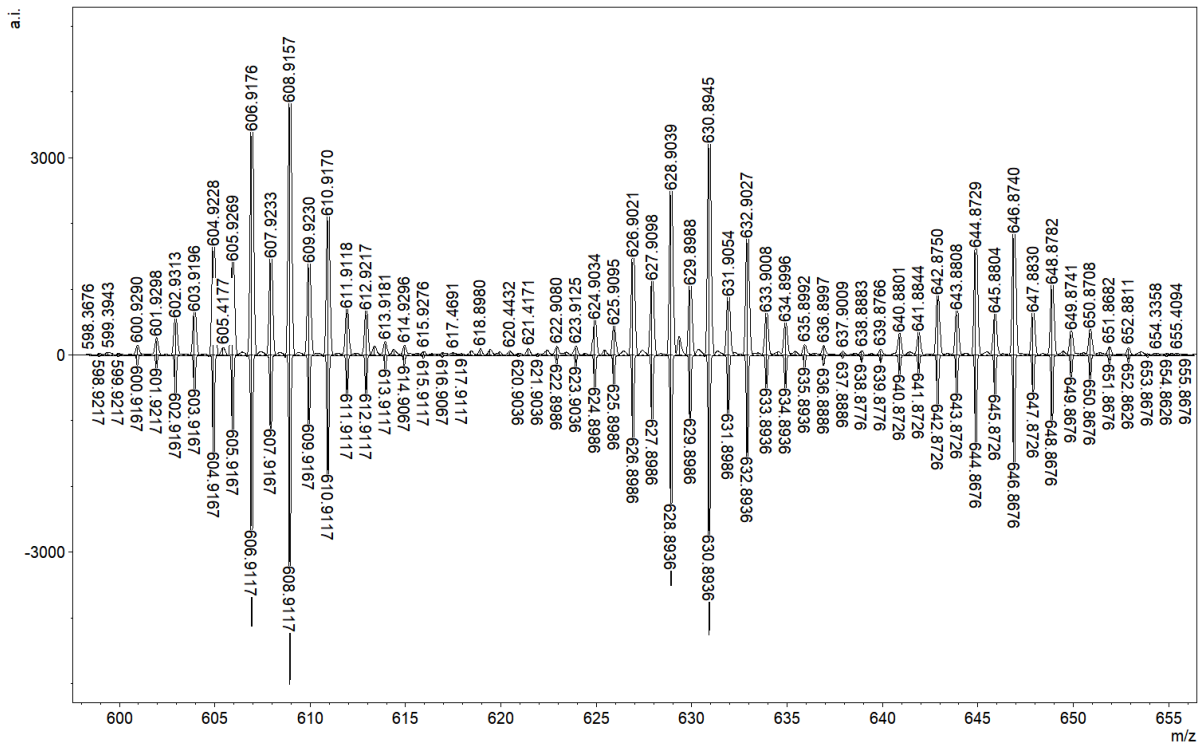

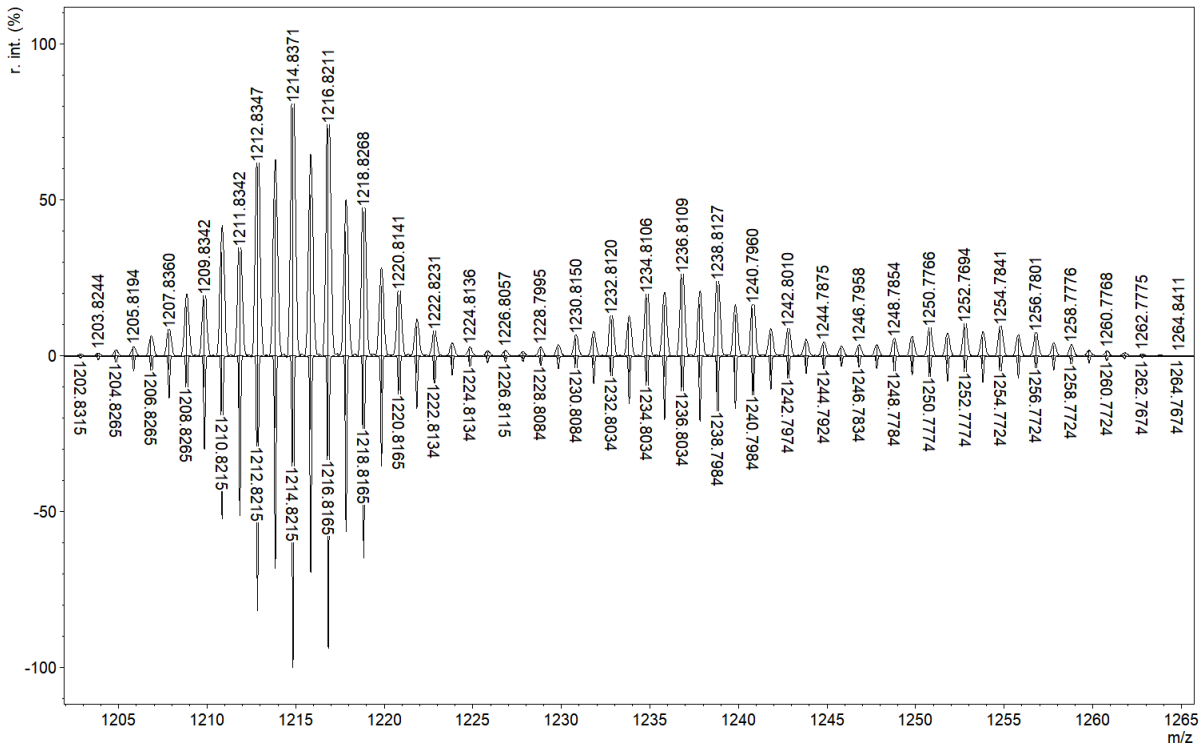

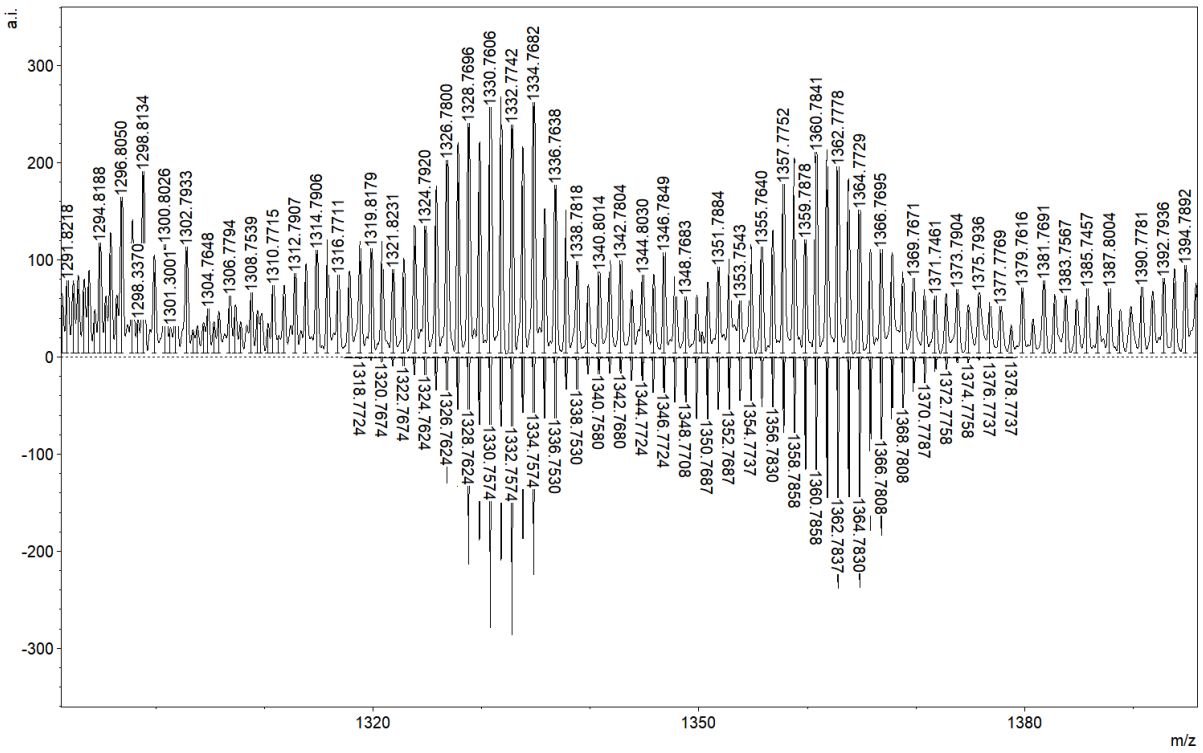
a.i.
m/z
1320
1350
1380

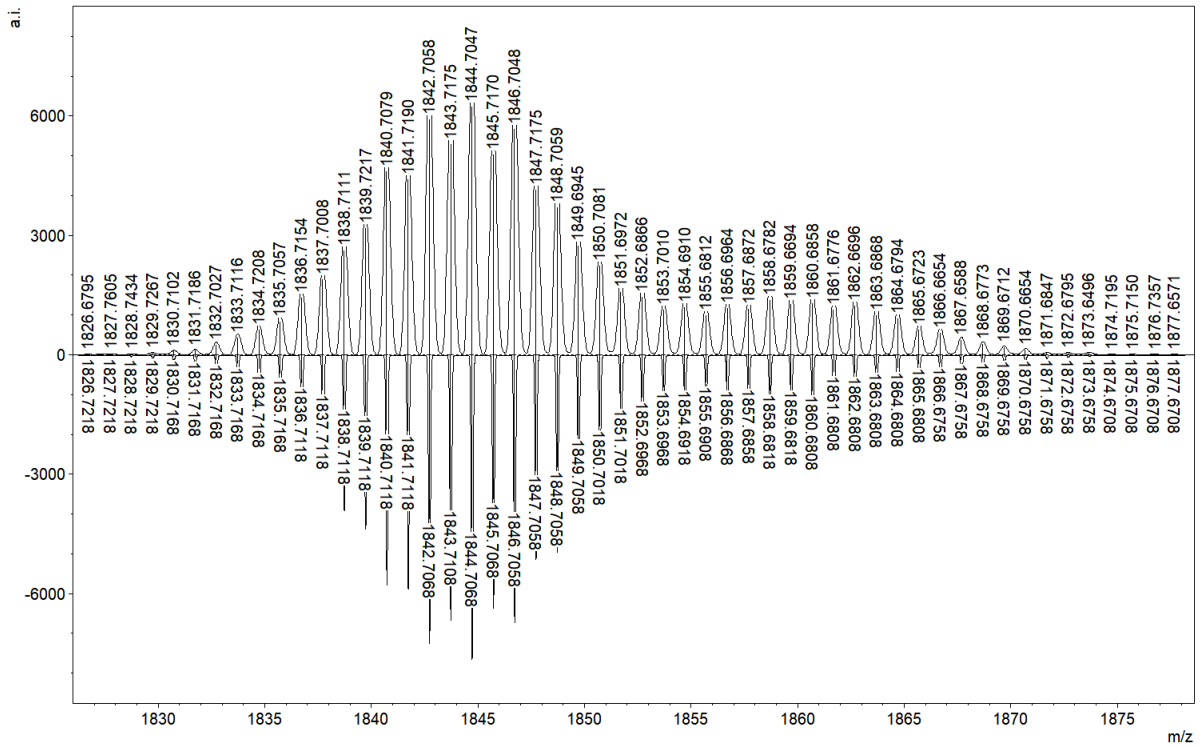
a.i.
m/z
1830
1835
1840
1845
1850
1855
1860
1865
1870
1875

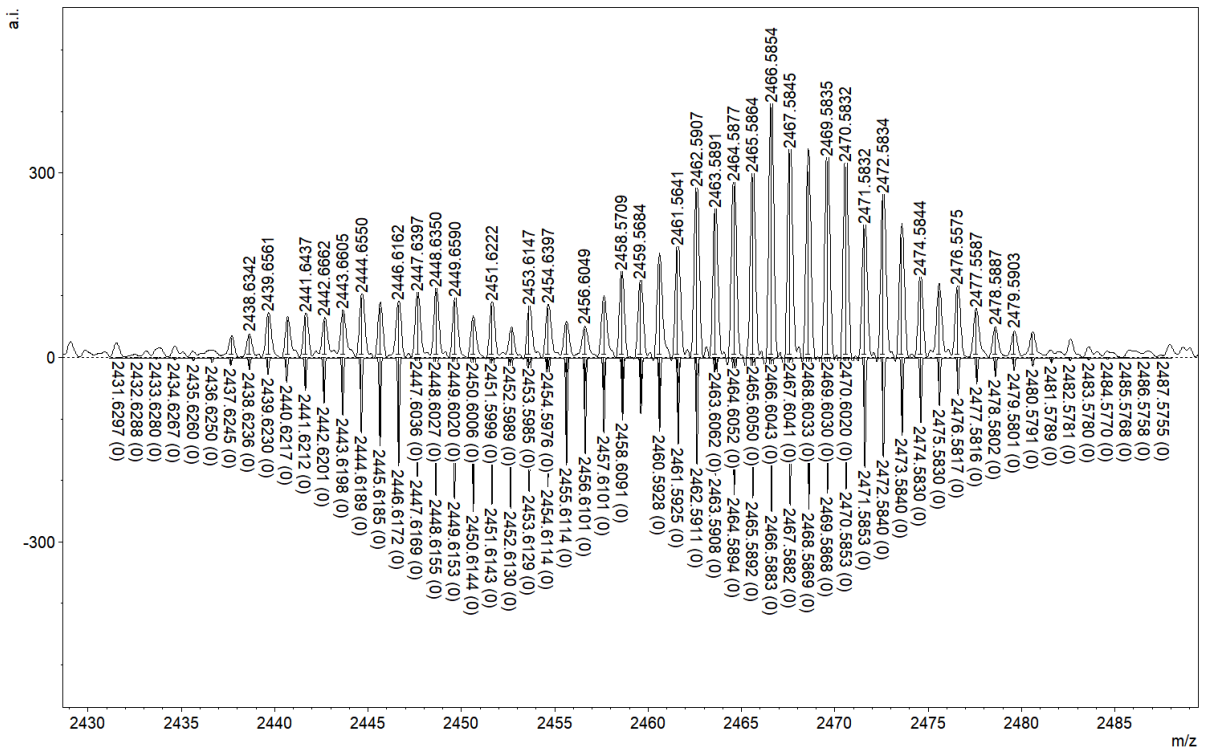

Figure S69. Full ESI$^-$ mass spectrum of [Ni-μ_2-κ_2-(Ni{κ_5-L^{Se}}$_2$)$_2$-μ_2-(OAc)$_2$] with a list of the assigned species.

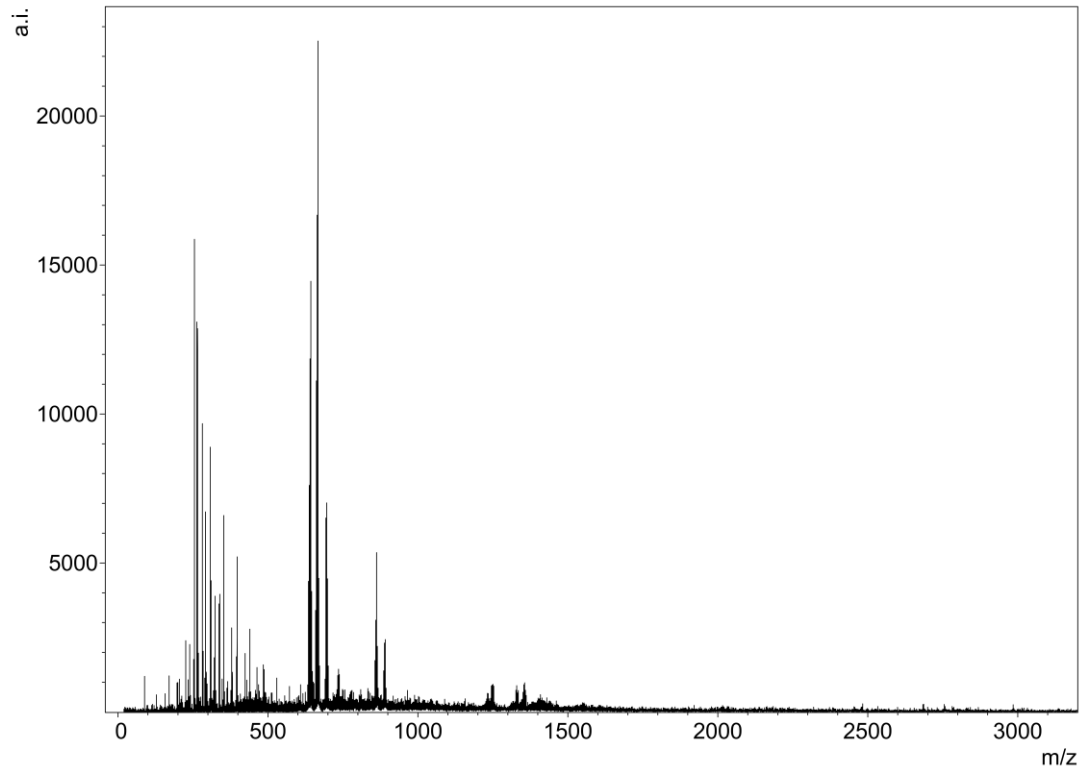

ESI$^-$ MS (m/z): 666.9196 ([Ni{L^{Se}}$_2$+OAc$^-$]$^-$ Calcd 666.9172, 100%), 696.9285 ([Ni{L^{Se}}$_2$+OCH$_2$+OAc$^-$]$^-$ Calcd 696.9187, 32%), 735.9218 (no unambiguous assignment, 7%), 863.1067 ([Ni{L^{Se}}$_2$+8MeOH-H$^+$]$^-$ Calcd 863.0948, 22%), 889.1420 (no unambiguous assignment, 12%), 1232.7831 ([Ni$_2${L^{Se}}$_4$+H$_2$O+H$^-$]$^-$ Calcd 1232.8301, 3%), 1250.7832 ([Ni$_2${L^{Se}}$_4$+Cl$^-$]$^-$ Calcd 1250.7784, 5%), 1330.7426 (no unambiguous assignment, 4%), 1356.7909 (no unambiguous assignment, 4%).

Figures S70-S76. Zoomed ESI$^-$ mass spectrum of [Ni-μ_2-κ_2-(Ni{κ_5-L^{Se}}$_2$)$_2$-μ_2-(OAc)$_2$] for selected regions. For the assignments see Figure S69 on the previous page.

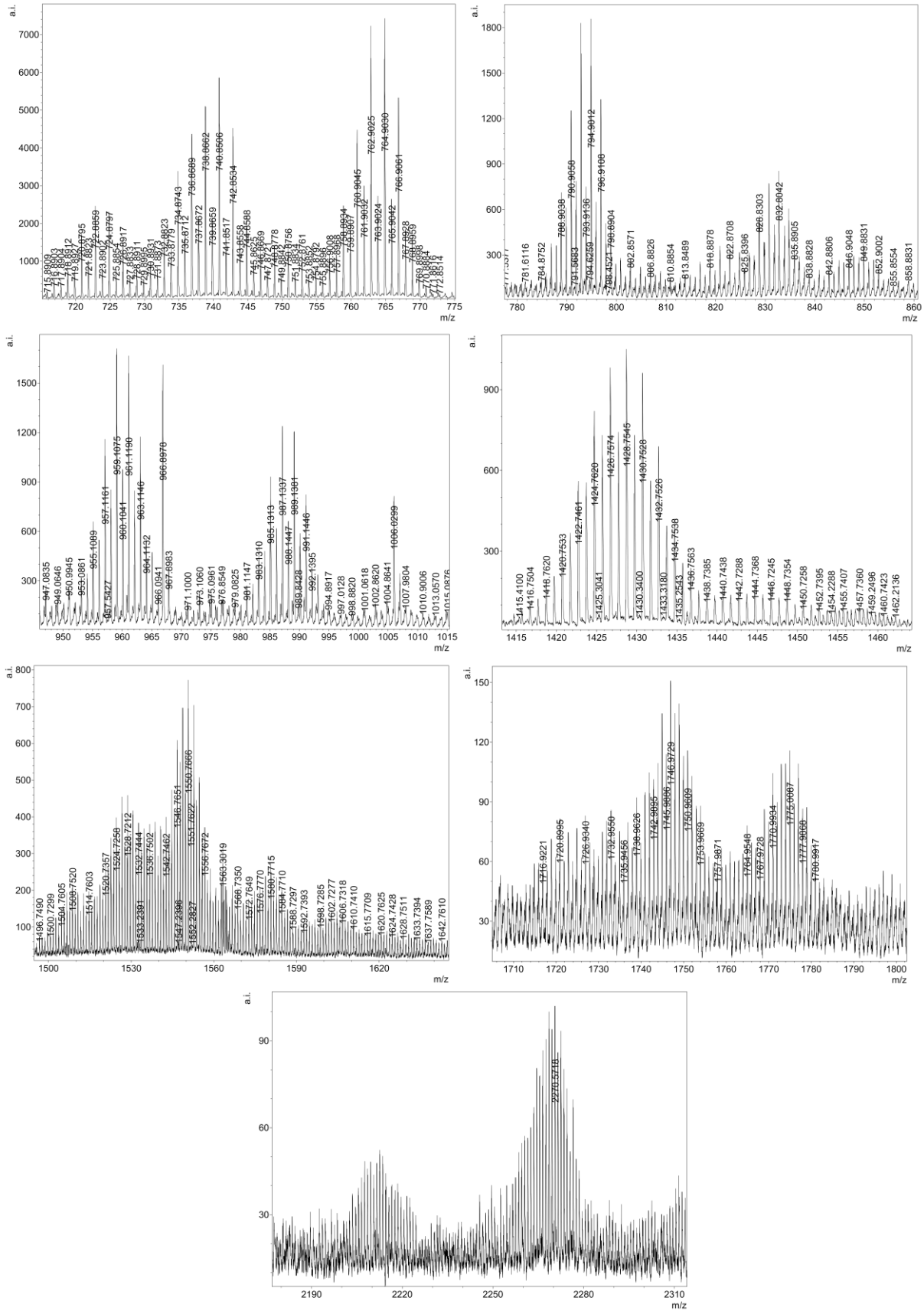

Figure S77. Predicted (down) vs. experimental (up) isotope patterns of main species in the ESI$^-$ mass spectrum of [Ni-μ_2-κ_2-(Ni{κ_5-L^{Se}}$_2$)$_2$-μ_2-(OAc)$_2$]. For the assignments see Figure S69 on page S42.

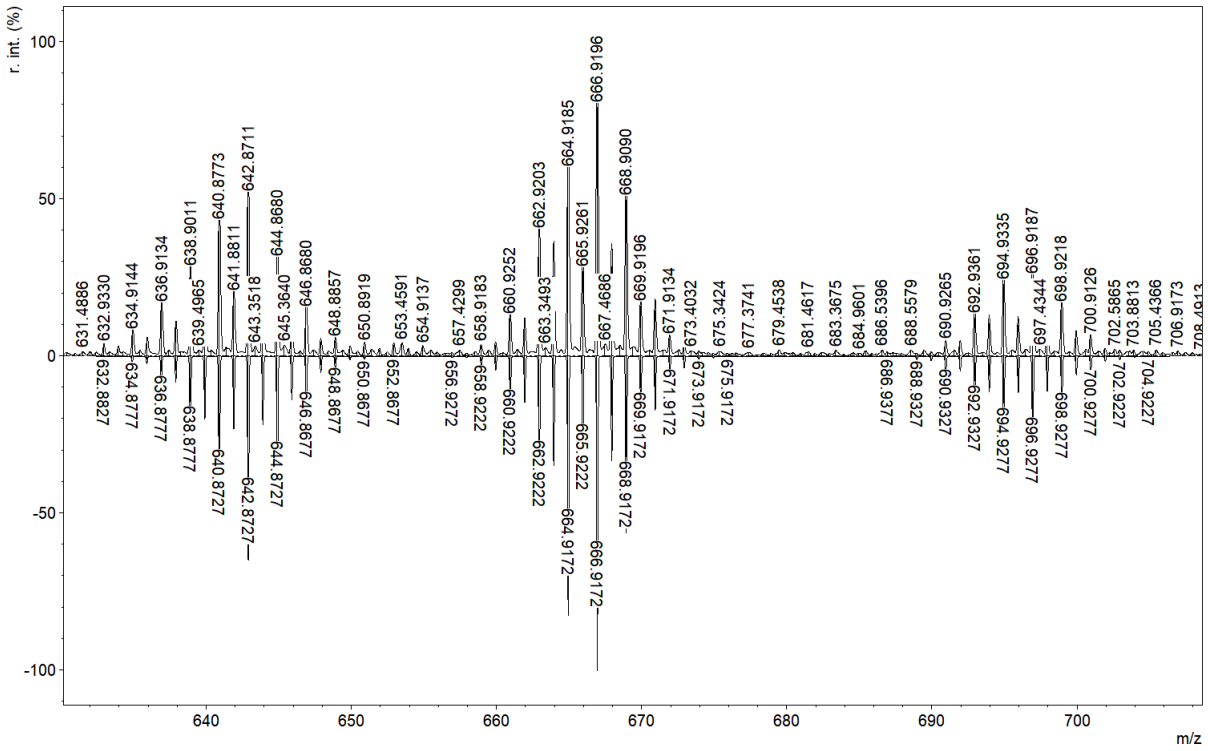

Figure S78. IR spectrum of the microcrystalline bulk of [Ni-μ_2-κ_2-(Ni{κ_5-L^{Te}}$_2$)$_2$-μ_2-(OAc)$_2$].

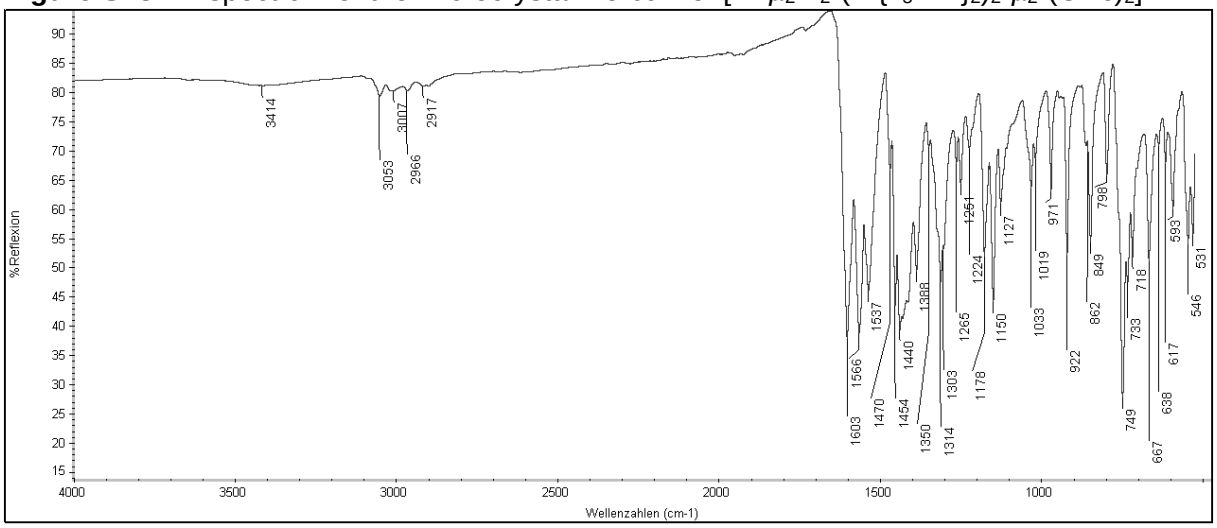

Figure S79. IR spectrum of vacuum-dried single crystals of [Ni-μ_2-κ_2-(Ni{κ_5-L^{Te}}$_2$)$_2$-μ_2-(OAc)$_2$].

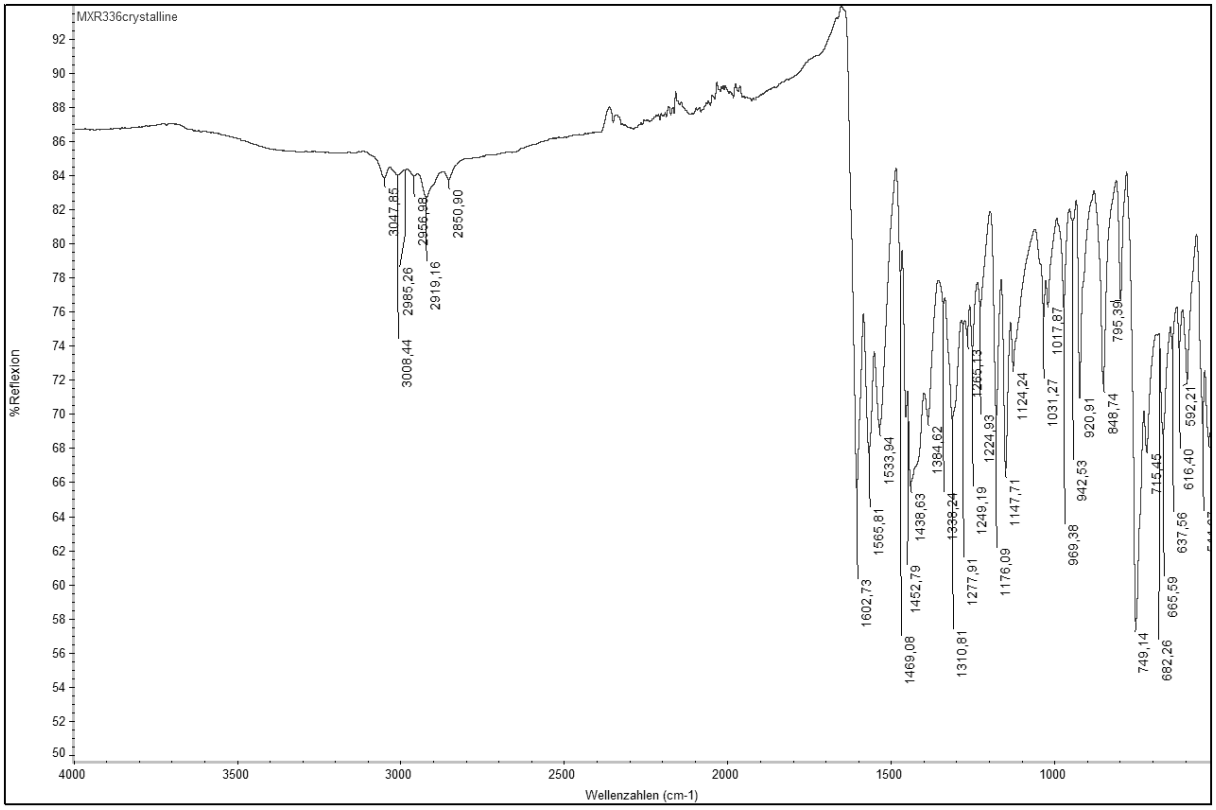

Figure S80. Full ESI$^+$ mass spectrum of [Ni-μ_2-κ_2-(Ni{κ_5-L^{Te}}$_2$)$_2$-μ_2-(OAc)$_2$] with a list of the assigned species.

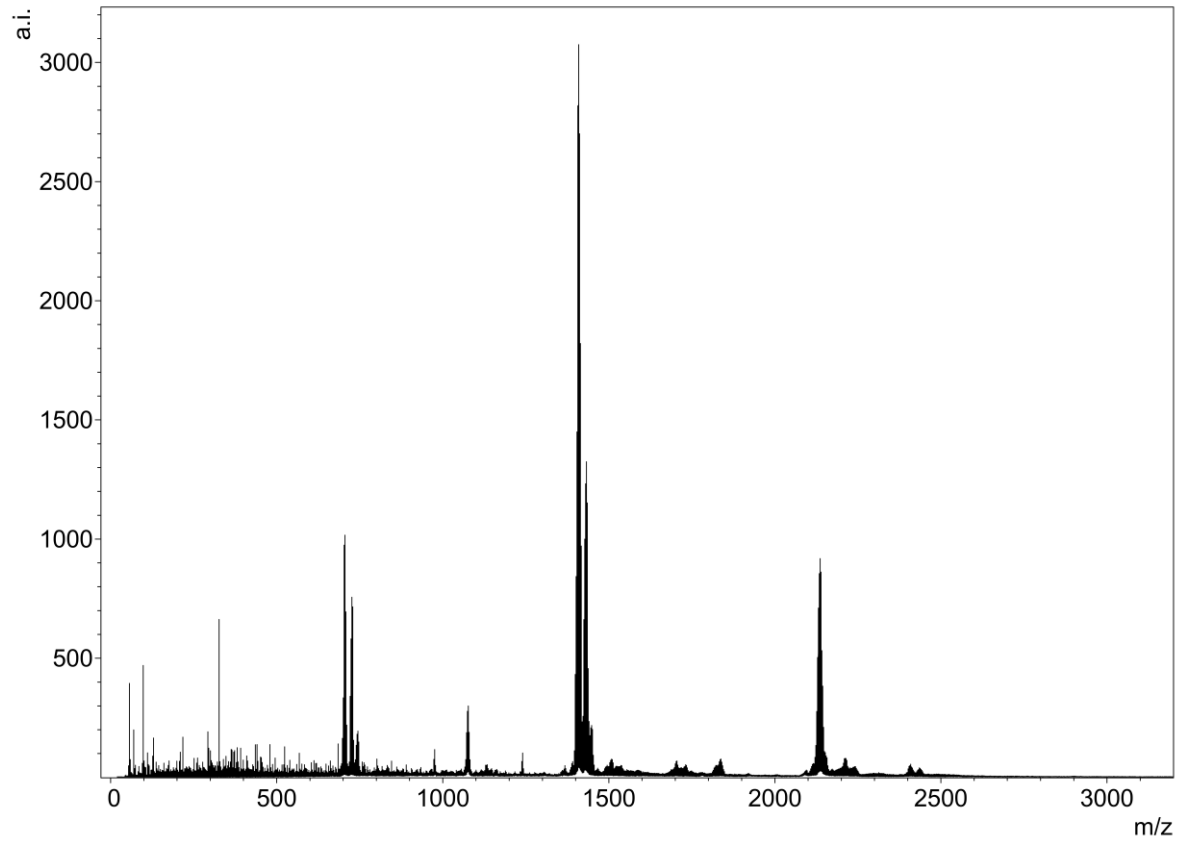

ESI$^+$ MS (m/z): 706.8956 ([Ni{L^{Te}}$_2$+H]$^+$ Calcd 706.8911, 34%), 726.8692 ([Ni{L^{Te}}$_2$+Na]$^+$ Calcd 728.8731, isotopic pattern skewed due to overlap, 25%), 744.8606 ([Ni{L^{Te}}$_2$+K]$^+$ Calcd 744.8470, 6%), 1068.8103

([(Ni$_3${L^{Te}}$_6$)$_3$+H+Na]$^{2+}$ Calcd 1068.8200, 2%), 1076.8102 ([Ni$_3${L^{Te}}$_6$+H+K]$^{2+}$ Calcd 1076.8073, 10%), 1410.7641 ([Ni$_2${L^{Te}}$_4$+H]$^+$ Calcd 1410.7713, 100%), 1432.7605 ([Ni$_2${L^{Te}}$_4$+Na]$^+$ Calcd 1432.7521, 38%), 1450.7208 ([Ni$_2${L^{Te}}$_4$+K]$^+$ Calcd 1450.7271, 7%), 2116.6550 ([Ni$_3${L^{Te}}$_6$+H]$^+$ Calcd 2116.6508, 2%), 2136.6394 ([Ni$_3${L^{Te}}$_6$+Na]$^+$ Calcd 2136.6327, 30%), 2152.6091 ([Ni$_3${L^{Te}}$_6$+K]$^+$ Calcd 2152.6077, 5%), 2100-2300 ([Ni$_3${L^{Te}}$_6$+2Cation+Anion or +NiAnion]$^+$ for Cation = H$^+$, Na$^+$, K$^+$ and Anion = Cl$^-$, OAc$^-$; each ca. 0.5-1%) {*with main signals at 2174.5845 (Ni$_3${L^{Te}}$_6$+H+HOAc]$^+$ Calcd 2174.6720), 2196.5903 ([Ni$_3${L^{Te}}$_6$+Na+HOAc]$^+$ Calcd 2196.6540), 2212.6199 ([Ni$_3${L^{Te}}$_6$+K+HOAc]$^+$ Calcd 2212.6278), 2234.5999 ([Ni$_3${L^{Te}}$_6$+K+NaOAc]$^+$ Calcd 2234.6097), 2250.6038 ([Ni$_3${L^{Te}}$_6$+K+KOAc]$^+$ Calcd 2250.5838)*}, 2408.8171 ([Ni$_5${L^{Te}}$_6$+3OAc]$^+$ Calcd 2408.5526), 2436.8530 ([Ni$_5${L^{Te}}$_6$+4OAc-OCH$_3$)]$^+$ Calcd 2436.5475).

Figures S81-S88. Zoomed ESI$^+$ mass spectrum of [Ni-μ_2-κ_2-(Ni{κ_5-L^{Te}}$_2$)$_2$-μ_2-(OAc)$_2$] for selected regions. For the assignments see Figure S80 on the previous page.

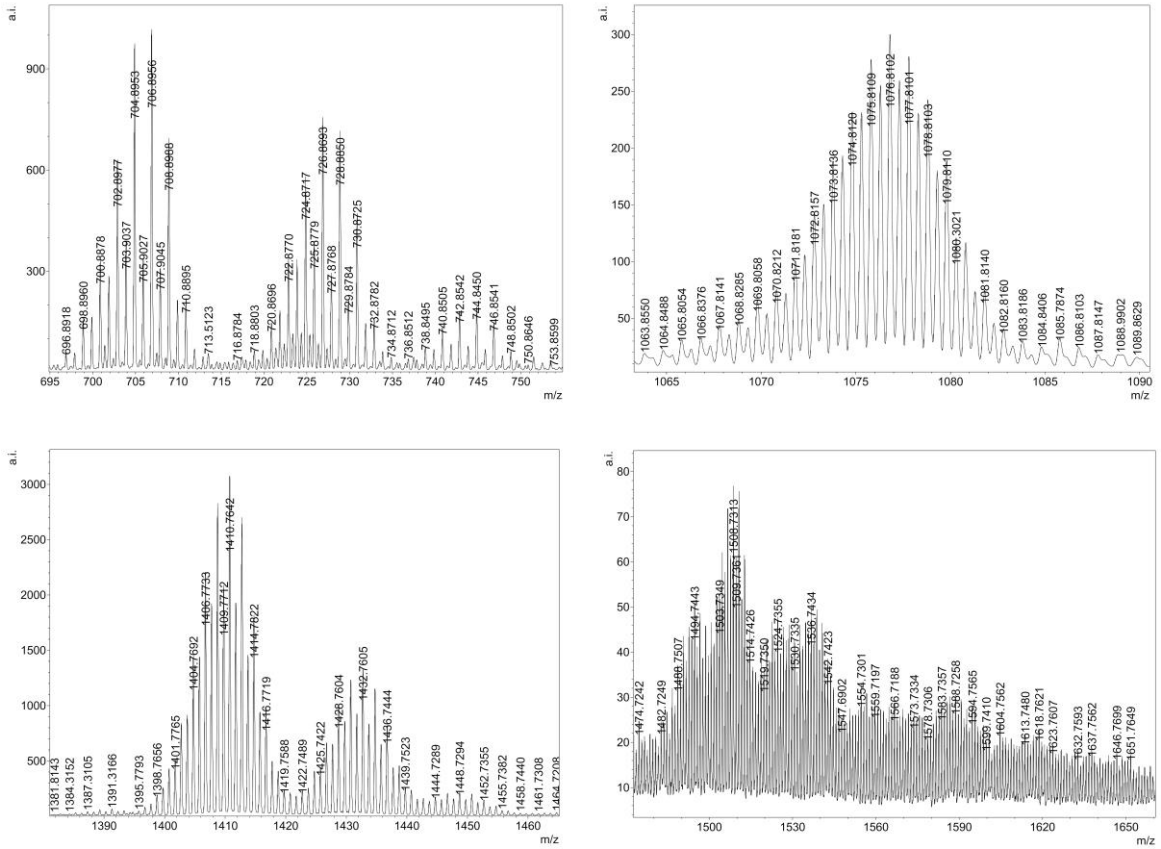

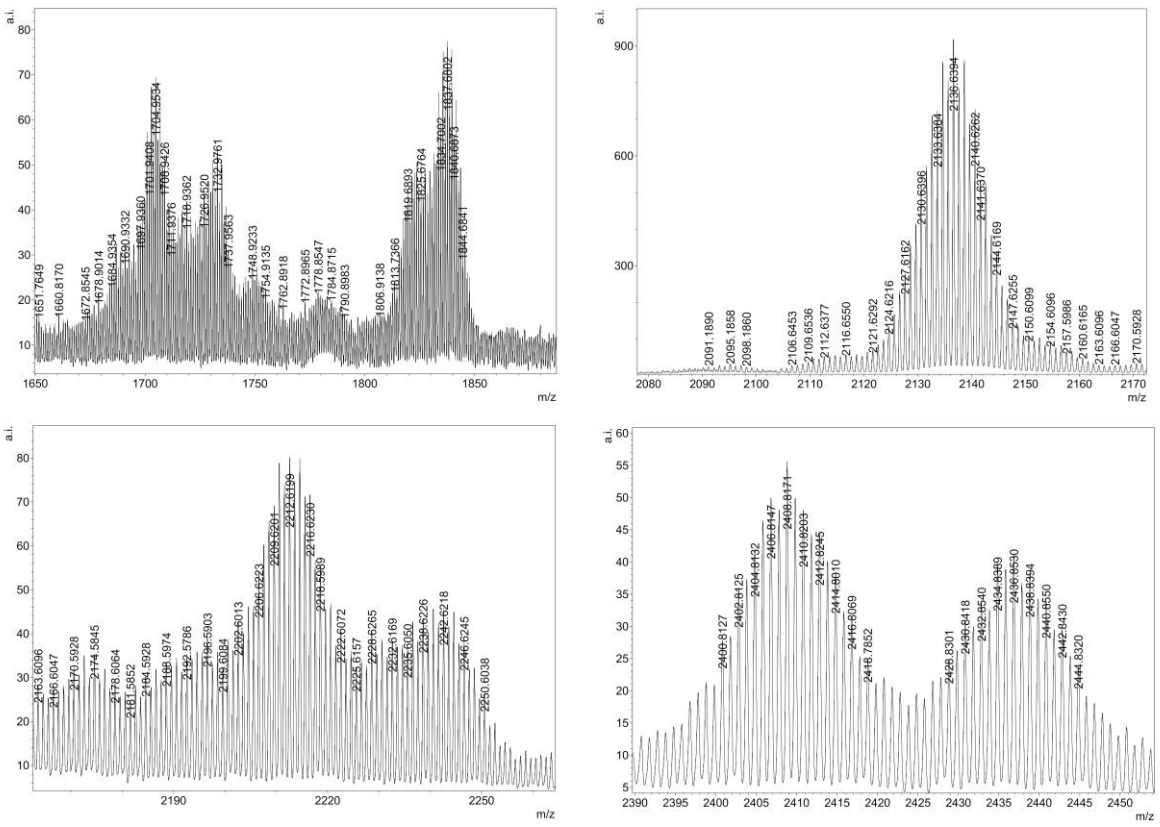

Figures S89-S94. Predicted (down) vs. experimental (up) isotope patterns of main species in the ESI⁺ mass spectrum of [Ni-μ_2-κ_2-(Ni{κ_5-L^{Te}}$_2$)$_2$-μ_2-(OAc)$_2$]. For the assignments see Figure S80 on page S45.

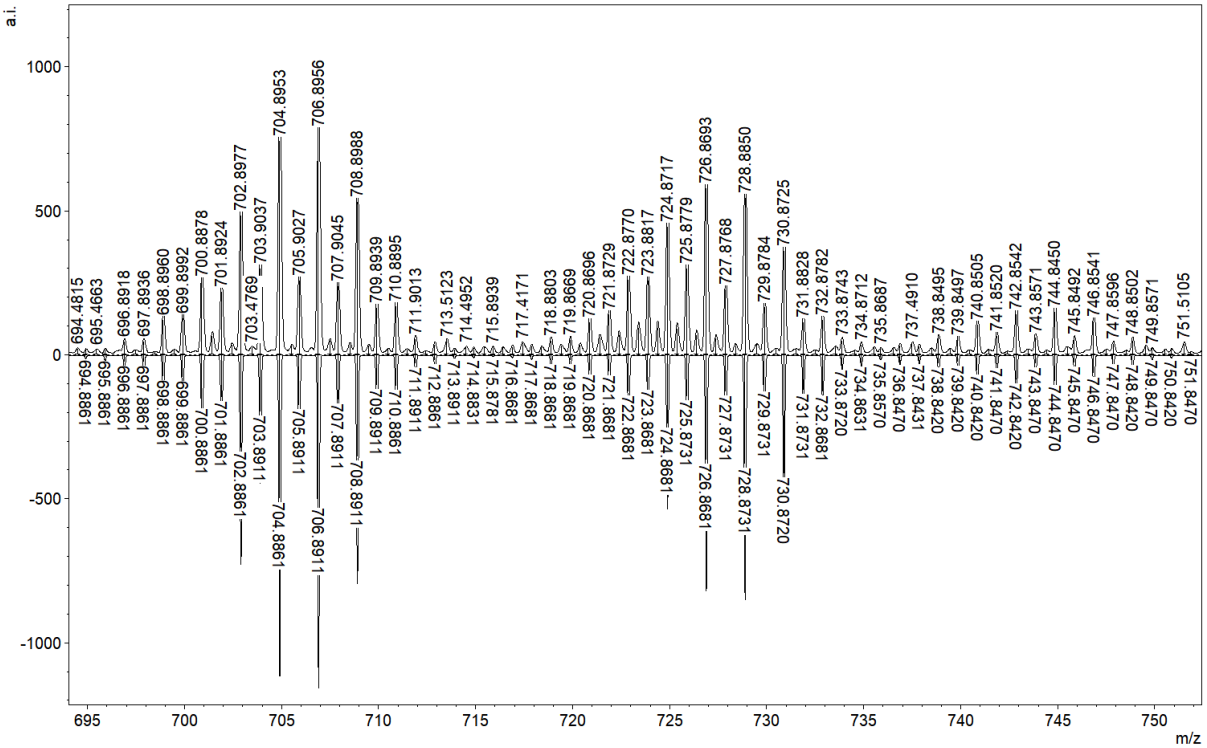

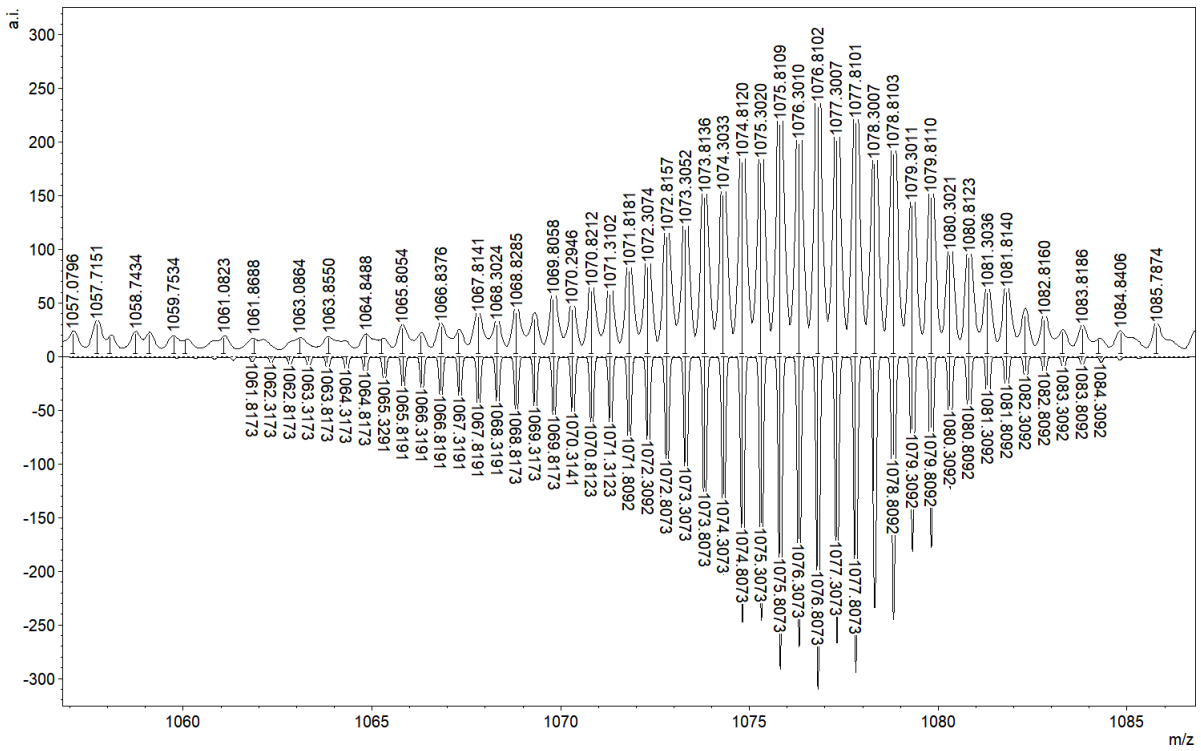
a.i.
m/z
1057.0796
1057.7151
1058.7434
1059.7534
1061.0823
1061.8688
1063.0864
1063.8550
1064.8488
1065.8054
1066.8376
1067.8141
1068.3024
1068.8285
1069.8058
1070.2946
1070.8212
1071.3102
1071.8181
1072.3074
1072.8157
1073.3052
1073.8136
1074.3033
1074.8120
1075.3020
1075.8109
1076.3010
1076.8102
1077.3007
1077.8101
1078.3007
1078.8103
1079.3011
1079.8110
1080.3021
1080.8123
1081.3036
1081.8140
1082.8160
1083.8186
1084.8406
1085.7874
1061.8173
1062.3173
1062.8173
1063.3173
1063.8173
1064.3173
1064.8173
1065.3291
1065.8191
1066.3191
1066.8191
1067.3191
1067.8191
1068.3191
1068.8173
1069.3173
1069.8173
1070.3141
1070.8123
1071.3123
1071.8092
1072.3092
1072.8073
1073.3073
1073.8073
1074.3073
1074.8073
1075.3073
1075.8073
1076.3073
1076.8073
1077.3073
1077.8073
1078.8092
1079.3092
1079.8092
1080.3092
1080.8092
1081.3092
1081.8092
1082.3092
1082.8092
1083.3092
1083.8092
1084.3092
1060
1065
1070
1075
1080
1085
300
250
200
150
100
50
0
-50
-100
-150
-200
-250
-300

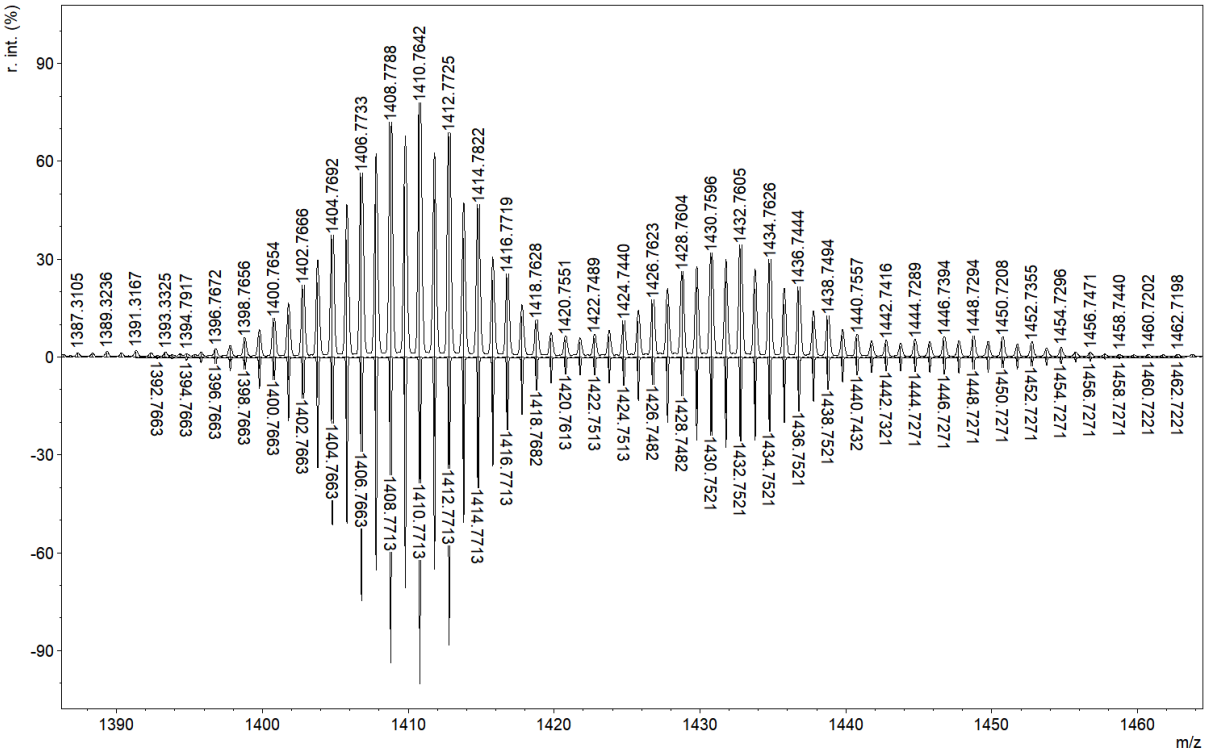
r. int. (%)
m/z
1387.3105
1389.3236
1391.3167
1393.3325
1394.7917
1396.7672
1398.7656
1400.7654
1402.7666
1404.7692
1406.7733
1408.7788
1410.7642
1412.7725
1414.7822
1416.7719
1418.7628
1420.7551
1422.7489
1424.7440
1426.7623
1428.7604
1430.7596
1432.7605
1434.7626
1436.7444
1438.7494
1440.7557
1442.7416
1444.7289
1446.7394
1448.7294
1450.7208
1452.7355
1454.7296
1456.7471
1458.7440
1460.7202
1462.7198
1392.7663
1394.7663
1396.7663
1398.7663
1400.7663
1402.7663
1404.7663
1406.7663
1408.7713
1410.7713
1412.7713
1414.7713
1416.7713
1418.7682
1420.7613
1422.7513
1424.7513
1426.7482
1428.7482
1430.7521
1432.7521
1434.7521
1436.7521
1438.7521
1440.7432
1442.7321
1444.7271
1446.7271
1448.7271
1450.7271
1452.7271
1454.7271
1456.7271
1458.7271
1460.7221
1462.7221
1390
1400
1410
1420
1430
1440
1450
1460
90
60
30
0
-30
-60
-90

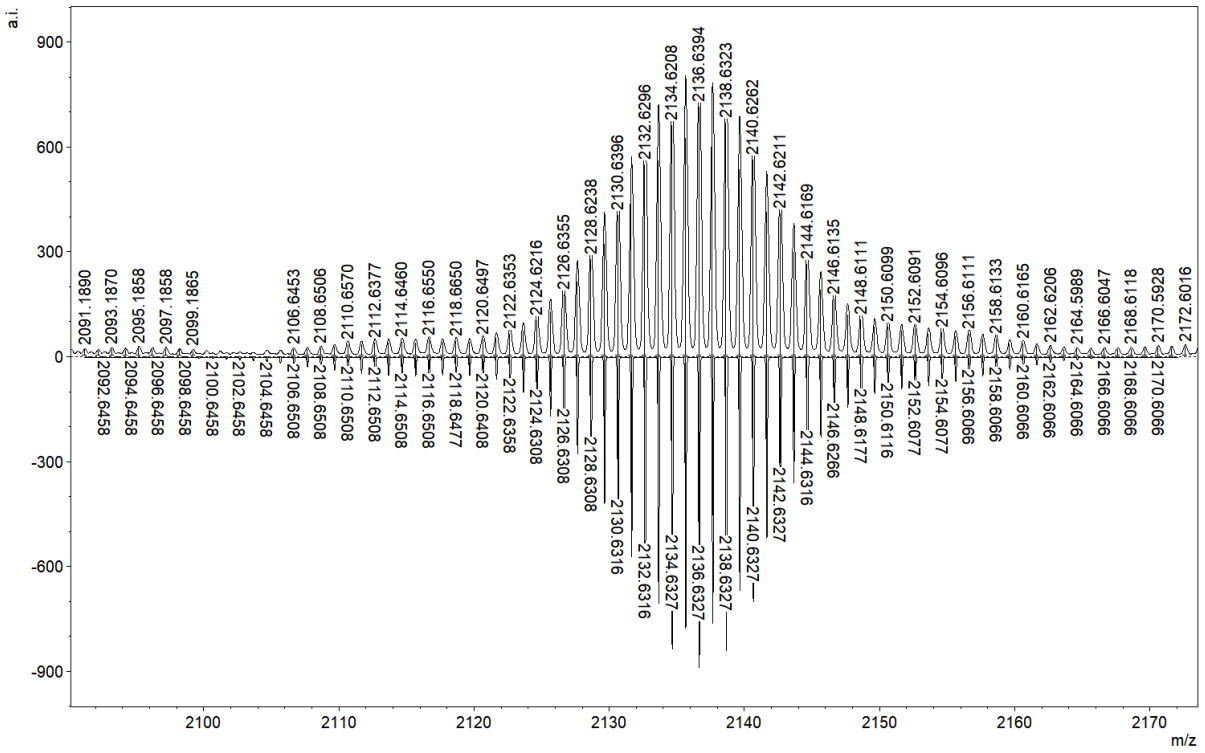
a.i.
900
600
300
0
-300
-600
-900
2091.1890
2093.1870
2095.1858
2097.1858
2099.1865
2106.6453
2108.6506
2110.6570
2112.6377
2114.6460
2116.6550
2118.6650
2120.6497
2122.6353
2124.6216
2126.6355
2128.6238
2130.6396
2132.6296
2134.6208
2136.6394
2138.6323
2140.6262
2142.6211
2144.6169
2146.6135
2148.6111
2150.6099
2152.6091
2154.6096
2156.6111
2158.6133
2160.6165
2162.6206
2164.5989
2166.6047
2168.6118
2170.5928
2172.6016
2092.6458
2094.6458
2096.6458
2098.6458
2100.6458
2102.6458
2104.6458
2106.6508
2108.6508
2110.6508
2112.6508
2114.6508
2116.6508
2118.6477
2120.6408
2122.6358
2124.6308
2126.6308
2128.6308
2130.6316
2132.6316
2134.6327
2136.6327
2138.6327
2140.6327
2142.6327
2144.6316
2146.6266
2148.6177
2150.6116
2152.6077
2154.6077
2156.6069
2158.6069
2160.6069
2162.6066
2164.6066
2166.6066
2168.6066
2170.6066
100
50
0
-50
-100
2160
2190
2220
2250
m/z

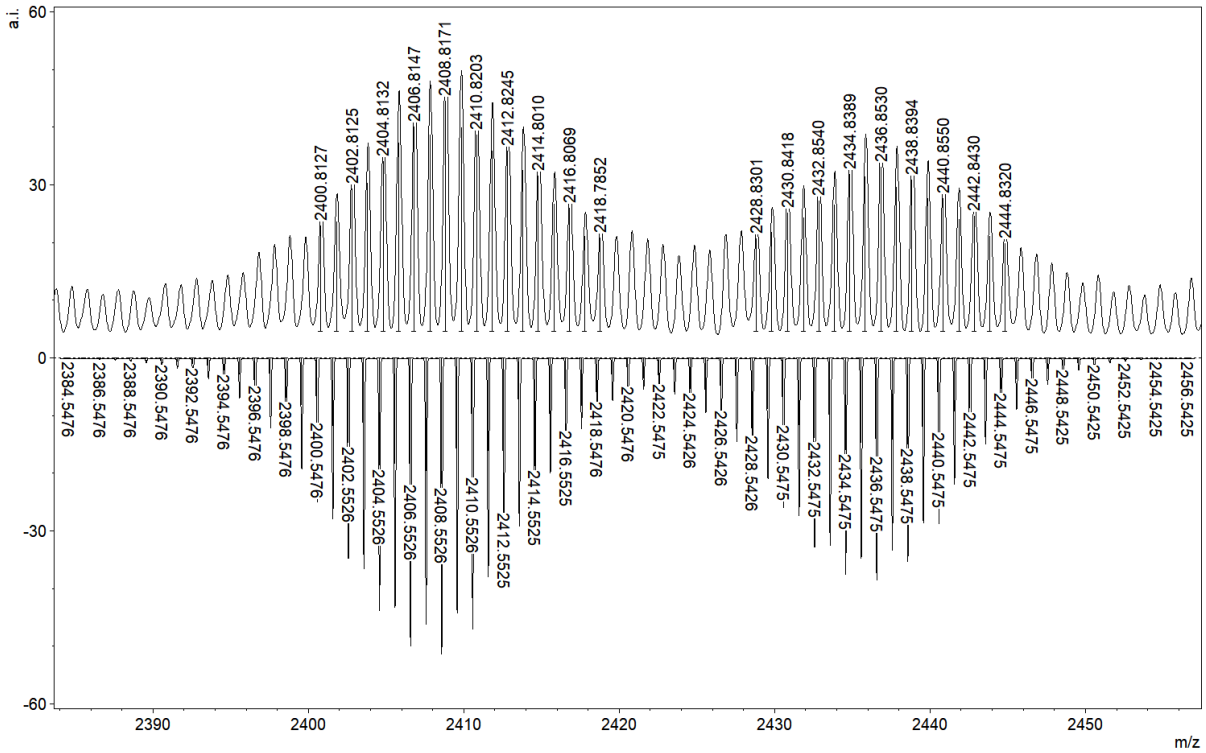

Figure S95. Full ESI$^-$ mass spectrum of [Ni-μ_2-κ_2-(Ni{κ_5-L^{Te}}$_2$)$_2$-μ_2-(OAc)$_2$] with a list of the assigned species.

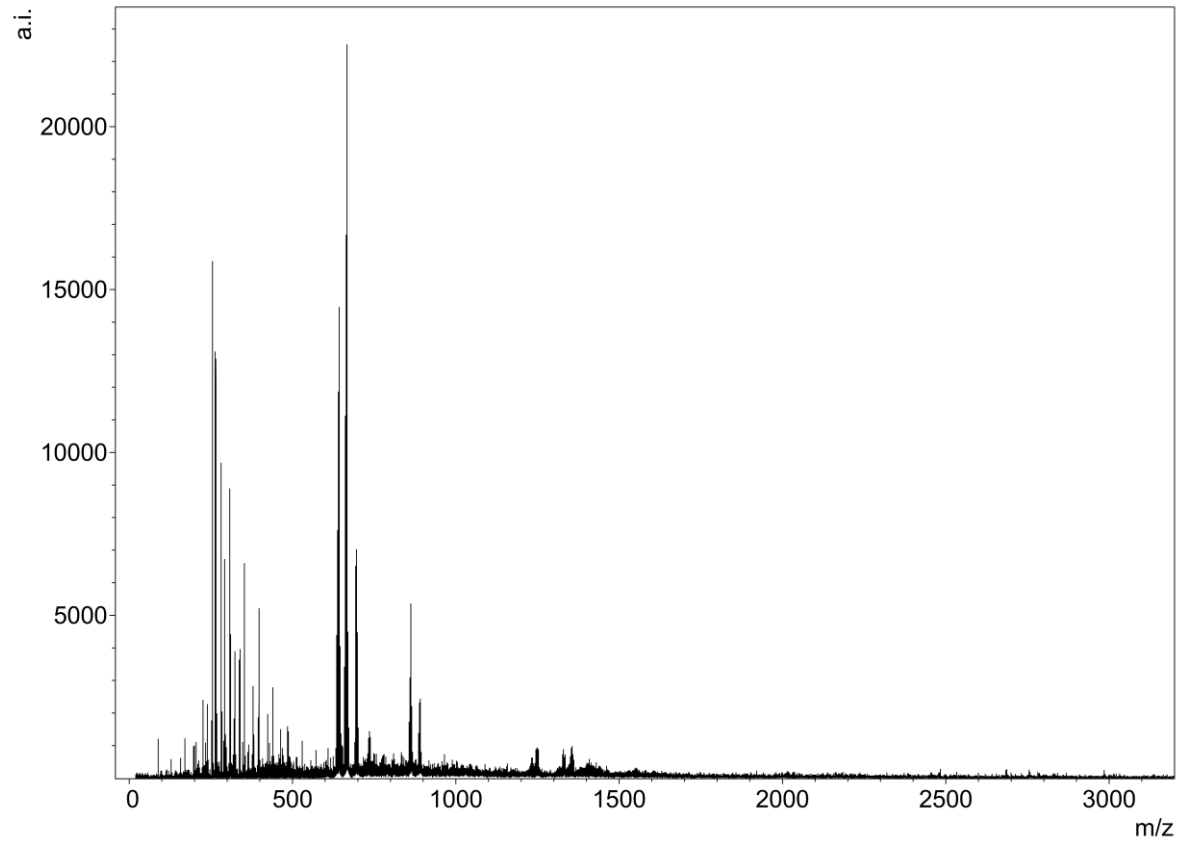

ESI$^-$ MS (m/z): 722.8859 ([Ni{L^{Te}}$_2$+OH$_2$+H$^-$]$^-$ Calcd 722.8989, 22%), 740.8506 ([Ni{L^{Te}}$_2$+Cl$^-$]$^-$ Calcd 740.8490, 53%), 764.9030 ([Ni{L^{Te}}$_2$+OAc$^-$]$^-$Calcd 764.8945, 68%), 794.9012 ([Ni{L^{Te}}$_2$+H$_2$CO+OAc$^-$]$^-$ Calcd 794.9051, 17%), 832.8042 ([Ni{L^{Te}}$_2$+MeOH+HCl+OAc$^-$]$^-$ Calcd 832.8965, 8%), 959.1075 ([Ni{L^{Te}}$_2$+7MeOH-H$^+$]$^-$ Calcd 959.0826, 16%), 987.1337 ([Ni{L^{Te}}$_2$+7MeOH+OAc$^-$]$^-$ Calcd 987.0775, 11%),

1428.7545 ($[Ni_2\{L^{Te}\}_4+OH_2+H^-]^-$ Calcd 1428.7805, 10%), 1444.7368 ($[Ni_2\{L^{Te}\}_4+Cl^-]$ Calcd 1444.7302, 2%), 1455.7407 $[Ni_3\{L^{Te}\}_8+CH_2O+2OAc^-]^{2-}$ Calcd 1455.8303, 1%), 1504.7605 ($[Ni_2\{L^{Te}\}_4+Ni+Cl^-]^-$ Calcd 1504.6640, 1%), 1508.7520 (no unambiguous assignment, 2%), 1528.7212 ($[Ni_2\{L^{Te}\}_4+Ni+OAc^-]^-$ Calcd 1528.7095, 4%), 1550.7666 ($[Ni_2\{L^{Te}\}_4+Na^++2OAc^-]^-$ Calcd 1550.7787, 7%), 1580.7715 ($[Ni_2\{L^{Te}\}_4+CH_2O+Na^++2OAc^-]^-$ Calcd 1580.7893, 3%), 1602.7277 ($[Ni_3\{L^{Te}\}_4+OH^-+2OAc^-]^-$ Calcd 1602.7253, 1%), 1746.9729 ($[Ni_2\{L^{Te}\}_5+CH_2]^-$ Calcd 1746.7513, 1%), 1775.0087 (no unambiguous assignment, 1%), 2212.5401 ($[Ni_4\{L^{Te}\}_6+K^+]^-$ Calcd 2212.5408, 0.5%), 2270.5718 ($[Ni_4\{L^{Te}\}_6+KOAc-H^+]^-$ Calcd 2270.5463, 1%).

Figures S96-S102. Zoomed ESI^- mass spectrum of [Ni-μ_2-κ_2-(Ni{κ_5-L^{Te}}$_2$)$_2$-μ_2-(OAc)$_2$] for selected regions. For the assignments see Figure S95 on the previous page.

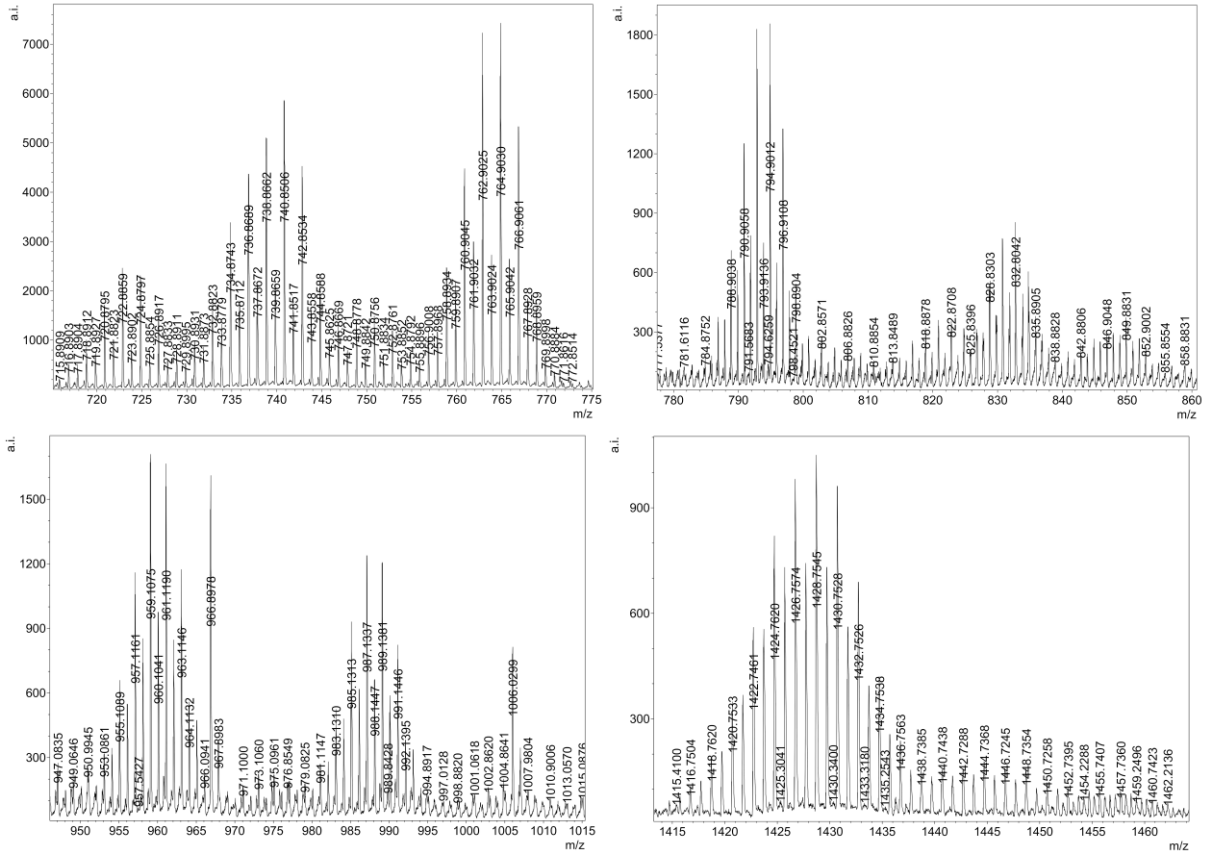

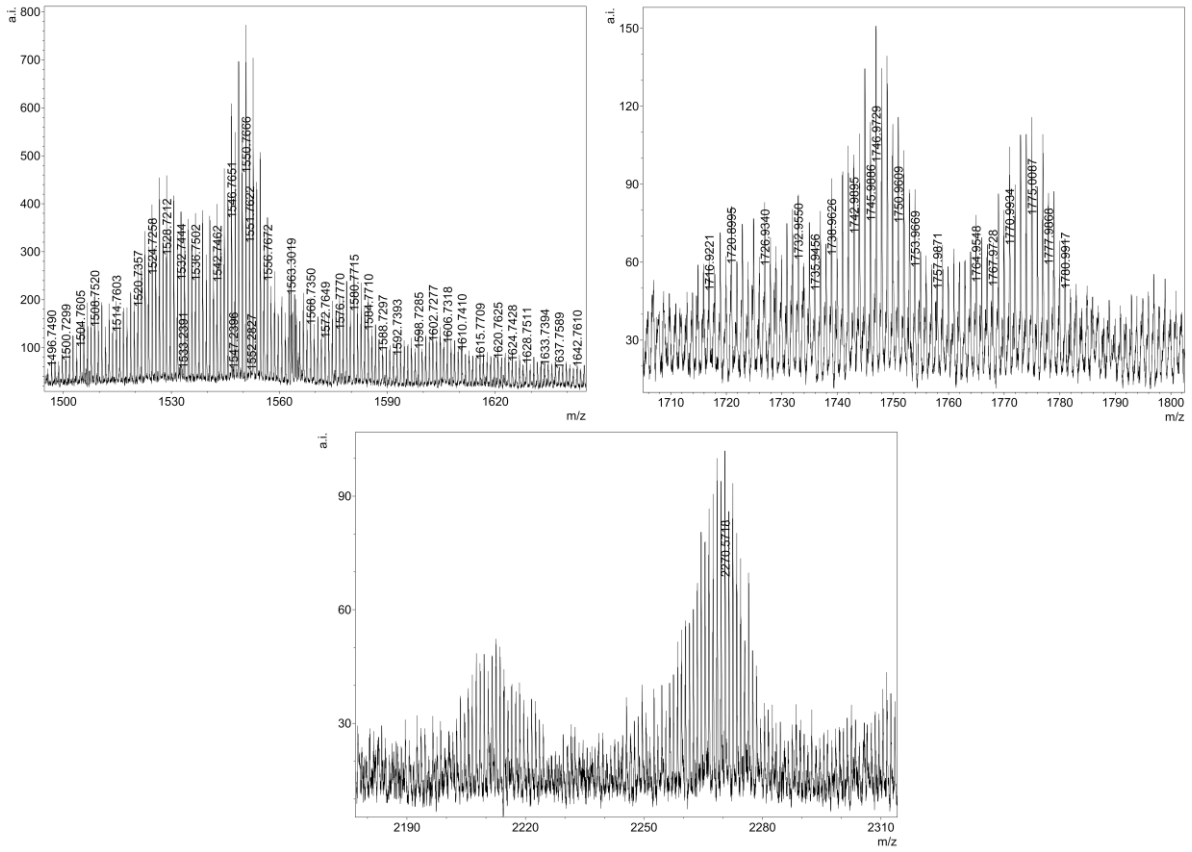

Figure S103. Predicted (down) vs. experimental (up) isotope patterns of main species in the ESI$^-$ mass spectrum of [Ni-μ_2-κ_2-(Ni{κ_5-L^{Te}}$_2$)$_2$-μ_2-(OAc)$_2$]. For the assignments see Figure S95 on page S50.

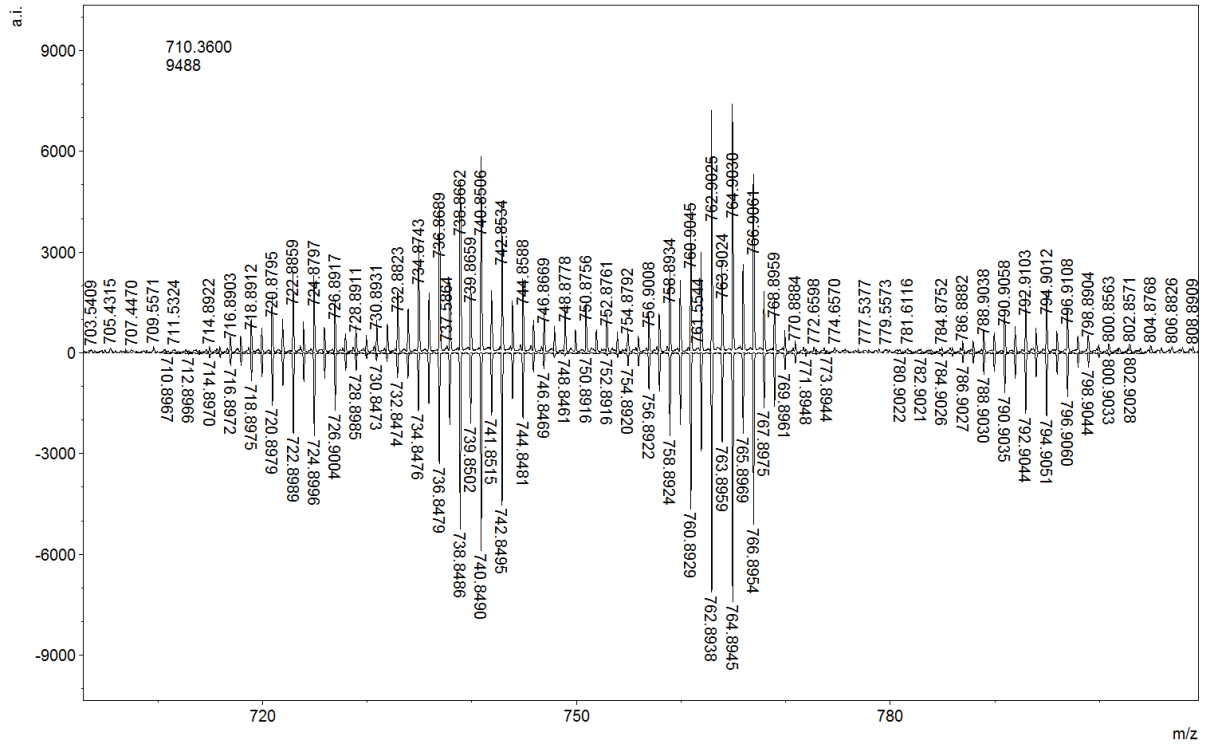

Figure S104. IR spectrum of crystalline [Ni_2-κ_5-(Ni_4-κ_6-μ_6-{($L'^{Te}_2O_3$)($L'^{Te}O_2$)$_2$}$_2$)-μ_2-(H_2O)$_2$].

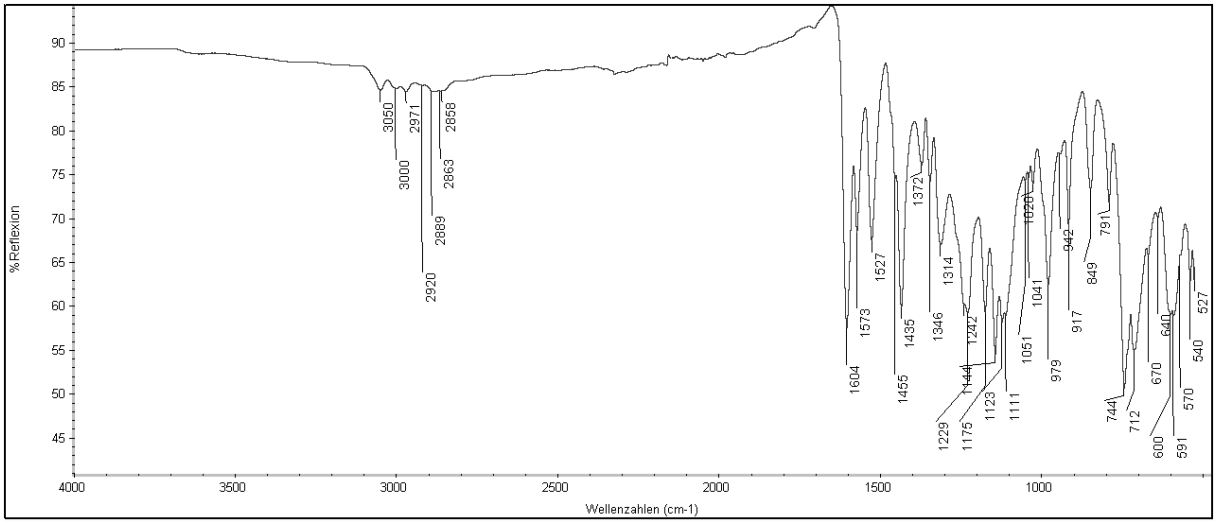

Figure S105. IR spectrum of amorphous [Ni_2-κ_5-(Ni_4-κ_6-μ_6-{($L'^{Te}_2O_3$)($L'^{Te}O_2$)$_2$}$_2$)-μ_2-(H_2O)$_2$].

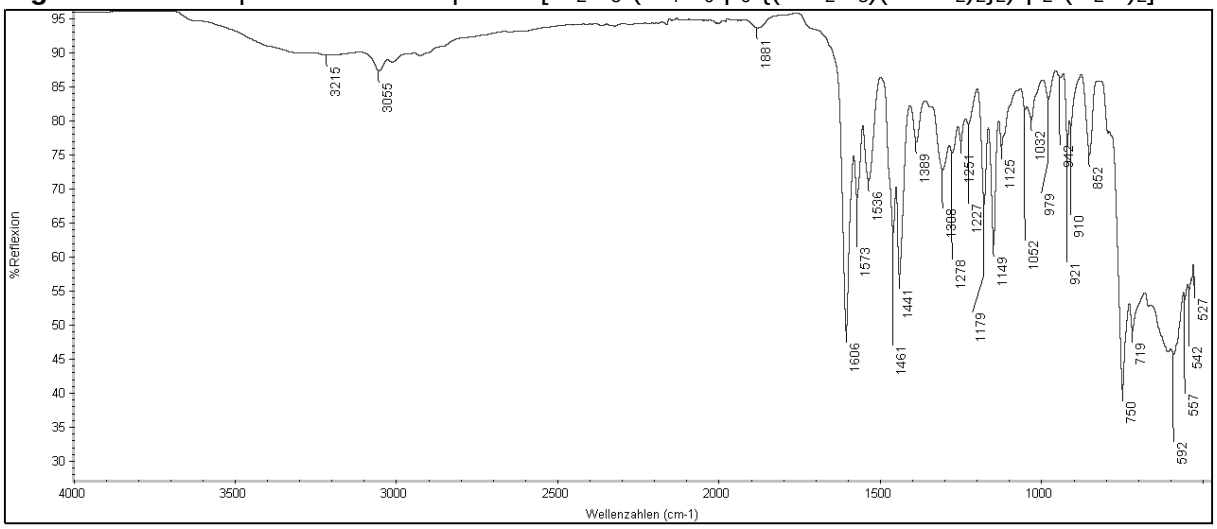

Part 3: Computational data

Figure S106. Optimized structure of cuboid-like $[Pd_4(L'^{Se})_4]$ in an implicit CH_2Cl_2 solvent model at the CAM-B3LYP level. The structure obtained is a distorted version of the gyrobifastigial isomer, which is also the final result when starting from a gyrobifastigial initial geometry.

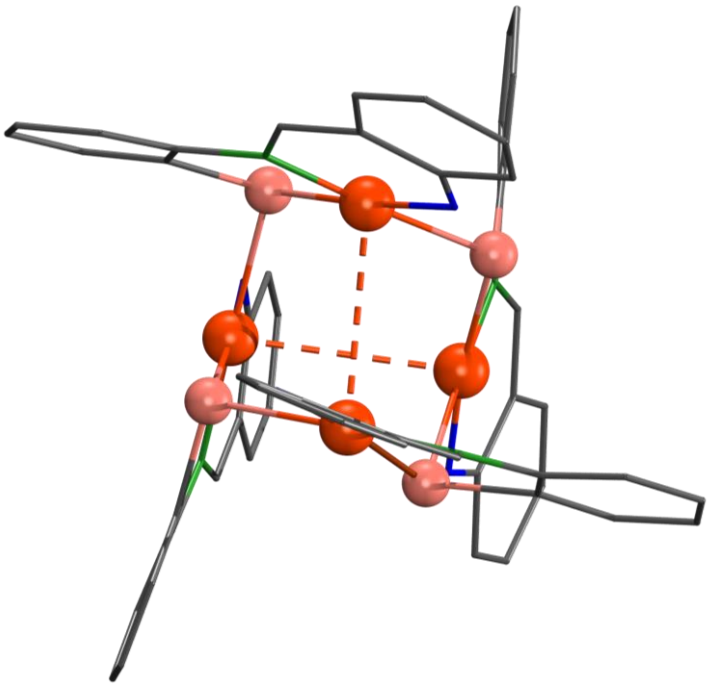

Figure S107. Optimized structure of cuboid-like $[Pd_4(L'^{Te})_4]$ in an implicit CH_2Cl_2 solvent model at the B3LYP level.

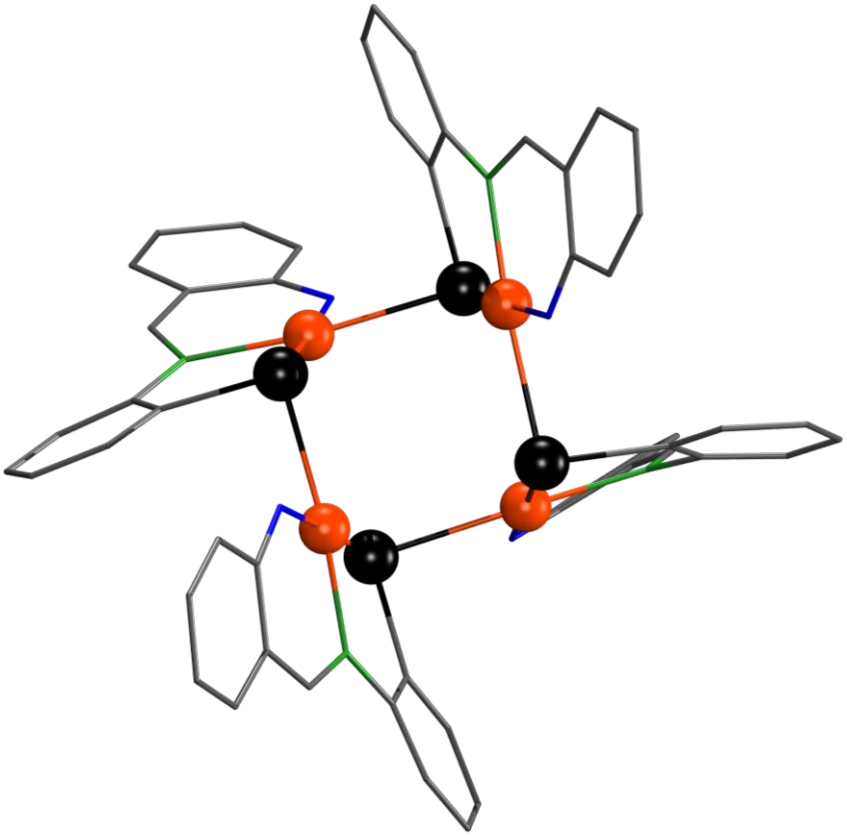

Figure S108. Optimized structure of cuboid-like $[Pd_4(L'^{Te})_4]$ in an implicit CH_2Cl_2 solvent model at the CAM-B3LYP level.

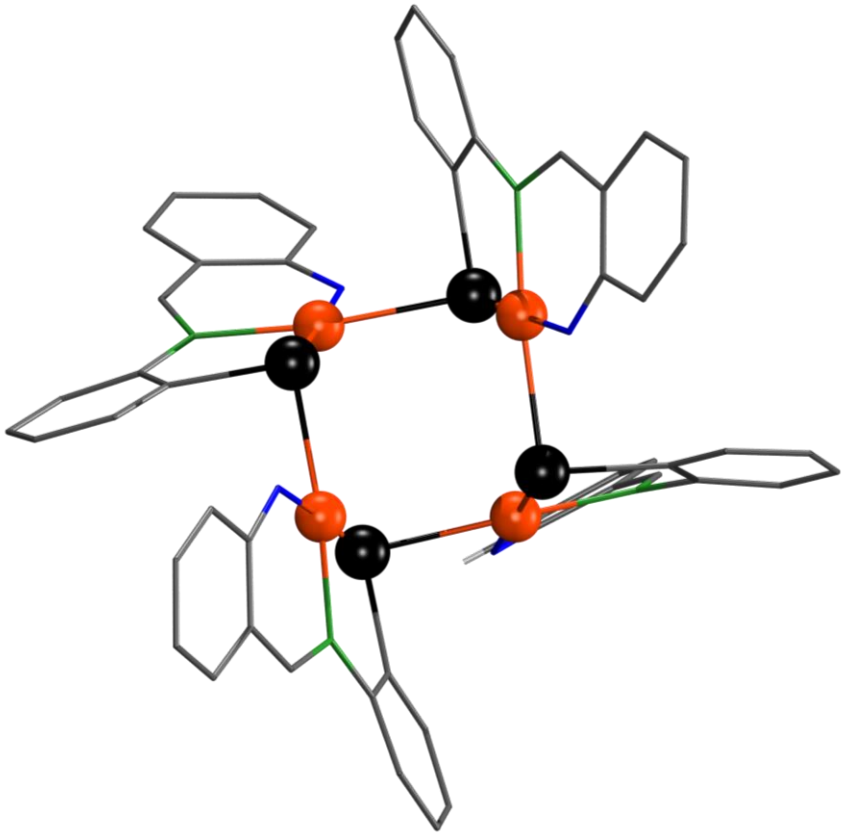

Figure S109. Optimized structure of cuboid-like $[Pd_4(L'^{Te})_4]$ in an implicit EtOH solvent model at the B3LYP level.

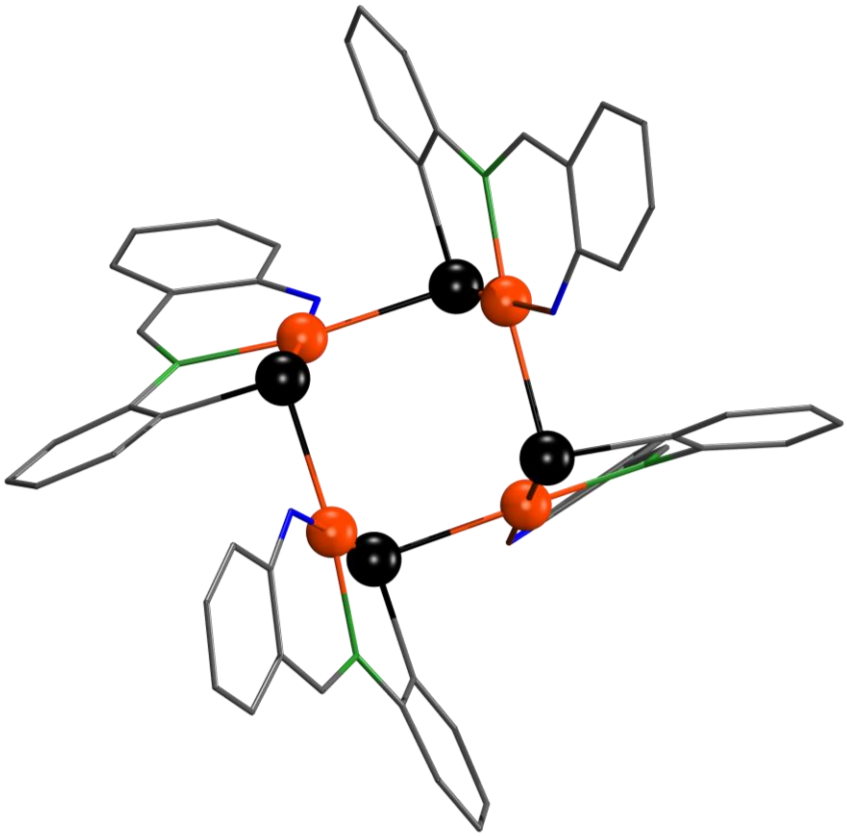

Figure S110. Optimized structure of cuboid-like $[Pd_4(L'^{Te})_4]$ at the B3LYP level in the gas phase.

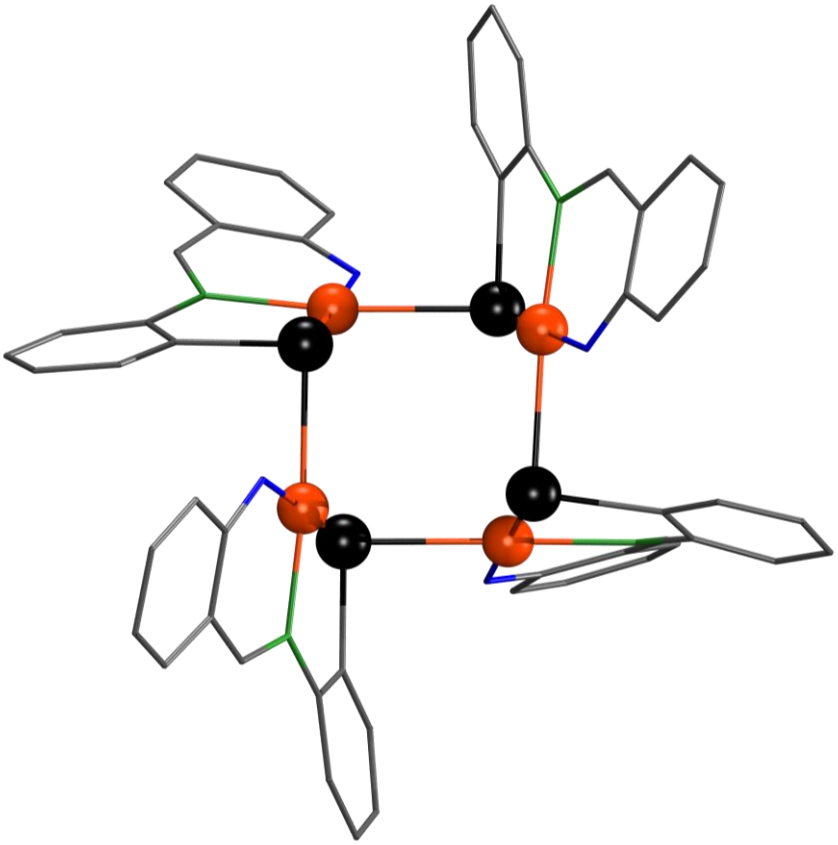

Figure S111. Optimized structure of gyrobifastigial $[Pd_4(L'^{Te})_4]$ in an implicit CH_2Cl_2 solvent model at the B3LYP level.

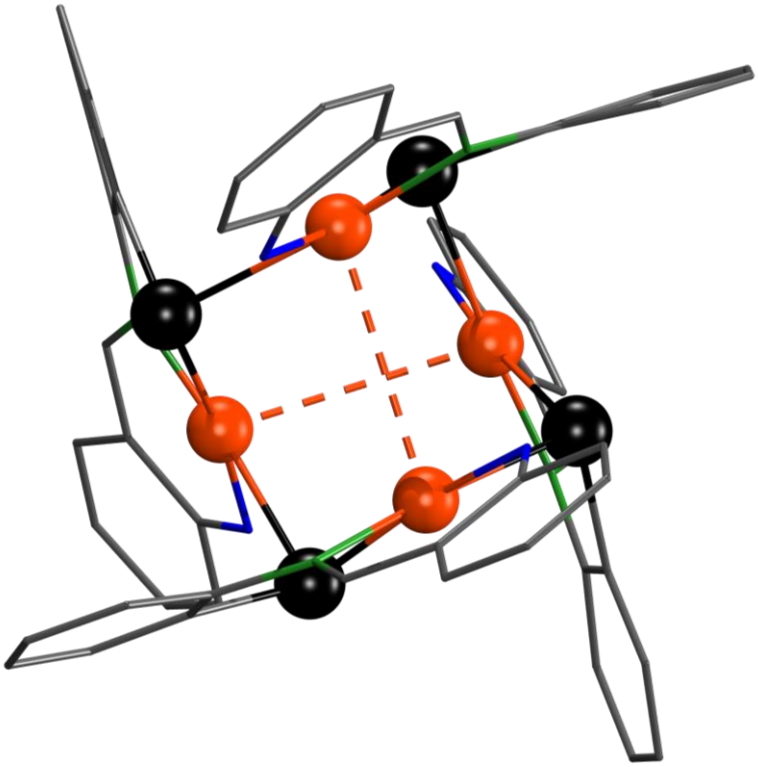

Figure S112. Optimized structure of gyrobifastigial $[Pd_4(L'^{Te})_4]$ in an implicit CH_2Cl_2 solvent model at the CAM-B3LYP level.

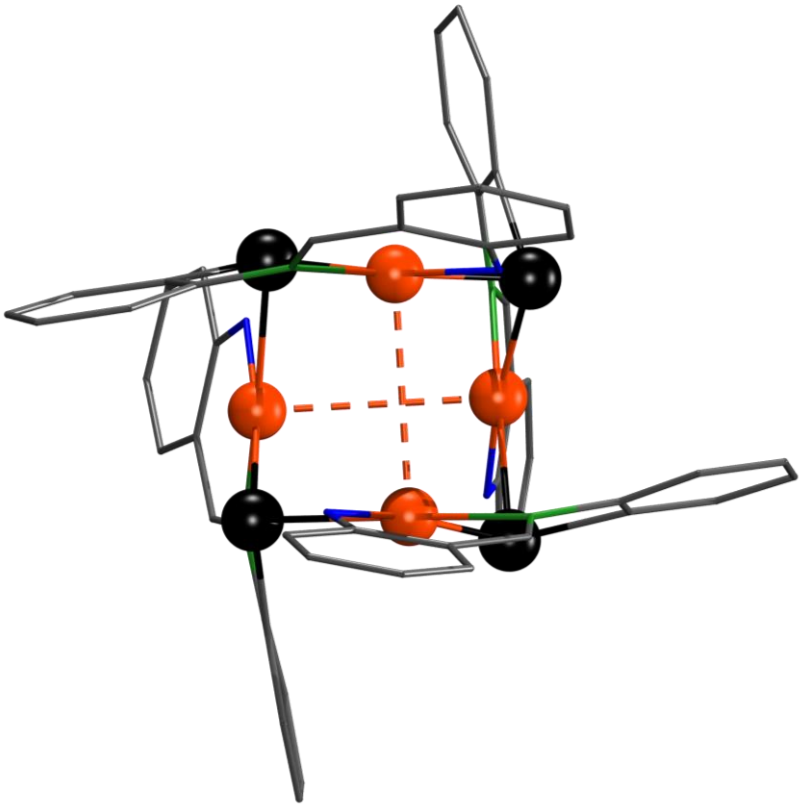

Figure S113. Optimized structure of gyrobifastigial $[Pd_4(L'^{Te})_4]$ in an implicit EtOH solvent model at the B3LYP level.

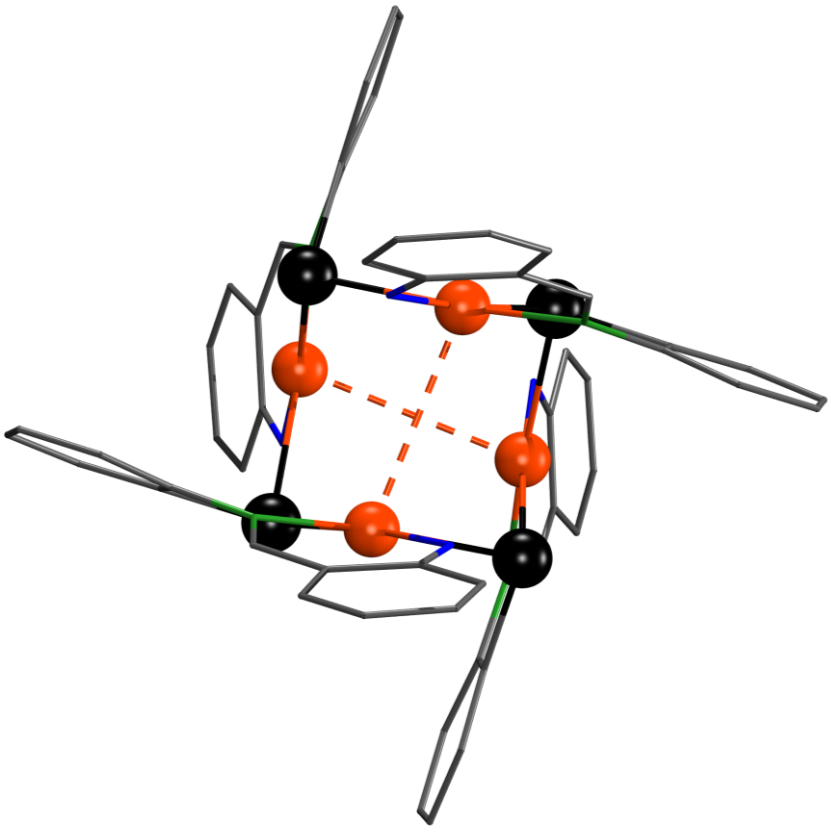

Part 4: Previous studies

Chart S1. Reference work on structurally characterized metal complexes containing salicylidene Schiff' base-substituted dichalcogenide ligands. Only complexes with disulfide ligands have previously been prepared. Softer metaion ions such as Ni^{II}, Mn^{II} and Fe^{III} form complexes with coordinated disulfide units,[1-9] while hard metal ions such as Ti^{IV} and V^{V} avoid the coordination by the disulfide unit.[10,11] Especially the metal ions with higher valency were found to cleave the disulfide moiety more often under formation of thiolato complexes.[10,11] Generally, the complexes show complex redox behavior that is attributed to the non-innocence of the ligands.[1,3,7,9-11] Furthermore, the nickel disulfide complexes showed an interesting and selective supramolecular sensing of the highly toxic wood preservatives chlorpyrifos and phosmet through increased fluorescence emission by the mono- and dimeric complexes respectively down to nanomolar concentrations of the toxin.[1,3]

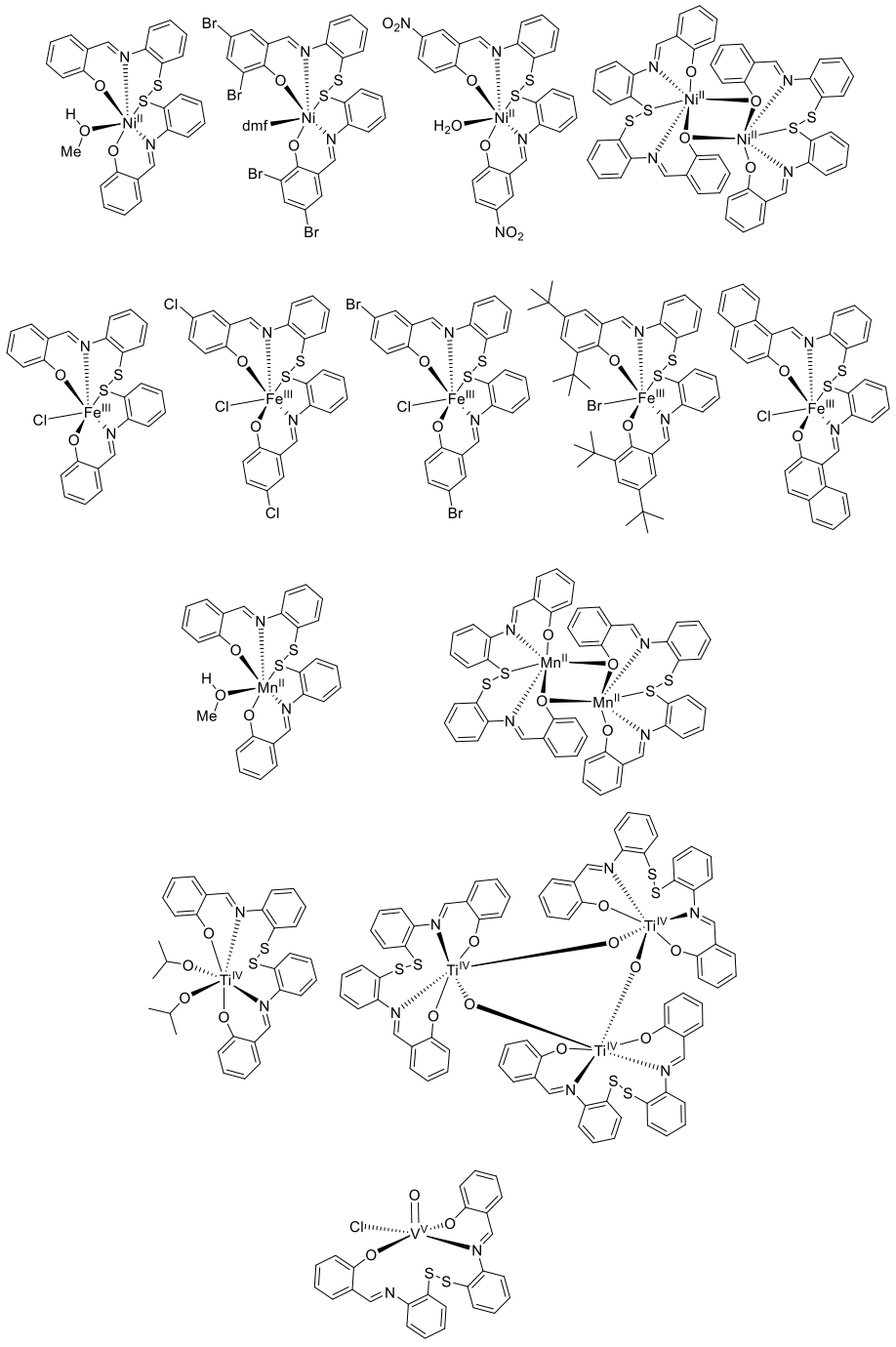

Part 5: References

1 Manzur, C.; Bustos, C.; Schrebler, R.; Carrillo, D.; Knobler, C. B.; Gouzerh, P.; Jeannin, Y. Synthesis, characterization and electrochemistry of nickel(II) complexes of Schiff base ligands containing a disulphide group. Crystal structure of [Ni{(*o*-$OC_6H_4CH{=}NC_6H_4)_2S_2$}(MeOH)]·MeOH. *Polyhedron*, **1989**, *8*(*18*), 2321-2330.

2 Cambridge Structural Database, Release 5.42, Update May **2021**: Xia, J.-H.; Liu, Z.; Jin, L.-X. *Wuji Huaxue Xuebao (Chin.) (Chin. J. Inorg. Chem.)* **2008**, *24*, 823.

3 Raj, P.; Singh, A.; Kaur, K.; Aree, T.; Singh, A.; Singh, N. Fluorescent Chemosensors for Selective and Sensitive Detection of Phosmet/Chlorpyrifos with Octahedral Ni^{2+} Complexes. *Inorg. Chem.* **2016**, *55*, 4874−4883.

4 Bertrand, J. A.; Breece, J. L. Preparation and Structure of Chloro(bis{salicylideniminephenyl}disulfido)iron(III). *Inorg. Chim. Acta* **1974**, *8*, 267-272.

5 Elmali, A.; Elerman, Y. Crystal Structure of Chloro(bis{5-chlorosalicylideniminephenyl}disulfido)iron(III) Complex. *Anal. Sci*. **2001**, *17*, 1137-1138.

6 Elmali, A.; Elerman, Y. Crystal Structure of Chloro(bis{5-bromosalicylideniminephenyl}disulfido)iron(III) Complex. *Anal. Sci*. **2002**, *18*, 1399-1400.

7 Roy, N.; Sproules, S.; Weyhermüller, T.; Wieghardt, K. Trivalent Iron and Ruthenium Complexes with a Redox Noninnocent (2-Mercaptophenylimino)-methyl-4,6-di-*tert*-butylphenolate(2-) Ligand. *Inorg. Chem*. **2009**, *48*, 3783-3791.

8 Elmali, A.; Elerman, Y.; Svoboda, I. {Bis[2-(2-oxido-1-naphthylmethylideneamino)phenyl] disulfide}chloroiron(III). *Acta Cryst. C* **2001**, *57*, 375-376.

9 Kessissoglou, D. P.; Butler, W. M.; Pecoraro, V. L. Characterization of Mono- and Binuciear Manganese(II) Schiff Base Complexes with Metal-Disulfide Ligation. *Inorg. Chem.* **1987**, *26*, 495-503.

10 Donzelli, A.; Metushi, I.; Potvin, P. G. Titanium(IV) Complexes of Disulfide-Linked Schiff Bases. *Inorg. Chem.* **2012**, *51*, 5138−5145.

11 Wang, D.; Behrens, A.; Farahbakhsh, M.; Gätjens, J.; Rehder, D. Formation, Preservation, and Cleavage of the Disulfide Bond by Vanadium. *Chem. Eur. J*. **2003**, *9*, 1805-1813.

A.11 Large Telluroxane Bowls Connected by a Layer of Iodine Ions

Authors	L. Kirsten, J. Fonseca Rodrigues, A. Hagenbach, A. Springer, N. R. Pineda, P. C. Piquini, M. Roca Jungfer, E. Schulz Lang, U. Abram
Journal	*Angew. Chem. Int. Ed.* **2021**, 60, *28*, 15517–15523
DOI	10.1002/anie.202103700 10.1002/ange.202103700
Link	https://onlinelibrary.wiley.com/doi/full/10.1002/anie.202103700
Detailed scientific contribution	Lars Kirsten, Ulrich Abram and Ernesto Schulz Lang designed the project. Lars Kirsten and Jessica Fonseca Rodrigues performed the synthesis and characterization of the compounds. Andreas Springer measured, simulated and interpreted the mass spectral data. Adelheid Hagenbach, Ulrich Abram and Jessica Fonseca Rodrigues calculated the X-ray structures. Maximilian Roca Jungfer, Nahum Ramirez Pineda and Paulo Cesar Piquini performed DFT calculations on the large telluroxane bowls. Ulrich Abram and Jessica Fonseca Rodrigues wrote the manuscript. Maximilian Roca Jungfer, Adelheid Hagenbach, Andreas Springer, Ernesto Schulz Lang and Ulrich Abram corrected the manuscript. Ernesto Schulz Lang and Ulrich Abram supervised the project, provided scientific guidance and suggestions and corrected the manuscript.
Estimated own contribution	25%

Return to publication 4.11.

Angewandte Chemie
Eine Zeitschrift der Gesellschaft Deutscher Chemiker

Supporting Information

Large Telluroxane Bowls Connected by a Layer of Iodine Ions

Lars Kirsten, Jessica Fonseca Rodrigues, Adelheid Hagenbach, Andreas Springer, Nahum R. Pineda, Paulo C. Piquini, Maximilian Roca Jungfer, Ernesto Schulz Lang, and Ulrich Abram**

anie_202103700_sm_miscellaneous_information.pdf

Supporting Information

Table of Contents

SUPPORTING INFORMATION

1. Experimental Procedures

Chemicals.
All chemicals were purchased commercially and used without further purification. Solvents were dried by standard methods. 3-(phenyltellanyl)propylamine, *N*-{3-(phenyltellanyl)propyl}picolinamide and Ph_2Te_2 were prepared according to literature procedures.[1,2]

Analytical and spectroscopic methods.
Elemental analyses were determined with an Heraeus Vario El III elemental analyser.
IR spectra between 4000 and 400 cm^{-1} were recorded on Shimadzu or ATR Nicolet iS10 Smart spectrometers. IR spectra in the range between 700 and 100 cm^{-1} were recorded on a Nexus 670 (Nicolet) instrument.
NMR spectra were recorded on a 400 MHz JEOL spectrometer. $SiMe_4$ and $TeMe_2$ were used as external standards.
All mass spectrometric experiments have been carried out on a Synapt G2-S HDMS system equipped with a Z-Spray ESI source (Waters Co., Milford, MA, USA).

Syntheses.
[(py)⊂{$(PhTe)_{19}O_{24}$}$_2I_{18}$] (**1a**): *N*-{3-(Phenyltellanyl)propyl}picolinamide (92 mg, 0.25 mmol) was dissolved in 5 ml CH_2Cl_2 and I_2 (63 mg, 0.25 mmol) in 10 ml CH_2Cl_2 was added. The resulting yellow-brown solution was stirred at room temperature for 10 min. The solvent was removed in vacuum. The residue was re-dissolved in a mixture of 5 ml CH_2Cl_2 and 5 ml MeOH and left on air for evaporation to dryness. Recrystallization from a CH_2Cl_2/$CHCl_3$/MeOH (v/v/v 3/8/3) mixture gave red-brown blocks. It is important to use the given solvent mixture and to perform the crystallization on air. Yield: 60 mg (84%). Elemental analysis: Calcd for $C_{233}H_{195}NO_{48}Te_{38}I_{18}$: C, 25.65; H, 1.80; N, 0.13%; Found: C, 25.21; H, 2.34; N, 0.96%. IR (cm^{-1}): 3044 (w), 1458 (m), 1431 (m), 1155 (w), 1090 (w), 1049 (w), 991 (w), 908 (m), 729 (s), 679 (s), 474 (m), 455 (w), 444 (w).

[{$(PhTe)_{19}O_{24}$}$_2I_{18}$] (**1b**): Method 1: Diphenylditellurid (82 mg, 0.2 mmol) was dissolved in 15 ml of CH_2Cl_2, a solution of iodine (48 mg, 0.19 mmol) in 15 ml of MeOH and 5 drops of water were added. After heating the mixture on reflux for 2 h, the solvents were removed in vacuum and the remaining brown solid was recrystallized from a mixture of CH_2Cl_2/$CHCl_3$/MeOH (v/v/v: 3/8/3) giving red-brown hexagons. Yield: 54 mg (47%).
Method 2: 3-(Phenyltellanyl)propylammonium hydrochloride (66 mg, 0.22 mmol) was dissolved in 3 ml of MeOH. A solution of iodine (64 mg, 0.25 mmol) in 5 ml of CH_2Cl_2 was slowly added. The resulting orange- red reaction mixture was stirred at room temperature for 30 min and evaporated to dryness. The remaining residue was recrystallized twice from CH_2Cl_2/$CHCl_3$/MeOH (v/v/v: 3/8/3) by slow evaporation on air. Yield: 64 mg (90%).
Elemental analysis: Calcd for $C_{228}H_{190}O_{48}Te_{38}I_{18}$: C, 25.28; H, 1.77%, Found: C, 25.54; H, 1.81%. IR (cm^{-1}): 3049 (w), 1476 (w), 1435 (m), 1180 (w), 1155 (w), 1055 (w), 1018 (w), 997(w), 912 (w), 733 (s), 685 (s), 664 (s), 619 (s), 603 (s), 474 (m), 459 (m), 386 (m), 315 (m), 283 (m), 245 (m) 195 (m), 139 (m). Raman (cm^{-1}): 3057 (w), 1574 (w), 1476 (w), 1183 (w), 1156 (w), 1018 (w), 998 (m), 733 (w), 700 (w), 659 (m), 612 (w), 461 (w), 434 (w), 407 (w), 282 (w), 250 (m), 173 (s), 150 (s). ^{1}H-NMR ($CDCl_3$; δ, ppm): 6.55 – 6.63 (m, 14H), 6.98 – 7.07 (m, 14H), 7.17 – 7.27 (m, 9H), 7.30 – 7.38 (m, 17H), 7.41 – 7.47 (m, 38H), 7.52 (dd, J = 5.7, 3.3 Hz, 38H), 7.54 – 7.59 (m, 8H), 7.69 (dd, J = 5.7, 3.3 Hz, 33H), 8.12 (dt, J = 8.5, 1.7 Hz, 19H, Ph). (+)-ESI MS data are presented separately in Chapter 3 of this Supporting Information.

[(MeOH)⊂{$(PhTe)_{19}O_{24}$}$_2I_{18}$] (**1c**): Diphenylditellurid (82 mg, 0.2 mmol) was suspended in 15 ml of MeOH and treated with a solution of iodine (48 mg, 0.19 mmol) in 15 ml of MeOH. After 5 min, 5 drops of water were added and the mixture was heated under reflux for 2 h. The solvent was evaporated to dryness. The remaining brown solid was recrystallized from a mixture of $CHCl_3$/MeOH (v/v: 3/4) giving red-brown hexagons. Yield: 54 mg (47%). Elemental analysis: Calcd for $C_{229}H_{194}O_{49}Te_{38}I_{18}$: C, 25.32; H, 1.80%. Found: C, 24.49; H, 1.95%. IR (cm^{-1}): 3048 (w), 1472 (m), 1435 (m), 1383 (w), 1196 (w), 1109 (w), 1055 (w), 991(m), 818 (w), 735 (s), 685 (s), 665 (s), 617 (s), 463 (m).

[{$(PhTe)_{18}O_{24}$}$_2${$Ca(H_2O)_2$}$_2I_{16}$] (**2**): Iodine (50 mg, 0.2 mmol) was dissolved in 15 ml of MeOH and added dropwise to a stirred solution of diphenylditellurid (82 mg, 0.2 mmol) in 15 ml of CH_2Cl_2. The resulting dark solution was stirred for 1 h at room temperature. The reaction mixture was charged on a CaO (50 g) filled frit (pore 2) and eluated with MeOH. The resulting orange yellow solution was brought to dryness. The solid residue was recrystallized from a mixture of CH_2Cl_2/$CHCl_3$/MeOH (v/v/v: 3/8/3) giving colorless hexagons. Yield: 19 mg (17%). Elemental analysis: Calcd for $C_{216}H_{188}O_{52}Ca_2Te_{36}I_{16}$: C, 25.14; H, 1.84%. Found: C, 25.01; H, 1.88%. IR (cm^{-1}): 3420 (w), 3049 (w), 1611 (w), 1574 (w), 1476 (m), 1435 (m), 1383 (w), 1329 (w), 1304 (w), 1269 (w), 1182 (w), 1155 (w), 1092 (w), 1059 (m), 1018 (w), 997 (w), 912 (w), 735 (s), 671 (s), 610 (s), 478 (s), 459 (m), 313 (m), 285 (m), 214 (m), 173 (m). Raman (cm^{-1}): 3057 (w), 1574 (w), 1477 (w), 1183 (w), 1157 (w), 1057 (w), 1018 (w), 998 (s), 740 (w), 705 (w), 685 (m), 661 (w), 643 (w), 612 (w), 462 (w), 410 (m), 340 (w), 282 (w), 251 (s), 208 (w), 161 (m), 110 (s). ^{1}H NMR ($CDCl_3$; δ, ppm): 1.55 (s, 8H, OH), 6.45 – 6.55 (m, 36H), 6.60 – 6.73 (m, 54H), 6.80 (t, J = 6.9 Hz, 10H), 6.93 – 7.04 (m, 18H), 7.09 – 7.15 (m, 12H), 7.43 (d, J = 8.0 Hz, 18H), 7.47 – 7.60 (m, 15H), 7.64 – 7.92 (m, 14H), 7.96 – 8.10 (m, 3H, Ph). (+)-ESI MS data are presented separately in Chapter 3 of this Supporting Information.

SUPPORTING INFORMATION

[{(PhTe)$_{18}$O$_{24}$}$_2${Y(NO$_3$)(H$_2$O)}$_2$I$_{16}$] (**3**): Diphenylditelluride (41 mg, 0.1 mmol) was dissolved in 5 ml of CH_2Cl_2 and iodine (25 mg, 0.1 mmol) in 5 ml of methanol was added dropwise. The resulting brownish solution was stirred for 30 minutes at room temperature and then Y(NO$_3$)$_3$·6H$_2$O (38 mg, 0.1 mmol) was added. There were no apparent changes in the color. The mixture was stirred for 3 hours and the solution was filtered over celite and dioxane (2 ml) was added for crystallization. After three days, yellow crystals were obtained. Yield: 27 mg (46%). Elemental analysis: Calcd for $C_{216}H_{184}O_{56}N_2I_{16}Te_{36}Y_2$: C, 24.69; H, 1.77; N, 0.27%. Found: C, 24.85; H, 1.91; N, 0.20%.IR (cm $^{-1}$): 3424 (s), 3050 (w), 1639 (w), 1618 (w), 1476 (w), 1434 (w), 1384 (w), 1056 (w), 997 (w), 734 (s), 685 (s), 664 (s), 617 (m), 480 (m). (+)-ESI MS data are presented separately in Chapter 3 of this Supporting Information.

[{(PhTe)$_{18}$O$_{24}$}$_2${La(NO$_3$)(H$_2$O)}$_2$I$_{16}$] (**4**): The synthesis was performed as described for compound **3** with La(NO$_3$)$_3$·6H$_2$O. Crystallization was achieved from the mother solution after addition of 2 ml of dioxane. Dark yellow crystals. Yield: 60%. Elemental analysis: Calcd for $C_{216}H_{184}O_{56}N_2I_{16}La_2Te_{36}$: C, 24.61; H, 1.76; N, 0.27%. Found: C, 24.49; H, 1.91; N, 0.24%. IR (cm^{-1}): 3453 (s), 3050 (w), 1631 (w), 1476 (w), 1434 (w), 1384 (w), 1268 (w), 1057 (w), 1018 (w), 997 (w), 734 (s), 685 (s), 662 (s), 608 (m), 479 (m), 457 (m).

[{(PhTe)$_{18}$O$_{24}$}$_2${Eu(NO$_3$)(H$_2$O)}$_2$I$_{16}$] (**5**): The synthesis was performed as described for compound **3** with Eu(NO$_3$)$_3$·5H$_2$O. Crystallization was achieved from the mother solution after addition of 2 ml of dioxane. Dark yellow crystals. Yield: 46%. Elemental analysis: Calcd for $C_{216}H_{184}O_{56}N_2Eu_2I_{16}Te_{36}$: C, 24.55; H, 1.76; N, 0.27%. Found: C, 25.08; H, 1.96; N, 0.27%. IR (cm^{-1}): 3450 (m), 3050 (w), 1634 (w), 1507 (w), 1476 (w), 1434 (w), 1384 (w), 1273 (w), 1057 (w), 997 (w), 734 (s), 685 (s), 665 (s), 609 (m), 481 (m), 458 (m).

[{(PhTe)$_{18}$O$_{24}$}$_2${Lu(NO$_3$)(H$_2$O)}$_2$I$_{16}$] (**6):** The synthesis was performed as described for compound **3** with Lu(NO$_3$)$_3$·xH$_2$O. Crystallization was achieved from the mother solution after addition of 2 ml of dioxane. Only a few orange red crystals of sufficient purity could be isolated. Yield: 6%. Elemental analysis: Calcd for $C_{216}H_{184}O_{56}N_2I_{16}Lu_2Te_{36}$: C, 24.44; H, 1.75; N, 0.26%. Found: C, 24.49; H, 1.90; N, 0.18%. IR (cm^{-1}): 3050 (w), 1574 (w), 1519 (w),1476 (w), 1434 (m), 1277 (w), 1182 (w), 1156 (w), 1056 (w), 1056 (m), 1018 (w), 998 (m), 914 (w), 730 (s), 659 (s), 598 (s).

2. X-Ray Crystallography

X-Ray diffraction studies have been performed with a STOE IPDS T2 or a BRUKER APEX-II CCD with Mo Kα radiation; λ = 0.71073 Å. Structure solution and refinement was done with the SHELX program package.[3]
Diffuse solvent molecules are contained in the voids between the large cluster molecules. They have been treated with the SQUEEZE option of the program PLATON.[4] Alternatively, an assignment of solvent molecules was undertaken as far as possible. However, only a small part of the diffuse electron density could be assigned unambiguously in this way. But it became obvious that the use of the SQUEEZE program had practically no influence on the bonding parameters inside the cluster molecules. For this reason, the structural discussion have been done with the more reliable data sets obtained with this option.

X-Ray crystal structure determination of [(py)⊂{(PhTe)$_{19}$O$_{24}$}$_2$I$_{18}$] (1a): Crystals suitable for X-ray diffraction were obtained by crystallization from a CH_2Cl_2/$CHCl_3$/MeOH (v/v/v: 3/8/3) mixture. Crystallographic data: $C_{233}H_{195}I_{18}NO_{48}Te_{38}$; FW = 10909.89 g/mol; 0.24x022x0.20 mm^3; red-brown block, monoclinic; $P2_1/c$; a = 22.197(1) Å, b = 40.283(1) Å, c = 39.115(2) Å; α = 90°, β = 98.85(1)°, γ = 90°; V = 34559(3) Å^3; Z = 4; Dx = 2.079 g cm^{-3}; μ = 4.810 mm^{-1}. 223632 reflections were measured by using STOE IPDS 2T at a temperature of 200 K. 38536 reflections were unique (R_{int} = 0.0801). Absorption correction with XRED32: T_{max} = 0.4409, T_{min} = 0.2598.[5] Non-hydrogen atoms were refined by using anisotropic displacement parameters. The positions of the hydrogen atoms were calculated for idealized positions. 2875 parameters were refined with 243 restraints. R1 = 0.051 for 38536 reflections with I > 2σ(I) and wR2 = 0.1449 for 73170 reflections, S = 0.732. Residual electron density was between -2.577 and 6.276 eÅ^{-3}. CCDC 1938245 contains the supplementary crystallographic data for this paper. These data can be obtained free of charge from The Cambridge Crystallographic Data Centre via www.ccdc.cam.ac.uk/data_request/cif.

X-Ray crystal structure determination of [{(PhTe)$_{19}$O$_{24}$}$_2$I$_{18}$] (1b): Crystals suitable for X-ray diffraction were obtained by crystallization from a CH_2Cl_2/$CHCl_3$/MeOH (v/v/v: 3/8/3) mixture. Crystallographic data: $C_{228}H_{190}I_{18}NO_{48}Te_{38}$; FW = 10830.79 g/mol; 0.24x022x0.20 mm^3; red-brown block, monoclinic; $P2_1/c$; a = 22.227(1) Å, b = 40.261(1) Å, c = 39.109(1) Å; α = 90°, β = 98.77(1)°, γ = 90°; V = 34589(2) Å^3; Z = 4; Dx = 2.080 g cm^{-3}; μ = 4.805 mm^{-1}. 184186 reflections were measured by using STOE IPDS 2T at a temperature of 200 K. 38536 reflections were unique (R_{int} = 0.094). Absorption correction with XRED32: T_{max} = 0.5873, T_{min} = 0.3594.[5] Non-hydrogen atoms were refined by using anisotropic displacement parameters. The positions of the hydrogen atoms were calculated for idealized positions. 2869 parameters were refined with 411 restraints. R1 = 0.0553 for 26922 reflections with I > 2σ(I) and wR2 = 0.1138 for 60762 reflections, S = 0.770. Residual electron density was between -3.276 and 4.133 eÅ^{-3}. CCDC 1938247 contains the supplementary crystallographic data for this paper. These data can be obtained free of charge from The Cambridge Crystallographic Data Centre via www.ccdc.cam.ac.uk/data_request/cif.

X-Ray crystal structure determination of [(0.5 MeOH)⊂{(PhTe)$_{19}$O$_{24}$}$_2$I$_{18}$] (1c): Crystals suitable for X-ray diffraction were obtained by crystallization from a CH_2Cl_2/$CHCl_3$/MeOH (v/v/v: 3/8/3) mixture. Crystallographic data: $C_{228.5}H_{192}I_{18}NO_{48.5}Te_{38}$; FW = 10846.81 g/mol; 0.28x027x0.10 mm^3; yellow-brown block, monoclinic; $P2_1/c$; a = 22.275(1) Å, b = 40.448(1) Å, c = 39.324(2) Å; α = 90°, β = 99.24(1)°, γ = 90°; V = 39970(2) Å^3; Z = 4; Dx = 2.060 g cm^{-3}; μ = 4.753 mm^{-1}. 225528 reflections were measured by using STOE IPDS 2T at a temperature of 200 K. 74115 reflections were unique (R_{int} = 0.0754). Absorption correction with XRED32: T_{max} = 0.4493, T_{min} = 0.2139.[5] Non-hydrogen atoms were refined by using anisotropic displacement parameters. The positions of the hydrogen atoms were calculated for idealized positions. 2926 parameters were refined with 232 restraints. R1 = 0.0452 for 36297 reflections with I > 2σ(I) and wR2 = 0.0988 for 74115 reflections, S = 0.677. Residual electron density was between -3.811 and 3.755 eÅ^{-3}. CCDC 1938244 contains the supplementary crystallographic data for this paper. These data can be obtained free of charge from The Cambridge Crystallographic Data Centre via www.ccdc.cam.ac.uk/data_request/cif.

X-Ray crystal structure determination of [{(PhTe)$_{19}$O$_{24}$}$_2${Ca(H$_2$O)$_2$}I$_{16}$] (2): Crystals suitable for X-ray diffraction were obtained by crystallization from a CH_2Cl_2/$CHCl_3$/MeOH (v/v/v: 3/8/3) mixture. Crystallographic data: $C_{216}H_{180}Ca_2I_{16}NO_{52}Te_{36}$; FW = 10311.75 g/mol; 0.12x012x0.06 mm^3; colorless octahedron, tetragonal; $P4_22_12$; a = 26.020(1) Å, b = 26.020(1) Å, c = 23.737(2) Å; α = 90°, β = 90°, γ = 90°; V = 16070(2) Å^3; Z = 2; Dx = 2.131 g cm^{-3}; μ = 4.832 mm^{-1}. 58630 reflections were measured by using STOE IPDS 2T at a temperature of 200 K. 14138 reflections were unique (R_{int} = 0.1177). Absorption correction with XRED32: T_{max} = 0.7721, T_{min} = 0.5794.[5] Non-hydrogen atoms were refined by using anisotropic displacement parameters. The positions of the hydrogen atoms were calculated for idealized positions. 575 parameters were refined with 486 restraints. R1 = 0.0592 for 9200 reflections with I > 2σ(I) and wR2 = 0.1451 for 14138 reflections, S = 0.809. Residual electron density was between -1.517 and 3.080 eÅ^{-3}. CCDC 1938246 contains the supplementary crystallographic data for this paper. These data can be obtained free of charge from The Cambridge Crystallographic Data Centre via www.ccdc.cam.ac.uk/data_request/cif.

X-Ray crystal structure determination of [{(PhTe)$_{19}$O$_{24}$}$_2${Y(NO$_3$)$_2$}$_2$I$_{16}$] (3): Crystals suitable for X-ray diffraction were obtained by crystallization from a CH_2Cl_2/MeOH/dioxane mixture. Crystallographic data: $C_{216}H_{180}I_{16}N_2O_{56}Te_{38}Y_2$, FW = 10501.43 g/mol; 0.2x02x0.2 mm^3; yellow block, monoclinic; $P2_1/n$; a = 22.761(5) Å, b = 39.189(4) Å, c = 37.811(4) Å; α = 90°, β = 91.01(1)°, γ = 90°;

SUPPORTING INFORMATION

V = 33722(9) $Å^3$; Z = 4; D_x = 2.068 g cm^{-3}; μ = 4.917 mm^{-1}. 808488 reflections were measured by using Bruker APEX-II CCD at a temperature of 120 K. 103852 reflections were unique (R_{int} = 0.099). Absorption correction with SADABS: T_{max} = 0.0988, T_{min} = 0.0431.[6] Non-hydrogen atoms were refined by using anisotropic displacement parameters. The positions of the hydrogen atoms were calculated for idealized positions. 2047 parameters were refined with 18 restraints. R1 = 0.0510 for 60821 reflections with I > 2σ(I) and wR2 = 0.1856 for 103852 reflections, S = 1.009. Residual electron density was between -5.028 and 4.976 $eÅ^{-3}$. CCDC 1938243 contains the supplementary crystallographic data for this paper. These data can be obtained free of charge from The Cambridge Crystallographic Data Centre via www.ccdc.cam.ac.uk/data_request/cif.

3. Mass Spectrometry

3.1. General Considerations

All experiments have been carried out on a Synapt G2-S HDMS system equipped with a Z-Spray ESI source (Waters Co., Milford, MA, USA). To allow accumulation of mass spectra over a longer period, a 11plus syringe pump (Harvard Apparatus, MA, USA) as well as gas-tight microliter syringes (100 or 250 µL, by Hamilton Bonaduz AG, Switzerland or Trajan Scientific and Medical, Australia) have been used.

Following solvents and chemicals have been used during the experiments: water and 2-propanol from ULC/MS – CC/SFC (Biosolve BV, Netherlands); dichloromethane: optigrade for HPLC and chloroform: picograde for residue analysis (both from LGC Standards GmbH, Germany); sodium iodide, ≥99.99% trace metal basis (Sigma-Aldrich Chemie GmbH, Germany).

Calibration procedure and general remarks on the measurements: Concentrations of approx. 1 mg/mL in dichloromethane (compounds **1b**, **2**) or chloroform (**3**) were injected into the instrument with a flow rate of 10 µL/min, allowing accumulation of mass spectra over a couple of minutes to compensate low intensities.
For external calibration, 2 mg/mL NaI in 1:1 2-propanol/water (m/z range 400 to 8,000) was used. External calibration was performed within 24 h of analysis. No internal calibration was possible since the low signal intensity as well as the wide isotopic pattern leading to overlaps as well as multiple charge states led to severe issues when performing the Automated Peak Detection/Lock Mass Correction. External calibration resulted - also affected by the low intensities in the single mass spectra - in a mass accuracy of about 10 ppm at a resolution (FWHM) of about 20,000 ("Res Mode"), although the isotopic pattern of the single chemical formulae partially overlap widely. The overlap can be deducted from lowered resolution, wider isotopic pattern and/or shoulders of the isotopic pattern, allowing assignment of e.g. the addition or loss of water. Please note that in all spectra the mass error is systematic, i.e., all experimental m/z values are shifted to higher (compounds **1b** and **2**) or lower (compound **3**) m/z than the calculated. Thus, the mass precision is higher than the absolute m/z error indicate since the variance is small.

Remarks on simulations and comparison of the experimental and calculated mass spectra
For data analysis, MassLynx vs. 4.1 SCN 941 (Waters Co., MA, USA) was used. Unfortunately, the software simplifies mass spectrometry too much: For any charge, it adds the mass of a hydrogen atom for each positive charge and subtracts it for each negative charge. Since for metal-organic compounds a positive charge is derived from anion stripping, this false, additional hydrogen must be subtracted when submitting the chemical composition for simulation. The software also reduces the number of peaks by cutting low abundant peaks and the sides of the isotopic distributions. This leads to significantly too narrow calculated isotopic patterns. Nevertheless, the maximum peaks of this extremely wide distributions are matching well to other simulations with a different software in terms of m/z value and peak height, typically with a mass difference of about 1 ppm between the simulations for this kind of complexes, which can mostly be attributed to not taking the electron mass into account in case of simulations by MassLynx. The alternative software used was the "Exact Mass Calculator" (Ver. 9.0.23) by Varian, Inc., now Agilent Technologies, CA, USA. One example of such an alternative simulation is given in Fig. S1.

Exact Mass Calculator (Ver 9.0.23)
Varian, Inc.

Base Formula: C228 H190 O48 I15 Te38 +3
Plus Adducts:
Minus Fragment Losses:
Isotopic Enrichment: C228H190O48I15Te38+
Monoisotopic m/z: 3511.74817
Monoisotopic Mass: 10535.24450
Average MW: 10450.41474

Calculated Isotope Distribution
Mass Resolving Power: 20,000

Peak	Mass	Rel. Abun.
A+246	3467.05778	0.19
A+247	3467.39123	0.24
A+248	3467.72471	0.30
A+249	3468.05816	0.38
A+250	3468.39164	0.48
A+251	3468.72510	0.60
A+252	3469.05857	0.75
A+253	3469.39204	0.92
A+254	3469.72551	1.14
A+255	3470.05898	1.39
A+256	3470.39245	1.70
A+257	3470.72592	2.07
A+258	3471.05939	2.50
A+259	3471.39287	3.01
A+260	3471.72633	3.61
A+261	3472.05982	4.31
A+262	3472.39328	5.12
A+263	3472.72678	6.06
A+264	3473.06024	7.13
A+265	3473.39374	8.36
A+266	3473.72720	9.74
A+267	3474.06082	11.30
A+268	3474.39416	13.06
A+269	3474.72779	15.02
A+270	3475.06112	17.19
A+271	3475.39476	19.57
A+272	3475.72809	22.19
A+273	3476.06174	25.03
A+274	3476.39507	28.10
A+275	3476.72871	31.39
A+276	3477.06205	34.90
A+277	3477.39569	38.61
A+278	3477.72903	42.50
A+279	3478.06267	46.57
A+280	3478.39614	50.78
A+281	3478.72966	55.06
A+282	3479.06313	59.43
A+283	3479.39665	63.79
A+284	3479.73013	68.17
A+285	3480.06364	72.43
A+286	3480.39712	76.60
A+287	3480.73064	80.55
A+288	3481.06413	84.31
A+289	3481.39764	87.74
A+290	3481.73113	90.87
A+291	3482.06464	93.56
A+292	3482.39814	95.87
A+293	3482.73165	97.66
A+294	3483.06515	98.99
A+295	3483.39866	99.75
A+296	3483.73217	100.00
A+297	3484.06567	99.65
A+298	3484.39919	98.79
A+299	3484.73269	97.34
A+300	3485.06622	95.42
A+301	3485.39972	92.95
A+302	3485.73325	90.07
A+303	3486.06675	86.72
A+304	3486.40029	83.05
A+305	3486.73379	79.02
A+306	3487.06746	74.75
A+307	3487.40083	70.30
A+308	3487.73450	65.70
A+309	3488.06787	61.03
A+310	3488.40156	56.33
A+311	3488.73493	51.67
A+312	3489.06861	47.10
A+313	3489.40199	42.65
A+314	3489.73567	38.38
A+315	3490.06905	34.29
A+316	3490.40274	30.46
A+317	3490.73625	26.87
A+318	3491.06980	23.53
A+319	3491.40333	20.47
A+320	3491.73688	17.68
A+321	3492.07041	15.17
A+322	3492.40396	12.92
A+323	3492.73749	10.92
A+324	3493.07104	9.17
A+325	3493.40459	7.64
A+326	3493.73813	6.31
A+327	3494.07169	5.18
A+328	3494.40523	4.22
A+329	3494.73879	3.41
A+330	3495.07234	2.73
A+331	3495.40590	2.17
A+332	3495.73945	1.71
A+333	3496.07302	1.34
A+334	3496.40657	1.04
A+335	3496.74015	0.80
A+336	3497.07369	0.61
A+337	3497.40729	0.46
A+338	3497.74083	0.34
A+339	3498.07456	0.25
A+340	3498.40798	0.19

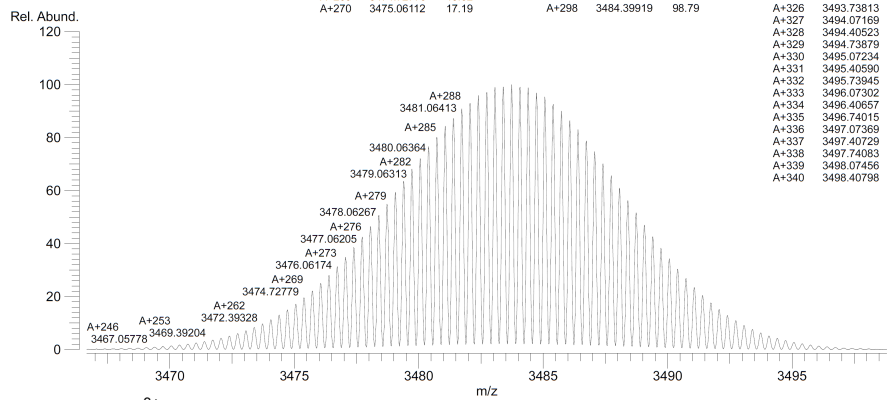

Fig. S1. Simulation of the $[M-3I]^{3+}$ of compound **1b**, $[\{(PhTe)_{19}O_{24}\}_2I_{18}]$, using the "Exact Mass Calculator", showing the capability of the software to depict a wider isotopic pattern as well as to simulate at different theoretical resolutions. For data analysis, we set the resolution to 30,000 as default.

3.2. Mass spectra of compound 1b, [{(PhTe)$_{19}$O$_{24}$}2I$_{18}$]

Original Data File Name:
00060_Kirsten_lk44b_CH2Cl2_a.raw

Experimental Settings:

Polarity	ES+
Capillary (kV)	3.3000
Source Temperature (°C)	80
Sampling Cone	40.0000
Source Offset	80.0000
Desolvation Temperature (°C)	250
Desolvation Gas Flow (L/Hr)	500.0
Nebuliser Gas Flow (Bar)	6.0

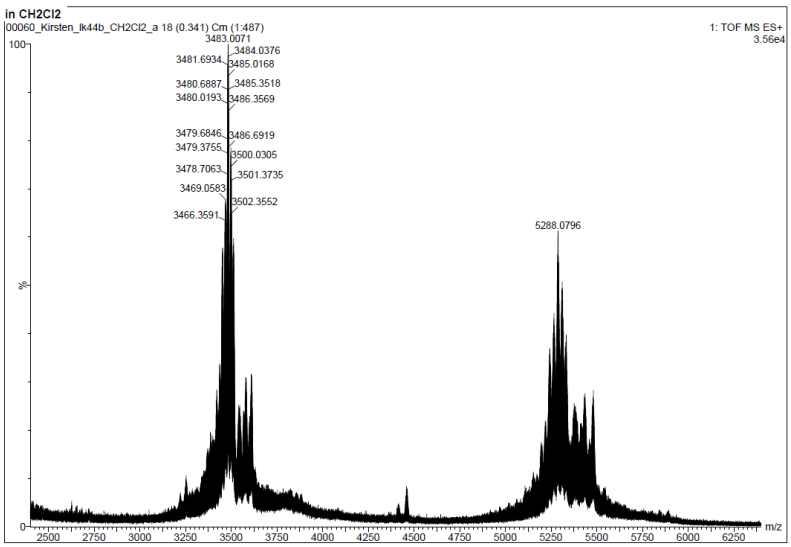

Fig. S2. (+)-ESI MS of compound **1b**, m/z range 2400 to 6400.

Fig. S2 shows the mass spectrum of the ions derived from the intact compound **1b**. At lower m/z, fragments of the compound have been detected, which show isotopic patterns characteristic for Te-containing compounds. The m/z range 3200 up to 3800 is characterized by triply charged species, while the corresponding doubly charged species are seen between m/z 5000 and 5550.
To rationalize the data evaluation, simulations of the chemical formulae are compared with the data derived experimentally (see also Overlays of simulated and experimental mass spectra are shown in Fig. 2 (main article, triply charged ions) and Fig. S3 (doubly charged ions). Table 1 (main article) and Table S1 summarize some assignments and comparisons of the calculated and experimental isotopic pattern depicted in Fig. 2 and Fig. S3 as well as other signals assigned for compound **1b**. Detailed illustrations of the experimental and simulated mass meaks are given in Fig. S4 and Fig. S5.
The given values correspond to the peaks with maximum abundance of the isotopic pattern as calculated by the MassLynx Vs. 4.1 SCN 941 software. While all major peak groups have been assigned, some additional peaks like the peaks between m/z 4300 and 4500 have not been assigned. Generally, they lack in intensity, resolution and do widely overlap each other.

Table S1: Comparison of experimental and calculated isotopic patterns of doubly charged ions in the (+) ESI MS of compound **1b**.

Ion	Chemical Formula	m/z$_{exp}$	m/z$_{calc}$	Δm/z (ppm)
$[M-2I]^{2+}$	$(C_{228}H_{190}O_{48}I_{16}Te_{38})^{2+}$	5288.556	5288.551	0.9
$[M-3I+Br]^{2+}$	$(C_{228}H_{190}O_{48}I_{15}Te_{38}Br)^{2+}$	5265.596	5265.558	7.2
$[M-3I+Cl]^{2+}$	$(C_{228}H_{190}O_{48}I_{14}Te_{38}Cl)^{2+}$	5243.097	5243.083	2.7
$[M-4I+2Br]^{2+}$	$(C_{228}H_{190}O_{48}I_{14}Te_{38}Br_2)^{2+}$	5241.580	5241.564	3.1
$[M-4I+Br+Cl]^{2+}$	$(C_{228}H_{190}O_{48}I_{14}Te_{38}BrCl)^{2+}$	5219.606	5219.589	3.2
$[M-5I+2Br+Cl]^{2+}$	$(C_{228}H_{190}O_{48}I_{13}Te_{38}Br_2Cl)^{2+}$	5196.073	5196.096	4.4
$[M-2I+H+Br]^{2+}$	$(C_{228}H_{191}O_{48}I_{16}Te_{38}Br)^{2+}$	5329.047	5329.014	6.2
$[M-2I+(CH_2Cl_2)]^{2+}$	$(C_{229}H_{192}O_{48}I_{16}Te_{38}Cl_2)^{2+}$	5308.034	5308.035	-0.2
$[M-3I+Br+(CH_2Cl_2)]^{2+}$	$(C_{229}H_{192}O_{48}I_{15}Te_{38}BrCl_2)^{2+}$	5331.533	5331.527	1.12

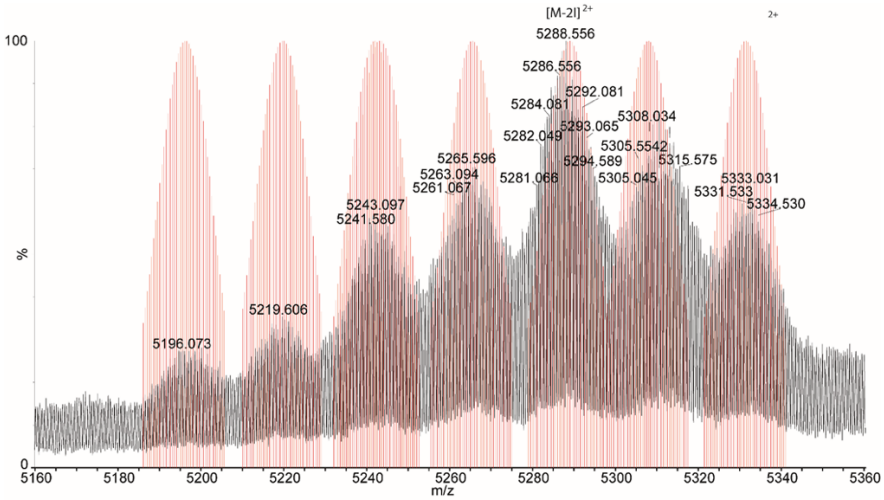

Fig S3. Region of doubly charged ions in the (+)ESI MS of compound **1b**, red: simulations, black: experimental data.

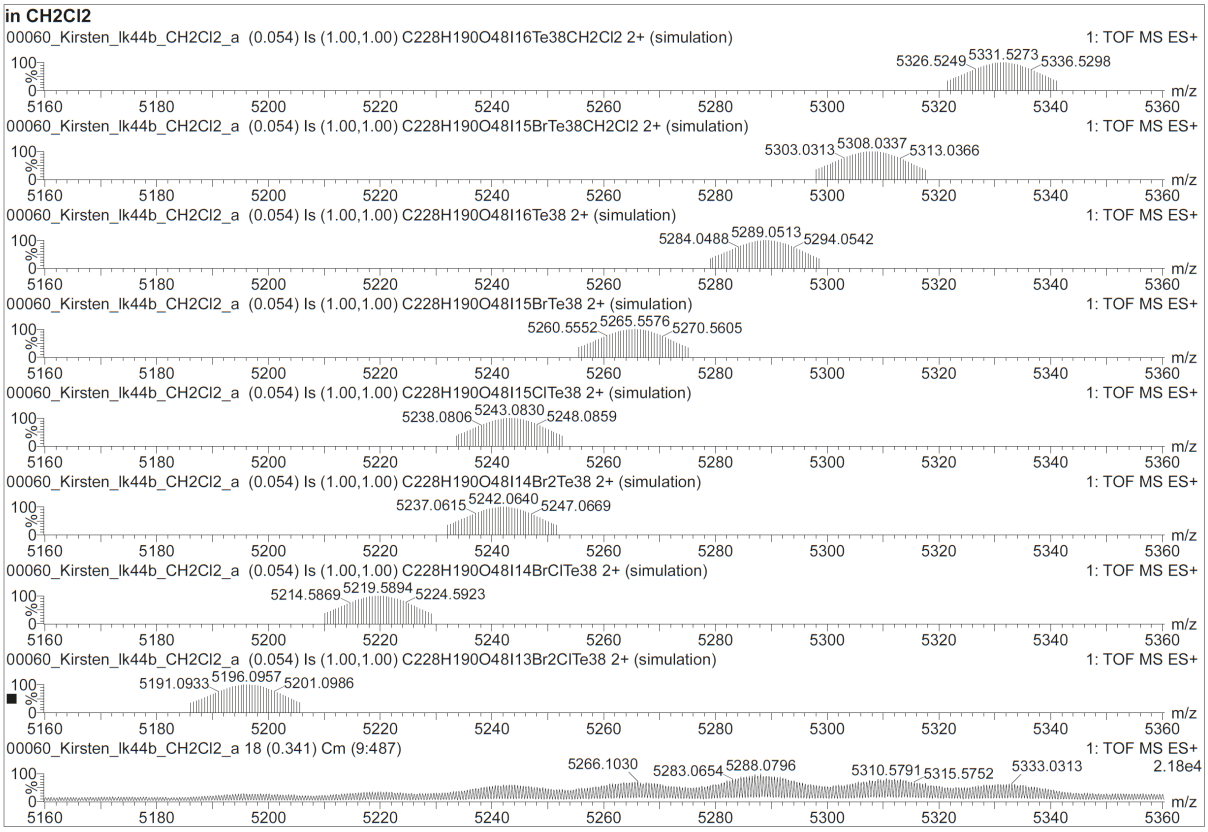

Fig. S4. Doubly charged ions of compound **1b** (simulations: top rows, experimental: bottom row).

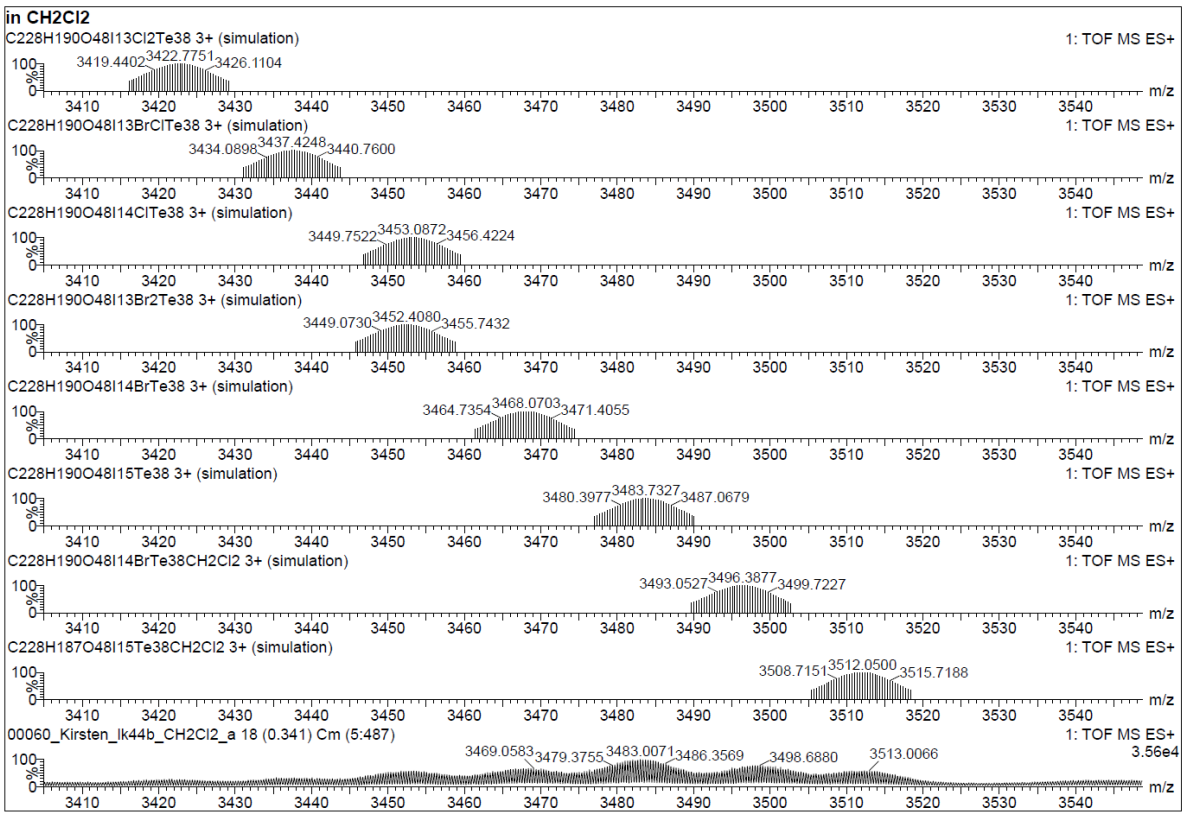

Fig. S5. Triply charged ions of compound **1b** (simulations: top rows, experimental: bottom row).

3.2. Mass spectra of compound 2, [{(PhTe)$_{18}${Ca(H$_2$O)$_2$}O$_{24}$}$_2$I$_{16}$]

Original Data File Name: 00101_Kirsten_CaBu_CH2Cl2_a.raw

Experimental Settings:

Polarity	ES+
Capillary (kV)	3.3000
Source Temperature (°C)	90
Sampling Cone	40.0000
Source Offset	80.0000
Desolvation Temperature (°C)	250
Desolvation Gas Flow (L/Hr)	500.0

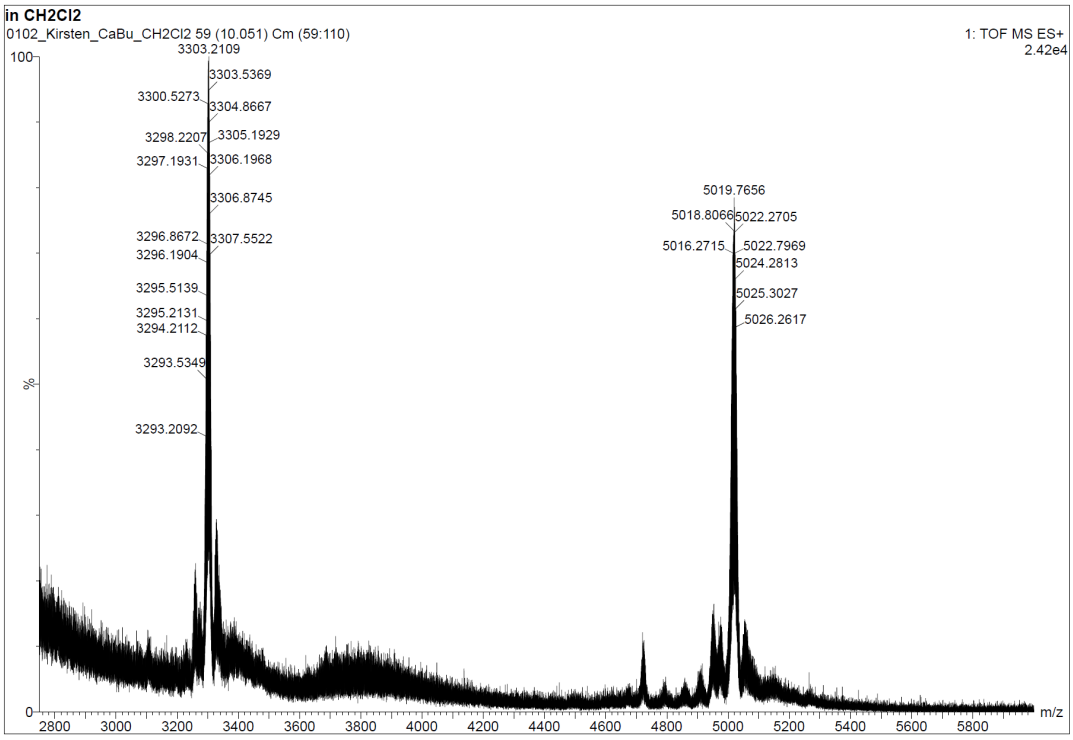

Fig. S6. (+)-ESI MS of compound **2**, m/z range 2750 to 6000.

Figure S6 shows the mass spectrum of the ions derived from the intact compound **2**. At lower m/z, the mass spectrum is dominated by organic impurities, e.g. with the plasticizer [Diisooctylphtalate+Na]$^+$, e.g. m/z 413.23. Just minor amounts of low mass Te-containing ions have been found. Nevertheless, peaks at m/z 1951, 4722 and broad areas of chemical noise (around m/z 2500 and 3800) might indicate partial decomposition in solution. The isotopic patterns caused by ions of the intact compound **2** are found in the m/z range 3220 to 3350 (triply charged species), while the corresponding doubly charged species are seen between m/z 4900 and 5100. Data evaluation was performed as described before. The wide isotopic pattern of the experimentally derived data seemingly is caused by loss of water moieties weakly bound to the Ca atoms, and once again one solvent molecule (dichloromethane) can fill the inner void of the cluster. Also, a minor amount of I$^-$ atoms is seemingly replaced by Cl- ions coming from the non-stabilized solvent, presumably containing traces of HCl.
A comparison of the experimental and calculated m/z values of assigned ions is found in Table S2, and comparisons of the assigned peaks with the simulated ones is presented in Fig. S7 (doubly charged ions) and Fig. S8 (triply charged ions).

Table S2. Comparison of the calculated and experimental isotopic pattern of compound **2**.

Ion	Chemical Formula	m/z$_{exp}$	m/z$_{calc}$	Δm/z (ppm)
[M-2I-2H$_2$O+CH$_2$Cl$_2$]$^{2+}$	(C$_{217}$H$_{186}$O$_{50}$Ca$_2$I$_{14}$Te$_{36}$Cl$_2$)$^{2+}$	5057.658	5057.651	1.4
[M-2I-H$_2$O]$^{2+}$	(C$_{216}$H$_{186}$O$_{51}$Ca$_2$I$_{14}$Te$_{36}$)$^{2+}$	5024.653	5024.681	-5.6
[M-2I-2H$_2$O]$^{2+}$	(C$_{216}$H$_{184}$O$_{50}$Ca$_2$I$_{14}$Te$_{36}$)$^{2+}$	5015.154	5015.176	4.4
[M-2I-3H$_2$O]$^{2+}$	(C$_{216}$H$_{182}$O$_{49}$Ca$_2$I$_{14}$Te$_{36}$)$^{2+}$	5006.230	5006.170	12.0
[M-3I-H$_2$O+Cl]$^{2+}$	(C$_{216}$H$_{186}$O$_{51}$Ca$_2$I$_{13}$Te$_{36}$Cl)$^{2+}$	4978.258	4978.212	9.2
[M-3I-2H$_2$O+Cl]$^{2+}$	(C$_{216}$H$_{184}$O$_{49}$Ca$_2$I$_{13}$Te$_{36}$Cl)$^{2+}$	4969.239	4968.208	6.2
[M-3I-2H$_2$O+CH$_2$Cl$_2$]$^{3+}$	(C$_{217}$H$_{186}$O$_{50}$Ca$_2$I$_{13}$Te$_{36}$Cl$_2$)$^{3+}$	3329.800	3329.830	9.0
[M-3I-H$_2$O]$^{3+}$	(C$_{216}$H$_{186}$O$_{51}$Ca$_2$I$_{13}$Te$_{36}$)$^{3+}$	3307.201	3307.152	14.8
[M-3I-2H$_2$O]$^{3+}$	(C$_{216}$H$_{184}$O$_{50}$Ca$_2$I$_{13}$Te$_{36}$)$^{3+}$	3301.530	3301.482	14.6
[M-4I-H$_2$O+Cl]$^{3+}$	(C$_{216}$H$_{186}$O$_{51}$Ca$_2$I$_{12}$Te$_{36}$Cl)$^{3+}$	3278.523	32878.515	2.4

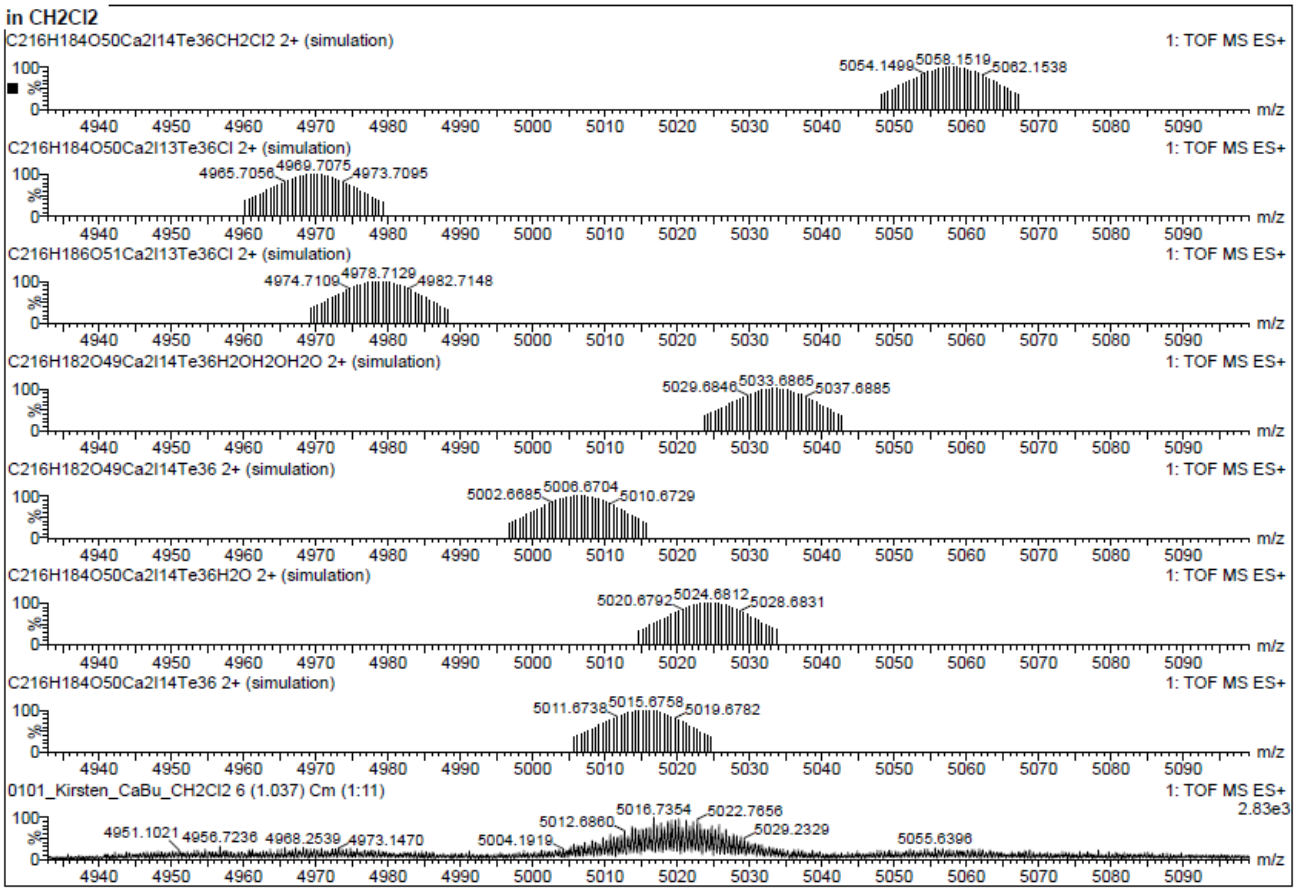

Fig. S7. Region of doubly charged ions in the (+)-ESI MS of compound **2**, top rows: simulations, bottom row: experimental data.

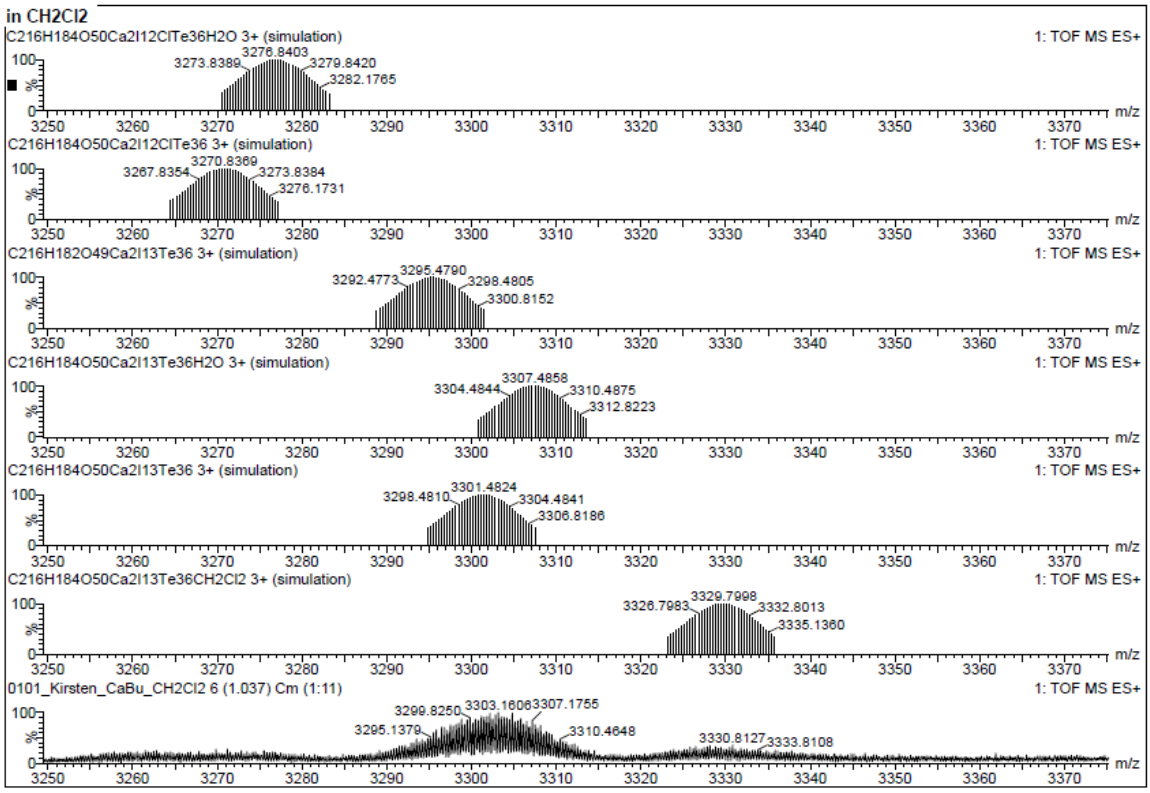

Fig. S8. Region of triply charged ions in the (+)-ESI MS pf compound 2, top rows: simulations, bottom row: experimental data.

3.3. Mass spectra of compound 3, $[\{(PhTe)_{18}\{Y(NO_3)(H_2O)\}O_{24}\}_2I_{16}]$

Original Data File Name: 1910_AR023_0166JF_2.raw

Experimental Settings:

Polarity	ES+
Capillary (kV)	3.3000
Source Temperature (°C)	100
Sampling Cone	40.0000
Source Offset	80.0000
Desolvation Temperature (°C)	280
Desolvation Gas Flow (L/Hr)	500.0

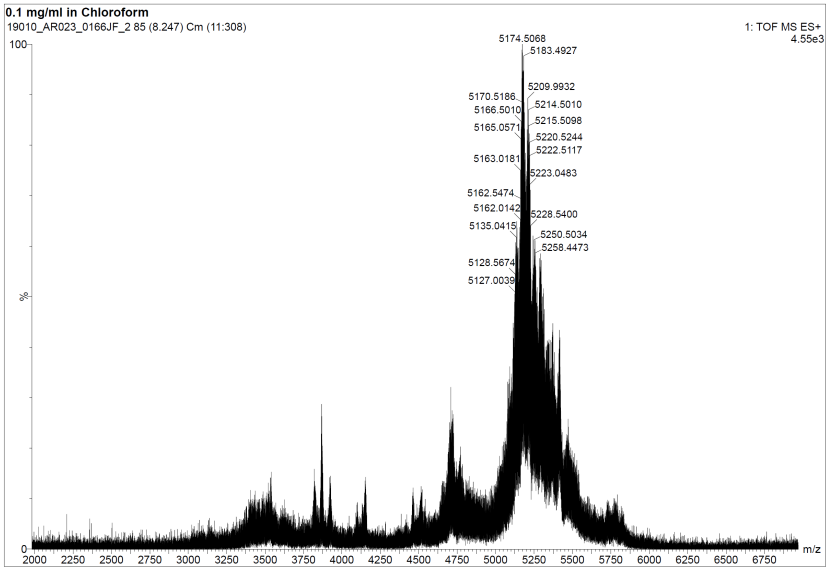

Fig. S9. (+)-ESI MS of compound **3**, m/z range 2000 to 6800.

Figure S9 shows the mass spectrum of the ions derived from the intact compound **3**. At lower m/z, the mass spectrum is dominated by organic impurities and small amounts of peaks with isotopic patterns typical for tellurium. Peak groups at m/z 410, 991, 1073 and 1473 as well as badly resolved peak distributions between m/z 3300 and 3700 indicate partial fragmentation and/or decomposition. The isotopic patterns caused by ions of the intact compound **3** are found between m/z 3350 and 3550 (triply charged species). All signals are close to noise level and show extensive peak splitting for the accumulated spectra. Since the quality criterion, S/N > 7, for these peaks is not fulfilled, a deeper analysis was not performed. Nevertheless, the corresponding doubly charged species are the peaks dominating the high-mass range of the mass spectrum (between m/z 5100 and 5400). Data evaluation was performed as described before. Note that the solvents used within the experiments do complicate the analysis. Dioxane was used during recrystallization and chloroform to dissolve the sample. Also, the water ligands of the Y^{3+} ions might be lost upon ionization and following collisions while desolvation and transfer to the detector, in total result in very broad isotopic patterns, much wider than what is expected for a "pure" isotopic pattern even for a cluster of that size. A list of the ions which are pointing towards a successful synthesis including experimental and calculated m/z values is found in Table S3, the comparison of the experimental data with simulations are presented in Fig. 10 and Fig. S11.

Table S3. Comparison of the calculated and experimental isotopic pattern of compound **3**.

Ion	Chemical Formula	m/z_{exp}	m/z_{calc}	Δm/z (ppm)
$[M-2I-H_2O]^{2+}$ (peak splitting)	$(C_{216}H_{182}N_2O_{55}I_{14}Te_{36}Y_2)^{2+}$	5117.005, 5117.067	5117.109	20.3, 8.2
$[M-2I]^{2+}$	$(C_{216}H_{184}N_2O_{56}I_{14}Te_{36}Y_2)^{2+}$	5126.066	5126.107	8.0
$[M-3I-H_2O+Cl+CCl_3H]^{2+}$	$(C_{217}H_{183}N_2O_{55}I_{13}Te_{36}Y_2Cl_4)^{2+}$	5131.038	5131.090	-10.5
$[M-3I+Cl+CCl_3H]^{2+}$	$(C_{217}H_{185}N_2O_{56}I_{13}Te_{36}Y_2Cl_4)^{2+}$	5140.080	5140.095	-2.9
$[M-2I-H_2O+C_4H_8O_2]^{2+}$	$(C_{220}H_{190}N_2O_{57}I_{14}Te_{36}Y_2)^{2+}$	5161.073	5161.128	-10.6
$[M-2I+C_4H_8O_2]^{2+}$	$(C_{220}H_{192}N_2O_{58}I_{14}Te_{36}Y_2)^{2+}$	5170.048	5170.133	16.7
$[M-2I-H_2O+CCl_3H]^{2+}$	$(C_{217}H_{183}N_2O_{55}I_{14}Te_{36}Y_2Cl_3)^{2+}$	5177.019	5177.058	7.5
$[M-2I+CCl_3H]^{2+}$	$(C_{217}H_{185}N_2O_{56}I_{14}Te_{36}Y_2Cl_3)^{2+}$	5186.063	5186.070	1.3
$[M-I+H]^{2+}$	$(C_{216}H_{185}N_2O_{56}I_{15}Te_{36}Y_2)^{2+}$	5190.002	5190.063	11.8
$[M-2I-H_2O+2C_4H_8O_2]^{2+}$	$(C_{224}H_{198}N_2O_{61}I_{14}Te_{36}Y_2)^{2+}$	5205. 583	5205. 654	13.6
$[M-2I+2C_4H_8O_2]^{2+}$ (peak splitting)	$(C_{228}H_{200}N_2O_{62}I_{14}Te_{36}Y_2)^{2+}$	5214.501, 5214.564	5214.660	30.5, 18.4
$[M-I-H_2O+H+C_4H_8O_2]^{2+}$ (peak splitting)	$(C_{220}H_{191}N_2O_{57}I_{15}Te_{36}Y_2)^{2+}$	5225.9512, 5226.0146	5226.085	25.6, 13.4
$[M-I+H+C_4H_8O_2]^{2+}$	$(C_{220}H_{193}N_2O_{58}I_{15}Te_{36}Y_2)^{2+}$	5234.034	5234.098	12.2
$[M-I+H+C_4H_8O_2+CCl_3H]^{2+}$	$(C_{221}H_{194}N_2O_{58}I_{15}Te_{36}Y_2Cl_3)^{2+}$	5295.015	5295.053	-7.2
$[M-I+H+C_4H_8O_2+CCl_3H-H_2O]^{2+}$	$(C_{221}H_{192}N_2O_{57}I_{15}Te_{36}Y_2Cl_3)^{2+}$	5286.028	5286.048	-3.8

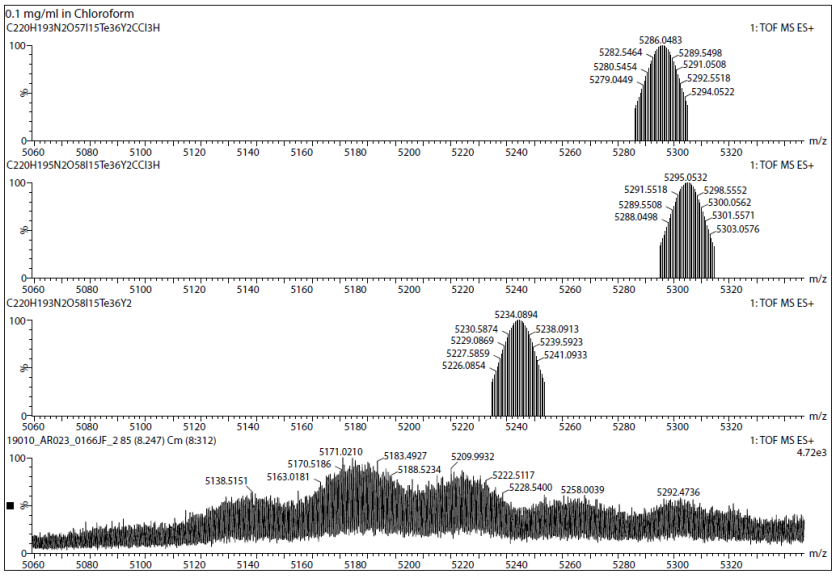

Fig. S10. (+)-ESI-MS of compound **3**, more simulations (top rows) and experimental data (bottom row).

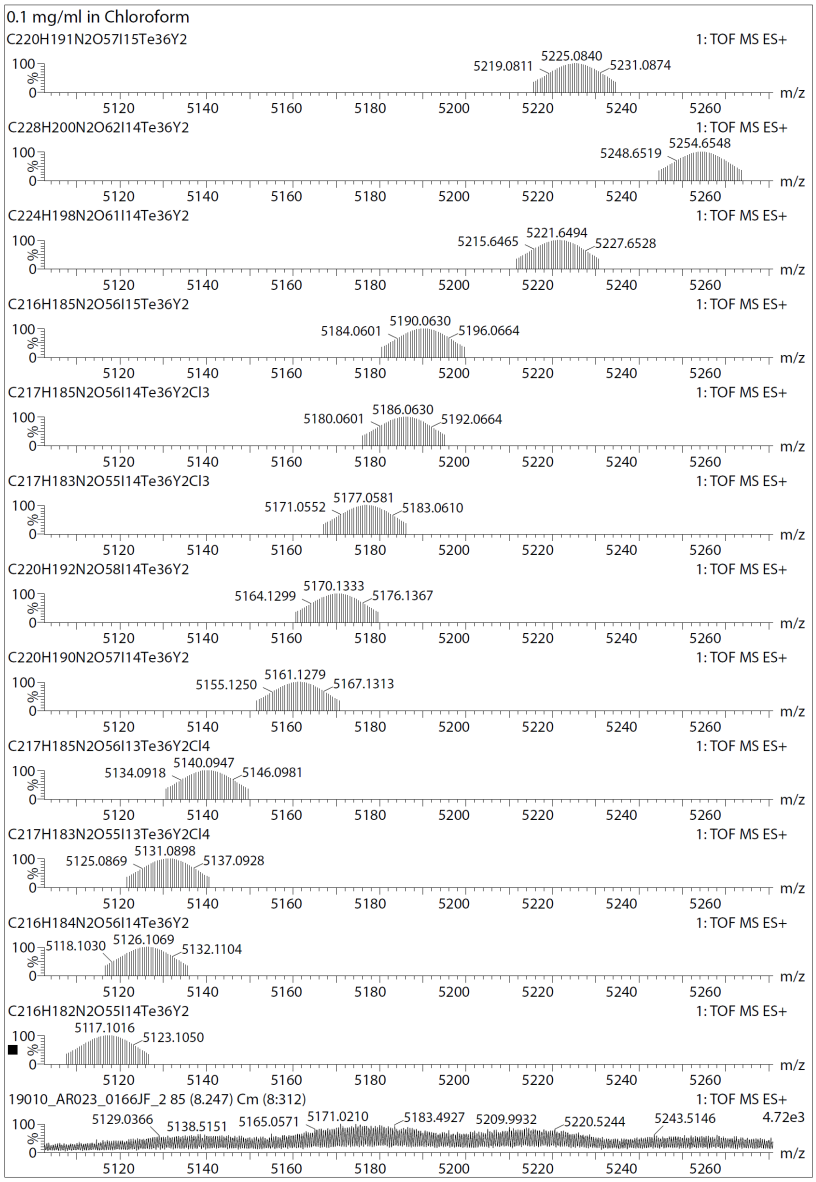

Fig. S11. (+)-ESI MS of compound **3**, simulations (top rows) and experimental data (bottom row).

4. Computational Chemistry

4.1. Computational details

The DFT calculations were performed using Gaussian 16.[7] The initial geometries for the optimizations were derived from the X-ray structures using Avogadro or GaussView.[8,9] The obtained geometries were reoptimized until the absence of imaginary frequencies verifying the true energetic minimum. The light atoms C and H were modelled by simple 3-21G basis functions,[10] while for O, Ca and I LANL2DZ was used.[11-12] For Te the even larger LANL2DZdp was employed.[1,13,14] For Ca, I and Te the corresponding effective core potential was used due to the excessive number of atoms involved in each computation. The basis sets were obtained from the Basis Set Exchange database.[15-17] Natural bond orbitals (NBOs) were obtained by the NBO6.0 implementation and are used in the description of the ground-state HOMO and LUMO orbitals. 40 potential excited states were considered in the following TD-DFT calculations with the same basis sets, however, a frozen noble gas core approximation was required for Ca and was therefore applied to both compounds to keep the results comparable. For $[\{(PhTe)_{19}O_{24}\}2I_{18}]$, the viability of this approach was verified by the non-frozen core calculation, which gave equivalent results. The natural transition orbitals (NTOs) corresponding to the most intense transitions were calculated using Gaussian 16. In all cases, the HOMO orbitals are located in the iodine layer, while the LUMO orbitals are located in the telluroxane hemispheres. The multifunctional wavefunction analyzer MultiWFN was used for topological evaluation and visualization of the electron density (ED), Laplacian and electron localization function (ELF) maps as well as the UV-VIS line spectra.[18] Avogadro was used to visualize the HOMOs and LUMOs of the ground state and those involved in the most intense transitions.[9]

4.2. Topological considerations and general bonding properties in the skeleton of the clusters

The analysis of the interactions of the iodine plane with the two shells of tellurium-oxygen atoms show effective interactions between the iodine and the tellurium atoms of the two telluroxane half-spheres. Figure S5a shows the plane formed by the 18 (12 + 6) iodine atoms and the external ring of tellurium atoms of one of the half-spheres. This ring is not planar. The interactions between the tellurium atoms and the iodine atoms of one of the external rings are represented by red dashed lines, whereas the interactions between the tellurium atoms with the atoms of the internal ring of iodine atoms are drawn as blue dashed lines. For these type of interactions 42 bond critical points (BCP) (3,-1) were found. Hence, each tellurium atom interacts with two iodine atoms of external iodine ring, and one of the internal iodine ring. The topological parameters characterizing these interactions are shown in Table S4. Three additional effective bonds were found for each tellurium atom (see Table S4 and Figure S12c). The Te-C interactions which complete the pseudo-octahedral geometry around the tellurium atoms are not shown.

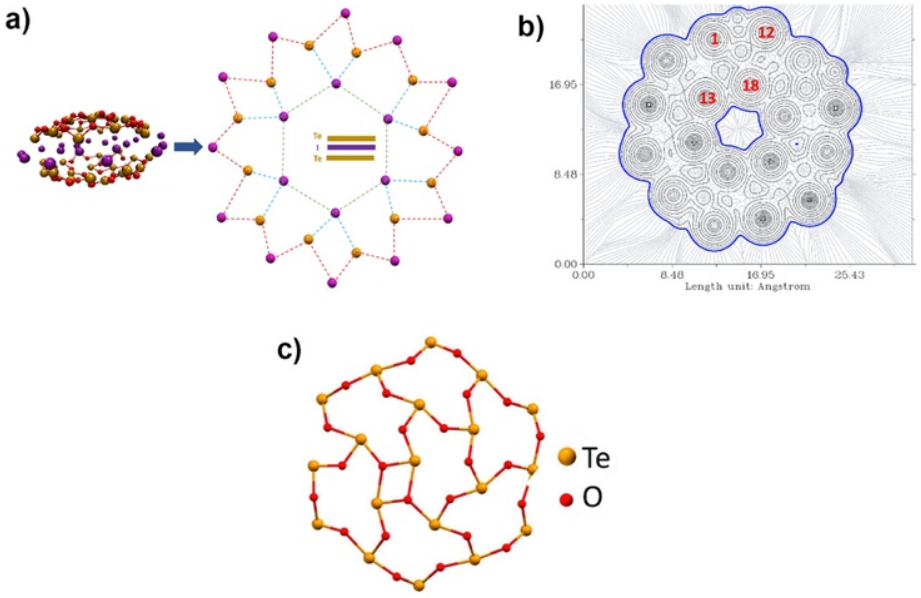

Fig. S12. (a) Scheme of the tellurium-iodine interactions, according to the topological analysis, (b) Electron density map of the plane formed by the iodine atoms, (c) Scheme of the Te-O half-shell according to the topological analysis.

Table S4. Topological parameters.

Contact (CP)	Density	Laplacian	Ellipticity	G(r)	V(r)	H(r)	V/G	E_{int}(kcal)	E_{inter}(KJ)
Te1-I505(23)	0,0276	0,0487	0,0262	0,0126	-0,0141	-0,0015	1,1211	-4,4373	-18,5659
Te1-I516(22)	0,0218	0,0445	0,0362	0,0108	-0,0110	-0,0002	1,0217	-3,4495	-14,4327
Te1-I517(35)	0,0145	0,0303	0,0356	0,0069	-0,0065	0,0004	0,9370	-2,0394	-8,5330
Te15-I514(1)	0,0092	0,0208	0,0662	0,0044	-0,0037	0,0007	0,8329	-1,1492	-4,8081
Te15-I517(24)	0,0153	0,0350	0,0203	0,0079	-0,0073	0,0006	0,9233	-2,2916	-9,5881
Te29-I506(3)	0,0226	0,0453	0,0257	0,0110	-0,0114	-0,0004	1,0355	-3,5879	-15,0119
Te29-I514(2)	0,0192	0,0403	0,0280	0,0095	-0,0093	0,0002	0,9791	-2,9037	-12,1492
Te29-I518(25)	0,0130	0,0283	0,0539	0,0063	-0,0057	0,0006	0,9055	-1,7952	-7,5112
Te42-I507(5)	0,0096	0,0217	0,0731	0,0046	-0,0039	0,0007	0,8469	-1,2308	-5,1495
Te42-I506(4)	0,0033	0,0084	-1,3653	0,0017	-0,0013	0,0004	0,7752	-0,4170	-1,7448
Te42-I518(26)	0,0157	0,0360	0,0432	0,0082	-0,0076	0,0006	0,9285	-2,3762	-9,9421
Te56-I508(7)	0,0208	0,0440	0,0306	0,0105	-0,0105	0,0000	1,0033	-3,3036	-13,8221

Te56-I507(6)	0,0218	0,0466	0,0421	0,0112	-0,0114	-0,0002	1,0154	-3,5656	-14,9186
Te56-I519(27)	0,0150	0,0332	0,0341	0,0076	-0,0070	0,0005	0,9277	-2,1983	-9,1976
Te69-I509(9)	0,0074	0,0170	0,1261	0,0035	-0,0029	0,0007	0,8093	-0,8987	-3,7600
Te69-I508(8)	0,0035	0,0087	-1,4934	0,0018	-0,0014	0,0004	0,7726	-0,4263	-1,7835
Te69-I519(28)	0,0143	0,0338	0,0236	0,0075	-0,0068	0,0007	0,9034	-2,1314	-8,9176
Te83-I510(11)	0,0210	0,0433	0,0259	0,0104	-0,0105	-0,0001	1,0097	-3,2858	-13,7478
Te83-I509(10)	0,0207	0,0439	0,0332	0,0104	-0,0104	0,0000	0,9984	-3,2628	-13,6515
Te83-I520(29)	0,0146	0,0323	0,0289	0,0073	-0,0067	0,0006	0,9234	-2,1162	-8,8542
Te96-I511(13)	0,0123	0,0283	0,0453	0,0062	-0,0055	0,0007	0,8835	-1,7240	-7,2131
Te96-I510(12)	0,0030	0,0076	-1,4065	0,0015	-0,0012	0,0076	0,7741	-0,3735	-1,5626
Te96-I520(30)	0,0141	0,0321	0,0247	0,0071	-0,0065	0,0007	0,9056	-2,0307	-8,4965
Te110-I515(15)	0,0223	0,0434	0,0229	0,0106	-0,0110	-0,0004	1,0381	-3,4642	-14,4944
Te110-I511(14)	0,0264	0,0522	0,0487	0,0133	-0,0145	-0,0012	1,0935	-4,5539	-19,0535
Te110-I521(31)	0,0128	0,0275	0,0512	0,0061	-0,0056	0,0006	0,9041	-1,7429	-7,2923
Te123-I512(17)	0,0085	0,0205	0,1775	0,0043	-0,0036	0,0008	0,8254	-1,1148	-4,6643
Te123-I515(16)	0,0070	0,0165	1,8235	0,0035	-0,0029	0,0006	0,8302	-0,9093	-3,8044
Te123-I521(32)	0,0162	0,0358	0,0130	0,0082	-0,0077	0,0005	0,9376	-2,4045	-10,0604
Te137-I513(19)	0,0170	0,0362	0,0359	0,0084	-0,0082	0,0003	0,9679	-2,5627	-10,7222
Te137-I512(18)	0,0323	0,0543	0,0427	0,0149	-0,0179	-0,0030	1,2019	-5,6150	-23,4932
Te137-I522(33)	0,0136	0,0290	0,0728	0,0066	-0,0060	0,0005	0,9189	-1,8897	-7,9064
Te150-I516(21)	0,0109	0,0257	0,0338	0,0055	-0,0047	0,0008	0,8498	-1,4660	-6,1338
Te150-I513(20)	0,0308	0,0480	0,0402	0,0132	-0,0158	-0,0026	1,2004	-4,9653	-20,7749
Te150-I522(34)	0,0189	0,0398	0,0396	0,0094	-0,0093	0,0001	0,9863	-2,9190	-12,2130
I517-I518(36)	0,0059	0,0137	0,0526	0,0029	-0,0023	0,0005	0,8157	-0,7364	-3,0810
I517-I522(41)	0,0043	0,0094	0,1368	0,0020	-0,0016	0,0004	0,8043	-0,4961	-2,0756
I518-I519(37)	0,0059	0,0136	0,1054	0,0029	-0,0023	0,0005	0,8165	-0,7345	-3,0730
I519-I520(38)	0,0052	0,0117	0,0712	0,0025	-0,0020	0,0005	0,8091	-0,6244	-2,6126
I520-I521(39)	0,0043	0,0095	0,0810	0,0020	-0,0016	0,0004	0,8037	-0,4992	-2,0888
I521-I522(40)	0,0046	0,0103	0,0692	0,0021	-0,0017	0,0004	0,8053	-0,5422	-2,2686
I517-I520(42)	0,0000	0,0094	-0,3929	0,0000	0,0000	0,0000	0,1994	-0,0002	-0,0006

Table S5. Topological parameters for the telluroxane half-shells.

Contact (CP)	Density	Laplacian	Ellipticity	G(r)	V(r)	H(r)	V/G	E_{int}(kcal)	E_{inter}(KJ)
Te1-O2(1)	0,1408	0,5144	0,0074	0,0712	-0,1344	-0,0632	0,1344	-42,1767	-176,4675
Te1-O3(2)	0,0585	0,3972	0,0508	0,0598	-0,1085	-0,0487	0,1085	-34,0363	-142,4080
Te1-C4(3)	0,1155	0,0299	0,0482	0,0246	-0,0796	-0,0550	0,0796	-24,9600	-104,4324
Te15-O2(4)	0,0910	0,2741	0,0143	0,0484	-0,0816	-0,0332	0,0816	-25,6136	-107,1671
Te15-O16(5)	0,0812	0,2260	0,0407	0,0448	-0,0723	-0,0275	0,0723	-22,6706	-94,8539
Te15-O17(6)	0,1422	0,4882	0,0645	0,0662	-0,1309	-0,0647	0,1309	-41,0835	-171,8934
Te15-C18(7)	0,1201	0,0407	0,0630	0,0255	-0,0840	-0,0584	0,0840	-26,3431	-110,2195
Te29-O16(8)	0,1318	0,4640	0,0238	0,0667	-0,1247	-0,0580	0,1247	-39,1150	-163,6570
Te29-O30(9)	0,1360	0,4876	0,0039	0,0681	-0,1284	-0,0603	0,1284	-40,2829	-168,5438
Te29-C31(10)	0,1206	0,0428	0,0742	0,0261	-0,0852	-0,0591	0,0852	-26,7392	-111,8769
Te42-O30(11)	0,0958	0,2998	0,0230	0,0509	-0,0869	-0,0360	0,0869	-27,2592	-114,0527
Te42-O43(12)	0,0801	0,2250	0,0447	0,0449	-0,0716	-0,0268	0,0716	-22,4792	-94,0531
Te42-O44(13)	0,1382	0,4589	0,0660	0,0632	-0,1258	-0,0626	0,1258	-39,4639	-165,1169
Te42-C45(14)	0,1238	0,0455	0,0228	0,0262	-0,0875	-0,0613	0,0875	-27,4610	-114,8970
Te56-O43(15)	0,1354	0,4779	0,0297	0,0678	-0,1281	-0,0603	0,1281	-40,1879	-168,1461
Te56-O57(16)	0,1327	0,4642	0,0108	0,0660	-0,1245	-0,0585	0,1245	-39,0507	-163,3881
Te56-C558(17)	0,1145	0,0317	0,0456	0,0249	-0,0790	-0,0541	0,0790	-24,7908	-103,7247
Te69-O67(18)	0,1028	0,3345	0,0238	0,0541	-0,0943	-0,0402	0,0943	-29,5932	-123,8179
Te69-O70(19)	0,0763	0,2132	0,0466	0,0438	-0,0682	-0,0244	0,0682	-21,4018	-89,5451
Te69-O71(20)	0,1414	0,4855	0,0671	0,0659	-0,1300	-0,0641	0,1300	-40,7913	-170,6710
Te69-C72(21)	0,1173	0,0198	0,0421	0,0241	-0,0805	-0,0564	0,0805	-25,2626	-105,6988
Te83-O70(22)	0,1355	0,4760	0,0182	0,0683	-0,1288	-0,0605	0,1288	-40,4106	-169,0780
Te83-O84(23)	0,1313	0,4667	0,0050	0,0659	-0,1232	-0,0573	0,1232	-38,6574	-161,7426
Te83-C85(24)	0,1155	0,0385	0,0706	0,0251	-0,0800	-0,0549	0,0800	-25,0930	-104,9889
Te96-O84(25)	0,1025	0,3314	0,0185	0,0539	-0,0940	-0,0401	0,0940	-29,4952	-123,4081
Te96-O97(26)	0,0814	0,2278	0,0541	0,0454	-0,0731	-0,0277	0,0731	-22,9399	-95,9807
Te96-O98(27)	0,1375	0,4747	0,0765	0,0641	-0,1255	-0,0614	0,1255	-39,3858	-164,7900
Te96-C99(28)	0,1243	0,0426	0,0211	0,0261	-0,0880	-0,0619	0,0880	-27,5975	-115,4679
Te110-O97(29)	0,1290	0,4328	0,0378	0,0633	-0,1201	-0,0568	0,1201	-37,6748	-157,6315
Te110-O111(30)	0,1292	0,4448	0,0054	0,0639	-0,1204	-0,0565	0,1204	-37,7679	-158,0210
Te110-C112(31)	0,1157	0,0301	0,0481	0,0248	-0,0799	-0,0550	0,0799	-25,0569	-104,8383
Te123-O111(32)	0,1066	0,3350	0,0067	0,0535	-0,0964	-0,0429	0,0964	-30,2538	-126,5819
Te123-O124(33)	0,0723	0,2038	0,0543	0,0433	-0,0653	-0,0220	0,0653	-20,4877	-85,7205
Te123-O125(34)	0,1323	0,4426	0,0743	0,0607	-0,1190	-0,0584	0,1190	-37,3451	-156,2521
Te123-C126(35)	0,1183	0,0258	0,0206	0,0246	-0,0817	-0,0571	0,0817	-25,6455	-107,3006
Te137-O124(36)	0,1365	0,4578	0,0349	0,0651	-0,1267	-0,0616	0,1267	-39,7500	-166,3140
Te137-O138(37)	0,1103	0,3646	0,0208	0,0565	-0,1011	-0,0446	0,1011	-31,7119	-132,6825
Te137-C139(38)	0,1154	0,0241	0,0523	0,0249	-0,0798	-0,0549	0,0798	-25,0508	-104,8127
Te150-O138(39)	0,1370	0,4913	0,0262	0,0667	-0,1274	-0,0607	0,1274	-39,9708	-167,2380
Te150-O151(40)	0,1058	0,3237	0,0582	0,0519	-0,0944	-0,0424	0,0944	-29,6052	-123,8683
Te150-C152(41)	0,1165	0,0309	0,0614	0,0253	-0,0811	-0,0558	0,0811	-25,4341	-106,4162
Te163-O151(42)	0,1346	0,4643	0,0767	0,0634	-0,1231	-0,0597	0,1231	-38,6240	-161,6029
Te163-O3(43)	0,1129	0,3610	0,0419	0,0573	-0,1046	-0,0473	0,1046	-32,8101	-137,2776
Te163-C164(44)	0,1166	0,0272	0,0476	0,0243	-0,0801	-0,0558	0,0801	-25,1351	-105,1652

Te175-O17(45)	0,0915	0,2656	0,0865	0,0478	-0,0817	-0,0339	0,0817	-25,6342	-107,2533
Te175-O176(46)	0,0881	0,2535	0,0737	0,0477	-0,0796	-0,0319	0,0796	-24,9769	-104,5034
Te175-O241(47)	0,1242	0,4064	0,0931	0,0570	-0,1105	-0,0535	0,1105	-34,6767	-145,0874
Te175-C177(48)	0,1136	0,0088	0,0368	0,0227	-0,0759	-0,0533	0,0759	-23,8139	-99,6372
Te188-O176(49)	0,1348	0,4574	0,0766	0,0627	-0,1229	-0,0602	0,1229	-38,5676	-161,3667
Te188-O189(50)	0,0934	0,2782	0,0596	0,0492	-0,0843	-0,0351	0,0843	-26,4551	-110,6880
Te188-O44(51)	0,0899	0,2626	0,0680	0,0483	-0,0812	-0,0330	0,0812	-25,4880	-106,6416
Te188-C190(52)	0,1233	0,0428	0,0232	0,0253	-0,0862	-0,0609	0,0862	-27,0479	-113,1685
Te201-O189(53)	0,1421	0,4899	0,0695	0,0666	-0,1316	-0,0649	0,1316	-41,2813	-172,7209
Te201-O202(54)	0,0862	0,2537	0,0721	0,0471	-0,0776	-0,0305	0,0776	-24,3480	-101,8721
Te201-O71(55)	0,0885	0,2586	0,0657	0,0477	-0,0797	-0,0320	0,0797	-25,0095	-104,6398
Te201-C203(56)	0,1148	0,0211	0,0339	0,0234	-0,0775	-0,0541	0,0775	-24,3303	-101,7981
Te214-O202(57)	0,1425	0,4774	0,0649	0,0668	-0,1328	-0,0660	0,1328	-41,6658	-174,3296
Te214-O215(58)	0,0584	0,1584	0,0726	0,0364	-0,0503	-0,0139	0,0503	-15,7762	-66,0078
Te214-O(59)	0,1004	0,3053	0,0560	0,0506	-0,0898	-0,0392	0,0898	-28,1649	-117,8420
Te214-C216(60)	0,1179	0,0367	0,0343	0,0248	-0,0814	-0,0566	0,0814	-25,5546	-106,9203
Te240-O215(61)	0,0556	0,1454	0,0949	0,0346	-0,0471	-0,0124	0,0471	-14,7652	-61,7775
Te240-O241(62)	0,1095	0,3445	0,0620	0,0536	-0,0984	-0,0448	0,0984	-30,8699	-129,1598
Te240-228(63)	0,1343	0,4422	0,0723	0,0628	-0,1237	-0,0609	0,1237	-38,8050	-162,3603
Te240-C242(64)	0,1226	0,0368	0,0399	0,0255	-0,0860	-0,0605	0,0860	-26,9867	-112,9122
Te227-O215(65)	0,1381	0,4628	0,0702	0,0648	-0,1279	-0,0630	0,1279	-40,1220	-167,8705
Te227-O228(66)	0,0651	0,1706	0,0937	0,0387	-0,0566	-0,0179	0,0566	-17,7599	-74,3074
Te227-O125(67)	0,1020	0,3146	0,0600	0,0510	-0,0910	-0,0400	0,0910	-28,5412	-119,4165
Te227-C229(68)	0,1153	0,0216	0,0342	0,0238	-0,0785	-0,0547	0,0785	-24,6219	-103,0179

The topological analysis of electron densities at the bond critical points of these interactions show positive Laplacians, which is characteristic of electrostatic interactions. Low ellipticities are found for electron density distributions along the interaction paths, revealing the stability of these distributions. Further, the larger kinetic energy (G) contributions of these interactions result in positive total energies (H) that are characteristic of non-covalent interactions. The average energy of the interactions between the tellurium atoms with the iodine atoms of the external iodine ring is -13 KJ/mol, while it is -8 KJ/mol for the interactions with iodine atoms of the internal ring.
The Te-C and Te-O interactions are also characterized by (3.-1) bond critical points. However, the dominant contribution for these interactions is now the potential energy (V), leading to negative total energies (H). It is characteristic of metallic bonds, what should be expected for metal-ligand bonds formed in transition metal complexes. The average energies of these interactions are -119 KJ/mol and -138 KJ/mol for Te-C and Te-O, respectively.

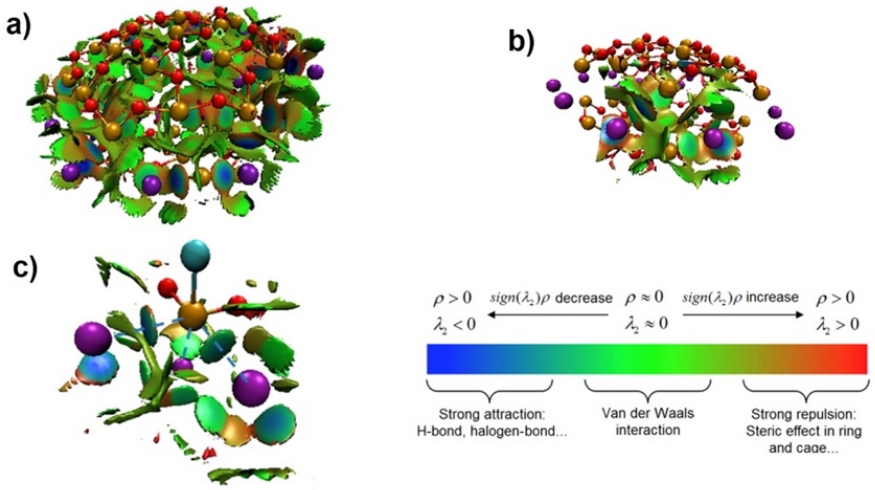

Fig. S13. a) Reduced density gradient a) total, b) only one tellurium region and c) pseudo-octahedral geometry of tellurium.

Figure S13a shows the reduced gradient density (RDG) surfaces for the non-covalent interactions between the iodine and tellurium atoms. The Figure reveals several van der Waals interactions (green color), and some strong interactions between the iodine and tellurion (blue regions).

4.3.Comparison between [{(PhTe)$_{19}$O$_{24}$}$_2$I$_{18}$] (1b) and [{(PhTe)$_{18}${Ca(H$_2$O)$_2$}O$_{24}$}$_2$I$_{16}$] (2)

4.3.1. Electron Localization and Delocalization in (1b) and (2)

The electron density in **1b** appears to be rather delocalized over the whole plane of iodine atoms since the Laplacian iso-lines between them in the Laplacian map rarely intersect. The delocalization appears to be more prominent than in the Ca-containing compound (*vide infra*). Figure S14 depicts a mapping of the Laplacian of the electron density (ED). In the inner iodine ring, there is an interaction between the six atoms indicated by (3,-1) critical points between them (orange). Nuclear position critical points (3,-3) are shown in brown. The iso-line shown in black resembles an iso density level of 0.001 and corresponds to the van der Waals radii of the atoms. It is evident, that the ED appears to be less fragmented compared to the Ca-containing compound as the major disturbance of the

Laplacian field is located in a regular hexagon in the center of the inner iodine ring. As a consequence, the ED is delocalized over a wider range of iodine atoms due to improved geometric restrains: the ELF map shows that the disturbance of the ED landscape by tellurium lone-pairs is insignificant in this compound. The deformation of the ELF indicates a delocalization between the iodine atoms in the inner and the outer ring. All iodine atoms are part of this delocalization. Generally, the electron density appears to be shared smooth and homogenous. The ground state HOMO and LUMO orbital also reflect this: the HOMO is delocalized over the six central iodine atoms of the inner ring, while the LUMO is spread over one whole telluroxane hemisphere. Details are shown in Figures S15 and S16.

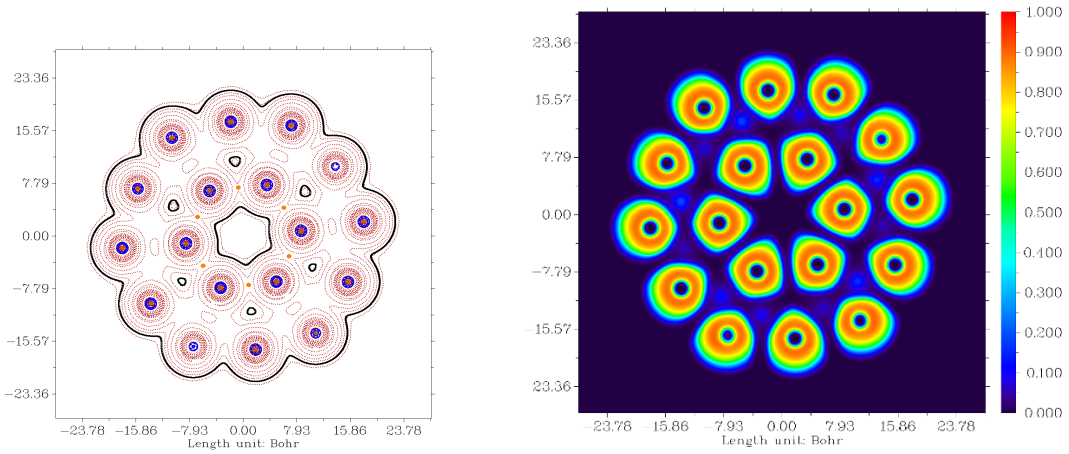

Fig. S14. Mapping of the Laplacian of the ED (left: positive = red, negative = blue) and the ELF (right) in [{(PhTe)$_{19}$O$_{24}$}$_2$I$_{18}$] (**1b**). Positive Laplacian values correspond to local charge depletion, negative values indicate local charge accumulation (areas, where the ED resides).

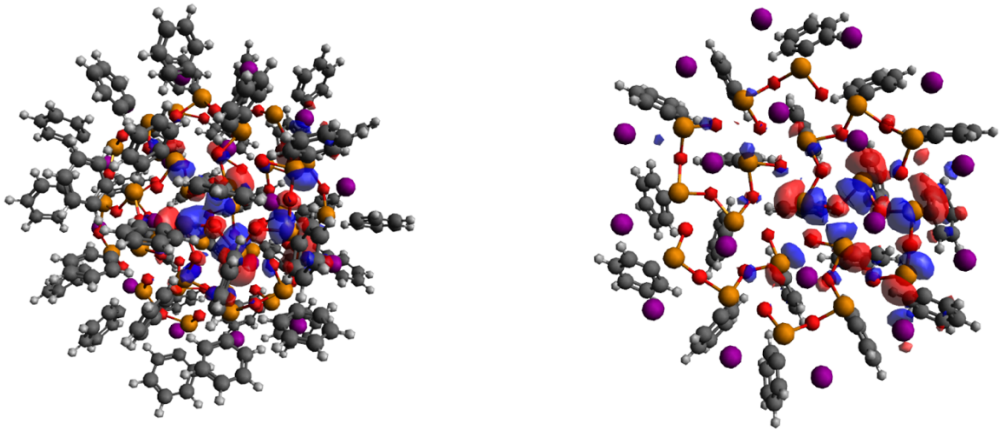

Fig. S15. Ring-shaped LUMO of the ground state of [{(PhTe)$_{19}$O$_{24}$}$_2$I$_{18}$] (**1b**) being localized at the tellurium and oxygen atoms of the inner and outer telluroxane rings of one half-shell.

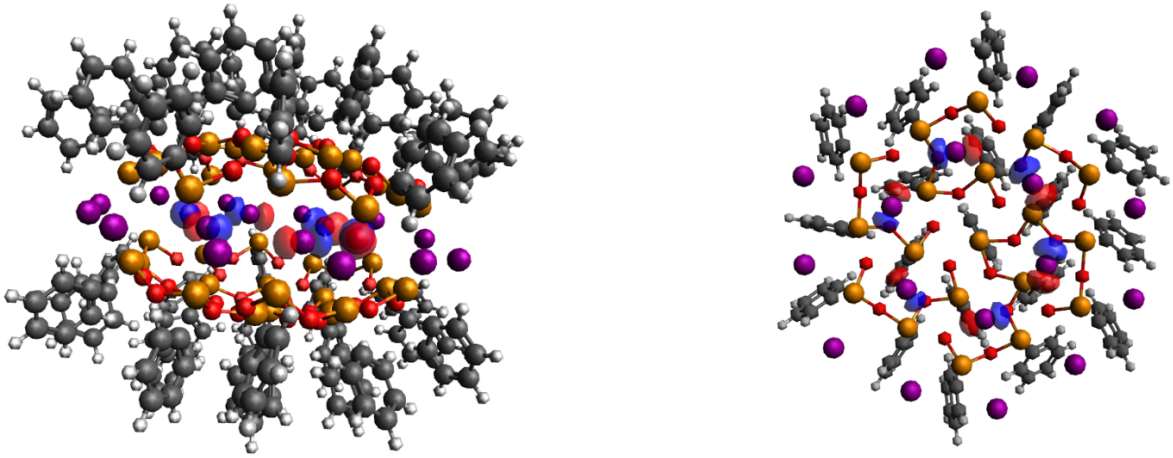

Fig. S16. Ring-shaped HOMO of the ground state of [{(PhTe)$_{19}$O$_{24}$}$_2$I$_{18}$] (**1b**) mainly localized at the six iodine atoms of the inner ring.

SUPPORTING INFORMATION

The electron density in [{(PhTe)$_{18}${Ca(H$_2$O)$_2$}O$_{24}$}$_2$I$_{16}$] (**2**) appears to be delocalized in the outer iodine ring as the Laplacian iso-lines are not intersecting the area between the outer ring iodine atoms. Additionally, only two of the inner ring iodine atoms participate. In the inner iodine ring, there are some interactions between the four iodine atoms indicated by (3,-1) critical points between them (orange).Critical points corresponding to nuclear positions (3,-3) are shown in brown. The iso-line shown in black resembles an iso density level of 0.001 and corresponds to the van der Waals radii of the atoms, revealing that there is nearly no free space in the middle of the iodine layer but four empty pockets disrupting the electron density between the iodine atoms in the iodine layer are clearly visible. The deformation of the ELF indicates a delocalization of the ED in the outer ring and a delocalization inside the central ring as has been observed for compound (**1b**). However, just as in the Laplacian map, the two rings exchange ED only via two iodine atoms with the central ring instead of all four. The remaining two iodine atoms of the inner ring are less involved as is also indicated by the Laplacian map (Fig. S17). The small blue dots between the iodine atoms of the outer ring that deform the ED towards less delocalization correspond to the free electron pairs at the terminal tellurium atoms, which indicates that the arrangement of the tellurium atoms affects the degree of delocalization not only in the telluroxane framework but also in the iodine layers.

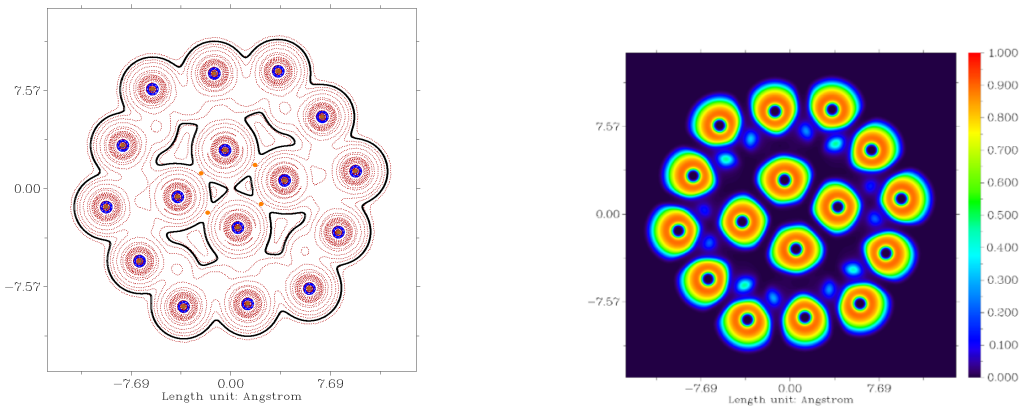

Fig. S17. Mapping of the Laplacian of the ED in [{(PhTe)$_{18}${Ca(H$_2$O)$_2$}O$_{24}$}$_2$I$_{16}$] (**2**) (left: positive = red, negative = blue) and the ELF (right). Positive Laplacian values correspond to local charge depletion, negative values indicate local charge accumulation (areas, where the ED resides).

Overall, these observations are also present in the structure of the corresponding HOMOs and LUMOs of [{(PhTe)$_{18}${Ca(H$_2$O)$_2$}O$_{24}$}$_2$I$_{16}$]. The HOMO in this compound is only localized on four neighboring and two additional, non-interacting, distant iodine atoms on the other side of the iodine plane. Thus, the HOMO is mainly localized in the outer iodine ring. The LUMO on the other hand resides on the tellurium-oxygen network and is mainly localized on the inner telluroxane ring. This situation is illustrated in Figures S18 and S19.

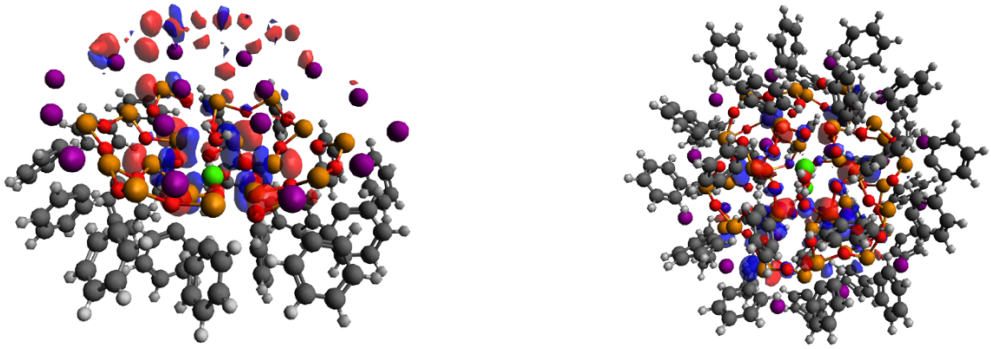

Fig. S18. Ring-shaped LUMO of the ground state of [{(PhTe)$_{18}${Ca(H$_2$O)$_2$}O$_{24}$}$_2$I$_{16}$] (**2**), being localized at the tellurium and oxygen atoms of the inner and outer telluroxane rings of one half-shell.

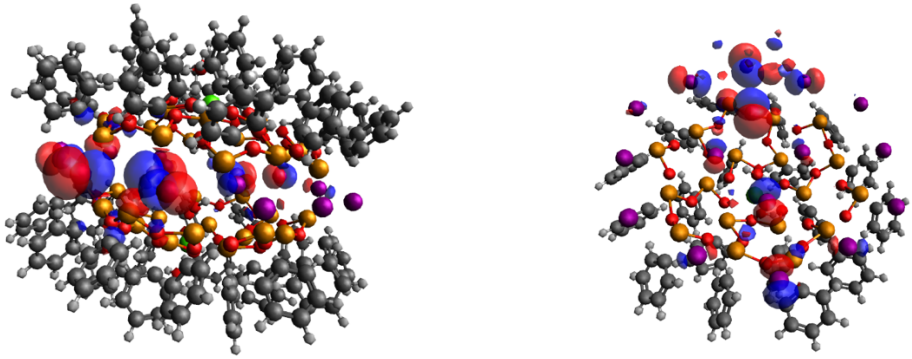

Fig. S19. Ring-shaped HOMO of the ground state of [{(PhTe)$_{18}${Ca(H$_2$O)$_2$}O$_{24}$}$_2$I$_{16}$] (**2**), being mainly localized at the six iodine atoms of the inner iodine ring.

4.3.2. UV/Vis spectra of [{(PhTe)$_{19}$O$_{24}$}$_2$I$_{18}$] (1b) and [{(PhTe)$_{18}${Ca(H$_2$O)$_2$}O$_{24}$}$_2$I$_{16}$] (2)

The main contributions within the visible absorption region of both complexes can be attributed to charge-transfer bands of iodine-centered p-orbitals into Te-O anti-bonding or Te-centered empty p-orbitals as can be concluded from the NTO calculations. Both compounds show a large degree of delocalization in their HOMO and LUMO orbitals. The degree of delocalization of the ground state LUMO is similar in both compounds. However, the ground state HOMO of [{(PhTe)$_{19}$O$_{24}$}$_2$I$_{18}$] (**1b**) is delocalized over the whole layer of iodine atoms. Contrarily, the HOMO of [{(PhTe)$_{18}${Ca(H$_2$O)$_2$}O$_{24}$}$_2$I$_{16}$] (**2**) is rather concentrated on the outer iodide ring, while the LUMO is still centered on the inner telluroxane ring. This potentially hinders the charge-transfer from iodide to the telluroxane resulting to even lower expected absorption coefficients.

Roughly two classes of transitions are visible in the simulated spectra of the two compounds: transitions with main contributions from the inner to the inner ring (or from the outer to the outer ring) and transitions with main contributions from the outer to the inner rings (or from the inner to the outer rings). This results in the two spectral bands in each spectrum (in one case a non-resolved shoulder is indicated) (Fig. S20).

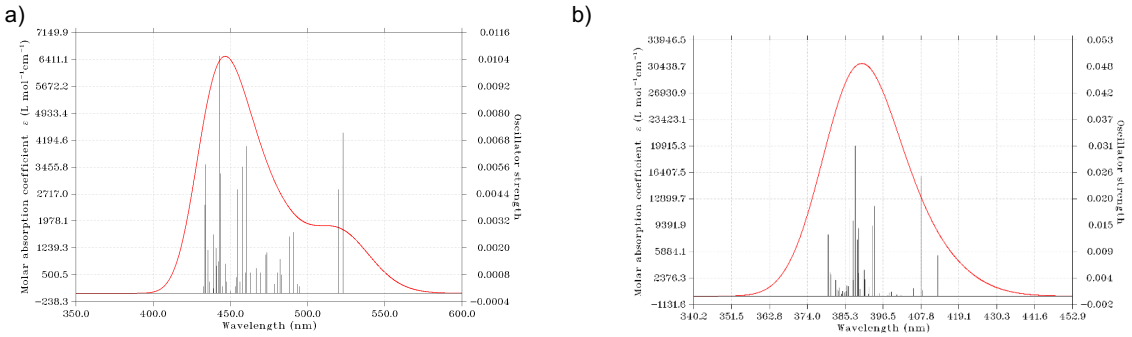

Fig. S20. Calculated UV/Vis spectra of [{(PhTe)$_{19}$O$_{24}$}$_2$I$_{18}$] (**1b**) and [{(PhTe)$_{18}${Ca(H$_2$O)$_2$}O$_{24}$}$_2$I$_{16}$] (**2**) with 0.2 eV halfwidth. N=40 transitions (black lines) were regarded for both compounds.

The overall more prominent delocalization of the electron density in [{(PhTe)$_{19}$O$_{24}$}$_2$I$_{18}$] (**1b**) results in smaller HOMO-LUMO gaps between the ground-state and the excited states compared to [{(PhTe)$_{18}${Ca(H$_2$O)$_2$}O$_{24}$}$_2$I$_{16}$] (**2**). Consequently, the HOMO and LUMO geometric arrangement and energy difference are much more favorable for the charge transfer compared to [{(PhTe)$_{18}${Ca(H$_2$O)$_2$}O$_{24}$}$_2$I$_{16}$] (**2**). This results in a shift of the corresponding absorption from the visible part of the spectrum into the near UV range, and can explain the fact that compound **2** appears almost colorless, while the compounds **1** with phenyltellurium-centered half-shells have a yellow-brown color.

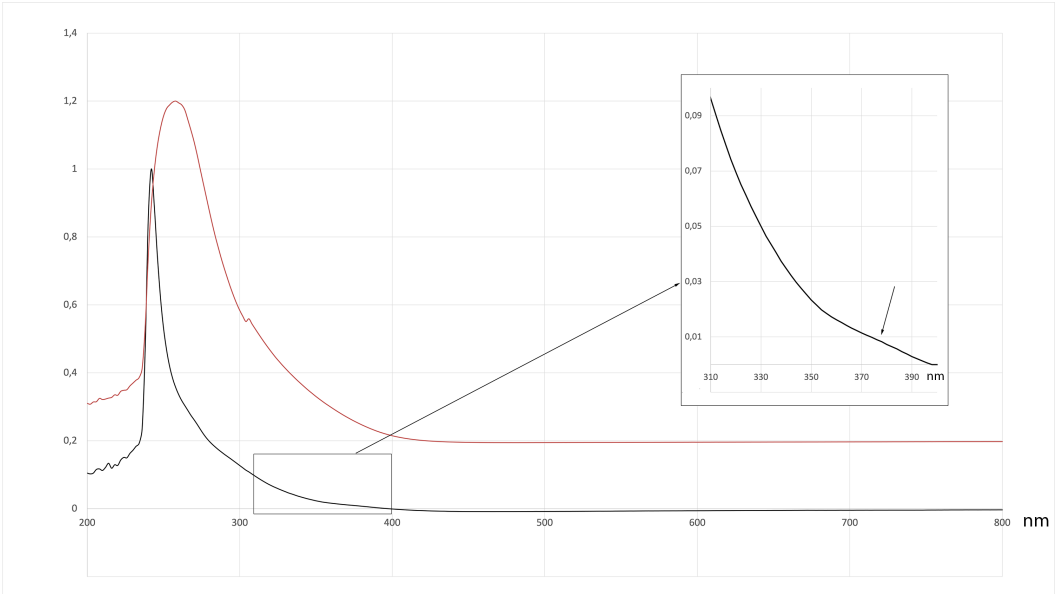

Fig. S21. Experimental UV/Vis spectra of [{(PhTe)$_{19}$O$_{24}$}$_2$I$_{18}$] (**1b**) (red) and [{(PhTe)$_{18}${Ca(H$_2$O)$_2$}O$_{24}$}$_2$I$_{16}$] (**2**) (black). Note the shoulder at approximately 380 nm, which corresponds to the calculated value (Fig. S13b). The corresponding band in the spectrum of **1b** is not resolved.

The calculated trend of the shift of the visible/near UV bands in the spectra of the telluroxane clusters when going from compounds **1** to the Ca^{2+}-centered compound **2** is also confirmed by the experimental spectra (Fig. S21). and may explain the unexpected 'decolorization' of the cluster when the central phenyltellurium building blocks are replaced by {Ca(H$_2$O)$_2$}$^{2+}$ units. Mainly contributing orbitals of of [{(PhTe)$_{19}$O$_{24}$}$_2$I$_{18}$] (**1b**) are shown in Figures S22 to S27, while the corresponding orbitals of [{(PhTe)$_{18}${Ca(H$_2$O)$_2$}O$_{24}$}$_2$I$_{16}$] (**2**) are illustrated in Figures S28 to S31.

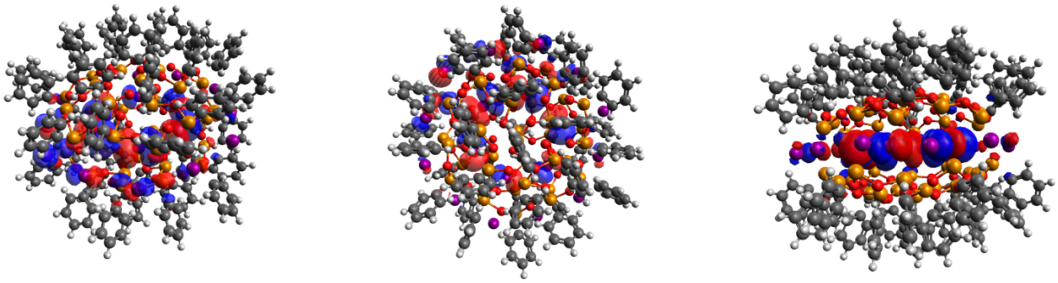

Fig. S22. HOMO of [{(PhTe)$_{19}$O$_{24}$}$_2$I$_{18}$] (**1b**) being involved in the 1st transition, corresponding to a major line of the line spectrum shown in Fig. S20a.

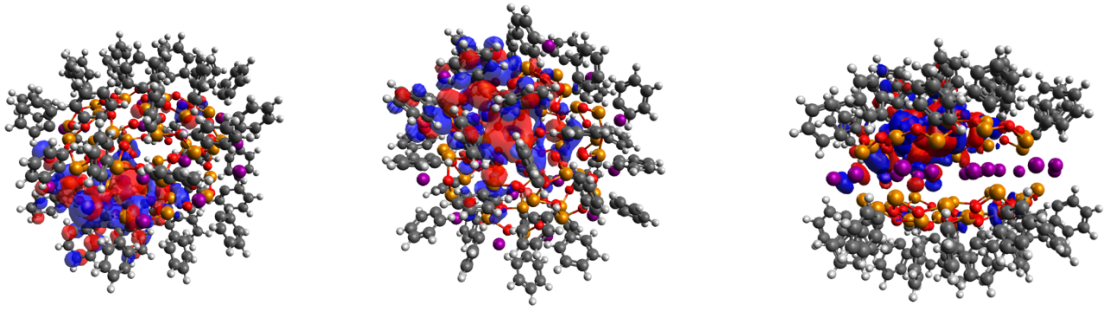

Fig. S23. LUMO of [{(PhTe)$_{19}$O$_{24}$}$_2$I$_{18}$] (**1b**) being involved in the 1st transition, corresponding to a major line of the line spectrum shown in Fig. S20a.

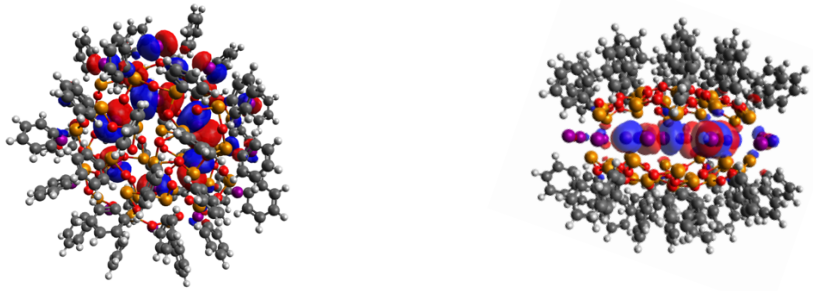

Fig. S24. HOMO of [{(PhTe)$_{19}$O$_{24}$}$_2$I$_{18}$] (**1b**) being involved in the 2nd transition, corresponding to a major line in the line spectrum shown in Fig. 20a.

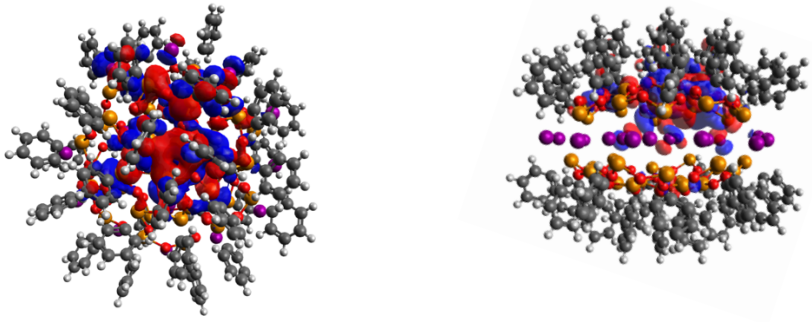

Fig. S25. LUMO of [{(PhTe)$_{19}$O$_{24}$}$_2$I$_{18}$] (**1b**) being involved in the 2nd transition, corresponding to a major line in the line spectrum shown in Fig. 20a.

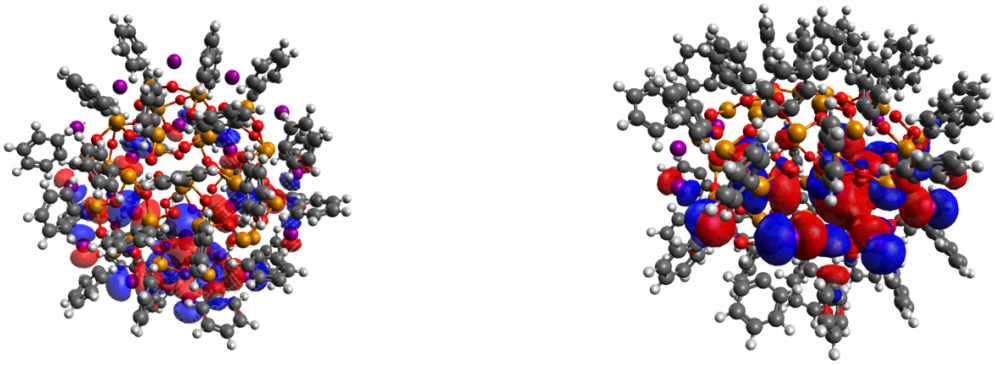

Fig. S26. HOMO of [{(PhTe)$_{19}$O$_{24}$}$_2$I$_{18}$] (**1b**) being involved in the 18th transition, corresponding to a major line in the line spectrum shown in Fig. S20a.

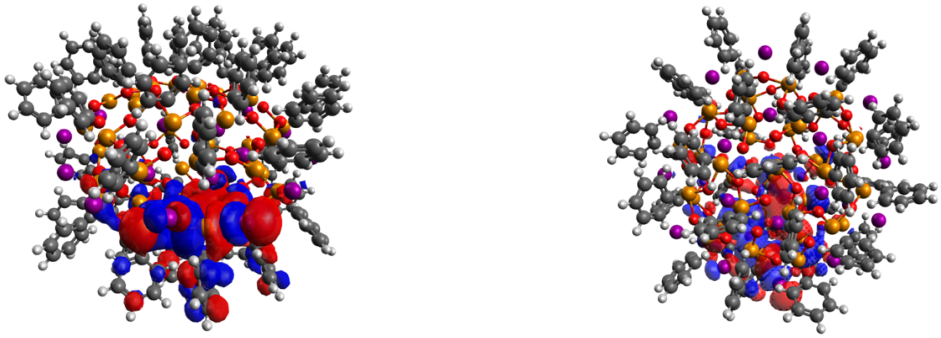

Fig. S27. LUMO of [{(PhTe)$_{19}$O$_{24}$}$_2$I$_{18}$] (**1b**) being involved in the 18th transition, corresponding to a major line in the line spectrum shown in Fig. S20a.

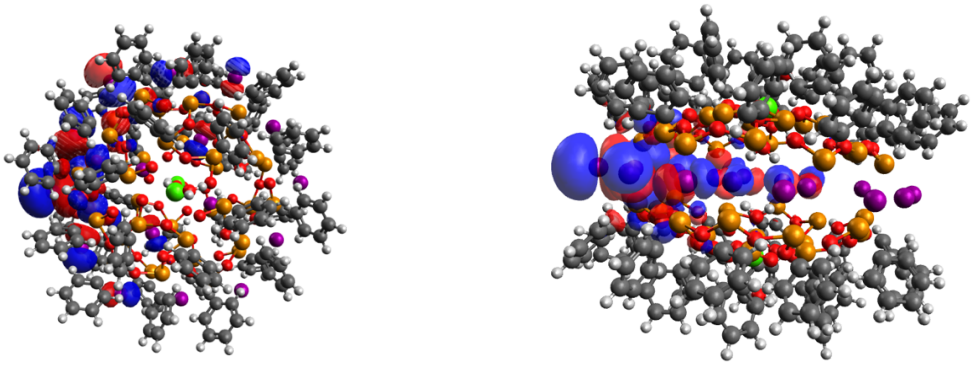

Fig.28. HOMO of [{(PhTe)$_{18}${Ca(H$_2$O)$_2$}O$_{24}$}$_2$I$_{16}$] being involved in the 14th transition, corresponding to a major line in the line spectrum shown in Fig. S20b.

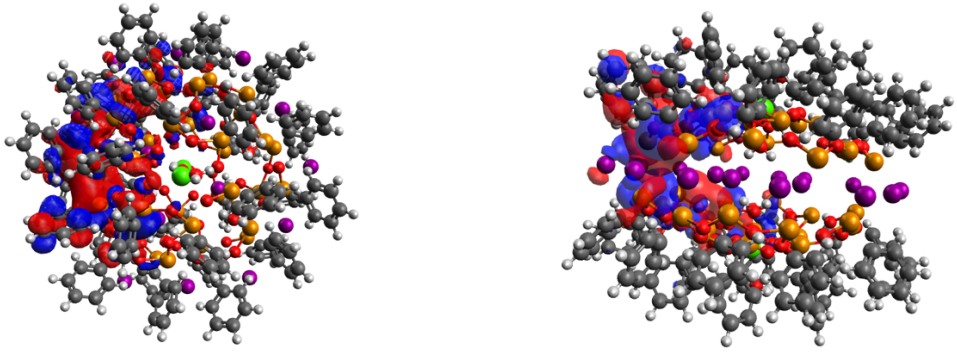

Fig. 29. LUMO of [{(PhTe)$_{18}${Ca(H$_2$O)$_2$}O$_{24}$}$_2$I$_{16}$] being involved in the 14th transition, corresponding to a major line in the line spectrum shown in Fig. S20b.

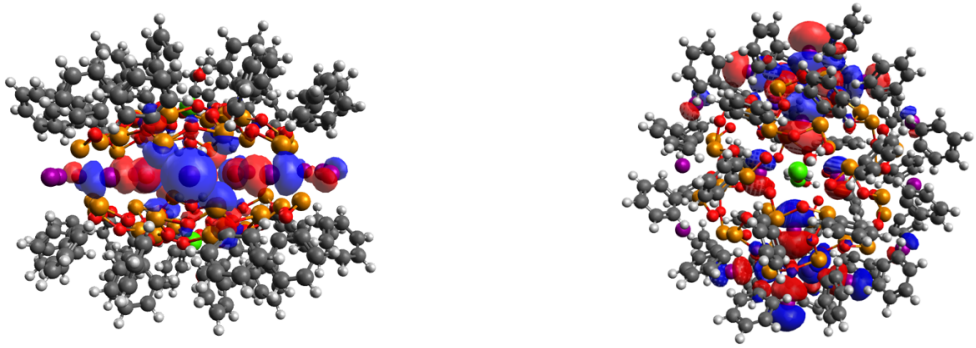

Fig. 30. HOMO of [{(PhTe)$_{18}${Ca(H$_2$O)$_2$}O$_{24}$}$_2$I$_{16}$] being involved in the 3rd transition, corresponding to a major line in the line spectrum shown in Fig. S20b.

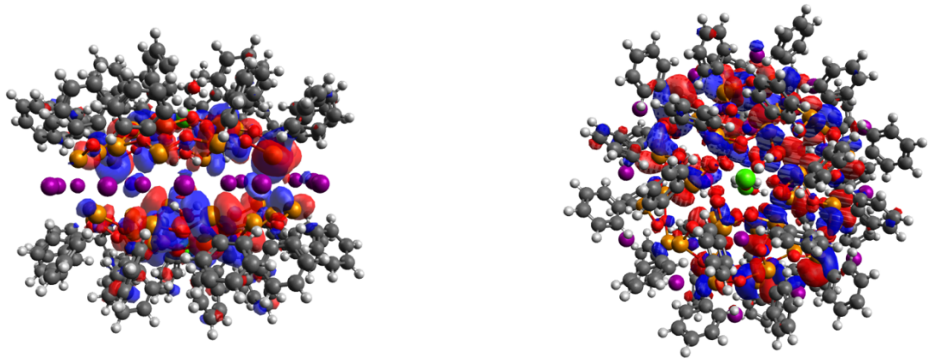

Fig. 31. LUMO of [{(PhTe)$_{18}${Ca(H$_2$O)$_2$}O$_{24}$}$_2$I$_{16}$] being involved in the 3rd transition, corresponding to a major line in the line spectrum shown in Fig. 20b.

4.4. Iodine-Hydrogen Interactions

An inspection of the X-ray diffraction data gives evidence for the formation of C-H….I hydrogen bonds between phenyl rings and iodine atoms of the outer ring (H…I distances between 2.9 and 2.1 Å) accompanied by weaker van der Waals interactions (H…I distances between 3.1 and 3.5 Å) in compounds **1** as well as in the metal-centered compounds **2** and **3**. Figure S32 illustrates this bonding situation for [{(PhTe)$_{19}$O$_{24}$}$_2$I$_{18}$] (**1b**). Additional weak interactions are established between adjacent clusters.

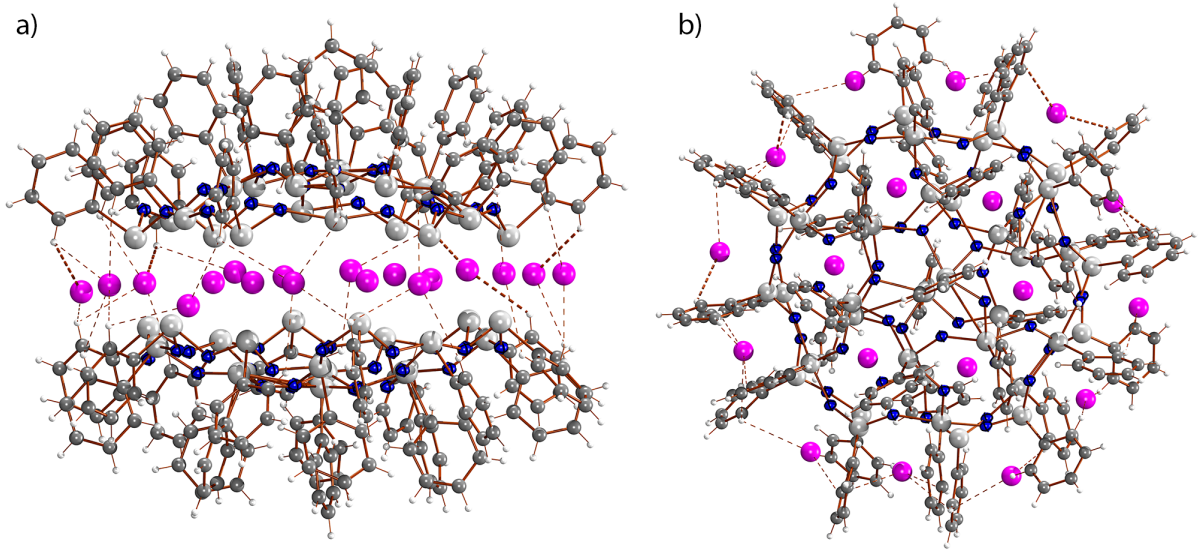

Fig. S32. a) Top view and b) side view of [{(PhTe)$_{19}$O$_{24}$}$_2$I$_{18}$] (**1b**) illustrating C-H…I interactions between the two telluroxane half-spheres and the central layer of iodine atoms. Thick dotted lines represent H…Te distances between 2.9 and 3.1 Å, thin dotted lines: 3.1 – 3.5 Å.

DFT calculations confirm the presence of attractive interactions by the detection of bond critical points between the outer ring iodine atoms and the *ortho*-protons of adjacent, outer phenyl groups of the telluroxane shells (Fig. S33). The phenyl tellurium units are tilted to accommodate such I···H interactions. No such interactions were found for the phenyl groups of the inner telluroxane rings.

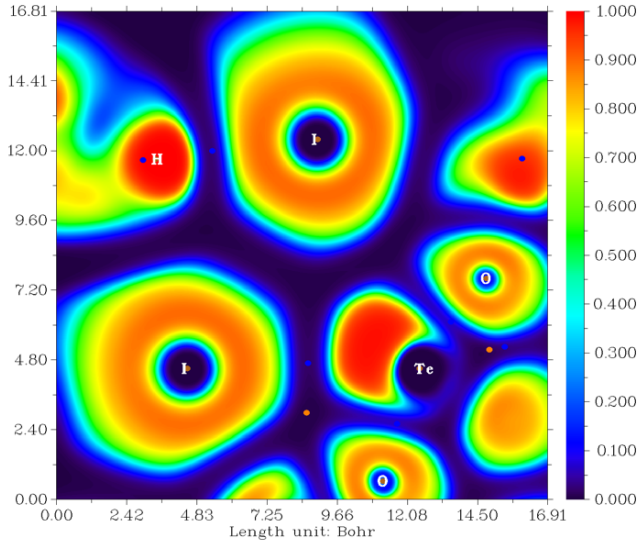

Fig. S33. ELF mapping with topological features enabled showing a bond critical point between an iodine atom of the outer iodine ring with an *ortho* protons of an outwards tilted phenyl tellurium unit in compound **1b**.

4.5. Symmetry Considerations

The symmetry of the complexes was assessed by using the program SHAPE to check symmetry relations between several potentially symmetry-connected tellurium and oxygen atoms.[17] Although the continuous shape measures for some separate parts of the compounds (e.g. the two inner tellurium rings in the non-calcium compound under neglection of the central non-symmetrical tellurium unit) indicate a distorted D_{6h} symmetry, the complexes do not show higher overall symmetry. In general we considered ideal structures for 12 vertex polyhedra (L12) with the corresponding point group symmetry: DP-12 dodecagon (D12h), HPY-12 hendecagonal pyramid (C11v), DBPY-12 decagonal bipyramid (D10h), HPR-12 hexagonal prism (D6h), HAPR-12 hexagonal antiprism (D6d), TT-12 truncated tetrahedron (Td), COC-12 cuboctahedron (Oh), ACOC-12 anticuboctahedron J27 (D3h), IC-12 icosahedron (Ih), JSC-12 Johnson square cupola J4 (C4v), JEPBPY-12 Johnson elongated pentagonal bipyramid J16 (D6h), JBAPPR-12 biaugmented pentagonal prism J53 (C2v), JSPMC-12 sphenomegacorona J88 (Cs).
Exemplarily, we provide in Table S6 the shape results for the 2 x 6 Te atoms and for the 2 x 6 O atoms of $[\{(PhTe)_{19}O_{24}\}_2I_{18}]$ (**1b**). It should be noted that the central tellurium atom, which is clearly situated apart from a potential symmetry center has been neglected. Nevertheless only low symmetric arrangements for the tellurium atoms could be found with Shape measures of 15 and larger. The arrangement of the oxygen atoms does not allow the assignment of any defined symmetry as all shape measures are at least 20.

Table S6. Results of the SHAPE analysis of $[\{(PhTe)_{19}O_{24}\}_2I_{18}]$ (**1b**).

Idealized Symmetry	Shape Measures for the 2 x 6 Te atoms	Shape Measures for the 2 x 6 O atoms
DP-12	34.06596	34.10939
HPY-12	28.9944	34.67684
DBPY-12	19.94072	31.19643
HPR-12	10.29372	22.30232
HAPR-12	14.01788	24.17939
TT-12	18.18921	3182371
COC-12	15.27656	29.85333
ACOC-12	14.56094	28.81741
IC-12	18.33491	31.95321
JSC-12	19.80717	26.45775
JEPBPY-12	19.80717	26.84524
JBAPPR-12	16.26094	27.08915
JSPMC-12	20.09786	26.35241

Also for compound **2** ($[\{(PhTe)_{18}\{Ca(H_2O)_2\}O_{24}\}_2I_{16}]$), for which a slightly higher crystallographic symmetry has been found, no defined cluster symmetry could be assigned. Shape measures of 11 and higher have been found by only considering the tellurium atoms. The corresponding results are summarized in Table S7.

Table S7. Results of the SHAPE analysis of [{$(PhTe)_{18}\{Ca(H_2O)_2\}O_{24}\}_2I_{16}$] (**2**).

Idealized Symmetry	Shape Measures for the 2 x 6 Te atoms
DP-12	34.41131
HPY-12	29.80747
DBPY-12	21.69781
HPR-12	11.83283
HAPR-12	14.83183
TT-12	19.37100
COC-12	16.86167
ACOC-12	15.74948
IC-12	19.59059
JSC-12	20.75132
JEPBPY-12	18.51887
JBAPPR-12	16.92545
JSPMC-12	20.24783

5. References

[1] L. Kirsten, Dissertation, FU Berlin, **2016**.

[2] H. J. Reich, M. L. Cohen, P. S. Clark, *Org. Synth.* **1979**, *59*, 141.

[3] G. M. Sheldrick, *Acta Cryst.* **2008***, A64*, 112.

[4] L. Spek, *Acta Cryst*. **2009**, *D65*, 148.

[5] X-RED32, A program for the absorption correction of reflection data, STOE & Cie GmbH, Darmstadt, Germany.

[6] G. M. Sheldrick, B. Blessing, Acta Cryst. 1995, A51, 33.

[7] M. J. Frisch, G. W. Trucks, H. B. Schlegel, G. E. Scuseria, M. A. Robb, J. R. Cheeseman, G. Scalmani, V. Barone, G. A. Petersson, H. Nakatsuji, X. Li, M. Caricato, A. V. Marenich, J. Bloino, B. G. Janesko, R. Gomperts, B. Mennucci, H. P. Hratchian, J. V. Ortiz, A. F. Izmaylov, J. L. Sonnenberg, D. Williams-Young, F. Ding, F. Lipparini, F. Egidi, J. Goings, B. Peng, A. Petrone, T. Henderson, D. Ranasinghe, V. G. Zakrzewski, J. Gao, N. Rega, G. Zheng, W. Liang, M. Hada, M. Ehara, K. Toyota, R. Fukuda, J. Hasegawa, M. Ishida, T. Nakajima, Y. Honda, O. Kitao, H. Nakai, T. Vreven, K. Throssell, J. A. Montgomery, Jr., J. E. Peralta, F. Ogliaro, M. J. Bearpark, J. J. Heyd, E. N. Brothers, K. N. Kudin, V. N. Staroverov, T. A. Keith, R. Kobayashi, J. Normand, K. Raghavachari, A. P. Rendell, J. C. Burant, S. S. Iyengar, J. Tomasi, M. Cossi, J. M. Millam, M. Klene, C. Adamo, R. Cammi, J. W. Ochterski, R. L. Martin, K. Morokuma, O. Farkas, J. B. Foresman, and D. J. Fox, Gaussian 16, Revision B.01, Gaussian, Inc., Wallingford CT, 2016.

[8] R. Dennington, T. A. Keith, J. M. Millam, GaussView, Version 6, Semichem Inc., Shawnee Mission, KS, 2016.

[9] M. D. Hanwell, D. E. Curtis, D. C. Lonie, T. Vandermeersch, E. Zurek, G. R. Hutchison; Avogadro: An open-source molecular builder and visualization tool. Version 1.2.0, and Avogadro: An advanced semantic chemical editor, visualization, and analysis platform" *J. Cheminformatics* **2012**, *4*, 17.

[10] J. S. Binkley, J. A. Pople, W. J. Hehre, *J. Am. Chem. Soc.* **1980**, *102*, 939.

[11] T. H. Dunning, P. J. Hay, Gaussian basis sets for molecular calculations in 'Methods of Electronic Structure Theory' ed. Henry F. Schaefer, *Modern Theoretical Chemistry*, **1977**, *3*, 1.

[12] P. J. Hay, W. R. Wadt, *J. Chem. Phys.* **1985**, *82*, 299.

[13] W. R. Wadt, P. J. Hay, *J. Chem. Phys.* **1985**, *82*, 284.

[14] C. E. Check, T. O. Faust, J. M. Bailey, B. J. Wright, T. M. Gilbert, L. S. Sunderlin, *J. Phys. Chem. A*, **2001**, *105*, 8111.

[15] B. P. Pritchard, D. Altarawy, B. Didier, T. D. Gibsom, T. L. Windus, *J. Chem. Inf. Model.* **2019**, *59*, 4814.

[16] D. Feller, J. Comput. Chem. 1996 17, 1571

[17] K. L. Schuchardt, B. T. Didier, T. Elsethagen, L. Sun, V. Gurumoorthi, J. Chase, J. Li, T. L. Windus, J. Chem. Inf. Model. 2007, 47, 1045.

[18] T. Lu, F. Chen*, J. Comput. Chem.*, **2012**, *33*, 580.

[19] (a) M. Llunell, D. Casanova, J. Cirera, P. Alemany, S. Alvarez, *SHAPE Program for the Stereochemical Analysis of Molecular Fragments by Means of Continuous Shape Measures and Associated Tools*. **2013**, version 2.1. (b) M. Pinsky, D. Avnir, *Inorg. Chem.* **1998**, *37*, 5575. (c) D. Casanova, J. Cirera, M. Llunell, P. Alemany, D. Avnir, S. Alvarez, *J. Am. Chem. Soc*. **2004**, *126*, 1755. (d) J. Cirera, E. Ruiz, S. Alvarez, *Chem. Eur. J.* **2006**, *12*, 3162.

5. Author Contributions

L. Kirsten developed the syntheses of compounds **1** and **2** and performed the spectroscopic measurements on these compounds. J. Fonseca synthesized compounds **3**, **4**, **5** and **6** and performed the spectroscopic measurements on these compounds. A. Hagenbach is the crystallographer, who did the corresponding measurements, data treatments and calculations. A. Springer contributed the acquisition, analysis and interpretation of the mass spectra. P. C. Piquini, N. R. Pineda and M. Roca Jungfer performed the DFT calculations. E. Schulz Lang and U. Abram developed the concept of the project, supervised the work and wrote the manuscript.